



UNIVERSITY OF
PLYMOUTH



Other Faculty of Science and Engineering Theses
Faculty of Science and Engineering Theses

2015

The development of microfluidic based processes

Stephen John Haswell

Let us know how access to this document benefits you

General rights

All content in PEARL is protected by copyright law. Author manuscripts are made available in accordance with publisher policies. Please cite only the published version using the details provided on the item record or document. In the absence of an open licence (e.g. Creative Commons), permissions for further reuse of content should be sought from the publisher or author.

Take down policy

If you believe that this document breaches copyright please [contact the library](#) providing details, and we will remove access to the work immediately and investigate your claim.

Follow this and additional works at: <https://pearl.plymouth.ac.uk/fose-theses-other>

Recommended Citation

Haswell, S. (2015) *The development of microfluidic based processes*. Thesis. University of Plymouth.

Retrieved from <https://pearl.plymouth.ac.uk/fose-theses-other/61>

This Thesis is brought to you for free and open access by the Faculty of Science and Engineering Theses at PEARL. It has been accepted for inclusion in Other Faculty of Science and Engineering Theses by an authorized administrator of PEARL. For more information, please contact openresearch@plymouth.ac.uk.



UNIVERSITY OF
PLYMOUTH

PEARL

PHD

The development of microfluidic based processes

Haswell, Stephen John

Award date:
2015

Awarding institution:
University of Plymouth

[Link to publication in PEARL](#)

All content in PEARL is protected by copyright law.

The author assigns certain rights to the University of Plymouth including the right to make the thesis accessible and discoverable via the British Library's Electronic Thesis Online Service (EThOS) and the University research repository (PEARL), and to undertake activities to migrate, preserve and maintain the medium, format and integrity of the deposited file for future discovery and use.

Copyright and Moral rights arising from original work in this thesis and (where relevant), any accompanying data, rests with the Author unless stated otherwise*.

Re-use of the work is allowed under fair dealing exceptions outlined in the Copyright, Designs and Patents Act 1988 (amended), and the terms of the copyright licence assigned to the thesis by the Author.

In practice, and unless the copyright licence assigned by the author allows for more permissive use, this means,

That any content or accompanying data cannot be extensively quoted, reproduced or changed without the written permission of the author / rights holder

That the work in whole or part may not be sold commercially in any format or medium without the written permission of the author / rights holder

* Any third-party copyright material in this thesis remains the property of the original owner. Such third-party copyright work included in the thesis will be clearly marked and attributed, and the original licence under which it was released will be specified. This material is not covered by the licence or terms assigned to the wider thesis and must be used in accordance with the original licence; or separate permission must be sought from the copyright holder.

The development of microfluidic based processes

By

Haswell S.J

A thesis and collection of works submitted to Plymouth University in partial fulfilment for the degree of

DOCTOR OF SCIENCE

Faculty of Science and Technology

July 2014

This thesis and copy of collected works has been supplied on condition that anyone who consults it is understood to recognise that its copyright rests with the author and that no quotation from the thesis and no information derived from it may be published without the author's prior consent.

Author's Declaration

At no time during the registration for the degree of Doctor of Science has the author been registered for any other University award without prior agreement of the Graduate Committee.

Work submitted for this research degree at Plymouth University has not formed part of any other degree, either at Plymouth University or at any other establishment.

A handwritten signature in black ink that reads "Stephen Haswell". The signature is written in a cursive style with a large initial 'S'.

Stephen John Haswell

10th July 2014

Acknowledgements

The collection of works presented here was only possible through the dedication and support of a great many talented and dedicated researchers, working for me, with me and around me, over the past twenty years. It to all these wonderful students and colleagues I must say thank you.

Contents

	Pages
Nature and significance of the submitted work	1-4
The candidate's contribution to the research and nature of joint work.	5-31
List of peer reviewed published papers	32-44
Copies of submitted papers	Appendix 1

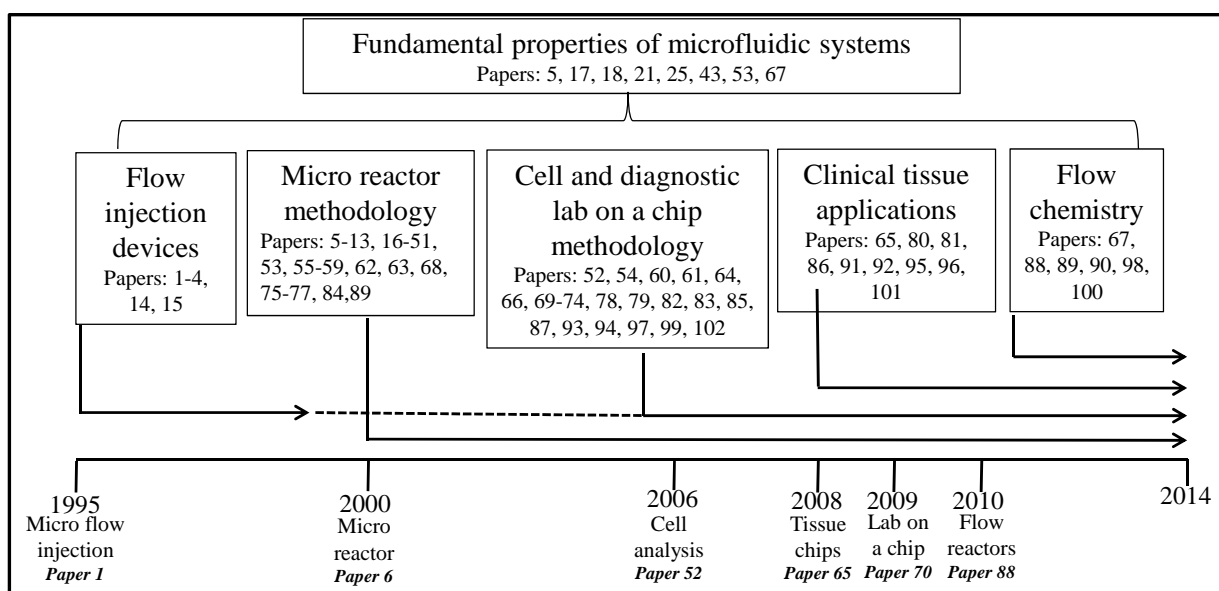
Nature and significance of the submitted work

Introduction

The work submitted for consideration of the award of a DSc represents a large sub section (102 of 210 published papers) of the candidates (Haswell) sustained research over a period of 20 years in the field of micro fluidic based processes. The candidate became aware of the potential of the field of research in 1986, when developing gas sensors, through the paper by Terry et al. published in IEEE Trans. Electron. Devices in 1979, in which the authors described a fully operational gas chromatography instrument produced on a silicon wafer using photolithographic and wet etching methodology. In the late 1980's the candidate adapted the work of Terry to produce etched patterned glass substrates which were used to develop a microfluidic flow injection device for determining orthophosphate based on electroosmotic pumping. This work represented one of the first analytical devices of its type to be reported in the literature (paper 1). Internationally, work in the field had been developing since the 1989 Transducers Conference where the term micro Total Analytical System was first used and by 1995 was concentrated in five centres based in Europe (Basel Switzerland, Twente The Netherlands) and North America (Berkeley California, Oak Ridge Tennessee, Alberta). In addition to analytical methodology, groups in Europe (Mainz Germany) and North America (MIT USA) were also exploring the generation of metal based micro reactor systems. The candidate attended and presented work at both the first micro total analytical systems conference in 1994 held in The Netherlands and the first International Conference on Microreaction Technology (IMRET) held in Frankfurt Germany in 1997. It is from this base the candidate established over a period of two decades an internationally recognized research activity in the field of microfluidics and lab on a chip technology.

Commentary

The figure below shows the research time line for the candidate's work which identifies five main areas of activity underpinned by a number of publications that address the more fundamental science associated with the research. Key milestone publications for each of the areas of research are also identified below on the time line.



The initial research into performing chemical reactions in a microfluidic device was based on analytical colorimetric analysis for phosphate (papers 1, 2,) and nitrite/nitrate (papers 4, 14) which together with a good review of the relevant literature (paper 2) established the practical and scientific platforms on which electrokinetic and hydrodynamic driven microfluidic research was established. The methodology used glass based devices as these offered chemical compatibility and good optical detection and were initially used to identify the operational characteristic of reactions performed in the absence of a large bulk solvent under continuous flow conditions. The results from these early fundamental studies are summarised in paper 21, which made a significant contribution in identifying and characterising the spatial and temporal control of reagents under a non-turbulent, diffusion limited mixing regime within reactor channels. Of the 79 cited references presented in paper 21, 30% came from the candidate's research with others (Jensen USA, Eherfeld Germany) contributing to define the fundamental operational criteria of micro reactor devices. This seminal paper which was directed at synthetic chemists has received 355 citations to date and has been instrumental in setting the research agenda in the field. The presence of industrial co-authors Pombo-Villar (Novartis Switzerland), Warrington and Wong (GSK UK) on this paper reflect the high level of industrial interest in the technology at the time and the subsequent investment made in the ongoing research. Many of the 58 papers published by the candidate in the field of micro reactors were the first to report chemical selectivity through the application of electrokinetic (papers 10, 16, 18, 25, 31, 39, 43, 46, 58) and hydrostatic flow gradients (papers 8, 17), paper 36 in particular describes a very elegant example of how localised concentrations gradients, accessed through flow

rate control, can be used to achieve stereo selective products. This is something of a holy grail for synthetic chemists and the work attracted considerable interest and funding from the pharmaceutical industry where product purity and selectivity are paramount. In addition the candidate's research reported early work for the immobilization of catalysts such as Pd, Pt, sulphated zirconia, zeolites and enzymes (papers 6, 34, 38, 41, 51, 75, 77), controlled microwave heating (papers 34, 37, 45), electro-synthesis (papers 47, 50, 57) and the monitoring of reactants and products (papers 30, 77, 100). A range of chemical reaction types were also reported for the first time in micro reactors and demonstrate the advantages meso/micro flow reactors in terms of stereo selective product control (paper 59), multi-step synthesis (paper 56) and *in situ* separations (paper 31). The 12 invited reviews and feature articles, many of which contain novel experimental results, serve also to summarise the impact of the candidate's research in the field (papers 2, 7, 12, 21, 27, 28, 29, 35, 40, 42, 44, 49) and demonstrated the relevance of the methodology to combinatorial, drug discovery and clean chemistry.

Based on the micro reactor experience gained by the candidate, research into using silica monolithic structures which offered favourable flow through characteristic (i.e. high flow rates with low backpressures) whilst maintaining the short diffusional distances and laminar flow properties, opened up the wider field of flow chemistry. The candidate was instrumental in describing the relationship between fabrication methodology and functional characteristics of silica monoliths (paper 90) and demonstrated how the cross-sectional area could be effectively be used to scale up reaction volumes without losing the intrinsic reaction properties of the micron scale environment (paper 88). In addition the research demonstrated that through the incorporation of on-line monitoring and feedback flow control the kinetics of reactions could be determined and product yield optimised (paper 100).

The concept of combining synthesis and biological screening into one device, introduced in paper 21, represented the early beginnings of research which eventually lead the candidate to establish research in the field of lab on a chip methodology. This early work focused mainly on cell based processing (papers 64, 66, 78, 87) and eventually generated an integrated microfluidic cell screening device for drug candidates synthesised in micro reactors (papers 52, 61). The lab on a chip idea was further developed by the candidate for a number of DNA based applications (papers 70

– 72, 74, 71, 79, 83, 93, 94, 102) which described leading work in the area of the real world to chip interface where the volumetric change is typically many orders of magnitude and matrix effects can be highly significant (papers 70, 72, 74, 83, 93, 94, 99). This body of work clearly demonstrated that the design of a real-world interface must be an integral component of the microfluidic device and requires a high degree of functionality to deal with sample/matrix type and downstream processing if the full potential of the technology is to be realised. Much of the candidate's research in the field of lab on a chip based technology for medical diagnostic application is reviewed in paper 85.

From experience gained from earlier cell based processing the candidate established collaborations with clinical colleagues to develop microfluidic based devices that would bio-mimic the fluidic transfer processes in living organisms. The first of such methodology was reported in paper 65 and lead to a number of studies which culminated in clinicians being able to design drug treatment regimens for cancer treatment at an individual level (papers 95, 101). A summary of the candidate research in this field and the potential clinical relevance for research and treatment is presented in paper 86.

The candidate's contribution to the research and nature of joint work

It is customary that publications in the field of chemical science appear with multiple authors who may include research students, academic colleagues and industry collaborators. Consequently, the quantitative contributions attributable to individual authors on each paper cannot be equitably determined and as such can only be shared amongst those named in each paper. However, the academic leadership, provision of funding and intellectual contribution has been predominantly that of the candidate. Notable exceptions are papers 41, 62, 69 and 82 where the candidate has collaborated in providing know-how rather than scientific leadership.

For clarification in this matter a statement of the originators of the published work, source of funding and role of associated authors is summarised for each submitted paper. Where the work involves PhD students the results reported may have been included in their thesis.

1. Daykin, R.N.C., and Haswell, S.J., Development of a micro flow injection manifold for the determination of orthophosphate, *Anal. Chim. Acta*, 1995, 313, 155-159.

Originator(s) of the published work: *Haswell*

Source of funding: *The Parliament of the Channel Islands – Haswell PI*

Role of associated authors: *Daykin undertook practical experiments as a PhD student supervised by Haswell.*

2. Haswell, S.J., Development and operating characteristics of micro flow injection analysis systems based on electroosmotic flow: A review, *Analyst*. 1997, 122, 1R-10R.

Originator(s) of the published work: *Haswell.*

3. Doku, G.N and Haswell, S.J., Further studies into the development of micro-FIA (μ FIA) system based on electroosmotic flow for the determination of phosphate as orthophosphate, *Anal. Chim. Acta*, 1999, 382. 1-13.

Originator(s) of the published work: *Haswell*

Source of funding: *Commonwealth Studentship*

Role of associated authors: *Doku undertook practical experiments as a PhD student supervised by Haswell.*

4. Greenway, G.M. Haswell S.J. and Petsul, P. H., Characterisation of a micro-total analytical system for the determination of nitrite with spectrophotometric detection, *Anal. Chim. Acta*, 1999, 387, 1-10.

Originator(s) of the published work: *Haswell*

Source of funding: *Government of Papua New Guinea – Haswell PI*

Role of associated authors: *Petsul undertook practical experiments as a PhD student co-supervised by Haswell and Greenway.*

5. Fletcher, P.D.I., Haswell, S.J. and Paunov, V.N., Theoretical considerations of chemical reactions in micro reactors operating under electrophoretic control, *Analyst*, 1999, 124, 1273-1282.

Originator(s) of the published work: *Haswell and Fletcher (75/25%)*

Role of associated authors: *Fletcher contributed knowledge on electrochemical and surface aspects of the paper and Paunov on the fundamentals of surface reactivity.*

6. Greenway, G.M., Haswell, S.J., Morgan, D.O., Skelton, V. and Styring, P, The use of novel micro reactors for high throughput continuous flow organic synthesis, *Sensors and Actuators B*, 2000, 63, 153-158.

Originator(s) of the published work: *Haswell*

Source of funding: *EPSRC - Glaxo SmithKline CASE studentship Haswell PI*

Role of associated authors: *Skelton undertook practical experiments as a PhD student co-supervised by Haswell and Greenway, Styring advised on the organic chemistry and Morgan was the industrial collaborator.*

7. Haswell, S.J. and Skelton, V., Chemical and biochemical micro reactors, *Trends in Anal. Chem.* 2000, 19, 389-395.

Originator(s) of the published work: *Haswell*

Source of funding: *EPSRC - Glaxo SmithKline CASE studentship - Haswell PI*

Role of associated authors: *Skelton co-authored this review as a PhD student.*

8. Haswell, S.J., O'Sullivan, B. and Styring, P., Kumada-Corriu reactions in a pressure-driven micro flow reactor, *Lab on a chip*, 2001, 1, 164-166.

Originator(s) of the published work: *Haswell*
Source of funding: *EPSRC – Grant GR/M73002 - Haswell PI*
Role of associated authors: *O’Sullivan undertook practical experiments as a post-doctoral research fellow supervised by Haswell, Styring advised on the organic chemistry.*

9. Doku, G.N., Haswell, S. J., McCreedy, T. and Greenway, G.M., Electric-field induced mobilisation of multiphase solution systems based on the nitration of benzene in a micro reactor, *Analyst*, 2001, 126, 14-20.

Originator(s) of the published work: *Haswell*
Source of funding: *Commonwealth Studentship – Haswell PI*
Role of associated authors: *Doku undertook practical experiments as a PhD student co-supervised by Haswell and McCreedy*

10. Skelton, V., Greenway, G.M., Haswell, S.J, Styring, P., Morgan, D.O., Warrington, B.H. and Wong, S., The generation of concentration gradients using electroosmotic flow in micro reactors allowing stereo-selectivity in chemical synthesis, *Analyst*, 2001, 126, 11-13.

Originator(s) of the published work: *Haswell*
Source of funding: *EPSRC - Glaxo SmithKline CASE studentship Haswell PI*
Role of associated authors: *Skelton undertook practical experiments as a PhD student co-supervised by Haswell and Greenway, Styring advised on the organic chemistry and Morgan, Warrington and Wong were the industrial collaborators.*

11. Skelton, V., Greenway, G.M., Haswell, S.J, Styring, P., Morgan, D.O., Warrington, B.H. and Wong, S., The preparation of a series of nitrostilbene ester compounds using micro reactor technology, *Analyst*, . 2001, 126, 7-10.

Originator(s) of the published work: *Haswell and Warrington (80/20%)*
Source of funding: *EPSRC - Glaxo SmithKline CASE studentship Haswell PI*
Role of associated authors: *Skelton undertook practical experiments as a PhD student co-supervised by Haswell and Greenway, Styring advised on the organic chemistry and Morgan, Warrington and Wong were the industrial collaborators.*

12. Haswell, S.J., Middleton, R.J., O'Sullivan, B., Skelton, V., Watts, P. and Styring, P., The application of micro reactors to synthetic chemistry, Chem. Comm., 2001, 391-398.

Originator(s) of the published work: *Haswell*

Source of funding: *EPSRC – Grant GR/M73002, and Glaxo SmithKline and Novartis - Haswell PI*

Role of associated authors: *This was a review co-authored by Skelton, O'Sullivan, Watts and Middleton post-doctoral research fellows supervised by Haswell, Styring advised on the organic chemistry.*

13. Watts, P., Wiles, C., S.J. Haswell, Pombo-Villar, E. and Styring, P., The synthesis of peptides using micro reactors, Chem. Comm., 2001, 990-991.

Originator(s) of the published work: *Haswell*

Source of funding: *Novartis - Haswell PI*

Role of associated authors: *Experimental work was carried out by Watts a post-doctoral research fellows supervised by Haswell, supported by Wiles a PhD student supervised by Haswell and Styring, Pombo-Villar was the industrial collaborator.*

14. Petsul, P.H., Greenway, G.M. and Haswell, S.J., The development of an on-chip micro flow injection analysis of nitrate with a cadmium reductor, Anal. Chim. Acta, 2001, 428, 155-161.

Originator(s) of the published work: *Haswell*

Source of funding: *Government of Papua New Guinea*

Role of associated authors: *Petsul undertook practical experiments as a PhD student co-supervised by Haswell and Greenway.*

15. Doku, G.N., Haswell, S.J., McCreedy, T. and Middleton, R.J., Preliminary studies into the direct interfacing of a microreactor to a gas chromatographic instrument, Analyst, 2001, 126, 133-135.

Originator(s) of the published work: *Haswell*

Source of funding: *Commonwealth Studentship – Haswell PI*

Role of associated authors: *Doku undertook practical experiments as a PhD student co-supervised by Haswell and McCreedy, assisted by Middleton a post-doctoral research fellow supervised by Haswell.*

16. Sands, M., Haswell, S.J., Kelly, S.M., Skelton, V., Morgan, D.O., Styring P. and Warrington, B., The investigation of an equilibrium dependent reaction for the formation of enamines in a microchemical system, *Lab on a chip*, 2001, 1, 64-65.

Originator(s) of the published work: *Haswell and Styring (50/50%)*

Source of funding: *EPSRC - Glaxo SmithKline CASE studentship Haswell PI*

Role of associated authors: *Sands undertook practical experiments as a PhD student co-supervised by Haswell and Styring, Skelton supported the work as a post-doctoral research fellow supervised by Haswell, Kelly advised on the reaction chemistry and Morgan and Warrington were the industrial collaborators.*

17. Broadwell, I., Fletcher, P.D.I., Haswell, S.J., McCreedy, T. and Zhang, X., Quantitative 3-dimensional profiling of channel networks within transparent 'lab-on-a-chip' micro reactors using a digital imaging method, *Lab on a Chip*, 2001, 1, 66-71.

Originator(s) of the published work: *Haswell and Fletcher (75/25%)*

Source of funding: *EPSRC – Grant GR/M74429 and Institute of Applied Catalysis - Haswell PI*

Role of associated authors: *Broadwell undertook practical experiments as a PhD student co-supervised by Haswell and Fletcher, Zhang supported the work as a post-doctoral research fellow supervised by Haswell, McCreedy advised on fabrication.*

18. Fletcher, P.D.I., Haswell, S.J. and Zhang, X.L., Electrical currents and liquid flow rates in micro reactors, *Lab on a chip*, 2001, 1, 115-121.

Originator(s) of the published work: *Haswell and Fletcher (75/25%)*

Source of funding: *EPSRC – Grant GR/M74429 - Haswell PI*

Role of associated authors: *Zhang undertook practical experiments as a post-doctoral research fellow supervised by Haswell, Fletcher advised on methodology.*

19. Wiles, C., Watts, P., Haswell, S.J. and Pombo-Villar, E., The aldol reaction of silyl enol ethers within a micro reactor, *Lab on a chip*, 2001, 1, 100-101.

Originator(s) of the published work: *Haswell*

Source of funding: *Novartis - Haswell PI*

Role of associated authors: *Experimental work was carried out by Wiles as PhD student supervised by*

Haswell supported by Watts a post-doctoral research fellow supervised by Haswell, Pombo-Villar was the industrial collaborator.

20. Watts, P., Wiles, C., Haswell, S. J., Pombo-Villar, E., Solution phase synthesis of beta-peptides using micro reactors, *Tetrahedron*, 2002, 58, 5427-5439.

Originator(s) of the published work: *Haswell*

Source of funding: *Novartis - Haswell PI*

Role of associated authors: *Experimental work was carried out by Watts a post-doctoral research fellows supervised by Haswell, supported by Wiles a PhD student supervised by Haswell and Pombo-Villar was the industrial collaborator.*

21. Fletcher, P.D.I., Haswell, S.J., Pombo-Villar, E., Warrington, B.H., Watts, P., Wong, S.Y.F., Zhang, X. L., Micro reactors: principles and applications in organic synthesis, *Tetrahedron*, 2002, 58, 4735-4757.

Originator(s) of the published work: *Haswell*

Source of funding: *Novarti and Galaxo SmithKline - Haswell PI*

Role of associated authors: *Review paper of earlier research co-authored by Watts and Zhang post-doctoral research fellows supervised by Haswell, and Pombo-Villar Warrington and Wong industrial collaborators.*

22. Wiles, C., Watts, P., Haswell, S.J., Pombo-Villar, E., The regioselective preparation of 1,3-diketones within a micro reactor, *Chem Comm.*, 2002. 1034-1035.

Originator(s) of the published work: *Haswell*

Source of funding: *EPSRC – grant GR/M74429 and Novartis - Haswell PI*

Role of associated authors: *Experimental work was carried out by Wiles as PhD student supervised by Haswell supported by Watts a post-doctoral research fellow supervised by Haswell, Pombo-Villar was the industrial collaborator.*

23. Wiles, C., Watts, P., Haswell, S.J. and Pombo-Villar, E., The regioselective preparation of 1,3-diketones, *Tetrahedron letters*, 2002, 2945-2948.

Originator(s) of the published work: *Haswell*
Source of funding: *Novartis - Haswell PI*
Role of associated authors: *Experimental work was carried out by Wiles as PhD student supervised by Haswell supported by Watts a post-doctoral research fellow supervised by Haswell, Pombo-Villar was the industrial collaborator.*

24. Watts, P., Wiles, C., Haswell, S.J., Pombo-Villar, E., Investigation of racemisation in peptide synthesis within a micro reactor, Lab on a chip, 2002, 2, 141-144.

Originator(s) of the published work: *Haswell*
Source of funding: *Novartis - Haswell PI*
Role of associated authors: *Experimental work was carried out by Watts a post-doctoral research fellows supervised by Haswell, supported by Wiles a PhD student supervised by Haswell, Pombo-Villar was the industrial collaborator.*

25. Fletcher, P.D.I., Haswell, S.J. and Zhang, X.L., Electrokinetic control of a chemical reaction in a lab-on-a- chip micro-reactor: measurement and quantitative modelling, Lab on a chip, 2002, 102-112.

Originator(s) of the published work: *Haswell and Fletcher (75/25%)*
Source of funding: *EPSRC – Grant GR/M74429 - Haswell PI*
Role of associated authors: *Zhang undertook practical experiments as a post-doctoral research fellow supervised by Haswell, Fletcher advised on methodology.*

26. Wiles, C., Watts, P., Haswell, S.J. and Pombo-Villar, E., 1,4-addition of enolates to alpha,beta-unsaturated ketones within a micro reactor, Lab on a chip, 2002, 62- 64.

Originator(s) of the published work: *Haswell*
Source of funding: *Novartis - Haswell PI*
Role of associated authors: *Experimental work was carried out by Wiles as PhD student supervised by Haswell supported by Watts a post-doctoral research fellow supervised by Haswell, Pombo-Villar was the industrial collaborator.*

27. Haswell, S.J. and Watts, P., Green chemistry: synthesis in micro reactors, Green Chem., 2003, 5, 240-249.

Originator(s) of the published work: *Haswell and Watts (50% each)*

Role of associated authors: *Co-authored review.*

28. Watts, P. and Haswell, S.J., Microfluidic combinatorial chemistry, Curr. Opin. Chem. Biol., 2003, 7, 380-387.

Originator(s) of the published work: *Haswell and Watts (50% each)*

Role of associated authors: *Co-authored review.*

29. Watts, P. and Haswell, S.J., Continuous flow reactors for drug discovery, Drug Discov. Today, 2003, 8, 586-593.

Originator(s) of the published work: *Haswell and Watts (50% each)*

Role of associated authors: *Co-authored review.*

30. Fletcher, P.D.I., Haswell, S.J. and Zhang, X.L., Monitoring of chemical reactions within micro reactors using an inverted Raman microscope spectrometer, Electrophoresis, 2003, 24, 3239-3245.

Originator(s) of the published work: *Haswell*

Source of funding: *EPSRC – Grant GR/R09800 - Haswell PI*

Role of associated authors: *Zhang undertook practical experiments as a post-doctoral research fellow supervised by Haswell, Fletcher advised on methodology.*

31. George, V., Watts, P., Haswell, S.J., and Pombo-Villar, E., On-chip separation of peptides prepared within a micro reactor, Chem. Comm. 2003, 23, 2886-2887.

Originator(s) of the published work: *Haswell*

Source of funding: *Novartis - Haswell PI*

Role of associated authors: *Experimental work was carried out by George a post-doctoral research fellow supervised by Haswell and supported by Watts a post-doctoral research fellow supervised by Haswell, Pombo-Villar was the industrial collaborator.*

32. Wiles, C., Watts, P., Haswell, S.J. and Pombo-Villar, E., Solution phase synthesis of esters within a micro reactor, Tetrahedron, 2003, 59, 10173-10179.

Originator(s) of the published work: *Haswell*

Source of funding: *Novartis - Haswell PI*
Role of associated authors: *Experimental work was carried out by Wiles as PhD student supervised by Haswell supported by Watts a post-doctoral research fellow supervised by Haswell, Pombo-Villar was the industrial collaborator.*

33. Wiles, C., Watts, P. and Haswell, S.J., The application of micro reactor technology for the synthesis of 1,2-azols, *Org. Proc. Res. Dev.*, 2004, 8, 28-32.

Originator(s) of the published work: *Haswell*
Source of funding: *Novartis - Haswell PI*
Role of associated authors: *Experimental work was carried out by Wiles as PhD student supervised by Haswell supported by Watts a post-doctoral research fellow supervised by Haswell.*

34. He, P., Haswell, S.J. and Fletcher, P.D.I., Microwave heating of heterogeneously catalysed Suzuki reactions in a micro reactor, *Lab on a chip*, 2004, 4, 38-41.

Originator(s) of the published work: *Haswell*
Source of funding: *EPSRC – Grant GR/S34106 - Haswell PI*
Role of associated authors: *He undertook practical experiments as a post-doctoral research fellow supervised by Haswell, Fletcher advised on methodology.*

35. Feng, X.Z., Haswell, S.J. and Watts, P., Organic synthesis in micro reactors, *Current Topics in Medicinal Chemistry*, 2004, 4, 707-727.

Originator(s) of the published work: *Haswell*
Source of funding: *EPSRC – Grant GR/S34267 - Haswell PI*
Role of associated authors: *Experimental work carried out by Feng a post-doctoral research fellow supervised by Haswell manuscript co-authored by Watts a post-doctoral research fellow supervised by Haswell.*

36. Wiles, C., Watts, P., Haswell, S.J. and Pombo-Villar, E., Stereoselective alkylation of an Evans auxiliary derivative within a pressure-driven micro reactor, *Lab on a Chip*, 2004, 4, 171-173.

Originator(s) of the published work: *Haswell*
Source of funding: *Novartis - Haswell PI*
Role of associated authors: *Experimental work was carried out by Wiles a PhD student supervised by Haswell*

supported by Watts a post-doctoral research fellow supervised by Haswell, Pombo-Villar was the industrial collaborator.

37. He, P., Haswell, S.J. and Fletcher, P.D.I., Microwave-assisted Suzuki reactions in a continuous flow capillary reactor, *Applied Catalysis A*, 2004, 274, 111-114.

Originator(s) of the published work: *Haswell*

Source of funding: *EPSRC – Grant GR/S34106 - Haswell PI*

Role of associated authors: *He undertook practical experiments as a post-doctoral research fellow supervised by Haswell, Fletcher advised on methodology.*

38. Wiles C., Watts P. and Haswell S.J., An investigation into the use of silica-supported bases within EOF-based flow reactors, *Tetrahedron*, 2004, 60, 8421-8427.

Originator(s) of the published work: *Haswell*

Source of funding: *EPSRC – Grant GR/S34106 - Haswell PI*

Role of associated authors: *Wiles and Watts undertook practical experiments as a post-doctoral research fellows supervised by Haswell.*

39. Watts P., Haswell S.J., Pombo-Villar E., Electrochemical effects related to synthesis in micro reactors operating under electrokinetic flow, *Chem. Eng. J.*, 2004, 101, 237-240.

Originator(s) of the published work: *Haswell*

Source of funding: *Novartis - Haswell PI*

Role of associated authors: *Experimental work was carried out by Watts a post-doctoral research fellow supervised by Haswell, Pombo-Villar was the industrial collaborator.*

40. Watts P. and Haswell S.J., Combinatorial synthesis in micro reactors, *Combinatorial Chem. & High Throughput Screening*, 2004, 7, 397-405.

Originator(s) of the published work: *Haswell*

Role of associated authors: *Review co-authored by Haswell and Watts a post-doctoral research fellow supervised by Haswell.*

41. Jonsson, C, Lundgren, S., Haswell, S.J. and Moberg, C., Asymmetric catalysis in a micro reactor – Ce, Yb and Lu catalysed enantioselective addition of trimethylsilyl cyanide to benzaldehyde, *Tetrahedron*, 2004, 60, 10515-10520.

Originator(s) of the published work: *Moberg (chemistry - 75%) Haswell (micro reactors -25%)*

Role of associated authors: *This paper describes a personal collaboration with Moberg in Sweeden who wanted to apply micro reactors to asymmetric synthesis Haswell produced micro reactor design and gave practical knowhow.*

42. Pennemann H., Watts P., Haswell S.J., Hessel V. and Lowe H., Benchmarking of microreactor applications, *Org. Proc. Res. Dev.*, 2004, 8 422-439.

Role of associated authors: *Collaborative review with leading group in Mainz Hessel, Lowe and Pennemann co-authored by Haswell and Watts a post-doctoral research fellow supervised by Haswell.*

43. Broadwell, I., Fletcher, P.D.I., Haswell, S.J., Zhang, X., Allen, R.W.K., MacInnes, J.M. and Du, X., Pressure-driven and electroosmotic flows and electrical currents in Lab-on-a-chip micro reactor devices, *Trends in Physical Chemistry*, 2004, Vol. 10, 117-133.

Originator(s) of the published work: *Haswell and Fletcher (75/25%)*

Source of funding: *EPSRC – Grant GR/M74429 and Institute of Applied Catalysis - Haswell PI*

Role of associated authors: *Broadwell undertook practical experiments as a PhD student co-supervised by Haswell and Fletcher, Zhang supported the work as a post-doctoral research fellow supervised by Haswell, collaborators from Sheffield also funded by a paired grant were Allen, MacInnes, and Du.*

44. Watts P. and Haswell S.J., The Application of Micro Reactors for Organic Synthesis, *Chem. Soc. Rev.*, 2005, 34, 235 – 246.

Originator(s) of the published work: *Haswell*

Role of associated authors: *Review co-authored by Haswell and Watts a post-doctoral research fellow supervised by Haswell.*

45. He, P., Haswell, S.J. and Fletcher, P.D.I., Efficiency, monitoring and control of microwave heating within a continuous flow capillary reactor, *Sensors & Actuators B*, 2005, 105, 516 – 520.

Originator(s) of the published work: *Haswell*

Source of funding: *EPSRC – Grant GR/S34106 - Haswell PI*

Role of associated authors: *He undertook practical experiments as a post-doctoral research fellow supervised by Haswell, Fletcher advised on methodology.*

46. Wiles C., Watts P. and Haswell S.J., Acid-catalysed synthesis and deprotection of dimethyl acetals in a miniaturised electrophoretic flow reactor, *Tetrahedron*, 2005, 61, 5209 – 5217.

Originator(s) of the published work: *Haswell*

Source of funding: *EPSRC – Grant GR/S34267 - Haswell PI*

Role of associated authors: *Wiles and Watts undertook practical experiments as a post-doctoral research fellows supervised by Haswell.*

47. He P., Watts P., Marken F., and Haswell S.J., Electrolyte free electro-organic synthesis: The cathodic dimerization of 4-nitrobenzyl bromides in a micro-gap cell, *Electrochem. Comm.*, 2005, 7, 918-924.

Originator(s) of the published work: *Haswell (75%) Marken (25%)*

Source of funding: *EPSRC – Grant GR/S34267 - Haswell PI*

Role of associated authors: *He undertook practical experiments as a post-doctoral research fellow supervised by Haswell, Watts assisted in chemical synthesis as a post-doctoral research fellow supervised by Haswell and Marken from Bath collaborated with supporting electrochemical expertise.*

48. Wiles C., Watts P., Haswell S.J. and Pombo-Villar E., The preparation and reaction of enolates within micro reactors, *Tetrahedron*, 2005, 61 10757-10773.

Originator(s) of the published work: *Haswell*

Source of funding: *Novartis and EPSRC – Grant GR/S34106 - Haswell PI*

Role of associated authors: *Wiles and Watts undertook practical experiments as a post-doctoral research fellows supervised by Haswell, Pombo-Villar was the industrial collaborator.*

49. Zhang, X. and Haswell, S.J., Materials matter in microfluidic devices, MRS bulletin, 2006, 31 (2) 95-99.

Originator(s) of the published work: *Haswell*

Role of associated authors: *Review co-authored by Haswell and Zhang a post-doctoral research fellow supervised by Haswell, on fabrication methodology for micro reactors.*

50. He, P., Watts, P., Marken, F. and Haswell, S.J., Self-supported and clean one-step cathodic coupling of activated olefins with benzyl bromide derivatives in a micro flow reactor Angew. Chem. Int. Ed., 2006, 45, 1-5.

Originator(s) of the published work: *Haswell (75%) Marken (25%)*

Source of funding: *EPSRC – Grant GR/S34267 - Haswell PI*

Role of associated authors: *He undertook practical experiments as a post-doctoral research fellow supervised by Haswell, Watts assisted in chemical synthesis as a post-doctoral research fellow supervised by Haswell and Marken from Bath collaborated with supporting electrochemical expertise.*

51. Wiles, C., Watts, P. and Haswell, S.J., Clean and selective oxidation of aromatic alcohols using silica-supported Jones' reagent in a pressure-driven flow reactor, Tetrahedron letters, 2006, 47 (30), 5261-5264.

Originator(s) of the published work: *Haswell*

Source of funding: *EPSRC – Grant GR/S34267 - Haswell PI*

Role of associated authors: *Wiles and Watts undertook practical experiments as a post-doctoral research fellows supervised by Haswell.*

52. Zhang, X., Yin, H., Cooper, J.M. and Haswell, S.J., A microfluidic based system for analysis of single cells based on Ca²⁺ flux, Electrophoresis, 2006, 27, 5093-5100.

Originator(s) of the published work: *Haswell (80%) Cooper (20%)*

Source of funding: *DTI MNT project 366 - Haswell PI*

Role of associated authors: *Zhang undertook practical experiments as a post-doctoral research fellow supervised by Haswell, Cooper was an academic collaborator from Glasgow and Yin was a post-doctoral research fellow supervised by Cooper.*

53. Zhang, X., Cooper, J.M., Monaghan, P.B. and Haswell, S.J., Continuous flow separation of particles within an asymmetric microfluidic device, *Lab on a Chip*, 2006, 6, 561-566.

Originator(s) of the published work: *Haswell*

Source of funding: *DTI MNT project 366 - Haswell PI*

Role of associated authors: *Zhang undertook practical experiments as a post-doctoral research fellow supervised by Haswell, Cooper was an academic collaborator from Glasgow and Monaghan was a post-doctoral research fellow supervised by Cooper.*

54. Yin, H., Zhang, X., Patrick, N., Klauke, N., Cordingley, H.C., Haswell, S.J. and Cooper, J.M., Influence of hydrodynamic conditions on quantitative cellular assays in microfluidic systems, *Anal. Chem.*, 2007, 79, 7139-7144.

Originator(s) of the published work: *Haswell (50%) Cooper (50%)*

Source of funding: *DTI MNT project 366 - Haswell PI*

Role of associated authors: *Zhang undertook practical experiments as a post-doctoral research fellow supervised by Haswell, Cooper was an academic collaborator from Glasgow and Yin and Klauke who supported the practical work were a post-doctoral research fellows supervised by Cooper, Cordingley and Patrick were industrial collaborators.*

55. He, P., Watts, P., Marken, F. and Haswell, S.J., Electrosynthesis of phenyl-2-propanone derivatives from benzyl bromides and acetic anhydride in an unsupported micro-flow cell electrolysis process, *Green Chem.*, 2007, 9, 20-22.

Originator(s) of the published work: *Haswell (75%) Marken (25%)*

Source of funding: *EPSRC – Grant GR/S34267 - Haswell PI*

Role of associated authors: *He undertook practical experiments as a post-doctoral research fellow supervised by Haswell, Watts assisted in chemical synthesis as a post-doctoral research fellow supervised by Haswell and Marken from Bath collaborated with supporting electrochemical expertise.*

56. Wiles, C, Watts, P., and Haswell S.J., The use of solid-supported reagents for the multi-step synthesis of analytically pure alpha, beta-unsaturated compounds in miniaturized flow reactors, *Lab on a chip*, 2007, 7, 322-330.

Originator(s) of the published work: *Haswell*
Source of funding: *EPSRC – Grant GR/S34267 - Haswell PI*
Role of associated authors: *Wiles and Watts undertook practical experiments as a post-doctoral research fellows supervised by Haswell.*

57. He, P., Watts, P., Marken, F. and Haswell, S.J., Scaling out of electrolyte free electrosynthesis in a micro-gap flow cell, Lab on a chip, 2007, 7, 141-143.

Originator(s) of the published work: *Haswell (75%) Marken (25%)*
Source of funding: *EPSRC – Grant GR/S34267 - Haswell PI*
Role of associated authors: *He undertook practical experiments as a post-doctoral research fellow supervised by Haswell, Watts assisted in chemical synthesis as a post-doctoral research fellow supervised by Haswell and Marken from Bath collaborated with supporting electrochemical expertise.*

58. Wiles C., Watts P. and Haswell S.J., The use of electroosmotic flow as a pumping mechanism for semi-preparative scale continuous flow synthesis, Chem. Comm., 2007, 966-968.

Originator(s) of the published work: *Haswell*
Source of funding: *EPSRC – Grant GR/S34267 - Haswell PI*
Role of associated authors: *Wiles and Watts undertook practical experiments as a post-doctoral research fellows supervised by Haswell.*

59. Wiles, C., Watts, P. and Haswell, S.J., An efficient, continuous flow technique for the chemoselective synthesis of thioacetals, Tet. Let., 2007, 48, 7362 - 7365.

Originator(s) of the published work: *Haswell*
Source of funding: *EPSRC – Grant GR/S34267 - Haswell PI*
Role of associated authors: *Wiles and Watts undertook practical experiments as post-doctoral research fellows supervised by Haswell.*

60. Yin H., Pattrick N., Zhang X, Klauke N., Cordingley H.C., Haswell S.J., Cooper J.M., Quantitative comparison between microfluidic and microtitre plate formats for cell-based assays, Anal. Chem., 2008, 80, 179-185.

Originator(s) of the published work: *Haswell (50%) Cooper (50%)*
Source of funding: *DTI MNT project 366 - Haswell PI*
Role of associated authors: *Zhang undertook practical experiments as a post-doctoral research fellow supervised by*

Haswell, Cooper was an academic collaborator from Glasgow and Yin and Klauke who supported the practical work were a post-doctoral research fellows supervised by Cooper, Cordingley and Patrick were industrial collaborators.

61. Zhang, X., Yin, H., Cooper, J.M., Haswell, S.J., Characterization of cellular chemical dynamics using combined microfluidic and Raman techniques, Analytical and Bioanalytical Chemistry, 2008, 390, 833-840.

Originator(s) of the published work: *Haswell (80%) Cooper (20%)*
Source of funding: *DTI MNT project 366 - Haswell PI*
Role of associated authors: *Zhang undertook practical experiments as a post-doctoral research fellow supervised by Haswell, Cooper was an academic collaborator from Glasgow and Yin was a post-doctoral research fellow supervised by Cooper.*

62. Yoon, T-H., Park, S-H., Min, K-I., Zhang, X., Haswell, S.J. and Kim, D-P., Novel inorganic polymer derived microreactors for organic microchemistry applications, Lab on a chip, 2008, 8, 1454-1459.

Originator(s) of the published work: *Kim (materials - 75%) Haswell (chemistry and micro reactors -25%)*
Role of associated authors: *This paper describes a personal collaboration with Kim in Korea who wanted to evaluate some novel polymers a suitable substrates for micro reactors Haswell contributed chemical and micro reactor design and practical knowhow.*

63. He, P., Greenway, G. and Haswell, S.J., The on-line synthesis of enzyme functionalized silica nanoparticles in a microfluidic reactor using polyethylenimine polymer and R5 peptide, Nanotechnology, 2008, 19, 315603 (7pp).

Originator(s) of the published work: *Haswell*
Source of funding: *EU – Grant NMP4 033254 - Haswell PI*
Role of associated authors: *He undertook practical experiments as a post-doctoral research fellow supervised by Haswell, Greenway advised on methodology.*

64. Zhang, X., Jones, P. and Haswell, S.J., Attachment and detachment of living cells on modified microchannel surfaces in a microfluidic-based lab-on-a-chip system, *Chem. Eng. J.*, 2008, 135, S82-S88.

Originator(s) of the published work: *Haswell*

Source of funding: *DTI MNT project 366 - Haswell PI*

Role of associated authors: *Jones an undergraduate project student undertook the practical work Zhang assisted as a post-doctoral research fellow supervised by Haswell.*

65. Hattersley, S.M., Dyer, C.E., Greenman, J. and Haswell, S.J., Development of a microfluidic device for the maintenance and interrogation of viable tissue biopsies, *Lab on a chip*, 2008, 8, 1842-1846.

Originator(s) of the published work: *Haswell (80%) Greenman (20%)*

Source of funding: *BBSRC – grant BB002722 - Haswell PI*

Role of associated authors: *Hattersley undertook the practical work as a PhD student supervised by Haswell and Greenman, Dyer advised on methodology.*

66. Garcia-Alonso, J., Greenway, G.M., Hardege, J.D. and Haswell, S.J., A prototype microfluidic chip using fluorescent yeast for detection of toxic compounds, *Biosens. and Bioelectronic.* 2009, 24 1508-1511.

Originator(s) of the published work: *Haswell (50%) Greenway (50%)*

Source of funding: *EU – grant TESS COLL-CT-2006 - Haswell PI*

Role of associated authors: *Garcia-Alonso undertook the practical work as a post-doctoral research fellow supervised by Haswell and Greenway, Hargege advised on methodology.*

67. Zhang, X.L., Coupland, P., Fletcher, P.D.I. and Haswell, S.J., Monitoring of liquid flow through microtubes using a micropressure sensor, *Chem. Eng. Res. Design*, 2009, 87, 19-24.

Originator(s) of the published work: *Haswell*

Source of funding: *EPSRC – Grant GR/M74429 - Haswell PI*

Role of associated authors: *Coupland an undergraduate project student undertook the practical work Zhang assisted as a post-doctoral research fellow supervised by Haswell, Fletcher advised on methodology.*

68. Wild, G.P., Wiles, C., Watts, P. and Haswell, S.J., The use of immobilized crown ethers as in-situ N-protecting groups in organic synthesis and their application under continuous flow, *Tetrahedron*, 2009, 65, 1618-1629.

Originator(s) of the published work: *Haswell*

Source of funding:

EPSRC – Grant GR/S34106 - Haswell PI

Role of associated authors:

Wild undertook practical experiments as a PhD student supervised by Haswell, Wiles and Watts supported the work as post-doctoral research fellows supervised by Haswell.

69. Shapiro, M.S., Haswell, S.J., Lye, G.J., Bracewell, D.G., Design and characterization of a microfluidic packed bed system for protein breakthrough and dynamic binding capacity determination, *Biotech. Progress*, 2009, 25, 277-285.

Originator(s) of the published work: *Bracewell (separations -70%) Haswell (chemistry and micro reactors -30%)*

Role of associated authors:

This paper describes a personal collaboration with Bracewell and Lye from London (UCL), Shapiro was a PhD student supervised by Bracewell and Lye Haswell contributed chemical and micro reactor design and practical knowhow.

70. Oakley, J.A., Shaw, K.J., Docker, P.T., Dyer, C.E., Greenman, J., Greenway, G.M. and Haswell, S.J., Development of a bi-functional silica monolith for electro-osmotic pumping and DNA clean-up/extraction using gel-supported reagents in a microfluidic device, *Lab on a chip*, 2009, 9, 1596-1600.

Originator(s) of the published work: *Haswell*

Source of funding:

EPSRC – Grant EP/D040930 - Haswell PI

Role of associated authors:

Oakley undertook the practical work as a PhD student supervised by Haswell and Greenman, Shaw a PhD student supervised by Haswell and Dyer and Docker a post-doctoral research fellow supervised by Haswell assisted in the work, Greenway advised on methodology.

71. Oakley, J.A., Robinson, S., Dyer, C.E., Greenman, J., Greenway, G.M. and Haswell, S.J., Development of a gel-to-gel electro-kinetic pinched injection method for an integrated micro-fluidic based DNA analyser, *Anal. Chim. Acta*, 2009, 652, 239-244.

Originator(s) of the published work: *Haswell*

Source of funding: *EPSRC – Grant EP/D040930 - Haswell PI*
Role of associated authors: *Oakley undertook the practical work as a PhD student supervised by Haswell and Greenman, with Robinson a project student supervised by Haswell. Shaw a PhD student supervised by Haswell and Dyer and Docker a post-doctoral research fellow supervised by Haswell assisted in the work, Greenway advised on methodology.*

72. Shaw, K.J., Thain, L., Docker, P.T., Dyer, C.E., Greenman, J., Greenway, G.M. and Haswell, S.J., The use of carrier RNA to enhance DNA extraction from microfluidic-based silica monoliths, *Anal. Chim. Acta*, 2009, 652, 231-233.

Originator(s) of the published work: *Haswell*
Source of funding: *EPSRC – Grant EP/D040930 - Haswell PI*
Role of associated authors: *Thain was a project student who carried out the experimental work supported by Shaw a PhD student supervised by Haswell and Dyer and Docker a post-doctoral research fellow supervised by Haswell assisted in the work, Greenman and Greenway advised on methodology.*

73. Dou, Y., Haswell, S.J., Greenman, J. and Wadhawan, J., Immobilized anthraquinone for redox mediation of horseradish peroxidase for hydrogen peroxide sensing, *Electrochem. Comm.*, 2009, 1976–1981.

Originator(s) of the published work: *Haswell (50%) Greenman (50%)*
Source of funding: *Heart Research UK grant – RG2538/07/10*
Role of associated authors: *Dou undertook the practical work as a post-doctoral research fellow supervised by Haswell and Greenman, Wadhawan advised on methodology.*

74. Shaw, K.J., Joyce D.A., Docker, P.T., Dyer, C.E., Greenman, J., Greenway, G.M. and Haswell, S.J., Simple practical approach for sample loading prior to DNA extraction using a silica monolith in a micro fluidic device, *Lab on a chip*, 2009, 9, 3430-3432.

Originator(s) of the published work: *Haswell*
Source of funding: *EPSRC – Grant EP/D040930 - Haswell PI*
Role of associated authors: *Shaw carried out the experimental work as a PhD student supervised by Haswell and Dyer, Joyce and Docker assisted in the work as post-doctoral research fellows*

supervised by Haswell, Greenman and Greenway advised on methodology.

75. He, P., Greenway, G. and Haswell, S.J., Development of enzyme immobilized monolith micro-reactors integrated with microfluidic electrochemical cell for the evaluation of enzyme kinetics, *Microfluid Nanofluid*, 2010, 8, 565-573.

Originator(s) of the published work: *Haswell*

Source of funding: *EU – Grant NMP4 033254 - Haswell PI*

Role of associated authors: *He undertook practical experiments as a post-doctoral research fellow supervised by Haswell, Greenway advised on methodology.*

76. He, P., Greenway, G. and Haswell, S.J., Development of a monolith based immobilized lipase micro-reactor for biocatalytic reactions in a biphasic mobile system, *Proc. Biochem.*, 2010, 45, 593-597.

Originator(s) of the published work: *Haswell*

Source of funding: *EU – Grant NMP4 033254 - Haswell PI*

Role of associated authors: *He undertook practical experiments as a post-doctoral research fellow supervised by Haswell, Greenway advised on methodology.*

77. He, P., Davies, J., Greenway, G. and Haswell, S.J., Measurement of acetylcholinesterase inhibition using bienzymes immobilized monolith micro-reactor with integrated electrochemical detection, *Anal. Chim. Acta*, 2010, 659, 9-14.

Originator(s) of the published work: *Haswell*

Source of funding: *EU – Grant NMP4 033254 - Haswell PI*

Role of associated authors: *Davies undertook practical experiments as a project student supported by He a post-doctoral research fellow supervised by Haswell, Greenway advised on methodology.*

78. Anderson, K., Cooper, J.M., Haswell, S.J., Marshall, D., Yin, H. and Zhang Z., Microfluidic-based measurements of cytochrome P450 enzyme activity of primary mammalian hepatocytes, *Analyst*, 2010, 135, 1282–1287.

Originator(s) of the published work: *Haswell (80%) Cooper (20%)*

Source of funding: *DTI MNT project 366 - Haswell PI*

Role of associated authors: *Zhang undertook practical experiments as a post-doctoral research fellow supervised by*

Haswell, Cooper was an academic collaborator from Glasgow and Yin was a post-doctoral research fellow supervised by Cooper, Anderson and Marshall were industrial collaborators.

79. Shaw, K.J., Docker, P.T., Yelland, J.V., Dyer, C.E., Greenman, J., Greenway, G.M. and Haswell, S.J., Rapid PCR amplification using a microfluidic device with integrated microwave heating and air impingement cooling, Lab on a chip, 2010, 10, 1725 – 1728.

Originator(s) of the published work: *Haswell*

Source of funding: *EPSRC – Grant EP/D040930 - Haswell PI*

Role of associated authors: *Shaw carried out the experimental work as a PhD student supervised by Haswell and Dyer, Docker assisted in the work as post-doctoral research fellow supervised by Haswell, Greenman and Greenway advised on methodology and Yelland was an industrial collaborator.*

80. Cheah L-T., Dou, Y-H., Seymour, A-M.L., Dyer, C.E., Haswell, S.J., Wadhawan, J.D. and Greenman, J., Microfluidic perfusion system for maintaining viable heart tissue with real-time electrochemical monitoring of reactive oxygen species, Lab on a chip, 2010, 10, 2720-2726.

Originator(s) of the published work: *Haswell (50%) Greenman (50%)*

Source of funding: *Heart Research UK grant – RG2538/07/10 and BBSRC grant – BB002722*

Role of associated authors: *Cheah undertook the practical work as a PhD student supervised by Haswell and Greenman, Dou supported the work as a post-doctoral research fellow supervised by Haswell and Greenman, Seymoure, Dyer and Wadhawan advised on methodology.*

81. Webster, A., Dyer, C.D., Haswell S.J. and Greenman, J., A microfluidic device for tissue biopsy culture and interrogation, Anal. Methods, 2010, 2, 1005–1007.

Originator(s) of the published work: *Haswell (80%) Greenman (20%)*

Source of funding: *BBSRC – grant BB002722 - Haswell PI*

Role of associated authors: *Webster undertook the practical work as a post-doctoral research fellow supervised by Haswell, Greenman and Dyer advised on methodology.*

82. Shapiro, M.S. Haswell, S.J., Lye, G.J. and Bracewell, D.G. Microfluidic chromatography for early stage evaluation of biopharmaceutical binding and separation conditions, *Separation Science and Technology*, 2011, 46, 185–194.

Originator(s) of the published work: *Bracewell (separations -70%) Haswell (chemistry and micro reactors -30%)*

Role of associated authors: *This paper describes a personal collaboration with Bracewell and Lye from London (UCL), Shapiro was a PhD student supervised by Bracewell and Lye Haswell contributed chemical and micro reactor design and practical knowhow.*

83. Shaw, K.J., Joyce, D.A., Docker, P.T., Dyer, C.E., Greenway, G.M., Greenman, J. and Haswell, S.J., Development of a real-world direct interface for integrated DNA extraction and amplification in a microfluidic device, *Lab on a Chip*, 2011, 11, 443–448.

Originator(s) of the published work: *Haswell*

Source of funding: *EPSRC – Grant EP/D040930 - Haswell PI*

Role of associated authors: *Shaw carried out the experimental work as a PhD student supervised by Haswell and Dyer, Joyce and Docker assisted in the work as post-doctoral research fellows supervised by Haswell, Greenman and Greenway advised on methodology.*

84. He, P., Greenway, G. and Haswell, S.J., Microfluidic synthesis of silica nanoparticles using polyethylenimine polymers, *Chem. Eng. J.* 2011, 167, 694–699.

Originator(s) of the published work: *Haswell*

Source of funding: *EU – Grant NMP4 033254 - Haswell PI*

Role of associated authors: *He undertook practical experiments as a post-doctoral research fellow supervised by Haswell, Greenway advised on methodology.*

85. Shaw, K. J., Birch, C., Hughes, E.M., Jakes, A.D., Greenman, J. and Haswell, S.J., Microsystems for personalized biomolecular diagnostics, *Eng. Life Sci.*, 2011, 11, 121–132.

Originator(s) of the published work: *Haswell*

Role of associated authors: *Review co-authored by Shaw a post-doctoral research fellow supervised by Haswell, Birch, Hughes and Jakes project*

*students and Greenman academic
colleague.*

86. Webster, A., Greenman, J., Haswell, S.J., Development of microfluidic devices for biomedical and clinical application, *Journal of Chemical Technology and Biotechnology*, 2011, 86. 10-17.

Originator(s) of the published work: *Haswell (80%) Greenman (20%)*
Source of funding: *BBSRC – grant BB002722 - Haswell PI*
Role of associated authors: *Review co-authored by Webster a post-doctoral research fellow supervised by Haswell and Greenman.*

87. Garcia-Alonso, J., Fakhrullin, R.F., Paunov, V.N., Shen, Z., Hardege, J.D., Pamme, N., Haswell, S.J., Greenway, G.M., Microscreening toxicity system based on living magnetic yeast and gradient chips, *Analytical and Bioanalytical Chemistry*, 2011, 400, 1009-1013.

Originator(s) of the published work: *Haswell (50%) Greenway (50%)*
Source of funding: *EU – grant TESS COLL-CT-2006 - Haswell PI*
Role of associated authors: *Fakhrullin and Garcia-Alonso undertook the practical work as a post-doctoral research fellows supervised by Haswell and Greenway, Hardege, Paunov, Shen and Pamme advised on methodology.*

88. He, P.; Haswell, S.J.; Fletcher, P.D.I.; Kelly, S.M. and Mansfield, A., Scaling up of continuous-flow, microwave-assisted, organic reactions by varying the size of Pd-functionalized catalytic monoliths, *Beilstein J. Org. Chem*, 2011, 7, 1150-1157.

Originator(s) of the published work: *Haswell*
Source of funding: *EPSRC – Grant EP/G027765 - Haswell PI*
Role of associated authors: *He undertook practical experiments as a post-doctoral research fellow supervised by Haswell, Fletcher and Kelly advised on methodology, Mansfield was the industrial collaborator.*

89. Betts, J.W., Kitney, S.P., Fu, Y., Peng, W-M., Kelly, S.M. and Haswell, S.J., Production of deuterium labelled (-)-epicatechin in a microreactor, *Chem, Eng. J.*, 2011, 167, 545-547.

Originator(s) of the published work: *Haswell*
Source of funding: *EPSRC – CASE with Unilever - Haswell PI*

Role of associated authors: *Betts undertook practical experiments as a PhD student supervised by Haswell and Kelly, Kitney supported as a post-doctoral research fellow supervised by Kelly, Peng and Fu were industrial collaborators.*

90. Fletcher, P.D.I.; Haswell, S.J, He, P., Kelly, S.M. and Mansfield, A., Permeability of silica monoliths containing micro-and nano-pores, *J. Porous Matter*, 2011, 18, 501-508.

Originator(s) of the published work: *Haswell*

Source of funding: *EPSRC – Grant EP/G027765 - Haswell PI*

Role of associated authors: *He undertook practical experiments as a post-doctoral research fellow supervised by Haswell, Fletcher and Kelly advised on methodology, Mansfield was the industrial collaborator.*

91. Woods, J., Docker, P.T., Dyer, C.E., Greenman, J., Haswell S.J., On-chip integrated labelling, transport and detection of tumour cells, *Electrophoresis*, 2011, 32, 3188–3195.

Originator(s) of the published work: *Haswell (80%) Greenman (20%)*

Source of funding: *BBSRC – grant BB002722 - Haswell PI*

Role of associated authors: *Woods undertook the practical work as a PhD student supervised by Haswell and Greenman, Docker gave technical support as a post-doctoral research fellow supervised by Haswell, Dyer advised on methodology.*

92. Hattersley, S. M., Greenman J. and Haswell S.J., Study of ethanol induced toxicity in liver explants using microfluidic devices, *Biomed. Microdevices*, 2011, 13, 1005-1014 .

Originator(s) of the published work: *Haswell (80%) Greenman (20%)*

Source of funding: *BBSRC – grant BB002722 - Haswell PI*

Role of associated authors: *Hattersley undertook the practical work as a PhD student supervised by Haswell and Greenman.*

93. Kemp, C., Birch, C., Shaw, K.J., Nixon, G.J., Docker, P.T., Greenman, J., Huggett, J.F., Haswell, S.J., Foy, C.A., and Dyer, C.E., Direct processing of clinically-relevant large volume samples for the detection of sexually transmitted infectious agents from urine on a microfluidic device, *Anal. Methods*, 2012, 4, 2141 – 2144.

Originator(s) of the published work: *Haswell (60%) and Nixon (40%)*
Source of funding: *EPSRC – Grant EP/D040930 - Haswell PI*
Role of associated authors: *Kemp carried out the experimental work as a post-doctoral research fellow supervised by Haswell, in collaboration with LGC London. Birch was a PhD student supervised by Haswell and Dyer, Shaw was a PhD student supervised by Haswell and Greenman who assisted in the work, Docker gave technical assistance and Nixon, Huggett and Foy were collaborators.*

94. Parton, J., Birch, C., Kemp, C., Haswell, S.J., Pamme, N. and Shaw, K.J., Integrated DNA extraction and amplification using electrokinetic pumping in a microfluidic device, *Anal. Methods*, 2012, 4, 96-100.

Originator(s) of the published work: *Haswell*
Source of funding: *EPSRC – Grant EP/D040930 - Haswell PI*
Role of associated authors: *Parton carried out the experimental work as a project student supported by Birch a PhD student supervised by Haswell, Shaw was a PhD student supervised by Haswell, Kemp was a post-doctoral research fellow supervised by Haswell and Pamme advised on methodology.*

95. Hattersley, S.M., Sylvester, D.C., Dyer, C.E., Stafford, N.D., Haswell, S.J. and Greenman, J., A microfluidic system for testing the responses of head and neck squamous cell carcinoma tissue biopsies to treatment with chemotherapy drugs, *Anal. Biomedical Eng.*, 2012, 40, 1277-1288.

Originator(s) of the published work: *Haswell (80%) Greenman (20%)*
Source of funding: *BBSRC – grant BB002722 - Haswell PI*
Role of associated authors: *Hattersley undertook the practical work as a PhD student supervised by Haswell and Greenman, Sylvester and Stafford gave clinical support and Dyer advised on methodology.*

96. Cheah, L.T., Fritsch, I., Haswell, S.J. and Greenman, J., Evaluation of heart tissue viability under redox-magnetohydrodynamics conditions: Toward fine-tuning flow in biological microfluidics applications, *Biotech. and Bioeng.*, 2012, 109, 1827-1834.

Originator(s) of the published work: *Haswell (50%) Fritsch (50%)*

Role of associated authors: *Cheah undertook the practical work as a PhD student supervised by Haswell and Greenman, Fritsch was a visiting academic from the USA who assisted in the work and developed the methodology used.*

97. Kashkary, L., Kemp, C., Shaw, K.J., Greenway, G.M. and Haswell, S.J., Improved DNA extraction efficiency from low level cell numbers using a silica monolith based micro fluidic device, *Anal. Chim. Acta*, 2012, 750, 127-131.

Originator(s) of the published work: *Haswell*

Source of funding: *EPSRC – Grant TS/100114X - Haswell PI*

Role of associated authors: *Kashkary carried out the experimental work as a PhD student supervised by Haswell and Greenway, Shaw and Kemp assisted in the work as post-doctoral research fellows supervised by Haswell.*

98. He. P., Haswell, S.J., Fletcher, P.D.I., Kelly, S.M. and Mansfield, A., Acetylation of alcohols and phenols using continuous-flow, tungstosilicic acid-supported monolith micro reactors with scale-up capability, *J. Flow Chem.*, 2012, 2, 47-51.

Originator(s) of the published work: *Haswell*

Source of funding: *EPSRC – Grant EP/G027765 - Haswell PI*

Role of associated authors: *He undertook practical experiments as a post-doctoral research fellow supervised by Haswell, Fletcher and Kelly advised on methodology, Mansfield was the industrial collaborator.*

99. Parton, J., Hassan, N.A., Brown, T.A., Haswell, S.J., Brown, K.A., Shaw, K.J., Sex identification of ancient DNA samples using a microfluidic device, *J. Archaeol. Sci.*, 2013, 40, 705-711.

Originator(s) of the published work: *Haswell (50%) and Brown K (50%)*

Source of funding: *EPSRC – Grant TS/100114X - Haswell PI*

Role of associated authors: *Parton carried out the experimental work as a PhD student supervised by Haswell, Shaw assisted in the work as post-doctoral research fellow supervised by Haswell. The work was collaboration with Manchester University where Hassan, Brown N and Brown K were based.*

100. Chaplain, G., Haswell, S.J., Fletcher, P.D.I., Kelly, S.M. and Mansfield, A., Development and evaluation of a Raman flow cell for monitoring continuous flow reactions, *Aust. J. Chem.*, 2013, 66, 208–212.

Originator(s) of the published work: *Haswell*

Source of funding: *EPSRC – Grant EP/G027765 - Haswell PI*

Role of associated authors: *Chaplain undertook practical experiments as a PhD student supervised by Haswell and Fletcher, Kelly advised on methodology, Mansfield was the industrial collaborator.*

101. Sylvester, D., Hattersley, S.M., Stafford, N.D., Haswell, S.J., Greenman, J., Development of microfluidic-based analytical methodology for studying the effects of chemotherapy agents on cancer tissue, *Current Anal. Chem.* 2013, 9, 2-8.

Originator(s) of the published work: *Haswell (80%) Greenman (20%)*

Source of funding: *BBSRC – grant BB002722 - Haswell PI*

Role of associated authors: *Hattersley undertook the practical work as a PhD student supervised by Haswell and Greenman, Sylvester and Stafford gave clinical support and Dyer advised on methodology.*

102. Shaw, K.J., Hughes, E.M., Dyer, C.E., Greenman, J., Haswell, S.J., Integrated RNA extraction and RT-PCR for semi-quantitative gene expression studies on a microfluidic device, *Lab. Invest.*, 2013, 93, 961-966.

Originator(s) of the published work: *Haswell*

Source of funding: *EPSRC – Grant TS/100114X - Haswell PI*

Role of associated authors: *Hughes carried out the experimental work as a project student supervised by Haswell, Shaw assisted in the work as post-doctoral research fellow supervised by Haswell. Greenman and Dyer advised on methodology.*

List of submitted papers

1. Daykin, R.N.C., and Haswell, S.J., Development of a micro flow injection manifold for the determination of orthophosphate, *Anal. Chim. Acta*, 1995, 313, 155-159.
Reprinted with permission from Elsevier
2. Haswell, S.J., Development and operating characteristics of micro flow injection analysis systems based on electroosmotic flow: A review, *Analyst*. 1997, 122, 1R-10R.
Reproduced with permission from The Royal Society of Chemistry. DOI: 10.1039/a606289j
3. Doku, G.N and Haswell, S.J., Further studies into the development of micro-FIA (μ FIA) system based on electroosmotic flow for the determination of phosphate as orthophosphate, *Anal. Chim. Acta*, 1999, 382. 1-13.
Reprinted with permission from Elsevier
4. Greenway, G.M. Haswell S.J. and Petsul, P. H., Characterisation of a micro-total analytical system for the determination of nitrite with spectrophotometric detection, *Anal. Chim. Acta*, 1999, 387, 1-10.
Reprinted with permission from Elsevier
5. Fletcher, P.D.I., Haswell, S.J. and Paunov, V.N., Theoretical considerations of chemical reactions in micro reactors operating under electrophoretic control, *Analyst*, 1999, 124, 1273-1282.
Reproduced with permission from The Royal Society of Chemistry. DOI: 10.1039/a903624e
6. Greenway, G.M., Haswell, S.J., Morgan, D.O., Skelton, V. and Styring, P, The use of novel micro reactors for high throughput continuous flow organic synthesis, *Sensors and Actuators B*, 2000, 63, 153-158.
Reprinted with permission from Elsevier
7. Haswell, S.J. and Skelton, V., Chemical and biochemical micro reactors, *Trends in Anal. Chem.* 2000, 19, 389-395.
Reprinted with permission from Elsevier
8. Haswell, S.J., O'Sullivan, B. and Styring, P., Kumada-Corriu reactions in a pressure-driven microflow reactor, *Lab on a chip*, 2001, 1, 164-166.
Reproduced with permission from The Royal Society of Chemistry. DOI: 10.1039/b104035a

9. Doku, G.N., Haswell, S. J., McCreedy, T. and Greenway, G.M., Electric-field induced mobilisation of multiphase solution systems based on the nitration of benzene in a micro reactor, *Analyst*, 2001, 126, 14-20.
Reproduced with permission from The Royal Society of Chemistry. DOI: 10.1039/b007585j
10. Skelton, V., Greenway, G.M., Haswell, S.J, Styring, P., Morgan, D.O., Warrington, B.H. and Wong, S., The generation of concentration gradients using electroosmotic flow in micro reactors allowing stereo-selectivity in chemical synthesis, *Analyst*, 2001, 126, 11-13.
Reproduced with permission from The Royal Society of Chemistry. DOI: 10.1039/b006727j
11. Skelton, V., Greenway, G.M., Haswell, S.J, Styring, P., Morgan, D.O., Warrington, B.H. and Wong, S., The preparation of a series of nitrostilbene ester compounds using micro reactor technology, *Analyst*, . 2001, 126, 7-10.
Reproduced with permission from The Royal Society of Chemistry. DOI: 10.1039/b006728h
12. Haswell, S.J., Middleton, R.J., O'Sullivan, B., Skelton, V., Watts, P. and Styring, P., The application of micro reactors to synthetic chemistry, *Chem. Comm.*, 2001, 391-398.
Reproduced with permission from The Royal Society of Chemistry. DOI: 10.1039/b008496o
13. Watts, P., Wiles, C., S.J. Haswell, Pombo-Villar, E. and Styring, P., The synthesis of peptides using micro reactors, *Chem. Comm.*, 2001, 990-991.
Reproduced with permission from The Royal Society of Chemistry. DOI: 10.1039/b102125g
14. Petsul, P.H., Greenway, G.M. and Haswell, S.J., The development of an on-chip micro flow injection analysis of nitrate with a cadmium reductor, *Anal. Chim. Acta*, 2001, 428, 155-161.
Reprinted with permission from Elsevier
15. Doku, G.N., Haswell, S.J., McCreedy, T. and Middleton, R.J., Preliminary studies into the direct interfacing of a microreactor to a gas chromatographic instrument, *Analyst*, 2001, 126, 133-135.
Reproduced with permission from The Royal Society of Chemistry. DOI: 10.1039/b009778k
16. Sands, M., Haswell, S.J., Kelly, S.M., Skelton, V., Morgan, D.O., Styring P. and Warrington, B., The investigation of an equilibrium dependent reaction for the formation of enamines in a microchemical system, *Lab on a chip*, 2001, 1, 64-65.

*Reproduced with permission from The Royal Society of Chemistry. DOI:
10.1039/b104036g*

17. Broadwell, I., Fletcher, P.D.I., Haswell, S.J., McCreedy, T. and Zhang, X., Quantitative 3-dimensional profiling of channel networks within transparent 'lab-on-a-chip' micro reactors using a digital imaging method, *Lab on a Chip*, 2001, 1, 66-71.

*Reproduced with permission from The Royal Society of Chemistry. DOI:
10.1039/b103280c*

18. Fletcher, P.D.I., Haswell, S.J. and Zhang, X.L., Electrical currents and liquid flow rates in micro reactors, *Lab on a chip*, 2001, 1, 115-121.

*Reproduced with permission from The Royal Society of Chemistry. DOI:
10.1039/b106339c*

19. Wiles, C., Watts, P., Haswell, S.J. and Pombo-Villar, E., The aldol reaction of silyl enol ethers within a micro reactor, *Lab on a chip*, 2001, 1, 100-101.

*Reproduced with permission from The Royal Society of Chemistry. DOI:
10.1039/b107861e*

20. Watts, P., Wiles, C., Haswell, S. J., Pombo-Villar, E., Solution phase synthesis of beta-peptides using micro reactors, *Tetrahedron*, 2002, 58, 5427-5439.

Reprinted with permission from Elsevier

21. Fletcher, P.D.I., Haswell, S.J., Pombo-Villar, E., Warrington, B.H., Watts, P., Wong, S.Y.F., Zhang, X. L., Micro reactors: principles and applications in organic synthesis, *Tetrahedron*, 2002, 58, 4735-4757.

Reprinted with permission from Elsevier

22. Wiles, C., Watts, P., Haswell, S.J., Pombo-Villar, E., The regioselective preparation of 1,3-diketones within a micro reactor, *Chem Comm.*, 2002, 1034-1035.

*Reproduced with permission from The Royal Society of Chemistry. DOI:
10.1039/b201220k*

23. Wiles, C., Watts, P., Haswell, S.J. and Pombo-Villar, E., The regioselective preparation of 1,3-diketones, *Tetrahedron letters*, 2002, 2945-2948.

Reprinted with permission from Elsevier

24. Watts, P., Wiles, C., Haswell, S.J., Pombo-Villar, E., Investigation of racemisation in peptide synthesis within a micro reactor, *Lab on a chip*, 2002, 2, 141-144.

*Reproduced with permission from The Royal Society of Chemistry. DOI:
10.1039/b203977j*

25. Fletcher, P.D.I., Haswell, S.J. and Zhang, X.L., Electrokinetic control of a chemical reaction in a lab-on-a-chip micro-reactor: measurement and quantitative modelling, *Lab on a chip*, 2002, 102-112.
Reproduced with permission from The Royal Society of Chemistry. DOI: 10.1039/b201685k
26. Wiles, C., Watts, P., Haswell, S.J. and Pombo-Villar, E., 1,4-addition of enolates to alpha,beta-unsaturated ketones within a micro reactor, *Lab on a chip*, 2002, 62- 64.
Reproduced with permission from The Royal Society of Chemistry. DOI: 10.1039/b202210a
27. Haswell, S.J. and Watts, P., Green chemistry: synthesis in micro reactors, *Green Chem.*, 2003, 5, 240-249.
Reproduced with permission from The Royal Society of Chemistry. DOI: 10.1039/b210539j
28. Watts, P. and Haswell, S.J., Microfluidic combinatorial chemistry, *Curr. Opin. Chem. Biol.*, 2003, 7, 380-387.
Reprinted with permission from Elsevier
29. Watts, P. and Haswell, S.J., Continuous flow reactors for drug discovery, *Drug Discov. Today*, 2003, 8, 586-593.
Reprinted with permission from Elsevier
30. Fletcher, P.D.I., Haswell, S.J. and Zhang, X.L., Monitoring of chemical reactions within micro reactors using an inverted Raman microscope spectrometer, *Electrophoresis*, 2003, 24, 3239-3245.
Reprinted with permission from John Wiley and Sons
31. George, V., Watts, P., Haswell, S.J., and Pombo-Villar, E., On-chip separation of peptides prepared within a micro reactor, *Chem. Comm.* 2003, 23, 2886-2887.
Reproduced with permission from The Royal Society of Chemistry. DOI: 10.1039/b310744b
32. Wiles, C., Watts, P., Haswell, S.J., and Pombo-Villar, E., Solution phase synthesis of esters within a micro reactor, *Tetrahedron*, 2003, 59, 10173-10179.
Reprinted with permission from Elsevier
33. Wiles, C., Watts, P. and Haswell, S.J., The application of micro reactor technology for the synthesis of 1,2-azols, *Org. Proc. Res. Dev.*, 2004, 8, 28-32.
Reprinted with permission from American Chemical Society
34. He, P., Haswell, S.J. and Fletcher, P.D.I., Microwave heating of heterogeneously catalysed Suzuki reactions in a micro reactor, *Lab on a chip*, 2004, 4, 38-41.

*Reproduced with permission from The Royal Society of Chemistry. DOI:
10.1039/b313057f*

35. Feng, X.Z., Haswell, S.J. and Watts, P., Organic synthesis in micro reactors, *Current Topics in Medicinal Chemistry*, 2004, 4, 707-727.

Publication removed due to copyright restrictions

36. Wiles, C., Watts, P., Haswell, S.J. and Pombo-Villar, E., Stereoselective alkylation of an Evans auxiliary derivative within a pressure-driven micro reactor, *Lab on a Chip*, 2004, 4, 171-173.

Reproduced with permission from The Royal Society of Chemistry. DOI:

10.1039/b400280f

37. He, P., Haswell, S.J. and Fletcher, P.D.I., Microwave-assisted Suzuki reactions in a continuous flow capillary reactor, *Applied Catalysis A*, 2004, 274, 111-114.

Reprinted with permission from Elsevier

38. Wiles C., Watts P. and Haswell S.J., An investigation into the use of silica-supported bases within EOF-based flow reactors, *Tetrahedron*, 2004, 60, 8421-8427.

Reprinted with permission from Elsevier

39. Watts P., Haswell S.J., Pombo-Villar E., Electrochemical effects related to synthesis in micro reactors operating under electrokinetic flow, *Chem. Eng. J.*, 2004, 101, 237-240.

Reprinted with permission from Elsevier

40. Watts P. and Haswell S.J., Combinatorial synthesis in micro reactors, *Combinatorial Chem. & High Throughput Screening*, 2004, 7, 397-405.

Publication removed due to copyright restrictions

41. Jonsson, C, Lundgren, S., Haswell, S.J. and Moberg, C., Asymmetric catalysis in a micro reactor – Ce, Yb and Lu catalysed enantioselective addition of trimethylsilyl cyanide to benzaldehyde, *Tetrahedron*, 2004, 60, 10515-10520.

Reprinted with permission from Elsevier

42. Pennemann H., Watts P., Haswell S.J., Hessel V. and Lowe H., Benchmarking of microreactor applications, *Org. Proc. Res. Dev.*, 2004, 8 422-439.

Reprinted with permission from American Chemical Society

43. Broadwell, I., Fletcher, P.D.I., Haswell, S.J., Zhang, X., Allen, R.W.K., MacInnes, J.M. and Du, X., Pressure-driven and electroosmotic flows and electrical currents in Lab-on-a-chip micro reactor devices, *Trends in Physical Chemistry*, 2004, Vol. 10, 117-133.

Publication removed due to copyright restrictions

44. Watts P. and Haswell S.J., The Application of Micro Reactors for Organic Synthesis, *Chem. Soc. Rev.*, 2005, 34, 235 – 246.
Reproduced with permission from The Royal Society of Chemistry. DOI: 10.1039/b313866f
45. He, P., Haswell, S.J. and Fletcher, P.D.I., Efficiency, monitoring and control of microwave heating within a continuous flow capillary reactor, *Sensors & Actuators B*, 2005, 105, 516 – 520.
Reprinted with permission from Elsevier
46. Wiles C., Watts P. and Haswell S.J., Acid-catalysed synthesis and deprotection of dimethyl acetals in a miniaturised electrophoretic flow reactor, *Tetrahedron*, 2005, 61, 5209 – 5217.
Reprinted with permission from Elsevier
47. He P., Watts P., Marken F., and Haswell S.J., Electrolyte free electro-organic synthesis: The cathodic dimerization of 4-nitrobenzyl bromides in a micro-gap cell, *Electrochem. Comm.*, 2005, 7, 918-924.
Reprinted with permission from Elsevier
48. Wiles C., Watts P., Haswell S.J., The preparation and reaction of enolates within micro reactors, *Tetrahedron*, 2005, 61 10757-10773.
Reprinted with permission from Elsevier
49. Zhang, X. and Haswell, S.J., Materials matter in microfluidic devices, *MRS bulletin*, 2006, 31 (2) 95-99.
Publication removed due to copyright restrictions
50. He, P., Watts, P., Marken, F. and Haswell, S.J., Self-supported and clean one-step cathodic coupling of activated olefins with benzyl bromide derivatives in a micro flow reactor *Angew. Chem. Int. Ed.*, 2006, 45 (25) 4146-4149.
Reprinted with permission from John Wiley and Sons
51. Wiles, C., Watts, P. and Haswell, S.J., Clean and selective oxidation of aromatic alcohols using silica-supported Jones' reagent in a pressure-driven flow reactor, *Tetrahedron letters*, 2006, 47 (30), 5261-5264.
Reprinted with permission from Elsevier
52. Zhang, X., Yin, H., Cooper, J.M. and Haswell, S.J., A microfluidic based system for analysis of single cells based on Ca²⁺ flux, *Electrophoresis*, 2006, 27, 5093-5100.
Reprinted with permission from John Wiley and Sons
53. Zhang, X., Cooper, J.M., Monaghan, P.B. and Haswell, S.J., Continuous flow separation of particles within an asymmetric microfluidic device, *Lab on a Chip*, 2006, 6, 561-566.

*Reproduced with permission from The Royal Society of Chemistry. DOI:
10.1039/b515272k*

54. Yin, H., Zhang, X., Patrick, N., Klauke, N., Cordingley, H.C., Haswell, S.J. and Cooper, J.M., Influence of hydrodynamic conditions on quantitative cellular assays in microfluidic systems, *Anal. Chem.*, 2007, 79, (7), 7139-7144.

Reprinted with permission from American Chemical Society

55. He, P., Watts, P., Marken, F. and Haswell, S.J., Electrosynthesis of phenyl-2-propanone derivatives from benzyl bromides and acetic anhydride in an unsupported micro-flow cell electrolysis process, *Green Chem.*, 2007, 9, 20-22.

*Reproduced with permission from The Royal Society of Chemistry. DOI:
10.1039/b610415k*

56. Wiles, C, Watts, P., and Haswell S.J., The use of solid-supported reagents for the multi-step synthesis of analytically pure alpha, beta-unsaturated compounds in miniaturized flow reactors, *Lab on a chip*, 2007, 7, 322-330.

*Reproduced with permission from The Royal Society of Chemistry. DOI:
10.1039/b615069a*

57. He, P., Watts, P., Marken, F. and Haswell, S.J., Scaling out of electrolyte free electrosynthesis in a micro-gap flow cell, *Lab on a chip*, 2007, 7, 141-143.

*Reproduced with permission from The Royal Society of Chemistry. DOI:
10.1039/b610411b*

58. Wiles C., Watts P. and Haswell S.J., The use of electroosmotic flow as a pumping mechanism for semi-preparative scale continuous flow synthesis, *Chem. Comm.*, 2007, 966-968.

*Reproduced with permission from The Royal Society of Chemistry. DOI:
10.1039/b614559k*

59. Wiles, C., Watts, P. and Haswell, S.J., An efficient, continuous flow technique for the chemoselective synthesis of thioacetals, *Tet. Let.*, 2007, 48, 7362 - 7365.

Reprinted with permission from Elsevier

60. Yin H., Patrick N., Zhang X, Klauke N., Cordingley H.C., Haswell S.J., Cooper J.M., Quantitative comparison between microfluidic and microtitre plate formats for cell-based assays, *Anal. Chem.*, 2008, 80, 179-185.

Reprinted with permission from American Chemical Society

61. Zhang, X., Yin, H., Cooper, J.M., Haswell, S.J., Characterization of cellular chemical dynamics using combined microfluidic and Raman techniques, *Analytical and Bioanalytical Chemistry*, 2008, 390, 833-840.

Reprinted with permission from Springer

62. Yoon, T-H., Park, S-H., Min, K-I., Zhang, X., Haswell, S.J. and Kim, D-P., Novel inorganic polymer derived microreactors for organic microchemistry applications, *Lab on a chip*, 2008, 8, 1454-1459.
Reproduced with permission from The Royal Society of Chemistry. DOI: 10.1039/b804726j
63. He, P., Greenway, G. and Haswell, S.J., The on-line synthesis of enzyme functionalized silica nanoparticles in a microfluidic reactor using polyethylenimine polymer and R5 peptide, *Nanotechnology*, 2008, 19, 315603 (7pp).
Publication removed due to copyright restrictions
64. Zhang, X., Jones, P. and Haswell, S.J., Attachment and detachment of living cells on modified microchannel surfaces in a microfluidic-based lab-on-a-chip system, *Chem. Eng. J*, 2008, 135, S82-S88.
Reprinted with permission from Elsevier
65. Hattersley, S.M., Dyer, C.E., Greenman, J. and Haswell, S.J., Development of a microfluidic device for the maintenance and interrogation of viable tissue biopsies, *Lab on a chip*, 2008, 8, 1842-1846.
Reproduced with permission from The Royal Society of Chemistry. DOI: 10.1039/b809345h
66. Garcia-Alonso, J., Greenway, G.M., Hardege, J.D. and Haswell, S.J., A prototype microfluidic chip using fluorescent yeast for detection of toxic compounds, *Biosens. and Bioelectronic*. 2009, 24 1508-1511.
Reprinted with permission from Elsevier
67. Zhang, X.L., Coupland, P., Fletcher, P.D.I. and Haswell, S.J., Monitoring of liquid flow through microtubes using a micropressure sensor, *Chem. Eng. Res. Design*, 2009, 87, 19-24.
Reprinted with permission from Elsevier
68. Wild, G.P., Wiles, C., Watts, P. and Haswell, S.J., The use of immobilized crown ethers as in-situ N-protecting groups in organic synthesis and their application under continuous flow, *Tetrahedron*, 2009, 65, 1618-1629.
Reprinted with permission from Elsevier
69. Shapiro, M.S., Haswell, S.J., Lye, G.J., Bracewell, D.G., Design and characterization of a microfluidic packed bed system for protein breakthrough and dynamic binding capacity determination, *Biotech. Progress*, 2009, 25, 277-285.
Reprinted with permission from Elsevier
70. Oakley, J.A., Shaw, K.J., Docker, P.T., Dyer, C.E., Greenman, J., Greenway, G.M. and Haswell, S.J., Development of a bi-functional silica monolith for electro-

osmotic pumping and DNA clean-up/extraction using gel-supported reagents in a microfluidic device, *Lab on a chip*, 2009, 9, 1596-1600.

Reproduced with permission from The Royal Society of Chemistry. DOI: 10.1039/b820553a

71. Oakley, J.A., Robinson, S., Dyer, C.E., Greenman, J., Greenway, G.M. and Haswell, S.J., Development of a gel-to-gel electro-kinetic pinched injection method for an integrated micro-fluidic based DNA analyser, *Anal. Chim. Acta*, 2009, 652, 239-244.
Reprinted with permission from Elsevier

72. Shaw, K.J., Thain, L., Docker, P.T., Dyer, C.E., Greenman, J., Greenway, G.M. and Haswell, S.J., The use of carrier RNA to enhance DNA extraction from microfluidic-based silica monoliths, *Anal. Chim. Acta*, 2009, 652, 231-233.
Reprinted with permission from Elsevier

73. Dou, Y., Haswell, S.J., Greenman, J. and Wadhawan, J., Immobilized anthraquinone for redox mediation of horseradish peroxidase for hydrogen peroxide sensing, *Electrochem. Comm.*, 2009, 1976–1981.
Reprinted with permission from Elsevier

74. Shaw, K.J., Joyce D.A., Docker, P.T., Dyer, C.E., Greenman, J., Greenway, G.M. and Haswell, S.J., Simple practical approach for sample loading prior to DNA extraction using a silica monolith in a micro fluidic device, *Lab on a chip*, 2009, 9, 3430-3432.
Reproduced with permission from The Royal Society of Chemistry. DOI: 10.1039/b913309g

75. He, P., Greenway, G. and Haswell, S.J., Development of enzyme immobilized monolith micro-reactors integrated with microfluidic electrochemical cell for the evaluation of enzyme kinetics, *Microfluid Nanofluid*, 2010, 8, 565-573.
Reprinted with permission from Springer

76. He, P., Greenway, G. and Haswell, S.J., Development of a monolith based immobilized lipase micro-reactor for biocatalytic reactions in a biphasic mobile system, *Proc. Biochem.*, 2010, 45, 593-597.
Reprinted with permission from Elsevier

77. He, P., Davies, J., Greenway, G. and Haswell, S.J., Measurement of acetylcholinesterase inhibition using bienzymes immobilized monolith micro-reactor with integrated electrochemical detection, *Anal. Chim. Acta*, 2010, 659, 9-14.
Reprinted with permission from Elsevier

78. Anderson, K., Cooper, J.M., Haswell, S.J., Marshall, D., Yin, H. and Zhang Z., Microfluidic-based measurements of cytochrome P450 enzyme activity of primary mammalian hepatocytes, *Analyst*, 2010, 135, 1282–1287.

*Reproduced with permission from The Royal Society of Chemistry. DOI:
10.1039/c0an00031k*

79. Shaw, K.J., Docker, P.T., Yelland, J.V., Dyer, C.E., Greenman, J., Greenway, G.M. and Haswell, S.J., Rapid PCR amplification using a microfluidic device with integrated microwave heating and air impingement cooling, *Lab on a chip*, 2010, 10, 1725 – 1728.

*Reproduced with permission from The Royal Society of Chemistry. DOI:
10.1039/c000357n*

80. Cheah L-T., Dou, Y-H., Seymour, A-M.L., Dyer, C.E., Haswell, S.J., Wadhawan, J.D. and Greenman, J., Microfluidic perfusion system for maintaining viable heart tissue with real-time electrochemical monitoring of reactive oxygen species, *Lab on a chip*, 2010, 10, 2720-2726.

*Reproduced with permission from The Royal Society of Chemistry. DOI:
10.1039/c004910g*

81. Webster, A., Dyer, C.D., Haswell S.J. and Greenman, J., A microfluidic device for tissue biopsy culture and interrogation, *Anal. Methods*, 2010, 2, 1005–1007.

*Reproduced with permission from The Royal Society of Chemistry. DOI:
10.1039/c0ay00293c*

82. Shapiro, M.S. Haswell, S.J., Lye, G.J. and Bracewell, D.G. Microfluidic chromatography for early stage evaluation of biopharmaceutical binding and separation conditions, *Separation Science and Technology*, 2011, 46, 185–194.

Reprinted with permission from Taylor & Francis

83. Shaw, K.J., Joyce, D.A., Docker, P.T., Dyer, C.E., Greenway, G.M., Greenman, J. and Haswell, S.J., Development of a real-world direct interface for integrated DNA extraction and amplification in a microfluidic device, *Lab on a Chip*, 2011, 11, 443–448.

*Reproduced with permission from The Royal Society of Chemistry. DOI:
10.1039/c0lc00346h*

84. He, P., Greenway, G. and Haswell, S.J., Microfluidic synthesis of silica nanoparticles using polyethylenimine polymers, *Chem. Eng. J.* 2011, 167, 694-699.

Reprinted with permission from Elsevier

85. Shaw, K. J., Birch, C., Hughes, E.M., Jakes, A.D., Greenman, J. and Haswell, S.J., Microsystems for personalized biomolecular diagnostics, *Eng. Life Sci.*, 2011, 11, 121–132.

Reprinted with permission from John Wiley and Sons

86. Webster, A., Greenman, J., Haswell, S.J., Development of microfluidic devices for biomedical and clinical application, *Journal of Chemical Technology and Biotechnology*, 2011, 86. 10-17.
Reprinted with permission from John Wiley and Sons
87. Garcia-Alonso, J., Fakhrullin, R.F., Paunov, V.N., Shen, Z., Hardege, J.D., Pamme, N., Haswell, S.J., Greenway, G.M., Microscreening toxicity system based on living magnetic yeast and gradient chips, *Analytical and Bioanalytical Chemistry*, 2011, 400, 1009-1013.
Reprinted with permission from Springer
88. He, P.; Haswell, S.J.; Fletcher, P.D.I.; Kelly, S.M. and Mansfield, A., Scaling up of continuous-flow, microwave-assisted, organic reactions by varying the size of Pd-functionalized catalytic monoliths, *Beilstein J. Org. Chem*, 2011, 7, 1150-1157.
Reprinted with permission from Beilstein Institute open access
89. Betts, J.W., Kitney, S.P., Fu, Y., Peng, W-M., Kelly, S.M. and Haswell, S.J., Production of deuterium labelled (-)-epicatechin in a microreactor, *Chem, Eng. J.*, 2011, 167, 545-547.
Reprinted with permission from Elsevier
90. Fletcher, P.D.I.; Haswell, S.J, He, P., Kelly, S.M. and Mansfield, A., Permeability of silica monoliths containing micro- and nano-pores, *J. Porous Matter*, 2011, 18, 501-508.
Reprinted with permission from Springer
91. Woods, J., Docker, P.T., Dyer, C.E., Greenman, J., Haswell S.J., On-chip integrated labelling, transport and detection of tumour cells, *Electrophoresis*, 2011, 32, 3188–3195.
Reprinted with permission from John Wiley and Sons
92. Hattersley, S. M., Greenman J. and Haswell S.J., Study of ethanol induced toxicity in liver explants using microfluidic devices, *Biomed. Microdevices*, 2011, 13, 1005-1014 .
Reprinted with permission from Springer
93. Kemp, C., Birch, C., Shaw, K.J., Nixon, G.J., Docker, P.T., Greenman, J., Huggett, J.F., Haswell, S.J., Foy, C.A., and Dyer, C.E., Direct processing of clinically-relevant large volume samples for the detection of sexually transmitted infectious agents from urine on a microfluidic device, *Anal. Methods*, 2012, 4, 2141 – 2144.
Reproduced with permission from The Royal Society of Chemistry. DOI: 10.1039/c2ay25075f

94. Parton, J., Birch, C., Kemp, C., Haswell, S.J., Pamme, N. and Shaw, K.J., Integrated DNA extraction and amplification using electrokinetic pumping in a microfluidic device, *Anal. Methods*, 2012, 4, 96-100.
Reproduced with permission from The Royal Society of Chemistry. DOI: 10.1039/c1ay05552f
95. Hattersley, S.M., Sylvester, D.C., Dyer, C.E., Stafford, N.D., Haswell, S.J. and Greenman, J., A microfluidic system for testing the responses of head and neck squamous cell carcinoma tissue biopsies to treatment with chemotherapy drugs, *Anal. Biomedical Eng.*, 2012, 40, 1277-1288.
Reprinted with permission from Springer
96. Cheah, L.T., Fritsch, I., Haswell, S.J. and Greenman, J., Evaluation of heart tissue viability under redox-magneto-hydrodynamics conditions: Toward fine-tuning flow in biological microfluidics applications, *Biotech. and Bioeng.*, 2012, 109, 1827-1834.
Reprinted with permission from John Wiley and Sons
97. Kashkary, L., Kemp, C., Shaw, K.J., Greenway, G.M. and Haswell, S.J., Improved DNA extraction efficiency from low level cell numbers using a silica monolith based micro fluidic device, *Anal. Chim. Acta*, 2012, 750, 127-131.
Reprinted with permission from Elsevier
98. He, P., Haswell, S.J., Fletcher, P.D.I., Kelly, S.M. and Mansfield, A., Acetylation of alcohols and phenols using continuous-flow, tungstosilicic acid-supported monolith micro reactors with scale-up capability, *J. Flow Chem.*, 2012, 2, 47-51.
Reprinted under open access
99. Parton, J., Hassan, N.A., Brown, T.A., Haswell, S.J., Brown, K.A., Shaw, K.J., Sex identification of ancient DNA samples using a microfluidic device, *J. Archaeol. Sci.*, 2013, 40, 705-711.
Reprinted with permission from Elsevier
100. Chaplain, G., Haswell, S.J., Fletcher, P.D.I., Kelly, S.M. and Mansfield, A., Development and evaluation of a Raman flow cell for monitoring continuous flow reactions, *Aust. J. Chem.*, 2013, 66, 208–212.
Reprinted under open access
101. Sylvester, D., Hattersley, S.M., Stafford, N.D., Haswell, S.J., Greenman, J., Development of microfluidic-based analytical methodology for studying the effects of chemotherapy agents on cancer tissue, *Current Anal. Chem.* 2013, 9, 2-8.
Publication removed due to copyright restrictions

102. Shaw, K.J., Hughes, E.M., Dyer, C.E., Greenman, J., Haswell, S.J., Integrated RNA extraction and RT-PCR for semi-quantitative gene expression studies on a microfluidic device, *Lab. Invest.*, 2013, 93, 961-966.

Reprinted with permission from Nature Publishing Group

Appendix 1

Copies of submitted papers

Note PDF copies of the publications 35, 40, 43, 49, 63 and 101 have been removed due to Copyright restrictions.

Letter

Development of a micro flow injection manifold for the determination of orthophosphate

R.N.C. Daykin, S.J. Haswell *

School of Chemistry, University of Hull, HU6 7RX Hull, UK

Received 22 June 1995; revised 14 July 1995; accepted 20 July 1995

Abstract

Fabrication of micro flow injection analysis (μ FIA) systems based on glass substrates using lithographic techniques and etching methodology has been found to produce a reliable manifold for orthophosphate analysis based on colorimetric detection. The channel dimensions used were 30 μ m deep and 325 μ m wide, and mobility of the reagents and analytes was achieved by exploiting electrokinetic mobility (at pH < 3) and electroosmotic flow (at pH > 3). Detection was facilitated through the use of fibre optics coupled to a LED photodiode system. The time for analysis for the μ FIA methods was found to be 3 min per analysis and the procedure had a limit of detection of 0.7 ppb (PO_4^{3-}) with R.S.D. values in the range 1–5%. The total volume of reactants in the μ FIA device was estimated to be 0.5 μ l.

Keywords: Flow injection; Micro flow injection analysis (μ FIA); Miniaturization; Phosphate

1. Introduction

Miniaturization of analytical systems offers considerable potential for overcoming many of the problems associated with traditional instrumental methods of analysis, namely the handling of large volumes of hazardous or costly reagents and the need for specialized bench and laboratory support facilities. Further the combination of such systems with sensor technology offers an attractive methodology for the realization of field devices. The interest in miniaturization has followed closely developments in micromachining technology which has allowed accu-

rate and reproducible manufacture of small scale systems. The main developments to date in miniaturized analytical systems, other than for specific sensor fabrication, have been in the field of separation science which benefits from increased speed of analysis and from the reduction in sample and reagent volumes (μ l). The focus of such systems has mainly been towards liquid separations in the form of capillary electrophoresis (CE) [1] which achieves separation of analytes in an applied electrical field as a function of analyte charge properties and in doing so exploits two main transport mechanisms: migration or electrokinetic mobility and electroosmotic flow (EOF) [2]. Migration represents the response of an ion to an applied electrical potential, under which anions move to a more positively charged electrode and cations to a more negative electrode. Electroos-

* Corresponding author.

mosis is a more complicated process dependent on the interaction between the carrier and the charge present on the surface of the capillary.

The application of electroosmotic pumping to facilitate flow in a miniature manifold has been discussed by Seiler et al. [3], who discuss the manipulation of flow in a microchannel system using multiple electrodes to control mixing of flow systems. The work reported two important results, firstly that both hydrodynamic and diffusion effects contribute to the creation of Venturi style streaming at side channels, i.e., that a solution in a channel perpendicular to that in which flow has been induced will be drawn into the flow. Secondly that the resistances calculated at constant applied voltage across a system of three intersecting channels obey Kirchoff's rules for a network of resistors, allowing the potential at a point in a system to be predicted from the conductivity and geometry of the system. This allows a valveless fluidic control to be achieved where mixing and flow direction can be controlled by manipulation of the voltage applied to the system.

Compared to conventional small bore flow injection systems [4] micro flow injection systems offer a more portable, robust and mechanically stable

methodology which has the potential of producing more reliable devices. Further, micro flow systems offer the possibility of single sample, multianalyte analysis, based on one device in either two or three dimensions with multiple chemical systems and detectors with computer control and data handling instead of the more linear geometry traditionally associated with small bore flow injection analysis.

Miniature systems using micromachined diaphragm pumps etched into silica have been reported [5] but these often suffer from problems of pump pulsing, and back pressure due to their size. In addition the complexity of manufacture which may require up to 5 layers of machined silica make such devices difficult to produce. With such systems it is also difficult and troublesome to produce multiple flows in different directions or where complex flow geometries may be required.

This paper will describe the fabrication of a μ FIA system for colorimetric determination of orthophosphate as the molybdenum blue complex. The preliminary results using micro flow technology are comparable to those obtained using an existing proven flow system [6] and some of the major operating parameters of the μ FIA device will be discussed.

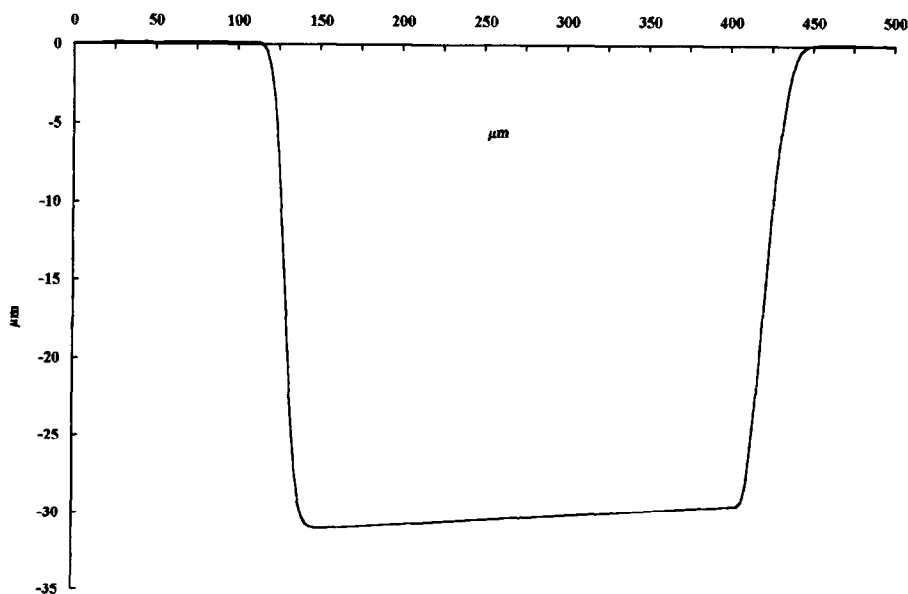


Fig. 1. Dektak scan of 50 μ m channel.

2. Experimental

2.1. Device fabrication

The devices were prepared according to the method given below. Each plate produced 25 devices of 5 different geometries, for each geometry 2 devices were prepared with a pre etch width of 50 μm , 2 with 30 μm and the final 1 with 20 μm channel width.

The plate (152.4 mm square), made from soda glass 3 mm thick was sputtered with a 0.1 μm thick layer of chrome and then spin coated with a 0.7 μm thick layer of AZ1350 positive photoresist (Shipley). The plate was covered with the photomask and exposed to UV light for 5 μs . The plate was then developed in CD351 photoresist developer (Shipley) at 30°C for 30–40 s with agitation. The developer was then washed off with deionised water and dried before etching the exposed chrome with CE8001 chrome etch (Shipley). When the channels had been clearly etched, the plate was removed from the bath of etching solution and washed with deionised water. The plate was again dried and placed in an oven at 120°C for 72 h to harden the photoresist and ensure total removal of solvents which might cause the photoresist to deform during the glass etching process. The plate was taken from the oven and immersed in the glass etching solution (1% hydrofluoric acid (BDH Merck AnalaR) with 5% ammonium fluoride (BDH Merck AnalaR)) at 70°C for 2 h with constant agitation. The plate was then removed from the bath and washed with deionised water. After drying the plate was exposed to strong UV light and then developed in CD351 for several hours to remove the remaining photoresist. The chrome layer was then stripped off using Microposit chrome etch 18 (Shipley). The plate was washed in deionised water, dried and then cut into separate 25.4 mm square base sections.

The channels in the prepared bases were measured using a Dektak 3 ST diamond stylus surface profiler. A typical trace obtained from this instrument is shown for a plate with a 2 h etch (Fig. 1). The channel width was initially 50 μm on the photomask, which when etched was expected to expand laterally by twice the depth removed [7], therefore for a required final depth of 20 μm , the

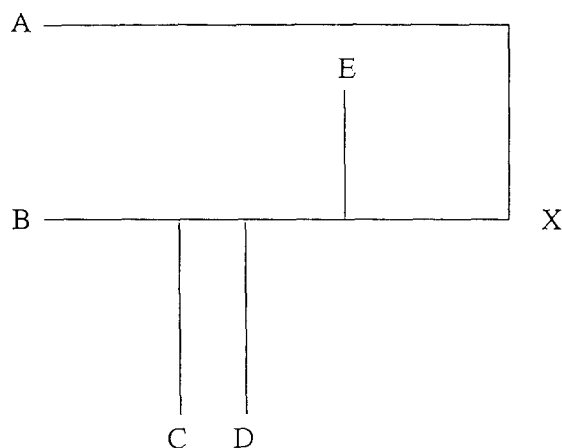


Fig. 2. Diagram of the micro flow injection analysis system. A = Ascorbic acid reservoir; B = ammonium heptamolybdate reservoir; C = unused reservoir; D = sample reservoir; E = sample waste reservoir.

expected width expansion of the channel would predictably be 40 μm as the acid undercuts the chrome. As seen from the Dektak profile the channel has expanded more than expected probably due to the use of soda glass rather than silica or quartz. The resulting etch for the first plate created a set of channels based on 50 μm pre etch widths, 30 μm deep with a maximum width of 325 μm .

For each plate a lid was prepared from 1 mm soda glass drilled with 2 mm diameter holes to provide reservoirs at points corresponding to the channel ends in the base sections. These lids were then fused onto the bases by heating in a muffle furnace at 575°C for 96 h and allowed to cool in the oven for a further 24 h.

The assembled devices had plastic reservoirs fitted to the holes in the lids to provide both a large reserve of reagent and a mechanical support for the platinum wire electrodes.

The different designs were produced to evaluate different flow and process geometries, however, the specific design used to demonstrate FIA methodology can be seen in Fig. 2. The device was used to construct a system for the detection of orthophosphate as the phosphomolybdate complex by spectrophotometric measurements.

The prepared devices were tested in a custom built isolation box with a non-conducting stage and

internal current and voltage metering across the two electrodes. The isolation box was fitted with a power cut-out preventing high voltage operation with the lid open and fibre optic cables (1 mm plastic) were used to carry optical signals between the device in the isolation box and the external light source and detector. A Farnell HiVolt XRV30/1.7 reversible polarity power supply (Farnell, Leeds) was used which enabled a power output up to 50 W with voltages up to 30 000 V and currents up to 1.7 mA to be selectable in constant stabilised current or voltage modes with an adjustable trip for overcurrent protection. This was connected via high purity copper conductors to 0.15 mm diameter platinum electrodes with a 10 mm exposed length for interfacing with the solutions in the reservoirs. The voltage was measured using an AVO analogue voltmeter (Avometer 8) connected in parallel with the device and the current measured on an AVO digital autoscaling multimeter (Avo multimeter M2036) with a low range of 0.00–300.00 μA . The light source was a red (700 nm peak output) high output LED (RS 564-015, RS Stores) rated at 3000 millicandela at 10 V which was matched with a photodetector with internal amplifier (850 nm peak sensitivity, RS 308-067, RS Stores) with the output range of 0–10 V dark voltage to LED direct reduced through the system to around 0–300 mV full scale deflection. The optical data was recorded on a chart recorder (Chessell BD-40-04, Kipp & Zonen, Netherlands).

2.2. Procedure

The ascorbic acid was made up at 5 g/l in order to establish a pH just below 3 and the ammonium heptamolybdate (0.005 M) made up in UHQ water, rather than nitric acid, at the original concentration which had a pH of 3.8 which was adjusted to pH 3.2 with 0.4 M nitric acid. The system was run with the molybdate reagent in reservoir B with the positive electrode and ascorbic acid in reservoir A with the negative electrode (Fig. 2). The phosphate was loaded into reservoir D and water placed in reservoir E and the electrical field applied from E(+) to D(-) which drew the sample into the main channel accompanied a slight change in the observed absorbance trace, this taking around 20–30 s. The electrodes were then restored to the original positions in reser-

voirs A and B and the field applied as before. The process was repeated up to 6 times before the reagents were replenished. A series of standards was prepared in the range 10–1000 ppb and a calibration model prepared.

3. Results and discussion

The initial studies of photolithographic micromachining of soda glass to create micro flow injection systems showed that it was a viable technique for the manufacture of micro flow systems to high, reproducible standards. From scanning electron microscopy examination the geometry of the junctions were found to be well defined despite channel spreading, indicating the ability to develop complex geometries using the manufacturing method described.

The ascorbic acid solution as used in the conventional system had a pH of 1.6 which was too acidic for the formation of EOF and the molybdate registered no reading on the pH meter ($< \text{pH } 1$) suggesting that the solution was extremely acidic, whilst the phosphate sample showed a pH of around 6.8. The acidity of the molybdenum solution thus explained the early difficulties experienced in moving the reagent and so it was decided to prepare the molybdenum solution in water instead of the acid so relying on the ascorbic acid to both oxidise the complex and provide the necessary conditions for reaction. In order to verify the chemistry of the system, these modified reagents when mixed 1:1 in a test tube gave an initial pH of 1.99, in the presence of phosphate the reaction proceeded rapidly and after around 2 min had reached an end point with a pH of 2.99, which was acceptable for EOF formation.

With the electrodes placed in their primary positions (A + B -) and the fibre optics applied along channel BX a current of 50 μA was applied. The molybdate was allowed to move by electroosmotic flow towards the positive electrode (A) while the ascorbic acid moved purely by electrokinetic mobility in the opposite direction. Observing at low current the change in absorbance when the system was first primed with reagents, it appeared that the ascorbic acid and molybdenum solutions were meeting after approximately 2 min in the vicinity of the

junction between reservoir E and the main channel. The electrodes were then moved to the sample loading positions (D + E –) and the current applied again for 1 min which gave rise to a slight increase and then drop in the absorbance reading. The electrodes were then returned to their original positions (A + B –) and the field restored. As the reaction reached completion, after about 60 s, the pH rose and the precipitate was carried by EOF out of the light path and away in the direction of the ascorbic acid reservoir. As soon as the precipitate was out of the light path and the detector had settled the process was repeated for a second sample and so on. It is interesting to note that the ascorbic acid moving under electrokinetic mobility is able to pass through the molybdenum which continued to migrate in the opposite direction under EOF in channel A. By changing the sample in reservoir A with a syringe a series of standards were run in replicate. The data obtained from the experiments with the micro system showed precision ranging from less than 5% R.S.D. at 10 ppb to less than 0.8% at 100 ppb orthophosphate for $n = 5$. The linear range of the micro system was found to be 10–100 ppb with the equation $\text{concentration/ppb} = (\text{absorbance/mV} - 10.922)/8.357$ giving a theoretical limit of detection of 0.7 ppb (calculated using $3 \times \text{S.D. of lowest standard}$).

Throughout the experiments the power delivered through the electrodes did not cause visible bubble formation at the electrodes, neither electrolysis nor boiling was observed except in the case of dilute (ca. 2 M) nitric acid which did exhibit bubble formation at the electrodes when used to backflush the channels to remove residual molybdenum blue.

The micro system offered the specific advantages of reduced reagent usage (total system volume approximately 0.5 μl , sample volume approximately 50 nl) and less corrosive reagents. In addition, the glass surface of the manifold was not effected by dilute acids and so the system does not require regular changing of components such as pump tubing and connectors as may be required in a conventional flow system. Potential interferences associated

with organic components in the system have yet to be fully explored but early indications suggest these will not pose a serious problem for the proposed methodology.

4. Conclusion

Miniaturization of chemical processes can offer considerable potential for the development of chemical measurement techniques in particular sensor technology. The present work has demonstrated that the fabrication of a μFIA manifold based on lithographic technology can produce a working device based on current chemistries and detection systems. The μFIA device fabricated out of glass had channels of 325 μm wide and 30 μm deep and used both electrokinetic and electroosmotic flow techniques to facilitate the mixing and mobility of reagents and products. The determination of orthophosphate as the phosphomolybdate complex was selected as a well understood process with which to evaluate the μFIA methodology. A more fundamental study of the reaction mechanisms, mixing properties and mechanisms of mobility has yet to be concluded, but the initial results from this and other work in the field show great promise

References

- [1] A. Manz, D.J. Harrison, E. Verpoorte and H.M. Widmer, *Adv. Chromatogr.*, 33 (1993) 1.
- [2] K.B. Oldham and J.C. Myland, *Fundamentals of Electrochemical Science*, Academic Press, Canada, 1994.
- [3] K. Seiler, Z.H.H. Fan, K. Fluri and D.J. Harrison, *Anal. Chem.*, 66 (1994) 3485.
- [4] J. Ruzicka and E.H. Hansen, *Flow Injection Analysis*, 2nd edn., Wiley, New York, 1988.
- [5] H.T.G. van Lintel, F.C.M. van de Pol and S. Bouwstra, *Sensors Actuators*, 15 (1988) 153.
- [6] J.J. Pauer, H.R. van Vliet and J.F. van Staden, *Water SA*, 14 (1988) 125.
- [7] D.J. Elliot, *Integrated Circuit Fabrication Technology*, McGraw-Hill, USA, 1982.

Critical Review

Development and Operating Characteristics of Micro Flow Injection Analysis Systems Based on Electroosmotic Flow

A Review

S. J. Haswell

School of Chemistry, University of Hull, Hull, UK HU6 7RX

Summary of Contents

Introduction
Fabrication
Pump Design
Injector Design
Reactor Design
Detector Design
Future Trends
Conclusion
References

Keywords: *Micro flow injection; electroosmotic flow; miniaturisation; micro total analytical system (μ TAS)*

Stephen J. Haswell is a Senior Lecturer in Analytical Chemistry at the University of Hull, UK. Following a period of five years working in the food and plastics industries, he undertook a Ph.D. in the area of atomic spectroscopy graduating in 1983 from the University of Plymouth. His current research activities are in the areas of μ FIA, micro-wave enhanced reaction chemistry, trace elemental speciation and chemometrics. He is author of over 100 research papers, books and patents and presenter of numerous national and international lectures on his research activities. The subject of this present review has become a great interest of the author over the past five years.



Introduction

Over the past 50 years, the design of instrumentation for the measurement of chemical, biological and physical parameters has brought analytical chemistry to a highly automated and technologically advanced science. It would be naive, however, to believe that the chemistries and physics associated with

present day analytical measurements, are in any way limited by current technology. On the contrary, laboratory based analysis has been almost exclusively designed, for the ergonomic needs of the human worker. There can be little doubt that this preoccupation with the physical size and operation of equipment, for laboratory based measurements, has significantly influenced the teaching and practice of analytical chemistry. If one considers the fundamental chemical and physical phenomena on which measurements are based, then it is apparent that one only requires a few molecules or atoms to be present for quantitative measurement to occur. In short, the physics and engineering of measurement science can be considered as oversized and in many cases over engineered to meet the needs of the chemical measurement.

Whilst instrumental design has relentlessly moved towards automation, the realization that the quality of analytical data can be profoundly influenced by factors such as sampling, sample storage, sample pretreatment and matrix interferences has led to the concept of the total analytical approach. This more holistic view of analysis, in which traceability and uncertainty prediction can be carried out, is often embodied in the concept of the 'total analytical system' (TAS).¹ There are, however, numerous disadvantages to TAS, including slow sample processing, lack of selectivity and high reagent consumption;² however, many such problems may be overcome through system miniaturisation. The term micro TAS (μ TAS) was first used at the Transducers 89 Conference.³ In its simplest sense, μ TAS involves the miniaturisation of all the functions found in an analytical method for example, pumps, valves, flow manifolds, mixing and reaction chambers, phase and analyte separation, detectors, control and communication electronics. One of the more exciting prospects of the μ TAS concept is the suggestion that the entire chemical measurement laboratory could be miniaturised onto a device of a few square centimetres.⁴ This type of miniaturisation has become possible largely through the adoption of microfabrication techniques developed in general by the microelectronics industry, and one can consider miniaturisation of chemical reactors and their corresponding instrumental requirements to be in a similar position to the microelectronics industry 30 years ago. Interestingly, it was from the heart of the microelectronics industry that Terry *et al.*⁵ were one of the first to demonstrate that integrated circuit (IC) technology could be used to fabricate a miniature GC instrument using a 5 in silicon wafer. Although the work of Terry and co-workers served to point the way, it was not until the advent of capillary electrophoresis (CE)^{1,6–8} and in particular, the exploitation of electroosmotic flow (EOF), that the realization of μ TAS came about some 10 years after the miniature GC work was first reported.

A significant research base has now built up in the area of μ TAS^{9–14} and the development of μ FIA over the past 5 years can be attributed to key research carried out by groups based in Basle, Switzerland,¹⁴ Texas Tech. University, USA,¹⁵ University of Alberta, Canada,¹⁶ the Oak Ridge National Laboratory, Tennessee, USA,¹⁷ and in a very modest way in the author's own laboratory.¹⁸ What follows is a review of the features present in a relatively small, but rapidly expanding research base, which can be exploited to develop micro flow injection analysis (μ FIA) systems, based on electroosmotic flow, to produce reliable sensor-type devices which incorporate mechanical and chemical robustness.

Fabrication

The fabrication of μ FIA systems has attracted various approaches in recent years, ranging from manifolds based around CE-type fused-silica capillaries,¹ to modular micro pump systems.^{19,20} This particular section, however, will focus specifically on fabrication methodology which leads to the production of a single integrated device, designed to use electroosmotic mobility for sample and reagent pumping.¹⁸ The discussion will focus almost exclusively on micro machined monolithic device fabrication, which adopts standard IC photolithographic, wet etching and bonding techniques to produce a planar structure.^{21,22} As the techniques used are based essentially on IC technology, they represent well established methodology, outlined schematically in Fig. 1. If one considers the current 'state-of-the-art' in IC fabrication, then it is clear that the challenge of producing μ FIA manifolds can in no way be considered as technologically demanding. From what follows, it will become clear that μ FIA device fabrication can be relatively simple and offer a reasonably high degree of flexibility in systems design.

The choice of a suitable substrate into which the channels of a μ FIA manifold can be etched is closely related to factors such as the fabrication method, the analytical chemistries involved

and the proposed pumping, injection and detection systems. The obvious candidate given the close relationship with IC technology is silicon,²³ which is amenable to the fabrication of structures in the nano- and micro-metre range. This crystalline material can be obtained in a very pure form, at relatively low cost, and offers good mechanical and chemical properties. Whilst silicon may seem an ideal microengineering candidate for μ FIA fabrication, it is by nature a conductor and so surface modifications will be required if electroosmotic pumping of samples and reagents is to be achieved. This can be carried out by coating the silicon with SiO₂ or Si₃N₄ to produce the required surface chemistries. Harrison *et al.*¹⁶ described the fabrication of such a manifold, in which the properties of silicon and oxide/nitride-modified layered surfaces were evaluated. They reported that the operating voltage achievable with such devices will be limited by the quality of the oxide insulating film produced. Nevertheless, the results are sufficient to demonstrate that silicon-based devices using a sandwich structure (*i.e.*, oxide–nitride–oxide) can sustain potentials in the range 400–1200 V before dielectric breakdown, which is certainly sufficient to generate EOF mobility for μ FIA systems. Although silicon does offer the attraction of producing high precision engineered μ FIA manifolds, with well characterised surfaces and the potential to integrate control and detection on to one substrate, other materials such as glass²⁴ and silica (quartz)²⁵ are also amenable to IC based fabrication techniques and will produce surfaces eminently suitable for EOF pumping. Judging from the reports in the literature, glass and silica have proved to be the most popular materials for device fabrication to date, but metal, plastic and ceramic substrates are also possible candidates for the manufacture of μ FIA systems.^{26,27}

In general, three basic concepts are required for the preparation of μ FIA systems: (i) a suitably prepared substrate, (ii) photolithographic equipment and (iii) wet etching and bonding facilities.²⁸ Prepared substrates based on glass, silica and silicon can be obtained commercially from photomask producers (*e.g.*, Alignrite, Wales, UK); these come ready coated with a metal film (0.1 μ m) such as chromium over which is spun a positive photoresist layer (0.7 μ m). These plates, which are typically 152.4 mm square (5 × 5 in) and 3 mm thick, can be used directly for manifold pattern transfer using photolithographic methods. A mask or negative of the final channel patterns required for the μ FIA system can be produced using CAD computer software.^{29,30} The mask pattern can be transferred to the photoresist film on the substrate, using basic photographic development equipment. For channels larger than 1 μ m, visible or UV light can be used to transfer the pattern from the mask to the photoresist (exposure times being approximately 5 μ s); however, to obtain good line definition and sub-micro patterning, X-ray or electron-beam (e-beam) photolithography will be required. Where facilities permit, e-beam photolithography offers at present one of the most flexible ways of producing μ FIA manifold designs; however, for most applications simple basic photographic equipment will suffice.

Once the pattern has been transferred to the photoresist film on the substrate, the plate can be developed and wet etched. If one uses the large plates as described, then multiple devices can be prepared; in our laboratory, for example, 25 manifolds of various geometries and channel widths are produced from one plate (Fig. 2).¹⁸ Workers in the field tend to prepare their own plates rather than using a commercial source and, although this adds additional steps to the fabrication process, it is not too technically demanding.^{29,30} As indicated previously, these are typically made from silica or glass on to which a thin metal film (0.05–0.1 μ m) of chromium, gold or a combination is produced, using sputtering or chemical vapour deposition (CVD) methods. The metal film is then spin coated with a layer of positive photoresist (approximately 0.5–2 μ m).

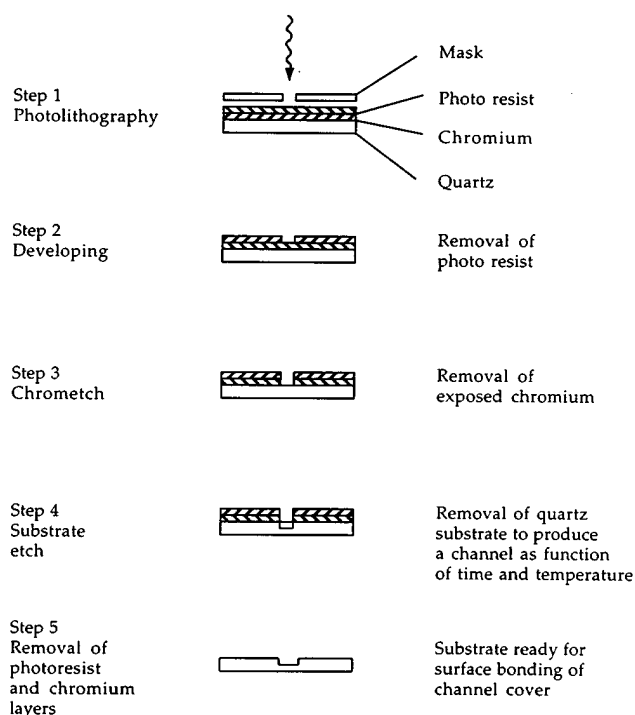


Fig. 1 Schematic diagram of the steps involved in the anisotropic etching technique for the fabrication of μ FIA devices. The arrow in Step 1 represents radiation.

Following the photolithographic transfer of the manifold pattern, the exposed photoresist and corresponding metal film are removed using commercially available reagents. The prepared plates may then be placed in an oven at 120 °C for 72 h to harden the photoresist and remove solvent residues from the plate.¹⁸ It should be noted that although the presence of a metal film on the glass is important for controlling the degree of surface etching that will occur, the exposed substrate will experience undercutting or sideways etching, which will proceed at a rate of approximately 2:1. Thus, as the etch goes down to 1 µm it spreads laterally 2 µm at the edges, producing channels, for which the width always exceeds the depth.³¹ Clearly, for a given substrate, the choice of the initial photomask line width and the time of etch will influence the size of the final channels produced.

Various reagents have been used for the wet etching of the substrate, but in general for glass and silica, hot (70 °C) dilute HF–NH₄F (1% HF + 5% NH₄F in water)^{18,29} will give an etch rate of approximately 0.3–0.5 µm min⁻¹, whereas dilute HF–HNO₃ produces an etch rate of between 0.5 and 0.8 µm min⁻¹ in Pyrex.³⁰ Silicon etching requires the use of reagents such as ethylenediaminepyrocatechol (115 °C, etch rate 2.5 µm min⁻¹) or KOH.¹⁶ Although indicative figures for etch rates can be obtained,^{31,32} it is strongly recommended that sample strips of the substrate are tested in the selected etchant to establish the rate of etching for a given system. It should be stressed that the final size of the µFIA channels will depend on the initial width of the lines on the photomask, the substrate material and mode of etching. During the etching process, agitation of the substrate or etchant is advisable otherwise asymmetric channel formation, *i.e.*, uneven etching on the bottom edge or side of the channel, may occur. It is usual, however, to obtain a channel profile that is wider at the top than the bottom. This effect, associated with undercutting, will vary as a function of the etch time, substrate type and reagents used. The surface quality of the etch is generally related to the types of material used. Good quality silica, for example, gives a well defined etch, whereas Pyrex or borosilicate glass can produce a rougher surface owing to the crystalline structure of the material. The real effect or significance of the surface properties in µFIA channels has not yet been fully characterised, but clearly the more controlled the etch, the more precise and smaller will be the channels that one can produce. What is not apparent from experimental results is the real influence that surface topography may have on the mobility and reactivity of reagents in a µFIA system. Rough or

poorly defined surfaces and intersections, of one or more channel, will increase the effect of turbulence and in turn promote dispersion, which in some instances may prove to be an advantage where mixing is required. This factor is particularly important in capillary systems where the Reynolds number is lower than the transitional values of 2000 or 2300 indicating laminar flow, thus minimal mixing will dominate.^{33–35} However, research indicates that at low Reynolds numbers microfluidic mixing cannot be simply classified as a laminar or turbulent model.³⁶ What is clear is that as channel sizes become smaller, surface effects will inevitably become more significant, which in turn will have an impact on fabrication and material specifications. Manz and Simon³⁷ demonstrated that for a 10-fold decrease in channel size, a 1000-fold decrease in reagent consumption and a 100-fold decrease in related time variables would be obtained. Pressure requirements of such a system will, however, increase by a factor of 100, but as indicated later this does not effect the voltage requirements for EOF.

Once an etched base has been produced, the top of the channels need to be sealed. Various bonding methods have been suggested, including glueing, low temperature bonding or annealing, high temperature fusion and anodic bonding.³⁸ The use of an adhesive in such systems can pose problems due to channel plugging and, although this may be overcome to some extent by using photosensitive dry films laminated on to the substrate surface as a protective coating,³⁹ the technique has found little real use in µFIA. Thermal bonding or annealing of top plates represents one of the simplest and therefore most widely used methods in device fabrication. These methods usually involve heating the substrate and top plate, which may be under slight pressure,³⁰ in an oven or furnace to near the upper annealing temperature. For glass and silica this is usually between 500 and 600 °C, whereas silicon will require higher temperatures of around 900 °C. The period of heating varies between 48 and 96 h, after which the device is slowly cooled (48–72 h) to minimize physical stress. For glass substrates, hydrolysing the surface with dilute NH₃–H₂O₂ followed by heating at 500 °C for 24 h²⁹ or 575 °C for 96 h¹⁸ has been demonstrated to achieve good reliable bonding. Slightly more complex temperature programmes have been suggested, but these are essentially slight modifications to the same basic method.³⁰ In order to keep the fabrication of a µFIA manifold as simple as possible and to increase the bonding success rate, it is advisable to use the same material (*i.e.*, similar thermal expansion coefficients) for both the base and top of the device, so minimizing stress features. The fabrication of multilayer devices can become complex and techniques using intermediate layers have been described in which more complex structures such as pumps and valves are required.^{40,41} One technique which has found particular favour with workers fabricating microvalves, micropumps and silicon devices generally is anodic bonding.^{42,43} In this process, ions such as sodium and oxygen are thought to migrate at elevated temperatures to electrodes placed on the outer surface of one of the layers, so increasing the electrostatic surface charge. The temperature and applied voltages used will depend on the materials in question, but for glass these are found to be 200–400 °C at 30–300 V and for silica 700–800 °C at 30 V applied for a period of 45 min. It might be necessary when employing anodic bonding to treat the surface with HF prior to bonding.

Holes or ports made in the top plate are commonly used as reagent or sample feeds into the manifold and can be generated either before¹⁸ or after^{29,30} the bonding process. The holes can simply be produced by using mechanical¹⁸ or ultrasonic¹⁶ drilling of the substrate and vary in diameter from 0.5–2 mm. At present, laser ablation, which offers an attractive method for hole production, has not been employed, but no doubt the technique will find its way into the literature before long. Plastic

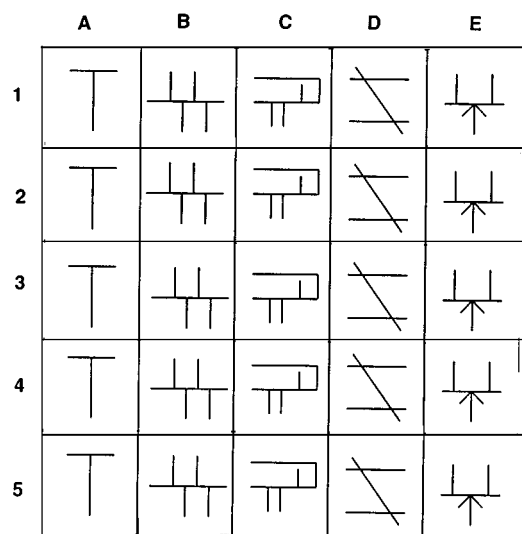


Fig. 2 Example of the photomask design used to produce five µFIA manifolds designs with variable line or channel widths. The line widths shown are A and E, 50, B, 30 and C, 10 µm.

reservoirs are usually glued to hold liquids and support the platinum electrodes when required. A photograph of a completed device used for phosphate and nitrite determination is shown in Fig. 3.

To date, only planar μ FIA systems have been reported based on the fabrication techniques described. The fabrication of three dimensional systems is, however, an attractive prospect and no doubt stacked systems will be produced as more sophisticated chemistries are exploited. Such systems based on micropumps have been reported in which multi-layers or modules are clamped or stuck together to produce a complete device.^{19,20}

Once a complete μ FIA manifold has been fabricated for use with EOF pumping, the success of the bonding process can be checked by filling the channels with a buffer⁴⁴ or weak acid¹⁸ and plotting the current–voltage relationship. This plot is generally found to be linear up to 10 kV in glass and silica, after which point dielectric breakdown of the substrate occurs. Any deviation in linearity at lower applied voltages is indicative of a device failure, associated with incomplete bonding.

Pump Design

In order to achieve reliable flow dynamics in an FIA manifold, which may contain numerous reagent streams, pulse free, constant flow characteristics must be maintained. It is not surprising therefore, to find that μ FIA systems also call for pulse free, variable nl min^{-1} – $\mu\text{l min}^{-1}$ flow control. Although a direct syringe or piston pump can be used with μ FIA systems,^{45,46} the closest equivalent to a conventional peristaltic FIA pump is the so called micropump, which usually takes the form of a pulsating one-way valve driven typically by a piezoelectric device.^{36,45,47–50}

Based on microengineering technology, micropumps have been employed in μ FIA manifolds consisting of channels 100 μm wide, 10 μm deep and 4 cm in total length.⁴⁷ When such small channel dimensions are employed, the hydrodynamics of the system can produce a pressure drop of 0.7 atm at a flow rate of 0.5 $\mu\text{l min}^{-1}$. However, diaphragm devices, commonly using microchemical silicon membranes, are only reliable up to back-pressures of 0.2 atm and so high pressure pumps or large channel dimensions are therefore required. High pressure pump designs using nickel rather than silicon check valves are now being developed using low temperature bonding techniques, incorporating intermediate photoresist layers to adhere the valve to the body of the pump.⁴⁷ These devices, which use a piezoelectric disc glued to the outer surface of the pump

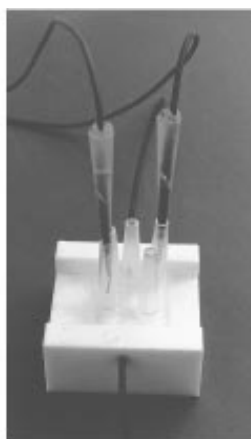


Fig. 3 A fully assembled μ FIA device showing the mounted plastic reservoirs which act as wells for the reagents and samples and support the platinum electrodes required for EOF pumping. The device is shown mounted in a rig which allows fibre optics (seen either side of the block) to be coupled into relevant sections or channels of the manifold.

housing, operate at many hundred Hertz, requiring around 300 V to produce flow rates in the range 20–300 $\mu\text{l min}^{-1}$. In an elaborate example, four such pumps have been used to drive reagents through a three-dimensional system constructed from silicon and glass at a flow rate of 1 ml min^{-1} , the channel dimensions being 600 μm wide and 200 μm deep in order to accommodate pressure effects.¹⁹ Diaphragm micropumps do have an important role to play in applications where electro-osmotic pumping is not applicable, owing to sample or reagent chemistries. It is essential, however, that micropumps remain chemically inert to the reagents and samples with which they may come into contact. In addition to piezoelectrically driven pumps, ultrasonic⁵¹ and other more exotic electrically activated pumps have also been described.^{36,52–54}

Electrophoresis embodies two basic electrokinetic components, electroosmotic and electrophoretic flow. These two components combine to give the total flow or velocity (v) in the following way:

$$\text{total flow rate} = v = (\mu_{\text{eo}} + \mu_{\text{ep}})E \quad (1)$$

where μ_{eo} = electroosmotic mobility, μ_{ep} = electrophoretic mobility and E = applied electric field.

At relatively low electric field strengths, electroosmotic mobility represents the larger component of the two processes; however, as the field strengths are increased the influence of the electrophoretic component (migration of analyte ions) increases also. For μ FIA, where bulk mobility is desired, one finds that field strengths around 300–400 V cm^{-1} are usually adequate; however, if separation is required, as in CE, then field strengths greater than 1 kV cm^{-1} are typically required. It is common for μ FIA systems based on EOF to operate with field strengths of the order of 80–300 V cm^{-1} , at which little or no analyte separation is observed. The generation of an EOF to pump reagents and samples through a μ FIA system is subject, however, to certain physico-chemical limitations. Firstly, in order to generate the EOF one must use a material which will yield negatively charged groups on the surface or walls of the channels when placed in contact with an appropriate liquid. Secondly, the liquid phase must dissociate to some extent in order to generate counter positive ions (notably H^+ ions). The combination of the negatively charged surface (typically SiO^-) and the H^+ ions in solution will form a diffuse double layer (sometimes referred to as the Gouy or Helmholtz layer). This diffuse double layer acts as a parallel-plate electric capacitor whose plates are d cm apart each carrying a charge e per cm^2 . The zeta potential (ξ) will be the potential difference between the plates, given by the general equation

$$\xi = 4\pi ed/\epsilon_r \quad (2)$$

where ϵ_r is the relative permittivity of the medium between the hypothetical plates. If an electrical field is now applied through the liquid phase, ions will migrate to their respective electrodes dominated by the positive ions (H^+) moving to the negative or ground electrode. As the ions move, they induce a drag on the bulk of the liquid, which in turn results in a corresponding net transfer of the solution to the negative electrode. Thus, in EOF the mobility of the solution is from the anode (positive electrode) to the cathode (negative electrode) or ground. In practice, the formation of the double layer is limited to the pH range 4–10. At lower pH values the cationic population becomes so high that the EOF is overrun by conductive flow and at pH values greater than 10 the cation population becomes too low to sustain the double layer. The zeta potential that is generated when the double layer forms will be influenced by changes in pH and ionic strength of the solutions in the channel, and this can affect the corresponding flow rate. Clearly, as one of the main attributes of a pump in FIA is to maintain a reproducible flow rate, the pH and ionic strength of the reagents

used in a μ FIA manifold need to be controlled, through the use of buffer systems. As the ionic strength increases, for example, a counter-ion effect will prevent the ions from migrating through the solution independent of the EOF. In general, it is therefore preferable to keep the total ionic strength of reagents and samples as low as possible.

Once an EOF has been generated, the flow establishes a flat, trapezoidal profile notably different from the parabolic (bullet) shape commonly associated with conventional FIA. Closer investigation of the μ FIA profile reveals that the edges of the profile (*i.e.*, closest to the wall surface) are slightly in advance of the bulk owing to the drag effect and the extent of this effect will be a function of the solution viscosity.⁵⁵ The fact that the flow profile, which offers minimal band broadening, does not contain the parabolic flow characteristics of a pressure or hydrodynamically pumped system, does have implications with respect to the mixing of reagents in the μ FIA reactor, where some dispersion will be necessary to achieve the desired chemical reactions. Thus EOF-pumped μ FIA can be considered to be more akin to segmented flow analysis rather than conventional FIA, in its flow characteristics.

In an EOF-pumped μ FIA system, the flow rate can be effectively controlled by varying the applied voltage as follows:

$$\text{flow rate } v = \frac{v}{L} \mu \quad (3)$$

where v = applied voltage (V), L = length of the channel (m) and μ = sum of the electroosmotic and electrophoretic mobility component under different conditions of pH and ionic strength.

The EOF and hence the flow rate in μ FIA, will be unaffected by capillary diameter up to channel sizes approaching 250 μ m, after which drag effects of the bulk solution may cause serious disruption to the EOF. The EOF produced in a channel can be considered, in the electrical sense, as a resistor, thus Joule heat will occur in the capillary. However, the almost negligible bulk properties of components in a channel, relative to the substrate, will ensure an effective dissipation of heat, which rarely poses a serious problem in μ FIA. If, however, the resistance is allowed to increase, for example when a highly viscous or an immobile solvent is present in a channel, heating can occur.

It should be stressed that an EOF can only be established if the double layer is formed, and this requires ions or dipoles to be present in the liquid stream. In the case, for example, where organic compounds or solvents may be present, such conditions may not be met. For example Zheng and Dasgupta⁵⁵ described some initial studies, using silica capillaries, to evaluate the suitability of an EOF in a μ FIA system for carrying out in-line analyte phase separation or solvent extraction. They described the use of a 50 cm \times 7.5 μ m id polyimide coated silica capillary to investigate various aqueous ionic complexes, based on well characterised cationic, anionic and neutral ion-pair chemistries. A quaternary ammonium salt, tetrabutylammonium perchlorate, was added to chloroform as a supporting electrolyte to assist in the mobilization process⁵⁶ and to catalyse phase transfer.⁵⁷ The results clearly indicated that organic solvent pumping was possible, when modified with the quaternary ammonium salt, but that migration of the ammonium ion occurred, creating a positive front end to the solvent slug. Bleeding of ions into the secondary aqueous buffer from the organic phase was also reported. Furthermore, they suggest that a thin interfacial layer of buffer is generated between the organic solvent and the capillary walls which enables the EOF to be generated. Investigations into solvent extraction indicated that the ion-pair complexes studied were either extracted into the organic phase or accommodated in the aqueous phase ahead of the organic slug interface. Not only were the findings of Zheng and

Dasgupta a significant contribution in terms of demonstrating phase extraction and organic solvent mobility using EOF in a μ FIA system, but they also clearly indicate that the migration of ions within a solvent under the influence of an electric field could lead to the development of gradient and separation techniques, complementary to CE, such as selective solvent extractions and matrix modification. Interestingly, the use of micellar electrokinetic capillary chromatography, described by Moore *et al.*,⁵⁸ suggests that multiphase systems could be developed for μ FIA applications, thus offering significant advantages for organic solvent based chemistries.

Although it is possible to use EOF as the primary pumping mechanism in a μ FIA manifold, it may be preferable or even necessary to isolate the pumping mechanism from the injector, reactor and detector components of the system. Such occasions might be, for example, when the chemistry of the method or detector system is not compatible with the electrical field required for direct EOF pumping. One such system has been described by Dasgupta and Liu⁴⁵ in which a section of polyimide-coated fused-silica tubing (40 cm \times 75 μ m id) was connected to a second capillary, *via* an isolating membrane. In the first channel a 2 mm borax buffer is pumped by direct EOF, with a field strength of around 40 V cm⁻¹. As the flow in the pumped capillary was electrically isolated from the second capillary it produced a hydrodynamic effect, sufficient to create a flow in the second channel, which could be varied between 1 nl min⁻¹ and 100 μ l min⁻¹. In this case the hydrodynamic effect of the EOF is exploited in a μ FIA manifold without the need for a direct electrical field.

Injector Design

The introduction or injection of a sample into an FIA manifold can generally be classified into two general types. The first is the timed or gated injection in which a sample is drawn into the FIA manifold, usually through a sampling probe, for a controlled period of time, after which the flow is switched back to the carrier stream. In this way, a variable volume can be injected into a manifold as a function of time. The second and more usual method of injection in FIA, is the introduction of a constant sample or reagent volume into a mobile carrier in a way that affords minimal flow dispersion. The most common approach for such systems is to use a rotary or slide valve, which contains a sample loop of a defined volume. It would therefore seem appropriate to have both these forms of sample injection available in μ FIA systems, and this is indeed found to be the case.

The injection of a sample into a μ FIA manifold can be performed using hydrodynamic/pneumatic pressure control,⁴⁶ miniaturised valves¹ or electrokinetic mobility based on EOF.^{15,18,59-62} Even the lowest volumes obtainable with traditionally based rotary-type valves⁶³ are clearly too large for practical use in μ FIA. However, Liu and Dasgupta¹ recently described the use of commercially available valves with an injection volume of 60 nl. It should be stressed, however, that most of the work relating to the introduction of small sample volumes (<20 nl) into capillary systems has been focused on CE methodology rather than addressing μ FIA systems. Of particular relevance to μ FIA systems is the development of the so-called valveless injection method, which uses EOF control in conjunction with specific capillary channel geometries.^{64,65}

The two simplest approaches to sample injection based on EOF are first to pump a sample for a given period of time into a flow channel and second to fill a defined volume (equivalent of a sample loop) built into the μ FIA manifold. In the former case, Zheng and Dasgupta⁵⁵ described a modified CE system in which an organic solvent was loaded for a given period of time into a μ FIA system consisting of a 50 cm \times 75 μ m id polyimide

coated fused-silica capillary. The solvent was introduced into the system by placing the capillary electrode in the solvent reservoir at 15 kV for 10 s. Following the injection step, the capillary electrode was switched to a borate buffer which subsequently pumped the solvent through the capillary to the detector. Using this approach, the authors reported an RSD of 0.51% associated with migration effects and 1.7% for the peak, suggesting that surface tension, viscosity and flow rate will influence this particular mode of injection. It should be noted that in this work, the authors were using the method described for introducing a solvent into the μ FIA system for the purpose of solvent extraction.

The second approach to sample introduction, based on defined volumes using EOF, falls into two categories, the X- and Z-type injections (Fig. 4). Of the two injection geometries, the X or cross design, has been most widely investigated. Depending on the geometry and electrical field used, the sample injection can be classified as 'floating' (gated) or 'pinched' (discrete), with the former occasionally being referred to as the continuous mode.^{59,60,64,65} Experimentally, the simplest of these two modes is the 'floating' method, as it only requires one pair of electrodes (Fig. 5). In this case the sample is pumped by an EOF from the sample reservoir (A the positive electrode) to the sample waste reservoir (B the negative electrode) along channel AB crossing part of channel CD. Note that the channel AB will have been filled prior to the sample introduction with a suitable buffer. The reservoirs C and D contain no electrodes and therefore have no applied field, hence their potential is floating relative to the field in channel AB. As the sample passes across the intercept of AB and CD, diffusion and eddy effects will allow some of the sample to migrate in the direction of both C and D [Fig. 5(a)]. Subsequently, on placing the electrodes in reservoirs C and D the field can be made to run in the CD direction, so any sample molecules in the intercept will be pumped towards D, the grounded reservoir [Fig. 5(b)], allowing the sample to pass *via* a detector on its way. Clearly, we can see that the leakage or migration of the sample solution into channel CD during injection and the possibility of dragging the stationary sample from channels A and B into D as a function of flow [Fig. 5(c)] will lead to an uncontrolled volume injection. Examples of this effect have been reported.^{59,60,64} The leakage observed into the main channel may not be a serious problem for certain applications and clearly it offers a simple method of operation, in which only one pair of electrodes are required. However, the quality of etch, surface topography and geometry of the channels concerned will influence the degree of diffusion using the 'floating' injection method.

The need, especially in CE, to have more precise control over the sample volume injected has led to the development of the so-called 'pinch' method (Fig. 5). In this case, the sample is once again pumped under an EOF from reservoir A to B, but this time reservoirs C and D are not electrically floating, but like A are given a positive potential, relative to the waste reservoir B

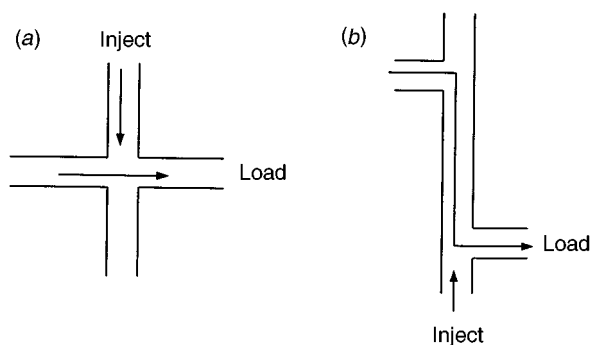


Fig. 4 Discrete volume injection using (a) the X and (b) the Z approach.

[Fig. 5(d)]. The effect of this is to draw buffer from channels C and D into B along with the sample from A. Under these flow dynamics, the sample gains a pinched or trapezoidal shape at the intercept of channels AB and CD. When the flow is redirected towards D [Fig. 5(e)], the sample volume, which may be only a few picolitres, is of a more precisely defined volume, less affected by diffusion effects. Jacobson *et al.*⁶⁰ have reported improvements in the RSD from 2.7 to 1.7% for a 90 μ l injection volume using the 'pinch' method, compared with the 'floating' approach. In this particular study, the applied voltages based on a 1 kV power supply were reservoir A 90, B 0, C 90 and D 100%, giving channel field strengths of 270, 20, 400 and 690 $V\ cm^{-1}$ in A, B, C and D, respectively. Clearly, operating the manifold in a multi-electrode configuration will reduce dispersion effects at intersections and allow improved control of the sample injection volume. The concept of the 'push-back distance' associated with surface diffusion has been used⁶⁶ to define the migration rate and shape of flow patterns at X-type intercepts. This approach to sample injection has considerable potential in controlling sample volumes as a function of applied field.

The larger volumes (9–22 nl) of the Z-type injection (Fig. 6) are introduced by pumping the sample between two reservoirs across a defined volume in a Z geometry. In the example shown, the sample is pumped from reservoir C or D to the waste reservoir D or E, so filling a defined volume in channel AX. The loaded sample can then be reacted with reagents in channel AX and moved to a detector or be monitored *in situ*. The Z mode of injection produces a larger volume than that obtained by the X mode, which in turn will be less influenced by the diffusional effects described previously.^{18,67} Recent work in the author's laboratory using the Z injection technique has indicated that

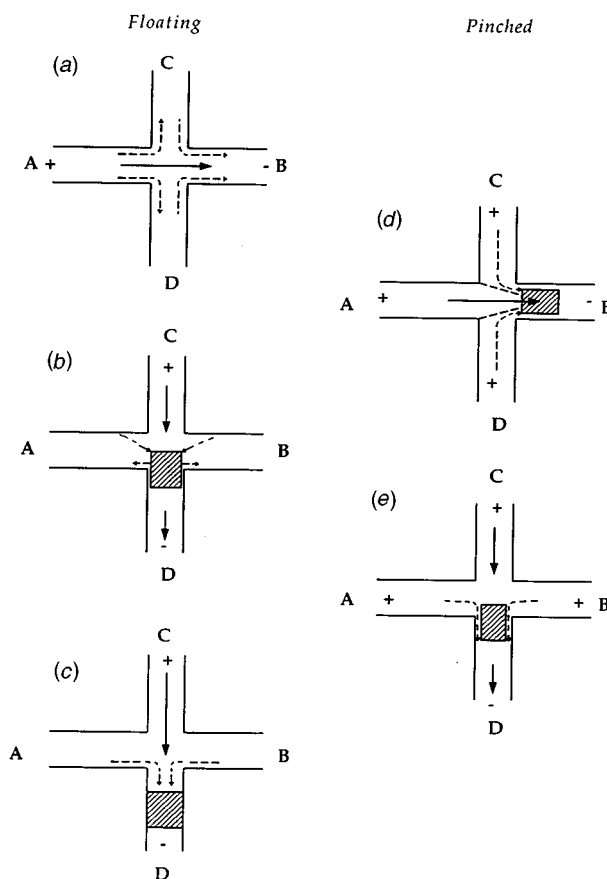


Fig. 5 Flow and dispersion characteristics of floating and pinched modes of injection.

pinch control offers no improvement in precision over the floating method.⁶⁸

The ability to matrix modify a sample in an injector system could be an attractive option in μ FIA and techniques such as synchronized cyclic capillary electrophoresis^{22,69} or sample fractionation⁶⁷ may offer considerable scope for such methodology. In these systems selected, analyte fractions can be separated from a more complex and possibly interfering matrix, owing to the variation in migration and flow direction under electrophoretic conditions. The switching of electrodes can be used to move components along channels and across channel intersections akin to shunting railway trucks, until the analytes required become isolated from matrix or interfering components. This aspect of sample manipulation is potentially very exciting for μ FIA system development and will no doubt be exploited in future applications.

Reactor Design

Having satisfactorily injected a sample into an FIA system, the next objective is usually to present the sample to a detector in an appropriate form as quickly as possible, using tube or channel geometries that minimize the dispersion of the sample slug. In μ FIA systems sample diffusion is known to be a function of the square root of the time after the injection of a sample.⁶⁹ There remains one additional and often complex step, however, that of achieving the appropriate chemistry or biochemistry necessary for the detection of the analyte of interest. This process typically requires the addition of at least one reagent and can include more complex steps such as in-line solid-phase extraction and multiphase separations.⁷⁰ Indeed, the complexity of the FIA manifold is only limited by the imagination or ingenuity of the analyst.

The first and perhaps the most important step in reactor design is a consideration of the physical and chemical characteristics that occur when two solutions combine at a channel junction in a μ FIA manifold. From the previous section, it is clear that even at Reynolds numbers less than 2000 some turbulent mixing takes place at channel intercepts and that the electrical potentials at which the channels are held can significantly influence the interfacial or mixing zone. Turbulent

mixing, for example, has been reported in channels 5.2 μ m deep and 57 μ m wide.⁷¹ The characterization of channel intersections indicates that leakage or diffusion of reagents from a 'floating' side stream into a channel in which EOF is present is around 2–5%, depending on the viscosity and flow rates.⁶⁴ This bleed occurs as a result of hydrodynamic effects, in which the molecules in the pumped stream entrain the stationary side channel molecules owing to frictional and eddy properties in a Venturi- or Bernoulli-type effect. What is interesting with such systems is that the flow characteristics in the main channel will have a flat, trapezoidal profile whereas the side channel, whose flow will be pressure driven, will have a parabolic profile. Hence the profiles of the merging streams may have a significant effect on the mixing characteristics at such an interface. As one of the main objectives of reagent addition in an FIA system is to induce mixing and so achieve the required reaction, some consideration needs to be given to this aspect of pumping in μ FIA systems.

In a valuable study, Seiler *et al.*⁴⁴ demonstrated that the individual electrical resistances in a series of interconnecting channels can be used to predict the flow characteristics, in a similar way to hydrodynamic estimations in conventional FIA. The basic concept considers the intercepting channels as electrical resistors and evokes Kirchhoff's rules,⁷² to predict the net flow of current which can be attributed to the flow dynamics of the device. One of the important findings of the work by Seiler *et al.*⁴⁴ is that by controlling channel voltages one is able to manipulate sample or buffer dilutions by adjusting flow rates, and this offers considerable scope for stopped-flow or reverse-flow operations. This effect was also recently demonstrated in our laboratory using a manifold previously described for phosphate analysis.¹⁸ Figure 6(a) illustrates how a sample of orthophosphate, held in reservoir D, is injected into channel AX using the Z technique, by pumping the sample to reservoir E. Thus the slug in channel AX defined by the intercepts DE represents the injected sample which reacts with ammonium heptamolybdate (0.01 M) in the presence of ascorbic acid (0.05 M) to produce molybdenum blue. Detection of the molybdenum blue is achieved by measuring the absorbance at 744 nm in a spectrophotometer coupled to the manifold by a fibre-optic system attached along channel AX (optical path 2 cm). Through the selection of different injection volumes [*i.e.*, C–D (9 nl), D–E (13 nl) and C–E (22 nl)] and variation in the positive voltage applied at reservoirs A and B relative to D or C, the absorbance signal was observed to decrease as the intercept 'pinch' potential applied across A–E and B–E became sufficient to dilute the formation of the coloured complex at each end of the injection slug.⁶⁸ In effect, the flow rate in channel A–B was being increased as a function of voltage, so diluting the flow from channels D–E, C–E or C–D into channel AX. Results obtained using this approach (Fig. 7) indicated that calibration based on one standard is possible and that the technique will have an important role to play in the development of future methodology.

Following the mixing of the reagent and analyte streams, some period of time is usually required to produce sufficient product, either for further reactions or for subsequent detection. Conventionally, this hold time is effected by using a coil or knotted reactor and/or a stopped-flow mode, in order to minimize dispersion whilst achieving the required reaction chemistries. In μ FIA it may be that owing to the more efficient interfacial nature of the mixing, *i.e.*, the need for less bulk mixing, reactions rates may increase; however, reactions are still likely to require a finite period of time for product production. A serpentine-type pattern or structure offers a very simple, but effective, use of space for extending channel length and is compatible with photolithographic fabrication techniques. The flow characteristics of serpentine channels have been studied and whilst disruption to the electroosmotic flow

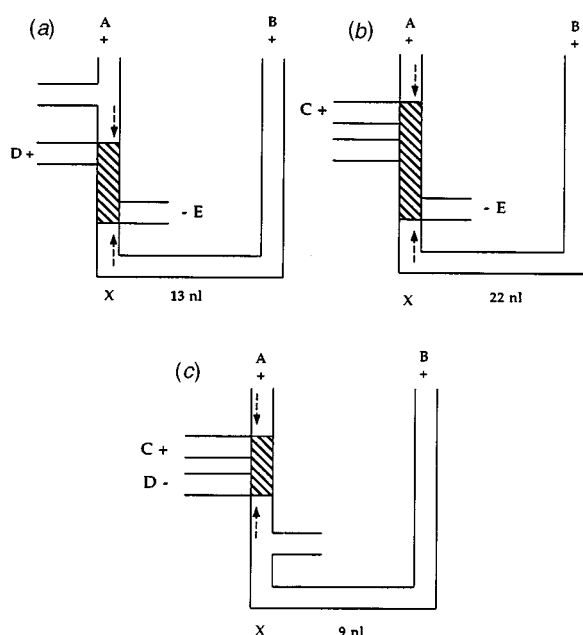


Fig. 6 Controlled dilution experiments using a pinch voltage.

was observed at the 90° bends, no significant band broadening has been found.⁶⁰ The particular design used had a total channel length of 17 cm operating with a field strength of 700 V cm⁻¹ and was used to perform electrophoretic separations. It would seem that using such an approach, time-dependent μ FIA reactions could be accommodated in a physically small area with minimal dispersion through the use of serpentine or spiral channels.⁶¹

Modification to the surface properties to induce selective flow characteristics, given the limitations of producing a double layer and hence EOF, has attracted some interesting approaches. These include the use of reversed-phase hydrophobic polymers,⁷³ surfactants,⁷⁴ silanals and quaternary ammonia groups.⁷⁵ In addition, the covalent bonding or immobilisation of glucose oxidase has been used to develop a glucose μ FIA method based on a serpentine geometry using a 260 cm long \times 100 μ m wide \times 70 μ m diameter reactor.⁷⁶

One of the interesting extensions of the μ FIA technology described is the development of electrochromatographic (EC) separations in which capillaries are packed with small particles (approximately 3 μ m) on which efficient separation can be achieved.⁷⁷ Using EOF as the primary pumping mechanism, EC can be mediated with reference to the zeta potential and hence separation is potentially possible through selection of the appropriate surface properties of a packing material. Thus the walls of the capillary act to facilitate the primary pumping mechanism and the packed chromatographic material offers enhanced electrophoretic separations.

In addition to surface modification, the physical effect of field flow fractionation may also be incorporated as a separation process in capillary systems.⁷⁸ In this case, an external force, *e.g.*, magnetism or gravity, is used to pull fractions to the wall of a channel; on removing the force, a gradual diffusion of the fractions in the sample occurs back into the flowing stream, usually based on molecular size.^{79,80} As yet field flow fractionation has not been widely studied in μ FIA systems, but the possibility of using field flow fractionation and modifying the zeta potential using a magnetic field might be an interesting subject for future research.

Detector Design

Much of the research reported to date in the area of μ FIA has focused on characterising the physical processes of reagent mobilisation and mixing in microchannel manifolds. Such work has relied heavily on imaging techniques, using, for example, charged coupled device (CCD) cameras⁶⁰ and microscopy-based techniques.^{30,44,61,81} In this section, consideration is given to the design of detectors suitable for direct integration

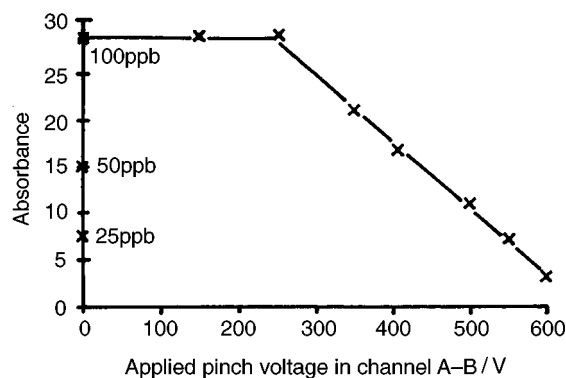


Fig. 7 Calibration based on 100 ppb PO₄ with dynamic applied pinch voltage. The equivalent absorbance values for 100, 50 and 25 ppb phosphate are indicated on the x-axis.

into EOF based μ FIA systems. The major detector systems used in conventional FIA are based on optical absorption/emission and electrochemical techniques,⁷⁰ and this is also found to be the case for μ FIA systems.^{82,83} Clearly, if electroosmotic based pumping is employed in the μ FIA manifold, then some care is required with the design of electrochemical detectors, but this does not pose any real serious limitations.⁸³ Not surprisingly, optical detection has proved to be the most attractive approach to on-device detection and various examples can be found in the literature,^{15,40,45,67} mainly associated with CE detectors.⁸⁴ One of the less obvious advantages of miniaturisation is the ability to introduce detector systems not readily available to conventional larger flow systems, such as mass-selective devices of the surface acoustic wave type.⁸⁵

Clearly, the design of a flow cell in terms of physical volume and optical geometry is very important in miniature systems if sensitivity, reliability and robustness are to be achieved. The incorporation of fibre optics as part of an optical detection system has proved to be of value, particularly with the advent of fibres with diameters of the order of 0.1 μ m.⁸⁶ In the area of optical detectors, some effort has gone into developing axially rather than perpendicularly oriented measurement cells.⁸⁷ Increasing the volume of the flow cell in a perpendicular viewing axis has been used to increase the optical pathlength,⁸⁸ whilst the use of multiple reflections axially in a flow cell has also been evaluated.⁸⁹ The first example led to severe dispersion effects and a subsequent loss in sensitivity and the second approach, based on a silicon device, suffered from signal loss due to scatter and absorption of light at the silicon surface.

One interesting approach to absorbance measurements is to consider the μ FIA channel as an extension of a fibre optic system.^{18,90} In this way, total internal reflection of light may be achieved and any photoactive species spatially present in the channel will undergo interaction with the photons present, to produce either a direct absorption measurement or a subsequent fluorescence effect. As with most absorption methods, it would be preferable to use a dual-channel system to improve stability and reduce scatter. Although a long pathlength is appealing for absorption measurements, emission-based techniques would benefit from a small spatial volumes in which the emission effect can be concentrated, and volumes less than 1 nl have been suggested.⁸⁹ The size of the detector cell is clearly related to the concentration and sensitivity of the method in question and a flow cell of 15 μ l has been reported to be adequate for chemiluminescent measurements of glucose and lactate in human serum.⁹¹ More recently Liang, *et al.*⁹² have described a UV cell with a parallel flow optical path of 120–140 μ m for absorbance and fluorescence detection at the end of a CE column, which would be most suitable for μ FIA applications.

Sequential detector arrays are an attractive approach in sensor design and lend themselves well to μ FIA systems.^{82,93} One such system⁸² has been described, based on electrochemical detectors, for liquid chromatographic separations of catecholamines and consisted of four photolithographically prepared ISFET sensors aligned sequentially in a 5 mm silicon channel 100 μ m wide and 70 μ m deep. The total volume of the detector was 20 μ l. Another device,⁹³ using a peristaltic pump to control flow rates, consisted of nine 5 μ m ISFET sensors housed in a 15 μ l cell, used for pH, potassium and calcium determinations in biological fluids. Although neither of these systems was used in μ FIA manifolds, they do illustrate the ability to develop array detectors compatible with μ FIA technology.

One of the most exciting prospects for μ FIA detector design is the ability to incorporate their fabrication into one integrated device. For example, miniature mass spectrometers (3 \times 3 \times 3 mm) have been produced based on fabrication technology that would be ideally suited for μ FIA.⁹⁴ Miniature spectroscopic systems are also becoming available^{95,96} and future developments in spectrometers incorporating opto-electronic systems

will undoubtedly bring valuable complementary technology for future μ FIA detector design.

Future Trends

The preceding sections have tried to focus on the basic concepts and developments relating to μ FIA systems based on EOF. Some indication has been given of the likely areas where current and future research may prove to be of great value. These include the fabrication of devices where there is considerable potential for the construction of stacked or three-dimensional systems, possibly using cold bonding and direct laser etching techniques. The mobilisation of reagents and analytes, based on EOF, requires more complete characterisation of flows and mixing effects at intersecting channels are to be effectively exploited.

The most important development if μ FIA technology is to be fully realised is the fabrication of self contained operational systems with proven application robustness. The close relationship of μ FIA technology with separation techniques such as capillary electrophoretic and micro-electrochromatographic separations may well lead to some form of hybrid system in the near future. The area perhaps where the greatest advances in μ FIA-based technology will be most readily realised is the biotechnology sector, where methodology and applications are complementary to miniature systems. Already examples are emerging of applications in DNA fragment analysis⁹⁷ and immunoassay methodology.⁹⁸ Developments, however, need to be focused not only on the integrated device which may be encapsulated and equipped with telecommunication for remote operation, but also to include interfacing to existing measurement systems such as MS or NMR, which would benefit from some form of sample pretreatment. One area which has not yet been considered in μ FIA systems is a return to the early gas-phase work started by Terry *et al.*⁵ Clearly there are some exciting possibilities in gas and multiphase systems yet to be realised.

Conclusion

Where has μ FIA and more generally μ TAS got to? In 1991, Manz *et al.*¹³ questioned whether the developments in μ TAS were 'a look into next century's technology or just a fashionable craze'. In their concluding remarks, the authors made some general comments relating to the uptake or acceptance of μ TAS technology, 'namely that changes are required in the political and cultural opinions of analytical work if appropriate financial support is to be forthcoming and that the research base must grow worldwide to foster both competitive and collaborative research'. Further, they identified that 'the market acceptance of the technology must be embraced through the design and production of μ TAS concepts'. Clearly, these requirements have been only partially fulfilled. An examination of the literature indicates that there has been a positive growth in the research base and this will obviously support the fundamental development of the science. What is less obvious is the political and more importantly the economic will to support the development of the technology, and this may yet be seen to be the most serious limitation to the growth of the science.

Although miniaturisation is conceptually appealing, there remain some important technical obstacles to overcome, such as the introduction of 'real' samples and the ability to deal with suspended particles. These limitations are not beyond the scope of present day membrane technology, and should pose no serious hindrance to the advancement of the science. Developments in the field of μ TAS since 1991 clearly point to the technique forming the basis of future methodology applicable to a wide range of applications ranging from measurement science to chemical synthesis in which μ FIA based on EOF flow will

play a significant role. The limitation in releasing the considerable potential that micro reactor technology can offer resides not in the technological challenge but in the imagination of our minds and only requires us to realize it.

References

- Liu, S., and Dasgupta, P. K., *Anal. Chim. Acta*, 1993, **283**, 739.
- Bogue, R., *Lab. Equip. Dig.*, 1995, February, 14.
- Manz, A., Effenhauser, C. S., Burggraf, N., Verpoorte, E. J. M., Raymond, D. E., and Widmer, H. M., *Analisis Mag.*, 1994, **22**, M25.
- Craston, D., and Cowen, S., *Chem. Br.*, 1996, October, 31.
- Terry, S. C., Jarman, J. H., and Angell, J. B., *IEEE Trans. Electron. Devices*, 1979, ED-26, 1880.
- Capillary Electrophoresis: Theory and Practice*, ed. Grossman, P. D., and Colburn, J. C., Academic Press, New York, 1992.
- Mikkers, F. E. P., Everaerts, F. M., and Verheggen, Th. P. E. M., *J. Chromatogr.*, 1979, **169**, 11.
- Jorgenson, J. W., and Lukacs, K. D., *Anal. Chem.*, 1981, **53**, 1298.
- Whalen-Pechersen, E. K., and Jurs, P. C., *Anal. Chem.*, 1981, **53**, 2184.
- Manz, A., Graber, N., and Widmer, H. M., *Sens. Actuators B*, 1990, **1**, 244.
- Advances in Chromatography*, ed. Brown, P. R., and Grushka, E., Marcel Dekker, New York, 1993, pp. 1–66.
- Micro Total Analysis Systems*, ed. van den Berg, A., and Bergveld, P., Kluwer, Dordrecht, 1995.
- Manz, A., Fettingner, J. C., Verpoorte, E. J. M., Lüdi, H., Widmer, H. M., and Harrison, D. J., *TrAC, Trends Anal. Chem. (Pers. Ed.)*, 1991, **5**, 144.
- Manz, A., Harrison, D. J., Verpoorte, E. M. J., Fettingner, J. C., Lüdi, H., and Widmer, H. M., *Chimia*, 1991, **45**, 103.
- Liu, S., and Dasgupta, P. K., *Anal. Chim. Acta*, 1992, **268**, 1.
- Harrison, D. J., Glavina, P. G., and Manz, A., *Sens. Actuators B*, 1993, **10**, 107.
- Jacobson, S. C., Hergenroder, R., Koulng, L. B., and Ramsey, J. M., *Anal. Chem.*, 1994, **66**, 2369.
- Daykin, R. N. C., and Haswell, S. J., *Anal. Chim. Acta*, 1995, **313**, 155.
- Verpoorte, E. J. M., Van der Schoot, B. H., Jeanneret, S., Manz, A., and de Rooij, N. F., in *Interfacial Design and Chemical Sensing*, ACS Symposium Series, American Chemical Society, Washington, DC, 1994, ch. 21, p. 244.
- Schomburg, W. K., Vollmer, J., Büstgens, J., Fahrenberg, J., Hein, H., and Manz, W., *J. Micromech. Microeng.*, 1994, **4**, 1.
- Sensors: a Comprehensive Survey*, ed. Grandke, T., and Ko, W. H., VCH, Weinheim, 1989, vol. 1, p. 107.
- Manz, A., Verpoorte, E. M. J., Effenhauser, C. S., Burggraf, N., Raymond, D. E. and Widmer, H. M., *Fresenius' J. Anal. Chem.*, 1994, **348**, 567.
- Woffenbittel, R. F., *Sens. Actuators A*, 1992, **30**, 109.
- Altmann, J. P., *Das Neue Lehrbuch de Glusälzerei*, Gentner, Stuttgart, 1963, p. 29.
- Daniel, J. S., and Delapierre, G., *J. Micromech. Microeng.*, 1991, **1**, 187.
- Becker, E. W., Ehrfeld, W., Hagmann, P., Maner, A., and Müchmeyer, D., *Microelectron. Eng.*, 1986, **4**, 35.
- Knapp, J., Andrae, G., and Petersohn, D., *Sens. Actuators A*, 1990, **21–23**, 1080.
- Kovacs, G. T. A., Petersen, K., and Albin, M., *Anal. Chem.*, 1996, **68**, 407A.
- Jacobson, S. C., Koutny, L. B., Herenroder, R., Moore, A. W., Jr., and Ramsey, J. M., *Anal. Chem.*, 1994, **66**, 3472.
- Fan, Z., and Harrison, D. J., *Anal. Chem.*, 1994, **66**, 177.
- Elliot, D. J., *Integrated Circuit Fabrication Technology*, McGraw-Hill, New York, 1982.
- Thin Film Processes*, ed. Vossen, J. L., and Keren, W., Academic Press, San Diego, 1978, ch. V-1, p. 401.
- van der Linden, W. E., *TrAC, Trends Anal. Chem. (Pers. Ed.)*, 1987, **6**, 37.
- Tyssen, R., *Anal. Chim. Acta*, 1980, **114**, 71.
- Hungerford, J., Thesis, University of Washington, 1986.
- Gravesen, P., Branebjerg, J., and Jensen, O. S., *J. Micromech. Microeng.*, 1993, **3**, 168.
- Manz, A., and Simon, N., *Anal. Chem.*, 1987, **59**, 74.

- 38 *Micro Total Analysis Systems*, ed. van den Berg, A., and Bergveld, P., Kluwer, Dordrecht, 1995, p. 165.
- 39 Shoji, S., and Esashi, M., *Sens. Actuators B*, 1992, **8**, 205.
- 40 Field, L. A., and Muller, R. S., *Sens. Actuators A*, 1990, **21–23**, 935.
- 41 Fung, C. D., Cheung, P. W., and Fleming, D. G., *Microachining and Micropackaging of Transducers*, Elsevier, Amsterdam, 1985.
- 42 Harz, M., *J. Micromech. Microeng.*, 1992, **2**, 161.
- 43 Esashi, M., Nakano, A., Shoji, S., and Hebiguchi, H., *Sens. Actuators A*, 1990, **21–23**, 931.
- 44 Seiler, K., Fan, Z. H., Fluri, K., and Harrison, D. J., *Anal. Chem.*, 1994, **66**, 3485.
- 45 Dasgupta, P. K., and Liu, S., *Anal. Chem.*, 1994, **66**, 1792.
- 46 Li, S. F. Y., *Capillary Electrophoresis*, Elsevier, New York, 1992.
- 47 Shaji, S., Esashi, M., van der Schoot, B., and de Rooij, N. F., *Sens. Actuators A*, 1992, **32**, 335.
- 48 Horowitz, P., and Hill, W., *The Art of Electronics*, Cambridge University Press, Cambridge, 2nd edn., 1989, p. 368.
- 49 van der Schoot, B. H., Jeanneret, S., van den Berg, A., and de Rooij, N. F., *Anal. Methods Instrum.*, 1993, **1**, 38.
- 50 Stewart, K. K., Beecher, G. R., and Hare, P. E., *Fed. Proc., Fed. Am. Soc. Exp. Biol.*, 1974, **33**, 1434.
- 51 Moriney, R. M., White, R. M., and Howe, R. T., *Proc. MEMS'91, Nara, Japan*, 1991, p. 277.
- 52 Richter, A., Plettner, A., Hofmann, K. A., and Sandmeier, H., *Proc. MEMS '91, Nara, Japan*, 1991, p. 271.
- 53 Osada, Y., Okuzzaki, H., and Hari, H., *Nature (London)*, 1992, **355**, 242.
- 54 Fuhr, G., Fiedler, S., Müller, T., Schnell, T., Glasser, H., Lisec, T., and Wagner, B., *Sens. Actuators A*, 1994, **41–42**, 230.
- 55 Zheng, H. J., and Dasgupta, P. K., *Anal. Chem.*, 1994, **66**, 3997.
- 56 Adams, R. N., *Electrochemistry at Solid Electrodes*, Marcel Dekker, New York, 1969.
- 57 Masson, D., Magdassi, S., and Sasson, Y., *J. Org. Chem.*, 1990, **55**, 2714.
- 58 Moore, A. W., Jr., Jacobson, S. C., and Ramsey, J. M., *Anal. Chem.*, 1995, **67**, 4184.
- 59 Jacobson, S. C., Hergenröder, R., Koutny, L. B., and Ramsey, J. M., *Anal. Chem.*, 1994, **66**, 1114.
- 60 Jacobson, S. C., Hergenröder, R., Koutny, L. B., Warmack, R. J., and Ramsey, J. M., *Anal. Chem.*, 1994, **66**, 1107.
- 61 Seiler, K., Harrison, D. J., and Manz, A., *Anal. Chem.*, 1993, **65**, 1481.
- 62 Manz, A., Effenhauser, C. S., Burggraf, N., Harrison, D. J., Seiler, K., and Fluri, K., *J. Micromech. Microeng.*, 1994, **4**, 257.
- 63 Tseida, T., Mizuno, T., and Akiyama, J., *Anal. Chem.*, 1987, **59**, 799.
- 64 Harrison, D. J., Manz, A., Fan, Z., Lüdi, H., and Widmer, H. M., *Anal. Chem.*, 1992, **54**, 1926.
- 65 Manz, A., Harrison, D. J., Verpoorte, E. M. J., Fellingner, J. C., Paulus, A., Lüdi, A., and Widmer, H. M., *J. Chromatogr.*, 1992, **593**, 253.
- 66 Effenhauser, C. S., Paulus, A., Manz, A., and Widmer, H. M., *Anal. Chem.*, 1994, **66**, 2949.
- 67 Effenhauser, C. S., Manz, A., and Widmer, H. M., *Anal. Chem.*, 1995, **67**, 2284.
- 68 Hasser, A., MSc Thesis, University of Hull, 1996.
- 69 Burggraf, N., Manz, A., Verpoorte, E. M. J., Effenhauser, C. S., Widmer, H. M., and de Rooij, N. F., *Sens. Actuators B*, 1994, **20**, 103.
- 70 Ruzicka, J., and Hansen, E. H., *Flow Injection Analysis*, Wiley, New York, 2nd edn., 1988.
- 71 Halliday, D., and Resnick, R., *Physics*, Wiley, New York, 1960.
- 72 Jacobson, S. C., Koutny, L. B., Hergenröder, R., Moore, A. W., Jr., and Ramsey, J. M., *Anal. Chem.*, 1994, **66**, 3472.
- 73 Monning, C. A., and Jorgenson, J. W., *Anal. Chem.*, 1991, **63**, 802.
- 74 Yao, X. W., Wu, D., and Regnier, F. E., *J. Chromatogr.*, 1993, **636**, 21.
- 75 Smith, J. T., and Rassel, Z. E., *J. High Resolut. Chromatogr.*, 1992, **15**, 573.
- 76 Marakami, Y., Suda, M., Yokogama, K., Tukeuchi, T., Tamiya, E., and Kurube, I., *Microchem.*, 1994, **49**, 319.
- 77 Tsuda, T., Nomura, K., and Nakagawa, G., *J. Chromatogr.*, 1982, **248**, 241.
- 78 Giddings, J. C., *Science*, 1993, **260**, 1456.
- 79 Widmer, H. M., and Koch-Kellner, L., *Chimia.*, 1989, **43**, 320.
- 80 Koch, L., Koch, T., and Widmer, H. M., *J. Chromatogr.*, 1990, **517**, 395.
- 81 Raymond, D. E., Manz, A., and Widmer, H. M., *Anal. Chem.*, 1994, **66**, 2858.
- 82 Sudfa, M., Sakuhara, R., and Karube, I., *Appl. Biochem. Biotechnol.*, 1994, **41**, 3.
- 83 Haber, C., Scilvestri, I., Böösli, S., and Seman, W., *Chimia*, 1991, **45**, 117.
- 84 Chervet, J. P., Ursem, M., Salzmann, J. P., and Vannoort, R. W., *LC-GC*, 1989, **7**, 515.
- 85 Wohltjen, J., *Sens. Actuators*, 1984, **5**, 305.
- 86 Ton, W., Zhang-You, S., Smith, S., Birnbaum, D., and Kopelman, R., *Science.*, 1992, **258**, 778.
- 87 Xi, X., and Yeing, F. S., *Anal. Chem.*, 1990, **62**, 1580.
- 88 Xue, Y., and Yeung, E. S., *Anal. Chem.*, 1994, **66**, 3575.
- 89 Verpoorte, E. M. J., Manz, A., Lüdi, H., Bruno, A. E., Maystre, F., Kruttiger, B., Widmer, H. M., van der Schoot, B. H., and de Rooij, N. F., *Sens. Actuators B*, 1992, **6**, 66.
- 90 Weigl, B. H., and Woelfbeis, O. S., *Anal. Chem.*, 1994, **66**, 3323.
- 91 Suda, M., Sakuhara, T., and Karube, I., *2nd Bioengineering Symposium, Tsukuba, Japan*, 1992, p. 113.
- 92 Liang, Z., Chiem, N., Ocvirk, G., Tang, T., Fluri, K., and Harrison, D. J., *Anal. Chem.*, 1996, **68**, 1040.
- 93 Arquint, P., Koudelka-Hep, M., van der Schoot, B. H., van der Wal, P., and de Rooij, N. F., *Clin. Chem.*, 1994, **40**, 1805.
- 94 *Micro Total Analysis Systems*, ed. van den Berg, A., and Bergveld, P., Kluwer, Dordrecht, 1995, p. 299.
- 95 Conzen, J. P., Bürch, J., and Ache, H. J., *Appl. Spectrosc.*, 1993, **47**, 753.
- 96 Ache, H. J., *Chem. Ind.*, 1993, **1**, 40.
- 97 Jacobson, S. C., and Ramsey, J. M., *Anal. Chem.*, 1996, **68**, 720.
- 98 Koutny, L. B., Schmalzing, D., Taylor, T. A., and Fuchs, M., *Anal. Chem.*, 1995, **68**, 18.

Paper 6/06289J

Received September 16, 1996

Accepted November 18, 1996



ELSEVIER

Analytica Chimica Acta 382 (1999) 1–13

ANALYTICA
CHIMICA
ACTA

Further studies into the development of a micro-FIA (μ FIA) system based on electroosmotic flow for the determination of phosphate as orthophosphate

G.N. Doku, S.J. Haswell*

Department of Chemistry, University of Hull, Hull, HU6 7RX, UK

Received 17 August 1998; received in revised form 12 November 1998; accepted 16 November 1998

Abstract

Photolithographic and wet etching techniques were used to fabricate a μ FIA manifold in a borosilicate glass substrate for the spectrophotometric determination of orthophosphate based on the molybdenum blue reaction, employing electroosmotic flow for both the mobilization of reagents and sample injection. The manifold channel dimensions were 200 μ m wide and 50 μ m deep. An evaluation of the electroosmotic flow characteristics (i.e. voltage, solution concentration/pH ranges and current–voltage relationships) for ascorbic acid, ammonium molybdate and orthophosphate standards, with and without borate buffer present, has been carried out. In addition, the effect that reaction precursors may have on the *in situ* spectrophotometric detection system is also discussed. Using the optimized operating conditions of 1.75% ascorbic acid and 0.6% ammonium molybdate in 10 mM borate buffer, the calibration model for phosphate standards was found to be linear ($y = 0.0036x + 0.0155$; correlation coefficient, $r^2 = 0.9952$) over the working range 1–10 μ gml⁻¹. A sampling rate of ca. 60 samples/h was achieved, with a detection limit of 0.1 μ gml⁻¹ for orthophosphate, with RSDs <5%. The reagent consumption was very low with the total reactant volume in the system estimated to be 0.6 μ l and a sample volume of 0.1 μ l being required. © 1999 Elsevier Science B.V. All rights reserved.

Keywords: Microflow-injection analysis; Miniaturization; Phosphate

1. Introduction

The development of microflow-injection analysis (μ FIA) systems based on microreactor manifolds [1–4] fabricated using photolithographic and wet etching [4] or laser ablation [5] techniques offer many attractive operational advantages. These include high portability, remote operation, reduced reagent and sample

consumption [6], minimal waste generation [7,8] and fast controllable analysis [8]. An example of a three-dimensional μ FIA system (22 \times 22 mm² planar micromachined silicon elements), based on a conventional FIA manifold developed by Spielman et al. [9] for phosphate detection, was described recently by Verpoorte et al. [10]. The system employed externally connected piezoelectrically driven silicon micropumps for reagent mobilisation, operating at flow rates of 0.03–0.2 ml/min which correspond to about one-tenth of those used in a conventional FIA system,

*Corresponding author. Tel.: +1-482-465475; fax: +1-482-466416; e-mail: S.J.Haswell@chem.hull.ac.uk

leading to a corresponding 270-fold reduction in reagent consumption. Sample volumes used with the microflow system were around 25 μl . To increase the sensitivity of the technique, since the analysis is carried out under non-equilibrium conditions, a stopped-flow mode was adopted, producing an analysis time of 4 min per sample. The sensitivity achieved with the μFIA system was comparable to that expected for a conventional system (5 μgml^{-1} phosphate as orthophosphate) [10].

In an attempt to exploit electroosmotic flow (EOF) rather than the hydrodynamic flow, as described by Verpoorte et al. [10], Daykin and Haswell [3] described the development of a μFIA system, also for the determination of orthophosphate. Channels 325 μm wide and 30 μm deep were etched into a glass substrate in which molybdate (pH 3.2) was mobilised by EOF; however, due to pH constraints (pH 1.6), it was necessary to pump the ascorbic acid by ion migration rather than EOF. The reagents were combined in a contra-flow manner and a Z-mode injection [4] was used to introduce the orthophosphate. On completion of the molybdenum blue reaction, the product was detected *in situ* using a fibre-optic configuration. The authors reported an RSD of <5% at 10 ppb, decreasing to <0.8% at 100 ppb for orthophosphate, where $n = 5$. The linear working range was found to be 10–100 ppb, and the system produced a limit of detection of 0.7 ppb.

This current work represents a further study into the development of a μFIA system for phosphate analysis, as first described by Daykin and Haswell [3], that utilises EOF control for all the reagents and samples used and considers potential detector problems associated with *in situ* measurements. The first section of the paper will, therefore, describe the use of EOF for the mobilisation of both, the ascorbic acid and ammonium molybdate reagents, together with on-chip sample injection of potassium dihydrogenphosphate. This will be followed by an evaluation of the influence spectrophotometrically active reaction precursors may have on the ability to detect reliably the molybdenum blue reaction product *in situ*.

In the example given, ascorbic acid solutions (pHs <3), which are initially colourless, turn yellowish, intensifying to a deep orange colour with time due to the low pH condition, degrading with the ascorbic acid [11]. Ammonium molybdate solutions (pH >3)

remain stable and colourless due to a self-buffering effect. At pH >3 (e.g. in the absence of excess mineral acid), a mixture of the two reagents (ascorbic acid and ammonium molybdate) produces an initial yellowish-green colour partly due to pH increase effect on the ascorbic acid and partly due to a slight preliminary direct reduction of some molybdenum(VI) to molybdenum(V) state, at pH >0.7. It is interesting to note, however, that the direct reduction of Mo (VI) to Mo (V) does not occur when phosphate is present [12]. This background colour of the reagent mixture (reaction precursor) has also been reported by other workers in the field [13] to be unstable and, therefore, the reagents are usually mixed in a conventional FIA manifold ahead of the sample injection point. In the case of the dominant phosphate–molybdenum blue reaction itself, the first stage of the reaction (formation of a yellow 12-molybdo(VI)phosphoric acid (12-MPA) complex) is fast, whilst the second (reduction of the molybdenum (VI) to a blue + 5 state (phosphomolybdenum blue, PMB) by ascorbic acid) is relatively slow [12,13]. Thus, the background yellow-green colour from the reaction precursor and all other optically active intermediate reaction products that might occur before the formation of the molybdenum blue, may contribute to an instability in the base line of the detection system prior to the formation of the final blue colour. In addition, the generation of an intermediate with different pH or ionic strength, to the reactants or product, may influence the EOF dynamics of the system, which in turn may also contribute to instabilities in the detector system.

In conventional FIA, the presence of such potential detection problems can be eliminated in numerous ways, for example, by ensuring that the full reaction is completed prior to detection or employing a dual beam spectrometer to compensate for background variations. In addition, with conventional FIA systems, measurements are not normally made directly at the point of injection, an option that may not be appropriate to μFIA systems. The incorporation of a dual optics systems in a μFIA system, whilst not difficult, would add to the complexities of the measurement process and, therefore, on-chip manifold design and integration of detection components are important considerations if simple systems are to be produced.

In order to address potential design problems with on-chip *in situ* detection, this paper will describe the spectrophotometric characteristics of premixing the ascorbic acid and ammonium molybdate reagents prior to the generation of the phosphate reaction product. Considerations will be given to the time-based instability of the reagent mixture and the buffering effects that a borate buffer may have on the generation of a stable phosphate reaction product.

2. Experimental

2.1. Reagents

All reagents and standards were of analytical grade unless otherwise stated. The primary reagents used were ammonium molybdate(VI)tetrahydrate ((NH₄)₆Mo₇O₂₄·4H₂O, 99.98%) supplied by BDH (Poole, Dorset); L-ascorbic acid (99%) supplied by Sigma-Aldrich (Gillingham, Dorset); potassium dihydrogenorthophosphate (KH₂PO₄), also supplied by BDH; and di-sodium tetraborate (Na₂B₄O₇, 98%) supplied by Hopkin and Williams, Essex. Water was obtained from an Elga (High Wycombe, UK) UHQ PS system and had a conductivity of 18 mΩ cm⁻¹.

2.2. Characterisation of electroosmotic flow

The main EOF characteristics monitored were applied voltage, current–voltage relationships and solution concentration/pH which were then selected to obtain parameters that gave good stable EOF. The pH of solutions were measured with the Ikamag RH Nr.361646 pH meter produced by Janke and Kunkel, GMBH, Germany.

A manifold consisting of channels 200 μm in diameter and 50 μm deep, (Fig. 1) was etched on a borosilicate glass chip (25 mm long, 25 mm wide and 3 mm thick), using the technology described previously [3]. A cover plate (25 mm long, 25 mm wide and 1 mm thick, also of borosilicate glass), into which 2 mm i.d. holes had been drilled to align with the ends of the channels, was annealed/bonded to the substrate chip. Plastic reservoirs were fixed at positions A to F with glass bonding glue (Loctite Glass Bond, Welwyn Garden City, UK) and dried in sunlight (UV lamp could also be used for the drying). This chip

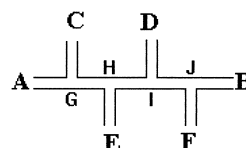


Fig. 1. μFIA manifold for determining flow characteristics of reagents. A, reagent reservoir; B, waste reservoir; and C–F, side channel reservoirs. AB, 18 mm; AG = GH = HI = IJ = JB = 3.5 mm; and CG = EH = DI = FJ = 8 mm.

was then used to evaluate the reagents EOF and side streaming characteristics.

A Farnell HiVolt XRV30/1.7 reversible polarity power supply (Farnell, Leeds) was used which offered a maximum power output of 50 W with variable voltages up to 30 000 V and currents up to 1.7 mA to be selected in constant stabilised current or voltage modes, with an adjustable trip for overcurrent protection. The power supply was connected via high-purity copper conductors to 0.15 mm diameter platinum electrodes with a 10 mm exposed length for interfacing with the solutions in the reservoirs. For safety, the electrode system was built in an isolation box fitted with a power cut-out preventing high voltage operation when the lid is open. The voltages applied across the electrodes and the internal currents generated within the solutions in the channels were monitored on an AVO digital autoscaling multimeter (Avo multimeter M2036, Thurnby Thunder Instruments, Huntingdon, UK) connected in parallel with the device.

The solution under investigation was placed in reservoir A and water or buffer in reservoir B, both to pre-marked levels. The reservoir levels of other reagent solutions in the side channel reservoirs C–F, perpendicular to the main channel AB were also recorded. The positive electrode was placed in A and the negative electrode in B, the other reservoirs were electrically left floating.

Initially, different concentrations of ascorbic acid (0.1–3%, pH 2.11–1.34) were run at different voltages (0.2–1.3 kV) over a period of 30 min and the change (decrease) in volume of ascorbic acid in reservoir A was measured by recording the new lower level, filling the reservoir to its original level and recording the addition required with a graduated 100 μl HPLC syringe. The voltage (V), current (I), time (min) and

volume changes (μl) were recorded and the flow rates ($\mu\text{l}/\text{min}$) calculated. The process was repeated to establish the flow characteristics for ammonium molybdate (0.1–3%, pH 3.86–5.03) and phosphate standard solutions ($1\text{--}40\ \mu\text{g ml}^{-1}$, pH 8.50–5.67).

The EOF characteristics of the ascorbic acid, ammonium molybdate and the orthophosphate were first determined without the presence of buffer to establish the natural EOF properties of these reagents. In a similar manner, the EOF characteristics of borate buffer (di-sodium tetraborate, 98% G.P.R. obtained from Hopkins and Williams, UK) solutions were studied to obtain an optimum buffer concentration that could be used in conjunction with the reagents and standards. In addition, the EOF characteristics of a mixture of the ascorbic acid and ammonium molybdate solution with buffer was also studied to establish any effects of reagent mixing in the channels on the EOF.

2.3. Reaction precursor studies

In order to establish the basic reaction characteristics and to simplify the analytical procedure for the proposed on-chip EOF methodology, the effects of mineral acid (HNO_3) on the generation of the background yellow-green reaction precursor, resulting from the reagent mixture, and on the molybdenum blue reaction product were evaluated. This was carried out by observing visually the background colour produced by the reagent mixture. For this part of the study, equal volumes ($1\ \text{cm}^3$) of the 1.75% ascorbic acid and 0.6% ammonium molybdate solutions

were mixed in a test tube and the background colour noted. To the yellow-green product produced, $0.5\ \text{cm}^3$ of the potassium dihydrogenphosphate solution ($5\ \mu\text{g ml}^{-1}$) was added in the presence, and absence, of nitric acid to observe whether a blue reaction product would be formed and if so how long it took to develop. In addition, the pH of the solutions produced was monitored to assess the possible influence of the presence of a mineral acid on the EOF.

The ascorbic acid and the ammonium molybdate reagents were also dissolved separately in 10 mM borate buffer with, and without, nitric acid being present to establish the effects of the buffer on the flow rates and reaction characteristics of the individual reagents. This was then followed by evaluating the same parameters for a buffered reagent mixture. The buffer-reagent mixture (1.75% ascorbic acid and 0.6% ammonium molybdate) was visually monitored, together with the unbuffered solutions, periodically for a number of days to see if any change in colour intensity occurred.

2.4. μFIA manifold with *in situ* detector

The μFIA manifold and detector setup for the phosphate analysis is shown in Fig. 2. In this section of the work, a glass chip (25 mm long, 8 mm wide and 3 mm thick) with etched channels (200 μm wide and 50 μm deep) was annealed/bonded to a thicker glass cover plate (25 mm long, 14 mm wide and 17 mm thick, both of borosilicate), into which 2 mm holes had been drilled to align with the ends of channels. The holes served as reservoirs for

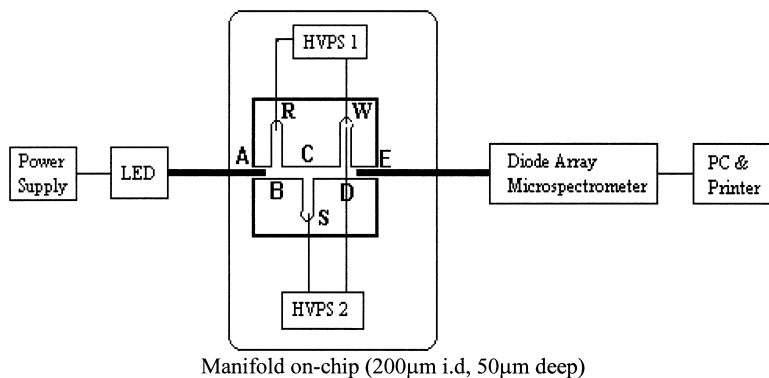


Fig. 2. μFIA manifold and detector setup for phosphate analysis. $AB = BC = DE = 3\ \text{mm}$; $CD = 4\ \text{mm}$, $BD = 7\ \text{mm}$; and $RB = SC = WD = 6\ \text{mm}$.

reagents/analyte and to support the platinum electrodes. This replaced the use of glued plastic reservoirs so as to produce a more robust and solution-tolerant device. In addition, side ports were created at each end of the main channel to allow axial access for optical fibres. Reaction signals were obtained spectrophotometrically by using the VIS-microspectrometer (operational wavelength range being 380–780 nm, supplied by microParts, Germany).

The light source was a high-output red (3000 mcd at 10 V, 700 nm peak output) light emitting diode (LED, RS 564-015, RS stores) with operating electronics built in house coupled to the chip also with fibre optic connector. The optical fibres taking light from the LED to the chip, and from the chip to the diode array detector, were 110 μm i.d. and made of silica housed in an outer plastic covering, giving a total o.d. of 125 μm . The fibre optics were attached to the chip by stripping off the covering plastic at the tips of the optic, which were then inserted axially (1–3 mm) into the channels on either side of the main reagent line whilst applying a positive pressure on the solution in one reservoir to create a continuous flow of solution in the channels, hence avoiding the trapping of any air bubbles in the channels and around the tips of the fibre optics. Excess liquid was then removed and an all-purpose clear adhesive (Bostic, Leicester, UK) followed by a thick layer of silicone rubber compound (RS Components, Northants, UK) glue were applied. The ends of the fibre optics, in this work, were not polished or prepared in any special way other than simply cleaving and stripping ≈ 3 mm of the fibre coating.

Output from the photodiode array detector (microParts) was coupled to a PC.

The supporting software (SpecView 3.0, microParts) was operated in two modes – Scan and Time drive modes. In both, the Scan and Time drive modes, the system was zeroed (zero reference) for a base line determination. Alignment of the fibre optics was carried out by observing a maximum transmission peak at the emission spectra, whilst moving the ends of the fibres. Once aligned, the fibres were fixed in place with adhesive. No definitive calculations have been carried out to date on the light losses in the system; however, this is currently under investigation. In the Time drive mode, the light transmission values for the peak maxima and two reference base wave-

lengths were monitored. In both these modes, the detector performed a pre-selected number of scans of the signal intensity received by the diode array detector. The scanned wavelength range selected for the phosphate analysis was 600–700 nm over which the blue phosphate reaction product absorbs well, with the maximum intensity being around 647 nm. Five scans were made over an integration time of 320 ms giving a total scanning time of 3 min. The Scan mode was primarily used to align the fibre optic and zero the detector whilst measurements were performed in the Time drive mode. The Time drive mode was chosen for in situ measurements because it acquires a signal intensity data in a continuous mode, which made it easier to observe reaction characteristics and interpret the precision and reproducibility of the analysis. By comparison, the Scan mode will only generate a full spectra for one injection over the selected wavelength range.

2.5. Optimisation of sample injection time (time-mode injection) for phosphate analysis

After priming the main reaction channel (R–W) with borate buffer (10 mM $\text{Na}_2\text{B}_4\text{O}_7$, pH 9.22), a fresh premixed reagent mixture of the 1.75% ascorbic acid and 0.6% of the ammonium molybdate was placed in the reagent reservoir R (Fig. 2). Buffer was placed in the sample reservoir S and suction was applied with a syringe at the waste reservoir W to facilitate the filling of the channels with the reagent and buffer solution. The sample reservoir S was then loaded with a $10 \mu\text{g ml}^{-1}$ phosphate standard. An electrical field HVPS 1 was then applied between R(+) and W(–) (400 V, $\cong 46 \mu\text{A}$) for 30 s to fill the main line completely with the reagent mixture and the spectrometer was then zeroed using both, the Scan and Time drive modes to obtain a baseline for the reagent blank. The electrical field HVPS 2 was then introduced across S(+) and W(–) (695 V, $\cong 16 \mu\text{A}$) for a range of times (60, 55, 50, 40, 30, 20 and 10 s) to inject the phosphate standard before the reagent flow was resumed to carry the sample plug towards the detector and, subsequently, to waste. The signals obtained were saved and the process repeated as necessary. In the injection process, the switching off and on of the reagent flow (RW) and the sample (SW) was performed simultaneously.

2.6. μ FIA calibration

A $20 \mu\text{g ml}^{-1}$ stock phosphate solution was prepared by weighing 0.088 g of the solid KH_2PO_4 and dissolving in 1 dm^3 of a 10 mM borate buffer solution. Serial dilutions of the stock $20 \mu\text{g ml}^{-1}$ solution were then carried out to prepare 1, 2.5, 5, 7.5 and $10 \mu\text{g ml}^{-1}$ phosphate standards. Using the procedure described in the injection optimisation above, six replicate injections/measurements were made for the different standards in turn, and the signal results obtained on PC were saved as before. Calibration was

achieved by plotting the absorbance vs. concentration for each standard.

3. Results and discussions

3.1. Flow characteristics in the μ FIA system

3.1.1. Ascorbic acid

The concentration range of ascorbic acid that gave the most stable flow rates was found to be 1.5–2.5% (Fig. 3(a), pH 1.5–1.9), with 1.75% (pH 1.77) giving

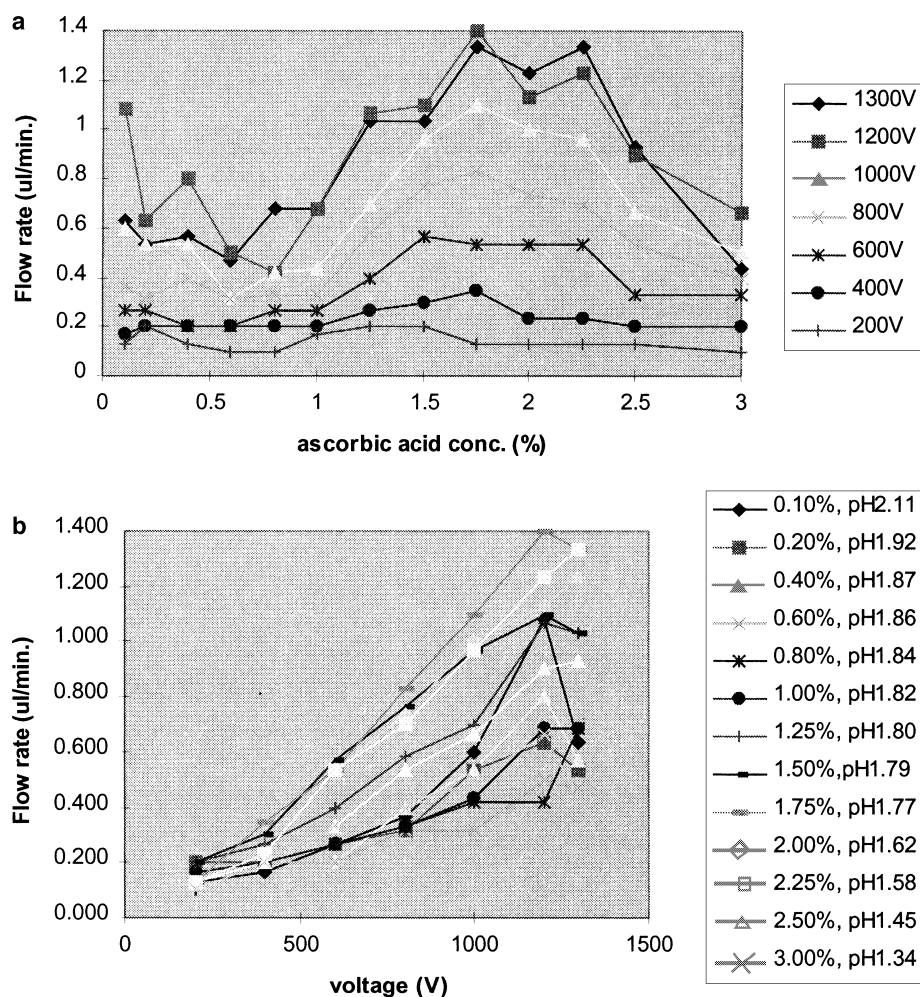


Fig. 3. (a) Plots of flow rate vs. ascorbic acid concentration for different voltages. (b) Plots of flow rate vs. voltage for different ascorbic acid concentrations.

the highest flow rate of 1.4 $\mu\text{l}/\text{min}$. At the operating pH 1.5–1.9, the ascorbic acid could not be assumed to be moving by EOF, due to the very low pH, but was undergoing a viscous drag induced by bulk electrophoretic mobility of the solution ions. Over the concentration range studied, the flow rates were found to increase quite steadily as a function of voltage from 0.2 kV up to a maximum at 1.2 kV (Fig. 3(b)). Beyond 1.2 kV, the flow was observed to drop due to the unstabilising effects of the high ionic strengths of the solutions used, and possibly, faster electrophoretic mobility of ions through the solution due to stronger attraction by the opposite electrode and, thus, leaving the bulk solution behind. The higher voltages were, however, associated with an increase in bubble generation observed in the reservoirs, caused by Joule heating. Beyond 2.25% ascorbic acid, the current was found to fluctuate considerably, due to increases in the thermal resistance caused by excessive bubbling which, in turn, aggravated the heating effect, eventually leading to solution evaporation. Consequently, reliable volume measurements became difficult to obtain. It was noted that bubbles occurred only at the negative electrode for ascorbic acid due to the generation of H_2 . The current fluctuation observed, at high voltages, made flow rate measurements by current–time monitoring [14] difficult with the chemistry used in this study. Thus, the simple volume change measurement procedure adopted, in this study, avoided current-based measurements. The current–time based technique for determining flow rates may, however, prove suitable at lower voltages (<1.2 kV) and this approach is worthy of further investigation.

In addition to flow rate increasing steadily with voltage over the 0–1.2 kV range (Fig. 3 (b)) (i.e. the electroosmotic flow generated is linearly proportional to the applied voltage), plots of current vs. voltage for the ascorbic acid 1.25–2.25% concentration range were also found to be linear, leading to correlation coefficients ≥ 0.9 and indicating that the volumetric flow rate is also linearly proportional to the current.

3.1.2. Ammonium molybdate

The concentration range of ammonium molybdate that was found to give reasonable EOF rates was 0.1–0.6% (Fig. 4(a), pH range 3.86–4.36) with the highest flow rates being obtained for 2% (pH 4.0) and 0.6%

(pH 4.36). The operating conditions suggest that the ammonium molybdate was moving by EOF. At concentrations higher than 0.6% (though within the EOF operating pH range of 3–10) bubbles were generated in both the reservoirs, leading to an increase in the resistance and a corresponding decrease in flow. However, the flow was observed to increase again for concentrations >1.5%; this was possibly due to an increase in pH to around 5.0 at 2.5% ammonium molybdate. The flow rate was, on average, higher for the ammonium molybdate (pH 3–5) than for ascorbic acid (pH 1.6–2.0) indicating a direct pH effect. For the concentration range used, the flow rate was found to increase quite steadily with an increase in voltage from 0.2 kV until it reached a maximum at 1.2 kV (Fig. 4(b)) and then a gradual decrease was observed for the same reasons as those given for ascorbic acid. It was concluded, therefore, that voltages up to 1.2 kV would be applicable to drive the ammonium molybdate solution.

Current–voltage plots were found to increase with increasing concentration from 0.1 to 0.6%, beyond which point the current/flow rate decreased for the 0.7 to 1.5% range then rose again for concentrations >1.5%, again indicating a current or current–voltage effect on the flow. It was more difficult to identify a flow rate–current linearity, compared with the flow rate–voltage linearity, which again was probably due to the slight current fluctuations and, therefore, to an inability to record accurate current values. In general, correlation coefficients were found to be better than 0.9 across the concentration range investigated.

As the concentration or applied voltage increases, the current increases, and as indicated previously bubble generation in both the reservoirs occurred beyond 2.0% ammonium molybdate, once again volume measurements became difficult. The bubbles occurred at both the negative and positive electrodes due to the generation of H_2 at the negative electrode and, possibly, the liberation of oxygen gas as a result of some aqueous electrolysis or the liberation of ammonia in the ammonium molybdate reservoir caused by thermal decomposition of some NH_4^+ ions.

3.1.3. Potassium dihydrogenphosphate

The phosphate standard solutions produced higher flow rates (Fig. 5(a)) than either the ascorbic acid or ammonium molybdate, across the standard working

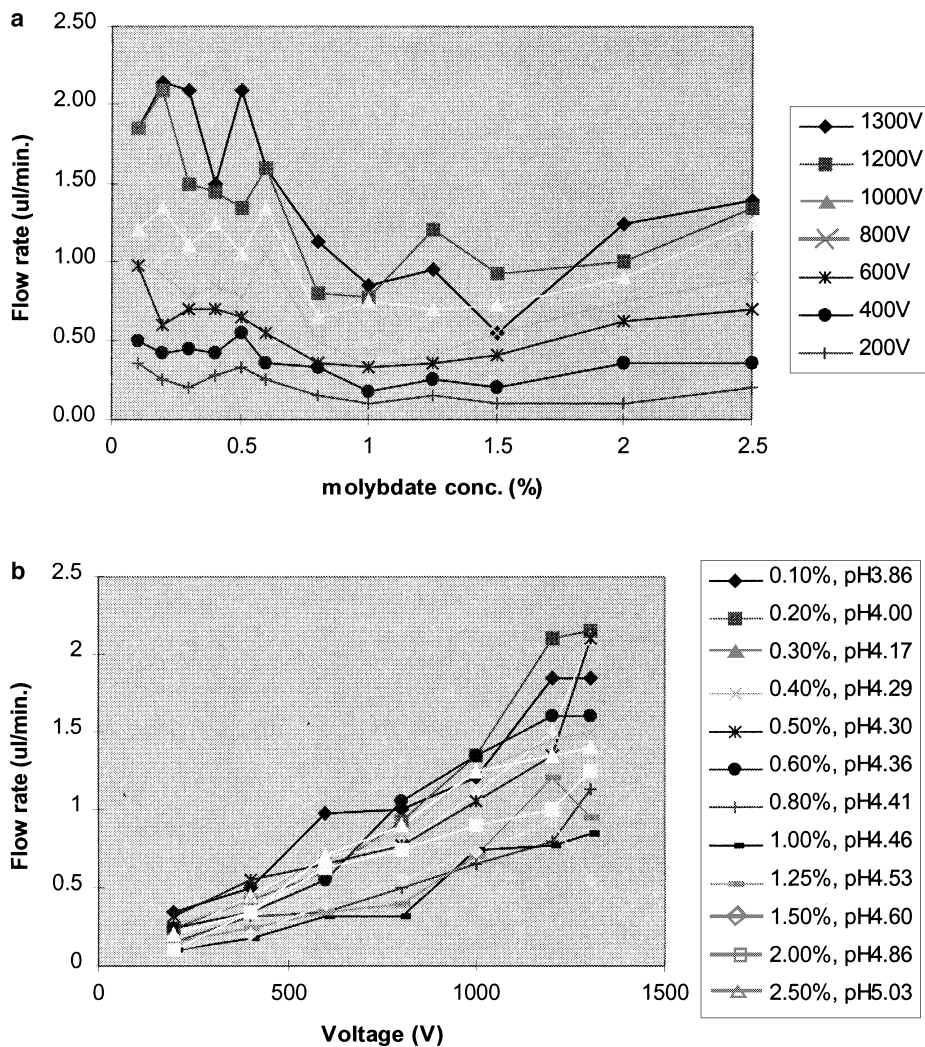


Fig. 4. (a) Plots of flow rate vs. molybdate concentration for different voltages. (b) Plots of flow rate vs. voltage for different molybdate concentrations.

concentration range of $1\text{--}10\ \mu\text{g ml}^{-1}$ (pH 8.5–6.67), with an optimum EOF operating pH range associated with $5\ \mu\text{g ml}^{-1}$ (pH 7.12) giving the highest flow rate, due to its pH and optimum ionic strength. Whilst the observed characteristics would enable a fast sample injection to be achieved by EOF and a corresponding high sample throughput rate, clearly the variation in flow and, hence, injection volume with time as a function of concentration will have implications for the calibration procedure. This apparent problem can, however, be effectively dealt with when buffer controlled systems are adopted as indicated below.

For the concentration range used, the flow rate increased with voltage over the range 0.2–1.3 kV (Fig. 5 (b)). Once again, correlation coefficients of the current–voltage models were >0.9 , indicating reasonable linearity between the current and the voltage and, therefore, the flow rate also increased with current.

Only a few bubbles were produced at both, negative and positive electrodes even at high concentrations or applied voltages because of the lower H^+ ion concentration and the absence of any potentially volatile components. Current fluctuations were, therefore, not

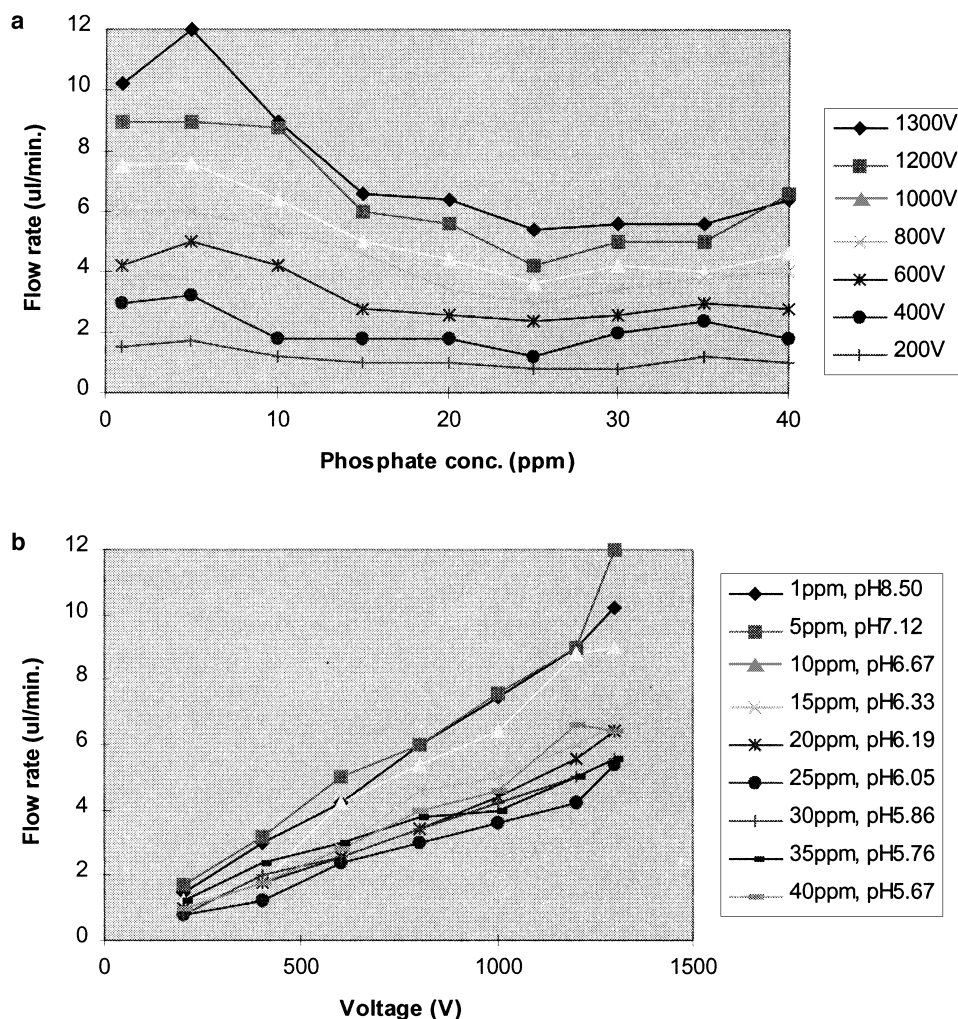


Fig. 5. (a) Plots of flow rate vs. phosphate concentration for different voltages. (b) Plots of flow rate vs. voltage for different phosphate concentrations.

evident and volume change measurements were relatively simple to make for the potassium dihydrogen-phosphate solution which produced no apparent Joule heating.

3.2. EOF characteristics of the buffer–reagent mixture

In order to achieve EOF control of the ascorbic acid, improve the quality of calibration data and simplify the reaction conditions used in the μ FIA system, a mixture of the optimum 1.75% ascorbic acid and 0.6%

ammonium molybdate was prepared in a 10-mM borate buffer (pH 9.22). The flow rate of the reagent mixture was found to increase steadily from 0.2 kV up to a maximum at 1.2 kV beyond which the flow rate dropped for the same reasons given for the ascorbic acid and ammonium molybdate. Therefore, voltages up to 1.2 kV for the reagent mixture were considered suitable to drive the solution. The reagent mixture prepared in buffer, however, did show a higher EOF than the individual reagents over the whole voltage range studied and, therefore, even voltages as low as 0.2 kV with a current of 20 μ A were found to be

sufficient to drive the reagent mixture at a flow rate of about 1 $\mu\text{l}/\text{min}$.

The most striking contribution/advantage observed from the buffer was the lack of fluctuations in the current and a more reliable flow control. The presence of the 10 mM borate buffer in the reagent solutions was found to have no detrimental effect on the reaction chemistry. Indeed, there was some evidence to suggest an apparent enhancement of the reaction signal.

3.3. Induced side channel flow characteristics

In order to establish the presence any Venturi-type side streaming effect, due to the reagent flow in the main channel AB, on solutions in perpendicular side channels CG, EH, DI and FJ, the side reservoirs C, D, E and F were filled with the same solution as was used in the main channel AB. This study was carried out in conjunction with the EOF characterisation of above-mentioned reagents.

The flow of each of the solutions (ascorbic acid, ammonium molybdate, potassium dihydrogenphosphate and the mixed buffer-reagent mixture) in the main flow channel AB was found to cause a very slight viscous drag (hydrodynamic effect) on side channel (CG, EH, DI and FJ) solutions. In qualitative terms, this addition of liquid was estimated to be <0.5% of the total transported material and was monitored by volume changes in both the side and collection reservoirs.

3.4. Reaction precursor studies

The observed change from initial colourless to yellowish, intensifying to a deep orange colour with time, of the ascorbic acid solutions (pHs <3, strongly reducing/antioxidant), is a chemical instability that might be induced by low lability to light/heat or easy oxidation by O_2 to dehydroascorbic acid (DHA). In an aqueous solution, this decomposition may lead to some sort of polymerisation, associated with the numerous functional groups on DHA which, in turn, increases the pH conditions and thus degrading the ascorbic acid [11].

In the ammonium molybdate solutions (pH 3.86–5.03), the Mo(VI) exists largely as a dimer in equilibrium with some monomer and polymer [12] which remain stable and colourless due to a self-buffering

effect. Results obtained for the molybdenum blue reaction are known to be independent of the age of the Mo(VI) solution and the original form of the Mo(VI) [12].

The yellow 12-molybdo(VI)phosphoric acid (12-MPA) complex, which is formed prior to the generation of the molybdenum blue reaction product, after adding phosphate to the ascorbic acid–ammonium molybdate reagent mixture, produces an absorption spectrum extending from 190 to 400 nm, which is less than the wavelength used to detect the molybdenum blue product (600–900 nm).

Thus, from an assessment of the above chemistries, it can be concluded that the main spectrophotometrically active reaction precursor most likely to affect the measurement process will be the initial yellow – green baseline colour of the ascorbic acid – ammonium molybdate mixture which absorbs weakly over a 190–900 nm range.

In order to reduce possible background detector effects associated with the generation of a yellow-green reaction precursor in the optical path of the detector, two approaches have been adopted. The first considered the use of mineral acid (HNO_3) to mask the generation of the coloured precursor, whilst the second examined various on-chip reagent mixture combinations to enable a zero baseline signal to be determined. Whilst excess HNO_3 was able to remove the background (base line) yellow-green colour of the reagent mixture and may reduce any direct reduction of Mo(VI) in the absence of phosphate, it also inhibited the appearance of the blue phosphate reaction product, suggesting that the use of excess HNO_3 should be avoided. This is in agreement with the results of Crouch and Malmstadt [12] who reported that, at nitric acid concentrations >0.3–0.5 N, the amount of molybdenum blue reaction product formed will be independent of the acidity but that the rate of formation will decrease sharply with increasing acidity. These observations were attributed to the nitric acid being associated with the reversible formation of the intermediate 12-MPA ($\text{H}_3\text{PO}_4 + 6 \text{Mo(VI)} \rightleftharpoons ((12\text{-MPA}) + 9\text{H}^+$, the Mo(VI) existing as a dimer) rather than the final reduction step. Thus, after the formation of the 12-MPA intermediate, the equilibrium will depend on the amounts of phosphate and molybdate initially present, any excess acid will favour the backward reaction.

Addition of phosphate to the yellow-green reagent mixture in the absence of acid (HNO_3), however, required some time (>1 min) for the reaction product to be produced. Such conditions would, therefore, necessitate a very low flow rate, implying a correspondingly low sample throughput rate. It was found that whilst a 0.4 M solution of HNO_3 did not totally remove the background yellow-green colour, it did promote the phosphate reaction enabling a blue colour to be formed within 10 s but with slightly lower colour intensity compared to when HNO_3 was not present at all. An appropriate amount of HNO_3 is, therefore, an advantage over either an excess or no HNO_3 being present in order to establish the required blue reaction product in a reasonable time frame. However, the low pH (<4) resulting from the use of acid will also have a limiting effect on the generation of EOF for the corresponding solutions. To compensate for this effect, the reagents were dissolved in a 10 mM borate buffer in the absence of mineral acid to promote EOF which, in addition, not only produced the yellow-green colour more slowly, compared to the non-buffer-dissolved mixture, but also generated a more intense blue reaction product. Thus, the use of a 10 mM borate buffer was identified as offering preferable reaction conditions which, in addition, enhanced the intensity of the reaction product.

The study carried out to investigate the generation of an unwanted yellow-green background effect indicated that premixing the phosphate and ascorbic acid solutions gave a clear/colourless mixture prior to adding the molybdate which subsequently generated blue phosphate reaction product. Thus, either the molybdate or the premixed phosphate/ascorbic acid could be pumped as the main reagent stream and the other solution injected accordingly, using a single line FIA. Premixing the phosphate and ammonium molybdate also gave a colourless solution mixture before adding the ascorbic acid to form the blue phosphate reaction product and, therefore, either combination could be pumped in the main channel with the other injected. In each instance, however, the yellow-green reaction precursor formed first before the blue phosphate reaction product.

In order to establish a simple single-line μFIA system for the determination of phosphate, it was decided that the phosphate standard/sample would be injected into a premixed reagents mixture stream

and, due to the generation of the reaction precursor yellow-green colour, the background reagent mixture signal would be determined and zeroed prior to measurement of the blue product, using an appropriate microspectrometer. The actual manifold used is shown in Fig. 2.

It should be noted that whilst this particular study is centred on producing a calibration model for phosphate, the conditions of pH <7 are also likely to enhance the potential for interference from silicate, arsenate, germanate, and tungstate, etc. and, therefore, in any 'real' analysis, an attempt should be made to avoid these interferences either by isolation of the interfering species or through the use of multivariate calibration models.

3.5. On-chip detection

3.5.1. Optimisation of sample chemistry and injection time for the phosphate analysis

From studies on the flow characteristic of the phosphate standards, it was clear that the injection time or corresponding volume (in time-based injection), will depend on the pH and, therefore, the EOF rate of the particular standard injected. In the absence of a pH buffer, standards/samples with lower phosphate concentrations would move at faster flow rates, due to a pH effect, than those with higher concentrations. Clearly such a situation would lead to an unsatisfactory method of sample injection, indicating the importance of using a pH buffer to control the EOF. The dissolution of the phosphate standards/samples (pH ranging from 6.67 to 8.50) in sodium borate buffer (10 mM), produced a buffered solution of around pH 8 which gave a standardised flow across the entire calibration range.

Using the injection mode described previously and the optical configurations shown in Fig. 2, the detector response resulting from the different injection times (10–60 s) for a $10 \mu\text{g ml}^{-1}$ phosphate standard are shown in Fig. 6 for which 50 s injection gave the highest peak intensity. It is important to note that whilst EOF, with a flat (trapezoidal or rectangular) flow profile characteristic, is the main mechanism for solution mobility, electrophoretic mobility will also occur, effecting the diffusion limiting reactions taking place in the interfacial zones between the reactants. Thus, the amount of reaction product formed and,

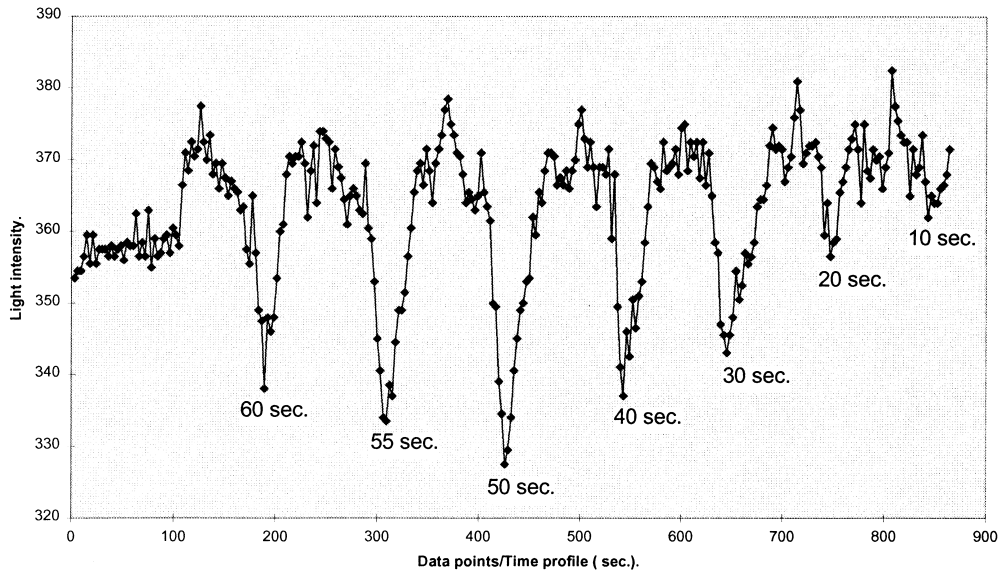


Fig. 6. Absorbance signals for different injection times of 10 ppm phosphate.

therefore, the sensitivity of detection will depend on the volume injected, the diffusion constants for the solutions present, the individual electrophoretic mobility for each component and the reactant concentrations. Thus, if insufficient reagent or standard is injected the response signal is reduced (i.e. <50 s);

however, if the injection volume delivers excess standard the unreacted solution seems to have a depressive effect on the detector response (i.e. >50 s), possibly due to a spectrophotometric effect of the unreacted potassium dihydrogenphosphate. It is estimated that a 50 s injection time, which is inclusive of the time

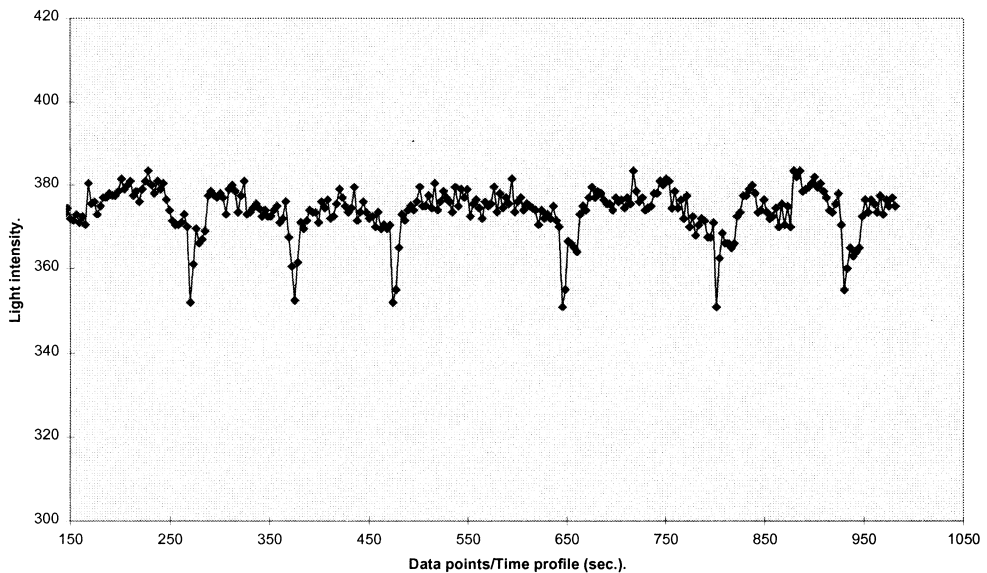


Fig. 7. Response signals for a 2.5 ppm phosphate.

required to form the molybdenum blue product, corresponds to $<0.1 \mu\text{l}$, but clearly the whole aspect of sample injection and reaction characteristics in μFIA systems requires a more detailed study and such work is currently in progress. It is also important to stress that, after injection, the reaction occurred only on resuming a reagent flow removing the need for a stopped-flow mode of analysis and indicates the relevance of electrophoretic mobility in such systems vs. diffusion-limited reactions. This latter observation serves also to support the case for further work to be carried out into the interfacial dispersion/mixing between reagents in such systems. Based on the experimental work carried out to-date, a 50 s injection time was used for the entire calibration procedure.

3.5.2. Calibration

Typical response signals for the $2.5 \mu\text{g ml}^{-1}$ standard are shown in Fig. 7. The calibration plot of absorbance vs. phosphate concentration was found to be linear with a correlation coefficient value of 0.9952 for the equation $y = 0.0036x + 0.0155$.

The calibration model for the μFIA produced a theoretical detection limit of $0.1 \mu\text{g ml}^{-1}$, calculated using $3 \times \text{SD}$ of the lowest standard and a precision ranging from 4.79 ($1 \mu\text{g ml}^{-1}$) to 2.94% ($10 \mu\text{g ml}^{-1}$ phosphate) RSD for $n = 6$. This slightly higher RSD of the system is thought to be more associated with the micro-detection system which might require the application of noise reduction techniques if higher precision and/or lower detection limits are required. There was no evidence of a serious chemical baseline effect suggesting that the single channel mode of detection will be suitable for future apparatus. The reaction/detection time for the μFIA system was 10–20 s which, together with the injection time gave a sampling rate of ca. 60 samples/h.

4. Conclusions

The current study has demonstrated that a μFIA methodology comparable in performance to conven-

tional FIA can be achieved for the detection of orthophosphate.

The μFIA system offered the specific advantages of reduced reagent usage (total system volume $\approx 0.6 \mu\text{l}$), reduced sample consumption (sample volume ca. $0.1 \mu\text{l}$), low waste generation and fast analysis times (60 analysis/h). In addition, the resistant nature of the glass chip material to acidic/corrosive solutions prevents the regular changing of components such as pump tubings, connectors, etc. encountered in conventional FIA systems.

References

- [1] A. Manz, C.S. Effenhauser, N. Burggraf, E.J.M. Verpoorte, D.E. Raymond, H.M. Widmer, *Analysis Mag.* 22 (1994) M25.
- [2] D. Craston, S. Cowen, *Chem. Br.*, 1996, Oct., p. 31.
- [3] R.N.C. Daykin, S.J. Haswell, *Anal. Chim. Acta.* 313 (1995) 155–159.
- [4] S.J. Haswell, *Analyst* 122 (1997) 1R.
- [5] M.A. Roberts, J.S. Rossier, P. Bercier, H. Girault, *Anal. Chem.* 69 (1997) 2035–2043.
- [6] R. Bogue, *Lab. Equip. Dig.*, 1995, p. 14.
- [7] S. Liu, P.K. Dasgupta, *Anal. Chim. Acta.* (1993) 283; 739.
- [8] A. Manz, D.J. Harrison, E. Verpoorte, H.M. Widmer, *Adv. Chromatogr.* 33 (1993) 1.
- [9] E.M.J. Verpoorte, B.H. Van der Schoot, S. Jeanneret, A. Manz, N.F. de Rooij, Silicon based chemical microsensors and microsystems, in *Interfacial Design and Chemical Sensing*, American Chemical Society Symposium Series, Chap. 21, 1994, p. 244.
- [10] A. Spielmann, M. Garn, S. Haemmerli, A. Manz, H.M. Widmer, *Proceedings of the Seminar of the Swiss Committee of Analytical Chemistry*, Bern, Switzerland, October 16, 1992, p. 49.
- [11] *Encyclopedia of Analytical Science*, vol. 9, Academic Press, UK, 1995, pp. 5376–5395.
- [12] S.R. Crouch, H.V. Malmstadt, *Anal. Chem.* 39 (1967) 1084–1089.
- [13] J. Ruzicka, E.H. Hanson, *Flow Injection Analysis*, second edn., Wiley, 1988, pp. 1–13.
- [14] X. Huang, M.J. Gordon, R.N. Zare, *Anal. Chem.* 60 (1988) 1837–1838.



ELSEVIER

Analytica Chimica Acta 387 (1999) 1–10

ANALYTICA
CHIMICA
ACTA

Characterisation of a micro-total analytical system for the determination of nitrite with spectrophotometric detection

G.M. Greenway^{*}, S.J. Haswell, P.H. Petsul

Department of Chemistry, University of Hull, Hull, HU6 7RX, UK

Received 17 August 1998; received in revised form 30 November 1998; accepted 8 December 1998

Abstract

A micro-total analytical system (μ TAS) is described for the determination of nitrite based on its reaction with sulphanilamide to form the diazonium salt which when coupled with *N*-(1-naphthyl) ethylene diamine yields an azo dye whose absorbance was measured at 526 nm. The reaction took place in an etched glass manifold containing channels 302 μ m wide and 115 μ m deep in which electro-osmotic flow was used to move the reagents. The absorbance of the product was measured in situ using a micro-spectrophotometric-fibre optic detection system. The electro-osmotic flow mixing characteristics of the reagents together with the production of the colorimetric complex have been investigated. In addition methods for obtaining sensitive detection in the micro-reactor are reported. Using the conditions established a linear calibration was obtained between 0 and 100 μ M with a correlation coefficient of 0.999. The RSD at 50 μ M NO_2^- was 2.6% ($n=6$) and the limit of detection obtained (3σ) was 0.20 μ M NO_2^- . © 1999 Elsevier Science B.V. All rights reserved.

Keywords: Micro flow injection analysis; Nitrite; Miniaturisation; μ TAS

1. Introduction

The presence of low level chemical species in the environment, an increasing need for good industrial process control, developments in clinical diagnostics and numerous areas have lead to the search for improved, less expensive and more robust methods for measuring low levels of chemical analytes. Micro-total analytical systems (μ TAS) have been suggested as a possible solution for such analysis as they are primarily concerned with the chemical reactions in small volumes of liquids where the measurement is

based on the reaction between more than one reagent, with subsequent determination being achieved in situ and an appropriate detector. These micro flow systems have the inherent advantages of being portable, requiring low reagent consumption, and are able to operate remotely [1]. The development of such systems has progressed more recently with the introduction of electro-osmotic flow that provides a flexible and robust method of moving fluids through microchannels of typically less than 200 μ m i.d. [2–4]. Fast controllable reactions have been shown to occur between picolitres of samples in such reactors [5] which to date have been mostly produced by photolithography techniques using substrates such as glass and silicon [5–7].

^{*}Corresponding author. Tel.: +44-01482-465475; fax: +44-01482-466416; e-mail: e.m.pickering@chem.hull.ac.uk

A range of different detection techniques have been investigated for μ TAS including spectrophotometry and electrochemistry [8,9]. Daykin and Haswell [8] for example reported the development of a micro flow injection system (μ FIA) for the determination of phosphate using spectrophotometric detection [8], whilst Fiehn et al. [9] have demonstrated the use of fluidic ISFET microsystem for the determination of pH, nitrate, ammonia, sodium and potassium based on a sensor technology using microfluidic injectors and diodes.

In this work a μ FIA has been investigated and developed for the determination of nitrite. Electro-osmotic flow has been used to mobilise reagents in an etched glass manifold to produce a coloured spectrophotometrically active analytical product. The absorbance of the product was measured in the manifold using a micro-spectrophotometric-fibre optic detection system. Nitrite was determined by its reaction with sulphanilamide to form the diazonium salt which was coupled with *N*-(1-naphthyl) ethylene diamine to yield an azo dye whose absorbance was measured at 526 nm.

2. Experimental

2.1. Reagents and materials

All the chemical standards and reagents used were analytical grade unless stated otherwise and the water used was high purity de-ionised (18 M Ω cm resistivity) (Elgastat UHQ PS, Elga, High Wycombe, UK). The sodium nitrite was supplied by Fisher Scientific (Loughborough, UK), ammonium chloride, hydrofluoric acid and ammonium fluoride being obtained from Merck (Poole Dorset, UK). The hydrochloric acid was supplied from Philip Harris (Shenstone, Lichfield, UK), and the sulphanilamide and *N*-(1-naphthyl) ethylene diamine (NED) was from Aldrich (Gillingham, Dorset, UK). Sodium formate and sodium acetate were from Avocado Research Chemical (Heysham, UK) and the nitric acid was R.P. NormapurTM, (Fontenay, S/Bois, France). The Microposit chrome etch 18 and photoresist remover 1112A were from Shipley (Coventry, UK). The glass for the micro-reactor chips and cover plates were both Superwhite Crown B70 borosilicate glass (Instrument Glasses,

Enfield, UK). The silica fibre optics were obtained from Optiflex (Doncaster, UK). Electronic components were from RS Components (Northants, UK).

The nitrite (10 mM NO₂⁻) stock solution was prepared from sodium nitrite. The pH of the ammonium chloride buffer (190 mM) was adjusted with ammonia to give a pH of 5. The sulphanilamide (1.16 mM) and *N*-(1-naphthyl) ethylene diamine (1.95 mM) were prepared as a mixed reagent in ammonium chloride buffer, with five drops of concentrated hydrochloric acid being used to dissolve the sulphanilamide.

2.2. Device fabrication

The photolithographic plates containing 25 devices of five different geometries were obtained from photo-mask producers (Alignrite, Wales, UK). The method of wet etching was a modified version of that described by Daykin and Haswell [8]. The glass plates were placed in 1% HF and 5% NH₄F at 70°C and agitated every 10 min for 1 min, followed by 1 min lateral stirring with a plastic rod during the etching process. The etching time for the manifold used in this work was 2 h after which the plate was removed from the bath and washed thoroughly with water. Before the etching solution was discarded the channels on the plates were measured using a DekTek³ST stylus surface profiler to ensure the required channel dimensions had been achieved. Three profiles were taken at three different locations along the channel and an average of the channel width, depth and area were recorded. With the required channel sizes achieved the etching solution was carefully discarded. The plates were then exposed to strong UV-light for 1–2 h before being dipped into a photoresist remover for 2–3 h to remove the photoresist. The plates were washed with tap water and any excess photoresist and the chrome layer were then stripped off with the Microposit chrome etch 18 with a final wash being carried out in de-ionised water. The etched plates were then cut into individual manifolds i.e. 25 (152 mm²) being obtained from the original plate.

In the work by Daykin and Haswell [8] the manifolds had thin glass cover plates with 2 mm i.d. holes thermally bonded onto the manifolds. The solution reservoirs were then stuck on to the cover plates. Many problems associated with mechanical and chemical stability were encountered with this approach and

therefore thick glass cover plates (17 mm) incorporating 2 mm i.d., predrilled holes as reservoirs were thermally bonded to the substrate so negating the need to glue reservoirs into the manifold. To achieve this the thick cover plate was carefully positioned such that the 2 mm holes (reservoir) were placed directly on the end of the etched channels in the substrate and were held firmly by Blu-tack (Bostik, Leicester, UK). The chip was placed on the silica support in the centre of a microwave ashing system (CEM microwave ashing system 300, NC, USA). During the bonding process the thicker cover plate was placed at the bottom to prevent the channel from being completely fused due to the weight of the cover plate pressing on the etched base plate. The thermal due to the weight of the cover plate pressing on the etched base plate. The thermal programme that was used was 75°C for 30 min, 150°C for 30 min, 680°C for 30 min, 650°C for 30 min, 570°C for 30 min, 505°C for 30 min after which the oven was allowed to return to room temperature. The bonded chip was tested for successful fusion by filling reservoirs with water and determining a linear current voltage relationship over the range 0–1 kV. If the chips became blocked in the development work they were cleaned with mineral acid.

2.3. Procedure

2.3.1. Determination of the reagent flow characteristics

To determine the flow characteristics of the reagents and reaction products a second manifold prepared as above with a channel size of 325 μm wide and 30 μm deep was used. In this work the applied voltage, concentration and pH of the reagents were the selected variables. A traditional FIA system using the method described by Daniel et al. [10] was first used to identify preliminary reaction conditions. These conditions are shown in Fig. 3. Using these conditions the optimum applied voltage and corresponding flow rates were determined for the individual reagents using the manifold shown in Fig. 1. With 560 mM NH_4Cl and a constant pH of 7.8 the NH_4Cl was placed in reservoir A whilst water was placed in reservoirs B and E. Reservoir E also acted as ground for the floating current. Voltage was applied across A(+) and B(–) which pumped the reagent from A to B for a period of 30 min. The volume of NH_4Cl in reservoir A was

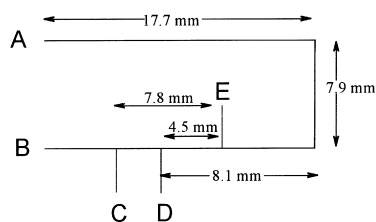


Fig. 1. Schematic diagram of the micro flow injection manifold for the determination of reagents flow characteristics. Channel size was 325 μm wide and 30 μm deep. The volume of the channel section from the junction BC to BE was 76 nl and BD to BE was 44 nl. A=sulphanilamide, B=ammonium chloride, C=*N*-(1-naphthyl) ethylene diamine, D=nitrite/nitrate/sample, E=waste.

measured by filling the reservoir to a premarked point bonding was with a micro syringe thereby replacing the amount that had been pumped out of the reservoir A. From the volume change over the 30 min the flow rate was calculated. The procedure was repeated again for the next chosen voltage until the optimum applied voltage was determined. Keeping the optimum applied voltage and the pH constant the optimum concentration of the NH_4Cl was determined and finally keeping the optimum applied voltage and concentration constant the optimum pH was determined. In a same manner, the flow characteristics of the sulphanilamide, NED, nitrite standards and mixed reagent were determined. The μFIA manifold and configuration for the final analytical measurements is shown in Fig. 2.

2.4. μFIA system

The μFIA system used is described schematically in Fig. 2 and was contained for experimental purposes in a custom built insulation box with two power supplies offering power outputs of up to 50 W with a maximum voltage of 1 kV (Advance Hivolt, West Sussex, UK). The current and voltage were monitored by a computing multimeter (model 1906, Thurlby Thandar Instrument, Huntingdon, Cambridgeshire, UK). A custom built light source with a green light emitting diode (LED) was attached using an SMA fitting to a 110 μm i.d., 125 μm o.d. silica fibre optic (Optiflex, Doncaster, UK) which transferred the light to and from the reaction channel in the micro-reactor. The receiving fibre optics carried the absorbed light into a computer controlled diode array micro-spectrometer with Spec-View windows software (microParts, Dortmund, Ger-

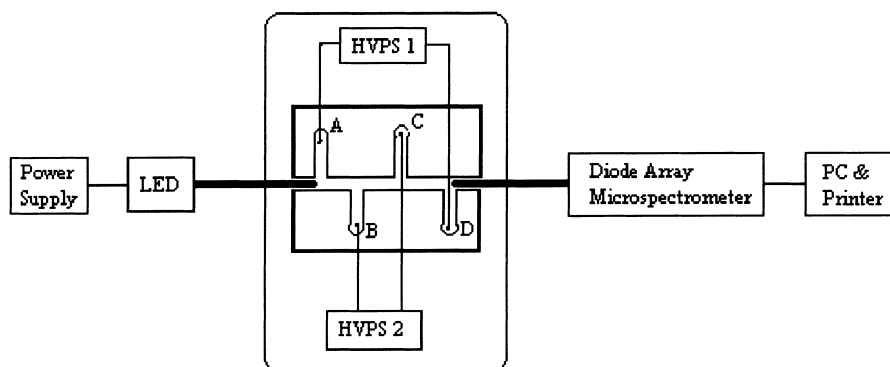


Fig. 2. A schematic of the micro flow injection manifold for the determination of nitrite using diode array microspectrometer. Microreactor chip enclosed in insulation box. Microchannel size of 302 μm wide and 115 μm deep with fibre optics (110 μm) indicated by the thick heavy line, HVPS 1 and 2 are high voltage power supplies. Reservoir A=mix reagent, B=nitrite/sample, C=waste 1, D=waste 2.

many). The fibres were prepared by removing the plastic coated covering at the ends of the fibre optics with NITRO[®]MORS all purpose paint-vanish remover (Winsford, UK). The bare ends of the fibre optics were then cleaned and cut with a quartz crystal. The fibre optics were carefully inserted into a water filled side channel of the chip and aligned using the diode array micro-spectrometer. The fibre optics were fixed in position by gluing with a general-purpose adhesive (Bostik, Leicester, UK) and silicon rubber glue (RS components, Northants, UK) and allowed to harden over night before being used.

3. Results and discussion

3.1. Characterisation of electro-osmotic flow properties of the reagents

The electro-osmotic flow characteristics of the reagents used in the colorimetric determination of nitrite were identified using the manifold shown in Fig. 1 according to the procedure described in Section 2. The buffer used in the original method was ammonium chloride. Despite this giving good electro-osmotic properties bubbles did occur around the electrodes due to formation of ammonia at voltage greater than 600 V. To overcome these difficulties several other buffering systems were investigated, however, the pH of the borate was found to be too high toward the end of the scale (9–10) whereby EOF is greatly reduced. The sodium acetate and sodium formate

buffers gave a low EOF due to their low pH (<3). In characterising the buffer flow a balance had to be established between the best conditions for EOF and the best conditions for the colorimetric reaction to occur.

3.1.1. Ammonium chloride

The flow characteristics of the NH_4Cl are shown in Fig. 3(a). An optimum voltage of 350 V was found to deliver a flow of 0.80 $\mu\text{l}/\text{min}$ NH_4Cl , however, any voltage between 250–400 V was clearly capable of delivering a suitable flow of NH_4Cl (Fig. 3(a1)). As the applied voltage was increased beyond 400 V the flow rate decreased and as the power increased above 600 V bubbles were formed around the electrodes and were being entrained into the channel forming air gaps and causing the current to fluctuate.

The most suitable concentration for NH_4Cl EOF was determined to be 190 mM (1% w/v), thereafter, as the concentration increased the flow decreased due to the ions migrating to the electrodes and leaving the bulk solution behind (Fig. 3(a2)). The flow rate for the reagent is also known to be dependent on the pH [11,12] with pH values between 4 and 10 being known to be suitable for EOF. In this study the highest flow rate was obtained at pH 6.8 (Fig. 3(a3)). The decrease in the flow observed at pH>7 was again due to bubble formation.

3.1.2. Sulphanilamide

The flow characteristics of sulphanilamide are shown in Fig. 3(b). The optimum applied voltage

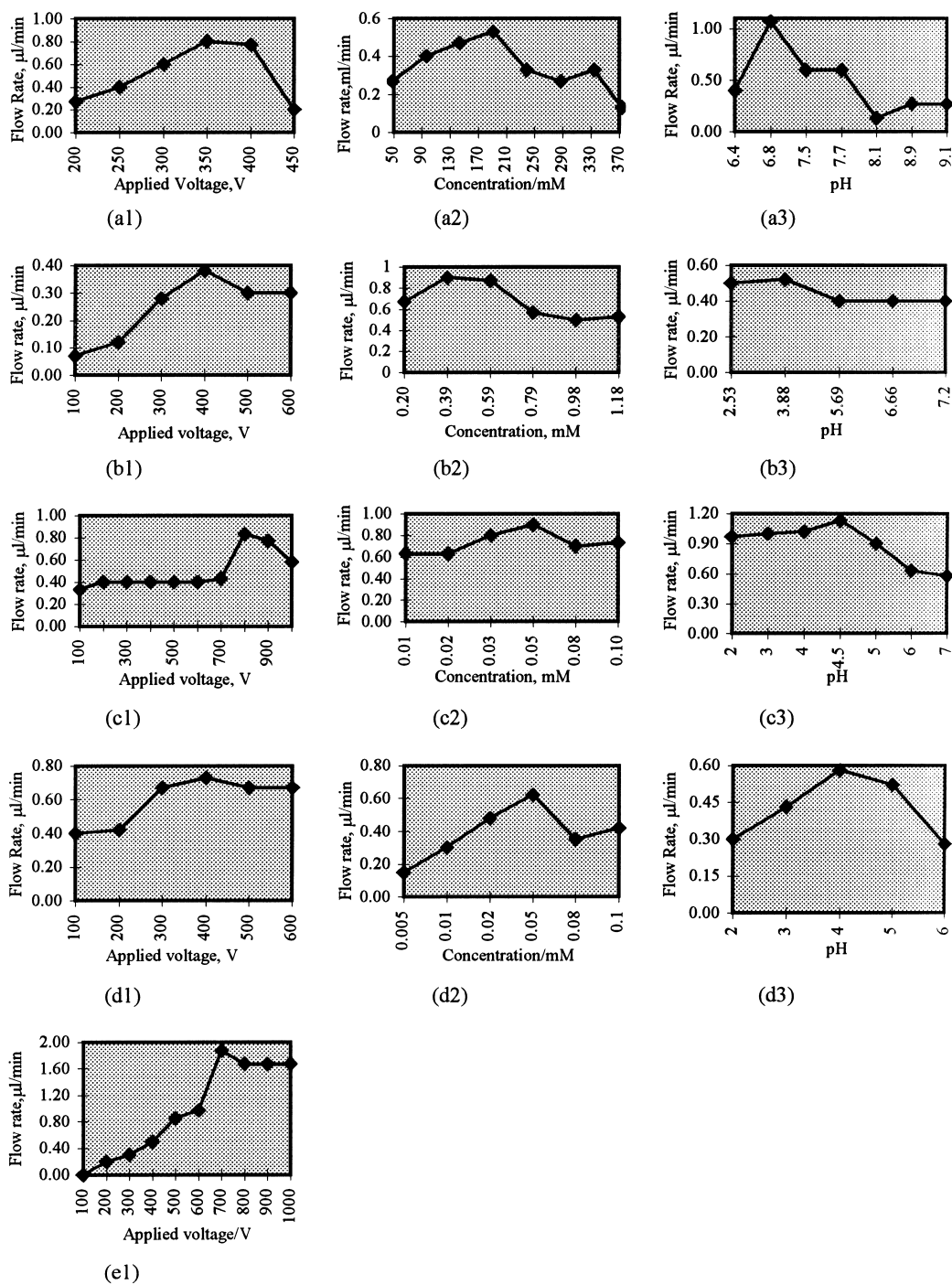


Fig. 3. Characterisation of electro-osmotic flow of reagents: (a) EOF of ammonium chloride, (a1) NH₄Cl: 560 mM, pH 7.8, (a2) 350 V, pH 7.8, (a3) 350 V, 190 mM; (b) EOF of sulphanilamide, (b1) sulphanilamide: 2.9 mM, pH 2.0, (b2) 400 V, pH 2.0, (b3) 400 V, 0.39 mM; (c) EOF of NED, (c1) NED: 5.4 mM, pH 4.0, (c2) 800 V, pH 4.0, (c3) 800 V, 0.05 mM; (d) EOF of nitrite, (d1) nitrite: 0.1 mM, pH 5.0, (d2) 400 V, pH 5.0, (d3) 400 V, 0.05 mM and (e) EOF of mixed reagent, (e1) mixed reagent: 1.16/1.95 mM, pH 4.0.

for moving sulphanilamide was found to be 400 V, however, the flow rate at this voltage was only 0.38 $\mu\text{l}/\text{min}$ (Fig. 3(b1)). The lower flow rates obtained at these applied voltages are due to a low EOF, a result mainly due to the acidic conditions of the reagent. The best concentration of sulphanilamide in terms of obtaining the highest flow rate was 0.39 mM (Fig. 3(b2)), however, the concentration range between 0.39 and 0.98 mM was not optimum for the reaction and the coloured azo dye was not formed. Higher concentrations causes resistance in the channel causing flow to reduce, however, a much higher concentration of 1.18 mM sulphanilamide was used because it immediately formed the coloured azo dye when added to the nitrite even at low flow rates. The optimum pH of 1.18 mM sulphanilamide was 3.9 and gave a flow rate of 0.52 $\mu\text{l}/\text{min}$ (Fig. 3(b3)). The diazotisation and coupling reaction is known to be pH sensitive and is better carried out at $\text{pH} < 4$. Thus, the conditions of 1.18 mM sulphanilamide at pH 3.9 offers good compromise conditions.

3.1.3. *N*-(1-naphthyl) ethylene diamine (NED)

The hydrophobicity of NED meant that a constant flow rate of 0.4 $\mu\text{l}/\text{min}$ was found over a large voltage range and only began to increase at voltages exceeding 800 V (Fig. 3(c1)).

Good flow control was achieved for the given concentration range (Fig. 3(c2)) at high voltages with the maximum flow rate obtained at 0.05 mM, however, a reaction between the 1.18 mM sulphanilamide and the 0.05 mM NED did not produce an immediate coloured azo dye. It was only at higher concentration ($> 1 \text{ mM}$) that an obvious coloured azo dye was formed. The optimum pH was 4.5 with a $\text{pH} > 5$ showing a decrease in flow rate (Fig. 3(c3)). This was important because it was found that when the pH of NED was > 5 the coupling reaction did not occur.

3.1.4. Nitrite standard

The voltage required to deliver a suitable flow rate for the nitrite standard was found to be between 300 and 600 V with 400 V being the optimum (Fig. 3(d1)). A linear flow was found between 0.005 and 0.05 mM NO_2^- , thereafter, the flow fluctuated (Fig. 3(d2)). The optimum concentration which gave the highest flow rate was 0.05 mM and the optimum pH was

4 (Fig. 3(d3)). In the analytical method ammonium chloride buffer at pH 4 controlled the EOF overriding these effects and ensuring reproducible injections.

3.1.5. Mixed reagents

To overcome the difficulties observed in moving the NED and sulphanilamide by EOF it was decided to premix the two reagents. A mixture of 1.18 mM sulphanilamide and 1.95 mM NED was prepared in 190 mM NH_4Cl at pH 4 to facilitate the movement yet still allow the required reaction to occur. The mixed reagent was colourless and stable for at least 12 h. The best applied voltage found to deliver a good flow rate (0.8 $\mu\text{l}/\text{min}$) for the mixed reagent was 600 V, although any voltages between 300 and 600 V would be indeed suitable (Fig. 3(e)). The increase in flow rate above 600 V lead once again to Joule heating and an increase in bubble formation with subsequent evaporation.

3.1.6. Reaction product (azo dye)

The product formed in the channel had a different flow characteristics to the reagent and analyte and therefore needed a different applied voltage to move it around in the channel. This was established by carrying out the reaction outside the reactor and introducing the product to the reservoir for the flow rate to be determined. The pH of the azo dye dropped to < 2 making it difficult to move by EOF. Although, applied voltages between 100 and 1000 V were used there was no evidence of the dye moving. It was observed that the coloured azo dye formed in the channel was not able to move to the detection point and that the coloured azo dye, when left for more than 2 days decolourised at applied voltages $> 400 \text{ V}$ indicating that any azo dye formed in the channel had to be moved by using lower applied voltages. To achieve appropriate analytical conditions a buffer system (NH_4Cl) was used to aid mobility of the coloured product.

3.2. Characterisation of detection method

3.2.1. Detector configuration

The detection system was designed to detect the absorbance of the azo dye product but this depended also on the arrangement of the fibre optics, the sensi-

tivity of the LED and the spectrophotometer detection system. It was found that the best results were obtained by actually ensuring that the ends of the fibres were carefully cut to give a defined flat surface so that the light coming out of this surface is not diffracted but intensely focus into the channel onto the receiving fibre optics. The light intensity is greatly improved when the ends of the fibre optics are glued into the channel and in direct contact with the solution providing a good alignment of the fibres as this was the key in obtaining acceptable sensitivity. The intensity of the green LED used was 0.25 candela with a viewing angle of 25° which meant that if the fibre optics surface was carefully cut there was no need for a focusing lenses.

3.2.2. Reagent mixing

As the absorbance efficiency is measured along the microchannel in which the reaction occurs (as shown in Fig. 2) signal intensity is dependent on the length of sample plug in the channel. Experiments were performed where the reaction was carried out outside the reactor and the product was introduced directly into the channel, thus ensuring complete mixing had occurred. In these experiments the absorbance was shown to be proportional to sample plug length in the region of 1–9 mm ($r^2=0.996$) with values up to 1.5 absorbance units for a 9 mm plug of 100 μM nitrite solution.

However, when the reaction took place in the micro-reactor the absorbances obtained were found to be much lower. This was due to the incomplete mixing of the reagents as they converged in the μFIA manifold. To understand the processes that were occurring it is important to realise that in this reaction the coloured product is formed almost immediately, but the colour then continues to intensify. The nitrite solution was introduced at a T-junction into the detection channel (which already contains the mixed reagent) as illustrated in Fig. 2. From the results obtained it appeared that once the coloured dye (product) has been formed by diffuse mixing at the interface between the solutions it effectively blocked further contact of the mixed reagent with the nitrite due to the lack of mixing in such systems (Reynold numbers <1). The product slug produced was less than 2 mm and was then diluted on the resumption of the reagent mixture giving a much lower absorbance than would be

expected. Further experiments with coloured dyes and different shaped intersections (T and Y) seemed to confirm mixing beyond that expected by natural diffusion was not occurring.

For the 'Y' type (45°) junction mixing there was some evidence of movement as far as the intersection and a close look at the intersection with a 9x eye piece magnifying glass confirmed the lack of mixing. At the intersection the two dyes formed distinctively two layers and did not mixed when water was pumped into the channel to help the mixing. This confirmed the suggestion that mixing was not occurring and therefore the reaction was as expected to be, a diffusion limited interfacial reaction. Thus it became apparent that the subsequent analytical procedure must accommodate the non-mixing or interfacial reaction characteristics of μFIA systems.

3.2.3. Optimisation of the injection time

The effect of the injection time of the 100 μM nitrite into the mixed reagent can be seen in Fig. 4. As can be seen from the graph an injection time <10 s was not long enough to inject a sufficient amount into the measurement channel and secondly an injection time >50 s was too long so that by the time the measurement was taken the coloured azo dye has moved out of the measurement channel leaving a new column of nitrite occupying the length of the main channel. The maximum absorbance was obtained at 30 s, although 20 and 40 s also gave good response. For this work 20 s injection was chosen for fast sample throughput.

3.2.4. Detection mode

The microspectrometer (Fig. 2) was supplied by microParts, Dortmund, Germany. This consist of a Hamamatsu S5463-256 photodiode array contained in a grey aluminium housing with a spectral range of 380–780 nm (dispersion of 0.12 nm/ μm). Light is introduced to the diode array via a fibre of 50 μm . The electronic components consisted of microcontroller (Siemens SAB 80C166), A/D converter (Burr Brown ADS 7807U), and had a resolution of 16 bits with integration times of 40–2560 ms possible. The system was used in the Scan mode for this work and Window software SpecView was used to collect the data, which was transferred into ASCII-File to be

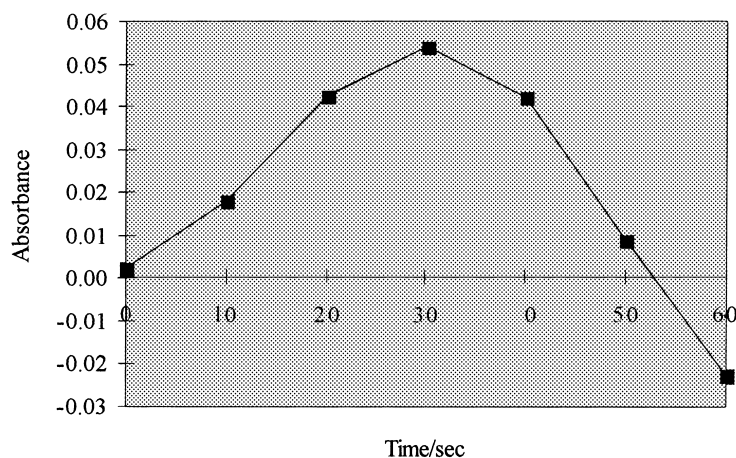


Fig. 4. Investigation of the sample injection time (scan mode), 100 μM nitrite was used with 3 absorbance reading taken ($n=3$) for each injection. Chosen $\lambda_{\text{max}}=526$ nm.

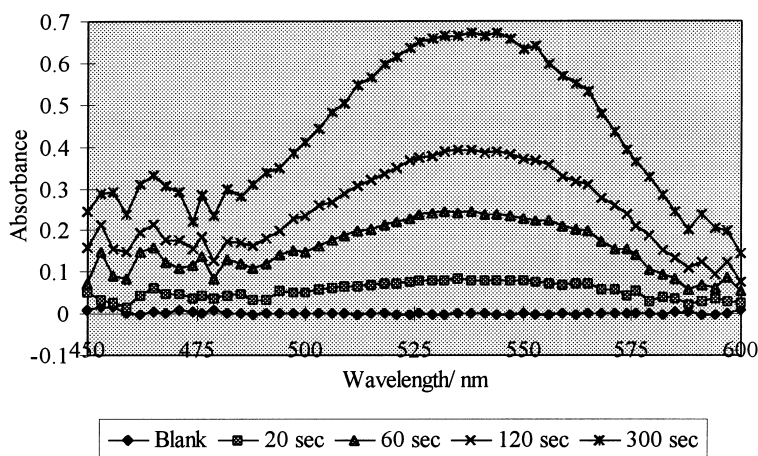


Fig. 5. Effect of changing the stop flow mode time on absorbance for injection of 100 μM NO_2^- (measurement recorded in scan mode).

analysed in an Excel spreadsheet. To optimise the absorbance signal the electro-osmotic flow was stopped when the product was in the channel (stop flow mode) and the dye allowed to increase in intensity, this allowed the signal to be adequately detected. The absorbance was found to increase the longer the product was in the channel until a steady state was reached but a hold time of 20 s was chosen as this gave acceptable limits of detection (Fig. 5). Subsequent work was carried out using a 30 s loading of the mixed reagents then 20 s injection of nitrite followed by 20 s in the stopped flow mode, the measurement was then made and the cycle repeated.

3.3. Analytical characteristics

Using the optimised conditions a calibration curve was obtained. The initial results using the manifold shown in Fig. 2 (Mode 1) with the two negative electrodes placed in reservoir C gave poor reproducibility ($r^2=0.973$) as can be seen in the r^2 value in Table 1. The reproducibility was increased by changing the set up of the electrodes in the manifold so that there were two negative waste reservoirs (Mode 2) to avoid the previous situation where the two negative electrodes were placed in the same reservoirs. In the new configuration (Fig. 2) the reservoir A(+) to

Table 1
Calibration details

Analytical parameters	μFIA		Conventional FIA
	Mode 1 ^a	Mode 2 ^b	
Equation ^c	$y=0.0014x+0.0118$	$y=0.0072x-0.0007$	$y=0.0048x-0.0008$
R^2	0.973	0.999	0.999
LOD (μM)	1.8	0.20	0.20
Standard (μM)	(RSD)		
1.0	7.9	8.7	4.0
10.0	14.6	5.3	1.4
50.0	11.5	2.6	0.6

^aMode 1: two negative electrodes in waste reservoir (C).

^bMode 2: two negative electrodes in separate waste reservoir (C+D).

^cWhere y is absorbance and x is concentration in μM.

reservoir D(–) was used to load the reagents and reservoirs B(+) to reservoir C(–) was used to inject the sample. In each calibration run, the absorbance measurement of the mixed reagent was zero reference (or blank corrected) to compensate any dye formation arising from trace nitrite before the nitrite standard was injected and measured. A linear calibration was obtained between 0 and 100 μM with an equation of the line being $y=0.0072x-0.0007$ where y is the absorbance and x is the concentration in μM with a correlation coefficient of 0.999. The limit of detection (3σ) was approximately 0.20 μM NO₂[–]. These results were comparable with those achieved by the conventional FIA in which the calibration was linear ($r^2=0.999$) between 0 and 100 μM and the LOD (3σ) was 0.20 μM (Table 1).

The reproducibility was not as good as for the conventional FIA system where the %RSD was below 5% for all standards. In the micro flow system although the RSD was 2.6% for the 50 μM NO₂[–] standard and 5.3% for the 10 μM NO₂[–] standard it decreased to 8.7% for the 1 μM NO₂[–] standard. This lack of reproducibility is thought to be due to the possibility of hydrodynamic flow competing with the EOF. To overcome this we are now investigating the reproducibility when the channel size in the micro reactor is reduced to 200 μm.

4. Conclusion

This paper has shown that it is possible to detect the nitrite by a spectrophotometric method in a micro flow

injection analysis system with acceptable sensitivity and reproducibility. In developing such a system a compromise has to be made between the conditions required for good EOF (for example a pH range between 2 and 9) and conditions required for the diazotisation reaction. The optimisation could be carried out more efficiently by measuring both the EOF and absorbance. The method enables a sampling rate of 50 samples/h with a significant reduction in reagent volumes and waste products. Further work needs to be carried out in the more fundamental area of reagent mixing and reaction characteristics to improve the system. Work is also currently being carried out to extend the method to the determination of nitrate by using in situ cadmium reduction of the nitrate to nitrite. Samples of natural waters will also be analysed after filtration through a 0.25 μm membrane filters.

Acknowledgements

The authors would like to acknowledge the contributions made to this work by other members of the micro-reactor group at Hull, especially, Lorna Nestrop and George Doku. They would also like to thank the Government of Papua New Guinea for the financial support to Peter Petsul.

References

- [1] S.J. Haswell, Analyst 122 (1997).
- [2] K. Seiler, Z.H. Fan, K. Fluri, D.J. Harrison, Anal. Chem. 66 (1994) 3485.

- [3] A. Meulemans, F. Delsenne, *J. Chromatogr. B* 660 (1994) 401.
- [4] N. Chiem, D.J. Harrison, *Anal. Chem.* 69 (1997) 373.
- [5] D.J. Harrison, A. Manz, Z. Fan, H. Ludi, H.M. Widmer, *Anal. Chem.* 64 (1992) 1926.
- [6] D.J. Harrison, Z. Fan, K. Seiler, *Anal. Chim. Acta* 283 (1993) 361.
- [7] D.J. Harrison, P.G. Glavina, *Sensors and Actuators B* 10 (1993) 10724.
- [8] R.N.C. Daykin, S.J. Haswell, *Anal. Chim. Acta* 313 (1995) 155.
- [9] H. Fiehn, S. Howitz, M.T. Pham, T. Vopel, M. Burger, T. Wegner, in: A. van den Berg, P. Bergveld (Eds.), *Micro Total Analysis Systems*, (1995) 289.
- [10] A. Daniel, D. Birot, M. Lehaitre, J. Poincin, *Anal. Chim. Acta* 308 (1995) 413.
- [11] M.F.M. Tavares, V.L. McGuffin, *Anal. Chem.* 67 (1995) 3687.
- [12] Q.H. Wan, *J. Phys. Chem. B* 101 (1997) 4860.

Theoretical considerations of chemical reactions in micro-reactors operating under electroosmotic and electrophoretic control

Paul D. I. Fletcher,* Stephen J. Haswell and Vesselin N. Paunov

Department of Chemistry, University of Hull, Hull, UK HU6 7RX.
E-mail: p.d.fletcher@chem.hull.ac.uk

Received 6th May 1999, Accepted 7th July 1999

Summary of contents

- 1 Introduction
- 2 Electroosmotic flow and electrophoresis in micro-reactor manifolds
- 3 Micro-reactor manifold configuration
- 4 Voltage conditions for loading, flow and injection
- 5 Control of chemical reactions under electroosmotic and electrophoretic flow
- 6 Example calculations
- 7 Conclusions and future outlook
- 8 Appendix
- 8.1 Numerical algorithm for the solution of eqns. (11)–(13)
- 8.2 Symbols
- 9 References

1 Introduction

Since the introduction of the concepts of micro flow injection analysis (μ FIA) and micro total analytical systems (μ TAS) nearly a decade ago;^{1–3} few researchers in the field of analytical science can fail to have been impressed by their impact, particularly in the area of DNA diagnostics.^{4–10} From the literature one is able to trace the pioneering developments of fabrication^{11–19} through detection^{20–26} and separation^{23,24,27–32} to sample preparation,^{5,33–35} culminating, for example, in a recent paper by Waters *et al.*³⁴ which describes a fully integrated μ TAS device for DNA characterisation. Whilst the majority of μ FIA and μ TAS studies have been focused on their application as capillary electrophoresis (CE) separation systems,^{23,24,27–32} the opportunity exists to extend such micro-reactor technology into the concept of ‘Lab-on-a-Chip’.^{36–39} In

this approach, the possibility exists of using a microfabricated system for the full characterisation of a wide range of chemical processes. Realisation of this goal requires a better understanding of the fluidics of chemically reacting systems in micro-reactors.

Whilst hydrodynamically pumped systems have been described in the literature,^{40–43} it has been the application of electrokinetic based fluidic pumping that has dominated previous studies.^{44–46} This clear trend can be attributed to



Stephen Haswell is Professor of Analytical Science at the University of Hull. His current research activities are in the areas of micro-reactor and μ FIA development, microwave enhanced reaction chemistry, trace elemental speciation and process analysis. He is author of over 100 research papers, a number of books and patents and is widely known nationally and internationally for his enthusiastic lectures. For a number of years one of the underlying principles of Professor Haswell's research has been to break down the sectorial walls which exist in science, in particular, the integration of analytical science with main line chemistry, physics, engineering and biology. Many of these ideals are encompassed in the development of micro-chemical processes and devices, part of which is reflected in this current review.
E-mail: S.J.Haswell@chem.hull.ac.uk



Paul Fletcher is Professor of Physical Chemistry at the University of Hull. He leads the Surfactant Science Group within the Department of Chemistry and his research interests include micro-reactors and the surface and colloid chemistry of surfactant systems such as micelles, monolayers, microemulsions, emulsions and foams and reactions in complex media. He has published over 100 papers in these areas.

E-mail: P.D.Fletcher@chem.hull.ac.uk



Vesselin N. Paunov is a Post-doctoral Fellow at the Department of Chemical Engineering at the University of Delaware. His research interests include surface forces and stability of foams and emulsions, wetting and spreading, capillary forces between colloidal particles, electrokinetic phenomena, phase behaviour and micro-structure of complex fluids, and computer modelling of physicochemical processes and micro-reactors. He has published over 25 papers in these areas.

E-mail: paunov@che.udel.edu

factors such as the experimental simplicity in achieving electroosmotic flow, *i.e.*, no moving parts, and minimal back-pressure effects, with the added dimension of superimposed electrophoretic separations. It follows, therefore, that a good basic understanding of the nature and capability of electrokinetic based devices is fundamental to the design and development of future applications. A number of theoretical and experimental studies of hydrodynamic and electrokinetic flow within μ FIA and μ TAS, including channel switching and velocity profile control, have been reported.^{47–52}

In this tutorial review, we describe the basic theoretical considerations governing liquid phase chemical reactions in micro-reactor manifolds using electrokinetic based fluidics. The calculations described demonstrate how the voltages applied may be used to control both the spatial (*i.e.*, lengthways along the channel long axis) and temporal evolution of chemical components and reaction products. The combination of spatial and temporal control of reactions, realisable in such micro-reactor manifolds (but not, for example, in microtitre wells), offers many potential advantages such as identifying the optimum detector position and the best point at which to perform reagent additions in catalytic systems. The purpose of this work is to review the quantitative theoretical basis for this type of control and to provide illustrative calculations to guide the design and development of novel micro-reactor systems.

The paper is organised as follows. First, the basic principles of electroosmotic flow (EOF) and electrophoresis are described. We then consider a specific micro-reactor manifold configuration and show how the operating voltages can be adjusted to control the loading, injection and flow phases necessary to investigate analytical type chemical reactions. The next section details the equations describing the spatial and temporal evolution of chemical reactions under EOF and electrophoretic control. Numerical results are then presented which illustrate the main features of the behaviour of chemical reactions under voltage control. Finally, the conclusions and the outlook for the future are discussed.

2 Electroosmotic flow and electrophoresis in micro-reactor manifolds

Fabrication of μ FIA or μ TAS micro-reactor manifolds involves creating a network of micron sized channels in a solid substrate surface using either wet etch, laser ablation, embossing, micromachining or microlithography techniques.^{11–19,53–56} Suitable substrates include materials such as glass, oxidised silicon and various plastics which support EOF. In most fabrication procedures a top cover is then bonded to the substrate using anodic or fusion bonding.^{53,56} Holes drilled through the top cover allow connection to the channels and also form the reagent reservoirs. Voltages to drive EOF are applied through electrodes placed within the reservoirs. With this form of fabrication the channels approximate to a rectangular cross-section with depths in the range 10–200 μ m, widths of 50–200 μ m and lengths in the centimetre range, as shown in Fig. 1. The reagent reservoirs are typically 1 mm in diameter and 1 cm in depth. A plan view of an entire micro-reactor manifold (as used in recent analytical studies^{57,58}) is shown in Fig. 1. For the purposes of this paper, we shall consider parameters appropriate to glass micro-reactor manifolds containing aqueous solutions of reactant species X and Y that react to form a product Z which can be detected colorimetrically.

For pure electroosmotic flow within a channel, the velocity profile across the channel is uniform except for the region very close to the channel wall.^{50,59,60} The thickness over which the velocity is non-uniform is of the order of the Debye length and is in the nanometer range. The linear liquid velocity far from the walls due to electroosmosis v_{os} is⁶⁰

$$v_{os} = -\frac{E\epsilon\epsilon_0\zeta}{\eta} \quad (1)$$

where E is the electric field (equal to the voltage divided by the distance between the electrodes for channels of uniform resistance per unit length), ϵ is the relative permittivity of the liquid, ϵ_0 is the permittivity of free space, ζ is the zeta potential of the channel/liquid interface and η is the liquid viscosity. The negative sign indicates that when ζ is negative, the diffuse charge in the liquid is positive and so the liquid flow is towards the negative electrode. The volumetric flow rate due to electroosmotic flow is $V_{os} = A_{channel}v_{os}$, where $A_{channel}$ is the cross-sectional area of the channel. The electric current I transported by the liquid is proportional to v_{os} according to

$$I = \frac{A_{channel}v_{os}\eta\lambda_0}{\epsilon\epsilon_0\zeta} \quad (2)$$

where λ_0 is the electrical conductivity of the liquid. Eqn. (2) neglects the possibility of surface conduction, which can be a complicating factor under some conditions.⁶⁰

It can be seen that the EOF is primarily controlled by the zeta potential at the channel wall/solution interface. For aqueous solutions in glass channels the zeta potential varies from zero at pH \approx 2 to about -100 mV at pH 7.^{61–64}

At fixed pH, the magnitude of ζ decreases with increasing concentration of most common electrolytes.^{61–64} It should be noted that the presence of species such as cationic surfactants, which adsorb strongly at the glass/water interface, can strongly influence ζ and hence the EOF.⁶⁵ The zeta potential is also sensitive to the nature of the glass and its treatment.⁶¹ For aqueous solutions around pH 7 (for which ζ is around -100 mV) with E of the order of 100 V cm^{-1} , v_{os} is of the order of mm s^{-1} .

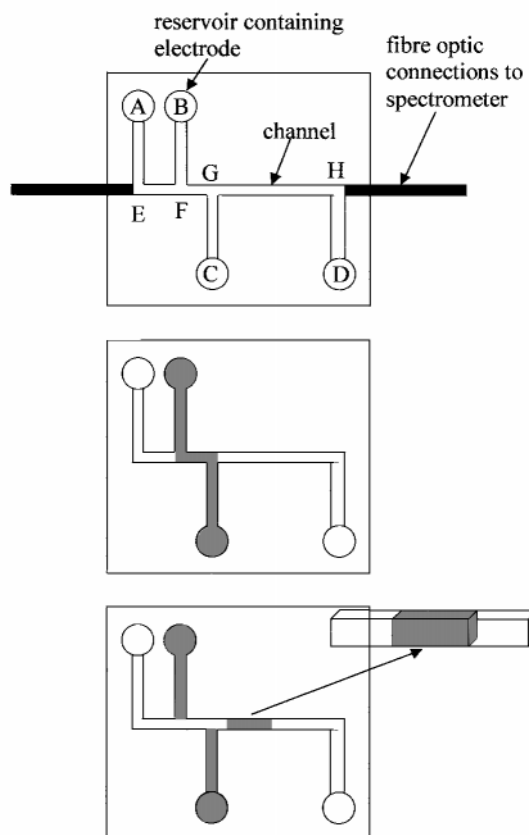


Fig. 1 Plan view of the basic micro-reactor configuration (not to scale). The reservoir diameters are typically 1 mm, the channel widths are typically 100 μ m and the side length of the microreactor is typically 2 cm. The middle diagram shows channel BC filled with Y. The bottom diagram shows the experimental configuration modelled here in which a stream of X containing a slug of Y (shown in 3D view in inset) is moving by EOF towards reservoir D.

Note that pure electroosmotic flow is only obtained in the absence of a pressure difference ΔP across the tube. If ΔP is not zero, one obtains a combination of electroosmotic and pressure driven flow. Since pressure driven flow (in a cylindrical channel) shows a parabolic velocity profile, a flat velocity profile across the channel is only obtained when ΔP is negligibly small. Experimentally, non-negligible pressure differences may be caused by a difference in liquid levels between the inlet and outlet reservoirs (Δh_{res}), by Laplace pressure differences resulting from the curved liquid menisci in the inlet and outlet reservoirs or by obstruction within the channel leading to a back-pressure.

The Laplace pressure change across the liquid menisci within the reservoirs is equal to $2\gamma/r$, where γ is the liquid/air surface tension and r is the radius of curvature of the liquid meniscus. As in capillary rise phenomena,⁶⁶ the radius of curvature of the liquid meniscus depends on both the radius of the reservoir containing the surface (r_r) and the contact angle θ made by the liquid with the reservoir wall according to $r = r_r/\cos\theta$. For pure water of tension 72 mN m^{-1} making a contact angle of 0° within a cylindrical reservoir of radius 1 mm, the Laplace pressure is approximately 140 Pa. The magnitude of this Laplace pressure, equivalent to the hydrostatic pressure exerted by a column of water of approximately 14 mm in height, can be significant in considerations of flow within micro-reactors.

Within a micro-reactor, a non-zero ΔP from Laplace effects arises only when the Laplace pressure differences across the inlet and outlet reservoirs are not equal. Since the liquid menisci within the inlet and outlet reservoir are normally similar, ΔP values from Laplace effects are generally expected to be considerably smaller than the value quoted above for a single meniscus. For a cylindrical reservoir containing an electrode, the meniscus shape is complex and the Laplace pressure will depend on the positioning of the electrode within the reservoir, the contact angles of the liquid with the electrode and the reservoir wall in addition to the tension. The value of ΔP arising from Laplace pressure differences can be minimised by matching reservoir diameters and electrode positioning for the inlet and outlet reservoirs as far as possible. The Laplace pressure can be reduced to zero if the reservoir diameter is made sufficiently large such that the liquid surface contains a flat region. This situation applies when the reservoir radius is much greater than the length scale over which the liquid meniscus is curved, *i.e.*, the capillary length equal to $\sqrt{\gamma/\Delta\rho g}$, where $\Delta\rho$ is the density difference between the liquid and air and g is acceleration due to gravity.

In order to ensure that 'pure' EOF is obtained within a channel, it is necessary to consider the limits of ΔP within which the pressure driven component of the total flow can be considered negligible relative to that from EOF. In the case that Laplace pressures and channel obstruction effects are absent, *i.e.*, ΔP arises only from hydrostatic pressure resulting from a difference in reservoir liquid height Δh_{res} ($\Delta P = \Delta h_{\text{res}}\Delta\rho g$), this can be estimated as follows. We consider the magnitude of Δh_{res} sufficient to produce a pressure driven volumetric flow rate V_{press} equal to V_{os} . We estimate V_{press} for laminar flow within a cylindrical channel of 'effective' radius r_{eff} such that $\pi r_{\text{eff}}^2 = A_{\text{channel}}$ and equate this with V_{os} :

$$V_{\text{press}} = \frac{\pi\Delta h_{\text{res}}\rho g r_{\text{eff}}^4}{8\eta l_{\text{channel}}} = V_{\text{os}} = \frac{V\epsilon\epsilon_0\zeta}{\eta l_{\text{channel}}} \quad (3)$$

where l_{channel} is the channel length held between the reservoirs and V is the voltage applied between the reservoirs. Rearrangement of eqn. (3) shows that, for V_{press} to be less than 10% of V_{os} , then

$$\Delta h_{\text{res}} \leq \frac{V\epsilon\epsilon_0\zeta}{10\rho g r_{\text{eff}}^2} \quad (4)$$

Inspection of eqn. (4) shows that for many μTAS operating conditions described in the literature, Δh_{res} may have to be less than 1 mm of water pressure in order to suppress pressure driven flow. Depending on the conditions (*e.g.*, whether the feed reservoir height is greater or less than the destination reservoir), the pressure driven flow may either accelerate or retard the EOF. For either acceleration or retardation, pressure driven flow will perturb the flat velocity profile expected for 'pure' EOF. Disturbances of EOF by pressure effects have been demonstrated experimentally by Boer *et al.*⁴⁶ Lack of proper control of these small pressure differences is expected to lead to irreproducible and erratic experimental results.

In addition to EOF, charged species within the channels move under the influence of the electric field by electrophoresis. The electrophoretic velocity v_{ph} of a species is given by⁶⁷

$$v_{\text{ph}} = \frac{zeED}{kT} \quad (5)$$

where z is the number of electronic charges on the species (positive for cations, negative for anions), e is the electronic charge (magnitude only), D is the diffusion coefficient, k is the Boltzmann constant and T is the absolute temperature. The total velocity of a particular species is simply the vector sum of that due to the electroosmosis and electrophoresis, *i.e.*, $v_{\text{total}} = v_{\text{ph}} + v_{\text{os}}$. For aqueous solutions in a glass channel (where ζ is negative), a positive value of v_{os} signifies movement towards the negative electrode. In this situation, the electrophoretic velocities of cations (z positive) are increased relative to v_{os} whereas the velocities of anions are decreased. For common small ions, the magnitudes of v_{ph} and v_{os} , both of which scale with E , are generally similar and in the mm s^{-1} range.

3 Micro-reactor manifold configuration

In this section we present explicit calculations for the simple micro-reactor manifold configuration shown as a plan view in Fig. 1. It consists of four reservoirs (A, B, C and D) each containing an electrode and connected by etched channels. The lengths of the different channel sections are specified here by reference to the letters marking the corner points as shown in Fig. 1. We shall consider a bimolecular, reversible reaction which, in analytical terms, could be the formation of a chromogenic complex:



The reaction has a forward, second-order rate constant k_f and reverse, first-order rate constant k_r . For the configuration shown, detection of the reaction progress is provided by optical absorbance measurements along the EH channel section situated between fibre optics connected to a spectrophotometer. Although the theoretical results presented here refer to the specific configuration of Fig. 1, the calculation approach may be easily modified to apply to a very wide range of manifold designs with more complex channel labyrinths and different detection systems.

The reactant species X and Y are introduced into the micro-reactor as follows. Initially, all reservoirs and channels are filled with solvent. The solution of reactant X is introduced into reservoir A and a suitable voltage is applied across the electrodes within the reservoirs A and D to fill the AD channel with X (the 'loading' phase). Reactant Y is introduced into reservoir B and a voltage across BC is used to fill the BC channel (the 'injection' phase) as shown in Fig. 1 (middle). For the experimental situation to be modelled, a voltage is reapplied across AD which mobilises the stream of X, now containing a slug of Y, in the EH channel (the 'flow' phase, Fig. 1, bottom). In fact, as will be discussed in detail in the next section, suitable voltages across *both* AD and BC must be applied simultane-

ously for the loading, flow and injection phases in order to achieve a 'clean' injection. The progress of the reaction of the slug of Y within the flowing stream of X is then monitored by the fibre optic spectroscopic detection systems and is considered in detail in the calculations presented later.

4 Voltage conditions for loading, flow and injection

As discussed by Seiler *et al.*,⁴⁹ dc circuit analysis (using Kirchhoff's rules) can be used to predict the variation with applied voltages of the electrical currents, and hence EOFs, in the different channel sections of a manifold. The manifold configuration of Fig. 1 can be represented as the equivalent dc circuit shown in Fig. 2. The circuit consists of two voltage sources V_{AD} and V_{BC} (supplied by the electrode pairs in reservoirs AD and BC, respectively) connected by the appropriate channel sections which form resistance elements R_{ij} , where the subscripts signify the particular channel section. The overall circuit contains two loops which both contain R_{FG} . We assume here that all channel sections have a uniform cross-sectional area and zeta potential and all contain liquid of identical conductivity. Under these conditions, easily achievable with solutions containing low concentrations of reacting species in a relatively high concentration of inert electrolyte, the resistance of a channel section is proportional to its length. We note that the approach could be extended to the more complex case where the resistance per unit length of the channel is not constant in different parts of the manifold. Neglecting surface conductivity, the electrical currents (proportional to the EOF velocity as discussed earlier) in the arms of loops 1 and 2 are I_1 and I_2 , respectively. The current in the FG channel section (common to both loops) is $I_1 + I_2$. Summing the product of current and resistances around each loop gives the following pair of equations:

$$\begin{aligned} V_{AD} &= (R_{AE} + R_{EF} + R_{GH} + R_{HD} + R_{FG})I_2 + R_{FG}I_1 \\ &= R_{loop2}I_2 + R_{FG}I_1 \\ V_{BC} &= (R_{CG} + R_{FB} + R_{FG})I_1 + R_{FG}I_2 \\ &= R_{loop1}I_1 + R_{FG}I_2 \end{aligned} \quad (7)$$

Solving the simultaneous equations and rearranging yields the following expressions for I_1 and I_2 :

$$\begin{aligned} I_1 &= \frac{V_{BC} - V_{AD}R_{FG}/R_{loop2}}{R_{loop1} - R_{FG}^2/R_{loop2}} \\ I_2 &= \frac{V_{AD} - V_{BC}R_{FG}/R_{loop1}}{R_{loop2} - R_{FG}^2/R_{loop1}} \end{aligned} \quad (8)$$

The current through the FG channel section is $I_1 + I_2$. Eqn. (8) allows the currents, and hence the EOF, in each channel section

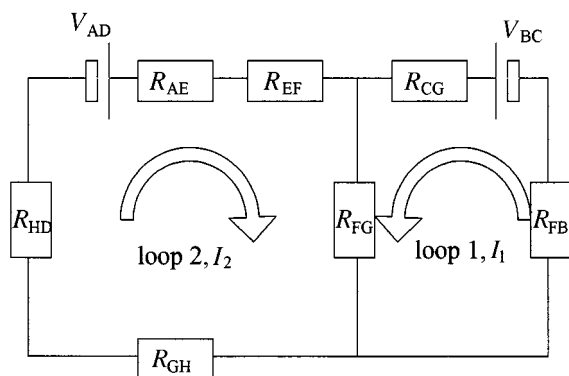


Fig. 2 The dc circuit equivalent to the micro-reactor configuration of Fig. 1. The rectangular boxes are the resistance elements arising from the channel sections marked by the subscripts.

to be calculated for any voltages provided that the resistances of the different channel sections are known.

For the loading and flow phases, we require EOF (*i.e.*, finite current I_2) between reservoirs A and D with zero EOF between reservoirs B and C (*i.e.*, current I_1 equal to zero) to avoid contamination of one reactant stream with the other. Similarly, for the injection phase, finite current I_1 and zero current I_2 are required. Inspection of eqn. (8) shows that, in order to obtain zero I_1 , the voltages V_{AD} and V_{BC} must obey the relationship

$$V_{BC} = V_{AD}R_{FG}/R_{loop2} = V_{AD}\text{length}_{FG}/\text{length}_{loop2} \quad (9)$$

The second equality is valid in the case that the resistance per channel length is constant. Similarly, to obtain zero I_2 , we require

$$V_{AD} = V_{BC}R_{FG}/R_{loop1} = V_{BC}\text{length}_{FG}/\text{length}_{loop1} \quad (10)$$

Hence, in order to obtain a 'clean' injection of a slug of reactant Y into a stream of X, both voltages V_{AD} and V_{BC} must be switched synchronously between the values required [and calculated using eqns. (9) and (10)] for the loading, injection and flow phases. This highlights the necessity for automated computer control of the applied voltages in micro-reactor devices.

It is, of course, possible to operate the micro-reactor such that the contents of reservoirs A and B are made to flow into the detection channel EH in different ratios controlled by the applied voltages (as opposed to the load, inject, flow sequence described above). Fig. 3 shows the ratio I_2/I_1 for different ratios of the applied voltages V_{AD}/V_{BC} at constant V_{BC} . Since the ratio of electrical currents is equal to the ratio of electroosmotic flow rates, the plot demonstrates that the mixing ratio of the flowing streams can be varied continuously by adjustment of the voltage ratio. (It should be noted that the current and voltage ratios in Fig. 3 are invariant with the absolute magnitudes of either current or voltages.) Fig. 3 also shows a similar plot in which the voltage V_{AD} is held constant. These calculations demonstrate that, in principle, the applied voltages can be used to vary

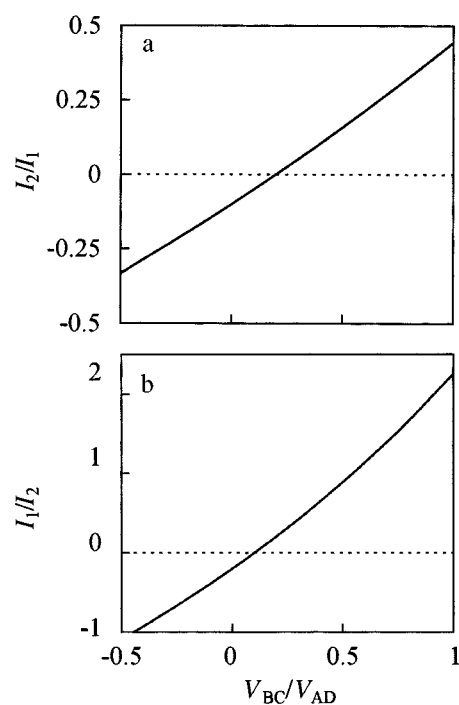


Fig. 3 Variation of I_2/I_1 with V_{AD}/V_{BC} (a) and I_1/I_2 with V_{BC}/V_{AD} (b). The calculations are for the micro-reactor configuration of Fig. 1 (assuming constant resistance per channel length) for channel lengths AE = CG = FB = HD = 10 mm, EF = FG = 5 mm and GH = 20 mm. The plots show the voltage ratios required (for this particular configuration) to obtain zero EOF in the injection circuit during loading/flow and zero EOF in the loading/flow circuit during injection.

continuously the ratio of concentrations of X and Y entering the detection channel. This type of micro-reactor manifold control can therefore be used, for example, to determine calibration data in analytical systems⁵³ or to investigate the concentration dependence of reaction kinetics under voltage control without refilling of the reservoirs.

It should be noted that this analysis, although revealing the basic principles, is somewhat simplistic in that hydrodynamic effects associated with the flows across manifold junctions and surface conductivity effects are neglected. More sophisticated modelling, as described, for example, in refs. 47, 48, 51 and 52, show that complex flow patterns around manifold junctions may significantly modify slug profiles obtained by the injection procedure. Additionally, non-zero surface conductivity would require modification of the equations presented here.

5 Control of chemical reactions under electroosmotic and electrophoretic flow

We take as the starting point a channel containing species X with a rectangular slug of reactant Y as would be obtained from a perfect load-inject-flow sequence (shown in Fig. 1). We assume here that species movement within the channel is controlled only by EOF and electrophoresis, *i.e.*, that pressure driven flow is absent. Under these conditions, the species' velocity profiles across the channel are flat (except for the region very close to the channel wall). Hence all concentrations vary only in the direction of the channel long axis x but are uniform in both orthogonal directions across the channel.

We consider a section of channel of length $2a$ centred at $x = 0$ and extending from $x = -a$ to $x = +a$. For the purpose of the numerical calculations, we adopt a moving coordinate system such that $x_{lab} = x + v_{os}t$, where x_{lab} is the x coordinate relative to the laboratory, v_{os} is the linear electroosmotic velocity and t is time. Initially the channel contains species X at concentration C_X^0 with a rectangular slug of species Y at concentration C_Y^0 . The slug of Y has a width of $2b$ and is initially centred at $x = 0$. As described above, X and Y can react reversibly to form product Z with forward rate constant k_f (second order) and reverse rate constant k_r (first order). The initial conditions are stated as follows:

$$\begin{aligned} -b \leq x \leq b: & \quad C_X = 0, \quad C_Y = C_Y^0 \quad \text{at } t = 0 \\ \pm b \leq x \leq \pm a: & \quad C_X = C_X^0, \quad C_Y = 0 \quad \text{at } t = 0 \\ -a \leq x \leq a: & \quad C_Z = 0, \quad \quad \quad \text{at } t = 0 \end{aligned} \quad (11)$$

Species X, Y and Z have diffusion coefficients D_X , D_Y and D_Z and move (relative to $x = 0$) with electrophoretic velocities v_{phX} , v_{phY} and v_{phZ} , respectively. We assume that all diffusion coefficients are invariant with concentration and that all thermal effects (arising, for example, from heats of reaction) are negligible. The concentrations of X, Y and Z are functions of both time and x according to the following set of equations:⁶⁸

$$\begin{aligned} \frac{\partial C_X}{\partial t} &= D_X \frac{\partial^2 C_X}{\partial x^2} - k_f C_X C_Y + k_r C_Z - v_{phX} \frac{\partial C_X}{\partial x} \\ \frac{\partial C_Y}{\partial t} &= D_Y \frac{\partial^2 C_Y}{\partial x^2} - k_f C_X C_Y + k_r C_Z - v_{phY} \frac{\partial C_Y}{\partial x} \\ \frac{\partial C_Z}{\partial t} &= D_Z \frac{\partial^2 C_Z}{\partial x^2} + k_f C_X C_Y - k_r C_Z - v_{phZ} \frac{\partial C_Z}{\partial x} \end{aligned} \quad (12)$$

These equations correspond to the simple reaction scheme of eqn. (6) but more complex reaction schemes are easily incorporated. The situation described here for micro-reactors is identical (from a theoretical point of view) with that of electrophoretically mediated microanalysis (EMMA) described both experimentally and theoretically by Regnier *et al.*^{69–72} Additionally, a related set of equations have been used recently

to describe the elution characteristics of species undergoing a first-order reaction in a capillary electrophoresis system.⁷³

The boundary conditions are taken to be that the concentrations of X, Y and Z are unperturbed from their initial values at $x = \pm a$, *i.e.*,

$$C_X(x = \pm a) = C_X^0, \quad C_Y(x = \pm a) = C_Z(x = \pm a) = 0 \quad (13)$$

The use of these boundary conditions restricts the analysis to conditions such that the zone of reaction is far from the channel ends. For the manifold configuration shown in Fig. 1, this is valid since we wish to simulate the concentration changes occurring in the detection channel section GH before the reaction zone moves round the corner into section HD. The series of eqns. (11)–(13) is solved numerically to obtain plots of C_X , C_Y and C_Z versus x_{lab} for different times. The numerical algorithm, outlined in the Appendix, was implemented in a Visual Basic program running in EXCEL on a PC.

6 Example calculations

We first model the time evolution of the concentration profiles for a reaction in which all species X, Y and Z are uncharged. All other conditions are specified in the legend of Fig. 4. In this case, all reaction species move together in the channel with the electroosmotic velocity v_{os} and mixing of the reactants occurs only by inter-diffusion between the X stream and slug of Y. Fig. 4 shows three 'snapshots' of the concentration profiles where it can be seen that product Z is formed only at the trailing and leading edges of the slug of Y where diffusional inter-mixing gives finite concentrations of both X and Y. Because the time

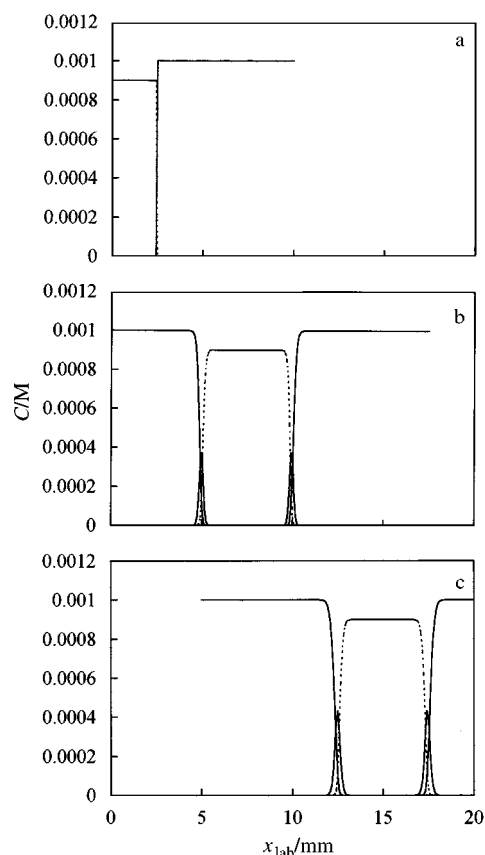


Fig. 4 Calculated concentration profiles for C_X (solid line), C_Y (dashed line) and product C_Z (solid line) for time = 0 (a), 15 (b) and 30 s (c). The parameters are $C_X^0 = 1$ mM, $C_Y^0 = 0.9$ mM, $C_Z^0 = 0$ mM, $D_X = 1 \times 10^{-9}$ m² s⁻¹, $D_Y = 0.7 \times 10^{-9}$ m² s⁻¹, $D_Z = 0.5 \times 10^{-9}$ m² s⁻¹, $v_{os} = 0.5$ mm s⁻¹, $k_f = 1000$ l mol⁻¹ s⁻¹, $k_r = 0$ s⁻¹, slug width ($2b$) = 5 mm and all electrophoretic velocities set equal to zero (*i.e.*, all species are uncharged).

required for reactant diffusion across the width of the slug of Y is long relative to the time the slug takes to traverse the detection channel EH, the extent of product formation is low.

The behaviour of charged reactant species is very different. We simulate the case in which X and Z both bear a positive charge and Y is uncharged. Within the electric field, the velocities of X and Z are accelerated relative to v_{os} whereas Y moves with velocity v_{os} . As seen in Fig. 5, the difference in electrophoretic velocities of the different species causes a displacement of the slug of Y relative to the 'gap' in the concentration profile of X. This gives a greatly increased mixing of X and Y (with concomitant formation of Z) at the trailing edge of the Y slug. The extent of product formation within the detection time is therefore greatly increased relative to that for the case of uncharged reagents. Changing the signs of the charges on both X and Z from positive to negative (calculations not shown) causes the product formation to occur at the leading (rather than the trailing) edge of the slug. We note here that it is not necessary for the species X and Y to have different sign charges to induce displacement of the slug of Y relative to the 'gap' in X. Even with the same (non-zero) charges, X and Y will have different electrophoretic velocities, and thus show displacement, so long as their diffusion coefficients are different [see eqn. (5)].

For the case in which X and Z bear charges, and Y is neutral as in Fig. 5, the extent of product formation is largely controlled by the relative rate of displacement of the concentration profiles of X and Y. In turn, this is determined by their relative electrophoretic velocities which, like v_{os} , scale with the applied electric field. Fig. 6 shows the effect of increasing the electric field which is modelled by increasing v_{os} whilst maintaining v_{ph} for the different species at constant ratios relative to v_{os} . The ordinate of Fig. 6 shows the integral of the product concentration profile, integrated over the detection channel length. (For

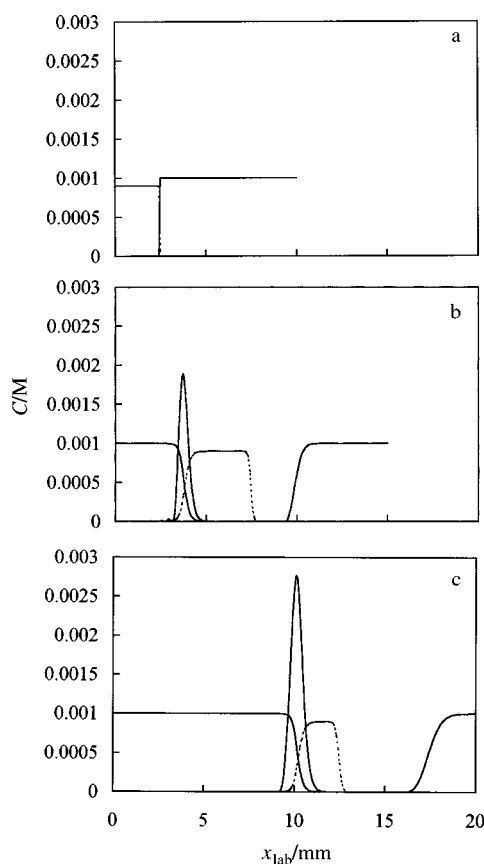


Fig. 5 Calculated concentration profiles for the conditions of Fig. 4 except that $v_{phX} = 0.5$, $v_{phY} = 0$ and $v_{phZ} = 0.25$ mm s⁻¹. This corresponds to the species X and Z both bearing a positive charge (which serve to accelerate their total motion) and Y being uncharged.

an optically absorbing species Z with the absorbance detection configuration of Fig. 1, the measured absorbance signal is proportional to this integral.) It can be seen that the applied voltage can be used to control the extent of product formation. The minimum value of product formation is obtained with zero voltage when the extent of product formation is determined only by inter-diffusion of X and Y without the aid of electrophoretic displacement of the concentration profiles. Sufficiently high applied voltage produces virtually complete displacement and complete conversion of Y to product.

As seen above, the time required for complete reaction of the Y slug is determined largely by the time taken for the slug to be displaced from the 'gap' in the concentration profile of X and should therefore decrease as the slug width is decreased. Simulation of this effect is shown in Fig. 7, where it can be seen that 100% product conversion can be achieved (at a particular applied voltage) by reducing the width sufficiently. Obviously, in the simulation shown, the total amount of product formed reduces as the initial width of the Y slug is decreased. However, it would of course be possible to inject multiple slugs of Y, so as to increase the total amount of product formation simultaneously with increasing the percentage conversion. We note here that techniques to produce very narrow slugs (μm) have been demonstrated experimentally.⁷⁴ At sufficiently small widths, diffusion alone would ensure complete reactant mixing and conversion of the Y slug to product.

We next examine the effects of varying the forward rate constant of the chemical reaction. As seen above, for the concentrations used in the simulation with $k_f = 1000$ l mol⁻¹ s⁻¹, the extent of chemical reaction is largely controlled by the time required for inter-mixing of the reagents. Under

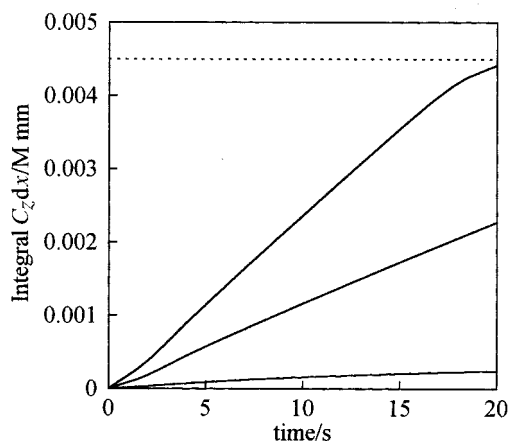


Fig. 6 Variation of the integral of the product concentration profile with time for different v_{os} equal to 0, 0.5 and 1 mm s⁻¹ for the curves in ascending order. The electrophoretic velocities were held at $v_{phX} = v_{os}$, $v_{phY} = 0$ and $v_{phZ} = v_{os}/2$ with other conditions as for Fig. 5. The horizontal dashed line corresponds to total conversion to product.

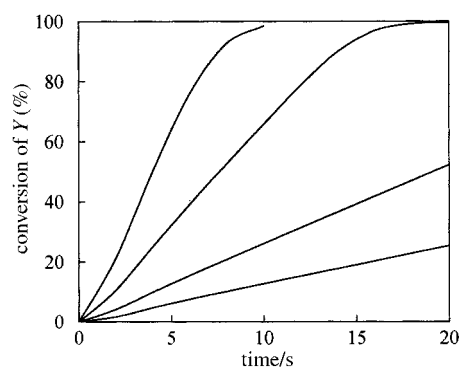


Fig. 7 Variation of percentage conversion of Y with time for (in ascending order) initial width of the slug of Y equal to 10, 5, 2 and 1 mm. All other conditions were as for Fig. 5.

these conditions, increasing k_f gives virtually no change in the extent of product formation (Fig. 8) since chemical reaction is already faster than the inter-mixing of X and Y. Reducing k_f to lower values causes product formation to decrease as the rate-determining step switches from mixing to the chemical reaction step. Concentration profiles for reactions where product formation is controlled either by mixing or by chemical reaction are compared in Fig. 9. We note here that the transition from

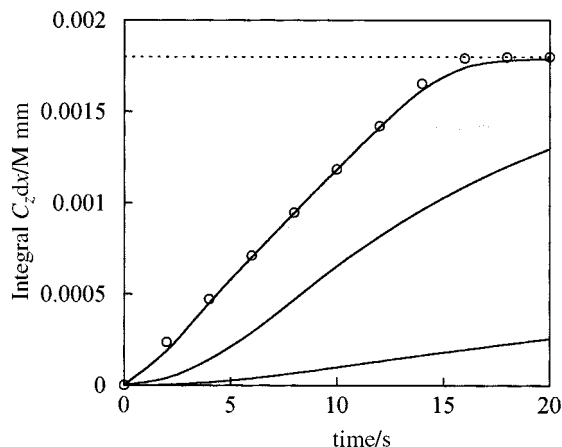


Fig. 8 Variation of integral $C_Z dx$ with time for (in ascending order) $k_f = 10, 100$ and $1000 \text{ l mol}^{-1} \text{ s}^{-1}$. The initial width of the slug of Y was 2 mm and all other conditions were as for Fig. 5. The open circles were calculated for $k_f = 10\,000 \text{ l mol}^{-1} \text{ s}^{-1}$ and correspond to the fast reaction limit under these conditions. The horizontal dashed line corresponds to total conversion to product.

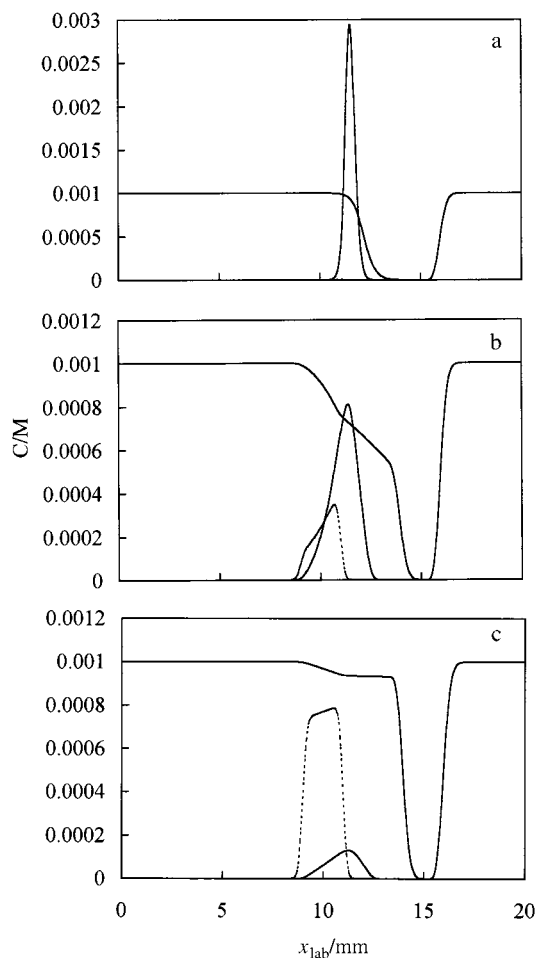


Fig. 9 Concentration profiles of X, Y (dashed line) and Z after 20 s for $k_f = 1000$ (a), 100 (b) and $10 \text{ l mol}^{-1} \text{ s}^{-1}$ (c). All other conditions were as for Fig. 8.

mixing rate control to chemical reaction rate control may be induced either by changing the forward rate constant or by changing the reactant concentrations since forward reaction rate is equal to the product $k_f C_X C_Y$.

The simulations highlight the importance of a number of time-scales in considering second-order chemical reactions in micro-reactor manifolds. Definitions of the time-scales appropriate to the manifold configuration discussed here are as follows:

$$t_{\text{diffusion}} = b^2/D \quad (14)$$

$$t_{\text{chemical}} = 1/k_f C_X^0 \quad (15)$$

$$t_{\text{displacement}} = 2b/|v_{\text{phX}} - v_{\text{phY}}| \quad (16)$$

$$t_{\text{detection}} = l_{\text{detection}}/(v_{\text{os}} + v_{\text{phY}}) \quad (17)$$

where $t_{\text{diffusion}}$ is the time required for inter-diffusional mixing of X and Y across the slug of Y (width $2b$) to occur. In this context, D is the mean of D_X and D_Y . t_{chemical} is the time required for chemical reaction between X and Y (under conditions when $C_X^0 > C_Y^0$). $t_{\text{displacement}}$ is the time required to displace completely the slug of Y from the 'gap' in the concentration profile of X. $t_{\text{detection}}$ is the time spent by the slug of Y within the detection channel of length $l_{\text{detection}}$. Consideration of the relative magnitudes of these times allows a crude prediction of the behaviour of a chemical reaction within a microreactor system. Virtually complete conversion to product is expected when $t_{\text{detection}} > t_{\text{displacement}}$ (or $t_{\text{diffusion}}$) and t_{chemical} . The extent of product formation is controlled by the applied voltage (by control of v_{ph}) when $t_{\text{detection}} < t_{\text{displacement}}$ and $t_{\text{displacement}} > t_{\text{chemical}}$. Under these conditions, the product formation is insensitive to the chemical reaction rate and the initial concentration of X but is controlled by the applied voltage. When $t_{\text{detection}} < t_{\text{chemical}}$ and $t_{\text{chemical}} > t_{\text{displacement}}$ or $t_{\text{diffusion}}$, product formation is sensitive to the chemical rate constant, the reactant concentrations and the applied voltage. These considerations apply to the simple load-inject-flow voltage control sequence described earlier. However, as demonstrated elegantly by Regnier's group in the context of EMMA, more complex voltage control sequences can be used to control the extent of reaction.^{69–72}

Finally, we consider the effect of introducing reversibility into the chemical reaction. Under conditions when the reaction reaches its final, equilibrium extent of product formation before exiting the detection channel section, the final value reached decreases with increasing k_r , as shown in Fig. 10. In this situation, when displacement and chemical reaction are complete, the final extent of product formation is primarily controlled by the equilibrium constant $K (= k_f/k_r)$ and C_X^0 .

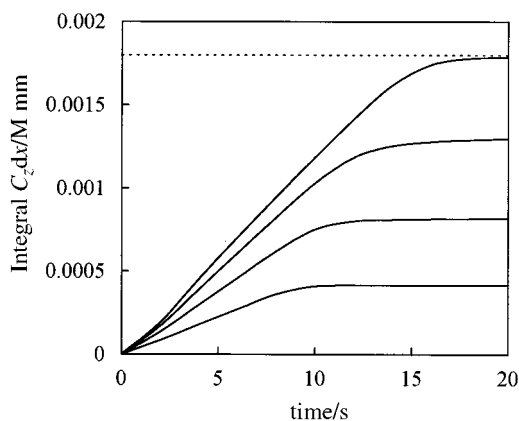


Fig. 10 Variation of integral $C_Z dx$ with time for $k_f = 10000 \text{ l mol}^{-1} \text{ s}^{-1}$ and (in ascending order) $k_r = 3, 1, 0.3$ and 0 s^{-1} . All other conditions were as for Fig. 8. The horizontal dashed line corresponds to total conversion to product.

The simulations illustrate that product formation in micro-reactor manifolds may (under different conditions) be sensitive to the applied voltage, the chemical rate constants, concentrations, diffusion constants and species charge. In principle, micro-reactor investigation of reactions can yield information on all these physico-chemical properties. For the simulations, the range of input parameters were chosen to be realistic for the type of reaction that may be studied. For example, in aqueous solution at pH 7 and 25 °C, the complex formation reaction $\text{Ni}^{2+} + \text{PADA}$ gives NiPADA^{2+} has $k_f = 1300 \text{ l mol}^{-1}\text{s}^{-1}$ and $k_r = 0.1 \text{ s}^{-1}$ where PADA is pyridine-2-azo-*p*-dimethylaniline.^{75,76} Ni^{2+} and the NiPADA complex both have a charge of +2 whereas PADA is uncharged. The value of D for Ni^{2+} is $1.25 \times 10^{-9} \text{ m}^2 \text{ s}^{-1}$.⁷⁷ Since PADA has a larger molecular volume than Ni^{2+} , it is expected to have a lower diffusion coefficient (approximately half). Similarly, the complex is expected to have a D value lower than that of either reactant. Hence the physico-chemical properties of the Ni–PADA reaction are such that the simulation parameters should correspond approximately to somewhere between those of the top two curves of Fig. 10. For the Ni–PADA reaction, the molar absorptivity of the complex product is approximately $32\,000 \text{ l mol}^{-1} \text{ cm}^{-1}$ at the wavelength corresponding to maximum absorption.⁷⁵ Using the spectrophotometric detection configuration described here, the integrated product concentration profile would produce a large absorbance signal, easily detectable with good precision.

7 Conclusions and future outlook

The theoretical principles and calculations described in this tutorial review provide the basis for understanding the behaviour of chemical reactions within micro-reactor manifolds with electrokinetic flow control. The aim has been to provide principles to guide the design and development of such systems and the main conclusions are as follows:

1. EOF is determined primarily by the zeta potential of the channel/solution interface and gives a uniform velocity profile across the channel except very close (nm) to the channel wall. Non-uniform velocity profiles may be caused by pressure gradients arising from unequal reservoir heights, Laplace pressure effects resulting from the liquid menisci within the reservoirs and non-uniformity of the cross-sectional areas and zeta potential of the channels. Non-uniform zeta potentials may arise owing to specific adsorption of reagents in different channel sections or when the different channel sections are constructed of different materials. These complicating factors require careful experimental control in order to obtain accurate, reproducible results in micro-reactor systems.

2. Analysis of the dc circuit equivalent to the micro-reactor configuration allows the proper calculation of the voltages required for a 'clean' injection of a reactant slug into a stream of a second reactant.

3. The temporal and spatial evolution of a chemical reaction under EOF and electrophoretic control is determined primarily by the relative magnitudes of $t_{\text{diffusion}}$, t_{chemical} , $t_{\text{displacement}}$ and $t_{\text{detection}}$. Proper adjustment of the relative magnitudes of these different time-scales allows the extent of product conversion to be controlled by the voltages applied to the micro-reactor device.

The potential power of micro-reactor manifolds lies in the fact that complex channel labyrinths can be accommodated within a small device and that they allow the investigation of chemical reactions to be made under computer control. From the results described here, measurement of the extent of product conversion under different voltage conditions should, in principle, yield quantitative information on reaction rate parameters and charge/diffusion properties of the reactant species. It is technically feasible to construct micro-reactor

manifolds in which many reactions could be investigated either in sequence or simultaneously using automated computer control. Such a development would go some way towards realising the 'Lab-on-a-Chip' concept and would provide a quantum leap in the rate of accumulation of physico-chemical information for analytical, general chemical, biochemical and catalytic reactions. Analogously to a conventional electronic chip, the main function of such a device would be rapid gathering and processing of chemical information.

In this paper, we have discussed a simple homogeneous liquid phase reaction, but many other possibilities can be envisaged. The areas of homogeneous and heterogeneous catalysis, in particular, could benefit from the high speed, high throughput experimentation possibilities of micro-reactors. In this connection, it has recently been demonstrated that glass frits may be incorporated within a micro-reactor channel.⁷⁸ Further, a palladium catalyst supported on such a frit has been used successfully to catalyse reactions within a manifold under EOF control.⁷⁹ It was demonstrated that the spatial and temporal control of reactants could be used to deliver a first reagent to a catalyst surface followed by a second reagent after a controllable time period. This type of detailed control is generally impossible (at least within the short time-scales achievable in micro-reactors) in the usual situation of stirring a reagent mixture over a slurry of catalyst. In analytical terms, such an approach could mean controlling the output from a chemiluminescent reaction accurately at a specific detector site.⁸⁰ Some of these possibilities are currently being pursued further in the authors' laboratories.

8 Appendix

8.1 Numerical algorithm for the solution of eqns. (11)–(13)

We use the fact that the diffusion–reaction eqns. (12) have virtually similar form:

$$\frac{\partial C_k}{\partial t} + v_{\text{ph}k} \frac{\partial C_k}{\partial x} = D_k \frac{\partial^2 C_k}{\partial x^2} + S_k(x, t) \quad (k = X, Y, Z) \quad (\text{A1})$$

where $S_k(x, t)$ are the source terms which depend on x and t through the rates of the respective chemical reactions. In our particular case of chemical reaction, eqn. (6), we have

$$S_X = S_Y = -S_Z = k_f C_Z(x, t) - k_r C_X(x, t) C_Y(x, t) \quad (\text{A2})$$

To find the evolution of the concentration profiles, $C_k(x, t)$, with time we use a semi-implicit Crank–Nicholson method for integration of eqns. (A1).^{81,82} For the convenience of readers we give here the details of the numerical scheme applied to eqns. (A1). To avoid overburden, we omit the subscript k in our further notations. The space and time are discretised as follows:

$$x_i = (i - 1)\Delta x, \quad t_j = (j - 1)\Delta t, \quad i = 1, 2, \dots, n; \\ j = 1, 2, \dots \quad (\text{A3})$$

where Δx and Δt are the spatial and time steps. Since eqns. (A1) are highly non-linear owing to the source terms, an appropriate linearisation is needed. In our calculations we apply the Crank–Nicholson scheme as follows:

$$\left(\frac{\partial C}{\partial t} \right)_i = \frac{1}{2} \left\{ D \left[\left(\frac{\partial^2 C}{\partial x^2} \right)_{i,j+1} + \left(\frac{\partial^2 C}{\partial x^2} \right)_{i,j} \right] - v_{\text{ph}} \left[\left(\frac{\partial C}{\partial x} \right)_{i,j+1} + \left(\frac{\partial C}{\partial x} \right)_{i,j} \right] \right\} + [S(x, t)]_{i,j} \quad (\text{A4})$$

where the non-linear terms, S , are estimated by using only information from the previous time step (j) or from the initial

conditions ($j = 0$). We remark that the coupling between the three eqns. (A1) comes from the source terms. That is why the resulting equations after the above discretisation are semi-decoupled in the framework of a single time step. Thus, the substitution of the partial derivatives in eqn. (A4) by finite difference approximations

$$\begin{aligned} \left(\frac{\partial C}{\partial t}\right)_i &= \frac{C_{i,j+1} - C_{i,j}}{\Delta t} + O(\Delta t) \\ \left(\frac{\partial C}{\partial x}\right)_i &= \frac{C_{i+1,j} - C_{i-1,j}}{2\Delta x} + O(\Delta x^2) \\ \left(\frac{\partial^2 C}{\partial x^2}\right)_i &= \frac{C_{i+1,j} - 2C_{i,j} + C_{i-1,j}}{\Delta x^2} + O(\Delta x^2) \end{aligned} \quad (\text{A5})$$

gives a system of linear equations describing each of the profiles in the next time ($j + 1$) step:

$$\beta(1 + a)C_{i+1,j+1} - (1 + 2\beta)C_{i,j+1} + \beta(1 - \alpha)C_{i-1,j+1} = \gamma_i, \quad i = 2, \dots, n - 1 \quad (\text{A6})$$

where

$$\alpha = \frac{v\Delta x}{2D}, \beta = \frac{D\Delta t}{2\Delta x^2}, \quad (\text{A7})$$

$$\gamma_i = S_{i,j}\Delta t - \beta(1 + \alpha)C_{i-1,j} - (1 - 2\beta)C_{i,j} - \beta(1 - \alpha)C_{i+1,j}$$

The implication of the boundary conditions, eqns. (11), requires that

$$C_{i,j+1} = C_{n,j+1} = C_0 \quad (\text{A8})$$

where $C_0 = C_X^0$ for X profile and $C_0 = 0$ for Y and Z profiles. Initially, stepwise profiles are used as an initial condition, according to eqns. (11). We solve the three-diagonal system of linear eqns. (A6) by using the Thomas algorithm⁸¹ to obtain the new concentration profiles ($j + 1$), which then are used to calculate γ_i for the next time step, *etc.* Once the spatial step-size Δx has been selected, the time step Δt is controlled to maintain the stability of the numerical method. We should stress that the accuracy of this numerical scheme decreases when the chemical reaction is much faster than the respective diffusion process ($t_{\text{diffusion}} \gg t_{\text{chemical}}$). In this case we recommend the use of the fully implicit Crank–Nicholson scheme.⁸¹

8.2 Symbols

A–D	reservoirs
a	half-length of channel
A_{channel}	cross-sectional area of channel
b	initial half-width of rectangular slug of reactant Y
C_X	concentration of species X
C_X^0	initial concentration of species X
D_X	diffusion coefficient of species X
E–H	channel corners
E	electric field
e	electronic charge
g	acceleration due to gravity
i, j	indices for space and time steps used in the numerical calculations
I_1	electrical current in loop 1
k	Boltzmann constant
K	equilibrium constant for reaction
k_f	second-order forward rate constant
k_r	first-order reverse rate constant
l_{channel}	channel length
$l_{\text{detection}}$	length of detection channel section
r	radius of curvature of liquid meniscus in reservoir
R_{AE}	resistance across channel section AE

$R_{\text{loop 1}}$	sum of resistances across channel sections comprising loop 1
$S(x, t)$	source terms
T	absolute temperature
t	time
t_{chemical}	time required for chemical reaction
$t_{\text{detection}}$	time required for Y slug to traverse the detection channel section
$t_{\text{diffusion}}$	time required for diffusion across the rectangular slug of Y
$t_{\text{displacement}}$	time required for displacement of slug of Y from ‘gap’ in X concentration profile
V_{AD}	applied voltage across reservoirs A and D
V_{os}	EOF driven volumetric flow rate
v_{os}	linear electroosmotic flow velocity
v_{phX}	electrophoretic velocity of species X
V_{press}	pressure driven flow rate
x	co-ordinate along channel normalised with respect to v_{os}
X, Y, Z	reactant species
x_{lab}	coordinate along channel in laboratory coordinates
z	number of electronic charges on an ionic species
Δh_{res}	height difference between reservoirs
ΔP	hydrostatic pressure difference between reservoirs
ϵ	relative permittivity
ϵ_0	permittivity of free space
γ	liquid/air surface tension
η	viscosity of liquid in the channel
λ_0	electrical conductivity of liquid
ρ	liquid density
ζ	zeta potential of the channel/liquid interface

9 References

- 1 A. Manz, D. J. Harrison, E. Verpoorte, J. C. Fetting, H. Lüdi and H. M. Widmer, *Chimia*, 1991, **45**, 103.
- 2 A. Manz, D. J. Harrison, E. Verpoorte and H. M. Widmer, *Adv. Chromatogr.*, 1993, **33**, 1.
- 3 A. Manz, C. S. Effenhauser, N. Barggraf, E. J. M. Verpoorte, D. E. Raymond and H. M. Widmer, *Analisis*, 1994, **22**, M25.
- 4 A. T. Woolley, and R. A. Mathies, *Anal. Chem.*, 1995, **67**, 3676.
- 5 A. T. Woolley, D. Hadley, P. Ladre, A. J. deMello, R. A. Mathies and M. A. Northrup, *Anal. Chem.*, 1996, **78**, 4843.
- 6 A. T. Woolley, G. F. Sensabaugh and R. A. Mathies, *Anal. Chem.*, 1997, **69**, 2181.
- 7 A. T. Woolley and R. A. Mathies, *Proc. Natl. Acad. Sci. USA*, 1994, **91**, 11348.
- 8 S. C. Jacobson and J. M. Ramsey, *Anal. Chem.*, 1996, **68**, 720.
- 9 P. C. Simpson, D. Roach, A. T. Woolley, T. Thorsen, G. F. Sensabaugh and R. A. Mathies, *Proc. Natl. Acad. Sci. USA*, 1998, **95**, 2256.
- 10 R. F. Service, *Science*, 1998, **282**, 399.
- 11 A. Manz, E. J. M. Verpoorte, C. S. Effenhauser, N. Barggraf, D. E. Raymond and H. M. Widmer, *Fresenius' J. Anal. Chem.*, 1994, **348**, 567.
- 12 H. Y. Wang, R. S. Foote, S. C. Jacobson, J. H. Schneibel and J. M. Ramsey, *Sens. Actuators B*, 1997, **45**, 199.
- 13 Z. H. Fan and D. J. Harrison, *Anal. Chem.*, 1994, **66**, 177.
- 14 D. J. Harrison, K. Fluri, N. Chiem, T. Tang and Z. Fang, *Sens. Actuators B*, 1996, **33**, 105.
- 15 D. J. Harrison, P. G. Glavina and A. Manz., *Sens. Actuators B*, 1993, **10**, 107.
- 16 M. A. Roberts, J. S. Rossier, P. Bercier and H. Girault, *Anal. Chem.*, 1997, **69**, 2035.
- 17 L. E. Locasico, *Anal. Chem.*, 1997, **69**, 4783.
- 18 W. Ehrfeld and H. Lehr, *Radiat. Phys. Chem.*, 1995, **45**, 349.
- 19 D. C. Duffy, J. Cooper McDonald, O. J. A. Schueller and G. M. Whitesides, *Anal. Chem.*, 1998, **70**, 4974.
- 20 H.-J. Ache, in *Micro Total Analytical Systems*, ed. A. van den Berg and P. Bergveld, Kluwer, Dordrecht, 1995, p. 47.

- 21 R. Vökel, H. P. Herzig, P. Nussbaum and R. Dändliker, *Opt. Eng.*, 1996, **35**, 3323.
- 22 E. Verpoorte, A. Manz, H. Lüdi, A. E. Bruno, F. Maystre, B. Krattiger, H. M. Widmer, B. H. van der Schoot and N. F. de Rooij, *Sens. Actuators B*, 1992, **6**, 66.
- 23 D. J. Harrison, K. Fluri, K. Seiler, Z. Fan, C. S. Effenhauser and A. Manz, *Science*, 1993, **261**, 895.
- 24 S. C. Jacobson and J. N. Ramsey, *Anal. Chem.*, 1996, **68**, 720.
- 25 C. S. Effenhauser, G. J. M. Bruin, A. Paulus and M. Ehrat, *Anal. Chem.*, 1978, **69**, 3451.
- 26 A. T. Woolley and R. A. Mathies, *Anal. Chem.*, 1995, **67**, 3676.
- 27 D. J. Harrison, A. Manz, Z. Fan, H. Lüdi and H. M. Widmer, *Anal. Chem.*, 1992, **64**, 1926.
- 28 N. Chiem and D. J. Harrison, *Anal. Chem.*, 1997, **69**, 373.
- 29 D. E. Raymond, A. Manz and H. M. Widmer, *Anal. Chem.*, 1996, **66**, 2858.
- 30 C. S. Effenhauser, A. Manz and H. M. Widmer, *Anal. Chem.*, 1995, **67**, 2284.
- 31 S. C. Jacobson and J. M. Ramsey, *Anal. Chem.*, 1997, **67**, 3212.
- 32 S. C. Jacobson, R. Hergenröder, L. B. Koutny and J. M. Ramsey, *Anal. Chem.*, 1994, **66**, 1114.
- 33 S. C. Jacobson, L. B. Koutny, R. Hergenröder, A. W. Moore and J. M. Ramsey, *Anal. Chem.*, 1994, **66**, 3472.
- 34 L. C. Waters, S. C. Jacobson, N. Kroutchinina, J. Khandurina, R. S. Foote and J. M. Ramsey, *Anal. Chem.*, 1998, **70**, 5172.
- 35 M. U. Kopp, A. J. deMello and A. Manz, *Science*, 1998, **280**, 1046.
- 36 C. S. Effenhauser and A. Manz, *Am. Lab.*, 1994, **26**, 15.
- 37 G. Blankenstein and U. D. Larsen, *Biosens. Bioelectron.*, 1998, **13**, 427.
- 38 S. Sundberg, A. Copsfill, R. Nagle, S. Gallagher, C. Chow, G. Wada, T. Nikiforov and J. W. Parce, *Am. Lab.*, 1998, **30**, 22.
- 39 R. Kniss, *Am. Lab.*, 1998, **30**, 40.
- 40 P. Graveson, J. Branebjerg and O. S. Jensen, *J. Micromech. Microeng.*, 1993, **3**, 168.
- 41 S. Shoji and M. Esashi, *J. Micromech. Microeng.*, 1994, **4**, 157.
- 42 P. K. Dasgupta and S. Liu, *Anal. Chem.*, 1994, **66**, 1792.
- 43 R. Zengerle, J. Ulrich, S. Kluge, M. Richter and A. Richter, *Sens. Actuators A*, 1995, **50**, 81.
- 44 A. Manz, C. S. Effenhauser, N. Burggraf, D. J. Harrison, K. Seiler and K. Fluri, *J. Micromech. Microeng.*, 1994, **4**, 257.
- 45 P. H. Paul, D. W. Arnold and D. J. Rakestraw, in *Micro Total Analysis Systems '98*, ed. D. J. Harrison and A. van den Berg, Kluwer, Dordrecht, 1998, p. 49.
- 46 G. Boer, A. Dodge, K. Fluri, B. H. van der Schoot, E. Verpoorte and N. F. de Rooij, in *Micro Total Analysis Systems '98*, ed. D. J. Harrison and A. van den Berg, Kluwer, Dordrecht, 1998, p. 53.
- 47 S. C. Jacobson, R. Hergenröder, L. B. Koutny, R. J. Warmack and J. M. Ramsey, *Anal. Chem.*, 1994, **66**, 1107.
- 48 S. C. Jacobson, R. Hergenröder, A. W. Moore and J. M. Ramsey, *Anal. Chem.*, 1994, **66**, 4127.
- 49 K. Seiler, Z. H. Fang, K. Fluri and D. J. Harrison, *Anal. Chem.*, 1994, **13**, 3485.
- 50 P. H. Paul, M. G. Garguilo and D. J. Rakeshaw, *Anal. Chem.*, 1998, **70**, 2459.
- 51 S. V. Ermakov, S. C. Jacobson and J. M. Ramsey, in *Micro Total Analysis Systems '98*, ed. D. J. Harrison and A. van den Berg, Kluwer, Dordrecht, 1998, p. 149.
- 52 N. A. Patankar and H. H. Hu, *Anal. Chem.*, 1998, **70**, 1870.
- 53 S. J. Haswell, *Analyst*, 1997, **122**, 1R.
- 54 L. J. Kricka and P. Wilding, in *Handbook of Clinical Automation, Robotics and Optimisation*, ed. G. J. Kost and J. Welsh, John Wiley & Sons, New York, 1996, p. 45.
- 55 G. T. A. Kovacs, *Micromachined Transducers Sourcebook*, WCB/McGraw-Hill, Boston, .
- 56 G. T. A. Kovacs, K. Petersen and M. Albin, *Anal. Chem.*, 1996, **68**, 407A.
- 57 G. N. Doku and S. J. Haswell, *Anal. Chim. Acta*, 1999, **382**, 1.
- 58 G. M. Greenway, S. J. Haswell and P. Petsul, *Anal. Chim. Acta*, 1999, **387**, 1.
- 59 C. L. Rice and R. Whitehead, *J. Phys. Chem.*, 1965, **69**, 4017.
- 60 R. A. Hunter, *Zeta Potential in Colloid Science*, Academic Press, London, 1981.
- 61 J. Jednacak, V. Pradvic and W. Haller, *J. Colloid Interface Sci.*, 1974, **49**, 16.
- 62 G. R. Wiese, R. O. James and T. W. Healy, *Discuss. Faraday Soc.*, 1971, **52**, 302.
- 63 A. Vernhet, M. N. Bellon-Fontaine and A. Doren, *J. Chim. Phys.*, 1994, **91**, 1728.
- 64 R. A. Van Wageningen and J. D. Andrada, *J. Colloid Interface Sci.*, 1979, **76**, 305.
- 65 M. P. Sidorova, I. A. Savina and L. E. Ermakova, *Colloid J.*, 1996, **53**, 380.
- 66 See, for example, A. W. Adamson and A. P. Gast, *Physical Chemistry of Surfaces*, John Wiley and Sons, New York, 5th edn., 1997, p. 10.
- 67 See, for example, P. W. Atkins, *Physical Chemistry*, Oxford University Press, Oxford, 5th edn., 1994, p. 840.
- 68 See, for example, W. Jost, *Diffusion in Solids, Liquids and Gases*, Academic Press, New York, 1952.
- 69 B. J. Harmon, D. H. Patterson and F. E. Regnier, *Anal. Chem.*, 1993, **65**, 2655.
- 70 B. J. Harmon, I. Leesong and F. E. Regnier, *Anal. Chem.*, 1994, **66**, 3797.
- 71 F. E. Regnier, D. H. Patterson and B. J. Harmon, *Trends Anal. Chem.*, 1995, **14**, 177.
- 72 D. H. Patterson, B. J. Harmon and F. E. Regnier, *J. Chromatogr.*, A, 1996, **732**, 119.
- 73 S. N. Semenov, *Anal. Commun.*, 1998, **35**, 411.
- 74 J. B. Knight, A. Vishwanath, J. P. Brody and R. H. Austin, *Phys. Rev. Lett.*, 1998, **80**, 3863.
- 75 M. A. Cobb and D. N. Hague, *J. Chem. Soc., Faraday Trans. 1*, 1972, **68**, 932.
- 76 A. D. James and B. H. Robinson, *J. Chem. Soc., Faraday, Trans. 1*, 1978, **74**, 10.
- 77 V. N. M. Lobo and J. L. Quaresma, *Handbook of Electrolyte Solutions, Part B*, Elsevier, Amsterdam, 1989.
- 78 P. D. Christensen, S. W. P. Johnson, T. McCreedy, V. Skelton and N. G. Wilson, *Anal. Commun.*, 1998, **35**, 341.
- 79 V. Skelton, S. J. Haswell, G. M. Greenway, P. Styring and D. O. Morgan, *Chem. Eur. J.*, submitted for publication.
- 80 G. M. Greenway, L. Nelstrop and S. N. Port, *Anal. Chim. Acta*, in press.
- 81 See, for example, W. H. Press, S. A. Teukolsky, W. T. Vetterling and B. P. Flannery, *Numerical Recipes in FORTRAN*, Cambridge University Press, Cambridge, 2nd edn., 1992.
- 82 V. N. Paunov, K. D. Danov, N. Alleborn, H. Raszclier and F. Durst, *Chem. Eng. Sci.*, 1998, **53**, 2839.

The use of a novel microreactor for high throughput continuous flow organic synthesis

Gillian M. Greenway^a, Stephen J. Haswell^{a,*}, David O. Morgan^b, Victoria Skelton^a, Peter Styring^a

^a Department of Chemistry, Faculty of Science and the Environment, The University of Hull, Hull HU6 7RX, UK

^b SmithKline Beecham Pharmaceuticals, Tonbridge, Kent TN11 9AN, UK

Abstract

The aim of this study was to investigate the performance characteristics of a flow injection microreactor with reference to both the chemistry and reactor design using a model system, the established synthesis of 4-cyanobiphenyl based on a modified Suzuki coupling of an aryl halide and an organoboron compound. The catalytic reaction was carried out in micro-channels (300 μm wide and 115 μm deep) etched into glass and sealed with a top plate. The mobility of the reagent solutions was achieved using electroosmotic flow (EOF) assisted by the incorporation of a microporous silica structure within the microreactor channels, which acted as both a micro-pump and an immobilisation technique for the catalyst bed (1.8% palladium on silica). The yield of 4-cyanobiphenyl was determined by GC–MS.

The synthesis of 4-cyanobiphenyl at room temperature in a flow injection microreactor, using a supported catalyst, without the addition of a base gave a product yield of $67 \pm 7\%$ ($n = 6$). This was achieved by injecting 4-bromobenzonitrile for 5 s, with a 25-s injection interval, into a continuous stream of phenylboronic acid. A series of injections were performed over a 25-min period and the product collected for analysis. Palladium contamination in the crude product was found to be in the range of 1.2–1.6 ppb, determined using ICP–MS, indicating a low leach rate from the immobilised catalyst.

A conventional laboratory batch scale method was also performed for the same synthesis using the identical conditions as those used in the flow injection microreactor, with and without the addition of a base, at both room and elevated temperatures (75–80°C) in an inert atmosphere under reflux for 8 h. The product yield for the non-optimised bulk reaction was 10% (determined by GC–MS), significantly lower than with the flow injection microreactor illustrating the potential of microreactors for clean efficient synthesis. © 2000 Elsevier Science S.A. All rights reserved.

Keywords: Microreactor; Synthesis design; Porosity; Heterogeneous catalysis; Palladium

1. Introduction

Over recent years a number of publications in analytical literature have described the development of the micro-total analytical system (μTAS) [1–3] with the main thrust of such work being directed towards the separation and characterisation of DNA [4–9]. These devices have been typically fabricated using a range of materials and manifold generation techniques creating a network of interconnecting channels, with typical cross-section of between 50 and 300 μm [10–13]. In general, such analytical devices have exploited the highly efficient separation capability of μTAS for the isolation and detection of analytes of interest. In

this study, whilst we adopt similar fabrication technology, i.e. photolithography and wet etching, to that used in μTAS the application of flow injection microreactors to solvent-based chemical synthesis introduces uniquely different modus operandi to that used in current analytical applications. To date there have been a limited number of reports describing gas phase catalytic reactions being performed in continuous flow injection microreactors [14], no reports have appeared to date describing a solvent-based reaction using a flow injection microreactor system.

The important features of flow injection microreactors of the type developed in this work are that they offer unique spatial and temporal control of reactant and products [15] whilst enabling rapid product production with desirable reaction kinetics. For the purpose of this study, the attributes of flow injection microreactors will be evalu-

* Corresponding author. Telefax: +44-1482-466416.

E-mail address: s.j.haswell@chem.hull.ac.uk (S.J. Haswell).

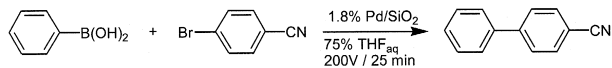


Fig. 1. Reaction scheme for the coupling of 4-bromobenzonitrile and phenylboronic acid in a microreactor under EOF.

ated with reference to both the chemistry and device design by using a modification of the well-established Suzuki reaction. One of the key features of such an approach for chemical synthesis is the ability to achieve highly selective, pure yields of products with minimal catalyst residues. Bench marking studies [16] have already indicated that such devices could be developed for a number of industrial process where a parallel scale-out approach could produce the bulk quantities required by the pharmaceutical and chemical industries.

The Suzuki–Miyaura synthesis is one of the most commonly used methods for the formation of carbon to carbon bonds in the chemical and pharmaceutical industry due to its selectivity in product formation [17]. The Suzuki coupling reaction of the aryl halide and organoboron requires a palladium catalyst to be present for which tetrakis(triphenylphosphine)palladium(0) has traditionally been used, producing a typical yield of 44–78% in dimethoxyethane (DME), benzene and tetrahydrofuran (THF) with reactions taking between 2–6 h [18]. Recently, Beller et al. [19] performed a Suzuki coupling of aryl halide and phenylboronic acid, reporting a yield of 83% using palladacycles as efficient catalysts, at 130°C. However, the degradation of the homogeneous catalyst system can result in undesirable by-products in the final product, for example triphenylphosphine oxide and palladium metal.

This paper will concentrate specifically on the Suzuki coupling reaction (Fig. 1), describing the method used to prepare the flow injection microreactor for the synthesis of 4-cyanobiphenyl. In this work electroosmotic flow (EOF) [15] has been used for the mobilisation of THF, which, like many organic solvents, exhibits very low natural EOF properties. However, a 75:25 mixture with water and the presence of a micro-porous silicate structure within the flow channels [20] was found to be sufficient to enhance the flow characteristics of the solvent. In addition to acting as a micro-pump, the micro-porous silicate structure was also used to immobilise the Pd/SiO₂ catalyst bed. The authors believe that this is the first paper to report on the combined use of EOF with the micro-porous silicate structure in a flow injection microreactor to perform the palladium-catalysed organic synthesis and as such illustrates the future potential of the methodology described.

2. Experimental

All reagents were of analytical grade, unless stated otherwise, and were used without further purification. Water was high purity, deionised (18 MΩ cm resistivity).

A flow injection microreactor, which included the immobilised catalyst (1.8% palladium on silica), was prepared in borosilicate glass using a photolithographic patterning technique and a modified wet etch technique, as described by Daykin and Haswell [10], generating a T channel geometry. In this case the plate was etched using a glass etching solution of 1% hydrofluoric acid (BDH Merck AnalaR) with 5% ammonium fluoride (BDH Merck AnalaR) at 70°C, for 2 h. The plate was then stripped of photoresist and chrome to produce a clean glass substrate with final channel geometries of 300 μm wide and 115 μm deep. The catalytic bed was generated by manually mixing 1.8% palladium on silica (kindly supplied by Johnson Matthey Chemicals) with the silica solution [20] and physically positioning the slurry in the channel as indicated in Fig. 2. The slurry was then heated in situ to 100°C for 1 h. The channels were then sealed by annealing to the patterned base plate, a 17 mm thick top plate (680°C) using a microwave furnace (CEM microwave ashing system 300). The top plate included 2 mm internal diameter pre-drilled holes aligned at the ends of each channel to act as reservoirs and supports for the platinum electrodes required to generate EOF.

The synthetic method used was adapted from that previously reported by Styring et al. [21]. The flow injection microreactor was operated in the following manner. A standard solution of phenylboronic acid (100 μl, 0.1 M Lancaster Synthesis) in 75% THF_(aq) (Fisher Scientific International) was added into reservoir B of the continuous flow microreactor (see Fig. 2). 4-Bromobenzonitrile (100 μl, 0.1 M, Lancaster Synthesis) in 75% THF_(aq) was introduced into reservoir A and 30 μl of 75% THF_(aq) only was introduced into reservoir C. Electrodes were then placed in each reservoir (A + B positive, C ground), which were then covered using laboratory film (Aldrich Chemical). An external voltage (in the range of 100–400 V) was then applied to channel B(+) relative to reservoir C(-). This induced a continuous flow of phenylboronic acid from B(+) to C(-). The periodic application of 200 V between reservoir A(+) and C(-) efficiently injected aliquots of 4-bromobenzonitrile into the continuous stream of phenylboronic acid. The total volume of solution in reservoir C at the end of each reaction was recorded and

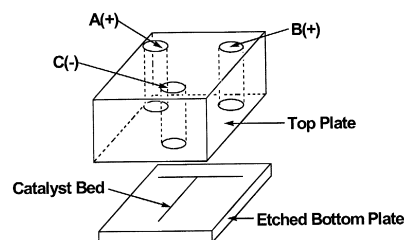


Fig. 2. Schematic diagram of the 'T'-shaped manifold used in the reactor for the Suzuki coupling.

samples taken for gas chromatography–mass spectrometry (GC–MS) and ICP–MS analysis. The GC–MS results were used to determine the reactor yield whilst the ICP–MS data was used to determine the concentration of Pd in the product, so indicating possible bleed from the immobilised catalyst bed. Three basic mixing techniques were investigated, as follows.

Study 1 investigated the effect of changing the volume of 4-bromobenzonitrile injected into the phenylboronic acid stream on the yield of 4-cyanobiphenyl. The phenylboronic acid solution (flow rate = $0.8 \mu\text{l min}^{-1}$) was moved continuously through the microreactor from B to C whilst sample plugs of 4-bromobenzonitrile (flow rate = $1.56 \mu\text{l min}^{-1}$) were injected every minute for a range of injection times (5, 20, 30, 40 and 50 s) from channel A. Repeated injections (25) for each injection time were carried out to generate sufficient product for analysis.

Study 2 investigated the effect on the yield of 4-cyanobiphenyl associated with the frequency between injections of 4-bromobenzonitrile into the phenylboronic acid flow. As in study 1, the phenylboronic acid solution was moved continuously through the microreactor (B to C) and multiple injections (5-s duration) of 4-bromobenzonitrile from channel A were carried out for a range of time intervals of 5, 15, 25, 30, 40 and 55 s to identify the maximum catalyst loading of the 4-bromobenzonitrile compound.

Study 3 investigated how the yield of 4-cyanobiphenyl changed when the flow rate of the continuous stream of phenylboronic acid was varied between 0.65 and $1.3 \mu\text{l min}^{-1}$. The flow rate was changed by applying voltages between 100 and 400 V across reservoirs B(+) and C(−). For this study, 5-s injections of 4-bromobenzonitrile moving at a flow rate of $1.56 \mu\text{l min}^{-1}$ were injected from reservoir A(+) every 25 s into the phenylboronic acid stream.

The products collected in reservoir C were analysed using GC–MS (Finnigan MAT 9001 GC–MS). The GC contained an RTX-5MS 35 m length column that was held at 70°C for 3 min. A ramp rate of 20°C per minute was employed up to 300°C and held for 5 min. The transfer line was heated to 250°C and the ion source temperature to 225°C with a helium carrier velocity of 40 cm s^{-1} . The mass spectrometry mass range used was 50 to 450 Da. The ICP–MS used was a VG Elemental PlasmaQuad II + fitted with a Cetac MCN nebuliser. Samples and standards were diluted in 2% HNO_3 to which internal standards (10 ppb Ga, Rh, Bi and Ho) were added. A calibration model for palladium was generated in the range 0–100 ppb.

The yield of 4-cyanobiphenyl was based on the reaction concept of micro-molar concentration levels. Initial solution preparation was at molar concentrations (0.1 M). For each reaction performed, a single flow injection microreactor was used rather than an array of reactors and therefore only a few micro-litres of product was generated for each analysis, approximately $35 \mu\text{l}$ in total (including the initial $30 \mu\text{l}$ of $\text{THF}_{(\text{aq})}$ placed in reservoir C). Yields were

calculated from a knowledge of the input weight of aryl bromide, the volume of solution in reservoirs A and C before and after the reaction, measurement of the concentration of arylbromide in reservoir A and C at the end of the reaction and the concentration of product in reservoir C. Concentrations were determined by GC measurement relative to authentic material.

2.1. Batch synthesis of 4-cyanobiphenyl

A solution of 4-bromobenzonitrile (0.4550 g, 0.1 M) and phenylboronic acid (0.3025 g, 0.1 M) in aqueous THF (75%, 50 ml total volume) was stirred at room temperature over 1.8% (w/w) Pd/SiO₂ (0.7585 g, 3 mol%) for 8 h. The progress of the reaction was monitored by GC. As no reaction was noted after this period, sodium carbonate (aq, 0.2 M, 20 ml) was added and the solution stirred for a further 8 h. The reaction temperature was then increased to reflux. After 8 h, GC–MS analysis revealed 10% conversion to the 4-cyanobiphenyl product (retention time 10.22 min, $[M]^+ = 179 \text{ Da}$).

3. Results and discussion

The initial stage of the catalytic cycle for the production of 4-cyanobiphenyl is the oxidative addition (Fig. 3) of an aryl bromide to palladium(0) to form a palladium(II) complex (Ar–Pd^{II}–Br). Matos and Soderquist [22] have reported that oxidative addition of bromobenzene to $[\text{Pd}(\text{PPh}_3)_4]$ can occur readily at room temperature, although immobilised metal catalysts have not been investigated. Transmetalation of the resulting Ar–Pd–Br with complex Ar'–B(OH)₂ gives the biaryl species (Ar'–Pd^{II}–Ar).

Conventionally, the Suzuki synthesis requires the addition of a base, commonly aqueous sodium carbonate [23], which activates the metal towards the reaction with the boronic acid. The synthesis of 4-cyanobiphenyl in this flow injection microreactor system is, however, unique in that the addition of a base was not required. This is thought to be due to the water associated with the aqueous

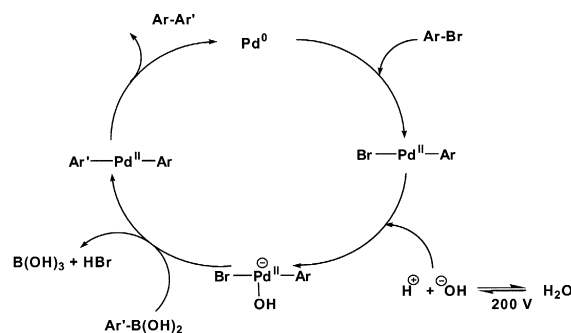


Fig. 3. Proposed catalytic cycle for the synthesis of biaryl systems using an immobilised palladium metal catalyst in a microreactor under EOF.

THF undergoing partial ionisation to form hydroxide species at the high surface feature generated by the silica frit in the flow injection microreactor channel. Clearly, the presence of free hydroxide ions batch reactions would be at a negligible concentration, but due to the high electrical field associated with the EOF generation and the presence of the palladium catalyst in the flow injection microreactor, it is postulated that a localised concentration effect is occurring around the palladium metal surface, negating the need for a base to be present i.e. in-situ base generation. Badone et al. [24] recently reported higher yields for similar coupling reactions, using a conventional laboratory system in an aqueous solvent system, however, the system still required an inorganic base to be present.

Initial studies indicated that the continuous diffusive mixing (rather than using the injection mode) of reagents did not produce any significant quantities of the 4-cyanobiphenyl. This may in part be attributed to the flow characteristics within the flow injection microreactor, which is essentially a non-turbulent laminar flow, resulting in diffusion-limited mixing. Thus, when two streams of reagents are moved under EOF in such a reactor, it is only at the reagent contact region that a reaction will proceed, which in turn leads to a low yield, i.e. the bulk of the reagents have not mixed and therefore cannot react. Additionally, the transmetallation mechanism described previously would suggest that if the 4-bromobenzonitrile is in too high a concentration, compared to the number of palladium sites available on the immobilised catalyst bed, and because of the continuous flow, the effective concentration of the $\text{Ar}'\text{-B}(\text{OH})_2$ available for the transmetallation

step would be reduced by dilution. The catalytic rate would therefore be reduced. However, injecting a sample plug of aryl halide into a continuous stream of the phenylboronic acid would decrease the effective concentration of the 4-bromobenzonitrile but increase the effective phenylboronic acid concentration on the catalyst surface and would therefore increase the interfacial regions for the reaction to occur.

Using this concept, the optimum injection lengths or volumes to allow complete diffusive mixing, the level of catalyst loading and the optimum voltage or flow rate were investigated in terms of the yield of 4-cyanobiphenyl.

Study 1 centred on one injection (of variable lengths) per minute across a total experimental time of 25 min. The higher the concentration of the aryl halide (longer injection times) the lower was the yield of 4-cyanobiphenyl obtained. Increasing the concentration of 4-bromobenzonitrile in turn caused a decrease in the effective concentration of $\text{Ar}'\text{-B}(\text{OH})_2$ due to dilution of the reaction system. The optimum injection length was found to be 5 s, which gave a yield of 14%. This injection time, which reflected the volume time for diffusive mixing, was used for the remainder of the investigations.

Study 2 investigated the effect of altering the proportion of the 4-bromobenzonitrile relative to the continuously flowing phenylboronic acid by varying the time delay between consecutive 5-s duration injections of the 4-bromobenzonitrile. The results obtained can be seen in Fig. 4. The initial section of the graph (5–20 s delay) indicate that catalyst saturation with 4-bromobenzonitrile is occurring due to the high injection rates which renders the

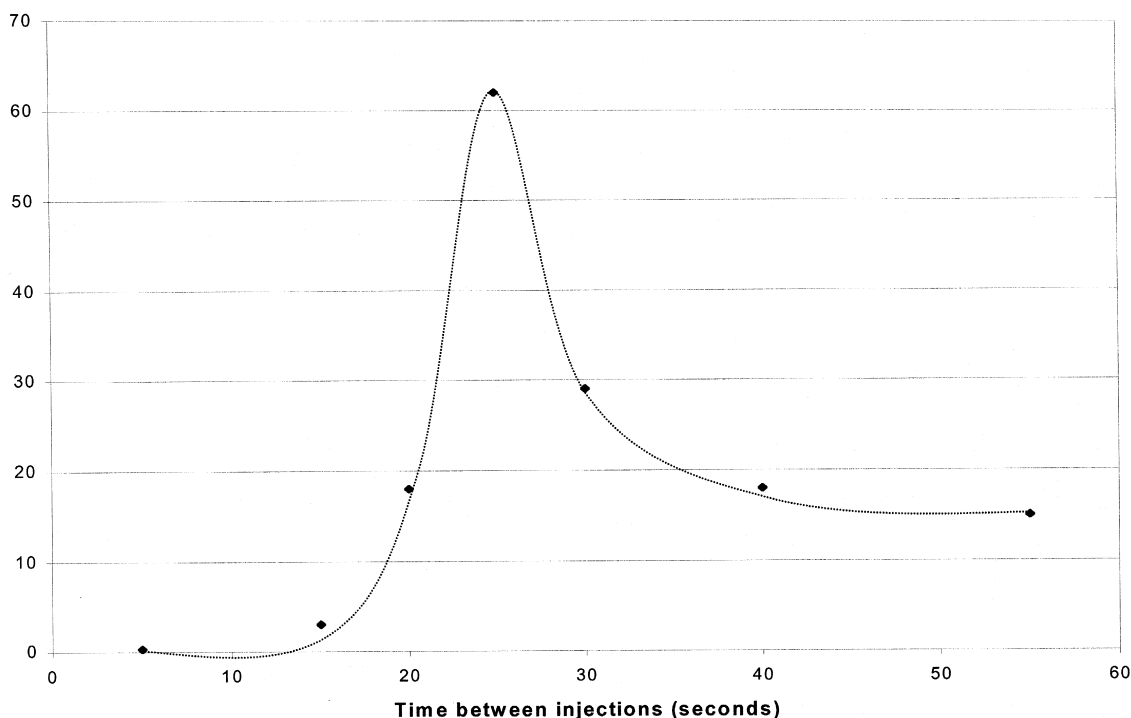


Fig. 4. Plot of the mean yield of 4-cyanobiphenyl for various time intervals between injections for 5 s injection of 4-bromobenzonitrile.

phenylboronic acid levels too low for any appreciable product to be formed. As the time between injections of the 4-bromobenzonitrile becomes too long (delay times of 30–55 s), the effective concentration of the 4-bromobenzonitrile becomes too low relative to the phenylboronic acid concentration for the reaction to produce appreciable yields. However, as the relative concentrations of the two reactants reaches an optimum at around 25 s injection interval for the 4-bromobenzonitrile, for a fixed 5-s injection time giving a yield of around 60%.

Study 3 compared the yield of 4-cyanobiphenyl obtained for various flow rates or voltages of the phenylboronic acid based on a fixed injection mode of 5-s injection, 25-s time interval for the 4-bromobenzonitrile. The results are presented in Fig. 5. The results indicate that at 200 V ($0.8 \mu\text{l min}^{-1}$), the flow rate of the phenylboronic acid gave a yield of 4-cyanobiphenyl between 49% and 68% whilst the other voltages investigated produced negligible yields. At 1.0 and $1.3 \mu\text{l min}^{-1}$ (300 and 400 V) the flow rate is too fast, reducing the residency time of the 4-bromobenzonitrile on the palladium catalyst. At lower voltages ($0.65 \mu\text{l min}^{-1}$), the flow rate is too small for effective transfer of the 4-bromobenzonitrile to occur efficiently.

In order to evaluate more fully the results obtained when using the flow injection microreactor, comparative batch reactions were performed, with and without added base, both at room and elevated temperature (75–80°C) using the solvent and reagents described for the microreactor system (i.e. not using the optimal bulk method). At room temperature, with and without the presence of a base,

the reaction did not yield any detectable quantities of the 4-cyanobiphenyl product, which suggests that the characteristic features of the flow injection microreactor and the immobilisation of the catalyst bed within the microreactor are highly efficient.

The same reaction was performed at elevated temperatures of 75–80°C with the addition of sodium carbonate (aq, 0.2 M, 20 ml water). Under these conditions the conversion of the reagents to 4-cyanobiphenyl after 8 h was found to be 10% by GC–MS analysis.

For many areas of applications such as the pharmaceutical industry, the levels of contamination in the final product from a palladium catalyst can be a serious problem dependent upon the product compound synthesised, particularly when homogeneous catalytic systems are used, which can lead to increased production costs. As the flow injection microreactor used in this study employed an immobilised heterogeneous Pd catalyst, ICP–MS analysis of the product was carried out to determine the levels of palladium leach. Results indicated that Pd was present in the range 1.2–1.6 ppb, in the crude product, which was indicative of a very low rate of leach from the catalytic bed.

In addition to direct palladium contamination, homogeneous catalyst can generate high levels of impurities such as triphenylphosphine oxide and often require regeneration due to the formation of colloidal palladium, which is difficult to isolate and recycle. Using a supported immobilised palladium catalyst not only allows immobilisation on a micro-porous silica structure within the flow injection microreactor but also prevents the diffusion of the catalyst into the product solution. This negates the costly process

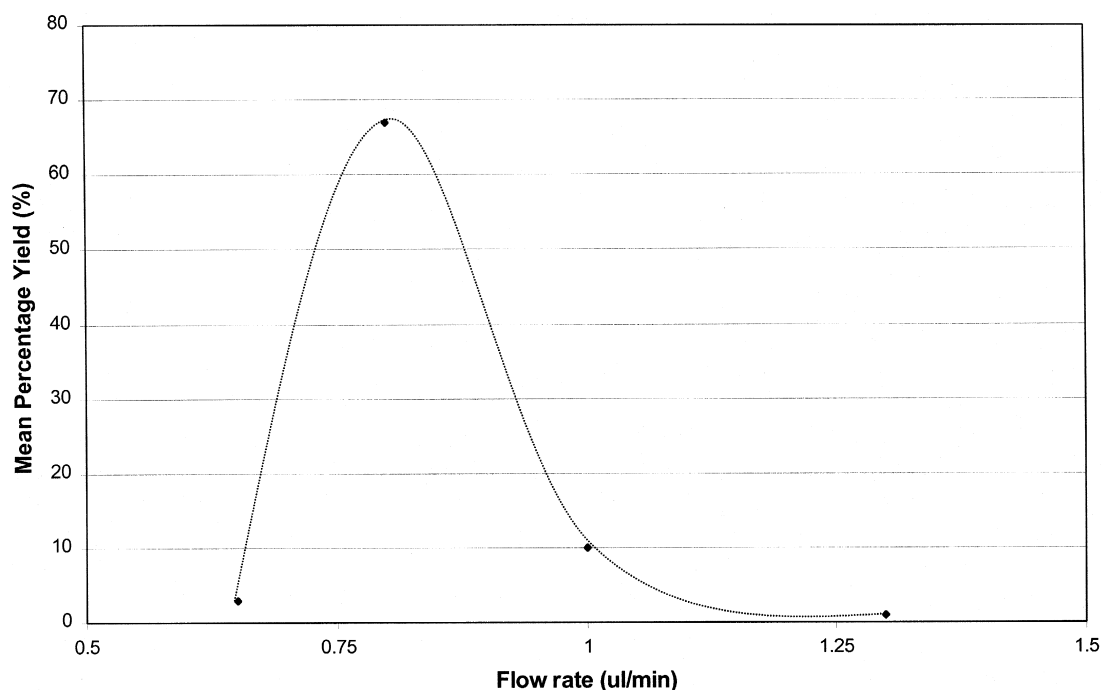


Fig. 5. Plot of the mean yield of 4-cyanobiphenyl against the flow rate of phenylboronic acid for 5 s injection of 4-bromobenzonitrile.

of removing the catalyst impurities and allows for long term catalyst activity. The current flow injection microreactors have been used for a large number of reactions (operating for over 35 h) with no apparent loss of catalytic activity. Whilst a more detailed study of catalytic performance is required, the chemistries involved do not suggest potential problems with long term stability of the immobilised palladium catalyst.

4. Conclusions

The synthesis of 4-cyanobiphenyl at room temperature without the addition of a base using a novel microreactor for high throughput continuous flow organic synthesis offers an efficient methodology, giving GC yields of $67 \pm 7\%$ with respect to the aryl halide with negligible presence of catalyst residues. The reaction was carried out using a supported catalyst (1.8% palladium on silica) which was immobilised within a flow injection microreactor manifold using a microporous silica frit.

It should be stressed that for the purpose of this study the reaction described was selected to simply illustrate the feasibility and identify any interesting features of performing such a reaction in a flow injection microreactor. The results suggest that further work should involve the enhancement of the yield of the 4-cyanobiphenyl through the development of a post-reaction separation system, which will allow the recycling of the starting materials so enhancing the yield and enabling isolation of a pure product. The development of in-situ fluorescence detection should also be considered, as natural fluorescence is observed by many liquid crystals, which can be generated by the Suzuki method.

Acknowledgements

We wish to thank the EPSRC and SmithKline Beecham for financial support to VS in the form of a CASE studentship. The palladium on silica catalyst was kindly supplied as a gift by Johnson Matthey.

References

- [1] A. Manz, D.J. Harrison, E. Verpoorte, J.C. Fettinger, H. Ludi, H.M. Widmer, Miniaturization of chemical analysis systems — a look into next century technology or just a fashionable craze, *Chimia* 45 (1991) 103.
- [2] A. Manz, D.J. Harrison, E. Verpoorte, H.M. Widmer, Planar chips technology for miniaturization of separation systems — a development perspective in chemical monitoring, *Adv. Chromatogr.* 33 (1993) 1.
- [3] A. Manz, C.S. Effenhauser, N. Barggraf, E. Verpoorte, D.E. Raymond, H.M. Widmer, Capillary electrophoresis integrated into a planar microstructure, *Anal. Mag.* 22 (1994) M25.
- [4] A.T. Woolley, R.A. Mathies, Ultra-high-speed DNA sequencing using capillary electrophoresis chips, *Anal. Chem.* 67 (1995) 3676.
- [5] A.T. Woolley, D. Hadley, P. Ladre, A.J. deMello, R.A. Mathies, M.A. Northrup, Functional integration of PCR amplification and capillary electrophoresis in a microfabricated DNA analysis device, *Anal. Chem.* 68 (1996) 4081.
- [6] A.T. Woolley, G.F. Sensabaugh, R.A. Mathies, High speed DNA genotyping using microfabricated capillary array electrophoresis chips, *Anal. Chem.* 69 (1997) 2181.
- [7] A.T. Woolley, R.A. Mathies, Ultra high speed DNA fragment separation using microfabricated capillary array electrophoresis chips, *Proc. Natl. Acad. Sci. U. S. A.* 91 (1994) 11348.
- [8] S.C. Jacobson, J.M. Ramsey, Integrated microdevice for DNA restriction fragment analysis, *Anal. Chem.* 68 (1996) 720.
- [9] P.C. Simpson, D. Roach, A.T. Woolley, T. Thorsen, R. Johnston, G.F. Sensabaugh, R.A. Mathies, High throughput genetic analysis using microfabricated 96-sample capillary array electrophoresis microplates, *Proc. Natl. Acad. Sci. U. S. A.* 95 (5) (1998) 2256.
- [10] R.N.C. Daykin, S.J. Haswell, Development of a micro flow injection manifold for the determination of orthophosphate, *Anal. Chim. Acta* 313 (1995) 155.
- [11] D.C. Duffy, J.C. McDonald, O.J.A. Schueller, G.M. Whiteside, Rapid prototyping of microfluidic systems in poly(dimethylsiloxane), *Anal. Chem.* 70 (1998) 4974.
- [12] Microchannel electrophoretic separation of DNA in injection molded plastic substrates, *Anal. Chem.* 69 (1997) 2626.
- [13] W. Ehrfeld, H. Lehr, Deep X-ray lithography for the production of 3-dimensional microstructures from metals, polymers and ceramics, *Radiat. Phys. Chem.* 45 (1995) 349.
- [14] Book of Abstracts, Proceedings of the IMRET 3 Conference, 1999, in preparation.
- [15] P.D.I. Fletcher, S.J. Haswell, V.N. Paunov, Theoretical considerations of chemical reactions in micro-reactors operating under electroosmotic and electrophoretic control, *Analyst* 124 (1999) 1273.
- [16] J.W. Ponton, Observations on hypothetical miniaturised, disposable chemical plant, in: W. Ehrfeld (Ed.), *Microreaction Technology*, Proceedings of the First International Conference on Microreaction Technology, Springer-Verlag, Berlin, 1998, p. 10, Part 1.
- [17] M. Moreno-Manas, M. Perez, R. Pleixats, Palladium-catalyzed Suzuki-type self-coupling of arylboronic acids. A mechanistic study, *J. Org. Chem.* 61 (1996) 2346.
- [18] N. Miyaura, A. Suzuki, Palladium-catalyzed cross-coupling reactions of organoboron compounds, *Chem. Rev.* 95 (1995) 2457.
- [19] M. Beller, H. Fischer, W. Herrmann, K. Ofele, C. Brossmer, Palladacycles as efficient catalyst for aryl coupling reactions, *Angew. Chem., Int. Ed. Engl.* 34 (17) (1995) 1848.
- [20] P.D. Christensen, S.W.P. Johnson, T. McCreedy, V. Skelton, N.G. Wilson, The fabrication of micro-porous silica structures for micro-reactor technology, *Anal. Commun.* 35 (1998) 341.
- [21] P. Styring, J.D. Vuijk, S.A. Wright, K. Takatoh, C. Dong, Inversion of chirality-dependent properties in helical liquid crystals: effects of structural modification, *J. Mater. Chem.* 4 (1994) 1365.
- [22] K. Matos, J.A. Soderquist, Alkylboranes in the Suzuki–Miyaura coupling: stereochemical and mechanistic studies, *J. Org. Chem.* 63 (1998) 461.
- [23] G.B. Smith, G.C. Dezeny, D.L. Hughes, A.O. King, T.R. Verhoeven, Mechanistic studies of the Suzuki cross-coupling reaction, *J. Org. Chem.* 59 (1994) 8151.
- [24] D. Badone, M. Baroni, R. Cardamone, A. Ielmini, U. Guzzi, Highly efficient palladium-catalyzed boronic acid coupling reactions in water: scope and limitations, *J. Org. Chem.* 62 (1997) 7170.

Chemical and biochemical microreactors

Stephen J. Haswell*, Victoria Skelton

Department of Chemistry, Faculty of Science and the Environment, University of Hull, Hull HU6 7RX, UK

Research into the fundamental and practical advantages of using micrometre scale reactors for chemical and biochemical applications is now growing at a considerable rate. This review tracks such developments, illustrating their inherent strengths and identifying areas where further development of a technology is poised to revolutionise significant areas of synthetic chemistry and biochemistry. ©2000 Elsevier Science B.V. All rights reserved.

Keywords: Microreactor; Gas phase; Heterocyclic chemistry; Catalysis; Biochemistry

1. Introduction

In recent years research and development of miniaturised chemical systems has grown dramatically, allowing the realisation of the micro total analytical system (μ -TAS), which the reader will find well-documented [1–6] and described, elsewhere in this issue of TrAC. In a less dramatic way the application of similar technology to that used for μ -TAS has also led to the development of so-called micro-chemical reactors [7–9]. However, simply reducing the size of a chemical reactor because technology is available goes beyond just being gimmicky and this review will attempt to illustrate some of the intrinsic features such as the spatial and temporal control of reagents and reactants that can be achieved under the diffusion-limited and unique thermal properties that exist at the micrometre scale [10].

Areas that have attracted most research to date have centred on gas and liquid phase reactions covering heterogeneous and homogeneous catalysis, catalytic oxidation, heterocyclic synthesis, and photochemical reactions. In particular, the processes described have clearly indicated the value

of using microreactor technology for solution-based chemistry and bio-application in areas such as chemical discovery and development. In addition we should not underestimate the relevance microreactors will have as tools for purely research and teaching applications across a wide range of scientific disciplines.

Microreactors exhibit numerous practical advantages when compared with traditional batch-scale synthesis, not least is the demand for a high standard of safety, which includes the transportation and storage of toxic, explosive or otherwise harmful materials. In such cases microreactors offer the capability to carry out production on site at the point of demand. The removal of potentially significant large-scale plant accidents associated with thermal runaway could also be envisaged due to the inherent thermal dissipation possible in microreactor devices. Indeed it has been demonstrated that reactions can be performed beyond their current explosive limits by adopting microreactor technology [11]. The whole aspect of heat management, enabling mass and heat transfer to be extremely rapid, leads inevitably to a higher level of reaction control and reactant manipulation at any one point within a device. In addition, the problems associated with traditional scale-up could be overcome by reactor scale-out producing the required quantity of raw material. Adopting a scale-out philosophy coupled with large-scale microreactor fabrication technology, it is possible to see how the optimisation of reaction conditions on a single device could be extended, allowing multiple numbers of single units referred to as 'parallel scale-out'. By adopting such an approach, the reaction efficiency and throughput capacity allowing the production of material on a supply and demand basis could be achieved without the need to redesign or validate the reaction methodology. Thus one can conclude that microreactors applied to the field of chemical and biochemical synthesis offer greater reaction control and selectivity, which in turn can be optimised through a scale-out methodology creating a safe and efficient approach to chemical discovery and production.

*Corresponding author. Tel.: +44 (1485) 465469;
Fax: +44 (1482) 466410.
E-mail: s.j.haswell@chem.hull.ac.uk

2. Microreactor fabrication and applications

Currently, microreactor devices are produced using a number of techniques, for example wet etching [12], injection moulding [13] and laser microforming [14] using a variety of materials, such as noble metals, polymers, ceramics, glass and silica. Noble metal devices are suitable for fast exothermic heterogeneously catalysed reactions and this has been successfully demonstrated for the partial oxidation of methane to syngas using a honeycomb, structured rhodium catalyst device [15]. Metal devices are commonly generated using microlamination techniques in which thin laminates of metal are stacked forming channels and partitions. The channels generated are achieved by pressure stamping or using photochemical machining techniques. Mobilisation of organic solutions in metal devices requires the use of micro-pressure pumping systems that can lead to an increase in internal pressure which may or may not be seen as an advantage for a number of reactions.

Glass and silica devices are suitable for a variety of applications allowing, for example, fast reaction screening for drug discovery applications and heterogeneously catalysed reactions. At the University of Hull, drug discovery screening applications are being developed in glass microreactors using model systems such as the Wittig synthesis based on aldehyde functionality [16]. In addition, heterogeneous catalytic reactions based around a modified Suzuki reaction have been investigated as these offer spatial and temporal delivery of reactants to the catalytic surface and in situ base generation to be exploited [17]. This type of device exhibits chemical inertness and temperature stability and can also mobilise aqueous and organic solution via electroosmotic flow (EOF) which has numerous advantages including minimal back pressure, no mechanically moving parts and therefore a corresponding high reliability with minimal hydrodynamic dispersion. In addition, the opportunity to exploit electrokinetic separation in conjunction with EOF offers considerable scope to temporally and spatially control of reaction intermediates and products [10].

3. World-wide development

This special issue of TrAC serves well to demonstrate that the whole area of microtechnology applied to chemical processes is a rapidly expanding area of research and there are now a number of growing research groups around the world focusing on chemical microreactor applications. Jensen's group from the Department of Chemical Engineering at the Massachusetts Institute of Technology has a particular interest in the safety aspects of reactions, especially the explosive and toxicity issues relating to the production of a variety of compounds at the point of demand. This has been demonstrated with the production of a microreactor for organic peroxides generated from acid chlorides [11]. In addition, advances in thin film metal membranes have allowed the development of a hydrogen flux device that has additional application for hydrogenation reactions [18]. With a similar emphasis on safety, Ehrfeld's group at the Institut für Mikrotechnik, Germany, has been a prime mover in developing microreactors for the reduction of exposure to hazardous materials. Recently a microreactor has been developed for the Andrusow reaction allowing the synthesis of the toxic material hydrogen cyanide [15] to be achieved. Success in controlling a high temperature reaction will now allow systems for a variety of similar high temperature reactions to be developed. Other work has centred on the direct fluorination of aromatic compounds in which greater product sensitivity was achieved [15].

The research group of Wegeng and Drost at the Pacific Northwest National Laboratories in Richland, WA, has generated a variety of applications for the development of an automotive fuel processor and heat pumps, microengineered devices for hydrogen-rich fuel streams and the development of microchannel contractors for gas absorption and microdevices for solvent extraction [15].

Other related applications include the fabrication of a multistep synthesis device by Orchid Biocomputers, USA, which will enable the synthesis of over 100 compounds to be performed simultaneously, the development by Bergveld of a microdialysis device and counterflow heat exchanger at the University of Twente, Netherlands [15] and developments in Sweden in the area of biocatalysis [19]. In addition, Yager's group from Washington State have extensively described the development and

fabrication of T-shaped manifolds for chemical reactions and sensors [20]. Karube's group has described the development of an enzyme-immobilised column with electrochemical flow cell for glucose detection using micromachining techniques [21]. In the UK, the Chemical Engineering Department at the University of Sheffield has been investigating the use of stacked gas-phase microchannels. The work, led by Ray Allen, has extensively modelled the fundamental parameters that affect the scaling of reactions [22] based on channel hydraulic diameter, reaction intensity and reactor proportions.

Finally, Haswell's group at the University of Hull has been working for a number of years on various areas of microreactor research, focusing in particular on establishing the practical capabilities of microreactor devices using already established synthetic chemistry reactions including the Suzuki catalytic-based reaction [17], and the characterisation of fluidic control demonstrated using the Wittig synthesis [16]. The group has a number of on-going projects looking at multi-stage synthesis and experimental design methods based on microreactor technology.

4. Research themes

In this section a selected number of examples have been chosen from the literature to illustrate the novelty microreactors can bring to the area of synthetic and bio-applications. The review is in no way meant to be definitive or wide ranging but will serve to illustrate some of the current developments that are occurring in a rapidly developing field.

Chambers et al. [23] have reported the development of a microreactor in which elemental fluorine has been used to allow both the selective fluorination and perfluorination of organic compounds in a simple controllable manner. The synthesis of fluorine-containing organic compounds has many inherent safety issues such as safe handling and temperature control. Chambers outlined the potential benefits of the microreactor used as being (i) a small inventory of fluorine in the reaction zone, (ii) an opportunity for good mixing and temperature control and (iii) simple reaction scale-up. Taking into account these criteria, Chambers designed the reactor outlined in Fig. 1. The microreactor is fabricated from a block of nickel in which a groove is machined (ca 500 μm) and sealed using a block of

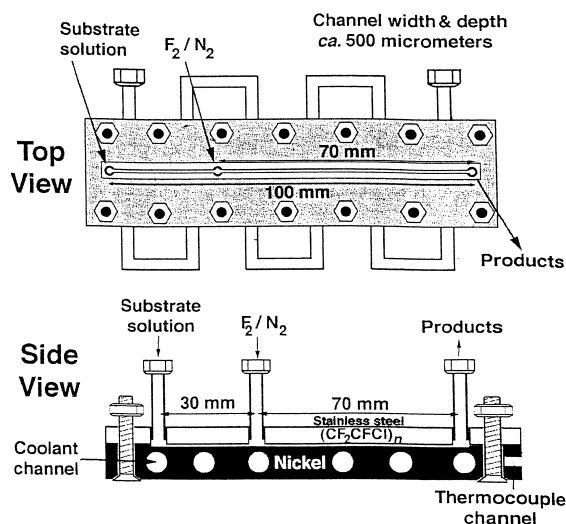


Fig. 1. Microreactor top and side view for elemental fluorine reactions.

polychlorotrifluoroethane. Liquid reactant and solvent delivery was achieved using pressure syringe pumps, whilst the fluorine in nitrogen was delivered from a small cylinder via a mass flow controller. Liquid-gas mixing was achieved using cylindrical flow and the products were trapped in polychlorotrifluoroethylene tubing and cooled. Residual gas was scrubbed using soda lime. The microreactor was shown to achieve the successful synthesis of a variety of selective fluorinations yielding 75% conversion derivatised from di(*m*-nitrophenyl)disulphide and for *p*-nitro systems 44% conversion was achieved using acetonitrile, 10% F_2 in N_2 (10 ml/min) at room temperature. Fluorination of β -dicarbonyl illustrated the catalytic effect by the fluorinated metal surface, giving a highly efficient conversion (step 5 to 6, 99%, step 7 to 8, 90% conversion) even though the overall yield was low (62%). The flow system obviously promotes the formation of the enol, which can be a limiting factor in large-scale reactors. Chambers also demonstrated that the microreactor could be used for perfluorination, which has many inherent safety issues. The overall product yield was 70% (stage 9 to 10, 52% conversion, yielding 91% and stage 11 to 12, 82% recovery, yielding 70%). The results obtained indicate a potential for elemental fluorine reactions to be achieved in the laboratory as well as on an industrial scale.

The group of Jensen et al. [18] has reported the development of a novel palladium membrane to allow for a controlled selective hydrogen flux.

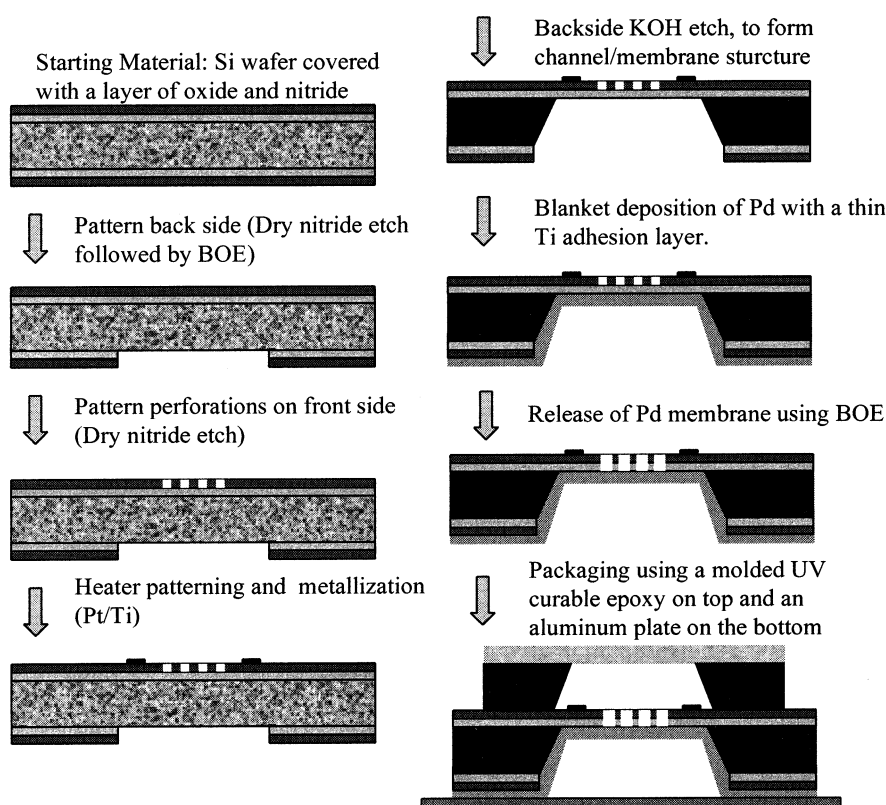


Fig. 2. Palladium membrane fabrication process.

The membrane was specifically designed for incorporation with microelectromechanical systems, microfluidic devices allowing hydrogen separation in palladium micromembranes resulting in two separate streams being generated. In addition the potential to perform hydrogen purification applications such as hydrogenation and dehydrogenation are possible with this form of a membrane reactor. Fig. 2 outlines the type of device fabrication used. The device is a two-channel flow system separated by a thin membrane layer that is fabricated from composite layers of perforated silicon nitride, silicon oxide that supports and insulates the palladium metal from the integrated temperature sensing and heater elements. The overall channel geometry is 1.2 cm long and slightly less than 700 μm wide. The extensive device fabrication method allows the use of arbitrarily thick or thin palladium films, due to the support being porous and so offering attractive cheaper metal alternatives. An intrinsic property of the device is the symmetric heater design, allowing a large area of the membrane to be heated whilst maximising the area in the centre for perforations and hydrogen flux. The micromembrane perme-

ability and selectivity were characterised as a function of the hydrogen pressure gradient and average membrane temperature. A mixture of hydrogen and nitrogen (1:9) together with pure hydrogen was fed into the device. At elevated temperatures, the membrane generated a notable exit drop in hydrogen concentration and increased nitrogen, indicating the presence of a selective hydrogen flux. In addition, a membrane separation factor of over 1800 was determined. At an average temperature of 500°C, a hydrogen flow rate of 0.5 sccm was observed for a single active heater segment, at a pressure of 0.1 atm, corresponding to a flux of 600 sccm/cm². These results indicated that the micro-fabricated membranes are potentially much more efficient than large-scale devices. Finally, the membrane's potential for hydrogenation and dehydrogenation was investigated using a hydrogen/nitrogen mixture exposed to air in the device. The hydrogen permeating through the membrane reacted with oxygen to form water, which condensed on the cold top of the surface.

At the Third International Conference on Micro-reaction Technology in Frankfurt am Main, Ger-

many, Worz et al. discussed the development of a high temperature hydrogen cyanide synthesis device using the synthetic Andrussov route [15]. The device was fabricated enabling the investigation of the influence of isothermal processing and extremely rapid cooling of a hot, reactive product gas and a highly exothermic reaction with extreme handling and exposure risks. The reaction was achieved in a 60 μm diameter microchannel, which allowed the reactant gas to be heated to 1000°C within 1 ms. The microreactor feasibility was compared with published results achieved in ceramic and metal monoliths with channel geometries of 0.5–1 mm. With the microreactor an increase in yield for hydrogen cyanide of up to 30% was obtained compared to standard methodology. The higher yields were attributed to the improved mass transfer because of the significant reduction in channel dimensions by at least one order of magnitude. In addition, the microreactor generated less than 2% ammonia and methane by-products compared to 59% ammonia and 27% methane in conventional reactors. The microreactor device demonstrated selective, high throughput conversion based on the Andrussov reaction, indicating that the device could easily be adapted allowing the development of a variety of high temperature reactions.

At the University of Hull, two solvent-based synthetic processes have been investigated as model systems to evaluate the potential of microreactors for such applications. The selected processes were heterogeneous catalysis based on a modified Suzuki synthesis [17] and homogeneous reactions based on Wittig chemistry [16]. The first example allowed an evaluation to be made of a flow injection-based methodology using the Suzuki reaction. The microreactor used was fabricated in borosilicate glass with channel geometries of 300 μm wide and 115 μm deep (Fig. 3). Reagent solutions

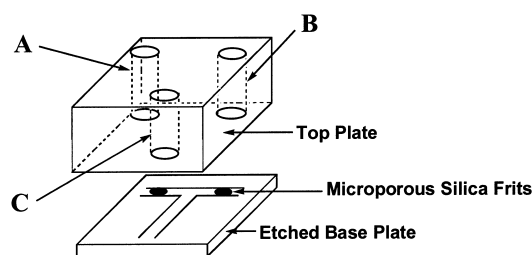


Fig. 3. Schematic diagram of the T-shaped manifold used in the reactor for the Suzuki coupling.

were mobilised via EOF assisted by the incorporation of a microporous silica structure [24], which was also used to immobilise the palladium as a heterogeneous catalyst bed. The synthesis of 4-cyanobiphenyl was achieved at room temperature, via in situ generation of base giving a product yield of $67 \pm 7\%$ ($n=6$). Conventional laboratory batch methodology using the same reaction criteria as used with the microreactor was performed, however the reaction was reflux for 8 h under an inert atmosphere, giving a non-optimised product of 10%. Further work is currently proceeding to improve the product yield in the microreactor by developing a post-reaction separation system, which allows the recycling of starting material and the isolation of a pure product.

The second reaction is based on Wittig chemistry [16] in which 2-nitrobenzyltriphenylphosphonium bromide and a variety of aldehydes, for example methyl-4-formylbenzoate in dry methanol and sodium methoxide, were reacted in a T-shaped manifold (300 μm wide and 100 μm deep). The microreactor is currently being evaluated for its potential to perform diverse generic chemistry for a variety of syntheses as this clearly has value in reaction optimisation and combinatorial applications. The reaction was optimised using EOF assisted by the incorporation of microporous silica frits, generating a product yield for 2:1 reaction stoichiometry of 70% (10% increase compared with traditional synthesis). This was achieved using continuous flow of both reagents through the microreactor for 20 min. Further reaction optimisation using a series of injections performed over a 20 min period gave a yield of 59% (1:1 stoichiometry, 11% increase over traditional batch synthesis). The optimised reaction was also investigated for a further four aldehydes, demonstrating the general applicability of the method. Fig. 4 shows a series of image captures using an optical microscope at which the coloured reaction intermediate (ylide) can be seen. In plate 1, the reagents are being moved by EOF from both the left- and right-hand side and a clear interface can be seen. Poor flow control however is observed due to the formation of the intermediate in the left-hand channel, which was readily corrected by the slight increase in the voltage applied to the left-hand electrode (plate 2). This allowed the reactants to move down the central channel due to the increase in flow of the reagent from the left-hand channel. As the reagents are pumped by EOF turning the power off sees the

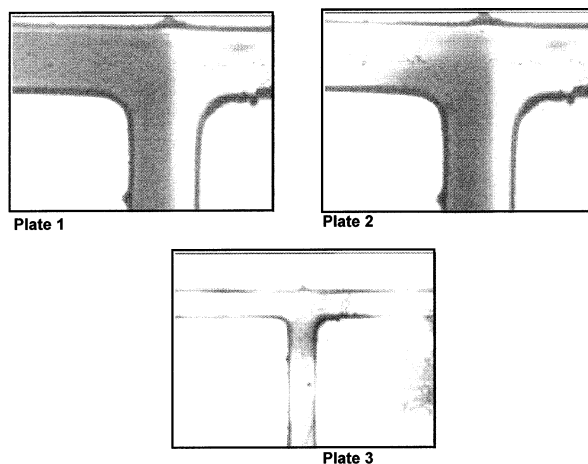


Fig. 4. A series of images captured using an optical microscope in which the coloured reaction intermediate (ylide) flow profile can be observed.

loss of colour rapidly (plate 3) thus demonstrating that the spatial position of a reaction can be controlled with relative ease. As indicated, the resulting optimised methodology is currently being developed for combinatorial screening implying increased analysis speed but also demonstrating diversity for a variety of reagents.

In the field of bio-catalysis, Laurell et al. [19] have investigated the use of porous silicon as a carrier matrix in microstructured enzyme reactors, increasing the surface area onto which enzymes could be coupled. The microreactor was fabricated using a flow-through cell comprising 32 channels, 50 μm wide, spaced 50 μm apart and 250 μm deep in silicon, p-type (20–70 $\Omega\text{ cm}$) generated by anisotropic wet etching. The porous matrix was generated by anodisation in hydrofluoric acid and ethanol, producing three different pore morphologies at 10, 50 and 100 mA/cm^2 current densities. Glucose oxidase was immobilised onto the three porous microreactors and onto the non-porous reference device. The enzyme activity was monitored using a colorimetric assay. The devices were used to study glucose turnover rates, which were deemed to be good and illustrated the potential value of using porous silicon as a support in enzyme reactors. Using the microreactor fabricated at 50 mA/cm^2 , they found that the enzyme activity was increased 100-fold compared with the reference reactor. The microreactor was also coupled with an FIA system allowing glucose monitoring. The system gave a linear response up to a 15 mM concentration of glucose.

Laurell et al. [25] further investigated the use of porous silicon by varying the matrix depth in micro enzyme reactors. Using p-type (20–70 $\Omega\text{ cm}$) orientated silicon, in which porous silicon was generated on a planar surface and on an isotropically pre-etched high aspect ratio parallel channel reactor, different silicon morphologies were generated for each sample type by varying the anodisation time, and two current densities. Standard methodology was used to immobilise the glucose oxidase on to the silicon surface, and the enzyme activity was monitored by colorimetric assay. In comparison to the identical non-porous material the results obtained for the silica matrices indicated a 170-fold increase in catalytic turnover for a reactor pore depth of 10 μm . Above this level, catalytic activity levelled out. The results clearly indicate the variation in catalytic activity with the difference in matrix depth for both the planar and reactor structures. In addition, work reported by Laurell [26] has demonstrated an increase in enzyme activity of up to 350 times, using the porous silicon as an enzyme carrier matrix.

5. Concluding remarks

From the examples given above we are already seeing evidence that microreactors can bring novelty and real practical advantages to reaction-based chemistry. The advantages come essentially from the thermal, spatial and temporal control possible in such devices, coupled with the capability to monitor reactions in situ while operating if necessary under controlled temperature, pressure and atmospheric conditions. In simple terms, microreactors reduce many of the practical difficulties associated with performing chemical reactions based on traditional methods. Indeed many of the experimental observations reported to date could not have been possible using conventional methodology. Work is currently under way by the authors and other leading research groups that will rapidly push the technology towards working devices for combinatorial and controlled multi-stage syntheses. In this context we should not forget the inherent advantage the technology offers in terms of being able to rapidly perform a reaction and screen for products with minimal practical intervention and reagent consumption. Issues over product volumes will always be raised when using microreactors but given the inherent practical advantages of the methodology,

these will no doubt already be attracting the necessary engineering and design developments to realise appropriate system scale-out. However many question the time it will take for this emerging technology to reach the market place. To this end one should not underestimate the role of the vendor organisations who will no doubt respond to reduce many of the cultural and practical difficulties associated with the technology due to the tremendous commercial potential that will catalyse this area of scientific research over the next few years.

References

- [1] S.J. Haswell, *Analyst* 122 (1997) 1R.
- [2] A. Manz, D.J. Harrison, E. Verpoorte, J.C. Fettinger, H. Ludi, H.M. Widmer, *Chimia* 45 (1991) 103.
- [3] A. Manz, D.J. Harrison, E. Verpoorte, H.M. Widmer, *Adv. Chromatogr.* 33 (1993) 1.
- [4] A. Manz, C.S. Effenhauser, N. Burggraf, E. Verpoorte, D.E. Raymond, H.M. Widmer, *Analysis Mag.* 22 (1994) M25.
- [5] D.J. Harrison, A. Van den Berg (Editors), *Proceedings of the Micro Total Analytical Systems '98 Workshop*, Kluwer Academic, Dordrecht, 1998.
- [6] A. Van den Berg, T.S.J. Lammerink, *Topics Curr. Chem.* 194 (1998) 21.
- [7] S. Cowen, *Chemistry and Industry*, 1999, no. 15, 584.
- [8] T. McCreedy, *Chemistry and Industry*, 1999, no. 15, 588.
- [9] D. Barrow, J. Cefai, S. Taylor, *Chemistry and Industry*, 1999, no. 15, 591.
- [10] P.D.I. Fletcher, S.J. Haswell, V.N. Paunov, *Analyst* 124 (1999) 1273.
- [11] R. Srinivasan, T.-M. Hsing, P.E. Berger, M.P. Harold, J.F. Ryley, J.J. Lerou, K.F. Jensen, M.A. Schmidt, *AIChE J.* 43 (1997) 3059.
- [12] R.N.C. Daykin, S.J. Haswell, *Anal. Chim. Acta* 313 (1995) 155.
- [13] H. Becker, W. Dietz, *Microfluidic Devices Syst.* 3515 (1998) 177.
- [14] M.A. Roberts, *Anal. Chem.* 69 (1997) 2626–2630.
- [15] *Proceedings of the IMRET 3 Conference*, in preparation, 1999.
- [16] G.M. Greenway, S.J. Haswell, D.O. Morgan, V. Skelton, P. Styring, B.H. Warrington, S.Y.F. Wong, *Sensors Actuators B, Proceedings of IMRET4 Conference*, March 5–9, 2000, p. 78.
- [17] G.M. Greenway, S.J. Haswell, D.O. Morgan, V. Skelton, P. Styring, *Sensors Actuators B* in press.
- [18] A.J. Franz, K.F. Jensen, M.A. Schmidt, *Palladium based micromembranes for hydrogen separation and hydrogenation/dehydrogenation reactions*, *Technical Digest, 12th International Conference of Microelectromechanical Systems, IEEE*, 1999, p. 38.
- [19] J. Drott, E. Rosengren, K. Lindstrom, T. Laurell, *J. Micro-mech. Microeng.* 7 (1997) 14.
- [20] P. Yager, et al. *Sensors Actuators A* 58 (1997) 13.
- [21] I. Karube, *Anal. Chem.* 65 (1993) 2731.
- [22] R.W.K. Allen, S. Hu, J.M. MacInnes, *Chem. Eng. Res. Des. A* (submitted).
- [23] R.D. Chambers, R.C.H. Spink, *Chem. Commun.* (1999) 883.
- [24] P.D. Christensen, S.W.P. Johnson, T. McCreedy, V. Skelton, N.G. Wilson, *Anal. Commun.* 35 (1998) 341.
- [25] J. Drott, E. Rosengren, K. Lindstrom, T. Laurell, *Mikrochim. Acta* 131 (1999) 115.
- [26] J. Drott, L. Rosengren, K. Lindstrom, T. Laurell, *Thin Solid Films* 330 (1998) 161.

Stephen Haswell is Professor of Analytical Science at the University of Hull. His current research activities are in the areas of microreactor and μ FIA applications, microwave-enhanced reaction chemistry, trace elemental speciation and process analysis. He is author of over 100 research papers, a number of books and patents and is widely known nationally and internationally for his enthusiastic lectures.

Vikki Skelton graduated from the University of Hull in 1997 with a BSc Honours degree in Chemistry with Analytical Chemistry and Toxicology. This included a year of industrial pharmaceutical experience in the analytical research and development department within Pfizer Central Research, Sandwich. Miss Skelton is currently studying towards a PhD at Hull University in collaboration with SmithKline Beecham Pharmaceuticals, along with a three-month industrial work placement investigating the role of microreactors for organic synthesis and combinatorial application.

Kumada–Corriu reactions in a pressure-driven microflow reactor

Stephen J. Haswell,*^a Brian O'Sullivan^a and Peter Styring^b

^a Department of Chemistry, University of Hull, Cottingham Road, Hull, UK HU6 7RX.

E-mail: s.j.haswell@chem.hull.ac.uk; Fax: +44 (0) 1482 466416; Tel: +44 (0) 1482 465475

^b Department of Chemical and Process Engineering, University of Sheffield, Sheffield, UK
S1 3JD

Received 8th May 2001, Accepted 13th June 2001

First published as an Advance Article on the web 21st August 2001

Reaction rates for the Kumada reaction (of Grignard reagents with aryl halides) catalysed by an immobilised nickel(II) catalyst have been shown to be enhanced when the reaction is carried out in a pressure driven microreactor (internal diameter 100–200 μm) rather than with conventional batch reaction techniques.

Introduction

Metal-catalysed carbon–carbon bond forming reactions are of great importance to the pharmaceutical and fine chemicals industries. Reactions such as the Heck¹ Sonogashira² and Suzuki³ couplings are well established as convenient routes to vinylaryl and biaryl compounds. Of similar importance is the Kumada–Corriu reaction,^{4,5} in which an aryl halide is oxidatively coupled with a homogeneous nickel(II) phosphine catalyst, and then reacts with a Grignard reagent to form biaryl or alkylaryl compounds. Murahashi *et al.*⁶ later extended the range of catalysts for this type of reaction with palladium phosphine complexes, and reported stereospecific transformations of (*E*)- and (*Z*)-bromostyrenes to their aryl-substituted derivatives. Since then, due in part to the mild reaction conditions and clean conversions, nickel- and palladium-catalysed cross-coupling reactions have become one of the most widely used methods for carbon–carbon bond formation.

One major disadvantage of the Kumada–Corriu reaction is the dependence on homogeneous catalysis, with attendant purification difficulties. Heterogeneous catalysts immobilised on an inert support such as polymer beads offer the possibility of cleaner simpler reactions, as it is possible to remove the catalyst prior to product purification, and recycle it if necessary. Recently, Styring and co-workers⁷ synthesised an unsymmetrical salen-type nickel(II) complex **1**, and used the acidic phenolic functional group to covalently bind it to the chloromethylstyrene group in Merrifield resin polymer beads (Scheme 1). The immobilised catalyst was air- and moisture-stable, could be re-used several times, and when used in a series of batch Kumada reactions, afforded yields of 70–95% under mild conditions.

Microreactors, in which microlitre quantities of reagents are manipulated, have been shown to confer many advantages over conventional scale chemistry.⁸ Heat transfer is improved and

mixing times reduced by orders of magnitude as a result of the decrease in linear dimensions. Whilst the size of an individual reactor may seem to preclude large-scale synthesis, it is possible to use multiple copies of the reactor to bypass the process development stage of 'scaling up', creating a high throughput system while maintaining the control and selectivity of the original system.

The microlitre flow rates involved in liquid-based micro-reactor research mean that high precision syringe pumps or HPLC pumps can be used as the back pressures present no serious problem. In this paper we describe how a microflow reactor containing an immobilised catalyst can effect rapid, clean production of biaryl compounds, with improved reaction rates compared to the equivalent batch reactions.

Experimental

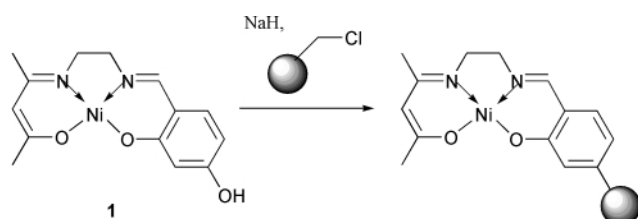
Immobilisation of [9-(2,4-dihydroxyphenyl)-5,8-diaza-4-methyl-nona-2,3,8-trienato] nickel(II) **1**

Merrifield resin (200–400 mesh, ≈ 1.7 mmol Cl (g resin)⁻¹, Fluka) was pre-swelled by soaking in *N,N*-dimethylformamide (DMF) for 30 min. The catalyst **1** (0.67 g, 2.1 mmol) was dissolved in a mixture of 40 ml dry DMF and 10 ml dry tetrahydrofuran (THF) and added dropwise to sodium hydride (0.08 g, 3 mmol, 60% suspension in mineral oil), then stirred at room temperature for 30 min. The suspension of Merrifield resin was added and the reaction mixture stirred for 18 h. On allowing the beads to settle, the supernatant liquid was pale, indicating that most of the complex had been immobilised on the resin. The resin was filtered off and washed with dichloromethane (3 \times 20 ml) and water (3 \times 20 ml). ICP analysis of different batches of the beads showed nickel loadings between 2 and 6% by weight.

In order to compare microreactor systems with batch reactions, Kumada reaction kinetics were studied under both sets of conditions.

Batch reactions

Batch reactions were carried out in a carousel synthesiser (Radley's). In a typical example, 4-bromoanisole (5 ml, 1.0 M in dry THF) was added over the immobilised catalyst and the



Scheme 1 The immobilisation of [9-(2,4-dihydroxyphenyl)-5,8-diaza-4-methyl-nona-2,3,8-trienato] nickel(II) onto Merrifield resin.

mixture stirred for 5 min to allow the beads to swell. Phenylmagnesium bromide (5 ml, 1.0 M in dry THF) was added *via* syringe and the mixture stirred at room temperature. Portions (0.5 ml) were removed *via* syringe at regular intervals and quenched using saturated aqueous sodium hydrogen carbonate. Samples of the aqueous phase were extracted into diethyl ether, which was analysed by GC-MS with reference to a 1.0 M standard solution of 4-methoxybiphenyl (Lancaster Synthesis) in THF. (Varian CPSIL8 column, 30 m, held at 50 °C for 4 min, then heated at 30 °C min⁻¹ to 250 °C, products identified by comparison of mass spectra and retention times with those of authentic materials). A graph of percentage conversion to the product against time is shown in Fig. 1(a).

Flow experiments

In order to establish the effectiveness of the immobilised catalyst resin in a capillary channel similar to that expected in a microreactor, flow reactors were constructed from lengths of clear polypropylene tubing with flanged ends (id 2 mm) or glass tubing (id 1 mm). The required amount of catalyst beads were held in place by plugs of glass wool (typical catalyst bed lengths ranged from 2 to 10 mm). Standard HPLC connectors allowed one end of the reactor to be connected to a disposable solvent-resistant syringe, while the other end was attached to a syringe needle leading to a quenching vessel containing ether and saturated aqueous sodium bicarbonate. A syringe pump (Har-

vard Apparatus, PHD 2000) was used to drive pre-determined volumes of a mixture of equimolar solutions of the aryl halide and the Grignard reagent through the reactor at known flow rates. Note that in the absence of any catalyst, no reaction occurred in the pre-mix over a 72 h period.

In the case of the reaction of 4-bromoanisole with phenylmagnesium bromide, a glass capillary was used connected to the reactor body using OmniFit connectors. A flow rate of 13.3 or 33.3 μl min⁻¹ was maintained using a syringe pump and the output stream passed directly into a flask containing a solution of saturated aqueous sodium hydrogen carbonate to quench the reaction. The aqueous solution was extracted into diethyl ether and analysed by GC as described above. Conversion was found to be independent of flow rate for each of the flow rates used, with 60 ± 2% conversion to the target compound and 20 ± 2% production of biphenyl being observed, leaving approximately 20% of the unreacted 4-bromoanisole.

Results and discussion

Batch reactions

The observed rate of reaction (k_{obs}) is first order with respect to the aryl bromide over the reaction profile. As the residence times in the microreactor are typically much shorter than in the batch process, then k_{obs} is also assumed to be first order and so comparisons were made using that assumption.

The stirred batch reaction is described by the first order design equation [eqn. (1)]. After 6 h the reaction has gone to 21% completion, achieving 72% completion after 24 h. A plot of $-\ln(1 - x_{\text{ArBr}})$ against time [Fig. 1(b)] where x_{ArBr} is the mole fraction of aryl bromide consumed or is the mole fraction of product produced and t the reaction time gives a rate constant, $k_{\text{obs}} = 1 \times 10^{-5} \text{ s}^{-1}$.

$$k_{\text{obs}} = -\frac{1}{t} \ln(1 - x_{\text{ArBr}}) \quad (1)$$

Flow reactors

For the reaction of 4-bromoanisole described above, the observed rate constant for the process at the highest flow rate was determined by applying the design equation [eqn. (2)] for a first order continuous flow process, where v_t is the flow rate and V is the reactor volume. k_{obs} was determined to be $0.033 \pm 0.002 \text{ s}^{-1}$ at $33.3 \mu\text{l min}^{-1}$. A list of k_{obs} values obtained in batch and flow reactors for a series of aryl halides reacted with phenylmagnesium bromide is given in Table 1.

$$k_{\text{obs}} = \frac{v_t}{V} \ln(1 - x_{\text{ArBr}}) \quad (2)$$

Comparison of the rates from continuous flow and batch reactions gives an enhancement of the rate of 3.4×10^3 (over three orders of magnitude) in the case of 4-bromoanisole. Less dramatic improvements are recorded for the iodoarenes. This can be rationalised in terms of the number of catalytic sites available at which reaction can occur. In the stirred batch process, although the beads are swollen and have a high porosity due to the solvent, reaction occurs essentially at the surface of the support, since the penetration of the reagents to the interior catalytic sites is governed by a slow diffusion process. In the constraints of the microreactor, where the beads are packed into the capillary, the reaction solution is driven through the pores under pressure and the number of catalytic sites available for reaction is increased. As we are unsure as to the exact availability of sites in the swollen state, the turnover frequency of the system would have little physical meaning. However, we

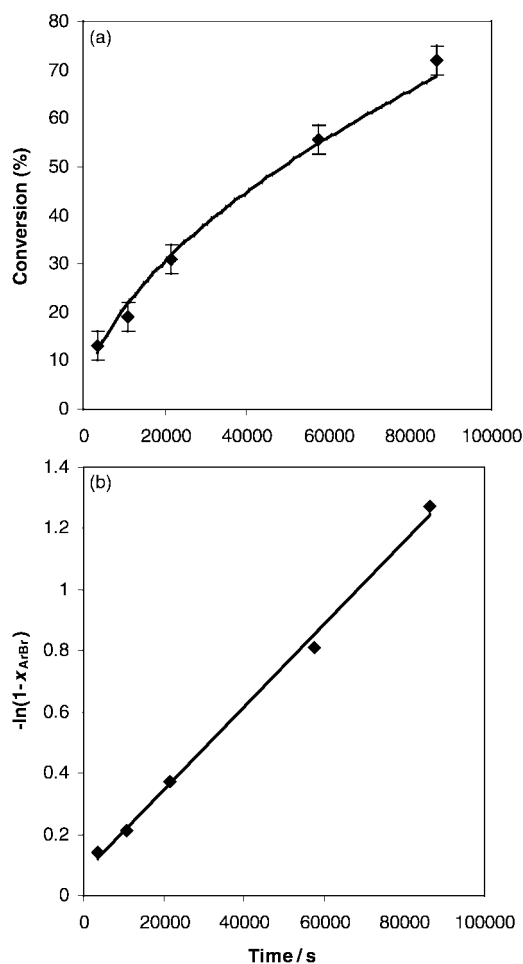


Fig. 1 (a) Profile of the first order batch reaction of 4-bromoanisole with phenylmagnesium bromide. (b) Plot of $-\ln(1 - x_{\text{ArBr}})$ against time for the same reaction, where x_{ArBr} is the mole fraction of 4-bromoanisole. The observed rate constant, k_{obs} , is found to be $1 \times 10^{-5} \text{ s}^{-1}$.

Table 1 Comparison of rate constants for a series of Kumada coupling reactions in flow reactors with the corresponding batch reaction

R	X	R'	Flow rate/ $\mu\text{l min}^{-1}$	Flow reactor rate constant $k/10^{-3} \text{ s}^{-1}$	Batch reactor rate constant $k/10^{-5} \text{ s}^{-1}$	Rate enhancement
CH ₃	I	Ph	25	2.67	3.50	76.3
OCH ₃	I	Ph	25	1.59	3.50 ^a	45.4
OCH ₃	I	CH ₃	25	2.67	3.35	79.3
CH ₃	I	CH ₃	25	1.05	6.73	15.6
OCH ₃	Br	Ph	33.3	33	1	3300

^a Rate constant estimated, since reaction complete (all of the 4-iodoanisole consumed) before first aliquot removed.

can clearly see the advantage gained by using a microreactor system. The enhanced rate means that yields obtainable after 24 h in a batch reaction can be realised in a matter of minutes using the capillary systems. In the reactors discussed, 0.62 mmol (116 mg) of product was produced in only 2 h. By scaling out the system, it is easily seen that yields of synthetic value can readily be obtained: for example 10 parallel reactors would yield 1.16 g of target material in the same time interval.

Conclusions

The enhanced reaction rates described above are solely due to the dimensions of the microreactor (since the reagents and catalyst are the same in batch and flow reactor). Although simple in design and concept, with easily replaceable catalyst beds and interchangeable reagent premixes, it provides a powerful tool in catalyst screening and a route to high throughput synthesis.

Acknowledgements

We acknowledge the University of Hull and the EPSRC Lab on a Chip Consortium for financial support.

References

- 1 H. A. Dieck and R. F. Heck, *J. Organomet. Chem.*, 1975, **93**, 259.
- 2 K. Sonogashira, *Comprehensive Organic Synthesis*, ed. B. M. Trost and I. Fleming, Pergamon, Oxford, 1991.
- 3 N. Miyaura and A. Suzuki, *Chem. Rev.*, 1995, **95**, 2457.
- 4 K. Tamao, K. Sumitani and M. Kumada, *J. Am. Chem. Soc.*, 1972, **94**, 4374. *★ This was one of the first papers to report the coupling reaction under discussion.*
- 5 R. J. P. Corriu and J. P. Masse, *Chem. Commun.*, 1972, 144. *★ This was one of the first papers to report the coupling reaction under discussion.*
- 6 M. Yamamura, I. Moritani and S. I. Murahashi, *J. Organomet. Chem.*, 1975, **91**, C39. *★ This paper extended the range of catalysts available for the Kumada–Corriu reaction.*
- 7 P. Styring, C. Grindon and C. M. Fisher, *Catal. Lett.*, 2001, submitted.
- 8 S. J. Haswell, R. J. Middleton, B. O'Sullivan, V. Skelton, P. Watts and P. Styring, *Chem. Commun.*, 2001, 391. *★ This is a useful review of recent developments in synthetic chemistry using microreactors.*

Electric field-induced mobilisation of multiphase solution systems based on the nitration of benzene in a micro reactor

G. N. Doku, S. J. Haswell,* T. McCreedy and G. M. Greenway

Department of Chemistry, University of Hull, Hull, UK HU6 7RX

Received 19th September 2000, Accepted 27th October 2000

First published as an Advance Article on the web 19th December 2000

This paper describes the electric field-induced flow characteristics of multiphase solutions in a micro reactor device using the nitration of benzene as a model process. Photolithographic and wet etching techniques were used to fabricate the micro reactor (channels, 200 μm id, 100 μm deep) in a borosilicate glass substrate. The results focus specifically on the flow parameters of reagents/reactants (*i.e.*, voltage, solution concentration and pH ranges and current–voltage relationships) used in this study. The benzene was introduced and mobilised by electroosmotic flow (EOF), as a microemulsion using an appropriate surfactant (sodium dodecyl sulfate), whilst the nitronium ions, produced *in situ* from mixed $\text{H}_2\text{SO}_4\text{--HNO}_3$ (the nitrating agent), underwent electrophoretic-induced (electrokinetic) mobility. A co-surfactant, butan-1-ol, was used owing to (a) its relative solubility in the aqueous surfactant solution, (b) its ability to aid the solubilization of benzene, (c) the provision of a water-rich (oil-in-water) rather than oil-rich (water-in-oil) microemulsion system and (d) its lack of significant adverse effects on the EOF. The optimum conditions used for the nitration of benzene within the micro reactor were a run of the microemulsion as main reagent stream, then three 30 s segmented injections of mixed acid, with a 5 s push of the microemulsion into the system after each injection, and then a 60 s stopped-flow reaction time before driving reaction product segments to a collection reservoir.

1. Introduction

Whereas the field of micro total analytical systems (μTAS), based on the use of electroosmotic flow (EOF) and electrophoretic separations,^{1–8} has gained much attention in recent years, the application of complementary micro reactor technology based on the electric field-induced mobility for chemical reactions^{9,10} and in particular organic synthesis¹¹ has attracted less attention. In addition, solutions employed to date in such systems have primarily been aqueous or single solvent phases. Early work, however, involving the nitration of nitrophenol, indicated that performing multiphase reactions in micro reactors was feasible.¹² Furthermore, this provisional research suggested that the position of the nitration and thus the isomers of nitrophenol produced may be influenced by the operating conditions used. In this work, the nitration of benzene using mixed acid, $\text{H}_2\text{SO}_4\text{--HNO}_3$, as the nitrating agent was used as a model process to investigate the ability to move multiphase solutions in a microreactor using electrically driven flow. The benzene was introduced into the system as a microemulsion using an appropriate surfactant, as this provided the necessary ionic character to mobilise the organic system under an electric field. In addition, the formation of the microemulsion droplets of the benzene would increase the surface area available to the nitrating agent, as the rate of nitration is determined not only by the chemical kinetics of the reaction, but also by the mass transfer between the two phases.¹³ The choice of a surfactant–co-surfactant system was based on an evaluation of what effects they will have on both the EOF and reaction mechanism. In addition, due consideration was given to the solubilization power of the surfactant–co-surfactant and the ease with which a water-rich (oil-in-water) rather than oil-rich (water-in-oil) microemulsion system can be formed in a stable manner.

2. Experimental

2.1. Reagents and materials

All reagents were of the analytical-reagent grade unless stated otherwise. The primary reagents used were disodium tetraborate (borax, 98%) (Merck, Poole, Dorset, UK), sodium dodecyl sulfate (SDS, 99%) (Lancaster Synthesis, UK), methanol (99.8%, 0.791 g ml^{-1}) (BDH, UK), ethanol (absolute) (bottled by U.O.H), propan-1-ol (99.5%) (BDH), butan-1-ol (99%) (BDH), pentan-1-ol (98%, 0.814 g ml^{-1}) (BDH), hexan-1-ol (98%, density 0.814 g ml^{-1}) (Aldrich, UK), octan-1-ol (99%) (Avocado, UK), decan-1-ol (0.83 g ml^{-1}) (BDH), benzene (99.8%, 0.878 g ml^{-1}) (Fisons, UK), sulfuric acid (98%) (Fisher Scientific, Loughborough, Leicestershire, UK) and nitric acid (68%) (Prolabo, Fontenay s/Bois, France). High purity distilled, de-ionised water (Elgastat UHQ PS system, Elga, High Wycombe, UK) with a conductivity of 18 ($\text{m}\Omega\text{ cm}$)^{–1} was used. Hydrofluoric acid (40%) and ammonium fluoride were obtained from Merck (Poole, Dorset, UK). Microposit chrome etch 18 and photoresist remover 1112A were purchased from Shipley (Coventry, UK). The glass for the micro reactor chips and cover-plates were both superwhite Crown B70 borosilicate glass (Instrument Glasses, Enfield, UK).

2.2. Chip device and instrumentation

The micro reactor consisted of channels 200 μm in diameter and 100 μm deep (Fig. 1), fabricated in borosilicate glass (25 mm long, 25 mm wide and 3 mm thick), using a wet-etching technique described previously.¹⁴ The glass chip was thermally bonded to a thicker glass cover-plate (25 mm long, 14 mm wide and 17 mm thick, also of borosilicate) containing 2 mm holes pre-drilled to align with the ends of channels which served as

reservoirs for reagents and analyte and to support the platinum electrodes used to apply voltages to the solutions.

A Farnell (Leeds, UK) HiVolt XRV30/1.7 reversible polarity power supply was used to supply the electric field to the system. This offered a maximum power output of 50 W with variable voltages up to 30 000 V and currents up to 1.7 mA to be selected in constant stabilised current or voltage modes, with an adjustable trip for overcurrent protection. The power supply was connected *via* high purity copper conductors to 0.15 mm diameter platinum electrodes with a 10 mm exposed length for interfacing with the solutions in the reservoirs. For safety, the electrode system was built in an isolation box fitted with a power cut-out preventing high voltage operation when the lid was opened. The voltages applied across the electrodes and the internal currents generated within the solutions in the channels were monitored on an AVO M2036 digital autoscaling multimeter (Thurnby Thunder Instruments, Huntingdon, UK) connected in parallel with the device.

Gas chromatography-mass spectrometry (GC-MS) with a GC970870-MS200478 system (Finnigan MAT GCQ, Austin, TX, USA), was used to analyse for benzene mobilised within the channel by the bulk flow of the microemulsion, and any benzene-nitrated products. The GC column used was a 35 m \times 0.25 mm id Rtx-5MS capillary (Crossbond 5% diphenyl-95% dimethylpolysiloxane stationary phase), stable to 360 °C; the carrier gas was helium at a flow rate of 40 cm³ s⁻¹. The temperatures used were: injector 250, detector 250 and oven 85 °C (held for 3 min) ramped at 30 °C min⁻¹ to 250 °C (held for 15 min).

2.3. Characterisation of electroosmotic flow

The main EOF characteristics monitored were applied voltage, current–voltage relationships and solution concentration and pH, which were then selected to obtain parameters for stable electric field-driven flow.

The solution under investigation was placed in reservoir R (Fig. 1) and water or buffer in reservoir W1, both to pre-marked levels. The reservoir levels of other reagent solutions in the side channel reservoirs S and W2 perpendicular to the main channel R–W1 were also recorded. The positive electrode was placed in R and the negative electrode in W1; the other reservoirs were electrically left floating.

Initially, different disodium tetraborate buffer solutions of concentrations 20 mM (pH 9.25), 15 mM (pH 9.24), 10 mM (pH 9.22) and 5 mM (pH 9.11) were run at different applied voltages (200–1200 V) over a period of 15 min and the change (decrease) in volume of buffer in reservoir R was measured by recording the difference in reagent level in the reservoir. This was done by filling the reservoir to its original level after each 15 min run and recording the addition required with a graduated 100 μ l HPLC syringe. The voltage (V), current (μ A), time (min) and volume

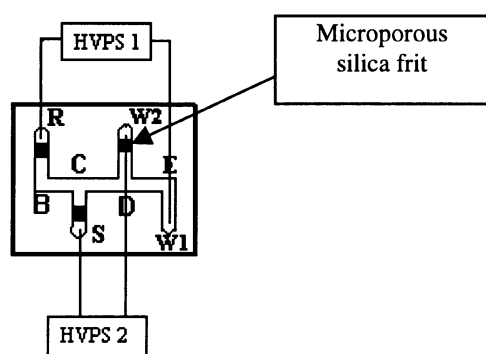


Fig. 1 Micro reactor design used for the nitration of benzene. BC = 3 mm, CD = DE = 4 mm, RB = SC = W2D = W1E = 5.5 mm, BE = 11 mm, RW1 22 mm, SW2 = 14 mm.

changes (μ l) were recorded and the flow rates (μ l min⁻¹) calculated to obtain an optimum buffer concentration that could be used in conjunction with the reagents having a pH > 4.

In a similar manner, the EOF properties of SDS solutions of concentrations 100 mM (pH 6.32), 50 mM (pH 6.05), 20 mM (pH 5.75), 15 mM (pH 5.80), 10 mM (pH 5.78) and 5 mM (pH 5.47) were studied to verify the effect of voltage and/or current on the flow. In addition, it was established which concentrations of the SDS could be used as the micellating or microemulsification surfactant in the buffer solution.

The above approach was repeated to establish the flow characteristics for different SDS–borate buffer solution mixtures containing 15 mM SDS (the SDS concentration that gave the best EOF properties) at different borate buffer concentrations, 5, 10, 15 and 20 mM, giving solution mixtures of pH 9.13, 9.24, 9.26 and 9.28, respectively. Finally, the buffer concentration was kept constant at 10 mM Na₂B₄O₇ (the buffer concentration that gave highest EOF rate) whilst the SDS concentration was varied to verify the effect of SDS concentration on the EOF of the mixture. In this case, the actual SDS concentrations and the pH of the solution mixtures were 5 mM (pH 9.06), 10 mM (pH 9.11), 15 mM (pH 9.24), 20 mM (pH 9.25), 50 mM (pH 9.28), 100 mM (pH 9.33) and 200 mM (pH 9.38).

A number of straight chain alcohols, methanol, ethanol, propan-1-ol, butan-1-ol, pentan-1-ol, 1-hexan-1-ol, octan-1-ol and decan-1-ol, were considered as possible co-surfactant agents but owing to solubility considerations only methanol to butanol were investigated. Initially, separate 10% v/v alcohol (methanol to butanol) mixtures with 10 mM borate buffer–SDS solution mixtures with various SDS concentrations (5–200 mM) were studied, to establish the effect of the presence of the alcohols on the EOF, and to establish how the SDS concentration in alcohol solution would affect the EOF. In a further study, the alcohol concentration was varied from 5 to 50% in separate 50 mM SDS–10 mM borate buffer solutions. This was followed by preparing separate 100 mM SDS–10mM borate buffer solutions to investigate the effect of alcohol concentration on the EOF and thus the possibility of using higher co-surfactant (alcohol) levels at higher surfactant (SDS) levels since this may be the only conditions under which some non-polar organic compounds would be solubilized.

Six microemulsion systems of the quaternary system, H₂O–SDS–butanol–benzene, one oil-rich (water-in-oil) and five water-rich (oil-in-water) with various water contents, were prepared by selecting various relative percentage weight ratios of each of the components from a Winsor IV phase diagram.¹⁵ The actual corresponding amounts (in weight or volume) were measured and mixed with gentle agitation and allowed to settle for 4 h to give clear or nearly clear microemulsion systems. The EOF properties of the different microemulsion systems were then studied at voltages ranging from 100 to 500 V to ascertain the trend in flow and the voltage–current characteristics as the mixture moved from the oil-rich to the more water-rich microemulsion systems. This was followed by evaluating the amounts of benzene moved by EOF for the five oil-in-water microemulsion systems (the oil-rich system did not exhibit any EOF) under an applied field of 100 V, by taking a 0.5 μ l aliquot of the resulting solution in the collection reservoir W1 (Fig. 1) and analysing it by GC-MS (single-ion MS monitoring at masses 76, 77, 78 and 79). A portion (0.5 μ l) of the remaining solution in the reagent reservoir R was similarly analysed to determine how much benzene was left in the reagent reservoir R after applying the electrical field.

A stock standard 11.22 M H₂SO₄–5.37 M HNO₃ solution was prepared and serial dilutions (dilution factors 1.333, 1.5, 1.666, 1.82, 2, 2.5, 3, 4, 5, ..., 10) were carried out to produce other mixtures of concentrations ranging from 8.42 M H₂SO₄–4.03 M HNO₃ to 1.22 M H₂SO₄–0.53 M HNO₃, which were used in similar electrokinetic flow studies at voltages ranging from

100–500 V to ascertain the trend in bulk flow and the effect of the acid concentration on the current.

The optimum acid concentration for the model nitration reaction and the maximum voltage and time of field application suitable for driving the mixed acid in the system, with microemulsion (containing organic components) also present, were investigated. For practical reasons, *i.e.*, minimising Joule heating effects and stabilising the current flow properties of the two reactants, it was necessary to select a set of compromised lower voltages than indicated in the univariate optimisation. It was therefore decided to pump the microemulsion at 90 V by EOF as the main reagent and inject the mixed acid at 200 V.

In a further experiment, microporous silica frits¹⁶ 0.5 mm in length were integrated into the channels R–B, C–S and W2–D (leaving the main reagent channel B–W1 free) to control hydrostatic pressure effects caused by imbalance in liquid levels in reservoirs, and to aid EOF.

2.4. Multiphase solution mobilisation and optimum operational conditions for the model nitration reaction (nitration of benzene)

The micro reactor manifold used for the multiphase solution mobilisation, based on the model nitration experiment (Fig. 1), contained four solution reservoirs (R, W1, S and W2). A Z-mode sample injection³ was used to introduce the mixed acid whilst running the microemulsion as the main reagent. The microreactor also contained 0.5 mm long microporous silica frits¹⁶ integrated into the channels R–B, C–S and W2–D.

After loading the reagent reservoir R and sample reservoir S with 10 mM borate buffer ($\text{Na}_2\text{B}_4\text{O}_7$, pH 9.22), and the waste reservoirs W1 and W2 also with buffer, the electrical fields HVPS 1 and HVPS 2 (400 V in each case) were applied one after the other to prime all channels with the blank buffer. The buffer in reservoir R was then replaced with a 92.5% water microemulsion and the sample reservoir S was loaded in a similar way with 6.17 M H_2SO_4 –2.95 M HNO_3 . Reservoirs W1 and W2 were loaded with the buffer. The electrical field HVPS 1 (90 V, $\approx 270 \mu\text{A}$) was applied between R (+) and W1 (–) for 5 min to fill the main reaction channel R–W1 with the microemulsion. A second voltage was then applied using the HVPS 2 (200 V, $\approx 300 \mu\text{A}$) across S (+) and W2 (–) for 5 min to fill the sample channel C–D completely with the mixed acid, driving any microemulsion between C and D to waste W2. The HVPS 1 (90 V, $\approx 270 \mu\text{A}$) was again applied across the R (+) and W1 (–) to drive any mixed acid and buffer along the main reaction channel to W1. After replacing the contents of reservoirs W1 and W2 with fresh 10 μl of buffer, the HVPS 2 [S (+), W2 (–)] was then applied for 180 s to inject the mixed acid into the microemulsion stream and, after allowing a 60 s stopped-flow mode as initial reaction time, the HVPS 1 was then applied across R (+) and W1 (–) again for 5 min to drive the reaction segment to the reservoir W1. A 100 μl HPLC syringe, pre-loaded with 6 μl of octane, was then used to transfer the reaction mixture in W1 to a 90 μl sample glass tube, followed by introduction of a further 6 μl of octane to assist in the extraction of any reaction products into the top organic layer.

Using fresh microemulsion and fresh mixed acid solution in each case, the process was repeated with different injection times between 0 and 120 s to verify the optimum continuous sample injection time for the process, and the corresponding reaction mixtures were collected separately. In this way, the amount of microemulsion fed into the system was kept constant whilst that of the mixed acid was varied. Before using the solutions, the 10 mM borate buffer, the 6.17 M H_2SO_4 –2.95 M HNO_3 and the 92.5% water microemulsion were cooled to 4 °C in a refrigerator to minimise the temperature effects associated with the exothermic nitration reaction. At injection times > 1

min, bubble generation was observed in the injection line S–W2 owing to excessive heating. In the injection process, the switching off and on of the microemulsion flow (R–W1) and the mixed acid reactant (S–W2) was performed simultaneously. Each of the mixtures produced was stirred with a small stainless steel rod, allowed to settle and 1 μl each of the octane extracted solutions was then analysed by GC–MS. In this part of the work, 0.5 μl of pure nitrobenzene and then pure octane were first injected in turn to determine the respective retention times and their MS data in full scan mode (mass 70–220).

Experiments based on a segmented mixed-acid injection coupled with a non-stopped-flow mode of operation, but with different segmented microemulsion run times, were also carried out to verify the effects of these conditions on the product yield. In these experiments, after priming all channels with the borate buffer, the main reaction line R–W1 was filled with the microemulsion, and the sample channel S–C was filled with the mixed acid, as before. Reservoirs W1 and W2 were each loaded with a fresh 10 μl of buffer. The HVPS 2 [S (+) W2 (–)] was then applied for 30 s (the optimum mixed-acid injection time) to inject the mixed-acid into the microemulsion stream and, without allowing any initial stopped-flow reaction time, the HVPS 1 [R (+) W1 (–)] was introduced for 30 s to run the microemulsion and drive the sample segment away from the injection point, followed by a further two 30 s mixed-acid injections with 30 s microemulsion runs between injections. Finally, the HVPS 1 was applied from R (+) to W1 (–) for 8 min to drive all sample segments to reservoir W1.

Using fresh microemulsion and fresh mixed acid solution in each case, the process was repeated with the same three times 30 s mixed-acid injection sequence but using different microemulsion run times of 0–25 s between injections and the corresponding reaction mixtures were collected separately. In this way, in addition to segmenting the injection and verifying the effect of non-stopped flow mode on the reaction, the amount of mixed acid introduced into the system was kept constant at three 30 s injection volumes, whilst the amount of microemulsion fed into the system was varied by altering the segmented microemulsion run times. The extraction of samples from the collection reservoir and subsequent GC–MS analysis were performed as described previously.

3. Results and discussion

3.1. EOF properties of buffer, surfactant and alcohol reagent systems

In order to establish the suitability of pumping a microemulsion in a borate buffer solution by EOF, the flow characteristics of the borate buffer were initially investigated to identify the optimum concentration required when used in conjunction with the surfactant SDS and other reagents. The anionic surfactant SDS was employed because it is known to solubilize benzene strongly,^{15,17–19} especially when employed with a co-surfactant such as an alcohol. In addition to providing an ionic character to the organic system, the small droplets (10 nm) produced increased the surface area available for the nitronium ion attack. SDS was also expected to exhibit an extra positive catalytic effect on the benzene reactions since it would exert an attraction on attacking electrophiles on to the surface of the droplet to aid attack on the solubilized benzene. It was expected that SDS molecules would not adsorb on the micro-channel surfaces of the microreactor, thus posing no adverse effects on the EOF, since the SDS and the glass surface are both negatively charged.

The borate buffer solutions alone all gave good EOF under applied voltage over the concentration range 5–20 mM studied, with the flow rate changing very little as a function of

concentration. The highest EOF of $2.6 \mu\text{l min}^{-1}$ was recorded for the 10 mM solution.

On the whole, the surfactant solutions alone also moved well by EOF within the voltage (200–1200 V) and concentration (5–100 mM) ranges studied, since SDS is an anionic surfactant and had no detrimental adsorption effects on the capillary surface. The 15 mM SDS solution gave the maximum flow rate of $2 \mu\text{l min}^{-1}$. Generally, the flow rates recorded for the surfactant solutions (pH 5–7) were lower ($1.2\text{--}2 \mu\text{l min}^{-1}$), however, than the $2.3\text{--}2.6 \mu\text{l min}^{-1}$ obtained for the borate buffer solutions (pH 9.13–9.33), owing to the lower pH and the slightly viscous nature of the surfactant solutions.

In order to use the surfactant (SDS) in a borate buffer solution, it was clearly necessary to establish the EOF parameters of the surfactant–buffer solution mixtures, across a range of different relative concentrations. Indeed, the dissolution of the SDS in the borate buffer solutions was found to improve the EOF rates, over the SDS solution systems without buffer, owing mainly to the pH buffering effect (pH 9.06–9.48 range) produced by the borate buffer. It was observed, however that beyond 100 mM SDS concentration, voltages >300 V resulted in higher and fluctuating currents, causing some degree of Joule heating to occur. SDS concentrations >100 mM were therefore thought to be a practical limitation. In Fig. 2, for example, the errors in the measured flow rates of the SDS–buffer mixtures (with no alcohol present) were in the range 1–2% RSD, with the error increasing as a function of the SDS concentration, possibly owing to the current fluctuations resulting from the increasing Joule heating effects.

The flow rates recorded for all the alcohol containing solution mixtures were slightly lower than those obtained for the mixtures without alcohol (Fig. 2). The presence of the alcohols resulted in a slight suppression of the EOF owing to their organic nature and possibly a slightly non-ionic surfactant adsorption property on the capillary wall. All four alcohols investigated (methanol, ethanol, propanol and butanol), however, gave nearly the same EOF properties, with butanol showing only a slight lowering of the EOF compared with the other alcohols. The errors in the measured flow rates of these alcohol containing mixtures were between 1.0 and 2.5% RSD for all four alcohols, with the error again increasing as a function of the SDS concentration. For all the four alcohols investigated, the EOF became suppressed as the alcohol concentration increased in both the 50 mM (Fig. 3) and the 100 mM SDS solutions (Fig. 4), owing to the increase in the organic character and viscosity of the solutions. In addition, it was possible that the alcohol was adsorbed on the capillary surface, so affecting the zeta potential of the system.²⁰ The general trend observed (Fig. 3 and 4) as the alcohol concentration increased was that the flow rate of the individual alcohol

systems all approached a convergence value at about 50% alcohol concentration. Beyond 40% alcohol concentration for the three most soluble alcohols (methanol, ethanol and propanol), the Joule heating and bubbling effects became more pronounced, especially at high SDS concentrations and applied voltages >600 V, owing to the higher volatility of these alcohols (methanol, ethanol and propanol). In these cases of different alcohol concentrations (Fig. 3 and 4), the errors in the flow rate measurements were between 2 and 3% RSD, with the error increasing slightly with increasing alcohol concentration. It is important to note, however, that in the SDS operating concentration range of 0–100 mM, as the concentration of alcohol or any other organic compounds increases, the SDS concentration must also be increased to ensure that sufficient ions are present in the medium to induce solution mobility under applied field.

The solubilizing properties of SDS–alcohol in a microemulsion increases substantially with increasing salinity.¹⁹ In this work, any additional salinity was expected to be provided by the sodium borate buffer employed.

3.2. EOF properties of the microemulsion systems

Of the four alcohols investigated for EOF purposes, butanol was selected because it has the highest threshold number¹⁵ of carbon atoms, $n_C = 4$, *i.e.*, where the unique Winsor IV domain is broadest and therefore there is more opportunity for changing the relative percentage composition of components without extending beyond the boundaries of the microemulsion domain. The percentage compositions obtained and the actual quantities of components measured to generate the microemulsion systems are shown in Table 1.

After mixing the components of the microemulsion and applying some agitation, clear microemulsion media were successfully obtained at room temperature. The time required for equilibration was, however, found to increase as the water

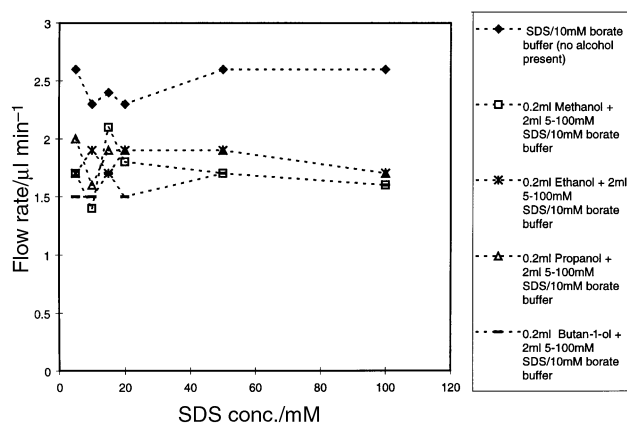


Fig. 2 Plots of flow rate versus SDS concentration for SDS–10 mM borate buffer solutions without alcohol, and flow rate versus SDS concentration for systems containing 10% v/v alcohols (methanol to butanol), at 800 V.

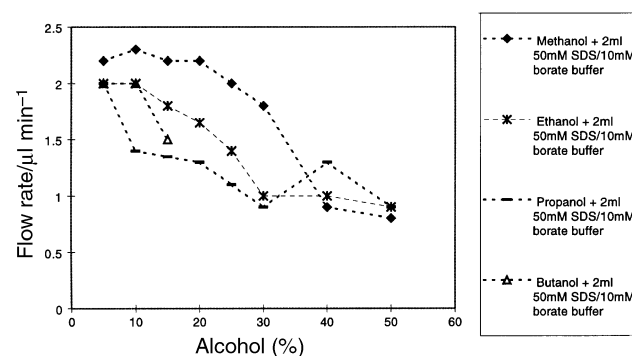


Fig. 3 Plots of flow rate versus alcohol concentration in 50 mM SDS–10 mM borate buffer, at 800 V.

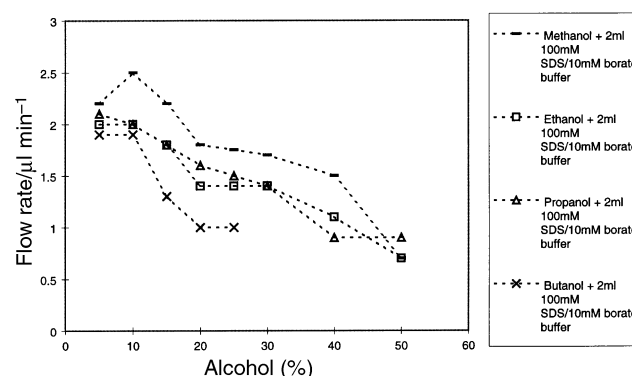


Fig. 4 Plots of flow rate versus alcohol concentration in 100 mM SDS–10 mM borate buffer, at 800 V.

content increased; thus, the oil-rich microemulsion systems 1 and 2 required between 1–4 h to become clear whereas the more water-rich systems 3, 4 and 5 required 8–12 h. In each case, the formation was found to be slightly endothermic and any foaming disappeared after the equilibration.

Fig. 5 shows the plots of the EOF rate *versus* voltage for the different microemulsion systems investigated for different percentage water content. The oil-rich microemulsion system 1 exhibited no bulk solution movement over the whole voltage range studied. This was thought to be owing to the high levels of SDS, alcohol and benzene components of the microemulsion which made the solution very oily (viscous) and interfered with the channel surface. With this oil-rich microemulsion system, the recorded currents were very high and fluctuated owing to high resistance, creating strong Joule heating in the system. It was found that, because the organic (benzene and butanol) additives generally decreased the vapour pressure of the whole mixture and the amount of SDS was substantial, evaporation occurred which precipitated the SDS in the reservoir, making its use impractical. The water-rich (oil-in-water) microemulsions showed a steady increase in the EOF, with a corresponding decrease in the current required. This trend was accompanied by a more stable current and less Joule heating, as the samples moved to more water-rich and lower organic/surfactant concentration systems. Voltages as low as 100 V and a current of 28 μ A were found to be sufficient to move the water-rich microemulsion solutions. The three most water-rich microemulsion systems (containing 85.0, 88.75 and 92.5% water, respectively) showed similar and steady EOF properties over the voltage range studied, but with decreasing current fluctuation and Joule heating effects. The errors in the flow rate measurements were between 1 and 2% RSD, with the error decreasing as the water content of the microemulsion increased.

3.3. Flow properties of the nitrating mixed-acid solutions

Fig. 6 shows the plots of the volumetric flow rate *versus* applied voltage for a range of acid concentrations at a fixed H_2SO_4 to HNO_3 ratio. The nitrating mixed-acid systems showed a steady decrease in flow rate as the concentration of the acids increased, with the highest concentration (11.22 M H_2SO_4 –5.37 M HNO_3) showing almost a zero flow rate within the micro reactor. Owing to the low pH (<2) and high ionic strength of the mixed-acid solutions, the bulk mobility observed for the less concentrated solutions was more likely to be induced by bulk ionic electrophoretic movement, rather than EOF. For the more dilute solutions with concentrations less than 5.61 M H_2SO_4 –2.68 M HNO_3 , voltages as low as 100 V appeared to be sufficient to move the solutions in the micro reactor. In addition, there was reduced Joule heating owing to the low electrical resistance. The errors in the flow rate measurements for the acid solutions were between 1.5 and 2.5% RSD, with the error decreasing as

the acid concentration decreased. In all cases, no evolution of brown nitrogen dioxide gas was noticed at the electrodes and in the channels.

Flow rates were determined by the simple volume change measurement procedure,²⁰ avoiding current²¹ and optical-

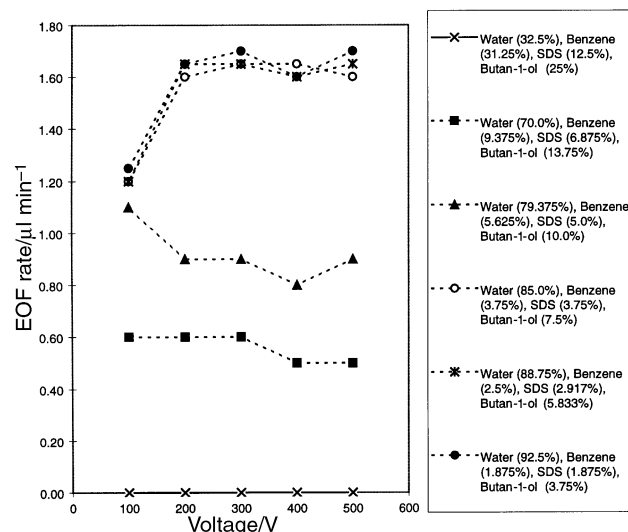


Fig. 5 Plots of flow rate *versus* voltage for the microemulsion systems with different percentage water contents.

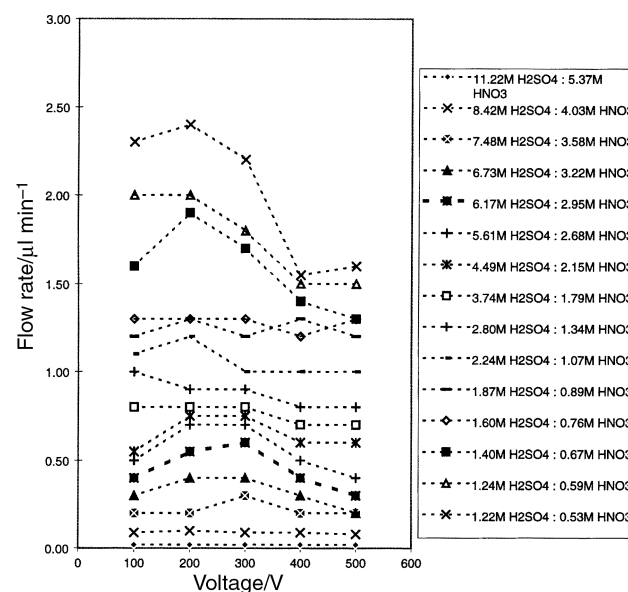


Fig. 6 Plots of flow rate *versus* voltage for the mixed-acid concentration levels.

Table 1 Percentage compositions and amounts of components in the microemulsion systems. C_S is the composition of the surfactant (SDS)–alcohol (ROH) combination of the ratio 1:2, C_H is the composition for the hydrocarbon (benzene) and C_W is the composition for the water in which 10 mM borate buffer is dissolved

Parameter	Oil-rich system	Water-rich (oil-in-water) system				
		1	2	3	4	5
C_W (%)	32.50 (2.6 g, 2.6 ml)	70.00 (10.18 g, 10.18 ml)	79.38 (15.88 g, 15.88 ml)	85.00 (26.7 g, 26.7 ml)	88.75 (30.43 g, 30.43 ml)	92.50 (49.33 g, 49.33 ml)
C_H (%)	31.25 (2.5 g, 2.9 ml)	9.38 (1.36 g, 1.58 ml)	5.63 (1.13 g, 1.31 ml)	3.75 (1.0 g, 1.16 ml)	2.50 (0.86 g, 0.99 ml)	1.88 (1.0 g, 1.16 ml)
C_S (%)	37.50	20.63	15.00	11.25	8.75	5.63
SDS (%)	12.50 (1.0 g)	6.88 (1.0 g)	5.00 (1.0 g)	3.75 (1.0 g)	2.92 (1.0 g)	1.88 (1.0 g)
ROH (%)	25.0 (2.0 g, 2.5 ml)	13.75 (2.0 g)	10.00 (2.0 g)	7.50 (2.0 g)	5.83 (2.0 g)	3.75 (2.0 g)
Total volume/ml	8.0	14.28	19.68	30.36	33.92	52.99

based²¹ methods which when applied to a two-phase system may pose some significant problems. For example, the presence of organic components in the aqueous phases and the employment of solutions with pH < 2 may result in some current irregularities, which would make flow rate measurements by current–time monitoring difficult. However, the integration of UV/visible optical detectors to allow flow rate measurements by more conventional approaches through the use of injected neutral marker²¹ is currently under investigation.

3.4. Characteristics of the nitration model reaction based on the electric field-induced mobilisation of the multiphase system

Ideally, the yield of reaction product should be calculated relative to the amount of reagent or sample injected into the reactor channel. However, this was difficult to achieve in this investigation as the nitronium ions injected are generated as reaction intermediates in the reversible interaction between H₂SO₄ and HNO₃. Hence, the yields of any benzene-nitrated products (as absolute gram amount and as percentage conversion) were calculated relative to a theoretical yield based on 100% conversion of the amount of benzene in an estimated volume of microemulsion interacting with the injected mixed acid at the reagent–sample interfaces initially created at the channel junction C (Fig. 1). The volume of the channel junction C was calculated to be 4 nl and the total amount of microemulsion interacting within the injected mixed acid at both sides of the injected slug was estimated to be approximately half (*i.e.*, 2 nl) of the volume of the channel junction.²²

Fig. 7 shows the percentage yield (calculated as percentage mass) for mono-, di- and trinitrobenzene obtained by injecting a slug of the mixed acid, for different periods of time, from reservoir S into the microemulsion filled main channel. During this process the flow was stopped for 60 s after each injection to allow the reaction to proceed.

The products formed were found to be dependent on the injection time and thus the corresponding volume of reactant acid introduced into the microemulsion stream. For the mononitrobenzene an injection slug of acid between 30 and 60 s proved to be optimal, giving a yield of 62–65%, but the less abundant di- and trinitrobenzene species increased slowly with a corresponding increase in acid injection time. It is important to note that whereas EOF, with a characteristic flat (trapezoidal or rectangular) flow profile, is the main mechanism for solution

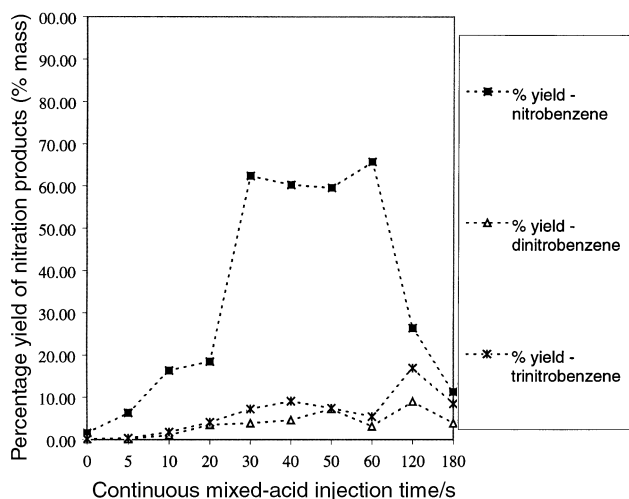


Fig. 7 Plots of the percentage yield for mono-, di- and trinitrobenzene obtained by varying the injection times of the mixed acid into the microemulsion filled main channel.

mobility, electrophoretic mobility will also occur, affecting the diffusion limiting reactions taking place in the interfacial zones between the reactants.²² The amount of reaction product formed would therefore depend not only on the volume injected but also on the diffusion constants for the solutions present, the individual electrophoretic mobility for each component and the reactant concentration. Thus, if insufficient acid is injected the nitrobenzene yield will be reduced (*i.e.*, <30 s). Attempts to deliver more acid by increasing the injection time (*i.e.*, >60 s) had a limiting effect on the amount of product obtained and this trend could possibly be due to an increase in Joule heating effects creating some in-channel bubbling during the injection, which eventually stopped the fluid flow. To prevent such excessive time-dependent Joule heating effects, a 30 s injection time, coupled with the 60 s initial stopped-flow mode reaction time, were chosen. This corresponds to <5 nl injected mixed-acid volume completely filling the reagent–sample channel junction C, and about 2 nl of microemulsion interacting with the acid at the interfaces between the microemulsion and the mixed-acid. To establish fully the optimum reaction conditions, experiments were carried out in which the mixed acid was segmented by different volumes of microemulsion, operating in a continuous flow mode. These results showed that the most appropriate injection sequence for this reaction was three 30 s segmented mixed-acid injections each immediately followed by a 5 s flush of microemulsion into the system. Clearly, however, the whole aspect of sample injection and reaction characteristics in μ FIA systems requires a more detailed study, which is currently in progress.

It is also important to stress that in the absence of any turbulent mixing, to disperse the injected mixed-acid slug in the relatively larger volume of microemulsion in the channel means that some concentrated mixed acid would still be in direct interfacial contact with the already formed nitrobenzene product. This situation could therefore lead to the possible formation of polynitration products. However, only traces of the di- and trinitrobenzene were formed owing to the deactivating nature of the nitro group already present on the benzene ring and the limited amount of mixed acid introduced as a sample into the benzene stream. Thus, kinetically, the formation of the polynitrated products was found to be, as expected, a function of both time and the amount of mixed acid introduced into the system. Shorter reaction times and less acid (or excess microemulsion) would favour the production of the mononitrobenzene, whereas a longer time and excess acid would favour the production of the polynitrated products.

Generally, any temperature gradients within the channels, resulting from the exothermic nature of the reaction and Joule heating effects, are expected to be minimal owing to the relatively small volume present. Locally high thermal effects may, however, still occur and the absence of active cooling may influence the reaction equilibrium to some extent, leading to decomposition of the reactants. In addition, the displacement of some of the surfactant SDS as sulfonic acid and the borate buffer as boric acid by the H₂SO₄–HNO₃, together with the presence of water and other side-reactions consuming some free hydrogen ions in solution, will act to suppress the generation of the electrophilic nitronium ion. As a consequence, the yields are expected to remain lower than that of the conventional industrial process. Other contributing factors to these low yields could be attributed to the product collection from the collection reservoir and the extraction efficiency of octane.

4. Conclusions

This investigation has demonstrated that it is possible to mobilise a non-polar liquid (benzene) under EOF by dissolving it in an oil-in-water microemulsion. It should be pointed out,

however, that other methods such as the addition of ion pairs (e.g., a quaternary ammonium salt)¹² and electrohydrodynamics²³ are possible options for mobilising relatively non-polar compounds. It was also possible to mobilise concentrated acid solutions by bulk electrokinetic mobility of solution ions at low pH.

The optimum conditions for the nitration of benzene in the microreactor developed were a run of the microemulsion as main reagent stream, then three 30 s segmented mixed-acid injections each immediately followed by a 5 s flush of microemulsion into the system. This was followed by a 60 s stopped-flow reaction time before driving all reaction product segments to the collection reservoir. An in-channel microporous silica frit integrated in the manifold system was found to be helpful in reducing hydrodynamic effects, so offering greater control over the fluidics.

Clearly, it is possible to use time, applied electric field and relative amount (feed rate) of reacting species (acid or microemulsion) to control the relative yields of the various products as required. The most important factors leading to the production of the mononitrobenzene were higher rates of microemulsion feed into the system, lower acid feed rate and shorter reaction times (60 s maximum). High interaction between the levels of SDS and the percentage of sulfuric or nitric acid (in the nitrating mixture) used were also found to influence the production of mononitrobenzene. Lower amounts of the di- and trinitrobenzene were found to occur owing to the deactivating nature of the nitro groups already present on the benzene ring and the limited amount of mixed acid introduced as a sample into the benzene stream serving as the main reagent.

The synthesis of the nitrated benzene compounds using such microtechnology indicated that the reaction itself was feasible on a small scale. The system operational variables such as the applied voltage and current, reagent concentrations and pH, relative flow rates of reactant species into the system, channel sizes, etc., which could influence chemical reactions on this small scale are important considerations in the manifold design if simple systems are to be realised. Control over the selectivity of reaction products, i.e., mono-, di- and trinitrobenzene, was not conclusive. The novel mixing characteristics and the high heat dissipating capability of the glass devices together with the direct close contact of reacting species in the channels in view

of the system miniaturisation could maximise the product yield.

5. References

- 1 A. Manz, N. Graber and H. M. Widmer, *Sens. Actuators B*, 1990, **1**, 244.
- 2 A. Manz, E. J. M. Verporte, C. S. Effenhauser, N. Burggraf, D. E. Raymond, D. J. Harrison and H. M. Widmer, *J. High Resolut. Chromatogr.*, 1993, **16**, 433.
- 3 S. J. Haswell, *Analyst*, 1997, **122**, 1R.
- 4 Z. Fan and D. J. Harrison, *Anal. Chem.*, 1994, **66**, 177.
- 5 S. C. Jacobson, L. B. Koutny, R. Herenroder, A. W. Moore, Jr. and J. M. Ramsey, *Anal. Chem.*, 1994, **66**, 3472.
- 6 D. E. Raymond, A. Manz and H. M. Widmer, *Anal. Chem.*, 1994, **66**, 2858.
- 7 A. T. Woolley and R. A. Mathies, *Anal. Chem.*, 1995, **67**, 3676.
- 8 D. Schmalzing, L. Koutny, A. Adourian, P. Belgrader, P. Matsudaira and D. Ehrlich, *Proc. Natl. Acad. Sci. USA*, 1998, **94**, 10 273.
- 9 S. J. Haswell and V. Skelton, *Trends Anal. Chem.*, 2000, **19**, 389.
- 10 P. D. Fletcher and S. J. Haswell, *Chem. Br.*, 1999, November, 38.
- 11 G. M. Greenway, S. J. Haswell, S. O. Morgan, V. Skelton and P. Styring, *Sens. Actuators B*, 2000, **63**, 153.
- 12 S. Bird, MSc Thesis, University of Hull, 1996.
- 13 L. F. Albright and C. Hanson, *Industrial and Laboratory Nitrations*, American Chemical Society, Washington, DC, 1976, p. 1.
- 14 R. N. C. Daykin and S. J. Haswell, *Anal. Chim. Acta*, 1995, **313**, 115.
- 15 K. L. Mittal and B. Lindman, *Surfactants in Solution*, Plenum Press, 1984, vol. 3, p. 1; K. L. Mittal and B. Lindman, *Surfactants in Solution*, Plenum Press, 1984, vol. 3, 1590.
- 16 P. D. Christenson, S. W. P. Johnson, T. McCreedy, V. Skelton and N. G. Wilson, *Anal. Commun.*, 1998, **35**, 34.
- 17 P. J. Jobe, V. C. Reinsborough and P. J. White, *Can. J. Chem.*, 1982, **60**, 279.
- 18 R. J. Hunter, *Introduction to Modern Colloidal Science*, Oxford Science, Oxford, 2nd edn., 1993, pp. 1–31; R. J. Hunter, *Introduction to Modern Colloidal Science*, Oxford Science, Oxford, 2nd edn., 1993, p. 227.
- 19 H. Kunieda and R. Aoki, *Langmuir*, 1996, **12**, 5796.
- 20 G. N. Doku and S. J. Haswell, *Anal. Chim. Acta*, 1999, **382**, 1.
- 21 J. E. Sandoval, *Anal. Chem.*, 1996, **68**, 2771.
- 22 P. D. I. Fletcher, S. J. Haswell and V. N. Paunov, *Analyst*, 1999, **124**, 1273.
- 23 S. E. McBride, R. M. Moroney and W. Chiang, in *Proceedings of the Micro Total Analysis Systems '98 Workshop*, ed. D. J. Harrison and A. van den Berg, Banff, Canada, October, 1998, p. 45.

The generation of concentration gradients using electroosmotic flow in micro reactors allowing stereoselective chemical synthesis

Victoria Skelton,^a Gillian M. Greenway,^a Stephen J. Haswell,^{*a} Peter Styring,^a David O. Morgan,^b Brian H. Warrington^c and Stephanie Y. F. Wong^c

^a Department of Chemistry, Faculty of Science and the Environment, University of Hull, Cottingham Road, Hull, UK HU6 7RX. E-mail: S.J.Haswell@chem.hull.ac.uk

^b SmithKline Beecham Pharmaceuticals, Old Powder Mills, Tonbridge, Nr. Leigh, Kent, UK TN11 9AN

^c SmithKline Beecham Pharmaceuticals, New Frontiers Science Park (North), Third Avenue, Harlow, Essex, UK CM19 5AW

Received 16th August 2000, Accepted 20th October 2000

First published as an Advance Article on the web 19th December 2000

The stereoselective control of chemical reactions has been achieved by applying electrical fields in a micro reactor generating controlled concentration gradients of the reagent streams. The chemistry based upon well-established Wittig synthesis was carried out in a micro reactor device fabricated in borosilicate glass using photolithographic and wet etching techniques. The selectivity of the *cis* (*Z*) to *trans* (*E*) isomeric ratio in the product synthesised was controlled by varying the applied voltages to the reagent reservoirs within the micro reactor. This subsequently altered the relative reagent concentrations within the device resulting in *Z/E* ratios in the range 0.57–5.21. By comparison, a traditional batch method based on the same reaction length, concentration, solvent and stoichiometry (*i.e.*, 1.0:1.5:1.0 reagent ratios) gave a *Z/E* in the range 2.8–3.0. However, when the stoichiometric ratios were varied up to ten times as much, the *Z/E* ratios varied in accordance to the micro reactor *i.e.*, when the aldehyde is in excess, the *Z* isomer predominates whereas when the aldehyde is in low concentrations, the *E* isomer is the more favourable form. Thus indicating that localised concentration gradients generated by careful flow control due to the diffusion limited non-turbulent mixing regime within a micro reactor, leads to the observed stereo selectivity for the *cis* and *trans* isomers.

Introduction

The controlled production of stereoselective products from organic reactions represents a significant development for the production of pharmaceutical drugs and the synthesis of polyunsaturated natural products. Such control, at the touch of a switch, has now been achieved so minimising the need for separation and purification of stereoisomers post-reaction. The micro reactor systems used exploit electroosmotic (EOF) and electrophoretic mobility to create a unique reaction environment in which localised diffusional mixing occurs in the presence of controlled electric fields.^{1–5} To demonstrate *Z/E* control we have used well-established Wittig chemistry in which 2-nitrobenzyltriphenylphosphonium bromide (0.01 M) is reacted with methyl 4-formylbenzoate (0.01 M) in dry methanol at a 1 to 1 stoichiometry to illustrate the experimental protocol. In the traditional batch synthesis, the kinetically favoured *cis* stereoisomer is produced with a typical *Z/E* ratio of 3.0. The reaction is normally performed at room temperature (25 °C) in the presence of an electrophilic phosphorous reagent (PPh₃) diluted by a polar, aprotic solvent.

Micro reactor—experimental

The micro reactor (Fig. 1) was fabricated in borosilicate glass using photolithography and wet etching⁶ techniques to produce appropriate channel geometries (200 μm wide and 100 μm deep). Microporous silica frits⁷ positioned in the subsidiary manifold channels and were used to minimise hydrodynamic

pressure improving the precision of electroosmotic pumping and electrophoretic mobility¹ of the solutions used. The network of interconnecting channels was subsequently annealed to a 17 mm top plate (680 °C) using a microwave furnace. The top plate included a series of 3 mm id pre-drilled holes (four reservoirs in total), which acted as reagent reservoirs and supported the gold electrodes. The final outer dimensions of the micro reactor were 20 mm × 20 mm square and 25 mm in depth.

Using a prototype power supply developed by Kingfield Electronics (Sheffield, UK) see Fig. 2, the Wittig reaction was investigated at a number of external applied voltages generating a variety of EOF rates. Using the Kingfield power supply, the micro reactor was positioned on the top plate of the unit into

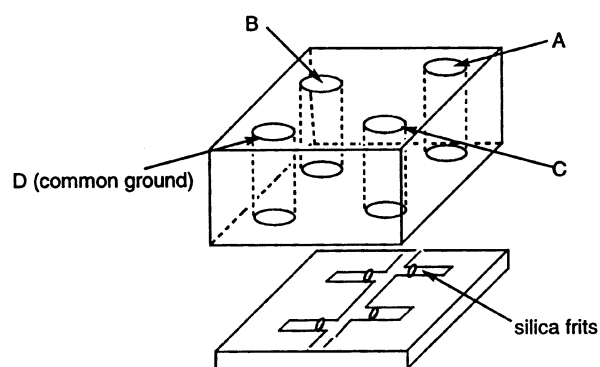


Fig. 1 Schematic diagram of the micro reactor used for the investigation of *Z/E* ratios in Wittig chemistry.

which a solution of 2-nitrobenzyltriphenylphosphonium bromide (0.01 M, 50 μL) in dry methanol (MeOH) was added to reservoir A. Sodium methoxide (0.015 M, 50 μL in MeOH) was added into reservoir B and methyl 4-formylbenzoate (0.01 M, 50 μL , in MeOH) was added to reservoir C. Finally, 40 μL of dry MeOH was added to reservoir D that was the collection reservoir and common ground for the system. Using multivariate experimental design,⁸ a number of chemical reactions were performed that investigated a series of voltages within the range 494 V to 754 V for a period of 20 min. Previous experimental design data suggested that the voltage region outlined above minimised the relative standard deviation between data points resulting in the models precision and potential prediction capability being high. In total, the multivariate experimental method designed produced 27 voltage combinations, which investigated the region 494 V to 754 V sufficiently. After each reaction combination was finished, the reagent volume in reservoir D was recorded and the product yield was determined using off-chip reversed phase high performance liquid chromatographic (HPLC) analysis (conditions: Phenomenex C18(2) 3 μm column, 75 \times 4.60 mm, mobile phase composition: 0.1% trifluoroacetic acid in water and 0.1% trifluoroacetic acid in acetonitrile (90% aqueous to 10% aqueous over 6 min) at 40 $^{\circ}\text{C}$, flow rate 3 $\mu\text{l min}^{-1}$).⁹ The compound yield was calculated using the knowledge of the input weight of the phosphonium salt, the volume of the solution in reservoirs A and D before and after the reaction, the measurement of the concentration of phosphonium salt in reservoirs A and D at the end of the reaction and the concentration of the products in reservoir D.

Batch reaction—experimental

For comparison purposes, a series of batch reactions were performed varying the concentration of the aldehyde. This was achieved by stirring the following reagents for 20 min at room temperature, 2-nitrobenzyltriphenylphosphonium bromide (0.01 M in 10 ml of MeOH) with sodium methoxide (0.015 M in MeOH) and the aldehyde, methyl 4-formylbenzoate at various concentrations. The concentration values investigated were 0.005 M, 0.01 M, 0.03 M, 0.05 M and 0.1 M. The yields were determined using the same HPLC method detailed above.

Results and discussion

In Fig. 3 we illustrated how applying a voltage of +494 V at reservoir A, increases the amount of ylide produced in the reaction channel. This is simply due to the negative potential difference (-166 V) between reservoirs A and B (with respect

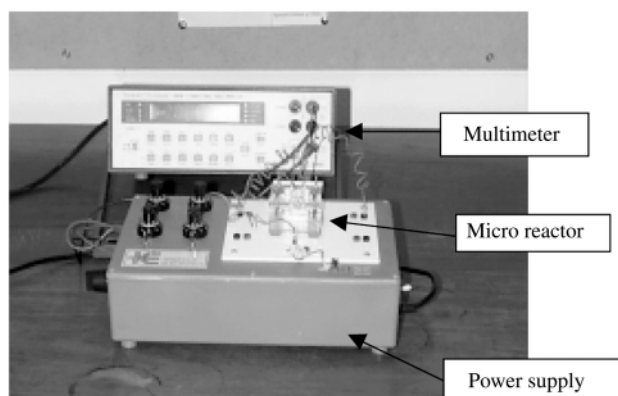


Fig. 2 The Kingfield electronics power supply.

to A), allowing the sodium methoxide (reservoir B) to ‘flow back’ towards reservoir A. The opposite trend applies when the voltage is increased at reservoir A (+694 V), giving a potential difference between reservoir A and B of +34 V, which reduces the amount of ylide intermediate formed due to the increased flow rate of 2-nitrotriphenylphosphonium bromide. Monitoring the current during the reaction indicated that the current in channel C was extremely small (0.01 μA) and could be classed as the system noise. However, a large current in the region of 50 to 70 μA was recorded between reservoir B and D in the main channel and this may be due to the formation of sodium bromide (step 1 by-product), which will influence locally the solution mobility and the stereoselectivity of the reaction product.

The lowest and highest *Z/E* ratios obtained in this particular data set were 0.57 (reservoir A: 495 V, reservoir B: 660 V and reservoir C: 678 V) and 5.21 (reservoir A: 550 V, reservoir B: 300 V and reservoir C: 500 V) respectively, which when compared with the *Z/E* ratio (≈ 3.0) obtained for a similar batch reaction (the same reaction length, concentration, stoichiometry and solvent system), illustrate the significant variation and control possible on the products produced. In the course of this work a number of additional aldehydes, detailed previously⁹ have been observed to also display stereoselectivity using the same basic Wittig chemistry and investigations are continuing in this area to establish the effective scope of the methodology described.

The origin of the *Z/E* selectivity can be rationalised in terms of the localised concentrations that occur within the capillary channel system of the micro reactor where diffusion limited non-turbulent mixing conditions predominate. This effect, which is supported by batch based experiments, illustrates the potential control and selectivity possible when using micro reactors for synthetic chemistry.¹ Thus when the solution velocity through the microchannels is high and hence the residency time or local concentration of the reagents in the channels is low, the *cis* isomer is kinetically favoured and hence the ylide reacts with the excess aldehyde to give the *cis*-oxaphosphotane. The *cis*-oxaphosphotane then quickly passes through the reaction channel before eliminating triphenylphosphine oxide to yield the *cis*-stilbene in excess. However, the formation of the *cis* isomer is not absolute and even at high field strengths some *trans* isomer is produced. As the residency time is increased, by reducing the applied electric field, the relative concentration of the ylide to aldehyde increases and the equilibrium position moves to the more thermodynamically favoured *trans*-oxaphosphotane, which is produced in excess. Again, the equilibrium between the two isomers ensures that there is never absolute selectivity of the *trans*-isomer, see Fig. 4. Experimental evidence to support the proposition that localised concentration gradients are being generated and controlled within a micro reactor is given in Fig. 5. This demonstrates that the variation in the *Z/E* ratios is dependant on the concentration of reactants. When the aldehyde is in excess, the *Z* isomer is the predominant product whereas if the

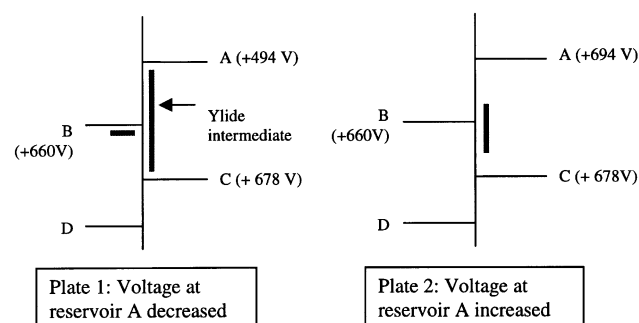


Fig. 3 The schematic representation of the spatial production of the ylide intermediate as a function of varying the applied voltage at reservoir A.

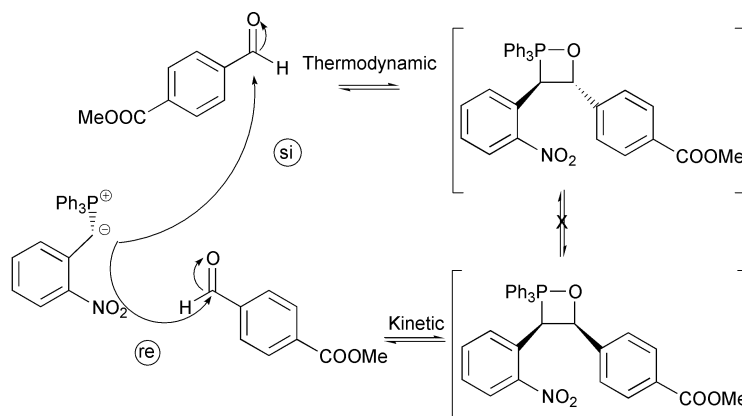


Fig. 4 The stereoselective mechanism for the Wittig chemistry within a micro reactor device.

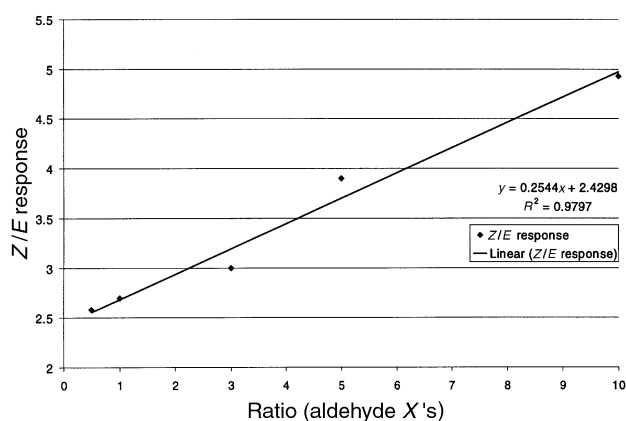


Fig. 5 Plot to show the effect of aldehyde concentration on the *Z/E* ratio.

phosphonium salt is in excess, the *E* isomer is the predominant product. This concentration effect is currently being investigated further within the author's laboratory looking at the fundamental kinetics of the reaction.

In conclusion, the micro reactor investigated using Wittig chemistry has demonstrated that stereoselective control of products can be induced using applied electrical fields in a micro reactor device. This was achieved by varying the voltage at reservoirs A, B and C, which allowed the precise control of the reagent concentration within the reactor channels. The micro reactor system described is currently being used in conjunction with statistical modelling techniques to predict the *Z/E* ratio with reference to the applied voltages at reservoirs A, B and C. The micro reactor developed offers considerable

potential for use in a number of chemical fields such as synthetic development and optimisation, combinatorial synthesis and drug discovery enabling rapid synthesis of a number of compounds with versatile selective control.

Acknowledgement

This work was financially supported by SmithKline Beecham Pharmaceuticals and EPSRC.

References

- 1 P. D. I. Fletcher, S. J. Haswell and V. N. Paunov, *The Analyst*, 1999, **124**, 1273.
- 2 B. H. Weigl and P. Yager, *Science*, 1998, **283**, 346.
- 3 A. E. Kamholz, B. H. Weigl, B. A. Finlayson and P. Yager, *Anal. Chem.*, 1999, **71**, 23.
- 4 P. J. A. Kenis, R. F. Ismagilov and G. M. Whitesides, *Science*, 1999, **285**, 83.
- 5 B. J. Harmon, I. Lessong and F. E. Regnier, *Anal. Chem.*, 1994, **66**, 3797.
- 6 R. N. C. Daykin and S. J. Haswell, *Analytical Chimica Acta*, 1995, **313**, 155.
- 7 P. D. Christensen, S. W. P. Johnson, T. McCreedy, V. Skelton and N.G. Wilson, *Anal. Commun.*, 1998, **35**, 341.
- 8 R. H. Myers and D. C. Montgomery, *Response Surface Methodology, Process and Product Optimisation Using Designed Experiments*, Wiley International Science, 1995.
- 9 V. Skelton, G. M. Greenway, S. J. Haswell, P. Styring, D. O. Morgan, B. H. Warrington and S. Wong, IMRET 4: 4th International Conference on Microreaction Technology, Topical conference proceedings, March 5–9 2000, Atlanta, GA.

The preparation of a series of nitrostilbene ester compounds using micro reactor technology

Victoria Skelton,^a Gillian M. Greenway,^a Stephen J. Haswell,^{*a} Peter Styring,^a David O. Morgan,^b Brian Warrington,^c Stephanie Y. F. Wong^c

^a Department of Chemistry, Faculty of Science and the Environment, University of Hull, Cottingham Road, Hull, UK HU6 7RX

^b SmithKline Beecham Pharmaceuticals, Old Powder Mills, Tonbridge, Nr Leigh, Kent, UK TN11 9AN

^c SmithKline Beecham Pharmaceuticals, New Frontiers Science Park (North), Third Avenue, Harlow, Essex, UK CM19 5AW

Received 16th August 2000, Accepted 19th October 2000

First published as an Advance Article on the web 27th November 2000

The synthesis of stilbene esters using Wittig chemistry has been used to illustrate the generic diversity micro reactors offer in terms of chemical control and rapid method development. The micro reactor consisted of a 'T' design based on channel geometries 200 μm wide and 100 μm deep, etched into borosilicate glass and sealed with a borosilicate top plate using a thermal bonding technique. The movement of the reagent and products was achieved using electroosmotic flow (EOF), assisted by the incorporation of micro porous silica frits within the micro-channels to allow accurate solution control. To optimise the operating conditions methyl 4-formylbenzoate, premixed with sodium methoxide, was reacted with 2-nitrobenzyl-triphenylphosphonium bromide in dry degassed MeOH using flow conditions for both reagents of 0.40 $\mu\text{L min}^{-1}$ for 20 min. A product yield of 70% (2:1 reaction stoichiometry with the aldehyde in excess) was obtained representing a 10% increase compared with the traditional batch synthesis. To demonstrate the capability of micro reactors to perform atom efficient synthesis a series of experiments based on an injection methodology (optimised to 30 s) were performed in the micro reactor at 1:1 stoichiometry resulting in a yield of 59%. Finally, the capability of micro reactors to perform a series of analogue reactions was investigated. The yields for a further three aldehydes indicated that the technology will be suitable for the development of automated device to support the generation of combinatorial libraries and rapid high throughput synthetic methods.

Introduction

In recent years, interest in developing total analytical system (μ -TAS) has grown considerably^{1–10} as the reality of achieving a faster and cheaper means of performing chemical analysis has been demonstrated. Interestingly, the principles demonstrated by μ -TAS can readily be exploited to develop reactors at the micron scale for the synthesis of organic compounds. Whilst such devices offer a rapid and practically attractive approach to synthesis, the real potential lies in the possibility of achieving novel reaction control and product formation.¹¹

A strong research base is now developing in the field of micro reactor technology with a particular emphasis on gas phase catalytic reactions,^{12,13} and a growing interest in solution based chemistry.¹⁴ This trend in micro reactor methodology is reflected in the growing number of papers appearing in associated conferences.¹⁵ Micro reactor fabrication can be achieved using a variety of mediums, for example glass, metals and silicon, however, glass substrates with typical cross sections between 50 and 300 μm have been preferred for organic synthesis due to the chemical inertness, temperature stability, optical transparency and the ability to support electroosmotic flow (EOF).¹⁶

For the purpose of this study, the evaluation of a glass based micro reactor for synthetic chemistry has been investigated using as an example, the Wittig chemistry commonly used for vitamin A synthesis.¹⁷ The reaction (Fig. 1) allows the formation of a carbon to carbon bond by the reaction of a phosphorane or phosphonium ylide and an aldehyde or ketone to form an alkene and phosphine oxide. The Wittig reaction was

investigated on a micro reactor with two specific aims, firstly to establish the criteria for achieving a solution based synthetic application and secondly, to investigate the potential for the technology to perform analogue-type chemistry. In this present case, the Wittig synthesis has been selected for its homogeneous solution properties, which produces a coloured intermediate (ylide) enabling solution profiling and diffusive mixing visualisation to be achieved, so gaining a greater understanding of system flow and reaction control.

Experimental

All reagents were of analytical grade, unless otherwise stated and were used without further purification. The micro reactor was fabricated using photolithographic techniques (200 μm wide and 100 μm deep) and the microchannels included microporous silica frits¹⁸ positioned as shown in Fig. 2. The channels were sealed by annealing the patterned base plate to a 17 mm thick top plate (680 $^{\circ}\text{C}$) using a microwave furnace (CEM microwave ashing system 300). The top plate included 3 mm internal diameter pre-drilled holes aligned at the ends of each channel to act as reservoirs and electrode supports. The final outer dimensions of the micro reactor were 20 mm \times 20 mm square and 25 mm in depth. In addition, the total length of the channels was 20 mm from reservoir A to C.

The synthetic method was adapted from that previously reported by Hughes *et al.*^{19–20} In this paper, 2-nitrobenzyl-triphenylphosphonium bromide was used as it produced a coloured intermediate (ylide), due to the presence of the nitro

functional group. Visual observation of the ylide enabled the reaction and the fluidics of the system to be monitored *via* a microscope and CCD camera. The yield was also determined using high performance liquid chromatography (Zorbax C18 3.5 μm , 75×4.5 mm id, mobile phase composition: 0.1% trifluoroacetic acid in water and 0.1% trifluoroacetic acid in acetonitrile, using a gradient system 90% aqueous to 10% aqueous over 6 min with a flow rate of 3 ml min^{-1} at 40°C).

Wittig synthesis based on 2:1 stoichiometry

Prior to synthesis, the microchannels were primed with dry methanol (MeOH) removing any excess moisture from the channels and the microporous silica frits to reduce a hydrolysis side reaction. A standard solution of 2-nitrobenzyltriphenylphosphonium bromide ($50 \mu\text{L}$, 0.01 M) in dry MeOH was added into reservoir A of the micro reactor. Methyl 4-formylbenzoate ($50 \mu\text{L}$, 0.02 M , 2 eq.) was premixed with sodium methoxide (0.015 M) and $50 \mu\text{L}$ of the premixed solution was introduced into reservoir B. Dry MeOH ($40 \mu\text{L}$, dry, degassed) was introduced into reservoir C. Gold electrodes were placed in each reservoir (A + B positive, C ground) and an external voltage of $100\text{--}700 \text{ V}$ was applied to channels A (+) and B (+) relative to reservoir C (−), see Fig. 2. This induced the continuous flow of methyl 4-formylbenzoate from B (+) to C (−) and 2-nitrobenzyltriphenylphosphonium bromide from A (+) to C. The total volume of the solutions in reservoir A and C at the end of each reaction was recorded and samples were taken for HPLC analysis. The flow rates over the voltage region 100 V to 700 V were determined using a volumetric approach with time. The yield obtained in the micro reactor was calculated from a knowledge of the input weight of 2-nitrobenzyltriphenylphosphonium bromide, the volume of solution in reservoirs A and C, before and after the reaction, measurement of the concentration of 2-nitrobenzyltriphenylphosphonium bromide in A and C at the end of the reaction and the concentration of the product in reservoir C.

Using the optimised conditions obtained, three additional aldehydes with various functional diversities (supplied by SmithKline Beecham Pharmaceuticals, Harlow) were used to demonstrate the potential of micro reactors to perform a variety of reactions. The aldehydes chosen were 3-benzyloxybenzaldehyde, 2-naphthaldehyde and 5-nitrothiophene-2-carboxaldehyde. Each aldehyde was reacted using the optimum conditions established for the aldehyde methyl 4-formylbenzoate. For comparison purposes, each aldehyde was reacted in a batch mode using the method outlined below.

Batch scale methodology

Batch synthesis was also performed at 2:1 and 1:1 stoichiometry in order to make a comparison of the yields obtained with the micro reactor *versus* traditional synthetic methods. This was achieved by stirring 2-nitrobenzyltriphenylphosphonium bromide (0.01 M in MeOH) with sodium methoxide (0.015 M in dry degassed methanol) and each aldehyde in turn at various stoichiometric ratios (concentrations 0.02 M and 0.01 M) at room temperature for 20 min. The reaction parameters set for the micro reactor and the batch system allows the comparison of the reaction length (20 min), concentration, and the solvent of choice. The solution was then evaporated to dryness, purified by Prep HPLC and the yield (g) recorded.

Wittig reaction based on 1:1 stoichiometry

Traditional batch syntheses are typically performed with an excess of reagent, in this particular case the aldehyde is in excess relative to the phosphonium bromide. To establish the operating features of the micro reactor, for the reduced reaction stoichiometry of 1:1, an injection profiling technique was adopted. This required the methyl 4-formylbenzoate solution to be continuously driven by EOF through the micro reactor from B to C whilst sample plugs of 2-nitrobenzyltriphenylphosphonium bromide were injected every min for a range of injection times (20 to 50 s) from channel A to C. Injection was initiated by the periodic application of an optimised voltage between A (+) and C (−) which injected slugs of the reagent (flow rate of $0.4 \mu\text{L min}^{-1}$ determined using volumetric flow rate with time). Repeat injections (20) for each injection time were carried out to generate sufficient product for off-chip analysis.

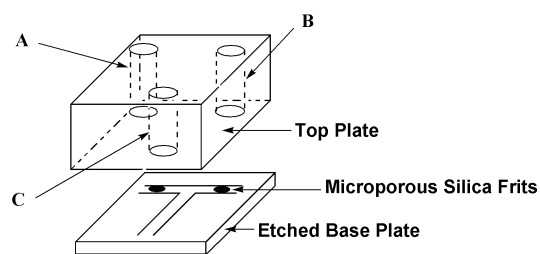


Fig. 2 Schematic of the T-shaped manifold used in the reactor for the Wittig synthesis.

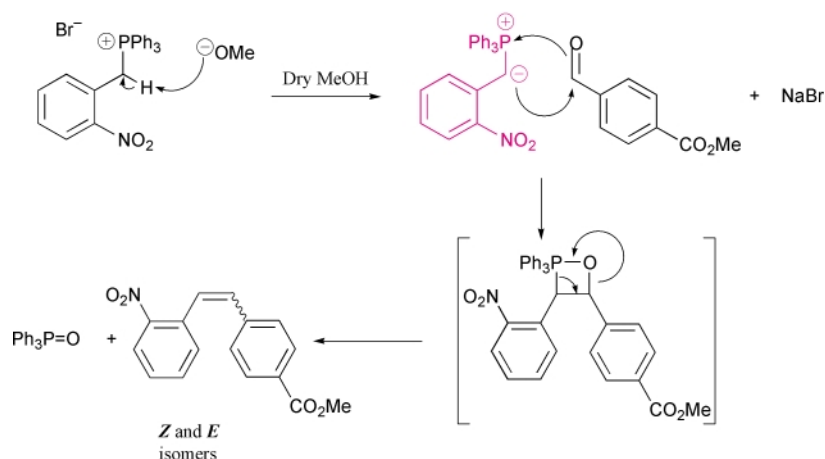


Fig. 1 Reaction scheme for the coupling of 2-nitrobenzyltriphenylphosphonium bromide and methyl 4-formylbenzoate in a micro reactor under EOF.

Results and discussion

The 2:1 stoichiometric study initially centred on evaluating the effect of reagent flow rates on the spatial location of the reaction intermediate by adjusting the voltage applied in reservoirs A and B relative to C. Whilst the initial data gave extremely high product yields several problems were experienced with the reaction. At high voltage (500–700 V) the purple colour observed from the ylide intermediate could clearly be seen being produced in reservoir C and the yields (approximately 50%) suggest the reaction was occurring in the reservoir rather than in the microchannels. Under such a regime, one of the fundamental benefits of the micro reactor, *i.e.*, the spatial control, was not being exploited. The yield however was comparable with that obtained for the traditional batch methodology. As the voltage (flow rates) was decreased to less than 400 V, the yield increased dramatically, on average from 30 to 70%. The variation in the RSD of the yield at 100 V was however greater than 5% associated error due to the irreproducible generation of the flow rates for both reagents. However, at 400 V an optimum pumping voltage (this equated to a flow rate of $0.4 \mu\text{L min}^{-1}$) was found which offered well-controlled flow conditions in which the reaction was contained within the channels of the micro reactor.

Fig. 3 summarises the results obtained for the micro reactor compared with the traditional batch process. In this case, the optimised micro reactor conditions were based on methyl 4-formylbenzoate (A), which gave an overall product yield of 70% compared to 60% obtained for the batch method performed in this study.

Using the optimum parameters established for methyl 4-formylbenzoate, Fig. 3 summarises the remaining results obtained for three additional aldehydes. For all the aldehydes tested the yield obtained in the micro reactor (2:1) were approximately half of those obtained by the traditional batch

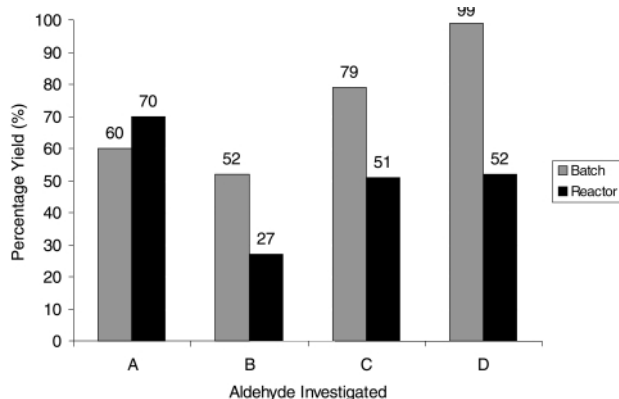


Fig. 3 Summary of the product yields obtained for both micro reactor and traditional batch methods for four aldehydes based on the optimisation with methyl 4-formylbenzoate using 2:1 stoichiometry. The aldehydes shown are methyl 4-formylbenzoate (A), 3-benzyloxybenzaldehyde (B), 2-naphthaldehyde (C) and 5-nitrothiophene-2-carboxaldehyde (D).

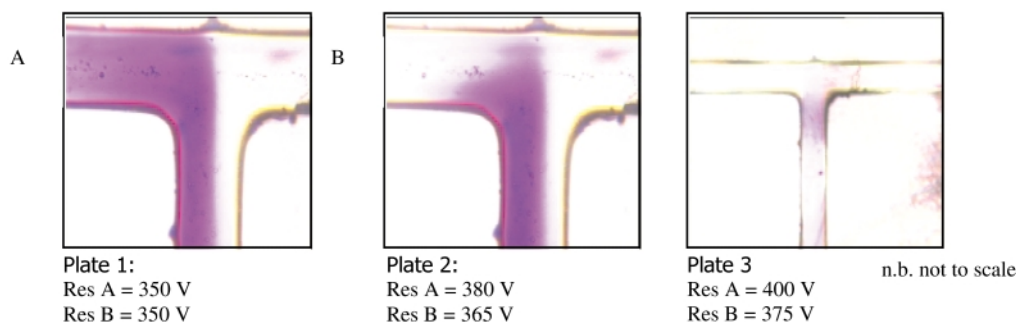


Fig. 4 Photographs obtained from an optical microscope showing the Wittig reaction ylide intermediate formation under variable flow control.

methodology. It is postulated that the reduction in yield may be due to the individual variation in flow dynamics through the micro reactor associated with each aldehyde, as described below.

Fig. 4 shows a series of photographs captured using an optical microscope. The images clearly indicate the diffusive flow profile of the reaction intermediate (ylide). Plate 1 shows the movement of reagents from the left (2-nitrobenzyltriphenylphosphonium bromide) and right hand (aldehyde and base) channels *via* EOF at 350 V. A clear diffusive reaction interface can be seen between the two reagents. However, due to poor flow control the formation of the ylide can be seen to be primarily occurring in the left-hand channel. This may be due to the zeta potential in the central channel being smaller than in the two feeder channels thus causing feedback of the reagent from B to A.^{21,22} In addition, the base, which is premixed with the aldehyde, has greater electrophoretic mobility compared to the aldehyde, see Plate 1 for ylide formation in the left hand channel. By slightly increasing the voltage and hence the flow rate in the left hand channel, the ‘over flow’ from the right hand channel can be corrected, see Plate 2. In this case the reaction can be spatially contained in the middle channel of the T reactor, see Fig. 2. Further adjustment of the voltages applied to the feed reservoirs allows complete diffusive mixing across the channel to be achieved, see Plate 3, demonstrating the EOF control possible in micro reactors. This small variation in reagent flow can significantly alter the position and the reaction conditions of the reagents in the channels. Thus when using a number of reagents, it is probable that each reagent will have a slightly different flow profile causing a disruption to the diffusive reaction interface. Such a situation will result in the reaction interface occurring in a non-optimum position for example, in either of the feed channels, where reaction conditions may not be ideal, resulting in reduced reaction yields. The results indicate that by *in situ* monitoring of the reaction and voltage feedback, an automated system could be developed enabling rapid method development and optimisation with high throughput synthetic capabilities.

The 1:1 stoichiometric study was carried out to investigate the effects on the overall solution yield of periodically injecting a known volume of 2-nitrobenzyltriphenylphosphonium bromide into a continuous stream of aldehyde, *e.g.* methyl 4-formylbenzoate. Previously, Fig. 3 illustrated a decrease in the yields for three of the aldehydes investigated in the micro reactor when compared to the traditional bulk reaction. By developing an injection profile (*i.e.* the optimisation of the injection time and interval) for the reaction, the surface area of the reaction is increased automatically which in theory should enhance the overall yield.¹³ In addition to increasing the overall yield, the fundamental features of the micro reactor, *i.e.*, spatial and temporal control needed to be investigated. This was easily achievable by reducing the stoichiometry of the reaction, which in turn enabled the micro reactor to be evaluated for reagent efficient chemistry.

Fig. 5 summarises the yields obtained for the traditional batch reaction and micro reactor scale based on a 1:1 stoichiometry.

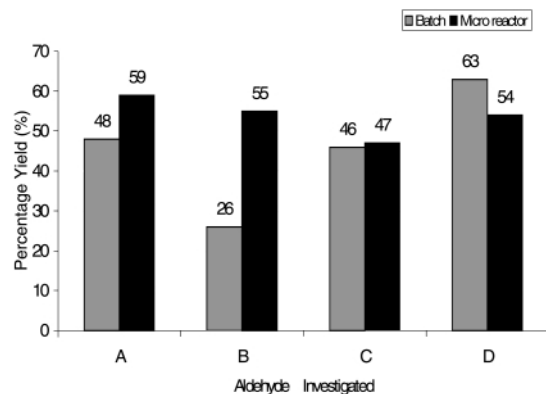


Fig. 5 Summary of the product yields obtained for both micro reactor and traditional batch methods for four aldehydes based on the optimisation with methyl 4-formylbenzoate using 1:1 stoichiometry. The aldehydes shown are methyl 4-formylbenzoate (A), 3-benzyloxybenzaldehyde (B), 2-naphthaldehyde (C) and 5-nitrothiophene-2-carboxaldehyde (D).

For the micro reactor the maximum yield of 59% was achieved using a 30 s injection length (*i.e.* one 30 s injection per min over a total of 20 min) from channel A into a continuous flow from B to C, see Fig. 2. Whilst there is a 10% reduction in the overall yield compared with the 2:1 reaction, the micro reactor under the injection optimised conditions still produced a high product yield at the chemically more favourable 1:1 stoichiometry. The 1:1 stoichiometry results in a lower reagent consumption and reduced work up and sample purification.

Using the optimum reaction (reservoirs A and B at 400 V with an injection length of 30 s from reservoir A) conditions based on methyl 4-formylbenzoate, once again the additional three test aldehydes were reacted. For the reaction with aldehyde B (3-benzyloxybenzaldehyde) in the micro reactor, a 29% increase in reaction efficiency was obtained compared with the batch reaction performed using the same concentrations, solvent and reaction time. For the reaction using aldehyde C (2-naphthaldehyde), the micro reactor yield was comparable with the traditional batch methodology. Aldehyde D (5-nitrothiophene-2-carboxaldehyde) gave a 9% decrease in reaction efficiency, which was an improvement over the 2:1 data (47% reduction).

The micro reactor device allows the synthesis of nitro stilbene esters, which are comparable with the reactions obtained in a more traditional fashion. With respect to the variation in yields for the remaining aldehydes tested, it is worth stressing that the micro reactors generated products rapidly and in sufficient quantities to determine the products of each reaction. This attribute of micro reactors clearly has important implications in establishing rapid analogue based high throughput chemistries and so representing a significant approach for future developments in the field.

Conclusions

The micro reactor has demonstrated the synthetic novelty to achieve the rapid synthesis of nitro stilbene esters, and hence the

potential generic diversity using simple homogeneous solution chemistry. The optimised micro reactor based on methyl 4-formylbenzoate on average gave a 10% increase in reaction efficiency for both 2:1 and 1:1 stoichiometry. In addition, the reactor could also be used as a tool for rapid reaction development and optimisation based on analogue chemistry.

Due to the diverse reaction features of the micro reactor, a combinatorial screening device is currently being investigated illustrating the potential to synthesise a combinatorial library and on-chip screening. If the micro reactor device could be coupled with a separation chip, the *Z* and *E* isomers could be purified from the solution making the device suitable for synthetic development.

Acknowledgements

We thank the EPSRC and SmithKline Beecham Pharmaceuticals for financial support to VS in the form of a CASE studentship.

References

- 1 S. Cowen, *Chem. Ind. (London)*, 1999, **15**, 584.
- 2 T. McCreedy, *Chem. Ind. (London)*, 1999, **15**, 588.
- 3 D. Barrow, J. Cefai and S. Taylor, *Chem. Ind. (London)*, 1999, **15**, 591.
- 4 S. J. Haswell, *Analyst*, 1997, **122**, 1R.
- 5 *Proceedings of the micro total analytical systems '98 workshop*, ed. D. J. Harrison and A. van den Berg, Kluwer Academic Publishers, Dordrecht, 1998.
- 6 A. Manz, D. J. Harrison, E. Verpoorte, J. C. Fetters, H. Ludi and H. M. Widmer, *Chimia*, 1991, **45**, 103.
- 7 A. Manz, D. J. Harrison, E. Verpoorte and H. M. Widmer, *Adv. Chromatogr.*, 1993, **33**, 1.
- 8 A. Manz, C. S. Effenhauser, N. Barggraf, E. Verpoorte, D. E. Raymond and H. M. Widmer, *Analysis Mag.*, 1994, **22**, M25.
- 9 D. J. Harrison, K. Fluri, K. Seiler, Z. H. Fan, C. S. Effenhauser and A. Manz, *Science*, 1993, **261**, 895.
- 10 S. C. Jacobson, R. Hergenroder, L. B. Koutny and J. M. Ramsey, *Anal. Chem.*, 1994, **66**, 1114.
- 11 P. D. I. Fletcher and S. J. Haswell, *Chem. Br.*, 1999, 38.
- 12 W. Ehrfeld and H. Lehr, *Radiat. Phys. Chem.*, 1995, **45**, 349.
- 13 R. D. Chambers and R. C. H. Spink, *Chem. Commun.*, 1999, **10**, 883.
- 14 G. M. Greenway, S. J. Haswell, D. O. Morgan, V. Skelton and P. Styring, *Sens. Actuators B*, 2000, **63**, 153.
- 15 IMRET 4: *4th International Conference on Microreaction Technology, Topical conference proceedings*, March 5–9 2000, Atlanta, GA.
- 16 P. D. I. Fletcher, S. J. Haswell and V. N. Paunov, *Analyst*, 1999, **124**, 1273.
- 17 J. McMurray, *Organic Chemistry*, 3rd edn., 1992, Wadsworth Inc.
- 18 P. D. Christensen, S. W. P. Johnson, T. McCreedy, V. Skelton, and N. G. Wilson, *Anal. Commun.*, 1998, **35**, 341.
- 19 I. Hughes, W. P. Nolan and R. A. Raphael, *J. Chem. Soc. Perkin Trans.*, 1990, **1**, 2475.
- 20 I. Hughes, *Tett. Lett.*, 1996, **37**(42), 7595.
- 21 R. S. Ramsey and J. M. Ramsey, *Anal. Chem.*, 1997, **69**, 1174.
- 22 L. Hu, D. J. Harrison and J. H. Masliyah, *Colloid Interface Sci.*, 1999, **215**, 300.

The application of micro reactors to synthetic chemistry

Stephen J. Haswell,^{*a} Robert J. Middleton,^a Brian O'Sullivan,^a Victoria Skelton,^a Paul Watts^a and Peter Styring^b

^a Department of Chemistry, University of Hull, Cottingham Road, Hull, UK HU6 7RX.

E-mail: s.j.haswell@chem.hull.ac.uk

^b Department of Chemical and Process Engineering, University of Sheffield, Mappin Street, Sheffield, UK S1 3JD

Received (in Cambridge, UK) 20th October 2000, Accepted 19th December 2000

First published as an Advance Article on the web 5th February 2001

A feature article describing the fundamental characteristics and emerging applications of micro technology in the field of synthetic chemistry.

Introduction

It is interesting to observe that despite the many advances made in synthetic chemistry over recent decades the basic practical methodology used remains unchanged. This situation arises primarily because reactions tend to be carried out on a bulk scale

using a batch approach which chemists feel comfortable manipulating. At the molecular level however, it makes little difference fundamentally whether a reaction takes place in a 10 ml or 10 pl container. By applying technology developed for the electronics industry, it is now possible to produce reactors in which one can manipulate and analyse materials on a micron to nanometer scale. It is our belief that so called micro reactor technology can do for synthetic chemistry what the solid-state transistor has done for computing, vastly increasing the versatility and the amount of chemical information that a single person can generate. In short it represents a paradigm shift, changing the way we think about the way we work.

Stephen Haswell is Professor of Analytical Chemistry at the University of Hull. His current research activities are in the areas of micro reactors including analytical developments, microwave enhanced reaction chemistry, trace elemental speciation and process analysis. He is author of over 100 research papers, a number of books and patents and is widely known nationally and internationally for his enthusiastic lectures. For a number of years one of the underlying principles of Professor Haswell's research has been to break down the sectorial walls which exist in science, in particular, the integration of analytical science with main line chemistry, physics, engineering and biology. Many of these ideals are encompassed in his research into micro-chemical reactors the subject of this feature article.

Robert Middleton obtained a B.Sc. (Hons) from the University of Nottingham and carried out postgraduate studies in synthetic organic chemistry with Professor David Knight at Cardiff University focusing on the synthesis of highly substituted tetrahydrofurans via electrophilic cyclisation. Now working at the University of Hull as part of the 'Lab on a Chip' Consortium, developing enzymatic and other catalytic reactions in micro reactors.

Brian O'Sullivan obtained a Ph.D. in physical organic chemistry from the University of Exeter, and has spent some time at the University of Reading researching heterogeneous catalysis and organic synthesis in supercritical fluids. He is currently working at the University of Hull as part of the 'Lab on a Chip' Consortium, studying metal-catalysed carbon-carbon bond forming reactions in micro reactors and using electro-osmotic flow to control reagent mobilisation. Brian is also interested in modelling currents within micro reactors, in order to achieve a greater understanding of the fundamental processes underlying this technology.

Victoria Skelton graduated from the University of Hull in 1997 with a B.Sc. Hons. degree in Chemistry with Analytical Chemistry and toxicology. This included a year of industrial pharmaceutical experience in the analytical research and development department within Pfizer Central Research, Kent. Vikki obtained her Ph.D. at Hull University in 2000, investigating the role of micro reactors for organic synthesis and combinatorial applications and has continued a collaboration with GlaxoSmithKline. She is currently developing a number of chemical reactions and detection systems in micro reactors in order to establish the physical and chemical requirements of such devices.

Paul Watts graduated from the University of Bristol in 1995 with a B.Sc. in chemistry. He continued his studies at Bristol, obtaining a Ph.D. in bio-organic chemistry in 1999 under the supervision of Professor Tom Simpson and Professor Chris Willis. His Ph.D. focussed on the synthesis of isotopically labelled compounds for use in the determination of biosynthetic pathways to polyketide-derived natural products of biological interest. Paul is currently researching methods of peptide synthesis using micro reactor technology at the University of Hull. The project is funded by Novartis Pharmaceuticals, Basel, Switzerland.

Peter Styring is Senior Lecturer in the Process Fluidics Group at the University of Sheffield, Department of Chemical and Process Engineering. Previously he was the Thorn-EMI-BNR and DERA Lecturer in Chemistry at the University of Hull between 1990-2000. Peter gained his B.Sc. and Ph.D. from the University of Sheffield, Department of Chemistry. He has a background in Liquid Crystal Chemistry but moved into the field of Chemical Micro Reactors in 1997 where he addresses aspects of high throughput organic chemistry and catalysis within miniaturised devices.

Basic concepts of micro reactors

A micro reactor is generally defined as a series of inter-connecting channels (10 to 300 microns in diameter) formed in a planar surface in which small quantities of reagents are manipulated. The reagents can be brought together in a specified sequence, mixed and allowed to react for a specified period of time in a controlled region. The product may then be analytically monitored and if necessary separated for further steps in a reaction, or collected for analysis or testing.

In what is basically a diffusion limited environment, where laminar flow characteristics dominate, the micro reactor confers many advantages over conventional scale chemistry. The decrease in linear dimensions allows heat transfer coefficients to exceed those of conventional heat exchangers by an order of magnitude.¹ Micromixers can reduce mixing times to milli- or nano-seconds.² The increased surface to volume ratio in micro reactors (10 000 to 50 000 m² m⁻³, compared to 1000 m² m⁻³ in conventional laboratory vessels) has implications for surface-catalysed reactions.³ Other properties include localised control of concentration gradients, separation of reaction products and the possibility of eliminating unwanted side reactions. For example, when Ehrfeld *et al.*⁴ prepared hydrogen cyanide in a micro reactor *via* the Andrussow route, the rapid cooling of the products by a micro heat exchanger prevented hydrolysis of the HCN to ammonia. Jensen and coworkers⁵ demonstrated that the synthesis of organic peroxides from acid chlorides and hydrogen peroxide may even be carried out beyond the 'explosion limit', as the transfer of heat energy from the area of reaction is rapid enough to prevent explosion.

In addition the small scales used reduce exposure to toxic or hazardous materials, and the enclosed nature of the micro reactors means greater ease of containment in the event of a runaway reaction. The greatest contribution to safety is the fact that hazardous materials can be synthesised as required at the point of use, in precisely defined quantities, thus eliminating the problems associated with transportation and storage.

Although the small size of the micro reactors would seem to preclude industrial scale synthesis, it has been shown⁶ that only 1000 micro reactors operating continuously could produce 1 kg of material in a day. This so called 'scaling out' concept has clear implications in process development where the costly and time-consuming process of going from lab to pilot plant to full-scale production is by-passed simply by optimising the reaction on a single chip and replicating it 1000 or 1 000 000 times. The main attraction of this approach is not only the elimination of the problems associated with the scaling up procedure but also the ability to maintain the high level of control and selectivity made possible through using micro reactor technology.

The micro total analysis systems (μ -TAS)

In recent years, research in the area of miniaturised analytical systems has become well established with a large rapidly growing number of publications reflecting this trend.⁷⁻¹⁴ The first fully miniaturised system fabricated was a gas chromatographic device reported by Terry *et al.*¹⁵ at Stanford University in 1979. This micro device was constructed using a silicon wafer, which included a sample inlet port, a 1.5 m long column, an injector and thermal conductivity detector allowing the separation of a mixture of hydrocarbons within 10 s. However, it took a further 10 years before Manz and colleagues¹⁶ at Ciba-Geigy laboratories in Switzerland fabricated a micro capillary electrophoresis device. The μ -TAS was fabricated from glass and allowed the rapid separation of two fluorescent dyes. During the past decade, the main research thrust in academia and industry has centred on the separation and characterisation of DNA.¹⁷⁻²² This has now led to commercially available micro analytical devices such as the DNA analyser from Agilent, formerly Hewlett-Packard. More recently, a number of research

groups worldwide have shifted the focus of research from μ -TAS to developing micro reactor technology building on the already existing μ -TAS concept. Some of the unique features of such devices will be described in the remainder of this paper but it is worth stressing that integration between μ -TAS and micro reactors is essential if chemical and biochemical reactions, at the micro scale or less, are to be effectively monitored and controlled.

Fabrication techniques

Many of the existing fabrication methods described for the μ -TAS systems have been successfully transferred to the field of chemical micro reactors.²³ A number of materials such as silicon, glass, quartz, metals and some polymers can be used to construct micro reactors. Glass and certain polymers have been particularly useful because of their physical properties and chemical inertness. These substrates also allow the mobilisation of organic reagent and aqueous solutions using a number of pumping mechanisms such as hydrodynamic pumping and electro-osmotic flow (EOF).²⁴⁻²⁶ A range of fabrication methods such as photolithography, hot embossing, powder blasting, injection moulding, laser micro forming and LIGA, from the German *Lithographie, Galvanioformung* (electroforming) and *Abformung* (moulding), are available and can be both versatile and relatively low cost processes.

Fig. 1 shows the steps that are involved in the popular technique of photolithography and wet etching to produce

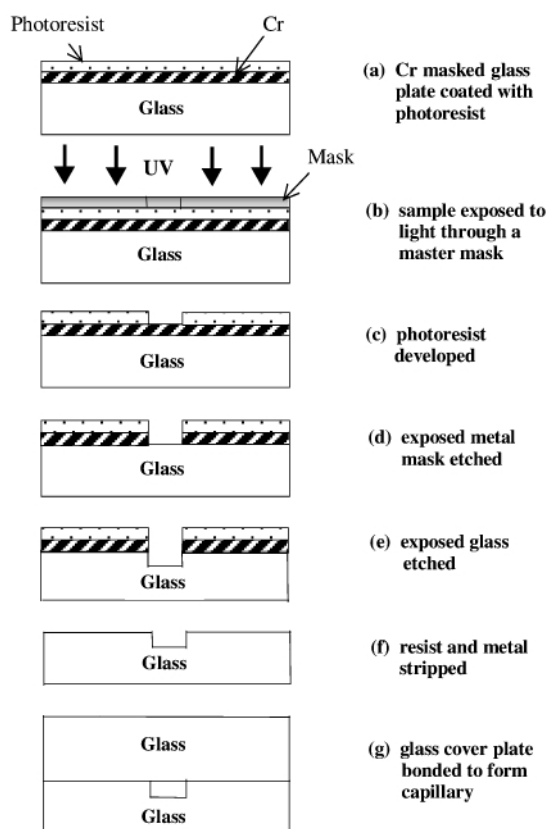


Fig. 1 Sequence of processes in photolithographic fabrication.

channels in a glass micro reactor. A thin layer of metal, such as chromium, is deposited on the surface of a glass plate to control the degree of undercutting during the etching process. A layer of positive photoresist is then spin coated on top of the chromium to a depth of 0.5 to 2.0 μ m. The pattern of the required network of interconnecting channels is transferred to the photoresist layer using photolithography. After exposure, the photoresist is developed and removed together with the chromium layer to

reveal the areas of glass to be etched. The plate is then heated to allow volatiles to evaporate, before performing the chemical etch. The channels are then etched using, for example, a mixture of 1% HF and 5% NH₄F in water at 65 °C, resulting in an etch rate of 0.3 to 0.5 μm min⁻¹. A glass top block, with pre-drilled holes to act as reservoirs and if necessary electrode supports, is aligned with the channel geometry and thermally bonded to the glass base plate, producing an all glass device. An example of such a micro reactor, produced by the photolithographic, wet etch and thermal bonding method outlined above is shown in Fig. 2. It should be noted that a range of alternative fabrication

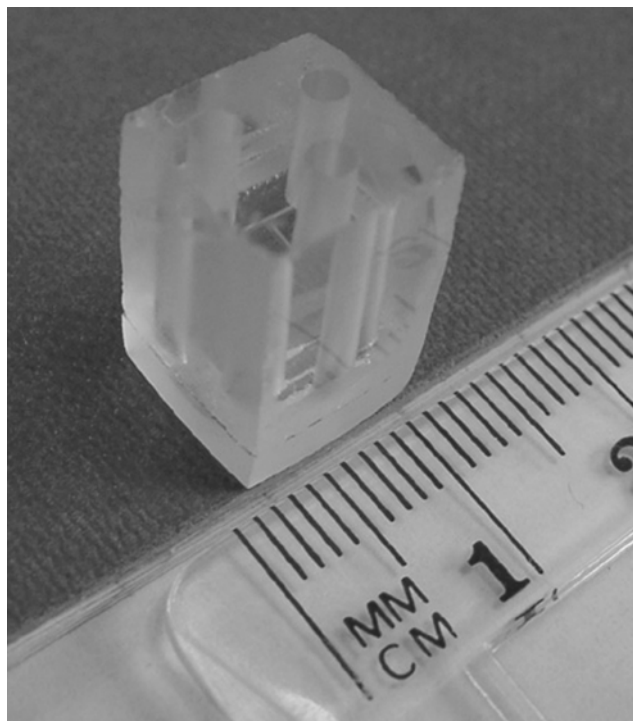


Fig. 2 A simple all-glass micro reactor.

techniques have been reported describing a number of different masking layers, etchant solutions, low temperature bonding, anodic bonding, and polymer based substrates. A recent review of these may be found in ref. 3.

Chemical control in micro reactors

Flow mechanics of liquids in micro channels

One of the main areas that liquid based micro reactor research has focused on to date has been the accuracy with which fluids in capillaries can be manipulated. Owing to the microlitre flow rates that are generally required, some groups have used methods such as syringe pumps, HPLC pumps and peristaltic pumps with high reproducibility being achieved through computer control. Syringe pumps can also be used to infuse and withdraw fluids through channels in both directions. These techniques provide a relatively quick and simple method for pumping reagents through a micro reactor in a controlled manner. However, these systems can build up high back-pressure due to capillary effects, which may lead to pulsing in the flow: this could be a particular problem when using peristaltic pumps.²⁴ Another problem is the cost associated with HPLC and syringe pumps. These pumps can also be intolerant of mixed-phase liquid systems, or systems that contain particulate matter.

Several companies have developed pumps specifically for micro reactor applications. These pumps are typically based on

a piezoelectric driven one way valve to mobilise liquids.²⁷ For example, the Institut für Mikrotechnik, Mainz has developed a membrane pump that operates with microlitre volumes, but can also pump at up to 0.4 ml min⁻¹. These pumps, which are very small, can deliver the microlitre volumes that are required for managing the movement of liquids in typical devices. However, as they have been constructed from a polymer, practical difficulties may arise when using organic solvents, and depending upon the micro channel geometry, excessive back pressures may be generated.

As one of the attractive features of using micro reactors is their capacity to perform high throughput parallel processing, the use of hydrodynamic pumping may become impractical due to the large number of different solutions that will be required within the reactor. To overcome the need therefore for a large number of pumps and to simplify the construction of micro fluidic systems, electro-osmotic flow (EOF) which has no moving parts, has proved to be a widely preferred method for reagent and solvent pumping.

EOF can be used to move reagents and solvents around a system of channels as a function of applied voltages, with a very high degree of control and allowing the processes to be readily automated. In addition, due to the high electric field (*e.g.* 200 V per centimetre of channel) associated with the EOF, variations in the electrophoretic mobility of individual species enables separation to be achieved. The combination of EOF and electrophoretic mobility can be used to both model and practically control the spatial and temporal position of components in a micro reactor system.²⁸

To illustrate the principles of EOF, one can consider a microchannel fabricated from a material (*e.g.* glass), having naturally negatively charged functional groups on its surface. If a liquid, displaying some degree of dissociation, is brought into contact with the material, positive counter ions will form a double layer such that the positively charged ions are attracted to the negatively charged surface. If an electric field is now applied through the liquid phase, the positive mobile ions will migrate to the negative electrode inducing a drag on the bulk liquid. In an aqueous buffered system (pH 3–9) the solution flows towards the cathode with volumetric flow rates in the order of nl min⁻¹ to μl min⁻¹ depending on the channel dimensions and applied field. The flow velocity achieved with EOF is given by eqn. (1)

$$v_{\text{EOF}} = \frac{V}{L}\mu$$

where V is the applied field, L is the length of the channel and μ is electro-osmotic mobility (dependent on factors such as zeta potential, ionic strength and pH).

Since V and L are controlled by the user, a very high level of control is achievable. Furthermore, this control can be automated and a relatively simple LabVIEW™ program, such as that developed at Hull which allows one to control the output from a power supply to a number of channels in a micro reactor (Fig. 3) has been developed. By varying the potentials across each channel section, it is possible to rapidly optimise the relative flows of different reagents, or to inject plugs of one reagent into a stream of another, or to introduce a number of reagents in a specified sequence for multi-step reactions.

Unlike conventional (hydrodynamic) flow systems, solutions that are moved by EOF have a flat velocity profile across the channel. This, together with an absence of back pressure effects and an inherent low Reynolds number, affords minimal band broadening and efficient electrophoretic separation of reactants and products.

Although EOF has mainly been used in applications with aqueous solutions, it is not restricted to these systems and EOF may be applied to reagents in polar solvents such as methanol, tetrahydrofuran, acetonitrile and dimethylformamide. For example, Harrison and coworkers²⁹ used EOF to achieve valveless

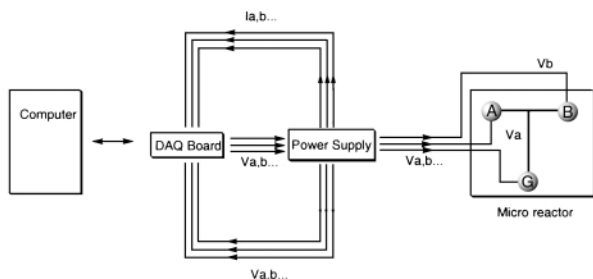
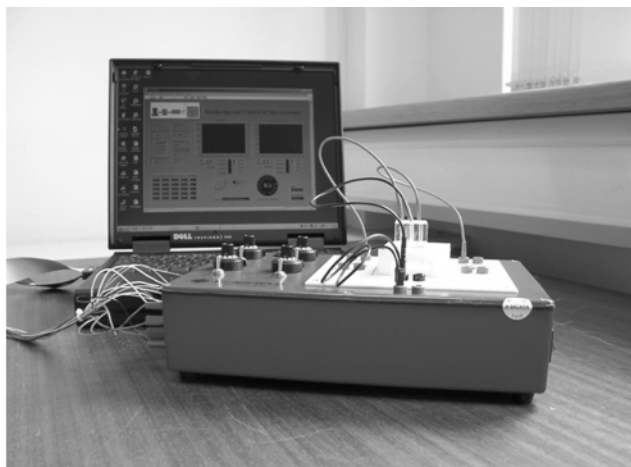


Fig. 3 An automated computer controlled chemical reaction, showing the hardware and a schematic of the system. Using the configuration shown, the duration and magnitude of voltage applied to each reservoir can be selected and the resulting current monitored.

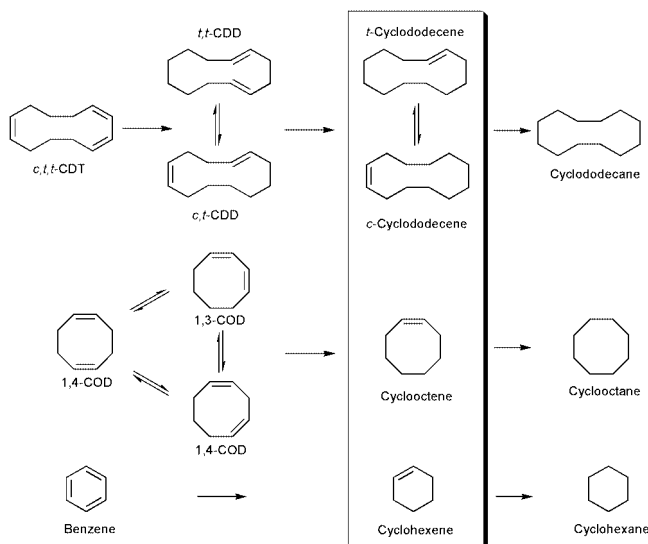
pumping of acetonitrile reagent solutions during the synthesis of an azo dye in a glass micro reactor. This degree of solvent choice greatly extends the types of EOF-controlled chemistry that can be carried out in micro reactors. Obviously the solvent systems used must exhibit some level of polarity, and strictly non-polar solvents cannot be pumped by EOF unless a polar modifier is added.

Applications of micro reactors in synthesis

The inherent benefits of micro reactors, namely rapid generation of small but detectable quantities of reaction products, efficient heat transfer and fluidic control, are now being applied successfully to synthetic chemistry. In theory, these factors might give a research worker using a micro reactor the ability to greatly increase the rate at which new compounds are produced. The work highlighted in this section demonstrates how some of the initial findings obtained by research groups developing micro reactor systems could be applied to high throughput synthesis. There are also some operating characteristics of the micro reactor environment that result in fundamental differences in chemistry. Of more immediate and perhaps significant impact to the research community is the opportunity micro reactors offer in terms of performing a large number (many hundreds) of reactions to explore and optimise a single reaction or a series of chemical reactions. For example, the capability to generate information about reaction conditions, kinetics and product selectivity is now readily accessible using micro reactors, an option not easily available using conventional methodology.

Micro reactor systems have so far been successfully deployed in gas and liquid phase chemistry, including catalyst testing. A recent example of the application of micro reactors to gas phase chemistry was reported at the IMRET 4 conference. Hönicke and coworkers reported the gas phase partial hydrogenation of cyclododeca-1,5,9-triene (CDT), cycloocta-1,5-diene (COD) and benzene over palladium and ruthenium/zinc catalysts (see

Scheme 1).³⁰ The micro reactor system consisted of alumina wafers with mechanically etched channels, which were then



Scheme 1 The mild reaction conditions and the unique mass transfer properties of micro reactors allow hydrogenation of cyclic trienes and dienes to industrially important monoalkenes (ref. 26).

activated by anodic oxidation and impregnation with an organic solution of palladium(II) acetylacetonate. This gave an 18 μm thick activated layer with 0.18 wt% palladium. Twenty four of these wafers were then stacked to give 672 micro channels with internal geometries of $200 \mu\text{m} \times 200 \mu\text{m} \times 30 \text{mm}$. A similar process was used for the construction of the Ru/Zn reactor, which contained 0.2 wt% each of ruthenium and zinc. The organic solvent was then removed *via* oxidation in air at 417 $^{\circ}\text{C}$ followed by hydrogen reduction at 150 $^{\circ}\text{C}$ to give the activated catalyst. Although palladium showed no conversion of benzene to cyclohexene, CDT was converted with high yield and selectivity to cyclododecene at 150 $^{\circ}\text{C}$, with the catalyst bed giving >80% conversion to cyclododecene for over 20 h. The COD conversion went from 75 to 100% at 150 $^{\circ}\text{C}$ by increasing the residence time in the reactor from 40 to 115 ms. This system proved to be robust, in that throughput could be increased ten-fold from 50 to 500 mg h^{-1} whilst conversion to cyclooctene remained above 80%. Partial hydrogenation of benzene by Ru/Zn was less successful with conversion falling rapidly, and only low yields of cyclohexene were obtained, with the major product being cyclohexane. This work shows that high conversions may be achieved given only a short residence time. By controlling the rate of flow, conversion rate and product yields may be selected or rapidly optimised. This micro reactor system also allows easy re-activation of the catalyst, and it would be readily possible to allow the mixture and velocity of gases to be adjusted automatically in real-time *via* feedback control from analysis of exhaust gases.

Micro reactors using heterogeneous catalysts have been applied in liquid-phase organic synthesis. An early, though still comparatively recent development was reported from the Micro Reactor Group in Hull by Greenway *et al.*³¹ The micro reactor utilised EOF to mobilise the reagents and allowed the catalytic synthesis of 4-cyanobiphenyl using a modified Suzuki coupling reaction (Scheme 2). The incorporation of micro porous silica frits³² within the reactor manifold enhanced EOF and allowed the immobilisation of the heterogeneous catalyst (1.8% palladium on silica). The catalyst immobilisation method produced a leaching rate in the region of ppb (1.2 to 1.6 ppb) removing the need for subsequent purification from metal residues. The micro reactor device was optimised using flow injection analysis principles producing a $67 \pm 7\%$ ($n = 6$) yield of the 4-cyanobiphenyl product at room temperature within 25 min.

The flow injection method adopted allowed the periodic injection of the aryl halide (5 s injection length with a 25 s injection interval) into a continuous flow of phenylboronic acid. Flow was maintained using an external applied voltage of 200 V. The yield obtained using the device was comparable with Suzuki reactions performed on a large (batch) scale using homogeneous catalysts. One of the interesting observations of this reaction was that, unlike conventional Suzuki couplings performed in a flask, base was not required. Although the reason for this is as yet unclear, it is thought that the applied electric field may be sufficient to cause localised ionisation of solvent water to H^+ and OH^- at the metal surface. It may be this so-formed hydroxide that performs the function of a conventional inorganic or amine base. However, the micro reactor demonstrated the potential application of such devices to perform chemical reactions, allowing high throughput screening, rapid method development or reaction optimisation.

The Hull group have also demonstrated that a superacid catalyst (sulfated zirconia) could be immobilised onto the surface of a polydimethylsiloxane (PDMS) micro reactor top plate. This was achieved by dusting the pre-cured PDMS surface with activated catalyst and baking the plate at 100 °C for 1 h. The PDMS top plate (containing the catalyst) was clamped to a glass base plate (with etched micro channels) and syringe pumps were used to mobilise the hexan-1-ol, which underwent dehydration to hex-1-ene. The micro reactor featured an *in situ* resistive heater wire cast into the PDMS top plate, which was operated at 155 to 160 °C.³³

An attractive feature of micro reactors is their ability to carry out chemical processes that may be hazardous. For example Burns and Ramshaw³⁴ at the University of Newcastle have described the nitration of toluene and benzene in stainless steel or PTFE micro reactors, demonstrating the approach is suited to a hazardous processes involving organic solvents and concentrated acids. In addition, they are also investigating the challenge of manipulating bi-phasic liquid–liquid systems and the control of product distribution to avoid hazardous trinitrated aromatic products. Their studies have yielded some elegant ways to control immiscible liquid layers in capillary systems that include (i) segmented flow, in which plugs of alternate phases travel down a capillary and (ii) parallel laminar flow, where similar amounts of two phases run together through the capillary producing an interfacial contact zone.

Burns and Ramshaw's studies on benzene nitration also demonstrated that conversion, while showing a near linear relationship with temperature, can be increased substantially by the use of smaller capillaries that enhance diffusion effects by reducing the size of the slugs of material in the channel. Halving the capillary diameter from 250 to 130 μm more than doubled the rate of nitration. Flow rates were also found to be important, with faster flow rates giving rise to higher conversion as they promoted internal circulation of the liquid plugs travelling down the capillary.

In comparison with conventional nitration techniques, the results showed that rate constants for the micro reactor process (1–8 min^{-1}) in 178 μm capillaries were similar to those in the published literature (1–5 min^{-1}). It is expected that further optimisation of the micro reactor device and its operation, particularly by increasing the sophistication of the technology to decrease droplet size, will result in substantial improvement to the efficiency of the devices.

To demonstrate the advantages that micro reactors offer when dealing with potentially hazardous reagents, Chambers and Spink³⁵ recently reported the development of a micro reactor fabricated from a block of nickel, which was used for the elemental fluorination of organic substrates. Conversions compare well with results from conventional reactors. The small amount of fluorine involved, together with the heat and mass transfer properties of the micro reactor, overcame many of the safety issues associated with this type of reaction.

Optimisation of catalytic processes

To demonstrate the testing and optimisation of catalytic processes, the Hull group has developed a simple procedure for the immobilisation and introduction of supported reagents in micro reactors (Fig. 4). Such configurations enable solutions to

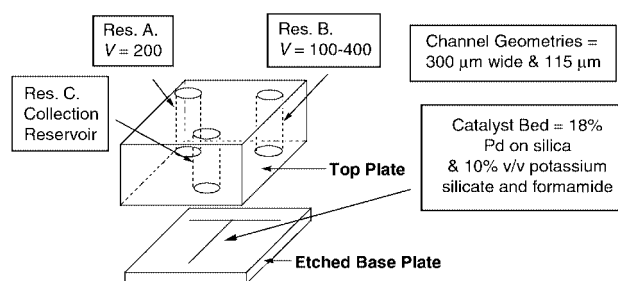
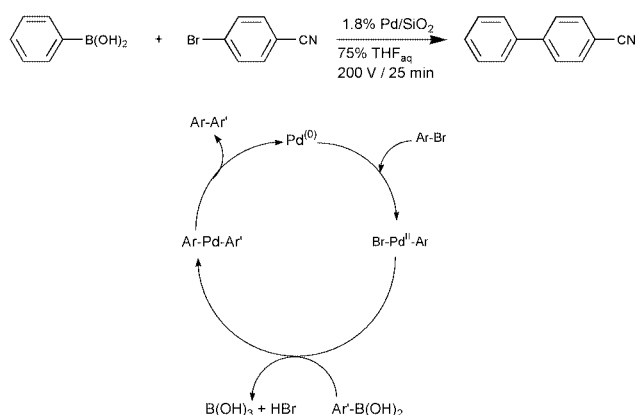


Fig. 4 A Hull micro reactor, configured for the Suzuki reaction. Reservoir A contains 100 μl of 4-bromobenzonitrile (0.1 M) and reservoir B 100 μl of phenylboronic acid (0.1 M), both in 75% THF_{aq} . Products from the reaction are taken from reservoir C and analysed by GCMS.

be passed over catalysts in either a continuous or plug mode with a high degree of fluidic control. Catalyst types under investigation include immobilised enzymes (such as lipases and esterase), metals, sulfated zirconia and zeolite-based materials. For example, in the case of an enzyme system based on porcine liver esterase, symmetrical diesters are passed over this catalyst bed to effect desymmetrisation to a chiral mono-ester, creating a high-throughput reactor for biocatalysis.

A second approach is to pulse several different reagents one by one over the catalyst bed. Given the computer-based flow-control possible with micro reactors, it is now relatively easy to achieve accurate and reproducible reaction sequencing. In the Suzuki reaction performed at Hull, the aryl halide and boronic acid were alternately pulsed over a catalyst bed of palladium on silica. This had the effect of increasing yields from < 5% to 68% by simulating the catalytic cycle (Scheme 2).³¹ The catalyst was



Scheme 2 The catalytic cycle of the Suzuki reaction.

flushed with the aryl bromide to drive the oxidative addition to the metal, and then flushed with boronic acid to effect conversion to the biphenyls.

Using a system of five continuous flow micro reactors, the Suzuki reaction has been carried out on an industrial scale by Merck in Germany, where researchers found improvements over conventional batch reactors.³⁰ For example, in the reaction of 3-bromobenzaldehyde with 4-fluorophenylboronic acid, 90% yields were reported for the micro reactors, compared with 50% in stirred flasks.

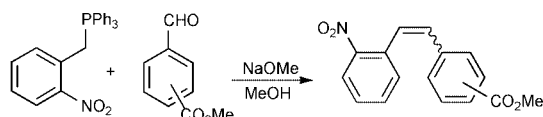
One of the chief limitations of the studies in Hull has been the high temperatures (680 °C) required to anneal the top glass plate

to the etched glass base plate as any organic material would be destroyed in these processes, hence metals on silica have been favoured as catalysts.

These early studies into catalytic processes demonstrate the potential of using micro reactor technology for a continuous production line approach to single compound production. However, the design of such devices could be easily modified to evaluate the performance of a catalyst across a broad range of substrates. Another opportunity would be in using multi-channel systems that would allow the evaluation of a number of different catalysts for a single reaction. These studies allow rapid evaluation of reaction conditions to allow the best catalyst for a given reaction to be studied, or the efficacy of a catalyst over a range of substrates to be evaluated.

Multi-step and analog based reactions

At the recent IMRET 4 conference, the Hull group reported a micro reactor device that allowed the synthesis of a number of nitrostilbene esters using a borosilicate micro reactor.³⁶ The micro reactor allowed the development of the Wittig reaction investigating a number of reaction features such as stoichiometry, stereochemistry and reaction diversity (Scheme 3).



Scheme 3 The Wittig reaction.

Initial investigations centred on using the device for synthetic method development and optimisation, allowing rapid reaction design in conjunction with EOF as the mobilisation method. With a 2:1 reaction stoichiometry (aldehyde in excess) a yield of 70% was achieved using the micro reactor in a continuous flow mode with an optimum voltage of 400 V. The micro reactor demonstrated an increase in reaction efficiency of 10% over the conventional batch method. The reaction stoichiometry was then reduced to 1:1 but the yield was poor (39%) so a flow injection technique was adopted. This resulted in the injection of the phosphonium salt into the continuous flow of the aldehyde compound at 400 V. A 59% yield was obtained, but more importantly it allowed a series of aldehydes to be reacted in sequential injections using the optimum conditions established at 1:1 stoichiometry. This demonstrated the micro reactors diversity and high through-put capability.

The above research has been extended to investigate the stereoselective control of the chemical reaction by applying electrical fields which generate controlled concentration gradients of the reagent streams.³⁷ The stereoselective synthesis of the *cis* (*Z*) and *trans* (*E*) isomers was controlled by varying the applied voltages to the reagent reservoirs within the device. The variation in the external applied voltage subsequently altered the relative reagent concentrations within the device producing *Z/E* ratios in the region of 0.57 to 5.21. In comparison, a traditional batch reaction was performed based on the same reaction length, concentration, solvent and stoichiometry resulting in a *Z/E* ratio of 3.0. The unique flow control created in the micro reactor system has allowed the localised concentration gradients, produced by a diffusion limited non-turbulent mixing regime, to generate the observed stereoselectivity. The control of these localised diffusion-limited concentration gradients is an important feature of micro reactors and one that can be effectively exploited for yield and product selectivity.

Multi-step reactions

So far, micro reactors appear to be limited to carrying out a single synthetic step. One of the thrusts of the research in Hull is to develop methodology that will give the chemist the ability

to look as multi-step reactions, culminating in target or diversity based synthesis.

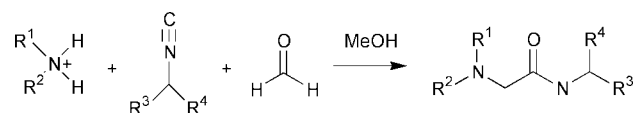
To extend the capability of performing multi step reactions in micro reactors, processes such as peptide synthesis represent a good model system. Peptides have been traditionally prepared combinatorially *via* solid supported techniques^{38,39} but this approach has the disadvantage that a fairly expensive polymer support is required and that the product requires post-synthetic cleavage. In addition, extra steps are added to the synthesis as a result of having to initially link the amino acid to the polymer support. The preparation of peptides in micro reactors, using solution phase chemistry, offers the possibility of overcoming such problems.

Using solution phase chemistry there are several methods that may be used to form peptide bonds such as diethyl azodicarboxylate⁴⁰ (DEAD) or carbodiimide reagents such as dicyclohexylcarbodiimide (DCC)⁴¹ or 1-(3-dimethylaminopropyl)-3-ethylcarbodiimide hydrochloride (EDCI).⁴² In addition acyl halides, anhydrides and azides may be utilised in the formation of peptide bonds.⁴³ Once the methodology for the formation of peptide bonds has been fully established, selective deprotection of either of the protecting groups will allow longer peptide chains to be assembled. This multi-step synthesis will clearly allow the rapid generation of libraries of peptides, which could then be used in determining their biological properties.

In situ detection methods in micro reactors

As indicated earlier, research focused on μ -TAS has developed a number of suitable detection methods for micron scale systems, with the most common method adopted being fluorescence. Other detection systems developed have included UV-VIS⁴⁴⁻⁴⁸ and electrochemical⁴⁹⁻⁵² detection offering sensitivity and simple detection with environmental micro systems. The information provided is however generally insufficient for structural characterisation of unknown chemical species. For the micro reactor system to become truly versatile, the development of hyphenated techniques and specialised equipment such as NMR and Raman spectrometry would allow direct, real time characterisation and spatial determination of concentration and pH information. Currently a range of analytical techniques are being investigated by a number of research groups. These include mass spectrometry (MS)⁵³ and near infrared (NIR).⁵⁴⁻⁵⁷

One area of analysis which has been readily reported in the literature is the hyphenation of micro reactor to mass spectrometers.⁵⁸⁻⁶¹ Lazar *et al.*⁵⁸ from Oakridge National Laboratories have coupled a micro fluidic device with a nanospray tip for electrospray ionisation, allowing dilute peptide and protein solutions to be characterised using a time of flight mass spectrometer. The hyphenated system allowed the capture of spectra within milliseconds (10 to 20 ms) resulting in 50 to 100 spectra per second. The second study by Mitchell *et al.*, presented at the recent Micro Total Analytical Systems conference,⁵⁹ described the detection of a multicomponent reaction using an electrospray ionisation (EIS)-MS. The multicomponent synthesis investigated was the Ugi reaction (Scheme 4) in which a solution of formaldehyde and pure



Scheme 4 The Ugi reaction.

solvent was infused through one of the inlets whilst a multicomponent mixture (isocyanide, amine salt) was also added. The hyphenated micro reactor-MS system allowed the real time detection of the synthetic Ugi coupling reaction.

Other detection systems reported have been NIR and Raman spectrometry. A miniaturised NIR spectroscopic system fabri-

cated in borosilicate glass has been developed by Ache.⁵⁶ The micro device contains a circular wave guide covered by a sensing membrane. In addition, the micro NIR system contained an incandescent light source, a NIR micro spectrometer with a self-focusing reflection grating and NIR diode. At the University of Michigan, Reshni and co-workers⁶² demonstrated one early example of Raman spectrometry on a micro device. The system was fabricated using a Raman microprobe stage coupled to a capillary electrophoresis chip. Traditionally, Raman spectroscopy has a limit of detection in the millimolar region, however Reshni's micro device achieved a limit of detection in the micromolar region and below. This was due to the addition of a preconcentration stage using isotachopheresis. This system has allowed the successful fingerprinting and quantification of reactions on-chip.

Commercialisation of micro reactor technology

A commercially available chemical synthesiser using micro reaction technology already exists, and is produced by IMM-Mainz. It consists of a pumping module, a micro-reactor that results in very efficient mixing of reagents, followed by a capillary to allow time for the reaction to go to completion. The outflow is then collected for further manipulation by the user. This could be just the first step along a road which will see the integration of automated reagent manipulation, reaction monitoring and product purification into a single instrument containing several interconnected micro reactors, or possibly a single micro reactor device. In common with microelectronic chips, once the facilities to fabricate micro reactors are in place, they become progressively cheaper to produce in quantity. This should make the production of chemicals in massive parallel arrays of reactors an economic possibility. It is likely that some of the peripheral equipment required will still represent a considerable cost, but this should be set against the potential increase in productivity per research worker. In addition, the effective production of molecules in terms of energy, safety and environmental impact will emerge as important factors in the future exploitation of micro reactor technology. One of the underlying features of any future commercially available automated synthesis system must be versatility. Research is now moving towards a 'plug and play' approach in which the reaction and detection configurations can be customised. The next couple of years will undoubtedly see significant development in this area of the technology. We should now prepare ourselves, including university courses for undergraduates, for the impact the micro reactor is going to have on the whole area of chemical research and production.

Acknowledgements

We wish to thank the EPSRC Lab-on-a-chip Consortium (B. O'S., R. J. M.), Novartis Pharmaceuticals (P. W.) and GlaxoSmithKline (V. S.) for financial support.

Further information

See the following websites:

<http://analyticalsciencehull.org/>

Further information about conferences relating to this topic may be found at the following websites:

IMRET 5 (Strasbourg, France, 27–30 May 2001):

<http://www.aiche.org/conferences/cosponsored/#2001>

μ-TAS 2001 (Monterey, CA, USA, 21–25 Oct 2001):

<http://www.casss.org/tas2001>

Notes and references

1 K. Schubert, W. Bier, J. Brandner, M. Fichtner, C. Franz and G. Linder, *Process Miniaturisation: 2nd International Conference on Micro-reaction Technology*, AIChE, New Orleans, 1998, p. 89.

- 2 J. B. Knight, A. Vishwanath, J. P. Brody and R. H. Austin, *Phys. Rev. Lett.*, 1998, **80**, 386.
- 3 W. Ehrfeld, V. Hessel and H. Löwe, *Microreactors*, Wiley-VCH, Weinheim, 2000, ch. 1.
- 4 W. Ehrfeld, V. Hessel, S. Kiesewalter, H. Löwe, T. Richter and J. Schiewe, *Proceedings of the Third International Conference on Microreaction Technology*, Frankfurt, Germany, 1999, p. 14.
- 5 T. M. Floyd, M. W. Losey, S. L. Firebaugh, K. F. Jensen and M. A. Schmidt, *Proceedings of the Third International Conference on Microreaction Technology*, Frankfurt, Germany, 1999, p. 171.
- 6 P. D. I. Fletcher and S. J. Haswell, *Chem. Br.*, 1999, **35**, 38.
- 7 S. J. Haswell, *Analyst*, 1997, **112**, 1R.
- 8 A. Manz, D. J. Harrison, E. Verpoorte, J. C. Fettingner, H. Ludi and H. M. Widmer, *Chimia*, 1991, **45**, 103.
- 9 A. Manz, D. J. Harrison, E. Verpoorte and H. M. Widmer, *Adv. Chromatogr.*, 1993, **33**, 1.
- 10 A. Manz, C. S. Effenhauser, N. Burggraf, E. Verpoorte, D. E. Raymond and H. M. Widmer, *Anal. Mag.*, 1994, **22**, M25.
- 11 *Proceedings of the Micro Total Analytical Systems 98' Workshop*, ed. D. J. Harrison and A. van den Berg, Kluwer Academic Press, Dordrecht, 1998.
- 12 A. van den Berg and T. S. J. Lammerink, *Top. Curr. Chem.*, 1998, **194**, 21.
- 13 D. J. Harrison, K. Fluri, K. Seiler, Z. H. Fan, C. S. Effenhauser and A. Manz, *Science*, 1993, **261**, 895.
- 14 S. C. Jacobson, R. Hergenroder, L. B. Koutny and J. M. Ramsey, *Anal. Chem.*, 1994, **66**, 1114.
- 15 S. C. Terry, J. H. Jerman and J. B. Angel, *IEEE Trans. Electron Devices*, 1979, **ED26**, 1880.
- 16 A. Manz, N. Graber and H. M. Widmer, *Sens. Actuators B*, 1990, **1**, 24.
- 17 A. T. Woolley, D. Hadley, P. Ladre, A. J. deMello, R. A. Mathies and M. A. Northrup, *Anal. Chem.*, 1996, **68**, 4081.
- 18 A. T. Woolley and R. A. Mathies, *Anal. Chem.*, 1996, **67**, 3676.
- 19 A. T. Woolley, G. F. Sensabaugh and R. A. Mathies, *Anal. Chem.*, 1997, **69**, 2181.
- 20 S. C. Jacobson and J. M. Ramsey, *Anal. Chem.*, 1996, **68**, 720.
- 21 C. S. Effenhauser, A. Paulus, A. Manz and H. M. Widmer, *Anal. Chem.*, 1994, **66**, 2949.
- 22 D. Schmalzing, A. Adourian, L. Koutny, L. Ziaoura, P. Matsudaria and D. Ehrlich, *Anal. Chem.*, 1998, **70**, 2303.
- 23 T. McCreedy, *TrAC*, 2000, **19**, 396.
- 24 D. M. Spence and S. R. Crouch, *Anal. Chem.*, 1998, **358**, 95.
- 25 B. H. Schoot, S. Jeanneret and A. Berg, *Anal. Methods Instrum.*, 1993, **1**, 38.
- 26 P. K. Das Gupta and S. Lui, *Anal. Chem.*, 1994, **66**, 1792.
- 27 H. T. G. van Lintel, F. C. M. van de Pol and S. Bouwstra, *Sens. Actuators*, 1988, **15**, 153.
- 28 S. J. Haswell, P. D. I. Fletcher and V. N. Paunov, *Analyst*, 1999, **124**, 1273.
- 29 H. Salimi-Moosavi, T. Tang and D. J. Harrison, *J. Am. Chem. Soc.*, 1997, **119**, 8716.
- 30 E. Dietzsch, D. Hönicke, M. Fichtner, K. Schubert and G. Weißmeier, *IMRET 4: 4th International Conference of Micro Reaction Technology Topical Conference Proceedings, AIChE Spring National Meeting, March 5–9 2000*, Atlanta GA, USA, p. 89.
- 31 G. M. Greenway, S. J. Haswell, D. O. Morgan, V. Skelton and P. Styring, *Sens. Actuators B*, 2000, **63**, 153.
- 32 P. D. Christensen, S. W. P. Johnson, T. McCreedy, V. Skelton and N. G. Wilson, *Anal. Commun.*, 1998, **35**, 341.
- 33 N. G. Wilson and T. McCreedy, *Chem. Commun.*, 2000, 733.
- 34 J. R. Burns and C. Ramshaw, *IMRET 4: 4th International Conference of Micro Reaction Technology Topical Conference Proceedings, AIChE Spring National Meeting, March 5–9 2000*, Atlanta GA, USA, p. 133.
- 35 R. D. Chambers and R. C. H. Spink, *Chem. Commun.*, 1999, 883.
- 36 V. Skelton, G. M. Greenway, S. J. Haswell, P. Styring, D. O. Morgan, B. H. Warrington and S. Y. F. Wong, *Analyst*, 2000, **126**, 7.
- 37 V. Skelton, G. M. Greenway, S. J. Haswell, P. Styring, D. O. Morgan, B. H. Warrington and S. Y. F. Wong, *Analyst*, 2000, **126**, 11.
- 38 R. B. Merrifield, *J. Am. Chem. Soc.*, 1963, **85**, 2149.
- 39 D. B. Whitney, J. P. Tam and R. B. Merrifield, *Tetrahedron*, 1984, **40**, 4237.
- 40 O. Mitsunobu, *Synthesis*, 1981, 1.
- 41 A. Hassner and V. Alexanian, *Tetrahedron Lett.*, 1978, 4475.
- 42 P. D. Bailey and K. D. Morgan, *Organonitrogen Chemistry*, Oxford University Press, 1996.
- 43 D. S. Perlow, J. M. Erb, N. P. Gould, R. D. Tung, R. M. Freidinger, P. D. Williams and D. F. Veber, *J. Org. Chem.*, 1992, **57**, 4394.
- 44 G. M. Greenway, S. J. Haswell and P. Petsul, *Anal. Chim. Acta*, 1999, **387**, 1.
- 45 G. N. Doku and S. J. Haswell, *Anal. Chim. Acta*, 1999, **382**, 1.

- 46 E. Verpoorte, A. Manz, H. Lüdi, A. E. Bruno, F. Maystre, B. Krattiger, H. M. Widmer, B. H. van der Schoot and N. F. de Rooij, *Sens. Actuators*, 1992, **6**, 66.
- 47 Z. Liang, N. Chiem, G. Ocvirk, T. Tang, K. Fluri and D.J. Harrison, *Anal. Chem.*, 1996, **68**, 1040.
- 48 H. Salimi-Moosavi, Y. Jiang, L. Lester, G. McKinnon and D. J. Harrison, *Electrophoresis*, 2000, **21**, 1291.
- 49 J.-J. Gau, E. H. Lan, B. Dunn and C.-H. Ho, *Micro Total Analysis Systems 2000*, ed. A. van den Berg, W. Olthius and P. Bergveld, Kluwer Academic Publishers, Dordrecht, 2000, p. 509.
- 50 A. T. Woolley, K. Q. Lao, A. N. Glazer and R. A. Mathies, *Anal. Chem.*, 1998, **70**, 684.
- 51 J. S. Rossier, M. A. Roberts, R. Ferrigno and H. H. Girault, *Anal. Chem.*, 1999, **71**, 4294.
- 52 R. S. Martin, A. J. Gawron, S. M. Lunte and C. S. Henry, *Anal. Chem.*, 2000, **72**, 3196.
- 53 A. Feustel, J. Muller and V. Reilling, *Micro Total Analysis Systems '95*, ed. A. van den Berg and P. Bergveld, Kluwer Academic Press, Dordrecht, 1995, p. 299.
- 54 J. P. Cozen, *Appl. Spectrosc.*, 1993, **37**, 753.
- 55 H. J. Ache, *Chem. Ind.*, 1993, **1**, 40.
- 56 H. J. Ache, *Micro Total Analysis Systems '95*, ed. A. van den Berg and P. Bergveld, Kluwer Academic Press, Dordrecht, 1995, p. 47.
- 57 R. J. Jackman, T. M. Floyd, M. A. Schmidt and K. Jensen, *Micro Total Analysis Systems 2000*, ed. A. van den Berg, W. Olthius and P. Bergveld, Kluwer Academic Publishers, Dordrecht, 2000, p. 155.
- 58 I. M. Lazar, R. S. Ramsey, S. Sundberg and J. M. Ramsey, *Anal. Chem.*, 1999, **71**, 3627.
- 59 M. C. Mitchell, V. Spikmans, F. Bessoth, A. Manz and A. de Mello, *Micro Total Analysis Systems 2000*, ed. A. van den Berg, W. Olthius and P. Bergveld, Kluwer Academic Press, Dordrecht, 2000, p. 463.
- 60 I. Ugi, R. Meyr, C. Fetzer and C. Steinbrückner, *Angew. Chem.*, 1959, **71**, 386.
- 61 J. Li, C. Wang, J. F. Kelly, D. J. Harrison and P. Thibault, *Electrophoresis*, 2000, **21**, 198.
- 62 K. A. Reshni, M. D. Morris, B. N. Johnson and M. A. Burns, *Micro Total Analysis Systems '98*, ed. A. van den Berg, W. Olthius and P. Bergveld, Kluwer Academic Press, Dordrecht, 1998, p. 109.

The synthesis of peptides using micro reactors†

Paul Watts,^a Charlotte Wiles,^a Stephen J. Haswell,^{*a} Esteban Pombo-Villar^b and Peter Styring^c^a Department of Chemistry, University of Hull, Cottingham Road, Hull, UK HU6 7RX.

E-mail: S.J.Haswell@chem.hull.ac.uk

^b Nervous System Research, WSJ-386.07.15, Novartis Pharma Ltd., CH4002, Basel, Switzerland^c Department of Chemical and Process Engineering, University of Sheffield, Mappin Street, Sheffield, UK S1 3JD

Received (in Cambridge, UK) 6th March 2001, Accepted 19th April 2001

First published as an Advance Article on the web 15th May 2001

We have demonstrated the first application of multi-step synthesis within a micro reactor and have shown that peptides may be prepared in quantitative yield in a period of 20 min, compared with batch reactions where only moderate yields (40–50%) were obtained in a 24 h period.

During the past ten years, there has been a rapid growth in the development of micro-Total Analytical Systems (μ -TAS)^{1–3} which exploit electroosmotic flow (EOF).⁴ The development of micro reactor devices for chemical synthesis based on complementary technology is less common. However, recent research has shown that Suzuki⁵ and Wittig⁶ reactions may be performed using micro reactor systems.⁷

Peptides have been commonly prepared *via* solid supported techniques since its introduction by Merrifield in 1963.⁸ Solid phase peptide synthesis is based on the addition of a protected amino acid residue to an insoluble polymeric support. The acid-labile Boc group⁹ and base-labile Fmoc group¹⁰ have been commonly used for *N*-protection. After removal of the protecting group the next protected amino acid may be added using either a coupling reagent or a pre-activated amino acid derivative. If this dipeptide is the desired product, it may be cleaved from the polymer support using various reagents, one of the more common methods being treatment with 25–80% HF.¹¹ If a longer peptide is required additional amino acids can be added by repeating further coupling reactions.

Solid phase peptide synthesis has the disadvantage that a fairly expensive polymer support is required. In addition, extra steps are added to the synthesis as a result of initially linking the amino acid to the support and finally having to remove the peptide from the polymer. In this paper a micro reactor has been used to prepare peptides using solution phase chemistry in an attempt to overcome some of the current problems associated with such syntheses.

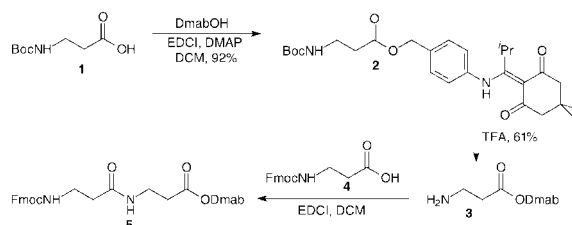
The micro reactor devices used in this work were prepared using standard procedures developed at Hull.¹² A schematic of a typical micro reactor produced using such fabrication techniques is shown in the graphical abstract.† Microporous silica frits¹³ were placed in the channels to prevent hydrodynamic flow occurring.

In the first instance a one-step reaction was considered in which an *N*-protected β -amino acid was reacted with an *O*-protected β -amino acid, to prepare the protected β -dipeptide. To enable the methodology to be applicable to the synthesis of more complex peptides, the use of orthogonal protecting groups was clearly required. After careful consideration, the base-labile Fmoc protecting group¹⁰ was selected for *N*-protection while the Dmab ester¹⁴ was chosen for protection of the carboxylic acid. Importantly, both protecting groups may be removed under mild conditions, since electroosmotic flow is retarded if the pH of the reaction is outside the range 3–10.

Commercially available Boc- β -alanine **1** was protected as the Dmab ester using an EDCI [1-(3-dimethylaminopropyl)-3-ethylcarbodiimide hydrochloride] and DMAP coupling reaction, to give the ester **2** in 92% yield in a bulk reaction (Scheme 1). Treatment of **2** with trifluoroacetic acid furnished the desired amine **3** in 61% yield, which was subsequently reacted with Fmoc- β -alanine **4** *via* a carbodiimide coupling reaction, to give a synthetic sample of dipeptide **5**.

Having prepared dipeptide **5**, it represented a synthetic target for preparation using the micro reactor. Prior to synthesis, the micro reactor channels were primed with anhydrous DMF to remove any air and moisture from the channels and the microporous silica frits. A standard solution of Fmoc- β -alanine **4** (50 μ l, 0.1 M) in anhydrous DMF was added to reservoir A, a solution of EDCI (50 μ l, 0.1 M) was placed in reservoir B and a solution of amine **3** (50 μ l, 0.1 M) was placed in reservoir C. Anhydrous DMF (40 μ l) was placed in reservoir D, which was used to collect the products of the reaction. Platinum electrodes were placed in each of the reservoirs (A, B and C positive, D ground) and an external voltage was applied to the channels inducing electroosmotic flow of the reagents. The reactions were conducted at rt for a period of 20 min, in order to acquire sufficient volume of product to determine the yield of the reaction. Analysis was achieved by high performance liquid chromatography (Jupiter C₁₈ 10 μ m, 4.6 \times 250 mm, obtained from Phenomenex), mobile phase composition: 0.1% TFA in water and 0.1% TFA in acetonitrile, using a gradient system of 30% aqueous to 70% aqueous over 20 min, with a flow rate of 2.5 ml min⁻¹ at rt).

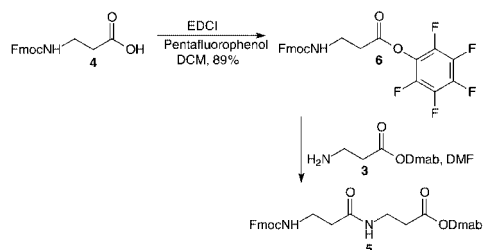
When stoichiometric quantities of the reagents were used only *ca.* 10% conversion to peptide **5** was achieved when a voltage of 700 V was applied to the reagents (A, B and C). However, by using two equivalents of EDCI (0.2 M solution) the yield of the reaction was increased to *ca.* 20%. By applying a stopped flow technique (2.5 sec injection length with flow stopped for 10 sec) the yield of the reaction was further increased to 50%. Since the yield of the reaction appeared to greatly depend on the number of equivalents of EDCI used, we wished to further investigate the effect of carbodiimide concentration on the reaction, however we found that EDCI was insoluble in DMF above 0.2 M concentrations. In further experiments DCC was used as the coupling reagent as it was considerably more soluble in DMF. Using 5 eq. of DCC (0.5 M solution in reservoir B) a 93% yield of dipeptide **5** was obtained using the optimised conditions described above.



Scheme 1 Synthesis of standard dipeptide derivative.

† Electronic supplementary information (ESI) available: schematic of a borosilicate glass micro reactor. See <http://www.rsc.org/suppdata/cc/b1/b102125g/>

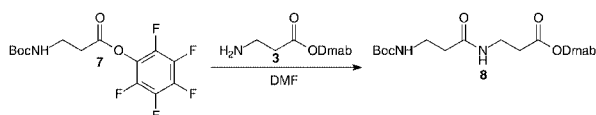
Another common method utilised in peptide bond formation involves the reaction of a pre-activated amino acid derivative, such as a pentafluorophenyl ester, with an amine.^{15,16} Fmoc- β -alanine **4** was activated as the pentafluorophenyl ester **6** via an EDCI coupling reaction (Scheme 2). The pentafluorophenyl ester **6** was stable and could be stored indefinitely in the freezer. The ester **6** was subsequently reacted in bulk with amine **3** to produce dipeptide **5**.



Scheme 2 Preparation and reaction of pentafluorophenyl esters of Fmoc protected amino acids.

Having prepared dipeptide **5** via the alternative pre-activated strategy, we wished to investigate if the reaction could be performed in a micro reactor. A standard solution of the pentafluorophenyl ester of Fmoc- β -alanine **6** (50 μ l, 0.1 M) in anhydrous DMF was added to reservoir A, a solution of amine **3** (50 μ l, 0.1 M) was placed in reservoir B and anhydrous DMF (40 μ l) was placed in reservoir D, which was used to collect the products of the reaction. It was found that using continuous flow of both reagents, where the ester **6** was maintained at 700 V and the amine **3** was maintained at 600 V, dipeptide **5** was produced in quantitative yield in just 20 min. This represented a significant increase in yield compared with the traditional batch synthesis where only 40–50% conversions were obtained.

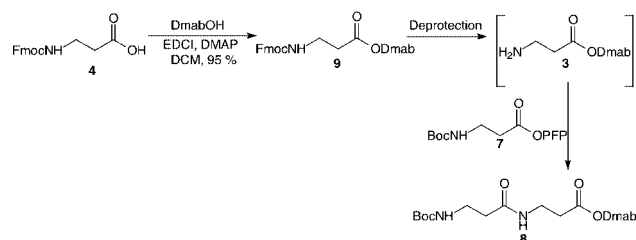
Similarly, the reaction between the pentafluorophenyl ester **7** of Boc- β -alanine and amine **3** was also investigated in the micro reactor (Scheme 3). In this case, when the reagents were mixed under a continuous flow regime, with both reagents maintained at 700 V, a quantitative yield of peptide **8** was observed. Importantly, this result demonstrates that both Boc and Fmoc protecting groups are suitable for use in the preparation of peptides using micro reactors.



Scheme 3 Reaction of pentafluorophenyl esters of Boc- β -alanine.

Having successfully demonstrated that peptide bonds could be formed in micro reactors using two common methods, we wished to show that we could extend the methodology to the preparation of longer chain peptides. Consequently, we needed to be able to conduct deprotection reactions in the micro reactor and subsequently perform further peptide bond forming reactions. Fmoc- β -alanine **4** was converted into the Dmab ester **9**, in a bulk reaction, using standard conditions (Scheme 4). It was proposed to convert ester **9** into amine **3** by deprotection of the Fmoc group in the micro reactor and subsequently react the amine 'in situ' with pentafluorophenyl ester **7**, to give the dipeptide **8**. Treatment of **9**, with 10 eq. of piperidine in DMF using the micro reactor, resulted in 60–70% deprotection over a 20 min period, to give amine **3**.¹⁷

Subsequently, a standard solution of the Dmab ester of Fmoc- β -alanine **9** (50 μ l, 0.1 M) in anhydrous DMF was added to reservoir A, a solution of piperidine (50 μ l, 1.0 M, 10 eq.) was placed in reservoir B and a solution of pentafluorophenyl ester **7** (50 μ l, 0.1 M) was placed in reservoir C, in an attempt to prepare dipeptide **8** using this multi-step approach. Anhydrous DMF (40 μ l) was placed in reservoir D, which was used to collect the products of the reaction. The HPLC of the reaction mixture showed that Fmoc deprotection had occurred, however



Scheme 4 Multi-step peptide synthesis.

no peptide was evident. It was however found that the excess piperidine used in the reaction was reacting with the pentafluorophenyl ester **7** to give amide **10**.

As a result, an alternative method of Fmoc deprotection was required that would not cause the aforementioned problem. Using the micro reactor, the Dmab ester of Fmoc- β -alanine **9** was reacted with one equivalent of DBU to give the free amine **3** which was then reacted with the pentafluorophenyl ester of Boc- β -alanine **7**, in an attempt to form the dipeptide **8**.

In this case, when the reagents were mixed using continuous flow, with the reagents maintained at 700 V, product **8** was observed in typically 25% yield. By comparing the flows of each reagent at this stage we were able to optimise the reaction. The Dmab ester of Fmoc- β -alanine **9** was maintained at 750 V while reacted with DBU at 800 V. The deprotected amine was then reacted, using continuous flow, with the pentafluorophenyl ester of Boc- β -alanine **7** to give a conversion of 96%, based on the amount of Dmab ester **9** present at the end of the reaction.

Having shown that more complex peptides could be produced by removal of the *N*-protecting group we wished to determine if we could remove the Dmab protecting group using hydrazine. Hence, a solution of the Dmab ester of Fmoc- β -alanine **9** (50 μ l, 0.1 M) in anhydrous DMF was added to reservoir A and a solution of hydrazine (50 μ l, 0.1 M) was placed in reservoir B. Anhydrous DMF (40 μ l) was placed in reservoir D, which was used to collect the products of the reaction. Using continuous flow of both reagents, maintained at 700 V, quantitative deprotection was observed to give carboxylic acid **4**.

We wish to thank Novartis Pharmaceuticals (P. W. and C. W.) for financial support. We are grateful to Dr Tom McCreedy (University of Hull) for help in fabricating the micro reactor devices.

Notes and references

- S. J. Haswell, *Analyst*, 1997, **112**, 1R.
- A. Manz, D. J. Harrison, E. Verpoorte and H. M. Widmer, *Adv. Chromatogr.*, 1993, **33**, 1.
- D. J. Harrison, K. Fluri, K. Seiler, Z. H. Fan, C. S. Effenhauser and A. Manz, *Science*, 1993, **261**, 895.
- P. D. I. Fletcher, S. J. Haswell and V. N. Paunov, *Analyst*, 1999, **124**, 1273.
- G. M. Greenway, S. J. Haswell, D. O. Morgan, V. Skelton and P. Styring, *Sensors & Actuators B*, 2000, **63**, 153.
- V. Skelton, G. M. Greenway, S. J. Haswell, P. Styring, D. O. Morgan, B. Warrington and S. Y. F. Wong, *Analyst*, 2001, **126**, 7.
- S. J. Haswell, R. J. Middleton, B. O'Sullivan, V. Skelton, P. Watts and P. Styring, *Chem. Commun.*, 2001, 391.
- R. B. Merrifield, *J. Am. Chem. Soc.*, 1963, **85**, 2149.
- P. Munster and W. Steglich, *Synthesis*, 1987, 223.
- B. Penke and J. Rivier, *J. Org. Chem.*, 1987, **52**, 1197.
- D. B. Whitney, J. P. Tam and R. B. Merrifield, *Tetrahedron*, 1984, **40**, 4237.
- T. McCreedy, *Anal. Chim. Acta*, 2001, **427**, 39.
- P. D. Christensen, S. W. P. Johnson, T. McCreedy, V. Skelton and N. G. Wilson, *Anal. Commun.*, 1998, **35**, 341.
- W. C. Chan, B. W. Bycroft, D. J. Evans and P. D. White, *J. Chem. Soc., Chem. Commun.*, 1995, 2209.
- L. Kisfaludy and I. Schon, *Synthesis*, 1983, 325.
- E. Atherton, L. R. Cameron and R. C. Sheppard, *Tetrahedron*, 1988, **44**, 843.
- L. A. Carpino and G. Y. Han, *J. Org. Chem.*, 1972, **37**, 3404.

The development of an on-chip micro-flow injection analysis of nitrate with a cadmium reductor

P.H. Petsul, G.M. Greenway*, S.J. Haswell

Department of Chemistry, University of Hull, Hull, HU6 7RX, UK

Received 13 August 1999; received in revised form 15 November 1999; accepted 26 November 1999

Abstract

The development of a method to determine nitrate by micro-flow injection analysis (μ FIA) is described, using electro-osmotic flow (EOF) control in a micro-chip with 300 μm wide and 115 μm deep channel wet etched in borosilicate glass. An *in situ* miniature copperised cadmium reductor column was produced by immobilisation within a micro-porous silica frit made from 10% formamide and 21% silicon dioxide. The reductor frit was located in the sample introduction reservoir of the device. Nitrate standards were placed in the sampling reservoir and an applied voltage of 50 V relative to a waste reservoir was used to move the nitrate ions through the reductor frit for μ FIA. Silica frits without copperised cadmium were also introduced into the interconnecting channels of the μ FIA device to promote EOF and minimise hydrodynamic movement of solutions. The nitrite produced on leaving the reductor frit was detected using the Griess diazo-coupling reaction. The reaction was monitored *in situ* using a micro-spectrometer. A calibration was obtained between 0.5 and 20 μM with a correlation coefficient of 0.985. The R.S.D. at 5 μM NO_3^- was 8.3% ($n = 6$) and the limit of detection (3σ) was 0.51 μM (0.026 $\mu\text{g ml}^{-1}$) NO_3^- . © 2001 Elsevier Science B.V. All rights reserved.

Keywords: μ FIA; Nitrate; Electro-osmotic flow; Copperised cadmium

1. Introduction

The determination of nutrients such as nitrate in natural waters is known to be of great environmental importance [1]. The World Health Organisation for example, through the Environmental Protection Agency (EPA), had set the maximum contamination levels of nitrate in drinking water at 10 $\mu\text{g ml}^{-1}$. To monitor nitrate accurately in environmental systems it is preferably to monitor the levels *in situ* and this can be analytically very challenging. Conventional

FIA methods for determining the nitrate are well documented [1–3], however, these systems are laboratory based and therefore samples have to be collected and brought to the laboratory. FIA systems have been adapted for shipboard and remote analysis [4,5] but these require frequent replenishment of reagent and considerable maintenance.

Micro-flow injection analysis (μ FIA) using EOF [6] to move reagents and samples around the manifolds overcomes many of the problems of portability and robustness associated with the traditional FIA systems. The amounts of reagents required for analysis are vastly reduced as flow rates and volumes in the nanolitre region are used. There are also no moving mechanical parts required if the reagents and samples are pumped using EOF.

* Corresponding author. Tel.: +44-1482-465475;
fax: +44-1482-466416.
E-mail address: g.m.greenway@chem.hull.ac.uk
(G.M. Greenway).

The most commonly adopted method for determining nitrate is based on reduction of nitrate to nitrite using reagent such as titanium III chloride [7], photoreduction [8] or metal reduction (cadmium for example) [9]. The nitrite is then determined spectrophotometrically using a diazo-coupling (Griess) reaction [9]. The copperised cadmium reductor is the most widely used reduction technique in FIA with good sensitivity between 1 and 20 $\mu\text{g l}^{-1}$ being obtained.

In μFIA systems nitrate has been determined electrochemically using ISFET's Islet's at levels down to 1×10^{-5} M [10]. In a previous paper we determined nitrite spectrophotometrically in a μFIA systems with limits of detection of 0.20 μM . The aim of this work was to determine nitrate in a μFIA by developing a method to reduce it to nitrite within the μFIA manifold. In carrying out this work we also investigated how frits or porous constriction within channels could be used in the manifold to control solution flow and retain reactants *in situ*.

2. Experimental

2.1. Instrumental and reagents

The light source for the spectrophotometric detection was a green light emitting diode (RS Components, Northants, UK) and the detector was a S2000 diode array fibre optic spectrometer (Ocean Optics, Inc., Anglia Instruments Ltd., Cambridge, UK). Its wavelength range was between 350 and 880 nm and its sensitivity was 86 photons counts with a resolution of approximately 0.3–10 nm full width at half maximum (FWHM).

Absorbance measurements were made along a micro-channel etched within manifold as shown in Fig. 1 and described previously for the analysis of nitrite [6]. The chip manifold was connected via 100 μm i.d. 125 μm o.d. fibre optics to both the spectrometer and light source using a fibre optic connectors (surface mounting assembly (SMA) 905, Optiflex, Doncaster, UK). The instrumentation was set-up as described previously [6], two multimeters were used to measure the current and voltages applied across the reservoirs (models 1705 and 1906, Thurby Thandar Instrument, Ltd., Huntingdon, Cambridge, UK). The chemicals

and reagents used for the determination of nitrite have already been described [6] with a slight modification in which sodium acetate was used instead of ammonia to adjust the pH of the mixed reagent solution (pH 4). The main reason for this was to reduce the pungent smell of ammonia and minimise bubbles generation.

The nitrate standard solutions were prepared from a stock solution of 0.082 g of dried potassium nitrate dissolved in 100 ml of 195 mM NH_4Cl solution. The reagents used to prepare the frits are described in the Section 2.2.

2.2. The fabrication of *in situ* frits in micro-channels

The micro-porous silica (frit) solution was prepared from 10% m/m formamide (Avocado Research Chemicals Ltd., Heysham, Lancashire, UK) and potassium silicate (21% SiO_2 , 9% K_2O , Prolabo, Manchester, UK) [11]. The frits in the micro-channels on the manifold were prepared by mixing 18 μl of formamide and a 140 μl of potassium silicate for 30 s. This mixture was then carefully placed into the side arm channels (Fig. 1) of the etched, unbonded manifold, using a Pasteur pipette. The frit reagent was prevented from invading the main channels by plugs of Blu-tack (Bostik, Leicester). The prepared base plate was then placed in an oven at 100°C for 1 h before being removed, cooled and cleaned. The etched unbonded base plate was then smoothed off with abrasive paper,

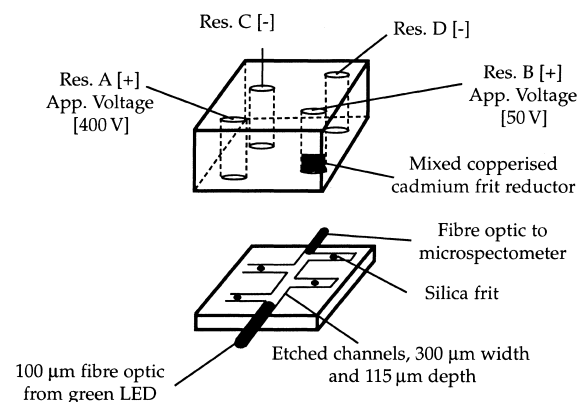


Fig. 1. Chip manifold for the reduction of nitrate. Dimension of the manifold are bottom etched substrate 26.2 mm \times 18.2 mm \times 3.1 mm, top cover plate was 27 mm \times 17.2 mm \times 17.2 mm. The main channel lengths were; intersection A–D was 11.2 mm and intersection B–C was 4.4 mm.

to remove any excess frit material and rinsed with distilled de-ionised water before being air-dried. The final manifold was then produced by thermal fusion of a top plate using the method already described [6]. Once the manifold was bonded the *in situ* frits (consisting of 90% porosity with $<10\ \mu\text{m}$ pore size) were rinsed and primed by placing distilled de-ionised water in the reservoirs (see Fig. 1) and applying pressure to drive the solution into the empty channels. A voltage of 50 V was then applied between reservoirs A/D and B/C for about 30–60 min to flush out excess reagents and air-trapped in the frit.

2.3. Preparation of the cadmium reductor frit in the μFIA manifold

Cadmium granules (30–80 mesh, $>99\%$) were obtained from Aldrich (Gillingham, Dorset, UK) and copper (II) sulphate 5 hydrate was from BDH Ltd. (Poole, UK). Both of these reagents were analytical grade. Fresh cadmium granules (50 mg) were coated with 40 mM copper sulphate for 10 min before being rinsed with distilled de-ionised water. A portion (3 mg) of the copperised cadmium was mixed with the potassium silicate frit reagents (described in the previous section) and then deposited into the bottom of reservoir B (see Fig. 1). The length of the mixed copperised cadmium frit was between 2 and 3 mm. During the deposition of the reductor into reservoir, water was placed in the other reservoirs and channels to ensure accurate placement of the cadmium/frit material. The chip manifold was placed in the oven at 100°C for 1 h for the frit to harden.

2.4. Procedure for flow rate studies through frits and reductors in straight capillaries (off-chip)

In addition to generating a copperised cadmium frit in the μFIA manifold three frits were generated in straight capillary tubes (1 mm i.d.) of 5, 10 and 250 mm lengths, respectively. The ends of the capillary tubes was inserted into two suba seals and attached to the glass reservoir wells and the optimum applied voltage (for maximum flow rate) was determined. The amount of reagent moved was determined and volume flow rates calculated. The experiments were repeated for a reductor in which the copperised cadmium reductor material (5 mm) sandwiched between

two 10 mm frits and for two reductors in which the copperised cadmium reductor material was physically trapped throughout the frit (16 and 40 mm) as described previously.

2.5. Procedure for the determination of nitrate

1.16 mM sulphanilamide and 1.95 mM *N*-(1-naphthyl) ethylene diamine, pH 4 was placed in reservoir A and the nitrate standard solution was placed in reservoir B over the mixed copperised cadmium frit (see Fig. 1). Reservoirs C and D contained distilled de-ionised water.

400 V was then applied between reservoirs A(+) and D(–) for 50 s using a power supply (HVPS 1) to load the main channel with the reagent mixture before simultaneously switching the HVPS 1 off and applying 50 V from the second power supply (HVPS 2) between B(+) and C(–) for 25 s to inject the reduced nitrate solution. There was then a 25 s hold (stop flow mode) after which the absorbance of the reaction mixture was measured.

3. Results and discussion

3.1. Use of frits to control flow

The chip manifold in this work was different to that used previously [6] in that frits had been placed in all the side channels connected to reservoirs. Theoretical studies [12] have shown that very small differences in the heights of the reservoirs in the μFIA manifold can cause hydrostatic flow resulting in loss of EOF control over the movement of reagents and samples. The addition of frits to the channels were used to reduced hydrostatic flow by restrictive flow through the 90% porous $<10\ \mu\text{m}$ pores which simultaneously enhanced and stabilised the EOF.

Frits of three different lengths were prepared in capillaries to investigate the relationship between solution flow rate and frit length. The results shown in Fig. 2 indicate that for the 5 and 10 mm frit there was a clear linear relationship between the applied voltage and flow rate in the range 0–50 V, after which point the flow rate is seen to deteriorate. A similar trend was also observed for the 250 mm frit over the range 0–100 V. In general a clear relationship exists

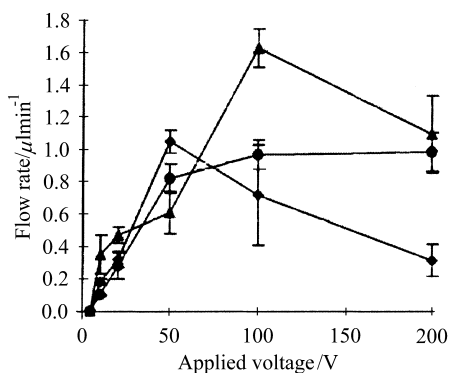


Fig. 2. The change in flow rate with increased applied voltages for different frit lengths. Each value represent an average of the replicates ($n = 3$), (▲) 250 mm frit; (●) 10 mm frit; (◆) 5 mm frit.

between the frit lengths in which the longer frit was found to generate a higher flow rate. This trend can be attributed to the numerous pore openings in the frit creating large surface areas to support the required electrical double layers for EOF as discussed by Christensen *et al.* [11]. The advantage of the longer frit was outweighed however, by the need to apply relatively high currents to induce flow which led to unwanted bubble formation due to Joule heating effects. From these initial frit studies it was found that for a good flow rate to be maintained the current needed to be held below $1000 \mu\text{A}$ and this was best achieved with the 5 and the 10 mm frit running below 50 V.

For practical reasons the 5 mm frits were subsequently used in the μFIA manifold but it remained important to ensure that such frit lengths would be sufficient to reduce hydrodynamic effects due to the pressure head differences caused by the changing levels of reagents in the various reservoirs. Verification of hydrostatic control was carried out by filling the reservoirs (A and D for example, in Fig. 1) with frits in place and monitoring the height change of the fluid over time. A voltage was then applied across reservoirs A and D so that liquid flowed through the connecting channel. The manifold was then sealed and left overnight and the relative heights of the reservoirs were noted the next morning. No movement of liquid was seen in the manifold containing frits however, in an identical manifold without frits, fluid from reservoir D readily flowed back to equilibrate the levels of buffer in the reservoirs once the EOF was turned off.

3.2. Development of reductor frit

An initial study to evaluate the effect on EOF placing a copperised cadmium reductor between two frits was carried out. The results indicated that no flow was obtained with this design of column due to the highly conducting nature of the metals within the column that severely affected the EOF. To overcome this problem a second type of reactor (a mixed reductor) was prepared in which the copperised cadmium was dispersed within the potassium silicate frit material. Two different lengths (16 and 40 mm) of the mixed reductor were produced in capillary tubes and the flow rates for a buffer in each of the tubes was obtained (Fig. 3).

The 16 mm mixed copperised cadmium frit indicated a much improved volume flow rate profile compared to the sandwiched reductor. In all cases the current was kept below $1000 \mu\text{A}$ and there was reproducible flow as can be seen by the error bars. The volume flow rates obtained were reasonably reproducible in a range between 20–100 V. An applied voltage of 50 V was selected for further work in the chip as this gave the most reproducible data and it was noted that at voltages below 50 V it was difficult to initiate the flow when the reductor was placed in the chip reservoir. Using the 40 mm mixed copperised cadmium frit a higher flow rate was observed compared to the 16 mm frit. It became apparent however, from these studies that the longer frit whilst giving higher flow rates, also required higher currents and

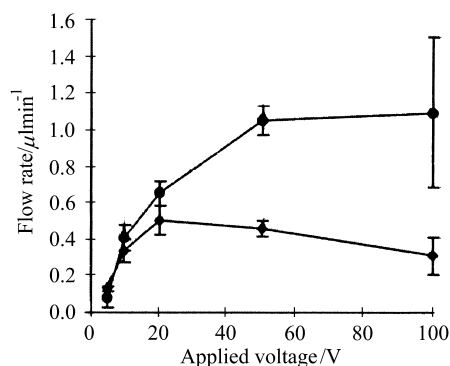


Fig. 3. The change in flow rate with increasing applied voltage for flow through the reductor in which the copperised cadmium was dispersed in the frit. Each value represent an average of the replicates ($n = 3$), (●) 16 mm reductor frit; (◆) 40 mm reductor frit.

this significantly affected the reproducibility of the flow due to heating and subsequent bubble formation as discussed previously. This effect is reflected in the size of the error bars at 100 V. At 200 V (not shown) no volume flow was recorded indicating channel blockage due to bubble generation.

3.3. On-chip reductor frit

Care had to be taken with the reductor frit because if the pH of solutions were allowed to become too acidic the copperised cadmium would dissolve. It was also necessary to have sufficient copperised cadmium present in the frit to ensure a high conversion rate of nitrate to nitrite. It was therefore decided to put the reductor frit in the sample reservoir B (Fig. 1) rather than in the channel. The reductor frit was 2.5 mm deep and had a diameter of 2.3 mm and contained 3 mg of copperised cadmium. The reductor frit was primed by soaking in buffer solution overnight. The copperised cadmium reductor frit was found to give a conversion rate of 95.9% nitrate to nitrite which is comparable with conventional flow injection reductor column [9]. The lifetime and stability of the copperised cadmium reductor in such devices is clearly important as it was noted that a continuous application of the voltage appeared to have degraded the surface by the de-colourisation of the copperised cadmium. In the work carried out using the straight capillaries a blue green colour was seen moving along the frit after two weeks

of operation. The blue green colour was attributed to hydroxides of copper which are found to decrease the performance of the reductant [3]. The reactor was used over a 2-week period with approximately 2000 samples being injected before deterioration of the copperised cadmium reductor column was noticed. Regeneration of the reductor column can however, be achieved by treatment with copper sulphate solution.

3.4. Conditions for the determination of nitrate

The initial investigation had shown that an applied voltage 50–100 V would give the most reproducible flow through the frits and that short frit lengths of 5 mm were adequate to control hydrostatic pressure effects. The nitrate standard was prepared in pH 4 buffer as used in conventional flow injection methods [9].

The reduction of nitrate to nitrite was achieved *in situ* and mobility of the sample was achieved by applying 50 V between B(+) and C(–) to generate EOF so moving the nitrate through the reductor frit at a flow rate of $0.3 \mu\text{l min}^{-1}$. The nitrite produced then flowed into the main channel containing the mixed reagent (sulphanilamide + (*N*-(1-naphthyl) ethylene diamine) for the diazo-coupling reaction. Mixing of the reactants in such a manifold is by diffusion (Reynolds number < 1). Applying the voltage for 25–40 s was found to give reasonable absorbance readings (Fig. 4a), however, 25 s was found to give the optimal absorbance value. At lower times 5–20 s,

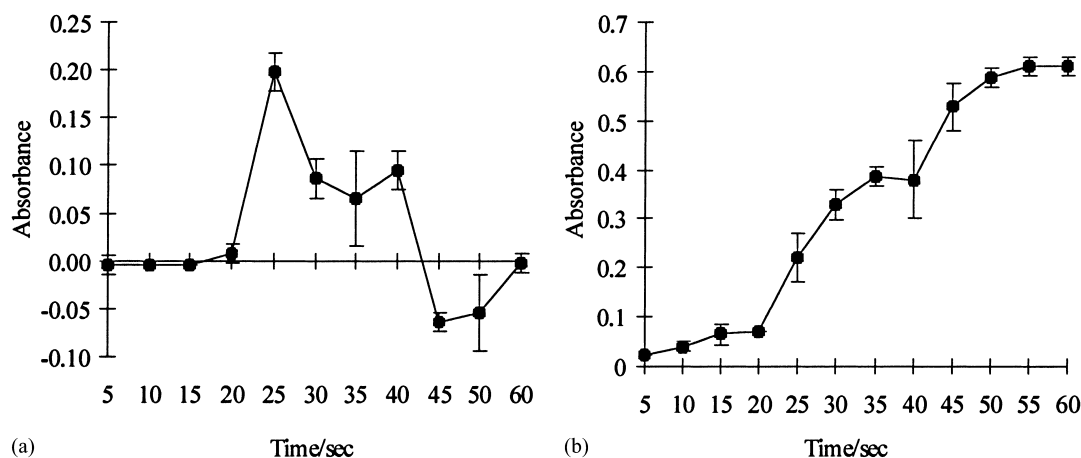


Fig. 4. (a) The change in absorbance as the injection time for the NO_3^- plug increased; (b) the change in absorbance as the holding time (stopped flow time) for the colour azo product increased. Each value represent an average of the replicates ($n = 3$).

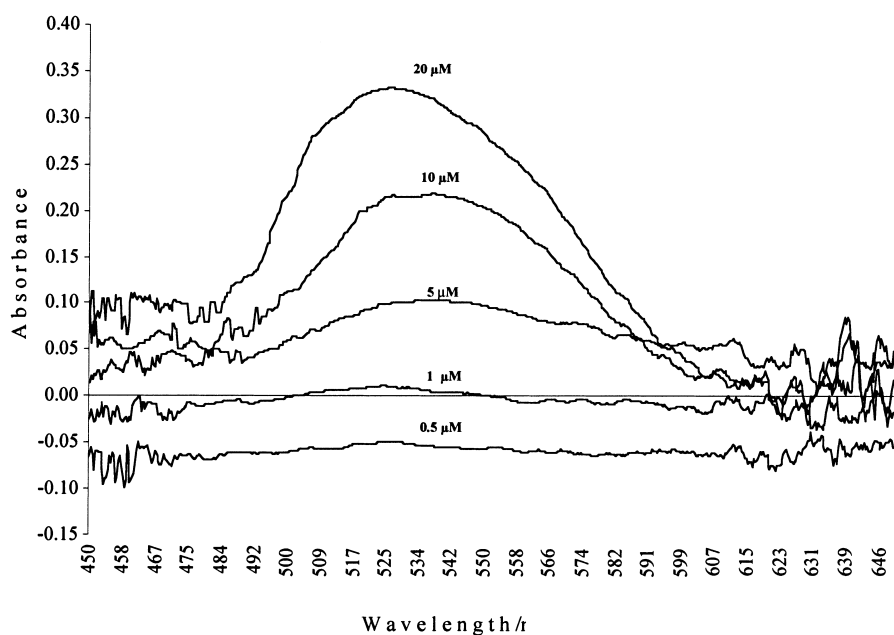


Fig. 5. Absorbance spectra for the nitrate determined by the μ FIA manifold.

only a small amount of NO_3^- were effectively getting into the main light path and beyond 40 s the coloured product had moved out of the light path. To allow full colour development a stop flow mode was used in which the product was held in the detector channel after injection for up to 1 min. Fig. 4b shows how the absorbance increased with time, 25 s was chosen as a compromise between obtaining sufficient sensitivity and having a high enough sample throughput ($20\text{--}30\text{ sample h}^{-1}$).

3.5. Analytical calibration

Fig. 5 shows the absorbance of the azo product between 450 and 646 nm. The maximum absorbance of the nitrite (reduced NO_3^-) was recorded at 526 nm. The spectrometer was zeroed when the mixed reagent without nitrite was in the channel. With the current system used an automated blank subtraction could not be achieved as there was only one channel in the device. A linear calibration was obtained between 0.5 and $20\ \mu\text{M}$ with a correlation coefficient of 0.985. The equation of the line was $y = 0.0125x + 0.0111$, where y is absorbance and x is concentration in

μM and the limits of detection (3σ) were $0.51\ \mu\text{M}$ ($0.026\ \text{mg ml}^{-1}$) ($n = 6$) which expressed in mass terms, would be approximately 20 pg. These results compare favourable with flow injection or sequential injection systems [1,3] however, the precision of the method at $5\ \mu\text{M NO}_3^-$ was found to be 8.3% R.S.D. which is not quite as good as that obtained for conventional FIA systems. Use of the frits in the system did not improve the reproducibility of the system over the previous system [6] however, they have prevented hydrodynamic flow. Poor mixing of the reagents at the intersection is one of the main causes of irreproducibility of the system. Currently work is being carried out to improve mixing by providing a combination of frit and open channels in the manifold design.

4. Conclusion

This paper has now shown that nitrate can be determined in a μ FIA manifold using a reductor frit to reduce the nitrate to nitrite. The sampling rate of this method was around 30 samples h^{-1} and the

consumption of reagents and amount of waste generated (approximately 2 μ l per analysis) is significantly lower than for conventional FIA systems. This work and previous work clearly demonstrated that nitrate and nitrite could be sequentially analysed by a combined μ FIA systems on the same device. The method currently lacks the reproducibility of conventional FIA systems, probably due to mixing problems, and further studies are continuing to improve this. The problem could be overcome by using a combination of frits and open channel to optimise the mixing zone or by adopting a micro-mixer design such as that described by Bessoth et al. [13].

Acknowledgements

The authors would like to thank other members of the miniaturisation group at Hull for their contribution. They would also like to extend the acknowledgement to the government of Papua New Guinea for supporting Peter Petsul financially.

References

- [1] A.A. Ensafi, A. Kazemzadeh, *Anal. Chim. Acta* 382 (1999) 15.
- [2] Z. Zhi-Qi, G. Lou-Jun, Z. Han-Ying, L. Qian-Guang, *Anal. Chim. Acta* 370 (1998) 59.
- [3] A. Cerda, M.T. Oms, R. Forteza, V. Cerda, *Anal. Chim. Acta* 371 (1998) 63.
- [4] D. Price, R.F.C. Mantoura, P.J. Worsfold, *Anal. Chim. Acta* 361 (1998) 189.
- [5] J.T.M. de Jong, J. den Das, U. Bathmann, M.H.C. Stoll, G. Kattner, *Anal. Chim. Acta* 377 (1998) 113.
- [6] G.M. Greenway, S.J. Haswell, P.H. Petsul, *Anal. Chim. Acta* 387 (1999) 1.
- [7] T. Aoki, M. Wakabayashi, *Anal. Chim. Acta* 308 (1995) 308.
- [8] S. Motomizu, M. Sanada, *Anal. Chim. Acta* 308 (1995) 406.
- [9] K. Horita, G.F. Wang, M. Satake, *Analyst* 122 (1997) 1569.
- [10] H. Fiehn, S. Howitz, M.T. Pham, T. Vopel, M. Burger, T. Wegner, in: A. van den Berg, P. Bergveld (Eds.), *Micro Total Analytical Systems*, Kluwer Academic Publishers, Dordrecht, 1995, p. 289.
- [11] P.D. Christensen, S.W.P. Johnson, T. McCreedy, V. Skelton, N.G. Wilson, *Anal. Commun.* 35 (1998) 341.
- [12] P.D.I. Fletcher, S.J. Haswell, V.N. Paunov, *Analyst* 124 (1999) 1273.
- [13] F.G. Bessoth, A.J. deMello, A. Manz, *Anal. Commun.* 36 (6) (1999) 213.

Preliminary studies into the direct interfacing of a microreactor to a gas chromatographic instrument

G. N. Doku, S. J. Haswell,* T. McCreedy and R. J. Middleton

Department of Chemistry, University of Hull, Hull, UK HU6 7RX

Received 6th December 2000, Accepted 10th January 2001

First published as an Advance Article on the web 19th January 2001

The paper reports on a preliminary study into the coupling of a microreactor to a GC-FID, using a standard GC needle as the interface between the microreactor and the injection port of a conventional GC. Using the injection needle as the ground electrode, electroosmotic flow was used to control the injection of reagent/sample into the GC. Photolithographic and wet etching techniques were used to fabricate the microreactor (channels 200 μm id, 100 μm deep) in a borosilicate glass substrate. The results of the effects of voltage and injection times on the response signal are presented. The critical obstacles to overcome were the backpressure posed by the carrier gas disrupting the liquid flow in the channels and reservoirs of the microreactor and the need to thermally insulate the microreactor, to prevent evaporation of solvent and reagents from the device.

1. Introduction

The development of so-called micro total analytical systems (μTAS), based on electroosmotic flow (EOF) and electrophoretic separations has gained much interest in recent years,^{1–9} however, the use of similar technology to construct microreactors for primarily organic-based chemical synthesis, has been less widely reported.^{10–15} The often complex nature of the chemistries performed and the demand for high throughput screening for combinatorial type applications, require rapid separations, detection and characterisation of intermediates and product to be carried out at or in a microreactor. Detection can be achieved relatively simply offline by taking a portion of the product collected from a sample reservoir and analysing it with a detection system such as the GC-MS.¹⁵ Online, at microreactor detection clearly requires some form of interface to be constructed between the reactor and the detection system, whilst on- or in-microreactor detection may be achieved by integrating part or all of the detection system into one device.

In terms of automation one of the simplest approaches to take, and one which exploits existing technology, is to directly couple the microreactor with a gas chromatograph (GC) or GC-MS. This paper reports on some preliminary results for coupling of a chemical microreactor to the injector of a conventional GC-FID instrument, employing electroosmotic flow as the reagent/sample injection mechanism. The interfacing of a microreactor directly to an MS has already been reported,^{13,14} however, there are potential limitations of such an approach associated with the overloading of the detector due to the relatively high concentrations of reagents present (*e.g.*, 1–0.1 mM) when performing synthetic reactions. One of the main advantages of the proposed methodology is the ability to control the injection volume and hence the amount of product and/or reactants injected into the analytical system. In addition, the opportunity to perform post-reactor separations based on conventional GC would be a relatively simple extension to the method described.

2. Experimental

2.1. Reagents and materials

The primary reagent used was *N,N*-dimethyl formamide (Lancaster, Eastgate, UK) of analytical reagent grade. Hydrofluoric acid (40%) and ammonium fluoride were used for etching the microreactor channels (Merck, Poole Dorset, UK). The hydrofluoric acid was diluted to 1% buffered with 5% ammonium fluoride. Microposit chrome etch 18 and photoresist remover 1112A were from Shipley (Coventry, UK). The glass for the microreactor chip and cover plate were both superwhite Crown B70 borosilicate glass (Instrument Glasses, Enfield, UK).

2.2. Chip device and instrumentation

The microreactor consisted of channels 200 μm in diameter and 100 μm deep (Fig. 1), fabricated in borosilicate glass base-plate (25 mm long, 14 mm wide and 3 mm thick), using a wet-etching technique described previously.¹⁶ The base-plate was thermally bonded to a thicker glass cover-plate (25 mm long, 14 mm wide and 17 mm thick, also of borosilicate) containing 2 mm holes pre-drilled to align with the ends of channels which served as reservoirs for the reagent and physical support for the platinum electrodes required to generate EOF.

Frits¹⁷ ranging from 2–3 mm in length were integrated into the channels R1-B, R2-C and R3-D (Fig. 1) to regulate the hydrostatic pressure within the microreactor, so preventing an imbalance of liquid levels in the individual reservoirs. In addition, the frits aid EOF and compensate for the backpressure generated by the GC injector carrier flow which, if not reduced, would cause disruption to the flow of reagents in the microreactor channels.

Interfacing the microreactor to the injection port of the GC was achieved using a GC needle (5.7 cm long, 75 μm id and 300 μm od) detached from a GC syringe (SGE, Australia). An access channel of approximately 300 μm id was created at position E (Fig. 1) in the microreactor and the interface needle was inserted (blunt end) 1.5 mm into the channel and sealed in place with a metallic silver adhesive. A coil of a high purity copper conductor was positioned 1.5 mm from the inserted end of the needle to provide a ground connection for the electric circuit, (RS, components, Northants, UK). The silver adhesive

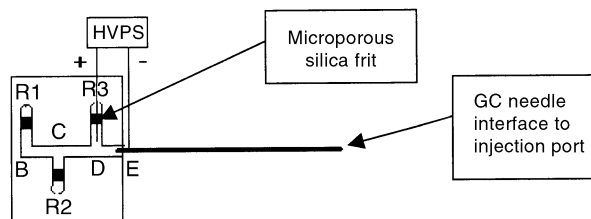


Fig. 1 Microreactor constructed from borosilicate glass with channel dimensions: 200 μm wide, 100 μm deep with R1B = R2C = R3D = 5.5 mm, BC = 3 mm, CD = DE = 4 mm, BE = 11 mm, showing position of the interface connection to a GC injection port and location of the high voltage power supply (HVPS).

was then coated with a quick set epoxy resin (RS, components, Northants, UK) to make the interface more physically stable. A 20 mm long, 0.15 mm in diameter platinum electrode, soldered to the high-purity copper conductor wire, with a 15 mm exposed length for interfacing with the solution in reservoir R3, was used as the positive electrode. The positive and the ground electrodes were connected *via* the copper cables to a power supply system, built in-house, capable of supplying up to 700V.

The GC was a standard Autosystem XL GC (Perkin Elmer, Beaconsfield, UK) with FID. As no separations were being performed in this preliminary study, a short (12 in long, 75 μm id) Rtx-5MS (Crossbond 5% diphenyl-95% dimethyl polysiloxane stationary phase) open capillary column, stable to 360 $^{\circ}\text{C}$, was used to connect the injector port with the FID detector. The carrier gas used was helium and the injector, detector and oven temperatures were 250, 250, and 250 $^{\circ}\text{C}$, respectively.

2.3. Reagent injection into GC

The channels in the microreactor, including the GC needle, were initially primed with the DMF by filling reservoir R1 with the reagent and applying a positive pressure with a syringe. This was then followed by filling all three reservoirs R1 to R3 with the DMF. A positive electrode was then placed in reservoir R3 whilst the grounded end of the injection needle was inserted into the injection port of the GC. EOF injection was achieved by switching the power supply on and off between the two electrodes described. The carrier gas flow was adjusted to minimise backpressure effects by visually monitoring bubble generation in the connecting channels.

Initially, an electric field R3 (+) E (-) of 700V was applied for 60 s followed by a waiting period of 60 s, to achieve a pulse injection of the DMF into the GC. This process was repeated consecutively ($n = 5$) to verify the repeatability of the injection process. Next, the applied voltage was kept constant whilst the injection time was varied with a sufficiently long waiting time between injections to allow each subsequent signal to return to the baseline. This was carried out to verify the effect of the injection time on the signal. Finally, the applied voltage was varied whilst keeping the injection time constant at 60 s to establish the effect of the voltage on the response signal. Once again, sufficient time between injections was allowed for the signal to return to the baseline.

3. Results and discussion

With a 3 mm microporous silica frit length in channel R3-D, a carrier gas pressure of 0.3-0.4 psi was found to be just enough to prevent a back flow of the DMF in the microreactor channel. It was possible, however, to increase the carrier gas pressure to around 10 psi by increasing the microporous frit length to 10 mm along the channel R2-E (Fig. 1). Extending the frit length also had the effect of decreasing tailing of the injection profiles, an essential factor for separation of complex mixtures. The porosity of the frit is also a crucial factor in this regard. Increasing the porosity of the frit, *e.g.*, by increasing the percentage formamide in the frit solution mixture,¹⁷ would enhance the liquid bulk flow but renders the system more susceptible to the carrier gas backpressure. Decreasing the porosity of the frit, by increasing the percentage of potassium silicate in the frit mixture, would decrease the liquid flow but offers greater resistance to the carrier gas backpressure. A 10 mm medium porosity frit (approximately 70% porous) with a pore size of 5–10 μm in a 250–300 μm id channel was found to give suitable operating conditions with respect to providing good EOF whilst minimising GC carrier gas backpressure effects.

Fig. 2 shows the FID signals obtained for a number of 60 s injections of DMF at 700 V, for a range of different time intervals between injections. A common trend seen in this data

is a rapid rise from a relatively low baseline of the first peak, followed by a general elevation in the baseline due to the conductive heating of the interface needle which is fixed in the heated injection port, causing bleed of the DMF into the GC. As the time between injections is increased, the baseline can be seen to become more constant but still elevated. The RSD, based on five injections (700 V, 60 s on with 60 s off), was found to be 1.7%. The results clearly indicate that a more careful study into the injection process, in particular thermal control of the interface, is required to reduce the baseline and improve the sensitivity of the technique. An investigation into the effect of varying injection time on the FID response signal (Fig. 3) indicated that as the injection time is increased the signal intensity and baseline also increased, indicating more DMF was being dispensed into the injector port. Finally, Fig. 4 shows the FID response for DMF as the voltage is decreased from 700 to 165 V), corresponding to a reduction in the flow rate of the solvent into the injector port.

4. Conclusion

The results presented in the paper have shown that it is feasible to link a chemical microreactor directly to the injection port of

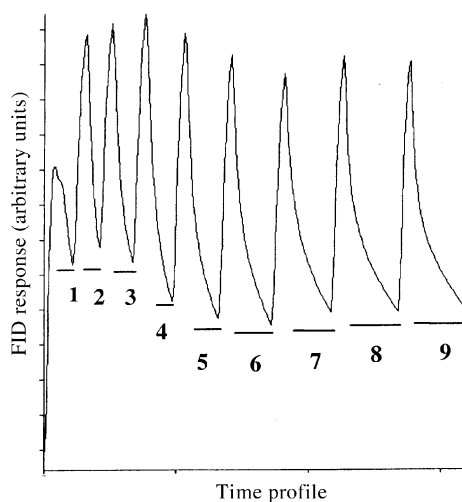


Fig. 2 FID signals obtained from repeated 700 V, 60 s pulse injections of DMF, increasing the time interval between injections: 1 = 60 s, 2 = 90 s, 3 = 120 s, 4 = 150 s, 5 = 180 s, 6 = 210 s, 7 = 240 s, 8 = 270 s, 9 = 300 s.

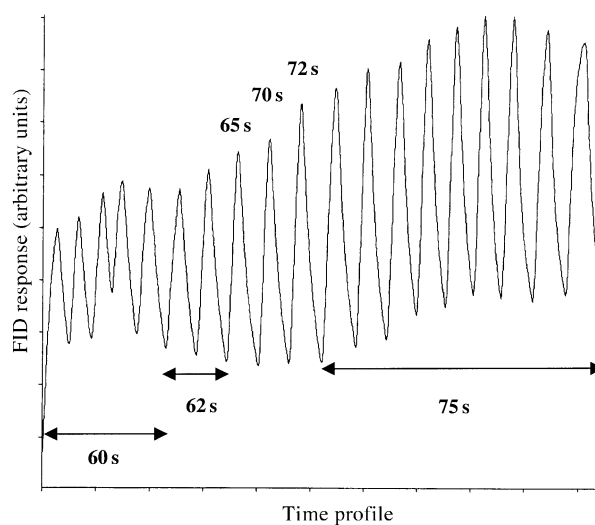


Fig. 3 FID signals obtained for different injection times at a constant voltage of 700 V.

a conventional GC, such that the injection of samples/reagents can be controlled. The injection can be performed using timed electroosmotic flow pulses, with sufficient backpressure control (up to 10 psi at present) of the GC carrier gas, this being achieved through the use of a porous frit positioned in the channels of the microreactor. Problems linked with the heating of the interface injector needle lead to an elevated FID baseline signal caused by a solvent bleed from the interface, leading in turn to an adverse effect on the detector sensitivity. Clearly, the technique could be extended to offer post-microreactor separations if an appropriate GC column were fitted to the system. In addition, the method would be equally amenable to GC-MS applications. Clearly, the construction of an appropriate interface between the microreactor and the injection port with

appropriate thermal control is an important consideration in the future development of the proposed interface.

5. References

- 1 A. Manz, N. Graber and H. M. Widmer, *Sens. Actuators*, 1990, **B1**, 244.
- 2 S. J. Haswell, *Analyst*, 1997, **122**, 1R.
- 3 Z. Fan and D. J. Harrison, *Anal. Chem.*, 1994, **66**, 177.
- 4 S. C. Jacobson, L. B. Kountny, R. Herenroder, A. W. Moore, Jr. and J. M. Ramsey, *Anal. Chem.*, 1994, **66**, 3472.
- 5 A. T. Woolley and R. A. Mathies, *Anal. Chem.*, 1995, **67**, 3676.
- 6 D. Schmalzing, L. Koutny, A. Adourian, P. Belgrader, P. Matsudaira and D. Ehrlich, *Proc. Natl. Acad. Sci. U. S. A.*, 1998, **94**, 10273.
- 7 G. N. Doku and S. J. Haswell, *Anal. Chim. Acta*, 1999, **382**, 1.
- 8 G. M. Greenway, S. J. Haswell and P. H. Petsul, *Anal. Chim. Acta*, 1999, **387**, 1.
- 9 P. D. I. Fletcher and S. J. Haswell, *Chem. Brit.*, Nov., 1999, 38.
- 10 S. J. Haswell and V. Skelton, *TrAC, Trends Anal. Chem. (Pers. Ed.)*, 2000, **19**, 389.
- 11 G. M. Greenway, S. J. Haswell, D. O. Morgan, V. Skelton and P. Styring, *Sens. Actuators*, 2000, **B63**, 153.
- 12 P. D. I. Fletcher, S. J. Haswell and V. N. Paunov, *Analyst*, 1999, **124**, 1273.
- 13 M. C. Mitchell, V. Spikmans, F. Bessoth, A. Manz and A. de Mello, *Proceedings of the Micro Total Analysis Systems 2000 Workshop*, ed. A. van den Berg, W. Olthuis and P. Bergveld, Kluwer Academic Publishers, Enschede, 2000, p. 463.
- 14 J. Li, C. Wang, J. F. Kelly, D. J. Harrison and P. Thibault, *Electrophoresis*, 2000, **21**, 198.
- 15 G. N. Doku, S. J. Haswell, T. McCreedy and G. M. Greenway, *Analyst*, 2001, **126**, 14.
- 16 R. N. C. Daykin and S. J. Haswell, *Anal. Chim. Acta*, 1995, **313**, 115.
- 17 P. D. Christenson, S. W. P. Johnson, T. McCreedy, V. Skelton and N. G. Wilson, *Anal. Commun.*, 1998, **35**, 34.

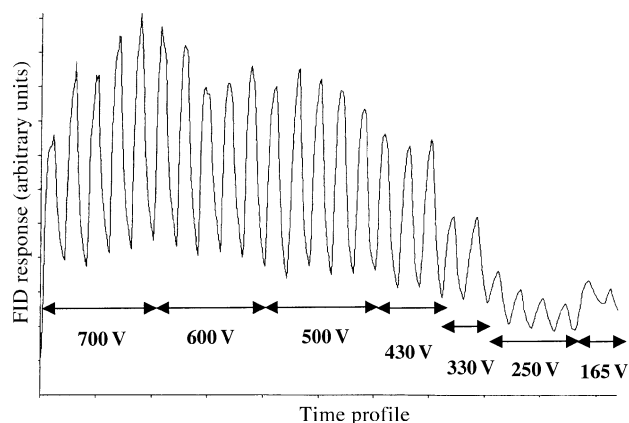


Fig. 4 FID signals obtained from 60 s pulse injections for a range of different voltages.

The investigation of an equilibrium dependent reaction for the formation of enamines in a microchemical system

Mike Sands,^a Stephen J. Haswell,^{*a} Stephen M. Kelly,^a Victoria Skelton,^a David O. Morgan,^b Peter Styring^c and Brian Warrington^d

^a Department of Chemistry, Faculty of Science and the Environment, University of Hull, Cottingham Road, Hull, UK HU6 7RX. E-mail: s.j.haswell@chem.hull.ac.uk; Fax: +44 (0) 1482 466416; Tel: +44 (0) 1482 465475

^b GlaxoSmithkline, Old Powder Mills, Tonbridge, Nr Leigh, Kent, UK TN11 9AN

^c Department of Chemical and Process Engineering, The University of Sheffield, Mappin Street, Sheffield, UK S1 3JD

^d GlaxoSmithkline, New Frontiers Science Park, Third Avenue, Harlow, Essex, UK CM19 5AW

Received 8th May 2001, Accepted 12th June 2001

First published as an Advance Article on the web 9th August 2001

The paper describes the equilibrium dependant reaction for the formation of enamines in a microchemical system utilising electroosmotic flow (EOF) for fluid mobilisation. The authors have shown that the reaction can be carried out without the presence of a Lewis acid catalyst, in addition the enamine intermediate was synthesised at room temperature using mild solvent conditions. A 42% conversion of cyclohexanone into the enamine has been achieved to date.

Introduction

The paper describes the equilibrium dependent reaction for the formation of enamines in a microchemical system utilising electroosmotic flow (EOF) for fluid mobilisation. The authors have shown that the reaction can be carried out without the presence of a Lewis acid catalyst, in addition the enamine intermediate was synthesised at room temperature using mild solvent conditions. The largest conversion of cyclohexanone into the enamine achieved has been 42%.

To date microreactors have been used to demonstrate a wide range of different chemistries.^{1–3} The benefits of using microreactors for synthetic applications has been clearly demonstrated using the Wittig reaction⁴ where not only the reaction yields were increased but also stereoselective control was possible. In this paper we intend to evaluate the Stork-enamine reaction in a microreactor for the synthesis of enamines.

The enamine reaction was first proposed by Stork *et al.* in 1954⁵ and allows the addition of an electrophile alpha to a carbonyl substituent. This carbon-carbon bond forming reaction can be used extensively over a wide range of chemistries. This presents an interesting challenge when performed in a microreactor due to the need for water removal from the reaction mixture to enable the enamine to be formed.

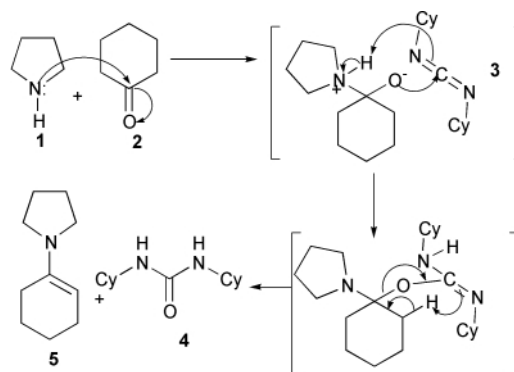
In order for equilibrium reactions to proceed, the removal of water can be achieved in one of two ways. Firstly, by the physical removal of water using molecular sieves, however this would introduce complications as molecular sieves may possibly disrupt EOF. In addition it would also cause problems with device design because of the need for immobilisation within the reaction channels. Alternatively chemical removal using a homogeneous drying agent can be achieved by a relatively simple operation to introduce it into a microreactor device. Thus the addition of 1,3-dicyclohexylcarbodiimide (DCC) to the reaction mixture to remove water has been investigated (see Scheme 1).

Experimental

The reaction was carried out using a T-chip fabricated in borosilicate glass with channels produced by photolithography and wet etching.⁶

A top plate of 17 mm borosilicate glass which included 3 mm pre-drilled holes was annealed at a temperature of 680 °C. Microporous silica structures were added into the annealed chip to reduce hydrodynamic effects.⁷ The final channel geometries were 200 µm wide at the top and 100 µm deep, with the overall outer dimensions of 20 mm × 20 mm and 25 mm in depth. EOF was generated and controlled *via* a computer/Labview interface developed by Kingfield electronics, Sheffield. An example of the chip used can be seen in Fig. 1.

All of the chemicals were purchased from Aldrich Fine Chemicals (Gillingham, Dorset). A solution of cyclohexanone (0.3 M, 50 µl) in anhydrous methanol with added DCC (approx 1 mg) was introduced into reservoir A. Pyrrolidine (0.3 M, 50 µl) in anhydrous methanol was added into reservoir B, whilst anhydrous methanol (30 µl) was added to reservoir C. Ranges



Scheme 1 General reaction scheme for the enamine formation using DCC.

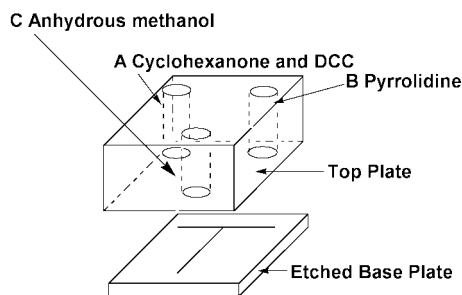


Fig. 1 Schematic of the 'T' microreactor used for the synthesis of the enamine intermediate. Positive voltages were applied to platinum wire electrodes placed reservoirs A & B relative to a ground electrode being placed in reservoir C.

and combinations of positive voltages were applied to the platinum wire electrodes placed in reservoirs A and B relative to the ground electrode situated in reservoir C. The variety of voltages applied was in the region from 300 to 1000 V.

The voltages were applied for a period of 40 min after which the content of reservoir C was analysed by gas chromatography coupled to a mass spectrometer (GC-MS). The GC-MS used was a Varian CP-3800 coupled to a Varian Saturn 2000 mass spectrometer. The column was a CP-Sil 8 (30 m capillary column). The following analysis conditions were employed: injector temperature 250 °C, helium flow rate 1 ml min⁻¹, oven temperature 50 °C held for 4 min, ramping to 250 °C over a period of 8 min and holding this temperature for 3.5 min. The use of GC-MS allowed the mass ion of *m/z* 151 to be identified at a retention time of 9.11 min. The retention time for the pure material had already been determined from batch reactions under similar conditions.

Results and discussion

Fig. 2 summarises the enamine yields obtained in the microreactor over a range of voltage combinations. Using an applied external voltage combination of 600 V at reservoir A (cyclohexanone) and 800 V at reservoir B (pyrrolidine) the largest yield of product obtained, based upon the percentage conversion of cyclohexanone to enamine, was 42% at room temperature, for which no catalyst was used. The yield obtained in the microreactor was comparable to that obtained using a batch Stork-enamine reaction performed using cyclohexanone, pyrrolidine and *p*-toluene sulfonic acid in methanol under Dean & Stark conditions.

The results presented represent preliminary findings, which demonstrates that enamine chemistry can be carried out in a mild solvent system at room temperature and in the absence of a Lewis acid catalyst in a microreactor. Product yields so far produced in the microreactor are comparable to those obtained by the bulk reaction, but the chip reaction negates the need for

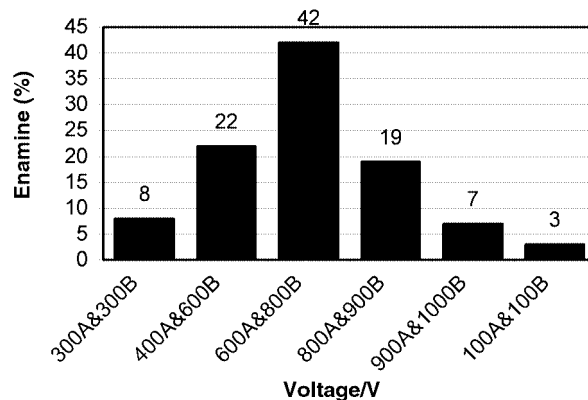


Fig. 2 The percentage conversion of enamine for a range of voltages. The letter after the value denotes the reservoir in which the voltage was applied.

Dean and Stark conditions. It is also carried out in the absence of a Lewis acid catalyst utilising a different solvent system and work is continuing to fully optimise the reaction. Once the reaction conditions have been optimised, the next stage will be to investigate the reaction using a wide range of suitable electrophiles. The initial product will then be hydrolysed back into the ketone. Once this part of the reaction has been optimised, some asymmetric synthesis can be carried out to investigate enantioselectivity in microchemical devices.

Acknowledgements

We thank the EPSRC and GlaxoSmithkline for financial support to MS in the form of a CASE studentship.

References

- 1 R. D. Chambers and R. C. H. Spink, *Chem. Commun.*, 1993, 883.
- 2 G. Vesper, G. Fredrick, M. Freygan and R. Zengerle, *Reaction Kinetics and the Development of Catalytic Processes*, ed. G. F. Froment and K. C. Waugh, Elsevier Science, Amsterdam, 1999
- 3 S. J. Haswell, R. J. Middleton, B. O'Sullivan, V. Skelton, P. Watts and P. Styring, *Chem. Commun.*, 2001, 391. * This references the work, carried out to date, that has been performed using microreactors.
- 4 V. Skelton, G. M. Greenway, S. J. Haswell, P. Styring, D. O. Morgan, B. H. Warrington and S. Y. F. Wong, *Analyst*, 2001, **126**, 11. * This was the first paper that described the use of microreactors to carry out specific solution based chemistries.
- 5 G. Stork, R. Terrell and J. Szmuszkowicz, *J. Am. Chem. Soc.*, 1954, **76**, 2029. * The first paper where the Stork-enamine reaction was described.
- 6 T. McCreedy, *Anal. Chim. Acta*, 2001, **427**, 39. * This paper describes the fabrication and manufacture of devices that can support EOF.
- 7 P. D. Christensen, S. W. P. Johnson, T. McCreedy, V. Skelton and N. G. Wilson, *Anal. Commun.*, 1998, **35**, 341. * This paper describes the fabrication and manufacture of devices that can support EOF.

Quantitative 3-dimensional profiling of channel networks within transparent 'lab-on-a-chip' microreactors using a digital imaging method

Ian Broadwell, Paul D. I. Fletcher,* Stephen J. Haswell, T. McCreedy and Xunli Zhang

Department of Chemistry, The University of Hull, Hull, UK HU6 7RX.
E-mail: P.D.Fletcher@chem.hull.ac.uk

Received 11th April 2001, Accepted 25th June 2001

First published as an Advance Article on the web 9th August 2001

We have developed a method for the quantitative 3-dimensional profiling of micron sized channel networks within optically transparent "lab-on-a-chip" microreactor devices. The method involves capturing digitised microscope images of the channel network filled with an optically absorbing dye. The microscope is operated in transmission mode using light filtered through a narrow bandpass filter with a maximum transmission wavelength matching the wavelength of the absorbance maximum of the dye solution. Digitised images of a chip filled with solvent and dye solution are analysed pixel by pixel to yield a spatially resolved array of absorbance values. This array is then converted to optical path length values using the Beer–Lambert law, thereby providing the 3D profile of the channel network. The method is capable of measuring channel depths from 10 to 500 μm (and probably even smaller depths) with an accuracy of a few percent. Lateral spatial resolution of less than 1 μm is achievable. It has been established that distortion of the measured profiles resulting from a mismatch in refractive index between the dye solution and the glass of the microreactors is insignificant. The method has been successfully used here to investigate the effects of thermal bonding and etch time on channel profiles. The technique provides a convenient, accurate and non-destructive method required to determine channel profiles; information which is essential to enable optimisation of the operating characteristics of microreactor devices for particular applications.

Introduction

There is increasing interest in the development of miniaturised microreactor devices for a wide range of analytical, chemical synthesis and other measurements as encompassed in the so-called 'lab-on-a-chip' concept. The microreactor designs developed and used by the Hull group consist of a network of micron-sized channels connecting a number of reagent reservoirs which also hold the electrodes used for electro kinetic pumping. Timed voltage sequences applied under computer control to the appropriate pairs of reservoir electrodes may be used to control the movement (and hence the chemical reactions) of reagents within particular regions of the channel network by a combination of electro-osmotic and electrophoretic effects. This enables control of the *spatial* and *temporal* evolution of chemical reactions in microreactors in a manner not achievable in conventional batch reactors. It has been demonstrated that this control can be used to alter the yields and selectivities of product mixtures for a range of different reactions performed in microreactors (see refs. 1–6 for recent progress in this area). The theoretical principles of electrokinetic control of chemical reactions in microreactors have been reviewed previously.⁷

The particular microreactor designs used in Hull (and by other researchers) are fabricated by etching a channel network into a glass base plate of typical dimensions 20 mm wide \times 20 mm deep \times 2 mm thick.^{5,8,9} The etched base plate is then thermally bonded to a thick glass upper plate (thickness typically 15 mm) containing pre-drilled holes of about 3 mm diameter which connect to the channel network and act as reagent reservoirs. In order to quantitatively predict and control the electrokinetic movement of reagents within the microreactors it is necessary to determine the full 3D profiles of the channel networks in the assembled microreactor devices. In addition, control and optimisation of the base etching and

thermal bonding processes also require methods for 3D profiling of both non-bonded and bonded base plates. A key consideration here is the possible extent to which the thermal bonding of the upper and base plates may distort the channel profile. For the open etched base plates before bonding, 3D profiles can be obtained using mechanical, stylus-based techniques. For such methods, care must be taken to avoid artefacts at the near vertical channel edges arising from the limited resolution and imperfections in the shape of the stylus tip. For the closed, bonded base plates, it is possible to obtain the channel profile by cutting the bonded device perpendicular to the channel axis followed by microscopically imaging the channel profile. This procedure has a number of disadvantages. Firstly, the device is destroyed by the measurement. Secondly, the channel profile is only obtained at a single point where the cut is made. Lastly, it is not a trivial matter to obtain the channel cross section accurately without artefacts due to 'chipping' of the edges arising from the cutting process. In order to meet the need for a rapid, accurate and non-destructive method for 3D profiling of both open and closed etched channel networks, we have developed a technique based on digital microscopic imaging of the channel network filled with an optically absorbing dye solution (see Fig. 1). The method is generally applicable for the quantitative 3-dimensional profiling of any voids fillable with dye solution which are present in a transparent solid. In this paper we describe the application of the method for the profiling of channel networks within a range of bonded and non-bonded microreactor devices.

The method described here is similar in principle to a range of (generally more complex) spectroscopic imaging techniques (UV/vis, IR, Raman) which have been developed for particular applications.^{10–16} The absorbance imaging method described here is simple to implement and provides *absolute* values of the channel depths.

Experimental

1 Materials

m-Cresol (Lancaster, 99%), glycerol (Lancaster, >99%), Patent Blue (Fluka standard reagent), Rose Bengal (Aldrich, dye content approx. 95%) were used without further purification. Water was purified by reverse osmosis.

2 Methods

An Axiovert S100 inverted microscope (Carl Zeiss) using transmission optics was employed to obtain digital micrographic images of the microreactors filled with either solvent or dye solutions. The light source was a 100 W tungsten lamp emitting over the wavelength range from approximately 400 to 800 nm. Wavelength selection appropriate to the particular dye solution used was achieved by incorporating an appropriate narrow band pass filter of the correct maximum transmission wavelength between the microscope objective and camera (Fig. 1). Transmittance spectra of the two filters used here (Chroma 11002, peak 546 nm full width at half maximum 10 nm and Edmund Scientific N43-136, peak 649, full width at half maximum 11 nm) are given in Fig. 2. Stray ambient light was reduced to negligible levels by use of a hood over the microscope. Microscope images were collected using a digital monochrome CCD camera (Hamamatsu C4742-95-12NRB) giving a digital output of a maximum of 1024×1024 pixels with 12 bit resolution of the light intensity in each pixel. The camera was connected to a PC and controlled by the digital image recording and analysis software AQM from Kinetic Imaging Ltd. Averaging of pixel intensities over 4×4 groups of pixels (' 4×4 binning') was used to yield a 256×256 array of intensity values. This procedure was found to provide the best compromise between rapid data acquisition, signal-to-noise ratio, spatial resolution and data file size. Scion Image software

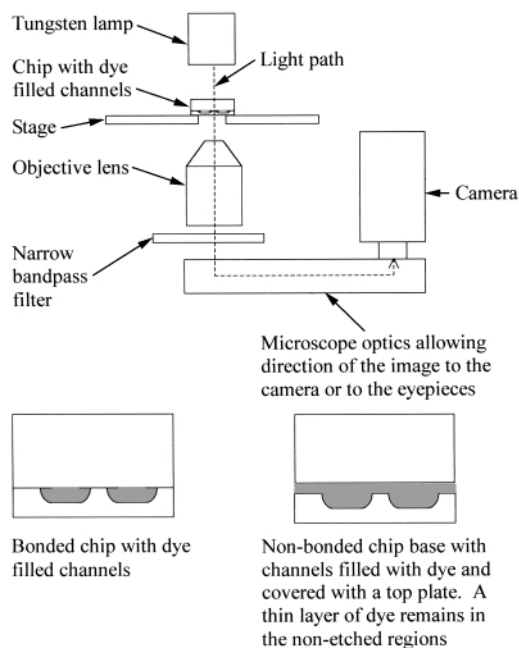


Fig. 1 Schematic diagram of the inverted optical microscope arrangement used for the 3D profiling of microreactor chip channel networks. The lower diagrams show side views of dye filled channels (shaded gray) in a bonded chip and in a non-bonded chip covered with a non-bonded top plate.

(Scion Corporation) was used to transfer the numerical image data into Microsoft EXCEL for subsequent conversion into absorbance values and hence pixel-by-pixel depth values.

As explained in detail below, for the profiling measurements by the imaging technique it is necessary to capture images of the microreactor filled with dye solution and filled with solvent. For the proper calculation of pixel-by-pixel absorbance values, it is essential that there is no movement of the microreactor between the capture of these two images. Hence, care was taken to ensure that the microreactor was firmly located in a fixed position on the microscope stage and filled with the appropriate liquid *in situ* using syringes. For 3D profiling of non-bonded base plates, the etched channels were filled with either solvent or dye solution and then covered with a non-bonded top plate. This procedure always gave a thin layer of dye in the non-etched regions of the base plate (see detail in Fig. 1). This small measured thickness of dye solution was subtracted from the derived values to obtain the true channel depths. Dye solution UV/Vis spectra and absorbance values required for calibration were recorded using a Unicam UV3 spectrophotometer using quartz cuvettes (Hellma) with accurate path lengths in the range 50–10000 μm .

Microreactor devices were fabricated according to published procedures.⁹ The base plate of chip 1 was etched using a solution comprising 250 ml of water, 12.5 g ammonium fluoride (Lancaster, 98%) and 7 ml of 40% HF solution in water (BDH Merck, AnalaR grade) for 25 min at 65 °C. The base was placed on a support in the etch solution with patterned side facing downwards within a heated ultrasonic bath (Ultrawave Scientific Supplies, Nottingham, UK). Ultrasound was applied in 1 min bursts at 5 min intervals. This procedure has been found to ensure that debris is effectively removed during the etch and that fresh etchant solution remains in good contact with the surface. Thermal bonding of chip 1 was made as follows. The base and upper plates were placed on a flat quartz plate in a conventional muffle furnace and a block of quartz of mass 70 g was placed on top to aid bonding. The oven temperature was then held at 575 °C for 3 h. Chip base 2 was etched similarly except that the etching temperature was 60 °C and the solution was stirred with a rod instead of using ultrasound. It was thermally bonded using an oven temperature of 570 °C for 3 h using a quartz top block of mass of 28 g. Chip bases 3–7 (non-bonded) were etched for variable times using an etch bath temperature of 60 °C with ultrasonication (non-continuous, 1 min on followed by 9 min off) to aid debris removal.

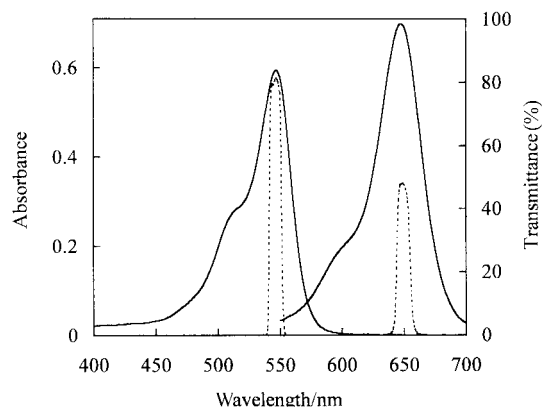


Fig. 2 Absorbance spectra of RB (1.0567 mM in water, $\lambda_{\text{max}} = 547$ nm) and PB solutions (0.8275 mM in 30.2 wt.% glycerol in *m*-cresol, $\lambda_{\text{max}} = 647$ nm). The path length was 100 μm . The dashed lines show the transmittance curves for the two narrow bandpass filters used in conjunction with the different dye solutions.

Results and discussion

1 Imaging procedure to obtain 3D profiles

The optical absorbance A of a solution is given by the Beer–Lambert law.

$$A = \log \left\{ \frac{I_{\text{ref}} - I_{\text{dark}}}{I_{\text{sol}} - I_{\text{dark}}} \right\} = C d \epsilon \quad (1)$$

where I_{ref} and I_{sol} are the transmitted light intensities recorded through the reference liquid (the solvent) and the dye solution respectively. I_{dark} is the detector signal recorded in the absence of incident light, C is the concentration of absorbing species in the solution, d is the optical path length and ϵ is the molar absorption coefficient. Using a dye solution for which the product $C\epsilon$ at the appropriate wavelength has been measured separately using a conventional spectrophotometer, determination of A for a channel filled with dye solution yields d which corresponds to the channel depth.

To obtain d , the following sequence of images was captured for each sample using the apparatus shown schematically in Fig. 1.

1. Image of the channels with zero incident illumination to obtain the array of I_{dark} intensities.
2. Image of the channels filled with solvent giving the array of I_{ref} intensities.
3. Image of the channels filled with dye solution giving the array of I_{sol} intensities.

For each measurement set, the incident light intensity and the camera gain were adjusted so that the maximum intensities in the I_{ref} array were close to the maximum value of 4095 allowed by the 12 bit resolution of the camera. It was monitored that, under the set conditions, the array of I_{dark} values did not exceed 200 or so. This procedure ensured that the full dynamic range allowed by the 12 bit resolution of the camera was used.

Solutions of two different dyes were used in this study. The spectra of RB (Rose Bengal) and PB (Patent Blue) solutions are shown in Fig. 2 and compared with the transmittance curves of the narrow band pass optical filters used in the microscope imaging. The water-soluble dye RB was used in aqueous solution for which the refractive index (RI) of approximately 1.33 is not matched to that of the glass (approximately 1.5). Because of this lack of RI matching, optical refraction is expected at the channel edges which may give some distortion of the measured channel profile. The profiling of non-bonded base plates requires that the dye solution be spread on the etched channel surface of the base before covering with a non-bonded top plate. In early experiments with RB and other dye solutions, problems were encountered due to significant evaporation of the dye solution during this procedure, resulting in uncontrolled changes in dye concentration. We developed the PB dye solution with the following characteristics required to optimise the 3D profiling method. The dye solution should be matched in RI with the glass of the microreactor chip and must be involatile. The dye must be highly soluble in the solvent in order that sufficiently high absorbance required to profile channels of low depth (*i.e.* small path lengths). It is advantageous if the absorbances of the dye solutions are proportional to concentration. This facilitates the optimisation of dye concentration necessary to minimise experimental uncertainties for different channel depths. The dye solutions should be chemically stable and the absorbance of the solvent should be negligible compared to that of the dye solution at the optimum wavelength.

These characteristics were fulfilled by PB solutions in a mixed solvent consisting of 30.2 wt.% glycerol in *m*-cresol. Fig. 2 shows the spectrum of a PB solution. Fig. 3 shows plots of absorbance at 647 nm *versus* PB concentration for different path lengths recorded using a conventional spectrophotometer. It is

clear that sufficiently high absorbance values can be obtained and that the Beer–Lambert law is obeyed with reasonable precision. For the PB solutions, full dissolution of the dye required treatment in an ultrasonic bath for several hours. Absorbance measurements over several weeks showed the dye solutions have adequate stability for reliable imaging measurements.

The accuracy with which d can be determined for each image array value (corresponding to a single ‘binned’ pixel group) depends on the value of the absorbance. For the setup used here, the typical experimental uncertainty in each of the intensity values I_{ref} , I_{sol} and I_{dark} was estimated from the variation in measured arrays of intensity values to be approximately ± 5 . The values for I_{dark} and I_{ref} using optimised settings for the incident light intensity and camera gain were typically 100 and 3500 respectively. Conversion of the uncertainties in the individual (binned) pixel intensities to the uncertainties in derived absorbance yields the plot shown in Fig. 4. The uncertainty in absorbance, and hence in depth d , is minimum for absorbance values of around 0.6 and is approximately 2%. Since absorbance is proportional to channel depth, the dye concentration used must be adjusted in order to achieve the optimum absorbance of 0.6 for the particular channel depth under study and an acceptable uncertainty of 2% in d .

An additional possible source of systematic error in the measurement of d arises from the fact that microscope objectives have a significant numerical aperture NA, meaning that light rays passing through the sample take on a variety of paths with different angles. A microscope objective lens accepts light over a cone in the angle range $\pm\alpha$ relative to the perpendicular. For an air objective, $NA = \sin\alpha$. Hence the actual path length experienced by a light will be the intensity weighted average for all angles between 0 and α . The maximum

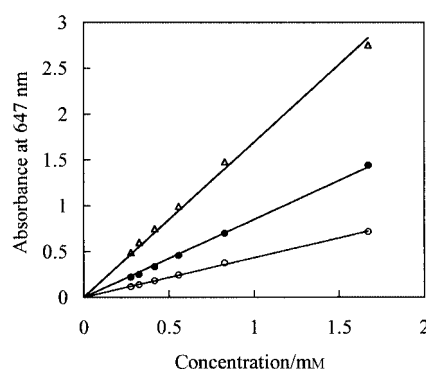


Fig. 3 Absorbance (647 nm, measured using a conventional spectrophotometer) *versus* PB concentration in glycerol–cresol mixed solvent for path lengths of 50 (open circles), 100 (filled circles) and 200 μm (open triangles).

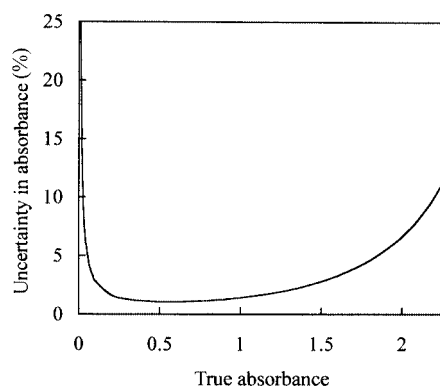


Fig. 4 Variation of percentage uncertainty in the measured absorbance with true absorbance for $I_{\text{dark}} = 100$ and $I_{\text{ref}} = 3500$. Uncertainties of ± 5 in each of the intensities I_{dark} , I_{ref} and I_{sol} were assumed.

error in the channel depth measurement can be estimated by calculation of the ratio $x_{\max} = (\text{true perpendicular path length} / \text{max light path length})$. The maximum light path length occurs for light rays at the maximum acceptance angle α and is equal to $\cos(\sin^{-1} \text{NA})$. The effective path length measured will differ from the perpendicular value by the intensity distribution weighted average $\langle x \rangle$ which will be intermediate between 1 and x_{\max} . As an approximate estimate of this effect, we take $\langle x \rangle$ to be $(1 + x_{\max})/2$. For the objective lenses used in this work with magnifications of 1.25, 2.5, 4 and $10\times$, the values of NA are 0.035, 0.075, 0.1 and 0.3 respectively. The corresponding values of $\langle x \rangle$ are 0.9997, 0.9986, 0.9975 and 0.9770. Thus, it can be seen that the errors in channel depth introduced by this effect are negligible so long as objectives of $10\times$ or less are used. Proper correction for the effect would be required when using objectives of higher magnification.

It was checked that the microscopic imaging method yielded reliable absorbance measurements. Images of dye filled rectangular capillaries of different path lengths (obtained from Camlab, UK) and a 1 mm cuvette were recorded and converted to absorbance. The absorbance of the 1 mm cuvette sample was also measured using a conventional spectrophotometer. The results, plotted in Fig. 5, show that the microscope absorbance values agree within the experimental uncertainties (mainly arising from the uncertainties ($\pm 7\%$, estimated microscopically) in the path lengths of the capillaries).

Fig. 6 shows a 3D profile image of a 7×7 mm area of chip 1 recorded using a $1.5\times$ objective lens. Even at this low magnification (required to image a large area) the spatial resolution is sufficient to allow details of the channel profiles and intersections to be seen clearly. The deep circular shape at $X = 7800, Y = 0$ mm corresponds to one of the reservoirs on the microreactor. When viewed on the computer screen using EXCEL software, the image can be fully rotated in 3D allowing examination from all angles. The time required for acquisition of the image set and subsequent data analysis to produce Fig. 6 was about 1 h.

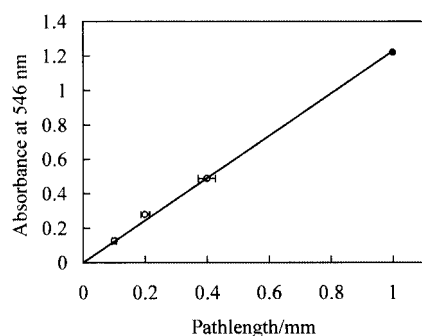


Fig. 5 Absorbance (546 nm, measured using the microscope imaging method) versus path length for dye filled capillaries or rectangular cross section (open circles) and a 1 mm path length cuvette (filled circle).

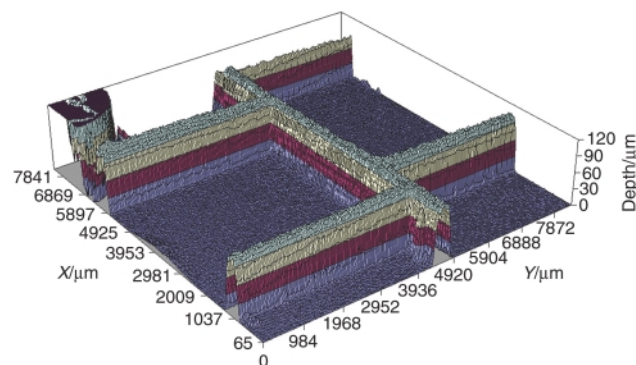


Fig. 6 3D profile image of a 7×7 mm area of the channel network of chip 1. The image was recorded using RB as the dye (non-RI matched).

Higher magnification images using a $10\times$ objective of a sub-area of chip 1 were recorded using both aqueous RB (non-RI matched) and glycerol-cresol PB dye (RI matched) solutions. The aim here was to determine whether non-RI matching between the dye solution and the glass of the microreactor produces significant distortion of the channel profiles due to refraction of the light at the channel edges. 2D 'slices' through the channels at corresponding positions in the two full 3D profiles are shown in Fig. 7. It can be seen that non-RI matching does not produce any significant distortion of the channel profiles. This conclusion is valid for aqueous RB solutions with an RI of approximately 1.33 as compared with approximately 1.52 for the glass. Although a higher level of mismatch in RI may produce significant distortion, it is important for many future microreactor applications to establish that use of aqueous solutions in glass microreactors in the context of imaging methods does not give significant distortion.

Fig. 8 shows an optical micrograph of one end of a channel which was etched right up to the edge of chip 1. This was done to enable us to compare the channel profile without the necessity for cutting the chip open. The dimensions of the channel end profile imaged in Fig. 8 shows reasonable agreement with those determined from the imaging measurements of Fig. 7.

2 Comparison of channel profiles before and after thermal bonding of the upper plate

Figs. 9a and 9b show 3D profile images recorded before and after thermal bonding of chip 2. The channel cross sections at corresponding positions in the two 3D images are compared in Fig. 10 where it can be seen that the effect of bonding has been to "squash" the channels from an initial depth of 55.3 down to 39.9 μm .

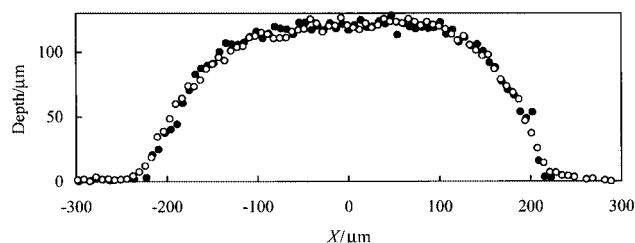


Fig. 7 Comparison of channel cross sectional profiles for chip 1 obtained using RB aqueous dye solution not RI matched to the glass (filled circles) and PB solution in glycerol-cresol mixed solvent which was RI matched to the glass (open circles). The two channel cross sections correspond to the same position in the channel network of chip 1.

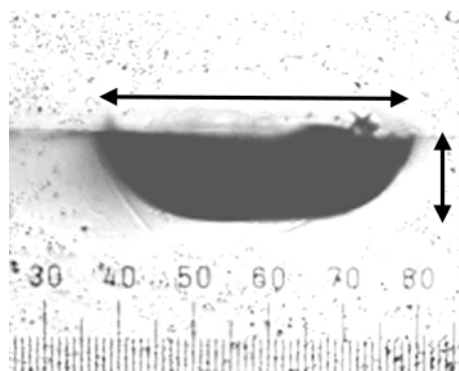


Fig. 8 Micrograph of a side view of a channel end in chip 1. The horizontal arrow length ($409 \mu\text{m}$) corresponds to the channel top width measured in Fig. 7. The vertical arrow length ($119 \mu\text{m}$) corresponds to the channel depth measured in Fig. 7.

The etching of glass, using the etch solution described above, proceeds at equal rates in all directions, *i.e.* the etching is isotropic. The etch depth d is controlled by the etch conditions and the etch time. Ideal isotropic etching through a channel mask of width m is expected to produce a channel profile comprising a rectangular shape of width m and depth d bounded by two quarter circle edges of radius equal to d . The expected channel width at the glass surface is equal to $(m + 2d)$. In practice, either prolonged etching or thermal bonding may produce a ‘smoothing’ of the channel edges away from the idealised quarter circle shape. In order to model the channel profiles, we first calculate the ideal isotropic etch profile using

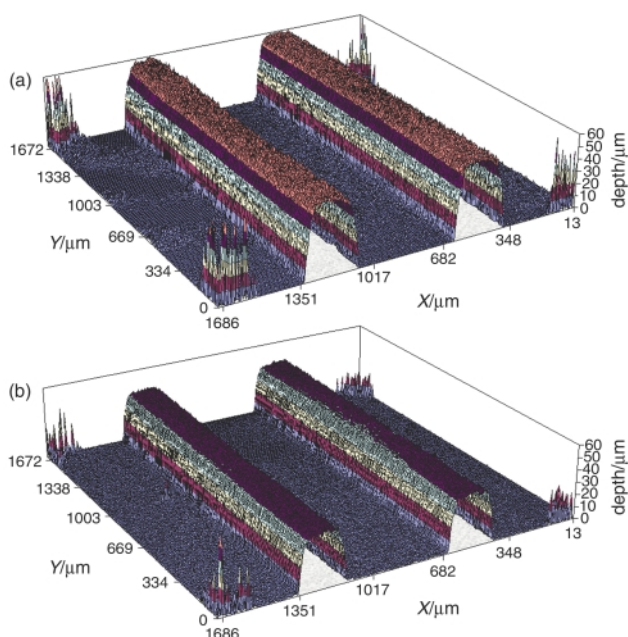


Fig. 9 Comparison of 3D profile images of a 1.7×1.7 mm area of chip 2 (a) before and (b) after thermal bonding of the base and upper plates. The images were recorded using PB as the dye (RI matched).

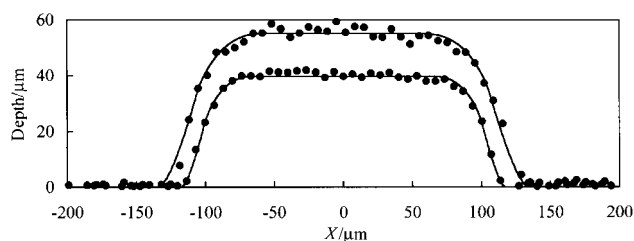


Fig. 10 Channel cross sectional profiles for chip 2 before (larger depth) and after thermal bonding (smaller depth) of the base and upper plates. The coordinates of the channel centres correspond to $X = 500$ and $Y = 615 \mu\text{m}$ in Fig. 9. The solid curves are best-fits to the model described in the text with the parameters listed in Table 1.

Table 1 Summary of measured channel profile parameters. Chip 1 (non-RI matched) was profiled using an RB solution in water. All other chips were profiled using PB solutions in glycerol–cresol mixed solvent which was RI matched to the glass of the chip

Chip	Depth/ μm	Apparent mask width/ μm	Actual mask width/ μm
Chip 1 (non-RI matched)	119.4	170.9	118
Chip 1 (RI matched)	119.2	173.8	118
Chip 2 (non-bonded)	55.3	129.0	128
Chip 2 (bonded)	39.9	138.2	128
Chip base 3 (24 min etch time)	50.1	126.0	128
Chip base 4 (36 min etch time)	62.8	137.1	128
Chip base 5 (48 min etch time)	85.7	157.3	128
Chip base 6 (96 min etch time)	173.4	145.2	128
Chip base 7 (120 min etch time)	189.8	126.9	128

the values of m and d . The ‘smoothing’ of the profile is then parameterised by incorporation into the model of a variable smoothing length δ . The channel depth at each X value is obtained by taking the depth calculated for the isotropic etch profile averaged over the range of X values corresponding to $\pm\delta$. Fitting of the experimental channel profiles then yields the best-fit values of m , d and smoothing length δ . A zero value of δ corresponds to no distortion from the idealised isotropic etch profile whereas a high value indicates that significant smoothing has occurred during either the etching or thermal bonding processes.

For the profiles of Fig. 10, the solid lines shows the best fits to the smoothed isotropic etch model. The derived parameters for chip 2 (shown in Table 1) show relatively low values of δ indicating little distortion from the isotropic etch profile. Thermal bonding in this case apparently *reduces* δ slightly. However, it can be seen in Fig. 10, that the difference in channel profile shapes corresponding to the best fit values of δ of 25 and 15 μm (for the non-bonded and bonded chips respectively) is rather small. In contrast to chip 2, the δ values for chip 1 (Table 1, where similar values are seen for non-RI and RI matching)

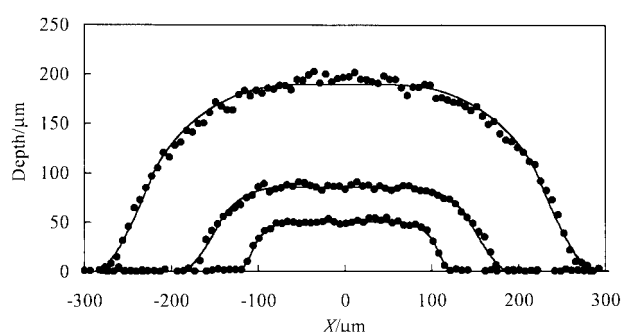


Fig. 11 Channel cross sectional profiles for chip bases with etch times of (in order of increasing depth) 24, 48 and 120 min. The solid curves are best-fits to the model described in the text with the parameters listed in Table 1.

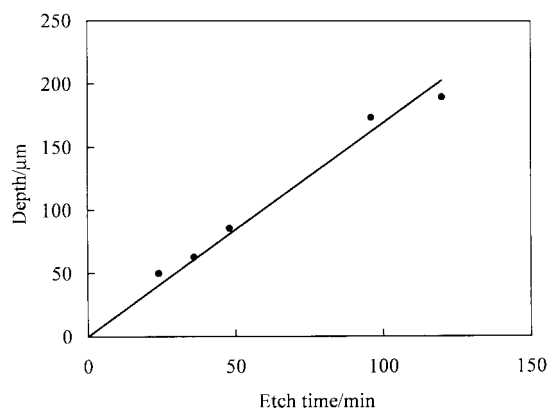


Fig. 12 Variation of channel depth with etch time under the conditions described in the text. The solid line corresponds to a mean etch rate of $1.7 \mu\text{m min}^{-1}$.

are high indicating that significant smoothing of the channels occurred during the fabrication of this chip. It is relevant to note here that chip 1 was bonded using a higher temperature and a larger top mass (added to aid bonding) than chip 2. Both factors might be expected to increase channel profile distortion during bonding. These examples serve to demonstrate the utility of the 3D profiling method coupled with the channel profile modelling in the characterisation of microreactors channel networks and the optimisation of their fabrication.

3 Channel profiles for different etch times

A series of microreactor bases were prepared using a constant mask width of 128 μm and etched for different times. Illustrative channel cross sectional profiles including fits to the smoothed isotropic etch model are plotted in Fig. 11. The variation of fitted depth with etch time (Fig. 12) indicates that the etch rate is approximately constant and equal to 1.7 $\mu\text{m min}^{-1}$. The mask widths derived from the fits to the measured channel profiles (Table 1) vary only slightly with etch time and are reasonably close to the actual mask width of 128 μm . The origin of the small differences between fitted and actual mask widths observed for some of the samples is unclear at present.

For each of the different chip bases, we have determined the standard deviation in channel depth over the flat region of the channels around the channel centre. The observed variability in channel depth can result from two causes. Firstly, variation can result from the random uncertainty in the microscope absorbance measurements and hence in the measured depths. Secondly, the channel surfaces may actually be rough giving a real point-to-point variation in depth. Fig. 13 shows a plot of the standard deviation in depth *versus* depth. The slope of the plot corresponds to the uncertainty (one standard deviation) in depth

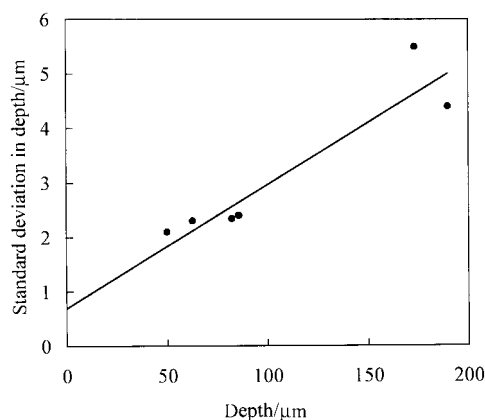


Fig. 13 Standard deviation in channel depth *versus* depth. The solid line corresponds to an uncertainty (one standard deviation) of 2.3% of the channel depth plus an intrinsic depth variability of 0.7 μm given by the intercept of the plot.

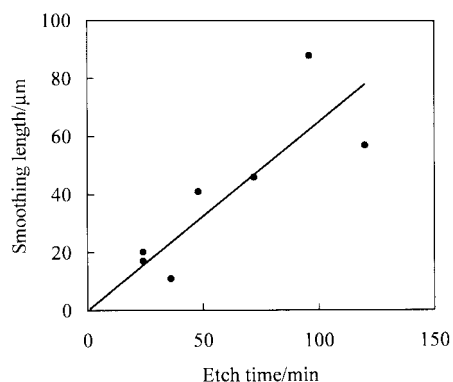


Fig. 14 Variation of fitted smoothing length δ with etch time.

being 2.3% of the measured depth. This level of uncertainty is reasonably consistent with the value expected from the analysis shown in Fig. 4. The intercept of Fig. 13 suggests that the actual roughness of the channel surfaces is of the order of 0.7 μm . Although plausible, the ‘scatter’ of the data of Fig. 13, makes this estimate rather uncertain.

Finally, Fig. 14 shows the variation of fitted smoothing length δ *versus* etch time. Although the uncertainty in δ is large, the results suggest that the distortion away from the ideal isotropic etch profile increases with increasing etch time.

Conclusions

We have developed a rapid, accurate and non-destructive technique to determine the 3D profiles of microreactor channel networks based on optical imaging of dye filled channels. The method is capable of measuring channel depths from 10 to 500 μm (and probably smaller depths) with an accuracy of a few percent and a spatial resolution of less than 1 μm . It has been established that distortion of the measured profiles resulting from a mismatch in refractive index between the dye solution and the glass of the microreactors are insignificant. The method has been successfully used to investigate the effects of thermal bonding and etch time on channel profiles.

The imaging method developed here could be applied to profile any solution-fillable voids within transparent solids. Furthermore, for microreactor channels where the depth (path length) has been measured, the technique may also be applied to determine the concentration profiles of either absorbing or fluorescent species in the channels with a time resolution of greater than 10 frames per second. This aspect is currently under active investigation in our laboratories.

Acknowledgements

We thank the Engineering and Physical Sciences Research Council of the UK for funding this study and the Institute of Applied Catalysis (iAC) for partial funding of the Studentship for Ian Broadwell.

References

- 1 S. J. Haswell, R. J. Middleton, B. O’Sullivan, V. Skelton, P. Watts and P. Styring, *Chem. Commun.*, 2001, 391.★ *This feature article gives a clear account of current work on synthesis in microreactors.*
- 2 V. Skelton, G. M. Greenway, S. J. Haswell, P. Styring, D. O. Morgan, B. H. Warrington and S. Y. F. Wong, *Analyst*, 2001, **126**, 7.
- 3 V. Skelton, G. M. Greenway, S. J. Haswell, P. Styring, D. O. Morgan, B. H. Warrington and S. Y. F. Wong, *Analyst*, 2001, **126**, 11.★ *This paper describes the first demonstration of the control of stereoselective product formation in a microreactor.*
- 4 G. N. Doku, S. J. Haswell, T. McCreedy and G. M. Greenway, *Analyst*, 2001, **126**, 14.
- 5 T. McCreedy and N. G. Wilson, *Analyst*, 2001, **126**, 21.
- 6 M. C. Mitchell, V. Spikemans and A. J. de Mello, *Analyst*, 2001, **126**, 24.
- 7 P. D. I. Fletcher, S. J. Haswell and V. N. Paunov, *Analyst*, 1999, **124**, 1273.★ *This tutorial review gives a clear account of the underlying principles of chemical reaction control in microreactors.*
- 8 T. McCreedy, *Trends Anal. Chem.*, 2000, **19**, 396.
- 9 T. McCreedy, *Anal. Chim. Acta*, 2001, **427**, 39.
- 10 P. J. Treado, A. Govil, M. D. Morris, K. D. Sternitzke and R. J. McCreedy, *Appl. Spectrosc.*, 1990, **44**, 1270.
- 11 S. C. Jacobson, R. Hergenroder, L. B. Koutny, R. J. Warmack and J. M. Ramsey, *Anal. Chem.*, 1994, **66**, 1107.
- 12 J. Wu and J. Pawliszyn, *Anal. Chem.*, 1994, **66**, 867.
- 13 E. N. Lewis, P. J. Treado, R. C. Reeder, G. M. Story, A. E. Dowrey, C. Marcott and I. W. Levin, *Anal. Chem.*, 1995, **67**, 3377.
- 14 Z. Wang and D. Scherson, *J. Electrochem. Soc.*, 1995, **142**, 4225.
- 15 E. T. Bergstrom, D. M. Goodal, B. Porkric and N. M. Allinson, *Anal. Chem.*, 1999, **71**, 4376.
- 16 B. L. McClain, J. Ma and D. Ben-Amotz, *Appl. Spectrosc.*, 1999, **53**, 1118.

Electrical currents and liquid flow rates in micro-reactors

Paul D. I. Fletcher,* Stephen J. Haswell and Xunli Zhang

Department of Chemistry, The University of Hull, Hull, UK HU6 7RX.
E-mail: P.D.Fletcher@hull.ac.uk

Received 17th July 2001, Accepted 18th September 2001
First published as an Advance Article on the web 5th October 2001

For micro-reactor devices in which liquids are pumped by electro-osmotic flow (EOF), *in situ* monitoring of the electrical currents in the channel networks provides a valuable diagnostic tool. We demonstrate here that the voltage–current characteristics of a micro-reactor channel network can be accurately modelled using measurements of the full 3-D geometry of the channel network, the liquid conductivity and the channel wall–liquid surface conductivity. It is shown that surface conductivity provides a significant contribution to the overall measured electrical currents in channel networks for which the ratio of surface area to volume is high. Following correction for surface conductivity, the electrical currents are proportional to the liquid volumetric flow rates measured in the different branches of the channel network. The constant of proportionality is related to the zeta potential of the channel wall–liquid surface. Measurements of the variation of electrical currents and volumetric flow rates as a function of the applied voltages allows the determination of the surface conductivity and zeta potential within the micro-reactor which enables the prediction of the voltages required to produce the desired flow rates in any channel section. *In situ* logging of the electrical currents, incorporated within the control system, allows continuous monitoring of the liquid flow rates during micro-reactor operation.

Introduction

There is increasing interest in the development of miniaturised micro-reactor devices for a wide range of analytical, chemical synthesis and other measurements as encompassed in the so-called ‘Lab-on-a-Chip’ concept. The particular micro-reactor designs developed and used by, *inter alia*, the Hull group consist of a network of micron-sized channels connecting a number of reagent reservoirs which also hold the electrodes used for electro-kinetic pumping. Timed voltage sequences applied under computer control to the appropriate pairs of reservoir electrodes may be used to control the movement of reagents within particular regions of the channel network by a combination of electro-osmotic and electrophoretic effects. This enables control of the *spatial* and *temporal* evolution of chemical reactions in micro-reactors in a manner not achievable in conventional batch reactors. It has been demonstrated that this control can direct the yields and selectivities of product mixtures for a range of different reactions (see refs. 1–7 for recent progress in this area). The theoretical principles of electrokinetic control of chemical reactions in microreactors have been reviewed previously.⁸

Electro-osmotic flow (EOF) produces a flat liquid velocity profile across the micro-reactor channels except in the regions very close (nm) to the channel walls.^{9,10} However, as explained in ref. 8, pressure driven flow caused by reservoir height differences plus differences in the Laplace pressures associated with the liquid menisci within the reservoir leads to a parabolic velocity profile. In order to obtain reproducible and predictable micro-reactor operation, it is advantageous to minimise the effects of pressure driven flow such that the EOF liquid flow rates are unaffected by the liquid reservoir heights and uncontrolled, variable velocity profiles are minimised. Specifically, the pressure driven flow contribution arising from (say) a 10 mm liquid height difference between reservoirs should be negligible in comparison with the EOF. For EOF, the linear liquid velocity is unaffected by channel cross sectional area (so long as channel diameters are much larger than the nm thickness of the diffuse layer of counter-ions at the channel wall interface)

whereas pressure driven flow is strongly suppressed by reducing the channel cross sectional dimensions. Hence, pressure driven flow can be reduced to negligible levels by including sections of high hydrodynamic resistance, *i.e.* small channel cross sectional area, within micro-reactor channel networks. For channels with typical dimensions of $50 \times 100 \mu\text{m}$ cross section and 10 mm length operating under EOF voltages of 200 to 1000 V, the EOF liquid volumetric flow rates are comparable in magnitude to the pressure driven flow arising from liquid reservoir height differences of only a few mm. In this situation, the actual flow rates result from contributions from both EOF and pressure driven flow and are highly sensitive to the reservoir heights. Virtually ‘pure’ EOF can be obtained by incorporation of one or more porous glass frits (typical porosity 10% and pore diameters of a few μm) which provide a high hydrodynamic resistance within the channel network and suppress pressure driven flow.¹¹

The fabrication and performance of frits, formed *in situ* within the channel networks as described in ref. 11, has been found to be rather irreproducible. An alternative method of incorporating regions of high hydrodynamic resistance uses a two-stage etching process as shown schematically in Fig. 1. For the simple T channel network used in this study, reservoirs A, B and C are linked by non-continuous large channels which are etched within the bottom plate. The breaks in the large channels are linked by rectangular grids of small channels which are etched on the lower side of the middle plate. The micro-reactor assembly is completed by thermal bonding of the ‘sandwich’ of bottom, middle and upper plates. Three holes drilled through the middle and upper plates connect to the ends of the large channel segments and form the reagent reservoirs. The strategy of using rectangular grids of small channels (as opposed to sections containing only a single small channel) is employed in order to avoid fabrication failure due to misalignment between the bottom and middle plates during thermal bonding.

For electrokinetic controlled operation of the micro-reactor, small Pt wire electrodes are placed in each reservoir and connected to a voltage supply and control box which, in turn, is operated under computer control using LabVIEW software.

Each voltage supply/control box allows timed sequences of voltages (0 to 1000 V) to be applied to up to 4 electrode pairs. In addition, the control system logs the values of voltage and electrical current between each electrode pair. Voltage supply to more than 4 electrode pairs, as required for complex channel networks, is easily achieved by using more than one voltage supply/control module. In this paper, starting from the channel network dimensions and the liquid conductivity, we describe a quantitative analysis of the electrical currents measured as a function of the applied voltages in the micro-reactor design shown in Fig. 1. The currents are then linked to the liquid flow rates measured as a function of the applied voltages. The importance of this analysis and its experimental validation lies in the fact that it provides the complete framework required to achieve the next step in micro-reactor control. At present, the input for the control software is simply the desired voltage–time sequences for each electrode pair. Using the analysis given here, it will be possible to input the desired liquid flow rates in the different channel sections directly into the control software. Following input of the relevant system parameters (micro-reactor geometry and liquid properties), the control software can then calculate the necessary voltage sequences required to achieve the inputted flow rate sequences.

EOF in micro-reactors has been used extensively in the last decade. Aspects of the modelling concepts used here and their application in micro-fluidic devices have been discussed previously in, for example, refs. 12–15. Novel devices allowing the control of EOF by application of an electric field perpendicular to the fluid flow have been fabricated.¹⁶ In addition, detailed modelling of the microscopic details of electro-osmotic fluid flow around channel junctions has been described.¹⁷

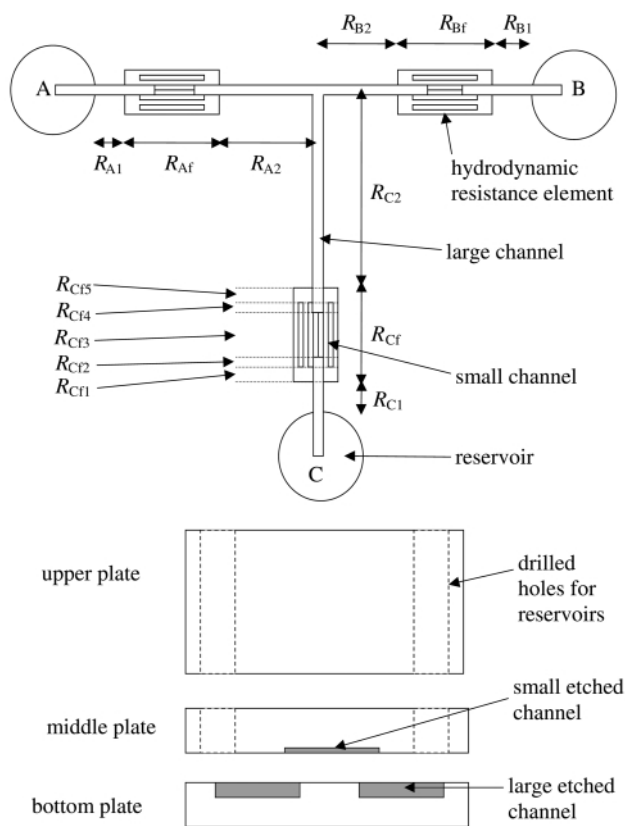


Fig. 1 Schematic diagram of the T shaped channel network of the micro-reactor showing the correspondence between channel sections and resistance elements. The lower diagram (not to scale) shows a side view before thermal bonding of the ‘sandwich’ construction.

Experimental

Materials

Rose Bengal (Aldrich, dye content approx. 95%) was used without further purification. Water was purified by reverse osmosis. Methanol (Aldrich, anhydrous, 99.8%), sodium methoxide (NaOMe, Aldrich, 0.5 M solution in methanol, A.C.S. reagent) and potassium chloride (BDH, AnalaR, >99.5%) were used as received.

Methods

An Axiovert S100 inverted microscope (Carl Zeiss) using transmission optics was employed to obtain digital micro-graphic images of the micro-reactor. Quantitative 3-D profiles of the channel network were obtained by analysis of micrograph images of the channels filled with dye solution according to the method described fully in ref. 18. In the present work, aqueous solutions of Rose Bengal (6 g dm^{-3}) were used and the images were obtained using a wavelength of 546 nm (selected using a narrow bandpass filter Chroma 11002, peak 546 nm full width at half maximum 10 nm) and a $10\times$ objective lens. For the normal optical micrographs, a $1.25\times$ objective was used to get a fuller view of the channel network.

The micro-reactor chip was fabricated according to published procedures¹⁹ with some variations. The bottom and middle plates were made from White Crown glass sheets pre-coated for etching (Align Rite, 3 mm thickness). Using an etch solution comprising 250 ml of water, 12.5 g ammonium fluoride (Lancaster, 98%) and 7 ml of 40% HF solution in water (BDH Merck, AnalaR grade), the bottom plate was etched for 10 min at 65 °C. The middle plate was etched for 1 min at 65 °C. Etching was carried out by placing the glass pieces on a support in the etch solution with patterned side facing downwards within a heated ultrasonic bath (Ultrawave Scientific Supplies, Nottingham, UK). Ultrasound was applied continuously to ensure that etch debris is effectively removed during the etch and that fresh etchant solution remains in good contact with the surface. The bottom and middle plates were thermally bonded together by placing them in a muffle furnace set at 570 °C for 3 h. A quartz block of mass 70 g was placed on top of the assembly to aid bonding. The top block was then bonded to the two bonded lower plates using the same procedure.

Electrokinetic control, voltage and current measurements of the micro-reactor were made using a home designed power supply which was constructed by Kingfield Electronics, UK. The power supply has four channels for voltage outputs, four channels for monitoring the electrical current of each channel and four channels to monitor the applied voltage for each channel. Programmed control of the timed voltage sequences to each channel and current and voltage logging was made using LabVIEW software (National Instruments). For the T shaped channel network used in this work, voltages were controlled, and the currents and voltages logged, for two channels only, *i.e.* between reservoirs A and C (ground) and between B and C (ground). Lengths of shiny Pt wire (Goodfellow, diameter 0.26 mm) were used as electrodes.

Liquid flow rates as a function of applied voltages were made by monitoring the changes in liquid heights over time for the reservoirs A, B and C. The reservoirs were connected to vertically-mounted, glass 0.5 ml graduated pipettes (Gallenkamp, approximately 1.2 mm internal diameter, 130 mm height) *via* plastic connecting tubes. The internal diameters of each pipette were measured accurately using a travelling microscope equipped with a digital clock gauge with 1 μm resolution (Mitutoyo). The electrodes were inserted through the sides of the connecting plastic tubes in order that they did not distort the liquid menisci positioned within the pipettes. The assembly was

sealed using Permabond epoxy glue. Complications arising from possible evaporation of the test liquids were avoided by layering a 3 mm depth of squalane (involatile and immiscible) on top of each liquid surface within the pipettes. Height changes of the solvent/squalane menisci were measured optically using the travelling microscope described above. The accuracy of the liquid height measurements was estimated by repeated measurements to be approximately $\pm 15 \mu\text{m}$.

The liquid conductivities were measured using a WTW GmbH model LF340 AC conductivity bridge operating at 1000 Hz and equipped with a graphite electrode dip cell with cell constant equal to 0.475 cm^{-1} .

All measurements were made at room temperature which was $22\text{--}25 \text{ }^\circ\text{C}$ and was measured separately for each experiment.

Results and discussion

Micro-reactor channel network geometrical parameters

The overall micro-reactor geometry is shown schematically in Fig. 1. Fig. 2 shows a microscope image of the central region of the channel network. As discussed below, the T shaped micro-reactor channel network filled with a conducting liquid can be analysed in terms of two connected DC circuits consisting of a number of resistance elements connected in series and parallel. Calculation of the electrical resistance of each element requires knowledge of the length and cross sectional area for every section. The different sections of the network, their resistance values and the corresponding DC circuit are defined in Figs. 1 and 3.

The lengths of the different channel sections were determined directly from a series of micrographs similar to Fig. 2. The different cross sectional profiles were obtained from full 3-D profile images such as that shown in Fig. 4 which shows the channel region where R_{C2} and R_{Cf} join. As shown in Fig. 5, the channel cross sections were fitted to an isotropic etch profile. For an isotropic etch of depth d under an etch mask width m , the resultant etched channel cross section is expected to consist of a rectangle of dimensions $(d \times m)$ with channel sides having a quarter circle shape with radius equal to d . The channel cross sectional area A is given by

$$A = (dm) + \frac{\pi d^2}{2} \quad (1)$$

As discussed in ref.18, the channel shapes in thermally bonded micro-reactors may be distorted from this idealised shape. However, the channel cross sectional area A estimated using

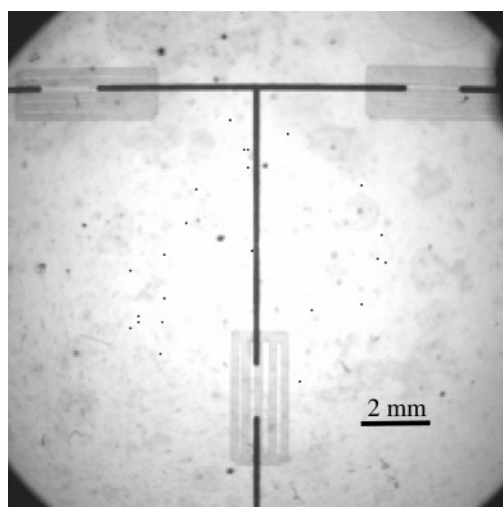


Fig. 2 Optical micrograph of the T shaped channel network. The image, recorded using a $1.25\times$ magnification objective, corresponds to an area of $14.6 \times 14.6 \text{ mm}$.

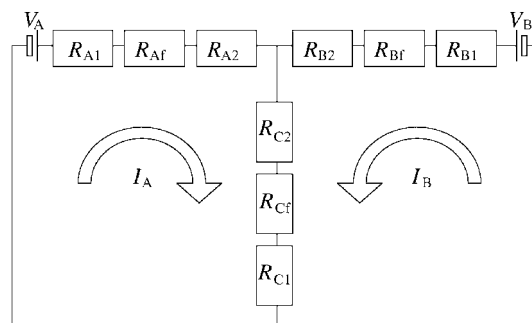


Fig. 3 The DC circuit equivalent the T shaped channel network.

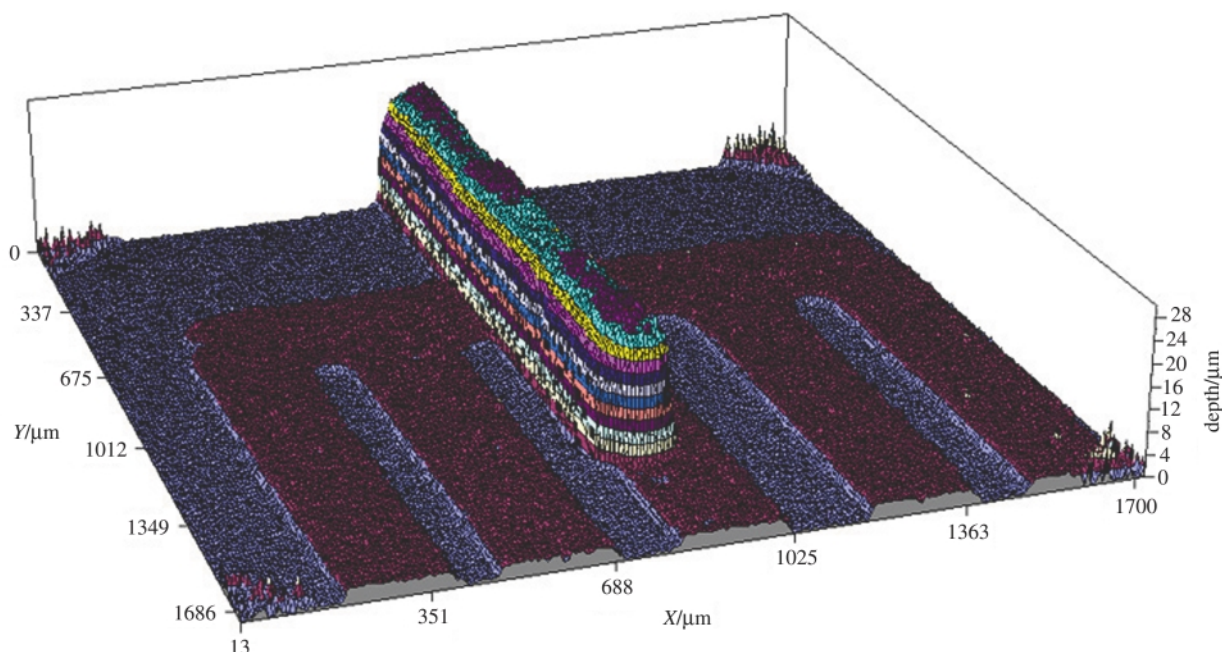


Fig. 4 Quantitative 3-D channel network profile in the region of the rectangular grid of small channels at R_{Cf} .

eqn. (1) with the best fit values of d and m is not significantly different to that obtained by integration of the fit to a slightly distorted channel profile. In the channel region shown in Fig. 4, the large channels have best-fit values of d and m of 24 ± 2 and $100 \pm 10 \mu\text{m}$ respectively. The small channels have $d = 2.4 \pm 0.2$ and $m = 210 \pm 20 \mu\text{m}$. Channel dimensions in different regions of the channel network (close to R_{Af} and R_{Bf}) were measured separately and found to be similar but not identical.

The regions of the rectangular grids of small channels, which have overlap with the large channels (*i.e.* R_{Af} , R_{Bf} and R_{Cf}), were each taken to consist of five different sections as shown in Fig. 3. Sections 1 and 5 correspond to the sections where the large channels overlap with the grid end borders. Sections 2 and 4 are the sections where the large channels overlap with the small channel zone. Section 3 contains only small channels. Values of the lengths and cross sectional areas for R_{A1} , R_{A2} , R_{B1} , R_{B2} , R_{C1} , R_{Cf} (sections 1–5) and R_{C2} are summarised in Table 1. Separately measured dimensions for the R_{Af} and R_{Bf} sections (not shown in Table 1) were found to be similar to the corresponding R_{Cf} sections. The full set of individual values were used in the data analysis.

The uncertainties in the channel lengths (Table 1) are relatively minor compared with those in d and m (approx. 10% in each) for the different channel sections. The uncertainties in the derived channel cross sectional areas are approximately 20%. The uncertainties in the channel dimensions, dominated by that in the area values, gives an approximate uncertainty of 20% in each of the derived resistance values used in the subsequent current–voltage analysis.

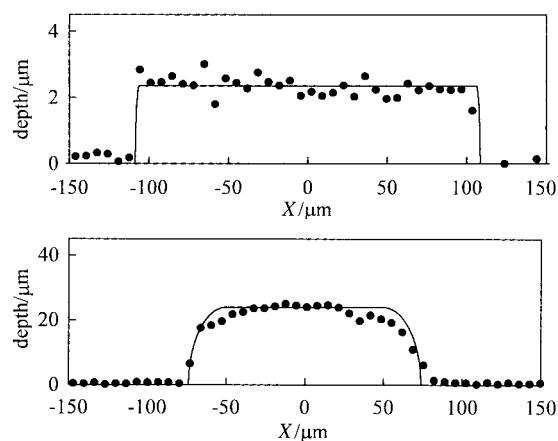


Fig. 5 Cross sectional profiles of the large (lower plot) and small channels (upper plot). In each case, the solid line shows a fit to the isotropic etch model.

Table 1 Lengths L and cross sectional areas A of the different channel section types as defined by the subscripts on the R values in Fig. 1. Cross sectional areas for the large channels, small channels and the border region are indicated by A_l , A_s and A_b respectively. The dimensions of the R_{Af} and R_{Bf} channel sections (not included here) were measured and found to be similar to the corresponding R_{Cf} sections

Channel section	Length/mm ± 0.05	Expression for A	$A/\mu\text{m}^2 \pm 20\%$
A1	1.53	A_l	3830
A2	2.74	A_l	3830
B1	0.81	A_l	4121
B2	3.06	A_l	4121
C1	7.18	A_l	3291
C2	7.02	A_l	3291
Cf1	0.30	$A_l + A_b$	7263
Cf2	0.83	$A_l + 5A_s$	5825
Cf3	1.53	$5A_s$	2534
Cf4	0.83	$A_l + 5A_s$	5825
Cf5	0.30	$A_l + A_b$	7263

Voltage–current characteristics of the micro-reactor

The resistance R of a channel of length L and cross sectional area A and filled with a liquid of conductivity κ is given by

$$R = \frac{L}{\kappa A} \quad (2)$$

For channels in which the ratio of surface area to volume is relatively high and the conductivity of the liquid is low, the surface conductivity of the channel wall–liquid interface becomes significant relative to that of the bulk liquid.^{9,10} For a resistance element with length L , cross sectional area A , cross sectional circumference C and surface conductivity κ_s , the resistance is

$$R = \frac{A}{\kappa_s CL} \quad (3)$$

For each resistance element, the components of the total resistance arising from the bulk liquid and the surface act in parallel. Hence, the overall resistance of each element is given by

$$R = \left(\frac{1}{\frac{\kappa A}{L} + \frac{\kappa_s CL}{A}} \right) \quad (4)$$

Using an independent measurement of the liquid conductivity κ and the geometrical parameters of the channel network, eqn. (4) enables the calculation of the resistances of all the different channel sections of the micro-reactor using only the surface conductivity κ_s as an adjustable parameter.

The DC circuit equivalent to the channel network (Fig. 3) contains two connected circuits. For each circuit, the applied voltage (relative to ground in reservoir C) is equal to the sum of the products of resistance and current in each limb of the circuit, according to

$$V_A = (R_A + R_C)I_A + R_C I_B \quad (5)$$

$$V_B = (R_B + R_C)I_B + R_C I_A \quad (6)$$

where $R_A = (R_{A1} + R_{Af} + R_{A2})$, $R_{Af} = (R_{Af1} + R_{Af2} + R_{Af3} + R_{Af4} + R_{Af5})$ and R_B and R_C refer to similar sums for the B and C limbs of the channel network. I_A corresponds to the current in the channel from the A reservoir to the channel intersection and I_B that for the channel from B to the intersection. The current from the intersection to the reservoir C is given by the sum of $I_A + I_B$. Solution of the two simultaneous equations provides expressions for I_A and I_B .

$$I_A = \frac{(R_B V_A + R_C V_A - R_C V_B)}{(R_A R_B + R_A R_C + R_B R_C)} \quad (7)$$

$$I_B = \frac{-(R_C V_A - R_A V_B - R_C V_B)}{(R_A R_B + R_A R_C + R_B R_C)} \quad (8)$$

The currents I_A and I_B were measured as functions of the voltages V_A and V_B . At constant set voltages, the currents were constant over 5 min and responded to a change in voltage within a few seconds. Fig. 6 shows the variation of the measured currents I_A and I_B (all values averaged over 5 min) with the voltage V_B for a constant voltage V_A equal to 300 V. The solution in the micro-reactor consisted of 40 mM sodium methoxide in methanol for which the conductivity was measured to be $2.46 \times 10^{-3} \text{ S cm}^{-1}$. The currents calculated using eqns. (7) and (8), incorporating the channel dimensions, the measured solution conductivity and a best fit value of κ_s of 0.095 nS show good agreement with the measured values. As can be seen from Fig. 6, it is necessary to include a contribution from surface conductivity in order to successfully model the measured currents. A similar level of agreement between theory and experiment was obtained for a 10 mM sodium methoxide

solution with a conductivity of $0.70 \times 10^{-3} \text{ S cm}^{-1}$ and a best-fit value of κ_s of 0.048 nS. Experimental values of surface conductivities show a wide variation. The values estimated here are smaller than most experimental values determined for the glass–water surfaces of a range of different systems but are similar in magnitude to theoretical estimates.⁹

The conclusion that it is necessary to include a non-zero surface conductivity to correctly predict the current–voltage curves requires some discussion of the uncertainties. The major uncertainty in the comparison of the measured and predicted currents arises from uncertainties of $\pm 20\%$ in the channel cross sectional areas which translate into approximately 20% uncertainties in the resistance values. The sensitivity of the fitting procedure to the uncertainties in the predicted resistance values was tested by setting the surface conductivity to zero and floating the values of R_A , R_B and R_C simultaneously to obtain a best fit. In order to obtain a fit to the measured data similar to that seen in Fig. 6, the floated values of R_A , R_B and R_C corresponded to reductions in the values of 9, 8 and 33% respectively. The same exercise was performed for the micro-reactor filled with 10 mM NaOMe for which the liquid conductivity was lower. In this case, reductions in R_A , R_B and R_C of 28, 13 and 46% were required to obtain a fit to the experimental data (having set the surface conductivity to zero). Overall, we conclude that the experimental data cannot be fitted within the estimated uncertainties without inclusion of the surface conductivity terms.

Electro-osmotic liquid flow rates

The volumetric liquid flow rate F by EOF pumping is proportional to the corresponding electrical current resulting from EOF according to^{8–10}

$$F = -I_{\text{EOF}} \left(\frac{\varepsilon \varepsilon_0 \zeta}{\eta \kappa} \right) \quad (9)$$

where I_{EOF} is the current from electro-osmotic flow (equal to the total current I minus the surface current I_s), ε is the relative dielectric constant of the liquid, ε_0 is the permittivity of free space, ζ is the zeta potential of the channel wall–liquid interface, η is the liquid viscosity and κ is the liquid conductivity.

Fig. 7 shows the measured reservoir height changes *versus* time for 10 mM NaOMe in methanol with $V_A = V_B = 300 \text{ V}$. The time plots are linear indicating that the volumetric flow

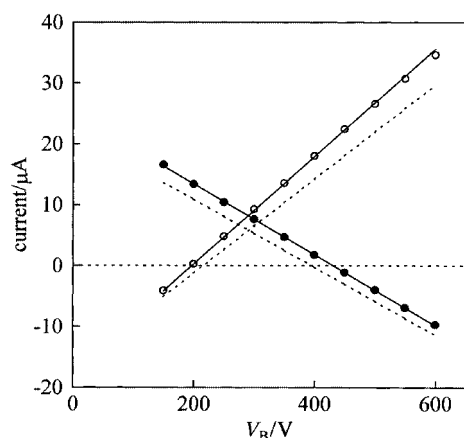


Fig. 6 Measured currents I_A (filled circles) and I_B (open circles) as a function of the voltage V_B at a constant voltage V_A equal to 300 V for the channel network filled with 40 mM NaOMe in methanol at 21.7 °C. The solid lines correspond to the currents calculated using the measured channel geometry and the solution conductivity ($2.46 \times 10^{-3} \text{ S cm}^{-1}$) and a best-fit value of the surface conductivity of 0.095 nS. The dashed lines show the currents calculated with the surface conductivity set to zero.

rates are independent of the relative reservoir heights, *i.e.* pressure driven flow resulting from differential reservoir heights is insignificant here. For V_A and V_B both equal to 300 V, liquid flows from reservoirs A and B (these heights both decline) towards C, for which the height increases. For each reservoir, multiplication of the rate of height change by the internal cross sectional area of the reservoir pipette yields the volumetric flow rates F_A , F_B and F_C . As required by mass conservation, F_C is found to be equal to $-(F_A + F_B)$. The volumetric flow rates F_A and F_B measured as a function of the voltage V_B at a fixed voltage V_A equal to 300 V are shown in Fig. 8. As predicted from eqn. (9), the forms of the plots in Fig. 8 are very similar to the plots of the currents I_A and I_B *versus* V_B in Fig. 6.

Fig. 9 shows the variation of the flow rates F_A , F_B and F_C plotted *versus* the corresponding electrical currents $I_{A,\text{EOF}}$, $I_{B,\text{EOF}}$ and $I_{C,\text{EOF}}$. The EOF currents were obtained from the measured total currents by subtraction of the surface conductivity contribution, calculated using the value of surface conductivity estimated from fits to the voltage–current data. The flow rates are proportional to EOF current and the solid line is calculated according to eqn. (9) using the following data taken either from the literature^{20,21} or measured independently; $\varepsilon = 32.6$, $\eta = 0.544 \text{ cP}$ and $\kappa = 0.74 \times 10^{-3} \text{ S cm}^{-1}$ (all at the measurement temperature of 25.3 °C). The value of ζ required to match the experimental data (-46 mV) is equal to that measured for the interface between glass and a 10 mM solution of KI in methanol.⁹

A similar analysis was made for a range of different electrolyte/solvent systems and the values of the zeta potentials and surface conductivities are summarised in Table 2. The zeta potentials estimated for the solutions are in reasonable agree-

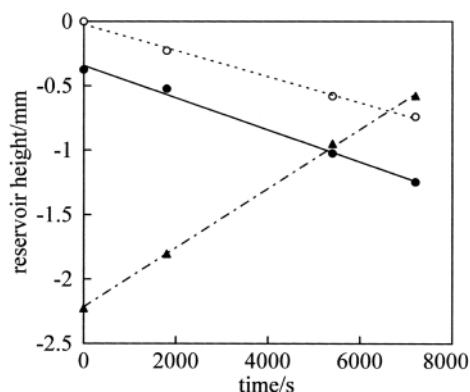


Fig. 7 Liquid heights *versus* time for reservoirs A (filled circles), B (open circles) and C (filled triangles) for 10 mM NaOMe in methanol at 25.3 °C. The voltages V_A and V_B were both equal to 300 V relative to reservoir C (ground).

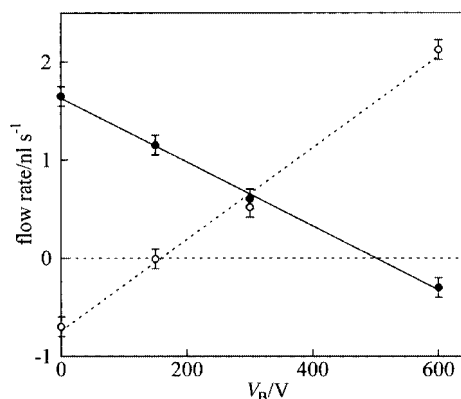


Fig. 8 Measured volumetric flow rates F_A (filled circles) and F_B (open circles) as a function of the voltage V_B at a constant voltage V_A equal to 300 V at 25.3 °C.

ment with literature values.^{9,22–29} It is relevant to note that caution must be exercised in comparing values of zeta potentials drawn from the literature. As shown in refs. 9, 22–29, different studies for glass–aqueous electrolyte interfaces show common features: the pH corresponding to zero zeta potential is equal to 2–3; the zeta potential becomes increasingly negative with increasing pH; and the zeta potential magnitude decreases with increasing electrolyte concentration. However, the absolute values of the zeta potentials for a particular glass–electrolyte solution commonly show a wide variation due to sensitivity to the exact nature of the glass used and the precise details of the measurement and data analysis methods (including correction for surface conductivity).

Conclusions and future outlook

We have demonstrated that the voltage–current characteristics of a micro-reactor channel network can be predicted with reasonable precision using complete 3-D channel network dimensional information and the measured liquid conductivity with the channel wall–liquid surface conductivity as the only adjustable parameter. The electrical currents due to EOF in the different limbs of the channel network are proportional to the corresponding volumetric liquid flow rates with the constant of proportionality dependent on the dielectric constant, viscosity and conductivity of the liquid and the zeta potential of the channel wall–liquid interface. Measurement of the volumetric flow rate within the channel network as a function of the electrical current provides a simple method to determine the zeta potential for solvent/reagent systems of interest for synthesis applications in micro-reactors for which literature data is absent. In this context, it is relevant to note that, although literature data for the zeta potential for different aqueous solutions at the glass surface is available, data for organic solvents is relatively scarce.^{9,22–29}

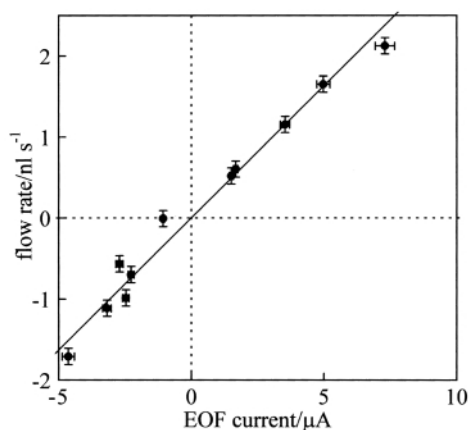


Fig. 9 Measured volumetric flow rates (F_A , F_B and F_C) versus the corresponding EOF electrical currents ($I_{A,EOF}$, $I_{B,EOF}$ and $I_{C,EOF}$) for 10 mM NaOMe at 25.3 °C. The solid line corresponds to theory using the parameters given in the text.

Table 2 Zeta potentials and surface conductivities estimated by analysis of measured flow rates and electrical currents for different electrolyte/solvent systems. Values of ζ shown in parentheses refer to literature values for fused silica with the same electrolyte solution²⁹

System	ζ /mV	κ_s /nS
10 mM NaOMe in methanol	–46	0.048
40 mM NaOMe in methanol	–21	0.095
1 mM KCl in water (pH 6)	approx. –90 (–80)	0.022
10 mM KCl in water (pH 6)	–60 (–50)	Neglected

Since the EOF electrical current is proportional to liquid flow rate, *in situ* logging of the total currents using the micro-reactor power supply and control system provides a useful diagnostic tool in several ways. Firstly, as noted above, combined measurements of flow rates and currents (corrected for surface conductivity) allows the measurement of zeta potentials for which literature data is absent. Secondly, micro-reactor operational problems arising from, for example, channel blockage and the formation of gas bubbles are easily detected. Thirdly, it is reasonably simple to incorporate the analysis given here within the micro-reactor control software to allow the user to directly input the desired sequences of *liquid flow rates* within specified sections of the channel network (as opposed to the present situation where voltages are inputted). Lastly, for chemical reactions in micro-reactors which produce a significant change in solution conductivity, current measurements can, in principle, provide a measure of the extent of reaction. Elucidation of such effects will require extension of the theoretical framework given here to allow for liquids having variable bulk and surface conductivities and zeta potentials within different channel sections. These aspects are currently under active development in our laboratories.

Acknowledgements

We thank the Engineering and Physical Sciences Research Council of the UK for funding this study. We are grateful to Dr T. McCreedy and Ms C. Clive of the University of Hull for assistance with the design and fabrication of the micro-reactor.

References

- S. J. Haswell, R. J. Middleton, B. O'Sullivan, V. Skelton, P. Watts and P. Styring, *Chem. Commun.*, 2001, 391. *This feature article gives a clear account of current work on synthesis in micro-reactors.*
- V. Skelton, G. M. Greenway, S. J. Haswell, P. Styring, D. O. Morgan, B. H. Warrington and S. Y. F. Wong, *Analyst*, 2001, **126**, 7.
- V. Skelton, G. M. Greenway, S. J. Haswell, P. Styring, D. O. Morgan, B. H. Warrington and S. Y. F. Wong, *Analyst*, 2001, **126**, 11. *This paper describes the first demonstration of the control of stereo-selective product formation in a micro-reactor.*
- G. N. Doku, S. J. Haswell, T. McCreedy and G. M. Greenway, *Analyst*, 2001, **126**, 14.
- T. McCreedy and N. G. Wilson, *Analyst*, 2001, **126**, 21.
- M. C. Mitchell, V. Spikemans and A. J. de Mello, *Analyst*, 2001, **126**, 24.
- P. Watts, C. Wills, S. J. Haswell, E. Pombo-Villar and P. Styring, *Chem. Commun.*, 2001, 990.
- P. D. I. Fletcher, S. J. Haswell and V. N. Paunov, *Analyst*, 1999, **124**, 1273. *This tutorial review gives a clear account of the underlying principles of chemical reaction control in micro-reactors.*
- J. Th. G. Overbeek, in *Colloid Science*, ed. H. R. Kruyt, Elsevier, Amsterdam, 1952, vol. 1, ch. V, p. 194.
- R. J. Hunter, *Zeta Potential in Colloid Science*, Academic Press, London, 1981.
- P. D. Christenson, S. W. P. Johnson, T. McCreedy, V. Skelton and N. G. Wilson, *Anal. Commun.*, 1998, **35**, 341.
- Z. H. Fan and D. J. Harrison, *Anal. Chem.*, 1994, **66**, 177.
- K. Seller, Z.H. Fan, K. Flurl and D. J. Harrison, *Anal. Chem.*, 1994, **66**, 3485.
- N. A. Polson and M. A. Hayes, *Anal. Chem.*, June 2001, 313A.
- T. E. McKnight, C. T. Culberson, S. C. Jacobson and J. M. Ramsey, *Anal. Chem.*, 2001, **73**, 4045.
- R. B. M. Schasfoort, S. Schlautmann, J. Hendrikse and A. van den Berg, *Science*, 1999, **286**, 942.
- S. V. Ermakov, S. C. Jacobson and J. M. Ramsey, *Anal. Chem.*, 2000, **72**, 3512.
- I. Broadwell, P. D. I. Fletcher, S. J. Haswell, T. McCreedy and X. Zhang, *Lab Chip*, 2001, **1**, 66.

- 19 T. McCreedy, *Anal. Chim. Acta*, 2001, **427**, 39.
- 20 *Handbook of Chemistry and Physics*, CRC Press, Boca Raton, 62nd edn., 1981.
- 21 J. Timmermans, *Physico-Chemical Constants of Pure Organic Compounds*, Elsevier, New York, vol. 1 (1950) and vol. 2 (1965).
- 22 M. Kosmulski and E. Matijevic, *Colloid Polym. Sci.*, 1992, **270**, 1046.
- 23 I. E. Valko, H. Siren and M.-L. Riekkola, *J. Microcolumn Sep.*, 1999, **11**, 199.
- 24 C. Schwer and E. Kenndler, *Anal. Chem.*, 1991, **63**, 1801.
- 25 P. B. Wright, A. S. Lister and J. G. Dorsey, *Anal. Chem.*, 1997, **69**, 3251.
- 26 G. R. Wiese, R. O. James and T. W. Healy, *Discuss. Faraday Soc.*, 1971, **52**, 302.
- 27 J. Jednacak, V. Pravdic and W. Haller, *J. Colloid Interface Sci.*, 1974, **49**, 16.
- 28 R. A. Van Wagenen and J. D. Andrade, *J. Colloid Interface Sci.*, 1980, **76**, 305.
- 29 P. J. Scales, F. Grieser, T. W. Healy, L. R. White and D. Y. C. Chan, *Langmuir*, 1992, **8**, 965.

The aldol reaction of silyl enol ethers within a micro reactor

Charlotte Wiles,^a Paul Watts,^a Stephen J. Haswell^{*a} and Esteban Pombo-Villar^b

^a Department of Chemistry, Faculty of Science and the Environment, University of Hull, Cottingham Road, Hull, UK HU6 7RX. E-mail: s.j.haswell@hull.ac.uk; Fax: +44 (0)1482 466416; Tel: +44 (0)1482 465475

^b Nervous Systems Research, WSJ-386.07.15, Novartis Pharma Ltd, CH4002 Basel, Switzerland

Received 31st August 2001, Accepted 15th October 2001

First published as an Advance Article on the web 6th November 2001

We have demonstrated the use of silyl enol ethers in the aldol reaction within a micro reactor. Quantitative conversion of the silyl enol ether to a β -hydroxyketone was observed in a 20 min period compared to traditional batch systems, where quantitative yields were only obtained when extended reaction times of 24 h were employed.

Introduction

Over the past three years, there has been a rapid growth in the development of micro reaction technology exploiting the technique of electroosmotic flow (EOF).¹ Recent research has demonstrated that along with multi-component reactions such as the Suzuki coupling² and the Wittig reaction,³ multi-step peptide synthesis can also be performed within a micro reactor.⁴

Enolates are often regarded as one of the most important intermediates in C–C bond formation. They are prepared by the removal of acidic protons α to a carbonyl using a base. In the late 1960's, Stork and Hudrlik demonstrated that an enolate could be transformed into a silyl enol ether and then converted back to the enolate.⁵ This technique therefore enabled the temporary trapping of enolates, while maintaining the stereo- and regiochemical features.⁶ Stork and Hudrlik described the regeneration of the enolate *via* the use of methyllithium, however, tetraalkylammonium fluorides have more recently found widespread use in desilylation reactions.⁷

This paper describes the aldol reaction of the silyl enol ethers of acetophenone and cyclohexanone with 4-bromobenzaldehyde using catalytic tetrabutylammonium fluoride (TBAF) within a micro reactor.

Experimental

Micro reactor methodology

The borosilicate micro reactor used in this work was prepared using a standard fabrication procedure developed at Hull.⁸ The reactions were carried out using a 4 channel micro reactor, illustrated in Fig. 1, with approximate channel dimensions of $100 \times 50 \mu\text{m}$ and outer dimensions of $20 \times 20 \times 25 \text{ mm}$. Micro porous silica frits were placed within the channels in order to

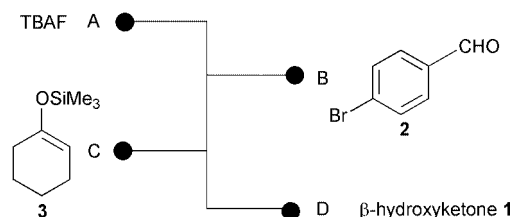


Fig. 1 Schematic of the micro reactor used in the synthesis of 1.

minimise hydrodynamic effects.⁹ An in-house LabVIEWTM program was used to set and monitor the voltages applied to platinum electrodes placed in the reservoirs (power supply was built by Kingfield electronics).

All micro reactions were carried out at room temperature over a period of 20 min to ensure a sufficient volume of product was generated for analysis. Reaction products were determined by GC-MS *via* the comparison of retention times and spectra with those obtained from synthetic standards **1** and **5**. Product conversions were calculated from the GC-MS with respect to the amount of starting material remaining in the sample.

Synthesis of the silyl enol ether of cyclohexanone 3

A solution of cyclohexanone (0.1 g, 1.02 mmol) in anhydrous THF (10 ml) was added dropwise to a stirred solution of lithium bis(trimethylsilyl)amide (LiHMDS) (1.02 ml, 1.0 M, 1.02 mmol) over a period of 30 min. The solution was then stirred for a further 15 min prior to the addition of chlorotrimethylsilane (0.13 ml, 1.20 mmol). The reaction mixture was concentrated *in vacuo* and the resulting residue dissolved in DCM. The inorganics were removed by filtration and the resulting solution concentrated *in vacuo*, yielding the silyl enol ether of cyclohexanone **3** (0.16 g, 93%); m/z (EI) 171 ($M^+ + 1$, 38%), 170 (70), 169 (65), 155 (100) and 127 (40).

Synthesis of the silyl enol ether of acetophenone 4

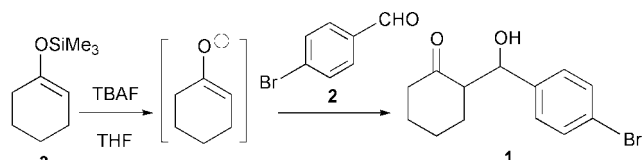
The silyl enol ether of acetophenone **4**, was prepared as for the enol ether of cyclohexanone above (0.79 g, 98%); m/z (EI) 193 ($M^+ + 1$, 92%), 192 (70), 191 (100), 177 (94) and 103 (26).

Preparation of 'anhydrous' tetrabutylammonium fluoride¹⁰

Tetrabutylammonium fluoride trihydrate (TBAF·3H₂O) was dried at room temperature over phosphorus pentoxide under vacuum (10 mm Hg) for 48 h to afford a gelatinous solid.

Synthesis of 1 *via* the silyl enol ether of cyclohexanone 3

The silyl enol ether of cyclohexanone **3** (0.1 g, 0.58 mmol) was added dropwise to a stirred solution of 'anhydrous' TBAF (0.015 g, 0.057 mmol) and 4-bromobenzaldehyde **2** (0.109 g, 0.58 mmol) in anhydrous THF (10 ml). The reaction mixture was stirred for 24 h and **3** extracted into ethyl acetate (3 \times 50 ml). The combined organic solvents were dried over magnesium sulfate and the product recrystallised from DCM/diethyl ether/hexane to afford a crystalline material **1** (0.16 g, 94%); m/z (EI) 267 ($M^+ + 1$, 15%), 266 (60), 264 (55) and 185 (100).



Scheme 1 Formation of **1** via the silyl enol ether of cyclohexanone **3**.

Synthesis of **5** via acetophenone and 4-bromobenzaldehyde **2**

Acetophenone (1.0 g, 8.26 mmol) was added dropwise to a stirred solution of LiHMDS (41.32 ml, 1.0 M, 41.32 mmol) and 4-bromobenzaldehyde (1.53 g, 8.27 mmol) in anhydrous THF (100 ml). The reaction mixture was stirred for 24 h and **5** extracted into ethyl acetate (3 × 50 ml). The combined organic solvents were dried over magnesium sulfate. Recrystallisation from DCM/hexane afforded a white crystalline material **5** (1.33 g, 56%); *m/z* (EI) 289 ($M^+ + 1$, 40%), 288 (100), 287 (77), 286 (90), 208 (65), 178 (25) and 105 (50).

Synthesis of **5** via the silyl enol ether of acetophenone **4**

The silyl enol ether of acetophenone **4** (0.09 g, 0.48 mmol) was added dropwise to a stirred solution of anhydrous TBAF (0.013 g, 0.05 mmol) and 4-bromobenzaldehyde **2** (0.089 g, 0.48 mmol) in anhydrous THF (100 ml). The reaction mixture was stirred for 5 h and the reaction mixture analysed by GC-MS and found to contain 100% **5** with respect to the silyl enol ether **4**; *m/z* (EI) 289 ($M^+ + 1$, 40%), 288 (100), 287 (77), 286 (90), 208 (65), 178 (25) and 105 (50).

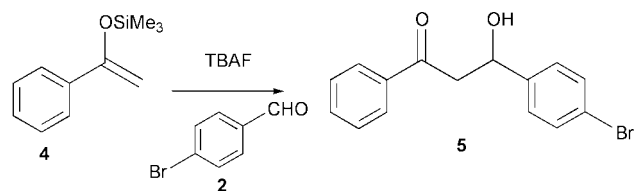
Results and discussion

In order to prepare β -hydroxyketone **1**, the enolate of cyclohexanone was formed using LiHMDS and subsequently reacted with 4-bromobenzaldehyde **2**. After a 24 h period only 20% conversion of cyclohexanone to product **1** had taken place. The reaction was then repeated using the silyl enol ether of cyclohexanone **3** resulting in a conversion of 100% with respect to the silyl enol ether **3** in 24 h (Scheme 1).

Having demonstrated that compound **1** could be prepared from the silyl enol ether **3**, this represented a synthetic target for preparation within a micro reactor (Fig. 1). Prior to the synthesis, the micro reactor was primed with anhydrous THF, in order to remove any air or moisture from the channels and microporous silica frits. A standard solution of TBAF (40 μ l, 0.1 M) in anhydrous THF was placed in reservoir A, a solution of 4-bromobenzaldehyde **2** (40 μ l, 1.0 M) in anhydrous THF in reservoir B and the silyl enol ether of cyclohexanone **3** (40 μ l, 1.0 M) was placed in reservoir C. The reaction products were collected in anhydrous THF in reservoir D. The reagents were manipulated within the device by the application of the following applied fields: 417, 455, 476 and 0 V cm^{-1} (A, B, C and D respectively). However, only 1% conversion of silyl enol ether **3** to product **1** was observed. Upon altering the applied field to 417, 341, 333 and 0 V cm^{-1} and hence increasing the proportion of TBAF, 100% conversion to product **1** was obtained.

Having demonstrated that the product **1** could be formed within a micro reactor, we wished to further demonstrate this technique using another ketone. In order to prepare a synthetic standard of **5**, the enolate of acetophenone was formed using LiHMDS and subsequently reacted with 4-bromobenzaldehyde.

After 24 h, 80% conversion to β -hydroxyketone **5** with respect to acetophenone had taken place. The reaction was



Scheme 2 Formation of **5** via the silyl enol ether of acetophenone **4**.

subsequently repeated using the silyl enol ether of acetophenone **4** and the resulting conversion of 100% with respect to the silyl enol ether **4** was obtained (Scheme 2).

A standard solution of TBAF (40 μ l, 0.1 M) in anhydrous THF was placed in reservoir A, a solution of 4-bromobenzaldehyde **2** (40 μ l, 1.0 M) in anhydrous THF in reservoir B and the silyl enol ether of acetophenone **4** (40 μ l, 1.0 M) was placed in reservoir C. The reaction products were collected in anhydrous THF in reservoir D. The reagents were manipulated within the device using the following applied fields: 375, 409, 381 and 0 V cm^{-1} to A, B, C and D respectively. This resulted in 100% conversion of the silyl enol ether of acetophenone **4** to product **5**.

Conclusions

In batch reactions, it has been shown that enhanced yields of β -hydroxyketones can be obtained via the use of silyl enol ethers, compared to the use of traditional lithium enolates. We subsequently demonstrated the formation of β -hydroxyketones within a micro reactor, whereby quantitative conversions were obtained in a 20 min period. This shows an improvement over traditional systems, where quantitative conversion was only observed if extended reaction times of 24 h were employed. Enhanced reaction rates of this type have previously been demonstrated by O'Sullivan *et al.* where enhancements of the order of 3.4×10^3 were reported as a result of miniaturisation.¹¹

Acknowledgements

We acknowledge Novartis Pharmaceuticals (C. W. and P. W.) for their financial support. We are grateful to Dr. Tom McCreedy for the device fabrication and Dr. Xunli Zhang for the automation of the power supply.

References

- P. D. I. Fletcher, S. J. Haswell and V. N. Paunov, *Analyst*, 1999, **124**, 1273.
- G. M. Greenway, S. J. Haswell, D. O. Morgan, V. Skelton and P. Styring, *Sens. Actuators B*, 2000, **63**, 153.
- V. Skelton, G. M. Greenway, S. J. Haswell, P. Styring, D. O. Morgan, B. Warrington and S. Y. F. Wong, *Analyst*, 2001, **126**, 7.
- P. Watts, C. Wiles, S. J. Haswell, E. Pombo-Villar and P. Styring, *Chem. Commun.*, 2001, 990.
- G. Stork and P. F. Hudrlik, *J. Am. Chem. Soc.*, 1968, **90**, 4462.
- I. Kuwajima and E. Nakamura, *Acc. Chem. Res.*, 1985, **18**, 181.
- E. Nakamura, T. Murofushi, M. Shimizu and I. Kuwajima, *J. Am. Chem. Soc.*, 1976, **98**, 2346.
- T. McCreedy, *Anal. Chim. Acta*, 2001, **427**, 39.
- P. D. Christensen, S. W. P. Johnson, T. McCreedy, V. Skelton and N. G. Wilson, *Anal. Commun.*, 1998, **35**, 341.
- I. Kuwajima, E. Nakamura and K. Hashimoto, *Org. Synth.*, 1982, **61**, 122. * Significant reference.
- S. J. Haswell, B. O'Sullivan and P. Styring, *Lab Chip*, 2001, **2** (DOI: 10.1039/b104035a).

Solution phase synthesis of β -peptides using micro reactors

Paul Watts,^a Charlotte Wiles,^a Stephen J. Haswell^{a,*} and Esteban Pombo-Villar^b

^aDepartment of Chemistry, Faculty of Science and the Environment, University of Hull, Cottingham Road, Hull HU6 7RX, UK

^bNervous System Research, WSJ-386.07.15, Novartis Pharma Ltd, CH4002 Basel, Switzerland

Received 19 March 2002; revised 22 April 2002; accepted 16 May 2002

Abstract—The synthesis of β -peptides has been successfully performed using a borosilicate glass micro reactor, in which a network of channels has been produced using a photolithographic and wet etching method. The reagents were mobilised by electroosmotic flow (EOF). The micro reactor was initially evaluated using a carbodiimide coupling reaction to form a dipeptide. The methodology has been extended such that the peptides may also be produced via the pentafluorophenyl ester derivatives of amino acids. It was found that performing the pentafluorophenyl ester reactions in the micro reactor resulted in an increase in the reaction efficiency over the traditional batch method. We postulate that the enhancement in rate of reaction is an electrochemical phenomenon, due to the reaction being performed in an electric field, which is unique to micro reactor systems. It has also been demonstrated that selective deprotection of the resultant dipeptides can be achieved. This approach has been used in the synthesis of a tripeptide. © 2002 Elsevier Science Ltd. All rights reserved.

1. Introduction

A micro reactor is generally defined as a series of inter-connecting channels (10–300 μm in diameter), formed in a planar surface, in which small quantities of reagents are manipulated. Thus reagents can be brought together in a specific sequence, mixed and allowed to react for a specified time in a controlled region of the reactor. During the past 10 years, there has been a rapid growth in the development of micro-Total Analytical Systems (μTAS)^{1–8} which exploit electroosmotic flow (EOF).^{9–12} The development of micro reactor devices for chemical synthesis based on complimentary technology is less common. However, recent research has shown that Suzuki,¹³ Wittig,^{14,15} diazo coupling reactions¹⁶ and enamines¹⁷ may be performed using micro chemical systems. In addition, we have demonstrated that peptide bonds may be prepared using such technology.¹⁸ The reactions performed in micro reactors have recently been reviewed by Haswell and co-workers.¹⁹

Micro reactors are advantageous because they allow the rapid optimisation of reactions and reduce exposure to hazardous chemicals. They also have the ability to generate reagents in situ, allowing the preparation and subsequent reaction of highly reactive or toxic intermediates. The ability to scale out the synthesis allows large quantities of chemicals to be prepared and it has been calculated that 1 kg of material could be produced in 24 h using 1000 micro reactors in parallel.²⁰ In addition, because EOF may be used to mobilise the solvents and reagents around the

micro reactor manifold, electrophoretic separation would enable isolation of pure products.²¹

To illustrate the principles of EOF, one can consider a micro channel fabricated from a material having negatively charged functional groups on the surface. If a liquid, displaying some degree of dissociation, is brought into contact with the surface, positive counter ions will form a double layer such that the positively charged ions are attracted to the negatively charged surface. Application of an electric field causes this layer to move towards the negative electrode, thus causing the bulk liquid to move within the channel (Fig. 1). Electroosmotic flow is not just restricted to aqueous systems and a range of organic solvents can be mobilised using the technique. A major advantage of EOF is that it gives a high degree of spacial and temporal control to reactants mixing under a diffusive regime. This high level of fluidic control and mixing has been attributed to the reactions^{13–19} reported in the literature. Electroosmotic flow also has the advantage that the direction and magnitude of the flow may be readily changed by altering the applied voltage, where the flow rates increase

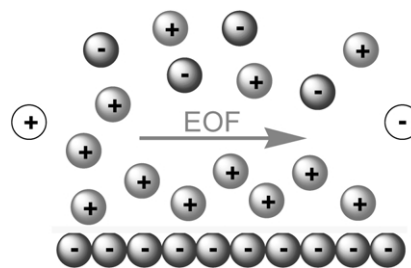


Figure 1. Principle of electroosmotic flow.

Keywords: β -peptides; electroosmotic flow; dipeptides.

* Corresponding author. Tel.: +44-1482-465469; fax: +44-1482-466416; e-mail: s.j.haswell@hull.ac.uk

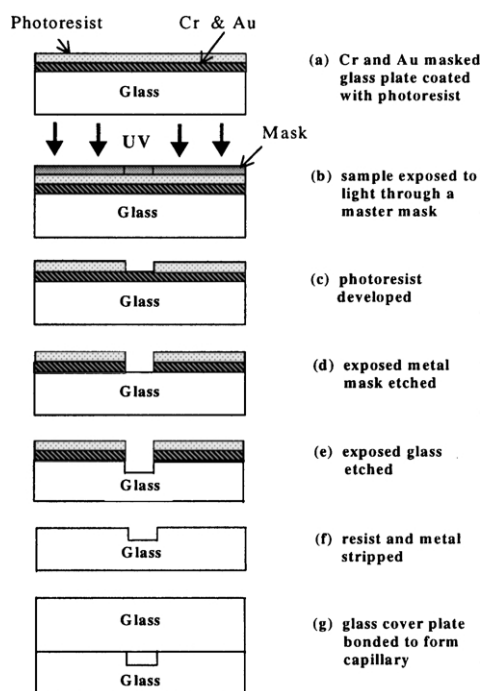


Figure 2. Sequence of processes in photolithographic fabrication.

with voltage. The flow rates, which are in the order of $\mu\text{l min}^{-1}$, are reproducible using EOF. In addition, the pumping technique has no mechanical or moving parts, hence it is highly suitable for operation in miniaturised systems. An automated power supply with multiple electrodes can support several pumping channels. Importantly, when using EOF, plugs of fluid are transported without significant hydrodynamic dispersion.

Following the discovery by Merrifield in 1963,²² peptides have been commonly prepared via solid supported techniques. Solid phase peptide synthesis (SPPS) is based on the addition of a protected amino acid residue to an insoluble polymeric support. The acid-labile Boc group²³ and base-labile Fmoc group²⁴ have been commonly used for *N*-protection. After removal of the protecting group the next protected amino acid may be added using either a coupling reagent or a pre-activated amino acid derivative. If this dipeptide is the desired product, it may be cleaved from the polymer support.^{25,26} If a longer peptide is required additional amino acids can be added by repeating further coupling reactions. Solid phase peptide synthesis is advantageous because of the ease of product purification. In addition the process is readily automated and has become common in the combinatorial synthesis of peptides. Solid

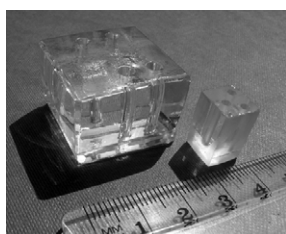


Figure 3. A borosilicate glass micro reactor.

phase peptide synthesis however, has the disadvantage that an expensive polymer support is required. Extra steps are also added to the synthesis as a result of initially linking the amino acid to the support and finally having to remove the peptide from the polymer. In this paper, a micro reactor has been used to prepare peptides using solution phase chemistry and the results are compared with traditional solid phase procedures.

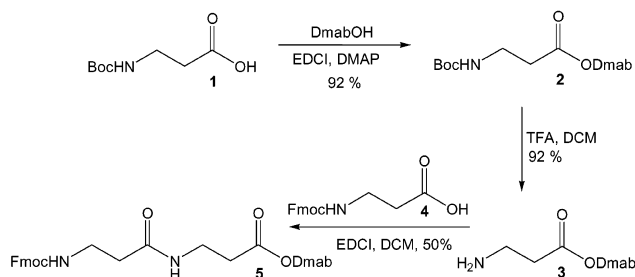
2. Fabrication and use of the micro reactors

A number of materials such as silicon, quartz, glass, metals and polymers have been used to construct micro reactors. Glass and certain polymers have been particularly useful because of their physical properties and chemical inertness. These substances allow the mobilisation of organic solvents and reagents using a number of pumping mechanisms such as hydrodynamic pumping and electroosmotic flow. A range of fabrication methods such as photolithography, hot embossing, powder blasting, injection moulding and laser micro forming alone, or in combination, have been reported in the literature.^{19,27,28}

The micro reactor devices used in this work were prepared using the popular technique of photolithography and wet etching to produce channels in a glass micro reactor (Fig. 2).²⁹ Firstly, a thin layer of metal, such as chromium, is deposited onto the surface of a borosilicate glass plate. This controls the degree of undercutting during the wet etching process. A layer of positive photoresist is then spin coated on top of the chromium to a depth of 0.5–2.0 μm . The pattern of the required network of inter-connecting channels is subsequently transferred to the photoresist layer using photolithography. After exposure, the photoresist is developed and removed, together with the chromium layer, to reveal the areas of glass to be etched. The plate is then heated to allow the volatiles to evaporate, before performing the chemical etch. The channels are etched using a mixture of 1% HF and 5% NH_4F in water at 65°C, resulting in an etch rate of 0.3–0.5 $\mu\text{m min}^{-1}$. A glass top block, with pre-drilled holes that act as reservoirs for reagents, is then aligned with the channel geometry and thermally bonded to the base plate, producing an all glass device (Fig. 3). Microporous silica frits³⁰ were placed in the channels to prevent hydrodynamic flow occurring.

3. Results and discussion

We selected to demonstrate the multi-step synthesis of peptides derived from β -amino acids for two reasons. Firstly, the simplest β -amino acids lack chiral centres, hence we avoid potential problems with racemisation and the generation of diastereomeric mixtures, which would complicate the analysis of the products in our initial studies. In addition, β -peptides have attracted much interest due to their structural^{31,32} and biological properties.³³ In particular, their stability to degradation by peptidases^{34,35} makes them potentially superior to the drugs derived from α -amino acids. Both solution and solid phase synthetic methods for these have been developed which would serve to benchmark the micro reactor synthesis.^{36,37}



Scheme 1. Synthesis of a standard dipeptide derivative.

In the first instance, a one-step reaction was considered in which an *N*-protected β -amino acid was reacted with an *O*-protected β -amino acid, to prepare the protected β -dipeptide. To enable the methodology to be applicable to the synthesis of more complex peptides, the use of orthogonal protecting groups was clearly required. As in SPPS, the base-labile Fmoc protecting group²⁴ was selected for *N*-protection while the Dmab ester³⁸ was chosen for protection of the carboxylic acid. Importantly, both protecting groups may be removed under mild conditions, since electroosmotic flow is retarded if the pH of the reaction is less than 3.^{9–12} We have already reported the application of micro reactors in the formation of peptide bonds,¹⁸ but here we give full experimental details for all procedures and also exemplify more complex examples.

Commercially available Boc- β -alanine **1** was protected as the Dmab ester using 1-(3-dimethylaminopropyl)-3-ethylcarbodiimide hydrochloride (EDCI) and 4-dimethylamino pyridine (DMAP), to give the ester **2** in 92% yield (Scheme 1). Treatment of **2** with trifluoroacetic acid furnished the desired amine **3** in 92% yield, which was subsequently reacted with Fmoc- β -alanine **4** via a carbodiimide coupling reaction, to give a synthetic sample of the target dipeptide **5** in 50% yield. Addition of a catalytic amount of DMAP resulted in appreciable quantities of Fmoc deprotection, hence DMAP was omitted in subsequent coupling reactions when the Fmoc protecting group was present.

Having prepared dipeptide **5**, it represented a synthetic target for preparation within the micro reactor. Prior to synthesis, the micro reactor channels were primed with anhydrous *N,N*-dimethylformamide (DMF) to remove any air and moisture from the channels and the microporous silica frits. A standard solution of Fmoc- β -alanine **4** (50 μ l, 0.1 M) in anhydrous DMF was added to reservoir A, a solution of EDCI (50 μ l, 0.1 M) in DMF was placed in

reservoir B and a solution of amine **3** (50 μ l, 0.1 M) in DMF was placed in reservoir C (Fig. 4). Anhydrous DMF (40 μ l) was placed in reservoir D, which was used to collect the products of the reaction. Platinum electrodes were placed in each of the reservoirs (A, B and C positive, D ground) and an external voltage was applied to the channels inducing electroosmotic flow of the reagents. The reactions were conducted at room temperature for a period of 20 min, in order to acquire sufficient volume of product to determine the conversion of the reaction by HPLC. Product conversions were based on the amount of carboxylic acid **4** remaining in the sample.

When stoichiometric quantities of the reagents were used only ca. 10% conversion to dipeptide **5** was achieved when a voltage of 700 V was applied to each of the reagents (A, B and C). By lowering the applied voltages to 500 V, hence reducing the flow rates and increasing the residence time of the reaction, no significant increase in conversion was observed. However, by using 2 equiv. of EDCI (0.2 M solution) an increase in conversion to ca. 20% was observed. By applying a stopped flow technique (2.5 s injection length with stopped flow for 5 s) thus further increasing the residence time of the reaction, the conversion was further increased to approximately 50%. Since the efficiency of the reaction appeared to be greatly dependent on the number of equivalents of EDCI used, we wished to further investigate the effect of carbodiimide concentration on the reaction, however we found that EDCI was insoluble in DMF above 0.2 M concentrations. In further experiments dicyclohexylcarbodiimide (DCC) was used as the coupling reagent as it was considerably more soluble in DMF. Using 5 equiv. of DCC (0.5 M solution in reservoir B) a conversion of 93% to dipeptide **5** was obtained, using the stopped flow regime described above. This represented a typical yield for a classic carbodiimide coupling reaction in SPPS.

We wished to demonstrate that alternative methods used in peptide synthesis, could also be applied to the synthesis within the micro reactors. Another common method utilised in peptide bond formation involves the reaction of a pre-activated amino acid derivative, such as a pentafluorophenyl ester, with an amine.^{39,40} Fmoc- β -alanine **4** was activated as pentafluorophenyl ester **6** via an EDCI coupling reaction, to give the product in 90% yield (Scheme 2). Subsequent treatment of ester **6** with amine **3** afforded dipeptide **5** in 46% yield in a bulk reaction, using DMF as solvent. The yield did not increase even when prolonged reaction times were employed.

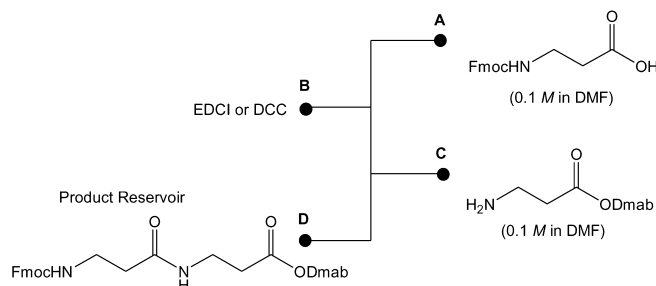
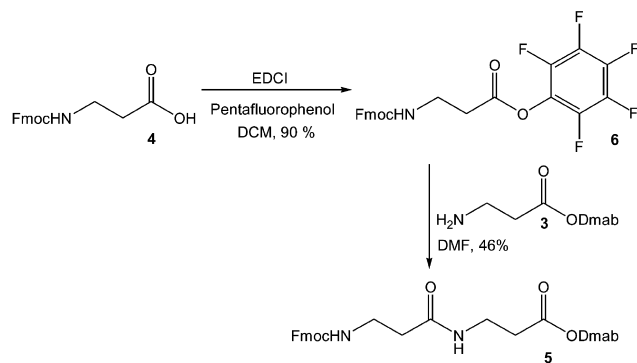


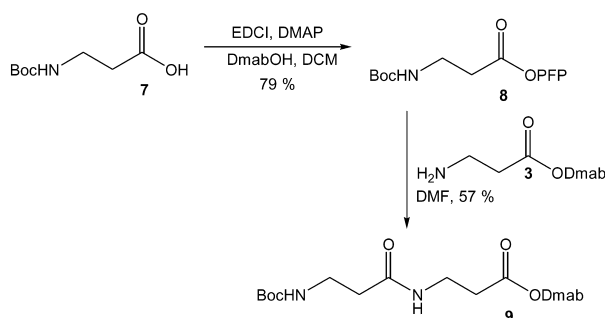
Figure 4. Schematic of the micro reactor used in carbodiimide coupling reactions.



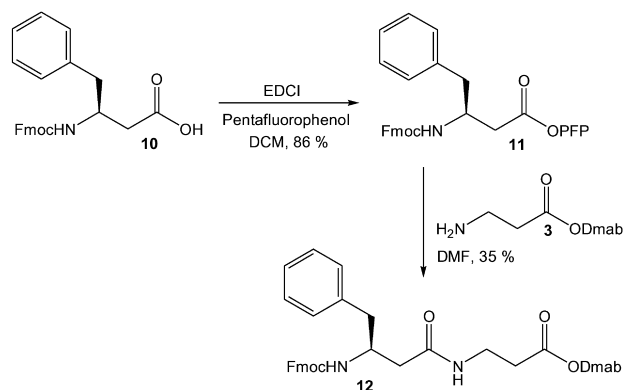
Scheme 2. Preparation and reaction of pentafluorophenyl esters of Fmoc protected amino acids.

Having prepared dipeptide **5** via the alternative pre-activated strategy, we wished to investigate if the reaction could be performed within a micro reactor. A standard solution of the pentafluorophenyl ester of Fmoc- β -alanine **6** (50 μ l, 0.1 M) in anhydrous DMF was added to reservoir A and a solution of amine **3** (50 μ l, 0.1 M) was placed in reservoir B. Anhydrous DMF (40 μ l) was placed in reservoir D, which was used to collect the products of the reaction. It was found that using continuous flow of both reagents, where the ester **6** was maintained at 700 V and the amine **3** was maintained at 600 V, dipeptide **5** was produced quantitatively in 20 min. Product conversions were based on the amount of pentafluorophenyl ester **6** remaining in the sample. This represented a significant increase in yield compared with solution phase synthesis, where lengthy reaction times are also required.

We were also interested to determine the effect of the protecting group on the reaction. Thus, Boc- β -alanine **7** was activated as pentafluorophenyl ester **8** via an EDCI coupling reaction, to give the product in 79% yield. The pentafluorophenyl ester **8** was reacted with amine **3** in DMF as solvent to give the dipeptide **9** in 57% yield (Scheme 3). Subsequently, the reaction between the pentafluorophenyl ester **8** of Boc- β -alanine and amine **3** was also investigated in the micro reactor. In this case, when the reagents were mixed using continuous flow, with both reagents maintained at 700 V, again quantitative conversion to dipeptide **9** was observed. The fact that pentafluorophenyl ester **8** needed to be maintained at a higher potential, in order to obtain a quantitative conversion, demonstrates that the different pentafluorophenyl esters **6** and **8** have



Scheme 3. Reaction of pentafluorophenyl ester of Boc- β -alanine.



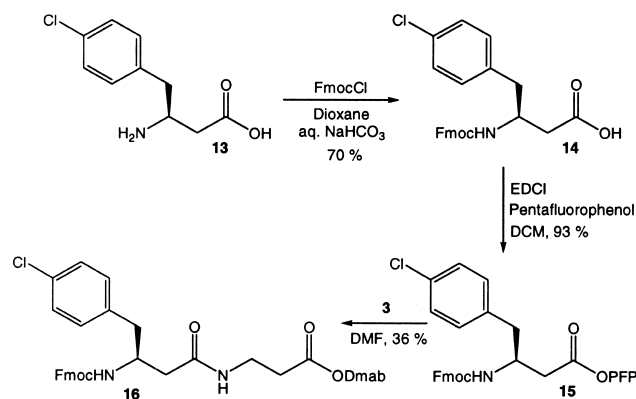
Scheme 4. Reaction of PFP ester of Fmoc-L- β -homophenylalanine.

different electroosmotic mobilities within the micro reactor channels.

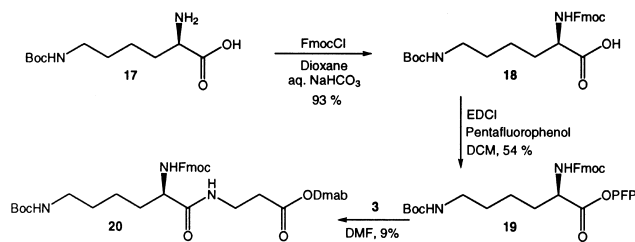
In order to demonstrate the generality of the technique we wished to demonstrate that a selection of peptides could be prepared. Thus, commercially available Fmoc-L- β -homophenylalanine **10** was converted into pentafluorophenyl ester **11** in 86% yield, under standard conditions. This was reacted with amine **3** to prepare a synthetic sample of dipeptide **12** in 35% yield (Scheme 4).

The reaction was subsequently investigated in the micro reactor. A solution of the pentafluorophenyl ester **11** in anhydrous DMF was added to reservoir A, a solution of amine **3** was placed in reservoir B and anhydrous DMF was placed in reservoir D. It was found that using continuous flow of both reagents, where the ester **11** was maintained at 900 V and the amine **3** was maintained at 600 V, dipeptide **12** was produced quantitatively in 20 min. As before this represented a significant increase in yield compared with bulk reaction.

Similarly L- β -homo-*p*-chlorophenylalanine **13** was reacted with 9-fluorenylmethyl chloroformate⁴¹ to effect *N*-protection affording carboxylic acid **14**, followed by an EDCI coupling reaction with pentafluorophenol to give the corresponding pentafluorophenyl ester **15**. The ester **15** was reacted with amine **3** in DMF, to prepare a synthetic sample of dipeptide **16** in 36% yield (Scheme 5).



Scheme 5. Reaction of pentafluorophenyl ester of Fmoc-L- β -homo-*p*-chlorophenylalanine.



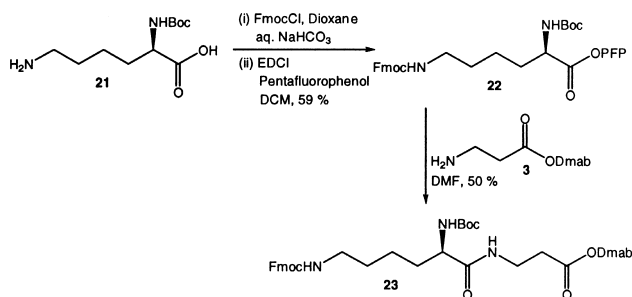
Scheme 6. Synthesis of peptides containing lysine.

The reaction was then transferred to the micro reactor. As in the previous example, it was found that using continuous flow of both reagents, where the ester **15** was maintained at 900 V and the amine **3** was maintained at 600 V, dipeptide **16** was produced quantitatively in 20 min.

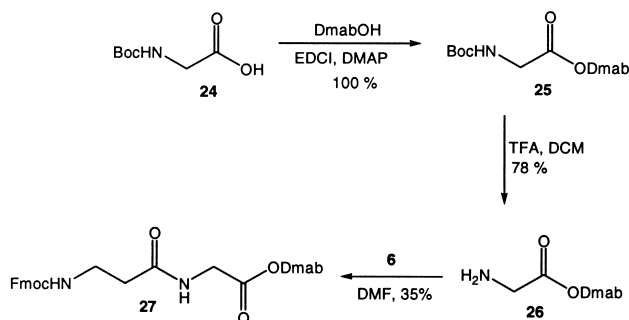
Having demonstrated the success of the technique using simple β -amino acids, we wished to perform the synthesis of more complex peptides. We selected to prepare peptides containing lysine, which contains two amine functionalities, which require orthogonal protection. Thus, commercially available *N* ϵ -Boc-L-lysine **17** was converted into pentafluorophenyl ester **19**, under standard conditions (Scheme 6). This was reacted with amine **3** to prepare a synthetic sample of dipeptide **20** in a disappointing 9% isolated yield.

The reaction was further investigated in the micro reactor. A solution of the pentafluorophenyl ester **19** in anhydrous DMF was added to reservoir A, a solution of amine **3** was placed in reservoir B and anhydrous DMF was placed in reservoir D. It was found that using continuous flow of both reagents, where the ester **19** was maintained at 1000 V and the amine **3** was maintained at 600 V, dipeptide **20** was produced quantitatively in 20 min.

Similarly *N* α -Boc-L-lysine **21** was converted into pentafluorophenyl ester **22**, in 59% yield (Scheme 7). This was reacted with amine **3** to prepare a synthetic sample of dipeptide **23** in 50% yield. The reaction was then transferred to the micro reactor. As in the previous example, it was found that using continuous flow of the reagents, where the ester **22** was maintained at 1000 V and the amine **3** was maintained at 600 V, dipeptide **23** was produced quantitatively. As expected, this result demonstrates that both pentafluorophenyl esters of lysine **19** and **22** have the same electrophoretic mobility within the channels of the micro reactor. Fmoc deprotection of the peptides **20** and **23** would prepare different amines, which could be used in further reactions.



Scheme 7. Synthesis of peptides containing lysine.



Scheme 8. Preparation of peptides containing glycine.

We were interested to observe that all reactions between pentafluorophenyl esters and amine **3** appeared to be faster in the micro reactor than when performed in a bulk reaction. However, bulk reactions were generally performed at much higher concentrations than micro reactions. In order to make comparison between rates we monitored the conversion of pentafluorophenyl ester **11** into peptide **12** at 0.05 M concentration, the same as used in the micro reaction studies (Scheme 8). Fig. 5 shows how conversion increases with time, the graph shows that after 20 min, the length of a micro reaction, only about 5% conversion to dipeptide was observed in the bulk reaction. Even after 400 h (ca. 16 days) only 70% conversion was attained. This result clearly shows that the rate of reactions is considerably enhanced when the reactions are conducted in a micro reactor. We postulate that the enhancement in rate of reaction is an electrochemical phenomenon, due to the reaction being performed in an electric field.

Having prepared numerous examples of peptides prepared from the Dmab ester of β -alanine **3**, we wished to demonstrate that other amines may be used in the synthesis of peptides. Thus, commercially available Boc-glycine **24** was protected as the Dmab ester via an EDCI/DMAP coupling reaction to give the ester **25** in 100% yield in a bulk reaction (Scheme 8). Treatment of **25** with trifluoroacetic acid furnished the desired amine **26** in 78% yield. This was subsequently reacted with pentafluorophenyl ester **6** to give a synthetic sample of the dipeptide **27** in 35% yield.

The reaction was subsequently investigated in the micro reactor. A solution of the pentafluorophenyl ester **6** in anhydrous DMF was added to reservoir A, a solution of amine **26** was placed in reservoir B and anhydrous DMF was placed in reservoir D, which was used to collect the

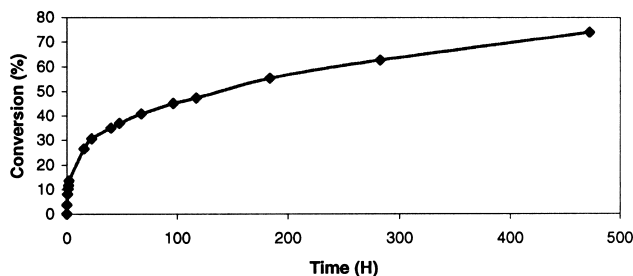
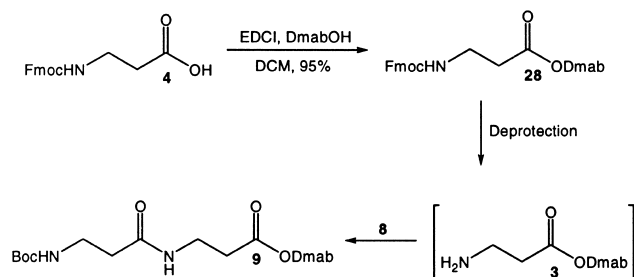


Figure 5. Conversion of pentafluorophenyl ester **11** to dipeptide **12** in a bulk reaction.



Scheme 9. Multi-step peptide synthesis.

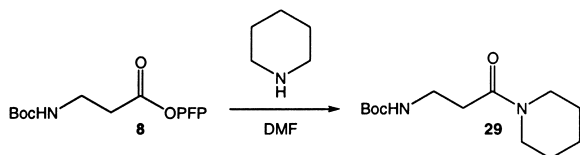
products of the reaction. It was found that using continuous flow of reagents, where both were maintained at 800 V, dipeptide **27** was produced quantitatively in 20 min.

Having extensively demonstrated that peptide bonds could be successfully formed when using a micro reactor, we wished to show that we could extend the methodology to the preparation of longer chain peptides. Consequently, we needed to be able to conduct deprotection reactions and subsequently perform further peptide bond forming reactions. Fmoc-β-alanine **4** was converted into the Dmab ester **28**, in a bulk reaction, using standard conditions (Scheme 9). It was proposed to convert ester **28** into amine **3** by deprotection of the Fmoc group and subsequently react the amine 'in situ' within the micro reactor with pentafluorophenyl ester **8**, to give the dipeptide **9**.

Several methods for the deprotection of the Fmoc group are reported in the literature, the most common method being treatment with 20% piperidine in DMF.^{42,43} The advantage of using piperidine in the reaction, is that the piperidine subsequently reacts with the dibenzofulvene, to form the DMF soluble piperidine adduct. This is advantageous, as precipitation or polymerisation of the dibenzofulvene within the micro reactor could cause blockage of the channels. Preliminary experiments revealed that treatment of **28**, with 10 equiv. of piperidine in DMF using continuous flow within the micro reactor, resulted in 60–70% deprotection over a 20 min period, to give amine **3**.

Subsequently, a standard solution of the Dmab ester of Fmoc-β-alanine **28** (50 μl, 0.1 M) in anhydrous DMF was added to reservoir A, a solution of piperidine (50 μl, 1.0 M) was placed in reservoir B and a solution of pentafluorophenyl ester **8** (50 μl, 0.1 M) was placed in reservoir C, in an attempt to prepare dipeptide **9** using this multi-step approach. Anhydrous DMF (40 μl) was placed in reservoir D, to collect the products of the reaction. The HPLC of the reaction mixture showed that Fmoc deprotection had occurred, however no dipeptide **9** was evident.

It was postulated that the excess piperidine was reacting



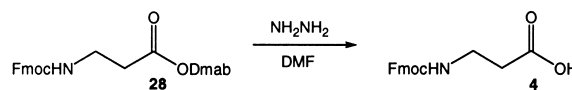
Scheme 10. Reaction of piperidine with pentafluorophenyl esters.

with the pentafluorophenyl ester. This was confirmed from a batch reaction, in which piperidine was reacted with the pentafluorophenyl ester of Boc-β-alanine **8** (Scheme 10). The only product isolated from the reaction was amide **29**, resulting from the nucleophilic attack of piperidine on the ester.

As a result, an alternative method of Fmoc deprotection was required that would not cause the aforementioned problem. Using the micro reactor, the Dmab ester of Fmoc-β-alanine **28** was reacted with 1 equiv. of 1,8-diazabicyclo[5.4.0]undec-7-ene (DBU)^{44,45} to give the free amine **3** which was then reacted with the pentafluorophenylester of Boc-β-alanine **8**, in an attempt to form the dipeptide **9**.

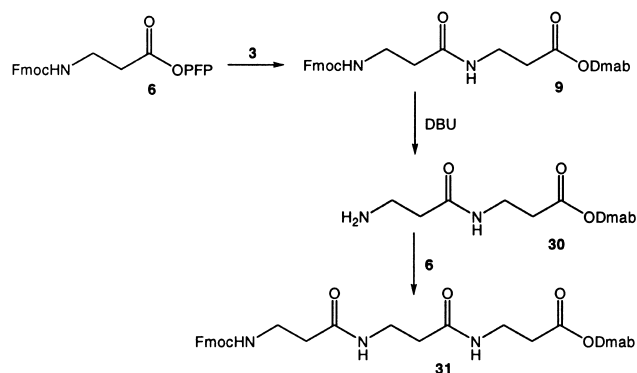
In this case, when the reagents were mixed using continuous flow, with the reagents maintained at 700 V, product **9** was observed in typically 25% yield. Surprisingly, when the reagents were mobilised using a stopped flow technique, the yield of product was actually reduced. By comparing the flows of each reagent at this stage we were able to optimise the reaction. The Dmab ester of Fmoc-β-alanine **28** was maintained at 750 V while reacted with DBU at 800 V. The deprotected amine was further reacted, using continuous flow, with the pentafluorophenyl ester of Boc-β-alanine **8**, maintained at 700 V, to give a conversion of 96%, based on the amount of Dmab ester **28** present at the end of the reaction. Importantly we have shown that deprotection may be achieved in micro reactions using just 1 equiv. of DBU, compared with 2% DBU used in SPPS.^{44,45}

Having shown that more complex peptides could be produced by removal of the *N*-protecting group we wished to determine if we could remove the Dmab protecting group using hydrazine.³⁸ Hence, a solution of the Dmab ester of Fmoc-β-alanine **28** (50 μl, 0.1 M) in anhydrous DMF was added to reservoir A, a solution of hydrazine (50 μl, 0.1 M) was placed in reservoir B and anhydrous DMF (40 μl) was placed in reservoir D. Using continuous flow of both reagents maintained at 700 V, quantitative deprotection was observed to give carboxylic acid **4** (Scheme 11). Again deprotection was achieved in the micro reactions using just 1 equiv. of hydrazine, compared with 2% solutions used in SPPS.³⁸ This suggests that reactions conducted within micro reactors are more molecule efficient.



Scheme 11. Removal of the Dmab protecting group.

Having successfully demonstrated that peptide bonds could be formed and that the protecting groups could be selectively removed, we wished to show that we could use the methodology in the preparation of tripeptides within micro reactor devices. Our initial target was the tripeptide of β-alanine **31**. We selected to initially investigate the synthesis of dipeptide **9** followed by the selective deprotection of the Fmoc group and subsequent reaction of amine **30** with another equivalent of pentafluorophenyl ester **6** (Scheme 12).



Scheme 12. Tripeptide synthesis.

A standard solution of the pentafluorophenyl ester of Fmoc- β -alanine **6** (50 μ l, 0.1 M) in anhydrous DMF was added to reservoir A and a solution of amine **3** (50 μ l, 0.1 M) was placed in reservoir B, such that dipeptide **9** could be prepared in the channel of the micro reactor (Fig. 6). A solution of DBU (50 μ l, 0.1 M) was placed in reservoir C to effect Fmoc deprotection and a second equivalent of pentafluorophenyl ester **6** was added to reservoir D. Anhydrous DMF (40 μ l) was placed in reservoir E, which was used to collect the products of the reaction. Using continuous flow of all reagents where reservoir A was maintained at 1000 V, reservoir B was at 1000 V, reservoir C was at 400 V and reservoir D was at 700 V, tripeptide **31** was prepared in 30% overall conversion, for the three step synthesis. Further work is currently underway to purify the tripeptide by electrophoretic separation.

4. Conclusion

We have demonstrated the application of micro reactors to perform multi-step synthesis, potentially allowing the high throughput synthesis of peptides. It has been demonstrated that peptide bonds may be prepared in high yield by either a carbodiimide coupling reaction or from pre-activated derivatives such as pentafluorophenyl esters. It was found that performing these reactions in the micro reactor resulted in an increase in the reaction efficiency over the traditional batch method. We propose that this enhancement in rate is an electrochemical phenomenon, due to the reaction being

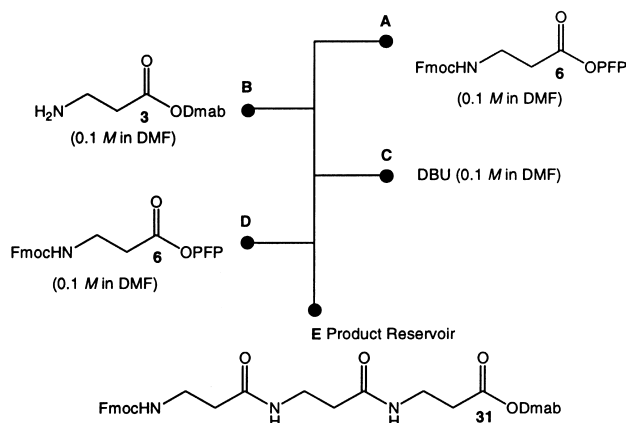


Figure 6. Schematic of the micro reactor used to prepare tripeptide.

performed in an electric field. It has also been demonstrated that selective deprotection of the resultant dipeptides can be achieved. The Fmoc group was successfully deprotected using 1 equiv. of DBU while the Dmab ester was removed by treatment with 1 equiv. of hydrazine. After deprotection further peptide bond forming reactions were performed, resulting in the synthesis of longer chain peptides. We have successfully used this approach in the synthesis of tripeptide **31**. Further studies are currently underway in our laboratories to increase the overall conversion of the multi-step reactions and to purify the peptides by electrophoretic separation.

5. Experimental

5.1. Micro reactions

Platinum electrodes were placed in each of the reservoirs of the micro reactor and an external voltage was applied to the channels inducing electroosmotic flow of the reagents. The power supply was manufactured by Kingfield Electronics (Sheffield, UK) and was controlled using LabVIEW™ software written by Dr X. Zhang (University of Hull).

The reactions were conducted at room temperature for a period of 20 min, in order to acquire sufficient volume of product to determine the conversion of the reaction. Reaction products were determined by HPLC via comparison with retention times and spectra with those obtained from synthetic standards. Analysis was achieved by high performance liquid chromatography (Jupiter C₁₈ 10 μ m, 4.6 \times 250 mm, mobile phase composition: 0.1% trifluoroacetic acid in water and 0.1% trifluoroacetic acid in acetonitrile, using a gradient system of 30% aqueous to 70% aqueous over 20 min, with a flow rate of 2.5 ml min⁻¹ at room temperature). Product conversions were based on the amount of carboxylic acid or pentafluorophenyl ester remaining in the sample.

5.2. Bulk reactions

All solvents were purchased as anhydrous solutions over molecular sieves from Fluka. Reagents were purchased from Aldrich and used as supplied. Amino acids were obtained from Bachem (UK) and Peptech. Column chromatography was carried out using Fluka silica gel 60 as the solid support. Compounds were eluted using various mixtures of ethyl acetate, hexane and methanol. Thin layer chromatography was performed using Merck Kieselgel 60 HF₂₅₄ aluminium backed TLC plates with various mixtures of ethyl acetate and hexane as the eluent. Visualisation of the plates was carried out by either exposure to short wave ultra violet light or by development in aqueous potassium permanganate (0.5%) and sodium hydrogen carbonate (2.5%) solution, followed by heating with a hot air gun.

Nuclear magnetic resonance (NMR) spectra were recorded as solutions in deuteriochloroform, unless otherwise stated, using tetramethylsilane (TMS) as internal standard. The spectra were recorded on Jeol GX270 or GX400 spectrometers. The chemical shift values for all spectra are given in

parts per million with coupling constants in Hertz. Mass spectra were recorded on a Thermo-Finnigan LCQ, using electrospray ionisation. Infrared spectra were recorded in the range 4000–600 cm^{-1} using a Perkin Elmer Paragon 1000 FT-IR spectrometer and peaks are reported (ν_{max}) in wavenumbers (cm^{-1}). Liquid samples were obtained as thin films and solid samples were dissolved in chloroform, on sodium chloride discs. Melting points were measured on a Gallenkamp melting point apparatus using open capillary tubes and are uncorrected. Elemental combustion analyses were measured using a Fisons Carlo Erba EA1108 analyser.

5.2.1. Boc- β -alanine-ODmab 2. A solution of EDCI (1.27 g, 6.62 mmol) and DMAP (72 mg, 0.59 mmol) in DCM (100 ml) was added to a stirred solution of Boc- β -alanine **1** (1.10 g, 5.81 mmol) and DmabOH (1.92 g, 5.83 mmol) in DCM (100 ml) at room temperature under nitrogen. After 24 h, the solvent was washed with dilute hydrochloric acid (50 ml) and the aqueous layer was further extracted with DCM (2 \times 50 ml). The combined organic extracts were dried over magnesium sulphate and concentrated in vacuo to give a solid, which was purified by column chromatography. Elution with 20% ethyl acetate in hexane gave *Boc- β -alanine-ODmab 2* (2.67 g, 92%) as a white solid; mp 78–80°C (from DCM/hexane); (Found C, 67.03; H, 7.79; N, 5.36. $\text{C}_{28}\text{H}_{40}\text{N}_2\text{O}_6$ requires C, 67.20; H, 8.00; N, 5.60%); ν_{max} (cm^{-1}) 3453, 3360, 2940, 1734, 1708, 1641, 1454 and 754; δ_{H} (399.6 MHz) 0.78 (6H, d, $J=6.6$ Hz, $\text{CH}(\text{CH}_3)_2$), 1.08 (6H, s, $\text{C}(\text{CH}_3)_2$), 1.43 (9H, s, $\text{C}(\text{CH}_3)_3$), 1.84 (1H, m, $\text{CH}(\text{CH}_3)_2$), 2.40 (2H, s, $\text{CH}_2\text{C}(\text{CH}_3)_2$), 2.49 (2H, s, $\text{CH}_2\text{C}(\text{CH}_3)_2$), 2.61 (2H, t, $J=6.1$ Hz, CH_2CO_2), 3.01 (2H, br d, $J=6.1$ Hz, $\text{CH}_2\text{CH}(\text{CH}_3)_2$), 3.43 (2H, dt, $J=6.1$ and 6.1 Hz, NHCH_2), 5.01 (1H, m, NHCH_2), 5.17 (2H, s, CO_2CH_2), 7.14 (2H, d, $J=8.4$ Hz, ArH), 7.41 (2H, d, $J=8.4$ Hz, ArH) and 15.30 (1H, s, ArNH); δ_{C} (100.4 MHz) 22.6, 28.3, 29.5, 30.0, 34.6, 36.1, 38.3, 52.3, 53.8, 65.5, 79.4, 100.5, 107.8, 126.7, 129.0, 135.3, 136.9, 155.7, 172.2, 176.4, 196.3 and 200.2; m/z 501 ($\text{M}^+ + 1$).

5.2.2. β -Alanine-ODmab 3. Trifluoroacetic acid (20 ml) was added to a solution of Boc- β -alanine-ODmab **2** (1.28 g, 2.56 mmol) in DCM (5 ml). After stirring for 30 min, the reaction mixture was concentrated in vacuo to remove the excess trifluoroacetic acid. The residue was dissolved in DCM (50 ml) and washed with saturated sodium hydrogen carbonate solution (50 ml). The aqueous solution was further extracted with DCM (2 \times 50 ml) and the combined organic extracts were dried over magnesium sulphate and concentrated in vacuo to give a solid which was recrystallised using DCM/Et₂O/hexane to give *β -alanine-ODmab* (as the TFA salt) **3** (1.21 g, 92%) as a pale yellow solid; mp 162–164°C; (Found C, 58.39; H, 6.50; N, 5.29. $\text{C}_{25}\text{H}_{33}\text{N}_2\text{O}_6\text{F}_3$ requires C, 58.37; H, 6.42; N, 5.45%); ν_{max} (cm^{-1}) 3451, 3251, 2960, 1730, 1672, 1648, 1450, 1195 and 755; δ_{H} (399.6 MHz) 0.77 (6H, d, $J=6.6$ Hz, $\text{CH}(\text{CH}_3)_2$), 1.08 (6H, s, $\text{C}(\text{CH}_3)_2$), 1.84 (1H, m, $\text{CH}(\text{CH}_3)_2$), 2.40 (2H, s, $\text{CH}_2\text{C}(\text{CH}_3)_2$), 2.49 (2H, s, $\text{CH}_2\text{C}(\text{CH}_3)_2$), 2.86 (2H, t, $J=6.4$ Hz, CH_2CO_2), 3.00 (2H, br d, $J=5.1$ Hz, $\text{CH}_2\text{CH}(\text{CH}_3)_2$), 3.26 (2H, t, $J=6.6$ Hz, NH_2CH_2), 5.01 (1H, m, NHCH_2), 5.17 (2H, s, CO_2CH_2), 7.14 (2H, d, $J=8.4$ Hz, ArH), 7.41 (2H, d, $J=8.4$ Hz, ArH), 8.42 (2H, br s, NH_2) and 15.31 (1H, s, ArNH); δ_{C} (100.4 MHz) 22.6, 28.2, 29.5, 30.0, 31.3, 35.3, 38.3, 52.3,

53.8, 66.1, 107.8, 126.7, 129.2, 134.8, 137.0, 171.0, 176.4, 196.3 and 200.2; m/z 401 ($\text{M}^+ + 1$).

5.2.3. Fmoc- β -alanine- β -alanine-ODmab 5. A solution of EDCI (91 mg, 0.47 mmol) in DCM (10 ml) was added to a stirred solution of Fmoc- β -alanine **4** (94 mg, 0.30 mmol) and amine **3** (130 mg, 0.33 mmol) in DCM (10 ml) at room temperature under nitrogen. After 24 h, the solvent was washed with dilute hydrochloric acid (20 ml) and the aqueous layer was further extracted with DCM (2 \times 50 ml). The combined organic extracts were dried over magnesium sulphate and concentrated in vacuo to give an oil which was purified by column chromatography. Elution with ethyl acetate gave *Fmoc- β -alanine- β -alanine-ODmab 5* (105 mg, 50%) as a colourless gum; δ_{H} (399.6 MHz) 0.77 (6H, d, $J=6.8$ Hz, $\text{CH}(\text{CH}_3)_2$), 1.08 (6H, s, $\text{C}(\text{CH}_3)_2$), 1.84 (1H, m, $\text{CH}(\text{CH}_3)_2$), 2.39 (2H, m, CH_2CO_2), 2.40 (2H, s, $\text{CH}_2\text{C}(\text{CH}_3)_2$), 2.49 (2H, s, $\text{CH}_2\text{C}(\text{CH}_3)_2$), 2.61 (2H, t, $J=6.4$ Hz, CH_2CO), 3.00 (2H, m, $\text{CH}_2\text{CH}(\text{CH}_3)_2$), 3.48 (2H, m, NHCH_2), 3.56 (2H, m, NHCH_2), 4.20 (1H, t, $J=6.8$ Hz, CHCH_2O), 4.37 (2H, d, $J=6.8$ Hz, CHCH_2O), 5.30 (2H, s, CO_2CH_2), 5.52 (1H, m, NH), 6.17 (1H, br t, NH), 7.12 (2H, d, $J=8.0$ Hz, ArH), 7.30 (2H, t, $J=7.6$ Hz, ArH), 7.39 (2H, t, $J=7.1$ Hz, ArH), 7.40 (2H, d, $J=8.0$ Hz, ArH), 7.59 (2H, d, $J=7.8$ Hz, ArH), 7.76 (2H, d, $J=7.8$ Hz, ArH) and 15.29 (1H, s, ArNH); δ_{C} (100.4 MHz) 22.6, 28.2, 29.6, 30.0, 31.9, 34.0, 34.9, 38.4, 47.2, 52.3, 53.7, 64.5, 65.8, 66.7, 107.8, 120.0, 125.1, 126.7, 127.1, 127.7, 129.1, 135.1, 137.0, 141.3, 143.9, 155.9, 172.1, 172.3, 176.5, 196.5 and 200.3; m/z 694 ($\text{M}^+ + 1$).

5.2.4. Fmoc- β -alanine-OPFP 6. A solution of EDCI (1.32 g, 6.88 mmol) in DCM (50 ml) was added to a stirred solution of Fmoc- β -alanine **4** (2.06 g, 6.62 mmol) and pentafluorophenol (1.22 g, 6.63 mmol) in DCM (100 ml) at room temperature under nitrogen. After 24 h, the solvent was washed with dilute hydrochloric acid (50 ml) and the aqueous layer was further extracted with DCM (2 \times 50 ml). The combined organic extracts were dried over magnesium sulphate and concentrated in vacuo to give a solid which was purified by column chromatography. Elution with 20% ethyl acetate in gave *Fmoc- β -alanine-OPFP 6* (2.85 g, 90%) as a white solid; mp 112–114°C (from EtOAc/hexane); (Found C, 60.06; H, 3.09; N, 2.67. $\text{C}_{24}\text{H}_{16}\text{NO}_4\text{F}_5$ requires C, 60.38; H, 3.35; N, 2.94%); ν_{max} (cm^{-1}) 3422, 1787, 1696, 1518, 1002 and 758; δ_{H} (399.6 MHz) 2.94 (2H, t, $J=6.1$ Hz, CH_2CO_2), 3.60 (2H, dt, $J=5.8$ and 6.1 Hz, NHCH_2), 4.22 (1H, t, $J=6.8$ Hz, CHCH_2O), 4.42 (2H, d, $J=6.8$ Hz, CHCH_2O), 5.22 (1H, m, NH), 7.31 (2H, t, $J=7.3$ Hz, ArH), 7.40 (2H, t, $J=7.3$ Hz, ArH), 7.58 (2H, d, $J=6.8$ Hz, ArH) and 7.76 (2H, d, $J=7.5$ Hz, ArH); δ_{C} (100.4 MHz) 33.8, 36.4, 47.2, 66.9, 120.0, 125.0, 127.0, 127.7, 136.6 (m, CF), 138.4 (m, CF), 139.1 (m, CF), 139.8 (m, CF), 140.8 (m, CF), 141.3, 142.2 (m, CF), 143.7, 156.3 and 168.3; m/z 478 ($\text{M}^+ + 1$).

5.2.5. Fmoc- β -alanine- β -alanine-ODmab 5. A solution of pentafluorophenyl ester **6** (181 mg, 0.38 mmol) and amine **3** (161 mg, 0.40 mmol) in DMF (2 ml) was stirred for 24 h. The DMF was removed in vacuo, the residue was dissolved in DCM (50 ml) and washed with dilute hydrochloric acid (20 ml). The aqueous layer was further extracted with DCM (2 \times 50 ml) and the combined organic extracts were dried

over magnesium sulphate and concentrated in vacuo to give a yellow oil which was purified by column chromatography. Elution with ethyl acetate gave *Fmoc-β-alanine-β-alanine-ODmab* **5** (121 mg, 46%) as a colourless oil. Spectroscopic data as reported.

5.2.6. Boc-β-alanine-OPFP 8. A solution of EDCI (2.35 g, 12.26 mmol) and DMAP (60 mg, 0.49 mmol) in DCM (100 ml) was added to a stirred solution of Boc-β-alanine **7** (2.28 g, 12.05 mmol) and pentafluorophenol (2.25 g, 12.22 mmol) in DCM (100 ml) at room temperature under nitrogen. After 24 h, the solvent was washed with dilute hydrochloric acid (50 ml) and the aqueous layer was further extracted with DCM (2×50 ml). The combined organic extracts were dried over magnesium sulphate and concentrated in vacuo to give a solid which was recrystallised using DCM and hexane to give *Boc-β-alanine-OPFP 8* (3.37 g, 79%) as a white solid; mp 56–57°C; (Found C, 47.27; H, 3.86; N, 3.61. C₁₄H₁₄NO₄F₅ requires C, 47.32; H, 3.94; N, 3.94%); ν_{\max} (cm⁻¹) 3374, 2989, 1797, 1691, 1518, 1097, 988 and 756; δ_{H} (399.6 MHz) 1.45 (9H, s, (CH₃)₃CO), 2.93 (2H, t, *J*=6.1 Hz, CH₂CO₂), 3.53 (2H, dt, *J*=6.1 and 6.1 Hz, NHCH₂) and 4.98 (1H, m, NH); δ_{C} (100.4 MHz) 28.4, 34.0, 36.0, 79.9, 136.6 (m, CF), 138.3 (m, CF), 139.2 (m, CF), 139.8 (m, CF), 140.8 (m, CF), 142.3 (m, CF), 155.8 and 168.5; *m/z* 356 (M⁺+1).

5.2.7. Boc-β-alanine-β-alanine-ODmab 9. A solution of pentafluorophenyl ester **8** (142 mg, 0.40 mmol) and amine **3** (176 mg, 0.44 mmol) in DMF (2 ml) was stirred for 48 h. The DMF was removed in vacuo, the residue was dissolved in DCM (50 ml) and washed with dilute hydrochloric acid (20 ml). The aqueous layer was further extracted with DCM (2×30 ml) and the combined organic extracts were dried over magnesium sulphate and concentrated in vacuo to give a yellow oil which was purified by column chromatography. Elution with ethyl acetate gave *Boc-β-alanine-β-alanine-ODmab 9* (129 mg, 57%) as a colourless oil; δ_{H} (399.6 MHz) 0.78 (6H, d, *J*=6.8 Hz, CH(CH₃)₂), 1.08 (6H, s, C(CH₃)₂), 1.43 (9H, s, C(CH₃)₃), 1.85 (1H, m, CH(CH₃)₂), 2.38 (2H, t, *J*=6.1 Hz, CH₂CO₂), 2.45 (4H, s, 2×CH₂C(CH₃)₂), 2.63 (2H, t, *J*=6.1 Hz, CH₂CO), 3.00 (2H, br d, *J*=6.1 Hz, CH₂CH(CH₃)₂), 3.38 (2H, m, NHCH₂), 3.56 (2H, dt, *J*=6.1 and 6.1 Hz, NHCH₂), 5.01 (1H, m, NHCH₂), 5.14 (1H, br s, NH), 5.17 (2H, s, CO₂CH₂), 6.21 (1H, br s, NH), 7.14 (2H, d, *J*=8.3 Hz, ArH), 7.41 (2H, d, *J*=8.3 Hz, ArH) and 15.30 (1H, s, ArNH); δ_{C} (100.4 MHz) 22.6, 28.2, 28.4, 29.5, 30.0, 34.0, 34.8, 36.3, 38.4, 53.0, 54.9, 65.7, 79.4, 107.8, 126.7, 129.1, 135.1, 137.0, 156.0, 171.4, 172.2, 176.4, 196.3 and 200.2; *m/z* 572 (M⁺+1).

5.2.8. Fmoc-L-β-homophenylalanine-OPFP 11. A solution of EDCI (0.37 g, 1.96 mmol) in DCM (50 ml) was added to a stirred solution of Fmoc-L-β-homophenylalanine **10** (0.43 g, 1.24 mmol) and pentafluorophenol (0.35 g, 1.91 mmol) in DCM (50 ml) at room temperature under nitrogen. After 24 h, the solvent was washed with dilute hydrochloric acid (50 ml) and the aqueous layer was further extracted with DCM (2×50 ml). The combined organic extracts were dried over magnesium sulphate and concentrated in vacuo to give a solid which purified by column chromatography. Elution with 20% ethyl acetate in hexane gave *Fmoc-L-β-homophenylalanine-OPFP 11* (0.55 g,

86%) as a white solid; mp 140–142°C (DCM/hexane); ν_{\max} (cm⁻¹) 3326, 1782, 1691, 1518, 993 and 754; δ_{H} (399.6 MHz) 2.83–3.05 (4H, m, CH₂CO₂ and CH₂Ph), 4.20 (1H, t, *J*=6.8 Hz, CHCH₂O), 4.36–4.42 (3H, m, CHCH₂O and CHNH), 5.13 (1H, d, *J*=8.8 Hz, NH), 7.19–7.33 (7H, m, ArH), 7.40 (2H, t, *J*=7.3 Hz, ArH), 7.55 (2H, d, *J*=7.3 Hz, ArH) and 7.76 (2H, d, *J*=7.3 Hz, ArH); δ_{C} (100.4 MHz) 36.8, 39.7, 47.1, 49.2, 66.8, 120.0, 125.0, 127.0, 127.1, 127.7, 128.8, 129.3, 136.6 (m, CF), 138.4 (m, CF), 136.8, 139.1 (m, CF), 139.8 (m, CF), 140.8 (m, CF), 141.3, 142.2 (m, CF), 143.8, 155.5 and 167.5; *m/z* 567 (M⁺+1).

5.2.9. Fmoc-L-β-homophenylalanine-β-alanine-ODmab 12. A solution of pentafluorophenyl ester **11** (171 mg, 0.30 mmol) and amine **3** (125 mg, 0.31 mmol) in DMF (2 ml) was stirred for 24 h. The DMF was removed in vacuo, the residue was dissolved in DCM (50 ml) and washed with dilute hydrochloric acid (20 ml). The aqueous layer was further extracted with DCM (2×50 ml) and the combined organic extracts were dried over magnesium sulphate and concentrated in vacuo to give a yellow oil which was purified by column chromatography. Elution with ethyl acetate gave *Fmoc-L-β-homophenylalanine-β-alanine-ODmab 12* (83 mg, 35%) as a cream solid; mp 116–118°C (DCM/hexane); ν_{\max} (cm⁻¹) 3432, 3316, 2951, 1734, 1686, 1556, 1445, 1166 and 756; δ_{H} (399.6 MHz) 0.76 (6H, d, *J*=6.8 Hz, CH(CH₃)₂), 1.08 (6H, s, C(CH₃)₂), 1.83 (1H, m, CH(CH₃)₂), 2.40 (2H, s, CH₂C(CH₃)₂), 2.49 (2H, s, CH₂C(CH₃)₂), 2.61 (2H, br t, CH₂CO₂), 2.87–2.99 (6H, m, CH₂CH(CH₃)₂, CH₂CO₂ and CH₂Ph), 3.54 (2H, m, CH₂NH), 4.18 (5H, t, *J*=7.0 Hz, CHCH₂O), 4.28–4.39 (2H, m, CHCH₂O and CHNH), 5.12 (2H, s, CO₂CH₂), 5.84 (1H, br d, *J*=8.4 Hz, NH), 6.28 (1H, m, NH), 7.09 (2H, d, *J*=7.3 Hz, ArH), 7.18–7.57 (13H, m, ArH), 7.76 (2H, d, *J*=7.3 Hz, ArH) and 15.28 (1H, s, ArNH); δ_{C} (100.4 MHz) 22.6, 28.2, 29.5, 30.0, 34.0, 34.9, 36.5, 38.3, 40.2, 47.2, 52.3, 53.7, 65.7, 66.7, 107.8, 120.0, 125.1, 126.7, 127.1, 127.7, 128.6, 129.1, 129.3, 135.0, 136.8, 137.8, 141.3, 143.9, 155.9, 162.6, 170.9, 172.2, 176.4, 196.4 and 200.2; *m/z* 784 (M⁺+1).

5.2.10. Fmoc-L-β-homo-*p*-chlorophenylalanine 14. A solution of 9-fluorenylmethyl chloroformate (0.37 g, 1.45 mmol) in dioxane (30 ml) was added to a stirred solution of L-β-homo-*p*-chlorophenylalanine **13** (0.30 g, 1.22 mmol) in saturated aqueous sodium hydrogen carbonate (50 ml). After stirring for 24 h the mixture was concentrated in vacuo and acidified using dilute hydrochloric acid (50 ml) and extracted using dichloromethane (3×50 ml). The combined organic extracts were dried over magnesium sulphate and concentrated in vacuo to give a solid which was recrystallised from DCM/hexane to give *Fmoc-L-β-homo-*p*-chlorophenylalanine 14* (0.37 g, 70%) as a white solid; mp 176–178°C; (Found C, 68.90; H, 5.16; N, 3.14. C₂₅H₂₂NO₄Cl requires C, 68.97; H, 5.06; N, 3.22%); ν_{\max} (cm⁻¹) 3326, 1682, 1652, 1537 and 737; δ_{H} (DMSO, 399.6 MHz) 2.47 (2H, d, *J*=6.1 Hz, CH₂CO₂), 2.84 (2H, d, *J*=6.6 Hz, CH₂Ph), 4.12–4.36 (4H, m, CHCH₂O and NH), 4.42 (2H, d, *J*=5.6 Hz, CHCH₂O), 6.63 (1H, d, *J*=8.0 Hz, NH), 7.15 (2H, d, *J*=8.1 Hz, ArH), 7.21 (2H, d, *J*=8.1 Hz, ArH), 7.31 (2H, dt, *J*=7.3 and 3.7 Hz, ArH), 7.40 (2H, t, *J*=7.3 Hz, ArH), 7.58 (2H, m, ArH) and 7.76

(2H, d, $J=7.6$ Hz, ArH); δ_C (100.4 MHz) 29.4, 38.4, 47.1, 49.4, 65.8, 119.8, 125.1, 127.0, 127.6, 128.2, 130.8, 131.7, 136.9, 141.0, 143.8, 155.6 and 173.0; m/z 436 ($M^+ + 1$).

5.2.11. Fmoc-L- β -homo-*p*-chlorophenylalanine-OPFP 15.

A solution of EDCI (0.20 g, 1.07 mmol) in DCM (20 ml) was added to a stirred solution of Fmoc-L- β -homo-*p*-chlorophenylalanine **14** (0.31 g, 0.71 mmol) and pentafluorophenol (0.14 g, 0.75 mmol) in DCM (20 ml) at room temperature under nitrogen. After 24 h, the solvent was washed with dilute hydrochloric acid (50 ml) and the aqueous layer was further extracted with DCM (2 \times 50 ml). The combined organic extracts were dried over magnesium sulphate and concentrated in vacuo to give a solid which was recrystallised using DCM and hexane to give Fmoc-L- β -homo-*p*-chlorophenylalanine-OPFP **15** (0.40 g, 93%) as a white solid; mp 160–162°C; ν_{\max} (cm^{-1}) 3322, 1777, 1687, 1520, 991, 758 and 741; δ_H (399.6 MHz) 2.86–3.01 (4H, m, CH_2CO_2 and CH_2Ph), 4.20 (1H, t, $J=5.6$ Hz, CHCH_2O), 4.30 (3H, m, CHNH), 4.42 (2H, d, $J=5.6$ Hz, CHCH_2O), 5.09 (1H, d, $J=9.0$ Hz, NH), 7.12 (2H, d, $J=7.6$ Hz, ArH), 7.26–7.32 (4H, m, ArH), 7.40 (2H, t, $J=7.3$ Hz, ArH), 7.54 (2H, d, $J=7.3$ Hz, ArH) and 7.76 (2H, d, $J=7.6$ Hz, ArH); δ_C (100.4 MHz) 36.8, 39.1, 47.2, 49.2, 66.8, 120.0, 125.0, 127.1, 127.8, 129.0, 130.6, 133.0, 135.3, 136.6 (m, CF), 138.4 (m, CF), 139.1 (m, CF), 139.8 (m, CF), 140.8 (m, CF), 141.4, 142.2 (m, CF), 143.8, 155.5 and 167.4; m/z 602 ($M^+ + 1$).

5.2.12. Fmoc-L- β -homo-*p*-chlorophenylalanine- β -alanine-ODmab 16.

A solution of pentafluorophenyl ester **15** (130 mg, 0.21 mmol) and amine **3** (102 mg, 0.26 mmol) in DMF (2 ml) was stirred for 24 h. The DMF was removed in vacuo, the residue was dissolved in DCM (50 ml) and washed with dilute hydrochloric acid (20 ml). The aqueous layer was further extracted with DCM (2 \times 50 ml) and the combined organic extracts were dried over magnesium sulphate and concentrated in vacuo to give a yellow oil which was purified by column chromatography. Elution with ethyl acetate gave Fmoc-L- β -homo-*p*-chlorophenylalanine- β -alanine-ODmab **16** (64 mg, 36%) as a white solid; mp 152–156°C (DCM/hexane); ν_{\max} (cm^{-1}) 3451, 3297, 2951, 1734, 1681 and 753; δ_H (399.6 MHz) 0.76 (6H, d, $J=6.7$ Hz, $\text{CH}(\text{CH}_3)_2$), 1.08 (6H, s, $\text{C}(\text{CH}_3)_2$), 1.83 (1H, m, $\text{CH}(\text{CH}_3)_2$), 2.40 (2H, s, $\text{CH}_2\text{C}(\text{CH}_3)_2$), 2.49 (2H, s, $\text{CH}_2\text{C}(\text{CH}_3)_2$), 2.60 (2H, br t, CH_2CO_2), 2.78–3.00 (6H, m, $\text{CH}_2\text{CH}(\text{CH}_3)_2$, CH_2CO_2 and CH_2Ph), 3.54 (2H, m, CH_2NH), 4.18 (5H, t, $J=6.7$ Hz, CHCH_2O), 4.30–4.39 (2H, m, CHCH_2O and CHNH), 5.13 (2H, s, CO_2CH_2), 5.80 (1H, br d, $J=8.2$ Hz, NH), 6.24 (1H, m, NH), 7.11 (2H, d, $J=7.6$ Hz, ArH), 7.22–7.56 (12H, m, ArH), 7.76 (2H, d, $J=7.6$ Hz, ArH) and 15.29 (1H, s, ArNH); δ_C (100.4 MHz) 22.6, 28.3, 29.6, 30.0, 34.0, 34.9, 36.5, 38.4, 39.4, 47.2, 52.3, 53.8, 65.8, 66.6, 107.8, 120.0, 125.1, 126.7, 127.1, 127.7, 128.7, 129.1, 130.6, 132.5, 135.0, 136.4, 137.0, 141.3, 143.9, 155.9, 162.6, 170.7, 172.2, 176.4, 196.4 and 200.3; m/z 818 ($M^+ + 1$).

5.2.13. N ϵ -Boc-N α -Fmoc-L-lysine 18. A solution of 9-fluorenylmethyl chloroformate (0.52 g, 2.02 mmol) in dioxane (50 ml) was added to a stirred solution of N ϵ -Boc-L-lysine **17** (0.45 g, 1.83 mmol) in saturated aqueous

sodium hydrogen carbonate (50 ml). After stirring for 24 h the mixture was concentrated in vacuo and acidified using dilute hydrochloric acid (100 ml) and extracted using dichloromethane (3 \times 100 ml). The combined organic extracts were dried over magnesium sulphate and concentrated in vacuo to give a solid which was recrystallised from DCM/hexane to afford N ϵ -Boc-N α -Fmoc-L-lysine **18** (0.80 g, 93%) as a white solid; mp 44–46°C (from DCM/hexane); ν_{\max} (cm^{-1}) 3422, 3336, 2970, 1705, 1648, 1516 and 757; δ_H (DMSO, 399.6 MHz) 1.25–1.41 (4H, m, CH_2CH_2), 1.36 (9H, s, $(\text{CH}_3)_3\text{CO}$), 1.51–1.68 (2H, m, CH_2), 2.89 (2H, m, CH_2NH), 3.89 (1H, m, CHCO_2H), 4.21 (1H, t, $J=6.1$ Hz, CHCH_2O), 4.27 (1H, d, $J=6.1$ Hz, CHCH_2O), 6.77 (1H, t, $J=5.6$ Hz, NHCH_2), 7.31 (2H, t, $J=7.3$ Hz, ArH), 7.41 (2H, t, $J=7.3$ Hz, ArH), 7.72 (2H, d, $J=7.6$ Hz, ArH), 7.88 (2H, d, $J=7.3$ Hz, ArH) and 12.56 (1H, br s, CO_2H); m/z 467 ($M^+ - 1$).

5.2.14. N ϵ -Boc-N α -Fmoc-L-lysine-OPFP 19.

A solution of EDCI (0.32 g, 1.68 mmol) in DCM (30 ml) was added to a stirred solution of N ϵ -Boc-N α -Fmoc-L-lysine **18** (0.74 g, 1.58 mmol) and pentafluorophenol (0.29 g, 1.60 mmol) in DCM (50 ml) at room temperature under nitrogen. After 24 h, the solvent was washed with dilute hydrochloric acid (50 ml) and the aqueous layer was further extracted with DCM (2 \times 50 ml). The combined organic extracts were dried over magnesium sulphate and concentrated in vacuo to give a solid, which was purified by column chromatography. Elution with 20% ethyl acetate in hexane gave N ϵ -Boc-N α -Fmoc-L-lysine-OPFP **19** (0.54 g, 54%) as a white solid; mp 100–102°C (from DCM/hexane); (Found C, 60.30; H, 4.81; N, 4.25. $\text{C}_{32}\text{H}_{31}\text{N}_2\text{O}_6\text{F}_5$ requires C, 60.57; H, 4.89; N, 4.42%); ν_{\max} (cm^{-1}) 3432, 3345, 2900, 1787, 1681, 1518, 993 and 753; δ_H (399.6 MHz) 1.28–1.59 (4H, m, CH_2CH_2), 1.44 (9H, s, $(\text{CH}_3)_3\text{CO}$), 1.91–2.09 (2H, m, CH_2), 3.16 (2H, m, CH_2NH), 4.24 (1H, t, $J=6.8$ Hz, CHCH_2O), 4.40–4.72 (4H, m, CHCH_2O , CHCO_2 and NH), 5.58 (1H, d, $J=7.8$ Hz, NH), 7.31 (2H, t, $J=7.3$ Hz, ArH), 7.40 (2H, t, $J=7.3$ Hz, ArH), 7.61 (2H, d, $J=7.3$ Hz, ArH) and 7.77 (2H, d, $J=7.6$ Hz, ArH); δ_C (100.4 MHz) 22.1, 28.4, 29.7, 31.4, 39.6, 47.1, 53.7, 67.2, 79.4, 120.0, 125.0, 127.1, 127.7, 136.6 (m, CF), 138.4 (m, CF), 139.1 (m, CF), 139.7 (m, CF), 141.0 (m, CF), 141.3, 142.3 (m, CF), 143.7, 155.9, 156.3 and 168.8; m/z 635 ($M^+ + 1$).

5.2.15. N ϵ -Boc-N α -Fmoc-L-lysine- β -Alanine-ODmab 20.

A solution of carboxylic acid **18** (142 mg, 0.30 mmol), amine **3** (131 mg, 0.33 mmol) and EDCI (95 mg, 0.50 mmol) in DCM (20 ml) was stirred under nitrogen. After 24 h, the solvent was washed with dilute hydrochloric acid (50 ml) and the aqueous layer was further extracted with DCM (2 \times 50 ml). The combined organic extracts were dried over magnesium sulphate and concentrated in vacuo to give an oil which was purified by column chromatography. Elution with ethyl acetate in gave N ϵ -Boc-N α -Fmoc-L-lysine- β -alanine-ODmab **20** (23 mg, 9%) as a colourless gum; ν_{\max} (cm^{-1}) 3432, 3336, 2951, 1667, 1551, 1450, 1166 and 748; δ_H (399.6 MHz) 0.77 (6H, d, $J=6.4$ Hz, $\text{CH}(\text{CH}_3)_2$), 1.08 (6H, s, $\text{C}(\text{CH}_3)_2$), 1.24–1.54 (6H, m, $\text{CH}_2\text{CH}_2\text{CH}_2$), 1.43 (9H, s, $(\text{CH}_3)_3\text{CO}$), 1.83 (1H, m, $\text{CH}(\text{CH}_3)_2$), 2.40 (2H, s, $\text{CH}_2\text{C}(\text{CH}_3)_2$), 2.49 (2H, s, $\text{CH}_2\text{C}(\text{CH}_3)_2$), 2.61 (2H, t, $J=5.6$ Hz, CH_2CO_2), 2.99 (2H,

br d, $J=5.3$ Hz, $\text{CH}_2\text{CH}(\text{CH}_3)_2$, 3.10 (2H, m, CH_2NH), 3.55 (2H, m, CH_2NH), 4.21 (2H, t, $J=6.8$ Hz, CHCH_2O), 4.39 (2H, m, CHCH_2O and CHCH), 4.69 (1H, m, NH), 5.09 (2H, s, CO_2CH_2), 5.56 (1H, m, NH), 6.70 (1H, m, NH), 7.09 (2H, d, $J=8.4$ Hz, ArH), 7.31 (2H, dt, $J=7.3$ and 1.1 Hz, ArH), 7.33 (2H, t, $J=8.4$ Hz, ArH), 7.40 (2H, t, $J=7.3$ Hz, ArH), 7.59 (2H, d, $J=7.3$ Hz, ArH), 7.76 (2H, d, $J=8.4$ Hz, ArH) and 15.28 (1H, s, ArNH); δ_{C} (100.4 MHz) 22.6, 28.3, 24.4, 29.6, 29.7, 30.0, 32.0, 33.9, 35.0, 38.4, 39.8, 47.2, 52.3, 53.8, 54.9, 60.4, 65.7, 67.1, 79.3, 107.8, 120.0, 125.1, 126.7, 127.1, 127.8, 129.1, 135.1, 136.9, 141.3, 143.8, 156.3, 171.8, 172.1, 176.5, 196.5 and 200.2; m/z 851 ($\text{M}^+ + 1$).

5.2.16. $N\alpha$ -Boc- $N\epsilon$ -Fmoc-L-lysine-OPFP 22. A solution of 9-fluorenylmethyl chloroformate (0.62 g, 2.40 mmol) in dioxane (30 ml) was added to a stirred solution of $N\alpha$ -Boc-L-lysine **21** (0.50 g, 2.05 mmol) in saturated aqueous sodium hydrogen carbonate (30 ml). After stirring for 24 h the mixture was concentrated in vacuo and acidified using dilute hydrochloric acid and extracted using dichloromethane (3×50 ml). The combined organic extracts were dried over magnesium sulphate and concentrated in vacuo to give an oil which was then reacted with EDCI (0.55 g, 2.86 mmol) and pentafluorophenol (0.41 g, 2.22 mmol) in DCM (100 ml). After 24 h, the solvent was washed with dilute hydrochloric acid (50 ml) and the aqueous layer was further extracted with DCM (2×50 ml). The combined organic extracts were dried over magnesium sulphate and concentrated in vacuo to give a solid, which was purified by column chromatography. Elution with 20% ethyl acetate in hexane gave $N\alpha$ -Boc- $N\epsilon$ -Fmoc-L-lysine-OPFP **22** (0.76 g, 59%) as a white solid; mp 146–148°C (from DCM/hexane); (Found C, 60.80; H, 5.19; N, 4.62. $\text{C}_{32}\text{H}_{31}\text{N}_2\text{O}_6\text{F}_5$ requires C, 60.57; H, 4.89; N, 4.42%); ν_{max} (cm^{-1}) 3413, 3336, 1787, 1686, 1518, 998 and 758; δ_{H} (399.6 MHz) 1.25–1.65 (4H, m, CH_2CH_2), 1.44 (9H, s, $(\text{CH}_3)_3\text{CO}$), 1.83–2.00 (2H, m, CH_2), 3.22 (2H, m, CH_2NH), 4.20 (1H, t, $J=6.8$ Hz, CHCH_2O), 4.37–4.83 (4H, m, CHCH_2O , CHCO_2 and NH), 5.58 (1H, d, $J=7.8$ Hz, NH), 7.30 (2H, t, $J=7.3$ Hz, ArH), 7.39 (2H, t, $J=7.3$ Hz, ArH), 7.58 (2H, d, $J=7.3$ Hz, ArH) and 7.76 (2H, d, $J=7.3$ Hz, ArH); δ_{C} (100.4 MHz) 22.3, 28.3, 29.6, 31.8, 40.4, 47.4, 53.4, 66.7, 77.4, 120.0, 125.1, 127.1, 127.7, 136.7 (m, CF), 138.4 (m, CF), 139.2 (m, CF), 139.9 (m, CF), 141.0 (m, CF), 141.4, 142.3 (m, CF), 144.0, 155.3, 156.7 and 169.2; m/z 635 ($\text{M}^+ + 1$).

5.2.17. $N\alpha$ -Boc- $N\epsilon$ -Fmoc-L-lysine- β -alanine-ODmab 23.

A solution of pentafluorophenyl ester **22** (184 mg, 0.293 mmol) and amine **3** (139 mg, 0.35 mmol) in DMF (2 ml) was stirred for 24 h. The DMF was removed in vacuo, the residue was dissolved in DCM (50 ml) and washed with dilute hydrochloric acid (20 ml). The aqueous layer was further extracted with DCM (2×50 ml) and the combined organic extracts were dried over magnesium sulphate and concentrated in vacuo to give a yellow oil which was purified by column chromatography. Elution with ethyl acetate gave $N\alpha$ -Boc- $N\epsilon$ -Fmoc-L-lysine- β -alanine-ODmab **23** (125 mg, 50%) as a pale yellow oil; ν_{max} (cm^{-1}) 3393, 2951, 1710, 1648, 1547, 1243, 1162 and 757; δ_{H} (399.6 MHz) 0.77 (6H, d, $J=6.7$ Hz, $\text{CH}(\text{CH}_3)_2$), 1.07 (6H, s, $\text{C}(\text{CH}_3)_2$), 1.34–1.63 (6H, m, $\text{CH}_2\text{CH}_2\text{CH}_2$), 1.42 (9H, s, $(\text{CH}_3)_3\text{CO}$), 1.83 (1H, m, $\text{CH}(\text{CH}_3)_2$), 2.40 (2H, s, $\text{CH}_2\text{C}(\text{CH}_3)_2$), 2.49 (2H, s,

$\text{CH}_2\text{C}(\text{CH}_3)_2$), 2.61 (2H, t, $J=5.6$ Hz, CH_2CO_2), 3.00 (2H, br d, $J=5.3$ Hz, $\text{CH}_2\text{CH}(\text{CH}_3)_2$), 3.18 (2H, m, CH_2NH), 3.55 (2H, m, CH_2NH), 4.02 (1H, m, NH), 4.20 (1H, m, CHCH_2O), 4.39 (2H, m, CHCH_2O), 5.09 (1H, m, NH), 5.18 (1H, m, NH), 5.30 (2H, s, CO_2CH_2), 6.75 (1H, m, NH), 7.12 (2H, d, $J=8.1$ Hz, ArH), 7.30 (2H, dt, $J=7.3$ and 0.9 Hz, ArH), 7.39 (4H, t, $J=8.4$ Hz, ArH), 7.59 (2H, d, $J=7.3$ Hz, ArH), 7.76 (2H, d, $J=8.1$ Hz, ArH) and 15.29 (1H, s, ArNH); δ_{C} (100.4 MHz) 22.6, 28.2, 24.3, 29.4, 29.5, 30.0, 31.9, 33.9, 34.9, 38.3, 40.3, 47.2, 52.3, 53.4, 53.7, 60.4, 65.6, 66.6, 80.1, 107.8, 119.9, 125.0, 126.7, 127.0, 127.7, 129.1, 135.2, 136.9, 141.3, 143.9, 156.6, 172.0, 172.2, 176.4, 196.4 and 200.2; m/z 851 ($\text{M}^+ + 1$).

5.2.18. Boc-glycine-ODmab 25. A solution of EDCI (0.95 g, 4.96 mmol) and DMAP (62 mg, 0.51 mmol) in DCM (50 ml) was added to a stirred solution of Boc-glycine **24** (0.82 g, 4.68 mmol) and DmabOH (1.55 g, 4.70 mmol) in DCM (100 ml) at room temperature under nitrogen. After 24 h, the solvent was washed with dilute hydrochloric acid (50 ml) and the aqueous layer was further extracted with DCM (2×50 ml). The combined organic extracts were dried over magnesium sulphate and concentrated in vacuo to give a solid which was purified by column chromatography. Elution with 20% ethyl acetate in hexane gave Boc-glycine-ODmab **25** (2.30 g, 100%) as a white solid; mp 50–52°C (from DCM/hexane); (Found C, 66.52; H, 7.97; N, 5.49. $\text{C}_{27}\text{H}_{38}\text{N}_2\text{O}_6$ requires C, 66.67; H, 7.82; N, 5.76%); ν_{max} (cm^{-1}) 3441, 3364, 2951, 1749, 1710, 1633, 1551 and 754; δ_{H} (399.6 MHz) 0.78 (6H, d, $J=6.6$ Hz, $\text{CH}(\text{CH}_3)_2$), 1.08 (6H, s, $\text{C}(\text{CH}_3)_2$), 1.45 (9H, s, $\text{C}(\text{CH}_3)_3$), 1.84 (1H, m, $\text{CH}(\text{CH}_3)_2$), 2.40 (2H, s, $\text{CH}_2\text{C}(\text{CH}_3)_2$), 2.49 (2H, s, $\text{CH}_2\text{C}(\text{CH}_3)_2$), 3.00 (2H, br d, $J=6.1$ Hz, $\text{CH}_2\text{CH}(\text{CH}_3)_2$), 3.99 (2H, d, $J=5.6$ Hz, NHCH_2), 5.07 (1H, m, NHCH_2), 5.21 (2H, s, CO_2CH_2), 7.14 (2H, d, $J=8.3$ Hz, ArH), 7.41 (2H, d, $J=8.3$ Hz, ArH) and 15.30 (1H, s, ArNH); δ_{C} (100.4 MHz) 22.5, 28.2, 29.5, 30.0, 38.3, 42.4, 52.2, 53.7, 66.1, 80.1, 107.8, 126.7, 129.1, 134.9, 137.0, 155.7, 170.2, 176.4, 196.3 and 200.2; m/z 487 ($\text{M}^+ + 1$).

5.2.19. Glycine-ODmab 26. Trifluoroacetic acid (20 ml) was added to a solution of Boc-glycine-ODmab **25** (0.43 g, 0.89 mmol) in DCM (10 ml). After stirring for 30 min, the reaction mixture was concentrated in vacuo to remove the excess trifluoroacetic acid. The residue was dissolved in DCM (50 ml) and washed with saturated sodium hydrogen carbonate solution (50 ml). The aqueous solution was further extracted with DCM (2×50 ml) and the combined organic extracts were dried over magnesium sulphate and concentrated in vacuo to give a solid which was recrystallised using DCM and hexane to give glycine-ODmab **26** (0.35 g, 78%) as a pale yellow solid; mp 132–136°C; (Found C, 57.51; H, 6.49; N, 5.53. $\text{C}_{24}\text{H}_{31}\text{N}_2\text{O}_6\text{F}_3$ requires C, 57.60; H, 6.20; N, 5.60%); ν_{max} (cm^{-1}) 3430, 2958, 1755, 1669, 1558 and 754; δ_{H} (DMSO, 399.6 MHz) 0.68 (6H, d, $J=6.8$ Hz, $\text{CH}(\text{CH}_3)_2$), 0.99 (6H, s, $\text{C}(\text{CH}_3)_2$), 1.70 (1H, m, $\text{CH}(\text{CH}_3)_2$), 2.38 (4H, s, $2\times\text{CH}_2\text{C}(\text{CH}_3)_2$), 2.96 (2H, br d, $J=6.1$ Hz, $\text{CH}_2\text{CH}(\text{CH}_3)_2$), 3.92 (4H, br s, NH_2CH_2), 5.28 (2H, s, CO_2CH_2), 7.33 (2H, d, $J=8.6$ Hz, ArH), 7.51 (2H, d, $J=8.6$ Hz, ArH) and 15.28 (1H, s, ArNH); δ_{C} (100.4 MHz) 22.3, 27.8, 28.8, 29.7, 37.3, 66.1, 107.1, 126.4, 129.1, 134.7, 136.5, 167.6, 175.0, 196.3 and 200.2; m/z 387 ($\text{M}^+ + 1$).

5.2.20. Fmoc- β -alanine-glycine-ODmab 27. A solution of pentafluorophenyl ester **8** (144 mg, 0.30 mmol) and amine **3** (50 mg, 0.10 mmol) in DMF (1 ml) was stirred for 48 h. The DMF was removed in vacuo, the residue was dissolved in DCM (50 ml) and washed with dilute hydrochloric acid (20 ml). The aqueous layer was further extracted with DCM (2 \times 30 ml) and the combined organic extracts were dried over magnesium sulphate and concentrated in vacuo to give a yellow oil which was purified by column chromatography. Elution with ethyl acetate gave *Fmoc- β -alanine-glycine-ODmab 27* (24 mg, 35%) as a colourless oil; δ_{H} (399.6 MHz) 0.69 (6H, d, $J=6.5$ Hz, $\text{CH}(\text{CH}_3)_2$), 1.00 (6H, s, $\text{C}(\text{CH}_3)_2$), 1.76 (1H, m, $\text{CH}(\text{CH}_3)_2$), 2.32 (2H, m, CH_2CO), 2.41 (2H, s, $\text{CH}_2\text{C}(\text{CH}_3)_2$), 2.50 (2H, s, $\text{CH}_2\text{C}(\text{CH}_3)_2$), 2.45 (2H, m, CH_2CO), 2.89 (2H, d, $J=5.8$ Hz, $\text{CH}_2\text{CH}(\text{CH}_3)_2$), 3.42 (2H, m, NHCH_2), 4.12 (1H, t, $J=6.8$ Hz, CHCH_2O), 4.27 (2H, d, $J=6.8$ Hz, CHCH_2O), 5.30 (2H, s, CO_2CH_2), 5.47 (1H, m, NH), 5.70 (1H, br t, NH), 7.04 (2H, d, $J=8.4$ Hz, ArH), 7.32 (2H, t, $J=7.3$ Hz, ArH), 7.31 (2H, t, $J=7.3$ Hz, ArH), 7.51 (2H, d, $J=7.3$ Hz, ArH), 7.67 (2H, d, $J=7.6$ Hz, ArH), 7.93 (2H, s, ArH) and 15.21 (1H, s, ArNH); δ_{C} (100.4 MHz) 22.6, 28.3, 29.6, 30.1, 32.0, 34.3, 35.4, 38.4, 47.3, 52.3, 53.8, 66.3, 66.7, 107.8, 120.0, 125.2, 126.8, 127.1, 127.7, 129.3, 134.8, 137.1, 141.3, 144.0, 156.6, 171.6, 172.1, 176.5, 196.6 and 200.3; m/z 680 ($\text{M}^+ + 1$).

5.2.21. Fmoc- β -alanine-ODmab 28. A solution of EDCI (0.41 g, 2.15 mmol) in DCM (20 ml) was added to a stirred solution of *Fmoc- β -alanine 4* (0.55 g, 1.78 mmol) and *DmabOH* (0.59 g, 1.80 mmol) in DCM (100 ml) at room temperature under nitrogen. After 24 h, the solvent was washed with dilute hydrochloric acid (50 ml) and the aqueous layer was further extracted with DCM (2 \times 50 ml). The combined organic extracts were dried over magnesium sulphate and concentrated in vacuo to give a solid which was purified by column chromatography. Elution with 20% ethyl acetate in hexane gave *Fmoc- β -alanine-ODmab 28* (1.05 g, 95%) as a white solid; mp 44–46°C (from DCM/hexane); (Found C, 73.61; H, 7.04; N, 4.33. $\text{C}_{38}\text{H}_{42}\text{N}_2\text{O}_6$ requires C, 73.31; H, 6.75; N, 4.50%); ν_{max} (cm^{-1}) 3451, 3365, 2951, 1720, 1638, 1450 and 756; δ_{H} (399.6 MHz) 0.77 (6H, d, $J=6.1$ Hz, $\text{CH}(\text{CH}_3)_2$), 1.08 (6H, s, $\text{C}(\text{CH}_3)_2$), 1.84 (1H, m, $\text{CH}(\text{CH}_3)_2$), 2.40 (2H, s, $\text{CH}_2\text{C}(\text{CH}_3)_2$), 2.49 (2H, s, $\text{CH}_2\text{C}(\text{CH}_3)_2$), 2.64 (2H, t, $J=6.1$ Hz, CH_2CO_2), 3.00 (2H, br d, $J=5.9$ Hz, $\text{CH}_2\text{CH}(\text{CH}_3)_2$), 3.51 (2H, dt, $J=6.1$ and 5.6 Hz, NHCH_2), 4.20 (1H, t, $J=7.1$ Hz, CHCH_2O), 4.40 (2H, d, $J=7.1$ Hz, CHCH_2O), 5.17 (2H, s, CO_2CH_2), 5.29 (1H, m, NH), 7.12 (2H, d, $J=8.1$ Hz, ArH), 7.30 (2H, dt, $J=7.6$ and 1.0 Hz, ArH), 7.39 (2H, t, $J=7.1$ Hz, ArH), 7.40 (2H, d, $J=8.1$ Hz, ArH), 7.59 (2H, d, $J=7.6$ Hz, ArH), 7.76 (2H, d, $J=7.6$ Hz, ArH) and 15.30 (1H, s, ArNH); δ_{C} (100.4 MHz) 22.6, 28.3, 29.6, 30.2, 34.4, 36.5, 38.3, 47.2, 52.3, 53.8, 65.7, 66.7, 107.8, 120.0, 125.0, 126.7, 127.0, 127.7, 129.0, 135.2, 137.0, 141.3, 143.9, 156.3, 172.1, 176.4, 196.4 and 200.2; m/z 623 ($\text{M}^+ + 1$).

5.2.22. Boc- β -alanine-piperidine 29. Piperidine (20 μl , 0.20 mmol) was added to a stirred solution of *Boc- β -alanine-OPFP 8* (33 mg, 0.09 mmol) in DMF (0.5 ml) under nitrogen. After 10 min the reaction was concentrated in vacuo and the residue was diluted with DCM (50 ml) and washed with dilute sodium hydroxide (20 ml) and dilute

hydrochloric acid (20 ml). The DCM was dried over magnesium sulphate and concentrated in vacuo to give *Boc- β -alanine-piperidine 29* (20 mg, 83%) as a yellow oil; δ_{H} (399.6 MHz) 1.42 (9H, s, $(\text{CH}_3)_3\text{CO}$), 1.51–1.67 (6H, m, $\text{CH}_2(\text{CH}_2)_3$), 2.49 (2H, t, $J=5.6$ Hz, CH_2CO), 3.36 (2H, t, $J=5.6$ Hz, CH_2N), 3.42 (2H, dt, $J=5.8$ and 5.6 Hz, NHCH_2), 3.55 (2H, t, $J=5.6$ Hz, CH_2N) and 5.35 (1H, m, NH); δ_{C} (100.4 MHz) 24.5, 25.6, 26.4, 28.4, 33.3, 36.4, 42.6, 46.4, 79.0, 156.1 and 169.8; m/z 257 ($\text{M}^+ + 1$).

5.2.23. Fmoc- β -alanine- β -alanine- β -alanine-ODmab 31. A solution of 9-fluorenylmethyl chloroformate (0.39 g, 1.92 mmol) in dioxane (10 ml) was added to a stirred solution of β -ALA- β -ALA (175 mg, 1.09 mmol) in saturated aqueous sodium hydrogen carbonate (10 ml). After stirring for 24 h the mixture was concentrated in vacuo and acidified using dilute hydrochloric acid and extracted using dichloromethane (3 \times 50 ml). The combined organic extracts were dried over magnesium sulphate and concentrated in vacuo to give an oil which was then reacted with EDCI (0.41 g, 2.13 mmol) and pentafluorophenol (0.42 g, 2.29 mmol) in DCM (50 ml). After 24 h, the solvent was washed with dilute hydrochloric acid (50 ml) and the aqueous layer was further extracted with DCM (2 \times 50 ml). The combined organic extracts were dried over magnesium sulphate and concentrated in vacuo to give a solid, which was used without further purification. The pentafluorophenyl ester was then added to amine **3** (48 mg, 0.12 mmol) in DMF (1 ml) and the reaction was stirred for 48 h. The DMF was removed in vacuo, the residue was dissolved in DCM (50 ml) and washed with dilute hydrochloric acid (20 ml). The aqueous layer was further extracted with DCM (2 \times 30 ml) and the combined organic extracts were dried over magnesium sulphate and concentrated in vacuo to give a yellow oil which was purified by column chromatography. Elution with 5% methanol in ethyl acetate gave *Fmoc- β -alanine- β -alanine- β -alanine-ODmab 31* (21 mg, 3% over three step synthesis) as a pale yellow gum; δ_{H} (399.6 MHz) 0.76 (6H, d, $J=6.7$ Hz, $\text{CH}(\text{CH}_3)_2$), 1.07 (6H, s, $\text{C}(\text{CH}_3)_2$), 1.83 (1H, m, $\text{CH}(\text{CH}_3)_2$), 2.39 (2H, t, $J=5.9$ Hz, CH_2CO), 2.39 (2H, s, $\text{CH}_2\text{C}(\text{CH}_3)_2$), 2.49 (4H, br s, $\text{CH}_2\text{C}(\text{CH}_3)_2$ and CH_2CO), 2.56 (2H, t, $J=5.9$ Hz, CH_2CO), 2.99 (2H, d, $J=4.5$ Hz, $\text{CH}_2\text{CH}(\text{CH}_3)_2$), 3.43–3.52 (6H, m, $3\times\text{NHCH}_2$), 4.19 (1H, t, $J=7.0$ Hz, CHCH_2O), 4.35 (2H, d, $J=7.0$ Hz, CHCH_2O), 5.11 (2H, s, CO_2CH_2), 5.72 (1H, br t, $J=5.6$ Hz, NH), 6.50 (1H, m, NH), 6.70 (1H, br t, NH), 7.11 (2H, d, $J=8.2$ Hz, ArH), 7.29–7.40 (6H, m, ArH), 7.58 (2H, d, $J=7.6$ Hz, ArH), 7.75 (2H, d, $J=7.6$ Hz, ArH) and 15.27 (1H, s, ArNH); δ_{C} (100.4 MHz) 22.6, 28.2, 29.6, 30.0, 34.0, 35.0, 35.5, 36.1, 37.2, 38.4, 47.2, 52.3, 53.7, 60.4, 65.8, 66.8, 107.8, 120.0, 125.1, 126.7, 127.1, 127.7, 129.1, 135.1, 137.0, 141.3, 143.9, 156.7, 171.8, 172.4, 176.5, 196.5 and 200.3; m/z 765 ($\text{M}^+ + 1$).

Acknowledgements

We wish to thank Novartis Pharmaceuticals (P. W. and C. W.) for financial support. We are grateful to Dr Tom McCreedy (University of Hull) for help in fabricating the micro reactor devices.

References

1. Haswell, S. J. *Analyst* **1997**, *112*, 1R.
2. Manz, A.; Harrison, D. J.; Verpoorte, E.; Fettingner, J. C.; Ludi, H.; Widmer, H. M. *Chimia* **1991**, *45*, 103.
3. Manz, A.; Harrison, D. J.; Verpoorte, E.; Widmer, H. M. *Adv. Chromatogr.* **1993**, *33*, 1.
4. Manz, A.; Effenhauser, C. S.; Burggraf, N.; Verpoorte, E.; Raymond, D. E.; Widmer, H. M. *Anal. Mag.* **1994**, *22*, M25.
5. *Proceedings of the Micro Total Analytical Systems 98' Workshop*; Harrison, D. J., van den Berg, A., Eds.; Kluwer Academic: Dordrecht, 1998.
6. van den Berg, A.; Lammerink, T. S. J. *Top. Curr. Chem.* **1998**, *194*, 21.
7. Harrison, D. J.; Fluri, K.; Seiler, K.; Fan, Z. H.; Effenhauser, C. S.; Manz, A. *Science* **1993**, *261*, 895.
8. Jacobson, S. C.; Hergenroder, R.; Koutny, L. B.; Ramsey, J. M. *Anal. Chem.* **1994**, *66*, 1114.
9. Spence, D. M.; Crouch, S. R. *Anal. Chem.* **1998**, *358*, 95.
10. Schoot, B. H.; Jeanneret, S.; Berg, A. *Anal. Meth. Instrum.* **1993**, *1*, 38.
11. Das Gupta, P. K.; Lui, S. *Anal. Chem.* **1994**, *66*, 1792.
12. Fletcher, P. D. I.; Haswell, S. J.; Paunov, V. N. *Analyst* **1999**, *124*, 1273–1282.
13. Greenway, G. M.; Haswell, S. J.; Morgan, D. O.; Skelton, V.; Styring, P. *Sens. Actuators, B* **2000**, *63*, 153.
14. Skelton, V.; Greenway, G. M.; Haswell, S. J.; Styring, P.; Morgan, D. O.; Warrington, B.; Wong, S. Y. F. *Analyst* **2001**, *126*, 7.
15. Skelton, V.; Greenway, G. M.; Haswell, S. J.; Styring, P.; Morgan, D. O.; Warrington, B.; Wong, S. Y. F. *Analyst* **2001**, *126*, 11.
16. Salimi-Moosavi, H.; Tang, T.; Harrison, D. J. *J. Am. Chem. Soc.* **1997**, *119*, 8716.
17. Sands, M.; Haswell, S. J.; Kelly, S. M.; Skelton, V.; Morgan, D. O.; Styring, P.; Warrington, B. H. *Lab on a Chip* **2001**, *1*, 64.
18. Watts, P.; Wiles, C.; Haswell, S. J.; Pombo-Villar, E.; Styring, P. *Chem. Commun.* **2001**, 990.
19. Haswell, S. J.; Middleton, R. J.; O'Sullivan, B.; Skelton, V.; Watts, P.; Styring, P. *Chem. Commun.* **2001**, 391.
20. Fletcher, P. D. I.; Haswell, S. J. *Chem. Br.* **1999**, *35*, 38.
21. Jacobson, S. C.; Hergenroder, R.; Koutny, L. B.; Ramsey, J. M. *Anal. Chem.* **1994**, *66*, 1114.
22. Merrifield, R. B. *J. Am. Chem. Soc.* **1963**, *85*, 2149.
23. Munster, P.; Steglich, W. *Synthesis* **1987**, 223.
24. Penke, B.; Rivier, J. *J. Org. Chem.* **1987**, *52*, 1197.
25. Whitney, D. B.; Tam, J. P.; Merrifield, R. B. *Tetrahedron* **1984**, *40*, 4237.
26. Chan, W. C.; White, P. D. *Fmoc Solid Phase Peptide Synthesis*; Oxford University Press: New York, 2000.
27. McCreedy, T. *TrAC* **2000**, *19*, 396.
28. *Micro Total Analysis Systems 2001*; Ramsey, J. M., van den Berg, A., Eds.; Kluwer Academic: Dordrecht, 2001.
29. McCreedy, T. *Anal. Chim. Acta* **2001**, *427*, 39.
30. Christensen, P. D.; Johnson, S. W. P.; McCreedy, T.; Skelton, V.; Wilson, N. G. *Anal. Commun.* **1998**, *35*, 341.
31. Daura, X.; Gademann, K.; Schaefer, H.; Jaun, B.; Seebach, D.; van Gunsteren, W. F. *J. Am. Chem. Soc.* **2001**, *123*, 2393.
32. Seebach, D.; Schreiber, J. V.; Abele, S.; Daura, X.; van Gunsteren, W. F. *Helv. Chim. Acta* **2000**, *83*, 34.
33. Dado, G. P.; Gellman, S. H. *J. Am. Chem. Soc.* **1994**, *116*, 1054.
34. Gademann, K.; Ernst, M.; Seebach, D.; Hoyer, D. *Helv. Chim. Acta* **2000**, *83*, 16.
35. Werder, M.; Hauser, H.; Abele, S.; Seebach, D. *Helv. Chim. Acta* **1999**, *82*, 1774.
36. Arvidsson, P. I.; Rueping, M.; Seebach, D. *Chem. Commun.* **2001**, 649.
37. Schreiber, J. V.; Seebach, D. *Helv. Chim. Acta* **2000**, *83*, 3139.
38. Chan, W. C.; Bycroft, B. W.; Evans, D. J.; White, P. D. *Chem. Commun.* **1995**, 2209.
39. Kisfaludy, L.; Schon, I. *Synthesis* **1983**, 325.
40. Atherton, E.; Cameron, L. R.; Sheppard, R. C. *Tetrahedron* **1988**, *44*, 843.
41. Johnson, T.; Quibell, M.; Owen, D.; Sheppard, R. C. *Chem. Commun.* **1993**, 369.
42. Carpino, L. A.; Han, G. Y. *J. Org. Chem.* **1972**, *37*, 3404.
43. Carpino, L. A.; Cohen, B. J.; Stephens, K. E.; Sadat-Aalae, S. J.; Tien, J.-H.; Langridge, D. E. *J. Org. Chem.* **1986**, *51*, 3732.
44. Wade, J. D.; Bedford, J.; Sheppard, C.; Tregear, G. W. *Pept. Res.* **1991**, *4*, 194.
45. Kates, S. A.; Nuria, A.; Sole, M.; Beyermann, M.; Barany, G.; Albericio, F. *Pept. Res.* **1996**, *9*, 106.

Tetrahedron report number 609

Micro reactors: principles and applications in organic synthesis

Paul D. I. Fletcher,^a Stephen J. Haswell,^{a,*} Esteban Pombo-Villar,^b Brian H. Warrington,^c
Paul Watts,^a Stephanie Y. F. Wong^c and Xunli Zhang^a

^aDepartment of Chemistry, Faculty of Science and the Environment, University of Hull, Cottingham Road, Hull HU6 7RX, UK

^bNervous System Research, WSJ-386.07.15, Novartis Pharma Ltd, CH4002 Basel, Switzerland

^cGlaxoSmithKline Pharmaceuticals, New Frontiers Science Park (North), Third Avenue, Harlow, Essex CM19 5AW, UK

Received 12 April 2002

Contents

1. Introduction	4735
2. Fabrication and physical characterisation of micro reactors	4736
2.1. Fabrication	4736
2.2. Determination of the 3D dimensions of the channel networks	4737
3. Operation of micro reactors using electrokinetic control	4739
3.1. Electroosmotic flow (EOF) and electrophoresis	4739
3.2. Control of reagent mobility in a channel network	4740
3.3. Reagent mixing and chemical reaction in a micro reactor	4743
4. Reactions performed in micro reactors	4745
4.1. Liquid phase reactions	4745
4.2. Catalytic reactions	4749
4.3. Gas phase reactions	4750
5. Potential applications of micro reactors	4752
6. Concluding remarks	4754

1. Introduction

The miniaturisation of chemical reactors offers many fundamental and practical advantages of relevance to today's chemical industry, who are constantly searching for controllable, information rich, high throughput, environmentally friendly methods of producing products with a high degree of chemical selectivity (see, for example, Refs. 1–9 for introductory overviews). Indeed, for some industries such as pharmaceuticals, an informatics based approach, that micro reactor chemistry can uniquely deliver, may be the trigger for a step change in process. In their simplest form, micro reactor devices consist of a network of micron-sized (typical dimensions are in the range 10–300 μm) channels etched into a solid substrate. For solution-based chemistry, the channel networks are connected to a series of reservoirs containing chemical reagents, products and/or waste to form the complete device

or 'chip' (derived from the concept of 'Lab-on-a-Chip') with overall dimensions of a few cm. Reagents can then be brought together in a specific sequence, mixed and allowed to react for a specified time in a controlled region of the reactor channel network using (most commonly) electrokinetic (electroosmotic and electrophoretic) and/or hydrodynamic pumping.

For electrokinetically-driven systems, electrodes are placed in the appropriate reservoirs to which specific voltage sequences can be delivered under automated computer control. This control offers a simple but effective method of moving and separating reactants and products within a micro reactor, without the need for moving parts. Hydrodynamic pumping exploits conventional or micro-scale pumps, notably syringe-type pumps, to manoeuvre solutions around the channel network but has the disadvantage of requiring either large external pumps or complex fabrication of small moving parts. Detection of chemical species can be either 'on-chip', using, for example, microscopic imaging of absorbance or fluorescence signals or 'off-chip' by either reservoir sampling or suitable connection to a conventional benchtop instrument such as an HPLC or mass spectrometer.

Keywords: micro reactors; organic synthesis; fabrication; electrokinetic; reaction modelling.

* Corresponding author. Tel.: +44-1482-465469; fax: +44-1482-466416; e-mail: s.j.haswell@hull.ac.uk

To date, the greatest research effort in the field of micro scale devices has been in the analytical arena. One of the main aims of this research is to develop a miniaturised total analytical system (μ -TAS).^{10–17} Optimally, such devices would automatically perform sampling, sample preparation, separation, detection and data processing in a fully-integrated manner. In addition to the advantages of high, automated throughput and low reagent consumption with increased safety of operation resulting from low reagent quantities, these devices offer potential as remote controlled systems, which could be placed in inaccessible locations for continuous monitoring of chemical or environmental processes. To date, the most popular area of μ -TAS research has been in the biomedical field, including the analysis of DNA and proteomics,^{18–25} and has resulted in the release of the first commercial analytical micro reactor device from Agilent, formerly Hewlett-Packard.

Alongside the continuing development of μ -TAS and related analytical applications, a concerted effort has now begun to establish the benefits that micro reactors can bring to the field of reaction chemistry. The ability to manipulate reagent concentrations in both space and time by electrokinetic voltage control within the channel network of a micro reactor, provides an additional level of reaction control which is not attainable in bulk stirred reactors where concentrations are generally uniform. The spatial and temporal control of chemical reactions in micro reactors, coupled with the features of very small reaction volumes (μm dimensions) and high surface interactions, is somewhat akin to the situation of reactions within biological cells. Nature exploits the organised distribution of reagents within the micron-sized sub-domains of cells to control and alter chemical reactivity relative to the situation of homogeneous solutions. Consistent with this notion, many reactions (as reviewed in Section 4) have been demonstrated to show altered reactivity, product yield and selectivity when performed in micro reactors as compared with conventional bench top glassware.

This review, covering key aspects of the fabrication and operation of micro reactors together with recent progress and potential applications in their use for chemical synthetic processes, is structured as follows. After this brief introduction, the fabrication of micro reactors is discussed in Section 2. Section 3 deals with the principles of electrokinetic operation of micro reactors and how the spatial and temporal evolution of reactions in micro reactors can be controlled. The range of liquid and gas phase reactions, including catalytic reactions, which have been performed in micro reactors is reviewed in Section 4. Potential applications and future directions are suggested in Section 5. Finally, conclusions and references are summarised.

2. Fabrication and physical characterisation of micro reactors

2.1. Fabrication

A number of materials such as silicon, quartz, glass, metals and polymers have been used to construct micro reactors.¹¹ Important considerations in material choice include chemi-

cal compatibility, ease and reproducibility of fabrication, whether or not the material supports electroosmotic flow (EOF) with the solvents of interest, and compatibility with detection methods. Glass is a popular choice since it allows EOF with many common solvents, is chemically inert, enables the use of visible light detection and fabrication methods are well established.

Depending on the material used, a range of channel micro-fabrication methods such as photolithography, hot embossing, powder blasting, injection moulding and laser micro forming are available.²⁶ For glass micro reactors, photolithographic fabrication of channel networks is performed as shown schematically in Fig. 1 and described in Refs. 27, 28. Firstly, the channel network is designed and printed on a large scale using suitable computer drawing software. A film negative of the desired final size is then prepared by photoreduction to form the optical mask. Commercially-supplied borosilicate glass photolithographic plates (thickness 3 mm) coated with a thin metal etch mask layer (normally chromium) plus an upper layer of positive photoresist (0.5–2.0 μm depth) are used for channel network fabrication. The pattern of the required network of interconnecting channels is transferred from the optical mask to the photoresist layer. After light exposure, the photoresist is developed and removed, together with the chromium layer, to reveal the areas of glass to be etched. Recent instrumental advances of this process will, however, shortly

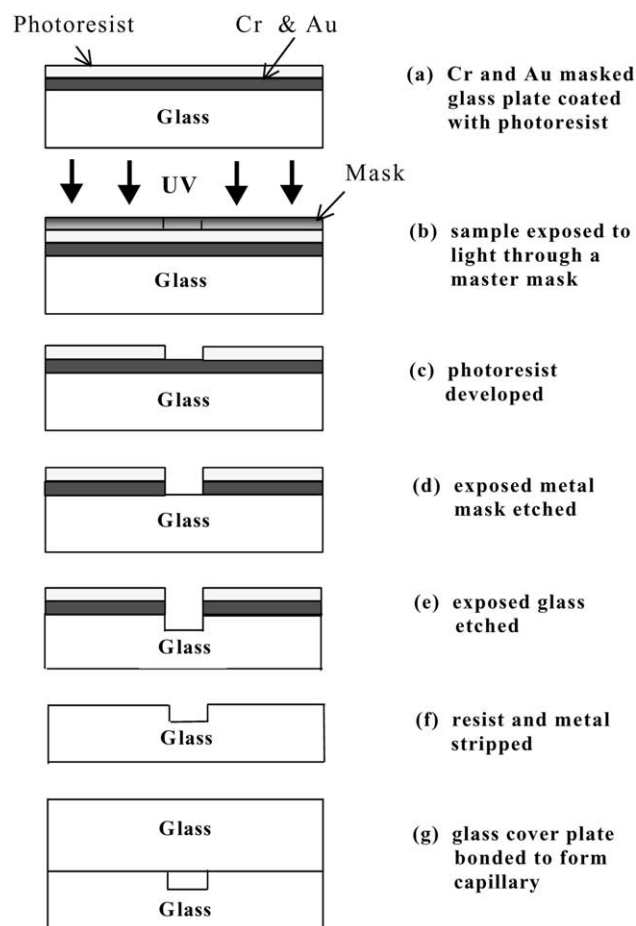


Figure 1. Photolithographic fabrication of channel networks in glass.

enable the direct production of negatives from computer drawings.²⁹ The patterned plate is then heated to allow the volatiles to evaporate, before performing the chemical etch. The channels are etched using a mixture of 1% HF and 5% NH₄F in water at 65°C, resulting in an etch rate of 0.3–0.5 μm min⁻¹. During etch it is important that the system is well agitated to ensure consistent supply of etchant to the surface plus removal of etch debris. In our laboratories, we have found that ultrasound irradiation during etch is effective.

In the procedure described above, glass is etched *isotropically*, i.e. the glass is etched away at equal rates in all directions from all points of exposed glass surface under the metal mask. The channel cross-sectional shape that results is shown in Fig. 2. For an initial optical mask channel width m and an etch depth d , the channel cross-section consists of a rectangle of dimensions $(d \times m)$ flanked by two quarter circles of radius d which undercut the mask. As shown in the micrograph of an exposed channel end, this theoretical channel shape is normally obtained in practice, although thermal bonding (discussed later) may result in some slight distortion. Note that, for isotropic etching, it is impossible to prepare channels the depth of which exceeds their width. Anisotropic materials, however, such as silicon, etch at different rates along different crystal planes. Etching of these materials therefore commonly produces V-shaped channels the geometry of which is related to the relative orientations of the etch mask and crystal planes, together with the differential etch rates.²⁶

The base plate containing the etched channel network must next be sealed by bonding to a 17 mm upper plate contain-

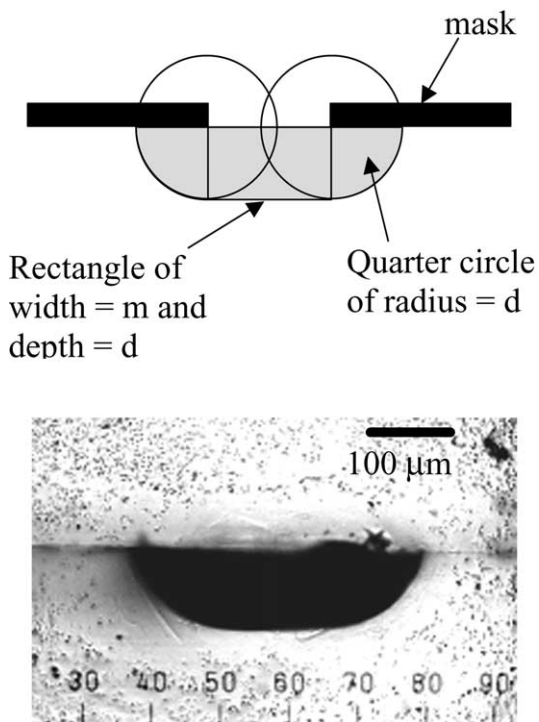


Figure 2. Diagram showing the relationship between mask width m , etch depth d and the channel profile (grey shaded area) for an isotropic etch in glass. The micrograph shows a channel end view in a bonded glass micro reactor.

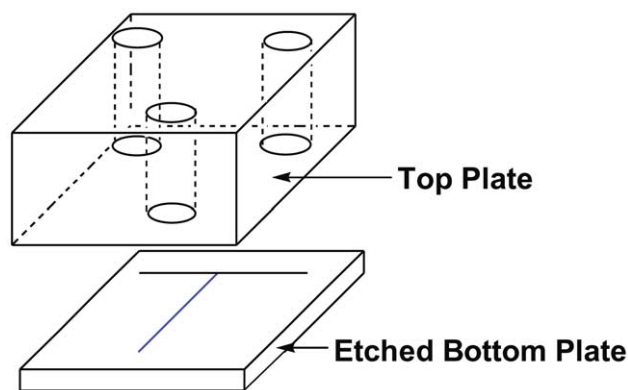


Figure 3. Exploded view of a micro reactor constructed from a base plate containing the etched channel network and thermally bonded to a thick upper plate containing reagent reservoirs.

ing pre-drilled holes to act as reservoirs for reagents. In our laboratories, the upper plate is aligned with the channel geometry and thermally bonded to the base plate (typically 575°C for 3 h).^{27,28} Thermal bonding is aided by placing a weighting block of non-adhering quartz of high softening temperature on the upper plate. A schematic of an all-glass device produced by the method described is shown in Fig. 3. For good thermal bonding, it is important to ensure that both the glass types of the upper and lower plates have the correct thermal softening and expansion properties. In addition, the surfaces to be bonded must be clean and flat.

2.2. Determination of the 3D dimensions of the channel networks

Having fabricated the micro reactor, it is essential to know the full set of dimensions in 3D of the channel network in order to establish volumetric flow rates and enable reaction characterisation. In the plane of the channel network, the lengths of the different channel sections are easily determined using optical microscopy. Channel profiles (depths and widths) can be determined using stylus profiling methods on the base plates before bonding. As mentioned earlier, however, thermal bonding can result in some degree of distortion of the channel profiles which can only be estimated by measurement of bonded devices. One approach for bonded chips is to cut the chip perpendicular to the channel axis followed by measurement of the channel profile using optical microscopy. This method is destructive and only enables the profile to be determined at a small number of pre-selected points. These disadvantages can be overcome by using a newly-developed method based on digital microscopic imaging of a dye solution-filled channel network.³⁰ As shown in Fig. 4, the chip is mounted on a transmission microscope operating with monochromatic light at a wavelength corresponding to the maximum absorbance of a dye solution within the channel network. Using a digital camera on the microscope, 256×256 arrays of pixel light intensity values are recorded for the chip filled with dye solution (I_{dye}), filled with solvent (I_{solvent}) and 'dark' images (I_{dark}). The data arrays are then converted to an array of absorbance values (Abs) using Eq. (1)

$$\text{Abs} = \log_{10} \left(\frac{I_{\text{solvent}} - I_{\text{dark}}}{I_{\text{dye}} - I_{\text{dark}}} \right) \quad (1)$$

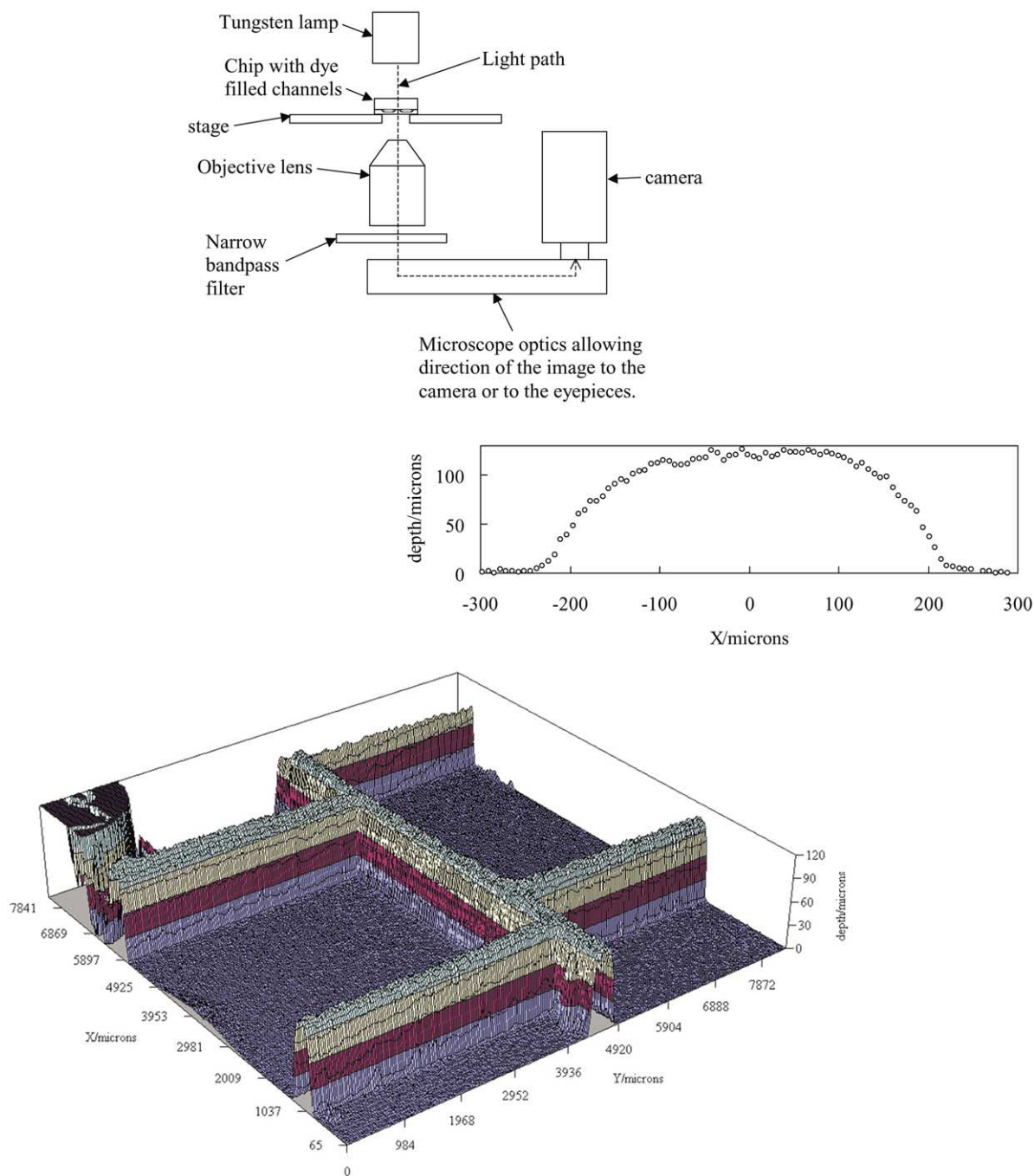


Figure 4. Digitised images taken using a transmission microscope can be used to produce full 3D profiles of a channel network. The inset plot shows a transverse slice across a channel.

Next by applying the Beer–Lambert Law $Abs = \epsilon cl$ (where ϵ is the extinction coefficient of the dye, c is the dye concentration and l is the optical path length), where the extinction coefficient (ϵ) and concentration (c) of the dye have been determined using a conventional UV/VIS spectrophotometer, the array of Abs values can be converted into an array of optical path-length values corresponding to the depth of each channel (l), and the etched depth for all X–Y positions within the chip images are obtained. Fig. 4 shows a full 3D profile measured in this way for a section of a channel network. Analysis of ‘slices’ through the full array of data enables the determination of the cross-

sectional channel profile within any part of the imaged network. Etched depths in the range from a few μm to hundreds of μm can be determined with a precision of a few percent. Having determined the path length l for the channel network, the concentration profile of a coloured (or fluorescent) reactant or product species can be similarly derived from digital camera images, an example of this approach being illustrated in Section 3.3. As will become more apparent in the later sections, the physical geometry of a micro reactor (i.e. cross-sectional profiles and channel intersections) is intrinsically linked to the chemical processes it supports. The influence of surface-to-bulk

effects, concentration (including pH) and thermal gradients, for example, are all affected by the material and geometry of the micro reactor.

3. Operation of micro reactors using electrokinetic control

3.1. Electroosmotic flow (EOF) and electrophoresis

Pumping of solutions around a channel network by EOF using voltages applied via electrodes placed in the reservoirs has several significant advantages over alternative pumping methods. It can be easily miniaturised since no mechanical moving parts are involved and the required voltage sequences can be readily applied under automated computer control. For a glass micro reactor, the channel wall-solution interface normally has a negative charge, arising from ionisation of surface groups that are immobile. This immobile surface charge attracts a diffuse layer (of thickness of the order of nm) of mobile, oppositely-charged counterions in the solution adjacent to the channel wall (cations for a negatively-charged glass channel wall). As shown schematically in Fig. 5, application of an electric field along the channel length causes the nm thick ‘skin’ of mobile cations to move towards the more negative electrode and drags all the intervening solution in the bulk of the channel with it. An important feature of EOF is that the liquid EOF velocity is constant across the channel except in the nm thick regions of the diffuse layer of counterions very close to the wall. Unlike EOF, pressure-driven flow produces a parabolic velocity profile with high velocities in the channel centre and slow velocities near to the wall, giving rise to increased ‘blurring’ of reagent zones along a channel length. Imaging of the different velocity profiles induced by EOF and pressure-driven flow has been described by Paul et al.³¹

The EOF fluid velocity v_{eof} is given by Eq. (2)^{32–34}

$$v_{\text{eof}} = \frac{E\varepsilon\varepsilon_0\zeta}{\eta} \quad (2)$$

where E is the electric field (voltage divided by electrode separation), ε is the relative dielectric constant of the liquid, ε_0 is the permittivity of free space, ζ is the zeta potential of the channel wall-solution interface and η is the liquid

viscosity. For the glass-aqueous solution interface, the value of ζ varies from -50 to -150 mV at pH 7 (dependent on ionic strength) but decreases to 0 at pH around 2.5.³⁵ The magnitude of the electric field applied in micro reactors (typically some hundreds of V cm^{-1}) gives EOF velocities in the range 0.1 – 1 mm s^{-1} for aqueous solutions at pH 7.

From Eq. (2), it can be seen that v_{eof} is proportional to the applied voltage and depends on the properties of both the liquid and the channel material. EOF is not obtained with semiconductor materials such as silicon and does not occur with low polarity solvents such as alkanes where no diffuse layer of surface counterions exists. The EOF velocity v_{eof} is independent of the channel cross-sectional dimensions whereas the EOF volumetric flow rate (given by the product of v_{eof} multiplied by the channel cross-sectional area) does depend on the channel dimensions. Additionally, it is important to note that the channel dimensions determine whether ‘pure’ EOF or a mixture of EOF and pressure-driven flow is actually obtained in practice. As indicated above, flow within a micro reactor produces liquid height differences between the reagent reservoirs which, in turn, may produce pressure-driven flow opposing the EOF and disturbing the flat velocity profile for pure EOF. As discussed in Ref. 36, pressure-driven flow arising from small (mm) reservoir height differences can be significant for relatively large channels but is suppressed for small channels where the hydrodynamic resistance is large. Overall, the channel dimensions must be designed to be sufficiently small such that pressure-driven flows are negligibly small relative to the EOF and errors arising from variable, pressure-driven flows (dependent on the reservoir liquid heights) are absent.

Under EOF voltage control, the solvent and any uncharged solutes move with a velocity v_{eof} . Within the electric field, charged solutes have an additional electrophoretic velocity v_{ph} which is given by Eq. (3)^{32,34}

$$v_{\text{ph}} = \frac{zeED}{kT} \quad (3)$$

where z is the charge number on the species, e is the electronic charge, D is the diffusion coefficient of the species, k is the Boltzmann constant and T is the absolute temperature. The magnitude of v_{ph} for typical micro reactor operating voltages is commonly comparable with v_{eof} . The total velocity of a charged species is given by the vector sum of v_{eof}

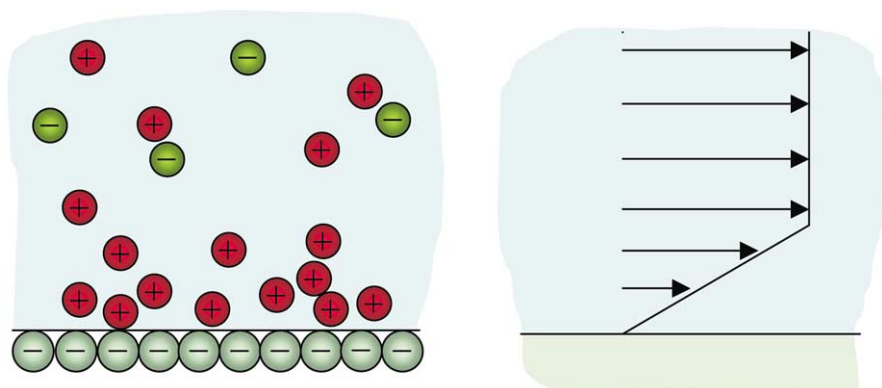


Figure 5. Voltage-driven movement of the diffuse layer of cations adsorbed at the negatively charged channel wall (left-hand figure) produces a flat EOF velocity profile across the channel except within the nm thick diffuse counterion layer (right-hand figure).

and v_{ph} . As noted above, the direction of EOF flow for aqueous solutions in a glass micro reactor is normally towards the more negative electrode. For a cationic solute species, v_{ph} will therefore be in the same direction as the EOF (i.e. towards the more negative electrode) and will move faster down the channel than the solvent and neutral species. Anionic solutes will be retarded and may, if the magnitude of v_{ph} is greater than v_{eof} , move in the opposite direction. In this way, electrophoretic separation of solutes occurs along with EOF in micro reactor channels when operated using electrokinetic control. The ability to use electrophoretic mobility to move charged reagents or species and products within a micro reactor independently of the solvent has been exploited in micro reactors and brings a rather novel concept to reaction chemistry. In the Wittig chemistry described in Section 4, for example, the charged base and phosphonium salt used to form the intermediate ylide move and mix rapidly by electrophoresis, negating the need to move and mix the solvent. In addition, in reactions where separation of the products and reactants in real time is advantageous, electrophoretic mobility is a distinct advantage. Differential electrophoretic mobilities have been exploited to selectively control product detection times in the capillary electrophoresis technique of electrophoretically-mediated microanalysis (EMMA).^{37–40}

3.2. Control of reagent mobility in a channel network

The strategy of using micro reactors to electrokinetically control the spatial and temporal evolution of chemical reactions relies on the ability to use voltage sequences to direct reagents to selected points at specified times within a channel network. For an intricate channel network with many reservoirs and electrodes, the relationships between the applied voltages and the liquid flow rates and solute mobilities in the different sections of the network can be very complex. The basic approach is to analyse the channel network in terms of an equivalent DC circuit where the different channel sections correspond to resistance elements and, as will be shown, the electrical currents are proportional to the volumetric liquid flow rates within the corresponding channel sections.^{36,41} As an illustrative example, we discuss the channel network shown in Fig. 6 where we wish to achieve a flow-inject-flow sequence to obtain a 'slug' of one reagent in a flowing stream of a second reagent. In the 'flow' mode, we require flow from reservoir A to D with zero flow from both B and C to D. In the 'inject' mode, we require flow from B to C with zero flow from A to D. To obtain both modes, a multichannel voltage supply operating under computer control using LabVIEW software is used to deliver the correct voltage sequences to the electrodes in reservoirs A, B and C (voltages V_A , V_B and V_C) relative to reservoir D, set to ground voltage. The control system used at Hull also enables computer logging of all voltages and currents during a run. The following analysis shows how the voltages are related to the electrical currents I_A , I_B and I_C which, in turn, are related to the liquid volumetric flow rates in the corresponding channel sections F_A , F_B and F_C .

We consider the simplest possible situation in which the channel network of Fig. 6 is filled with a liquid of uniform electrical conductivity κ and the zeta potential of the

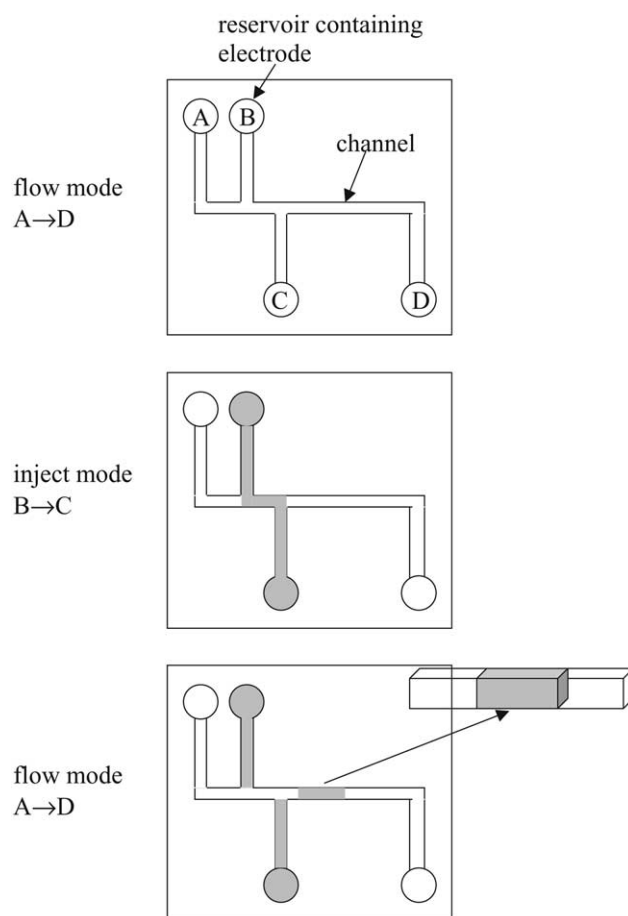


Figure 6. Double T-junction channel network and flow-inject-flow required to achieve a slug of one reagent within a flowing stream of a second reagent.

channel wall is equal in all channel sections. Experimentally, this situation can be achieved even when mixing different reactant solutions by ensuring a high background ('swamping') concentration of inert electrolyte in the different reagent solutions to be mixed. For the sake of simplicity

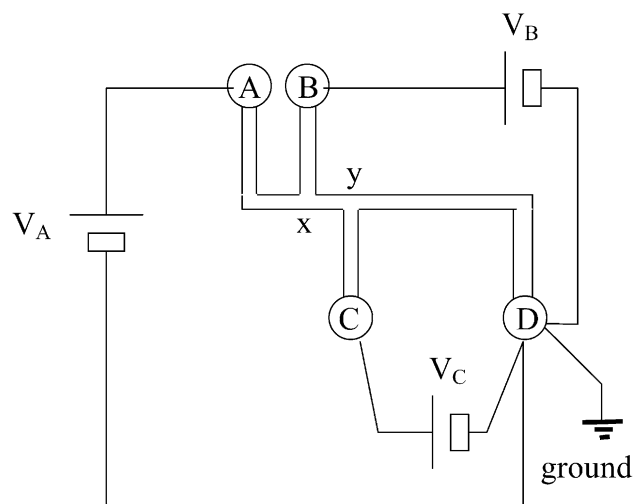


Figure 7. DC circuit used to drive the channel network of Fig. 6. Reservoir voltages (relative to ground in D) are V_A , V_B and V_C and x and y denote the channel junctions. The electrical current in channel section Ax is I_A , section Bx is I_B , section Cy is I_C , section xy is $(I_A + I_B)$ and section yD is $(I_A + I_B + I_C)$.

we ignore the (normally small) contribution to the overall conductivity of a channel section which arises from surface conduction.^{32–34,41} With these approximations, the electrical resistance of the i th channel section R_i is given by Eq. (4)

$$R_i = \frac{L_i}{\kappa A_i} \quad (4)$$

where L_i and A_i are the length and cross-sectional area of the i th channel section. The DC circuit used to drive flow in the channel network of Fig. 6 is shown in Fig. 7 and serves to define the current values in the different channel sections. In each of the limbs of the coupled circuit, the applied voltages are equal to the sum of the products of the resistances and currents and one ends up with a series of $(n-1)$ simultaneous equations where n is the number of reservoirs containing electrodes (it is $n-1$ since one electrode is set to ground). For the channel network considered here, we have the three equations incorporated in Eq. (5)

$$\begin{aligned} V_A &= R_{Ax}I_A + R_{xy}(I_A + I_B) + R_{yD}(I_A + I_B + I_C) \\ V_B &= R_{Bx}I_B + R_{xy}(I_A + I_B) + R_{yD}(I_A + I_B + I_C) \end{aligned} \quad (5)$$

$$V_C = R_{Cy}I_C + R_{yD}(I_A + I_B + I_C)$$

where R_i is the resistance of the i th channel section. Solving these simultaneous equations (achieved most easily using a software package such as MathCAD) yields the corresponding expressions for the electrical currents shown in Eq. (6)

$$\begin{aligned} I_A &= \frac{(R_{Cy}R_{xy} + R_{Cy}R_{yD} + R_{Bx}R_{yD} + R_{xy}R_{yD} + R_{Cy}R_{Bx})V_A - (R_{Cy}R_{yD} + R_{Cy}R_{xy} + R_{xy}R_{yD})V_B - R_{Bx}R_{yD}V_C}{R_{Cy}R_{Bx}R_{Ax} + R_{Cy}R_{xy}R_{Bx} + R_{Cy}R_{xy}R_{Ax} + R_{Cy}R_{yD}R_{Bx} + R_{Cy}R_{yD}R_{Ax} + R_{Bx}R_{yD}R_{Ax} + R_{xy}R_{yD}R_{Bx} + R_{xy}R_{yD}R_{Ax}} \\ I_B &= \frac{-(R_{Cy}R_{xy} + R_{Cy}R_{yD} + R_{Bx}R_{yD})V_A - (R_{Cy}R_{xy} + R_{Cy}R_{yD} + R_{Cy}R_{Ax} + R_{xy}R_{yD} + R_{yD}R_{Ax})V_B - R_{Ax}R_{yD}V_C}{R_{Cy}R_{Bx}R_{Ax} + R_{Cy}R_{xy}R_{Bx} + R_{Cy}R_{xy}R_{Ax} + R_{Cy}R_{yD}R_{Bx} + R_{Cy}R_{yD}R_{Ax} + R_{Bx}R_{yD}R_{Ax} + R_{xy}R_{yD}R_{Bx} + R_{xy}R_{yD}R_{Ax}} \\ I_C &= \frac{-(R_{Bx}R_{yD})V_A - (R_{yD}R_{Ax})V_B - (R_{Bx}R_{Ax} + R_{yD}R_{Ax} + R_{xy}R_{Ax} + R_{xy}R_{Bx} + R_{Bx}R_{yD})V_C}{R_{Cy}R_{Bx}R_{Ax} + R_{Cy}R_{xy}R_{Bx} + R_{Cy}R_{xy}R_{Ax} + R_{Cy}R_{yD}R_{Bx} + R_{Cy}R_{yD}R_{Ax} + R_{Bx}R_{yD}R_{Ax} + R_{xy}R_{yD}R_{Bx} + R_{xy}R_{yD}R_{Ax}} \end{aligned} \quad (6)$$

The volumetric liquid flow rate in the i th channel section F_i is proportional to the corresponding electrical current I_i according to Eq. (7),^{32–34}

$$F_i = -I_i \left(\frac{\varepsilon \varepsilon_0 \zeta}{\eta \kappa} \right) \quad (7)$$

In order to determine the voltages required to achieve a particular pattern of flow rates (e.g. flow or inject modes described above), all the resistance values of the different channel sections, filled with the liquid of interest, must be known. This can be done by measuring the currents as a function of the various voltages within the micro reactor and computer fitting the resistance values. Alternatively, one can measure the liquid conductivity (using a conventional conductivity meter) and all the channel dimensions and calculate the required resistances according to Eq. (4). Calibration measurements of liquid flow rates within the micro reactor as a function of different set currents yield the value of ζ and then enable the conversion of measured currents (logged during a run) to liquid flow rates from Eq. (7).

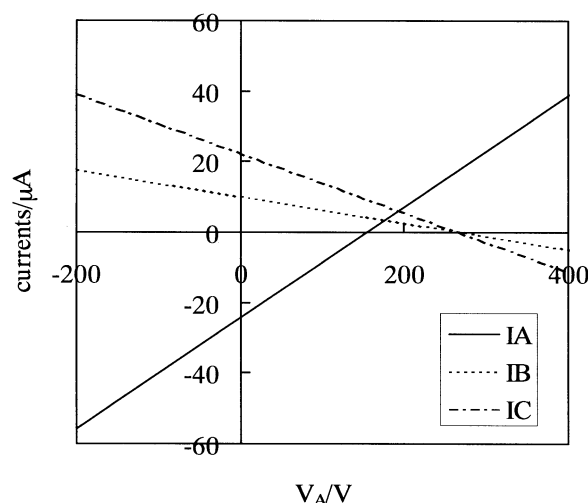


Figure 8. Illustrative plots of electrical currents versus V_A for V_B and V_C both set to 200 V. The data refer to the channel network of Fig. 6 filled with 50 vol% ethanol/water containing 35 mM phosphate buffer at pH 7.5.

Representative plots of electrical currents versus one of the voltages (with the remaining voltages being fixed) are shown in Fig. 8. The current values are typically in the μA range and, as expected from Ohm's law, they are proportional to the voltage. However, because of the linking together of the different limbs of the overall circuit, the

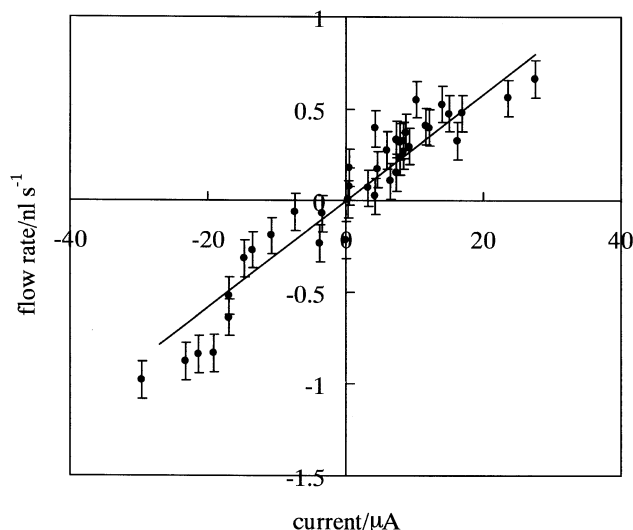


Figure 9. Correlation between measured volumetric liquid flow rates and the corresponding electrical currents for the channel network of Fig. 6 filled with 50 vol% ethanol/water containing 35 mM phosphate buffer at pH 7.5.

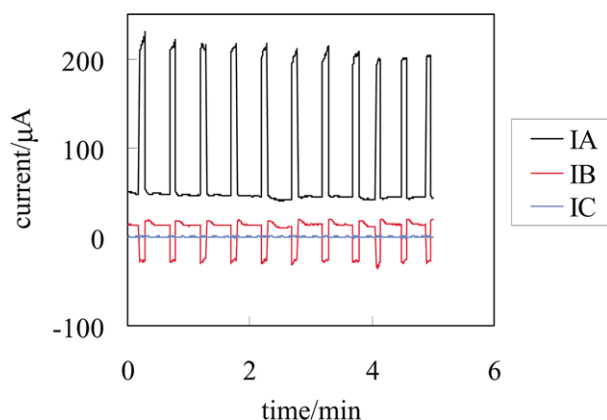
Table 1. Voltages, electrical currents, volumetric flow rates and liquid EOF velocities for flow and injection modes in the system of Fig. 9

Variable	Flow mode (A→D)	Inject mode (B→C)
V_A (V)	225	1
V_B (V)	169	86
V_C (V)	169	-38
I_A (μA)	15 (set)	0 (set)
I_B (μA)	0 (set)	8 (set)
I_C (μA)	0 (set)	-8 (set)
F_A (nl s^{-1})	0.45	0
F_B (nl s^{-1})	0	0.24
F_C (nl s^{-1})	0	-0.24
v_{eof} (A) (mm s^{-1})	0.05	0
v_{eof} (B) (mm s^{-1})	0	0.03
v_{eof} (C) (mm s^{-1})	0	-0.03

voltages required to produce zero current in a particular channel section are determined by a complex function of all resistance and voltage values. An example of the linear correlation between the electrical current and liquid flow rates in corresponding channel sections is shown in Fig. 9. Applying this type of information, Table 1 lists the calculated voltage settings required to achieve flow and injection modes with set flow rates for the system shown in Fig. 9.

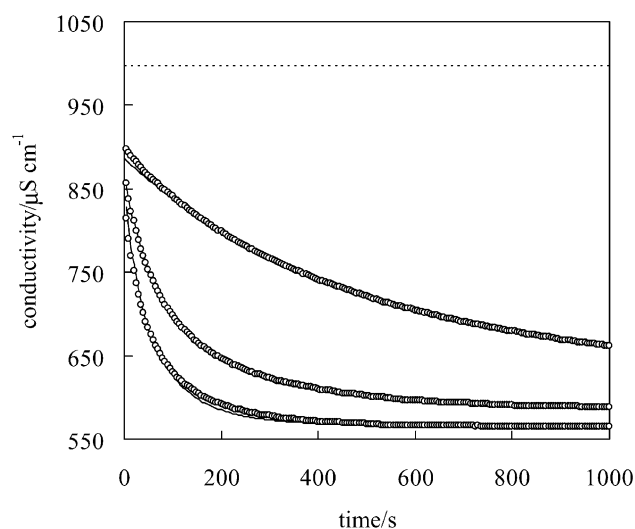
Full details of this entire procedure are described in Ref. 41 where it is demonstrated that measurement of the liquid conductivity κ , zeta potential ζ and all channel dimensions enables the correct calculation of the voltages needed to achieve any set of flow rates.

Several notes of caution about this analysis should be emphasised. Firstly, the study described in Ref. 41 indicates that correction of the overall electrical current for surface conduction along the channel walls is sometimes required. The surface conduction may become non-negligible when the bulk conductivity of the liquid is relatively low. Secondly, the analysis given here applies to the situation when the liquid conductivity and the zeta potential are uniform throughout the channel network. Mixing of reagent solutions which possess different conductivities and/or which have different zeta potentials with the channel walls

**Figure 10.** Electrical current oscillations due to electrolytic formation and subsequent dissolution of gas bubbles in the micro reactor channel network of Fig. 6.

will produce moving channel zones with non-uniform properties and EOF mobilities. Obviously, this situation requires a considerably more complex analysis. Lastly, the simplified analysis presented here, although sufficient to illustrate the main features of flow control, takes no account of flow inertial effects and the non-uniformity of the electrical field around channel junctions. At a microscopic level, the effects cause complex local flow patterns in these regions, which can be modelled using sophisticated fluid dynamics software. Interested readers are referred to Refs. 42–46 for progress in this field.

In addition to its use in determining the required electrokinetic flow control parameters, the routine, in situ monitoring of electrical currents in channel networks provides useful diagnostic information on micro reactor operation. Firstly, the observation of a current dropping to zero in a branch of the channel network can indicate the position of a channel blockage. Secondly, application of an excessive voltage across a channel network can cause electrochemical reactions that may result in the release of gas bubbles. Fig. 10 shows an example of a current trace where a series of regular 'spikes' were caused by the liberation and subsequent dissolution of hydrogen bubbles at an electrode. Electrolysis occurs in micro reactors when the overall voltage difference between an electrode pair (typically several hundred V) is sufficiently high or the electrical resistance of the relevant channel section is low such that the voltage change across an electrode/solution interface (typically a fraction of a V) exceeds the redox potential required for an electrochemical reaction. Lastly, when chemical reactions occur in a micro reactor and result in a change of conductivity of the solution, in situ current monitoring can, in principle, be exploited to monitor the extent of a reaction within the channel network. Fig. 11 shows the change in conductivity observed during the progress of a Wittig reaction, where methanol is used as the solvent.

**Figure 11.** Conductivity changes which occur during the Wittig reaction of 2-nitrophenylphosphonium bromide (NTPB) (5 mM), sodium methoxide base (7.5 mM) and 0, 15, and 30 mM methyl 4-formylbenzaldehyde (MFB) in methanol at 20°C. The reaction proceeds via the fast reversible formation of the ylid which then either decomposes or reacts to form an adduct with MFB. The horizontal line shows the conductivity of the reagents in the absence of the formation of the ylid intermediate.

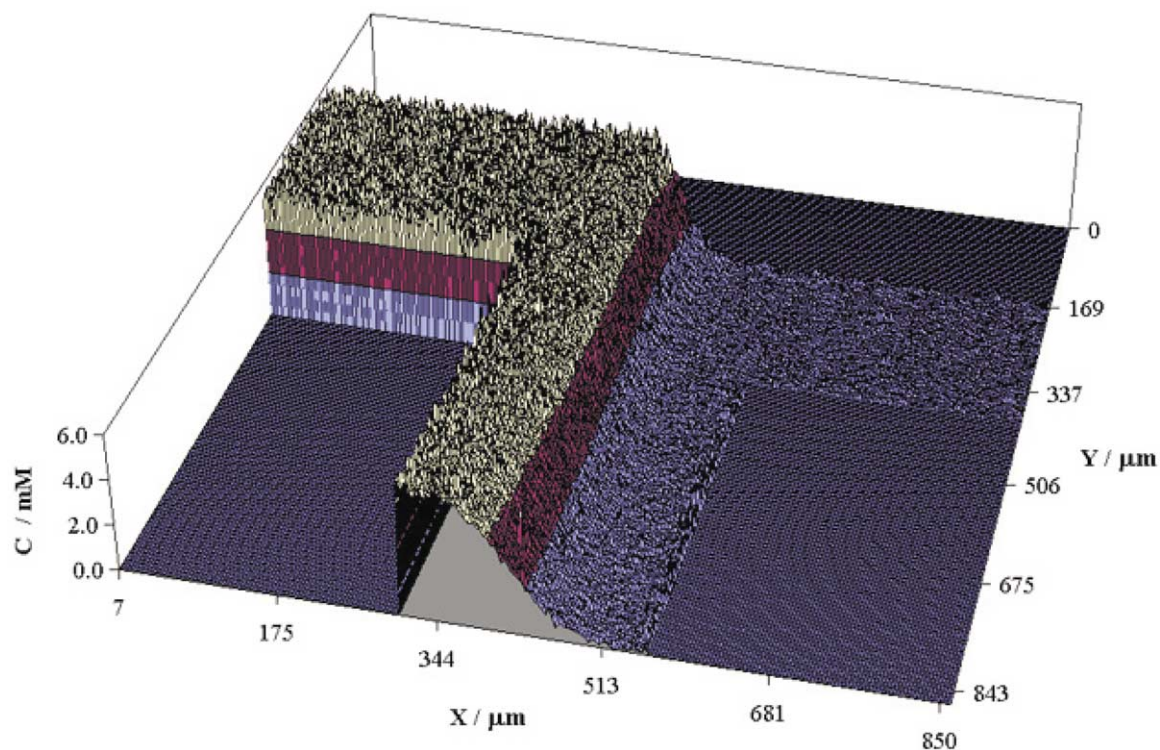


Figure 12. 3D plot of dye concentration versus position within a T-junction. The dye solution enters from the left and is combined with solvent entering from the right. The flow velocity down the ‘leg’ of the T is 0.48 mm s^{-1} . Detailed analysis of the diffusional broadening of the dye-solvent interface seen as the laminar streams move down the channel (corresponding to different times after contact) yields the diffusion coefficient of the dye ($1.0 \times 10^{-10} \text{ m}^2 \text{ s}^{-1}$ in this example).

3.3. Reagent mixing and chemical reaction in a micro reactor

Except for unimolecular reactions, two or more reactant solutions must be mixed as a necessary first step to achieving reaction. Two main modes of mixing are possible which have very different characteristics. The first mode, denoted ‘diffusive mixing’, is illustrated in Fig. 12 which shows the 3D concentration profile resulting when a dye solution (entering from the left channel) is combined with solvent entering from the right-hand channel of a T-junction. The two solutions flow together down the leg of the T. For typical EOF conditions, the linear fluid velocities are of the order of $0.1\text{--}1 \text{ mm s}^{-1}$. The Reynolds number R_e (equal to $D_e v \rho / \eta$ where D_e is the effective channel diameter, v is the velocity, ρ is the liquid density and η is the liquid viscosity) for such flow is <10 , well below the transition from laminar to turbulent flow which occurs at R_e values of around 2500. The co-flowing reagent streams therefore retain their laminar flow pattern and mixing occurs only by inter-diffusion. From the 3D concentration plot of the dye, it can be seen that only a small extent of diffusional mixing occurs in the time between the first contact of the solution streams’ (at the top edge of the image) flow to a position corresponding to the bottom edge of the image. For the flow velocity used (0.48 mm s^{-1}), this time corresponds to approximately 2 s. In this mode of mixing, at very long times the reagent concentrations are diluted by a ratio equal to the ratio of the flow rates of the incoming streams. A crude estimate of the time required for mixing across the complete width of the channel (w) is given by $t \approx 5w^2/D$, where D is the diffusion coefficient of the solute species.

For a typical channel width of $100 \mu\text{m}$ and a value of D of $5 \times 10^{-10} \text{ m}^2 \text{ s}^{-1}$, this time is of the order of 100 s. It can be seen that the mixing of two streams flowing at 1 mm s^{-1} in a typical channel length of a few cm will normally be very incomplete. Imaging of the diffusive broadening of the concentration gradient perpendicular to the laminar-flowing streams at different times has in fact been used to determine diffusion coefficients of absorbing or fluorescent species.⁴⁷

Complete mixing by diffusion can be achieved by using slow (or stopped) flow to increase the contact time. Alternatively, faster flow or smaller channel cross-sections, within long channels (generally folded to reduce overall device size), will achieve the same result. Elegant designs of networks containing cascades of T-junctions connected by suitably long, tortuous channels have been used to produce output channels giving simultaneously a series of fully-mixed dilutions of the original input solution.^{48,49} This type of multiple output is useful when using a micro reactor to determine, for example, a calibration plot of detector signal versus the concentration of an analyte species. The fact that the laminar flows of reagent streams inter-diffuse only relatively slowly has been exploited by using chemically-reactive reagent streams. Reactions between appropriate reagents at the interface between laminar, co-flowing streams of the reactants have been used, for example, to deposit very thin lines of metals (plus a range of other species) at the channel base as a novel means of fabricating ‘nanowires’ in specified locations.⁵⁰

The second mode of mixing, ‘slug injection’, is illustrated in Fig. 6. Using a pair of offset T-junctions and the

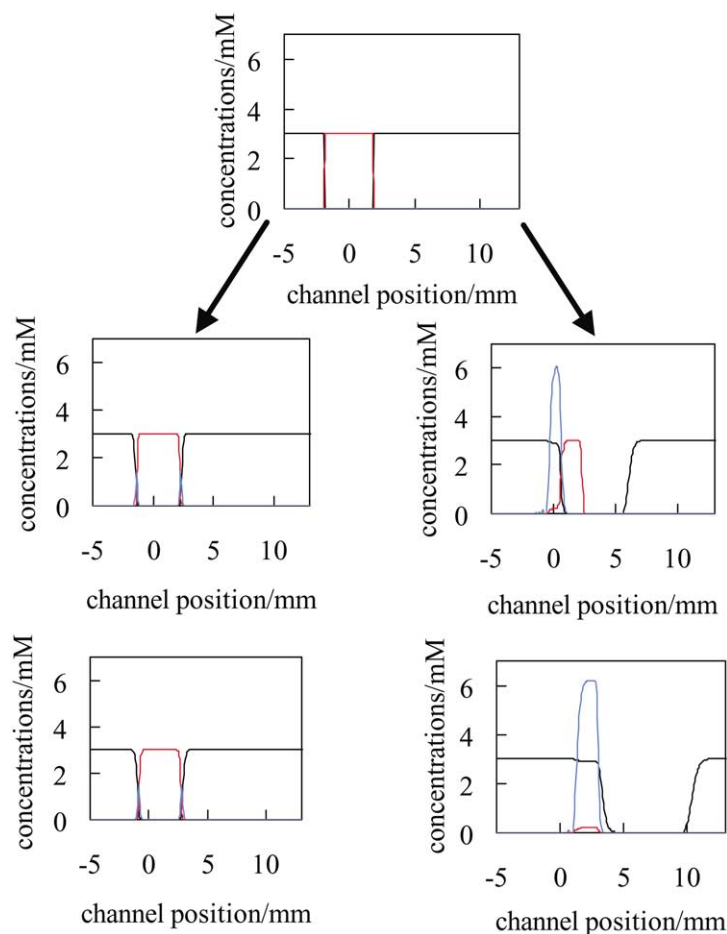


Figure 13. Time snapshots at 0, 10 and 20 s of the concentration profiles of reactants X (red) and Y (black) and product Z (blue). The top plot shows the initial configuration of a rectangular slug of X in a stream of Y, centred at channel position=0. The left-hand plots correspond to $v_{\text{eof}}=0.05 \text{ mm s}^{-1}$ with v_{ph} of all species=0 (diffusive mixing only). The right-hand plots correspond to $v_{\text{eof}}=0.05 \text{ mm s}^{-1}$ and $v_{\text{ph}}(\text{X})=0$, $v_{\text{ph}}(\text{Y})=0.76 \text{ mm s}^{-1}$ and $v_{\text{ph}}(\text{Z})=0.23 \text{ mm s}^{-1}$. In this case, mixing of X and Y occurs mainly as a result of the different electrophoretic velocities.

‘flow-inject-flow’ sequence described earlier, a slug of one reagent is produced within a flowing stream of a second reagent. We illustrate the main features of this mode by considering the behaviour of a slug of a reagent X in a flowing stream of a reagent Y where X and Y can chemically react to give product Z. We consider the situation where the reactant concentrations and the reaction rate constant are such that chemical reaction occurs fast, i.e. virtually immediately the reagents are locally mixed in a particular channel section. Using the simulation procedure described in Ref. 36, we are able to calculate the concentrations of all the species X, Y and Z as a function of the distance x along the flow channel length for different times after the production of the initial rectangular slug of X in the stream of Y. Input variables include the initial concentrations of X, Y and Z, the forward and reverse rate constants for the reaction $\text{X}+\text{Y}=\text{Z}$, the EOF velocity and the electrophoretic velocities of X, Y and Z. The first simulation (Fig. 13) shows a series of time snapshots for the situation in which the electrophoretic velocities of X, Y and Z are all zero (corresponding to these species all being uncharged). In this case, all species move with velocities equal to v_{eof} and mixing (and hence reaction) occurs only by inter-diffusion at the leading and trailing edges of the slug of X. For the wide slug and the short time shown in Fig. 11, the inter-diffusion and therefore

the extent of the reaction, is low. The time for diffusional mixing across the slug (approximately $5 w_s^2/D$, where w_s is the slug width) can be made shorter by reducing the slug width. In order to maximise the conversion to products, a series of many narrow slugs is therefore more effective than a single, broad slug. Elegant methods to achieve very narrow slug widths have been described.⁴⁴

In the second simulation shown in Fig. 13, v_{ph} for X is set to zero, but v_{ph} for Y and Z are set to positive values corresponding to these species bearing positive charges. Y now moves slowly with a velocity v_{eof} whereas X moves faster with a velocity $v_{\text{eof}}+v_{\text{ph}}$. In this situation, the slug of X becomes displaced relative to the concentration ‘gap’ in Y and mixing of X and Y therefore occurs relatively rapidly as a result of the different electrophoretic mobilities of the two species and results in reaction at the trailing edge of the slug of X. It should be noted that, in contrast to the diffusive mixing mode discussed above, mixing by differential electrophoretic mobilities does not result in dilution of the localised reagent concentrations. Fig. 14 shows the experimental realisation of this type of mixing and reaction. A slug of the uncharged ligand, pyridine-azo-dimethylaniline (PADA), is injected into a flowing stream of Ni^{2+} ions. As seen in the measured concentration profiles along the channel length, fast complexation to form the NiPADA^{2+}

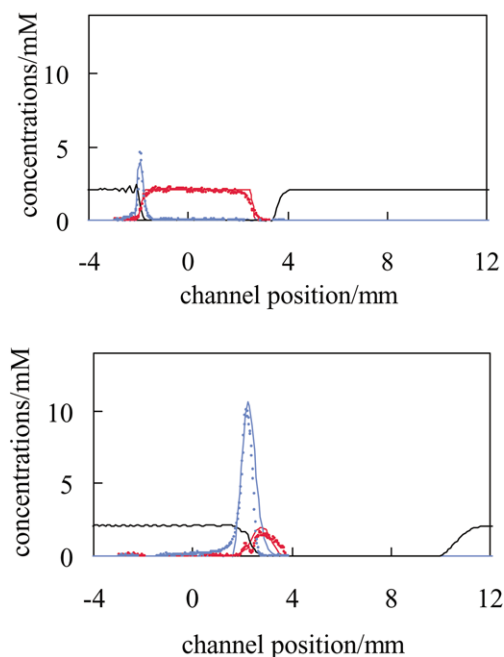
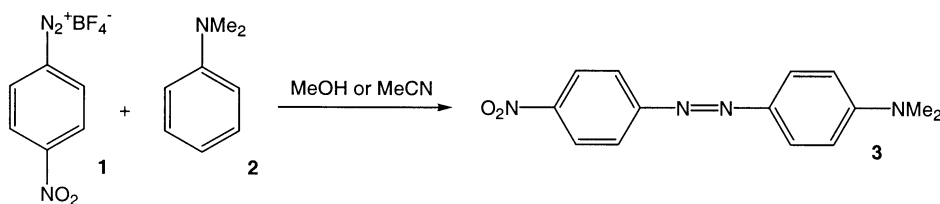


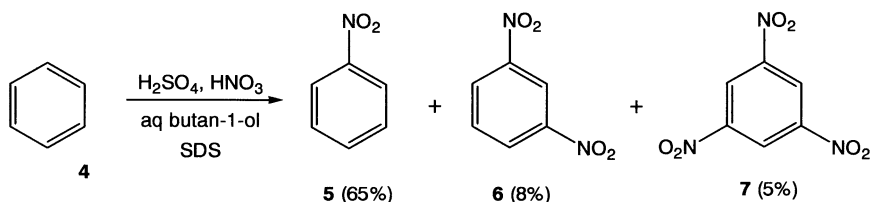
Figure 14. Comparison of simulated (solid lines) and measured (data points) concentration profiles for the reaction between Ni^{2+} ions (black) and a slug of the ligand PADA (red) to form the NiPADA^{2+} complex (blue) at the trailing edge of the PADA slug. Concentration profiles of the coloured PADA and complex species were determined by analysis of digitised video images. The concentration profiles correspond to 10 (upper plot) and 70 s (lower plot) after PADA slug injection.

complex occurs at the trailing edge of the PADA slug and can be successfully modelled using the kinetic rate parameters measured for the forward (complexation) and reverse (complex dissociation) reactions.⁵¹

Following the time sequence shown in Fig. 14, it is possible to reverse the flow which moves the NiPADA^{2+} complex product peak back into the concentration gap of Ni^{2+} . Since the complex formation reaction is reversible, the complex dissociates via the back reaction into PADA and Ni^{2+} . This example, using a mechanistically very simple reaction, demonstrates the type of spatial and temporal control of chemical reactions that is achievable in micro reactors,



Scheme 1.



Scheme 2.

but not in bulk solution reactors where all concentrations are uniform. The potential for detailed control of complex, multistep reactions is only just beginning to be explored. As discussed below, the empirical results for a wide range of reactions performed in micro reactors indicate that voltage control can alter the product yields and selectivity for many reactions. The full elucidation and optimisation of these effects will require detailed analysis using the principles described above. In addition to applications involving the control of synthetic reactions, micro reactors also have potential as ‘chemical information chips’. Comparison of experimental concentration profile data for reactions for which diffusion coefficients, electrophoretic mobilities and rate constants are unknown with simulations such as those shown in Figs. 13 and 14 should enable the determination of the relevant physicochemical properties. Micro reactors therefore potentially offer a significant new tool in the armouries of both synthetic and physical chemists.

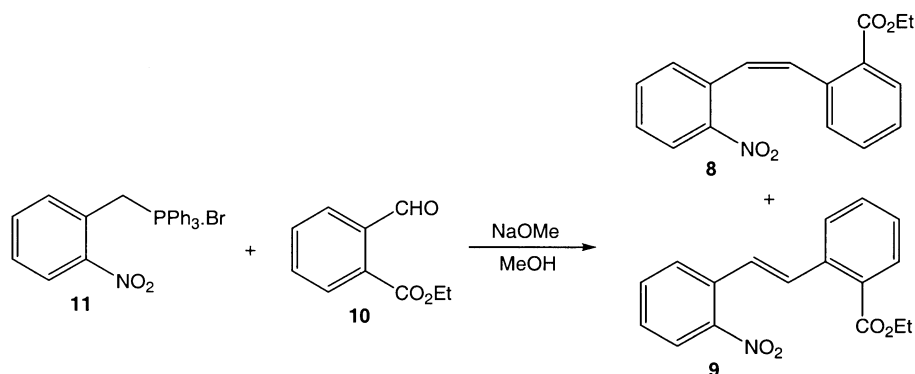
4. Reactions performed in micro reactors

4.1. Liquid phase reactions

Salimi-Moosavi et al.⁵² have demonstrated the synthesis of diazo dyes within a micro reactor. The authors have reacted 4-nitrobenzenediazonium tetrafluoroborate **1** with *N,N*-dimethylaniline **2** in a micro reactor fabricated from glass, to give the red diazo compound **3** (Scheme 1). The reagents were mobilised in the reactor using EOF in either a protic (methanol) or an aprotic (acetonitrile) solvent, to give conversions of 37 and 22%, respectively.

Nitration reactions in organic synthesis are problematic because of the use of excess quantities of concentrated nitric and sulphuric acids. The reactions are extremely exothermic and it is hence difficult to control the temperature of such reactions when performed on a large scale. As a result, micro reactors have a considerable attraction for these reactions because the reactor enables excellent temperature control of the reaction.

Doku et al.⁵³ have reported the nitration of benzene **4** in a



Scheme 3.

borosilicate glass micro reactor. The benzene was mobilised by electroosmotic flow as a microemulsion using the surfactant, sodium dodecyl sulphate (SDS). The nitronium ions, which were produced in situ by mixing sulphuric and nitric acids, underwent electrophoretic-induced mobility. A co-solvent, butan-1-ol, was used to enhance the solubility of the benzene in the aqueous system. The authors report that mononitration occurs in 65% conversion to give nitrobenzene **5** (Scheme 2) and that approximately 8% of 1,3-dinitrobenzene **6** and 5% of 1,3,5-trinitrobenzene **7** were obtained. Importantly, Doku demonstrated that it is possible to mobilise a non-polar liquid, such as benzene, using EOF by dissolving it in a microemulsion.

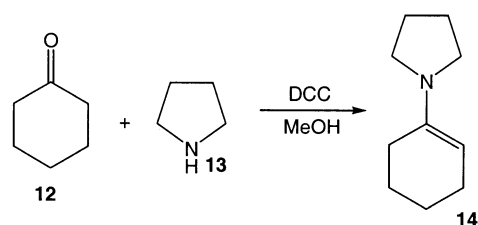
Burns and Ramshaw⁵⁴ have also investigated the nitration of benzene and toluene in a micro reactor. They have reported that the conversion has a linear relationship with temperature. More interestingly, they have demonstrated that the conversion can be considerably increased by reducing the dimensions of the micro reactor channels. They found that halving the capillary diameter from 250 to 130 μm more than doubled the rate of nitration. The flow rates were additionally determined to be critical, with faster flow rates giving higher conversions. The authors postulate that the increased flows promoted increased mixing within the channels.

Skelton and co-workers have reported the application of micro reactors, prepared from borosilicate glass, for the Wittig reaction.^{55,56} The authors used the micro reactor to prepare the *cis*- and *trans*-nitrostilbene esters **8** and **9** using the Wittig reaction (Scheme 3). A number of features such as stoichiometry and stereochemistry were investigated. When 2 equiv. of the aldehyde **10** to the phosphonium salt **11** were used in the reaction, a conversion of 70% was achieved. The micro reactor demonstrated an increase in reaction efficiency of 10% over the traditional batch synthesis. The reaction stoichiometry was subsequently reduced to 1:1, but using a continuous flow of reagents, as above, the conversion was poor (39%). The conversion was increased to 59% using an injection technique, where slugs of the phosphonium salt **11** were injected into a continuous flow of the aldehyde **10**.

The research was further extended to investigate the stereochemistry of the reaction. The ratio of isomers **8** and **9** was controlled by altering the applied voltages to the reagent

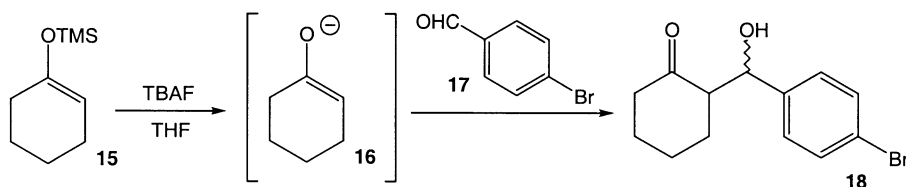
reservoirs within the device. The variation in the external voltage subsequently altered the relative reagent concentration within the device, producing *Z/E* ratios in the region 0.57–5.21. In comparison, the authors report that, when a traditional batch synthesis was performed based on the same reaction time, concentration, solvent and stoichiometry, a *Z/E* ratio of approximately 3:1 was observed. This demonstrated that significant control was possible in a micro reactor compared with batch reactions.

Sands and co-workers⁵⁷ have recently reported the preparation of enamines in a micro reactor. Enamines are traditionally prepared under Dean and Stark conditions, where the ketone and secondary amine are heated to reflux in toluene. These conditions remove the water from the reaction to produce the equilibrium-dependent enamine. Using the micro reactor, cyclohexanone **12** was reacted with pyrrolidine **13** using methanol as the solvent, in the presence of dicyclohexylcarbodiimide (DCC), to form the enamine **14** in 42% conversion at room temperature (Scheme 4). The authors postulate that the DCC reacts with the water that is produced in the reaction.

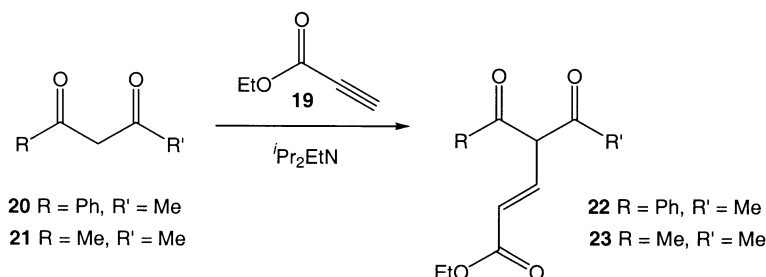


Scheme 4.

Wiles et al.⁵⁸ have recently demonstrated the use of silyl enol ethers in the aldol reaction within a micro reactor. Quantitative conversion of the silyl enol ethers to β -hydroxyketones was observed in 20 min compared to traditional batch systems, where quantitative yields were only obtained when extended reaction times of up to 24 h were employed. One example involved the treatment of the TMS enol ether **15** with tetra-*n*-butylammonium fluoride (TBAF) to generate the tetra-*n*-butylammonium enolate **16** in situ, followed by condensation with *p*-bromobenzaldehyde **17** to give the β -hydroxyketone **18** in 100% conversion (Scheme 5).



Scheme 5.



Scheme 6.

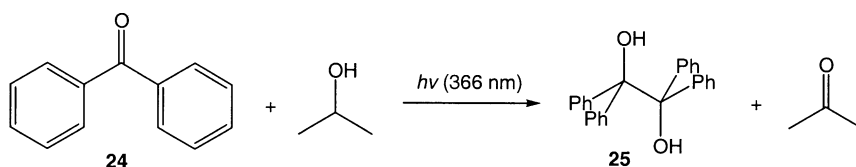
Wiles et al.⁵⁹ have reported the preparation of the enolates from a series of 1,3-diketones using an organic base, and their subsequent reaction with a variety of Michael acceptors such as **19** to afford 1,4-addition products within a micro reactor (Scheme 6).

When using a continuous flow of the reagents **19** and **20**, 15% conversion to the adduct **22** was observed, compared with 56% when the diketone **21** was reacted with **19** forming the Michael adduct **23**. The authors, however, demonstrated enhancements in conversions through the application of the stopped flow technique. This procedure involved the mobilisation of reagents through the device for a designated period of time, using an applied field, and the flow was subsequently paused by the removal of the applied field, prior to re-applying the field. Using the regime of 2.5 s on and 5 s off, the conversion to the product **22** was improved to 34%, while lengthening the stopped flow period to 10 s, resulted in a further increase to 100%. This was compared to the preparation of **23**, in which the regime of 2.5 s on and 5 s off resulted in an increase in conversion to 95%. This demonstrated that the enolate of 2,4-pentanedione **21** was

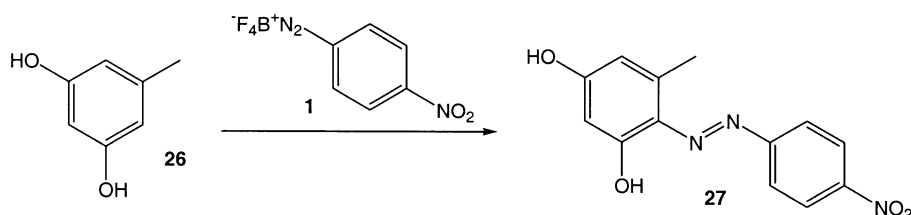
more reactive than the corresponding enolate of benzoyl acetone **20**. The authors propose that the observed increase in conversion, when using the technique of stopped flow, was due to an effective increase in residence time within the device and hence an increase in the diffusive mixing of the reagent streams.

Jenson et al.⁶⁰ have reported a photochemical reaction within a micro reactor. The reactor was fabricated by bonding a patterned silicon wafer to a quartz wafer, the advantage of this fabrication technique being that the quartz substrate allows reaction and detection using UV light of lower wavelengths than permitted by Pyrex substrates.

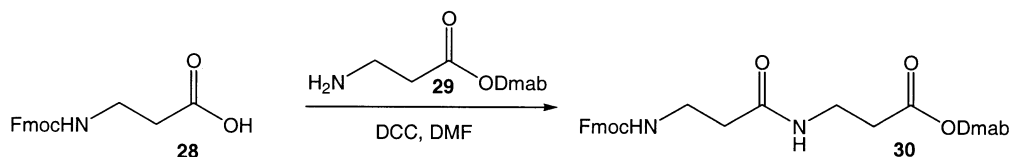
The authors investigated the pinacol formation reaction of benzophenone **24** in propan-2-ol (Scheme 7). The reaction is known to follow a radical reaction pathway,⁶¹ and it is reported that the longer the residence time of the reaction, the greater the conversion to benzopinacol **25**. The authors report that there was no detectable product formation for flow rates $>10 \mu\text{l min}^{-1}$. With reduced flow rates, having larger residence times, the conversion improves because the



Scheme 7.



Scheme 8.



Scheme 9.

amount of light absorbed increases, and there is therefore sufficient time for the excited species to diffuse and react with the benzophenone. The authors report conversions of up to 60% when using flow rates of 4 $\mu\text{l min}^{-1}$.

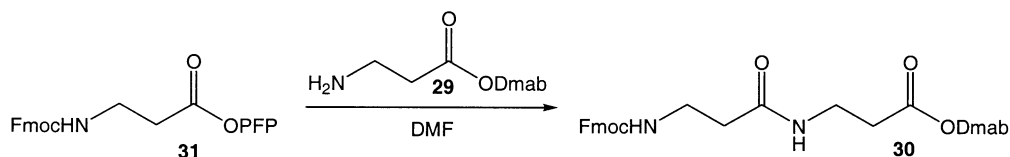
Hisamoto and co-workers⁶² have described the first example of a phase transfer reaction in a micro reactor. These authors have successfully conducted a phase transfer diazo coupling reaction in which a solution of 5-methylresorcinol **26** in ethyl acetate was reacted with an aqueous solution of 4-nitrobenzenediazonium tetrafluoroborate **1** to form the azo dye **27** (Scheme 8). Syringe pumps were used to move the reagents around the reactor manifold and the authors report that the product was isolated in 100% yield.

Watts et al. have recently demonstrated the first example of a multistep synthesis in a micro reactor where they have used their micro reactor devices in peptide synthesis.⁶³ The authors evaluated their device using a carbodiimide coupling reaction of Fmoc-β-alanine **28** with the amine **29** to give the dipeptide **30** (Scheme 9). When stoichiometric quantities of the reagents were used, only ca 10% conversion to dipeptide the **30** was achieved. By using two equiv of DCC, however, an increase in conversion to ca 20% was observed and by applying a stopped flow technique (2.5 s injection length with stopped flow for 10 s), the conversion of the reaction was further increased to approximately 50%. Using five equiv of DCC, a conversion of up to 93% of the dipeptide **30** was obtained using the stopped flow technique.

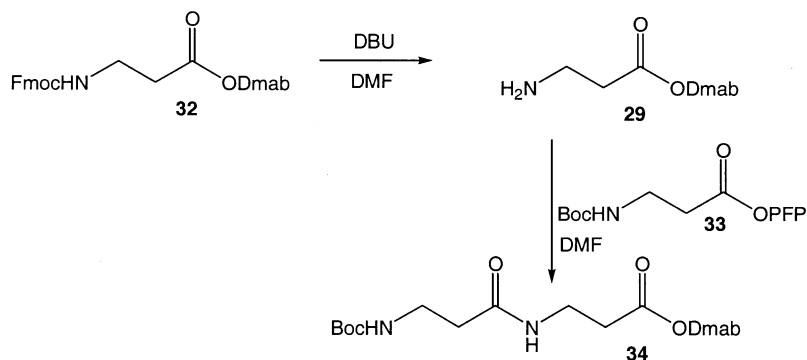
The authors also demonstrated that the dipeptide could be prepared from pre-activated carboxylic acids. They report that the reaction of the pentafluorophenyl (PFP) ester of Fmoc-β-alanine **31** with the amine **29** gave the dipeptide **30** quantitatively in 20 min (Scheme 10). This represented a significant increase in yield compared with the traditional batch synthesis, where only a 50% yield was obtained in 24 h.

Having demonstrated that peptide bonds could be successfully formed when using a micro reactor, the authors then found that they could extend the methodology to the preparation of longer-chain peptides. Using the micro reactor, the Dmab ester of Fmoc-β-alanine **32** was reacted with one equiv of piperidine or 1,8-diazabicyclo(5.4.0)undec-7-ene (DBU) to give the free amine **29** in quantitative conversion. This is in comparison to the solid phase peptide synthesis where 20% piperidine in DMF is frequently employed.^{64,65} The authors then reacted the amine in situ with the pentafluorophenyl ester **33** to give the dipeptide **34** (Scheme 11) in 96% overall conversion.

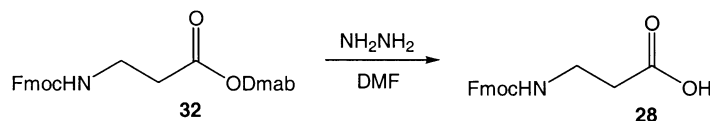
Having shown that more complex peptides could be produced by removal of the *N*-protecting group, the authors then demonstrated that they could remove the Dmab ester using hydrazine. The reaction of the Dmab ester **32** with 1 equiv. of hydrazine gave quantitative deprotection to afford the carboxylic acid **28** (Scheme 12). This is in comparison to the solid phase peptide synthesis where 2% hydrazine in DMF is generally used to effect deprotection.⁶⁶



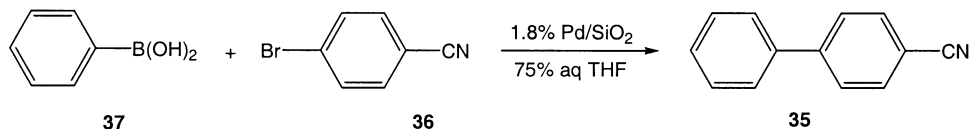
Scheme 10.



Scheme 11.



Scheme 12.



Scheme 13.

4.2. Catalytic reactions

Greenway et al. have demonstrated the Suzuki reaction within a micro reactor device.⁶⁷ This represented an example of heterogeneous catalysis where 1.8% palladium on silica was placed in the central channel of the micro reactor. The catalyst was immobilised between microporous silica frits prepared from potassium silicate and formamide. The micro reactor was optimised using flow injection analysis principles, producing a conversion of 67% of the cyanobiphenyl **35** product at room temperature. The flow injection method adopted allowed the periodic injection of the aryl halide **36** into a continuous flow of the phenylboronic acid **37** (Scheme 13). Traditionally, tetrahydrofuran (THF) is used as the solvent in this reaction. As has been found with many organic solvents, however, THF has very low natural EOF properties and for this reason, it was mixed with water (75:25) for use in the experiment. The yields obtained were comparable with Suzuki reactions on a batch scale using homogeneous catalysis. Importantly, there were negligible levels of the palladium catalyst in the product, which was demonstrated using inductively coupled-mass spectrometry (ICP-MS), this illustrating that the catalyst was not leaching from the reactor.

One of the interesting observations of the reaction was that, unlike conventional Suzuki reactions, an additional base was not required. Although the exact reason for this is not clear, it is postulated that the electric field may be sufficient to cause ionisation of the water at the metal surface. It is feasible that the hydroxide formed in this way may be sufficient to perform the function of the conventional organic or inorganic base. Alternatively, it has been subsequently proposed that a more basic environment may be formed at the surface of the micro reactor.

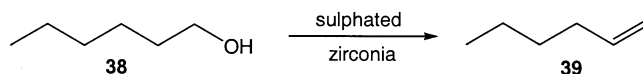
Wilson and McCreedy⁶⁸ have reported the use of a micro reactor to perform the dehydration of hexan-1-ol to hex-1-ene, using a sulphated zirconia catalyst. The micro reactor was fabricated from a glass plate, which was etched using photolithography. A PDMS top block, with pre-drilled holes to act as reservoirs for the reagents, was then aligned with the channel geometry. In order to introduce the catalyst into

the micro reactor, it was dusted over the surface of the PDMS face before the base plate was joined to the top plate. This process immobilised the catalyst, while simultaneously increasing its surface area. The overall effect was to produce a catalytically-active wall of the microchannel. A heater, fabricated from Nichrome wire, was also immobilised in the top plate. Pumping was produced with a syringe pump and the products were analysed by gas chromatography (GC). The conversion of hexan-1-ol **38** to hex-1-ene **39** was between 85 and 95% and no additional products were detected (Scheme 14). This yield is extremely good when compared to the 30% yield expected for the industrially used process.

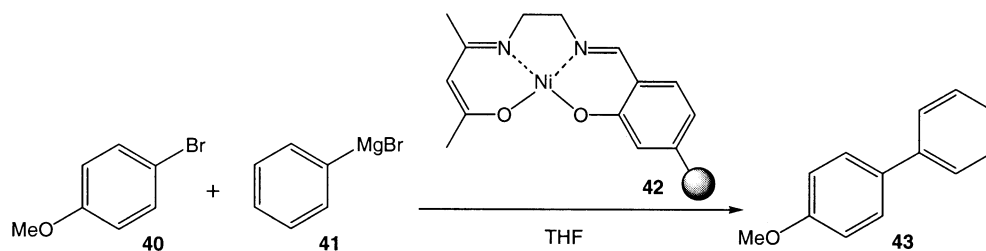
The reaction was also applied to ethanol. At a reaction temperature of 155°C and using a syringe pump at a flow rate of 3 $\mu\text{l min}^{-1}$, the product collected was found to contain 68% ethene, 16% ethane and 15% methane, together with trace amounts of ethanol. When electroosmotic pumping was used, the flow rate obtained was between 0.9 and 1.1 $\mu\text{l min}^{-1}$ at a field strength of 200 V cm^{-1} . The only detectable product was methane, indicating that the reaction had progressed beyond dehydration to complete cracking of the ethanol. Additionally, trace amounts of methanol were present in the product. It is proposed that the slow flow rate of the electroosmotic pumping method results in longer residence times in the reactor, this offering a significant advantage over the syringe pump. EOF however cannot be applied to all reactions because organic reactants, such as hexanol, exhibit no natural EOF under an applied potential.

O'Sullivan et al.⁶⁹ have recently investigated the Kumada–Corriu reaction in a pressure-driven micro reactor. The reactor was constructed by placing a plug of catalyst into a length of polypropylene tubing. The catalyst was held in place using plugs of glass wool. Standard HPLC connectors allowed one end of the tubing to be connected to a syringe. A syringe pump was used to drive a pre-mixed solution containing equimolar quantities of the aryl halide and Grignard reagent through the reactor.

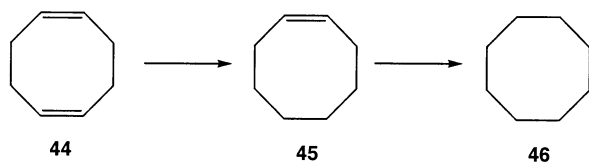
The authors reacted *p*-bromoanisole **40** with phenylmagnesium bromide **41**, in the presence of the nickel catalyst **42**,



Scheme 14.



Scheme 15.



Scheme 16.

which was supported on Merrifield resin, to give 4-methoxybiphenyl **43** (Scheme 15). When the reaction was conducted in the micro reactor, an enhanced reaction rate was observed compared to the batch reactions. Since the concentrations were the same in the both cases, the authors postulate that the dimensions of the micro reactor are solely responsible for the enhanced rate of reaction.

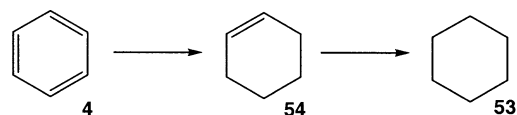
4.3. Gas phase reactions

Hönicke and co-workers⁷⁰ have reported the gas phase partial oxidation of cyclic dienes, to their corresponding monoalkeneses, over palladium and ruthenium/zinc catalysts. The micro reactors consisted of aluminium wafers, with mechanically-etched channels, which were activated by anodic oxidation to obtain a porous oxide layer, which was used as the catalyst support. Impregnation of an organic solution of palladium(II) acetylacetonate resulted in micro-channels consisting of an 18 μm thick layer of 0.18% Pd catalyst. The wafers were then stacked in a stainless steel housing to form a micro reactor consisting of 672 micro-channels for a stream of reagents to pass through. The authors used the device to investigate the hydrogenation of 1,5-cyclooctadiene **44** to cyclooctene **45** (Scheme 16). The diene **44** was vapourised and mixed with hydrogen, before being passed through the micro reactor at a temperature of 150°C. By increasing the residence time of the reaction from 35 to 115 ms the authors report that the conversion increased from 75 to 99.5%. Although the increased residence time resulted in increased quantities of cyclooctane

46 being formed, the selectivity of cyclooctene **45** decreased from 99.5 to 98% under these conditions.

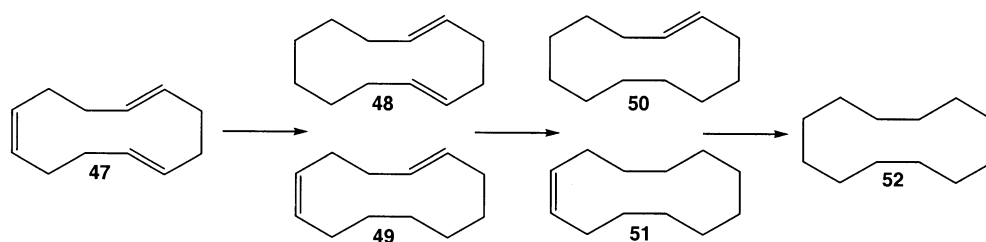
The authors used the same device to investigate the hydrogenation of *c,t,t,1,5,9*-cyclododecatriene **47** to the cyclododecenes **48** and **49** (Scheme 17). At a temperature of 150°C, a selectivity of 85 to 90% was reported, where the conversion was approximately 90%. The selectivity of this reaction was lower than the previous example because of the formation of the by-products **50–52**. It was demonstrated, however, that there was a selectivity advantage of the micro reactor compared to a fixed-bed reactor.

The catalytic hydrogenation of benzene **4** was also investigated (Scheme 18), but complete reduction to cyclohexane **53** was observed to take place when using the Pd catalyst. The authors report that hydrogenation of benzene to cyclohexene **54** was accomplished using a micro reactor system consisting of a ruthenium/zinc catalyst, which was incorporated into the micro reactor using the same methodology, but the conversions were reported to be low (ca 10%), with a maximum selectivity of 36%.

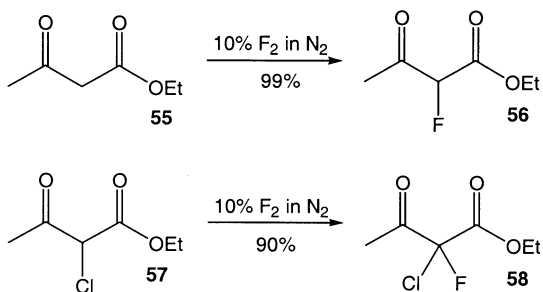


Scheme 18.

The use of elemental fluorine in organic synthesis is problematic as a result of the difficulties associated with the safe handling of gaseous fluorine.^{71,72} In addition, fluorination reactions are generally extremely exothermic and it is difficult to control the temperature of such reactions when performed on a large scale. Micro reactors have a considerable attraction for direct fluorination processes because there is only a small amount of fluorine in the reactor at any given time. The micro reactor enables



Scheme 17.



Scheme 19.

excellent temperature control of the reaction as well as an opportunity for scale up, by the simultaneous use of many such reactors.

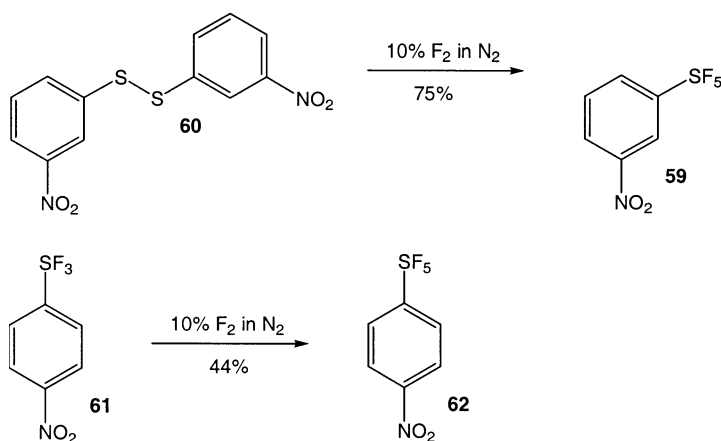
Chambers and Spink^{73,74} have reported the use of micro reactors for the fluorination and perfluorination of organic compounds using elemental fluorine. A nickel or copper micro reactor was used for the investigation and the liquid reactants and solvents were introduced into the reaction chamber via a syringe using a syringe-pump. Fluorine, in a nitrogen carrier gas, was introduced from a cylinder using a mass-flow controller. The liquid-gas mixing proceeded via 'cylindrical flow', where the liquid forms an outer cylinder coating the reactor surface with the gas flowing through the centre. This flow regime has enormous benefits in that it provides very large surface-to-volume ratios for the liquid phase, producing a very efficient reaction over a short distance. The products were trapped in a tube, which was cooled with either a salt/ice bath (0°C) or an acetone/carbon dioxide bath (-78°C). The fluorination of β-dicarbonyl compounds proceeded with a high efficiency using 10% fluorine in nitrogen at 5°C and with formic acid as the solvent. Ethyl acetoacetate **55** was fluorinated in 99% conversion to give ethyl 2-fluoroacetoacetate **56** while

ethyl 2-chloroacetoacetate **57** was fluorinated in 90% conversion, yielding ethyl 2-chloro-2-fluoroacetoacetate **58** (Scheme 19). Importantly, under these conditions, no perfluorination of the substrates was observed, with only the monofluorinated derivatives being isolated. The authors report that the bulk fluorination of ethyl 2-chloroacetoacetate **57** gives only a low conversion to **58**,⁷⁵ illustrating that the flow system is more efficient. This illustrates the catalytic effect of the fluorinated metal surface.

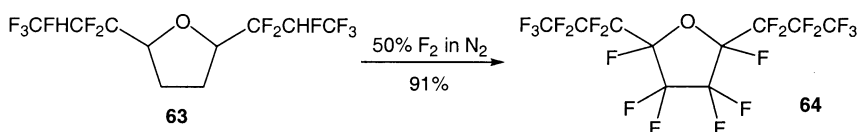
The sulphur pentafluoride derivative **59** was prepared in 75% yield by the reaction of the disulphide **60** with 10% fluorine in nitrogen, using acetonitrile as the solvent (Scheme 20). Similarly, treatment of the trifluoride **61** with excess fluorine gave the sulphur pentafluoride derivative **62** in 44% yield.

Perfluorination reactions were found to require an additional heating stage for the reaction to go to completion. The reaction of the tetrahydrofuran derivative **63** with 50% fluorine in nitrogen at 280°C gave the perfluorinated compound **64** in 91% yield (Scheme 21). In conventional reactions, cobalt trifluoride would be used to perfluorinate hydrocarbons.⁷⁶ Some of the reactions carried out by the authors, however, required much lower temperatures than would be expected if this compound was used.

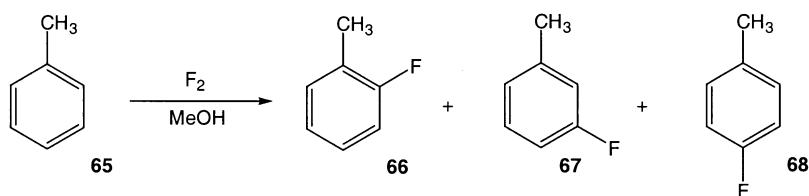
Jenson has demonstrated the direct fluorination of aromatic compounds in a micro reactor, a process difficult to perform on a conventional scale.⁷⁷ The reactor was fabricated from silicon and capped with Pyrex using anodic bonding. The surfaces of the reactor, which were in contact with the reagents, were coated with a nickel film using a metal deposition technique. The authors have used the micro reactor in the fluorination of toluene **65** at room temperature (Scheme 22). Using 10 equiv. of fluorine, in methanol as the solvent, the authors report an 80% conversion to give



Scheme 20.



Scheme 21.



Scheme 22.

the monofluorinated toluenes. The substitution pattern of the *ortho*-**66**, *meta*-**67** and *para*-**68** isomers was determined to be 4:1:2 by GC.

Srinivasan et al.⁷⁸ performed the partial oxidation of ammonia using a silicon-based micro reactor. Integrated heaters as well as flow and temperature sensors were fabricated into the sub-mm flow channels. The platinum catalyst was deposited in the reaction channel by electron-beam evaporation via a shadow mask. The gaseous reactants were fed from cylinders into the micro reactor by external mass-flow controllers, which maintained the desired flow rates. The product composition was continuously monitored using a mass spectrometer. The authors reported a change in the micro reactor exhaust composition over a range of temperatures and flow rates and they also demonstrated that the conversion and selectivity behaviour of conventional reactors could be reproduced in a micro reactor.

The effective heat transfer of micro reactors provides very accurate temperature control for both exothermic and endothermic reactions, thus eliminating undesired side reactions. An example has been reported by Hessel et al.,⁷⁹ who demonstrated that a micro reactor could be used to prepare hydrogen cyanide via the Andrussow route. In traditional laboratory reactions, the hydrogen cyanide is reported to hydrolyse to ammonia. The use of a microheat exchanger in this experiment, however, prevented this further reaction occurring.

As a final summary to this section, we list in Table 2 the reactions that are currently being investigated in micro reactors.

5. Potential applications of micro reactors

This review has summarised a small yet significant area of scientific research that is poised to challenge our understanding and future applications of reaction chemistry. To date, the outcome of the reported research has confirmed that micro reactor methodology is applicable to performing both gas and liquid phase reaction chemistry. But the question which remains are: is there more beyond just doing smaller than what can already be performed by traditional methodology? From the work cited in this article, the evidence is that the unique *modus operandi* of micro reactors, namely the low-volume spatial and temporal control of reactants and products in a laminar flow diffusive mixing environment in which distinctive thermal and concentration gradients exist, offers a novel method for the chemical manipulation and generation of products. In short, micro reactors are new tools with which to generate molecules and increase our knowledge of complex chemical processes.

The technology is still in its early development stage and it would be presumptuous at this point to expand too far on the potential applications that micro reactors will find, but some early trends are clear. In the authors' experience, reactions

Table 2. Reactions conducted in a micro reactor

Reaction	Chip material	Solvent	Conversion (%)	Comments	Reference
Suzuki	Glass	aq THF	67	EOF	67
Kumada coupling	Polypropylene	THF	60	Syringe pump	69
Aldol	Glass	THF	100	EOF	58
Nitration	Glass	Benzene	65	EOF	53
Wittig	Glass	MeOH	39–59	EOF	55, 56
Enamine	Glass	MeOH	42	EOF	57
Ugi four component coupling	Glass	MeOH		EOF	
Peptide synthesis	Glass	DMF	100	EOF	63
Synthesis of pyridazinones	Glass	EtOH/AcOH	30	EOF	
Synthesis of amides from amines and acid chlorides	Glass	DCM	77	EOF	
Diazo coupling	Glass	MeOH, MeCN	37, 22	EOF	52
Aminothiazole synthesis	Glass	NMP	58–100	EOF	
Knoevenagel	Glass	MeOH/H ₂ O	59–68	EOF	
Hantzsch thiazole synthesis	Glass	NMP	58–100	EOF	
Michael addition	Glass	EtOH	95–100	EOF	59
S _N 2 alkyl halide	Glass	DMF/H ₂ O	25	EOF	
Dehydration	Glass/PDMS	EtOH	85–95	EOF or syringe pump	68
Photochemical	Silicon/quartz	(CH ₃) ₂ CHOH	60	Syringe pump	60
Phase transfer	Glass	EtOAc	100	Syringe pump	62
Fluorination	Ni or Cu	Nitrogen gas	90–99	Syringe pump	73, 74
Fluorination	Silicon/pyrex	MeOH	80	Syringe pump	77

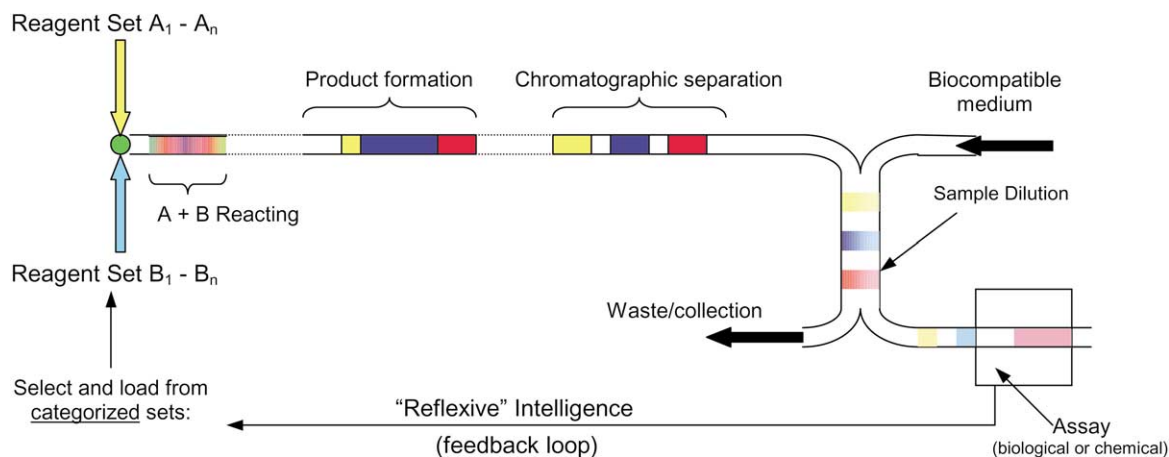


Figure 15. Integration of a micro reactor with a biological assay system.

performed in a micro reactor invariably generate relatively pure products in high yield, in comparison to the equivalent bulk reactions, in much shorter times and in sufficient quantities to perform full instrumental characterisation. One of the immediate and obvious applications is therefore in drug and process discovery, where the generation of compounds either with different reagents or under variable conditions is an essential factor. In addition, the opportunity to establish optimal chemical processes including reaction and formulation is an exciting capability of the technology, which could readily be married to appropriate analytical monitoring. An interesting twist to the chemistry carried out to date in the author's laboratories is not just the opportunity to separate reactants and products in real time but also the capability to manufacture and use reagents in situ. Perhaps more intriguing, is what new angles micro reactors bring to reaction chemistry and these are only now just emerging. Extending the heterogeneous catalyst work already described^{64–66} one can see how immobilised or supported reagents could be placed within a device to impart functionality to a reaction whilst maintaining spatial and temporal control. This concept could be extended to consider self-assembly methods for generating surface-specific properties such as shape and energy or colloidal-based processes. Such concepts could also be easily extended to include biological functionality and integration. One intriguing aspect of electrokinetically-operated micro reactors is anecdotal electrochemical effect that will undoubtedly yield novel chemistries in the next few years.

This review would not be complete without some estimate of the impact of this technology. The success of pharmaceutical companies resides largely on synthesis and screening of novel chemical entities representative of the universe of drug-like compounds, which may be of the order of 10^{200} compounds or about 10^{40} chemotypes, and to optimise selected leads to marketable drugs. Clearly, such a lead-generation task is beyond terrestrial resources. In an industry where development costs are extraordinarily high and attrition rates from lead generation onwards are about 98%, careful lead selection and ruthless pressure to shorten optimisation cycle times are, therefore, critical for survival. In addition to this diligence, new technology that would enable a cost-neutral upward step-change in the number of lead candidates (and thus choice of a better lead) and/or

optimisation speed (to reduce time to market and extend patent life) would provide a distinct competitive advantage. The ability of the micro reactor to provide the opportunity for a range of controls over the chemistry environment, directly through device resident actuators, has already been described. A microchannel system also provides a potential separation column and a non-turbulent environment for partition between solvents. Integration of a micro reactor device, via purification and optional phase exchange elements, to one of the many highly sensitive microchannel-based biological assay systems may therefore not only be possible, but may also address some of the industries' potential requirements. Apart from the greatly reduced reaction times demonstrated for the micro reactors, handling times to assay and chemical reagent costs are virtually eliminated. In fact, with computer control and access to a range of categorised reagents, real-time prospecting to find and enhance leads may be possible. This paradigm is shown diagrammatically in Fig. 15.

In lead optimisation using conventional batch technology, irrespective of whether parallel or iterative mode is chosen, validation and optimisation of reactions tends to be the rate-limiting step. Based on the model described in Fig. 15, however, it can be seen that, if the biological assay was replaced by a chemical assay, and the conditions not the reagents are varied, then an auto-optimisation could be carried out. Replication of the optimised channel as a parallel bundle could then provide a means of amplifying the amounts of material generated, even up to the quantities required for *in vivo* biology. In effect, chemistry is probably poised for the same sort of revolution that has taken place in electronics, biochemical screening and molecular biology, to name but a few examples. This is essentially a realisation that the desired product is usually information rather than a tangible, storable product, although here we can see that micro reactors can deliver both. This could enable the 'Moore's Law' environment for data generation required to support a cheminformatic approach to chemical lead discovery that is truly the counterpart of the bioinformatic discovery of biological targets from the human genome. It may also, at last, disconnect the chemist from the sheer slow drudgery of manual chemistry!

Clearly the mass of material generated in the type of micro

reactor described is very low and with continuous use could produce up to 1 g/day. The engineering aspects of parallel scaling out, ie maintaining the advantages of a small reaction zone whilst achieving volume, have been elaborated. This aspect of volume production together with the concept of make and use (i.e. no inventory) and localised distribution rather than bulk manufacture, storage, shipping and delivery are important factors. Perhaps the more compelling driver to develop localised production facilities based on micro reactors is the economic benefits of efficient flexible production that is responsive to market demands.

6. Concluding remarks

Accept it or not, micro reactor chemistry exists and is currently showing great promise as a novel method on which to build new chemical technology and processes. One of the current barriers to testing the methodology would seem to be system availability and the authors are currently planning to make the technology more accessible to the wider community. From whichever camp, sceptic or enthusiast, in the scientific community, the real value of micro reactors needs to be established and readers wishing to express their views on this topic are invited to contact the authors of this review.

Acknowledgements

We wish to thank EPSRC, UK (X. Z.) and Novartis Pharmaceuticals (P. W.) for financial support.

References

- Bradley, D. *Eur. Chem.* **1999**, *1*, 17.
- Fletcher, P. D. I.; Haswell, S. J. *Chem. Br.* **1999**, 35, 38.
- Cowen, S. *Chem. Ind.* **1999**, 584.
- McCreedy, T. *Chem. Ind.* **1999**, 588.
- Barrow, D.; Cefai, J.; Taylor, S. *Chem. Ind.* **1999**, 591.
- Cooper, J.; Disley, D.; Cass, T. *Chem. Ind.* **2001**, 653.
- Haswell, S. J.; Middleton, R. J.; O'Sullivan, B.; Skelton, V.; Watts, P.; Styring, P. *Chem. Commun.* **2001**, 5, 391.
- IMRET 5: Proceedings of the Fifth International Conference on Microreaction Technology*; Matlosz, M., Ehrfeld, W., Baselt, J. P., Eds.; Springer: Berlin, 2002.
- Ehrfeld, W.; Hessel, V.; Löwe, H. *Microreactors: New Technology for Modern Chemistry*; Wiley-VCH: Weinheim, Germany, 2000.
- Haswell, S. J. *Analyst* **1997**, *112*, 1R.
- Manz, A.; Harrison, D. J.; Verpoorte, E.; Fettingner, J. C.; Ludi, H.; Widmer, H. M. *Chimia* **1991**, *45*, 103.
- Manz, A.; Harrison, D. J.; Verpoorte, E.; Widmer, H. M. *Adv. Chromatogr.* **1993**, *33*, 1.
- Manz, A.; Effenhauser, C. S.; Burggraf, N.; Verpoorte, E.; Raymond, D. E.; Widmer, H. M. *Anal. Mag.* **1994**, *22*, M25.
- Proceedings of the Micro Total Analytical Systems '98 Workshop*; Harrison, D. J., van den Berg, A., Eds.; Kluwer Academic: Dordrecht, 1998.
- van den Berg, A.; Lammerink, T. S. J. *Top. Curr. Chem.* **1998**, *194*, 21.
- Harrison, D. J.; Fluri, K.; Seiler, K.; Fan, Z. H.; Effenhauser, C. S.; Manz, A. *Science* **1993**, *261*, 895.
- Jacobson, S. C.; Hergenroder, R.; Koutny, L. B.; Ramsey, J. M. *Anal. Chem.* **1994**, *66*, 1114.
- Woolley, A. T.; Hadley, D.; Ladre, P.; DeMello, A. J.; Mathies, R. A.; Northrup, M. A. *Anal. Chem.* **1996**, *68*, 4081.
- Woolley, A. T.; Mathies, R. A. *Anal. Chem.* **1995**, *67*, 3676.
- Woolley, A. T.; Sensabaugh, G. F.; Mathies, R. A. *Anal. Chem.* **1997**, *69*, 2181.
- Jacobsen, S. C.; Ramsey, J. M. *Anal. Chem.* **1996**, *68*, 720.
- Effenhauser, C. S.; Paulus, A.; Manz, A.; Widmer, H. M. *Anal. Chem.* **1994**, *66*, 2949.
- Schmalzing, D.; Adourian, A.; Koutny, L.; Ziaqura, L.; Matsudaria, P.; Ehrlich, D. *Anal. Chem.* **1998**, *70*, 2303.
- Spence, D. M.; Crouch, S. R. *Anal. Chem.* **1998**, 358, 95.
- Schoot, B. H.; Jeanneret, S.; Berg, A. *Anal. Meth. Instrum.* **1993**, *1*, 38.
- Madou, M. *Fundamentals of Microfabrication*; CRC: Boca Raton, 1997.
- McCreedy, T. *TrAC* **2000**, *19*, 396.
- McCreedy, T. *Anal. Chim. Acta* **2001**, *427*, 39.
- Katana 5040 High End Image Setter. For information see: www.screen.co.uk.
- Broadwell, I.; Fletcher, P. D. I.; Haswell, S. J.; McCreedy, T.; Zhang, X. *Lab on a Chip* **2001**, *1*, 66.
- Paul, P. H.; Garguilo, M. G.; Rakestraw, D. J. *Anal. Chem.* **1998**, *70*, 2459.
- Overbeek, J. Th. G. *Colloid Science*; Kruyt, H. R., Ed.; Elsevier: Amsterdam, 1952; Vol. 1, p 195 Chapter V.
- Rice, C. L.; Whitehead, R. *J. Phys. Chem.* **1965**, *69*, 4017.
- Hunter, R. J. *Zeta Potential in Colloid Science*; Academic: London, 1981.
- Jednacak, J.; Pravidic, V.; Haller, W. *J. Colloid Interface Sci.* **1974**, *49*, 16.
- Fletcher, P. D. I.; Haswell, S. J.; Paunov, V. N. *Analyst* **1999**, *124*, 1273–1282.
- Harmon, B. J.; Patterson, D. H.; Regnier, F. E. *Anal. Chem.* **1993**, *65*, 2655.
- Harmon, B. J.; Leesong, I.; Regnier, F. E. *Anal. Chem.* **1994**, *66*, 3797.
- Regnier, F. E.; Patterson, D. H.; Harmon, B. J. *TrAC* **1995**, *14*, 177.
- Patterson, D. H.; Harmon, B. J.; Regnier, F. E. *J. Chromatogr. A* **1996**, *732*, 119.
- Fletcher, P. D. I.; Haswell, S. J.; Zhang, X. *Lab-on-a-Chip* **2001**, *2*, 115.
- Jacobson, S. C.; Hergenroder, R.; Koutny, L. B.; Warmack, R. J.; Ramsey, J. M. *Anal. Chem.* **1994**, *66*, 1107.
- Ermakov, S. V.; Jacobson, S. C.; Ramsey, J. M. In *Micro Total Analysis Systems '98*; Harrison, D. J., Van den Berg, A., Eds.; Kluwer: Dordrecht, 1998; p 149.
- Knight, J. B.; Vishwanath, A.; Brody, J. P.; Austin, R. H. *Phys. Rev. Lett.* **1998**, *80*, 3863.
- Patankar, N. A.; Hu, H. H. *Anal. Chem.* **1998**, *70*, 1870.
- Ermakov, S. V.; Jacobson, S. C.; Ramsey, J. M. *Anal. Chem.* **2000**, *72*, 3512.
- Kamholz, A. E.; Weigl, B. H.; Finlayson, B. A.; Yager, P. *Anal. Chem.* **1999**, *71*, 5340.
- Jacobson, S. C.; McKnight, T. E.; Ramsey, J. M. *Anal. Chem.* **1999**, *71*, 4455.
- Polson, N. A.; Hayes, M. A. *Anal. Chem.* **2001**, *73*, 313A.
- Kenis, P. J. A.; Ismagilov, R. F.; Whitesides, G. M. *Science* **1999**, 285, 83.
- James, A. D.; Robinson, B. H. *J. Chem. Soc., Faraday Trans. 1* **1978**, *74*, 10.

52. Salimi-Moosavi, H.; Tang, T.; Harrison, D. J. *J. Am. Chem. Soc.* **1997**, *119*, 8716.
53. Doku, G. N.; Haswell, S. J.; McCreedy, T.; Greenway, G. M. *Analyst* **2001**, *126*, 14.
54. Burns, J. R.; Ramshaw, C. G. IMRET 4: Fourth International Conference of Micro Reaction Technology Topical Conference Proceedings AIChE Spring National Meeting, March 5–9, Atlanta GA, USA, 2000; p 133.
55. Skelton, V.; Greenway, G. M.; Haswell, S. J.; Styring, P.; Morgan, D. O.; Warrington, B.; Wong, S. Y. F. *Analyst* **2001**, *126*, 7.
56. Skelton, V.; Greenway, G. M.; Haswell, S. J.; Styring, P.; Morgan, D. O.; Warrington, B.; Wong, S. Y. F. *Analyst* **2001**, *126*, 11.
57. Sands, M.; Haswell, S. J.; Kelly, S. M.; Skelton, V.; Morgan, D. O.; Styring, P.; Warrington, B. H. *Lab on a Chip* **2001**, *1*, 64.
58. Wiles, C.; Watts, P.; Haswell, S. J.; Pombo-Villar, E. *Lab on a Chip* **2001**, *1*, 100.
59. Wiles, C.; Watts, P.; Haswell, S. J.; Pombo-Villar, E. *Lab on a Chip* **2002** in press.
60. Lu, H.; Schmidt, M. A.; Jenson, K. F. *Lab on a Chip* **2001**, *1*, 22.
61. Pitts, J. N.; Letsinger, R. L.; Taylor, R. P.; Patterson, J. M.; Recktenwald, G.; Martin, R. B. *J. Am. Chem. Soc.* **1959**, *81*, 1068.
62. Hisamoto, H.; Saito, T.; Tokeshi, M.; Hibara, A.; Kitamori, T. *J. Chem. Soc., Chem. Commun.* **2001**, 2662.
63. Watts, P.; Wiles, C.; Haswell, S. J.; Pombo-Villar, E.; Styring, P. *J. Chem. Soc., Chem. Commun.* **2001**, 990.
64. Carpino, L. A.; Han, G. Y. *J. Org. Chem.* **1972**, *37*, 3404.
65. Carpino, L. A.; Cohen, B. J.; Stephens, K. E.; Sadat-Aalae, S. Y.; Tien, J.-H.; Langridge, D. E. *J. Org. Chem.* **1986**, *51*, 3732.
66. Chan, W. C.; Bycroft, B. W.; Evans, D. J.; White, P. D. *J. Chem. Soc., Chem. Commun.* **1995**, 2209.
67. Greenway, G. M.; Haswell, S. J.; Morgan, D. O.; Skelton, V.; Styring, P. *Sens. Actuators, B* **2000**, *63*, 153.
68. Wilson, N. G.; McCreedy, T. *J. Chem. Soc., Chem. Commun.* **2000**, 733.
69. Haswell, S. J.; O'Sullivan, B.; Styring, P. *Lab on a Chip* **2001**, *1*, 164.
70. Dietzsch, E.; Hönicke, D.; Fichtner, M.; Schubert, K. IMRET 4: 4th International Conference of Micro Reaction Technology Topical Conference Proceedings, AIChE Spring National Meeting, March 5–9, 2000; p 89.
71. Rozen, S. *Acc. Chem. Res.* **1996**, *21*, 307.
72. Purrington, S. T.; Kagen, B. S.; Patrick, T. B. *Chem. Rev.* **1986**, *86*, 997.
73. Chambers, R. D.; Spink, R. C. H. *J. Chem. Soc., Chem. Commun.* **1999**, 883.
74. Chambers, R. D.; Holling, D.; Spink, R. C. H.; Sandford, G. *Lab on a Chip* **2001**, *1*, 132.
75. Chambers, R. D.; Greenhall, M. P.; Hutchinson, J. *Tetrahedron* **1996**, *52*, 1.
76. Chambers, R. D.; Grievson, B.; Drakesmith, F. G.; Powell, R. L. *J. Fluorine Chem.* **1985**, *29*, 323.
77. de Mas, N.; Jackman, R. J.; Schmidt, M. A.; Jenson, K. F. IMRET 5: Proceedings of the Fifth International Conference on Microreaction Technology, Springer: Berlin, 2002; p 60.
78. Srinivasan, R.; Hsing, I.-M.; Berger, P. E.; Jensen, K. F.; Firebaugh, S. L.; Schmidt, M. A.; Harold, M. P.; Lerou, J. J.; Ryley, J. F. *AIChE J.* **1997**, *43* (11), 3059.
79. Hessel, V.; Ehrfeld, W.; Golbig, K.; Hofman, C.; Jungwirth, S.; Löwe, H.; Richter, T.; Storz, M.; Wolf, A. IMRET 3: Proceedings of the Third Conference on Microtechnology, 2000; p 151.

Biographical sketch



Paul Fletcher is Professor of Physical Chemistry at the University of Hull. He leads the Surfactant & Colloid Research Group within the Department of Chemistry (see www.hull.ac.uk/scg) and his research interests include micro-reactors, microwaves and the surface and colloid chemistry of surfactant systems such as micelles, monolayers, microemulsions, emulsions and foams and reactions in complex media. He has published over 120 papers in these areas.



Stephen J. Haswell is Professor of Analytical Chemistry at the University of Hull. His current research activities are in the areas of micro reactors including analytical developments, microwave enhanced reaction chemistry, trace elemental speciation and process analysis. He is author of over 100 research papers, a number of books and patents and is widely known nationally and internationally for his enthusiastic lectures. For a number of years one of the underlying principles of Professor Haswell's research has been to break down the barriers that exist in science, in particular, the integration of analytical science with main line chemistry. Many of these ideals are encompassed in his research into micro chemical reactors, the subject of this article.



Esteban Pombo-Villar, Ph.D., C.Chem FRSC. Born in Bogotá, Colombia, May 24, 1958. Studies at the National University of Colombia, Bogotá, then at the University of Warwick, and University of Newcastle upon Tyne. M.Sc. and Ph.D. studies with Professor B. T. Golding, post-doctoral studies at ETH-Zurich with Professor A. Eschenmoser. Chaired the ECSOC-2 (1998) and ECSOC-3 (1999) electronic conferences, former Editor-in-Chief of *Molecules*. Employed with Sandoz Pharma as laboratory Head in Nervous System Research from 1988, now in Novartis Pharma AG, in Basel, Switzerland, where he is Manager of External Collaborations for Nervous System Research.



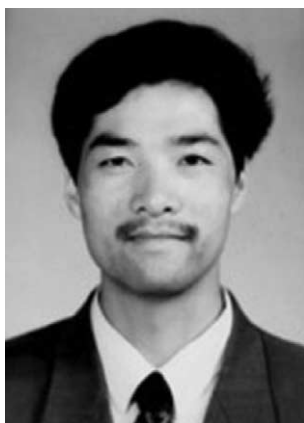
Brian H. Warrington has worked in various drug discovery roles and projects in GlaxoSmithKline Pharmaceuticals and its forebears since 1965. Since 1996 his interests have concentrated on high throughput technologies for chemical synthesis and drug discovery. Currently, he is VP Technology Development, Chemistry for GSK.



Paul Watts graduated from the University of Bristol in 1995 with a first class B.Sc. in chemistry. He continued his studies at Bristol, obtaining a Ph.D. in bio-organic chemistry under the supervision of Professor Tom Simpson FRS and Professor Chris Willis. His Ph.D. focussed on the synthesis of isotopically labelled compounds, for use in determination of biosynthetic pathways to polyketide-derived natural products. Paul subsequently worked as a postdoctoral research associate, with Professor Steve Haswell, at the University of Hull. During this period Paul investigated organic synthesis in micro reactors. In February 2002, Paul was appointed as a lecturer at the University of Hull. He is interested in organic chemistry and electrosynthesis in micro reactors.



Stephanie Y. F. Wong is a Senior Scientist at GlaxoSmithKline Pharmaceuticals in the Technology Development Department. She has worked in the pharmaceutical industry for over 10 years in several therapeutic areas and on targets such as nitric oxide synthase and serotonin receptors. Since the start of 1998 she has been working in the microfluidics area (Microsystems Technology) on novel methods to enhancing the drug discovery and optimisation process.



Xunli Zhang graduated from Northwest University in Xi'an, China, with a B.Sc. and an M. Eng. in Chemical Engineering. He obtained his Ph.D., studying on heterogeneous catalysis using microwave and conventional heating, from Imperial College of Science, Technology and Medicine of the University of London in 2000. Dr Xunli Zhang is currently working at the University of Hull in the Microreactor Research Group, aiming to model the behaviour of fluidics and chemical reactions in microreactors, develop methods of monitoring and control of microreactors, and integrate automated micro chemical systems.

The regioselective preparation of 1,3-diketones within a micro reactor

Charlotte Wiles,^a Paul Watts,^a Stephen J. Haswell^{*a} and Esteban Pombo-Villar^b^a Department of Chemistry, Faculty of Science and the Environment, University of Hull, Cottingham Road, Hull, UK HU6 7RX. E-mail: s.j.haswell@hull.ac.uk; Fax: 01482 466416; Tel: 01482 465475^b Nervous Systems Research, WSJ-386.07.15, Novartis Pharma Ltd, CH4002 Basel, Switzerland

Received (in Cambridge, UK) 6th February 2002, Accepted 2nd April 2002

First published as an Advance Article on the web 11th April 2002

We demonstrate a simple method for the regioselective preparation of 1,3-diketones within a micro reactor from silyl enol ethers where the products are free from both competing *O*-acylation and diacylation products.

Over the past three years, there has been a rapid growth in the development of micro reaction technology exploiting the technique of electroosmotic flow (EOF).¹ Recent research has demonstrated that along with multi-component reactions such as the Suzuki coupling² and the Wittig reaction,³ multi-step peptide synthesis can also be performed within a micro reactor.⁴

The enolate has been described as the most important intermediate in C–C bond formation. Its ambident nature however, allows the formation of bonds at either the carbon or the oxygen. In the case of acylation, this can result in the formation of a mixture of *O*- and *C*-acylated products which are difficult to separate, often resulting in low yields.⁵ A large amount of work has been undertaken in order to explore and understand the reaction conditions that promote the regioselective acylation of enolates, these include; the nature of the counter ion, reaction temperature, solvent, stoichiometry of reagents, order of reagent addition and type of acylating reagent.^{6,7} Although careful selection of the aforementioned conditions has been shown to influence the regioselectivity of the acylation, the 1,3-diketones produced remain contaminated with small amounts of *O*-acylated products.^{8,9,10} The procedure is however, still regarded as being heavily substrate dependent.¹¹

We recently demonstrated a simple technique for the regioselective preparation of uncontaminated 1,3-diketones in high to excellent conversions (> 95%) via the reaction of silyl enol ethers with acyl fluorides (1 h) and cyanides (24 h) in the presence of a catalytic amount of *anhydrous* TBAF (tetrabutylammonium fluoride).¹² We found that α -substituted ketones react with both acyl fluorides and cyanides to give 100% *C*-acylated products compared with non α -substituted ketones which gave 100% *O*-acylated products when reacted with acyl fluorides and *C*-acylated products when reacted with acyl cyanides. In this paper we wish to demonstrate the regioselective acylation of silyl enol ethers within a micro reactor using catalytic amounts of *anhydrous* TBAF. We also report reduced reaction times within a micro reactor in comparison to traditional batch reactions.

The borosilicate micro reactor used in this work was prepared using a standard fabrication procedure developed at Hull.¹³ The reactions were carried out using a 4 channel micro reactor, as illustrated in Fig. 1, with approximate channel dimensions of 100 × 50 μ m and outer dimensions of 20 × 20 × 25 mm. Micro porous silica frits were placed within the channels in order to minimise hydrodynamic effects.¹⁴ An in-house LabVIEWTM program was used to set and monitor the voltages applied to platinum electrodes placed in the reservoirs (power supply was built by Kingfield electronics).

All micro reactions were carried out under fume extraction in order to minimise exposure to the reagents used. The micro reactions were performed over a period of 20 min in order to ensure a sufficient volume of product was generated for analysis

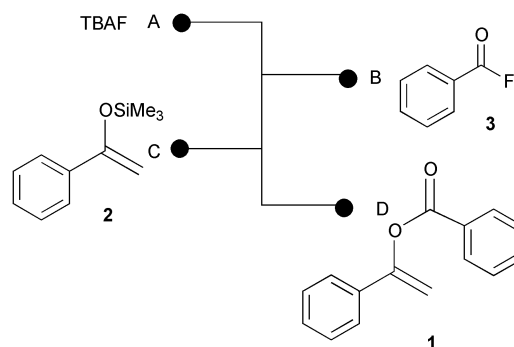


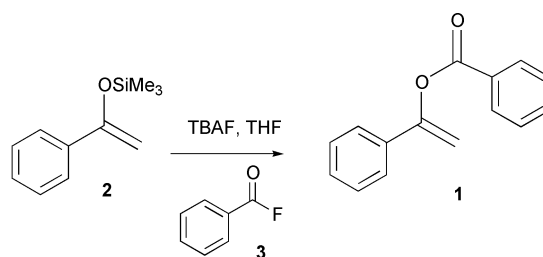
Fig. 1 Schematic of the micro reactor used in the synthesis of **1**.

(Typical flow rates of 0.3–0.4 μ l min⁻¹ were observed from each reservoir). Reaction products were determined by GC-MS via the comparison of retention times and spectra with those obtained from synthetically prepared standards.¹²

A synthetic standard of product **1** was prepared via the dropwise addition of the enol ether of acetophenone **2** (0.1 g, 0.52 mmol) to a stirred solution of *anhydrous* TBAF (0.014 g, 0.05 mmol) and benzoyl fluoride **3** (0.06 g, 0.52 mmol) in anhydrous THF (10 ml) (Scheme 1). The reaction mixture was stirred for 1 h, subsequent analysis by GC-MS showed that 100% conversion of the silyl enol ether of acetophenone **2** to the product **1** had been achieved.

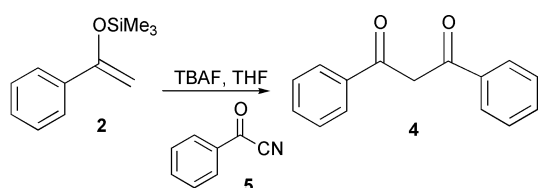
Having demonstrated that **1** could be prepared from the silyl enol ether **2**, this represented a synthetic target for preparation within a micro reactor (Fig. 1). Prior to the synthesis, the micro reactor was primed with anhydrous THF in order to remove any air or moisture from the channels and micro porous silica frits. A standard solution of TBAF (40 μ l, 0.1 M) in anhydrous THF was placed in reservoir A, a solution of benzoyl fluoride **3** (40 μ l, 1.0 M) in anhydrous THF in reservoir B and the silyl enol ether of acetophenone **2** (40 μ l, 1.0 M) in anhydrous THF was placed in reservoir C. The reaction products were collected in anhydrous THF in reservoir D over a period of 20 min. The reagents were manipulated within the device by the application of the following applied fields; 333, 455, 333 and 0 V cm⁻¹, resulting in 100% conversion to **1** (no products of *C*-acylation **4** or diacylation were observed).

Having successfully demonstrated the *O*-acylation of acetophenone within a micro reactor, we wished to also demonstrate that *C*-acylation was possible.



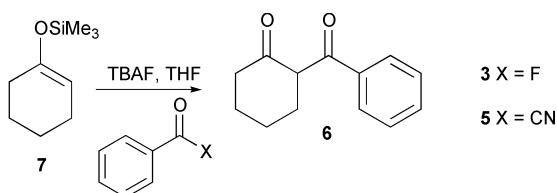
Scheme 1 Formation of **1** via the silyl enol ether of acetophenone **2**.

A synthetic standard of dibenzoylmethane **4** was prepared *via* the reaction of the silyl enol ether of acetophenone **2** and benzoyl cyanide **5** (Scheme 2). In order to obtain high conversion of the enol ether **2** to the product **4**, extended reaction times of 24 h were necessary. This is due to the reduced reactivity of benzoyl cyanide **5** compared with benzoyl fluoride **3**. Under the conditions stated above, 98% conversion with respect to the enol ether **2** was observed in bulk. Using a micro reactor, a standard solution of TBAF (40 μ l, 0.1 M) in anhydrous THF was placed in reservoir A, a solution of benzoyl cyanide **5** (40 μ l, 1.0 M) in anhydrous THF in reservoir B and the silyl enol ether of acetophenone **2** (40 μ l, 1.0 M) was placed in reservoir C. The reaction products were collected in anhydrous THF in reservoir D over a period of 20 min. The reagents were manipulated within the device using the following applied fields; 416, 318, 476 and 0 V cm^{-1} , this resulted in 100% conversion of the enol ether **2** to product **4**. In order to demonstrate the generality of the technique, the silyl enol ethers of propiophenone and cyclohexanone were also investigated.



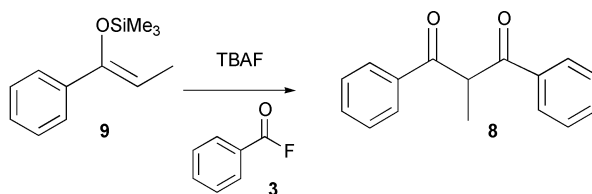
Scheme 2 Formation of **4** *via* the silyl enol ether of acetophenone **2**.

A synthetic standard of 2-benzoylcyclohexanone **6** was prepared *via* the reaction of the silyl enol ether of cyclohexanone **7** and benzoyl fluoride **3** (Scheme 3). Within 1 h, 100% conversion with respect to the silyl enol ether **7** was obtained in bulk. A standard solution of TBAF (40 μ l, 0.1 M) in anhydrous THF was placed in reservoir A, a solution of benzoyl fluoride **3** (40 μ l, 1.0 M) in anhydrous THF in reservoir B and the silyl enol ether of cyclohexanone **7** (40 μ l, 1.0 M) was placed in reservoir C. The reaction products were collected in anhydrous THF in reservoir D over a period of 20 min. The reagents were manipulated within the device using the following applied fields; 208, 409, 357 and 0 V cm^{-1} . This resulted in 100% conversion of the silyl enol ether of cyclohexanone **7** to product **6**. The reaction was repeated using benzoyl cyanide (40 μ l, 1.0 M) and the following applied fields; 208, 409, 381 and 0 V cm^{-1} , this resulted in 100% conversion of the enol ether of cyclohexanone **7** to 2-benzoylcyclohexanone **6**.



Scheme 3 Preparation of 2-benzoylcyclohexanone **6** *via* the silyl enol ether of cyclohexanone **7**.

We subsequently extended the technique to the preparation of product **8** within a micro reactor. A synthetic standard of **8** was prepared *via* the reaction of the silyl enol ether of propiophenone **9** with benzoyl fluoride **3** (Scheme 4). After stirring for 1 h, the reaction mixture was analysed by GC-MS and 99% of the



Scheme 4 Preparation of **8** *via* the silyl enol ether of propiophenone **9**.

silyl enol ether **9** was converted to product **8**. Using a micro reactor, a standard solution of TBAF (40 μ l, 0.1 M) in anhydrous THF was placed in reservoir A, a solution of benzoyl fluoride **3** (40 μ l, 1.0 M) in anhydrous THF in reservoir B and the silyl enol ether of propiophenone **9** (40 μ l, 1.0 M) was placed in reservoir C. The reaction products were collected in anhydrous THF in reservoir D over a period of 20 min. The reagents were manipulated within the device using the following applied fields; 375, 455, 405 and 0 V cm^{-1} . This resulted in 100% conversion of the silyl enol ether of propiophenone **9** to product **8**.

In conclusion, we have developed a simple, room temperature route to the regioselective formation of uncontaminated 1,3-diketones or *O*-acylated products depending upon the acylating reagents used. In all instances, no competing diacylation products were observed. The use of ammonium enolates is also advantageous as it removes the effect of a metal counter ion along with the observed reactions between aminated bases and acylating reagents.

In the preparation of β -hydroxyketones from silyl enol ethers we previously demonstrated that enhancements in both reaction rates and conversion are observed when using micro reactors.¹⁵ This work therefore re-emphasises the increase in reaction rates. Typically, the formation of **4** in batch required extended reaction times of 24 h due to reduced reagent reactivity however, when transferred to a micro reactor, quantitative conversions were observed in minutes.

Notes and references

- P. D. I. Fletcher, S. J. Haswell and V. N. Paunov, *Analyst*, 1999, **124**, 1273.
- G. M. Greenway, S. J. Haswell, D. O. Morgan, V. Skelton and P. Styring, *Sens. Actuators, B*, 2000, **63**, 153.
- V. Skelton, G. M. Greenway, S. J. Haswell, P. Styring, D. O. Morgan, B. Warrington and S. Y. F. Wong, *Analyst*, 2001, **126**, 7.
- P. Watts, C. Wiles, S. J. Haswell, E. Pombo-Villar and P. Styring, *J. Chem. Soc., Chem. Commun.*, 2001, 990.
- H. House, R. Auerbach, M. Gall and N. P. Peet, *J. Org. Chem.*, 1972, **38**, 514.
- M. W. Rathke and J. Dietch, *Tetrahedron Lett.*, 1971, 2953.
- A. R. Katritzky and A. Pastor, *J. Org. Chem.*, 1999, 3679.
- R. E. Tirpak and M. W. Rathke, *J. Org. Chem.*, 1982, **47**, 5099.
- I. Kopka and M. W. Rathke, *J. Org. Chem.*, 1981, **46**, 3771.
- H. T. Black, S. M. Arrivo, J. S. Schumm and J. M. Knobloch, *J. Org. Chem.*, 1987, **52**, 5425.
- G. Stork and P. F. Hudrlik, *J. Am. Chem. Soc.*, 1968, **90**, 4462.
- C. Wiles, P. Watts, S. J. Haswell and Esteban Pombo-Villar, *Tetrahedron Lett.*, 2002, **43**, 2945.
- T. McCreedy, *Anal. Chim. Acta*, 2001, **427**, 39.
- P. D. Christensen, S. W. P. Johnson, T. McCreedy, V. Skelton and N. G. Wilson, *Anal. Commun.*, 1998, **35**, 341.
- C. Wiles, P. Watts, S. J. Haswell and Esteban Pombo-Villar, *Lab on a Chip*, 2001, **1**, 100.



The regioselective preparation of 1,3-diketones

Charlotte Wiles,^a Paul Watts,^a Stephen J. Haswell^{a,*} and Esteban Pombo-Villar^b

^aDepartment of Chemistry, Faculty of Science and the Environment, University of Hull, Cottingham Road, Hull HU6 7RX, UK

^bNervous Systems Research, WSJ-386.07.15, Novartis Pharma Ltd., CH4002, Basel, Switzerland

Received 28 November 2001; revised 18 February 2002; accepted 1 March 2002

Abstract—The regioselectivity of the acylation of Li enolates and silyl enol ethers is reported using acyl halides and acyl cyanides. We illustrate a simple method for the preparation of 1,3-diketones via the silyl enol ether in excellent yields, free from competing *O*-acylation and diacylation products. © 2002 Elsevier Science Ltd. All rights reserved.

The enolate has been described as the most important intermediate in C–C bond formation. Its ambident nature however, allows the formation of bonds at either the carbon or the oxygen. In the case of acylation, this can result in the undesirable formation of a mixture of *O*- and *C*-acylated products which are difficult to separate, often resulting in low yields.¹ A large amount of work has been undertaken in order to explore and understand the reaction conditions that promote the regioselective acylation of enolates, these include; the nature of the counterion, reaction temperature, solvent, stoichiometry of reagents, order of reagent addition and type of acylating reagent.^{2,3} Although careful selection of the aforementioned conditions has been shown to influence the regioselectivity of the acylation, the 1,3-diketones produced remain contaminated with small amounts of *O*-acylated product.^{4,5} The procedure is still therefore regarded as being heavily substrate dependant.⁶

In the late 1960s, Stork et al. demonstrated that an enolate could be transformed into a silyl enol ether and then converted back to the enolate.⁶ The technique therefore enables the temporary trapping of an enolate while maintaining the regio- and stereochemical features.^{7,8} Stork described the regeneration of enolates via the use of methyl lithium. However, more recently *anhydrous* fluoride salts⁹ and reagents such as potassium ethoxide¹⁰ have found use in desilylation reactions. Beck et al. demonstrated the *C*-acylation of Li enolates generated by the treatment of silyl enol ethers with methyl lithium.¹¹ This technique proved advantageous as it removed the undesirable reaction between the

acylating reagent and amide base (LDA), previously observed by Rathke et al.² Howard and co-workers¹² have also demonstrated the *C*-acylation of Li enolates (generated using LDA) using acyl cyanides.^{13,14} Using this methodology, no competing *O*-acylation, diacylation or reactions of the enolate with the cyanide group were reported.

Although many techniques have demonstrated the formation of C–C bonds via the use of Li enolates and silyl enol ethers, there are few that enable the preparation of clean *O*-acylated products. Noyori et al. however demonstrated the selective *O*-acylation of silyl enol ethers using stoichiometric amounts of the expensive fluoride source, tris(dimethylamino)sulfonium difluorotrimethyl silicate (TASF).¹⁵ Limat and co-workers, subsequently demonstrated the use of a catalytic amount of tetrabutylammonium fluoride trihydrate to afford enol esters in good yields.¹⁶

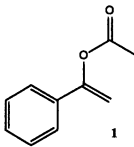
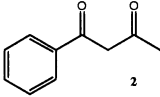
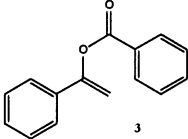
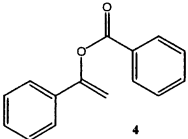
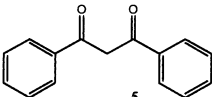
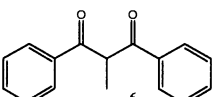
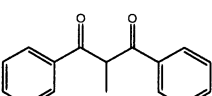
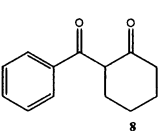
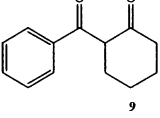
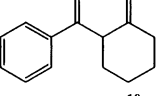
We report here a simple procedure for the regioselective acylation of ketones from their respective Li enolates (prepared using LiHMDS)¹⁷ and silyl enol ethers^{18,19} using a series of acylating reagents. The enolates are regenerated from the silyl enol ethers using a catalytic amount of *anhydrous* TBAF.²⁰ This effectively means that the enolate formed is ‘naked’ i.e. remains relatively unaffected by its counterion, in this case the ‘soft’ ammonium ion.⁷ As Table 1 illustrates, the products were isolated in good to excellent yields.

As Table 1 illustrates, the acylation of the Li enolate of acetophenone with acetyl chloride results in the formation of the *O*-acetylated product **1**.²¹ *O*-Acylation **3**²³ was also observed when using the reagent benzoyl chloride (Table 1), no contamination from competing

Keywords: acylation; silyl enol ethers; enolates; regioselectivity.

* Corresponding author.

Table 1. Products obtained from the acylation of a series of Li enolates and their respective silyl enol ethers

Entry	Ketone	Acylation Reagent	Product	Yield % ^a (Li Enolate)	Conversion % ^{b, c} (Enol ether)
1	Acetophenone	Acetyl chloride		89 ²¹	-
2	Acetophenone	Acetyl cyanide		92 ²²	97
3	Acetophenone	Benzoyl chloride		56 ²³	-
4	Acetophenone	Benzoyl fluoride		80	100
5	Acetophenone	Benzoyl cyanide		93 ²⁴	98
6	Propiophenone	Benzoyl chloride		95 ²⁵	-
7	Propiophenone	Benzoyl fluoride		96	99
8	Cyclohexanone	Benzoyl chloride		71 ²⁶	-
9	Cyclohexanone	Benzoyl fluoride		70	100
10	Cyclohexanone	Benzoyl cyanide		89	95

^a Yields calculated based on the ketone, products generated from the lithium enolate.

^b Conversions were calculated by GC-MS based on the amount of product with respect to the residual silyl enol ether.

^c No results are reported for the acylation of silyl enol ethers using acyl chlorides as no reactions were observed.

C-acylation was observed in either reaction. Subsequent reactions of the Li enolate of acetophenone with acetyl cyanide and benzoyl cyanide however, resulted in the formation of the C-acylated products, benzoyl acetone **2**²² and dibenzoylmethane **5**,²⁴ respectively. Again no contamination occurred from competing O-acylation (**1** and **3**).²³

Upon treatment of the silyl enol ether of acetophenone with acetyl chloride and benzoyl chloride, no reactions were observed. This phenomenon was also noted by Olofson et al. whereby the use of chloroformates in place of fluoroformates impeded the synthesis of enol carbonates from silyl enol ethers.²⁷ The acyl chlorides were therefore replaced by their respective acyl fluoride and again, O-acylation was observed **4**. Treatment of the silyl enol ether of acetophenone with benzoyl cyanide resulted in C-acylation and the preparation of dibenzoylmethane **5**.²⁴ As Table 1 illustrates, the acylation of propiophenone²⁵ (**6** and **7**) and cyclohexanone²⁶ (**8**, **9** and **10**) via both the Li enolates and their respective silyl enol ethers resulted in the formation of the C-acylated product regardless of the acylating reagent used.

The regioselectivity of both the acylations of Li enolates and silyl enol ethers was found to be dependent upon the type of ketone used i.e. α -substituted ketones gave C-acylated products and non α -substituted resulted in O-acylation with acyl halides and C-acylation with acyl cyanides. In all cases, the products were found to be 100% C- or O-acylated, no mixtures were observed. In comparison to the use of acyl cyanides, the treatment of a Li enolate with an acyl cyanide showed an increase in yield. An increase in conversion was also observed when using the silyl enol ether approach, compared to the direct acylation of the Li enolate.

In conclusion, the use of silyl enol ethers is advantageous as it removes the effect of a metal counterion along with the observed reactions between aminated bases and acylating reagents. The procedure provides a simple, room temperature, route to the formation of uncontaminated 1,3-diketones or O-acylated products in high yields.

Acknowledgements

We acknowledge Novartis Pharmaceuticals (C.W. and P.W.) who financially supported this research.

References

1. House, H.; Auerbach, R. A.; Gall, M.; Peet, N. P. *J. Org. Chem.* **1972**, *38*, 514.
2. Rathke, M. W.; Deitch, J. *Tetrahedron Lett.* **1971**, 2953.
3. Katritzky, A. R.; Pastor, A. *J. Org. Chem.* **1999**, 3679.
4. Tirpak, R. E.; Rathke, M. W. *J. Org. Chem.* **1982**, *47*, 5099.
5. The NMR and mass spectral data obtained from the silyl enol ethers were in accordance with published data. (a) Kopka, I.; Rathke, M. W. *J. Org. Chem.* **1981**, *46*, 3771; (b) Black, H. T.; Arrivo, S. M.; Schumm, J. S.; Knobloch, J. M. *J. Org. Chem.* **1987**, *52*, 5425.
6. Stork, G.; Hudrlik, P. F. *J. Am. Chem. Soc.* **1968**, *90*, 4462.
7. Kuwajima, I.; Nakamura, E. *Acc. Chem. Res.* **1985**, *18*, 181.
8. Kuwajima, I.; Nakamura, E.; Hashimoto, K. *Org. Synth.* **1982**, *61*, 122.
9. Nakamura, E.; Murofushi, T.; Shimizu, M.; Kuwajima, I. *J. Am. Chem. Soc.* **1976**, *98*, 2346.
10. Yu, W.; Jin, Z. *Tetrahedron Lett.* **2001**, *42*, 369.
11. Beck, A. K.; Hoestra, S. M.; Seebach, D. *Tetrahedron Lett.* **1977**, 1187.
12. Howard, A. S.; Meerholz, C. A.; Michael, J. P. *Tetrahedron Lett.* **1979**, *15*, 1339.
13. Renger, B.; Hugel, H.; Wykypiel, W.; Seebach, D. *Chem. Ber.* **1978**, *111*, 2630.
14. Taylor, E. C.; Andrade, J. G.; John, K. C.; McKillop, A. *J. Org. Chem.* **1978**, *43*, 2280.
15. Noyori, R.; Nishida, I.; Sakata, J. *J. Am. Chem. Soc.* **1983**, *105*, 1598.
16. Limat, D.; Schlosser, M. *Tetrahedron* **1995**, *51*, 5799.
17. *Example of a typical Li enolate procedure*: cyclohexanone (1.00 g, 10.20 mmol) was added dropwise to a stirred solution of lithium bis(trimethylsilyl)amide (LiHMDS) (10.20 ml, 1.0 M, 10.20 mmol) in THF (100 ml) over a period of 30 min. The resulting solution was stirred for a further 15 min prior to the addition of benzoyl fluoride (1.11 ml, 10.20 mmol) in THF (10 ml). The reaction mixture was stirred for 15 min and subsequently extracted using ethyl acetate (3×50 ml). The combined organic solvents were dried over magnesium sulfate and concentrated in vacuo. Purification was achieved using silica gel chromatography. Elution with 10% ethyl acetate in hexane yielded 2-benzoylcyclohexanone (1.44 g, 70%).
18. *Example of a typical silyl enol ether preparation*: A solution of cyclohexanone (0.10 g, 1.02 mmol) in anhydrous THF (10 ml) was added dropwise to a stirred solution of LiHMDS (1.02 ml, 1.0 M, 1.02 mmol) over a period of 30 min. The solution was then stirred for a further 15 min prior to the addition of chlorotrimethylsilane (0.13 ml, 1.20 mmol). The reaction mixture was concentrated in vacuo and the resulting residue dissolved in DCM (50 ml). The inorganics were removed by filtration and the resulting solution concentrated in vacuo to yield the silyl enol ether of cyclohexanone (0.16 g, 93%).
19. *Example of a typical acylation using a silyl enol ether*: The silyl enol ether of cyclohexanone (0.10 g, 0.59 mmol) was added dropwise to a stirred solution of anhydrous TBAF (0.015 g, 0.059 mmol) and benzoyl fluoride (0.06 ml, 0.59 mmol) in anhydrous THF (10 ml). The reaction mixture was extracted into ethyl acetate (3×50 ml) and the combined organic solvents dried over magnesium sulfate. Purification was achieved using silica gel chromatography. Elution with 10% ethyl acetate in hexane gave 2-benzoyl cyclohexanone (100% conversion, calculated by GC-MS, with respect to residual silyl enol ether).

20. *Anhydrous* tetrabutylammonium fluoride was prepared from TBAF·3H₂O, purchased from Aldrich. The TBAF·3H₂O was dried over phosphorous pentoxide under vacuum (10 mm Hg) for 48 h to afford a gelatinous solid. The use of TBAF·3H₂O proved unsuccessful as a catalytic desilylation agent as the added moisture resulted in the protonation of the enolate, converting it back to the corresponding ketone.
21. Compound **1**: δ_{H} (400 MHz, CDCl₃/TMS) 2.24 (3H, s, CH₃), 4.87 (1H, d, *J* 2.2, CHH), 5.33 (1H, d, *J* 2.2, CHH), 7.29 (2H, m, Ar) and 7.33 (3H, m, Ar); *m/z* (EI) 163 (M⁺+1, 26%), 162 (65), 161 (100) and 105 (50).
22. Compound **2**: δ_{H} (400 MHz, CDCl₃/TMS) 2.19 (3H, s, CH₃), 6.17 (2H, s, CH₂), 7.43 (3H, m, Ar) and 7.86 (2H, m, Ar); δ_{C} (100 MHz, CDCl₃/TMS) 25.9 (CH₃), 96.8 (CH₂), 125.6 (CH), 128.7 (CH), 132.4 (CH), 134.9 (C), 183.4 (CO) and 194.0 (CO); *m/z* (EI) 163 (M⁺+1, 100%), 162 (30), 161 (35), 105 (45) and 77 (10).
23. Compound **3**: δ_{H} (400 MHz, CDCl₃/TMS) 5.16 (1H, d, *J* 2.3, CHH), 5.59 (1H, d, *J* 2.3, CHH), 7.35 (3H, m, Ar) and 7.95 (7H, m, Ar); δ_{C} (100 MHz, CDCl₃/TMS) 102.4 (CH₂), 125.0 (CH), 128.7 (CH), 128.8 (CH), 130.2 (CH), 133.7 (CH), 134.4 (C) and 134.7 (C); *m/z* (EI) 225 (M⁺+1, 5%), 224 (20), 105 (100) and 77 (20).
24. Compound **5**: δ_{H} (400 MHz, CDCl₃/TMS) 6.84 (2H, s, CH₂), 7.51 (6H, m, Ar) and 7.98 (4H, m, Ar); δ_{C} (100 MHz, CDCl₃/TMS) 93.3 (CH₂), 127.3 (CH), 128.8 (CH), 132.6 (CH), 135.6 (C) and 185.9 (CO); *m/z* (EI) 225 (M⁺+1, 25%), 224 (50), 223 (75), 105 (100) and 77 (75).
25. Compound **6**: δ_{H} (400 MHz, CDCl₃/TMS) 1.59 (1H, d, *J* 7.0, CH₃), 5.28 (3H, q, *J* 7.0, CH), 7.96 (6H, m, Ar) and 7.45 (4H, m, Ar); δ_{C} (100 MHz, CDCl₃/TMS) 14.5 (CH₃), 51.1 (CH₂), 128.6 (CH), 129.0 (CH), 130.0 (CH), 133.6 (C) and 197.3 (CO); *m/z* (EI) 239 (M⁺+1, 2%), 238 (10) and 105 (100).
26. Compound **8**: δ_{H} (400 MHz, CDCl₃/TMS) 1.74 (2H, m, CH₂), 1.98 (2H, m, CH₂), 2.28 (2H, m, CH₂), 2.54 (2H, m, CH₂), 4.38 (1H, m, CH), 7.44 (2H, m, Ar), 7.54 (1H, m, Ar) and 7.89 (2H, m, Ar); δ_{C} (100 MHz, CDCl₃/TMS) 23.2 (CH₂), 23.5 (CH₂), 27.4 (CH₂), 30.1 (CH₂), 58.9 (CH), 128.6 (CH), 128.7 (CH), 133.3 (CH), 136.6 (C), 197.7 (CO) and 208.7 (CO); *m/z* (EI) 203 (M⁺+1, 15%), 202 (30), 201 (28), 105 (100) and 77 (55).
27. Olofson, R. A.; Cuomo, J. *Tetrahedron Lett.* **1980**, 819.

Investigation of racemisation in peptide synthesis within a micro reactor

Paul Watts,^a Charlotte Wiles,^a Stephen J. Haswell*^a and Esteban Pombo-Villar^b

^a Department of Chemistry, University of Hull, Cottingham Road, Hull, UK HU6 7RX.

E-mail: s.j.haswell@hull.ac.uk; Fax: 01482 466416; Tel: 01482 465475

^b Nervous System Research, WSJ-386.07.15, Novartis Pharma Ltd, CH4002 Basel, Switzerland

Received 24th April 2002, Accepted 30th May 2002

First published as an Advance Article on the web 17th June 2002

We demonstrate that peptides derived from α -amino acids may be prepared in a micro reactor. The peptides were prepared in 20 min with quantitative conversion, compared to batch reactions which require prolonged reaction times. We illustrate that by using dilute reagent concentrations and short reaction times, less racemisation is observed in micro reactions than in bulk reactions.

Introduction

A range of multi-component reactions such as the Sukuki,¹ Wittig,^{2,3} Aldol condensation⁴ and Michael addition⁵ have been performed in micro reactors under electroosmotic flow (EOF) conditions.^{6,7} In addition, we recently demonstrated that pentafluorophenyl ester **1** could be converted into dipeptide **2** with 100% conversion (Scheme 1) within a micro reactor.^{8,9} In comparison, when the reaction was performed at the same concentration and temperature in a bulk reaction only 75% conversion was obtained after nearly 500 h (Fig. 1).

Whilst rate enhancements associated with reactions within micro reactor devices are generally attributed to diffusive mixing under non-turbulent conditions,¹⁰ in this current example the enhanced rate of reaction is also associated with the reaction occurring within an electric field, previously described in ref. 9.

To date, only the synthesis in a micro reactor of peptides containing β -amino acids has been reported.^{8,9} These amino acids do not have chiral centres, hence potential problems with racemisation are avoided. In addition, β -peptides have attracted much interest due to their structural^{11,12} and biological properties.¹³ In particular, their stability to degradation by peptidases^{14,15} makes them potentially superior to the drugs derived from α -amino acids. However, many peptides also contain α -amino acid residues which are prone to racemisation. We were therefore interested to investigate if the low reagent concentrations and reduced reaction times, observed in micro reactors, would effect the levels of racemisation occurring.

In bulk reactions, peptides are commonly derivitised as their Moshers amide¹⁶ and ¹⁹F-NMR is used to calculate the amount of racemisation occurring. However, micro reactors currently produce ng– μ g quantities of product, which is insufficient for such NMR analysis. Hence it was necessary to use a GC-MS method to calculate the degree of racemisation.

In this paper, a micro reactor has been used to prepare peptide derivatives using solution phase chemistry to evaluate the level

of racemisation that occurs when reactions are conducted within micro reactors.

Results and Discussion

As a model reaction we investigated racemisation of *R*-2-phenylbutyric acid **3**. The acid **3** was reacted with *R*- and *S*-methylbenzylamine **4** and **5** to prepare synthetic samples of the diastereomers **6** and **7** with 97 and 95% yield respectively (Scheme 2). It was demonstrated that these products were

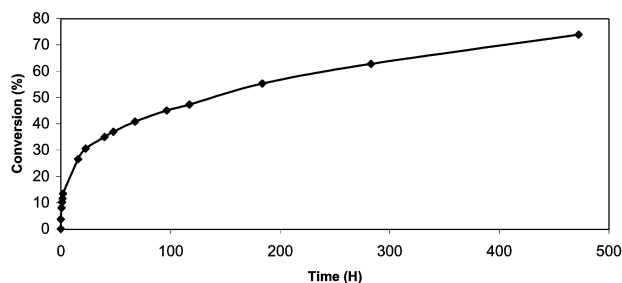
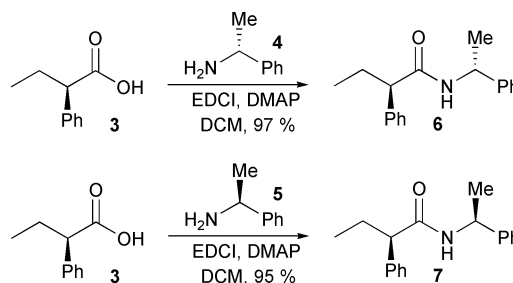
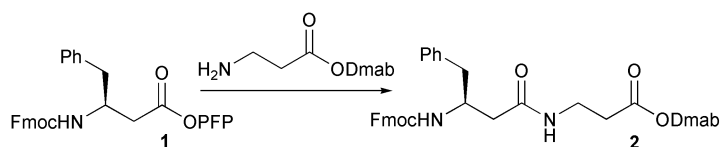


Fig. 1 Conversion of PFP ester **1** into dipeptide **2** in bulk reaction.



Scheme 2 Preparation of amides of *R*-2-phenylbutyric acid.



Scheme 1 Synthesis of a β -peptide.

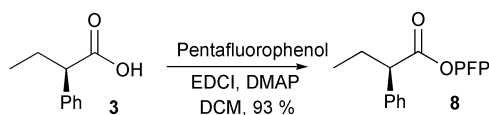
separable by gas chromatography and the results indicated that up to 6.2% racemisation occurred in the bulk reactions.

Having established a method to separate the diastereomers it was now possible to quantify if racemisation occurred when the reaction was performed in a micro reactor. The micro reactions were conducted using the pentafluorophenyl ester **8** of *R*-2-phenylbutyric acid **3**, which was prepared *via* a 1-(3-dimethylaminopropyl)-3-ethylcarbodiimide hydrochloride (EDCI) coupling reaction with 93% yield (Scheme 3). The pentafluorophenyl ester derivative **8** was used, based on previous results.^{8,9}

Prior to synthesis the micro reactor was primed with anhydrous *N,N*-dimethylformamide (DMF), in order to remove any air and moisture from the channels and the micro porous silica frits. A standard solution of pentafluorophenyl ester **8** (30 μ l, 0.1 M) in DMF was placed in reservoir A and a solution of *S*- α -methylbenzylamine **5** (30 μ l, 0.1 M) was placed in reservoir B. The reaction products were collected in reservoir C, which contained anhydrous DMF (30 μ l) (Fig. 2).

It was found that using continuous flow of both reagents (0.1 M), where the ester **8** was maintained at 600 V and the amine **5** was maintained at 1000 V, the product **7** was prepared quantitatively in 20 min. Under these conditions it was found that $4.2 \pm 1.1\%$ ($n = 5$) racemisation occurred. The reaction was also investigated at a higher concentration (0.5 M) and as expected it was found that the amount of racemisation increased to $7.8 \pm 1.0\%$ ($n = 6$).

Having demonstrated that racemisation of a simple chiral carboxylic acid could be monitored, the racemisation of the α -amino acid, alanine was investigated. Boc-*D*-alanine **9** was reacted with *S*- α -methylbenzylamine **5** *via* an EDCI coupling reaction, to prepare a synthetic sample of amide **10** with 61% yield (Scheme 4). Similarly Boc-*L*-alanine **11** was converted into amide **12** with 84% yield and it was shown that diastereomeric amides **10** and **12** were also separable by gas chromatography.



Scheme 3 Preparation of pentafluorophenyl ester.

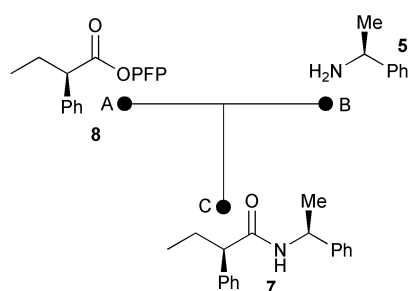
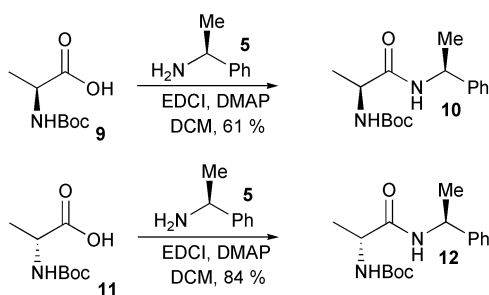


Fig. 2 Schematic of micro reactor.



Scheme 4 Preparation of amides of alanine.

In the micro reactor, a standard solution of the pentafluorophenyl ester **13** of Boc-*D*-alanine (30 μ l, 0.1 M) in DMF was placed in reservoir A and a solution of *S*- α -methylbenzylamine **5** (30 μ l, 0.1 M) was placed in reservoir B. The reaction products were collected in reservoir C, which contained anhydrous DMF (30 μ l). It was found that using continuous flow of both reagents (0.1 M), where the ester **13** and the amine **5** were both maintained at 1000 V, the product **10** was prepared quantitatively in 20 min. Under these conditions it was found that $5.6 \pm 0.8\%$ ($n = 5$) racemisation occurred.

Conclusions

In conclusion, we have demonstrated that peptides derived from α -amino acids may be prepared in a micro reactor. We have shown that the peptide bonds may be prepared in 20 min with quantitative yield, compared to batch reactions which generally require prolonged reaction times of up to 24 h to achieve high yields.

We have shown that the amount of racemisation is highly dependant upon the concentration of the reagents. When the reaction was conducted at 0.1 M concentration, the amount of racemisation was slightly less than in the bulk reactions. Further studies are currently underway within our laboratories to investigate racemisation in more complex peptides and to purify the peptides by electrophoretic separation.¹⁷

Experimental

Micro reactions

The borosilicate glass micro reactor used in this work was prepared using standard fabrication procedures developed at the University of Hull.¹⁸ The micro reactor had approximate channel dimensions of $100 \times 50 \mu\text{m}$ and outer dimensions of $20 \times 20 \times 25 \text{ mm}$. Micro porous silica frits were placed within the channels to minimise hydrodynamic effects.¹⁹ An in-house LabVIEW™ program was used to set and monitor the voltages applied to platinum electrodes, which were placed in the reagent reservoirs (power supply built by Kingfield Electronics, UK).

All micro reactions were carried out at room temperature over a period of 20 min to ensure a sufficient volume of product for analysis. Reaction products were determined by GC-MS *via* comparison of retention times and spectra with those obtained from synthetic standards. A Varian CP-3800 coupled to a Varian Saturn 2000 mass spectrometer fitted with a CP-Sil 8 column (30 m) was used for the analysis (injector temperature 250 $^{\circ}\text{C}$; helium flow rate 1 ml min^{-1} ; oven held at 60 $^{\circ}\text{C}$ for 1 min then ramped to 270 $^{\circ}\text{C}$ at 25 $^{\circ}\text{C} \text{ min}^{-1}$). Product conversions were calculated with respect to the amount of amino acid remaining in the sample.

Bulk reactions

All solvents were purchased as anhydrous solutions over molecular sieves from Fluka. Reagents were purchased from Fluka or Aldrich and used as supplied. Column chromatography was carried out using Fluka silica gel 60 as the solid support. Compounds were eluted using various mixtures of ethyl acetate and hexane. Nuclear magnetic resonance (NMR) spectra were recorded as solutions in deuteriochloroform (CDCl_3), using tetramethylsilane (TMS) as internal standard. The spectra were recorded on Jeol GX270 or GX400 spectrometers. The chemical shift values for all spectra are given in parts per million with coupling constants in Hertz. Mass spectra were recorded using a Varian Saturn 2000 mass spectrometer.

Synthetic standards of all products were prepared using the following procedure: A solution of EDCI (*ca.* 1.3 eq.) and 4-dimethylaminopyridine (DMAP, *ca.* 0.1 eq.) in dichloromethane (DCM, 10 ml) was added to a stirred solution of the carboxylic acid (1 eq.) and α -methylbenzylamine or pentafluorophenol (*ca.* 1.3 eq.) in DCM (20 ml) at room temperature under nitrogen. After 24 h, the solvent was washed with dilute hydrochloric acid (20 ml) and the aqueous layer was further extracted with DCM (2 \times 50 ml). The combined organic extracts were dried over magnesium sulfate and concentrated *in vacuo* to give the product which was purified by column chromatography.

R- α -methylbenzylamide of R-phenylbutyric acid 6

The reaction was carried out according to the general procedure using EDCI (271 mg, 1.41 mmol), DMAP (11 mg, 0.09 mmol), R-2-phenylbutyric acid **3** (227 mg, 1.38 mmol) and R- α -methylbenzylamine **4** (203 mg, 1.67 mmol). Elution with 20% ethyl acetate in hexane gave amide **6** (358 mg, 97%) as a white solid; δ_{H} (400 MHz) 0.89 (3H, t, *J* 7.6, CH₃CH₂), 1.41 (3H, d, *J* 6.7, CH₃CH), 1.77 (1H, m, CH₃CHH), 2.18 (1H, m, CH₃CHH), 3.27 (1H, t, *J* 7.6, CHCH₂), 5.08 (1H, dq, *J* 7.8 and 6.7, CHCH₃), 5.84 (1H, br d, *J* 7.8, NH) and 7.18–7.35 (10H, m, Ar); δ_{C} (100 MHz) 12.3, 21.9, 26.3, 48.5, 55.0, 125.7, 127.0, 127.1, 127.9, 128.4, 128.6, 140.0, 143.2 and 172.5; *m/z* (EI) 267 (M⁺, 65 %), 252 (5), 119 (45), 105 (100), 91 (95) and 77 (27).

S- α -methylbenzylamide of R-phenylbutyric acid 7

The reaction was carried out according to the general procedure using EDCI (219 mg, 1.14 mmol), DMAP (14 mg, 0.11 mmol), R-2-phenylbutyric acid **3** (141 mg, 0.86 mmol) and S- α -methylbenzylamine **5** (121 mg, 1.00 mmol). Elution with 20% ethyl acetate in hexane gave amide **7** (217 mg, 95%) as a white solid; δ_{H} (400 MHz) 0.84 (3H, t, *J* 7.3, CH₃CH₂), 1.41 (3H, d, *J* 7.0, CH₃CH), 1.77 (1H, m, CH₃CHH), 2.15 (1H, m, CH₃CHH), 3.22 (1H, t, *J* 7.6, CHCH₂), 5.08 (1H, dq, *J* 7.6 and 7.0, CHCH₃), 5.80 (1H, br d, *J* 7.6, NH) and 7.21–7.36 (10H, m, Ar); δ_{C} (68 MHz) 12.3, 21.5, 26.5, 48.7, 55.1, 126.0, 127.1, 127.2, 127.9, 128.6, 128.7, 140.1, 143.3 and 172.6; *m/z* (EI) 267 (M⁺, 57 %), 252 (5), 119 (40), 105 (95), 91 (100) and 77 (30).

Pentafluorophenyl ester of R-phenylbutyric acid 8

The reaction was carried out according to the general procedure using EDCI (331 mg, 1.73 mmol), DMAP (29 mg, 0.24 mmol), R-2-phenylbutyric acid **3** (254 mg, 1.55 mmol) and pentafluorophenol (364 mg, 1.98 mmol). Elution with 10% ethyl acetate in hexane gave ester **8** (476 mg, 93%) as a colourless oil; δ_{H} (400 MHz) 1.00 (3H, t, *J* 7.4, CH₃CH₂), 1.94 (1H, m, CH₃CHH), 2.25 (1H, m, CH₃CHH), 3.81 (1H, t, *J* 7.6, CH₃CH) and 7.30–7.41 (5H, m, Ar); δ_{C} (68 MHz) 11.9, 26.7, 52.8, 127.9, 128.0, 128.9, 136.1 (m), 137.2, 137.6 (m), 139.2 (m), 139.8 (m), 141.3 (m), 142.9 (m) and 170.1; *m/z* (EI) 301 (M⁺-CH₃CH₂, 2%), 119 (100) and 91 (27).

S- α -methylbenzylamide of Boc-D-alanine 10

The reaction was carried out according to the general procedure using EDCI (255 mg, 1.33 mmol), DMAP (7 mg, 0.06 mmol), Boc-D-alanine **9** (177 mg, 0.94 mmol) and S- α -methylbenzylamine **5** (144 mg, 1.19 mmol). Elution with 30% ethyl acetate in hexane gave amide **10** (167 mg, 61%) as a white solid; δ_{H} (400

MHz) 1.32 (3H, d, *J* 7.0, CH₃CH), 1.41 (9H, s, (CH₃)₃C), 1.46 (3H, d, *J* 7.0, CH₃CH), 4.18 (1H, br s, NH), 5.05 (1H, q, *J* 7.0, CH₃CH), 5.21 (1H, d, *J* 7.0, CH₃CH), 6.85 (1H, br s, NH) and 7.20–7.31 (5H, m, Ar); δ_{C} (100 MHz) 17.8, 22.0, 28.2, 48.6, 49.9, 80.0, 126.0, 127.1, 128.5, 143.2, 155.7 and 171.7; *m/z* (EI) 293 (M⁺+1, 2 %), 237 (100), 193 (32), 120 (40) and 105 (45).

S- α -methylbenzylamide of Boc-L-alanine 12

The reaction was carried out according to the general procedure using EDCI (283 mg, 1.48 mmol), DMAP (5 mg, 0.04 mmol), Boc-L-alanine **11** (220 mg, 1.16 mmol) and S- α -methylbenzylamine **5** (140 mg, 1.16 mmol). Elution with 30% ethyl acetate in hexane gave amide **12** (286 mg, 84%) as a white solid; δ_{H} (400 MHz) 1.31 (3H, d, *J* 6.8, CH₃CH), 1.42 (9H, s, (CH₃)₃C), 1.46 (3H, d, *J* 7.0, CH₃CH), 4.19 (1H, br s, NH), 5.08 (1H, q, *J* 6.8, CH₃CH), 5.28 (1H, d, *J* 7.0, CH₃CH), 6.84 (1H, br s, NH) and 7.21–7.33 (5H, m, Ar); δ_{C} (100 MHz) 18.2, 21.9, 28.3, 48.6, 50.0, 79.9, 126.0, 127.2, 128.6, 143.1, 155.6 and 171.9; *m/z* (EI) 293 (M⁺+1, 2%), 237 (100), 193 (30), 120 (37) and 105 (32).

Pentafluorophenyl ester of Boc-D-alanine 13

The reaction was carried out according to the general procedure using EDCI (733 mg, 3.82 mmol), DMAP (10 mg, 0.08 mmol), Boc-D-alanine **9** (677 mg, 3.58 mmol) and pentafluorophenol (699 mg, 3.80 mmol). Elution with 20% ethyl acetate in hexane gave ester **13** (1.10 g, 86%) as a white solid; δ_{H} (400 MHz) 1.47 (9H, s, (CH₃)₃C), 1.59 (3H, d, *J* 7.3, CH₃CH), 4.66 (1H, m, CHCH₃) and 5.03 (1H, br d, *J* 6.5, NH); δ_{C} (68 MHz) 18.2, 28.2, 49.2, 80.6, 136.0 (m), 137.8 (m), 139.2 (m), 139.7 (m), 141.5 (m), 142.9 (m), 154.9 and 169.8; *m/z* (EI) 300 (100) and 256 (62).

Acknowledgements

We wish to thank Novartis Pharmaceuticals (P.W. and C.W.) for financial support. We are grateful to Dr Tom McCreedy (University of Hull) for help in fabricating the micro reactor devices.

References

- 1 G. M. Greenway, S. J. Haswell, D. O. Morgan, V. Skelton and P. Styring, *Sens. Actuators, B*, 2000, **63**, 153.
- 2 V. Skelton, G. M. Greenway, S. J. Haswell, P. Styring, D. O. Morgan, B. Warrington and S. Y. F. Wong, *Analyst*, 2001, **126**, 7.
- 3 V. Skelton, G. M. Greenway, S. J. Haswell, P. Styring, D. O. Morgan, B. Warrington and S. Y. F. Wong, *Analyst*, 2001, **126**, 11.
- 4 C. Wiles, P. Watts, S. J. Haswell and E. Pombo-Villar, *Lab Chip*, 2001, **1**, 100.
- 5 C. Wiles, P. Watts, S. J. Haswell and E. Pombo-Villar, *Lab Chip*, 2002, **2**, 62.
- 6 P. D. I. Fletcher, S. J. Haswell and V. N. Paunov, *Analyst*, 1999, **124**, 1273.
- 7 S. J. Haswell, R. J. Middleton, B. O'Sullivan, V. Skelton, P. Watts and P. Styring, *Chem. Commun.*, 2001, 391.
- 8 P. Watts, C. Wiles, S. J. Haswell, E. Pombo-Villar and P. Styring, *Chem. Commun.*, 2001, 990.
- 9 P. Watts, C. Wiles, S. J. Haswell and E. Pombo-Villar, *Tetrahedron*, 2002, in press.
- 10 P. D. I. Fletcher, S. J. Haswell, E. Pombo-Villar, B. H. Warrington, P. Watts, S. Y. F. Wong and X. Zhang, *Tetrahedron*, 2002, in press.
- 11 X. Daura, K. Gademann, H. Schaefer, B. Jaun, D. Seebach and W. F. van Gunsteren, *J. Am. Chem. Soc.*, 2001, **123**, 2393.
- 12 D. Seebach, J. V. Schreiber, S. Abele, X. Daura and W. F. van Gunsteren, *Helv. Chim. Acta*, 2000, **83**, 34.
- 13 G. P. Dado and S. H. Gellman, *J. Am. Chem. Soc.*, 1994, **116**, 1054.

- 14 K. Gademann, M. Ernst, D. Seebach and D. Hoyer, *Helv. Chim. Acta*, 2000, **83**, 16.
- 15 M. Werder, H. Hauser, S. Abele and D. Seebach, *Helv. Chim. Acta*, 1999, **82**, 1774.
- 16 J. A. Dale, D. L. Dull and H. S. Mosher, *J. Org. Chem.*, 1969, **34**, 2543.
- 17 S. C. Jacobsen, R. Hergenroder, L. B. Koutny and J. M. Ramsey, *Anal. Chem.*, 1994, **66**, 1114.
- 18 T. McCreedy, *Anal. Chim. Acta*, 2001, **427**, 39.
- 19 P. D. Christensen, S. W. P. Johnson, T. McCreedy, V. Skelton and N. G. Wilson, *Anal. Commun.*, 1998, **35**, 341.

Electrokinetic control of a chemical reaction in a lab-on-a-chip micro-reactor: measurement and quantitative modelling†

Paul D. I. Fletcher,* Stephen J. Haswell and Xunli Zhang

Department of Chemistry, The University of Hull, Hull, UK HU6 7RX.

E-mail: P.D.Fletcher@hull.ac.uk

Received 14th February 2002, Accepted 15th April 2002

First published as an Advance Article on the web 30th April 2002

We have investigated the complex formation/dissociation reaction between Ni^{2+} ions and the ligand pyridine-2-azo-*p*-dimethylaniline (PADA) in a glass micro-reactor operating under electrokinetic control. An *in situ*, microscope-imaging technique was used to determine the spatial and temporal evolution of the reaction within the channel network of the micro-reactor. Using appropriately controlled voltage sequences, a 'slug' of PADA was injected into a stream of Ni^{2+} solution. Under the experimental reaction conditions used, Ni^{2+} ions are mixed with the PADA as a consequence of the species' different electrokinetic mobilities allowing the complex formation to occur at the trailing edge of the PADA slug. Following complex formation, reversal of the flow results in the partial re-formation of free PADA by dissociation of the complex, demonstrating that voltage control can be used to drive the reaction either forwards or backwards. We discuss the methods whereby all the parameters required to predict the spatial and temporal evolution of the reaction in the micro-reactor can be either measured or estimated. Based on the estimated parameters, model calculations of the concentration profiles as a function of time show good agreement with the measured data.

Introduction

There is a growing interest in the development of miniaturised micro-reactor devices for a wide range of chemical and measurement applications encompassed by the so-called 'Lab-on-a-Chip' concept. The particular micro-reactor designs developed and used by, *inter alia*, the Hull group consist of a network of micron-sized channels connecting a number of reagent reservoirs which also hold the electrodes used for electrokinetic pumping. Timed voltage sequences applied under computer control to the appropriate reservoir electrodes are used to control the movement of reagents within particular regions of the channel network by a combination of electro-osmotic and electrophoretic effects. This enables control of the *spatial* and *temporal* evolution of a chemical reaction in a micro-reactor in a manner not achievable in a conventional bulk reactor where reagent concentrations are uniform. For a range of different reactions in micro-reactors, it has been demonstrated that voltage control can, in many cases, alter the yields and selectivities of product mixtures.^{1–11} However, for the reactions studied to date, detailed knowledge of solvent flow rates and reagent velocities within the channel networks as a function of the applied electrode voltages has been lacking with the result that data interpretation has been somewhat speculative. As discussed in a review of the theoretical principles of electrokinetic control of reactions in micro-reactors,¹² the prediction and control of the spatial and temporal evolution of a reaction in a channel network requires knowledge of the detailed 3D geometry of the channels, the dependence of the electrical currents and electroosmotic flow rates in the different channel

sections as a function of the applied voltages, the electrophoretic mobilities and diffusion coefficients of all species involved in the reaction together with the kinetic rate law and rate constants for the reaction. The aims of the study described here are to estimate all these physico-chemical parameters for a selected reaction and to quantitatively validate predictions of the spatial and temporal evolution of concentrations by comparison with experimental data.

The chemical reaction selected for this study was the reversible formation of a complex between Ni^{2+} ions and the bidentate ligand pyridine-2-azo-*p*-dimethylaniline (PADA). This choice was dictated by three considerations. Firstly, the reaction is relatively simple with no complications from side-reactions. Secondly, the kinetic rate law and rate constants are known from the literature^{13,14} and are such that the reaction occurs in the micro-reactor within an experimentally convenient time frame. Lastly, both PADA and the complex show strong and reasonably widely separated absorbance bands in the visible spectral range which enable the use of an *in situ* microscope imaging technique to determine their spatial concentration profiles in the micro-reactor as a function of time. The water-based solvent mixture for the reaction contained 30 vol% ethanol (required to achieve sufficient PADA solubility) and 50 mM tris buffer at pH 7.5. Under these conditions, the nickel ion is present as Ni^{2+} , PADA is uncharged and the complex is NiPADA^{2+} . The overall concentration of tris buffer was such that the ionic strength and electrical conductivity of the solvent mixture, nickel, PADA and complex solutions were approximately constant (within 10%). This condition of high background electrolyte greatly simplifies the analysis of the electrical current–voltages relationships. The ranges of voltages applied in this study were restricted to values low enough such that the electrolytic formation of gas bubbles was not observed. Electrolytic bubble generation (observed at higher voltages than those used here) was easily detected in the micro-reactor through large effects on the electrical currents.

This paper is organised as follows. Following the Experimental section, the Results and Discussion section starts with a description of the 3D geometry of the micro-reactor channel

† Electronic supplementary information (ESI) available. The first video file (run2 PADA 450nm.avi) shows a video sequence of gray images recorded at 450 nm where PADA has maximum absorbance. The sequence shows the PADA injection followed by reaction when the 'flow' mode is restarted. The second file (run2 Complex 550nm.avi) shows the corresponding image sequence recorded at 550 nm where the complex has maximum absorbance. The videos do not correspond to real time; they consist of a series of 'snapshots' run in sequence. The actual time sequences are detailed in Figs. 11 and 12. See <http://www.rsc.org/suppdata/lc/b2/b201685k/>

network. The relationships between the applied voltages and the measured currents and liquid flow rates are then discussed. The next section deals with the estimation of electrophoretic mobilities and diffusion coefficients for all the species participating in the reaction. In the final Results and Discussion section, the channel network flow configurations used to initiate the reaction are described together with measured concentration profiles as a function of time. The measured profiles are then compared with calculated curves based on the parameters estimated in earlier sections. Finally, the main conclusions are summarised.

Experimental

Materials

Water was purified by reverse osmosis and by passage through a Milli-Q Reagent system. Ethanol (absolute AR grade, Fisher Scientific), $\text{Ni}(\text{NO}_3)_2 \cdot 6\text{H}_2\text{O}$ (99%, Acros Organics), PADA (99%, Sigma), Rose Bengal (dye content 95%, Aldrich) and tris buffer (tris(hydroxymethyl)methylamine, AnalaR grade, BDH) were used without further purification.

Methods

The micro-reactor chip was fabricated according to published procedures^{15,16} with minor variations. For the channel network used in this study (Fig. 1), reservoirs A, B, C and D are linked by non-continuous large channels which are etched within the bottom plate. The breaks in the large channels are linked by rectangular grids of small channels which are etched on the lower side of the middle plate. The grids of small channels have a high resistance to hydrodynamic flow and act to suppress pressure driven flow resulting from differences in the reservoir heights. The micro-reactor assembly is completed by thermal bonding of the ‘sandwich’ of the bottom, middle and a 20 mm thick upper plate. Holes drilled through the middle and upper plates connect to the ends of the large channel segments and form the reagent reservoirs. The strategy of using rectangular grids of small channels (as opposed to sections containing only a single small channel) is employed in order to avoid fabrication failure due to misalignment between the bottom and middle plates during thermal bonding.

The bottom and middle plates were made from White Crown glass sheets pre-coated for photolithographic etching (Align

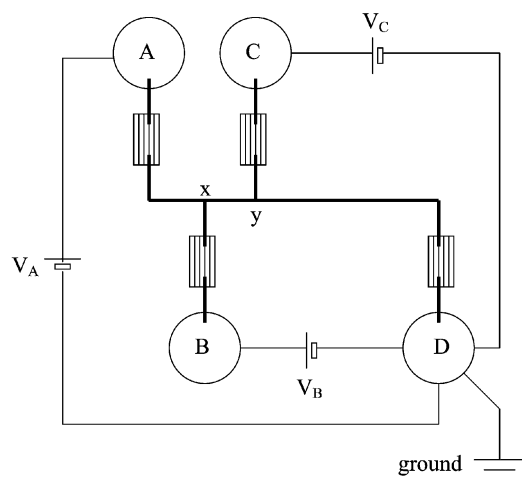


Fig. 1 Diagram of the micro-reactor channel network and reservoirs. The thick lines show the large channels which are connected by grids of small channels which act as hydrodynamic resistance elements. The thin lines show the external electrical connections and applied voltages.

Rite, 3 mm thickness). The channel network design was drawn in large scale, photoreduced and transferred to the photoresist layer using a standard UV exposure unit (Mega Electronics, Cambridge, UK). Using an etch solution comprising 250 ml of water, 12.5 g ammonium fluoride (98%, Lancaster) and 7 ml of 40% HF solution in water (AnalaR grade, BDH Merck), the bottom plate was etched for 10 min at 65 °C. The middle plate was etched for 1 min at 65 °C. Etching was carried out by placing the glass pieces on a support in the etch solution with patterned side facing downwards within a heated ultrasonic bath (Ultrawave Scientific Supplies, Nottingham, UK). Ultrasound was applied continuously to ensure that etch debris is effectively removed during the etch and that fresh etchant solution remains in good contact with the surface. The bottom and middle plates were thermally bonded together by placing them in a muffle furnace set at 570 °C for 3 h. A quartz block of mass 70 g was placed on top of the assembly to aid bonding. The top block was then bonded to the two bonded lower plates using the same procedure.

An Axiovert S100 inverted microscope (Carl Zeiss) using transmission optics was employed to obtain both conventional micrographs and quantitative absorbance images of the micro-reactor. The absorbance imaging method is described fully in ref. 17. Briefly, at a fixed wavelength selected by insertion of a narrow bandpass filter in the microscope light path, digitised 256×256 arrays of camera pixel transmission intensity values are collected for the sample system (the chip containing an absorbing solution), the same chip filled with solvent and a ‘dark’ image. The intensity arrays are I , I_0 and I_d respectively. The combined set of intensity arrays are then converted to a single array of absorbance values A using $A = \log_{10}\{(I_0 - I_d)/(I - I_d)\}$. From the Beer-Lambert law ($A = Ecd$ where d is the path length, c is the concentration of the absorbing species and E is the extinction coefficient at the relevant wavelength), the array of absorbance values yields either the path length d (equal to the channel depth) or the concentration at that pixel position. Quantitative 3D profiles of the channel network in the assembled device were obtained using this analysis for micrographic absorbance images of the channels filled with aqueous solutions of Rose Bengal (2.1 g l^{-1}). A wavelength of 550 nm, selected using a narrow bandpass filter (Edmund Scientific N43-126, peak 550 nm, full width at half maximum 10 nm) was used. Concentration profiles of PADA (wavelength of maximum absorbance $\lambda_{\text{max}} = 450 \text{ nm}$) and the NiPADA²⁺ complex ($\lambda_{\text{max}} = 550 \text{ nm}$) were determined by similar analysis of micrographic absorbance images obtained using the appropriate narrow bandpass optical filter and using the values of d measured in the profiling work. For PADA, the Edmund Scientific N43-111 (peak 450 nm, full width at half maximum 10 nm) was used; for the complex, the Edmund Scientific N43-126 (peak 550 nm, full width at half maximum 10 nm) was used.

Electrokinetic control, voltage and current measurements of the micro-reactor were made using a home designed power supply which was constructed by Kingfield Electronics, UK. The power supply has four channels for voltage outputs, four channels for monitoring the electrical current of each channel and four channels to monitor the voltages delivered to each channel. Programmed control of the timed voltage sequences applied to each channel plus current and voltage logging was made using LabVIEW software (National Instruments). For the chip design used here (Fig. 1), voltages were controlled, and the currents and voltages logged for three channels only, *i.e.* between reservoirs A and D (ground), B and D (ground) and between C and D (ground). Lengths of shiny Pt wire (Goodfellow, diameter 0.26 mm, length 20 mm) were used as electrodes.

Liquid flow rates as a function of the applied voltages were determined as described in ref. 16, by monitoring the changes in liquid heights over time for the reservoirs A, B, C and D. The

reservoirs were connected to vertically mounted, glass 0.5 ml graduated pipettes (Gallenkamp, approximately 1.2 mm internal diameter, 130 mm height) *via* plastic connecting tubes. The internal diameters of each pipette were measured accurately using a travelling microscope equipped with a digital clock gauge with 1 μm resolution (Mitutoyo). The electrodes were inserted through the sides of the connecting plastic tubes in order that they did not distort the liquid menisci within the pipettes. The accuracy of the liquid height measurements was estimated by repeated measurements to be $\pm 15 \mu\text{m}$.

Liquid conductivities were measured using a WTW GmbH model LF340 AC conductivity bridge operating at 1000 Hz and equipped with a graphite electrode dip cell with cell constant equal to 0.475 cm^{-1} . All measurements were made at room temperature equal to $24 \pm 1 \text{ }^\circ\text{C}$.

Results and discussion

Micro-reactor geometry

The overall micro-reactor geometry and the external electrical connections, voltages and reservoir labels are shown schematically in Fig. 1. Each different section of the network of large cross sectional area channels contains a channel break which is spanned by a grid of channels of low cross sectional area. The grids of small channels have a high resistance to hydrodynamic flow and hence act to suppress pressure driven flow arising from hydrostatic pressure gradients resulting from small differences in liquid heights between the different reservoirs. It was confirmed that such pressure driven flows were negligible by observation of the lack of liquid reservoir height changes over an hour following the deliberate creation of high initial reservoir height differences of 25 mm. Since pressure driven flow was found to be negligible, species' mobility within the micro-reactor under electrokinetic operation results *only* from electro-osmosis and electrophoresis. Fig. 2 shows an optical micro-

graph of the channel network in the region of the channel intersections at positions x and y which, as will be seen later, is where the reaction occurs.

An illustrative example of a quantitative 3D profile, corresponding to the channel network in the region where a large channel intersects with a grid of small channels, is shown in Fig. 3. 'Slices' through the data array perpendicular to the long axes of the channels give the cross sectional profiles of the large and small channels. Since the etching of glass by HF proceeds isotropically, for an etch of depth d under an etch mask of width m , the etched channel cross section is expected to consist of rectangle of dimensions $(d \times m)$ with channel sides having a quarter circle shape with radius equal to d .¹⁷ The channel cross sectional area A_{channel} is given by

$$A_{\text{channel}} = (dm) + \frac{\pi d^2}{2} \quad (1)$$

As discussed in ref. 17, the channel shapes in micro-reactors following thermal bonding are generally slightly distorted from

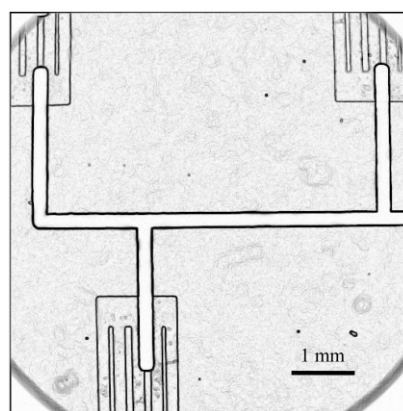


Fig. 2 Optical micrograph of the channel network in the region of the x - y channel section.

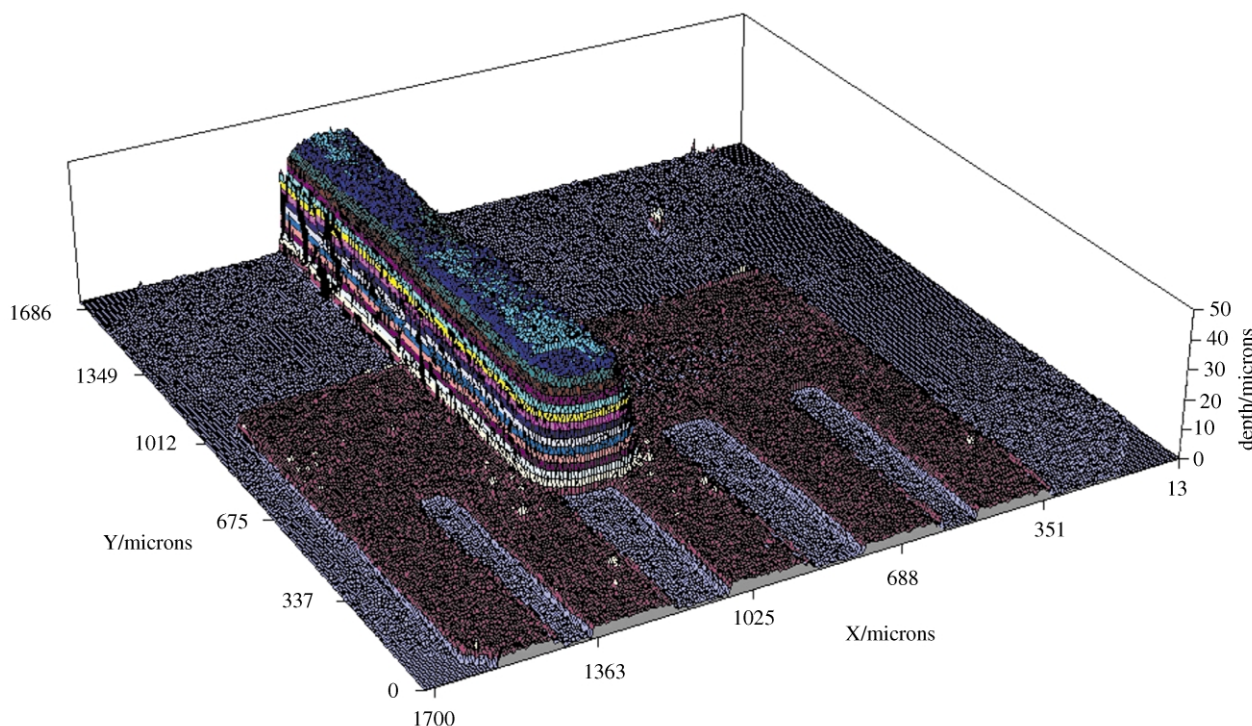


Fig. 3 3D channel profile in the region of overlap between the large channel and the grid of small channels.

this idealised shape. However, the channel cross sectional area A_{channel} estimated using eqn. 1 with the best-fit values of d and m is not significantly different to that obtained by integration of the fit to a slightly distorted channel profile. The large channels have best-fit values of d and m of 38 ± 2 and $146 \pm 5 \mu\text{m}$ respectively. The small channels have $d = 3.1 \pm 0.5$ and $m = 183 \pm 5 \mu\text{m}$.

Voltages, currents and flow rates

The electrokinetic mobilities of reagent and solvent species within the different sections of the channel network are related to the corresponding electrical currents.^{16,18,19} Hence, it is necessary to establish the relationship between the applied reservoir voltages (V_A , V_B and V_C relative to ground in reservoir D) and the electrical currents. The currents in the channel network (Fig. 1) are defined as follows. I_A is the current flowing from reservoir A $\rightarrow x$, I_B is from B $\rightarrow x$ and I_C is from C $\rightarrow y$. The current flowing from $x \rightarrow y$ is $(I_A + I_B)$ and that from $y \rightarrow D$ is $(I_A + I_B + I_C)$. The electrical resistance R of a channel section of length L and cross sectional area A and filled with a liquid of conductivity κ is given by¹⁶

$$R = \frac{L}{\kappa A} \quad (2)$$

In this study, we have used a high concentration of background electrolyte (50 mM tris buffer) such that the liquid conductivity is approximately constant and independent of the local concentrations of the reaction species (Ni^{2+} , PADA and complex). In addition, because the bulk liquid conductivity is relatively high (approximately $1000 \mu\text{S cm}^{-1}$), corrections to eqn. 2 arising from surface conductivity are relatively small and are neglected here.^{16,18} Under these conditions, the electrical resistances of the different channel sections are proportional to the channel lengths and inversely proportional to the channel cross sectional areas. For the channel network of Fig. 1, one expects the resistances of the grids of small channels to be large relative to the same length of a large channel.

The DC circuit equivalent to the channel network (Fig. 1) contains three connected circuit loops. For each circuit loop, the applied voltage (relative to ground in reservoir D) is equal to the sum of the products of resistance and current in each channel section according to

$$V_A = R_{Ax}I_A + R_{xy}(I_A + I_B) + R_{yD}(I_A + I_B + I_C) \quad (3)$$

$$V_B = R_{Bx}I_B + R_{xy}(I_A + I_B) + R_{yD}(I_A + I_B + I_C) \quad (4)$$

$$V_C = R_{Cy}I_C + R_{yD}(I_A + I_B + I_C) \quad (5)$$

where the R values refer to the resistance of the channel section denoted by the subscript. Solution of the three simultaneous equations provides expressions for I_A , I_B and I_C .

$$I_A = \frac{(R_{Cy}R_{xy} + R_{Cy}R_{yD} + R_{Bx}R_{yD} + R_{xy}R_{yD} + R_{Cy}R_{Bx})V_A - (R_{Cy}R_{yD} + R_{Cy}R_{xy} + R_{xy}R_{yD})V_B - R_{Bx}R_{yD}V_C}{R_{Cy}R_{Bx}R_{Ax} + R_{Cy}R_{xy}R_{Bx} + R_{Cy}R_{xy}R_{Ax} + R_{Cy}R_{yD}R_{Bx} + R_{Cy}R_{yD}R_{Ax} + R_{Bx}R_{yD}R_{Ax} + R_{xy}R_{yD}R_{Bx} + R_{xy}R_{yD}R_{Ax}} \quad (6)$$

$$I_B = \frac{-(R_{Cy}R_{xy} + R_{Cy}R_{yD} + R_{Bx}R_{yD})V_A - (R_{Cy}R_{xy} + R_{Cy}R_{yD} + R_{Cy}R_{Ax} + R_{xy}R_{yD} + R_{yD}R_{Ax})V_B - R_{Ax}R_{yD}V_C}{R_{Cy}R_{Bx}R_{Ax} + R_{Cy}R_{xy}R_{Bx} + R_{Cy}R_{xy}R_{Ax} + R_{Cy}R_{yD}R_{Bx} + R_{Cy}R_{yD}R_{Ax} + R_{Bx}R_{yD}R_{Ax} + R_{xy}R_{yD}R_{Bx} + R_{xy}R_{yD}R_{Ax}} \quad (7)$$

$$I_C = \frac{-(R_{Bx}R_{yD})V_A - (R_{yD}R_{Ax})V_B - (R_{Bx}R_{Ax} + R_{yD}R_{Ax} + R_{xy}R_{Ax} + R_{xy}R_{Bx} + R_{Bx}R_{yD})V_C}{R_{Cy}R_{Bx}R_{Ax} + R_{Cy}R_{xy}R_{Bx} + R_{Cy}R_{xy}R_{Ax} + R_{Cy}R_{yD}R_{Bx} + R_{Cy}R_{yD}R_{Ax} + R_{Bx}R_{yD}R_{Ax} + R_{xy}R_{yD}R_{Bx} + R_{xy}R_{yD}R_{Ax}} \quad (8)$$

The resistance values were determined by measurements of the currents I_A , I_B and I_C for a series of different set values of the voltages V_A , V_B and V_C . At constant set voltages, the currents were constant over 5 min and responded to a change in voltage within a second. Each data series was simultaneously fitted to eqn. 6–8 using the EXCEL Solver function to obtain the best-fit resistance values. For a data set covering a wide range of applied voltages in reservoirs A, B and C, a comparison of the currents measured and those calculated using the set of best-fit resistance values is shown in Fig. 4. It can be seen that all currents can be reliably predicted within the experimental uncertainty of $\pm 0.5 \mu\text{A}$. Resistance values for the reaction solvent system (30 vol% ethanol in water containing 50 mM tris buffer, pH 7.5 and conductivity = $1028 \mu\text{S cm}^{-1}$ and the same solution also containing 2.1 mM Ni^{2+} ions, conductivity = $1194 \mu\text{S cm}^{-1}$) are summarised in Table 1. The properties of the solvent mixture were unaffected by the addition of 2.1 mM PADA. The magnitudes of R_{Ax} , R_{Bx} and R_{Cy} (all containing a grid of small channels plus a similar length of large channel) are all similar and larger than R_{xy} (containing no grid of small channels). The resistance R_{yD} is the largest as it contains a grid of small channels plus the largest length of large channel.

The volumetric liquid electroosmotic flow rate F in a particular channel section is proportional to the electrical

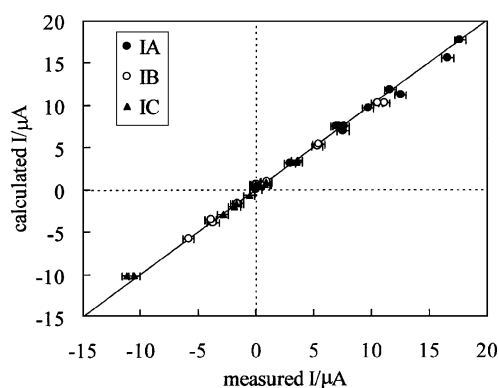


Fig. 4 Comparison of measured currents with those calculated using eqns. (6)–(8) with the resistance values listed in Table 1 for solution 1. The data set corresponds to applied voltages ranges of V_A : 30 to 340, V_B : 80 to 320 and V_C : -110 to 270 V. The solid line shows a slope of unity.

Table 1 Electrical resistance values (units $\text{M}\Omega$) for the micro-reactor channel sections indicated by the subscripts when filled with either solution 1 or solution 2. Solution 1 contained 30 vol% ethanol in water, 50 mM tris buffer, pH 7.5 and conductivity = $1028 \mu\text{S cm}^{-1}$. Solution 2 had the same composition plus 2.1 mM Ni^{2+} ions with conductivity = $1194 \mu\text{S cm}^{-1}$

Channel section	Solution 1	Solution 2
R_{Ax}	9.44	8.13
R_{xy}	3.12	2.68
R_{yD}	15.0	12.9
R_{Bx}	8.77	7.55
R_{Cy}	10.8	9.28

current in the corresponding channel section according to^{12,16,18,19}

$$F = -I \left(\frac{\varepsilon \varepsilon_0 \zeta}{\eta \kappa} \right) \quad (9)$$

where I is the current, ε is the relative dielectric constant of the liquid, ε_0 is the permittivity of free space, ζ is the zeta potential of the channel wall–liquid interface, η is the liquid viscosity and κ is the liquid conductivity. Fig. 5 shows an example of measured reservoir height changes used to determine flow rates. For the set voltages corresponding to Fig. 5, liquid flows out of reservoir A (the height decreases) into reservoirs B and D for which the heights increase. Reservoir C has virtually zero flow. As expected, the algebraic sum of all the flows is zero, *i.e.* the total volume of liquid is conserved.

Fig. 6 shows plots of volumetric flow rate *versus* the corresponding electrical current for solutions 1 and 2. For solution 1 (containing no Ni^{2+} ions) significant flow is observed and, as expected from eqn. 9, the plot is linear. For 30 vol% ethanol in water, the relative dielectric constant is 64 and the viscosity is 0.975 cP. These values were estimated by taking the volume fraction weighted mean of the values for water and ethanol.^{20–22} Substitution of these values and the slope of Fig. 6 into eqn. 9 yields a value of -7 ± 2 mV for the zeta potential of the channel wall–solution interface. This value is rather low when compared with literature values for the interface between glass and water of this pH containing electrolytes such as NaCl or KCl for which values (somewhat dependent on the exact type

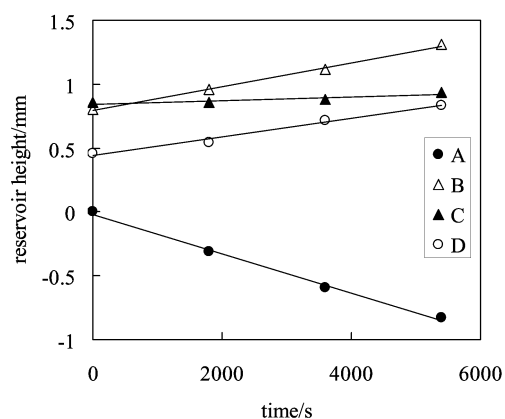


Fig. 5 Plots of reservoir height changes *versus* time for the micro-reactor filled with 30 vol% ethanol in water plus 50 mM tris buffer at pH 7.5. Applied voltages were $V_A = 337.5$, $V_B = 120$ and $V_C = 102$ V and measured currents were $I_A = 17.7$, $I_B = -5.8$ and $I_C = -2.8$ μA . The calculated value of $I_D (= I_A + I_B + I_C) = 9.0$ μA .

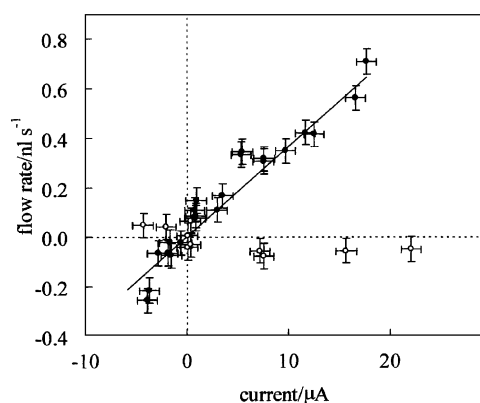


Fig. 6 Plots of flow rates *versus* current for 30 vol% ethanol in water plus 50 mM tris buffer (filled circles) and the same solvent mixture plus 2.1 mM Ni^{2+} (open circles). The solid line corresponds to a zeta potential of -7 mV.

of glass involved) are typically in the range -30 to -80 mV.^{16,18,23–30} The low value of the zeta potential observed here may be a consequence of adsorption of the tris buffer to the channel wall. For solution 2, containing 2.1 mM Ni^{2+} , the zeta potential is further reduced to 0 ± 2 mV, suggesting that specific adsorption of Ni^{2+} ions is occurring. For solutions containing 2.1 mM PADA (not shown), the flow rates were identical to the solvent mixture without added reagents.

Estimation of electrophoretic mobilities and diffusion coefficient measurement

As discussed previously,¹² for the modelling of chemical reactions in a micro-reactor operating under electrokinetic control, one must take account of EOF (electroosmotic flow), electrophoresis, diffusion and chemical reaction. Within the electric field present in the micro-reactor, uncharged species, including the solvent, undergo diffusion and EOF with velocity v_{eof} . The value of v_{eof} is given by^{18,19}

$$v_{\text{eof}} = -\frac{E_f \varepsilon \varepsilon_0 \zeta}{\eta} \quad (10)$$

where E_f is the electric field. Within a channel section where the current is I , the cross sectional area is A_{channel} and the liquid conductivity is κ , the local value of $E_f = I/A_{\text{channel}}\kappa$. Hence, knowledge of the current–voltage relationships and the channel cross sectional area enables the estimation of v_{eof} for any channel section with any voltage settings. Charged species move with a velocity equal to the vector sum of v_{eof} and the electrophoretic velocity v_{ph} . The electrophoretic velocity v_{ph} is given by^{18,19}

$$v_{\text{ph}} = \frac{zeE_f D}{kT} = \frac{IzeD}{A_{\text{channel}}\kappa kT} \quad (11)$$

where ze is the charge on the species, D is the diffusion coefficient, k is the Boltzmann constant and T is the absolute temperature. From eqn. (11), it can be seen that v_{ph} can be estimated provided that the diffusion coefficient is known. For the reaction modelling described later, the values of D for PADA (uncharged), Ni^{2+} and the NiPADA^{2+} complex are, in any case, required to take account of diffusion. The D values for the charged species can be used additionally to obtain the required electrophoretic velocities.

We first describe the measurement of D for the uncharged PADA using a method based on EOF within a micro-reactor. Using the simple T shaped channel network micro-reactor described fully in ref. 16, EOF was used to combine a flowing stream of PADA with a flowing stream of solvent down the ‘leg’ of the T. For the EOF conditions used, the typical linear velocities are of the order of 0–1 mm s^{-1} . The Reynolds number (Re equal to $D_e v_{\text{eof}} \rho / \eta$ where D_e is the effective channel diameter and ρ is the liquid density) for such flow is typically less than 1, well below the transition point from laminar to turbulent flow which occurs at Re of approximately 2500. Thus, the flowing dye and solvent streams retain their integrity when combined and mix only by diffusion as they flow together. Fig. 7 shows an example of a measured concentration profile in the region of the channel junction when a PADA solution is combined with a solvent stream. From Fig. 7, it can be seen that the interface between the co-flowing streams is noticeably broadened as one goes from low Y values (corresponding to short times after stream combination) to large Y values (corresponding to long times after stream combination). Analysis of this diffusional broadening yields the diffusion coefficient of the PADA.

Using images such as those shown in Fig. 7, PADA concentration profiles perpendicular to the channel length (*i.e.* $[\text{PADA}]$ *versus* X position) corresponding to different times

after stream combination were obtained by taking ‘slices’ of the data at different Y values. Y values were converted to times after stream combination using the EOF velocities measured as described earlier. Measurements were made at two different velocities, 0.48 and 0.78 mm s^{-1} . For short times, such that the PADA concentrations at the channel edges remain equal to their initial values, the concentration as a function of X and time t is given by³¹

$$c(X,t) = \frac{1}{2}c_0 \operatorname{erfc}\left\{\frac{X}{2\sqrt{Dt}}\right\} \quad (12)$$

where c_0 is the unperturbed PADA concentration far from the PADA–solvent interface, D is the diffusion coefficient and erfc is the error-function complement. The time corresponding to each Y position was calculated according to

$$t = \frac{(Y - Y_0)}{v_{\text{eof}}} \quad (13)$$

where Y is the measured Y position of the concentration profile (see Fig. 7) and Y_0 is an adjustable Y shift to take account of the fact that the Y position corresponding to $t = 0$ is uncertain for the channel intersection geometry used here. The four concentration profiles of Fig. 8, corresponding to two different values of Y and two values of v_{eof} , were globally fitted to eqn. 12 and 13 using D and Y_0 as adjustable parameters. It can be seen that the fitted lines show good agreement with the experimental data using a fitted value of D for PADA of $4.0 \times 10^{-10} \text{ m}^2 \text{ s}^{-1}$. The best-fit value of Y_0 was found to be $-252 \mu\text{m}$ which gives the time values for each concentration profile derived from the data of Fig. 7. The value of Y_0 indicates that time zero, corresponding to a vertical step change in PADA concentration apparently occurs at $Y = -252 \mu\text{m}$, *i.e.* outside the region of the channel intersection. A more realistic interpretation is probably that the PADA concentration profile is actually slightly distorted from the ideal vertical step profile at the point at which the solutions meet, thereby giving the appearance of slightly more diffusion than expected at short times. The procedure of using a global fit

of the set of concentration profiles was found to be robust, *i.e.* constant best-fit values were obtained for widely differing initial guesses of D and Y_0 . The use of several concentration profiles, corresponding to different times after contact, overcomes the problem of the uncertainty in the channel position corresponding to time zero.

The diffusion coefficient of Ni^{2+} ion was estimated using literature values for the single ion molar conductivity as follows. At 25 °C, the molar conductivity λ_m of Ni^{2+} in aqueous solutions of NiCl_2 is $106.1 \text{ cm}^2 \text{ S mol}^{-1}$ at infinite dilution and decreases to $72.8 \text{ cm}^2 \text{ S mol}^{-1}$ at a concentration of 0.05 M.³² According to the Nernst-Einstein equation³¹

$$D = \frac{\lambda_m kT}{z^2 e^2} \quad (14)$$

the value of D for Ni^{2+} is $7.03 \times 10^{-10} \text{ m}^2 \text{ s}^{-1}$ at infinite dilution and decreases to $4.83 \times 10^{-10} \text{ m}^2 \text{ s}^{-1}$ at 0.05 M due to a combination of ionic relaxation and electrophoretic effects as described by Debye–Hückel–Onsager theory.³³ For the reaction solvent containing 30 vol% ethanol in water and 0.05 M tris buffer, the viscosity is slightly higher than that of water at 25 °C. Assuming that D scales inversely with viscosity and that the relaxation and electrophoretic retardation effects in the reaction solvent are equal to those in 0.05 M NiCl_2 , we estimate D for Ni^{2+} to be approximately $4.5 \times 10^{-10} \text{ m}^2 \text{ s}^{-1}$. For NiPADA^{2+} , the value of D at infinite dilution is expected to be slightly lower than that for PADA because of the increase in molecular volume due to ion binding. Assuming D for NiPADA^{2+} (at infinite dilution) to be $3.0 \times 10^{-10} \text{ m}^2 \text{ s}^{-1}$ (*i.e.* 75% of the value for PADA) and that the fractional reduction in D for NiPADA^{2+} due to relaxation and electrophoretic effects is similar to that calculated for Ni^{2+} , leads to an approximate estimate of $2 \times 10^{-10} \text{ m}^2 \text{ s}^{-1}$ for D of the complex.

In situ imaging of the reaction

The complex formation reaction between Ni^{2+} and PADA can be written as

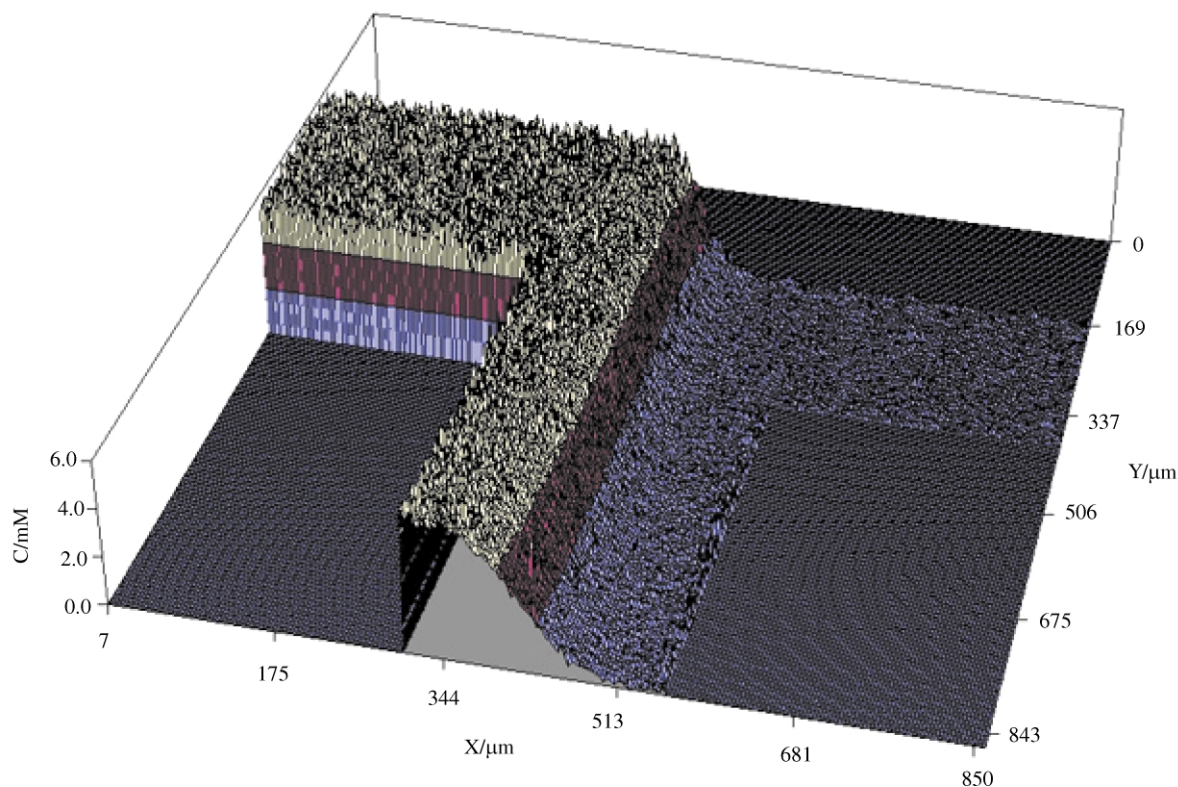


Fig. 7 PADA concentration profile for a T shaped channel network. PADA solution enters from the top left corner and solvent enters from the right.



where k_f is the second-order, forward rate constant and k_r is the reverse, first-order rate constant. The rate law for the reaction is

$$\frac{d[\text{complex}]}{dt} = k_f[\text{Ni}^{2+}][\text{PADA}] - k_r[\text{complex}] \quad (16)$$

At 25 °C and pH 7.5, the rate constants k_f and k_r are 1300 M⁻¹ s⁻¹ and 0.1 s⁻¹ respectively.^{13,14}

The reaction was performed in the micro-reactor as shown schematically in Fig. 9. Initially, all channels were filled with 30 vol% ethanol in water containing 0.05 M tris buffer. The same solvent mixture containing 2.1 mM Ni²⁺ was loaded into reservoir A using a micro-syringe. Using appropriate controlling voltages, the channel connecting reservoir A to D was filled with Ni²⁺ solution (by electrophoresis) whilst maintaining zero flow from/to reservoirs B and C. This flow pattern is denoted ‘flow mode’. Solvent mixture containing 2.1 mM PADA was then loaded into reservoir B. Using control voltages for the ‘injection mode’, the channel connecting reservoirs B and C

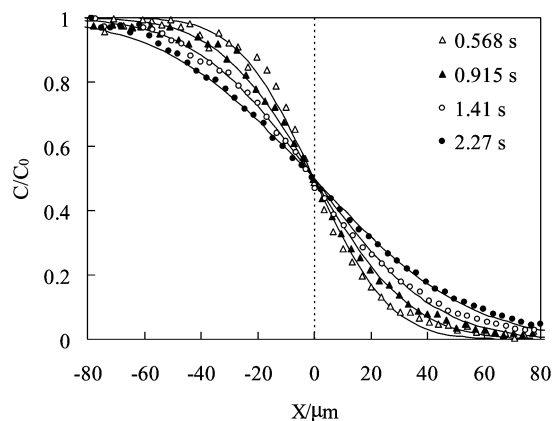


Fig. 8 PADA concentration profiles across the interface between co-flowing streams of PADA solution and solvent. The solid lines show the global best-fit to the profiles corresponding to the different times shown in the key.

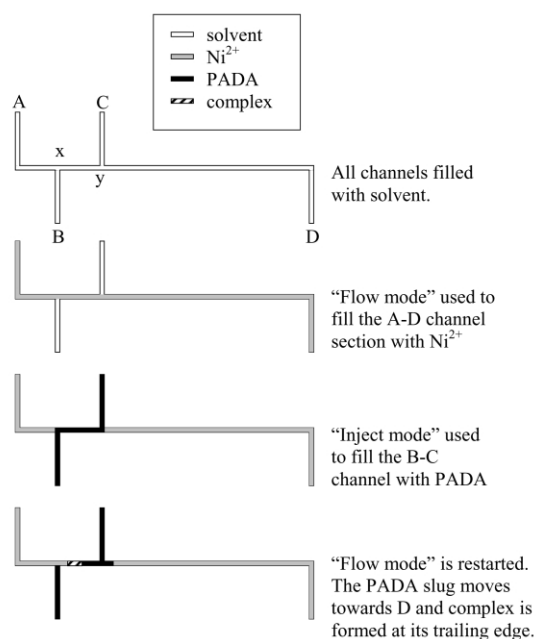


Fig. 9 Schematic diagram showing the formation of a ‘slug’ of PADA solution within a stream of Ni²⁺ solution following a ‘flow-inject-flow’ sequence.

was filled (by EOF) with PADA solution whilst maintaining zero flow from/to reservoirs A and D. Following the flow-inject sequence, the A–D channel section is filled with Ni²⁺ solution except for the x–y channel section which contains a ‘slug’ of PADA. Mixing of the Ni²⁺ and PADA, and hence reaction, is initiated by restarting the flow mode between A and D. Voltages and currents corresponding to the ‘flow’ and ‘inject’ modes are summarised in Table 2.

As seen in the spectra of Fig. 10,¹⁴ the complex formation between Ni²⁺ and PADA produces a colour change in the visible wavelength range from the yellow colour of PADA ($\lambda_{\text{max}} = 450$ nm) to the purple colour of the NiPADA²⁺ complex ($\lambda_{\text{max}} = 550$ nm). For the reaction measurements in the micro-reactor, each kinetic run was performed twice, once using a wavelength in the absorbance-imaging microscope of 450 nm and once at 550 nm. Hence, each run yielded a series of 256 × 256 arrays of values of the optical absorbances at 450 and 550 nm (A_{450} and A_{550}) corresponding to each camera pixel position for each time frame collected. As seen in Fig. 10, the spectra of the PADA and complex overlap significantly and hence both species absorb at both 450 and 550 nm. The values of A_{450} and A_{550} were used to derive the concentrations of PADA and the complex using the Beer-Lambert law as follows. At each wavelength, the absorbance is given by the sum of contributions from PADA and the complex according to

$$A_{450} = d \left(E_{450}^{\text{PADA}} [\text{PADA}] + E_{450}^{\text{complex}} [\text{complex}] \right) \quad (17)$$

$$A_{550} = d \left(E_{550}^{\text{PADA}} [\text{PADA}] + E_{550}^{\text{complex}} [\text{complex}] \right) \quad (18)$$

where d is the optical path length (equal to the channel depth), E is the extinction coefficient of the superscripted species at the subscripted wavelength and the square brackets denote concentrations. Solution of the two simultaneous equations yields

$$[\text{complex}] = \frac{\left(\frac{A_{550}}{E_{550}^{\text{PADA}}} - \frac{A_{450}}{E_{450}^{\text{PADA}}} \right)}{d \left(\frac{E_{550}^{\text{complex}}}{E_{550}^{\text{PADA}}} - \frac{E_{450}^{\text{complex}}}{E_{450}^{\text{PADA}}} \right)} \quad (19)$$

Table 2 Control voltages and electrical currents corresponding to the ‘flow’, and ‘inject’ modes in the micro-reactor (see Figs. 9 and 11)

	Flow mode	Inject mode
V_A/V	225	31
V_B/V	160	120
V_C/V	134	−110.5
$I_A/\mu\text{A}$	7.2	0
$I_B/\mu\text{A}$	0	11.1
$I_C/\mu\text{A}$	0	−11.1

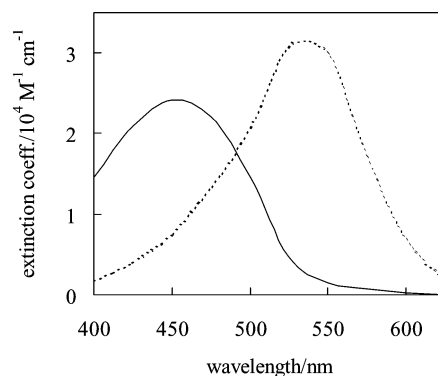


Fig. 10 Absorbance spectra of PADA (solid line) and the NiPADA²⁺ complex (dashed line). Because of the peak overlap, both species show significant absorbance at both observation wavelengths used in the micro-reactor (450 and 550 nm).

$$[\text{PADA}] = \frac{\left(\frac{A_{550}}{E_{550}^{\text{complex}}} - \frac{A_{450}}{E_{450}^{\text{complex}}} \right)}{d \left(\frac{E_{550}^{\text{PADA}}}{E_{550}^{\text{complex}}} - \frac{E_{450}^{\text{PADA}}}{E_{450}^{\text{complex}}} \right)} \quad (20)$$

Fig. 11 shows a series of time snapshots of the concentration profiles of PADA and complex along the A–D channel in the vicinity of the x – y intersections where the rectangular slug of PADA is formed. During PADA injection (upper plots) from reservoir B to C, the PADA concentration builds up at the intersection point x and spreads towards y . Using the data of Fig. 5, the expected value of v_{eof} for the PADA solution is 0.052 mm s^{-1} for the inject mode current applied ($11.1 \mu\text{A}$). Although the moving front of the PADA slug during injection shows considerable distortion (upper left plot of Fig. 11), an approximate value of v_{eof} can be estimated using a plot (not shown) of the PADA front position (taken to correspond to $[\text{PADA}] = 1 \text{ mM}$) versus time. The value for v_{eof} of 0.043 mm s^{-1} estimated in this way is similar to, but significantly smaller than 0.052 mm s^{-1} . In addition to the observed distortion of the PADA solution

front, the PADA solution also spreads back along the channel section A– x in addition to filling the x – y section. As seen in Fig. 11 (left hand upper plot), the length of the x – y channel section is 3.8 mm whereas the final width of the PADA slug is 5.0 mm . This observed ‘leakage’ of the PADA slug, giving an increase of approximately 20% in the final slug width, is the probable origin of the 20% reduction in the EOF velocity of the PADA slug front noted earlier. The right hand upper plot of Fig. 11 shows that a small amount of complex is formed during injection at a channel position of -2.5 mm , corresponding to the length of A– x channel section filled with ‘leaked’ PADA.

Following injection, when the flow mode (with current of $7.2 \mu\text{A}$) is restarted at 180 s , the EOF velocity of the Ni^{2+} stream containing the slug of PADA is uncertain. For the Ni^{2+} filled sections of the A–D channel, v_{eof} is zero whereas v_{eof} for the PADA filled section (around x – y) is expected to be 0.034 mm s^{-1} . As discussed in the literature,^{34–36} for a channel with non-uniform EOF velocities, the flat velocity profile expected for uniform EOF is distorted since EOF in one zone produces pressure driven flow in the second zone and the overall mean velocity is intermediate between the uniform values for the

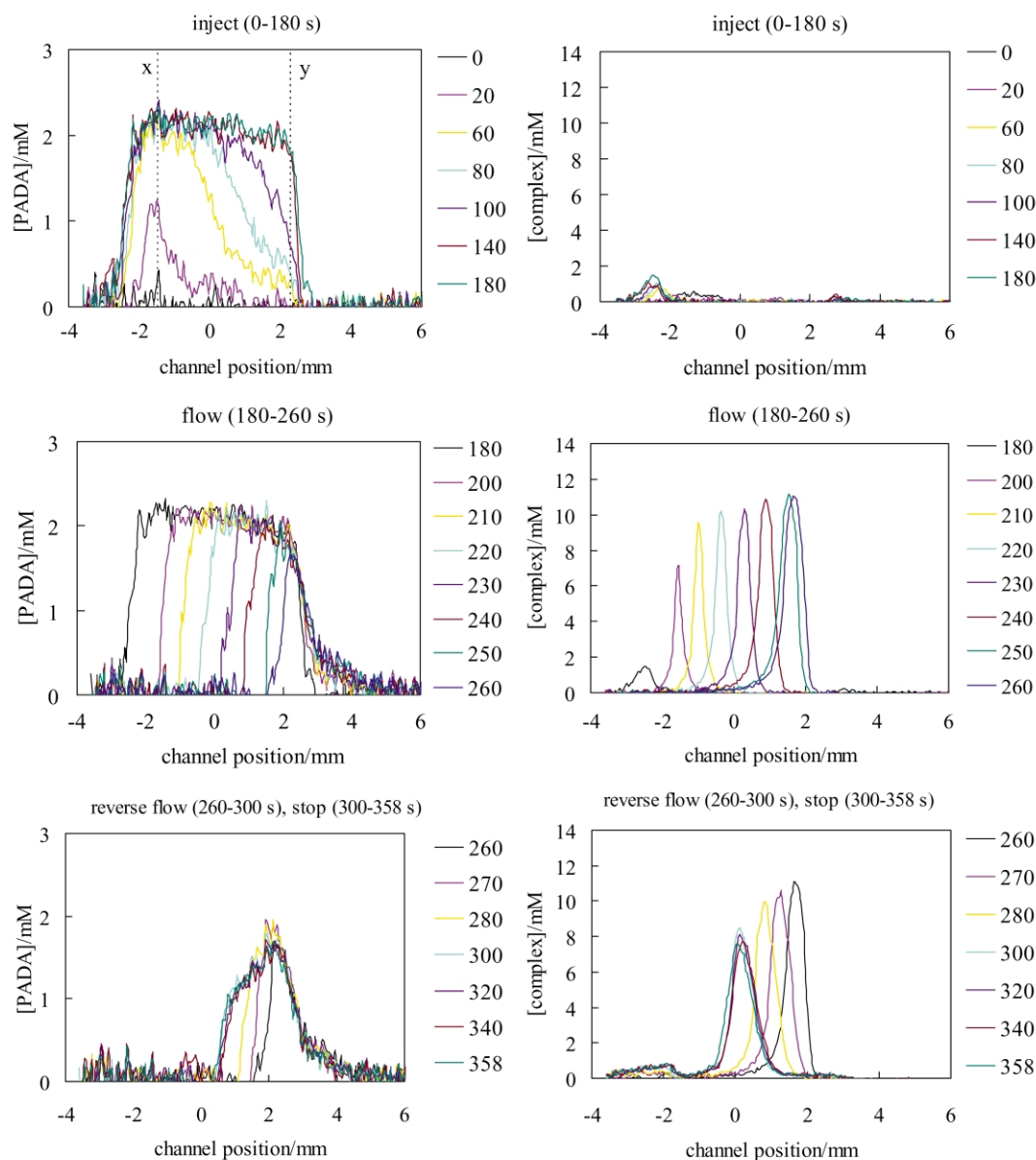


Fig. 11 Concentration profiles of PADA and the complex along the x – y channel section. Following filling of the A–D channel section with Ni^{2+} solution using ‘flow mode’, the slug of PADA is formed using ‘inject mode’ for 0 to 180 s (upper plots). ‘Flow mode’ is restarted for 180–260 s which results in the consumption of the PADA slug and the formation of a peak of complex (middle plots). ‘Reverse flow’ mode (260–300 s) and ‘stop mode’ is then used to return the complex peak to channel position zero and leads to the partial reversal of the reaction (bottom plots). In the upper left plot, the vertical dashed lines show the positions of the x and y channel intersections and serve to relate the channel position scale to the chip geometry.

different sections. In agreement with this latter expectation, we find that the average value of v_{eof} is approximately 0.01 mm s^{-1} for the reaction conditions used here, *i.e.* intermediate between the velocities expected for the PADA and Ni^{2+} solution zones. For the profiles shown in the middle plots of Fig. 11 (180–260 s), the Ni^{2+} moves by electrophoresis from left to right through the PADA slug. Hence, the PADA slug is eroded from the trailing edge and a peak of complex grows and shifts to channel positions closer to the leading edge of the PADA slug. Further detailed discussion of this reaction sequence is postponed to the section dealing with quantitative model comparison.

The bottom series of plots of Fig. 11 show the effect of reversing the flow such that the peak of complex is moved back to channel position zero. The flow reversal was effected by manually switching the electrodes between reservoirs A and D, thereby making A the ground voltage. Voltages and currents were $V_{\text{D-A}} = 225$, $V_{\text{B-A}} = 160$ and $V_{\text{C-A}} = 136 \text{ V}$, $I_{\text{D-A}} = 6.0$, $I_{\text{B-A}} = 6.8$ and $I_{\text{C-A}} = 1.1 \text{ }\mu\text{A}$ (the additional subscripts indicate that the values are relative to ground at reservoir A instead of relative to reservoir D as ground as in the rest of this paper). From the current values, it can be seen that, along with reversal of the flow along the A–D channel, significant flow from/to reservoirs B and C also occurs in this situation. Following the flow reversal from 260–300 s, all flow was then stopped for 58 s by setting all applied voltages to zero. Following this flow sequence, the complex peak is positioned in the approximate centre of the zone containing zero Ni^{2+} and hence the complex is expected to partially dissociate back to free PADA. As seen in the plots, the complex peak diminishes and the PADA peak is partially restored. Full restoration of the PADA is not expected since the Ni^{2+} concentration liberated by partial dissociation of the complex coupled with the high value of the reaction equilibrium constant ($K = k_f/k_r = 13000 \text{ M}^{-1}$) is sufficient to maintain an equilibrium concentration of complex. Although a detailed analysis has not been undertaken, this data set has been included here to provide an illustration of the point that voltage control can be used successfully to drive the reaction both forwards and backwards.

Comparison with modelling

Finally, we compare calculated and measured concentration profiles for the reaction phase occurring during the re-application of the flow mode following injection of the PADA slug. Although this sequence corresponds to the middle plots of Fig. 11, it is worth noting that the data analysed was actually obtained in a second independent run which shows good agreement with the first. For the calculations, the starting position is taken to be a perfectly rectangular slug of PADA of width 5 mm centred at channel position 0 (located approximately midway between x – y , see the left hand upper plot of Fig. 11 for the slug position relative to x and y) within a stream of Ni^{2+} . The EOF velocity is taken to be uniform for all channel positions and the electrokinetic velocities of all species are taken to be the vector sum of v_{eof} plus the appropriate value of v_{ph} . In fact, as noted above, the EOF is not uniform. However, the mean EOF velocity (intermediate between 0 for Ni^{2+} and 0.03 mm s^{-1} for PADA) is an order of magnitude smaller than the electrophoretic velocities of Ni^{2+} and the complex and so this non-uniformity is not expected to have a large effect under the reaction conditions used.

The numerical calculations take account of EOF, electrophoresis, diffusion and chemical reaction. The concentrations of Ni^{2+} , PADA and complex are functions of both time and channel position x according to the following set of equations¹²

$$\frac{\partial C_{\text{Ni}}}{\partial t} = D_{\text{Ni}} \frac{\partial^2 C_{\text{Ni}}}{\partial x^2} - k_f C_{\text{Ni}} C_{\text{PADA}} + k_r C_{\text{complex}} - v_{\text{phNi}} \frac{\partial C_{\text{Ni}}}{\partial x} \quad (21)$$

$$\frac{\partial C_{\text{PADA}}}{\partial t} = D_{\text{PADA}} \frac{\partial^2 C_{\text{PADA}}}{\partial x^2} - k_f C_{\text{Ni}} C_{\text{PADA}} + k_r C_{\text{complex}} - v_{\text{phPADA}} \frac{\partial C_{\text{PADA}}}{\partial x} \quad (22)$$

$$\frac{\partial C_{\text{complex}}}{\partial t} = D_{\text{complex}} \frac{\partial^2 C_{\text{complex}}}{\partial x^2} + k_f C_{\text{Ni}} C_{\text{PADA}} - k_r C_{\text{complex}} - v_{\text{phcomplex}} \frac{\partial C_{\text{complex}}}{\partial x} \quad (23)$$

Details of the full numerical procedure for the solution of this coupled set of differential equations are given in ref. 12. The situation described here for micro-reactors is identical (from a theoretical point of view) to that of electrophoretically mediated microanalysis (EMMA) described both experimentally and theoretically by the group of Regnier *et al.*^{37–40}

Calculated and measured concentration profiles are compared in Fig. 12. The full set of calculation parameters is summarised in Table 3 and compared with independent estimates of each parameter used. Overall, the calculations successfully capture the main features of the measured profiles. In particular, the fact that the reaction of a stream of 2.1 mM Ni^{2+} with a slug of 2.1 mM PADA produces a relatively narrow peak of complex with maximum concentration of 12 mM is predicted successfully. Detailed features that are *not* captured include the following. The concentration profiles at the edges of the PADA slug are not predicted accurately, probably due to two main effects. Firstly, the initial slug of PADA is not perfectly rectangular due to flow distortion of the slug around the channel corners during the injection phase (see Fig. 11). Although visualisation and computer modelling of this type of detailed effect have been discussed in the literature,^{41–45} such calculations are extremely computer intensive and thus have only been attempted for the (relatively) simple case of liquids not including a variety of different species undergoing chemical reaction. Secondly, under the conditions of this experiment, additional distortion of the slug edges beyond that predicted by diffusion alone is expected to occur due to the non-uniformity of the EOF mobility along the channel length. The second feature of the profiles seen in this work which was not predicted is that the initial width of the slug of PADA (5 mm) is wider than the gap between the channel intersections x – y (3.8 mm). During injection, the PADA ‘leaks’ from x – y into the A– x channel section. Currently, we have no clear explanation for this effect.

Conclusions

We set out in this study to demonstrate and validate by comparison with experiment the full set of measurement and data analysis tools required for the control and prediction of the spatial and temporal evolution of a chemical reaction within the channel network of a micro-reactor device. These tools include (1) the proper design of the channel network to ensure the absence of uncontrolled pressure driven flow, (2) full 3D quantitative profiling of the channel network using absorbance imaging, (3) measurement and modelling of the relationship between currents and applied voltages, (4) measurement of the liquid flow rates and their correlation with currents to determine zeta potentials and hence EOF for any applied voltages, (5) measurement of diffusion coefficients within a micro-reactor, (6) estimation of electrophoretic mobilities from conductivity data, (7) *in situ*, microscopic absorbance imaging of concentration profiles and (8) modelling of the full concentration profiles. Combining and applying these tools, we have demonstrated that predictable control of the spatial and temporal evolution of the (relatively simple) reaction between Ni^{2+} and PADA can be

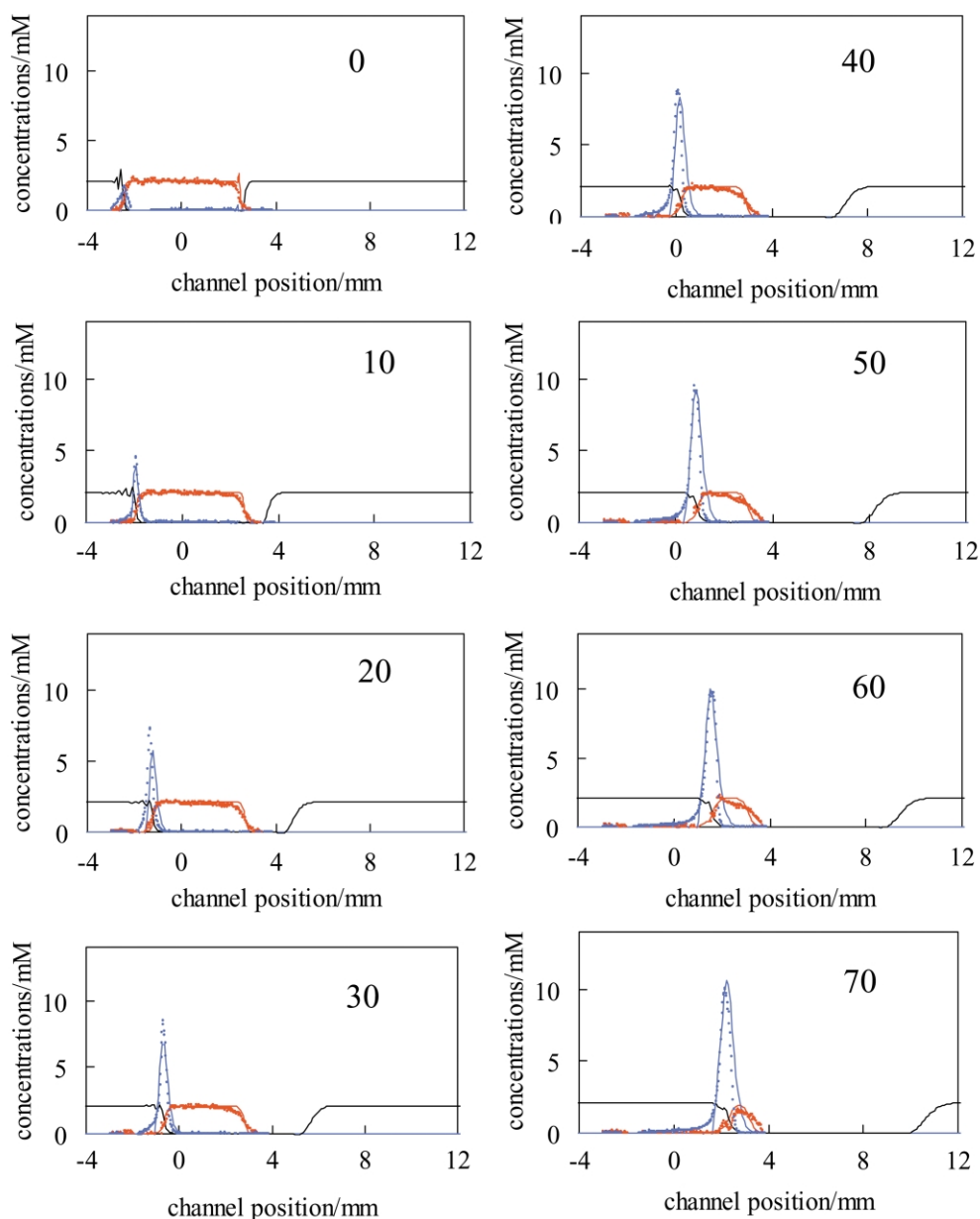


Fig. 12 Comparison of calculated concentration profiles of Ni^{2+} (solid black lines), PADA (red solid lines) and complex (blue solid lines) with measured profiles for PADA (red points) and complex (blue points). The numbers noted in each plot correspond to the time in seconds elapsed in 'flow mode' following the formation of the PADA slug using a 'flow-inject' sequence. The parameters used in the model calculations are summarised in Table 3.

Table 3 Summary of parameters used in the modelling of the concentration profiles of Fig. 12 showing the comparison with independent estimates. For the conversion of measured absorbances to concentrations, the optical path length (equal to the channel depth, 38 μm) was measured and the necessary extinction coefficients were taken from the spectra of Fig. 10

Parameter	Input value	Independent estimation
$I_A/\mu\text{A}$	7.2	measured
$I_B/\mu\text{A}$	0	measured
$I_C/\mu\text{A}$	0	measured
$D_{\text{PADA}}/\text{m}^2 \text{ s}^{-1}$	4.0×10^{-10}	measured
$D_{\text{Ni}}/\text{m}^2 \text{ s}^{-1}$	4.4×10^{-10}	$\approx 4.5 \times 10^{-10}$ estimated from the molar conductivity of 0.05 M NiCl_2 in water with a small correction for the viscosity of the reaction solvent.
$D_{\text{complex}}/\text{m}^2 \text{ s}^{-1}$	2.4×10^{-10}	$\approx 2.1 \times 10^{-10}$ estimated assuming D_{complex} at zero ionic strength is $0.75 \times D_{\text{PADA}}$ with correction for relaxation and electrophoretic retardation at finite ionic strength as for Ni^{2+} .
$v_{\text{phPADA}}/\text{mm} \text{ s}^{-1}$	0	zero charge
$v_{\text{phNi}}/\text{mm} \text{ s}^{-1}$	0.215	≈ 0.26 derived from estimate of D_{Ni} .
$v_{\text{phcomplex}}/\text{mm} \text{ s}^{-1}$	0.117	≈ 0.12 derived from estimate of D_{complex} .
mean $v_{\text{eof}}/\text{mm} \text{ s}^{-1}$	0.01	intermediate between measured values of 0 for Ni^{2+} and 0.03 $\text{mm} \text{ s}^{-1}$ for PADA.
$k_f/\text{M}^{-1} \text{ s}^{-1}$	1300	literature value ^{9,10}
k_r/s^{-1}	0.1	literature value ^{9,10}
initial PADA slug width/mm	5.0	larger than the x - y distance of 3.8 mm

reliably achieved to a level that captures most of the main features. Fundamentally, the ability to control the micron-scale spatial and temporal evolution of reactions (not achievable in bulk reactors where concentrations are generally uniform) is a key feature of micro-reactor technology which has some analogies with the control exerted on biochemical reactions by the micron-scale structures of living cells. Exploitation of this effect, *e.g.* by controlling a complex, multi-step reaction such that reaction occurs in a position where the local concentration of a key intermediate is high, to control and alter chemical reactivity is a potentially fruitful avenue which is under active investigation in our Laboratories.

Acknowledgements

We thank the Engineering and Physical Sciences Research Council of the UK for funding this study. We are grateful to Dr. T. McCreedy and Ms. C. Clive of the University of Hull for assistance with the design and fabrication of the micro-reactor.

References

- H. Salimi-Moosavi, T. Tang and D. J. Harrison, *J. Am. Chem. Soc.*, 1997, **119**, 8716.
- W. Ehrfeld, V. Hessel and H. Lehr, *Top. Curr. Chem.*, 1998, **194**, 233.
- J. R. Burns and C. Ramshaw, *Trans. IchemE*, 1999, **77A**, 206.
- J. R. Burns and C. Ramshaw, *Lab Chip*, 2001, **1**, 10.
- S. J. Haswell, R. J. Middleton, B. O'Sullivan, V. Skelton, P. Watts and P. Styring, *Chem. Commun.*, 2001, 391.
- V. Skelton, G. M. Greenway, S. J. Haswell, P. Styring, D. O. Morgan, B. H. Warrington and S. Y. F. Wong, *Analyst*, 2001, **126**, 7.
- V. Skelton, G. M. Greenway, S. J. Haswell, P. Styring, D. O. Morgan, B. H. Warrington and S. Y. F. Wong, *Analyst*, 2001, **126**, 11.
- G. N. Doku, S. J. Haswell, T. McCreedy and G. M. Greenway, *Analyst*, 2001, **126**, 14.
- T. McCreedy and N. G. Wilson, *Analyst*, 2001, **126**, 21.
- M. C. Mitchell, V. Spikemans and A. J. de Mello, *Analyst*, 2001, **126**, 24.
- P. Watts, C. Wills, S. J. Haswell, E. Pombo-Villar and P. Styring, *Chem. Commun.*, 2001, 990.
- P. D. I. Fletcher, S. J. Haswell and V. N. Paunov, *Analyst*, 1999, **124**, 1273.
- M. A. Cobb and D. N. Hague, *J. Chem. Soc. Faraday Trans. 1*, 1972, **68**, 932.
- A. D. James and B. H. Robinson, *J. Chem. Soc. Faraday Trans. 1*, 1978, **74**, 10.
- T. McCreedy, *Anal. Chim. Acta*, 2001, **427**, 39.
- P. D. I. Fletcher, S. J. Haswell and X. Zhang, *Lab Chip*, 2001, **1**, 115.
- I. Broadwell, P. D. I. Fletcher, S. J. Haswell, T. McCreedy and X. Zhang, *Lab Chip*, 2001, **1**, 66.
- J. Th. G. Overbeek, in *Colloid Science*, ed. H. R. Kruyt, Elsevier, Amsterdam, 1952, vol. 1, ch. V, p. 194.
- R. J. Hunter, *Zeta Potential in Colloid Science*, Academic Press, London, 1981.
- Handbook of Chemistry and Physics*, CRC Press, Boca Raton, 62nd edn., 1981.
- J. Timmermans, *Physico-Chemical Constants of Pure Organic Compounds*, Elsevier, New York, 1950, vol. 1, 1965, vol. 2.
- The dielectric constant of ethanol was obtained from the microwave spectrum for pure ethanol measured in our laboratories.
- M. Kosmulski and E. Matijevic, *Colloid Polym. Sci.*, 1992, **270**, 1046.
- I. E. Valko, H. Siren and M.-L. Riekkola, *J. Microcolumn Sep.*, 1999, **11**, 199.
- C. Schwer and E. Kenndler, *Anal. Chem.*, 1991, **63**, 1801.
- P. B. Wright, A. S. Lister and J. G. Dorsey, *Anal. Chem.*, 1997, **69**, 3251.
- G. R. Wiese, R. O. James and T. W. Healy, *Discuss. Faraday Soc.*, 1971, **52**, 302.
- J. Jednacak, V. Pravidic and W. Haller, *J. Colloid Interface Sci.*, 1974, **49**, 16.
- R. A. Van Wagenen and J. D. Andrade, *J. Colloid Interface Sci.*, 1980, **76**, 305.
- P. J. Scales, F. Grieser, T. W. Healy, L. R. White and D. Y. C. Chan, *Langmuir*, 1992, **8**, 965.
- J. Crank, *The Mathematics of Diffusion*, Clarendon Press, Oxford, 1956.
- V. M. M. Lobo and J. L. Quaresma, *Handbook of Electrolyte Solutions Part B*, Elsevier, Amsterdam, 1989, p. 1914.
- See, for example, P. W. Atkins, *Physical Chemistry*, 5th edn., Oxford University Press, Oxford, 1994, p. 849.
- J. K. Towns and F. E. Regnier, *Anal. Chem.*, 1992, **64**, 2473.
- C. T. Culberson, R. S. Ramsey and J. M. Ramsey, *Anal. Chem.*, 2000, **72**, 2285.
- A. E. Herr, J. I. Molho, J. G. Santiago, M. G. Mungal, T. W. Kenny and M. G. Garguilo, *Anal. Chem.*, 2000, **72**, 1053.
- B. J. Harmon, D. H. Patterson and F. E. Regnier, *Anal. Chem.*, 1993, **65**, 2655.
- B. J. Harmon, I. Leesong and F. E. Regnier, *Anal. Chem.*, 1994, **66**, 3797.
- F. E. Regnier, D. H. Patterson and B. J. Harmon, *Trends Anal. Chem.*, 1995, **14**, 177.
- D. H. Patterson, B. J. Harmon and F. E. Regnier, *J. Chromatogr., A*, 1996, **732**, 119.
- S. C. Jacobson, R. Hergenroder, L. B. Koutny, R. J. Warmack and J. M. Ramsey, *Anal. Chem.*, 1994, **66**, 1107.
- S. V. Ermakov, S. C. Jacobson and J. M. Ramsey, in *Micro Total Analysis Systems '98*, ed. D. J. Harrison and A. Van den Berg, Kluwer, Dordrecht, 1998, p. 149.
- J. B. Knight, A. Vishwanath, J. P. Brody and R. H. Austin, *Phys. Rev. Lett.*, 1998, **80**, 3863.
- N. A. Patankar and H. H. Hu, *Anal. Chem.*, 1998, **70**, 1870.
- S. V. Ermakov, S. C. Jacobson and J. M. Ramsey, *Anal. Chem.*, 2000, **72**, 3512.

1,4-Addition of enolates to α,β -unsaturated ketones within a micro reactor

Charlotte Wiles,^a Paul Watts,^a Stephen J. Haswell^{*a} and Esteban Pombo-Villar^b

^a Department of Chemistry, Faculty of Science and the Environment, University of Hull, Cottingham Road, Hull, UK HU6 7RX. E-mail: s.j.haswell@hull.ac.uk; Fax: +44 (0)1482 466416; Tel: +44 (0)1482 465475

^b Nervous Systems Research, WSJ-386.07.15, Novartis Pharma Ltd, CH4002 Basel, Switzerland

Received 4th March 2002, Accepted 28th March 2002
First published as an Advance Article on the web 19th April 2002

We demonstrate the formation of a series of diketone enolates and their subsequent reaction with α,β -unsaturated carbonyl compounds in order to prepare a variety of Michael adducts. In all cases, the conversions observed within a micro reactor were greater than those obtained in batch.

Introduction

Over the past three years, there has been a rapid growth in the development of micro reaction technology exploiting the technique of electroosmotic flow (EOF).¹ Recent research has demonstrated that along with multi-component reactions such as the Suzuki coupling² and the Wittig reaction,³ multi-step peptide synthesis can also be performed within a micro reactor.^{4,5}

We have recently demonstrated the formation of enolates within a micro reactor using a class of reagents known as silyl enol ethers.^{6,7} The enolates were generated *in situ* using tetrabutylammonium fluoride and subsequently reacted with a series of aldehydes and acylating reagents, resulting in the preparation of β -hydroxy ketones, 1,3-diketones and *O*-acylated ketones. We were therefore interested in the preparation of enolates *via* the direct treatment of a ketone with a base and subsequently investigated the area of 1,4-additions.

Conjugate additions of enolates to α,β -unsaturated carbonyl compounds are generally known as Michael additions or 1,4-additions. The enolates of 1,3-diketone systems are traditionally formed using bases such as sodium ethoxide,⁸ we however observed a reaction between the Michael acceptor and the sodium ethoxide. As 1,3-dicarbonyl compounds are more acidic than mono substituted ketones (*e.g.* acetophenone), the protons can be abstracted using relatively weak bases (pK_a 9–13). We therefore investigated the use of an organic base, diisopropylethylamine. Here we demonstrate the preparation of enolates from a series of 1,3-diketones using an organic base, and their subsequent reaction with a variety of Michael acceptors to afford 1,4-addition products within a micro reactor.

Experimental

Micro reactor methodology

The borosilicate glass micro reactor used in this work was prepared using a standard fabrication procedure developed at Hull.⁹ The reactions were carried out using a 4 channel micro reactor, illustrated in Fig. 1, with approximate channel dimensions of $100 \times 50 \mu\text{m}$ and outer dimensions of $20 \times 20 \times 25 \text{ mm}$. Micro porous silica frits were placed within the channels in order to minimise hydrodynamic effects.¹⁰ An in-house LabVIEWTM program was used to set and monitor the voltages

applied to platinum electrodes placed in the reservoirs (power supply was built by Kingfield electronics). All micro reactions were carried out at room temperature over a period of 20 min to ensure a sufficient volume of product was generated for analysis. Reaction products were determined by GC-MS *via* the comparison of retention times and spectra with those obtained from synthetic standards **1**, **5**, **7** and **9** (Varian GC (CP-3800) coupled to a Varian MS (2000), CP-Sil 8 column (30 m), injector temperature 200 °C, helium flow rate 1 ml min⁻¹, oven temperature 50 °C for 4 min then ramped to 250 °C at 30 °C min⁻¹). Product conversions were calculated from the GC-MS with respect to the amount of respective diketone remaining in the sample. The synthetic standards were prepared using the following procedures:

Synthesis of the **1** using 2,4-pentanedione **2**

2,4-Pentanedione **2** (0.50 g, 5.00 mmol) was added to a stirred solution of ethyl propiolate **4** (0.49 g, 5.00 mmol) and diisopropylethylamine **3** (1.29 g, 10.00 mmol) in ethanol (50 ml), the reaction mixture was subsequently stirred overnight. The reaction mixture was concentrated *in vacuo* and subsequently purified by silica gel chromatography. Elution with 7% ethyl acetate in hexane yielded the title compound **1** as a colourless oil (0.88 g, 89%); δ_{H} (400 MHz, CDCl₃/TMS) 1.34 (3H, t, *J* 7.0, CH₂CH₃), 2.13 (6H, s, 2 \times CH₃), 4.24 (2H, t, *J* 7.0 CH₂CH₃), 4.4–4.45 (1H, m, COCHCO), 5.74 (1H, d, *J* 16.9, CH) and 7.39 (1H, d, *J* 16.9, CH); δ_{C} (100 MHz, CDCl₃/TMS) 14.3 (2 \times CH₃), 18.5 (CH₂CH₃), 61.6 (CH₂CH₃), 61.8 (COCHCO), 125.4 (CH), 141.8 (CH), 165.4 (2 \times CO) and 203.5 (CO₂); *m/z* (EI) 199 (M⁺+1, 15%), 198 (27), 181 (20), 153 (30), 124 (100) and 109 (20).

Synthesis of **5** using benzoyl acetone **6**

Benzoyl acetone **6** (0.25 g, 1.54 mmol) was added to a stirred solution of ethyl propiolate **4** (0.15 g, 1.54 mmol) and diisopropylethylamine **3** (0.40 g, 3.00 mmol) in ethanol (25 ml),

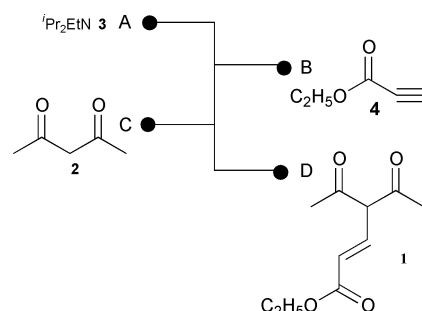


Fig. 1 Schematic of the micro reactor used in the synthesis of **1**.

the resulting reaction mixture was subsequently stirred overnight. The reaction mixture was concentrated *in vacuo* and subsequently purified by silica gel chromatography. Elution with 5% ethyl acetate in hexane yielded the title compound **5** as a pale yellow oil (0.31 g, 78%); δ_{H} (400 MHz, CDCl_3/TMS) 1.34 (3H, t, J 7.2, CH_2CH_3), 1.96 (3H, s, CH_3), 4.07–4.12 (3H, m, CH_2CH_3 and COCHCO), 5.47 (1H, d, J 16.8, CH), 7.69 (1H, d, J 16.8, CH), 7.69 (1H, m, Ar), 7.80 (2H, m, Ar) and 7.93 (2H, m, Ar); δ_{C} (100 MHz, CDCl_3/TMS) 14.2 (CH_3), 19.1 (CH_2CH_3), 60.7 (CH_2CH_3), 96.7 (COCHCO), 125.2 (CH), 128.6 (Ar, CH), 128.7 (Ar, CH), 129.7 (Ar, CH), 135.2 (Ar, C_0), 142.9 (CH), 165.5 (CO), 195.8 (CO) and 204.2 (CO_2); m/z (EI) 261 (M^++1 , 10%), 260 (15), 181 (40) and 105 (100).

Synthesis of **7** using diethyl malonate **8**

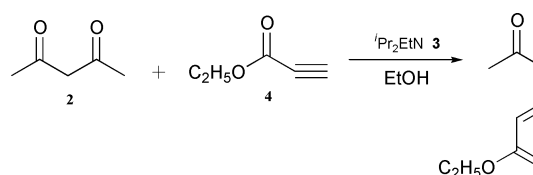
Diethyl malonate **8** (0.50 g, 3.10 mmol) was added to a stirred solution of ethyl propiolate **4** (0.30 g, 3.10 mmol) and diisopropylethylamine **3** (0.80 g, 6.20 mmol) in ethanol (50 ml), the reaction mixture was subsequently stirred overnight. The reaction mixture was concentrated *in vacuo* and subsequently purified by silica gel chromatography. Elution with 5% ethyl acetate in hexane yielded the title compound **7** as a colourless oil (0.73 g, 91%); δ_{H} (400 MHz, CDCl_3/TMS) 1.27 (3H, t, J 7.0, CH_2CH_3), 1.29 (3H, t, J 7.4, CH_2CH_3), 1.31 (3H, t, J 7.4, CH_2CH_3), 4.19–4.27 (7H, m, $3 \times \text{CH}_2\text{CH}_3$ and COCHCO), 5.88 (1H, d, J 16.4, CH) and 7.28 (1H, d, J 16.4, CH); δ_{C} (100 MHz, CDCl_3/TMS) 18.6 ($3 \times \text{CH}_2\text{CH}_3$), 61.5 ($3 \times \text{CH}_2\text{CH}_3$), 64.0 (COCHCO), 123.5 (CH), 143.0 (CH), 169.1 ($2 \times \text{CO}$) and 203.5 (CO_2); m/z (EI) 259 (M^++1 , 5%), 258 (15), 257 (50), 255 (95), 227 (100), 212 (80), 182 (23), 167 (50), 109 (40) and 81 (15).

Synthesis of **9** using 2,4-pentanedione **2**

2,4-Pentanedione **2** (0.50 g, 5.00 mmol) was added to a stirred solution of methyl vinyl ketone **10** (0.35 g, 5.00 mmol) and diisopropylethylamine **3** (1.29 g, 10.00 mmol) in ethanol (50 ml), the reaction mixture was subsequently stirred overnight. The reaction mixture was concentrated *in vacuo* and subsequently purified by silica gel chromatography; elution with 10% ethyl acetate in hexane yielded the title compound **9** as a colourless oil (0.77 g, 89%); δ_{H} (400 MHz, CDCl_3/TMS) 2.08 (2H, dt, J 7.0, CH_2), 2.10 (3H, s, CH_3), 2.20 (6H, s, $2 \times \text{CH}_3$), 2.46 (2H, t, J 7.0, CH_2CO) and 3.39 (1H, J 7.0, COCHCO); δ_{C} (100 MHz, CDCl_3/TMS) 29.3 ($2 \times \text{CH}_3$), 30.0 (CH_3), 37.9 (CH_2), 40.5 (CH_2CO), 66.9 (COCHCO), 191.2 (CH_2COCH_3) and 204.2 ($2 \times \text{CO}$); m/z (EI) 171 (M^++1 , 5%), 170 (1), 153 (15), 128 (25), 110 (20), 95 (40), 71 (25), 58 (10) and 43 (100).

Results and discussion

In order to prepare product **1**, the enolate of 2,4-pentanedione **2** was formed using diisopropylethylamine **3** and subsequently reacted with ethyl propiolate **4**. After a 24 h period, 89% conversion of 2,4-pentanedione **2** to product **1** had taken place. Although there are two isomers of product **1**, both in batch and within a micro reactor, the major product (>99%) formed was the *trans* product **1** (Scheme 1).

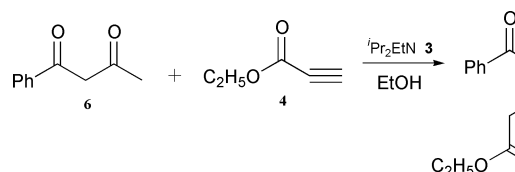


Scheme 1 Formation of **1** via the deprotonation of 2,4-pentanedione **2**.

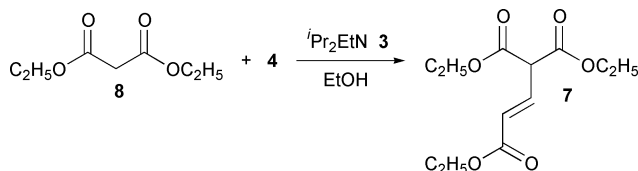
Having demonstrated that compound **1** could be prepared from 2,4-pentanedione **2** using the organic base diisopropylethylamine **3**, this represented a synthetic target for preparation within a micro reactor (Fig. 1). Prior to the synthesis, the micro reactor was primed with absolute ethanol, in order to remove any air or moisture from the channels and microporous silica frits. A standard solution of diisopropylethylamine **3** (40 μl , 5.0 M) in EtOH was placed in reservoir A, a solution of ethyl propiolate **4** (40 μl , 5.0 M) in EtOH in reservoir B and 2,4-pentanedione **2** (40 μl , 5.0 M) was placed in reservoir C. The reaction products were collected in EtOH in reservoir D. The reagents were manipulated within the device by the application of the following applied fields; 417, 318, 333 and 0 V cm^{-1} (A, B, C and D respectively). Using continuous flow of the reagents, resulted in 56% conversion of **2** to **1**. However, when the technique of stopped flow was employed, whereby the fields are applied for 2.5 s and then turned off for 5.0 s, 95% conversion of **2** to **1** was observed. In both cases, the reactions were performed for a period of 20 min, therefore the observed improvement in conversion can be attributed to the increased residence time within the micro reactor. Also by stopping the flow within the device, there is an increase in diffusion between the reagent streams allowing a higher degree of mixing which results in higher conversion of **2** to product **1**.^{11,12} The enhancements observed within a micro reactor compared with batch are summarised in Table 1.

Having demonstrated that the product **1** could be formed within a micro reactor, we wished to further demonstrate this technique using another diketone. In order to prepare a synthetic standard of **5**, the enolate of benzoyl acetone **6** was formed using diisopropylethylamine **3** and subsequently reacted with ethyl propiolate **4**. After 24 h, 78% conversion of **6** to compound **5** was observed in batch, the reaction was therefore transferred to the micro reactor (Scheme 2).

A standard solution of diisopropylethylamine **3** (40 μl , 5.0 M) in EtOH was placed in reservoir A, a solution of ethyl propiolate **4** (40 μl , 5.0 M) in EtOH in reservoir B and benzoyl acetone **6** (40 μl , 5.0 M) was placed in reservoir C. The reaction products were collected in EtOH in reservoir D. The reagents were manipulated within the device by the application of the following applied fields; 417, 318, 333 and 0 V cm^{-1} (A, B, C



Scheme 2 Formation of **5** via the deprotonation of benzoyl acetone **6**.



Scheme 3 Formation of **7** via the deprotonation of diethyl malonate **8**.

Table 1 Comparison of conversions obtained in batch with those obtained within a micro reactor

Reaction method	Product conversion (%)			
	1	5	7	9
Batch	89	78	91	89
^a Continuous flow	56	15	40	13
^a 2.5 on/5.0 off	95	34	100	95
^a 5.0 on/10.0 off	N/A	100	N/A	N/A

^a Reactions performed within a micro reactor.

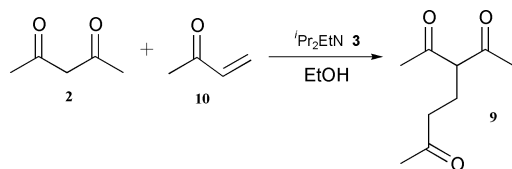
and D respectively). Using the continuous flow approach, resulted in 15% conversion of **6** to **5**. However, when the technique of stopped flow was employed, 2.5 s on and then 5.0 s off for a period of 20 min, 34% conversion was observed. This was subsequently increased to 100% conversion when using the regime of 2.5 s applied voltage and 10 s turned off. The technique was further demonstrated by the preparation of the Michael adduct **7** of diethyl malonate **8** within a micro reactor. Using diisopropylethylamine **3**, the enolate of diethyl malonate **8** was formed and subsequently reacted with ethyl propiolate **4** to form the product **7**. After 24 h, 91% conversion of the diethyl malonate **8** to the adduct **7** had taken place (Scheme 3).

Using the following procedure, the reaction was subsequently transferred to a micro reactor: A standard solution of diisopropylethylamine **3** (40 μ l, 5.0 M) in EtOH was placed in reservoir A, a solution of ethyl propiolate **4** (40 μ l, 5.0 M) in EtOH in reservoir B and diethyl malonate **8** (40 μ l, 5.0 M) was placed in reservoir C. The reaction products were collected in EtOH in reservoir D. The reagents were manipulated within the device by the application of the following applied fields; 417, 386, 381 and 0 V cm⁻¹ (A, B, C and D respectively). Using the continuous flow approach, resulted in 40% conversion of **8** to **7**. However, when the technique of stopped flow was employed, whereby the fields were applied for 2.5 s and then turned off for a further 5.0 s, 100% conversion of **8** to **7** was observed.

As the generality of the technique has been demonstrated through the use of the highly reactive alkynic Michael acceptor **4**, we further illustrated the technique using a less reactive alkenic acceptor methyl vinyl ketone **10**. A synthetic standard of **9** was prepared by the formation of the enolate of 2,4-pentanedione **2** using diisopropylethylamine **3**, subsequent reaction with methyl vinyl ketone **10** resulted in the formation of the Michael adduct **9**. After 24 h, 89% conversion of **2** to **9** was observed in batch, the reaction was therefore transferred to a micro reactor (Scheme 4).

A standard solution of diisopropylethylamine **3** (40 μ l, 5.0 M) in EtOH was placed in reservoir A, a solution of methyl vinyl ketone **10** (40 μ l, 5.0 M) in EtOH in reservoir B and 2,4-pentanedione **2** (40 μ l, 5.0 M) was placed in reservoir C. The reaction products were collected in EtOH in reservoir D. The reagents were manipulated within the device by the application of the following applied fields; 417, 455, 476 and 0 V cm⁻¹ (A, B, C and D respectively), continuous flow resulted in 13% conversion. Using the stopped flow approach (2.5 on/5.0 off), resulted in 95% conversion of **2** to **9**.

Interestingly, the flow regimes implemented with these reactions illustrated the varying reactivities of the respective diketone enolates *i.e.* when using continuous flow, 56% conversion of 2,4-pentanedione **2** to the adduct **1** was observed, compared with benzoyl acetone **6** whereby 15% conversion to **5** was obtained. In order to increase the conversion, the technique of stopped flow was implemented whereby the reaction of 2,4-pentanedione **2** required 2.5 s on and 5.0 s off (95%) compared with 2.5 s on and 10.0 s off for the reaction with



Scheme 4 Formation of **9** via the deprotonation of 2,4-pentanedione **2**.

benzoyl acetone **6** (100%). Thus demonstrating that the enolate of 2,4-pentanedione **2** is more reactive than that of benzoyl acetone **6**.

Conclusions

In conclusion, we have demonstrated the formation of a series of enolates within a micro reactor using the organic base, diisopropylethylamine. The enolates were subsequently reacted with α,β -unsaturated carbonyl compound in order to prepare a variety of Michael adducts. In all cases, the observed conversion within a micro reactor is greater than that obtained in batch, in one instance an increase of 22% was observed.

We have also illustrated enhancements in conversion through the application of the stopped flow technique. This was particularly highlighted in the synthesis of **5** whereby continuous flow resulted in an optimised conversion of 15%, by applying the regime of 2.5 s applied field and 5.0 s stopped flow, this increased to 34% and subsequently by increasing the time that the flow was stopped to 10.0 s, the conversion was further increased to 100%. We propose that the observed increase in conversion when utilizing stopped flow is due to an effective increase in residence time within the device and hence an increase in the diffusive mixing of the reagent streams.

We have therefore demonstrated the successful transfer of a reaction from batch, where it typically takes hours, to a micro reactor where it takes seconds or minutes.

Acknowledgements

We acknowledge Novartis Pharmaceuticals (C.W. and P.W.) for their financial support. We are grateful to Dr. Tom McCreedy for the device fabrication.

References

- 1 P. D. I. Fletcher, S. J. Haswell and V. N. Paunov, *Analyst*, 1999, **124**, 1273.
- 2 G. M. Greenway, S. J. Haswell, D. O. Morgan, V. Skelton and P. Styring, *Sens. Actuators B*, 2000, **63**, 153.
- 3 V. Skelton, G. M. Greenway, S. J. Haswell, P. Styring, D. O. Morgan, B. Warrington and S. Y. F. Wong, *Analyst*, 2001, **126**, 7.
- 4 P. Watts, C. Wiles, S. J. Haswell, E. Pombo-Villar and P. Styring, *J. Chem. Soc., Chem. Commun.*, 2001, 990.
- 5 P. Watts, C. Wiles, S. J. Haswell, E. Pombo-Villar and P. Styring, *Imret 5: Proceedings of the Fifth International Conference on Microreaction Technology*, 2001, p. 508.
- 6 C. Wiles, P. Watts, S. J. Haswell and E. Pombo-Villar, *Lab Chip*, 2001, **1**, 100.
- 7 C. Wiles, P. Watts, S. J. Haswell and E. Pombo-Villar, *J. Chem. Soc., Chem. Commun.*, in the press.
- 8 E. D. Bermann, D. Ginsburg and R. Pappo, *Org. React.*, 1959, **10**, 179.
- 9 T. McCreedy, *Anal. Chim. Acta*, 2001, **427**, 39.
- 10 P. D. Christensen, S. W. P. Johnson, T. McCreedy, V. Skelton and N. G. Wilson, *Anal. Commun.*, 1998, **35**, 341.
- 11 P. D. I. Fletcher, S. J. Haswell, T. McCreedy and X. Zhang, *Lab Chip*, submitted for publication.
- 12 X. Zhang, X. Z. Feng, P. D. I. Fletcher and S. J. Haswell, in *Micro Total Analysis Systems 2001*, ed. J. M. Ramsey and A. van den Berg, 2001, p. 371.



Green chemistry: synthesis in micro reactors

Stephen J. Haswell and Paul Watts*

Department of Chemistry, University of Hull, Cottingham Road, Hull, UK HU6 7RX.
E-mail: p.watts@hull.ac.uk

Received 25th October 2002

First published as an Advance Article on the web 10th February 2003

The importance of minimizing the impact that chemical processing has on the environment is growing, with an increased appreciation of the need to reduce pollution and the depletion of our finite environmental resources. Optimal use of material, energy and consequent waste management can be recognised as important factors for environmental protection. In the case of minimising waste there are two approaches, the traditional approach aims at reducing waste at the end of the pipeline, for example, decreasing emission by catalytic incineration of exhaust fumes. The second approach is based on minimising waste at the source. In this case, innovative procedures have to be employed to change both the method and the technology used throughout the production cycle. The miniaturisation of chemical reactors offers many fundamental and practical advantages of relevance to the pharmaceutical and fine chemicals industry, who are constantly searching for controllable, information rich, high throughput, environmentally friendly methods of producing products with a high degree of chemical selectivity. Indeed, for pharmaceutical companies an informatics-based approach, that micro reactor chemistry can uniquely deliver, may be the trigger for a step change in processes. This review explores how miniaturisation may revolutionise chemical synthesis, highlighting in particular the environmental benefits of this new technology, which include solvent free mixing, *in situ* reagent generation and integrated separation techniques. Furthermore, the possibility of preparing the chemicals in the required volume at point of use, negates the need to store and transport hazardous materials.

1 Introduction

In their simplest form, micro reactor devices consist of a network of micron-sized channels (typical dimensions are in the range 10–300 μm) etched into a solid substrate (see, for example refs. 1–9 for introductory overviews). For solution-based chemistry, the channel networks are connected to a series of reservoirs containing chemical reagents and products to form the complete device or ‘chip’ with overall dimensions of a few cm.

Reagents can be brought together in a specific sequence, mixed and allowed to react for a specified time in a controlled region of the channel network using electrokinetic (electro-osmotic and electrophoretic) or hydrodynamic pumping. For electrokinetically-driven systems, electrodes are placed in the appropriate reservoirs to which specific voltage sequences can be delivered under automated computer control. This control offers a simple but effective method of moving and separating reactants and products within a micro reactor, without the need for moving parts. Hydrodynamic pumping uses conventional, or micro-scale pumps (notably syringe pumps) to manoeuvre solutions around the channel network, however this technique has the disadvantage of requiring either large external pumps or complex fabrication of small moving parts.

The largest research effort in the field of micro scale devices to date has been in analytical science, where the aim has been to develop a Miniaturised Total Analytical System ($\mu\text{-TAS}$).^{10–17} Alongside the continuing development of $\mu\text{-TAS}$ and related analytical applications, a concerted effort has now begun to establish the benefits that micro reactors can bring to the field of reaction chemistry. For example, the ability to manipulate reagent concentrations in both space and time within the channel network of a micro reactor, provides an additional level of reaction control which is not attainable in bulk stirred reactors where concentrations are generally uniform. Furthermore, the spatial and temporal control of chemical reactions

in micro reactors, coupled with the features of very small reaction volumes and high surface interactions, is somewhat akin to the situation of reactions within biological cells. Nature exploits the organised distribution of reagents within the micron-sized sub-domains of cells to control and alter chemical reactivity relative to the situation of homogeneous solutions, in a rapid and efficient manner. Consistent with this notion, many reactions have been demonstrated to show altered reactivity, product yield and selectivity when performed in micro reactors as compared with conventional bench top glassware.

To date, the outcome of the reported research has confirmed that micro reactor methodology is applicable to performing both gas and liquid phase reaction chemistry. From the work cited in this review article, the evidence is that the unique *modus operandi* of micro reactors, namely the low-volume spatial and

Green Context

Traditional chemical manufacturing is heavily based on economy of scale with large reactors and associated plants requiring large process batches and associated large scale transport and storage of raw materials and products. All these large scale features present health and safety problems which can lead to major disasters as well as unacceptable levels of risk to operators and the neighbouring community. Microreactor chemistry shows great promise as a novel method on which to build new chemical technology and processes. The desired product is often produced in higher yield and purity, and more quickly. Reactions are much easier to control thus minimising risk and side reactions. Furthermore, solvent free mixing, *in-situ* reagent generation and integrated separation techniques can all help green the chemistry.

JHC

temporal control of reactants and products in a laminar flow diffusive mixing environment in which distinctive thermal and concentration gradients exist, offers a novel method for the chemical manipulation and generation of products. In short, micro reactors are new, safe and more atom efficient tools with which to generate molecules and increase our knowledge of complex chemical processes.

The technology is still in its early development stage and it would be presumptuous at this point to expand too far on the potential applications that micro reactors will find, but some early trends are clear. In the authors' experience, reactions performed in a micro reactor invariably generate relatively pure products in high yield, in comparison to the equivalent bulk reactions, in much shorter times and in sufficient quantities to perform full instrumental characterisation. One of the immediate and obvious applications is therefore in drug and process discovery, where the generation of compounds either with different reagents or under variable conditions is an essential factor. In addition, the opportunity to establish optimal chemical processes including reaction and formulation is an exciting capability of the technology, which could be integrated to appropriate analytical instrumentation. An interesting twist to the chemistry carried out to date in the authors' laboratories is not just the opportunity to separate reactants and products in real time but also the capability to manufacture and use reagents *in situ*. In this review, a brief description of the fabrication and operation of micro reactors is outlined, followed by a detailed description of the type of reactions that can be performed in micro reactors. The environmental significance of performing the reaction in micro reactors, compared with traditional techniques, is subsequently highlighted.

2 Fabrication of micro reactors

A number of materials such as silicon, quartz, glass, metals and polymers have been used to construct micro reactors.¹¹ Important considerations in material choice include chemical compatibility, ease and reproducibility of fabrication, whether or not the material supports electroosmotic flow (EOF) with the solvents of interest and compatibility with detection methods. Glass is a popular choice since it allows EOF with many common solvents, is chemically inert, enables the use of visible light detection and fabrication methods are well established.

Depending on the material used, a range of channel microfabrication methods such as photolithography, hot embossing, powder blasting, injection moulding and laser micro forming are available.¹⁸ For glass micro reactors, photolithographic fabrication of channel networks is performed as shown schematically in Fig. 1 and described in refs. 19 and 20. First, the channel network is designed and printed using suitable computer drawing software and a film negative of the desired final size is then prepared by photoreduction to form the optical mask. Commercially supplied borosilicate glass photolithographic plates (thickness 3 mm) coated with a thin metal etch mask layer (normally chromium) plus an upper layer of positive photoresist (0.5–2.0 μm depth) are used for channel network fabrication. The pattern of the required network of inter-connecting channels is transferred from the optical mask to the photoresist layer. After light exposure, the photoresist is developed and removed, together with the chromium layer, to reveal the areas of glass to be etched. The channels are then etched using a mixture of 1% HF and 5% NH_4F in water at 65 $^\circ\text{C}$, resulting in an etch rate of 0.3–0.5 $\mu\text{m min}^{-1}$. During the etching process it is important that the system is well agitated to ensure consistent supply of etchant to the surface plus removal of etch debris.

The base plate containing the etched channel network must next be sealed by bonding to an upper plate (17 mm thick)

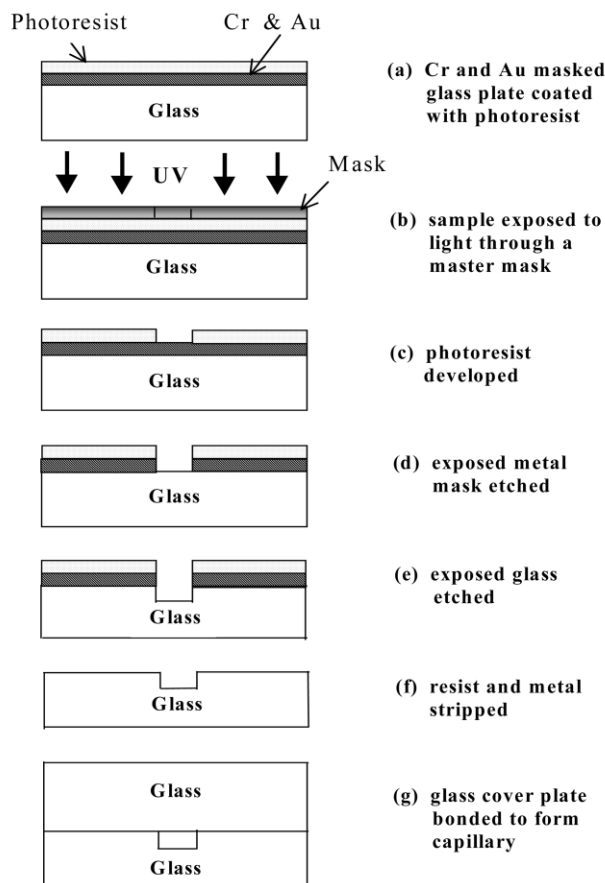


Fig. 1 Photolithographic fabrication of micro reactors.

containing pre-drilled holes which act as reservoirs for reagents and products. In our laboratories, the upper plate is aligned with the channel geometry and thermally bonded to the base plate (typically 575 $^\circ\text{C}$ for 3 h).^{19,20} Thermal bonding is aided by placing a weighting block of non-adhering quartz of high softening temperature on the upper plate. A photograph of an all-glass device produced by the method described is shown in Fig. 2. For good thermal bonding, it is important to ensure that

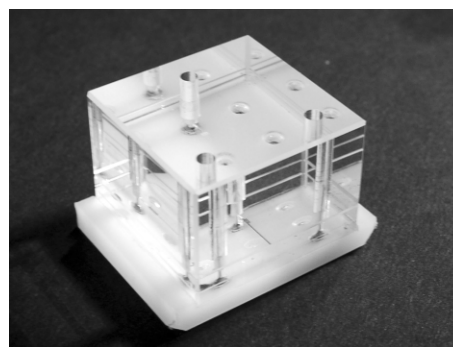


Fig. 2 A borosilicate glass micro reactor.

both the glass types of the upper and lower plates have the correct thermal softening and expansion properties. In addition, the surfaces to be bonded must be clean and flat.

More recently the thermal bonding of ceramic adaptors has enabled hydrodynamic pumping to be more effectively realised.¹⁹ Fig. 3 shows a glass micro reactor with ceramic adaptors enabling HPLC type fittings to be connected directly to the chip.

Fabrication in polymeric materials, whilst attractive from an engineering and cost perspective, does pose a number of reagent compatibility issues. However, recently, the UK Lab on a Chip

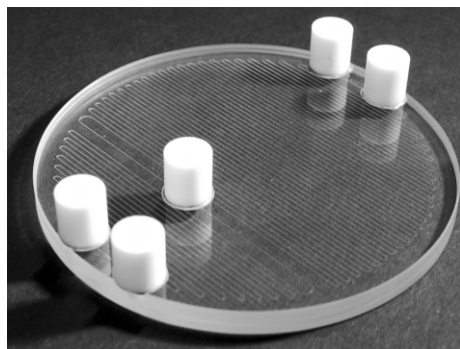


Fig. 3 Micro reactor with ceramic fittings.

Consortium project demonstrated that polymer devices with channels fabricated in SU-8 (an epoxy resin) coated on a polymer support (such as methacrylate) is relatively robust to chemical attack. The first generation of such devices (Fig. 4) are

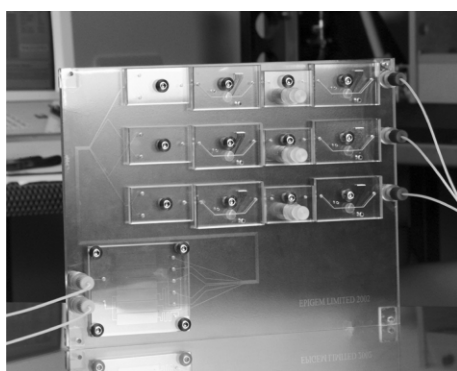


Fig. 4 Micro reactors fabricated from polymers (Photograph courtesy of Epigem Ltd.).

now being evaluated. This methodology has the advantage that the non-wetted bulk of the chip can, if desired, be fabricated from low cost commodity polymers.

Of all the fabrication media, perhaps metals are the most robust in terms of engineering requirements and more specifically, micro mixers have been constructed and applied in chemical processing. This subject is extensively reviewed in ref. 9.

3 Operation of micro reactors using electrokinetic control

Pumping of solutions around a channel network by EOF, using voltages applied *via* electrodes placed in the reservoirs, has several significant advantages over hydrodynamic based pumping methods.^{21–24} It can be easily miniaturised since no mechanical moving parts are involved and the required voltage sequences can be readily applied under automated computer control. For a glass micro reactor, the channel wall–solution interface normally has a negative charge, arising from ionisation of surface groups, which are immobile. This immobile surface charge attracts a diffuse layer (of thickness of the order of nm) of mobile, oppositely charged counter-ions in the solution adjacent to the channel wall (cations for a negatively-charged glass channel wall). As shown schematically in Fig. 5, application of an electric field along the channel length causes the nm thick ‘skin’ of mobile cations to move towards the more negative electrode, which drags all the intervening solution in the bulk of the channel with it. An important feature of EOF is that the liquid EOF velocity is constant across the channel except in the nm thick regions of the diffuse layer of counter-

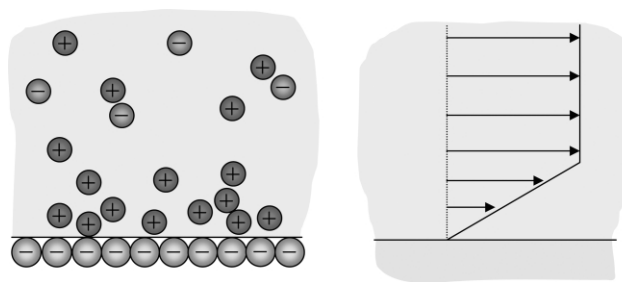


Fig. 5 Profile of electroosmotic flow.

ions very close to the wall. Unlike EOF, pressure-driven flow produces a parabolic velocity profile with high velocities in the channel centre and slow velocities near to the wall, giving rise to increased ‘blurring’ of reagent zones along a channel length. Imaging of the different velocity profiles induced by EOF and pressure-driven flow has been described by Paul *et al.*²⁵ It should however be emphasised, that under EOF control, charged solutes move with an electrophoretic velocity in addition to the EOF of the solvent.

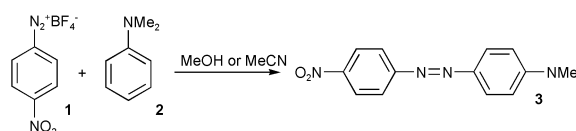
It should be stressed, that for EOF to be achieved polar solvent types need to be used (*e.g.* methanol, DMF, DMSO *etc.*). Clearly this limitation could reduce the scope of micro reactor applications, however the authors are currently developing a combined electrokinetic/hydrodynamic pumping method for manipulating reactants, intermediates and products within a micro reactor device. Such a system offers wider solvent and reagent capability, whilst still enabling the electrophoretic mobility of chemical species to be exploited.

4 Reactions performed in micro reactors

The following section reviews the chemical reactions that have been performed within micro reactor systems to date. The review is divided into three sections, concentrating on solution phase synthesis, catalysed reactions and finally gas phase synthesis.

4(a) Liquid phase reactions

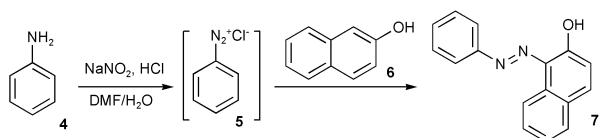
The diazotization of aromatic amines is an industrial process of great importance, however the dangers of diazotization are well known. The explosive nature of diazonium salts necessitates extreme care hence the low volume associated with micro reactors affords a safe route to perform such reactions. Salimi-Moosavi *et al.*²⁶ have demonstrated the synthesis of diazo dyes within a micro reactor. The authors have reacted 4-nitrobenzenediazonium tetrafluoroborate **1** with *N,N*-dimethylaniline **2** in a micro reactor fabricated from glass, to give the red diazo compound **3** (Scheme 1). The reagents were mobilised in



Scheme 1

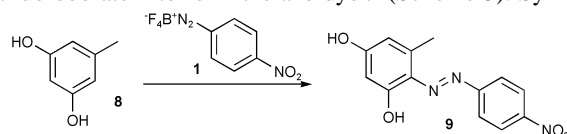
the reactor, using EOF in either a protic (methanol) or an aprotic (acetonitrile) solvent, to give conversions of 37 and 22%, respectively.

In comparison Wootton *et al.*²⁷ have demonstrated the synthesis of azo dyes using hydrodynamic pumping within a micro reactor. The authors demonstrated that aniline **4** could be converted into the diazonium salt **5** before being reacted *in situ* with β -naphthol **6** to form the azo dye **7** in up to 52% overall conversion (Scheme 2).



Scheme 2

Hisamoto *et al.*²⁸ have described the first example of a phase-transfer reaction in a micro reactor. The authors have successfully conducted a phase-transfer diazo coupling reaction in which a solution of 5-methylresorcinol **8** in ethyl acetate was reacted with an aqueous solution of 4-nitrobenzenediazonium tetrafluoroborate **1** to form the azo dye **9** (Scheme 3). Syringe

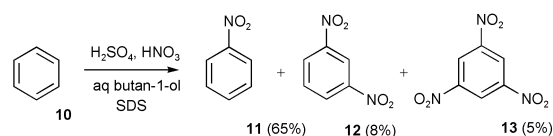


Scheme 3

pumps were used to move the reagents around the reactor manifold and the authors report that the product was isolated in 100% yield.

Nitration reactions also represent an important but hazardous process, in which the use of excess quantities of concentrated nitric and sulfuric acids are used. The reactions are extremely exothermic and it is hence difficult to control the temperature of such reactions when performed on a large scale. As a result, micro reactors have a considerable attraction for these reactions because the reactor enables not only excellent temperature control of the reaction but also product selectivity.

Doku *et al.*²⁹ have reported the nitration of benzene **10** in a borosilicate glass micro reactor. The benzene was mobilised by electroosmotic flow as a microemulsion using the surfactant, sodium dodecyl sulfate (SDS). The nitronium ions, which were produced *in situ* by mixing sulfuric and nitric acids, underwent electrophoretic-induced mobility (*i.e.* the ions not the reagents moved). A co-solvent, butan-1-ol, was used to enhance the solubility of the benzene in the aqueous system. The authors report that mononitration occurs in 65% conversion to give nitrobenzene **11** (Scheme 4) and that approximately 8% of

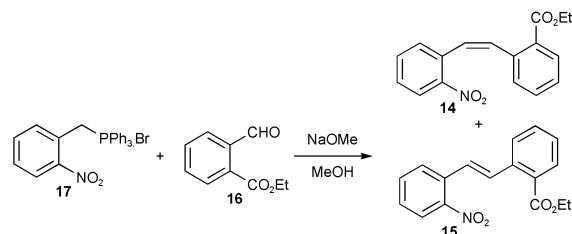


Scheme 4

1,3-dinitrobenzene **12** and 5% of 1,3,5-trinitrobenzene **13** were obtained. Importantly, Doku *et al.* demonstrated that it is possible to mobilise a non-polar liquid, such as benzene, using EOF by dissolving it in a two-phase microemulsion system.

Burns and Ramshaw³⁰ have also investigated the nitration of benzene and toluene in a micro reactor. They have reported that the conversion has a linear relationship with temperature. More interestingly, they have demonstrated that the conversion may be increased, by reducing the dimensions of the micro reactor channels. They found that reducing the capillary diameter from 250 to 130 nm more than doubled the rate of nitration. The flow rates were additionally determined to be critical, with faster flow rates giving higher conversions. The authors postulate that the increased flows promoted increased mixing within the channels.

Skelton *et al.* have reported the application of micro reactors, prepared from borosilicate glass, for the Wittig reaction.^{31,32} The authors used the micro reactor to prepare the *cis*- and *trans*-nitrostilbene esters **14** and **15** using the Wittig reaction (Scheme 5). A number of features such as stoichiometry and stereochemistry were investigated. When two equivalents of the aldehyde **16** to the phosphonium salt **17** were used in the reaction, a conversion of 70% was achieved. The micro reactor

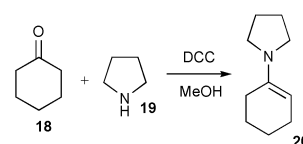


Scheme 5

demonstrated an increase in reaction efficiency of 10% over the traditional batch synthesis. The reaction stoichiometry was subsequently reduced to 1:1, but using a continuous flow of reagents, as above, the conversion was poor (39%). The conversion was increased to 59% using an 'injection' technique, where 'slugs' of the phosphonium salt **17** were injected into a continuous flow of the aldehyde **16**.

The research was further extended to investigate the stereochemistry of the reaction. The ratio of isomers **14** and **15** was controlled by altering the voltages applied to the reagent reservoirs within the device, which in turn affected the EOF and electrophoretic mobility of the reagents. The variation in the external voltage subsequently altered the relative reagent concentration within the device, producing *cis/trans* ratios in the region 0.57–5.21. In comparison, the authors report that, when a traditional batch synthesis was performed based on the same reaction time, concentration, solvent and stoichiometry, a *cis/trans* ratio of approximately 3:1 was observed. This demonstrated that significant control was possible in a micro reactor compared with batch reactions.

Sands *et al.*³³ have recently reported the preparation of enamines in a micro reactor. Enamines are traditionally prepared under Dean and Stark conditions, where the ketone and secondary amine are heated to reflux in toluene. These conditions remove the water from the reaction to produce the equilibrium-dependent enamine. Using the micro reactor, cyclohexanone **18** was reacted with pyrrolidine **19** using methanol as the solvent, in the presence of dicyclohexylcarbodiimide (DCC), to form the enamine **20** in 42% conversion at room temperature (Scheme 6). Clearly the use of



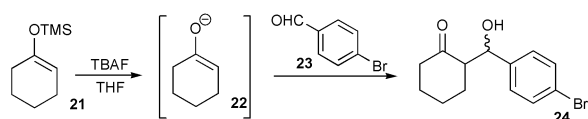
Scheme 6

methanol as solvent at room temperature, compared with the traditional conditions, represents a more environmentally friendly procedure. In this case also, the electrophoretic mobility of the product is thought to be greater than that of water, so enabling product separation and purification *in situ*.

Carbanion chemistry is one of the most common methods of C–C bond formation used in the pharmaceutical industry. In such reactions large volumes of highly pyrophoric bases are frequently employed. In addition, large quantities of heat are frequently generated which means that careful control of the temperature, to prevent by-product formation, is required. Hence, micro reactors have a considerable attraction for these reactions because the reactor enables excellent temperature control of the reaction.

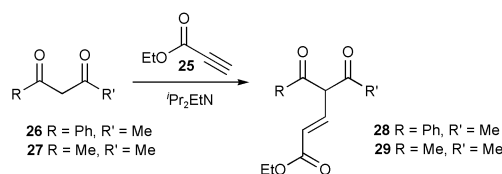
Wiles *et al.*³⁴ have recently demonstrated the use of silyl enol ethers in the aldol reaction within a micro reactor. Quantitative conversion of the silyl enol ethers to β -hydroxyketones was observed in 20 min compared to traditional batch systems, where quantitative yields were only obtained when extended reaction times of up to 24 h were employed. One example involved the treatment of the TMS enol ether **21** with tetra-*n*-butylammonium fluoride (TBAF), to generate the tetra-*n*-

butylammonium enolate **22** *in situ*, followed by condensation with *p*-bromobenzaldehyde **23** to give the β -hydroxyketone **24** in 100% conversion (Scheme 7).



Scheme 7

Wiles *et al.*³⁵ have also reported the preparation of the enolates from a series of 1,3-diketones using an organic base and their subsequent reaction with a variety of Michael acceptors such as **25** to afford 1,4-addition products within a micro reactor (Scheme 8).

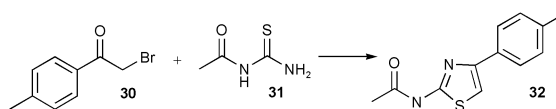


Scheme 8

When using a continuous flow of the reagents **25** and **26**, 15% conversion to the adduct **28** was observed, compared with 56% when the diketone **27** was reacted with **25** forming the Michael adduct **29**. The authors, however, demonstrated enhancements in conversions through the application of the stopped flow technique. This procedure involved the mobilisation of reagents through the device for a designated period of time, using an applied field, and the flow was subsequently paused by the removal of the applied field, prior to re-applying the field. Using the regime of 2.5 s on and 5 s off, the conversion to the product **28** was improved to 34%, while lengthening the stopped flow period to 10 s, resulted in a further increase to 100%. This was compared to the preparation of **29**, in which the regime of 2.5 s on and 5 s off resulted in an increase in conversion to 95%. This demonstrated that the enolate of 2,4-pentanedione **27** was more reactive than the corresponding enolate of benzoyl acetone **26**. The authors propose that the observed increase in conversion, when using the technique of stopped flow, was due to an effective increase in residence time within the device corresponding to the different kinetics associated with these reactions. This approach is clearly relevant to those wishing to study reaction kinetics of such reactions.

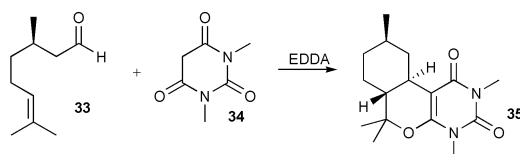
Although the previous result demonstrates the ease with which reaction conditions may be optimised, it is still sometimes necessary to heat reactions in order to achieve high yields of products. Industrially, special equipment is required when performing large-scale reactions at elevated temperature. However, Garcia-Egido *et al.*³⁶ at GlaxoSmithKline have demonstrated the synthesis of 2-aminothiazoles using a Hantzsch synthesis within a micro reactor. The paper represents the first example of a heated reaction using an organic solvent, within a glass micro reactor under EOF conditions. During the experiments the T-shaped micro reactor was heated to 70 °C using a Peltier heater, which was aligned with the channels and the heat generated by the device was applied to the base of the micro reactor. Reaction of α -bromoketone **30** with thiourea **31**, using *N*-methylpyrrolidine (NMP) as solvent, resulted in the preparation of aminothiazole **32** in up to 85% conversion (Scheme 9).

Fernandez-Suarez *et al.*³⁷ have reported the synthesis of cycloadducts in a micro reactor using hydrodynamic driven flow. The reactions consisted of Knoevenagel condensation of an aldehyde **33** with a 1,3-diketone **34** in the presence of



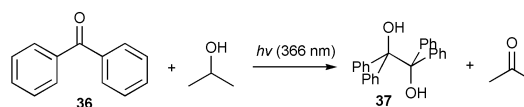
Scheme 9

ethylenediamine acetate (EDDA) as catalyst, in aqueous methanol as solvent. The reaction intermediate underwent an intramolecular hetero-Diels–Alder reaction to form cycloadduct **35** in 60–68% conversion (Scheme 10).



Scheme 10

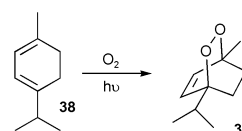
Environmentally attractive photochemically induced reactions are problematic on a large scale because many chemical species strongly absorb the light, effectively reducing the path length, even when powerful irradiation is used. Hence better results are obtained when the desired reaction is scaled down in size and Jenson and coworkers³⁸ have reported a photochemical reaction within a micro reactor. The reactor was fabricated by bonding a patterned silicon wafer to a quartz wafer, the advantage of this fabrication technique being that the quartz substrate allows reaction and detection using UV light of lower wavelengths than permitted by Pyrex substrates. The authors investigated the pinacol formation reaction of benzophenone **36** using propan-2-ol as solvent (Scheme 11). The reaction is



Scheme 11

known to follow a radical reaction pathway³⁹ and it is reported that the longer the residence time of the reaction, the greater the conversion to benzopinacol **37**. The authors report that there was no detectable product formation for flow rates greater than 10 $\mu\text{l min}^{-1}$. With reduced flow rates, having larger residence times, the conversion improves because the amount of light absorbed increases and there is therefore sufficient time for the excited species to diffuse and react with the benzophenone. The authors report conversions of up to 60% when using flow rates of 4 $\mu\text{l min}^{-1}$.

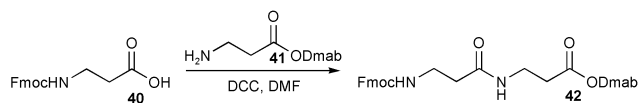
Using a similar approach Wootton *et al.*⁴⁰ investigated the photochemical generation of singlet oxygen within micro reactors. The technique allows the generation of singlet oxygen without the inherent dangers of forming large quantities of potentially explosive oxygenated solvents. The singlet oxygen was formed within the reactor channel by irradiation with a 20 W, 6 V tungsten lamp. The authors have used the aforementioned conditions to convert α -terpinene **38** into ascaridole **39** (Scheme 12) in greater than 80% conversion. For safety,



Scheme 12

nitrogen degassing of the product mixture was undertaken as soon as the solution was collected, hence avoiding accumulation of oxygenated solvents.

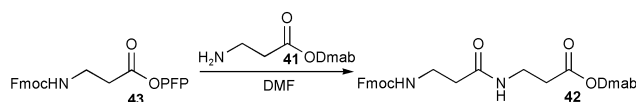
Watts *et al.* have recently demonstrated the first example of a multi-step synthesis in a micro reactor where they have used their devices in peptide synthesis.^{41,42} The authors evaluated the reactor using a carbodiimide coupling reaction of Fmoc- β -alanine **40** (Fmoc = fluorenylmethoxycarbonyl) with the amine **41** to give the dipeptide **42** (Scheme 13). When stoichiometric



Scheme 13

quantities of the reagents were used, only *ca.* 10% conversion to the dipeptide **42** was achieved. By using two equivalents of dicyclohexylcarbodiimide (DCC), however, an increase in conversion to *ca.* 20% was observed and by applying a stopped flow technique (2.5 s injection length with stopped flow for 10 s), the conversion of the reaction was further increased to approximately 50%. Using five equivalents of DCC, a conversion of up to 93% of the dipeptide **42** was obtained using the stopped flow technique.

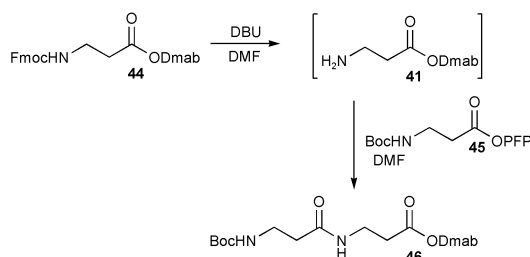
The authors also demonstrated that the dipeptide could be prepared from pre-activated carboxylic acids.^{41,42} They report that the reaction of the pentafluorophenyl (PFP) ester of Fmoc- β -alanine **43** with the amine **41** gave the dipeptide **42** quantitatively in 20 min (Scheme 14). This represented a



Scheme 14

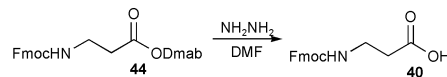
significant increase in yield compared with the traditional batch synthesis, where only a 50% yield was obtained in 24 h.

Having demonstrated that peptide bonds could be successfully formed when using a micro reactor, the authors then found that they could extend the methodology to the preparation of longer-chain peptides. Using the micro reactor, the Dmab ester (Dmab = 4-[N-(1-(4,4-dimethyl-2,6-dioxocyclohexylidene)-3-methylbutyl)-3-amino]benzyl) of Fmoc- β -alanine **44** was reacted with one equivalent of piperidine or 1,8-diazabicyclo(5.4.0)undec-7-ene (DBU)^{43,44} to give the free amine **41** in quantitative conversion. This is in comparison to solid phase peptide synthesis where 20% piperidine in DMF is frequently employed, which demonstrates the atom efficiency of reactions performed within the devices. The authors then reacted the amine *in situ* with the pentafluorophenyl ester **45** to give the dipeptide **46** (Scheme 15) in 96% overall conversion.



Scheme 15

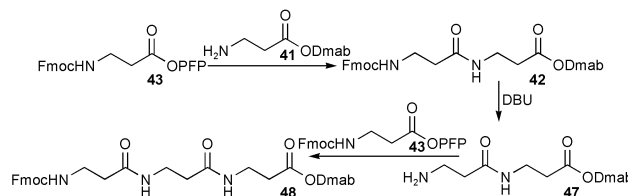
Having shown that more complex peptides could be produced by removal of the *N*-protecting group, the authors then demonstrated that they could remove the Dmab ester using hydrazine. The reaction of the Dmab ester **44** with one equivalent of hydrazine resulted in quantitative deprotection, to afford the carboxylic acid **40** (Scheme 16). This is in



Scheme 16

comparison to the solid phase peptide synthesis where 2% hydrazine in DMF is generally required to effect complete deprotection.⁴⁵

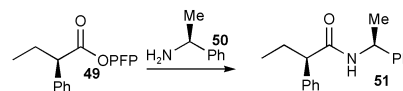
The authors have further extended the approach to the synthesis of tripeptide **48**.⁴² Reaction of pentafluorophenyl ester **43** with amine **41** formed dipeptide **42**, which was reacted with DBU to effect Fmoc deprotection. The amine **47** was then reacted *in situ* with another equivalent of pentafluorophenyl ester **43** to prepare tripeptide **48** in 30% overall conversion (Scheme 17). The approach clearly demonstrates that inter-



Scheme 17

mediates may be generated *in situ* and used in subsequent reactions. Although in the above examples the intermediates are relatively non-toxic, it is postulated that the approach may be used to generate highly toxic reagents *in situ*, that one would rather not use in a large-scale synthesis.

Having demonstrated that peptide bonds could be successfully formed when using a micro reactor, the authors then investigated racemisation in peptides derived from α -amino acids.⁴⁶ Reaction of the pentafluorophenyl ester of (*R*)-2-phenylbutyric acid **49**, at 0.1 M concentration, with α -methylbenzylamine **50**, gave the product **51** in quantitative conversion with 4.2% racemisation (Scheme 18). Importantly

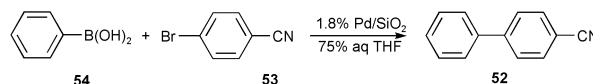


Scheme 18

there was less racemisation than observed in the batch reaction at the same concentration and temperature. The reduced level of racemisation was attributed to the reduced reaction times observed within the micro reactors.

4(b) Catalytic reactions

Greenway *et al.* have demonstrated the Suzuki reaction within a micro reactor.⁴⁷ This represented an example of heterogeneous catalysis where 1.8% palladium on silica was placed in the central channel of the micro reactor. The catalyst was immobilised between microporous silica frits prepared from potassium silicate and formamide. The micro reaction was optimised using flow injection analysis principles, producing a conversion of 67% of cyanobiphenyl **52** at room temperature. The flow injection method adopted allowed the periodic injection of the aryl halide **53** into a continuous flow of the phenylboronic acid **54** (Scheme 19). Traditionally, tetra-



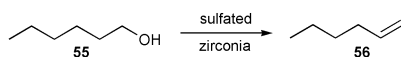
Scheme 19

hydrofuran (THF) is used as the solvent in this reaction, however as has been found with many organic solvents THF has

very low natural EOF properties and for this reason, it was mixed with water (75:25) for use in the reaction. The yields obtained were comparable with Suzuki reactions on a batch scale using homogeneous catalysis. Importantly, there were negligible levels of the palladium catalyst in the product, which was demonstrated using inductively coupled-mass spectrometry (ICP-MS), this illustrating that the catalyst was not leaching from the reactor.

One of the interesting observations of the reaction was that, unlike conventional Suzuki reactions, an additional base was not required. Although the exact reason for this is not clear, it is postulated that the electric field may be sufficient to cause ionisation of the water at the catalyst surface. It is feasible that the hydroxide formed in this way may be sufficient to perform the function of the conventional organic or inorganic base. Alternatively, it has been subsequently proposed that a more basic environment may be formed at the surface of the micro reactor. Once again this effect could have wider implications in the field of clean chemistry.

Wilson and McCreedy⁴⁸ have reported the use of a micro reactor to perform the dehydration of hexan-1-ol to hex-1-ene, using a sulfated zirconia catalyst. The micro reactor was fabricated from a glass plate, which was etched using photolithography. A PDMS top block, with pre-drilled holes to act as reservoirs for the reagents, was then aligned with the channel geometry. In order to introduce the catalyst into the micro reactor, it was dusted over the surface of the PDMS face before the base plate was joined to the top plate. This process immobilised the catalyst, while simultaneously increasing its surface area. The overall effect was to produce a catalytically-active wall of the microchannel. A heater, fabricated from Nichrome wire, was also immobilised in the top plate. Pumping was produced with a syringe pump and the products were analysed by gas chromatography (GC). The conversion of hexan-1-ol **55** to hex-1-ene **56** was between 85 and 95% with no additional products being detected (Scheme 20). This yield is

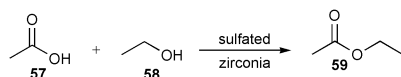


Scheme 20

extremely good when compared to the 30% yield expected for the industrially used process.

The reaction was also applied to ethanol. At a reaction temperature of 155 °C and using a syringe pump at a flow rate of 3 $\mu\text{l min}^{-1}$, the product collected was found to contain 68% ethene, 16% ethane and 15% methane, together with trace amounts of ethanol. When electroosmotic pumping was used, the flow rate was between 0.9 and 1.1 $\mu\text{l min}^{-1}$ at a field strength of 200 V cm^{-1} . The only detectable product was methane, indicating that the reaction had progressed beyond dehydration to complete cracking of the ethanol. Additionally, trace amounts of methanol were present in the product. It is proposed that the slow flow rate of the electroosmotic pumping, resulted in longer residence times in the reactor. EOF however cannot be applied to all reactions because organic reactants, such as hexanol, exhibit no natural EOF under an applied potential.

The authors used the same device to investigate esterification reactions, where a 1 : 1 mixture of acetic acid **57** and ethanol **58** was pumped through the micro reactor using a syringe pump at a flow rate of 2 $\mu\text{l min}^{-1}$ to produce ethyl acetate **59** (Scheme 21).⁴⁹ By increasing the temperature of the reaction from room temperature to 180 °C, the conversion of the reaction was

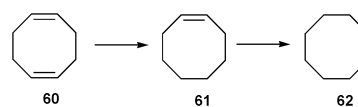


Scheme 21

increased to about 30%. Although the preliminary yield was not great, the procedure has environmental advantages compared to the traditional conditions used in esterification reactions.

4(c) Gas phase reactions

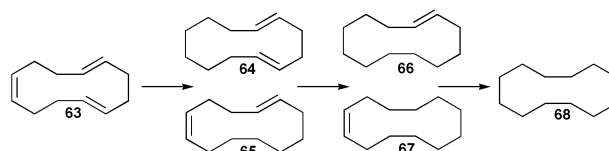
Hönicke and coworkers⁵⁰ have reported the gas phase partial oxidation of cyclic dienes, to their corresponding monoalkenes, over palladium and ruthenium/zinc catalysts. The micro reactors consisted of aluminium wafers, with mechanically-etched channels, which were activated by anodic oxidation to obtain a porous oxide layer, which was used as the catalyst support. Impregnation of an organic solution of palladium(II) acetylacetonate resulted in microchannels consisting of an 18 μm thick layer of 0.18% Pd catalyst. The wafers were then stacked in a stainless steel housing to form a micro reactor consisting of 672 microchannels for a stream of reagents to pass through. The authors used the device to investigate the hydrogenation of 1,5-cyclooctadiene **60** to cyclooctene **61** (Scheme 22). The diene **60** was vapourised and mixed with



Scheme 22

hydrogen, before being passed through the micro reactor at a temperature of 150 °C. By increasing the residence time of the reaction from 35 to 115 ms the authors report that the conversion increased from 75 to 99.5%. Although the increased residence time resulted in increased quantities of cyclooctane **62** being formed, the selectivity of cyclooctene **61** decreased from 99.5 to 98% under these conditions. The procedure represented a novel method for the immobilisation of potentially toxic catalysts, hence the process has possible environmental advantages.

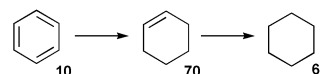
The authors used the same device to investigate the hydrogenation of *cis,trans,trans*-1,5,9-cyclododecatriene **63** to the cyclododecenes **64** and **65** (Scheme 23). At a temperature of



Scheme 23

150 °C, a selectivity of 85 to 90% was reported, where the conversion was approximately 90%. The selectivity of this reaction was lower than the previous example because of the formation of the by-products **66**, **67** and **68**. It was demonstrated, however, that there was a selectivity advantage of the micro reactor compared to a fixed-bed reactor.

The catalytic hydrogenation of benzene **10** was also investigated (Scheme 24), but complete reduction to cyclohexane **69**



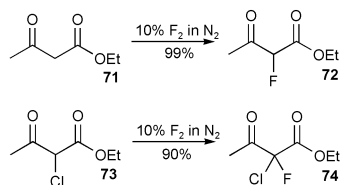
Scheme 24

was observed to take place when using the Pd catalyst. The authors report that hydrogenation of benzene to cyclohexene **70** was accomplished using a micro reactor system consisting of a ruthenium/zinc catalyst, which was incorporated into the micro reactor using the same methodology, but the conversions were

reported to be low (*ca* 10%), with a maximum selectivity of 36%.

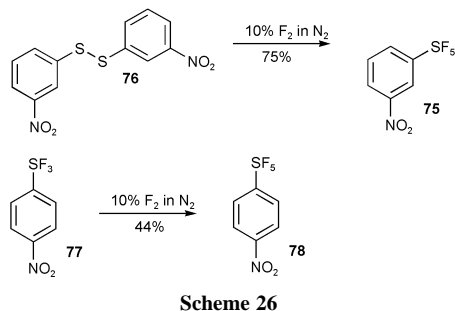
The use of elemental fluorine in organic synthesis is problematic as a result of the difficulties associated with the safe handling of gaseous fluorine.^{51,52} In addition, fluorination reactions are generally extremely exothermic and it is difficult to control the temperature of such reactions when performed on a large scale. Micro reactors have considerable attraction for direct fluorination processes because there is only a small amount of fluorine in the reactor at any given time. The micro reactor enables excellent temperature control of the reaction as well as an opportunity for scale up, by the simultaneous use of many such reactors.

Chambers and Spink^{53,54} have reported the use of micro reactors for the fluorination and perfluorination of organic compounds using elemental fluorine. A nickel or copper micro reactor was used for the investigation and the liquid reactants and solvents were introduced into the reaction chamber *via* a syringe using a syringe-pump. Fluorine, in a nitrogen carrier gas, was introduced from a cylinder using a mass-flow controller. The liquid-gas mixing proceeded *via* 'cylindrical flow', where the liquid forms an outer cylinder coating the reactor surface with the gas flowing through the centre. This flow regime has enormous benefits in that it provides very large surface-to-volume ratios for the liquid phase, producing a very efficient reaction over a short distance. The products were trapped in a tube, which was cooled with either a salt/ice bath (0 °C) or an acetone/carbon dioxide bath (−78 °C). The fluorination of β -dicarbonyl compounds proceeded with a high efficiency using 10% fluorine in nitrogen at 5 °C and with formic acid as the solvent. Ethyl acetoacetate **71** was fluorinated in 99% conversion to give ethyl 2-fluoroacetoacetate **72** while ethyl 2-chloroacetoacetate **73** was fluorinated in 90% conversion, yielding ethyl 2-chloro-2-fluoroacetoacetate **74** (Scheme 25). Importantly, under these conditions, no perfluorination of



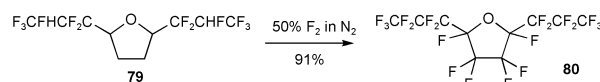
the substrates was observed, with only the monofluorinated derivatives being isolated. The authors report that the bulk fluorination of ethyl 2-chloroacetoacetate **73** gives only a low conversion to **74**,⁵⁵ illustrating that the flow system is more efficient. This illustrates the catalytic effect of the fluorinated metal surface.

Sulfur pentafluoride derivative **75** was prepared in 75% yield by the reaction of the disulfide **76** with 10% fluorine in nitrogen, using acetonitrile as the solvent (Scheme 26). Similarly,



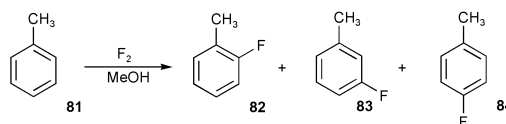
treatment of the trifluoride **77** with fluorine gave sulfur pentafluoride derivative **78** in 44% yield.

Perfluorination reactions were found to require an additional heating stage for the reaction to go to completion. The reaction of the tetrahydrofuran derivative **79** with 50% fluorine in nitrogen at 280 °C gave the perfluorinated compound **80** in 91% yield (Scheme 27). In conventional reactions, cobalt trifluoride



would be used to perfluorinate hydrocarbons.⁵⁶ Some of the reactions carried out by the authors, however, required much lower temperatures than would be expected if this compound was used.

Jenson and coworkers have also demonstrated the direct fluorination of aromatic compounds in a micro reactor, a process difficult to perform on a conventional scale.⁵⁷ The reactor was fabricated from silicon and capped with Pyrex using anodic bonding. The surfaces of the reactor, which were in contact with the reagents, were coated with a nickel film using a metal deposition technique. The authors have used the micro reactor in the fluorination of toluene **81** at room temperature (Scheme 28). Using ten equivalents of fluorine, in methanol as



the solvent, the authors report an 80% conversion to give the monofluorinated toluenes. The substitution pattern of the *ortho*-**82**, *meta*-**83** and *para*-**84** isomers was determined to be 4 : 1 : 2 by GC.

Srinivasan *et al.*⁵⁸ performed the partial oxidation of ammonia using a silicon-based micro reactor. Integrated heaters as well as flow and temperature sensors were fabricated into the sub-mm flow channels. The platinum catalyst was deposited in the reaction channel by electron-beam evaporation *via* a shadow mask. The gaseous reactants were fed from cylinders into the micro reactor by external mass-flow controllers, which maintained the desired flow rates. The product composition was continuously monitored using a mass spectrometer. The authors reported a change in the micro reactor exhaust composition over a range of temperatures and flow rates and they also demonstrated that the conversion and selectivity behaviour of conventional reactors could be reproduced in a micro reactor.

The effective heat transfer of micro reactors provides very accurate temperature control for both exothermic and endothermic reactions, thus eliminating undesired side reactions. An example has been reported by Hessel *et al.*,⁵⁹ who demonstrated that a micro reactor could be used to prepare hydrogen cyanide *via* the Andrussov route. In traditional laboratory reactions, the hydrogen cyanide is reported to hydrolyse to ammonia. The use of a micro heat exchanger in this experiment, however, prevented this further reaction.

5 Concluding remarks

Micro reactor chemistry is currently showing great promise as a novel method on which to build new chemical technology and processes in which the reactions generally produce the desired product in higher yield and purity, in shorter periods of time, compared with traditional batch reactions. The technology is still in its early development and it would be presumptuous to expand too far on the potential applications that micro reactors will find, but some early trends are clear. One of the immediate and obvious applications is in combinatorial chemistry and drug

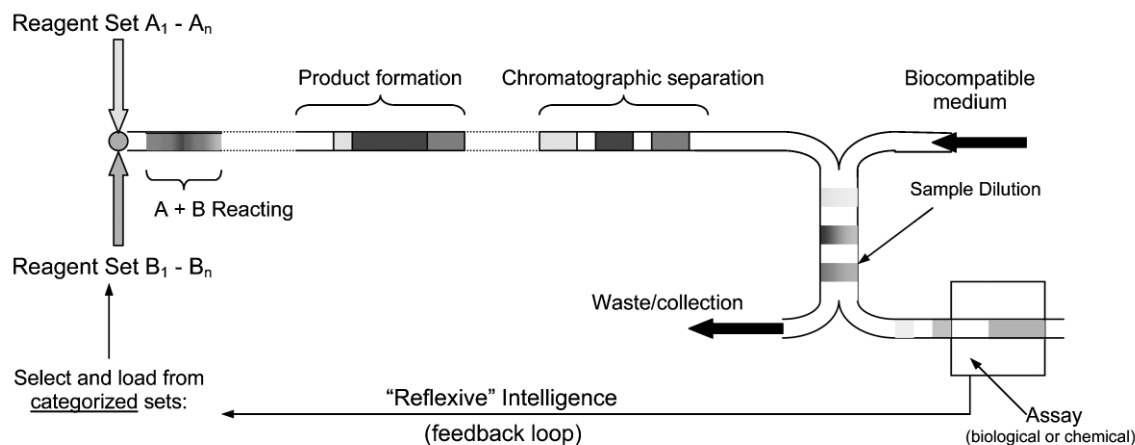


Fig. 6 Integration of a micro reactor with a biological assay system.

discovery, where the generation of compounds with different reagents or under variable conditions is an essential factor. Perhaps more intriguing, is what new angles micro reactors bring to reaction chemistry and these are only now just emerging. For example, extending the heterogeneous catalyst work already described one can see how immobilised or supported reagents could be placed within a device to impart functionality to a reaction whilst maintaining spatial and temporal control. In addition, a microchannel system also provides a potential separation column and integration of a micro reactor device to one of the many highly sensitive microchannel-based biological assay systems may therefore not only be possible, but may also address some of the pharmaceutical industries' potential requirements. Apart from the greatly reduced reaction times demonstrated for the micro reactors, handling times to assay and chemical reagent costs may be virtually eliminated. This paradigm is shown diagrammatically in Fig. 6.

Reactions within the micro reactors are found to be more atom efficient, which is of significant environmental importance as this reduces the quantities of raw materials required and minimises waste. Furthermore, the technology allows the temperature of reactions to be controlled, enabling reactions to be conducted safely, where explosion may be observed if the reaction was conducted on a batch scale.

The use of solvent for purification of products is often the largest contributor to waste in a chemical process. Research is currently underway to investigate the purification of chemicals within the micro reactors by exploiting the electrophoretic mobility of the chemical species, which would not require any solvent to be moved within the reactor. This process may be further enhanced through the use of supercritical fluid and ionic liquids, which would be compatible with current micro reactor devices.

In terms of Green Chemistry, micro reactors clearly offer considerable potential in performing safer and more efficient chemical reactions by the use of novel methodologies such as solvent free mixing, *in situ* reagent generation and integrated separation techniques. The capability of producing a parallel network of micro reactors, the so called 'scaling out' of the process, offers a clear route to generating product volume on demand, at the point of use, so reducing the need to store and transport hazardous or reactive chemicals. This is where micro reactors make the greatest contribution to the public's perception of environmentally clean chemistry.

References

- 1 D. Bradley, *Eur. Chem.*, 1999, **1**, 17.
- 2 P. D. I. Fletcher and S. J. Haswell, *Chem. Br.*, 1999, **35**, 38.
- 3 S. Cowen, *Chem. Ind. (London)*, 1999, 2nd Aug., 584.
- 4 T. McCreedy, *Chem. Ind. (London)*, 1999, 2nd Aug., 588.
- 5 D. Barrow, J. Cefai and S. Taylor, *Chem. Ind. (London)*, 1999, 2nd Aug., 591.
- 6 J. Cooper, D. Disley and T. Cass, *Chem. Ind. (London)*, 2001, 15th Oct., 653.
- 7 P. D. I. Fletcher, S. J. Haswell, E. Pombo-Villar, B. H. Warrington, P. Watts, S. Y. F. Wong and X. Zhang, *Tetrahedron*, 2002, **58**, 4735.
- 8 *IMRET 5: Proceedings of the Fifth International Conference on Microreaction Technology*, ed. M. Matlosz, W. Ehrfeld and J. P. Baselt, Springer, Berlin, 2002.
- 9 W. Ehrfeld, V. Hessel and H. Löwe, *Microreactors: New Technology for Modern Chemistry*, Wiley-VCH, Weinheim, 2000.
- 10 S. J. Haswell, *Analyst*, 1997, **112**, 1R.
- 11 A. Manz, D. J. Harrison, E. Verpoorte, J. C. Fettinger, H. Ludi and H. M. Widmer, *Chimia*, 1991, **45**, 103.
- 12 A. Manz, D. J. Harrison, E. Verpoorte and H. M. Widmer, *Adv. Chromatogr.*, 1993, **33**, 1.
- 13 A. Manz, C. S. Effenhauser, N. Burggraf, E. Verpoorte, D. E. Raymond and H. M. Widmer, *Anal. Mag.*, 1994, **22**, 25M.
- 14 *Proceedings of the Micro Total Analytical Systems '98 Workshop*, ed. D. J. Harrison and A. van den Berg, Kluwer Academic Press, Dordrecht, 1998.
- 15 A. van den Berg and T. S. J. Lammerink, *Top. Curr. Chem.*, 1998, **194**, 21.
- 16 D. J. Harrison, K. Fluri, K. Seiler, Z. H. Fan, C. S. Effenhauser and A. Manz, *Science*, 1993, **261**, 895.
- 17 S. C. Jacobson, R. Hergenroder, L. B. Koutny and J. M. Ramsey, *Anal. Chem.*, 1994, **66**, 1114.
- 18 M. Madou, *Fundamentals of Microfabrication*, CRC Press, Boca Raton, FL, 1997.
- 19 T. McCreedy, *TrAC, Trends Anal. Chem.*, 2000, **19**, 396.
- 20 T. McCreedy, *Anal. Chim. Acta.*, 2001, **427**, 39.
- 21 J. Th. G. Overbeek in *Colloid Science*, ed. H. R. Kruyt, Elsevier, Amsterdam, 1952, vol. 1, ch. V, p. 195.
- 22 C. L. Rice and R. Whitehead, *J. Phys. Chem.*, 1965, **69**, 4017.
- 23 R. J. Hunter, *Zeta Potential in Colloid Science*, Academic Press, London, 1981.
- 24 J. Jednacak, V. Pradic and W. Haller, *J. Colloid Interface Sci.*, 1974, **49**, 16.
- 25 P. H. Paul, M. G. Garguilo and D. J. Rakestraw, *Anal. Chem.*, 1998, **70**, 2459.
- 26 H. Salimi-Moosavi, T. Tang and D. J. Harrison, *J. Am. Chem. Soc.*, 1997, **119**, 8716.
- 27 R. C. R. Wootton, R. Fortt and A. J. de Mello, *Lab Chip*, 2001, **2**, 5.
- 28 H. Hisamoto, T. Saito, M. Tokeshi, A. Hibara and T. Kitamori, *Chem. Commun.*, 2001, 2662.
- 29 G. N. Doku, S. J. Haswell, T. McCreedy and G. M. Greenway, *Analyst*, 2001, **126**, 14.
- 30 J. R. Burns and C. G. Ramshaw, *IMRET 4: 4th International Conference of Micro Reaction Technology Topical Conference Proceedings, AIChE Spring National Meeting*, March 5–9, 2000, Atlanta, GA, USA, p. 133.
- 31 V. Skelton, G. M. Greenway, S. J. Haswell, P. Styring, D. O. Morgan, B. Warrington and S. Y. F. Wong, *Analyst*, 2001, **126**, 7.
- 32 V. Skelton, G. M. Greenway, S. J. Haswell, P. Styring, D. O. Morgan, B. Warrington and S. Y. F. Wong, *Analyst*, 2001, **126**, 11.
- 33 M. Sands, S. J. Haswell, S. M. Kelly, V. Skelton, D. O. Morgan, P. Styring and B. H. Warrington, *Lab Chip*, 2001, **1**, 64.

- 34 C. Wiles, P. Watts, S. J. Haswell and E. Pombo-Villar, *Lab Chip*, 2001, **1**, 100.
- 35 C. Wiles, P. Watts, S. J. Haswell and E. Pombo-Villar, *Lab Chip*, 2002, **2**, 62.
- 36 E. Garcia-Egido, S. Y. F. Wong and B. H. Warrington, *Lab Chip*, 2002, **2**, 170.
- 37 M. Fernandez-Suarez, S. Y. F. Wong and B. H. Warrington, *Lab Chip*, 2002, **2**, 31.
- 38 H. Lu, M. A. Schmidt and K. F. Jenson, *Lab Chip*, 2001, **1**, 22.
- 39 J. N. Pitts, R. L. Letsinger, R. P. Taylor, J. M. Patterson, G. Recktenwald and R. B. Martin, *J. Am. Chem. Soc.*, 1959, **81**, 1068.
- 40 R. C. R. Wootton, R. Fortt and A. J. de Mello, *Org. Proc. Res. Dev.*, 2002, **6**, 187.
- 41 P. Watts, C. Wiles, S. J. Haswell, E. Pombo-Villar and P. Styring, *Chem. Commun.*, 2001, 990.
- 42 P. Watts, C. Wiles, S. J. Haswell and E. Pombo-Villar, *Tetrahedron*, 2002, **58**, 5427.
- 43 L. A. Carpino and G. Y. Han, *J. Org. Chem.*, 1972, **37**, 3404.
- 44 L. A. Carpino, B. J. Cohen, K. E. Stephens, S. Y. Sadat-Aalae, J-H. Tien and D. E. Langridge, *J. Org. Chem.*, 1986, **51**, 3732.
- 45 W. C. Chan, B. W. Bycroft, D. J. Evans and P. D. White, *J. Chem. Soc., Chem. Commun.*, 1995, 2209.
- 46 P. Watts, C. Wiles, S. J. Haswell and E. Pombo-Villar, *Lab Chip*, 2002, **2**, 141.
- 47 G. M. Greenway, S. J. Haswell, D. O. Morgan, V. Skelton and P. Styring, *Sens. Actuators B*, 2000, **63**, 153.
- 48 N. G. Wilson and T. McCreedy, *Chem. Commun.*, 2000, 733.
- 49 T. McCreedy and N. G. Wilson, *Analyst*, 2001, **126**, 21.
- 50 E. Dietzsch, D. Hönicke, M. Fichtner, K. Schubert and G. Weißmeier, *IMRET 4: 4th International Conference of Micro Reaction Technology Topical Conference Proceedings, AIChE Spring National Meeting*, March 5–9, 2000, Atlanta, GA, USA, p. 89.
- 51 S. Rozen, *Acc. Chem. Res.*, 1996, **21**, 307.
- 52 S. T. Purrington, B. S. Kagen and T. B. Patrick, *Chem. Rev.*, 1986, **86**, 997.
- 53 R. D. Chambers and R. C. H. Spink, *Chem. Commun.*, 1999, 883.
- 54 R. D. Chambers, D. Holling, R. C. H. Spink and G. Sandford, *Lab Chip*, 2001, **1**, 132.
- 55 R. D. Chambers, M. P. Greenhall and J. Hutchinson, *Tetrahedron*, 1996, **52**, 1.
- 56 R. D. Chambers, B. Grievson, F. G. Drakesmith and R. L. Powell, *J. Fluorine Chem.*, 1985, **29**, 323.
- 57 N. de Mas, R. J. Jackman, M. A. Schmidt and K. F. Jenson, *IMRET 5: Proceedings of the Fifth International Conference on Micro-reaction Technology*, Springer, Berlin, 2002, p. 60.
- 58 R. Srinivasan, I-M. Hsing, P. E. Berger, K. F. Jensen, S. L. Firebaugh, M. A. Schmidt, M. P. Harold, J. J. Lerou and J. F. Ryley, *AIChE J.*, 1997, **43**(11), 3059.
- 59 V. Hessel, W. Ehrfeld, K. Golbig, C. Hofman, S. Jungwirth, H. Lowe, T. Richter, M. Storz and A. Wolf, *IMRET3: Proceedings of the third conference on microtechnology*, 2000, , 151.

Microfluidic combinatorial chemistry

Paul Watts* and Stephen J Haswell

Microreactors are finding increasing application in the field of combinatorial chemistry. In the past few years, microreactor chemistry has shown great promise as a novel method on which to build new chemical technology and processes. It has been conclusively demonstrated that reactions performed within microreactors invariably generate relatively pure products in high yield. One of the immediate and obvious applications is therefore in combinatorial chemistry and drug discovery.

Addresses

Department of Chemistry, University of Hull, Cottingham Road, Hull, HU6 7RX, UK

*e-mail: p.watts@hull.ac.uk

Current Opinion in Chemical Biology 2003, 7:380–387

This review comes from a themed issue on

Combinatorial chemistry

Edited by Samuel Gerritz and Andrew T Merritt

1367-5931/03/\$ – see front matter

© 2003 Elsevier Science Ltd. All rights reserved.

DOI 10.1016/S1367-5931(03)00050-4

Abbreviations

DBU 1,8-diazabicyclo[5.4.0]undec-7-ene

DCC *N,N*-dicyclohexylcarbodiimide

DMF dimethylformamide

EOF electroosmotic flow

Introduction

Microreactors consist of a network of micron-sized channels (typical dimensions are in the range 10–300 µm) etched into a solid substrate (see, for example, [1–9] for introductory overviews). They may be fabricated from a range of materials including glass, silicon, quartz, metals and polymers using a variety of fabrication techniques including photolithography, hot embossing, powder blasting, injection moulding and laser microforming [10]. For glass microreactors, photolithographic fabrication of channel networks is performed as shown schematically in Figure 1 [11,12].

For solution-based chemistry, the channel networks are connected to a series of reservoirs containing chemical reagents to form the complete device with overall dimensions of a few centimetres, as illustrated in Figure 2. Reagents can be brought together in a specific sequence, mixed and allowed to react for a specified time in a controlled region of the channel network using either electrokinetic (electroosmotic and electrophoretic) or hydrodynamic pumping. For electrokinetically driven

systems, electrodes are placed in the appropriate reservoirs to which specific voltage sequences can be delivered under automated computer control [13–16]. This control offers a simple but effective method of moving and separating reactants and products within a microreactor, without the need for moving parts. In comparison, hydrodynamic pumping uses conventional or microscale pumps (notably syringe pumps) to manoeuvre solutions around the channel network; however, this technique has the disadvantage of requiring either large external pumps or complex fabrication of small moving parts.

A concerted effort has now begun to establish the benefits that microreactors can bring to the field of reaction chemistry. For example, the ability to manipulate reagent concentrations in both space and time within the channel network of a microreactor provides an additional level of reaction control that is not attainable in bulk stirred reactors, where concentrations are generally uniform [17**]. Consistent with this notion, many reactions have been demonstrated to show altered reactivity, product yield and selectivity when performed in microreactors as compared with conventional bench-top glassware [18**].

To date, the outcome of the reported research has confirmed that microreactor methodology is applicable to performing both gas- and liquid-phase reaction chemistry [18**]. From the work cited in this article, the evidence is that the unique *modus operandi* of microreactors, namely the low-volume spatial and temporal control of reactants and products in a laminar flow diffusive mixing environment in which distinct thermal and concentration gradients exist, offers a novel method for the chemical manipulation and generation of products. In short, microreactors are new, safe and more atom-efficient tools with which to generate molecules and increase our knowledge of complex chemical processes.

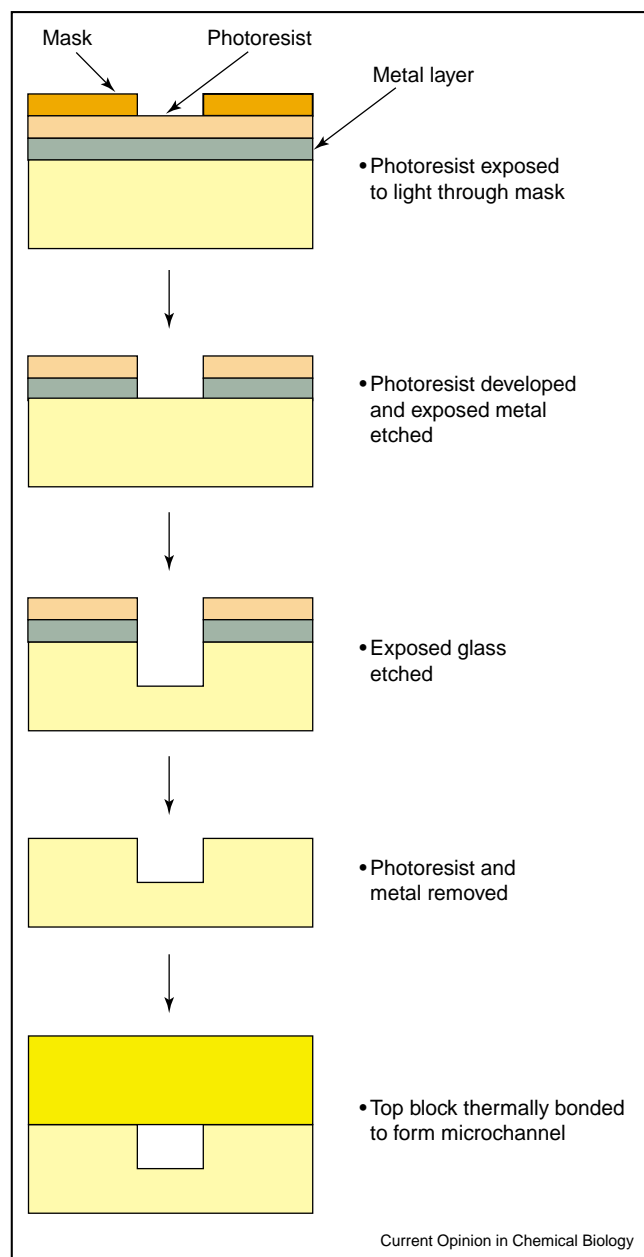
Reactions performed in microreactors

Most reactions that have been performed in microreactors have been conducted simply to demonstrate proof of principle. A summary of the reactions that have been performed in microreactors to date is presented in Table 1 and these are reviewed in detail in [18**].

This section reviews reactions that have been performed within microreactor systems specifically with combinatorial applications.

Skelton and co-workers [19*,20*] have reported the application of microreactors, prepared from borosilicate glass, for the Wittig reaction. They used the microreactor to

Figure 1



Photolithographic fabrication of microreactors.

prepare the *cis*- and *trans*-nitrostilbene esters **1** and **2** using the Wittig reaction (Figure 3a). Several features such as stoichiometry and stereochemistry were investigated. When two equivalents of the aldehyde **3** to the phosphonium salt **4** were used in the reaction, a conversion of 70% was achieved. The microreactor demonstrated an increase in reaction efficiency of 10% over the traditional batch synthesis. The reaction stoichiometry was subsequently reduced to 1:1, but using continuous flow of reagents, as above, the conversion was poor (39%). The

Figure 2



A borosilicate glass microreactor.

conversion was increased to 59% using an 'injection' technique, where 'slugs' of **4** were injected into a continuous flow of the aldehyde **3**.

The research was further extended to investigate the stereochemistry of the reaction. The ratio of isomers **1** and **2** was controlled by altering the voltages applied to the reagent reservoirs within the device, which in turn affected the electroosmotic flow (EOF) and electrophoretic mobility of the reagents. The variation in the external voltage subsequently altered the relative reagent concentration within the device, producing *Z/E* ratios in the region 0.57–5.21. In comparison, the authors report that when a traditional batch synthesis was performed using the same reaction time, concentration, solvent and stoichiometry, a *Z/E* ratio of approximately 3:1 was observed. This demonstrated that significant control was possible in a microreactor compared with batch reactions. The authors also demonstrated that the microreactor could be used as a tool for the rapid reaction development and optimisation based on analogue chemistry by using other aldehydes in the reaction [19*,20*].

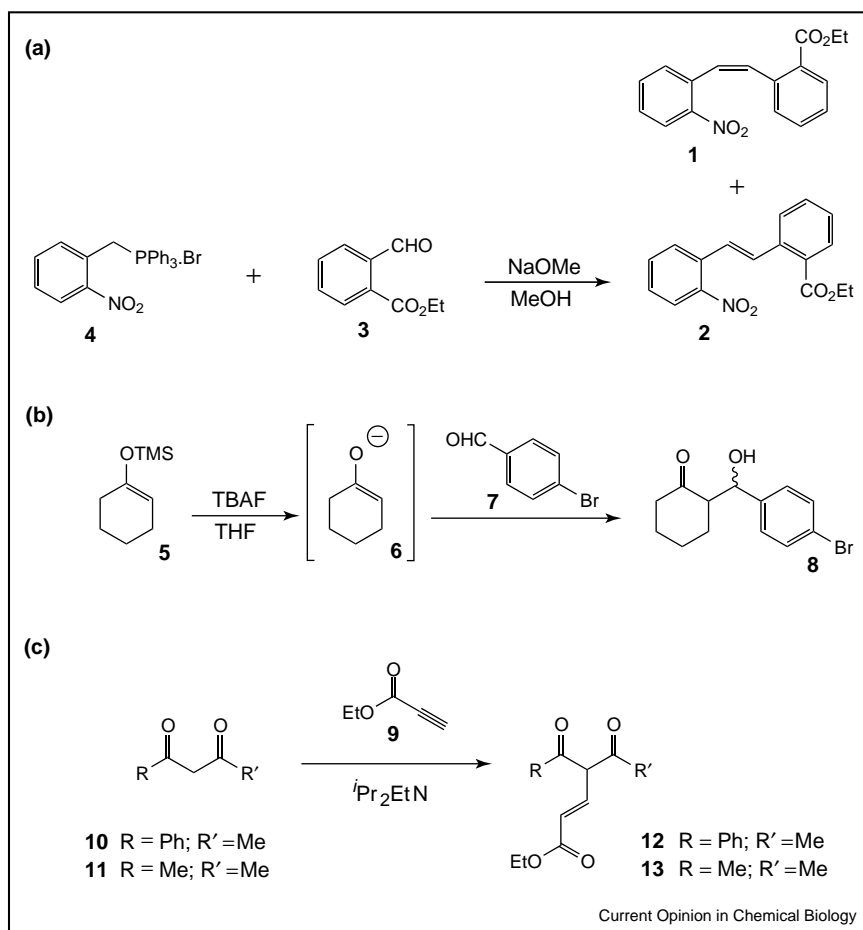
Carbanion chemistry is one of the most common methods of C–C bond formation used in the pharmaceutical industry. The temperature of the reaction often governs the stereochemistry of the product, hence microreactors have a considerable attraction because the reactor enables excellent temperature control to be attained. Wiles *et al.* [21*] have recently demonstrated the use of silyl enol ethers in the aldol reaction within a microreactor. Quantitative conversion of the silyl enol ethers to

Table 1

Reactions conducted in a microreactor.

Reaction	Chip material	Solvent	Conversion (%)	Comments	Refs
Suzuki	Glass	Aq THF	67	EOF	[28]
Kumada coupling	Polypropylene	THF	60	Syringe pump	[29]
Nitration	Glass	Benzene	65	EOF	[30]
Enamine	Glass	MeOH	42	EOF	[31]
Diazo coupling	Glass	MeOH	37	EOF	[32]
		MeCN	22		
Diazotisation	Glass	DMF/H ₂ O	52	Syringe pump	[33]
Photocyanation	Polymer	Pyrene/H ₂ O	73	Syringe pump	[34]
Dehydration	Glass/PDMS	EtOH	85–95	EOF or syringe pump	[35]
Esterification	Glass/PDMS	EtOH	30	Syringe pump	[36]
Photochemical	Silicon/quartz	(CH ₃) ₂ CHOH	60	Syringe pump	[37]
Photochemical	Glass	MeOH	80	Syringe pump	[38]
Phase transfer	Glass	EtOAc	100	Syringe pump	[39]
Fluorination	Ni or Cu	Nitrogen gas	90–99	Syringe pump	[40,41]
Fluorination	Silicon/Pyrex	MeOH	80	Syringe pump	[42]
Oxidation	Al	None	75–99	Syringe pump	[43]

Figure 3



Reactions performed within microreactors. (a) The Wittig reaction. (b) The aldol reaction. (c) Michael addition.

β -hydroxyketones was observed in 20 min in the microreactor, compared with traditional batch systems where quantitative yields were only obtained when extended reaction times of up to 24 h were employed. One example involved the treatment of the trimethylsilyl enol ether **5** with tetra-*n*-butylammonium fluoride (TBAF), to generate the tetra-*n*-butylammonium enolate **6** *in situ*, followed by condensation with *p*-bromobenzaldehyde **7** to give the β -hydroxyketone **8** in 100% conversion (Figure 3b). The reaction has also been successfully achieved using a variety of other silyl enol ethers and aldehydes, which demonstrates that microreactors may be used in the synthesis of combinatorial libraries.

Similarly, Wiles *et al.* [22^{*}] have also reported the preparation of the enolates from a series of 1,3-diketones using an organic base and their subsequent reaction with a variety of Michael acceptors such as **9** to afford 1,4-addition products within a microreactor (Figure 3c).

When using a continuous flow of reagents **9** and **10**, 15% conversion to the adduct **12** was observed, compared with 56% when the diketone **11** was reacted with **9** forming the Michael adduct **13**. The authors, however, demonstrated enhancements in conversions through the application of the stopped-flow technique. This procedure involved the mobilisation of reagents through the device for a designated period of time, using an applied field, and the flow was subsequently paused by the removal of the applied field, before re-applying the field. Using the regime of 2.5 s on and 5 s off, the conversion to the product **12** was improved to 34%, whereas lengthening the stopped-flow period to 10 s, resulted in a further increase to 100%. This was compared to the preparation of **13**, in which the regime of 2.5 s on and 5 s off resulted in an increase in conversion to 95%. This demonstrated that the enolate of 2,4-pentanedione **11** was more reactive than the corresponding enolate of benzoyl acetone **10**. The authors propose that the observed increase in conversion, when using the technique of stopped flow, was due to an effective increase in residence time within the device corresponding to the different kinetics associated with these reactions. This approach is clearly relevant to those wishing to study the kinetics of such reactions and the results demonstrate the ease with which reactions may be optimised in microreactors when conducting combinatorial synthesis.

Although the previous result demonstrates the ease with which reaction conditions may be optimised, it is still sometimes necessary to heat reactions to achieve high yields of products. Industrially, special equipment is required when performing large-scale reactions at elevated temperature. However, Garcia-Egido *et al.* [23^{**}] have demonstrated the synthesis of a series of 2-aminothiazoles using a Hantzsch synthesis within a microreactor. The paper represents the first example of a

heated solution-based organic reaction within a glass microreactor under EOF conditions. The T-shaped microreactor was heated to 70°C using a Peltier heater, which was aligned with the channels, and the heat generated by the device was applied to the base of the microreactor. Reaction of α -bromoketones such as **14** with a thiourea derivative such as **15**, using *N*-methylpyrrolidinone as solvent, resulted in the preparation of the aminothiazoles **16** in up to 85% conversion (Figure 4a).

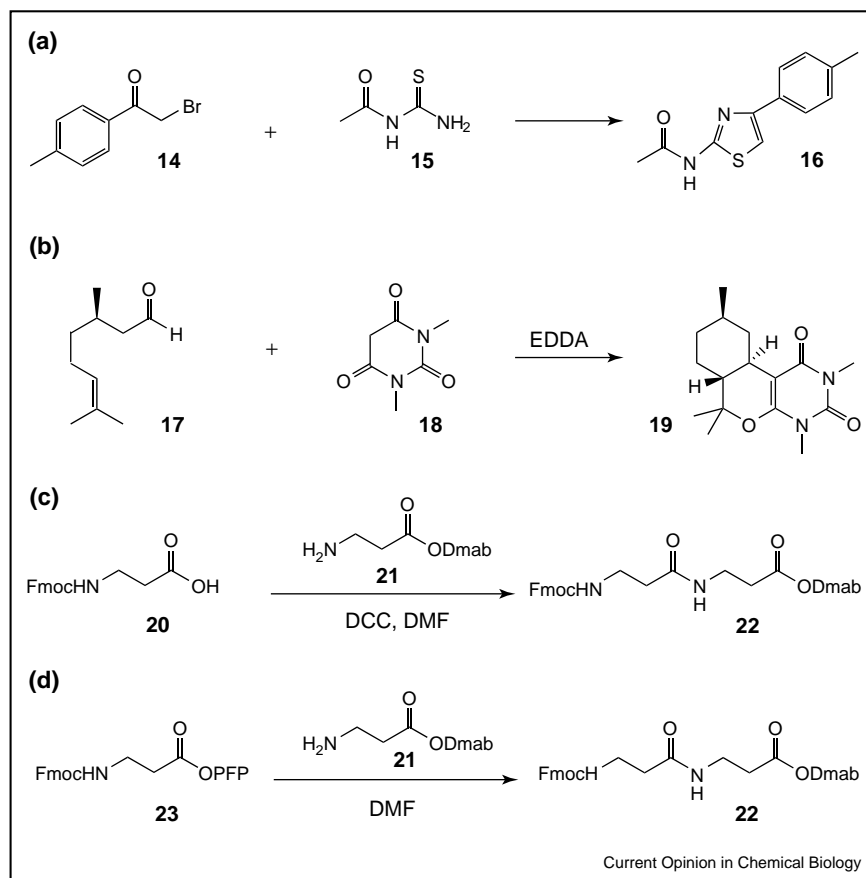
Fernandez-Suarez *et al.* have reported the synthesis of cycloadducts in a microreactor using hydrodynamic driven flow [24^{*}]. The reactions consisted of Knoevenagel condensation of an aldehyde **17** with a 1,3-diketone **18** with ethylenediamine acetate (EDDA) as catalyst, in aqueous methanol as solvent. The reaction intermediate underwent an intramolecular hetero-Diels-Alder reaction to form cycloadduct **19** in 60–68% conversion (Figure 4b). Initially, four different compounds were prepared individually but the research was extended to a multi-reaction experiment where all compounds were prepared in a single run.

Watts *et al.* [25,26^{**}] have recently demonstrated the first example of a multi-step synthesis in a microreactor, using their devices in peptide synthesis. The authors evaluated the reactor using a carbodiimide coupling reaction of Fmoc- β -alanine **20** with the amine **21** to give the dipeptide **22** (Figure 4c). When stoichiometric quantities of the reagents were used, only *ca* 10% conversion to dipeptide **22** was achieved. By using two equivalents of *N,N*-dicyclohexylcarbodiimide (DCC), however, an increase in conversion to *ca.* 20% was observed, and by applying a stopped flow technique (2.5 s injection length with stopped flow for 10 s) the conversion of the reaction was further increased to approximately 50%. Using five equivalents of DCC, a conversion of up to 93% of **22** was obtained using the stopped-flow technique.

The authors also demonstrated that the dipeptide could be prepared from pre-activated carboxylic acids [25,26^{**}]. They reported that the reaction of the pentafluorophenyl (PFP) ester of Fmoc- β -alanine **23** with the amine **21** gave the dipeptide **22** quantitatively in 20 min (Figure 4d). This represented a significant increase in yield compared with the traditional batch synthesis, where only a 50% yield was obtained in 24 h.

Having demonstrated that peptide bonds could be successfully formed when using a microreactor, the authors then found that they could extend the methodology to the preparation of longer-chain peptides. Using the microreactor, the Dmab ester of Fmoc- β -alanine **24** was reacted with one equivalent of piperidine or 1,8-diazabicyclo[5.4.0]undec-7-ene (DBU) to give the free amine **21** in quantitative conversion. This is in comparison with solid-phase peptide synthesis where 20%

Figure 4



Reactions performed within microreactors. (a) Hantzsch reaction. (b) Cycloadduct formation. (c,d) Peptide bond formation reactions.

piperidine in dimethylformamide (DMF) is frequently employed, which demonstrates the atom efficiency of reactions performed within the devices. The authors then reacted the amine *in situ* with the pentafluorophenyl ester **25** to give the dipeptide **26** (Figure 5a) in 96% overall conversion.

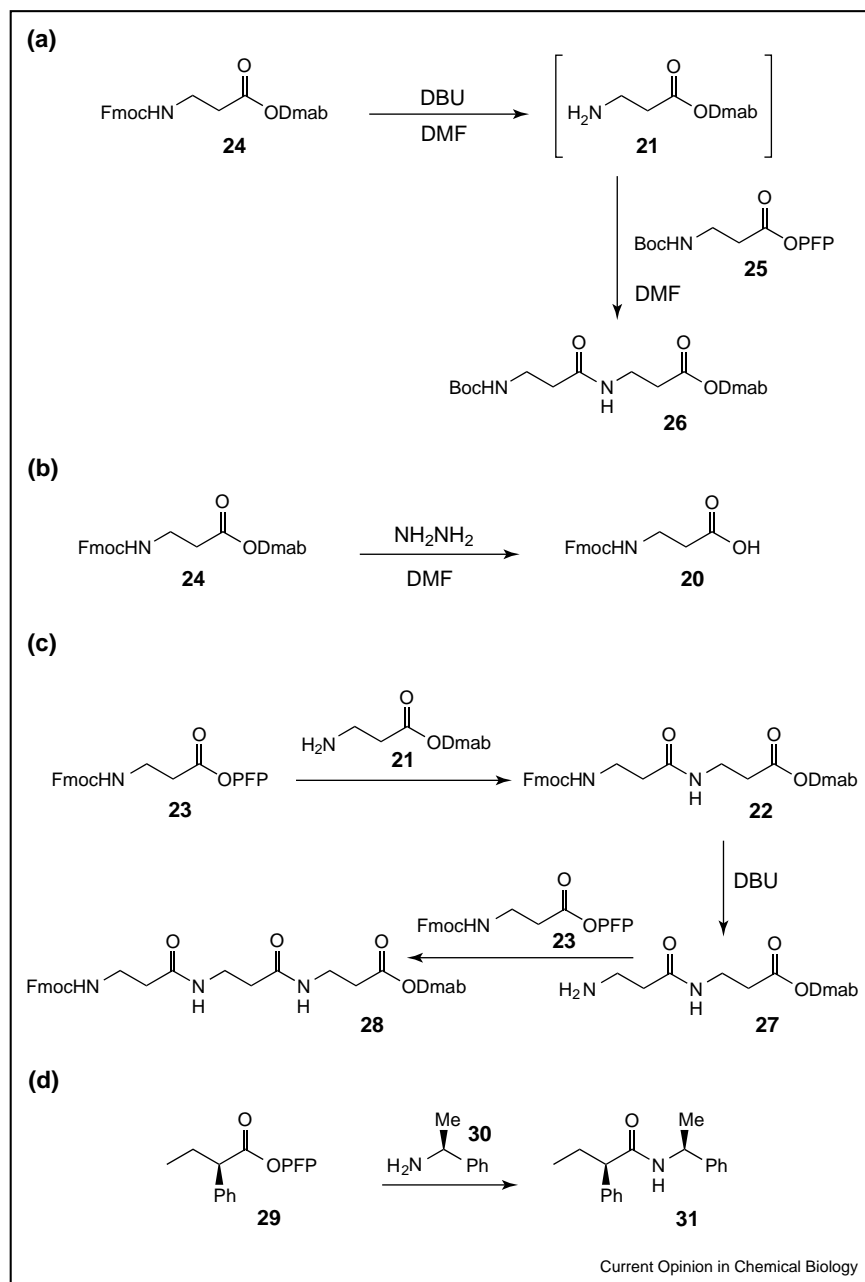
Having shown that more complex peptides could be produced by removal of the N-protecting group, the authors then demonstrated that they could remove the Dmab ester using hydrazine. The reaction of the Dmab ester **24** with one equivalent of hydrazine resulted in quantitative deprotection, to afford the carboxylic acid **20** (Figure 5b). This is in comparison to solid-phase peptide synthesis where 2% hydrazine in DMF is generally required to effect complete deprotection.

The authors have further extended the approach to the synthesis of tripeptide **28** [26^{••}]. Reaction of pentafluorophenyl ester **23** with amine **21** formed dipeptide **22**, which was reacted with DBU to effect Fmoc deprotection. The amine **27** was then reacted *in situ* with another

equivalent of pentafluorophenyl ester **23** to prepare tripeptide **28** in 30% overall conversion (Figure 5c). The approach clearly demonstrates that intermediates may be generated *in situ* and used in subsequent reactions, enabling the combinatorial synthesis of peptides, which are of biological and pharmaceutical interest.

Having demonstrated that peptide bonds could be successfully formed when using a microreactor, the authors then investigated racemisation in peptides derived from α -amino acids [27]. Reaction of the pentafluorophenyl ester of *R*-2-phenylbutyric acid **29**, at 0.1 M concentration, with α -methylbenzylamine **30**, gave the product **31** in quantitative conversion with 4.2% racemisation (Figure 5d). Importantly, there was less racemisation than observed in the batch reaction at the same concentration and temperature. The reduced level of racemisation was attributed to the reduced reaction times observed within the microreactors. This demonstrates that there would be real advantages to performing combinatorial chemistry in microfluidic reactors compared with traditional batch systems.

Figure 5



Peptide synthesis within microreactors.

Conclusions

Microreactor chemistry is currently showing great promise as a novel method on which to build new chemical technology and processes. Reactions performed in a microreactor invariably generate relatively pure products in high yield, in comparison to the equivalent bulk reactions, in much shorter times and in sufficient quantities to perform full instrumental characterisation. One of the immediate and obvious applications is therefore in combinatorial chemistry and drug discovery, where the

generation of compounds either with different reagents or under variable conditions is an essential factor. An interesting twist to the chemistry carried out to date is not just the opportunity to separate reactants and products in real time but also the capability to manufacture and use reagents *in situ*.

The success of pharmaceutical companies resides largely on the ability to synthesise novel chemical entities and to optimise the production of marketable drugs. In an

industry where development costs are extraordinarily high and attrition rates from lead generation onwards are about 98%, careful lead selection and ruthless pressure to shorten optimisation times are crucial for survival, microreactor technology could certainly help meet these criteria.

References and recommended reading

Papers of particular interest, published within the annual period of review, have been highlighted as:

- of special interest
- of outstanding interest

1. Bradley D: **Chemical reduction**. *Eur Chem* 1999, **1**:17-20.
2. Fletcher PDI, Haswell SJ: **Downsizing synthesis**. *Chem Br* 1999, **35**:38-41.
3. Cowen S: **Chip service**. *Chem Ind* 1999:584-586.
4. McCreedy T: **Reducing the risks of synthesis**. *Chem Ind* 1999:588-590.
5. Barrow D, Cefai J, Taylor S: **Shrinking to fit**. *Chem Ind* 1999:591-594.
6. Cooper J, Disley D, Cass T: **Lab-on-a-chip and microarrays**. *Chem Ind* 2001:653-655.
7. Haswell SJ, Middleton RJ, O'Sullivan B, Skelton V, Watts P, Styring P: **The application of micro reactors to synthetic chemistry**. *Chem Commun* 2001:391-398.
8. Matlosz M, Ehrfeld W, Baselt JP (Eds): *IMRET 5: Proceedings of the Fifth International Conference on Microreaction Technology*. Berlin: Springer; 2002.
9. Ehrfeld W, Hessel V, Löwe H: *Microreactors: New Technology for Modern Chemistry*. Weinheim: Wiley-VCH; 2000.
10. Madou M: *Fundamentals of Microfabrication*. Boca Raton, FL: CRC Press; 1997.
11. McCreedy T: **Fabrication techniques and materials commonly used for the production of micro reactors and micro total analytical systems**. *TrAC* 2000, **19**:396-401.
12. McCreedy T: **Rapid prototyping of glass and PDMS microstructures for micro total analytical systems and micro chemical reactors by microfabrication in the general laboratory**. *Anal Chim Acta* 2001, **427**:39-43.
13. Overbeek J: **Electrokinetic phenomena**. In *Colloid Science*. Edited by Kruyt HR. Amsterdam: Elsevier; 1952:195-244.
14. Rice CL, Whitehead R: **Electrokinetic flow in a narrow cylindrical capillary**. *J Phys Chem* 1965, **69**:4017-4024.
15. Hunter RJ: *Zeta Potential in Colloid Science*. London: Academic Press; 1981.
16. Jednacak J, Pravdic V, Haller W: **The electrokinetic potential of glasses in aqueous electrolyte solutions**. *J Colloid Interface Sci* 1974, **49**:16-23.
17. Fletcher PDI, Haswell SJ, Zhang X: **Electrokinetic control of a chemical reaction in a lab-on-a-chip micro reactor: measurement and quantitative modelling**. *Lab on a Chip* 2002, **2**:101-112.
This paper demonstrates the spatial and temporal control achievable when performing a reaction in a microreactor under electrokinetic flow. Specifically, Ni²⁺ ions are reacted with a ligand to produce a complex. The results demonstrate that Ni²⁺ ions have a greater electrophoretic velocity than the neutral ligand.
18. Fletcher PDI, Haswell SJ, Pombo-Villar E, Warrington BH, Watts P, Wong SYF, Zhang X: **Micro reactors: principles and applications in organic synthesis**. *Tetrahedron* 2002, **58**:4735-4757.
This review article gives a detailed account of the fabrication and operation of microreactors. The paper gives a detailed account of all gas phase, liquid phase and catalysed reactions performed in microreactors to date.
19. Skelton V, Greenway GM, Haswell SJ, Styring P, Morgan DO, Warrington B, Wong SYF: **The preparation of a series of nitrostilbene ester compounds using micro reactor technology**. *Analyst* 2001, **126**:7-10.
This paper uses a borosilicate glass microreactor, operating under electrokinetic control, to prepare a range of stilbenes using the Wittig reaction. A range of starting materials are used, demonstrating that it is possible to prepare a combinatorial library of derivatives using the microreactor systems.
20. Skelton V, Greenway GM, Haswell SJ, Styring P, Morgan DO, Warrington B, Wong SYF: **The generation of concentration gradients using electroosmotic flow in micro reactors allowing stereoselective chemical synthesis**. *Analyst* 2001, **126**:11-13.
This paper uses a borosilicate glass microreactor, operating under electrokinetic control, to prepare stilbenes using the Wittig reaction. It discusses how the Z/E ratio of isomers changes depending on the electrokinetic parameters used.
21. Wiles C, Watts P, Haswell SJ, Pombo-Villar E: **The aldol reaction of silyl enol ethers within a micro reactor**. *Lab on a Chip* 2001, **1**:100-101.
This paper illustrates how a selection of enolates may be prepared *in situ* within microreactor devices. The enolates are subsequently reacted with a range of aldehydes to form a variety of aldol products in high yield.
22. Wiles C, Watts P, Haswell SJ, Pombo-Villar E: **1,4-Addition of enolates to α,β -unsaturated ketones within a micro reactor**. *Lab on a Chip* 2002, **2**:62-64.
This paper prepares a range of Michael adducts by reaction of a selection of diketones with an organic base in a microreactor. The paper illustrates that microreactors may be used to study the kinetics of reactions.
23. Garcia-Egido E, Wong SYF, Warrington BH: **Synthesis of a three-member array of cycloadducts in a glass microchip under pressure driven flow**. *Lab on a Chip* 2002, **2**:170-174.
This paper demonstrates that an array of compound may be simultaneously produced within microreactor devices operating under pressure-driven flow. This methodology may be used for a combinatorial library of compounds.
24. Fernandez-Suarez M, Wong SYF, Warrington BH: **A Hantzsch synthesis of 2-aminothiazoles performed in a heated microreactor system**. *Lab on a Chip* 2002, **2**:31-33.
This paper reports a convenient method of heating a reaction in a microreactor by aligning a Peltier heating device with the fluidic channels. It is demonstrated how such devices may be applied to combinatorial chemistry.
25. Watts P, Wiles C, Haswell SJ, Pombo-Villar E, Styring P: **The synthesis of peptides using micro reactors**. *Chem Commun* 2001:990-991.
26. Watts P, Wiles C, Haswell SJ, Pombo-Villar E: **Solution phase synthesis of β -peptides using micro reactors**. *Tetrahedron* 2002, **58**:5427-5439.
This paper illustrates that a series of peptide derivatives may be prepared *in situ* within microreactor devices. The methodology has been extended such that tripeptides may be prepared by careful control of protecting-group chemistry. The paper illustrates that reactions in microreactors are considerably faster than in batch reactions and an electrochemical effect is reported.
27. Watts P, Wiles C, Haswell SJ, Pombo-Villar E: **Investigation of racemisation in peptide synthesis within a micro reactor**. *Lab on a Chip* 2002, **2**:141-144.
28. Greenway GM, Haswell SJ, Morgan DO, Skelton V, Styring P: **The use of a novel microreactor for high throughput continuous flow organic synthesis**. *Sens Actuators B Chem* 2000, **63**:153-158.
29. Haswell SJ, O'Sullivan B, Styring P: **Kumada-Corriu reactions in a pressure-driven microflow reactor**. *Lab on a Chip* 2001, **1**:164-166.
30. Doku GN, Haswell SJ, McCreedy T, Greenway GM: **Electric field-induced mobilisation of multiphase solution systems based on the nitration of benzene in a micro reactor**. *Analyst* 2001, **126**:14-20.
31. Sands M, Haswell SJ, Kelly SM, Skelton V, Morgan DO, Styring P, Warrington BH: **The investigation of an equilibrium dependent reaction for the formation of enamines in a microchemical system**. *Lab on a Chip* 2001, **1**:64-65.

32. Salimi-Moosavi H, Tang T, Harrison DJ: **Electroosmotic pumping of organic solvents and reagents in microfabricated reactor chips.** *J Am Chem Soc* 1997, **119**:8716-8717.
33. Wootton RCR, Fortt R, de Mello AJ: **On-chip generation and reaction of unstable intermediates – monolithic nanoreactors for diazonium chemistry: azo dyes.** *Lab on a Chip* 2002, **2**:5-7.
34. Ueno K, Kitagawa F, Kitamura N: **Photocyanation of pyrene across an oil/water interface in a polymer microchannel chip.** *Lab on a Chip* 2002, **2**:231-234.
35. Wilson NG, McCreedy T: **On-chip catalysis using a lithographically fabricated glass microreactor—the dehydration of alcohols using sulfated zirconia.** *Chem Commun* 2000:733-734.
36. McCreedy T, Wilson NG: **Microfabricated reactors for on-chip heterogeneous catalysis.** *Analyst* 2001, **126**:21-23.
37. Lu H, Schmidt MA, Jenson KF: **Photochemical reactions and on-line UV detection in microfabricated reactors.** *Lab on a Chip* 2001, **1**:22-28.
38. Wootton RCR, Fortt R, de Mello AJ: **A microfabricated nanoreactor for safe, continuous generation and use of singlet oxygen.** *Organic Process Res Dev* 2002, **6**:187-189.
39. Hisamoto H, Saito T, Tokeshi M, Hibara A, Kitamori T: **Fast and high conversion phase-transfer synthesis exploiting the liquid-liquid interface formed in a microchannel chip.** *Chem Commun* 2001:2662-2663.
40. Chambers RD: **Spink RCH: microreactors for elemental fluorine.** *Chem Commun* 1999:883-884.
41. Chambers RD, Holling D, Spink RCH, Sandford G: **Elemental fluorine. Part 13. gas-liquid thin film microreactors for selective direct fluorination.** *Lab on a Chip* 2001, **1**:132-137.
42. de Mas N, Jackman RJ, Schmidt MA, Jenson KF: **Microchemical systems for direct fluorination of aromatics.** In *IMRET 5: Proceedings of the Fifth International Conference on Microreaction Technology*. Edited by Matlosz M, Ehrfeld W, Baselt JP. Berlin: Springer; 2002:60-67.
43. Dietzsch E, Hönicke D, Fichtner M, Schubert K, Weißmeier G: **The formation of cycloalkenes in the partial gas phase hydrogenation of c,t,t 1,5,9-cyclodecatriene, 1,5-cyclooctadiene and benzene in micro channel reactors.** In *IMRET 4: Proceedings of the Fourth International Conference on Microreaction Technology*. Edited by Matlosz M, Ehrfeld W, Baselt JP. Berlin: Springer; 2000:89-93.

Continuous flow reactors for drug discovery

Paul Watts and Stephen J. Haswell

To develop a new generation of drugs, pharmaceutical companies need to be able to synthesize and screen novel chemicals with enhanced speed. New technology that would enable a cost-neutral increase in the number of potential drug candidates would provide a distinct competitive advantage. The miniaturisation of chemical reactors offers many fundamental and practical advantages of relevance to the pharmaceutical industry, which is constantly searching for controllable, information-rich, high-throughput and environmentally friendly methods of producing compounds with a high degree of chemical selectivity. This article reviews the current and future applications of micro reactors that could enhance the drug discovery process.

Paul Watts*
Stephen J. Haswell
Department of Chemistry
University of Hull
Cottingham Road
Hull
UK, HU6 7RX
*e-mail: P.Watts@hull.ac.uk

▼ The success of pharmaceutical companies resides largely on their ability to synthesize novel chemical entities (NCEs) and to optimize the production of marketable drugs. In an industry where development costs are extraordinarily high, it is important to develop new technology that enables the rapid synthesis and screening of NCEs. The miniaturization of chemical reactors offer many advantages of relevance to the pharmaceutical industry, which is constantly searching for high-throughput methods of producing products with a high degree of chemical selectivity [1–8]. This review illustrates how miniaturization of chemical reactors could revolutionize medicinal chemistry and the pharmaceutical industry through the implementation of innovative technology.

In their simplest form, micro reactors consist of a network of micron-sized channels (10–300 μm in diameter) etched into a solid substrate. Several materials, such as silicon, quartz, glass, metals and polymers, have been used to construct micro reactors [9]. Important considerations when choosing a material include chemical compatibility, the ease and reproducibility of fabrication, whether the

material supports electroosmotic flow (EOF) [10–13] with the solvents of interest and compatibility with detection methods. Glass is a popular choice because it allows EOF with many common solvents, it is chemically inert, it enables the use of a range of visible-light detection methods and the fabrication techniques are well established. Depending on the material used, a range of fabrication methods, such as photolithography, hot embossing, powder blasting, injection moulding and laser micro-forming, where the channels are etched into the material using high-powered lasers, are available [9,14]. For glass micro reactors, which are ideal for synthetic chemistry, photolithographic fabrication of the channel network is performed [15,16].

For solution-based chemistry, the channel networks are connected to a series of reservoirs containing chemical reagents to form the complete device with overall dimensions of a few cm. In the micro reactor, reagents can be brought together in a specific sequence, mixed and allowed to react for a specified time in a controlled region of the channel network using electrokinetic or hydrodynamic pumping. For electrokinetically driven systems, electrodes are located in the appropriate reservoirs (Fig. 1), which allows the sequential application of voltages under automated computer control. This control offers a simple but effective method of moving and separating reactants and products within a micro reactor, without the need for moving parts. Hydrodynamic pumping, by comparison, exploits conventional or micro-scale pumps, notably syringe-type pumps, to manoeuvre solutions around the channel network.

Until recently, the greatest research effort in the field of micro-scale devices has been in analytical science. One of the main aims of this research is to develop a so-called miniaturized

Abbreviations

Boc:	<i>tert</i> -butoxycarbonyl
DBU:	1,8-Diazabicyclo[5.4.0]undec-7-ene
DCC:	<i>N,N</i> -Dicyclohexylcarbodiimide
Dmab:	4-[<i>N</i> -(1-(4,4-dimethyl-2,6-diocyclohexylidene)-3-methylbutyl)amino]benzyl
DMF:	<i>N,N</i> -Dimethylformamide
EDDA:	Ethylenediamine acetate
EtOAc:	Ethyl acetate
EtOH:	Ethanol
Fmoc:	9-Fluorenylmethoxycarbonyl
MeOH:	Methanol
NaNO ₂ :	Sodium nitrite
NaOMe:	Sodium methoxide
NMP:	<i>N</i> -Methyl-2-pyrrolidinone
^t Pr ₂ EtN:	Diisopropylethylamine
TBAF:	tetra- <i>n</i> -butylammonium fluoride
THF:	Tetrahydrofuran
TMS:	Trimethylsilyl

total analytical system (μ -TAS) [17–24]. To date, the most popular area of μ -TAS research has been in the biomedical field, particularly in genomics and proteomics, where it has been used in the analysis of both DNA and proteins [25–32] and has resulted in the release of several commercial devices. Alongside the continuing development of μ -TAS, a concerted effort has been underway to establish the benefits that micro reactors can bring to the field of reaction chemistry. The ability to manipulate reagent concentrations in both space and time by electrokinetic voltage control

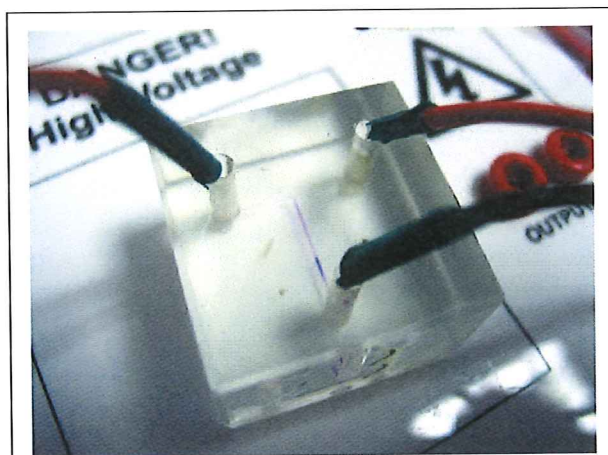


Figure 1. Reaction in process within a micro reactor under electroosmotic flow (EOF) control. The platinum electrodes in the reservoirs are used to apply voltages to the reagents, which are placed within the reservoirs. The product is collected in the final reservoir, which contain a ground electrode.

within the channel network of a micro reactor provides a level of reaction control that is not attainable in bulk-stirred reactors, where concentrations are generally uniform. Many chemical reactions have been demonstrated to show improved reactivity, product yield and selectivity when performed in micro reactors, compared with those generated using conventional laboratory practices.

The outcome of the reported research has confirmed that micro reactor methodology is applicable to performing both gas and liquid-phase reaction chemistry [33]. The evidence is that the unique *modus operandi* of micro reactors, namely the low-volume spatial and temporal control of reactants and products in a diffusive mixing environment, in which distinctive thermal and concentration gradients exist, offers a novel method for chemical manipulation and generation of products. In short, micro reactors are new tools with which to generate molecules and to increase our knowledge of complex chemical processes. When compared with the equivalent bulk reactions, reactions performed in a micro reactor invariably generate purer products in a higher yield and in much shorter times. Therefore, one of the obvious applications is in drug and process discovery, where the generation of compounds, either with different reagents or under variable conditions, is an essential factor.

Performing chemical reactions within a microfluidic system also provides the opportunity to perform real-time separations. Therefore, integration of a micro reactor device, via a purification step, with one of the many highly sensitive microchannel-based biological assay systems would provide a drug discovery tool. This level of integrated functionality within one device clearly addresses some of the pharmaceutical industry's requirements for rapid compound production and screening (Fig. 2). Apart from the greatly reduced reaction times demonstrated for the micro reactors, handling times and assay and chemical reagent costs are virtually eliminated with this proposed technology.

Chemical reactions performed in micro reactors

To date the majority of reactions that have been performed in micro reactors have been single-step processes, conducted simply to demonstrate that it is possible to perform chemical synthesis within such devices. A summary of the reactions that have been performed in micro reactors is presented in Table 1 and these are reviewed in detail in ref [33].

To prepare compounds that are of interest to the pharmaceutical industry it is important to demonstrate that multi-step reactions may be performed within such devices. In addition, it is imperative to demonstrate that by using different reagents as the starting materials, combinatorial

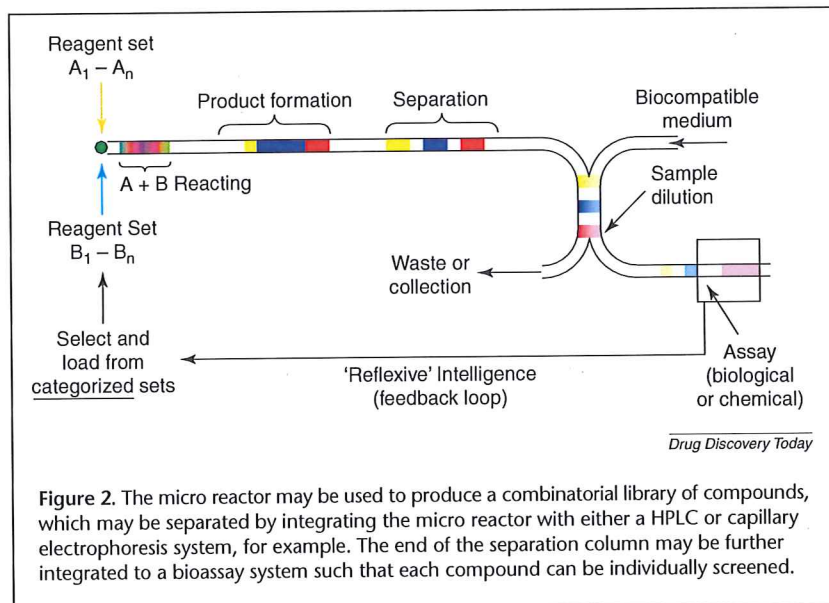


Figure 2. The micro reactor may be used to produce a combinatorial library of compounds, which may be separated by integrating the micro reactor with either a HPLC or capillary electrophoresis system, for example. The end of the separation column may be further integrated to a bioassay system such that each compound can be individually screened.

libraries of compounds can be rapidly generated. A summary of the reactions performed in micro reactors that meet these criteria is reviewed in detail below.

Combinatorial synthesis in micro reactors

Wittig reactions

Skelton and colleagues have reported the application of micro reactors to the Wittig reaction [34,35]. The authors used the micro reactor to prepare the *cis*- and *trans*-nitrostilbene esters **1** and **2** via this reaction (Scheme 1). Several

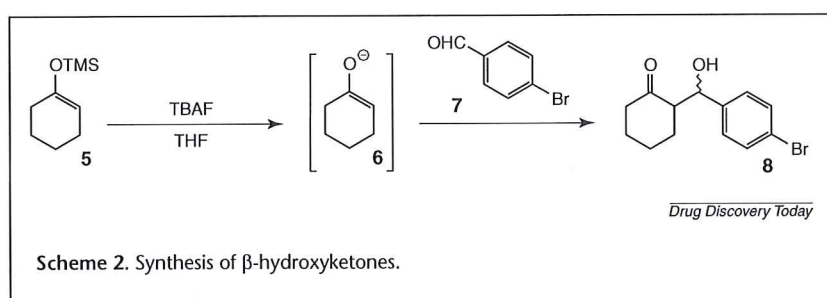
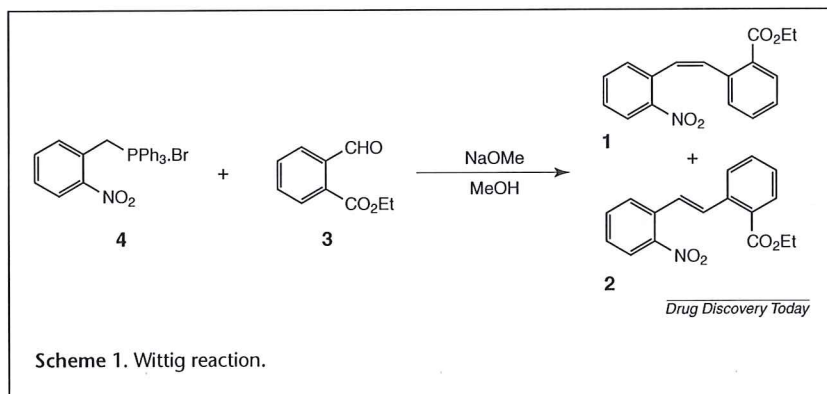
reagent reservoirs within the device, which in turn affected the EOF and electrophoretic mobility of the reagents. The variation in the external voltage subsequently altered the relative reagent concentrations within the device, producing *Z/E* ratios (the ratio of *cis*- and *trans*-isomers) in the region of 1:9. By comparison, when a traditional batch synthesis was performed using the same reaction time, concentration, solvent and stoichiometry, a *Z/E* ratio of approximately 3:1 was observed. This demonstrated that significant control was possible in a micro reactor compared

features, such as stoichiometry and stereochemistry, were investigated. When two equivalents of the aldehyde **3** to the phosphonium salt **4** were used in the reaction, a conversion of 70% was achieved, which represented an increase in reaction efficiency of 10% over the traditional batch synthesis. The reaction stoichiometry was subsequently reduced to 1:1, but using continuous flow of the reagents, the conversion was only 39%. This was increased to 59% using an injection technique, where slugs of the phosphonium salt **4** were injected into a continuous flow of the aldehyde **3**. The research was further extended to investigate the stereochemistry of the reaction, where the ratio of isomers **1** and **2** was controlled by altering the voltages applied to the

Table 1. Single step reactions performed in micro reactors

Reaction	Chip material	Solvent	Conversion (%)	Pumping mechanism	Ref
Suzuki	Glass	aq THF	67	EOF	[45]
Kumada coupling	Polypropylene	THF	60	Syringe pump	[46]
Nitration	Glass	benzene	65	EOF	[47]
Enamine formation	Glass	MeOH	42	EOF	[48]
Diazo coupling	Glass	MeOH	37	EOF	[49]
		MeCN	22		
Photocyanation	Polymer	pyrene/H ₂ O	73	Syringe pump	[50]
Dehydration	Glass/PDMS	EtOH	85–95	EOF or syringe pump	[51]
Esterification	Glass/PDMS	EtOH	30	Syringe pump	[52]
Photochemical	Silicon/quartz	(CH ₃) ₂ CHOH	60	Syringe pump	[53]
Photochemical	Glass	MeOH	80	Syringe pump	[54]
Phase transfer	Glass	EtOAc	100	Syringe pump	[55]
Fluorination	Ni or Cu	Nitrogen gas	90–99	Syringe pump	[56,57]
Fluorination	Silicon/Pyrex	MeOH	80	Syringe pump	[58]
Oxidation	Al	none	75–99	Syringe pump	[59]

Abbreviations: EOF, electroosmotic flow; PDMS, polydimethylsiloxane; THF, tetrahydrofuran.



with batch reactions. The authors also demonstrated that the micro reactor could be used as a tool for rapid reaction development and optimization based on analogue chemistry by using different aldehydes in the reaction [35].

Carbanion chemistry

Carbanion chemistry is the most common method of C–C bond formation, however the temperature of such reactions often governs the stereochemistry of the product. Therefore, micro reactors have a considerable attraction because of their excellent temperature control. Wiles and colleagues have demonstrated the use of silyl enol ethers in the aldol reaction within a micro reactor [36] where quantitative conversion of the silyl enol ethers to β -hydroxyketones was observed in 20 min in the micro reactor, compared with traditional batch systems where quantitative yields were only obtained when extended reaction times of up to 24 h were employed. One example involved the treatment of trimethylsilyl (TMS) enol ether **5** with tetra-*n*-butylammonium fluoride (TBAF), to generate the tetra-*n*-butylammonium enolate **6** *in situ*, followed by condensation with *p*-bromobenzaldehyde **7** to give the β -hydroxyketone **8** in a 100% conversion (Scheme 2). The reaction was successfully performed using a variety of other silyl enol ethers and aldehydes, which demonstrates that micro reactors can be used in the rapid synthesis of combinatorial libraries.

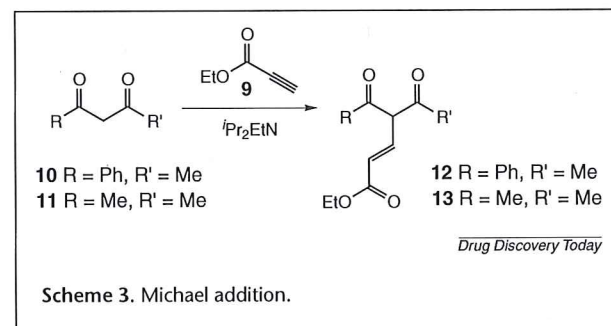
Wiles and co-workers [37] have also reported the preparation of the enolates from a series of 1,3-diketones using

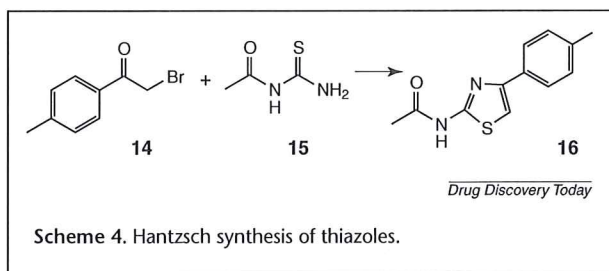
an organic base and their subsequent reaction with a variety of Michael acceptors, such as **9**, to afford 1,4-addition products within a micro reactor (Scheme 3). When using a continuous flow of the reagents **9** and **10**, 15% conversion to the product **12** was observed, compared with 56% when the diketone **11** was reacted with **9** forming the Michael adduct **13**. The authors demonstrated enhancements in the conversions through the application of the stopped-flow technique. This procedure involved the mobilization of reagents through the device for a designated period of time, using an applied field before the flow was subsequently paused by the removal of the applied field, before re-application of the field. Using the regime of 2.5 s on and 5 s off, the conversion to **12** was improved to 34%, whereas lengthening the stopped-flow period to 10 s resulted

in a further increase to 100%. This was compared with the preparation of **13**, in which the regime of 2.5 s on and 5 s off resulted in an increase in conversion to 95%. This demonstrated that the enolate of 2,4-pentanedione **11** was more reactive than the corresponding enolate of benzoyl acetone **10**. The authors propose that the observed increase in conversion when using the technique of stopped-flow was due to an effective increase in residence time within the device corresponding to the different kinetics associated with these reactions.

Hantzsch reactions

Special equipment is required when performing large-scale reactions at elevated temperature. However, the synthesis of a series of 2-aminothiazoles using a Hantzsch reaction within a micro reactor has been demonstrated [38]. During the experiments, the T-shaped micro reactor was heated to





Scheme 4. Hantzsch synthesis of thiazoles.

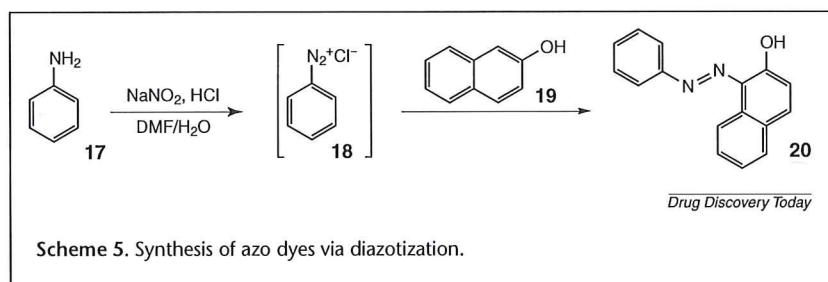
70°C using a Peltier heater, which was aligned with the channels and the heat generated by the device was applied to the base of the micro reactor. The reaction of α -bromoketone 14 with the thiourea derivative 15, using *N*-methyl-2-pyrrolidinone (NMP) as solvent, resulted in the preparation of aminothiazole 16 in a 85% conversion (Scheme 4). A range of aminothiazole derivatives were prepared using alternative α -bromoketones as starting materials.

Whereas the above examples represent sequential combinatorial synthesis, Kikutani and co-workers have recently reported an example of parallel synthesis within a micro reactor [39]. The authors used their micro reactor to synthesize a range of amides, by reaction of a selection of amines with a diverse range of acid chlorides via a phase transfer reaction.

Multi-step synthesis in micro reactors

Diazotization reactions

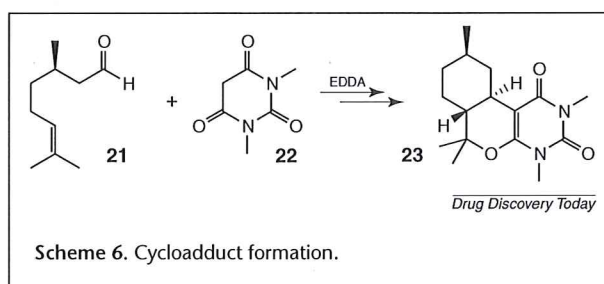
Diazotization of aromatic amines is an industrially important yet dangerous process. The explosive nature of diazonium salts necessitates extreme care in reaction processing. Therefore, the small volume of micro reactors affords a safe route to perform hazardous reactions. Wootton and colleagues [40] have demonstrated the synthesis of azo compounds using hydrodynamic pumping within a micro reactor. The authors demonstrated that aniline 17 could be converted into the diazonium salt 18 before being reacted *in situ* with β -naphthol 19 to form the azo dye 20 in up to a 52% overall conversion (Scheme 5). The ability to prepare and react diazonium salts *in situ* clearly demonstrates the versatility of micro reactor technology.



Scheme 5. Synthesis of azo dyes via diazotization.

Condensation reactions

The synthesis of cycloadducts in a micro reactor using hydrodynamic-driven flow has been reported [41]. The reaction consisted of Knoevenagel condensation of an aldehyde 21 with a 1,3-diketone 22 in the presence of ethylenediamine acetate (EDDA) as catalyst, using aqueous methanol as a solvent. The reaction intermediate underwent a spontaneous intramolecular hetero-Diels-Alder reaction to form cycloadduct 23 in a 60–68% conversion (Scheme 6).



Scheme 6. Cycloadduct formation.

Peptide synthesis

Watts and co-workers have recently demonstrated multi-step synthesis of peptides in a micro reactor [42,43]. The authors evaluated the reactor using a carbodiimide coupling reaction of Fmoc- β -alanine 24 with the amine 25 to give the dipeptide 26 in up to 93% conversion (Scheme 7).

The authors also demonstrated that the dipeptide could be prepared from pre-activated carboxylic acids [42,43]. The reaction of the pentafluorophenyl (PFP) ester of Fmoc- β -alanine 27 with amine 25 gave a 100% yield of dipeptide 26 in 20 min (Scheme 8). This represented a significant increase in yield compared with the traditional batch synthesis, where only a 50% yield was obtained in 24 h.

Having demonstrated that peptide bonds could be successfully formed when using a micro reactor, the authors then found that they could extend the methodology to the preparation of longer chain peptides. Using the micro reactor, the 4-[*N*-(1-(4,4-dimethyl-2,6-dioxocyclohexylidene)-3-methylbutyl)amino]benzyl (Dmab) ester of Fmoc- β -alanine 28 was reacted with one equivalent of 1,8-diazabicyclo [5.4.0]undec-7-ene (DBU) to give the free amine 25 in a quantitative conversion. The authors then reacted the amine *in situ* with the pentafluorophenyl ester 29 to give the dipeptide 30 (Scheme 9) in a 96% overall conversion.

Having shown that more complex peptides could be produced by removal of the *N*-protecting group, the authors then demonstrated that they could remove the Dmab ester using hydrazine.

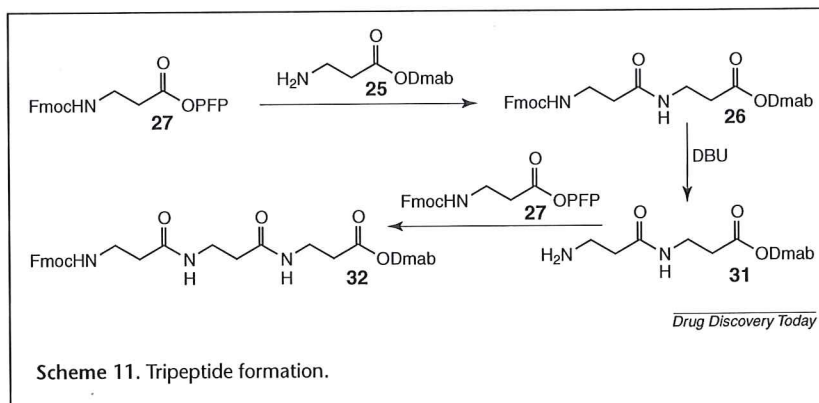
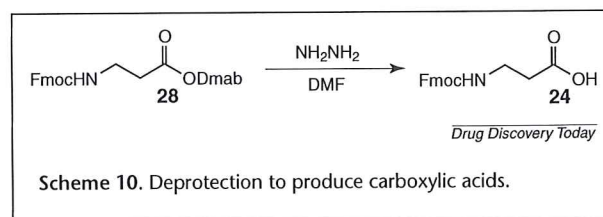
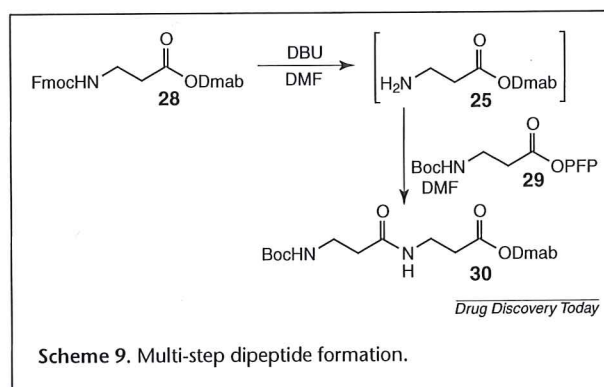
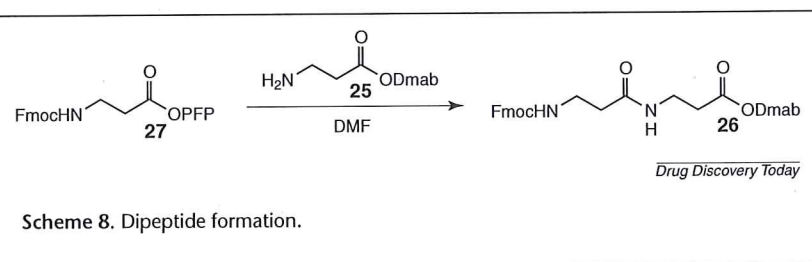
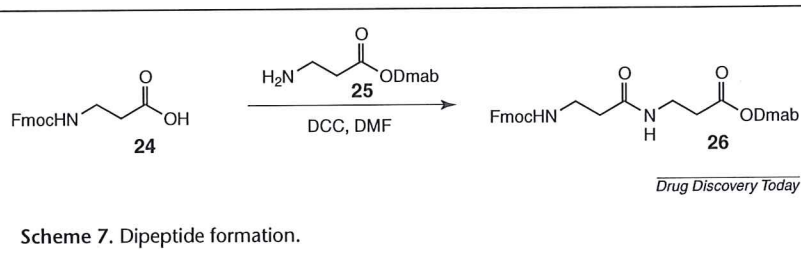
The reaction of the Dmab ester **28** with one equivalent of hydrazine resulted in quantitative deprotection, producing the carboxylic acid **24** (Scheme 10). Solid phase peptide synthesis, by comparison, generally requires 2% hydrazine in *N,N*-dimethylformamide (DMF) to effect complete deprotection.

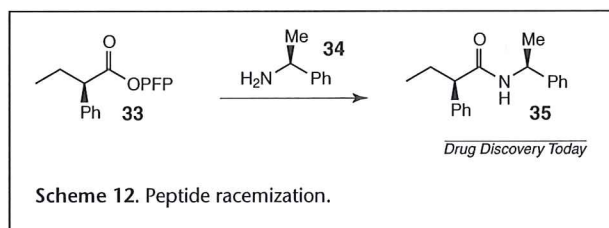
Watts and co-workers have further extended this approach to the synthesis of tripeptide **32** [58]. The reaction of pentafluorophenyl ester **27** with amine **25** formed dipeptide **26**, which was reacted with DBU to effect 9-fluorenylmethoxycarbonyl (Fmoc) deprotection. The amine **31** was then reacted *in situ* with another equivalent of pentafluorophenyl ester **27** to prepare tripeptide **32** in a 30% overall conversion (Scheme 11). This approach clearly demonstrates that intermediates can be generated *in situ* and used in subsequent reactions, thus enabling the combinatorial synthesis of peptides, which are of biological and pharmaceutical interest.

These same authors then investigated racemization in peptides derived from α -amino acids [44]. The reaction of the pentafluorophenyl ester of *R*-2-phenylbutyric acid **33** with α -methylbenzylamine **34**, gave the amide **35** in quantitative conversion with 4.2% racemization (Scheme 12). Importantly, there was less racemization than was observed in the batch reaction at the same concentration and temperature. The reduced level of racemization was attributed to the reduced reaction times observed within the micro reactors. This demonstrates that there would be significant advantages to performing such reactions in micro reactors compared with traditional batch systems.

Conclusions

Micro reactor chemistry is currently showing great promise as a novel method on which to build new chemical technology and processes. Reactions performed in micro reactors invariably generate pure products in a high yield, in shorter periods of time than the equivalent batch reactions and in sufficient quantities to perform full characterization. Therefore, one of the obvious applications is in combinatorial chemistry and drug discovery, where the generation of compounds with either different reagents or under variable





conditions is an essential factor. In short, micro reactor technology has the potential to revolutionize the pharmaceutical industry because the number of potential drug candidates that can be prepared and screened can be considerably increased, hence the likelihood of developing new drugs is considerably enhanced.

References

- Bradley, D. (1999) Chemical reduction. *Eur. Chem.* 1, 17–20
- Fletcher, P.D.I. and Haswell, S.J. (1999) Downsizing synthesis. *Chem. Br.* 35, 38–41
- Cowen, S. (1999) Chip service. *Chem. Ind.* 8, 584–586
- McCreedy, T. (1999) Reducing the risks of synthesis. *Chem. Ind.* 8, 588–590
- Barrow, D. *et al.* (1999) Shrinking to fit. *Chem. Ind.* 8, 591–594
- Cooper, J. *et al.* (2001) Lab-on-a-chip and microarrays. *Chem. Ind.* 10, 653–655
- Haswell, S.J. *et al.* (2001) The application of micro reactors to synthetic chemistry. *Chem. Commun.* 5, 391–398
- Matlosz, M. *et al.* eds (2002) *IMRET 5: Proc. 5th Int. Conf. Microreact. Technol.*, Springer, Berlin
- Ehrfeld, W. *et al.* (2000) *Microreactors: New Technology for Modern Chemistry*, Wiley-VCH
- Overbeek, J. (1952) *Chap. V: Th.G. in Colloid Science* (Vol. 1) (Kruyt, H.R., ed.), pp. 195–244, Elsevier
- Rice, C.L. and Whitehead, R. (1965) Electrokinetic flow in a narrow cylindrical capillary. *J. Phys. Chem.* 69, 4017–4024
- Hunter, R.J. (1981) *Zeta Potential in Colloid Science*, Academic Press
- Jednacak, J. *et al.* (1974) The electrokinetic potential of glasses in aqueous electrolyte solutions. *J. Colloid Interface Sci.* 49, 16–23
- Madou, M. (1997) *Fundamentals of Microfabrication*, CRC Press
- McCreedy, T. (2000) Fabrication techniques and materials commonly used for the production of micro reactors and micro total analytical systems. *TRAC* 19, 396–401
- McCreedy, T. (2001) Rapid prototyping of glass and PDMS microstructures for micro total analytical systems and micro chemical reactors by microfabrication in the general laboratory. *Anal. Chim. Acta* 427, 39–43
- Haswell, S.J. (1997) Development and operating characteristics of micro flow injection analysis systems based on electroosmotic flow. *Analyst* 122, 1R–10R
- Manz, A. *et al.* (1991) Miniaturization of chemical analysis systems – a look into next century technology or just a fashionable craze. *Chimia (Aarau)* 45, 103–105
- Manz, A. *et al.* (1993) Planar chip technology for miniaturization of separating systems – a developing perspective in chemical monitoring. *Adv. Chromatogr.* 33, 1–66
- Freemantle, M. (1999) Downsizing chemistry. *CEN* 2, 27–36
- Harrison, D.J. and van den Berg, A., eds (1998) *Proceedings of the Micro Total Analytical Systems '98 Workshop*, Kluwer Academic Press
- van den Berg, A. and Lammerink, T.S.J. (1998) Micro total analysis systems: microfluidic aspects, integration concept and applications. *Top. Curr. Chem.* 194, 21–49
- Harrison, D.J. *et al.* (1993) Micromachining a miniaturized capillary electrophoresis-based chemical-analysis system on a chip. *Science* 261, 895–897
- Jacobson, S.C. *et al.* (1994) High-speed separations on a microchip. *Anal. Chem.* 66, 1114–1118
- Woolley, A.T. *et al.* (1996) Functional integration of PCR amplification and capillary electrophoresis in a microfabricated DNA analysis device. *Anal. Chem.* 68, 4081–4086
- Woolley, A.T. and Mathies, R.A. (1995) Ultra-high-speed DNA sequencing using capillary electrophoresis chips. *Anal. Chem.* 67, 3676–3680
- Woolley, A.T. *et al.* (1997) High-speed DNA genotyping using microfabricated capillary array electrophoresis chips. *Anal. Chem.* 69, 2181–2186
- Jacobsen, S.C. and Ramsey, J.M. (1996) Integrated microdevice for DNA restriction fragment analysis. *Anal. Chem.* 68, 720–723
- Effenhauser, C.S. *et al.* (1994) High-speed separation of antisense oligonucleotides on a micromachined capillary electrophoresis device. *Anal. Chem.* 66, 2949–2953
- Schmalzing, D. *et al.* (1998) DNA sequencing on microfabricated electrophoretic devices. *Anal. Chem.* 70, 2303–2310
- Spence, D.M. and Crouch, S.R. (1997) Factors affecting zone variance in a capillary flow injection system. *Anal. Chem.* 69, 165–169
- Service, R.F. (1998) Microchip arrays put DNA on the spot. *Science* 282, 396
- Fletcher, P.D.I. *et al.* (2002) Micro reactors: principles and applications in organic synthesis. *Tetrahedron* 58, 4735–4757
- Skelton, V. *et al.* (2001) The preparation of a series of nitrostilbene ester compounds using micro reactor technology. *Analyst* 126, 7–10
- Skelton, V. *et al.* (2001) The generation of concentration gradients using electroosmotic flow in micro reactors allowing stereoselective chemical synthesis. *Analyst* 126, 11–13
- Wiles, C. *et al.* (2001) The aldol reaction of silyl enol ethers within a micro reactor. *Lab Chip* 1, 100–101
- Wiles, C. *et al.* (2002) 1,4-Addition of enolates to α,β -unsaturated ketones within a micro reactor. *Lab Chip* 2, 62–64
- Garcia-Egido, E. *et al.* (2002) Synthesis of a three-member array of cycloadducts in a glass microchip under pressure driven flow. *Lab Chip* 2, 170–174
- Kikutani, K. *et al.* (2002) Glass microchip with three-dimensional microchannel network for 2 x 2 parallel synthesis. *Lab Chip* 2, 188–192
- Wootton, R.C.R. *et al.* (2002) On-chip generation and reaction of unstable intermediates - monolithic nanoreactors for diazonium chemistry: Azo dyes. *Lab Chip* 2, 5–7
- Fernandez-Suarez, M. *et al.* (2002) A Hantzsch synthesis of 2-aminothiazoles performed in a heated microreactor system. *Lab Chip* 2, 31–33
- Watts, P. *et al.* (2001) The synthesis of peptides using micro reactors. *J. Chem. Soc. Chem. Commun.* 1, 990–991
- Watts, P. *et al.* (2002) Solution phase synthesis of β -peptides using micro reactors. *Tetrahedron* 58, 5427–5439
- Watts, P. *et al.* (2002) Investigation of racemisation in peptide synthesis within a micro reactor. *Lab Chip* 2, 141–144
- Greenway, G.M. *et al.* (2000) The use of a novel microreactor for high throughput continuous flow organic synthesis. *Sensors & Actuators B.* 63, 153–158
- Haswell, S.J. *et al.* (2001) Kumada-Corriu reactions in a pressure-driven microflow reactor. *Lab Chip* 1, 164–166
- Doku, G.N. *et al.* (2001) Electric field-induced mobilisation of multiphase solution systems based on the nitration of benzene in a micro reactor. *Analyst* 126, 14–20
- Sands, M. *et al.* (2001) The investigation of an equilibrium dependent reaction for the formation of enamines in a microchemical system. *Lab Chip* 1, 64–65

- 49 Salimi-Moosavi, H. *et al.* (1997) Electroosmotic pumping of organic solvents and reagents in microfabricated reactor chips. *J. Am. Chem. Soc.* 119, 8716–8717
- 50 Ueno, K. *et al.* (2002) Photocyanation of pyrene across an oil/water interface in a polymer microchannel chip. *Lab Chip* 2, 231–234
- 51 Wilson, N.G. and McCreedy, T. (2000) On-chip catalysis using a lithographically fabricated glass microreactor—the dehydration of alcohols using sulfated zirconia. *J. Chem. Soc. Chem. Commun.* 1, 733–734
- 52 McCreedy, T. and Wilson, N.G. (2001) Microfabricated reactors for on-chip heterogeneous catalysis. *Analyst* 126, 21–23
- 53 Lu, H. *et al.* (2001) Photochemical reactions and on-line UV detection in microfabricated reactors. *Lab Chip* 1, 22–28
- 54 Pitts, J.N. *et al.* (1959) Photochemical reactions of benzophenone in alcohols. *J. Am. Chem. Soc.* 81, 1068–1077
- 55 Hisamoto, H. *et al.* (2001) Fast and high conversion phase-transfer synthesis exploiting the liquid–liquid interface formed in a microchannel chip. *J. Chem. Soc. Chem. Commun.* 1, 2662–2663
- 56 Chambers, R.D. and Spink, R.C.H. (1999) Microreactors for elemental fluorine. *J. Chem. Soc. Chem. Commun.* 1, 883–884
- 57 Chambers, R.D. *et al.* (2001) Elemental fluorine. Part 13. Gas–liquid thin film microreactors for selective direct fluorination. *Lab Chip* 1, 132–137
- 58 de Mas, N. *et al.* (2002) *IMRET 5: Proceedings of the Fifth International Conference on Microreaction Technology* 60–67, Springer, Berlin
- 59 Srinivasan, R. *et al.* (1997) Micromachined reactors for catalytic partial oxidation reactions. *AIChE J.* 43, 3059–3069

Contributions to Drug Discovery Today

Drug Discovery Today publishes topical information on all aspects of drug discovery – molecular targets, lead identification, lead optimization and associated technologies, drug delivery, gene therapy, vaccine development and clinical trials – together with overviews of the current status of compound classes and approaches in specific therapeutic areas or disease states. Areas of pharmaceutical development that relate to the potential and viability of drug candidates are also included, as are those relating to the strategic, organizational and logistic issues underlying pharmaceutical R&D.

Authors should aim for topicality rather than comprehensive coverage. Ultimately, articles should improve the reader's understanding of the field addressed and should therefore assist in the increasingly important decision-making processes for which drug discovery and development scientists are responsible.

Most articles appearing in *Drug Discovery Today* are commissioned. However, suggestions and proposals for Reviews or shorter items for the Editorial, Monitor or Update sections are welcomed; in the first instance, a tentative title and brief outline of the proposed article should be supplied. Typically, full reviews will extend to 4000 words with up to 60 references. Update and Monitor items (news, letters and views, reports of new technological advances, conferences, experimental methods, and critical assessment of important new literature and other media) do not usually exceed 1500 words, and one or two figures plus up to ten references can be included. The Editorial represents a personal perspective on contemporary issues and controversies affecting R&D and the pharmaceutical industry.

Please note that publication of Review articles is subject to satisfactory expert peer and editorial review. The publication of Update and Editorial articles is subject to satisfactory editorial review. In addition, personal perspectives published in *Drug Discovery Today* do not represent the view of the journal or its editorial staff

If you would like to contribute to the *Reviews*, *Monitor* or *Editorial* sections of *Drug Discovery Today* in the future, please submit your proposals to: Dr Steve Carney, Editor, *Drug Discovery Today*, Elsevier, 84 Theobald's Road, London, UK WC1X 8RR, e-mail: s.carney@elsevier.com.

If you would like to contribute to the *Update* section, please submit your proposals to: Dr Joanna Clough, News Editor, *Drug Discovery Today*, Elsevier, 84 Theobald's Road, London, UK WC1X 8RR, e-mail: j.owens@elsevier.com

Paul D. I. Fletcher
Stephen J. Haswell
Xunli Zhang

Department of Chemistry,
The University of Hull,
Hull, UK

Monitoring of chemical reactions within microreactors using an inverted Raman microscopic spectrometer

An inverted Raman microscope spectrometer has been used to profile the spatial evolution of reactant and product concentrations for a chemical reaction within a microreactor operating under hydrodynamic flow control. The Raman spectrometer was equipped with a laser source at wavelength of 780 nm, confocal optics, a holographic transmission grating, and a charge-coupled device (CCD) detector. The microreactor consisted of a T-shaped channel network etched within a 0.5 mm thick glass bottom plate that was thermally bonded to a 0.5 mm thick glass top plate. The ends of the channel network were connected to reagent reservoirs that were linked to a syringe pump for driving the solutions by hydrodynamic pumping within the channels. The microchannels were 221 μm wide and 73 μm deep. The synthesis of ethyl acetate from ethanol and acetic acid was investigated as a model system within the microreactor as Raman scattering bands for each reactant and product species were clearly resolved. Raman spectral intensities of each band were proportional to concentration for each species and hence all concentrations could be quantitatively measured after calibration. By scanning specific Raman bands within a selected area in the microchannel network at given steps in the X-Y plane, spatially resolved concentration profiles were obtained under steady-state flow conditions. Under the flow conditions used, different positions within the concentration profile correspond to different times after contact and mixing of the reagents, thereby enabling one to observe the time dependence of the product formation. Raman microscopy provides a useful complementary technique to UV/VIS absorbance and fluorescence methods for the *in situ* monitoring and analysis of chemical reaction species having their lowest S_0 - S_1 absorption bands too far in the UV to be of use, due to their probable overlap with the bands from other reactant, product and solvent molecules.

Keywords: Microreactor / Miniaturization / Monitoring of chemical reactions / Raman microscopic spectroscopy / Synthesis of ethyl acetate

DOI 10.1002/elps.200305532

1 Introduction

The development of miniaturized microreactors based on the so-called "Lab-on-a-Chip" concept has witnessed an explosive growth in recent years [1–4]. Such miniaturized devices represent the ability to "shrink" conventional bench chemical reactors to a size of a few square centimetres with major advantages of speed, performance, integration, portability, sample/solvent quantity, automation, hazard control, and cost. These merits are important for a variety of applications in analytical chemistry, biochemistry, clinical diagnosis, medical chemistry and industrial chemistry [5, 6]. A microreactor is generally

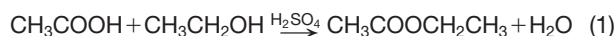
defined as a device consisting of a number of interconnecting capillary channels in which small quantities of a liquid or gas are moved in a specified sequence, mixed and allowed to react for a specified period of time. For a liquid-based microreactor, the typical cross-sectional dimensions of the channels used are normally in a range of 10–500 μm . The movement of reagents and products in microreactors can be achieved in a number of ways including micropumping and electrokinetic mobilisation by electroosmotic flow coupled with electrophoresis [7].

To analyse the reagents within a microchannel, a wide range of analytical methods have been examined with UV/VIS absorbance and fluorescence techniques being the most common [5]. Raman spectroscopy offers a number of advantages over other spectroscopic techniques for chemical analysis and has in recent years been used

Correspondence: Prof. S. J. Haswell, Department of Chemistry, The University of Hull, Hull HU6 7RX, UK
E-mail: s.j.haswell@hull.ac.uk
Fax: +44-(0)1482-466416

effectively for process analysis monitoring [8–11]. It enables the analysis of a wide range of organic species which possess no UV/VIS chromophores and, since Raman spectra are “information rich”, can be used to identify unknown species. Since water is almost Raman “transparent”, this technique is ideally suited for analyzing aqueous based reaction media whereas infrared (IR) methods fail in this case owing to the strong adsorption by water. The major disadvantage of Raman is that, relative to UV/VIS methods, the sensitivity is poor and hence either high concentrations, long data acquisition times or the use of specialist surface or resonance enhancement techniques are required. The use of an inverted microscope optical systems in combination with a charged coupled device (CCD) detector allows Raman spectroscopy to be used for measurement of several Raman spectra simultaneously for chemical reactants and products within a microreactor. The use of confocal optics also provides discrimination between points of different depths within the sample. Raman laser excitation sources covering a range of wavelengths from 496 to 1064 nm have been used for studies of bulk reaction systems involving liquid and solid-phase reactions. Longer wavelength sources in the near-IR region are advantageous to suppress unwanted fluorescence background signal [8].

The aim of the current study was to develop an *in situ* chemical imaging technique using Raman spectroscopic microscopy to obtain spatially resolved concentration profiles of reactant and product species within a microreactor. The reaction selected for this study was the esterification of ethanol and acetic acid catalysed by H^+ , resulting in the products ethyl acetate and water, see Eq. (1).



This reaction was chosen because (i) it is relatively simple with no side reactions, and (ii) the kinetics of the reaction are known from the literature [12].

2 Materials and methods

2.1 Chemicals

Ethanol (absolute, A. R. grade) and ethyl acetate (99%) were obtained from Fisher Scientific (Springfield, NJ, USA). Acetic acid (99.8%) was provided by Vickers Laboratories (Pudsey, West Yorkshire, England). Sulphuric acid (97.5%, A. R. grade) was obtained from Aldrich (Milwaukee, WI, USA) and used as catalyst for the synthesis of ethyl acetate using ethanol and acetic acid. All the above chemicals were used as received.

2.2 Fabrication of microreactors

The microreactor consisted of a bottom plate of Pyrex glass (thickness, 0.5 mm) containing an etched microchannel which was thermally bonded to a top glass plate (also 0.5 mm thick). The microchannel network was fabricated by a powder blasting technique in which an Al_2O_3 particle jet was directed through a nozzle towards the glass surface for mechanical material removal [13]. The particle diameters were in the range of 3–30 μm and the jet was at a speed of about 100 $m \cdot s^{-1}$ which was set using an applied pressure of 5×10^5 Pa. The desired pattern of the microchannel network was obtained by scanning the nozzle over the target glass surface coated with an electroplated copper mask patterned with the network design. The blasting time was adjusted to control the channel depth. Figure 1 shows a schematic plan view of the entire T-shaped channel network and reservoirs together with an optical micrograph of the junction section. The ends of the channel network were connected to holes (2 mm in diameter) drilled through the top plate at appropriate positions. Lengths of plastic tubing were

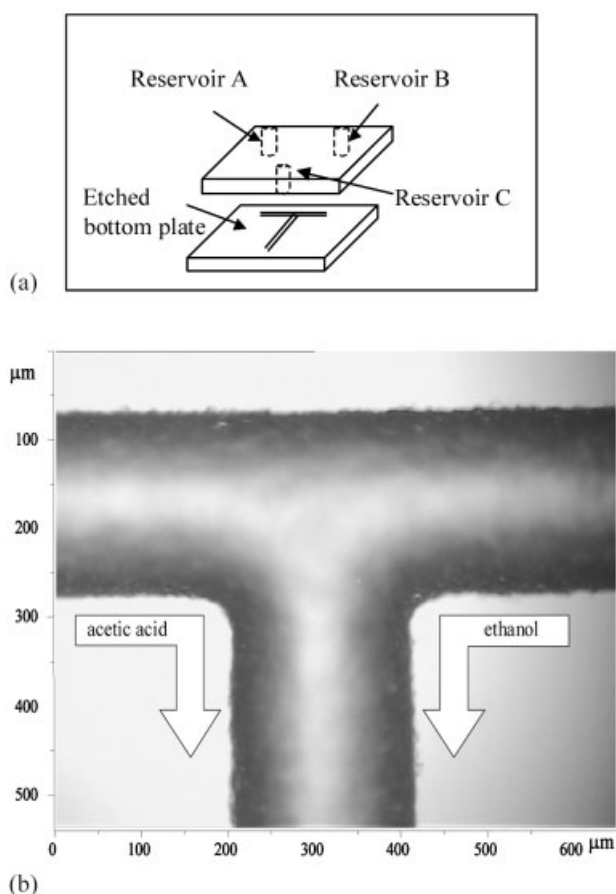


Figure 1. (a) Schematic plan view showing reservoir positions and (b) optical micrograph of the T-shaped channel network in the region of the T-junction.

attached over the holes in the top plate to form the reagent reservoirs A, B, and C. The reservoirs filled with the appropriate solutions were then connected to syringe pumps to drive the reagents through the channel network.

2.3 Instrumentation

Raman microscope spectrometer: All Raman spectra were acquired with a LabRam inverted microscope spectrometer, manufactured by Jobin Yvon Ltd. This spectrometer was equipped with dual laser sources at wavelengths of 780 and 633 nm, confocal optics, a holographic transmission grating, and a charge coupled device (CCD) detector with 1024×256 pixels. The instrument included a precision motorized XY sample stage for automated chemical imaging at spatial resolution down to less than $1 \mu\text{m}$ and extensive software support (LabSpec 4.02) for data processing. In this study, an Olympus objective lens of $10 \times$ magnification, 10.0 mm working distance, and numerical aperture (NA) of 0.3 was used (Olympus UPLFL 37542). A grating with 950 grooves/mm, a confocal aperture of $500 \mu\text{m}$, an entrance slit of $1000 \mu\text{m}$, and the 780 nm excitation laser were selected for the experiments. The Raman spectrometer wavelength range was calibrated using the center frequency of the silicon band from a silicon sample (520.2 cm^{-1}). Using these conditions, spectra of adequate signal/noise from the pure liquid reagents contained in channels of $70 \mu\text{m}$ depth required an acquisition time of 5 s. **Liquid pumping:** A dual channel syringe pump (PHD 2000; Harvard Apparatus, South Natick, MA, USA) was used to pump the two reactants into reservoirs A and B of the T-shaped network. Unreacted reagents and product flowed into reservoir C.

Heating microscope stage: A Microstat heated stage, supplied by Brunel Microscopes Ltd, UK, was mounted directly onto the microscope stage to heat the microreactor. The heating plate with a round aperture (diameter, 4.4 mm) for transmitted illumination was controlled via a controlling unit for temperatures up to 50°C with an accuracy of 0.5°C .

3 Results and discussion

3.1 Microchannel profiling

The T-junction of the microreactor channel network, where the reactants mixed and reacted, is shown in Fig. 1. To determine the average liquid linear velocity in the channel, it was necessary to profile the channel cross section. An optical microscope absorbance imaging technique [14] of the channel network filled with dye solution was used to obtain the quantitative 3-D profile of the T-junction region (see Fig. 2). "Slices" through the data array perpendicular to the long axes of the channels give the cross sectional profiles of the three channels (see Fig. 3). It was observed that the cross sectional shape of the channel etched by powder blasting consisted of a trapezoidal shape in which the bottom of the channel was slightly rounded. This shape was markedly different from the cross sectional shape obtained for a channel produced by isotropic wet etching of glass which consists of a rectangle flanked by quarter circles [14]. By fitting the channel profile (Fig. 3) it was obtained that the best-fit values of the etch mask width (m), the depth at the edge of the channel bottom (d), the radius of the curved

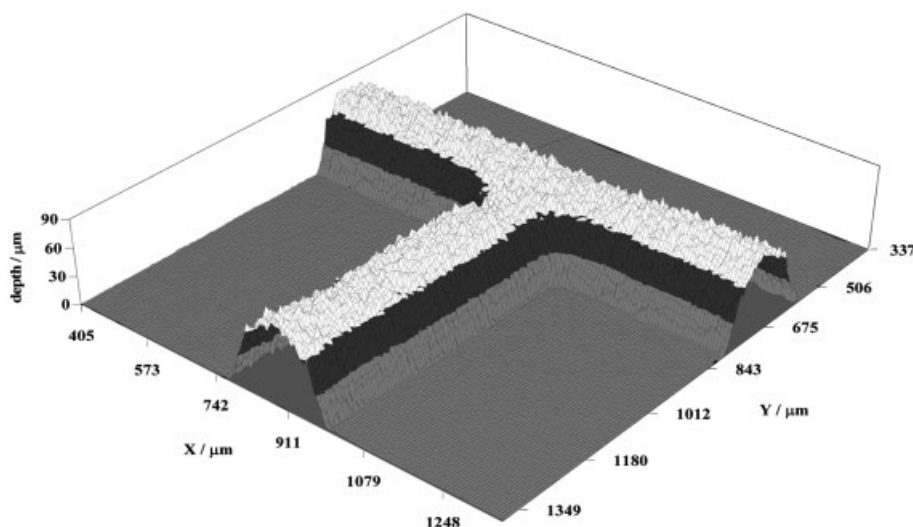


Figure 2. 3-D channel profile in the region of the T-junction determined using microscope visible absorbance imaging of the microreactor filled with a dye solution.

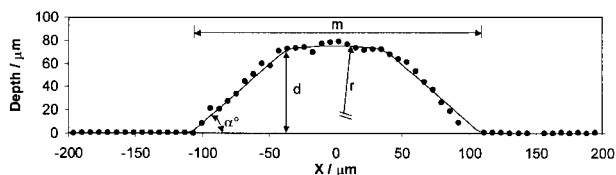


Figure 3. Cross sectional channel profile “sliced” from the 3-D plot in Fig. 2.

channel bottom (r), with origin shifted a depth (y_0), and the angle between the channel sidewall and the horizontal plane (α) were 221 ± 2 , 71 ± 2 , 202 ± 1 , $127 \pm 1 \mu\text{m}$, and 45° , respectively. These parameters enabled the calculation of the channel cross sectional area. It can be noticed from Figs. 1–3 that the surfaces and edges of the channels were not smooth. The roughness, typically in the range of $0.2\text{--}2.5 \mu\text{m}$, was a consequence of the high speed Al_2O_3 particle blasting method since hydrogen fluoride (HF) solution etching of glass produces relatively smooth channels [15].

3.2 Chemical imaging in microchannels

Figure 4 shows the reference Raman spectra for ethanol, acetic acid, and ethyl acetate which were obtained by filling the channels with each pure liquid. Background spectra measured using the empty microchannel were subtracted in each case. It was found that ethanol had a main characteristic band at 882 cm^{-1} , acetic acid had two at 620 and 893 cm^{-1} , and ethyl acetate had three characteristic bands at 376 , 632 , and 845 cm^{-1} . These characteristic bands obtained were in good agreement with literature values [9], and were used as fingerprints for chemical imaging of the three compounds within microreactors. Based on these spectra, a scan region from 200 to 1450 cm^{-1} was used in most of the experimental runs to cover all the main characteristic bands and also minimize the acquisition time.

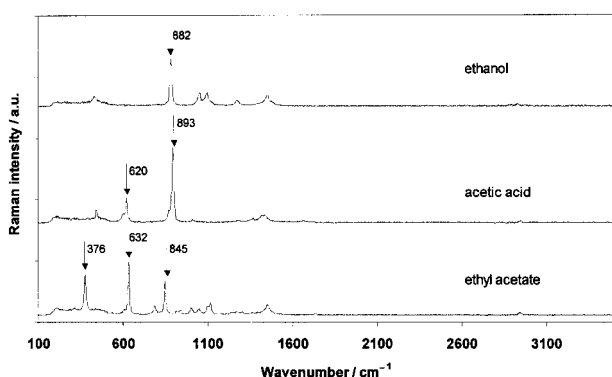


Figure 4. Raman spectra of ethanol, acetic acid, and ethyl acetate.

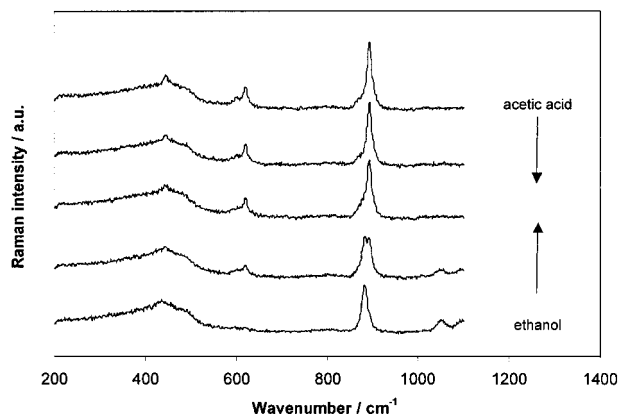


Figure 5. Raman spectra taken at different positions across the downstream channel containing co-flowing streams of acetic acid and ethanol.

We next describe the spatial imaging of mixtures of ethanol and acetic acid in the T-junction region of the channel network. Acetic acid was pumped from reservoir A down the left channel and ethanol from reservoir B down the right channel, both at constant flow rates of $0.1 \mu\text{L} \cdot \text{min}^{-1}$. No acid catalyst was included and hence no ethyl acetate product formation is expected in this case. Since the flow in the microchannels is laminar (the Reynolds number for the flow is less than 1, well below the threshold value of 2500 at which the transition to turbulent flow occurs), the two solutions meet at the T-junction and then flow side-by-side in the downstream channel towards the outlet reservoir C. Mixing occurs only by interdiffusion across the interface between the co-flowing laminar streams [16]. Raman mapping of the T-junction region was made by programming the movement of the automated microscope stage in both X and Y directions. Using step sizes of $17.73 \mu\text{m}$ and $25.09 \mu\text{m}$ in the X and Y directions, respectively, an array of 21×15 spectra was recorded. Figure 5 shows a series of illustrative spectra taken across the interface region when acetic acid and ethanol were co-flowing side by side. The spectra stacked in the figure, from top to bottom, were taken from five positions across the channel in X direction $35.46 \mu\text{m}$ apart and the middle spectrum was from the central position. The transition from the channel region filled with acetic acid (bands at 893 and 620 cm^{-1}) to that filled with ethanol (band at 882 cm^{-1}) can be clearly seen.

Using the complete array of spectra, a 3-D plot of Raman intensities for the band of 893 cm^{-1} for acetic acid across the T-junction was obtained and the result is shown in Fig. 6a. Similarly, the corresponding 3-D plot for ethanol using the band at 882 cm^{-1} is shown in Fig. 6b. The contact between the two liquids and the formation of co-flowing laminar streams down the leg of the T towards reser-

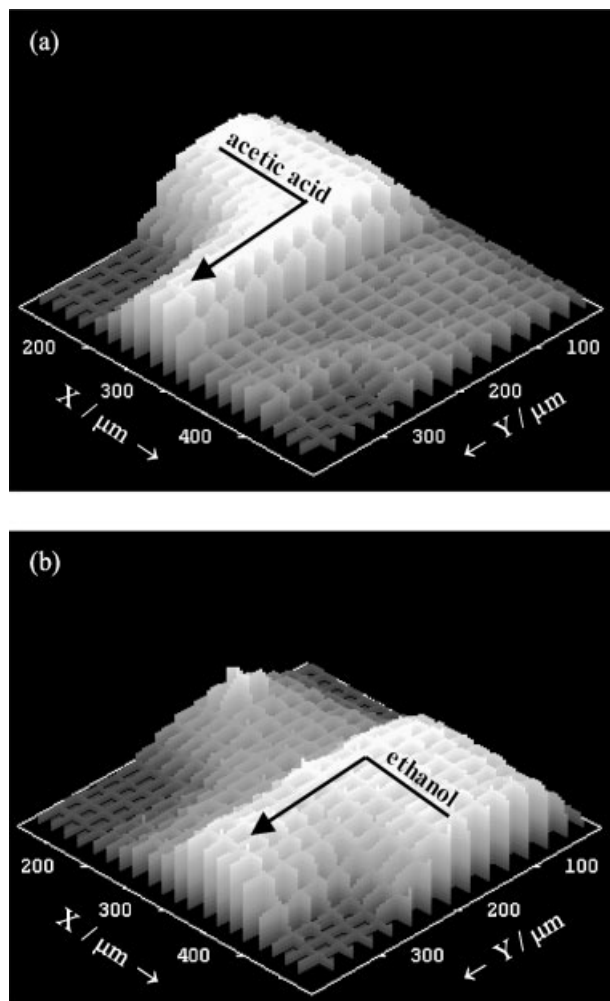


Figure 6. 3-D plots of Raman intensity (without background subtraction) in the T-junction region for specific bands; (a) 893 cm^{-1} from acetic acid, and (b) 882 cm^{-1} from ethanol.

voir C can be clearly seen. It was noticed that a “spike” appeared in the left side channel (see Fig. 6b) where only acetic acid is present. This “spike” of apparent high Raman intensity, shown as an example, was likely caused by a defect in the glass structure giving a high fluorescent signal since it appeared in the same position for several runs. This “spike” and some additional background noise have been removed by subtracting a blank spectrum recorded for water-filled channels in the further data processing. In principle, the chemical mapping can be achieved with different spatial resolution down to less than $1\text{ }\mu\text{m}$ by changing the step sizes applied to the microscope stage. However, finer spatial resolution must be balanced against considerations of the size of the final array of spectra and the total acquisition time (5 s for each X–Y location).

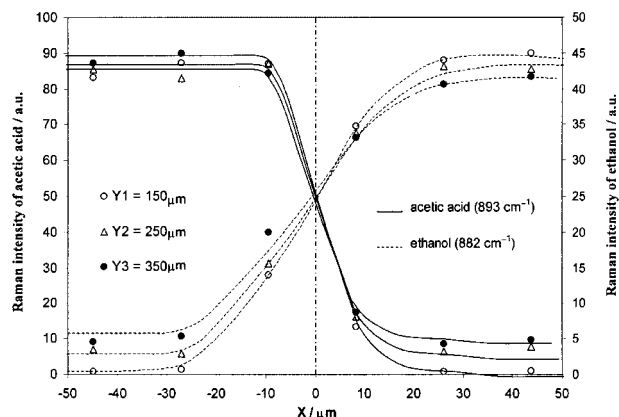


Figure 7. Raman intensity profiles across the downstream channel for acetic acid at 893 cm^{-1} and ethanol at 882 cm^{-1} at different Y positions corresponding to different times after first contact between the reagent streams.

“Slicing” of the 3-D images in Fig. 6 across the X axis yields the Raman intensity profile at the specific band across the channel at different Y positions. The different Y positions correspond to different times after contact between the two solutions according to

$$t = \frac{Y - Y_0}{v} \quad (2)$$

where Y is the measured position in the Y direction (see Fig. 6), Y_0 is at the middle of the top channels where the two reactants were assumed to first contact each other, and v is the average linear velocity of liquid flowing in the Y direction. The average velocity v can be calculated by dividing the set volumetric flow rate by the channel cross sectional area. For the combined flow rate used here ($0.2\text{ }\mu\text{L}\cdot\text{min}^{-1}$), the mean liquid velocity was $0.323\text{ mm}\cdot\text{s}^{-1}$. Figure 7 shows three Raman intensity profiles across the co-flowing streams of ethanol and acetic acid corresponding to three positions in the Y direction ($Y = 150, 250,$ and $350\text{ }\mu\text{m}$, respectively). These Y positions correspond to times after contact of the two liquids of 0.46, 0.77, and 1.08 s, respectively. As seen in Fig. 7, a slight broadening of the interface between the ethanol and acetic acid, due to diffusional inter-mixing, occurs over this time scale.

3.3 Monitoring of a chemical reaction within microreactor

The synthesis of ethyl acetate from ethanol and acetic acid was performed in the microreactor under identical flow conditions to those described above except that 5% (by volume) of sulphuric acid was added into the

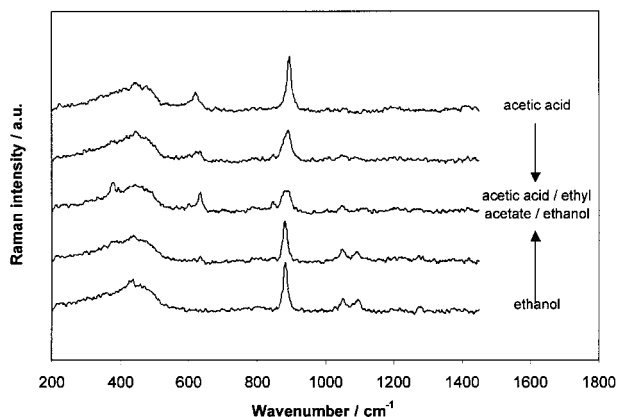


Figure 8. Raman spectra taken at different positions across the downstream channel containing co-flowing streams of acetic acid plus catalyst and ethanol. Reaction to form ethyl acetate occurs at the interface between the reactant streams.

acetic acid as catalyst. In addition, the Microstat heating plate was mounted between the microscope stage and the microreactor to increase the temperature to 37.5°C. Using the Raman mapping method described above, an array of spectra covering the T-junction region was obtained in order to monitor the spatial and temporal evolution of the reaction. Figure 8 shows examples of the stacked Raman spectra obtained at different X positions across the down stream channel where ethanol and acetic acid with catalyst were co-flowing at a temperature of 37.5°C. The characteristic Raman bands of 632 and 845 cm^{-1} for ethyl acetate product together with the bands for ethanol and acetic acid (the middle spectrum in Fig. 8) are observed in the interface region between the ethanol and acetic acid streams where mixing and the esterification reaction occurs. At the channel edges only the bands due to either acetic acid (the upper spectrum in Fig. 8) or ethanol (the bottom spectrum in Fig. 8) are seen.

To profile the concentrations, the relationships between solution concentrations and corresponding Raman intensities (the characteristic peak heights, in practice) must be obtained. This calibration was carried out by recording the Raman spectra of mixed solutions of varying concentrations for all the species involved in the reaction under exactly the same conditions as used for the reaction. Figure 9 shows the calibration results for acetic acid, ethyl acetate, and ethanol with characteristic bands of 893, 632, and 882 cm^{-1} , respectively. In each case, a linear relation between the solution concentration and the Raman intensity is observed as expected [8]. It was also confirmed that the additional reaction product (water) showed negligible Raman scattering.

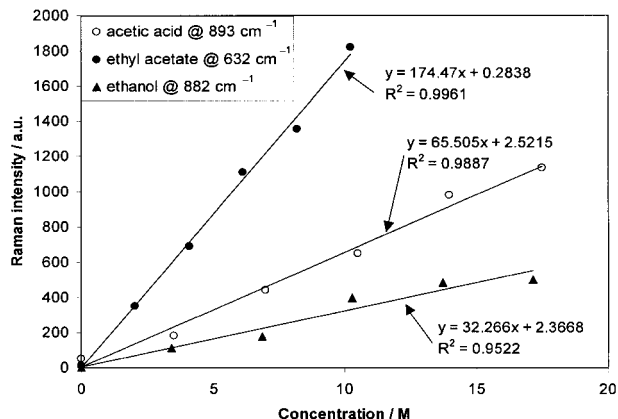


Figure 9. Calibration results of Raman intensity vs. concentration for ethanol, acetic acid and ethyl acetate.

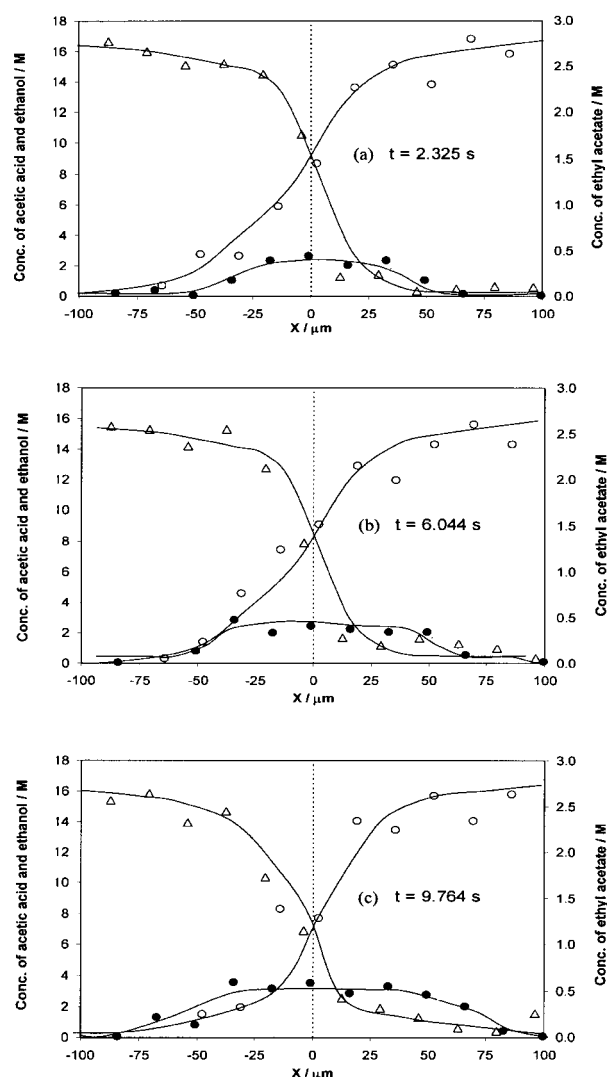


Figure 10. Concentration profiles for (Δ) acetic acid, (\circ) ethanol, and (\bullet) ethyl acetate across the downstream channel at different Y positions corresponding to the times shown on the plot.

The calibration plots were used in conjunction with the array of Raman spectra to obtain the concentration profiles of the reactants and product across the downstream microchannel at three Y positions ($Y = 750, 1950,$ and $3150 \mu\text{m}$ respectively), corresponding to times after contact of the two reactants of 2.3, 6.0, and 9.8 s, respectively. As shown in Fig. 10, the concentrations of the reactants and ethyl acetate product depend on both X position (relating to the diffusional mixing of the reactants between the co-flowing streams) and Y (corresponding to increasing time for reaction). It was also observed that the asymmetric nature of the product concentration profile (see Fig. 10). This was likely due to the difference in diffusion speeds and viscosities of different species in the mixture region. Optimization of the reaction in the microreactor thus requires careful consideration of both mass transfer and reaction kinetic processes. The Raman concentration imaging method described here is a valuable tool needed to test and validate mathematical models of organic reactions in these systems.

4 Concluding remarks

The results presented here demonstrate the utility of Raman spectroscopy microscope for profiling the spatial and temporal evolution of chemical reactions within a microreactor. As shown by this example, this technique provides *in situ* information on the progress of fluidics (*i.e.*, flow properties), mixing and reactions within channel networks, and can be used to optimize reactions in microreactors. However, some points should be taken into consideration concerning the recording of Raman spectra from samples within microreactors. (i) The material and thickness of the bottom glass plate should be selected carefully to minimise the background fluorescence signals from the glass, even though confocal optics are used. In general, a quartz glass plate with thickness of 0.5–1 mm yields acceptable signal:background ratios. (ii) For some chemicals, especially in the small volumes within microchannels, the Raman signals are very weak and so require long accumulation times (up to a few minutes) and high concentrations. In some cases, surface

or resonance enhancement may be used to improve the inherently low sensitivity of Raman scattering. Alternatively, long spectral accumulation times can be used for steady-state flow conditions (as in this work). Even with these limitations, this method is expected to find applications *in situ* chemical imaging in microreactor channel networks, particularly for aqueous solvent systems which enable good transmission of Raman signals.

The Engineering and Physical Sciences Research Council (EPSRC) of the UK is thanked for funding this study.

5 References

- [1] Manz, A., Fettinger, J. C., Verpoorte, E., Ludi, H., Widmer H. M., Harrison, D. J., *Trends Anal. Chem.* 1991, 10, 144–147.
- [2] Ehrfeld, W. (Ed.), *Microreaction Technology*, Springer, Berlin 1998.
- [3] Manz, A., Becker, H. (Eds.), *Microsystem Technology in Chemistry and Life Sciences*, Springer, Berlin 1998.
- [4] Jensen, K. F., *Chem. Eng. Sci.* 2001, 56, 293–303.
- [5] Ramsey, J. M., van den Berg, A. (Eds.), *5th μ -TAS Symposium*, Monterey, October 21–25, Kluwer Academic Publishers, London 2001.
- [6] Fletcher, P. D. I., Haswell, S. J., Warrington, B. H., Watts, P., Zhang, X. L., *Tetrahedron* 2002, 58, 4735–4757.
- [7] Fletcher, P. D. I., Haswell, S. J., Zhang, X. L., *Lab Chip* 2001, 1, 115–121.
- [8] Lewis, I. R., Edwards, H. G. M. (Eds.), *Handbook of Raman Spectroscopy – From the Research Laboratory to the Process Line*, Marcel Dekker, New York 2001.
- [9] Svensson, O., Josefson, M., Langkilde, F. W., *Chemometr. Intell. Lab. Syst.* 1999, 49, 49–66.
- [10] Mestl, G., *J. Mol. Catal. A: Chem.* 2000, 158, 45–65.
- [11] Zangmeister, C. D., Pemberton, J. E., *J. Am. Chem. Soc.* 2000, 122, 2289–2296.
- [12] Glasstone, S., *Physical Chemistry, 2nd Ed*, Macmillan and Co. Ltd, London 1962, pp. 1073–1074.
- [13] Schlautmann, S., Wensink, H., Schasfoort, R., Elwenspoek, M., van den Berg, A., *J. Micromech. Microeng.* 2001, 11, 386–389.
- [14] Broadwell, I., Fletcher, P. D. I., Haswell, S. J., McCreedy, T., Zhang, X. L., *Lab Chip* 2001, 1, 66–73.
- [15] McCreedy, T., *Anal. Chim. Acta* 2001, 427, 39–43.
- [16] Reyes, D. R., Iossifidis, D., Auroux, P. A., Manz, A., *Anal. Chem.* 2002, 74, 2623–2636.

On-chip separation of peptides prepared within a micro reactor

Vinod George,^a Paul Watts,^a Stephen J. Haswell*^a and Esteban Pombo-Villar^b^a Department of Chemistry, University of Hull, Cottingham Road, Hull, UK HU6 7RX.

E-mail: S.J.Haswell@hull.ac.uk; Fax: +44 1482 466416; Tel: +44 1482 465469

^b Nervous Systems Research, WSJ-386.07.15, Novartis Pharma Ltd., CH4002, Basel, Switzerland

Received (in Cambridge, UK) 4th September 2003, Accepted 7th October 2003

First published as an Advance Article on the web 22nd October 2003

We have demonstrated that peptides may be electrophoretically separated from unreacted reagents within an integrated micro reactor.

Over the past five years there has been a rapid growth in the development of micro reactor technology exploiting the technique of electroosmotic flow (EOF).¹ Recent research has demonstrated that a selection of gas and liquid phase reactions may be successfully performed within micro reactors where the products are inherently produced in higher yield and purity in much shorter periods of time compared with traditional batch reactions.^{2,3}

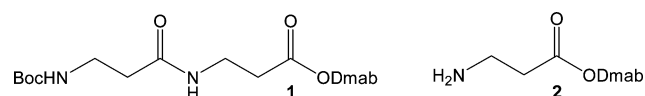
The authors have recently reported an extensive study on the synthesis of peptides within micro reactors, in which multi step reactions may be performed in high overall conversion in much shorter periods of time when compared with batch reactions at the same concentration and temperature.^{4,5} Furthermore, the reduced levels of racemisation in reactions involving α -amino acid derivatives is attributed to the reduced reaction times.⁶

The previous work concentrated on the reaction of a variety of pentafluorophenyl esters of Boc (*tert*-butoxycarbonyl) and Fmoc (9-fluorenylmethoxycarbonyl) protected amino acids within a micro reactor. In all dipeptide-forming reactions it was demonstrated that 100% conversion of the pentafluorophenyl ester to the peptide was achieved with just residual amine still present in the reaction mixture. In this paper we report the on-chip separation of the peptide from the unreacted amine by exploitation of their different electrophoretic mobilities.

The borosilicate glass micro reactors used in this work were fabricated by Micro Chemical Systems Ltd.⁷ In both micro reactor designs the channels had a width and depth of 200 μm and 65 μm respectively. In order to prevent hydrodynamic flow a restriction (3 μm in diameter) was fabricated at the entrance to each channel.⁸ Platinum electrodes were integrated into the reservoirs through the bottom glass plate (Fig. 1). The glass reactor is connected to a MDK™ power supply in order to initiate electrokinetic flow, where the voltages may be controlled either manually or from a computer controlled panel. This modified power supply system (Fig. 1) is advantageous over the previously used assembly^{4,5} as it has a wider range of operating voltages (± 1500 V). Prior to use, the micro reactors were primed with anhydrous *N,N*-dimethylformamide (DMF) to remove air and moisture from the channels.

As mentioned above, peptide bond forming reactions within the micro reactor generally produce a dipeptide contaminated with only residual amounts of amine. Consequently an initial

study was carried out to investigate the electrophoretic separation of peptide **1** from an equal concentration of amine **2** (Dmab is 4- $\{N$ -[1-(4,4-dimethyl-2,6-dioxocyclohexylidene)-3-methylbutylamino]benzyl).



A solution of dipeptide **1** (25 μl , 0.1 M) and amine **2** (25 μl , 0.1 M) dissolved in anhydrous DMF was premixed and placed in reservoir G (ground electrode) of a micro reactor (Fig. 2). Anhydrous DMF (25 μl) was placed in reservoir A, and an external voltage was applied in order to induce electrokinetic flow of the dipeptide **1** from the ground reservoir G to reservoir A (separated by 3 cm). The experiment was conducted at room temperature for a period of 20 minutes (the contents of reservoir A were analysed by HPLC, using a Jupiter C₁₈ 10 μm column, 4.6 \times 250 mm, with a mobile phase composition of 0.1% TFA in water and 0.1% TFA in acetonitrile, using a gradient system of 30% aqueous to 70% aqueous in 20 minutes with a flow rate of 2.5 ml min⁻¹ at room temperature).

When various voltages (Table 1) were applied across the reservoirs, the peptide **1** was found to move from the ground reservoir G to reservoir A, with a corresponding decrease in the volume of DMF in reservoir A and increase in G. We therefore postulate that the DMF is moving from A to G under electroosmotic flow whilst the peptide **1** moves in the opposite direction *via* its electrophoretic mobility. The analysis illustrates that peptide **1** has moved to reservoir A (at the higher voltage) which leads to preconcentration of the amine **2** in reservoir G (ground), which could potentially be recycled in subsequent reactions.

Having demonstrated that it is possible to separate the desired peptide **1** from the amine **2**, a reactor was designed to enable the synthesis of the peptide **1** by reaction of the amine **2** with the pentafluorophenyl (PFP) ester **3** (Scheme 1), followed by subsequent separation within a single device (Fig. 3).

A solution of amine **2** (50 μl , 0.1 M) in DMF was added to reservoir A and a solution of ester **3** (50 μl , 0.1 M) in DMF was



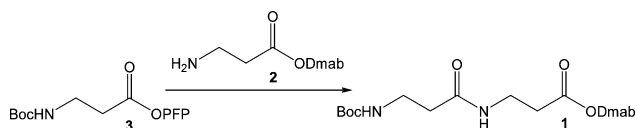
Fig. 2 Micro reactor design for separation.

Table 1 HPLC analysis of **1** and **2** in reservoir A at various voltages

Entry	Voltage/V	Amine (%)	Peptide (%)
1	800	—	100
2	900	—	100
3	1000	—	100
4	1100	—	100
5	1200	—	100
6	1300	—	100
7	1400	—	100
8	1500	—	100



Fig. 1 MDK™ Power supply and micro reactor; electrodes were fabricated within the base plate of the micro reactor.



Scheme 1 Synthesis of dipeptide 1.

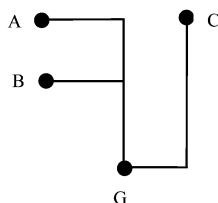


Fig. 3 Micro reactor design for synthesis and separation.

placed in reservoir B and anhydrous DMF (20 μ l) was placed in the ground reservoir G and reservoir C. A continuous voltage of 1000 V and 900 V was applied for 10 min across reservoirs A and B respectively to collect the dipeptide product 1 in reservoir G. HPLC analysis indicated that the peptide was produced in greater than 92% conversion at the ground reservoir. The dipeptide was then electrophoretically mobilised from the ground reservoir G to reservoir C by applying a voltage of 1500 V at reservoir C for a further 10 min to collect the pure dipeptide (Table 2) which showed no trace of any amine 2 or pentafluorophenyl ester 3.

In summary we have reported for the first time a facile method of separating a peptide from a reaction mixture using the reverse electrokinetic flow technique within a micro reactor.

Table 2 HPLC analysis of reservoir C

Entry	Peptide conversion (%)	Reservoir C		
		2 (%)	3 (%)	1 (%)
1	93	0	0	100
2	92	0	0	100
3	96	0	0	100
4	95	0	0	100

We wish to thank Novartis Pharmaceuticals for financial support. We are grateful to Micro Chemical Systems (MCS), Hull for providing the MDK™ power supply and micro reactor.

Notes and references

- P. D. I. Fletcher, S. J. Haswell and V. N. Paunov, *Analyst*, 1999, **124**, 1273.
- P. D. I. Fletcher, S. J. Haswell, E. Pombo-Villar, B. H. Warrington, P. Watts, S. Y. F. Wong and X. Zhang, *Tetrahedron*, 2002, **58**, 4735.
- T. Schwalbe, V. Autze and G. Wille, *Chimia*, 2002, **56**, 636.
- P. Watts, C. Wiles, S. J. Haswell, E. Pombo-Villar and P. Styring, *Chem. Commun.*, 2001, 990.
- P. Watts, C. Wiles, S. J. Haswell and E. Pombo-Villar, *Tetrahedron*, 2002, **58**, 990.
- P. Watts, C. Wiles, S. J. Haswell and E. Pombo-Villar, *Lab. Chip*, 2002, **2**, 141.
- See <http://www.microchemicalsystems.com>.
- P. D. I. Fletcher, S. J. Haswell and X. Zhang, *Lab. Chip*, 2002, **2**, 102.

Solution phase synthesis of esters within a micro reactor

Charlotte Wiles,^a Paul Watts,^a Stephen J. Haswell^{a,*} and Esteban Pombo-Villar^b

^aDepartment of Chemistry, The University of Hull, Cottingham Road, Hull HU6 7RX, UK

^bNovartis Institute for BioMedical Research, WSJ-386.07.15, CH4002 Basel, Switzerland

Received 5 September 2003; revised 24 September 2003; accepted 23 October 2003

Abstract—A range of techniques are demonstrated for the solution phase synthesis of esters within an EOF-based borosilicate glass micro reactor, including the use of mixed anhydrides and the in situ preparation of acyl halides.

© 2003 Elsevier Ltd. All rights reserved.

1. Introduction

Over the past five years, interest in the miniaturisation of chemical synthesis has grown rapidly with the desire to miniaturise being driven by the need for greater process control.¹ Due to the predictable thermal and mass transportation properties observed within a micro reactor a high degree of reaction control is obtained.² Also, the inherently high surface to volume ratio obtained is advantageous, enabling heat generated by exothermic reactions to be dissipated rapidly, reducing the likelihood of thermal runaway. Using an approach referred to as scale-out or numbering-up,³ a reaction is firstly optimised within the laboratory using a single micro reactor and in order to increase production volume, the number of reactors employed is simply increased. Consequently, a reaction is only optimised once and all subsequent reactors are controlled using the same operating conditions, making the technique cost effective, time saving and flexible. With these factors in mind, micro reaction technology is of particular interest to the pharmaceutical industry, where long term objectives include the desire to perform multiple functions such as synthesis, screening, detection and biological evaluation on a single integrated device, resulting in an overall reduction in the time taken to discover new lead compounds and put them into production.⁴

In the context of this paper, a micro reactor is defined as a device containing a series of interconnecting channels formed in a planar substrate, with dimensions in the range of 10–400 μm .⁵ Depending on the application of the device, a range of substrates have been employed,⁶ however due to its compatibility with organic solvents, high mechanical strength, temperature resistance and optical transparency, borosilicate glass is the chosen substrate for the work

described herein. The device consists of a borosilicate glass base plate, containing an etched channel network; and a top block, containing 3 mm drilled holes to form the reagent reservoirs.⁷ Thermal bonding of the two layers affords a sealed micro reactor, with typical dimensions in the range of 2.5 cm \times 2.5 cm \times 2.0 cm (Fig. 1). In order to perform a reaction, reagents are brought together within the micro channel using a suitable pumping mechanism, in this case electroosmotic flow (EOF),⁸ reacted for a specified period of time and the reaction products collected in the product reservoir and analysed using a suitable chromatographic technique. Using this approach, a number of groups have successfully synthesised a range of compounds, including; azo dyes,⁹ stilbene esters,^{10,11} peptides,¹² 1,3-diketones¹³ and α,β -unsaturated carbonyl compounds,¹⁴ demonstrating reduced reaction times, enhanced conversions and reaction stereoselectivity.



Figure 1. A typical borosilicate glass micro reactor.

For many years, functional group incompatibility remained a problem for synthetic chemists, until Emil Fischer¹⁵ developed the notion that an otherwise reactive group could be temporarily rendered inert by the use of a 'protecting group'. In complex systems, such as the synthesis of peptides,¹² there is often a need for more than one protecting group, it is therefore crucial that the groups can be added

Keywords: micro reactor; synthesis; esters.

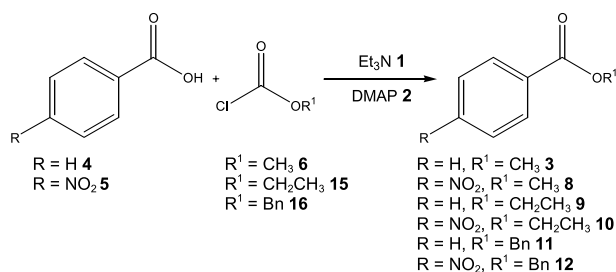
* Corresponding author. Tel.: +44-1-482-465-469; fax: +44-1-482-466-416; e-mail: s.j.haswell@hull.ac.uk

and removed selectively. The widespread use of carboxyl groups in organic synthesis has led to a great deal of work in the field of carboxyl protection.¹⁶ Although many techniques are available within the literature for the transformation of carboxylic acids to esters, there remains a need for mild and rapid techniques that enable the efficient protection of the carboxyl group in base sensitive molecules.¹⁷ Many of the existing techniques however are not suitable for use within an electrokinetic environment due to the extremes of pH (acid/base catalysed) and elevated reaction temperatures employed. Consequently, the catalytic conversion of mixed anhydrides to esters, demonstrated by Kim et al.¹⁸ was of considerable interest, as the reaction was found to proceed rapidly and in high yield, whilst employing mild reaction conditions.

2. Results and discussion

2.1. Use of alkyl chloroformates within a micro reactor

In order to investigate the use of alkyl chloroformates within a micro reactor and highlight any advantages associated with the use of this technique, a series of synthetic standards were prepared and characterised in batch (Scheme 1). The alkyl chloroformate was added to a stirred solution of carboxylic acid and triethylamine **1** at 0°C, after stirring for 5 min DMAP **2** was added (0.5 equiv.) to afford the respective ester. Although the reaction is traditionally performed in DCM, this solvent exhibits no electroosmotic mobility therefore alternative solvent systems were investigated. As solvents such as DMF are incompatible with alkyl chloroformates, prior to transferring the reaction from batch to a micro reactor, the reaction was investigated using anhydrous MeCN. As Table 1 illustrates, comparable conversions were obtained for the preparation of benzoic acid methyl ester **3** in both DCM and MeCN, consequently all synthetic standards were prepared using anhydrous MeCN as solvent.



Scheme 1. Preparation of an array of esters using alkyl chloroformates.

Table 1. Comparison of conversions obtained for the preparation of benzoic acid methyl ester **3** using anhydrous MeCN and DCM

Solvent	Conversion (%)	
	30 min	24 h
DCM	44	67
MeCN	46	69

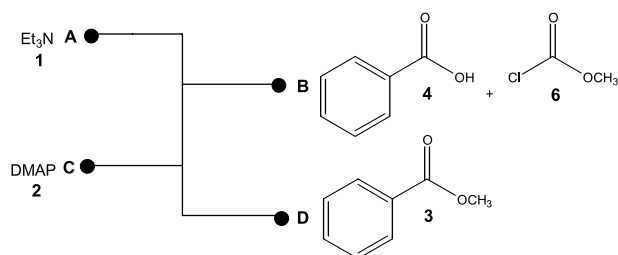
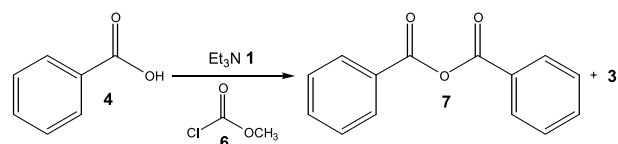


Figure 2. Schematic of the reactor manifold used to synthesise benzoic acid methyl ester **3**.

Using the reaction manifold illustrated in Figure 2, the preparation of benzoic acid methyl ester **3** was investigated within a micro reactor; a standard solution of triethylamine **1** (40 μl , 1.0 M) in anhydrous MeCN was placed in reservoir A, a solution of benzoic acid **4** and methyl chloroformate **6** (40 μl , 1.0 M) in anhydrous MeCN in reservoir B, a solution of DMAP **2** (40 μl , 0.5 M) in anhydrous MeCN in reservoir C and the reaction products collected in anhydrous MeCN in reservoir D over a period of 20 min. The reagents were manipulated within the device using the following applied fields, 276, 400, 318 and 0 V cm^{-1} (A, B, C and D respectively). Analysis of the reaction products by GC–MS illustrated 100% conversion of benzoic acid **4** to the ester **3**.

The reaction was subsequently repeated without DMAP **2** in order to investigate whether or not the ester **3** could be prepared in the absence of a catalyst; a standard solution of triethylamine **1** (40 μl , 1.0 M) in anhydrous MeCN was added to reservoir A, a solution of benzoic acid **4** (40 μl , 1.0 M) in anhydrous MeCN in reservoir B, a solution of methyl chloroformate **6** (40 μl , 1.0 M) in reservoir C and the reaction products were collected in anhydrous MeCN at reservoir D. The reagents were manipulated using the following applied fields, 276, 400, 400 and 0 V cm^{-1} . Although subsequent analysis of the reaction products by GC–MS illustrated ester **3** formation (ca. 20% conversion), the reaction mixture also contained a significant quantity of benzoic anhydride **7** (Scheme 2), a phenomenon previously reported by Kim et al.¹⁹ As a result of this observation, all subsequent micro reactions were performed using 0.5 equiv. of DMAP **2**.



Scheme 2. Preparation of the by-product benzoic anhydride **7**.

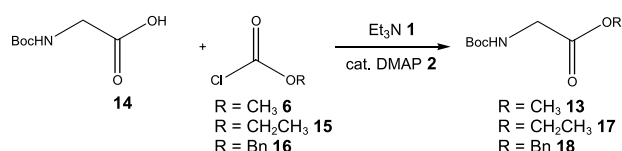
In order to further demonstrate the technique, the preparation of 4-nitrobenzoic acid methyl ester **8** was investigated. A standard solution of triethylamine **1** (40 μl , 0.5 M) in anhydrous MeCN was placed in reservoir A, a solution of 4-nitrobenzoic acid **5** and methyl chloroformate **6** (40 μl , 0.5 M) in anhydrous MeCN in reservoir B, a solution of DMAP **2** (40 μl , 0.25 M) in anhydrous MeCN in reservoir C and the reaction products collected in anhydrous MeCN in reservoir D. The reagents were manipulated within the device using the following applied fields, 345, 400, 455 and 0 V cm^{-1} , to afford 100% conversion of 4-nitrobenzoic acid

Table 2. Comparison of the conversions obtained for the preparation of esters **3–12** in a micro reactor with those in batch

Product No.	Conversion (%)		Applied field ($V\text{ cm}^{-1}$)
	Batch	Micro reaction	
3	67	100	276, 400, 318, 0
8	95	100	345, 400, 455, 0
9	100	95	345, 400, 455, 0
10	93	98	385, 396, 386, 0
11	80	91	345, 200, 455, 0
12	98	100	345, 400, 455, 0

5 to the methyl ester **8**. Using the aforementioned methodology, the technique was extended to the preparation of ethyl esters **9** and **10**, and benzyl esters **11** and **12**. In all cases, compared to the esterification of benzoic acid **4**, reduced reagent concentrations were employed for all 4-nitrobenzoic acid **5** micro reactions due lower reagent solubility in anhydrous MeCN. As [Table 2](#) illustrates, in all cases, comparable conversions were obtained within a micro reactor compared to the batch technique.

As previously mentioned, the protection of the carboxyl group is an important transformation used in the synthesis of peptides, the technique was therefore extended to the preparation of a series of Boc-glycine esters ([Scheme 3](#)). Using the following procedure, Boc-glycine methyl ester **13** was subsequently prepared within a micro reactor; a standard solution of triethylamine **1** (40 μl , 1.0 M) in anhydrous MeCN was placed in reservoir A, a solution of Boc-glycine **14** and methyl chloroformate **6** (40 μl , 1.0 M) in anhydrous MeCN was placed in reservoir B, a solution of DMAP **2** (40 μl , 0.5 M) in anhydrous MeCN in reservoir C and the reaction products collected at reservoir D in anhydrous MeCN. The reagents were manipulated within the device using the following applied fields, 385, 417, 364 and 0 $V\text{ cm}^{-1}$, resulting in 100% conversion of Boc-glycine **14** to Boc-glycine methyl ester **13**. The technique was further exemplified using ethyl chloroformate **15** and benzyl chloroformate **16** to afford the respective ethyl ester **17** and benzyl ester **18** in quantitative conversion. As [Tables 2 and 3](#) illustrate, we have successfully transferred a simple room temperature technique for the preparation of esters from batch to a micro reactor, demonstrating enhanced or equivalent conversions compared to those obtained in

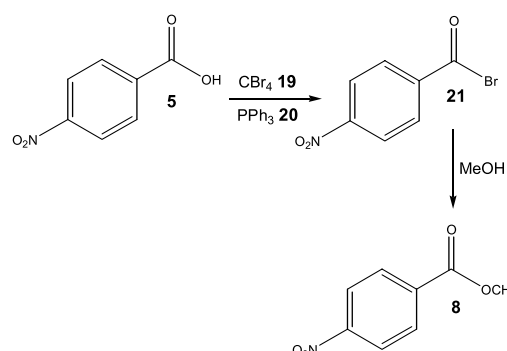
**Scheme 3.** Preparation of Boc-glycine esters **13**, **17** and **18**.**Table 3.** Conversions obtained for the preparation of Boc-glycine esters

Product No.	Conversion (%)		Applied field ($V\text{ cm}^{-1}$)
	Batch	Micro reaction	
13	100	100	385, 417, 364 and 0
17	100	100	385, 417, 364 and 0
18	100	100	385, 417, 364 and 0

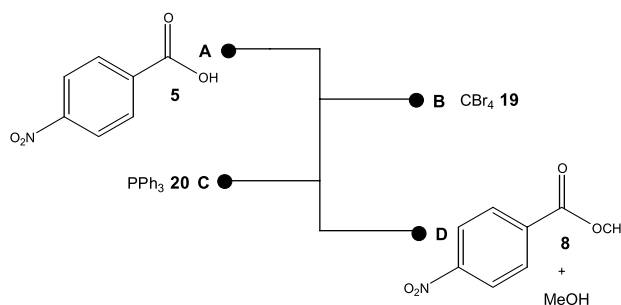
batch. In all cases when employing DMAP **2**, no undesirable anhydride formation was observed.

2.2. In situ preparation of an acyl bromide

Having successfully demonstrated the synthesis of esters via the mixed anhydride approach, the investigation was extended to incorporate the preparation of esters via an acyl halide. As [Scheme 4](#) illustrates, treatment of 4-nitrobenzoic acid **5** with CBr_4 **19**/ PPh_3 **20** (1:2),^{19–21} enabled the preparation of the acyl halide 4-nitrobenzoyl bromide **21**. Subsequent quenching of the acyl bromide **21** with anhydrous MeOH afforded the methyl ester **8** in 100% conversion over the two-step synthesis.

**Scheme 4.** Preparation of an acyl bromide using CBr_4 **19**/ PPh_3 **20**.

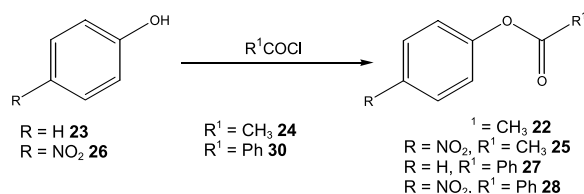
Using the manifold illustrated in [Figure 3](#), the in situ preparation of an acyl halide and subsequent ester formation was investigated. A standard solution of 4-nitrobenzoic acid **5** (40 μl , 0.2 M) in anhydrous MeCN was placed in reservoir A, a solution of CBr_4 **19** (40 μl , 0.2 M) in anhydrous MeCN in reservoir B and a solution of PPh_3 **20** (40 μl , 0.4 M) in anhydrous MeCN in reservoir C. In order to detect the formation of 4-nitrobenzoyl bromide **21** as the methyl ester **8**, the reaction products were collected in anhydrous MeOH at reservoir D. Manipulation of the reagents within the device using the following applied fields, 385, 417, 455 and 0 $V\text{ cm}^{-1}$, resulted in a disappointing 11% conversion to the methyl ester **8** with respect to residual 4-nitrobenzoic acid **5**. The low conversion obtained compared to batch is attributed to the poor electroosmotic flow exhibited by the PPh_3 **20**, therefore in order to improve reagent flow, the concentration of PPh_3 **20** was reduced. Using 0.2 M standard solutions, the reagents were mobilised using the applied fields, 385, 417, 455 and 0 $V\text{ cm}^{-1}$, whereby 6% conversion to the ester **8** was obtained.

**Figure 3.** Schematic of the manifold used for the synthesis of ester **8**.

Although initial studies illustrate poor conversion within the micro reactor (11%), attributed to poor mobilisation of the PPh₃ **20**, further investigations into solvent system, concentration of reagents and pumping mechanism are required in order to fully evaluate the feasibility of this approach within a micro reactor. Alternatively, polymer-supported PPh₃ could be used with the added advantage being that resulting products are free from triphenylphosphine oxide. Through investigating the above parameters, the in situ generation and subsequent reaction of acyl halides should prove to be a synthetically useful transformation within a micro reactor.

2.3. Preparation of phenolic esters within a micro reactor

Phenyl acetate **22** formed via the acetylation of phenol **23**, Scheme 5 is a synthetically useful compound as subsequent Fries rearrangement leads to the pharmaceutically important hydroxyacetophenone.²² Having successfully demonstrated the preparation of esters using the mixed anhydride technique, the investigation was extended to the preparation of phenolic esters. Due to the acidity of the phenolic proton, the preparation of phenolic esters can be performed using relatively mild conditions, therefore having previously demonstrated the mobilisation of triethylamine **1** by EOF, the organic base was again investigated.



Scheme 5. Preparation of a series of phenolic esters.

Using the following procedure, the preparation of acetic acid phenyl ester **22** was investigated; a standard solution of triethylamine **1** (40 μ l, 2.0 M) in anhydrous MeCN was placed in reservoir A, a standard solution of phenol **23** (40 μ l, 2.0 M) in anhydrous MeCN was placed in reservoir B, a solution of acetyl chloride **24** (40 μ l, 2.0 M) in anhydrous MeCN in reservoir C (Fig. 4). The reagents were manipulated within the device using the following applied fields, 345, 400, 364 and 0 V cm⁻¹ and the reaction products collected in anhydrous MeCN at reservoir D. Analysis of the reaction products by GC–MS illustrated 100% conversion of phenol **23** to the ester **22** had occurred.

Having successfully demonstrated the preparation of acetic acid phenyl ester **22**, the preparation of acetic acid 4-nitrophenyl ester **25** was investigated. Again, a standard

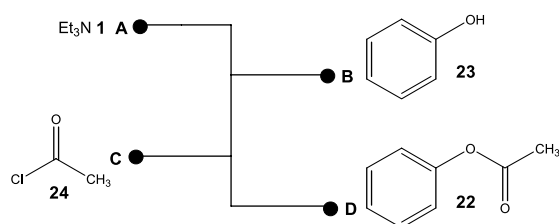


Figure 4. Schematic of the reaction manifold used for the preparation of acetic acid phenyl ester **22**.

Table 4. Conversions obtained for the preparation of phenolic esters

Product No.	Conversion (%)		Applied field (V cm ⁻¹)
	Batch	Micro reaction	
22	93	100	345, 400, 364, 0
25	73	77	345, 375, 455, 0
27	96	100	308, 333, 364, 0
28	74	87	259, 308, 364, 0

solution of triethylamine **1** (40 μ l, 1.0 M) in anhydrous MeCN was placed in reservoir A, a solution of 4-nitrophenol **26** (40 μ l, 1.0 M) in anhydrous MeCN was placed in reservoir B, a solution of acetyl chloride **24** (40 μ l, 1.0 M) in anhydrous MeCN was placed in reservoir C and the reaction products collected in anhydrous MeCN at reservoir D. The reagents were manipulated within the device using the following applied fields, 345, 375, 455 and 0 V cm⁻¹, whereby 77% conversion to the ester **25** was observed (with respect to residual 4-nitrophenol **26**). As the preparation of acetic acid phenyl esters proved successful, the study was extended to the preparation of benzoic acid phenyl esters **27** and **28** whereby 100% and 87% conversion were obtained respectively. As Table 4 illustrates, in all cases, enhancements in conversion were obtained compared to batch.

3. Conclusions

Previous work by Wilson et al.²³ demonstrated catalytic esterification within a heated PDMS/glass micro reactor by incorporating a solid acid catalyst into the channel network. Operating the device at 180°C enabled 35% conversion of a 1:1 ethanol and ethanoic acid solution to ethyl acetate to be obtained using pressure-driven flow. Compared to the work described herein, this approach is disadvantageous, as elevated reaction temperatures are required to enable relatively moderate conversions to be obtained. This investigation therefore focussed on the preparation of an array of esters within a micro reactor at room temperature.

In conclusion we have demonstrated a range of techniques for the preparation of esters within an EOF-based, borosilicate glass micro reactor. With the exception of the in situ preparation of acyl bromides, excellent conversions were obtained for all examples investigated. Further studies are currently underway within our laboratories in order to improve the conversions obtained for the in situ preparation of an acyl halide via the use of diphenyldibromophosphorane and to utilise the chemistry in more complex natural product synthesis.

4. Experimental

4.1. Materials and methods

All solvents were purchased as anhydrous grade over molecular sieves from Fluka Chemie. Reagents (analytical grade) were purchased from Sigma-Aldrich and unless otherwise stated, were used without purification. Nuclear magnetic resonance (NMR) spectra were recorded as

solutions in deuteriochloroform (CDCl_3), using tetramethylsilane (TMS) as an internal standard. The spectra were recorded on a Joel GX400 spectrometer and the chemical shifts are given in parts per million (ppm) with coupling constants in Hertz (Hz). Elemental combustion analyses were performed using a Fisons Carlo Erba EA1108 analyser. Gas Chromatography–Mass Spectrometry data was obtained using a Varian GC (CP-3800) coupled to a Varian MS (2000) with a CP-Sil 8 (30 m) column (Phenomenex) and ultra high purity helium (99.999% Energas) carrier gas. Samples were analysed using the following method, injector temperature 200°C , helium flow rate 1 ml min^{-1} , oven temperature 50°C for 4 min then ramped to 250°C at $30^\circ\text{C min}^{-1}$, with a 3.0 min filament delay.

4.2. Micro reactor methodology

The reactions described herein were carried out using a 4 channel borosilicate glass micro reactor, as illustrated in Figure 2, with channel dimensions of $350\ \mu\text{m}$ (wide) $\times 52\ \mu\text{m}$ (deep) $\times 2.5\ \text{cm}$ (long).^{8,24} In order to minimise the effect of pressure gradients within the micro channels, micro porous silica frits were placed within the channels.²⁵ In order to mobilise reagents by EOF, platinum electrodes (0.5 mm o.d. $\times 2.5\ \text{cm}$) were placed within the reagent reservoirs and voltages applied using a Paragon 3B high voltage power supply (HVPS) (capable of applying 0–1000 V to four pairs of outputs) (Kingfield electronics, Sheffield, UK). Automation of the HVPS using an in-house LabVIEW™ program enabled complex sequences of voltages to be investigated. To enable the results obtained to be applied to devices of different dimensions, voltages are reported as applied fields (V cm^{-1}) i.e. voltage/channel length. In order to monitor the progress of the reaction, experiments were conducted over a period of 20 min, after which the product reservoir was analysed by GC–MS whereby comparison of the amount of product with respect to residual starting material enabled the progression of the reaction to be determined.

4.3. Batch reactions

4.3.1. General procedure for the preparation of esters using alkyl chloroformates. A typical experimental procedure is as follows: Alkyl chloroformate in MeCN (0.5 ml per mmol) was added to a stirred solution of carboxylic acid (1 equiv.) and triethylamine **1** (1 equiv.) in MeCN (0.5 ml per mmol) under N_2 at 0°C . The reaction mixture was stirred for a further 5 min prior to the addition of DMAP **2** (0.5 equiv.) in MeCN (1 ml per mmol). After stirring overnight, the reaction mixture was concentrated in vacuo and the residue diluted with DCM (100 ml). The organic portion was washed with saturated sodium hydrogen carbonate (50 ml) followed by dilute hydrochloric acid (50 ml, 0.1 M). The combined organic extracts were dried (MgSO_4) and concentrated in vacuo to afford the ester. Residual DMAP **2** was subsequently triturated using DCM/hexane, to afford the respective ester.

4.3.2. Benzoic acid methyl ester **3.**²⁶ Using methyl chloroformate **6** (0.16 ml, 2.05 mmol), benzoic acid **4** (0.25 g, 2.05 mmol) and DMAP **2** (0.13 g, 1.0 mmol),

benzoic acid methyl ester **3** was obtained (0.19 g, 68%) as a colourless oil; spectroscopic data as previously reported in the literature.

4.3.3. 4-Nitrobenzoic acid methyl ester **8.**²⁷ Using methyl chloroformate **6** (0.12 ml, 1.50 mmol), 4-nitrobenzoic acid **5** (0.25 g, 1.50 mmol) and DMAP **2** (0.09 g, 0.75 mmol), 4-nitrobenzoic acid methyl ester **8** was obtained (0.26 g, 97%) as a pale yellow solid; spectroscopic data as previously reported in the literature.

4.3.4. Benzoic acid ethyl ester **9.**²⁷ Using ethyl chloroformate **15** (0.20 ml, 2.10 mmol), benzoic acid **4** (0.25 g, 2.10 mmol) and DMAP **2** (0.13 g, 1.05 mmol), benzoic acid ethyl ester **9** was obtained (0.29 g, 95%) as a pale yellow oil; spectroscopic data as previously reported in the literature.

4.3.5. 4-Nitrobenzoic acid ethyl ester **10.**²⁷ Using ethyl chloroformate **15** (0.14 ml, 1.50 mmol), 4-nitrobenzoic acid **5** (0.25 g, 1.50 mmol) and DMAP **2** (0.09 g, 0.75 mmol), 4-nitrobenzoic acid ethyl ester **10** was obtained (0.27 g, 93%) as a yellow solid; spectroscopic data as previously reported in the literature.

4.3.6. Benzoic acid benzyl ester **11.**²⁸ Using benzyl chloroformate **16** (0.29 ml, 2.05 mmol), benzoic acid **4** (0.25 g, 2.05 mmol) and DMAP **2** (0.12 g, 1.0 mmol), benzoic acid benzyl ester **11** was obtained (0.37 g, 85%) as a colourless oil; spectroscopic data as previously reported in the literature.

4.3.7. 4-Nitrobenzoic acid benzyl ester **12.**²⁸ Using benzyl chloroformate **16** (0.21 ml, 1.50 mmol), 4-nitrobenzoic acid **5** (0.25 g, 1.50 mmol) and DMAP **2** (0.09 g, 0.75 mmol), 4-nitrobenzoic acid benzyl ester **12** was obtained (0.35 g, 90%) as a colourless oil; spectroscopic data as previously reported in the literature.

4.3.8. *tert*-Butoxycarbonylaminoacetic acid methyl ester **13.**²⁸ Using methyl chloroformate **6** (0.11 ml, 1.42 mmol), Boc-glycine **14** (0.25 g, 1.42 mmol) and DMAP **2** (0.09 g, 0.71 mmol), the title compound **13** was obtained (0.26 g, 93%) as a colourless oil; spectroscopic data as previously reported in the literature.

4.3.9. *tert*-Butoxycarbonylaminoacetic acid ethyl ester **17.** Using ethyl chloroformate **15** (0.14 ml, 1.42 mmol), Boc-glycine **14** (0.25 g, 1.42 mmol) and DMAP **2** (0.09 g, 0.71 mmol), the title compound **17** was obtained (0.27 g, 93%) as a colourless oil. (Found C, 52.93; H, 8.83; N, 7.03; $\text{C}_9\text{H}_{18}\text{O}_4\text{N}$ requires C, 52.90; H, 8.89; N, 6.86%); δ_{H} (400 MHz, CDCl_3/TMS) 1.28 (3H, t, $J=7.0\ \text{Hz}$, CH_2CH_3), 1.45 (9H, s, $3\times\text{CH}_3$), 3.90 (2H, d, $J=5.6\ \text{Hz}$, NHCH_2CO), 4.21 (2H, q, $J=7.0\ \text{Hz}$, CH_2CH_3) and 5.11 (1H, br s, NH); δ_{C} (100 MHz, CDCl_3/TMS) 14.1 (CH_2CH_3), 28.3 ($3\times\text{CH}_3$), 42.4 ($\text{C}(\text{CH}_3)_3$), 61.3 (CH_2CH_3), 79.9 (NHCH_2CO), 155.7 (CO) and 170.4 (CONH); m/z (E.I.) 204 (M^++1 , 3%), 203 (5), 148 (100) and 104 (15); GC–MS $R_{\text{T}}=5.69\ \text{min}$.

4.3.10. *tert*-Butoxycarbonylaminoacetic acid benzyl ester **18.** Using benzyl chloroformate **16** (0.20 ml, 1.42 mmol), Boc-glycine **14** (0.25 g, 1.42 mmol) and DMAP **2** (0.09 g, 0.71 mmol), the title compound **18** was obtained (0.36 g,

96%) as a colourless oil. (Found C, 63.38; H, 7.42; N, 5.47 C₁₄H₂₀O₄N requires C, 63.14; H, 7.57; N, 5.26%); δ_{H} (400 MHz, CDCl₃/TMS) 1.44 (9H, s, 3×CH₃), 3.95 (2H, d, $J=5.6$ Hz, COCH₂NH), 5.08 (1H, br s, NH), 5.17 (2H, s, CH₂Ph) and 7.36 (5H, m, Ar); δ_{C} (100 MHz, CDCl₃/TMS) 28.3 (3×CH₃), 42.5 (C(CH₃)₃), 67.0 (CH₂Ph), 80.0 (NHCH₂CO), 128.4 (2×CH), 128.5 (2×CH), 128.6 (CH), 135.2 (C₀), 155.7 (CO) and 170.3 (OCONH); m/z (E.I) 266 (M⁺+1, 1%), 265 (1), 256 (75), 166 (100) and 91 (25); GC–MS $R_{\text{T}}=7.56$ min.

4.3.11. Acetic acid phenyl ester 22.²⁹ Purified sodium hydride **29** (0.06 g, 2.33 mmol) in THF (5 ml) was added to a stirred solution of phenol **23** (0.20 g, 2.13 mmol) in THF (20 ml), after stirring at room temperature for 10 min, acetyl chloride **24** (0.17 g, 2.13 mmol) was added; the reaction mixture was stirred for a further 1 h prior to concentrating in vacuo. The aqueous layer was neutralised with sodium hydrogen carbonate (50 ml) and the product extracted into DCM (3×50 ml). The combined organic extracts were dried (MgSO₄) and concentrated in vacuo to afford, after recrystallisation (DCM/hexane), the ester **22** (0.26 g, 90%) as a cream solid; spectroscopic data as reported in the literature.

4.3.12. Acetic acid 4-nitrophenyl ester 25.³⁰ Purified sodium hydride **29** (0.10 g, 3.96 mmol) in THF (5 ml) was added to a stirred solution of 4-nitrophenol **26** (0.50 g, 3.59 mmol) in THF (20 ml), after stirring at room temperature for 10 min, acetyl chloride **24** (0.26 ml, 3.66 mmol) was added. The reaction mixture was stirred for a further 1 h and subsequently concentrated in vacuo, the aqueous layer was neutralised with sodium hydrogen carbonate (50 ml) and the product extracted into DCM (3×50 ml). The combined organic extracts were dried (MgSO₄) and concentrated in vacuo to afford, after recrystallisation (DCM/hexane), acetic acid-4-nitrophenyl ester **25** (0.43 g, 65.0%) as a colourless solid; spectroscopic data as previously reported in the literature.

4.3.13. Benzoic acid phenyl ester 27.²⁹ Purified sodium hydride **29** (0.06 g, 2.33 mmol) was added to a stirred solution of phenol **23** (0.20 g, 2.13 mmol) in THF (2 ml), after stirring at room temperature for 10 min, benzoyl chloride **30** (0.25 ml, 2.15 mmol) was added. The reaction mixture was stirred for 1 h and subsequently concentrated in vacuo, the aqueous layer was neutralised with sodium hydrogen carbonate (50 ml) and the product extracted into DCM (3×50 ml). The combined organic extracts were dried (MgSO₄) and concentrated in vacuo to afford, after recrystallisation (DCM/hexane), the ester **27** (0.41 g, 98%) as a pale yellow solid; spectroscopic data as previously reported in the literature.

4.3.14. Benzoic acid 4-nitrophenyl ester 28.³⁰ Purified sodium hydride **29** (0.10 g, 3.96 mmol) in THF (10 ml) was added to a stirred solution of 4-nitrophenol **26** (0.50 g, 3.59 mmol) in THF (25 ml). The reaction mixture was stirred for 10 min prior to quenching with benzoyl chloride **30** (0.50 g, 3.60 mmol). The reaction mixture was stirred for a further 1 h and subsequently concentrated in vacuo, the aqueous layer was neutralised with sodium hydrogen carbonate (50 ml) and the reaction products extracted into

DCM (3×50 ml). The combined organic extracts were dried (MgSO₄) and concentrated in vacuo to afford, after recrystallisation (DCM/hexane), the ester **28** (0.85 g, 97%) as a cream solid; spectroscopic data as previously reported in the literature.

Acknowledgements

Full financial support provided by Novartis (C.W. and P.W.) is gratefully acknowledged.

References

- Jensen, K. F. *Chem. Eng. Sci.* **2001**, *56*, 293.
- Schwalbe, T.; Volker, A.; Wille, G. *Chimia* **2002**, *56*, 636.
- Ehrfeld, W.; Hessel, V.; Lowe, H. *Microreactors: New Technology for Modern Chemistry*; Wiley-VCH: New York, 2000.
- Fletcher, P. D. I.; Haswell, S. J.; Pombo-Villar, E.; Warrington, B. H.; Watts, P.; Wong, S. Y. F.; Xhang, X. *Tetrahedron* **2002**, *58*, 4735.
- Haswell, S. J.; Middleton, R. J.; O'Sullivan, B.; Skelton, V.; Watts, P.; Styring, P. *J. Chem. Soc., Chem. Commun.* **2001**, 391.
- Duffy, D. C.; McDonald, J. C.; Schueller, O. J. A.; Whitesides, G. M. *Anal. Chem.* **1998**, *70*, 4974.
- McCreeady, T. *Anal. Chim. Acta* **2001**, *427*, 39.
- Fletcher, P. D. I.; Haswell, S. J.; Paunov, V. N. *Analyst* **1999**, *124*, 1273.
- Salimi-Moosavi, H.; Tang, T.; Harrison, D. J. *J. Am. Chem. Soc.* **1997**, *68*, 2515.
- Skelton, V.; Greenway, G. M.; Haswell, S. J.; Styring, P.; Morgan, D. O.; Warrington, B. H.; Wong, S. Y. F. *Analyst* **2001**, *126*, 7.
- Skelton, V.; Greenway, G. M.; Haswell, S. J.; Styring, P.; Morgan, D. O.; Warrington, B. H.; Wong, S. Y. F. *Analyst* **2001**, *126*, 11.
- Watts, P.; Wiles, C.; Haswell, S. J.; Pombo-Villar, E. *Tetrahedron* **2002**, *58*, 5427.
- Wiles, C.; Watts, P.; Haswell, S. J.; Pombo-Villar, E. *J. Chem. Soc., Chem. Commun.* **2002**, 1034.
- Wiles, C.; Watts, P.; Haswell, S. J.; Pombo-Villar, E. *Lab Chip* **2002**, *2*, 62.
- Kocienski, P. J. *Protecting Groups*; Wiley: New York, 1994.
- Haslam, E. *Tetrahedron* **1980**, *36*, 2409.
- Pizey, J. S. *Synthetic Reagents*; Wiley: New York, 1974; Vol. 2. p 65.
- Kim, S.; Kim, Y. C.; Lee, J. I. *Tetrahedron Lett.* **1983**, *24*, 3365.
- Posner, G. H.; Loomis, G. L.; Sawaya, H. S. *Tetrahedron Lett.* **1975**, *16*, 1373.
- Rabinowitz, R.; Marcus, R. *J. Am. Chem. Soc.* **1962**, *84*, 1312.
- Gavina, F.; Luis, S. V.; Ferrer, P.; Costero, A. M.; Alberto Marco, J. J. *J. Chem. Soc., Chem. Commun.* **1985**, 296.
- Olah, G. H.; Grant, J. L.; Westerman, P. W. *J. Org. Chem.* **1975**, *40*, 2103.
- McCreeady, T.; Wilson, N. G. *Analyst* **2001**, *126*, 21.
- Broadwell, I.; Fletcher, P. D. I.; Haswell, S. J.; McCreeady, T.; Zhang, X. *Lab Chip* **2001**, *1*, 66.

25. Christensen, P. D.; Johnson, S. W. P.; McCreedy, T.; Skelton, V.; Wilson, N. G. *Anal. Commun.* **1998**, 35, 341.
26. Johnstone, R. A. W.; Price, P. J. *Tetrahedron* **1985**, 41, 2493.
27. Hans, J. J.; Driver, R. W.; Burke, S. D. *J. Org. Chem.* **2000**, 65, 2114.
28. Matt, T.; Seebach, D. *Helv. Chim. Acta* **1998**, 81, 1845.
29. Bradamate, S.; Pagani, G. A. *J. Org. Chem.* **1980**, 45, 114.
30. Highet, R. J.; Highet, P. F. *J. Org. Chem.* **1965**, 30, 902.

The Application of Microreactor Technology for the Synthesis of 1,2-Azoles

Charlotte Wiles, Paul Watts, and Stephen J. Haswell*

Department of Chemistry, The University of Hull, Cottingham Road, Hull HU6 7RX, UK

Esteban Pombo-Villar

Novartis Institute for BioMedical Research, WSJ-386.07.15, CH4002 Basel, Switzerland

Abstract:

We demonstrate the successful synthesis of an array of 1,2-azoles within a borosilicate glass microreactor whereby conversions in the range of 98–100% were obtained. In terms of large-scale production, this corresponds to 0.339 g day^{-1} per microreactor when employing reagent concentrations of 1.0 M.

Introduction

Current production technology is based on the scale-up of successful lab-scale reactions in order to achieve large-scale production. This approach is however fundamentally flawed as at each stage of the scale-up, modifications made to the reactor vessel result in changes to the surface-to-volume ratio, which in turn have a profound effect on thermal and mass-transport properties of the reaction. As a result of these variations it is often necessary to re-optimize the process at each stage of the scale-up process. Consequently, the route from bench to production is both costly and time-consuming. It is therefore postulated that through the application of microreaction technology, the transfer of reactions from the laboratory to production will be both rapid and cost-effective.

The desire to miniaturise chemical synthesis has been driven by the need for greater process control as a means of increasing not only product purity but also reactor safety.¹ Using an approach referred to as scale-out or numbering-up,² a reaction is first optimised within the laboratory using a single microreactor, and to increase production volume, the number of reactors employed is simply increased. Consequently, a reaction is only optimised once, and all subsequent reactors are controlled using the same operating conditions. This approach is therefore both cost-effective, time saving, and flexible, enabling changes in production volume by simply increasing or decreasing the number of reactors employed. With these factors in mind, microreaction technology is of particular interest to the pharmaceutical industry, where long-term objectives include the desire to perform multiple functions such as synthesis, screening, detection, and biological evaluation within a single integrated device, resulting in an overall reduction in the time taken to discover new lead compounds and put them into production.

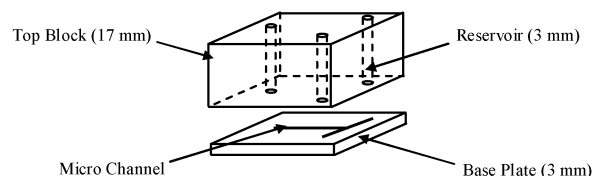


Figure 1. Exploded view of a borosilicate glass microreactor.

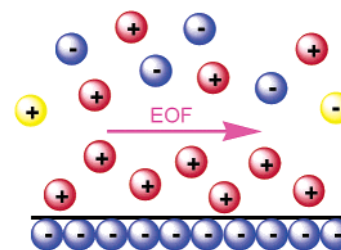


Figure 2. Schematic illustrating the principle of electroosmotic flow.

Microreactors. In the context of this paper, a microreactor is defined as a device containing a series of interconnecting channels formed in a planar substrate, with dimensions in the range $10\text{--}400 \mu\text{m}$. Microreactors may be fabricated from glass, quartz, ceramics, polymers, and metals; however, due to its compatibility with organic solvents, high mechanical strength, temperature resistance, and optical transparency, borosilicate glass is the chosen substrate for the work described herein. As Figure 1 illustrates, the microreactor consists of a borosilicate glass base plate, containing an etched channel network, and a top block, containing the reagent reservoirs. Thermal bonding of the two layers affords a sealed microreactor, with typical dimensions in the range of $2.5 \text{ cm} \times 2.5 \text{ cm} \times 2.0 \text{ cm}$.³

To perform a reaction, reagents are brought together within the microchannel using a suitable pumping mechanism, reacted for a specified period of time, collected in the product reservoir, and analysed using a suitable technique. Although examples of pressure-driven systems have been reported within the literature, owing to its simplicity, the technique of electroosmotic flow (EOF) is frequently employed.⁴ As Figure 2 illustrates, when an ionisable surface such as glass, quartz, or Teflon comes in contact with a suitable solvent system, the surface is neutralised with a diffuse layer of positive ions from the bulk liquid. A

(1) Jensen, K. F. *Chem. Eng. Sci.* **2001**, *56*, 293.

(2) Ehrfeld, W.; Hessel, V.; Lowe, H. *Microreactors: New Technology for Modern Chemistry*; Wiley-VCH: New York, 2000.

(3) McCreedy, T. *Anal. Chim. Acta* **2001**, *427*, 39.

(4) Fletcher, P. D. I.; Haswell, S. J.; Paunov, V. N. *Analyst* **1999**, *124*, 1273.

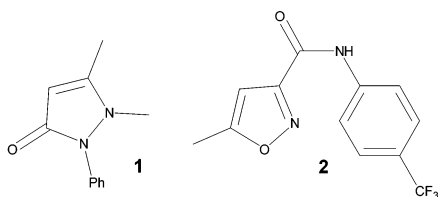


Figure 3. Some heterocyclic compounds of pharmaceutical interest.

proportion of the counterions are adsorbed onto the surface, resulting in the formation of an immobile layer, and the remaining positive ions form a transient double layer. Application of an electric field causes the double layer to move towards the negative electrode, inducing bulk flow within the microchannel.

With respect to fluidic manipulation, the use of EOF is advantageous as it is easy to use, requires no mechanical parts, enables reproducible pulse-free flow, and generates minimal backpressure. Therefore, with respect to scale-out, the technique is advantageous as multiple reagent streams can be controlled by a single power supply, maintaining the simplicity of the technique.

Advantages of Miniaturisation. As previously mentioned, the main advantage associated with the miniaturisation of chemical synthesis is the increased reactor control obtained, owing to the predictable thermal and mass transportation properties observed within the laminar flow environment.

In traditional large-scale reactor vessels, fluctuations in temperature are difficult to correct as any alterations made take time to have an effect on the system as a whole. In comparison, changes on the microscale are observed almost immediately. Along with increasing the rate of thermal mixing, decreasing the reactor dimensions results in an inherently high surface-to-volume ratio. Consequently, heat generated by exothermic reactions can be dissipated rapidly, reducing the likelihood of thermal runaway or hot-spot formation. As a result of the uniform reactor conditions obtained, a high degree of reaction control is observed.⁵ Previous work has successfully demonstrated the ability to synthesise a range of compounds within an EOF-based microreactor including azo dyes, stilbene esters, peptides, 1,3-diketones and α,β -unsaturated carbonyl compounds, demonstrating both reduced reaction times and enhanced conversions compared to those observed in batch.⁶

1,2-Azole Synthesis. Heterocyclic compounds represent an important group of organic compounds, with many of them exhibiting significant biological activity, including anti-rheumatic agents such as antipyrine, **1**, and leflunomide, **2** (Arava) (Figure 3). To compare the use of a microreactor with traditional batch techniques, the reactions were initially performed in batch, enabling the products to be characterised.

Results and Discussion

As Scheme 1 illustrates, treatment of a 1,3-diketone with hydrazine monohydrate **3** (1.1 equivalents) in THF affords

Scheme 1. General reaction scheme illustrating the preparation of a series of 1,2-azoles

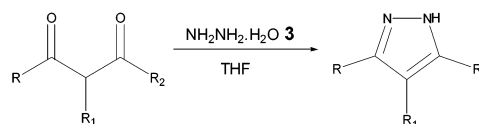


Table 1. Summary of the conversions obtained for the batch-scale preparation of 1,2-azoles 4–8

product no.	R–	R ₁ –	R ₂ –	conversion/% ^a
4	CH ₃	H	CH ₃	62
5	Ph	H	CH ₃	63
6	–(CH ₂) ₄ –		Ph	72
7	Ph	H	Ph	64
8	Ph	CH ₃	CH ₃	71

^a Conversion based on GC–MS analysis of the crude reaction mixture after 1 h.

the respective 1,2-azoles **4–8** in excellent yield within a batch reaction. Using this methodology, a series of synthetic standards were prepared, representing synthetic targets for preparation within a microreactor. Analysis of the crude reaction mixture by GC–MS enabled the proportion of 1,2-azole to be determined with respect to residual 1,3-diketone i.e. percent conversion (Table 1).

Using the experimental setup illustrated in Figure 4, the preparation of 3,5-dimethyl-1*H*-pyrazole, **4**, was initially investigated by using the solvent system THF. A standard solution of 2,4-pentanedione **9** (40 μ L, 0.1 M) in THF was placed in reservoir A, a solution of hydrazine monohydrate **3** (40 μ L, 0.1 M) in THF was placed in reservoir B, and the reaction products were collected in THF at reservoir C. The reagents were manipulated within the device using the following applied fields, 292, 318, and 0 V cm⁻¹ (A, B, and C respectively); analysis of the reaction products by GC–MS demonstrated 100% conversion of the 1,3-diketone **9** to 3,5-dimethyl-1*H*-pyrazole, **4**. The reaction was subsequently repeated using the solvent system DMF, whereby application of the following applied fields, 318, 318, and 0 V cm⁻¹ again resulted in quantitative conversion to pyrazole **4**. The use of different applied fields compared to those employed for THF is attributed to the different physical properties exhibited by the solvents and hence slightly different electroosmotic mobilities.⁷

To increase the volume of product synthesised, the reagent concentrations were increased by a factor of 10; a standard solution of 1-phenylbutane-1,3-dione **10** (40 μ L, 1.0 M) in THF was placed in reservoir A and a solution of hydrazine monohydrate **3** (40 μ L, 1.0 M) in THF in reservoir B; the reaction products were collected in THF at reservoir C. The reagents were manipulated within the device using the following applied fields, 364, 341, and 0 V cm⁻¹, resulting in quantitative conversion of the 1,3-diketone **10** to 3-methyl-5-phenyl-1*H*-pyrazole, **5**. Using the same reaction conditions, the reaction was repeated in DMF, whereby 100% conversion to the pyrazole **5** was again obtained. The reaction was subsequently repeated using the diketones, 2-benzoylcyclo-

(5) Schwalbe, T.; Volker, A.; Wille, G. *Chimia* **2002**, *56*, 636.

(6) Fletcher, P. D. I.; Haswell, S. J.; Pombo-Villar, E.; Warrington, B. H.; Watts, P.; Wong, S. Y. F.; Zhang, X. *Tetrahedron* **2002**, *58*, 4735.

(7) Rice, C. L.; Whitehead, R. *J. Phys. Chem.* **1965**, *69*, 4017.

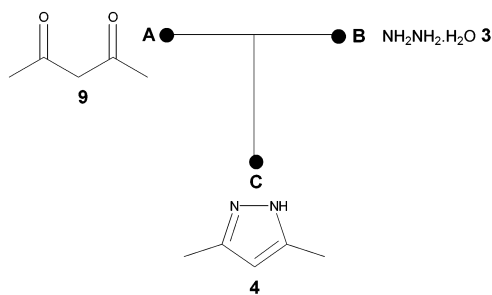


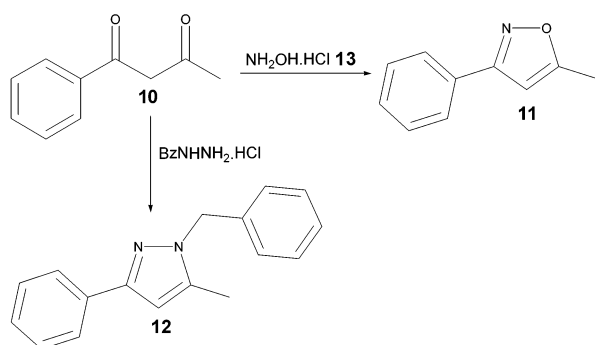
Figure 4. Schematic of the microreactor used to synthesize 1,2-azoles.

Table 2. Comparison of the conversions obtained for the preparation of 1,2-azoles 4–12 in batch and a microreactor

product no.	conversion/%		applied field/V cm ⁻¹
	batch	microreactor	
4	62	100 ^a (100) ^a	292, 318, and 0
5	63	100 ^a (100) ^a	364, 341, and 0
6	72	100 ^a	260, 303, and 0
7	64	100 ^a	386, 364, and 0
8	71	98 ^a	409, 386, and 0
11	52	98 ^a	292, 318, and 0
12	76	42 ^a (100) ^c	364, 341, and 0

^a Reaction performed using THF. ^b Reaction performed using DMF. ^c Reaction performed using stopped flow regime.

Scheme 2. Preparation of an isoxazole 11 and a substituted pyrazole 12



hexanone, 1,3-diphenylpropane-1,3-dione, and 2-methyl-1-phenylbutane-1,3-dione to afford 3-phenyl-4,5,6,7-tetrahydro-2*H*-indazole 6, 3,5-diphenyl-1*H*-pyrazole 7, and 3,4-dimethyl-5-phenyl-1*H*-pyrazole 8 in 100, 100, and 98% conversion respectively (Table 2).

Having successfully demonstrated the preparation of an array of pyrazoles, the technique was extended to the synthesis of an isoxazole 11 and a substituted pyrazole 12 (Scheme 2). A standard solution of 1-phenylbutane-1,3-dione 10 (40 μ L, 1.0 M) in THF was placed in reservoir A and a solution of hydroxylamine hydrochloride 13 (40 μ L, 1.0 M) in THF in reservoir B, and the reaction products were collected in reservoir C. Manipulation of the reagents using the following applied fields, 296, 409, and 0 V cm⁻¹ resulted in 98% conversion to 5-methyl-3-phenylisoxazole 11.

Using the following procedure, the substituted pyrazole, 1-benzyl-3-methyl-5-phenyl-1*H*-pyrazole 12, was synthesised within a microreactor. A standard solution of phen-

ylbutane-1,3-dione 10 (40 μ L, 1.0 M) in THF was placed in reservoir A and a solution of benzyl hydrazine hydrochloride 14 (40 μ L, 1.0 M) in THF in reservoir B, and the reaction products were collected in reservoir C. Manipulation of the reagents using the following applied fields, 318, 318, and 0 V cm⁻¹ resulted in 42% conversion to pyrazole 12. This was later increased to 100% by employing a stopped-flow regime. The technique involved the application of a field for 2.5 s and no field for 5.0 s; these steps were subsequently repeated over a period of 20 min and served to increase the reagents' residence time within the device (Table 2).⁸

As Table 2 illustrates, compared to traditional batch techniques, the use of a microreactor is advantageous because not only are excellent conversions obtained in all cases, but the reaction times involved are also decreased from typically hours to seconds.

Since conducting this investigation, Garcia-Egido et al.⁹ demonstrated the preparation of a pyrazole library (21 compounds) within a pressure-driven system. The authors employed a serpentine reactor, with channel dimensions in the range of 100 μ m \times 25 μ m \times 3 m, coupled to an LC–UV–MS. To prepare an array of compounds, 2.5 μ L slugs of reagent were introduced into the device at 1 μ L min⁻¹ and mobilised throughout the channel network using methanol as the driving solvent. Using 0.01 M diketone and 0.8 M hydrazine monohydrate 3 solutions and a residence time of 210 s enabled the sequential preparation of a range of pyrazoles in moderate to high conversion (35–99%). However, compared to the system discussed herein, the pressure-driven approach is disadvantageous as the device is relatively large (6 \times 2.5 cm), the reaction requires a lengthy equilibration time (10 min) to ensure stable flow, and the reactions are performed using 81 equiv of hydrazine monohydrate 3. Although the quantities of reagents employed are reduced due to the desire to prepare small quantities of each compound, the use of an 81-fold excess of hydrazine monohydrate 3 is unnecessary with respect to both product purification and environmental concerns, i.e., disposal.

Using the preparation of 5-methyl-3-phenylisoxazole 11 as a model and employing 1.0 M standard solutions, the EOF-based device can synthesise 0.339 g day⁻¹ (based on 98% conversion and an average flow rate of 1.5 μ L min⁻¹). Therefore, if 1000 microreactors were operated in parallel, 339.0 g day⁻¹ could be synthesised, compared to the pressure-driven system whereby 2.5 \times 10⁻⁶ g of product is prepared per 2.5 μ L aliquot injected. Therefore, if only a small amount of compound is required for biological evaluation, devices of the kind used by Garcia-Egido et al.⁹ can be employed as a means of preparing a large number of samples, i.e., libraries, in a short period of time. Alternatively the approach of scale-out can be employed as a means of preparing fine chemicals or pharmaceuticals on a large-scale, demonstrating the flexibility associated with microreaction technology.

(8) Wiles, C.; Watts, P.; Haswell, S. J.; Pombo-Villar, E. *Lab Chip* 2002, 2, 62.

(9) Garcia-Egido, E.; Spikmans, V.; Wong, S. Y. F.; Warrington, B. H. *Lab Chip* 2003, 3, 73.

Summary

In conclusion, we have demonstrated a simple, stoichiometric technique for the preparation of an array of 1,2-azoles within an EOF-based microreactor, whereby excellent conversions were obtained in all cases.

Experimental Section

Materials and Methods. All materials (analytical grade) were purchased from Aldrich and were used without purification. All NMR spectra were recorded as solutions in deuteriochloroform (CDCl_3) using tetramethylsilane (TMS) as an internal standard. The spectra were recorded on a Joel GX400 spectrometer and the chemical shifts given in parts per million (ppm) with coupling constants in Hertz (Hz). The following abbreviations are used to report NMR data: s = singlet, d = doublet, t = triplet, br s = broad singlet, m = multiplet, and C_0 = quaternary carbon. Gas chromatography–mass spectrometry (GC–MS) was performed using a Varian GC (CP-3800) coupled to a Varian MS (2000) with a CP-Sil 8 (30 m) column (Phenomenex) and ultrahigh purity helium (99.999%, Energas) carrier gas. Samples were analysed using the following method: injector temperature 200 °C, helium flow rate 1 mL min^{-1} , oven temperature 50 °C for 4 min and then ramped to 250 °C at 30 °C min^{-1} , with a 3.0 min filament delay.

Microreactor Methodology. The reactions described herein were carried out using a three-channel microreactor, as illustrated in Figure 1, with channel dimensions of 350 μm (wide) \times 52 μm (deep) \times 2.5 cm (long).¹⁰ To minimise the effect of pressure gradients within the microchannels, microporous silica frits were placed within the channels.¹¹ To mobilise reagents by EOF, platinum electrodes (0.5 mm o.d. \times 2.5 cm) were placed within the reagent reservoirs and voltages applied using a Paragon 3B high-voltage power supply (HVPS) (capable of applying 0–1000 V to four pairs of outputs) (Kingfield Electronics). Automation of the HVPS using an in-house LabVIEW program enabled complex sequences of voltages to be investigated. To enable the results obtained to be applied to devices of different dimensions, voltages are reported as applied fields (V cm^{-1}), i.e. voltage/channel length. To monitor the progress of the reaction, experiments were conducted over a period of 20 min, after which the product reservoir was analysed by GC–MS, whereby comparison of the amount of product with respect to residual starting material enabled the progression of the reaction to be determined.

General Procedure for the Preparation of 1,2-Azoles in Batch. A typical experimental procedure was as follows: Hydrazine monohydrate **3** (1.1 equiv) in THF (2 mL mmol^{-1}) was added via a syringe to a stirred solution of 1,3-diketone in THF (2 mL mmol^{-1}) over a period of 30 min. After stirring overnight, the reaction mixture was concentrated in vacuo prior to the addition of water (50 mL), and the reaction products were extracted into ethyl acetate (3 \times 50 mL). The

combined extracts were dried (MgSO_4) and concentrated in vacuo, whereby purification by silica gel chromatography (7–10% ethyl acetate in hexane) afforded the respective 1,2-azole.

3,5-Dimethyl-1H-pyrazole (4):¹² (0.48 g, 100%) as a pale yellow solid; δ_{H} (400 MHz, CDCl_3/TMS) 2.19 (6H, s, 2 \times CH_3), 5.75 (1H, s, CH), and 7.25 (1H, br s, NH); δ_{C} (100 MHz, CDCl_3/TMS) 12.2 (2 \times CH_3), 104.0 (CH), and 144.4 (2 \times CN); m/z (EI) 97 ($\text{M}^+ + 1$, 100%) and 96 (5); GC–MS retention time $R_{\text{T}} = 7.35$ min.

3-Methyl-5-phenyl-1H-pyrazole (5):¹³ (0.49 g, 100%) as a pale yellow solid; δ_{H} (400 MHz, CDCl_3/TMS) 2.35 (3H, s, CH_3), 6.36 (1H, s, CH), and 7.29–7.62 (5H, m, Ar) (NH not observed); δ_{C} (100 MHz, CDCl_3/TMS) 11.8 (CH_3), 102.2 (CH), 125.7 (CH), 127.0 (2 \times CH), 128.0 (CH), 128.6 (CH), 132.3 (C_0), 143.2 (CNCH₃), and 149.9 (CN); m/z (EI) 159 ($\text{M}^+ + 1$, 75%), 158 (100), and 77 (5); GC–MS retention time $R_{\text{T}} = 10.43$ min.

3-Phenyl-4,5,6,7-tetrahydro-2H-indazole (6):¹⁴ (0.49 g, 94%) as a pale yellow oil; δ_{H} (400 MHz, CDCl_3/TMS) 1.85 (4H, m, 2 \times CH_2), 2.74 (2H, t, J 5.7, CH_2), 2.86 (2H, t, J 5.7, CH_2), 7.46 (3H, m, Ar), 7.80 (2H, m, Ar), and 12.14 (1H, br s, NH); δ_{C} (100 MHz, CDCl_3/TMS) 21.4 (3 \times CH_2), 22.7 (CH_2), 114.4 (C_0), 127.5 (C_0), 127.6 (2 \times CH), 129.2 (2 \times CH), 129.9 (CH), 142.4 (CN), and 145.4 (CN); m/z (EI) 199 ($\text{M}^+ + 1$, 100%), 198 (5), and 170 (10); GC–MS retention time $R_{\text{T}} = 12.71$ min.

3,5-Diphenyl-1H-pyrazole (7):¹³ (0.42 g, 86%) as a pale yellow solid; δ_{H} (400 MHz, CDCl_3/TMS) 7.13 (1H, s, CH), 7.49 (6H, m, Ar), 7.96 (4H, m, Ar), and 9.96 (1H, br s, NH); δ_{C} (100 MHz, CDCl_3/TMS) 100.2 (CH), 126.0 (4 \times CH), 127.6 (2 \times C_0), 128.6 (4 \times CH), 129.3 (2 \times CH), and 147.0 (2 \times CN); m/z (EI) 221 ($\text{M}^+ + 1$, 20%), 220 (100), and 77 (25); GC–MS retention time $R_{\text{T}} = 14.98$ min.

3,4-Dimethyl-5-phenyl-1H-pyrazole (8):¹⁵ (0.45 g, 93%) as a pale yellow solid; δ_{H} (400 MHz, CDCl_3/TMS) 2.13 (3H, s, CH_3), 2.25 (3H, s, CH_3), 7.22 (3H, m, Ar), 7.32 (2H, m, Ar), and 18.29 (1H, s, NH); δ_{C} (100 MHz, CDCl_3/TMS) 10.9 (CH_3), 31.4 (CH_3), 127.4 (2 \times CH), 127.9 (2 \times CH), 128.7 (CH), 130.9 (C_0), 141.9 (CNCH₃), and 146.8 (CN); m/z (EI) 173 ($\text{M}^+ + 1$, 70%), 172 (100), and 77 (15); GC–MS retention time $R_{\text{T}} = 10.72$ min.

5-Methyl-3-phenylisoxazole (11).¹⁶ Hydroxylamine hydrochloride **13** (0.21 g, 3.09 mmol) was dissolved in THF (10 mL) and added dropwise to a stirred solution of 1-phenylbutane-1,3-dione **10** (0.50 g, 3.09 mmol) in THF (10 mL). After stirring overnight, the reaction mixture was concentrated in vacuo prior to the addition of water (50 mL), and the reaction products were extracted into ethyl acetate (3 \times 50 mL). The combined organic extracts were dried (MgSO_4), concentrated in vacuo, and purified by silica gel chromatography. Elution with 10% ethyl acetate in hexane

(10) Broadwell, I.; Fletcher, P. D. I.; Haswell, S. J.; McCreedy, T.; Zhang, X. *Lab Chip* **2001**, *1*, 66.

(11) Christensen, P. D.; Johnson, S. W. P.; McCreedy, T.; Skelton, V.; Wilson, N. G. *Anal. Chem.* **1963**, *35*, 341.

(12) Barluenga, J.; Muniz, L.; Iglesias, M. J.; Gotor, V. *J. Chem. Soc., Perkin Trans. 1* **1984**, 611.

(13) Texier-Boullet, F.; Klein, B.; Hamelin, J. *Synthesis* **1986**, 409.

(14) Bunnelle, W. H.; Singam, P. R.; Narayanan, B. A.; Bradshaw, C. W.; Liou, J. S. *Synthesis* **1997**, 439.

(15) Tensmeyer, L. G.; Ainsworth, C. *J. Org. Chem.* **1996**, *31*, 1878.

(16) Werner, A.; Sanchez-Migallon, A.; Fruchier, A.; Elguero, J.; Fernandez-Castano, C.; Foces-Foces, C. *Tetrahedron* **1995**, *51*, 4779.

afforded 5-methyl-3-phenylisoxazole **11** (0.46 g, 93%) as a pale yellow solid; δ_{H} (400 MHz, CDCl_3/TMS) 2.34 (3H, s, CH_3), 6.35 (1H, s, CH), 7.42 (3H, m, Ar), and 7.74 (2H, m, Ar); δ_{C} (100 MHz, CDCl_3/TMS) 11.5 (CH_3), 100.2 (CH), 125.7 (2 \times CH), 127.6 (C_0), 128.9 (2 \times CH), 130.0 (CH), 160.34 (CN), and 169.6 (CO); m/z (EI) 160 ($\text{M}^+ + 1$, 30%), 159 (100), 105 (50), and 77 (10); GC–MS retention time, $R_{\text{T}} = 9.56$ min.

1-Benzyl-3-methyl-5-phenyl-1H-pyrazole (12).¹⁷ Benzyl hydrazine hydrochloride **14** (0.61 g, 3.09 mmol) was dissolved in THF (10 mL) and added dropwise to a stirred solution of 1-phenylbutane-1,3-dione **10** (0.50 g, 3.09 mmol) in THF (10 mL). After stirring overnight, the reaction mixture was concentrated in vacuo prior to the addition of water (50 mL), and the reaction products were extracted into ethyl acetate (3 \times 50 mL). The combined organic extracts were

(17) Bromilow, J.; Brownlee, R. T. C.; Craik, D. J.; Sadek, M.; Taft, R. W. *J. Org. Chem.* **1980**, *45*, 2429.

dried (MgSO_4), concentrated in vacuo, and subsequently purified by silica gel chromatography. Elution with 7% ethyl acetate in hexane afforded 1-benzyl-3-methyl-5-phenyl-1H-pyrazole **12** (0.74 g, 97%) as a pale yellow oil; δ_{H} (400 MHz, CDCl_3/TMS) 2.34 (3H, s, CH_3), 5.28 (2H, s, CH_2), 6.14 (1H, s, CH), 7.03 (2H, m, Ar), and 7.22–7.38 (8H, m, Ar); δ_{C} (100 MHz, CDCl_3/TMS) 13.7 (CH_3), 52.2 (CH_2), 106.2 (CH), 126.7 (2 \times CH), 127.1 (CH), 127.8 (4 \times CH), 128.2 (3 \times CH), 130.9 (C_0), 132.4 (C_0), 145.0 (CN), and 148.4 (CN); m/z (EI) 249 ($\text{M}^+ + 1$, 100%), 248 (20), 91 (15), and 77 (10); GC–MS retention time, $R_{\text{T}} = 12.02$ min.

Acknowledgment

Full financial support provided by Novartis (C.W. and P.W.) is gratefully acknowledged.

Received for review September 3, 2003.

OP034125A

Microwave heating of heterogeneously catalysed Suzuki reactions in a micro reactor

Ping He, Stephen J. Haswell* and Paul D. I. Fletcher

Department of Chemistry, The University of Hull, Hull, UK HU6 7RX.

E-mail: S.J.Haswell@hull.ac.uk

Received 17th October 2003, Accepted 5th November 2003

First published as an Advance Article on the web 2nd December 2003



The Suzuki cross-coupling reaction of aryl halides with phenylboronic acid to form biaryls has been used to illustrate the development of a microwave based technique capable of delivering heat locally to a heterogeneous Pd-supported catalyst located within a micro reactor device. A 10–15 nm gold film patch, located on the outside surface of the base of a glass micro reactor, was found to efficiently assist in the heating of the catalyst when irradiated with 5–7 W of microwave power at 2.45 GHz. Using a hydrodynamically pumped system, reactant–catalyst contact times of less than 60 s were found to give conversions for different substrates which were in the range 50–99%. Two methods of loading catalysts into the micro reactor were investigated which required either 1.5 or 6 mg of material.

Introduction

To date the majority of liquid based chemical syntheses carried out in lab-on-a-chip micro reactors have involved homogeneous reactions performed at room temperature.¹ As discussed in ref. 1, the ability to spatially control localized concentrations of reactant, intermediates and products within the micro-channel networks of micro reactors enables a level of reaction control (including rates, yields and product selectivities) which is not achievable in bulk reactors where concentrations are generally uniform. In addition to the control of local concentrations, the ability to deliver localized heating^{2–3} and the more effective use of *in situ* supported reagents such as catalysts would add a further dimension of reaction control and hence extend the range of potential applications of micro reactors. Accordingly, in this paper we describe a microwave (MW) based localized heating technique used in conjunction with an immobilized palladium catalyst to perform a number of exemplary Suzuki based reactions⁴ within a hydrodynamically pumped micro reactor.

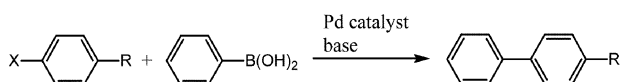
The palladium-catalyzed cross coupling of aryl halides with aryl boronic acids was selected for this study because of its relevance as a popular method for the selective formation of carbon–carbon bonds^{4–5} (see Scheme 1). Such Suzuki reactions are commonly performed using a homogeneous soluble palladium catalyst, however, recovery of such homogeneous catalysts can prove difficult at the aqueous work-up stage.⁶ Developing a methodology based on a heterogeneous catalyst in a continuous flow micro reactor type operation offers many advantages over homogeneous batch based methods. These include effective product isolation from the catalysts reaction zone and improved control of the catalyst–reactant contact time leading to more rapid optimization of both yield and product selectivity. In addition, the solid phase catalysts which are required only in mg quantities, can be readily tested under reaction conditions and are easily recovered for reuse if required.

The use of MW heating in organic synthesis^{7–8} including Suzuki reactions^{9–11} has attracted considerable interest in the past few years where the main benefits are reported to be significant rate-enhancements and increased product yields.^{11–13} These features have attracted interest from the drug discovery and medicinal chemistry communities^{14–15} who are also interested in the high

throughput, rapid optimization, small volume and intrinsically safe operating characteristics of micro reactors. Coupling the use of MW heating with micro reactor based synthesis potentially combines a number of advantages of each technology and hence may have good potential in applications involving the synthesis of fine chemicals. One obvious problem with the direct heating of liquid phase reagent solution in a micro reactor channel of micron depth is the limited absorption of MW energy directly by the channel contents. Even for polar species which show (relatively) strong absorption of MW, efficient absorption typically requires a liquid depth in the order of a cm for MWs at 2.45 GHz.¹⁶ However, this shortcoming can be overcome by exploiting the absorption of MWs by either supported metal catalysts within a channel and/or thin metallic films¹⁶ located on the surface of a micro reactor. Positioning of the MW absorbing species or patch in or on the micro reactor enables localized heating over a prescribed length of a channel and, through careful control of the substrate amount/thickness, selected local temperatures may be reliably generated.¹⁶ In the present study, direct MW heating of a catalyst and the combined MW heating of a catalyst and a thin gold film on the outer surface of the micro reactor are evaluated as methodologies for the efficient localized heating of a micro reactor device.

Experimental

The reactions were conducted in glass micro reactors supplied by Micro Chemical Systems Ltd (Hull). Two linear channel designs (see Fig. 1) were used in which a premixed reactant solution containing an aryl halide (0.1 M), phenylboronic acid (0.12 M) and K₂CO₃ (0.3 M) with dimethylformamide (DMF) and H₂O (3:1 volume ratio) mixture as solvent, was pumped from an input reservoir to a collection reservoir through a catalyst bed. PEEK tubing (outer diameter OD = 1.58 mm, inner diameter ID = 0.18



Scheme 1 General reaction scheme for palladium catalysed Suzuki cross-coupling.

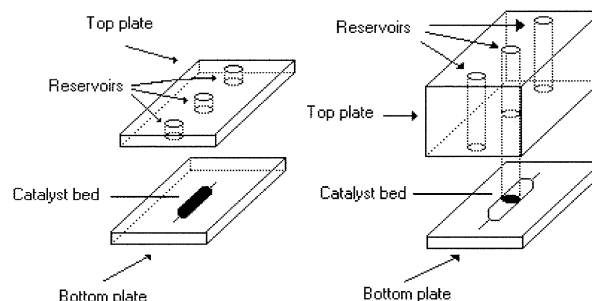


Fig. 1 Schematic diagram of the linear channel micro reactor designs and catalyst packing strategies used to perform Suzuki based reactions.

mm) was fitted to the inlet and outlet reservoirs and sealed using Torr seal (Varian). The end of the inlet tube was connected to a Harvard PHD 2000 syringe pump which delivered the homogeneous reaction solution to the reactor. The end of the outlet tube was connected to a sample vial which was placed in an ice bath and used to collect the reaction products.

In design A, the top and bottom plates of the micro reactor were both 3 mm thick. The catalyst channel was 1.5 mm wide, 80 μm deep and 15 mm long and connected to the inlet and outlet reservoirs by channels which were 130 μm wide and 50 μm deep. Design B used a 10 mm thick top plate and a 3 mm bottom plate with a catalyst channel which was 1.5 mm wide, 50 μm deep and 15 mm long, *i.e.* 20 μm shallower than that of design A. The catalyst channel again used channels which were 130 μm wide and 50 μm deep to connect to the inlet and outlet reservoirs. For both micro reactor designs, the catalyst was introduced as a dry powder through the central port (3 mm in diameter) and then located in the micro reactor channel using the air pressure generated from a hand held syringe. This packing procedure only took a few minutes to complete, as did the removal of the wet catalyst achieved by drawing the slurry out through the central port again with a syringe. During reaction, the central port was blanked off with a tightly fitting PEEK rod. The catalyst consisted of particles of size 45–63 μm (selected by sieving). These catalyst particles fitted within the catalyst channel of design A to create a monolayer of particles (requiring 1.5 mg) over the entire catalyst channel area. During the continuous flow maintained during reaction, the particles were retained by the keystone effect.¹⁷ The catalyst particles were too large to fit within the depth of the catalyst channel of design B and were located within the central reservoir in the form of a plug about 0.5–1 mm in height (requiring 6 mg). As required, an area (15 \times 1.5 mm) on the outside of the bottom plate corresponding to the region of catalyst packing was sputter coated with gold to a thickness of either 10 or 15 nm using a SEMPREP 2 Sputter Coater (Nanotech Ltd.). During MW irradiation no electrical sparking was observed from the film, however, caution may be required if thicker or larger areas of metalization are used.

The micro reactor was heated in the cavity of a Discover MW system from CEM, which is capable of delivering 0–300 W of MW power at 2.45 GHz. An IR temperature sensor located in the base of the Discover enabled determination of the temperature at the base of the micro reactor. It should be emphasized that this temperature refers to the lower exterior surface of the micro reactor and not the actual reaction zone within the catalyst channel. The measured temperature of each reaction was mediated by variation of the MW heating power (power time mode) in conjunction with different solution flow rates. The residence times of the solutions within the catalyst bed were measured by timing the movement of the liquid front during first filling.

During a reaction run, product samples were collected in a cooled (0 $^{\circ}\text{C}$) product vial for 5 min. This collection period was found to be long enough to obtain a representative sample for subsequent analysis. Samples were weighed, a known amount of dodecane was added as an internal standard and then treated with 1 M aqueous NaOH to remove unreacted phenylboronic acid. The remaining organic material was then extracted, washed three times with distilled water, collected and dried over MgSO_4 . Samples were then analysed for both aryl halide reactant and biaryl product using a GC instrument (Shimadzu GC-17A) equipped with a capillary column (CP SIL 8 CB, 30 m length, Chrompack). Pressure of carrier gas (helium) was 600 kPa and injector temperature was set to 250 $^{\circ}\text{C}$. The GC column temperature was held initially at 70 $^{\circ}\text{C}$ for 4 min, ramped at 20 $^{\circ}\text{C min}^{-1}$ to reach 240 $^{\circ}\text{C}$ which was then held for 12 min. The retention times for starting materials and products are summarized in Table 1.

The retention times for all compounds were verified using pure materials obtained as indicated below. All analysis was carried out in duplicate with replicates agreeing to within a 5% variation. Conversions were calculated from GC data by determining the

quantity of aryl halide present in the collection vial after reaction using internal standard method. Overall mass balances were checked using the GC data for the product and were correct to within a few percent.

The reagents and solvents 4-bromobenzonitrile (Aldrich, 99%), 4-cyanobiphenyl (Aldrich, 99%), 4-bromonitrobenzene (Aldrich, 99%), 4-nitrobiphenyl (Aldrich, 99%), 4-bromobenzaldehyde (Aldrich, 99%), biphenylaldehyde (Aldrich, 99%), 4-iodoanisole (Aldrich, 98%), 4-methoxybiphenyl (Aldrich, 99%), 4-iodotoluene (Aldrich, 99%), 4-methylbiphenyl (Aldrich, 99%), benzonitrile (Aldrich, 99%), biphenyl (Aldrich, 99%), phenylboronic acid (Aldrich, 97%), dodecane (Aldrich, 99%), *N,N*-dimethylformamide (DMF, Fluka, 99%), dichloromethane (DCM, Fisher, 99%), MgSO_4 (Fisher, 99%) and K_2CO_3 (Lancaster, 99%) were used without further purification. The catalysts Pd supported on alumina ($\text{Pd}/\text{Al}_2\text{O}_3$) and Pd anchored on polymer (Pd–polymer) were supplied by Johnson Matthey and contained 5 wt% Pd for the $\text{Pd}/\text{Al}_2\text{O}_3$ and 4 wt% Pd for Pd–polymer.

Results and discussion

The first set of experiments were carried out using the micro reactor with a catalyst plug (design B) and 5 selected substrates, in order to evaluate the potential of the proposed methodology. It should be noted that, in order to maintain comparable temperature ranges for each reaction, monitored by the optical detector in the base of the Discover instrument, the applied MW power was varied. As shown in Fig. 2, the gold films became less efficient at absorbing the MW power and reaching a high temperature following MW exposure during a larger number of 5 min heating cycles.

The appearance of the gold film changed from dark grey to an increasingly lighter grey following repeated heated cycles. This observation suggested that the films became progressively thinner, probably due to evaporation of the gold, rather than “peeling” away from the glass surface of the micro reactor. For the experiments

Table 1 Retention times for starting materials and products obtained by GC analysis

Compound	Retention time/min
4-Bromobenzonitrile	9.4
4-Cyanobiphenyl	13.2
4-Bromonitrobenzene	10.3
4-Nitrobiphenyl	14.0
4-Bromobenzaldehyde	9.2
4-Biphenylaldehyde	13.1
4-Iodoanisole	10.0
4-Methoxybiphenyl	12.6
4-Iodotoluene	8.4
4-Methylbiphenyl	11.5
Benzonitrile	6.5
Biphenyl	10.6
Dodecane	8.8

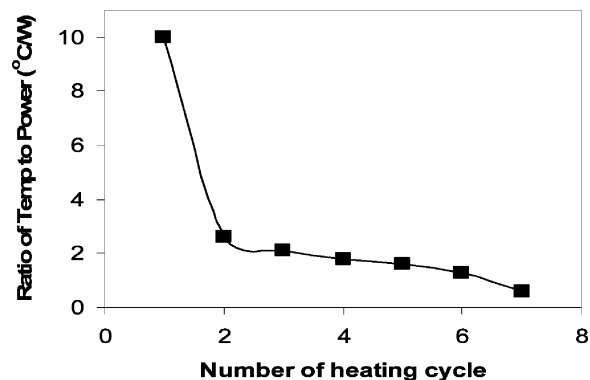


Fig. 2 Variation of the MW absorption efficiency (expressed as the ratio IR sensor temperature/MW power) following repeated 5 min heating cycles. The gold film was 15 nm thick initially.

here, the first heating cycle was ignored and all reaction measurements refer to heating cycles 2–4 where the gold films are more constant. As noted earlier, the MW power was adjusted for each run so as to obtain a constant temperature as measured by the IR sensor.

Some preliminary measurements were made using heating patch films of different materials. For the same MW power and film thickness, the measured temperatures were in the order Au > Pt ≈ Pd > C. This ranking sequence correlates with the electrical conductivities of the materials, *i.e.* the more conducting, the better the MW absorption and the higher the temperature reached. It was observed that improved MW heating could be obtained with Pt by using thicker films. Further work is proceeding to find the best choice of metal material and film thickness which optimizes heating performance, metal film stability and its adhesion to the glass surface of the micro reactor. The results presented in Table 2 for different aryl halide reactants indicate that deactivated species such as 4-bromonitrobenzene and 4-bromobenzonitrile are more reactive than activated substrates and give correspondingly high conversions. This is consistent with a mechanism in which electron withdrawing groups favor oxidative addition of aryl halides to a Pd(0) species.²

Having established that the proposed methodology was able to generate significant product, the effects of different heating methods on product yield were measured using 4-bromobenzonitrile as aryl halide reactant. As seen in Table 3, no conversion is detected under the reaction conditions used at room temperature. In the second heating method, the micro reactor was immersed in an oil bath at 130 °C. Reactants from a reservoir at room temperature were then pumped through the micro reactor and a 65% conversion was obtained. The third heating method used the MW absorption by the alumina supported catalyst without any metal film heating patch. In this case, 150 W of MW power were required to produce

Table 2 Conversion for a range of aryl halides reacted in micro reactor design B. Reaction mixture consisting of aryl halide (0.1 M), phenyl boronic acid (0.12 M), K₂CO₃ (0.3 M) in a DMF (75 vol%)/H₂O (25 vol%) mixed solvent was pumped continuously through the catalyst channel at 5 μl min⁻¹. The solution–catalyst contact time was 36 s. The gold film was 15 nm initial thickness and 6 mg of 5 wt% Pd/Al₂O₃ catalyst was used

Aryl halide		MW power/W	Temp/°C	Conv ^a %
X	R			
Br	NO ₂	50	90–98	98
Br	CN	55	90–102	99
Br	CHO	40	90–96	75
I	OCH ₃	80	90–100	75
I	CH ₃	55	90–98	58

^a Conversions were calculated from GC data based on the amount of aryl halide present in the collection vial after reaction. Only cross-coupling product was produced.

Table 3 Conversion for different heating methods using micro reactor design B. Reaction mixture consisting of 4-bromobenzonitrile (0.1 M), phenyl boronic acid (0.12 M), K₂CO₃ (0.3 M) in a DMF (75 vol%)/H₂O (25 vol%) mixed solvent was pumped continuously through the catalyst channel at 5 μl min⁻¹. The solution–catalyst contact time was 36 s. The gold film was 15 nm initial thickness and 6 mg of 5 wt% Pd/Al₂O₃ catalyst was used

Heating method	MW power/W	Temp/°C	Conv ^a %
Room temperature	0	25	0
Oil bath	0	130	65
MW heating only	150	94–98	71
MW heating plus gold coating	55	90–102	99

^a Conversions were calculated from GC data based on the amount of 4-bromobenzonitrile present in the collection vial after reaction. Only cross-coupling product was produced.

a temperature of around 95 °C as sensed on the external micro reactor surface by the IR sensor. The localized temperature at the catalyst surface is hard to estimate under these conditions as it is simultaneously cooled by the reagent flow and heated by MW absorption into (mainly) the alumina catalyst support. In the fourth method, MW energy was absorbed into both the catalyst and the gold film heating patch situated underneath the catalyst channel. The more efficient MW absorption is clearly evident by the reduced MW power required to achieve the measured temperature of around 95 °C. In all cases a flow rate of 5 μl min⁻¹ was used and it can be seen that the best conversion (virtually 100%) is obtained at relatively low MW power when MW absorption into both the catalyst and gold coating is used. Because of the coupled effects of reagent flows, energy absorption and conduction, it is difficult to estimate the localized temperature within the reaction zone. On the basis that the conversion is an effective measure of the localized temperature experienced by the reaction (*i.e.* the MW effect is purely thermal), the data of Table 3 suggest that MW absorption into both catalyst support and gold film is both effective and efficient in focusing heating energy into the small reaction zone within the micro reactor.

A comparison between the two catalyst packing modes (design A and B) was carried out in order to evaluate the proposed methodology. As seen in Table 4, product yields were generally similar for the two packing designs. However design A, using a slightly longer residence time (lower flow rate), did need less mass of catalyst and was found to require significantly less MW energy. Although somewhat uncertain due to the variation in gold film properties (Fig. 2), the apparently more efficient heating of design A is attributed to the fact that the catalyst is present as a thin particle monolayer to which heat transfer from the gold patch is more effectively achieved. The results also indicate that a system using a catalyst particle monolayer design plus a relatively low powered MW system (5 W, see Table 4) can be used to achieve good product yields in systems requiring localized temperatures in excess of 100 °C. Noting that the present system is very far from being optimized, these first results are very encouraging.

Finally, in order to evaluate the suitability of the proposed packing methodology to deal with polymeric based catalysts, a Pd anchored polystyrene support was used in a B design micro reactor. Using the design B micro reactor with the substrate 4-bromobenzonitrile, reagent concentrations as listed in Tables 2–4, 3 mg of both catalysts, 3 μl min⁻¹ flow rate, a catalyst contact time of 32 s and a MW power of 55 W giving a measured temperature range of 90–100 °C which gave a 75% conversion for the Pd–polystyrene and 72% for Pd–alumina. Despite having a 20% lower loading of

Table 4 Comparison of conversion for a range of aryl halides reacted in micro reactor designs A and B. Reaction mixture consisting of aryl halide (0.1 M), phenyl boronic acid (0.12 M), K₂CO₃ (0.3 M) in a DMF (75 vol%)/H₂O (25 vol%) mixed solvent was pumped continuously through the catalyst channel at the flow rates shown. The gold film was 15 nm initial thickness, 6 mg of 5 wt% Pd/Al₂O₃ catalyst was used for design B and 1.5 mg for design A

Substrate	Flow/μl min ⁻¹	MW power/W	Packing design	Conv %
	/Contact time/s	/Temp/°C		
Br–C ₆ H ₄ –NO ₂	5/36	50/90–98	B	98
Br–C ₆ H ₄ –NO ₂	3/44	7/90–105	A	90
Br–C ₆ H ₄ –CN	5/36	55/90–102	B	99
Br–C ₆ H ₄ –CN	3/44	5/90–108	A	92
Br–C ₆ H ₄ –CHO	5/36	40/90–96	B	75
Br–C ₆ H ₄ –CHO	3/44	50/80–90	A	72 ^a

^a A 10 nm gold film was used for this run which is therefore not strictly comparable. Use of a 15 nm gold film at a measured temperature range of 90–103 °C achieved with 10 W MW power gave an overall conversion of 98%. However, 50% of the conversion was biphenyl side product.

metal than the alumina supported catalyst, the Pd–polystyrene catalyst gives a comparable product yield. When using the polymer supported catalyst, it was found that filling the channel of micro reactor design A was practically very difficult due to the particle shape, size and texture however, filling design B with the polymeric based catalyst was virtually straightforward.

Conclusions

In order to more fully exploit the use of micro reactor technology in chemical and biochemical synthesis, methods for the controlled localized heating and the utilization of highly intensive surface properties need to be established. Whilst micro reactor based heating may be achieved using for example localized electrical resistance,^{2–3} in this work a contactless technique based upon MW induced heating has been used. In this way the controlled heating of a reaction can be achieved using selective MW absorption into both a catalyst and an externally applied gold film. It was found that at present the 10–15 nm film of gold used, whilst mechanically stable, did appear to evaporate and work in this area to generate a more robust film is in progress. In addition, a simple and practical technique is described for the loading and removal of an alumina and polymer supported metal catalyst from a micro reactor device. Whilst a Suzuki type reaction was used to illustrate the methodology, the results clearly point the way to developing a wider range of chemical methods and process applications of micro reactor technology.

Acknowledgements

We thank CEM Microwave Technology Ltd. and the Engineering and Physical Sciences Research Council for funding and Mr.

Sinclair of the University of Hull for the preparation of the gold coatings.

References

- 1 P. D. I. Fletcher, S. J. Haswell, E. Pombo-Villar, B. H. Warrington, P. Watts, S. Y. F. Wong and X. Zhang, *Tetrahedron*, 2002, **58**, 4735.
- 2 M. U. Kopp, A. J. de Mello and A. Menz, *Science*, 1998, 1046.
- 3 D. S. Yoon, Y.-S. Lee, Y. Lee, H. J. Cho, S. W. Sung, K. W. Oh, J. Cha and G. Lim, *J. Micromech. Microeng.*, 2002, **12**, 813.
- 4 N. Miyaura and A. Suzuki, *Chem. Rev.*, 1995, **95**, 2457.
- 5 S. Kotha, K. Lahiri and D. Kashinath, *Tetrahedron*, 2002, **58**, 9633.
- 6 J. H. Clark, *Green Chem.*, 1999, **1**, 1.
- 7 P. Lidstrom, J. Tierney, B. Wathey and J. Westman, *Tetrahedron*, 2001, **57**, 9225.
- 8 L. Perreux and A. Loupy, *Tetrahedron*, 2001, **57**, 9199.
- 9 C. G. Blettner, W. A. Konig, W. Stenzel and T. Schotten, *J. Org. Chem.*, 1999, **64**, 3885.
- 10 N. E. Leadbeater and M. Marco, *J. Org. Chem.*, 2003, **68**, 888.
- 11 M. Larhed and A. Hallberg, *J. Org. Chem.*, 1996, **61**, 9582.
- 12 D. Villemin and F. Caillot, *Tetrahedron Lett.*, 2001, **42**, 639.
- 13 N. Kuhnert and T. N. Danks, *Green Chem.*, 2001, **3**, 98.
- 14 (a) B. Wathey, J. Tierney, P. Lidstrom and J. Westman, *Drug Discov. Today*, 2002, **7**, 373; (b) M. Larhed and A. Hallberg, *Drug Discov. Today*, 2001, **6**, 406.
- 15 J. L. Krstenansky and I. Cotterill, *Curr. Opin. Drug Discov. Dev.*, 2000, **4**, 454.
- 16 P. He, P. D. I. Fletcher and S. J. Haswell, Proceedings of Conference and Workshop on Micro Total Analytical and Chemical Systems, April 7–9, 2003, Hull, UK.
- 17 G. A. Lord, D. B. Gordon, P. Myers and B. W. King, *J. Chromatogr., A*, 1997, **768**, 9.

Stereoselective alkylation of an Evans auxiliary derivative within a pressure-driven micro reactor

Charlotte Wiles,^a Paul Watts,^{*a} Stephen J. Haswell^a and Esteban Pombo-Villar^b

^a Department of Chemistry, The University of Hull, Cottingham Road, Hull, UK HU6 7RX

^b Novartis Institute for BioMedical Research, WSJ-386.07.15, CH4002, Basel, Switzerland

Received 8th January 2004, Accepted 8th March 2004

First published as an Advance Article on the web 17th March 2004

A simple technique for the diastereoselective alkylation of a metal stabilised enolate is demonstrated within a pressure-driven micro reactor whereby enhanced diastereoselectivities were obtained compared to batch.

Introduction

The preparation of compounds with specific stereochemistry is of great interest to pharmaceutical companies, as often one enantiomer exhibits biological activity whereas the other may be inactive or even harmful. One approach is to start with an enantiomerically pure material and to ensure that all steps in the synthesis retain their stereochemistry; this can however be extremely difficult. Alternatively a chiral auxiliary, such as those employed by Evans *et al.*,¹ can be used in order to prepare enantiomerically pure compounds. Using this approach, many examples of synthetically important compounds have featured in the literature including the synthesis of thiorphan² (enkephalinase inhibitor) and vancomycin (an antibiotic used to treat multi-drug resistant infections).³

Owing to the predictable thermal and mass transportation properties observed within the laminar flow environment of a micro reactor, one of the main advantages associated with miniaturisation is reactor control.^{4,5} In traditional large-scale reactor vessels, fluctuations in temperature are difficult to correct as any alterations made take time to have an effect on the system as a whole. In comparison, changes on the micro scale are observed almost immediately.⁵ Along with increasing the rate of diffusive mixing, decreasing the reactor dimensions also results in an inherently high surface to volume ratio, enabling heat generated by exothermic reactions to be dissipated rapidly.⁶ As a result of the uniform reactor conditions obtained, a high degree of reaction control is observed. With these factors in mind, micro reaction technology is of particular interest to the pharmaceutical industry, where long term objectives include the desire to perform multiple functions such as synthesis, screening, detection and biological evaluation on a single integrated device, resulting in an overall reduction in the time taken to discover new lead compounds and transfer them to production.

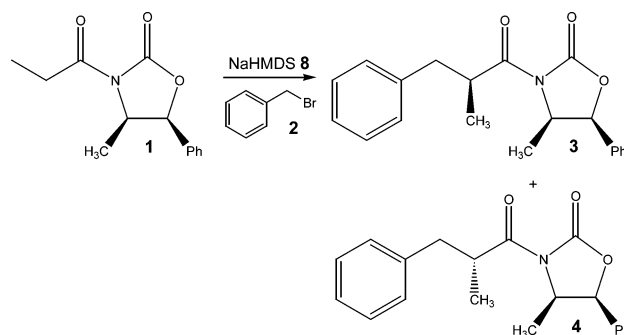
Previous work has demonstrated the preparation of a range of synthetically useful compounds,⁷ demonstrating many of the advantages associated with the miniaturisation of chemical synthesis, including: reduced reaction times, enhanced conversions and the ability to continuously purify reaction products.⁸ With these factors in mind, we extended our investigation of C–C bond forming reactions within a micro reactor⁹ to incorporate diastereoselective synthesis (Scheme 1).¹⁰

Experimental

Micro reactor methodology

The micro reactor described herein was purchased from Micro Chemical Systems Ltd. (Hull, UK) and consisted of a two-layer borosilicate glass device with ceramic fittings (Macor) located over each of the etched micro channels (152 μm (wide) \times 51 μm (deep) \times 2.3 cm (long)).

As Fig. 1 illustrates, PTFE or fused silica tubing (178 μm od \times 2.5 cm) was attached to the micro reactor using PEEK microtight fittings (Upchurch Scientific); subsequent attachment to a gas-tight syringe (Hamilton) resulted in a pressure-tight connection. The advantage of this attachment technique compared to the use of glue/resins¹¹ is that should any blockages occur within the tubing, the device could be disassembled and new tubing fitted. Also, if glue were used, degradation of the connection would result after prolonged contact with organic solvents *i.e.* CO₂-solvent bath. To accommodate the alkylation of 4-methyl-5-phenyl-3-propionyloxazolidin-2-one **1**, a PEEK microtee (Upchurch Scientific) connector was incorporated into the system, enabling 3 inputs and an output (Fig. 2). The magnitude of flow was controlled using two displacement pumps (MD-1001, Bioanalytical Systems Inc.) capable of delivering fluid at flow rates of 1–100 $\mu\text{l min}^{-1}$. All micro reactions were conducted over a period of 20 min to ensure a sufficient volume of product was generated for analysis by GC-MS (Varian GC (CP-3800) coupled to a Varian MS (2000), 30 m CP-Sil 8 column (Phenomenex), injector temperature 200 $^{\circ}\text{C}$, helium flow rate 1 ml min^{-1} , oven temperature 60 $^{\circ}\text{C}$ for 1 min then



Scheme 1 Alkylation of *N*-acetyl oxazolidinone **1** to afford diastereomers **3** and **4**.

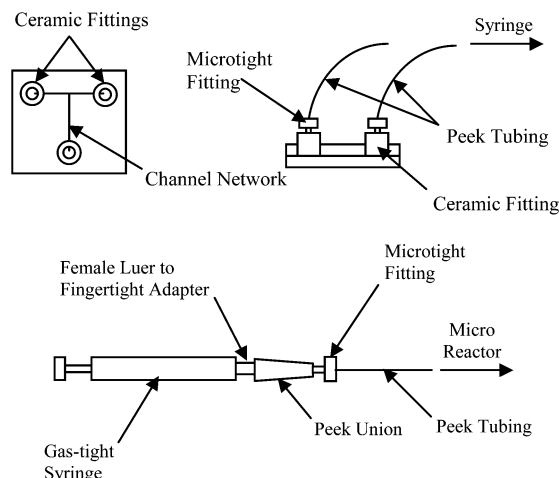


Fig. 1 Schematic of the connectors used to interface the micro reactor to a displacement pump.

ramped to 270 °C at 25 °C min⁻¹). Reaction products were determined *via* the comparison of retention times and spectra with those obtained from a series of synthetic standards. Analysis of the crude reaction mixtures by GC-MS enabled the proportion of product to be determined with respect to residual starting material *i.e.* % conversion.

Results and discussion

Using methodology established by Evans *et al.*,¹ the enolate of 4-methyl-5-phenyl-3-propionyloxazolidin-2-one **1** was alkylated using benzyl bromide **2**, to afford diastereomers **3** and **4** in an overall yield of 68% and a ratio of 85 : 15 (**3** : **4**) (Scheme 1).

Having successfully prepared a series of synthetic standards at -100 °C, the reaction was subsequently repeated at room temperature (25 °C) and -78 °C in order to investigate the effect of reaction temperature on product diastereoselectivity. As expected, performing the reaction at room temperature is undesirable as both diastereoselectivity and conversion are poor (Table 1). This observation is attributed to the decomposition of a large proportion of the *N*-acyl oxazolidinone enolate **5** and subsequent alkylation of the anion **6** to afford 3-benzyl-4-methyl-5-phenyloxazolidin-2-one **7** (Scheme 2). Although performing the reactions at -78 °C initially appears advantageous as a greater conversion to product is obtained, compared with reactions conducted at -100 °C, reduced diastereoselectivity and increased enolate decomposition is observed. Consequently, all further investigations were carried out at -100 °C.

Due to the excellent thermal and mass transportation properties observed within micro fluidic devices, it was postulated that

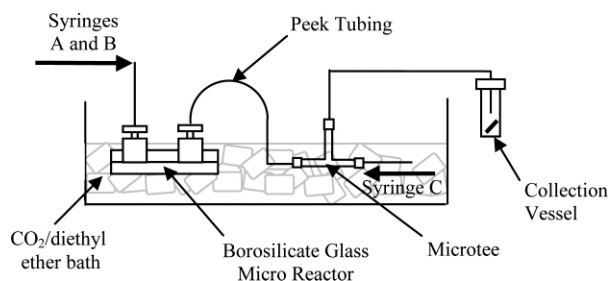
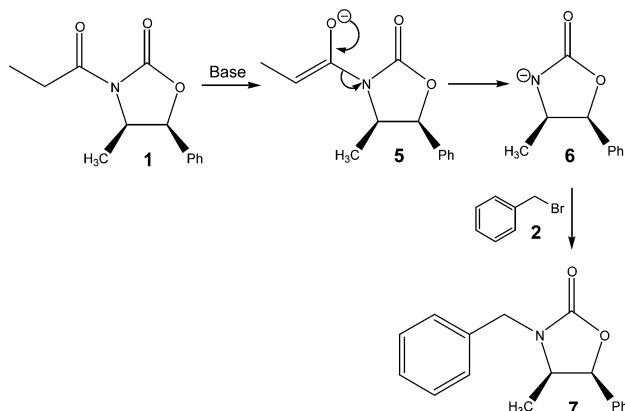


Fig. 2 Schematic of the reduced temperature set-up.

Table 1 Effect of reaction temperature on diastereoselectivity in batch

Reaction temp./°C	Conversion (%) ^a (3 + 4)	Ratio (3 : 4)	Decomposition (%) ^a (7)
25	17	69 : 31	53
-78	59	75 : 25	24
-100	31	85 : 15	10

^a Determined by GC-MS analysis of reaction mixture after 30 min.



Scheme 2 Decomposition of the enolate **5** to afford by-product **7**.

product diastereoselectivity could be further improved as a result of conducting the reaction in a micro reactor.

Although many reactions have been demonstrated within micro reactors at temperatures ranging from 4 °C to 300 °C,⁶ few authors, with the exception of Yoshida and Schwalbe,¹² report reactions performed at reduced temperatures. Using the following experimental procedure, the preparation of diastereomers **3** and **4** was investigated within a pressure-driven system; a standard solution of NaHMDS **8** (0.5 M) in anhydrous THF was added from syringe A at 50 µl min⁻¹, a solution of 4-methyl-5-phenyl-3-propionyloxazolidin-2-one **1** (0.5 M) in anhydrous THF was added from syringe B at 50 µl min⁻¹ and a solution of benzyl bromide **2** (0.5 M) in anhydrous THF was added from syringe C at 50 µl min⁻¹ (Fig. 2). In order to maintain the reactor temperature, the micro reactor was placed within a CO₂-ether bath and the reaction products collected at room temperature. To ensure the results obtained were representative of the reaction occurring within the micro fabricated device, the reaction products were collected in a stirred vial where they were quenched immediately. Using this approach, the chiral enolate **5** was formed within the central micro channel and subsequently reacted with benzyl bromide in the microtee to afford diastereomers **3** and **4**, in 31% conversion and a ratio of 94 : 6 (**3** : **4**). Reducing the flow rates to 20 and 10 µl min⁻¹ respectively enabled the effect of residence time on product conversion and diastereoselectivity to be investigated. As Table 2 illustrates, as the flow rate was decreased, both product conversion and diastereoselectivity increased enabling diastereoselectivities >91 : 9 to be obtained.

Using the aforementioned approach, the diastereoselective synthesis of ((2*S*, 4*R*, 5*S*)-3-(2'-methyl-3'-phenylpropionyl)-4-methyl-5-phenyloxazolidin-2-one **3** was demonstrated in a micro reactor whereby diastereoselectivities of >91 : 9 (**3** : **4**) were obtained compared to 85 : 15 in batch. Although the technique remains unoptimised at 10 µl min⁻¹, increased conversions of up to 10% were obtained when using the pressure-driven system compared to traditional batch techniques, demonstrating 41% conversion to diastereomers **3** and **4**. The fact that unreacted *N*-acyl oxazolidinone **1** was detected by GC-MS (59%) indicates incomplete enolate formation rather than decomposition, therefore by increasing the residence time within the initial part of the device, it is proposed that conversion could be further increased. The technique is also advantageous as no decomposition product **7** was observed when performing the reaction in a micro reactor compared with >10% in batch. These observations are attributed to the ability to accurately control both residence time and temperature of the reaction mixture within the micro fluidic device.

Conclusions

In summary, we have demonstrated a simple technique for the diastereoselective alkylation of metal stabilised enolates using a pressure-driven micro reactor at -100 °C, whereby increased conversions and diastereoselectivity were observed compared to batch. Further work is currently under way within our laboratories to improve the product conversions obtained and demonstrate the scope of this technique.

Table 2 Effect of flow rate on product diastereoselectivity and conversion within a pressure-driven micro reactor

Flow rate/µl min ⁻¹	Conversion (%) ^a (3 + 4)	Ratio (3 : 4)	Decomposition (%) ^a (7)
50	31	94 : 6	0
20	38	91 : 9	0
10	41	91 : 9	0

^a Conversion and diastereoselectivity based on *n* = 10.

Acknowledgements

Full financial support provided by Novartis Pharmaceuticals (C. W. and P. W.) is gratefully acknowledged.

References

- 1 D. A. Evans, J. Bartroli and T. L. Shih, *J. Am. Chem. Soc.*, 1981, **103**, 2127.
- 2 D. A. Evans, D. A. Evrard, S. D. Rychnovsky, T. Fruh, W. G. Whittingham and K. M. DeVries, *Tetrahedron Lett.*, 1992, **33**, 1189.
- 3 D. A. Evans, D. J. Mathre and W. L. Scott, *J. Org. Chem.*, 1985, **50**, 1830.
- 4 K. F. Jensen, *Chem. Eng. Sci.*, 2000, **56**, 293.
- 5 T. Schwalbe, A. Volker and G. Wille, *Chimia*, 2002, **56**, 636.
- 6 W. Ehrfeld, V. Hessel and H. Lowe, *Microreactors: New Technology for Modern Chemistry*, Wiley-VCH, New York, 2000.
- 7 (a) P. D. I. Fletcher, S. J. Haswell, E. Pombo-Villar, B. H. Warrington, P. Watts, S. Y. F. Wong and X. Zhang, *Tetrahedron*, 2002, **58**, 4735; (b) H. Salimi-Moosavi, T. Tang and D. J. Harrison, *J. Am. Chem. Soc.*, 1997, **68**, 2515; (c) P. Watts, C. Wiles, S. J. Haswell and E. Pombo-Villar, *Chem. Commun.*, 2002, 1034; (d) G. N. Doku, S. J. Haswell, T. McCreedy and G. M. Greenway, *Analyst*, 2001, **119**, 8716; (e) H. Lu, M. A. Schmidt and K. F. Jensen, *Lab Chip*, 2002, **2**, 31; (f) H. Hisamoto, M. Saito, M. Tokeshi, A. Hibara and T. Kitamori, *Chem. Commun.*, 2001, 2662; (g) R. D. Chambers and R. C. H. Spink, *Chem. Commun.*, 1999, 883; (h) V. Skelton, G. M. Greenway, S. J. Haswell, P. Styring, D. O. Morgan, B. H. Warrington and S. Y. F. Wong, *Analyst*, 2001, **126**, 7.
- 8 (a) M. Tokeshi, T. Minagawa and T. Kitamori, *Anal. Chem.*, 2000, **72**, 1711; (b) H. Hisamoto, T. Horiuchi, K. Uchiyama, M. Tokeshi, A. Hibara and T. Kitamori, *Anal. Chem.*, 2001, **73**, 5551.
- 9 (a) C. Wiles, P. Watts, S. J. Haswell and E. Pombo-Villar, *Lab Chip*, 2001, **1**, 100; (b) C. Wiles, P. Watts, S. J. Haswell and E. Pombo-Villar, *Chem. Commun.*, 2002, 1034; (c) C. Wiles, P. Watts, S. J. Haswell and E. Pombo-Villar, *Lab Chip*, 2002, **2**, 141; (d) C. Wiles, P. Watts, S. J. Haswell and E. Pombo-Villar, *Abstr. Pap. Am. Chem.*, 2002, *ORGN* 105.
- 10 D. A. Evans, M. D. Ennis and D. J. Mathre, *J. Am. Chem. Soc.*, 1982, **104**, 1737.
- 11 N. H. Bings, C. Wang, C. D. Skinner, C. L. Colyer, T. Thibault and D. J. Harrison, *Anal. Chem.*, 1999, **71**, 3292.
- 12 (a) S. Suga, M. Okajima, K. Fujiwara and J. Yoshida, *J. Am. Chem. Soc.*, 2001, **123**, 7941; (b) T. Schwalbe, V. Autze and G. Willie, *Chimia*, 2002, **56**, 636.

Microwave-assisted Suzuki reactions in a continuous flow capillary reactor

Ping He, Stephen J. Haswell*, Paul D.I. Fletcher

Department of Chemistry, University of Hull, Hull HU6 7RX, UK

Received in revised form 26 May 2004; accepted 27 May 2004

Available online 7 July 2004

Abstract

Suzuki cross-coupling reaction of aryl halides with phenylboronic acid to form biaryls has been used to illustrate the development of a microwave-based technique capable of delivering heat locally to a solid Pd-supported catalyst located within a continuous flow capillary reactor. The strong inherent absorption of a thin layer of gold metal on the outside surface of the capillary enabled effective heating to be carried out in the region of the catalyst, enhancing the rate of reaction to give product yields greater than 70% with catalyst/reactant contact times of less than 60 s using a hydrodynamically pumped system.

© 2004 Elsevier B.V. All rights reserved.

Keywords: Microwave; Suzuki reaction; Heterogeneous catalysis; Continuous flow capillary reactor

1. Introduction

In recent years the use of emerging techniques such as microwave heating [1] and miniaturised continuous flow reactor technology (microreactors) for organic synthesis [2] has attracted considerable interest, particularly within the pharmaceutical and fine chemical communities, where the benefits associated with rate enhancements, higher yields and greater product selectivity have been reported [3–5]. The coupling therefore of microwave heating with a capillary-based flow through reactor, in which chemical synthesis can be performed, offers the possibility of realising many of the individual advantages associated with these two techniques combined into one integrated system. One obvious problem however with attempting to couple microwave energy directly into the reactants contained within a capillary system is the very low absorption and hence heating that will occur due to the small volumes of material present [6]. Even for polar species which show (relatively) strong absorption of microwaves, efficient absorption typically requires a liquid depth in the order of a cm for microwaves at 2.45 Gz to be efficiently absorbed. This

shortcoming can be overcome by exploiting the absorption of microwaves by either supported metal catalysts within the capillary reactor and/or thin metallic films located on the surface of such a system [6].

In this present study, Suzuki reactions [7] have been performed using Pd supported on silica and alumina to demonstrate the utility of the proposed methodology. The Suzuki reaction (palladium-catalysed cross-coupling of aryl halides with aryl boronic acids) has now become one of the most widely used methods for the selective formation of carbon–carbon bonds, in particular for the formation of biaryls [7,8], which represent important intermediate materials in the pharmaceutical and fine chemicals industries. Such Suzuki reactions are commonly performed using a homogeneous soluble palladium complex catalyst; however, recovery of such homogeneous catalysts can prove difficult at the aqueous work-up stage [9]. Solid Pd-supported catalyst has been successfully used for Suzuki reactions and showed comparable or better activity than soluble palladium complexes [10–12]. Developing a methodology based on a heterogeneous catalyst in a continuous flow capillary reactor-type operation offers many advantages over homogeneous batch-based methods. These include effective product isolation from the catalysts and improved control of the catalyst–reactant contact time leading to more rapid optimization of both product selectivity and yield. In addition,

* Corresponding author. Tel.: +44 1482 465469; fax: +44 1482 466416.

E-mail address: s.j.haswell@hull.ac.uk (S.J. Haswell).

tion, the solid-phase catalysts which are only required in mg quantities, can be readily tested under reaction conditions and are easily recovered for reuse if required.

In this work we demonstrate that the proposed methodology offers controlled localised microwave heating of reactants in a continuous flow capillary reactor leading to significant enhancements in the rate of reaction to give high product yields with catalyst/reactants contact times of less than 60 s.

2. Experimental

The experimental setup is shown schematically in Fig. 1. The flow reactor consisted of a U-shaped glass capillary of inner diameter 800 μm , outer diameter 1.2 mm and total length 138 mm. The capillary was mounted within the cavity of a Discover microwave system (CEM Ltd.) which is capable of delivering 0–300 W of microwave power at 2.45 GHz. The microwave cavity was fitted with an infrared sensor which was aligned so as to monitor the temperature of the external surface of the lower part of the U-shaped capillary. The capillary was connected via two two-way connectors and PTFE tubing to an external syringe pump (Harvard PHD 2000). The catalyst particles (355–420 μm , selected by sieving) were loaded in the U-tube and prevented from moving along the tube by insertion of a glass rod (outer radius 300 mm) at the end of the catalyst bed. Reactant solution, containing an aryl halide (0.1 M), phenylboronic acid (0.12 M), base (0.25 M) in a solvent mixture consisting of 75 vol.% dimethylformamide (DMF) in water, was pumped through the reactor using the syringe pump. For the different pump flow rates, the residence times of the solutions within the catalyst bed were directly measured by timing the movement of the liquid front during first filling. As required, the bottom section of the U-tube (15 mm length) was sputter-coated with gold to the required thickness using a SEMPREP 2 sputter Coater (Nanotech Ltd.). During a reaction run, product samples were collected after the required flow period, weighed and a known amount of dode-

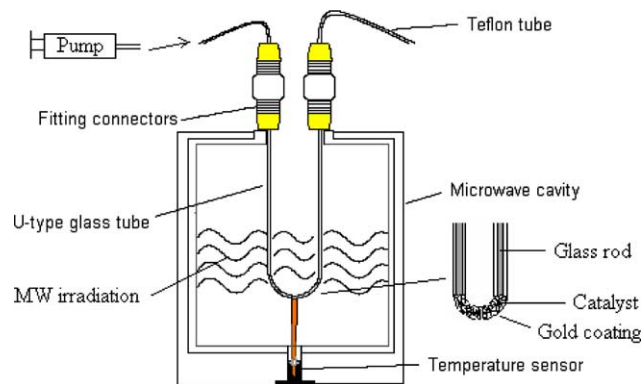


Fig. 1. Schematic diagram of the setup for microwave-assisted coupling reactions.

cane was added as an internal standard. Samples were treated with 1 M aqueous NaOH to remove unreacted PBA, the remaining organic material was then extracted, washed three times with distilled water, collected and dried over MgSO_4 . Treated samples were analysed for biaryl product plus benzonitrile and biphenyl side products using a GC (Shimadzu GC-17A) equipped with a capillary column (CP SIL 8 CB, 30 m length, Chrompack). The GC column temperature was held initially at 70 $^\circ\text{C}$ for 4 min, ramped at 20 $^\circ\text{C}/\text{min}$ to reach 240 $^\circ\text{C}$ which was then held for 12 min. Conversions were calculated from GC data by determining the quantity of aryl halide present in the collection vial after reaction. Overall mass balances were checked using the GC data for the product and were correct within a few percent.

The reagents and solvents 4-bromobenzonitrile (BBN, Aldrich, 99%), 4-bromonitrobenzol (BNB, Aldrich, 99%), 4-bromobenzaldehyde (BBA, Aldrich, 99%), 4-iodoanisole (IA, Aldrich, 98%), 4-iodotoluene (IT, Aldrich, 99%), phenylboronic acid (PBA, Aldrich, 97%), dodecane (Aldrich, >99%), *N,N*-dimethylformamide (DMF, Fluka, >99%), dichloromethane (DCM, Fisher, >99%), MgSO_4 (Fisher, >99%), K_2CO_3 (Lancaster, >99%) and NaOH (BDH, 98%) were used without further purification. The catalysts Pd supported on silica (Pd/SiO_2) and alumina ($\text{Pd}/\text{Al}_2\text{O}_3$) were supplied by Johnson Matthey and contained 2 wt.% Pd for the Pd/SiO_2 and 5 wt.% Pd for the $\text{Pd}/\text{Al}_2\text{O}_3$.

3. Results and discussion

Experiments were initially carried out to evaluate an appropriate catalyst and base for the proposed reaction. For this, two solid catalysts (Pd/SiO_2 and $\text{Pd}/\text{Al}_2\text{O}_3$) and two bases (NaOH and K_2CO_3) were selected for the coupling reaction of BBN with PBA to form 4-cyanobiphenyl (CBP). As seen from Table 1, the product yield when using Pd/SiO_2 and K_2CO_3 as a base increases with temperature up to ap-

Table 1
Evaluation of the catalyst support and appropriate base for the coupling reaction of 4-bromobenzonitrile and phenylboronic acid

Catalyst	Base	MW power (W)	IR sensor temperature ($^\circ\text{C}$)	Yield (%)
Pd/SiO_2	K_2CO_3	0	Room temperature	0
Pd/SiO_2	K_2CO_3	50	46	14
Pd/SiO_2	K_2CO_3	150	66	37
Pd/SiO_2	K_2CO_3	170	80	26
Pd/SiO_2	NaOH	150	66	0 (83 ^a)
$\text{Pd}/\text{Al}_2\text{O}_3$	K_2CO_3	60	55	59
$\text{Pd}/\text{Al}_2\text{O}_3$	K_2CO_3	90	80	99 ^b

Reaction mixture consisting of 4-bromobenzonitrile (0.1 M), phenylboronic acid (0.12 M), base (0.25 M) in a DMF (75 vol.%) / H_2O (25 vol.%) mixed solvent was pumped continuously through the capillary reactor at 0.04 ml min^{-1} . The solution–catalyst contact time was 15 s. The gold film used was 15 nm thick and 8 mg of catalyst was used.

^a Benzonitrile is only product.

^b Containing 9% biphenyl and 15% benzonitrile.

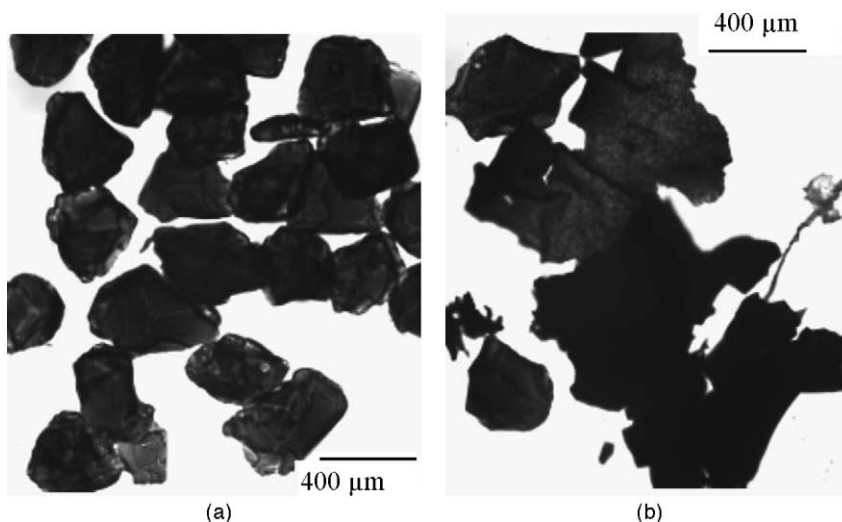


Fig. 2. Images of Pd/SiO₂ before (a) and after (b) microwave irradiation. Aggregation of the catalyst particles are clearly seen in image (b) which in turn deactivates the catalyst.

proximately 37% at 66 °C and then decreases to about 26% as the temperature is increased to around 80 °C. At this higher temperature, aggregation of Pd/SiO₂ catalysts was observed and this is attributed to the condensation of SiO₂ under basic condition which deactivates the catalyst (see Fig. 2). Such condensation between alumina particles was not observed when using the Pd/Al₂O₃-supported catalyst. In addition, measurements of the microwave-induced heating of the catalyst alone indicated that the Pd/Al₂O₃ catalyst absorbed microwaves better than the Pd/SiO₂ catalyst giving a higher local temperature at the catalyst surface. As a result, Pd/Al₂O₃ catalyst was found to give a 59% product yield at an IR sensor temperature of 55 °C rising to 75% at 80 °C, showing a greater reactivity for the Pd/Al₂O₃-supported catalyst as obtained using the Pd/SiO₂. It can also be seen from Table 1 that when NaOH (0.25 M) was used as the base the undesired product benzonitrile (through debromination) at 83% conversion was generated. This result indicates that the use of a strong base, such as NaOH, leads to the debromination of 4-bromobenzonitrile to give an undesired by-product. The carbonate ($pK_a = 10.3$) however is clearly a sufficiently

strong base to form the C₆H₅-B(OH)₃⁻ intermediate required for cross-coupling to give the desired product (pK_a of PBA = 8.8). Based on this initial evaluation, further investigations focused on using Pd/Al₂O₃ as the catalyst with K₂CO₃ as a base.

The results summarized in Table 2 show a comparison of heating methods and the corresponding effect of contact time on product yield. The data show that no product conversion is detected at room temperature and that heating the capillary reactor by immersion in an isothermal oil bath at 65 °C produced almost no product. Increasing the oil bath temperature to 100 °C with a contact time of 1200 s gave a 61% yield of the product. When the capillary reactor was heated using microwave absorption (250 W) by the alumina-supported catalyst only (i.e. without the presence of a gold metal film) a temperature of around 59 °C was determined by the IR sensor focused on the external capillary reactor surface at the lowest point of the U-tube and a 37% product yield was obtained for a contact time of 15 s. This yield was improved to 43% for a contact time of 60 s. Clearly, the localized temperature at the catalyst surface is

Table 2
Evaluation of the heating mode and time on the coupling reaction of 4-bromobenzonitrile and phenylboronic acid

Heating method	Flow (μl min ⁻¹)/contact time (s)	MW power (W)	IR sensor temperature (°C)	Yield (%)
Room temperature	0.01/60	0	25	0
Oil bath	0.04/15	0	65	1
Oil bath	Bulk ^a /1200	0	100	61
MW heating no Au film	0.04/15	250	58–60	37
MW heating no Au film	0.01/60	250	58–60	43
MW heating plus gold coating	0.04/15	60	55–63	59
MW heating plus gold coating	0.01/60	90	55–63	91 ^b

Reaction mixture consisting of 4-bromobenzonitrile (0.1 M), phenylboronic acid (0.12 M), K₂CO₃ (0.25 M) in a DMF (75 vol.%) / H₂O (25 vol.%) mixed solvent was pumped continuously through the capillary reactor. The gold film used was 15 nm thick and 8 mg of Pd/Al₂O₃ catalyst was used.

^a Bulk reaction.

^b Containing 5% biphenyl and 12% benzonitrile.

Table 3

Comparison of activities on replicated reuse of Pd/Al₂O₃ catalyst on the Suzuki reaction of 4-bromobenzonitrile and phenylboronic acid using a capillary without gold coating

Reuse of Pd/Al ₂ O ₃	Power (W)	Temperature (°C)	Yield (%)
1	250	60	43
2	250	62	42
3	250	64	41
4	250	64	42

Reaction mixture consisting of 4-bromobenzonitrile (0.1 M), phenylboronic acid (0.12 M), K₂CO₃ (0.25 M) in a DMF (75 vol.)/H₂O (25 vol.%) mixed solvent was pumped continuously through the capillary reactor and 8 mg of Pd/Al₂O₃ catalyst was used.

hard to estimate under these conditions as it is simultaneously cooled by the reagent flow and heated by microwave absorption into (mainly) the Pd/Al₂O₃ catalyst. Finally when the microwave energy was absorbed by both the catalyst and a gold film situated on the outside of the capillary in the region of the catalyst zone a more efficient absorption of microwaves occurred enabling the microwave power to be reduced from 250 W, as used in the case of the catalyst alone, to less than 100 W. Under these conditions a temperature of around 59 °C was obtained together with a 59% yield of product for contact time of 15 s rising to 91% for a contact time of 60 s. It can be clearly seen that the best product yield is obtained at relatively low microwave power when microwave absorption by both the catalyst and gold coating is used. Due to the coupled effects of reagent flows, energy absorption and conduction, it is difficult to estimate the localized temperature within the reaction zone. On the basis that the product conversion is an effective measure of the localized temperature experienced by the reaction (i.e. the microwave effect is purely thermal), the data in Table 2 suggest that microwave absorption into both catalyst support and gold film is both effective and efficient in focusing heating energy into the small reaction zone within the capillary reactor. It is also seen that, as expected, increasing contact time between catalyst and reactants improves the product yield. The stability of Pd/Al₂O₃ was also investigated and the deactivation of the catalyst was not observed over a short number of runs (Table 3).

To demonstrate the applicability of the proposed methodology for the rapid evaluation of a catalyst, a range of different aryl halides were evaluated. The results presented in Table 4 indicate that deactivated substrates are more reactive than activated substrates and give correspondingly high product yields. This is consistent with a mechanism in which electron-withdrawing groups favour oxidative addition of aryl halides to a Pd(0) species [7]. This set of results clearly demonstrates the advantages that the proposed methodology offers in terms of high throughput synthesis, where pure products can be generated in high yields with a catalyst contact time of less than 1 min.

Table 4

Product conversion for a range of aryl halides reacted in the capillary flow reactor

Aryl halide		MW power (W)	Yield (%)
X	R		
Br	NO ₂	150	74
Br	CN	90	59
Br	CHO	150	54
I	OCH ₃	250	32
I	CH ₃	150	30

Reaction mixture consisting of aryl halide (0.1 M), phenyl boronic acid (0.12 M), K₂CO₃ (0.25 M) in a DMF (75 vol.)/H₂O (25 vol.%) mixed solvent was pumped continuously through the reactor at 0.04 μl min⁻¹. The solution–catalyst contact time was 15 s. The gold film was 15 nm thick and 8 mg of Pd/Al₂O₃ catalyst was used. The sensor temperature was approximately constant at 50 ± 5 °C.

4. Conclusions

We have demonstrated that the controlled heating of a reaction can be achieved using selective microwave absorption by both a catalyst within a capillary channel and a gold film placed on the outside surface of a capillary reactor. Using a heterogeneously catalysed Suzuki reaction to demonstrate the utility of the proposed methodology, catalyst, base, substrate, heating and flow effects could be evaluated quickly and effectively. In this particular work a Pd/Al₂O₃ catalyst used in conjunction with a K₂CO₃ base was found to give over 70% yield of the product in 15 s using 150 W of microwave power. Whilst a Suzuki-type reaction was used to illustrate the methodology, the results clearly point the way to developing a wider range of rapid chemical evaluation methods and process based on capillary flow reactor technology.

References

- [1] P. Lidstrom, J. Tierney, B. Wathey, J. Westman, *Tetrahedron* 57 (2001) 9225.
- [2] P.D.I. Fletcher, S.J. Haswell, E. Pombo-Villar, B.H. Warrington, P. Watts, S.Y.F. Wong, X. Zhang, *Tetrahedron* 58 (2002) 4735.
- [3] M. Larhed, A. Hallberg, *J. Org. Chem.* 61 (1996) 9582.
- [4] D. Villemin, F. Caillot, *Tetrahedron Lett.* 42 (2001) 639.
- [5] N. Kuhnert, T.N. Danks, *Green Chem.* 3 (2001) 98.
- [6] (a) P. He, P.D.I. Fletcher, S.J. Haswell, in: *Proceedings of the International Conference and Workshop on Micro Total Analytical and Chemical Synthesis*, Hull, UK, 7–9 April 2003.;
(b) P. He, P.D.I. Fletcher, S.J. Haswell, *Lab Chip* 4 (2004) 38.
- [7] N. Miyauro, A. Suzuki, *Chem. Rev.* 95 (1995) 2457.
- [8] S. Kotha, K. Lahiri, D. Kashinath, *Tetrahedron* 58 (2002) 9633.
- [9] J.H. Clark, *Green Chem.* 1 (1999) 1.
- [10] A. Corma, H. Garcia, A. Leyva, *Appl. Catal. A: Gen.* 236 (2002) 179.
- [11] H. Bulut, L. Artok, S. Yilmaz, *Tetrahedron Lett.* 44 (2003) 289.
- [12] E.B. Mubofu, J.H. Clark, D.J. Macquarrie, *Green Chem.* 3 (2001) 23.



An investigation into the use of silica-supported bases within EOF-based flow reactors

Charlotte Wiles, Paul Watts* and Stephen J. Haswell

Department of Chemistry, Faculty of Science and the Environment, The University of Hull, Cottingham Road, Hull, HU6 7RX, UK

Received 6 April 2004; revised 8 June 2004; accepted 1 July 2004

Abstract—Using a series of silica-supported bases, we demonstrate the synthesis of eight condensation products within an EOF-based flow reactor; in all cases, high yields (>99%) and product purity are obtained.

© 2004 Elsevier Ltd. All rights reserved.

1. Introduction

Increased demand for the rapid preparation of small molecule libraries has led to renewed interest in the development of clean and efficient techniques for the synthesis of organic compounds. With this in mind, the miniaturisation of reaction technology is of particular interest to the pharmaceutical industry, where long term objectives include the desire to perform multiple functions such as synthesis, detection, screening and biological evaluation within a single integrated device, resulting in an overall reduction in the time taken to discover new lead compounds and put them into production.¹ To date, numerous compounds have been successfully synthesised within micro fabricated devices with many groups demonstrating advantages over traditional batch techniques such as greater reaction control, leading to increased conversions, selectivities and reduced reaction times.² Although many groups have begun the task of transferring synthetic methodology from batch to micro reactors, few have addressed the problems associated with product purification in continuous systems.³ In order to tackle these problems, we were interested in the use of solid-supported reagents.⁴

1.1. Solid-supported reagents

Compared to solid-phase techniques,⁵ where reaction intermediates are immobilised and cannot be fully characterised until cleaved from the support, the use of solid-supported reagents means that reaction products remain in solution, enabling reaction progress to be monitored. As the technique couples the advantages of both solid and solution-

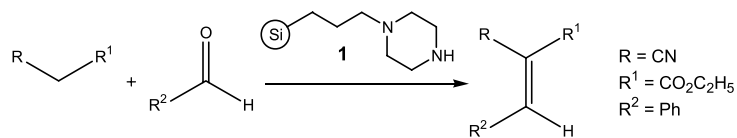
phase synthesis, the use of solid-supported reagents means that excess reagent can be employed in order to drive the reaction to completion, while the reagent can be easily removed from the reaction mixture. With the obvious similarities to solid-phase synthetic methodology, polymers have found widespread use in the preparation of solid-supported reagents;^{6,7} other materials however include zeolites,⁸ clays⁹ and silicas.¹⁰ Unlike certain polymers, silica exhibits no swelling in organic solvents and is thermally, chemically and mechanically stable; consequently, its use as a support is becoming more widespread. Due to the non-porous nature of the support, functionalisation is limited to the surface and as a result, reaction rate is not limited by reagent diffusion whilst enabling controlled, reproducible loading. In order to prevent any undesirable adsorption of materials onto the silica, any unfunctionalised silanol groups are end-capped. With this in mind, we were interested in investigating the incorporation of silica-supported reagents for continuous synthesis in a miniaturised flow reactor.

1.2. Knoevenagel condensation

The Knoevenagel reaction is defined as the condensation of an aldehyde or ketone with compounds that possesses an active methylene group. The reaction is brought about using organic bases such as primary or secondary amines.¹¹ The active methylene groups employed include nitro, cyano and acyl groups and in most cases, two groups are required in order to provide sufficient activation. As [Scheme 1](#) illustrates, the primary product formed is the unsaturated product although, in some cases, further reaction may take place with a second molecule of the activated methylene compound resulting in a Michael addition to afford the bis product. With careful selection of the starting materials, enantioselective¹² and diastereoselective¹³ condensation

Keywords: Silica supported base; Knoevenagel reaction; Flow reactor.

* Corresponding author. Tel.: +44-1482-465471; fax: +44-1482-466416.; e-mail: p.watts@hull.ac.uk



Scheme 1. General scheme illustrating the reaction of activated methylenes and aldehydes with a functionalised silica gel **1**.

products may be obtained. The main disadvantage associated with the Knoevenagel condensation is that the reactions do not proceed to completion and require purification to remove the organic base and its salt. Many alternatives exist, including acid catalysed condensations,¹⁴ dry grind,¹⁵ the use of microwave irradiation,¹⁶ zeolites,¹⁷ aluminium oxides¹⁸ and the use of amino functionalised polymers¹⁹ and silica gels.²⁰

It was therefore proposed that by incorporation of a series of supported bases into a micro-fabricated device, that product purity could be increased while simultaneously maintaining the advantages associated with miniaturisation. Firstly, in order to compare the use of supported reagents within a flow reactor with traditional batch techniques, the reactions were initially performed in batch using both silica-supported and solution phase bases.

2. Results and discussion

As Scheme 1 illustrates, treatment of an activated methylene with a base **1** in the presence of an aldehyde, results in the preparation of an unsaturated product (Fig. 1).

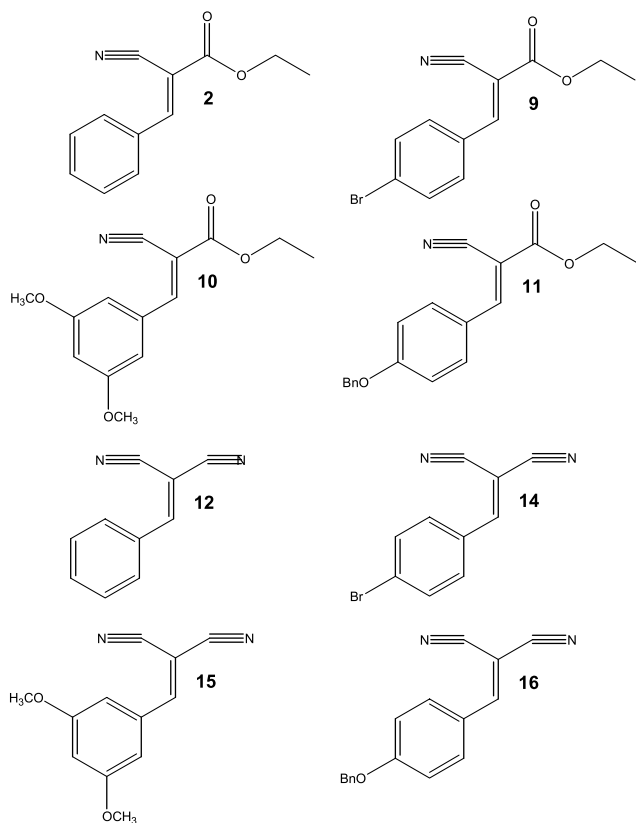


Figure 1. Synthetic targets for preparation in a miniaturised device.

Prior to investigating the incorporation of a silica-supported base within a flow reactor, using the preparation of 2-cyano-3-phenyl acrylic acid ethyl ester **2** as a model reaction, the rate of reaction was compared to a solution phase base at room temperature. As Figure 2 illustrates, compared to piperazine **3**, the rate of conversion is markedly reduced when 3-(1-piperazino)propyl-functionalised silica gel **1** is employed.

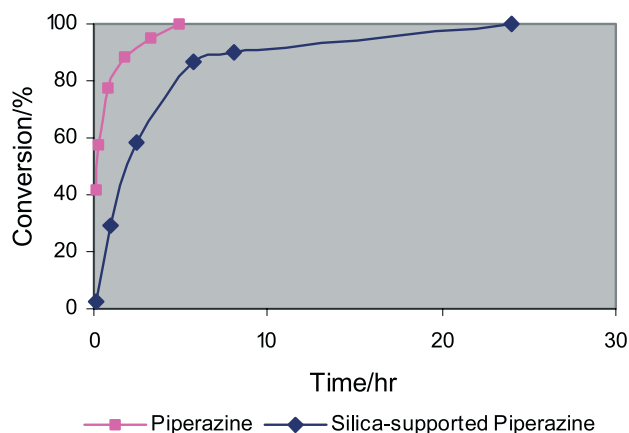


Figure 2. Graph illustrating the rate of conversion when employing solution-phase organic bases compared with solid-phase bases.

Having demonstrated the successful synthesis of 2-cyano-3-phenyl acrylic acid ethyl ester **2** using 3-(1-piperazino)propyl-functionalised silica gel **1**, the next step was to investigate reagent longevity. As Figure 3 illustrates, recycling the reagent results in a significant decrease in conversion to 2-cyano-3-phenyl acrylic acid ethyl ester **2**. As the reaction is base catalysed and the reagent is end-capped to prevent fouling, the increase in reaction time was attributed to a loss of reagent as a result of recycling. In order to confirm this, the reaction was again investigated

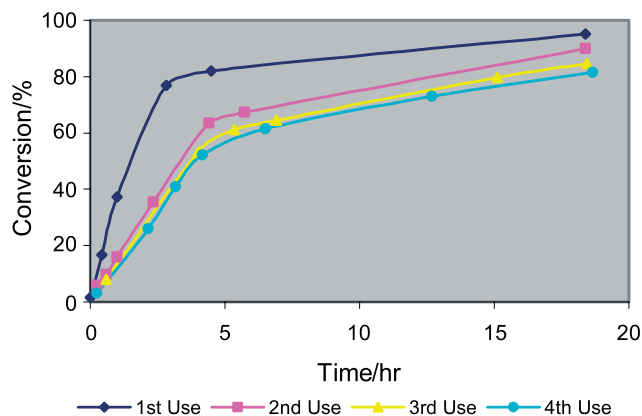


Figure 3. Graph illustrating the effect of recycling a solid supported reagent on the rate of conversion.

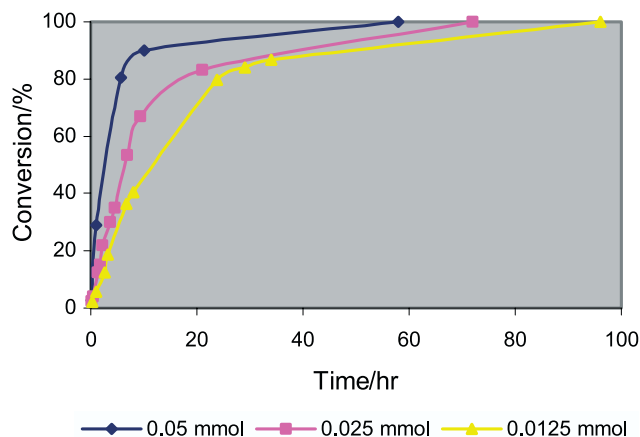


Figure 4. Graph illustrating the effect of base amount on the rate of conversion.

using varying amounts of 3-(1-piperazino)propyl-functionalised silica gel **1** (0.05–0.0125 mmol). As **Figure 4** illustrates, as the quantity of base employed is decreased, the reaction time required increases, confirming the reduction in reaction rate is due to reagent loss. Having demonstrated the ability to recycle 3-(1-piperazino)propyl-functionalised silica gel **1**, the next step was to demonstrate its use in a micro fabricated device.

In order to evaluate the use of silica-supported reagents within an EOF-based system, a miniaturised flow reactor was investigated (**Fig. 5**). This approach not only enabled the reagents to be packed with ease but also provided a relatively inexpensive, versatile system. Although examples of pressure-driven systems have been reported within the literature, owing to its simplicity, the technique of electroosmotic flow (EOF) is demonstrated. The technique is advantageous as it is simple to use, requires no mechanical parts, enables reproducible pulse-free flow and most importantly, with respect to packed systems, generates minimal back-pressure.²¹ As **Figure 6** illustrates, when an ionisable surface such as glass, quartz or Teflon, comes in contact with a suitable solvent system, the surface is neutralised with a diffuse layer of positive ions from the bulk liquid. A proportion of the counterions are adsorbed onto the surface, resulting in the formation of an immobile layer, and the remaining positive ions form a transient

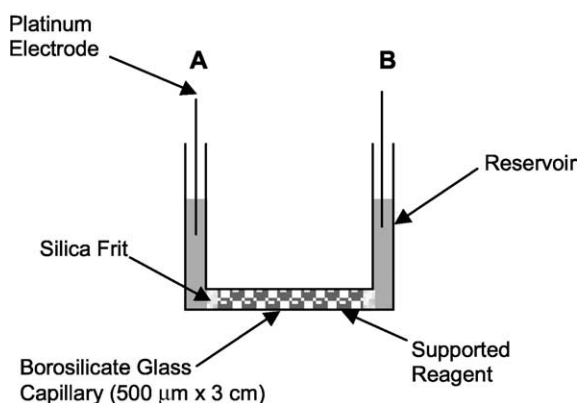


Figure 5. Schematic of the reaction set-up used for the evaluation of solid-supported reagents.

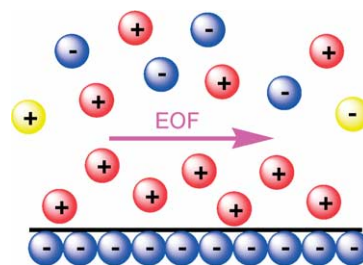


Figure 6. Schematic illustrating the principle of electroosmotic flow.

double layer. Application of an electric field causes the double layer to move towards the most negative electrode, inducing bulk flow within the microchannel.

To perform a reaction, the starting materials are passed over a silica-supported reagent using EOF, reacted for a specified time, collected in the product reservoir and analysed using a chromatographic technique. As **Figure 5** illustrates, 5 mg of 3-(1-piperazino)propyl-functionalised silica gel **1** (4.75×10^{-3} mmol) was packed into a borosilicate glass capillary ($500 \mu\text{m} \times 3 \text{ cm}$) and in order to prevent loss of the reagent, micro porous silica frits were placed at either end.²² The capillary was then primed with MeCN to remove any air, ensuring the formation of a complete circuit, and the capillary attached to two glass reservoirs. The reagents were manipulated through the device via the application of a voltage to the platinum electrodes placed in the reagent reservoirs. As **Figure 7** illustrates, a 1:1 mixture of benzaldehyde **4** and ethylcyanoacetate **5** ($40 \mu\text{l}$, 1.0 M) in MeCN was placed in reservoir A and MeCN in reservoir B ($40 \mu\text{l}$). Application of 333 and 0 V cm^{-1} resulted in the mobilisation of the reaction mixture through the packed bed at a flow rate of $0.5 \mu\text{l min}^{-1}$.

After 20 min, the reaction products were collected in reservoir B, diluted with MeCN and analysed by GC-MS, whereby 98.3% conversion to 2-cyano-3-phenyl acrylic acid ethyl ester **2** was obtained with respect to residual benzaldehyde **4** (**Fig. 8**). Consequently, in order to demonstrate the use of the aforementioned device for the continuous synthesis of 2-cyano-3-phenyl acrylic acid ethyl ester **2**, the reactor was run continually over a period of 4.75 h (14 runs), whereby 0.025 g (0.124 mmol, 98.9%) of product **2** was prepared. As **Table 1** illustrates, reproducible conversions of greater than 98% were obtained demonstrating device stability and reagent longevity. After analysis by GC-MS, the reaction products were collected and concentrated in vacuo, the crude product was then analysed by NMR. As **Figure 9** illustrates, NMR confirms the successful

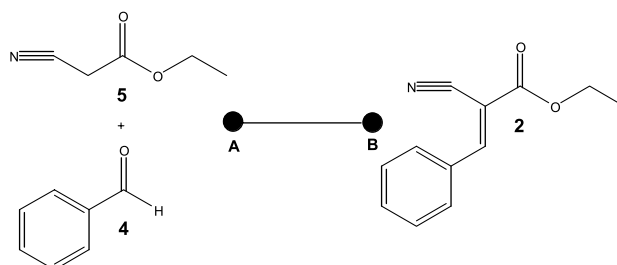


Figure 7. Schematic of the preparation of 2-cyano-3-phenyl acrylic acid ethyl ester **2** in an EOF-based miniaturised device.

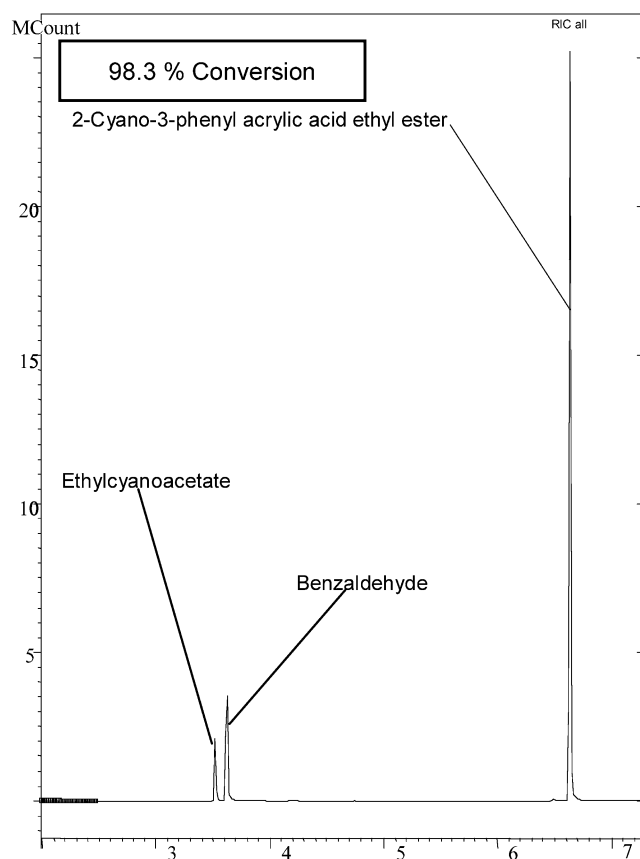


Figure 8. Chromatogram illustrating the synthesis of 2-cyano-3-phenyl acrylic acid ethyl ester **2** within a micro reactor (98.3% conversion).

Table 1. Table illustrating device reproducibility over 4.7 h

Run No.	Conversion (%)
1	98.3
2	98.5
3	98.3
4	98.3
5	98.4
6	99.2
7	99.1
8	99.1
9	100.0
10	99.6
11	99.3
12	100.0
13	100.0
14	99.2

Mean = 99.1%, % RSD = 0.65

synthesis of 2-cyano-3-phenyl acrylic acid ethyl ester **2** in high purity within a micro fabricated device without the need for further purification. Having demonstrated the ability to synthesise 2-cyano-3-phenyl acrylic acid ethyl ester **2**, the technique was repeated using 4-bromobenzaldehyde **6**, 3,5-dimethoxybenzaldehyde **7**, 4-benzyloxybenzaldehyde **8**, to afford the respective condensation products **9**, **10** and **11** in 99.5, 94.7 and 95.1% conversion respectively (Table 2).

Having successfully demonstrated the preparation of an array of condensation products, the technique was extended to the synthesis of 2-benzylidene malononitrile **12**. Using the aforementioned methodology, a 1:1 mixture of malononitrile **13** and benzaldehyde **4** (40 μ l, 1.0 M) in MeCN was placed in reservoir A and MeCN in reservoir B (40 μ l). As malononitrile **13** exhibits a greater electroosmotic mobility cf. ethylcyanoacetate **5**, the applied field was

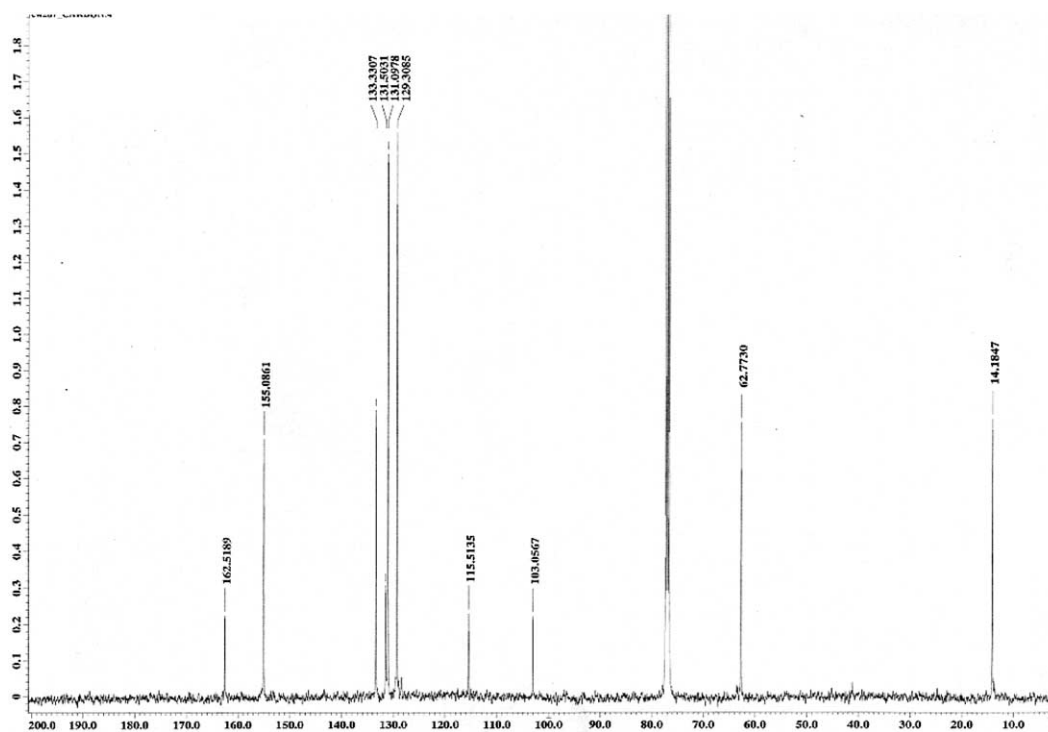


Figure 9. ^{13}C NMR of 2-cyano-3-phenyl acrylic acid ethyl ester **2** synthesised using a micro fabricated device.

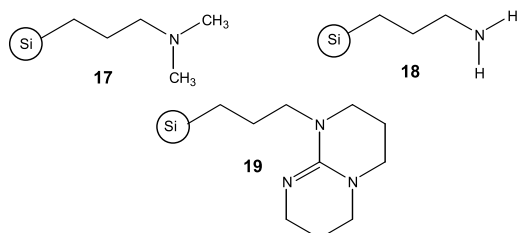
Table 2. Summary of the conversions obtained in a micro fabricated device using 3-(1-piperazino)propyl-functionalised silica gel **1**

Product No.	Applied Field (V cm ⁻¹)	Flow Rate (μl min ⁻¹)	Conversion ^a (%)
2	333	0.5	99.1
9	333	0.3	99.5
10	333	0.3	94.7
11	333	0.5	95.1
12	167	1.0	96.9
14	167	0.5	96.3
15	167	0.7	97.8
16	167	1.0	99.7

^a ≥ 10 replicates were performed for each compound.

reduced in order to obtain comparable flow rates. Application of 167 and 0 V cm⁻¹ resulted in the mobilisation of the reaction mixture through the packed bed, at a flow rate of 1.0 μl min⁻¹, resulting in 96.9% conversion to 2-benzylidene malononitrile **12**. This was subsequently repeated using 4-bromobenzaldehyde **6**, 3,5-dimethoxybenzaldehyde **7**, 4-benzyloxybenzaldehyde **8**, to afford 2-(4-bromobenzylidene)-malononitrile **14** (96.9%), 2-(3,5-dimethoxybenzylidene)-malononitrile **15** (96.3%) and 2-(4-benzyloxybenzylidene)-malononitrile **16** (97.3%) respectively (Table 2). Again, ¹H and ¹³C NMR spectra were obtained for all compounds synthesised within the device demonstrating excellent product purity. In all cases, no by-product formation was observed by GC-MS or NMR spectroscopy. The technique was subsequently repeated using the reagents; 3-(dimethylamino)propyl-functionalised silica gel **17** (1.50 mmol N g⁻¹), 3-aminopropyl-functionalised silica gel **18** (1.00 mmol N g⁻¹) and 3-(1,3,4,6,7,8-hexahydro-2H-pyrimido[1,2-*a*]-pyrimidino)-propyl-functionalised silica gel **19** (2.4 mmol N g⁻¹) (Fig. 10) whereby 99.4, 100 and 99.3% conversion to 2-cyano-3-phenyl acrylic acid ethyl ester **2** were obtained.

Previous work by Macquarrie et al.,²³ demonstrated the use of a 3-aminopropyl-functionalised silica surface in a heated, pressure-driven, aluminium micro reactor. Operating the device at 98 °C enabled 70% conversion of a 1:1 ethylcyanoacetate **5** and benzaldehyde **4** to 2-cyano-3-phenyl acrylic acid ethyl ester **2**. Compared to the work described herein, this approach is disadvantageous as solvent-free techniques are only suitable for the preparation of low viscosity compounds. Also, the elevated reaction temperatures employed, compromises device simplicity. This investigation therefore focussed on the preparation of an array of condensation products at room temperature, within an EOF-based micro fabricated device (Table 3).

**Figure 10.** Schematic of 3-(dimethylamino)propyl-functionalised silica gel **17**, 3-aminopropyl-functionalised silica gel **18** and 3-(1,3,4,6,7,8-hexahydro-2H-pyrimido[1,2-*a*]pyrimidino)propyl-functionalised silica gel **19**.**Table 3.** Comparison of the conversions obtained for the synthesis of 2-cyano-3-phenyl acrylic acid ethyl ester **2** using silica-supported bases **1**, **17**, **18** and **19**

Base	Applied field (V cm ⁻¹)	Flow rate (μl min ⁻¹)	Conversion ^a (%)
1	333	0.5	99.1
17	333	0.35	99.4
18	333	.35	100.0
19	333	0.80	99.3

^a ≥ 10 replicates were performed for each compound.

Using four silica-supported bases, 3-(1-piperazino)propyl-functionalised silica gel **1**, 3-(dimethylamino)propyl-functionalised silica gel **17**, 3-aminopropyl-functionalised silica gel **18** and 3-(1,3,4,6,7,8-hexahydro-2H-pyrimido[1,2-*a*]pyrimidino)propyl-functionalised silica gel **19**, enabled the synthesis of an array of condensation products in excellent conversions when the device was operated at flow rates of <1.0 μl min⁻¹. This technique is therefore suitable for the rapid synthesis of small quantities of compound for biological screening or the preparation of larger quantities by scaling-out.²⁴ The ability to prepare pure compounds in sufficient quantities to obtain structural information is also advantageous as it negates the need to prepare synthetic standards, whilst demonstrating the preparation of compounds of analytical purity. Compared to standard batch techniques employing solid supported reagents, the use of a continuous flow reactor is advantageous as reagents can be recycled without any loss upon filtration, resulting in more consistent conversions over extended periods of operation (Table 1 cf. Fig. 3). Localised concentration gradients enable reactions to be driven to completion without the need to employ large quantities of reagent, that is, 5 mg (4.75 × 10⁻⁴ mmol) in a micro reactor enables conversions in excess of 95% to be attained in minutes compared with >95 h in batch (Fig. 4, 0.0125 mmol).

3. Conclusions

In conclusion, we have demonstrated the successful incorporation of a series of silica-supported bases within an EOF-based micro-fabricated device, enabling the synthesis and characterisation of eight condensation products. Using the methodology described herein, further studies are currently underway within our laboratories to extend both the type of reagent and support employed, enabling more complex syntheses to be demonstrated.

4. Experimental

4.1. Materials and methods

All materials (analytical grade) were purchased from Aldrich and were used without purification. All NMR spectra were recorded as solutions in deuteriochloroform (CDCl₃) using tetramethylsilane (TMS) as an internal standard. The spectra were recorded on a Joel GX400 spectrometer and the chemical shifts are given in parts per million (ppm) with coupling constants given in Hertz (Hz). The following abbreviations are used to report NMR data; s=singlet, d=doublet, t=triplet, br s=broad singlet, m=

multiplet and C_0 = quaternary carbon. Gas chromatography-mass spectrometry (GC-MS) was performed using a Varian GC (CP-3800) coupled to a Varian MS (2000) with a CP-Sil 8 (30 m) column (Phenomenex) and ultra high purity helium (99.999% Energas) carrier gas. Samples were analysed using one of the following methods; Method A: injector temperature 250 °C, helium flow rate 1.0 ml min⁻¹, oven temperature 60 °C for 1.0 min and then ramped to 270 °C at 35 °C min⁻¹, with a 3.0 min filament delay or; Method B: injector temperature 250 °C, helium flow rate 1.0 ml min⁻¹, oven temperature 60 °C for 1.0 min and then ramped to 270 °C at 20 °C min⁻¹, with a 3.0 min filament delay.

4.2. Batch reactions

4.2.1. General procedure for the solution-phase synthesis of Knoevenagel condensation products in batch. Piperazine **3** (0.09 g, 0.1 mmol) was added to a stirred solution of activated methylene (1.0 mmol) and aldehyde (1.0 mmol) in anhydrous MeCN (10 ml mmol⁻¹). After stirring overnight, the reaction mixture was concentrated in vacuo prior to the addition of dilute HCl (50 ml, 0.1 M) and the reaction products extracted into DCM (3 × 50 ml). The combined extracts were dried (MgSO₄) and concentrated in vacuo, subsequent recrystallisation from DCM/hexane afforded the respective condensation product.

4.2.2. General procedure for the solid-phase synthesis of Knoevenagel condensation products in batch. 3-(1-Piperazino)propyl-functionalised silica gel **1** (1.9 mmol N g⁻¹, 200–400 mesh) (0.10 g, 0.1 mmol) was added to a stirred solution of activated methylene (1.0 mmol) and aldehyde (1.0 mmol) in anhydrous MeCN (10 ml mmol⁻¹). After stirring overnight, the reaction mixture was filtered and the filtrate concentrated in vacuo to afford the respective condensation product.

4.3. Micro-scale methodology

The reactions described herein were carried out using a single capillary device, as illustrated in Figure 5, with capillary dimensions of 500 μm i.d. × 3.0 cm. To hold the supported reagent in place, micro porous silica frits were placed at either end of the capillary.²² To mobilise reagents by EOF, platinum electrodes (0.5 mm o.d. × 2.5 cm) were placed within the reagent reservoirs and voltages applied using a Paragon 3B high-voltage power supply (HVPS), capable of applying 0–1000 V to four pairs of outputs (Kingfield Electronics). Automation of the HVPS was achieved using an in-house LabVIEW™ program. To enable the results obtained to be attained using devices of different dimensions, voltages are reported as applied fields (V cm⁻¹), that is, voltage/capillary length. To monitor the progress of the reaction, experiments were conducted over a period of 20 min, after which, the product reservoir was analysed by GC-MS, whereby comparison of the amount of product with respect to residual aldehyde enabled the percentage conversion to be determined. In order to obtain NMR data on the compounds synthesised in the flow system, the reactors were operated continuously for 3–5 h, after which the reaction products were concentrated in vacuo and the crude compound analysed.

4.3.1. 2-Cyano-3-phenyl acrylic acid ester 2²⁵. (0.0253 g, 98.9%) as a white solid; δ_H 1.41 (3H, t, $J=7.0$ Hz, CH₂CH₃), 4.39 (2H, q, $J=7.0$ Hz, CH₂CH₃), 7.53 (3H, m, Ar), 7.99 (2H, m, Ar) and 8.26 (1H, s, CH); δ_C 14.2 (CH₃), 62.8 (CH₂), 103.1 (C₀CN), 115.5 (CN), 129.3 (2 × CH), 131.0 (2 × CH), 131.5 (C₀), 133.3 (CH), 155.1 (CH) and 162.5 (CO); m/z (EI) 202 (M⁺ + 1, 70%), 201 (100), 172 (80), 156 (90), 128 (75), 102 (55), 77 (50) and 51 (50); GC-MS retention time (Method A) $R_T=6.63$ min.

4.3.2. 3-(4-Bromophenyl)-2-cyano acrylic acid ethyl ester 9²⁶. (0.0118 g, 99.5%) as a white solid; δ_H 1.40 (3H, t, $J=7.3$ Hz, CH₂CH₃), 4.39 (2H, q, $J=7.3$ Hz, CH₂CH₃), 7.65 (2H, d, $J=8.7$ Hz, Ar), 7.86 (2H, d, $J=8.7$ Hz, Ar) and 8.19 (1H, s, CH); δ_C 14.2 (CH₃), 62.9 (CH₂), 103.7 (C₀CN), 115.3 (CN), 128.3 (C₀Br), 130.3 (C₀), 132.3 (2 × CH), 132.7 (2 × CH), 153.6 (CH) and 162.3 (CO); 281 (M⁺ + 1, 90%), 280 (45), 279 (100), 251 (25), 200 (20), 154 (10), 127 (25), 100 (20) and 76 (20); GC-MS retention time (Method B) $R_T=10.84$ min.

4.3.3. 3-(3,5-Dimethoxyphenyl)-2-cyano acrylic acid ethyl ester 10²⁷. (0.0109 g, 99.5%) as a white solid; δ_H 1.40 (3H, t, $J=7.0$ Hz, CH₂CH₃), 3.85 (6H, s, 2 × OCH₃), 4.39 (2H, q, $J=7.0$ Hz, CH₂CH₃), 6.65 (1H, m, Ar), 7.15 (2H, m, Ar) and 8.17 (1H, s, CH); δ_C 14.2 (CH₃), 55.7 (2 × OCH₃), 62.8 (CH₂), 103.4 (C₀CN), 106.2 (CH), 108.6 (2 × CH), 115.6 (CN), 133.1 (C₀), 155.2 (CH), 161.1 (2 × C₀) and 162.5 (CO); 262 (M⁺ + 1, 20%), 261 (100), 189 (55), 161 (25) and 77 (10); GC-MS retention time (Method A) $R_T=8.06$ min.

4.3.4. 3-(4-Benzyloxyphenyl)-2-cyano acrylic acid ethyl ester 11. (0.0211 g, 99.1%) as a cream solid (Found C, 74.51; H, 5.77; N, 4.62. C₁₉H₁₇O₃N requires C, 74.25; H, 5.58; N, 4.56%); δ_H 1.39 (3H, t, $J=7.3$ Hz, CH₂CH₃), 4.37 (2H, q, $J=7.3$ Hz, CH₂CH₃), 5.15 (2H, s, CH₂), 7.00 (2H, d, $J=8.7$ Hz, Ar), 7.40 (5H, m, Ar), 7.99 (2H, d, $J=8.7$ Hz, Ar) and 8.17 (1H, s, CH); δ_C 14.2 (CH₃), 62.5 (CH₂), 70.4 (C₀CH₂), 99.5 (C₀), 115.6 (2 × CH), 124.6 (CN), 127.5 (2 × CH), 128.4 (CH), 128.8 (2 × CH), 133.7 (2 × CH), 135.8 (C₀), 154.4 (CH), 162.9 (OC₀) and 163.1 (CO); 308 (M⁺ + 1, 5%), 307 (20), 91 (100) and 65 (20); GC-MS retention time (Method B) $R_T=12.35$ min.

4.3.5. 2-Benzyldiene-malononitrile 12²⁵. (0.0154 g, 100%) as a pale yellow solid; δ_H 7.55 (2H, m, Ar), 7.64 (1H, m, Ar), 7.79 (1H, s, CH) and 7.91 (2H, m, Ar); δ_C 83.0 (C₀), 112.6 (CN), 113.7 (CN), 129.7 (2 × CH), 130.8 (2 × CH), 131.0 (C₀), 134.7 (CH) and 159.9 (CH); 155 (M⁺ + 1, 20%), 154 (100), 127 (20) and 76 (10); GC-MS retention time (Method A) $R_T=5.84$ min.

4.3.6. 2-(4-Bromobenzylidene)-malononitrile 14²⁸. (0.0349 g, 99.9%) as a pale yellow solid; δ_H 7.69 (2H, d, $J=8.4$ Hz, Ar), 7.72 (1H, s, CH) and 7.77 (2H, d, $J=8.4$ Hz, Ar); δ_C 83.6 (C₀), 112.3 (CN), 113.5 (CN), 129.7 (C₀Br), 130.0 (C₀), 131.8 (2 × CH), 133.1 (2 × CH) and 158.4 (CH); 235 (M⁺ + 1, 70%), 234 (100), 233 (95), 232 (90), 153 (25) and 77 (10); GC-MS retention time (Method B) $R_T=9.65$ min.

4.3.7. 2-(3,5-Dimethoxybenzylidene)-malononitrile 15²⁵.

(0.0240 g, 99.2%) as a yellow solid; δ_{H} 3.84 (6H, s, OCH₃), 6.70 (1H, m, Ar), 7.03 (2H, m, Ar) and 7.69 (1H, s, CH); δ_{C} 55.7 (2×OCH₃), 83.2 (C₀), 107.3 (CH), 108.3 (2×CH), 112.7 (CN), 113.7 (CN), 132.4 (C₀), 160.1 (CH) and 161.3 (2×C₀OCH₃); 215 (M⁺+1, 25%), 214 (100), 186 (55), 171 (20), 155 (20), 142 (15), 114 (10) and 76 (10); GC-MS retention time (Method A) $R_{\text{T}}=7.50$ min.

4.3.8. 2-(4-Benzyloxybenzylidene)-malononitrile 16²⁹. (0.0235 g, 99.6%) as a pale yellow solid; δ_{H} 5.17 (2H, s, CH₂), 7.08 (2H, d, $J=9.0$ Hz, Ar), 7.39 (5H, m, Ar), 7.64 (1H, s, CH) and 7.90 (2H, d, $J=9.0$ Hz, CH); δ_{C} 70.6 (CH₂), 78.8 (C₀), 113.3 (CN), 114.4 (CN), 116.0 (2×CH), 124.2 (C₀), 127.5 (2×CH), 128.6 (CH), 128.9 (2×CH), 133.5 (2×CH), 135.5 (C₀), 158.8 (CH) and 163.9 (OC₀); 261 (M⁺+1, 5%), 260 (5), 114 (10) and 91 (100); GC-MS retention time (Method B) $R_{\text{T}}=11.97$ min.

Acknowledgements

Full financial support provided by the EPSRC (Grant No. GR/S34106/01) is gratefully acknowledged. Mike Bailey (University of Hull) is also acknowledged for assistance in the device fabrication.

References

- Fletcher, P. D. I.; Haswell, S. J.; Pombo-Villar, E.; Warrington, B. H.; Watts, P.; Wong, S. Y. F.; Zhang, X. *Tetrahedron* **2002**, *58*, 4735.
- Schwalbe, T.; Volker, A.; Wille, G. *Chimia* **2002**, *56*, 636.
- Brody, J.; Yager, P. *Sens. Actuators A* **1997**, *58*, 13.
- (a) McKillop, A.; Young, D. W. *Synthesis* **1979**, 422. (b) McKillop, A.; Young, D. W. *Synthesis* **1979**, 481.
- Terrett, N. K.; Gardner, M.; Gordon, D. W.; Kobylecki, R. J.; Steele, J. *Tetrahedron* **1995**, *51*, 8135.
- Ley, S. V.; Baxendale, I. R.; Bream, R. N.; Jackson, P. S.; Leach, A. G.; Longbottom, D. A.; Nesi, M.; Scott, J. S.; Storer, R. I.; Taylor, S. J. *J. Chem. Soc., Perkin Trans. 1* **2000**, 3815.
- Shuttleworth, S. J.; Allin, S. M.; Sharma, P. K. *Synthesis* **1997**, 1217.
- Sen, S. E.; Smith, S. M.; Sullivan, K. A. *Tetrahedron* **1999**, *55*, 12657.
- Varma, R. S. *Tetrahedron* **2002**, *58*, 1235.
- Singh, R. P.; Subbarao, H. N.; Dev, S. *Tetrahedron* **1980**, *37*, 846.
- Jones, G. *Org. React.* **1967**, *15*, 204 and references therein.
- Togni, A.; Pastor, S. D. *J. Org. Chem.* **1990**, *55*, 1649.
- Trost, B. M.; Florez, J.; Jebaratnam, D. J. *J. Am. Chem. Soc.* **1987**, *109*, 613.
- Rappoport, Z.; Patai, S. *J. Chem. Soc., Perkin Trans. 1* **1962**, 731.
- McCluskey, A.; Robinson, P. J.; Hill, T.; Scott, J. L.; Edwards, J. K. *Tetrahedron Lett.* **2002**, *43*, 3117.
- Cruz de la, P.; Diez-Barra, E.; Loupy, A.; Langa, F. *Tetrahedron Lett.* **1996**, *37*, 1113.
- Lai, S. M.; Martin-Aranda, R.; Yeung, K. L. *J. Chem. Soc., Chem. Commun.* **2003**, 218.
- Texier-Boulett, F.; Foucod, A. *Tetrahedron Lett.* **1982**, *23*, 4927.
- Simpson, J.; Rathbone, D. L.; Billington, D. C. *Tetrahedron Lett.* **1999**, *40*, 7031.
- Angeletti, E.; Canepa, C.; Martinetti, G.; Venturello, P. *J. Chem. Soc., Perkin Trans. 1* **1989**, 105.
- Fletcher, P. D. I.; Haswell, S. J.; Paunov, V. N. *Analyst* **1999**, *124*, 1273.
- Christensen, P. D.; Johnson, S. W. P.; McCreedy, T.; Skelton, V.; Wilson, N. G. *Anal. Commun.* **1998**, *35*, 341.
- Jackson, T.; Clark, J. H.; Macquarrie, D. J.; Brophy, J. H. *Green Chem.* **2004**, *6*, 193.
- Ehrfeld, W.; Hessel, V.; Lowe, H. *Microreactors: New Technology for Modern Chemistry*; VCH: Wiley, 2000.
- Choudray, B. M.; Lakshmi Kantam, M.; Kavita, B.; Venkat Reddy, C.; Figueras, F. *Tetrahedron* **2000**, *56*, 9357.
- Shen, Y.; Yang, B. *Synth. Commun.* **1989**, 3069.
- Arya, V. P.; Ghate, S. P. *Indian J. Chem.* **1971**, *9*, 1209.
- Obrador, E.; Castro, M.; Tamariz, J.; Zepeda, G.; Miranda, R. *Synth. Commun.* **1998**, 4649.
- Cornelis, A.; Lambert, S.; Laszlo, P. *J. Org. Chem.* **1977**, *42*, 381.

Electrochemical effects related to synthesis in micro reactors operating under electrokinetic flow

Paul Watts^{a,*}, Stephen J. Haswell^a, Esteban Pombo-Villar^b

^a Department of Chemistry, University of Hull, Cottingham Road, Hull HU6 7RX, UK

^b Novartis Institute for Biomedical Research, WSJ-386.07.15, CH 4002, Basel, Switzerland

Abstract

We have demonstrated that peptides may be prepared in quantitative conversion in a micro reactor by reaction of the pentafluorophenyl (PFP) ester derivatives of protected amino acids. It was found that performing these reactions in a micro reactor operating under electrokinetic control resulted in an increase in reaction efficiency compared with the traditional batch method. By addition of an electrode to batch reactions, we propose that the enhancement in reaction rate is due to an electrochemical effect.

© 2003 Elsevier B.V. All rights reserved.

Keywords: Pentafluorophenyl ester; Micro reactor; Electrokinetic flow

1. Introduction

Micro reactors generally consist of a series of interconnecting channels formed in a planar surface, in which small quantities of reagents are manipulated [1,2]. To perform a chemical reaction, reagents are brought together in a laminar or slug flow diffusive mixing regime and are allowed to react for a specified time in a controlled region of the reactor. The ability to manipulate reagent concentrations and reaction interfaces in both space and time within the channel network provides a level of reaction control, which is not attainable in traditional bulk reactors. The spatial and temporal control of reactions in the chemically intensive environment of micro reactors, coupled with the features of very small reaction volumes and high surface interactions has been demonstrated to give faster reactions and improved product yields, with greater product selectivity compared with conventional bench top methodology [3–12].

To illustrate the principles of electroosmotic flow (EOF) [13], one can consider a micro channel fabricated from a material having negatively charged functional groups on the surface. If a liquid, displaying some degree of dissociation, is brought into contact with the surface, positive counterions will form a double layer. Application of an electric field causes this layer to move towards the negative electrode, thus causing the bulk liquid to move within the channel (Fig. 1).

Importantly, when using EOF plugs of fluid are transported without significant hydrodynamic dispersion, which is not the case with hydrodynamic pumping.

When operating micro reactors under electrokinetic control, two unique processes occur which influence the reaction properties that are fundamentally different to those associated with bulk reactions. The first mechanism relates to properties associated with the electroosmotic and electrophoretic mobilities of solvents and individual species, which in addition to offering excellent spatial and temporal control, enables localised thermal, electric field and concentration gradients to be generated in pre-defined sections of a channel network. The second process is more specifically associated with the presence of an electrical field and relates to the possibility of performing electrochemically based processes within a micro reactor channel.

In order to exploit more fully the electrochemical effects within the channels of a micro reactor, operating under electrokinetic control, high voltages (typically up to 1500 V) need to be applied across electrodes placed in the reagent reservoirs. The conductivities for common solvents are of the order of $500 \mu\text{S cm}^{-1}$, with the result that the electrical resistances of the channel sections are typically of the order of tens of megaohms. Hence, nearly all the voltage drop occurs within the channel of the reactor. This has the consequence that the voltage drop across the electrode–solution interface is usually very small and may or may not be sufficient to drive an electrochemical reaction. The micro reactor situation is therefore very different to the usual electrochemical cell in which a small voltage (e.g. 2 V) is

* Corresponding author. Tel.: +44-1482-465471;

fax: +44-1482-466416.

E-mail address: p.watts@hull.ac.uk (P. Watts).

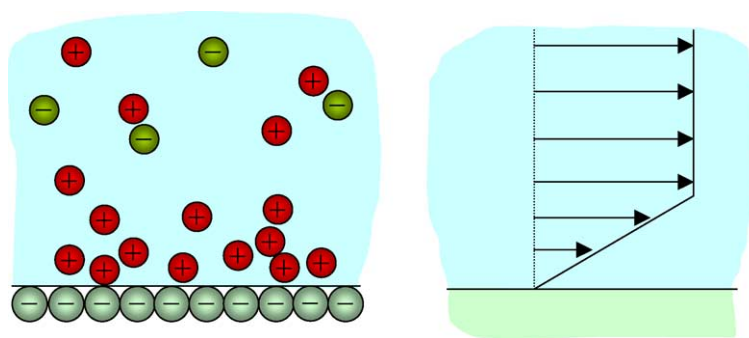


Fig. 1. Principle of electroosmotic flow.

mainly localised across the electrode–solution interfaces in a cell where the resistance of the intervening solution is low [14,15]. Experimental observations when using micro reactors show that electrochemical reactions can be induced at high voltages, particularly when the resistance of the channel section between the electrodes is relatively low. Thus, at low operating voltages when electrochemical effects are absent, the progress of chemical reactions in micro reactors are controlled solely by the localised concentrations. At high operating voltages, additional effects due to electrochemical processes may be present. In this paper, we report the effect of reaction rates when performed in micro reactors operating under electrokinetic control. It should be noted that Yoshida and coworkers [16,17] have recently reported electrochemical reactions in micro reactors, however, they hydrodynamically pumped the reactants through an electrochemical cell.

2. Experimental

The borosilicate glass micro reactors used in this work were prepared using standard fabrication procedures developed at Hull [18]. The reactions were carried out in a T-shaped micro reactor with approximate channel dimensions of $200 \text{ mm} \times 50 \text{ }\mu\text{m}$ and outer dimensions of $20 \text{ mm} \times 20 \text{ mm} \times 25 \text{ mm}$. Micro porous silica frits were placed within the channels in order to minimise hydrodynamic effects [19]. Prior to synthesis, the micro reactor channels were primed with anhydrous solvent to remove air and moisture from the channels and the micro porous silica frits. Platinum electrodes were placed in each of the reservoirs of the micro reactor and an external voltage was applied to the channels inducing electroosmotic flow of the reagents. The power supply was manufactured by Kingfield Electronics (Sheffield, UK) and was controlled using LabVIEW™ software.

The reactions were conducted at room temperature for a period of 20 min, in order to acquire sufficient volume of product to determine the conversion of the reaction. Reaction products were determined by HPLC via comparison with retention times and spectra with those obtained from synthetic standards. Analysis was achieved by high performance liquid chromatography (Jupiter C_{18} $10 \text{ }\mu\text{m}$, $4.6 \text{ mm} \times 250 \text{ mm}$, mobile phase composition: 0.1% trifluoroacetic acid in water

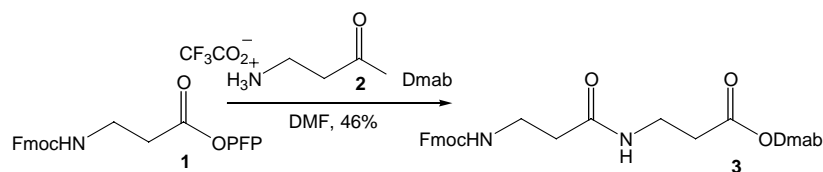
and 0.1% trifluoroacetic acid in acetonitrile, using a gradient system of 30% aqueous to 70% aqueous over 20 min, with a flow rate of 2.5 ml min^{-1} at room temperature). Product conversions were based on the amount of pentafluorophenyl (PFP) ester remaining in the sample.

3. Results

We have recently demonstrated that the multi-step synthesis of peptides may be performed within micro reactors [20,21]. In a series of examples we demonstrated that peptide bonds were produced in quantitative conversion in much shorter periods of time when prepared in the micro reactor environment in comparison to batch reactions. Furthermore, when reactions involving α -amino acids were conducted less racemisation was observed compared with batch reactions and this is attributed to the enhanced speed of the reactions [22]. In this paper, we report a more detailed study on the aforementioned observations.

In a batch reaction between pentafluorophenyl ester **1** and amine **2** we found that dipeptide **3** was produced in 46% yield, using *N,N*-dimethylformamide (DMF) as solvent (Scheme 1).

In a micro reactor a standard solution of the pentafluorophenyl ester of Fmoc- β -alanine **1** ($50 \text{ }\mu\text{l}$, 0.1 M) in anhydrous DMF was added to reservoir A, a solution of amine **2** ($50 \text{ }\mu\text{l}$, 0.1 M) was placed in reservoir B and anhydrous DMF ($40 \text{ }\mu\text{l}$) was placed in reservoir C, which was used to collect the products of the reaction (Fig. 2). Platinum electrodes were placed in each of the reservoirs (A and B positive, C ground) and an external voltage was applied to the channels inducing electroosmotic flow of the reagents. The reactions were conducted at room temperature for a period of 20 min, in order to acquire sufficient volume of product to determine the conversion of the reaction by HPLC. It was found that using continuous flow of both reagents in the micro reactor, where reservoir A was maintained at 700 V and reservoir B was maintained at 600 V, dipeptide **3** was produced in 100% conversion in 20 min. This represented a significant increase in conversion compared with the traditional batch synthesis, for which 46% yield was obtained in 24 h.



Scheme 1. Preparation and reaction of PFP esters.

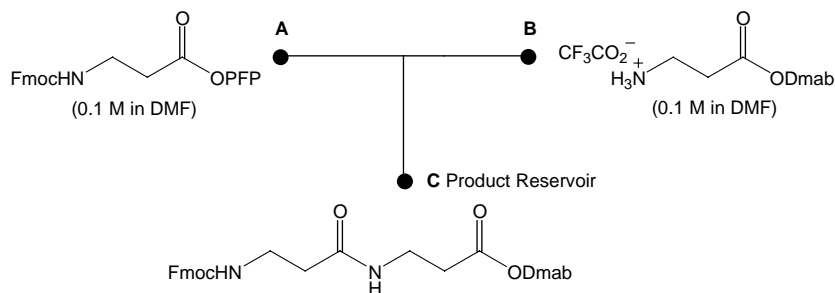
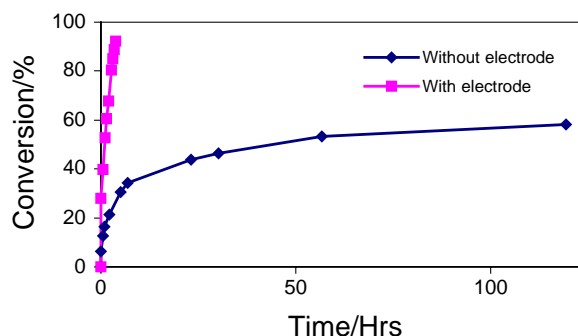


Fig. 2. Schematic of micro reactor manifold.

We were interested to observe that the reaction between pentafluorophenyl ester **1** and amine **2** appeared to be much faster in a micro reactor than when performed in batch. However, batch reactions are generally performed at much higher concentrations than in micro reactors. In order to make meaningful comparison between rates of reaction we monitored the conversion of pentafluorophenyl ester **1** (200 μ l, 0.1 M) and amine **2** (200 μ l, 0.1 M) into peptide **3**, at the same concentration as used in the micro reactor studies. It can be seen from Fig. 3, that the bulk reaction is very slow with approximately 60% conversion to product in approximately a week. The data suggests that in 20 min, the duration of a micro reactor reaction, only 10% conversion to dipeptide should be obtained.

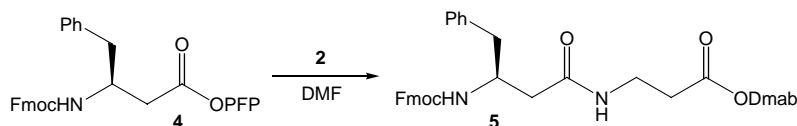
In an attempt to further understand the enhancement in rate of reaction the pentafluorophenyl ester **1** (200 μ l, 0.1 M) and amine **2** (200 μ l, 0.1 M) were again mixed, but in this case a 10 V electrode and a ground electrode were placed in the reaction mixture. The two electrodes were approximately 5 mm apart. It can be seen from Fig. 3, that the electrodes have the effect of enhancing the rate of reaction such that 90% conversion was obtained in under 4 h. The data also illustrates that less than 30% conversion was observed in 4 h when the electrodes were absent. This implies that the enhancement in rate of reaction is due to an electrochemical phenomenon.

It should be emphasised that the voltage was set at 10 V in order to produce a current (ca. 5 μ A) similar to that ob-

Fig. 3. Reaction of PFP ester **1** (0.1 M) with amine **2** (0.1 M) in a batch reaction at room temperature, with and without electrodes.

served within the micro reactor situation. Nevertheless, the reaction conducted within the micro reactor, operating under electrokinetic control, still appears to be even faster than the batch reaction performed under electrochemical control. This can be attributed to the effect of increased diffusional mixing within the micro reactor environment.

To illustrate that rate enhancement was always observed in such reactions the pentafluorophenyl ester **4** of Fmoc-L- β -homo phenylalanine was reacted with amine **2** to prepare a synthetic sample of dipeptide **5** in 35% yield in a batch reaction (Scheme 2). The reaction was subsequently investigated in the micro reactor. A solution of the pentafluorophenyl ester **4** in anhydrous DMF (50 μ l, 0.1 M) was



Scheme 2. Batch reaction to study reaction kinetics.

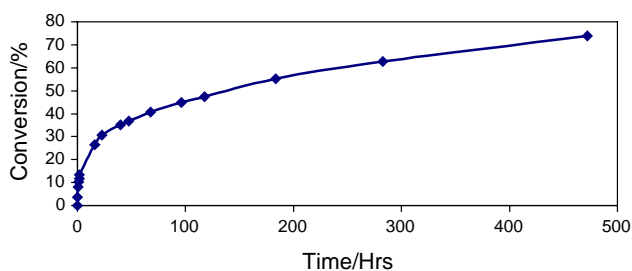


Fig. 4. Conversion of PFP ester **4** (0.1 M) to dipeptide **5** in a batch reaction at room temperature.

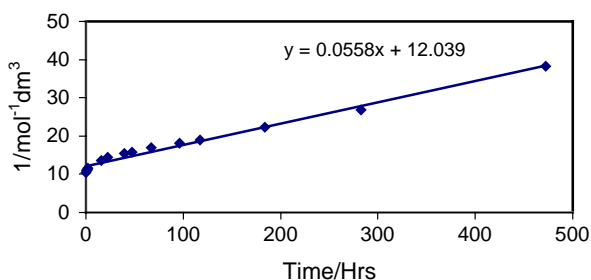


Fig. 5. Graph of pentafluorophenyl ester **1** concentration during the reaction to produce dipeptide **5**.

added to reservoir A, a solution of amine **2** (50 μ l, 0.1 M) was placed in reservoir B and anhydrous DMF was placed in reservoir C (40 μ l) to collect the product of the reaction. It was found that using continuous flow of both reagents, where the ester **4** was maintained at 900 V and the amine **2** was maintained at 600 V, dipeptide **5** was produced in 100% conversion in a 20 min period. Again this represented a significant increase in conversion compared with the batch reaction.

We monitored the conversion of pentafluorophenyl ester **4** into peptide **5**, where 0.1 M solutions of reagents were mixed in a batch reaction. It can be seen from Fig. 4, that the batch reaction is very slow with approximately 70% conversion to product in 500 h. The data in Fig. 4 was subsequently used to calculate how the concentration of the pentafluorophenyl ester **4** changes during the reaction. Fig. 5 illustrates that the reaction is indeed second order as expected, which implies that no other chemical species are involved in the reaction.

4. Conclusions

We have demonstrated that peptide bonds may be prepared in high conversion from pre-activated derivatives of

amino acids such as pentafluorophenyl esters. It was found that performing these reactions in the micro reactor resulted in an increase in the reaction efficiency over the traditional batch method. By addition of an electrode to batch reactions we have demonstrated that the enhancement in rate of reaction is due to an electrochemical phenomenon. Subsequent analysis of amine **2** showed that the compound was actually the trifluoroacetate salt rather than the free amine as originally thought. It is proposed that the salt is converted into the free amine at the electrode, consequently the more reactive amine leads to a faster reaction. Nevertheless, the reaction is still faster when performed within the micro reactor rather than in batch which is attributed to the faster mixing which occurs within micro fluidic systems.

References

- [1] W. Ehrfeld, V. Hessel, H. Löwe, *Microreactors: New Technology for Modern Chemistry*, Wiley-VCH, 2000.
- [2] M. Madou, *Fundamentals of Microfabrication*, CRC Press, Boca Raton, 1997.
- [3] P.D.I. Fletcher, S.J. Haswell, E. Pombo-Villar, B.H. Warrington, P. Watts, S.Y.F. Wong, X. Zhang, *Tetrahedron* 58 (2002) 4735.
- [4] G.M. Greenway, S.J. Haswell, D.O. Morgan, V. Skelton, P. Styring, *Sens. Actuators B* 63 (2000) 153.
- [5] N.G. Wilson, T. McCreedy, *Chem. Commun.* (2000) 733.
- [6] V. Skelton, G.M. Greenway, S.J. Haswell, P. Styring, D.O. Morgan, B.H. Warrington, S.Y.F. Wong, *Analyst* 126 (2001) 7.
- [7] V. Skelton, G.M. Greenway, S.J. Haswell, P. Styring, D.O. Morgan, B.H. Warrington, S.Y.F. Wong, *Analyst* 126 (2001) 11.
- [8] R.D. Chambers, R.C.H. Spink, *Chem. Commun.* (1999) 883.
- [9] E. Garcia-Egido, S.Y.F. Wong, B.H. Warrington, *Lab on a Chip* 2 (2002) 170.
- [10] M. Fernandez-Suarez, S.Y.F. Wong, B.H. Warrington, *Lab on a Chip* 2 (2002) 31.
- [11] H. Lu, M.A. Schmidt, K.F. Jenson, *Lab on a Chip* 1 (2001) 22.
- [12] R.C.R. Wootton, R. Fortt, A.J. de Mello, *Org. Process Res. Dev.* 6 (2002) 187.
- [13] P.D.I. Fletcher, S.J. Haswell, V.N. Paunov, *Analyst* 124 (1999) 1273.
- [14] J. Utlej, *Chem. Soc. Rev.* 26 (1997) 157.
- [15] K.D. Moeller, *Tetrahedron* 56 (2000) 9527.
- [16] S. Suga, M. Okajima, K. Fujiwara, J. Yoshida, *J. Am. Chem. Soc.* 123 (2001) 7941.
- [17] J. Yoshida, S. Suga, *Chem. Eur. J.* 8 (2002) 2651.
- [18] T. McCreedy, *Anal. Chim. Acta* 427 (2001) 39.
- [19] P.D. Christensen, S.W.P. Johnson, T. McCreedy, V. Skelton, N.G. Wilson, *Anal. Commun.* 35 (1998) 341.
- [20] P. Watts, C. Wiles, S.J. Haswell, E. Pombo-Villar, P. Styring, *Chem. Commun.* (2001) 990.
- [21] P. Watts, C. Wiles, S.J. Haswell, E. Pombo-Villar, *Tetrahedron* 58 (2002) 5427.
- [22] P. Watts, C. Wiles, S.J. Haswell, E. Pombo-Villar, *Lab on a Chip* 2 (2002) 5427.



Asymmetric catalysis in a micro reactor—Ce, Yb and Lu catalysed enantioselective addition of trimethylsilyl cyanide to benzaldehyde

Christina Jönsson,^a Stina Lundgren,^a Stephen J. Haswell^b and Christina Moberg^{a,*}

^aDepartment of Chemistry, Organic Chemistry, Royal Institute of Technology, SE-100 44 Stockholm, Sweden

^bDepartment of Chemistry, University of Hull, Cottingham Road, HU6 7RX, UK

Received 24 June 2004; revised 3 August 2004; accepted 23 August 2004

Available online 21 September 2004

Abstract—A T-shaped micro reactor was used for the optimisation of reaction conditions for the enantioselective silylcyanation of benzaldehyde catalysed by lanthanide–pybox complexes. Compared to a conventional batch procedure, higher conversion was observed within shorter reaction time. The micro reactor process involving Lu(III) afforded essentially the same enantioselectivity as the batch process (73 vs 76% ee), whereas the enantioselectivity was lower in the micro reactor for catalysts containing Yb(III) (53 compared to 72%). Ce(III) provided very low selectivity in both types of processes (1 and 11% ee, respectively). A study of the effect of additives showed that the enantioselectivity in the Yb catalysed reaction performed in the micro reactor could be increased to 66%, whereas only a minor improvement, to 78% ee, was observed in the reaction with Lu.

© 2004 Elsevier Ltd. All rights reserved.

1. Introduction

Asymmetric metal catalysis constitutes a powerful method for the preparation of chiral compounds in enantiomerically pure form.¹ Although highly selective catalysts have been found for a large number of catalytic processes, the structure of the catalyst and the reaction conditions usually need to be optimised for each particular reaction and for each particular substrate. To achieve this in an efficient manner, procedures based on combinatorial chemistry and parallel synthesis techniques involving high throughput screening are frequently used today.² As screening of large numbers of reaction parameters and reaction conditions often requires large quantities of reagents and consumables, downsizing of reactions,³ enabling fast screening with minimal consumption of reagents, is desirable. For this reason, various types of micro reactors have been constructed.⁴

A micro reactor can consist of sensors, pumps, valves and mixers, integrating chemistry with mechanics, electronics, optics and analysis. The mobilisation of the reagents/solvents within the device is usually achieved by external

pumps (syringe pumps or microfabricated pumps) or by electroosmosis.⁵ The use of an electroosmotic flow (EOF) is well-explored⁶ and some of the most recent applications within the field of organic synthesis using EOF are multi-step syntheses of peptides,⁷ Wittig reactions⁸ and aldol condensations,⁹ as well as metal catalysed reactions such as Suzuki couplings.¹⁰

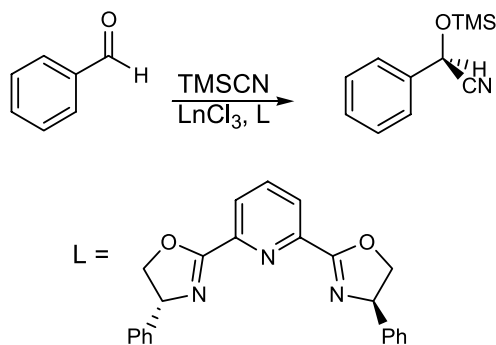
Whilst both homogeneous¹¹ and heterogeneous^{8,12} catalysis have been performed using micro reactor technology, asymmetric catalysis has not yet been explored. In this communication we describe lanthanide catalysed silylcyanations of benzaldehyde performed in a micro reactor under electroosmotic control. Cyanohydrins are important building blocks in synthetic organic chemistry as they can both be incorporated into complex molecules and easily be transformed into other types of compounds.¹³ We selected a relatively robust cyanohydrin synthesis, a process catalysed by lanthanide(III) complexes of 2,6-bis(oxazolin-2-yl)pyridine (pybox)¹⁴ derivatives.¹⁵ In a micro reactor, where the mobilisation of the reagents was achieved by EOF, reaction parameters such as applied voltage, reagent concentrations, reaction time and catalyst loading were optimised. The effect of additives on the conversion and the enantioselectivity was also studied. The results obtained using the micro reactors were compared to those obtained using the conventional batch technique.

Keywords: Asymmetric metal catalysis; Lanthanide; Pybox; Silylcyanations; Micro reactor.

* Corresponding author. Tel.: +46-8-790-9036; fax: +46-8-791-2333; e-mail: kimo@kth.se

2. Results and discussion

The enantioselective addition of trimethylsilyl cyanide to benzaldehyde in the presence of 2–8 mol% of 2,6-bis(4-(*R*)-phenyloxazolin-2-yl)pyridine and LnCl_3 to yield a scalemic mixture of a chiral silylated cyanohydrin, with the (*R*)-enantiomer as the major product (Scheme 1), was carried out in a micro reactor.



Scheme 1. Enantioselective addition of trimethylsilyl cyanide to benzaldehyde.

A T-shaped borosilicate micro reactor, operating in a continuous mode using electroosmotic flow, with two inlets (A and B, Fig. 1) and one outlet (C), was employed for the catalytic reactions. Voltages were applied between A (+ve) and C (–ve), and B (+ve) and C (–ve). The reaction volumes used were 100 μL .

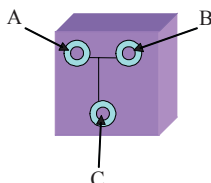


Figure 1. A schematic of the micro reactor consisting of two inlets (A and B) and one outlet (C).

The enantioselectivity of the catalytic reaction studied varied with the reaction conditions. The value reported in the literature for reactions employing YbCl_3 , 89% ee,¹⁵ could not be repeated by us; in our hands merely 84% ee was observed.¹⁶ To facilitate analysis of the product and to avoid clogging, non-optimal reaction conditions were used for initial reactions in the micro reactor. Suitable conditions were found with more concentrated solutions and a lower

amount of the catalyst (1.84 mmol of benzaldehyde per mL acetonitrile compared to 0.2 mmol/mL and 1–8 mol% catalyst instead of 10 mol%). Under these conditions 52–53% ee was achieved (Table 1). The results obtained were compared to those of the analogous reactions run under conventional batch conditions using the same concentration of reagents. Reactions performed in the micro reactor resulted in ee values about 10–20% lower than those achieved in batch reactions, whereas the reactivity was similar or even higher in the micro reactor process. The results of the catalytic reaction were rather insensitive to the amount of catalyst loading, permitting a decrease of the amount of catalyst down to 2 mol% without any significant decrease in reactivity (Table 1).

To explore the usefulness of the micro reactor for optimising the reaction conditions, the effect of additives on the selectivity and reactivity of the catalytic reaction was studied. It was found that each additive (Yb:additive molar ratio 1:1) influenced reactions run in the micro reactor and under conventional conditions in a similar manner, although lower selectivity was always found for the micro reactor reactions. Of the additives employed, only tritylamine had a positive effect on the enantioselectivity affording the product with 66 and 81% ee in micro reactor and batch processes, respectively, compared to 53 and 72% ee for reactions without any additive (Chart 1).

The silylcyanation is known to be catalysed by pybox complexes with other lanthanides as well, although amongst the elements investigated, Yb was found to result in highest enantioselectivity.¹⁵ A correlation between the ionic radius of the lanthanide ion and the enantioselectivity has been observed in a related catalytic procedure.¹⁷ We therefore decided to study reactions with Ce(III), with larger ionic radius than Yb(III), and also Lu(III), having a smaller ionic radius. These ions were not previously tested in this catalytic reaction. CeCl_3 was found to result in only low enantioselectivity, 11% in a batch process and only 1% ee in the micro reactor. In contrast, we were pleased to find that a catalyst prepared from LuCl_3 afforded the product with 76% ee in the batch reaction and with only slightly lower enantioselectivity in the micro reactor process (73% ee). The conversions in the Ce and Lu catalysed reactions in the micro reactor were lower (82 and 89%, respectively) than that in the Yb catalysed process.

In order to study whether higher conversion in the Lu catalysed reaction could be achieved, the reaction

Table 1. Results collected during optimisation of experimental conditions of the Yb catalysed reaction within the micro reactor

Catalyst loading	Concentration of reagent	Collection after 30 min; Voltage: A, B	Conversion. I for batch; II for micro reactor	Ee; I for batch; II for micro reactor
2 mol%	1.84 mmol per mL solvent	12 μL A: 240 V B: 440 V	I: 99% II: 95%	I: 70% II: 52%
4 mol%	1.84 mmol per mL solvent	13 μL A: 280 V B: 390 V	I: 92% II: 98%	I: 72% II: 53%
8 mol%	1.84 mmol per mL solvent	12 μL A: 270 V B: 400 V	I: 100% II: 99%	I: 72% II: 52%

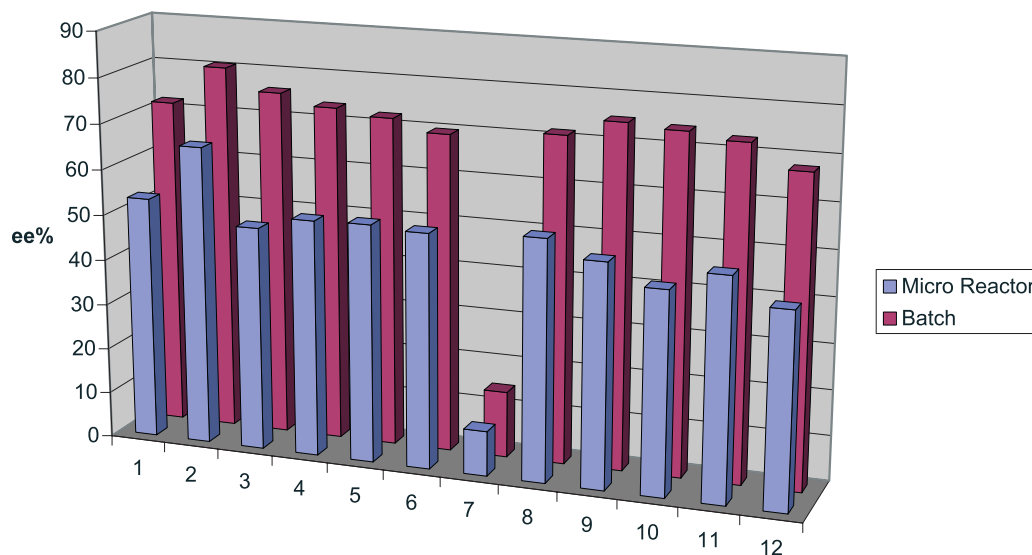


Chart 1. The influence of additives on the enantioselectivity of the YbCl₃ catalyzed reaction. All reactions were carried out in acetonitrile at room temperature using 1.2 equiv TMSCN, 8 mol% pybox ligand, 4 mol% YbCl₃ and 4 mol% of the additive. 1: No additive; 2: Tritylamine; 3: Neomenthol; 4: L-Menthol; 5: R-(−)-2-Butanol; 6: Diethyl ether; 7: Sparteine; 8: R-1-Ethylphenylamine; 9: Methanol; 10: Ethanol; 11: Water; 12: *tert*-Butanol. The ee was determined by GC analysis using a chiral column (Chiraldex, G-TA).

conditions were optimised by varying the voltages. Each reaction was run for 30 min. The highest conversion was achieved when the applied voltages were 140 V on inlet A and 220 V on inlet B (97%) (Chart 2). Higher voltages resulted in lower conversion. The conversion achieved in batch reaction using the same stock solutions was 87% after 30 min.

In order to achieve further optimisation, the effect of additives was studied for the Lu catalyzed reaction (Chart 3). In contrast to the situation with Yb(III), the enantioselectivity in the Lu(III) catalyzed reaction was not improved by the addition of tritylamine or additives such as *N*-oxides and phosphine oxides, which are known to

enhance the selectivity for related reactions.¹⁸ Addition of *D*-menthol resulted in a slight improvement of the enantioselectivity (to 78% ee).

In order to verify that the catalytic reaction really occurred in the channel of the micro reactor and not in the outlet reservoir, some further experiments were performed. In the first experiment, the results from a batch reaction performed under conditions mimicking those in the outlet reservoir were compared to the results obtained using the micro reactor system. The standard solutions (4 mol%) used in the batch reaction were diluted three times since, when the reaction mixture in the micro reactor reaches the outlet reservoir, it is mixed with an additional 20 μ L of acetonitrile

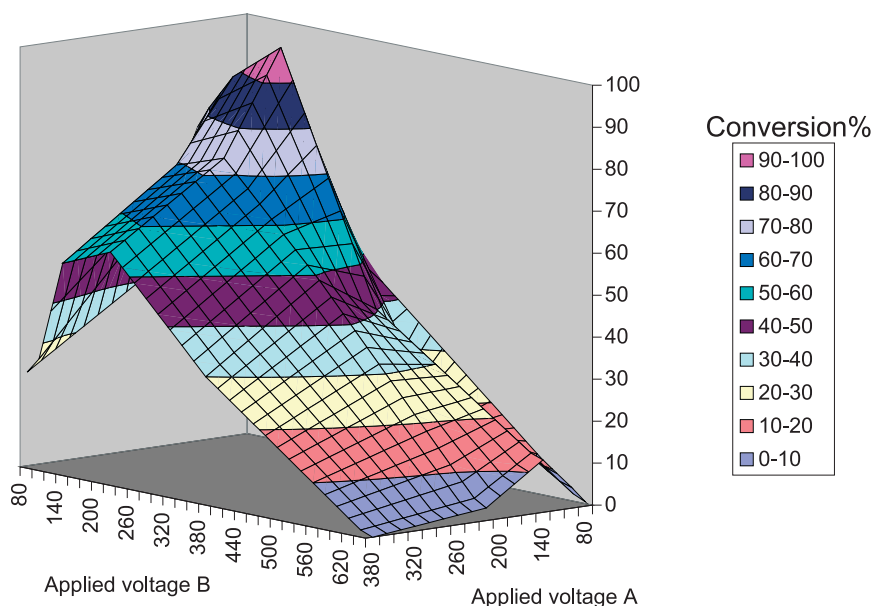


Chart 2. Results collected during optimisation of experimental conditions of the Lu catalyzed reaction within the micro reactor. All reactions were carried out in acetonitrile at room temperature using 1.2 equiv TMSCN, 8 mol% pybox ligand and 4 mol% LuCl₃.

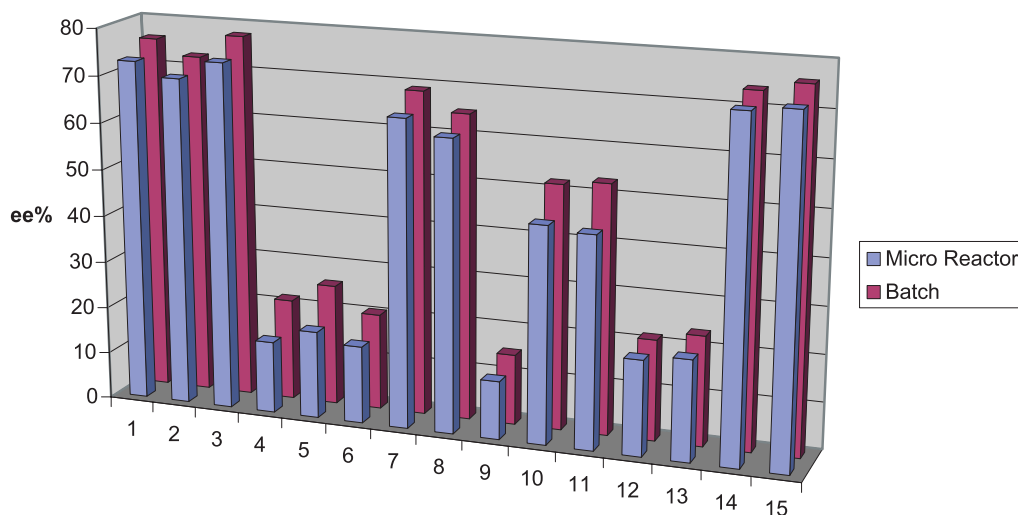


Chart 3. The influence of additives on the enantioselectivity of the LuCl_3 catalysed reaction. All reactions were carried out in acetonitrile at room temperature using 1.2 equiv TMSCN, 8 mol% pybox ligand, 4 mol% LuCl_3 and 4 mol% of the additive. 1: No additive; 2: L-Menthol; 3: D-Menthol; 4: *N,N*-Dimethylaniline *N*-oxide; 5: Pyridine *N*-oxide; 6: Tritylamine; 7: Neomenthol; 8: *R*-(-)-2-Butanol; 9: (-)-Sparteine; 10: *R*-(+)-1-Ethylphenylamine; 11: *S*-(-)-1-Ethylphenylamine; 12: Triphenylphosphine oxide; 13: Dimethylphenylphosphine oxide; 14: THF; 15: Diethyl ether. The ee was determined by GC analysis using a chiral column (Chiraldex, G-TA).

and the collection in that reservoir is between 8 and 15 μL (i.e. a total volume of 28–35 μL). In batch, this resulted in a conversion of 37% after 30 min, as compared to conversions around 98% within the same period of time in the micro reactor, indicating that the catalytic reaction indeed occurs in the channels of the micro reactor.

In the second experiment the reaction time in the outlet reservoir of the micro reactor was increased. The reaction mixture was run through the micro reactor channels for a period of 10 min, after which the flow was halted and the reaction mixture was allowed to stand for an additional 20 min in the outlet reservoir. GC analyses directly after halting the flow and 20 min later showed the conversions to be around 91 and 93%, respectively. Running the batch reaction for 10 min resulted in 45% conversion. These results provide further indication that the reaction indeed takes place in the channel network. In addition, if the reaction had occurred in the outlet reservoir, the reaction outcome would not have been influenced by the applied voltages.

The fact that the selectivity was lower for the Yb catalysed reaction performed in the micro reactor than for batch reactions run under the same conditions, may be due to several reasons. Slow diffusion of the lanthanide complex or decomposition of the chiral ligand may be reasons for the low enantioselectivity observed, although this should have influenced the Lu catalysed reaction in a similar manner. Another reason could be that Yb, which is known to be quite oxophilic,¹⁹ binds to oxygen in the silicon oxide surface of the channels, thereby forming achiral ytterbium complexes which may catalyse a non-enantioselective reaction to give racemic product. This assumption is in agreement with recent investigations showing lutetium to be less oxophilic than ytterbium,²⁰ explaining why the selectivity for the Lu catalysed reaction was less affected by the conditions in the micro reactor.

3. Conclusions

In this study we have shown that it is possible to use a flow-through micro reactor for asymmetric catalysis employing a homogenous chiral metal complex and that EOF can be used to pump relatively large metal complexes within a micro reactor device. It was demonstrated that the catalytic reaction indeed takes place in the channels of the micro reactor and not in the collection reservoir. The reactivity achieved using optimal micro reactor operating conditions was higher than that observed in analogous batch reactions. Lower enantioselectivity was observed for the Yb catalysed reaction in the micro reactor than for that of a similar batch reaction. Finally, it was demonstrated that a flow-through micro reactor could be used for screening of additives, making this type of micro reactor a promising tool for optimisation studies.

4. Experimental

4.1. General

The micro reactor used in this study was fabricated in borosilicate glass following a standard procedure developed at Hull University.^{10,21} A T-shaped micro reactor design with three reservoirs, two inlets (A and B) and one outlet (C, Fig. 1), with approximate channel dimensions of $100 \times 50 \mu\text{m}$ and outer dimensions of $20 \times 20 \times 25 \text{ mm}$ was used. The chemicals used were purchased from Aldrich or Strem, or prepared according to literature procedures. In order to trap the metal complexes, all reaction mixtures were passed through a plug of silica, using dry acetonitrile as eluent, prior to analysis. Conversions were determined by GC/MS and the enantiomeric excesses by GC (Chiraldex, G-TA (gamma cyclodextrin trifluoroacetyl), 30 m \times 0.25 m).²²

4.1.1. Synthesis of 2,6-bis(4-(*R*)-phenyloxazolin-2-yl)pyridine.

(*R*)-Phenylglycinol (4.85 g, 35.4 mmol) and

dimethyl 2,6-pyridine dicarboxylate (3.45 g, 17.7 mmol) were heated at 120 °C for 16 h. Tosyl chloride (6.8 g, 34.8 mmol), Et₃N (10 mL), and CH₂Cl₂ (20 mL) were added. The reaction mixture was refluxed for 20 h. The reaction mixture was diluted with CH₂Cl₂ (20 mL), washed with water, dried (MgSO₄), and the solvent was evaporated. The product was purified by recrystallisation from ethanol. Yield: 92%. Spectral data were in accordance with those previously published.²³

4.2. General procedure for preparation of standards solutions

In order to allow simultaneous addition of reagents into the separate inlets, two standard solutions, S1 and S2, were prepared: S1: Phenyl-pybox (25 mg, 0.068 mmol, 4 mol%) was added to anhydrous LnCl₃ (0.034 mmol) in dry acetonitrile (0.22 mL) and the mixture was stirred for 1 h at rt. Benzaldehyde (86.25 µL, 0.85 mmol) was then added and the solution was finally cooled to 0 °C. S2: TMSCN (136.3 µL, 1.02 mmol) was dissolved in dry acetonitrile (0.22 mL) and the solution was cooled to 0 °C. The standard solutions could be used for 2–3 days without any loss of activity of the catalytic complex, in agreement with the previous observations.¹² For the additive study, 4% of the selected compound was added to S1 1 h before use.

4.3. General procedure for batch reaction

Equal amounts of standard solutions S1 and S2 were added to a dry round-bottomed flask. The reaction mixture was allowed to warm to rt while stirring under air for 10–30 min before analysis.

4.4. General procedure for micro reactor based reaction

The channels of the micro reactor were primed with dry acetonitrile prior to the addition of standard solutions S1 and S2, (50 µL of each) to reservoirs A and B, and the addition of dry acetonitrile (20 µL) to the collection reservoir, C. EOF was generated by applying appropriate voltages to platinum electrodes (A and B ranging from 150 to 750 V, C set to ground) placed in each reservoir using a power supply supplied by Kingfield electronics, Sheffield. Reactions were performed over a 10–30 min period in order to ensure that a sufficient volume of the reaction product was present in reservoir C for analysis. The micro reactor was primed with dry acetonitrile prior to each experiment in order to remove any residue from the system.

Acknowledgements

Financial support from the Swedish Foundation for Strategic Research (the Nanochemistry Program) is gratefully acknowledged.

References and notes

- Ojima, I. *Catalytic Asymmetric Synthesis*; Wiley: New York, 2000. Noyori, R. *Asymmetric Catalysis in Organic Synthesis*; Wiley: New York, 1994. Seyden-Penne, J. *Chiral Auxiliaries and Ligands in Asymmetric Synthesis*; Wiley: New York, 1995. Jacobsen, E. N.; Pfaltz, A.; Yamamoto, H. In *Comprehensive Asymmetric Catalysis*; Springer: Berlin, 1999; Vol. 1–3.
- Shimizu, K. D.; Snapper, M. L.; Hoveyda, A. H. *Chem. Eur. J.* **1998**, *4*, 1885–1889. Bein, T. *Angew. Chem., Int. Ed. Engl.* **1999**, *38*, 323–326. Porte, A. M.; Reibenspies, J.; Burgess, K. *J. Am. Chem. Soc.* **1998**, *120*, 9180–9187. Reetz, M. T. *Angew. Chem., Int. Ed.* **2001**, *40*, 284–310. Traverse, J. F.; Snapper, M. L. *Drug Discovery Today* **2002**, *7*, 1002–1012. Gennari, C.; Piarulliu, U. *Chem. Rev.* **2003**, *103*, 3071–3100.
- Freemantle, M. *Chem. Eng. News Febr.* **1999**, *22*, 27–36.
- Haswell, S. J.; Middleton, R. J.; O'Sullivan, B.; Skelton, V.; Watts, P.; Styring, P. *Chem. Commun.* **2001**, 391–398. DeWitt, S. H. *Curr. Opin. Chem. Biol.* **1999**, *3*, 350–356. Fletcher, P. D. I.; Haswell, S. J.; Pombo-Villar, E.; Warrington, B. H.; Watts, P.; Wong, S. Y. F.; Zhang, X. *Tetrahedron* **2002**, *58*, 4735–4757. Watts, P.; Haswell, S. J. *Curr. Opin. Chem. Biol.* **2003**, *7*, 380–387.
- Whitesides, G. M.; Strook, A. D. *Phys. Today* **2001**, *54*, 42–48.
- Fletcher, P. D. I.; Haswell, S. J.; Paunov, V. N. *Analyst* **1999**, *124*, 1273–1282.
- Watts, P.; Wiles, C.; Haswell, S. J.; Pombo-Villar, E.; Styring, P. *Chem. Commun.* **2001**, 990–991. Watts, P.; Wiles, C.; Haswell, S. J.; Pombo-Villar, E.; Styring, P. *Chem. Commun.* **2001**, 990–991.
- Skelton, V.; Greenway, G. M.; Haswell, S. J.; Styring, P.; Morgan, D. O.; Warrington, B. H.; Wong, S. Y. F. *Analyst* **2001**, *126*, 7–10. Skelton, V.; Greenway, G. M.; Haswell, S. J.; Styring, P.; Morgan, D. O.; Warrington, B. H.; Wong, S. Y. F. *Analyst* **2000**, *126*, 11–13.
- Wiles, C.; Watts, P.; Haswell, S. J.; Pombo-Villar, E. *Lab on a Chip* **2001**, *1*, 100–101.
- Greenway, G. M.; Haswell, S. J.; Morgan, D. O.; Skelton, V.; Styring, P. *Sens. Actuators B* **2000**, *63*, 153–158.
- Suga, S.; Okajima, M.; Fujiwara, K.; Yoshida, J.-i. *J. Am. Chem. Soc.* **2001**, *123*, 7941–7942. Mitchell, M. C.; Spikmans, V.; de Mello, A. J. *Analyst* **2001**, *126*, 24–27. Mitchell, M. C.; Spikmans, V.; Manz, A.; de Mello, A. J. *J. Chem. Soc., Perkin Trans. 1* **2001**, *5*, 514–518. Sands, M.; Haswell, S. J.; Kelly, S. M.; Skelton, V.; Morgan, D. O.; Styring, P.; Warrington, B. *Lab on a chip* **2001**, *1*, 64–65.
- Wilson, N. G.; McCreedy, T. *Chem. Commun.* **2000**, 733–734. Wilson, N. G.; McCreedy, T. *Analyst* **2001**, *126*, 21–23.
- Gregory, R. J. H. *Chem. Rev.* **1999**, *99*, 3649–3682. North, M. *Tetrahedron: Asymmetry* **2003**, *14*, 147–176.
- Nishiyama, H. *Adv. Catal. Proc.* **1997**, *2*, 153–188. Desimoni, G.; Faita, G.; Quadrelli, P. *Chem. Rev.* **2003**, *103*, 3119–3154.
- Aspinall, H. A.; Greeves, N.; Smith, P. M. *Tetrahedron Lett.* **1999**, *40*, 1763–1766. Aspinall, H. A.; Dwyer, J. L. M.; Greeves, N.; Smith, P. M. *J. Alloys Compd.* **2000**, *303*–304, 173–177.
- Lundgren, S.; Lutsenko, S.; Jönsson, C.; Moberg, C. *Org. Lett.* **2003**, *5*, 3663–3665.
- Schaus, S. E.; Jacobsen, E. N. *Org. Lett.* **2000**, *2*, 1001–1004.
- Chen, F.; Feng, X.; Qin, B.; Zhang, G.; Jiang, Y. *Org. Lett.* **2003**, *5*, 949–952. Hamashima, Y.; Kania, M.; Shibasaki, M. *J. Am. Chem. Soc.* **2000**, *122*, 7412–7413. Vogl, E. M.; Gröger, H.; Shibasaki, M. *Angew. Chem., Int. Ed.* **1999**, *28*, 1570–1577. Shibasaki, M.; Kanai, M. *Chem. Pharm. Bull.* **2001**, *49*, 511–524.
- Cotton, S. A. In *Encyclopedia of Inorganic Chemistry*; King, R. B., Ed.; Wiley: Chichester, 1994; Vol. 7, p 3595.

20. Tsuruta, H.; Yamaguchi, K.; Imamoto, T. *Tetrahedron* **2003**, *59*, 10419–10438.
21. Christensen, P. D.; Johnson, S. W. P.; McCreedy, T.; Skelton, V.; Wilson, N. G. *Anal. Commun.* **1998**, *35*, 341–343.
22. Belokon', Y. N.; Caveda-Cepas, S.; Green, B.; Ikonnikov, N. S.; Khrustalev, V. N.; Larichev, V. S.; Moscalenko, M. A.; North, M.; Orizu, C.; Tararov, V. I.; Tasinazzo, M.; Timofeeva, G. I.; Yashkina, L. V. *J. Am. Chem. Soc.* **1999**, *121*, 3968–3973.
23. Nishiyama, H.; Kondo, M.; Nakamura, T.; Itoh, K. *Organometallics* **1991**, *10*, 500–508.

Reviews

Benchmarking of Microreactor Applications

Helmut Pennemann,^{*,†} Paul Watts,^{*,‡} Stephen J. Haswell,[‡] Volker Hessel,[†] and Holger Löwe[†]

Institut für Mikrotechnik Mainz GmbH, Carl-Zeiss-Strasse 18-20, 55129 Mainz, Germany, and Department of Chemistry, University of Hull, Cottingham Road, Hull HU6 7RX, United Kingdom

Abstract:

At present, the aims of the investigations with microchemical processing devices are changing from simply proving feasibility for one chemical reaction towards more in-depth scientific studies and industrial piloting. In this way, large data sets are gathered, providing multifaceted information on the topic. To enable industrial exploitation of the technology, future investigations should aim to complete the economic evaluation of the methodology for plant engineering. Hence, commercially oriented studies have to be undertaken, not with the aim to further broaden the scope of information, but rather to achieve a new system-oriented level of know-how. Since this involves the interaction of many parties with many different skills, it is a bridging function that is needed to bring the vast amount of findings documented to a compact format and to compare it to the state of the art in the chemicals-producing industry. Accordingly, this contribution reviews many chemical reactions carried out in either credit-card-sized microdevices or in larger microflow processing tools for reasons of screening/analysis and organic synthesis/industrial piloting, respectively. Quantities which characterize the process itself, the product on a molecular and supramolecular level, and the downstream processing are compared for both microreactor and conventional processing, benchmarking the performance of microflow devices at minute and large throughput levels.

Introduction

Microchannel process devices gain interest not only for academic investigations but also for uses in the chemical industry.^{1–9} MEMS (*microelectro mechanical systems*)-based chips with a microchannel architecture in one plane serve for chemical screening or analysis (Figure 1); precision-engineered microflow devices having a three-dimensional

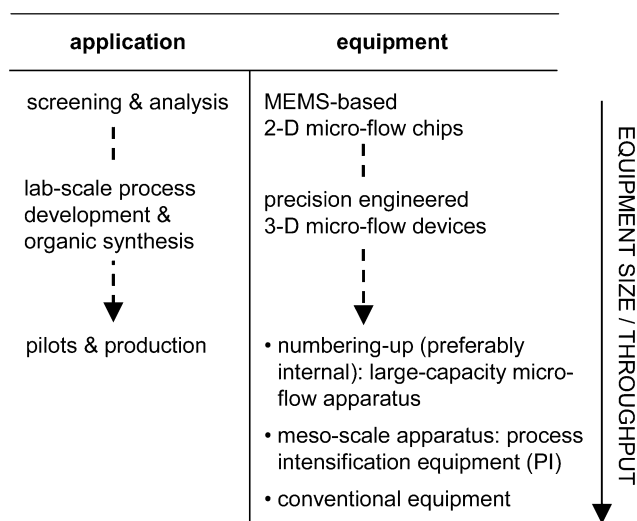


Figure 1. Stages of microreaction technology.

(3D) microchannel architecture are used for lab-scale development or organic synthesis, as the investigations may refer to the process itself or the material to be produced, respectively. Pilot operation and production with chemical microprocessing apparatus is not directly evident for a large number of cases since the companies involved keep this as secret as possible. However, the increasing practice can be deduced from the growing number of industrial patents, the larger number of industrial participants at microreactor conferences, and the increasing sales of the supplier companies in the field. This feeling that the business is expanding steers the foundation of platforms worldwide which promotes a breakthrough in the microreaction technology.

However, the way to achieve this is not clear at present. Hence, in the future, probably a multitude of processing solutions will cope with the tasks, which differ in scale as the most distinctive feature (the *multiscale concept*). This includes the simple numbering up of microchannels, done preferentially in an internal manner, mesoscale processing, preferably by process intensification (PI) equipment, or even using conventional equipment. Concerning the first approach, one has to be aware that the first large-capacity devices such as microflow mixers and heat exchangers have been reported, achieving liquid throughputs in the $\text{m}^3 \text{h}^{-1}$ range.^{10–14}

However, newcomers still consider the technique to be inscrutable, due to its interdisciplinary nature, and fear unforeseen consequences of an abrupt change in their way of processing, when switching from large batch tanks to

* To whom correspondence should be addressed. E-mail: pennemann@imm-mainz.de; p.watts@hull.ac.uk.

[†] Institut für Mikrotechnik Mainz GmbH.

[‡] University of Hull.

- (1) Ehrfeld, W.; Hessel, V.; Löwe, H. *Microreactors*; Wiley-VCH: Weinheim, 2000.
- (2) Hessel, V.; Hardt, S.; Löwe, H. *Micro Chemical Process Engineering*; Wiley-VCH: Weinheim, 2004.
- (3) Jensen, K. F. *Chem. Eng. Sci.* **2001**, *56*, 293.
- (4) Gavriilidis, A.; Angeli, P.; Cao, E.; Yeong, K. K.; Wan, Y. S. S. *Trans. Inst. Chem. Eng.* **2002**, *80/A*, 3.
- (5) Hessel, V.; Löwe, H. *Chem. Eng. Technol.* **2003**, *26*, 13.
- (6) Hessel, V.; Löwe, H. *Chem. Eng. Technol.* **2003**, *26*, 391.
- (7) Hessel, V.; Löwe, H. *Chem. Eng. Technol.* **2003**, *26*, 531.
- (8) Fletcher, P. D. I.; Haswell, S. J.; Pombo-Villar, E.; Warrington, B. H.; Watts, P.; Wong, S. Y. F.; Zhang, X. *Tetrahedron* **2002**, *58*, 4735.
- (9) Haswell, S. J.; Watts, P. *Green Chem.* **2003**, *5*, 240.

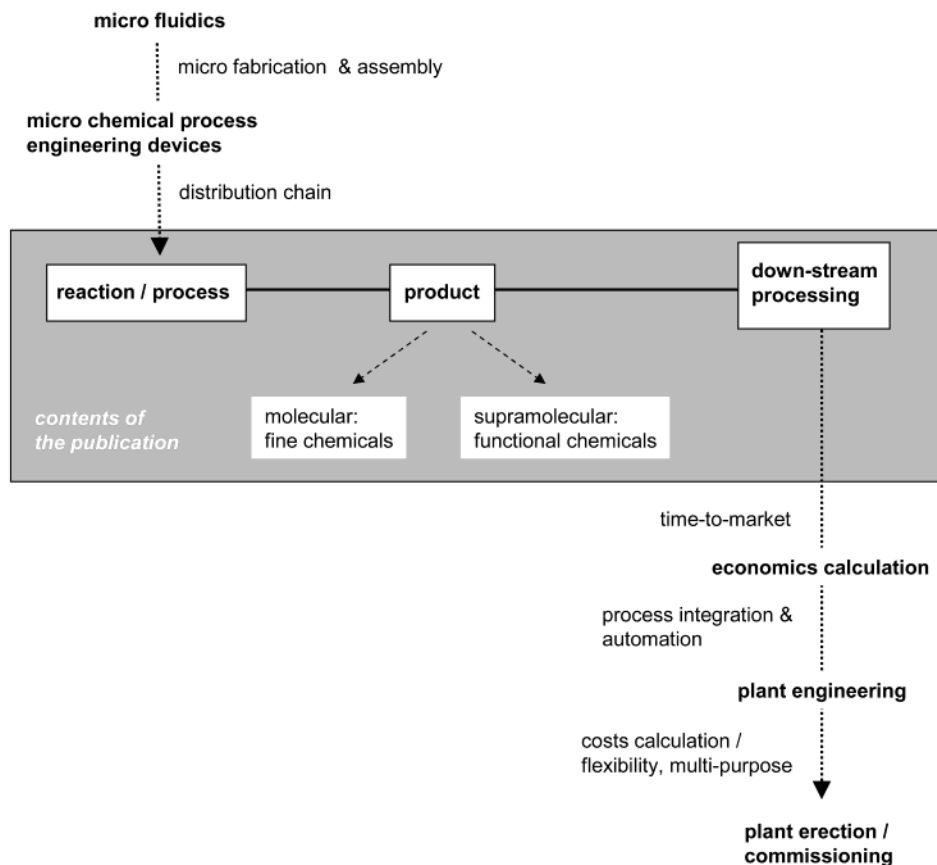


Figure 2. Contents of the present publication.

smaller continuous-flow devices (see also the Conclusions of this article and Table 27). Nobody wants to take the lead on his own; thus, the situation can be described as “wait-and-see”. While more and more decision makers believe in the performance of the microprocessing devices themselves and do not consider the technology to be immature any more, they ask at the same time for a complete picture of the processing, i.e., including a detailed engineering design and economics calculation (Figure 2).

For such a comprehensive view, initially all performance data are required. Most initial investigations were concerned with comparing selectivity and space-time yields, thus proving the feasibility of carrying out a chemical reaction in a microchannel. When the devices changed from scientists’ playthings to accepted professional processing tools, this led to further requests on more in-depth data, e.g., with regard to loss of catalyst during longer runs, spectra and morphology of crystallites, and product purity. Besides specification on molecular quantities, information on supramolecular properties was now desired. Having raised commercial interest in this way, one nowadays is faced with questions on outlining a whole production process scenario, e.g., regarding the impact of other processing operations (i.e., separation), energy efficiencies of the process, consequential costs for equipment, process controllability and safety, overall profitability of the process and multipurpose flexibility. This includes such detailed aspects as how using the microreactor affects and simplifies downstream separation or how much this may help to decrease the amount of coolant water, for instance. It therefore stands to reason that we need more

information and preferably more qualified data on microreactor processing, the latter being based on existing knowledge of chemical processes in industry. Accordingly, qualified data should first of all allow benchmarking of microreactor information.

After five years of intensive research with now more than 1000 publications (among them about 450 peer-reviewed) microreactor benchmarking can be done with regard to the following: (1) the reaction/process, (2) the product properties, and (3) the impact on downstream processing (Figure 2). These issues will be addressed in this publication; however, giving an economic calculation or details on the plant engineering behind the technique is out of the scope of this paper.

Typical parameters which can be derived from the reaction/process are the experimental protocol of an organic reaction (e.g., temperature or reaction time), performance parameters of the process (e.g., selectivity or space-time yield), product features (e.g., isomer ratios or particle size distribution), and finally features of downstream processing (e.g. energy efficiency or safety measures) (Figure 3).

In the following sections, the benchmarking of these parameters will be discussed for microreactor vs conventional processing. It will be given as a short text for each reaction and will be summarized as a table, comparing the performance data of a microreactor with those of traditional chemical apparatus. The reactions are put into two classes, one referring to small-scale applications and one to lab- and pilot-scale synthesis. The first class have flow rates typically up to several milliliters per hour, and the flow rates of the

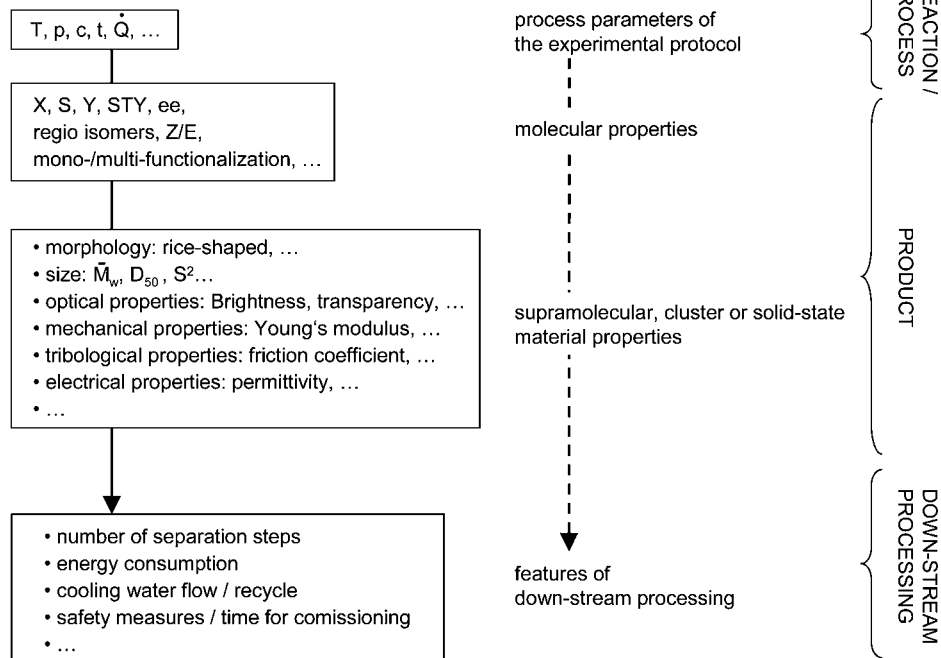


Figure 3. Parameters suitable for benchmarking of microreactors.¹⁵

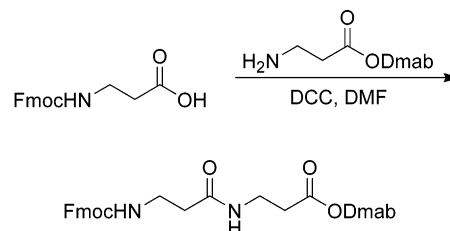
latter range from several milliliters per hour up to several tens of liters per hour (Table 1).

Microreactors Used for Small-Scale Applications: Liquid Reactions

Peptide Synthesis. Peptides and peptide-related molecules are present in many pharmaceutically important compounds, and consequently, the pharmaceutical industry is particularly interested in developing improved methodology for their preparation.

Watts et al. have recently demonstrated multistep peptide synthesis in a borosilicate glass microreactor operating under electrokinetic control.^{16,17} The authors evaluated their device using a carbodiimide coupling reaction of Fmoc- β -alanine with an amine to give the dipeptide (Scheme 1). When stoichiometric quantities of the reagents were used, approximately 10% conversion to the dipeptide was achieved. By using two equivalents of DCC however, an increase in

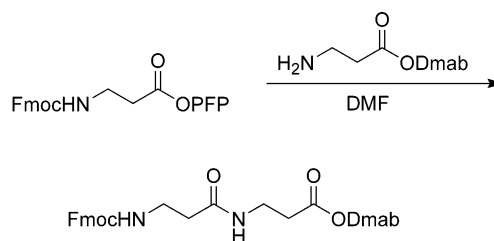
Scheme 1. Dipeptide synthesis with β -amino acids



conversion to 20% was observed, and by applying a stopped-flow technique (2.5 s injection length with stopped-flow for 10 s), the conversion of the reaction was further increased to approximately 50%. Using five equivalents of DCC, a conversion of up to 93% for the dipeptide was obtained using the stopped-flow technique described, as summarized in Table 2.

The authors also demonstrated that the dipeptide could be prepared from preactivated carboxylic acids.^{16,17} They report that the reaction of the pentafluorophenyl (PFP) ester of Fmoc- β -alanine with the amine gave the dipeptide quantitatively in 20 min (Scheme 2). This represented a significant increase in yield compared with the traditional batch synthesis, where only a 60% yield was obtained in 120 h.

Scheme 2. Dipeptide synthesis with activated β -amino acids



- Schubert, K.; Brandner, J.; Fichtner, M.; Linder, G.; Schyguilla, U.; Wenka, A. *Microscale Thermophys. Eng.* **2001**, *5*, 17.
- Löb, P.; Dresse, K. S.; Hessel, V.; Hardt, S.; Hofmann, C.; Löwe, H.; Schenk, R.; Schönfeld, F.; Werner, B. *Chem. Eng. Technol.* **2003**. In press.
- Haynes, B. S.; Wegeng, R. S. In *Topical Conference Proceedings; IMRET 6*, 6th International Conference on Microreaction Technology, AIChE Spring National Meeting, March 11–14, 2002, New Orleans, LA; American Institute of Chemical Engineers: New York, NY, 2002; pp 223–237.
- Edge, A. M.; Pearce, I.; Phillips, C. H. In *Proceedings of 1st International Conference on Process Intensification for the Chemical Industry*; Green, A., Ed.; BHR Group Conference Series, Vol. 38, pp 175–189; Professional Engineering Publishing Ltd., 1997.
- Information about Atotech's heat exchanger can be found on the homepage (<http://www.atotech.com>) or in a patent: Breuer, N.; Meyer, H. (Atotech Deutschland GmbH). WO 98/37457, Priority: February 20, 1997.
- T : temperature, p : pressure, c : concentration, t : reaction time, \dot{Q} : flow rate, X : conversion, S : selectivity, Y : yield, STY : space-time yield, ee : enantiomeric excess, Z/E : isomers with a C=C-bond, \bar{M}_w : weight-average molecular weight, D_{50} : median particle diameter, S^2 : mean square radius of gyration.
- Watts, P.; Wiles, C.; Haswell, S. J.; Pombo-Villar, E.; Styring, P. *Chem. Commun.* **2001**, 990.
- Watts, P.; Wiles, C.; Haswell, S. J.; Pombo-Villar, E. *Tetrahedron* **2002**, *58*, 5427.

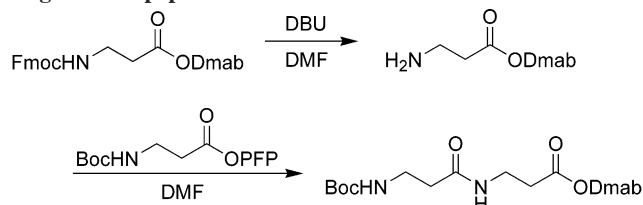
Table 1. Summary of the published parameters and properties of organic reactions in microreactors

	small-scale applications								lab-scale synthesis																
	peptide synthesis	Suzuki reaction	Kumada–Corriu reaction	aldol reaction	Michael addition	enamine synthesis	Hantzsch reaction	dehydration reactions	hydrogenation reactions	hydrolysis & transglycosylation	diazotation & diazo coupling	aromatic nitration	nitration of urea derivatives	phenylboronic acid formation	Sonogashira coupling	polyacrylate formation	addition of organometallic reagents	cumene hydroperoxide rearrangement	methylation of aromatics	oxidation of ethanol	photo chlorination of alkyl aromatics	chlorination of acetic acid	hydrogenation of nitro compounds	fluorination of aromatics	fluorination of non-aromatics
process parameter	temperature				x	x		x			x	x	x	x	x	x	+	x	x	x	x	x	x	x	x
	pressure																+		x		x	x	x		
	reactant concentration	x			+	+	+				x		+	+			x		x			x	x	x	x
	flow rate			+							x	x	x	x	x	x			x	x	x	x	x	x	x
	reaction time	x	x	x	x	x	x	x	x	x	x	x	x		x	x	+	x	x	x		x		+	
	reaction rate			+					x		x														
	interfacial area									x														+	
	heat transfer area																	x							
molecular properties	conversion	x	x	x	x	x	x	x	x	x	x										x		x	x	x
	yield					+							x	x			x	x	x		x		x	x	
	selectivity											x								x	x		x	x	
	space-time yield																		x	x				+	
	isomeric ratio	x									x													x	
supramolecular properties	color strength									x															
	brightness									x															
	transparency									x															
	particle size									x															
	molecular weight distribution														x										
d.-s. proc.^a	recycle ratio																	x					x		
	purification												x									x			

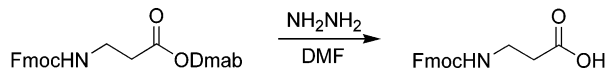
Table 2. Benchmark of the microreactor

	microreactor	batch reactor
1. DCC coupling reactions (5 equiv)		
reaction time	20 min	24 h
conversion	up to 93%	92%
2. active ester coupling reaction		
reaction time	20 min	120 h
conversion	100%	60%
3. deprotection chemistry (DBU or hydrazine)		
reaction time	20 min (1 equiv)	several hours (100 equiv)
conversion	100%	100%

Having demonstrated that peptide bonds could be successfully formed using a microreactor, the authors then found that they could extend the methodology to the preparation of longer-chain peptides.¹⁸ Using the microreactor, the Dmab ester of Fmoc- β -alanine was reacted with one equivalent of piperidine or 1,8-diazabicyclo(5.4.0)undec-7-ene (DBU) to give the free amine in quantitative conversion. This is in comparison to the solid-phase peptide synthesis where 20% piperidine in DMF is frequently employed. The authors then reacted the amine in situ with a pentafluorophenyl ester derivative to give the dipeptide (Scheme 3) in 96% overall conversion.

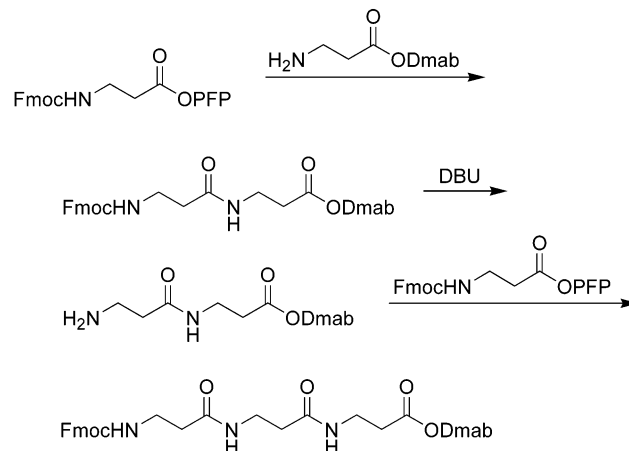
Scheme 3. Methodology for the preparation of longer-chain peptides

Having shown that more complex peptides could be produced by removal of the *N*-protecting group, the authors then demonstrated that they could remove the Dmab ester using hydrazine.¹⁸ The reaction of the Dmab ester with one equivalent of hydrazine gave quantitative deprotection to afford the carboxylic acid (Scheme 4). This is in comparison

Scheme 4. Deprotection by hydrazinolysis

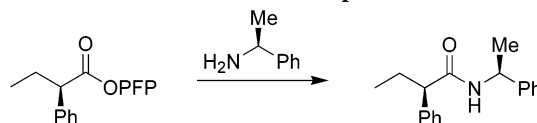
to the solid-phase peptide synthesis where 2% hydrazine in DMF is generally used to effect deprotection.

The authors have further extended the approach to the synthesis of tripeptides. Reaction of a pentafluorophenyl ester with an amine formed a dipeptide, which was reacted with DBU to effect Fmoc deprotection. The amine was then reacted in situ with another equivalent of the pentafluorophenyl ester to prepare the tripeptide in 30% overall conversion (Scheme 5). The approach clearly demonstrates that intermediates may be generated in situ and used in

Scheme 5. Synthesis of tripeptides

subsequent reactions. Although in the above examples the intermediates are relatively nontoxic, it is postulated that the approach may be used to generate highly toxic reagents in situ, consequently, this is an approach that one would like to use in a large-scale synthesis.

Synthesis of peptides containing α -amino acids is far more problematic as a result of racemization. Having demonstrated that peptide bonds could be successfully formed when using a borosilicate glass microreactor, the authors then investigated racemization in a model compound, namely α -phenylbutyric acid.¹⁹ Reaction of the pentafluorophenyl ester of *R*-2-phenylbutyric acid (0.1 M concentration) with α -methylbenzylamine gave the product in quantitative conversion with 4.2% racemization (Scheme 6). Significantly this was less

Scheme 6. Racemization control experiment

racemization than observed in the batch reaction at the same concentration and temperature. The reduced level of racemization was attributed to the reduced reaction times observed within the microreactors.

Furthermore, the authors have reported that it is possible to purify the reaction mixture within the microreactor by exploiting the differential electrophoretic mobilities of the individual components of the reaction mixture.²⁰

Suzuki Reaction. Heterogeneous catalysis is of significant industrial importance for the synthesis of fine chemicals and pharmaceuticals. However, to isolate the product it is necessary to remove the catalyst from the reaction mixture, which further complicates the procedure. Consequently, microreactors involving the use of immobilized catalysts represent a method to overcome this problem.

Greenway et al. have demonstrated the Suzuki reaction within a borosilicate glass microreactor in which electro-osmotic flow was used as the pumping mechanism.²¹ The

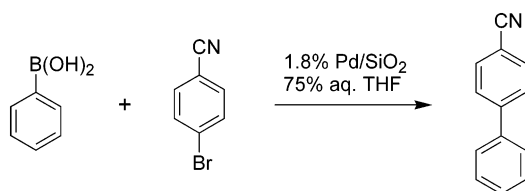
(18) Watts, P.; Wiles, C.; Haswell, S. J.; Pombo-Villar, E.; Styring, P. In *Topical Conference Proceedings*; IMRET 5, 5th International Conference on Microreaction Technology, AIChE Spring National Meeting; Matlosz, M., Ehrfeld, W., Baselt, J. P., Eds.; Springer-Verlag: Berlin, 2001; pp 508–519.

(19) Watts, P.; Wiles, C.; Haswell, S. J.; Pombo-Villar, E. *Lab Chip* **2002**, *2*, 141.

(20) George, V.; Watts, P.; Haswell, S. J.; Pombo-Villar, E., *Chem. Commun.* **2003**, 2886.

catalyst, 1.8% palladium on silica, was immobilized between microporous silica frits prepared from potassium silicate and formamide. The boronic acid derivative was reacted with an aryl bromide to give a 68% conversion to cyanobiphenyl at room temperature within the microreactor (Scheme 7).

Scheme 7. Suzuki coupling



Traditionally, tetrahydrofuran (THF) is used as the solvent in this reaction; however, as has been found with many organic solvents, THF has very low natural EOF properties, and for this reason it was mixed with water (75:25) for use in these experiments. The yields obtained were comparable with those from Suzuki reactions on a batch scale using homogeneous catalysis. Importantly, there were negligible levels of the palladium catalyst in the product, demonstrating the environmental benefits of the technology (Table 3).

Table 3. Benchmark of the microreactor

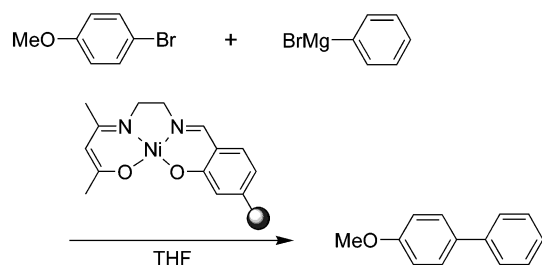
	microreactor	batch reactor
reaction time	6 s	8 h
conversion	68%	60%
solvent	water/THF (1:3)	THF

One of the interesting observations of the reaction was that, unlike conventional Suzuki reactions, an additional base was not required. Although the exact reason for this is unclear, it is postulated that the electric field may be sufficient to cause ionization of the water at the metal surface. It is feasible that the hydroxide formed in this way may be sufficient to perform the function of the conventional base.

Kumada–Corriu Reaction. In another example of heterogeneous catalysis, O’Sullivan et al. have recently investigated the Kumada–Corriu reaction in a pressure-driven microreactor.²² The reactor was constructed by placing a plug of catalyst into a length of polypropylene tubing. A syringe pump was used to drive a premixed solution containing equimolar quantities of the aryl halide and Grignard reagent through the reactor.

The authors reacted *p*-bromoanisole with phenylmagnesium bromide, in the presence of the nickel catalyst which was supported on Merrifield resin, to give 4-methoxybiphenyl (Scheme 8). When the reaction was conducted in the

Scheme 8. Kumada–Corriu reaction



microreactor, an enhanced reaction rate was observed compared to that of the batch reactions (Table 4). Since the

Table 4. Benchmark of the microreactor

	microreactor	batch reactor
reaction time	10 min	25 h
conversion	60%	70%

concentrations were the same in the both cases, the authors postulated that the dimensions of the microreactor were solely responsible for the enhanced rate of reaction.

Aldol Reaction. Carbanion chemistry is one of the most common methods of C–C bond formation used in the pharmaceutical industry. In such reactions, large volumes of highly pyrophoric bases are frequently employed. In many cases the selectivity of the reaction is temperature dependent; consequently, microreactors have a considerable attraction for these reactions because the reactor enables excellent temperature control of the reaction.

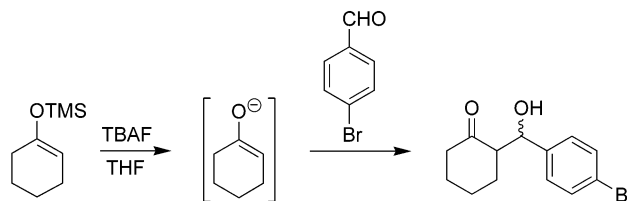
Wiles et al. have recently demonstrated the use of silyl enol ethers in the aldol reaction within a borosilicate glass microreactor operating under electrokinetic control.²³ Quantitative conversion of the silyl enol ethers to β -hydroxyketones was observed in 20 min compared to traditional batch systems, where quantitative yields were only obtained when extended reaction times of up to 24 h were employed (Table 5). One example involved the treatment of the TMS enol

Table 5. Benchmark of the microreactor

	microreactor	batch reactor
reaction time	20 min	24 h
conversion	100%	100%

ether with tetra-*n*-butylammonium fluoride (TBAF) to generate the tetra-*n*-butylammonium enolate in situ, followed by condensation with *p*-bromobenzaldehyde to give the β -hydroxyketone in 100% conversion (Scheme 9).

Scheme 9. Aldol reaction



Michael Addition. Another example of enolate-type chemistry performed within a microreactor has been reported by Wiles et al.²⁴ The authors reported the preparation of enolates from a series of 1,3-diketones using an organic base

(21) Greenway, G. M.; Haswell, S. J.; Morgan, D. O.; Skelton, V.; Styring, P., *Sensors Actuators B* **2000**, *63*, 153.

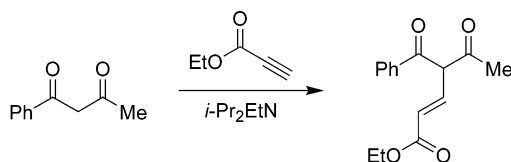
(22) Haswell, S. J.; O’Sullivan, B.; Styring, P. *Lab Chip* **2001**, *1*, 164.

(23) Wiles, C.; Watts, P.; Haswell, S. J.; Pombo-Villar, E. *Lab Chip* **2001**, *1*, 100.

(24) Wiles, C.; Watts, P.; Haswell, S. J.; Pombo-Villar, E. *Lab Chip* **2002**, *2*, 62.

and their subsequent reaction with a variety of Michael acceptors to afford 1,4-addition products within a microreactor (Scheme 10).

Scheme 10. Michael addition



When using a continuous flow of the reagents, 15% conversion to the adduct was observed. The authors, however, demonstrated enhancements in conversions through the application of the stopped-flow technique. This procedure involved the mobilization of reagents through the device for a designated period of time, using an applied field, and the flow was subsequently paused by the removal of the applied field, prior to reapplying the field. Using the regime of 2.5 s on and 5 s off, the conversion to the product was improved to 34%, while lengthening the stopped-flow period to 10 s, resulted in a further increase to 100% (Table 6). The authors

Table 6. Benchmark of the microreactor

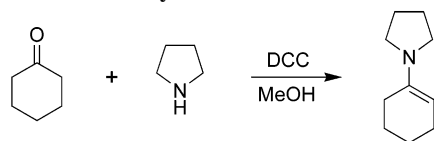
	microreactor	batch reactor
reaction time	20 min	24 h
conversion	100%	89%

proposed that the observed increase in conversion, when using the technique of stopped-flow, was due to an effective increase in residence time within the device and hence an increase in the diffusive mixing of the reagent streams.

Enamine Synthesis. Sands and co-workers have recently reported the preparation of enamines within a microreactor.²⁵ Enamines are traditionally prepared under Dean and Stark conditions, where the ketone and secondary amine are heated to reflux in toluene. These conditions remove the water from the reaction to produce the equilibrium-dependent enamine; however, it is difficult to perform the reaction on a large scale. To remove the water from the reaction by distillation it is necessary to use a high-boiling point solvent and to heat the reaction at typically 120 °C, which clearly requires large amounts of energy.

By using a borosilicate glass microreactor operating under electrokinetic control cyclohexanone was reacted with pyrrolidine using methanol as the solvent to form the enamine (Scheme 11) in 42% conversion at room temperature (Table

Scheme 11. Enamine synthesis



7), rather than at the elevated temperatures discussed above. To assist in removing the water, one equivalent of DCC was used in the reaction. Clearly, the use of methanol as solvent

(25) Sands, M.; Haswell, S. J.; Kelly, S. M.; Skelton, V.; Morgan, D.; Styring, P.; Warrington, B. *Lab Chip* **2001**, *1*, 64.

Table 7. Benchmark of the microreactor

	microreactor	batch reactor
reaction time	20 min	not reported (probably several hours)
conversion	42%	not reported
temperature	25 °C	120 °C

at room temperature, compared with the traditional conditions, represents a more environmentally friendly procedure. In this case also, the electrophoretic mobility of the product is thought to be greater than that of water, thus enabling product separation in situ. Consequently exploitation of the individual electrophoretic mobilities of the individual reactants and products enables control of the thermodynamics of the reaction.

Hantzsch Reaction. Industrially, special equipment is required when performing large-scale reactions at elevated temperature, such as reflux condensers. Consequently, the ability to use microreactors at elevated temperatures using the scale-out principle is of commercial interest.

Garcia-Egido et al. have demonstrated the synthesis of a series of 2-aminothiazoles using a Hantzsch reaction within a microreactor.²⁶ During the experiments the T-shaped microreactor was heated to 70 °C using a Peltier heater, which was aligned with the channels, and the heat generated by the device was applied to the base of the microreactor. Reaction of an α -bromoketone with a thiourea derivative, using NMP as solvent, resulted in the preparation of an aminothiazole in 85% conversion (Scheme 12 and Table 8).

Scheme 12. Hantzsch reaction

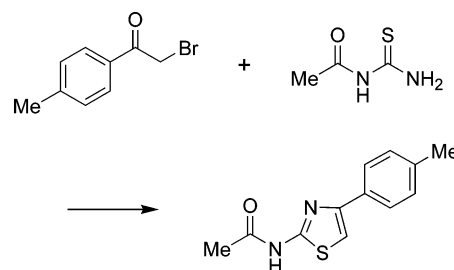


Table 8. Benchmark of the microreactor

	microreactor	batch reactor
reaction time	30 min	not reported
conversion	85%	up to 99%
temperature	70 °C	70 °C

A range of aminothiazole derivatives were prepared using alternative α -bromoketones as starting materials.

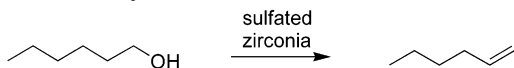
Dehydration Reactions. Wilson and McCreeley have reported the use of a microreactor to perform the dehydration of alcohols using a sulfated zirconia catalyst.²⁷ The microreactor was fabricated from a glass plate, which was etched using photolithography. A PDMS top block, with predrilled holes to act as reservoirs for the reagents, was then aligned

(26) Garcia-Egido, E.; Wong, S. Y. F.; Warrington, B. H. *Lab Chip* **2002**, *2*, 31.

(27) Wilson, N. G.; McCreeley, T. *Chem. Commun.* **2000**, 733.

with the channel geometry. To introduce the catalyst into the microreactor, it was dusted over the surface of the PDMS face before the base plate was joined to the top plate. This process immobilized the catalyst, while simultaneously increasing its surface area. The overall effect was to produce a catalytically active wall of the microchannel. A heater, fabricated from Nichrome wire, was also immobilized in the PDMS top plate. Pumping was produced with a syringe pump, and the products were analyzed by gas chromatography (GC). The conversion of hexan-1-ol to hex-1-ene was between 85 and 95%, and no additional products were detected (Scheme 13). This yield is extremely good when

Scheme 13. Dehydration of alcohols



compared to the 30% expected for the industrially used process (Table 9).

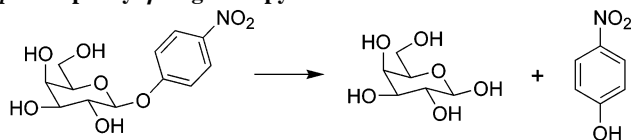
Table 9. Benchmark of the microreactor

	microreactor	batch reactor
reaction time	20 min	not reported
conversion	85–95%	30%

The reaction was also applied to ethanol. At a reaction temperature of 155 °C and using a syringe pump at a flow rate of 3 $\mu\text{L min}^{-1}$, the product was found to contain 68% ethene, 16% ethane, and 15% methane, together with trace amounts of ethanol. When electroosmotic pumping was used, the flow rate obtained was between 0.9 and 1.1 $\mu\text{L min}^{-1}$ at a field strength of 200 V cm^{-1} . The only detectable product was methane, indicating that the reaction had progressed beyond dehydration to complete cracking of the ethanol. Additionally, trace amounts of methanol were present in the product. It is proposed that the slow flow rate of the electroosmotic pumping method results in longer residence times in the reactor, thus offering a significant advantage over the syringe pump. Electroosmotic flow (EOF), however, cannot be applied to all reactions because organic reactants, such as hexanol, exhibit no natural EOF under an applied potential.

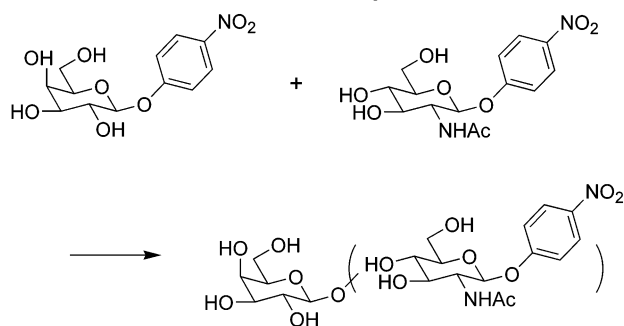
Hydrolysis and Transglycosylation of β -D-Galactopyranoside Derivatives. Two enzyme-catalyzed reactions were carried out in a microchip reactor by Kanno et al. At first *p*-nitrophenyl- β -D-galactopyranoside was hydrolyzed with a β -galactosidase from *Escherichia coli* (Scheme 14) and a

Scheme 14. Hydrolysis of *p*-nitrophenyl- β -D-galactopyranoside



transgalactosylation of a *p*-nitrophenyl-2-acetamide-2-deoxy- β -D-glucopyranoside was carried out (Scheme 15).²⁸

Scheme 15. Transglycosylation of β -D-galactopyranoside



As a microreactor, a mechanically fabricated microchip made of PMMA was used. The chip consisted of a two-plate assembly. One plate featured the microchannels having a cross section of 200 $\mu\text{m} \times 200 \mu\text{m}$ and length of 40 cm, and the second plate covered the microchannel. The microchip is designed for contacting two liquids, whereas the mixing is realized by a micro Y-piece. For temperature control a hot plate is used.

For the hydrolysis, the *p*-nitrophenyl- β -D-galactopyranoside solution and the enzyme solution were pumped into the microchip using microsyringes with identical flow rates (several $\mu\text{L min}^{-1}$). The microchannel was maintained at 37 °C. After leaving the microchip, the reaction mixture was quenched into hot water to inactivate the enzyme. The resulting raw product was analyzed by LC–MS. For the second experiment, the transgalactosylation, the pure *p*-nitrophenyl- β -D-galactopyranoside solution was replaced by a mixture of *p*-nitrophenyl- β -D-galactopyranoside and nitrophenyl-2-acetamide-2-deoxy- β -D-glucopyranoside.

Due to different flow rates, the residence times of the reaction mixture inside the microchip were varied. It was found that the hydrolysis of *p*-nitrophenyl- β -D-galactopyranoside (Scheme 14) in the microchip was 5 times faster than in a batch reactor. According to this, a higher conversion was determined by the use of the microchip reactor (Table 10). Although the reaction rate of the transgalactosylation

Table 10. Comparison of the microchip reactor with respect to a microtest tube concerning the hydrolysis and transgalactosylation of β -D-galactopyranoside derivatives

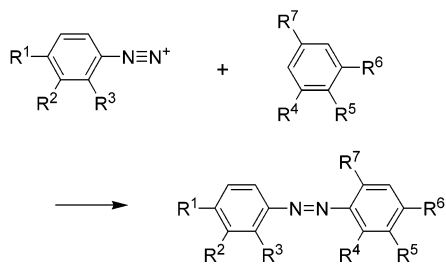
	microchip reactor (continuous)	microtest tube (batch)
1. hydrolysis		
reaction rate	5 times faster than batch	
conversion	0.16 (after 8 min)	0.01 (after 8 min)
2. transgalactosylation		
reaction rate	faster than batch	
conversion	0.04 (after 11 min)	0.01 (after 10 min)

(Scheme 15) is comparably low, an acceleration of the latter could be detected in the case of the microchip reactor.

Microreactors Used for Lab- and Pilot-Scale Synthesis: Liquid or Liquid/Liquid Reactions

Diazotization and Diazo Coupling. Previous publications refer to various process conditions. Salimi-Mososavi et al. conducted diazotization reactions under EOF, while Wootton

(28) Kanno, K.; Maeda, H.; Izumo, S.; Ikumo, M.; Takeshita, K.; Tashiro, A.; Fujii, M. *Lab Chip* 2002, 2, 15.

Table 11. Diazo coupling in various microreactors

entry	ref	R ¹	R ²	R ³	R ⁴	R ⁵	R ⁶	R ⁷
1	25	NO ₂	H	H	H	H	NMe ₂	H
2	26)	H	H	H	naphthyl	H	OH	
3	26	H	Me	H	naphthyl	H	OH	
4	26	H	H	Me	naphthyl	H	OH	
5	27	NO ₂	H	H	OH	H	OH	Me
6	28	substituents not disclosed						

et al. used a microreactor operating under hydrodynamic flow conditions for a similar reaction (Table 11, No. 1–4).^{29,30} In comparison, Hisamoto et al. realized the azo chemistry using phase-transfer synthesis in a glass microchip (Table 11, No. 5).³¹ A first attempt to transfer a microreactor-based azo-pigment process from lab scale into a pilot-plant process was described by Wille et al. (Table 11, No. 6).³²

Whereas the experimental results obtained within microchip reactors based on EOF were not compared with those from batch experiments, the publication referring to the glass microchip published by Hisamoto et al. provides such information (Table 11, No. 5).³¹ The latter reactor consisted of a microchannel (cross section: 250 μm × 100 μm, length: 3 cm) fabricated on a glass chip. The contacting of the two phases was realized by a micro Y-piece on the chip, which ensured the formation of a stable two-phase flow consisting of two lamellae.

To determine the efficiency of the glass-chip reactor (Table 11, No. 5) the diazo coupling was carried out in the microreactor and a glass vessel (diameter: 3.5 cm). In the first case syringe pumps were used to realize a total flow rate of 10 μL min⁻¹ for each phase. The macro-scale benchmark test using a glass vessel was carried out with 10 mL of both phases and different stirring conditions. The product was analyzed by reversed phase HPLC.

Using the glass-chip reactor (Table 11, No. 5) it was found that the conversion is close to 100% within 2.3 s, whereas the strongest stirring of the glass vessel leads to approximately 80% conversion after 10 min (Table 12). This is in accordance with the specific interface surface area of the microreactor, which is twice as high as that of the glass vessel. Furthermore, the high conversion in connection with the short reaction time demonstrates that the phase-transfer

(29) Salimi-Moosavi, H.; Tang, T.; Harrison, D. J. *J. Am. Chem. Soc.* **1997**, *119*, 8716.

(30) Wootton, R. C. R.; Fortt, R.; de Mello, A. J. *Lab Chip* **2002**, *2*, 5.

(31) Hisamoto, H.; Saito, T.; Tokeshi, M.; Hibara, A.; Kitamori, T. *Chem. Commun.* **2001**, 2662.

(32) Wille, C.; Autze, V.; Kim, H.; Nickel, U.; Oberbeck, S.; Schwalbe, T.; Unverdorben, L. In *Topical Conference Proceedings; IMRET 6*, 6th International Conference on Microreaction Technology, AIChE Spring National Meeting, March 11–14, 2002, New Orleans, LA; American Institute of Chemical Engineers: New York, NY, 2002; pp 7–17.

Table 12. Diazo coupling in a strong stirred vessel as benchmark for the glass microchip

	glass microchip	strong stirred glass vessel
conversion	~100%	80%
reaction time	2.3 s	~10 min
interfacial area	80 cm ⁻¹	40 cm ⁻¹

conditions in the glass-chip reactor were instrumental in suppressing the formation of the bis-azo product, a literature-known side reaction.

As a microreactor for the lab-scale and pilot-plant azo-pigment process (Table 11, No. 6) the standard laboratory reactor CYTOS provided by CPC, Germany was used.³² The latter was stacked-plate units comprising of mixing and reaction zones, as well as including an integrated heat exchanger. For the pilot plant a numbering-up concept by connecting three reactors in parallel was realized.

The laboratory-scale reactor (Table 11, No. 6) was used with flow rates of 20 and 80 mL min⁻¹, leading to residence times of several seconds. In the case of the pilot plant the total flow rate was increased up to 500 mL min⁻¹, resulting in an output of 10 t a⁻¹. All experiments were carried out at laminar flow as well as isothermal conditions. Although preliminary experiments have indicated that the diazotization and the pigmentation step can also be carried out in a microreactor, only the results of the diazo coupling are described. The coupling of two azo pigments, one red and one yellow, were investigated. In the case of the first one, a homogeneous diazo solution was used, and a pigment suspension was formed in the course of the reaction. In contrast, the yellow pigment was synthesized starting with a suspended diazo solution which resulted also in a suspended pigment solution.

Concerning the red pigment synthesized in a lab-scale reactor (Table 11, No. 6) an increased brightness and transparency were determined, which were mainly based on a smaller particle size of the pigments. Even better results were achieved for the yellow pigment, whose color strength was increased by up to 139% (Table 13). For the latter

Table 13. Comparison of the diazo coupling in the microreactor (lab-scale) with respect to the traditional batch reactor

	microreactor red pigment	microreactor yellow pigment
color strength	119%	139%
brightness	5 steps glossier	6 steps glossier
transparency	5 steps more transparent	6 steps more transparent
particle size: D ₅₀ (σ)	(not given)	<250 nm (1.5)/batch: 598 nm (2.0)

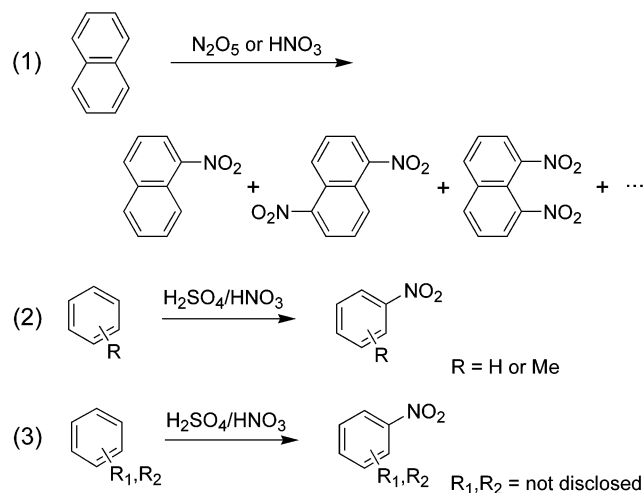
pigment, a particle size less than 250 nm was found which is significantly smaller compared with that from the batch process (598 nm).

A further reduction of the particle size D₅₀ down to 90 nm was achieved by applying the yellow pigment process to the pilot-scale microreactor. Due to the smaller particles,

the color strength of the pigments was increased by up to 149%.

Nitration of Aromatics. Previously investigated reactions refer to the nitration of naphthalene, by Antes et al.^{33,34} (Scheme 16, No. 1), of benzene and toluene (Scheme 16,

Scheme 16. Nitration reactions carried out in different microreactors



No. 2) by Burns et al.,^{35,36} and substituted aromatic compounds (Scheme 16, No. 3) by Dummann et al.³⁷

Antes et al. used three micromixers which were connected to tubular reactors (PTFE capillary of length: up to 150 cm) (Scheme 16, No. 1). The micromixers were based on different mixing principles such as multilamination (interdigital micromixer, Institut für Mikrotechnik Mainz GmbH, Germany (IMM)), split-recombine (silicon-based micromixer, University of Ilmenau, Germany), and T-piece mixing (glass micromixer, mgt mikroglas technik Mainz, Germany (mgt)).

The nitrations (Scheme 16, No. 1) were carried out at -10 to 50 °C using gaseous dinitrogen pentoxide as a nitration agent, or at 30 °C using fuming HNO_3 diluted in dichloromethane. Typical residence times were in the range of 15 – 45 s using a flow rate of 1 mL min^{-1} . After a quenching and an extraction step, the product composition was determined by HPLC and GC analysis.

If gaseous dinitrogen pentoxide was used for the nitration (Scheme 16, No. 1), the highest conversion was achieved by the interdigital micromixer, resulting in dinitrated naphthalene as the main product. By applying fuming nitric acid as the nitration agent, the selectivity changed to the mono-

substituted product, whereas the highest yield was obtained using the glass microreactor. Overall, the results indicate that the selectivity was sensitive to the reaction conditions as well as to which microreactor was used. A brief comparison of these results with those from batch processes is given in Table 14.

Table 14. Nitration of naphthalene in a batch reactor as benchmark for the microreactor

	microreactor	batch reactor
typical reaction temperature for nitrations using N_2O_5	30 °C	-50 to -20 °C
product ratio: 1,5-dinitro:1,8-dinitro	1:2.8	1:3.6
product ratio: 1-mono-nitro:2-mono-nitro	32:1	20:1

To generate a liquid/liquid slug flow various T-pieces (i.d.: 0.5 or 0.8 mm) connected to a capillary reactor (i.d.: 127 , 178 , or 254 μm ; length: 45 – 135 cm)^{35,36} and Y-pieces (inner diameter: 0.5 – 1 mm) connected to a capillary reactor (i.d.: 0.5 – 1 mm, length: 1 – 8 m)³⁷ were used (Scheme 16, Nos. 2 and 3). The latter reactor featured a heating jacket, which allowed isothermal operation of the reactor.

The nitrations of benzene and toluene^{35,36} (Scheme 16, Nos. 2 and 3) were carried out in a temperature range of 60 – 90 °C using different ratios of nitric acid and sulfuric acid (H_2SO_4 : 70 – 85 wt %) as nitration agents, and different acid/organic solution ratios ($2:1$ to $7:1$). The nitration studies published by Dummann et al. were carried out with mixtures of concentrated sulfuric and nitric acid as a nitration agent and various undisclosed substrates.³⁷ An isothermal capillary reactor was used to realize reactions temperatures in a range of 60 – 120 °C. The reactor was operated at 4 bar using total flow rates in the range of 9 – 36 mL h^{-1} . A GC was used for the analysis.

For the nitration of benzene and toluene (Scheme 16, Nos. 2 and 3) it was found that the reaction rate could be increased by several parameters, e.g. a smaller inner diameter of the tube implying a better mass transfer, a higher sulfuric acid ratio, and a low acid/organic solution ratio. If two of the experiments were compared with patent data, it can be seen that the capillary reactor-based process is competitive (Table 15).^{35,36} Especially the high reaction rate in the case of the capillary reactor promises room for improvement if smaller inner diameters are used.

By investigating the nitration reaction in a capillary reactor, Dummann et al. confirmed the published reaction mechanism, which explains the detection of two by-products, a dinitrated and a phenolic one. Further experiments at 60 and 120 °C outline that the amount of by-products can be decreased at lower temperatures. The use of various flow rates show that the by-product composition can be affected by the flow velocity.³⁷

Nitration of Urea Derivatives. Due to application of nitrated N,N' -dialkyl ureas as new energetic plasticizers, the nitration step was investigated in two microreactors by Antes et al.^{33,38,39} It was found that the direct nitration of N,N' -diethyl urea resulted in a mixture of mono- and dinitro

(33) Antes, J.; Tuercke, T.; Marioth, E.; Schmid, K.; Krause, H.; Loebbecke, S. *Topical Conference Proceedings: IMRET 4, 4th International Conference on Microreaction Technology*, AIChE Spring National Meeting, March 5–9, 2000, Atlanta, GA; American Institute of Chemical Engineers: New York, NY, 2000; pp 194–200.

(34) Löbbecke, S.; Antes, J.; Tuercke, T.; Marioth, E.; Schmid, K.; Krause, H. In *Proceedings of the 31st International Annual Conference ICT: Energetic Materials-Analysis, Diagnostics and Testing*, June 27–30, 2000, Karlsruhe, Germany.

(35) Burns, J. R.; Ramshaw, C. *Trans. Inst. Chem. Eng.* **1999**, *77*, 206.

(36) Burns, J. R.; Ramshaw, C. In *Topical Conference Proceedings: IMRET 4, 4th International Conference on Microreaction Technology*, AIChE Spring National Meeting, March 5–9, 2000, Atlanta, GA; American Institute of Chemical Engineers: New York, NY, 2000; pp 133–140.

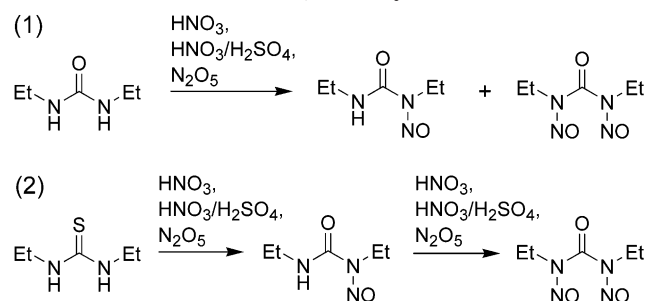
(37) Dummann, G.; Quitmann, U.; Gröschel, L.; Agar, D. W.; Wörz, O.; Morgenschweis, K. *Catal. Today* **2003**, *79–80*, 433.

Table 15. Comparison of the performance of the micro T-piece/capillary reactor with published patent data concerning the nitration of aromatics

type of nitration process	inlet/°C	outlet/°C	H ₂ SO ₄ /wt %	conversion/%	by-product/ppm	time/s	rate/min ⁻¹
traditional equipment	80	128	60.6	89.5	1000	120	0.9
traditional equipment	80	134	65.2	99.1	2090	120	2.1
traditional equipment	95	120	69.5	90.0	1750	25	4.6
T-piece and 178 μm capillary	90	90	77.7	94.0	4600	24.4	5.9
T-piece and 178 μm capillary	90	90	72.2	60.7	<1000	26.1	1.6

derivatives (Scheme 17, No. 1), which is in accordance to the batch process. Furthermore, a new two-step route to the dinitrated products using thiourea derivatives as the starting compounds was described (Scheme 17, No. 2).

Scheme 17. Nitration of *N,N'*-dialkyl urea derivatives



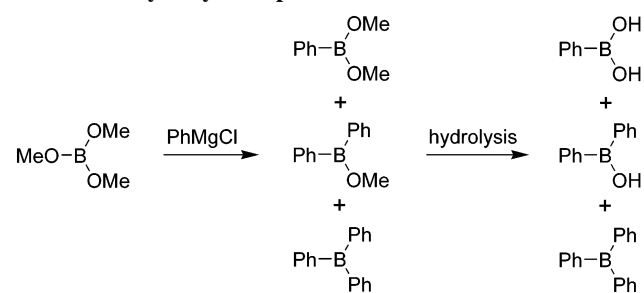
The silicon-based microreactors described in the former section “nitration of aromatics” were used. The nitration was carried out at defined temperatures between 0–20 °C using various nitrating agents such as nitric acid, mixtures of nitric and sulfuric acid, and dinitrogen pentoxide. PTFE capillaries of different lengths were used as residence time loops to realize different reaction times (0.6–82 s).

In accordance with the batch process, the nitration of *N,N'*-diethyl urea in a microreactor resulted in a mixture of mononitro and dinitro derivatives (Scheme 17, No. 1). In comparison, the nitration of corresponding thioureas was successfully carried out in a two-step procedure, resulting at first in the mononitro urea derivative with nearly 100% selectivity (Scheme 17, No. 2). By a second nitration step the respective dinitro derivative was obtained. The latter process was transferred to a batch process using sodium nitrate and sulfuric acid as a nitrating agent, and similar results were achieved, albeit the heat management could be more easily realized in a microreactor setup.

Phenylboronic Acid Formation. The formation of phenylboronic acid by Grignard addition of phenylmagnesium chloride to trimethyl borate was investigated in three micromixers by Hessel et al. and Koch et al. (Scheme 18).^{40,41}

To ensure a fast mixing of the substrate solutions, both were contacted by various micromixers. Two mixers made of glass and stainless steel respectively, featured an inter-

Scheme 18. Grignard addition to trimethyl borate and the consecutive hydrolysis step



digital channel structure and a geometric focusing section to generate a multilamellae flow with thin lamellae. The third micromixer was based on the split-recombine principle of fluid lamellae and was made of stainless steel. As residence time loops, different tubular reactors were applied. In a typical lab-scale setup the glass micromixer⁴⁰ was connected to a PTFE tube (length: 70 cm, i.d.: 2 mm). The caterpillar mixer⁴⁰ was used with various stainless steel tubular reactors of 100 cm length (i.d.: 0.7–21.2 mm), resulting in residence times in the range of 1–120 s. The flow rates were chosen with respect to the micromixer.⁴² The temperature range was varied between –12 up to 50 °C. Analogous investigations were carried out by Koch et al. using the stainless steel micromixer.⁴¹ The reaction temperature was varied in the range of –20–30 °C, and residence times between 5 and 180 s were realized by applying different flow rates.

The best results for each microreactor are listed in Table 16. It was found that the experimental setups based on micromixers provided higher yields than the batch process using traditional laboratory glassware. Furthermore, the amount of the disubstituted by-product can be decreased from 11% (batch process) down to 0.6% in the case of the stainless steel micromixer.⁴¹ Besides a detailed analysis of by-products, also the fouling in the microstructured devices was addressed by Hessel et al.⁴⁰ It was found that the glass mixer can be operated for 15 min only as long as deposition of a white precipitate was visible.

In addition, it is reported that, by achieving high purity of the crude product (99.2%), downstream processing could be considerably facilitated. The previously required distil-

(38) Antes, J.; Tuercke, T.; Marioth, E.; Schmid, K.; Krause, H.; Loebbecke, S. In *Topical Conference Proceedings; IMRET 4*, 4th International Conference on Microreaction Technology, AIChE Spring National Meeting, March 5–9, 2000, Atlanta, GA; American Institute of Chemical Engineers: New York, NY, 2000; pp 194–200.

(39) Löbbecke, S.; Antes, J.; Tuercke, T.; Marioth, E.; Schmid, K.; Krause, H. In *Proceedings of the 31st International Annual Conference ICT: Energetic Materials-Analysis, Diagnostics and Testing*, June 27–30, 2000, Karlsruhe, Germany.

(40) Hessel, V.; Löwe, H.; Hofmann, C.; Schönfeld, F.; Wehle, D.; Werner, B. In *Topical Conference Proceedings; IMRET 4*, 4th International Conference on Microreaction Technology, AIChE Spring National Meeting, March 5–9, 2000, Atlanta, GA; American Institute of Chemical Engineers: New York, NY, 2000; pp 39–54.

(41) Koch, M.; Wehle, D.; Scherer, S.; Forstinger, K.; Meudt, A.; Hessel, V.; Werner, B.; Löwe, H. (Clariant GmbH). DE 10140857, Frankfurt, Priority: August 21, 2001.

(42) Flow rates: glass mixer: 3.3–25 mL min⁻¹, caterpillar mixer: 23–167 mL min⁻¹.

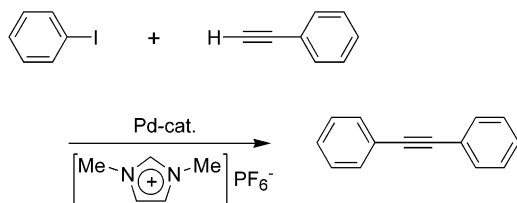
Table 16. Comparison of the Grignard addition using different microreactors and traditional laboratory glass ware

	interdigital glass mixer ⁴⁰	caterpillar mixer ⁴⁰	stainless steel interdigital micromixer ⁴¹	traditional glass ware ⁴¹
yield: PhB(OH) ₂	83% ^a	89% ^a	95% ^b	83% ^b
by-product yield: Ph ₂ B(OH)	1.4%	0%	0.6%	13.8%
temperature	22 °C	10 °C	20 °C	20 °C
residence time	8 s	10 s	5 s	not given

^a Determined by HPLC. ^b Isolated yield.

lation step is not needed anymore; instead, purification can be performed by crystallization or extraction. The latter two processes are favorably performed at room temperature, while distillation requires an additional energy supply, rendering the whole process more costly.

Sonogashira Coupling. The coupling reaction was based on a transition metal-catalyzed conversion of aryl halides and monosubstituted acetylenes to disubstituted acetylenes. A copper-free catalyst for this reaction was found by Fukuyama et al. (Scheme 19).⁴³ The latter was used in the

Scheme 19. Pd-catalyzed coupling of iodo benzene and phenyl acetylene

connection with an ionic liquid as the solvent to realize a continuous catalyst recycling system.

The coupling reaction was carried out in an interdigital micromixer having a microstructured mixing device (30 microchannels, width: 40 μm, depth: 200 μm) to generate a multilamellae flow. Furthermore, a T-shaped tubular reactor made of glass (length: 40 mm, i.d.: 2 mm) was used.

The low flow rates of 1.7 μL min⁻¹ for both the substrate solution containing the aryl halide and the acetylene and the Pd-catalyst dissolved in an ionic liquid was realized by syringe pumps. After the liquids were contacted at 110 °C, the reaction mixture was extracted, and the yield was determined by GC analysis.

Concerning catalyst recycling, the results indicate that the microflow system provides yields nearly equal to those of the batch setup using traditional glassware (20 mL round-bottomed flask) (Table 17). In contrast a continuous process

Table 17. Comparison of a microflow system with respect to a batch process in traditional laboratory glass ware concerning the Sonogashira coupling

	microflow system/%	batch process/%
yield of the first run	93	96
yield of the second run	83	80

based on a T-shaped tubular reactor resulted in a low conversion of the substrate.

Formation of Polyacrylates. A radical polymerization of acrylates was investigated by Bayer et al. (Scheme 20).^{44,45}

Scheme 20. Radical polymerization of acrylates

Since fouling limited the continuous polymerization process of a lab-scale tubular reactor, investigations were carried to enhance the homogenization of the monomer and initiator by a micromixer.

The setup for polymerization consisted of a tubular reactor (i.d.: 5–20 mm, length: 23–60 m) with static mixers inside and a premixing device. For the latter a Sulzer SMX or a mixer array, a numbering-up version of the stainless steel interdigital micromixer from IMM comprising 10 mixing units, was used.

The polymerization of acrylates was carried out with various monomers and initiators (preferential ratio 9:1) which were not disclosed. As typical reaction conditions, a reaction temperature up to 150 °C and a pressure up to 16 bar were mentioned. The flow rate was adjusted in the range of 6–8 kg h⁻¹ which resulted in a typical residence time of 40 min. The molecular weight distribution was determined by size exclusion chromatography.

In comparison to the Sulzer SMX, it was found that the use of a micromixer array as a premixing device led to an important improvement of the polymerization process. Due to an enhancement of the mixing of monomer and initiator, no molecular weights > 6 × 10⁴ g mol⁻¹ were found, which prevented fouling inside the tubular reactor (Table 18).

Addition of Organometallic Reagents. The addition of organometallic reagents to carbonyl compounds was the target reaction of Krummradt et al. (Scheme 21).⁴⁶ The investigations included the optimization of process parameters using various micro- and ministructured devices.

For the lab-scale experiments the micromixer array from IMM comprising 10 mixing units which generate a multi-

(43) Fukuyama, T.; Shinmen, M.; Nishitani, S.; Sato, M.; Ryu, I. *Org. Lett.* **2002**, *4*, 1691.

(44) Bayer, T.; Pysall, D.; Wachsen, O. In *Topical Conference Proceedings; IMRET 3, 3rd International Conference on Microreaction Technology*, AIChE Spring National Meeting; Ehrfeld, W., Ed.; Springer-Verlag: Berlin, 2000; pp 165–170.

(45) Pysall, D.; Wachsen, O.; Bayer, T.; Wulf, S. (Axiva GmbH). DE 19816886 C1, Priority: April 17, 1998.

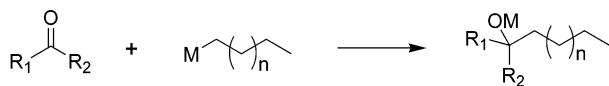
(46) Krummradt, H.; Koop, U.; Stoldt, J. In *Topical Conference Proceedings; IMRET 3, 3rd International Conference on Microreaction Technology*, AIChE Spring National Meeting; Ehrfeld, W., Ed.; Springer-Verlag: Berlin, 2000; pp 181–186.

Table 18. Comparison of premixers concerning the polymerization of acrylates

	micromixer	Sulzer SMX
molecular weight distribution	$2 \times 10^2 - 6 \times 10^4 \text{ g mol}^{-1}$	$2 \times 10^2 - 7 \times 10^6 \text{ g mol}^{-1}$
modality of the distribution	bimodal	trimodal
fouling	not found	fouling because of high-weight molecules

Table 19. Comparison of various reactors concerning the addition of organometallic reagents to carbonyl compounds

reactor type	surface/volume ratio/ $\text{m}^2 \text{ m}^{-3}$	$T/^\circ\text{C}$	residence time	yield/%
flask (0.5 L) (lab-scale)	80	-40	0.5 h	88
stirred vessel (6 m^3) (production-scale)	4	-20	5 h	72
micromixer (lab-scale)	10000	-10	<10 s	95
minimixer (pilot-scale)	4000	-10	<10 s	92
5 parallel minimixer (production-scale)	5×4000	-10	<10 s	92

Scheme 21. Addition of organometallic reagents to carbonyl compounds

lamellae flow was applied. Due to the deposition of solids inside the microreactor a mini-structured mixing unit was designed and used for the pilot-scale experiments. Finally a numbering-up concept containing five minireactors was realized for the production process.

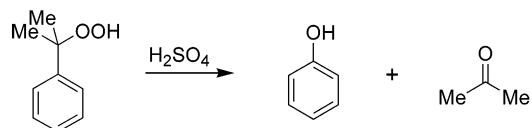
The process optimization was carried out with the micromixer-array-based lab-scale setup. Two flow rates of 6.7 and 33.3 mL min^{-1} were used at different temperatures in the range of -10 to -40 $^\circ\text{C}$ and at various substrate concentrations.

The best results for the lab-scale experiments were obtained at a temperature of -10 $^\circ\text{C}$ using the higher flow rate. A comparison of this result with those from other experiments carried out in a flask, a stirred vessel, and in the minireactors is summarized in Table 19. It is evident that the continuously operating micro- and mini-structured reactors result in much higher yields than the batch reactor. This was enabled by shorter reaction times which prevented side reactions and more efficient heat management by a larger surface/volume ratio.

Although the yield gained by the mini-structured mixer was a little bit smaller than that of the micromixer, the minimixer was applied to the production process. Besides the still high surface/volume ratio and the short residence time, the latter device could better face the fouling issue.

Cumene Hydroperoxide Rearrangement. The synthesis of phenol and acetone by means of the acid-catalyzed rearrangement of cumene hydroperoxide was described in a patent by Weber et al. (Scheme 22).⁴⁷

To contact the cumene hydroperoxide and the catalyst solution a multichannel reactor made of stainless steel was used. After splitting both feed streams into a multitude of reaction channels, two channels, one from each stream, were rejoined again. A typical cross section of the microchannels was 100 $\mu\text{m} \times 5000 \mu\text{m}$. The dimensions of the cooling

Scheme 22. Acid-catalyzed rearrangement of cumene hydroperoxide

channels of the integrated heat exchanger also had a depth of 500 μm and a width of 5000 μm . Referring to the volume of the reaction channels, the specific heat-transfer area amounted to 10000 $\text{m}^2 \text{ m}^{-3}$, which ensured sufficient heat transfer even if the cooling circuit failed.

The experiments were carried out with technical solution of 67 wt % cumene hydroperoxide and sulfuric acid as the catalyst. The catalyst feed stream was adjusted until the residual cumene hydroperoxide content was reduced to 1 wt %.

In the case of the microreactor the amount of high-boiling substances in the product stream was reduced down to 0.1 wt %. Conventional processing at a recycle ratio of 17 resulted in 0.21 wt % high-boiling substances (Table 20).

Table 20. Rearrangement of cumene hydroperoxide in a traditional tubular reactor as benchmark for the microreactor

	microreactor	traditional tubular reactor
yield	0.5% higher than the traditional process	
high-boiling substances	0.12 wt %	0.21 wt %
recycle ratio	2	17

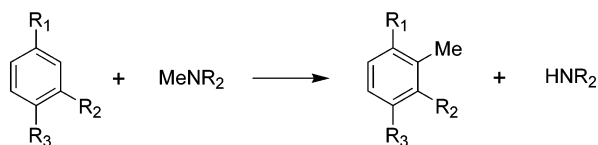
Methylation of Aromatics. The methylation of substituted aromatics was carried out by Wörz using tertiary methylamine (Scheme 23).⁴⁸ Since this process is proprietary, the nature of the substituents was not disclosed.

The reactor used for the methylation consisted of three parts. At first, both substrates were contacted in a short tubular pre-reactor (i.d.: 1 mm). Subsequently, the product

(47) Weber, M.; Tanger, U.; Kleinloh, W. (Phenolchemie GmbH & Co. KG). WO 01/30732, Priority: October 22, 1999.

(48) Wörz, O. In *Topical Conference Proceedings*; IMRET 5, 5th International Conference on Microreaction Technology, AIChE Spring National Meeting; Matlosz, M., Ehrfeld, W., Baselt, J. P., Eds.; Springer-Verlag: Berlin, 2001; pp 377-386.

Scheme 23. Methylation of aromatics by tertiary methylamines



stream was divided into two parts, and both partial streams were guided into a micromixer array (microchannels: 40 μm) provided by IMM to ensure a complete homogenization. Third, a tubular postreactor (i.d.: 1 mm) completed the reaction. The methylation was conducted at 0 $^{\circ}\text{C}$ and was completed within a total residence time of 6 s.

Compared with a former investigated semi-batch process, an equal yield of 95% was achieved by the micromixer-based setup (Table 21). However, two major advantages were

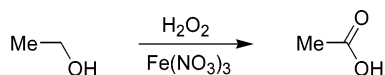
Table 21. Methylation of aromatics in a semi-batch process as benchmark for the micromixer-based process

	micromixer-based process	semi-batch process
yield	95%	95%
temperature	0 $^{\circ}\text{C}$	-70 $^{\circ}\text{C}$
reaction time	6 s	15 min

achieved: the reaction temperature was increased from -70 $^{\circ}\text{C}$ (semi-batch) up to 0 $^{\circ}\text{C}$, and the reaction time was diminished from 15 min down to 6 s.

Oxidation of Ethanol to Acetic Acid. The synthesis of acetic acid by the highly exothermic oxidation of ethanol was investigated by Kraut et al. (Scheme 24).⁴⁹ The reaction

Scheme 24. Synthesis of acetic acid by catalytic oxidation of ethanol



was catalyzed by ferric nitrate using hydrogen peroxide as the oxidant.

As a microdevice a modular microreactor composed of micromixers and microreactors was used. The latter were built as cross-flow heat exchangers. The section for the reactants consisted of 169 channels with a cross section of 150 $\mu\text{m} \times 300 \mu\text{m}$ and a length of 6 cm. The section used for the thermo fluid featured 1960 channels with a cross section of 150 $\mu\text{m} \times 300 \mu\text{m}$ and a length of 1.8 cm.

The experiments were performed using flow rates between 0.2 to 0.9 kg h^{-1} ethanol, 0.015 to 0.05 kg h^{-1} catalyst solution containing aqueous solutions of 1 mol L^{-1} ferric nitrate and 1 mol L^{-1} acetic acid, and 0.3 to 4 kg h^{-1} hydrogen peroxide solution (35%). The reactants were mixed successively by micromixers and passed through a series of four reaction modules (ignition, reaction, quenching) with cross-flow guided thermo fluids. The inlet temperatures of the modules were set to 70–115 $^{\circ}\text{C}$. To prevent boiling, the

(49) Kraut, M.; Nagel, A.; Schubert, K. In *Topical Conference Proceedings; IMRET 6, 6th International Conference on Microreaction Technology, AIChE Spring National Meeting, March 11–14, 2002, New Orleans, LA; American Institute of Chemical Engineers: New York, NY, 2002; pp 352–356.*

pressure was adjusted in the range of 3–5 bar. Analysis was performed by in-line NIR flow-cell measurement.

As summarized in Table 22, a yield and a selectivity of

Table 22. Oxidation of ethanol in a continuous stirred tank as benchmark for the microreactor

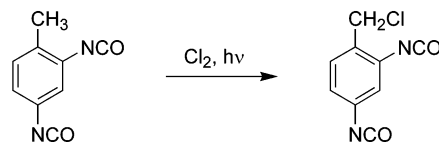
	microreactor	continuous stirred tank
residence time	3 s	1760 s
pressure	3–5 bar	atmospheric
conversion	>99%	30–95% (oscillating)
selectivity	>99%	>99%
reaction volume	3 cm^3	2900 cm^3
throughput	4300 $\text{cm}^3 \text{h}^{-1}$	5930 $\text{cm}^3 \text{h}^{-1}$
space-time yield	500 h^{-1}	0.7–2.0 h^{-1}

>99% was obtained. On the basis of temperature measurements of the thermo fluids and the mass throughput a power output of 2.8–3.1 kW was found which is in good accordance with the theoretical value of 3.13 kW. A benchmark of the microreactor-based setup and a continuous stirred tank reactor for this oxidation process is given in Table 22.

Microreactors Used for Lab- and Pilot-Scale Synthesis: Gas/Liquid and Gas Reactions

Side-Chain Chlorination of Alkyl Aromatics. The side-chain chlorination of toluene-2,4-diisocyanate was investigated by Ehrich et al. in terms of a photochemical reaction (Scheme 25).⁵⁰ The reaction was started by irradiation to generate chlorine radicals from gaseous chlorine.

Scheme 25. Photo chlorination of toluene-2,4-diisocyanate



The nondispersive gas/liquid contacting of the photochlorination was carried out in a falling film microreactor comprising a vertically orientated reaction plate with 32 microchannels (width: 600 μm , depth: 300 μm , length: 66 mm). The latter was used to generate a small liquid film. Furthermore, the microreactor featured an integrated heat exchanger for heating and a quartz window to allow an irradiation of the microchannels by an external light source.

The flow rates of the reactants were adjusted in the range of 14 to 56 mL min^{-1} for the chlorine and 0.12 to 0.57 mL min^{-1} for the solution of toluene-2,4-diisocyanate in tetrachloroethane. The latter resulted in residence times of 4.8–13.7 s. By the use of an integrated heat exchanger, the reactor was held at a temperature of 130 $^{\circ}\text{C}$. The raw product was analyzed by GC.

The highest conversion (81%) was obtained at the highest residence time. Furthermore, it was found that the amount of unidentified by-products was increased at higher residence times. In contrast, the amount of product resulting from an electrophilic chlorination reaction (by-product) was diminished. Hence, the best result was achieved at a residence

(50) Ehrich, H.; Linke, D.; Morgenschweis, K.; Baerns, M.; Jähnisch, K. *Chimia* **2002**, *56*, 647.

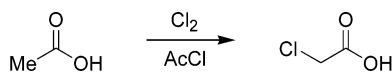
time of 8.9 s, resulting in a conversion of 55% and a selectivity of 80%. In comparison, a traditional glass vessel resulted in a conversion of 65%, but the selectivity of the desired product was reduced down to 45% (Table 23).

Table 23. Photochlorination in a glass vessel as benchmark for the falling film microreactor

	falling film microreactor	glass vessel
reaction time	8.9 s	30 min
space-time yield	401 mol L ⁻¹ h ⁻¹	1.3 mol L ⁻¹ h ⁻¹
conversion	55%	65%
selectivity (product)	80%	45%
selectivity (by-product)	5%	54%

Chlorination of Acetic Acid. The synthesis of monochloroacetic acid by the chlorination of acetic acid in the presence of acetyl chloride was described by Wehle et al. (Scheme 26).⁵¹

Scheme 26. Chlorination of acetic acid



The reaction was carried out in a microreactor comprising different microstructured plates for the flow distribution and gas/liquid contacting. Typically, the reaction channels had a width of 1000 μm and depth of 300 μm. An integrated heat exchanger ensured an appropriate heat management.

The conversion of acetic acid with chlorine was carried out at 170–190 °C. At a pressure of 4–6 bar chlorine gas was passed into the reactor in a co-current or counter-current direction. The chlorine flow rate was adjusted such that the chlorine content of the waste stream was smaller than 0.1%. A typical liquid flow rate of 50 g min⁻¹ was chosen.

Compared to the traditional process, which required a further crystallization step to remove the unwanted 3.5% dichloroacetic acid, the amount of this by-product could be decreased down to 0.01% using the microreactor-based process. Due to the stacked plate design a numbering up approach could be easily realized by assembling two reactors. The latter resulted in a yield of 85% for the monochloroacetic acid with 0.1% of the dichloro product (Table 24).

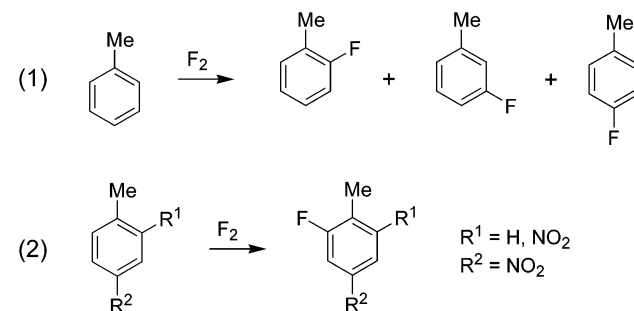
Table 24. Comparison of the microcapillary reactor with respect to a traditional bubble column concerning the chlorination of acetic acid

	microcapillary reactor	microcapillary reactor (2×)	bubble column
flow rate	50 g min ⁻¹	100 g min ⁻¹	
yield:	90%	85%	85%
monochloroacetic acid			
by-product yield:	<0.05%	<0.1%	3.5%
dichloroacetic acid			

Fluorination of Aromatics. A microbubble column,^{52–54} a falling film microreactor,^{52–54} and a silicon-based micro-

channel reactor^{55,56} were used by Jähnisch et al. and de Mas et al., respectively, for the direct fluorination of toluene. In both reactors the fluorination was carried out with elemental fluorine diluted in a nitrogen carrier gas, and pure or dissolved toluene (Scheme 27, No. 1). Furthermore, Cham-

Scheme 27. Direct fluorination of aromatics



bers et al. demonstrated the fluorination of 4-nitrotoluene and 2,4-dinitrotoluene (Scheme 27, No. 2).⁵⁷

Jähnisch et al. demonstrated the fluorination in two microreactors made of stainless steel. The microbubble column was composed of a dispersion device which ensured a uniform distribution of the gas and liquid flow to the reaction plate with a number of microchannels (width: 50 μm and depth: 50 μm or width: 300 μm, depth: 100 μm). For cooling, integrated heat exchangers were located on both sides of the reaction plates. The falling film microreactor featured a microstructured plate having 300 μm wide and 100 μm deep channels. A thin film of several 10 μm thickness was generated by means of gravity forces. de Mas et al. used a microreactor made by silicon microfabrication having two microchannels with a triangular cross section (width: 435 μm, depth: 305 μm, length: 2 cm). The inner volume of the reactor amounted to 2.7 μL. Chambers et al. fabricated a channel reactor, composed of nickel block with three parallel 0.5 mm wide and 0.5 mm deep channels covered by plastic plate. An integrated heat exchanger beneath the reaction channels allowed an adequate temperature control.

When using the microbubble column and the falling film microreactor the experiments were conducted at –50 to 15 °C, using liquid flow rates of 185–327 μL min⁻¹ and molar fluorine ratios from 0.2 to 2 equiv. The product mixture was analyzed by GC.

- (52) Jähnisch, K.; Baerns, M.; Hessel, V.; Ehrfeld, W.; Haverkamp, W.; Löwe, H.; Wille, C.; Guber, A. *J. Fluorine Chem.* **2000**, *105*, 117.
- (53) Jähnisch, K.; Baerns, M.; Hessel, V.; Haverkamp, V.; Löwe, H.; Wille, C. In *Proceedings of the 37th ESF/EUCHEM Conference on Stereochemistry*, April 13–19, 2002, Bürgenstock, Switzerland.
- (54) Hessel, V.; Ehrfeld, W.; Golbig, K.; Haverkamp, V.; Löwe, H.; Storz, M.; Wille, C.; Guber, A.; Jähnisch, K.; Baerns, M. In *Topical Conference Proceedings; IMRET 3, 3rd International Conference on Microreaction Technology, AIChE Spring National Meeting*; Ehrfeld, W., Ed.; Springer-Verlag: Berlin, 2000; pp 526–540.
- (55) de Mas, N.; Günther, A.; Schmidt, M. A.; Jensen, K. F. *Ind. Eng. Chem. Res.* **2003**, *42*, 698.
- (56) de Mas, N.; Jackman, R. J.; Schmidt, M. A.; Jensen, K. F. In *Topical Conference Proceedings; IMRET 5, 5th International Conference on Microreaction Technology, AIChE Spring National Meeting*; Matlosz, M., Ehrfeld, W., Baselt, J. P., Eds.; Springer-Verlag: Berlin, 2001; pp 60–67.
- (57) Chambers, R. D.; Holling, D.; Spink, R. C. H.; Sandford, G. *Lab Chip* **2001**, *1*, 132.

(51) Wehle, D.; Dejmek, M.; Rosenthal, J.; Ernst, H.; Kampmann, D.; Trautschold, S.; Pechatschek, R. DE 10036603 A1, Priority: July 27, 2000.

Table 25. Direct fluorination in a laboratory bubble column as benchmark for a microbubble column, a falling film microreactor, and silicon-based microchannel reactor

	microbubble column ⁵²	falling film microreactor ⁵²	laboratory bubble column ⁵²	silicon-based microchannel reactor ⁵⁵
temperature	-15 °C	-16 °C	-17 °C	rt
fluorine ratio	0.54 equiv	2.0 equiv	1.0 equiv	2.5 equiv
conversion	26%	76%	34%	58%
yield	11%	28%	8%	14%
selectivity	42%	37%	22%	24%

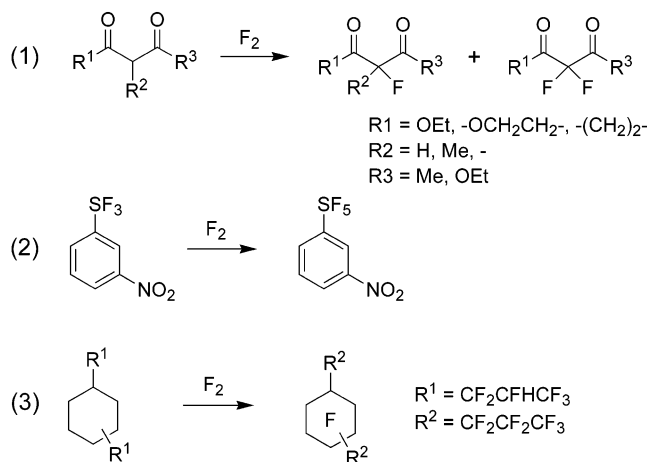
As a typical distribution of monofluorinated isomers a ortho:meta:para ratio of 5:1:3 was found. The experimental results with the highest yields are listed in Table 25. Both microreactors exceed the results gained by laboratory bubble column (volume: 20 mL), whereas the better results were achieved by the falling film microreactor.

The experiments of de Mas et al. were conducted at room temperature and nearly atmospheric pressure using flow velocities of 1.4 m s⁻¹ for gas flow and 5.6 × 10⁻³ m s⁻¹ for the liquid flow. The fluorine ratio was varied from 1 to 5 equiv. The best result is given in Table 25.

Chambers et al. applied flow rates of 50 and 100 μL min⁻¹ for the dissolved substrate, and typically 10 mL min⁻¹ for the fluorine/nitrogen mixture (10%). The reaction temperature was set to 5 °C. In the fluorination of 4-nitrotoluene a conversion of 40% was achieved. GC analysis resulted in a purity of 70%. The fluorination of 2,4-dinitrotoluene resulted in a conversion of 44%, whereas the purity amounted to 78%.

Fluorination of Non-aromatics. The fluorination of non-aromatics, namely the fluorination of 1,3-dicarbonyl compounds, the fluorination of sulfur trifluoride derivatives and the perfluorination of alkanes (Scheme 28) was also investigated by Chambers et al.^{57,58}

Scheme 28. Direct fluorination of nonaromatics



The reactions were carried out in a single-channel reactor having a 0.5 mm wide and 0.5 mm deep channel covered by a plastic plate. A numbered-up version with three parallel channels was fabricated to demonstrate the scale-up possibilities. In both cases an integrated heat exchanger beneath the reaction channel ensured the temperature control.

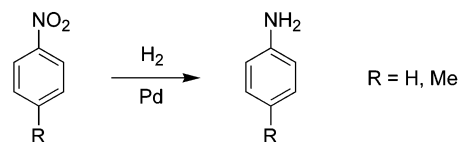
(58) Chambers, R. D.; Spink, R. C. H. *Chem. Commun.* **1999**, *10*, 883.

The experiments were conducted typically at 5 °C using liquid flow rates in the range of 4.2–83.3 μL min⁻¹. A mixture of 10% fluorine in nitrogen (typical flow rate: 10 mL min⁻¹) was used as the gaseous reactant.

It was demonstrated that the single-channel reactor provided conversions up to 98% (Scheme 28: R₁ = OEt, R₂ = H, R₃ = CH₃), whereas the three-channel device gave lower conversions up to 59% (Scheme 28: R₁ = OEt, R₂ = H, R₃ = CH₃). The fluorination of the sulfur trifluoride derivative led to a crude product which contained the pentafluorinated product in a ratio of 56%. The perfluorinated alkane was obtained with a purity of 70%.

Hydrogenation of Aromatic Nitro Compounds. The hydrogenation of aromatic nitro compounds, e.g., *p*-nitrotoluene and nitrobenzene, was investigated by Födisch et al.^{59,60} (Scheme 29, R = Me) and by Yeong et al.^{61,62} respectively (Scheme 29, R = H).

Scheme 29. Hydrogenation of aromatic nitro compounds



Födisch et al. used a stack of microstructured platelets which had 6 × 14 channels having a width of 300 μm, a depth of 700 μm, and a length of 400 μm. The aluminum platelets were anodically oxidized, and palladium was deposited using an electrochemical or chemical method. The reactor housing was used either with the stack of platelets or without this stack as a conventional fixed bed reactor.

Hydrogenation experiments were carried out at 70 °C and 20 bar. As a liquid reactant a 10% *p*-nitrotoluene solution in 2-propanol was used. To increase the conversion the reaction mixture was partly recycled in the loop reactor. In the case of the microreactor the recycle ratio was set to 43%. The residence time amounted to 280 s.

The experimental results illustrate that the chemical deposition of palladium resulted in a more efficient catalyst

(59) Födisch, R.; Hönicke, D.; Xu, Y.; Platzer, B. In *Topical Conference Proceedings; IMRET 5, 5th International Conference on Microreaction Technology*, AIChE Spring National Meeting; Matlosz, M., Ehrfeld, W., Baselt, J. P., Eds.; Springer-Verlag: Berlin, 2001; pp 470–478.

(60) Födisch, R.; Reschetilowski, W.; Hönicke, D. In *Proceedings of the DG MK-Conference on the Future Role of Aromatics in Refining and Petrochemistry*; Erlangen, Germany, 1999; pp 231–238.

(61) Yeong, K. K.; Gavrilidis, A.; Zapf, R.; Hessel, V. *Catal. Today* **2003**, *81*, 641.

(62) Yeong, K. K.; Gavrilidis, A.; Zapf, R.; Hessel, V. *Chem. Eng. Sci.* Manuscript submitted.

than the electrochemical deposition. In the first case using a recycle ratio of 43 a nearly quantitative conversion (98%) of *p*-nitrotoluene in combination with a *p*-toluidine selectivity of 100% was achieved in the microchannel reactor (Table 26). If the microchannel reactor is compared at smaller

Table 26. Comparison of a microchannel reactor with respect to a fixed bed reactor concerning the hydrogenation of aromatic nitro compounds

	conversion/ %	residence time/s	recycle ratio	<i>p</i> -nitrotoluene flow/geometric surface area/ g h ⁻¹ cm ⁻²
microchannel reactor	98	280	43	0.013
microchannel reactor	58	85	21	0.045
fixed bed	85	90	21	1.7 × 10 ⁻⁶
coated aluminum wires	89	260	21	0.045

recycle ratios with a conventional fixed bed catalyst or with coated aluminum wires, it turned out that the conversion of the microreactor is lower. The latter was ascribed to an unequal distribution of gas and liquid in the microchannels.

Yeong et al. demonstrated the hydrogenation of nitrobenzene in a falling film microreactor. To generate a thin liquid film the reactor was equipped with a microstructured plate having 64 parallel, 300 μm wide, 100 μm deep, and 65 mm long channels. The temperature control was ensured by an integrated heat exchanger which is located behind the reaction plate. For a visual inspection of the liquid film, e.g. measuring the film thickness, the reactor housing was equipped with an inspection glass. Experiments were conducted at 60 °C and 1–6 bar pressure using liquid flow rates in the range of 0.2–3 mL min⁻¹. The analysis was carried out with a GC.

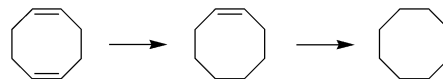
Because the liquid flow rate affected the thickness of the liquid film and the residence time, a dependency of the nitrobenzene conversion on liquid flow rate and the hydrogen pressure was ascertained. The best conversions greater than 85% were obtained at low flow rates of 0.5 mL min⁻¹. Furthermore, different catalyst preparation methods (Pd sputtering, UV-decomposition, wet impregnation, incipient wetness) were compared in long-term experiments, whereas the catalyst prepared by incipient wetness retained a nearly stable activity.

Hydrogenation Reactions. The use of gas-phase reactions in organic synthesis is problematic as a result of the difficulties associated with the safe handling of gaseous reagents. In addition, many such reactions are generally extremely exothermic, and it is difficult to control the temperature of such reactions when performed on a large scale. Microreactors have considerable attraction for such processes because there is only a small amount of reactants in the reactor at any given time. The microreactor enables excellent temperature control of the reaction as well as an opportunity for scale-up, by the simultaneous use of many such reactors.

Hönicke and co-workers have reported the gas-phase partial oxidation of cyclic dienes, to their corresponding

monoalkenes, over palladium and ruthenium/zinc catalysts.⁶³ The microreactors consisted of aluminium wafers, with mechanically etched channels, which were activated by anodic oxidation to obtain a porous oxide layer, which was used as the catalyst support. Impregnation of an organic solution of palladium(II) acetylacetonate resulted in microchannels consisting of an 18 μm thick layer of 0.18% Pd catalyst. The wafers were then stacked in a stainless steel housing to form a microreactor consisting of 672 microchannels for a stream of reagents to pass through. The authors used the device to investigate the hydrogenation of 1,5-cyclooctadiene to cyclooctene (Scheme 30). The diene was

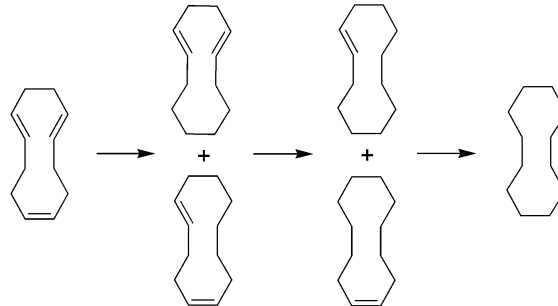
Scheme 30. Hydrogenation of cyclooctadiene



vaporized and mixed with hydrogen before being passed through the microreactor at a temperature of 150 °C. By increasing the residence time of the reaction from 35 to 115 ms the authors reported that the conversion increased from 75 to 99.5%. Although the increased residence time resulted in increased quantities of cyclooctane being formed, the selectivity of cyclooctene decreased from 99.5 to 98% under these conditions.

The authors used the same device to investigate the hydrogenation of *c,t,t,1,5,9*-cyclododecatriene to cyclododecene derivatives (Scheme 31). At a temperature of 150 °C, a

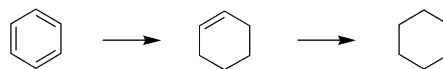
Scheme 31. Hydrogenation of cyclododecatriene



selectivity of 85–90% was reported, where the conversion was approximately 90%. The selectivity of this reaction was lower than the previous example because of the formation of the by-products. It was demonstrated, however, that there was a selectivity advantage of the microreactor compared to that of a fixed-bed reactor.

The catalytic hydrogenation of benzene was also investigated (Scheme 32), but complete reduction to cyclohexane

Scheme 32. Hydrogenation of benzene



was observed to take place when using the Pd catalyst.⁶³

(63) Dietzsch, E.; Hönicke, D.; Fichtner, M.; Schubert, K.; Weissmeier, G. *Topical Conference Proceedings; IMRET 4, 4th International Conference on Microreaction Technology, AIChE Spring National Meeting, March 5–9, 2000, Atlanta, GA; American Institute of Chemical Engineers: New York, NY, 2000; pp 89–99.*

The authors reported that hydrogenation of benzene to cyclohexene was accomplished using a microreactor system consisting of a ruthenium/zinc catalyst, which was incorporated into the microreactor using the same methodology, but the conversions were reported to be low (ca. 10%), with a maximum selectivity of 36%.

Conclusions

A large range of reactions have been carried out in microflow devices with success, among them many of the famous and industrially relevant organic processes. It is necessary to significantly change the experimental protocol of such reactions in order to adapt them to the needs of chemical microprocess engineering. Most prominent, the residence time of reactions has been notably shortened, usually by orders of magnitude, with the result that formerly hour-long processes may now be completed within seconds (Table 27).

Table 27. Comparison of process parameters in batch and microreactors with exemplary citations

parameter	batch quantity	microreactor quantity	exemplary citations
concentrated	c_b	$c_{mr} = c_b (< c_b)$	40, 41
temp	T_b	$T_{mr} = T_b + x \times 10 \text{ }^\circ\text{C}^a$	34, 40, 46
time	t_b	$t_{mr} \ll t_b$	23, 46, 50
pressure	p_b	$p_{mr} = p_b (> p_b)$	41, 49
volume	V_b	$V_{mr} \ll V_b (V_{mr} \gg V_b)$	49, 52

^a $x = 1-5$.

Since this task cannot be accomplished for every process by improving mass and heat transfer on its own (and undoubtedly can fail for some reactions), operation at higher temperatures is mandatory for some organic reactions in microreactors. This increase in reaction temperature may have other desired implications. When performing formerly cryogenic processes at ambient temperature, this may notably reduce energy costs. Typically, reactions may be carried out at temperatures up to 50 °C higher than done in a conventional way (albeit examples with larger gaps are still possible). Reactant concentrations (and pressure in the case of processing gaseous species) may be maintained or even

increased; however, to avoid fouling in the tiny microchannels a slight reduction in concentration is generally advised. The sample volumes are nowadays flexible in a surprisingly large range when using microflow devices, and many systems are commercially available.

The microreactor benchmarking was described above in a multifaceted manner. The discussion was grouped per reaction. It is difficult at this stage to draw general, at best deductive, conclusions. Each chemical process and each company demands unique profiles and specifications. In addition, the data set is far from being complete. A more in-depth scenario is provided in a more extended volume, but still cannot give top-down conclusions.² As one of the most striking facets it is very clear that microreactors give rise to a number of increases in selectivity and conversion, albeit the unsuccessful examples are not reported in open literature. It is also evident that by good mixing other parameters can be improved, such as the molecular weight of a polymer or the size, morphology, and distribution of a powder. There could be more “facets” added to this list; this information was largely given in the main section of this article and does not need to be repeated. In this sense, it is intended for this article to give the general information and to provide an overall impression of the field.

Finally, all this information must be used to build plants with microflow devices and to profit from the new technology. Otherwise the technology will stay at a level of an “innovation”, “plaything”, or whatever. Since the learning curve is large, the market is conservative, and the tool is not the solution to anything, it becomes increasingly apparent that “micro” should be only placed where it is needed and not where it may be technically feasible. To determine the “need”, benchmarking with documentation and analysis is the proper way. Finally, a market has to be served and the tool has to be brought into application.

Acknowledgment

We thank Steffen Hardt for his valuable contributions for specifying the quantities for description of the chemical processes and the products generated thereby.

Received for review November 28, 2003.

OP0341770

The application of micro reactors for organic synthesis

Paul Watts* and Stephen J. Haswell

Received 25th September 2004

First published as an Advance Article on the web 1st February 2005

DOI: 10.1039/b313866f

This *tutorial review* describes how micro reactors are being applied to synthetic chemistry covering a wide range of applications, from the preparation of nanograms of material for drug discovery and screening to the multi-tonne production of fine chemicals. This article explores how miniaturisation may revolutionise chemical synthesis and demonstrates that products are generated in higher yield and purity compared to the equivalent bulk reactions, in much shorter periods of time.

Introduction

In their simplest form, micro reactors consist of a network of micron-sized channels (typical dimensions are in the range 10–500 μm) etched into a solid substrate.¹ For synthetic chemistry, the channel networks are connected to a series of reservoirs containing chemical reagents (or products) to form the complete device or ‘chip’. Reagents can be brought together in a specific sequence, mixed and allowed to react for a specified time in a controlled region of the channel network using various pumping techniques; including electrokinetic (electroosmotic and electrophoretic) or hydrodynamic pumping. For electrokinetically-driven systems, electrodes are placed in the appropriate reservoirs to which specific voltage sequences can be delivered under automated computer control.² This control offers a simple but effective method of moving and separating reactants and products within a micro reactor, without the need for moving parts. In comparison, hydrodynamic pumping uses conventional, or micro-scale

pumps (notably syringe pumps) to manoeuvre solutions around the channel network, however this technique has the disadvantage of requiring either large external pumps or the complex fabrication of small moving parts within the device.

To date, research in the area has confirmed that micro reactor methodology is applicable to performing both gas and liquid phase reactions. From the work cited in this review article, the low-volume spatial and temporal control of reactants and products in a laminar flow diffusive mixing environment, in which distinctive thermal and concentration gradients exist, offers a novel method for chemical manipulation and product generation. Often, reactions performed within a micro reactor invariably generate relatively pure products in high yield, in comparison to the equivalent bulk reactions, in much shorter times and in sufficient quantities to perform full structural characterisation. One of the immediate and obvious applications is therefore in drug and process discovery, where the generation of compounds with either different reagents or under variable conditions is an essential factor. In addition, the opportunity to establish optimal chemical processes is an exciting capability of the technology,

*P.Watts@hull.ac.uk



Paul Watts

Paul Watts graduated from the University of Bristol in 1995 with a first class BSc in chemistry. He continued his studies at Bristol, obtaining a PhD in bio-organic chemistry under the supervision of Professor Tom Simpson FRS and Professor Chris Willis. His PhD focussed on the synthesis of isotopically labelled compounds, for use in determination of biosynthetic pathways to polyketide-derived natural products. Paul subsequently worked as a

postdoctoral research associate, with Professor Steve Haswell, at the University of Hull. During this period he investigated organic synthesis in micro reactors. In February 2002, he was appointed as a lecturer at the University of Hull. He is interested in organic chemistry and electrosynthesis in micro reactors and has published 30 papers in the area.



Stephen J. Haswell

Stephen Haswell is Professor of Analytical Chemistry at the University of Hull. His current research activities are in the areas of micro reactors including analytical developments, microwave enhanced reaction chemistry, trace elemental speciation and process analysis. He is author of over 120 research papers, a number of books and patents and is widely known nationally and internationally for his enthusiastic lectures. For a number of years one of the

underlying principles of Professor Haswell's research has been to break down the barriers that exist in science, in particular, the integration of analytical science with main line chemistry. Many of these ideals are encompassed in his research into micro chemical reactors, the subject of this article.

which could be integrated with appropriate analytical instrumentation. An interesting twist to the chemistry reported is not just the opportunity to separate reactants and products in real time, but also the ability to manufacture and use reagents *in situ*; an important issue when using highly toxic or explosive reagents, for example. In short, micro reactors are new, safe and more atom efficient tools with which to generate molecules and to increase our knowledge of complex chemical processes. In this review, a brief description of the fabrication and operation of micro reactors is outlined, followed by a detailed description of the types of reaction that have been performed in micro reactors and the benefits observed.

Fabrication of micro reactors

A number of materials such as silicon, quartz, glass, metals and polymers have been used to construct micro reactors.¹ Depending on the material used, a range of channel micro-fabrication methods such as photolithography, hot embossing, powder blasting, injection moulding and laser micro forming are available.^{1,3} However, the most important considerations for synthetic applications include chemical compatibility with the substrate, as well as the ease and reproducibility of fabrication. Furthermore if electrokinetic pumping is required special surface characteristics are essential as detailed below. Another issue which should be considered when *in situ* analysis is required is the compatibility of the material with the detection method to be used.

For organic chemistry glass is the most popular choice since it allows electroosmotic flow (EOF) with many common solvents, it is chemically inert, enables the use of visible light detection methods and fabrication procedures are well established. For glass micro reactors, photolithographic fabrication of channel networks is performed as shown schematically in Fig. 1.^{4,5} Firstly, the channel network is designed and printed using suitable computer drawing software and a film negative of the desired final size is prepared by photoreduction to form the optical mask. Recent instrumental advances of this process also enable the direct production of the mask from computer drawings.⁶ Commercially available borosilicate glass photolithographic plates (typically a few mm in thickness) coated with a thin metal layer (normally chromium) plus an upper layer of positive photoresist (0.5–2.0 μm depth) are used for channel network fabrication. The pattern of the required network of interconnecting channels is transferred from the optical mask to the photoresist layer. After light exposure, the photoresist is developed and removed, together with the chromium layer, to reveal the areas of glass to be etched. The channels are then etched using a mixture of 1% HF and 5% NH_4F in water at typically 65 °C, resulting in an etch rate of approximately 0.5 $\mu\text{m min}^{-1}$. During the etching process, it is important that the system is well agitated to ensure a consistent supply of etchant to the surface.

The base plate containing the etched channel network must next be sealed by bonding to an upper plate containing pre-drilled holes which act as reservoirs (or connecting conduits) for reagents and products. The most common method of bonding the two pieces of glass is thermal bonding at typically

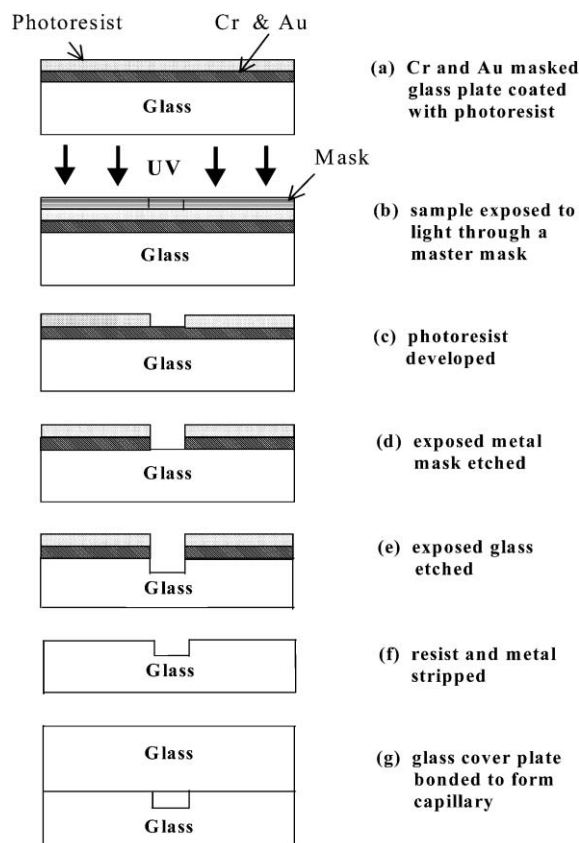


Fig. 1 Photolithographic fabrication of micro reactors.

575 °C for a few hours, using either a conventional or microwave furnace.^{4,5} A photograph of an all-glass device produced by this method is shown in Fig. 2. For good thermal bonding, it is important to ensure that both glass types have the correct thermal softening and expansion properties. In addition, the surfaces to be bonded must be clean and flat. Importantly, the advantage of using thermal bonding to seal the device is that no adhesives are required, as these are not generally resistant to organic solvents and reagents.

If hydrodynamic pumping is required it is possible to thermally bond ceramic HPLC-type adaptors to the glass device (Fig. 3) or use commercially available quartz capillaries. Connecting syringe pumps to such devices is relatively easy and enables the reactor to be incorporated with a HPLC system, for example. This type of micro reactor is ideal for reaction optimisation.

Of all the fabrication media, perhaps metal is the most robust in terms of engineering requirements and more specifically, micro mixers have been constructed and applied in chemical processing. This subject is extensively reviewed in ref. 1. However in the authors' experience, chemists generally prefer to use glass reactors if possible.

Operation of micro reactors

For a newcomer to the field of micro reactor technology, the easiest way to operate a device is by hydrodynamic control, using syringe pumps to manoeuvre solutions around the channel network. However, this approach has the

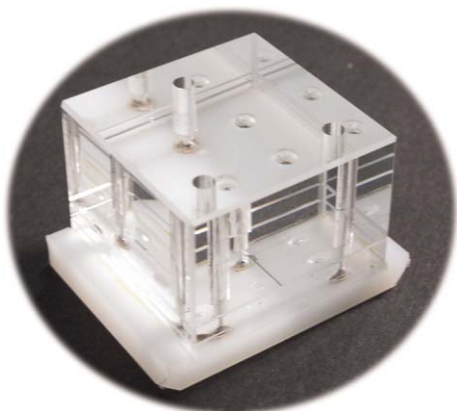


Fig. 2 A glass micro reactor suitable for electrokinetic control. The electrodes may either be placed in the reservoirs from above or may be fabricated into the base of the device.

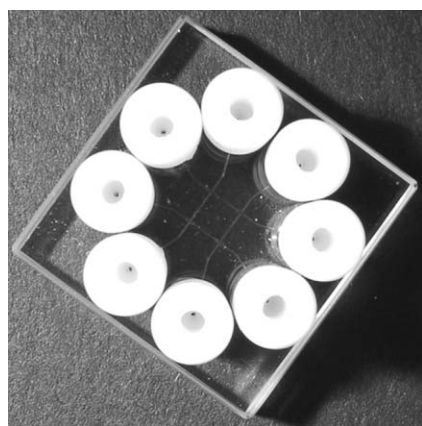


Fig. 3 A glass micro reactor fitted with ceramic HPLC adaptors.

disadvantage of requiring either large external pumps or the complex fabrication of small moving parts within the reactor itself. It should also be emphasised that although this approach is relatively easy if reacting just two solutions, it becomes far more complex to accurately control the fluidics when introducing more than three reagents into the device; in these situations much more care is required when designing the exact dimensions of the reactor channels.

A more elegant way of pumping solutions around a channel network is by electroosmotic flow (EOF),⁷ using voltage sequences applied *via* electrodes placed within the reagent reservoirs. This method has several significant advantages over hydrodynamic based pumping methods,⁸ as it can be easily miniaturised as no moving parts are involved and the required voltage sequences can be readily applied under automated computer control. For a glass micro reactor, the

channel wall-solution interface normally has a negative charge, arising from ionisation of surface groups, which are immobile. This immobile surface charge attracts a diffuse layer (of thickness in the order of nm) of mobile, oppositely charged counterions in the solution adjacent to the channel wall (cations for a negatively-charged glass channel wall). As shown schematically in Fig. 4, application of an electric field along the channel length causes the nm thick layer of mobile cations to move towards the more negative electrode, which drags all of the intervening solution in the bulk of the channel with it. An important feature of EOF is that the liquid velocity is constant across the channel, except in the nm thick regions of the diffuse layer of counterions very close to the wall. Unlike EOF, pressure-driven flow produces a parabolic velocity profile with high velocities in the channel centre and slow velocities near to the wall, giving rise to increased blurring of reagent zones along a channel length.⁸

It should be stressed that for EOF to be achieved, polar solvent types need to be used. The EOF fluid velocity v_{eof} is given by eqn. (1)²

$$v_{\text{eof}} = - \frac{E \epsilon \epsilon_0 \zeta}{\eta} \quad (1)$$

where E is the electric field (voltage divided by electrode separation), ϵ is the relative dielectric constant of the liquid, ϵ_0 is the permittivity of free space, ζ is the zeta potential of the channel wall-solution interface and η is the liquid viscosity. Consequently it can be deduced that solvents which possess a high dielectric constant (*i.e.* polar solvents) and low viscosity (η) will have a higher flow rate, as illustrated in Table 1 and Fig. 5.

It can be seen from Fig. 5, that the solvent flow rate is directly proportional to the field strength applied; as a result the flow rates within the channels can be easily controlled. Clearly this limitation prevents non polar solvents such as hexane and dichloromethane from being used in EOF

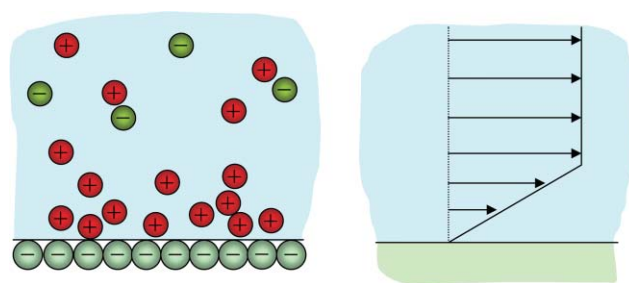


Fig. 4 Voltage-driven movement of the diffuse layer of cations adsorbed at the negatively charged channel wall (left-hand Figure) produces a flat EOF velocity profile across the channel except within the nm thick diffuse counterion layer (right-hand Figure).

Table 1 Relationship between magnitude of EOF and solvent properties

Solvent	Dielectric constant	Viscosity/cP	Polarity index/P	Flow rate/ $\mu\text{l min}^{-1}$
MeCN	37.5 (20 °C)	0.38	5.8	5.30
DMF	36.7 (25 °C)	0.92	6.4	1.67
EtOH	24.6 (25 °C)	1.10	5.2	0.90
THF	7.58 (25 °C)	0.55	4.0	1.00

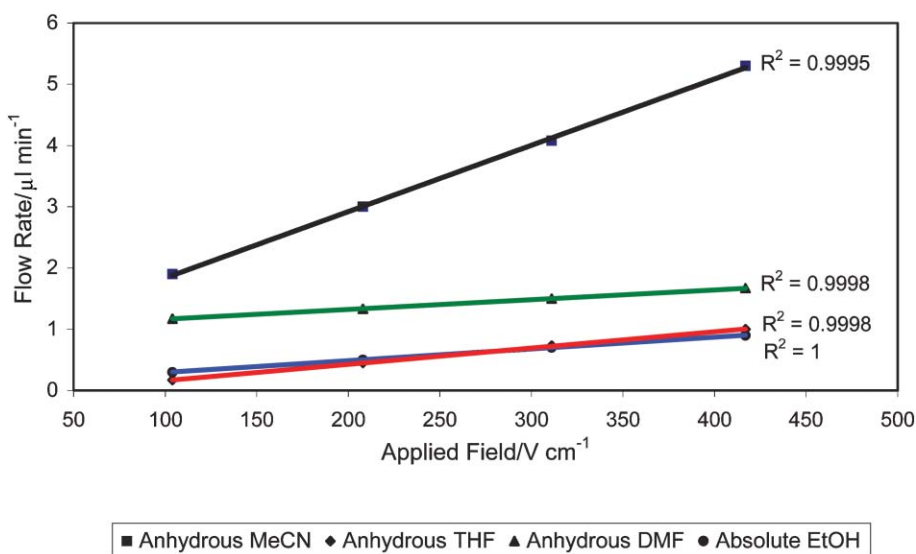


Fig. 5 Flow rates within a micro reactor for a range of common solvents.

controlled micro reactors, however research is currently underway to use combined hydrodynamic and EOF driven systems to overcome this problem.

It should however be emphasised, that under EOF control, charged solutes move with an electrophoretic velocity in addition to the electroosmotic velocity of the solvent. An elegant example of this was demonstrated by Fletcher *et al.* who reacted Ni^{2+} ions (from $\text{Ni}(\text{NO}_3)_2$) with pyridine-2-azop-*p*-dimethylaniline (PADA) within an EOF based micro reactor to produce a $[\text{NiPADA}]^{2+}$ complex.⁹ The authors reacted 2mM Ni^{2+} with 2mM PADA, which in a batch reaction would produce product (assuming a 100% conversion) of 1 mM concentration; however within the micro reactor they report that the product was produced in 12 mM concentration. The explanation for this is that the positively charged Ni^{2+} ions move with a higher electrophoretic velocity than the neutral PADA molecules, hence the Ni^{2+} ions move through the PADA solution, leading to preconcentration of the product within the channel.

Reactions performed in micro reactors

The following section reviews a number of chemical reactions that have been performed within micro reactors to date. The review is divided into two sections on how micro reactor technology may be used to make small quantities of product for use in the drug discovery process and secondly how micro reactor methodology may be applied to large scale chemical manufacture.

Small scale manufacture

The success of pharmaceutical companies resides largely on the synthesis and screening of novel chemical entities representative of the universe of drug-like compounds, which may be of the order of 10^{200} compounds or about 10^{40} chemotypes; and to optimise selected leads to marketable drugs. In an industry where development costs are extraordinarily high and attrition rates from lead generation onwards are about 98%, careful

lead selection and ruthless pressure to shorten optimisation cycle times are therefore critical for survival. In addition to this diligence, new technology that would enable a cost-neutral upward step-change in the number of lead candidates (and thus choice of a better lead with enhanced therapeutic effects and reduced side effects) and optimisation speed (to reduce time to market and extend patent life) would provide a distinct competitive advantage. A microchannel system also provides a potential separation column and a non-turbulent environment for partition between solvents. Integration of a micro reactor device, *via* purification to one of the many highly sensitive microchannel-based biological assay systems is not only possible, but may also address many of the industries' potential requirements. Apart from the greatly reduced reaction times demonstrated for the micro reactors, handling times to assay and chemical reagent costs are virtually eliminated. This paradigm is shown diagrammatically in Fig. 6.

In lead optimisation using conventional batch technology, validation and optimisation of reactions tends to be the rate-limiting step. Based on the model described in Fig. 6 however, it can be seen that if the biological assay was replaced by an analytical measurement and the conditions not the reagents are varied, then reaction optimisation could be easily carried out.

In a move to achieve this aim, Garcia-Egido *et al.* have recently reported the synthesis of a combinatorial library of pyrazoles within a glass micro reactor operated using hydrodynamic control.¹⁰ A T-shaped micro reactor was used to react seven 1,3-dicarbonyl compounds **1** with three hydrazine derivatives **2** to produce a library of twenty-one pyrazoles **3** (Scheme 1). The automated system consisted of an autosampler to introduce the reagents into the chip, a HPLC pump to move the reagents through the micro reactor and a dilution system to enable a small sample to be diverted to an LC-MS instrument for analysis. Other than in a few cases most of the pyrazoles were obtained in 99% conversion, but clearly the chromatography step allowed the reaction mixtures to be purified to produce analytically pure compounds. The final step would be to couple the output of the chromatography

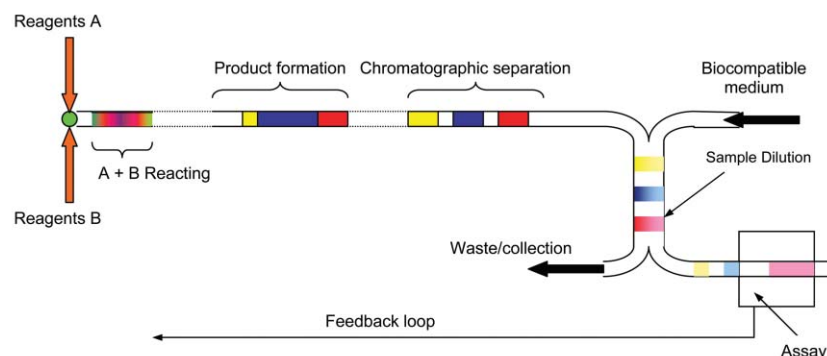
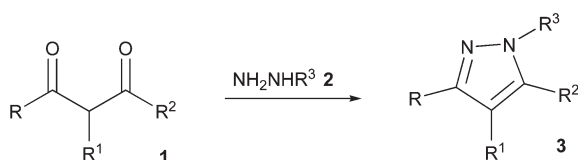


Fig. 6 Integration of a micro reactor with a biological assay system.

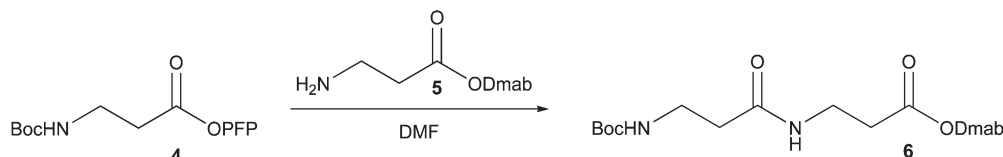


Scheme 1

column to a miniaturised bioassay system to enable *in situ* screening to be performed.

Although the above system is excellent in achieving combinatorial synthesis for the desired application, cynics argue that the overall system is hardly miniaturised; the micro reactor itself is tiny but the overall system is still composed of large bench top instrumentation. This is where EOF-based systems are potentially advantageous (as long as the solvent and/or reagents move by EOF) as external pumps are not necessary and purification could be achieved using on-chip electrophoretic separation rather than using large external instrumentation (such as the HPLC described above); it should be pointed out that the concept of miniaturisation started in analytical chemistry and separations using this technology are well established.¹¹

In a move to develop an EOF based system, Watts *et al.* have demonstrated the first example of multi-step synthesis in a micro reactor where they have used the micro reactors in peptide synthesis.^{12–14} The authors demonstrated that the dipeptide could be prepared from pre-activated carboxylic acids. They report that the reaction of the pentafluorophenyl (PFP) ester of Boc- β -alanine **4** with the amine **5** (Dmab is 4-[*N*-(1-(4,4-dimethyl-2,6-dioxocyclohexylidene)-3-methylbutyl)-amino]benzyl) gave the dipeptide **6** quantitatively in 20 min (Scheme 2). This represented a significant increase in yield compared with the traditional batch synthesis, where only a 50% yield was obtained in 24 h. The authors then used the



Scheme 2

methodology to consecutively react alternative pentafluorophenyl esters and amines to produce a library of peptides.¹³

Although the dipeptide bond forming reactions produced the dipeptide in 100% conversion based on consumption of the pentafluorophenyl ester, the product was still contaminated with residual amine as well as pentafluorophenol, the by-product of the reaction. George *et al.*¹⁵ have reported that the dipeptide may be separated from the reaction mixture using the device in Fig. 7, where the reaction mixture is collected in the ground reservoir during the synthesis and then the peptide is purified by electrophoresis and collected in reservoir D. Hence this methodology enables the synthesis and separation to be efficiently conducted within an integrated micro reactor without the need to have large peripheral equipment attached. However, further research is still needed to investigate integration of bioassay devices to this type of system.

Having demonstrated that peptide bonds could be successfully formed using a micro reactor; the authors then extended the methodology to the preparation of longer-chain peptides. Using the micro reactor, the Dmab ester of Fmoc- β -alanine **7** was reacted with one equivalent of piperidine or 1,8-diazabicyclo[5.4.0]undec-7-ene (DBU) to give the free amine **5** in quantitative conversion. This is in comparison to solid phase peptide synthesis where 20% piperidine in DMF is frequently employed, which demonstrates the atom efficiency of reactions performed within the devices. The authors then reacted the amine *in situ* with the pentafluorophenyl ester **4** to give the dipeptide **6** (Scheme 3) in 96% overall conversion.¹³

Having shown that more complex peptides could be produced by removal of the *N*-protecting group, the authors then demonstrated that they could remove the Dmab ester using hydrazine. The reaction of the Dmab ester **7** with one equivalent of hydrazine resulted in quantitative deprotection, to afford the carboxylic acid **8** (Scheme 4). This is in comparison to the solid phase peptide synthesis where 2% hydrazine in DMF is generally required to effect complete

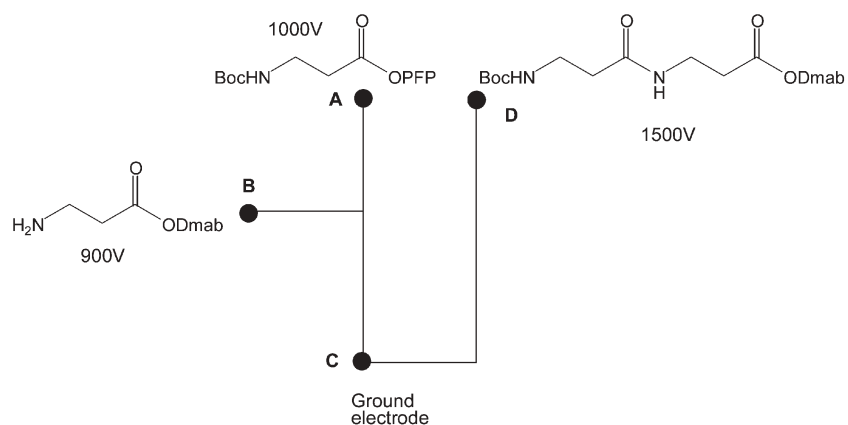
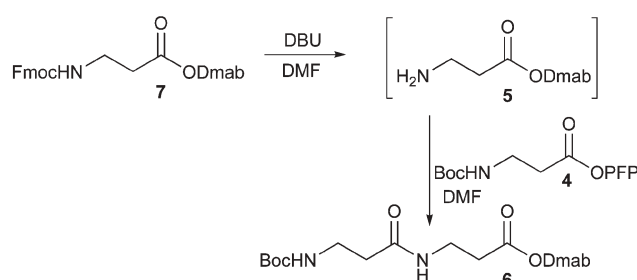
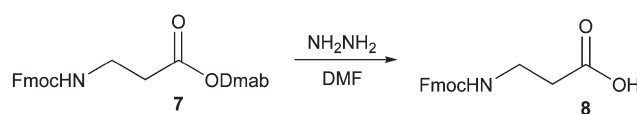


Fig. 7 Micro reactor design for simultaneous synthesis and separation of dipeptide.



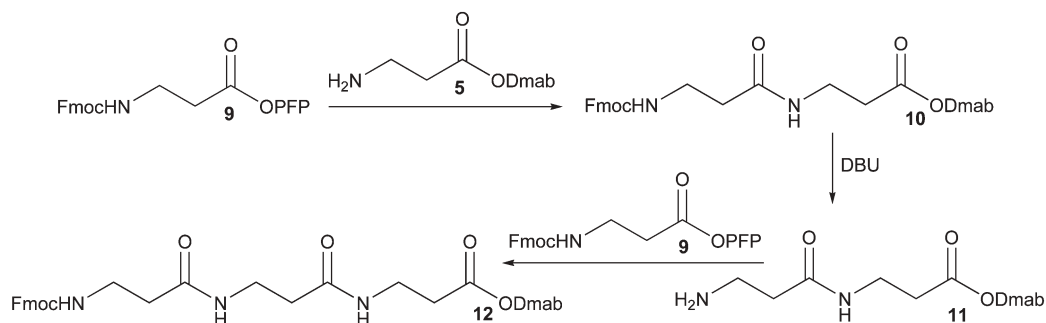
Scheme 3



Scheme 4

deprotection.¹³ From an environmental perspective the use of stoichiometric quantities of reagents in such reactions is clearly desirable, furthermore it makes the reaction mixtures easier to purify as excess reagents are eliminated.

The authors have further extended the approach to the synthesis of tripeptides, such as **12**.¹³ Reaction of pentafluorophenyl ester **9** with amine **5** formed dipeptide **10**, which was reacted with DBU to effect Fmoc deprotection. The amine **11** was then reacted *in situ* with another equivalent of pentafluorophenyl ester **9** to prepare tripeptide **12** in 30% overall

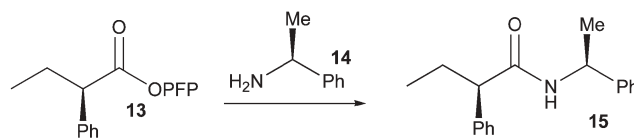


Scheme 5

conversion (Scheme 5). The approach clearly demonstrates that intermediates may be generated *in situ* and used in subsequent reactions. Although in the above examples the intermediates are relatively non-toxic, it is postulated that the approach may be used to generate highly toxic or explosive reagents *in situ*, that one would rather not use in organic synthesis.

Having demonstrated that peptide bonds could be successfully formed when using a micro reactor, the authors then investigated racemisation in peptide bond forming reactions derived from α -amino acids.¹⁶ Reaction of the pentafluorophenyl ester of (*R*)-2-phenylbutyric acid **13**, at 0.1M concentration, with α -methylbenzylamine **14**, gave the product **15** in quantitative conversion with 4.2% racemisation (Scheme 6). Importantly this represented less racemisation than observed in the batch reaction at the same concentration and temperature. The reduced level of racemisation was attributed to the reduced reaction times observed within the micro reactors.

While investigating different types of reactions within micro reactors, in order to expand the range of reactions that may be

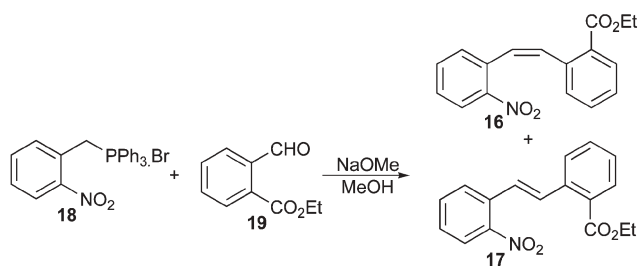


Scheme 6

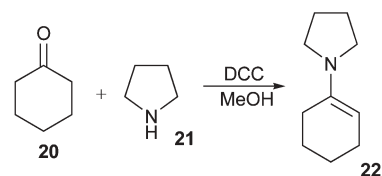
performed within such devices, various interesting results have been reported and these are discussed below.

Skelton and coworkers have reported the application of micro reactors for the Wittig reaction.^{17,18} The authors used the micro reactor to prepare the *cis*- and *trans*-nitrostilbene esters **16** and **17** using the Wittig reaction (Scheme 7). A number of features such as stoichiometry and stereochemistry were investigated. When two equivalents of the aldehyde **19** to the phosphonium salt **18** were used in the reaction, a conversion of 70% was achieved. The micro reactor demonstrated an increase in reaction efficiency of 10% over the traditional batch synthesis. The reaction stoichiometry was subsequently reduced to 1 : 1, but using a continuous flow of reagents, as above, the conversion was poor (39%). The conversion was increased to 59% using an injection technique, where slugs of the phosphonium salt **18** were injected into a continuous flow of the aldehyde **19**. The research was further extended to investigate the stereochemistry of the reaction. The ratio of isomers **16** and **17** was controlled by altering the voltages applied to the reagent reservoirs, which in turn affected the EOF and electrophoretic mobility of the individual reagents, meaning that the stoichiometry of the mixture was different. The variation in the external voltage subsequently altered the relative reagent concentrations within the device, producing *cis/trans* ratios in the region 0.57 to 5.21. In comparison, the authors report that, when a traditional batch synthesis was performed based on the same reaction time, concentration, solvent and stoichiometry, a *cis/trans* ratio of approximately 3 : 1 was observed in all cases. This demonstrated that significant control was possible in a micro reactor compared with batch reactions.

Sands and coworkers¹⁹ reported the preparation of enamines in a micro reactor. Enamines are traditionally prepared under Dean and Stark conditions, where the ketone and secondary amine are heated to reflux in toluene. These conditions remove the water from the reaction to produce the equilibrium-dependent enamine. Using the micro reactor, cyclohexanone **20** was reacted with pyrrolidine **21** to form the enamine **22** in 42% conversion at room temperature (Scheme 8). Clearly the use of methanol as solvent at room temperature, compared with the traditional Dean–Stark conditions, represents a more environmentally friendly procedure. In this case, the electrophoretic mobility of the product is thought to be greater than that of water, so enabling *in situ* separation of the by-product, which drives the equilibrium forward.



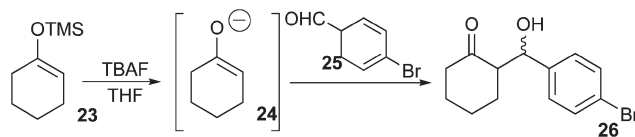
Scheme 7



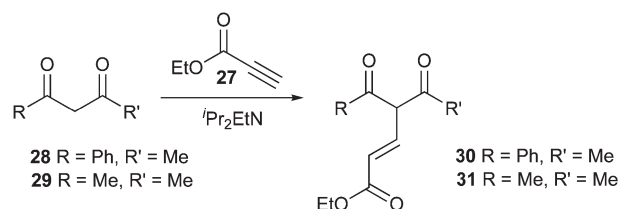
Scheme 8

Carbanion chemistry is one of the most common reactions used in organic synthesis, however large quantities of heat are frequently generated which means that careful control of the temperature, to prevent by-product formation, is required. Hence, micro reactors have a considerable attraction for these reactions because the reactor enables excellent temperature control of the reaction. Wiles *et al.*²⁰ have demonstrated the use of silyl enol ethers in the aldol reaction within a micro reactor. Quantitative conversion of the silyl enol ethers to β -hydroxyketones was observed in 20 min compared to traditional batch systems, where quantitative yields were only obtained when extended reaction times of up to 24 h were employed. One example involved the treatment of the TMS enol ether **23** with tetra-*n*-butylammonium fluoride (TBAF), to generate the tetra-*n*-butylammonium enolate **24** *in situ*, followed by condensation with *p*-bromobenzaldehyde **25** to give the β -hydroxyketone **26** in 100% conversion (Scheme 9). It should be emphasised that the air sensitive enolate was generated *in situ* within a sealed micro reactor and only had a lifetime of a few seconds before it was reacted with the aldehyde, consequently it was found that the reaction could be conducted on the open bench top without any problems.

Wiles *et al.*²¹ have also reported the preparation of the enolates from a series of 1,3-diketones using an organic base and their subsequent reaction with a variety of Michael acceptors such as **27** to afford 1,4-addition products within a micro reactor (Scheme 10). When using a continuous flow of the reagents **27** and **28**, 15% conversion to the adduct **30** was observed, compared with 56% when the diketone **29** was reacted with **27** forming the Michael adduct **31**. The authors, however, demonstrated enhancements in conversions through the application of the stopped flow technique. This procedure involved the mobilisation of reagents through the device for a



Scheme 9

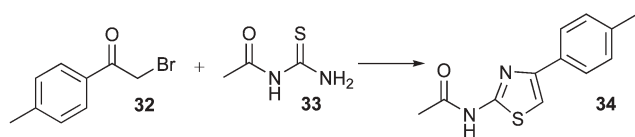


Scheme 10

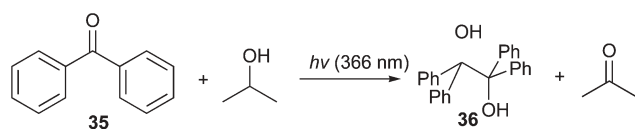
designated period of time, using an applied field, and the flow was subsequently paused by the removal of the applied field, prior to re-applying the field. Using the regime of 2.5 s on and 5 s off, the conversion to the product **30** was improved to 34%, while lengthening the stopped flow period to 10 s, resulted in a further increase to 100%. This was compared to the preparation of **31**, in which the regime of 2.5 s on and 5 s off resulted in an increase in conversion to 95%. The authors propose that the observed increase in conversion, when using the technique of stopped flow, was due to an effective increase in residence time within the device. This approach clearly shows the ease by which reactions can be optimised within micro reactors. Furthermore, in batch reactions it was found that a significant amount of by-product arose from reaction of the base with the Michael acceptor, however because the reagents were introduced sequentially within the micro reactor this was not observed.

Industrially, special equipment is required when performing large-scale reactions at elevated temperature. However, Garcia-Egido *et al.*²² have demonstrated the synthesis of 2-aminothiazoles using a Hantzsch synthesis within a heated micro reactor. The paper represents the first example of a heated reaction using an organic solvent within a glass micro reactor under EOF conditions. During the experiments the T-shaped micro reactor was heated to 70 °C using a Peltier heater. Reaction of α -bromoketone **32** with thiourea **33**, using NMP as solvent, resulted in the preparation of aminothiazole **34** in up to 85% conversion (Scheme 11).

Jenson *et al.*²³ have reported photochemical reactions within micro reactors. The reactor was fabricated by bonding a patterned silicon wafer to a quartz wafer, the advantage of this fabrication technique being that the quartz substrate allows reaction and detection using UV light of lower wavelengths than permitted by glass substrates. The authors investigated the pinacol reaction of benzophenone **35** in propan-2-ol (Scheme 12). The reaction is known to follow a radical reaction pathway and it is reported that the longer the residence time of the reaction, the greater the conversion to benzopinacol **36**. The authors report that there was no detectable product formation for flow rates $>10 \mu\text{l min}^{-1}$. With reduced flow rates (corresponding to larger residence times) the conversion improves because the amount of light absorbed increases, and there is therefore sufficient time for the excited species to diffuse and react with the benzophenone.



Scheme 11



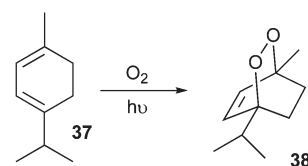
Scheme 12

The authors report conversions of up to 60% when using flow rates of $4 \mu\text{l min}^{-1}$.

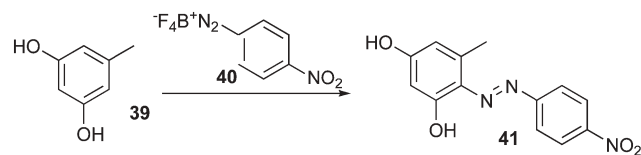
Wootton *et al.*²⁴ also report the ease of photochemistry to generate singlet oxygen *in situ* within a micro reactor. The technique allows the generation of singlet oxygen without the inherent dangers of forming large quantities of potentially explosive oxygenated solvents. The singlet oxygen was formed within the reactor channel by irradiation with a 20 W, 6 V tungsten lamp. The authors then used the aforementioned conditions to convert α -terpinene **37** into ascaridole **38** (Scheme 13) in greater than 80% conversion. For safety, nitrogen degassing of the product mixture was undertaken as soon as the solution was collected, hence avoiding accumulation of oxygenated solvents.

Hisamoto and coworkers²⁵ have described the first example of a phase transfer reaction in a micro reactor. These authors have successfully conducted a phase transfer diazo coupling reaction in which a solution of 5-methylresorcinol **39** in ethyl acetate was reacted with an aqueous solution of 4-nitrobenzenediazonium tetrafluoroborate **40** to form the azo dye **41** (Scheme 14). Syringe pumps were used to move the reagents around the reactor manifold and the authors report that the product was isolated in 100% yield and greater than 95% purity as a result of the phase transfer conditions. This example of phase transfer illustrates that the extraction of compounds into the bioassay system discussed earlier (Fig. 6) is indeed feasible.

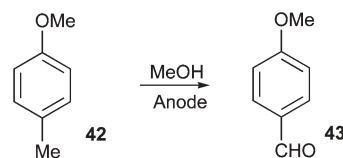
Several research groups have developed micro reactors for electrochemical synthesis. Löwe *et al.*²⁶ reported a micro reactor in which electrodes were fabricated within the flow channels and the system was used for the conversion of 4-methoxytoluene **42** to 4-methoxybenzaldehyde **43** (Scheme 15). By experimentally varying the voltage the selectivity was increased to 86% with a conversion of 88%.



Scheme 13



Scheme 14



Scheme 15

In contrast to the batch reaction it was possible to perform the reaction without a supporting electrolyte which makes product isolation easier.

Similarly, Suga *et al.*^{27,28} have developed micro reactors for the generation of highly reactive acyliminium ions which could be reacted with nucleophiles to produce C–C bonds. The reactor was cooled to $-78\text{ }^{\circ}\text{C}$ using integrated cooling channels. For example heterocycle **44** was converted into carbocation **45** *in situ* within the reactor before being reacted with nucleophile **46** to produce alkylated product **47** (Scheme 16). The micro reactor was used to produce a library of compounds in greater than 60% yield and in higher selectivities than in batch reactions.

Greenway *et al.* have demonstrated the Suzuki reaction within a micro reactor.²⁹ This represented an example of heterogeneous catalysis where 1.8% palladium on silica was placed in the central channel of the device. The catalyst was immobilised between microporous silica frits. The micro reaction was optimised using flow injection analysis principles, producing a conversion of 67% of cyanobiphenyl **48** at room temperature. The flow injection method allowed the periodic injection of the aryl halide **49** into a continuous flow of the phenylboronic acid **50** (Scheme 17). Traditionally, tetrahydrofuran (THF) is used as the solvent in this reaction, however as has been found with many organic solvents THF has very low natural EOF properties and for this reason, it was mixed with water (75 : 25) for use in the reaction. The yields obtained were comparable with Suzuki reactions on a batch scale using homogeneous catalysis. Importantly, there were negligible levels of the palladium catalyst in the product, which was demonstrated using inductively coupled-mass spectrometry (ICP-MS), this illustrating that the catalyst was not leaching from the reactor.

One of the interesting observations of the reaction was that, unlike conventional Suzuki reactions, an additional base was not required. Although the exact reason for this is not clear, it is postulated that the electric field may be sufficient to cause ionisation of the water at the catalyst surface. It is feasible that the hydroxide formed in this way may be sufficient to perform the function of the conventional organic or inorganic base.

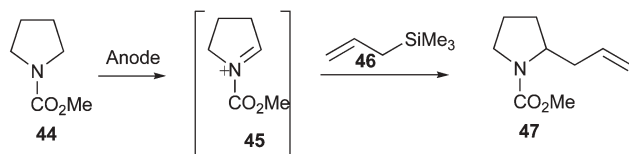
As an extension to the above work, He *et al.* have reported the same Suzuki reaction in a micro reactor which was placed within a microwave cavity.³⁰ In this case the authors report that the conversion was increased from 67% to 99%. The authors report that in order to get effective heating of the

catalyst, a 10 nm thick layer of gold was placed under the catalyst bed. The authors used the device to prepare a range of biaryls in greater than 70% conversion.

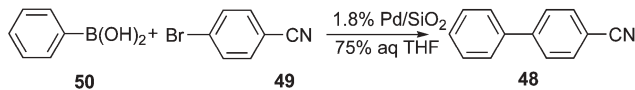
Kanno *et al.*³¹ have reported the use of enzymes within micro reactors operated by hydrodynamic pumping. Hydrolysis of *p*-nitrophenyl- β -D-galactopyranoside **51** was conducted using a β -galactosidase enzyme from *E. coli* to produce sugar **52** in quantitative conversion (Scheme 18). The reactor was maintained at $37\text{ }^{\circ}\text{C}$ using a hot plate. It was found that the hydrolysis of *p*-nitrophenyl- β -D-galactopyranoside within the micro reactor was five times faster than in a batch reactor. The paper also reports the transgalactosylation of a *p*-nitrophenyl-2-acetamide-2-deoxy- β -D-glucopyranoside using an enzymatic reaction.

Micro reactors are also showing a significant level of interest in the evaluation of catalysts. Dietzsch and coworkers³² have reported the gas phase hydrogenation of cyclic dienes, to their corresponding monoalkenes, over a variety of catalysts. The micro reactors consisted of aluminium wafers, with mechanically-etched channels, which were activated by anodic oxidation to obtain a porous oxide layer, which was used as the catalyst support. For example, impregnation of an organic solution of palladium(II) acetylacetonate resulted in microchannels consisting of an 18 μm thick layer of 0.18% Pd catalyst. The wafers were then stacked in a stainless steel housing to form a micro reactor consisting of microchannels for a stream of reagents to pass through. The authors used the device to investigate the hydrogenation of 1,5-cyclooctadiene **53** to cyclooctene **54** (Scheme 19). The diene **53** was vaporised and mixed with hydrogen, before being passed through the micro reactor at a temperature of $150\text{ }^{\circ}\text{C}$. By increasing the residence time of the reaction from 35 to 115 ms the authors report that the conversion increased from 75 to 99.5%. Although the increased residence time resulted in increased quantities of cyclooctane **55** being formed, the selectivity of cyclooctene **54** decreased from 99.5 to 98% under these conditions. A microstructured mesh micro reactor has been reported by de Bellefon and co-workers for use in catalyst screening experiments.³³

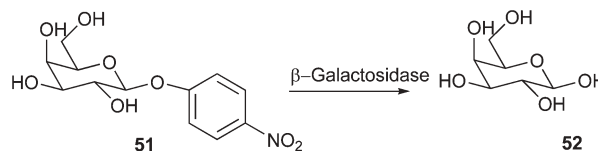
Wagner *et al.*³⁴ have reported the use of micro reactors in the preparation and growth of colloidal gold nanoparticles. Critically it was demonstrated that such particles could be handled in microfluidic channels without causing blockages. The authors report that the size distribution of



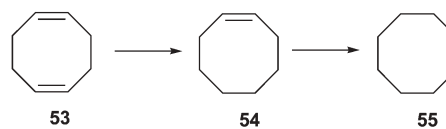
Scheme 16



Scheme 17



Scheme 18



Scheme 19

the nanoparticles may be readily controlled by simply altering the flow rates of the solutions through the channel.

Similarly Takagi *et al.*³⁵ have used micro reactors in the preparation of titania nanoparticles. Mixing of tetraisopropoxide and aqueous isopropanol solutions within a micro reactor enabled the preparation of mono-modal spherical particles of titania with a narrow size distribution. The authors reported that it was possible to prepare particles in the size range of 40–150 nm depending on the size of the micro reactor channels used.

Large scale manufacture

Current production technology is based on the scaling-up of successful laboratory scale reactions by firstly constructing a pilot plant, followed by a final increase in scale to enable production. This approach is however fundamentally flawed as at each stage changes are made to the overall surface to volume ratio of the reactors, which in turn affects mass and heat transfer processes. These variations in reactor conditions therefore result in changes to the process, meaning that it is necessary to evaluate the process and reoptimise it at each stage of scale up. Consequently the route from bench to large scale production is both costly and time consuming. It is therefore postulated that through the application of micro reactor technology, the transfer from laboratory to production would be both rapid and cost effective as processes would initially be optimised on a single device and in order to increase the production capacity more devices would be employed; a technique referred to as numbering up or scale out. With the number of techniques amenable to mass production increasing, the commercial availability of parallel reactors is starting to be realised. Along with the ability to reduce the transfer time between initial discovery and production, the scale out approach is also advantageous as it enables access to an array of features not commonly used in traditional scale out approaches, such as reduced reaction times and the ability to work in the explosive limit.

From a production perspective, the scale out approach is advantageous as it enables changes in production volume by simply increasing or decreasing the number of devices employed, therefore meeting the customer demand. Also through the use of generic reactor designs custom syntheses could be performed with relative ease. Compared to a production plant whereby reactors are configured for a single function, this flexibility is both advantageous and cost effective. In principle, all the reactions discussed in the previous section are suitable for scale out if required, but for illustrative purposes two specific examples are discussed in detail.

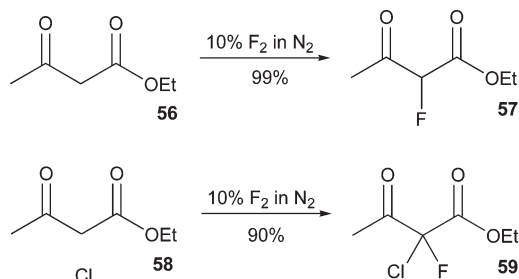
The diazotization of aromatic amines is an industrial process of great importance, however the dangers of diazotization are well known. The explosive nature of diazonium salts necessitates extreme care; hence the low volume associated with micro reactors affords a safe route to perform such reactions.

As a 'micro reactor' for the lab-scale diazo synthesis the standard laboratory reactor CYTOS produced by CPC, Germany was used.³⁶ This was constructed from stacked units comprising of mixing and reaction zones, as well as an

integrated heat exchanger. To make larger quantities of product the scale-up concept of connecting three reactors in parallel was realized. The laboratory-scale reactor was used with flow rates of 20 ml min⁻¹ and 80 ml min⁻¹ leading to residence times of several seconds. In the case of the pilot plant the total flow rate was increased up to 500 ml min⁻¹ resulting in an output of 10 t per year. Other industrial scale reactions using similar equipment have been reported in the literature.³⁷

The use of elemental fluorine in organic synthesis is problematic as a result of the difficulties associated with the safe handling of gaseous fluorine. In addition, fluorination reactions are generally extremely exothermic and it is difficult to control the temperature of such reactions when performed on a large scale. Micro reactors have considerable attraction for direct fluorination processes because there is only a small amount of fluorine in the reactor at any given time. The micro reactor enables excellent temperature control of the reaction as well as an opportunity for scale up, by the simultaneous use of many such reactors.

Chambers and Spink^{38,39} have reported the use of micro reactors for the fluorination and perfluorination of organic compounds using elemental fluorine. A nickel or copper micro reactor was used for the investigation and the liquid reactants and solvents were introduced into the reaction chamber *via* a syringe using a syringe-pump. Fluorine, in a nitrogen carrier gas, was introduced from a cylinder using a mass-flow controller. The liquid-gas mixing proceeded *via* cylindrical flow (sometimes called annular flow), where the liquid forms an outer cylinder coating the reactor surface with the gas flowing through the centre. This flow regime has enormous benefits in that it provides very large surface-to-volume ratios for the liquid phase, producing a very efficient reaction over a short distance. The products were trapped in a tube, which was cooled with either a salt/ice bath (0 °C) or an acetone/carbon dioxide bath (-78 °C). The fluorination of β -dicarbonyl compounds proceeded with a high efficiency using 10% fluorine in nitrogen at 5 °C and with formic acid as the solvent. Ethyl acetoacetate **56** was fluorinated in 99% conversion to give ethyl 2-fluoroacetoacetate **57** while ethyl 2-chloroacetoacetate **58** was fluorinated in 90% conversion, yielding ethyl 2-chloro-2-fluoroacetoacetate **59** (Scheme 20). Importantly, under these conditions, no perfluorination of the substrates was observed, with only the monofluorinated derivatives being isolated. The authors report that the bulk fluorination of ethyl 2-chloroacetoacetate **58** gives only a low conversion to **59**,⁴⁰ illustrating that the flow system is more



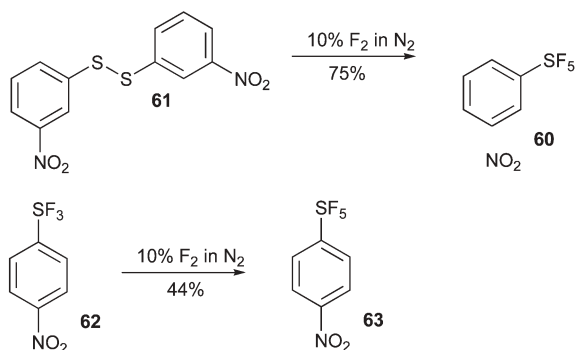
Scheme 20

efficient. This illustrates the catalytic effect of the fluorinated metal surface.

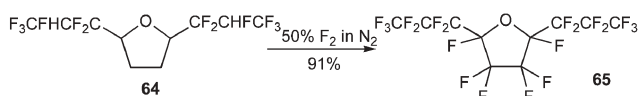
Sulfur pentafluoride derivative **60** was prepared in 75% yield by the reaction of the disulfide **61** with 10% fluorine in nitrogen, using acetonitrile as the solvent (Scheme 21). Similarly, treatment of the trifluoride **62** with fluorine gave sulfur pentafluoride derivative **63** in 44% yield.

Perfluorination reactions were found to require an additional heating stage for the reaction to go to completion. The reaction of the tetrahydrofuran derivative **64** with 50% fluorine in nitrogen at 280 °C gave the perfluorinated compound **65** in 91% yield (Scheme 22). In conventional reactions, cobalt trifluoride would be used to perfluorinate hydrocarbons.⁴¹ Some of the reactions carried out by the authors, however, required much lower temperatures than would be expected if this compound was used.

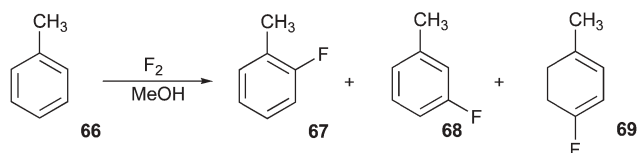
Jensen *et al.* have also demonstrated the direct fluorination of aromatic compounds in a micro reactor, a process difficult to perform on a conventional scale.⁴² The reactor was fabricated from silicon and capped with Pyrex using anodic bonding. The surfaces of the reactor, which were in contact with the reagents, were coated with a nickel film using a metal deposition technique. The authors have used the micro reactor in the fluorination of toluene **66** at room temperature (Scheme 23). Using methanol as the solvent, the authors report an 80% conversion to give the monofluorinated toluenes. The substitution pattern of the *ortho*-**67**, *meta*-**68** and *para*-**69** isomers was determined to be 4:1:2 by GC.



Scheme 21



Scheme 22



Scheme 23

Conclusions

Micro reactor chemistry is currently showing great promise as a novel method on which to build new chemical technology and processes in which the reactions generally produce the desired product in higher yield and purity, in shorter periods of time, compared with traditional batch reactions. The technology is still in its early development and it would be presumptuous to expand too far on the potential applications that micro reactors will find, but some early trends are clear. One of the immediate and obvious applications is in combinatorial chemistry and drug discovery, where the generation of compounds with different reagents or under variable conditions is an essential factor. Perhaps more intriguing, is what new angles micro reactors bring to reaction chemistry and these are only now just emerging. For example, extending the heterogeneous catalyst work already described one can see how immobilised or supported reagents could be placed within a device to impart functionality to a reaction whilst maintaining spatial and temporal control.

In addition, a microchannel system also provides a potential separation column and integration of a micro reactor device to one of the many highly sensitive microchannel-based biological assay systems may therefore not only be possible, but may also address some of the pharmaceutical industries' potential requirements. Apart from the greatly reduced reaction times demonstrated for the micro reactors, handling times to assay and chemical reagent costs may be virtually eliminated. Other emerging areas for the technology include catalyst screening and nanoparticle production.

Reactions within the micro reactors are found to be more atom efficient, which is of significant environmental importance as this reduces the quantities of raw materials required and minimises waste. Furthermore, the technology allows the temperature of reactions to be controlled, enabling reactions to be conducted safely, where explosion may be observed if the reaction was conducted on a batch scale. This is where scale out to produce large volumes of products is advantageous.

Paul Watts* and Stephen J. Haswell

Department of Chemistry, University of Hull, Cottingham Road, Hull, UK HU6 7RX. E-mail: P.Watts@hull.ac.uk; Fax: +44 (0)1482 466416; Tel: +44 (0)1482 465471

References

- W. Ehrfeld, V. Hessel and H. Löwe, *Microreactors: New Technology for Modern Chemistry*, Wiley-VCH, 2000.
- P. D. I. Fletcher, S. J. Haswell, E. Pombo-Villar, B. H. Warrington, P. Watts, S. Y. F. Wong and X. Zhang, *Tetrahedron*, 2002, **58**, 4735.
- M. Madou, *Fundamentals of Microfabrication*, CRC Press, Boca Raton, 1997.
- T. McCreedy, *TrAC*, 2000, **19**, 396.
- T. McCreedy, *Anal. Chim. Acta.*, 2001, **427**, 39.
- See: www.screen.co.uk.
- P. D. I. Fletcher, S. J. Haswell and V. N. Paunov, *Analyst*, 1999, **124**, 1273.
- P. H. Paul, M. G. Garguilo and D. J. Rakestraw, *Anal. Chem.*, 1998, **70**, 2459.
- P. D. I. Fletcher, S. J. Haswell and X. Zhang, *Lab Chip*, 2002, **2**, 102.
- E. Garcia-Egido, V. Spikmans, S. Y. F. Wong and B. H. Warrington, *Lab Chip*, 2003, **3**, 73.

- 11 R. E. Oosterbroek and A. van den Berg, *Lab-on-a-Chip: Miniaturised Systems for (Bio)Chemical Analysis and Synthesis*, Elsevier, Amsterdam, 2003.
- 12 P. Watts, C. Wiles, S. J. Haswell, E. Pombo-Villar and P. Styring, *Chem. Commun.*, 2001, 990.
- 13 P. Watts, C. Wiles, S. J. Haswell and E. Pombo-Villar, *Tetrahedron*, 2002, **58**, 5427.
- 14 P. Watts, S. J. Haswell and E. Pombo-Villar, *Chem. Eng. J.*, 2004, **101**, 237.
- 15 V. George, P. Watts, S. J. Haswell and E. Pombo-Villar, *Chem. Commun.*, 2003, 2886.
- 16 P. Watts, C. Wiles, S. J. Haswell and E. Pombo-Villar, *Lab Chip*, 2002, **2**, 141.
- 17 V. Skelton, G. M. Greenway, S. J. Haswell, P. Styring, D. O. Morgan, B. Warrington and S. Y. F. Wong, *Analyst*, 2001, **126**, 7.
- 18 V. Skelton, G. M. Greenway, S. J. Haswell, P. Styring, D. O. Morgan, B. Warrington and S. Y. F. Wong, *Analyst*, 2001, **126**, 11.
- 19 M. Sands, S. J. Haswell, S. M. Kelly, V. Skelton, D. O. Morgan, P. Styring and B. H. Warrington, *Lab Chip*, 2001, **1**, 64.
- 20 C. Wiles, P. Watts, S. J. Haswell and E. Pombo-Villar, *Lab Chip*, 2001, **1**, 100.
- 21 C. Wiles, P. Watts, S. J. Haswell and E. Pombo-Villar, *Lab Chip*, 2002, **2**, 62.
- 22 E. Garcia-Egido, S. Y. F. Wong and B. H. Warrington, *Lab Chip*, 2002, **2**, 170.
- 23 H. Lu, M. A. Schmidt and K. F. Jenson, *Lab Chip*, 2001, **1**, 22.
- 24 R. C. R. Wootton, R. Fortt and A. J. de Mello, *Org. Process Res. Dev.*, 2002, **6**, 187.
- 25 H. Hisamoto, T. Saito, M. Tokeshi, A. Hibara and T. Kitamori, *J. Chem. Soc., Chem. Commun.*, 2001, 2662.
- 26 K. Jahnisch, V. Hessel, H. Lowe and M. Baerns, *Angew. Chem. Int. Ed.*, 2004, **43**, 406.
- 27 S. Suga, M. Okajima, K. Fujiwara and J. Yoshida, *J. Am. Chem. Soc.*, 2001, **123**, 7941.
- 28 J. Yoshida and S. Suga, *Chem. Eur. J.*, 2002, **8**, 2651.
- 29 G. M. Greenway, S. J. Haswell, D. O. Morgan, V. Skelton and P. Styring, *Sens. Actuators B*, 2000, **63**, 153.
- 30 P. He, S. J. Haswell and P. D. I. Fletcher, *Lab Chip*, 2004, **4**, 38.
- 31 K. Kanno, H. Maeda, S. Izumo, M. Ikuno, K. Takeshita, A. Tashiro and M. Fujii, *Lab Chip*, 2002, **2**, 15.
- 32 E. Dietzsch, D. Hönicke, M. Fichtner, K. Schubert and G. Weißmeier, *IMRET 4: 4th International Conference of Micro Reaction Technology Topical Conference Proceedings, AIChE Spring National Meeting*, March 5–9 2000, Atlanta GA, USA, p 89.
- 33 R. Abdallah, V. Meille, J. Shaw, D. Wenn and C. de Bellefon, *Chem. Commun.*, 2004, 372.
- 34 J. Wagner, T. Kirner, G. Mayer, J. Albert and J. M. Kohler, *Chem. Eng. J.*, 2004, **101**, 251.
- 35 M. Takagi, T. Maki, M. Miyahara and K. Mae, *Chem. Eng. J.*, 2004, **101**, 269.
- 36 C. Wille, H. P. Gabski, T. Haller, L. Unverdorben and R. Winter, *Chem. Eng. J.*, 2004, **101**, 179.
- 37 T. Schwalbe, V. Autze and G. Wille, *Chimia*, 2002, **56**, 636.
- 38 R. D. Chambers and R. C. H. Spink, *J. Chem. Soc., Chem. Commun.*, 1999, 883.
- 39 R. D. Chambers, D. Holling, R. C. H. Spink and G. Sandford, *Lab Chip*, 2001, **1**, 132.
- 40 R. D. Chambers, M. P. Greenhall and J. Hutchinson, *Tetrahedron*, 1996, **52**, 1.
- 41 R. D. Chambers, B. Grievson, F. G. Drakesmith and R. L. Powell, *J. Fluorine Chem.*, 1985, **29**, 323.
- 42 N. de Mas, A. Gunther, M. A. Schmidt and K. F. Jenson, *Ind. Eng. Chem. Res.*, 2003, **42**, 698.

Efficiency, monitoring and control of microwave heating within a continuous flow capillary reactor

Ping He, Stephen J. Haswell*, Paul D. I. Fletcher

Department of Chemistry, University of Hull, Hull HU67RX, UK

Received 27 April 2004; received in revised form 5 July 2004; accepted 22 July 2004

Available online 25 September 2004

Abstract

We describe a method of monitoring temperature within a continuous flow capillary reactor (800 μm , outer diameter 1.2 mm and total length 138 mm) by measuring the change in electrical conductivity of a solution undergoing heating due to interaction with microwave energy. The method has been used to determine the extent of microwave heating as a function of liquid flow rate for solvents of differing microwave absorption properties. Deposition of gold metal on the outside surface of a glass capillary reactor was found to improve the efficiency of the microwave heating process. The alkylation of 2-pyridone with benzyl bromide, performed in DMF solution containing 0.01N NaBr, has been used to illustrate the suitability of the proposed methodology for monitoring the reaction temperature.
© 2004 Elsevier B.V. All rights reserved.

Keywords: Continuous flow capillary reactor; Microwave heating; Organic synthesis; Thermal measurement

1. Introduction

In recent years, the use of microwave-based heating in organic synthesis has proved to be a popular methodology [1] leading to numerous examples in which significant reductions in reaction times and enhancements in product conversions and selectivity are possible [2–4]. Interestingly, most of the work reported to date has been a batch rather than flow through technique and the opportunity of combining microwave heating with a capillary based flow reactor could offer an attractive route to high throughput reaction evaluations. In developing such methodology, however, two important issues need to be address. Firstly obtaining a direct temperature measurement from within a reacting solution, which can be difficult using conventional methods such as thermocouples and optical probes and secondly achieving controllable efficient heating of a capillary reactor using a microwave field. Whilst the use of current monitoring has

previously been used to determine the average temperature of a buffer in electrokinetic systems [5,6], its application to a hydrodynamically pumped microwave heated capillary system has not been reported. In addition to current measurement a number of optical temperature monitoring techniques have been reported, in which thermal measurements or imaging have been obtained through the use of a temperature-dependent fluorophores added to the system [5,6]. Whilst this approach overcomes the spatial limitation of the current measurement approach, which will only give an average determination of temperature, the necessity to image fluorophore emission from a reaction medium and their removal from products would be a severe disadvantage for chemical synthesis applications.

In this paper, we describe an electrical conductivity (EC) method for *in situ* temperature monitoring within a gold coated capillary flow reactor under microwave irradiation. The method has been used to measure the microwave heating characteristics of different solvents as a function of flow rate within a capillary flow reactor and to monitor thermal conditions during a reaction. To illustrate the relevance of

* Corresponding author. Tel.: +44 1482 465469; fax: 44 1482 466416.
E-mail address: s.j.haswell@hull.ac.uk (S.J. Haswell).

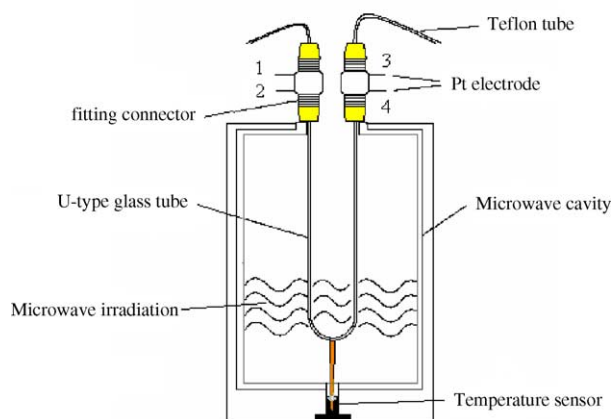


Fig. 1. Schematic diagram of the capillary flow reactor fitted within the microwave cavity showing the positions of the IR temperature sensor and the electrodes 1–4 used to monitor the different temperature values.

this proposed methodology, the alkylation of 2-pyridone with benzyl bromide has been used.

2. Experimental

The experimental set-up is shown schematically in Fig. 1. The flow reactor consisted of a U-shaped glass capillary of inner diameter 800 μm , outer diameter 1.2 mm and total length 138 mm. The capillary was mounted within the cavity of a Discover microwave system from CEM. This provided microwave radiation of 2.45 GHz and total power in the range 0–300 W, which was incident on the lower section of the U-shaped capillary. The microwave cavity was fitted with an infrared sensor, which was aligned so as to monitor the temperature of the external surface of the lower part of the U-shaped capillary. The capillary was connected via two, two-way connectors and PTFE tubing to an external syringe pump (Harvard, model PHD 2000). The two-way connectors were fitted with two Pt wire electrodes (0.4 mm outer diameter), which are labelled 1–4 in Fig. 1. Measurement of the conductivity between electrodes 1 and 2 was used to determine the temperature of the inlet tube section, between electrodes 3 and 4 for the outlet section and between electrodes 2 and 4 for the average temperature of the main U-shaped section. The conductance values between the different electrode pairs were measured using a Wayne Kerr 6430A precision component analyser operating at 40 Hz and 10 V. Conductance values were converted to conductivity values using calibration measurements (with solutions of known conductivity values) of the cell constants corresponding to the different capillary sections. Repeated measurements of the cell constants were found to be reproducible within 1% and showed good agreement with values calculated according to the measured lengths and cross-sectional areas of the capillary sections.

In order to convert measured conductivities into the corresponding temperatures, the solution conductivities were

measured as a function of temperature using a PTI-18 conductivity meter fitted with a conventional dip-cell. Solutions were thermostatted to ± 0.1 °C using a Grant LTD6 circulatory thermostat.

Water was purified by reverse osmosis and by passage through a Milli-Q reagent water system. The solvents dimethylformamide (DMF, Lancaster, 99%) and *N*-methyl formamide (NMF, Lancaster, 99%), NaBr (Fisher Chemicals, 99%) and KCl (BDH, AnalaR grade) were used without further purification. Immediately prior to microwave heating experiments, test solutions were degassed by briefly boiling under reduced pressure with ultrasound treatment. This was done to avoid bubble formation within the capillary.

The outer surface of the capillaries were coated with metal using a SEMPREP 2 Sputter Coater (Nanotech Ltd.). The areas not requiring coating were masked off with tape before placing on a water-cooled table within the vacuum chamber. Metal was sputtered in an atmosphere of argon at a pressure of 200 mTorr and an HT current of 20 mA being applied to the metal target. These settings were kept constant for all the coatings described here. The coating thickness was controlled at the time of sputtering; for example, 90 s sputtering was estimated to yield a thickness of 10–12 nm and 180 s produced a thickness of 20–22 nm. Both sides of the capillaries were coated by sputtering once, turning the capillary over and sputtering a second time.

For the alkylation reaction, 2-pyridone solutions (0.5 M, Lancaster, 98+%) was premixed with benzyl bromide (0.5 M, Lancaster, 99%) in a DMF solution containing 0.01N NaBr and pumped using a syringe pump (Harvard PHD 2000) through the U-capillary reactor heated by microwave irradiation. The residence times of the solutions within the heating zone defined by the gold coating were directly measured by timing the movement of the liquid front during first filling. The products from each reaction run were collected in a glass vial for a period of 90 s, weighed and a known amount of dodecane (10 μl , Aldrich, 99+%) was added as an internal standard. Samples were treated with distilled water to remove unreacted 2-pyridone and extracted with dichloromethane (Fisher, AR). The extract was then washed three times with distilled water, collected and dried over MgSO_4 (Fisher, 99+%). Samples were then analysed for benzyl bromide and alkylation product using a GC instrument (Shimadzu GC-17A) equipped with a capillary column (CP SIL 8 CB, 30 m length, Chrompack). Pressure of carrier gas (helium) was 600 kPa and injector temperature was set to 280 °C. The GC column temperature was held initially at 70 °C for 4 min, ramped at 20 °C/min to reach 240 °C, which was then held for 12 min.

3. Results and discussion

Initial measurements were made to establish a suitable microwave absorbent film that could easily be deposited on the outside surface of the glass capillary reactor. From Table 1, it

Table 1
Temperatures measured on the external capillary surface using the IR sensor for different metal films under MW irradiation

Metal	Sensor temperature (°C)	Resistivity ($\mu\Omega$ cm)
Carbon	66	1375
Platinum	98	10.6
Gold	>200	2.3

NMF is used as solvent and flow rate 0.1 ml min^{-1} . The thicknesses of metal films were all 20 nm. MW power was 50 W and heating time 20 s.

can be seen that, for the same MW power and film thickness, the measured temperatures based on the integrated instrument IR sensor were in the order $\text{Au} > \text{Pt} > \text{C}$. This ranking sequence correlates with the electrical conductivities of the materials, i.e., the more conducting the better the MW absorption and the higher the temperature reached. Therefore, gold was selected for producing heating patch films.

Plots of conductivity versus temperature for 0.01 M NaBr solutions in water, DMF and NMF are shown in Fig. 2. Over this temperature range, the relationship is virtually linear and the fitted values of slopes and intercepts of the plots were used to convert measured conductivity values to the corresponding temperatures.

Conductance values recorded for a liquid flowing in the capillary during microwave irradiation were converted to conductivity (using the measured cell constants) and then to temperature (using the calibration data of Fig. 2). As noted previously, conductance measured between electrodes 1 and 2 gives the inlet temperature, electrodes 3 and 4 give the outlet temperature and electrodes 2 and 4 provide the average liquid temperature over the length of capillary within the microwave cavity. An additional temperature value provided by the IR sensor reading corresponds to the temperature on the external surface of the lowest part of the capillary.

Steady-state values of the four different temperatures are plotted versus liquid flow rate for 0.01 M NaBr in DMF, water and NMF in Fig. 3(a–c). The incident microwave power was 50 W. For each solvent, the characteristic shapes of the

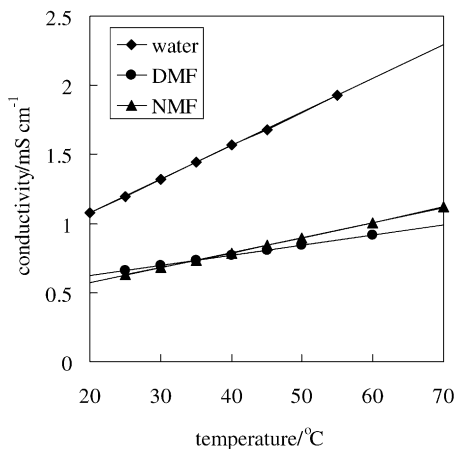


Fig. 2. Calibration plots of conductivity vs. temperature for 10 mM NaBr solutions in the three solvents.

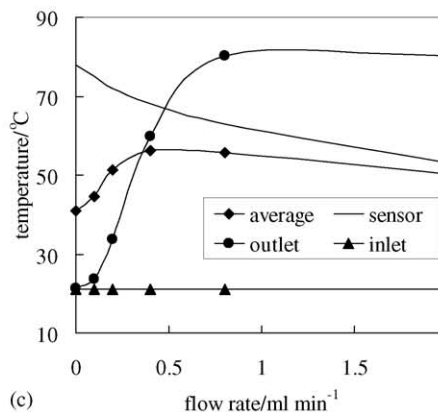
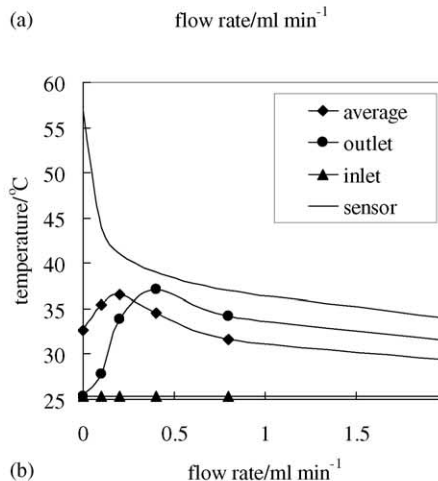
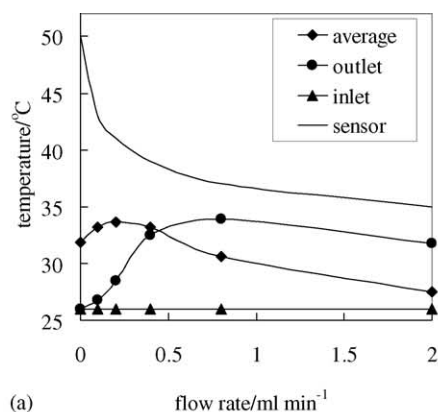


Fig. 3. Plots of temperature (average, outlet, inlet and sensor) vs. liquid flow rate for (a) DMF, (b) water and (c) NMF in uncoated capillaries with a microwave power of 50 W.

different plots can be explained as follows. Firstly, the inlet temperature is unaffected by the microwaves and simply remains constant at the external, ambient temperature. The temperature of the outlet is low at slow flow rates as the liquid cools in the long travel time between the microwave irradiation zone and the outlet. Increasing the flow rate corresponds to less time for cooling and also less exposure time to the incident microwaves. The net result of these competing effects is that the outlet temperature passes through a maximum value with increasing flow rate. The average temperature

(i.e., the average over the capillary length between electrodes 2 and 4) behaves similarly except that the flow rate corresponding to the maximum temperature is shifted. The sensor temperature, measured in the microwave zone, decreases monotonically with increasing flow rate due to the decrease in exposure time of the flowing liquid to the incident microwaves.

For fixed sample geometry and microwave incident intensity, the heating rate of a sample depends on the density ρ , heat capacity C_p and the dielectric loss ε'' of the sample according to [7]:

$$\frac{dT}{dt} \propto \frac{\varepsilon''}{\rho C_p} \quad (1)$$

For the three solvents shown in Fig. 3, the densities and heat capacities are similar and hence, to a first approximation, the relative heating rates are proportional to ε'' . For a microwave frequency of 2.45 GHz, the values of ε'' at room temperature are approximately 6, 9 and 75 for DMF, water and NMF, respectively [8–10]. From Fig. 3, the corresponding values of maximum temperature rise (ΔT_{\max} is taken to be the maximum average temperature minus the inlet temperature) are 8, 12 and 37 °C, respectively. It can be seen that the microwave heating correlates with ε'' , highly polar solvents such as NMF couple strongly with microwaves and heating much more than weakly polar solvents such as DMF. However, it is important to note that even for solvents, which absorb microwaves very strongly, the efficiency of the heating (i.e., the power absorbed relative to the total incident power) in this type of micro-flow system is very low. From the data of Fig. 3 for NMF, a maximum of only approximately 0.5 W is converted into heat in the liquid, i.e., only about 1% of the total microwave power.

Higher temperatures can be achieved by using higher microwave powers. For the relatively-weakly absorbing DMF, the ΔT_{\max} increases from 8 °C at 50 W incident microwave power to 16 °C at 100 W and 21 °C at 150 W. For the different powers, it remains true that the overall efficiency of converting the microwave energy to heat is lower for DMF than for the stronger absorbing NMF (discussed above). For

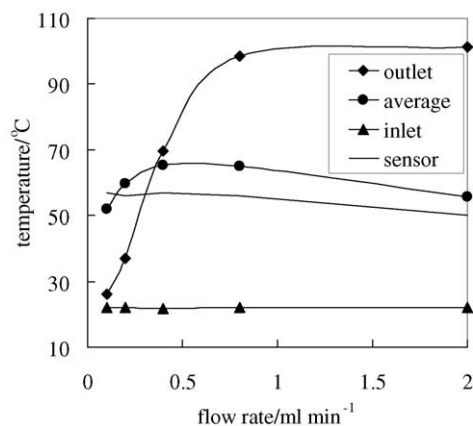


Fig. 4. Temperature (average, outlet, inlet and sensor) vs. liquid flow rate for NMF with microwave power of 10 W in a capillary coated with a gold film of 20 nm thickness and 50 mm length.

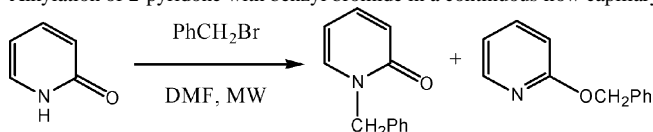
non-polar solvents showing virtually no microwave absorption at 2.45 GHz, the heating efficiency will be zero.

Microwave absorption efficiency can be greatly improved by coating the outer surface of the capillary with gold. Fig. 4 shows the temperature plots versus flow rate for NMF within a capillary coated with gold (20 nm thickness, coated length 50 mm) with a microwave power of 10 W. In the absence of gold coating (Fig. 3a), the ΔT_{\max} is approximately 37 °C for a microwave power of 50 W. From Fig. 4, the ΔT_{\max} is approximately 47 °C for a microwave power of only 10 W. From the measured temperature value, the gold coating has increased the microwave power absorption efficiency to approximately 10%.

The alkylation reaction of 2-pyridone with benzyl bromide was carried out to demonstrate the suitability of the proposed methodology to monitor online the reaction temperature under microwave heating in a continuous flow capillary reactor. From Table 2 it can be seen that whilst no product was detected at room temperature, under the same flow conditions and with microwave irradiation, with and without the presence of a gold film, product was produced. Measurement of the average reaction temperature, determined by the conductivity measured between electrodes 2 and 4, was found to give

Table 2

Alkylation of 2-pyridone with benzyl bromide in a continuous flow capillary reactor under microwave (MW) heating



Heating method	Flow (ml min ⁻¹)/ residence time (s)	MW power (W)/IR sensor temperature (°C)	Measured temperature (°C)		Yield (%)
			Outlet	Average	
RT	0.05/48	0/20	22	22	0
MW heating, no Au coating	0.05/48	250/69	91	70	19
MW heating plus gold coating ^a	0.05/48	220/69	92	70	29

Reaction mixture consisting of 2-pyridone (0.5 M), benzyl bromide (0.5 M) and NaBr (0.01 M) in a DMF solvent was pumped continuously through the capillary reactor.

^a Gold coating was of 10 nm thickness and 5 cm length.

a similar value to that obtained using the IR sensor probably the external capillary surface. However, the outlet temperature, determined by the conductivity measured between electrodes 3 and 4, indicated that the actual temperature within the reaction zone inside the capillary was higher than determined by the IR sensor or the average conductivity measurements. The presence of a localised hot zone within the capillary reactor, particularly when using the gold film, is confirmed by a higher yield of product even when no apparent difference in the average (sensor and current) was observed due to significant thermal loss between the reaction zone and outlet. Whilst this result demonstrates the limitation of the proposed technique to obtain spatial measurements, the technique was found to be comparable in usefulness to the current IR sensor and offered the opportunity to monitor an output value within the capillary reactor, which is not currently possible with existing methodology.

4. Conclusions

Conductivity measurements of electrolyte solutions can be used to monitor the mean temperatures of the solvent and reaction matrix within different sections of a capillary under microwave irradiation. The temperatures achievable are dependent on the microwave power, the flow rate and the magnitude of ϵ'' at the microwave frequency. However, even for solvents such as NMF, which is a strong absorber of 2.45 GHz microwaves, the overall heating efficiency is very low, typically less than 1% for an 800 μm diameter capillary. An effective method to overcome this limitation is to coat the exterior surface of the capillary with gold. This method can be used to achieve at least ten-fold increases in efficiencies, and enables reductions in reaction time and enhancements in the product yield.

Acknowledgements

We thank Ms. J. Halder, University of Hull for the preparation of the metal coatings and the Engineering and Physical Sciences research Council, UK for funding.

References

- [1] L. Perreux, A. Loupy, A tentative rationalization of microwave effects in organic synthesis according to the reaction medium and mechanistic considerations, *Tetrahedron* 57 (2001) 9199.
- [2] D. Villemin, F. Cailot, Microwave mediated palladium-catalysed reactions on potassium fluoride/alumina without use of solvent, *Tetrahedron Lett.* 42 (2001) 639.
- [3] A. Loupy, A. Petit, J. Hamelin, F. Texier-Boullet, P. Jacquault, D. Mathe, New solvent-free organic synthesis using focused microwaves, *Synthesis* (1998) 1213.
- [4] R.S. Varma, Solvent-free organic syntheses: using supported reagents and microwave irradiation, *Green Chem.* 1 (1999) 43.
- [5] W.A. Gobie, C.F. Ivory, Thermal model of capillary electrophoresis and a method for countereacting thermal band broadening, *J. Chromatogr. A* 516 (1990) 191.
- [6] D. Ross, M. Gaitan, L.E. Locascio, Temperature measurement in microfluidic systems using a temperature-dependent fluorescent dye, *Anal. Chem.* 73 (2002) 4117.
- [7] See, for example, *Microwave-enhanced Chemistry*, in: H.M. Kingston, S.J. Haswell, (Eds.), ACS, Washington DC, 1997.
- [8] J. Lou, T.A. Hatton, P.L. Laibinis, Effective dielectric properties of solvent mixtures at microwave frequencies, *J. Phys. Chem.* 101 (1997) 5262.
- [9] U. Kaatze, Microwave dielectric properties of liquids, *Radiat. Phys. Chem.* 45 (1995) 549.
- [10] J. Barthel, R. Buchner, B. Wurm, The dynamics of liquid formamide, *N*-methylformamide, *N,N*-dimethylformamide, and *N,N*-dimethylacetamide—A dielectric relaxation study, *J. Mol. Liq.* 98-99 (2002) 51.



Acid-catalysed synthesis and deprotection of dimethyl acetals in a miniaturised electroosmotic flow reactor

Charlotte Wiles, Paul Watts* and Stephen J. Haswell

Department of Chemistry, The University of Hull, Cottingham Road, Hull, HU6 7RX, UK

Received 28 February 2005; accepted 23 March 2005

Available online 13 April 2005

Abstract—Through incorporating a series of polymer-supported acid catalysts into a miniaturised EOF-based flow reactor, we demonstrate a clean and efficient technique for the protection of aldehydes as their respective dimethyl acetal. In addition, we also report the acid catalysed deacetalisation of 11 dimethyl acetals to their respective aldehyde. In all cases, the compounds described are obtained in high yield (>95%) and excellent purity (>99%) without the need for further product purification.

© 2005 Elsevier Ltd. All rights reserved.

1. Introduction

As a result of increasing environmental pressure, the chemical industry as a whole are exploring many routes to improve both the cleanliness and efficiency of many synthetic processes. One such approach is the application of micro reaction technology, which enables reactions to be performed more rapidly, efficiently and selectively than traditional batch-scale reactions. Although many groups have demonstrated the advantages of synthesising small organic compounds in micro fabricated devices, few have addressed the problems associated with purification of reaction products prepared using continuous flow systems.¹ In order to address this, we recently investigated the use of silica-supported catalysts in a micro fabricated device whereby analytically pure products were synthesised.²

Compared to solid-phase techniques,³ where reaction intermediates and products cannot be fully characterised until they are cleaved from the support, the use of solid-supported reagents is advantageous as reaction products remain in solution thus enabling the reaction to be monitored with time.⁴ Additionally, as the supported reagent can be easily removed from the reaction mixture, excess amounts can be employed in order to drive the reaction to completion. Although solid-supported reagents have many advantages over their solution phase counterparts, one main limitation is the support degradation that occurs as a result of stirring or shaking. Therefore by

performing reactions in continuous flow reactors, such as the one described herein, the support material undergoes minimal physical degradation, resulting in extended reagent lifetime and system reproducibility.^{5–7}

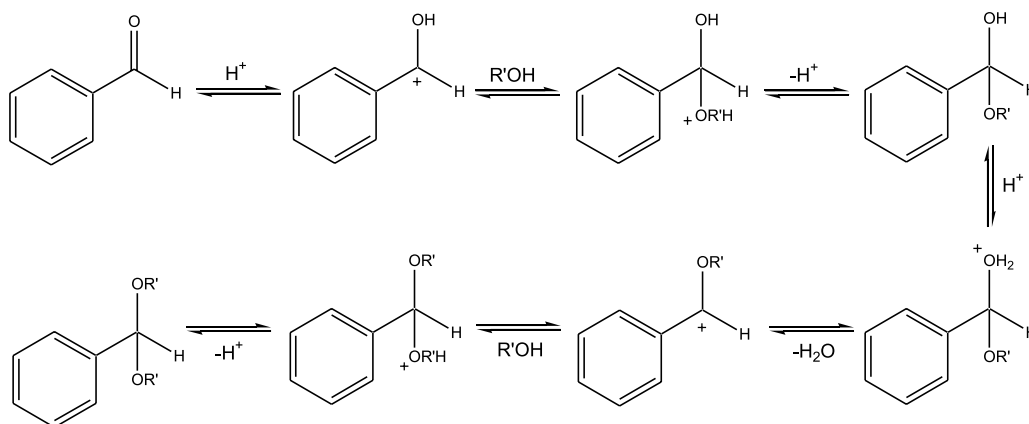
Automation of this technique would therefore, enable the high-throughput synthesis of analytically pure compounds, suitable for the fine chemical industry or combinatorial applications. With these factors in mind, we propose that by incorporating a series of solid-supported acid catalysts into miniaturised flow reactors, problems such as corrosion of reactor vessels, generation of acidic waste and the inability to recover/recycle the catalyst can be addressed. In order to demonstrate the advantages associated with the proposed technique, the acid catalysed synthesis of dimethyl acetals and their deprotection was investigated.

1.1. Acid catalysed acetalisation

Acetals are one of the most common carbonyl protecting groups, prepared by the treatment of aldehydes (or ketones) with alcohols (or orthoformates) in the presence of an acid catalyst (Scheme 1). Although triflic acid and *p*-toluenesulfonic acid are generally used, other catalysts include ferric chloride,⁸ ammonium nitrate⁹ rhodium(III) complexes¹⁰ and ethanolic hydrogen chloride.¹¹ In addition, numerous examples of solid-supported acid catalysts have been applied to the synthesis of acetals, these include, Amberlite resin,¹² Amberlyst-15 (dry),¹³ polymer-supported lanthanides,¹⁴ and Nafion-H.^{15,16} As Scheme 1 illustrates, hydrolysis of an acetal with an aqueous acid, affords the respective carbonyl compound. Consequently, as

Keywords: Acetals; Micro reactor; Deprotection.

* Corresponding author. Tel.: +44 1482 465471; fax: +44 1482 466416; e-mail: p.watts@hull.ac.uk



Scheme 1. Schematic illustrating the acid catalysed acetalisation of an aldehyde.

neither the forward or reverse reaction is base catalysed, acetals are frequently employed as protecting groups.

1.2. How are reactions performed?

To conduct a reaction, the starting materials are passed over a solid-supported reagent or catalyst and the reaction products are collected at the outlet (Fig. 1). The reaction mixture is then analysed by GC–MS whereby conversion of starting material to product is determined. If any residual starting material is observed the reaction is repeated, this time passing the reagents over the support at a slower flow rate, thus having the effect of increasing the reagents residence time within the reactor. When successfully optimised, the devices are operated continuously in order to prepare sufficient quantity of product for analysis by NMR spectroscopy and if required, elemental analysis. Using this approach, work-up is extremely simple, consisting of concentrating the reaction product in vacuo followed by analysis. By optimising the flow rate, and hence residence time within the reactor, it is possible to obtain complete conversion of starting materials to product in a single pass through the device (Scheme 3).

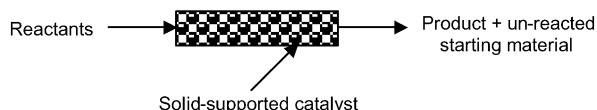


Figure 1. Schematic illustrating the use of solid-supported catalysts in a continuous flow reactor.

1.3. Pumping mechanism

Although examples of pressure-driven micro fluidic systems have featured widely in the literature,¹⁷ owing to its simplicity, the evaluation of polymer-supported acid catalysts was carried out using electroosmotic flow (EOF). The advantages of using this approach are, it is simple to use, requires no mechanical parts, enables reproducible pulse-free flow, generates minimal back-pressure, can alter both the direction and magnitude of flow and can be easily automated. Of the many positive features associated with the use of EOF, in this case, the generation of minimal backpressure and reproducible flow are the most important.

1.4. Principle of electroosmotic flow

When an ionisable surface such as glass,¹⁸ quartz¹⁹ or teflon,²⁰ comes in contact with a suitable solvent system, the surface is neutralised with a diffuse layer of positive ions from the bulk liquid. A proportion of the counterions are adsorbed onto the surface resulting in an immobile layer and the remaining ions form a transient double layer (Fig. 2). Application of an electric field causes the double layer to move towards the oppositely charged electrode, inducing bulk flow within the channel/capillary.

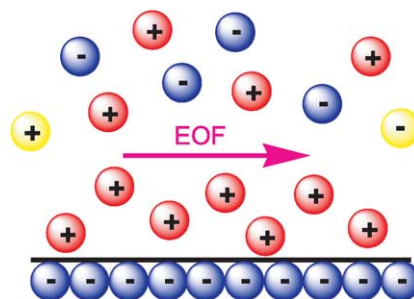


Figure 2. Schematic illustrating the principle of electroosmotic flow for a negatively charged glass surface.

As electrokinetic flow is a surface phenomenon, the physical properties of the fluid have a direct bearing on the flow rates observed (Eq. 1), consequently the technique is typically employed for polar, low viscosity solvent systems. In addition, in order to preserve the diffuse double layer, the solutions must be $> \text{pH } 2$. Below this, no EOF is observed as an immobile layer replaces the diffuse positive ions. Consequently, performing reactions that require acidic reagents can be problematic, in order to circumvent this problem we recently demonstrated an alternative approach to the synthesis of esters²¹ and McCreey et al.²² reported

$$v_{\text{eof}} = -\frac{E\epsilon\epsilon_0\zeta}{\eta}$$

v_{eof} = electroosmotic flow velocity, E = applied field, ϵ = relative dielectric constant of the fluid, ϵ_0 = the permittivity of free space, ζ = zeta potential and η = viscosity.

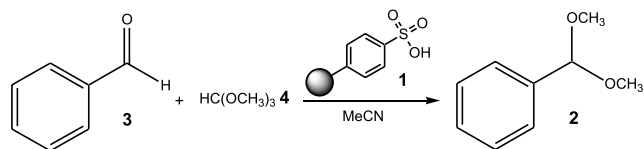
Equation 1. Determination of electroosmotic flow (EOF) velocity.²⁴

the use of a sulphated zirconia catalyst for the dehydration of alcohols. More recently, Crocker et al.²³ reported the use of amine functionalised electrokinetic micro pumps for the mobilisation of acidic solutions (0.1% TFA in H₂O/MeCN) whereby nl min⁻¹ flow rates were obtained. Therefore, by incorporating polymer-supported acids into micro fabricated devices, we are able to conduct reactions that otherwise could not be performed efficiently within EOF-based devices.

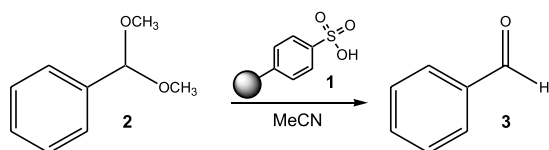
2. Results and discussion

2.1. Synthesis of dimethyl acetals using Amberlyst-15

Amberlyst-15 (dry) **1** is a sulfonic acid based cation exchange resin that has been widely employed for the preparation of acetals, ketals, tetrahydropyranyl ethers and enol ethers.²⁵ Using the synthesis of dimethoxymethyl benzene **2** as a model reaction, we investigated the use of Amberlyst-15 **1** in a micro fabricated device (Scheme 2).



Scheme 2. General scheme illustrating the acid catalysed synthesis of dimethoxymethyl benzene **2** using Amberlyst-15 **1**.



Scheme 3. Deacetalisation of dimethoxymethyl benzene **2** using Amberlyst-15 **1**.

Using EOF, the starting materials are passed over Amberlyst-15 **1**, the reaction mixture is then collected at the outlet and analysed by GC–MS. As Figure 3 illustrates, Amberlyst-15 **1** (dry) (2.5 mg, 1.05×10^{-2} mmol) was packed into a borosilicate glass capillary (500 μ m \times 3.0 cm) and held in place using micro porous silica frits.²⁶ The capillary was then primed with MeCN to remove any

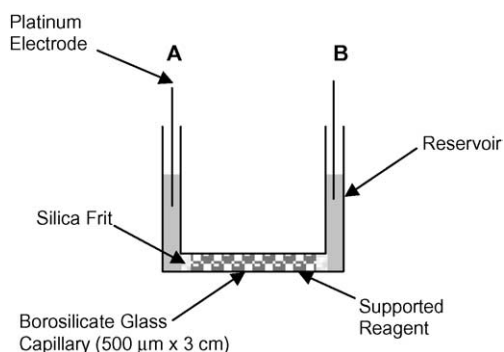


Figure 3. Schematic of the reaction set-up used for the evaluation of the polymer-supported acid catalysts.

air, ensuring the formation of a complete circuit, and the capillary attached to two glass reservoirs. The reagents were manipulated through the device via the application of a voltage to the platinum electrodes placed in the reagent reservoirs. As Figure 4 illustrates, benzaldehyde **3** and trimethylorthoformate **4** (40 μ l, 1.0 and 2.0 M, respectively) in MeCN was placed in reservoir A and MeCN in reservoir B (40 μ l). Application of 333 and 0 V cm⁻¹ respectively, resulted in the mobilisation of the reaction mixture at a flow rate of 1.75 μ l min⁻¹. After 10 min, the reaction products were collected from reservoir B, diluted with MeCN, and analysed by GC–MS, whereby 100% conversion to dimethoxymethyl benzene **2** was obtained with respect to residual benzaldehyde **3**. In order to demonstrate both system reproducibility and the continuous synthesis of dimethoxymethyl benzene **2**, the reaction was repeated a further 14 times (2.5 h), whereby conversions of >99.6% were obtained (Table 1). After analysis by GC–MS, all reaction products were collected and concentrated in vacuo, to afford dimethoxymethyl benzene **2** as a pale yellow oil (0.025 g, 96.6%). In order to confirm product purity, the crude reaction mixture was analysed by NMR spectroscopy, whereby no residual aldehyde was observed.

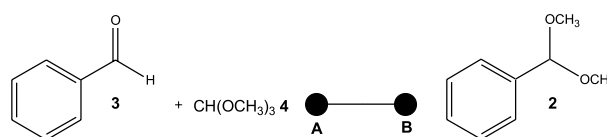


Figure 4. Schematic illustrating the manifold set-up used for the synthesis of dimethyl acetal **2** in an EOF-based micro reactor.

Table 1. Illustration of system stability over 15 runs for the synthesis of dimethoxymethyl benzene **2**

Run No.	Conversion (%)
1	100.0
2	99.58
3	99.68
4	99.83
5	99.87
6	99.69
7	99.65
8	99.75
9	99.70
10	99.74
11	99.71
12	99.63
13	99.90
14	100.0
15	99.80

Mean = 99.8%, % RSD = 0.13

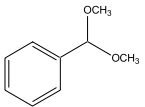
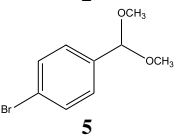
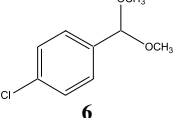
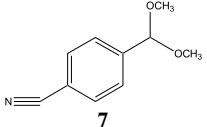
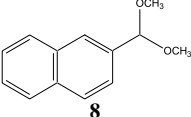
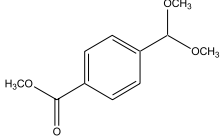
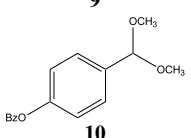
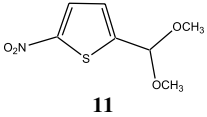
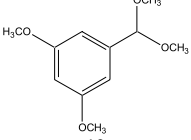
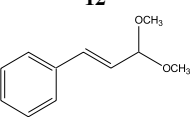
In summary, we have synthesized 0.165 mmol of dimethoxymethyl benzene **2** using 1.05×10^{-2} mmol of Amberlyst-15 **1**. This result not only demonstrates the successful incorporation of supported acids into an EOF-based device, but also the ability to recycle the supported reagent (> 16 times) without any loss of activity. Although the activity of Amberlyst-15 **1** is also retained in batch, this approach is advantageous as macroreticular resins are difficult to recycle due to support degradation observed as a result of mechanical agitation; therefore limiting the number of times they can be recycled. In order to confirm that the observed reaction was due to the presence of a solid-

supported acid catalyst and not as a result of conducting the reaction in an electric field, the reaction was repeated in the absence of a catalyst.

Again, using the experimental set-up illustrated in Figure 3, unfunctionalised polystyrene beads (2% cross-linked with divinylbenzene) were packed into the device. A mixture of benzaldehyde **3** and trimethylorthoformate **4** (40 μl , 1.0 and 2.5 M, respectively) in MeCN was placed in reservoir A and MeCN in reservoir B (40 μl). Application of 100 and

0 V cm^{-1} , respectively, resulted in the mobilisation of the reaction mixture at a flow rate of 1.75 $\mu\text{l min}^{-1}$.²⁷ After 10 min, the reaction products from reservoir B were diluted with MeCN and analysed by GC–MS, whereby no acetal formation was detected. Having confirmed that the reaction was due to the catalytic activity of the Amberlyst-15 **1**, we went on to investigate generality of the technique, preparing dimethyl acetals **5–13** (Table 2). In all cases, no measurable by-products were observed by GC–MS or NMR spectroscopy.

Table 2. Summary of the conversions obtained for the synthesis of dimethyl acetals **2,5–13**

Product	Flow rate ($\mu\text{l min}^{-1}$)	Conversion ^a (%)	RSD (%)	Yield (%)
 2	1.75	99.77	0.13	96.6
 5	1.00	99.92	0.22	96.8
 6	1.60	99.78	0.15	98.0
 7	2.00	99.64	0.90	97.5
 8	1.40	99.83	0.26	95.2
 9	0.60	99.86	0.08	95.3
 10	0.35	99.70	0.15	98.13
 11	2.00	99.88	0.93	97.5
 12	0.50	99.84	0.24	98.4
 13	1.30	99.65	0.29	95.4

^a ≥ 15 replicates were performed for each compound.

2.2. Other supported acid catalysts

Having demonstrated the successful incorporation of Amberlyst 15 **1** into an EOF-based miniaturised flow reactor, the investigation was extended to the use of ytterbium (III) polystyrylsulfonate **14** and polymer supported *p*-toluenesulfonic acid **15**.

Using the aforementioned methodology, 2.5 mg of ytterbium (III) polystyrylsulfonate **14** (2.0×10^{-3} mmol) was packed into a micro fabricated device. Again, a solution of benzaldehyde **3** and trimethylorthoformate **4** (40 μ l, 1.0 and 2.5 M, respectively) in MeCN was placed in reservoir A and MeCN in reservoir B (40 μ l). Application of 333 and 0 V cm^{-1} respectively, resulted in mobilisation of the reaction mixture at 0.40 $\mu\text{l min}^{-1}$ (Table 3). After 10 min, the reaction products were collected, diluted with MeCN and analysed by GC–MS; whereby 99.7% conversion to dimethoxymethyl benzene **2** was observed. The reaction was repeated a further 14 times, whereby 0.010 g (94.7%) of dimethoxymethyl benzene **2** was obtained. Due to the slower flow rate observed with catalyst **14** cf. Amberlyst-15 **1**, less product is prepared over the same period of time (0.010 g cf. 0.025 g) however the catalyst is recycled > 32 times. The catalyst was subsequently evaluated for the synthesis of dimethyl acetals **2**, **5–13** whereby conversions of greater than 99.7% and yields greater than 94.9% were obtained (Table 3).

Table 3. Summary of the conversions obtained for the synthesis of dimethyl acetals using ytterbium (III) polystyrylsulfonate resin **14**

Product	Flow rate ($\mu\text{l min}^{-1}$)	Conversion ^a (%)	RSD (%)	Yield (%)
2	0.40	99.72	0.13	94.7
5	0.40	99.96	0.06	98.8
6	0.28	99.97	0.08	96.3
7	0.52	99.92	0.05	96.8
8	0.40	99.87	0.15	97.7
9	0.40	99.72	0.06	97.2
10	0.70	99.88	0.03	98.7
11	0.55	99.83	0.08	95.5
12	0.95	99.83	0.12	98.6
13	0.90	99.64	0.14	96.1

^a ≥ 15 replicates were performed for each compound.

Finally, polymer-supported *p*-toluenesulfonic acid **15** (2.5 mg, 5.3×10^{-3} mmol) was evaluated, whereby again conversions of greater than 99.7% with respect to residual aldehyde were obtained for dimethyl acetals **2**, **5** and **13** (Table 4).

2.3. Deacetalisation

One of the most important aspects of protecting a functional group is the ability to cleanly and efficiently remove it without affecting other moieties within the molecule. As previously mentioned, the hydrolysis of acetals, to afford their respective carbonyl derivative, is promoted in the presence of aqueous acids such as hydrochloric,²⁸ sulfuric,²⁹ acetic³⁰ and *p*-toluenesulfonic acid.³¹ However, more recently, supported acids such as Amberlyst-15 **1** have been reported as efficient catalysts for the transformation whereby excellent yields were obtained.³² In addition, Amberlyst-15 **1** has been shown to hydrolyse isomerisable

Table 4. Summary of the conversions obtained for the synthesis of dimethyl acetals using polymer supported *p*-toluenesulfonic acid **15**

Product	Flow rate ($\mu\text{l min}^{-1}$)	Conversion ^a (%)	RSD (%)	Yield (%)
2	1.10	99.80	0.20	96.8
5	0.30	99.86	0.27	96.0
6	1.40	99.85	0.19	97.6
7	0.79	99.93	0.21	95.9
8	1.00	99.77	0.21	98.3
9	0.70	99.74	0.12	95.8
10	0.60	99.64	0.25	95.7
11	5.00	99.87	0.17	97.8
12	1.00	99.85	0.15	94.9
13	1.70	99.70	0.11	98.5

^a ≥ 15 replicates were performed for each compound.

acetals with no detectable epimerisation compared to 20% when aqueous HCl was employed. With this in mind, the investigation was extended to the deacetalisation of a series of dimethyl acetals to afford their respective aldehyde in the presence of Amberlyst-15 **1**.

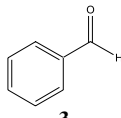
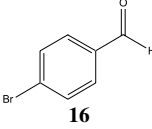
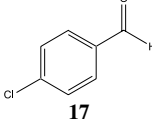
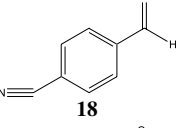
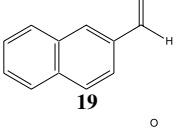
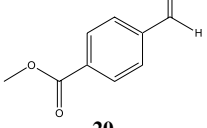
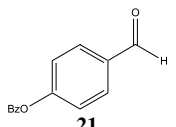
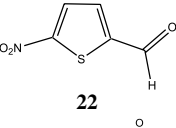
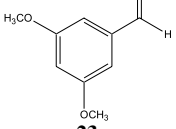
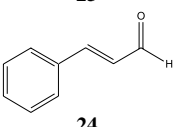
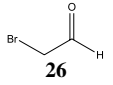
In order to investigate the deacetalisation, a solution of dimethoxymethyl benzene **2** (40 μ l, 1.0 M) in MeCN was placed in reservoir A and MeCN in reservoir B (40 μ l). Application of 167 and 0 V cm^{-1} respectively, resulted in mobilisation of the reaction mixture through the packed-bed at 0.40 $\mu\text{l min}^{-1}$ (Table 5). After 10 min the reaction products were collected, diluted with MeCN and analysed by GC–MS; whereby 100% conversion to benzaldehyde **3** was observed with respect to residual dimethoxymethyl benzene **2**. The reaction was repeated a further 14 times, whereby 0.011 g (94.8%) of benzaldehyde **3** was obtained. The procedure was subsequently repeated for the remaining nine dimethyl acetals, affording the respective aldehydes in greater than 99.7% conversion and 94.8% yield (Table 5).

In addition to demonstrating the deacetalisation of acetals **2**, **5–13**, we extended the investigation to look at the in situ regeneration of volatile reagents (Scheme 4). Using commercially available bromoacetaldehyde dimethyl acetal **25**, the synthesis of bromoacetaldehyde **26** was investigated using Amberlyst-15 **1** in an EOF-based flow reactor. Bromoacetaldehyde dimethyl acetal **25** (40 μ l, 1.0 M) in MeCN was placed in reservoir A and MeCN (40 μ l) in reservoir B. Application of 167 V cm^{-1} resulted in mobilisation of bromoacetaldehyde dimethyl acetal **25** at a flow rate of 0.25 $\mu\text{l min}^{-1}$. After 10 min, the reaction mixture was analysed by GC–MS, whereby 100% conversion of dimethyl acetal **25** to bromoacetaldehyde **26** was obtained. Compared to the standard batch approach, this technique is advantageous as it enables us to regenerate what is a volatile compound at the point of use, therefore enabling more efficient reactions to be performed.

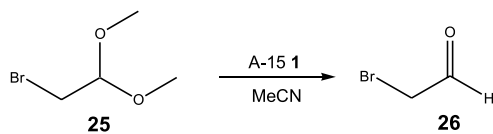
3. Conclusions

Compared to standard batch techniques, the approach described herein, is advantageous as supported reagents can be recycled without the need for filtration, resulting in more consistent results between reactions. Also, the absence of stirring or shaking greatly reduces mechanical degradation of the reagent, enabling the catalyst to be employed

Table 5. Summary of the conversions obtained for the deacetalisation of dimethyl acetals **2**, **5–13** and **25** using Amberlyst-15 **1**

Product	Flow rate ($\mu\text{l min}^{-1}$)	Conversion ^a (%)	RSD (%)	Yield (%)
 3	0.50	100.0	0.00	94.8
 16	1.00	99.85	0.10	99.5
 17	0.65	100.0	0.00	99.3
 18	0.80	99.93	0.03	99.0
 19	0.80	99.71	0.08	97.2
 20	0.50	99.81	0.01	98.6
 21	0.30	99.93	0.03	99.6
 22	0.53	100.0	0.00	99.7
 23	0.50	99.85	0.19	97.7
 24	0.55	99.99	0.02	98.5
 26	0.25	100.0	0.00	—

^a ≥ 15 replicates were performed for each compound.

**Scheme 4.** Synthesis of bromoacetaldehyde **26** using A-15 **1**.

for longer. In addition, the formation of localised concentration gradients enable reactions to be driven to completion without the need to employ large quantities of supported catalyst (typically <2.5 mg is used). Consequently, reaction conditions can be optimised rapidly enabling small quantities of analytically pure compounds to be prepared in min; alternatively, larger quantities of materials can be

synthesised by simply operating numerous reactors in parallel.³³ Applying the methodology described herein, further studies are currently underway within our laboratories to extend both the type of reagent and support employed, enabling more complex syntheses to be evaluated.

4. Experimental

All solvents were purchased as puriss grade ($\geq 99.5\%$) over molecular sieves ($\text{H}_2\text{O} < 0.005\%$) from Fluka and unless otherwise stated reagents purchased from Sigma-Aldrich and Lancaster were used as received. Ytterbium (III) polystyrylsulfonate resin **14** (0.8 mmol g^{-1}) was purchased from Novabiochem. Ytterbium (III) polystyryl sulfonate resin **14**, polymer bound *p*-toluenesulfonic acid **15** (2.0 mmol g^{-1}) and Amberlyst-15 **1** (4.2 mmol g^{-1}) were ground and sieved (Endcotts) to afford 38 and $75 \mu\text{m}$ particles. All NMR spectra were recorded as solutions in deuteriochloroform (CDCl_3) using tetramethylsilane (TMS) as an internal standard. The spectra were recorded on a Joel GX400 spectrometer and the chemical shifts given in parts per million (ppm) with coupling constants given in Hertz (Hz). The following abbreviations are used to report NMR data; s = singlet, d = doublet, t = triplet, br s = broad singlet, m = multiplet and C_0 = quaternary carbon. Elemental analyses were performed using a Fisons Carlo Erba EA1108 CHN analyser. Gas Chromatography–mass spectrometry (GC–MS) was performed using a Varian GC (CP-3800) coupled to a Varian MS (Saturn 2000) with a CP-Sil 8 (30 m) column (Zebron ZB-5, Phenomenex) and ultra high purity helium (99.999%, Energas) carrier gas. Samples were analysed using the following method; injector temperature 250°C , helium flow rate 1.0 ml min^{-1} , oven temperature 50°C for 4 min and then ramped to 270°C at $30^\circ\text{C min}^{-1}$, with a 3.0 min filament delay.

4.1. Micro-scale methodology

The reactions described herein were carried out using a single capillary device, as illustrated in Figure 3, with dimensions of $500 \mu\text{m}$ (i.d.) $\times 3.0 \text{ cm}$ (length). To hold the polymer-supported reagent in place, micro porous silica frits were placed at either end of the capillary.²⁶ To mobilise reagents by EOF, platinum electrodes ($0.5 \text{ mm o.d.} \times 2.5 \text{ cm}$) were placed within the reagent reservoirs and voltages applied using a Paragon 3B high-voltage power supply (HVPS), capable of applying 0–1000 V to four pairs of outputs (Kingfield Electronics). Automation of the HVPS was achieved using an in-house LabVIEW™ program. To enable the results obtained to be achieved using devices of different capillary dimensions, voltages are reported as applied fields (V cm^{-1}) that is voltage/capillary length. To monitor the progress of the reaction, experiments were conducted over a period of 10 min, after which the contents of the product reservoir was analysed by GC–MS. Comparison of the amount of product with respect to residual aldehyde enabled the percentage conversion to be determined. In order to obtain NMR data of the compounds synthesised in the flow system, the reactor was operated continuously for 2.5–3.5 h (depending on the observed flow rate). After, which the reaction products were collected, concentrated in vacuo, dissolved in CDCl_3/TMS and

analysed by NMR spectroscopy. In some cases, the products were subjected to elemental analysis.

4.1.1. Dimethoxymethyl benzene 2.³⁴ (0.025 g, 96.6%) as a pale yellow oil; δ_{H} (400 MHz, CDCl_3) 3.33 (6H, s, $2 \times \text{OCH}_3$), 5.40 (1H, s, CH), 7.37 (3H, m, $3 \times \text{Ar}$) and 7.45 (2H, m, $2 \times \text{Ar}$); δ_{C} (100 MHz, CDCl_3) 52.7 (OCH_3), 103.2 (CH), 126.7 ($2 \times \text{CH}$), 128.2 ($2 \times \text{CH}$), 128.5 (CH) and 134.5 (C_0); 153 ($\text{M}^+ + 1$, 2%), 152 (3), 151 (5), 122 (10), 121 (100), 77 (30) and 51 (10); GC–MS retention time $R_{\text{T}} = 8.03 \text{ min}$.

4.1.2. 1-Bromo-4-dimethoxymethyl benzene 5.³⁵ (0.034 g, 96.8%) as a colourless oil; δ_{H} (400 MHz, CDCl_3) 3.49 (6H, s, $2 \times \text{OCH}_3$), 5.30 (1H, s, CH), 7.69 (2H, d, $J = 8.7 \text{ Hz}$, $2 \times \text{Ar}$) and 7.76 (2H, d, $J = 8.7 \text{ Hz}$, $2 \times \text{Ar}$); δ_{C} (100 MHz, CDCl_3) 50.9 ($2 \times \text{OCH}_3$), 102.3 (CH), 129.8 (C_0Br), 131.0 ($2 \times \text{CH}$), 132.5 ($2 \times \text{CH}$) and 135.1 (C_0); 232 ($\text{M}^+ + 1$, 5%), 201 (100), 200 (90) and 77 (15); GC–MS retention time $R_{\text{T}} = 8.78 \text{ min}$.

4.1.3. 1-Chloro-4-dimethoxymethyl benzene 6.³⁵ (0.044 g, 98.0%) as a pale yellow oil; δ_{H} (400 MHz, CDCl_3) 3.31 (6H, s, $2 \times \text{OCH}_3$), 5.37 (1H, s, CH), 7.34 (2H, d, $J = 8.7 \text{ Hz}$, $2 \times \text{Ar}$) and 7.40 (2H, d, $J = 8.7 \text{ Hz}$, $2 \times \text{Ar}$); δ_{C} (100 MHz, CDCl_3) 52.6 ($2 \times \text{OCH}_3$), 102.3 (CH), 128.2 ($2 \times \text{CH}$), 129.5 ($2 \times \text{CH}$), 134.3 (C_0Cl) and 136.7 (C_0); 187 ($\text{M}^+ + 1$, 2%), 185 (3), 157 (30), 165 (20), 155 (100) and 75 (20); GC–MS retention time $R_{\text{T}} = 9.05 \text{ min}$.

4.1.4. 1-Cyano-4-dimethoxymethyl benzene 7. (0.042 g, 97.5%) as a pale yellow oil (Found C, 68.00; H, 6.11; N, 7.88. $\text{C}_{10}\text{H}_{11}\text{O}_2\text{N}$ requires C, 67.78; H, 6.26; N, 7.90%); δ_{H} (400 MHz, CDCl_3) 3.33 (6H, s, $2 \times \text{OCH}_3$), 5.45 (1H, s, CH), 7.58 (2H, d, $J = 8.3 \text{ Hz}$, $2 \times \text{Ar}$) and 7.67 (2H, d, $J = 8.3 \text{ Hz}$, $2 \times \text{Ar}$); δ_{C} (100 MHz, CDCl_3) 52.7 ($2 \times \text{OCH}_3$), 101.8 (CH), 117.7 (CN), 118.7 (C_0CN), 127.6 ($2 \times \text{CH}$), 132.1 ($2 \times \text{CH}$) and 143.2 (C_0); 178 ($\text{M}^+ + 1$, 2%), 177 (2), 176 (5), 146 (100) and 75 (10); GC–MS retention time $R_{\text{T}} = 9.66 \text{ min}$.

4.1.5. 2-Dimethoxymethyl naphthalene 8. (0.080 g, 95.2%) as a pale yellow oil (Found C, 77.21; H, 7.16; $\text{C}_{13}\text{H}_{14}\text{O}_2$ requires C, 77.20; H, 6.98%); δ_{H} (400 MHz, CDCl_3) 3.37 (6H, s, $2 \times \text{OCH}_3$), 5.56 (1H, s, CH), 7.50 (2H, m, $2 \times \text{Ar}$), 7.61 (2H, m, $2 \times \text{Ar}$), 7.94 (2H, m, $2 \times \text{Ar}$) and 8.34 (1H, m, Ar); δ_{C} (100 MHz, CDCl_3) 52.8 ($2 \times \text{OCH}_3$), 103.2 (CH), 124.4 (CH), 126.1 ($2 \times \text{CH}$), 126.2 (CH), 127.7 (CH), 128.1 (CH), 128.3 (CH), 133.4 (C_0), 133.5 (C_0) and 135.5 (C_0); 203 ($\text{M}^+ + 1$, 3%), 201 (5), 172 (20), 171 (100), 126 (5) and 75 (10); GC–MS retention time $R_{\text{T}} = 10.70 \text{ min}$.

4.1.6. 4-Dimethoxymethylbenzoic acid methyl ester 9.³⁶ (0.018 g, 95.3%) as a pale yellow oil; δ_{H} (400 MHz, CDCl_3) 3.33 (6H, s, $2 \times \text{OCH}_3$), 3.90 (3H, s, OCH_3), 5.44 (1H, s, CH), 7.53 (2H, d, $J = 8.3 \text{ Hz}$, $2 \times \text{ArH}$) and 8.05 (2H, d, $J = 8.3 \text{ Hz}$, $2 \times \text{ArH}$); δ_{C} (100 MHz, CDCl_3) 52.2 (COOCH_3), 52.7 ($2 \times \text{OCH}_3$), 102.4 (CH), 126.8 ($2 \times \text{Ar}$), 129.5 ($2 \times \text{Ar}$), 130.2 (C_0), 143.0 (C_0COOCH_3) and 166.9 (CO); 211 ($\text{M}^+ + 1$, 2%), 210 (1), 179 (100) and 77 (5); GC–MS retention time $R_{\text{T}} = 10.21 \text{ min}$.

4.1.7. 1-Benzyloxy-4-dimethoxymethyl benzene 10. (0.200 g, 98.1%) as a pale yellow oil (Found C, 74.32; H,

7.23; $C_{16}H_{18}O_3$ requires C, 74.40; H, 7.02%; δ_H (400 MHz, $CDCl_3$) 3.31 (6H, $2 \times OCH_3$), 5.06 (2H, s, OCH_2), 5.14 (1H, s, CH), 7.07 (2H, d, $J=8.7$ Hz, $2 \times Ar$), 7.39 (5H, m, $5 \times Ar$) and 7.83 (2H, d, $J=8.7$ Hz, $2 \times Ar$); δ_C (100 MHz, $CDCl_3$) 52.6 ($2 \times OCH_3$), 70.3 (OCH_2), 103.1 (CH), 114.5 ($2 \times CH$), 127.9 ($2 \times CH$), 128.6 ($2 \times CH$), 128.7 ($2 \times CH$), 136.9 (C_0), 158.9 (C_0O); 259 ($M^+ + 1$, 1%), 258 (2), 257 (3), 228 (25), 227 (100), 91 (5) and 75 (15); GC–MS retention time $R_T=12.48$ min.

4.1.8. 2-Dimethoxymethyl-5-nitrothiophene 11.³⁵ (0.039 g, 97.5%) as a pale yellow oil; δ_H (400 MHz, $CDCl_3$) 3.50 (6H, s, $2 \times OCH_3$), 5.61 (1H, s, CH), 7.71 (1H, d, $J=4.2$ Hz, Ar) and 7.97 (1H, d, $J=4.2$ Hz, Ar); δ_C (100 MHz, $CDCl_3$) 52.7 ($2 \times OCH_3$), 98.8 (CH), 124.5 (CH), 128.4 (CH), 149.8 (C_0) and 151.2 (C_0NO_2); 203 (M^+ , 1%), 202 (5), 187 (10), 172 (100), 157 (10), 142 (10), 97 (5) and 75 (%); GC–MS retention time $R_T=10.23$ min.

4.1.9. 1-Dimethoxymethyl-3,5-dimethoxybenzene 12. (0.030 g, 98.4%) as a colourless oil (Found C, 62.52; H, 7.41. $C_{11}H_{16}O_4$ requires C, 62.25; H, 7.60%); δ_H (400 MHz, $CDCl_3$) 3.34 (6H, s, $2 \times OCH_3$), 3.80 (6H, s, $2 \times OCH_3$), 5.30 (1H, s, CH), 6.43 (1H, t, $J=2.2$ Hz, $2 \times Ar$) and 6.62 (2H, d, $J=2.2$ Hz, $2 \times Ar$); δ_C (100 MHz, $CDCl_3$) 52.9 ($2 \times OCH_3$), 55.4 ($2 \times OCH_3$), 100.8 (CH), 103.1 (CH), 104.5 ($2 \times CH$), 140.5 (C_0) and 160.7 ($2 \times C_0OCH_3$); 213 ($M^+ + 1$, 5%), 212 (20), 182 (100), 134 (5) and 75 (5); GC–MS retention time $R_T=10.32$ min.

4.1.10. 3,3-Dimethoxypropenyl benzene 13.³⁶ (0.022 g, 95.4%) as a yellow oil; δ_H (400 MHz, $CDCl_3$) 3.38 (6H, s, $2 \times OCH_3$), 4.96 (1H, d, $J=4.9$ Hz, CH), 6.16 (1H, dd, $J=4.9$, 16.0 Hz, $CHCH(OCH_3)_2$), 6.72 (1H, d, $J=16.0$ Hz, Ar) 7.30 (2H, m, $2 \times Ar$), 7.43 (2H, m, $2 \times Ar$) and 7.57 (1H, m, Ar); δ_C (100 MHz, $CDCl_3$) 52.8 ($2 \times OCH_3$), 102.9 (CH), 126.8 ($2 \times CH$), 128.5 ($2 \times CH$), 129.1 (CH) and 133.6 (C_0); 179 ($M^+ + 1$, 3%), 178 (20), 177 (15), 147 (100), 115 (10) and 77 (5); GC–MS retention time $R_T=9.56$ min.

The purity of aldehydes **3**, **16–24** synthesized in the miniaturized flow reactor was determined based on the comparison of GC–MS data with that obtained for commercially available standards.

4.1.11. Benzaldehyde 3. (0.011 g, 94.8%) as a colourless solid; 107 ($M^+ + 1$, 20%), 106 (15), 105 (100), 77 (25) and 51 (20); GC–MS retention time $R_T=6.87$ min.

4.1.12. 4-Bromobenzaldehyde 16. (0.027 g, 99.5%) as a white solid; 186 ($M^+ + 1$, 20%), 185 (100), 184 (75), 157 (15), 155 (15), 77 (20) and 50 (25); GC–MS retention time $R_T=9.51$ min.

4.1.13. 4-Chlorobenzaldehyde 17. (0.014 g, 99.3%) as a white solid; 142 ($M^+ + 1$, 20%), 141 (98), 140 (50), 139 (100), 110 (10) and 77 (10); GC–MS retention time $R_T=8.18$ min.

4.1.14. 4-Cyanobenzaldehyde 18. (0.015 g, 99.0%) as a colourless solid; 132 ($M^+ + 1$, 15%), 131 (20), 130 (100), 103 (7), 102 (45), 76 (20) and 50 (20); GC–MS retention time $R_T=8.85$ min.

4.1.15. 2-Naphthaldehyde 19. (0.018 g, 97.2%) as a white solid; 157 ($M^+ + 1$, 25%), 156 (75), 155 (100), 128 (10), 127 (15), 126 (20) and 102 (5); GC–MS retention time $R_T=10.16$ min.

4.1.16. Methyl-4-formylbenzoate 20. (0.012 g, 98.6%) as a pale orange solid; 165 ($M^+ + 1$, 50%), 164 (55), 163 (50), 133 (100), 105 (25) and 77 (10); GC–MS retention time $R_T=9.46$ min.

4.1.17. 4-Benzyloxybenzaldehyde 21. (0.013 g, 99.6%) as a white solid; 213 ($M^+ + 1$, 100%), 212 (74), 107 (10) and 91 (25); GC–MS retention time $R_T=11.98$ min.

4.1.18. 5-Nitro-2-thiophenecarboxaldehyde 22. (0.017 g, 99.7%) as a pale yellow solid; 158 ($M^+ + 1$, 75%), 157 (70), 156 (80), 141 (100), 127 (25), 112 (20), 99 (45), 98 (50), 71 (40) and 55 (25); GC–MS retention time $R_T=9.38$ min.

4.1.19. 3,5-Dimethoxybenzaldehyde 23. (0.015 g, 97.7%) as a white solid; 167 ($M^+ + 1$, 25%), 166 (100), 135 (25), 79 (10) and 64 (15); GC–MS retention time $R_T=9.75$ min.

4.1.20. trans-Cinnamaldehyde 24. (0.010 g, 98.5%) as a yellow oil; 133 ($M^+ + 1$, 10%), 132 (40), 131 (100), 103 (55), 77 (45) and 50 (25); GC–MS retention time $R_T=8.98$ min.

4.1.21. Bromoacetaldehyde 26. 125 ($M^+ + 1$, 5%), 124 (4), 123 (7), 96 (100), 95 (25), 94 (100), 81 (25), 80 (2), 79 (25), 42 (30); GC–MS retention time $R_T=2.69$ min.

Acknowledgements

We gratefully acknowledge the financial support of the EPSRC (C.W.) (Grant No. GR/S34106/01). Mike Bailey (The University of Hull) is also acknowledged for his assistance in the device fabrication.

References and notes

1. Brody, J.; Yager, P. *Sens. Actuators, A* **1997**, *58*, 13.
2. Wiles, C.; Watts, P.; Haswell, S. J. *Tetrahedron* **2004**, *60*, 8421.
3. Terrett, N. K.; Gardner, M.; Gordon, D. W.; Kobylecki, R. J.; Steele, J. *Tetrahedron* **1995**, *51*, 8135.
4. (a) McKillop, A.; Young, D. W. *Synthesis* **1979**, 422. (b) McKillop, A.; Young, D. W. *Synthesis* **1979**, 481.
5. Hodge, P. *Curr. Opin. Chem. Biol.* **2003**, *7*, 362.
6. Wan, Y. S. S.; Chau, J. L. H.; Gavriilidis, A.; Yeung, K. L. *J. Chem. Soc., Chem. Commun.* **2002**, 878.
7. Lai, S. M.; Martin-Aranda, R.; Yeung, K. L. *J. Chem. Soc., Chem. Commun.* **2003**, 218.
8. Shwernk, E. *J. Am. Chem. Soc.* **1938**, *60*, 1702.
9. van Allan, J. A. *Org. Synth. Coll.* **1963**, *4*, 21.
10. Ott, J.; Ramos Tombo, G. M.; Schmid, B.; Venanzi, L. M.; Wang, G.; Ward, T. R. *Tetrahedron Lett.* **1989**, *30*, 6151.
11. Patwardhan, S. A.; Dev, S. *Synthesis* **1974**, 348.

12. Stenberg, V. I.; Vesley, G. F.; Kubik, D. *J. Org. Chem.* **1971**, *36*, 2550.
13. Patwardhan, S. A.; Dev, S. *Synthesis* **1974**, 349.
14. Yu, L.; Chen, D.; Li, J.; Wang, P. G. *J. Org. Chem.* **1997**, *62*, 3575.
15. Olah, G. A.; Iyer, P. S.; Prakash, G. K. S. *Synthesis* **1986**, 513.
16. Olah, G. A.; Narang, S. C.; Mediar, D.; Salem, G. F. *Synthesis* **1981**, 282.
17. Kunz, U.; Schonfeld, H.; Kirschning, A.; Solodenko, W. *J. Chromatogr., A* **2003**, *1006*, 241.
18. Schwer, C.; Kenndler, E. *Anal. Chem.* **1991**, *63*, 1801.
19. Jacobson, S. C.; Moore, A. W.; Ramsey, J. M. *Anal. Chem.* **1995**, *67*, 2059.
20. Reijenga, J. C.; Aben, G. V. A.; Verheggen, Th.P.E. M.; Everaerts, F. M. *J. Chromatogr.* **1983**, *260*, 241.
21. Wiles, C.; Watts, P.; Haswell, S. J.; Pombo-Villar, E. *Tetrahedron* **2003**, *59*, 10173.
22. McCreedy, T.; Wilson, N. G. *Analyst* **2001**, *126*, 21.
23. Patel, K.; Crocker, R. *8th International Conference on Miniaturised Systems for Chemistry and Life Sciences*, 2004; Vol. 1, p 590.
24. Rice, C. L.; Whitehead, R. *J. Phys. Chem.* **1965**, *69*, 4017.
25. (a) Gupta, S. K. *J. Org. Chem.* **1976**, *41*, 2642. (b) Bongini, A.; Cardillo, G.; Orena, M.; Sanri, S. *Synthesis* **1979**, 618.
26. Christensen, P. D.; Johnson, S. W. P.; McCreedy, T.; Skelton, V.; Wilson, N. G. *Anal. Commun.* **1998**, *35*, 341.
27. As an increased flow rate of $\sim 4.0 \mu\text{l min}^{-1}$ was observed at 333 V cm^{-1} , the applied field was reduced to 100 V cm^{-1} in order to obtain comparable flow rates to those observed for Amberlyst-15 **1**.
28. Tanis, S. P.; Nakanishi, K. *J. Am. Chem. Soc.* **1979**, *101*, 4398.
29. Cameron, A. F. B.; Hunt, J. S.; Oughton, J. F.; Wilkinson, P. A.; Wilson, B. M. *J. Chem. Soc.* **1953**, 3864.
30. Oliveto, E. P.; Gerold, C.; Hershberg, E. B. *J. Am. Chem. Soc.* **1954**, *76*, 6113.
31. Howard, W. L.; Lorette, N. B. *J. Org. Chem.* **1960**, *25*, 525.
32. Coppola, G. M. *Synthesis* **1984**, 1021.
33. Ehrfeld, W.; Hessel, V.; Lowe, H. *Microreactors: New Technology for Modern Chemistry*; VCH-Wiley: New York, 2000.
34. Rosenberg, G. M.; Brinker, H. U. *J. Org. Chem.* **2003**, *68*, 4819.
35. Creary, X.; Aldridge, T. *J. Org. Chem.* **1991**, *56*, 4280.
36. Clerici, A.; Pastor, N.; Porto, O. *Tetrahedron* **1998**, *54*, 15679.

Electrolyte free electro-organic synthesis: The cathodic dimerisation of 4-nitrobenzylbromide in a micro-gap flow cell

Ping He ^a, Paul Watts ^a, Frank Marken ^b, Stephen J. Haswell ^{a,*}

^a Department of Chemistry, University of Hull, Hull HU6 7RX, UK

^b Department of Chemistry, University of Bath, Claverton Down, Bath BA2 7AY, UK

Received 20 May 2005; accepted 15 June 2005

Available online 8 August 2005

Abstract

The electrochemical reduction of 4-nitrobenzylbromide is studied in *N,N*-dimethylformamide solution in the presence and in the absence of intentionally added supporting electrolyte. By conventional voltammetry it is shown that an ECE-type reaction occurs with formation of the dimer 4,4'-dinitrodibenzyl irrespective of the presence of supporting electrolyte. Next, a micro-gap flow cell is characterised and employed for the preparative electro-reduction in the absence of supporting electrolyte. Excellent yields of the dimer are obtained and explained based on a self-propagation mechanism.

© 2005 Elsevier B.V. All rights reserved.

Keywords: Micro-flow cell; 4-Nitrobenzylbromide; Electro-reduction; Platinum

1. Introduction

Preparative electrochemistry can provide a clean and versatile method for the synthesis of organic compounds as the addition of electrons to or the removal of electrons from neutral organic substrates can be activated under relatively mild reaction conditions. As the electrons are not bound to a reagent, the pollution of the environment by spent reagents can be minimised. However, the common use of supporting electrolytes in electro-synthesis has been a problem in realizing such clean processes because the recovery of the supporting electrolyte may create problems and can be costly. Whilst solid polymer electrolyte membranes [1] have been developed for electrolyte-free electrolysis, an approach based on micro-fluidic systems could prove particularly attractive for electro-organic synthetic methods [2a]. Indeed industrial processes do already employ cells with relative

small interelectrode gap (~ 1 mm) [21] in order to minimise energy losses.

Recently, micro-gap flow cell devices have received significant research interest [2] because of the small anode–cathode gap, high electrode surface area to volume ratio, a uniform current distribution, and the continuous production of products. In the thin-gap flow cell geometry, working and counter electrodes can be placed facing each other and the inter-electrode gap is typically in the range of a few tens up to approximately 500 μm . This electrode geometry reduces the total value of the ohmic resistance of a cell by orders of magnitude compared to those observed in conventional cells. Therefore, it is possible to eliminate the need for supporting electrolyte depending on the residual intrinsic conductivity of the organic solvents. Electrode processes which by definition involve charge carrier formation and transport may be regarded as “self-supported” as long as the inter-electrode distance is similar to the diffusion layer thickness. The elimination of supporting electrolyte in turn reduces costs and in some cases simplifies the chemistry. This methodology also opens up the possibility to couple processes at anode

* Corresponding author. Fax: +0 1482 466416.

E-mail address: s.j.haswell@hull.ac.uk (S.J. Haswell).

and cathode to give new reaction pathways in “paired” organic electro-syntheses [2b]. The control of reaction conditions can be readily achieved via the reaction parameters potential, current density, and residence time.

Many types of thin-gap flow cells have been proposed for electro-organic synthesis including the segmented thin-gap flow cell [2c], multisectioned porous electrode flow-through cell [2f,2g,2i,2j], the coplanar interdigitated micro-band electrode cell [2k], and the miniaturized parallel channel electrochemical reactor [2d,2h]. However, all of these approaches have involved the use of supporting electrolytes or relatively low conversion without intentionally added supporting electrolyte [2d,2h]. Recently, Yoshida and coworkers [2a] reported a flow-through porous thin-gap electrode micro-reactor permitting operation without supporting electrolyte. The control of the applied potential in this reactor was however a problem due to the ohmic drop in the current flow direction which results in a natural tendency for current density to be concentrated in the portion of the porous electrode nearest the counter electrode [2g]. This non-uniformity in the current distribution can have a considerable impact on the process feasibility and performance. Marken and coworkers [2e] reported a micro-gap flow cell for the reduction of tetraethylethylenetetra-carboxylate also allowing operation without supporting electrolyte. Relatively low flow rates (1.9 $\mu\text{l}/\text{min}$) were necessary to obtain high yields of the product. Whilst the electro-synthesis approach in the absence of intentionally added supporting electrolyte has received only limited attention to date, its ability to deliver clean electro-organic syntheses is attractive in terms of green chemical methodology and timely in view of the recent surge in micro-reactor synthesis applications.

In the present study, the electrochemical reduction of 4-nitrobenzylbromide [3a,3b] is chosen to demonstrate the utility of the proposed methodology. This reaction is studied first by cyclic voltammetry in the presence and in the absence of intentionally added electrolyte and then at conventional and micro-gap flow cell electrodes. Electro-synthetic reactions under optimised conditions in *N,N*-dimethylformamide (DMF) in the absence of intentionally added supporting electrolyte are shown to give very high yields of the dimeric product, 4,4'-dinitrobenzyl. The reaction was carried out in a preparative micro-gap flow cell by simply pumping the starting material 4-nitrobenzylbromide dissolved in DMF through the cell and isolation of the product by solvent evaporation.

2. Experimental

The cyclic voltammetric (CV) experiments were carried out with an Autolab PGSTAT30 system (Eco Chemie, The Netherlands) in both a conventional

three-electrode cell and in micro-gap flow cells. In this work electrolyte (0.1 M *n*-Bu₄NBF₄) was added to assist in interpreting the voltammograms produced. For the conventional cell, either a Pt disc (diameter 0.5 mm) or a Pt micro-disc (diameter 0.025 mm) were used as the working electrode, a Pt wire and silver wire (both diameter 0.1 mm) were used as the counter and the reference electrode, respectively. In some experiments an Ag|AgCl (3 M KCl) electrode (Cypress Systems, USA) was used as the reference electrode and externally placed upstream near the inlet of the micro-gap flow cell. For the micro-gap flow cell, two equally sized Pt foils (squares of 5 mm width and length, 0.05 mm thickness) were used for the working and the counter electrodes. A Harvard PHD 2000 syringe pump was used to pump solution flow through the cell system at controlled flow rate. The diffusion coefficients in DMF (at $22 \pm 2^\circ\text{C}$) for ferrocene, 4-nitrobenzyl bromide and 4,4'-dinitrobenzyl were determined independently by steady state micro-electrode voltammetry at a 25 micrometer diameter Pt disc electrode [2e] (estimated error $\pm 5\%$) and by comparison with the literature value for ferrocene in DMF [4]. The diffusion coefficients were found to be $1.0 \times 10^{-9} \text{ m}^2 \text{ s}^{-1}$ for ferrocene, $1.0 \times 10^{-9} \text{ m}^2 \text{ s}^{-1}$ for 4-nitrobenzyl bromide, and $0.83 \times 10^{-9} \text{ m}^2 \text{ s}^{-1}$ for 4,4'-dinitrobenzyl.

The micro-gap flow cells were easy and convenient to build by simply clamping all components together with a suitable spacer. As shown in Fig. 1, the cell consisted of two glass plates (3 cm length, 2 cm width, 6 mm thickness) forming the bottom and top with two holes connecting PEEK tubes (i.d. 0.24 mm) which acted as the flow inlet and outlet. Two equally sized Pt foils (5 mm width and length, 50 μm thickness, Goodfellow Cambridge Limited, purity 99.99%) were used as working and counter electrodes and a PTFE spacer (BOHLENDER GmbH, Germany) with rectangular window (3 mm width and 19 mm length) generated the reaction flow cell. A small amount of silicone adhesive sealant (Ambersil Ltd., UK) was used for sealing the outside area around glass and the Pt foil to avoid leakage. PTFE spacers with thicknesses of 120 and 250 μm were employed. After assembly, the cell height was calibrated by flowing a solution of 1 mM ferrocene in 0.1 M NBu₄BF₄-DMF and analysing the limiting current I_{lim} with the expression $I_{\text{lim}} = 0.925nFc \left(\frac{DA}{h}\right)^{2/3} (V_f)^{1/3}$. In this expression, n is the number of electrons transferred per reacting molecule, D denotes the diffusion coefficient, A is the electrode area, V_f is the volume flow rate, and h is the cell half height. For the two spacers the inter-electrode distance was found to be $2h = 160 \mu\text{m}$ and $2h = 320 \mu\text{m}$.

The electrochemical reduction of 4-nitrobenzyl bromide was chosen to test the proposed micro-gap flow cell configuration in the presence and absence of supporting electrolyte. During typical reaction runs,

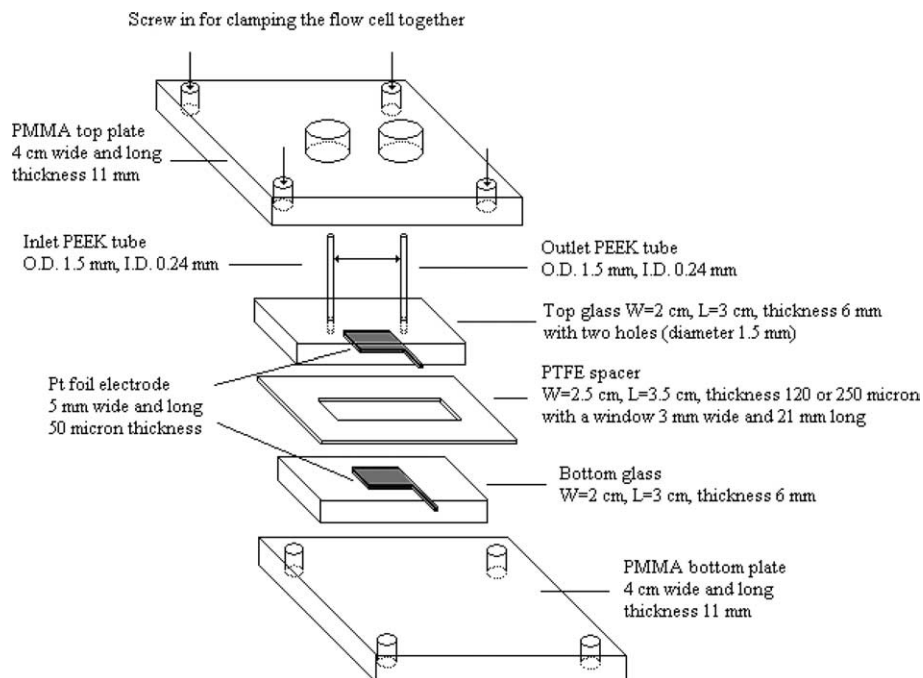


Fig. 1. Schematic representation of the micro-gap flow cell.

product samples were collected in a cooled (0 °C) product vial for a duration of 5 min. Samples were analysed by GC/MS (Varian 2000) equipped with a capillary column (CP SIL 8CB, 30 m length, Chrompack). The GC column temperature was held initially at 70 °C for 4 min, ramped at 20 °C/min to reach 240 °C which was then held for 12 min. The internal standard method was used for the quantitative determination of product yields with decane as an internal standard added to the reactant solution prior to reaction.

The reagents 4-nitrobenzyl bromide (Aldrich, 99%), 4-nitrotoluene (Aldrich, 99%), 4,4'-dinitrodibenzyl (Aldrich, >80%), tetrabutylammonium tetrafluoroborate (Aldrich, 99%) and ferrocene (Aldrich, 99%) were used without further purification. The solvents used were *N,N*-dimethylformamide (DMF, Fluka, ≥99%, stored over molecular sieve, H₂O ≤ 0.01%) and tetrahydrofuran (THF, Fluka, 99.5). DMF was further dried over molecular sieve 3A (Lancaster, 1–2 mm beads) for 72 h prior to use and kept in a desiccator [5]. THF was purified by distilling with sodium and benzophenone prior to use. All solutions were degassed with argon (Pureshield Argon, BOC gases, UK) before measurements.

3. Results and discussion

The cyclic voltammetric (CV) behaviour of 4-nitrobenzyl bromide, 4,4'-dinitrodibenzyl and 4-nitrotoluene in DMF with 0.1 M *n*-Bu₄NBF₄ as the supporting electrolyte has been investigated and data are shown in Fig. 2. 4-NBB exhibits two cathodic peaks (processes P1 and

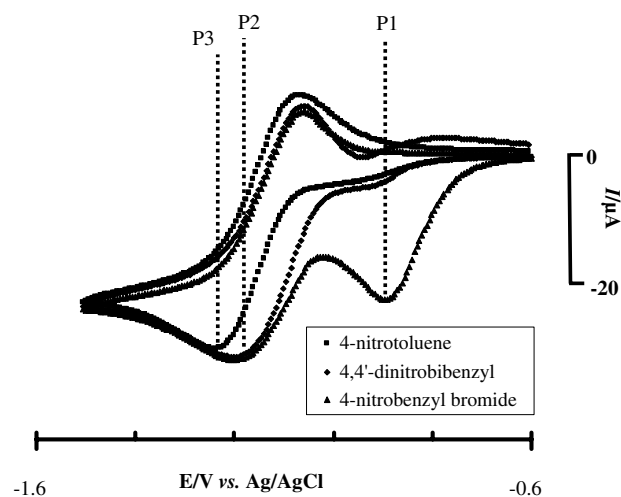


Fig. 2. Cyclic voltammograms in 0.1 M *n*-Bu₄NBF₄-DMF at scan rate of 80 mV/s, the concentration is 3 mM for 4-nitrobenzyl bromide, 2.5 mM for 4,4'-dinitrodibenzyl and 3.0 mM for 4-nitrotoluene.

P2) near -0.89 and -1.2 V on the cathodic sweep. After reversal of the potential scan direction at -1.5 V, only one oxidation wave corresponding to the re-oxidation of the product is seen at -1.07 V. By comparison of 4-nitrobenzyl bromide CV characteristics with those of the two possible products of the cathodic process (4,4'-dinitrodibenzyl and 4-nitrotoluene), the final product for cathodic reduction of 4-nitrobenzyl bromide is determined to be the dimer 4,4'-dinitrodibenzyl (see Fig. 2). This result was confirmed by GC/MS analysis of the products. It is interesting to note that in spite of the lower diffusion coefficient for 4,4'-dinitrodibenzyl and the lower

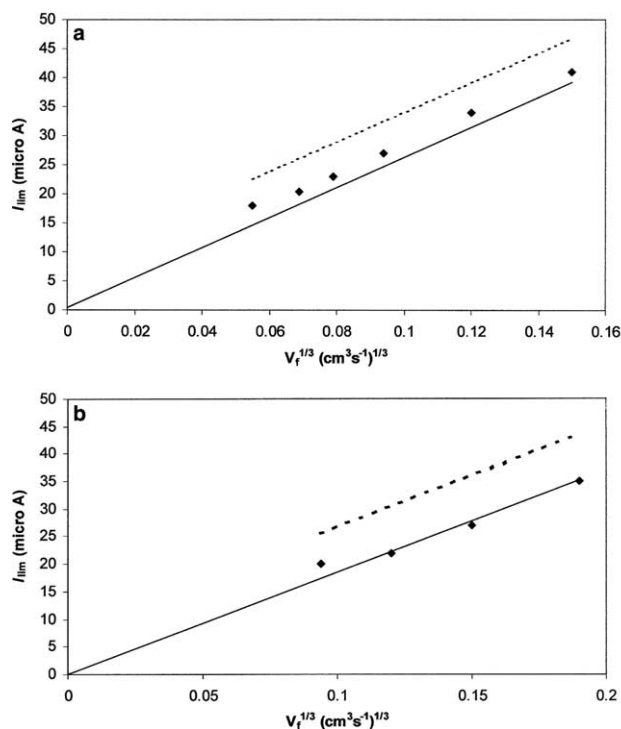


Fig. 5. Plot of limiting current versus cube root of the flow rate with (a) the exposed area of 12.5 mm² and electrode-gap of 160 μm and (b) the exposed area of 15 mm² and electrode-gap of 320 μm. Square: experimental limiting current; bold line: theoretical limiting current for the diffusion only case which was calculated with Eq. (1); dashed line: the theoretical limiting current for diffusion with feedback [6].

create a flow cell with electrode area $A = 15 \text{ mm}^2$ and cell height $2h = 320 \text{ μm}$, the voltammetric behaviour (Fig. 4(b)) is seen to be similar to that observed in the thinner spacer flow cell. Well-defined limiting currents are detected while the traces between forward and backward scan become widened a little and the limiting current is found to be smaller than that observed with the thinner gap cell. At a lower flow rate of 20 μl/min, the CV response becomes similar to typical stationary CV responses. The experimental limiting currents are also consistent with diffusion control, as seen in Fig. 5(b).

The diffusion controlled limiting current under flow conditions in a channel flow cell may be given in the following equation:

$$I_{\text{lim}} = 0.925nFc \left(\frac{DA}{h} \right)^{2/3} (V_f)^{1/3}, \quad (1)$$

where I_{lim} is the limiting current, n refers to the number of electrons transferred at the electrode, F is Faraday constant (96,485 C/mol), A is the exposed area of the working electrode, D and c refer to the diffusion coefficient and the concentration of reactant in the solution, h and V_f refer to half cell height and volume flow rate. Theoretical lines based on this equation are shown in Fig. 5. The deviation to higher currents in particular for the thinner spacer suggests a small contribution from

“feedback” currents due to reactants diffusing between anode and cathode. For efficient electrolysis these currents have to be minimised.

For stirred solution voltammetry, the limiting current at a uniformly accessible electrode may be expressed in terms of the Nernst diffusion layer thickness, δ , as given in the following equation:

$$I_{\text{lim}} = \frac{nFDAc}{\delta}. \quad (2)$$

The diffusion layer thickness is an important parameter and may be helpful for identifying coupling phenomena between cathode and anode diffusion layers, which can have implications for chemical reaction occurring in electrochemical cells. By combining Eqs. (1) and (2) the diffusion layer thickness within the micro-gap flow cell can be determined. The new equation (3) shows that the diffusion layer thickness is linearly dependent on the inverse cube root of volume flow rate. (It has to be emphasised that for channel flow systems the diffusion layer thickness δ gradually increases toward the trailing end of the electrode and the condition of uniform accessibility is not fulfilled.)

$$\delta = 1.081(DA)^{1/3}(h)^{2/3}(V_f)^{-1/3}. \quad (3)$$

It is interesting to consider the case in which the two diffusion zones start to couple. In this case, the δ value is set to the inter-electrode distance. The flow rate corresponding to this case is found to be 1.4 μl/min for the 160 μm gap cell and 0.8 μl/min for the 320 μm gap cell. These values are in agreement with results from Eq. (4) [2e] giving flow rates of 1.1 and 0.7 μl/min, respectively. All experiments carried out here are conducted under conditions of weak coupling where “feedback” currents between the anode and cathode become detectable but do not lead to significant efficiency losses.

$$V_f^{\text{diffusion-FB}} \approx \frac{DA}{8h}. \quad (4)$$

Next, synthetic experiments were conducted in order to isolate and identify products and to optimise yields for the reductive dimerisation of 4-nitrobenzyl bromide. The electrochemical reduction of 4-nitrobenzyl bromide was conducted in preparative cells with electrode area of 45 mm² and with electrode-gaps of 160 and 320 μm without the addition of an electrolyte. A two-electrode configuration was used for preparative experiments with 10 mM 4-nitrobenzyl bromide in DMF being continuously pumped through the cell at a constant applied current. The applied potential required about 4–10 V for limiting current conditions corresponding to currents of 0.6–2.5 mA. For preparative electrolysis, the dimer 4,4'-dinitrodibenzyl is the principle product but small amount of the monomeric product 4-nitrotoluene were also observed. The formation of this product can be ex-

Table 1

Preparative electrolysis in micro-flow cells with two-electrode geometry for the reduction of 10 mM 4-nitrobenzyl bromide in DMF without intentionally added supporting electrolyte

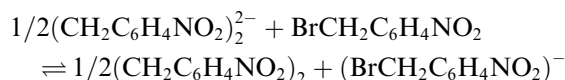
Entry	Electrode gap (μm)	Current (mA)	Flow rate (μl/min)	Residence time (s)	Conversion (%)	Product distribution	
						R–R	R–H
1	160	0.8	20	22	99	68	32
2	160	1.3	40	11	95	69	31
3	320	0.6	20	44	70	93	7
4	320	1.2	20	44	91	91	9
5	320	0.6	40	22	58	94	6
6	320	2.5	40	22	92	91	9
7 ^a	320	2.5	40	22	100	76	24

The potential was adjusted to allow the current flow to be consistent with the second plateau for the reduction process.

^a Co-solvents DMF and THF were used in the ratio of 3–1.

plained by the formation of the neutral radical 4-nitrobenzyl bromide which abstracts hydrogen atom from the solvent after failing to find a reaction partner for dimerisation. Table 1 summarizes the conversion and product distribution for a range of conditions. It can be seen that the conversion and product distribution are strongly dependent on the electrode gap, the flow rate and the applied current. For the 160 μm gap cell (entries 1 and 2), a conversion of more than 90% can be obtained with more than 30% 4-nitrotoluene being produced. The applied voltage was 4.0 V for producing a current of 0.8 mA with a flow rate of 20 μl/min and 4.8 V for producing 1.3 mA current at a flow rate of 40 μl/min. The current efficiency calculated based on Faraday's Law is more than 80% in these cases. However, the increased cathodic formation of the monomeric product suggests some degree of interference from the anode reaction. It is very likely that products formed at the anode, e.g., protons, will interfere with the process at the cathode in particular further downstream where the diffusion layer overlap becomes more significant.

For the 320 μm gap cells (entries 3–6), higher voltages were required to obtain sufficiently high conversions (>90%). Interestingly, more than 90% of the dimer product 4,4'-dinitrodibenzyl are obtained in these cases. When a co-solvents containing DMF and THF (THF is well known to be a source of hydrogen atoms in H-abstraction reactions [7]) in 3:1 ratio was used (entry 7), the amount of monomeric product 4-nitrotoluene obtained increased to 20–30%. This implies that the H-atom abstraction process is competing with the dimerisation. Under the conditions used here, the residence time in the cell was found to be in the range of 11–44 s for the starting materials to be completely converted. It is surprising that a good balance can be found between efficiency losses due to “feedback” currents and efficiency losses due to incomplete reaction. This can be explained by the fact that the 4,4'-dinitrodibenzyl dianion produced at the cathode can react (even in the solution) to produce more of the anion radical [8] as indicating below



Therefore, this reaction may be regarded as “self-propagating” (the dimeric dianion triggers the formation of more product) and the formation of the dimeric product becomes highly efficient. A more detailed study of reaction layer for ECE process, the diffusion layer and the current density across the cell will be required to fully understand the processes in the cells.

4. Conclusion

We have demonstrated that the electrochemical reduction of 4-nitrobenzyl bromide can be conducted efficiently in a micro-gap flow cell and in the absence of intentionally added supporting electrolyte. The dimer is the principle product of the reaction but the tendency to form the monomeric product 4-nitrotoluene increases with decreasing inter-electrode gap. The “self-propagating” nature of the overall process contributes to the clean formation of high yields of the dimer product 4,4'-dinitrodibenzyl.

Acknowledgement

We thank the Engineering and Physical Sciences Research Council for funding.

References

- [1] (a) J. Jörissen, *J. Appl. Electrochem.* 33 (2003) 969; (b) S.S. Vaghela, G. Ramachandiraiah, P.K. Ghosh, D. Vasudevan, *J. Appl. Electrochem.* 32 (2002) 1189; (c) D. Hoorman, C. Kubon, J. Jörissen, L. Kröner, H. Pütter, *J. Electroanal. Chem.* 507 (2001) 215.
- [2] (a) R. Horcajada, M. Okajima, S. Suga, J. Yoshida, *Chem. Commun.* (2005) 1303; (b) D. Horii, M. Atobe, T. Fuchigami, F. Marken, *Electrochem. Commun.* 7 (2005) 35;

- (c) S. Rode, S. Altmeyer, M. Matlosz, *J. Appl. Electrochem.* 34 (2004) 671;
- (d) M. Küpper, V. Hessel, H. Löwe, W. Stark, J. Kinkel, M. Michel, H. Schmidt-Traub, *Electrochim. Acta* 48 (2003) 2889;
- (e) C.A. Paddon, G.J. Pritchard, T. Thiemann, F. Marken, *Electrochem. Commun.* 4 (2002) 825;
- (f) T. Bechtold, A. Turcanu, *J. Electrochem. Soc.* 149 (2002) D7;
- (g) C. Vallieres, M. Matlosz, *J. Electrochem. Soc.* 146 (1999) 2933;
- (h) A. Ziogas, M. Küpper, H. Löwe, W. Ehrfeld, in: *IMRET3: Micro-reaction Technology: Industrial Processes*, Springer, Berlin, 1998, p. 136;
- (i) T. Bechtold, E. Burts, A. Turcanu, O. Bobleter, *J. Appl. Electrochem.* 27 (1997) 1021;
- (j) M. Matlosz, *J. Electrochem. Soc.* 142 (1995) 1915;
- (k) C. Belmont, H.H. Girault, *J. Appl. Electrochem.* 24 (1994) 719;
- (l) D. Pletcher, F.C. Walsh, *Industrial Electrochemistry*, Chapman & Hall, London, 1993.
- [3] (a) J.G. Lawless, D.E. Bartak, M.D. Hawley, *J. Am. Chem. Soc.* 91 (1969) 7121;
- (b) D.E. Bartak, M.D. Hawley, *J. Am. Chem. Soc.* 94 (1972) 640.
- [4] S.R. Jacob, Q. Hong, B.A. Coles, R.G. Compton, *J. Phys. Chem. B* 103 (1999) 2963.
- [5] R.D. Burfield, R.H. Smithers, *J. Org. Chem.* 43 (1978) 3966.
- [6] For sufficiently small cell height (or slow flow rate), feedback current is possibly produced, leading to an over-all increase in limiting current. In this case, total limiting current is equal to the limiting current for diffusion only plus feedback current I_{FB} which is calculated based on $\frac{nFDAc}{2h}$ (see reference [2e]).
- [7] T. Nishino, T. Watanabe, M. Okada, Y. Nishiyama, N. Sonada, *J. Org. Chem.* 67 (2002) 966.
- [8] J. Pinson, J.M. Saveant, *J. Am. Chem. Soc.* (1978) 1506.

The preparation and reaction of enolates within micro reactors

Charlotte Wiles,^a Paul Watts,^{a,*} Stephen J. Haswell^a and Esteban Pombo-Villar^b

^a*Department of Chemistry, The University of Hull, Cottingham Road, Hull HU6 7RX, UK*

^b*Novartis Institute for BioMedical Research, WSJ-386.07.15, CH4002 Basel, Switzerland*

Received 4 April 2005; revised 26 July 2005; accepted 18 August 2005

Available online 13 September 2005

Abstract—Over the past 5 years, interest in the miniaturisation of chemical synthesis has grown rapidly, however in order to facilitate transfer of the technology from its current position as a research tool to industrial applications, a core understanding of the challenges associated with transferring reactions from the macro to the micro domain is required. This paper therefore aims to broach this problem by investigating the application of micro reactors to a range of commonly employed synthetic reactions including acylation, aldol, alkylation, 1,4-conjugate addition (Michael addition) and the Knoevenagel condensation. Comparison of the results obtained with traditional batch techniques enable us to highlight some of the advantages associated with micro reaction technology.

© 2005 Elsevier Ltd. All rights reserved.

1. Introduction

Although less common than their analytical counterparts,¹ miniaturised devices capable of performing chemical synthesis, termed micro reactors, have recently received widespread interest from both industry and academia. The desire to miniaturise synthetic reactions has been driven by a need for greater process control, not only as a means of increasing product purity and plant productivity, but also reactor safety.^{2,3} With these factors in mind, the micro reactor group at Hull have successfully demonstrated the application of miniaturised systems to a range of solution phase chemistries, contributing greatly to the initial evaluation of micro reactors for synthetic applications.^{4,5} This paper follows a series of communications and aims to illustrate, in detail, the challenges associated with the transfer of reactions from the macro to the micro domain, laying the foundations necessary for the ultimate goal of performing novel synthetic procedures in micro fabricated devices.^{6–11}

In this context, we define a micro reactor as a device that contains a series of interconnecting channels with cross-sectional dimensions in the range of 10–500 μm . Depending on the end use of the device, a range of substrates have been employed, these include; silicon, glass, quartz, ceramics, polymers and metals.¹² However, due to its compatibility with organic solvents, high mechanical strength,

temperature resistance and optical transparency, borosilicate glass is the chosen substrate for the work described herein. As **Figure 1** illustrates, the devices consist of a borosilicate glass base plate, containing an etched channel network, and a top block through which reagents are delivered. Thermal bonding of the two layers affords a sealed micro reactor, with typical dimensions of 2.5 cm \times 2.5 cm \times 2.0 cm for electroosmotic devices¹³ and 2.5 cm \times 2.5 cm \times 0.6 cm for pressure driven applications. Using a suitable pumping mechanism, reagents are brought together within the micro channels, where they are reacted for a specified period of time, prior to collection and analysis. In order to manipulate reagents and products within micro fabricated devices accurate pumping mechanisms are

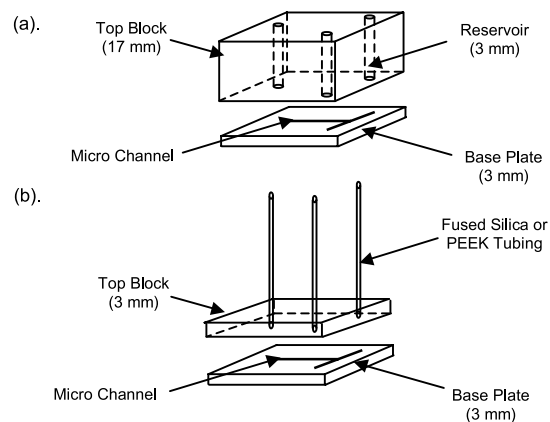


Figure 1. Exploded view of borosilicate glass micro reactors for (a) electroosmotic and (b) pressure-driven applications.

Keywords: Micro reactor; Enolate synthesis.

* Corresponding author. Tel.: +44 1482 465471; fax +44 1482 466416; e-mail: p.watts@hull.ac.uk

required, these are loosely categorised as either mechanical or non-mechanical.¹⁴

1.1. Non-mechanical pumping

In the early 1990's, Manz and co-workers¹⁵ described the use of electrokinetic flow in a miniaturised flow injection system, a concept further investigated by Dasgupta et al.¹⁶ Harrison and co-workers¹⁷ later applied the principle to the mobilisation of fluorescein labelled amino acids in a glass reactor manifold, whereby valve-less control of fluid at a T-shaped intersection was observed. In comparison to the use of mechanical micro pumps, field induced flow is advantageous as the electric field acts as a pump and a valve, enabling both the direction and magnitude of flow to be controlled.¹⁸

1.1.1. Scope and limitations of electrokinetic flow. Electrokinetic flow comprises of two physical effects; electroosmotic flow (EOF), which is responsible for the velocity of the solvent system as a whole, and electrophoretic flow (EPF), which is an additional velocity effect experienced by charged species within the solvent system. As Figure 2 illustrates, when an ionisable surface such as glass, quartz or Teflon comes into contact with a suitable solvent system, the surface is neutralised with a diffuse layer of positive ions from the bulk liquid.¹² A proportion of the counterions are adsorbed onto the surface, resulting in the formation of an immobile layer, and the remaining positive ions form a transient double layer. Application of an electric field causes the double layer to move towards the most negative electrode, inducing bulk flow within the micro channel.

Although the use of EOF has been well documented within the literature, the manipulation of fluid within open channel networks is inherently irreproducible due to hydrodynamic pressure effects.¹⁹ Consequently, in order to obtain reproducible controlled flow, it is important to ensure that non-uniformities in velocity profile (that arise as a result of different reservoir heights) are excluded or minimised. One such approach is the fabrication of micro porous silica frits (MPS frits) within the micro channels.²⁰ The porous silica structure acts to reduce the cross sectional area of the micro channel in a specific region, therefore minimising pressure effects while maintaining EOF.²¹ Alternatively, Fletcher et al.²² recently reported the fabrication of a series of narrow channels (restrictions) at strategic points within the main channel network, thus providing the necessary regions of resistance. Clearly, compared to the use of micro porous silica frits, the fabrication of restrictions is more amenable to the large-scale manufacture of micro fluidic devices.

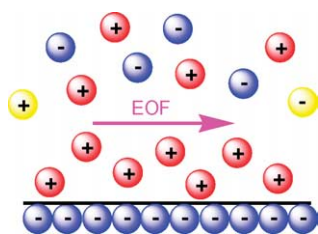


Figure 2. Schematic illustrating the principle of electroosmotic flow.

Table 1. Summary of the flow rates obtained for a series of commonly employed organic solvents

Applied field (V cm ⁻¹)	Average flow rate (μl min ⁻¹) ^a			
	MeCN	THF	DMF	EtOH
417	5.30	1.00	1.67	0.90
311	4.08	0.73	1.50	0.70
208	3.00	0.45	1.33	0.50
104	1.90	0.17	1.17	0.30

^a ≥ 10 measurements were made at each applied field.

$$v_{\text{eof}} = -\frac{E \varepsilon \varepsilon_0 \zeta}{\eta} \quad (1)$$

v_{eof} = electroosmotic flow velocity, E = applied field, ε = relative dielectric constant of the fluid, ε_0 = the permittivity of free space, ζ = zeta potential and η = viscosity.

Equation 1. Determination of the electroosmotic flow velocity.²³

While EOF has generally been associated with the manipulation of aqueous systems for analytical applications,²³ we have more recently demonstrated the mobilisation of polar solvent systems such as MeOH and DMF.²⁴ With this in mind, the flow rates of a series of common organic solvents were investigated over a range of applied fields (V cm⁻¹) (Table 1 and Fig. 3). As Table 2 illustrates, the electroosmotic flow rate is largely determined by the dielectric constant, polarity and viscosity of the solvent system (Eq. 1).²⁵ Consequently, the technique is restricted to the use of solvents such as alcohols, tetrahydrofuran, dimethylformamide, acetonitrile and aqueous systems.

1.2. Mechanical pumping

Most mechanical or reciprocating pumps are based on the movement of a piston or membrane, resulting in the delivery of fluids or gases in discrete aliquots. Due to the wide array of primary sources actuation of a membrane can be achieved using a variety of techniques including piezoelectric²⁶ and shape memory alloys.²⁷ As the pumping mechanism is independent of the device material any fluid can be mobilised, the flow is however, often pulsed (exceptions have been demonstrated²⁸). Alternatively, external displacement pumps such as syringe pumps have found widespread use, at a research level, due to their ability to deliver stable, bi-directional flow. The main challenge

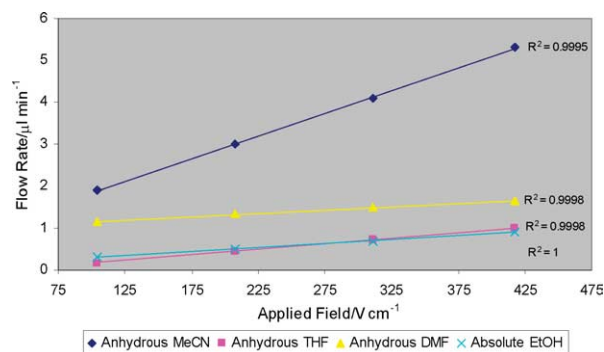


Figure 3. Graph illustrating the relationship between flow rate and applied field for a range of organic solvents.

Table 2. Relationship between the magnitude of EOF and the physical properties of a range of common organic solvents

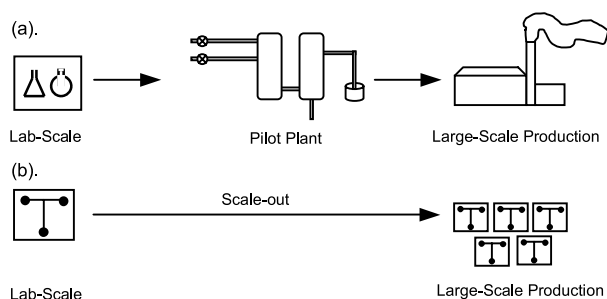
Solvent	Dielectric constant	Viscosity (cP)	Polarity index (<i>P</i>)	Flow rate ($\mu\text{l min}^{-1}$)
MeCN	37.50 (20 °C)	0.38	5.8	5.30
DMF	36.71 (25 °C)	0.92	6.4	1.67
EtOH	24.55 (25 °C)	1.10	5.2	0.90
THF	7.58 (25 °C)	0.55	4.0	1.00

associated with the use of displacement pumps is obtaining low dead volume, leak free connections between the pump and device.²⁹ The mechanism is currently very cumbersome resulting in a system whereby the pumps dwarf the device. The low tolerance to particulates also results in the generation of high back-pressure within the system. In addition, the control of multiple inputs represents a challenge, as careful balancing of the flow rates and internal pressures is required.³⁰ Consequently, we believe that electrokinetic pumping is advantageous as it enables us to obtain reproducible, pulse-free, low flow rates without the generation of high back-pressures. As the pumping mechanism requires no moving parts, the technique is simple to use and free from component wear and tear making it ideal for the continuous manipulation of fluid within miniaturised systems. Therefore, unless otherwise stated, electroosmotic flow is employed for the manipulation of reagents and reaction products within the micro fabricated devices described herein.

1.3. Advantages of miniaturisation

Current production technology is based on the scale-up of successful bench-scale processes to a pilot plant, followed by a final increase in scale to achieve mass production. This approach is however fundamentally flawed as at each stage of scale-up, reactor modifications result in changes to the surface to volume ratio, which in turn have a profound effect on the thermal and mass transportation properties of the reaction. As a result of these variations, it is often necessary to re-optimize the process at each stage of scale-up; consequently the route from bench to production is both costly and time-consuming. It is therefore proposed that through the application of micro reaction technology, the transfer of reactions from the laboratory to production will be both rapid and cost effective as processes would initially be optimised on a single device and in order to increase production capacity, more devices would be employed.³ Therefore instead of the traditional approach of scaling-up the reactor vessel, the approach of scale-out or numbering-up would be employed (Fig. 4).

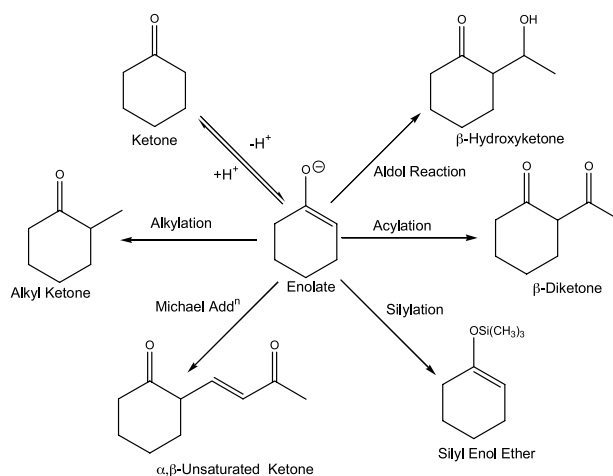
From a production perspective, the scale-out approach is advantageous as it enables changes in production volume to be met by simply increasing or decreasing the number of devices employed, therefore meeting customer demand. Additionally, the use of generic reactor designs, such as those described herein, would enable custom syntheses to be performed with relative ease. Compared to a production plant where reactors are generally configured/optimised for a single function, this flexibility is both advantageous and cost effective. In addition, the predictable thermal and mass transportation properties observed within a laminar flow

**Figure 4.** Schematic illustrating the (a) traditional, versus (b) miniaturised approaches to mass production.

environment result in increased reactor control.² In traditional large-scale reactor vessels, fluctuations in temperature and concentration are difficult to rapidly address as any alterations made take time to have an effect on the system as a whole. Along with increasing the rate of mixing, decreasing the reactor dimensions results in an inherently high surface to volume ratio. Consequently, heat generated by exothermic reactions can be dissipated rapidly, reducing the likelihood of thermal runaway or hot spot formation. As a result of the uniform reactor conditions obtained, extended reaction times are no longer required in order to obtain high conversions, resulting in fewer, but more often, no side reactions.^{2,6}

2. Results and discussion

As a result of the importance of enolate chemistry in the pharmaceutical industry, the synthesis of 1,3-diketones, β -hydroxyketones, α,β -unsaturated ketones and 1,4-addition products (Scheme 1), has been used to demonstrate the key advantages associated with micro reaction technology, these include; rapid reaction optimisation, reduced reaction time, enhanced conversions, reduced by-product formation, in-situ generation of reactive intermediates and the ability to synthesise compounds that require no further purification.

**Scheme 1.** Illustration of the reaction diversity exhibited by an enolate.

2.1. The regioselective acylation of silyl enol ethers^{7,8}

The preparation and subsequent acylation of enolates is a fundamental transformation used in organic synthesis; their ambident nature however, allows the formation of bonds at either the carbon or the oxygen. This often results in the undesirable formation of a mixture of both *O*- and *C*-acylated products, which can prove difficult to separate, resulting in low yields.³¹ Consequently, a large amount of work has been undertaken in order to explore and understand those reaction conditions that promote the regioselective acylation of enolates; that is, the nature of the counterion, reaction temperature, solvent; stoichiometry of reagents, order of reagent addition and type of acylating reagent employed.³²

Although careful selection of the aforementioned conditions has been shown to influence reaction regioselectivity, many of the 1,3-diketones prepared remain contaminated with small amounts of *O*-acylated product.³³ With this in mind, we recently demonstrated a simple technique for the regioselective synthesis of 1,3-diketones, free from any competing *O*-acylation or diacylation products. The procedure involved regeneration of enolates from silyl enol ethers³⁴ using a catalytic quantity of ‘anhydrous’ tetra-*n*-butylammonium fluoride (TBAF) **1**, followed by acylation using acyl halides (1 h) or acyl cyanides (24 h).⁸ Using this approach, α -substituted ketones were found to give *C*-acylated products when treated with either acyl halides or cyanides, whereas non α -substituted ketones reacted to give *O*-acylation with acyl halides and *C*-acylation with acyl cyanides. Based on these findings, the catalytic desilylation approach was further investigated within an EOF-based micro reactor.⁷

Prior to performing an EOF-based micro reaction it is important to consider what reagent concentration, flow rate (a function of applied field) and length of experiment to use. As one of the aims of micro reaction technology is to synthesise compounds more efficiently, the use of higher reagent concentrations is desirable as this enables a greater quantity of product to be synthesised in a shorter time; consequently the limiting factor is reagent solubility (Section 2.5.2). When employing EOF, the flow rate is dependant on both the applied field and the physical properties of the reagents; as a result applied fields vary to ensure that equal flow of reagents is obtained from all reservoirs. Finally, the length of experiment is chosen in order to obtain a sufficient quantity of product for off-line analysis by GC–MS and does not reflect the residence time of reagents within the micro reactor channel; unless otherwise stated reactions are performed for 20 min.

In order to perform the acylation reaction, solutions of ‘anhydrous’ TBAF **1** (40 μ l, 0.1 M), benzoyl fluoride **2** (40 μ l, 1.0 M) and trimethyl(1-phenylvinyl)oxy)silane **3** (40 μ l, 1.0 M) in anhydrous THF were placed in reservoirs A, B and C, respectively, (Fig. 5). The reagents were then manipulated within the device, using the following applied fields 333, 455, 333 and 0 V cm⁻¹ (to reservoirs A, B, C and D, respectively), and the reaction products collected in reservoir D. Analysis of the reaction mixture by off-line GC–MS showed that 100.0% conversion of silyl enol ether

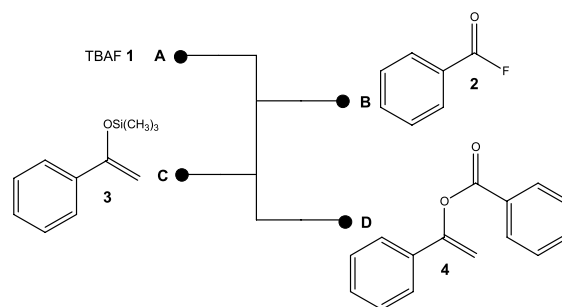


Figure 5. Schematic of the reactor manifold used for the synthesis of benzoic acid 1-phenylvinyl ester **4**.

3 to benzoic acid 1-phenylvinyl ester **4** had occurred and crucially, no *C*-acylated **5** or diacylated products were detected. Having successfully demonstrated the micro-scale synthesis of benzoic acid 1-phenylvinyl ester **4**, the kinetically slower *C*-acylation reaction (24 h in batch) was investigated.

Substitution of benzoyl fluoride **2** with benzoyl cyanide **6** (40 μ l, 1.0 M) enabled the synthesis of 1,3-diphenylpropane-1,3-dione **5** to be investigated using the same micro reactor manifold. Manipulation of the reagents using 417, 318, 476 and 0 V cm⁻¹, resulted in 100.0% conversion of the enol ether **3** to 1,3-diphenylpropane-1,3-dione **5**, again no competing *O*-acylated **4** or diacylated products were observed. The generality of the technique was subsequently demonstrated using trimethyl(1-phenyl-propenyloxy)silane **7** and cyclohex-1-enyloxy(trimethylsilane) **8** to afford 2-methyl-1,3-diphenylpropane-1,3-dione **9** and 2-benzoyl-cyclohexanone **10**, respectively. Again, all standard solutions were prepared in anhydrous THF and the reagents introduced into the reactor as follows; ‘anhydrous’ TBAF **1** (40 μ l, 0.1 M) in reservoir A, acylating reagent (40 μ l, 1.0 M) in reservoir B, the enol ether (40 μ l, 1.0 M) in reservoir C and the reaction products collected in reservoir D. Manipulation of the reagents using the applied fields reported in Table 3 resulted in 100.0% conversion to the respective 1,3-diketone. In summary, we have demonstrated a simple, regioselective technique for the acylation of an array of tetra-*n*-butylammonium enolates in an EOF-based micro reactor (Table 3); demonstrating an approach, which is clearly suited to the generation of combinatorial libraries.

2.2. The synthesis of β -hydroxyketones using silyl enol ethers⁹

Having successfully demonstrated the use of silyl enol ethers as enolate precursors with respect to regioselective acylation, the investigation was extended to incorporate the synthesis of β -hydroxyketones. In the mid 1970’s, Noyori

Table 3. Comparison of the conversions obtained for the acylation of silyl enol ethers in batch and in a micro reactor

Product no.	Conversion (%)		Applied field (V cm ⁻¹)
	Batch	Micro reaction	
4	100.0	100.0	333, 455, 333 and 0
5	95.0	100.0	417, 318, 476 and 0
9	100.0	100.0	375, 455, 405 and 0
10	100.0	100.0	208, 409, 357 and 0

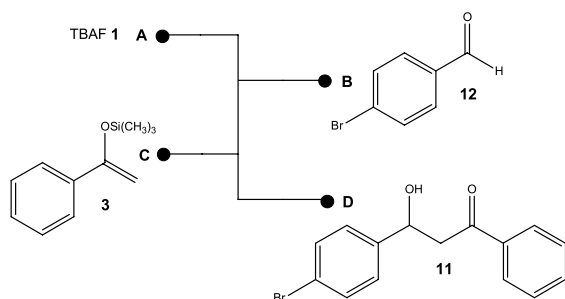


Figure 6. Schematic of the micro reactor manifold used for the synthesis of 3-(4-bromophenyl)-3-hydroxy-1-phenylpropan-1-one **11**.

et al.³⁵ demonstrated the aldol reaction of silyl enol ethers as a means of circumventing the dehydration step frequently associated with the aldol condensation. As the resulting β -hydroxyketone is a versatile synthon finding application for example in the synthesis of natural products derived from polyketide biosynthetic pathways, we investigated their synthesis in an EOF-based micro reactor.

The synthesis of 3-(4-bromophenyl)-3-hydroxy-1-phenylpropan-1-one **11** was investigated using anhydrous THF as the solvent system. As Figure 6 illustrates, ‘anhydrous’ TBAF **1** (40 μ l, 0.1 M) was placed in reservoir A, 4-bromobenzaldehyde **12** (40 μ l, 1.0 M) was placed in reservoir B and trimethyl(1-phenylvinyl)oxy)silane **3** (40 μ l, 1.0 M) in reservoir C. Manipulation of the reagents using 375, 409, 381 and 0 V cm^{-1} resulted in 100.0% conversion of the silyl enol ether **3** to 3-(4-bromophenyl)-3-hydroxy-1-phenylpropan-1-one **11**. Using the aforementioned procedure, the reaction was subsequently repeated using cyclohex-1-enyl(trimethylsilyl)oxy)cyclohexane **8** (40 μ l, 1.0 M), whereby application of 417, 455, 476 and 0 V cm^{-1} resulted in only 1.0% conversion of the enol ether **8** to 2-[(4-bromophenyl)-hydroxymethyl]cyclohexanone **13**. Upon altering the applied fields to 417, 341, 333 and 0 V cm^{-1} , and hence increasing reagent residence time within the device, the conversion to product **13** was increased to 100.0% wrt residual enol ether **8**. As Table 4 illustrates, compared to traditional batch techniques, enhancements in conversion were obtained as a result of performing the reactions within a micro reactor; in the case of 3-(4-bromophenyl)-3-hydroxy-1-phenylpropan-1-one **11**, an increase of 20.0% was observed. Along with a reduction in reaction times, the technique is highly desirable as no dehydration products were detected.

2.2.1. Alternative silylation technique. The use of preformed enolates, in the form of silyl enol ethers,^{36,37} has allowed us to successfully demonstrate the regeneration and subsequent reaction of a series of enolates within a micro reactor (Sections 2.1 and 2.2). This approach can however be disadvantageous when base sensitive molecules are employed as poor conversions result in products often contaminated with inorganic salts.³⁸ In order to circumvent these problems, many groups have investigated mild and efficient alternatives.^{39,40} Nakamura and co-workers⁴¹ demonstrated the use of ethyltrimethylsilylacetate (ETSA) **14** and ‘anhydrous’ TBAF **1** for the *O*-silylation of ketones and alcohols under nearly neutral conditions. As Scheme 2 illustrates, TBAF **1** acts catalytically with the

Table 4. Summary of the conversions obtained for the synthesis of β -hydroxyketones **11** and **13** in batch and a micro reactor

Product no.	Conversion (%)		Applied field (V cm^{-1})
	Batch	Micro reaction	
11	80.0	100.0	375, 409, 381 and 0
13	93.0	1.0	417, 341, 333 and 0
13	93.0	100.0	333, 455, 333 and 0

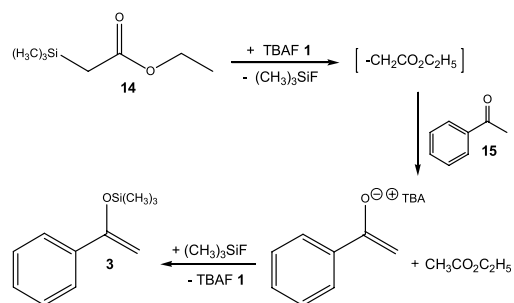
only by-product of the reaction being ethyl acetate. Consequently, this approach was of particular interest as the reaction conditions are mild and no inorganic residues are formed during the reaction.

Prior to transferring the technique to a micro reactor, the synthesis of trimethyl(1-phenylvinyl)oxy)silane **3** was investigated in batch. Reaction of ETSA **14** and acetophenone **15** in the presence of ‘anhydrous’ TBAF **1** (0.1 equiv) afforded 56.2% conversion to enol ether **3** after only 20 min. Surprisingly however, after 2 h only 6.0% trimethyl(1-phenylvinyl)oxy)silane **3** remained; an observation that is attributed to competing desilylation and protonation of the tetra-*n*-butylammonium enolate. Obviously when performing the reaction in batch, the limited lifetime of the enol ether is disadvantageous, however by transferring the reaction to a micro reactor we believed that the spatial control obtained would enable us to synthesise the enol ether, generate the tetra-*n*-butyl ammonium enolate and react it to afford the desired product in high conversion.

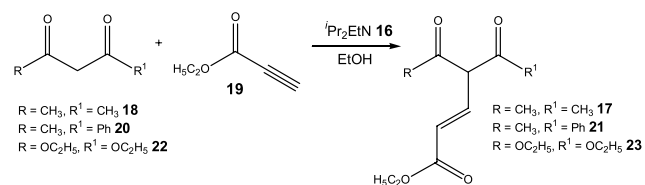
In order to demonstrate the technique, the synthesis of trimethyl(1-phenylvinyl)oxy)silane **3** and its subsequent reaction to afford benzoic acid 1-phenylvinyl ester **4**, was selected as a model reaction. A premixed solution of acetophenone **15** and ETSA **14** (40 μ l, 1.0 M) in anhydrous THF was placed in reservoir A, a solution of ‘anhydrous’ TBAF **1** (40 μ l, 0.1 M) in THF in reservoir B and a solution of benzoyl fluoride **2** (40 μ l, 1.0 M) in THF in reservoir C. Manipulation of the reagents using 417, 417 and 0 V cm^{-1} , resulted in 100.0% conversion of acetophenone **15** to product **3**, demonstrating the potential of this technique for the in-situ synthesis of silyl enol ethers and their subsequent reaction within the micro fluidic device.

2.3. Michael addition⁶

Following the successful synthesis of a series of β -hydroxyketones, 1,3-diketones and *O*-acylated ketones within an EOF-based micro reactor, we were interested in extending



Scheme 2. Preparation of trimethyl(1-phenylvinyl)oxy)silane **3** using ETSA **14**/TBAF **1**.

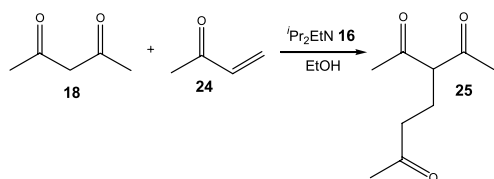


Scheme 3. Synthesis of Michael adducts **17**, **21** and **23** using diisopropylethylamine **16**.

the investigation to include the preparation of 1,3-diketone enolates. In order to demonstrate their synthetic utility, a series of 1,4-conjugate additions were investigated (Scheme 3). With the extensive range of donor and acceptor compounds featured within the literature serving to demonstrate the synthetic scope associated with the Michael reaction,^{42,43} the investigation concentrated on the reaction of 1,3-diketones (donor) and α,β -unsaturated carbonyl compounds (acceptor). As the protons of 1,3-dicarbonyl compounds are relatively acidic (^{MeCN}p*K*_{BH+} 9–13), deprotonation was achieved using the organic base diisopropylethylamine **16**.

Prior to investigating the reactions within a micro reactor, synthetic standards of the target products were synthesised. (*E*)-4-Acetyl-5-oxohex-2-enoic acid ethyl ester **17** was prepared in 89.0% yield via the dropwise addition of 2,4-pentanedione **18** to a stirred solution of ethyl propiolate **19** and diisopropylethylamine **16** in absolute EtOH. Analysis of the product by ¹H NMR, indicated that the Michael adduct **17** formed was predominantly the trans isomer (>99.0% selectivity). With this in mind, the reaction was subsequently repeated using 1-phenylbutane-1,3-dione **20** to afford (*E*)-4-benzoyl-5-oxohex-2-enoic acid ethyl ester **21** in 77.0% yield and diethyl malonate **22** to give (*E*)-4-ethoxycarbonylpent-2-enedioic acid ethyl ester **23** in 82.5% yield. The generality of the technique was examined using the alkenic acceptor methyl vinyl ketone **24**, whereby 3-acetylheptane-2,6-dione **25** was obtained in 91.0% yield (Scheme 4).

Using absolute EtOH as the solvent system, the synthesis of (*E*)-4-acetyl-5-oxohex-2-enoic acid ethyl ester **17** was investigated in a micro reactor (Fig. 7). Diisopropylethylamine **16** (40 μ l, 5.0 M), 2,4-pentanedione **18** (40 μ l, 5.0 M) and ethyl propiolate **19** (40 μ l, 5.0 M) were manipulated within the device using 417, 318, 333 and 0 V cm⁻¹. Off-line analysis of the reaction mixture showed 56.0% conversion of 2,4-pentanedione **18** to (*E*)-4-acetyl-5-oxohex-2-enoic acid ethyl ester **17**, with the remaining 44.0% being unreacted starting material **18**. This was subsequently increased to 95.0% by employing stopped flow (Flow Regime B) (for a detailed discussion of flow regimes see Section 4.2.2). The increase in conversion was



Scheme 4. Synthesis of 3-acetylheptane-2,6-dione **25** using diisopropylethylamine **16**.

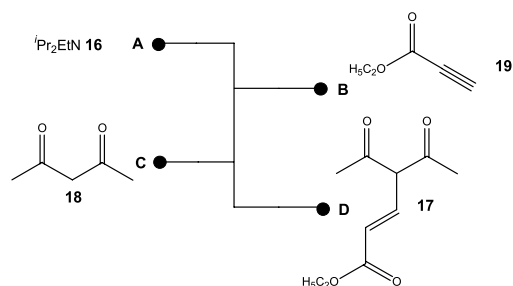


Figure 7. Schematic of the micro reactor manifold used for the synthesis of (*E*)-4-acetyl-5-oxohex-2-enoic acid ethyl ester **17**.

originally attributed to an increase in diffusive mixing between the reagent streams,⁶ this is however, unlikely as micro-scale reactions are often regarded as being rate limited, not diffusion limited.² As both reactions were performed over the same period of time, the observed increase in conversion is attributed to an increase in residence time within the micro reactor.

Based on these initial observations, the synthesis of (*E*)-4-benzoyl-5-oxohex-2-enoic acid ethyl ester **21** was subsequently investigated using absolute EtOH as the solvent system. Standard solutions of diisopropylethylamine **16** (40 μ l, 5.0 M), ethyl propiolate **19** (40 μ l, 5.0 M) and 1-phenylbutane-1,3-dione **20** (40 μ l, 5.0 M) were manipulated within the device using the following applied fields, 417, 318, 333 and 0 V cm⁻¹. Employing Flow Regime A resulted in 15.0% conversion of 1-phenylbutane-1,3-dione **20** to (*E*)-4-benzoyl-5-oxohex-2-enoic acid ethyl ester **21**, with the remaining 85.0% being unreacted diketone **20**. Again, application of a stopped flow regime (Flow Regime B) resulted in an increase in conversion to 34.0%, which was further increased to 100.0% by employing a longer period of stopped flow (Flow Regime C). The technique was further exemplified using the synthesis of (*E*)-4-ethoxycarbonylpent-2-enoic acid ethyl ester **23**, whereby Flow Regime A (417, 386, 381 and 0 V cm⁻¹) resulted in 40.0% conversion to product **23** compared to 100.0% as a result of employing Flow Regime B.

Having successfully demonstrated a number of conjugate additions using the alkyne acceptor ethyl propiolate **19**, the synthesis of 3-acetylheptane-2,6-dione **25** was subsequently investigated using methyl vinyl ketone **24** (Scheme 4). Using absolute EtOH as the solvent system, diisopropylethylamine **16** (40 μ l, 5.0 M), 2,4-pentanedione **18** (40 μ l, 5.0 M) and MVK **24** (40 μ l, 5.0 M) were manipulated within the device (417, 455, 476 and 0 V cm⁻¹) and the reaction products collected in reservoir D. As a result of employing Flow Regime A, 13.0% conversion to product **25** was obtained, this was further increased to 96.0% conversion as a result of employing Flow Regime B (Table 5).

To summarise, using the Michael addition as a model reaction, we have demonstrated the ability to rapidly optimise reactions by employing a range of flow regimes in an EOF-based micro reactor. In addition, it must also be noted that as a result of the increased reaction control obtained within the micro fluidic device, no by-products were detected; compared to batch, where a competing

Table 5. Comparison of the effect of flow regime on conversion to Michael adduct in an EOF-based micro reactor

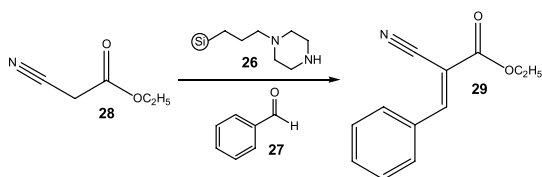
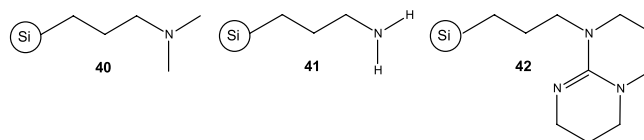
Product no.	Conversion (%)		
	Flow regime A	Flow regime B	Flow regime C
17	56.0	95.0	—
21	15.0	34.0	100.0
23	40.0	100.0	—
25	13.0	96.0	—

reaction between the base **16** and the Michael acceptor **19** was frequently observed.⁴⁴

2.4. The use of solid-supported bases for the synthesis of analytically pure condensation products¹⁰

Due to the widespread pharmaceutical interest in the Knoevenagel condensation (Scheme 5), we investigated the synthesis of α,β -unsaturated compounds in an EOF-based micro reactor. As the reactions are base catalysed, one of the main disadvantages is that the reaction products require purification in order to remove the organic base and its salt. With this in mind, we proposed that by incorporating a series of supported bases (Fig. 8) into a micro fabricated device, product purity could be increased while simultaneously maintaining the advantages associated with reaction miniaturisation. In order to evaluate the use of supported reagents within an EOF-based system, a miniaturised flow reactor was designed (Fig. 9). This approach not only enabled reagents to be packed with ease but also provided a relatively inexpensive, versatile system. Using the set-up illustrated in Figure 9, 5 mg of 3-(1-piperazino)propyl-functionalised silica gel **26** (4.75×10^{-3} mmol) was packed into a borosilicate glass capillary (500 $\mu\text{m} \times 3.0$ cm) and micro porous silica frits placed at both ends, the capillary was then placed between two glass reservoirs. A 1:1 mixture of benzaldehyde **27** and ethyl cyanoacetate **28** (40 μl , 1.0 M) in MeCN was placed in reservoir A and MeCN in reservoir B (40 μl).

Application of 333 and 0 V cm^{-1} resulted in the mobilisation of the reaction mixture through the packed bed at a flow rate of 0.5 $\mu\text{l min}^{-1}$. Operating the device continually for 4.75 h (14×20 min runs) resulted in the synthesis of 0.025 g (0.124 mmol, 98.9%) of 2-cyano-3-phenyl acrylic acid ethyl ester **29**. The 'crude' reaction products were then analysed by NMR spectroscopy to confirm product purity.¹⁰ The generality of the technique was subsequently investigated using 4-bromobenzaldehyde **12**, 3,5-dimethoxybenzaldehyde **30** and 4-benzyloxybenzaldehyde **31**. As Table 6 illustrates, the respective condensation products **32**, **33**, and **34** were obtained in >95.0% conversion. In addition, we investigated the condensation of malononitrile **35** with the aforementioned aldehydes to afford condensation products

**Scheme 5.** General scheme illustrating the use of a functionalized silica gel **26**, in the Knoevenagel condensation.**Figure 8.** Schematic illustrating the silica-supported bases investigated.

36 (96.9%), **37** (96.3%), **38** (97.8%) and **39** (99.7%), respectively.

Using the synthesis of unsaturated ketone **29** as a model reaction, we also investigated the use of other supported bases, namely; 3-(dimethylamino)propyl-functionalised silica gel **40**, 3-aminopropyl-functionalised silica gel **41** and 3-(1,3,4,6,7,8-hexahydro-2H-pyrimido[1,2-a]-pyrimidin-9-yl)propyl-functionalised silica gel **42** (Fig. 8) whereby 99.4, 100.0 and 99.3% conversion to the desired product 2-cyano-3-phenyl acrylic acid ethyl ester **29** was observed. Compared to standard batch techniques, the approach described is advantageous as the supported reagents can be recycled with ease, enabling more consistent results to be obtained. In addition, the generation of localised concentration gradients enables reactions to be driven to completion without the need to employ large quantities of catalyst. In summary, we have demonstrated the successful incorporation of a series of silica-supported bases within an EOF-based device, enabling the synthesis and characterisation of eight condensation products whereby no additional product purification was required.

2.5. Enolate alkylation

Following the successful preparation of a range of 1,3-diketone enolates using both solution phase and solid-supported organic bases, the next step was to evaluate the preparation of enolates directly from ketones such as acetophenone **15**. This was firstly demonstrated using organic peralkylated polyaminophosphazene bases (Section 2.5.1) and secondly using inorganic bases (Section 2.5.2–2.5.3).

2.5.1. Phosphazene bases. Over the past 30 years, research has been undertaken in order to increase the inherent strength ($\text{p}K_{\text{BH}^+}$) of organic bases⁴⁵ and although a few examples are commercially available, such as heptamethylisobiguanide,⁴⁶ however they were not well received by synthetic chemists.⁴⁷ The field was however transformed in the early 1990's by Schwesinger and co-workers^{48,49} with

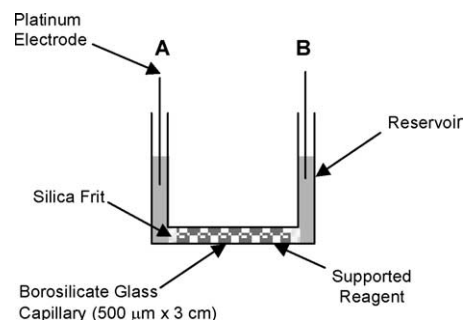
**Figure 9.** Schematic of the reaction set-up used for the evaluation of solid-supported reagents, in a miniaturized system.

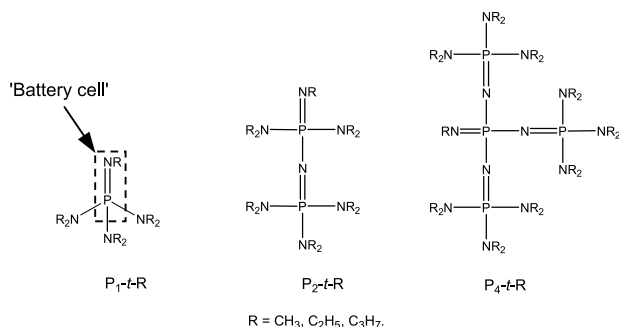
Table 6. Summary of the conversions obtained in a micro fabricated device using 3-(1-piperazino)propyl-functionalised silica gel **26**

Product no.	Applied field (V cm ⁻¹)	Flow rate (μl min ⁻¹)	Conversion ^a (%)
29	333	0.5	99.1
32	333	0.3	99.5
33	333	0.3	94.7
34	333	0.5	95.1
36	167	1.0	96.9
37	167	0.5	96.3
38	167	0.7	97.8
39	167	1.0	99.7

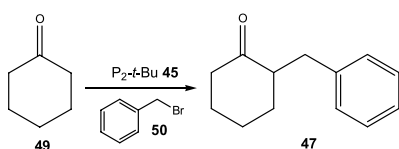
^a ≥ 10 replicates were performed for each compound.

the synthesis of a series of strong, uncharged bases, termed peralkylated polyaminophosphazenes or simply phosphazenes (Fig. 10).⁵⁰ Compared to traditional organic bases such as diisopropylethylamine **16** and 1,8-diazabicyclo[5.4.0]undec-7-ene (DBU) **43**, the peralkylated phosphazene bases demonstrate a dramatic increase in basicity, of between 14.9 and 30.6 p*K*_{BH+} units, representing base strengths more commonly associated with inorganic bases such as *n*-butyllithium **44** (Table 7).⁵¹

In order to demonstrate enolate formation within a micro reactor, the synthesis of 2-benzylcyclohexanone **47** was selected as a model reaction (Scheme 6). As a means of identifying any advantages associated with the miniaturisation of this technique, the reaction was initially performed in batch. As Table 8 illustrates, despite the fact that 2-benzylcyclohexanone **47** was successfully synthesised

**Figure 10.** General structure of a series of peralkylated polyaminophosphazenes bases.**Table 7.** Comparison of base strength as a function of charge delocalization for a range of organic bases

Base	MeCN p <i>K</i> _{BH+}	Charge delocalisation
DBU 43	24.3	2
P ₁ - <i>t</i> -Bu	26.9	5
P ₂ - <i>t</i> -Bu 45	33.5	9
P ₃ - <i>t</i> -Bu	38.6	13
P ₄ - <i>t</i> -Bu 46	42.6	17

**Scheme 6.** Preparation of 2-benzylcyclohexanone **47** using P₂-*t*-Bu **45**.**Table 8.** Comparison of the proportion of by-product formed in batch and a micro reactor for the alkylation of cyclohexanone **49**

Base	Conversion ratio 47:48 ^a	
	Batch	Micro reaction
P ₂ - <i>t</i> -Bu 45	40.0:7.0	84.0:0.0
P ₄ - <i>t</i> -Bu 46	15.0:40.0	N/A

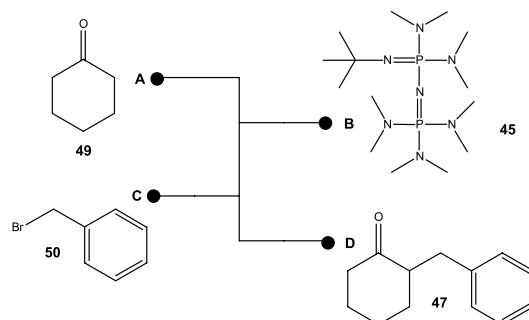
^a Remainder is unreacted starting material.

using both P₂-*t*-Bu **45** and P₄-*t*-Bu **46**, the reaction mixtures were found to contain appreciable amounts of the dialkylated product 2,2-dibenzylcyclohexanone **48**. With this in mind, we investigated the synthesis of 2-benzylcyclohexanone **47** in an EOF-based micro reactor.

Using anhydrous THF as the solvent system, cyclohexanone **49** (40 μl, 0.25 M) was placed in reservoir A, P₂-*t*-Bu **45** (40 μl, 0.25 M) in reservoir B and benzyl bromide **50** (40 μl, 0.25 M) in reservoir C (Fig. 11). The reagents were mobilised within the device using the following applied fields, 417, 455, 476 and 0 V cm⁻¹ and the reaction products collected in anhydrous THF (40 μl) at reservoir D. Analysis of the reaction products by GC–MS illustrated 84.0% conversion to product **47** (with respect to residual cyclohexanone **49**) demonstrating a significant increase in conversion compared to that obtained in batch (44.0%). The technique also proved advantageous as no dialkylation products **48** were detected when the reaction was performed in a micro reactor. This observation is attributed to the reduced reaction times employed in a micro reactor, i.e. the reaction mixture is removed from the reactor and quenched prior to the 2nd alkylation. The spatial control obtained within such a device therefore enabled by-product formation to be eliminated, enabling the synthesis of uncontaminated products.⁵²

In spite of the array of examples featured within the literature, chemists remain hesitant to employ phosphazene bases, in preparative scale reactions, due to their cost (typically £21 g⁻¹). To some extent, this has been addressed by the availability of polymer-supported derivatives, which enable their efficient separation and recovery from a reaction mixture.⁵³ Incorporation of these supported bases into a micro fabricated device (Section 2.4) would enable the continuous synthesis of base free reaction products coupled with enhanced reaction control.

In summary, using the synthesis of 2-benzylcyclohexanone **47** as a model reaction, we have demonstrated significant

**Figure 11.** Schematic of the reactor manifold used for the synthesis of 2-benzylcyclohexanone **47**.

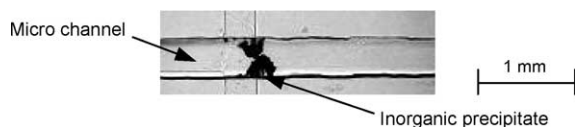


Figure 12. Optical microscope image of a blocked micro channel, caused by the precipitation of an inorganic base.

enhancements in conversion compared to batch, i.e. 84.0% cf. 40.0%, along with significantly enhancing product selectivity. In addition, the use of phosphazene bases enabled us to demonstrate the synthesis of previously inaccessible carbanions within an EOF-based micro reactor.

2.5.2. Inorganic bases. Although we have described numerous techniques for the preparation of enolates within a micro reaction environment, we are yet to discuss their preparation using inorganic bases. Again, the synthesis of 2-benzylcyclohexanone **47** was used as a model reaction for the investigation of the following bases; lithium bis(trimethylsilyl)amide **51**, sodium bis(trimethylsilyl)amide **52**, potassium bis(trimethylsilyl)amide **53**, sodium *tert*-butoxide **54**, potassium *tert*-butoxide **55**, lithium *tert*-butoxide **56**, lithium 2,2,6,6-tetramethylpiperidine **57**, lithium diisopropylamide **58**, lithium phenoxide **59**, sodium methoxide **60** and sodium ethoxide **61**.

Due to their inherent ionic nature, many reagents used in organic synthesis are largely insoluble in non-polar organic solvents. In this case, the relative insolubility of inorganic bases within solvents such as THF, DMF and MeCN (0.05–1.0 M) proved problematic, as blockage formation within the micro channels resulted in retardation of EOF (Fig. 12). These observations were initially surprising as Skelton et al.⁵⁴ had previously demonstrated the use of NaOMe **60** in MeOH, within an EOF-based device, for the synthesis of a range of stilbenes. The mobilisation of NaOMe **60** was inferred via the generation of a purple coloured intermediate (ylide) within the micro channel and the subsequent off-line detection of the respective stilbene ester. We however postulate that the base was successfully mobilised as a result of its enhanced solubility within the polar solvent system employed. Consequently, in order to further investigate the mobilisation of inorganic bases by EOF, a means of ensuring greater solubility was required.

2.5.3. Enhanced base solubility using crown ethers. In 1967, Pedersen et al.⁵⁵ demonstrated the complete dissolution of potassium permanganate in benzene by employing a stoichiometric quantity of the cyclic ether, 18-crown-6 **62**. A phenomenon that was later attributed to the separation of the metal ion from its associated ions, rendering the salt soluble in the non-polar media. With this in mind, we postulated that by solvating inorganic bases with their respective crown ether, increased solubility could be achieved; enabling their electro osmotic mobilisation in solvents such as THF. In order to evaluate this approach, we again used the preparation of 2-benzylcyclohexanone **47** in THF as a model reaction. As Figure 13 illustrates, a solution of cyclohexanone **49** and benzyl bromide **50** (40 μ l, 1:1) was placed in reservoir A and a solution of base and crown ether (40 μ l, 1:1) was placed in reservoir B. The reagents were manipulated within the device using 417, 455 and

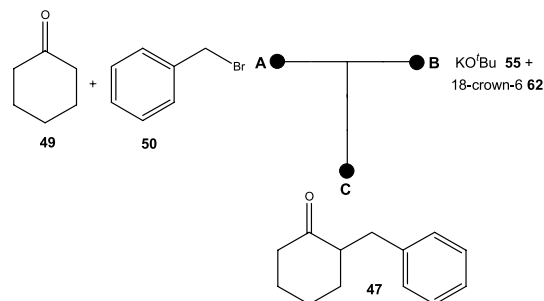


Figure 13. Typical reactor manifold used for the determination of inorganic base flow by EOF.

0 V cm⁻¹ and the reaction products collected in reservoir C. As the aim of the investigation was to rationalise the problems associated with the mobilisation of inorganic bases by EOF, at this stage, the detection of 2-benzylcyclohexanone **47** (and the respective crown ether) by GC–MS was considered indicative of base mobilisation. Consequently, conversions and optimised reaction conditions are not provided. In accordance with the literature, 18-crown-6 **62** was investigated for potassiated bases, 15-crown-6 **63** for sodiated bases and 12-crown-4 **64** for lithiated bases.⁵⁵

Using the aforementioned methodology, 0.5–1.0 M solutions of KHMDS **53**, NaO^tBu **54** and KO^tBu **55** were successfully mobilised by EOF. Extension of the technique to NaHMDS **52**, LiO^tBu **56** and LiHMDS **51** however, proved problematic as over the course of the micro reaction, the contents of reservoir B became turbid, resulting in the partial blockage of the micro channel; an observation attributed to decomposition of the base. In order to prevent base decomposition, the reagent reservoirs were covered with a series of PTFE bungs, as illustrated in Figure 14. Using this approach, reagent turbidity was prevented, enabling the successful mobilisation of NaHMDS **52** and LiO^tBu **56** by EOF.⁵⁶ In contrast, no electrokinetic flow was observed for LiHMDS **51**; with all solutions forming a gelatinous precipitate within the reagent reservoir and micro channel.

Due to the widespread application of the base sodium hydride **65**, its mobilisation by EOF was also investigated, however as NaH **65** is not strong enough to provide complete deprotonation of cyclohexanone **49**, the benzylation of phenol **66** was employed as a model reaction (Scheme 7). Using either anhydrous THF or MeCN as the solvent system, NaH **65** and 15-crown-5 **63** (40 μ l, 0.5 M) were placed in reservoir A, phenol **66** (40 μ l, 0.5 M) in reservoir B and benzyl bromide **50** (40 μ l, 0.5 M) in reservoir C (Fig. 15). The reagents were manipulated within the micro reactor using applied fields, 417, 455, 476 and

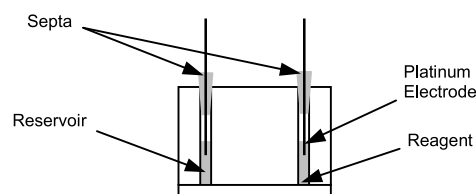
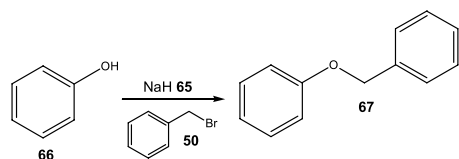


Figure 14. Schematic illustrating the reaction set-up used for moisture/air sensitive micro reactions.



Scheme 7. Synthesis of benzyloxybenzene **67** using NaH **65**.

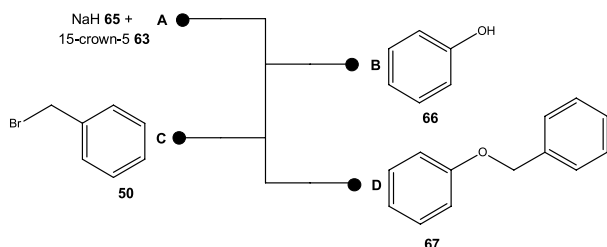


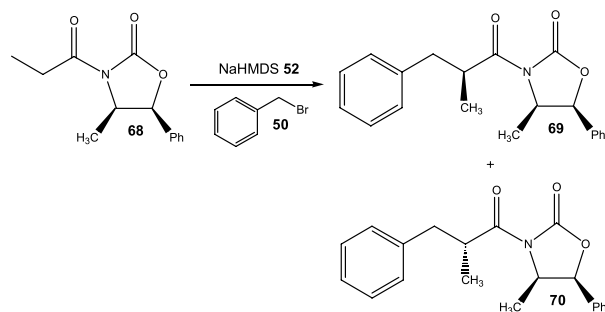
Figure 15. Schematic illustrating the reaction manifold used for the synthesis of benzyloxybenzene **67**.

0 V cm⁻¹ (500, 588, 769 and 0 V cm⁻¹ when employing MeCN) and the reaction products collected in reservoir D. The detection of benzyloxybenzene **67** and 15-crown-5 **63** was indicative of base mobilisation. In summary, as a result of increasing inorganic base solubility, by the addition of a stoichiometric quantity of crown ether, we have successfully demonstrated the electrokinetic mobilisation of six inorganic bases and their subsequent use for the synthesis of 2-benzylcyclohexanone **47** (Table 9).

2.6. Diastereoselective alkylation¹¹

The preparation of compounds with specific stereochemistry is of great interest to pharmaceutical companies as often one enantiomer exhibits biological activity whereas the other may be inactive or even harmful. With this in mind, one such approach for the synthesis of enantiomerically pure compounds is the use of chiral auxiliaries.⁵⁷

Based on initial observations by Skelton et al.,⁵⁴ where product stereoselectivity was found to be influenced as a result of synthesising a series of stilbene esters in a micro reactor, the effect on reaction diastereoselectivity was of interest. In order to investigate the factors that affect product diastereoselectivity, the reactions were initially performed in batch, enabling the preparation and characterisation of synthetic standards (Scheme 8). Using methodology established by Evans et al.⁵⁸ the enolate of 4-methyl-5-phenyl-3-propionyloxazolidinone **68** was alkylated, using



Scheme 8. Diastereoselective alkylation of 4-methyl-5-phenyl-3-propionyl oxazolidinone **68**.

benzyl bromide **50**, to afford diastereomers **69** and **70** in an overall yield of 68.0% and a ratio of 85:15 (**69**:**70**) (at -100 °C). Although Evans et al.⁶⁹ report greater diastereoselectivities, in practise they are difficult to reproduce. With this in mind, it was postulated that due to the excellent thermal and mass transportation properties observed within micro fluidic devices, product diastereoselectivity, and reaction reproducibility, could be improved as a result of conducting the reaction in a micro reactor.

Although many reactions have been demonstrated within micro reactors at temperatures ranging from 4 to 300 °C,⁵⁹ few authors with the exception of Yoshida⁶⁰ and Schwalbe,² report reactions performed at reduced temperatures. Using the following experimental procedure, the synthesis of diastereomers **69** and **70** was investigated within a pressure-driven system; a standard solution of NaHMDS **52** (0.5 M) in anhydrous THF was added from syringe A (50 μl min⁻¹), a solution of 4-methyl-5-phenyl-3-propionyloxazolidinone **68** (0.5 M) in anhydrous THF was added from syringe B (50 μl min⁻¹) and a solution of benzyl bromide **50** (0.5 M) from syringe C (50 μl min⁻¹). In order to maintain the reactor temperature, the device was submerged within a CO₂-ether bath and the reaction products collected at room temperature (Fig. 16). To ensure results obtained were representative of reactions occurring within the micro fabricated device, the reaction products were quenched upon collection. Using this approach, the chiral enolate was formed within the central micro channel and reacted with benzyl bromide in the microtee, to afford diastereomers **69** and **70** in 31.0% conversion and a ratio of 94:6 (**69**:**70**). In order to increase the conversion obtained, the flow rate was firstly reduced to 20 μl min⁻¹ and finally to 10 μl min⁻¹, resulting in an increase in conversion to 38.0% and 41.0% respectively. Most importantly however, the observed diastereoselectivity increased to from 94:6 to 99:1

Table 9. Mobilisation of inorganic base/crown ether complexes by EOF

Base	Crown ether	Applied field (V cm ⁻¹)	EOF
KO ^t Bu 55	18-Crown-6 62	417, 455 and 0	✓
KHMDS 53	18-Crown-6 62	417, 455 and 0	✓
NaO ^t Bu 54	15-Crown-5 63	417, 455 and 0	✓
NaHMDS 52	15-Crown-5 63	417, 455 and 0	✓
NaH 65	15-Crown-5 63	417, 455, 476 and 0	✓
NaH 65 ^a	15-Crown-5 63	500, 588, 769 and 0	✓
LiO ^t Bu 56	12-Crown-4 64	417, 455 and 0	✓
LiHMDS 51	12-Crown-4 64	417, 455 and 0	×

^a Performed in anhydrous MeCN.

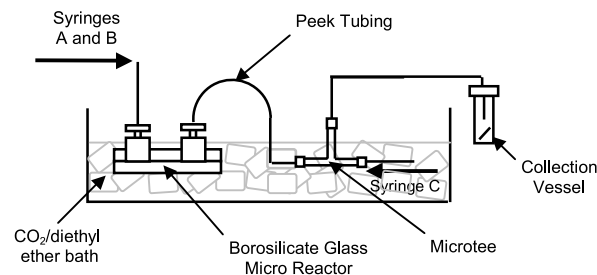


Figure 16. Schematic of the reaction set-up used for the evaluation of reduced temperature micro reactions.

Table 10. Effect of flow rate on product diastereoselectivity and conversion in a pressure-driven micro reactor

Flow Rate ($\mu\text{l min}^{-1}$)	Conversion (%)	Ratio (69:70)	Decomposition 71 (%)
50	31	94:6	0
20	38	99:1	0
10	41	99:1	0

(Table 10). Although these results represent initial observations and currently remain unoptimised, compared to traditional batch techniques the approach described is advantageous as no decomposition products, 3-benzyl-4-methyl-5-phenyloxazolidin-2-one **71** and 4-methyl-5-phenyloxazolidin-2-one **72**, were detected. We attribute this observation to the ability to accurately control both residence time and temperature of the reaction mixture within the micro fluidic device.

Consequently we propose that by either increasing the residence time within the device or reducing the reagent concentrations, that product conversion could be further increased. In summary, we have demonstrated a simple technique for the diastereoselective alkylation of a metal stabilised enolate, using a pressure-driven micro reactor at $-100\text{ }^{\circ}\text{C}$, whereby increased diastereoselectivity was observed compared to batch.

3. Conclusions

In order to demonstrate the application of micro reaction technology to chemical synthesis, the preparation and reaction of enolates was selected as it enabled a range of reactions to be investigated while maintaining a common element, i.e. deprotonation followed by nucleophilic substitution. Due to initial problems encountered with the mobilisation of inorganic bases by EOF, the use of preformed enolates, in the form of silyl enol ethers, was investigated. Using this approach, a series of tetra-*n*-butylammonium enolates were prepared using anhydrous TBAF **1** and subsequently reacted to afford 1,3-diketones, phenyl vinyl esters and β -hydroxyketones. The technique was subsequently extended to the use of organic bases whereby the Michael addition and alkylations were employed as model reactions. In addition, we demonstrated the synthesis of two carbanions using solid-supported organic bases and their subsequent reaction in the Knoevenagel condensation. Based on these observations, the use of inorganic bases was reinvestigated, this time enhancing base solubility by the addition of a stoichiometric quantity of crown ether, resulting in their successful electrokinetic mobilization. Inorganic bases were also successfully employed in a pressure-driven system demonstrating the diastereoselective alkylation of an Evans auxiliary derivative.

In conclusion, using the preparation and reaction of carbanions and enolates, we have demonstrated numerous advantages associated with micro reaction technology including; rapid reaction optimization, reduced reaction times, enhanced conversions, reduced by-product formation and the ability to generate reagents in-situ, whilst

demonstrating some of the challenges associated with performing organic synthesis within micro fabricated devices.

4. Experimental procedures

4.1. Materials and methods

All materials (analytical reagent grade) were obtained from commercial suppliers and unless otherwise stated were used without further purification. Sodium hydride **65** (60% dispersion in mineral oil) was washed free of any mineral oil using *n*-hexane, to afford the purified reagent as a pale grey solid. Column chromatography was performed using Kieselgel silica gel 60 (Fluka) as the solid support and compounds eluted using mixtures of ethyl acetate and *n*-hexane of varying polarity. Thin-layer chromatography was carried out using Kieselgel 60, HF₂₅₄ aluminium backed TLC plates (Merck), with mixtures of ethyl acetate and hexane as eluent. Visualisation was achieved using one of the following methods: exposure to short wave ultra violet light (λ 254 nm), or; development in an aqueous potassium permanganate (0.5%) and sodium carbonate (2.5%) solution, followed by heating with a hot air gun.

All NMR spectra were recorded as solutions in deuteriochloroform (CDCl_3) using tetramethylsilane (TMS) as an internal standard. The spectra were recorded on a Jeol GX400 spectrometer and the chemical shifts given in parts per million (ppm) with coupling constants in Hertz (Hz). The following abbreviations are used to report NMR data: s=singlet, d=doublet, t=triplet, q=quartet, dt=doublet of triplets, m=multiplet and C₀=quaternary carbon. Elemental analyses were performed using a Fisons Carlo Erba EA1108 CHN analyser. Infra-red spectra were recorded ($4000\text{--}600\text{ cm}^{-1}$) using a Perkin Elmer Paragon 1000 FT-IR spectrometer and peaks (ν_{max}) reported in wavenumbers (cm^{-1}). Gas-Chromatography–Mass Spectrometry (GC–MS) was performed using a Varian GC (CP-3800) coupled to a Varian MS (2000) with a CP-Sil 8 (30 m) column (Phenomenex) and ultra high purity helium (99.999%, Energas) carrier gas. Samples were analysed using one of the following methods. *Method A.* Injector temperature $200\text{ }^{\circ}\text{C}$, helium flow rate 1 ml min^{-1} , oven temperature $50\text{ }^{\circ}\text{C}$ for 4 min then ramped to $250\text{ }^{\circ}\text{C}$ at $30\text{ }^{\circ}\text{C min}^{-1}$, with a 3 min filament delay. *Method B.* Injector temperature $200\text{ }^{\circ}\text{C}$, helium flow rate 1 ml min^{-1} , oven temperature $50\text{ }^{\circ}\text{C}$ for 1 min then ramped to $250\text{ }^{\circ}\text{C}$ at $30\text{ }^{\circ}\text{C min}^{-1}$, with a 3 min filament delay. *Method C.* Injector temperature $250\text{ }^{\circ}\text{C}$, helium flow rate 1 ml min^{-1} , oven temperature $60\text{ }^{\circ}\text{C}$ for 1 min then ramped to $270\text{ }^{\circ}\text{C}$ at $35\text{ }^{\circ}\text{C min}^{-1}$, with a 3 min filament delay and. *Method D.* Injector temperature $250\text{ }^{\circ}\text{C}$, helium flow rate 1 ml min^{-1} , oven temperature $60\text{ }^{\circ}\text{C}$ for 1 min then ramped to $270\text{ }^{\circ}\text{C}$ at $20\text{ }^{\circ}\text{C min}^{-1}$, with a 3 min filament delay. All known compounds prepared had spectroscopic data consistent with the literature.

The electroosmotic micro reactions described herein were carried out using in-house fabricated borosilicate glass micro reactors with channel dimensions of $350\text{ }\mu\text{m}$ (wide) \times $53\text{ }\mu\text{m}$ (deep). In order to minimise the effect of pressure gradients within the micro channels, micro porous silica frits were placed within the channels.²⁹ To mobilise

reagents by EOF, platinum electrodes (0.5 mm o.d. × 2.5 cm) were placed within the reagent reservoirs and voltages applied using a Paragon 3B high voltage power supply (capable of applying 0–1000 V to four outputs) (Kingfield electronics, Sheffield, UK). Automation of the HVPS using an in-house LabVIEW™ program enabled complex sequences of voltages to be investigated. To enable the results obtained to be applied to devices of different dimensions, voltages are reported as applied fields (V cm^{-1}), i.e. voltage/channel length. Prior to commencing an electroosmotic micro reaction, the micro channels were filled with anhydrous solvent in order to remove air from the micro porous silica frits and to ensure a complete circuit is formed.

The pressure driven micro reactions were performed using a device purchased from Micro Chemical Systems Ltd (Hull, UK), which consisted of a two layer borosilicate glass device with ceramic fittings (Macor) located over each of the etched micro channels ($152 \mu\text{m}$ (wide) × $51 \mu\text{m}$ (deep)). PTFE tubing ($178 \mu\text{m}$ o.d. × 2.5 cm (Supelco)) was attached to the micro reactor using PEEK microtight fittings (Upchurch Scientific); subsequent attachment to a gas-tight syringe (Hamilton) resulted in a pressure tight connection. In order to employ three input solutions and a single output, a PEEK microtee (Upchurch scientific) was incorporated into the system. The magnitude of flow was controlled using two displacement pumps (MD-1001, Bioanalytical Systems Inc.) capable of delivering fluid at flow rates of $1\text{--}100 \mu\text{l min}^{-1}$. To monitor the progress of both EOF and pressure-driven micro reactions, experiments were conducted over a period of 20 min, after which the product reservoir was analysed by GC–MS, whereby comparison of the amount of residual starting material enabled the progression of the reaction to be determined.

4.2. Micro-scale methodology

4.2.1. Typical procedure for an electroosmotic micro reaction. After priming with THF, a standard solution of ‘anhydrous’ TBAF **1** ($40 \mu\text{l}$, 0.1 M) in anhydrous THF was placed in reservoir A, a solution of benzoyl cyanide **6** ($40 \mu\text{l}$, 1.0 M) in anhydrous THF was placed in reservoir B and a solution of trimethyl(1-phenylvinyl)oxy)silane **3** ($40 \mu\text{l}$, 1.0 M) in anhydrous THF was placed in reservoir C. The reaction products were manipulated within the device by applying an electric field to the platinum electrodes placed in each reservoir. In this case, the following applied fields were employed, 417, 318, 476 and 0 V cm^{-1} . The reaction products were collected in reservoir D, in anhydrous THF ($40 \mu\text{l}$), over a period of 20 min and analysed off-line by GC–MS. The progress of the reaction was subsequently determined by calculating the proportion of starting material converted to product (% conversion); 100% conversion to 1,3-diphenylpropane-1,3-dione **5** was observed in this case.

4.2.2. Electroosmotic flow regimes. *Flow Regime A:* Application of a constant applied field is referred to as continuous flow (unless otherwise stated this flow regime was employed); *Flow Regime B:* In this case, the field is applied for 2.5 s and no field for 5 s, the steps are subsequently cycled over a period of 20 min; *Flow Regime*

C: As for Flow Regime B, with an applied field for 5 s and no field for 10 s.

4.3. Batch reactions

4.3.1. ‘Anhydrous’ tetra-*n*-butylammonium fluoride **1.** Tetra-*n*-butylammonium fluoride trihydrate (TBAF· $3\text{H}_2\text{O}$) **73** was dried over phosphorus pentoxide under vacuum (10 mmHg) for 48 h to afford ‘anhydrous’ TBAF **1** as a gelatinous, colourless solid.

4.3.2. General procedure 1: synthesis of silyl enol ethers. The ketone in THF (2 ml per mmol) was added dropwise to a stirred solution of LiHMDS **51** (1.1 equiv) in THF (10 ml per mmol) over a period of 30 min at room temperature. The resulting solution was stirred for a further 15 min prior to the addition of chlorotrimethylsilane **74** (1.0 equiv) in THF (1 ml per mmol). In order to remove any residual inorganic material, the reaction mixture was concentrated in vacuo and the residue dissolved in DCM (5 ml per mmol). The reaction mixture was then filtered and the filtrate concentrated in vacuo to afford the silyl enol ether, which was stored at $-10 \text{ }^\circ\text{C}$ and used without further purification.

4.3.3. General procedure 2: acylation using acyl halides. The silyl enol ether in anhydrous THF (2 ml per mmol) was added dropwise to a stirred solution of ‘anhydrous’ TBAF **1** (0.1 equiv) and acyl halide (1.0 equiv) in anhydrous THF (10 ml per mmol) under N_2 , over a period of 30 min. After stirring for a further 30 min, the reaction mixture was concentrated in vacuo prior to the addition of dilute NaOH (50 ml, 0.1 M). The reaction products were extracted into ethyl acetate ($3 \times 50 \text{ ml}$) and the combined organic extracts were dried (MgSO_4), prior to concentrating in vacuo. The product was subsequently purified by silica gel chromatography.

4.3.4. General procedure 3: acylation of using acyl cyanides. The silyl enol ether in anhydrous THF (2 ml per mmol) was added dropwise to a stirred solution of ‘anhydrous’ TBAF **1** (0.1 equiv) and acyl cyanide (1.0 equiv) in anhydrous THF (10 ml per mmol) under N_2 , over a period of 30 min. After stirring overnight, the reaction mixture was concentrated in vacuo prior to the addition of dilute NaOH (50 ml, 0.1 M). The reaction products were extracted into ethyl acetate ($3 \times 50 \text{ ml}$) and the combined organic extracts were dried (MgSO_4), prior to concentrating in vacuo. The product was subsequently purified by silica gel chromatography.

4.3.5. General procedure 4: aldol reaction of silyl enol ethers. The silyl enol ether in anhydrous THF (2 ml per mmol) was added dropwise to a stirred solution of ‘anhydrous’ TBAF **1** (0.1 equiv) and 4-bromobenzaldehyde **12** (1.0 equiv) in anhydrous THF (10 ml per mmol) under N_2 , over a period of 30 min. After stirring overnight, the reaction mixture was concentrated in vacuo prior to the addition of distilled water (50 ml). The reaction products were extracted into ethyl acetate ($3 \times 50 \text{ ml}$) and the combined organic extracts were dried (MgSO_4), prior to concentrating in vacuo. The product was subsequently purified by silica gel chromatography.

4.3.6. General procedure 5: Michael addition. The 1,3-diketone in absolute EtOH (4 ml per mmol) was added to a stirred solution of Michael acceptor (1.0 equiv) and diisopropylethylamine **16** (2 equiv) in absolute EtOH (5 ml per mmol) and the reaction mixture stirred overnight. The reaction mixture was concentrated in vacuo and subsequently purified by silica gel chromatography to afford the respective product.

4.3.7. General procedure 6: Knoevenagel condensation. 3-(1-Piperazino)propyl-functionalised silica gel **26** (1.9 mmol N g⁻¹, 200–400 mesh) (0.10 g, 0.1 mmol) was added to a stirred solution of activated methylene (1.0 mmol) and aldehyde (1.0 mmol) in anhydrous MeCN (10 ml per mmol). After stirring overnight, the reaction mixture was filtered and the filtrate concentrated in vacuo to afford the respective condensation product.

4.3.8. Trimethyl(1-phenylvinyl)silane 3.⁸ The reaction was carried out in accordance with general procedure 1 using acetophenone **15** (0.50 g, 4.13 mmol), LiHMDS **51** (0.77 g, 4.58 mmol) and chlorotrimethylsilane **74** (0.39 ml, 4.13 mmol) to give trimethyl(1-phenylvinyl)silane **3** (0.79 g, 98.0%) as a pale yellow oil; GC–MS retention time (Method A) R_T = 8.55 min.

4.3.9. Benzoic acid 1-phenylvinyl ester 4.⁸ The reaction was carried out in accordance with general procedure 2 using trimethyl(1-phenylvinyl)silane **3** (0.10 g, 0.52 mmol), TBAF **1** (0.014 g, 0.05 mmol) and benzoyl fluoride **2** (0.06 ml, 0.52 mmol) to afford benzoic acid 1-phenylvinyl ester **4** (0.12 g, 99.0%) as a pale yellow oil; GC–MS retention time (Method A) R_T = 11.36 min.

4.3.10. 1,3-Diphenylpropane-1,3-dione 5.^{8,61} The reaction was carried out in accordance with general procedure 3 using trimethyl(1-phenylvinyl)silane **3** (0.10 g, 0.52 mmol), TBAF **1** (0.02 g, 0.05 mmol) and benzoyl cyanide **6** (0.07 g, 0.59 mmol) to afford 1,3-diphenylpropane-1,3-dione **5** (0.11 g, 98.0%) as a white solid; GC–MS retention time (Method A) R_T = 12.67 min.

4.3.11. Trimethyl(1-phenylpropenyloxy)silane 7.^{8,62} The reaction was carried out in accordance with general procedure 1 using propiophenone **75** (1.00 g, 7.48 mmol), LiHMDS **51** (1.37 g, 8.21 mmol) and chlorotrimethylsilane **74** (1.04 ml, 7.48 mmol) to give trimethyl(1-phenylpropenyloxy)silane **7** (1.47 g, 96.0%) as a pale yellow oil; GC–MS retention time (Method A) R_T = 8.92 min.

4.3.12. Cyclohex-1-enyloxy(trimethylsilane) 8.^{8,37} The reaction was carried out in accordance with general procedure 1 using cyclohexanone **49** (1.00 g, 10.20 mmol), LiHMDS **51** (1.88 g, 11.22 mmol) and chlorotrimethylsilane **74** (0.95 ml, 10.20 mmol) to afford cyclohex-1-enyloxy(trimethylsilane) **8** (1.60 g, 93.0%) as a pale yellow oil; GC–MS retention time (Method A) R_T = 7.40 min.

4.3.13. 2-Methyl-1,3-diphenylpropane-1,3-dione 9.^{8,61} The reaction was carried out in accordance with general procedure 2 using trimethyl(1-phenylpropenyloxy)silane **7** (0.10 g, 0.48 mmol), TBAF **1** (0.013 g, 0.05 mmol) and

benzoyl fluoride **2** (0.07 ml, 0.48 mmol) to afford 2-methyl-1,3-diphenylpropane-1,3-dione **9** (0.11 g, 96.0%) as a pale yellow oil; GC–MS retention time (Method A) R_T = 11.67 min.

4.3.14. 2-Benzoylcyclohexanone 10.^{8,63} The reaction was carried out in accordance with general procedure 2 using cyclohex-1-enyloxy(trimethylsilane) **6** (0.10 g, 0.59 mmol), TBAF **1** (0.0015 g, 0.06 mmol) and benzoyl fluoride **2** (0.06 ml, 0.59 mmol) to give 2-benzoylcyclohexanone **10** (0.12 g, 99.0%) as a white solid; GC–MS retention time (Method A) R_T = 11.20 min.

4.3.15. 2-Benzoylcyclohexanone 10.^{8,63} The reaction was carried out in accordance with general procedure 3 using cyclohex-1-enyloxy(trimethylsilane) **8** (0.10 g, 0.59 mmol), TBAF **1** (0.0015 g, 0.06 mmol) and benzoyl cyanide **6** (0.08 g, 0.59 mmol) to give 2-benzoylcyclohexanone **10** (0.11 g, 94.0%) as a white solid; GC–MS retention time (Method A) R_T = 11.20 min.

4.3.16. 3-(4-Bromophenyl)-3-hydroxy-1-phenylpropan-1-one 11.⁶⁴ The reaction was carried out in accordance with general procedure 4 using trimethyl(1-phenylvinyl)silane **3** (0.09 g, 0.48 mmol), TBAF **1** (0.013 g, 0.048 mmol) and 4-bromobenzaldehyde **12** (0.09 g, 0.48 mmol) to afford 3-(4-bromophenyl)-3-hydroxy-1-phenylpropan-1-one **11** (0.13 g, 87.0%) as a white crystalline solid; GC–MS retention time (Method A) R_T = 14.71 min.

4.3.17. 2-[(4-Bromophenyl)hydroxymethyl]cyclohexanone 13.⁶⁵ The reaction was carried out in accordance with general procedure 4 using cyclohex-1-enyloxy(trimethylsilane) **7** (0.11 g, 0.65 mmol) and 4-bromobenzaldehyde **12** (0.12 g, 0.65 mmol) to afford 2-[(bromophenyl)hydroxymethyl]cyclohexanone **13** (0.16 g, 94.0%) as a cream solid; δ_H 1.31 (1H, m, CH), 2.33 (1H, m, CH), 1.51 (1H, m, CH), 1.71 (1H, m, CH), 1.86 (3H, m, 3×CH), 2.08 (1H, m, CH), 2.33 (1H, m, CHOH), 7.69 (2H, d, J = 6.8 Hz, Ar) and 7.74 (2H, d, J = 6.8 Hz, Ar); δ_C 24.8 (CH₂), 27.0 (CH₂), 27.7 (CH₂), 30.7 (CH₂), 42.6 (CH), 67.9 (CHOH), 127.5 (2×CH), 128.6 (2×CH), 131.4 (C₀), 140.4 (C₀Br) and 191.1 (CO); 267 (M⁺ + 1, 15%), 266 (60), 264 (55) and 185 (100); GC–MS retention time (Method A) R_T = 12.45 min.

4.3.18. (E)-4-Acetyl-5-oxohex-2-enoic acid ethyl ester 17. The reaction was carried out in accordance with general procedure 5 using 2,4-pentanedione **18** (0.50 g, 5.00 mmol), diisopropylethylamine **16** (1.29 g, 10.00 mmol) and ethyl propiolate (0.49 g, 5.00 mmol). The reaction mixture was concentrated in vacuo and subsequently purified by silica gel chromatography. Elution with 7% ethyl acetate in hexane afforded (E)-4-acetyl-5-oxohex-2-enoic acid ethyl ester **17** (0.88 g, 89.0%) as a colourless oil. (Found C, 60.78; H, 7.25, C₁₀H₁₄O₄ requires C, 60.60; H, 7.12%); $\nu_{\max}/\text{cm}^{-1}$ 1667, 1703, 1740 and 2970; δ_H 1.34 (3H, t, J = 7.0 Hz, CH₂CH₃), 2.13 (6H, s, CH₃), 4.24 (2H, q, J = 7.0 Hz, CH₂CH₃), 4.24 (1H, J = 7.0 Hz, COCHCO), 5.74 (1H, d, J = 16.9 Hz, CH) and 7.39 (1H, d, J = 16.9 Hz, CH); δ_C 14.3 (2×CH₃), 18.5 (CH₂CH₃), 61.6 (CH₂CH₃), 61.8 (COCHCO), 125.4 (CH), 141.8 (CH), 165.4 (2×CO) and 203.5 (CO₂); 199 (M⁺ + 1, 15%), 198 (27), 181 (20), 153

(30), 124 (100) and 109 (20); GC–MS retention time (Method B) R_T = 10.21 min (trans).

4.3.19. (*E*)-4-Benzoyl-5-oxohex-2-enoic acid ethyl ester

21. The reaction was carried out in accordance with general procedure 5 using 1-phenylbutane-1,3-dione **20** (0.25 g, 1.54 mmol), ethyl propiolate **19** (0.15 g, 1.54 mmol) and diisopropylethylamine **16** (0.40 g, 3.00 mmol). The reaction mixture was concentrated in vacuo and subsequently purified by silica gel chromatography. Elution with 5% ethyl acetate in hexane afforded (*E*)-4-benzoyl-5-oxohex-2-enoic acid ethyl ester **21** (0.31 g, 77.0%) as a pale yellow oil. (Found C, 69.48; H, 6.42, $C_{15}H_{16}O_4$ requires C, 69.22; H, 6.20%); ν_{max}/cm^{-1} 1183, 1676, 1721 and 2929; δ_H 1.34 (3H, t, J = 7.3 Hz, CH_2CH_3), 1.96 (3H, s, CH_3), 4.23 (3H, m, CH_2CH_3 and $COCHCO$), 5.47 (1H, d, J = 16.8 Hz, CH), 7.69 (1H, d, J = 16.8 Hz, CH), 7.70 (1H, m, Ar), 7.80 (2H, m, Ar) and 7.93 (2H, m, Ar); δ_C 14.2 (CH_3), 19.1 (CH_2CH_3), 60.7 (CH_2CH_3), 96.7 ($COCCO$), 125.2 (CH), 128.6 ($2 \times CH$), 128.7 ($2 \times CH$), 129.7 (CH), 135.2 (C_0), 142.9 (CH), 165.5 (CO), 195.8 (CO) and 204.2 (CO_2); 261 ($M^+ + 1$, 10%), 260 (15), 181 (40) and 105 (100); GC–MS retention time (Method C) R_T = 12.45 min.

4.3.20. (*E*)-4-Ethoxycarbonylpent-2-enedioic acid ethyl ester

23. The reaction was carried out in accordance with general procedure 5 using diethyl malonate **22** (0.50 g, 3.10 mmol), ethyl propiolate **19** (0.30 g, 3.10 mmol) and diisopropylethylamine **16** (0.80 g, 6.20 mmol). The reaction mixture was concentrated in vacuo and subsequently purified by silica gel chromatography. Elution with 5% ethyl acetate in hexane afforded (*E*)-4-ethoxycarbonylpent-2-enedioic acid ethyl ester **23** (0.60 g, 82.5%) as a colourless oil; δ_H 1.29 (9H, t, J = 7.4 Hz, $3 \times CH_2CH_3$), 4.19–4.27 (7H, m, $3 \times CH_2CH_3$ and $COCHCO$), 5.88 (1H, d, J = 16.4 Hz, CH) and 7.28 (1H, d, J = 16.4 Hz, CH); δ_C 18.6 ($3 \times CH_2CH_3$), 61.5 ($3 \times CH_2CH_3$), 64.0 ($COCHCO$), 123.5 (CH), 143.0 (CH), 169.1 ($2 \times CO$) and 203.5 (CO_2); 259 ($M^+ + 1$, 5%), 258 (15), 257 (50), 255 (95), 227 (100), 212 (80), 182 (23), 167 (50), 109 (40) and 81 (15); GC–MS retention time (Method B) R_T = 10.85 min.

4.3.21. 3-Acetylheptane-2,6-dione

25. The reaction was carried out in accordance with general procedure 5 using 2,4-pentanedione **18** (0.50 g, 5.00 mmol), methyl vinyl ketone **24** (0.35 g, 5.00 mmol) and diisopropylethylamine **16** (1.29 g, 10.00 mmol). The reaction mixture was concentrated in vacuo and subsequently purified by silica gel chromatography. Elution with 10% ethyl acetate in hexane afforded 3-acetylheptane-2,6-dione **25** (0.77 g, 91.0%) as a colourless oil; δ_H 2.08 (2H, dt, J = 7.0, 7.0 Hz, CH_2), 2.10 (3H, s, CH_3), 2.20 (6H, s, CH_3), 2.46 (2H, t, J = 7.0 Hz, CH_2CO) and 3.39 (1H, t, J = 7.0 Hz, $COCHCO$); δ_C 29.3 ($2 \times CH_3$), 30.0 (CH_3), 37.9 (CH_2), 40.5 (CH_2CO), 66.9 ($COCHCO$), 204.2 ($2 \times CO$) and 207.1 (CO); 171 ($M^+ + 1$, 5%), 170 (1), 153 (15), 128 (25), 110 (20), 95 (40) and 43 (100); GC–MS retention time (Method B) R_T = 8.79 min.

4.3.22. 2-Cyano-3-phenyl-acrylic acid ethyl ester

29.⁶⁶ The reaction was carried out in accordance with general procedure 6 using benzaldehyde **27** (0.106 g, 1.00 mmol), ethyl cyanoacetate **28** (0.113 g, 1.00 mmol) and 3-(1-

piperazino)propyl functionalised silica gel (0.100 g, 0.10 mmol) to afford the product **29** (0.195 g, 97.0%) as a white crystalline solid; GC–MS retention time (Method C) R_T = 6.63 min.

4.3.23. 2-Benzylcyclohexanone

47.⁶⁷ Cyclohexanone **49** (0.50 g, 5.10 mmol) in THF was added dropwise to a stirred solution of KO^tBu **55** (0.63 g, 5.61 mmol) in THF (100 ml) over a period of 30 min to afford a yellow enolate solution. The reaction mixture was stirred for a further 15 min prior to the addition of benzyl bromide **50** (0.61 ml, 5.10 mmol). After stirring overnight, the reaction mixture was concentrated in vacuo and the residual oil dissolved in ethyl acetate (50 ml) and washed with distilled water (50 ml). The aqueous layer was further extracted using ethyl acetate (2×50 ml) and the combined organic extracts dried ($MgSO_4$) and concentrated in vacuo. Purification was achieved by silica gel chromatography, whereby elution with 2.5% ethyl acetate in hexane afforded 2-benzylcyclohexanone **47** (0.85 g, 89.0%) as a pale yellow oil; GC–MS retention time (Method C) R_T = 10.36 min.

4.3.24. 2,2-Dibenzylcyclohexanone

48.⁶⁸ Cyclohexanone **49** (0.25 g, 2.60 mmol) in THF (10 ml) was added dropwise to a stirred solution of KO^tBu **55** (0.63 g, 5.61 mmol) in THF (100 ml) over a period of 30 min to afford a yellow enolate solution. The reaction was stirred for a further 15 min prior to the addition of benzyl bromide **50** (0.61 ml, 5.10 mmol). After stirring overnight, the reaction mixture was concentrated in vacuo and the residual oil dissolved in ethyl acetate (50 ml) and washed with water (50 ml). The aqueous layer was further extracted using ethyl acetate (2×50 ml) and the combined organic extracts and the combined organic extracts dried ($MgSO_4$). Purification was achieved by silica gel chromatography, whereby elution with 20% ethyl acetate in hexane afforded 2,2-dibenzylcyclohexanone **48** (0.71 g, 85.0%) as a yellow oil; GC–MS retention time (Method A) R_T = 14.50 min.

4.3.25. Benzyloxybenzene

67.⁶⁹ NaH **65** (0.13 g, 5.33 mmol) in THF (10 ml) was added dropwise to a stirred solution of phenol **66** (0.50 g, 5.32 mmol) in THF (50 ml) and stirred for 5 min prior to the addition of benzyl bromide **50** (0.63 ml, 5.32 mmol). After stirring overnight, the reaction mixture was concentrated in vacuo and the residue diluted with DCM (50 ml) prior to washing with dilute sodium hydroxide (50 ml, 0.1 M). The aqueous layer was further extracted using DCM (2×50 ml) and the combined organic extracts dried ($MgSO_4$) and concentrated in vacuo. Purification was achieved by silica gel chromatography, whereby elution with 11% ethyl acetate in hexane afforded benzyloxybenzene **67** (0.70 g, 71.0%) as a pale yellow oil; GC–MS retention time (Method A) R_T = 10.14 min.

4.3.26. 4-Methyl-5-phenyloxazolidin-2-one

71.⁷⁰ Diphenyl carbonate **76** (10.60 g, 49.49 mmol), (1*S*, 2*R*) (+) norephedrine hydrochloride **77** (8.44 g, 44.97 mmol) and anhydrous potassium carbonate **78** (6.84 g, 49.49 mmol) were stirred at 100 °C for 6 h. The reaction mixture was subsequently cooled to 70 °C, methanol (100 ml) was added and the mixture heated to reflux for a further 30 min. The reaction mixture was concentrated in vacuo and subjected to an aqueous work up. The product was dissolved into DCM

(1 × 150 ml) and the organic layer washed with sodium hydroxide (2 × 150 ml, 1.0 M) and hydrochloric acid (2 × 150 ml, 1.0 M). The organic extract was subsequently dried (MgSO₄) and concentrated in vacuo to afford 4-methyl-5-phenyloxazolidin-2-one **71** (5.96 g, 75.0%) as an analytically pure light brown solid, which was used without further purification; GC–MS retention time (Method B) R_T = 8.54 min.

4.3.27. 4-Methyl-5-phenyl-3-propionyloxazolidin-2-one 68.⁷¹ *n*-Butyllithium **44** in hexane (4.97 ml, 2.5 M, 12.43 mmol) was added dropwise to a stirred solution of 4-methyl-5-phenyloxazolidin-2-one **71** (2.00 g, 11.30 mmol) in THF (50 ml) under N₂. The solution was maintained at –78 °C for 30 min prior to the addition of propionyl chloride **79** (1.96 ml, 22.47 mmol) and the reaction mixture warmed to room temperature and stirred overnight. The reaction mixture was concentrated in vacuo and subjected to an aqueous work up. The organic layer was neutralised using sodium hydrogen carbonate and the product extracted into DCM (3 × 50 ml), the combined organic extracts were dried (MgSO₄) and concentrated in vacuo. Purification of the residue by silica gel chromatography (9% ethyl acetate in hexane) afforded the title compound **68** (2.58 g, 98.0%) as a pale yellow gum; GC–MS retention time (Method B) R_T = 8.82 min.

4.3.28. (2′S,4R,5S)-2-(2′-methyl-3′-phenylpropionyl-4-methyl)-5-phenyloxazolidin-2-one 69.⁵⁸ NaHMDS **52** (2.63 ml, 1.0 M, 2.63 mmol) was added dropwise to a stirred solution of 4-methyl-5-phenyl-3-propionyloxazolidin-2-one **68** (0.50 g, 2.15 mmol) in THF (50 ml) under N₂ at –78 °C, the enolate was formed over a period of 20 min prior to the addition of benzyl bromide **50** (0.31 ml, 2.60 mmol). The reaction mixture was maintained at –78 °C for 40 min prior to quenching with distilled water (10 ml). The reaction mixture was concentrated in vacuo and subjected to an aqueous work up. The reaction products were extracted into DCM (4 × 50 ml), dried (MgSO₄) and concentrated in vacuo to afford a pale yellow oil. Purification was achieved by silica gel chromatography (10% ethyl acetate in hexane) to afford the diastereomer **69** (0.48 g, 59.0%) as a pale yellow oil; GC–MS retention time (Method B) R_T = 12.16 min.

4.4. Micro-scale reactions¹⁰

4.4.1. 2-Cyano-3-phenyl acrylic acid ester 29.⁶⁶ White solid (0.025 g, 98.9%); GC–MS retention time (Method C) R_T = 6.63 min.

4.4.2. 3-(4-Bromophenyl)-2-cyano acrylic acid ethyl ester 32.⁷² White solid (0.012 g, 99.5%); GC–MS retention time (Method D) R_T = 10.84 min.

4.4.3. 3-(3,5-Dimethoxyphenyl)-2-cyano acrylic acid ethyl ester 33.⁷³ White solid (0.011 g, 99.5%); δ_H 1.40 (3H, t, J = 7.0 Hz, CH₂CH₃), 3.85 (6H, s, 2 × OCH₃), 4.39 (2H, q, J = 7.0 Hz, CH₂CH₃), 6.65 (1H, m, Ar), 7.15 (2H, m, Ar) and 8.17 (1H, s, CH); δ_C 14.2 (CH₃), 55.7 (2 × OCH₃), 62.8 (CH₂), 103.4 (C₀CN), 106.2 (CH), 108.6 (2 × CH), 115.6 (CN), 133.1 (C₀), 155.2 (CH), 161.1 (2 × C₀) and 162.5 (CO); 262 (M⁺ + 1, 20%), 261 (100), 189 (55), 161

(25) and 77 (10); GC–MS retention time (Method C) R_T = 8.06 min.

4.4.4. 3-(4-Benzyloxyphenyl)-2-cyano acrylic acid ethyl ester 34. (0.021 g, 99.1%) as a cream solid (Found C, 74.51; H, 5.77; N 4.62, C₁₉H₁₇O₃N requires C, 74.25; H, 5.58; N, 4.56%); δ_H 1.39 (3H, t, J = 7.3 Hz, CH₂CH₃), 4.37 (2H, q, J = 7.3 Hz, CH₂CH₃), 5.15, (2H, s, CH₂), 7.00 (2H, d, J = 8.7 Hz, Ar), 7.40 (5H, m, Ar), 7.99 (2H, d, J = 8.7 Hz, Ar) and 8.17 (1H, s, CH); δ_C 14.2 (CH₃), 62.5 (CH₂), 70.4 (C₀CN), 77.8 (CH₂O), 99.5 (C₀), 115.6 (2 × CH), 124.6 (CN), 127.5 (2 × CH), 128.4 (CH), 128.8 (2 × CH), 133.7 (2 × CH), 135.8 (C₀), 154.4, (CH), 162.9 (OC₀) and 163.1 (CO); 308 (M⁺ + 1, 5%), 307 (20), 91 (100) and 65 (20); GC–MS retention time (Method D) R_T = 12.35 min.

4.4.5. 2-Benzylidene-malononitrile 36.⁶⁶ Pale yellow solid (0.015 g, 100%); GC–MS retention time (Method C) R_T = 5.84 min.

4.4.6. 2-(4-Bromobenzylidene)-malononitrile 37.⁷⁴ Pale yellow solid (0.035 g, 99.9%); GC–MS retention time (Method D) R_T = 9.65 min.

4.4.7. 2-(3,5-Dimethoxybenzylidene)-malononitrile 38.⁶⁶ Yellow solid (0.024 g, 99.2%); GC–MS retention time (Method C) R_T = 7.50 min.

4.4.8. 2-(4-Benzyloxybenzylidene)-malononitrile 39.⁷⁵ Pale yellow solid (0.024 g, 99.6%); GC–MS retention time (Method D) R_T = 11.97 min.

Acknowledgements

We wish to thank Novartis Pharmaceuticals (P.W. and C.W.) and the EPSRC (C.W.) (Grant No. GR/S34106/01) for financial support. We are grateful to Dr. Tom McCreedy and Mr. Mike Bailey (The University of Hull) for help in fabricating the micro reactor devices.

References and notes

- Gisin, M.; Thommen, C. *Anal. Chim. Acta* **1986**, *190*, 165–176.
- Schwalbe, T.; Volker, A.; Wille, G. *Chimia* **2002**, *56*, 636–646.
- Jahnisch, K.; Hessel, V.; Löwe, H.; Baerns, M. *Angew. Chem., Int. Ed.* **2004**, *43*, 406–446.
- Fletcher, P. D. I.; Haswell, S. J.; Pombo-Villar, E.; Warrington, B. H.; Watts, P.; Wong, S. Y. F.; Zhang, X. *Tetrahedron* **2002**, *58*, 4735–4757.
- Watts, P.; Haswell, S. J. *Chem. Soc. Rev.* **2005**, *34*, 235–246.
- Wiles, C.; Watts, P.; Haswell, S. J.; Pombo-Villar, E. *Lab Chip* **2002**, *2*, 62–64.
- Wiles, C.; Watts, P.; Haswell, S. J.; Pombo-Villar, E. *Chem. Commun.* **2002**, 1034–1035.
- Wiles, C.; Watts, P.; Haswell, S. J.; Pombo-Villar, E. *Tetrahedron Lett.* **2002**, *43*, 2945–2948.

9. Wiles, C.; Watts, P.; Haswell, S. J.; Pombo-Villar, E. *Lab Chip* **2001**, *1*, 100–101.
10. Wiles, C.; Watts, P.; Haswell, S. J.; Pombo-Villar, E. *Tetrahedron* **2004**, *60*, 8421–8427.
11. Wiles, C.; Watts, P.; Haswell, S. J.; Pombo-Villar, E. *Lab Chip* **2004**, *4*, 171–173.
12. Ehrfeld, W.; Hessel, V.; Löwe, H. *Microreactors: New Technology for Modern Chemistry*; Wiley-VCH: New York, 2000.
13. McCreedy, T. *Anal. Chim. Acta* **2001**, *427*, 39–43.
14. (a) Reyes, D. R.; Iossifidis, D.; Auroux, P. A.; Manz, A. *Anal. Chem.* **2002**, *74*, 2626–2636. (b) Reyes, D. R.; Iossifidis, D.; Auroux, P. A.; Manz, A. *Anal. Chem.* **2002**, *74*, 2637–2652. (c) Woias, P. In *Microfluidics and BioMEMS*, Mastrangelo, C. H.; Becker, H., Eds. SPIE Conference Proceedings 2001, **2001**, 4560, 39.
15. Manz, A.; Fettingner, J. C.; Ludi, H.; Widmer, H. M.; Harrison, J. D. *Trends Anal. Chem.* **1991**, *10*, 144–149.
16. Dasgupta, P. K.; Lui, S. *Anal. Chem.* **1994**, *66*, 1792–1798.
17. Seller, K.; Fan, Z. H.; Fluri, K.; Harrison, D. J. *Anal. Chem.* **1994**, *66*, 3485–3491.
18. Manz, A.; Effenhauser, C. S.; Buggraf, N.; Harrison, J. D.; Seiler, K.; Fluri, K. *J. Micromech. Microeng.* **1994**, *4*, 257.
19. Boer, G.; Dodge, A.; Fluri, K.; van der Schoot, H.; Verpoorte, E.; de Rooij, N. F. In *Micro Total Analysis Systems*; Ramsey, J. M., van den Berg, A., Eds.; Kluwer: Dordrecht, 1998; pp 53–56.
20. Christensen, P. D.; Johnson, S. W. P.; McCreedy, T.; Skelton, V.; Wilson, N. G. *Anal. Commun.* **1998**, *35*, 341–342.
21. Zeng, S.; Chen, C.; Mikkelsen, J. C., Jr.; Santiago, J. G. *Sens. Actuators, B* **2001**, *79*, 107–114.
22. Fletcher, P. D. I.; Haswell, S. J.; Zhang, X. *Lab Chip* **2002**, *2*, 102–112.
23. Rice, C. L.; Whitehead, R. *J. Phys. Chem.* **1965**, *69*, 4017–4024.
24. Haswell, S. J.; Middleton, R. J.; O'Sullivan, B.; Skelton, V.; Watts, P.; Styring, P. *J. Chem. Soc., Chem. Commun.* **2001**, 391–398.
25. Snyder, L. R. *J. Chromatogr. A* **1974**, *92*, 223–230.
26. Smits, J. G. *Sens. Actuators, A* **1990**, *21*, 203–206.
27. Makino, E.; Mitsuya, T.; Shibata, T. *Sens. Actuators, A* **2001**, *88*, 256–262.
28. Shoji, S.; Nakagakawa, S.; Esashi, M. *Sens. Actuators, B* **1990**, *21*, 189–192.
29. (a) Bings, N. H.; Wang, C.; Skinner, C. D.; Colyer, C. L.; Thibault, P.; Harrison, D. J. *Anal. Chem.* **1999**, *71*, 3292–3296. (b) Nittis, V.; Fortt, R.; Legge, C. H.; de Mello, A. J. *Lab Chip* **2001**, *1*, 148–152. (c) Gray, B. L.; Collins, S. D.; Smith, R. L. In *Micro total analysis systems*, Ramsey, J. M., van den Berg, A., Eds. Kluwer: Enschede, 2001; Vol. 1, pp 153–158.
30. Kikuntani, Y.; Hibara, A.; Uchiyama, K.; Hisamoto, H.; Tokeshi, M.; Kitamori, T. *Lab Chip* **2002**, *2*, 193–196.
31. House, H.; Auerbach, R. A.; Gall, M.; Peet, P. *J. Org. Chem.* **1972**, *38*, 514–522.
32. Deitch, J.; Rathke, M. W. *Tetrahedron Lett.* **1971**, *12*, 2953–2956.
33. Rathke, M. W.; Tirpak, R. E. *J. Org. Chem.* **1982**, *47*, 5099–5102.
34. (a) Kuwajima, I.; Nakamura, E. *Acc. Chem. Res.* **1985**, *18*, 181–187. (b) Kuwajima, I.; Nakamura, E.; Hashimoto, K. *Org. Synth.* **1982**, *61*, 122–128.
35. Noyori, R.; Yokoyama, K.; Sakata, J.; Kuwajima, I.; Nakamura, E.; Shimizu, M. *J. Am. Chem. Soc.* **1977**, *97*, 1265–1266.
36. Howard, A. S.; Meerholz, C. A.; Michael, J. P. *Tetrahedron Lett.* **1979**, *15*, 1339–1340.
37. House, H. O.; Czuba, L. J.; Gall, M.; Olmstead, H. D. *J. Org. Chem.* **1969**, *34*, 2324–2336.
38. Veysoglu, T.; Mitscher, L. A. *Tetrahedron Lett.* **1981**, *22*, 1299–1302.
39. Morita, T.; Okamoto, Y.; Sakurai, H. *Tetrahedron Lett.* **1980**, *21*, 835–838.
40. Kita, Y.; Haruta, J.; Segawa, J.; Tamura, Y. *Tetrahedron Lett.* **1979**, *20*, 4311–4314.
41. Nakamura, E.; Murofushi, T.; Shimizu, M.; Kuwajima, I. *J. Am. Chem. Soc.* **1976**, *98*, 2346–2348.
42. LeBel, N. A.; Cherluck, R. M.; Curtius, E. A. *Synthesis* **1973**, 678–679.
43. Cooke, M. P., Jr.; Pollock, C. M. *J. Org. Chem.* **1993**, *58*, 7474–7481.
44. Picquet, M.; Bruneau, C.; Dixneuf, P. H. *Tetrahedron* **1999**, *55*, 3937–3948.
45. Oediger, H.; Moller, F.; Eiter, K. *Synthesis* **1972**, 591–598.
46. Flynn, K. G.; Nenortas, D. R. *J. Org. Chem.* **1963**, *28*, 3527–3530.
47. Barton, D. H. R.; Elliot, J. D.; Gero, S. D. *J. Chem. Soc., Perkin Trans. 1* **1982**, 2085–2090.
48. Schwesinger, R.; Willaredt, J.; Schlemper, H.; Keller, M.; Schmidt, D.; Fritz, H. *Chem. Ber.* **1994**, *127*, 2435–2454.
49. Schwesinger, R.; Schlemper, H.; Hasenfrazt, C.; Willaredt, J.; Dambacher, T.; Breuer, T.; Ottaway, C.; Fletschinger, M.; Boele, J.; Fritz, H.; Putzas, D.; Roter, H. W.; Bordwell, F. G.; Satish, A. V.; Ji, J.; Peters, E.; Peters, K.; von Schnering, H. G.; Walz, L. *Liebigs Ann. Chem.* **1996**, 1055–1081.
50. Schwesinger, R.; Hasenfrazt, C.; Schlemper, H.; Walz, E.; Peters, E.; Peters, K.; von Schnering, H. G. *Angew. Chem., Int. Ed. Engl.* **1993**, *32*, 1361–1363.
51. Schwesinger, R. *Angew. Chem., Int. Ed. Engl.* **1987**, *26*, 1164–1167.
52. In addition, we investigated the manipulation of a stronger phosphazene derivative, P₄-t-Bu **46** (0.25 M in anhydrous THF), by EOF. Application of 417 V cm⁻¹, resulted in the successful mobilisation of the reagent at a flow rate of 0.15 μl min⁻¹. Analysis of the product reservoir by TLC confirmed the successful transfer of P₄-t-Bu **46** from reservoir B–D.
53. O'Donnell, M. J.; Zhou, C.; Scott, W. L. *J. Am. Chem. Soc.* **1996**, *118*, 6070–6071.
54. (a) Skelton, V. *An Investigation of Synthetic and Combinatorial Reactions in Miniaturised Devices*. PhD Thesis, The University of Hull, **2000**, 114. (b) Skelton, V.; Greenway, G. M.; Haswell, S. J.; Styring, P.; Morgan, D. O.; Warrington, B. H.; Wong, S. Y. F. *Analyst* **2001**, *126*, 7–10. (c) Skelton, V.; Greenway, G. M.; Haswell, S. J.; Styring, P.; Morgan, D. O.; Warrington, B. H.; Wong, S. Y. F. *Analyst* **2001**, *126*, 11–13.
55. Pederson, C. J. *J. Am. Chem. Soc.* **1967**, *89*, 7017–7036.
56. Alternatively micro-scale reactions could be performed in an inert atmosphere, i.e. glove-box purged with N₂.
57. Evans, D. A.; Bartroli, J.; Shih, T. L. *J. Am. Chem. Soc.* **1981**, *103*, 2127–2129.
58. Evans, D. A.; Ennis, M. D.; Mathre, D. J. *J. Am. Chem. Soc.* **1982**, *104*, 1737–1739.
59. Ehrfeld, W.; Hessel, V.; Löwe, H. *Microreactors: New Technology for Modern Chemistry*; Wiley-VCH: New York, 2000.
60. Suga, S.; Okajima, M.; Fujiwara, K.; Yoshida, J. *J. Am. Chem. Soc.* **2001**, *123*, 7941–7942.

61. Barluenga, J.; Jardon, J.; Gotor, V. *J. Org. Chem.* **1985**, *50*, 802–804.
62. Heathcock, C. H.; Buse, C. T.; Kieschick, W. A.; Pirrung, M. C.; Sohn, J. E.; Lampe, J. *J. Org. Chem.* **1980**, *45*, 1066–1081.
63. Hermanson, J. R.; Gunther, M. L.; Michael, I.; Belletine, J. L.; Pinhas, A. R. *J. Org. Chem.* **1995**, *60*, 1900–1903.
64. Marx, A.; Yamamoto, H. *Angew. Chem., Int. Ed.* **2000**, *39*, 178–182.
65. Huitric, A. C.; Kumler, W. D. *J. Am. Chem. Soc.* **1956**, *78*, 1147–1151.
66. Choudray, B. M.; Lakshmi-Kantam, M.; Kavita, B.; Venkat Reddy, C.; Figueras, F. *Tetrahedron* **2000**, *56*, 9357–9364.
67. House, H. O.; Gall, M.; Holmstead, H. D. *J. Org. Chem.* **1971**, *36*, 2361–2371.
68. Bates, R. B.; Taylor, S. R. *J. Org. Chem.* **1993**, *58*, 4469–4470.
69. Forrester, J.; Ray, R. V. H.; Newton, L.; Preston, N. P. *Tetrahedron* **2001**, *57*, 2871–2884.
70. Evans, D. A.; Matre, D. J. *J. Org. Chem.* **1985**, *50*, 1830–1835.
71. Pettit, G. R.; Burkett, D. D.; Barkoczy, J.; Breneman, G. L.; Pettit, W. E. *Synthesis* **1996**, 719–725.
72. Shen, Y.; Yang, B. *Synth. Commun.* **1989**, 3069–3072.
73. Arya, V. P.; Ghate, S. P. *Indian J. Chem.* **1971**, *9*, 1209–1212.
74. Obrador, E.; Castro, M.; Tamariz, J.; Zepeda, G.; Miranda, R. *Synth. Commun.* **1998**, 4649–4664.
75. Cornelis, A.; Lambert, S.; Laszlo, P. *J. Org. Chem.* **1977**, *42*, 381–382.

DOI: 10.1002/anie.200600951

Self-Supported and Clean One-Step Cathodic Coupling of Activated Olefins with Benzyl Bromide Derivatives in a Micro Flow Reactor**

Ping He, Paul Watts, Frank Marken, and Stephen J. Haswell*

Electrosynthesis offers a clean and versatile method for the generation of anion and cation radical intermediates.^[1] The addition of electrons to, or the removal of electrons from, neutral organic substrates can be achieved under relatively mild reaction conditions and may lead to powerful electro-synthetic strategies. A possible role of electro-synthesis in “green chemistry” has been highlighted by several authors,^[2] particularly in combination with the recently emerging microreactor technology.^[3a–c] Microreactors have numerous practical advantages including safe operating, easy modulation, and easy scale-up for industrial production when compared with batch reactors.^[3d,e] The combination of electro-synthesis with microreactors has made electrochemistry more accessible even in the absence of electrolyte.^[4]

In synthetic chemistry, C–C-bond-formation processes are of considerable importance and new methods are constantly sought with the aim of obtaining clean, simple, and efficient synthetic routes. Herein, we describe a C–C-bond-formation method based on the electro-reductive coupling of activated olefins and benzyl bromide derivatives. The coupling products such as 2-benzyl succinic acid dimethyl ester are important classes of compounds owing to their utility as intermediates in the synthesis of important targets such as natural antibiotics,^[5a] pyrrolidines,^[5b] metalloproteinase inhibitors,^[5c] inhibitors towards human leukocytes,^[5d] cephalotaxine,^[5e] and monoesters of alkylated succinic acids.^[5f] Several methods have been reported^[5b,g,h] for this class of compounds, most of which involve multi-step processes and require the presence of metal catalysts. Alternatively, a photochemical procedure based on electron transfer to a photo-sensitizer has been proposed for the coupling of methylbenzene and dimethylsuccinate,^[5i] but the method resulted in a complex mixture of reaction products. In contrast, the process described herein is based on a clean one-step cathodic coupling process carried out under micro-

reactor flow through conditions to generate higher yields of products when compared with conventional synthetic methods. Considerable benefits of the novel electrochemical process are 1) simple operation, 2) no need for chemical reagents or electrolytes, 3) simple work-up, and 4) a surprisingly high yield.

Initially, the coupling of dimethyl fumarate with benzyl bromide was selected for study by cyclic voltammetry experiments. Both dimethyl fumarate and dimethyl maleate are known to be reduced in one-electron processes, both leading to the dimethyl fumarate radical anions as the intermediate followed by slow hydrodimerization.^[6] The reduction of benzyl bromide is usually found to be chemically irreversible leading to the formation of dibenzyl products. The one-electron reduction of benzyl bromide proceeds through the benzyl radical intermediate. The two-electron reduction of benzyl bromide to give a benzyl carbanion may occur at sufficiently negative potentials, at mercury pool electrodes,^[7] or in the presence of electrophilic reagents such as protons. Figure 1 A shows typical (conventional) cyclic voltammograms for the reduction of benzyl bromide (curve a), dimethyl fumarate (curve b), and dimethyl fumarate in the presence of benzyl bromide (curve c). The reduction of dimethyl fumarate occurs as a reversible one-electron process. In the presence of benzyl bromide, the peak current of the reduction wave for dimethyl fumarate remains and the re-oxidation wave after reversal of the scan direction completely disappears. A complete loss of the anodic peak reveals a rapid chemical reaction of the dimethyl fumarate radical anion with benzyl bromide. From the peak current in Figure 1 A (and based on additional microelectrode experiments, see Supporting Information), the process can be identified as a one-electron process. As will be shown below, on a longer time scale during the course of electrolysis, transfer of a second electron occurs and is attributed to a further unidentified processes.

During the main electrode reaction, the interaction of the primary fumarate radical anion and benzyl bromide is believed to lead to rapid C–C coupling. The coupling, followed by loss of bromide, occurs only if a sufficient driving force for this process is available. The parameter ΔE ($E_{1/2,df} - E_{1/2,bb}$) describes the potential difference for the reduction of the dimethyl fumarate (df) and for benzyl bromide (bb) and is obtained here as an approximate measure of the energy balance in the intermolecular electron transfer. If ΔE becomes too high, the energy for the C–Br bond heterolysis will be insufficient.

Preparative microreactor electrolyses were conducted in a flow cell (see Figure 2) to isolate and identify products by using GC/MS as well as ¹H and ¹³C NMR spectroscopy and to optimize yields for the coupling of dimethyl fumarate (or dimethyl maleate) with benzyl bromide. The solution containing 5 mM dimethyl fumarate (or dimethyl maleate) and 5 mM benzyl bromide in DMF (*N,N*-dimethylformamide) was continuously pumped through the cell in which two platinum electrodes with a working area of 45 mm² were positioned with an inter-electrode gap of 160 μ m or 320 μ m. The coupling reactions were conducted galvanostatically and product samples were collected in a product vial for 5 min. Table 1 summarizes the conversion and product distribution for the

[*] Dr. P. He, Dr. P. Watts, Prof. S. J. Haswell
Department of Chemistry
University of Hull, Hull, HU6 7RX (UK)
Fax: (+44) 148-246-6416
E-mail: s.j.haswell@hull.ac.uk

Dr. F. Marken
Department of Chemistry
University of Bath, Bath, BA2 7AY (UK)

[**] We thank the EPSRC for funding.

Supporting information for this article is available on the WWW under <http://www.angewandte.org> or from the author.

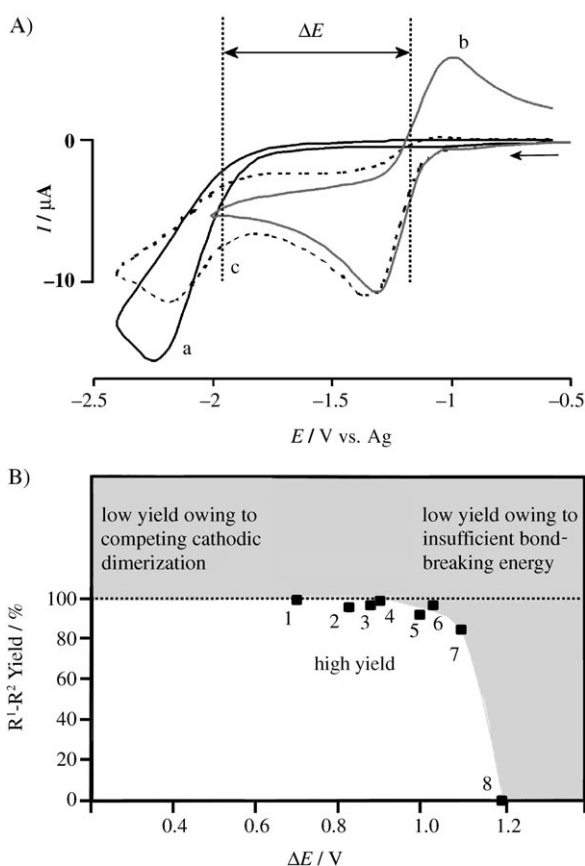


Figure 1. A) Cyclic voltammograms (scan rate 10 V s^{-1}) obtained at a platinum disc electrode (diameter 0.5 mm) immersed in $0.1 \text{ M } n\text{Bu}_4\text{NBF}_4/\text{DMF}$ for: a) 3 mM benzyl bromide, b) 3 mM dimethyl fumarate, and c) 3 mM dimethyl fumarate in the presence of 3 mM benzyl bromide. The parameter ΔE when compared to the energy for heterolytic C–Br bond fission allows the driving force for the reaction to be assessed (see text). B) Plot of the yield of the $\text{R}^1\text{--R}^2$ coupling product (see Table 1) versus the gap in halfwave potential for: 1) dimethyl fumarate/benzyl bromide, 2) dimethyl fumarate/4-bromobenzyl bromide, 3) dimethyl fumarate/1-phenylethylbenzyl bromide, 4) fumaronitrile/benzyl bromide, 5) dimethyl fumarate/4-methoxybenzyl bromide, 6) fumaronitrile/4-bromobenzyl bromide, 7) maleic anhydride/bisbromomethylbenzene, 8) maleic anhydride/benzyl bromide.

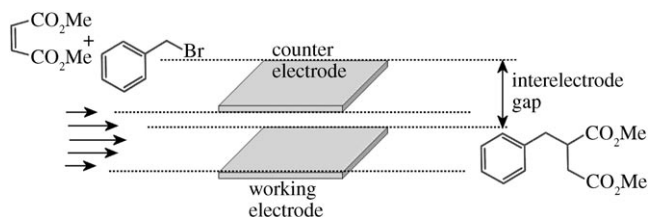


Figure 2. Schematic representation of the C–C coupling reaction during electrosynthesis in a microreactor. A flow of reagents through a rectangular duct with the working and counter electrodes facing each other results in the formation of products.

range of conditions employed in this study. Both conversion and product distribution are strongly dependent on the electrode gap, the flow rate, and the applied current. For a $320\text{-}\mu\text{m}$ inter-electrode gap (Table 1, entries 1 and 2), 47%

and 77% conversion to the desired coupling product can be achieved with significant homo-coupling side products. An increase in current was found to enhance only homo-dimerization of the olefin or benzyl bromide. For an inter-electrode gap of $160 \mu\text{m}$ (Table 1, entries 3–7), relatively lower voltages ($4\text{--}4.4 \text{ V}$) were required to obtain sufficiently high levels of conversion ($>95\%$). Interestingly, unwanted dimerization of olefins was found to be less than 2% plus a very small amount of toluene (from debromination of benzyl bromide) and no dimerization of benzyl bromide was detected. The best result obtained was 98% of 2-benzyl dimethylsuccinate with only 2% of the homo-dimer tetramethyl butanetetracarboxylate and toluene at a flow rate of 10 or $15 \mu\text{L min}^{-1}$ (Table 1, entries 5 and 6, respectively). At higher flow rates, the possibility of homo-dimerization of the olefin was observed (Table 1, entry 7).

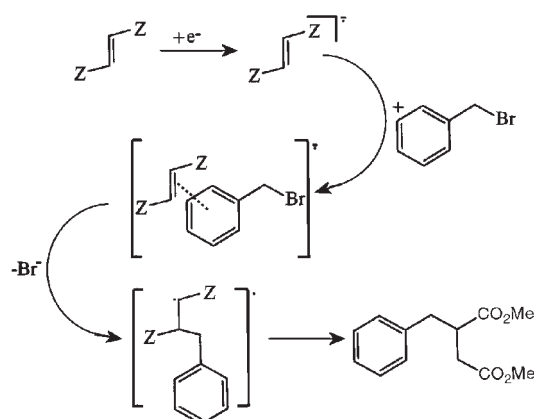
This electrochemical procedure was also scaled up in a “parallel” microreactor cell containing two equally sized sets of electrodes. Again, dimethyl fumarate was completely converted to give the cross-coupling product 2-benzyl dimethylsuccinate with only 2% of olefin dimer and toluene. In this case, a volumetric flow rate equivalent to $30 \mu\text{L min}^{-1}$ (i.e. $15 \mu\text{L min}^{-1} \times 2$ flow cells) was achieved, which is double the flow rate of the single cell and hence producing twice the quantity of the product in a given time. Other benzyl bromide derivatives such as 4-methoxybenzyl bromide, 4-methylbenzyl bromide, 4-bromobenzyl bromide, 4-iodobenzyl bromide, and 1-phenylethyl bromide were also examined for coupling reactions with dimethyl fumarate using the same microreactor as that used in entry 3 in Table 1. All preparative electrolyses gave excellent yields (94%) of cross-coupling products with very small amount of olefin dimer and debrominated products (Table 1, entries 8–12). The formation of bromine due to oxidation of bromide was not observed presumably owing to the limited overlap of diffusion layers within the flow cell. Current efficiencies for all processes are typically 40–50%. These data suggest that overall two moles of electrons are consumed for each mole of product formed by electrolysis. Cyclic voltammetry data (short time scale) do not show evidence for the transfer of the second electron. However, the time scale for the electrolysis process is different and the second electron transfer may occur in the later stages of the process, for example, involving solvent.

From the results obtained, it can be seen that the presence of benzyl bromide suppresses olefin hydrodimerization, indicating that the reaction between olefin radical anion and benzyl bromide is fast. The neutral benzyl radical intermediate,^[4d] which is short-lived^[8] and known to either dimerize (to give bibenzyl) or to abstract a hydrogen atom to produce toluene,^[9] appears to be an unlikely free intermediate. The absence of bibenzyl and only a small amount of toluene indicate fast direct coupling of the dimethyl fumarate radical anion with benzyl bromide. Scheme 1 describes a plausible reaction pathway. The mild conditions employed during electrolysis are consistent with a one-electron pathway, and a related transition metal complex mediated reduction of benzyl bromide also has been shown to proceed through a one-electron pathway.^[10] However, in this particular study it is not clear whether the final step proceeds through a second-

Table 1: Data for the preparative electrolysis of activated olefins in the presence of benzyl bromides in a micro flow cell without intentionally added supporting electrolyte.^[a]

No.	<i>I</i> [mA]	Olefin R ¹	R ² -Br R ²	Flow [μL min ⁻¹]	Conv. [%] ^[b]	Distribution [%] R ¹ -R ² others ^[c]	
1	0.6	dimethyl maleate	benzyl	20	47	89	11
2	1.5	dimethyl maleate	benzyl	20	77	70	30
3	0.6	dimethyl maleate	benzyl	10	100	98	2
4	0.6	dimethyl maleate	benzyl	15	100	98	2
5	0.6	dimethyl fumarate	benzyl	10	100	98	2
6	0.6	dimethyl fumarate	benzyl	15	100	98	2
7	0.6	dimethyl fumarate	benzyl	20	100	94	6
8	0.6	dimethyl fumarate	4-methoxybenzyl	10	100	94	6
9	0.6	dimethyl fumarate	4-methylbenzyl	10	100	94	6
10	0.6	dimethyl fumarate	4-bromobenzyl	10	100	99	1
11	0.6	dimethyl fumarate	4-iodobenzyl	10	100	99	1
12	0.6	dimethyl fumarate	1-phenylethyl	10	100	98	2
13	0.5	fumaronitrile	benzyl	10	100	96	4
14	0.5	fumaronitrile	4-methylbenzyl	10	100	93	7
15	0.5	fumaronitrile	4-bromobenzyl	10	100	95	5
16	0.3	maleic anhydride	dibromide	10	82	84	16 ^[d]

[a] Olefin 5 mm, halide 5 mm, solvent DMF; the electrode gap is 320 μm for entries 1 and 2, and 160 μm for entries 3–16. [b] Conversion was determined based on the quantity of olefin before and after reaction using *n*-decane as an internal standard. [c] Other products result from dimerization of olefin and debromination of benzyl bromides; no dimerization of benzyl bromides is detected except for entry 2. [d] Other side products are 1,2-dimethylbenzene and 2-methylbenzyl bromide.



Scheme 1. Plausible mechanistic reaction pathway for the C–C coupling process.

electron transfer process or not and this will require further study.

Further coupling reactions between fumaronitrile and benzyl bromides as well as between maleic anhydride and 1,2-bis(bromomethyl)benzene were investigated. Formally equivalent (but more laborious and less effective) conventional synthetic reactions have been described in the literature, for example, a photochemical process in the presence of organometallic catalysts for the coupling of benzyl bromide with fumaronitrile,^[11] a sacrificial zinc approach,^[12a] a photochemical approach,^[12b] and a direct Diels–Alder reaction^[12c,d] for coupling of maleic anhydride with dibromides. Interestingly, in a flow microreactor cell excellent yields (> 93 %) for coupling of fumaronitrile and bromides (Table 1, entries 13–15) and 84 % yields for coupling of maleic anhydride and

1,2-bis(bromomethyl)benzene (Table 1, entry 16) can be obtained.

For the proposed mechanism, the differences between the approximate reduction halfwave potentials for the olefin and benzyl bromide, ΔE , may be understood as part of a thermodynamic cycle.^[13] It is observed that conversion is dependent on the reduction potential difference ΔE . For the coupling reaction of dimethyl fumarate and benzyl bromide with ΔE of 0.7 V up to 100 % conversion can be achieved, and for the coupling reaction of dimethyl fumarate and 4-methoxybenzyl bromide with ΔE of 1.1 V 91 % conversion are obtained at a flow rate of 15 μL min⁻¹ under the same conditions. It is also observed that coupling reactions of benzyl chloride with dimethyl fumarate, and that of maleic anhydride with all benzyl bromide derivatives ($\Delta E > 1.2$ V) except 1,2-bis(bromomethyl)benzene ($\Delta E = 1.1$ V) fail to produce any cross-coupling products. The benzyl bromides are recovered unreacted. A schematic plot of maximum yield versus ΔE (Figure 1B) suggests a threshold of $\Delta E \approx 1.1$ V for successful coupling. This value is in approximate agreement (ΔE is slightly high due to uncertainty in half wave potential for the benzyl bromide reduction) with the value expected for dissociation of the C–Br bond: $\Delta E = 0.85$ V (the gas phase bond energy for benzyl bromide is $D_0 = 82$ kJ mol⁻¹).^[14]

We have demonstrated that clean microreactor-based electrosyntheses in the absence of supporting electrolyte are feasible even with very simple cell geometries. The height of the microfluidic cell and the flow rate have been shown to be crucial for the minimization of unwanted side products and optimization of yields. More work will be required for a better understanding of the spatial distribution of reagents, the electron transfer process in microreactor systems, as well as for the optimization and scale up of processes in the microreactor cell. For an energy-efficient use of microreactor electrosynthesis, the resistive losses during electrosynthesis will need further investigation and better electrode designs may help in optimizing the efficiency of the process. It is very likely that clean one-step electrochemical coupling processes in microfluidic reactors are applicable for a wider range of reactions.

Experimental Section
 Cyclic voltammetric (CV) experiments were carried out with an Autolab PGSTAT30 system in a conventional three-electrode cell and in the presence of supporting electrolyte. A Pt disc (diameter 0.5 mm), a Pt wire, and a silver wire (both diameter 0.1 mm) were used as the working electrode, the counter electrode, and the

reference electrode, respectively. For preparative microreactor electrolyses, a Harvard PHD 2000 syringe pump was used to pump the reaction solution containing olefin (5 mM) and benzyl bromide (5 mM) in DMF without the addition of electrolyte through the microreactor cell in which two platinum foil electrodes with a working area of 45 mm² were positioned with an inter-electrode distance of 160 μm and 320 μm.^[4d] All reactions were conducted galvanostatically and product samples were continuously collected 5 times and each run took 5 min. Reactions were analyzed by GC (Shimadzu GC-17 A, FID, column CPSIL8) using decane as an internal standard. The replicate analysis shows RSD less than 5%. The products were also identified using ¹H and ¹³C NMR spectroscopy (Jeol GX400) in CDCl₃ as well as mass spectrometry (Varian 2000).

Received: March 10, 2006

Published online: ■ ■ ■ ■ ■, ■ ■ ■ ■ ■

Keywords: C–C coupling · electrochemical synthesis · flow cells · microreactors · olefins

- [1] J. Utley, *Chem. Soc. Rev.* **1997**, 26, 157.
- [2] a) P. T. Anastas, T. C. Williamson, *Green Chemistry*, Oxford University Press, Oxford, **1998**, pp. 167; b) E. Steckhan, T. Arns, W. R. Heineman, G. Hilt, D. Hoorman, J. Jorissen, L. Kroner, B. Lewall, H. Putter, *Chemosphere* **2001**, 43, 63; c) D. Pletcher, N. L. Weinberg, *Chem. Eng.* **1992**, 99, 98.
- [3] a) *Microreaction Technology* (Ed.: W. Ehrfeld), Springer, Berlin, **1998**; b) W. Ehrfeld, V. Hessel, H. Löwe, *Microreactors: New Technology for Modern Chemistry*, Wiley-VCH, Weinheim, **2000**; c) V. Hessel, S. Hardt, H. Löwe, *Chemical Micro Process Engineering*, Wiley-VCH, Weinheim, **2004**; d) S. Taghavi-Moghadam, A. Kleemann, K. G. Golbig, *Org. Process Res. Dev.* **2001**, 5, 652; e) T. Kawaguchi, H. Miyata, K. Ataka, K. Mae, J. Yoshida, *Angew. Chem.* **2005**, 117, 2465; *Angew. Chem. Int. Ed.* **2005**, 44, 2413.
- [4] a) C. A. Paddon, G. J. Pritchard, T. Thiemann, F. Marken, *Electrochem. Commun.* **2002**, 4, 825; b) D. Horii, M. Atobe, T. Fuchigami, F. Marken, *Electrochem. Commun.* **2005**, 7, 35; c) R. Horcajada, M. Okajima, S. Suga, J. Yoshida, *Chem. Commun.* **2005**, 1303; d) P. He, P. Watts, F. Marken, S. J. Haswell, *Electrochem. Commun.* **2005**, 7, 918.
- [5] a) J. P. Devlin, W. D. Ollis, J. E. Thorpe, R. S. Wood, B. J. Broughton, P. J. Warren, K. R. H. Wooldbridge, D. E. Wright, *J. Chem. Soc. Perkin Trans. 1* **1975**, 830; b) N. A. Porter, D. M. Scott, I. J. Rosenstein, B. Giese, A. Veit, H. G. Zeitz, *J. Am. Chem. Soc.* **1991**, 113, 1791; c) D. E. Levy, F. Lapiere, W. Liang, W. Ye, C. W. Lange, X. Li, D. Grobelny, M. Casabonne, D. Tyrrell, K. Holme, A. Nadzan, R. E. Galardy, *J. Med. Chem.* **1998**, 41, 199; d) W. C. Groutas, M. J. Brubaker, M. A. Stanga, J. C. Castrisos, J. P. Crowley, E. J. Schatz, *J. Med. Chem.* **1989**, 32, 1607; e) R. B. Bates, R. S. Cuther, R. M. Freeman, *J. Org. Chem.* **1977**, 42, 4162; f) G. Sabitha, R. Srividya, J. S. Yadav, *Tetrahedron* **1999**, 55, 4015; g) S. C. Bergmeier, K. A. Ismail, *Synthesis* **2000**, 1369; h) R. Ballini, G. Bosica, D. Fiorini, P. Righi, *Synthesis* **2002**, 681; i) M. Mella, M. Fagnoni, A. Albini, *Eur. J. Org. Chem.* **1999**, 9, 2137.
- [6] a) C. Degrand, H. Lund, *Nouv. J. Chim.* **1977**, 1, 35; b) E. A. Casanova, M. C. Dutton, D. J. Kalota, J. H. Wagenknecht, *J. Electrochem. Soc.* **1993**, 140, 2565.
- [7] a) J. G. Lawless, D. E. Bartak, M. D. Hawley, *J. Am. Chem. Soc.* **1969**, 91, 7121; b) D. E. Bartak, M. D. Hawley, *J. Am. Chem. Soc.* **1972**, 94, 640; c) J. Grimshaw, *Electrochemical Reactions and Mechanisms in Organic Chemistry*, Elsevier, Amsterdam, **2000**, pp. 98–103; d) *Organic Electrochemistry* (Eds.: H. Lund, O. Hammerich), Marcel Dekker, New York, **2001**, and references therein.
- [8] D. Zhou, H. Carrero, J. F. Rusling, *Langmuir* **1996**, 12, 3067.
- [9] a) “Acyclic Aliphatic Halides”: M. D. Hawley in *Encyclopedia of Electrochemistry of the Elements, Organic Section, Vol. 14* (Eds.: A. J. Bard, H. Lund), Marcel Dekker, New York, **1980**, pp. 83–103; b) O. R. Brown, H. R. Thirsk, B. Thornton, *Electrochim. Acta* **1971**, 16, 495; c) C. P. Andrieux, A. L. Gorande, J. M. Saveant, *J. Am. Chem. Soc.* **1992**, 114, 6892.
- [10] a) D. Zhou, H. Carrero, J. F. Rusling, *Langmuir* **1996**, 12, 3067; b) C. P. Andrieux, A. Le Gorande, J. M. Savéant, *J. Am. Chem. Soc.* **1992**, 114, 6892; c) A. J. Fry, A. H. Singh, *J. Org. Chem.* **1994**, 59, 8172; d) N. Sadler, S. L. Scott, A. Bakac, J. H. Espenson, M. S. Ram, *Inorg. Chem.* **1989**, 28, 3951.
- [11] B. Giese, G. Thoma, *Helv. Chim. Acta* **1991**, 74, 1135.
- [12] a) B. H. Han, B. P. Hee, *J. Org. Chem.* **1982**, 47, 751; b) A. Ouchi, Y. Koga, *Chem. Commun.* **1996**, 17, 2075; c) J. H. P. Utley, Y. Gao, J. Gruber, R. Lines, *J. Mater. Chem.* **1995**, 5, 1297; d) A. Ouchi, Z. Li, M. Sakuragi, T. Majima, *J. Am. Chem. Soc.* **2003**, 125, 1104.
- [13] J. H. P. Utley, S. Ramesh, X. Salvatella, S. Szunerits, M. Motevalli, M. F. Nielsen, *J. Chem. Soc. Perkin Trans. 2* **2001**, 153.
- [14] A. Freedman, S. C. Yang, M. Kawasaki, R. Bersohn, *J. Chem. Phys.* **1980**, 72, 1028.

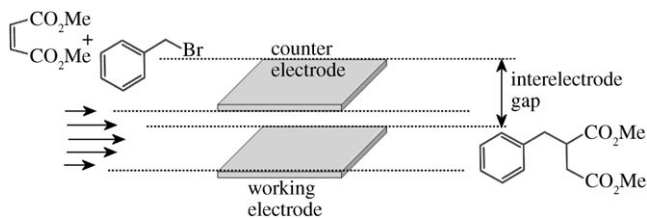
Communications

Microreactors

P. He, P. Watts, F. Marken,
S. J. Haswell*



Self-Supported and Clean One-Step
Cathodic Coupling of Activated Olefins
with Benzyl Bromide Derivatives in a
Micro Flow Reactor



Currently coupled: A clean microreactor-based electrosyntheses in the absence of supporting electrolyte is demonstrated and shown to feature very simple cell geometries. As exemplified for the coupling reaction of various olefins with

benzyl bromides, the height of the microfluidic cell and the flow rate are crucial for the minimization of unwanted side products and optimization of yields (see picture).

Clean and selective oxidation of aromatic alcohols using silica-supported Jones' reagent in a pressure-driven flow reactor

Charlotte Wiles, Paul Watts* and Stephen J. Haswell

The Department of Chemistry, Faculty of Science and the Environment, The University of Hull, Cottingham Road, Hull HU6 7RX, United Kingdom

Received 18 April 2006; revised 12 May 2006; accepted 24 May 2006

Abstract—By exploiting the high surface to volume ratio obtained within continuous flow reactors, we are able to oxidise selectively an array of primary alcohols to either the aldehyde or carboxylic acid, depending on the flow rates employed, demonstrating a degree of reaction control unattainable in traditional stirred reactors.

© 2006 Elsevier Ltd. All rights reserved.

The selective oxidation of primary and secondary alcohols to aldehydes and ketones is a fundamental synthetic transformation¹ that can be achieved using a plethora of reagents; of these, chromium(VI) reagents are among the most efficient. The synthetic utility of the technique is however often marred by concomitant over-oxidation, leading to the formation of complex reaction mixtures. In addition, chromium(VI) based reagents are largely viewed as being undesirable, due to the generation of toxic residues and acidic waste-water. To address the problem of chromium contamination, numerous supported analogues have been developed enabling the spent oxidising agent to be filtered from the reaction products;² in addition, the use of a co-oxidant enables the oxidising agent to be recycled.³ The complete removal of such materials from reaction products can, however, prove problematic due to mechanical degradation of the support as a result of prolonged stirring/agitation. In addition, the use of solid-supported oxidising agents can require long reaction times⁴ and elevated reaction temperatures,⁵ whilst being low-yielding.⁶

With this in mind, continuous flow reactors have found use as powerful synthetic tools enabling operational flexibility, reduced reaction times and system automation, resulting in a technique that is suitable for both high-throughput synthesis and lead generation. The main drawback of the technique, however, is how to purify the reaction products prepared in continuous

flow systems. By coupling the advantages associated with solid-supported reagents with those of flow reaction methodology, the problems associated with reagent

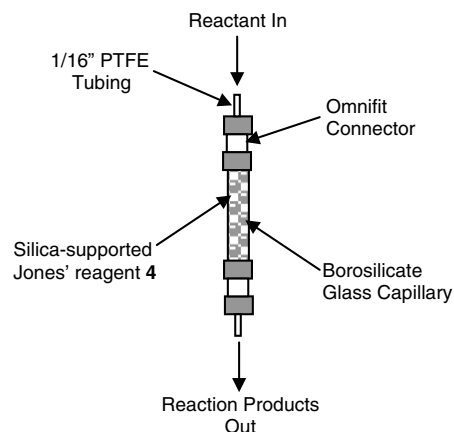
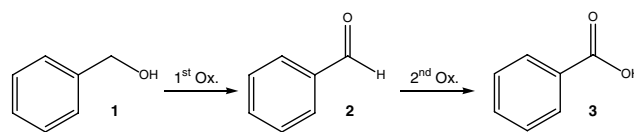


Figure 1. Schematic illustrating the flow reactor used for the selective oxidation of primary alcohols.



Scheme 1. Schematic illustrating the oxidation of benzyl alcohol 1 to afford benzaldehyde 2 and benzoic acid 3.

Keywords: Selectivity; Continuous flow; Oxidation; Jones' reagent.

* Corresponding author. E-mail: p.watts@hull.ac.uk

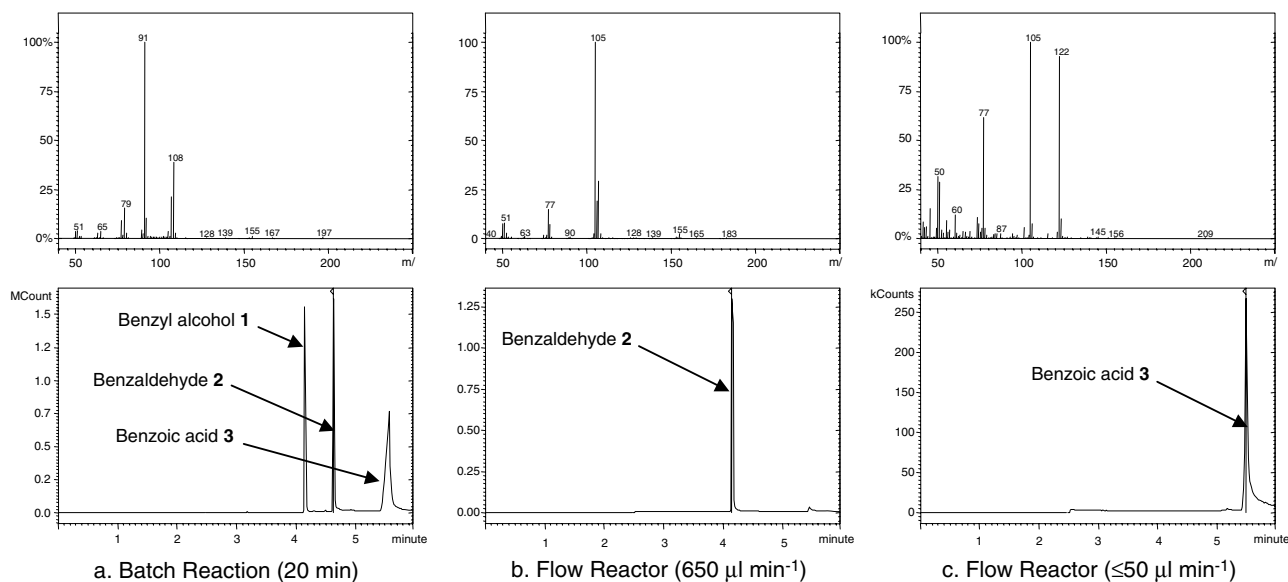


Figure 2. Gas chromatograms and mass spectra illustrating the products synthesised in (a) a stirred batch reactor, (b) a flow reactor operated at $650 \mu\text{l min}^{-1}$ and (c) a flow reactor operated at $50 \mu\text{l min}^{-1}$.

Table 1. Summary of the results obtained for the oxidation of an array of primary alcohols, using silica-supported Jones' reagent **4**, in a flow reactor

Entry	Primary alcohol	Flow rate ($\mu\text{l min}^{-1}$)	Product distribution	
			Aldehyde ^a (%)	Carboxylic acid ^a (%)
1	Benzyl alcohol 1	650	100 (99.1) ^b	0
		50	0	100 (99.6)
2	3,5-Dimethoxybenzyl alcohol	650	100 (99.5)	0
		50	0	100 (99.3)
3	4-Bromobenzyl alcohol	650	100 (99.0)	0
		50	0	100 (98.3)
4	4-Chlorobenzyl alcohol	650	100 (99.3)	0
		50	0	100 (99.4)
5	4-Cyanobenzyl alcohol	650	100 (98.5)	0
		50	0	100 (99.0)
6	Methyl-4-formylbenzyl alcohol	650	100 (99.2)	0
		50	0	100 (99.6)
7	4-Methylbenzyl alcohol	650	100 (99.2)	0
		50	0	100 (95.6)
8	4-Benzyloxybenzyl alcohol	650	100 (99.5)	0
		50	0	100 (99.8)
9	4-Aminobenzyl alcohol	650	100 (100)	0
		50	0	100 (99.8)
10	4-Dimethylaminobenzyl alcohol	650	100 (99.3)	0
		50	0	100 (99.6)
11	Biphenyl-4-yl methanol	650	100 (99.7)	0
		50	0	100 (99.5)
12	(5-Nitrothiophen-2-yl)-methanol	650	100 (99.8)	0
		50	0	100 (99.7)
13	2-Benzyloxybenzyl alcohol	650	100 (99.7)	0
		50	0	100 (99.8)
14	2-Naphthalen-2-yl-methanol	650	100 (99.9)	0
		50	0	100 (99.9)
15	4-Acetylbenzyl alcohol	650	100 (99.8)	0
		50	0	100 (99.8)

^a $n = \geq 15$.

^b The number in parentheses represents the % isolated yield.

recovery/recycle are readily overcome enabling the continuous synthesis of compounds in both high purity and excellent yield.

Building on our recent syntheses of analytically pure α,β -unsaturated compounds⁷ and dimethyl acetals in continuous flow reactors,⁸ we report herein the prelimin-

ary results obtained for the selective oxidation of primary (and secondary) alcohols in a pressure-driven flow reactor (Fig. 1).

As Scheme 1 illustrates, when a primary alcohol **1** is oxidised, precautions must be taken to ensure that the desired aldehyde **2** is not further oxidised to the corresponding carboxylic acid **3**. In practice, this can be achieved by distillation of the aldehyde as it forms, this technique is however restricted to molecules of low molecular weight.

We therefore proposed that by conducting the reaction in a continuous flow reactor, where the residence time of a reagent can be carefully controlled, selective oxidation of the primary alcohol could be achieved. In addition to the obvious advantage of enhanced product selectivity, in the case of acidic oxidants, such as Jones' reagent (H_2CrO_4), the use of silica-supported analogues proves advantageous as heavy metal contamination of the product is avoided, as even in its reduced form, the chromium residues are retained by the support.⁹ Unlike previous examples where EOF-based flow reactors have been employed,¹⁰ due to solvent incompatibilities with the supported oxidising agent **4**,[†] a simple pressure-driven system was constructed.

In order to perform a flow reaction, 0.150 g (0.150 mmol) of silica-supported Jones' reagent **4** was packed into a borosilicate glass flow reactor (0.3 cm (i.d.) \times 3.0 cm (length)) and a solution of benzyl alcohol **1** (0.01 M in DCM) pumped through the reactor, using a syringe pump (Harvard Apparatus), at the desired flow rate. The reaction products were collected from the reactor outlet at 1 min time intervals and analysed by GC-MS (number of samples (n) = ≥ 15). After chromatographic analysis, the reaction products were combined, concentrated in vacuo, the 'crude' product dissolved in CDCl_3 and analysed by NMR spectroscopy; all known compounds prepared had spectroscopic data consistent with the literature. In order to confirm product purity and reagent **4** stability, the reaction products were also analysed by ICP-MS; whereby $\leq 6.9 \times 10^{-5}\%$ w/w Cr was detected in all samples.

As Figure 2b illustrates, when operating the flow reactor at $650 \mu\text{l min}^{-1}$, providing a reagent residence time of 9.7 s,¹¹ over-oxidation to benzoic acid **3** was successfully prevented and quantitative conversion of benzyl alcohol **1** to benzaldehyde **2** was obtained.

Interestingly, when the reactor was operated at $300 \mu\text{l min}^{-1}$ (residence time = 21 s), the reaction products contained a mixture of unreacted starting material **1**, benzaldehyde **2** and benzoic acid **3**, replicating the

Table 2. Summary of the results obtained for the oxidation of secondary alcohols, using silica-supported Jones' reagent **4**, in a flow reactor

Entry	Secondary alcohol	Conversion ^a (%)	Yield ^b (%)
1	1-Phenylpropan-1-ol	100	100
2	1-Phenylethanol	100	100
3	1-(4-Aminophenyl)ethanol	100	98.8
4	Diphenylmethanol	100	99.6
5	1-(4-Iodophenyl)ethanol	100	99.6
6	1-(4-Nitrophenyl)ethanol	100	100
7	1-(4-Hydroxyphenyl)ethanol	100	99.3
8	1-Phenylbutan-1-ol	100	100
9	1-(4-Methylphenyl)ethanol	100	99.5
10	1-(4-Bromophenyl)ethanol	100	99.2
11	1,3-Diphenylpropan-1-ol	100	100
12	1-(4-Chlorophenyl)ethanol	100	99.0
13	Cyclopentanol	100	99.2
14	Cyclohexanol	100	100
15	2-Methylcyclohexanol	100	99.7

^a $n \geq 15$.

^b Flow reactor operated at $650 \mu\text{l min}^{-1}$.

lack of reaction control exhibited in the stirred, batch reactor (Fig. 2a). However, by further reducing the flow rate to $\leq 50 \mu\text{l min}^{-1}$ (residence time = ≥ 126 s), quantitative conversion to the carboxylic acid **3** was observed (Fig. 2c). Having demonstrated the ability to synthesise selectively either benzaldehyde **2** or benzoic acid **3** in excellent yield and purity (Table 1), the reaction was repeated using an array of substituted primary alcohols. As illustrated in Table 1, excellent selectivity was obtained for all primary alcohols investigated; importantly, no functional group incompatibilities were observed.

In order to demonstrate the versatility of the aforementioned methodology, a series of secondary alcohols was subsequently oxidised within the flow reactor. As Table 2 illustrates, in all cases, quantitative conversion of the alcohol to the respective ketone was observed, affording all products in excellent yield and purity; again no substrate dependency was observed.

Finally, the oxidation of aliphatic primary alcohols (C_2 – C_8) was investigated; however, in all cases leaching of oxidising agent from the silica support was observed (indicated by colouration of the reaction products), an observation that was attributed to an increase in the polarity of the reactant stream, compared to that observed for the primary aromatic alcohols. Consequently, this particular supported oxidising agent is limited to the oxidation of aromatic alcohols in a flowing system; this could however be overcome by the use of covalently bound oxidising agents.

Owing to the unique reaction conditions obtained as a result of incorporating supported reagents into continuous flow reactors, we have demonstrated the ability to oxidise selectively an array of primary alcohols to their respective aldehydes (residence time = 9.7 s) or carboxylic acids (residence time = 126 s), depending on the flow rate employed (Table 1).

[†] When the flow reactions were performed using water, acetonitrile, tetrahydrofuran or diethyl ether as the reaction solvent, chromium release was observed (determined by a distinct orange colouration of the product stream). In comparison, when performing the reaction in dichloromethane, no colouration of the reaction products was observed (confirmed by ICP-MS analysis of the product stream, $\leq 6.9 \times 10^{-7}\%$ w/w Cr).

Using this approach, we have successfully synthesised 15 aromatic aldehydes and their respective carboxylic acids, along with the oxidation of 15 secondary alcohols; in all cases, excellent yields and product purities were obtained, irrespective of functionality (Table 2).

In conclusion, the strategy employed herein provides a route to product selectivity and system reproducibility that is unobtainable in traditional stirred or shaken reactors. With these factors in mind, further investigations are currently underway within our laboratories to explore the use of co-oxidants, enabling the solid-supported oxidising agent to be recycled.

Acknowledgements

Full financial support provided by the EPSRC (Grant No. GR/S34106/01) (C.W.) is gratefully acknowledged. Mike Bailey and Bob Knight are also thanked for their assistance with device fabrication and ICP-MS analysis, respectively.

Supplementary data

Supplementary data associated with this article can be found, in the online version, at [doi:10.1016/j.tetlet.2006.05.157](https://doi.org/10.1016/j.tetlet.2006.05.157).

References and notes

1. (a) Hudlicky, M. *Oxidation in Organic Chemistry*; American Chemical Society: Washington, 1990; (b) Lee, D. G. *The Oxidation of Organic Compounds by Permanganate Ion and Hexavalent Chromium*, Open Court, **1980**.
2. Ley, S. V.; Baxendale, I. R.; Bream, R. N.; Jackson, P. S.; Leach, A. G.; Longbottom, D. A.; Nesi, M.; Scott, J. S.; Storer, R. I.; Taylor, S. J. *J. Chem. Soc., Perkin. Trans. 1* **2000**, 3815–4195, and references cited therein.
3. Kobayashi, S.; Miyamura, H.; Akiyama, R.; Ishida, T. *J. Am. Chem. Soc.* **2005**, *127*, 9251–9254.
4. Zhang, G. S.; Shi, Q. Z.; Chen, M. F.; Cai, K. *Synth. Commun.* **1994**, *27*, 953–955.
5. (a) Caineli, G.; Cardillo, G.; Orena, M.; Sandri, S. *J. Am. Chem. Soc.* **1976**, *98*, 6737–6738; (b) Brunelet, T.; Jouilleau, C.; Gelbard, G. *J. Org. Chem.* **1986**, *51*, 4016–4022.
6. Santaiello, E.; Ponti, F.; Manzocchi, A. *Synthesis* **1978**, 534–535.
7. Wiles, C.; Watts, P.; Haswell, S. J. *Tetrahedron* **2004**, *60*, 8421–8427.
8. Wiles, C.; Watts, P.; Haswell, S. J. *Tetrahedron* **2005**, *61*, 5209–5217.
9. Ali, M. H.; Wiggan, C. J. *Synth. Commun.* **2001**, *31*, 1389–1397.
10. Wiles, C.; Watts, P.; Haswell, S. J. *Abstr. Pap. Am. Chem. Soc.* **2005**, ORGN 699.
11. The total volume of the flow reactor, once packed, was determined experimentally to be 105 μl . Therefore when operating the reactor at flow rates of 650, 300 and 50 $\mu\text{l min}^{-1}$, residence times of 9.7, 21 and 126 s were obtained, respectively.

Xunli Zhang¹
Huabing Yin²
Jon M. Cooper²
Stephen J. Haswell¹

¹Department of Chemistry,
The University of Hull,
Hull, UK

²Department of Electronics and
Electrical Engineering,
University of Glasgow,
Glasgow, UK

Received June 26, 2006
Revised August 16, 2006
Accepted August 18, 2006

Research Article

A microfluidic-based system for analysis of single cells based on Ca²⁺ flux

A microfluidic format-based system has been developed for *in situ* monitoring of the calcium flux response to agonists using Chinese hamster ovary (CHO) cells. The assay is based on measuring the fluorescent intensity of the calcium-sensitive indicator, Fluo-4 AM, and was performed in a modified glass chip channel, whose surface was functionalised using a silanisation method with 3-aminopropyltriethoxysilane (APTS) (enabling the cells to be immobilised on the channel surface). CHO cells calcium flux response was measured for different agonists over a range of concentrations. Cells and reagents were introduced into the chip in a continuous flow as a series of plugs in a given sequence.

Keywords: Calcium flux / CHO K-1 cells / Fluorescent measurement / Microfluidics / Lab-on-a-chip
DOI 10.1002/elps.200600390

1 Introduction

The development of miniaturised microfluidic systems for chemical and/or biochemical analysis based on the so-called 'Lab-on-a-Chip' concept has witnessed considerable growth over the last decade [1–5]. Such microsystems represent the ability to 'shrink' conventional bench chemical systems to a size of a few square centimetres with major advantages of speed, performance, integration, portability, sample/solvent quantity, automation, hazard control and cost. These merits are important for a variety of applications in analytical chemistry, biochemistry, clinical diagnosis, medical chemistry and industrial chemistry [6, 7]. Consequently, numerous micro-total analysis systems (μ -TAS) and microreactor systems have been developed, and many more are currently under investigation [4].

Currently, the on-chip analysis of biological systems is attracting great interest with particular emphases being placed on the manipulation of cells and cell-based analyses [8–17]. Among the variety of cell-based bioassays that are possible, methods for determining calcium flux have been popular (calcium being an important cellular messenger [12, 18] whose mechanistic pathways have been intensively studied in pharmacology [19–25]). The

calcium flux assay is normally carried out by measuring the change in light intensity of a calcium-sensitive fluorescent dye which is preloaded into the cell [26]. Visible light-excitable indicators are commonly used, which generally exhibit a few tens- to a hundred-fold increase in fluorescence emission intensity upon binding Ca²⁺, without a significant shift in wavelength [26].

In this study, a new format of microfluidic-based system has been developed for the *in situ* monitoring of Chinese hamster ovary (CHO) cell's calcium flux response to agonists by measuring the fluorescent intensity of the calcium-sensitive indicator, Fluo-4 AM. The modification of the chip channel surface using a silanisation method, enabled CHO cells to be immobilised on the channel surface for *in situ* fluorescence monitoring of their response to different agonists present at a range of concentrations.

2 Materials and methods

2.1 Microfluidic chip fabrication

Figure 1 shows the chip used which consists of a circular chamber with two inlet channels and one outlet channel. The depth for all the channels was 50 μ m, with a width of 150 μ m. The diameter of the analysis chamber was 600 μ m, providing a total working volume of 0.0141 μ L.

The microchip was produced according to published procedures [27, 28] with minor adaptations. Briefly, the channel network was fabricated based on a photolithographic fabrication method. The channel network was

Correspondence: Professor Steve Haswell, Department of Chemistry, The University of Hull, Hull HU6 7RX, United Kingdom

E-mail: S.J.Haswell@Hull.ac.uk

Fax: +44-0-1482-466410

Abbreviations: APTS, 3-aminopropyltriethoxysilane; CHO, Chinese hamster ovary

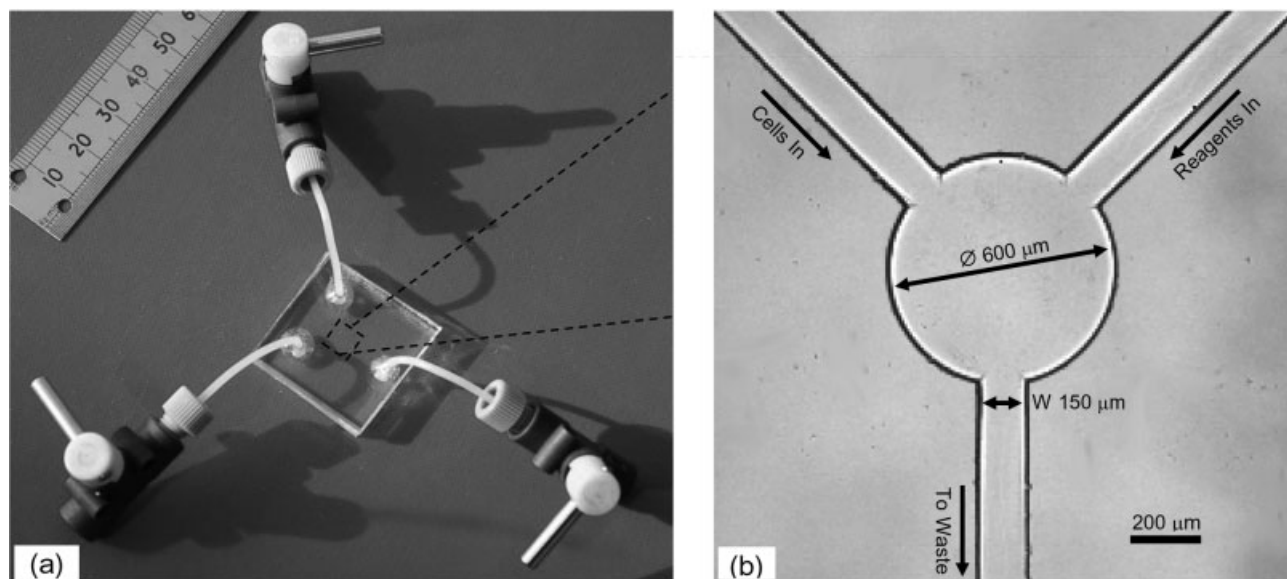


Figure 1. (a) Example of chip with tubing and on-off valves connected, and (b) outline of chip channel network.

first designed using AutoCAD LT 2005 drawing software (Autodesk, Farnborough GU14 6FG, UK). A film negative of the desired fluidic network was then prepared by a commercial photo mask manufacturer (J. D. Photo Tools, Oldham OL8 1EZ, UK) to form the optical mask. B-270 glass photolithographic plates (thickness of 3 mm) coated with a thin chromium metal mask layer, plus an upper layer of positive photoresist, supplied by Telic (Telic Company, Valencia, CA, USA), were used for channel network fabrication. With UV exposure, the pattern of interconnecting channels was transferred from the optical mask to the photoresist layer which was then developed and removed, together with the chromium layer, to reveal the channel areas of glass to be etched. The channels were etched using a mixture of 1% w/w HF and 5% w/w NH_4F in water at 65°C for 15 min, resulting in an etch channel network with a depth of 50 μm .

The base plate containing the etched channel network was sealed by thermally bonding an upper glass plate (also 3 mm thick) containing predrilled holes (diameter 1.5 mm) in order to link the ends of the channels with tubing. The upper plate was aligned with the channel geometry. Bonding was aided by placing a 90-g block of stainless steel on the upper plate.

2.2 Microchannel surface modification

To carry out cell-based bioassay at the single cell level, the immobilisation of cells at the desired location is important. The most commonly used method to either improve or prevent the adhesion of cells on the substrate

is to coat the substrate surface with appropriate agents [29]. In this experiment, the glass microchannel surface was treated with a solution of 2% v/v 3-aminopropyltriethoxysilane (APTS) (99%, Sigma-Aldrich Company Ltd, Dorset, UK) in acetone in the presence of a trace (0.1%) of water (which was sufficient to catalyse the surface modification process). The modification was carried out by continuously flowing APTS solution through the channel at a flow rate of 10 $\mu\text{L}/\text{min}$ for 10 min at room temperature. The microchannels were then rinsed by continuously flowing distilled water at a flow rate of 20 $\mu\text{L}/\text{min}$ for 5 min and dried by blowing N_2 through the channel network. It has been reported that the chemical reaction between the glass surface and the silanisation reagent allows amino groups to be linked by covalent bonds to the silicon atoms of the glass, leaving the glass surface positively charged, which in turn enhances the adhesion of cells which are generally negatively charged [29].

2.3 Cell culture and assay reagents

CHO-K1 (Chinese hamster ovary, *Cricetulus griseus*) cells were supplied by ATCC/LGC Promochem (ATCC® No. CCL-61™, LGC Promochem, Middlesex, UK). The cells were cultured routinely in DMEM/F-12 medium without L-glutamine (Cat. No. 21331–020, Invitrogen Ltd., Paisley, UK), which was supplemented with fetal bovine serum (Cat. No. 16000–044, Invitrogen Ltd.) to a final concentration of 10%, and L-glutamine (Cat. No. 25030–032, Invitrogen Ltd.) to a final concentration of 4 mM. An incubator was used at 37°C supplying 5% CO_2 . The

concentration of cells used in loading the chips during this experiment was in the range of 7.5×10^6 cells/mL.

A wash solution consisting of a modified Tyrodes buffer was used to wash the cells and to prepare the dye labelling and test solutions. The Tyrodes buffer was composed of 145 mM NaCl, 2.5 mM KCl, 10 mM HEPES, 10 mM D-glucose and 1.2 mM MgCl₂. CaCl₂ (99.5%, BDH AnalaR, 150 mM dissolved in Tyrodes buffer) and probenecid Sigma; (98%, 0.834 M dissolved in 1 M NaOH aqueous solution) were then added to Tyrodes giving final concentrations of 1.5 mM and 2.5 mM for CaCl₂ and probenecid, respectively. The dye labelling solution was made by adding Fluo-4 AM solution (1 mM Fluo-4 AM in DMSO, Invitrogen Molecular Probes, F14217) into wash solution giving a final concentration of 2 μM. Ionomycin test solutions were made by adding ionomycin stock (1 mM in DMSO) into wash solutions for desired concentrations. Ionomycin was obtained from Calbiochem (Cat. No. 407952, Calbiochem of EMD Biosciences, San Diego, CA, USA) and DMSO from Sigma-Aldrich (99%, P/N. D2650). The UTP (uridine triphosphate) test solutions were made by adding UTP stock (1 mM dissolved in ddH₂O) into wash solutions for desired concentrations. UTP was obtained from Sigma-Aldrich (90%, P/N. U6875).

2.4 Instrumentation and image analysis

An Axiovert S100 inverted microscope (Carl Zeiss, Hertfordshire, UK) using both transmission and fluorescent optics coupled with a monochrome CCD digital camera (C4742-95-12NRB, Hamamatsu Photonics, Hertfordshire, UK) was used to obtain both conventional micrographs and digital videos of the microchip. An AQM Hamamatsu ORCA I software (Kinetic Imaging, Nottingham, UK) was used for image acquisition and analysis. By selecting areas (cells) in successive video images, a light intensity profile *versus* time was obtained. Since the excitation and emission wavelengths of Fluo-4 AM were 494 and 516 nm respectively [26], a Chroma blue filter set (P/N. 11001, Chroma Technology Corp, Rockingham, USA) was selected which consisted of an Exciter D470/40, an Emitter E515LP and a beam splitter Dichroic 495DCLP.

Two KDS 200 syringe pumps (KD Scientific Inc., Holliston, MA, USA) were used to deliver cells in suspension and test solutions. ETFE (ethylene tetrafluoroethylene) polymer tubing with an inner diameter of 250 μm (P/N. 1529), on-off valves (P/N. P-782) and appropriate fittings and connectors, all obtained from Upchurch (Upchurch Scientific Inc., Oak Harbor, WA, USA), were used for plumbing to link the chip and the syringes.

3 Results and discussion

3.1 Labelling and loading cells on chip

Labelling of cells with a fluorescent probe is normally carried out by suspending cells in a labelling solution for a pre-determined period of time. In this study, after centrifugation and washing with the wash solution for removing the media, cells were resuspended in 1 mL of the 2 μM Fluo-4 AM labelling solution and kept at room temperature in the dark. After about 30 min, it was found that adequate fluorescent Ca²⁺ probes had been taken into cells for detection.

Labelled cells were loaded on chip by introducing a plug of cells contained in the labelling solution which was inserted and carried by a stream of wash solution (30 μL/min) into the chip. Once a steady state of cell stream was obtained in the circular chamber area, all the three on-off valves (Fig. 1a) were closed at the same time. This allowed cells to settle down and become immobilised on the channel surface of the chip after a period of 30 min at room temperature in the dark.

It was noted that this procedure allowed cells to be distributed evenly on the bottom of the chamber where they remained due to electrostatic forces (Fig. 2a). It was also observed that the cell attachment on surface was strong enough to resist the shear force produced by flowing in either the wash solution or test solution at a flow rate of 5 μL/min.

It should be noted that, in microfluidic systems with cells attached on the surface, some level of flow rate optimisation is required since it can clearly influence the environment around the cells and may cause them to be washed off the surface due to shear stress effects. At slow flow rates, the low linear velocity will require longer time periods for the reagent to completely fill the circular chamber. As a result, cells in different positions within the chamber will experience exposure to reagents at significantly different times. Increasing flow rates in order to shorten the fill time will, however, increase the shear stress effect experienced by the cells, which in turn may affect their physical and/or biochemical behaviour [30]. Shear stresses are generally measured as the ratio of the shearing force to the area over which it is applied. For the etched channels which have an approximately rectangular crosssection [28], the shear stress under laminar flow conditions can be expressed as [30–32]

$$\tau = \frac{6\mu Q}{wd^2} \quad (1)$$

where τ is the shear stress in dyne/cm², μ is the fluid viscosity in dyne·s·cm⁻² or poise, Q is the volumetric flow rate in cm³/s and w and d are the flow path width and depth in cm, respectively.

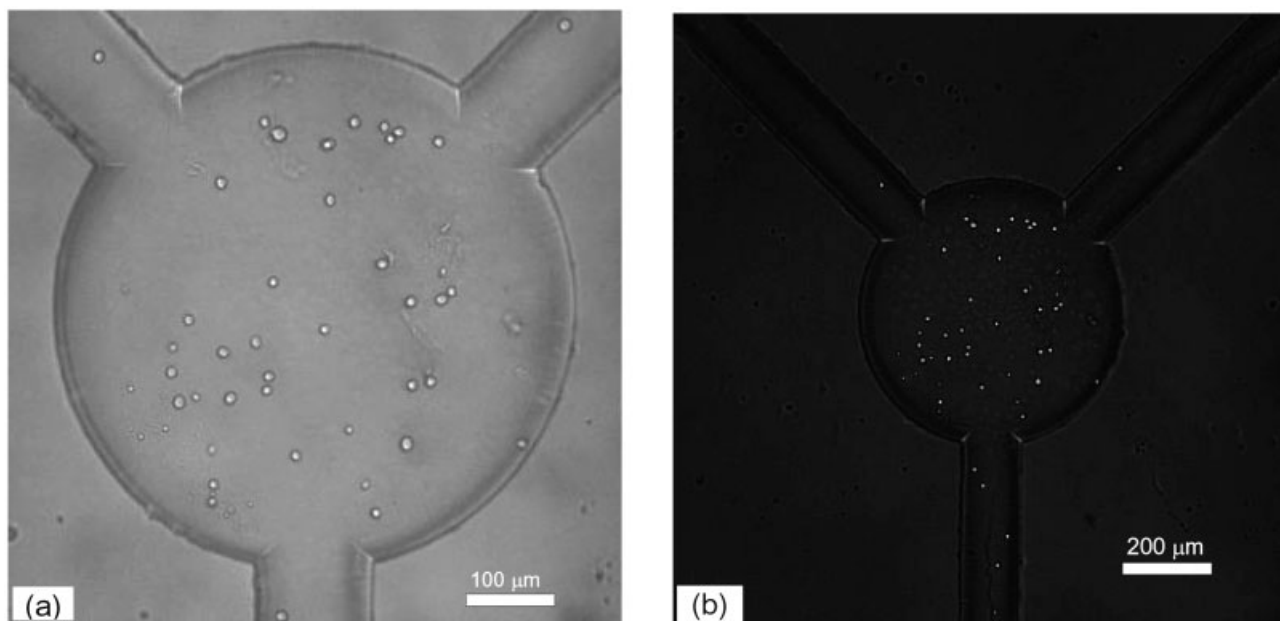


Figure 2. CHO cells loaded on chip in (a) bright-field view and (b) fluorescent view.

When the system was operated at a flow rate of 5 $\mu\text{L}/\text{min}$, the time for the fluid to fill the circular chamber was estimated to be 0.17 s, subjected to an assumption of plug flow conditions. By using Eq. (1), the shear stress was determined to be in the range of 13.9 dyne/cm^2 (at both the inlet and outlet channels) dropping to 3.5 dyne/cm^2 (at the largest crosssection of the chamber). Since only a few cells were close to the channel entrance/exit, most of the cells in the central area of the chamber were subjected to a relatively low shear stress (less than 10 dyne/cm^2) at which no significant effects were expected [30].

3.2 *In situ* monitoring of calcium flux response

After the cells were immobilised on the chip, the stimulation reagent (ionomycin or UTP) was introduced into the chip at a flow rate of 5 $\mu\text{L}/\text{min}$ *via* the reagent inlet channel. The video recorder was started at the same time with a scan rate of one frame/s under the fluorescent conditions. Figure 2b shows a snap of the fluorescent image where a weak transmission light was also applied for a better visibility of the channel network.

Upon the introduction of the ionomycin solution, an increase in the fluorescent intensity for almost all cells present was observed. Fluorescent signals were recorded and plotted *versus* time. Ten cells were selected randomly over the view field for data acquisition (Fig. 3). It should be noted that the fluorescent curves have been normalised for comparison. It can be seen that the fluo-

rescent intensity achieved its maximum and then declined gradually. A similar trend was found for both ionomycin concentrations of 20 μM (Fig. 3a) and 160 μM (Fig. 3b), except that the peak height and the time needed for reaching the peak were different.

It has been reported previously that the calcium indicator, Fluo-4 AM, exhibits a relatively high fluorescence emission and the fluorescent intensity is proportional, within a certain range, to the concentration of Ca^{2+} which results from the cells' response to a variety of stimuli [24, 26]. In this case, when the commonly used calcium flux-evoking stimulus was introduced, it triggered the so-called store-regulated calcium uptake (SRCU) process [12, 33–35]. When ionomycin permeated into CHO cells it caused cells to release Ca^{2+} from internal stores into the cytosol and the released Ca^{2+} would quickly combine with the calcium indicator, Fluo-4 AM. The reason for the signal decline following its maximum is unclear, although it is possible that an efflux of Ca^{2+} and/or the calcium indicator from the cell may occur, which in turn will reduce the fluorescent signal observed in the cell [36].

It was also observed that of the 50 cells in the view field (Fig. 2), *ca.* 10% did not show significant calcium flux response to the stimulation, suggesting that *ca.* 90% of the cell population were viable under the conditions used. The data shown in Fig. 3 were based on the calcium flux response from ten responding cells and the average response is shown as the black solid curve in Fig. 3. An error range of $\pm 10\%$ of the average is also shown in the

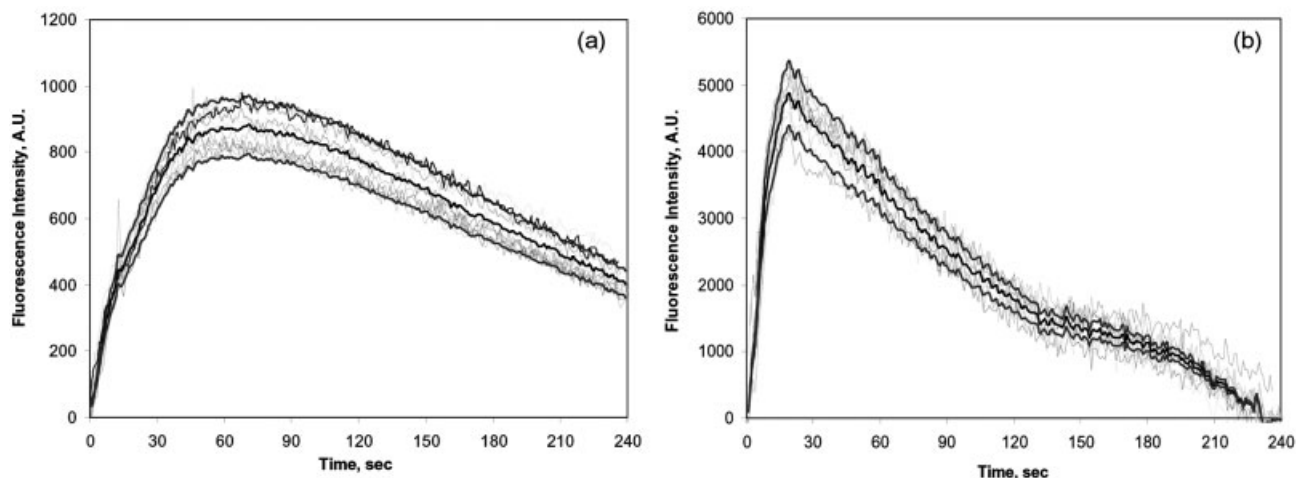


Figure 3. Fluorescent intensity as a function of time when ionomycin at two concentration levels of (a) 20 μM and (b) 160 μM was introduced into a chip by continuous flow. The black solid curve in the middle shows the average fluorescent intensity of ten cells, while the other two thick solid curves define the error range of $\pm 10\%$ of the average.

figure (the two red solid curves). It can be seen that for both ionomycin concentrations there were about two out of ten cells beyond the defined error range. This observation indicated that the proposed method can give a reasonably reliable statistical analysis based on signal cell measurements. The analysis also showed that a small number of cells, ten in this case, can still provide a statistic result with reasonable confidence, 90%, which is likely to be improved if more cells are analysed.

To ensure an even concentration distribution of the reagent over the circular chamber is achieved within a short time period (estimated to be approximately 0.17 s at a flow rate of 5 $\mu\text{L}/\text{min}$), the flow pattern was examined by flowing in a fluorescent dye solution (10 μM resorufin aqueous solution) *via* the reagent inlet channel. It was observed that the solution was distributed over more than 90% of the chamber area within 200 ms, where the lowest concentration point was close to the entrance of the cell inlet channel (about 100 μm away from the entrance). Based on Fick's law [37], a water molecule takes approximately 500 ms to cross a distance of 50 μm (where the self-diffusion coefficient of water at 25°C is $2.30 \times 10^{-9} \text{ m}^2/\text{s}$) [38], suggesting that the fluidic component will become homogeneous in the chamber within one second.

3.3 Effects of varying agonist concentration

Using the same *in situ* monitoring method under identical fluidic conditions, the effect of agonist concentration on calcium flux was examined at different ionomycin concentration levels. The results are illustrated in Fig. 4. It can

be seen that with higher agonist concentrations the corresponding fluorescent intensity became notably higher. The relationship between the calcium flux response and the agonist concentration is also plotted (inset in Fig. 4).

A four-parameter logistic model has frequently been used in biochemical and biomedical studies for the correlation between stimulation and response [39–43]. This model was also used for fitting the experimental data shown in Fig. 4.

$$y = \frac{A - D}{1 + (x/C)^B} + D \quad (2)$$

where y is the calcium flux fluorescent response (arbitrary unit) and x is the stimulant agonist concentration (μM). A and D are the lower and upper asymptotes, B is the slope of the curve and C is the central point of the linear portion of the curve. By fitting the experimental data to the four-parameter logistic model, the best-fit of the four parameters have been found to be 269.4, 1.9, 67.1 and 5762.2, respectively. It is believed that the four parameters in this model are related to certain physical and/or biochemical factors in the process [41], and as such the model is commonly used to obtain the IC_{50} or EC_{50} values in drug testing (IC_{50} represents the concentration of a drug that is required for 50% inhibition *in vitro*, whereas EC_{50} represents the plasma concentration required for obtaining 50% of a maximum effect *in vivo* [44]). However, to define the correlation in this system, further study is required.

It was also observed that different times were required to reach the maximum fluorescent intensity for different concentration stimuli, whilst a higher concentration of

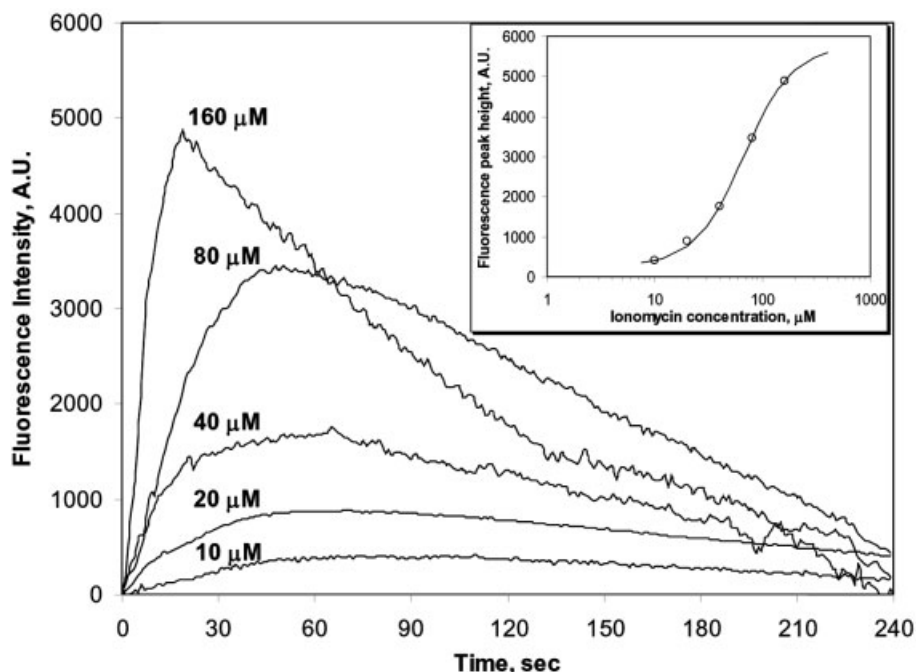


Figure 4. Average fluorescent intensity as a function of time for five ionomycin concentrations, and (inset) the relationship between the fluorescent intensity peak height and concentration where the solid curve is the best-fit using a four-parameter logistic model.

ionomycin gave a faster response. This was due to the effect of agonist concentration on both mass transfer (as diffusion into or within the cell) and/or its interaction within the cell. With a higher agonist concentration, the overall reaction was accelerated. This acceleration can, in turn, result in the release of calcium in a shorter time frame.

3.4 Comparison of effects of different agonists

It has been reported that the addition of UTP can also elicit rapid increases in Ca^{2+} in CHO cells and this was attributed to calcium mobilisation from intracellular stores and calcium entry across the plasma membrane [21]. In this study, using the same procedure as for the ionomycin test, a UTP solution with a concentration of 80 μM was used to measure the calcium flux response. Figure 5 shows the comparison of the two agonists at the same concentration measured under identical conditions. It can be seen that both curves show a similar trend, except that the UTP gave a stronger stimulation than ionomycin. It has been reported that UTP could induce calcium flux responses similar to ionomycin [45] although the cellular reaction mechanism was thought to be different [46].

Since it is of interest to investigate the effect from different stimuli simultaneously or in a given sequence [45–47], the proposed microfluidic-based system could provide the possibility to apply different stimulation test solutions to a selected area of cells in a controllable manner, *i.e.*, simultaneously or as a series of plugs in a given sequence

without mechanically disturbing cells. Future studies will investigate both (i) the historical effects of having previously exposed the cell to other agonists, on any given response, being measured; and (ii) longer term effects due to the mechanical effects of flow (shear-stress) on stretch receptors within the CHO cell.

4 Concluding remarks

The proposed microfluidic-based format for *in situ* monitoring of calcium flux in CHO cells has been shown to give rapid response to two agonists, namely ionomycin and UTP, by measuring the fluorescent intensity of the calcium-sensitive indicator, Fluo-4 AM. The chip channel surface was modified using a silanisation method enabling CHO cells to be immobilised through electrostatic affinity on the channel surface for further analysis. Since the microfluidic-based system allowed reagents to be introduced into the chip in a continuous flow format, it exhibited the ability of introducing different stimulation test solutions as a series of plugs in a given sequence without mechanically disturbing the immobilised cells. In addition, the microscope-based imaging system allowed measurements to be carried out on single cells but due to statistical limitations a mean of ten cell results was used in this study. On the other hand, there are some limitations associated with this system. For example, it can only be used for examining cells over a short time period (minutes) in order to minimise the loss of the specific signalling

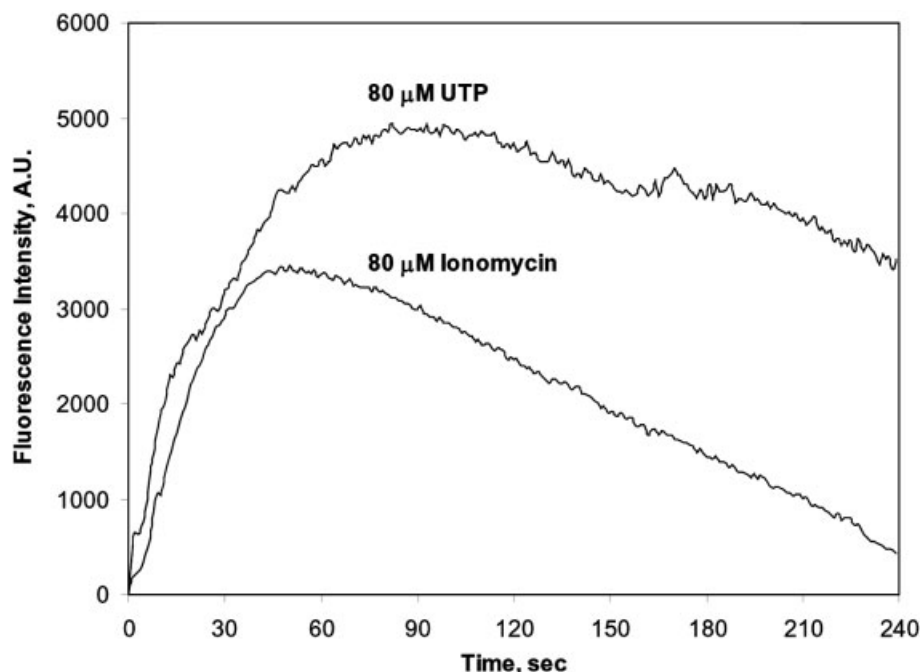


Figure 5. Comparison of calcium flux response to ionomycin and UTP.

ability. During the image acquisition, the position of the specific cell needs to remain stationary. Furthermore, as a general requirement, a robust system needs a reasonably high level of automation.

We thank Ms. Huguette Savoie of the Department of Chemistry at the University of Hull for help with the cell culture. We also thank Dr. Hayley Cordingly and Dr. Nicki Patrick from GSK (Harlow, UK) for the helpful discussion of the results. The DTI (MNT Project 366) of UK is acknowledged for funding this research.

5 References

- [1] Janasek, D., Franzke, J., Manz, A., *Nature* 2006, 442, 374–380.
- [2] Andersson, H., van den Berg, A., *Sens. Actuators B* 2003, 92, 315–325.
- [3] Fletcher, P. D. I., Haswell, S. J., Zhang, X., *Electrophoresis* 2003, 24, 3239–3245.
- [4] Jensen, K. F., Han, J., Harrison, D. J., Voldman, J. (Eds.), *Ninth International Conference on Miniaturized Systems for Chemistry and Life Sciences (TAS 2005)*, October 9–13, 2005 Boston, MA, USA, Kluwer Academic Publishers, Dordrecht, The Netherlands 2005.
- [5] Huh, D., Gu, W., Kamotani, Y., Grotberg, J. B., Takayama, S., *Physiol. Meas.* 2005, 26, R73–R98.
- [6] Fletcher, P. D. I., Haswell, S. J., Pombo-Villar, E., Warrington, B. H. et al., *Tetrahedron* 2002, 58, 4735–4757.
- [7] Manz, A., Becker, H. (Eds.), *Microsystem Technology in Chemistry and Life Sciences*, Springer, Berlin 1998.
- [8] Dittich, P. S., Manz, A., *Nat. Rev. Drug Discov.* 2006, 5, 210–218.
- [9] Yi, C., Li, C.-W., Ji, S., Yang, M., *Anal. Chim. Acta* 2006, 560, 1–23.
- [10] Sadani, Z., Wacogne, B., Pieralli, C., Roux, C., Gharbi, T., *Sens. Actuators A* 2005, 121, 364–372.
- [11] Xia, F., Jin, W., Yin, X., Fang, Z., *J. Chromatogr. A* 2005, 1063, 227–233.
- [12] Li, X., Li, P. C. H., *Anal. Chem.* 2005, 77, 4315–4322.
- [13] Ramser, K., Enger, J., Goksoy, M., Hanstorp, D. et al., *Lab Chip* 2005, 5, 431–436.
- [14] Nam, K.-H., Chang, W.-J., Hong, H., Lim, S.-M. et al., *Biomed. Microdevices* 2005, 7, 189–195.
- [15] Zhang, Z. L., Crozatier, C., Le Berre, M., Chen, Y., *Microelectron. Eng.* 2005, 78–79, 556–562.
- [16] Li, P. C. H., de Camprieux, L., Cai, J., Sanger, M., *Lab Chip* 2004, 4, 174–180.
- [17] Wheeler, A. R., Thronset, W. R., Whelan, R. J., Leach, A. M. et al., *Anal. Chem.* 2003, 75, 3581–3586.
- [18] Takahashi, A., Camacho, P., Lechleiter, J. D., Herman, B., *Physiol. Rev.* 1999, 79, 1089–1125.
- [19] Rollins, B. J., Walz, A., Baggiolini, M., *Blood* 1991, 78, 1112–1116.
- [20] Iredale, P. A., Martin, K. F., Hill, S. J., Kendall, D. A., *Eur. J. Pharmacol.* 1992, 226, 163–168.
- [21] Iredale, P. A., Hill, S. J., *Br. J. Pharmacol.* 1993, 110, 1305–1310.
- [22] Iredale, P. A., Alexander, S. P. H., Hill, S. J., *Br. J. Pharmacol.* 1994, 111, 1252–1256.
- [23] Vernino, S., Rogers, M., Radcliffe, K. A., Dani, J. A., *J. Neurosci.* 1994, 14, 5514–5524.
- [24] McCarthy, S. T., Younger, J. P., Owen, W. G., *Biophys. J.* 1994, 67, 2076–2089.
- [25] M. Rogers, Dani, J. A., *Biophys. J.* 1995, 68, 501–506.
- [26] Gee, K. R., Brown, K. A., Chen, W. N., Bishop-Stewart, J. et al., *Cell Calcium* 2000, 27, 97–106.
- [27] McCreedy, T., *Anal. Chim. Acta* 2001, 427, 39–43.

- [28] Broadwell, I., Fletcher, P. D. I., Haswell, S. J., McCreedy, T., Zhang, X., *Lab Chip* 2001, 1, 66–71.
- [29] Kiernan, J., *Microscopy Today* 1999, 7, 20–24.
- [30] Ainslie, K. M., Garanich, J. S., Dull, R. O., Tarbell, J. M., *J. Appl. Physiol.* 2005, 98, 242–249.
- [31] Jacobs, C. R., Yellowley, C. E., Davis, B. R., Zhou, Z. *et al.*, *J. Biomech.* 1998, 31, 969–976.
- [32] Schneider, T. W., Schessler, H. M., Shaffer, K. M., Dumm, J. M., Younce, L. A., *Biomed. Microdevices* 2001, 3:4, 315–322.
- [33] Pressman, B. C., Fahim, M., *Annu. Rev. Pharmacol. Toxicol.* 1982, 22, 465–490.
- [34] Mason, M. J., Grinstein, S., *Biochem. J.* 1993, 296, 33–39.
- [35] Morgan, A. J., Jacob, R., *Biochem. J.* 1994, 300, 665–672.
- [36] Peng, L. X. Y., Li, P. C. H., *Anal. Chem.* 2004, 76, 5282–5292.
- [37] Fick, A., *Ann. Phys. Chem.* 1855, 94, 59–86.
- [38] Mills, R., *J. Phys. Chem.* 1973, 77, 685–688.
- [39] Ratkovsky, D. A., Reedy, T. J., *Biometrics* 1986, 42, 575–582.
- [40] Jung, M., Michaud, J. C., Steinberg, R., Barnouin, M. C. *et al.*, *Neuroscience* 1996, 74, 403–414.
- [41] Cloutier, M., Gagnon, Y., Gascon-Barre, M., Brossard, J. H., D'Amour, P., *J. Endocrinol.* 1997, 155, 133–141.
- [42] Ugur, O., Onaran, H. O., *Biochem. J.* 1997, 323, 765–776.
- [43] Vale, C., Fonfria, E., Bujons, J., Messeguer, A. *et al.*, *Neuroscience* 2003, 117, 397–403.
- [44] <http://www.fda.gov/>. Last access on July, 2006.
- [45] Poulsen, A. N., Klausen, T. L., Pedersen, P. S., Willumsen, N. J., Frederiksen, O., *Eur. J. Physiol.* 2005, 450, 227–235.
- [46] Carraway, R. E., Hassan, S., Cochrane, D. E., *J. Pharmacol. Exp. Ther.* 2004, 309, 92–101.
- [47] De Smedt, F., Missiaen, L., Parysi, J. B., Vanweyenberg, V. *et al.*, *J. Biol. Chem.* 1997, 272, 17367–17375.

Continuous flow separation of particles within an asymmetric microfluidic device

Xunli Zhang,^a Jon M. Cooper,^b Paul B. Monaghan^b and Stephen J. Haswell*^a

Received 27th October 2005, Accepted 2nd March 2006

First published as an Advance Article on the web 13th March 2006

DOI: 10.1039/b515272k

A microfluidic based device has been developed for the continuous separation of polymer microspheres, taking advantage of the flow characteristics of systems. The chip consists of an asymmetric cavity with variable channel width which enables continuous amplification of the particle separation for different size particles within the laminar flow profile. The process has been examined by varying the sample inlet position, the sample to media flow rate ratio, and the total flow rate. This technique can be applied for manipulating both microscale biological and colloidal particles within microfluidic systems.

1. Introduction

The development of miniaturized micro chemical systems based on the so-called “Lab-on-a-Chip” concept has witnessed an explosive growth over the last decade.^{1–3} Such micro systems represent the ability to “shrink” conventional bench chemical systems to a size of a few square centimetres with major advantages of speed, performance, integration, portability, sample/solvent quantity, automation, hazard control, and cost. These merits are important for a variety of applications in analytical chemistry, biochemistry, clinical diagnosis, medical chemistry and industrial chemistry.^{4,5} New research fields of microfluidics, microreaction technology, micromixing, microheat exchanging and microseparation have now spun off from conventional chemistry and chemical technology. As a result, numerous micro-total-analysis-systems (μ -TAS) and micro reactor systems have been developed, and more are still under investigation.³

Sorting and separating of microparticles and biological cells has been an area of particular interest to a number of industrial and academic research groups as it represents an important step in many chemical and biological processes. A range of techniques have been reported for the separation of such particles which have included mechanical sieving, sedimentation, and so-called elution-based separation.^{6–9} The mechanical sieving and sedimentation methods are generally used to separate relatively large particles ($>1\ \mu\text{m}$), whilst elution-based techniques allow separation of particles in a smaller size range. Examples of those techniques include hydrodynamic chromatography, size exclusion chromatography and electrophoretic techniques. In addition, field-flow fractionation (FFF) which is based on the introduction of an external force field has attracted some recent interest in the field of microfluidics. Since this method was pioneered by Giddings in 1960's,⁷ it has been used to separate a range of

samples including polymers, biological macromolecules, synthetic and environmental particles, and living cells.⁸ This technique has been proved being efficient and also flexible for different reagents by choosing appropriate external force fields, and new methods based on the same principle are still being developed.⁶ In recent years, alongside the continuing development of miniaturized total analytical systems (μ -TAS) and micro reactor systems, effort has been made to separate micro-litre sample amounts of suspensions of particles and cells in Lab-on-a-Chip micro devices.^{9–15} Most of the studies involved the use of external force fields including dielectric (polarisability),⁹ acoustic,¹⁰ magnetic,¹¹ thermal,¹² optical^{13,14} and centrifugal¹⁵ forces. Clearly, the requirement of external forces increases the complexity of the device and may limit the application for some specific reagents such as biological samples. Consequently, researchers have been paying attention to the development of physical methods (without external forces) by making use of the laminar flow profile inside microchannels.^{16–19} In these systems, particles are carried by the laminar flow stream and the designed flow profile along the microchannel can be used to enhance the separation further.

In this study, we develop a new format of microfluidic based device for the continuous separation of microspheres. The chip consists of an asymmetric cavity with a variable channel width which enables continuous amplification of the separation of particles in different sizes along the laminar flow profile. The main design and operation parameters of the process have been examined.

2. Experimental

2.1. Materials

Water was purified by reverse osmosis and by passage through a Milli-Q Reagent Water System (Millipore, Watford, UK). Polystyrene latex microspheres with diameters of 10 μm and 25 μm were manufactured by Alfa Aesar, A Johnson Matthey Company (Ward Hill, MA, USA), and were supplied as 2.5 wt% dispersion in water. HISTOPAQUE[®]-1119, supplied by Aldrich (Poole, Dorset, UK), was a solution containing

^aDepartment of Chemistry, The University of Hull, Hull, United Kingdom HU6 7RX. E-mail: S.J.Haswell@Hull.ac.uk; Fax: +44 (0) 1482 466410; Tel: +44 (0) 1482 465469

^bDepartment of Electronics and Electrical Engineering, University of Glasgow, Glasgow, United Kingdom G12 8QQ

polysucrose and sodium diatrizoate, adjusted to a density of 1.119 g cm^{-3} . This medium was generally used to separate a range of viable mononuclear cells from the plasma by centrifugation which facilitates the mononuclear cells to form a distinct layer at the plasma-HISTOPAQUE[®] interface.²⁰ In this study Histopaque[®]-1119 was used to adjust the fluid density to minimize the microparticles sedimentation during flowing. The fluid media was prepared by mixing water with Histopaque[®]-1119, which was calculated to produce a desired density of 1.05 g cm^{-3} to match the polymer particle density.

2.2. Microdevice design and fabrication

Fig. 1 shows the outline of the chip design. The channel network consists of an asymmetric cavity with 3 inlet and 3 outlet channels. The key parameters for the chip design are shown in the figure. The depth for all the channels was $68 \mu\text{m}$. The microchip was fabricated according to published procedures²¹ with minor adaptations. The chip consisted of a polymer sheet with microchannels fabricated on the surface and a glass sheet to act as a cover plate.

To fabricate the channels a silicon mould was first constructed onto which the polydimethylsiloxane (PDMS) was poured and cured. The silicon mould was fabricated using the inductively coupled plasma (ICP) STS[™] process. A silicon wafer was first cleaned in acetone for 10 min with ultrasonication and then rinsed under a stream of de-ionised water for 5 min followed by drying under a stream of nitrogen. The wafer was then spin-coated with a layer of adhesion promoter (hexamethyldisilane, HMDS), followed by coating AZ4562 positive tone photoresist at $4000 \text{ rev min}^{-1}$ for 30 s resulting in about $6 \mu\text{m}$ thick polymer film. The wafer was baked at $90 \text{ }^\circ\text{C}$ for 120 s, and once cooled, the photoresist layer was patterned by a 25 s exposure to a photomask. The channel network patterns was thus transferred into the photoresist.

In all cases, the photomask, a negative photo film, was produced by drawing the channel designs using AutoCAD (Autodesk, Farnborough, Hampshire, UK) software and then transferring onto to a polyester film. After exposure, the wafer was developed in AZ400K developer solution (1 : 4 v/v in water) for approximately 2 min and rinsed in water. Once dried under a stream of nitrogen, the exposed silicon was etched under the following conditions: SF_6 , 130 sccm; C_4F_8 , 85 sccm; O_2 , 10 sccm; APC, 74%; pressure, 33 mTorr; power, 600 W coil, 12 W platen; temperature, $20 \text{ }^\circ\text{C}$, which gave an etch rate of $2.2 \mu\text{m min}^{-1}$.

After etching, the remaining photoresist was stripped in acetone, and then the silicon wafer was mounted onto to a glass support to improve its robustness. Finally, the silicon mould was silanized by placing the wafer in a petri dish with a few drops of HMDS overnight in order to aid the removal of the moulded PDMS sheet.

In order to make a moulded PDMS sheet, PDMS (Sylgard 184 Silicone Elastomer, manufactured by Dow Corning, Midland, Michigan, USA) was mixed in a 1 : 10 v/v ratio of curing agent to base oligomers and poured over the silicon mould. This was left for 1 h to allow the sample to degas, and was then baked in an oven at $75 \text{ }^\circ\text{C}$ for 2 h. Once cooled the PDMS structure was peeled away from the mould. Fluid access holes were then punched through the PDMS sheet (thickness: 4 mm) with a modified gauge 21 syringe needle, resulting in interconnect holes with a diameter of approximately $500 \mu\text{m}$. The chips were then cleaned in ethanol with ultrasonication for 5 min followed by a rinse in water and drying under a stream of nitrogen. The cross section of the micro channels produced using this method has been found to be nearly rectangular.²¹

To seal the microfluidic structure, a glass cover plate (thickness: 1.5 mm) was bonded to the PDMS sheet. Before bonding both the PDMS and glass were exposed in the ICP

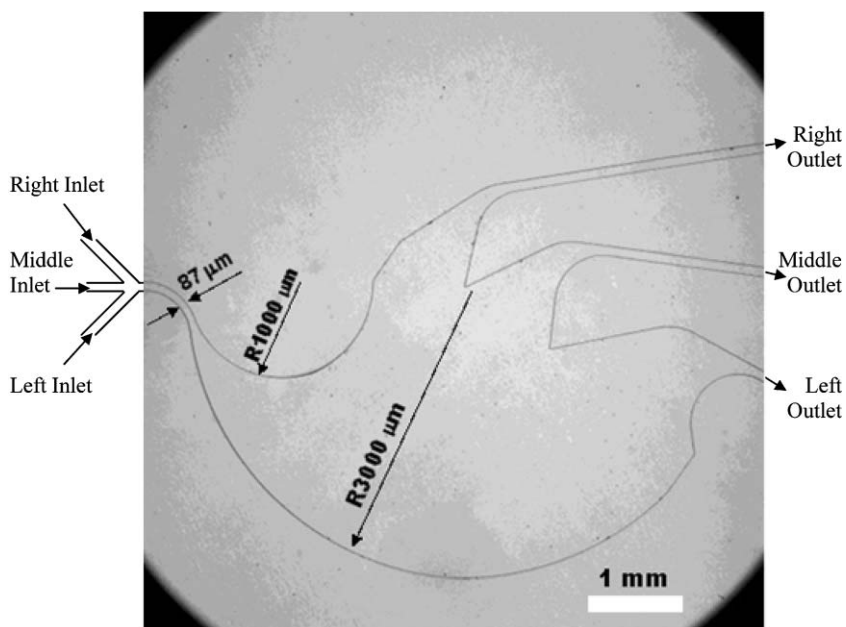


Fig. 1 Micrograph of the chip design and the channel network which is fabricated on a PDMS sheet with 6 interconnect holes, and the PDMS sheet is bonded to a glass cover.

system for 10 s (power, 100 W coil, 5 W platen; 100% O₂, 100 sccm; APC, 91. 5%; pressure, 80 mTorr). After exposure, the two surfaces were brought into contact and were allowed to rest to enable bonding to proceed, and the device was ready for use.

2.3. Instrumentation and image analysis

An Axiovert S100 inverted microscope (Carl Zeiss, Welwyn Garden City, Hertfordshire, UK) using transmission optics coupled with a monochrome CCD digital camera (Hamamatsu C4742-95-12NRB) was used to obtain both conventional micrographs and digital videos of the microchip which was placed horizontally on the microscope stage above the objective lens. Thus, the look direction in all the images obtained from this microscope is from the bottom of the microfluidic chip. The microscopic video images were then analyzed using IrfanView software. By tracking a particle in successive video images a velocity vector was obtained. Two KDS 200 syringe pumps (KD Scientific Inc., Holliston, MA, USA) were used to deliver the media and the sample containing microparticles. PEEK polymer tubing and connectors (Upchurch Scientific Inc., Oak Harbor, WA, USA) were used for plumbing to link the chip and the syringes.

3. Results and discussion

3.1. Flow characterisation

Whilst flow characteristics within channels with given channel widths under pressure driven flow has been intensively studied, the flow pattern and velocity profile within an asymmetric cavity still need to be characterised in order to demonstrate the separation principle and optimise the operation conditions. This was carried out by flowing media containing particles within the cavity at a given flow rate, and then tracking the flowing particles in successive video images taken at given time intervals (100 ms).

Fig. 2 shows the polymer microspheres (dia. 10 μm) flowing in the asymmetric cavity when the particles were carried by media and introduced *via* the middle inlet, with no additional fluid flow from either the left or right inlet. The input flow rate

was maintained at 1.375 $\mu\text{l min}^{-1}$. It can be seen that the particles were dispersed evenly within the media, in which they were flowing. To visualise the flow pattern five particles (marked in Fig. 2 (a)) were tracked as they progressed within the cavity producing results illustrated by Fig. 2 (b). It should be noted that the co-ordinate shown in the figure (and thereafter) are in accordance with that in the original digital image where the origin is at the top-left corner. From Fig. 2 (b) it can be seen that, as expected, the flow pattern in general follows the cavity shape. Specifically, when the particles were flowing in the x direction, the distance between them was increased across the y direction. This observation is indicative that particles can be separated within the asymmetric cavity based on the nature of the laminar flow field, given the appropriate particle position at the cavity entrance. The unique feature of this separation is its continuous amplification along the cavity, which suggests that a high resolution of separation can be reached.

Focused on the five particles chosen, the behaviour of the flow velocity within the cavity was also examined, and a flow velocity profile was obtained by locating each particle at a given time. Fig. 2 (c) shows that when the five particles are assumed to start flowing at the same time and position, and the time interval between the dashed lines is 100 ms. The main features of the flow velocity profile can be summarized as follows:

(i) The flow velocity decreases along the cavity, which is reflected by the reducing distance between the dashed lines. This decrease in the linear flow velocity is mainly due to the increase in the cross section area as it becomes wider along the flow direction;

(ii) A deformed symmetric parabolic flow velocity profile was created under pressure driven flow conditions, where the fluid/wall boundary velocity tends to be zero and the velocity maxima is obtained in the channel centre. This is generally in line with the observation obtained in a symmetric cross section channel.²² However, the two sidewalls in the asymmetric cavity are neither symmetric nor in parallel, and it is this irregularity that results in the parabolic flow velocity profile to be deformed;

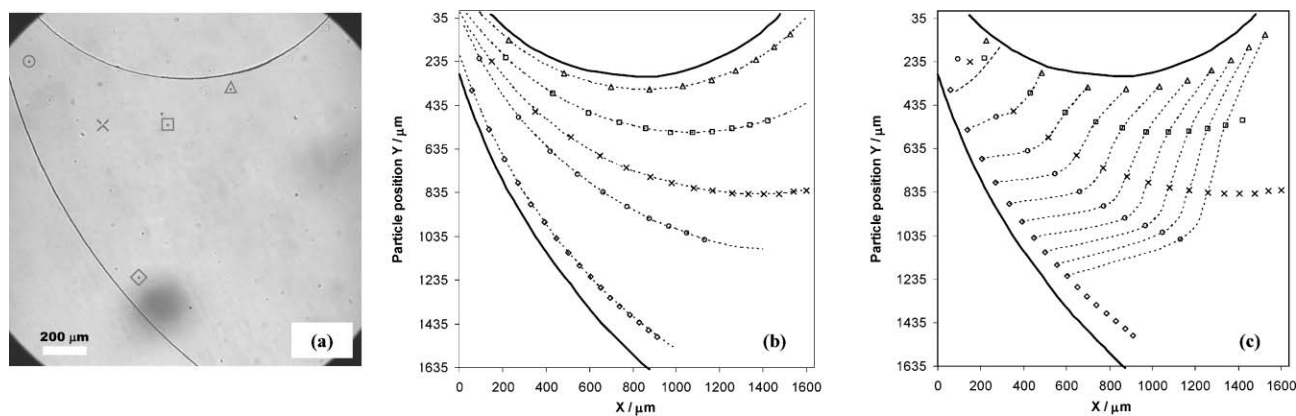


Fig. 2 Polymer microspheres (dia. 10 μm) flowing, carried by the media within the asymmetric cavity (a) where five particles are chosen, marked with different symbols accordingly for obtaining the flow pattern (b), and the flow velocity profile (c) by tracking particles in successive video images. Two solid curves define the cavity area.

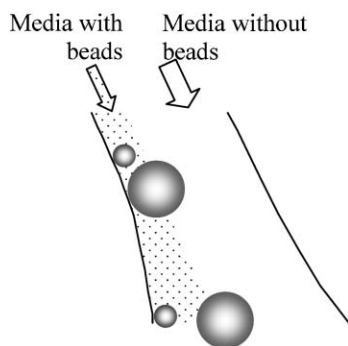


Fig. 3 The principle of the particle separation.

(iii) The deformation of the parabolic flow profile was pronounced along the cavity, a fact that was likely to be related to the development state of the flow profile. Generally, when the fluid enters a channel or pipe it needs a certain time period to develop the flow field because of the “entrance effect”²³ mainly caused by the sudden change of the channel geometry. Once developed, a parabolic velocity profile is obtained in the case of a symmetric straight channel. As can be seen in the asymmetric cavity, the cavity geometry is continuously changing that the flow within the entire cavity is underdeveloped, or continuously developing. As a result, the parabolic feature becomes more significant with flowing towards the wider area.

3.2. Effects of particle sample inlet positions

As discussed above, as the particles of different sizes contained in a stream of media were placed in appropriate positions in the flow field they can be separated continuously following the flow profile, thus the initial entry position of the particle is important for separation. Fig. 3 diagrammatically shows the principle of the separation at the entry section where a relatively narrow stream of media containing particle mixture is introduced along the left sidewall and the rest channel is occupied by media without particles. When the left side stream is narrow, all of the particles can be forced to flow along the

channel sidewall. In that case, particles in different sizes are passively placed in different distances between the spheres centre and the sidewall according to their diameters. This distance difference also forces the particles into different flowing tracks; the smaller being close to the sidewall and the larger, farther away, which consequently initialises the separation. While the laminar flow continues within the horn-shape cavity the separation is further amplified.

Fig. 4 (a) shows an example micrograph taken during the separation where the media containing particles was introduced *via* the left inlet at a flow rate of $1 \mu\text{l min}^{-1}$ and the media without particles *via* the middle and right inlets at a total flow rate of $2.75 \mu\text{l min}^{-1}$ in total. It can be seen that the particles were flowing within the laminar flow field in different tracks according to their sizes and were being separated continuously along the flow direction. It also shows that the flow pattern, flow velocity and separation effect are all agreed with that described and discussed previously for the expected observations.

Yamada *et al.*¹⁷ has studied the particle separation based on a different principle within a chip with a suddenly enlarged channel linked to a much narrower neck, which suggested that the “pinched” entrance section is then key to the separation results. In contrast, in our study, it was not necessary for the entrance channel to be small as long as the fluid stream that contains the particle mixture was narrow enough to position the particles at a different distance from the sidewall.

Based on the analysis and observation, the separation principle should also apply when the particle-containing media is introduced *via* the right inlet along the smaller curved sidewall. In this case, the flowing track which carries the smaller particles is expected to be close to the sidewall (Fig. 4 (b)). In contrast, when the particle-containing media enters the cavity *via* the middle inlet while the media without particles are flowing along both sides, this separation effect was lost (Fig. 4 (c)).

To quantitatively compare the effect of the inlet positions of the particle sample, a relatively large number of particles were analysed statistically to obtain their position in y direction when they passed across the detection line, the dashed line

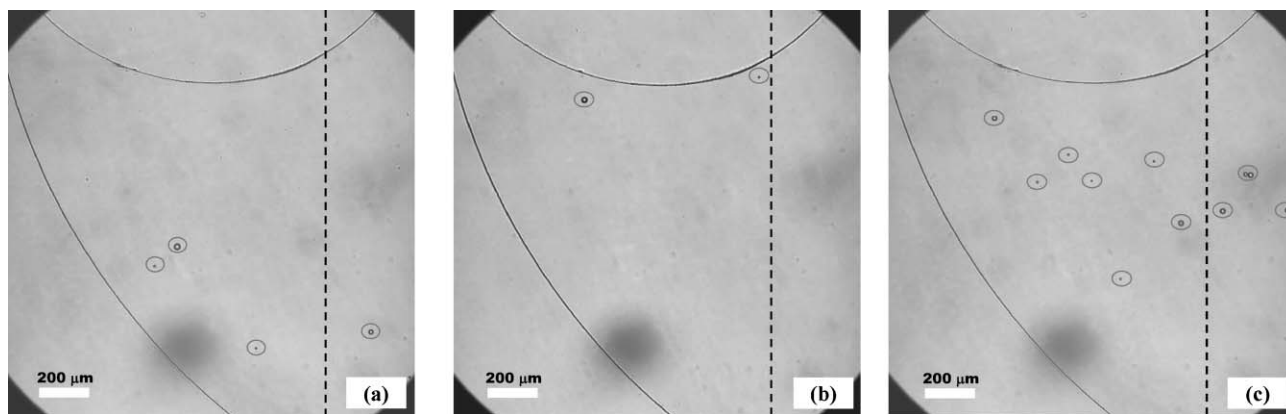


Fig. 4 Micrographs of the separation process when (a) the media with particles was introduced from the left inlet whilst the media without particles entered *via* both middle and right inlets, (b) the media with particles was introduced from the right inlet whilst the media without particles entered *via* both middle and left inlets, and (c) the media with particles was introduced from the middle inlet whilst the media without particles entered *via* both left and right inlets. The dashed line ($x = 1277.3 \mu\text{m}$) shows a reference for detection.

Table 1 Comparison of separation results for particles introduced *via* different inlets

	Left inlet		Middle inlet		Right inlet	
	d10 ^b	d25 ^c	d10 ^b	d25 ^c	d10 ^b	d25 ^c
Distance from upper sidewall ^a /μm						
Mean/μm	1227.7	1026.7	649.3	614.1	141.4	298.2
Range (±)/μm	+169.9	+57.9	+106.5	+122.5	+113.0	+128.7
	-159.0	-175.2	-235.2	-113.8	-110.6	-174.7
Separation ^d /μm	201.0		35.1		-156.7	

^a Particles distance from the small curved sidewall in *y* direction when passing across the reference line ($x = 1277.3 \mu\text{m}$) shown in Fig. 4.

^b Particles in a diameter of $10 \mu\text{m}$. ^c Particles in a diameter of $25 \mu\text{m}$. ^d Average distance between d10 and d25 particles when passing across the reference line.

Table 2 Comparison of separation results for different flow rate ratios (0.250 : 1–0.875 : 1) of media with particles to media without particles

	0.250 : 1		0.364 : 1		0.500 : 1		0.667 : 1		0.875 : 1	
	d10	d25	d10	d25	d10	d25	d10	d25	d10	d25
Distance from upper sidewall/μm										
Mean/μm	1283.3	807.9	1381.7	1180.8	1268.2	1145.0	1130.1	1029.0	1097.3	1014.4
Range (±)/μm	+136.7	+62.8	+169.9	+57.9	+98.3	+33.0	+338.5	+101.1	+505.4	+125.3
	-131.5	-90.5	-159.0	-175.2	-61.4	-24.5	-214.0	-84.1	-254.6	-79.0
Separation/μm	475.3		201.0		123.1		101.1		83.0	

shown in Fig. 4. The results are summarized in Table 1, which shows that the best separation was obtained when the particle sample was introduced *via* the left inlet. An average distance of $201 \mu\text{m}$ between large and small particles was created when they passed across the reference line ($x = 1277.3 \mu\text{m}$). The right inlet introduction of the particle sample can also result in separation but to a much lesser extent. As discussed above, this was mainly due to the relatively smaller change of flow field compared to that near the big curved sidewall. No significant separation was found when the particle sample was delivered through the middle inlet.

3.3. Effects of varying flow rate ratio

It has been demonstrated that a narrow stream of particle-containing media is essential to initialise the separation by placing the particles in different flow tracks according to their sizes. That can be created by changing the channel width of the asymmetric cavity entrance (which is impractical once the chip is fabricated). An operational way to reach this condition is to change the flow rate ratio, *i.e.*, the flow rate of the media containing particles compared to the flow rate of the media without particles. This variation of flow rates in turn changes the effective width of the stream of particle-containing media.

Table 2 summarizes the results obtained for a range of flow rate ratios between 0.250 : 1 and 0.875 : 1 when the particle sample was introduced *via* the left inlet and the media without particles was delivered *via* both middle and right inlets. The overall flow rate of the three streams was kept at a constant of $3.75 \mu\text{l min}^{-1}$. The flow rate of the media containing particle sample was varied from 0.75 to $1.75 \mu\text{l min}^{-1}$ while the other two inlets were controlled in a range of 3.0 to $2.0 \mu\text{l min}^{-1}$ in total. The average separated distance between large and small particles was plotted as a function of flow rate ratio in Fig. 5. It can be seen that the separation was significantly affected by the flow rate ratio. In general, a better separation was obtained when the flow rate ratio was decreased. That effect was enhanced when the ratio was below 0.4 : 1, which was reflected

on the dramatic increase in the average distance between the big particles and the smalls.

By varying flow rate ratios, R , the width of the particle carrier stream, W_{carr} , is altered according to the following equation.

$$W_{\text{carr}} = \frac{R}{1+R} W_{\text{chan}} \quad (1)$$

where W_{chan} is the entrance channel width of $87 \mu\text{m}$. As can be seen from Fig. 5, there is a critical flow rate ratio of 0.4 : 1 which corresponds to the carrier stream width of $24.86 \mu\text{m}$. This is in good agreement with the larger particle diameter of $25 \mu\text{m}$, suggesting that a minimum particle-containing stream width, which is equal to the big particle diameter, should be maintained in order to obtain a separation.

It was also observed that the flow rate ratio had a more significant effect on the small particles travelling distance in *y* direction. When the width of the particle-containing stream

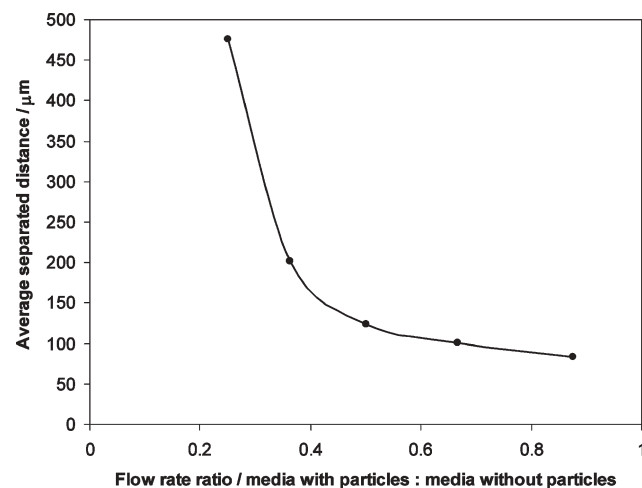


Fig. 5 Average separated distance between big and small particles as a function of flow rate ratio.

Table 3 Comparison of separation results for different total flow rates (2.80–5.60 $\mu\text{l min}^{-1}$)

Distance from upper sidewall/ μm	2.80 $\mu\text{l min}^{-1}$		3.75 $\mu\text{l min}^{-1}$		5.60 $\mu\text{l min}^{-1}$	
	d10	d25	d10	d25	d10	d25
Mean/ μm	1168.0	1009.6	1227.7	1026.7	1175.0	1068.7
Range (\pm)/ μm	+181.8	+59.1	+169.9	+57.9	+225.8	+118.2
	–137.6	–59.1	–159.0	–175.2	–138.2	–143.7
Separation/ μm	158.3		201.0		106.3	

was increased, the small particles contained in that stream also spreaded in a wider area compared to the larger ones, which again was reflected on changes in both the small particles distance from the lower sidewall and their covering range (see the maximum and minimum ranges in Table 2).

3.4. Effects of total flow rates

At a constant flow rate ratio of 0.364 : 1 (media with particles relative to media without particles) while the particle sample was introduced *via* the left inlet, the effect of varying total flow rate was also examined. The total flow rate was controlled at three levels of 2.80, 3.75 and 5.60 $\mu\text{l min}^{-1}$. The results are compared in Table 3.

It can be seen that the influence of the total flow rate on the separation was insignificant, which indicated that the flow profile remained unaltered with the change of total flow rates under the experimental conditions. Thus, a higher total flow rate can be operated to obtain a high throughput without the cost of separation efficiency. This observation is in line with that obtained by Yamada *et al.*¹⁷

It was also interesting to note from Table 3 that the large particles were moving towards the large circle sidewall. This was reflected by an increase in the distance to the small circle sidewall, from 1009.7 to 1068.7 μm , when the total flow rate was increased from 2.813 to 5.625 $\mu\text{l min}^{-1}$. The change was likely due to the centrifugal effect with a higher velocity flow along the curved cavity which, however, still needs more investigation.

4. Conclusions

A microdevice has been designed and fabricated with an asymmetric cavity. This device has been used to separate polymer microspheres of two sizes, 10 and 25 μm . The process is based on the microfluidic profile within the asymmetric cavity, which can amplify the separation in a continuous manner along the flow profile. The results showed that the introduction of the particle sample *via* the left inlet along the large circle sidewall gave the best separation. It was also found that a narrower stream width of particles gave a better separation which can be obtained by varying the flow rate ratio, but a minimum particle-containing stream width equal to the large particle diameter should be maintained in order to obtain a reasonable separation. No significant effect of total flow rate on the separation result was observed which however

suggested that a higher sample throughput is reachable. This technique can in principle be applied for manipulating both microscale biological and colloidal particles within microfluidic systems.

References

- 1 A. Manz, J. C. Fettinger, E. Verpoorte, H. Ludi, H. M. Widmer and D. J. Harrison, *Trends Anal. Chem.*, 1991, **10**, 144–149.
- 2 K. F. Jensen, *Chem. Eng. Sci.*, 2001, **56**, 293–303.
- 3 *8th International Conference on Miniaturized Systems for Chemistry and Life Sciences (MicroTAS 2004)*, ed. T. Laurell, J. Nilsson, K. Jensen, D. J. Harrison and J. P. Kutter, Malmö, Sweden, September 26–30, 2004, Royal Society of Chemistry, Cambridge, UK, 2004.
- 4 P. D. I. Fletcher, S. J. Haswell, E. Pombo-Villar, B. H. Warrington, P. Watts, S. Y. F. Wong and X. Zhang, *Tetrahedron*, 2002, **58**, 4735–4757.
- 5 *Microsystem Technology in Chemistry and Life Sciences*, ed. A. Manz and H. Becker, Springer, Berlin, 1998.
- 6 P. Vastamaki, M. Jussila and M.-L. Riekkola, *Analyst*, 2005, **130**, 427–432.
- 7 J. C. Giddings, *Sep. Sci.*, 1966, **1**, 123–125.
- 8 *Field-Flow Fractionation Handbook*, ed. M. Schimpf, K. Caldwell and J. C. Giddings, John Wiley & Sons, Inc., New York, 2000.
- 9 J. Auerswald and H. F. Knapp, *Microelectron. Eng.*, 2003, **67–68**, 879–886.
- 10 T. Lilliehorn, U. Simu, M. Nilsson, M. Almqvist, T. Stepinski, T. Laurell, J. Nilsson and S. Johansson, *Ultrasonics*, 2005, **43**, 293–303.
- 11 N. Pamme and A. Manz, *Anal. Chem.*, 2004, **76**, 7250–7256.
- 12 J. Janca, I. A. Ananieva, A. Y. Menshikova, T. G. Evseeva and J. Dupak, *J. Chromatogr., A*, 2004, **1046**, 167–173.
- 13 M. P. MacDonald, S. Neale, L. Paterson, A. Richies, K. Dholakia and G. C. Spalding, *J. Biol. Regul. Homeostatic Agents*, 2004, **18**, 200–205.
- 14 J. Kruger, K. Singh, A. O'Neill, C. Jackson, A. Morrison and P. O'Brien, *J. Micromech. Microeng.*, 2002, **12**, 486–494.
- 15 J. Kim, S. H. Jang, G. Jia, J. V. Zoval, N. A. Da Silva and M. J. Madou, *Lab Chip*, 2004, **4**, 516–522.
- 16 J. Oakey, J. Allely and D. W. M. Marr, *Biotechnol. Prog.*, 2002, **18**, 1439–1442.
- 17 M. Yamada, M. Nakashima and M. Seki, *Anal. Chem.*, 2004, **76**, 5465–5471.
- 18 S. Ookawara, R. Higashi, D. Street and K. Ogawa, *Chem. Eng. J.*, 2004, **101**, 171–178.
- 19 J. Takagi, M. Yamada, M. Yasuda and M. Seki, *Lab Chip*, 2005, **5**, 778–784.
- 20 M. Slifkin and R. Cumbie, *J. Clin. Microbiol.*, 1992, **30**, 2722–2724.
- 21 F. T. Docherty, P. B. Monaghan, R. Keir, D. Graham, W. E. Smith and J. M. Cooper, *Chem. Commun.*, 2004, 118–119.
- 22 Y. J. Kang, C. Yang and X. Y. Huang, *Microfluid Nanofluid*, 2005, **1**, 168–176.
- 23 J. O. Wilkes and S. G. Bike, *Fluid Mechanics for Chemical Engineers*, Prentice Hall PTR, Upper Saddle River, 1998.

Influence of Hydrodynamic Conditions on Quantitative Cellular Assays in Microfluidic Systems

Huabing Yin,[†] Xunli Zhang,[‡] Nicola Patrick,[§] Norbert Klauke,[†] Hayley C. Cordingley,[§] Stephen J. Haswell,[‡] and Jonathan M. Cooper^{*†}

Department of Electronics and Electrical Engineering, University of Glasgow, Glasgow, G12 8LT, U.K., Department of Chemistry, University of Hull, Hull, HU6 7RX, U.K., and Technology Development, GlaxoSmithKline Pharmaceuticals, Harlow, CM19 5AW, U.K.

This study demonstrates the importance of the hydrodynamic environment in microfluidic systems in quantitative cellular assays using live cells. Commonly applied flow conditions used in microfluidics were evaluated using the quantitative intracellular Ca²⁺ analysis of Chinese hamster ovary (CHO) cells as a model system. Above certain thresholds of shear stress, hydrodynamically induced intracellular Ca²⁺ fluxes were observed which mimic the responses induced by chemical stimuli, such as the agonist uridine 5'-triphosphate tris salt (UTP). This effect is of significance given the increasing application of microfluidic devices in high-throughput cellular analysis for biophysical applications and pharmacological screening.

Cell-based assays have been performed in a variety of sectors in the life sciences, particularly those associated with biotechnology and the pharmaceutical industries. Many cellular assays use intact cells to obtain functional information on cell signaling pathways as well as kinetic data related to drug absorption, metabolism, and toxicity. In recent years there have been rapid developments in cell-based assays in microfluidic systems, particularly in the area of lab-on-a-chip, enabling the efficient analysis of complex biological phenomenon within microscale systems.¹ Clearly, the generation of quantitatively reliable information on-chip, which is a true reflection of the cell's response to a drug or an analyte, remains an important challenge within the biopharmaceutical industry.

To date, microfluidic devices have been constructed to study either single-cell or population responses to a variety of factors such as exposure to agonists, electrical stimulation, or variations in the solution composition that may be quiescent or flowing. In general, hydrodynamic forces (or shear stresses) are more significant within microfluidic systems,² compared to open quiescent microtiter plates. Several studies have already shown that

shear stress can have a range of effects dependent on both the cell type and the local hydrodynamic environment.^{3–7} For example, the severity of shear stress can influence the metabolism of hepatocytes³ and the morphology and metabolism of shear-sensitive endothelia cells.^{6,7} Outside of the microfluidic environment shear stress has also been found to modulate ion channel (i.e., K⁺, Ca²⁺) activation in mechanosensitive cell types, such as endothelial cells⁸ and bone cells.⁹ Furthermore, it has been observed that Ca²⁺ flux is modulated in artificially constructed bilayers by changes in shear stress.¹⁰ This latter observation suggests that similar variations in Ca²⁺ flux may exist even for cell types that are generally regarded as non-mechano-sensitive, when they are subjected to the fluid flow regimes found in microfluidic devices where moderate to high shear stresses can readily exist.

The importance of having an understanding of the fundamental reasons behind variations in cellular-based Ca²⁺ flux can be appreciated since Ca²⁺ is generally regarded as a universal intracellular messenger, regulating a diverse range of processes, such as gene transcription, muscle contraction, and cell proliferation,¹¹ with localized changes reported in a variety of diseases.¹² As a consequence, Ca²⁺ measurement is now one of the most important validation assays in high-throughput drug screening in the pharmaceutical industry.¹³ To date, however, there has only been limited published work on the measurement of intracellular Ca²⁺ in microfluidic or lab-on-a-chip systems, with examples of

* To whom correspondence should be addressed. Phone: +44(0)141-330-4931. Fax: +44(0)141-330-6002. E-mail: jmcooper@elec.gla.ac.uk.

[†] University of Glasgow, Glasgow.

[‡] University of Hull, Hull.

[§] GlaxoSmithKline Pharmaceuticals.

(1) El-Ali, J.; Sorger, P. K.; Jensen, K. F. *Nature* **2006**, *442*, 403–442.

(2) Walker, G.; Zeringue, H. C.; Beebe, D. J. *Lab Chip* **2004**, *4*, 91–97.

(3) Tanaka, Y.; Yamato, M.; Okano, T.; Kitamori, T.; Sato, K. *Meas. Sci. Technol.* **2006**, *17*, 3167–3170.

(4) Jacobs, C. R.; Yellowley, C. E.; Davis, B. R.; Zhou, Z.; Cimbala, J. M.; Donahue, H. J. *J. Biomech.* **1998**, *31*, 969–976.

(5) Keane, J. T.; Ryan, D.; Gray, P. *Biotechnol. Bioeng.* **2003**, *81*, 211–220.

(6) Gray, B. L.; Lieu, D. K.; Collins, S. D.; Smith, R. L.; Barakat, A. I. *Biomed. Microdevices* **2002**, *4*, 9–16.

(7) Nollert, M. U.; Diamond, S. L.; McIntire, L. V. *Biotechnol. Bioeng.* **1991**, *38*, 588–602.

(8) Li, Y.; Haga, H.; Chien, S. *J. Biomech.* **2005**, *38*, 1949–1971.

(9) Klein-Nulend, J.; Bacabac, R. G.; Mullender, M. G. *Pathol. Biol.* **2005**, *53*, 576–580.

(10) Chakravarthy, S. R.; Giorgio, T. D. *Biochim. Biophys. Acta Biomembranes* **1992**, *1112*, 197–204.

(11) Bootman, M. D.; Collins, T. J.; Peppiatt, C. M.; Prothero, L. S.; MacKenzie, L.; De Smet, P.; Travers, M.; Tovey, S. C.; Seo, J. T.; Berridge, M. J.; Ciccolini, F.; Lipp, P. *Cell Dev. Biol.* **2001**, *12*, 3–10.

(12) Rizzuto, R.; Pozzan, T. *Nat. Genet.* **2003**, *34*, 135–141.

(13) Monteith, G. R.; Bird, G. St. J. *Trends Pharmacol. Sci.* **2005**, *26*, 218–223.

such work focusing on excitable chondrocyte cells^{14,15} and the myocyte cells.^{16–18} Fundamental studies to evaluate on-chip intracellular Ca²⁺ analysis as a reliable method for general biophysical and pharmacological screening applications are less well represented in the literature, especially when a non-mechano-sensitive cell type is used.

In order to ascertain whether Ca²⁺ fluxes are induced when non-mechano-sensitive cells are subjected to different shear stresses in a microfluidic environment, we conducted a quantitative evaluation of variations in Ca²⁺ flux within Chinese hamster ovary (CHO) cells (generally regarded as a non-mechano-sensitive cell) immobilized from a loaded cell suspension. Here, *immobilized cells* differ from *adherent cells* in that the latter are cultured and then spread over a substrate. One pragmatic reason for immobilizing the cell within the channel is that the process fixes its position, thereby helping with signal tracking (intracellular Ca²⁺ levels will change in both space and amplitude over fast time scales¹¹).

This Ca²⁺ flux was measured using the Ca²⁺ sensitive fluorescence indicator, and experiments were performed within a platform comprising a microfluidic manifold clamped to a preprepared substrate. This allowed the manifold to be sterilized and substrates chemically modified prior to integration. The particular silane and collagen surface modifications described below were found to provide an effective means to both immobilize cells on-chip and maintain their viability.

MATERIALS AND METHODS

Cell Culture. All cell culture media and serum were supplied by Invitrogen Corporation. The CHO cell line was supplied from GSK. CHO cells were cultured in 25 cm² tissue culture flasks at 37 °C in a humidified atmosphere with 5% CO₂/95% air. The cells were incubated in DMEM/F12 medium supplemented with 10% fetal calf serum and 4 mM L-glutamine. All chemicals were supplied by Sigma Limited (Poole, U.K.), unless otherwise indicated.

Cells were grown to near confluence in the culture flasks and then suspended with 0.05% trypsin–EDTA solution. The concentration of suspended cells was determined using a hemocytometer, before being introduced into the microfluidic chip. The viability of cells was determined using the 0.4% trypan blue solution. An average measurement of the percent viable cells in four randomly selected fields of view was used as a measure of cell viability.

Cell Loading and Immobilization. Cells in suspension at a concentration of about 2.5 × 10⁶ cells/mL were pumped into a microfluidic channel at a flow rate of 1 μL/min. Once in the channel, they were left undisturbed for 30 min to allow attachment to the channel surface. Subsequently, unattached cells were washed away at a flow rate of 1 μL/min. Adhesion experiments were performed to investigate the density of attached cells over a range of shear stresses, starting at low flow rates and then increasing. During a given measurement, a continuous flow was

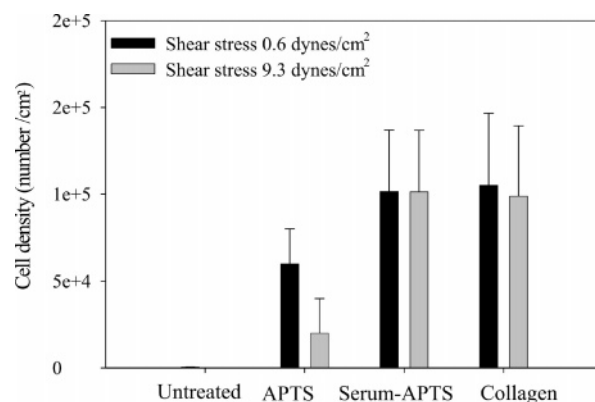


Figure 1. Comparison of immobilized cell densities on differently modified microfluidic channels at both low (black) and elevated shear stresses (gray). Statistical results of three independent experiments for each condition. The seeding density was 2.5 × 10⁶ cells/mL.

maintained for 2 min, during which time the chip was imaged in situ. This was followed by a 1 min quiescent period, before retesting the cells at a higher flow rate (inducing progressively higher shear stresses). In all cases, the maximum Reynolds number was less than 0.1, indicating that flow was laminar in nature.

Images were taken at the center of the channels, away from the side walls, to ensure the full development of the flow profile. Cell number and morphology in the field of view were recorded in real time using bright-field phase contrast microscopy. Cell densities attached on the surfaces were determined by dividing the number of cells left in the field of view after each step by the surface area of the field of view.

Intracellular Ca²⁺ Flux. In order to quantitatively evaluate the intracellular Ca²⁺ level, a well-established fluorescence intensity measurement using Fluo-4 AM Ca²⁺ indicator dye was employed in this study.¹⁹ This involved labeling cells with the dye and subsequently monitoring any change in fluorescence intensity as the cells responded to shear stress.

Cell Labeling. The Ca²⁺ fluorescent dye solution comprised 2 μM Fluo-4 AM (Invitrogen Molecular Probes) in a Tyrode buffer. The Tyrode buffer was prepared from a stock containing 145 mM NaCl, 2.5 mM KCl, 10 mM HEPES, 10 mM D-glucose, 1.2 mM MgCl₂, pH 7.4. Final concentrations of 2.5 mM probenecid and 1.5 mM CaCl₂ were added shortly before the buffer was used. Suspended cells were centrifuged and washed with the Tyrode buffer at 100g for 5 min to remove the medium. They were resuspended in the labeling buffer to a concentration of ~2.5 × 10⁶/mL and incubated at 37 °C for 10 min.

Signal Recording. Fluorescence imaging was used to record the change of intracellular Ca²⁺ level using the Fluo-4 AM labeled cells. The labeled suspended CHO cells were loaded into microfluidic channels and left undisturbed in darkness for 30 min to allow further incorporation of the dye into cells and for cell attachment to the substrate surface to occur. It was found that such a labeling procedure provided a strong fluorescence signal from within cells. Importantly, the cell-permeable Fluo-4 AM ester fluoresces only after it enters the cells, giving low background signals.¹⁹ After this 30 min incubation, Tyrode buffer was then

(14) Chao, P. H. G.; West, A. C.; Hung, C. T. *Am. J. Physiol.: Cell Physiol.* **2006**, *291*, C718–C725.

(15) Donahue, S. W.; Donahue, H. J.; Jacobs, C. R. *J. Biomech.* **2003**, *36*, 35–43.

(16) Klauke, N.; Smith, G. L.; Cooper, J. M. *Biophys. J.* **2006**, *91*, 2543–2551.

(17) Li, X.; Li, P. C. H. *Anal. Chem.* **2005**, *77*, 4315–4322.

(18) Werdich, A. A.; Lima, E. A.; Ivanov, B.; Ges, I.; Anderson, M. E.; Wikswo, J. P.; Baudenbacher, F. *J. Lab. Chip* **2004**, *4*, 357–362.

(19) Takahashi, A.; Camacho, P.; Lechleiter, J. D.; Herman, B. *Physiol. Rev.* **1999**, *79*, 1089–1125.

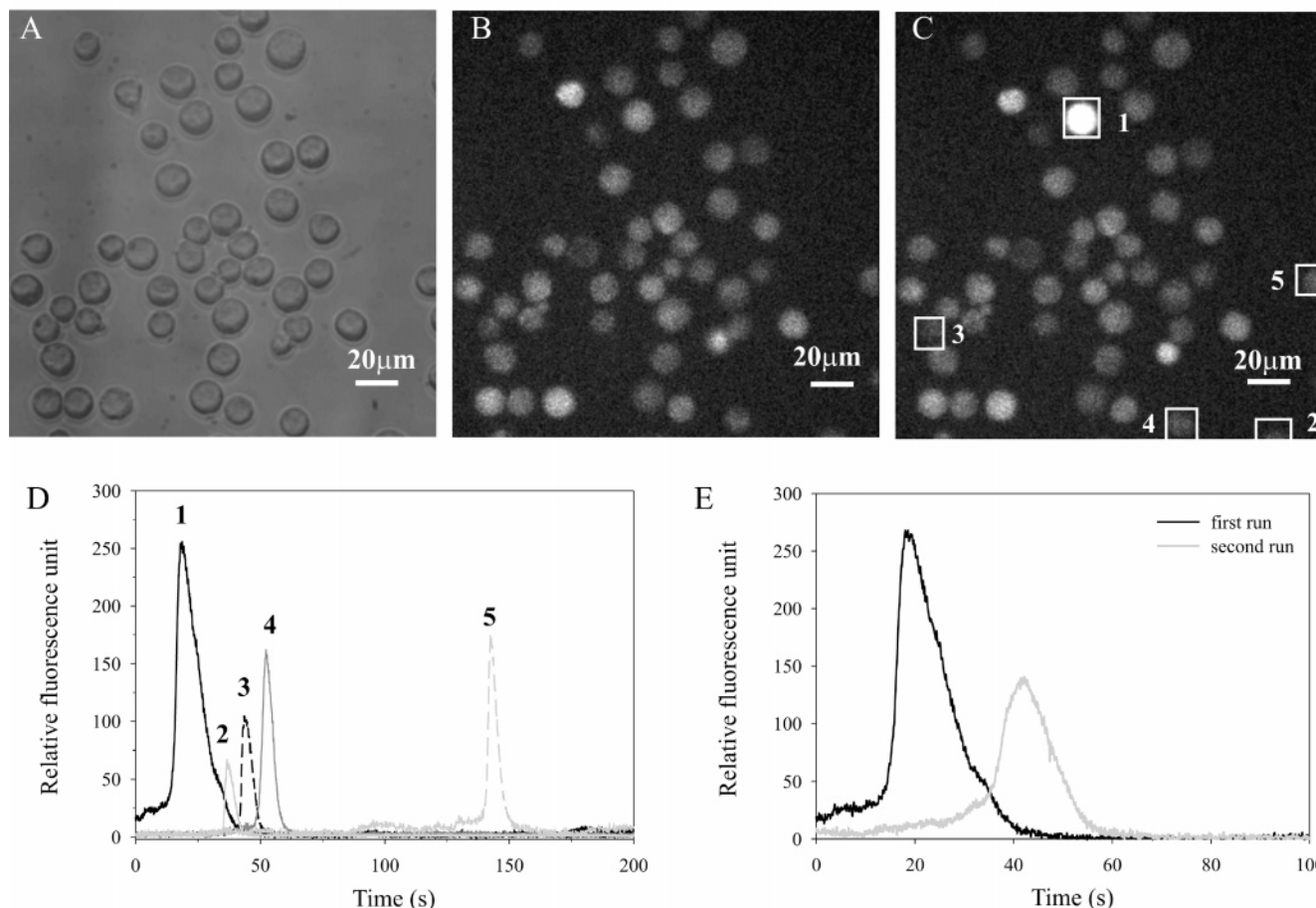


Figure 2. Shear-stress-induced intracellular Ca^{2+} transient measured from spherical suspended cells. Transmitted light image (A) and fluorescent images (B and C) of cells in the center of the $500\ \mu\text{m}$ wide microfluidic channel. The fluorescent image (B) represents background in the absence of any flow, while the fluorescent image (C) shows one cell (cell 1) responding to shear stress at $9.3\ \text{dynes/cm}^2$ 16 s after the onset of flow. During the 2 min of recording, five cells respond to the shear stress (each is surrounded by a square, and the sequence is shown in the Supporting Information). The Ca^{2+} -sensitive fluorescent dye Fluo-4 was used to indicate intracellular Ca^{2+} flux. (D) Corresponding relative fluorescence unit profile of the responding cells in (C), showing the temporal (transient) nature and magnitude of the response. For the purpose of comparison, the relative fluorescence unit was plotted after subtraction of the particular quiescent baseline fluorescence unit to an individual cell. Panel E shows a representative example of the recovery of the response of cells after shear stress was resumed in the second run. A representative profile of cell 1 in (C) is shown.

flowed across the attached cells at successively higher rates, which gave an increase in shear stress. At each flow rate, continuous flow was maintained for 6 min during which time three different intracellular regions were recorded for 2 min each. After each recording, the cells were maintained in quiescent buffer for 1 min, before performing the next measurement at a higher flow rate.

Data Acquisition and Analysis. Both transmission and fluorescent images were recorded using a Zeiss Axiovert inverted fluorescence microscope coupled to a monochrome cooled CCD digital camera (Andor iXon, Andor Technology). A filter set, containing an exciter D475/40, an emitter E510, and a beam splitter Dichroic 495, was used for the fluorescence imaging. The intensity of the excitation light was adjusted using neutral density filters ($\text{OD} = 1$) to minimize photobleaching of the dye. Real-time fluorescence recordings were made for 3 min at a rate of 10 frames per second with a nominal gain of 200. Confocal images were recorded using a Zeiss LSM 510 Meta confocal system with 488 nm argon ion laser using a $\times 63$ oil immersion lens. Z-stacks were recorded to measure cell size in three dimensions.

The fluorescence intensity of whole discrete individual cells was obtained using the Andor iQ1.4 image software. The maxi-

um responding amplitude (simplified as response) was calculated accordingly: The cell's response was expressed as $(F_{\text{peak}} - F_0)/F_0 \times 100\%$, where F_{peak} is the peak fluorescence intensity and F_0 the baseline.¹⁹ For all the measurements, fluorescence intensity was background subtracted using the fluorescence intensity of an adjacent cell-free region. The baseline fluorescence intensity (F_0) was taken as an average initial value over 10 s before applying either shear stress or UTP solutions.

RESULTS AND DISCUSSION

The overall aim of this work was to assess the potential use of microfluidics as a reliable method for high-throughput cellular functional assay. In order to provide a suitable platform for such a study, it was necessary to design a device capable of accurately and reliably testing cell responses under different flows and different chemical stimuli. The particular requirements of this study, included the generation of statistically meaningful information, the creation of uniform, well-controlled flow profiles around cell, and the production of a disposable device (or disposable cell-contact part) to reduce the potential for contamination. The resulting microfluidic platform (Supporting Information Figure S1)

was then used to assess the effect of commonly used hydrodynamic conditions on quantitative intracellular Ca^{2+} cellular assay.

Microfluidic Device Design and Fabrication. The microfluidic device developed for this study is shown in Supporting Information Figure S1, parts A and B. The substrate was modified using a biocompatible adhesion matrix to increase the likelihood of cell attachment and enhance viability. The sealing mechanism maintained the integrity of this adhesion matrix layer in the microchannel. Leakage from the chip was tested using a colored dye, and it was found that the device formed in this way remained robust even with shear stresses of 120 dynes/cm^2 (Supporting Information video 1). Note: none of the experiments using cells as discussed below involved shear stresses that exceeded 10 dynes/cm^2 , as calculated from eq 1.

Many reported microfluidic devices for cellular assays have channels $10\text{--}100 \text{ }\mu\text{m}$ wide and less than $50 \text{ }\mu\text{m}$ high,²⁰ leading to shear stresses in the range of many tens of dynes/cm^2 even with low flow rates of $2 \text{ }\mu\text{L/min}$. The actual shear stress on such cells may, in fact, be even higher due to a high cell radius/channel height ratio.²¹ In general, rapid on-chip cellular measurement requires a sufficiently fast flow rate for cell or reagent delivery. To take into account both the speed of the reagent delivery and the resultant shear stress, hydrodynamic conditions that lead to low shear stresses of less than 10 dynes/cm^2 were assessed in this study.

To estimate hydrodynamic mechanical loading on the cells, the effects of cell topology and microchannel design were also taken into account. Gaver and Kute have previously demonstrated that the actual mechanical stress on an attached round-shaped cell was significantly greater than that experienced in a cell-free system when the ratio of cell size to channel height (R/H) was over 0.25 .²¹ Lu et al. found that when $R/H = 0.16$, the average shear stress on a nonflat cell was comparable to that of an empty channel.²²

In this study, after cell attachment for 30 min, the mean diameter of CHO cells (from base membrane to cell top) was $\sim 10.5 \text{ }\mu\text{m}$, as determined by confocal microscopy. The channel height of the chips chosen for this study was $140 \text{ }\mu\text{m}$ ($R/H < 0.1$), so avoiding any amplification of mechanical stress (as predicted by others^{21,22}). In other words, when R/H is very small, the shear stress on the cell is equivalent to the wall shear stress.

The wall shear stress, which takes into account both flow rate and the geometry of chips, was used in the study as the nominal mechanical loading on cells, according to eq 1:²²

$$\tau = -\frac{12v\nu}{h} \quad (1)$$

where τ is shear stress (dynes/cm^2), ν is liquid viscosity (g/cm-s), v is linear velocity (cm/s), and h is the flow channel height. As illustrated in eq 1, increases in flow rate lead to a proportional increase in shear stress for fixed geometry systems.

Surface Modification for Cell Immobilization. When using unmodified glass substrates to construct the base of microfluidic

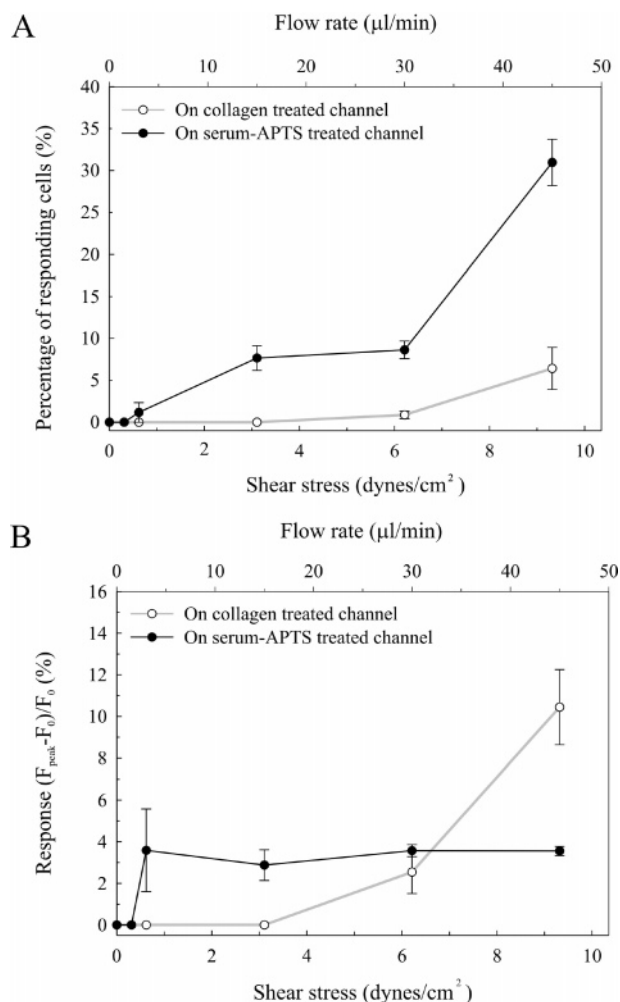


Figure 3. Shear-induced Ca^{2+} flux as a function of shear stress. (A) Figure shows the dependence of responding population to the shear stress; panel B shows the amplitude as a function of shear stress. The flow rates and the corresponding shear stresses were shown on the top and the bottom of the x-axis, respectively. The error bar is the standard error ($n = 270$).

channels, it was found that few cells attached, even at a low flow rate of $1 \text{ }\mu\text{L/min}$ and high loading density of $1 \times 10^7 \text{ cells/mL}$. Modification with collagen and APTS silane was used to enhance cell attachment. The surface modification process was optimized off-chip (Supporting Information). Initial attachment of CHO cells on the modified surfaces was examined by plating the substrates for 30 min with serum-free CHO suspended cells at a seeding density of $2.5 \times 10^6 \text{ cells/mL}$, followed by rinsing with serum-free culture medium. Attachment densities were higher on the collagen-treated surface compared to untreated glass. It was observed that such an enhancement was significantly higher on a surface treated with collagen at concentrations $> 0.4 \text{ mg/mL}$, Supporting Information Figure S2A, although there was no significant further enhancement at higher concentrations. Overnight incubation of the attached cells with serum-free culture medium also showed an enhancement in cell growth after the collagen treatment (Supporting Information Figure S2B), suggesting the role of an improved biocompatible extracellular matrix. An off-chip-modified substrate was used to construct the device, since this provided a flexible way of integrating different surface

(20) Andersson, H.; van den Berg, A. *Sens. Actuators, B* **2003**, *92*, 315–325.

(21) Gaver, D. P.; Kute, S. M. *Biophys. J.* **1998**, *75*, 721–733.

(22) Lu, H.; Koo, L. Y.; Wang, W. M.; Lauffenburger, D. A.; Griffith, L. G.; Jensen, K. F. *Anal. Chem.* **2004**, *76*, 5257–5264.

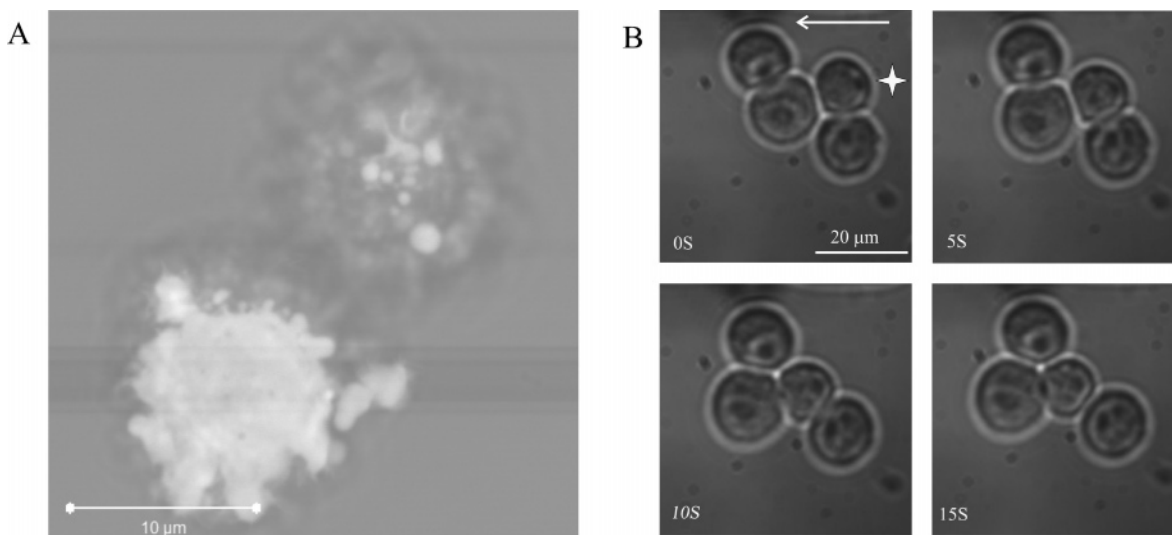


Figure 4. (A) Fluorescence confocal images show the different degree of attachment of two cells, 15 min after loading onto the substrates. Cells were washed and loaded with $2 \mu\text{M}$ calcein AM for fluorescence imaging. The images were taken on the plane near the substrate. The contact area that cells forms with the substrate is indicated by the fluorescence intensity. The large difference in the contact area of two cells indicates an inherent heterogeneity in cell attachment. The heterogeneity persists for at least 2 h. (B) Time series of bright-field images showing cell movement due to high shear stress (9.3 dynes/cm^2). The white star indicates the moving cell. In both (A) and (B), surfaces had been treated with serum–APTS silane. The white arrow indicates flow direction.

functionalizations with microfluidics. No leakage was found over the range of shear stresses investigated.

The densities of attached cells in the resultant microchannels under various hydrodynamic conditions were investigated, and the results are shown in Figure 1. After initial loading of cells at a low shear stress of $\sim 0.6 \text{ dyn/cm}^2$, cell attachment densities increased by 2 orders of magnitude on an APTS silane treated substrate, and by an additional factor of 2 on a collagen-treated substrate, in comparison to that obtained on an unmodified glass substrate. More than half of the cells attached on the APTS silane treated surface were lost at a shear stress of $\sim 9.3 \text{ dynes/cm}^2$, whereas most ($>95\%$) cells on the collagen-treated surface remained. However, both cell attachment density and adhesion strength were enhanced if the APTS silane treated surface was first primed with a serum containing culture medium. This latter modification achieved a similar performance to that of a collagen-treated surface and is possibly due to the adsorption of soluble proteins, such as fibronectin (or other attachment factors) onto the positively charged APTS silane modified glass surface.²³ Both collagen and serum–APTS silane treatment of microchannels promoted rapid cell attachment and enhanced immobilization density, allowing statistical studies to be made.

Intracellular Ca^{2+} Flux Induced by Shear Stress. Reliable functional information can only be obtained from viable cells. The viability of cells on the collagen-modified surface under the highest shear stress of $\sim 9.3 \text{ dynes/cm}^2$ was found to be over 96%, which was virtually identical to that determined before loading ($96.7 \pm 0.6\%$). We found that even a brief exposure to low levels of shear stress induced an intracellular Ca^{2+} flux in the CHO cells, although no gross morphological changes were observed. A representative series of fluorescence images of shear-induced Ca^{2+} flux of CHO cells at 9.3 dynes/cm^2 are shown in Figure 2, parts Band C. After the onset of the flow, a fraction of the cells start to respond,

resulting in transients ($\sim 20 \text{ s}$) of high levels of intracellular Ca^{2+} concentration, as indicated in the fluorescence intensity profile (Figure 2D). The Ca^{2+} flux within each of the cells was different with respect to its point of initiation, its amplitude, and the frequency of oscillation of its response (details shown in Supporting Information video_2). No cell responded when the fluid flow was stopped. In some cases, cells were found to respond to stimulation when the same, or an increased, shear stress was resumed, although the amplitude of the response was always reduced, Figure 2E.

Characteristics of Shear-Induced Intracellular Ca^{2+} Flux.

To understand the nature of shear-induced intracellular Ca^{2+} flux and the relationship of cell response to shear stress, further statistical studies were carried out over a range of shear stress from 0.01 to 9.3 dynes/cm^2 . The use of either serum–APTS silane modified or collagen-modified substrates for the construction of chips gave rise to a high density of attached suspended cells (~ 40 to ~ 50 cells in a field of view of $200 \times 200 \mu\text{m}^2$).

Six different regions comprising over 270 cells were recorded to permit a statistically meaningful evaluation which showed that there was a threshold for shear-induced intracellular Ca^{2+} transition of CHO cells whether attached on serum–APTS silane treated surfaces ($>0.31 \text{ dynes/cm}^2$) or on collagen-treated surfaces ($>3.1 \text{ dynes/cm}^2$), as shown in Figure 3A. In both cases there was a clear trend showing that the percentage of the cell population that was responding increased with increased shear stress, although the amplitude of the responses varied. This latter variation was constant over the range of shear stress studied, once the Ca^{2+} response was triggered. In addition, cells attached on a serum–APTS silane treated surface had a higher percentage of responding population than those on the collagen-treated surface, even though cell densities attached on both surface types were similar (Figure 3B).

(23) Steele, J. G.; Dalton, B.; Johnson, G.; Underwood, P. *Biomaterials* **1995**, *16*, 1057–1067.

The intracellular Ca^{2+} transition can be activated through a variety of mechanisms, such as ligand-gated ion channels or via membrane depolarisation.¹¹ In this series of experiments, there were no chemical stimuli present, and the observed shear-induced intracellular Ca^{2+} flux in a nonexcitable CHO cell may therefore be directly related to mechanically triggered channel opening¹¹ due to membrane depolarization. Using confocal microscopy, we found that the extent of cell attachment (measured as the “in contact” surface area) on the same chip showed a degree of variability, ranging from ~ 10 to $110 \mu\text{m}^2$. A z-slice taken at the level of the substrate revealed the area of attachment, and a representative example is shown in Figure 4A. At low levels of shear stress, on both collagen and serum-ATPS treated surfaces, no sign of cell movement or distortion was observed in any cells in the field of view. At higher levels of shear stress (i.e., 9.3 dynes/cm^2) those less firmly attached cells were moved in the direction of flow and cell membranes showed visible deformation (as shown in Figure 4B). This may explain the increased population of responding cells with increasing shear stress, although deformation did not necessarily lead to intracellular Ca^{2+} release, as shown in Figure 2 and the Supporting Information video_2.

The observed quantitative difference in shear-induced intracellular Ca^{2+} flux for cells attached on serum-APTS silane treated and collagen-treated microchannels also suggested a possible influence of focal adhesion strength, as illustrated in a number of other studies.^{24,25} Undoubtedly, the biophysical mechanisms responsible for these observations are complex and will form the basis of future studies. However, the phenomenon clearly demonstrates the high probability of hydrodynamic influence on cellular functionality, even for cells that are generally regarded as being nonmechanically sensitive, such as CHO cells.

Implications of Shear-Induced Intracellular Ca^{2+} Flux. It is well-known that the presence of chemical stimuli, such as uridine 5'-triphosphate tris salt (UTP), can induce intracellular Ca^{2+} flux. Figure 5 shows a typical intracellular Ca^{2+} flux in response to $1 \mu\text{M}$ UTP (black trace), and the shear-induced response in the absence of UTP (gray trace). Clearly, these two responses are similar, suggesting that the shear stress mimics the responses that can be induced by UTP. The possibility therefore exists that shear-induced intracellular Ca^{2+} flux could bias information in microfluidic assays involving the functional screening of chemical stimuli (for example, agonists generally used for activation of ligand-gated ion channels). Careful on-chip evaluation is therefore essential, in order to ensure that cells are being assessed under conditions that reveal a genuine response to the analytes of interests.

(24) Allen, L. T.; Tosetto, M.; Miller, I. S.; O'Connor, D. P.; Penney, S. C.; Lynch, I.; Keenan, A. K.; Pennington, S. R.; Dawson, K. A.; Gallagher, W. M. *Biomaterials* **2006**, *27*, 3096–3108.

(25) Keselowsky, B. G.; Collard, D. M.; Garcia, A. J. *J. Biomed. Mater. Res.* **2003**, *66A*, 247–259.

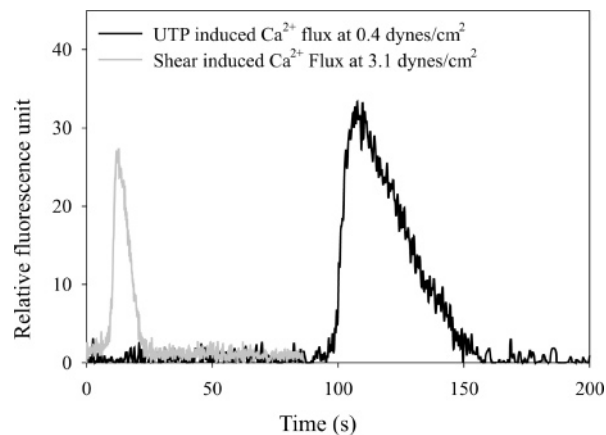


Figure 5. Comparison of shear-induced Ca^{2+} flux at a shear stress of 3.1 dynes/cm^2 with agonist UTP ($1 \mu\text{M}$) induced Ca^{2+} flux. The UTP solution was delivered at $2 \mu\text{L/min}$ (shear stress at 0.4 dynes/cm^2), which was below the threshold of shear stress inducing intracellular Ca^{2+} flux. At this shear stress, no Ca^{2+} flux was observed in the absence of UTP. Both peaks present similar transient responses and amplitude, which could lead to biased interpretation (i.e., shear-induced Ca^{2+} flux could be mistaken for a UTP-induced effect).

CONCLUSIONS

A systematic evaluation of a quantitative functional assay using immobilized spherical nonmechanically sensitive CHO cells in a microfluidic system was investigated. The device enabled a high density of immobilized, viable cells to be analyzed on-chip. By using intracellular Ca^{2+} analysis of CHO cells as a model system, we found that the microenvironment of the microfluidic device, particularly that of shear stress, could exert a significant influence on cell functionality. The possibility of this effect leading to biased information on functional cellular analysis exists. Careful on-chip assessment is therefore vital in future applications of microfluidics and lab-on-a-chip in biomedical and pharmaceutical fields. Further quantification of cell response to agonists (i.e., UTP) on-chip in comparison with traditional pharmaceutical method is ongoing.

ACKNOWLEDGMENT

The DTI is acknowledged for funding this research. We also acknowledge Epigem Ltd. for fabrication of the sealing block. We also thank Drs. Andrew Glidle, Paul Monaghan, and Helen Sedgwick for helpful discussions.

SUPPORTING INFORMATION AVAILABLE

Detailed information on microfluidics fabrication and surface modification; one video clip of the leakage test on the formed device and one video clip of the shear-induced Ca^{2+} flux at shear stress of 9.3 dynes/cm^2 . This material is available free of charge via the Internet at <http://pubs.acs.org>.

Received for review May 31, 2007. Accepted June 7, 2007.

AC071146K

Electrosynthesis of phenyl-2-propanone derivatives from benzyl bromides and acetic anhydride in an unsupported micro-flow cell electrolysis process†

Ping He,^a Paul Watts,^a Frank Marken^b and Stephen J. Haswell^{*a}

Received 20th July 2006, Accepted 26th October 2006

First published as an Advance Article on the web 3rd November 2006

DOI: 10.1039/b610415k

A simple process for the synthesis of phenyl-2-propanone is described based on a one-step electrochemical acylation reaction, involving the direct electroreductive coupling of benzyl bromides and acetic anhydride in a micro-flow electrolysis cell, equipped with micro-gap Pt electrodes. The technique offered yields typically in excess of 80% with corresponding high levels of product selectivity. The electrochemical process was also scaled-up by connecting four identical micro electrochemical cells in parallel to increase product throughput.

Phenyl-2-propanone, commonly referred to as P2P, is probably the most popular intermediate for the manufacture of amphetamine and methamphetamine,¹ and represents a versatile intermediate for the synthesis of pharmaceuticals, agrochemicals and fragrances. Due to the relatively simple structure of the compound and because of its common use,¹ a number of synthetic routes for its production have been developed. Most of these methods require the presence of a catalyst based on organometallic complexes,² metal acetates,³ metal halides,⁴ or Grignard reagents⁵ to give overall yields of up to 70%. There remains however scope for greener and cleaner methods based, for example, on electrochemical technology to be more effectively exploited. In 1977, Shono⁶ described a novel electrosynthesis process based on the reduction of benzyl chlorides in the presence of carboxylic acid chlorides in acetonitrile or *N,N*-dimethylformamide media, and using a conventional two compartment cell with a ceramic diaphragm and 1 M supporting electrolyte. Yields varied between 29 and 73% depending on the starting materials. In 1986, a patent^{7a} reported a process for the synthesis of P2P by electrochemical reduction of benzyl chlorides in the presence of acetic anhydride using an undivided electrolysis cell equipped with a sacrificial anode (*i.e.* Mg, Al, Zn), organic solvent (*N,N*-dimethylformamide, acetonitrile, tetrahydrofuran), and supporting electrolyte to give yields of 55% to 64%. In 1994, this process was further modified to use the electrochemical arylation of α -chloroketones with arylhalides in the presence of a catalytic nickel complex.^{7c} All of these cited electrochemically based processes suffer, however, from complicated work up and generate only modest yields.

^aDepartment of Chemistry, University of Hull, Hull, UK HU6 7RX.

E-mail: s.j.haswell@hull.ac.uk

^bDepartment of Chemistry, University of Bath, Bath, UK BA2 7AY

† Electronic supplementary information (ESI) available: Experimental procedures, P2P syntheses described in literature and characterization. See DOI: 10.1039/b610415k

Micro reactor methodology has been shown to have numerous practical advantages (when compared with batch reactors),⁸ including a safe operating environment, good process control, and the capability to scale-up for industrial production. In addition electrosyntheses in micro reactors has been shown to offer higher yields, in the absence of a supporting electrolyte,⁹ which reduces costly work up and purification steps.

In this present study we describe a simple and clean process for the synthesis of P2P based on a one-step electrochemical acylation reaction by direct electroreductive coupling of benzyl bromides and acetic anhydride in a micro-flow electrolysis cell equipped with micro-gap Pt electrodes. The reaction occurs in DMF solvent without supporting electrolyte to generate excellent yields of the products when compared with conventional synthetic methods. Notable benefits of this novel electrochemical process include (i) simple operation, (ii) no need for electrolytes, (iii) minimum product work-up, and (iv) high yield and selectivity of products.

Initially, the acylation reaction of benzyl bromide with acetic anhydride was studied by cyclic voltammetry at conventional Pt-disc (diameter 0.5 mm) and micro Pt-disc electrodes (diameter 25 μ m) to establish the reaction mechanism. The electroreduction of benzyl bromide is chemically irreversible, leading to the formation of either toluene *via* a two-electron reduction¹⁰ or dibenzyl formally *via* a one-electron reduction. Fig. 1 shows cyclic voltammograms obtained in DMF for (i) the reduction of acetic anhydride, (ii) the reduction of benzyl bromide, and (iii) the

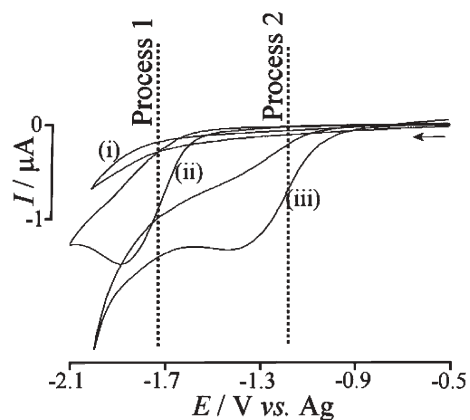


Fig. 1 Cyclic voltammograms (scan rate of 0.1 V s⁻¹) obtained at a 0.5 mm diameter platinum disc electrode immersed in 0.1 M *n*-Bu₄NBF₄-DMF for (i) 60 mM acetic anhydride, (ii) 3 mM benzyl bromide, and (iii) 3 mM benzyl bromide in the presence of 60 mM acetic anhydride.

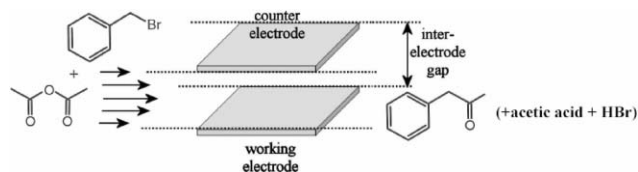


Fig. 2 Schematic representation of the acylation reaction during micro reactor electrosynthesis. A flow of reagents through a rectangular cavity with working and counter electrode facing each other results in the formation of products.

reduction of benzyl bromide in the presence of excess acetic anhydride.

The irreversible reduction of benzyl bromide (Process 1) occurs as a two-electron process (see ESI†). In the presence of acetic anhydride, a new reductive peak appears (Process 2) at more positive potential position. The peak current for Process 2 increases with increasing amounts of acetic anhydride (for 15 mM to 60 mM) whilst the peak current for Process 1 gradually decreases. The overall mechanism remains a two-electron transfer, with Process 2 being observed only at platinum electrode surfaces and not at glassy carbon or gold (see ESI†). The ratio of peak currents for Processes 1 and 2 is scan rate dependent, consistent with a fast preceding chemical step coupled to electron transfer at the platinum surface. Acetyl from acetic anhydride is likely to act as a “trap” for a benzyl anion intermediate formed at the platinum electrode surface.

Preparative micro reactor electrolysis was conducted in a rectangular cavity micro-flow cell (see Fig. 2) with products being determined off-line by using GC/MS and ¹H-NMR. The reaction medium, containing 5 mM benzyl bromide in DMF with varied amount of acetic anhydride, was continuously pumped through the cell, in which two platinum electrodes with a working area of 45 mm² each were positioned with an inter-electrode gap of 160 μm to produce a 7.2 μl cell volume.

The electro-acylation reactions were conducted galvanostatically and product samples were collected for a 30 minute period. Table 1 summarizes the conversion and product distribution for the range of conditions employed in this study.

From Table 1 it can be seen (Entry 1–4) that the conversion and product distribution are dependent on the molar ratio of benzyl

bromide to acetic anhydride and the applied current (or potential). Voltages between 5–5.4 V were required to obtain sufficiently high levels of conversion (>85%) in most cases. The best result obtained was 81% of phenyl-2-propanone with 9% of toluene at a flow rate of 10 μl min⁻¹ (corresponding to 43 s contact time, see Entry 4). Lower ratios of acetic anhydride to benzyl bromide led to the formation of more toluene (Entry 2–3), and even the formation of the dibenzyl product (Entry 1).

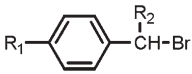
Other benzyl bromide derivatives such as 1-phenylethyl bromide, 4-methylbenzyl bromide, 4-methoxybenzyl bromide, and 4-bromobenzyl bromide were also examined (see Entry 5–8 in Table 1) for the acylation reaction with acetic anhydride. It is noted that the presence of Br⁻ and CH₃O⁻ groups on the benzyl bromides promote the formation of the debromination products (see Entry 7–8), compared to CH₃- and H- groups. In contrast, in the presence of an electron donating group (see Entry 5–6) yields are improved. The formation of bromine due to oxidation of bromide (as a follow up anodic process) was not observed, presumably due to the limited overlap of diffusion layers within the flow cell. The diffusion layer thickness for the process can be estimated based on eqn (1).

$$\delta = \sqrt[3]{\frac{DAh^2}{V_f}} \quad (1)$$

In this equation the diffusion layer thickness is obtained based on the diffusion coefficient *D*, the electrode area *A*, the half height of the cell *h*, and the volume flow rate *V_f*. For a diffusion coefficient of 10⁻⁹ m² s⁻¹ and under conditions employed here, the diffusion layer thickness is estimated as δ = 120 μm, which is approaching the inter-electrode distance.

Current efficiencies for all processes are typically around 20–25%, consistent with an overall transfer of 4 electrons per benzyl bromide, but background currents in the presence of acetic anhydride are likely to be responsible for the low yield (see Fig. 1). This observation is consistent with literature reports.^{7a,b} The electrochemical process was also scaled-up by connecting four identical micro electrochemical cells in parallel. In this case, a similar level of product yield was obtained with a four-fold increase in the quality of the product formation. In summary, micro-flow electrosynthesis offers a surprisingly simple and

Table 1 Data for preparative electrolysis of benzyl bromides (BB) in the presence of acetic anhydride (AA) in DMF in a micro-flow cell without intentionally added supporting electrolyte^a

Entry	Current/mA			AA/BB ^b (mol/mol)	Conv. (%) ^c	Distribution (%)	
		R ₁	R ₂			P2P ^d	DBr ^e
1	0.8	H	H	10	87	61	26 ^f
2	0.8	H	H	20	85	62	23
3	1.1	H	H	20	92	66	26
4	1.1	H	H	40	90	81	9
5	1.1	CH ₃	H	40	93	87	6
6	1.1	H	CH ₃	40	98	96	2
7	1.3	CH ₃ O	H	40	99	83	16
8	1.1	Br	H	40	73	51	22

^a 5 mM benzyl bromides, acetic anhydride concentration as shown in the Table, electrode gap is 160 μm, electrode area 45 mm², flow rate 10 μl min⁻¹ corresponding to 43 s contact time. ^b Molar concentration ratio. ^c The conversion was determined based on the quality of benzyl bromide before and after reaction using *n*-decane as an internal standard. ^d P2P represents P2P or its derivatives. ^e DBr is debromination yield for benzyl bromides. ^f Side products include debromination of benzyl bromide (16%) and dimer formation (10%).

low waste access to phenyl-2-propanone derivatives which is readily optimized and can be scaled-up. It is very likely that in future a wider range of chemical processes will be identified to be suitable for this kind of simple and clean micro-reactor technology.

Acknowledgements

We thank EPSRC for funding (Project No. GR/S34106)

Notes and references

- 1 A. C. Allen and T. S. Cantrell, *Synthetic reductions in clandestine amphetamine and methamphetamine laboratories: A Review*, Forensic Science International, Elsevier, 1989, vol. 42, p. 183.
- 2 (a) R. Ballini, *Synthesis*, 1994, 723; (b) S. Inaba and R. D. Rieke, *Tetrahedron Lett.*, 1983, **24**, 2451; (c) S. Inaba and R. D. Rieke, *J. Org. Chem.*, 1985, **50**, 1373.
- 3 (a) M. E. Kurz, V. Baru and P. N. Nguyen, *J. Org. Chem.*, 1984, **49**, 1603; (b) A. C. Allen, M. L. Stevensen, S. M. Nakamura and R. A. Ely, *J. Forensic Sci.*, 1992, **37**, 301.
- 4 (a) K. Lee and D. Y. Oh, *Tetrahedron Lett.*, 1988, **29**, 2977; (b) K. Okabe, T. Ohwada, T. Ohta and K. Shudo, *J. Org. Chem.*, 1989, **54**, 733.
- 5 (a) P. Canonne, G. B. Foscolos and G. Lemay, *Tetrahedron Lett.*, 1980, **21**, 155; (b) K. Okabe, T. Ohwada, T. Ohta and K. Shudo, *J. Org. Chem.*, 1972, **37**, 3369.
- 6 T. Shono, *Chem. Lett.*, 1977, 1021.
- 7 (a) M. D. Moingeon and J. Chaussard, *US Pat.*, 4 629 541, 1986; (b) E. D'Incan, S. Sibille, J. Périchon, M. D. Moingeon and J. Chaussard, *Tetrahedron Lett.*, 1986, **27**, 4175; (c) M. Durandetti, S. Sibille, J.-Y. Nédélec and J. Périchon, *Synth. Commun.*, 1994, **24**, 145.
- 8 (a) S. Taghavi-Moghadam, A. Kleemann and K. G. Golbig, *Org. Process Res. Dev.*, 2001, **5**, 652; (b) T. Kawaguchi, H. Miyata, K. Ataka, K. Mae and J. Yoshida, *Angew. Chem., Int. Ed.*, 2005, **44**, 2413.
- 9 (a) C. A. Paddon, G. J. Pritchard, T. Thiemann and F. Marken, *Electrochem. Commun.*, 2002, **4**, 825; (b) R. Horcajada, M. Okajima, S. Suga and J. Yoshida, *Chem. Commun.*, 2005, 1303; (c) P. He, P. Watts, F. Marken and S. J. Haswell, *Electrochem. Commun.*, 2005, **7**, 918; (d) P. He, P. Watts, F. Marken and S. J. Haswell, *Angew. Chem., Int. Ed.*, 2006, **45**, 4146.
- 10 (a) J. Grimshaw, *Electrochemical Reactions and Mechanisms in Organic Chemistry*, Elsevier, Amsterdam, 2000, pp. 98–103; (b) *Organic Electrochemistry*, ed. H. Lund and O. Hammerich, Marcel Dekker, New York, 2001.

The use of solid-supported reagents for the multi-step synthesis of analytically pure α,β -unsaturated compounds in miniaturized flow reactors†‡

Charlotte Wiles, Paul Watts* and Stephen J. Haswell

Received 16th October 2006, Accepted 18th December 2006

First published as an Advance Article on the web 8th January 2007

DOI: 10.1039/b615069a

Micro reaction technology offers a safe, controllable and information rich technique suitable for the long-term production of pharmaceutical agents and fine chemicals. To date however, few of the syntheses performed using this technology have addressed the problems associated with product purification. With this in mind, we report herein the incorporation of multiple supported reagents into EOF-based miniaturized flow reactors for the two-step synthesis of analytically pure compounds. Using this approach, the successful synthesis of 20 α,β -unsaturated compounds in excellent yields (>99.1%) and purities (>99.9%) has been achieved, illustrating significant improvements compared to traditional batch techniques.

1 Introduction

Under increasing environmental and financial pressure, the chemical industry as a whole has begun exploring numerous ways of improving both the cleanliness and efficiency of many synthetic processes. One such approach is the application of micro reaction technology, whereby miniaturized reactor vessels provide controllable, information rich systems that enable reactions to be performed more rapidly,² efficiently³ and selectively⁴ than traditional batch-scale reactions. With these factors in mind, the use of micro reaction technology is of particular interest to the pharmaceutical industry where long term objectives include the desire to perform multiple functions (such as synthesis, detection, screening⁵ and biological evaluation) within a single integrated device, resulting in an overall reduction in the time taken to discover lead compounds and subsequently transfer them to production.

Although the past ten years has seen a rapid growth in the field of micro reaction technology, with many groups demonstrating the successful synthesis of small organic compounds,^{6–11} few have addressed the problems associated with the purification of reaction products prepared in continuously flowing systems.^{12,13} In order to tackle this problem, we recently demonstrated the incorporation of solid-supported catalysts into miniaturized flow reactors, where the advantages of solid-supported catalysts/reagents were coupled with those of reaction miniaturization.^{14,15}

As solid-supported reagents are designed to work in a similar manner to their solution phase counterparts, little reaction optimization is usually required in order to implement their use.^{16,17} In comparison to solution phase reagents,

however, the use of solid-supported analogues is advantageous, as they enable reaction products to be isolated with ease; consequently, supported reagents are often employed in a large excess in order to drive reactions to completion. Furthermore, by employing more than one supported reagent in the same reaction vessel, multiple transformations can be achieved.¹⁸ Although solid-supported reagents clearly have many advantages over solution phase reagents, drawbacks of the technique include increased reaction times and mechanical degradation of the support (as a result of stirring or agitating the reaction mixture) which can make reagent recovery/recycling difficult. Consequently, by performing reactions in flow reactors,¹⁹ the supported reagent undergoes minimal degradation, leading to extended reagent lifetimes, increased system reproducibility and simplified product isolation (Fig. 1).

In addition, from a production point of view, reaction miniaturization is advantageous, as syntheses can be readily transferred from a laboratory scale to mass production with ease. Using an approach referred to as scale-out or numbering-up,^{20,21} reactions are firstly optimized within a single micro reactor, then, in order to increase production volume, the number of reactors employed is simply increased. In comparison to current production technology, scale-out is advantageous, as the thermal and mass transportation properties of the original micro reaction are maintained, facilitating the rapid transfer of a synthetic route from the laboratory scale where a single reactor is used, to mass production where multiple reactors are employed; for this approach to be

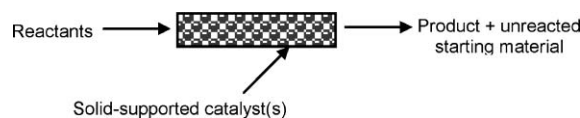


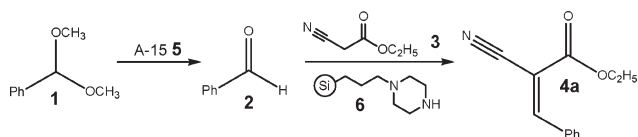
Fig. 1 Schematic illustrating the principle of employing solid-supported reagents in continuous flow reactors.

Department of Chemistry, University of Hull, Hull, UK HU6 7RX.

E-mail: p.watts@hull.ac.uk

† See ref. 1.

‡ Electronic supplementary information (ESI) available: Experimental details and compound characterisation. See DOI: 10.1039/b615069a



Scheme 1 General reaction scheme illustrating the multi-step synthesis of an α,β -unsaturated compound **4a**.

successful, it is important that individual reactors can be operated reproducibly. This work therefore builds on the successful base-catalyzed synthesis of α,β -unsaturated compounds¹⁴ and the acid-catalyzed synthesis (also deprotection) of dimethyl acetals,¹⁵ by increasing reaction complexity, enabling multi-step syntheses to be performed. As Scheme 1 illustrates, the proposed reaction sequence involves the acid-catalyzed deprotection of a dimethyl acetal **1** followed by the *in situ* base-catalyzed condensation of the aldehyde **2** with an activated methylene **3** to afford the respective α,β -unsaturated compound **4a**.²²

2 General procedure for the synthesis of α,β -unsaturated compounds in a flow reactor

A typical procedure for the synthesis of α,β -unsaturated compounds in a miniaturized flow reactor consisted of passing a solution of dimethyl acetal and activated methylene (1.0 M respectively in MeCN) through a solid-supported acid catalyst (whereby deprotection of the dimethyl acetal afforded the respective aldehyde) followed by a solid-supported base catalyst (where the aldehyde and activated methylene condensed) to afford the desired α,β -unsaturated compound. The reaction mixture was subsequently analyzed by GC-MS, and the conversion of starting materials to product determined, *i.e.* % conversion. If any residual starting materials were detected the reaction was repeated, this time passing the starting materials over the supported catalysts at a slower flow rate; thus having the effect of increasing reagent residence time within the reactor. Once successfully optimized, the devices were operated for 2.5 h, after which work-up of the reaction product consisted simply of concentrating the sample *in vacuo*. The purity of the 'crude' product was subsequently evaluated by NMR spectroscopy, and, in the case of previously unreported compounds, elemental analysis performed; in all cases, no additional product purification was found to be necessary.

In order to mobilize reagents and products through the packed bed, electroosmotic flow (EOF) was selected as the pumping mechanism as it is simple to use, provides reproducible pulse-free flow, enables both the magnitude and direction of flow to be altered with ease and generates minimal back-pressure; an important feature with respect to the use of solid-supported reagents.²³ While EOF is widely associated with the manipulation of aqueous systems, more recently it has been applied to polar organic systems such as MeOH, MeCN and DMF.²⁴ In comparison to mechanical pumping techniques, electroosmotic systems are advantageous as they consist simply of the flow reactor and a power supply; automation of the system therefore enables the

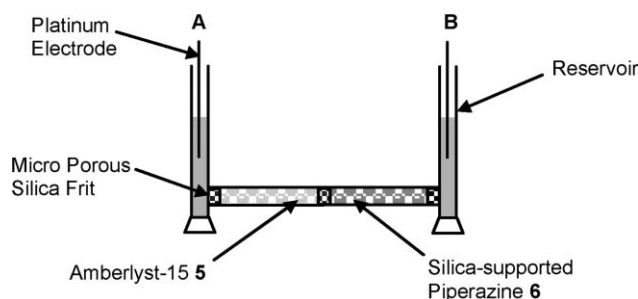


Fig. 2 Schematic illustrating the use of two solid-supported catalysts in an EOF-based continuous flow reactor.

reaction set-up to be housed within a fume-cupboard and operated remotely.

2.1 Experimental set-up used for the evaluation of solid-supported reagents in miniaturized flow reactors

In order to evaluate the use of multiple supported reagents within an EOF-based system for the synthesis of α,β -unsaturated ketones (Scheme 1), a series of miniaturized flow reactors were constructed. As previously demonstrated,^{14,15} reactions were performed using a single capillary borosilicate glass reactor, as illustrated in Fig. 2, with capillary dimensions of 500 μm (i.d.) \times 3.0 cm (length). To hold the solid-supported reagents in place, a micro porous silica frit (MPS frit)²⁵ was placed at one end of the capillary and the Amberlyst-15 **5** (2.5 mg, 0.105 mmol) dry packed against it, the acid catalyst **5** was then held in place with another MPS frit positioned in 1.5 cm along the capillary (Fig. 2). The silica-supported base **6** (2.5 mg, 4.25×10^{-3} mmol) was subsequently dry packed up to the second MPS frit, which was again held in place by a third MPS frit. The packed capillary was subsequently primed with MeCN to remove any air, ensuring the formation of an electrical circuit. A leak-tight connection between the packed capillary and the borosilicate glass reagent reservoirs was achieved using PTFE thread seal tape (75 μm \times 12 mm \times 12 m). To mobilize reagents by EOF, platinum electrodes (500 μm (o.d.) \times 2.5 cm (length)) were placed within the reservoirs and voltages applied using a Paragon 3B high-voltage power supply (HVPS), capable of applying 0 to 1000 V to four pairs of outputs (Kingfield Electronics, UK); automation of the HVPS was achieved using LabViewTM software. Typical applied fields ranged from 167 to 333 V cm^{-1} ; enabling flow rates of between 0.40 and 1.05 $\mu\text{l min}^{-1}$ to be achieved.²⁶

3 Results and discussion

3.1 Synthesis of 2-cyano-3-phenyl acrylic acid ethyl ester **4a**

Using the set-up illustrated in Fig. 2 and 3, a solution of dimethoxymethyl benzene **1** and ethyl cyanoacetate **3** (40.00 μl , 1.0 M in MeCN) was placed in reservoir A and MeCN (40.00 μl) in reservoir B. Application of 333 V cm^{-1} to the solution in reservoir A and 0 V cm^{-1} to reservoir

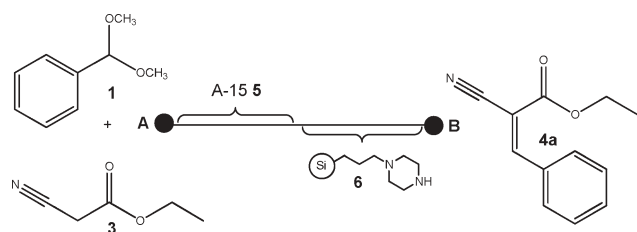


Fig. 3 Schematic illustrating the multi-step synthesis of 2-cyano-3-phenyl acrylic acid ethyl ester **4a** in an EOF-based miniaturized flow reactor.

B (ground electrode) resulted in the electroosmotic mobilization of reagents **1** and **3** through the packed bed at a rate of $0.50 \mu\text{l min}^{-1}$ (throughput of 6.0 mg h^{-1}). After 10 min, the reaction products collected from reservoir B were analyzed by GC-MS, confirming that 99.98% conversion to 2-cyano-3-phenyl acrylic acid ethyl ester **4a** had occurred.²⁷

In order to demonstrate the reproducibility of the experimental set-up, the reaction was repeated a further 14 times (2.5 h in total), resulting in an average conversion of 99.99% (Table 1, % RSD = 3.5×10^{-3} , $n = 15$). After analysis by GC-MS, the reaction products were combined and concentrated *in vacuo* to afford 2-cyano-3-phenyl acrylic acid ethyl ester **4a** as a white solid (0.0150 g, 99.40%). In order to confirm product purity, the 'crude' product **4a** was analyzed by NMR spectroscopy; whereby no residual starting materials **1**, **2** and **3**, or by-products, were detected.

To confirm that the observed reaction was in fact attributed to the presence of both acid and base catalysts within the flow reactor, the synthesis of 2-cyano-3-phenyl acrylic acid ethyl ester **4a** was evaluated in the absence of Amberlyst-15 **5** and 3-(1-piperazino)propyl-functionalized silica gel **6**. Firstly, the base catalyst **6** was replaced with silica gel (Kieselgel 60), and a 1 : 1 mixture of dimethyl acetal **1** and ethyl cyanoacetate **3** mobilized through the reactor at a flow rate of $0.50 \mu\text{l min}^{-1}$; after 10 min, the

Table 1 Illustration of system stability over 15 runs (2.5 h) for the synthesis of 2-cyano-3-phenyl acrylic acid ethyl ester **4a**

Run no.	Conversion (%) ^a
1	99.98
2	99.99
3	99.99
4	99.99
5	99.99
6	99.99
7	99.99
8	99.99
9	99.99
10	99.99
11	99.99
12	99.99
13	99.99
14	99.98
15	99.99

Mean = 99.99%, % RSD = 3.5×10^{-3}

^a Calculated with respect to residual aldehyde **2**

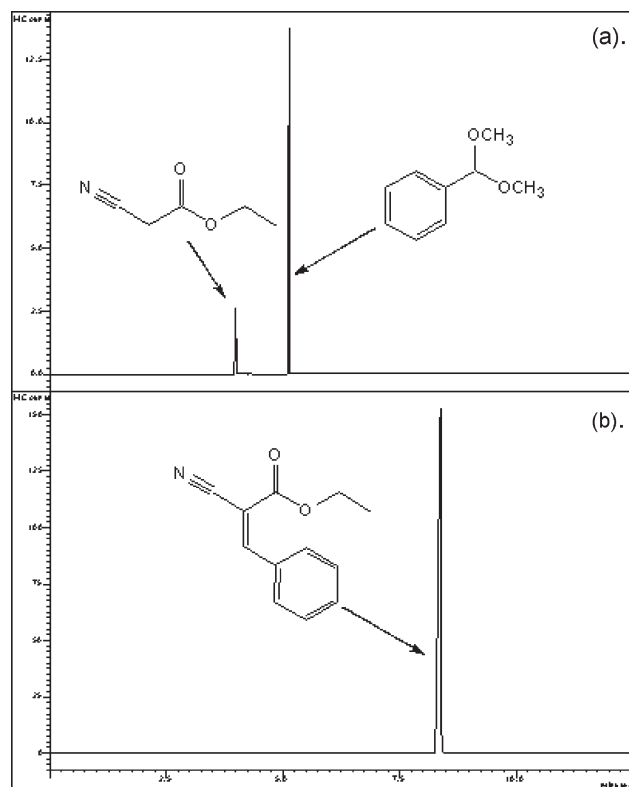


Fig. 4 Gas chromatograms illustrating the complete conversion of (a) dimethoxymethyl benzene **1** and ethyl cyanoacetate **3** to (b) 2-cyano-3-phenyl acrylic acid ethyl ester **4a** within a miniaturized flow reactor.

reaction products were diluted with MeCN and analysed by GC-MS. As expected, the reaction products only contained benzaldehyde **2** (due to acid catalyzed deprotection of dimethyl acetal **1**) and ethyl cyanoacetate **3**; importantly no 2-cyano-3-phenyl acrylic acid ethyl ester **4a** was detected. The effect of the acid catalyst **5** was subsequently investigated by replacing Amberlyst-15 **5** with polystyrene beads (2% cross-linked with divinylbenzene), again the stock solution was passed through the polystyrene beads and 3-(1-piperazino)propyl-functionalized silica gel **6**; analysis of the reaction products confirmed that the starting materials **1** and **3** remained unchanged.

Finally, the reaction was repeated using polystyrene beads and silica gel; again, as expected, analysis of the reaction products confirmed that no reaction had occurred. In summary, it was concluded that the observations presented in Table 1 are in fact attributed to the acid-catalyzed deprotection of dimethoxymethyl benzene **1**, followed by the base-catalyzed condensation of benzaldehyde **2** and ethyl cyanoacetate **3** to afford 2-cyano-3-phenyl acrylic acid ethyl ester **4a**; and importantly, not as a result of performing the reaction in an electric field.

In order to compare the efficiency of miniaturized flow reactors with traditional batch techniques, the synthesis of 2-cyano-3-phenyl acrylic acid ethyl ester **4a** was subsequently performed using the traditional one-pot approach. In brief, 3-(1-piperazino)propyl-functionalized silica gel **6**

(2.5 mg, 4.25×10^{-3} mmol) and Amberlyst-15 **5** (2.5 mg, 1.05 mmol) were added to a solution containing dimethoxymethyl benzene **1** (0.011 g, 0.075 mmol) and ethyl cyanoacetate **3** (0.08 g, 0.075 mmol) in MeCN (75.0 μ l) (1.0 M respectively) and stirred for 2.5 h. In order to monitor the progress of the reaction, aliquots of the reaction mixture (1.0 μ l in 100.0 μ l MeCN) were analyzed every 10 min, by GC-MS. As Fig. 5 illustrates, after 30 min complete deprotection of dimethoxymethyl benzene **1** to benzaldehyde **2** was achieved, however even after a further 1.5 h only 2.9% conversion to 2-cyano-3-phenyl acrylic acid ethyl ester **4a** had occurred. In comparison, by performing the reaction in a miniaturized flow reactor, with a residence time of 1.0 min, 0.015 g (0.075 mmol, 99.40%) of 2-cyano-3-phenyl acrylic acid ethyl ester **4a** was synthesized in excellent purity over the same 2.5 h period. In addition, by employing scale-out methodology, the quantity of material synthesized can be increased by simply employing an array of reactors in parallel.

The observed reduction in reaction time can be partly explained by the formation of localized concentration gradients within the flow reactor, as although only small quantities of catalyst are employed (2.5 mg per reagent), when the starting materials are passed through the reactor they are, in fact, exposed to a large excess of catalyst. In addition, within a packed reactor, the diffusion distance between any starting materials and the supported catalyst is greatly decreased compared to within traditional stirred reactors; consequently, conversions >99% can be achieved in minutes, in contrast with >24 h in a traditional stirred reactor. Furthermore, compared to the one-pot approach, the preparation of packed columns is also advantageous, as the supported catalysts remain spatially resolved (Fig. 2) enabling their reuse either separately or in alternative reaction sequences.

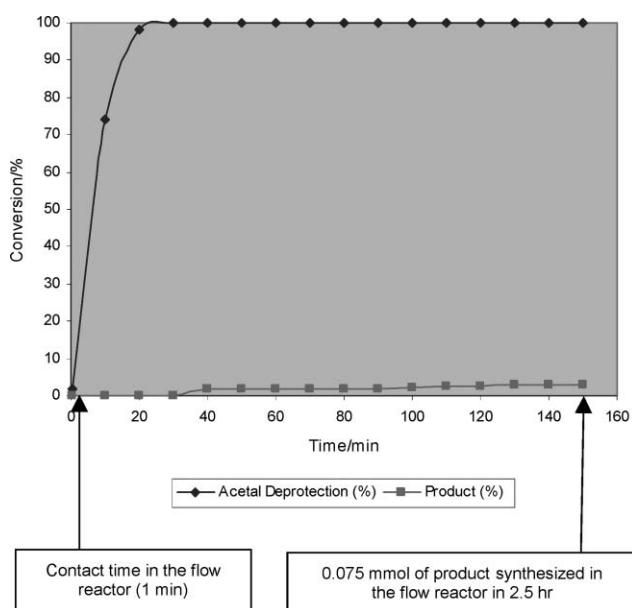


Fig. 5 Graph illustrating the progress of a two-step reaction using the one-pot approach.

3.2 Synthesis of α,β -unsaturated compounds in an EOF-based miniaturized flow reactor

Using the synthesis of 2-cyano-3-phenyl acrylic acid ethyl ester **4a** as a model reaction, the advantages associated with incorporating multiple supported catalysts into miniaturized flow reactors have been clearly illustrated. As a means of demonstrating the versatility of this technique, the investigation was extended to demonstrate the reactions of substituted aldehydes. Again, Amberlyst 15 **5** and 3-(1-piperazino)propyl-functionalized silica gel **6** were employed as the catalysts, enabling the synthesis of α,β -unsaturated ketones **4a** to **4j** in excellent yield (Table 2). The generality of the technique was further investigated, employing malononitrile **7** as the activated methylene, and, as Table 3 illustrates, α,β -unsaturated compounds **8a** to **8j** were again synthesized in excellent yields (>99.2%). Evaluation of the resulting 'crude' products by GC-MS and NMR spectroscopy once more confirmed that all products were synthesized in analytical purity without the need for additional purification steps.

3.3 Catalyst turnover

As previously mentioned, when employing solid-supported reagents, in either stirred or shaken reactor vessels, degradation of the support material can lead to problems with reagent recovery and reuse; as a means of overcoming this problem, we investigated the use of miniaturized continuous flow reactors. Using this approach, a combinatorial array of α,β -unsaturated compounds were synthesized in excellent yield and purity (Tables 2 and 3), whereby separation of the reaction products from the supported catalyst was achieved with ease. With this in mind, our attention turned to assessing the recyclability of the supported catalysts employed in the aforementioned device. In order to ascertain the technique's efficiency, the same 2.5 mg portions of Amberlyst-15 **5** and 3-(1-piperazino)propyl-functionalized silica gel **6** were used for the synthesis of all 20 α,β -unsaturated compounds. As illustrated by Table 4, this equates to the synthesis of 2.13 mmol of α,β -unsaturated product using only 1.05×10^{-2} mmol of acid **5** and 4.25×10^{-3} mmol of base **6**, demonstrating catalyst turnovers of 203 and 501 times, respectively. Most importantly, over the course of the investigation, no sign of reagent degradation or reduced reaction efficiency was observed; consequently, the flow reactor will be employed in further studies. Notably, although the catalysts remain active in a traditional stirred reactor, to perform 20 separate syntheses using the same portion of catalytic material (5 mg in total) would be unfeasible due to difficulties associated with the filtration and recovery of small quantities of supported material.

In summary, by incorporating multiple solid-supported catalysts into a miniaturized flow reactor an array of α,β -unsaturated compounds have been synthesized in excellent yield and purity without the need for additional, off-line, purification steps. In addition, we have demonstrated the ability to recycle solid-supported catalysts, enabling reaction reproducibility that is currently unobtainable in traditional stirred/shaken reactors (Table 4).

Table 2 Summary of the conversions obtained for the synthesis of α,β -unsaturated ketones **4a** to **4j** using Amberlyst-15 **5** and 3-(1-piperazino)propyl-functionalized silica gel **6** in a miniaturized flow reactor

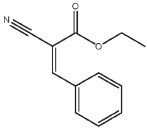
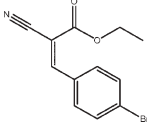
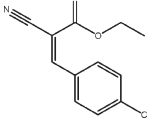
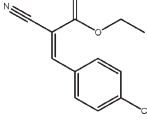
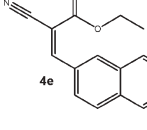
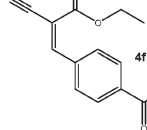
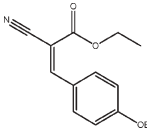
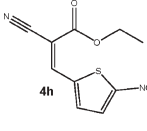
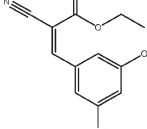
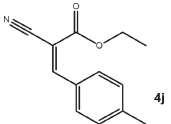
Product	Flow rate/ $\mu\text{l min}^{-1}$	GC-MS purity (%) ^a	Yield (%)
 4a	0.50 (1.00) ^b	99.99 (3.0×10^{-3}) ^c	99.40 (0.0150) ^d
 4b	0.80 (0.63)	99.99 (1.2×10^{-3})	99.76 (0.0338)
 4c	0.65 (0.77)	99.99 (1.25×10^{-3})	99.56 (0.0227)
 4d	0.84 (0.60)	99.99 (8.0×10^{-4})	99.65 (0.0284)
 4e	0.84 (0.60)	99.99 (8.0×10^{-4})	99.80 (0.0298)
 4f	0.65 (0.77)	100.00 (0.0)	99.68 (0.0253)
 4g	0.48 (1.04)	99.99 (2.6×10^{-4})	99.10 (0.0219)
 4h	0.75 (0.67)	99.99 (6.0×10^{-4})	99.65 (0.0234)
 4i	0.55 (0.91)	99.99 (8.0×10^{-4})	99.53 (0.0213)

Table 2 Summary of the conversions obtained for the synthesis of α,β -unsaturated ketones **4a** to **4j** using Amberlyst-15 **5** and 3-(1-piperazino)propyl-functionalized silica gel **6** in a miniaturized flow reactor (*Continued*)

Product	Flow rate/ $\mu\text{l min}^{-1}$	GC-MS purity (%) ^a	Yield (%)
	0.89 (0.56)	99.99 (2.5×10^{-3})	99.30 (0.0284)

^a GC-MS conversion determined with respect to residual aldehyde. ^b the number in parentheses represents the period of time, in min, that the starting materials are in contact with each supported reagent. ^c the number in parentheses represents the RSD, whereby $n = 15$. ^d the number in parentheses represents the isolated yield in g.

Table 3 Summary of the conversions obtained for the synthesis of α,β -unsaturated compounds **8a** to **8j** using Amberlyst-15 **5** and 3-(1-piperazino)propyl-functionalized silica gel **6** in a miniaturized flow reactor

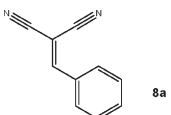
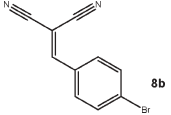
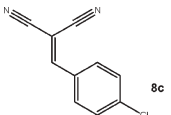
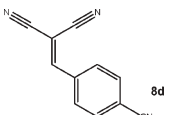
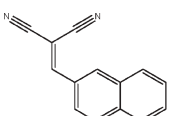
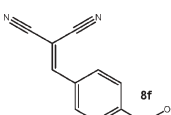
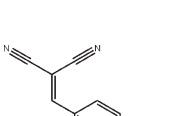
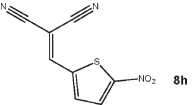
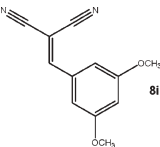
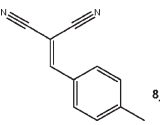
Product	Flow rate/ $\mu\text{l min}^{-1}$	GC-MS purity (%) ^a	Yield (%)
	0.53 (0.94) ^b	99.99 (7.0×10^{-4}) ^c	99.42 (0.0121) ^d
	0.95 (0.53)	99.99 (5.0×10^{-4})	99.36 (0.0312)
	0.65 (0.77)	99.99 (4.6×10^{-4})	99.40 (0.0179)
	0.83 (0.60)	99.99 (7.0×10^{-4})	99.55 (0.0222)
	0.84 (0.60)	99.99 (2.6×10^{-3})	99.22 (0.0255)
	0.67 (0.75)	99.99 (1.06×10^{-4})	99.53 (0.0211)
	0.40 (1.25)	100.00 (0.0)	99.36 (0.0155)

Table 3 Summary of the conversions obtained for the synthesis of α,β -unsaturated compounds **8a** to **8j** using Amberlyst-15 **5** and 3-(1-piperazino)propyl-functionalized silica gel **6** in a miniaturized flow reactor (*Continued*)

Product	Flow rate/ $\mu\text{l min}^{-1}$	GC-MS purity (%) ^a	Yield (%)
 8h	1.04 (0.48)	100.00 (0.0)	99.90 (0.0263)
 8i	0.50 (1.00)	99.99 (5.6×10^{-4})	99.66 (0.0177)
 8j	1.05 (0.50)	99.99 (2.5×10^{-4})	99.62 (0.0319)

^a GC-MS conversion determined with respect to residual aldehyde. ^b the number in parentheses represents the period of time, in min, that the starting materials are in contact with each supported reagent. ^c the number in parentheses represents the RSD, whereby $n = 15$. ^d the number in parentheses represents the isolated yield in g.

3.4 Catalyst screening

Having demonstrated the ability to continuously synthesize an array of α,β -unsaturated compounds within an EOF-based flow reactor, the investigation was extended to look at the use of other solid-supported acids and bases. As illustrated in Table 5, nine combinations of polymer-supported acids (Amberlyst-15 **5**, polymer-supported *p*-toluenesulfonic acid **9** and ytterbium polystyrylsulfonate(III) **10**) and silica-supported bases (3-(1-piperazino)propyl-functionalized silica gel **6**, 3-(dimethylamino)propyl-functionalized silica gel **11** and 3-(1,3,4,6,7,8-hexahydro-2*H*-pyrimidino)propyl-functionalized silica gel **12**) were packed into a series of miniaturized flow reactors (Fig. 6).

In order to evaluate these catalyst combinations, the synthesis of 2-cyano-3-phenyl acrylic acid ethyl ester **4a** was again selected as the model reaction. To perform a reaction, a solution of dimethoxymethyl benzene **1** and ethyl cyanoacetate **3** (40 μl , 1.0 M in MeCN) was placed in reservoir A and MeCN (40 μl) in reservoir B; application of 333 and 0 V cm^{-1} , respectively, resulted in mobilization of the reagents through the packed-bed at flow rates in the range of 0.4 to 0.5 $\mu\text{l min}^{-1}$ (Table 5). All reaction products were subsequently analyzed by GC-MS after 10 min ($\geq 99.99\%$ conversion w.r.t. residual benzaldehyde **2**) and the reactors operated for a total of 2.5 h (15 runs) per catalyst combination. In all cases, concentration of the reaction products *in vacuo* afforded 2-cyano-3-phenyl acrylic acid ethyl ester **4a** as a white crystalline solid ($\geq 99.26\%$ yield).

Table 4 Illustration of reagent recycling demonstrated in a miniaturized EOF-based flow reactor

	Supported reagent/mmol	Product/mmol	Turnover number
Amberlyst-15 5	1.05×10^{-2}	2.13	203
3-(1-Piperazino)propyl-functionalized silica gel 6	4.25×10^{-3}	2.13	501

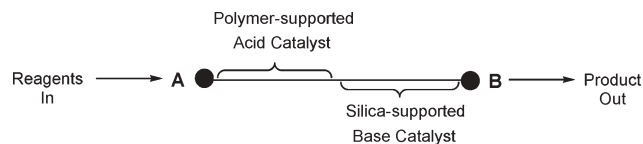


Fig. 6 Schematic illustrating the reaction set-up used to screen the solid-supported catalysts.

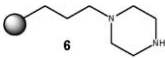
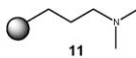
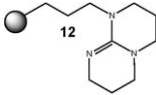
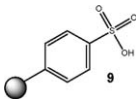
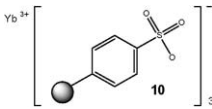
These results not only demonstrate the generality of the technique with respect to the nature of catalyst used but also the support material employed.

4 Conclusions

In conclusion, we have demonstrated a simple and efficient technique for the incorporation of multiple supported reagents into miniaturized flow reactors, resulting in a system suitable for the continuous flow synthesis of analytically pure compounds; using this approach, 20 α,β -unsaturated compounds (**4a–4j** and **8a–8j**) were synthesized in near quantitative yield and purity *via* a two-step synthesis.

Compared to standard batch techniques, the application of miniaturized flow reactors proved advantageous, as it is possible to synthesize compounds in high yield and purity without the need for additional purification steps. Furthermore, the ease with which supported reagents are

Table 5 Illustration of the results obtained for the synthesis of 2-cyano-3-phenyl acrylic acid ethyl ester **4a** using various polymer-supported acids and silica-supported bases

			
Amberlyst-15 5	0.50 ^a 99.99% ^b 3.0×10^{-3c} 99.40% ^d 0.0150 g ^e	0.45 99.99% 9.6×10^{-4} 99.26% 0.0134 g	0.49 99.99% 7.4×10^{-4} 99.32% 0.0148 g
	0.47 99.99% 5.1×10^{-4} 99.30% 0.0140 g	0.42 99.99% 4.9×10^{-4} 99.53% 0.0126 g	0.41 99.99% 7.4×10^{-4} 100.0% 0.0123 g
	0.45 99.99% 3.5×10^{-4} 99.27% 0.0136 g	0.40 99.99% 7.4×10^{-4} 99.50% 0.0120 g	0.50 99.99% 6.1×10^{-4} 99.34% 0.0150 g

^a Electroosmotic flow rate ($\mu\text{l min}^{-1}$). ^b Average GC Conversion ($n = \geq 15$). ^c % RSD ($n = \geq 15$). ^d Yield (%). ^e Isolated yield (g).

recycled provides reaction reproducibility unobtainable in traditional stirred or shaken reactor vessels. In addition, the formation of localized concentration gradients within the flow reactor enables reactions to be driven to completion more rapidly than in stirred/shaken reactors, a point clearly illustrated in Fig. 4.

Consequently, whether milligrams of a compound are required for biological evaluation or tonnes for the production of fine chemicals, the flexibility associated with micro reaction technology enables these differences in scale to be bridged with ease.

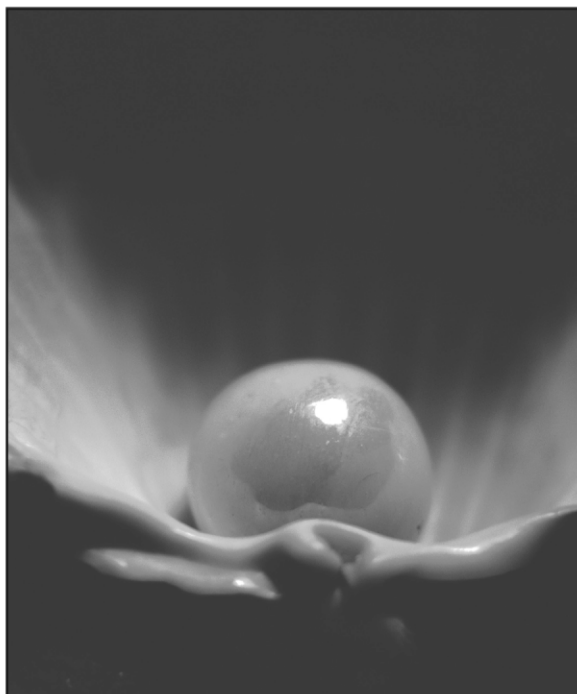
Acknowledgements

Financial support from the EPSRC (C.W.) (Grant No. GR/S34106/01) is gratefully acknowledged. We also thank Mike Bailey (The University of Hull) for assistance with device fabrication.

References

- C. Wiles, P. Watts and S. J. Haswell, *Abstr. Pap. Am. Chem. Soc.*, 2005, ORGN 699.
- O. Worz, K. P. Jackel, Th. Richter and A. Wolf, *Chem. Eng. Sci.*, 2001, **40**, 2555–2562.
- M. Uneo, H. Hisamoto, T. Kitamori and S. Kobayashi, *Chem. Commun.*, 2003, 936–937.
- (a) A. Nagaki, M. Togai, S. Suga, N. Aoki, K. Mae and J. Yoshida, *J. Am. Chem. Soc.*, 2005, **127**, 11666–11675; (b) A. Nagaki, K. Kawamura, T. Ando, M. Sawamoto and J. Yoshida, *J. Am. Chem. Soc.*, 2004, **126**, 14702–14703; (c) C. Wiles, P. Watts and S. J. Haswell, *Abstr. Pap. Am. Chem. Soc.*, 2005, ORGN 293.
- M. Bartolini, V. Cavrini and V. Andrisano, *J. Chromatogr., A*, 2005, 135–144.
- K. Jahnisch, V. Hessel, H. Lowe and M. Baerns, *Angew. Chem., Int. Ed.*, 2004, **43**, 406–446.
- H. Krummradt, U. Kopp and J. Stoldt, *Microreaction Technology-IMRET 3: Proceedings of the 3rd International conference on Microreaction Technology*, ed. W. Ehrfeld, Springer, Berlin, 2000, 7.
- E. Garcia-Egido, V. Spikmans, S. Y. F. Wong and B. H. Warrington, *Lab Chip*, 2003, **3**, 73–76.
- C. Wiles, P. Watts and S. J. Haswell, *Org. Process Res. Dev.*, 2004, **8**, 28–32.
- E. van Meenen, K. Moonen, D. Acke and C. V. Stevens, *Arkivoc*, 2006, 31–45.
- X. Zhang, E. S. M. Lai, R. Martin-Aranda and K. L. Yeung, *Appl. Catal., A*, 2004, **261**, 109–118.
- (a) Y. Kikutani, M. Tokeshi, K. Sato and T. Kitamori, *Pure Appl. Chem.*, 2002, **74**(12), 2299–2309; (b) E. Angeletti, C. Canepa, G. Martinetti and P. Venturello, *Tetrahedron Lett.*, 1988, **29**, 2261–2264.
- Y. Kikutani, T. Horiuchi, K. Uchiyama, H. Hisamoto, M. Tokeshi and T. Kitamori, *Lab Chip*, 2002, **2**, 188–192.
- C. Wiles, P. Watts and S. J. Haswell, *Tetrahedron*, 2004, **60**, 8421–8427.
- C. Wiles, P. Watts and S. J. Haswell, *Tetrahedron*, 2005, **61**, 5209–5217.
- S. V. Ley, I. R. Baxendale, G. Brusotti, M. Caldarelli, A. Massi and M. Nesi, *Farmaco*, 2002, **57**, 321–330.
- (a) A. McKillop and D. W. Young, *Synthesis*, 1979, 401–480; (b) A. McKillop and D. W. Young, *Synthesis*, 1979, 481–500; (c) B. J. Cohen, M. A. Kraus and A. Patchornik, *J. Am. Chem. Soc.*, 1981, **103**, 7620–7629.
- J. J. Parlow, *Tetrahedron Lett.*, 1995, **36**, 1395–1396.
- (a) P. Hodge, *Curr. Opin. Chem. Biol.*, 2003, **7**, 362–373; (b) Y. S. S. Wan, J. L. H. Chau, A. Gavriilidis and K. L. Yeung, *Chem. Commun.*, 2002, 878–879; (c) S. M. Lai, R. Martin-Aranda and K. L. Yeung, *Chem. Commun.*, 2003, 218–219; (d) E. Vickerstaffe, B. H. Warrington, M. Ladlow and S. V. Ley, *Org. Biomol. Chem.*, 2003, **1**, 2419–2422; (e) A. Kirschning, W. Solodenko and K. Mennecke, *Chem.–Eur. J.*, 2006, **12**, 5972.
- W. Ehrfeld, V. Hessel and H. Lowe, *Microreactors: New Technology for Modern Chemistry*, Wiley-VCH, New York, 2000.
- Y. Kikutani, A. Hibara, K. Uchiyama, H. Hisamoto, M. Tokeshi and T. Kitamori, *Lab Chip*, 2002, **2**, 193.

- 22 G. Jones, *Organic Reactions*, Wiley, New York, 1967, **15**, 204–599.
- 23 C. L. Rice and R. Whitehead, *J. Phys. Chem.*, 1965, **69**, 4017–4024.
- 24 C. Wiles, P. Watts, S. J. Haswell and E. Pombo-Villar, *Tetrahedron*, 2005, **61**, 10757–10773.
- 25 P. D. Christensen, S. W. P. Johnson, T. McCreedy, V. Skelton and N. G. Wilson, *Anal. Commun.*, 1998, **35**, 341–343.
- 26 The total volume of the flow reactor was calculated to be 0.5 μl ; therefore when operating the reactor at flow rates in the range of 0.40 to 1.05 $\mu\text{l min}^{-1}$ contact times of 1.25 to 0.5 min were obtained.
- 27 In all cases, the acid-catalyzed deprotection of the dimethyl acetal was found to proceed in quantitative conversion; consequently, the percentage conversion to the α,β -unsaturated compound was based on residual aldehyde.



Looking for that **special** chemical biology research paper?

TRY this free news service:

Chemical Biology

- highlights of newsworthy and significant advances in chemical biology from across RSC journals
- free online access
- updated daily
- free access to the original research paper from every online article
- also available as a free print supplement in selected RSC journals.*

*A separately issued print subscription is also available.

Registered Charity Number: 207890

22030681

RSC Publishing

www.rsc.org/chembiology

Scaling out of electrolyte free electrosynthesis in a micro-gap flow cell

Ping He,^a Paul Watts,^a Frank Marken^b and Stephen J. Haswell^{*a}

Received 20th July 2006, Accepted 20th October 2006

First published as an Advance Article on the web 30th October 2006

DOI: 10.1039/b610411h

The electro-reductive coupling of activated olefins and benzyl bromide derivatives has been selected to compare the performance of single and multiple channel (scaled-out) micro-gap electrochemical flow reactors. Two working electrode configurations were evaluated; in the first a single set of electrodes was used in conjunction with a multiple flow manifold to give two and four separate flow channels; in the second independent electrodes were used within the same flow manifold. Problems with shunt currents and Joule heating in the first configuration meant that only the second configuration was reliable, giving results comparable to those obtained for the single flow cell. Excellent yields of the coupling products such as 2-benzyl-succinic acid dimethyl ester and derivatives were obtained. This demonstrates micro reactor scale-out for unsupported electrosyntheses.

Introduction

Electrosynthesis offers a potentially clean and versatile methodology for the generation of anion and cation radical intermediates in organic synthesis under relatively mild reaction conditions.¹ At present, however, the main disadvantage of using micro reactor based methodology is the low quantities of product produced. In order to overcome this problem, whilst maintaining the practical and chemical advantages, the concept of scale-out can be employed.² Scale-out systems have included multisectioned flow-through porous electrodes,^{2a} coplanar platinum interdigitated microband electrodes^{2b} and a miniaturized parallel plate electrochemical cell.^{2c} However, all of these cited electrochemical cells have involved the use of supporting electrolytes or relatively low conversion without intentionally added supporting electrolyte.

In this note, the electro-reductive coupling of activated olefins and benzyl bromide derivatives has been selected to compare the performance of single and multiple channel micro-gap flow reactors.³

Experimental

Construction of micro-gap flow electrochemical cells

The details of constructing a single channel electrochemical cell have been described previously.⁴ In brief, a single channel cell consisted of two glass plates (3 cm length, 2 cm width, 6 mm thickness) in which two holes are drilled in the top plate to enable PEEK tubes (id 0.24 mm) to be connected in order to allow inlet and outlet flow. Two equally sized Pt foils (4 mm width and 15 mm length, 50 μm thickness, Goodfellow Cambridge Limited, purity 99.99%) were used as the working and counter electrodes, and two PTFE spacers (120 μm thick, Bohlender GmbH, Germany) with a rectangular flow reaction zone (3 mm width and 15 mm length) were used to produce the single channel cell with a working area of 45 mm² and

inter-electrode distance of 160 μm . Scaling out systems were made with multiple channels and using two distinct cell configurations. In the first configuration, a single set of electrodes was used in conjunction with a multiple flow manifold to give two (see Fig. 1(a)) and four separate flow channels. In the second configuration, independent electrodes were used within the same flow manifold (see Fig. 1(b)). In the first configuration, the electrode width was 8 mm and 16 mm for making two channels and four channels, respectively. In the second configuration, each channel was built by using the same procedures as that for making single cells (see above).

The electrochemical coupling of an activated olefin with benzyl bromide

For electrosynthesis in single reaction channel cells, the procedure described previously⁴ was employed. For 2 and 4 independent reaction channel cells, each cell was connected in parallel linkage and each circuit consisted of a power supply (BPS4000, CALEX Electronics Ltd.), an ammeter and a voltmeter (TTi1906 Computing Multimeter, RS Components). A solution containing 5 mM activated olefin and 5 mM benzyl bromide in DMF (*N,N*-dimethylformamide, Fluka, 99%, stored over molecular sieve, H₂O \leq 0.01%, which was further dried over molecular sieve 3A (Lancaster, 1–2 mm beads) for 72 h prior to use and kept in a desiccator⁵) was continuously pumped (Harvard PHD 2000 syringe pump) through the reaction cell in which two platinum electrodes with a working area of 45 mm² were positioned with an inter-electrode gap of 160 μm (see Fig. 2). During typical electrosynthesis runs, product samples were collected in a vial from each channel for 5 min in order to obtain sufficient material for subsequent GC/MS analysis. The conditions for GC/MS analysis and identification of products using ¹H and ¹³C NMR analysis were described previously.^{4a}

Resistance measurements (80 mA, 6430A Precision component analyzer, Wayne Kerr) for independent sets of electrodes were performed and indicate that each cell has resistance of typically 1.5 k Ω (for DMF/5 mM benzylbromide/5 mM dimethylfumate) and the total resistance for 2 and 4 parallel connections is 750 Ω and 375 Ω , respectively. The total resistance for ten cells in

^aDepartment of Chemistry, University of Hull, Hull, UK HU6 7RX

^bDepartment of Chemistry, University of Bath, Bath, UK BA2 7AY.

E-mail: s.j.haswell@hull.ac.uk

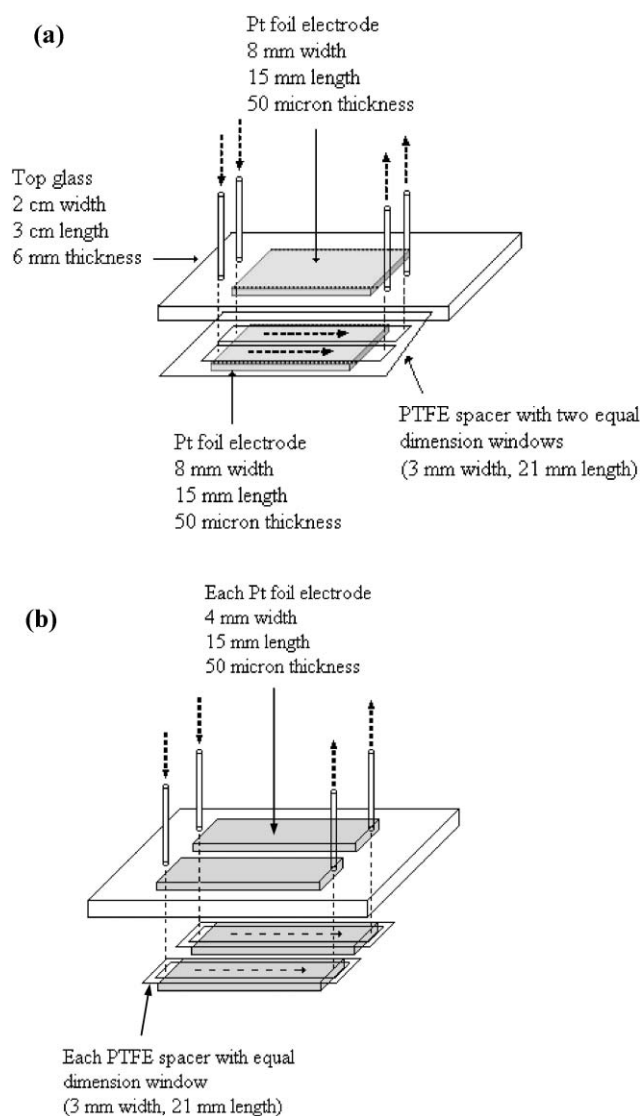


Fig. 1 Schematic representation of scale out of micro-gap flow cell showing (a) a single pair of electrodes and (b) independent electrode configuration for a multiple double flow system. The arrows show reagent flow direction.

parallel connection would be 150 Ω , compared to 170 Ω total resistance for ten cells in series connection reported for a similar system.^{2a} However, resistance effects under no electrolyte conditions are complicated and the current distribution within individual cells may have effects on the local resistance.

Table 1 Data for preparative electrolysis of activated olefins in the presence of benzyl bromides in a micro flow cell without intentionally added supporting electrolyte^a

Entry	Olefin R ¹	R ² -Br R ²	Cell	Flow/ $\mu\text{l min}^{-1}$	Yield (R ¹ -R ²) (%) ^b
1	Dimethylfumarate	Benzyl	Single	10	98
2	Dimethylfumarate	4-Methoxybenzyl	Single	10	94
3	Dimethylfumarate	4-Methylbenzyl	Single	10	94
4	Dimethylfumarate	4-Bromobenzyl	Single	10	99
5	Dimethylfumarate	1-Phenylethyl	Single	10	98

^a Olefin is 5 mM, halide is 5 mM, solvent is DMF, electrode gap is 160 μm , voltage is 4–4.4 V to maintain constant current of 0.6 mA. ^b Yield was determined using GC based on the quantity of the product after reaction using *n*-decane as an internal standard. Side products include dimerization of olefin and debromination of benzyl bromides, no dimerization of benzyl bromides is detected.

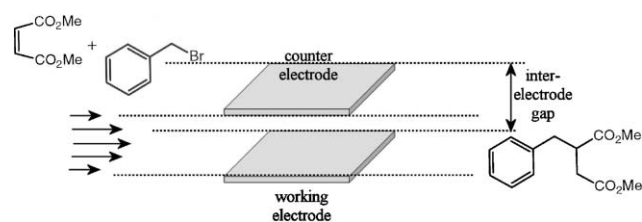


Fig. 2 Schematic representation of the C–C coupling reaction during micro reactor electrosynthesis. A flow of reagents through a rectangular duct with working and counter electrode facing each other results in the formation of products.

Results and discussion

Initially, experiments were conducted for the coupling of an activated olefin with benzyl bromide at constant current (under conditions employed here constant current and constant potential modes give essentially the same results) in the absence of intentionally added supporting electrolyte in a single channel cell at 10 $\mu\text{l min}^{-1}$ flow rate of reactant solution. Under these conditions voltages of typically 4–4.4 V (applied between working and counter electrodes) are applied to maintain a current of 0.6 mA. Table 1 summarizes the typical product yields. It can be seen that sufficiently high levels of product (yield >93%) can be obtained. Interestingly, it was noted that the unwanted dimerization of olefins was occurring to an extent of less than 2%. A very low amount of toluene (from debromination of benzyl bromide) was observed and no dimerization of benzyl bromide was detected. No obvious detrimental anode processes occurred at the counter electrode (*i.e.* the oxidation of bromide ions formed during the coupling reaction to produce bromine, was minimal^{4a}).

In order to further explore the reactant flow within the micro reactor, we estimate the average residence time and the approximate inter-diffusion time for reactants travelling between the two electrodes. At a flow rate of 10 $\mu\text{l min}^{-1}$, the residence time and the average linear velocity are about 43 s and 0.35 mm s^{-1} , respectively. Using the Einstein–Smoluchowski equation⁶ ($d_{\text{diff}} = \sqrt{2Dt}$; d_{diff} = distance travelled by diffusion, D = diffusion coefficient, t = time) the diffusion time across the electrode gap is estimated as typically 12–13 s. This suggests that inter-diffusion is possible. High conversion is probably due to effective inter-diffusion of the dimethylfumarate radical anion and benzyl bromide, and reactive electron transfer between the dimethylfumarate radical anion and benzyl bromide.^{4a}

To further evaluate the scale out methodology, the same coupling reactions were conducted using double and quadruple

Table 2 Data for preparative electrolysis of activated olefins in the presence of benzyl bromides in a double micro flow cell and multiple cells without intentionally added supporting electrolyte^a

Entry	Olefin R ¹	R ² -Br R ²	Cell ^b	Electrode/reactor number ^c	Flow ^d $\mu\text{l min}^{-1}$	Product (R ¹ -R ²) yield (%)			
						Cell-1	Cell-2	Cell-3	Cell-4
1	Dimethylfumarate	Benzyl	D	1/2	20	98	97	—	—
2	Dimethylfumarate	4-Methoxybenzyl	D	1/2	20	93	94	—	—
3	Dimethylfumarate	4-Methylbenzyl	D	1/2	20	93	94	—	—
4	Dimethylfumarate	4-Bromobenzyl	D	1/2	20	99	99	—	—
5	Dimethylfumarate	1-Phenylethyl	D	1/2	20	98	97	—	—
6	Dimethylfumarate	Benzyl	M2	2/2	20	98	98	—	—
7	Dimethylfumarate	4-Methoxybenzyl	M2	2/2	20	94	94	—	—
8	Dimethylfumarate	4-Methylbenzyl	M2	2/2	20	94	95	—	—
9	Dimethylfumarate	4-Bromobenzyl	M2	2/2	20	99	99	—	—
10	Dimethylfumarate	1-Phenylethyl	M2	2/2	20	98	98	—	—
11	Dimethylfumarate	Benzyl	M4	4/4	40	98	98	97	98
12	Dimethylfumarate	4-Methoxybenzyl	M4	4/4	40	93	94	93	94
13	Dimethylfumarate	4-Methylbenzyl	M4	4/4	40	95	93	94	93
14	Dimethylfumarate	4-Bromobenzyl	M4	4/4	40	99	98	99	99
15	Dimethylfumarate	1-Phenylethyl	M4	4/4	40	98	97	97	98
16	Dimethylfumarate	Benzyl	Q4 ^e	1/4	40	70	20	30	65

^a Olefin is 5 mM, halide is 5 mM, solvent is DMF, electrode gap is 160 μm . For the double cell (D) experiments, voltage was 3.5–4 V to maintain constant current of 0.6 mA. For multiple cell experiments (M), each cell has similar voltage value to the single cell in order to maintain a constant current of 0.6 mA. ^b When using the double cell geometry, a single electrode was divided into two single flow cells. In multiple cell geometry, two and four independent electrodes were used for generating 2 (M2) and 4 (M4) parallel flow cells. ^c The values present the number of electrode and reactor used in the cell configuration. ^d The flow value represents the total flow rate. ^e The quadruple flow cell with a single electrode (configuration 1).

micro-gap flow cells (see Fig. 1). The individual flow rates for each of the quadruple cells were measured and found to vary by less than 5% compared to each other and the single channel device. The cells were operated in two distinct configurations as described in the experimental section. It is important to stress that the two and four parallel flow cells used allowed the geometry, flow rate, and applied potentials of the previously optimised single flow cell to be maintained. Using the double and quadruple micro-gap flow cells the coupling reactions were carried out using both electrode configurations and the results are summarised in Table 2. Comparison with Table 1 indicates that the double and quadruple flow cells show the same level of product yield as that obtained with the single cell under the same conditions. However, volumetric flow rates equivalent to 20 $\mu\text{l min}^{-1}$ (*i.e.* 10 $\mu\text{l min}^{-1} \times 2$ flow cells) and 40 $\mu\text{l min}^{-1}$ (*i.e.* 10 $\mu\text{l min}^{-1} \times 4$ flow cells) could be achieved. This demonstrates that scale-out can be achieved without loss of performance compared to that obtained for a single cell. The performance however of the quadruple flow cell configured with only one set of electrodes was poor (configuration 1, Entry 16 in Table 2). This is due presumably to shunt currents (localised resistance changes) and a pronounced Joule heating effect.^{2d} These problems lead to the generation of bubbles and disruption to the flow. No such problems were observed in the second configuration with electrode current individually controlled.

Conclusions

In this preliminary scale-out study, it has been demonstrated that electrosynthesis in a multi-channel micro-gap electrochemical flow cell is possible in the absence of intentionally added supporting electrolyte. The micro flow electrochemical reactor can be easily multiplexed to generate a number of parallel flow cells (scale-out) which offer the performance of

the single cell whilst increasing the volumetric throughput of the system.

References

- 1 J. Utley, *Chem. Soc. Rev.*, 1997, **26**, 157; P. T. Anastas and T. C. Williamson, *Green Chemistry*, Oxford University Press, Oxford, 1998, p. 167; E. Steckhan, T. Arns, W. R. Heineman, G. Hilt, D. Hoorman, J. Jorissen, L. Kroner, B. Lewall and H. Putter, *Chemosphere*, 2001, **43**, 63; D. Pletcher and N. L. Weinberg, *Chem. Eng.*, 1992, **99**, 98; *Microreaction Technology*, ed. W. Ehrfeld, Springer, Berlin, 1998; W. Ehrfeld, V. Hessel and H. Löwe, *Microreactors: New Technology for Modern Chemistry*, Weinheim, Wiley-VCH, 2000; V. Hessel, S. Hardt and H. Löwe, *Chemical Micro Process Engineering*, Weinheim, Wiley-VCH, 2004; D. Horii, M. Atobe, T. Fuchigami and F. Marken, *J. Electrochem. Soc.*, 2006, **153**, 143.
- 2 (a) C. Vallieres and M. Matlosz, *J. Electrochem. Soc.*, 1999, **146**, 2933; (b) C. Belmont and H. H. Girault, *J. Appl. Electrochem.*, 1994, **24**, 719; (c) S. Rode, S. Altmeyer and M. Matlosz, *J. Appl. Electrochem.*, 2004, **34**, 671; (d) M. Küpper, V. Hessel, H. Löwe, W. Stark, J. Kinkel, M. Michel and H. Schmidt-Traub, *Electrochim. Acta*, 2003, **48**, 2889.
- 3 (a) J. P. Devlin, W. D. Ollis, J. E. Thorpe, R. S. Wood, B. J. Broughton, P. J. Warren, K. R. H. Wooldbridge and D. E. Wright, *J. Chem. Soc., Perkin Trans. 1*, 1975, 830; (b) N. A. Porter, D. M. Scott, I. J. Rosenstein, B. Giese, A. Veit and H. G. Zeitz, *J. Am. Chem. Soc.*, 1991, **113**, 1791; (c) D. E. Levy, F. Lapierre, W. Liang, W. Ye, C. W. Lange, X. Li, D. Grobelyny, M. Casabonne, D. Tyrrell, K. Holme, A. Nadzan and R. E. Galaray, *J. Med. Chem.*, 1998, **41**, 199; (d) W. C. Groutas, M. J. Brubaker, M. A. Stanga, J. C. Castrisos, J. P. Crowley and E. J. Schatz, *J. Med. Chem.*, 1989, **32**, 1607; (e) R. B. Bates, R. S. Cuther and R. M. Freeman, *J. Org. Chem.*, 1977, **42**, 4162; (f) G. Sabitha, R. Sridivya and J. S. Yadav, *Tetrahedron*, 1999, **55**, 4015; (g) S. C. Bergmeier and K. A. Ismail, *Synthesis*, 2000, 1369; (h) R. Ballini, G. Bosica, D. Fiorini and P. Righi, *Synthesis*, 2002, 681; (i) M. Mella, M. Fagnoni and A. Albini, *Eur. J. Org. Chem.*, 1999, **9**, 2137.
- 4 (a) P. He, P. Watts, F. Marken and S. J. Haswell, *Angew. Chem., Int. Ed.*, 2006, **45**, 4146; (b) P. He, P. Watts, F. Marken and S. J. Haswell, *Electrochem. Commun.*, 2005, **7**, 918.
- 5 R. D. Burfield and R. H. Smithers, *J. Org. Chem.*, 1978, **43**, 3966.
- 6 I. Levine, *Physical Chemistry*, McGraw-Hill, 2nd edn, 1983.

The use of electroosmotic flow as a pumping mechanism for semi-preparative scale continuous flow synthesis

Charlotte Wiles, Paul Watts* and Stephen J. Haswell

Received (in Cambridge, UK) 6th October 2006, Accepted 24th November 2006

First published as an Advance Article on the web 11th December 2006

DOI: 10.1039/b614559k

By employing a series of reactions we demonstrate the use of electroosmotic flow as a continuous pumping mechanism suitable for semi-preparative scale synthesis, affording an array of small organic compounds, of analytical purity, with yields ranging from 0.57–1.71 g h⁻¹.

One of the slowest steps associated with lead compound generation is the efficient synthesis and purification of small organic compounds, in particular those used to introduce diversity into combinatorial libraries. At present, the majority of synthetic transformations performed in research laboratories employ techniques, and glassware, that has remained largely unchanged for decades. Furthermore, the use of long standing protocols can mean that such reactions are performed using un-optimised reaction conditions, the outcome of which is largely operator dependent. Consequently, when target compounds are identified and prepared for transfer to production, the synthetic route frequently requires re-optimization, not only to address changes in scale, but also to enable the process to be operated under a more efficient continuous flow regime.

Owing to the pharmaceutical importance of α,β -unsaturated compounds, we were interested in developing a simple synthetic technique that would enable the rapid production of gram quantities of analytically pure material, using continuous flow methodology. Whilst a range of green approaches have been investigated for the synthesis of such analogues, the use of water¹ or ionic liquids² as reaction media demands that a formal work-up be performed in order to isolate, and where possible recycle, the catalyst. To circumvent this problem, numerous authors have reported the use of solid-supported bases, which can simply be filtered from the reaction mixture.³ However, difficulties with the technique arise due to mechanical degradation of the support upon prolonged stirring, or shaking, of the reaction mixture in a batch mode.

In the late 1980s, Venturello and co-workers⁴ reported the Knoevenagel condensation under continuous flow, using a vertical, double jacketed glass column packed with aminopropyl functionalised silica gel. Reactions were performed by simply placing a solution of aldehyde and activated methylene at the top of the column, where it passed through the catalyst under gravity (as in a liquid chromatographic process). Collection of the reaction mixture at the outlet, followed by evaporation of the solvent system, afforded the desired product and any unreacted starting

materials. Although this technique illustrated advantages associated with continuous flow syntheses, namely the ease of product isolation and catalyst recycle, the technique employed large volumes of solvent (30 ml mmol⁻¹) and provided no control over flow rate. This inability to readily alter a reagent's residence time led to incomplete product conversions when less reactive analogues were employed, resulting in the need for additional off-line purification. To address this shortfall, continuous flow techniques have evolved to employ pressure-driven flow (in the form of HPLC or displacement pumps), enabling the rate at which reagents pass through the packed beds to be controlled.⁵ Using this approach, an array of synthetic transformations have been demonstrated including hydrogenations,⁶ oxidations,⁷ reductions,⁸ Diels–Alder reactions,⁹ Suzuki couplings¹⁰ and Michael additions,¹¹ culminating in the ability to perform automated multi-step syntheses, as illustrated by Ley and co-workers¹² for the synthesis of (\pm)-oxomaritidine. Whilst the aforementioned examples serve to illustrate the versatility of continuous flow systems, in order for the technique to become more widely adopted problems such as irreproducible flow (especially at low flow rates), back-pressure generation and cumbersome operating systems, need to be addressed.

Having recently demonstrated the ability to synthesise milligram quantities of analytically pure compounds in a series of miniaturised electroosmotic flow (EOF) based reactors,¹³ we were interested in exploring methodologies capable of increasing the throughput of the system. One option was to scale-out the technique, *i.e.*, increase the number of optimised micro-reactor units employed, while an alternative approach was to simply increase the size of the catalyst bed.

To date, EOF has largely found use as a pumping mechanism for the manipulation of nl to μ l quantities of material within micron-sized capillaries and channel networks.¹⁴ However, as the volumetric flow rate is largely dependent upon the cross-sectional area of a channel, increasing the size of the channel enables the flow rate to be readily increased. As such reactions are diffusion limited, increasing the size of a reaction channel can be detrimental to reaction efficiency as it leads to inefficient mixing. This is, however, not the case when employing packed catalyst beds, as the diffusion distance between the liquid phase and the solid-supported catalyst, or reagent, remains the same irrespective of the overall bed size. Unlike simple pressure-driven systems where packed-bed size is limited by a reactor's tolerance to pressure, electroosmotic systems generate minimal back-pressure and therefore have the potential to be scaled-up with ease. In addition, the absence of mechanical pump drivers greatly reduces the footprint of the reaction set-up, which simply consists of a power supply (16 cm (w) \times 6 cm (d) \times 27 cm (l)) and a flow reactor

Department of Chemistry, Faculty of Science and the Environment, The University of Hull, Cottingham Road, Hull, HU6 7RX, UK.
E-mail: P.Watts@hull.ac.uk.; Fax: +44 (0)1482 466410;
Tel: +44 (0)1482 465471

(6 cm (w) × 1 cm (d) × 6 cm (l)). Automation of the system also enables the reactors to be operated remotely from a safe working distance, reducing the amount of valuable fume cupboard space required. Using this approach, we investigated the ability to scale-up our previously optimised reaction set-up which employed a 0.5 mm (id) capillary to a 3.0 mm (id) capillary, the results of which are reported herein.

As Fig. 1 illustrates, the reaction set-up employed consists of a borosilicate glass capillary (3.0 mm (id), 3.0 cm (length)), fritted at both ends to retain the solid-supported reagent, attached to two borosilicate glass reagent reservoirs *via* rubber stoppers (No. 9, Suba Seal). To perform a reaction, the packed-bed is primed with anhydrous acetonitrile (MeCN) (to form a complete electrical circuit) and platinum electrodes (0.25 mm (od) × 2.5 cm (length)) are then placed in reservoirs A and B, respectively. A solution of starting material is then placed in reservoir A and an aliquot of solvent placed in reservoir B. The reaction mixture is subsequently passed through the packed-bed by application of a positive voltage to reservoir A (167 to 300 V cm⁻¹) and the reaction products collected in reservoir B (0 V cm⁻¹). Unless otherwise stated, reactions are carried out for 10 min, after which the contents of reservoir B are removed and analysed, off-line, by GC-MS. Once optimised, the reactors are operated continuously for a period of 1 h (2.5 h in some instances), the reaction products collected, concentrated *in vacuo* and the crude product dissolved in CDCl₃ prior to purity evaluation by NMR spectroscopy.

To assess the reactor's performance, we firstly investigated the incorporation of silica-supported piperazine (0.100 g, 1.70 mmol g⁻¹) into the packed-bed, demonstrating the Knoevenagel condensation of two activated methylenes with a series of aldehydes (Table 1). Employing an applied field of 200 V cm⁻¹, a pre-mixed solution of aldehyde and activated methylene (both 1.0 M in anhydrous MeCN) was placed in reservoir A and passed through the packed-bed at flow rates in the range from 48.3 to 62.1 μl min⁻¹, depending on the aldehyde employed. In all cases, optimised reaction conditions afforded the desired α,β-unsaturated product (*trans*-isomer only) in excellent product purity (>99.9%) and yield (>98.8%), demonstrating reactor stability over ≥15 runs. To further demonstrate the feasibility of operating such reactors continuously, the syntheses of 3-(4-bromophenyl)-2-cyanoacrylic acid ethyl ester and 2-(4-bromobenzylidene)malononitrile were investigated over an extended 2.5 h period, affording 2.30 g (99.4%) and 1.70 g (99.8%) of analytically pure material, respectively.

Based on the results presented in Table 1, it can be seen that the use of continuous flow reactors not only leads to enhanced

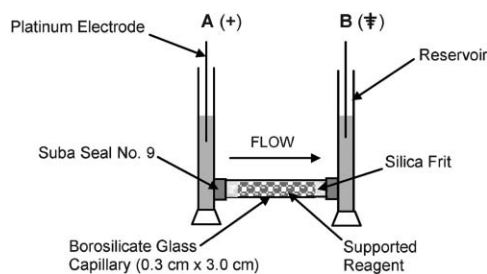


Fig. 1 Schematic illustrating the reaction set-up used for the continuous flow synthesis of small organic compounds by EOF.

Table 1 Summary of the results obtained for the synthesis of α,β-unsaturated compounds in an EOF-based continuous flow reactor (unless stated otherwise, all reactions were conducted for 1 h)

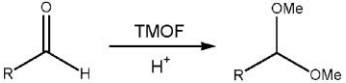
R ¹	R ²	R ³	R ⁴	Flow rate ⁻¹ /μl min	Conv. (%) ^a	Yield /g
H	H	H	CO ₂ Et	62.0	99.9	0.75 (99.7) ^b
H	CO ₂ Me	H	CO ₂ Et	56.1	100.0	0.87 (99.8)
OMe	H	OMe	CO ₂ Et	50.1	99.9	0.78 (99.9)
H	OBn	H	CO ₂ Et	51.1	99.9	0.94 (99.7)
H	Br	H	CO ₂ Et	55.1	99.9	2.30 ^c (99.4)
H	H	H	CN	62.1	99.9	0.57 (99.4)
H	CO ₂ Me	H	CN	60.4	99.9	0.76 (98.8)
OMe	H	OMe	CN	55.7	100.0	0.71 (99.2)
H	OBn	H	CN	48.4	99.9	0.75 (99.4)
H	Br	H	CN	48.3	100.0	1.70 ^c (99.8)

^a n = 15. ^b Number in parentheses represents % yield. ^c Reaction conducted for 2.5 h.

product purity but also to a dramatic reduction in reaction time, affording near quantitative yields with residence times in the range of 0.15–0.19 min.† The generality of the technique was subsequently evaluated by incorporating polymer supported diazabicyclo[2.2.2]octane (1.45 mmol N g⁻¹), 3-(dimethylamino)propyl (1.50 mmol N g⁻¹), 3-aminopropyl (1.70 mmol N g⁻¹) and 3-(1,3,4,6,7,8-hexahydro-2H-pyrimido[1.2.1]-pyrimidino)propyl (2.40 mmol N g⁻¹) functionalised silica gels into the flow reactor, whereby 3-(4-bromophenyl)-2-cyano-3-phenylacrylic acid ethyl ester was obtained in excellent yield and purity (>99.0%). Compared with the gravity-based system reported by Venturello and co-workers,⁴ the approach described here is also advantageous as it represents a significant reduction in solvent usage, requiring only 1 ml mmol⁻¹ of product, *cf.* 30 ml mmol⁻¹. In addition, as the products synthesised are obtained in excellent purity, no subsequent off-line chromatographic purification is needed, further reducing the environmental burden associated with the technique.

In addition to the base-catalysed syntheses discussed, the study also investigated the feasibility of performing acid catalysed reactions in such continuous flow systems. Based on our previous experience of solid-supported acid catalysts, the synthesis of dimethyl acetals was selected as a model reaction. In brief, reactions were performed by mobilising a pre-mixed solution of aldehyde and trimethylorthoformate (1.0 M and 2.5 M, respectively, in MeCN) through a packed bed, containing Amberlyst-15 (0.075 g, 0.315 mmol), upon application of 300 and 0 V cm⁻¹, to reservoirs A and B respectively. Again, the reaction products were

Table 2 Synthesis of dimethylacetals in a wide bore, EOF-based, continuous flow reactor (unless stated otherwise, all reactions were conducted for 1 h)



Starting material	Flow rate/ $\mu\text{l min}^{-1}$	Conv. (%) ^a	Yield/g
Benzaldehyde	139.0	100.0	1.26 (99.2) ^b
4-Cyanobenzaldehyde	124.0	99.8	1.31 (99.2)
4-Chlorobenzaldehyde	120.0	99.9	1.33 (99.5)
4-Benzyloxybenzaldehyde	111.0	99.9	1.71 (99.7)
3,5-Dimethoxybenzaldehyde	112.0	99.9	1.42 (99.4)
2-Naphthaldehyde	126.0	99.9	1.52 (99.8)
Methyl-4-formylbenzoate	121.0	99.9	1.52 (99.4)
5-Nitro-2-thiophenecarboxaldehyde	123.0	99.9	1.50 (99.8)
<i>trans</i> -Cinnamaldehyde	113.0	99.9	1.20 (99.4)
4-Bromobenzaldehyde	105.0	99.6	3.64 (99.7) ^c

^a $n = 15$. ^b Number in parentheses represents % yield. ^c Reaction conducted for 2.5 h.

Table 3 Evaluation of the catalytic activity of an acid and a base catalyst employed within the EOF-based flow reactor

	Catalyst/ mmol	Product/ mmol	Turnover number
Silica-supported piperazine	0.17	42.00	247
Amberlyst-15	0.32	80.71	256

^a Based on the data presented herein (catalysts remain active).

collected at 10 min intervals and analysed off-line by GC-MS. Once optimised, reactions were operated continuously for 1 h and the products isolated by evaporation of the reaction solvent: the purity of the 'crude' material was subsequently evaluated by NMR spectroscopy. Employing flow rates in the range of 111.0–139.0 $\mu\text{l min}^{-1}$ resulted in optimal conversion of an array of aldehydes to their respective dimethylacetal (Table 2), obtaining greater product purity compared with analogous batch reactions. This observation is attributed to the unique reaction conditions attained within continuous flow reactors, which enable reaction products to be removed from the reactor prior to, in this case, competing acid-catalysed deprotection occurring. Again, extended operation was demonstrated for the synthesis of 1-bromo-4-dimethoxymethylbenzene, affording a space time yield of 1.46 g h^{-1} . Furthermore, system generality was demonstrated *via* the incorporation of additional solid-supported Lewis acid catalysts, including silica-supported sulfonic acid (1.50 mmol g^{-1}), polymer supported *para*-toluene sulfonic acid (2.00 to 3.50 mmol g^{-1}), ytterbium polystyryl sulfonate(III) (0.80 mmol g^{-1}), whereby excellent yields and purities were obtained in all cases.

Based on the data presented herein it can be concluded that the catalysts remain active over prolonged periods of time, enabling catalytic turnovers in excess of 247 times to be attained (Table 3).

The scope of the technique was subsequently extended to evaluate the feasibility of performing continuous flow, multi-step syntheses. As Fig. 2 illustrates, the model reaction selected involved an acid-catalysed acetal deprotection, followed by a base-catalysed condensation, of the *in situ* generated aldehyde with

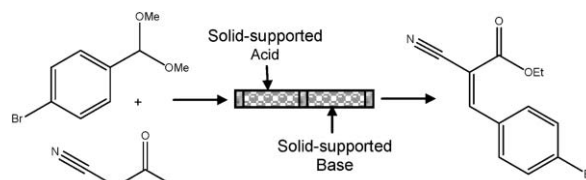


Fig. 2 Schematic illustrating the multi-step synthesis of 3-(4-bromophenyl)-2-cyanoacrylic acid ethyl ester in an EOF based, continuous flow reactor.

ethylcyanoacetate, to afford 3-(4-bromophenyl)-2-cyanoacrylic acid ethyl ester. To perform a reaction, a pre-mixed solution of 1-bromo-4-dimethoxymethylbenzene and ethylcyano acetate (1.00 M in MeCN) was placed in reservoir A and pumped through a packed-bed containing Amberlyst-15 (0.036 g, 0.151 mmol) and silica-supported piperazine (0.050 g, 0.085 mmol). By ensuring that each step of the reaction proceeds to completion, multiple reaction steps can be performed in series, without the need to purify the reaction intermediates. Consequently, operation of the reactor at an optimised flow rate of 54.9 $\mu\text{l min}^{-1}$ afforded 3-(4-bromophenyl)-2-cyanoacrylic acid ethyl ester in excellent purity (100.0% by GC-MS) with a system throughput of 0.926 g h^{-1} .

From the examples presented, it can be seen that EOF is a versatile pumping technique that affords accurate, pulse-free reagent delivery, enabling reactions to be readily optimised. Furthermore, the ease with which the supported reagents are recycled provides reaction reproducibility and catalyst lifetimes unobtainable in traditional agitated reaction systems.

Full financial support provided by the EPSRC (C.W.) (Grant No. GR/S34106/01) is gratefully acknowledged.

Notes and references

[†] The total volume of the flow reactor was found to be 9.0 μl , therefore when operating at 50.0 $\mu\text{l min}^{-1}$ a residence time of 0.18 min is obtained.

- A. Pande, K. Ganesan, A. K. Jain, P. K. Gupta and R. M. Malhotra, *Org. Process Res. Dev.*, 2005, **9**, 133.
- D. W. Morrison, D. C. Forbes and J. H. Davis, *Tetrahedron Lett.*, 2001, **42**, 6053.
- (a) J. Simpson, D. L. Rathbone and D. C. Billington, *Tetrahedron Lett.*, 1999, **40**, 7031; (b) F. Texier-Boulett and A. Foucod, *Tetrahedron Lett.*, 1982, **23**, 4927.
- (a) E. Angelletti, C. Canepa, G. Martinetti and P. Venturello, *Tetrahedron Lett.*, 1988, **29**, 2261; (b) E. Angelletti, C. Canepa, G. Martinetti and P. Venturello, *J. Chem. Soc., Perkin Trans. 1*, 1989, 105.
- A. Kirschning, W. Solodenko and K. Mennecke, *Chem.-Eur. J.*, 2006, **12**, 5972.
- (a) R. V. Jones, L. Godorhazy, N. Varga, D. Szalay, L. Urge and F. Darvas, *J. Comb. Chem.*, 2006, **8**(1), 110; (b) N. Yoswathananont, K. Nitta, Y. Nishiuchi and M. Sato, *Chem. Commun.*, 2005, 40.
- C. Wiles, P. Watts and S. J. Haswell, *Tetrahedron Lett.*, 2006, **47**, 5261.
- S. Itsuno, K. Ito, T. Maruyama, N. Kanda, A. Hirao and S. Nakahama, *Bull. Chem. Soc. Jpn.*, 1986, **59**, 3329.
- K. Kamahori, K. Ito and S. Itsuno, *J. Org. Chem.*, 1996, **61**, 8321.
- I. R. Baxendale, C. M. Griffiths-Jones, S. V. Ley and G. K. Tranmer, *Chem.-Eur. J.*, 2006, **12**, 4407.
- F. Bonfils, I. Cazaux, P. Hodge and C. Caze, *Org. Biomol. Chem.*, 2006, **4**, 493.
- I. R. Baxendale, J. Deeley, C. M. Griffiths-Jones, S. V. Ley, S. Saaby and G. K. Tranmer, *Chem. Commun.*, 2005, 2566.
- (a) C. Wiles, P. Watts and S. J. Haswell, *Tetrahedron*, 2005, **61**, 5209; (b) C. Wiles, P. Watts and S. J. Haswell, *Tetrahedron*, 2004, **60**, 8421.
- S. J. Haswell, *Analyst*, 1997, **112**, 1R.

An efficient, continuous flow technique for the chemoselective synthesis of thioacetals

Charlotte Wiles, Paul Watts* and Stephen J. Haswell

Department of Chemistry, The University of Hull, Cottingham Road, Hull HU6 7RX, UK

Received 22 June 2007; revised 3 August 2007; accepted 6 August 2007

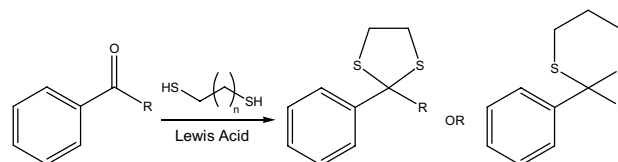
Available online 10 August 2007

Abstract—By optimizing a reagent's residence time within a packed-bed reactor, it is possible to overcome selectivity issues frequently encountered in stirred reaction vessels. This important feature is demonstrated for the chemoselective protection of 4-acetylbenzaldehyde whereby 1-[4-(1,3-dithian-2-yl-phenyl)]ethanone is obtained in excellent yield and purity. In addition, the generality of the technique is highlighted via the protection of numerous aldehydes and ketones affording the respective thioacetal/ketal in excellent yield (>99.1%) and purity (>99.9%), with space–time yields in the range of 0.44–1.10 g h⁻¹.

© 2007 Elsevier Ltd. All rights reserved.

1,3-Dithianes are versatile reagents employed in the formation of C–C bonds, with the conjugate addition of lithiated 1,3-dithianes to α,β -unsaturated ketones, aldehydes, esters, and lactones widely reported in modern organic synthesis.¹ Additionally, *S,S*-acetals form an important class of carbonyl protecting groups that, unlike their respective oxygen containing analogues, are hydrolytically stable and tolerant to a wide pH range.² Due to their overwhelming stability to an array of reaction conditions, deprotection is not easily achieved. Consequently, many approaches have been reported with reagent selection determined by the sensitivity and stability of the particular substrate.

Owing to the synthetic utility of 1,3-dithianes and 1,3-dithiolanes, many techniques have been described for their preparation based on the condensation of a carbonyl compound with the respective dithiol (Scheme 1). To promote the reaction, an array of Lewis or Bronsted acid catalysts have been reported including zinc or magnesium triflate,³ titanium tetrachloride,⁴ boron trifluoride,⁵ and lithium perchlorate,⁶ frequently in conjunction with an excess of dithiol (0.1–5.0 equiv). Subsequent purification is therefore required, not only to remove the excess thiolating agent, but also the acid catalyst, prior to performing subsequent reaction steps.



Scheme 1. General reaction scheme illustrating the protection of carbonyl moieties as their respective 1,3-dithiolane ($n = 1$) or 1,3-dithiane ($n = 2$).

The use of heterogeneous catalysts, such as Amberlyst-15 (A-15) 1,⁷ natural kaolinitic clay,⁸ silica-supported *p*-toluenesulfonic acid^{9,10} addressed the problem of catalyst recovery, whereby employing a simple filtration at the end of the reaction enables isolation, and potential recovery/reuse, of the catalyst. Again, an excess of dithiol is often employed, demanding additional purification steps to be performed. Although solid-supported reagents and catalysts have many advantages over their solution phase analogues, one limitation is mechanical degradation of the support (due to stirring or agitation of reaction mixtures) which leads to reduced reagent lifetimes and difficulties with efficient reagent recycle. Consequently, by performing reactions within continuous flow reactors,¹¹ such as the one described herein, the support undergoes minimal mechanical stress, affording extended reagent lifetimes, along with ease of catalyst recycling and reproducibility between reactions. Furthermore, automation of the technique offers increased reaction control, reduced operator dependency and facilitates rapid reaction optimization.

* Corresponding author. Tel.: +44 1482 465471; fax: +44 1482 466416; e-mail: p.watts@hull.ac.uk

In pursuit of an atom efficient technique for the protection of carbonyl moieties, we investigated the continuous flow synthesis of 1,3-dithianes and 1,3-dithiolanes, proposing that careful optimization of the reaction conditions would allow the synthesis and isolation of analytically pure products, by simply removing the reaction solvent.

To manipulate reactants and products within the flow reactor, the pumping mechanism selected was electroosmotic flow (EOF) as compared to pressure-driven (PD) flow, EOF generates minimal back-pressure; a particularly important feature for packed-bed reactors. EOF therefore enables reaction systems to be scaled without being limited by the reactor's pressure tolerance, a frequently encountered problem in PD systems. The technique also enables precise control over flow rate, as it is not limited by an incremental stepper motor, thus affording pulse-free flow. In addition, the absence of mechanical pump drivers reduces the footprint of the set-up, which simply consists of a power supply. Again, automation of the system enables remote operation of the reactors, reducing greatly the amount of valuable fume cupboard space required to perform such reactions. While EOF has predominantly been employed as a pumping mechanism within miniaturized reaction systems for the manipulation of μl quantities of material,¹² we recently reported its use within a flow reactor of millimeter dimensions, enabling access to flow rates in the range of 0.1–500.0 $\mu\text{l min}^{-1}$.¹³

As Figure 1 illustrates, the reaction set-up employed herein consists of a borosilicate glass capillary (3.0 mm (i.d.) \times 30.0 mm (length)), packed with A-15 1 (0.055 g, 0.231 mmol) attached to borosilicate glass reagent reservoirs via two rubber septa (No. 9, Suba Seal). To perform a reaction, the packed-bed is filled with anhydrous MeCN (to form a complete electrical circuit) and a solution containing the reactants is then placed in reservoir A along with an aliquot of solvent in reservoir B. Platinum electrodes (0.5 mm (o.d.) \times 2.5 cm (length)) are placed in each reservoir and the reaction mixture pumped through the packed-bed by application of a positive voltage (50–200 V cm^{-1}) to reservoir A; the reaction products are subsequently collected in reservoir B (0 V cm^{-1}) (Fig. 2). Unless otherwise stated optimization reactions are performed for 10 min, prior to analy-

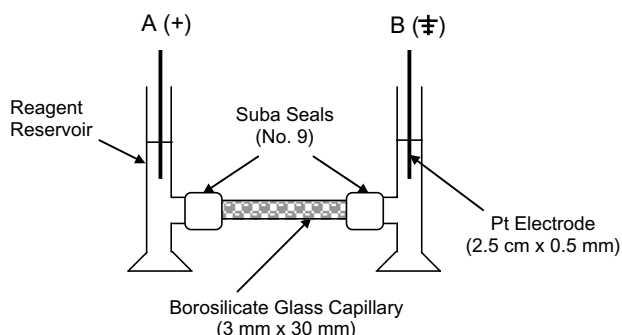


Figure 1. Schematic illustrating the reaction set-up used for the continuous flow synthesis of 1,3-dithianes and 1,3-dithiolanes.

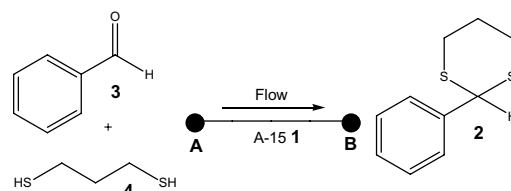


Figure 2. Schematic illustrating the continuous flow synthesis of 2-phenyl-1,3-dithiane 2.

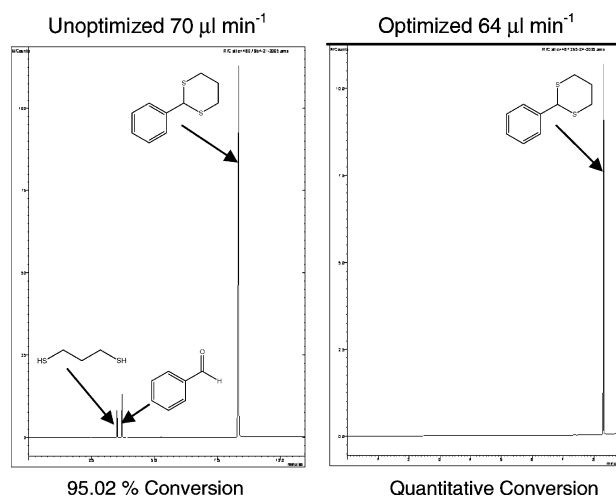


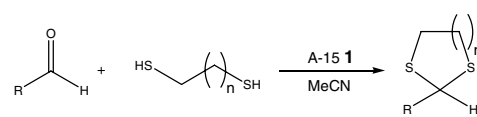
Figure 3. Gas chromatograms illustrating the difference between an optimized and an unoptimized system for the synthesis of 2-phenyl-1,3-dithiane 2, under continuous flow.

sis by GC–MS whereby the percentage conversion of carbonyl compound to product is determined. Once optimized (Fig. 3), the reactor is operated continuously for 1 h, after which the reaction products are removed from reservoir B, concentrated in vacuo and the crude product dissolved in CDCl_3 prior to additional purity evaluation by NMR spectroscopy.

Using the set-up illustrated in Figures 1 and 2, the reactor's performance was assessed using the synthesis of 2-phenyl-1,3-dithiane 2 as a model reaction. Employing an applied field of 200 V cm^{-1} , a pre-mixed solution of benzaldehyde 3 and 1,3-propanedithiol 4 (1.0 M, 1:1 in MeCN) was pumped through the packed-bed at a flow rate of 63.7 $\mu\text{l min}^{-1}$ (residence time = 75.4 s) and the reaction products evaluated every 10 min, off-line by GC–MS (Fig. 3). Typical reaction data from the optimization process afforded quantitative conversion of benzaldehyde 3 to 2-phenyl-1,3-dithiane 2 (99.992%). In addition, the reaction reproducibility ($5.0 \times 10^{-3}\%$ RSD) obtained over 2.5 h confirms effective recycle of the acid catalyst, generating 9.42 mmol of product 2 with 0.231 mmol of catalyst; representing a turnover of 41 times, so far.

Having established the ability to perform a model thioacetalization under continuous flow conditions, the next step was to evaluate the generality of the technique, firstly investigating the protection of an array of substituted aldehydes as the respective 1,3-dithiane. As

Table 1. Summary of the results obtained for the thioacetalization of ten substituted aldehydes under continuous flow conditions (200 V cm⁻¹)



Aldehyde	<i>n</i> ^a	Flow rate (μl min ⁻¹)	Yield ^b (g)	Yield (%)
Benzaldehyde	2	63.7	1.96 ^c	99.97
	1	63.4	0.69	99.97
4-Bromobenzaldehyde	2	61.4	1.01	99.92
	1	61.2	0.96	99.96
4-Chlorobenzaldehyde	2	61.7	0.85	99.91
	1	61.9	0.80	99.95
4-Cyanobenzaldehyde	2	65.4	0.87	99.94
	1	64.6	0.80	99.96
4-Benzyloxybenzaldehyde	2	61.1	1.10	99.22
	1	60.9	1.05	99.93
4-Methylbenzaldehyde	2	69.7	0.88	99.97
	1	69.0	0.81	99.93
4-Biphenylcarboxaldehyde	2	63.0	1.02	99.06
	1	63.0	0.97	99.97
2-Naphthaldehyde	2	60.4	0.89	99.94
	1	60.2	0.84	99.98
2-Furaldehyde 5	2	67.9	0.76	99.92
	1	67.5	0.69	99.97
3,5-Dimethoxybenzaldehyde	2	67.9	1.04	99.91
	1	67.7	0.982	99.93

^a 1,2-Ethanedithiol **6** (*n* = 1) and 1,3-propanedithiol **4** (*n* = 2).

^b Unless otherwise stated, reactions were performed for 1 h.

^c Reaction conducted for 2.5 h.

Table 1 illustrates, employing a stoichiometric quantity of dithiol, and an average residence time of 76 s (~62.9 μl min⁻¹), afforded the respective dithiane, in excellent yield and purity. Importantly no sign of substituent effect was observed, with even difficult to protect compounds such as 2-furaldehyde **5** being reacted with ease. Furthermore, substitution of 1,3-propanedithiol **4** with 1,2-ethanedithiol **6** afforded the synthesis of 1,3-dithiolanes in excellent yields and purities, employing analogous reaction conditions to those previously optimized for the 1,3-dithianes. Compared to a typical batch reaction, the use of a flow reactor enabled a dramatic reduction in reaction time, from 24 h to 76 s; an observation, which is attributed to the high surface-to-volume ratio obtained between the catalyst and reactants. Furthermore, the use of a closed reaction system, such as the one described herein, facilitates the efficient reaction of odorous compounds, affording reaction products of excellent purity without the need for additional purification.

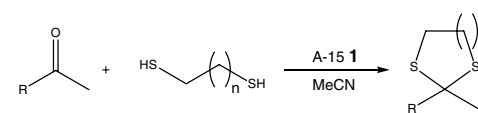
As the preparation of thioketals is kinetically less favorable than their respective thioacetals, extended reaction times are frequently employed (24–120 h), along with an excess of the dithiol or extreme reaction temperatures.⁷

Based on the encouraging results summarized in Table 1, our investigation progressed on to the protection of ketones, determining whether the aforementioned reductions in reaction time were also attainable for the

synthesis of thioketals. Utilizing a comparable technique to that employed for the thioacetalizations, a pre-mixed solution of ketone and dithiol (1.0 M, 1:1 in MeCN) was mobilized through the packed-bed, using an applied field of 50 V cm⁻¹. As the results in Table 2 demonstrate, in all cases excellent yields were obtained, with throughputs in the range of 0.44–0.70 g h⁻¹. Importantly, no substituent effects were observed, with even highly substituted ketones, which are normally difficult to protect, proving facile in this system.

Having demonstrated the different reaction conditions required to quantitatively protect both aldehydic and ketonic moieties within a continuous flow reactor, we investigated the ability to chemoselectively protect an aldehyde in the presence of a ketone (Scheme 2). Under reaction conditions previously optimized for the protection of aldehydes, a pre-mixed solution of 4-acetylbenzaldehyde **7** and 1,3-propanedithiol **4** (1.0 M) in MeCN was mobilized through the packed-bed (200 V cm⁻¹) at a flow rate of 65.2 μl min⁻¹, affording 1-[4-1,3-dithian-2-yl-phenyl]ethanone **8** in quantitative yield. Conducting the reaction under such flow conditions, afforded superior results compared to those obtained in an analogous batch reaction, enabling selectivity toward protection of the formyl group. As Figure 4 illustrates, in an analogous batch reaction (24 h), incomplete conversion of 4-acetylbenzaldehyde **7** to the respective 1,3-dithiane **8** was observed, along with competing di-protection to afford 2-[4-1,3-dithian-2-yl-phenyl]-2-methyl-1,3-dithiane **9**.

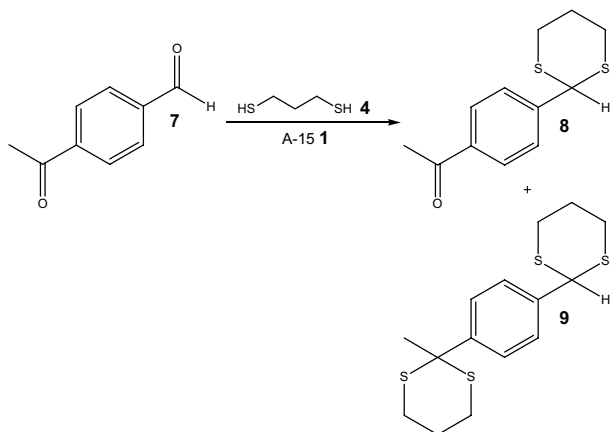
Table 2. Summary of the results obtained for the protection of ketones, under continuous flow, as their respective thioketal (50 V cm⁻¹)



Ketone	<i>n</i> ^a	Flow rate (μl min ⁻¹)	Yield ^b (g)	Yield (%)
Acetophenone	2	41.5	0.52	99.57
	1	41.3	0.48	99.96
Propiophenone	2	40.2	0.54	99.97
	1	40.3	0.51	99.96
Butyrophenone	2	41.6	0.59	99.90
	1	41.6	0.56	99.90
Cyclohexanone	2	42.2	0.47	99.62
	1	42.1	0.44	99.98
Benzophenone	2	40.2	0.57	99.81
	1	40.1	0.65	99.91
4-Nitroacetophenone	2	40.9	0.63	99.95
	1	41.0	0.59	99.95
2-Methoxyacetophenone	2	40.9	0.59	99.93
	1	41.9	0.57	99.93
4-Chloroacetophenone	2	40.9	0.60	99.87
	1	40.8	0.60	99.91
4-Hydroxyacetophenone	2	42.2	0.57	99.76
	1	42.1	0.53	99.83
4-Bromoacetophenone	2	40.2	0.70	99.94
	1	40.1	0.66	99.97

^a 1,2-Ethanedithiol **6** (*n* = 1) and 1,3-propanedithiol **4** (*n* = 2).

^b Unless otherwise stated reactions were performed for 1 h.



Scheme 2. Possible reaction products obtained from the protection of 4-acetylbenzaldehyde **7** as its respective 1,3-dithiane **8**.

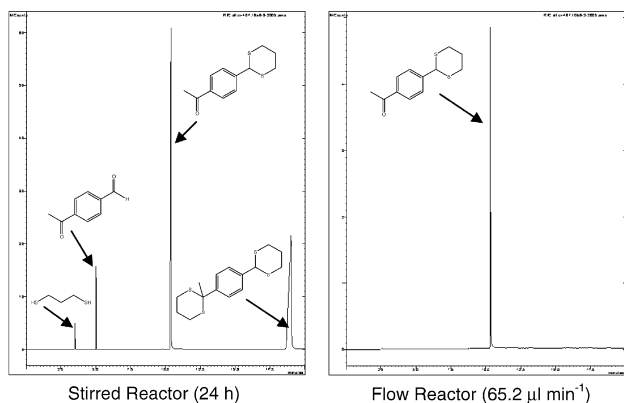


Figure 4. Gas chromatograms illustrating the chemoselectivity obtained in a flow reactor compared to a traditional stirred reactor.

Further to the excellent isolated yields obtained when conducting reactions under continuous flow, an additional advantage of the technique is the ability to recycle the solid-supported catalyst with ease. This is illustrated herein whereby 128.5 mmol of thioacetals and ketals were synthesized using 0.231 mmol of catalyst, representing an impressive turnover number of 556, with no sign of degradation to date. Although A-15 1 is capable of being turned over this number of times in batch, it is a difficult undertaking when using traditional reaction methodology as the catalyst must be filtered from the reaction mixture in order to be re-used. In addition, the mechanical degradation that the catalyst undergoes

when used repeatedly increases the difficulties associated with efficient filtration.

In conclusion, we have developed a simple and efficient technique that enables the chemoselective protection of aldehydes, based solely on reactant residence time within a packed-bed reactor.

Acknowledgements

The authors acknowledge the EPSRC (C.W.) (Grant No. GR/S34106/01) for full financial support of this project and Mr. Mike Bailey (The University of Hull) for assistance with device fabrication.

Supplementary data

Supplementary data associated with this article can be found, in the online version, at doi:10.1016/j.tetlet.2007.08.027.

References and notes

- (a) Seebach, D. J. *Synthesis* **1969**, 17; (b) Corey, E. J.; Seebach, D. J. *J. Org. Chem.* **1966**, *31*, 4097; (c) Bulman Page, P. C.; van Niel, M. B.; Prodger, J. *Tetrahedron* **1989**, *45*, 7643; (d) Yus, M.; Najera, C.; Foubelo, F. *Tetrahedron* **2003**, *59*, 6147, and references cited therein.
- (a) Greene, T. W.; Wuts, P. G. M. *Protective Groups in Organic Synthesis*, second ed.; Wiley: New York, 1991.
- Corey, E. J.; Shimoji, K. *Tetrahedron Lett.* **1983**, *24*, 169.
- Kumar, V.; Dev, S. *Tetrahedron Lett.* **1983**, *24*, 1289.
- Wilson, G. E., Jr.; Huang, M. G.; Schloman, W. W. *J. Org. Chem.* **1968**, *33*, 21343.
- Tietze, L. F.; Weigand, B.; Wulff, C. *Synthesis* **2000**, 69.
- Perni, R. B. *Synth. Commun.* **1989**, *19*, 2383.
- Ponde, D.; Sudalai, B. A.; Ravindranathan, T.; Deshpande, V. H. *Tetrahedron Lett.* **1996**, *37*, 4605.
- Ali, M. H.; Gomes, M. G. *Synthesis* **2005**, *8*, 1326.
- Kitamori, Y.; Hojo, M.; Masuda, R.; Kimura, T.; Yoshida, T. *J. Org. Chem.* **1986**, *51*, 1427.
- (a) Jas, G.; Kirschning, A. *Chem. Eur. J.* **2003**, *9*, 5708; (b) Kirschning, A.; Solodenko, W.; Mennecke, K. *Chem. Eur. J.* **2006**, *12*, 5972; (c) Hodge, P. *Curr. Opin. Chem. Biol.* **2003**, *1*, 2419.
- Haswell, S. J. *Analyst* **1997**, *112*, 1R.
- Wiles, C.; Watts, P.; Haswell, S. J. *Chem. Commun.* **2007**, 966.

Quantitative Comparison between Microfluidic and Microtiter Plate Formats for Cell-Based Assays

Huabing Yin,[†] Nicola Pattrick,[‡] Xunli Zhang,[§] Norbert Klauke,[†] Hayley C. Cordingley,[‡] Steven J. Haswell,[§] and Jonathan M. Cooper^{*,†}

Department of Electronics, University of Glasgow, Glasgow, G12 8LT, UK, Department of Chemistry, University of Hull, Hull, HU6 7RX, UK, and GlaxoSmithKline Pharmaceuticals, Harlow, CM19 5AW, UK

In this paper, we compare a quantitative cell-based assay measuring the intracellular Ca^{2+} response to the agonist uridine 5'-triphosphate in Chinese hamster ovary cells, in both microfluidic and microtiter formats. The study demonstrates that, under appropriate hydrodynamic conditions, there is an excellent agreement between traditional well-plate assays and those obtained on-chip for both suspended immobilized cells and cultured adherent cells. We also demonstrate that the on-chip assay, using adherent cells, provides the possibility of faster screening protocols with the potential for resolving subcellular information about local Ca^{2+} flux.

The development of robust methods for high-throughput screening (HTS) is important for the rapid assessment of a drug's activity.¹ Traditionally, such measurements, which involve recording the average response of tens of thousands of cells in microtiter plates, have been performed with automated fluid handling robots.² Although robotic operation can reduce sample handling errors, effective washing, evaporation, and relative volumetric errors are significant concerns in microtiter plate operation, particularly when the well volume is decreased.³

As a consequence, recently there has been considerable interest in trying to translate microtiter-based measurements into microfluidic platforms. Such miniaturized microfluidic systems can provide better precision in generating sample concentrations and improved efficiency in washing.⁴ Chip-based assays also use smaller numbers of cells, have a low volume of operation (sub-microliter or nanoliter), and have general flexibility in the control of hydrodynamic conditions under which the assay is performed.^{5,6} However, the uptake of microfluidics by the pharmaceutical industry in cell screening, and its potential to become a versatile and robust method for pharmacological assessment of new

medicines, relies on the ability to generate comparable quantitative information on-chip, with respect to that obtained using current technology (i.e., standard multiwell plates).

Within the pharmaceutical industry, ligand-gated ion channels represent >40% of the targets for drug discovery. Many of these channels are modulated by calcium ions, and as such, the intracellular measurement of Ca^{2+} flux remains one of the preferred ways to determine the activity of new drug candidates.⁷ Building upon this established work, we use the activity of the agonist, uridine 5'-triphosphate (UTP), which binds to G-coupled protein receptors and triggers the release of internal Ca^{2+} from a cell's endoplasmic reticulum,⁸ as a model assay to quantitatively compare new microfluidic formats with established microtiter plate assay procedures.

To date, there has been limited work on the measurement of intracellular Ca^{2+} in microfluidic systems^{9–14} and even fewer fundamental studies that evaluate quantitative on-chip cellular assays. We have previously demonstrated that commonly applied hydrodynamic conditions in microfluidics can activate mechanosensitive ion channels leading to an intracellular Ca^{2+} flux¹⁵ (an observation that has profound implications for assay optimization on chip, as the local hydrodynamic conditions have the potential to induce cell responses that mimic pharmacological effects). In order to demonstrate the broad applicability of chip-based assays as a HTS assay, it is important that equivalent information can be obtained in microfluidic systems.

In this paper, we evaluate functional ligand-based ion channel microfluidic assays using both suspended and adherent cells (cultured on-chip) and under appropriate hydrodynamic conditions compare them with traditional microtiter well-plate assays. We show that measuring Ca^{2+} flux from low numbers of discrete single cells, used in the microchannel format, can provide robust

* To whom correspondence should be addressed. Telephone: +44(0)141-330-4931. Fax: +44(0)141-330-6002. E-mail: jmcooper@elec.gla.ac.uk.

[†] University of Glasgow.

[‡] GlaxoSmithKline Pharmaceuticals.

[§] University of Hull.

(1) Drews, J. *Science* **2000**, *287*, 1960–1964.

(2) Monteith, G. R. and Bird, G. St. J. *Trends Pharmacol. Sci.* **2005**, *26*, 218–223.

(3) Dunn, D. A.; Feygin, I. *Drug Discovery Today* **2000**, *5*, S84–S91.

(4) Warrick, J.; Meyvantsson, I.; Ju, J. I.; Beebe, D. J. *Lab Chip* **2007**, *7*, 316–321.

(5) Carlo, D.; Lee, L. P. *Anal. Chem.* **2006**, *78*, 7918–7925.

(6) Martin, R.; Root, P and Spence, D. *Analyst* **2006**, *131*, 1197–1206.

(7) Worley III, J. F.; Main, M. J. *Rep. Channels* **2002**, *8*, 269–282.

(8) Conigrave, A. D.; Jiang, L. *Cell Calcium* **1995**, *17*, 111–119.

(9) Vilkner, T.; Janasek, D.; Manz, A. *Anal. Chem.* **2004**, *76*, 3373–3386.

(10) Klauke, N.; Smith, G. L.; Cooper, J. M. *Biophys. J.* **2006**, *91*, 2543–2551.

(11) Li, X.; Li, P. C. H. *Anal. Chem.* **2005**, *77*, 4315–4322.

(12) Werdich, A. A.; Lima, E. A.; Ivanov, B.; Ges, I.; Anderson, M. E.; Wikswo, J. P.; Baudenbacher, F. J. *Lab Chip* **2004**, *4*, 357–362.

(13) Yang, M. S.; Li, C. W.; Yang, J. *Anal. Chem.* **2002**, *74*, 3991–4001.

(14) Wheeler, A. R.; Thronset, W. R.; Whelan, R. J.; Leach, A. M.; Zare, R. N.; Liao, Y. H.; Farrell, K.; Manger, I. D.; Daridon, A. *Anal. Chem.* **2003**, *75*, 3581–3586.

(15) Yin, H. B.; Zhang, X. L.; Pattrick, N.; Klauke, N.; Cordingley, H. C.; Haswell, S. J.; Cooper, J. M. *Anal. Chem.* **2007**, *79*, 7139–7144.

pharmacological information, which is in excellent agreement with data obtained from larger populations of cells.

MATERIALS AND METHODS

Cell Culture. The Chinese hamster ovary (CHO)-K1 cell line was from ATCC (the American Type Culture Collection). CHO cells were cultured in 25-cm² tissue culture flasks at 37 °C in a humidified atmosphere with 5% CO₂/95% air. The cells were incubated in DMEM/F12 medium (Invitrogen) supplemented with 10% fetal calf serum and 4 mM L-glutamine, were grown to near confluence in the culture flasks, and then were suspended with 0.05% trypsin–EDTA solution. Prior to being introduced into the microfluidic chip or the microtiter plate, the concentration of suspended cells was determined using a hemocytometer. The viability of cells was determined using 0.4% Trypan Blue solution.

Microfluidic Device Fabrication. We developed a reusable microfluidic device, which comprised a glass substrate that could be sealed against a microfluidic gasket, formed by molding a poly-(dimethylsiloxane) (PDMS) elastomer against a silicon master. The substrate could be modified prior to assembly to promote the rapid attachment of a high density of viable cells; see below. Microchannels were 500 μm wide, 140 μm high, and 15 mm long, providing a local environment in which we were able to mitigate against local shear stress, at appropriate flow rates.¹⁵

Substrate Modification. The substrate was modified prior to assembly with collagen to enhance the immobilization of cells, as described previously.¹⁵ These collagen-modified glass substrates were stored in sterilized foil at 4 °C before being mechanically sealed against a 5-mm PDMS gasket, to form an enclosed microfluidic chip. The gasket was sufficiently thick that the channel geometry did not deform during sealing.

The microfluidic devices were connected to a KDS 260 syringe pump (KD Scientific Inc.) using ethylenetetrafluoroethylene polymer tubing with an inner diameter of 250 μm. On–off valves (with appropriate fittings and connectors) obtained from Upchurch Scientific Inc. were used to control flow. Tests were carried out with a colored dye solution to show that the chip did not leak even when using flow rates as high as 400 μL/min.

Well Plate Assay. A traditional measurement of CHO cell's response to UTP in a standard microtiter format was used as a standard reference. Intracellular Ca²⁺ level was quantified using Ca²⁺-sensitive Fluo-4 AM indicator dye.¹⁶ Cell labeling and washing buffers are described in detail in the Supporting Information. Briefly, 50 μL of a cell suspension (at a concentration of 2 × 10⁶ cells/mL) was seeded per well (~10 000 cells/well) in a 384-well plate and incubated overnight at 37 °C in a humidified atmosphere with 5% CO₂/95% air. After removal of the medium, the adherent cells were washed with the Tyrode buffer and incubated with 50 μL of the Fluo-4 AM labeling buffer for an hour at 37 °C in a humidified atmosphere with 5% CO₂/95% air. The labeling buffer was then replaced with 40 μL of fresh Tyrode buffer to minimize the buffering effect of the dye within the cells. Ten seconds after starting recording the fluorescent intensity of cells, either using fluorescence microscopy or using a fluorometric imaging plate reader (FLIPR), 10 μL of UTP test solution (at a range of concentrations between 10 nM and 10 μM) was added to each

well. The induced changes in fluorescence intensity were recorded and calculated to reflect the changes in [Ca²⁺].^{16,17}

On-Chip Assay Using Suspended Cells. On-chip analysis of suspended cells required their loading and immobilization inside microfluidic channels, so that they did not move while tracking rapid changes in intracellular Ca²⁺ flux. The procedure for labeling suspended cells was modified from that used for the well plate assay in order to minimize the adverse effects of long periods of incubation of cells with dye. Suspended cells were centrifuged at 100g for 5 min to remove the medium and then washed with Tyrode buffer before being resuspended in the labeling buffer to a concentration of ~2.8 × 10⁶ cells/mL. Following incubation at 37 °C for 10 min, the labeled suspended cells were loaded on-chip at a flow rate of 1 μL/min. Once in the channel, they were left undisturbed for 10 min to allow attachment to the collagen-modified channel surface. Any unattached or loosely attached cells were washed away at a higher flow rate (5 μL/min). UTP agonist test solutions in Tyrode buffer were then introduced into the microfluidic platform at the selected flow rates with UTP concentrations from 10 nM to 10 μM.

On-Chip Assay Using Adherent Cells. The use of adherent cells in microfluidics requires on-chip culture. To avoid bacterial contamination, the valves, connections, and PDMS chips were all sterilized using 70% ethanol and were then dried prior to assembly. A sterilized microfluidic device was constructed using a presterilized collagen-modified substrate, as described previously.¹⁵ The microfluidic channel was first primed with sterilized medium. Freshly harvested cell suspensions at different concentrations were then pumped into the microfluidic chip at 1 μL/min. Once in the microchannel, the cells were left undisturbed for 10 min, before being washed in medium. All operations were performed in a class II biological laminar hood. The cell–chip (as a closed system) was then transferred into an incubator at 37 °C in a humidified atmosphere with 5% CO₂/95% air. The system was continually perfused with medium at a rate of 0.5 μL/min overnight. Once cells were confluent inside the microfluidic device, the medium was replaced with Tyrode buffer at a flow rate of 20 μL/min. Finally, the labeling buffer (as above) was introduced and incubated for 30 min for uniform labeling to occur. After further washing with Tyrode buffer, cells were challenged with UTP concentrations over the same range as above.

Data Acquisition and Analysis. Both transmission and fluorescence images were recorded using a Zeiss Axiovert inverted fluorescence microscope coupled to a monochrome cooled CCD digital camera (Andor iXon^{EM}, Andor Technology.). A filter set, containing an exciter D475/40, an emitter E510, and a beam splitter Dichroic 495, was used for the fluorescence imaging. The intensity of the excitation light was adjusted by a neutral density filter (OD = 1) to minimize photo bleaching of the dye. Real-time fluorescence recordings were made for 3 min at a rate of 10 frames/s using an X40 water immersion lens. The CCD field of view was 200 μm × 200 μm.

In situ fluorescence measurements of the response of adherent cells in the microfluidic device were carried out using a confocal microscope (Zeiss LSM 510) with a X63 oil immersion lens and a 488-nm excitation laser. Real-time recordings of the field of view

(16) Takahashi, A.; Camacho, P.; Lechleiter, J. D.; Herman, B. *Physiol. Rev.* **1999**, *79*, 1089–1125.

(17) Smart, D.; Jerman, J. C.; Brough, S. J.; Rushton, S. L.; Murdock, P. R.; Jewitt, F.; Elshourbagy, N. A.; Ellis, C. E.; Middlemiss, D. N.; Brown, F. *Br. J. Pharmacol.* **1999**, *128*, 1–3.

(202 $\mu\text{m} \times 202 \mu\text{m}$) were made at both 4 frames/s and as line scans of a single cell recorded at a rate of 0.0075 s/line.

The fluorescence intensity of whole discrete individual cells was calculated using the Andor iQ1.4 image software. The maximum responding amplitude (simplified as response) was calculated as follows; the cell's response was expressed as $(F_{\text{peak}} - F_0)/F_0 \times 100\%$, where F_{peak} is the peak fluorescence intensity and F_0 the baseline. All fluorescence measurements were background subtracted.¹⁶ The baseline fluorescence intensity (F_0) was taken as the average background value over 10 s before applying UTP solutions. All measurements were made in triplicate, and standard errors are given unless noted.

RESULTS AND DISCUSSION

Studies Involving the Comparison of Cell Populations and Single Cells. There has been much debate about the relative merit of the use of single cells, particularly in microfluidic devices, compared with that of population studies in microtiter plate assays when evaluating pharmacological responses.¹⁸ For example, in a typical 384 titer plate, up to 10 000 cells may be used per well, which when incubated overnight will give a confluent layer, as shown in Supporting Information, Figure S1A. Upon the addition of an agonist such as UTP, a proportion of the cells respond, as indicated by an increase in fluorescence intensity (Supporting information Figure S1B). Using a FLIPR, the average response of the whole population in a well is obtained and subsequently used in any data manipulation.¹⁷ In our study, a wide range of UTP concentrations were tested using this procedure in order to obtain a dose–response curve, as shown in Figure 1A. Subsequently, the pEC_{50} ($-\log(\text{EC}_{50})$) values were determined using standard sigmoidal curve-fitting methods.¹⁷ A mean value of pEC_{50} from 64 duplicated dose–response experiments (i.e., 16 duplicates on 4 individual plates) was 6.2, which corresponds to a mean EC_{50} value of 0.65 μM . This latter value is the concentration of agonist that provokes a response exactly midway between the baseline and maximum response. In pharmacological studies, it is used as a quantitative measure of the agonist's activity.

The microtiter plate format using a population of cells has obvious limitations, including the lack of information from individual cells and a susceptibility to optical artifacts (due to reagent addition, for example). Moreover, attempts at parallel quantification are limited by the reproducibility and uniformity of the cell monolayer in individual wells. Notably, with other types of cells, i.e., primary cells, a heterogeneous culture is generally produced, and in these circumstances, the formation of uniform cell monolayers remains a significant challenge.

In contrast, the microfluidic approach described here provides the capability to reveal heterogeneous information from individual cells as well as cell ensembles. In order to understand how many single cells were needed to produce a comparable measurement to the traditional microtiter using a cell population assay, we performed a statistical study using the response of individual plated CHO cells within a well plate. Using a fluorescence microscope, the average responses of random selected discrete cells, in groups of 10–125, were recorded from within the microtiter well to obtain the dose–response curves and, subse-

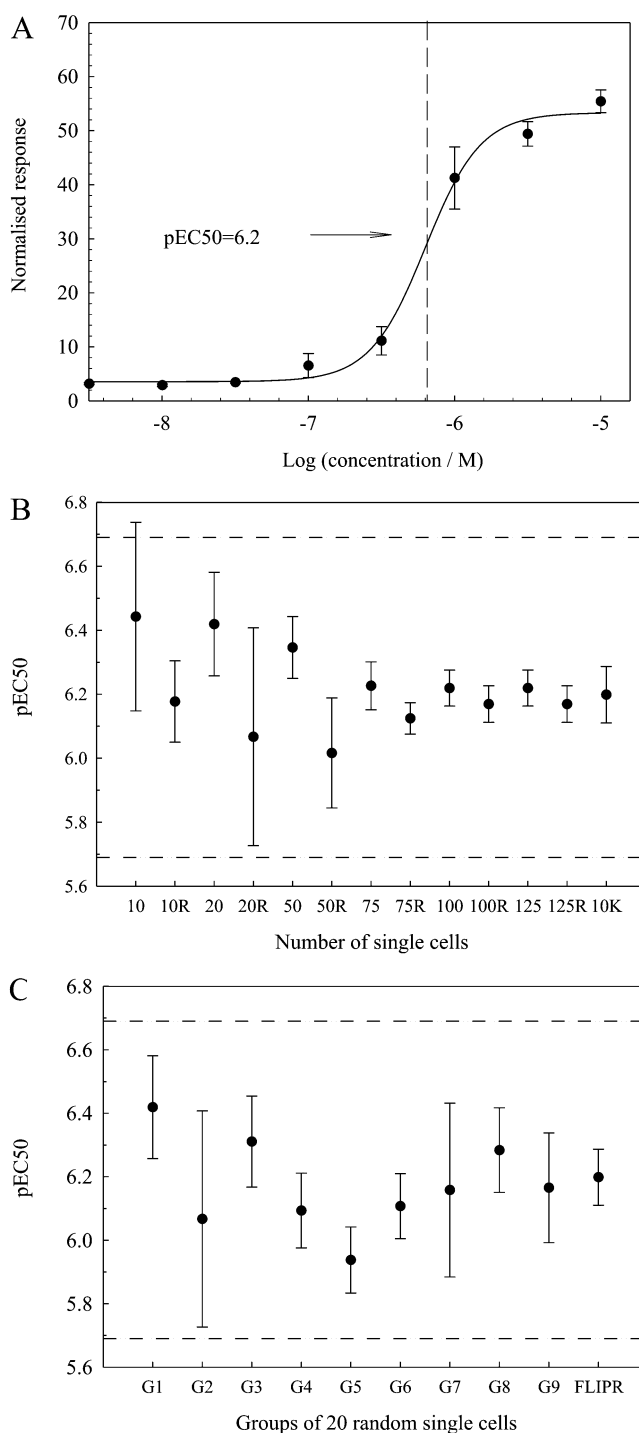


Figure 1. Population response vs single-cell response in quantitative study. (A) A representative dose–response curve from multi-well plates using 10 000 cells/well by FLIPR. pEC_{50} ($-\log(\text{EC}_{50})$) was determined by fitting a sigmoid to the concentration–response curve (<http://www.graphpad.com/curvefit>).¹⁵ Data were normalized to the average maximum value. The mean pEC_{50} from 64 duplicate experiments is 6.20 (± 0.03), which corresponds to a mean EC_{50} value of 0.65 μM . (B) Single-cell study using a range of cell numbers. The suffix “R” indicates a duplicate measurement. The acceptable range of the pEC_{50} in industry equals the mean value of pEC_{50} from the FLIPR test 6.2 (± 0.5), as indicated by the dotted lines. Any pEC_{50} of a single-cell study with its 95% confidence limit falling into this range was considered reliable. (C) Statistical analysis of a single-cell study using groups of 20 cells randomly selected from within the microtiter plate. Error bar is the 95% confidence limit.

(18) Wolff, M.; Joerg Wiedenmann, J.; Nienhaus, J. U.; Valler, M.; Heilker, R. *Drug Discovery Today* 2006, 11, 1054–1061.

quently, to determine the pEC_{50} values. The pEC_{50} values were then plotted against the number of individual cells measured and analyzed by a Monte Carlo statistical method, as shown in Figure 1B. The mean pEC_{50} value of 6.2 from the population study using 10 000 cells was used as a reference. Any pEC_{50} value whose 95% confidence limit was within the range of 6.2 ± 0.5 was considered reliable.¹⁹ As shown in Figure 2B, all pEC_{50} values obtained from ≥ 20 cells were within the accepted range. An analysis of 9 groups of 20 randomly chosen single cells further demonstrated that all the obtained pEC_{50} values fall within the accepted deviation; see Figure 1C. In summary, the data show that measurements of 20 single cells were sufficient to produce a reliable assay that was comparable to the standard FLIPR measurement of 10 000 cells in the well plate format.

On-Chip Quantification Using Suspended Cells. The introduction of cells into microfluidic devices was generally carried out from a cell suspension, with cells becoming trapped inside a device^{20–22} or flowed-through the device for the purpose of handling or detection, i.e., flow cytometry. In most cases, the whole process is rapid, as there is no requirement for culturing the cells. An aim of this work was to assess the potential for using suspended cells (without culture) to give a quantitative Ca^{2+} flux assay on-chip. Due to the rapid intracellular Ca^{2+} flux induced by UTP, it was necessary to immobilize the cells in the microchannel during signal measurement. The microchannel surface was therefore first treated with collagen to achieve high immobilization densities.¹⁵ As shown in Supporting Information Figure S2A, up to 50 single cells (in an area of 0.04 mm^2) could be imaged simultaneously, which allows a random selection of 20 cells for the analysis. UTP concentrations were delivered rapidly and uniformly over cells in the microfluidic channel. At a low flow rate of $2 \mu\text{L}/\text{min}$ (i.e., a fluid velocity of $479 \mu\text{m}/\text{s}$), it took ~ 400 ms to exchange the solution in the field of view of the X40 objective. In the standard well plate, the buffer solution is quiescent, and the desired UTP concentration at the cell surface was produced by convective mixing of a small quantity of stock UTP solution within the bulk solution within the well (normally, $50 \mu\text{L}$ per well for a 384-well plate). In contrast, microfluidic delivery of the drug is both quicker and leads to a more uniform drug distribution across the cell layer. Less than $2 \mu\text{L}$ of UTP solution is needed to replace the buffer in the microchannel in this study. Supporting Information Figure S2B shows how a cell layer within the microfluidic device responds to $1 \mu\text{M}$ UTP.

Using the above procedure, quantitative analysis of the response of CHO cells to a wide range of UTP concentrations was assessed on-chip and compared with the 384-well plate. The response of 20 randomly chosen individual cells was measured using fluorescence microscopy. It was known that cells become desensitized after the addition of UTP, and as a consequence, in a microtiter plate it was always necessary to perform parallel assays. Therefore, in order to directly compare data from the traditional microtiter plate with the microfluidic devices, we configured the microchannel as an array of microfluidic structures.

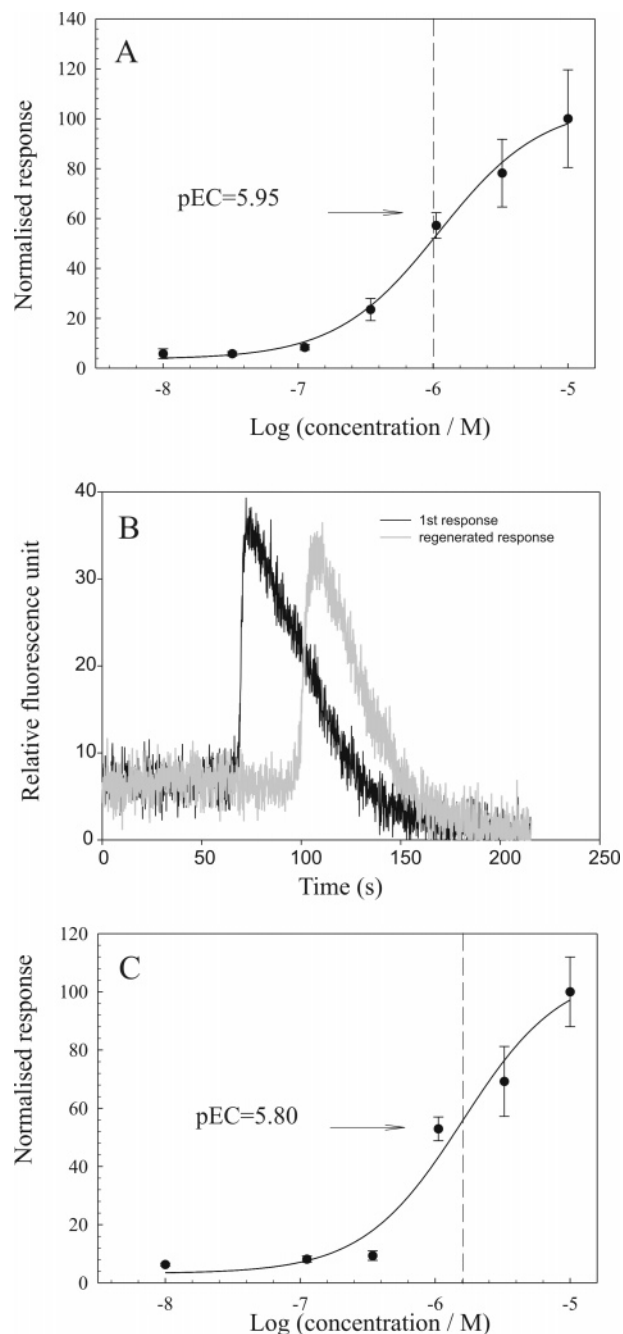


Figure 2. On-chip analysis using suspended cells. (A) A representative concentration–response curve achieved by parallel on-chip analysis at a flow rate of $2 \mu\text{L}/\text{min}$. The response of ~ 20 single cells was averaged for a given concentration. The average pEC_{50} obtained from triplicates of on-chip analysis at a flow rate of $2 \mu\text{L}/\text{min}$ is 6.02 ± 0.11 , which corresponds to a mean EC_{50} value of $1.0 \mu\text{M}$. (B) Sequential on-chip analysis shows that the cell response can be regenerated after buffer washing. In both runs, cells were stimulated with $1 \mu\text{M}$ UTP. (C) A representative concentration–response curve achieved by sequential on-chip analysis as in (B) at a flow rate of $2 \mu\text{L}/\text{min}$. The average pEC_{50} value from three duplicate experiments is 5.77 ± 0.10 , giving a mean EC_{50} of $1.7 \mu\text{M}$. Data were analyzed as in Figure 1. The error bars correspond to the standard error.

Using these devices, we then compared the UTP dose–response curves under a variety of hydrodynamic flow conditions.

Initially, a low flow rate of $2 \mu\text{L}/\text{min}$ (shear stress $0.4 \text{ dyn}/\text{cm}^2$) was used to deliver UTP. The dose–response curve generated on-chip showed a sigmoidal relationship, as is commonly

(19) GSK internal publication. Patrick, N.; Cordingley, H. C. Technology Development, GlaxoSmithKline Pharmaceuticals, 2006.

(20) Yang, M.; Li, C. W.; Yang, J. *Anal. Chem.* **2002**, *74*, 3991–4001.

(21) Khademhosseini, A.; Yeh, J.; Jon, S.; Eng, G.; Suh, K. Y.; Burdick, J. A.; Langer, R. *Lab Chip* **2004**, *4*, 425–430.

(22) Folch, A.; Toner, M. *Annu. Rev. Biomed. Eng.* **2000**, *2*, 227–256.

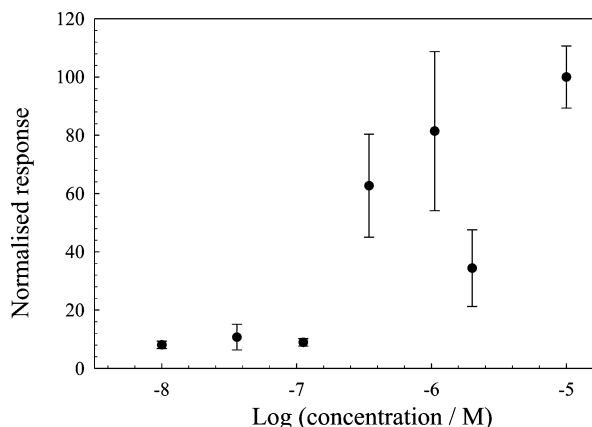


Figure 3. Influence of high shear stress on dose–response curves for suspended cells. A representative concentration–response curve from a parallel on-chip analysis at a flow rate of $20 \mu\text{L}/\text{min}$. The response of ~ 20 single cells was averaged for a given concentration. Since a sigmoid curve did not fit the data well, an estimation of pEC_{50} similar to that in Figure 2 was not possible.

obtained in the traditional well-plate assay, Figure 2A. The pEC_{50} value determined on-chip was 6.02 ± 0.11 , which corresponds to a mean EC_{50} value of $1.0 \mu\text{M}$. To assess the difference between such a parallel on-chip measurement and the standard FLIPR measurement, the p -value from a t -test was determined to be 0.45. This is much greater than that required for the on-chip mean to be within the 95% confidence limit for the microtiter plate (i.e., p -value > 0.05).

We also showed that, within the microfluidic format, a rapid exchange of UTP solution can be readily achieved without disturbing the immobilized cells, enabling the sequential testing of the *same* cells. This is of considerable interest for the experimentalist wishing to track the dose–response of an individual cell to a range of agonist concentrations. Again, using a flow rate of $2 \mu\text{L}/\text{min}$ to deliver the UTP solutions, it was found that cells which had become desensitized in a previous test now responded to the same UTP concentration (Figure 2B), after Tyrode buffer washing sequences. The dose–response curve achieved using such sequential UTP/Tyrode washing steps, starting at a low UTP (10 nM) concentrations and increasing to $10 \mu\text{M}$, provided similar quantitative information ($\text{pEC}_{50} = 5.77 \pm 0.10$, corresponding mean $\text{EC}_{50} = 1.7 \mu\text{M}$) to the traditional well-plate assay, Figure 2C. When compared to the standard FLIPR measurement, the p -value is 0.09, which again shows that there is no significant difference between the means of the two types of tests.

Importantly, low flow rates were used in the above measurement, since as we have previously shown, shear stress induced by flow rates over a certain threshold ($3.1 \text{ dyn}/\text{cm}^2$ for the collagen-modified channel) can induce intracellular Ca^{2+} flux.¹⁵ In this context, it is important to note that when UTP solutions are delivered at a flow rate of $20 \mu\text{L}/\text{min}$ (shear stress $4.1 \text{ dyn}/\text{cm}^2$), Figure 3, the dose–response curve cannot be fitted using a standard sigmoid relationship. This implies that the hydrodynamic conditions are influencing the cellular response significantly possibly through activation of mechano-sensitive channels.

On-Chip Assays Using Adherent Cells. In contrast to using suspended cells (described above), intra- and intercellular signaling can best be studied using adherent cells, which, when they

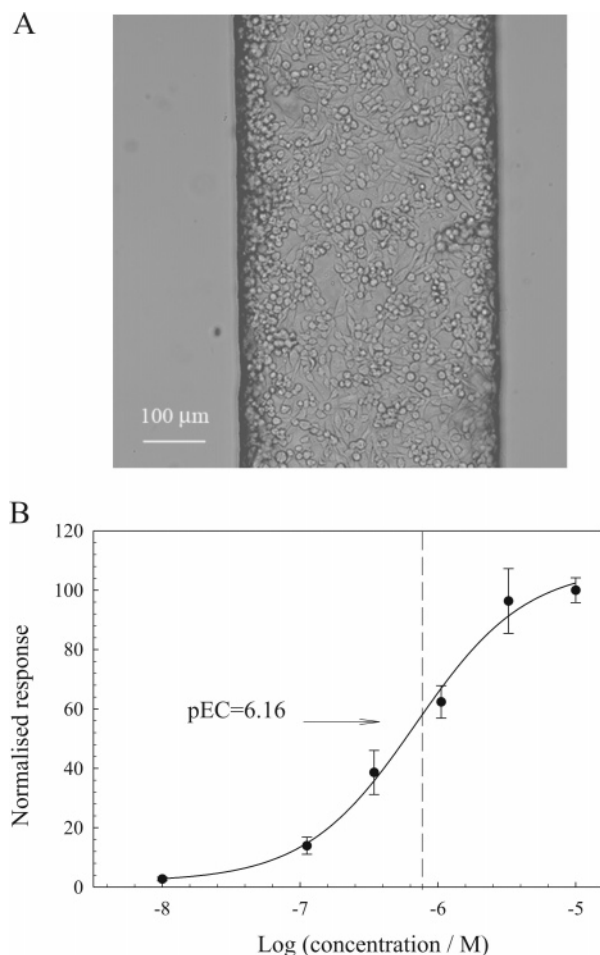


Figure 4. On-chip analysis using adherent cells. (A) A monolayer of adherent cells forms inside the microfluidic channel after 8-h on-chip perfusion at a flow rate of $0.5 \mu\text{L}/\text{min}$. (B) A representative concentration–response curve achieved by sequential on-chip analysis at a flow rate of $20 \mu\text{L}/\text{min}$. Data were analyzed as in Figure 2. The average pEC_{50} value from three duplicate experiments is 6.15 ± 0.08 , giving a mean EC_{50} of $0.7 \mu\text{M}$.

form confluent monolayers, generally give stronger and more uniform signaling. In order to create confluent monolayers of adherent cells inside a microfluidic channel, it was necessary to perform on-chip cell culture, a task that has generally been proven to be difficult as the sterility, the continuous supply of gases, and of medium all need to be controlled carefully.²³ The microfluidic chip developed in this study, however, not only provides a simple way to assemble a sterilized chip but also allows for ready diffusion of gases into the medium, through the PDMS gasket. Low densities of cells ($2 \times 10^6/\text{mL}$) were sufficient for seeding the cells inside a collagen-treated microfluidic channel, prior to cell culture. After overnight perfusion with medium at $0.5 \mu\text{L}/\text{min}$, cells developed into a confluent monolayer with almost 100% viability, Figure 4A.

The effect of shear stress on the on-chip cultured adherent cells was assessed in the same manner as in the study of the suspended cells. No shear-induced Ca^{2+} flux was observed even at high shear stress of $20 \text{ dyn}/\text{cm}^2$ (data not shown). In contrast

(23) Yamamura, S.; Kishi, H.; Tokimitsu, Y.; Kondo, S.; Honda, R.; Ramachandra, S.; Omori, R.; Tamiya, E.; Muraguchi, A. *Anal. Chem.* **2005**, *77*, 8050–8056.

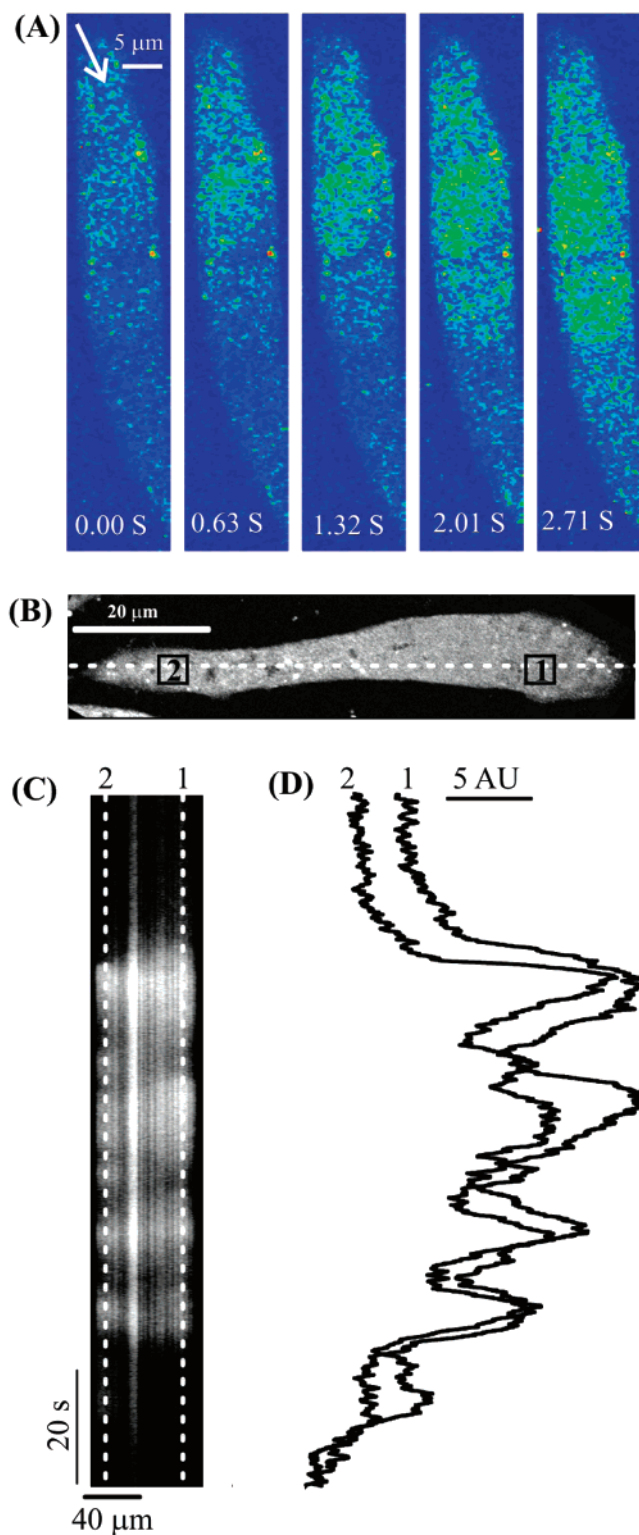


Figure 5. On-chip analysis of intracellular Ca^{2+} wave propagation. (A) Series of confocal images of intracellular Ca^{2+} flux propagation inside a single cell upon delivery of $1 \mu\text{M}$ UTP solution. The white arrow indicates the flow direction. The Ca^{2+} flux peak travels inside the single cell following the flow direction. (B)-(D) Time course record of Ca^{2+} flux along a fixed line across a single cell upon delivery of $1 \mu\text{M}$ UTP solution. (B) indicates the line position inside the cell. ROI 1 indicates the front end of the cell to the flow direction; ROI 2 indicates the far end. (C) The 4 distinct fluorescence bands demonstrate Ca^{2+} waves inside the single cell during the 5-min recording. (D) Relative fluorescence profiles from ROIs 1 and 2 show the Ca^{2+} flux arrives at ROI 2 is after that generated at ROI 1.

to the suspended cells, this lower sensitivity to shear stress of the adherent cells can be attributed to their well-formed cytoskeleton, which may serve to reduce the distortion of the cell membrane. With the high tolerance of the adherent cells to shear stress, it was found that substantially higher flow rates could be used for fast cell screening without compromising the cell response. For example, an on-chip sequential assay of the adherent cells in response to UTP was performed in a manner identical to that study using suspended cells (Figure 2C), but at a higher flow rate of $20 \mu\text{L}/\text{min}$ (shear stress of $4 \text{ dyn}/\text{cm}^2$). These assay conditions substantially shortened the total assay time, and the pEC_{50} value from measurements performed in triplicate was 6.15 ± 0.08 ($n = 60$), Figure 4B. The determined p -value of 0.85 was substantially higher than the p -values from the on-chip assays using suspended cells (0.45 and 0.09), suggesting an excellent comparability between the on-chip assay using adherent cells and the traditional microtiter-plate method.

On-Chip Monitoring Intracellular Signals Using Adherent Cells. Confocal analysis of adherent cells on chip was used to reveal information on the nature of intracellular Ca^{2+} flux. The arrival of a $1 \mu\text{M}$ UTP dose at $20 \mu\text{L}/\text{min}$ and reaching the cell (arrowed) resulted in a Ca^{2+} wave which “traveled” within a cell in the same direction as the flow rate, Figure 5. Control experiments using Tyrode buffer at the same flow rate induced no Ca^{2+} flux. This phenomenon was further revealed by imaging a line scan across a cell in the direction of UTP delivery (Figure 5B). For the purpose of analysis, a line was constructed between two positions inside the cell, ROI 1 and ROI 2. Four distinct fluorescence peaks were observed along this line, corresponding to a succession of Ca^{2+} waves within the isolated cell, Figure 5C. The relative fluorescence profile from ROI 2 clearly lags behind the one from ROI 1, as shown in Figure 5D. This observation demonstrates the potential of an on-chip assay to resolve local information at a subcellular level, providing a tool for studying the mechanism of signal trafficking and cell pathology. Clearly, the spatial nature of the response would be difficult to observe using a traditional microtiter plate.

CONCLUSIONS

A systematic evaluation of a quantitative functional assay using both suspended CHO cells and on-chip cultured cells in a microfluidic system was investigated. By using intracellular Ca^{2+} analysis of CHO cells as a model system, we found that it was possible to show a close correlation between the suspended CHO cell dose–response for the agonist UTP on-chip and that achieved in a traditional microtiter plate. The use of adherent cells in microfluidics demonstrated a lower susceptibility to the influence of hydrodynamic conditions, providing fast and reliable screening data when compared with that from microtiter plate. The system also demonstrated its potential in controlling and revealing subcellular events.

The outcome of the work quantitatively demonstrated the promise of microfluidics in HTS applications. Information equivalent to that obtained from the microtiter plate has been achieved on-chip with a reduced assay volume and smaller amounts of cells. The precise and multiple delivery of liquid over cells using microfluidics provides additional opportunity to develop new assays, for example, in applications where sequential or dynamic change of cellular microenvironments is difficult to achieve using

microtiter plates. In future, the integration of other microfluidic subunits (such as valves and diluters) or sensors (electrochemical or optical) on-chip may further improve sample handling and analysis, leading to an integrated high-throughput and high-content cell screen.

ACKNOWLEDGMENT

The DTI, IRC in Bionanotechnology, and Royal Society of Edinburgh are acknowledged for supporting aspects of this research and Huabing Yin. We also thank Drs Andrew Glidle, and Paul Monaghan for helpful discussions.

SUPPORTING INFORMATION AVAILABLE

Detailed information on buffers for Ca^{2+} flux assay. Description on assembly of microfluidic chips. Representative fluorescence images of CHO cell response to UTP in a traditional well-plate assay and in an on-chip assay. This material is available free of charge via the Internet at <http://pubs.acs.org>.

Received for review September 18, 2007. Accepted October 16, 2007.

AC701958Z

Characterization of cellular chemical dynamics using combined microfluidic and Raman techniques

Xunli Zhang · Huabing Yin · Jon M. Cooper ·
Stephen J. Haswell

Received: 13 July 2007 / Revised: 14 August 2007 / Accepted: 17 August 2007 / Published online: 12 September 2007
© Springer-Verlag 2007

Abstract The integration of a range of technologies including microfluidics, surface-enhanced Raman scattering and confocal microspectroscopy has been successfully used to characterize *in situ* single living CHO (Chinese hamster ovary) cells with a high degree of *spatial* (in three dimensions) and *temporal* (1 s per spectrum) resolution. Following the introduction of a continuous flow of ionomycin, the real time spectral response from the cell was monitored during the agonist-evoked Ca^{2+} flux process. The methodology described has the potential to be used for the study of the cellular dynamics of a range of signalling processes.

Keywords Microfluidics · Chinese hamster ovary (CHO) cells · Confocal microspectroscopy · Surface-enhanced Raman scattering (SERS) · Dynamic monitoring

Introduction

The advance of miniaturized microfluidic systems for chemical and/or biochemical applications based on so-

called Lab-on-a-Chip technology has demonstrated that such micro systems represent the ability to “shrink” conventional bench systems to the size of a few square centimetres with major advantages of speed, performance, integration, portability, reduced sample/solvent quantity, automation, hazard control and lower cost [1–6]. These merits are important for a variety of applications in analytical chemistry, biochemistry, clinical diagnosis, medical chemistry and industrial chemistry [1, 2]. Consequently, numerous micro total analysis systems (μ -TAS) and micro reactor systems have been developed, and many more are currently under investigation [2].

For the study of cellular and subcellular systems, a wide range of analytical methods have been used with fluorescence techniques being the most common. In addition, fluorescence-based imaging is a highly attractive methodology for the study of organelle dynamics, identifying subcellular compartments and monitoring biological kinetics [7]. Over the last two decades, Raman spectroscopy has become an increasingly important technology with ability to study the biophysics and biochemical processes involving cells [4, 8–12]. Since Raman spectroscopy is based on vibrational transitions where frequency shifts are associated with specific molecular vibrations within the sample of interest, it enables the identification of polarizable bio/chemical species, the elucidation of molecular structure and the investigation of interface reactions, all in a non-destructive manner. In addition, unlike fluorescence-based techniques, Raman spectroscopy does not require labelling dyes and since water is almost Raman “transparent”, the technique is ideally suited for analysing cell-based biological systems. Coupling a Raman spectrometer with a confocal microscope enables the acquisition of full spectral information with a high spatial ($<1 \mu\text{m}$) resolution in three dimensions. Raman spectroscopy, however, suffers from an

X. Zhang · S. J. Haswell (✉)
Department of Chemistry, The University of Hull,
Hull HU6 7RX, UK
e-mail: S.J.Haswell@Hull.ac.uk

H. Yin · J. M. Cooper
Department of Electronics and Electrical Engineering,
University of Glasgow,
Glasgow G12 8QQ, UK

Present address:

X. Zhang
School of Engineering Sciences, University of Southampton,
Southampton SO17 1BJ, UK

inherent poor level of sensitivity compared for example to fluorescence, which can be 12–14 orders of magnitude more sensitive. As a consequence, despite advances in detector technologies, the technique can be less than ideal for the direct detection of intracellular components present at low concentrations, which may take from a few tens of seconds to a few minutes for spectral acquisition [12]. With the unexpected discovery of surface-enhanced Raman scattering (SERS) by Fleischman et al. [13], Raman intensity can now be dramatically increased (a factor of up to 10^5 – 10^{10}) with the inclusion of metallic nano structures either on a substrate surface or in a colloidal solution [8]. For cellular and subcellular analysis with SERS, colloid nanoparticles (e.g. silver or gold) are normally loaded into cells by different means such as general incubation (fluid-phase uptake) or ultrasonication-assisted uptake [14, 15]. Due to its chemical inactivity, gold nanoparticles are generally regarded to be more suitable for incorporation within living cells [14].

To analyse living cells using Raman spectroscopy, the cells are usually fixed at a specific location. The most commonly used method for cell fixation is to seed or grow cells on a substrate, e.g. a microscope cover slide. Other approaches such as optical tweezers have also been reported [9]. However, the conventional batch operation in a static system limits the in situ Raman analysis, especially when a series of reagent treatments are required. With those limitations in mind, the development of microfluidic and associated Lab-on-a-Chip technologies provides unique opportunities for delivering and immobilizing cells on a microchannel surface, prior to introducing different reagents with a continuous flow in a given sequence [3, 4] whilst under spectroscopic investigation.

In this study, we report the successful integration of a range of techniques including microfluidics, surface-enhanced Raman scattering (SERS) and confocal microspectroscopy which enables in situ characterization of single living CHO cells with high *spatial* and *temporal* resolution. By using the microfluidic methodology, cells and reagents were introduced into the chip in a continuous flow as a series of plugs in a given sequence where agonist (ionomycin) evoked intracellular Ca^{2+} fluxes and the cell's real time spectral response was recorded.

Materials and methods

Confocal Raman microspectroscopy

All Raman spectra were acquired with a LabRam inverted microscope spectrometer, manufactured by Jobin Yvon Ltd. Figure 1 shows the schematic of the experimental setup. The spectrometer was equipped with dual laser sources at

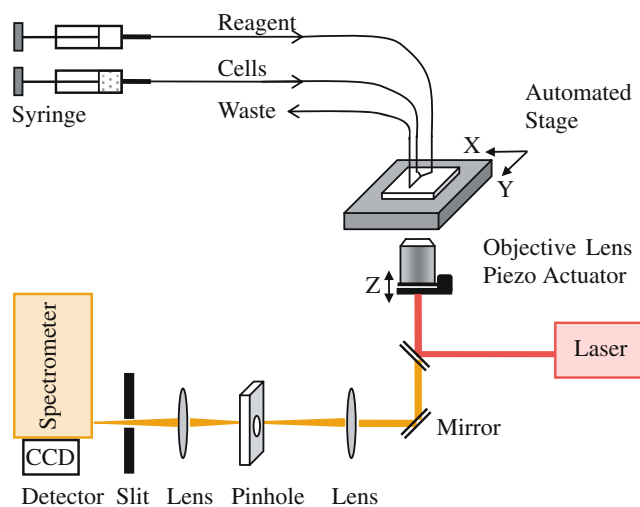


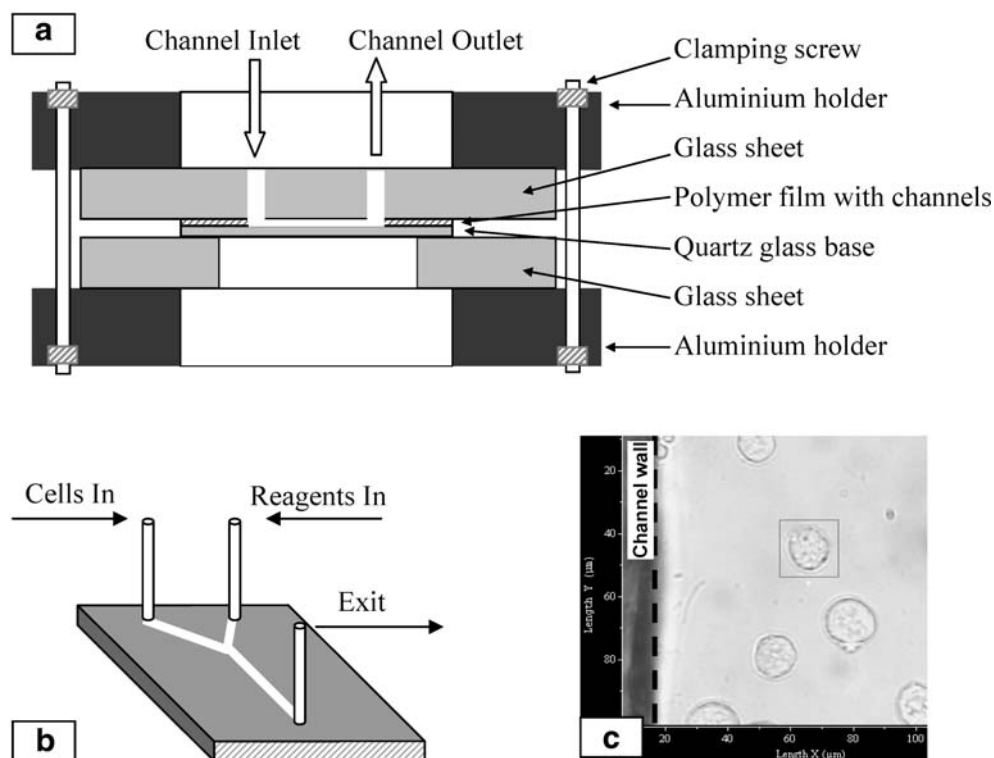
Fig. 1 Schematic of experimental setup

wavelengths of 780 nm (diode laser, 70 mW) and 633 nm (He–Ne laser, 20 mW), confocal optics, a holographic transmission grating, and a charge coupled device (CCD) detector with $1,024 \times 256$ pixels. The instrument included a precision motorized X–Y sample stage for automated mapping at spatial resolution down to less than $1 \mu\text{m}$ and extensive software support (LabSpec 4.18) for data processing. In this study, an objective lens of $\times 50$ magnification, 17-mm working distance and numerical aperture (NA) of 0.45 was used (L Plan SLWD 50, Nikon, Japan). This objective lens was mounted on a PI-721.10 piezo actuator (Physik Instrumente, Germany) for automatic focussing of the microscope objective at different depths in the Z direction enabling 3D mapping. A grating with $1,800 \text{ grooves mm}^{-1}$, a confocal aperture of $300 \mu\text{m}$ and an entrance slit of $150 \mu\text{m}$ were selected for the experiments. The Raman spectrometer wavelength range was calibrated using the centre frequency of the silicon band from a silicon sample (520.2 cm^{-1}). Using these conditions, a typical acquisition time of 1 s was used to collect SERS spectra from cells within the microchannel.

Microfluidic device fabrication

The microfluidic device was constructed using a manifold clamping method according to published procedures with some adaptations [16–18]. The assembly of the device is illustrated in Fig. 2a. Briefly, the microchip consisted of a PARAFILM® sheet (thickness $130 \mu\text{m}$, American National Can Company, US) with a channel network and two glass plates which sandwiched the polymer film. The Y-shaped channel network (Fig. 2b) cut through the film was $500\text{-}\mu\text{m}$ wide. The top glass plate (B-270, $25 \times 25 \times 3 \text{ mm}$) had three holes (diameter 1.5 mm) drilled through at appropriated positions in order to link the ends of the channels with inlet/

Fig. 2 (a) Assembly of microfluidic device and (b) Y-shaped channel network (channel depth 100 μm , width 500 μm) with cells loaded (c) for examination



outlet tubing. The bottom glass plate was a thin quartz coverslip (22×22 mm, Agar Scientific Ltd, UK) which had a thickness of 250 μm in order to minimise the glass background during Raman measurements. This sandwich chip was then clamped using two aluminium frames with screws. The windows on the frames were designed for tubing connections (through top frame) and for optical passage (through bottom frame).

Two KDS 200 syringe pumps (KD Scientific Inc., USA) were used to deliver cells in suspension and test solutions into the microchip channel (Fig. 2c). Ethylene tetrafluoroethylene (ETFE) polymer tubing with an inner diameter of 250 μm , on-off valves, and appropriate fittings and connectors, all obtained from Upchurch (Upchurch Scientific Inc., USA), were used for plumbing to link the chip and the syringes.

Cell culture and assay reagents

CHO-K1 (Chinese hamster ovary, *Cricetulus griseus*) cells were supplied by ATCC/LGC Promochem (ATCC[®] No. CCL-61[™], LGC Promochem, UK). The cells were cultured routinely in DMEM/F-12 medium without L-glutamine (Invitrogen Ltd, UK) which was supplemented with fetal bovine serum (Invitrogen Ltd) to a final concentration of 10%, and L-glutamine (Invitrogen Ltd) to a final concentration of 4 mM. An incubator was used at 37 $^{\circ}\text{C}$ supplying 5% CO_2 . The concentration of cells used in loading the chips during this experiment was in the range of 7.5×10^6 cells mL^{-1} .

A wash solution consisting of a modified Tyrodes buffer was used to wash the cells and to prepare the test solution. The Tyrodes buffer was composed of 145 mM NaCl, 2.5 mM KCl, 10 mM HEPES, 10 mM D-glucose and 1.2 mM MgCl_2 . CaCl_2 (99.5%, BDH AnalaR, 150 mM dissolved in Tyrodes buffer) and probenecid (98%, Sigma, 0.834 M dissolved in 1 M NaOH aqueous solution) were then added to the Tyrodes buffer giving final concentrations of 1.5 mM and 2.5 mM for CaCl_2 and probenecid, respectively. Ionomycin test solutions were made by adding ionomycin stock (1 mM in DMSO) into wash solutions for a concentration of 50 μM . Ionomycin was obtained from

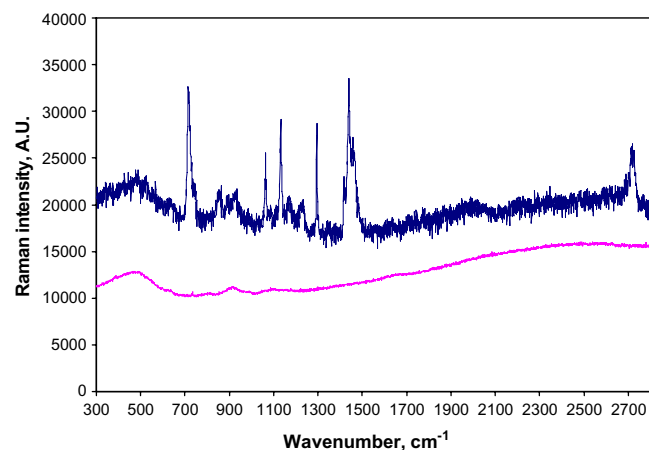


Fig. 3 Raman spectra from cells following incubation in medium with gold colloid (upper spectrum) and without gold colloid (lower spectrum)

Calbiochem (Calbiochem of EMD Biosciences, Inc., USA), and DMSO from Sigma–Aldrich (99%, D2650). The flow rate for the introduction of ionomycin test solution into the microchip was $2 \mu\text{L min}^{-1}$.

Gold colloid with a particle size of 50 nm (EM.GC50), suspended in water, was supplied by BBInternational Ltd, UK. The gold nanoparticles were introduced into cells by a passive uptake method where the cells were incubated with gold colloid solution at desired concentration (20% colloid solution, v/v) and room temperature for 50 mins. Prior to loading into the microfluidic chip, the cells were washed with wash solution to remove the culture media and gold nanoparticles outside cells. The cells were re-suspended in the wash solution for measurements.

Results and discussion

SERS effects

After loading cells into the microfluidic channel, Raman spectra were taken from a selected single cell (Fig. 2c). By using the near-infrared laser excitation (780 nm) the optical and thermal effects of laser illumination on the living cells were minimised [19, 20]. In addition, using a near-infrared laser can significantly reduce the fluorescence interference background and light scattering from the quartz base plate. It has been reported that silver or gold nanoparticles with an individual size in the range of 20–60 nm can yield significant enhancement of Raman scattering for cellular

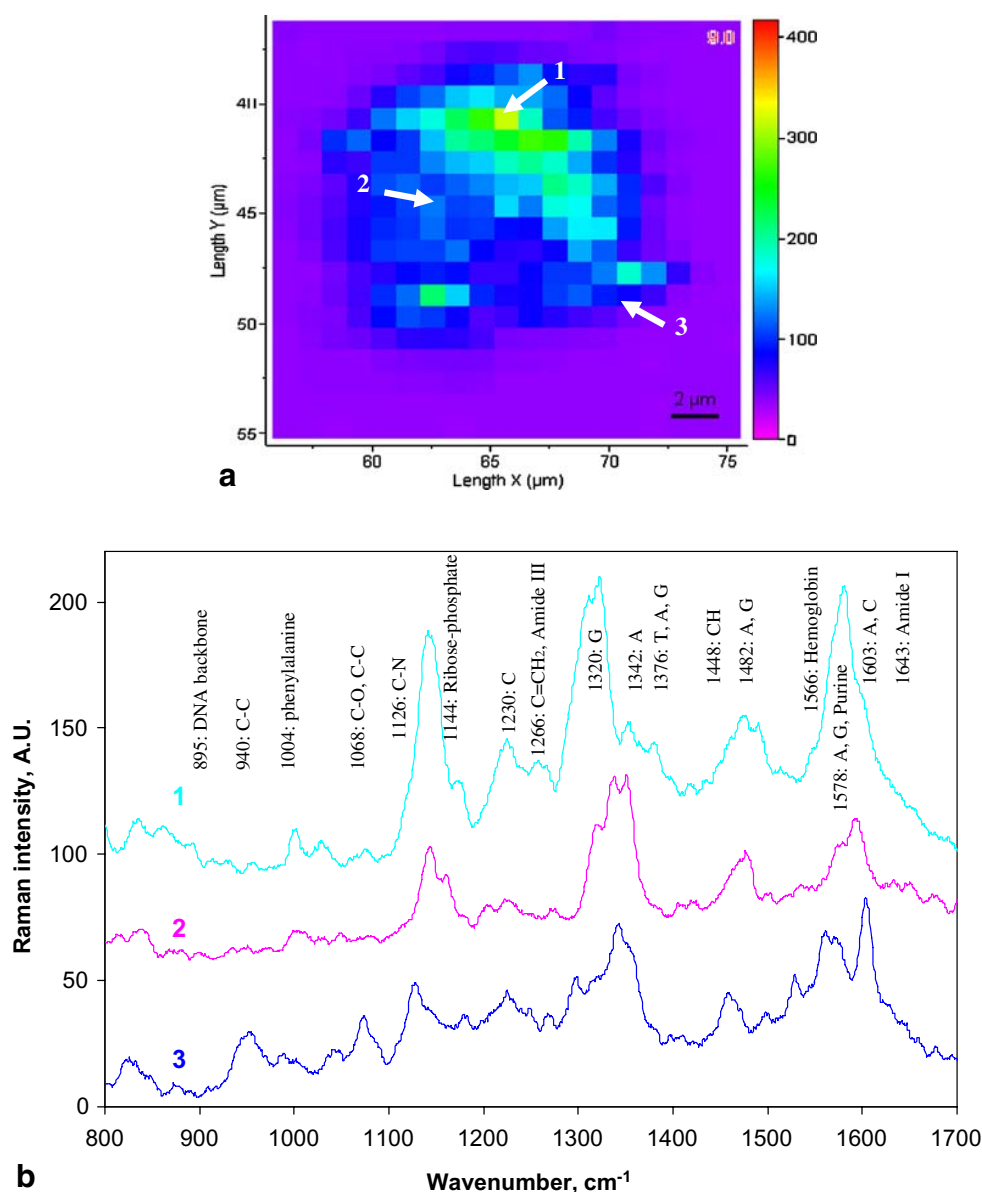


Fig. 4 **a** Spectral mapping of a single CHO cell on an X - Y plane and **b** corresponding spectra from three positions in the area of nucleus, cytoplasm and membrane, respectively

Table 1 Band assignment for Raman spectra of CHO cells

Bands (cm^{-1})	Assignments		
	DNA/RNA	Proteins	Lipids
830	Phosphodiester BkB [12, 23, 24]	Tyr [12, 23, 24]	
895	Phosphodiester BkB, deoxyribose [12, 23, 24]		
940		ν (C–C), α -helix [9, 12, 23]	
1,004		Phenylalanine [9, 12, 23]	
1,065	ν (C–O) [12, 23]	ν (C–C) chian [25]	
1,126		ν (C–N) BkB [9, 12, 23]	ν (C–C) chain [25]
1,144	Ribose–phosphate [12, 23]		
1,157	Ribose–phosphate [20, 26]		
1,176	T, C, G [9, 12, 23, 24]	Phenylalanine [12, 23]	
1,230	C [12, 23, 24]		
1,266		Amide III [25]	δ (C=CH ₂) [25]
1,295			δ (CH ₂) [25]
1,320	G [24]		
1,342	A [12, 23, 24]		
1,376	T, A, G [9, 12, 23, 24]		
1,448		δ (CH) [9, 12, 23]	δ (CH) [9, 12, 23]
1,482	A, G [12, 23, 24]		
1,566		Hemoglobin [25]	
1,578	A, G, purine [12, 23, 24]		
1,603	A, C [24]		
1,643		Amide I [27]	

Abbreviations: *BkB* DNA sugar–phosphate backbone, *Tyr* tyrosine, *A* adenine, *T* thymine, *G* guanine, *C* cytosine, ν stretching vibrations, δ deformation vibrations

analysis when nanoparticles are introduced into cells [14]. This has been confirmed in this study by using gold nanoparticles with a size of 50 nm.

Figure 3 shows a typical spectrum (upper) taken from a cell incubated with gold colloid solution. The spectrum was recorded in the range from 300 to 2,800 cm^{-1} with an acquisition time of 1 s. We observed that with the introduction of gold nanoparticles the Raman spectra were clearly detectable under those conditions. For comparison, a spectrum obtained from a cell incubated in medium without

gold colloid solution is also shown in Fig. 3 (lower). It can be seen that even though the spectra acquisition time was increased to 10 s it was still unable to obtain a good quality spectrum without gold nanoparticles present. This observation confirmed the significant enhancement of Raman scattering with the presence of gold nanoparticles which also enabled a fast spectra acquisition although the exact mechanism of the SERS enhancement of Raman signals is not fully understood [21]. The introduction of gold nanoparticles therefore significantly shortened signal acquisition times mainly owing to the increase in sensitivity which in turn allowed an array of spectra to be obtained in a relatively short time period.

Characterization of single living cells by 3D mapping

Using the SERS technique described above it was possible to obtain spectra from a single living cell which represented a “fingerprint” from which various chemical constituents in the cell can be assigned. Combined with an automated microscope stage which offers spatial resolution (i.e. 1 μm), mapping of an entire cell area at a specific plane was carried out. It has been suggested from previous studies that most of the spectral bands associated with living cells occur in the range 800–1,700 cm^{-1} [11, 22, 23], hence this range was used in this study for mapping. Figure 4a shows an “image” of Raman spectra obtained from the middle layer across the single cell by mapping an area of $21 \times 21 \mu\text{m}^2$ with a spatial step of 1 μm in both *X* and *Y* directions. The mapping provided information on the distribution of selected bands, as seen in Fig. 4b in the range from 1,290 to 1,370 cm^{-1} , which represent most of the significant bands associated with DNA and proteins within a cell’s nucleus and cytoplasm [11, 23].

In general, the Raman spectra of single CHO cells showed contributions from all its cellular components

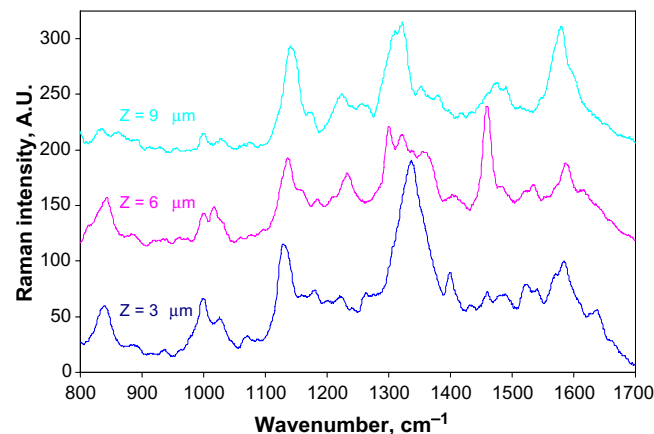


Fig. 5 Raman spectra taken at three levels along the *Z* direction in the nucleus area

including nucleic acids, proteins, lipids and carbohydrates. Table 1 summarises the band assignment for the Raman spectra taken from CHO cells based on the published data [8, 9, 12, 23–27]. Comparison of the spectra taken from different positions across the cell on an X – Y plane (Fig. 4) indicated that strong peaks from the nucleus spectrum corresponding to DNA sugar–phosphate backbone (895 and $1,142$ cm^{-1}), and bases G ($1,320$ and $1,487$ cm^{-1}), A ($1,420$ and $1,578$ cm^{-1}), T ($1,176$ and $1,376$ cm^{-1}) and C ($1,420$ cm^{-1}) were noticeably reduced in the cytoplasm

and membrane spectra (Table 1). This change was expected as the nucleus contains high densities of DNA, whilst the cytoplasm also had significant quantities of RNA contributing to the corresponding peaks. As expected, the spectrum taken from membrane area showed significant peaks corresponding to lipids ($1,068$ and $1,453$ cm^{-1}).

Using the confocal optics of the microscope system, the chemical concentration distribution in the Z axis at three levels in the nucleus was examined (Fig. 5) and indicated that the main peaks positions were generally identical but the

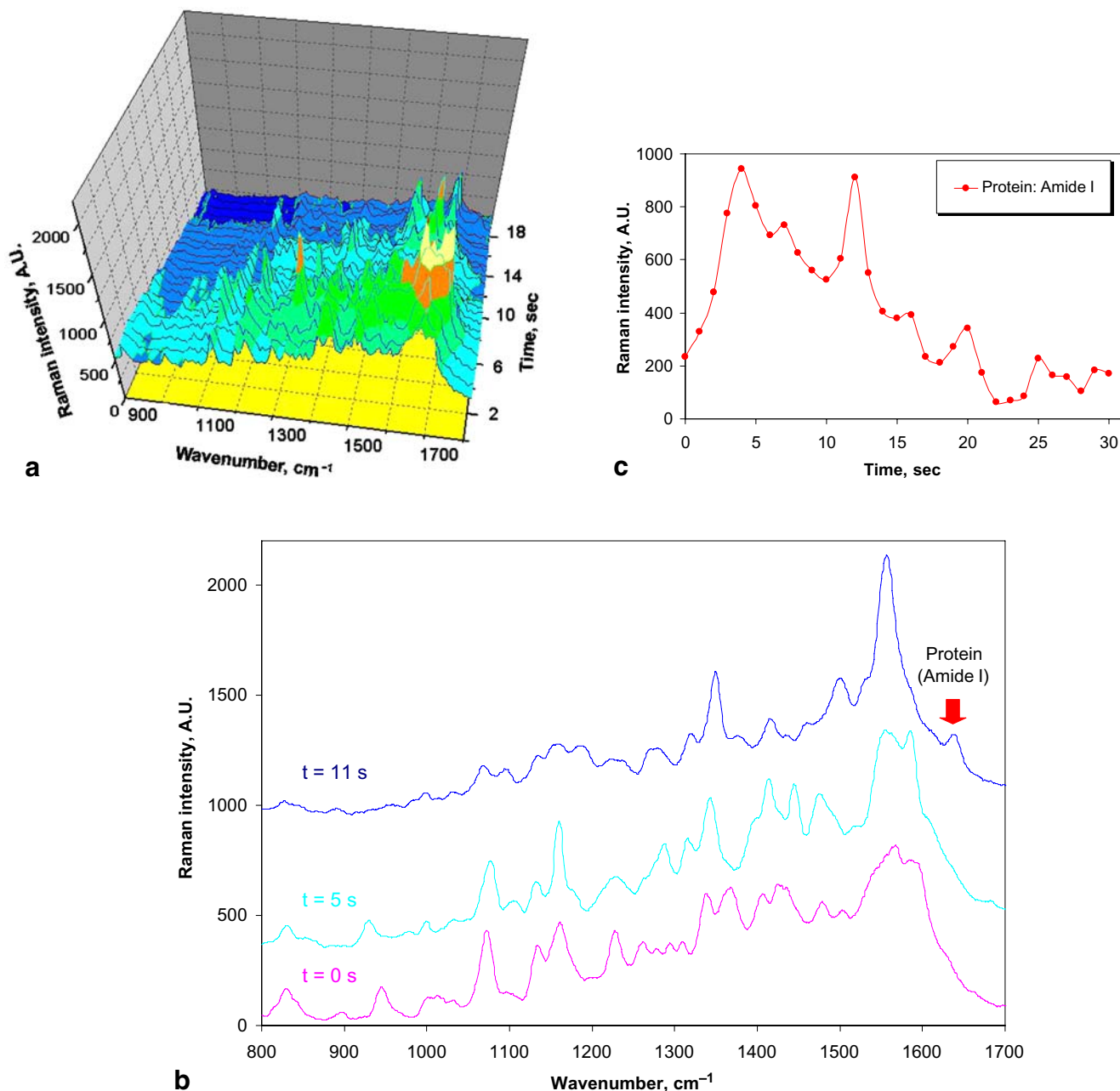


Fig. 6 In situ monitoring of cellular dynamics by recording a series of Raman spectra (**a**) from a specific area at an interval of 1 s. The first spectrum, at time 0, was taken when no agonist was introduced (**b**);

c shows the time profile of the peak at $1,643$ cm^{-1} corresponding to the change of amide I

peak heights were markedly different, indicating a concentration difference. From Fig. 5a significant a peak was observed at $1,320\text{ cm}^{-1}$ on the spectrum taken from $Z=3\text{ }\mu\text{m}$ (near to the bottom of the cell) which was assigned to DNA bases G [23], whilst the peak at $1,450\text{ cm}^{-1}$ from $Z=6\text{ }\mu\text{m}$ indicated a strong deformation from a C–H stretch in proteins [8, 12, 23]. Thus, by collecting spectra from different spatial positions, it provided an approach to build a 3D mapping of the distribution of chemicals within a single cell.

It should be noted that the spectra taken from different positions are distinct in terms of both Raman band amplitudes and band positions. This spectral variation can be attributed to the native chemical inhomogeneity within a cell. However, the possibility of non-uniform distribution of gold nanoparticles within the cell cannot be excluded [15]. In addition, this non-uniform distribution can also take place during the time-resolved monitoring because dynamic processes inside the cell can lead to local fluctuations of the particle densities and hence changes of the spectra. To further develop this spectroscopic technique for both qualitative and quantitative analysis, technologies need to be explored in order to deliver and position nanoparticles within cells in a controllable format for a uniform distribution. Nevertheless, it is still possible using this promising methodology to examine a specific point within a cell in a dynamic way with time, especially when applying stimulation, e.g. an agonist, under microfluidic control conditions.

In situ monitoring of cellular chemical dynamics

Finally, we monitored the chemical dynamics of the cell when exposed to the agonist ionomycin [3, 28]. After loading cells into the chip channel, a 40-min period of settlement was allocated before introducing the ionomycin solution at a constant flow rate of $2\text{ }\mu\text{L min}^{-1}$. Whilst focussed on a region close to the cell nucleus, a series of spectra were taken at an interval of 1 s in the range from 800 to $1,700\text{ cm}^{-1}$ (Fig. 6a). It can be seen from the spectra (Fig. 6b) that most of the peaks corresponding to nucleic acids, proteins and lipids remain visible with time but the peak heights vary noticeably, indicating the concentration change of these compounds. One of the most significant changes is the appearance of a peak at $1,643\text{ cm}^{-1}$ which can be assigned to amide I [27]. The time profile of this peak (Fig. 6c) reveals the concentration change of amide I within the cell, showing a similar trend to that of the Ca^{2+} flux evoked by the agonist ionomycin [3] which is commonly used in biomedical research to stimulate the intracellular production of proteins such as interferon [29]. Since amide I contributes spectrally to the Raman spectrum of interferon, it follows that the in situ monitoring of such molecules could in future be used to produce characteriza-

tion of protein expression dynamics at subcellular levels. Clearly, more studies are required in order to understand the mechanism and cause of the concentration change of amide I within the cell when exposed to agonist ionomycin.

Conclusions

The SERS technique has been used for characterisation of single CHO (Chinese hamster ovary) cells with a microfluidic device where gold nanoparticles were introduced into cells for Raman enhancement. The use of an inverted microscope optical systems in combination with a charge coupled device (CCD) detector allows the measurement of Raman spectra for simultaneous analysis of bio/chemical species within cells. In addition to a precision automated X – Y sample stage, the confocal optics provides discrimination between points of different depths within the cell, enabling chemical mapping in three dimensions. By using microfluidic methodology, the cell manipulation and reagent delivery were performed in a controllable manner. By introducing cells and test reagent into the chip in a continuous flow as a series of plugs in a given sequence, it enabled the in situ chemical characterization of single CHO cells with a high degree of *spatial* and *temporal* resolution. This allows the real time monitoring of the dynamics of the agonist-evoked Ca^{2+} flux response. The approach described has the potential to be used for the study of the spatial dynamics of a range of intercellular processes.

Acknowledgements We thank Ms Huguette Savoie of the Department of Chemistry at the University of Hull for help with the cell culture. The DTI (MNT Project 366) is acknowledged for funding this research.

References

1. Janasek D, Franzke J, Manz A (2006) *Nature* 442:374–380
2. Kitamori T, Fujita H, Hasebe S (eds) Proceedings of the 10th international conference on miniaturized systems for chemistry and life sciences (μ -TAS 2006), Tokyo, Japan, 5–9 November 2006
3. Zhang X, Yin H, Cooper JM, Haswell SJ (2006) *Electrophoresis* 27:5093–5100
4. Ramser K, Enger J, Goksor M, Hanstorp D, Logg K, Kall M (2005) *Lab Chip* 5:431–436
5. Huh D, Kamotani Y, Grotberg JB, Takayama S (2005) *Physiol Meas* 26:R73–R98
6. Monaghan PB, McCarney KM, Ricketts A, Littleford RE, Docherty F, Smith WE, Graham D, Cooper JM (2007) *Anal Chem* 79:2844–2849
7. Olson KJ, Ahmadzadeh H, Arriaga EA (2005) *Anal Bioanal Chem* 382:906–917
8. Lee S, Kim S, Choo J, Shin SY, Lee YH, Choi HY, Ha S, Kang K, Oh CH (2007) *Anal Chem* 79:916–922

9. Jess PRT, Garcés-Chávez V, Smith D, Mazilu M, Paterson L, Riches A, Herrington CS, Sibbett W, Dholakia K (2006) *Opt Express* 14:5779–5791
10. Krafft C, Knetschke T, Funk RHW, Salzer R (2006) *Anal Chem* 78:4424–4429
11. van Manen H-J, Kraan YM, Roos D, Otto C (2005) *PNAS* 102:10159–10164
12. Puppels GJ, de Mul FF, Otto C, Greve J, Robert-Nicoud M, Arndt-Jovin DJ, Jovin TM (1990) *Nature* 347:301–303
13. Fleischman M, Hendra PJ, McQuillan AJ (1974) *Chem Phys Lett* 26:163–166
14. Kneipp J, Kneipp H, McLaughlin M, Brown D, Kneipp K (2006) *Nano Lett* 6:2225–2231
15. Kneipp K, Haka AS, Kneipp H, Badizadegan K, Yoshizawa N, Boone C, Shafer KE, Motz JT, Dasari RR, Feld MS (2002) *Appl Spectrosc* 56:150–154
16. He P, Watts P, Marken F, Haswell SJ (2005) *Electrochem Commun* 7:918–924
17. Katak AS, Gale BK, Lvov Y, Jone SA (2003) *Biomed Microdev* 5:207–215
18. Ma N, Koelling KW, Chalmers JJ (2002) *Biotech Bioeng* 80:428–437
19. Nottingher I, Jones JR, Verrier S, Bisson I, Embanga PP, Edwards P, Polak JM, Hench LL (2003) *Spectroscopy* 17:275–278
20. Nottingher I, Verrier S, Romanska H, Bishop AE, Polak JM, Hench LL (2002) *Spectroscopy* 16:43–51
21. Chowdhury MH, Gant VA, Trache A, Baldwin AM, Meininger GA, Coté GL (2006) *J Biomed Opt* 11:24004
22. Nottingher I, Verrier S, Haque S, Polak JM, Hench LL (2003) *Biopolymers* 72:230–240
23. Puppels GJ, Garritsen HSP, Segers-Nolten GMJ, Mul FFM, de Greve J (1991) *Biophys J* 60:1046–1056
24. Ruiz-Chica AJ, Medina MA, Sánchez-Jiménez F, Ramírez FJ (2004) *Nucleic Acids Res* 32:579–589
25. Krafft C, Sobottka SB, Schackert G, Salzer R (2005) *Analyst* 130:1070–1077
26. Overman SA, Aubrey KL, Reilly KE, Osman O, Hayes SJ, Serwer P, Thomas GJ Jr (1998) *Biospectroscopy* 4:S47–S56
27. Williams RW (1985) *J Biol Chem* 260:3937–3940
28. Gergely L, Cook L, Agnello V (1997) *Clin Diagn Lab Immunol* 4:70–74
29. Osna N, Elliott K, Khan MM (2001) *Int Immunopharmacol* 1:135–145

Lab on a Chip

Miniaturisation for chemistry, biology & bioengineering

www.rsc.org/loc

Volume 8 | Number 9 | September 2008 | Pages 1409–1588

Published on 15 July 2008. Downloaded by Deakin University on 06/07/2014 23:41:34.



ISSN 1473-0197

RSC Publishing

Kim
New microreactor polymers

Kamm
3D Cell culture platform

Sohn
Protein functionalized pore

Austin
Crossing microfluidic streams

Novel inorganic polymer derived microreactors for organic microchemistry applications

Tae-Ho Yoon,^a Sang-Hee Park,^a Kyoung-Ik Min,^a Xunli Zhang,^b Stephen J. Haswell^c and Dong-Pyo Kim^{*a,d}

Received 19th March 2008, Accepted 19th June 2008

First published as an Advance Article on the web 15th July 2008

DOI: 10.1039/b804726j

Microreactors fabricated with optically transparent inorganic polymers from two types of precursors using a UV-microimprinting process demonstrated reliable solvent resistance and capability for performing three model organic synthetic reactions, which were compared with batch systems and glass based microreactors.

Introduction

During the last two decades, significant development in the fields of miniaturized systems, so-called microfluidics or lab-on-a-chip technologies, has been achieved and spread widely over diverse areas such as bioengineering, optics and electronics. One of the main driving forces behind such work is the unique characteristics of microreactors, compared with that of conventional reaction vessels, including a high surface-to-volume ratio, diffusion dominated mass transfer, and the capability for spatial and temporal control of reaction reagents and products.^{1,2} In particular, the high surface-to-volume ratio is beneficial for heat transfer enhancement allowing one to utilize the full potential of catalysts during highly endothermic or exothermic reaction while avoiding formation of high thermal gradients.³ In addition, the small dimensions of the reactor channel ensure a short radial diffusion time leading to a narrow residence time distribution.⁴ This is advantageous for consecutive processes since high selectivity to the desired intermediate can be achieved.

Currently, a wide variety of materials, including metal, silicon, glass and polymers, have been used to fabricate microfluidic devices, such as microchips or microreactors.⁵ Silicon has been used widely in the field of MEMS applications by means of a semiconductor process with high manufacture costs using dry and wet etching. In the meantime, polymers such as PDMS and PMMA have been widely used in a range of microfluidic systems owing to their convenient and cheap process based on soft lithography techniques. However, the properties of these polymers, including low mechanical strength and poor solvent resistance against most non-aqueous solutions, restrict their applications in particular for organic reaction systems. Thus, there has been an increasing need to develop novel materials with reliable durability for the fabrication of microfluidic devices by adopting the well-developed facile fabrication process, leading to

potential replacement of current glass or metal based microfluidic devices for versatile applications. We have recently reported the development of polyvinylsilazane inorganic polymer and the feasibility for the fabrication of glass-like microchannels and substrates using a simple and cost effective UV-microimprinting process which is followed by a sequential photocuring and thermal cross-linking step.^{6,7} It has been demonstrated that such cured polyvinylsilazane exhibits high optical transparency and organic solvent resistance.

In this paper, we report further the development of microreactors using two types of commercially available inorganic polymers, namely polyvinylsilazane and allylhydropolycarbosilane, based on a micro-imprinting lithography fabrication technique, and their applications for organic synthesis. Three model organic chemical reactions have been selected; synthesis of 3,5-dimethylpirazole, exothermic Diels–Alder cyclo-addition and Knoevenagel reaction, which are carried out in commonly used organic solvents including THF, acetonitrile and DMF. It is believed that, to our knowledge, this is the first attempt to demonstrate these organic reactions within polymer-based microreactors. The microchemical performance of two inorganic polymer microchannels is preliminarily evaluated in comparison to those of glass-based microreactors and batch reaction systems. The results indicate that the novel inorganic polymer-based microreactors can provide an economic and versatile platform for both aqueous and non-aqueous chemistry applications.

Materials and methods

The microreactor was fabricated by UV-imprinting techniques with PDMS (polydimethylsiloxane, Sylgard 184, Dow Corning, USA) replica molds which were prepared using the conventional soft lithography method with silicon wafer fabricated with SU-8 photoresist (Microchem, USA) as reported in the literature.⁸ To fabricate the microreactor, allylhydridopolycarbosilane (AHPCS, SMP-10[®], Starfire systems, USA) and polyvinylsilazane (PVSZ, KION VL-20[®], Clariant, USA) (Fig. 1) with low viscosity were used directly or with dilution using tetrahydrofuran (THF, Sigma-Aldrich, USA), depending on the coating thickness. In addition, 2 wt% of dicumylperoxide (Sigma-Aldrich, USA) and Irgacure 500 (Ciba Specialty, Japan) as a thermal and a photo initiator, respectively, were mixed into the

^aDepartment of Finechemical Engineering, Chungnam National University, Daejeon, 305-764, South Korea

^bBioengineering Group, School of Engineering Sciences, University of Southampton, Southampton, SO17 1BJ, UK

^cDepartment of Chemistry, The University of Hull, Hull, HU6 7RX, UK

^dCenter for Ultramicrochemical Process Systems (CUPS), KAIST, 305-701, South Korea

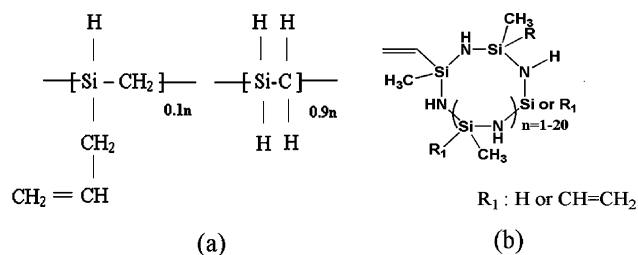


Fig. 1 Polymeric structures of (a) allylhydridopolycarbosilane (AHPCS) and (b) polyvinylsilazane (PVSZ).

inorganic polymers. The solvent resistance of the cured AHPCS was investigated by the identical method as reported for cured PVSZ.^{6,9} The samples were prepared in the PDMS cast with 1×1 cm (width \times length) and 1 mm of thickness and soaked in the diverse solvents for 24 h. Finally, the swelling ratio, D/D_0 , where D and D_0 are the lateral width of sample in solvent for 24 h and that of the dried sample, respectively, was examined. For the optical transmittance with the UV-VIS spectrophotometer (Avantes, Netherland), the inorganic polymer films with ~ 10 μm spun-coated on glass slides and cured at 100 – 160 $^\circ\text{C}$ in nitrogen atmosphere were used. In addition, PDMS films having the same thickness were prepared as a reference sample. The fabrication processes of the inorganic polymer derived microchannel was illustrated in Fig. 2. To prevent the unwanted adhesion between stamps and inorganic polymers, a mold release agent (Kion mold release, Clariant, USA), diluted with hexane, was spin-coated on the PDMS stamp at a spin rate of 2000 rpm for 30 s, which was then baked at 70 $^\circ\text{C}$ for 5 h and ready for use. Microchannels were created by placing the stamp with relief structures (typically 50 μm high and 380 – 500 μm wide) on the viscous inorganic polymer layer which was formed by dropping the liquid inorganic polymer on a pre-cleaned glass slide under nitrogen atmosphere. Subjected to a UV exposure (ELC-4100 UV light system) for 20 min the liquid inorganic

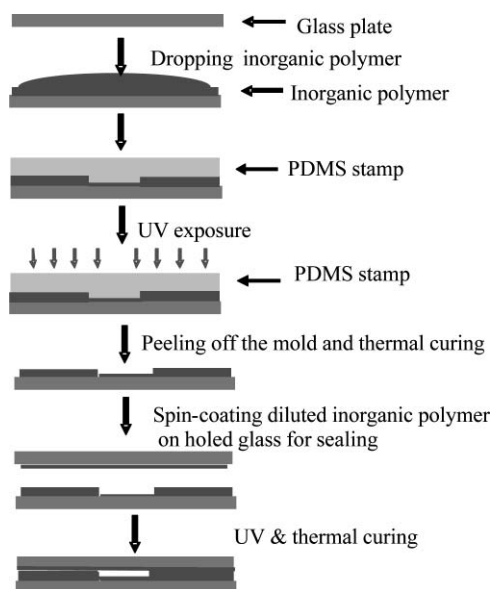


Fig. 2 Schematic fabrication process of inorganic polymer derived microchannel between glass slides.

polymer was cured and solidified. After peeling off the PDMS stamp, the patterned microchannel was thermally post-cured for 3 h at either 160 $^\circ\text{C}$ for AHPCS (polyallylhydridocarbosilane), or 150 $^\circ\text{C}$ for PVSZ (polyvinylsilazane) at a heating and cooling rate of 2.5 $^\circ\text{C min}^{-1}$ under nitrogen atmosphere. To close the microchannel using the same material, a thin polymer film (3 – 4 μm) was spin-coated on a top glass slide which was then gently placed on the patterned structure. A sequential UV exposure and thermal curing under the identical conditions described above resulted in an irreversible sealing of the microchannel. The holes (diameter 1.5 mm) on either side of the supporting bare glass slides were mechanically drilled through to connect the microchannel with tubing. Thus, a microreactor with microchannels (typical dimensions: 500 μm wide, 50 μm deep, 2 – 16 cm long) within an inorganic polymer layer which was sandwiched between two glass slides was fabricated. The microreactors were then connected to pumping devices *via* PFPE tubes ($1/16$ " OD, Upchurch, USA). To secure the connection between the holes on the supporting glass and the tube, a ceramic sealing (Torrseal, USA) material was used. The morphology or topography of the fabricated microchannel was determined by SEM (FE-SEM, XL30SFEG, Philips, Netherland, 5 kV) and a digital imaging technique (AQM image acquisition software).¹⁰

In order to evaluate the performance of the inorganic polymer derived microreactors, three organic synthetic reactions (Fig. 3) were carried out, namely, synthesis of 3,5-dimethylpirazole, exothermic Diels–Alder cyclo-additions and Knoevenagel condensation, under different reaction conditions.^{11,12} All chemicals used were purchased from Sigma-Aldrich and used without additional purification. All liquid samples were pressure-driven into the channel using syringe pumps (KDS 100, KD Scientific Inc., Holliston, MA, USA) at flow rates in the range 0.67 – 60 $\mu\text{l min}^{-1}$. The quantitative analysis of products was performed with a GC-MS (Gas chromatography-mass analyzer, Varian GC (CP-3800) coupled to a Varian MS (2000), USA), capillary column (DB-35MS, 0.25 $\mu\text{m} \times 30$ m $\times 0.32$ mm) and a GC-FID (Shimadzu, GC 17A, Japan, capillary column 30 m, Zebtron ZB 5, Phenomenex, USA). Fig. 3 shows the three reaction schemes. During the reaction of 3,5-dimethylpirazole synthesis, 0.1 M acetylacetone in THF solution, and 0.1 M hydrazine monohydrate in THF solution, were introduced into the Y shaped channel at an equal flow rate ranging from 0.76 to 10 $\mu\text{l min}^{-1}$ (Fig. 3(a)). For comparison, this reaction was run within a glass made microreactor having identical channel design and dimensions. It was also carried out in a batch format using a glass vial.^{11–13} The catalyzed Diels–Alder cycloaddition was performed by flowing in a mixture of 1 mM of ethylacrylate and 2,3-dimethyl-1,3-butadiene with THF *via* one inlet of the Y shaped channel, and a solution of 2.5 mol% of AlCl_3 in THF *via* the other inlet (Fig. 3(b)), whilst the temperature of the microreactor was kept constant at 45 $^\circ\text{C}$ using a hotplate (Fisher Scientific, USA). The Knoevenagel reaction (Fig. 3(c)) was carried out within an extended Y channel allowing a longer residence time for reaction where ethyl cyanoacetate mixed with piperazine (v/v, $10 : 1$) in THF was introduced from one inlet and the benzaldehyde solution from the other. This was also compared with batch reaction results.

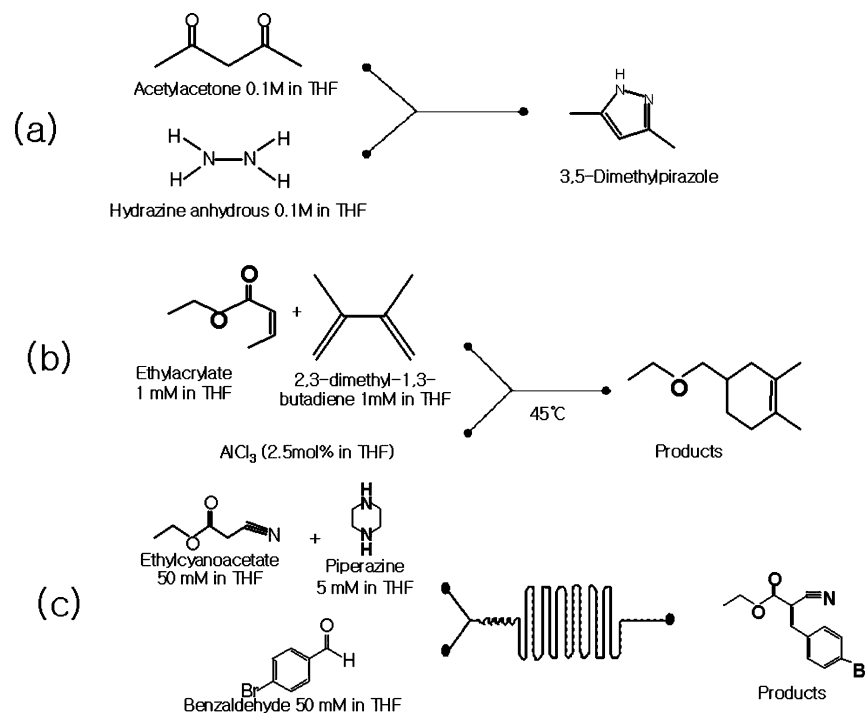


Fig. 3 Reaction schemes for (a) synthesis of 3,5-dimethylpirazole, (b) Diels–Alder cycloaddition and (c) Knoevenagel reaction.

Results and discussion

Solvent resistance and optical transparency

Solvent resistance of the structural material used is an essential characteristic for developing microfluidic devices applicable for non-aqueous as well as aqueous mediums. This has been examined with a range of solvents including water and different solvents. Table 1 summarises the results with AHPCS samples cured for 3 h at two temperature levels of 100 °C and 160 °C. It was observed that temperature had significant effects on the solvent resistance performance; samples cured at 100 °C showed

Table 1 Solvent resistance test of two inorganic polymers AHPCS and PVSZ cured at either 100 or 150 °C for 3 h

	AHPCS		PVSZ	
	N ₂ cured at 100 °C ^a , 3 h	N ₂ cured at 160 °C ^a , 3 h	N ₂ cured at 100 °C ^a , 3 h	N ₂ cured at 150 °C ^a , 3 h
Acetone	0.99	1.01	Crack	0.98
Ethanol	1.01	1.00	1.00	1.00
Hexane	1.12	1.02	1.22	1.03
Methanol	1.00	1.00	Crack	1.00
THF	Crack	0.99	Crack	Crack
Toluene	1.26	0.99	Crack	0.99
Acetonitrile	1.00	1.00	1.00	1.00
DMF	1.00	1.00	1.00	1.00
Water	1.00	1.00	0.97	1.00

^a Solvent resistances were evaluated with two inorganic polymers AHPCS and PVSZ cured at different temperatures. ^b Numbers listed in this table refer to experimentally measured swelling ratio = D/D_0 , where D and D_0 are length of cured polymer in solvent and length of dried cured polymer, respectively.

low resistance to a part of the solvents used and in particular, cracking in THF. In contrast the samples cured at 160 °C for 3 h exhibited good stability in all solvents showing insignificant defects. This temperature effect can be attributed to the polymer's chemical structures; a higher temperature was favorable to form extensive cross-linked structure *via* hydrosilylation and dehydro-coupling reaction routes where active Si–H and allyl functional groups of the AHPCS reacted with the presence of thermal initiator, dicumyl peroxide.¹⁴

Previous studies indicated that the higher dense network structure with Si–C backbones in AHPCS can provide a stronger solvent resistance.¹⁵ The test with PVSZ samples showed similar temperature effect; PVSZ cured at a higher temperature of 150 °C for 3 h exhibited excellent solvent resistance against almost all the solvents used except less resistance to THF causing slight changes in sample dimensions by swelling, subject to 24 h soaking. This observation was in line with the previous studies on PVSZ polymers.⁶ Based on these test results it is suggested that both AHPCS and PVSZ can be good candidate polymers in terms of organic solvent resistance, for the fabrication of microreactors for organic chemical applications owing to the ceramic characteristics. The wettability of the cured inorganic polymer was analyzed by contact angle measurement, and the contact angle with water was noted to be around 101°, suggesting a highly hydrophobic nature of the surface as reported in previous work.⁶ It might come from the fact that both AHPCS and PVSZ have been widely used as preceramic precursors for the preparation of high temperature stable SiC and SiCN ceramic materials.^{16,17} It has even been claimed that the cured PVSZ polymer can act as a thermally protective coating.¹⁵

The optical transmittance of the two types of inorganic polymers coated on glass substrates was measured across the UV-Visible range under different curing conditions. The results are depicted in Fig. 4. The measurement from a PDMS sample is also shown for comparison. It can be seen from Fig. 4 that both cured inorganic polymers AHPCS and PSVZ showed a high transmittance (over 90%), which is close to that of PDMS sample.⁶ It was observed that the AHPCS samples cured at a higher temperature (160 °C) showed a slightly lower transmittance which was attributed to its color change from transparent to yellow tinge. Nevertheless, the optical transparency of these inorganic polymers is promising for their applications in the fabrication of microreactors, in particular when incorporating photo-induced chemistry and/or optical detections.

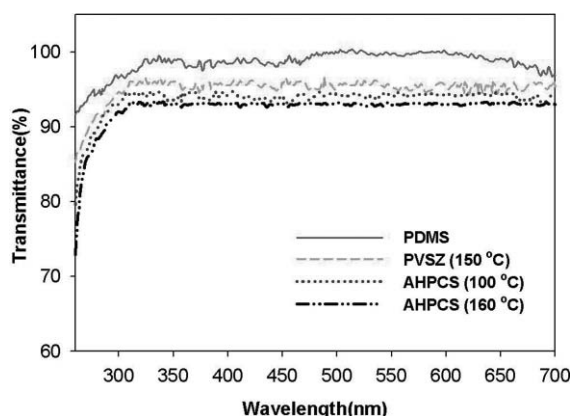


Fig. 4 Comparative UV-Vis transmittance of PDMS and inorganic polymers AHPCS and PVSZ cured at different temperatures.

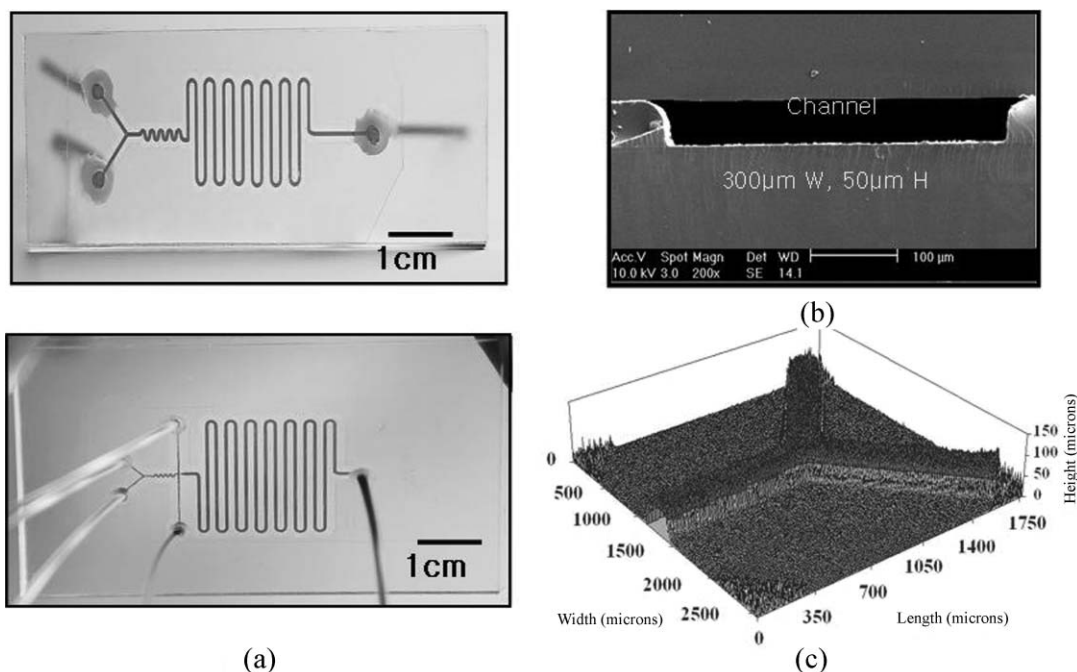


Fig. 5 (a) Image of microreactor devices fabricated with AHPCS (upper) and PVSZ (lower), (b) SEM image of the cross-section and (c) topographical image of the Y-junction using profiler.

Microchemical performance of inorganic polymer microchannels

Fig. 5(a) shows the inorganic polymer derived microreactors fabricated with AHPCS and PVSZ with about 80% of production yields. It is obvious that the inorganic polymer microreactors on glass slides displayed high optical transparency where the channel layout can be clearly seen. A cross section of the the sealed microchannel, taken by SEM, is shown in Fig. 5(b) and a topographical 3D-image of the microchannel Y-junction is displayed in Fig. 5(c) showing smooth surface along the overall channel and homogenous shape with insignificant deformation from the bonding step.

In order to test the stability of the completed microreactors fabricated, various solvents were continuously pumped through the microchannels for several hours in a range of flow rates up to $10 \mu\text{l min}^{-1}$. It was confirmed that both types of microreactors were stable; neither leakage nor damage was observed with 4 h continuous flow of alcohols and acetone containing red dye to aid observation. However, THF solvent did cause partial delamination and leakage in the PVSZ based microreactor after 1 h running, which corresponded to the swelling observed (Table 1). On the other hand, the AHPCS based microreactor was stable as repeatedly used under all solvents given in Table 1. In addition, the chemical stability was confirmed by analysing THF solvent which was kept for 1 h in the AHPCS derived microchannel, using a GC-MS. It should be noted that the solvent resistance and chemical stability are remarkable in contrast to that of commonly used PDMS microchannels which can be operated only under mild aqueous conditions, including ethanol mixture for a short working period.¹⁸ These inorganic polymer reactors also showed advantages over cyclic olefin copolymer (COC) based plastic microreactors which are not suitable for non-polar solvents such as hexane or toluene.^{19,20}

Table 2 Synthesis of 3,5-dimethylpirazole with AHPCS derived microreactor, glass microreactor and batch reactor

Flow rate/ $\mu\text{l min}^{-1}$	Residence time	AHPCS(%)	Glass(%)	Batch, %
10.0	5.0 s	13.6	10.2	
5.0	10.0 s	30.4	32.9	
0.76	65.7 s	63.6	59.0	
	5 min			55.3

Synthesis of 3,5-dimethylpirazole

3,5-Dimethylpirazole is a useful pharmaceutical heterocyclic intermediate in biological research, and there have been attempts to synthesize it using glass based microreactors in THF medium.¹¹ In this study we performed this reaction within an AHPCS derived microreactor with Y shaped channel (50 μm deep, 500 μm wide and 2 cm long). The reaction was also carried out in a glass based microreactor with identical channels, and in a batch system for comparison. The experimental results are summarized in Table 2. It can be seen that in both polymer and glass microreactors with continuous flow the product yield remarkably increased when the fluid residence time was increased. For example, a change in residence time within AHPCS microreactor from 5.0 s to 65.7 s resulted in a yield jump from 13.6% to 63.6%. This was likely due to the fact that a longer residence time allowed more time for a better mixing by diffusion of the two co-flowing reactant streams. In contrast, a noticeably longer reaction time of 300 s within a batch reaction vial (ID, 1 cm; volume 1.57 ml), resulted in a yield of only 55.3%. These results indicate that the inorganic polymer derived microreactors performances were comparable with glass made microreactors for organic synthesis at room temperature.

Catalyzed Diels–Alder cycloaddition

The Diels–Alder cycloaddition is one of the well studied in organic chemistry and has been carried out under a variety of reaction conditions within glass based reactor with both organic solvents and catalysts involved (Fig. 3(b)). In this study, the exothermic reaction was performed within a AHPCS microreactor (Y-shaped channel, 500 μm wide, 50 μm high and, 30 mm long) with THF solvent. Again the result was compared with that obtained from a batch reactor. The results are shown in Table 3. It was observed that, similar to the reaction above, the synthetic yields of product were gradually increased from 68.0 to 82.3 and 100% as the fluid residence time was extended from 12.5 to 25 and 100 s, respectively. During repeated use

Table 3 Experimental results of Diels–Alder reaction in AHPCS derived microreactor and batch reactor

Flow rate/ $\mu\text{l min}^{-1}$	Residence time	AHPCS(%)	Batch(%)
4	12.5 s	68.0	
2	25.0 s	82.3	
0.5	100.0 s	100	
	6 h		82.0

for 6 h, the AHPCS microreactor had been preserved with no mechanical failure or chemical deflections, and maintained reliable microreaction chemistry as listed in Table 3. In contrast, the bulk batch system performed in a small size vial gave a yield of only 82.0% in spite of a much longer reaction time of 6 h. In addition, the polymer microreactor demonstrated a good thermal performance with insignificant temperature changes during the exothermic reaction, which is attributed to the high surface-to-volume ratio enabling a fast heat dissipation from the reaction fluids to the reactor body. In contrast, a poor heat transfer in the batch reaction vessel led to a rapid heat-up of the reactor up to 60 °C without delay after the reactants were mixed. This temperature increase, in turn, affected the exothermic reaction progress resulting in a lower conversion.

Knoevenagel condensation

This reaction was carried out in both PVSZ and AHPCS microreactors which had identical channel design (Fig. 3(c)) with a 160 mm long reaction main channel (width: 500 μm , depth: 50 μm). The Knoevenagel condensation reaction was investigated in both microreactors under a wide variety of reaction conditions in terms of temperature, flow rate and solvent. The experimental results are summarized in Table 4 for product yields, namely 4-(4-bromophenyl)-3-ethoxy-2-oxo-but-3-enitrile.

It was found that the effect of fluid residence time (or flow rate) was similar to that observed in the two reactions described above; a longer residence time resulted in a higher yield. This applied to all the solvents used and all three temperature levels set. An increase in reaction temperature, in most cases, showed a higher yield with a given flow rate in most of the solvents used except insignificant changes in methanol solvent. It was interestingly noted that the different solvents selected had significant effects on the reaction. For example, under identical conditions (flow rate 40 $\mu\text{l min}^{-1}$ at room temperature) in ACN a yield of 48.5% was observed whilst a more than doubled figure, 90.1%, was obtained in methanol. It was found that the order of yields obtained from different kinds of solvents is as follows:

Table 4 Summarized performance of Knoevenagel condensation reaction as a function of flow rate, solvent and reaction temperature

Flow rate (retention time)		5 $\mu\text{L min}^{-1}$ (30 s)			10 $\mu\text{L min}^{-1}$ (15 s)			20 $\mu\text{L min}^{-1}$ (8 s)			40 $\mu\text{L min}^{-1}$ (4 s)		
		Temperature			Temperature			Temperature			Temperature		
Solvent	Material	RT	40 °C	60 °C	RT	40 °C	60 °C	RT	40 °C	60 °C	RT	40 °C	60 °C
Ethanol	PVSZ	95.5	98.1	99.5	93.1	96.4	98.2	87.3	95.1	95.0	85.7	94.1	93.8
Methanol		96.8	95.6	—	95.3	94.5	—	91.4	91.4	—	90.1	90.1	—
DMF		70.5	77.5	78.5	63.7	70.8	72.5	56.0	63.5	65.4	51.4	55.8	60.2
ACN		65.0	66.8	70.4	61.7	62.3	65.3	54.2	58.7	61.2	48.5	53.3	56.5
THF	AHPCS	89.1			86.3			85.3			80.1		

ethanol > methanol > THF > DMF > ACN. This sequence is indicative that the effect of solvent is likely due to polarity differences in different solvents. However, in order to confirm and further quantify this effect more studies need to be put forward.

After beginning the experiments, inorganic polymer chip was monitored over 8 hours to check for defects occurring from chemical instability. In the case of the PVSZ based microreactor some delamination showed under THF solvent, but the one made from AHPCS was preserved without any leakage of product and deformity of channel shape. These kinds of experiments were not reported with PDMS or plastic based microreactor but with glass microreactor. Similarly, when this reaction was carried out in a batch reactor a lower yield was obtained; a yield of 50.6% was observed in a bulk reaction vial (ID = 1 cm, working volume 1.57 ml) with ethanol, despite a long reaction time of 20 min.

Conclusions

The imprint lithography technique, which has advantages in terms of low-cost and mass production, has been employed for the fabrication of inorganic polymer-based microreactors in a cheap and simple manner. Such microreactors produced by this technique demonstrated reliable microchemical characteristics with high optical transparency, strong organic solvent resistance and stabilities for running organic synthesis reactions. Three model organic synthetic reactions, namely synthesis of 3,5-dimethylpirazole, exothermic Diels–Alder cyclo-additions and Knoevenagel condensation have been successfully carried out under different reaction conditions. It was demonstrated that the microchemistry performance of the inorganic polymer based microreactors was well in accordance with that of glass made microreactors, and both were significantly advantageous over batch reaction systems. These novel inorganic polymer derived microreactors proved to be promising for organic microchemistry applications.

Acknowledgements

This work was financially supported by the 2008 National Research Lab (NRL) Project [R0A20040001036702007] administered by the Korean Ministry of Science and Technology (MOST). We thank Dr Charlotte Wiles and Dr Lan-Young Hong for their kind cooperation.

Notes and references

- 1 X. Zhang and S. J. Haswell, *MRS Bull.*, 2006, **31**, 95.
- 2 D. S. Kim, S. W. Lee, T. H. Kwon and S. S. Lee, *J. Micromech. Microeng.*, 2004, **14**, 798.
- 3 G. Kolb and V. Hessel, *Chem. Eng. J.*, 2004, **98**, 1.
- 4 St. Walter, St. Malmberg, B. Schmidt and M. A. Liauw, *Catal. Today*, 2005, **110**, 15.
- 5 W. Ehrfeld, V. Hessel, H. Löwe, *Microreactors: New Technology for Modern Chemistry*, Wiley-VCH, Weinheim, Germany, 11, 2000.
- 6 A. Asthana, Y. Asthana, I. K. Sung and D. P. Kim, *Lab Chip*, 2006, **6**, 1200.
- 7 J. H. Park, P. A. Tuan, J. J. Lee and D. P. Kim, *Polymer (Korea)*, 2006, **30**, 407.
- 8 M. J. Madou, *Fundamentals of microfabrication; The science of miniaturization*, 2nd edn., CRC Press, 2002.
- 9 J. N. Lee, C. Park and G. M. Whitesides, *Anal. Chem.*, 2003, **75**, 6544.
- 10 I. Broadwell, P. D. I. Fletcher, S. J. Haswell, T. McCreedy and X. L. Zhang, *Lab Chip*, 2001, **1**, 66.
- 11 B. Koc, Yigit Kaymakçioğlu and S. Rollas, *Il Farmaco*, 2002, **57**, 595.
- 12 F. Fringuelli, R. Girotti, F. Pizzo and L. Vaccaro, *Org. Lett.*, 2006, **8**, 2487.
- 13 C. Wiles, P. Watts and S. J. Haswell, *Tetrahedron*, 2004, **60**, 8421.
- 14 W. Z. Xia and W. D. Cook, *Polymer*, 2003, **44**, 79.
- 15 Technical report, Clariant, <http://www.clariant.com>.
- 16 T. H. Yoon, H. J. Lee, J. Yan and D. P. Kim, *J. Ceram. Soc. Jpn.*, 2006, **114**, 473.
- 17 D. Klaffke, R. Wasche, N. Janakiraman and F. Aldinger, *Wear*, 2006, **260**, 711.
- 18 J. Ng. Lee, C. Park and G. M. Whitesides, *Anal. Chem.*, 2003, **75**, 6544.
- 19 J. Y. Shin, J. Y. Park, C. Liu and J. S. He, *Pure Appl. Chem.*, 2005, **77**, 801.
- 20 Technical report, TOPAS, <http://www.topas.com>.

Provided for non-commercial research and education use.
Not for reproduction, distribution or commercial use.



This article was published in an Elsevier journal. The attached copy is furnished to the author for non-commercial research and education use, including for instruction at the author's institution, sharing with colleagues and providing to institution administration.

Other uses, including reproduction and distribution, or selling or licensing copies, or posting to personal, institutional or third party websites are prohibited.

In most cases authors are permitted to post their version of the article (e.g. in Word or Tex form) to their personal website or institutional repository. Authors requiring further information regarding Elsevier's archiving and manuscript policies are encouraged to visit:

<http://www.elsevier.com/copyright>



Attachment and detachment of living cells on modified microchannel surfaces in a microfluidic-based lab-on-a-chip system

Xunli Zhang¹, Paul Jones, Stephen J. Haswell*

Department of Chemistry, The University of Hull, Hull HU6 7RX, United Kingdom

Abstract

The attachment/detachment of living cells on modified microfluidic channel surfaces has been investigated using a “lab-on-a-chip” system. Cell attachment was mediated using surface modifications of the microchannel based on three different reagents, namely, 3-aminopropyltriethoxysilane (APTES), glutaraldehyde and collagen, whilst the detachment was carried out by flowing media through the microchannel at increasing flow rates. All three surface modification methods showed significant improvement for Chinese hamster ovary (CHO) cells’ attachment, compared to that for an unmodified glass surface. The attachment/detachment of an additional four cell types, namely, T47D, U937, CaCo2 and NCTC 2544 cells, were also examined using the APTES modified channel surface. The observation of cell deformation suggested that the control of a shear stress within an optimal range enhances the cell adhesion to the surface. A theoretical model for fitting the measured detachment data is reported based on flow shear stress and the contribution from both surface adhesion bonds and hydrodynamic viscous stresses. It was demonstrated that the microfluidic system provided an easy and controllable approach to examine the attachment/detachment of a range of cells on different modified surfaces.

© 2007 Elsevier B.V. All rights reserved.

Keywords: Living cells; Microfluidics; Surface modification; Shear stress; Cell detachment

1. Introduction

The development of miniaturized “lab-on-a-chip” systems for chemical and/or biological applications has increasingly attracted interest over the last decade [1–5]. Such microfluidic-based microsystems represent the potential to “shrink” conventional bench chemical systems to the size of a few square centimetres with major advantages in terms of speed, performance, integration, portability, sample/solvent quantity, automation, hazard control and cost. These advantages are important for a variety of applications in analytical chemistry, biochemistry, clinical diagnosis, medical chemistry and industrial chemistry [6,7]. Consequently, numerous micrototal-analysis-systems (μ -TAS) and microreactor systems have been developed, and many more are currently under investigation [4].

For the study of biochemical or biomedical systems involving living cells, it is often a requirement that cells are delivered and remain at a desired location for examination and from where they can subsequently be removed. Our previous studies have demonstrated that microfluidics allows reagents and parti-

cles including cells to be manipulated and delivered to desired locations with programmable sequences within microchannel networks [5,6,8,9]. The location and then removal of cells from a given area generally involve an attachment/detachment process between cells and the substrate surface which can be mediated by channel geometry and flow rate (shear stress). The attachment of cells on a surface is normally performed by allowing cells to settle down without fluidic disturbance for a certain period of time. In some cases a chemical or biochemical modification of either cell surfaces or substrate surfaces can enhance the adhesion [10]. To remove cells from the substrate surface appropriate washing solutions are employed to break the bonds or cellular ‘glue’ that attaches the cells to the substrate and to each other by using proteolytic enzymes such as trypsin and dispase [11,12]. Whilst these methods are commonly used for batch or static operations, the shear stress caused by a fluid flowing along the substrate has been used as an effective approach to detach cells from the surface [13], which can be operated in either a continuous-flow or a paused-flow format [14] in a highly controllable manner [15,16]. The kinetics and mechanics of cell adhesion on substrate surfaces under shear stresses have been studied since the 1980s [17,18]. However, most of this work has been carried out from a mechanical engineering point of view. For instance, two commonly used models are based on either peeling-off-adhesive-tape or receptor–ligand-binding processes

* Corresponding author. Tel.: +44 1482 465469; fax: +44 1482 466410.

E-mail address: S.J.Haswell@Hull.ac.uk (S.J. Haswell).

¹ Present address: School of Engineering Sciences, University of Southampton, Southampton SO17 1BJ, United Kingdom.

[19]. The mechanism, however, of attachment/detachment of living cells on a substrate surface represents a much more complicated system especially when the physical–biological interaction, involving hydrodynamics, adhesion strength and cell deformation is considered. More recently, research has been directed towards the interface of biology and material science for the study of interaction between cells and substrates under physiologically relevant shear stress conditions [20–23]. Furthermore, some dynamic surfaces using self-assembled monolayers have been developed allowing real-time control of the presentation of ligands in order to sequentially release and attach cells to a substrate [24,25].

In the present study, the attachment/detachment behaviour of living cells on modified microchannel surfaces has been studied by exploring the fluidic properties of a microfluidic-based “lab-on-a-chip” system. The microchannel surface was modified using three different surface modification reagents, namely, 3-aminopropyltriethoxysilane (APTES), glutaraldehyde and collagen to enhance cell adhesion. The attachment/detachment of Chinese hamster ovary (CHO) cells to these modified surfaces were investigated. In addition, four other cell types, namely, T47D (breast tumour cells), U937 (human lymphoma cells), CaCo2 (human colon adenocarcinoma epithelial cells) and NCTC 2544 (keratinocytes cells), were also examined using a silanized channel surface. The deformation of cells under shear stress within microfluidic channels was also studied. A theoretical model for fitting the experimental data has been developed by taking account of shear stresses and the contribution from both surface adhesion bonds and cells deformability.

2. Experimental

2.1. Microfluidic chip fabrication

The microchip was fabricated according to published procedures [26,27] with minor adaptations. Briefly, the channel network was fabricated based on a photolithographic fabrication method. The channel network was designed using AutoCAD LT 2005 drawing software (Autodesk, Farnborough GU14 6FG,

UK). A film negative of the desired final size was then prepared by a commercial photo mask manufacturer (J.D. Photo Tools, Oldham OL8 1EZ, UK) to form the optical mask. B-270 glass photolithographic plates (thickness of 3 mm) coated with a thin chromium metal mask layer plus an upper layer of positive photoresist, supplied by Telic (Telic Company, Valencia, CA 91355, USA), were used for channel network fabrication. With UV exposure, the pattern of interconnecting channels was transferred from the optical mask to the photoresist layer which was then developed and removed, together with the chromium layer, to reveal the channel areas of glass to be etched. The channels were etched by using a mixture of 1% (w/w) HF and 5% (w/w) NH_4F in water at 65°C for 20 min, resulting in an etch channel network with a depth of $60\ \mu\text{m}$.

A base plate containing the etched channel network was sealed by bonding to an upper plate (also 3 mm thick) containing predrilled holes (diameter 1.5 mm) in order to link the ends of the channels with external tubing. The upper plate was aligned with the channel geometry and thermally bonded to the base plate by heating in a conventional furnace at a temperature of 575°C for 3 h. Thermal bonding was aided by placing a 90 g block of stainless steel on the upper plate. After bonding, ETFE (ethylene tetrafluoroethylene) polymer tubing with an inner diameter of $250\ \mu\text{m}$ was inserted into the drilled holes on the top plate and epoxy glue was used to secure the joint. On–off valves were connected to the other end of the tubing. The ETFE tubing (P/N. 1529) and on–off valves (P/N. P-782) were obtained from Upchurch (Upchurch Scientific Inc., Oak Harbor, WA, USA).

Fig. 1 shows the chip setup and configuration used, which consists of a double-T network with two inlet channels and two outlet channels. The geometry of the channel network is shown in the micrograph (Fig. 1b). The depth for all the channels was $60\ \mu\text{m}$.

2.2. Microchannel surface modification

The presence of surface modification to assist in the immobilisation of cells was located in a specific area in the microchannel

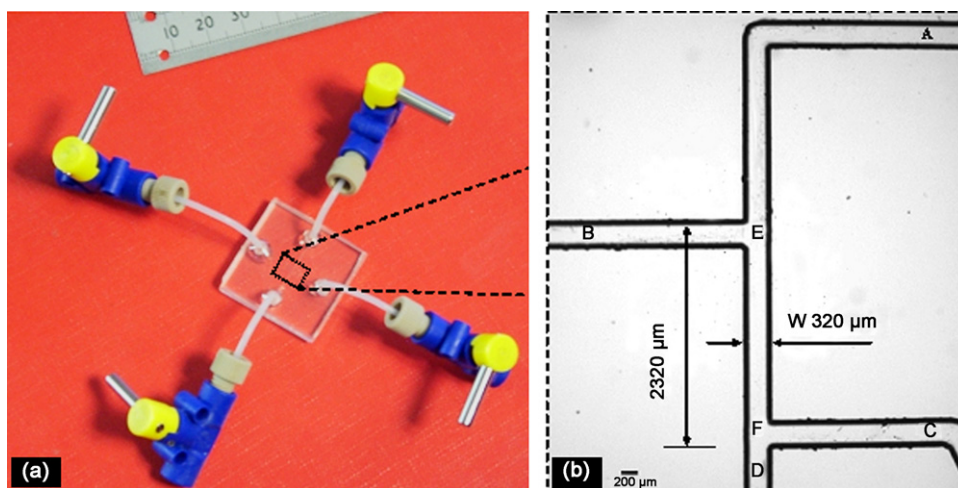


Fig. 1. (a) Glass chip with tubing and on–off valves and (b) outline of channel network.

between points E and F (Fig. 1b). Three modification agents were used, 3-aminopropyltriethoxysilane (APTES), glutaraldehyde and collagen. In order to modify the selected channel area on the chip, the modification reagent was directed from B to C while channels A and D were closed. This flow pattern allows only the channel section between junctions E and F along the main channel to be modified.

2.2.1. Silane coating

To silanize the selected area on the microchannel surface, a solution of 10% (v/v) 3-aminopropyltriethoxysilane or APTS (99%, Sigma–Aldrich Company Ltd., Dorset SP8 4XT, UK) in ethanol was infused across the channel B–C at a flow rate of $10 \mu\text{L min}^{-1}$ for 30 min. The microchannels were then rinsed by continuously flowing 60% ethanol followed by DI water, both at a flow rate of $5 \mu\text{L min}^{-1}$ for 30 min. The channel network was then dried by blowing N_2 through.

2.2.2. Glutaraldehyde coating

Following the silanization step, a second layer of glutaraldehyde was coated which was obtained from Sigma–Aldrich as 50 wt.% solution in water. To perform the coating, 6% (v/v) glutaraldehyde solution in 0.01 M phosphate-buffered saline (PBS, with 0.0027 M potassium chloride, 0.137 M sodium chloride, pH 7.4, Fluka) was infused at a flow rate of $5 \mu\text{L min}^{-1}$ for 1 h across the selected microchannel section between junctions E and F along the main channel (Fig. 1b). The microchannels were then washed by continuously flowing 60% ethanol at a flow rate of $5 \mu\text{L min}^{-1}$ for 30 min. The channel network was then dried by blowing N_2 through.

2.2.3. Collagen coating

Following the silanization and glutaraldehyde coating steps, a collagen coating was performed on the top of the previous coatings. The agent was prepared by dissolving 1.0 mg collagen, type I from calf skin supplied by Sigma–Aldrich, in 1 mL acetic acid (0.1N) at room temperature, followed by adjusting pH to 8.3 with 0.1N NaOH. After the solution was filtered through a $0.2 \mu\text{m}$ filter, it was infused across the selected area within the microchannel network at a flow rate of $15 \mu\text{L min}^{-1}$ for 30 min. The channel was then washed by continuously flowing PBS buffer at a flow rate of $5 \mu\text{L min}^{-1}$ for 30 min. The channel network was then dried by blowing N_2 through.

2.3. Cell culture

CHO-K1 (Chinese Hamster Ovary, *Cricetulus griseus*) cells were supplied by ATCC/LGC Promochem (ATCC[®] No. CCL-61[™], LGC Promochem, Middlesex TW11 0LY, UK). T47D, U937, CaCo2 and NCTC 2544 cells were obtained from the Medical Research Laboratory of the University of Hull. All cells were cultured in DMEM/F-12 medium (Cat. No. 21331-020, Invitrogen Ltd., Paisley PA4 9RF, UK) with a minor modification for each cell type according to the published procedures [15,28–31], respectively. A humidified incubator was used at

37°C supplying 5% CO_2 in air. The concentration of cells used in this experiment was in the range of 7.5×10^6 cells mL^{-1} .

2.4. Instrumentation, image analysis and experimental procedures

Two KDS 200 syringe pumps (KD Scientific Inc., Holliston, MA 01746, USA) were used to deliver cells in suspension and carrier media. ETFE polymer tubing, on–off valves, and appropriate fittings and connectors were all obtained from Upchurch (Upchurch Scientific Inc., Oak Harbor, WA, USA). The viscosity of the media was measured using a modified Ubbelohde viscometer tube. All the measurements were carried out at room temperature.

An Axiovert S100 inverted microscope (Carl Zeiss, Hertfordshire AL7 1JQ, UK) using both transmission and fluorescent optics coupled with a monochrome CCD digital camera (C4742-95-12NRB, Hamamatsu Photonics, Hertfordshire AL7 1BW, UK) was used to obtain both conventional micrographs and digital videos of the microchip. AQM Hamamatsu ORCA I software (Kinetic Imaging, Nottingham NG8 6PE, UK) was used for image acquisition and analysis.

To deliver cells to the selectively modified area, channel surface between junctions E and F (Fig. 1b), cells in suspension were injected from inlet B to outlet C while channels A and D were closed. Following the infusion of cells into the chip all channels were closed in order to allow the cells settle down over a 30 min period without fluidic disturbance. To measure the cell detachment from the channel surface, the carrier media was introduced from channel A to D while channels B and C remained closed. The flow rate was incrementally increased, i.e., 1, 2, 5, $10 \mu\text{L min}^{-1}$, and after each adjustment of the flow rate, an additional running period of 2 min was given to allow the chip to equilibrate at the programmed flow rate.

At each of the flow rates used two snap images covering the selected area were taken and subsequently analysed. The cell detachment was calculated as a percentage of cells removed from the surface as a result of the induced shear force. After a series of images had been acquired, the cells were counted for the selected area on the channel surface. The extent of cell detachment from the channel surface was calculated as a percentage of the initial cell number (Eq. (1))

$$\text{detachment}(\%) = \frac{\text{initial cell number} - \text{remaining cell number}}{\text{initial cell number}} \times 100 \quad (1)$$

3. Results and discussion

3.1. Effects of surface modification on cell attachment/detachment under shear stress

Shear stresses are generally measured as the ratio of the shearing force to the area over which it acts. For the etched channels which have an approximately rectangular cross-section [27], the

Table 1
Summary of experimental conditions and corresponding shear stresses

Fluid viscosity, μ (dyn s cm ⁻²)	0.01045
Channel depth, h (cm)	0.006
Channel width, w (cm)	0.032
Flow rate, Q (μ L min ⁻¹)	Shear stress, τ (dyn cm ⁻²)
0	0
1	0.9
5	4.5
10	9.1
20	18.1
60	54.4
90	81.6
110	99.8
150	136.1
190	172.4
230	208.6
290	263.1
350	317.5

wall shear stress under laminar flow conditions is calculated as [14,32,33]

$$\tau = \frac{6\mu Q}{wd^2} \quad (2)$$

where τ is the shear stress in dyn cm⁻², μ the fluid viscosity in dyn s cm⁻² or P, Q the volumetric flow rate in cm³ s⁻¹ and w and d are the channel width and depth in cm, respectively. Table 1 summarizes the experimental conditions and corresponding shear stresses calculated using Eq. (2).

Fig. 2 shows the detachment of CHO cells as a function of shear stress for an unmodified and three modified channel surfaces. The results showed that all the modified surface resulted in a significant retention of cells, compared to the unmodified surface. It can be seen that, in general, with an increase in shear stress, induced by increasing flow rate, more cells were detached from the channel surface. However, when the shear stress was increased above a certain point the detachment tended to reach

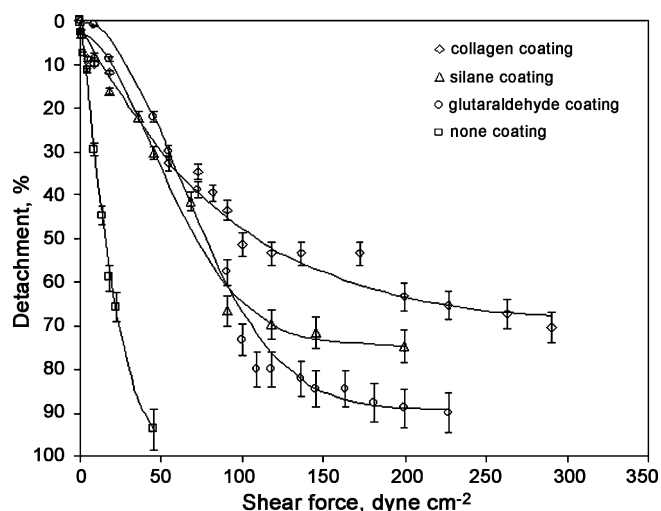


Fig. 2. Detachment percentage of CHO cells from the four types of modified microchannel surface as a function of shear stress. The solid curves are calculation results based on the theoretical model, and the error bars show a 95% confidence.

a stable level indicating that the remaining cells attached to the surface in a firm manner. More details will be discussed in later sections in order to understand further about this observed trend. It was also found that surfaces modified by collagen provided the strongest attachment.

Generally, any forces between the cell surface and the channel surface can contribute to the attachment/detachment of cells, including hydrodynamic viscous forces, electrostatic affinity, chemical bonds and/or biological complex binding. In the silanization process with APTES, it has been reported that the chemical reaction between the glass surface and the silanization reagent allows amino groups to link by covalent bonds to the silicon atoms of the glass [10], and will leave the glass surface positively charged. Since the surface of cells is generally charged negatively, the electrostatic force can enhance the adhesion of cells to the positively charged channel surface.

Glutaraldehyde has been commonly used to fix cells whilst preserving their original shape and rendering them rigid [34]. This approach has been used notably for blood cells [35,36]. It has also been used as a pre-treatment for substrate surface to facilitate further modification [15]. It has been reported that the cell fixation process can result in an increase in cell's adhesion to the substrate [37]. In this study, glutaraldehyde was used to modify the channel instead of the cells' surface. The results (Fig. 2) confirm the enhancement of cell adhesion, although its mechanism remains unclear while some explanation has been proposed. Burks has found differences in zeta potentials of bacteria following glutaraldehyde treatment [35]. Brown et al. [37] found that glutaraldehyde caused yeast cells to become more hydrophobic. It is generally accepted however that glutaraldehyde can stiffen cells by cross-linking proteins and amino acids in the peptidoglycan layer [38].

Collagen is present as a major component of the extracellular matrix in many tissues and can influence cell proliferation, differentiation and migration [39]. Although the effects from collagen on cell behaviour are not fully understood, it is clear that it can be used to enhance the attachment contact or properties of cell with surface. Based on the biochemistry of collagen, the collagen monomer, tropocollagen, is a rigid rod-shaped molecule consisting of three polypeptide chains (α -chains) wound around each other to form a triple helix [40]. It is this particular structure that plays a big part interacting with the receptors on the cell surface, affecting cell surface glycosyltransferases, and influencing the mobility of proteins in the plane of the membrane [39].

To detach a cell from the surface by a fluid flow, a certain level of input fluid energy is required and distributed for two purposes (a) to overcome the hydrodynamic viscous resistance and (b) break adhesion bonds on the cell–substrate interface [13]. The hydrodynamic resistance can be generally treated in a similar way as for rigid, non-biological particles in fluidics. In contrast, the binding system on the cell–substrate interface is more complicated, as discussed above, which strongly depends on the cell's biological behaviour and activities in addition to their physical properties. Based on these assumptions, a simplified mathematical model has been used

$$P = P_{\max} - (P_{\max} - P_0) e^{-(\tau/a)^b} \quad (3)$$

Table 2

Four parameters obtained by best-fitting the experimental data into the model for CHO cells on four types of surfaces

	P_{\max}	P_0	a	b
Collagen coating	70.17	1.44	89.13	1.05
Silane coating	74.83	2.96	68.87	1.80
Glutaraldehyde coating	89.24	0.12	85.05	2.01
No coating	101.25	0.02	21.02	1.25

where τ is the shear stress in dyn cm^{-2} , P_{\max} the highest level of percentage detachment when high shear stresses are applied, P_0 the initial percentage detachment when the flow starts (being 0 in most cases). a provides a reference shear stress scale and b , the exponent reflects a threshold for cell removal which is a combination of contribution from cell–substrate affinity, cells deformability and hydrodynamic viscous affect. The four parameters have been obtained by best-fitting the experimental data, and are summarized in Table 2.

It is generally assumed that particles are “washed off” surfaces as fluid flow rates are increased because the hydrodynamic force can weaken the adhesion/attachment. This is indeed true for most of rigid mechanical particles. However, for a range of biological cells it has been reported that a threshold of fluid shear stress is required to sustain cell rolling on a substrate surface [41,42] and a maximum cell attachment is obtained. This has been mainly attributed to the chemical and/or biological bonds between the surfaces, and the deformation of cells which enlarges the cell–substrate contact area. In this study, an induction range was also observed, especially for cells with glutaraldehyde-coated surface (Fig. 2), indicating that cells were detached at a relatively low rate in the lower shear stress range. This effect is reflected on the b value in the model (Eq. (3)); a greater b value is an indication that a higher threshold is required.

3.2. Comparison of different cell types under shear stresses

It has been shown that all of the three surface modification agents investigated in this study can significantly enhance the attachment of CHO cells to the microchannel surface with collagen providing the strongest attachment. However as silanization proved to be the simplest surface modification method, in practice, it was used in this part of the work to study the attachment/detachment of a further four types of human cells, of general interest in biomedical research. The measured detachments of cells as a function of shear stress are depicted in Fig. 3. The calculated results based on the model (Eq. (3)) are also shown as the solid curves. By best-fitting into the experimental data the values of the four parameters in the model were determined and are summarised in Table 3.

It was observed that T47D cells from human breast tumours showed the strongest attachment to the channel surface whilst, in contrast, U937 human blood lymphoma cells appeared to be non-adherent with a lowest threshold. These results are in line with the general observation where breast cancer cells T47D are very adherent and tend to spread and attach to other tissues [43], whilst untreated monocytic U937 cells are unable to

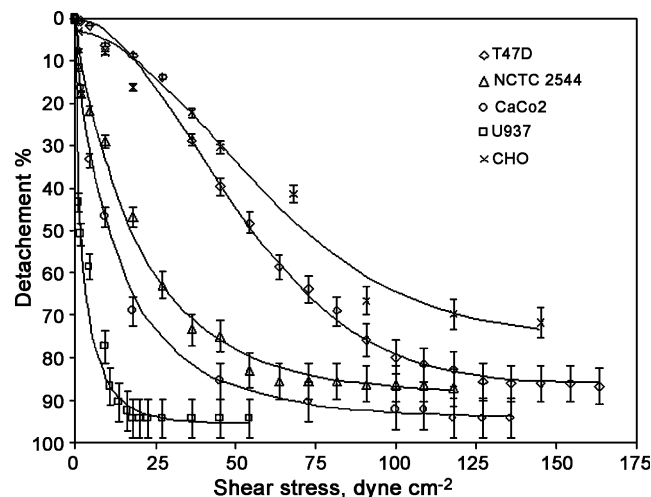


Fig. 3. Detachment percentage of five cell types on silanized microchannel surface as a function of shear stress. The solid curves are calculation results based on the theoretical model, and the error bars show a 95% confidence.

Table 3

Four parameters obtained by best-fitting the experimental data into the model for four cell types (in addition to CHO cell) on silanized channel surface

	P_{\max}	P_0	a	b
T47D	86.00	0.01	59.64	1.81
NCTC 2544	88.66	0.09	21.43	0.88
CaCo2	94.01	0.00	14.65	0.77
U937	95.54	0.00	2.78	0.64

adhere to glass surfaces [44,45]. The human colon adenocarcinoma epithelial cells CaCo2 and skin-derived keratinocytes cells NCTC 2544 also showed some degree of adherence.

3.3. Cell deformation under shear stresses within microchannels

As discussed above, in addition to effects from cell–surface adhesion (chemically, or biologically) and hydrodynamic viscous factors, the deformation of cells under shear stresses is also important in the attachment/detachment process as it may lead to artifacts associated with cell differential. Fig. 4 shows a series of snap images for a single CHO cell within a microchannel under different conditions. It can be seen that the cell tended to spread on the surface after a period of settling down (Fig. 4b) and that the contact area with the surface increased. With a low shear stress applied (Fig. 4c), the contact area was enlarged further, and an increase in shear stress enhanced the cell deformation more significantly (Fig. 4d). After the flow was stopped the deformation recovered remarkably quickly (Fig. 4e).

Clearly, under shear stresses in a certain range, the cell appeared to be more “flat” to the surface aligning along in the direction of flow, decreasing the encountering cross-section area in both dimensions. Consequently, this deformation can reduce the fluid energy to the cell because a flattened cell will influence less disturbances to the flow and hence smaller shear stresses on the cell surface. In addition, the cell deformation can result in a larger contact area between the cell and the substrate surface.

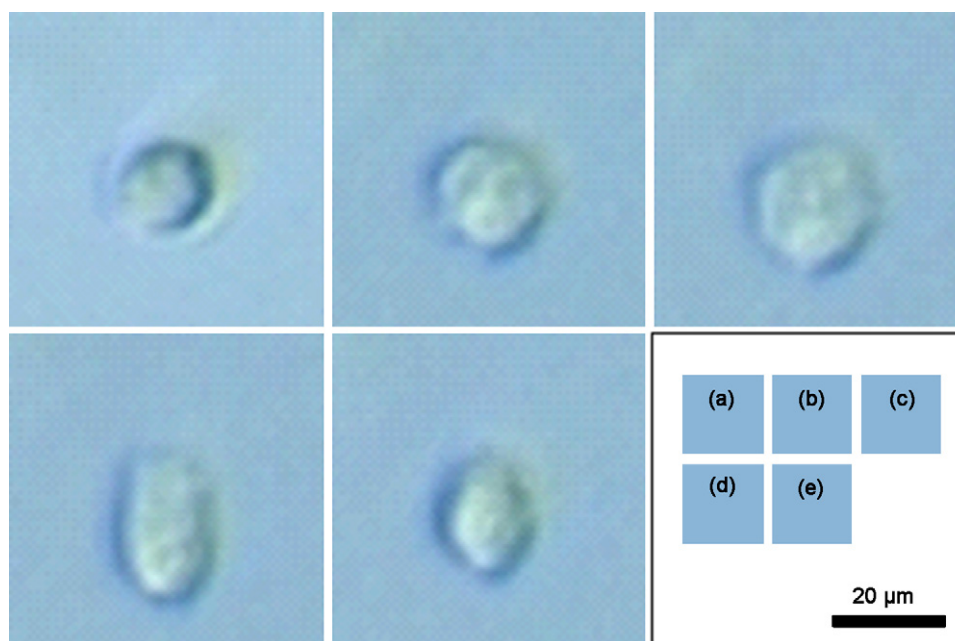


Fig. 4. Micrographs of a single CHO cell within a microchannel under different flow conditions. (a) The cell was delivered to position by injection flow, (b) followed by a 40 min settling, then subject to (c) a low shear stress of 11 dyn cm^{-2} and (d) a high shear stress of 274 dyn cm^{-2} by flowing in the media, and finally (e) the shear stress was released by stopping the flow.

It has been found that the contact area between the cell and the substrate could be nearly doubled under high wall shear stresses [13]. As a result, a higher shear stress was required to detach the cell from the surface. The observation of cell deformation under flow conditions can significantly contribute to the explanation for the existence of the threshold of shear stress to detach cells from surfaces. As can be seen from Fig. 5, that when encountering cross-section area with flow decreased, the contact area or adherent bonds (Fig. 5b) with substrate increased, so requiring more energy to detach the cell from the substrate surface.

It was also interesting to note that the cell recovered remarkably well from deformation when the shear stress was released which is probably due to the general surface effect where the cell tends to keep spherical due to its surface tension. It should be noted however that biochemical responses to shear stresses cannot be excluded. Frangos et al. reported that some cell functions may be modulated by membrane stresses induced by such artifacts as blood flow [46]. In addition, a recent investigation on the influence of hydrodynamic conditions on CHO cells activity in a microfluidic system found that a shear stress of 3.1 dyn cm^{-2} can cause a detectable fluorescence signal to be generated associated with intracellular Ca^{2+} transition within cells [47]. Clearly,

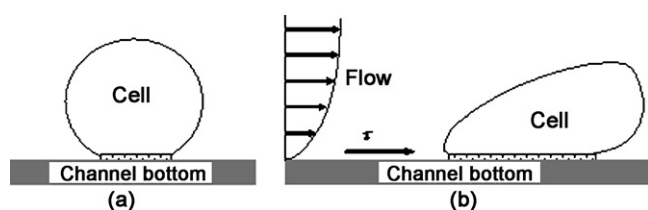


Fig. 5. Schematic of the cross-section of cells (a) attached on the surface of the microchannel bottom and (b) subject to a shear stress caused by the laminar flow.

to distinguish active actions from passive effects on the process of cell's deformation and its recovery, more investigation is required.

4. Conclusions

The behaviour of attachment/detachment of living cells on modified microfluidic channel surfaces has been studied in a “lab-on-a-chip” system for a range of cells with surfaces modified using different methods. The attachment was performed by modification of the microchannel surface using three different surface modification reagents, namely, 3-aminopropyltriethoxysilane (APTES), glutaraldehyde and collagen. It was found that surfaces modified by collagen provided the strongest attachment for CHO cells whilst the silanization was the simplest method to use practically. The detachment of other four types of cells, namely, T47D, U937, CaCo2 and NCTC 2544 cells, were also examined on a silanized channel surface. The observation of cell deformation suggested that the application of a shear stress in a certain range could enhance the cell adhesion to the surface mainly due to the enlargement of contact area between cells and the microchannel surface. A theoretical model for fitting the measured detachment data has been developed by taking account of shear stresses and the contribution from both surface adhesion bonds and hydrodynamic viscous stresses. It was demonstrated that the microfluidic system provided an easy and controllable approach to examine the attachment/detachment of a range of cells on different surfaces.

Acknowledgements

We thank Ms. Huguette Savoie of the Department of Chemistry at the University of Hull for help with the cell culture.

The Medical Research Laboratory of the University of Hull is acknowledged for providing the cells.

References

- [1] P.S. Dittrich, K. Tachikawa, A. Manz, *Anal. Chem.* 78 (2006) 3887–3907.
- [2] H. Andersson, A. van den Berg, *Lab Chip* 6 (2006) 467–470.
- [3] D. Huh, W. Gu, Y. Kamotani, J.B. Grothberg, S. Takayama, *Physiol. Meas.* 26 (2005) R73–R98.
- [4] K.F. Jensen, J. Han, D.J. Harrison, J. Voldman (Eds.), *Proceedings of the Ninth International Conference on Miniaturized Systems for Chemistry and Life Sciences (μ TAS 2005)*, October 9–13, Boston, MA, USA, 2005.
- [5] P.D.I. Fletcher, S.J. Haswell, X. Zhang, *Electrophoresis* 24 (2003) 3239–3245.
- [6] P.D.I. Fletcher, S.J. Haswell, E. Pombo-Villar, B.H. Warrington, P. Watts, S.Y.F. Wong, X. Zhang, *Tetrahedron* 58 (2002) 4735–4757.
- [7] A. Manz, H. Becker (Eds.), *Microsystem Technology in Chemistry and Life Sciences*, Springer, Berlin, 1998.
- [8] P.D.I. Fletcher, S.J. Haswell, X. Zhang, *Lab Chip* 2 (2002) 102–112.
- [9] X. Zhang, J.M. Cooper, P.B. Monaghan, S.J. Haswell, *Lab Chip* 6 (2006) 561–566.
- [10] J. Kiernan, *Microsc. Today* 7 (1999) 20–24.
- [11] R.I. Freshney, *Culture of Animal Cells: A Manual of Basic Technique*, 3rd ed., Wiley-Liss, New York, 1994, pp. 153–157.
- [12] J.A. McAteer, W.H.J. Douglas, *Monolayer cell culture techniques*, in: W.B. Jakoby, I.H. Pastan (Eds.), *Methods in Enzymology*, vol. 58: Cell Culture, Academic Press, New York, 1979, pp. 132–140.
- [13] C. Dong, X.X. Lei, *J. Biomech.* 33 (2000) 35–43.
- [14] C.R. Jacobs, C.E. Yellowley, B.R. Davis, Z. Zhou, J.M. Cimbala, H.J. Donahue, *J. Biomech.* 31 (1998) 969–976.
- [15] B.J. Kirby, A.R. Wheeler, R.N. Zare, J.A. Fruetel, T.J. Shepodd, *Lab Chip* 3 (2003) 5–10.
- [16] H. Lu, L.Y. Koo, W.M. Wang, D.A. Lauffenburger, L.G. Griffith, K.F. Jensen, *Anal. Chem.* 76 (2004) 5257–5264.
- [17] R. Shalak, P.R. Zarda, K.-M. Jan, S. Chien, *Biophys. J.* 35 (1981) 771–781.
- [18] G.I. Bell, M. Dembo, P. Bongrand, *Biophys. J.* 45 (1984) 1051–1064.
- [19] C. Zhu, *J. Biomech.* 33 (2000) 23–33.
- [20] C. Dong, M. Slattery, S.L. Liang, *Front. Biosci.* 10 (2005) 379–384.
- [21] E. Decave, D. Rieu, J. Dalous, S. Fache, Y. Brechet, B. Fourcade, M. Satre, F. Bruckert, *J. Cell Sci.* 116 (2003) 4331–4343.
- [22] L.G. Braddon, D. Karoyli, D.G. Harrison, R.M. Nerem, *Tissue Eng.* 8 (2002) 695–708.
- [23] H.G. Craighead, C.D. James, A.M.P. Turner, *Curr. Opin. Solid State Mater. Sci.* 5 (2001) 177–184.
- [24] W.-S. Yeo, M.N. Yousaf, M. Mrksich, *J. Am. Chem. Soc.* 125 (2003) 14994–14995.
- [25] T. Shimizu, M. Yamato, A. Kikuchi, T. Okano, *Biomaterials* 24 (2003) 2309–2316.
- [26] T. McCreedy, *Anal. Chim. Acta* 427 (2001) 39–43.
- [27] I. Broadwell, P.D.I. Fletcher, S.J. Haswell, T. McCreedy, X. Zhang, *Lab Chip* 1 (2001) 66–71.
- [28] K.-H. Nam, W.-J. Chang, H. Hong, S.-M. Lim, D.-I. Kim, Y.-M. Koo, *Biomed. Microdev.* 7 (2005) 189–195.
- [29] S. Hardy, G.G. St-Onge, É. Joly, Y. Langelier, M. Prentki, *J. Biol. Chem.* 280 (2005) 13285–13291.
- [30] T. Sergen-Engelen, V. Delistrie, Y.J. Schneider, *Biochem. Pharmacol.* 46 (1993) 1393–1401.
- [31] L. Lo Muzio, G. Pannone, S. Staibano, M.D. Mignogna, R. Serpico, S. Fanali, G. De Rosa, A. Piattelli, M.A. Mariggio, *Oral Oncol.* 38 (2002) 64–72.
- [32] T.W. Schneider, H.M. Schessler, K.M. Shaffer, J.M. Dumm, L.A. Younce, *Biomed. Microdev.* 3:4 (2001) 315–322.
- [33] K.M. Ainslie, J.S. Garanich, R.O. Dull, J.M. Tarbell, *J. Appl. Physiol.* 98 (2005) 242–249.
- [34] Ph. Lavalle, J.-F. Stoltz, B. Senger, J.-C. Voegel, P. Schaaf, *Proc. Natl. Acad. Sci.* 93 (1996) 15136–15140.
- [35] G.A. Burks, S.B. Velegol, E. Paramonova, B.E. Lindenmuth, J.D. Feick, B.E. Logan, *Langmuir* 19 (2003) 2366–2371.
- [36] G. Kampf, R. Blob, H. Martiny, *J. Hosp. Infect.* 57 (2004) 137–143.
- [37] W.R. Brown, R.W. Lovitt, C.J. Wright, *J. Colloid Interf. Sci.* 237 (2001) 54–61.
- [38] D. Hopwood, *Histochem. J.* 4 (1972) 267–303.
- [39] S.L. Schor, J. Court, *J. Cell Sci.* 38 (1979) 267–281.
- [40] M. Grant, D.S. Jackson, *Essays Biochem.* 12 (1976) 77–113.
- [41] E.B. Finger, K.D. Puri, R. Alon, M.B. Lawrence, U.H. von Andrian, T.A. Springer, *Nature* 379 (1996) 266–269.
- [42] M.B. Lawrence, G.S. Kansas, E.J. Kunkel, K. Ley, *J. Cell Biol.* 136 (1997) 717–727.
- [43] A. Lostumbo, D. Mehta, S. Setty, R. Nunez, *Exp. Mol. Pathol.* 80 (2006) 46–53.
- [44] M.C. Shepherd, G.S. Baillie, D.I. Stirling, M.D. Houslay, *Brit. J. Pharmacol.* 142 (2004) 339–351.
- [45] F. Monczor, N. Fernandez, E. Riveiro, A. Mladovan, A. Baldi, C. Shayo, C. Davio, *Biochem. Pharmacol.* 71 (2006) 1219–1228.
- [46] J.A. Frangos, S.G. Eskin, L.V. McIntire, C.L. Ives, *Science* 227 (1985) 1477–1479.
- [47] H. Yin, X. Zhang, N. Patrick, N. Klauke, H.C. Cordingley, S.J. Haswell, J.M. Cooper, *Anal. Chem.*, in press.

Development of a microfluidic device for the maintenance and interrogation of viable tissue biopsies†

Samantha M. Hattersley,^{a,b} Charlotte E. Dyer,^b John Greenman^b and Stephen J. Haswell^a

Received 2nd June 2008, Accepted 19th August 2008

First published as an Advance Article on the web 1st October 2008

DOI: 10.1039/b809345h

A microfluidic based experimental methodology has been developed that offers a biomimetic microenvironment in which pseudo *in vivo* tissue studies can be carried out under *in vitro* conditions. Using this innovative technique, which utilizes the inherent advantages of microfluidic technology, liver tissue has been kept in a viable and functional state for over 70 h during which time on-chip cell lysis has been repeatedly performed. Tissue samples were also disaggregated *in situ* on-chip into individual primary cells, using a collagenase digestion procedure, enabling further cell analysis to be carried out off-line. It is anticipated that this methodology will have a wide impact on biological and clinical research in fields such as cancer prognosis and treatment, drug development and toxicity, as well as enabling better fundamental research into tissue/cell processes.

Introduction

Traditional *in vitro* tissue culture as a model of human disease represents a poor substitute for the *in vivo* environment,¹ often leading to experimental artifacts associated with the handling and or the presence of adverse culture conditions.^{2,3} For example, conventional tissue culture methods typically supply nutrients and growth factors in batches, which then decrease as metabolism occurs leading to a build-up of waste products. Hence, the levels of nutrients and waste products vary considerably in conventional culture methods, which contrasts with the tightly regulated homeostatic systems *in vivo*.^{4–6} Under normal physiological conditions the flow within vascular capillaries and tissues is known to have Reynolds numbers < 100, resulting in predominantly diffusion based characteristics, over spatial distances of approximately 100 μm ,^{6,7} within which cellular metabolite uptake, gaseous exchange and waste removal occurs.⁸

Given that the flow and spatial parameters which exist in tissue are very similar to those of the microfluidic environment, the opportunity to carry out continuous perfusion of tissue samples^{8,9} would seem to offer a more attractive experimental approach than is currently possible using the turbulent fluidic conditions present in a standard batch culture system.¹⁰ The benefits of microfluidic techniques for cell/tissue culture that have been demonstrated previously include laminar flow conditions, small length scales, large surface to volume ratios, diffusion dominant

transport, portability, reusability or disposability and reduced cost.^{11,12} In addition, by exploiting the flow conditions present in a microfluidic device, unprecedented spatial and temporal control over materials entering and leaving an experimental system can be achieved.^{13,14} Accordingly the ability to place a viable tissue biopsy in a microfluidic device could offer the opportunity to control, probe and monitor complex cell functions in diseased and healthy tissue whilst maintaining *in vivo* architecture.^{12,15–17}

The use of microfluidic devices to create tissue-like 3D micro-architectures from cells has already attracted some interest and have included: hepatocyte arrays, which mimic physiological liver mass transport,¹⁸ cardiac tissue-like structure with anisotropic properties,¹⁹ modeling of the alveolo-pulmonary barrier²⁰ and multicellular spheroids established from several different cell lines.²¹ In addition, agglomerations of different established cell lines^{22,23} have also been used to create tissue-like constructs in which fibroblasts and hepatocytes are combined in a gel and allowed to proliferate in a microfluidic chamber for up to 24 h.²⁴ The encapsulation of AML-12 murine hepatocytes in agarose hydrogel through which a microfluidic channel has been formed has also been used to create a synthetic tissue construct.⁷

The culture of *ex vivo* tissue in microfluidic devices has, however, been far less well documented and is currently restricted to brain tissue using either a hollow SU-8 microneedle system²⁵ to perfuse 400 μm hippocampal rat brain tissue or a three-layer polydimethylsiloxane (PDMS) device incorporating medullary brain slices from neonatal rats.²⁶ Using these approaches cell viability was found to be lost after 4 h at 36 °C in the case of the SU-8 device, and 3 h in the PDMS system.

In this paper, we describe an innovative approach to study tissue which exploits the benefits of the microfluidic environment to create pseudo *in vivo* conditions *in vitro*.

^aDepartment of Chemistry, University of Hull, Cottingham Road, Hull, HU6 7RX, UK. E-mail: s.j.haswell@hull.ac.uk; Tel: 441482465469

^bPostgraduate Medical Institute, University of Hull, Cottingham Road, Hull, HU6 7RX, UK. E-mail: j.greenman@hull.ac.uk; Fax: 441482466032; Tel: 44 1482466996

† In honour of Andreas Manz on his retirement as Chair of the *Lab on a Chip* Editorial Board.

Experimental

Microfluidic set-up

The microfluidic device was fabricated from glass using photolithographic and wet etching techniques.²⁷ The overall device (Fig. 1) consisted of two thermally bonded glass layers of 1 mm (base layer) and 3 mm (top layer) thickness.

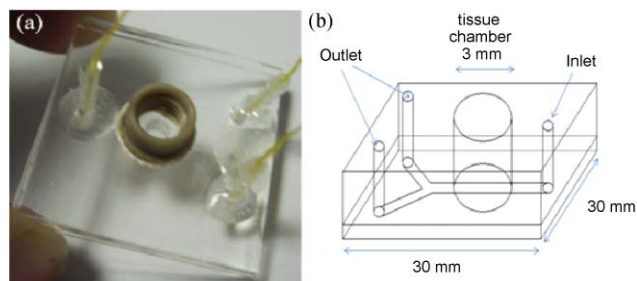


Fig. 1 Microfluidic device used for maintaining and probing tissue samples. (a) Photograph showing the open microport and connecting tubing in place and (b) schematic of device.

The top layer included a 3 mm diameter hole into which a tissue sample was placed and three 1.5 mm diameter inlets into which tubing was connected, one for the medium/reagent inlet and two for medium/reagent outlet. These were drilled using traditional glass drilling techniques. A microport fitting (Anachem, UK) was attached to the surface of the top glass layer such that the circular tissue cavity could be sealed using an English threaded adapter (Anachem, UK). The adapter was filled with PDMS (Dow Corning, UK) to allow gaseous exchange to occur.²⁸ The channel network was etched into the bottom glass layer to produce channels of 190 μm width and 70 μm depth and featured two outlet channels to aid post-tissue flow. A Baby Bee syringe pump (Bioanalytical Systems Inc., UK) was connected to the device *via* 1/16" Tefzel tubing (Anachem, UK). The entire system was placed in an incubator at 37 $^{\circ}\text{C}$.

Animal and tissue preparation

A male rat (Wistar, B & K Universal Ltd, UK) was used for all experiments. The animal was fed and watered *ad libitum* until anaesthetized (10 ml kg^{-1} of 10 mM sodium thiopentone, intraperitoneal) and killed under a Schedule 1 procedure prior to liver extraction. The liver was immediately sectioned into pieces approximately 1 cm^3 and placed in 1 ml cryovials (Alpha Laboratories, UK) which were then plunged into liquid nitrogen.

The microfluidic system was sterilized prior to use by pumping 70% (v/v) ethanol/water through the device for 15 min at 10 $\mu\text{l min}^{-1}$ followed by a rinse with autoclaved, distilled water. The device was then primed with Williams Media E (WME) (Gibco, UK) supplemented with 1% (w/v) penicillin/streptomycin (Sigma, UK) at a flow rate of 20 $\mu\text{l min}^{-1}$ and set in a 37 $^{\circ}\text{C}$ incubator. The frozen tissue was removed from the cryovial, cut into approximately 4 mm^3 sized sections, weighed and placed into the tissue cavity pre-filled with medium. The ratio of microfluidic chamber to tissue sample volume was

approximately 1 : 0.8. The cavity was sealed using the threaded adapter and the flow rate reduced to 2 $\mu\text{l min}^{-1}$. A visual check was made to ensure no bubbles were trapped in the chamber; any bubbles observed were removed using a sterile hypodermic needle. The eluent from both outlets of the microfluidic device was collected for a period of 30 min and then combined in 0.5 ml microcentrifuge tubes for analysis.

Analysis

To quantify cell viability a colorimetric cytotoxicity assay (Cytotoxicity Detection Kit Plus, LDH, Roche, UK) was carried out following the manufacturer's protocol with the exception that all test samples were diluted 1 : 10 prior to analysis. The results are expressed as an average determined from triplicate samples.

To assess the functionality of the tissue within the microfluidic device production of albumin and urea was investigated. Albumin levels in the eluent were determined by enzyme-linked immunosorbant assay (ELISA) (Bethyl Laboratories Inc., USA) according to the manufacturer's guidelines. A 96-well flat bottom ELISA plate (SLS, UK) was coated overnight with primary sheep anti-rat albumin antibody diluted in 0.05 M carbonate-bicarbonate buffer, pH 9.6 (Sigma, UK) at 4 $^{\circ}\text{C}$. A wash solution containing 50 mM Tris, 0.14 M NaCl, and 0.05% (v/v) Tween 20, pH 8.0 (Sigma, UK) was used after each step. Plates were subsequently blocked with 50 mM Tris, 0.14 M NaCl, containing 1% (w/v) Bovine Serum Albumin (BSA) pH 8.0 for 30 min at ambient temperature. The rat serum reference standards were diluted in 50 mM Tris, 0.14 M NaCl and 0.05% (v/v) Tween 20, pH 8.0 and incubated on the plate with eluent samples for 1 h. Next, the plates were incubated with Horse Radish Peroxidase-conjugated detection antibody 1 : 5000 in 50 mM Tris, 0.14 M NaCl and 0.05% (v/v) Tween 20, pH 8.0 for 1 h. Finally, a colorimetric reaction was carried out by the addition of 50 μl undiluted Tetramethyl benzidine solution (Sigma, UK). The reaction was stopped with 25 μl of 2 M sulfuric acid (Sigma, UK) and the absorbances were measured at $\lambda = 450 \text{ nm}$. Urea concentrations in the media were determined using a colorimetric assay (QuantiChrom™ Urea Assay Kit, BioAssay Systems, USA) carried out following the manufacturer's protocol.

To visualise cell architecture following perfusion for up to 70 h in the microfluidic device the tissue was removed, embedded on a cork tile covered with Tissue-Tek® (Sakura, Netherlands) and plunged immediately in liquid nitrogen cooled 2-methyl butane solution (Sigma, UK). Frozen sections (12 μm thick) were cut using a Microm HM505E cryostat. The samples were fixed with 10% formalin and stained with Hematoxylin and Eosin (H & E).

For the determination of the long term viability of tissue, samples were prepared and placed in the microfluidic device as described above. To induce cell rupture a solution of 10% lysis buffer (Cytotoxicity Detection Kit Plus LDH) was introduced (2 $\mu\text{l min}^{-1}$) for 30 min at 18.5, 21.5 and 24 h; after each exposure WME was re-introduced into the microfluidic system.

To analyze individual primary cells isolated from tissue held within the microfluidic device, the tissue was enzymatically disaggregated. The perfusion method, which was modified from

Bayliss and Skett,²⁹ used Eagle's Balanced Salt Solution (EBSS) (Gibco, UK) in place of WME. EBSS flow was sustained for 5 min at $5 \mu\text{l min}^{-1}$ to flush WME media from the device and the sample was then perfused at $2 \mu\text{l min}^{-1}$ for 20 min with an 8.3 mM solution of ethylene glycol bis-(β -aminoethyl ether) *N,N,N',N'*-tetra acetic acid (EGTA) (Sigma, UK), to chelate extracellular calcium. After EGTA treatment the tissue was perfused with EBSS at $2 \mu\text{l min}^{-1}$ for a further 10 min to remove any chelator, as EGTA is known to inhibit collagenase action. Collagenase (0.48 U ml^{-1}) (Sigma, UK) was dissolved in EBSS (pH 7.4) (2 ml) with the addition of 0.4 mg trypsin inhibitor (Sigma, UK) and 2 mM calcium chloride (Sigma, UK). The tissue was then perfused with this collagenase solution for 2 h at $2 \mu\text{l min}^{-1}$. The perfusate was allowed to drain to waste. Following collagenase treatment the microfluidic device was removed from the incubator while still connected to the perfusate system and set on an ice pack. Ice-cold dispersal buffer containing 10 mM HEPES, 142 mM NaCl, 7 mM KCl, 5% (w/v) BSA in water and adjusted to pH 7.4, $40 \mu\text{g ml}^{-1}$ DNase I and 5 mM magnesium chloride (Sigma, UK) was then perfused through the tissue sample at $500 \mu\text{l min}^{-1}$ for 2 min. The enzymatically disaggregated cells were collected in 1.5 ml micro centrifuge tubes and centrifuged at 100g for 5 min. The supernatant containing cell debris was removed by aspiration. The cells were resuspended in the dispersal buffer containing $40 \mu\text{g ml}^{-1}$ DNase I and 5 mM magnesium chloride by gentle swirling of the tube. Centrifugation was then repeated and a final wash of the cell preparation was repeated in the absence of DNase I and magnesium chloride. The cells were then resuspended in WME (1 ml) and maintained at 4°C . To quantify cell viability equal volumes of 2% (w/v) Trypan Blue (Sigma, UK) and cell solution were mixed and the cell count enumerated using a haemocytometer. Counts were measured in duplicate and the percentage viability determined.

Calcein AM (Molecular Probes, UK) fluorescence ($\lambda_{\text{ex}} = 494 \text{ nm}$, $\lambda_{\text{em}} = 517 \text{ nm}$) and 2.04 mM Lavacell (Active Motif, Belgium) fluorescence ($\lambda_{\text{ex}} = 405, 488 \text{ and } 532 \text{ nm}$, $\lambda_{\text{em}} = 610 \text{ nm}$) were used as a measure of cell function. Non-viable cells were identified by uptake of propidium iodide (PI) (Sigma, UK) ($\lambda_{\text{ex}} = 536 \text{ nm}$, $\lambda_{\text{em}} = 617 \text{ nm}$), which stains the nuclei of cells which have ruptured cell membranes. The *in situ* imaging of tissue was carried out using a laser-scanning inverted confocal microscope (Nikon Eclipse TE2000-E, Nikon) equipped with Helium/Neon and Argon lasers running Lazershop 2000 software. When interrogating tissue with fluorescent probes, $10 \mu\text{M}$ calcein AM was first perfused through the system ($2 \mu\text{l min}^{-1}$ for 40 min) followed by a ten minute flush with EBSS, after which 3.75 mM PI was pumped through the device ($2 \mu\text{l min}^{-1}$ for 10 min). Finally a further EBSS wash of the tissue was carried out prior to image collection.

A Quant-iTTM PicoGreen[®] dsDNA Assay Kit (Invitrogen, UK) was used to monitor DNA release from tissue samples. PicoGreen[®] ($\lambda_{\text{ex}} = 485 \text{ nm}$, $\lambda_{\text{em}} = 538 \text{ nm}$) was diluted 1 in 400 in $1\times$ Tris EDTA buffer and $50 \mu\text{l}$ was added to $2 \mu\text{l}$ of the tissue media and then fluorescence intensity was measured using a FLUOstar OPTIMATM plate reader. DNA standards, 10, 5, 2.5, 1.25, 0.625 and $0.312 \text{ ng } \mu\text{l}^{-1}$ were used to generate a calibration curve. Medium rather than tissue supernatant was used to determine the level of background fluorescence.

Results and discussion

Establishing on-chip tissue viability and functionality

H & E staining shows retention of normal tissue architecture and fluorescence imaging using LavacellTM shows cell viability (Fig. 2). The ability of the tissue biopsy to continue to produce both albumin and urea (Fig. 3) demonstrated that the fluidic properties and geometric size of a microfluidic device are adequate for maintaining tissue viability and function, for at least 70 h.

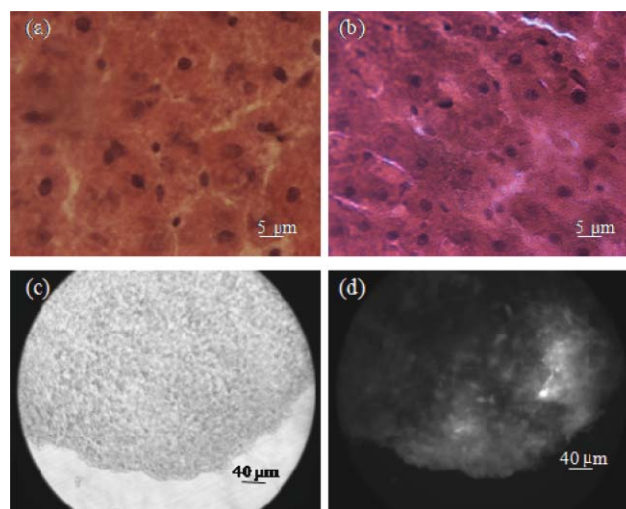


Fig. 2 H & E stained cryostat section of tissue before culture in the microfluidic device (a) and after 71 h (b) using $40\times$ magnification. Brightfield (c) and epi-fluorescence images (d) of rat liver tissue, after incubation with LavacellTM, following maintenance in a microfluidic device for 53 h; showing the edge of the tissue distinguished from background. A $10\times$ objective was used.

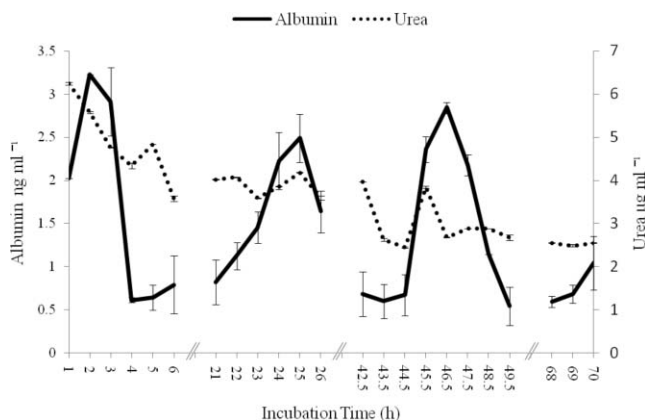


Fig. 3 Albumin and urea synthesis within a microfluidic device per mg of liver tissue. Albumin concentration is represented by the continuous line and urea levels by the dashed line. Breaks in lines signify periods when samples were not collected and analysed. The mean of replicate experiments is plotted.

Histomorphology was analysed before and after tissue culture in the microfluidic device. The fresh-frozen sections were stained with H & E to visualize changes within the tissue architecture

(Fig. 2). Tissue sections taken through the full depth of samples were analysed for structural changes. The cell nuclei of the hepatocytes have maintained their rounded appearance, with little or no shrinkage after 70 h of culture in a microfluidic device. The cell membranes can be seen in several places, with the hepatocytes preserving their original hexagonal shape. In addition there is no discernible loss of the extracellular matrix between the cells.

Eluents were analysed for the levels of albumin and urea. Albumin is the most abundant protein in blood plasma and is produced by hepatocytes. It maintains osmotic pressure of blood and is a carrier of low water soluble molecules such as bile salts and free fatty acids. Production of urea is a cycle of biochemical reactions that, in mammals, only occurs in hepatocytes. Ammonia, an extremely toxic waste product has to be converted into a less potent product, urea. The conversion of ammonia to urea takes five steps; two in the mitochondria and three in the cytoplasm of hepatocytes. Urea production has been commonly used as a specific marker of liver function.³⁰ Preliminary results (Fig. 3) demonstrate that albumin concentrations vary in a cyclical manner, peaking every 24 h period. Urea concentration, after an initial drop, remained relatively stable during perfusion up to 71 h.

On-chip cell disaggregation

Following *in situ* collagenase disaggregation of primary cells from the tissue, viability was determined using Trypan blue exclusion. The results indicated that $78\% \pm 2.4$ ($n = 3$) of cells were alive which is comparable to values expected from traditional disaggregation methods.²⁹ A two hour collagenase disaggregation treatment, which offered a relatively gentle method of cell removal, resulted in approximately 30 000 cells being released; based on haemocytometer measurements.

Fluorescent images of tissue, before and after collagenase disaggregation, were obtained using calcein and propidium iodide (PI) probes that stain live and apoptotic/necrotic cells respectively (Fig. 4). The images confirm that both live and dead cells are removed using this procedure and indicate that the 'new' tissue surface generated has a greater proportion of live to apoptotic/necrotic cells.

On-chip tissue probing

In order to characterize tissue response to transient exposure to lysis buffer during prolonged maintenance on-chip, LDH and Picogreen[®] assays were carried out to monitor cell rupture. As the effect of the lysis buffer is both transient and diffusion-dependent a series of response peaks for both LDH and double stranded DNA (Picogreen[®]) are observed (Fig. 5).

This response is seen to diminish with repeated exposure to lysis buffer, due to the tissue mass being reduced as peripheral layers of cells are removed. In addition it can be seen that within one hour of probing the tissue, LDH and double stranded DNA levels return to background. Based on agar plate cultures no evidence of bacterial contamination of either media or tissue was found which may have contributed to a false positive response.

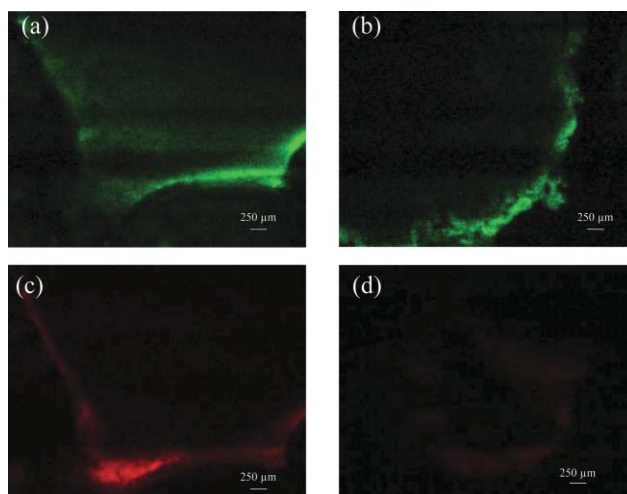


Fig. 4 Fluorescent images of liver tissue after staining with calcein and propidium iodide (PI). The green fluorescence is caused by retention of cleaved fluorescent probe, calcein, in the cytosol of viable cells. The red fluorescence is associated with PI intercalating with DNA having entered the cells through damaged membranes. Tissue pre-(a), (c) and post-disaggregation (b), (d) was probed with calcein and PI respectively. Changes in the tissue edge shape are evident after enzymatic treatment. Data shown are representative of four independent experiments. Scanning resolution was 1024×1024 using a $4\times$ objective.

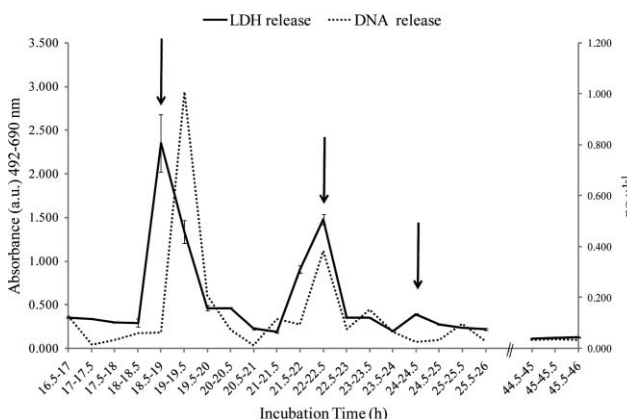


Fig. 5 LDH release from primary rat liver tissue in a microfluidic device with transient exposure to lysis buffer. The tissue was exposed to a continuous flow of lysis buffer for 30 min at 18.5, 21.5 and 24 h of incubation (indicated by arrows on the figure). After each exposure, WME was reapplied to the system for a further 2 h to allow tissue recovery.

Conclusions

Perhaps one of the most innovative aspects of the proposed methodology is its direct application to primary tissue samples which offers a unique approach to performing experiments in a pseudo *in vivo* environment. This contrasts with work in the field of tissue engineering which endeavours to construct replicate tissue micro-architectures.³¹⁻³³ Accordingly the proposed tissue-based microfluidic methodology is expected to have a wide impact on biological and clinical research in fields such as cancer prognosis and treatment, drug development and toxicity, as well as enabling better fundamental research into tissue/cell processes. In addition the direct use of tissue offers a more

clinically relevant experimental system which can potentially replace less attractive, animal based models.

Acknowledgements

The authors acknowledge Ann Lowry, Jane Woods, Jenny Foster and Kirsty Shaw for their technical support in this work and the University of Hull for SMH studentship funding and financial support from BBSRC (BB/E002722).

References

- 1 V. Jung, B. Wullich, J. Kamradt, M. Stockle and G. Unteregger, *Toxicol. in Vitro*, 2007, **21**, 183–190.
- 2 A. Thompson, K. Brennan, A. Cox, J. Gee, D. Harcourt, A. Harris, M. Harvie, I. Holen, A. Howell, R. Nicholson, M. Steel and C. Streuli, *Breast Cancer Res.*, 2008, **10**.
- 3 Y. Sambuy, I. De Angelis, G. Ranaldi, M. L. Scarino, A. Stammati and F. Zucco, *Cell Biol. Toxicol.*, 2005, **21**, 1–26.
- 4 J. Warrick, I. Meyvantsson, J. I. Ju and D. J. Beebe, *Lab Chip*, 2007, **7**, 316–321.
- 5 G. M. Walker, H. C. Zeringue and D. J. Beebe, *Lab Chip*, 2004, **4**, 91–97.
- 6 L. Kim, Y. C. Toh, J. Voldman and H. Yu, *Lab Chip*, 2007, **7**, 681–694.
- 7 Y. Ling, J. Rubin, Y. Deng, C. Huang, U. Demirci, J. M. Karp and A. Khademhosseini, *Lab Chip*, 2007, **7**, 756–762.
- 8 J. T. Nevill, R. Cooper, M. Dueck, D. N. Breslauer and L. P. Lee, *Lab Chip*, 2007, **7**, 1689–1695.
- 9 L. Kim, M. D. Vahey, H. Y. Lee and J. Voldman, *Lab Chip*, 2006, **6**, 394–406.
- 10 H. M. Yu, C. M. Alexander and D. J. Beebe, *Lab Chip*, 2007, **7**, 726–730.
- 11 I. Meyvantsson and D. J. Beebe, *Annu. Rev. Anal. Chem.*, 2008, **1**, 423–449.
- 12 J. El-Ali, P. K. Sorger and K. F. Jensen, *Nature*, 2006, **442**, 403–411.
- 13 X. L. Zhang, H. B. Yin, J. M. Cooper and S. J. Haswell, *Anal. Bioanal. Chem.*, 2008, **390**, 833–840.
- 14 S. Takayama, E. Ostuni, P. LeDuc, K. Naruse, D. E. Ingber and G. M. Whitesides, *Chem. Biol.*, 2003, **10**, 123–130.
- 15 D. B. Weibel and G. M. Whitesides, *Curr. Opin. Chem. Biol.*, 2006, **10**, 584–591.
- 16 J. Nakanishi, T. Takarada, K. Yamaguchi and M. Maeda, *Anal. Sci.*, 2008, **24**, 67–72.
- 17 C. M. Puleo, H. C. Yeh and T. H. Wang, *Tissue Eng.*, 2007, **13**, 2839–2854.
- 18 M. Y. Zhang, P. J. Lee, P. J. Hung, T. Johnson, L. P. Lee and M. R. K. Mofrad, *Biomed. Microdevices*, 2008, **10**, 117–121.
- 19 M. Yang and X. Zhang, *Sens. Actuators, A*, 2007, **135**, 73–79.
- 20 D. D. Nalayanda, C. M. Puleo, W. B. Fulton, T. H. Wang and F. Abdullah, *Exp. Lung Res.*, 2007, **33**, 321–335.
- 21 D. Kloß, M. Fischer, A. Rothermel, J. C. Simon and A. A. Robitzki, *Lab Chip*, 2008, **8**, 879–884.
- 22 S. R. Khetani and S. N. Bhatia, *Nat. Biotechnol.*, 2008, **26**, 120–126.
- 23 M. H. Wu, S. B. Huang, Z. F. Cui, Z. Cui and G. B. Lee, *Sens. Actuators, B*, 2008, **129**, 231–240.
- 24 B. A. Bruzewicz, P. A. McGuigan and G. M. Whitesides, *Lab Chip*, 2008, **8**, 663–671.
- 25 Y. Choi, M. A. McClain, M. C. LaPlaca, A. B. Frazier and M. G. Allen, *Biomed. Microdevices*, 2007, **9**, 7–13.
- 26 A. J. Blake, T. M. Pearce, N. S. Rao, S. M. Johnson and J. C. Williams, *Lab Chip*, 2007, **7**, 842–849.
- 27 I. Broadwell, P. D. I. Fletcher, S. J. Haswell, T. McCreedy and X. L. Zhang, *Lab Chip*, 2001, **1**, 66–71.
- 28 B. J. Kane, M. J. Zinner, M. L. Yarmush and M. Toner, *Anal. Chem.*, 2006, **78**, 4291–4298.
- 29 M. K. Bayliss, P. Skett, in *Human Cell Culture Protocols*, ed. G. E. Jones, Humana Press, 1996.
- 30 S. Peters, H. P. Haagsman and K. van Norren, *Toxicol. in Vitro*, 2008, **22**, 1094–1098.
- 31 E. W. K. Young, A. R. Wheeler and C. A. Simmons, *Lab Chip*, 2007, **7**, 1759–1766.
- 32 A. Khademhosseini and R. Langer, *Biomaterials*, 2007, **28**, 5087–5092.
- 33 A. P. Golden and J. Tien, *Lab Chip*, 2007, **7**, 720–725.



Short communication

A prototype microfluidic chip using fluorescent yeast for detection of toxic compounds

Javier García-Alonso*, Gillian M. Greenway, Joerg D. Hardege, Stephen J. Haswell

Faculty of Science, The University of Hull, Hull HU6 7RX, England, United Kingdom

ARTICLE INFO

Article history:

Received 14 April 2008

Received in revised form 25 July 2008

Accepted 29 July 2008

Available online 13 August 2008

Keywords:

Microfluidic chip

GFP

Toxicity screening

Yeast

ABSTRACT

A microfluidic chip has been developed to enable the screening of chemicals for environmental toxicity. The microfluidic approach offers several advantages over macro-scale systems for toxicity screening, including low cost and flexibility in design. This design flexibility means the chips can be produced with multiple channels or chambers which can be used to screen for different toxic compounds, or the same toxicant at different concentrations. *Saccharomyces cerevisiae* containing fluorescent markers are ideal candidates for the microfluidic screening system as fluorescence is emitted without the need of additional reagents. Microfluidic chips containing eight multi-parallel channels have been developed to retain yeast within the chip and allow exposure of them to toxic compounds. The recombinant yeast used was GreenScreen™ which expresses green fluorescent proteins when is exposed to genotoxins. After exposure of the yeast to target compounds, the fluorescence emission was detected using an inverted microscope. Qualitative and quantitative comparisons of the fluorescent emission were performed. Results indicated that fluorescent intensity per area significantly increases upon exposure to methyl-methanesulfonate, a well known genotoxic compound.

The microfluidic approach reported here is an excellent tool for cell-based screening and detection of different toxicities. The device has the potential for use by industrial manufacturers to detect and reduce the production and discharge of toxic compounds, as well as to characterise already polluted environments.

© 2008 Elsevier B.V. All rights reserved.

1. Introduction

The requirement for toxicity testing of chemical substances is of growing concern as most manufactured chemical products are formulations or mixtures of substances and the toxicity of each formulation could change depending on particle sizes, volatility, etc. The new EU REACH (Registration, Evaluation, Authorisation and registration of CHemicals) regulations will mean much more testing is required, and unless rapid, meaningful screening tests can be developed, animal testing will inevitably be used. Both, *in vivo* and *in vitro* bioassays are currently used to study toxic effects in whole organisms or at cell level, respectively.

For toxicity testing, miniaturized systems have many advantages including small sample and reagent volumes and a biomimetic microenvironment within microfluidic systems ideal for microor-

ganism maintenance. Accordingly, the microfluidic environment with its inherent high surface area-to-volume ratio, provides a tool that creates a more *in vivo*-like cellular microenvironment *in vitro* than current methodology offers. The ability to control the spatial distribution within a microfluidic device readily allows for the isolation of single cells or small groups of cells and their interactions with other stimuli can be monitored (Inoue et al., 2001). Wet-etching channel geometries in glass and sealing with elastomeric siloxane polymers such as poly-dimethylsiloxane (PDMS) to generate a PDMS-glass microfluidic chip offers an ideal method for the prototyping of microfluidic chips as they have low fabrication costs and good chemical compatibility with most biological fluids. In addition, the integration of optical and/or electrochemical detectors onto the microfluidic system forms a complete device or “chip” with overall dimensions of a few centimetres (Watts and Haswell, 2005).

A number of elegant microfluidic cell based handling applications have been described for drug development, tissue engineering, molecular diagnostics and biosensors (Cho et al., 2003; MacDonald et al., 2003; Rhee et al., 2004; Zeringue et al., 2004). Microfluidic systems have also been used to analyse single cells, including bacterial, fungal, yeast and mammalian cells

* Correspondence address: Sensory and Chemical Ecology Group, Department of Biology, Faculty of Science, The University of Hull, Cottingham Road, Hull HU6 7RX, England, United Kingdom. Tel.: +44 1482 465521; fax: +44 1482 465458.

E-mail address: j.garcia-alonso@hull.ac.uk (J. García-Alonso).

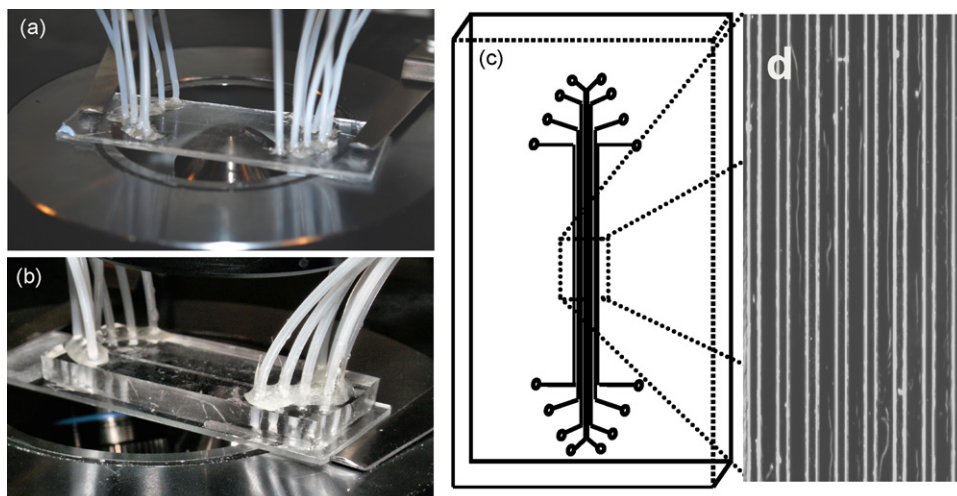


Fig. 1. Microchips with 8 multi-parallel channels. (a) Glass-glass device and (b) PDMS-glass chip on an inverted microscope. (c) Scheme showing the design of the chips. (d) Microphotography of the channels (40 \times magnifications).

(Tourovskaja et al., 2004; Werdich et al., 2004; Shackman et al., 2004).

Despite the advantages of using yeast (i.e. a robust eukaryotic cell line) and their widespread use in biotechnology, few microsystems have been developed using yeast. Incorporating cells within a microfluidic device would allow fast high throughput screening to test different metabolic responses to toxicants/drugs on a cellular level (e.g. human cell lines) as well as an organismal level (e.g. yeasts and bacteria).

Toxicity screening using yeast is widely used for different target compounds, such as genotoxic chemicals (Cahill et al., 2004) endocrine disrupting chemicals (EDCs, Michellini et al., 2005) or oxidative stress factors (de Souza and Geibel, 1999). Recombinant budding yeast (*Saccharomyces cerevisiae*) containing fluorescent markers such as green or red fluorescent protein (GFP or RFP) are ideal candidates for microscreening, because they fluoresce without the addition of substrates. GreenScreen™ yeast cells have been genetically modified to express the GFP whenever the cells repair damaged DNA. This yeast is being used to simultaneously detect genotoxicity and cytotoxicity (Cahill et al., 2004). Under genotoxic conditions, the fluorescence emission increases, whilst cytotoxicity is determined by a reduction in cell proliferation as compared to an untreated control. GreenScreen™ has been employed for screening both industrial products and for environmental samples (Gompel et al., 2005; Knight et al., 2004).

In this paper we describe a simple microfluidic based toxicity screening test, using glass and polydimethylsiloxane (PDMS)-glass microchips with viable recombinant yeast and fluorescence quantification. The device was designed to have a low cost and to be used by non-experts in small- to medium-sized enterprises to screen chemicals that had not been previously evaluated for their toxicity in aquatic environment.

2. Materials and Methods

2.1. Microchips

Glass (Fig. 1a) and PDMS-glass microchips (Fig. 1b) incorporating eight 20 mm long parallel channels (40 μ m wide and 80 μ m deep) were fabricated by wet-etching the glass using a technique similar to a previously published method (McCreeley, 2001). Briefly, the design was drawn using autoCAD software and transferred, by a commercial process (J.D. Phototools, Oldham, UK) to

a film photomask. Crown white glass (B270) plates coated with chrome and photoresist (Telic Co., CA, USA) were contacted with a photomask design and exposed to UV radiation. The plates were then treated with photoresist developer followed by chrome etch solution (Rohm-Haas Ltd., UK). The exposed glass channels were etched at a rate of 4 μ m per minute in a 1% hydrofluoric acid/5% ammonium fluoride solution at 65 $^{\circ}$ C. After a thorough cleaning process, the etched plates were thermally bonded (595 $^{\circ}$ C for 3 h) to top-plates with drilled access holes. The fabrication of the PDMS-glass microchips used the same methodology as described above for the glass base plates. The upper layer of PDMS (5 mm) was produced by polymerisation and was then hardened for 2 h at 90 $^{\circ}$ C before being plasma bonded to the 2 mm glass base plate (Fig. 1b).

TFZL tubes (i.d. 1/16 in., Upchurch Scientific) were used to connect the microfluidic channels to pumps and the recombinant yeast was pumped inside the chambers using a 250/500 μ l syringes (SGA) connected to the system with a two-way valve. The specific assay culture media for keeping the cells alive was then pumped into the microfluidic device at a very low flow rate of 0.1 μ l min^{-1} using two pumps (KDS-200CE, kdScientific®).

2.2. Recombinant Yeast and Reagents

The GreenScreen™ yeast strains, specialist resuscitation and assay media were supplied by Gentronix Ltd. (Manchester, UK). A DNA repair-competent strain of the brewer's yeast *S. cerevisiae* was employed as the host strain for a reporter of DNA repair activity (the "test" strain). The reporter consisted of a fusion of the DNA damage-inducible promoter from an endogenous DNA repair gene, RAD54, with a gene encoding a yeast enhanced green fluorescent protein (yEGFP). The yeast cells are genetically modified to express a yeast enhanced GFP under the control of a copy of the promoter from the native yeast gene RAD54. RAD54 is known to be specifically up regulated by the cells in response to DNA damage. Thus, on exposure to a genotoxic agent the cells become increasingly fluorescent as GFP accumulates. A second "control" strain was used to correct for cellular or test article auto-fluorescence. The control strain contained a disabled reporter plasmid, and thus was unable to express GFP despite being identical to the test strain in every other way. Methyl methanesulfonate (MMS #M4016) as a genotoxic standard and dimethyl sulfoxide (DMSO #D8418) as diluent were purchased from Sigma-Aldrich.

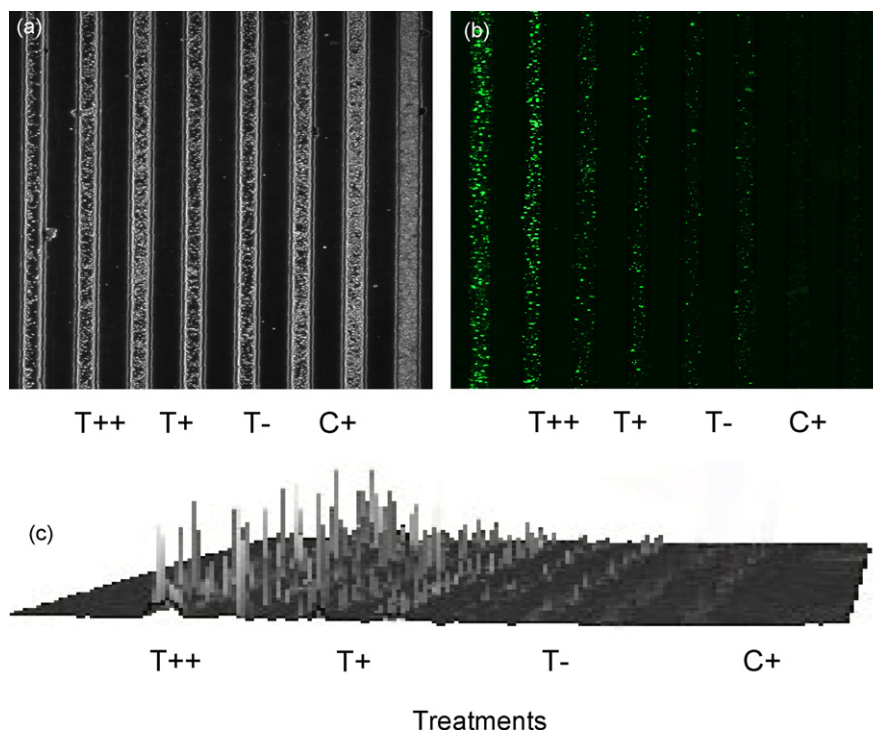


Fig. 2. Recombinant yeast in the chips upon exposure to MMS in DMSO at final concentration of 2% DMSO. (a) Common light microscopy showing yeast in the channels. (b) Fluorescent microscopy of the same yeast showing fluorescent emission. (c) 3D plot of the fluorescence emission. T++, Test strain with high concentration of MMS; T+, low concentration of MMS; T-, with diluent alone (culture media containing 2% DMSO); C+, control strain with low concentration of MMS. Magnification: 40 \times (bar indicates 200 μ m).

2.3. Bioassay and Fluorescence Quantification

Prior to the assay, yeast was grown in 20 ml resuscitation media for 72 h in an orbital incubator (200 rpm) at 30 °C in order to reach a stationary phase with a concentration approximately 1×10^7 cells per ml determined by optical density (OD) in a spectrophotometer at 620 nm. 100 μ l aliquots of the yeast in the media were then pumped into each channel. The yeast settled in the channels and then the culture media (with or without the addition of MMS) was passed over the cells at flow rate of approximately $0.1 \mu\text{l min}^{-1}$ for 14–16 h at 25 °C. Six of the channels (see Fig. 2a) were filled with a test strain of yeast, then two of these channels received fresh culture medium containing a high concentration of MMS (0.005%, T++), two received a low concentration of MMS (0.0002%, T+), and two received the diluent (2% DMSO, T-). The last two channels contained the control strain with the low concentration of MMS (C+), thus totalling 8 parallel channels.

After exposure of yeast to MMS, the flow of culture media was stopped and the yeast was excited at 485 nm and the fluorescence emission detected at 520 nm under an inverted microscope (Olympus IX71) using a 4 \times objective (UPLFLN). The induction of GFP fluorescence was compared to the constitutive expression of GFP which proceeds in normal, healthy cells as they maintain DNA integrity. Qualitative analyses were performed by 3D-surface plotting (Cell DTM) of the fluorescence (each step = 10 pixels; Fig. 2c). Fluorescence emission was quantified as intensity per area. Ten squares (5000 μm^2) were analysed per channel obtaining mean intensity (20 squares per treatment). For each square, approximately 200 yeast cells were imaged. Comparisons of the fluorescence intensity was performed by analyses of variance (ANOVA) followed by Dunnett's T_3 post hoc test, using SPSS 15.0 software. Genotoxicity was corroborated when significant dif-

ferences appeared ($p < 0.05$) between those cells exposed to MMS and those under 2% DMSO only.

3. Results

3.1. Retention of Yeast in the Microfluidic Device

The microfluidic chip used was designed to carry out bioassays with yeast. Fig. 1 shows that it was possible to perform a toxicity bioassay by placing the prototype microchip under an inverted microscope, such that all the channels could be observed at the same time at 40 times magnification. Both the glass and PDMS-glass microchips were able to retain the cells within the microchannels (Fig. 2a). Most of the cells were retained by gravity with some attaching to the walls of the channel while others moved slowly through the bottom of the channel. For retention to be achieved, however, only a very low flow rate of the culture medium ($\leq 0.1 \mu\text{l min}^{-1}$) could be used due to the small size of the yeast cells, otherwise they were swept out of the system at higher flow rates. Fluorescence emission could be measured from both glass and PDMS-glass microchips.

3.2. Genotoxicity Bioassay

A genotoxicity bioassay was demonstrated in the microfluidic chip (Figs. 2 and 3). Qualitative analysis of the fluorescence emission, using a 3D plot, clearly discriminates the basal fluorescence emission compared to that developed in exposed cells (Fig. 2c). The selected area for fluorescence intensity quantification could clearly differentiate the cells exposed to MMS compared to the control cells. The control strain C+, showed the lowest values in arbitrary units of 75.57 ± 15 . The test strain exposed to DMSO alone (T-) was 305.18 ± 35 , while T+ increased fluorescence to 377.39 ± 64 and T++

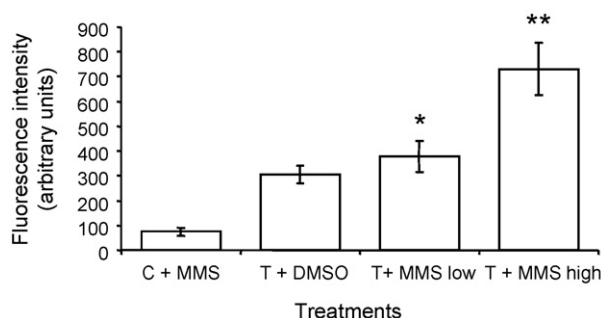


Fig. 3. Fluorescence quantification (mean \pm S.D.) of intensity per 5000 μm^2 . T++, High concentration of MMS; T+, test strain with low concentration of MMS; T-, test strain with diluent alone (culture media containing 2% DMSO); C+, control strain with low concentration of MMS. Asterisk (*) denote significant level at $p < 0.05$ and asterisks (**) denote significant level at $p < 0.001$ of exposed to MMS compared to the control.

presented the largest signal of 730.97 ± 107 . The intensity of the fluorescence was greatly different when yeasts were exposed to MMS in high toxicant concentration ($p < 0.001$) and also at low toxicant concentration ($p < 0.05$, ANOVA, $F_{(3,78)} = 334.509$) compared to the control (Fig. 3).

4. Discussion

The microfluidic approach described here was found to be an excellent tool for cell-based screening to test and detect different toxic effects. The three-dimensional plot of fluorescence gives a rapid qualitative indication of the effect of the toxic chemical on the yeast which is useful for the non-expert toxicologist (Fig. 2c).

A key point to make regarding yeast is their robustness compared to bacterial or mammalian cells. These yeast cells are an eukaryote alternative and possess several advantages over bacteria in microbial biosensor development: they tolerate a wide range of pH, can survive temperatures from freezing to over 40 °C, and have a wide tolerance of osmolarity/ionic strength (Walmsley and Keenan, 2000).

The glass microchips are robust and can be sterilised, while the PDMS-glass chips have low cost of production, they are disposable polymer chips which could be mass produced by using fabrication techniques such as hot embossing. New designs are being developed with various channel architectures in order to improve yeast retention within the channels. In parallel channels, yeast cells are retained only if the system is running at very low flow rates, and completely sealed to avoid undesired air bubbles.

Cytotoxicity analysis via the number of cells per treatment (i.e. absorbance measured at 620 nm) could not be carried out under the microscope with the current system, although the microfluidic systems could be adapted for this toxicity assay. The plan would be

to build a low cost, dedicated fluorescent and optic system for both genotoxicity and cytotoxicity.

The data presented in our preliminary tests clearly show the response upon exposure to toxins (Fig. 3) and highlights that such screening devices based on microfluidics are very promising in the development of rapid screening tests. Future work involves cross-validation of the integrated microfluidic system with standard 96-well plate and fluorescent microplate reader methodology for genotoxicity.

5. Conclusions

A toxicity screening test using fluorescent yeasts was performed in a microfluidic device. Miniaturization of toxicity screening methods is a very promising alternative in the future.

The further development of this low cost approach with simple optical detection would allow small- to medium-sized enterprises to comply with the new EU REACH (Registration, Evaluation, Authorisation and registration of Chemicals) regulations by allowing them to decide whether they require further costly tests. It would also have additional applications for environmental monitoring.

Acknowledgements

Thanks to S. Clark and Z. Shen (University of Hull) for technical support with the chip manufacturing and A. Knight (Gentronix, Manchester) for kindly supplying the yeast cells. This work was funded by European Commission, TESS COLL-CT-2006 project (6th Framework Programme).

References

- Cahill, P.A., Knight, A.W., Billington, N., Barker, M.G., Walsh, L., Keenan, P.O., Williams, C.V., Tweats, D.J., Walmsley, R.M., 2004. *Mutagenesis* 19, 105–119.
- Cho, B.S., Schuster, T.G., Zhu, X., Chang, D., Smith, G.D., Takayama, S., 2003. *Analytical Chemistry* 75, 1671–1675.
- de Souza Pereira, R., Geibel, J., 1999. *Molecular and Cellular Biochemistry* 201, 17–24.
- Gompel, J.V., Woestenborghs, F., Beerens, D., Mackie, C., Cahill, P.A., Knight, A.W., Billington, N., Tweats, D.J., Walmsley, R.M., 2005. *Mutagenesis* 20, 449–454.
- Inoue, I., Wakamoto, Y., Moriguchi, H., Okano, K., Yasuda, K., 2001. *Lab on a Chip* 1, 50–55.
- Knight, A.W., Keenan, P.O., Goddard, N.J., Fielden, P.R., Walmsley, R.M., 2004. *Journal of Environmental Monitoring* 6, 71–79.
- MacDonald, M.P., Spalding, G.C., Dholakia, K., 2003. *Nature* 426, 421–424.
- McCreedy, T., 2001. *Analytica Chimica Acta* 427, 39–43.
- Michellini, E., Leskinen, P., Virta, M., Kart, M., Roda, A., 2005. *Biosensors and Bioelectronics* 20, 2261–2267.
- Rhee, S.W., Taylor, A.M., Tu, C.H., Cribbs, D.H., Cotman, C.W., Jeon, N.L., 2004. *Lab on a Chip* 5, 102–107.
- Shackman, J.G., Dahlgren, G.M., Peters, J.L., Kennedy, R.T., 2004. *Lab on a Chip* 5, 56–63.
- Tourovskaya, A., Figueroa-Masot, X., Folch, A., 2004. *Lab on a Chip* 5, 14–19.
- Walmsley, R.M., Keenan, P., 2000. *Biotechnology BioProcess Engineering* 5, 387–394.
- Watts, P., Haswell, S.J., 2005. *Chemical Society Reviews* 34, 235–246.
- Werdich, A.A., Lima, E.A., Ivanov, B., Ges, I., Anderson, M.E., Wikswo, J.P., Baudenbacher, F.J., 2004. *Lab on a Chip* 4, 357–362.
- Zeringue, H.C., Rutledge, J.J., Beebe, D.J., 2004. *Lab on a Chip* 5, 86–90.



Contents lists available at ScienceDirect

Chemical Engineering Research and Design

IChemE

journal homepage: www.elsevier.com/locate/cherd

Monitoring of liquid flow through microtubes using a micropressure sensor

Xunli Zhang^{a,b,*}, Paul Coupland^a, Paul D.I. Fletcher^a, Stephen J. Haswell^a

^a Department of Chemistry, The University of Hull, Hull HU6 7RX, UK

^b Bioengineering Group, School of Engineering Sciences, University of Southampton, Southampton SO17 1BJ, UK

A B S T R A C T

The pressure-driven liquid flow through microtubes was studied in a range of very low Reynolds numbers (<0.15) by monitoring the pressure change *in situ*. Cylindrical microtubes with diameters ranging from 50 μm to 500 μm were examined and two types of tube material, namely PEEK polymer and fused silica were compared. A good linear relation for the pressure drop *versus* flow rate was obtained. Apparent deviations between the measured slopes with those calculated using conventional theory were attributed to uncertainties in the calculated values which are dominated by the uncertainties in the microtube diameters. It was found that a period of stabilisation time was required for reaching a steady flow after the syringe pump was switched on/off or to a different flow rate. The stabilisation time was likely due to the compressibility of the fluid. Insignificant difference between PEEK polymer and fused silica microtubes in terms of flow resistance was observed. The *in-situ* measurement of pressure drops provides a convenient approach for monitoring fluid flow through microtubes and detecting dimensional changes within microchannels in Lab-on-a-Chip and microreactor systems.

© 2008 The Institution of Chemical Engineers. Published by Elsevier B.V. All rights reserved.

Keywords: Microtube; Laminar flow; Pressure sensor; Liquid flow monitoring

1. Introduction

The increasing interest in the development of miniaturized micro chemical systems has led to the emergence of micro chemical engineering, a new field of research embracing microfabrication, microfluidics, microreaction technology, and their applications in chemical syntheses and analytical measurements (Viovy, 2007; Schütte et al., 2006; Ehrfeld et al., 2000; Jensen, 2001; Zhang et al., 2006, 2008). Such systems have feature sizes in a range of 1–1000 μm , and reaction channels are usually integrated with microsensors and microactuators. In these systems, understanding and controlling microfluidics is key to controlling reagent delivery, mixing, separation, and heat and mass transfer. In general, most microchemical systems studies to date have employed either electrokinetic mobilization or hydrodynamic (pressure driven) pumping of reagents. In previous studies we have demonstrated the successful modelling and control of microfluidics driven by electrokinetic (i.e. voltage driven electroosmosis and electrophoresis) forces for the control of the *spatial* and *tem-*

poral evolution of chemical reactions (Fletcher et al., 2002). However, to create some complex flow patterns desired by certain chemical processes in the microreactor channel network, a pressure-driven flow is required.

There have been a number of studies on the microscale flow behaviour in the laminar flow regime under pressure-driven flow conditions. Most of the work has focused on comparing flows for a range of fluids measured in microchannels of different shapes with predictions based on conventional theory developed for macroscopic scale pipes (Tuckerman and Pease, 1981; Peiyi and Little, 1983; Wilding et al., 1994; Papautsky et al., 1999, 2001; Mala and Li, 1999; Brutin and Tadriss, 2003; Choi et al., 1991; Yu et al., 1995; Pfahler et al., 1990; Xu et al., 2000; Weilin et al., 2000; Sharp et al., 2000, 2002; Koo and Kleinstreuer, 2003; Jiang et al., 1995; Spence and Crouch, 1998). The initial work on microfluidics for an electronic chip cooling system with water through microchannels fabricated directly on silicon chips was conducted by Tuckerman and Pease (1981). Following that, a number of studies have been carried out with fluid flows in microchannels or microtubes and

* Corresponding author. Tel.: +44 23 8059 8748; fax: +44 23 8059 3016.

E-mail address: XL.Zhang@soton.ac.uk (X. Zhang).

Received 24 October 2007; Accepted 28 June 2008

Table 1 – The specifications of the microtubes used

Inner diameter (i.d.) (μm)	Outer diameter (o.d.) (μm)	Material	Colour	Upchurch part number
50	360	PEEK	Natural	1570
75	360	PEEK	Black	1573
100	360	PEEK	Red	1571
150	360	PEEK	Yellow	1572
250	1/16"	PEEK	Blue	1531B
500	1/16"	PEEK	Orange	1532
75	360	Fused silica	Natural	FS-175

some significant disagreements have been observed between experiments and conventional theory used in macroscale fluidics. Peiyi and Little (1983) measured the friction factors for gas flow in microchannels and found that the measured values were larger than that predicted by conventional theory for macroscale pipes. They attributed these differences to the large relative roughness of the microchannel surface. Similar increases in friction factors have also been observed by other researchers (Wilding et al., 1994; Papautsky et al., 1999; Mala and Li, 1999; Brutin and Tadrist, 2003). Papautsky et al. (1999) developed a numerical model based on micropolar fluid theory which augmented the laws of classical continuum mechanics by incorporating the effects of fluid molecules on the continuum. Their model showed better predictions for water flows in microchannels than the classical theory. A roughness-viscosity model was proposed by Mala and Li (1999) to interpret the experimental results. Brutin and Tadrist (2003) suggested that a modification of local viscosity due to the fluid ionic coupling with the surface might be accountable for the increase in friction factors. In the meantime, other researchers have found that the friction factors were lower than those predicted by theory (Choi et al., 1991; Yu et al., 1995; Pfahler et al., 1990), and most of the deviation was attributed to the uncertainty of the microchannel dimensions. In addition to the effect from the microscale tubes and errors from channel dimension determinations, other factors including viscosity variations due to temperature changes or surface roughness, entrance effects, and possible geometric non-uniformities, e.g., a contraction and/or bend at the inlet to the microchannel, have been taken into account for the explanation of the deviation from theory (Papautsky et al., 2001; Xu et al., 2000; Weilin et al., 2000; Sharp et al., 2002; Koo and Kleinstreuer, 2003). On the other hand, some experiments have shown good agreements with the conventional theory (Tuckerman and Pease, 1981; Jiang et al., 1995; Spence and Crouch, 1998; Sharp et al., 2000).

The aim of the present study was to obtain further understanding of the behaviour of the liquid flow driven by a syringe pump under microfluidic conditions. Microtubes with inner diameters ranging from 50 μm to 500 μm were examined; a range which is similar to that of microreactor channels. Three main aspects of the liquid flow were examined. Firstly, the relationships between pressure drops and flow rates were examined for the different microtube diameters. Secondly, we measured the times required to achieve steady flows and pressure drops when the pump flow rate was altered. This aspect is particularly relevant to attempting fast switching of flows between different limbs of a microreactor channel network, and controlling integrated on-chip valving. Thirdly, we examined the viability and usefulness of continuous, in-situ monitoring of the pressure drop across the channel lengths.

2. Experimental

The experimental apparatus consisted of a syringe pump, a micropressure sensor, a series of lengths of microtubes with connectors, and a data acquisition system with PC. The syringe pump (Model 200, kdScientific Inc., USA) was controlled by the computer using a LabVIEW™ software program via RS232 serial ports, and can deliver liquid at flow rates ranging from 0.001 mL/h to 2.203 mL/min with a 1 mL luer-lock gas-tight glass syringe (i.d. 4.61 mm, SGE, Australia). The volumetric flow rate was set by the computer via the pump's control system and the average volumetric flow rate was confirmed by a weighing method.

A miniature threaded pressure sensor (Model EPX-V01-35B, Entran® Sensors & Electronics, Fairfield, NJ, USA), powered by a 10 VDC power supply, was used to measure the pressure in a range of 0–35 bar above atmosphere. The output signal of the sensor in millivolts (125 mV/FS) was collected by the computer using a LabVIEW™ software program via the data acquisition interface card (DAQ Card-6024E, National Instruments, USA). The data acquisition frequency was set at 20 scans/s, which were then averaged over every second. The pressure sensor was connected to the microtube inlet with a P775 MicroTee (Upchurch Scientific Inc., USA) connector where the outlet of the microtube was open to atmosphere. The pressure sensor was zeroed against atmosphere so the pressure measured was equal to the pressure difference between the microtube inlet and outlet, which is often referred to as the pressure drop.

The microtubes used in this study were supplied by Upchurch Scientific Inc., USA, and made of two types of material, namely PEEK™ (polyetheretherketone) polymer and fused silica. All the microtube sections examined were cut to a length of 25 cm for comparison. The specifications of the microtubes used are summarized in Table 1. MicroTight Unions (Upchurch P720) were used to directly connect two pieces of microtube with o.d. 360 μm . For a connection between o.d. 1/16" and o.d. 360 μm tubes a MicroTight Adapter (Upchurch P770) was used.

Squalane was chosen as the test fluid in this study in view of its biomedical applications (Allison, 1999; Hilgers et al., 1999; Shahiwala and Amiji, 2008). Squalane is a linear hydrocarbon precursor of cholesterol found in many tissues, notably the livers of sharks (Squalus) and other fishes (Allison, 1999). It has been used in pharmaceuticals and as a skin lubricant, as an ingredient in suppositories (Allison, 1999; Hilgers et al., 1999). In recent years, its applications associated with lipophilic drug delivery and vaccine studies have increasingly attracted attention while studies have shown that (squalane) oil-in-water emulsions can elicit both humoral and cellular immune responses (Shahiwala and Amiji, 2008). Squalane is generally considered as a Newtonian fluid (Chaomleffel et al., 2007), and studies on its viscosity under different conditions have been

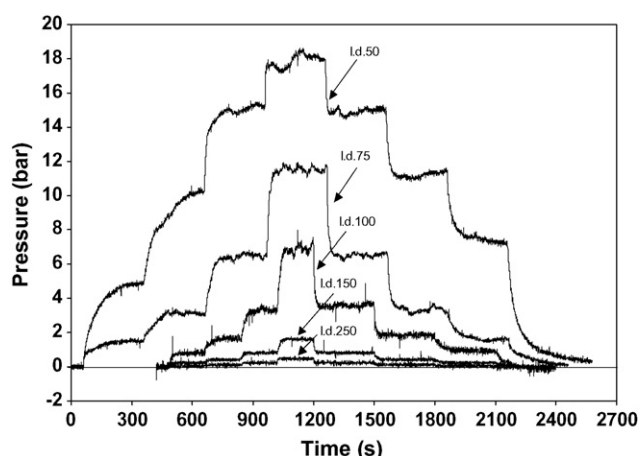


Fig. 1 – Pressure versus time when the flow rate was raised then lowered step by step for microtubes with different diameters (Flow rate cycles: PEEK tubes with i.d. 250, i.d. 150 and i.d. 100, 0-2-4-8-16-8-4-2-0 $\mu\text{L}/\text{min}$; PEEK tube with i.d. 75, 0-2-4-8-12-8-4-2-0 $\mu\text{L}/\text{min}$; PEEK tube with i.d. 50, 0-2-4-6-8-6-4-3-0 $\mu\text{L}/\text{min}$).

reported in a number of publications (de Ruijter et al., 1998; Kumagai et al., 2007; Ling and Shaw, 2008). The viscosity was found to be sensitive to temperature, e.g., 35.6 mPas at 20 °C and 23.01 mPas at 30 °C, and the relationship can be found in reference (de Ruijter et al., 1998). In this study squalane was supplied by Aldrich and used without further treatment (http, 2008a). All measurements were carried out at 25.0 °C.

3. Results and discussion

3.1. Pressure drops at different flow rates

Pressure drops across microtube sections with different diameters were monitored as the flow rate was raised step by step and then decreased in steps to investigate the relationship between pressure drops and flow rates. The results are depicted in Fig. 1.

As the flow rate was raised, in general, the pressure drop increased in response to a higher level and tended to be stable after a period of stabilisation time. When the flow rate was reduced step by step the pressure drop also decreased and tended to reach a lower stable level again after a period of time. The pressure drop at the stable level was found to be reproducible when the flow rate was cycled up and down. Fig. 2 shows the relation of the pressure drop at the stable level to the flow rate for microtubes with different inner diameters in a flow rate range of 0–16 $\mu\text{L}/\text{min}$. It can be seen from Fig. 2 that the pressure drop across a length of microtube increases linearly with flow rate.

Pressure-driven fluidics on macroscale has been extensively studied and the well-known Hagen–Poiseuille equation for laminar flow in a circular pipe can be represented by

$$\frac{P}{F} = \frac{128\mu L}{\pi D^4} \quad (1)$$

when the Reynolds number, Re , is in the laminar flow range,

$$Re = \frac{Du\rho}{\mu} < 2000 \quad (2)$$

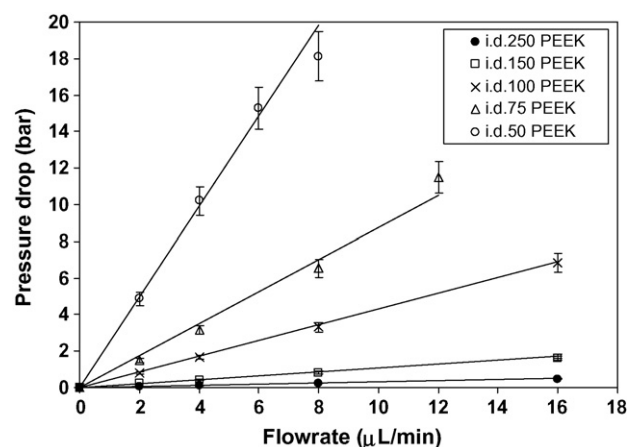


Fig. 2 – Pressure drop as a function of flow rate for microtubes with different diameters.

where P is the pressure drop across a length L of pipe with an inner diameter D , F is the volumetric flow rate, u is the average linear velocity, μ is the fluid viscosity, and ρ , the fluid density. Under the experimental conditions in the present study, the Reynolds number is below 1 indicating that the flow is restrictively in the laminar flow range.

In agreement with Eq. (1), the measured pressure drop increases linearly with flow rate (Fig. 2) for all tube diameters tested. However, calculated values of the slopes of the plots of Fig. 2 (i.e. P/F) using Eq. (1) and the microtube manufacturers' values for the inner diameters deviate from the measured values of P/F . In previous studies similar deviations have been observed (Wilding et al., 1994; Papautsky et al., 1999, 2001; Mala and Li, 1999; Brutin and Tadrist, 2003; Choi et al., 1991; Yu et al., 1995; Pfahler et al., 1990; Xu et al., 2000; Weilin et al., 2000; Sharp et al., 2002; Koo and Kleinstreuer, 2003) and a range of models (mainly based on surface roughness and non-uniform fluid viscosities very close to channel walls) have been developed to account for the observations. Here we note that $(P/F) \propto D^{-4}$ and so a relatively small fractional uncertainty in D leads to a large uncertainty in the calculation of P/F . Using the tube inner diameter tolerances specified by the manufacturer (Table 1, http, 2008b) the uncertainties in P/F were estimated. Fig. 3 compares measured and calculated P/F val-

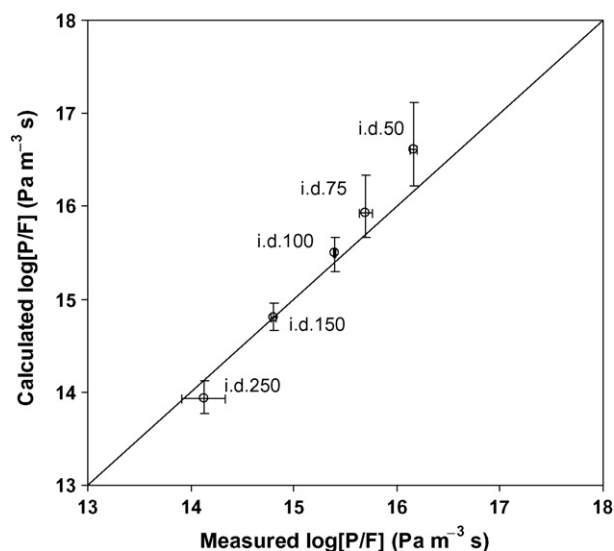


Fig. 3 – Comparison of calculated and measured $\log[P/F]$ for microtubes with different inner diameters.

ues with the estimated uncertainties and it can be seen that the apparent discrepancies are all within the estimated uncertainties. However, possible contributions to the deviation due to departures from non-circularity of the microtube cannot be excluded even it is unlikely to determine that along the entire tube length. Although the uncertainties are relatively large, particularly for the smaller tube diameters, there is no significant evidence for special microscale fluidic behaviour in this case.

3.2. Effects of changing pumping conditions

It has been seen from Fig. 1 that a stabilisation period prior to reaching a steady state flow always existed after the pump was switched on/off or to a different flow rate. This phenomenon was also observed by other researchers and generally believed to be the time for reaching a pressure equilibration in the whole flow system including the syringe used (Weilin et al., 2000; Spence and Crouch, 1998). Clearly, this introductory time is problematic for control and change of flow conditions in an instantaneous way, where special flow patterns such as slugs or pulses of reagents are usually required in microreactor systems or integrated on-chip valving is being used.

Fig. 4 shows the pressure changes at different flow rates when the pump was switched on for 5 min and then off where a PEEK tube with an inner diameter of 75 μm was used. It can be seen from the figure that the variation of the stabilisation time became more significant as the pump was switched on/off with different flow rate settings and, consequently, the pressure in the flow system was altered. It is found that the relation of the introductory time τ to the pressure can be represented by

$$P = P_0 + \Delta P \left[1 - \text{Exp} \left(-\frac{t - t_0}{\tau} \right) \right] \quad (3)$$

where P_0 is the pressure at time t_0 when the pumping conditions are altered, i.e., on/off or changing flow rates. ΔP is the pressure difference between two adjacent stable pressure levels. By fitting the measured pressure profiles to this model,

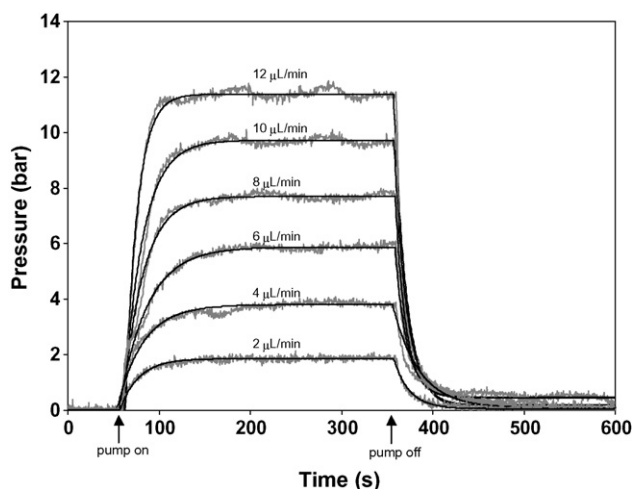


Fig. 4 – Pressure versus time at different flow rates for PEEK tubing with an inner diameter of 75 μm when the pump was switched on/off. The gray dash lines show the measured data and the black solid curves are the best-fits to the model described in the text.

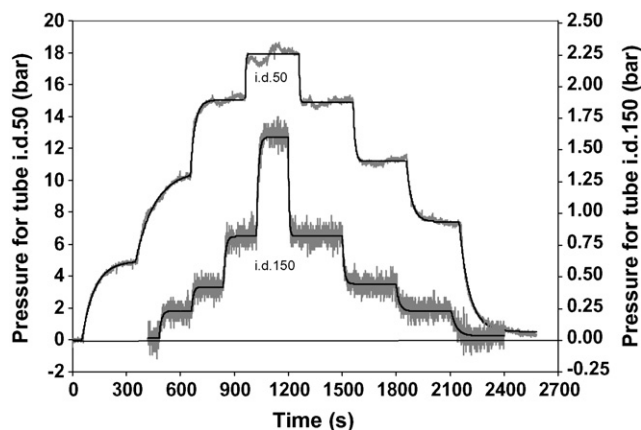


Fig. 5 – Pressure versus time when the flow rate was raised and then lowered step by step for the microtube with inner diameters of 50 μm and 150 μm (Flow rate cycles: i.d. 50 μm tube, 0-2-4-6-8-6-4-3-0; i.d. 150 μm tube, 0-2-4-8-16-8-4-2-0 $\mu\text{L}/\text{min}$). The gray dash lines show the measured data and the black solid curves are the best-fits to the model.

the introductory time τ for different flow rate was obtained. The best-fit results are shown in Fig. 4 as the solid curves. This model was also applied to the experimental data shown in Fig. 1 where the pressure corresponding to the flow rate was cycled up and down. The solid curves in Fig. 5 show two examples of the best-fit results for the microtubes with inner diameters of 50 μm and 150 μm .

In general, the volume of most fluids varies in response to the pressure change at a given temperature and this thermo-physical property of fluids is referred to as its compressibility C_{comp} . The effect of compressibility on the flow stability is believed in most cases to be negligible in macroscale liquid flow systems where a relatively high volumetric flow rate is applied. In microscale flow systems, however, the volume variation due to pressure change could result in significant variation in the instant flow rate for the liquid flow. Thus, the stabilisation time for reaching a steady state flow is likely to be the relaxation time for building a pressure equilibration in the whole liquid flow system, and the relaxation time τ can be represented by

$$\tau = \frac{\Delta V}{F_{\text{mean}}} = \frac{\Delta P C_{\text{comp}} V}{F_{\text{mean}}} \quad (4)$$

where ΔV is the volumetric variation due to a pressure change ΔP . V is the volume of the whole liquid flow system and F_{mean} , the mean volumetric flow rate during the pressure change. Although the volume of the whole liquid system is varying during the liquid flow it is possible to determine the system volume in a short period of time with a known flow rate setting. Based on the results shown in Figs. 4 and 5 for the relaxation time, the best fitting of the liquid compressibility could be obtained according to Eq. (4). Fig. 6 shows the relation of the relaxation time τ versus $\Delta P V / F_{\text{mean}}$. The best-fit value for the liquid compressibility C_{comp} is found to be $2.3135 \times 10^{-4} \text{ bar}^{-1}$ under the experimental conditions. Although the deviation is relatively big, this result is in rough agreement with the compressibility of other hydrocarbons that is typically on the order of 10^{-4} to 10^{-5} bar^{-1} at a temperature of 25 $^{\circ}\text{C}$ (Lide, 2003).

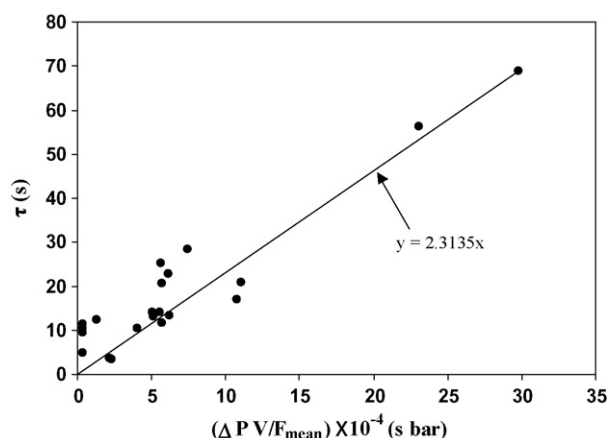


Fig. 6 – Relaxation time τ versus $(\Delta P V/F_{\text{mean}})$.

3.3. Comparison of PEEK polymer and fused silica microtubes

The effect of material properties in particular the surface roughness of tubes on pressure drops was found to be important under turbulent flow conditions but insignificant under laminar flow conditions in macroscale tubes. In the laminar flow regime on microscale, the assumption that the effect from the tube material is negligible in terms of flow resistance is still under discussion in the literature (Peiyi and Little, 1983; Wilding et al., 1994; Papautsky et al., 1999; Mala and Li, 1999; Brutin and Tadrist, 2003; Jiang et al., 1995; Spence and Crouch, 1998; Sharp et al., 2000). In this present study, two types of microtubes, which are commonly used in microreactor research laboratories, made of either PEEK polymer or fused silica were compared for different flow rates where the two microtubes were cut to a same length. The results are illustrated in Fig. 7. It can be seen from the figure that insignificant difference between the two types of material in terms of pressure drop was observed.

This insignificance was also observed by Brutin and Tadrist (2003), and they suggested that with small Reynolds number of less than 100 the effect from the surface roughness on the pressure drop was negligible although this effect was found notable on the transition from laminar to turbulent regime. On the other hand, Mala and Li (1999) observed the dependence of the flow behaviour on the material of the microtubes, where fused silica microtubes required higher pressure gra-

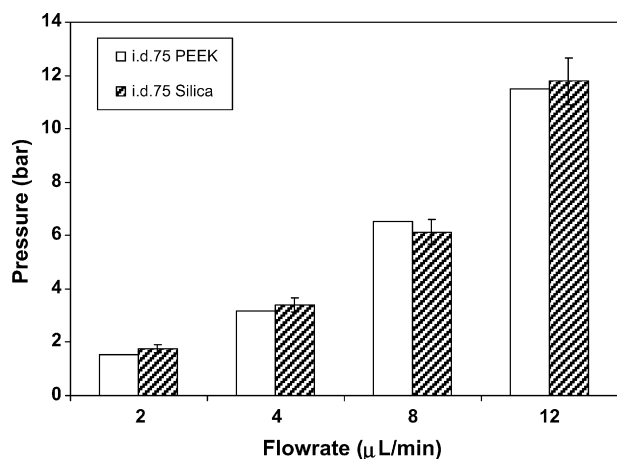


Fig. 7 – Comparison of pressure drops for a same length of microtubes made of PEEK polymer and fused silica.

dients compared to the stainless steel microtubes under the same conditions. The effect of the roughness on the surface of microchannels was also believed, by Peiyi and Little (1983) and Papautsky et al. (1999), to be the cause of deviations of the pressure drop from the conventional theory prediction.

3.4. Monitoring of liquid flow through a series of microtubes

As noted above, the measured pressure drop for liquid flow is very sensitive to the tube diameter and this can give rise to apparent discrepancies between microfluidics and macroscale theory. However, if there are no complications due to rough surfaces, measuring the pressure drop can provide a sensitive and non-destructive method of estimating the dimensions of channel sections. During the filling of an empty microtube, the measured pressure drop increases in proportion to the filled length and the pressure drop per unit of filled length depends on the channel cross section dimensions in the section of interest.

To investigate this aspect, we have monitored the pressure drop as a function of time as squalane is pumped at a constant volumetric flow rate though a series of three connected tube sections of different dimensions. The three sections were 26.5 cm of 250 μm i.d., 11 cm of 500 μm i.d. and 44 cm of 150 μm i.d. The time needed for the liquid to fill each section is given by

$$t = \frac{L}{u} = \frac{L\pi D^2}{4F} \quad (5)$$

For a fixed flow rate of 15 $\mu\text{L}/\text{min}$, the tube section filling times are 52 s, 86 s and 31 s respectively and 26 s, 45 s and 15.5 s for a flow rate of 30 $\mu\text{L}/\text{min}$. Fig. 8 shows the pressure drop as a function of time along the three pieces of microtubes with inner diameters of 250 μm , 500 μm and 150 μm , respectively. It can be seen that the plot clearly indicates the changes in tube dimensions experienced by the moving liquid front. It is also seen that the plot scales as expected with the set volumetric flow rate. Using Eqs. (1), (3) and (4), the curve of pressure versus time was calculated and is compared with the measured data in Fig. 8. The agreement is good indicating that the relaxation time considerations derived initially for changing pump flow rates also apply to considerations of time dependent changes in hydrodynamic resistance to flow. Thus, the measurement of pressure drop along a microtube could be used for in-situ monitoring of liquid passing through the microtube. Moreover, if

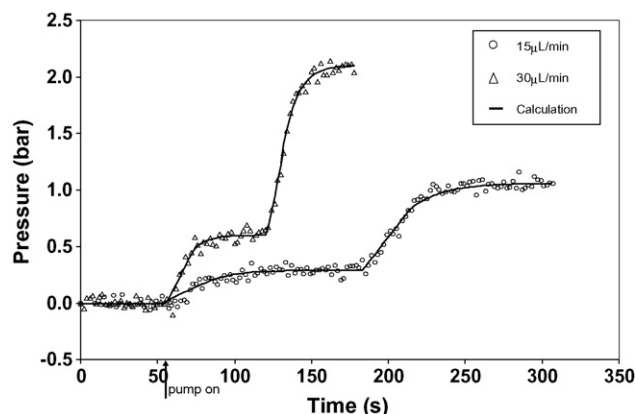


Fig. 8 – Pressure drop versus time for a series of three pieces of tubes with different diameters.

the sensitivity and accuracy of the sensor and data acquisition system are high enough, a change in the microchannel dimension could be detected with a sudden pressure variation.

4. Conclusions

The liquid flow driven by a syringe pump within microtubes in a range of very low Reynolds numbers (< 0.15) was investigated by monitoring the pressure change *in situ*. Cylindrical microtubes with diameters ranging from 50 μm to 500 μm were examined and two types of tube material, namely PEEK polymer and fused silica were compared. A good linear relation for the pressure drop versus flow rate was obtained. Apparent deviations between the measured slopes with those calculated using conventional theory were attributed to uncertainties in the calculated values which are dominated by the uncertainties in the microtube diameters. It was found that a period of stabilisation was required for reaching a steady flow after the syringe pump was switched on/off or to a different flow rate. The stabilisation time was likely due to the compressibility of the fluid. These relatively long stabilisation times (tens of seconds, contrasting sharply with ms flow switching times by electrokinetic pumping) have implications for pressure-driven flow control in Lab-on-a-chip microreactor applications where interconnecting tubing or on-chip pumping/valving is used. By comparing the two types of microtubes made of either PEEK polymer or fused silica, insignificant difference was found between the two types of material in terms of flow resistance. This approach of *in-situ* monitoring of pressure drop in microchannel liquid flow systems provides a simple and effective means of monitoring the liquid flow and can be used as a non-destructive method to characterize the local dimensions of the channel sections. Conversely, the method would also enable the detection of viscosity changes in specific channel sections. In addition to miniaturizing viscosity measurements of pure liquids, viscosity changes would enable *in-situ* detection of diverse processes such as protein denaturation and emulsion instability.

Acknowledgement

The financial support provided by the UK's Engineering and Physical Sciences Research Council (EPSRC) is acknowledged.

References

- Allison, A.C., 1999, Squalene and squalane emulsions as adjuvants. *Methods*, 19: 87–93.
- Brutin, D. and Tadrist, L., 2003, Experimental friction factor of a liquid flow in microtubes. *Phys Fluids*, 15: 653–661.
- Chaomleffel, J.-P., Dalmaz, G. and Vergne, P., 2007, Experimental results and analytical film thickness predictions in EHD rolling point contacts. *Tribology Int*, 40: 1543–1552.
- S.B. Choi, R.F. Barron, R.O., (1991). Warrington, Proc. ASME, DSC Vol. 32, Atlanta, Dec. 1–6.
- de Ruijter, M., Koelsch, P., Voue, M., De Coninck, J. and Rabe, J., 1998, Effect of temperature on the dynamic contact angle. *Colloids Surf A: Physicochem Eng Aspects*, 144: 235–243.
- Ehrfeld, W., Hessel, V. and Lowe, H., (2000). *Microreactors*. (Wiley-VCH, Weinheim).
- Fletcher, P.D.I., Haswell, S.J. and Zhang, X., 2002, Electrokinetic control of a chemical reaction in a lab-on-a-chip micro-reactor: measurement and quantitative modeling. *Lab Chip*, 2: 102–112.
- Hilgers, L.A.Th., Lejeune, G., Nicolas, I., Fochesato, M. and Boon, B., 1999, Sulfolipo-cyclodextrin in squalane-in-water as a novel and safe vaccine adjuvant. *Vaccine*, 17: 219–228. <http://www.sigmaaldrich.com>. <http://www.upchurch.com>.
- Jensen, K.F., 2001, Microreaction engineering – is small better? *Chem Eng Sci*, 56: 293–303.
- Jiang, X.N., Zhou, Z.Y., Yao, J., Li, Y. and Ye, X.Y., 1995, Micro-fluid flow in microchannel, In *Proc. Transducers 95*, pp. 317–320.
- Koo, J. and Kleinstreuer, C., 2003, Liquid flow in microchannels: experimental observations and computational analyses of microfluidics effects. *J Micromech Microeng*, 13: 568–579.
- Kumagai, A., Tomida, D. and Yokoyama, C., 2007, Measurements of the liquid viscosities of mixtures of isobutane with squalane to 30 MPa. *Int J Thermophys*, 28: 1111–1119.
- Lide, D.R., (2003). *CRC Handbook of Chemistry and Physics* (84th ed.). (CRC Press, London).
- Ling, G.H. and Shaw, M.T., 2008, Reversible thermal gelation of soft semi-crystalline polyethylene microparticles with surface interactions in squalane. *Polymer Eng Sci*, 48: 329–335.
- Mala, G.M. and Li, D., 1999, Flow characteristics of water in microtubes. *Int J Heat Fluid Flow*, 20: 142–148.
- Papautsky, I., Brazzle, J., Ameen, T. and Frazier, A.B., 1999, Laminar fluid behavior in microchannels using micropolar fluid theory. *Sens Actuators A: Phys*, 73: 101–108.
- Papautsky, I., Ameen, T. and Frazier, A.B., 2001, A review of laminar single-phase flow in microchannels, In *Proc. Int. Mech. Eng. Cong. Expos. ASME*, pp. 1–9.
- Peiyi, W. and Little, W.A., 1983, Measurement of friction factors for the flow of gases in very fine channels used for microminiature Joule-Thomson refrigerators. *Cryogenics*, 23: 273–277.
- Pfahler, J., Harley, J., Bau, H. and Zemel, J., 1990, Liquid transport in micron and submicron channels. *Sens Actuators A: Phys*, 22: 431–434.
- Schütte, R., Matlosz, M., Renken, A., & Liauw, M. (eds) 2006, *Proceedings of the 9th International Conference on Microreaction Technology (IMRET9)*.
- Shahiwala, A. and Amiji, M.M., 2008, Enhanced mucosal and systemic immune response with squalane oil-containing multiple emulsions upon intranasal and oral administration in mice. *J Drug Target*, 16: 302–310.
- Sharp, K.V., Adrian, R.J. and Beebe, D.J., 2000, Sharp, K.V., Adrian, R.J., Santiago, J.G. and Molho, J.I., (2002). Gad-el-Hak, M. (Ed.), *The MEMS Handbook* (CRC Press, London), 6.1–6.38 (Chapter 6)
- Spence, D.M. and Crouch, S.R., 1998, An investigation of internal pressures in capillary flow injection systems. *Anal Chim Acta*, 358: 95–101.
- Tuckerman, D.B. and Pease, R.F.W., 1981, High-performance heat sinking for VLSI. *IEEE Electron Dev Lett EDL-2*, 126–129.
- Viovy, J.-L. (ed) 2007, *Proceedings of the 11th International Conference on Miniaturized Systems for Chemistry and Life Sciences (μ -TAS 2007)*.
- Weilin, Q., Mala, G.M. and Donqing, L., 2000, Pressure-driven water flows in trapezoidal silicon microchannels. *Int J Heat Mass Transfer*, 43: 353–364.
- Wilding, P., Pfahler, J., Bau, H.H., Zemel, J.N. and Kricka, L.J., 1994, Manipulation and flow of biological fluids in straight channels micromachined in silicon. *Clin Chem*, 40: 43–47.
- Xu, B., Ooi, K.T., Wong, N.T. and Choi, W.K., 2000, Experimental investigation of flow friction for liquid flow in microchannels. *Int Comm Heat Mass Transfer*, 27: 1165–1176.
- Yu, D., Warrington, R., Barron, R. and Ameen, T., 1995, Zhang, X., Cooper, J.M., Monaghan, P.B. and Haswell, S.J., 2006, Continuous flow separation of particles within an asymmetric microfluidic device. *Lab Chip*, 6: 561–566.
- Zhang, X., Jones, P. and Haswell, S.J., 2008, Attachment and detachment of living cells on modified microchannel surfaces in a microfluidic based lab-on-a-chip system. *Chem Eng J*, 135: S82–S88.



The use of immobilized crown ethers as in-situ N-protecting groups in organic synthesis and their application under continuous flow

Gareth. P. Wild^a, Charlotte Wiles^{a,b}, Paul Watts^{a,*}, Stephen J. Haswell^a

^aDepartment of Chemistry, University of Hull, Cottingham Road, Hull, HU6 7RX, UK

^bChemtrix BV, Burgemeester Lemmensstraat 358, 6163JT Geleen, The Netherlands

ARTICLE INFO

Article history:

Received 10 October 2008

Received in revised form 26 November 2008

Accepted 11 December 2008

Available online 24 December 2008

ABSTRACT

In addition to their high affinity for inorganic cations, crown ethers have been shown to efficiently sequester ammonium ions, forming a stable adduct via hydrogen bonding. Using this principle, several authors have reported the use of crown ethers as protecting groups for amines however to date, their widespread use has been somewhat precluded by the difficulties associated with removal of the crown ether from the resulting reaction mixture. In order to address this problem, we report the preparation of an immobilized 18-crown-6 ether derivative and its incorporation into a flow reactor, demonstrating the ability to use and recycle the reagent for the chemoselective O-acylation and alkylation of bifunctional compounds such as 4-(2-aminoethyl)phenol and 4-nitrophenol.

© 2009 Elsevier Ltd. All rights reserved.

1. Introduction

When conducting the synthesis of polyfunctionalized molecules it is often necessary to render one or more of the functionalities within the molecule temporarily inert in order to allow the selective reaction of another group. This process is achieved by appending a blocking group, which is stable to the reaction conditions under investigation whilst being readily removed; such a moiety is termed as a protecting or protective group.¹ While the use of protecting groups has enabled access to a vast library of complex molecules over the years, by removing functional group incompatibilities, their use can be disadvantageous as the introduction and removal of such groups generates additional synthetic steps. This can lead to increased costs and contribute to reductions in overall yield, along with the need to perform complex purifications in order to remove any protecting group residues from the final material. Furthermore, the deprotection strategy must be carefully selected in order to ensure that the product is obtained in the desired form i.e. as the free functionality or as a salt.

1.1. The use of crown ethers in organic synthesis

In addition to the propensity of crown ethers to form complexes with metal ions (Li⁺, Na⁺, K⁺, Rb⁺, Cs⁺) and promote solubility in non-polar media, Pederson² also reported their ability to form complexes with ammonium ions (R-NH₃⁺). Further work by

Bushmann and Mutihac³ compared the degree of ammonium ion complexation with various functionalized and un-functionalized crown ethers, concluding that 18-crown-6 ethers afforded superior complexation cf. to smaller crown ethers. As depicted in Figure 1, unlike metal ions, the ammonium ion is held above the cavity of the crown ether in a tetrahedral configuration via hydrogen bonding⁴ with stabilization achieved due to distribution of the positive charge on the ammonium ion over the hydrogen atoms. The geometry of the complexed ammonium ion also leaves the remainder of the molecule unhindered and available to take part in subsequent reactions as demonstrated by Kunishima et al.^{4b}

In the early 1990s, Mascagni and Hyde⁵ exploited this phenomena for the synthesis of peptides and oligomers, proposing that the non-covalent nature of the interaction between the crown ether and the ammonium ion would provide a mild protection strategy for amines. Employing dibenzo-18-crown-6 ether (DB-18-c-6) and an array of alanine salts (HCl, TFA and *p*-TSA), the effect of solvent polarity on a coupling reaction was evaluated. During this investigation it was observed that tosylate salts formed the most stable complexes (*p*-TSA>TFA>HCl) and that complex stability increased with decreasing solvent polarity; an observation that was

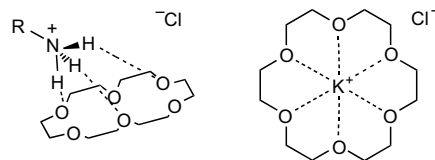


Figure 1. Schematic illustrating the modes of complexation observed for ammonium ions versus metal ions with 18-c-6 ether.

* Corresponding author. Tel.: +44 1482 465471.

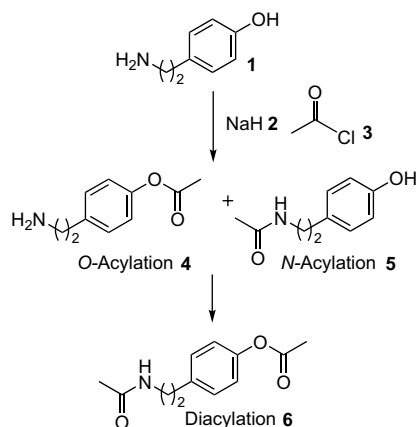
E-mail address: p.watts@hull.ac.uk (P. Watts).

attributed to a reduction in competition between solvation of the cation and coordination by the crown ether.⁵ Consequently, subsequent coupling reactions were performed in DCM and found to afford the desired complexed tripeptide in 80% yield, with the remainder comprising of mixed oligomers; the formation of which was attributed to partial decomplexation of the peptide during the reaction.⁶ The authors subsequently reported the decomplexation of another tripeptide using aq KCl, exploiting the crown ethers affinity for metal ions to force out the ammonium ion and leaving the crown ether complexed with potassium, as depicted in Figure 1. Although this approach demonstrated the key components of a protecting group strategy, namely the ability to protect an amino acid, perform a coupling reaction and deprotect the resulting peptide, the use of stoichiometric quantities of crown ether proved disadvantageous due to difficulties associated with its removal from the reaction product. As such, isolation of the peptide, regeneration of the crown ether cavity and subsequent re-use of the crown ether were not demonstrated by the authors.

Based on the preliminary observations made by Mascagni et al.^{5,6} it was proposed that the preparation of an immobilized 18-crown-6 ether derivative would facilitate the process of amine deprotection, along with product isolation and subsequent crown ether regeneration. With this in mind, our aim was to develop a non-covalent protecting group strategy using an immobilized 18-crown-6 ether derivative and combine it with continuous flow methodology, developed within our group, to demonstrate efficient O-acetylation/alkylation of substituted 1° amines.

2. Results and discussion

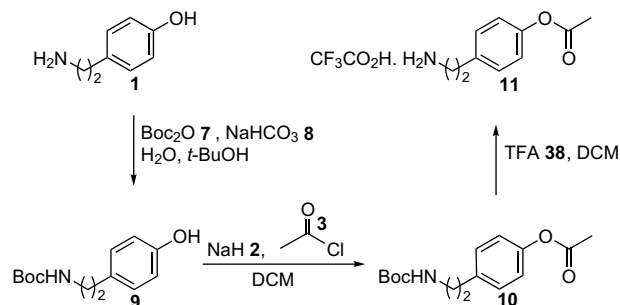
Owing to the highly basic and nucleophilic nature of an amine group, protection is essential in reactions such as acylations and alkylations. This is illustrated for the bifunctional compound tyramine **1**, which contains both aromatic alcohol and aliphatic amine functionalities. As depicted in Scheme 1, failure to protect the amine group and direct the reaction to the phenolic group upon treatment of tyramine **1** with NaH **2** (1.0 equiv) and acetyl chloride **3** (1.2 equiv) results in a complex mixture containing the desired tyramine acetate (4-(2-aminoethyl)-phenyl acetate) **4** (23%), along with tyramine *N*-acetate (*N*-[2-(4-hydroxyphenyl)ethyl]-acetamide) (12%) **5**, tyramine diacetate (acetic acid 4-(2-acetylami-noethyl)-phenyl ester) (20%) **6** and residual starting material **1** (45%).



Scheme 1. Schematic illustrating the potential reaction products obtained when acetylating tyramine **1**.

In order to benchmark the developed non-covalent protecting group strategy against existing covalent approaches, the acetylation of tyramine **1** was subsequently performed using the acid

labile *tert*-butoxycarbonyl (Boc) protecting group. As depicted in Scheme 2, the reaction sequence firstly involved the protection of tyramine **1**, using di-*tert*-butyl dicarbonate **7** in the presence of NaHCO₃ **8**, which afforded the intermediate Boc-tyramine **9** as a white solid (93% yield). Subsequent acylation, with acetyl chloride **3** (1.2 equiv) in the presence of NaH **2** (1.0 equiv) afforded the desired Boc-tyramine acetate **10** as a pale yellow gum (69% yield).



Scheme 2. Schematic of the covalent protecting group strategy employed to synthesize tyramine acetate TFA salt **11**.

Although the use of a protecting group afforded a chemoselective route to the O-acetylation of tyramine **4**, in addition to increasing the number of reaction steps employed in the synthetic pathway, removal of the protecting group proved problematic, affording a mixture of tyramine acetate TFA salt **11** (69%), tyramine TFA salt **12** (16%) and Boc-tyramine acetate **10** (15%) as determined by HPLC. In an analogous manner to the direct acetylation of tyramine **1** (Scheme 1), the use of a protecting group afforded a complex reaction mixture, largely due to problems associated with the efficient removal of the Boc-protecting group. Furthermore, in order to isolate the desired tyramine acetate **4** it was necessary to free-base the TFA salt **11** thus incurring additional reaction steps.

2.1. Evaluation of immobilized crown ethers as non-covalent protecting groups

In order to evaluate the use of an immobilized crown ether as a protecting group, preliminary investigations were conducted using the commercially available di-*tert*-butylcyclohexano-18-crown-6 ether on an inert chromatographic support (0.37 mmol g⁻¹) (Eichrom Technologies, France). To assess the potential of di-*tert*-butylcyclohexano-18-c-6 as a non-covalent protecting group, the ability of the material to complex tyramine HCl **13** and subsequently decomplex tyramine **1** was firstly investigated. This was achieved by stirring the crown ether with tyramine HCl **13** in MeOH, prior to filtration, under suction, to remove any uncomplexed tyramine HCl **13**. To confirm sequestration had occurred, the immobilized complex was treated with methanolic KCl **14**, to induce decomplexation, and the resulting filtrate analyzed by HPLC. Initial results were pleasing and detection of tyramine **1** confirmed the ability of the material to complex tyramine HCl **13** and release tyramine **1** from the crown ether cavity. To demonstrate re-use of the supported crown ether, the cavity was regenerated and the above procedure repeated; unfortunately, upon analysis of the filtrate no tyramine **1** was detected. Employing a fresh portion of the solid-supported crown ether again confirmed sequestration of tyramine HCl **13** and release of the amine **1**. It was therefore postulated that during the regeneration step the crown ether, which was only adsorbed onto the solid support, leached from the support and therefore could not be efficiently recycled or employed in a continuous system.

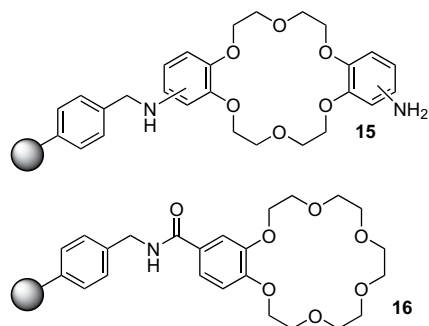


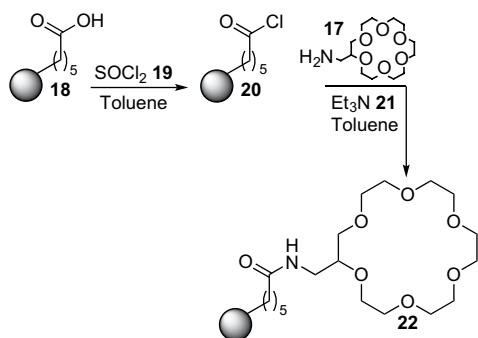
Figure 2. Illustration of two immobilized crown ethers that was found to complex metal ions but not ammonium ions.

2.1.1. Preparation of an immobilized crown ether

To address if desorption of the crown ether was the problem, we evaluated the covalent immobilization of three 18-crown-6 ether derivatives and subsequently evaluated the materials towards the sequestration of ammonium salts under continuous flow. With this in mind, several immobilization techniques were employed, with starting materials including diamino-dibenzo-18-crown-6 ether and carboxybenzo-18-crown-6 ether to afford crown ethers **15** and **16**, respectively, as depicted in **Figure 2**.

Unfortunately, due to the increased ring strain observed as a result of immobilization, neither material was able to complex ammonium ions, a process, which is reliant on hydrogen bonding (**Fig. 1**), however, both materials successfully sequestered potassium permanganate (0.12 mmol g^{-1} and 0.98 mmol g^{-1} , respectively) confirming the presence of active crown ether moieties.

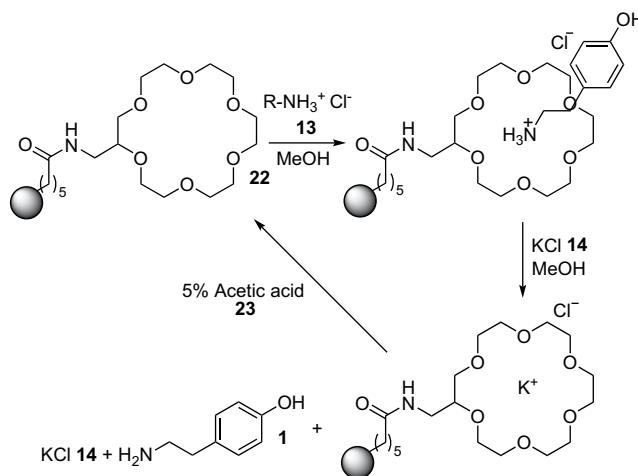
Owing to the reliance of ammonium ion complexation on hydrogen bonding (**Fig. 1**), it is imperative for the immobilized crown ether to be free of strain in order to form a stable complex. With this in mind, a further attempt was made to prepare a covalently bound 18-crown-6 ether with no ring strain, this was achieved by employing aminomethyl-18-crown-6 ether (AM-18-c-6) **17** as a precursor. As **Scheme 3** illustrates, treatment of carboxypolystyrene **18** with thionyl chloride **19** afforded the immobilized acid chloride **20**, to which was added Et_3N **21** followed by AM-18-c-6 **17** to afford immobilized AM-18-c-6 **22**.



Scheme 3. Synthetic protocol employed for the covalent immobilization of AM-18-c-6 **17** to carboxypolystyrene **18**.

To evaluate the materials ability to sequester ammonium ions, the crown ether **22** was stirred at room temperature in a methanolic solution of tyramine HCl **13**, filtered under suction and washed with MeOH prior to treatment with methanolic KCl **14** to release any complexed tyramine HCl **13** as the free amine **1**. Analysis of the filtrate by HPLC confirmed the presence of tyramine **1** and elemental analysis of the crown ether **22**, coupled with sequestration of KMnO_4 followed by ICP-MS analysis, confirmed the material to have a loading of 0.37 mmol g^{-1} .

Having identified the presence of active crown ether cavities on the solid-support **22**, the ability to recycle the material was subsequently investigated, with removal of the potassium cation achieved using methanolic acetic acid **23**. Once successfully regenerated, the cycle was repeated a further four times and unlike the commercially available di-*tert*-butylcyclohexano-18-c-6, all subsequent cycles yielded tyramine **1**, with an 11.4% RSD ($n=5$) (**Scheme 4**).



Scheme 4. Reaction scheme illustrating the complexation of tyramine HCl **13**, using immobilized AM-18-c-6 **22**, and subsequent decomplexation and cavity regeneration.

Although the material was able to be recycled, illustrating the robustness required for continuous processing, the irreproducible quantities of tyramine **1** recovered were still undesirable. In order to identify the origin of any irreproducibility, an aliquot of immobilized crown ether was taken at each stage of the process and subjected to elemental analysis. As **Table 1** illustrates, the decomplexation step was found to be 100% efficient and as such, the gradual decrease in the proportion of tyramine **1** recovered was attributed to loss of immobilized crown ether **22** upon filtration and washing.

Table 1

Elemental analyses illustrating the efficient complexation and decomplexation achieved using immobilized crown ether **22**

Polymeric material	N (%)	N (mmol g^{-1})
Blank 18	0.00	0.00
Immobilized AM-18-c-6 22	0.52	0.37
Complexed	0.97	0.69
Decomplexed	0.52	0.37

2.1.2. Continuous flow evaluation of crown ether

In order to address the irreproducibility associated with the batch process and develop an efficient, re-useable system for the non-covalent protection of amines, the incorporation of the immobilized crown ether into a continuous flow reactor was

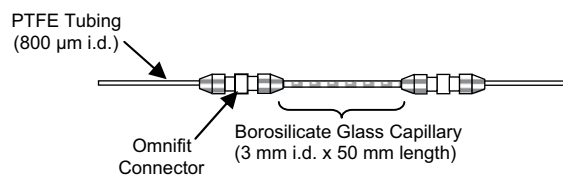


Figure 3. Schematic of the continuous flow reactor used herein for the evaluation of an immobilized crown ether **22**.

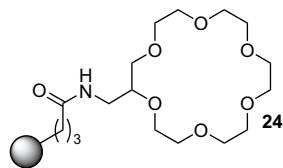


Figure 4. SILICA AM-18-c-6 **24** prepared via the acid chloride.

investigated. It was proposed that such an approach would enable material **22** to be recycled with ease as solutions of the various reactants would be pumped through crown ether **22** in order to conduct the desired reaction step; thus removing the main source of error observed thus far, loss of material upon filtration.

As Figure 3 illustrates, the flow reactor comprised of a borosilicate glass capillary (50 mm (length)×3 mm (i.d.)) packed with ~0.15 g of immobilized crown ether **22**. Reactant solutions were passed through the reactor using a syringe pump and reaction products collected in a sample vial prior to off-line analysis by HPLC.⁷ To increase the reproducibility of the technique further, reactants were introduced into the system via a Rheodyne valve (200 μL sample loop).

Employing a solvent stream of MeOH, tyramine HCl **13** (0.3 M, 6.0×10^{-2} mmol) was introduced into the flow reactor, containing immobilized AM-18-c-6 **22** (0.15 g, 5.6×10^{-2} mmol) at a flow rate of $100 \mu\text{L min}^{-1}$. Decomplexation was again achieved using KCl **14** in MeOH (0.3 M, 6.0×10^{-2} mmol) and the column purged with 5% acetic acid **23** in MeOH to regenerate the crown ether **22**. Using this approach, 0.35 mmol g^{-1} of tyramine **1** was released with an RSD of 4.3% ($n=10$), demonstrating a dramatic increase in reproducibility cf. the 11.4% obtained in batch.

While the use of MeOH was found to be ideal for complex formation, decomplexation and cavity regeneration, the solvent is not suitable for the reactions under investigation herein. As such, a series of alternative solvents were investigated, these included DMF, THF, DCM and MeCN. Unfortunately, when this series of common organic solvents were employed, the immobilized AM-18-c-6 **22** was observed to swell, leading to blockages within the reactor and inconsistencies in the volume of solution passing through the packed bed at any one time. This observation was attributed to the low degree of crosslinking within the carboxypolystyrene **18** (1% DVB) employed as a solid support and was confirmed by packing the reactor with polystyrene crosslinked with 2% DVB whereby no swelling was observed. Regrettably, carboxypolystyrene **18** was not available with a higher degree of crosslinking and as such, 3-carboxypropyl functionalized silica gel was evaluated as an alternative, non-swelling support material.

2.1.3. Preparation and evaluation of SILICA AM-18-c-6

Having successfully immobilized AM-18-c-6 **17** onto carboxypolystyrene **18** via the acid chloride, an analogous approach was employed for the derivatization of 3-carboxypropyl functionalized silica gel, as depicted in Figure 4, affording a loading of

0.16 mmol g^{-1} . Prior to performing a reaction, material's **24** stability to DMF, THF, DCM and MeCN was evaluated and unlike immobilized crown ether **22**, all solvents were able to be pumped through the reactor at $100 \mu\text{L min}^{-1}$ with no sign of swelling or restricted flow over a period of 8 h. Having demonstrated the materials stability, its ability to complex tyramine HCl **13** and release tyramine **1** was evaluated. Employing a solvent stream of MeOH, tyramine HCl **13** (0.12 M, 2.4×10^{-2} mmol) was introduced into the flow reactor, containing SILICA AM-18-c-6 **24** (0.15 g, 2.4×10^{-2} mmol) at a flow rate of $100 \mu\text{L min}^{-1}$. Decomplexation was again achieved using KCl **14** in MeOH (0.12 M, 2.4×10^{-2} mmol) and the column washed with 5% acetic acid **23** in MeOH to regenerate the crown ether **24**. Using this approach, a loading of 0.16 mmol g^{-1} was obtained, which was in agreement with ICP-MS analysis performed on the respective potassium complex.

2.1.4. Evaluation of complex stability

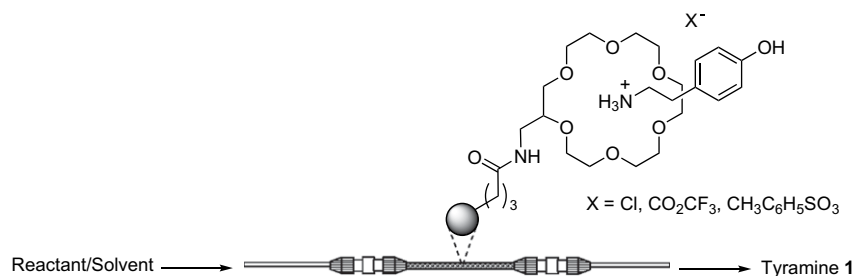
Once complexed, it was important to determine how stable the ammonium salt was to various solvents and reactants that may be employed in the derivatization of the complexed material. To ensure the investigation provided general conclusions for this non-covalent protecting group strategy, three ammonium salts were investigated (tyramine HCl **13**, then tyramine TFA **12** and finally tyramine *p*-TSA **25**). As before, complexation was achieved by injecting a 200 μL plug of the tyramine salt under investigation (0.12 M, 2.4×10^{-2} mmol) into a continuous MeOH stream ($100 \mu\text{L min}^{-1}$) (Scheme 5), which ensured complete washing of the resin prior to evaluating the stability of the complex under the selected reaction condition, followed by decomplexation with KCl **14** in MeOH (0.12 M, 2.4×10^{-2} mmol) and analysis by HPLC (Tables 2–5).

2.1.4.1. Solvent stability. To determine the stability of the ammonium salts of tyramines **12**, **13** and **25**, each solvent illustrated in Table 2 was pumped through the reactor at $100 \mu\text{L min}^{-1}$ for 5 min prior to analysis of the reactor effluent by HPLC; all solvents were evaluated five times and the average result is presented. With the

Table 2

Evaluation of complex stability to a series of common organic solvents ($n=5$)

Solvent	Stability of complex (%)		
	Tyramine HCl 13	Tyramine TFA 12	Tyramine <i>p</i> -TSA 25
Acetone	100	100	100
Methanol	100	100	100
Ethanol	100	100	100
Dichloromethane	100	100	100
Diethyl ether	100	100	100
Hexane	100	100	100
Toluene	100	100	100
Water	100	100	100
Acetonitrile	100	100	100
Tetrahydrofuran	100	100	100
DMF	18	34	44



Scheme 5. Set-up used to evaluate the stability of tyramine HCl **13**, TFA **12** and *p*-TSA **25** salts to an array of reactants and solvents.

Table 3
Summary of the stability of tyramine HCl **13**, TFA **12** and *p*-TSA **25** to a variety of common amines in MeOH (*n*=5)

Amine	<i>pK_b</i>	Stability of complex (%)		
		13	12	25
3° Et ₃ N 21	11.06	100	100	100
3° DIEA	10.50	48	54	69
3° <i>N</i> -Methylpiperidine	10.08	51	53	68
3° TMEDA 26	6.10	0	0	0
3° Lutidine	6.75	100	100	100
2° Diethylamine	11.09	27	48	89
2° Piperazine	9.82	37	47	57
2° Piperidine	11.22	40	54	81
2° Diisopropylamine	11.05	57	61	73
2° Dimethylamine	10.73	50	58	69
1° Aniline	4.63	27	58	78
1° Benzylamine	9.33	50	64	73
1° 2-Phenylethylamine	9.58	39	61	53
1° 3-Phenylpropylamine	9.68	49	57	63

Table 4
Stability of tyramine HCl **13** complexed SILICA AM-18-c-6 **24** when exposed to a plethora of common reactants

Substrate type	Compound	Stability of complex (%)
Cation/anion	KOH	0
Cation/anion	NaOH	0
Cation/anion	LiOH	0
Cation/anion	KCl	0
Cation/anion	NaCl	0
Cation/anion	LiCl	0
Cation/anion	K ₂ CO ₃	46
Cation/anion	Na ₂ CO ₃	0
Cation/anion	Li ₂ CO ₃	50
Reactant	Acetyl chloride 3	100
Reactant	Acetic anhydride 26	100
Reactant	DMAP	47
Reactant	DCC	45
Reactant	EDCI	50
Reactant	Methyl iodide 27	0
Acid	TFA 38	100
Acid	HCl	100
Acid	Acetic acid 23	100
Acid	Sulfuric acid	100

Table 5
Summary of the ammonium salts evaluated under continuous flow and their ability to form complexes with SILICA AM-18-c-6 **24**

Effect	Amine	Complexation (%)
Cation	Tyramine <i>p</i> -TSA 25	100
Cation	Tyramine TFA 12	100
Cation	Tyramine HCl 13	100
No cation	Tyramine 1	0
Free amine	Aniline	0
Free amine	Benzylamine	0
Free amine	2-Phenylethylamine	0
Free amine	3-Phenylpropylamine	0
Chain length	Aniline HCl	100
Chain length	Benzylamine HCl	100
Chain length	Phenylethylamine HCl	100
Chain length	Phenylpropylamine HCl	100
Chain length	4-Aminophenol HCl 35	100
Steric	L-β-Alanine benzyl ester HCl 29	0
Steric	(S)-(-)-2-Amino-3-phenyl-1-propanol HCl 30	0
Functionality	Benzamide HCl 31	0

exception of DMF, the complexes were found to be stable to all solvents investigated and interestingly, the proportion of tyramine **1** displaced by DMF ranged from 66 to 82% depending on the ammonium salt under investigation. The results from this study herein suggest therefore that the basic nature of DMF induces decomplexation, thus removing the protecting capacity of the crown ether and potentially resulting in undesirable reaction of the free amine functionality. Mascagni and Hyde^{5a} also observed this trend, *p*-TSA>TFA>HCl, suggesting that stability increased as a function of cation conjugation.

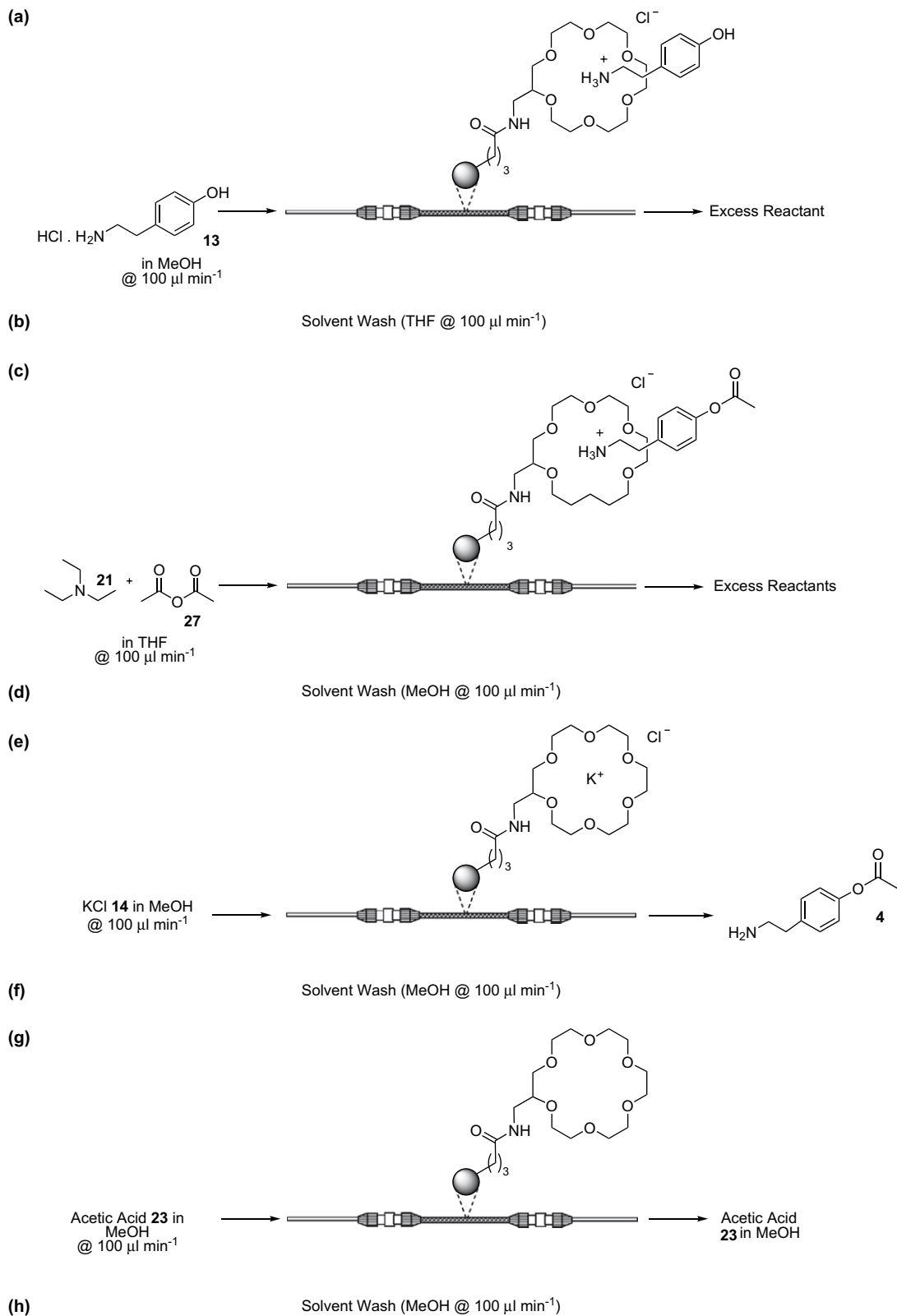
2.1.4.2. Complex stability in the presence of amines. In addition to the use of organic solvents, many reactions that require the protection of amine functionalities involve the use of compounds containing other amine moieties; as such it was important to identify, which of those reagents were compatible with the protecting group strategy under investigation. Using the aforementioned complexation strategy, the effect of an array of amines (0.12 M, 2.4×10⁻² mmol) on the complex stability was investigated, with the data presented in Table 3 highlighting an obvious trend of increased complex stability towards 3° amines; with 1° amines causing the greater degree of destabilization. This general trend of complex stability, 1°<2°<3°, has some obvious exceptions such as lutidine and Et₃N **21**, which have no destabilizing effect, an observation that is attributed to their steric bulk. As a result, however, these bases may be useful as reagents in future reactions, such as in the deprotonation of the phenolic moiety in the model reaction.

Interestingly, *N,N,N',N'*-tetramethylethylenediamine **26** (TMEDA) was found to afford quantitative decomplexation for all three salts **12**, **13** and **25**; an observation that compares favourably with reports by Hyde et al.^{5b} who found diisopropylethylamine (DIEA) induced decomplexation of an ammonium salt. In comparison to TMEDA **26**, however, DIEA afforded only 31–52% decomplexation, depending upon the salt employed. As such, the advantages of TMEDA **26** as a decomplexation agent are discussed in Section 2.1.5.

2.1.4.3. Stability to common reactants and by-products. Further to investigating the complex stability to possible bases and solvents, it was also important to consider other reagents common to synthetic reactions that require the protection of amines. Table 4 illustrates the stability of the tyramine HCl **13** complexed with SILICA AM-18-c-6 **24** when exposed to a plethora of possible reactants (0.12 M, 2.4×10⁻² mmol) such as those used for peptide couplings, acetylations and methylations.

Common reagents for acylation (acetyl chloride **3**, acetic anhydride **27**) and alkylation (methyl iodide **28**) were observed to have no destabilizing effect, however, reagents employed in coupling reactions such as DMAP, DCC and EDCI were all found to cause varying degrees of decomplexation. This is an observation that would go some way towards explaining the poor reaction control reported by Mascagni et al.,⁵ as upon deprotection, the amino acid could take part in random solution phase couplings to afford oligomers.

Entries 1–9 (Table 4) were investigated for the purpose of gaining further understanding into the decomplexation process as well as identifying possible reagents for use in future reactions; all solutions evaluated were saturated in MeOH. Of the three metal salts investigated, lithium was found to have the least affinity for the 18-c-6 ether due to its small cation size, followed by sodium. In addition to decomplexation, potassium hydroxide was found to be unsuitable for use with the solid-supported crown ether **24** as it was found to cleave AM-18-c-6 **17** from the support (confirmed by ICP-MS analysis). In comparison to the metal alkoxides, carbonates are weaker inorganic bases, which exhibit relatively poor dissociation in solution, resulting in a lower concentration of available

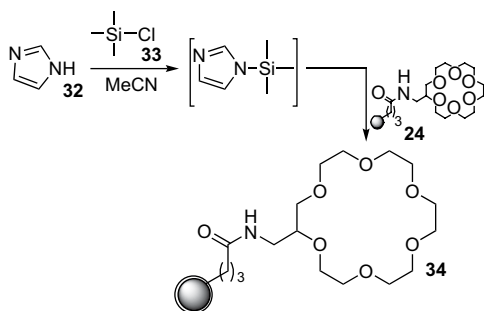


Scheme 6. Schematic illustrating the reaction steps used to evaluate the synthesis of tyramine acetate **4** under continuous flow.

metal ions, which leads to the observed increase in complex stability.

In addition, acid catalyzed reactions are also commonly employed and thus a range of acids, which are known to remove inorganic ions from crown ether cavities, were tested for their

effect on ammonium complex stability, this time focusing on the tyramine HCl **13** complex as it had been shown to be the least stable of the three salts evaluated thus far. As Table 4 illustrates, it was pleasing to see that the acids evaluated were found to have no effect on the complex stability and thus could be



Scheme 7. Schematic illustrating the end-capping protocol employed to prepare TMS SILICA 18-c-6 **34**.

employed as reactants alongside this non-covalent protecting group strategy.

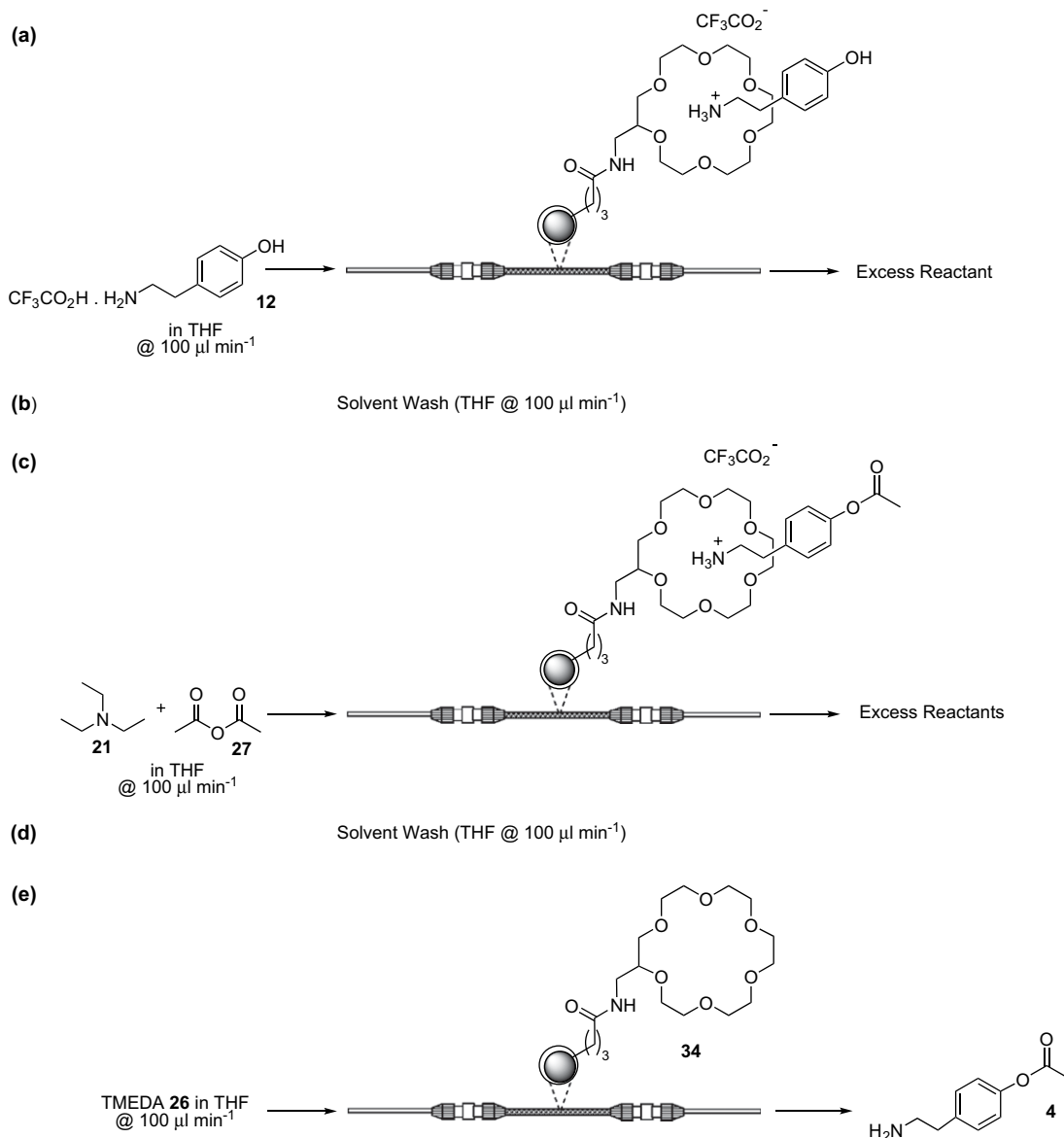
2.1.4.4. Generality of complexation. Recognizing the need for the technique to *N*-protect compounds other than tyramine **1**, a general study was undertaken in order to evaluate factors such as

chain length, steric hindrance, as well as the effect of counterions. Again MeOH was used as the reaction solvent ($100 \mu\text{L min}^{-1}$), reactant concentrations of 0.12 M ($2.4 \times 10^{-2} \text{ mmol}$) were employed, methanolic KCl **14** (0.12 M , $2.4 \times 10^{-2} \text{ mmol}$) afforded decomplexation and the reaction products were analyzed off-line by HPLC.

Table 5 summarizes the results obtained and confirms initial observations whereby no complexation is observed for free amines. In keeping with previous findings the HCl salts of all amines investigated, independent of chain length or aromaticity, were found to complex efficiently. The issue of steric hindrance on complexation was also evaluated, employing α - β -alanine benzyl ester HCl **29** and (*S*)-(-)-2-amino-3-phenyl-1-propanol HCl **30**, in both cases no complexation was observed. Benzamide HCl **31** also failed to complex due to resonance effects experienced by the carbonyl group, which reduces hydrogen bonding between the crown ether and results in the formation of an unstable complex.

2.1.5. The selective acetylation of tyramine

Having successfully developed a supported crown ether **24** capable of sequestering ammonium ions and subsequently evaluated



Scheme 8. Summary of the protocol employed for the continuous flow acetylation of tyramine **1**, using TMS SILICA AM-18-c-6 **34**.

the stability of the complex to a range of common reaction conditions, the final step of the investigation was to perform a reaction on the exposed phenolic moiety. When conducting the acetylation of tyramine in batch, NaH **2** was employed as the base (Scheme 1), however, when employing a crown ether as the protecting group, the presence of sodium is undesirable due to its ability to deprotect the amine (Table 4), consequently Et₃N **21** and acetic anhydride **27** were selected suitable as reactants for the transformation.

With this in mind, Scheme 6 summarizes the proposed reaction sequence for the continuous flow acetylation of tyramine **1**, comprising of N-protection (step (a)), followed by O-acetylation (step (c)), deprotection (step (e)) and crown ether regeneration (step (g)) all punctuated with solvent wash (steps (b), (d), (f) and (h)). Upon evaluation of the reaction under continuous flow, it was disappointing to observe that analysis of the reaction products obtained from step (c) (Scheme 6), afforded only tyramine **1** (2.4×10^{-2} mmol). Therefore, in order to promote the acetylation (step (c)), a range of flow rates (10 – $200 \mu\text{L min}^{-1}$), hence reaction times, were subsequently investigated; unexpectedly all flow rates failed to prepare the desired product **4**. Based on this observation it was postulated that the THF flush performed between reaction steps was not removing MeOH from the reactor prior to the introduction of the acetylating reagents and hence the volume of THF was increased (from 1 mL to 2 mL), however, all subsequent reactions failed, yielding only un-reacted tyramine **1** (2.4×10^{-2} mmol).

As Mascagni⁵ and the work conducted within our laboratory had shown analogous reactions to be possible in the solution phase, the only remaining explanation for the reaction failing was an interaction between the reagents and the solid-support itself, resulting in either quenching or adsorption of the reactants. Consequently, the SILICA AM-18-c-6 **24** was treated with imidazole **32** and chlorotrimethylsilane **33** in MeCN to afford trimethylsilane (TMS) end-capped SILICA AM-18-c-6 **34** (Scheme 7), rendering the support hydrophobic (represented as a white sphere around the solid support).⁸

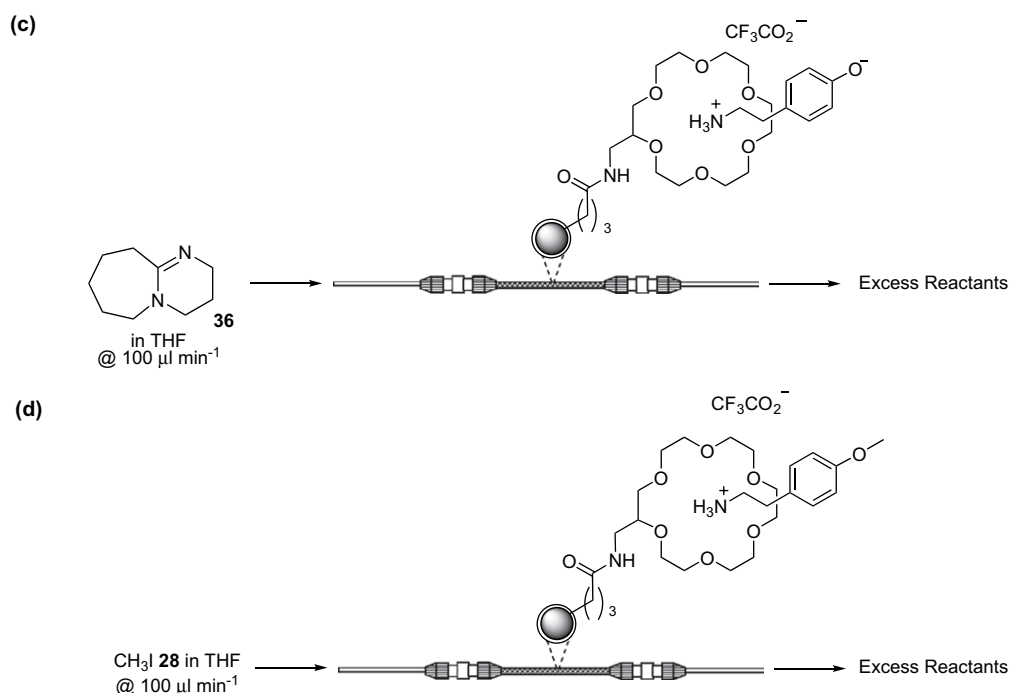
The TMS modified material **34** was subsequently filtered, washed with acetone and oven dried prior to packing into the flow

reactor (0.15 g, 2.4×10^{-2} mmol). At this stage, the reaction sequence illustrated in Scheme 6 was repeated, affording 42% conversion to tyramine acetate **4** and 58% un-reacted tyramine **1**; quantified via internal standardization with biphenyl. Although a proportion of the N-protected tyramine had been successfully acetylated and no N- or di-acetylation was observed, the detection of un-reacted tyramine **1** was again attributed to the presence of residual MeOH, owing to its use as a reaction solvent for the complexation and decomplexation steps ((a) and (e)). Consequently, all efforts to remove MeOH from the process were, therefore, investigated.

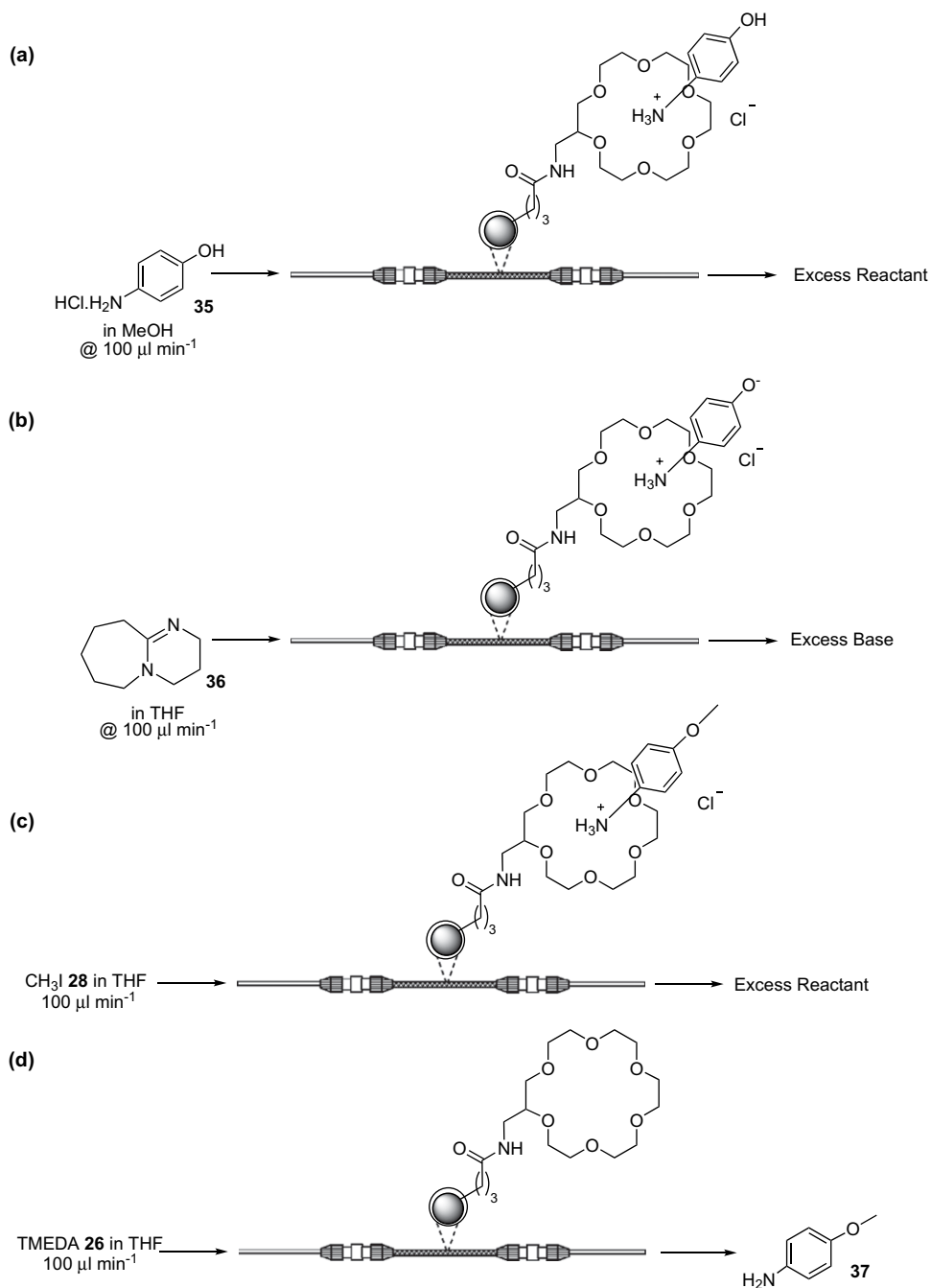
To achieve this, two approaches were investigated, the first involved exploring an alternative decomplexation strategy as KCl **14** was found to be insoluble in THF. As Table 3 illustrates, TMEDA **26** (0.12 M, 2.4×10^{-2} mmol) was shown to quantitatively decomplex all three salts evaluated and owing to its increase solubility in THF cf. KCl **14** it provided an alternative means of decomplexation (% RSD=4.4 ($n=5$)). Furthermore, by employing an organic base, the regeneration steps (f), (g) and (h) illustrated in Scheme 6 became unnecessary as TMEDA **26** destabilized the complexed amine without residing within the cavity, thus reducing the reaction cycle to complexation, reaction and decomplexation. Using the modified decomplexation strategy, the reaction was repeated and found to afford 63% conversion to tyramine acetate **4** and 27% residual tyramine **1**. At this stage, the complexation step (a) was the only methanolic step remaining, which proved necessary due to the insolubility of tyramine HCl **13** in non-polar solvents. To circumvent this, tyramine TFA **12** was employed, which was found to be extremely soluble in THF, alongside TMEDA **26** as illustrated in Scheme 8. Using the refined protocol, complete removal of MeOH from the reaction enabled 100% conversion of tyramine TFA **12** to tyramine acetate **4**, affording 2.4×10^{-2} mmol reaction⁻¹ (4.3 mg) (Scheme 8).

2.1.6. Further reactions of N-protected compounds

Having demonstrated the ability to complex a bifunctional compound and selectively O-acetylate it under continuous flow (Scheme 8), the next step of the investigation was to evaluate the



Scheme 9. Schematic illustrating the consecutive reaction steps required for the synthesis of 2-(4-methoxyphenyl)ethylamine.



Scheme 10. Summary of the reaction protocol employed for the continuous flow synthesis of 4-methoxyphenylamine **37**.

generality of the protecting group strategy. With the ability to complex other bifunctional compounds previously illustrated (Table 5), this prompted us to investigate the acetylation of 4-aminophenol. Once again, the use of MeOH as a complexation solvent for 4-aminophenol HCl **35** ($0.12\ \text{M}$, $2.4\times 10^{-2}\ \text{mmol}$) was found to be problematic, affording only 84% conversion to 4-aminophenyl acetate. Replacing MeOH with THF and employing the protocol depicted in Scheme 8, quantitative conversion to 4-aminophenyl acetate was obtained, again affording a throughput of $2.4\times 10^{-2}\ \text{mmol}\ \text{reaction}^{-1}$.

2.1.6.1. Alkylations. Having acetylated two bifunctional compounds, the scope of the technique was extended to the O-alkylation of tyramine TFA **12** and 4-aminophenol HCl **35**, to afford the

respective methyl esters. However, unlike the acylations, where a pre-mixed solution was employed to achieve deprotonation and acetylation, the reagents selected for the alkylation, namely methyl iodide **28** and 1,8-diazabicyclo[5.4.0]undec-7-ene (DBU) **36**,^{9,10} could potentially react together. As such, the steps were performed separately, as illustrated in Scheme 9, employing DBU **36** ($0.12\ \text{M}$, $2.4\times 10^{-2}\ \text{mmol}$) in THF at $100\ \mu\text{L}\ \text{min}^{-1}$, followed by methyl iodide **28** ($0.12\ \text{M}$, $2.4\times 10^{-2}\ \text{mmol}$) in THF at $100\ \mu\text{L}\ \text{min}^{-1}$. Decomplexation was again achieved using TMEDA **26** and analysis of the reaction products by HPLC confirmed quantitative conversion of tyramine TFA **12** to 2-(4-methoxyphenyl)ethylamine.

Using analogous reaction conditions to those reported for the alkylation of tyramine **1**, the methylation of 4-aminophenol HCl **35** ($0.12\ \text{M}$, $2.4\times 10^{-2}\ \text{mmol}$) was investigated and afforded 100%

conversion of the starting material to 4-methoxyphenylamine **37** (2.4×10^{-2} mmol) (Scheme 10), with no *N*-methylation or dimethylation observed.

In addition to the generality observed for both the complex formation and subsequent reaction of the protected compounds, it must be noted that a full 12 months after the initial investigation was performed, the alkylation of 4-aminophenol HCl **35** was repeated using the same aliquot of TMS SILICA AM-18-c-6 **34** and found to afford analogous results, demonstrating long term stability of the immobilized crown ether **34**.

3. Conclusions

Owing to the complex nature of conventional covalent protecting group chemistry, it was the aim of this work to devise a non-covalent protecting group strategy, which would enable the facile *N*-protection of bifunctional compounds, thus removing the selectivity issues associated with the reaction of bifunctional amines. 18-Crown-6 ethers have been shown to efficiently complex ammonium salts and examples of reactions employing these complexes have been reported within the literature. Application of the technique to the protection of amines was, however, limited due to problems largely associated with the removal of the crown ether from the resulting reaction product. It was, therefore, proposed that through the immobilization of an 18-crown-6 ether derivative, that many of the issues that have prevented adoption of this technique could be overcome.

Having investigated a range of immobilization strategies and crown ether derivatives, it was found that the covalent immobilization of AM-18-c-6 **17** onto 3-carboxypropyl functionalized silica gel (0.16 mmol g^{-1}) combined the properties of efficient complexation and suitability for use in a continuous flow reactor. Using the aforementioned material, a plethora of ammonium salts were complexed (Table 5) and their stability to a wide range of solvents (Table 3) and reactants (Table 4) was evaluated.

Once the scope and limitations of the operating conditions had been evaluated, reaction of the complexed tyramine salt was performed and found to afford the selective *O*-acetylation, providing an efficient route to the synthesis of tyramine acetate **4** cf. the laborious route required when employing covalent protecting groups (Scheme 2). Having demonstrated the quantitative conversion of tyramine TFA salt **12** to the free tyramine acetate **4**, the investigation was extended to *O*-alkylation, demonstrating again the selective synthesis of 2-(4-methoxyphenyl)ethylamine in quantitative conversion, with no sign of competing di-alkylation or *N*-alkylation products. The generality of the technique was subsequently explored using 4-aminophenol HCl **35**, which enabled the facile synthesis of 4-aminophenyl acetate and 4-methoxyphenylamine **37** in quantitative yield, respectively. In all cases, the free amine was afforded and products were obtained in higher purity than those prepared using conventional *N*-protecting group strategies.

In summary, the work described herein presents a broad investigation into the viability of immobilized crown ethers as a replacement for traditional covalent *N*-protecting group chemistry and combines their use with continuous flow technology to afford a technique that has potential for future automation.

4. Experimental section

4.1. Reagents and materials

Unless otherwise stated, the chemicals employed herein were used as received and purchased from Sigma Aldrich, Acros and Avocado. Where available, reactions were performed using puriss grade solvents, which were stirred over molecular sieves ($<0.005\%$

H_2O) (Fluka, UK), with the exception of DCM and *tert*-butanol, which were of laboratory grade (Fisher Scientific, UK). All chromatography employed HPLC grade solvents (Fisher Scientific) and purified water ($5 \text{ M}\Omega \text{ cm}^{-1}$) was prepared by reverse osmosis and ion exchange using a water purifier (Elgast, UK) fitted with an Option 4 cartridge. PTFE tubing ($1/16''$ o.d. $\times 800 \mu\text{m}$ i.d.), female luer-lok fittings (Tefzel), $1/16''$ unions (Tefzel), o-rings (Viton), gas-tight syringes (5 mL and 10 mL, Hamilton, UK) and Omnifit connectors employed for the flow reactor system were sourced from Supelco (UK) and Kinesis (UK). Borosilicate glass capillary (3 mm i.d.) (Duran[®], UK) was cut into the desired 50 cm lengths and flame polished.

4.2. Instrumentation

Nuclear magnetic resonance (NMR) spectra were recorded at room temperature as solutions in either deuterated chloroform (CDCl_3) or deuterated MeOH (CD_3OD) using TMS as the internal standard. All spectra were recorded on a Jeol GX400 spectrometer and the chemical shifts given in parts per million (ppm) with coupling constants in hertz (Hz). Elemental analyses were performed using a Fisons (UK) Carlo Erba EA1108 analyser, with measurements repeated until concurrent data was obtained, typically $n=2$. Matrix-Assisted Laser Desorption Ionization (MALDI)-Mass Spectrometry was performed using a Bruker Reflex 4 instrument operated in reflector mode. Inductively Coupled Plasma-Mass Spectrometry (ICP-MS) measurements were made at 257.61 nm and 766.49 nm using a Perkin Elmer (UK) Optima 5300DV instrument. Melting points were obtained using a Stuart Scientific (UK) SMP10 apparatus and are reported uncorrected. High Performance Liquid Chromatography (HPLC) data was obtained using a Jasco (UK) modular system comprising of a LV-1580-03 solvent selector, a DG-1580-53 degasser, two PU-1580 pumps, an HG-1580-32 mixer, a UV-1575 detector and an AS-1555 autosampler. Analytical measurements were made using a Jupiter 10 μm C18, 300 A ($250 \times 4.60 \text{ mm}$) column (Phenomenex, UK). Reagents and solutions were delivered to the continuous flow reactor using a Harvard syringe pump (UK) capable of delivering liquids at flow rates ranging from 0.1 to $1000.0 \mu\text{L min}^{-1}$ based on a 5 mL gas-tight syringe. Where necessary, aliquots of reactants were introduced into the continuous flow reactor using a Rheodyne injector valve, model 7125 (Supelco, UK).

4.3. HPLC method

Using a gradient elution at a flow rate of 1.5 mL min^{-1} , the aqueous portion of the mobile phase was decreased from 60% to 40% over a period of 7 min and then maintained at 40% for the remaining 30 min of the method. Both the organic phase (MeOH) and aqueous phases contained 0.1% TFA. An injection volume of $20 \mu\text{L}$ was employed and biphenyl used as the internal standard.

4.4. Preparation of silica gel immobilized aminomethyl-18-crown-6 ether **24**

Thionyl chloride **19** (0.37 mL, 5.11 mmol) was added to a stirred solution of oven dried 3-carboxypropyl functionalized silica gel (1.06 g, 1.6 mmol g^{-1} , 200–400 mesh) in toluene (20 mL) and the reaction mixture heated to reflux for 3 h. The resulting silica supported acid chloride was concentrated in vacuo to afford a free flowing white solid, which was subsequently redispersed in toluene (20 mL), prior to the addition of 2-aminomethyl-18-crown-6 ether **17** (0.50 g, 1.70 mmol), followed by triethylamine **21** (0.26 mL, 1.86 mmol). The reaction mixture was stirred overnight, under N_2 , prior to filtration under vacuum. The supported crown ether **24** was then washed (H_2O , acetone and DCM) and oven dried, at 90°C , to

afford a free flowing white powder (1.08 g, 72.2%); ICP-MS 0.162 mmol g⁻¹.

4.5. Silanisation of SILICA AM-18-c-6 **24** to afford TMS SILICA AM-18-c-6 **34**

Imidazole **32** (1.36 g, 20.00 mmol) and chlorotrimethylsilane **33** (2.51 mL, 20.00 mmol) were added to a stirred solution of SILICA AM-18-c-6 **24** (0.50 g, 0.16 mmol g⁻¹) in MeCN (10 mL) under N₂. After stirring at room temperature for 1 h, the reaction mixture was filtered under suction and washed with MeCN (20 mL), acetone (20 mL) and DCM (20 mL) prior to oven drying at 60 °C to afford a free flowing white powder **34**.

4.6. Flow reactor set-up

As illustrated in Figure 3, the syringe driver was interfaced to inlet 2 of the Rheodyne valve (7125) using a series of commercially available connectors and a length of PTFE tubing (800 μm i.d.). Interconnects were made between the PTFE tubing and the luer lock gas-tight syringes using a female to male 10–32 (Tefzel) luer, a 1/16" union (Tefzel) and a 1/16" HPLC connector (PEEK). The flow reactor comprised of a borosilicate glass capillary (50 mm (length)×3 mm (i.d.)), packed with ~0.15 g of the immobilized crown ether under investigation, the inlet of which was connected to the Rheodyne valve via outlet 3. The stainless steel sample loop (200 μL) was positioned across outlets 1 and 4, with excess reactants diverted to waste via outlet 6 of the valve and reaction products collected in a sample vial (1.5 mL) at the reactor outlet.

4.7. General flow reaction protocol

Prior to performing a flow reaction, the solvent under investigation (THF, MeOH or DCM) was driven through the packed-bed reactor at 100 μL min⁻¹ to waste.

4.7.1. Crown ether complexation

To prepare the immobilized crown ether complex, the sample loop was filled with a solution of the ammonium salt under investigation (200 μL) with the valve in the load position. Once filled, the valve was turned to the inject position and the solvent stream diverted through the sample loop and the ammonium salt pumped through the packed bed at 100 μL min⁻¹ and the reactant stream diverted to waste.

4.7.1.1. Acetylation of the ammonium complex. To acetylate the immobilized crown ether complex, a pre-mixed solution of acetic anhydride **27** and Et₃N **21** (200 μL) in THF was pumped through the reactor at 100 μL min⁻¹, which facilitated both deprotonation of the phenolic moiety and the subsequent acetylation in a single step. THF was then pumped through the system for 2 min, prior to initiating decomplexation.

4.7.1.2. Alkylation of the ammonium complex. To alkylate the immobilized crown ether complex, a solution of DBU **36** (200 μL) in THF was pumped through the reactor at a flow rate of 100 μL min⁻¹, followed by THF for 2 min prior to the introduction of the alkylating agent (200 μL) in THF at 100 μL min⁻¹. This process was found to enable deprotonation of the phenolic moiety and subsequent alkylation; throughout this step, the reaction products were diverted to waste.

4.7.2. Decomplexation of the immobilized product

The decomplexing agent, KCl **14** in MeOH (200 μL) or TMEDA **26** in THF (200 μL), was pumped through the packed bed at a flow rate of 100 μL min⁻¹ and at this point, the reactant stream was diverted

from waste to sample collection; the reaction products were analyzed off-line by HPLC.

4.7.3. Regeneration of the immobilized crown ether

In the cases where KCl **14** in MeOH was employed for the decomplexation step, the immobilized crown ether cavity was regenerated using methanolic acetic acid **23** (200 μL, 5% v/v). In this case, the reactor effluent was again diverted to waste and the system purged with the reaction solvent for 2 min prior to repeating the aforementioned steps.

4.8. Flow synthesis of 4-(2-aminoethyl)phenyl acetate **4**

Using the general flow procedure detailed above, tyramine acetate **4** was synthesized under continuous flow. To achieve this, tyramine TFA **12** (200 μL, 0.12 M, 2.4×10⁻² mmol), in THF, was introduced into a continuous stream of THF (100 μL min⁻¹) via a Rheodyne valve. To ensure the tyramine salt **12** had passed through the system containing TMS SILICA AM-18-c-6 **34** (0.15 g, 2.4×10⁻² mmol) before introducing additional reactants, THF was pumped through the system for 2 min. Reaction of the phenolic moiety was achieved via introduction of a pre-mixed solution of acetic anhydride **27** and Et₃N **21** (200 μL, 0.12 M, 2.4×10⁻² mmol) at a flow rate of 100 μL min⁻¹. The system was again purged with THF (2 min), prior to initiating decomplexation using TMEDA **26** (200 μL, 0.12 M, 2.4×10⁻² mmol), in THF, at 100 μL min⁻¹. At this point the solvent stream was diverted from waste to sample collection and the reaction products collected prior to off-line analysis by HPLC; whereby comparison with a synthetic standard¹⁰ (HPLC, t_R=6.3 min) confirmed quantitative conversion of tyramine TFA **12** to 4-(2-aminoethyl)phenyl acetate **4** with a throughput of 4.3×10⁻² g reaction⁻¹ (2.3×10⁻² mmol).

4.9. Flow synthesis of 4-aminophenyl acetate

Using the general flow protocol detailed above, 4-aminophenyl acetate was synthesized under continuous flow. To achieve this, 4-aminophenol HCl **35** (200 μL, 0.12 M, 2.4×10⁻² mmol), in THF, was introduced into a continuous stream of THF (100 μL min⁻¹) via a Rheodyne valve. To ensure salt **35** had passed through the system before introducing additional reagents, THF was pumped through the system for 2 min. Reaction of the phenolic moiety was achieved via introduction of a pre-mixed solution of acetic anhydride **27** and Et₃N **21** (200 μL, 0.12 M, 2.4×10⁻² mmol) at a flow rate of 100 μL min⁻¹. The system was purged with THF (2 min) prior to initiating decomplexation using TMEDA **26** (200 μL, 0.12 M, 2.4×10⁻² mmol), in THF, at 100 μL min⁻¹. At this point the solvent stream was diverted from waste to sample collection and the reaction products collected prior to off-line analysis by HPLC. Comparison with a synthetic standard (HPLC, t_R=3.2 min) confirmed quantitative conversion of 4-aminophenol HCl **35** to 4-aminophenyl acetate, with a throughput of 2.3×10⁻² mmol reaction⁻¹.

4.10. Flow synthesis of 2-(4-methoxyphenyl)ethylamine

Using the general flow procedure detailed above, tyramine TFA **12** (200 μL, 0.12 M, 2.4×10⁻² mmol) in THF was introduced into a continuous THF stream (100 μL min⁻¹) via a Rheodyne valve. To ensure tyramine salt **12** had passed through the system containing TMS SILICA AM-18-c-6 **34** (0.15 g, 2.4×10⁻² mmol), before introducing further reagents, THF (100 μL min⁻¹) was pumped through for 2 min. The first of the reaction steps incorporated a 200 μL plug of DBU **36** (0.12 M, 2.4×10⁻² mmol), followed by methyl iodide **28** (200 μL, 0.12 M, 2.4×10⁻² mmol); both of which were passed through the flow reactor at 100 μL min⁻¹, facilitating the deprotonation of the phenolic moiety and methylation in consecutive steps. Again 2 min

was allowed before initiating decomplexation via a 200 μL plug of TMEDA **26** (0.12 M, 2.4×10^{-2} mmol) at 100 $\mu\text{L min}^{-1}$. At this point, the solvent stream was diverted from waste to sample collection and the reaction products analyzed off-line by HPLC ($t_{\text{R}}=6.1$ min) whereby 100% conversion to 3-(4-methoxyphenyl)ethylamine was obtained (2.3×10^{-2} mmol reaction $^{-1}$).

4.11. Flow synthesis of 4-methoxyphenylamine **37**

4-Aminophenol HCl **35** (200 μL , 0.12 M, 2.4×10^{-2} mmol) in THF was introduced into a continuous THF stream (100 $\mu\text{L min}^{-1}$) via the Rheodyne valve. To ensure 4-aminophenol salt **35** has passed through the system containing TMS SILICA AM-18-c-6 **34** (0.15 g, 2.4×10^{-2} mmol), before introducing further reagents, THF (100 $\mu\text{L min}^{-1}$) was pumped through the reactor for 2 min. The reaction steps firstly incorporated a 200 μL plug of DBU **36** (0.12 M, 2.4×10^{-2} mmol), followed by methyl iodide **28** (200 μL , 0.12 M, 2.4×10^{-2} mmol); both of which were pumped at a flow rate of 100 $\mu\text{L min}^{-1}$, facilitating the deprotonation and methylation of the complexed phenolic derivative. Again, 2 min was allowed before initiating decomplexation via a 200 μL plug of TMEDA **26** (0.12 M, 2.4×10^{-2} mmol). At this point the solvent stream was diverted from waste to sample collection and the reaction products analyzed off-line by HPLC, affording 100% conversion with a throughput of 2.4×10^{-2} mmol reaction $^{-1}$; HPLC, $t_{\text{R}}=5.7$ min.

Acknowledgements

The authors wish to acknowledge the EPSRC (G.P.W. and C.W.) (Grant No. GR/S34106/01) for full financial support of the

work described herein. Eichrom Technologies (France) are thanked for their kind donation of di-*tert*-butylcyclohexano-18-crown-6 ether. Mr. Bob Knight, Dr. Kevin Welham and Mr. Mike Bailey (The University of Hull) are also thanked for their assistance with ICP-MS, MS and flow reactor fabrication, respectively.

Supplementary data

Supplementary data associated with this article can be found in the online version, at [doi:10.1016/j.tet.2008.12.052](https://doi.org/10.1016/j.tet.2008.12.052).

References and notes

1. Wuts, P. G. M.; Greene, T. W. *Greene's Protective Groups in Organic Synthesis*, 4th ed.; Wiley Interscience: New Jersey, NJ, 2007.
2. Pederson, C. J. *J. Am. Chem. Soc.* **1967**, *89*, 7017.
3. Buschmann, H.-J.; Mitihac, L. *Anal. Chim. Acta* **2002**, *466*.
4. (a) Batinic-Haberele, I.; Crumbliss, A. L.; Spasojevic, I.; Bartsch, R. A. *J. Chem. Soc., Dalton Trans.* **1995**, 2503; (b) Kunishima, M.; Hioki, K.; Moriya, T.; Morita, J.; Ikuta, T.; Tani, S. *Angew. Chem., Int. Ed.* **2006**, *45*, 1.
5. Mascagni, P.; Botti, P.; Ball, H. L.; Rizzi, E.; Lucietto, P.; Pinori, M. *Tetrahedron* **1995**, *51*, 5447; (a) Mascagni, P.; Hyde, C. B. *Tetrahedron Lett.* **1990**, *31*, 339; (b) Mascagni, P.; Hyde, C. B.; Welham, K. J. *J. Chem. Soc., Perkin Trans. 2* **1989**, 2011; Mascagni, P.; Hyde, C. B.; Charalambous, M. A.; Welham, K. J. *J. Chem. Soc., Perkin Trans. 2* **1987**, 323.
6. Mascagni, P.; Botti, P.; Ball, H. L.; Rizzi, E.; Lucietto, P.; Pinori, M. *Tetrahedron* **1995**, *51*, 5447.
7. The reactor volume was determined experimentally to be 35 μL .
8. Verzele, M.; Dewaele, C.; Mussche, P. *J. High Resolut. Chromatogr.* **1982**, *5*, 616.
9. Mai, D. *Synth. Commun.* **1986**, *16*, 331.
10. See, [Supplementary data](#) for additional experimental details.

Design and Characterization of a Microfluidic Packed Bed System for Protein Breakthrough and Dynamic Binding Capacity Determination

Michael S. Shapiro

The Advanced Centre for Biochemical Engineering, Dept. of Biochemical Engineering, University College London, London WC1E 7JE, U.K.

Steve J. Haswell

Dept. of Chemistry, University of Hull, Hull HU6 7RX, U.K.

Gary J. Lye and Daniel G. Bracewell

The Advanced Centre for Biochemical Engineering, Dept. of Biochemical Engineering, University College London, London WC1E 7JE, U.K.

DOI 10.1021/bp.99

Published online January 8, 2009 in Wiley InterScience (www.interscience.wiley.com).

*A 1.5 μL ion exchange chromatography column to accommodate resins used for biopharmaceutical processing has been designed to produce breakthrough curves and to quantify dynamic and maximum protein binding capacities. Channels within a glass chip were fabricated using photolithography and isotropic etching. The design includes a 1 cm long microfluidic column in which compressible, polydispersed porous agarose beads (70 μm mean diameter) were packed using a keystone method where particles aggregate in a narrow channel. The depth of the column is such that two bead layers exist. The fabrication technique used forms Cartesian geometries as opposed to circular cross sections found in standard columns. The voidage was therefore higher than standard values when measured by 3D confocal microscopy. In conjunction with microscopic techniques, the column allows visualization of events within the bed such as adsorption profiles that would otherwise be difficult to observe. In this work, the binding of fluorescently labeled protein during isocratic loading was used to generate breakthrough from the microcolumn. Useful breakthrough curves were achieved using mobile phase velocities from 60 to 270 cm h^{-1} . Calculated dynamic binding capacities were compared well with previously published data on conventional scale columns. The microfluidic chromatography column described here thus allows study of process scale chromatography behavior at scales 20,000 times smaller than in current practice. The work described in this article is representative of the proof of principle of a potentially powerful tool for the generation of microfluidic process bed data for the biopharmaceutical industry. © 2009 American Institute of Chemical Engineers *Biotechnol. Prog.*, 25: 277–285, 2009*

Keywords: microfluidic, protein breakthrough, ion exchange

Introduction

Ion exchange chromatography is the most ubiquitous unit operation in the bioprocessing sector. The procedure is based upon electrostatic interactions. A charged stationary phase will interact, bind, and separate an oppositely charged macromolecule such as a protein or DNA present in the mobile phase. Cation exchange occurs where the stationary phase is negatively charged and the macromolecule in the mobile phase is positively charged.^{1,2} An important parameter to assess column performance, when

considering this type of chromatographic operation is breakthrough or frontal chromatography, i.e., the process where the column becomes saturated with solute. Large-scale columns are usually run to maximize yield by reduction of losses during loading as determined from the breakthrough curve.²

The biopharmaceutical sector is a rapidly expanding business in which increased competition is placing pressure on companies to improve purification process performance.³ In addition, there is also a growing variety of stationary phase materials now available from suppliers. Pharmaceutical companies frequently have limited time and material to make a full assessment of suitable resins for a given purification process. Microfluidic technologies allow for a thorough investigation of the experimental space using minimal

Additional Supporting Information may be found in the online version of this article.

Correspondence concerning this article should be addressed to D. G. Bracewell at d.bracewell@ucl.ac.uk.

amounts of protein. In addition to adsorbent type, any number of parameters such as the buffer type, pH, flow rate, etc., may be investigated.⁴ This is possible by employing the parallel architecture of microfluidic systems to increase throughput. Moreover, events can be visualized within the bed that would be difficult to observe using larger scale systems such as adsorption profiles across the bed. Additionally, confocal microscopy may be used to determine bead packing structure using glass microfluidic chips.

A number of approaches to microscale chromatography operation and evaluation have been described in the literature. An automated microscale system using adsorbents located in robot pipette tips, for example, has been created reducing the scale of the chromatographic step by 1,000 times from the laboratory scale. This was exemplified for virus-like particle purification.⁵ Another system involves confocal microscopy⁶ of individual beads in a batch manner to measure diffusion of a protein into a porous bead and relating the information obtained to frontal chromatography behavior. Shallow bed chromatography systems can also be used to estimate chromatographic parameters. A column containing 5–10 μL of polymeric beads is connected to a valve allowing the interchanging of buffers or samples from different reservoirs.⁷ All these studies have produced impressive results, however, none truly operates as a chromatography column in the conventional sense.

Equally, although research into microfluidic chip-based chromatography is extensive, there has been little concern for the evaluation of neither preparative chromatography beads nor operation under the conditions found in conventional scale columns. Packed chromatography microchips have been fabricated using a variety of beads and methods including hydrodynamic chromatography,⁸ shear-driven chromatography,⁹ and electrochromatography.^{10–12} In many of the analytical technologies, nonporous incompressible silica beads are used with diameters ranging from 1.5 to 4 μm (although Blom et al.⁸ used polymeric based beads). Process scale ion exchange beads due to the mode of use are usually porous and compressible beads with larger diameters ranging from 30 to 150 μm . These beads are used as they are able to operate at relatively high flow rate ranges and low pressures and can tolerate low levels of particulates that may be encountered in a process stream.

When using beads in microfluidic channels, the simplest method for packing involves using a chemical, such as latex¹³ for an ion exchange chromatography system or octadecyl coating for electrochromatography,¹⁰ to bond the beads to create an open-tubular format. Other options are specifically designed for electrochromatography, in which the beads are pumped in using an electroosmotic pumping system into a weir where the beads settle.¹² Using electric currents with agarose, porous beads may destabilize the matrix and possibly destroy them.¹⁴

In this work, a novel microfluidic method for quantifying protein breakthrough, frontal adsorption chromatography using standard preparative scale beads (ion exchange) in a glass microchip is described. A 1.5 μL chromatography column was packed with preparative beads, and breakthrough curves at varying linear velocities were recorded using fluorescence detection. This microfluidic system allows for the visualization of beads within the column, which aids a more detailed understanding of the binding phenomena controlling larger scales of operation.

Materials and Methods

Materials

All chemicals were purchased from Sigma-Aldrich (Dorset, UK) apart from the fluorescein-5-isothiocyanate (FITC) which was purchased from Invitrogen (Paisley, UK) and were of the highest purity available. The chromatography resin, Sulfopropyl (SP) Sepharose Fast Flow, was bought from GE Healthcare UK (Buckinghamshire, UK). All tubing, the connectors, and the MilliGAT pump were purchased from Presearch (Hampshire, UK). All buffers were prepared using analytical-grade water (Millipore, Watford, UK).

Design of the chip

The microchip was fabricated according to published procedures¹⁵ with minor adaptations. Briefly, the channel network was fabricated based on a photolithographic fabrication method. The channel network was designed using AutoCAD LT 2005 software (Autodesk, Farnborough, UK). A film negative of the desired final size was then prepared by a commercial photo mask manufacturer (J.D. Photo Tools, Oldham, UK) to form the optical mask. B-270 glass photolithographic plates (thickness of 3 mm) coated with a thin chromium metal mask layer plus an upper layer of positive photoresist, supplied by Telic (Telic Company, Valencia, CA), were used for channel network fabrication. With UV exposure, the pattern of interconnecting channels was transferred from the optical mask to the photoresist layer, which was then developed and removed, together with the chromium layer, to reveal the channel areas of glass to be etched. The channels were etched by using a mixture of 1% (w/w) HF and 5% (w/w) NH_4F in water at 65°C for 15 min, resulting in an etch channel network with a depth of $\sim 50 \mu\text{m}$.

The base plate containing the etched channel network was sealed by bonding to an upper plate (also 3-mm thick) containing predrilled holes (diameter 360 μm) to link the ends of the channels with tubing. The upper plate was aligned with the channel geometry and thermally bonded to the base plate by heating in a furnace at 575°C for 3 h. Thermal bonding was aided by placing a 90 g block of stainless steel on the upper plate.

Figure 1a displays a schematic diagram of a single channel in the chip, and Figure 1b shows a picture of a chip with four parallel microfluidic chromatography columns. The column dimensions were 10 mm \times 1 mm \times 0.15 mm, whereas the input and output channel dimensions were 15 mm \times 0.2 mm \times 0.075 mm. The column was limited to these dimensions due to fabrication specifications, whereas the dimensions of the input channel ensured there was limited dead volume. Connections were made using 125 μm Teflon FEP Tubing (Presearch) between the injection valve and the chip. To seal the tubing in place, epoxy resin (Sigma-Aldrich) was used.

Packing the chip

The packing procedure involved dilution of a 20% (v/v) slurry of matrix in 20% (v/v) ethanol in analytical-grade water. The beads were sieved using 38 and 106 μm sieves (VWR Leicestershire, UK) since larger beads block the channels and smaller beads may block the entrance and exit of the chip. SP Sepharose Fast Flow sieved and unsieved was then compared with Jupiter 300 silica high-performance

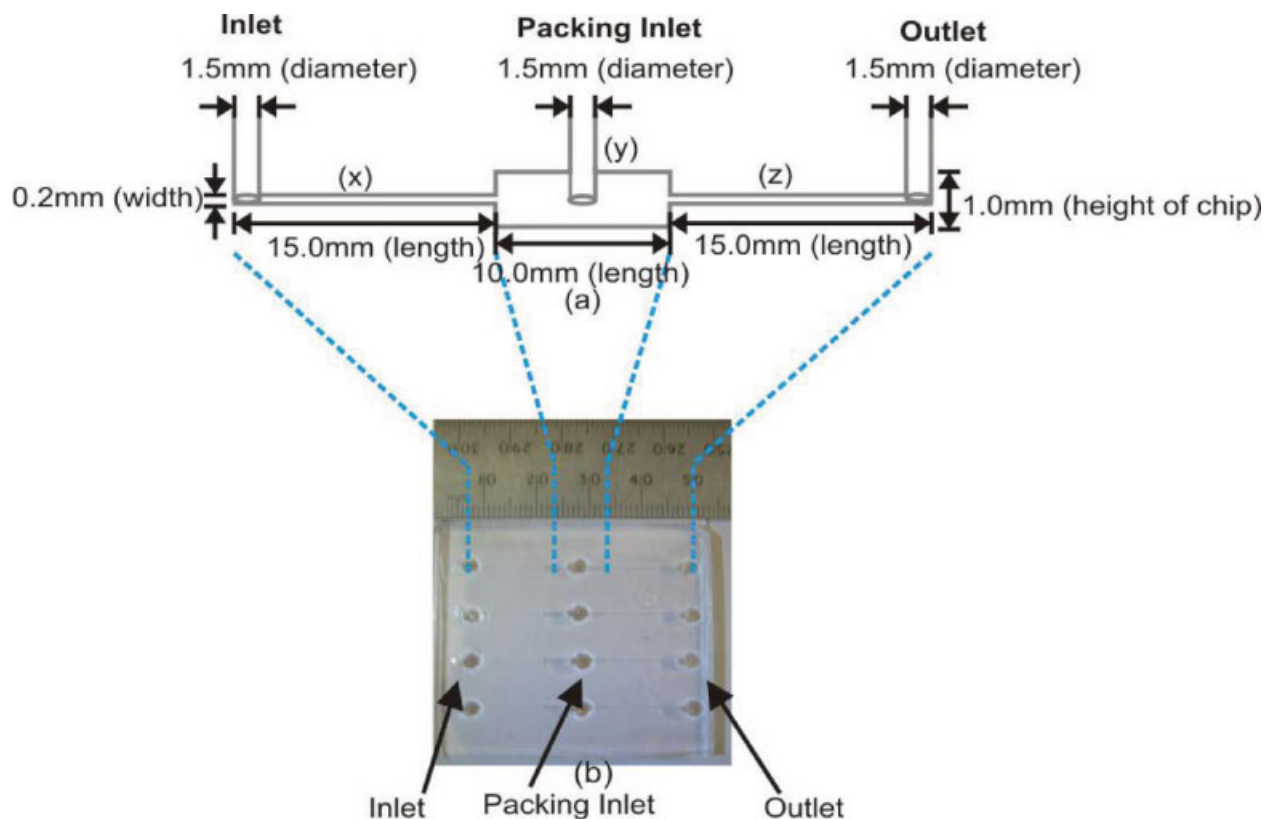


Figure 1. (a) Schematic diagram of a single microfluidic column as used in this work, where (x) is the input into the column, (y) is the microcolumn, and (z) is the outlet of the column, while (b) is a photograph of a chip with four parallel columns (x and z, inlet and exit channels) are etched to a depth of 75 μm , y (the microcolumn) is etched to a depth of 150 μm .

SP Sepharose Fast Flow beads are packed into the middle chamber using a syringe containing 20% (v/v) bead solution in 20% (v/v) ethanol in analytical grade water. Dashed lines in (b) indicate sections of the channel that relate to the dimensions in (a).

liquid chromatography beads (Phenomenex, Cheshire, UK) and their size distribution determined by laser light scattering using a Malvern Mastersizer (Malvern Instruments, Worcestershire, UK).

A 2 mL plastic syringe with an adapted micropipette tip was used to ensure a sealed connection between the syringe and the tip and equally between the tip and the drilled hole. This was used to pack the microfluidic column. The matrix was manually pressurized into the packing chamber using the drilled hole in the center of the microfluidic column (see Figure 1a), until it fills over a 5 minute time interval. Liquid was then allowed to flow out of the inlet and outlet channels, the resin then keystoneed inside the chip. Keystoneing is where matrix particles will aggregate in narrow channels due to tapered columns, or as in this case differences in depths within columns.¹⁶ The difference in depths ensured that the matrix particles remained in place without the need for a frit. The packing inlet was sealed by using a plastic rod specifically designed for the hole. To clean and dry the chip channel, the syringe can be used to suck air from all holes. The quality of the packed microfluidic column was then checked using a Leica DMRA2 microscope (Leica Microsystems, Milton Keynes, UK) and QWin Software to ensure that there was no resin particles that blocked the inlet and outlet channels.

Fluid handling

Figure 2 displays a schematic diagram of the experimental setup used in this work. A MilliGAT pump was employed

for the purpose of pumping all liquid through a motorized injection valve and into the chip. The pump was able to accurately pump from 0.6 to 600,000 $\mu\text{L min}^{-1}$ and could accurately deliver at 10 nL volumes suitable for this work.

A small internal volume Rheodyne Valve 7010 (0.5 mm ID) was used for all the chromatography work while 500 μL PEEK tubing was used as an injection loop. The injection volume could be readily varied by changing the size of the sample loop. There is a motorized actuator that allowed simple insertion of the liquid into the connecting tubing from the chip.

Preparation of fluorescently labeled lysozyme

The preparation of fluorescently labeled lysozyme was performed using the manufacturer's instructions with slight modifications. Briefly, a solution of 3 mg mL^{-1} of lysozyme (14.6 kDa, pI 11.0¹⁷) was prepared in 0.1 M sodium bicarbonate buffer pH 9. 10 mg mL^{-1} of fluorescein-5-isothiocyanate (FITC) (excitation wavelength: 494 nm and emission wavelength: 520 nm) was dissolved in dimethyl sulfoxide (DMSO). A molar ratio 0.5:1 (derived from labeling experiments of varying molar ratios) was added to the lysozyme mixture and left to bind for 1 h. Fluorescently labeled lysozyme was dialyzed into 0.05 M Tris buffer pH 8. The concentration of labeled lysozyme was then analyzed by taking readings at 280 and 494 nm using a spectrophotometer (Thermo Fisher Scientific, Basingstoke, UK). Equation 1 was used to determine the concentration¹⁸:

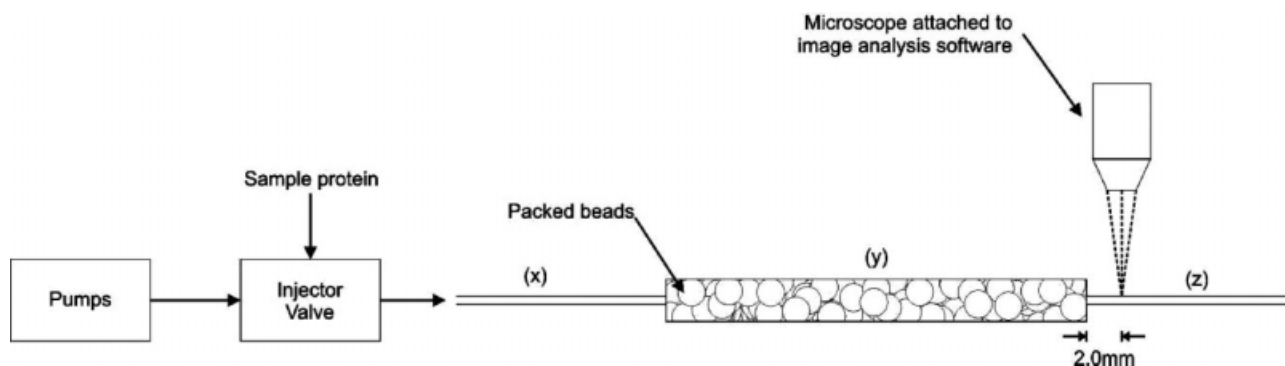


Figure 2. Schematic diagram of the experimental setup.

A highly accurate MilliGAT pump was used to pump 0.05 M sodium phosphate pH 5.5 into a motorized injector valve and then into the chip. 500 μL of 1 mg mL^{-1} lysozyme (20% (v/v) was fluorescently labeled) in buffer was injected into the inlet stream using the injector valve. 15 cm of 125 μm of Teflon FEP tubing connected the injector valve to the drilled hole for the inlet channel and was sealed using epoxy resin. The nomenclature used is the same as in Figure 1, where (x) is the inlet line, (y) is the microcolumn, and (z) is the outlet of the column.

$$c = \frac{(A_{280} - (0.3 \times A_{494}))DF \times m}{\epsilon} \quad (1)$$

where c is the concentration of fluorescently labeled lysozyme, A is the absorbance, DF is the dilution factor, 0.3 is a correction factor used to offset any dye absorption at 280 nm based on the manufacturer's instructions, m is the molecular weight of lysozyme, and ϵ is the molar absorptivity of the protein (37,900 $\text{M}^{-1} \text{cm}^{-1}$), which was also validated experimentally.

On-chip fluorescence detection

Leica QWin software was used for all image analysis. To facilitate fluorescence quantification, the integration time (the resolution time of the image analyzer) was adjusted depending on the level of fluorescent lysozyme. A time-interval program was developed to record the average fluorescence intensity in the outlet channel every 3 s in order to produce the necessary concentration–time data for breakthrough analysis.

Confocal microscopy and voidage calculation

The packed microfluidic column was also subjected to confocal microscopy imaging.^{19,20} A Leica DMI confocal microscope recorded 35 depth images over a 1-mm² area. VolocityTM software (Improvision, Coventry, UK) was then used to render the pictures into a three-dimensional image. The voidage, ϵ_b (the percentage of empty space between the packing) is defined as follows:

$$\epsilon_b = \frac{V_b - V_c}{V_b} \quad (2)$$

where V_b is the volume of empty bed and V_c is the total volume of the packing. The volume of the empty bed was calculated from the dimensions shown in Figure 1. The total volume of the packing was calculated from counting the number of beads in three recorded areas, averaging the number, and was then multiplied by the average measured bead volume.

Microfluidic column breakthrough measurements

A 1.5 μL microfluidic column packed with SP Sepharose Fast Flow was equilibrated with five column volumes (CV) of 0.05 M sodium phosphate buffer pH 5.5 (start buffer). 1 mg mL^{-1} total lysozyme solution (0.8 mg mL^{-1} unlabeled lysozyme and 0.2 mg mL^{-1} fluorescently labeled lysozyme in the same buffer) was pumped isocratically at linear velocities of 60, 150, 220, and 270 cm h^{-1} (1.33, 3.67, 5.33, and 6.67 $\mu\text{L min}^{-1}$, respectively) calculated for the microfluidic column packed bed by using the cross-sectional area at that point. Breakthrough was monitored as described in the “On-chip fluorescence detection” section. Once breakthrough was achieved, the column was cleaned, removing the resin present and repacked with fresh resin. Alternatively, another channel was packed for use.

To measure the influence of the dead volume within the system and quantify diffusion effects, a nonbinding solution of 1 mg mL^{-1} lysozyme in 0.05 M Tris pH 8 was pumped through a microfluidic column containing Quaternary amine (Q) Sepharose Fast Flow (GE Healthcare) isocratically at 270 cm h^{-1} . The peak was monitored using the Leica QWin Image Analyzer. The appearance of the first shoulder of the peak was the maximum amount of dead volume and diffusion within the system. This volume was then subtracted from all the volumes of the breakthrough curves.

Dynamic protein binding capacity was calculated at 5, 10, and 100% breakthrough. All data were normalized in terms of c/c_0 , where c is the concentration of effluent material at each time point and c_0 is the highest value of recorded effluent concentration. Equation 3 displays the calculation used to find the capacity (Q)²¹:

$$Q = \frac{(M_{\text{in}} - V_{\text{retained}} \int_{c_{\text{in}}}^{c_0} dc)}{V_{\text{beads}}} \times \frac{\epsilon_m}{\epsilon_s} \quad (3)$$

where M_{in} is the total protein mass into the column, V_{retained} and V_{beads} are the volume retained through the system and the volume of the beads packed in the column, respectively, and ϵ_s and ϵ_m are the voidages in a standard column and in the microfluidic column, respectively. The voidage was normalized in this way to allow comparison with larger scale published results. Data presented are the average of at least three breakthrough curves determined at different flow rates.

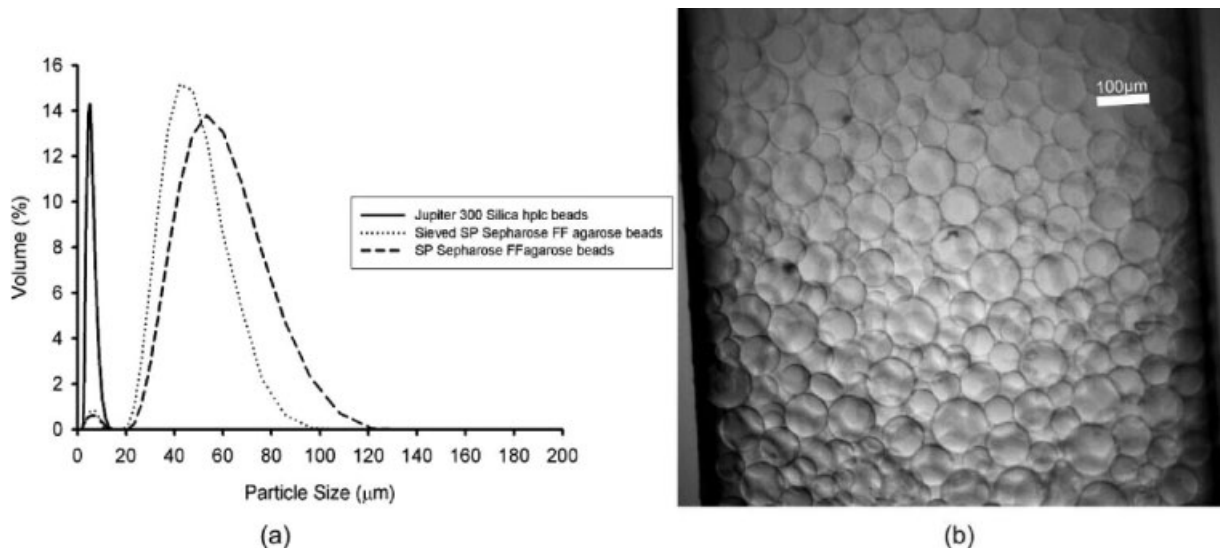


Figure 3. (a) Size distributions showing the difference between nonporous beads commonly used in analytical HPLC and the preparative scale SP Sepharose Fast Flow beads (sieved and unsieved). (b) Photograph of the packed SP Sepharose Fast Flow sieved beads from a two-dimensional perspective using a standard light microscope.

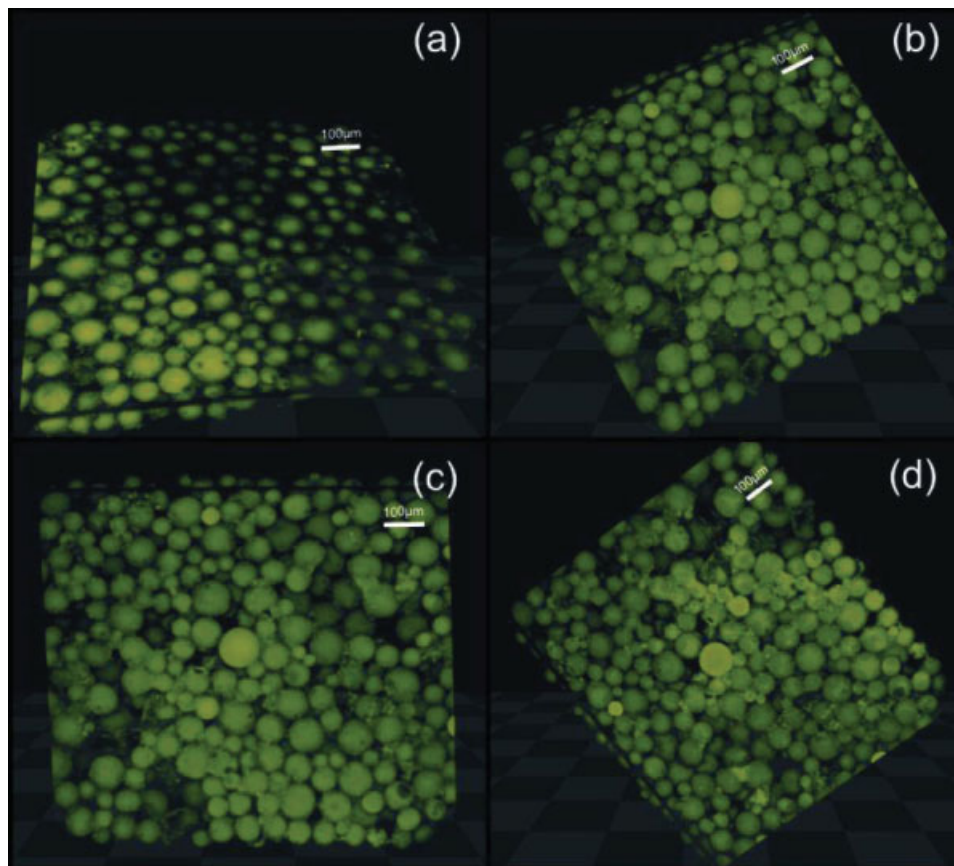


Figure 4. Confocal microscope images of the microfluidic packed bed in a three-dimensional plane. (a) Planar perspective, (b) a 45° angle from the top of the bed, (c) a side image of the top of the bed, and (d) a 45° angle of the end of the bed. These images provide additional insight into the structure of the bed clearly showing voids that contribute to the increased voidage of the bed when compared with larger scale columns. Supporting information Figure 1 displays a video of the packed microcolumn.

Results and Discussion

Determination and assessment of the voidage of the packed microcolumn

The microfluidic columns were packed as described in the “Packing the chip” section. SP Sepharose Fast Flow is a

polydispersed matrix. It has a volume-average particle diameter of 90 μm, although the actual range is between 10 and 150 μm (see Figure 3a). The averaged bead diameters after sieving were measured to be 70 μm with a d_{10} of 40 μm and a d_{90} of 100 μm using laser light scattering. The difference between a standard nonporous HPLC resin and the sieved

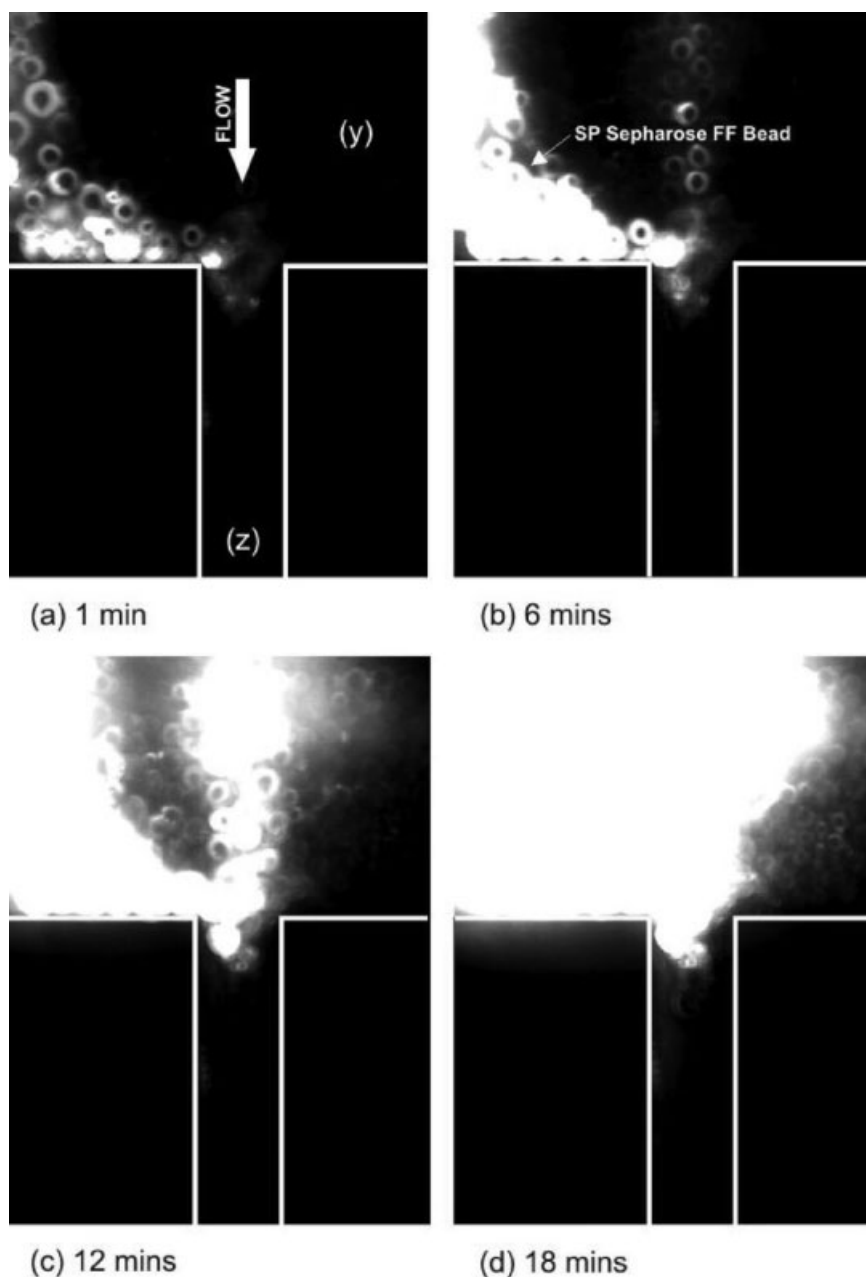


Figure 5. Fluorescent light microscope images displaying flow distribution and binding of fluorescently labeled lysozyme to SP Sepharose Fast Flow at the end of the column at a mobile phase velocity of 270 cm h^{-1} .

The white lines indicate the walls of the column. The white arrow present in image (a) shows the direction of flow, while the labels correspond to those present in Figure 1 where (y) is the packed column and (z) is the outlet of the column. There is initially binding down one wall of the bed, shown in (b) and (c), but by 30 min binding occurs throughout the entire cross-section of the bed.

and unsieved process resins are also shown in Figure 3a. The nonporous resin is a monodispersed matrix with an average particle diameter of $5 \mu\text{m}$. This variation between nonporous and porous resins provides evidence toward the complexity of packing the larger porous beads.

Figure 3b displays a two-dimensional photograph of the packing of the sieved SP Sepharose Fast Flow beads. There is clearly more than one layer of beads. The standard method to assess the quality of chromatography packing is to inject a pulse of a noninteracting solute through the column.²² As the volume of the adjacent equipment was $2 \mu\text{L}$, compared with the volume of the packed bed which is $1.5 \mu\text{L}$, volumes of injected solutes would become overly dispersed producing long tails that were problematic to analyze. The peak produced was not Gaussian and therefore could not be analyzed

using the standard method. Instead, the bed was subjected to confocal microscopy to provide an understanding of the three-dimensional arrangement of beads.

Figure 4 shows the confocal microscopy images of the same microfluidic packed bed over a 1-mm^2 area. Two layers of packing are clearly seen. Voids that were not visible using standard two-dimensional photography were made more apparent. Aggregation can also occur which may be due to electrostatic charges and differences due to sizes. As bead diameters may be as large as $150 \mu\text{m}$, they may block smaller beads from packing into specific areas of the bed, therefore producing voids and increasing the voidage of the bed.

These voids affect the overall column voidage as described in the "Confocal microscopy and voidage

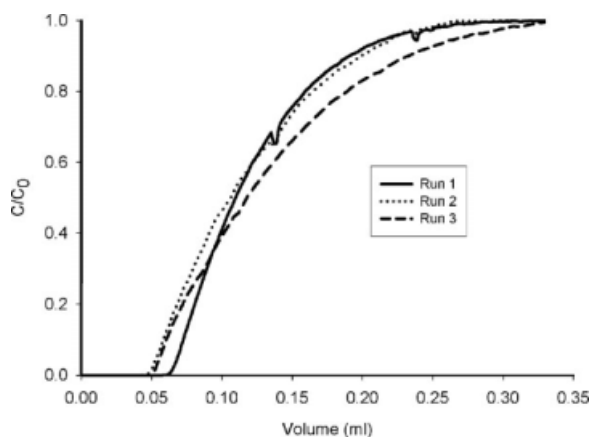


Figure 6. Reproducibility of lysozyme breakthrough curve determination based on three runs at 270 cm h^{-1} using three separately packed columns.

The graphs represent normalized lysozyme elution concentration as a function of time. The average maximum dynamic binding capacity calculated is 110.7 mg mL^{-1} matrix with a relative standard deviation of 11%.

calculation” section. In standard chromatography columns, the bed voidage is usually estimated to be between 0.3 and 0.4,²³ as the column contains at least tens of bead layers and is of a circular geometry. However, the microfluidic packed bed described here has a rectangular cross section and principally only contains two bead layers. Based on Eq. 2, the voidage in the microfluidic packed bed described here was estimated to be 0.55. This value is substantially higher than standard values suggesting that the voids resulting from packing a column of only a bilayer in depth may have an effect on the measurement of breakthrough.

Flow characteristics of the mobile phase through the packed column

The quality of the packing of the microfluidic column will inevitably affect the quality of the measured breakthrough curve. Figure 5 displays the stages of breakthrough at the fastest linear velocity, 270 cm h^{-1} . The images show some channeling of the solute to the left-hand side of the microfluidic column during the initial stages of breakthrough. In a purely plug flow system, mobile phase material would partition into the stationary phase evenly throughout the column culminating in an even signal emanating from the column that would be picked up using the detector. In this column, especially at the two faster linear velocities, there appears to be some deviation from idealized plug flow. This phenomenon is expected to produce shallower breakthrough curves in a 15-cm column. Holland et al.²⁴ developed MRI scans of a column (1.60 cm ID and 2.5 cm height) with bead diameters ranging between 15 and $70 \mu\text{m}$. Nonideal conditions were observed in their case as well, implying that there is a lack of plug flow present even at this larger scale.

Reproducibility of protein breakthrough curves

Figure 6 indicates the reproducibility of 1 mg mL^{-1} lysozyme breakthrough experiments in the form of the normalized concentration as a function of the volume retained for triplicate experiments. The curves are slightly shallower than would be expected, as explained in the “Determination and assessment of the voidage of the packed microcolumn” sec-

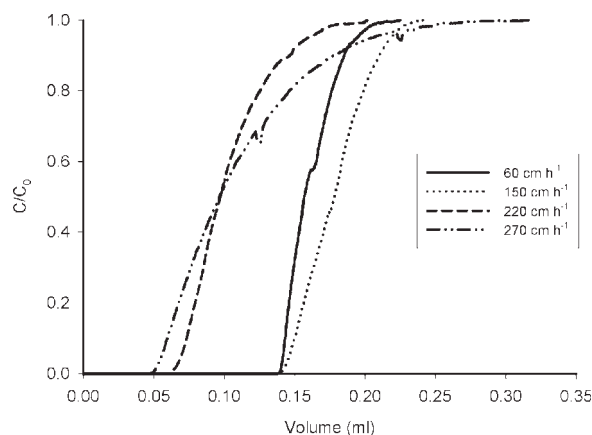


Figure 7. Lysozyme breakthrough curves at a range of linear velocities.

The load time for breakthrough volume to reach $250 \mu\text{L}$ (180 CV) for the velocities 60, 150, 220, and 270 cm h^{-1} was 190, 70, 50, and 35 min, respectively, implying that equilibrium would not be reached for the faster velocities.⁶

tion, due to channeling of flow at the bed outlet. The three curves can be considered to be reproducible. The average maximum capacity calculated for this column based on a voidage of 0.55 (see Eq. 3) was 110.7 mg mL^{-1} matrix with a relative standard deviation of 10.5%. This variation is low enough to validate the method for binding capacity qualification.

Breakthrough at varying linear velocities

Figure 7 displays representative lysozyme breakthrough curves at different linear velocities. The two faster flow rates display different profiles to the slower flow rates. Experiments at velocities less than 150 cm h^{-1} took a long time and were difficult to reproduce. This could be due to the increased importance of the wall effects at the longer residence times. However, good, reproducible data were obtained at the highest flow rates. The maximum capacities produced are still comparable with other studies, as shown in Table 1. This may be due to the fact that some of the deviations from ideality exist at the larger scale but are more difficult to visualize, but can be detected using a microfluidic device.²⁴

There are a number of important issues underpinning the reproducibility and accurate quantification when using the microfluidic column. First, the packed column is highly dependent on the cleanliness of the channel area. Any small material including dust may affect the flow behavior, which may lead to dispersed material and hence lengthened breakthrough curves.²⁸ Additionally, over repeated breakthrough curve determination, using the same resin, protein can foul the microfluidic channels as well as the tubing causing blockages.²⁹ To avoid this problem, the column was repacked after each breakthrough; however, this brought separate challenges. As only two bead layers were in evidence inside the column, each column when repacked may provide a different packing structure, which is potentially a source of variability in the breakthrough profile. Wall support is in evidence within the microfluidic column that would not be available at a larger scale because of the presence of the bilayer of beads. Natural compression observed in larger columns may not be present within this microfluidic column.

Table 1. Comparison of Microfluidic Column Operating Conditions and Measured Dynamic Binding Capacities with Other Published Data: Error Values Represent 1 Standard Deviation about the Mean. (\approx Represents Approximate Binding Capacities due to Variation in Column Packing Characteristics)

Reference	Column Type	Linear Velocity (cm h ⁻¹)	Buffer	pH	Load Concentration (mg mL ⁻¹)	Maximum Binding Capacity (mg mL matrix ⁻¹)	10% Dynamic Binding Capacity (mg mL matrix ⁻¹)
This work	1.5 μ L column	270	50 mM sodium phosphate	5.5	1	117.4 \pm 10.5	59.5 \pm 11.0
This work	1.5 μ L column	220	50 mM sodium phosphate	5.5	1	96.4 \pm 46.8	50.0 \pm 29.5
This work	1.5 μ L column	150	50 mM sodium phosphate	5.5	1	\approx 175	\approx 145
This work	1.5 μ L column	60	50 mM sodium phosphate	5.5	1	\approx 160	\approx 140
25	2 mL column	77	100 mM sodium acetate	5	1	120	
26	0.79 mL column	245	100 mM sodium acetate	5	1	111.6	
27	2 mL column	185	16.7 mM MES + 16.7 mM HEPES + 16.7 mM sodium acetate	5.5	1		110

Methods to improve packing reproducibility are therefore of interest.

An additional issue was the nonspecific binding that occurred between the mobile phase containing lysozyme and the channel walls. Additionally, the large surface area permits more nonspecific binding than other geometries at a larger scale. Nonspecific binding may affect and alter the signal produced for breakthrough; however, the amount of protein that bound to the channel walls was minimal in comparison with the breakthrough curves. The flow distribution pictures in Figure 5 display little evidence of nonspecific binding, as fluorescence would be viewed as bound to the walls and external to the beads. However, this extra fluorescence is not present in these images.

Quantification of dynamic binding capacities at each linear velocity and comparison with published results

Table 1 displays all calculated dynamic binding capacities for each linear velocity measured using Eq. 3. The maximum capacity varies between 96 and 175 mg mL⁻¹ matrix, whereas at 10% of the dynamic capacity, the variation is between 50 and 145 mg mL⁻¹ matrix, in which the slower flow rates present higher capacities. This latter trend is viewed as a standard observation in previous literature.²⁷

Additionally, Table 1 displays comparisons with previously published data. At 220 cm h⁻¹ there is a larger error due to reasons explained in "Breakthrough at varying linear velocities" section as well as due to the increasing residence time. For SP Sepharose Fast Flow beads in this system, the 220 cm h⁻¹ run appears to show differing levels of mass transfer occurring over repeated breakthroughs. This may indicate that this flow rate is highly sensitive to these effects.

The measured maximum capacity is close in absolute value to that published from Hasim and Chu.²⁶ Their study uses a linear velocity of 245 cm h⁻¹, and a model is used for the estimation of parameters based on experimental breakthroughs. Skidmore et al.,²⁵ however, used parameters from batch studies to fit a modeled breakthrough profile to a breakthrough curve produced using a 2 mL column. Both studies used short columns from 2 to 5 cm in length. As explained previously, channeling is likely to be present in such short lengths of columns. Values at 10% dynamic binding capacity are recorded around 60 mg mL⁻¹ matrix compared with 110 mg mL⁻¹ matrix quoted by Staby et al.²⁷ The column used for their work had a length of 10 cm, which would be reflected in an improved breakthrough curve. In addition, channeling should decrease

when compared with the smaller lengths of column. Generally, the difference between the published data collected on the breakthrough of lysozyme and the measured data presented is small.

Conclusion

The microfluidic chromatography system described here represents the current limit of scale down for process chromatography. It enables the generation of breakthrough curves and thereafter the calculation of the maximum protein binding capacities as well as dynamic binding capacities that are vital parameters for bioprocess design. The system also allows for the visualization of events within a packed chromatography bed that are not possible at larger scales. The chip system does not possess a conventional geometry for a chromatography system, as there is a Cartesian geometry and contains only a bilayer of beads. The voidage calculated from confocal microscopy images is 0.55 when compared with a standard column which has a voidage of 0.3–0.4. However, the system has been shown to work effectively over a range of linear velocities irrespective of the voidage and geometry. Maximum capacities calculated were recorded to be in the range of 95–170 mg mL⁻¹ matrix. These values were found to be close to those published previously. To extend the utility of the microfluidic chromatography system for the bioprocess industry, future work will examine the system's ability to produce a chromatographic separation. The work described in this article is representative of the proof of principle of a potentially powerful tool for the generation of microfluidic process bed data for the biopharmaceutical industry.

Acknowledgments

This work was supported by the Engineering and Physical Sciences Research Council (EPSRC) via the Innovative Manufacturing Research Centre (IMRC) in Bioprocessing at UCL, a Life Sciences Interface and Innovative Manufacturing program. The IMRC is part of The Advanced Centre of Biochemical Engineering, UCL, with collaboration from a range of academic partners and biopharmaceutical and biotechnology companies.

Literature Cited

- Levison PR. Large-scale ion-exchange column chromatography of proteins—comparison of different formats. *J Chromatogr B*. 2003;790:17–33.

2. Cramer SM, Natarajan V. Chromatography-ion exchange. In Flinkinger MC, Drew SW, editors. *Encyclopaedia of Bioprocess Technology—Fermentation, Biocatalysis, and Bioseparation*. New York: Wiley; 1999; Chapter 1–5:612–627.
3. Low D, O’Leary R, Pujar NS. Future of antibody purification. *J Chromatogr B*. 2007;848:48–63.
4. Micheletti M, Lye GJ. Microscale bioprocess optimisation. *Curr Opin Biotechnol*. 2006;17:611–618.
5. Wenger MD, DePhillips P, Price CE, Bracewell DG. An automated microscale chromatography purification of virus-like particles as a strategy for process development. *Biotechnol Appl Biochem*. 2007;47:131–139.
6. Dziennik SR, Belcher EB, Barker GA, Lenhoff AM. Effect of ionic strength on lysozyme uptake rates in cation exchangers. I. Uptake in SP Sepharose FF. *Biotechnol Bioeng*. 2005;91:139–153.
7. Hahn R, Tscheliessnig A, Zochling A, Jungbauer A. Shallow bed adsorption: theoretical background and applications. *Chem Eng Technol*. 2005;28:1241–1251.
8. Blom MT, Chmela E, Oosterbroek RE, Tijssen R, van der Berg A. On-chip hydrodynamic chromatography separation and detection of nanoparticles and biomolecules. *Anal Chem*. 2003;75:6761–6768.
9. Vervoot N, Clicq D, Baron GV, Desmet G. Experimental Van Deemter plots of shear-driven liquid chromatographic separations in disposable microchannels. *J Chromatogr A*. 2003;987:39–48.
10. Gottschlich N, Jacobson SC, Culbertson CT, Ramsey JM. Two dimensional electrochromatography/capillary electrophoresis on a microchip. *Anal Chem*. 2001;73:2669–2674.
11. Soper SA, Henry AC, Viadva B, Galloway M, Wabuyele M, McCarley RL. Surface modification of polymer-based microfluidic devices. *Anal Chim Acta*. 2002;470:87–99.
12. Jemere AB, Oleschuk RD, Ouchen F, Fajuyigbe F, Harrison DJ. An integrated solid-phase extraction system for sub-picomolar detection. *Electrophoresis*. 2002;23:3537–3544.
13. Murrhly JP, Breadmore MC, Tan A, McEnery M, Alderman J, O’Mathuna C, O’Neill AP, O’Brien P, Advoldvic N, Haddad PR, Glennon JD. Ion chromatography on-chip. *J Chromatogr A*. 2001;924:233–238.
14. Svec F, Fréchet JMJ. Molded rigid monolithic porous polymers: an inexpensive, efficient and versatile alternative to beads for the design of materials for numerous applications. *Ind Eng Chem Res*. 1999;38:34–48.
15. Fletcher PDI, Haswell SJ, Pombo-Villar E, Warrington BH, Watts P, Wong SYF, Zhang X. Micro reactors: principles and applications in organic synthesis. *Tetrahedron*. 2002;58:4735–4757.
16. Ceriotti L, de Rooij NF, Verpoorte E. An integrated fritless column for on-chip capillary electrochromatography with conventional stationary phases. *Anal Chem*. 2002;74:639–647.
17. Fasman GD. *Practical Handbook of Biochemistry and Molecular Biology*. Boca Raton: CRC Press; 1989.
18. Molecular Probes Inc. *FlouReporter^(R) FITC Protein Labelling Kit (F6434)*, Eugene, USA. 2004.
19. Dziennik SR, Belcher EB, Barker GA, DeBergalis MJ, Fernandez SE, Lenhoff AM. Nondiffusive mechanisms enhance protein uptake rates in ion exchange particles. *Proc Natl Acad Sci USA*. 2002;100:420–425.
20. Siu SC, Boushaba R, Topoyassakul V, Graham A, Choudhury S, Moss G, Titchener-Hooker NJ. Visualising fouling of a chromatographic matrix using confocal scanning laser microscopy. *Biotechnol Bioeng*. 2006;95:714–723.
21. Sin SC, Baldascini H, Hearle DC, Hoare M, Titchener-Hooker NJ. Effect of fouling on the capacity and breakthrough characteristics of a packed bed ion exchange chromatography column. *Bioprocess Biosyst Eng*. 2006;28:405–414.
22. Rathore AS, Kennedy RM, O’Donnell JK, Bemberis I, Kaltenbrunner O. Qualification of a chromatographic column why and how to do it. *Biopharm Int*. 2003;3:30–40.
23. DePhillips P, Lenhoff AM. Pore size distributions of cation-exchange adsorbents determined by inverse size-exclusion chromatography. *J Chromatogr A*. 2000;883:39–54.
24. Holland DJ, Sederman AJ, Mantle MD, Gladden LF, Middelberg APJ. Quantitative magnetic resonance imaging of urea and lysozyme in protein chromatography. *J Chromatogr A*, 2004; 1033:311–319.
25. Skidmore GI, Horstmann BJ, Chase HA. Modelling single-component protein adsorption to the cation exchanger S Sepharose FF. *J Chromatogr*. 1990;498:113–128.
26. Hashim MA, Chu KH, Tsan PS. Modelling of protein adsorption in a fixed-bed: single and two-solute breakthrough behaviour. *Chem Eng Commun*. 1997;161:45–63.
27. Staby A, Sand M, Hansen RG, Jacobson JH, Anderson LA, Gerstenberg M, Bruus UK, Jensen IH. Comparison of chromatographic ion-exchange resins IV. Strong and weak cation-exchange resins and heparin resins. *J Chromatogr A*. 2005; 1069:65–77.
28. Heeter GA, Liapis AI. Frontal chromatography of proteins effect of axial dispersion on column performance. *J Chromatogr A*. 1998;796:157–164.
29. Mukhopadhyay R. When microfluidic devices go bad—how does fouling occur in microfluidic devices, and what can be done about it? *Anal Chem*. 2005;77:429A–432A.

Manuscript received Jul. 29, 2008, and revision received Aug. 11, 2008

Development of a bi-functional silica monolith for electro-osmotic pumping and DNA clean-up/extraction using gel-supported reagents in a microfluidic device

Jennifer A. Oakley,^{*a} Kirsty J. Shaw,^a Peter T. Docker,^a Charlotte E. Dyer,^b John Greenman,^b Gillian M. Greenway^a and Stephen J. Haswell^{*a}

Received 17th November 2008, Accepted 20th February 2009

First published as an Advance Article on the web 11th March 2009

DOI: 10.1039/b820553a

A silica monolith used to support both electro-osmotic pumping (EOP) and the extraction/elution of DNA coupled with gel-supported reagents is described. The benefits of the combined EOP extraction/elution system were illustrated by combining DNA extraction and gene amplification using the polymerase chain reaction (PCR) process. All the reagents necessary for both processes were supported within pre-loaded gels that allow the reagents to be stored at 4 °C for up to four weeks in the microfluidic device. When carrying out an analysis the crude sample only needed to be hydrodynamically introduced into the device which was connected to an external computer controlled power supply *via* platinum wire electrodes. DNA was extracted with 65% efficiency after loading lysed cells onto a silica monolith. Ethanol contained within an agarose gel matrix was then used to wash unwanted debris away from the sample by EOP (100 V cm⁻¹ for 5 min). The retained DNA was subsequently eluted from the monolith by water contained in a second agarose gel, again by EOP using an electric field of 100 V cm⁻¹ for 5 min, and transferred into the PCR reagent containing gel. The eluted DNA in solution was successfully amplified by PCR, confirming that the concept of a complete self-contained microfluidic device could be realised for DNA sample clean up and amplification, using a simple pumping and on-chip reagent storage methodology.

Introduction

Microfluidic devices, which form the basis of 'lab on a chip' applications, not only offer many sample handling advantages but also hold the potential for developing truly portable, automated devices through process and systems integration.^{1,2} In addition, due to their relatively low cost, the possibility of producing versatile yet disposable devices is a distinct advantage for clinical and forensic applications.³⁻⁵ In order to produce reliable and robust microfluidic based devices, the integration of pumps, detectors, together with separation and other on-chip processes remains challenging.

Accordingly work relating to the integration of sample clean up, extraction, PCR amplification and separation/detection onto a single chip has attracted considerable interest. Easley *et al.* for example have described a fully integrated genetic analysis system incorporating each of these steps, for the rapid screening of infectious pathogens, using hydrodynamic pumping to move samples and reagents around the device.⁵ A similar system was also reported by Liu *et al.* in which rapid short tandem repeat typing for forensic purposes was reported.⁶ The development of a hand held integrated system for the rapid detection of the avian influenza virus H5N1, has been described by Pipper *et al.* using

a system that enables the purification and pre-concentration of RNA for real-time PCR to be carried out.⁷ In terms of commercial systems, the GeneXpert® System produced by Cepheid offers a fully integrated automated commercial system for nucleic acid analysis.

One of the main obstacles however in developing a fully integrated device is the high degree of control required when attempting to move a sample from one area or process to another on a single device. Differences for example in the depths and widths of channels and chambers, which might be necessary to accommodate the various processes required, can cause changes in hydrodynamic pressure and alter the fluidic flow profile. Introducing a system of valves and barriers has met with some success but the system becomes complex and the loss of analyte and reagents on surfaces can become significant.⁸⁻¹⁰ In addition, the control of both forward and back pressure in devices of different channel geometries especially when a solid support may be present can prove challenging. Grover *et al.* discussed some of the problems associated with using valves and micro pumps in integrated systems,¹⁰ and Vilkner *et al.* compiled a review discussing developments in micro total analysis systems (μTAS), including methods of non-mechanical micro-pumping, *e.g.* electro-kinetic micro-pumps.¹¹

Hydrodynamic based micro-pumping and electro-kinetic movement in integrated microfluidic devices have been well reported in the literature as a method for fluidic manipulation.¹²⁻¹⁶ Gui *et al.* for example discuss an electro-osmotic pumping mechanism for a continuous flow PCR chip. In this relatively easy to operate system the authors showed greater potential for

^aDepartment of Chemistry, The University of Hull, Cottingham Road, Kingston upon Hull, HU6 7RX, UK; Fax: +01482 466410; Tel: +01482 465475

^bPostgraduate Medical Institute, The University of Hull, Cottingham Road, Kingston upon Hull, HU6 7RX, UK. E-mail: S.J.Haswell@hull.ac.uk; Fax: +01482 466410; Tel: +01482 465469

integration over hydrodynamic pumping.¹⁷ EOP was induced across a parallel silica based monolith which prevented the solution pumped across the monolith from flowing backwards due to hydrodynamic forces, generating a flow of approximately $0.6 \mu\text{L min}^{-1}$.¹⁸ Kim *et al.* have reported the use of a borosilicate glass and low ion density liquids to achieve much higher flow rates,¹⁹ whilst Reichmuth *et al.* describe the use of a zwitterionic additive, trimethylammonio propane sulfonate (TMAPS), to enhance the performance of the EOP and reported a three-fold increase in flow rate.²⁰ This increase in performance allows for the potential to reduce voltage and power requirements, thus facilitating the development of portable hand held integrated micro total analytical systems. These and other novel methods to control the flow of an integrated PCR device have been reviewed by Zhang *et al.*^{21,22} who discuss the advances and trends in micro pumps, micro valves and micro mixers within PCR microfluidic chips, over the last decade.

A further difficulty encountered, however, when trying to develop a lab on a chip device is the introduction of reagents in a timely and cost effective manner. One possible solution could be to introduce them mechanically at the time of manufacturing, however this raises the issue of how to maintain the integrity of the reagents during long periods of dormancy, a particular problem with PCR reagents. Klatser *et al.* developed and commercialised a stabilised freeze-dried PCR mix which included all the components used in a PCR reaction suitable for this purpose, claiming stability for a year at -20°C and 4 weeks at 4°C .²³ In addition commercially available 'PCR pellets' have been developed where the necessary PCR reagents are contained within a $1 \mu\text{L}$ gel bead (REAX™ MASTERMIX 25 PCR Beads, Q Chip Life Science, Q Chip Ltd, Cardiff MediCentre, Heath Park, Cardiff, Wales, UK), to which only the addition of water and the DNA sample is required to create the reaction solution. These pellets have been shown to be stable for three months when stored at 4°C , and for two months when stored at room temperature.

In this paper we report on the development of an approach which addresses both the pumping and reagent storage issues through the use of a silica monolith for EOP coupled with the presence of preloaded capillary channels containing stabilized reagents within a gel matrix, designed for DNA extraction and PCR amplification. This work represents the first steps towards the development of a self-contained, integrated DNA extraction, amplification and analysis system.

Experimental

Reagents

Low melting point agarose gel (gelling point of 36°C), guanidine hydrochloride, ethidium bromide and EDTA were purchased from Sigma Aldrich (Poole, Dorset, UK). Tris(hydroxymethyl) aminomethane was purchased from Fisher Scientific UK Ltd (Loughborough, Leicestershire, UK). The standard electrophoresis grade agarose gel, deoxyribonucleotide triphosphates (dNTPs), $10\times \text{NH}_4$ buffer, bovine serum albumin (BSA), and magnesium chloride were all purchased from Bioline Ltd (The Edge Business Centre, London, UK). The Hot Start *Taq* DNA polymerase, GoTaq®, was purchased from Promega (Hampshire, UK). The forward and reverse D16S539 (Forward;

5'-ACTCTCAGTCCTGCCGAGGT-3', Reverse; 5'TGTGTG-TGCATCTGTAAGCATG-3', product size of 300–360 base pairs) and Amelogenin (Forward; 5'-CCCTGGGCTCTGT-AAAGAATAGTG-3', Reverse; 5'-ATCAGAGCTTAAA-CTGGGAAGCTG-3', product size of 106 base pairs) oligonucleotide primers were ordered to specification from MWG Biotech (Ebersberg, Germany). The DNA template was extracted from a sample provided by a volunteer, using a QIAamp® DNA Micro Kit, (Qiagen House, West Sussex, UK). The silica based monolith was manufactured from potassium silicate (9% K_2O , 21% SiO_2) purchased from Prolabo (Merck, supplied by VWR International Ltd), and formamide (98%) purchased from Avocado Research Chemicals Ltd (Morecambe, UK). Quant-iT™ PicoGreen® dsDNA Assay kit used to quantify eluted DNA was purchased from Invitrogen Ltd (Paisley, Scotland, UK). Other chemicals used were of analytical grade and all solutions were prepared with deionised water (Millipore Ltd, Livingston, UK).

Instrumentation

Experimentation was performed in a microfluidic device (Fig. 1), wet etched in borosilicate glass and fabricated in-house.²⁴ The electric potentials for EOP were generated using a Paragon 3B power supply unit (0–1000 V DC), custom built by Kingfield Electronics Ltd (Chesterfield, Derbyshire, UK). The power supply was controlled using LabView software (version 5.0), written and supplied by National Instruments Corporation Ltd (Newbury, Berkshire, UK). Platinum wire, diameter $500 \mu\text{m}$, acted as electrode contacts and was supplied by Johnson Matthey (London, UK). Hydrodynamic pumping was

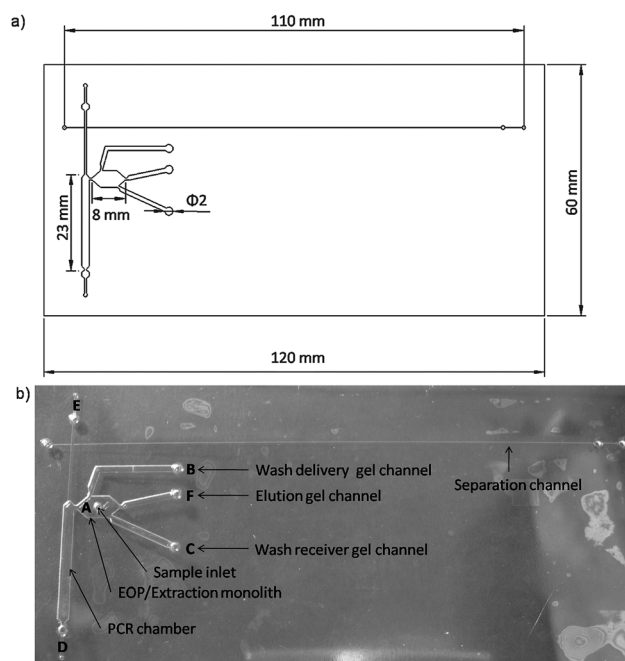


Fig. 1 (a) Schematic and photograph (b) of the integrated chip capable of DNA clean up, extraction, PCR amplification and capillary electrophoretic separation; B–F indicates the positioning of platinum electrodes.

performed using a KDS200 Syringe Infusion Pump (Kd Scientific, Holliston, Massachusetts, USA).

The PCR reagents stability was tested by performing PCR amplification in a TECHNE TC-312 Thermal Cycler (Barloworld Scientific, Bibby Scientific Ltd, Staffordshire UK). For qualitative analysis, the resulting PCR products were separated by agarose slab gel electrophoresis in which 115 V was applied for 45 min, using a Horizontal Electrophoresis tank, SCIE PLAS with MD-250N OmniPAC MIDI power supply (SCIE PLAS, Warwickshire, UK). After staining with $0.5 \mu\text{g ml}^{-1}$ ethidium bromide the separated products were visualised using a UV transilluminator (Syngene, Synoptics Ltd, Cambridge, UK). The DNA extracted by EOP elution was also quantified using a POLARStar OPTIMA plate reader (BMG LABTECH Ltd, Aylesbury, UK), used in conjunction with the Quant-iT™ PicoGreen® dsDNA Assay kit.

Preparation of microfluidic device

The silica EOP/extraction monolith, formed in the hexagonal structure of the chip (Fig. 1), was manufactured from a 10 : 1 ratio of potassium silicate and formamide mixture and allowed to cure at 95°C for 12 hours. The monolith was then activated by hydrodynamic pumping $1 \times \text{TE}$ buffer at a flow rate of $5 \mu\text{l min}^{-1}$ for 30 minutes. The agarose wash delivery gel was made by dissolving low melting point agarose gel in deionised water to give a concentration of 3% (w/v) ($0.0030 \text{ g agarose in } 100 \mu\text{l deionised water}$) and heated to 75°C .

Once the gel was formed and still molten, $100 \mu\text{l}$ of 80% ethanol and 20% 1 M sodium chloride solution was added. The gel was then introduced into the wash delivery gel channel at port B where it solidified trapping the ethanol wash.

The wash receiver gel was prepared by dissolving low melting point agarose gel in deionised water to produce a concentration of 0.75% (w/v), and heated to 75°C for 10 minutes after which it was injected into the wash receiver gel channel through port C whilst still molten, then allowed to cool. A 0.75% (w/v) elution gel was similarly prepared and injected into the elution gel channel through port F whilst still molten, and allowed to cool.

The optimal PCR gel was prepared by dissolving low melting point agarose gel in deionised water to produce a concentration of 1.5% (w/v), and heated to 75°C for 10 minutes. Once the gel was formed and whilst still molten the PCR reagents were added ($1 \times \text{NH}_4$ buffer, $1.5 \mu\text{M}$ BSA, $1 \mu\text{M}$ forward primer, $1 \mu\text{M}$ reverse primer, $200 \mu\text{M}$ dNTPs, 1.5 mM MgCl_2 and 1 Unit of GoTaq®) and mixed. The PCR gel was then injected into the PCR chamber through port D whilst still molten and on cooling the gel retained the PCR reagents.

Once all channels were filled with gel-supported reagents platinum wire electrodes were secured in place at ports B–F and the chip was then ready for operational use.

DNA collection and loading

DNA was extracted from buccal cells collected from the cheek of a volunteer, quantified, and diluted to create a standard concentration of $5 \text{ ng } \mu\text{l}^{-1}$. DNA standard solution ($5 \mu\text{l}$) was then mixed with $120 \mu\text{l}$ of guanidine hydrochloride and loaded

hydrodynamically on to the monolith through the sample inlet A and out to channel C using a flow rate of $5 \mu\text{l min}^{-1}$.

DNA sample wash

To remove any cellular debris introduced during the DNA sample loading process, an ethanol wash across the monolith was performed. An evaluation of applied electric fields ($50\text{--}200 \text{ V cm}^{-1}$ across electrodes placed at ports B and C) was performed to establish the optimum EOP movement of the ethanol sodium chloride solution in the gel (Fig. 2). The optimum electric field was determined as that which enabled the fastest flow rate of solution whilst incurring minimal gel damage (*i.e.* where the physical structure of the gel began to deteriorate), which was found to be 100 V cm^{-1} .

DNA elution into PCR reagent gel

In order to establish the optimal EOP conditions for eluting the washed DNA by water contained within the elution gel held in the elution gel channel, a range of applied voltage sequences between electrodes F to D were investigated (Table 1). It was found that an electric field of 100 V cm^{-1} across electrodes D and F for 5 minutes gave optimal results. The experiments were performed on an ice block to maintain the integrity of the PCR reagents. Once the EOP movement was complete, the PCR gel was removed from the channel by pressure injection, collected and amplified in a thermal cycler. The resulting products were separated by slab agarose gel electrophoresis and observed using the UV transilluminator.

PCR gel stability

The same method described above was used to prepare PCR reagent gels of differing reagent and gel concentrations in order to determine the most appropriate conditions to facilitate successful PCR amplification, whilst maintaining reagent stability. The short and long term stability of the optimal reagent gel was also investigated by storing the PCR gel for known periods of time at room temperature and at 4°C .

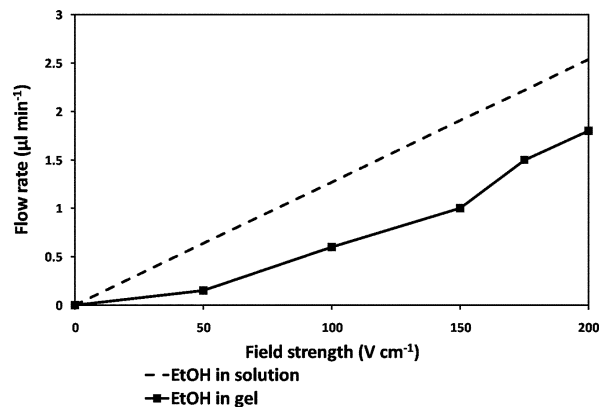


Fig. 2 Flow rates achieved for EOP movement of ethanol solution in gel across a silica monolith at increasing field strengths, compared to that obtained for ethanol free solution.

Table 1 Summary of the voltage sequences to control the elution of DNA from a silica monolith into a PCR reagent gel^a

	Electrode D	Electrode E	Electrode F	Time
Sequence 1	Ground	50 V cm ⁻¹	50 V cm ⁻¹	5 min
Sequence 2	Ground	100 V cm ⁻¹	100 V cm ⁻¹	10 min
Sequence 3	Ground	50 V cm ⁻¹	50 V cm ⁻¹	5 min
	50 V cm ⁻¹	Ground	Ground	20 s
Sequence 4	Ground	100 V cm ⁻¹	100 V cm ⁻¹	5 min
	100 V cm ⁻¹	Ground	Ground	20 s
Sequence 5	Ground	—	100 V cm ⁻¹	5 min
	100 V cm ⁻¹	—	Ground	10 s
Sequence 6	Ground	—	100 V cm ⁻¹	10 min
	100 V cm ⁻¹	Ground	—	10 s
Sequence 7	Ground	—	100 V cm ⁻¹	5 min
	100 V cm ⁻¹	Ground	—	10 s

^a Sequences 3–7 are two step processes, incorporating a reverse shunting step. (Refer to Fig. 1 for electrode positions in relation to sequence)

Results and discussion

DNA sample wash

In order to prepare the DNA sample for PCR amplification, cellular debris trapped in the monolith pores after the loading process, was washed away using the ethanol solution stored in the wash gel channel by applying an electric field of 100 V cm⁻¹ across electrodes B and C for 5 minutes. Ethanol was used in this instance because iso-propanol, which is typically used for the wash step in DNA extraction clean-up,²⁵ did not move under EOP. When comparing the flow rate of ethanol solution with that of ethanol gel (Fig. 2), it was noted that the relationship between field strength and flow rate for the ethanol in gel was non-linear due to the interference effect of the cross polymer network on the bulk flow of liquid. In addition, it can be seen that as expected, the flow rate of ethanol solution was found to be more rapid than that obtained from the same solution in gel format. However, the agarose gel was found to be capable of delivering the ethanol wash across the monolith at an acceptably efficient flow rate. Therefore enabling the removal of cellular debris from the monolith which would have a detrimental effect on the PCR process, as proven by the successful PCR amplification of the cleaned sample.

DNA elution into PCR reagent gel

Based on slab gel electrophoresis, qualitative analysis of PCR products was obtained to establish the efficiency of DNA elution for sequences presented in Table 1. The results indicated DNA recovery increased with each sequence investigated. Accordingly sequence 7 gave a recovery of 65% DNA based on data obtained using the PicoGreen[®] quantification method. The residual 35% was found to be present at the positive electrode F (22%), probably due to electrophoretic movement, with 13% being detected in the ethanol wash. Increasing the electric field beyond 100 V cm⁻¹ was found to damage the physical structure of the gel whilst offering no notable improvement in the extraction efficiency.

For successful PCR amplification 1–10 ng of genomic DNA is required,²⁶ therefore for a recovery rate of 65% a biological sample containing at least 1.5 ng of genomic DNA is required. The DNA

extracted from the monolith by EOP was found to be of sufficient quantity and quality for PCR amplification of the Amelogenin loci to be carried out, as determined by the presence of a PCR product band at the target base pair size (not shown). The results also established that the reagents present in gel-form remained stable even when a relatively high electric field was applied.

PCR gel stability

In order to assess the stability of the gel-supported reagents a series of agarose gel concentrations were investigated (10%, 5%, 3%, 1.5%, 1% and 0.75% (w/v)). As the results obtained for the 5% and 10% concentrations were poor, due to adverse viscosity effects hindering the flow/mixing of DNA and PCR reagents within the gel matrix, these samples were excluded from further study. Of the concentrations evaluated the visualisation of the results for solutions 0.75–3% are presented in Fig. 3. The results indicate that the PCR amplification was successful for each experiment, as all PCR bands were of the target base pair size. In addition, it was determined that the PCR amplification process was more successful when using a lower concentration of agarose, suggested by the presence of stronger UV absorbance bands on the gel. Preliminary tests, however, indicated that concentrations above 1.5% agarose gel were necessary in order to provide long term functional preservation of the reagents. Accordingly 1.5% gel was identified as most suitable both in terms of PCR reagent stability and flow/mixing characteristics.

Gel storage stability tests (Fig. 4) identified that at room temperature the reagents were rendered completely unusable after 1 hour, as indicated by the absence of a PCR product band at the target base pair size. However, stability tests did indicate that storage for 30 minutes at room temperature still permitted generation of PCR products. The storage tests indicated that for optimal results the pre-loaded device should be maintained in a cool environment until time of use.

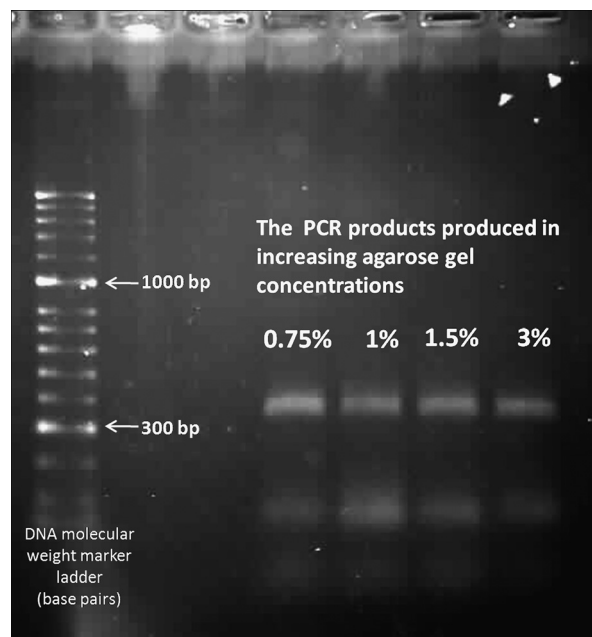


Fig. 3 UV transilluminator image of D16S539 PCR products obtained from the stability testing of the concentration of reagent support gel.

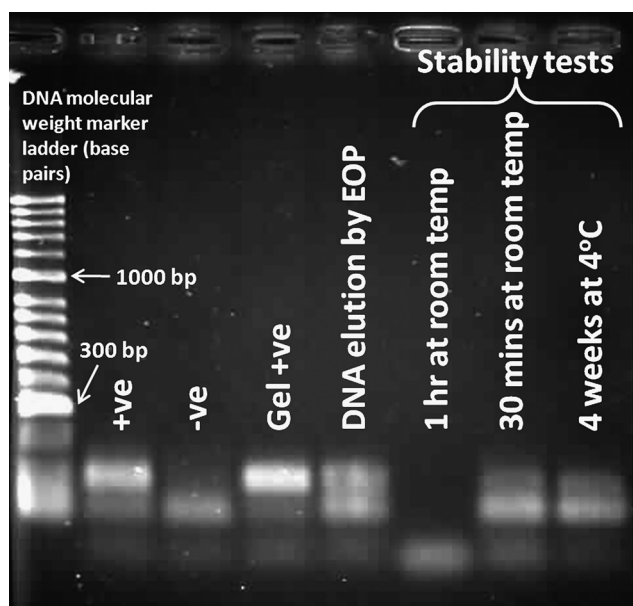


Fig. 4 UV transilluminator image of Amelogenin PCR products following EOP of DNA into PCR reagents in gel. Positive and negative controls are samples of the PCR reagents with and without DNA template respectively. The 'gel positive' and 'DNA elution by EOP' are control samples of PCR reagents in gel and DNA, pre- and post-experimentation respectively. Stability tests; gel left at room temperature for 1 hour, gel left at room temperature for 30 minutes and gel stored at 4 °C for four weeks.

Conclusions

This paper reports the successful application of EOP through a gel supported reagent matrix, supported by a silica monolith which additionally acted as the extraction surface for DNA clean up and elution prior to PCR amplification. It was determined that PCR could successfully be performed in the specifically designed PCR reagent agarose gel, even after the application of an electric field of 100 V cm⁻¹. Stability testing indicated that the agarose gel containing all the reagents necessary for PCR was stable for up to four weeks, when stored at 4 °C.

The incorporation of pre-loaded reagent gels into a microfluidic device offers an attractive methodology compatible with the aim of developing integrated, self-contained, lab on a chip technology. Work is currently in progress to establish a fully integrated device capable of DNA extraction, amplification and analysis.

Acknowledgements

Financial support from Engineering and Physical Sciences Research Council (EPSRC) (EP/D040930)

References

- 1 P. J. Obeid and T. K. Christopoulos, *Analytica Chimica Acta*, 2003, **494**, 1–9.
- 2 F. C. Huang, C. S. Liao and G. B. Lee, *Electrophoresis*, 2006, **27**, 3297–3305.
- 3 D. Erickson, D. Sinton and D. Q. Li, *Lab on a Chip*, 2004, **4**, 87–90.
- 4 P. Liu, S. H. I. Yeung, K. A. Crenshaw, C. A. Crouse, J. R. Scherer and R. A. Mathies, *Forensic Science International: Genetics*, 2008, **2**, 301–309.
- 5 C. J. Easley, J. M. Karlinsey, J. M. Bienvenue, L. A. Legendre, M. G. Roper, S. H. Feldman, M. A. Hughes, E. L. Hewlett, T. J. Merkel, J. P. Ferrance and J. P. Landers, *Proceedings of the National Academy of Sciences of the United States of America*, 2006, **103**, 19272–19277.
- 6 P. Liu, T. S. Seo, N. Beyor, K. J. Shin, J. R. Scherer and R. A. Mathies, *Anal. Chem.*, 2007, **79**, 1881–1889.
- 7 J. Pipper, M. Inoue, L. F. P. Ng, P. Neuzil, Y. Zhang and L. Novak, *Nature Medicine*, 2007, **13**, 1259–1263.
- 8 E. T. Lagally, C. A. Emrich and R. A. Mathies, *Lab on a Chip*, 2001, **1**, 102–107.
- 9 E. T. Lagally and R. A. Mathies, *Journal of Physics D-Applied Physics*, 2004, **37**, R245–R261.
- 10 W. H. Grover, A. M. Skelley, C. N. Liu, E. T. Lagally and R. A. Mathies, *Sensors and Actuators B-Chemical*, 2003, **89**, 315–323.
- 11 T. Vilknor, D. Janasek and A. Manz, *Anal. Chem.*, 2004, **76**, 3373–3385.
- 12 J. P. Landers, *Anal. Chem.*, 2003, **75**, 2919–2927.
- 13 P. S. Dittrich, K. Tachikawa and A. Manz, *Anal. Chem.*, 2006, **78**, 3887–3907.
- 14 T. Bayraktar and S. B. Pidugu, *International Journal Of Heat And Mass Transfer*, 2006, **49**, 815–824.
- 15 M. C. Breadmore, *Electrophoresis*, 2007, **28**, 254–281.
- 16 D. P. Wu, J. H. Qin and B. C. Lin, *Journal of Chromatography A*, 2008, **1184**, 542–559.
- 17 L. Gui and C. L. Ren, *Anal. Chem.*, 2006, **78**, 6215–6222.
- 18 F. Q. Nie, M. Macka, L. Barron, D. Connolly, N. Kent and B. Paull, *Analyst*, 2007, **132**, 417–424.
- 19 D. Kim, J. D. Posner and J. G. Santiago, *Sensors and Actuators A-Physical*, 2008, **141**, 201–212.
- 20 D. S. Reichmuth, G. S. Chirica and B. J. Kirby, *Sensors and Actuators B-Chemical*, 2003, **92**, 37–43.
- 21 C. S. Zhang, J. L. Xu, W. L. Ma and W. L. Zheng, *Biotechnology Advances*, 2006, **24**, 243–284.
- 22 C. S. Zhang, D. Xing and Y. Y. Li, *Biotechnology Advances*, 2007, **25**, 483–514.
- 23 P. R. Klatser, S. Kuijper, C. W. van Ingen and A. H. J. Kolk, *Journal of Clinical Microbiology*, 1998, **36**, 1798–1800.
- 24 P. D. I. Fletcher, S. J. Haswell, E. Pombo-Villar, B. H. Warrington, P. Watts, S. Y. F. Wong and X. L. Zhang, *Tetrahedron*, 2002, **58**, 4735–4757.
- 25 J. M. Butler, *Journal of Forensic Sciences*, 2006, **51**, 253–265.
- 26 J. M. Butler, *Forensic DNA Typing*, Elsevier, 2005, p. 67.



Development of a gel-to-gel electro-kinetic pinched injection method for an integrated micro-fluidic based DNA analyser

Jennifer A. Oakley^a, Sarah Robinson^a, Charlotte E. Dyer^b, John Greenman^b, Gillian M. Greenway^{a,*}, Stephen J. Haswell^a

^a Department of Chemistry, The University of Hull, Cottingham Road, Kingston upon Hull, HU6 7RX, United Kingdom

^b Postgraduate Medical Institute, The University of Hull, Cottingham Road, Kingston upon Hull, HU6 7RX, United Kingdom

ARTICLE INFO

Article history:

Received 31 March 2009

Received in revised form 23 July 2009

Accepted 24 July 2009

Available online 3 August 2009

Keywords:

Electro-kinetic injection

Micro-fluidics

DNA analysis

Integration

Gel matrix

ABSTRACT

An integrated gel supported micro-fluidic system is reported, in which PCR products can be efficiently injected into a capillary electrophoresis device. The gel supported system is designed to provide greater stability to reagents during long periods of dormancy, enabling the mass production of one use chips encapsulating all required reagents at the time of manufacturing. This simultaneously diminishes the risk of sample contamination, and reduces the amount of external hardware required for auxiliary flow control, thus increasing the potential for portability. After PCR amplification was performed in a polysaccharide gel matrix, the PCR product was injected into the separation gel polymer matrix by executing a capillary-based electro-kinetic pinched injection across a gel-to-gel interface. The gel-to-gel system delivered a precise and accurate plug into the separation polymer, which offered more stable electro-kinetic control of the sample compared to solution based methodology even when bubbles were present in the system. Suitable voltage control was proven to provide a repeatable electro-kinetic injection of PCR product sufficient for an on-chip separation of multiple loci by capillary electrophoresis.

© 2009 Elsevier B.V. All rights reserved.

1. Introduction

Micro-fluidic devices, which offer the benefits of high sample throughput and low sample volume, are attractive as they introduce the possibility of integrating multiple processes onto one device [1], which in turn can lead to automated systems that will increase the integrity of an analytical measurement [2]. DNA analysis is one such technique that would benefit greatly from the integration of processes such as sample clean up, extraction, PCR amplification, separation and detection. Current methods in place to perform such practices are laborious, with a single analysis taking several hours moving from one process 'station' to another, in addition issues such as misplacement, contamination and chain of custody are problems which would be avoidable if analysis could be performed on one device at point of need. There are a number of reviews published that discuss in detail various work undertaken in the field of integration and miniaturisation of DNA analysis, including Wu et al., Horsman et al., and Cruces-Blanco et al. [3–5].

Integration of different processes onto one device has proven difficult in past attempts, and providing meaningful and repro-

ducible analytical results difficult to attain [6–9]. One of the reasons such integration has proved difficult to implement, however, is the high degree of complexity associated with successfully coupling the macro to micro interface necessary for introducing reactants and samples into the micro-fluidic system. A solution to this problem would be to incorporate the reactants into the device at the time of manufacture, sealing them inside so only the sample needs to be introduced at point of analysis.

A pre-loaded liquid based system can be problematic, however in terms of stability of the reagents when exposed to long periods of dormancy in the micro-fluidic device, so substantially reducing the shelf life of such a device for commercial uses. Previous work has suggested that the stability of certain volatile reagents can be greatly increased by encapsulating them in a protective polymer solution [10,11].

We previously demonstrated the advantage of this approach for integrating the process of DNA clean up and extraction in a micro-fluidic device [12]. All the reagents necessary for both the processes were supported within the pre-loaded gels, which could be stored for 4 °C for up to four weeks. The crude sample of lysed cells was introduced hydro-dynamically onto a silica monolith contained within a chip in order to extract the DNA. Ethanol contained within an agarose gel matrix on chip was then used to wash unwanted debris away from the sample by electro-osmotic pumping (EOP). The retained DNA was then eluted from the monolith by water

* Corresponding author. Tel.: +44 1482 465475; fax: +44 1482 466410.

E-mail address: g.m.greenway@hull.ac.uk (G.M. Greenway).

retained within a second on chip agarose gel, again using EOP. The eluted DNA was then successfully amplified by PCR.

The next step in the integration process would be the electrokinetic (EK) injection of the PCR product into a separation channel to allow separation and detection. Controlling the injection, for example, of a sample into capillary channels is key to obtaining reproducible electrophoretic separations [13,14], and reliable detection resolution. However, producing an accurate, reproducible injection can prove challenging, when addressing issues such as large volumes of sample lost during sample placement and clearance stages of an injection and bias complicating the injection process.

In general, injections into a micro-fluidic device can be controlled either pneumatically, hydro-dynamically, by suction, pressure, gravity, or alternatively, electro-kinetically [2,8,15–17]. The latter intrinsically lends itself to more precise and accurate control of sample introduction over hydro-dynamic systems, whilst at the same time removing the need for external pumps, actuators, valves, etc. Accordingly a number of different forms of EK injection have been reported; Zhang et al. for example, described a form of pressure pinched injection, where a combination of negative pressure, electro-kinetic, hydrostatic, and geometric forces were used to control the quantity of the sample injected. The approach described claims to provide a highly accurate and reproducible injection, though it involves a complicated procedure involving extensive instrumentation [17]. Another common approach is the gated injection where a small sample volume is diverted from a continuous flowing stream into a side channel. To control the injection, a negative charge is applied to the cross channel perpendicular to the separation channel creating a gate, which directs or withdraws the sample stream away from the separation channel. The gated approach is simple to operate and requires fairly simple channel geometry, however a large volume of sample can be required to maintain a steady flow in which a reproducible plug could be directed from the main stream. In addition, the application of a divergent electric field can create an interference effect upon the separation field. This method was modified by Wenclawiak and Puschl, who used a high powered laser to bleach sections of the sample stream, creating a succession of very short sample plugs in the channel, thereby generating an optically gated injection [18].

The principle of the pinched EK injection, specifically in 'T' geometry, is that a plug of a controllable size is pulled into the separation channel, from a sample source aligned with the separation channel entrance. Once a plug of controlled size is contained in the separation channel, the remaining sample is prevented from entering the separation channel by creating an opposing electric field at the entrance and exit of the channel, such that excess sample is drawn away from the separation channel. The advantage of the pinched injection is that problems associated with continuous sample leakage during the separation process can be addressed; the pull back of the remaining sample efficiently prevents leakage of excess sample passing down the separation channel, so reducing the peak tailing and the sample background.

A disadvantage of EK injection however, is Joule heating which occurs when high voltage differences are applied to small volumes of liquids, which can generate a large amount of heat in the liquid. This problem can be reduced or negated by finding a means to dissipate the heat, such as the use of buffers or the addition of a higher viscosity body into the system such as a polymer matrix [19].

Leading on from our previous work, to complete the integrated DNA analysis it was necessary to efficiently inject the DNA products from the agarose gel filled PCR chamber into the separation matrix ready for CE separation. An EK pinched injection was investigated because, an optimised voltage profile can provide a sample plug with a precisely determined shape and size, in addition to the sim-

ilarity of its implementation, making the EK pinched injection an appealing option for the integrated device. Schmalzing et al. credit the ultra fast separation capabilities of their system to the extremely short injection plugs achieved by an electro-kinetic injection across a suitably designed geometry [20].

Whilst gel-to-gel electro elution of species has been utilised in protein analysis, for example 2-D gel electrophoresis and blotting techniques, it has not been widely used in micro-fluidic systems. Thiatrong et al. recently developed an in-line affinity capture sample injection in which a photo-polymerised oligonucleotide-modified acrylamide capture gel was used to eliminate band broadening and achieve 100% efficiency of injection. The modified gel captured the entirety of the sample, which was then thermally released by melting the gel, before being electrically eluted into the CE channel [21]. The advantage of this system was that the entire sample would be injected but this did require energy to melt the gel which adds complexity to the process and may be problematic for portable systems where it is essential to preserve energy requirements to a minimum.

In this study, we describe how a gel-to-gel based approach impacts the EK pinched injection technique and subsequent separation of DNA by capillary electrophoresis; we describe how the introduction of a gel based system can increase the general robustness of the technique by overcoming disrupted flow problems that may occur due to complicated solution injections or Joule heating when bubbles or voids form.

2. Experimental

2.1. Reagents

Low melting point agarose gel (gelling point of 36°C), EDTA, polyethylene oxide (molecular weight 8,000,000), 40% *N,N*-dimethylacrylamide solution (for electrophoresis, stark filtered), acryloyl chloride, dihexylamine, triethylamine, azobis(4-cyanopentetic acid), and dichloromethane were purchased from Sigma-Aldrich (Poole, Dorset, UK). Tris(hydroxymethyl)aminomethane was purchased from Fisher Scientific UK Ltd. (Loughborough, Leicestershire, UK). The standard electrophoresis grade agarose gel, deoxyribonucleotide triphosphates (dNTPs), 10× NH₄ buffer, bovine serum albumin (BSA), and magnesium chloride were all purchased from Bioline Ltd. (The Edge Business Centre, London, UK). The Hot Start *Taq* DNA polymerase, GoTaq[®], was purchased from Promega (Hampshire, UK). The forward and reverse vWA (forward; 5'-GGACAGATGATAAATACATAGGATGGATGG-3', reverse; 5'-GCCCTAGTGGATGATAAGAATAATCAGTATGTG-3', product size of approximately 150–200 bp) and FGA (forward; 5'-GGCTGCAGGGCATAACATTA-3', reverse; 5'-ATTCTATGACTTTGCCG-TTCAGGA-3', product size of approximately 210–280 bp), both labelled with 5' TAMRA 5', oligonucleotide primers were ordered to specification from MWG Biotech (Ebersberg, Germany). The DNA template was extracted from a sample provided by a volunteer, using a QIAamp[®] DNA Micro Kit, (Qiagen House, West Sussex, UK). Other chemicals used were of analytical grade and all solutions were prepared with distilled water (Millipore Ltd., Livingston, UK).

2.2. Instrumentation

Experimentation was performed in a micro-fluidic device (Fig. 1) [12], wet etched in borate-silicate glass and fabricated in-house [22].

The electro-kinetic movement was generated via the application of electric potentials to platinum electrodes placed in reservoirs A–D. The electric potentials were generated by a Paragon 3B power supply unit (4 × 0 – 1000 V D.C.), which was custom built by King-

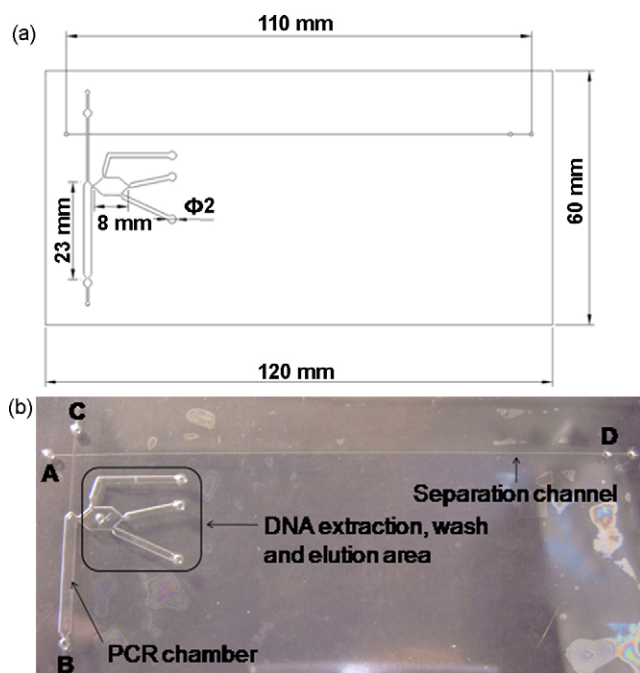


Fig. 1. (a) Schematic of the integrated chip design capable of DNA clean up, extraction, PCR amplification and capillary electrophoretic separation and (b) photograph of the device; A–D indicates the positioning of platinum electrodes.

field Electronics Ltd., Chesterfield, Derbyshire, UK. In addition, an H Series compact, regulated power supply (0–10,000 V D.C.) supplied by *EMCO High Voltage Corporation* (Sutter Creek, California, USA) was used. Both the Paragon 3B and the H Series power supply units were controlled using LabView software (version 5.0), written and supplied by *National Instruments Corporation Ltd.* (Newbury, Berkshire, UK). Platinum wire, diameter 500 μm , acted as electrode contacts and was supplied by *Johnson Matthey* (London, UK). Visualisation of the movement of the fluorescently labelled PCR products was recorded with a Zeiss Axiovert S 100 fluorescence microscope coupled to an ORCA-ER Hamamatsu digital camera. Laser induced fluorescent measurements were also recorded with an Ocean Optics S2000 fiber optic spectrometer, supported by 001Base32 Spectrometer Operating Software, *Ocean Optics Inc.* (Dunedin, Florida, USA), and a diode pumped green laser (*CrystaLaser*[®], Reno, Nevada, USA). The separation polymers used were polyethylene oxide (PEO) gel, (made up to a concentration of 2.5% (w/v) in $1 \times$ Tris-EDTA buffer by the prolonged stirring method, detailed by Fung et al.) [23] and linear poly(acrylamide-co-dihexyl-acrylamide) according to a method described by Chiesl et al. [24].

2.3. Procedures

The micro-fluidic device was cleaned and prepared by flushing through with 1 M hydrochloric acid followed by 1 M sodium hydroxide and deionised water before drying. The separation polymer was loaded into the separation channel by pressure injection into port D. Before performing a gel-to-gel injection a voltage profile capable of performing a suitable EK injection of DNA products in solution into the gel separation was identified. The fluorescently labelled PCR product sample intended for injection was prepared in solution by diluting 9.8 μL of sample, into 10.2 μL of deionised water. The sample was then introduced into the micro-fluidic device by pressure injection into port A in order to ensure equal filling of sample matrix into both arms of the cross bar (B–C). The presence of the separation polymer provided enough resistance

to ensure the PCR product sample was not introduced into the separation channel. Finally platinum wire electrodes were secured into place in ports A–D (Fig. 1).

Once the micro-fluidic device was prepared the sample and separation matrices were inspected by eye to ensure no bubbles or debris, that could cause interruption to the applied electric field, had been introduced by the injection process. The voltage profile was automatically applied from a preset program entered through the LabView software. Systematic stepwise changes of voltages at the different electrodes were investigated with visual assessment of the results. The voltage profile selected (as given in Table 1) gave a reproducible plug injection approximately 5 s long with sample diffusion and tailing greatly reduced.

The next step was to investigate a gel-to-gel injection of the PCR products from the PCR chamber to the separation channel. The agarose gel utilised in the PCR chamber was prepared by dissolving 0.0029 g of low melting point agarose in 100 μL of DNA/RNA-free water, creating a gel concentration of 2.94% (w/v). The solution was then heated in a water bath at 75 $^{\circ}\text{C}$ for 10 min to allow the gel to form. For optimisation experiments the PCR products were added to the molten gel, 10.2 μL of the gel was added to 9.8 μL of the PCR, and mixed. The final gel solution, which had a concentration of 1.5% (w/v), was injected into the micro-fluidic device whilst in molten form by pressure injection into port A and the electrodes secured into place. The voltage profile was then modified from that used for the solution injection to identify a suitable profile that would perform a comparable EK injection in agarose gel (given in Table 1). Later in the work to test integration of the device the PCR was performed on chip (conditions as described in our previous publication) [12] and the resulting products injected into the separation channels.

3. Results and discussion

3.1. Characterisation of solution to gel and the gel-to-gel based electro-kinetic injections

3.1.1. Solution to gel injection

By making systematic stepwise changes to the voltages at electrodes placed in channels A–D and visually assessing the result on a fluorescent microscope a voltage profile was obtained that provided a satisfactory EK injection from solution to gel which gave a narrow plug of DNA products. These results were used as a comparison for the gel-to-gel injection process.

3.1.2. Gel-to-gel injection

When the voltage profile optimised for solution based injection was applied to EK injection from the agarose gel into the separation gel (PEO), the injection proved unsuccessful as no fluorescent PCR product was seen to move into the separation channel (as shown in Fig. 2).

In Fig. 2, step 1, the PCR products were not pulled into the separation channel (i.e. towards D); furthermore, after the initial injection the excess sample is usually pulled away from the entrance to the separation channel to prevent diffusion and sample leakage and this can be seen in steps 2 and 3, however in step 4 the process is not completed because the applied voltage degraded the gel at electrode B and electrical contact was disrupted. The two most probable reasons for the failure of the injection into the separation chamber in step 1 are either a miss match in the viscosities of the loading and separation gels, or the interface between the two different gel types had a detrimental effect on the electric field strength across the channel.

Examination of the current profiles acquired for the solution and gel injections (Fig. 3a and b), however, indicated that the electric

Table 1
The voltages and times required for the optimised electro-kinetic injection of sample contained within a 1.5% (w/v) agarose gel made with TE buffer, into PEO separation polymer.

	Applied voltage (V)				Applied time (s)
	Electrode A	Electrode B	Electrode C	Electrode D	
Step 1: initial injection of sample	1	2400	600	1100	5
Step 2: concentration of sample and 'pull back' of excess	1	3600	900	825	10
Step 3: clearance of excess from separation channel opening	1	3600	900	1237.5	30
Step 4: concentration of sample in separation channel	1	3200	800	1237.5	5

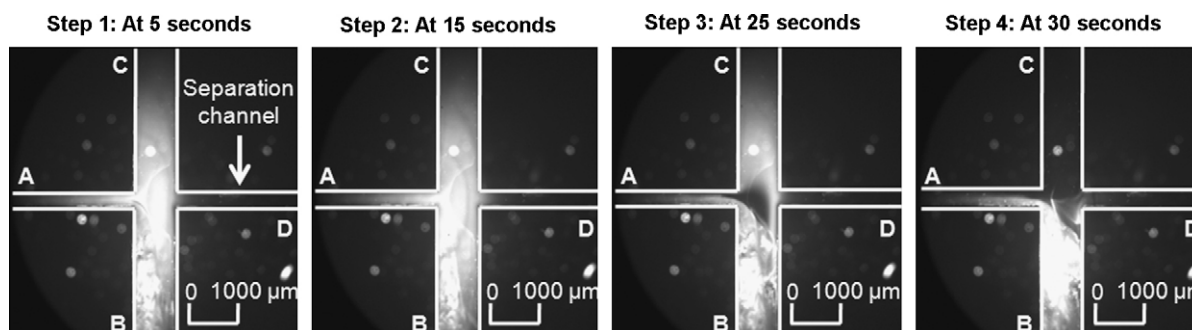


Fig. 2. Visualisation of the unsuccessful electro-kinetic injection of fluorescent PCR product contained within agarose gel.

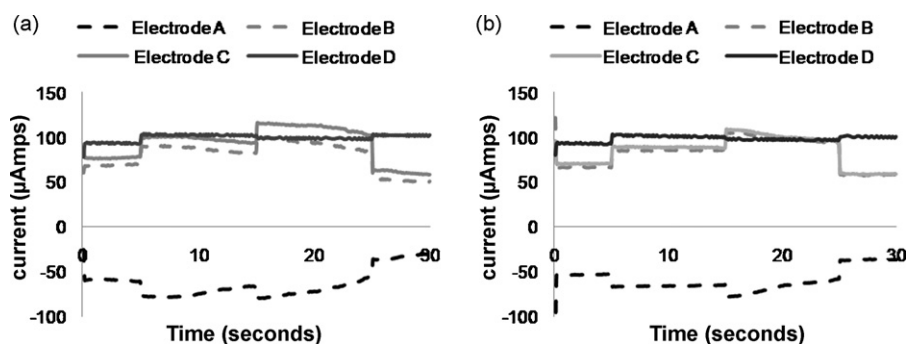


Fig. 3. The current profile acquired from the EK injection: (a) in solution and (b) in 1.5% (w/v) agarose gel.

currents generated within the system were in fact almost identical, the only difference being the flatter and more even nature of the profile observed for the gel system. This evidence suggested that the increased viscosity of the gel has not influenced the applied electric field, other than producing a stabilising effect. The observed hindrance to the injected PCR products is therefore more likely to be attributable to a physical resistance caused by the higher viscosity agarose gel matrix compared to that of a solution based sample. This would suggest that the same fundamental mechanism of movement would apply in both the gel and the solution, the only difference being that the physical influence of the gel requires higher voltages and longer time periods for similar movement to occur.

It was therefore necessary to change the voltage profile for the gel-to-gel EK injection and as previously, systematic stepwise changes to the voltages at the different electrodes were made and the results inspected visually until a narrow reproducible plug of DNA products was obtained. The optimal voltages are given in Table 1 and Fig. 4 show a successful gel-to-gel injection.

This time in step 1 the PCR products can be seen to be entering the separation channel (towards D) and in step 4 the sample can be seen to be focussed into a sharp plug. The new voltage profile given in Table 1 also indicates a higher field strength was required to move the same sample through the agarose gel matrix.

This increase in field strength can be explained from Eq. (1) which describes electrophoretic mobility (μ_{ep}) (where q is the net

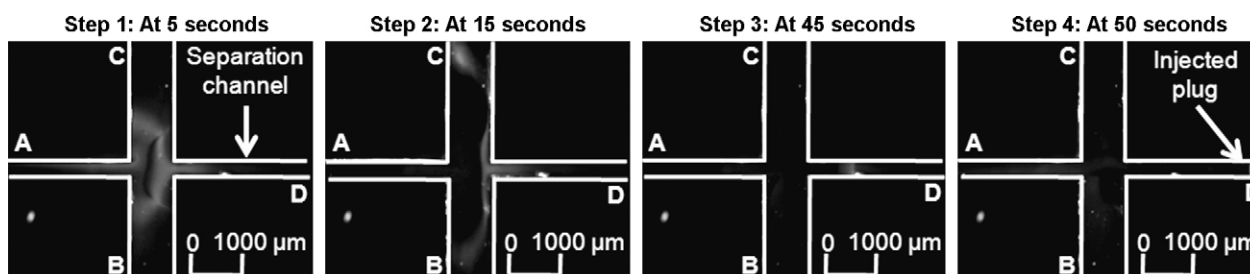


Fig. 4. Visualisation of a successful electro-kinetic injection in agarose gel matrix. Operating voltages and times are given in Table 1.

charge, f is the translational friction coefficient, v is the migration velocity of the component and E is the electric field) and the Hückel equation [25] (Eq. (2)), which is a modified form of the electrophoretic mobility equation, that takes into account electrophoretic movement of a species in a polymer solution (μ_0), (where η is the solvent viscosity and q is the polyion's charge and R the polyion's radius).

$$\mu_{ep} = \frac{q}{f} = \frac{v}{E} \quad (1)$$

$$\mu_0 = \frac{q}{6\pi\eta R} \quad (2)$$

The electrophoretic mobility is expressed in terms of charge over the translational friction coefficient, however the additional consideration of a polymer solution necessitates the introduction of not only the viscosity of the solvent but also the radius of the polyions. In both equations whilst the charge could be the same the added effect of viscosity and the radius of the polyions will alter the electrophoretic mobility within the gel considerably.

To investigate the reproducibility of the gel-to-gel injection repeat injections were made under a range of conditions, including alteration of injection time, injection voltage and polymer concentration. To evaluate the injection process the detector was placed at a fixed point 5 mm distance from the entrance to the separation channel and electropherograms were obtained (fluorescence intensity against time). The half peak width for the injected PCR products was then measured and found to give 7.7% RSD ($n=3$) for the optimal conditions indicated in Table 1. (Repeated experiments were performed on the same device, the reagent debris from each experiment was removed and the device was cleaned and reloaded as described).

As indicated earlier, controlling the injection of a sample into a capillary channel is key to obtaining reproducible electrophoretic separations with reliable detection resolution. In order to improve the resolution of the CE separation, having established the optimal agarose to PEO injection technique, other separation polymers were investigated including LPA-co-DHA [26]. When the voltage profile given in Table 1 was applied for an injection into this matrix, it was found that the difference in viscosity between the separation gels PEO and LPA-co-DHA resulted once again in the optimised voltage profile for the gel-to-gel injection being no longer valid. When the profile optimised for the PEO was applied to LPA-co-DHA, it was found lower voltages applied to electrodes B and C were satisfactory compared to PEO separations. This is thought to occur due to the low resistance afforded by the less viscous PEO separation matrix providing a preferential field for the sample, a higher force is required to alter the direction of the movement of the sample after the initial sample pull down action (step 1).

Once the successful gel-to-gel injection (LPA-co-DHA) had been obtained with good precision, 2.9% RSD ($n=3$), separations of the PCR products could be carried out and an example is shown in Fig. 5 in which PCR products vWA and FGA are seen to be separated with a peak resolution of 2.7.

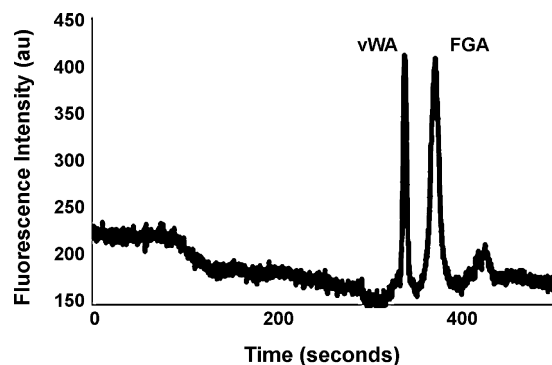


Fig. 5. Electropherogram, separation of PCR products (vWA and FGA) in 3% LPA-co-DHA, injection field of 90 V cm^{-1} for 5 s, separation field of 275 V cm^{-1} .

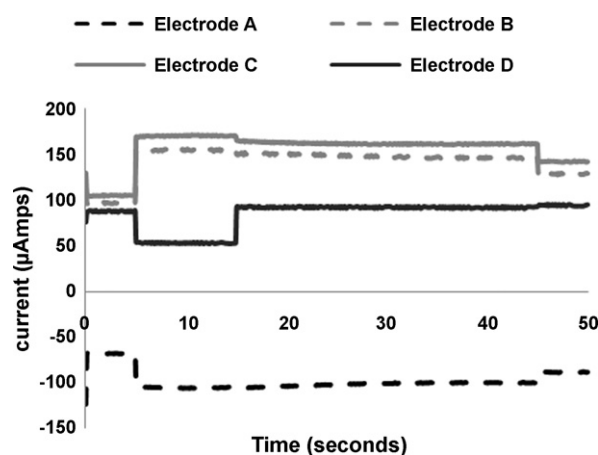


Fig. 6. The current profile acquired from the optimised EK injection in 1.5% agarose gel.

3.2. Robustness of a gel supported injection

It can clearly be seen in Fig. 3b and Fig. 6 that for gel-to-gel injections the current profiles acquired are smoother when compared to the solution to gel injection (Fig. 3a); this suggests a greater degree of electrical stability in the system.

The increased stability of the gel was further displayed when an electro-kinetic injection was successfully carried out with a void or a bubble, introduced into the system as an artefact of reagent introduction (Fig. 7).

In the solution based system, a bubble present during the EK injection can severely compromise the fluidic movement and often lead to failure of the process. Fig. 7 shows a gel-to-gel EK injection in the presence of a void or a bubble. In step 1 a large void or bubble can be seen in the channel leading to B, however the PCR products can be seen to have entered the separation channel in the same way as Fig. 4. In steps 2 and 3 the excess sample is still cleared away

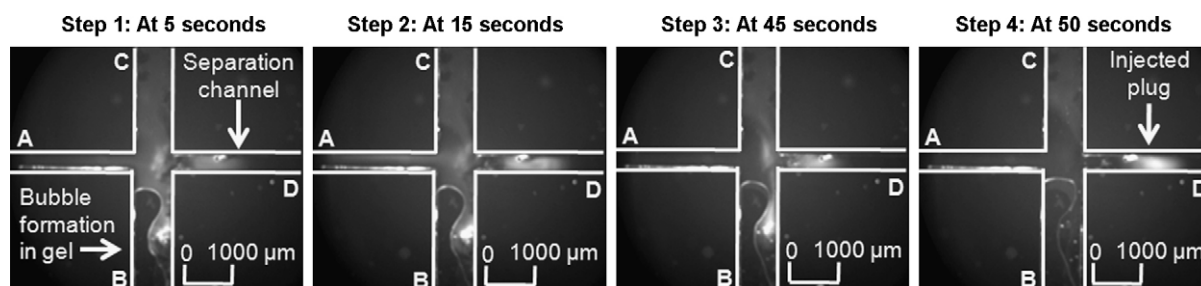


Fig. 7. Visualisation of a successful electro-kinetic injection in agarose gel matrix with a bubble present. Operating voltages and times are given in Table 1.

from the separation channel despite having to move around the bubble. By step 4 for the excess sample has gone and the sample plug can be seen moving down the separation. The sample plug is more diffuse with a wider diameter, however it can clearly be seen that a successful injection of sample can be made, despite the presence of a bubble or void. The success of an injection with a bubble or void present was found to be dependent on the placement of the disruption in the gel, if it occurs between the interface of the separation matrix and sample containing gel, or in the vicinity of the junction at that point, then this would disrupt the electric field and the injection would be unsuccessful.

4. Conclusions

This paper reports the successful optimisation and application of a gel-to-gel electro-kinetic injection of a sample from a gel supported matrix into a polymer gel separation matrix. The work has identified the importance viscosity plays on a gel-to-gel system for electro-kinetic injections, compared to a solution injection, indicating much higher electric fields were required to achieve identical movement within a sample gel matrix. Interestingly, the opposite effect was noted when the viscosity of the separation gel was increased, the electric field required to clear excess sample from separation channel entrance was found to be much lower with the higher viscosity separation gel than the low viscosity separation gel.

Evidence of an increase in control and robustness for a gel supported injection over solution based introduction has been demonstrated. In addition, an interesting aspect of this work discovered that the presence of a bubble or void in the sample gel did not cause the problems of excess Joule heating observed in sample solution based systems. Although disruptions in the continuity of the gel altered the pathway of the injection mechanism substantially, the robustness of the system allowed the current to still be maintained and an injection achieved. It is important to remember that if this disruption occurred in a solution only fluidic system, a break in the electric field would have severely compromised the injection process.

These results will support the development of a fully integrated portable gel based DNA analyser on a micro-fluidic device. The use of both applied voltages and gels leads to several advantages for integration including simplification of instrumentation with no need for moving parts and reduction of macro to micro interfacing and power requirements. The gels allow the storage of the reactants at the time of manufacture along with increasing the robustness of the EK injection.

Acknowledgements

Financial support from Engineering and Physical Sciences Research Council (EPSRC) (EP/D 040930), and for technical support the authors would like to acknowledge Dr. Peter Docker, Dr. Abigail Webster and Kirsty Shaw.

References

- [1] P.J. Obeid, T.K. Christopoulos, *Analytica Chimica Acta* 494 (2003) 1–9.
- [2] F.C. Huang, C.S. Liao, G.B. Lee, *Electrophoresis* 27 (2006) 3297–3305.
- [3] D.P. Wu, J.H. Qin, B.C. Lin, *Journal of Chromatography A* 1184 (2008) 542–559.
- [4] K.M. Horsman, J.M. Bienvenue, K.R. Blasler, J.P. Landers, *Journal of Forensic Sciences* 52 (2007) 784–799.
- [5] C. Cruces-Blanco, L. Gamiz-Gracia, A.M. Garcia-Campana, *TRAC—Trends in Analytical Chemistry* 26 (2007) 215–226.
- [6] R.G. Blaze, P. Kumaresan, R.A. Mathies, *Proceedings of the National Academy of Sciences of the United States of America* 103 (2006) 7240–7245.
- [7] C.L. Bliss, J.N. McMullin, C.J. Backhouse, *Lab on a Chip* 7 (2007) 1280–1287.
- [8] C.J. Easley, J.M. Karlinsey, J.M. Bienvenue, L.A. Legendre, M.G. Roper, S.H. Feldman, M.A. Hughes, E.L. Hewlett, T.J. Merkel, J.P. Ferrance, J.P. Landers, *Proceedings of the National Academy of Sciences of the United States of America* 103 (2006) 19272–19277.
- [9] R.T. Zhong, X.Y. Pan, L. Jiang, Z.P. Dai, J.H. Qin, B.C. Lin, *Electrophoresis* 30 (2009) 1297–1305.
- [10] P.R. Klatser, S. Kuijper, C.W. van Ingen, A.H.J. Kolk, *Journal of Clinical Microbiology* 36 (1998) 1798–1800.
- [11] M. Hori, H. Fukano, Y. Suzuki, *Biochemical and Biophysical Research Communications* 352 (2007) 323–328.
- [12] J. Oakley, K. Shaw, P. Docker, C. Dyer, J. Greenman, G.M. Greenway, S.J. Haswell, *Lab on a Chip* 9 (2009) 1596–1600.
- [13] D. Belder, M. Ludwig, L.W. Wang, M.T. Reetz, *Angewandte Chemie—International Edition* 45 (2006) 2463–2466.
- [14] S.C. Jacobson, R. Hergenroder, L.B. Koutny, R.J. Warmack, J.M. Ramsey, *Analytical Chemistry* 66 (1994) 1107–1113.
- [15] A.M. Leach, A.R. Wheeler, R.N. Zare, *Analytical Chemistry* 75 (2003) 967–972.
- [16] J.M. Karlinsey, J. Monahan, D.J. Marchiarullo, J.P. Ferrance, J.P. Landers, *Analytical Chemistry* 77 (2005) 3637–3643.
- [17] L. Zhang, X.F. Yin, Z.L. Fang, *Lab on a Chip* 6 (2006) 258–264.
- [18] B.W. Wenclawiak, R. Puschl, *Analytical Letters* 39 (2006) 3–16.
- [19] L. Gui, C.L. Ren, *Langmuir* 24 (2008) 2938–2946.
- [20] D. Schmalzing, L. Koutny, A. Adourian, P. Belgrader, P. Matsudaira, D. Ehrlich, *Proceedings of the National Academy of Sciences of the United States of America* 94 (1997) 10273–10278.
- [21] N. Thaitrong, N.M. Toriello, N.D. Bueno, R.A. Mathies, *Analytical Chemistry* 81 (2009) 1371–1377.
- [22] P.D.I. Fletcher, S.J. Haswell, E. Pombo-Villar, B.H. Warrington, P. Watts, S.Y.F. Wong, X.L. Zhang, *Tetrahedron* 58 (2002) 4735–4757.
- [23] E.N. Fung, H.M. Pang, E.S. Yeung, *Journal of Chromatography A* 806 (1998) 157–164.
- [24] T.N. Chiesl, K.W. Putz, M. Babu, P. Mathias, K.A. Shaikh, E.D. Goluch, C. Liu, A.E. Barron, *Analytical Chemistry* 78 (2006) 4409–4415.
- [25] J. Zhang, Y.M. Wang, D.H. Liang, Q.C. Ying, B. Chu, *Macromolecules* 38 (2005) 1936–1943.
- [26] C.P. Fredlake, D.G. Hert, C.W. Kan, T.N. Chiesl, B.E. Root, R.E. Forster, A.E. Barron, *Proceedings of the National Academy of Sciences of the United States of America* 105 (2008) 476–481.



The use of carrier RNA to enhance DNA extraction from microfluidic-based silica monoliths

Kirsty J. Shaw^a, Lauren Thain^a, Peter T. Docker^a, Charlotte E. Dyer^b, John Greenman^b, Gillian M. Greenway^a, Stephen J. Haswell^{a,*}

^a Department of Chemistry, University of Hull, Cottingham Road, Hull, HU6 7RX, United Kingdom

^b Postgraduate Medical Institute, University of Hull, Cottingham Road, Hull, HU6 7RX, United Kingdom

ARTICLE INFO

Article history:

Received 5 February 2009

Accepted 24 March 2009

Available online 31 March 2009

Keywords:

DNA extraction

Carrier RNA

Silica monoliths

Microfluidics

ABSTRACT

DNA extraction was carried out on silica-based monoliths within a microfluidic device. Solid-phase DNA extraction methodology was applied in which the DNA binds to silica in the presence of a chaotropic salt, such as guanidine hydrochloride, and is eluted in a low ionic strength solution, such as water. The addition of poly-A carrier RNA to the chaotropic salt solution resulted in a marked increase in the effective amount of DNA that could be recovered (25 ng) compared to the absence of RNA (5 ng) using the silica-based monolith. These findings confirm that techniques utilising nucleic acid carrier molecules can enhance DNA extraction methodologies in microfluidic applications.

© 2009 Elsevier B.V. All rights reserved.

1. Introduction

The isolation of DNA from biological samples constitutes the first step in a variety of bioanalytical techniques, for example the polymerase chain reaction (PCR) which performs optimally when using purified DNA free from potential inhibitors of the amplification reaction. In many instances, such as forensic investigations, biological samples are limited both in terms of quantity and quality therefore retrieving the maximum amount of DNA possible from the original sample is crucial. DNA purification is commonly achieved by employing solid-phase extraction methodology, whereby the DNA is adsorbed onto a solid support, potential contaminants are removed by washing and the purified DNA eluted from the support. One of the practical advantages of using adsorption-based methodology is that it facilitates pre-concentration of the DNA, which is important when dealing with a limited amount of sample material.

One example of solid-phase DNA extraction methodology, used in many commercially available DNA extraction kits such as the QIAamp[®] DNA Micro Kit [Qiagen, UK], involves the use of silica as the solid-phase to which the DNA binds in the presence of chaotropic agents, such as guanidine hydrochloride. Chaotropic salts have a disruptive effect on the three-dimensional macromolecular structure of DNA, by interfering with intra-molecular interactions, thereby facilitating binding of DNA to the silica sur-

face. In addition, the chaotrope also acts to lyse cells and inactivate deoxyribonucleases, which enzymatically digest DNA. Following DNA adsorption to the solid-phase support, any cellular or proteinaceous debris is removed using an alcohol wash. Finally the DNA is eluted in a low ionic strength buffer such as water [1] in which it can then be used in downstream applications.

Alternative solid-phase DNA extraction methodologies include the use of ion exchange chromatography [2], which exploits the anionic nature of the DNA by capturing DNA molecules on a positively charged column such as those containing diethylaminoethyl (DEAE) groups, for example QIAGEN Genomic-tip System [Qiagen, UK]. By altering the pH and salt concentration of the buffers used, the binding, wash stringency and elution of DNA can be controlled. In addition, liquid–liquid DNA extraction techniques are also available, such as phenol–chloroform extraction but these tend to be more laborious and so are less extensively used.

Whilst commercially available kits, such as the QIAamp[®] DNA Micro Kit [Qiagen, UK] are widely used for DNA extraction and provide the gold standard [3], there is increasing interest in performing DNA analysis in miniaturised microfluidic systems. Such miniaturised systems offer many advantages over conventional benchtop laboratory systems, including reduced reagent volumes and shorter analysis times. More importantly, however, they facilitate direct integration of DNA extraction with other techniques such as PCR.

Early work incorporating solid-phase DNA extraction methods into microfluidic devices utilised silica beads held in place by adapting the device geometry, for example the inclusion of a weir to trap the silica beads [4]. Typical DNA extraction efficiencies, given as the amount of DNA eluted expressed as a percentage of the total

* Corresponding author. Tel.: +44 01482 465469.

E-mail address: s.j.haswell@hull.ac.uk (S.J. Haswell).

DNA added to the system, when using silica beads in a microfluidic device are in the region of 70% [1].

More recently microfluidic devices have incorporated silica-based monoliths, which provide a larger surface area for DNA adsorption and offer favourable properties in terms of fluid dynamics. Silica-based monoliths can be produced by either thermal activation [5] or photo-initiation [6]. Each method of production has its own advantages and range of compatible substrates which can be used. The use of monoliths for DNA extraction has been shown to offer higher DNA extraction efficiencies [6] and greater reproducibility compared with bead-based systems [4], with reported DNA extraction efficiencies for silica-based monoliths of up to 85%, depending on the type of biological sample used as the starting material [5–7].

Despite the high DNA extraction efficiencies reported when using monoliths instead of beads as the solid-phase, there are techniques available to potentially further improve the recovery of DNA including the use of carrier molecules such as RNA [8], salmon sperm DNA [9] or glycogen [10]. As part of phenol–chloroform DNA extraction methodologies, glycogen can be used as a co-precipitant to increase the precipitation of DNA in the presence of alcohol. Carrier molecules have also been used in solid-phase DNA extraction procedures, for example, the addition of poly-A carrier RNA to the extraction matrix in commercially available Qiagen DNA kits increases the amount of DNA recovered during the extraction phase by an average of 24% [3].

The use of carrier molecules to improve DNA extraction efficiencies has not yet been applied to microfluidic systems. The work presented here is an investigation of the potential for carrier RNA to enhance DNA extraction on thermally activated silica monoliths in order to evaluate its compatibility with microfluidic systems.

2. Materials and methods

Silica-based monoliths, of 2 mm in length, were produced by mixing a solution of aqueous potassium silicate (K_2SiO_3 [21% SiO_2 , 9% K_2O]) [VWR International, UK] with formamide [Alfa Aesar, UK], in a 10:1 (v/v) ratio which was then injected into a glass capillary with an internal diameter of 0.65 mm [11]. The solution was cured at 90 °C overnight to produce the solid monolith (Fig. 1).

A 30 min pre-treatment of the monolith with TE buffer (10 mM Tris, 1 mM EDTA adjusted to pH 6.7 [Sigma–Aldrich, UK]) at $5 \mu L \text{ min}^{-1}$ was required prior to performing DNA extraction in order to activate the silica surface and produce optimal DNA

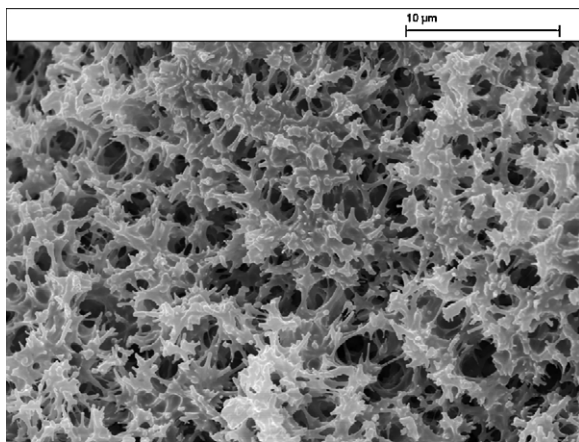


Fig. 1. Scanning electron micrograph image of the surface of a thermally activated silica monolith at 10,000 \times resolution, showing the large surface area available for DNA binding and also the porous structure which allows flow of solutions through the microfluidic device.

extraction efficiency. DNA was first extracted from human buccal cells, using QIAamp[®] DNA Micro Kits [Qiagen, UK], to obtain genomic DNA of a known concentration. An aliquot of DNA was then added to a solution of 5 M guanidine hydrochloride (GuHCl) [Sigma–Aldrich, UK] with varying amounts of poly-A carrier RNA ($1 \mu g \mu L^{-1}$) [Qiagen, UK]. The DNA solution was flowed through the monolith at $2.5 \mu L \text{ min}^{-1}$. An 80% isopropanol wash, administered at $5 \mu L \text{ min}^{-1}$, was subsequently used to remove any remaining proteins/cellular contaminants that might interfere with downstream applications. The purified, pre-concentrated DNA was then eluted from the monolith in ultrapure water at $1 \mu L \text{ min}^{-1}$. All solutions from the loading, washing and elution phases were collected in $2 \mu L$ aliquots and placed in a sealed 96 well microtitre plate to prevent evaporation of solutions.

Since carrier RNA will co-elute with the DNA, it is important to use a DNA specific detection method rather than measuring the total nucleic acid concentration. The concentration of DNA was, therefore, determined using a Quant-iT[™] PicoGreen[®] assay [Invitrogen, UK]. Standards of known DNA concentration were made up in the appropriate media for each phase, i.e. guanidine hydrochloride, isopropanol or water, to enable accurate quantitation. The PicoGreen[®] solution was diluted, according to the manufacturer's instructions, in $1 \times$ TE buffer and then $100 \mu L$ added to each $2 \mu L$ aliquot collected from the DNA extraction process. All measurements were carried out on a FLUOstar OPTIMA microplate reader [BMG LabTech, UK]. DNA extraction efficiencies were calculated based on the amount of DNA recovered during the elution step as a percentage of the initial amount of DNA added to the system.

To assess the quality and integrity of the extracted DNA the collected fractions were analysed by using PCR to amplify a specific microsatellite target sequence. The PCR reaction mixture comprised of: $1 \times$ NH_4 buffer [Bioline, UK], 1 mM $MgCl_2$ [Bioline, UK], 200 μM each dNTPs [Bioline, UK], 1 μM forward primer [MWG, Germany], 1 μM reverse primer [MWG, Germany], 1 unit Taq DNA polymerase [Bioline, UK] and 10 μg bovine serum albumin [New England BioLabs, UK]. Forward and reverse primers with the following sequences 5'-GTGGGCTGAAAAGCTCCCGATTAT-3' and 5'-GTGATTCCCATTTGGCC TGTTCCTC-3' were designed for the amplification of THO1 microsatellite locus [12]. Samples were then amplified using a Techne TC-312 thermal cycler for 28 cycles, each cycle comprising heating steps of: 94 °C for 30 s, 59 °C for 30 s and 72 °C for 30 s.

3. Results and discussion

The effect of the ratio of carrier RNA to DNA was determined by adding varying amounts of $1 \mu g \mu L^{-1}$ carrier RNA to a 25 ng aliquot

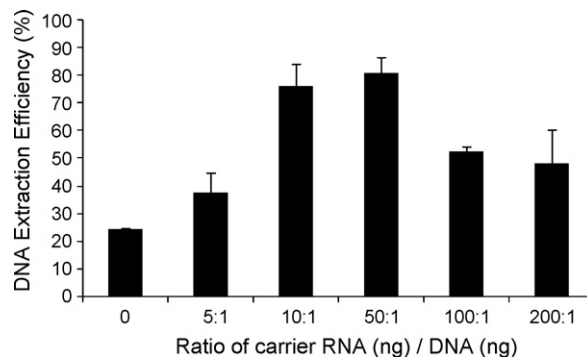


Fig. 2. The ratio of carrier RNA (ng) to DNA (ng) was varied to determine the effects on the amount of DNA recovered during the elution step. DNA extraction efficiencies were calculated as the percentage of DNA recovered during the elution step compared with the amount initially added onto the monolith ($n = 3$).

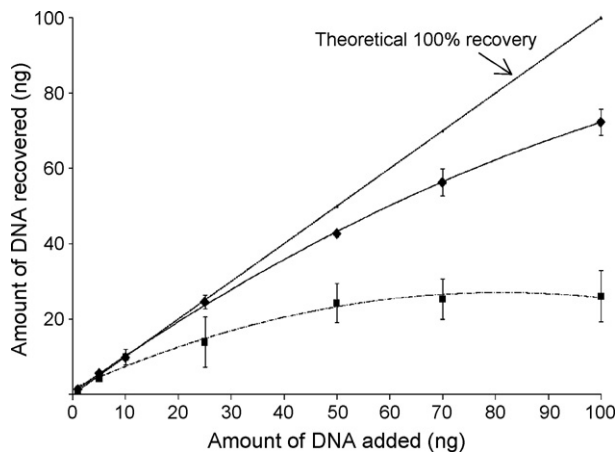


Fig. 3. Amount of DNA recovered from the monolith during the elution step compared with the amount of DNA initially added. Samples with carrier RNA (◆) (ratio 10:1, RNA:DNA) were compared to those with no carrier RNA added (■) ($n=3$).

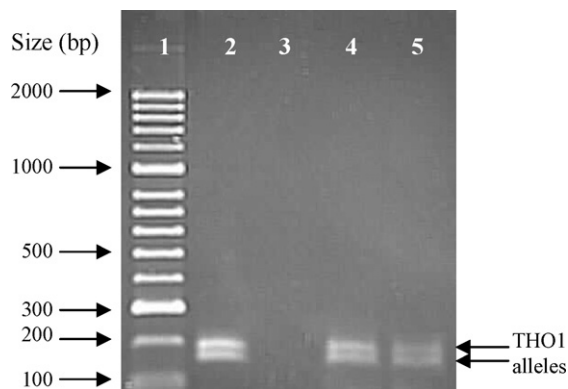


Fig. 4. Agarose gel showing PCR products amplified from DNA extracted using silica-based monoliths within a microfluidic device. Lane 1: DNA size ladder; lane 2: positive control using genomic DNA extracted with QIAamp® DNA Micro Kit; lane 3: negative control containing no DNA; lane 4: amplified DNA extracted using silica monolith with carrier RNA; lane 5: amplified DNA extracted using silica monolith with no carrier RNA.

of DNA in GuHCl solution and calculating the DNA extraction efficiencies (Fig. 2). The efficiency of the DNA extraction process was highest when carrier RNA to DNA ratios of between 10:1 and 50:1 were used.

Having investigated the effect of varying the ratio of carrier RNA to DNA, the influence of varying the amount of starting DNA used, ranging from 1 to 100 ng, was investigated. A comparative set of experiments was carried out in which the samples did not have any carrier RNA added (Fig. 3). When RNA was added at the ratio of 10:1, the DNA extraction efficiency can be seen to follow the ideal 100% recovery up to 25 ng of total added DNA. In comparison however,

without carrier RNA the DNA extraction efficiency only follows the ideal recovery up to 5 ng of DNA. The results therefore indicate that more efficient DNA recoveries can be achieved over a larger mass range when carrier RNA is present in the binding solution.

PCR analysis was carried out on the eluted DNA not only to confirm the integrity of the DNA but also to establish that the carrier RNA had no adverse effects on downstream applications. After 28 cycles of amplification the PCR products were analysed using conventional slab gel electrophoresis. The results showed successful amplification of the target THO1 locus indicating that the extracted DNA is of sufficient quality for amplification and furthermore that the carrier RNA does not inhibit the reaction (Fig. 4).

4. Conclusions

It has been demonstrated that the inclusion of carrier RNA markedly increases DNA extraction efficiency on thermally activated silica-based monoliths in a microfluidic device, confirming that this methodology is suitable for microfluidic applications. Carrier RNA was found to have a more pronounced effect on increasing the DNA extraction efficiency when smaller amounts of DNA were added to the system. It is hypothesised that on the silica matrix there are always a certain number of sites which will irreversibly bind nucleic acids. By including carrier RNA in the binding solution it can sacrificially bind to these sites and so the loss of important DNA is minimised leading to greater recoveries [3]. No adverse effects on downstream applications such as PCR were observed to be associated with the inclusion of carrier RNA.

Acknowledgement

The authors acknowledge EPSRC grant EP/D040930 for supporting this research.

References

- [1] H.J. Tian, A.F.R. Huhmer, J.P. Landers, *Anal. Biochem.* 283 (2000) 175.
- [2] P.R. Levisona, S.E. Badgera, P. Hathib, M.J. Davies, I.J. Bruce, *J. Chromatogr. A* 827 (1998) 337.
- [3] R. Kishore, W.R. Hardy, V.J. Anderson, N.A. Sanchez, M.R. Buoncristiani, *J. Forensic Sci.* 51 (2006) 1055.
- [4] K.A. Wolfe, M.C. Breadmore, J.P. Ferrance, M.E. Power, J.F. Conroy, P.M. Norris, J.P. Landers, *Electrophoresis* 23 (2002) 727.
- [5] Q.R. Wu, J.M. Bienvenue, B.J. Hassan, Y.C. Kwok, B.C. Giordano, P.M. Norris, J.P. Landers, *J.P. Ferrance, Anal. Chem.* 78 (2006) 5704.
- [6] J. Wen, C. Guillo, J.P. Ferrance, J.P. Landers, *Anal. Chem.* 78 (2006) 1673.
- [7] J. Wen, C. Guillo, J.P. Ferrance, J.P. Landers, *J. Chromatogr. A* 1171 (2007) 29.
- [8] S.J. Read, *J. Clin. Pathol.: Mol. Pathol.* 54 (2001) 86.
- [9] L.A. Schiffner, E.J. Bajda, M. Prinz, J. Sebestylen, R. Shaler, T.A. Caragine, *Croat. Med. J.* 46 (2005) 578.
- [10] E.M. Heath, N.W. Morken, K.A. Campbell, D. Tkach, E.A. Boyd, D.A. Strom, *Arch. Pathol. Lab. Med.* 125 (2001) 127.
- [11] P.D. Christensen, S.W.P. Johnson, T. McCreedy, V. Skelton, N.G. Wilson, *Anal. Commun.* 35 (1998) 341.
- [12] U. Ricci, I. Sani, M. Klintschar, N. Cerri, F. De Ferrari, M.L.G. Uzielli, *Croat. Med. J.* 44 (2003) 299.



Immobilized anthraquinone for redox mediation of horseradish peroxidase for hydrogen peroxide sensing

Yuehua Dou^{a,b}, Stephen Haswell^a, John Greenman^b, Jay Wadhawan^{a,*}

^a Department of Physical Sciences (CHEMISTRY), The University of Hull, Cottingham Road, Kingston-upon-Hull HU6 7RX, United Kingdom

^b Centre for Biomedical Research, Postgraduate Medical Institute, The University of Hull, Cottingham Road, Kingston-upon-Hull HU6 7RX, United Kingdom

ARTICLE INFO

Article history:

Received 20 July 2009

Received in revised form 15 August 2009

Accepted 18 August 2009

Available online 22 August 2009

Keywords:

Hydrogen peroxide

Biosensor

Anthraquinone

Horseradish peroxidase

ABSTRACT

The detection of hydrogen peroxide is detailed using horseradish peroxidase and anthraquinone. Both species are immobilized on a glassy carbon electrode substrate. This dual immobilization gives rise to lower detection limits compared with the situation when either of the species is immobilized. Detection limits of 40 nM are reported within physiologically-relevant media.

© 2009 Elsevier B.V. All rights reserved.

1. Introduction

Horseradish peroxidase (HRP) is a stable and readily-available haeme peroxidase found in horseradish roots containing an iron(III) prosthetic group (haemin), and which catalyses the oxidation of a plethora of compounds by hydrogen peroxide [1]. Accordingly, it is an important enzyme in amperometric bioelectroanalysis [2], for which the simplest peroxide biosensor consists of a layer of HRP adsorbed onto an electrode surface, with the applied electrode poised lower than 0.6 V vs. SCE. However, since the redox active site is relatively deeply buried in the polypeptide of HRP, and that numerous glycosylation sites exist on the surface of the native form of HRP, the direct long-range electron transfer (ET) is relatively slow [3]. In contrast, mediated ET between the electrode and the electron-accepting prosthetic group of the enzyme is more efficient *c.f.* direct ET [2], so that the former process can be used to determine the mediator concentration at constant peroxide levels; *mutatis mutandis* the converse. It is this latter route (*q.v.* Scheme 1 in Ref. [4]) that we wish to examine in this article for the proof-of-concept development of an HRP-based biosensor of fast response, good stability and good reproducibility which may be useful in the understanding of biological stress (such as ischaemic injury of the heart) [5,6].

Our approach follows earlier work [7,8], except that we covalently attach an anthraquinone (AQ) monolayer on an electrode surface, and allow the HRP to adsorb onto this layer [9,10]. We prefer this method of protein immobilization to direct attachment [11], as it is thought not to affect the enzyme activity, whilst allowing for a distribution in the conformational orientation of the enzyme [10]. Although AQ-derivatives are known to mediate peroxide reduction directly [12], the use of HRP has the advantage of “amplifying” the response, thence leading to enhanced sensitivity. Nevertheless, the “blocking” of the AQ-layer by enzyme adsorption may reduce the extent of this reaction. Of course, our approach is limited by inhibition due to HRP-mediated O₂-reduction [13,14].

2. Experimental

2.1. Reagents

Water, with a resistivity greater than 18 MΩ cm, was taken from an Elgastat system (Vivendi, UK). HRP (EC 1.11.1.7) type-I (50–150 units mg⁻¹) and type-VI (250–330 units mg⁻¹), hydrogen peroxide (30 vol.%), tetrabutylammonium perchlorate (electrochemical grade), and chemicals for the preparation of phosphate (PBS, 10 mM PBS with 0.1 M NaCl) and Britton–Robinson (BR, 0.04 M BR with 0.1 M KCl) buffers were purchased from Sigma–Aldrich (UK). Acetonitrile and fast-red-AL-salt were respectively obtained from Fischer (UK) and Acros (UK). All chemicals were used as received.

* Corresponding author. Tel.: +44 (0) 14 82 46 63 54; fax: +44 (0) 14 82 46 64 16.
E-mail address: j.wadhawan@hull.ac.uk (J. Wadhawan).
URL: <http://www.hull.ac.uk/chemistry/wadhawan> (J. Wadhawan).

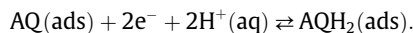
2.2. Instrumentation

Electrochemical experiments employed a three-electrode cell using a glassy carbon (GC) disc electrode (diameter 3.0 mm, BAS, UK) as working electrode with a platinum spiral counter electrode and Ag–AgCl–3 M NaCl (aq) reference electrode (BAS, UK), controlled by a μ -AUTOLAB-type-III potentiostat (Eco-Chemie, The Netherlands). Electrolytes were degassed with nitrogen (BOC, UK) prior to experimentation, and were thermostatted at 22 ± 1 °C except where specified. Square wave voltammetry (SWV) was undertaken in the range $-0.1 \leq E/V \leq -1.2$, at a frequency of 25.0 Hz, 5.0 mV amplitude. Hydrogen peroxide aliquot additions were of at least 0.02 μ M concentrations.

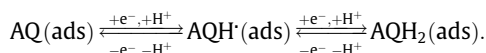
The GC electrode was polished using diamond lapping compounds of decreasing particle size (1.0, 0.3 and 0.1 μ m, Kemet, UK) followed by sonication in water for 5 min. AQ-modification was achieved by reduction of 2.0 mM fast-red-AL-salt in 0.1 M Bu₄NClO₄–MeCN during 20-reduction–oxidation cycles [15,16]. HRP films were physisorbed to this layer after immersion [9] of the AQ-modified electrode in 4.0 mg (mL)⁻¹ HRP–0.1 M PBS (pH 7.0) overnight at 4.0 °C. Electrodes were stored over this solution at this temperature. All protein-modified electrodes were cycled ($v = dE/dt = 0.1$ V s⁻¹) between -0.2 and 1.2 V in 0.1 M PBS (pH 7.0) until the voltammograms stabilized, prior to measurement.

3. Results and discussion

Fig. 1a depicts cyclic voltammograms (CVs) of the AQ-modified GC electrode immersed in aqueous solution of different proton concentration. At pH 1, a single pair of broad redox waves are observed, as anticipated [16] consistent with the known two-electron reduction pathways of anthraquinone species in Eigen-acid media:



Decreasing the solution proton concentration causes the waves to split due to stabilization of an intermediate semiquinone species within the classical square reduction scheme [17]:



Accordingly, such changes affect the overall electrode kinetics of the reduction, as inferred from the changes in the voltammetric waveshapes and the shifts in the potential of the observed voltammetric peaks with changing timescales (*q.v.* Fig. 1a(i)). The two-electron, two-proton transfer in acidic media enables the determination of the electrode coverage (Γ_{AQ}) on application of Faraday's Laws ($\Gamma_{\text{AQ}} = \frac{\int idE}{nFSv}$) to be $4.6 \pm 1.5 \times 10^{-10}$ mol cm⁻², in agreement with literature results [16]. In all cases, as expected

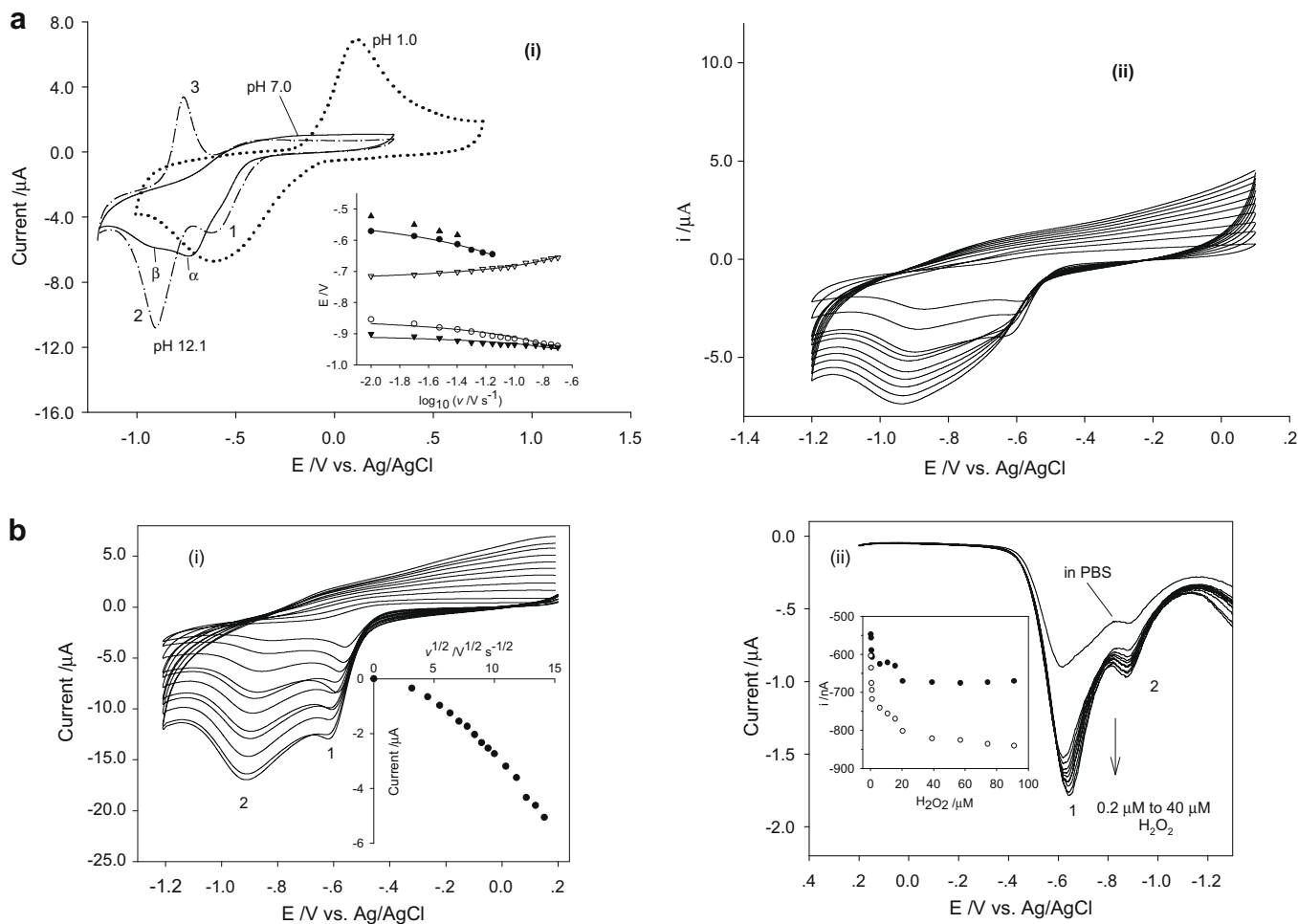


Fig. 1. (a) CVs of an AQ-modified GC electrode immersed in (i) BR buffer at pH 1.0, 7.0 and 12.1 ($v = 0.1$ V s⁻¹); inset depicts the variation of the peak potentials with experimental timescale, key: (●, ○) correspond to peaks α and β at pH 7.0; (▲, ▼, ▽) refer to peaks 1, 2 and 3, respectively at pH 12.1, and (ii) in PBS (pH 7.0). (b) Voltammograms of an AQ-modified GC electrode immersed in PBS (pH 7.0) containing: (i) 0.1 mM H₂O₂; variable scan rate CVs are illustrated – the inset shows the variation of the cathodic current with timescale; (ii) various amounts of H₂O₂; SWVs are depicted, with the inset illustrating the increase in cathodic currents at peak 1 (●) and 2 (○). Average gradients: 3.5 nA (μ M)⁻¹ (1.0–15.0 μ M, $R^2 = 0.986$) at -0.65 V; 1.4 nA (μ M)⁻¹ (1.0–20.0 μ M, $R^2 = 0.924$) and 0.6 nA (μ M)⁻¹ (20.0–100.0 μ M, $R^2 = 0.996$) at -0.89 V.

for adsorbed species, the two-electron peak reduction current is proportional to the voltage sweep rate (*q.v.* Fig. 1a(ii) for pH 7.0, from which the surface coverage is deduced, assuming electrochemical reversibility, to be $2.0 \pm 1.2 \times 10^{-10} \text{ mol cm}^{-2}$, in approximate agreement with that estimated above). We will only

be interested in the response of such electrodes at pH 7.0 hereafter, since these conditions are physiologically-relevant and optimal for enzyme activity. It suffices to note that the final two-electron product is the fully protonated quinol (for which [18] $pK_{a_1}^{25^\circ\text{C}} = 9.00$; $pK_{a_2}^{25^\circ\text{C}} = 12.05$).

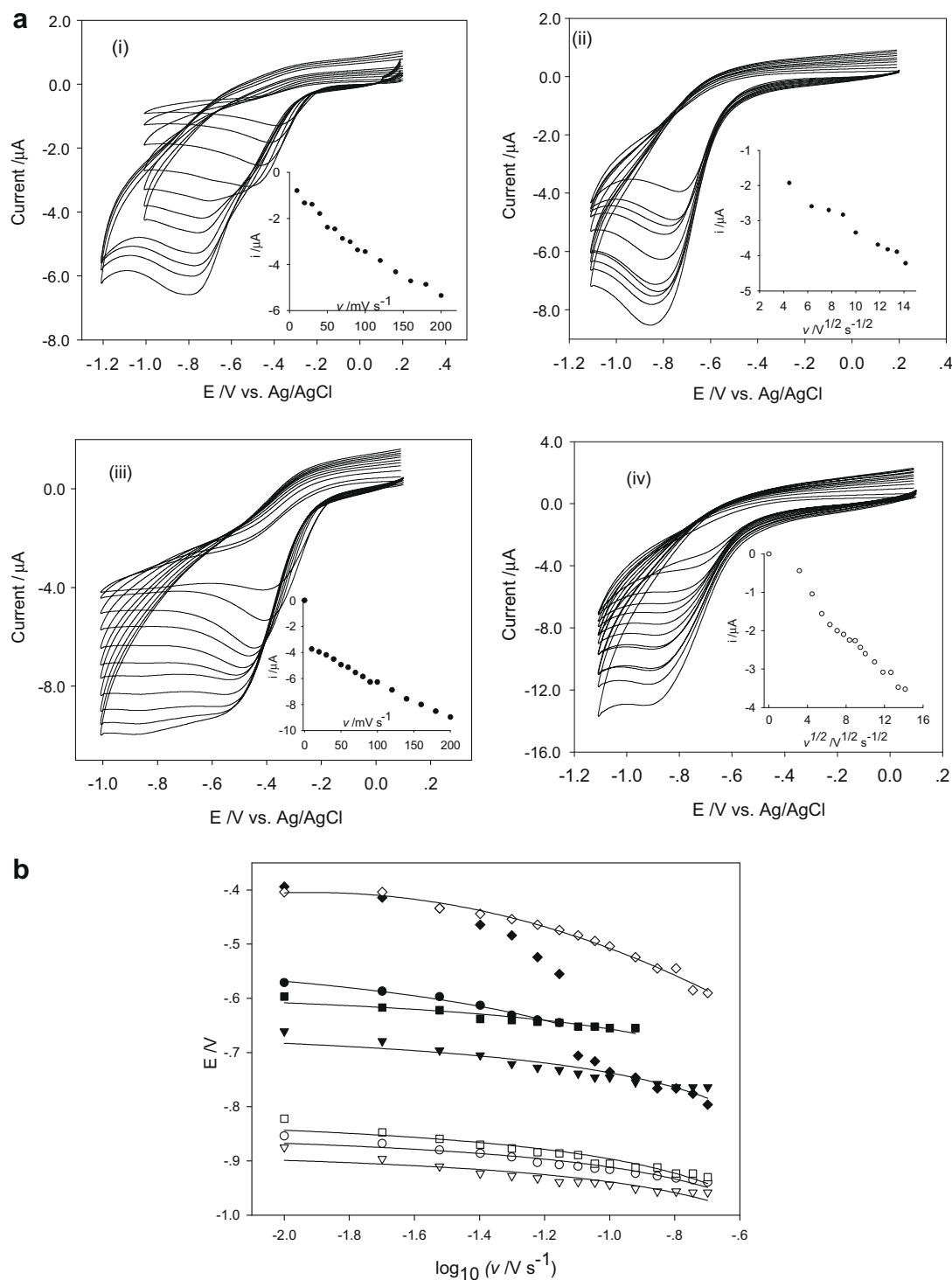


Fig. 2. (a) Representative CVs ($10 \leq v / \text{mV s}^{-1} \leq 250$) illustrating the voltammetry of an HRP-modified GC electrode immersed in PBS (pH 7.0) in the absence (panels (i) and (iii)) and presence (panels (ii) and (iv)) of H_2O_2 (at a concentration of 0.1 mM). The insets illustrate the variation of the cathodic currents with the experimental timescale. HRP-type-I, (i) and (ii); HRP-type-VI, (iii) and (iv). (b) Variation of the CV peak reduction potential with experimental timescale. Key: (\bullet , \circ) AQ-modified GC electrode immersed in BR (pH 7.0) for peaks α and β (*q.v.* Fig. 1a(i)); (\blacklozenge) HRP-I/GC and (\blacklozenge) HRP-VI/GC immersed in PBS (pH 7.0) (*q.v.* Fig. 2a); (\blacktriangledown , \blacktriangledown) HRP-I/AQ/GC at 1 and 2; (\blacksquare , \square) HRP-VI/AQ/GC at 1 and 2 immersed in PBS (pH 7.0) (*q.v.* Fig. 3a(i) and (ii)). (c) SWV of HRP-modified GC electrodes immersed in PBS (pH 7.0) in the absence, (i), and presence, (ii) and (iii), of H_2O_2 . HRP-type-I, (i) and (ii); HRP-type-VI, (iii). In (i), peaks at -0.37 V decrease with scan number, but increase at -0.75 V . Inset of (ii) illustrates the calibration of current on HRP-I/GC with H_2O_2 concentration, gradient of $1.46 \text{ nA } (\mu\text{M})^{-1}$, $R^2 = 0.998$; inset of (iii) is the H_2O_2 -dependence of the currents at peak 1 and 2 in range $2.0 \leq [\text{H}_2\text{O}_2] / \mu\text{M} \leq 150.0$.

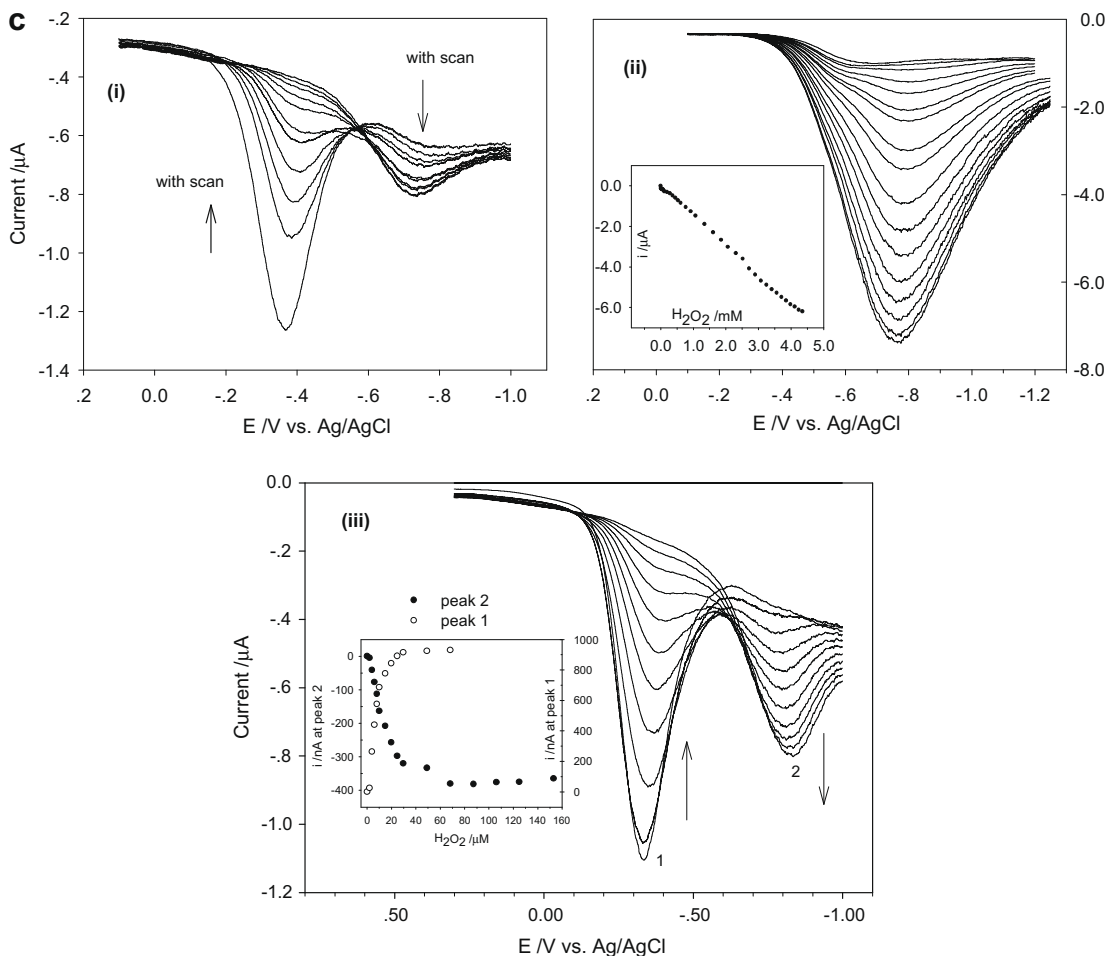


Fig. 2 (continued)

This anthraquinone-modified electrode allows for the redox catalysis of hydrogen peroxide, as suggested by earlier work [12]. Such effects are illustrated in Fig. 1b. The absence of the surface modification results in a broad voltammetric wave corresponding to hydrogen peroxide reduction (for $[H_2O_2] > 20 \mu M$, data not shown; the combination of surface anthraquinone and hydrogen peroxide results in sharper signals and more current passed during each anthraquinone wave. Moreover, the peak potentials shift negatively with decreasing experimental timescale as expected for such behaviours [19,20]. SWV (*q.v.* Fig. 1b(ii)) suggests that several linear regions in the current/concentration plot exist, to a lower level of $0.2 \mu M$.

Fig. 2a shows voltammograms corresponding to the reduction of adsorbed protein films of HRP. These two broad waves are seen to be apparently quasi-reversible – the peak potentials shift to more negative values whilst the peak current increases with decreasing timescale (*q.v.* Fig. 2a(i), (iii) and b), but chemically irreversible forming a new species detected voltammetrically at $-0.75 V$ [3]. There is a noticeable difference between types-I and VI HRP: the latter is reduced more easily, yet gives rise to larger currents (at constant enzyme coverage) presumably due to its greater activity. The presence of hydrogen peroxide dramatically changes the voltammetry (Fig. 2a(ii), (iv) and b) – the narrower peaks coupled with a square-root scan rate dependence of the peak current are indicative of redox catalysis, as has been described [21]. As before, kinetics of this process [20] have not been deduced owing to the complex reaction pathways involved. Nevertheless, the square wave voltammetry current at $-0.8 V$ is linear with $[H_2O_2] < 4.0 mM$ (type-I HRP) or $[H_2O_2] < 30.0 \mu M$ (type-VI HRP),

q.v. Fig. 2c. This difference between these two enzymes was observed to be consistent; we attribute the underlying cause to be statistical effects in the orientation of the adsorbed protein [10].

Fig. 3a illustrates voltammograms of the combined anthraquinone/HRP surface modification. These sharp adsorbed waves follow increase with scan rate, and are suggestive of the mediated reduction of HRP. In the presence of hydrogen peroxide, both voltammetric waves increase in size (*q.v.* Fig. 3b), with greater sensitivity being observed at $37^\circ C$ rather than room temperature, as expected, with linearity in the current-concentration plot observed for $0.015 \leq [H_2O_2]/mM \leq 2.0$ (type-I HRP) and $0.2 \leq [H_2O_2]/\mu M \leq 1.0$ (type-VI HRP), the latter giving an estimated limit of detection (based on $3s_b/b$) of $0.04 \mu M$. It is important to note that the perceived reaction pathway results in inhibition at high peroxide concentrations depending on the enzyme activity [4], as observed in Fig. 3b.

4. Conclusions

An amperometric biosensor for the detection of hydrogen peroxide has been reported. Noticeable differences in enzyme type have been established, in particular in sensitivity and range of linear response. In particular, we note that the use of a type-VI sensor may be appropriate for study of hydrogen peroxide released from a single cell under oxidative stress injury, since the measured extracellular concentration [22] is as low as $10 nM$. In contrast, use of a type-I sensor may be of interest for highlighting conditions of myocardial-ischaemia, for which hydrogen peroxide concentra-

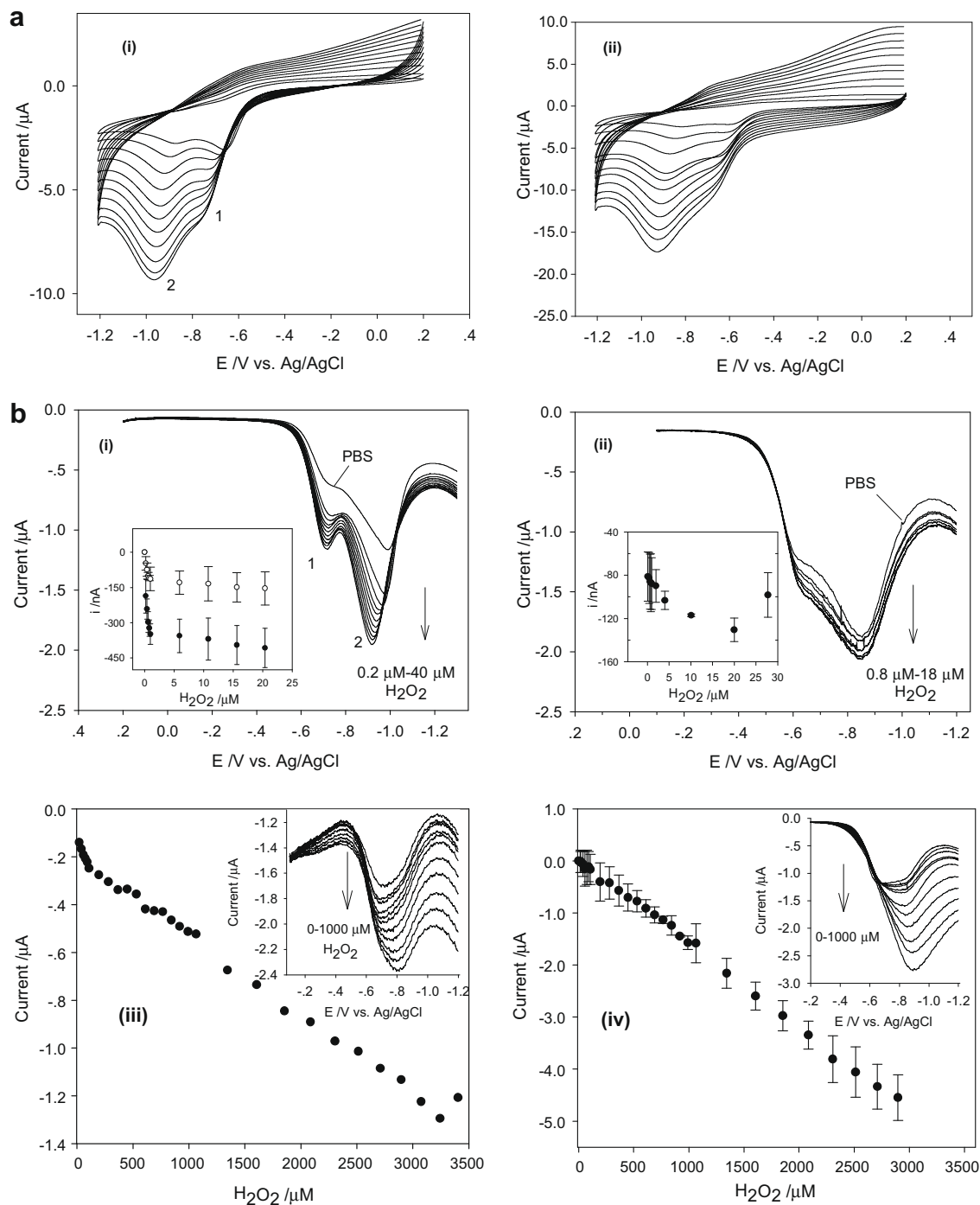


Fig. 3. (a) Typical CVs ($10 \leq v/mV s^{-1} \leq 250$) of a GC electrode covalently bound to AQ and onto which HRP is adsorbed immersed in PBS (pH 7.0); (i) HRP-type-I; (ii) HRP-type-VI. (b) Representative SWVs for HRP/AQ/GC immersed in PBS (pH 7.0) containing H_2O_2 at 22 °C, (i) and (iii) and 37 °C (ii) and (iv); HRP-type-VI, (i) and (ii), HRP-type-I, (iii) and (iv). Inset (i) calibration: 205 and 97 $nA (\mu M)^{-1}$, 0.2–1.0 μM , $R^2 = 0.997$ (peak 1, ●, and 2, ○, respectively); inset (ii) calibration at -0.62 V: 7.7 $nA (\mu M)^{-1}$, 1.0–15.0 μM , $R^2 = 0.983$; (iii) calibration: 0.3 $nA (\mu M)^{-1}$, 20.0–2000.0 μM , $R^2 = 0.994$; (iv) calibration: 2.0 $nA (\mu M)^{-1}$, 15.0–2000.0 μM , $R^2 = 0.993$.

tions are [5,6] between 3.0 μM and 1.0 mM. Indeed, long-term storage of the electrode at 4 °C immersed in PBS (pH 7.0) demonstrated a 93% response after 45 days. A future work will examine the performance of these sensing systems in human heart perfusion studies.

Acknowledgement

We thank HeartResearch UK for funding through the Novel and Emerging Technology scheme.

References

- [1] H.B. Dunford, J.S. Stillman, *Coord. Chem. Rev.* 19 (1976) 187.
- [2] T. Ruzgas, E. Csöregi, J. Emnéus, L. Gorton, G. Marko-Varga, *Anal. Chim. Acta* 330 (1996) 123.
- [3] P.N. Bartlett (Ed.), *Bioelectrochemistry*, Wiley, Chichester, 2008.
- [4] B. Limoges, J.-M. Savéant, D. Yazidi, *J. Am. Chem. Soc.* 125 (2003) 9192.
- [5] J. Slezak, N. Tribulova, J. Pristacova, B. Uhrík, T. Thomas, N. Khaper, N. Kaul, P.K. Singalt, *Am. J. Pathol.* 147 (1995) 772.
- [6] M.J. Shattock, A.S. Manning, D.J. Hearse, *Pharmacology* 24 (1982) 118.
- [7] B.R. Horrocks, D. Schnidtké, A. Heller, A.J. Bard, *Anal. Chem.* 65 (1993) 3605.
- [8] N. Mogharrab, H. Ghourchian, *Electrochem. Commun.* 7 (2005) 466.

- [9] F.A. Armstrong, J.N. Butt, A. Sucheta, *Meth. Enzymol.* 227 (1993) 479.
- [10] C. Léger, P. Bertrand, *Chem. Rev.* 108 (2008) 2379.
- [11] A.-E. Radi, X. Muñoz-Berbel, M. Cortina-Puig, J.-L. Marty, *Electroanalysis* 21 (2009) 696.
- [12] I. Cruz-Vieira, O. Fatibello, *Talanta* 52 (2000) 681.
- [13] B. Sljukić, C.E. Banks, S. Mentus, R.G. Compton, *Phys. Chem. Chem. Phys.* 6 (2004) 992.
- [14] K. Tammeveski, K. Kontturi, R.J. Nichols, R.J. Potter, D.J. Schiffrin, *J. Electroanal. Chem.* 515 (2001) 101.
- [15] P. Allongue, M. Delamar, B. Pesbat, O. Fagebaume, R. Hitmi, J. Pinson, J.-M. Savéant, *J. Am. Chem. Soc.* 119 (1997) 201.
- [16] N.S. Lawrence, M. Pagels, S.F.J. Hackett, S. McCormack, A. Meredith, T.G.J. Jones, G.G. Wildgoose, R.G. Compton, L. Jiang, *Electroanalysis* 19 (2007) 424.
- [17] C. Amatore, in: H. Lund, O. Hammerich (Eds.), *Organic Electrochemistry*, fourth ed., Marcel Dekker, New York, 2000, p. 1.
- [18] J. Revenga, F. Rodríguez, J. Tijero, *J. Electrochem. Soc.* 141 (1994) 330.
- [19] C.P. Andrieux, J.-M. Savéant, *J. Electroanal. Chem.* 93 (1978) 163.
- [20] M.E.G. Lyons, *Sensors* 1 (2001) 215.
- [21] G. Presnova, V. Grigorenko, A. Egorov, T. Ruzgas, A. Lindgren, L. Gorton, T. Börchers, *Faraday Discuss.* 116 (2000) 281.
- [22] B. Chance, H. Sies, A. Boveris, *Physiol. Rev.* 59 (1979) 527.

Simple practical approach for sample loading prior to DNA extraction using a silica monolith in a microfluidic device

Kirsty J. Shaw,^a Domino A. Joyce,^a Peter T. Docker,^a Charlotte E. Dyer,^b John Greenman,^b Gillian M. Greenway^a and Stephen J. Haswell^{*a}

Received 6th July 2009, Accepted 24th August 2009

First published as an Advance Article on the web 21st September 2009

DOI: 10.1039/b913309g

A novel DNA loading methodology is presented for performing DNA extraction on a microfluidic system. DNA in a chaotropic salt solution was manually loaded onto a silica monolith orthogonal to the subsequent flow of wash and elution solutions. DNA was successfully extracted from buccal swabs using electro-osmotic pumping (EOP) coupled with *in situ* reagents contained within a 1.5% agarose gel matrix. The extracted DNA was of sufficient quantity and purity for polymerase chain reaction (PCR) amplification.

Introduction

Isolating deoxyribonucleic acid (DNA) from other cellular components in order to perform subsequent analysis and/or the pre-concentration of a dilute sample are the main objectives of DNA extraction methodologies. For example, DNA extraction is critical for bioanalytical applications based on blood samples in which haem protein is a known inhibitor of PCR.¹ Solid-phase extraction protocols in which DNA is adsorbed onto a solid support, usually silica-based, are commonly employed. The use of chaotropic agents, such as guanidine hydrochloride, not only facilitates binding of DNA to the silica surface but also acts to lyse cells and inactivate deoxyribonucleases (DNases).² Any cellular debris is then removed from the system using an alcohol wash. Finally the DNA is eluted in a low ionic strength buffer such as Tris-EDTA (TE) buffer or water. This method has the added advantage that it allows pre-concentration of the DNA, which is of particular relevance where samples are limited, such as those available in forensic cases.

Solid-phase extraction methodology commonly employs a packed column or membrane such as those in the commercially available Qiagen™ DNA extraction kits.³ To replicate this type of system within a microfluidic device it is vital to create a large surface area to which the DNA can be adsorbed. The silica solid-phase can exist in a variety of forms such as immobilised particles, microfabricated pillars or monoliths as recently reviewed by Wen *et al.*⁴ The use of sol-gels of monoliths not only provides a large surface area for adsorption but also offers favourable properties in terms of reproducibility when incorporated into microfluidic devices.⁵

When performing DNA extraction in microfluidic systems, the required reagents are commonly moved within the device using hydrodynamic or electrokinetic pumping, allowing accurate control of flow rates. More recently, DNA extraction devices

have emerged which rely on centrifugal forces to move solutions hydrodynamically through the microfluidic device. For example, pathogen-specific DNA extraction using antibody-conjugated magnetic beads was performed on a compact disc (CD) platform, incorporating target pathogen capture, washing and cell lysis to extract the DNA.⁶ Whilst such methods for controlling movement of solutions work very well, the sample is typically loaded onto the extraction matrix using the same direction of flow as the wash and elution solutions, which can lead to practical difficulties when producing sealed interfaces between the macro- and micro-scale. By dispensing with mechanically-driven connections, the interfacing between different systems becomes easier as does the practical and engineering design of the system.

The work reported here demonstrates a practical approach to the introduction of a biological sample onto a silica monolith using the sample inlet employed for loading of the monolith solution. The wash and elution steps for DNA extraction are then performed in an orthogonal direction through the microfluidic device.

Experimental

Microfluidic device manufacture

All glass microfluidic devices were produced using standard photolithography and wet etching techniques to produce the design shown in Figure 1.⁷ The features were etched to a depth of 250 µm using hydrofluoric acid. In order to allow the microfluidic device to be loaded with reagents and enable connection to electrodes for EOP, 1 mm holes were drilled for the inlets and outlet. The etched glass surface was then thermally bonded to a second 1 mm glass wafer to produce the complete microfluidic device.

Silica-based monoliths were produced by mixing potassium silicate solution (21% SiO₂ and 9% K₂O (VWR International, UK)) and formamide (Alfa Aesar, UK) in a 10:1 ratio.⁸ In order to make sure the monolith was only produced in the DNA extraction chamber, the entire device was first filled with glycerol (Sigma-Aldrich, UK). The monolith solution was then

^aDepartment of Chemistry, University of Hull, Cottingham Road, Hull, UK HU6 7RX. E-mail: s.j.haswell@hull.ac.uk; Fax: +44 (0)1482 466410; Tel: +44 (0)1482 465475

^bPostgraduate Medical Institute, University of Hull, Cottingham Road, Hull, UK HU6 7RX; Fax: +44 (0)1482 466996; Tel: +44 (0)1482 466996

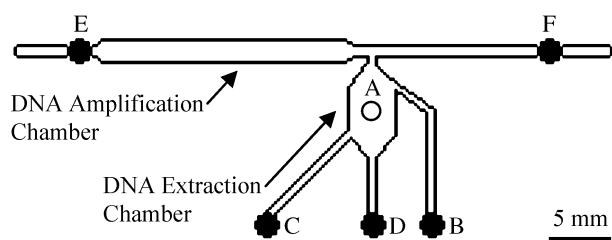


Fig. 1 Schematic of the microfluidic device incorporating the DNA extraction chamber with an adjacent chamber providing the potential for integrated DNA amplification. There is an inlet at the top of the DNA extraction chamber for loading of both the solid-phase matrix and DNA in loading solution (A○). The position of the holes for carbon electrodes for EOP is shown (B–F●).

injected into the DNA extraction chamber, displacing the glycerol, and the microfluidic device placed in an oven at 90 °C for 15 min. After this initial heating step, the remaining glycerol was removed and the microfluidic device placed back in the oven overnight for complete polymerisation to occur. Once polymerised, the monoliths were washed with ethanol to remove any unreacted solution. Prior to DNA extraction the monoliths were washed with 10 mM TE buffer at 5 μ l/min for 30 min.

For EOP, the wash and elution reagents were encapsulated in 1.5% (w/v) low melting temperature (LMT) agarose gels (Sigma-Aldrich, UK) and pre-loaded into the relevant channels on the microfluidic device. The wash gel, produced by dissolving 0.015 g LMT agarose in a solution of 500 μ l of ethanol, 400 μ l of distilled water and 100 μ l of 1 M NaCl (Sigma-Aldrich, UK) was injected into channel B. The elution gel, produced by dissolving 0.015 g LMT agarose in 1 ml 10 mM TE buffer, was injected into channel D. Injection molded carbon-containing polystyrene plugs were then fitted into the 1 mm reagent loading holes and attached to platinum electrodes, through which a voltage could be delivered using an external power supply.

DNA extraction

Buccal cells were collected from volunteers using an OmniSwab™ (Whatman, UK) scraped along the inside of the cheek. The buccal swab was then added to a 1 ml solution of 5 M guanidine hydrochloride (GuHCl) (Sigma-Aldrich UK) in 10 mM TE buffer and incubated at room temperature for 5 min. A 50 μ l aliquot of the DNA in loading buffer was then manually injected onto the monolith using a displacement pipette and capillary action, with any excess sample collected in the waste channel (C) which gave relatively low hydrodynamic resistance. Once the biological sample was added the hole was sealed using a polystyrene plug to prevent leaking/contamination.

When using EOP, the ethanol gel contained in channel B was used to wash the monolith by applying a voltage of 100 V/cm between electrodes B and C. The DNA was then eluted using the 10 mM TE buffer gel contained in channel D by applying a voltage of 100 V/cm between electrodes D and E. The eluted DNA was then removed from the microfluidic device through port E prior to analysis.

Analysis of extracted DNA

Quantification of the DNA obtained from the extraction procedure was carried out using a Quant-iT™ PicoGreen® double stranded (ds) DNA Assay Kit (Invitrogen, UK) and a FLUOstar Optima Plate Reader (BMG Labtech, UK).

PCR amplification of the extracted DNA was performed using a PCR reaction mixture composed of the following: 1x NH_4 buffer, 1 mM MgCl_2 , 200 μ M each dNTPs, 1 μ M forward primer, 1 μ M reverse primer, 1 unit *BIOTaq*™ DNA polymerase and 10 μ g bovine serum albumin. Forward and reverse primers were designed for amplification of the Amelogenin locus with the following sequences: 5'-CCCTGGGCTCTGTAAAGAATAG TG-3' and 5'-ATCAGAGCTTAAACTGGGAAGCTG-3'.⁹ All PCR reagents were purchased from Bionline, UK except for the primers which were custom-made by Eurofins MWG Operon, Germany. The samples were then amplified using a Techne TC-312 thermal cycler for 28 cycles, each cycle comprising heating steps of: 94 °C for 30 s, 59 °C for 30 s and 72 °C for 30 s. An initial denaturing step of 94 °C for 5 min and a final extension step of 60 °C for 45 min were also included.

PCR products were analysed using slab-gel electrophoresis. A 1.5% (w/v) agarose gel was prepared by dissolving 1.5 g agarose (Bionline, UK) in 100 ml 0.5 \times TBE buffer (0.09 M Tris-HCl (Sigma-Aldrich, UK), 0.09 M boric acid (Fisher Scientific) and 0.002 M EDTA in distilled water). PCR products were mixed with loading dye (MBI Fermentas, Canada) and added to the gel, along with a DNA molecular weight standard, Hyperladder II (Bionline, UK), before being subjected to electrophoresis at 120 V until adequate separation was achieved. Gels were then stained using 0.5 μ g/ml ethidium bromide (CLP, UK) in 0.5 \times TBE buffer for 20 min and then visualized using a UV trans-illuminator.

Results and discussion

DNA was successfully extracted from a solution of GuHCl containing buccal cells by manually pipetting the sample onto a monolith which was then washed and eluted using EOP. The average DNA concentration in the eluent was 0.44 ng/ μ l. The extracted DNA was assessed for quantity and integrity using PCR. Successful amplification of the target locus, producing PCR products of the expected size (106 bp) from DNA extracted using EOP, indicated that the eluted DNA was of sufficient quality for downstream applications (Fig. 2).

The results confirm that the monolith-based sample loading procedure coupled with preloaded reagents and EOP represent a suitable combination of techniques for DNA extraction on a microfluidic device. Optimum DNA elution was obtained using an applied voltage of 100 V/cm for 10 min. In addition, extraction based on hydrodynamic pumping was carried out, using established methodology,¹⁰ to evaluate the effectiveness of the sample loading procedure. The hydrodynamic pumping DNA extraction efficiency was found to be 72% compared to that of 52% with the optimised EOP protocol, which correlates with DNA extraction efficiencies reported in the literature ranging from 30% to 84% for λ -phage DNA.^{11,12} The difference in the DNA extraction efficiencies between the hydrodynamic and electro-osmotic pumping system presented here can be attributed

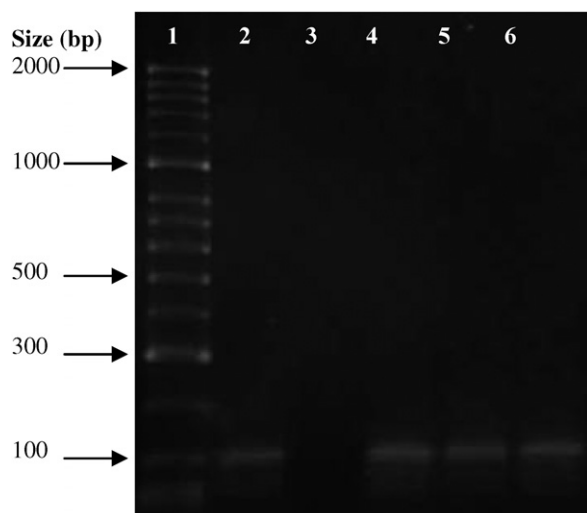


Fig. 2 Example of an agarose gel showing PCR products of the expected size (106 bp) for amplification of the Amelogenin locus from female genomic DNA where samples are: (1) DNA size ladder; (2) positive PCR control containing DNA extracted using a QIAamp® DNA Micro Kit; (3) negative PCR control containing no DNA; (4–6) replicate samples showing PCR products of DNA extracted from the microfluidic device using EOP.

to the different flow rates achieved and the opposing electrophoretic force which acts upon the DNA when using EOP. Despite this slightly lower recovery, the DNA extraction efficiency of EOP was still sufficient for subsequent PCR and also enables a proportion of the DNA to be retained upon the monolith for subsequent analysis, particularly useful for forensic samples.

Conclusion

The manual loading method described offers a simple practical means of introducing liquid samples onto microfluidic systems. The inlet above the DNA extraction chamber serves two purposes: firstly it allows the monolith solution to be introduced prior to polymerisation and secondly, it enables the loading of a DNA sample into the microfluidic device. Following sample addition, DNA extraction was successfully performed using EOP, producing DNA of PCR-amplifiable quantity and quality.

By simply using a pipette to achieve manual injection of a biological sample, *via* capillary action, to facilitate DNA adsorption prior to performing a DNA extraction protocol, no external connection is required. In addition, the use of disposable pipette tips provides a cost effective means of adding samples to a microfluidic system with minimal risk of contamination.

Incorporation of all the necessary reagents for performing DNA extraction on the microfluidic device creates a ready-to-use system. Indeed the need for complex interfaces or macro to micro connections is eliminated in this system, which only requires the presence of simple electrodes to control reagent movement. This in turn leads to a more robust microfluidic system for DNA extraction.

Acknowledgements

The authors would like to thank Dr S. Clark at the University of Hull for manufacture of the microfluidic devices, Professor N. Goddard at the University of Manchester for the kind gift of polymer electrodes and the EPSRC (EP/D040930) for financial support.

References

- 1 I. G. Wilson, *Appl. Environ. Microbiol.*, 1997, **63**, 3741–3751.
- 2 R. Boom, C. J. A. Sol, M. M. M. Salimans, C. L. Jansen, P. M. E. Wertheimvanden and J. Vandernoordaa, *J. Clin. Microbiol.*, 1990, **28**, 495–503.
- 3 Qiagen, ed. Qiagen, Qiagen, 2003.
- 4 J. Wen, L. A. Legendre, J. M. Bienvenue and J. P. Landers, *Anal. Chem.*, 2008, **80**, 6472–6479.
- 5 K. A. Wolfe, M. C. Breadmore, J. P. Ferrance, M. E. Power, J. F. Conroy, P. M. Norris and J. P. Landers, *Electrophoresis*, 2002, **23**, 727–733.
- 6 Y. K. Cho, J. G. Lee, J. M. Park, B. S. Lee, Y. Lee and C. Ko, *Lab Chip*, 2007, **7**, 565–573.
- 7 T. McCreedy, *TrAC, Trends Anal. Chem.*, 2000, **19**, 396–401.
- 8 P. D. Christensen, S. W. P. Johnson, T. McCreedy, V. Skelton and N. G. Wilson, *Anal. Commun.*, 1998, **35**, 341–343.
- 9 U. Ricci, I. Sani, M. Klintschar, N. Cerri, F. De Ferrari and M. L. G. Uzielli, *Croatian Med. J.*, 2003, **44**, 299–305.
- 10 K. J. Shaw, L. Thain, P. T. Docker, C. E. Dyer, J. Greenman, G. M. Greenway and S. J. Haswell, *Anal. Chim. Acta*, 2009, DOI: 10.1016/j.aca.2009.03.038.
- 11 T. Poeckh, S. Lopez, A. Overta Fuller, M. J. Solomon and R. G. Larson, *Anal. Biochem.*, 2008, **373**, 253–262.
- 12 R. T. Zhong, D. Liu, L. F. Yu, N. Ye, Z. P. Dai, J. H. Oin and B. C. Lin, *Electrophoresis*, 2007, **28**, 2920–2926.

Development of enzyme immobilized monolith micro-reactors integrated with microfluidic electrochemical cell for the evaluation of enzyme kinetics

Ping He · Gillian Greenway · Stephen J. Haswell

Received: 5 May 2009 / Accepted: 27 June 2009 / Published online: 24 July 2009
© Springer-Verlag 2009

Abstract This paper describes a simple and efficient method for producing an on-chip enzyme immobilized monolith micro-reactor that integrates a microfluidic electrochemical cell for rapid characterization of enzymatic kinetics. The monolith was generated using a sol-gel method, followed by PEI functionalization and enzyme immobilization via electrostatic attraction between electronegative enzymes and electropositive PEI polymers. Using the proposed immobilization strategy, a glucose oxidase (GOD) immobilized monolith micro-reactor has been produced with the controllable porosity that gives better enzyme kinetics compared to previously reported devices. This can be attributed to a favourable enzyme-substrate affinity in which more than 98% of the immobilized enzyme remains in an active conformation. The kinetic studies conducted have identified that a similar value of the k_{cat} is obtained for immobilized GOD (13.4 s^{-1}) and GOD free in solution (14 s^{-1}) whilst the immobilized Michaelis constant $K_{\text{m(app)}}$ (7.2 mM) is ~ 4 times lower than GOD in solution (25 mM). In addition, the immobilized GOD exhibits increased stability, retaining at least 95% of the initial activity when stored of 30 days at 4°C, compared to only 60% for GOD in solution. Furthermore, the same enzyme immobilization strategy has been used for choline oxidase immobilization and similar kinetics to choline oxidase in solution were observed, once again indicating better maintenance of the enzyme conformation provided by the proposed method.

Keywords Micro-reactor · Monolith · Immobilization · Kinetics · Glucose oxidase · Choline oxidase

1 Introduction

The use of integrated enzymatic micro-reactors has attracted a growing interest in recent years due to their ability to facilitate the characterization of reaction kinetics which in turn allows for faster screening of enzymatic reaction parameters including substrate concentration, new biocatalysts and feedstock (Verpoorte 2003; Krenková and Foret 2004; Girelli and Mattei 2005; Urban et al. 2006; Peterson 2005). To date, enzyme immobilization methods in a micro-reactor configuration have focused mainly on one of three strategies: (i) direct attachment of enzymes to a modified surface (Guo et al. 2003; Mao et al. 2002; DeLouise and Miller 2005; Gleason and Carbeck 2004; Holden et al. 2004; Thomsen et al. 2007; Koh and Pishko 2005; Honda et al. 2006; Tokeshi et al. 2003), (ii) attachment of enzymes to beads (packed-bed) (Wang et al. 2000; Seong and Crooks 2002; Park et al. 2003; Nomura et al. 2004; Vodopivec et al. 2003; Kerby et al. 2006; Seong et al. 2003) and (iii) the immobilization of enzymes onto monoliths (Peterson et al. 2002; Mersal and Bilitewski 2005; Kato et al. 2005; Sakai-Kato et al. 2003; Kawakami et al. 2005; Ota et al. 2007; Legido-Quigley et al. 2003; Hilder et al. 2002). There have been, however, a number of reported drawbacks associated with both direct surface attachments and the packed bead approach, including long diffusion times (Krenková and Foret 2004) and the loss of enzyme activity owing to altered structural conformation and/or steric hindrance resulting from covalent bonding, cross-linking and the encapsulation associated with these methods (Guo et al. 2003; Mao et al. 2002; DeLouise and

P. He · G. Greenway · S. J. Haswell (✉)
Department of Chemistry, University of Hull,
Hull HU6 7RX, UK
e-mail: s.j.haswell@hull.ac.uk

Miller 2005; Peterson et al. 2002; Mersal and Bilitewski 2005; Kato et al. 2005; Sakai-Kato et al. 2003; Kawakami et al. 2005; Ota et al. 2007). Accordingly, a high enzyme load is generally required with these approaches to alleviate the limitations indicated (Park and Clark 2002; Luckarift et al. 2004; Lei et al. 2002; Demers et al. 2001). In addition, packed-bed micro-reactors often generate increased backpressure that gives rise to leaking or blocking problems, making the maintenance of micro-reactors stable conditions difficult (Honda et al. 2006; Tokeshi et al. 2003), which has led in turn to special reaction chamber designs for lowering backpressure (Kerby et al. 2006; Seong et al. 2003). In recent years, monolith micro-reactor devices (continuous beds) have emerged as an attractive alternative to packed beads for the analysis of proteins, peptides and nucleic acids because of good porosity control and minimal backpressure effects (Verpoorte 2003; Krenková and Foret 2004; Girelli and Mattei 2005; Urban et al. 2006; Peterson 2005). Generally, silicon alkoxides such as TMOS (tetramethoxysilane) and MTMOS (methyltrimethoxysilane) can be used to generate silica-based monoliths but current approaches usually require the addition of other additives, i.e. PEG (polyethylene glycol) and dextrin to stabilize the structure (Kato et al. 2005; Sakai-Kato et al. 2003) and fabrication can be time consuming (ca. 3–15 days) (Kato et al. 2005; Sakai-Kato et al. 2003; Kawakami et al. 2005). In addition, large molecules such as proteins may not be able to diffuse through the nanopores of a hydrogel network (Sakai-Kato et al. 2003). To date, the maximum percentage of active enzymes immobilized has been around 75% compared to the equivalent enzyme in solution, indicating that at least 25% of the enzyme is immobilized in an inactive conformation (Mao et al. 2002; DeLouise and Miller 2005; Honda et al. 2006; Vodopivec et al. 2003; Kerby et al. 2006; Sakai-Kato et al. 2003).

In order to improve on the current immobilization efficiency, we propose a new approach for enzyme immobilization that involves the on-chip preparation of macroporous silica-monoliths within a glass microfluidic channel, followed by modification with PEI (polyethylenimine) and enzyme immobilization via electrostatic attraction between electronegative enzymes and electro-positive PEI polymers. In addition, the on-chip integration of an appropriate electrochemical detection system could provide rapid evaluation of enzyme activity. Two enzymes, glucose oxidase (GOD) and choline oxidase, have been immobilized separately within a PEI-coated silica monolith micro-reactor and enzymatic kinetics have been evaluated. The proposed method not only offers the advantages of simple, low cost and shorter preparation times compared to existing methods (Kato et al. 2005; Sakai-Kato et al. 2003; Kawakami et al. 2005) but also favours the maintenance of

the active conformation and stability of the immobilized enzymes.

2 Experimental

2.1 Materials

Glucose oxidase from *Aspergillus niger* (GOD, MW 160 kDa), choline oxidase from *Alcaligenes* sp. (CHO, MW 72 kDa), choline chloride (CH, 99%) and tris(hydroxymethyl)aminomethane (Tris, 99%) were purchased from the Sigma-Aldrich. Polyethylenimine (PEI, 99%, molecular weight 423, 800, 2000, 10000 and 25000, respectively), KCl (99%), D-Glucose (99%), HCl (37%), tetramethoxysilane (TMOS, 99%) and methyltrimethoxysilane (MTMOS, 99%) were purchased from Fluka. Milli-Q water (18 M Ω cm) was used to prepare all aqueous solutions.

2.2 Preparation of silica-monoliths in the micro-reactors

Glass micro-reactor devices were fabricated in house using standard photolithography technology followed by wet etching and thermal bonding (Fletcher et al. 2002) and comprised a channel in which a monolith was produced and an electrochemical detector integrated. A photograph of the micro-reactor system used is shown in Fig. 1. The dimensions of the channels were 600 μ m wide, 50 μ m deep and 20 mm long for the monolith channel and 1.5 mm wide, 50 μ m deep and 20 mm long for electrochemical detection channel. The connecting channel between the monolith and detector was 100 μ m wide, 50 μ m deep and 5 mm long. The silica-monoliths were prepared from two precursors, TMOS and MTMOS using a sol-gel method modified from that reported by Kawakami (Kawakami et al. 2005). A mixture containing 18 μ l of TMOS and 69 μ l of MTMOS (at 1:4 molar ratio) was added to dilute HCl solution (8 μ l of 1 mM HCl and 13.2 μ l water) and allowed to hydrolyse for 15 min under sonication at room temperature to form a homogeneous sol. A 4.2 μ l aliquot of sol was mixed with 17.8 μ l of water and 22 μ l of 0.2 M (pH 7) Tris-HCl buffer, and the resultant liquid mixture was immediately loaded into the monolith channel and allowed to polymerize for 15 h at room temperature followed by vacuum drying for 1 h to form a silica monolith with a porosity of 0.67 (void volume ca 0.4 μ l).

2.3 Measurement of the porosity of silica monolith

The porosity (ϵ) of silica monoliths was estimated using Eq. 1 where d is the density of water by first measuring the

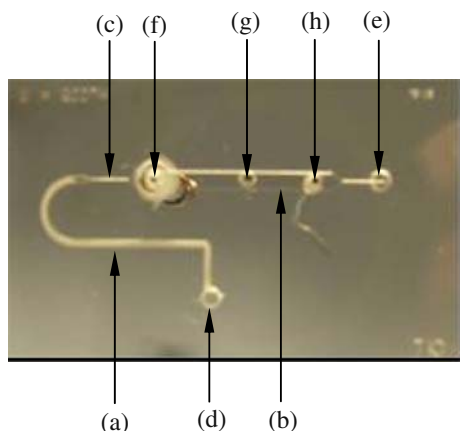


Fig. 1 Photograph of micro-reactor system: (a) silica monolith, 600 μm wide, 50 μm deep and 20 mm long; (b) electrochemical detection channel, 1.5 mm wide, 50 μm deep and 20 mm long; (c) link channel, 100 μm wide, 50 μm deep and 5 mm long; (d) inlet, 1.5 mm diameter; (e) outlet, 1.5 mm diameter; (f) working electrode (Pt disc, 0.5 mm diameter); (g) Pt wire (1 mm diameter) counter electrode and (h) Ag/AgCl (1 mm diameter) reference electrode. A working buffer solution was continuously pumped into the monolith micro-reactor through a plastic tube (0.5 mm diameter) that connected the syringe pump with the inlet of the monolith micro-reactor

weight of water filled into an empty capillary (W_T) and then into a monolith filled capillary (W_M). The measurements were normally carried out five times and an average taken.

$$\epsilon = \frac{(W_M/d)}{(W_T/d)} = \frac{W_M}{W_T} \quad (1)$$

2.4 Modification of silica monolith with PEI and enzyme immobilization

The silica-monoliths were loaded with PEI solution (concentration 10 mg/ml in 0.1 M neutral Tris–HCl buffer) and kept in a fridge (4°C) for at least 2 h followed by vacuum drying for 1 h. PEI-modified monolith was then washed with 0.05 M neutral Tris–HCl buffer to remove loosely bound PEI and vacuum drying for 1 h to generate the PEI-coated silica-monolith. An enzyme solution (i.e. GOD 4.8 mg/ml (0.1 U/ μl) or CHO 3.3 mg/ml (0.05 U/ μl) in 0.05 M neutral Tris–HCl buffer) was then loaded into the monolith (required ca. 0.4 μl of enzyme solution to fully fill the monolith) using a micropipette. The monolith was then placed in a fridge (4°C) for 1 h followed by vacuum drying for 30 min to generate the enzyme immobilized monolith micro-reactor. Three electrodes were then placed into the holes in the detection channel of the device and sealed by using epoxy resin. Before kinetic measurements were carried out, the micro-reactor was washed for 5 min with a working buffer solution that was collected.

2.5 Evaluation of solution and immobilized enzyme activity

The enzyme kinetic measurements were carried out on-chip to evaluate the performance of the immobilized enzyme by comparing the data obtained to a solution only system. In order to evaluate the immobilized enzyme activity a continuous flow micro-reactor system that consisted of a syringe pump (PHD 2000, Harvard), a syringe (1 ml), a micro-injector with a sample loop of 2.5 μl and an enzyme immobilized monolith micro-reactor equipped with on-chip amperometric detector was used. A working buffer solution was continuously pumped into the monolith through a plastic tube (0.5 mm I.D.) that connected the syringe pump with the inlet of the monolith. The detector was constructed from a Pt disc-working electrode (0.5 mm diameter), a Pt wire counter electrode (1 mm diameter) and a Ag/AgCl (1 mm diameter) reference electrode and aligned as shown in Fig. 1.

A series of substrate concentrations (0.25, 0.5, 0.75 and 1 mM) were injected onto the monolith using a 6-port valve injector. The carrier (0.05 M neutral Tris–HCl buffer containing 10 mM KCl) held at a constant flow rate and the H_2O_2 product formed during enzyme reaction was amperometrically measured using the on-chip electrochemical cell according to Eqs. 2 and 4 for GOD and Eqs. 3 and 4 for CHO.

Enzymatic reactions:



Electrode reaction:



All amperometric measurements were obtained using a PalmSens Electrochemical Sensor interface (IVIUM Technologies, The Netherlands) with a computer at a fixed electrode potential (650 mV vs. Ag/AgCl) at room temperature. It should be noted that the detection technique used is applicable not only for enzymes producing H_2O_2 but also has wider applicability for enzymes giving redox products measurable with bare electrodes.

Based on flow rates of 5, 7.5 and 10 $\mu\text{l}/\text{min}$ for the buffer carrier stream, the enzyme kinetics were determined using the electrochemical Eadie–Hofstee equation in Lineweaver–Burk form (Eq. 5) under steady-state conditions (Kaku et al. 1994; Arai et al. 1998):

$$\frac{1}{j} = \frac{K_{m(\text{app})}}{j_{\text{max}}} \frac{1}{[S]} + \frac{1}{j_{\text{max}}} \quad (5)$$

where $K_{m(\text{app})}$ was the apparent Michaelis constant, j the current intensity, j_{max} the maximum current intensity and

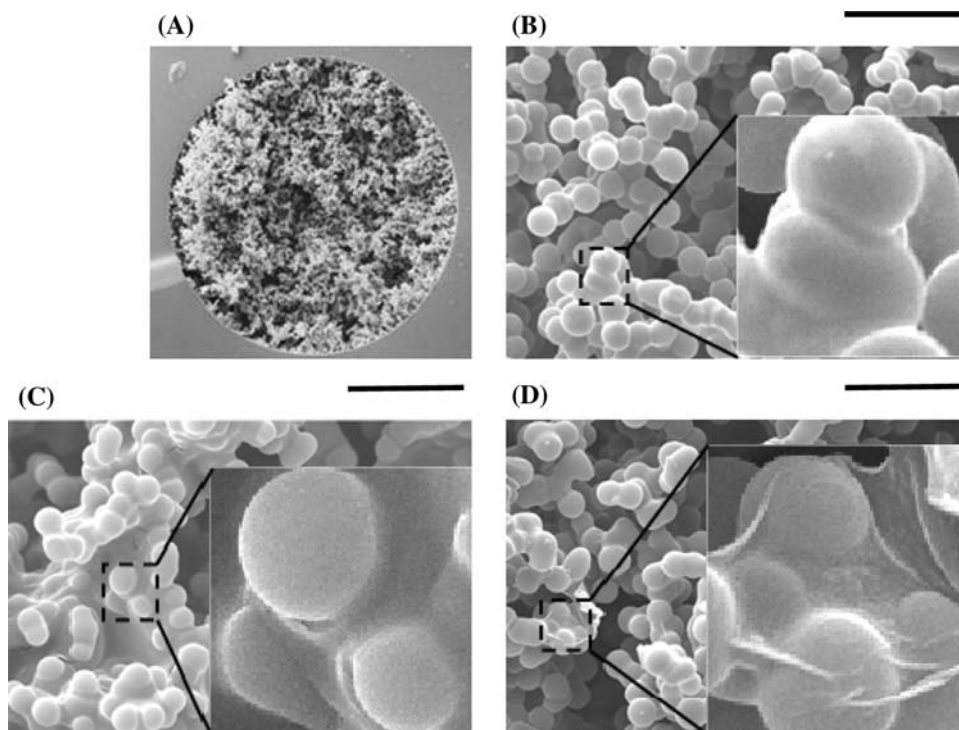
[S] the substrate concentration. The $K_{m(\text{app})}$ and j_{max} values could be directly obtained from the Lineweaver–Burk plots and the V_{max} values were determined from j_{max} values according to a standard H_2O_2 -current calibration curve divided by average contact times of 2.4, 3.2 and 4.8 s for the flow rate of 10, 7.5 and 5 $\mu\text{l}/\text{min}$, respectively. The standard H_2O_2 -current calibration curves (linear range from 0.005 to 10 mM) were obtained by injecting a series of different concentrations of freshly prepared H_2O_2 in working buffer solution after kinetic measurements were taken. The contact times were calculated from the measured void volume of the monolith (0.4 μl for porosity 0.67 ± 0.04) divided by flow rates. The k_{cat} was determined from Eq. 6.

$$V_{\text{max}} = k_{\text{cat}}[E] \quad (6)$$

where, [E] was immobilized GOD or CHO concentration in a monolith micro-reactor. The quantity of enzyme immobilized was determined from the difference between the amount of enzymes in the enzyme solution and that collected from washings which was measured using a GeneQuant instrument (Pharmacia Biotech) at 280 nm (He et al. 2008). All measurements were normally repeated at least three times and data was then presented as mean and standard deviation values.

For comparative purposes, batch-based enzymatic reactions were also carried out and the activity of GOD and CHO in free solution was determined by the method previously reported (He et al. 2008).

Fig. 2 SEM images of the cross-section of silica monoliths formed in a capillary of 0.5 mm diameter: **a** low magnification; **b** silica-monolith at high magnification; **c** PEI-coated silica-monolith and **d** GOD immobilized on the surface of PEI-coated silica-monolith. (scale bar 20 μm)



2.6 Scanning electron microscopy

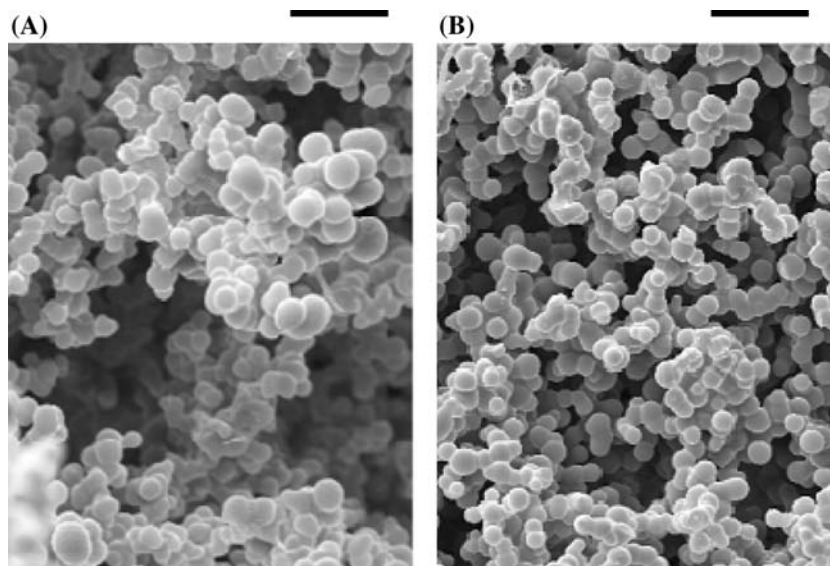
Due to the practical difficulty of cutting and so losing a micro-reactor device to obtain a perfect cross-section of the silica monolith, a glass capillary of similar channel geometry was used to observe the type of monolith being produced on-chip. Each sample was sputter-coated with a thin layer of gold-platinum (thickness approximately 2 nm) using a SEMPREP 2 Sputter Coater (Nanotech Ltd.). Once sputtered, samples were imaged on a Cambridge S360 scanning electron microscopy (SEM) operated at fixed voltage (20 kV).

3 Results and discussion

3.1 Effect of silica-monolith porosity as a function of sol volume used in the polymerization process

SEM images (see Fig. 2a–b) of the cross-section of the silica-monoliths formed in a glass capillary (0.5 mm diameter) revealed that the monoliths consisted of fused particles of 3–6 μm in diameter, forming a macroporous structure that could minimize backpressure effect in a continuous-flow system. In addition, the monolith porosity could be selectively changed by controlling the volume of the silicic acid solution used, for example, the measured porosity was reduced from 0.67 to 0.33 (see Fig. 3a–b) by increasing the volume of sol from 4.2 (silicic acid 0.52 M)

Fig. 3 SEM images of the cross-section of silica monoliths formed in a capillary of 0.5 mm diameter with: **a** silicic acid 0.52 M; **b** silicic acid 1.57 M (scale bar 20 μm)



to 12.6 μl (silicic acid 1.57 M) in the polymerization reactions.

3.2 Functionalization of silica-monolith with PEI polymers and enzymes

As indicated, the use of PEI polymers for enzyme immobilization can promote the enzyme activity by avoiding the formation of covalent bonds and/or encapsulation processes. PEI polymers have been found to have the ability to carry proteins in aqueous media via the electrostatic attraction between the positively charged polymers and the negatively charged proteins (He et al. 2008; Laarz and Bergström 2000; Han et al. 1999). PEI is a cationic polyelectrolyte and acts as a weak base owing to the pH-dependent protonation of its amine groups in water. At $\text{pH} \approx 2$, approximately 70% of the amine groups are protonated, thus carrying positive charges that decrease with increasing pH and approach zero at $\text{pH} \approx 11.5$ (Deere et al. 2002). In this study, silica and the enzymes used have low isoelectric point (pI) values, i.e. 5.4 for GOD, 3–4 for CHO and ca. 2 for silica, meaning that at neutral pH enzymes and silica are electronegative species whilst PEI polymer represents an electropositive species. Therefore, by using electrostatic attraction, PEI polymers can be readily coated on the surface of silica-monolith (see Fig. 2c), thus enabling enzymes to be efficiently immobilized on the PEI-coated monolith (see Fig. 2d).

3.3 Effects of reaction parameters on enzyme immobilization

Several reaction parameters, i.e. PEI polymer molecular weight (MW) and concentration, buffer type and

concentration for the enzyme immobilization have been investigated to optimize the performance of the immobilized enzyme. The influence of PEI polymer MW and concentration on the activity of immobilized enzymes are presented in Table 1. It can be seen from Table 1 that the performance of immobilized enzymes can be significantly affected by both the PEI polymer MW and concentration. A significant reduction in the response current, which is proportional to the enzyme activity, was observed for PEI MW 25000 at a concentration of 20 mM, probably due to steric hindrance produced by the larger polymer and high concentrations. The effect of buffer on the performance of immobilized enzymes is attributed to the ionic strength of buffer solutions (Laarz and Bergström 2000; Han et al. 1999; Deere et al. 2002). Experiments indicated that washing with water and 0.05 M neutral Tris–HCl buffer with 10 mM KCl (ionic strength 0.057 mM) failed to release any immobilized enzymes, even at high flow rates

Table 1 Response current of monolith micro-reactors coated with different molecular weights (MW) and concentrations of PEI polymer

PEI MW	PEI concentration (mg/ml)	Response current (nA) ^a
423	10	0
800	10	2.7 \pm 0.2
2,000	10	18.5 \pm 1
10,000	10	29.5 \pm 2
25,000	10	13.8 \pm 2
10,000	5	19.3 \pm 2
10,000	20	16.8 \pm 0.5

Flow rate of buffer was 10 $\mu\text{l}/\text{min}$ and substrate concentration 1 mM

^a Mean value \pm SD

(30 $\mu\text{l}/\text{min}$). However, washing with 0.1 M phosphate buffer (ionic strength 0.6 mM) could release at least 95% of immobilized enzymes. Using a high concentration of KCl (i.e. 0.1 M with 0.05 M Tris–HCl, ionic strength 0.15 mM) also gradually washed out the immobilized enzymes. This observation was consistent with reports in the literature (Laarz and Bergström 2000; Han et al. 1999; Deere et al. 2002). The reaction conditions for the best performance of the immobilized enzymes were to be PEI MW 10000 and concentration 10 mg/ml in 0.05 M neutral Tris–HCl buffer containing 10 mM KCl. Using these optimal conditions, maximum enzyme immobilization was found to be approximately 100 mg per gram of silica-monolith. It should be noted that enzyme release, however, occurred at flow rates greater than 40 $\mu\text{l}/\text{min}$, leading to the loss of enzyme activity.

3.4 Evaluation of the kinetic parameters for free and immobilized GOD and CHO enzymes

The kinetic parameters obtained from the ($1/j$ vs. $1/[S]$) double-reciprocal plots for both the immobilized (see Fig. 4a) and solution-based GOD are summarized in Table 2. The K_m for GOD free in solution was found to be 25 ± 2 mM, which agreed well with the reported value (27 mM) (Rogers and Brandt 1971). The $K_{m(\text{app})}$ for immobilized GOD was, however, found to be around 7 mM, which is nearly 4 times lower than the K_m for GOD in solution. This value of the $K_{m(\text{app})}$ was also smaller than 22 mM reported for GOD entrapped in a silica sol–gel membrane (Wang et al. 1998), 20 mM for GOD bound to self-assembled monolayer electrode (Murthy and Sharma 1998), 25 mM for GOD-polypyrrole (Vidal et al. 1998) and 11.8 mM for GOD immobilized on silica hybrid sol–gel film (Liu and Sun 2007). The $K_{m(\text{app})}$ generally relates to the diffusion of the substrate from bulk solution into the enzyme's substrate binding site with a lower $K_{m(\text{app})}$ indicating a smaller diffusion limitation (DeLouise and Miller 2005). From Table 2, effects of flow rates on $K_{m(\text{app})}$ were also obtained. Values for the immobilized $K_{m(\text{app})}$ were found to be independent of flow rates, which differed from the packed-bed methodology where the immobilized $K_{m(\text{app})}$ showed dependence on flow rates due to a mass transfer limitation effect (Kerby et al. 2006; Seong et al. 2003). A similar value of the k_{cat} for immobilized GOD (13.4 s^{-1}) and GOD free in solution (14 s^{-1}) was observed, indicating that good maintenance of the enzyme conformation was being provided by the proposed method. Comparison between values of the V_{max} for GOD in solution and the immobilized GOD in PEI-coated monolith micro-reactor indicates that the immobilized V_{max} (23.6 mM/min) is about 74 times higher than the solution V_{max} (0.32 mM/min). Quantitative analysis of enzyme

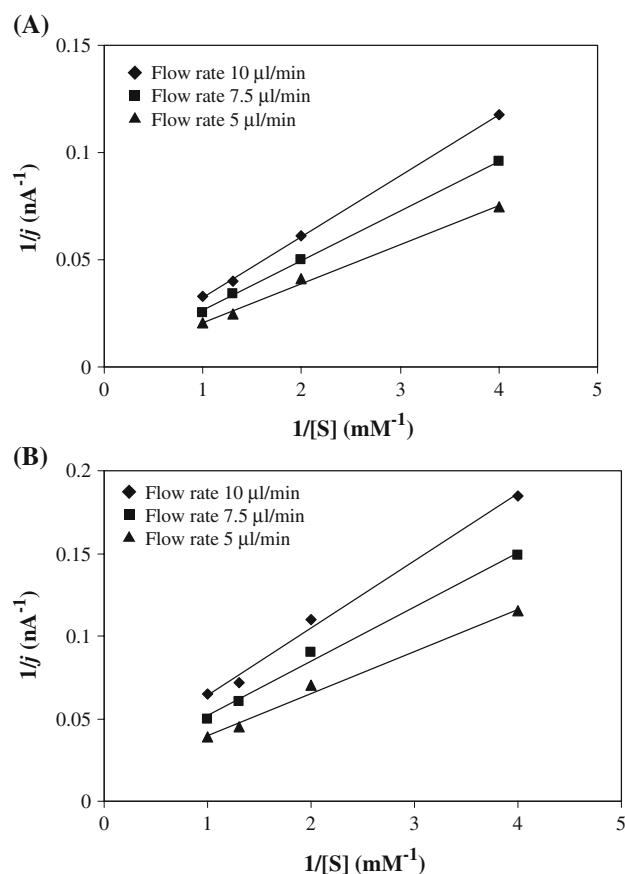
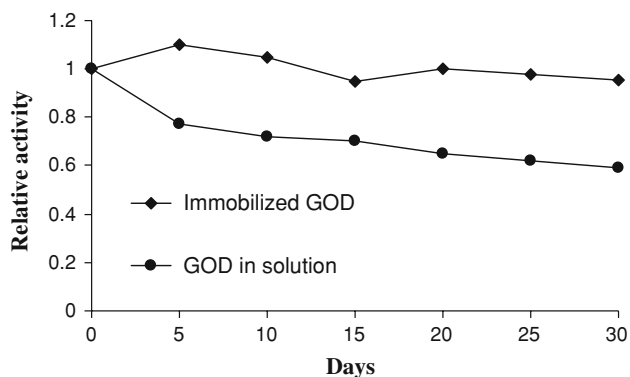


Fig. 4 The ($1/j$ vs. $1/[S]$) double-reciprocal plots for GOD (a) and CHO (b) immobilized in the PEI-coated silica-monolith micro-reactor system with different flow rates

presented in a monolith micro-reactor of 0.4 μl void volume revealed that ca. 1.89 μg of GOD was immobilized, giving a GOD concentration of approximately 0.029 mM in the micro-reactor which corresponded to at least 98% of the enzymes being immobilized. Comparison to a GOD concentration of 3.7×10^{-4} mM in 0.8 ml buffer solution, the ratio of the immobilized GOD concentration to the solution GOD concentration is therefore 78, which is in good agreement with the ratio (74) of the immobilized V_{max} to the solution V_{max} , indicated above. This observation also indicates that GOD is immobilized in a similar active conformation to GOD in solution. The GOD kinetic measurements were also carried out using PEI-coated monolith micro-reactor with lower porosity (0.33) and the kinetic parameters were found to be almost similar to those obtained for the micro-reactor with the porosity of 0.67 (see Table 2). The stability of the immobilized GOD during operation and storage was also examined. The activity of the immobilized GOD and GOD in solution as a function of storage time is shown in Fig. 5. A continuous run of 1 day did not lead to any significant decrease in the enzyme activity and after subsequent storage at 4°C for 30 days the

Table 2 The kinetic parameters $K_{m(\text{app})}$, V_{max} and k_{cat} for enzyme immobilized in PEI-coated silica-monolith and enzyme in solution

	Flow rate ($\mu\text{l}/\text{min}$)	$K_{m(\text{app})}$ (mM) ^a	V_{max} (mM/min) ^a	k_{cat} (s^{-1}) ^a
GOD in the monolith ^b	5	7.3 ± 0.2	23.9 ± 0.2	13.5 ± 0.5
	7.5	7.2 ± 0.2	23.6 ± 0.3	13.4 ± 0.4
	10	7.3 ± 0.2	23.5 ± 0.3	13.3 ± 0.5
GOD in the monolith ^c	5–10	6.7 ± 0.6	23.4 ± 0.2	13.2 ± 0.2
GOD in solution	0	25 ± 2	0.32 ± 0.02	14 ± 0.3
CHO in the monolith ^c	5	1.8 ± 0.2	8.3 ± 0.2	3.0 ± 0.1
	7.5	1.7 ± 0.4	8.0 ± 0.4	2.9 ± 0.1
	10	1.7 ± 0.3	7.8 ± 0.4	2.8 ± 0.2
CHO in solution	0	2.1 ± 0.2	0.15 ± 0.01	3 ± 0.3

^a Mean value \pm SD^b The porosity was 0.67 ± 0.04 ^c The porosity was 0.33 ± 0.02 **Fig. 5** Stability of the immobilized GOD and the GOD in solution. Both GOD immobilized monolith micro-reactor and GOD in working buffer solution were stored at 4°C, substrate was 1 mM and flow rate 10 $\mu\text{l}/\text{min}$

activity of the immobilized GOD retained at least 95% of the initial activity compared to only 60% of the initial activity for GOD in solution.

In addition to GOD, the same enzyme immobilization strategy was used for CHO immobilization. CHO is a catabolic enzyme that offers a model system for the study of choline oxidation, an important metabolic process in both prokaryotes and eukaryotes. The kinetic parameters obtained from the ($1/j$ vs. $1/[S]$) double-reciprocal plots (see Fig. 4b) for immobilized CHO in a monolith micro-reactor with porosity of 0.33 and solution-based CHO with choline chloride as the substrate are also summarized in Table 2. Comparisons between the kinetic parameters of the immobilized CHO in PEI-coated monolith micro-reactor and CHO free in solution revealed that the $K_{m(\text{app})}$ value (1.7 mM) for the immobilized CHO was slightly smaller than that (2.1 mM) for free CHO in solution and a

similar value of the k_{cat} for the immobilized (2.9 s^{-1}) and solution (3.0 s^{-1})-based CHO was obtained. As with immobilized GOD, the immobilized $K_{m(\text{app})}$ for CHO was also found to be independent of flow rates. These results indicate slightly favourable mass transfer and less influence on the CHO conformation by electrostatic interaction between the CHO and the PEI-coated monolith. Comparisons between value of the V_{max} for the immobilized CHO (8.0 mM/min) and CHO in solution (0.15 mM/min) and the concentrations for the immobilized CHO in the PEI-coated monolith micro-reactor (0.046 mM in monolith void volume of 0.2 μl) and CHO in solution (8.2×10^{-4} mM in 0.8 ml of buffer solution) showed a good agreement between the ratio (53) of the immobilized V_{max} to the solution V_{max} and the ratio (56) of the concentration of the immobilized CHO to the CHO in solution, once again indicating that CHO was immobilized in a similar active conformation to CHO in solution. As a control the immobilization of GOD and CHO in a silica monolith micro-reactor in the absence of PEI did not form detectable H_2O_2 because the silica monolith micro-reactor could not be efficiently immobilized enzymes in the absence of PEI when loading a limited volume of enzyme solution into the silica monolith micro-reactor. It should also be noted that the both micro-reactors with porosity of 0.67 and 0.33 did not create any backpressure problems (i.e. leakage or blockage) at flow rates less than 30 $\mu\text{l}/\text{min}$. However, further reduction of porosity decreased enzyme immobilization efficiency, leading to a reduction in enzyme activity. Finally, regeneration of the micro-reactor devices could be achieved by simply adding 1 M NaOH solution and heating at 60–90°C for 15 min to dissolve and totally remove the used silica-monoliths. The performance of monolith micro-reactors produced by using new microchip and regenerated microchip was highly reproducible ($97 \pm 3\%$, $n = 5$).

4 Conclusions

The method described in the present work has the following significant advantages: (1) monolith preparation is simple and the porosity can be controlled; (2) micrometer-size flow-through pores give low pressure drop and fast mass transfer kinetics; (3) enzymes such as GOD and CHO can be immobilized in their active conformation on the surface of the PEI-coated monolith via electrostatic attractions between electronegative enzyme and electro-positive PEI, so efficiently maintaining the biological activity compared to covalent bonding and encapsulation processes; (4) the on-chip electrochemical detection provides the opportunity for fast and convenient monitoring the activity of the immobilized enzymes and (5) the microchip devices can be regenerated simply by adding

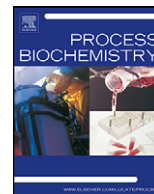
1 M NaOH solution to dissolve and remove the used silica-monoliths. Accordingly, the immobilized enzyme in PEI-coated monolith exhibit almost similar k_{cat} to GOD in solution with the $K_{\text{m(app)}}$ being ~ 4 times lower and the $V_{\text{max}} \sim 70$ times higher compared to GOD in solution, indicating better maintenance of the conformation of GOD by proposed immobilization method and favourable enzyme concentration in the micro-reactor environment. Similar kinetic behaviour was also observed for CHO immobilized in the PEI-coated monolith where analogous values for k_{cat} and $K_{\text{m(app)}}$ but with the $V_{\text{max}} \sim 50$ times higher compared to CHO in solution were obtained, once again indicating better maintenance of the conformation of CHO by proposed method and favourable enzyme concentration in the micro-reactor environment. In addition, the immobilized enzyme exhibited increased stability during continuous use and storage compared to enzyme in solution. This method also provides the flexibility to regenerate micro-reactor or to use disposal monolithic capillary micro-reactor.

Acknowledgments We acknowledge the EU for funding through project NMP4-CT-2006-033254.

References

- Arai G, Noma T, Hayashi M, Yasumori I (1998) Electrochemical characteristics of D-amino acid oxidase immobilized in a conductive redox polymer. *J Electroanal Chem* 452:43–48
- Deere J, Magner E, Wall JG, Hodnett BK (2002) Mechanistic and structural features of protein adsorption onto mesoporous silicates. *J Phys Chem B* 106:7340–7347
- DeLouise LA, Miller BL (2005) Enzyme immobilization in porous silicon: quantitative analysis of the kinetic parameters for glutathione-S-transferases. *Anal Chem* 77:1950–1956
- Demers N, Agostinelli E, Averill-Bates DA, Fortier G (2001) Immobilization of native and poly(ethylene glycol)-treated ('PEGylated') bovine serum amine oxidase into a biocompatible hydrogel. *Biotechnol Appl Biochem* 33:201–207
- Fletcher PDI, Haswell SJ, Pombo-Villar E, Warrington BH, Watts P, Wong SYF, Zhang X (2002) Micro reactors: principles and applications in organic synthesis. *Tetrahedron* 58:4735–4757
- Girelli AM, Mattei E (2005) Application of immobilized enzyme reactor in on-line high performance liquid chromatography: a review. *J Chromatogr B* 819:3–16
- Gleason NJ, Carbeck JD (2004) Measurement of enzyme kinetics using microscale steady-state kinetic analysis. *Langmuir* 20:6374–6381
- Guo Z, Xu S, Lei Z, Zou H, Guo B (2003) Immobilized metal-ion chelating capillary microreactor for peptide mapping analysis of proteins by matrix assisted laser desorption/ionization-time of flight-mass spectrometry. *Electrophoresis* 24:3633–3639
- Han Y-J, Stucky GD, Butler A (1999) Mesoporous silicate sequestration and release of proteins. *J Am Chem Soc* 121:9897–9898
- He P, Greenway G, Haswell SJ (2008) The on-line synthesis of enzyme functionalized silica nanoparticles in a micro-reactor using poly ethylenimine polymer and R5 peptide. *Nanotechnol* 19:315603
- Hilder EF, Svec F, Fréchet JM (2002) Polymeric monolithic stationary phases for capillary electrochromatography. *Electrophoresis* 23:3934–3953
- Holden MA, Jung S-Y, Cremer PS (2004) Patterning enzymes inside microfluidic channels via photoattachment chemistry. *Anal Chem* 76:1838–1843
- Honda T, Miyazaki M, Nakamura H (2006) Facile preparation of an enzyme-immobilized microreactor using a cross-linking enzyme membrane on a microchannel surface. *Adv Synth Catal* 348:2163–2171
- Kaku T, Karan HI, Okamoto Y (1994) Amperometric glucose sensors based on immobilized glucose oxidase-polyquinone system. *Anal Chem* 66:1231–1235
- Kato M, Inuzuka K, Sakai-Kato K, Toyo'oka T (2005) Monolithic bioreactor immobilizing trypsin for high-throughput analysis. *Anal Chem* 77:1813–1818
- Kawakami K, Sera Y, Sakai S, Ono T, Ijima H (2005) Development and characterization of a silica monolith immobilized enzyme micro-bioreactor. *Ind Eng Chem Res* 44:236–240
- Kerby MB, Legge RS, Tripathi A (2006) Measurements of kinetic parameters in a microfluidic reactor. *Anal Chem* 78:8273–8280
- Koh WG, Pishko M (2005) Immobilization of multi-enzyme microreactors inside microfluidic devices. *Sens Actuators B* 106:335–342
- Krenková J, Foret F (2004) Immobilized microfluidic enzymatic reactors. *Electrophoresis* 25:3550–3563
- Laarz E, Bergström L (2000) Dispersing WC-Co powders in aqueous media with polyethylenimine. *Int J Refract Metals Hard Mater* 18:281–286
- Legido-Quigley C, Marlin ND, Melin V, Manz A, Smith NW (2003) Advances in capillary electrochromatography and micro-high performance liquid chromatography monolithic columns for separation science. *Electrophoresis* 24:917–944
- Lei C, Shin Y, Liu J, Ackerman E (2002) Entrapping enzyme in a functionalized nanoporous support. *J Am Chem Soc* 124:11242–11243
- Liu S, Sun Y (2007) Co-immobilization of glucose oxidase and hexokinase on silicate hybrid sol-gel membrane for glucose and ATP detections. *Biosens Bioelectron* 22:905–911
- Luckarift HR, Spain JC, Naik RR, Stone MO (2004) Enzyme immobilization in a biomimetic silica support. *Nat Biotechnol* 22:211–213
- Mao H, Yang T, Cremer PS (2002) Design and characterization of immobilized enzymes in microfluidic systems. *Anal Chem* 74:379–385
- Mersal GAM, Bilitewski U (2005) Development of monolithic enzymatic reactors in glass microchips for the quantitative determination of enzyme substrates using the example of glucose determination via immobilized glucose oxidase. *Electrophoresis* 26:2303–2312
- Murthy ASN, Sharma J (1998) Glucose oxidase bound to self-assembled monolayers of bis(4-pyridyl) disulfide at a gold electrode: amperometric determination of glucose. *Anal Chim Acta* 363:215–220
- Nomura A, Shin S, Oulad MO, Kauffmann JM (2004) Preparation, characterization, and application of an enzyme-immobilized magnetic microreactor for flow injection analysis. *Anal Chem* 76:5498–5502
- Ota S, Miyazaki S, Matsuoka H, Morisato K, Shintani Y, Nakanishi K (2007) High-throughput protein digestion by trypsin-immobilized monolithic silica with pipette-tip formula. *J Biochem Biophys Methods* 70:57–62
- Park CB, Clark DS (2002) Sol-gel encapsulated enzyme arrays for high-throughput screening of biocatalytic activity. *Biotechnol Bioeng* 78:229–235

- Park SS, Cho SI, Kim MS, Kim YK, Kim BG (2003) Integration of on-column immobilized enzyme reactor in microchip electrophoresis. *Electrophoresis* 24:200–206
- Peterson DS (2005) Solid supports for micro analytical systems. *Lab Chip* 5:132–139
- Peterson DS, Rohr T, Svec F, Fréchet JMJ (2002) Enzymatic microreactor-on-a-chip: protein mapping using trypsin immobilized on porous polymer monoliths molded in channels of microfluidic devices. *Anal Chem* 74:4081–4088
- Rogers MJ, Brandt KG (1971) Interaction of D-glucal with a niger glucose oxidase. *Biochem* 10:4624–4630
- Sakai-Kato K, Kato M, Toyo'oka T (2003) Creation of an on-chip enzyme reactor by encapsulating trypsin in sol–gel on a plastic microchip. *Anal Chem* 75:388–393
- Seong GH, Crooks RM (2002) Efficient mixing and reactions within microfluidic channels using microbead-supported catalysts. *J Am Chem Soc* 124:13360–13361
- Seong GH, Heo J, Crooks RM (2003) Measurement of enzyme kinetics using a continuous-flow microfluidic system. *Anal Chem* 75:3161–3167
- Thomsen MS, Pölt P, Nidetzky B (2007) Development of a microfluidic immobilized enzyme reactor. *Chem Commun* 252:7–2529
- Tokeshi M, Kikutani Y, Hibara A, Sato K, Hisamoto H, Kitamori T (2003) Chemical processing on microchips for analysis, synthesis, and bioassay. *Electrophoresis* 24:3583–3594
- Urban PL, Goodall DM, Bruce NC (2006) Enzymatic microreactors in chemical analysis and kinetic studies. *Biotechnol Adv* 24:42–57
- Verpoorte E (2003) Beads and chips: new recipes for analysis. *Lab Chip* 3:60N–68N
- Vidal J-C, Garcia E, Castillo J-R (1998) Electropolymerization of pyrrole and immobilization of glucose oxidase in a flow system: influence of the operating conditions on analytical performance. *Biosens Bioelectron* 13:371–382
- Vodopivec M, Podgornik A, Berovič M, Štrancar A (2003) Characterization of CIM monoliths as enzyme reactors. *J Chromatogr B* 795:105–113
- Wang B, Li B, Deng Q, Dong S (1998) Amperometric glucose biosensor based on sol–gel organic-inorganic hybrid material. *Anal Chem* 70:3170–3174
- Wang C, Oleschuk R, Ouchen F, Li J, Thibault P, Harrison DJ (2000) Integration of immobilized trypsin bead beds for protein digestion within a microfluidic chip incorporating capillary electrophoresis separations and an electrospray mass spectrometry interface. *Rapid Commun Mass Spectrom* 14:1377–1383



Development of a monolith based immobilized lipase micro-reactor for biocatalytic reactions in a biphasic mobile system

Ping He, Gillian Greenway, Stephen J. Haswell*

Department of Chemistry, University of Hull, Hull HU6 7RX, UK

ARTICLE INFO

Article history:

Received 1 October 2009

Received in revised form 6 December 2009

Accepted 10 December 2009

Keywords:

Micro-reactor
Immobilized lipase
Monolith
Biphasic system
Hydrolysis reaction
Enzyme kinetics

ABSTRACT

This paper reports a simple method for producing macroporous silica-monoliths with controllable porosity that can be used for the immobilization of lipases to generate an active and stable micro-reactor for biocatalysis. A range of commercially available lipases has been examined using the hydrolysis reactions of 4-nitrophenyl butyrate in water–decane media. The kinetic studies performed have identified that a similar value for k_{cat} is obtained for the immobilized *Candida antarctica* lipase A (0.13 min^{-1}) and the free lipase in solution (0.12 min^{-1}) whilst the immobilized apparent Michaelis constant K_m (3.1 mM) is 12 times lower than the free lipase in solution (38 mM). A 96% conversion was obtained for the immobilized *C. antarctica* lipase A compared to only 23% conversion for the free lipase. The significant higher conversions obtained with the immobilized lipases were mainly attributed to the formation of a favourable biphasic system in the continuous flowing micro-reactor system, where a significant increase in the interfacial activation occurred. The immobilized *C. antarctica* lipase A on the monolith also exhibited improved stability, showing 64% conversion at 80 °C and 70% conversion after continuous running for 480 h, compared to 40 and 20% conversions under the same temperature and reaction time for the free lipase.

© 2009 Elsevier Ltd. All rights reserved.

1. Introduction

Due to the existence of the interfacial activation lipases (triacylglycerol acylhydrolase, EC 3.1.1.3) represent versatile group of enzymes with various biocatalytic activities which include triacylglycerols hydrolysis, esterification, trans-esterification, alcoholysis and acidolysis to yield a wide range of useful biological and chemical derivatives [1–5]. Furthermore, lipases are also enantioselective catalysts and can be used for the resolution of chiral compounds and the synthesis of high-value pharmaceutical intermediates [6–8]. However, the high cost of lipase makes enzymatically driven processes in the soluble homogenous form economically unattractive. A practical solution to this problem is to use an immobilized lipase that can significantly reduce the cost and increase the ratio of product to lipase used [9,10]. The use of an appropriate immobilization method may promote enzyme-support multipoint or multi-subunit interactions and enhance enzyme stabilization. Such a method of immobilization will also enhance other lipase properties including activity [11,12] whilst facilitating the separation of products from the enzyme, and optimization of

lipase/substrate contact time by using continuous flow systems [2,10–13]. Traditional methods for lipase immobilization are largely based on lipase adsorption onto hydrophobic polymers such as polypropylene, alkyl-agarose, polyacrylate and polystyrene, lipase stability can, however, still be significantly affected by the polymer surfaces and activity is typically limited by surface coverage [14–16]. Recently, hydrophobic sol–gel supports, obtained by using alkyl-modified silane ($\text{RSi}(\text{OCH}_3)_3$), have been reported for the entrapment of lipases [17,18]. Since lipases are interface-active enzymes with lipophilic domains, lipophilic interactions between hydrophobic parts of gel and lipase favour the stabilization of the open form of the lipase which offers in turn enhanced activity [11,12]. However, if the substrate is large or hydrophilic, the near presence of the hydrophobic support surface may generate some steric hindrances, reducing the activity of the lipase. More recently chemical covalent bonding and cross-linking as well as physical encapsulation processes have been reported for the enzyme immobilization but these methods can still cause structural deformation of the enzyme or introduce steric hindrance to the catalytic sites, leading to reduction in enzyme activity [19–23].

The use of micro-reactors in conjunction with enzymatic processes is now attracting increasing attention due to their ability to spatially control localized concentration of reactants, intermediates and products within the flow region of such systems

* Corresponding author. Tel.: +44 01482 465469; fax: +44 01482 466410.
E-mail address: s.j.haswell@hull.ac.uk (S.J. Haswell).

offering a significant reduction in both reagent consumption and operating costs [24]. In addition, chemical and biological processing at the microscale offers a number of reaction and practical benefits that are unattainable when using a macroscale configurations [25–27]. However, packed-bed micro-reactors often generate increased backpressure that gives rise to leaking or blocking problems [28,29]. Recently, silica-based monoliths have been used as an attractive alternative to packed columns for the analysis of proteins, peptides and nucleic acids as they offer low diffusion resistance during mass transfer, controllable porosity and low back pressure compared to packed column reactors [30–35]. The preparation of these monoliths by sol–gel chemistry however usually requires the addition of other additives such as polyethylene glycol (PEG) and dextrin to stabilise the structure [21,22] and fabrication can be time consuming (ca. 3–15 days) [21,22].

In this paper we report a simple method for generating a stable monolith for the immobilization of lipase with in a micro-reactor device. The macroporous silica-monoliths with controllable porosity were prepared within a capillary from two precursors tetramethoxysilane (TMOS) and methyltrimethoxysilane (MTMOS) using a sol–gel method, followed by lipase immobilization *via* multipoint interactions between lipase and the surface of silica-monoliths to generate immobilized lipase micro-reactors based on a range of commercially available lipases. Through multipoint immobilization the lipases can be immobilized in an active conformation that significantly enhances thermal and reactive stability. In addition, the use of mobile water–decane biphasic system for the hydrolysis reaction of 4-nitrophenyl butyrate can significantly increase the lipase interfacial activation. Kinetic parameters, i.e. apparent Michaelis constant K_m and turnover number k_{cat} for the free and immobilized lipase were determined. An evaluation of the stability for the free and immobilized lipase at elevated temperatures and over extended run times was also carried out.

2. Experimental

2.1. Materials

Six lipases (EC 3.1.1.3) including *Aspergillus niger* lipase (ANL), *Burkholderia* sp. Lipase (BCL), *Candida antarctica* lipase A (CAL), *C. antarctica* lipase B (CBL), *Penicillium camemberti* lipase (PCL) and *C. antarctica* lipase A cross-linked enzyme aggregate (CLEA–CAL) were purchased from Sigma–Aldrich (UK) and used without further purification. Decane ($\geq 99\%$), 4-nitrophenyl butyrate (4-NPB, $\geq 98\%$) and 4-nitrophenol (4-NP, $\geq 98\%$) were also obtained from Sigma–Aldrich. Polyethyleneimine (PEI, molecular weight 10,000), KCl (99%), HCl (37%), tetramethoxysilane (TMOS, 99%) and methyltrimethoxysilane (MTMOS, 99%) were purchased from Fluka. Glass capillary (0.6 \pm 0.05 mm ID and 25 mm length) was obtained from Brand GMBH (Germany). Milli-Q water (18 M Ω cm) was used to prepare all aqueous solutions.

2.2. Preparation of silica-monoliths within a capillary

Silica-monoliths were prepared from two precursors TMOS and MTMOS by using a sol–gel method [36]. In a typical preparation, 18 μ l of TMOS and 69 μ l of MTMOS (at 1:4 molar ratio) were added to dilute HCl solution (8 μ l of 1 mM HCl and 13.2 μ l water) and allowed to hydrolyse for 15 min under sonication at room temperature to form a homogeneous sol of silicic acid. A 12.6 μ l aliquot of sol was then mixed with 9.4 μ l of water and 22 μ l of 0.2 M (pH 7) Tris–HCl buffer, and the resultant liquid mixture was immediately loaded into a capillary (4 cm length) and allowed to polymerize for 15 h at room temperature, followed by vacuum drying for 1 h to form a silica-monolith with void volume of 10 \pm 1 μ l.

2.3. Lipase immobilization

An aqueous solution (lipase in 0.05 M pH 7 Tris–HCl buffer, final lipase concentration 0.1–1 mg/ml) was pumped through a monolith micro-reactor at flow rate of 10 μ l/min for 10 min, then the monolith micro-reactor was kept in a fridge (4 $^{\circ}$ C) for 1 h, followed by vacuum drying for 30 min to give a monolith immobilized lipase micro-reactor (note: after an initial evaluation of a range of lipase substrates only monoliths based on immobilized *C. antarctica* lipase A (CAL–monolith) were used in this paper). Before measurement was taken, the micro-reactor was washed with 0.05 M neutral Tris–HCl buffer (flow rate 10 μ l/min) for 5 min to remove untrapped lipase and washing liquid was collected.

2.4. Assay of the free solution and immobilized lipase activity

4-NPB, a well-known substrate for lipase hydrolysis activity, was used as the substrate in this work to evaluate the performance of free solution and immobilized lipase in the media consisted of 0.05 M pH 7 Tris–HCl buffer and decane solvent. The solubility of the reactant 4-NPB, the product 4-NP and lipases was checked in both water and decane solvent, it was found that the reactant 4-NPB was dissolved in the organic phase (decane) whilst the product 4-NP and lipase (for solution based reactions only) were present in water phase.

The assay for free lipase activity was carried out at the desired temperature (usually room temperature 25 $^{\circ}$ C) under agitation (with a magnetic stirrer at 100 rpm) in 1 ml final volume, containing 0.4 ml of organic phase (1–15 mM 4-NPB in decane) and 0.6 ml of aqueous phase (free lipase in 0.05 M pH 7 Tris–HCl buffer). After a given time (1, 2.5, 5, 10 and 15 min), aqueous phase samples (10–100 μ l) were removed by a pipette and mixed with a 0.1 M neutral Tris–HCl buffer solution to quench the reaction (final volume 1 ml in a disposable plastic UV–vis cuvette). The production of 4-NP was determined using an UV–vis spectrophotometer (Chemspec M508) by reading absorbance at 400 nm and using a calibration curve of 4-NP concentration versus absorbance. The conversion was calculated using Eq. (1):

$$\text{Conversion} = \frac{C_p}{C_0} \times 100 \quad (1)$$

where C_0 was initial concentration of 4-NPB and C_p concentration of 4-NP in the samples collected at a given time. All data reported are average values from at least triplicate measurements and with standard error less than 6%.

A schematic of the apparatus used for the evaluation of the immobilized lipase activity is shown in Fig. 1 and consists of two syringe pumps for controlling flow rate of the aqueous and organic solutions, a capillary mixer, and a monolith immobilized lipase micro-reactor. An aqueous solution (0.05 M neutral Tris–HCl buffer) without lipase present and an organic solution (1–15 mM 4-NPB in decane) were separately pumped through the capillary mixer and monolith micro-reactor with the product being collected from the outlet of the micro-reactor under steady-state condition. The organic phase was then removed by a pipette and the aqueous phase was treated and analysed using the same methodology as described above for the assay of the free lipase activity.

2.5. Determination of lipase loading in the immobilized monolith micro-reactor

The quantity of the immobilized lipase was determined by calculating the difference between the amount of lipase in the initial loading solution and that in the residual solution collected after the entrapping process, which was quantified using a calibration curve of lipase activity versus lipase concentration within a linear range. The quantity of immobilized lipase reported is an average value from at least triplicate measurements with a standard error less than 5%.

3. Results and discussion

3.1. Initial solution study into the catalytic activity of different lipases and effect of water content

The activity of the different lipases and the effect of water content were first investigated in order to aid the selection of lipase and determine the optimum water content to use in the immobilization methodology. Six commercially available lipases including CAL, BCL, ANL, PCL, CBL and CLEA–CAL were examined in

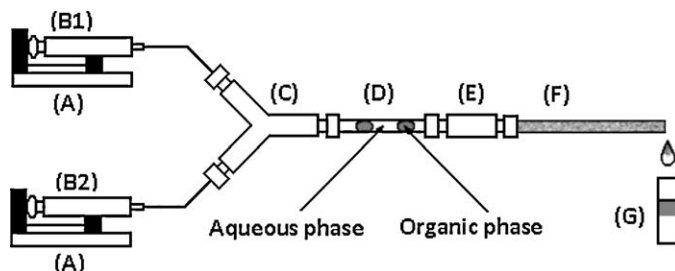


Fig. 1. Schematic diagram of the reaction system used to assay immobilized lipase activity, consisting of (A) syringe pump, (B1) syringe (volume 1 ml) for organic solution and (B2) syringe (volume 1 ml) for buffer solution, (C) small PEEK Y-shape connector (pore size 0.5 mm diameter), (D) the capillary mixer (0.6 mm ID and 3 cm length), (E) 2-way PEEK connector (pore size 0.5 mm diameter), (F) the monolith micro-reactor (0.6 mm ID and 4 cm length), (G) sample collection vial. Within the capillary mixer, water was the continuous phase and the organic solution the segmented phase. The length of the organic plugs was ca. 1.5 mm.

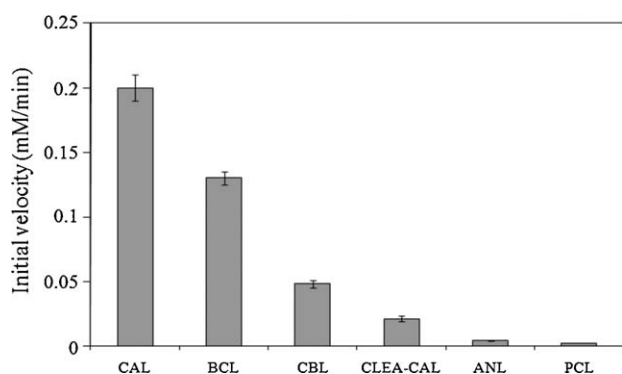


Fig. 2. Initial velocity obtained from different lipases in solution-based reactions. CAL = *Candida antarctica* lipase A, BCL = *Burkholderia* sp lipase, CBL = *Candida antarctica* lipase B, CLEA = *Candida antarctica* lipase A cross-linked enzyme aggregate, ANL = *Aspergillus niger* lipase, PCL = *Penicillium camemberti* lipase, lipase concentration = 1 mg/ml, 4-NPB concentration = 4 mM, the volume ratio of aqueous phase to organic phase was 1, reaction temperature, 25 °C.

Table 1
Effect of water to decane ratio on the CAL lipase activity.^a

Interfacial area (mm ²)	Ratio of water to decane in volume	Initial velocity (mmol/min)
229.5 ^b	3:1	0.029 ± 0.001
229.5 ^b	3:2	0.045 ± 0.002
229.5 ^b	3:3	0.035 ± 0.002
437.2 ^c	3:2	0.0675 ± 0.003

^a 4-NPB = 5 mM, CAL = 1.5 mg, total volume = 1.0 ml.

^b The diameter of the reaction tube was 17.1 mm.

^c The diameter of reaction tube was 23.6 mm.

free solution batch-based reactions. The initial velocity obtained from the different lipases is presented in Fig. 2, from which it can be seen that the CAL represents the best lipase for the hydrolysis of 4-NPB in water–decane media, accordingly CAL was subsequently used for all further immobilization experiments. The difference in activity observed for the various lipases investigated is attributed to different substrate specificities. It was also found that higher stirring speeds reduce the activity of the lipase due to the production of more bubbles that can reportedly inactivate enzyme activity [11]. However, in the case where CLEA–CAL particles were used, the lower activity is attributed more to the fact that most of the particles tended to be present in the lower water phase, resulting in the immobilized enzyme molecules having poor contact with the substrates in the organic phase.

For hydrolytic reactions, water is required not only as a substrate but also for structural integrity of the lipase, however, the effect of water is known also to depend on the amount of enzyme, polarity of the solvent, solid support and type of reaction [37]. In this study the effect of water was examined by evaluating

the initial velocity of the free CAL as a function of water to decane ratio. As indicated in Table 1, the initial velocity was found to increase with increasing interfacial area with the maximum initial velocity being obtained at a water to decane ratio of 3:2. These findings were attributed to favourable lipase interfacial activation. The ratio of 3:2 was therefore used for all further immobilization experiments.

3.2. Evaluation of the kinetic parameters for the free and immobilized CAL in a biphasic system

Kinetic constants for the free CAL were determined using Lineweaver–Burk double reciprocal plot. Kinetic constants for the immobilized CAL were obtained from Lilly–Hornby model (Eq. (2)), which was developed for packed-bed reactor systems [38]:

$$C_{in} - C_{out} = K_m \ln \frac{C_{out}}{C_{in}} + \frac{V_{max} V_{void}}{Q} \quad (2)$$

where K_m was the apparent Michaelis constant, V_{max} the maximum velocity, C_{in} and C_{out} the reactant concentration at the inlet and outlet, V_{void} the void volume of the monolith micro-reactor and Q the volume flow rate. The K_m values could be directly obtained from a slope of the plot and V_{max} was calculated from the Y-axis intercept. The values of V_{void} (10 μ l) and Q (10 μ l/min) were measured and the turnover number k_{cat} was determined ($V_{max}/[\text{lipase}]$). The Lilly–Hornby and Lineweaver–Burk plots obtained for the immobilized and the free CAL are shown in Fig. 3a and b and the kinetic constants calculated are summarized in Table 2. It can be seen that the immobilized K_m is 3.1 mM for the CAL–monolith. This value was found to be 12 times lower than the K_m for the free CAL in solution (38 mM), indicating a favourable affinity between substrate and enzyme's substrate binding site. A similar value of the k_{cat} was obtained for the CAL–monolith (0.13 min^{-1}) and the free CAL (0.12 min^{-1}), indicating that both the free and immobilized lipases were activated in a similar way [36]. However, it was observed that the k_{cat} values were reduced to 0.029 min^{-1} for CAL–monolith when using higher lipase loadings (4.4 mg/ml). In this case the reduction in the k_{cat} can be attributed to both lipase aggregation and the possibility of pores blocking at higher lipase loadings, decreasing specific lipase activity and accessibility of the substrate to the biphasic system. Although higher lipase loadings gave lower k_{cat} values, higher conversions were obtained using higher lipase loadings compared to lower lipase loadings. For example, CAL–monolith with lipase load of 4–5 mg/ml gave a conversion of approximately 70–75% compared to ca. 40% conversion with lipase load of 0.55 mg/ml at flow rate of 2.5 μ l/min (1.5 μ l/min of 0.05 M neutral Tris–HCl buffer and 1 μ l/min of 1 mM 4-NPB in decane).

The free and immobilized CAL activities were also examined using the same loading of lipase (see Table 3). The immobilized lipase was found to give a conversion of 96%, which was four times

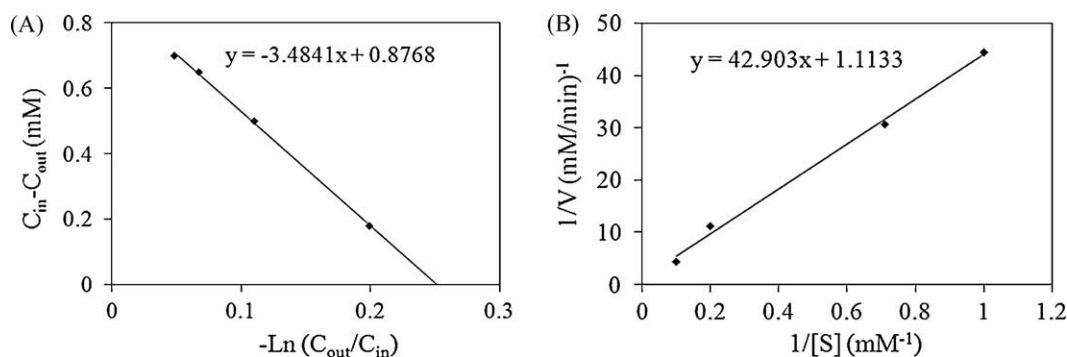


Fig. 3. (a) The Lilly–Hornby plots obtained for the CAL–Monolith (1.1 mg/ml). (b) The Lineweaver–Burk double reciprocal plot obtained for the free CAL (1 mg/ml).

Table 2
The kinetic parameters K_m and k_{cat} for the immobilized and free CAL.

Lipase	Lipase loading (mg/ml)	Reaction kinetics	
		K_m (mM)	k_{cat} (min^{-1})
CAL–monolith	1.1	3.1 ± 0.2	0.13 ± 0.01
CAL–monolith	4.4	3.0 ± 0.2	0.029 ± 0.002
Free	1.0	38 ± 4	0.12 ± 0.01

Table 3
Activity of the free and immobilized CAL obtained using the same CAL loadings.

Lipase	Lipase loading (mg/ml)	Conversion (%)	
		8 min	16 min
CAL–monolith ^a	3.6	77 ± 2.5^b	96 ± 4.5^c
Free CAL in solution ^d	3.6	13.9 ± 0.6	24.3 ± 1.4

^a Organic phase = 1 mM 4-NPB in decane, aqueous phase = 0.05 M pH 7 Tris–HCl buffer, length of micro-reactor = 8 cm.

^b Flow rate of organic phase = 1 $\mu\text{l}/\text{min}$, flow rate of aqueous phase = 1.5 $\mu\text{l}/\text{min}$.

^c Flow rate of organic phase = 0.5 $\mu\text{l}/\text{min}$, flow rate of aqueous phase = 0.75 $\mu\text{l}/\text{min}$.

^d Organic phase = 1 mM 4-NPB in 400 μl of decane, aqueous phase = 600 μl of 0.05 M pH 7 Tris–HCl buffer.

higher than that (23.4%) for the free lipase in solution. This trend was mainly attributed to the favourable biphasic system formed in the continuous flow micro-reactor system in which the aqueous phase represented the continuous phase and the organic solution the segmented phase (ca. 1.5 mm long) surrounded by the aqueous buffer. The calculation revealed that the surface to volume ratio was 8 mm^{-1} in the flow system compared to only 0.23 mm^{-1} for the batch-based reaction. This significant increase in interfacial area could therefore enhance the lipase activation, giving consequently higher reaction conversions. It was also observed that when a longer contact time (>16 min) is used in the continuous flow system the production of the product is reduced due to the reversible reaction, i.e. the intensity of the reverse reaction increased with the increase in the production of the product.

3.3. Thermal stability and reaction life time of the free and immobilized CAL

The thermal stability of the free and immobilized CAL was examined by determining lipase activity (conversion) as a function of reaction temperature (heating was provided by an isothermal water bath), and the reaction was carried out in a closed vial with a 30 s reaction time to prevent evaporation of solvents. Fig. 4 shows

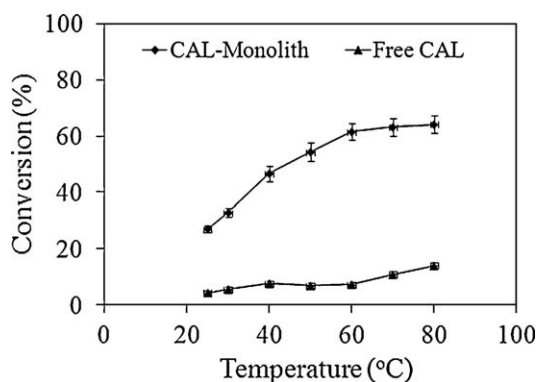


Fig. 4. Effect of the reaction temperature on the free and immobilized CAL activity: (◆) the immobilized CAL at flow rate of 2.5 ml/min (1.5 ml/min of 0.05 M pH 7 Tris–HCl buffer and 1 ml/min of 5 mm 4-NPB in decane); (▲) the free CAL using a closed vial, reaction time 30 s, 5 mm 4-NPB in 400 ml of decane, 0.05 M pH 7 Tris–HCl buffer 600 ml.

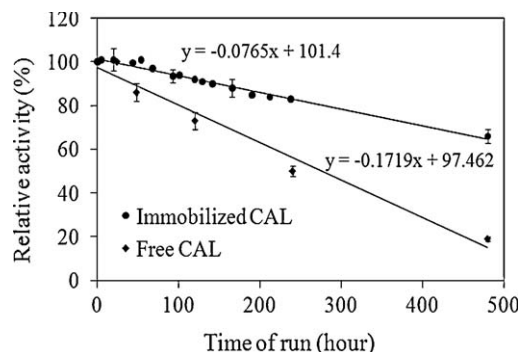


Fig. 5. Stability of the activity for the free and immobilized CAL as a function of reaction time: (●) hydrolysis was carried out using free CAL (1.1 mg/ml) in solution at room temperature and 4-NPB 1 mM in decane; (◆) 0.05 M pH 7 Tris–HCl buffer (1.5 ml/min) and 1 mM 4-NPB in decane (1 ml/min) continuously pumped through an immobilized CAL–monolith micro-reactor (8 cm long and immobilized CAL 0.102 mg) giving a contact time ca. 8 min, samples were collected to determine the conversion.

changes in conversion of the free and immobilized CAL with temperature. The maximum activity of the free CAL appeared at 30 °C, which was consistent with results reported by Liu et al. [39]. On the other hand, the immobilized CAL exhibited better thermal stability and gave higher conversions compared to the free CAL, resulting in an increase from 27 to 61% with increasing temperature from 25 to 60 °C with a slight increase to 64% when the temperature was increased to 80 °C.

The reactive stability of the free and immobilized CAL was also observed as function of continuous reaction time at room temperature (25 °C). As shown in Fig. 5, immobilized CAL exhibited better stability during 480 h of continuous run compared to the free CAL. For the free CAL, full activation was only observed for 24 h then the activity gradually decreased with time to 19% after 480 h of continuous operation. The half-life (time of obtaining half of initial activity) was estimated from linear regression of all data to be 672 h for the immobilized CAL and 276 h for free CAL. The higher thermal and reactive stability for the immobilized lipase could be attributed to multiple interactions between hydrophobic surface of silica–monolith and lipase including hydrophobic interaction, hydrogen bond or ionic interaction [16].

4. Conclusions

A simple method has been reported for producing macroporous silica–monoliths that can be used for lipase immobilization to generate active and stable immobilized lipase micro-reactors for biocatalysis. Different lipases exhibited varied activity for the hydrolysis of 4-NPB in water–decane media and the activity followed the sequence of CAL > BCL > CBL > CLEA–CAL > ANL > PCL. The lipase activity for the biphasic system was significantly affected by the ratio of water to decane and the interfacial area. Significantly higher conversions were obtained in the continuous flow micro-reactor system and these have been attributed to favourable formation of the biphasic system that significantly enhanced the lipase interfacial activation. A kinetic study identified that the immobilized apparent K_m constant (3.1 mM) is 12 times lower than that obtained for the free CAL (38 mM) and a similar value of the k_{cat} is obtained for the immobilized lipase (0.13 min^{-1}) and the free lipase in solution (0.12 min^{-1}), indicating that the immobilization method used can maintain the entrapped/immobilized lipases in the active conformation in both the free and immobilized forms. However, higher lipase loadings reduced the immobilized k_{cat} due to lipase aggregation and pore blocking which decreased the lipase specific activity and the accessibility of the substrate to the biphasic

system. The monolith immobilized lipase also exhibited significant thermal and reactive stability at both elevated temperatures and during long term continuous runs. This can be attributed to the multipoint or multisubunit interactions occurring between the hydrophobic surface of the silica-monolith and lipase.

Acknowledgement

We acknowledge the EU for funding through project NMP4-CT-2006-033254.

References

- [1] Fernandez-Lafuente R, Armisen P, Sabuquillo P, Fernández-Lorente G, Guisán JM. Immobilization of lipases by selective adsorption on hydrophobic supports. *Chem Phys Lipids* 1998;93:185–97.
- [2] Balcão VM, Paiva AL, Malcata FX. Bioreactors with immobilized lipases: state of the art. *Enzyme Microb Technol* 1996;18:392–416.
- [3] Paiva AL, Balcão VM, Malcata FX. Kinetics and mechanisms of reactions catalyzed by immobilized lipases. *Enzyme Microb Technol* 2000;27:187–204.
- [4] Soni K, Madamwar D. Ester synthesis by lipase immobilized on silica and microemulsion based organogels (MBGs). *Process Biochem* 2001;36:607–11.
- [5] Nagayama K, Yamasaki N, Imai M. Fatty acid esterification catalyzed by *Candida rugosa* lipase in lecithin microemulsion-based organogels. *Biochem Eng J* 2002;12:231–6.
- [6] Singh S, Kumar S, Chimni SS. Enantioselective resolution of 3-phenylthio-2-propanol with *Humicola lanuginosa* lipase. *Biotechnol Lett* 2000;22:1237–41.
- [7] Miyazawa T, Yukawa T, Koshihata T, Ueji S, Yanagihara R, Yamada T. Enzymatic resolution of 2-phenoxy-1-propanols through the enantioselective acylation mediated by *Achromobacter* sp. lipase. *Biotechnol Lett* 2001;23:1547–50.
- [8] Lee YS, Hong JH, Jeon NY, Won K, Kim BT. Highly Enantioselective acylation of *rac*-alkyl lactates using *Candida antarctica* lipase B. *Org Process Res Dev* 2004;8:948–51.
- [9] Sharma R, Chisti Y, Banerjee UC. Production, purification, characterization, and applications of lipases. *Biotechnol Adv* 2001;19:627–62.
- [10] Villeneuve P, Muderhwa JM, Graille JM, Hass MJ. Customizing lipases for biocatalysis: a survey of chemical, physical and molecular biological approaches. *J Mol Catal B Enzymol* 2000;9:113–48.
- [11] Mateo C, Palomo JM, Fernandez-Lorente G, Guisán JM, Fernandez-Lafuente R. Improvement of enzyme activity, stability and selectivity via immobilization techniques. *Enzyme Microb Technol* 2007;40:1451–63.
- [12] Fernandez-Lafuente R. Stabilization of multimeric enzymes: strategies to prevent subunit dissociation. *Enzyme Microb Technol* 2009;45:405–18.
- [13] Tischer W, Wedekind F. Immobilized enzymes: methods and applications. *Top Curr Chem* 1999;200:95–126.
- [14] Malcata FX, Reyes HR, Garcia HS, Hill Jr CG, Amundson CH. Immobilized lipase reactors for modification for fats and oils—a review. *J Am Oil Chem Soc* 1990;67:890–910.
- [15] Ruckenstein E, Wang X. Lipase immobilized on hydrophobic porous polymer supports prepared by concentrated emulsion polymerization and their activity in the hydrolysis of triacylglycerides. *Biotechnol Bioeng* 1993;42:821–8.
- [16] Bastida A, Sabuquillo P, Amisen P, Fernández-Lafuente R, Huget J, Guisán JM. A single step purification, immobilization, and hyperactivation of lipases via interfacial adsorption on strongly hydrophobic supports. *Biotechnol Bioeng* 1998;58:486–93.
- [17] Reez MT, Zonta A, Simpelkamp J. Efficient immobilization of lipases by entrapment in hydrophobic sol–gel materials. *Biotechnol Bioeng* 1996;49:527–34.
- [18] Chen JP, Lin WS. Sol–gel powders and supported sol–gel polymers for immobilization of lipase in ester synthesis. *Enzyme Microb Technol* 2003;32:801–11.
- [19] Peterson DS, Rohr T, Svec F, Fréchet JM. Enzymatic microreactor-on-a-chip: protein mapping using trypsin immobilized on porous polymer monoliths molded in channels of microfluidic devices. *Anal Chem* 2002;74:4081–8.
- [20] Mersal GAM, Bilitewski U. Development of monolithic enzymatic reactors in glass microchips for the quantitative determination of enzyme substrates using the example of glucose determination via immobilized glucose oxidase. *Electrophoresis* 2005;26:2303–12.
- [21] Kato M, Inuzuka K, Sakai-Kato K, Toyo'oka T. Monolithic bioreactor immobilizing trypsin for high-throughput analysis. *Anal Chem* 2005;77:1813–8.
- [22] Kawakami K, Sera Y, Sakai S, Ono T, Ijima H. Development and characterization of a silica monolith immobilized enzyme micro-bioreactor. *Ind Eng Chem Res* 2005;44:236–40.
- [23] Ota S, Miyazaki S, Matsuoka H, Morisato K, Shintani Y, Nakanishi K. High-throughput protein digestion by trypsin-immobilized monolithic silica with pipette-tip formula. *J Biochem Biophys Methods* 2007;70:57–62.
- [24] Pennemann H, Watts P, Haswell SJ, Hessel V, Lowe H. Benchmarking of microreactor applications. *Org Process Res Dev* 2004;8:422–39.
- [25] Fletcher PDI, Haswell SJ, Pombo-Villar E, Warrington BH, Watts P, Wong SYF, et al. Micro reactors: principles and applications in organic synthesis. *Tetrahedron* 2002;58:4735–57.
- [26] Barry R, Ivanov D. Microfluidics in biotechnology. *J Nanobiotechnol* 2004;2:2.
- [27] Woodcock LL, Wiles C, Greenway GM, Watts P, Wells A, Eyley S. Enzymatic synthesis of a series of alkyl esters using novozyme 435 in a packed-bed, miniaturized, continuous flow reactor. *Biocatal Biotrans* 2008;26:466–72.
- [28] Honda T, Miyazaki M, Nakamura H. Facile preparation of an enzyme-immobilized microreactor using a cross-linking enzyme membrane on a micro-channel surface. *Adv Synth Catal* 2006;348:2163–71.
- [29] Tokeshi M, Kikutani Y, Hibara A, Sato K, Hisamoto H, Kitamori T. Chemical processing on microchips for analysis, synthesis, and bioassay. *Electrophoresis* 2003;24:3583–90.
- [30] Verpoorte E. Beads and chips: new recipes for analysis. *Lab Chip* 2003;3:60N–8N.
- [31] Krenková J, Foret F. Immobilized microfluidic enzymatic reactors. *Electrophoresis* 2004;25:3550–63.
- [32] Giirelli AM, Mattei E. Application of immobilized enzyme reactor in on-line high performance liquid chromatography: a review. *J Chromatogr B* 2005;819:3–16.
- [33] Urban PL, Goodall DM, Bruce NC. Enzymatic microreactors in chemical analysis and kinetic studies. *Biotechnol Adv* 2006;24:42–57.
- [34] Peterson DS. Solid supports for micro analytical systems. *Lab Chip* 2005;5:132–9.
- [35] Josic D, Buchacher A, Jungbauer A. Monoliths as stationary phases for separation of proteins and polynucleotides and enzymatic conversion. *J Chromatogr B* 2001;752:191–205.
- [36] He P, Greenway GM, Haswell SJ. Microfluid Nanofluid; 2009. doi: 10.1007/s10404-009r-r0476-8.
- [37] Hirata H, Higuchi K. Enzyme reaction in organic solvent *Candida cylindracea* lipase catalyzed transesterification between tri-*n*-butyltin and 1-octanol in various organic solvents. *J Jpn Oil Chem Soc* 1987;36:643–9.
- [38] Lilly MD, Hornby WE, Crook EM. The kinetics of carboxymethylcellulose-ficin in packed beds. *Biochem J* 1966;100:718–23.
- [39] Liu X, Guan Y, Shen R, Liu H. Immobilization of lipase onto micron-size magnetic beads. *J Chromatogr B* 2005;822:91–7.



Measurement of acetylcholinesterase inhibition using bienzymes immobilized monolith micro-reactor with integrated electrochemical detection

Ping He, Joanna Davies, Gillian Greenway, Stephen J. Haswell*

Department of Chemistry, University of Hull, Hull HU6 7RX, UK

ARTICLE INFO

Article history:

Received 22 September 2009

Received in revised form

13 November 2009

Accepted 20 November 2009

Available online 3 December 2009

Keywords:

Micro-reactor

Immobilized enzymes

Monolith

Acetylcholinesterase

Enzyme inhibition

Pesticides

Electrochemical detection

ABSTRACT

This paper reports a simple μ -FIA based method for the rapid evaluation of acetylcholinesterase inhibition based on bienzymes immobilized monolith micro-reactor, with integrated electrochemical detection. The monolith was prepared inside a micro-fluidic device from two precursors TMOS and MTMOS using a sol-gel method, followed by PEI polymer functionalization and subsequent enzyme immobilization via electrostatic attraction between electronegative enzymes and electropositive PEI polymers. A bienzyme system containing co-immobilized acetylcholinesterase and choline oxidase was used for the evaluation of enzyme inhibition induced by malaoxon, eserine and methomyl analytes. The proposed method, which gave a LOD of 0.5, 0.2 and 1.0 μ M for malaoxon, eserine and methomyl repeatedly, was found to offer several advantages over existing systems including efficient enzyme immobilization, minimal reagent consumption and rapid analysis capability.

© 2009 Elsevier B.V. All rights reserved.

1. Introduction

Cholinesterases (e.g. acetylcholinesterase (AChE) and butyrylcholinesterase (BuChE)) are known to play an important role in central and peripheral nervous system impulse transmission processes [1], a property that has lead such compounds to be used in a number of clinico-diagnostic and pharmaco-therapeutic applications [2–3]. In addition, cholinesterase inhibition is widely used for environmental, agricultural and military detection of carbamate and organophosphate pesticides as well as nerve agents [4–7]. Such compounds therefore, can by their nature, also represent severe environmental and health risks and have been linked to many diseases such as carcinogenic processes, fertility disorders, cytogenic effects, neurological diseases and respiratory and immunological dysfunction [8]. The traditional methods used for the determination of the cholinesterase activity include UV- and IR-spectroscopy, liquid chromatography (LC), gas chromatography (GC) and mass spectrometry (MS) with often different combinations of these methods being reported in the literature [4–6]. The main drawback however of these approaches, is that they are highly dependent on laboratory base techniques which may require slow and sometimes sophisticated analytical methodology [9]. As a result, many biosensors based on cholinesterase-inhibition

have been developed for identifying and detecting samples in the field. Most of these are based on a bioelectrocatalytic principle where enzymes are immobilized onto suitable electrodes (e.g. platinum and carbon) and the levels of pesticides for example, are determined by measuring the variation of the enzyme activity as a function of their concentration. The features of these biosensors have been described, evaluated and discussed in a number of recent review papers [10–15]. The main disadvantages however of the enzyme electrode based biosensor approach include the high number of steps required for the preparation and measurement procedures, the instability of the response and short life-times [13].

To improve sample throughput or allow online monitoring of the inhibition processes, flow-injection analysis (FIA) systems have proved to be a popular approach and capable of performing continuous analysis. The FIA systems usually consist of a packed enzymatic reactor column combined with different detection system e.g. electrochemistry or UV spectroscopy [13–16]. The performance of the FIA systems are however very dependent on the methods used for creating the immobilized enzymatic component. Currently, chemical covalent bonding and cross-linking as well as physical encapsulation processes are the most popular methods for the enzyme immobilization but these methods can cause structural deformation of the enzyme or introduce steric hindrance to the catalytic sites, leading to reduction in enzyme activity [17–21]. In addition, packed column reactors often generate increased back-pressure that gives rise to leaking or blocking problems [22–23].

* Corresponding author. Tel.: +44 1482 465469.

E-mail address: s.j.haswell@hull.ac.uk (S.J. Haswell).

The use of micro-fluidic devices as analytical systems has attracted increasing attention in recent years due to their significant reduction of reagent consumption and low operating costs as well as high throughput capability [24]. As demonstrated in earlier publications, undertaking chemical and biological processes at the micro-scale offers benefits that are generally unattainable with a macro scale process configuration [25–26]. Recently, silica-based monoliths, coupled with micro-fluidic devices, have been used as an attractive alternative to packed columns for the analysis of proteins, peptides and nucleic acids with special features of low diffusion resistance during mass transfer, controllable porosity and low back pressure compared to packed columns [27–32]. However, the preparation of these monoliths usually requires the addition of other additives, i.e. PEG (polyethylene glycol) and dextrin to stabilise the structure [19–20] and the fabrication can be time considerable (ca. 3–15 days) [19–20]. In addition, large molecules such as proteins may not be able to diffuse through nanopores of the hydrogel network [33].

Recently the authors described the development of a silica based, immobilized enzyme micro-reactor, with an integrated micro-fluidic electrochemical detector for the rapid evaluation of enzyme kinetics. In this work a similar approach has been used to determine pesticide (e.g. eserine, malaoxon and methomyl) inhibition in a μ FIA device based on the co-immobilization of acetylcholinesterase (AChE), choline oxidase (CHO) using a monolith structure. Compared to the mono-enzyme system the bienzyme approach was expected to offer better selectivity [34–37] and through the system miniaturization a significant reduction in enzyme consumption and an increase in sample throughput can be expected [19–20].

2. Materials and methods

2.1. Materials

Acetylcholinesterase from *electric eel* (AChE, EC 3.1.1.7, MW 280 kDa), choline oxidase from *Alcaligenes species* (CHO, EC 1.1.3.17, MW 72 kDa), acetylcholine chloride (ACh, 99%) and tris(hydroxymethyl)aminomethane (Tris, 99%) were purchased from Sigma–Aldrich. Three pesticides eserine, malaoxon, and methomyl were also obtained from Sigma–Aldrich. Polyethylenimine (PEI, molecular weight 10,000), KCl (99%), HCl (37%), tetramethoxysilane (TMOS, 99%) and methyltrimethoxysilane (MTMOS, 99%) were purchased from Fluka. Milli-Q water (18 M Ω cm) was used in the preparation of all aqueous solutions.

2.2. Micro-fluidic device fabrication, preparation of silica-monoliths, enzyme immobilization and detection

Glass micro-fluidic devices were fabricated in house using standard photolithography technology followed by wet etching and thermal bonding [25]. The device used comprised of a channel in which a monolith could be generated and a region where the electrodes for the amperometric detector could be located. A schematic of the micro-fluidic device is shown in Fig. 1A. The dimensions of the channels were 600 μ m wide, 50 μ m deep and 20 mm long for the monolith channel and 1.5 mm wide, 50 μ m deep and 20 mm long for electrochemical detection channel. The connecting channel between the monolith and detector was 100 μ m wide, 50 μ m deep and 5 mm long. The preparation of silica-monoliths and the monolith functionalization with PEI polymer were carried out using similar methods to those reported previously [38]. In a typical preparation, 18 μ l of TMOS and 69 μ l of MTMOS (at 1:4 molar ratio) were added to dilute HCl solution (8 μ l of 1 mM HCl and 13.2 μ l water) and allowed to hydrolyse for 15 min under sonication at

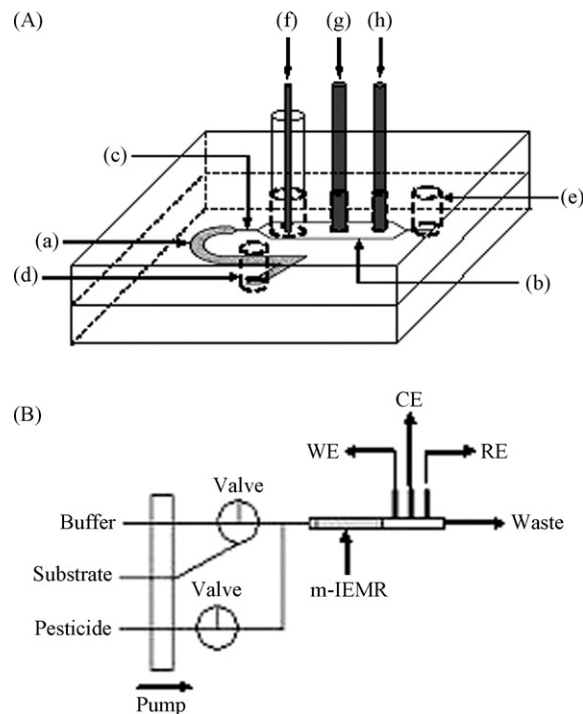


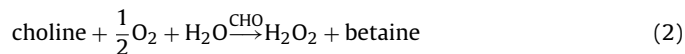
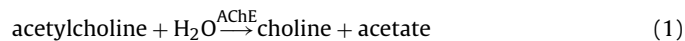
Fig. 1. Schematic of the micro-fluidic device: (a) monolith channel, 600 μ m wide, 50 μ m deep and 20 mm long; (b) electrochemical detection channel, 1.5 mm wide, 50 μ m deep and 20 mm long; (c) link channel, 100 μ m wide, 50 μ m deep and 5 mm long; (d) inlet, 1.5 mm diameter, to which syringe a pump was linked through a plastic tube (0.5 mm diameter); (e) outlet, 1.5 mm diameter; (f) working electrode (WE, Pt disc, 0.5 mm diameter), (g) Pt wire (1 mm diameter) counter electrode (CE) and (h) Ag/AgCl (1 mm diameter) reference electrode (RE).

room temperature to form a homogeneous sol of silicic acid. A 4.2 μ l aliquot of sol was mixed with 17.8 μ l of water and 22 μ l of 0.2 M (pH 7) Tris–HCl buffer, and the resultant liquid mixture was immediately loaded into the monolith channel and allowed to polymerize for 15 h at room temperature, followed by vacuum drying for 1 h to form a silica-monolith which was subsequent functionalization with PEI solution (concentration 10 mg ml⁻¹ in 0.1 M neutral Tris–HCl buffer) to generate the PEI-coated silica-monolith. For enzyme immobilization an enzyme solution (i.e. AChE 0.01–0.1 U μ l⁻¹ and CHO 0.025–0.25 U μ l⁻¹ in 0.05 M neutral Tris–HCl buffer) was loaded into the monolith (required ca. 0.4 μ l of enzyme solution to fully filled the monolith) using a micropipette. The monolith was then kept in a fridge (4 °C) for 1 h followed by vacuum drying for 30 min to generate a monolith immobilized enzyme micro-reactor where enzymes were efficiently immobilized via electrostatic interaction between electronegative enzymes and electropositive PEI polymers [38–40]. The amperometric detector was constructed from a Pt disc-working electrode (0.5 mm diameter), a Pt wire counter electrode (1 mm diameter) and a Ag/AgCl (1 mm diameter) reference electrode which were placed into the holes in the detection channel (Fig. 1a) of the device and sealed by using epoxy resin. Before measurements were carried out, using a PalmSens Electrochemical Sensor (IVIUM Technologies, The Netherlands) at a fixed electrode potential (650 mV versus Ag/AgCl, room temperature), the micro-reactor was washed for 5 min with a working buffer solution (0.05 M pH 7 Tris–HCl buffer containing 10 mM KCl) and the washings collected.

2.3. Enzyme activity assay and measurements of free and immobilized enzyme inhibition

Enzyme activity was measured using the μ FIA system shown in Fig. 1B, which consisted of a syringe pump (PHD 2000, Harvard), a

micro-injector with a sample loop of 2.5 μl , three-way valves and the monolith immobilized enzyme micro-reactor equipped with on-chip amperometric detector. The product H_2O_2 formed during enzyme reactions was detected according to Eqs. (1)–(3). The substrate acetylcholine (ACh) was first hydrolysed to produce choline and acetate in the presence of AChE (see Eq. (1)), the choline formed, was then oxidized in the presence of CHO to form hydrogen peroxide and betaine (see Eq. (2)). The hydrogen peroxide produced, which was proportional to the enzyme activity, was then recorded as a current response (see Eq. (3)).



The initial free enzyme activity (I_0) was measured by pumping the buffer carrier stream ($10 \mu\text{l min}^{-1}$) into the flow-injection system and making successive acetylcholine chloride injections (0.5–5 mM). A defined volume (ca. 0.4 μl) of sample containing different concentrations of pesticides was then loaded into the monolith immobilized enzyme micro-reactor and incubated for 20 min at room temperature, in accordance with standard methodology [12] followed by washing for 2 min with buffer solution at flow rate of $10 \mu\text{l min}^{-1}$. Subsequent injection of acetylcholine chloride (0.5–5 mM) were then introduced into the monolith immobilized enzyme micro-reactor. The response current (I_i) was recorded and the percentage inhibition of enzyme ($I\%$) was calculated from Eq. (4).

$$I\% = \frac{I_0 - I_i}{I_0} \times 100 \quad (4)$$

The measurements for free AChE inhibition were performed in a small vial (1 ml) which contained 1 μl of $1.0 \text{ U } \mu\text{l}^{-1}$ of AChE and 2.5 μl of $1.0 \text{ U } \mu\text{l}^{-1}$ of CHO, to which different volumes of a standard pesticide was added to give the required concentrations in a total volume of 800 μl buffer solution. After an incubation time of 20 min at room temperature, 5 μl aliquots of acetylcholine chloride standards were added to the vial in order to generate a range of substrate concentrations (0.25–5.0 mM). Three electrodes were then placed in the solution to record the current response.

3. Results and discussion

3.1. Evaluation of the immobilized enzyme inhibition and detection system

The determination of pesticide levels based on single AChE amperometric sensors, where the substrate acetylthiocholine iodide is catalytically hydrolysed in the presence of AChE to produce thiocholine that can be amperometrically measured by anodic oxidation has been reported in literature [41–43]. However, the anodic oxidation of thiocholine provokes a passivation of the platinum electrode due to their interaction with the sulphur containing compounds [43]. In this study, AChE was co-immobilized with CHO in a PEI-coated monolith micro-reactor and the effect of an inhibitor on the enzyme system was studied by measuring enzyme velocity at a variety of substrate concentration in the presence and absence of an inhibitor. The use of the bienzyme reaction system therefore avoids passivation of the electrode resulting from the use of a single enzyme. The substrate concentration and the amount of enzymes immobilized can however affect the performance of the monolith immobilized enzyme micro-reactor. For instance, at higher concentrations of the substrate and enzyme more hydrogen peroxide will be produced which in turn will increase the current detected. Accordingly, it was found that the inhibitor substantially reduced

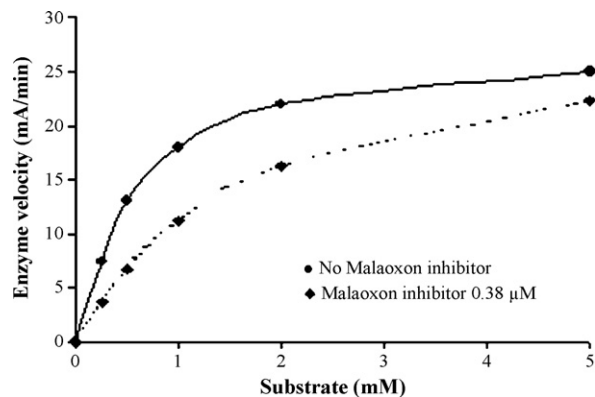


Fig. 2. The effect of an inhibitor on enzyme velocity measured for a variety of substrate concentrations in the presence and absence of the inhibitor.

enzyme velocity at lower concentrations of substrate, but did not appear to alter significantly the enzyme velocity at higher substrate concentrations, as indicated shown in Fig. 2. The highest sensitivity to inhibitors was found when the monolith micro-reactor contained low amounts of enzyme. In this work ca. 0.01–0.1 U of AChE and 0.025–0.25 U of CHO were co-immobilized in a monolith micro-reactor and the substrate concentrations ranged from 0.5 to 5.0 mM. Flow rate was also found to have a significant influence on the enzyme activity, with smaller flow rates yielding more product due to a longer contact time of the substrate with the enzymes in the monolith micro-reactor but this in turn lead to a longer analytical time. In order to reach a reasonable compromise between sensitivity and response time a flow rate of $10 \mu\text{l min}^{-1}$ was selected, giving a total analysis time of 2.5 min for one injection. Fig. 3 shows the variation in inhibition as a function of the inhibition time. It can be seen that enzymes are completely inhibited within 20 min which is comparable to many current techniques [12]. The amperometric response was found to be linear for both the immobilized ($Y = 95.2X + 0.2$, $R^2 = 0.9983$) and free ($Y = 820.73X + 30.503$, $R^2 = 0.9995$) enzyme systems whilst the limits of detection (Table 1), which varied slightly between different pesticides, were found to be approximately 10 times lower for the free AChE in solution, which is attributed to possible steric hindrance in the micro-reactor environment.

In general studies on the inhibition of enzymatic reactions are based on evaluating the experimental data according to the Lineweaver–Burk double reciprocal plot and/or the Dixon method [44]. For the Lineweaver–Burk method the data obtained from the amperometric measurements were treated based on the electro-

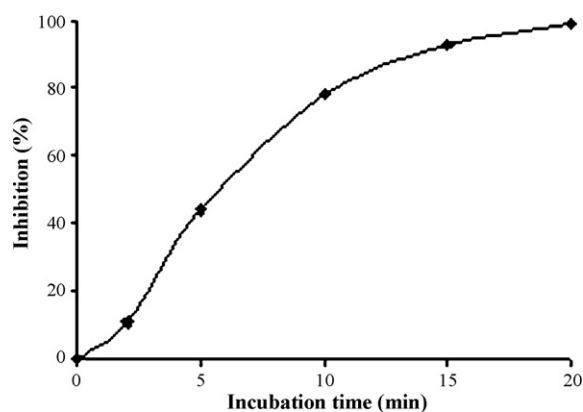


Fig. 3. AChE inhibition from methomyl in solution as a function of incubation time. For each measurement methomyl of 0.98 μg was added to 800 μl of 0.05 M neutral Tris–HCl buffer containing 1 U AChE and 2.5 U CHO as well as 10 mM KCl.

Table 1
The kinetic constants of K_m and K_i as well as the LOD for AChE-CHO immobilized monolith and free AChE-CHO in solution.^a

	Immobilized AChE-CHO			Free AChE-CHO		
	Malaoxon	Eserine	Methomyl	Malaoxon	Eserine	Methomyl
K_i (μM) _{L-B} ^b	3.9 ± 0.2	1.0 ± 0.09	10.6 ± 0.6	0.3 ± 0.01	0.2 ± 0.01	0.7 ± 0.04
K_i (μM) _{Dixon} ^c	3.5 ± 0.2	1.4 ± 0.1	9.8 ± 0.5	0.3 ± 0.01	0.2 ± 0.01	0.6 ± 0.03
K_m (mM) ^d		1.0 ± 0.1			0.8 ± 0.05	
LOD (μM) ^e	0.5	0.2	1.0	0.05	0.02	0.12

^a 0.05 M neutral Tris-HCl buffer contained 10 mM KCl was used, flow rate of buffer carrier was 10 $\mu\text{L}\cdot\text{min}^{-1}$ and measurements were carried out at room temperature (25 °C).

^b The values of K_i were determined by the Lineweaver–Burk plot.

^c The values of K_i were determined by Dixon method.

^d K_m was determined by Lineweaver–Burk plot in the absence of pesticide.

^e The LOD was determined as three times the background signal.

chemical Eadie-Hofstee equation in Lineweaver–Burk (Eqs. (5) and (6)) form under steady-state conditions [45–46]:

$$\frac{1}{j} = \frac{1}{j_{\max}} + \frac{K_m\text{-obs}}{j_{\max}} \cdot \frac{1}{[S]} \quad (5)$$

$$K_m\text{-obs} = K_m \left[1 + \frac{[I]}{K_i} \right] \quad (6)$$

where j was the current intensity, j_{\max} the maximum current intensity in the absence of inhibitor, $[S]$ and $[I]$ the substrate and inhibitor concentration, K_m and K_i the apparent Michaelis constant and the inhibition constant, and $K_m\text{-obs}$ the observed K_m are defined by Eq. (6). The Dixon method is a graphical method based on a plot of $(1/j)$ versus inhibitor concentration $[I]$, which only requires the determination of two or three substrate concentrations using a series of inhibitor concentrations at each substrate concentration to obtain the values of K_i . Fig. 4a and b shows typical plots obtained according to the Lineweaver–Burk form and the Dixon method for the enzyme inhibition induced by malaoxon. It can be seen that the plots of $(1/j)$ versus $(1/[S])$ (Fig. 4a) for each inhibitor concentration gives different slopes for the same value of j_{\max} and the slope is increased by factors of $(1 + [I]/K_i)$ whilst plots of $(1/j)$ versus $([I])$ (Fig. 4b) from each set of reactions show a series of lines that intersect at the same ordinate intercept (j_{\max} remaining constant). The similar linear relationship was also observed for enzyme inhibition induced by eserine and methomyl, as shown in plots of ($K_m\text{-obs}$ versus $[I]$) (see Fig. 5a). These characteristics indicate a typical competitive inhibition [44] induced by malaoxon, eserine and methomyl in which the addition of more substrate overcomes the competitive inhibition of the enzyme catalytic rate, as seen in Fig. 2.

The kinetic characterization of enzyme inhibition in this study indicated typical competitive inhibition, where the addition of more substrate will reduce competition from the inhibitor and overcome the inhibition of the enzyme catalytic rate.

The kinetic constants K_m and K_i can be obtained from the plots of $([I])$ versus $K_m\text{-obs}$ where the Y-axis intercept equals the K_m and the X-axis intercept equals the negative K_i . For the Dixon plots the value of K_i can be determined by the value of $[I]$ at the intersection where the value of $[I]$ is equal to the negative K_i , as indicated in Fig. 4b. The inhibition of free AChE by eserine, methomyl and malaoxon were also performed in a small vial and experimental data was also treated according to Lineweaver–Burk double reciprocal plot or Dixon method. Plots of $([I])$ versus $K_m\text{-obs}$ for free AChE in solution are shown in Fig. 5b. The kinetic constants of K_m and K_i obtained from the Lineweaver–Burk and Dixon plots for the immobilized AChE-CHO and free AChE-CHO in solution are summarized in Table 1.

It can be seen that the values of the K_i constant determined by the Lineweaver–Burk plot are similar to those obtained from the Dixon method, indicating that both methods give similar values for

free and immobilized enzyme systems however the Dixon method did offer a more straightforward approach. It can also be seen that the Michaelis constant K_m (1.0 mM) for the immobilized enzyme is similar to that (0.8 mM) obtained for the free enzyme in solution. Nevertheless, the inhibition constants of eserine, malaoxon and methomyl for the immobilized enzyme are approximately 5–7, 11–13 and 15–16 times higher than those observed for the free enzyme in solution, indicating that the inhibitors appear to be more easily dissociated from the inhibitor binding sites for the inhibition of immobilized AChE for these particular pesticides within monolith micro-reactor environment when compared to the inhibition of free AChE. Again, this is probably due to limited space and/or steric hindrance existed in monolith micro-reactor environment that

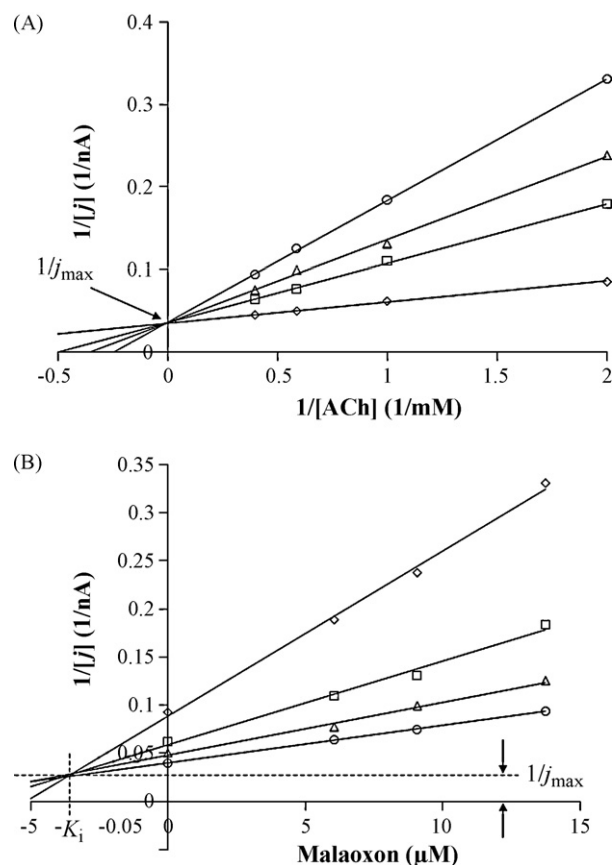


Fig. 4. (A) Lineweaver–Burk plots for malaoxon inhibition of the immobilized AChE obtained based on the electrochemical Eadie-Hofstee equation at different malaoxon concentration: (\diamond) 0 μM , (\square) 6 μM , (\blacktriangle) 9.1 μM , (\circ) 13.7 μM . (B) Dixon plots for malaoxon inhibition of the immobilized AChE at different substrate ACh concentration: (\diamond) 0.5 μM , (\square) 1 mM, (\blacktriangle) 1.7 mM, (\circ) 2.5 mM.

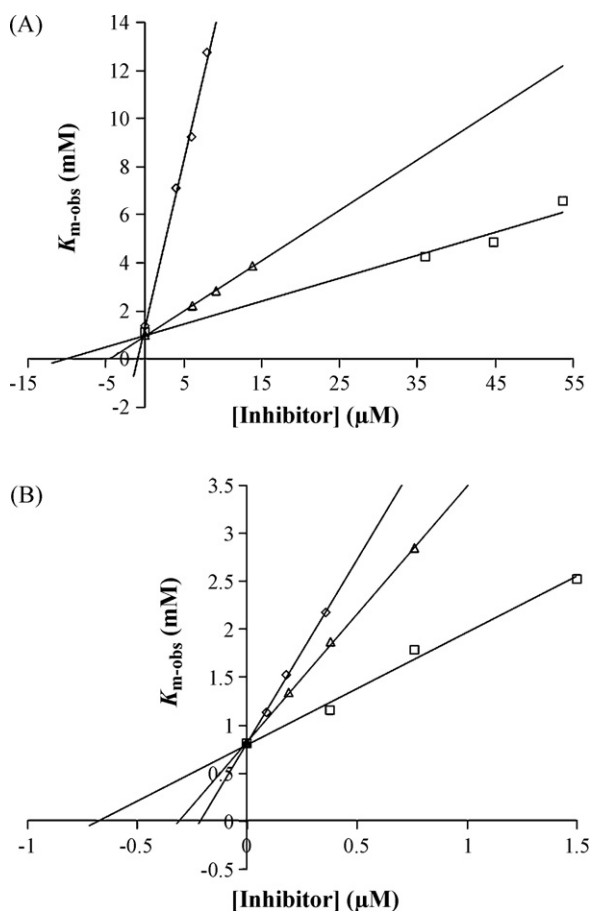


Fig. 5. Plots of observed K_m (K_{m-obs}) versus inhibitor concentration obtained for (A) immobilized enzyme and (B) free enzyme in solution at different inhibitor concentrations: (\diamond) eserine, (\square) methomyl and (\blacktriangle) malaoxon.

results in weaker inhibitor binding, leading in turn to an increase in the dissociation constant. However, the K_i values obtained in this study are several tens of times lower than those reported in literature [37,47]. For example, the K_i value of 3.5–3.9 μM for malaoxon obtained in this study is almost 4 times lower than the 14 μM obtained from a flow through microreactor containing magnetic particles immobilized AChE using glutaraldehyde method [37] and slightly lower than the 5.6 μM obtained from the immobilized AChE on a controlled pore glass capillary [47]. In the case of eserine the K_i value of 1.1 μM obtained in this study is 45 times lower than the 50 μM obtained from the packed bed immobilized enzyme reactor [48]. These results indicate that the monolith immobilized enzyme micro-reactors offer a more sensitive detection system compared to the immobilized enzyme reactors previously reported in the literature.

3.2. Stability of immobilized enzyme and regeneration of micro-fluidic devices

The stability of the immobilized enzymes during operation and storage was also examined. It was found that a continuous run of 1 day did not lead to any significant decrease in the enzyme activity and after subsequent storage at 4 $^{\circ}\text{C}$ for a week the activity of the immobilized AChE retained ca. 85% of the initial activity compared to only 33% of the initial activity for free AChE in solution after storage of 1 day and total loss activity after storage of 5 days. However, after two weeks storage the immobilized AChE retained only ca. 50% of the initial activity.

4. Conclusions

A μ -FIA system incorporating an immobilized enzyme micro-reactor with a micro-fluidic electrochemical detection has been shown to enable enzymes to be immobilized in an active conformation such that the screening of pesticides through induce enzyme inhibition can be detected in a rapid sensitive fashion. The method described includes minimal preparation time and reagent consumption as well as low operating cost. Comparison of the inhibition constant K_i between free and immobilized AChE indicates that inhibitor binding within monolith micro-reactor environment is less strong due to limited space and/or steric hindrance that may exist within the monolith micro-reactor environment which in turn leads to an increase in inhibition constant. However, the K_i values obtained in this study are several to tens times lower than those reported currently in the literature. The method presented in this study is at present based on standard pesticide solutions, however work is currently being planned to extend the methodology to measure enzyme inhibition on real samples.

Acknowledgement

We acknowledge the EU for funding through project NMP4-CT-2006-033254.

References

- [1] F. Villatte, V. Marcel, S. Estrada-Mondaca, D. Fournier, *Biosens. Bioelectron.* 13 (1998) 157.
- [2] D.R. Liston, J.A. Nielsen, A. Villalobos, D. Chapin, S.B. Jones, S.T. Hubbard, I.A. Shalaby, A. Ramirez, D. Nason, W.F. White, *Eur. J. Pharmacol.* 486 (2004) 9.
- [3] R. Moretti, P. Torre, R.M. Antonello, T. Cattaruzza, G. Cazzato, *Am. J. Alzheimer's Dis. Dementia* 19 (2004) 333.
- [4] T. Cairus, J. Sherma (Eds.), *Emerging Strategies for Pesticide Analysis*, CRC Press, Boca Raton, FL, 1992.
- [5] J. Sherma, *Anal. Chem.* 65 (1993) 40R.
- [6] W. Fresenius, K.E. Quentin, W. Schneider (Eds.), *Water Analysis*, Springer, Heidelberg, 1988.
- [7] G. Liu, Y. Lin, *Anal. Chem.* 78 (2006) 835.
- [8] *Public Health Impact of Pesticides Used in Agriculture*, World Health Organization, Geneva, 1990.
- [9] E. Onelli, A. Mosca, *Life Chem. Rep.* 110 (1994) 189.
- [10] N. Jaffrezic-Renault, *Sensors* 1 (2001) 60.
- [11] G. Turdean, I.C. Popescu, L. Oniciu, *Can. J. Chem.* 80 (2002) 315.
- [12] S. Solé, A. Merkoçi, S. Alegret, *Crit. Rev. Anal. Chem.* 33 (2003) 89.
- [13] S. Solé, A. Merkoçi, S. Alegret, *Crit. Rev. Anal. Chem.* 33 (2003) 127.
- [14] M. Stoytcheva, R. Zlatev, B. Valdez, J. Magnin, Z. Velkova, *Biosens. Bioelectron.* 22 (2006) 1.
- [15] A. Amine, H. Mohammadi, I. Bourais, G. Palleschi, *Biosens. Bioelectron.* 21 (2006) 1405.
- [16] J. Salamoun, J. Remien, *J. Pharm. Biomed. Anal.* 10 (1992) 931.
- [17] D.S. Peterson, T. Rohr, F. Svec, J.M.J. Fréchet, *Anal. Chem.* 74 (2002) 4081.
- [18] G.A.M. Mersal, U. Bilitewski, *Electrophoresis* 26 (2005) 2303.
- [19] M. Kato, K. Inuzuka, K. Sakai-Kato, T. Toyo'oka, *Anal. Chem.* 77 (2005) 1813.
- [20] K. Kawakami, Y. Sera, S. Sakai, T. Ono, H. Ijima, *Ind. Eng. Chem. Res.* 44 (2005) 236.
- [21] S. Ota, S. Miyazaki, H. Matsuoka, K. Morisato, Y. Shintani, K. Nakanishi, *J. Biochem. Biophys. Methods* 70 (2007) 57.
- [22] T. Honda, M. Miyazaki, H. Nakamura, *Adv. Synth. Catal.* 348 (2006) 2163.
- [23] M. Yokeshi, Y. Kikutani, A. Hibara, K. Sato, H. Hisamoto, T. Kitamori, *Electrophoresis* 24 (2003) 3583.
- [24] N.T. Nguyen, S. Wereley, *Fundamental and Application of Micro Fluidics*, Artech House Publishers, London, 2002.
- [25] P.D.I. Fletcher, S.J. Haswell, E. Pombo-Villar, B.H. Warrington, P. Watts, S.Y.F. Wong, X. Zhang, *Tetrahedron* 58 (2002) 4735.
- [26] R. Barry, D. Ivanov, *J. Nanobiotechnol.* 2 (2004) 2.
- [27] E. Verpoorte, *Lab Chip* 3 (2003) 60N.
- [28] J. Krenková, F. Foret, *Electrophoresis* 25 (2004) 3550.
- [29] A.M. Girelli, E. Mattei, *J. Chromatogr. B* 819 (2005) 3.
- [30] P.L. Urban, D.M. Goodall, N.C. Bruce, *Biotechnol. Adv.* 24 (2006) 42.
- [31] D.S. Peterson, *Lab Chip* 5 (2005) 132.
- [32] D. Josic, A. Buchacher, A. Jungbauer, *J. Chromatogr. B* 752 (2001) 191.
- [33] K. Sakai-Kato, M. Kato, T. Toyo'oka, *Anal. Chem.* 75 (2003) 388.
- [34] L. Campanella, S. DeLuca, M.P. Sammartino, M. Tomassetti, *Anal. Chim. Acta* 385 (1999) 59.
- [35] R. Kindervater, W. Kunnecke, R. Schmid, *Anal. Chim. Acta* 234 (1990) 113.
- [36] F. Botrè, G. Lorenti, F. Mazzei, G. Simonetti, F. Porcelli, C. Botrè, G. Scibona, *Sens. Actuators B* 18–19 (1994) 689.

- [37] A. Günther, U. Bilitewski, *Anal. Chim. Acta* 300 (1995) 117.
- [38] Ping He, Gillian Greenway, Stephen J. Haswell, *Microfluid. Nanofluid.* (2009), doi:10.1007/s10404-009-0476-8.
- [39] E. Laarz, L. Bergström, *Int. J. Refr. Met. Hard Mater.* 18 (2000) 281.
- [40] Y. Han, G.D. Stucky, A. Butler, *J. Am. Chem. Soc.* 121 (1999) 9897.
- [41] G.S. Nunes, P. Skladal, H. Yamanaka, D. Barcelo, *Anal. Chim. Acta* 362 (1998) 59.
- [42] M. Stoytcheva, *Electroanalysis* 7 (1995) 560.
- [43] E.B. Nikol'skaya, G.A. Evtyugin, *Zh. Anal. Khim.* 47 (1992) 1358.
- [44] A. Cornish-Bowden (Ed.), *Fundamentals of Enzyme Kinetics*, Portland Press, London, 1995.
- [45] T. Kaku, H.I. Karan, Y. Okamoto, *Anal. Chem.* 66 (1994) 1231.
- [46] G. Arai, T. Noma, M. Hayashi, I. Yasumori, *J. Electroanal. Chem.* 452 (1998) 43.
- [47] D. Krstic, M. Colovic, M.B. Kralj, M. Franko, K. Krinulovic, P. Trebse, V. Vasic, *J. Enzyme Inhibit. Med. Chem.* 23 (2008) 562.
- [48] H.R. Luckarift, G.R. Johnson, J.C. Spain, *J. Chromatogr. B* 843 (2006) 310.

Microfluidic-based measurements of cytochrome P450 enzyme activity of primary mammalian hepatocytes

Keith Anderson,^a Jonathan M. Cooper,^b Stephen J. Haswell,^c Damian Marshall,^a Huabing Yin^b and Xunli Zhang^{*cd}

Received 24th January 2010, Accepted 19th March 2010

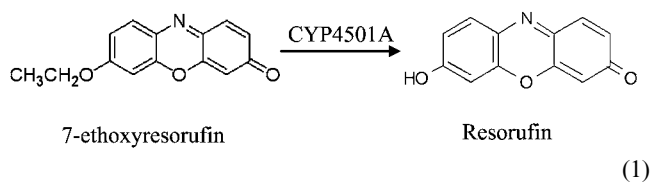
First published as an Advance Article on the web 17th April 2010

DOI: 10.1039/c0an00031k

A microfluidic-based system was developed for the *in situ* monitoring of the 7-ethoxyresorufin O-dealkylation (EROD) activity of primary rat hepatocytes by measuring the fluorescent intensity of both cells and their surrounding media. The microfluidic chip was designed to allow the cell suspension and test reagent to be introduced in a layer-by-layer flow format, thereby resulting in a short mixing time by diffusion. A good linear relationship was obtained between the resorufin concentration up to 30 μM and fluorescent intensity over the chip's circular chamber area. The EROD activity was determined with 3-methylcholanthrene (3-MC)-induced hepatocytes. The inhibition effect of α -naphthoflavone was also examined on EROD activity resulting in an IC_{50} value of 12.98 μM .

1. Introduction

Hepatic cytochrome P450 (CYP450) is a family of variant enzymes that catalyses the oxidative metabolism of a wide variety of exogenous chemicals including drugs, carcinogens, toxins and endogenous compounds such as steroids, fatty acids and prostaglandins.^{1,2} The quantitative determination of CYP450 enzymatic activity in mammalian hepatocytes is a commonly used method for drug screening and detecting general toxicity where CYP activity can be induced or inhibited by specific test compounds.^{3–5} One of the commonly used assays for CYP450 enzymatic activity is 7-ethoxyresorufin O-dealkylation (EROD), which is based on the conversion of 7-ethoxyresorufin (7-ER) to resorufin, a reaction catalysed by CYP4501A enzymes (eqn (1)).^{6–8} Since the product is fluorescent, the kinetics of the reaction can be quantified by the measurement of fluorescence intensity during the reaction, which is directly related to CYP4501A enzymatic activity.



The determination of EROD activity is typically carried out in a multi-well (e.g., 96-well) plate using a fluorescence reader to record the signal associated with resorufin.^{5,7} Although the

commonly used multi-well system can provide useful information on cell behaviour, function and genotype, based on the average measurements of cell populations, it is incapable of measuring the kinetics of enzyme reactions occurring within individual cells. In the case of EROD process, it involves both reaction (eqn (1)) and subsequent mass transport steps where fluorescent resorufin produced transfers by diffusion across the cell membrane towards the outside, and a closer examination of the reaction step is important for understanding the enzymatic reaction kinetics and mechanism. However, conventional methods of cell observation are unable to distinguish between these two steps.

In recent years, there has been an increasing awareness of the importance of cell heterogeneity in clinical diagnostics, which has been reflected in the shift from studying large cell populations (to obtain average cell responses) to single cell measurements.^{9–11} The development of single cell-based analysis not only provides complementary information on a cell population but can also help reveal the actual functional interaction of biomolecules at both a cellular and tissue level.^{12,10}

Over the past two decades, significant developments in the field of miniaturised systems, so-called microfluidics or lab-on-a-chip technologies, have seen the methodology influence diverse areas of applications relating to analytical chemistry, biochemistry, clinical diagnosis, medical chemistry and industrial chemistry.^{13,14} It has been demonstrated that such microsystems represent advantages over conventional bench systems in terms of speed, performance, reduced sample/solvent quantity, integration and automation. Of particular relevance to cell analysis is the small length scale used in which fluidics are restricted to diffusive mixing under laminar flow, thereby enabling precise fluidic control to create a biomimetic cell microenvironment. The microfluidic control also provides unique opportunities for delivering and locating single cells within microchips with an appropriate micro-geometry design. In addition, coupling with microscope-based imaging techniques allows the detection and measurement of single cell and subcellular levels *in situ*.¹⁵

^aLGC Limited, Queens Road, Teddington, Middlesex, TW11 0LY, UK

^bDepartment of Electronics and Electrical Engineering, University of Glasgow, Glasgow, G12 8QQ, UK

^cDepartment of Chemistry, The University of Hull, Hull, HU6 7RX, UK

^dBioengineering Group, School of Engineering Sciences, University of Southampton, Southampton, SO17 1BJ, UK. E-mail: X.L.Zhang@soton.ac.uk; Fax: +44 (0) 23 8059 3016; Tel: +44 (0) 23 8059 5099

Consequently, a wide range of microfluidic-based methodologies has been developed for cell manipulation, culture and analysis including hepatocytes.^{4,16}

The aim of this feasibility study is to develop a microfluidic-based system that enables the *in situ* monitoring of EROD activity using primary rat hepatocytes by measuring the fluorescent intensity of both single cells and the surrounding media. The inhibition of EROD activity will be examined using α -naphthoflavone (α -NF) as a CYP1A inhibitor over a range of concentrations (0–40 μ M).

2. Materials and methods

2.1. Microfluidic chip fabrication

The microfluidic device was produced according to published procedures with minor adaptations.^{17,18} Briefly, the channel network was fabricated using a photolithographic fabrication method. The channel network was first designed using AutoCAD drawing software (Autodesk, Farnborough, UK). A film negative of the desired fluidic network was then prepared by a commercial photo mask manufacturer (J.D. Photo Tools, Oldham, UK) to form the optical mask. B-270 glass photolithographic plates (thickness of 3 mm) coated with a thin chromium metal mask layer plus an upper layer of positive photoresist, supplied by Telic (Telic Company, Valencia, USA), were used for channel network fabrication. With UV exposure, the pattern of interconnecting channels was transferred from the optical mask to the photoresist layer, which was then developed and removed together with the chromium layer to reveal the channel areas of glass to be etched. The channels were etched using a mixture of 1% (w/w) HF and 5% (w/w) NH_4F in water at 65 °C.

The fabricated microchannel network consisted of a circular chamber (for cell holding and monitoring) with two inlet channels and one outlet channel (Fig. 1a). To create two layers of sheet flow in the main inlet channel and the chamber, the inlet channels were etched separately on two glass plates, which were then bonded face-to-face. Channels on each glass plate were etched to a depth of 35 μ m, resulting in a total depth of 70 μ m for the main channel and the chamber. The width for all the channels was 150 μ m, and the circular chamber had a diameter of 900 μ m, providing a working volume of 0.0445 μ l. The main purpose of using lay-by-layer sheet flow instead of side-by-side flow was to reduce the diffusion distance in order to shorten the diffusive mixing time whilst providing a relatively large field of view.

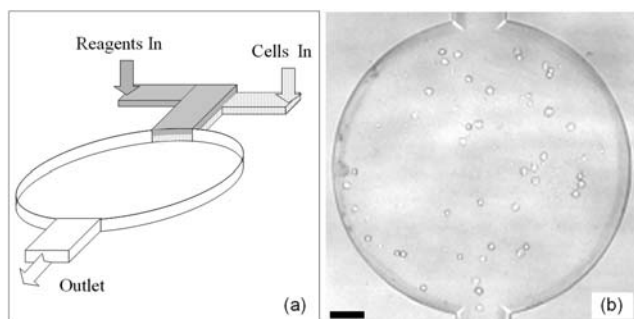


Fig. 1 Schematic of chip design (a) and hepatocytes in suspension loaded onto the chip in the circular chamber (b). Scale bar: 100 μ m.

Three holes (dia. 1.5 mm) were drilled through the upper glass plate to link the ends of the channels with tubing. The upper plate was then aligned with the channel geometry on the base plate and thermally bonded by placing it in a muffle furnace set at 570 °C for 3 h. A 90 g block of stainless steel was placed onto the upper plate to assist bonding.

2.2. Cell culture and assay reagents

Preserved rat hepatocytes were supplied by Abcellute (Abcellute Ltd, Cardiff, UK) and maintained at a temperature of 10 °C during transportation. Both 3-methylcholanthrene (3-MC)-induced (72 h) hepatocytes and controls were supplied. The preserved hepatocytes were then reactivated with the reactivation medium and wash medium, which were supplied with the cells, using the Abcellute protocol ABC-REC-S. The concentration of cells used for loading the chip during the experiment was in the range of 1×10^6 cells ml^{-1} . The viability of hepatocytes was assessed prior to introduction on the chip using the trypan blue exclusion method with a haemocytometer.

The buffer solution was prepared by adding one pot of KHB (Krebs-Heinslett buffer) powder to 1 l of distilled water in a volumetric flask supplemented by amikacin (84 μ g ml^{-1}), calcium chloride (1 mM), gentamicin (84 μ g ml^{-1}), HEPES (20 mM), heptanoic acid (4.2 μ M) and sodium bicarbonate (28.5 mM), and then adjusted to pH 7.4 with either 1 M NaOH or 1 M HCl. Other chemicals were used as received, including 7-ER, resorufin, 3,3'-methylenebis(4-hydroxycoumarin) (or dicumarol), α -NF, acetonitrile and dimethyl sulfoxide (DMSO). All these materials were supplied by Sigma-Aldrich (Dorset, UK). To make the test reagent, dicumarol was first dissolved in DMSO and then diluted, together with 7-ER, in buffer to the desired concentration. The blank was DMSO only (at the equivalent concentration) added to the buffer.

2.3. Instrumentation and image analysis

An Axiovert S100 inverted microscope (Carl Zeiss, UK) using both transmission and fluorescent optics coupled with a monochrome CCD digital camera (C4742-95-12NRB, Hamamatsu Photonics, UK) was used to obtain both conventional micrographs and digital videos. AQM Hamamatsu ORCA I software (Kinetic Imaging, Nottingham, UK) was used for image acquisition and analysis. By selecting areas (*e.g.*, cells or whole chamber) in successive video images a light intensity profile *versus* time was obtained. A Chroma green filter set (P/N 11002, Chroma Technology Corp, Rockingham, USA) was selected, which consists of an Exciter D546/10, an Emitter E590LP and a beam splitter Dichroic 565DCLP.

Two KDS 200 syringe pumps (KD Scientific Inc., Holliston, USA) were used to deliver cells in suspension and test reagents. ETFE (ethylene tetrafluoroethylene) polymer tubing with an inner diameter of 250 μ m and outer diameter of 1/16" (P/N 1529), on/off valves (P/N P-782) and appropriate fittings and connectors, all obtained from Upchurch (Upchurch Scientific Inc., Oak Harbor, USA), were used for plumbing to link the chip and syringes.

To maintain the chip temperature during measurements, a heated microscope stage (Model 14472, World Precision

Instruments Ltd, Stevenage, UK) with an aperture of 6 mm in diameter was used and the temperature was controlled in the range of 37 ± 0.5 °C. When the cells were loaded onto the chip, the measurement of EROD activity was carried out by taking a series of digital images as a video clip covering the whole circular chamber area of the chip under the fluorescent conditions. The scan rate of the video was set to be one frame every two minutes with an exposure time of 20 ms. To minimise the photo bleaching effect, a shutter was inserted into the light path which was open (for 2 s) only when taking each image frame. All fluorescent images were taken under the same conditions for comparison and data analysis.

3. Results and discussion

3.1. Cell loading

Hepatocytes in suspension and the test reagent were introduced into the chip at a flow rate of $15 \mu\text{l min}^{-1}$ via the two inlet channels, in a continuous flow, layer-by-layer format (Fig. 1a). The test reagent was composed of $40 \mu\text{M}$ 7-ER and $80 \mu\text{M}$ dicumarol in buffer, where dicumarol was added to prevent the disappearance of resorufin fluorescence since the product resorufin (eqn (1)) can be further reduced through metabolism by cytosolic oxidoreductases.^{7,19} Once a steady flow had been established, the on/off valves on all three inlet and outlet tubes were closed simultaneously,¹⁷ and the measurement process started. Fig. 1b shows the hepatocytes retained in the chip chamber in bright-field view after loading.

It can be seen from Fig. 1 that the delivery procedure allowed hepatocytes to be distributed reasonably evenly on the bottom of the chamber, whereas the test reagent solution was placed in the top layer above the cell/media. When the flow was stopped and all the valves were closed, cells in the chamber tended to settle down and attach to the bottom surface within about 10 s, and diffusive mixing occurred based on Fick's law,²⁰ which defines the relationship between the distance travelled, d , by a molecule and the time, t :

$$d = \sqrt{2Dt} \quad (2)$$

where D is the diffusion coefficient. Using this equation, the time needed for a resorufin molecule to diffuse across a distance of $70 \mu\text{m}$, *i.e.*, the chamber depth, is estimated to be 5.1 s, based on the diffusion coefficient value of $4.80 \times 10^{-10} \text{ m}^2 \text{ s}^{-1}$ as determined by Schilling *et al.*²¹ Compared to the typical measurement time of 20 min this time for diffusion was not expected to cause significant errors for kinetic measurements.

It was also observed that the hepatocytes were distributed as an attached monolayer within the $70 \mu\text{m}$ deep chamber where the size of the hepatocytes was in the range of $10\text{--}20 \mu\text{m}$ in diameter. This monolayer distribution clearly simplified the process of image analysis and made it possible to select either a single cell or the surrounding media (outside the cell) for further analysis based on the fluorescent intensity. In addition, the cell viability assessment before and after passing through the chip without reaction over a given time period was not significantly different between the samples on the chip and in the batch micro-well plate.

3.2. Single cell monitoring

Upon the reaction taking place an increase in fluorescent intensity from the resorufin was observed for almost all hepatocytes. Fig. 2 shows the plot of fluorescent intensity of 12 individual cells randomly selected as a function of time (the fluorescent curves have been normalised for comparison). It was found that the fluorescent intensity for all cells showed a similar profile with some variations; fluorescent intensity increased approximately linearly for the first 10–12 min, reaching a maximum and then followed by a relatively stable period (and a gradual decline for some cells).

The fluorescent intensity of most cells (about nine out of 12) fell in a standard deviation of $\pm 15\%$ compared with the average. This intensity difference was probably because of the variation in cell size. By examining the cell morphology (Fig. 1b), it was found that the cell size distribution for the majority of cells (about 80%) was within the range of $\pm 20\%$ compared with the average, which corresponds closely to the maxima for the cells' fluorescent intensities; the highest fluorescent intensity corresponds to the largest cell size and the lowest fluorescent intensity to the smallest cell size, although the variation in activity for individual cells cannot be ruled out.

However, the variation in the time needed for each single cell to reach the maximum fluorescence was indicative of alterations in reaction rates among individual cells. This method, therefore, can provide a useful tool for the measurement of the kinetics of enzyme reactions occurring within individual cells. It was also shown that the chip-based measurement required a remarkably low number of cells, which can be a major advantage when screening limited amounts of cell samples.²²

3.3. *In situ* measurement of EROD activity

As discussed above, the measurement of EROD activity is based on the conversion of 7-ER (which is delivered with the test reagent) to fluorescent resorufin.^{23,24} This reaction was catalysed by cytochrome CYP1A, the expression of which was induced by 3-MC. Since the biocatalytic conversion of 7-ER to resorufin occurred inside hepatocytes, temporarily, the increase in fluorescent intensity started within hepatocytes and was followed by the fluorescent intensity increase in the surrounding media as

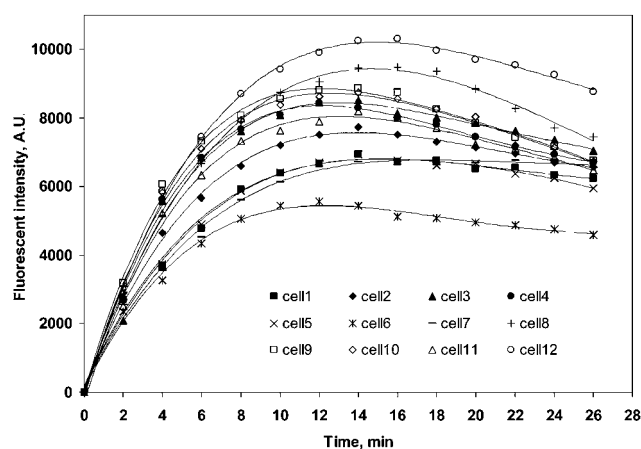


Fig. 2 Fluorescent intensity of single cells ($n = 12$) vs. time.

resorufin diffused outside cells. *Spatially*, the accumulation of the fluorescent intensity, both inside and outside hepatocytes, represented the total amount of resorufin produced.

This process was detected, both *temporarily* and *spatially*, by monitoring fluorescent intensity changes over the chip chamber area while the reaction progressed with time. Fig. 3 shows two example snapshots at reaction time zero and 10 min to compare the fluorescent intensity changes in both cells and the surrounding media. It can be seen clearly that at the beginning of the reaction resorufin production started showing significant fluorescence within the cells only (Fig. 3a). With the increase in resorufin concentration inside the cells, resorufin diffusion across the cell membrane towards the outside became more significant, resulting in a bright fluorescence in the media within the whole chamber (Fig. 3b).

Fig. 4 compares the integrated fluorescent intensities from cells, the surrounding media and the whole circular chamber. It was seen that the integrated fluorescent intensity of all cells was just about 10% of that from the surrounding media, although the cell area was generally brighter. To obtain the total amount of the resorufin produced during the process, the fluorescent intensity from the whole circular chamber area was used because it represents the analyte in both cells and media, which could be converted to a concentration-dependant calibration model.

To correlate the fluorescent intensity with the resorufin concentrations within the chamber, a calibration method was carried out in which the fluorescent intensity was measured over the whole circular chamber area with a wide range of resorufin concentrations. It was observed that the fluorescent intensity gave a good linear relationship ($\text{Int} = 1.7554 \times \text{Conc} - 0.0095$) with the resorufin concentration in the range of 0–30 μM (Fig. 5). Above that concentration, the fluorescent intensity tended to be lower than predicted, which was thought to be caused by the saturation of the CCD detector. Since the working concentration was normally in the range of a few μM the linear correlation was considered suitable for determining the resorufin concentration in this study. Using the calibration curve the resorufin concentration profile was obtained. Fig. 5 shows a plot of the resorufin concentration as a function of time. It can be seen that the general trend followed the profile of the fluorescent intensity. The blank result is also included for comparison, which indicated no significant increase in fluorescent intensity.

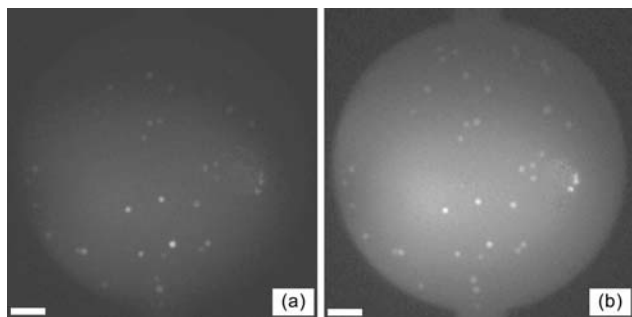


Fig. 3 Fluorescent intensity variations in both cells and media during the reaction of EROD at time zero (a) and 10 min (b). Scale bar: 100 μm . (A weak transmission light was applied for a better visibility of the chamber and channel).

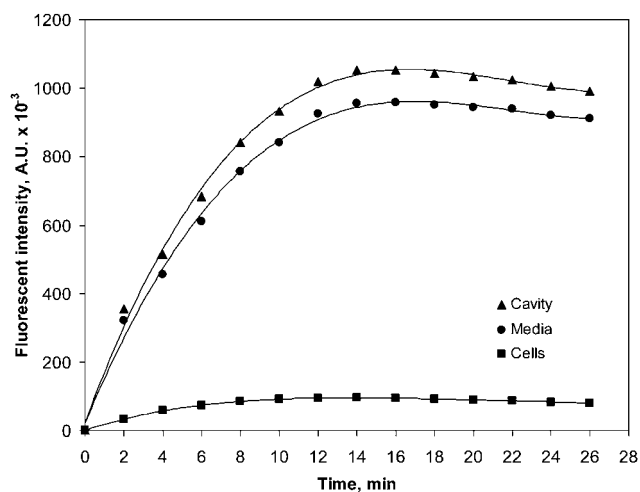


Fig. 4 Integrated fluorescent intensity from areas covering the cells, media or whole circular chamber.

3.4. Inhibition of EROD activity

CYP1A enzymes are active in the biotransformation of both endogenous substances and xenobiotics.²⁵ They can activate innocuous promutagens into their mutagenic and/or carcinogenic forms through the production of highly reactive epoxide intermediates that can bind potently to DNA and initiate carcinogenesis.²⁶ Thus, the examination of the inhibition of CYP1A enzymatic activity is important in the studies of toxicology and drug metabolism, whereas hepatic microsomal EROD activity is an indicator of CYP1A.²⁷

In this study, the effect of a model CYP1A inhibitor α -NF was examined on the 3-MC-induced rat hepatocytes when various concentrations of α -NF were added to the test reagent for a range of concentrations (0–40 μM). EROD activity was measured using the procedure described above under identical fluidic conditions, and the results are summarised in Fig. 6. It was found that with higher inhibitor concentrations the corresponding fluorescent intensity became lower, as expected. When the concentration of α -NF reached 40 μM , no significant EROD

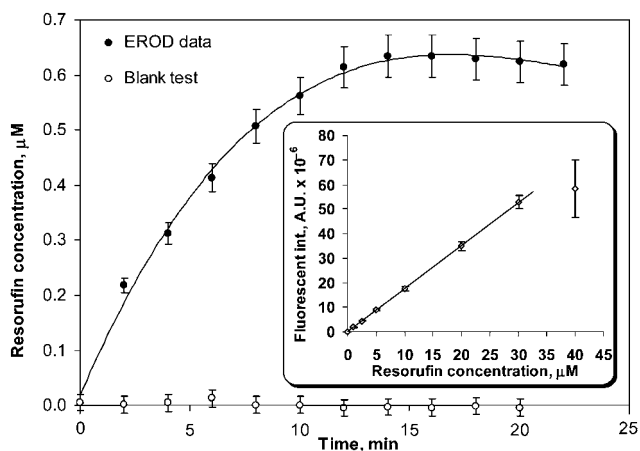


Fig. 5 Resorufin production as a function of time, and (inset) the calibration of fluorescent intensity vs. resorufin concentration.

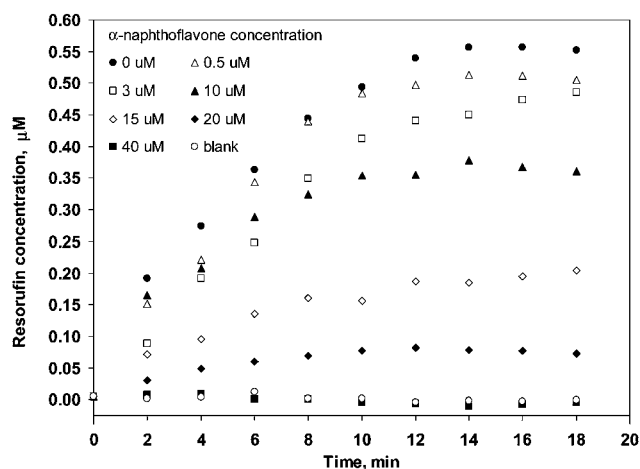


Fig. 6 Resorufin production as a function of time with inhibitor α -NF at different concentrations.

activity was observed, which was comparable with the result of the blank test. The relationship between the inhibition effect and inhibitor α -NF concentration is plotted in Fig. 7, where the inhibition effect is expressed as a percentage of the EROD activity remaining.

In biochemical and biomedical studies for dose-response relationships, a four-parameter logistic model has frequently been used to obtain the IC_{50} value in drug testing (IC_{50} represents the concentration of an inhibitor at which 50% of the maximal response is observed).^{28,29} This model was employed for fitting the experimental data shown in Fig. 6:

$$y = \frac{A - D}{1 + (x/C)^B} + D \quad (3)$$

where y is the EROD activity remaining as a percentage and x is the inhibitor α -NF concentration (μ M). A and D are the upper and lower asymptotes, respectively. B is the slope of the curve (or Hill slope) and C is the central point of the linear portion of the curve, *i.e.*, IC_{50} . By fitting the experimental data to the four-parameter logistic model, the best fit of the four parameters was found to be 98.63, -2.27 , 3.36 and 12.98, respectively.

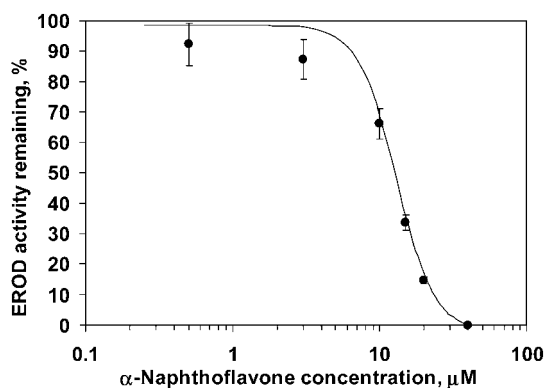


Fig. 7 Effects of various concentrations of inhibitor α -NF. The inhibition effect is expressed as percentage of EROD activity remaining.

4. Conclusions

A microfluidic-based system was developed for the *in situ* monitoring of EROD activity for primary rat hepatocytes by measuring the fluorescent intensity of both single cells and their surrounding media. The glass microfluidic chip enabled the cell suspension and test reagent to be introduced in a layer-by-layer flow format, thereby resulting in a short mixing time by diffusion. A calibration showed a good linear relationship between the resorufin concentration up to 30 μ M and fluorescent intensity. EROD activity was measured with 3-MC-induced hepatocytes, and the inhibition effect of α -NF was also examined on EROD activity.

Acknowledgements

Financial support from the UK DTI and UKIERI† is gratefully acknowledged.

References

- 1 M. J. Gomez-Lechon, J. V. Castell and M. T. Donato, *Chem.-Biol. Interact.*, 2007, **168**, 30–50.
- 2 T. Lynch and A. Price, *Am. Fam. Physician*, 2007, **76**, 391–396.
- 3 H. N. Chaobal and E. D. Kharasch, *Clin. Pharmacol. Ther.*, 2005, **78**, 529–539.
- 4 C. A. Schumann, A. Dorrenhaus, J. Franzke, P. Lampen, P. S. Dittrich, A. Manz and P. H. Roos, *Anal. Bioanal. Chem.*, 2008, **392**, 1159–1166.
- 5 H. L. Tsang, S. C. Wu, C. K. Wong, C. K. Leung, S. Tao and M. H. Wong, *Environ. Int.*, 2009, **35**, 1040–1047.
- 6 M. D. Burke and R. T. Mayer, *Drug Metab. Dispos.*, 1974, **2**, 583–588.
- 7 A. Behrens, K. Schirmer, N. C. Bols and H. Segner, *Mar. Environ. Res.*, 1998, **46**, 369–373.
- 8 G. Zamaratskaia and V. Zlabek, *Sensors*, 2009, **9**, 2134–2147.
- 9 S. Lindstrom, M. Hammond, H. Brismar, H. Andersson-Svahn and A. Ahmadian, *Lab Chip*, 2009, **9**, 3465–3471.
- 10 X. Li, X. Xue and P. C. H. Li, *Integr. Biol.*, 2009, **1**, 90–98.
- 11 S.-W. Lee, J. Y. Kang, I.-H. Lee, S.-S. Ryu, S.-M. Kwak, K.-S. Shin, C. Kim, H.-I. Jung and T.-S. Kim, *Sens. Actuators, A*, 2008, **143**, 64–69.
- 12 L. Charon, A. R. Wheeler and L. Lilge, in *Encyclopedia of Micro- and Nanofluidics*, ed. D. Q. Li, Springer, Heidelberg, Editon edn, 2008, vol. 3, pp. 1851–1859.
- 13 O. Hofmann, P. Miller, P. Sullivan, T. S. Jones, J. C. deMello, D. D. C. Bradley and A. J. deMello, *Sens. Actuators, B*, 2005, **106**, 878–884.
- 14 A. L. Paguirigan and D. J. Beebe, *BioEssays*, 2008, **30**, 811–821.
- 15 X. L. Zhang, H. B. Yin, J. M. Cooper and S. J. Haswell, *Anal. Bioanal. Chem.*, 2008, **390**, 833–840.
- 16 P. Chao, T. Maguire, E. Novik, K. C. Cheng and M. L. Yarmush, *Biochem. Pharmacol.*, 2009, **78**, 625–632.
- 17 X. L. Zhang, H. B. Yin, J. M. Cooper and S. J. Haswell, *Electrophoresis*, 2006, **27**, 5093–5100.
- 18 T. McCreedy, *Anal. Chim. Acta*, 2001, **427**, 39–43.
- 19 K. Behnia, S. Bhatia, N. Jastromb, U. Balis, S. Sullivan, M. Yarmush and M. Toner, *Tissue Eng.*, 2000, **6**, 467–479.
- 20 A. Fick, *Ann. Phys. Chem.*, 1855, **94**, 59–86.
- 21 E. A. Schilling, A. E. Kamholz and P. Yager, *Anal. Chem.*, 2002, **74**, 1798–1804.

† This document is an output partially from the UKIERI (UK-India Education and Research Initiative) project funded by the Department for Innovation, Universities and Skills (DIUS), the FCO, British Council, Department of Science and Technology, Government of India, The Scottish Government, Department of Learning, Northern Ireland, Welsh Assembly, GSK, BP, SHELL and BAE for the benefit of the UK and Indian Higher Education Sector. The views expressed are not necessarily those of the funding bodies.

-
- 22 S. Lindström, R. Larsson and H. A. Svahn, *Electrophoresis*, 2008, **29**, 1219–1227.
- 23 M. T. Donato, E. Herrero, M. J. Gomezlechón and J. V. Castell, *Toxicol. Vitro*, 1993, **7**, 481–485.
- 24 D. D. Vakharia, N. Liu, R. Pause, M. Fasco, E. Bessette, Q. Y. Zhang and L. S. Kaminsky, *Drug Metab. Dispos.*, 2001, **29**, 999–1006.
- 25 D. L. Anger, M. A. Petre and D. J. Crankshaw, *Br. J. Pharmacol.*, 2005, **145**, 926–933.
- 26 F. J. Gonzalez and H. V. Gelboin, *Drug Metab. Rev.*, 1994, **26**, 165–183.
- 27 P. V. Nerurkar, S. S. Park, P. E. Thomas, R. W. Nims and R. A. Lubet, *Biochem. Pharmacol.*, 1993, **46**, 933–943.
- 28 O. Ugur and H. O. Onaran, *Biochem. J.*, 1997, **323**, 765–776.
- 29 Y. I. Yagi, K. Abe, K. Ikebukuro and K. Sode, *Biochemistry*, 2009, **48**, 10255–10266.

Rapid PCR amplification using a microfluidic device with integrated microwave heating and air impingement cooling†

Kirsty J. Shaw,^a Peter T. Docker,^a John V. Yelland,^b Charlotte E. Dyer,^c John Greenman,^c Gillian M. Greenway^a and Stephen J. Haswell^{*a}

Received 6th January 2010, Accepted 6th April 2010

First published as an Advance Article on the web 23rd April 2010

DOI: 10.1039/c000357n

A microwave heating system is described for performing polymerase chain reaction (PCR) in a microfluidic device. The heating system, in combination with air impingement cooling, provided rapid thermal cycling with heating and cooling rates of up to 65 °C s⁻¹ and minimal over- or under-shoot (± 0.1 °C) when reaching target temperatures. In addition, once the required temperature was reached it could be maintained with an accuracy of ± 0.1 °C. To demonstrate the functionality of the system, PCR was successfully performed for the amplification of the Amelogenin locus using heating rates and quantities an order of magnitude faster and smaller than current commercial instruments.

Introduction

PCR is a commonly used biochemical tool for the amplification of DNA and features thermal cycling between two or three distinct temperatures to achieve the denaturing of the DNA, primer annealing and DNA extension.

In order to increase sample processing and facilitate the integration of PCR with other techniques, the speed of processing is very important. In addition, a reduction in the volume required for PCR is advantageous as it not only increases speed but also reduces the amount of reagents required therefore reducing the cost of analysis. Since the early development of PCR in microfluidic systems, either as a stand-alone technique¹ or as an integrated process,² numerous examples of miniaturised PCR have been reported which can be found in substantial reviews on the subject.^{3–6}

A wide variety of heating and cooling methods have been reported in the literature for achieving thermal cycling. Broadly speaking these methods can be divided into contact and non-contact forms. Commonly used contact heating methods include block heaters *e.g.* Peltier heaters, or the deposition of thin film resistive heaters *e.g.* platinum, on the exterior of the microfluidic device. While Peltier heaters are widely used to achieve thermal cycling for DNA amplification as they produce reliable heating, they suffer from relatively slow temperature ramp rates.³

Non-contact heating methods described for DNA amplification in microfluidic systems include the use of infrared⁷ and halogen lamps.⁸ Induction heating has been shown to provide a low power consumption method for performing thermal cycling with a temperature stability of ± 0.2 °C.^{9,10} An alternating

electric current induced Joule heating method has also been described where platinum electrodes are used to transfer an electric current directly into the PCR solution, producing heating and cooling rates of 15 °C s⁻¹.¹¹

The use of microwaves for dielectric heating of liquids within microfluidic devices has previously been shown to have the potential for thermal cycling but the technology has not been fully exploited to demonstrate actual DNA amplification.^{12–14} Issadore *et al.*, for example, reported a system whereby droplets are flowed through a microwave heater, which relies on integrated metal electrodes that run parallel to the fluidic channel to deliver the microwave power.¹² The use of direct sample coupling of microwave heating has also been demonstrated for PCR, with the emphasis of this work being on the thermal cycling of relatively large volumes of liquid rather than miniaturisation. For example, Orrling *et al.* presented a microwave heating system capable of performing PCR in a 15 ml reaction volume for increased sample processing.¹⁵ A total of 33 cycles were used to amplify a 53 bp fragment in 2 hours and 7 minutes. Despite successful amplification of the target product, this system was only capable of heating and not cooling therefore the sample required manual transfer into a thermally controlled block for each annealing step.

The work presented here demonstrates the successful use of a tuned microwave cavity for direct substrate heating, configured to perform both heating and air impingement cooling resulting in rapid thermal cycling, enabling DNA amplification on a microfluidic device.

Experimental

Microwave cavity and power source

A custom built re-entrant microwave cavity operating at 8 GHz was used to directly heat the glass microfluidic device (Fig. 1). The copper cavity was connected *via* a coaxial coupling loop to the microwave power source, a CPI VZM6991 series 8–18 GHz 20 W travelling wave tube amplifier [CPI, US] capable of

^aDepartment of Chemistry, University of Hull, Cottingham Road, Hull, UK HU6 7RX. E-mail: s.j.haswell@hull.ac.uk; Fax: +44 (0)1482 466410; Tel: +44 (0)1482 465475

^bExxel Amplifiers Ltd., 4 Pinfold Lane, Norfolk, UK IP26 5LH

^cCentre for Biomedical Research, University of Hull, Cottingham Road, Hull, UK HU6 7RX

† Electronic supplementary information (ESI) available: Details of temperature measurement technique used; description of the microwave cavity and power source developed. See DOI: 10.1039/c000357n

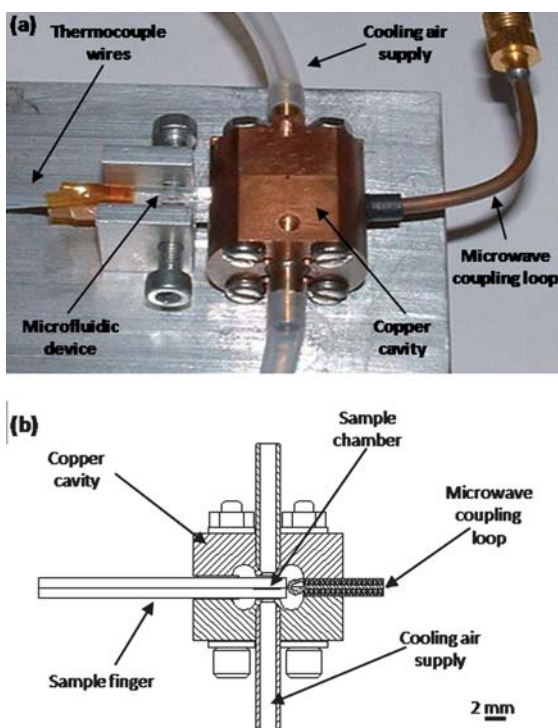


Fig. 1 Photograph (a) and schematic cross-section (b) of the re-entrant cylindrical microwave cavity.

delivering power levels up to 10 W and driven by a HP3850B microwave signal generator [Hewlett Packard, US].

After inserting a microfluidic device into the cavity the resonant frequency was determined at low power using a HP8719D network analyser [Hewlett Packard, US] by observing the resonance dip in the reflected power signal. The frequency was noted and transferred to the HP3850B signal generator. Coupling into the cavity was adjusted for a minimum of 10 dB return loss by varying the insertion depth of the coupling loop. The mean power consumption of the cavity during a typical heating cycle was found to be under 500 mW (for further details see ESI†).

Air impingement cooling was provided from a compressed air cylinder and controlled by the actuation of a solenoid valve which delivered short pulses of air to aid the transition between the denaturation and annealing temperatures.

Temperature measurement

A 75 μm type-k (Chromel-Alumel) junction thermocouple was inserted through the etched channels leading to the PCR chamber. By positioning the thermocouple junction in the centre of the PCR chamber, true sample measurement could be ensured. A digital display on the control system allows the temperature to be monitored in real-time, while a PicoScope 2200 [Pico@ Technology Ltd., UK] was used to record the thermal cycling (for further details see ESI†). To ensure direct heating of the thermocouple was not occurring in the ac electric field associated with the microwaves, the microwave generator was (temporarily) 100% square wave amplitude modulated and the low level dc signal (around 40 $\mu\text{V } ^\circ\text{C}^{-1}$) of the thermocouple was monitored. The resulting oscilloscope temperature trace showed only the

expected triangular heating and cooling waveform, with no step discontinuity occurring at the modulation switching points, thus confirming the adequacy of the screening and filtering used.

In order to check the accuracy of the thermocouple measurement a microfluidic device with a thermocouple in position was placed into an isothermal block with a glass thermometer and found to give complete agreement within the tolerances of the thermometer used, ± 0.5 $^\circ\text{C}$. Furthermore, the calculated error for the thermocouple electronics was ± 0.4 $^\circ\text{C}$, assuming that the thermocouples, the Pt resistance thermometer and all the resistors used were in tolerance.

Thermocycler

The thermocycler was designed for rapid throughput with maximum flexibility and portability; it is therefore self-contained and functions without an external computer. Hold times at the DNA denaturation, primer annealing and DNA extension temperatures are adjustable from 1 to 99 seconds, and from 1 to 999 seconds at initial and final hold temperatures if required. The target temperatures are all adjustable and displayed numerically to a resolution and an accuracy of ± 0.1 $^\circ\text{C}$. Time and temperature settings can be adjusted during cycling if necessary (for further details see ESI†).

Production of microfluidic device

Borosilicate glass microfluidic devices of cross-section 5 mm \times 2 mm were produced using standard photolithography and wet etching techniques.¹⁶ The DNA amplification chamber (3 mm diameter, 100 μm deep), which had a volume of 0.7 μl , was connected to inlet and outlet ports *via* etched channels (200 μm wide and 100 μm deep), which also served to allow access for the thermocouple (Fig. 2). To create a sealed device the etched glass plate was thermally bonded to a top plate which had 360 μm holes drilled in it to act as reagent and sample inlets. The thermocouple was threaded into the microfluidic device by hand from the open channel end after fabrication.

The internal glass surfaces of the microfluidic device were silanised to prevent DNA polymerase adsorption.¹⁷ A solution of 290 μl of trichloro(1*H*,1*H*,2*H*,2*H*-perfluorooctyl) silane in 5 ml of 2,2,4-trimethylpentane was flowed through the microfluidic device for 10 minutes at 5 $\mu\text{l min}^{-1}$.¹⁸ Following this solutions of 2,2,4-trimethylpentane, acetone and distilled water were sequentially used to wash the microfluidic device.

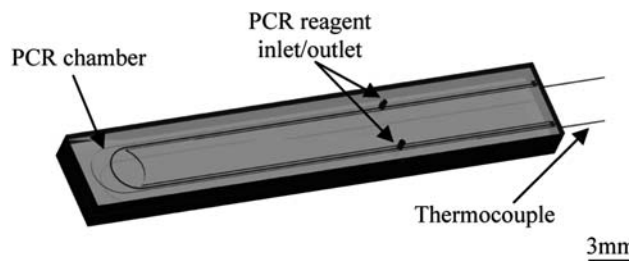


Fig. 2 Schematic showing the microfluidic device design, showing a type-k junction thermocouple which has been threaded along the channel length into the PCR chamber.

DNA amplification

Saliva was collected, from male and female volunteers, using a 0.9% (w/v) saline solution mouthwash which was swilled around the mouth. A 1 ml aliquot of the mouthwash was placed in a 1.5 ml microcentrifuge tube and centrifuged at 14 000 rpm for 3 minutes. The supernatant was removed and the pellet subjected to DNA extraction using a QIAamp® DNA Micro Kit [Qiagen, UK] following standard protocols.

The extracted DNA (1 ng) was added to a PCR reagent solution composed of the following: 1× reaction buffer [Promega, UK], 2 mM MgCl₂ [Promega, UK], 200 μM each dNTPs [Bioline, UK], 0.5 μM forward primer, 0.5 μM reverse primer, 10 mg ml⁻¹ bovine serum albumin [NEB, UK], 0.01% (w/v) poly(vinylpyrrolidone) [Sigma-Aldrich, UK], 0.1% (v/v) Tween-20 [Sigma-Aldrich, UK] and 1 U GoTaq® DNA polymerase [Promega, UK] made up in purified water. Forward and reverse primers were custom-made for the Amelogenin locus (Forward: 5'-JOE-CCCTGGGCTCTGTAAAGAA-3', Reverse: 5'-ATC-AGAGCTTAACTGGGAAGCTG-3') [Eurofins MWG Operon, Germany].¹⁹ PCR control samples were run in parallel on a TC-312 thermal cycler [Techne, UK].

Analysis of PCR products

PCR products were analysed by capillary electrophoresis using an ABI Prism 310 Genetic Analyser [Applied Biosystems, UK]. The samples were collected from the DNA amplification chamber and added to 12 μl of Hi-Di™ formamide [Applied Biosystems, UK] and 0.5 μl GeneScan™ 500 ROX™ DNA size standard [Applied Biosystems, UK]. The solutions were heated to 95 °C for 5 minutes to denature the DNA and then snap-cooled on ice prior to loading on the ABI Prism 310 Genetic Analyser. Standard protocols for DNA fragment analysis were followed, using POP-4 [Applied Biosystems, UK] as the separation matrix.

Results and discussion

Microwave cavity and power source

The microwave heating system was designed to have an impedance mismatch between the substrate and sample in order to heat the glass of the microfluidic device and not the sample itself. This was achieved by combining the device geometry, electrical characteristics and very low sample volume and ionic strength together with the radio frequency (RF) field. For example as the sample solution was not simply water but a mixture of buffer and PCR reagents its ionic strength would make the solution sufficiently conducting to effectively act as a short circuit in its axial direction so supporting the preferential match of the transverse impedance of the glass with the impedance of the microwave cavity. Evidence that it was indeed direct heating of the glass substrate as opposed to heat conduction from the sample was established by the fact that heating rates were the same with or without the sample being present.

Whilst indirect microwave heating of the sample *via* the glass may seem to offer little advantage over simpler methods such as surface contact resistive heating, the uniformity of microwave heating throughout the volume of the glass rather than *via* the

surface removes the delay in the thermal control loop, thus allowing far more rapid yet stable temperature control. The cooling process of two impinging air jets is, however, susceptible to the thermal delay of the glass, as it is its outer surface and not its bulk volume that is cooled. The air cooling was therefore excluded from the temperature control system by cooling to just below the target temperature then maintaining that temperature by the feedback controlled microwave heating. This also eliminated any need for proportional control of the cooling air flow, thus allowing a simple on-off solenoid valve to be used.

Thermal cycling profile

Using feedback controlled microwave heating coupled with air impingement cooling, the system showed minimal thermal overshoot or undershoot at any of the three set temperatures. Once the microwave system had reached a set temperature the variation was less than ±0.1 °C. The ramp rates for heating and cooling exceeded 65 °C s⁻¹, allowing very fast transitions between temperatures (Fig. 3). Note that the cooling rate is slower than the heating rate.

The thermocycler of the microwave system was designed to include an initial denaturing step, essential when using Hot-Start Taq DNA polymerases, and a final extension step to ensure complete adenylation of the PCR products. The time and temperature of these steps were adjustable in the same way as for the three amplification steps.

DNA amplification

DNA amplification of the Amelogenin locus was carried out using the microwave heating system described. Amelogenin is used to distinguish between male (XY) and female (XX), yielding PCR products of 106 bp (X) and 112 bp (Y). For PCR experiments, a 2 minute initial heating step at 95 °C was carried out to ensure complete denaturation of the DNA and to activate the Hot-Start GoTaq DNA polymerase. Thermal cycling between DNA denaturation (94 °C), primer annealing (59 °C) and DNA extension (72 °C) temperatures was performed for 28 cycles.

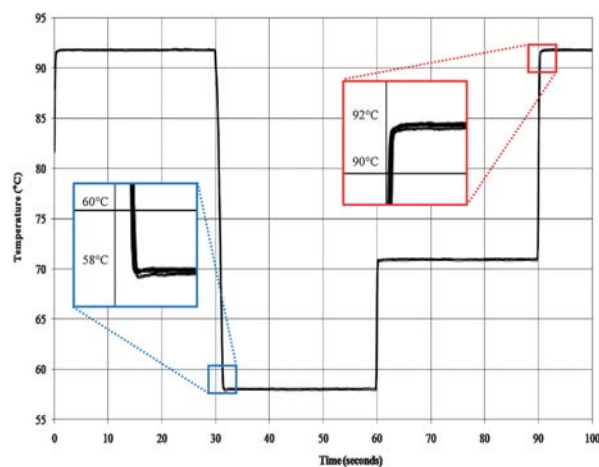


Fig. 3 Graph showing the thermal cycling profile of the microwave heating system based on selected temperatures of 92 °C, 58 °C and 71 °C. The image comprises 5 overlaid thermal cycles demonstrating the reproducibility of the system.

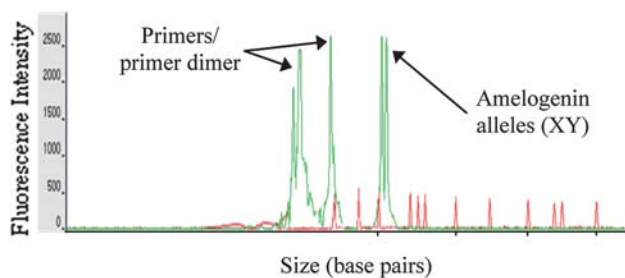


Fig. 4 Electropherogram showing PCR products from amplification of the Amelogenin locus, using DNA extracted from a male volunteer, on a microfluidic device using microwave heating. A DNA size standard was also included to enable accurate sizing of the PCR products.

Samples were then analysed using capillary electrophoresis. Successful PCR amplification, of DNA from both male and female donors, was achieved using the microwave system (Fig. 4).

Conclusions

The microwave heating system developed was found to have a response speed orders of magnitude faster than that of current commercial systems. This fast thermal transition capability enabled 28 cycles to be performed in 42 minutes. This represents a considerable time saving on previously reported microwave PCR systems where 33 cycles took 127 minutes.¹³ Further work aims to reduce the hold times at each temperature to achieve DNA amplification which will be no longer thermally limited but restricted for example by the processivity of the DNA polymerase, where an average DNA polymerase enzyme adds 60–100 nucleotides per second.

Acknowledgements

The authors acknowledge Exxel Amplifiers Ltd. for providing the microwave heating system, Dr Steve Clark for microfluidic

device manufacture, Mark Tarn for production of microfluidic device graphics and the EPSRC for funding EP/D040930.

References

- 1 M. A. Northrup, M. T. Ching, R. M. White and R. T. Watson, Seventh international conference on solid state sensors and actuators, *Transducers*, 1993, 924–926.
- 2 A. T. Woolley, D. Hadley, P. Landre, A. J. deMello, R. A. Mathies and M. A. Northrup, *Anal. Chem.*, 1996, **68**, 4081–4086.
- 3 C. S. Zhang, J. L. Xu, W. L. Ma and W. L. Zheng, *Biotechnol. Adv.*, 2006, **24**, 243–284.
- 4 C. S. Zhang and D. Xing, *Nucleic Acids Res.*, 2007, **35**, 4223–4237.
- 5 P. A. Aurox, Y. Koc, A. deMello, A. Manz and P. J. R. Day, *Lab Chip*, 2004, **4**, 534–546.
- 6 L. Chen, A. Manz and P. J. R. Day, *Lab Chip*, 2007, **7**, 1413–1423.
- 7 J. P. Ferrance, Q. R. Wu, B. Giordano, C. Hernandez, Y. Kwok, K. Snow, S. Thibodeau and J. P. Landers, *Anal. Chim. Acta*, 2003, **500**, 223–236.
- 8 C. Ke, H. Berney, A. Mathewson and M. M. Sheehan, *Sens. Actuators, B*, 2004, **102**, 308–314.
- 9 D. Pal and V. Venkataraman, *Sens. Actuators, A*, 2002, **102**, 151–156.
- 10 Y. Lao, F. E. H. Tay, G. Xu, D. Hartono and Y. Y. Lee, *Int. J. Comput. Eng. Sci.*, 2003, **4**, 651–654.
- 11 S. Stern, C. Brooks, M. Strachan, A. Kopf-Sill and J. W. Parce, *Inter Society Conference on Thermal Phenomena*, 2002, 1033–1038.
- 12 D. Issadore, K. J. Humphry, K. A. Brown, L. Sandberg, D. A. Weitz and R. M. Westervelt, *Lab Chip*, 2009, **9**, 1701–1706.
- 13 J. J. Shah, S. G. Sundaresan, J. Geist, D. R. Reyes, J. C. Booth, M. V. Rao and M. Gaitan, *J. Micromech. Microeng.*, 2007, **17**, 2224–2230.
- 14 A. Kempitiya, D. A. Borca-Tasciuc, H. S. Mohamed and M. M. Hella, *Appl. Phys. Lett.*, 2009, **94**, 064106.
- 15 K. Orrling, P. Nilsson, M. Gullbergh and M. Larhed, *Chem. Commun.*, 2004, 790–791.
- 16 T. McCreedy, *TrAC, Trends Anal. Chem. (Pers. Ed.)*, 2000, **19**, 396–401.
- 17 I. Erill, S. Campoy, N. Erill, J. Barbe and J. Aguilo, *Sens. Actuators, B*, 2003, **96**, 685–692.
- 18 H. Hartshorne, C. J. Backhouse and W. E. Lee, *Sens. Actuators, B*, 2004, **99**, 592–600.
- 19 B. E. Krenke, A. Tereba, S. J. Anderson, E. Buel, S. Culhane, C. J. Finis, C. S. Tomsey, J. M. Zachetti, A. Masibay, D. R. Rabbach, E. A. Amriott and C. J. Sprecher, *J. Forensic Sci.*, 2002, **47**, 773–785.

Microfluidic perfusion system for maintaining viable heart tissue with real-time electrochemical monitoring of reactive oxygen species†

Lih-Tyng Cheah,^{‡a} Yue-Hua Dou,^{‡a} Anne-Marie L. Seymour,^b Charlotte E. Dyer,^a Stephen J. Haswell,^c Jay D. Wadhawan^c and John Greenman^{*a}

Received 7th April 2010, Accepted 26th July 2010

DOI: 10.1039/c004910g

A microfluidic device has been developed to maintain viable heart tissue samples in a biomimetic microenvironment. This device allows rat or human heart tissue to be studied under pseudo *in vivo* conditions. Effluent levels of lactate dehydrogenase and hydrogen peroxide were used as markers of damaged tissue in combination with *in situ* electrochemical measurement of the release of reactive oxygen species (ROS). The parameters for perfusion were optimized to maintain biopsies of rat right ventricular or human right atrial tissue viable for up to 5 and 3.5 hours, respectively. Electrochemical assessment of the oxidation current of total ROS, employing cyclic voltammetry, gave results in real-time that were in good agreement to biochemical assessment using conventional, off-chip, commercial assays. This proof-of-principle, integrated microfluidic device, may be exploited in providing a platform technology for future cardiac research, offering an alternative approach for investigating heart pathophysiology and facilitating the development of new therapeutic strategies.

Introduction

Studies of cardiac physiology and biochemistry have traditionally used *in vitro* perfusion systems such as the Langendorff retrograde perfusion.^{1,2} This model has been widely used for a diverse range of studies of the heart, including molecular and cellular alterations, as well as evaluating therapeutic interventions.

The main alternative approaches for studying the pathophysiology of heart diseases are based on cell or tissue culture. However, the concern for all *in vitro* cell manipulation studies is that the cells behave differently in culture flasks,³ as the microenvironment experienced *in vitro* is clearly different from those *in vivo*. In addition, there is a further complication with adult cardiomyocytes as these can only be maintained as primary cell cultures, not immortal cell lines. Tissues and organs have complex three-dimensional systems *in situ*, including a complex network of extra-cellular matrix, *e.g.* elastin, laminin, collagen and fibronectin. In addition, cells inhabit a closely packed spatio-temporal environment where any cell is always communicating and interacting with multiple other cell types, responding to local concentrations of a plethora of molecules, such as cytokines, enzymes and nutrients. Accordingly in an *in vitro* cell culture environment, many, if not all of these signals are missing.

Microfluidics offers an approach that can circumvent many of the limitations of *in vitro* cell culture methodology. For example,

by continuously supplying enriched media to heart tissue biopsies *in vitro*, whilst removing waste products and gases produced by cellular processes.^{4,5} Several groups have developed microfluidic devices for studying cardiomyocyte functions, with Li and Li being the first, investigating cell contraction.⁶ A single cardiomyocyte was retained within a V-shaped structure of the chip. Analysis of intracellular [Ca²⁺] following ionomycin stimulation was measured using the calcium-sensitive dye, Fluo-4 AM ester. Subsequently, Li *et al.* developed a microfluidic chip with improved cell retention properties and used this to monitor calcium mobilization in single cardiomyocytes, in real-time, as a part of a drug screening application.⁷ Cheng *et al.* developed a multi-functional microfluidic platform with a microelectrode array to stimulate the cell and monitor lactate release by electrochemical (EC) probes.⁸ This analysis was used in conjunction with *in situ* microscopy and fluorescence detection of extracellular pH and cellular Ca²⁺ concentrations during cell contraction. However tissue, with its highly complex structures, presents a greater technological challenge in terms of maintaining essential supplies of oxygen and nutrients, whilst removing waste products. The benefits of studying a more holistic representation of the complex cell–cell and cell–stroma interactions are a greater relevance for physiological and clinical studies.

Reactive oxygen species (ROS) play a major role in ischemia–reperfusion injury, ageing, neurodegenerative disorders and many other diseases.^{9,10} ROS can cause the oxidation of membrane phospholipids, DNA and proteins, subsequently impairing mitochondrial function. ROS can be measured by various means, such as chemiluminescence,^{11,12} fluorescence,^{13,14} infrared¹⁵ and electron spin resonance spectroscopy.¹⁶ Electrochemical methods, however, provide a direct means of analysing the concentration of free radicals in solution at the specific site where the sensing electrode is positioned, with minimal disturbance to the sample under investigation.¹⁷ Fast cyclic voltammetry has been carried out previously to capture the transient

^aCentre for Biomedical Research, Hull York Medical School, University of Hull, Cottingham Road, Kingston-Upon-Hull, HU6 7RX, UK

^bDepartment of Biological Sciences, Hull York Medical School, University of Hull, Cottingham Road, Kingston-Upon-Hull, HU6 7RX, UK

^cDepartment of Physical Sciences, University of Hull, Cottingham Road, Kingston-Upon-Hull, HU6 7RX, UK. E-mail: j.greenman@hull.ac.uk; Tel: +44 (0)1482466032

† Electronic supplementary information (ESI) available: Supplementary Information. See DOI: 10.1039/c004910g

‡ These authors contributed equally to this work.

signals of extracellular nitric oxide or nitric oxide synthase (NOS) in brain slices.^{18,19} Recently, triple potential-step chronoamperometry has been developed to measure simultaneously ROS and reactive nitrogen species (RNS).²⁰

Several groups have reported electrochemical sensors integrated with microfluidic devices to determine changes in ROS. A microfabricated Pt electrode was platinised to increase electrochemical sensitivity and used to detect ROS and RNS released from macrophage cells following continuous microinjection of a calcium ionophore.²¹ Electrochemical measurement has also been used to detect lactate released from heart cells⁷ and in saliva.²² Hitherto, electrochemical monitoring of ROS during perfusion of viable heart tissue biopsies has not been reported.

Here, a microfluidic chip based perfusion system has been designed and optimised to maintain viable and functioning heart tissue samples. Analysis of tissue was performed on-chip by electrochemical measurements and verified off-chip by biochemical methods, as a route towards developing the next generation of user-friendly devices to maintain and analyse tissue to address clinically relevant issues.

Experimental

Experimental models

All procedures conform to the UK Animals (Scientific Procedures) Act 1986. Wistar rats (B&K Universal Ltd., Grimston, UK) were housed under a 12:12 hour light–dark cycle and provided with food and water *ad libitum*. Animals were anaesthetized *via* intraperitoneal injection of 0.5 mL 100 g⁻¹ sodium thiopentone (25 mg mL⁻¹, Link Pharmaceuticals Ltd., West Sussex, UK). In brief, hearts were rapidly excised and the aorta was cannulated. A piece of right ventricular tissue (approximately 2 × 4 × 4 mm³) was taken and placed directly into the chamber of the perfusion device filled with buffer. At the end of the experiment, the wet weight of the heart tissue sample was recorded.

Human heart tissue biopsies were supplied by Mr S. Griffin (Consultant Cardiothoracic Surgeon). Ethics and Hospital Trust approvals were obtained from Hull and East Yorkshire Local Research Ethics Committee (07/H1304/105) and Hull and East Yorkshire NHS Trust (R0568), respectively. Samples were taken from patients undergoing coronary artery bypass surgery (CABG). Heart biopsies were immersed in freshly prepared cardioplegic solution at 4 °C (Martindale Pharmaceuticals, UK), transported to the laboratory and mounted in the perfusion chamber within 60 minutes.

Fabrication of microfluidic perfusion device

A microfluidic perfusion chamber with a capacity of 400 μL was constructed from polydimethylsiloxane (PDMS) (Dow Corning, USA) and a polystyrene Petri dish (35 mm in diameter) (Fig. 1). Briefly, the chamber was moulded around the diamond-shaped end of a 1 mL syringe barrel that was attached to a silicon wafer using an instant adhesive (Henkel Loctite Adhesives Ltd., UK). Mixed and degassed PDMS monomer and initiator (w/w, 10 : 1) were poured over the syringe end and cured at 75 °C for two hours to form a mould. The PDMS chamber was stripped off the template and five holes (1–3 mm in diameter) were punched to

Fabrication of microfluidic perfusion device

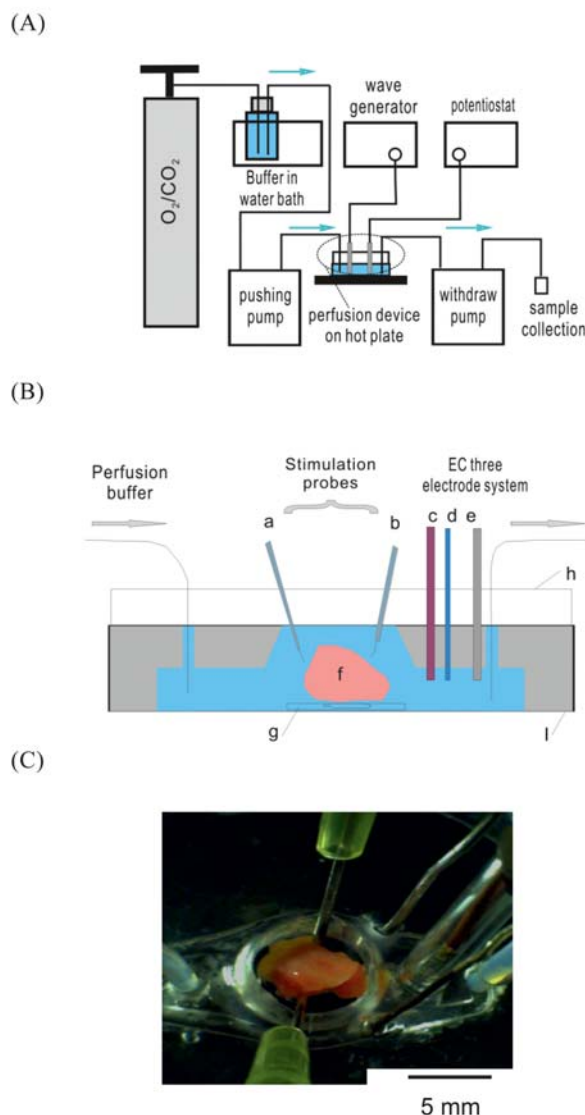


Fig. 1 Schematics of the experimental setup (A and B): stimulation electrodes (a and b); working, reference and counter electrodes (c–e); tissue in chamber with Krebs–Henseleit buffer (supplemented with 5 mM glucose, 100 Units mL⁻¹ penicillin and 100 μg mL⁻¹ streptomycin, f); tissue holder (PDMS, g). Petri dish lid as the chamber cover and holder for electrodes and tubes (h). Polystyrene Petri dish (i). Photograph of the device with tissue (without the chamber lid) (C).

allow for the inlet, and outlet Teflon™ tubings (1.0 mm ID × 1.6 mm OD, VWR Int. Ltd.), and electrodes. The PDMS was bonded with the Petri dish after oxygen plasma treatment at 350 V, 20 mA, P_{O₂} 8 mbar for 50 s (SPEEDIVAC, Model 12E6/1405 Edwards High Vacuum Ltd., UK). This device provided a 7 mm chamber at its centre into which a heart biopsy was placed and positioned on a 37 °C hotplate (WIS1, World Precision Instruments, UK). Both the inlet and outlet were connected to peristaltic pumps at a flow rate of 120 μL min⁻¹, and the heart tissue was electrically stimulated *via* two platinum wire electrodes anchored in the chamber lid using a programmable, square wave, function generator (TG1010A, Thurlby Thandar Instruments Ltd., UK).

Experimental protocols

Prior to each experiment, the microfluidic system was sterilised with 70% (v/v) ethanol/water by perfusion at 120 $\mu\text{L min}^{-1}$ and rinsed with sterilised double distilled water for 10 minutes, respectively. The microfluidic device was then primed with Krebs–Henseleit buffer (KH, 118 mM NaCl, 25 mM NaHCO_3 , 4.8 mM KCl, 1.2 mM KH_2PO_4 , 1.2 mM MgCl_2 and 2.5 mM CaCl_2) for 15 minutes. In this paper KHG represents KH buffer plus 5 mM glucose. The addition of 100 Unit mL^{-1} penicillin and 0.1 mg mL^{-1} streptomycin (final concentration) to KHG buffer formed KHGB. All constituents were purchased from Sigma-Aldrich (UK) in the highest purity grade commercially available and used without further purification. Buffers were filtered using a 0.22 μm syringe filter (Millipore Corporation, USA) and oxygenated with 95% O_2 -5% CO_2 continuously at 37 $^\circ\text{C}$.

Right ventricular tissue from rat or right atrial tissue biopsies from patients were perfused with KHGB for up to 5 hours followed by 30 minutes to one hour with 2% (v/v) Triton X100 (BDH, England) in KHGB. Triton X100 is a non-ionic surfactant able to solubilise phospholipid membranes,²³ releasing the intracellular enzymes. In some experiments, 95% N_2 -5% CO_2 saturated KHGB was used as an alternative method of inducing damage.

Assessment of tissue functions

1 Tissue viability. Viability was evaluated using calcein-acetoxymethyl ester (Calcein AM; Invitrogen, UK) and propidium iodide (PI; Sigma-Aldrich, UK). Calcein AM is a modified carboxylic acid containing an additional ester group that permits entry into cells. The ester is hydrolysed within viable cells altering hydrophobicity; the resulting carboxylate is both fluorescent and membrane impermeable. Conversely, PI only enters cells when the plasma membrane is disrupted where it intercalates with the double-stranded DNA and fluoresces, thus providing a measure of dead or dying cells. Following perfusion for various time periods, cardiac tissue sections were incubated with 50 μL of 10 μM calcein AM ($\lambda_{\text{ex}} = 494$ nm and $\lambda_{\text{em}} = 517$ nm) in phosphate buffered saline (PBS, pH 7.4) for 1 hour. The tissue was then washed with PBS and incubated with 50 μL of 3.75 mM PI ($\lambda_{\text{ex}} = 536$ nm and $\lambda_{\text{em}} = 617$ nm) in PBS for 10 minutes. After a final wash with PBS, the cardiac tissue section was examined under a laser-scanning inverted confocal microscope (Nikon Eclipse TE2000-E).

2 Lactate dehydrogenase measurement. Cell damage was determined *via* release of lactate dehydrogenase (LDH),²⁴ using a commercial colorimetric assay (Cytotoxicity Detection Kit^{plus}, Roche, UK). Effluent samples were collected for 2 min (approximately 240 μL in total) at 5 min intervals during perfusion from the outlet tube (see Fig. 1(A)). To measure LDH, samples (50 μL) were incubated with 50 μL of reaction mixture containing diaphorase/ NAD^+ , iodotetrazolium chloride and sodium lactate for 30 min at room temperature in 96-well plates. The reaction was terminated by adding 50 μL of stop solution (1 M HCl) per well, and absorbance measured at 492 nm using a microplate reader (BioTek Instruments, Inc., USA). All samples were assayed in triplicate.

3 Detection of H_2O_2 . The concentration of H_2O_2 in the effluent was determined using a commercial Amplex Red Hydrogen Peroxide assay kit (Invitrogen Molecular Probes, UK). A standard curve ranging from 0 to 5 μM H_2O_2 was generated for each experiment. Samples (50 μL) were incubated with 50 μL of reaction mixture containing 100 μM Amplex Red reagent and 0.2 U mL^{-1} horseradish peroxidase (EC. 1.11.1.7, one unit of enzyme will form 1.0 mg purpurogallin from pyrogallol in 20 seconds at pH 6.0 and 20 $^\circ\text{C}$) for 30 minutes at room temperature. Absorbance at 562 nm was measured using a microplate reader (BioTek Instruments Inc.). All results were corrected for background absorbance and expressed as the average of duplicate samples.

4 Electrochemical monitoring of the total ROS. Electrochemical measurements were performed with the three-electrode system integrated onto the perfusion chip by a PalmSens potentiostat (PalmSens Instruments, Netherlands). This in-house produced system comprised one Pt disk electrode (250 μm in diameter) sealed in a glass tube (3 mm OD) which served as a working electrode (WE), a Pt wire as a counter electrode and Ag wire with a layer of AgCl operating as a reference electrode. Note that the saline buffer is sufficient to ensure that this reference maintains a constant potential. The AgCl layer was electrochemically coated by placing Ag wire in 100 mM NaCl solution and holding the potential at 0.45 V *vs.* Ag/AgCl (3 M NaCl) for 10 min until the oxidation current tailed to a residual. Potentials are reported *versus* this reference electrode unless otherwise stated. Prior to use, the working electrode was polished with 0.3 μm and 0.1 μm alumina slurry on polishing pads (Kemet International Ltd., Kent, UK), respectively and then successively cleaned in 10% (v/v) HNO_3 and water in an ultrasonic bath. During tests, refreshing of the electrode surface was carried out by wiping the WE on a polishing cloth and rinsing with water. During *in situ* measurements, cleaning of the WE was carried out by electrochemical methods, such as differential pulse voltammetry (DPV) or cyclic voltammetry. During perfusion, cyclic voltammetry was conducted between -0.8 V and 1.0 V at a scan rate of 0.1 V s^{-1} and followed by a square wave voltammetry (SWV) scan from -0.55 V to 1.0 V with a frequency of 25 Hz, amplitude of 25 mV and a step of 5 mV. The first scan of cyclic voltammetry data was used for “non-polishing-mode” analysis while the second scan was used when polishing was undertaken, due to the enhanced sharpness of the feature in the second cycle. The electrochemical measurement was carried out when the stimulation pulse (E_s) was switched off to obviate the deterioration in voltammograms.

Results and discussion

Perfusion system and viability assessment of tissue

1 Establishment of an optimal perfusion system. The dimensions of the tissue samples were optimised so that sufficient oxygen was supplied to the heart tissue sample. Samples with dimensions of approximately $4 \times 2.5 \times 2$ mm^3 were evenly labelled with calcein AM with little PI staining after perfusion for 5 hours (Fig. 2(A)). Larger heart tissue biopsies had a greater distance for oxygen and nutrient permeation from the edge to the

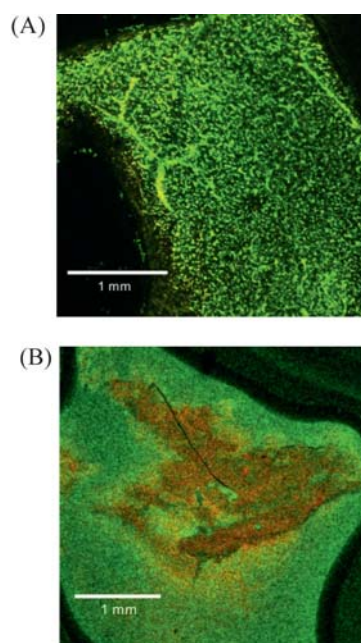


Fig. 2 Representative confocal microscopy images of cardiac tissue sections treated with calcein AM (green fluorescence) and PI (red fluorescence) following 5 h incubation and an hour treatment with 2% (v/v) Triton X100. Tissue size in (A) $\sim 4 \times 2.5 \times 2 \text{ mm}^3$; (B) $\sim 5 \times 3.5 \times 2 \text{ mm}^3$. A $10\times$ objective lens was used. The images were $400\text{--}500 \mu\text{m}$ from the bottom surface of the tissues.

core of the tissue sample; and thus the central region was strongly stained with PI but with a reduced calcein signal (Fig. 2(B)). Flow rates $<100 \mu\text{L min}^{-1}$ meant that the collection of sufficiently sized aliquots took too long for repeated analysis, whereas flow rates $\geq 200 \mu\text{L min}^{-1}$ disturb the tissue and stimulation probes preventing reproducible assessment; see later and ESI† for EC optimisation. A flow rate of $120 \mu\text{L min}^{-1}$ was established as the standard flow rate for all subsequent experiments.

2 Establishment of on-chip electrical stimulation parameters.

The heart tissue in the current study was stimulated electrically to mimic the *in vivo* situation. It was found that the excitation threshold for rat tissue to start beating and be maintained for at least 1 min was 1.0 V cm^{-1} at 2 Hz. Normally, the stimulation regime using square monophasic pulses, for a whole rat heart, occurs for a duration of 5 ms at a frequency of 5 Hz and amplitude of $1.5\text{--}2 \text{ V}$;²⁵ or for approximately 3 ms at a frequency between 0.5 and 1 Hz with a field strength of $5\text{--}6 \text{ V cm}^{-1}$ for single rat ventricular cardiomyocytes.^{26,27} For rat tissue samples of the sizes described in Fig. 2 stimulation started at 0.8 V cm^{-1} and 2 Hz and the electric field was incrementally increased until all or part of the tissue commenced beating. At 1 V cm^{-1} the beating was observed to last more than 1 min. Bubbles due to solvent breakdown formed when the electrical field was $\geq 12 \text{ V cm}^{-1}$. A standardized frequency of 1.5 Hz with an electric field of $3\text{--}4 \text{ V cm}^{-1}$ was chosen in order to obtain prolonged heart beating.

The contractile function of tissue in the perfusion device became more pronounced, and generally lasted for longer periods of time when the calcium concentration in the KH buffer

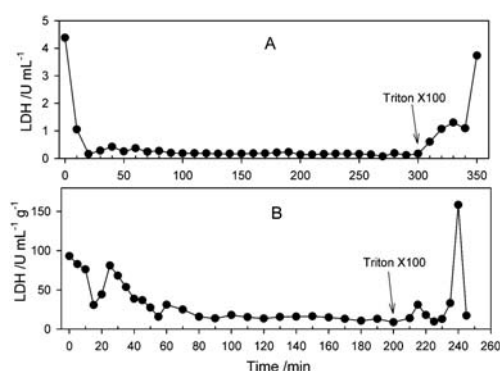


Fig. 3 LDH level in rat (A) or human (B) tissue. Tissues were perfused with oxygenated KHGB until 300 min in (A), and 200 min in (B), followed by 2% (v/v) Triton X100 in KHGB. Stimulation pulse, 4 V cm^{-1} ; 1.5 Hz. The LDH concentration was calculated in U mL^{-1} in (A) and subsequently standardised against the wet weight of human tissue (B). (Representation of three and eleven experiments in (A) and (B), respectively.)

was increased from 1.25 to 2.5 mM. The latter concentration was used as standard for all subsequent experiments.

The optimized conditions ($3\text{--}4 \text{ V cm}^{-1}$, 1.5 Hz, 2.5 mM calcium chloride) maintained the heart tissue with regular contractions for up to 5 hours. Contraction of the electrically excited heart tissue sample was observed *via* a microscope camera (Veho, UK) during the perfusion of the majority of rat tissue biopsies, but only about 40% of human tissue samples showed this trend. The key determinant of damage was LDH release, measured in effluent samples and following incubation of the tissue with Triton X100 at the end of the perfusion period in the device. An alternative method of inducing injury was through perfusion with media containing 95% N_2 -5% CO_2 . It was observed that rat tissue ceased functioning within 10 min after incubation in KHG buffer saturated with this gas, associated with a marked increase in LDH release, similar to that observed after incubation with Triton X100 (Fig. 3).

3 Viability in perfusion device as assessed by LDH release.

Biopsies from right ventricular rat tissue were maintained in a viable state for at least 5 hours (Fig. 3A), whereas for human right atrial tissues, a period of 3.5 hours was the maximum tested (Fig. 3B). LDH activities were high initially in every experiment, most likely due to damage caused when samples were taken and transported to the microdevice. Following this initial peak, the LDH levels remained at low levels, suggesting a recovery from the acute injury due to sufficient supplies of nutrients, oxygen and appropriate electrical stimulation in the flow perfusion chamber. When oxygen was removed from the buffer, electrical stimulation was stopped, or the biopsy was treated with Triton X100, the LDH levels showed a sharp increase within 10–15 minutes, verifying the viability of tissue prior to induction of damage.

The current work here is distinct from tissue engineering constructs in microfluidic systems, which generate new tissues to restore, maintain, or enhance tissue function. The methodology described here allows direct experimentation on primary clinical samples under *in vivo* conditions. Similar work has been

demonstrated by our group using liver tissue²⁸ and colorectal tumour biopsies,²⁹ both of which were kept viable for over 70 hours in the microfluidic environment. The liver tissue produced albumin and urea during perfusion, whereas the colorectal tissue produced vascular endothelial growth factor in response to hypoxia, demonstrating that both cell types were functional and responded in a similar manner to tissue *in vivo*.

ROS monitoring by electrochemistry

ROS or NOS can be measured by various kinds of chemical means.^{11–16} Electrochemical measurement has distinct advantages in terms of sensitivity and speed for real-time assessment, *in situ*. Previously H₂O₂ has been reported to be released at a rate of 50 nmol g⁻¹ min⁻¹ two minutes after an ischaemia/reperfusion episode.³⁰ Following previous work in our laboratory regarding the development of a hydrogen peroxide biosensor, preliminary studies indicated that this enzyme-modified electrode could be employed to measure H₂O₂ using the current methodology.³¹ Given that the half-life of H₂O₂ is longer than that of the other ROS and NOS, we chose to employ direct H₂O₂ oxidation at Pt electrodes as the validation of part of ROS.

1 Species confirmation and identification of the monitoring window. Details regarding the amperometric monitoring of ROS are given in ESI 1†; in summary it was observed that potentials of +0.72 V vs. Ag/AgCl allowed for the oxidative detection of ROS.^{21,32}

2 Control tests. Monitoring the current change continuously in the perfusion system is a challenge because many parameters can cause interference with the electrochemical measurements. The cleanliness of the WE, the presence or absence of oxygen and nitrogen in different stages of the perfusion, Triton X100 and the stimulation for maintenance of the heart “beat” were the main interfering parameters.

Two modes of control test for EC measurement were studied: non-polishing and polishing of the electrode in the relevant buffers. In the first mode, the WE was scanned initially in KH solution from -0.8 V to 1.0 V until a stable response was observed; the electrode remained in place within the chamber during perfusion without cleaning prior to voltammetric measurement. In the second control the WE was polished and rinsed with water before each measurement; Fig. 4 illustrates these results. It was found that the “on/off” stimulation pulse caused fluctuations in the background current measured using cyclic voltammetry or SWV. When no stimulation pulse was applied, the baseline was relatively noise-free and stable with a low standard deviation (Fig. 4a, and ESI 2, Table S1†).

Higher variances of oxidation current (I_O) were observed when electrical stimulation was applied, as expected (region 40–80 min in Fig 4). Glucose and antibiotics were not responsible for this because further tests in KH and KHG buffers suggested a similar fluctuation within this period (Fig. 4b and c). When electrical stimulation is applied ionic species will redistribute around the pulse probes to form electrical double layers, which may alter the background current of a voltammetric measurement each time this stimulation is turned on. In order to mitigate this effect EC measurement was delayed for 5 seconds after the pulse ceased to

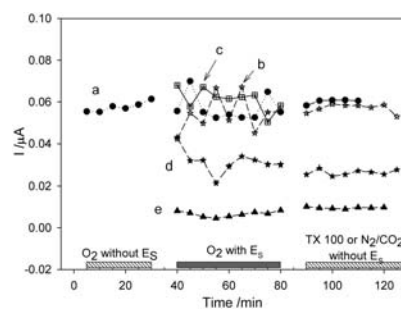


Fig. 4 Control tests in different buffer solutions using polished electrodes. Between 0–30 min and 90–125 min, no stimulation pulse; 40–80 min, stimulation pulse on while not conducting EC measurement. I_O at 0.72 V in cyclic voltammetry in KHGB buffer with Triton X100 from the 90th min (a, solid circle), in KHG with 95% N₂-5% CO₂ from the 90th min (b, empty star) and in KH (c, square-cross). I_O at 0.3 V in SWV with 95% N₂-5% CO₂ from 90 min, in KHG (d, solid star), and KHGB (e, solid triangle). Flow rate: 120 $\mu\text{L min}^{-1}$ for all perfusions. (Representative of three independent experiments.)

ensure sufficient time for the double layer around the electrode to resettle in the presence of freshly flowing buffer.

3 Study of induction of injury and *in situ* EC measurement. In Triton X100–KHGB with no electrical stimulation (90 to 125 min), the background current I_O at 0.72 V in cyclic voltammetry fluctuated by up to $\pm 10\%$ compared with those between 40 and 80 min without Triton X100; whilst in 95% N₂-5% CO₂–KHGB, I_O increased less than 6% on average (Fig. 4). The surfactant was reported to enhance efficiently the electron transfer between solution and electrode surface due to its strong adsorption on the hydrophobic electrode surface.³³ Since the use of Triton X100 in tissue-free buffer caused an increased signal of up to 10%, the tissue would be considered alive before the assault only when the current measured in EC increased by more than 15%.

In order to achieve *in situ* EC measurement, a non-polished electrode was first used. The baseline was found to be smooth and stable when there were no electrical stimulation periods but suffered poor reproducibility and a decreasing baseline when stimulation pulses were switched on. The average I_O decreased more than 20% with addition of Triton X100, and the relative standard deviation was 12% on average. The WE also became easily contaminated during voltammetry scans. This was confirmed by using a Pt disk electrode in *N,N,N',N'*-tetramethyl-*p*-phenylenediamine solutions (TMPD, Sigma) before and after cyclic voltammetry scans in KHGB and KH (ESI 3, Fig. S2†). Distorted voltammograms were observed in the range of 0.05 V to -0.02 V in the TMPD solution after scans in KH buffers. However, when operating in the non-polishing mode, it was necessary to minimise disturbances of the device once established, hence a method for cleaning the electrode *in situ* by electrochemistry was designed. DPV and cyclic voltammetry, which scan to high potentials (from -0.5 V to 1.5 V with the E_S -on), were demonstrated to clean the WE effectively *in situ*, when fouling was observed by increased reduction currents around 0.8 V in cyclic voltammograms.

In order to increase the sensitivity of the EC measurement and shorten the record time, thus limiting any potential disruption of

the perfusion, measurement of ROS by SWV was also studied. Generally, the average I_0 at 0.25 V in SWV was smaller than that in cyclic voltammetry (Fig. 4 (d, KHG) and (e, KHGB)). This lower current at 0.25 V in KHGB is due to the presence of antibiotics ((d) in Fig. S1A, inset†), which may induce electrode surface blocking after the SWV scan. This can be found in 90–125 min area when 95% N₂-5% CO₂ took the place of O₂ and electrical stimulation was off; the standard deviation was better than in cyclic voltammetry, whilst the variance of I_0 after N₂ treatment was $\pm 20\%$, higher than in cyclic voltammetry.

4 ROS results compared with LDH and H₂O₂ assays. Fig. 5A shows the results of LDH and *in situ* EC measurement of ROS in real time. The electrode was cleaned by the EC method described above. The profile of LDH release (measured off-chip) and EC agreed well, with relatively high levels in the early stage of the perfusion, this then decreased and remained low until a sharp increase was induced with the addition of Triton X100. The electrode was cleaned by DPV with scans from -0.8 V to 1.5 V before the 25th, 55th, 140th and 190th min, when the WE was contaminated (an early sign was increased cathodic current around 0.8 V in cyclic voltammetry). The decrease of signal at the 55th and 190th min accordingly is likely to be due to this action. It was noted that the length of time between obtaining the biopsy and placing this in the chamber was correlated with electrode contamination, *i.e.* when placed in the device within 5 minutes, little electrode contamination was observed; unfortunately the human tissue had to be transported from the hospital site and took up to 60 min from biopsy to device.

Fig. 5B shows the comparison of LDH, H₂O₂ release with total ROS by electrochemical measurement in a polishing mode. During perfusion, cyclic voltammetry and SWV measurements

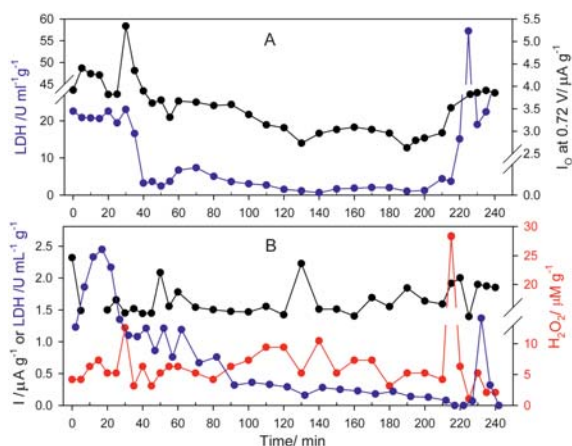


Fig. 5 Comparison of LDH, H₂O₂ and total ROS by EC in human sample perfusion. (A) Release of LDH (blue circles) and ROS by cyclic voltammetry (filled circles). *In situ* electrode cleaning by DPV, scanning from -0.5 V to 1.5 V before the 25th, 55th, 140th and 190th min. (B) LDH (blue circles), H₂O₂ (red circles) from Amplex Red assay and ROS by cyclic voltammetry (filled circles) with perfusion. The electrode was polished before each scan. Perfusion with 95% O₂-5% CO₂-KHGB with E_s until the 200th min then electrical stimulation was turned off and the sample was incubated with Triton X100-KHGB in (A), or 95% N₂-5% CO₂-KHGB in (B). Stimulation pulse: 4 V cm⁻¹, 1.5 Hz; EC measurements were carried out with the pulse off. (Representative of three independent experiments.)

took 1.5 min, while it took 2 min to collect sufficient effluents for H₂O₂ assay and another 2 min for LDH analysis. Taking these small differences into account, the LDH release matched the H₂O₂ levels, except between 100 and 160 min where there was a raised level of H₂O₂, with only minor fluctuations in LDH. However, the I_0 in cyclic voltammetry and SWV agreed well with the H₂O₂ assay results in the main, especially at 130 min where LDH did not detect damage (see ESI 4, Fig. S3† for SWV results).

The [H₂O₂] at 220 min was determined to be 1.18 μM from the off-chip biochemical assay and 3 μM by electrochemical means after calibration with standard H₂O₂ in the flow system (ESI 5, Fig. S4†), indicating that the total ROS included H₂O₂ plus additional ROS. As stated above it has been reported that H₂O₂ was released from rat heart tissue at a rate of 50 nmol g⁻¹ min⁻¹ two minutes after an ischaemia/reperfusion incident.³⁰ Given the chamber size of the device used in this work was 0.4 mL, with a tissue weight of 0.03 g, these parameters would give an H₂O₂ concentration of approximately 3.75 μM min⁻¹ for our tissue. In contrast, a release rate of 3×10^{-18} mol s⁻¹ per cell for H₂O₂ by human neutrophils has been reported.³⁴ Assuming an average rat or human cardiomyocyte from the ventricle has a volume $30\,000$ μm³ (this varies considerably with age and sex)³⁵ and tissue biopsy dimensions of $2 \times 4 \times 4$ mm³ would give a calculation of 0.48 μM min⁻¹ for H₂O₂. These values do not take into account differences in cell type, nature of the cell sample, *i.e.* in the tissue a restricted number of cells are initially exposed to the Triton X100, or stimulation method, however the production rates are of a similar scale. Interestingly the H₂O₂ release occurred prior to LDH, indicating that oxidative damage preceded membrane damage and LDH release.

It was found that 95% N₂-5% CO₂ was a good alternative to Triton X100 for inducing cell damage, due to the gas having less effect on the background current in cyclic voltammetry. It induced a similar release of LDH 10 min earlier than Triton X100 did (the 240th min in Fig. 3B and the 230th min in Fig. 5B). However, the LDH rise was smaller than that caused by the detergent treatment. This is most likely due to Triton acting directly on the cell membranes rather than an indirect effect associated with a lack of oxygen. It is hypothesised that longer periods of perfusion with the 95% N₂-5% CO₂ media would result in a similar level of cell rupture and LDH release.

Conclusions

A microfluidic device has been developed for heart tissue perfusion with real-time electrochemical monitoring of ROS release. Having optimized the perfusion and stimulation conditions, it is possible to maintain viable tissue biopsies from rat and human tissue for up to 300 min, a typical time frame for current *in vitro* models. *In situ*, real-time electrochemical measurement of total ROS was achieved, matching the release of LDH determined off-chip. Both cyclic voltammetry and square wave voltammetry have been utilised to monitor ROS levels and the concentrations detected have been verified by biochemical assay of H₂O₂. In summary, this study describes a novel method to monitor continuously the change of ROS and other factors in heart tissue biopsies, and will facilitate investigations of normal

and pathological cardiac functions *ex vivo*, whilst mimicking the *in vivo* environment.

Acknowledgements

Thanks are given to Mr Steven Griffin (Castle Hill Hospital) for providing the human cardiac biopsies. This study was supported by Heart Research UK (RG2538/07/10) and BBSRC (BB/E002722/1).

References

- 1 H. Zimmer, *News Physiol. Sci.*, 1998, **13**, 203–210.
- 2 A. Akki, K. Smith and A.-M. L. Seymour, *Mol. Cell. Biochem.*, 2008, **311**, 215–224.
- 3 S. Zhang, *Nat. Biotechnol.*, 2004, **22**, 151–152.
- 4 J. H. Yeon and J. Park, *Biochip J.*, 2007, **1**, 17–27.
- 5 P. J. Hung, P. J. Lee, P. Sabounchi, R. Lin and L. P. Lee, *Biotechnol. Bioeng.*, 2005, **89**, 1–8.
- 6 X. Li and P. C. H. Li, *Anal. Chem.*, 2005, **77**, 4315–4322.
- 7 X. Li, J. Huang, G. F. Tibbits and P. C. H. Li, *Electrophoresis*, 2007, **28**, 4723–4733.
- 8 W. Cheng, N. Klauke, H. Sedgwick, G. L. Smith and J. M. Cooper, *Lab Chip*, 2006, **6**, 1424–1431.
- 9 E. J. Lesnefsky, S. Moghaddas, B. Tangler, J. Kerner and C. L. Hoppel, *J. Mol. Cell. Cardiol.*, 2001, **33**, 1065–1089.
- 10 W. Dröge, *Physiol. Rev.*, 2002, **82**, 47–95.
- 11 C. Lu, G. Song and J. Lin, *TrAC, Trends Anal. Chem.*, 2006, **25**, 985–995.
- 12 R. Mahfouz, R. Sharma, J. Lachner, N. Aziz and A. Agarwal, *Fertil. Steril.*, 2009, **92**, 819–827.
- 13 J. R. Henderson, D. A. Fulton, C. J. McNeil and P. Manning, *Biosens. Bioelectron.*, 2009, **24**, 3608–3614.
- 14 H. Li, Q. Li, X. Wang, K. Xu, Z. Chen, X. Gong, X. Liu, L. Tong and B. Tang, *Anal. Chem.*, 2009, **81**, 2193–2198.
- 15 A. Chandrasekaran and M. Packirisamy, *J. Biomed. Opt.*, 2009, **14**(5), 054050.
- 16 N. Weissmann, N. Kuzkaya, B. Fuchs, V. Tiyerili, R. U. Schäfer, H. Schütte, H. A. Ghofrani, R. T. Schermuly, C. Schudt, A. Sydykov, B. Egemnazarow, W. Seeger and F. Grimminger, *Respir. Res.*, 2005, **6**, 86.
- 17 C. Amatore, S. Arbault, C. Bouton, K. Coffi, J. C. Drapier, H. Ghandour and Y. H. Tong, *ChemBioChem*, 2006, **7**(4), 653–661.
- 18 S. J. Starkey, A. L. Grant and R. M. Hagan, *Br. J. Pharmacol.*, 2001, **134**, 1084–1092.
- 19 J. J. O'Connor and C. O'Neill, *Sensors*, 2008, **8**, 5516–5534.
- 20 C. Amatore, S. Arbault and A. Koh, *Anal. Chem.*, 2010, **82**(4), 1411–1419.
- 21 C. Amatore, S. Arbault, Y. Chen, C. Crozatier and I. Tapsoba, *Lab Chip*, 2007, **7**, 233–238.
- 22 C. G. J. Schabmueller, D. Loppow, G. Piechotta, B. Schütze, J. Albers and R. Hintsche, *Biosens. Bioelectron.*, 2006, **21**, 1770–1776.
- 23 P. S. C. Preté, S. V. P. Malheiros, N. C. Meirelles and E. de Paula, *Biophys. Chem.*, 2002, **97**, 1–5.
- 24 A. J. Racher, D. Looby and J. B. Griffiths, *Cytotechnology*, 1990, **3**, 301–307.
- 25 M. L. Field, A. Azzawi, P. Styles, C. Henderson, A.-M. L. Seymour and G. K. Radda, *Cell Calcium*, 1994, **16**, 87–100.
- 26 N. Klauke, G. Smith and J. Cooper, *Lab Chip*, 2007, **7**, 731–739.
- 27 N. Klauke, G. Smith and J. Cooper, *Biophys. J.*, 2003, **85**, 1766–1774.
- 28 S. M. Hattersley, C. E. Dyer, J. Greenman and S. J. Haswell, *Lab Chip*, 2008, **8**, 1842–1846.
- 29 A. Webster, C. E. Dyer, S. J. Haswell and J. Greenman, *Anal. Methods*, 2010, **2**, 1005–1007.
- 30 J. Slezak, N. Tribulova, J. Pristacova, B. Uhrík, T. Thomas, N. Khaper, N. Kaul and P. K. Singalt, *Am. J. Pathol.*, 1995, **147**, 772–781.
- 31 Y. Dou, S. Haswell, J. Greenman and J. Wadhawan, *Electrochem. Commun.*, 2009, **11**, 1976–1981.
- 32 R. Kohen, *J. Pharmacol. Toxicol. Methods*, 1993, **29**, 185–193.
- 33 S. Zhang, K. Wu and S. Hu, *Talanta*, 2002, **58**, 747–754.
- 34 S. Shleev, J. Wettero, K. E. Magnusson and T. Ruzgas, *Cell Biol. Int.*, 2008, **32**, 1486–1496.
- 35 S. E. Campbell, K. Rakusan and A. M. Gerdes, *Basic Res. Cardiol.*, 1989, **84**, 247–258.

A microfluidic device for tissue biopsy culture and interrogation

Abigail Webster,^a Charlotte E. Dyer,^b Stephen J. Haswell^a and John Greenman^{*b}

Received 4th May 2010, Accepted 23rd June 2010

DOI: 10.1039/c0ay00293c

This communication reports the development of a microfluidic device capable of maintaining the long-term culture of viable tissue biopsies. Tissue-based models will enable evaluation of cell–cell and cell–matrix interactions within multi-cellular systems. The device demonstrated is a prototype, fabricated with the capacity to receive biopsy samples up to 2 mm³, from various tissue sources. Presently, this system has been tested with human colorectal tissue biopsies, for periods in excess of 3 days. The response of normal colorectal tissue and neoplastic biopsies to hypoxia was assayed by the release of vascular endothelial growth factor (VEGF) into the media, which was measured off-chip. As anticipated, the hypoxia induced a greater VEGF response in the tumour biopsies than the non-malignant tissue.

The application of microfluidic devices to the analysis of biological samples is a rapidly developing field. Culturing tissue biopsies in a microfluidic device will provide a more holistic model for detecting cellular response to changes, such as drug stimuli, because the device can accurately reproduce many of the key parameters of the *in vivo* environment. Compared with a traditional cell culture model, biopsy tissue retains the complex cell–cell and cell–matrix communication/interaction; furthermore tissue biopsies are far less likely to undergo surface marker changes, a phenomenon that occurs over time with cell culture as essentially a portion of the tissue in its native state is being studied. Advances in 3D culturing¹ and tumour spheroid models² have been reported recently as it is believed these will provide superior models of tumour response to anticancer drugs in preclinical *in vitro* experiments. Whilst a great deal of literature describes cell culture within microfluidic devices,^{3,4} relatively few report whole tissue based methodology due to the difficulty in culturing this type of sample. Previous work within this area has largely been restricted to culturing ultra-thin brain tissue slices in polydimethylsiloxane (PDMS) devices for a maximum of 3 h.^{5–7} Culturing tissue biopsies, not cells, in excess of 24 hours would generally be considered long-term.⁸

The most important factors when culturing cells or tissue are temperature, sterility, nutrients (*via media*) and gas supply. Gas saturation of media is essential as media require pH stabilisation using CO₂, while gas concentrations, especially O₂, are vital to the normal functioning of cellular processes. Tissue hypoxia, resulting from inadequate oxygen supply, compromises cellular functions and in tumours can be described as a pathophysiological consequence of a functionally and structurally disturbed microcirculation. Hypoxia not only affects tumour cells directly, but is also an important

parameter to be considered when investigating drug treatments, *i.e.* hypoxic regions within the tumour microenvironment will alter the local pH and drug sensitivity.⁹ During cancer progression, the neoplastic tissue grows too large for diffusion to supply the nutrient needs of the inner cell mass. The neoplastic tissue releases a variety of factors including vascular endothelial growth factor (VEGF), a fundamental neovascularisation factor,¹⁰ which is required to stimulate angiogenesis and thus create new supply routes that will provide the rapidly dividing tumour mass with essential nutrients. Overexpression of VEGF has been demonstrated in almost all solid tumours including colonic neoplasms.¹¹ Critically low gaseous supply can be generated in the laboratory to mimic the process by creating a hypoxic environment, and tumours release VEGF in response to this stimulation.¹² Hence, VEGF is a useful biomarker for monitoring the response of normal and neoplastic tissue biopsies to changes in the microenvironment within the tissue cavity of the prototype device due to changes in the gassing regime.

Results and discussion

The microfluidic device was designed using AutoCAD software and was fabricated in-house according to published procedures¹³ with some adaptation. Briefly, the channel network (50 μm deep) was fabricated by photolithography on B270 super white crown glass (1 mm thick). A 3 mm top-plate was predrilled with 1.25 mm diameter holes to accommodate the tubing and a central 3 mm tissue cavity (Fig. 1A). The two plates were then thermally bonded in a muffle furnace. A flat bottomed nanoport assembly with an internal diameter of 6.4 mm (Upchurch Scientific, UK) was adhered to the top-plate over the tissue cavity, using thermally activated glue according to the manufacturer's instructions, to enable easy access for insertion or removal of tissue biopsies (Fig. 1B).

The experimental assembly offers a high degree of fluidic and gas saturation control and the potential for manipulating the tissue microenvironment. The device was attached to a peristaltic pump (Minipuls 3, Gilson, France) that provided in-line filtered (Millipore 0.22 μm PES membrane, Millipore Ireland), gas-saturated media of known concentrations (Fig. 1C). A 30 ml reservoir of Dulbecco's Modified Eagle Medium (DMEM) supplemented with 10% (v/v) fetal calf serum and penicillin/streptomycin (10 unit per ml) (Invitrogen, UK) was gassed with 75% O₂/20% N₂/5% CO₂. Prior to each experiment, a microdevice was primed with this medium.

Temperature was kept at a constant 37.5 ± 0.2 °C using a hotplate (Stuart CB160), monitored with an optical temperature probe (OpSens, Hart Scientific, UK) located directly under the tissue chamber. pH stabilisation of the media was achieved using 5% CO₂ in both gas mixtures and was verified by measuring the pH of the media after it had flowed through an empty, sterile microdevice. The pH was stable at 7.4 when no tissue was present in the device, minor fluctuations in pH were seen when the device contained tissue, which

^aDepartment of Chemistry, University of Hull, Cottingham Rd, Hull, UK

^bDivision of Cancer, Postgraduate Medical Institute, University of Hull, Hull, UK. E-mail: j.greenman@hull.ac.uk; Fax: +44 (0)1482466996; Tel: +44 (0)1482466032

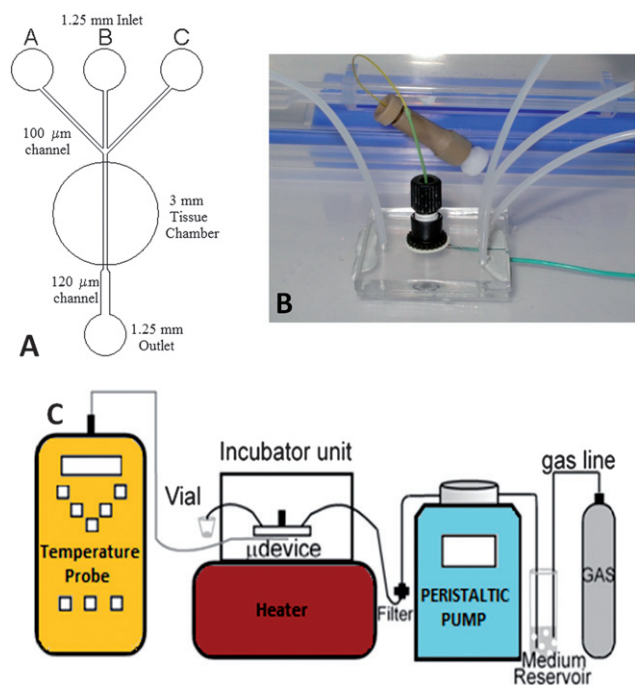


Fig. 1 (A) Channel schematic of the device. (B) Photograph showing the glass microdevice with attached nanoport. (C) General schematic of the assembly showing the pumping system, gassing to media reservoir and flow of the system.

was most probably due to changes caused by the tissue and the factors released.

Tissue was taken following ethics approval from Hull and East Yorkshire Local Research Ethics Committee 07/H1304/105 and NHS Trust R0568. Colorectal tissue biopsies, normal and neoplastic, were sectioned and a sample weighing approx. 5–10 mg was then placed in the device. The control was tissue taken from the distal region of the tumour biopsy. The tissue was perfused with supplemented DMEM at a flow rate of $1 \mu\text{l min}^{-1}$. After a period of normoxia (18 h), this was replaced by perfusion with an aliquot of supplemented DMEM saturated with 95% $\text{N}_2/5\% \text{CO}_2$, at the same flow rate, to generate a hypoxic environment. After approximately 26 h the medium was changed to supplemented DMEM that had been O_2 purged and normoxia was restored for 22 h, finishing with a second (4 h) period of hypoxia. During this time, aliquots of the supernatant were collected at 2 h intervals after flow over the tissue, however overnight samples were collected for a 16 h period. The supernatant was frozen immediately after collection and analysed for VEGF release using a commercial ELISA (R&D Systems, UK). Samples were measured in triplicate and the results were normalised for VEGF concentration per mg of tissue.

The tumour tissue responded to the hypoxic conditions of the gas regime with an enhanced production of VEGF, as measured by ELISA. The normal tissue also responded with a release of VEGF, but at lower levels, which is in accord with the expected *in vivo* response as colorectal neoplastic tissue is known to overexpress VEGF.¹¹ The release of VEGF was reduced when the gaseous microenvironment was restored to normoxia, and subsequently a reduction in the amount of VEGF was seen in the supernatant, these results are shown in Fig. 2.

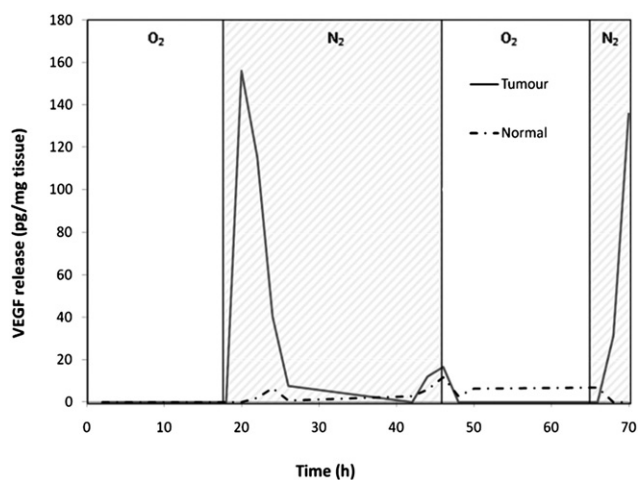


Fig. 2 Results from the ELISA showing the expression of VEGF in response to changes in the gas regime. The tumour tissue shows a greater increase of VEGF release than seen with the normal tissue after the hypoxic period (N_2/CO_2 gassed media). Hypoxic periods are indicated by cross-hatched N_2 areas on the graph. Data shown are representative of 3 similar experiments.

Summary

Initial testing of this experimental system has shown adequate gas saturation and sterile media delivery, which enables the long-term culturing of tissue. It is expected that the microfluidic device will now be used to investigate chemotherapeutic drugs that prevent proliferation and/or induce apoptosis by assaying VEGF and other relevant biomarkers. For the majority of *in vitro* studies, apart from those on blood cells, tissues are disaggregated and cultured as individual cell populations, with the concomitant loss of cell organisation and interaction with a tissue-specific extracellular matrix. With the advent of tissue engineering the complexity and importance of the 3D structure has become very apparent for normal¹⁴ and disease processes.¹⁵ Furthermore, it is acknowledged that many of the 3D models or co-cultures cannot yet represent the natural or pathophysiological state, although many studies are in progress to address this problem.¹⁶ The simplistic and flexible design of the current system offers a device that will be capable of real time analytical interrogation of various tissue types, supporting a variety of diverse applications in which a microfluidic tissue device can be used to guide drug treatment selection in a clinical setting. This will be particularly valuable for diseases where a cocktail of drugs are required, for example in cancer therapy. This research is timely in driving towards less animal-reliant testing in the pharmaceutical industry and more personalised care in the medical arena. It also offers the potential for development of point-of-care units capable of assessing the suitability of drug treatments prior to administration to patients, providing more cost effective and, more importantly, clinically effective treatments.

Acknowledgements

We gratefully acknowledge the support of the BBSRC (Grant no. BB/E002722/1), members of the Academic Surgical Unit for tissue biopsies and Dr Leigh Madden for invaluable discussions and advice.

References

- 1 J. Vukasinovic, D. K. Cullen, M. C. Laplaca and A. Glezer, *Biomed. Microdevices*, 2009, **11**, 1155–1165.
- 2 Y. S. Torisawa, A. Takagi, Y. Nashimoto, T. Yasukawa, H. Shiku and T. Matsue, *Biomaterials*, 2007, **28**, 559–566.
- 3 B. G. Chung, J. W. Park, J. S. Hu, C. Huang, E. S. Monuki and N. L. Jeon, *BMC Biotechnol.*, 2007, **7**, 60.
- 4 J. H. Wittig, A. F. Ryan and P. M. Asbeck, *J. Neurosci. Methods*, 2005, **144**, 79–89.
- 5 A. J. Blake, T. M. Pearce, N. S. Rao, S. M. Johnson and J. C. Williams, *Lab Chip*, 2007, **7**, 842–849.
- 6 Y. Choi, M. A. McClain, M. C. LaPlaca, A. B. Frazier and M. G. Allen, *Biomed. Microdevices*, 2007, **9**, 7–13.
- 7 P. A. Passeraub, A. C. Almeida and N. V. Thakor, *Biomed. Microdevices*, 2003, **5**, 147–155.
- 8 S. M. Hattersley, C. E. Dyer, J. Greenman and S. J. Haswell, *Lab Chip*, 2008, **8**, 1842–1846.
- 9 O. Tredan, C. M. Galmarini, K. Patel and I. F. Tannock, *J. Natl. Cancer Inst.*, 2007, **99**, 1441–1454.
- 10 T. Tokunaga, Y. Oshika, Y. Abe, Y. Ozeki, S. Sadahiro, H. Kijima, T. Tsuchida, H. Yamazaki, Y. Ueyama, N. Tamaoki and M. Nakamura, *Br. J. Cancer*, 1998, **77**, 998–1002.
- 11 L. F. Brown, B. Berse, R. W. Jackman, K. Tognazzi, E. J. Manseau, H. F. Dvorak and D. R. Senger, *Am. J. Pathol.*, 1993, **143**, 1255–1262.
- 12 K. Toshio, K. Yasuhiko, T. Shinji, O. Seiji, M. Norimasa, K. Eijiro, I. Masanori and C. Kazuaki, *Int. J. Cancer*, 2003, **105**, 176–181.
- 13 T. McCreedy, *Anal. Chim. Acta*, 2001, **427**, 39–43.
- 14 L. G. Griffith and A. S. Melody, *Nat. Rev. Mol. Cell Biol.*, 2006, **7**, 211–224.
- 15 P. Friedl and K. Wolf, *Nat. Rev. Cancer*, 2003, **3**, 362–374.
- 16 M. P. Schwartz, B. D. Fairbanks, R. E. Rogers, R. Rangarajan, M. H. Zaman and K. S. Anseth, *Integr. Biol.*, 2010, **2**, 32–40.

This article was downloaded by: [Deakin University Library]

On: 06 July 2014, At: 17:51

Publisher: Taylor & Francis

Informa Ltd Registered in England and Wales Registered Number: 1072954 Registered office: Mortimer House, 37-41 Mortimer Street, London W1T 3JH, UK



Separation Science and Technology

Publication details, including instructions for authors and subscription information:

<http://www.tandfonline.com/loi/lst20>

Microfluidic Chromatography for Early Stage Evaluation of Biopharmaceutical Binding and Separation Conditions

Michael S. Shapiro^a, Stephen J. Haswell^b, Gary J. Lye^a & Daniel G. Bracewell^a

^a The Advanced Centre for Biochemical Engineering, Department of Biochemical Engineering, University College London, Torrington Place, London, UK

^b Department of Chemistry, University of Hull, Hull, UK

Published online: 18 Jan 2011.

To cite this article: Michael S. Shapiro, Stephen J. Haswell, Gary J. Lye & Daniel G. Bracewell (2010) Microfluidic Chromatography for Early Stage Evaluation of Biopharmaceutical Binding and Separation Conditions, Separation Science and Technology, 46:2, 185-194, DOI: [10.1080/01496395.2010.511641](https://doi.org/10.1080/01496395.2010.511641)

To link to this article: <http://dx.doi.org/10.1080/01496395.2010.511641>

PLEASE SCROLL DOWN FOR ARTICLE

Taylor & Francis makes every effort to ensure the accuracy of all the information (the "Content") contained in the publications on our platform. However, Taylor & Francis, our agents, and our licensors make no representations or warranties whatsoever as to the accuracy, completeness, or suitability for any purpose of the Content. Any opinions and views expressed in this publication are the opinions and views of the authors, and are not the views of or endorsed by Taylor & Francis. The accuracy of the Content should not be relied upon and should be independently verified with primary sources of information. Taylor and Francis shall not be liable for any losses, actions, claims, proceedings, demands, costs, expenses, damages, and other liabilities whatsoever or howsoever caused arising directly or indirectly in connection with, in relation to or arising out of the use of the Content.

This article may be used for research, teaching, and private study purposes. Any substantial or systematic reproduction, redistribution, reselling, loan, sub-licensing, systematic supply, or distribution in any form to anyone is expressly forbidden. Terms & Conditions of access and use can be found at <http://www.tandfonline.com/page/terms-and-conditions>

Microfluidic Chromatography for Early Stage Evaluation of Biopharmaceutical Binding and Separation Conditions

Michael S. Shapiro,¹ Stephen J. Haswell,² Gary J. Lye,¹ and Daniel G. Bracewell¹

¹The Advanced Centre for Biochemical Engineering, Department of Biochemical Engineering, University College London, Torrington Place, London, UK

²Department of Chemistry, University of Hull, Hull, UK

Optimization of separation conditions for biopharmaceuticals requires evaluation of a large number of process variables. To miniaturize this evaluation a microfluidic column (1.5 µL volume and 1 cm height) was fabricated and packed with a typical process scale resin. The device was assessed by comparison to a protein separation at conventional laboratory scale. This was based upon measurement of the quality of packing and generation of breakthrough and elution curves. Dynamic binding capacities from the microfluidic column compared well with the laboratory scale. Microfluidic scale gradient elution separations also equated to the laboratory column three orders of magnitude larger in scale.

Keywords breakthrough; elution; ion exchange; microfluidics

INTRODUCTION

Ion exchange chromatography is a commonly used separation process within the biopharmaceutical industry. The charged stationary phase will interact, bind, and separate an oppositely charged macromolecule such as a protein or DNA present in the mobile phase. Cation exchange occurs where the stationary phase is negatively charged and the macromolecule in the mobile phase has a net positive charge, while the opposite situation occurs in the case of anion exchange chromatography (1,2). In assessing chromatographic performance, plate analysis combined with frontal and elution chromatography is commonly used (2). Frontal chromatography (or breakthrough) is the process by which the column becomes saturated with the biological macromolecule contained within the mobile phase, while elution chromatography involves the separation of solutes using a step or linear gradient, usually via increased salt concentration (2).

Biopharmaceuticals represent an internationally important and growing industry sector (3). This is especially

highlighted in the field of chromatography where there are an ever increasing number of stationary phase materials available from suppliers each offering improved separations and recovery yields. During bioprocess development biopharmaceutical companies generally have restricted time and resources to analyse each of these resins for a specific purification process. Microfluidic scale chromatography columns, requiring minimal quantities of resin and product molecule, offer potential advantages in this respect. Additionally, many experimental variables such as protein concentration, buffer type, pH, flowrate, etc. may be investigated in systems that have the possibility to be used in parallel and in Lab-on-a-chip formats. Possibilities include sample preparation and eluate analysis on a single microfluidic chip (4).

There have been a number of approaches described in the literature recently to small-scale chromatography evaluation. The majority relate to 96-well microtiter filter plate technologies (micro-batch adsorption) (5) as well as resin-packed micro-pipette tips (micro-tip columns) (6,7). Additionally, more conventional mini columns have also been described (8). In each case parallelization of experimentation is achieved by integration with a laboratory liquid handling robot. Fig. 1 summarizes the available technologies (9) and also compares the scales of operation to the microfluidic approach established here.

Micro-batch adsorption is operated using a batch mode such that the resin is contained within the microwell plate while the remaining liquid is captured by using aspiration or filtration. Linear gradients cannot be performed using this technique; however, pseudo linear gradients have been developed using a series of increasing ionic strength batch adsorption steps (10). This approach has been applied to both breakthrough and elution chromatography yielding results that can compare favorably with laboratory scale columns (11–15). Micro-pipette tip systems also operate in batch mode; however, the solute containing fluid is moved in both directions through the resin bed by repeated automated aspiration and dispensing of the sample. This

Received 31 March 2010; accepted 26 July 2010.

Address correspondence to Daniel G. Bracewell, Department of Biochemical Engineering, Torrington place, London WC1E 7JE, United Kingdom. Tel.: +44 (0)207 679 2374; Fax: +44 (0)207 209 0703. E-mail: d.bracewell@ucl.ac.uk

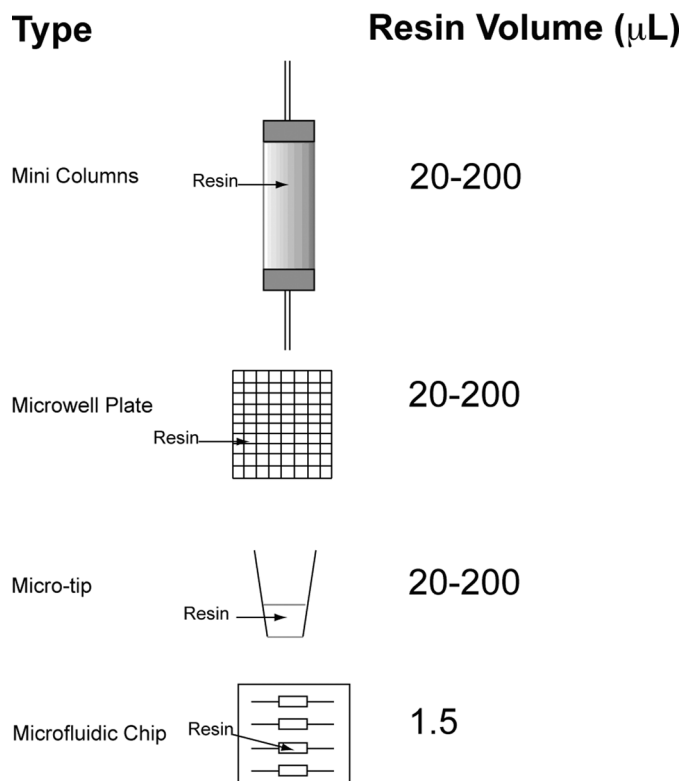


FIG. 1. A selection of the microscale chromatography technologies currently available. The first three are designed for use with a laboratory automation platform, while the fourth is the microfluidic chip presented here.

approach offers enhanced solute mass transfer under flow conditions and we have recently demonstrated its application to the miniaturization of virus-like particle purification (6). The more conventional mini columns (50, 100, 200 μL) resemble most closely standard laboratory chromatography columns. They are operated as part of a 96 microwell plate system where the mobile phase is pumped through the column in one direction. Such systems have been successfully used for the determination of dynamic binding capacity and elution chromatography of proteins (8).

While offering certain advantages none of these technologies truly operate as a chromatography column offering continuous mobile flow with either linear or gradient elution. Previously, we described the fabrication and flow characterization of a microfluidic chromatography column that has the necessary flow characteristics and which operates at at least a 20,000-fold smaller scale than standard laboratory scale columns. Dynamic binding capacities were generated that were comparable with those found within the literature (16) for laboratory scale columns. In this work study of the 1.5 μL microfluidic column is extended to both dynamic binding and separation studies with model protein solutions of either lysozyme or a mixture of hen egg

white proteins. The column is packed with a polydisperse 6% agarose process resin, Sepharose 6FF, in order to resemble the columns used in the ultimate large scale applications. In this way the work is distinct from the small scale columns used in proteomics studies which are based on very small, monodisperse resins and which separate only digested protein fragments rather than whole proteins (17). When compared to results obtained on conventional laboratory scale columns the microfluidic column shows almost quantitative agreement in dynamic binding capacity and gives a good indication of separation conditions.

MATERIALS AND METHODS

Materials

All chemicals were purchased from Sigma-Aldrich (Dorset, UK), apart from the fluorescein-5-isothiocyanate (FITC) which was purchased from Invitrogen (Paisley, UK), and were of the highest purity available. The chromatography resins, Sulfopropyl (SP) and Quaternary Amine Sepharose (Q) Fast Flow, were bought from GE Healthcare UK Ltd (Buckinghamshire, UK). Chicken eggs were purchased locally from Tesco (London, UK). All tubing, the connectors and the MilliGAT pump, were purchased from Presearch (Hampshire, UK). All buffers were prepared using analytical grade water (Millipore, Watford, UK).

Packing and HETP Measurements for the Laboratory Scale Columns

The 2 or 30 mL columns of Q or SP Sepharose Fast Flow (6% agarose) were gravity settled and flow packed at a velocity of 300 cm h^{-1} into an XK 16/20 Column to a height of 15 cm. To gravity pack, the bottom adaptor was placed on the bottom of the XK column then 30–35 mL of SP Sepharose Fast Flow in 20% (v/v) ethanol was poured into the column. The adaptor was opened to allow the ethanol to drip out. More matrix was then gently poured into the top of the column to ensure the height reached 17 cm. Once the matrix had formed a stable bed, the bottom adaptor was sealed and further addition of 20% (v/v) ethanol was added to the top of the column until a meniscus was formed. The top adaptor was connected to an AKTA Basic (GE Healthcare) and was placed at a 45° angle onto the top of the bed. Then, using a flowrate of 0.5 mL min^{-1} of ethanol to avoid air bubbles, the bottom adaptor was opened to ready the column for flow packing. The flowrate was slowly increased to 10 mL min^{-1} (300 cm h^{-1}) until the column had compressed to 15 cm, then the top adaptor was placed on top of the bed. The packing quality was then tested by producing a conductivity peak using a 100 μL sample loop filled with 2 M NaCl at 0.5 mL min^{-1} . The HETP and asymmetry of the peak were then calculated.

Laboratory Column Breakthrough Measurements

Each SP Sepharose 6FF column was equilibrated with 5 Column Volumes (CVs) of 0.05 M sodium phosphate buffer pH 5.5 (start buffer). This buffer system was selected to have a large buffering pH range; however, at pH 5.5 it is limited, and to ensure capacity results were not impacted by this selection they were validated against a sodium acetate system. Lysozyme (1 mg mL^{-1}) from egg white in the same buffer was continually pumped through at either 9, 7.5, 5, or 2 mL min^{-1} (270 , 225 , 150 , and 60 cm h^{-1} calculated on the basis of an XK 16/20 column). When breakthrough was achieved, the column was washed with 5 CVs of the start buffer, and then the lysozyme was eluted from the column using 5 CVs of 0.05 M sodium phosphate and 1 M NaCl buffer (elution buffer) at the same pH. The column was then regenerated with 5 CVs of 1 M sodium hydroxide and equilibrated with the start buffer. Dynamic binding capacity was then calculated at 5, 10, and 100% capacity by calculating the area under the breakthrough curve, subtracting the mass of protein adsorbed from that in the feed and then dividing the result by the column volume.

Laboratory Column Elution Measurements

Egg white was separated from the egg yolk and 1 in 2 diluted using 0.05 M Tris/HCl pH 8. The mixture was stirred overnight at 4°C to remove glycosylated proteins by precipitation, then centrifuged at 10000 RPM for 30 minutes (18–20).

Each Q Sepharose 6FF column was equilibrated with 5 CVs of 0.05 M Tris/HCl pH 8 and then run isocratically at 2, 5, 7.5, or 9 mL min^{-1} (linear velocities of 60, 150, 220, and 270 cm h^{-1}). For the 2 mL column, injection volumes of 0.13, 0.33, 0.67, and 1.33 mL were used while for the 30 mL column, volumes of 2, 5, 10, and 20 mL were used. Two CVs were used for the injection process using either standard loops with PEEK tubing or for larger volumes,

a superloop. The superloop is a pressurized cylinder which can be connected to the pump as a standard loop. It is used for injections of 10 mL and above. Fifteen CVs were used for the linear gradient based on 0.05 M Tris/HCl, 0.3 M NaCl pH 8 and then 5 CVs were used for the final wash step in which the elution buffer was used. The column was then re-equilibrated for 5 CVs using 0.05 M Tris/HCl pH 8. Experiments were also performed using a linear gradient of 0.05 M Tris/HCl, 0.3 M NaCl pH 8 over 150 CVs to facilitate comparison with the microfluidic column results.

Microfluidic Column Fabrication and Operation

Details of microfluidic column fabrication are described in our previous work (16). Briefly, the glass chip was fabricated using standard photolithography and wet etching techniques. The column length, width, and depth were constant at 10 mm, 1000 μm , and 150 μm . The packing procedure involved the dilution of a 20% (v/v) slurry of resin in 20% (v/v) aqueous ethanol. Beads were sieved using 38 and 106 μm (VWR Leicestershire, UK) mesh to reduce the size range in order to prevent blockages. Beads were packed into the microfluidic column using a 2 mL plastic syringe with an adapted micropipette tip. The matrix was manually pressurized into the packing chamber and held in position due to a keystone effect. The quality of the packed microfluidic column was then checked using a Leica DMRA2 microscope (Leica Microsystems, Milton Keynes UK) and QWin Software to ensure that there were no resin particles that blocked the inlet and outlet channels. MilliGAT pumps were used throughout this work in the experimental setup outlined in Fig. 2. These pumps are able to accurately pump from $0.6\text{--}6 \times 10^6 \mu\text{L min}^{-1}$ and can accurately dispense 10 μL of liquid. A small internal volume Rheodyne Valve was used for all injections into the microfluidic column.

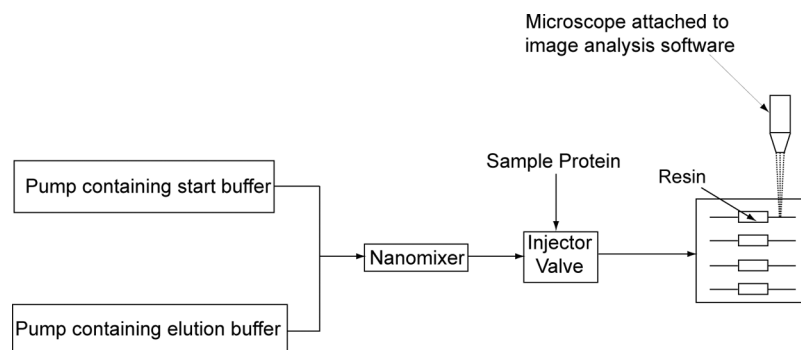


FIG. 2. Schematic diagram of the experimental system used for microfluidic elution chromatography. Two precision MilliGAT pumps were used to pump the start buffer (0.05 M Tris/HCl pH 8) and elution buffer (0.05 M Tris/HCl/0.3 M NaCl pH 8) through the nanomixer and injection valve and into the microfluidic column containing Q Sepharose FF beads. A sample of $1 \mu\text{L}$ of 1 mg mL^{-1} lysozyme, 3.6 mg mL^{-1} conalbumin and 15 mg mL^{-1} ovalbumin in start buffer was injected onto the microfluidic column once equilibrated with start buffer (20% (v/v) of each protein was fluorescently labelled using FITC).

All protein solutions contained 20% (v/v) of the protein fluorescently labelled using fluorescein-5-ithocyanate (FITC). The preparation of the fluorescently labelled proteins was performed using the manufacturer's instructions with slight modifications (21) as described previously (16). Leica QWin software was used as the image analysis software where fluorescence quantification was analyzed by altering the resolution time depending on the level of fluorescence. A time interval programme was developed to record the average fluorescence intensity in the outlet channel every 3 seconds (16).

Breakthrough measurements occurred using 1 mg mL^{-1} lysozyme in 0.05 M sodium phosphate buffer pH 5.5 (start buffer). The buffer was pumped at linear velocities of 60, 150, 220, and 270 cm h^{-1} (1.33, 3.67, 5.33, and $6.67 \mu\text{L min}^{-1}$ respectively) calculated for the microfluidic packed bed using the crosssectional area of the column. Column dead volume was analyzed using 1 mg mL^{-1} lysozyme in 0.05 M Tris/HCl pH 8 using Quarternary amine (Q Sepharose FF) beads. Dynamic protein binding capacity was calculated at 5, 10, and 100% breakthrough. All data was normalized in terms of c/c_o where c is the lysozyme concentration in the effluent at each time point and c_o is the highest value of recorded effluent concentration. Equation (1) was used to calculate the binding capacity (Q) (22):

$$Q = \frac{(M_{in} - V_{retained} \int_{c_{in}}^{c_o} dc)}{V_{beads}} \times \frac{\epsilon_m}{\epsilon_s} \quad (1)$$

Here M_{in} is the total protein mass into the column, $V_{retained}$ and V_{beads} are the volume retained through the system and the volume of the beads packed in the column respectively and ϵ_s and ϵ_m are the voidages in a standard column and in the microfluidic column respectively. The voidage was normalized in this way to allow comparison with larger scale published results. Data presented is the average of at least three breakthrough curves determined at different flowrates.

Microfluidic Column HETP Measurements

The experimental procedure used was the same as for the breakthrough measurements, except the fluorescent light microscope detection occurred at either end of the microfluidic column which now contained sieved Q Sepharose Fast Flow beads (average diameter of $70 \mu\text{m}$). The variance and HETP (23) were then calculated from the intensity readings produced. A volume of $0.4 \mu\text{L}$ (the smallest volume available) of 1 mg mL^{-1} lysozyme (20% (v/v) fluorescently labelled) in 0.05 M Tris/HCl pH 8 was injected into the microfluidic column. The method was validated against the laboratory scale method described earlier to ensure no interactive effects between the protein and column.

Microfluidic Column Elution Measurements

A $1.5 \mu\text{L}$ microfluidic column packed with sieved Q Sepharose Fast Flow was equilibrated with 5 CVs of 0.05 M Tris/HCl pH 8 (start buffer). A concentration of 1 mg mL^{-1} lysozyme, 3.6 mg mL^{-1} conalbumin, and 15 mg mL^{-1} ovalbumin proteins (20% (v/v) of each labelled with FITC) was pumped through in the start buffer. Elution was carried out using the same method outlined in the laboratory column elution measurements. The peaks were monitored using the Leica fluorescent microscope as shown in Fig. 2. In order to achieve the gradient, 0.2 mg mL^{-1} fluorescently labelled lysozyme was used in place of the elution buffer allowing the monitoring of the gradient using the Leica microscope. The gradient used for the separations was 0.05 M Tris/HCl pH 8 with 0.3 M NaCl over 150 CVs over 16 step changes.

RESULTS AND DISCUSSION

Determination and Assessment of Column Packing

Initial experiments focused on measurement of the HETP of the three columns in order to assess the quality of resin packing. The HETP for the 30 mL (15 cm height) and 2 mL (1 cm height) columns were calculated to be 389.9 and $350.7 \mu\text{m}$ at a linear velocity of 30 cm h^{-1} while the variance (σ^2) for each was 1.83 and 0.10 mL^2 . The variance for the 2 mL column gave a lower plate number due to the reduced height and increased complexity involved in packing the column. The asymmetry of the 30 and 2 mL columns were 0.65 and 2 respectively. Ideal peak symmetry should be achieved for a well-packed chromatography column. The values reported here display under and over packing respectively; however, the results produced were adequate for comparisons with the microfluidic column (24).

Table 1 displays the measured peak asymmetry, the calculated variance of the peak, the HETP and the HETP/d_p (diameter of the resin particle) as a function of mobile phase linear velocity for the $1.5 \mu\text{L}$ microfluidic column. Values were calculated from the width at 50% of the maximum height of the peak using the standard plate analysis (23). Although the peaks used for analysis were not Gaussian, due to tailing, standard peak analysis was considered useful as a method to compliment the confocal microscopy analysis developed previously (16). The asymmetry values for all peaks were two to three times the value of a Gaussian peak (unity). The variance calculated over the column was smaller than expected since laminar flow and diffusive mixing throughout the extra-column system appear to be the dominating factor. The volume of the adjacent equipment was $2 \mu\text{L}$, compared to the volume of the packed bed which was $1.5 \mu\text{L}$, producing dispersed peaks. The data presented, however, does show that variance and HETP may still be calculated within a

TABLE 1

Influence of mobile phase linear velocity on microfluidic chromatography column performance. Peak symmetry, σ^2 and the HETP and HETP/ d_p determined using 0.4 μL of 0.2 mg mL^{-1} fluorescently labelled lysozyme in 0.05 M Tris/HCl buffer pH 8 (non-binding conditions). Asymmetry and σ^2 were calculated from the values obtained before and after the packed microfluidic column. Errors represent one standard deviation around the mean

Linear velocity (cm h^{-1})	σ^2 (mL^2)	HETP (μm)	HETP/ d_p	Asymmetry
60	$1.41 \times 10^{-6} \pm 4.35 \times 10^{-7}$	945 ± 290	13.52 ± 4.16	2.98 ± 0.56
105	$1.44 \times 10^{-6} \pm 1.70 \times 10^{-7}$	1050 ± 175	15.00 ± 2.52	2.64 ± 0.31
150	$1.21 \times 10^{-6} \pm 0$	1035 ± 35.30	14.79 ± 0.50	2.90 ± 0.36
220	$1.09 \times 10^{-6} \pm 2.74 \times 10^{-7}$	970 ± 95.80	13.88 ± 1.37	3.05 ± 0.30
270	$1.12 \times 10^{-6} \pm 0$	1010 ± 0	14.44 ± 0	3.10 ± 0.22

microfluidic system. In Table 1, σ^2 can be considered to be constant at around $1.5 \times 10^{-6} \text{ mL}^2$.

The HETP data are also presented in Table 1. As the variance is directly proportional to the HETP (23) a similar level of error is observed. The value for the HETP can be considered to be around 1 mm, while the HETP/ d_p is around 14. In conventional terms, this value would be indicative of poor packing especially when compared with the laboratory scale 15 cm column (experimentally determined to have a HETP/ d_p of 4). However, the 2 mL column produced a similar value to the microfluidic column due to similar heights.

The voidage in the microfluidic column was 0.55 (as calculated and presented previously (16)) which implies that there are more voids present in the microfluidic packed system than in a standard column. When considering the assessment of microfluidic column packing the plate test results are best interpreted in conjunction with a three dimensional image of the packing, as shown within Fig. 3. In practice the packing was good enough for the binding and elution studies given that there was only 1.5 μL of packing and that on average it is only 2 beads high.

Laboratory Scale Column Breakthrough Profiles

As a basis for later comparison with the microfluidic column, Fig. 4 displays the breakthrough curves for all 4 flowrates as a function of the volume retained for (a) the 30 mL (15 cm height) column and (b) the 2 mL (1 cm height) column. Breakthrough curves for the 30 mL column (Fig. 4(a)) are consistent and independent of mobile phase linear velocity. They show near perfect representations of breakthrough curves with a constant pattern front (25,26). This was expected and is due to a number of factors including the use of low concentrations of a model protein and the fact that lysozyme is a protein with a high isoelectric point (11.1) that adsorbs with high affinity (27).

For the 2 mL column (Fig. 4(b)) there is some variation of the breakthrough curves with increasing linear velocity; however, in general the flow rates are consistent. At the

higher flowrates the residence time in the column would be reduced leading to proportionally less time for the protein to interact with the matrix particles. Additionally, as shown in Table 2 there was a decreased number of theoretical plates. However, the breakthrough curves are highly consistent and accurate over the range required.

The breakthrough curves determined here in both the laboratory scale columns are similar to those described in the literature (28,29) using lysozyme with the same Sepharose FF resin. The reported values of maximum dynamic binding capacity were also similar to those calculated and reported here in Table 1 ($\sim 120 \text{ mg mL}^{-1}$ matrix $^{-1}$).

Microfluidic Scale Column Breakthrough Profiles

In our previous work on chip fabrication and analysis of fluid flow within the column initial breakthrough studies

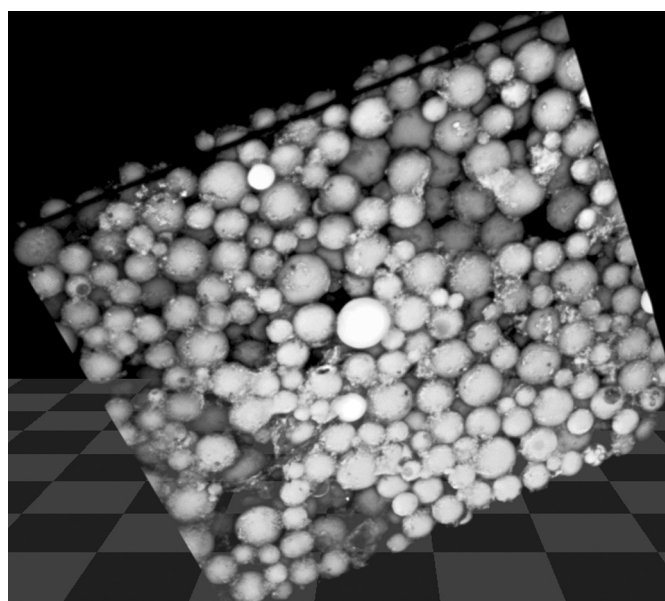


FIG. 3. Confocal microscope image of a section of the microfluidic packed bed rendered in a 3 dimensional plane. The perspective is of a 45° angle from the top of the bed (average particle diameter 70 μm).

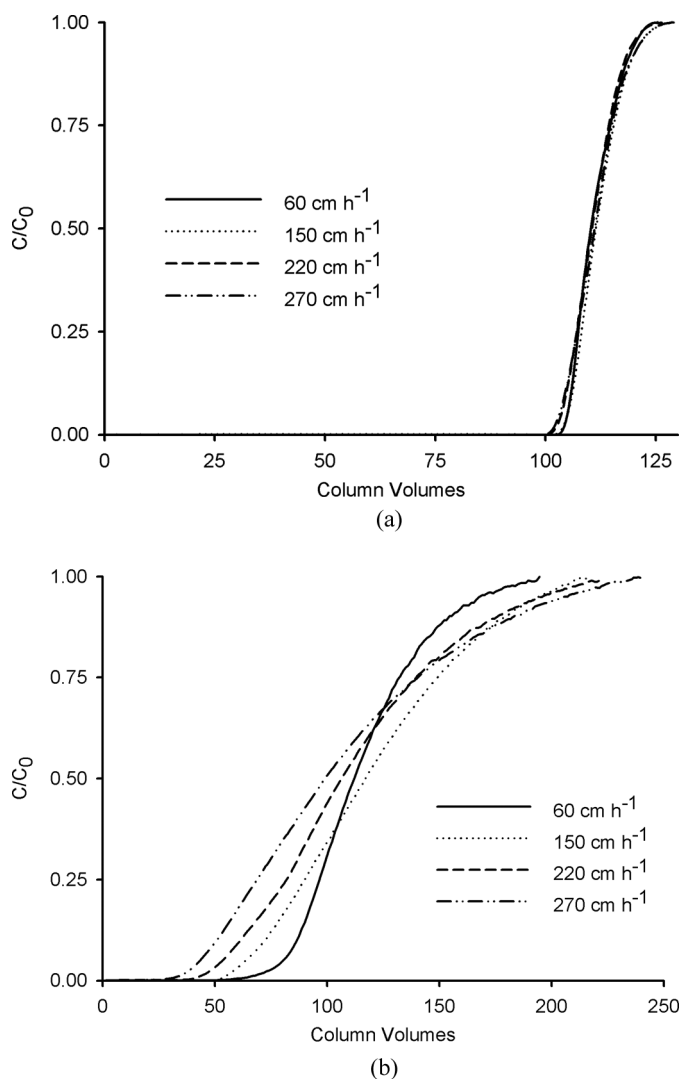


FIG. 4. Influence of mobile phase velocity on dynamic binding capacity of laboratory scale chromatography columns. Breakthrough curves of 1 mg mL^{-1} lysozyme using (a) 30 mL (15 cm height) and (b) 2 mL (1 cm height) XK 16/20 columns containing SP Sepharose Fast Flow in 0.05 M sodium phosphate pH 5.5.

on the microfluidic column were also reported. Here comparisons are made between breakthrough profiles determined on the microfluidic column and the two laboratory scale columns at an identical linear velocity of 270 cm h^{-1} . The voidage for the $1.5 \mu\text{L}$ column was 0.55 as opposed to 0.4 which was present in the standard laboratory columns (as is also standard in general chromatography columns) (16). Instead of the standard column volumes employed in previous figures, the resin column volumes was used where the column volume was multiplied by the bed voidage, so as to standardize the results.

As shown in Fig. 5, the microfluidic and the 2 mL laboratory scale columns are very similar in terms of breakthrough profile shape and the column residence time. This agreement is considered excellent given the 1300-fold difference in scale and is probably related to the columns having the same length. The breakthrough curve for the 30 mL column is a near perfect representation of a breakthrough curve which was considered to be an excellent basis to make comparisons with other scales.

Table 2 presents a comparison of the calculated maximum and 5% dynamic binding capacities for both laboratory scale columns and the microfluidic column at different mobile phase linear velocities. Values of the maximum binding capacity are in reasonable agreement between the microfluidic and laboratory scale, as suggested by the breakthrough profiles shown in Fig. 5. Although the shape of the breakthrough curve was different, the calculated maximum binding capacity for the 30 mL column was similar to the microfluidic column.

Calculated dynamic binding capacities (at 5% capacity) were not as similar between the various scale columns as were the maximum binding capacities. This may have been due to non-specific binding and channelling through the column (16). Overall, the capacities calculated are in reasonable agreement with previously published data and laboratory scale data (28,29). This provides a further confirmation that the microfluidic chromatography column does offer a useful methodology for the determination of breakthrough curves and binding capacities using considerably reduced quantities of material.

TABLE 2
Comparison of maximum and 5% dynamic binding capacities for the microfluidic and laboratory scale columns

Dynamic binding capacity (mg mL^{-1} matrix $^{-1}$)	Linear velocity (cm h^{-1})											
	1.5 μL Column				2 mL Column				30 mL Column			
	60	150	220	270	60	150	220	270	60	150	220	270
5%	140	144	50.3	55.7	79.8	57.3	53.5	39.6	105	105	103	103
Maximum	160	175	96.4	117	116	121	113	108	116	112	104	111

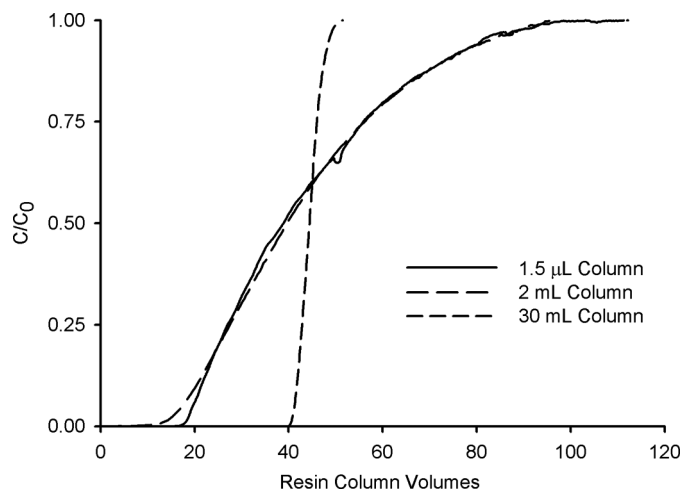


FIG. 5. Comparison of lysozyme breakthrough curves determined on the 1.5 μL (1 cm height) and 2 μL (1 cm height) microfluidic chromatography columns compared to the laboratory scale 30 mL (15 cm height) column. Experiments performed at a linear velocity of 270 cm h^{-1} . Note the ~ 1300 fold difference in scale.

Laboratory Scale Column Elution Profiles

Figure 6 displays the egg white separation data generated using the two laboratory scale columns. Three peaks are clearly shown in each profile, the first being lysozyme, which is unretained, and two further peaks which are not fully resolved. In Fig. 6(a) for the 30 mL column conalbumin and ovalbumin represent the second and third peak respectively. There is some evidence that resolution using smaller injection volumes produced better resolution, as the column has sufficient time to remove the proteins over the linear gradient. In Fig. 6(b) when using 1.33 mL as the injection volume for the 2 mL column, no resolution was obtained between the second two peaks. This is almost certainly due to the reduction in the residence time in this much shorter column. The lack of resolution on both columns could be due to the fact that the isoelectric points for both proteins are comparatively close to each other. Conalbumin has a pI of 6.5, while ovalbumin has a pI of 4.7 (30) which could lead to some competitive binding. A longer bed height or a longer linear gradient would most likely improve resolution of the two proteins when using the same flowrates. The fact that there was incomplete resolution between peaks, however, does not detract from the ability to obtain useful insights from these columns on how the conalbumin-ovalbumin peaks alter with changing bed heights and potentially different mobile phase conditions i.e., pH, ionic strength etc.

Microfluidic Scale Elution Profiles

In assessing the utility of the microfluidic column in early stage bioprocess development it is important to not only assess binding capacity (Table 2) but also the degree

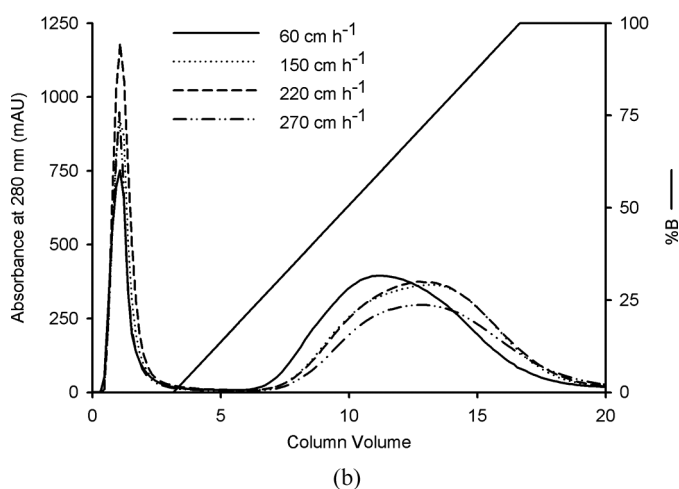
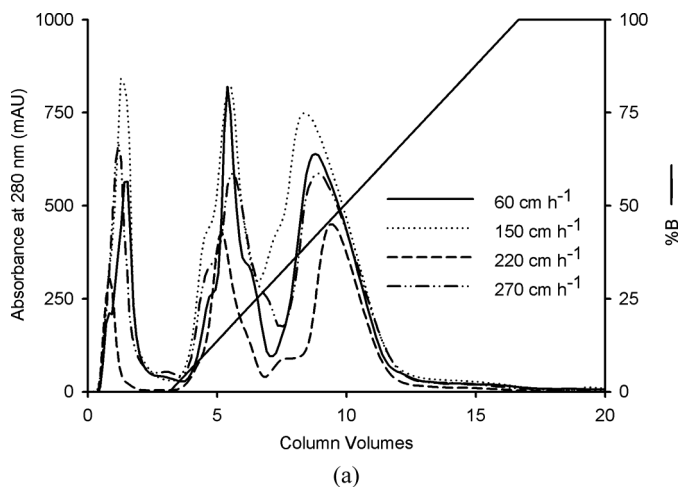


FIG. 6. Influence of mobile phase velocity on laboratory scale separation of a ternary protein mixture. (a) a 20 mL injection of 30 mg mL^{-1} egg white proteins (3.6% (w/w) lysozyme, 12% (w/w) conalbumin and 54% (w/w) ovalbumin) in 0.05 M Tris/HCl buffer pH 8 using a 30 mL column; (b) 1.33 mL injection of egg white protein using a 2 mL column. The first peak is lysozyme, then conalbumin and finally ovalbumin. Proteins were eluted using 0.05 M Tris/HCl/0.3 M NaCl pH 8 and the resin used was Q Sepharose Fast Flow.

of resolution that could potentially be obtained on the ultimate, large scale manufacturing column. One of the main technical challenges of achieving linear gradient separations at this scale is the production of the gradient. This could be due to local flow instabilities at nano flowrate changes explained below.

To visualize the linear gradient required for separation, fluorescently labelled lysozyme was used as buffer B instead of a salt gradient. Results were then overlaid over the separation data. Separation of egg white proteins was then instituted. Column volumes in this case were not quoted in terms of the resin column volume because the comparison required referred to the linear gradient of the separation which was not present when using breakthrough curves.

To institute a linear gradient at the microfluidic flowrates used here, nano flowrate changes are required. Very low flowrate changes are difficult to maintain as they are affected by factors such as temperature, variation in the piston seal quality over time, and there may be solvent compressibility problems (31). Extremely small air bubbles in the liquid that compress in a piston based pump could also cause instabilities within local velocities. Velocities then even out as the pressure reaches atmospheric pressure at the exit (32). The small scale of the microfluidic column therefore ensures that accurate gradients are difficult to obtain. The chip version developed by Brennen et al. (31) have developed gradients over minutes at nano-liter flow rates.

Irrespective of these technical challenges however, a separation of three proteins using a linear gradient was achieved on the microfluidic column as shown in Figs. 7 and 8. Figure 7 shows elution of the non-binding lysozyme peak first followed by a broader second peak being a mixture of conalbumin and ovalbumin. There is a shoulder evident on this second peak (at around 100 column volumes), which is most likely to be from conalbumin while the main body of the peak is ovalbumin.

Figure 8(a) provides a close-up view of this shoulder and peak. In order to verify if the degree of separation achieved is likely to be representative of large scale separations, it was necessary to generate comparative 2 mL column data (i.e., 1 cm length at the laboratory scale) using a similar 150 column volume gradient as shown in Fig. 8(b). Although the height of the conductivity when the curve returns to the baseline differs between the scales, the length of the gradient is the same.

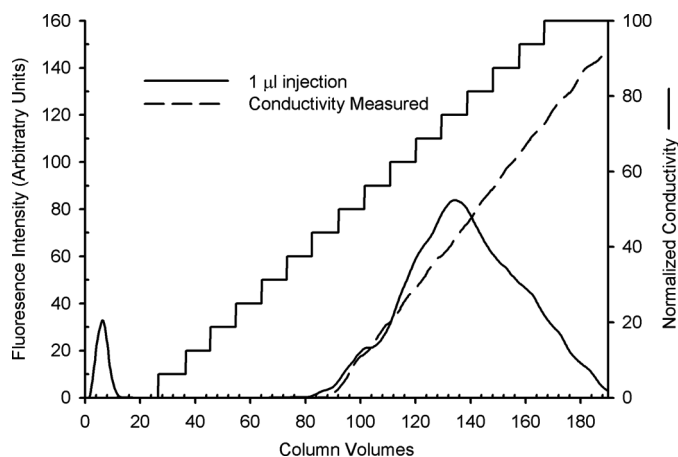


FIG. 7. Influence of mobile phase linear velocity on separation of a ternary protein mixture. A microfluidic column egg white protein separation using a series of 16 steps to produce a gradient over 150 column volumes. The same buffer conditions were used as in the standard scale chromatography column system. An injection of 1 μL volume was used containing 1 mg mL^{-1} lysozyme, 3.6 mg mL^{-1} conalbumin and 16.2 mg mL^{-1} ovalbumin in a fluorescently labelled solution with the standard buffer.

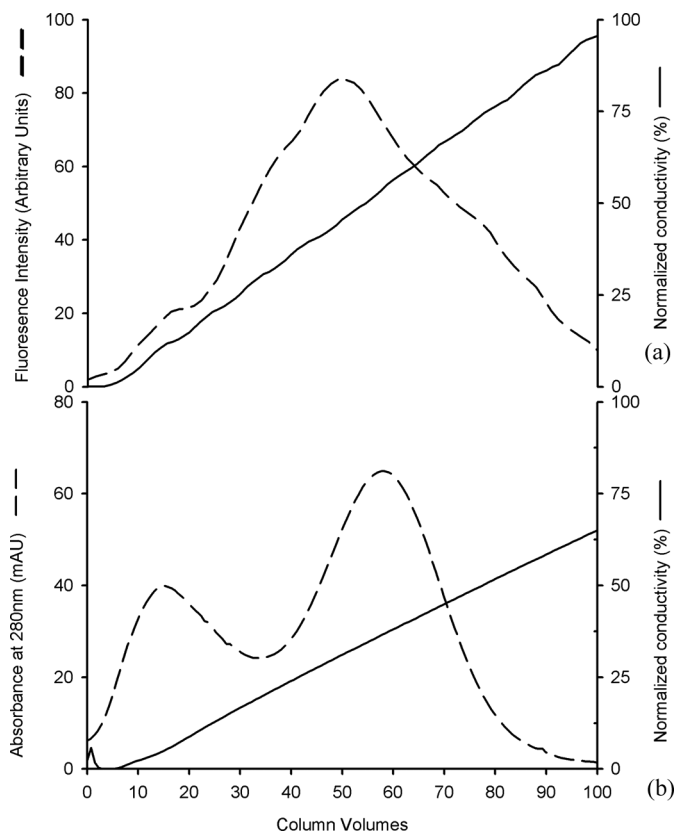


FIG. 8. Comparison of both scales of the ternary protein separation at the elution stage using 150 column volumes. Linear gradient separation of the three egg white proteins using (a) the microfluidic column and (b) the 2 mL column. Both columns were run at 270 cm h^{-1} , while the injection volume used for the 2 mL column was 1.33 mL.

Although full resolution was not observed between the conalbumin and ovalbumin peaks when using 150 column volumes with the 2 mL column, the data in Figs. 7 and 8 represents a first step in the generation of elution profiles of ion exchange chromatography using a microfluidic column.

Comparison with Other Microscale Chromatography Techniques

As shown in Fig. 1 the performance and potential industrial application of the microfluidic column established here needs to be considered against other similar technologies for high throughput chromatographic process screening. The other systems presented use complex liquid handling systems facilitating the use of many different chromatographic separations at once. The advantage of the approach presented within this paper is the use of extremely small volume (1.5 μL) chromatography columns. The microfluidic system is capable of developing into the use of highly parallel chromatography columns using true flowrate conditions. All other systems within the literature

operate using batch conditions or with the use of pseudo linear gradients. The advantage of the microfluidic system is that it is capable of producing separations using true linear gradients as well as parallel conditions.

CONCLUSIONS

The data presented here displays positive initial results on the performance of a 1.5 μL microfluidic chromatography column packed with process scale chromatography resin. Results in terms of packing quality and performance (HETP) and frontal and elution chromatography between the microfluidic column and laboratory scale 2 mL and 30 mL columns showed good quantitative agreement both in terms of maximum dynamic binding capacity and also separation of binding and non-binding proteins. Protein requirement has decreased 10,000-fold for breakthrough analysis and 3000-fold for elution between the microfluidic and the 30 mL column. Therefore the work described in this paper is representative of the proof of principle of a potentially powerful tool for the generation of microfluidic process bed data for the biopharmaceutical industry and is useful for early stage bioprocess development.

ACKNOWLEDGEMENTS

The work was supported by the Engineering and Physical Sciences Research Council (EPSRC) via the Innovative Manufacturing Research Centre (IMRC) in Bioprocessing at UCL, a Life Sciences Interface and Innovative Manufacturing program. The IMRC is part of The Advanced Centre of Biochemical Engineering, UCL with collaboration from a range of academic partners and biopharmaceutical and biotechnology companies.

REFERENCES

- Levison, P.R. (2003) Large-scale ion-exchange column chromatography of proteins – Comparison of different formats. *J. Chromatogr. B.*, 790 (1–2): 17.
- Cramer, S.M.; Natarjan, V. (1999) Chromatography – ion exchange. In: *Encyclopaedia of Bioprocess Technology – Fermentation, Biocatalysis and Bioseparation*, Flinkinger, M.C.; Drew, S.W., eds.; John Wiley & Sons: New York, p. 612.
- Low, D.; O'Leary, R.; Pujar, N.S. (2007) Future of antibody production. *J. Chromatogr. B.*, 848 (1): 48.
- Micheletti, M.; Lye, G.J. (2006) Microscale bioprocess optimisation. *Curr. Opin. Biotechnol.*, 17 (6): 611.
- Kelley, B.D.; Tobler, S.A.; Brown, P.; Coffman, J.L.; Godavarti, R.; Iskra, T.; Switzer, M.; Vunnum, S. (2008) Weak partitioning chromatography for anion exchange purification of monoclonal antibodies. *Biotechnol. Bioeng.*, 101 (3): 553.
- Wenger, M.D.; DePhillips, P.; Price, C.E.; Bracewell, D.G. (2007) An automated microscale chromatography purification of virus-like particles as a strategy for process development. *Biotechnol. Appl. Biochem.*, 47 (2): 131.
- Bensch, M.; Wierling, P.S.; von Lieres, E.; Hubbuch, J. (2005) High throughput screening of chromatographic phases for rapid process development. *Chem. Eng. Technol.*, 28 (11): 1274.
- Wiendahl, M.; Wierling, P.S.; Nielsen, J.; Christensen, D.F.; Krarup, J.; Staby, A.; Hubbuch, J. (2008) High throughput screening for the design and optimization of chromatographic processes – Miniaturization, automation and parallelization of breakthrough and elution studies. *Chem. Eng. Technol.*, 31 (6): 893.
- Chhatre, S.; Titchener-Hooker, N.J. (2009) Microscale methods for high-throughput chromatography development in the pharmaceutical industry. *J. Chem. Technol. Biotechnol.*, 84 (7): 927.
- Rege, K.; Pepsin, M.; Falcon, B.; Steele, L.; Heng, M. (2006) High-throughput process development for recombinant protein purification. *Biotechnol. Bioeng.*, 93 (4): 618.
- Kelley, B.D.; Switzer, M.; Bastek, P.; Kramarczyk, J.F.; Molnar, K.L.; Yu, T.N.; Coffman, J.L. (2008) High-throughput screening of chromatographic separations: IV. Ion-exchange. *Biotechnol. Bioeng.*, 100 (5): 950.
- Wensel, D.L.; Kelley, B.D.; Coffman, J.L. (2008) High-throughput screening of chromatographic separations: III Monoclonal antibodies on ceramic hydroxyapatite. *Biotechnol. Bioeng.*, 100 (5): 839.
- Dziennik, S.R.; Belcher, E.B.; Barker, G.A.; Lenhoff, A.M. (2005) Effect of ionic strength on lysozyme uptake rates in cation exchangers. I: Uptake in SP Sepharose FF. *Biotechnol. Bioeng.*, 91 (2): 139.
- Dziennik, S.R.; Belcher, E.B.; Barker, G.A.; DeBergalis, M.J.; Fernandez, S.E.; Lenhoff, A.M. (2002) Nondiffusive mechanisms enhance protein uptake rates in ion exchanger particles. *Proc. Natl. Acad. Sci. USA.*, 100 (2): 420.
- Kramarczyk, J.F.; Kelley, B.D.; Coffman, J.L. (2008) High-throughput screening of chromatographic separations: II. Hydrophobic interactions. *Biotechnol. Bioeng.*, 100 (4): 707.
- Shapiro, M.S.; Haswell, S.J.; Lye, G.J.; Bracewell, D.G. (2009) Design and characterization of a microfluidic packed bed system for protein breakthrough and dynamic binding capacity determination. *Biotechnol. Prog.*, 25 (1): 277.
- de Mello, A. (2002) On-chip chromatography: The last twenty years. *Lab Chip.*, 2 (3): 48N.
- Vachier, M.C.; Piot, M.; Awadé, A.C. (1995) Isolation of hen egg white lysozyme, ovotransferrin and ovalbumin, using a quarternary ammonium bound to a highly crosslinked agarose matrix. *J. Chromatogr. B.*, 664 (1): 201.
- Awadé, A.C.; Efstathiou, T. (1999) Comparison of three liquid chromatographic methods for egg-white protein analysis. *J. Chromatogr. B.*, 723 (1–2): 69.
- Guerin-Dubiard, C.; Pasco, M.; Hietanen, A.; del Bosque, A.Q.; Nau, F.; Croguennec, T. (2005) Hen egg white fractionation by ion-exchange chromatography. *J. Chromatogr. A.*, 1090 (1–2): 58.
- Molecular Probes Inc., *FlourReporter[®] FITC Protein Labelling Kit (F6434)*. 2004.
- Sin, S.C.; Baldascini, H.; Hearle, D.C.; Hoare, M.; Titchener-Hooker, N.J. (2006) Effect of fouling on the capacity and breakthrough characteristics of a packed bed ion exchange chromatography column. *Bioprocess. Biosyst. Eng.*, 28 (6): 405.
- Harrison, R.G.; Todd, P.; Rudge, S.R.; Petrides, D.P. (2003) *Bioseparations Science and Engineering*; Oxford University Press.
- G.E. Healthcare. (2007) Appendix 3: Column packing and preparation. In: *Ion Exchange Chromatography and Chromatofocusing*
- Cooney, D.O.; Lightfoot, E.N. (1965) Existence of asymptotic solutions to fixed-bed separations and exchange equations. *Ind. Eng. Chem. Fundam.*, 4 (2): 233.
- Tejeda-Mansi, A.; Montesinos, R.M.; Guzmán, R. (2001) Mathematical analysis of frontal affinity chromatography in particle and membrane configuration. *J. Biochem. Biophys. Meth.*, 49 (1–3): 1.

27. Figueiredo, K.; Salim, V.; Alves, T.; Pinto, J. (2005) Lysozyme adsorption on to different surfaces: A comparative study. *Adsorption*, 11 (3–4): 131.
28. Skidmore, G.L.; Hortsmann, B.J.; Chase, H.A. (1990) Modelling single-component protein adsorption to the cation exchanger S sepharose^(R) FF. *J. Chromatogr. A.*, 498: 113.
29. Staby, A.; Sand, M.; Hansen, R.G.; Jacobsen, J.H.; Anderson, L.A.; Gerstenberg, M.; Bruus, U.K.; Jensen, I.H. (2005) Comparison of chromatographic ion-exchange resins: IV. Strong and weak cation-exchange resins and heparin resins. *J. Chromatogr. A.*, 1069 (1): 65.
30. Ehsani, N.; Parkkinen, S.; Nyström, M. (1997) Fractionation of natural and model egg-white protein solutions with modified and unmodified polysulfone UF membranes. *J. Membr. Sci.*, 123 (1): 105.
31. Brennen, R.A.; Yin, H.; Killeen, K.P. (2007) Microfluidic gradient formation for nanoflow chip LC. *Anal. Chem.*, 79 (24): 9302.
32. Zhou, X.; Furushima, N.; Terashima, C.; Tanaka, H.; Kurano, M. (2001) New micro-flow pumping system for liquid chromatography. *J. Chromatogr. A.*, 913 (1–2): 165.

Development of a real-world direct interface for integrated DNA extraction and amplification in a microfluidic device

Kirsty J. Shaw,^a Domino A. Joyce,^b Peter T. Docker,^a Charlotte E. Dyer,^c Gillian M. Greenway,^a John Greenman^c and Stephen J. Haswell^{*a}

Received 27th August 2010, Accepted 15th October 2010

DOI: 10.1039/c0lc00346h

Integrated DNA extraction and amplification have been carried out in a microfluidic device using electro-osmotic pumping (EOP) for fluidic control. All the necessary reagents for performing both DNA extraction and polymerase chain reaction (PCR) amplification were pre-loaded into the microfluidic device following encapsulation in agarose gel. Buccal cells were collected using OmniSwabs [Whatman™, UK] and manually added to a chaotropic binding/lysis solution pre-loaded into the microfluidic device. The released DNA was then adsorbed onto a silica monolith contained within the DNA extraction chamber and the microfluidic device sealed using polymer electrodes. The washing and elution steps for DNA extraction were carried out using EOP, resulting in transfer of the eluted DNA into the PCR chamber. Thermal cycling, achieved using a Peltier element, resulted in amplification of the Amelogenin locus as confirmed using conventional capillary gel electrophoresis. It was demonstrated that the PCR reagents could be stored in the microfluidic device for at least 8 weeks at 4 °C with no significant loss of activity. Such methodology lends itself to the production of 'ready-to-use' microfluidic devices containing all the necessary reagents for sample processing, with many obvious applications in forensics and clinical medicine.

Introduction

Nucleic acid purification and amplification are important biochemical tools for genetic analysis. In many instances, such as forensic or clinical investigations, biological samples are limited both in terms of quantity and quality, accordingly retrieval of sufficient amounts of high enough quality DNA from the original sample without contamination is crucial. The use of solid-phase DNA extraction methodology is highly suited to such samples as it also enables pre-concentration of nucleic acids. Genomic regions of interest can then be amplified from this template DNA using PCR, facilitating simplified detection, for example through the incorporation of fluorescently labelled primers.

A wide variety of DNA purification protocols have been successfully adapted to work in a microfluidic environment. Silica-based, solid-phase methodology has been commonly employed in which nucleic acids adsorb onto the silica in the presence of a chaotropic salt. Cellular or proteinaceous debris can then be removed using an alcohol wash, and the nucleic acids subsequently eluted in a low ionic strength solution enabling direct transfer to downstream applications. In addition to silica-based methodologies, a range of other nucleic acid extraction techniques have been successfully applied to microfluidic

systems, such as the use of organic polymeric monoliths and ion-exchange resins, each suited for different applications.¹

PCR in microfluidic systems has been widely reported in the literature and the reader is directed for more information to substantial reviews which look in detail at the diverse variety of amplification systems which exist.^{2–4} Whilst the integration of PCR with downstream analysis techniques (mainly capillary gel electrophoresis) has received significant interest, much less focus has been placed on the integration with pre-PCR procedures such as DNA extraction; important when dealing with crude biological samples.⁵ This is in part because of the difficulties associated with confining the solid-phase extraction matrix within a specific location in the microfluidic device, preventing contamination of the template DNA with potential inhibitors from the DNA extraction process *e.g.* isopropanol, and isolating any surface coating required for the prevention of DNA polymerase adsorption onto the internal glass surfaces of the PCR chamber.⁶

A number of approaches designed to overcome the challenges associated with developing microfluidic devices for integrated DNA extraction and amplification have been evaluated. Silica-coated or surface-charge switchable magnetic particles can be used to facilitate nucleic acid movement within microfluidic systems. For example, Pippert *et al.*⁷ used superparamagnetic particles to move viral RNA between aqueous droplets in a microfluidic environment. Each droplet, separated by an oil carrier phase, contained a different reagent solution for sequential nucleic acid purification and reverse transcription (RT)-PCR. Alternatively, the particles can be retained within one or more chambers on a microfluidic device using an external magnet, allowing the various biological sample, DNA extraction and PCR solutions to be pumped over the solid-phase surface.^{8,9}

^aDepartment of Chemistry, University of Hull, Cottingham Road, Hull, UK HU6 7RX. E-mail: s.j.haswell@hull.ac.uk; Fax: +44 (0)1482 466410; Tel: +44 (0)1482 465475

^bDepartment of Biological Sciences, University of Hull, Cottingham Road, Hull, UK HU6 7RX

^cCentre for Biomedical Research, University of Hull, Cottingham Road, Hull, UK HU6 7RX

This enables nucleic acids present in the biological sample to bind to the particles during the extraction process, allowing them to be directly transferred into a chamber containing PCR reagents. However, it has been shown that performing PCR in the presence of magnetic beads can decrease the amplification efficiency by as much as 50%.¹⁰

Another approach is to combine the flow of DNA eluted from a solid-phase extraction matrix with a concentrated PCR reagent mixture from a side channel and direct the combined solutions into a PCR chamber for amplification.^{11,12} Direct elution of RNA, from immobilised silica beads, using a nucleic acid sequence-based amplification (NASBA) reagent mixture has also been demonstrated, although in this instance the enzymes required for NASBA were added to the amplification chamber in a separate step following RNA elution.¹³

The use of mechanical external syringe pumps to facilitate flow of solutions through such integrated devices allows accurate control of flow rates but requires the use of miniaturised fittings to provide an interface to the microfluidic device, which in turn brings problems associated with large dead volumes (important when dealing with expensive reagents such as DNA polymerase) and labour intensive assembly.¹⁴ The use of dynamic EOP, however, eliminates the need for moving parts enabling easier integration of pumping methodology into the microfluidic device. A recent review by Wang *et al.*¹⁵ demonstrated the flexibility of electro-osmotic pumps for a variety of uses including microflow injection analysis and microfluidic chromatography systems. EOP has recently been demonstrated by the authors to be a suitable pumping technique for performing DNA extraction on a microfluidic device, using a dual function monolith which not only provides the solid-phase for DNA extraction but also acts as support for electro-osmotic flow (EOF) whilst reducing the reverse hydrodynamic flow of solutions.¹⁶

In addition to integrating pumping mechanisms onto microfluidic devices, the storage of reagents within such devices lends itself to the development of truly portable miniaturised systems. Long-term storage of reagents on microfluidic devices for performing nucleic acid-based reactions has received limited attention in the literature but in recent years the need for such capability has become apparent if truly portable, integrated microfluidic systems are to be developed. In terms of DNA extraction, storage of liquid reagents for washing and elution has been achieved by using valve actuated reservoirs¹⁷ or glass ampoules.¹⁸ The latter requires the application of a local mechanical force to break the ampoules and centrifugal force to ensure release of reagents to the desired location in the microfluidic device.¹⁸ An alternative approach has been described by Yobas *et al.*,¹⁹ who presented a self-contained cartridge which can be connected to a microfluidic device and contains all the necessary reagents for performing nucleic acid extraction. In this case a magnetic planar peristaltic pump was used to move reagent plugs, separated by air spaces, around the system. Whilst representing an advance in the development of 'ready-to-use' microfluidic technology, no long-term storage of the reagents was evaluated as the cartridges were used immediately following preparation. The use of a cartridge for reagents also represents an extra component in addition to the microfluidic device increasing the complexity of operation.

The storage of essential components for nucleic acid amplification within microfluidic devices has focussed on the drying of PCR reagents within amplification chambers. For example, by freeze-drying PCR reagents onto the internal surfaces of a PCR chamber, successful DNA amplification can be performed after six months storage at $-20\text{ }^{\circ}\text{C}$.²⁰ However, when the PCR reagents were stored at higher temperatures, of $4\text{ }^{\circ}\text{C}$ or room temperature, DNA polymerase was found to be half or completely inactive respectively. Furthermore, Kim *et al.*, have demonstrated that PCR reagents can be dried at room temperature and passivated using a protective paraffin layer which melts during thermal cycling facilitating release and hydration of the reagents.²¹ More recently, the same group have combined this form of dry reagent storage with liquid storage of reagents for upstream DNA extraction.²² Whilst the drying of PCR reagents within microfluidic devices eliminates the need for reagent loading at point-of-use, offering several advantages including reduced risk of contamination and increased portability, there are problems relating to decreased DNA polymerase activity as a result of the drying methodology utilised.²¹

The work presented here describes an integrated DNA extraction and amplification methodology in which all the required reagents are pre-loaded onto the microfluidic device by encapsulating them in agarose gel. A bi-functional thermally activated silica-based monolith was used as the solid-phase for DNA extraction and as a pump for electro-osmotic movement. The efficiency of the DNA extraction process was evaluated along with the effectiveness of encapsulation of PCR reagents in a gel-based format for storage on the microfluidic device.

Experimental

Microfluidic device

All glass microfluidic devices were produced using standard photolithography and wet etching techniques to generate the design shown in Fig. 1.²³

The features were etched to a depth of $50\text{ }\mu\text{m}$ using a 1% hydrofluoric acid/5% ammonium fluoride solution at $65\text{ }^{\circ}\text{C}$ for 10 minutes. In order to allow electrodes to be connected to the microfluidic device, 3 mm diameter holes were drilled in a 3 mm thick top plate which was then thermally bonded to the etched glass wafer (1 mm thick) to produce the complete microfluidic device. Injection moulded carbon-containing polystyrene plugs [N. Goddard, Manchester University, UK] were fitted into the holes and then brought into contact, *via* pogo-pins, with electrodes housed in the custom-made control instrument [JLS Designs Ltd, UK] shown in Fig. 2.

The internal glass surfaces of the PCR chamber were silanised to prevent DNA polymerase adsorption. A solution of $290\text{ }\mu\text{l}$ of trichloro(1*H*,1*H*,2*H*,2*H*-perfluorooctyl)silane [Sigma-Aldrich, UK] in 5 ml of 2,2,4-trimethylpentane [Fisher Scientific, UK] was flowed through the microfluidic device for 10 minutes at $5\text{ }\mu\text{l min}^{-1}$. Following this, solutions of 2,2,4-trimethylpentane, acetone and distilled water were sequentially used to wash the microfluidic device for a total of 5 minutes each at $5\text{ }\mu\text{l min}^{-1}$.²⁴

The channels of the DNA extraction chamber were incubated with a 5% hexadimethrine bromide (Polybrene, PB) [Sigma-Aldrich, UK] solution for 15 minutes and then dried under

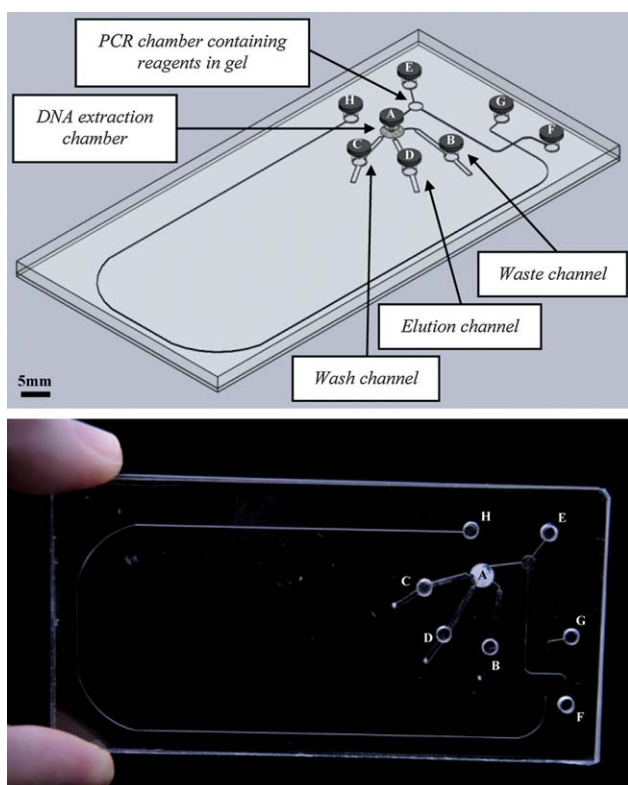


Fig. 1 Schematic (top) and photograph (bottom) of the microfluidic device showing the thermally activated silica monolith (A) within the microfluidic device, the position of the carbon electrodes (B–H) and the locations of the gel encapsulated reagents. The additional channel between electrodes G and H provides the potential for future integration with capillary electrophoresis for detection of PCR products.

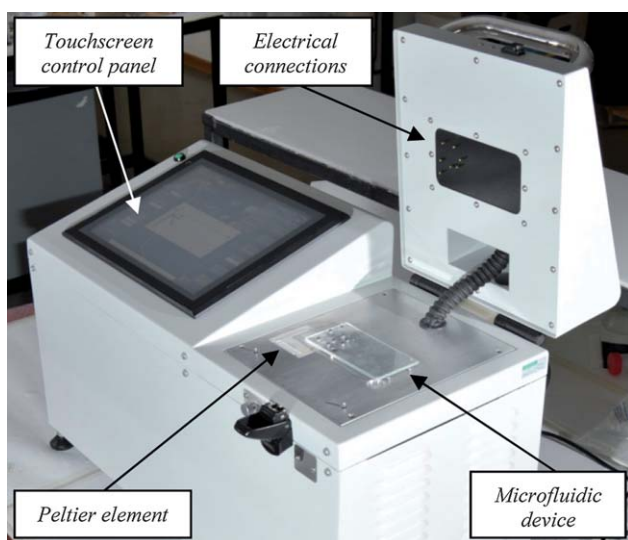


Fig. 2 Photograph of the control instrument, showing position of the microfluidic device, Peltier element, electrical connections and touchscreen control panel.

vacuum. This created a positively charged surface reversing the normal direction of EOP so that bulk movement occurs from cathode to anode.

The thermally activated silica-based monolith was produced by mixing potassium silicate solution (21% SiO₂ and 9% K₂O [VWR International, UK]) and formamide [Alfa Aesar, UK] in a 10 : 1 ratio.²⁵ In order to ensure the monolith was only produced in the DNA extraction chamber, the entire device was first filled with glycerol [Sigma-Aldrich, UK]. The monolith solution was then injected into the DNA extraction chamber, displacing the glycerol, and the microfluidic device placed in an oven at 90 °C for 15 minutes. After this initial heating step, the remaining glycerol was removed and the microfluidic device placed back in the oven overnight for complete polymerisation to occur. Once polymerised, the monoliths were washed with ethanol to remove any unreacted solution and glycerol residue. Prior to DNA extraction the monoliths were washed with 10 mM TE buffer (10 mM Tris and 1 mM EDTA in distilled water, adjusted to pH 6.7 using hydrochloric acid [Sigma-Aldrich, UK]) at 5 μl min⁻¹ for 30 minutes.

All the necessary reagents for performing DNA extraction and amplification were encapsulated in 1.5% (w/v) low-melting temperature (LMT) agarose [Sigma-Aldrich, UK] for pre-loading and storage in the microfluidic device. The wash gel contained 50% (v/v) ethanol in 100 mM sodium chloride for increased electro-osmotic movement,¹⁶ and the elution gel was made up using 10 mM TE buffer. For single locus amplification PCR reagents were added to a molten agarose solution (in which the concentration of the agarose gel was varied in the initial experiments²⁶): 1× GoTaq[®] buffer, 2 mM MgCl₂, 1 unit GoTaq[®] Hot Start DNA polymerase [Promega, UK], 10 mg ml⁻¹ bovine serum albumin [NEB Inc., UK], 0.01% (w/v) poly(vinylpyrrolidone), 0.1% (v/v) Tween-20 [Sigma-Aldrich, UK], 200 μM each deoxyribonucleotide triphosphate [Biolone, UK] and 0.1 μM Amelogenin forward and reverse primers²⁷ [Eurofins MWG Operon, Germany]. The molten wash, elution and PCR gel solutions were injected by positive pressure into the relevant locations on the microfluidic device through electrode loading holes C, D and E respectively, prior to electrode fitting (Fig. 1).

DNA extraction and amplification

Buccal swab DNA samples were collected using an OmniSwab[™] [Whatman, UK] which was gently scraped along the inside of the cheek. The tip of the swab was then added to a binding/lysis solution of 5 M guanidine hydrochloride (GuHCl) [Sigma-Aldrich, UK] in 10 mM TE buffer previously added (20 μl) to the DNA extraction chamber (port A in Fig. 1). A carbon containing polystyrene plug was then placed into port A which enabled the DNA present in the binding/lysis solution to be displaced onto the surface of the silica monolith with the residual liquid passing into channel B shown in Fig. 1. An ethanol wash was used to remove any cellular or proteinaceous debris from the sample by applying a voltage of 100 V cm⁻¹ between electrodes at B and C resulting in EOP of the ethanol wash gel contained in channel C (Fig. 1). The DNA retained on the monolith was then eluted into the chamber pre-loaded with PCR reagents by applying a voltage of 100 V cm⁻¹ from electrodes D to E resulting in EOP of the elution solution contained in channel D (Fig. 1). During this step the PCR reagents were cooled to 4 °C using a thermoelectric Peltier element to prevent adverse thermal effects that may arise

from Joule heating. DNA amplification was then performed using the same Peltier system, which provided both the heating and cooling required for thermal cycling, according to the following program: a Hot-Start step of 95 °C for 2 minutes, followed by 35 cycles of 94 °C for 30 seconds, 60 °C for 30 seconds and 72 °C for 30 seconds, with a 7 minute final extension at 60 °C. Control PCR samples were run on a Techne TC-312 thermal cycler, at the same temperatures and hold-times as the Peltier system.

DNA quantification

Quantification of the DNA obtained from the extraction procedure was performed using a Quant-iT™ PicoGreen® double stranded (ds) DNA Assay Kit [Invitrogen, UK]. To each 2 µl aliquot of sample from the DNA extraction process, 100 µl of the PicoGreen® working stock solution was added, based on manufacturer's protocol, in a black microtitre plate. DNA standards were used to provide a calibration curve at the following concentrations: 10, 5, 2.5, 1.25, 0.625, 0.3125 and 0.15625 ng µl⁻¹. A blank containing no DNA was also used to account for any background fluorescence. All samples were analysed using a FLUOstar Optima Plate Reader [BMG Labtech, UK].

Analysis of PCR products

PCR products were analysed off-chip by capillary electrophoresis using an ABI Prism 310 Genetic Analyser [Applied Biosystems, UK]. The PCR-amplified DNA samples were collected from the DNA amplification chamber (Fig. 1) and added to 12 µl of Hi-Di™ formamide and 0.5 µl GeneScan™ 500 ROX DNA size standard [Applied Biosystems, UK]. The solutions were then heated to 95 °C for 5 min to denature the DNA before being snap-cooled and electrokinetically injected into the capillary.

Results and discussion

DNA recovery direct from buccal swabs

In order to reduce the complexity of sample introduction into the microfluidic device the direct transfer of DNA from the buccal swab to the extraction monolith was evaluated. This was carried out by placing the buccal swab tip (Fig. 3, section A) directly into port A, indicated in Fig. 1, which had been pre-loaded with 20 µl of binding/lysis solution. The buccal swab tip was left in the binding/lysis solution for varying amounts of time and the amount of DNA present in the lysate analysed. Optimum yields were produced when the swab tip remained in the binding/lysis solution for a total of 10 minutes (Fig. 4).

In order to ensure that the tip of the swab would yield sufficient amounts of DNA for analysis, the DNA yields for each segment of the swab were analysed. The average DNA concentration for each segment (A–G, as shown in Fig. 3) was found to be 0.576 ± 0.086 ng µl⁻¹, indicating that all sections of the buccal swab, including the tip, were equally effective in retaining DNA and could be used for analysis.

Previous work by the authors has shown that DNA extraction can be successfully performed using conventional EOP across a silica-based monolith.²⁸ Here DNA was eluted using an applied voltage of 100 V cm⁻¹ resulting in DNA extraction efficiencies of



Fig. 3 Photograph showing the individual buccal swab segments that were analysed.

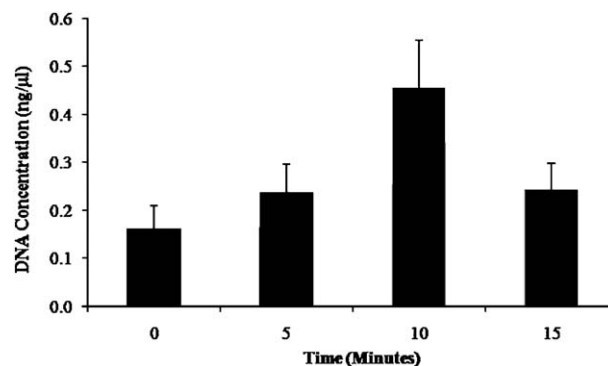


Fig. 4 Graph showing the effect of time on DNA recovery from buccal swab tips using a 5 M GuHCl lysis solution (error bars indicate standard deviation, $n = 6$).

approximately 52%. Despite sufficient DNA being recovered for PCR amplification, the DNA extraction efficiency was limited by the anionic nature of the DNA. As conventional EOF creates bulk movement in the direction of the cathode it opposes the natural electrophoretic migration of the DNA therefore reducing the overall mobility of the DNA. By reversing the direction of EOF, *i.e.* creating a positively charged surface, both EOF and electrophoresis work together to move DNA to the anode resulting in a more efficient process.

To this end, DNA extraction from monoliths using EOP in channels treated with PB was evaluated. The average DNA extraction efficiency obtained using an applied voltage of 100 V cm⁻¹ was found to be 74.5% (with a standard deviation of 20.3%) representing an increased yield as compared with conventional forward EOP (data not shown).

Encapsulation of PCR reagents in LMT agarose gel

A range of final agarose gel concentrations, ranging from 0 to 2.5% (w/v), for encapsulating the PCR reagents were evaluated. Conventional aqueous PCR reagent solutions, containing no agarose gel, were used as control samples. All samples were amplified in a standard bench top thermal cycler and the relative fluorescence intensities of the PCR products, as determined by capillary electrophoresis, were compared.

Comparable PCR efficiencies were demonstrated when using agarose gel concentrations between 0 and 1.5%. However, at agarose gel concentrations of 2% or greater there was a significant decrease in the signal intensity observed, most likely due to high viscosity of the gel matrix slowing the diffusion rate of reactants during the primer annealing and DNA extension phases of the reaction.²⁶ Accordingly, a 1.5% agarose gel was identified as optimal for maintaining a high PCR efficiency, with

the gel providing increased mechanical stability for reagent storage (Fig. 5).

Once the optimum agarose gel concentration had been established the stability of PCR reagents contained within the matrix was examined. All the necessary reagents for PCR, excluding the DNA, were incorporated into a 1.5% (w/v) agarose gel solution and stored at room temperature, 4 °C or −20 °C for up to 8 weeks. DNA was added immediately prior to analysis and the stability was determined by measuring the relative fluorescence intensity of the PCR products obtained (Fig. 6).

The results indicated that storage of the encapsulated PCR reagents at room temperature was not a viable option as the signal intensity is drastically reduced after just 24 hours. Reagents stored at either 4 °C or −20 °C, however, retain the ability to support PCR amplification of DNA at the same efficiency for at least 8 weeks. By storing the microfluidic device under these conditions, all the necessary reagents for performing PCR amplification of specific target loci can be pre-loaded onto the device.

Integration of DNA extraction and amplification

Following optimisation of the individual processes on the microfluidic device, integration of the two processes was evaluated for DNA extraction and amplification of a single target locus (Amelogenin). A small section of buccal swab was placed in port A directly above the silica monolith, along with 20 µl of binding/lysis solution, before being sealed using a polystyrene plug. The entire microfluidic device was then placed inside the control instrument. Following a 10 minute incubation step at room temperature, voltages were applied to achieve movement of the reagents stored on the microfluidic device for both washing of the monolith and subsequent DNA elution. Once the DNA had been transferred into the PCR chamber, which contained all the necessary reagents for amplification, thermal cycling was performed using the Peltier heating/cooling system. Successful amplification of the target locus directly from a buccal swab using the self-contained microfluidic device was confirmed using conventional capillary gel electrophoresis (Fig. 7).

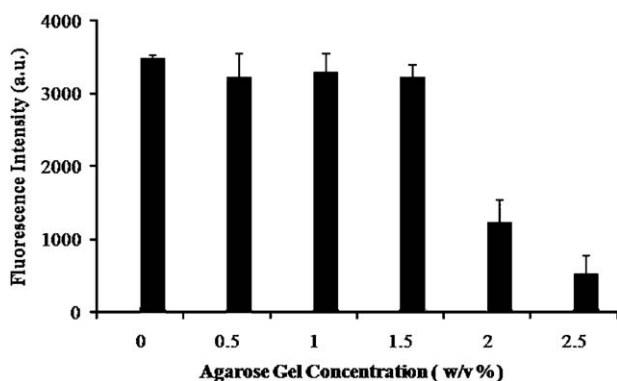


Fig. 5 Amplification of a single locus (Amelogenin) from male DNA with PCR reagents encapsulated in different concentrations of agarose gel. Samples were analysed using capillary electrophoresis and the peak heights of the two alleles (XY) at the Amelogenin locus recorded providing the fluorescence intensity measurements (error bars indicate standard deviation, $n = 3$).

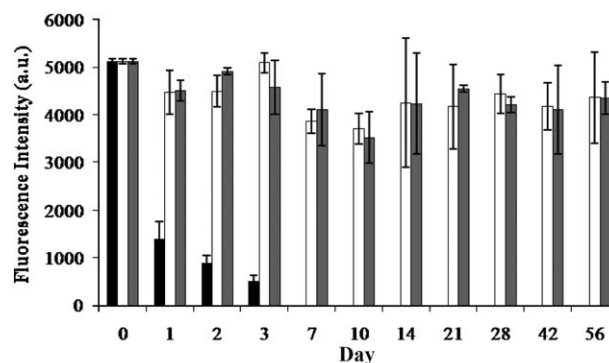


Fig. 6 Relative fluorescence intensities, as determined by capillary electrophoresis, from amplification of a single locus (Amelogenin) when PCR reagents (without DNA) were stored at different temperatures: room temperature (black bar), 4 °C (white bar) and −20 °C (grey bar) (error bars indicate standard deviation, $n = 3$).

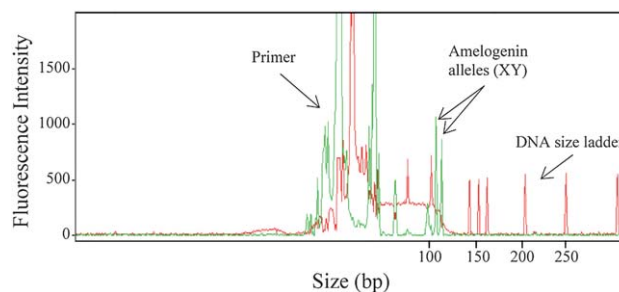


Fig. 7 Electropherogram showing PCR products from amplification of the Amelogenin locus ($X = 104$ bp and $Y = 110$ bp), using DNA extracted from a male volunteer, on the 'ready-to-use' microfluidic device as confirmed on an ABI Prism 310 Genetic Analyser.

Conclusion

This paper reports the successful integration of direct DNA extraction and PCR amplification on a single, self-contained microfluidic device. All the necessary extraction and PCR reagents were pre-loaded onto the device in specific compartments and no external pumps were required as movement was achieved using EOP. In this novel system, a bi-functional silica monolith provided both a solid-phase for DNA extraction and a pump for EOP. An evaluation of the encapsulation of PCR reagents for storage on the microfluidic device showed a final concentration of 1.5% (w/v) agarose gel provided the greatest degree of reagent stability. The gel loaded with reagents could be stored at 4 °C for at least 8 weeks and no interference with the amplification process was observed. Storing the reagents on the device reduces the size of the system footprint by eliminating the need for any external reservoirs of solutions and their mechanical manipulation. The approach developed also serves to increase the reproducibility of the analysis process as any handling errors related to preparing reagents and flowing them into the device will be reduced.

Using reverse EOF in combination with electrophoretic flow improved DNA extraction efficiencies. The use of EOP also resulted in an effective pumping method for performing DNA

extraction and amplification, eliminating the need for complex mechanical interfaces. It has been demonstrated, by successful amplification of the target locus from the eluted DNA, that no detrimental electrophoretic effects on the PCR reagents are observed. By reducing user intervention and simplifying the pumping interface the proposed system exhibits reduced potential for introducing contamination, a particularly important consideration when dealing with clinical or forensic samples. In conclusion, the work presented here offers the potential for creating 'ready-to-use' microfluidic devices that can be used in fully automated systems for rapid sample processing. By combining the current methodology with PCR product detection, *via* real-time PCR or capillary electrophoresis, on a single device a complete "sample in-answer out" system could be generated.

Acknowledgements

The authors would like to thank Dr S. Clark at the University of Hull for manufacture of the microfluidic devices, Prof. N. Goddard at the University of Manchester for the kind gift of polymer electrodes, JLS Designs Ltd. for development of the prototype control system and the EPSRC (EP/D040930) for financial support.

References

- 1 J. Wen, L. A. Legendre, J. M. Bienvenue and J. P. Landers, *Anal. Chem.*, 2008, **80**, 6472–6479.
- 2 Y. Zhang and P. Ozdemir, *Anal. Chim. Acta*, 2009, **638**, 115–125.
- 3 C. S. Zhang, J. L. Xu, W. L. Ma and W. L. Zheng, *Biotechnol. Adv.*, 2006, **24**, 243–284.
- 4 P. A. Auroux, Y. Koc, A. deMello, A. Manz and P. J. R. Day, *Lab Chip*, 2004, **4**, 534–546.
- 5 L. Chen, A. Manz and P. J. R. Day, *Lab Chip*, 2007, **7**, 1413–1423.
- 6 J. P. Ferrance, Q. R. Wu, B. Giordano, C. Hernandez, Y. Kwok, K. Snow, S. Thibodeau and J. P. Landers, *Anal. Chim. Acta*, 2003, **500**, 223–236.
- 7 J. Pipper, M. Inoue, L. F.-P. Ng, P. Neuzil, Y. Zhang and L. Novak, *Nat. Med. (N. Y., NY, U. S.)*, 2007, **13**, 1259–1263.
- 8 K. Y. Lien, C. J. Liu, Y. C. Lin, P. L. Kuo and G. B. Lee, *Microfluid. Nanofluid.*, 2009, **6**, 539–555.
- 9 Y. Zhang, S. Park, S. Yang and T.-H. Wang, *Biomed. Microdevices*, 2010, **12**, 1043–1049.
- 10 R. H. Liu, J. N. Yang, R. Lenigk, J. Bonanno and P. Grodzinski, *Anal. Chem.*, 2004, **76**, 1824–1831.
- 11 J. M. Bienvenue, L. A. Legendre, J. P. Ferrance and J. P. Landers, *Forensic Sci. Int.: Genet.*, 2010, **4**, 178–186.
- 12 N. C. Cady, S. Stelick, M. V. Kunnavakkam and C. A. Batt, *Sens. Actuators, B*, 2005, **107**, 332–341.
- 13 I. K. Dimov, J. L. Garcia-Cordero, J. O'Grady, C. R. Poulsen, C. Viguier, L. Kent, P. Daly, B. Lincoln, M. Maher, R. O'Kennedy, T. J. Smith, A. J. Ricco and L. P. Lee, *Lab Chip*, 2008, **8**, 2071–2078.
- 14 K. H. Han, R. D. McConnell, C. J. Easley, J. M. Bienvenue, J. P. Ferrance, J. P. Landers and A. B. Frazier, *Sens. Actuators, B*, 2007, **122**, 337–346.
- 15 X. Y. Wang, C. Cheng, S. L. Wang and S. R. Liu, *Microfluid. Nanofluid.*, 2009, **6**, 145–162.
- 16 J. A. Oakley, K. J. Shaw, P. T. Docker, C. E. Dyer, L. Furuberg, G. M. Greenway and S. J. Haswell, *Lab Chip*, 2009, **9**, 1596–1600.
- 17 T. Baier, T. E. Hansen-Hagge, R. Gransee, A. Crombé, S. Schmahl, C. Paulus, K. S. Drese, H. Keegan, C. Martin, J. J. O'Leary, L. Furuberg, L. Solli, P. Grønn, I. M. Falang, A. Karlgård, A. Gulliksen and F. Karlsen, *Lab Chip*, 2009, **9**, 3399–3405.
- 18 J. Hoffmann, D. Mark, S. Lutz, R. Zengerle and F. Von Stetten, *Lab Chip*, 2010, **10**, 1480–1484.
- 19 L. Yobas, L. F. Cheow, K.-C. Tang, S.-E. Yong, E. K.-Z. Ong, L. Wong, W. C.-Y. Teo, H. Ji, S. Rafeah and C. Yu, *Biomed. Microdevices*, 2009, **11**, 1279–1288.
- 20 M. Brivio, Y. Li, A. Ahlford, B. G. Kjeldsen, J. L. Reimers, M. Bu, A.-C. Syvanen, D. D. Bang and A. Wolff, *MicroTAS 2007*, Paris, France, 2007, pp. 59–61.
- 21 J. Kim, D. Byun, M. G. Mauk and H. H. Bau, *Lab Chip*, 2009, **9**, 606–612.
- 22 D. Chen, M. Mauk, X. Qiu, C. Liu, J. Kim, S. Ramprasad, S. Ongagna, W. R. Abrams, D. Malamud, P. L. A. M. Corstjens and H. H. Bau, *Biomed. Microdevices*, 2010, **12**, 705–719.
- 23 T. McCreedy, *TrAC, Trends Anal. Chem.*, 2000, **19**, 396–401.
- 24 H. Hartshorne, C. J. Backhouse and W. E. Lee, *Sens. Actuators, B*, 2004, **99**, 592–600.
- 25 P. D. Christensen, S. W. P. Johnson, T. McCreedy, V. Skelton and N. G. Wilson, *Anal. Commun.*, 1998, **35**, 341–343.
- 26 X. Leng, W. Zhang, C. Wang, L. Cui and C. J. Yang, *Lab Chip*, 2010, **10**, 2841–2843.
- 27 B. E. Krenke, A. Tereba, S. J. Anderson, E. Buel, S. Culhane, C. J. Finis, C. S. Tomsey, J. M. Zchetti, A. Masibay, D. R. Rabbach, E. A. Amiot and C. J. Sprecher, *J. Forensic Sci.*, 2002, **47**, 773–785.
- 28 K. J. Shaw, D. A. Joyce, P. T. Docker, C. E. Dyer, J. Greenman, G. M. Greenway and S. J. Haswell, *Lab Chip*, 2009, **9**, 3430–3432.



Microfluidic synthesis of silica nanoparticles using polyethylenimine polymers

Ping He, Gillian Greenway, Stephen J. Haswell*

Department of Chemistry, University of Hull, Hull HU6 7RX, UK

ARTICLE INFO

Article history:

Received 12 April 2010

Received in revised form 17 August 2010

Accepted 17 August 2010

Keywords:

Microfluidics

Silica nanoparticles

PEI polymer

ABSTRACT

A microfluidic reactor system for the synthesis of silica nanoparticles has been developed from commercially available ETFE tubing (0.17–1.0 mm diameter) connected in series to support the hydrolysis, nucleation and particle growth based on a sol–gel method in the presence of PEI polymer at room temperature. Two microfluidic reactor configurations, laminar flow and segmented flow, have been evaluated. Both microfluidic reactors produce particles with narrower size distributions and higher particle yields compared to batch based process. In addition, microfluidic methods offer the possibility to tune particle sizes and size distributions by varying the operation variables such as flow rate, reactor tube diameter and residence time.

© 2010 Elsevier B.V. All rights reserved.

1. Introduction

The synthesis of silica nanoparticles, which underpins a wide range of potential applications covering material science, biotechnology and drug delivery, health-care, sensors, chromatography, catalysis, paints and paper coating [1] has reached the world market demand of 1.5 million metric tons in 2010 [2]. Current industrial processes which provide relatively little control over size and composition are also energy intensive and generally involve harsh reaction conditions such as high temperatures and acidic or basic media in the presence of an organic solvent [3]. By contrast, marine organisms such as diatoms and sponges make elaborate silica structures at ambient conditions and neutral pH from the low amount of silicon found in seawater. In recent years work has been undertaken to mimic this biosilicification process through the use of polypeptides isolated from marine organisms [4] and artificial polyamines [5] to rapidly precipitate silica spheres of several hundreds of nanometers in diameter from hydrolysed tetramethoxysilane solutions at neutral pH.

In order to improve the control over particle generation continuous methodology rather than batch based reactions to generate silica nanoparticles has also been evaluated [6]. The use of microfluidic reactors has for example been used to rapidly produce inorganic and organic nanoparticles [7] because such reactions are extremely sensitive to the reaction conditions such as high temperature and caustic precursors which are more controllable in a microfluidic device [8]. In these methods microfluidic reactors provide the capability of controlling particle size, shape, and composition [8], which is not achievable when using batch based

reactions. Recently, a microfluidic method has been reported for the generation of silica nanoparticles [9] in which single-phase laminar flow and two-phase (air–liquid) segmented flow microreactors were used to control the particle sizes and size distributions by varying flow velocity and residence time. Using this method colloidal silica particles were synthesized using the Stöber process which involves a high concentration of base (i.e. 2M NH_3) and alcohol solvent [10]. The yield of particles was not however provided, and the deposition of particles on the channel walls occurred, leading clogging and unstable reactor conditions were reported.

In this current paper, a simple microfluidic reactor system is proposed for performing continuous hydrolysis, nucleation and particle growth in the presence of polyethylenimine polymers. The microfluidic reactors presented in this study is built by simply connecting commercially available ETFE tubes, fittings and connectors together enabling reaction tubes to be replaced, which minimizes effect of particle deposition within the reaction tube whilst maintaining constant flow conditions. Using polyethylenimine polymers as nucleation catalysts, silica nanoparticles can be rapidly precipitated at room temperature. Two reactor configurations, a single-phase continuous flow microreactor (CFMR) and a two-phase (gas–liquid) segmented flow microreactor (SFMR), will be evaluated for continuous hydrolysis and condensation of tetramethoxysilane. The effects of some operation variables such as reactor tube diameter, pH and flow rate on particle sizes and distribution together with yield will be evaluated and results compared with those obtained from small-scale batch based process.

2. Methods and materials

Tetramethoxysilane (TMOS, 99%), sodium dihydrogen phosphate anhydrous (99%), sodium phosphate dibasic anhydrous (99%), polyethylenimine (PEI, 99%, molecular weight 423, 800,

* Corresponding author.

E-mail address: s.j.haswell@hull.ac.uk (S.J. Haswell).

2000, 10,000 and 25,000) and HCl (37%), were purchased from the Sigma–Aldrich. ETFE tubing was purchased from VWR International and fittings and connectors (pore size 0.5 mm diameter) were purchased from Upchurch. Milli-Q water (18 M Ω cm) was used to prepare all aqueous solutions.

2.1. Construction of microfluidic reactors

Currently, most microfluidic reactors are fabricated by photolithographic process and the reactor channels are not readily changeable after fabrication has been completed. The microfluidic reactors used in the present work were fabricated using readily available commercial components such as PEEK Y-shape and cross connectors as well as ETFE tubing. The practical advantages of this method for fabricating microfluidic reactors include simplicity and component replaceability. Fig. 1A shows a CFMR system that consists of two PEEK Y-shape connectors and ETFE tubing for hydrolysis and silicification reactions. Fig. 1B shows a SFMR system that consists of a PEEK Y-shape connector and a PEEK cross connector as well as ETFE tubing. Syringe pumps (KD Scientific) were used for controlling flow rates of the reagents and air (in the SFMR system). Reaction times for TMOS hydrolysis and silicification can be adjusted by altering the length of the tubing and flow rate.

2.2. Batch based silica synthesis

A typical reagent mixture of 250 μ l of 0.2 M sodium phosphate buffer, 200 μ l of Milli-Q water, 25 μ l of PEI (100 mg/ml) and 25 μ l of 1 M TMOS solution (which was pre-hydrolysed in 1 mM HCl for 10 min) was added in the above sequence into a polypropylene vial. In the final reaction mixture (volume = 500 μ l), the concentration of phosphate buffer, PEI and TMOS was 0.1 M, 5 mg/ml and 0.05 M respectively. After adding the freshly hydrolysed TMOS, the solution became cloudy within tens of seconds and a reaction time of 5 min was used. After which the mixture was centrifuged at 14,000 rpm for 1 min, the supernatant was collected and the pellets were washed three times by re-dispersing in Milli-Q water and re-centrifuging, and finally dispersed in 500 μ l of Milli-Q water. The reagent concentrations used for batch based synthesis were also chosen for the microfluidic synthesis in order to compare the performance of the two synthetic methods.

2.3. Continuous flow microreactor (CFMR) based silica synthesis

The set up for the CFMR synthesis of silica nanoparticles can be seen in Fig. 1A, in which TMOS (0.15 μ l/min) and 1 mM HCl (1.85 μ l/min) are individually pumped into a small Y-shape connector (M1) where the two reagents mix and pass through the ETFE

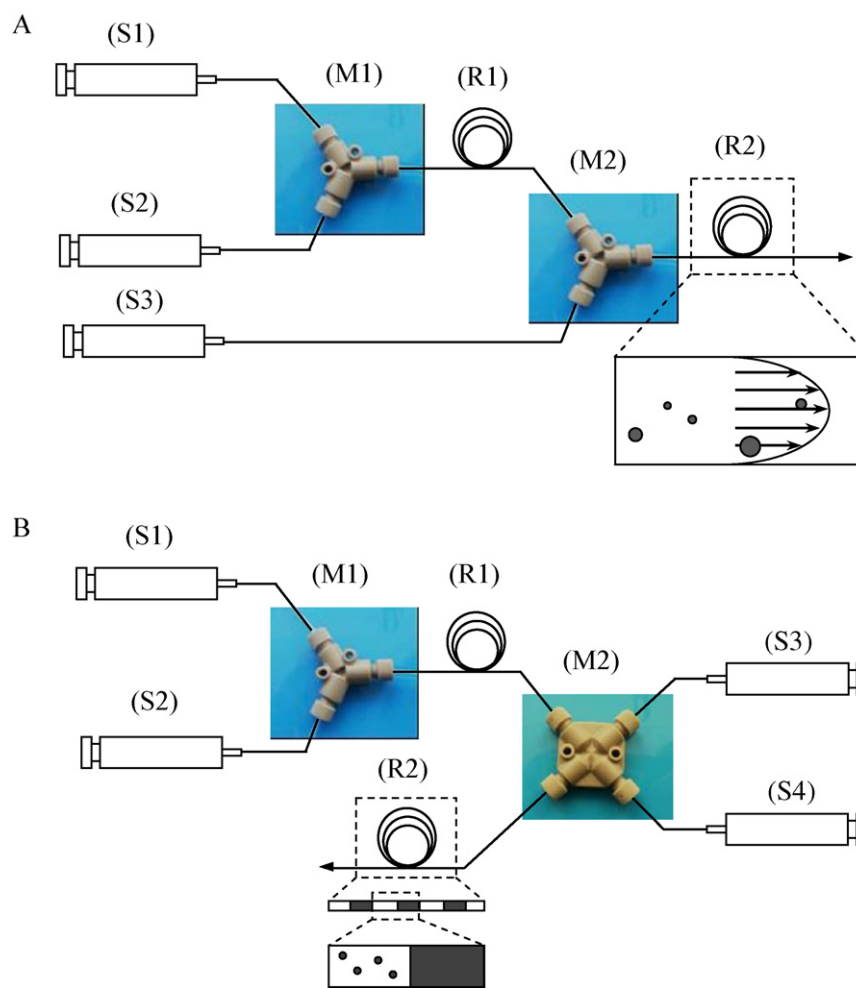


Fig. 1. Schematic diagram of microfluidic reactor systems for the particle synthesis. (A) CFMR system: (S1) syringe (volume 1 ml) for TMOS, (S2) syringe (volume 1 ml) for 1 mM HCl, (S3) syringe (volume 1 ml) for PEI polymer in Tris–HCl buffer solution, (M1) and (M2) PEEK Y-shape mixers (pore size 0.5 mm diameter), (R1) reaction tube (0.17 mm diameter) for hydrolysis, (R2) reaction tube (0.5 mm diameter) for silica precipitation. (B) SFMR system: (S1) syringe (volume 1 ml) for TMOS, (S2) syringe (volume 1 ml) for 1 mM HCl, (S3) syringe (volume 20 ml) for air injection, (S4) syringe for PEI polymer in Tris–HCl buffer solution, (M1) PEEK Y-shape mixers (pore size 0.5 mm diameter), (M2) PEEK 4-way mixer, (R1) reaction tube (0.17 mm diameter) for hydrolysis, (R2) reaction tube (0.5 mm diameter) for silica precipitation.

tubing (R1, diameter 0.17 mm) to complete the 10 min hydrolysis reaction. The use of online hydrolysis of TMOS rather than pre-hydrolysed TMOS enabled a more reproducible hydrolysis time to be achieved compared to the batch synthesis. PEI in phosphate buffer (18 $\mu\text{l}/\text{min}$) was then introduced and mixed with hydrolysed TMOS at a small Y-shape mixer (M2) and finally passed through ETFE tubing (R2, diameter 0.5–1.0 mm) to perform silicification over a period of 5 min. A sintered funnel with a membrane (10 nm pore size), connected to a vacuum pump, was used to immediately remove reaction media in order to effectively quench the reaction and isolate the particles formed. The liquid sample was collected and the particles were physically collected by carefully removing the membrane and transferring it to a 1.5 ml polypropylene vial in which the particles were re-suspended in Milli-Q water and washed three times using the procedure described previously.

2.4. Segmented flow microreactor (SFMR) based silica synthesis

The SFMR system for the synthesis of silica nanoparticles is shown in Fig. 1B. Air–liquid segmented flow was used to generate small plugs within the ETFE tubing, which acted as compartments for the silicification reaction. TMOS (0.15 $\mu\text{l}/\text{min}$) and 1 mM HCl (1.85 $\mu\text{l}/\text{min}$) were separately pumped into a small Y-shape connector (M1) where the two reagents mixed and passed along an ETFE tubing (R1, diameter 0.17 mm) to complete the hydrolysis reaction over a period of 10 min. Air–liquid segmented flow was generated using a small PEEK cross connector (M2) in which air (20 $\mu\text{l}/\text{min}$) was pumped into the middle inlet of the cross connector through a SEG gastight syringe, hydrolysed TMOS solution and PEI in phosphate buffer (pH 7.0) solution (18 $\mu\text{l}/\text{min}$) were introduced from two side inlets. The reaction streams passed through ETFE tubing (R2, diameter 0.5 mm) to complete silicification reac-

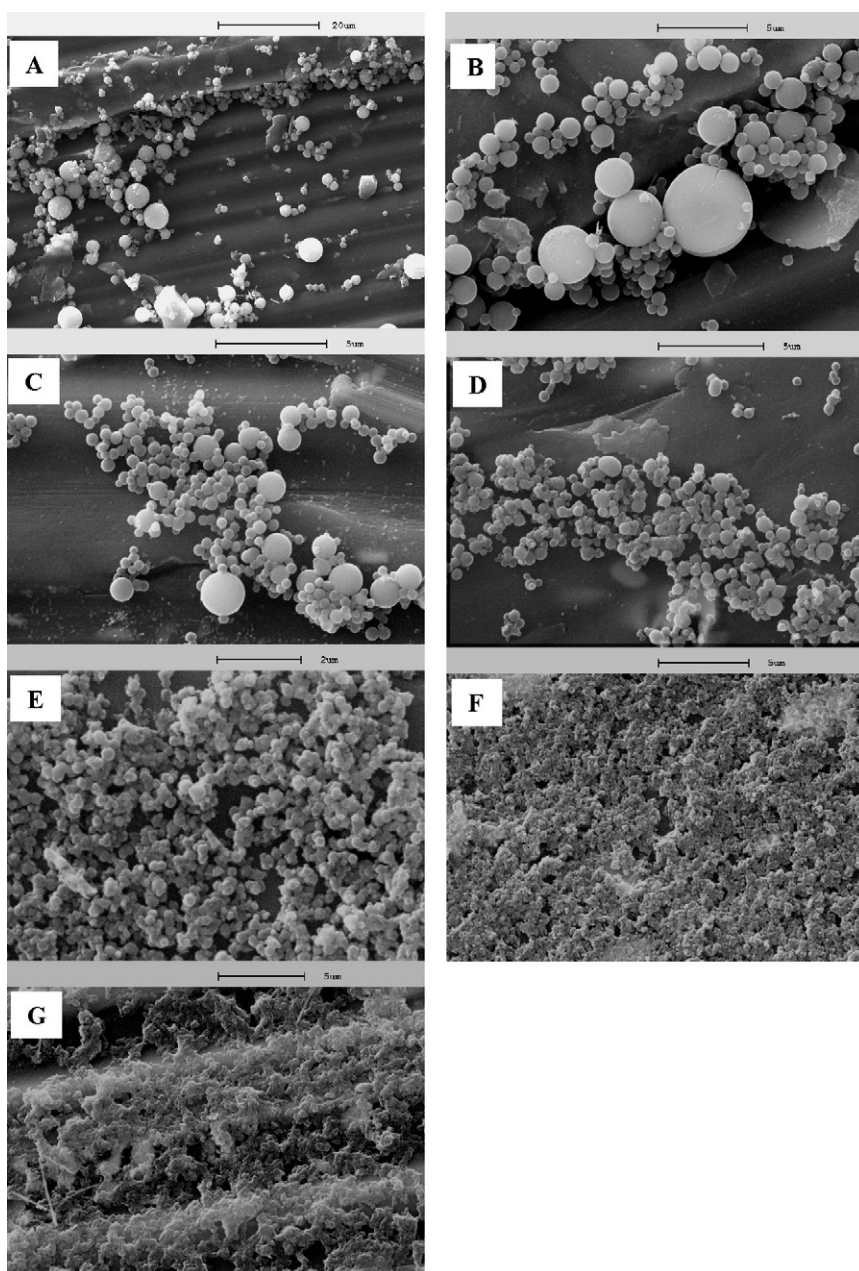


Fig. 2. SEM images of silica spheres obtained using batch based process. (A) pH 6.0; (B) pH 6.5; (C) pH 7.0; (D) pH 7.5; (E) pH 8.0; (F) Phosphate buffer (pH 7.5) first mixed with TMOS then PEI added to; (G) PEI first mixed with TMOS then phosphate buffer (pH 7.5) added to.

tion in a period of 5 min. Sample collection and treatment were the same as the procedures used for the CFMR based synthesis.

2.5. Silica quantitation

The silica produced was quantitated using the β -silicomolybdate method developed by Iler [11]. Briefly, individual samples obtained from total reaction volume of 500 μ l were dissolved in 0.5 M NaOH solution and incubated at 95 °C (oil bath) for 30 min to ensure complete dissolution. After which the liberated PEI polymers in solution were removed from the solution by centrifuging at 14,000 rpm for 1 min. 100 μ l of supernatant was added to the molybdate solution to form the bright yellow product that was monitored by UV–vis spectrophotometry at 410 nm and quantitated from a standard curve of silicate standards.

3. Results and discussion

In this study the synthesis of silica particles was first performed using a batch based process in the presence of PEI polymers. SEM images of silica particles (Fig. 2) produced at different pH and yield (Fig. 3) indicate that the diameter of silica spheres significantly decreases with increasing pH of the silicic acid solution whilst the yield increases. The properties of silica spheres precipitated in the presence of PEI polymer, using batch based process are shown in Table 1. At present, the mechanism of polyamine-induced silica condensation and precipitation is not completely understood, but it has been suggested by several groups [4d, 4i, 5e] that the PEI could act as an acid-base catalyst in which deprotonated residues (acting as the “base”) accept a proton from a silicic acid molecule to form a reactive silanolate group and protonated residues (acting as the “acid”) that facilitate the release of a water from the silicic acid substrate. In addition, electrostatic interaction between negatively charged silica species and positively charged PEI molecule may lead to a supramolecular assembly that encapsulates the PEI molecules within the silica nanospheres. As the TMOS was pre-hydrolysed the size of the particles formed was found to be directly determined by the nucleation and growth processes where nucleation is the reaction of the monomer with unreacted monomer and growth is the reaction of the monomer with existing particles. Accordingly, the

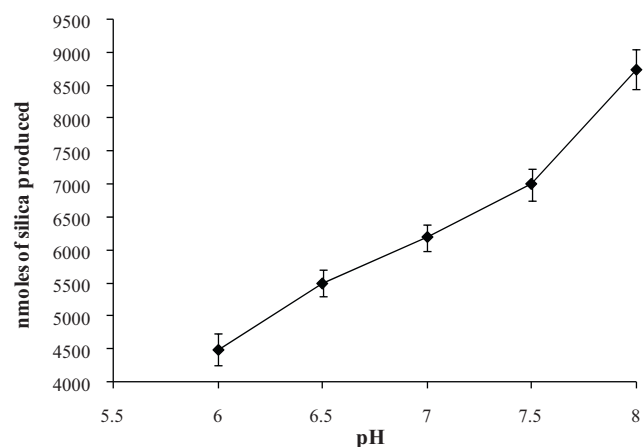


Fig. 3. Production of silica particles as function of buffer pH values.

Table 1

Properties of silica nanoparticles obtained from batch, CFMR and SFMR synthesis.

Reactor	pH	Mean size (nm)	Standard deviation	Yield (%)
Batch	6.0	1100	90.2	18 ± 5
Batch	6.5	802	50.2	22 ± 3
Batch	7.0	493	23.5	25 ± 3
Batch	7.5	476	12.4	28 ± 3
Batch	8.0	228	3.4	35 ± 3
CFMR ^a	6.5	176	5.5	59 ± 6
CFMR ^b	6.5	73	3.0	62 ± 6
CFMR ^a	7.5	53	1.1	65 ± 7
SFMR ^c	6.5	63	1.1	58 ± 6

^a TMOS = 0.15 μ l/min, 1 mM HCl = 1.85 μ l/min, PEI-buffer = 20 μ l/min, residence time = 5 min.

^b TMOS = 0.075 μ l/min, 1 mM HCl = 0.09 μ l/min, PEI-buffer = 10 μ l/min, residence time = 5 min.

^c TMOS = 0.15 μ l/min, 1 mM HCl = 1.85 μ l/min, PEI-buffer = 20 μ l/min, air injection = 20 μ l/min, residence time = 5 min.

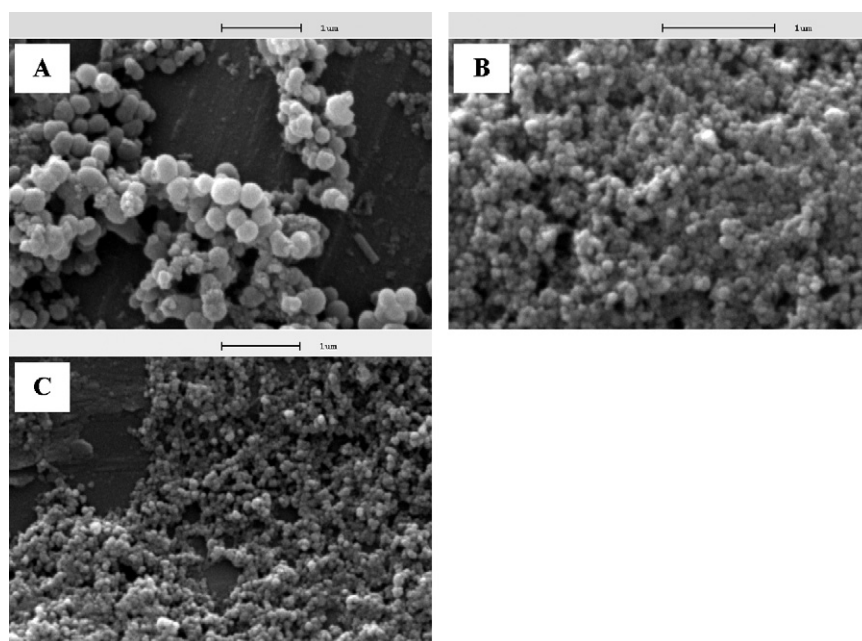


Fig. 4. SEM images of silica particles obtained using microfluidic reactors. (A) CFMR synthesis at pH 6.5; (B) CFMR synthesis at pH 7.5; (C) SFMR synthesis at pH 6.5.

nucleation rate is a second-order reaction dependant on the concentration of the monomer whereas growth is first order. Factors that promote nucleation must result in smaller particles whilst fac-

tors that favour growth should have the opposite effect [12]. From Table 1 it can be seen that at a low pH (i.e. 6.0) the monomer is consumed in the reaction with existing particles (particle growth), rather than with unreacted monomer (nucleation), giving significantly larger particles and considerably broader size distributions. However, at high pH (i.e. 8.0) nucleation dominates the reaction, producing smaller particles with narrower size distributions and higher silica yields. Other parameters were also investigated and it was found that PEI molecular mass (423–10,000) and concentration (2–10 mg/ml) and silicic acid concentration (0.05–0.1 M in final solution) have no significant effect on diameter of silica spheres and morphology of silica spheres produced (data not shown). However, the order of mixing reagents was found to be important for the formation of silica spheres (Fig. 2D, F and G).

To compare the effect of microfluidic reactors on the particle size and aggregation behaviour with batch based process, silica precipitation was carried out in both CFMR and SFMR systems using the same conditions as those used in the batch synthesis. SEM images of silica particles obtained from the CFMR and SFMR systems are shown in Fig. 4 and their characteristics are summarized in Table 1. It can be seen that microfluidic reactors always produce significantly smaller particles with narrower size distributions and twice the silica yield compared to batch based synthesis. The particle characteristics observed in microfluidic reactor systems, i.e. sizes, yields and size distributions, can be attributed to the fast kinetics for nucleation or the decrease in the particle size dispersion. In terms of chemical synthesis reactions in microliter to nanoliter volumes have demonstrated enhanced reaction yield and kinetics [13] this being due to the high concentration of active (hydrolysed) monomers, monomer–monomer reaction present and hence the rate of growth is low, giving smaller particles. Under laminar flow (CFMR case) the axial dispersion coefficient (E_A) of particles suspended in a cylindrical tube can be expressed by Taylor dispersion Eq. (1).

$$E_A = D + \frac{U^2 R^2}{48D} \quad (1)$$

Here, U is the average velocity in the reaction tube, R the radius of the reaction tube, and D the diffusion coefficient of the particles, which is given by Stokes–Einstein relation (2).

$$D = \frac{k_B T}{6\pi\mu r_p} \quad (2)$$

Here k_B is the Boltzmann constant, T the absolute temperature and μ the fluid viscosity. Substituting the radius of the reaction tube (0.25 mm) for the tube radius in Eq. (1) and a radius of 88 nm (corresponding to mean size 176 nm, see Table 1) for the calculation of particle diffusivity, we can make the following observation on the axial dispersion effect. The small diffusivity of silica spheres ($\approx 10^{-12}$ m²/s) implies that the axial dispersion is dominated by the convective term in Eq. (1), thus the axial dispersion coefficient varies as the square of ($U \times R$). As the Reynolds number is proportional to $U \times R$, this implies that the axial dispersion coefficient varies with the second power of the Reynolds number. Normally, the Reynolds number in microfluidic reactors is very small (0.01–10), that is to say, the microfluidic reactor systems give smaller dispersion coefficients, which in turn lead to narrow distribution of residence times and consequently, lower particle size distribution, the particle size dispersion therefore becomes smaller. Indeed, at the same pH values as the batch processes, the CFMR system produced significantly smaller particles (mean size 176 nm for pH 6.5 and 53 nm for pH 7.5) with narrower size distributions (SD 5.5 for pH 6.5 and 1.1 for pH 7.5) and double increase in silica yield (59% for pH 6.5 and 65% for pH 7.5) (see Fig. 4A and B and Table 1).

For the SFMR system, introduction of gas into the inlet of the reaction tube continuously separates liquid feed into small por-

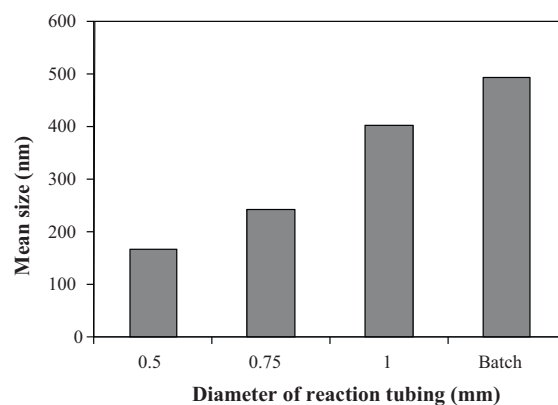


Fig. 5. Effect of reactor tube diameter on mean size of silica nanoparticles obtained at pH 7.

tions, as shown in Fig. 4B. Hence an SFMR process is equivalent to many small batch reactors passing through the tube at constant velocity. As re-circulation occurs within each slug, all the segmented batches experience the same amount of mixing and the residence time which eliminates dispersion of the particles, leading to more uniform particles [9].

Comparison of the silica spheres obtained under SFMR conditions (Fig. 4C) with those under CFMR conditions (Fig. 4A) indicates that the SFMR silica spheres were found to have smaller mean size, narrower size distribution and similar silica yield relative to the CFMR. For example, the SFMR system gave mean size of 63 nm, SD of 1.1 and 58% silica yield compared to a mean size of 176 nm, SD of 5.5 and 59% silica yield obtained from the CFMR system (see Table 1). It was also found that under CFMR conditions a decrease in flow rate by a factor of 2 for the liquid and gas, produced smaller particles (mean size = 73 nm) with narrower size distribution (SD = 3.0) and a slightly higher yield (62%) whilst having no obvious effect on particle size and size distribution for the SFMR synthesis (data not shown).

Under CFMR conditions, the effect of reaction tube diameter on particle size was also investigated. Results (Fig. 5) indicate that the particle sizes can be controlled by using different tube diameters with an increase in reactor diameter from 0.5 to 0.75 and 1.0 mm generating silica spheres with increasing mean size of 167 nm to 241 nm and 402 nm respectively, compared to mean size of 492 nm obtained for batch based reaction. This is in agreement with the discussion on Eq. (1) where smaller diameters of the reaction tubes give smaller axial dispersions, leading to smaller particles.

It should be noted that the deposition of silica particles was observed around 1–2 cm from the inlet when carrying out the microfluidic synthesis after approximately 2 h. The deposition of particles formed in the reaction channel is a common phenomenon [9], which leads to clogging and unstable reactor conditions. For our microfluidic systems the reaction tubes can be simply replaced, minimizing effect of the particle deposition on the synthesis. Finally, there was no indication that pulsation or jetting occurred under the reaction conditions used.

4. Conclusions

It has been demonstrated that microfluidic methods for the synthesis of silica nanoparticles offer the possibility to tune particle sizes and size distributions by varying the operation variables such as flow rate and residence time. A significantly narrow size distribution of silica particles can be obtained by using microfluidic reactors in the presence of PEI polymer at room temperature compared to batch based synthesis. The SFMR conditions yield fine particles of better quality than the CFMR due to the elimination of axial disper-

sion effect under the SFMR conditions. Compared to a conventional batch system, microfluidic reactors enable a controllable process in terms of size and size distribution for the production of silica particles. For the microfluidic reactor systems presented in this work the reaction tubes can be simply replaced, minimizing effect of the particle deposition on the synthesis and potential channel blockage.

References

- [1] (a) C.J. Brinker, J.W. Scherer, *Sol-Gel Science, The Physics and Chemistry of Sol-Gel Processing*, Academic Press, Boston, 1990;
- (b) R.K. Iler, *The Chemistry of Silica*, John Wiley and Sons, New York, 1979.
- [2] According to a report (2006) of World Market for Precipitated silica by Notch Consulting Group, Amherst, MA (<http://www.thefreelibrary.com/Demand+for+precipitated+silica+to+rise+4%25-a0119376710>).
- [3] D.J. Belton, S.V. Patwardhan, V.V. Annenkov, E.N. Danilovtseva, C.C. Perry, From biosilicification to tailored materials: optimizing hydrophobic domains and resistance to protonation of polyamines, *Proc. Natl. Acad. Sci. U.S.A.* 105 (2008) 5963–5968.
- [4] (a) N. Kröger, R. Deutzmann, M. Sumper, Polycationic peptides from diatom biosilica that direct silica nanosphere formation, *Science* 286 (1999) 1129–1132;
- (b) K. Shimizu, D.E. Morse, The biological and biomimetic synthesis of silica and other polysiloxanes, in: *Biomimetalization: From Biology to Biotechnology and Medical Application*, Wiley-VCH, New York, 2000, p. 207;
- (c) N. Kröger, R. Deutzmann, M. Sumper, Silica-precipitating peptides from diatoms. The chemical structure of silaffin-A from *Cylindrotheca fusiformis*, *J. Biol. Chem.* 276 (2001) 26066–26070;
- (d) N. Kröger, R. Deutzmann, C. Bergsdorf, M. Sumper, Species-specific polyamines from diatoms control silica morphology, *Proc. Natl. Acad. Sci. U.S.A.* 97 (2000) 14133–14138;
- (e) F. Noll, M. Sumper, N. Hampp, Nanostructure of diatom silica surfaces and of biomimetic analogues, *Nano Lett.* 2 (2002) 91–95;
- (f) P.J. Lopez, C. Gautier, J. Livage, T. Coradin, Mimicking biogenic silica nanostructures formation, *Curr. Nanosci.* 1 (2005) 73–83;
- (g) S.V. Patwardhan, N. Mukherjee, M. Steinitz-Kannan, S.J. Clarson, Bioinspired synthesis of new silica structures, *Chem. Commun.* (2003) 1122–1123;
- (h) R.R. Naik, P.W. Whitlock, F. Rodrigues, L.L. Brott, D.D. Glawe, S.J. Clarson, M.O. Stone, Controlled formation of biosilica structures *in vitro*, *Chem. Commun.* (2003) 238–239;
- (i) M.R. Knecht, D.W. Wright, Functional analysis of the biomimetic silica precipitating activity of the R5 peptide from *Cylindrotheca fusiformis*, *Chem. Commun.* (2003) 3038–3039.
- [5] (a) S.V. Patwardhan, N. Mukherjee, S.J. Clarson, The use of poly-L-lysine to form novel silica morphologies and the role of polypeptides in biosilicification, *J. Inorg. Organomet. Polym.* 11 (2001) 193–198;
- (b) S.V. Patwardhan, S.J. Clarson, Silicification and biosilicification Part 1. Formation of silica structures utilizing a cationically charged synthetic polymer at neutral pH and under ambient conditions, *Polym. Bull.* 48 (2002) 367–371;
- (c) S.V. Patwardhan, S.J. Clarson, Silicification and biosilicification, *Silicon Chem.* 1 (2002) 207–214;
- (d) M.R. Knecht, D.W. Wright, Amine-Terminated dendrimers as biomimetic templates for silica nanosphere formation, *Langmuir* 20 (2004) 4728–4732;
- (e) T. Mizutani, H. Nagase, N. Fujiwara, H. Ogoshi, Silicic acid polymerization catalyzed by amines and polyamines, *Bull. Chem. Soc. Jpn.* 71 (1998) 2017–2022.
- [6] (a) T. Yonemoto, M. Kubo, T. Doi, T. Tadaki, Continuous synthesis of titanium dioxide fine particles using a slug flow ageing tube reactor, *Chem. Eng. Res. Des.* 75 (1997) 413–419;
- (b) T. Ogihara, M. Iizuka, T. Yanagawa, N. Ogata, K. Yoshida, Continuous reactor system of monosized colloidal particles, *J. Mater. Sci.* 27 (1992) 55–62;
- (c) C.H. Kaiser, M. Hanson, H. Giesche, J. Kinkel, K.K. Unger, *Fine Particles Science and Technology*, Kluwer Academic Publishers, Amsterdam, 1996, pp. 71–84.
- [7] (a) T. Nisisako, T. Torii, T. Takahashi, Y. Takizawa, Synthesis of monodisperse bicolored janus particles with electrical anisotropy using a microfluidic co-flow system, *Adv. Mater.* 18 (2006) 1152–1156;
- (b) Z.H. Nie, W. Li, M. Seo, S.Q. Xu, E. Kumacheva, Janus and ternary particles generated by microfluidic synthesis: design, synthesis and self-assembly, *J. Am. Chem. Soc.* 128 (2006) 9408–9412;
- (c) R.F. Shepherd, J.C. Conard, S.K. Rhodes, D.R. Link, M. Marquez, D.A. Weitz, J.A. Lewis, Microfluidic assembly of homogeneous and janus colloid-filled hydrogel granules, *Langmuir* 22 (2006) 8618–8622;
- (d) S. Takeuchi, P. Garstecki, D.B. Weibel, G.M. Whitesides, An axisymmetric flow-focusing microfluidic device, *Adv. Mater.* 17 (2005) 1067–1072;
- (e) S. Xu, Z. Nie, M. Seo, P. Lewis, E. Kumacheva, H.A. Stone, P. Garstecki, D.B. Weibel, I. Gitlin, G.M. Whitesides, Generation of monodisperse particles by using microfluidics: control over size, shape, and composition, *Angew. Chem. Int. Ed.* 44 (2005) 724–728.
- [8] (a) B.K.H. Yen, N.E. Stoot, K.F. Jensen, M.G. Bawendi, A Continuous-flow microcapillary reactor for the preparation of a size series of CdSe nanocrystals, *Adv. Mater.* 15 (2003) 1858–1862;
- (b) B.K.H. Yen, A. Günther, M.A. Schmidt, K.F. Jensen, M.G. Bawendi, A microfabricated gas-liquid segmented flow reactor for high-temperature synthesis: the case of CdSe quantum dots, *Angew. Chem. Int. Ed.* 44 (2005) 5447–5451;
- (c) E.M. Chan, A.P. Alivisatos, R.A. Mathies, High-temperature microfluidic synthesis of CdSe nanocrystals in nanoliter droplets, *J. Am. Chem. Soc.* 127 (2005) 13854–13861;
- (d) J.A. Schwartz, J.V. Vykoukal, P.R.C. Gascoyne, Droplet-based chemistry on a programmable micro-chip, *Lab Chip* 4 (2004) 11–17;
- (e) J.B. Edel, R. Fortt, J.C. deMello, A.J. deMello, Microfluidic routes to the controlled production of nanoparticles, *Chem. Commun.* (2002) 1136–1137;
- (f) H. Nakamura, Y. Yamaguchi, M. Miyazaki, M. Uehara, H. Maeda, P. Mulvaney, Continuous preparation of CdSe nanocrystals by a microreactor, *Chem. Lett.* (2002) 1072–1074;
- (g) I. Shestopalov, J.D. Tice, R.F. Ismagilov, Multi-step synthesis of nanoparticles performed on millisecond time scale in a microfluidic droplet-based system, *Lab Chip* 4 (2004) 316–321;
- (h) S. Krishnadasan, J. Tovilla, A.J. deMello, J.C. deMello, On-line analysis of CdSe nanoparticle formation in a continuous flow chip-based microreactor, *J. Mater. Chem.* 14 (2004) 2655–2660;
- (i) H. Song, D.L. Chen, R.F. Ismagilov, Reactions in droplets in microfluidic channels, *Angew. Chem. Int. Ed.* 45 (2006) 7336–7356.
- [9] S.A. Khan, A. Günther, M.A. Schmidt, K.F. Jensen, Microfluidic synthesis of colloidal silica, *Langmuir* 20 (2004) 8604–8611.
- [10] W. Stöber, A. Fink, E. Bohn, Controlled growth of monodisperse silica spheres in the micron size range, *J. Colloid Interface Sci.* 26 (1968) 62–69.
- [11] R.K. Iler, *The Chemistry of Silica*, Wiley, New York, 1979, pp. 96–98.
- [12] (a) T. Matsoukas, E. Gulari, Dynamics of growth of silica particles from ammonia-catalyzed hydrolysis of tetra-ethyl-orthosilicate, *J. Colloid Interface Sci.* 124 (1988) 252–261;
- (b) G.H. Bogush, C.F. Zukoski IV, Studies of the kinetics of the precipitation of uniform silica particles through the hydrolysis and condensation of silicon alkoxides, *J. Colloid Interface Sci.* 142 (1991) 1–18.
- [13] (a) P.D.F. Fletcher, S.J. Haswell, E. Pombo-Villar, B.H. Warrington, P. Watts, S.Y.F. Wong, X. Zhang, Micro reactors: principles and applications in organic synthesis, *Tetrahedron* 58 (2002) 4735–4757;
- (b) P. He, S.J. Haswell, P.D.F. Fletcher, Microwave heating of heterogeneously catalysed Suzuki reactions in a micro reactor, *Lab Chip* 4 (2004) 38–41;
- (c) P. He, P. Watts, F. Marken, S.J. Haswell, Self-supported and clean one-step cathodic coupling of activated olefins with benzyl bromide derivatives in a micro flow reactor, *Angew. Chem. Int. Ed.* 45 (2006) 4146–4149;
- (d) K.F. Jensen, Microreaction engineering – is small better? *Chem. Eng. Sci.* 56 (2001) 293–303;
- (e) H. Pennemann, P. Watts, S.J. Haswell, V. Hessel, H. Lowe, Benchmarking of microreactor applications, *Org. Process Res. Dev.* 8 (2004) 422–439;
- (f) J.R. Burns, C. Ramshaw, The intensification of rapid reactions in multiphase systems using slug flow in capillaries, *Lab Chip* 1 (2001) 10–15;
- (g) E.T. Lagally, C.A. Emrich, R.A. Mathies, Fully integrated PCR-capillary electrophoresis microsystem for DNA analysis, *Lab Chip* 1 (2001) 102–107.

Kirsty J. Shaw¹
 Christopher Birch¹
 Elizabeth M. Hughes²
 Adam D. Jakes²
 John Greenman³
 Stephen J. Haswell¹

Review

Microsystems for personalized biomolecular diagnostics

The development of microfluidic methodology that can be used in conjunction with drug screening and biomolecular diagnostics offers a route to evidence-based personalized medical care. Ideally, all personal diagnostics are best carried out in a rapid and frequent manner and a microfluidic interface can provide appropriate methodology. The ability to perform genetic analysis or biomarker detection at point-of-care would allow the clinician to decide on the most informed course of treatment. Microfluidic systems for biomolecular analysis at all levels, from genes to whole tissue biopsies, have been proposed. Much of the work presented here is at an early stage of development but will consider the range of design considerations together with the plethora of potential applications of integrated microfluidic technology.

Keywords: Diagnostics / Healthcare / Integration / Microfluidics / Personalized medicine

Received: October 1, 2010; *revised:* January 25, 2011; *accepted:* February 18, 2011

DOI: 10.1002/elsc.201000175

¹Department of Chemistry,
 University of Hull,
 Cottingham Road, Hull, UK

²Hull and York Medical
 School, University of Hull,
 Cottingham Road, Hull, UK

³PostGraduate Medical
 Institute, University of Hull,
 Cottingham Road, Hull, UK

1 Introduction

The aims of personalized medicine are to predict how an individual will respond to a particular drug or medical intervention such that the therapeutic efficacy is maximized while reducing unwanted side effects. To achieve this, the correct selection of drug formulation and dosage, for example, all need to be determined, leading to a gradual lowering of mass development of pharmaceuticals and an increase in production of a range of more specified drugs. This extended knowledge on a molecular level can further serve to pre-diagnose the development of a disease, within a particular individual based on genomic and proteomic information [1]. A recent article by Bates reviews current clinical progress in personalized medicine and summarizes future perspectives in the field [2]. Specifically, the review demonstrates that the main thrust of personalized medicine is focused in oncology. Cancer arises when disrupted cell signaling pathways cause a significant growth advantage over their neighboring cells resulting in the development of a tumor mass. However, the genetic changes that define these variations are not universal to all cases of cancer, even for tumors of the

same location within the body. By isolating this genetic information, it is possible to gather information about the disease in its *in vivo* state and location, while also obtaining further details on how it will progress and respond to drug intervention.

The move towards personalized medicine has been driven by the knowledge that, for a given disease, each individual person will respond in a unique way to treatment. Broadly speaking, personalized diagnostic medicine can be divided into four main steps: evaluating an individual's predisposition for genetic disorders possibly enabling preventative treatment; screening and early disease diagnosis; targeting therapeutic treatments based on molecular characteristics of disease; and preventing adverse drug reactions. To enable truly personalized medical treatment, these steps can be performed individually, in parallel or in series.

By using genetic analysis, it is possible to predict an individual's predisposition to a certain disease, usually by single nucleotide polymorphism (SNP) analysis, allowing administration of preventative therapies, e.g. statins for people at risk of developing coronary artery disease [3]. An example of a targeted therapeutic in use is Herceptin[®] (trastuzumab) for the treatment of breast cancers, which overexpress human epidermal growth factor receptor (EGFR) 2 (HER-2/neu), as identified using a complementary diagnostic test, Hercep-Test[™] (Dako, Denmark). Alternatively, the prescription of medications based on genetic data can be used to avoid drugs that demonstrate absent or incomplete efficacy in certain individuals in the population, e.g. 40–70% of the population for 2-agonists [1]. Drug development in the pharmaceutical industry can take advantage of the molecular basis of a disease in order to direct therapeutic agents at the right population.

Correspondence: Dr. Kirsty J. Shaw (k.j.shaw@hull.ac.uk), Department of Chemistry, University of Hull, Cottingham Road, Hull, Yorkshire HU6 7RX, UK

Abbreviations: CRP, C-reactive protein; CTC, circulating tumor cell; EGFR, epidermal growth factor receptor; EpCAM, epithelial cell adhesion molecule; HPV, human papilloma virus; IgV_H, immunoglobulin heavy-chain variable region; PDMS, poly(dimethylsiloxane); POC, point-of-care; RT-PCR, reverse transcription-PCR; SNP, single nucleotide polymorphism

This is achieved by selecting optimal drug targets and dosage, predicting which individuals will respond well to the drugs and those who will experience toxic effects, as a result the overall cost of treatment is reduced with more effective healthcare. Adverse drug reactions are caused by the failure to predict drug toxicity in individuals, which can have a severe health impact and a corresponding, often substantial, related economic cost. Both drug efficacy and adverse reactions are dependent upon a complex interaction of genetic and non-genetic factors, including genetic variation in the drug target, disease pathway genes and drug metabolizing enzymes. For example, SNP variation in the cytochrome P450 system is associated with toxicity due to differences in drug metabolism [4].

Biotechnological advances in the post-genomic era enable the possibility of managing diseases, such as cancer, by combining molecular profiles with conventional clinical observation to provide the best possible course of treatment for the individual patient. Biomarkers can be examined for risk assessment, treatment response, prediction and prognosis [5]. Various manifestations of cancer are immensely heterogeneous with respect to metastatic potential and resistance to treatment, for example, the interstitial lung disease associated with non-small cell lung cancer can vary greatly and require a wide range of chemotherapy treatments [6]. A proteomic fingerprint obtained using biomarkers can serve to eliminate treatments proven to be ineffective and isolate an effective treatment without the need for a trial and error approach. However, early detection can require as many as four or more biomarkers to identify a susceptible individual with confidence [6, 7]. The Tumor Marker Guidelines Committee of the American Society of Clinical Oncology has published a short list of acceptable biomarkers; the list is limited as the markers must show sufficient robustness to provide reliable prognosis and determination of the optimum course of treatment. The ability to be able to provide these biomolecular profiles at the point-of-care (POC) through the use of microfluidic systems would be invaluable.

The field of microfluidics has rapidly expanded in the past decade, driven by the need for so-called micro-total-analysis or Lab-on-a-Chip (LOC) systems, in which multiple processes are integrated into a single device. Utilizing microfluidic platforms to miniaturize bio(chemical) processes has many inherent advantages. Importantly, for diagnostics, this includes a reduction in the amount of sample, which maybe limited, for example, in the case of a section from a tissue biopsy. Of particular importance in dealing with clinical samples, microfluidics offers spatial and temporal fluidic control in a biomimetic environment allowing *in vivo* conditions to be created *in vitro*. Speed of analysis within microfluidic devices is faster than conventional laboratory-based diagnostic tests and can be further enhanced by parallel processing, enabling production of results “while-you-wait.” Both material selection and kinetic mechanisms are important variables that can be adapted to suit the specific requirements of the assay. Manufacturing capabilities provide the potential for mass production of cheap, disposable microfluidic devices, which can be used as part of fully integrated portable systems for POC analysis [8]. Analysis of clinical samples at POC also brings with it a number of other considerations, such as who will

operate the system and what resources will they have available to them. Diagnostic tests that are to be used in developing countries or in remote areas may not have access to refrigeration and so any reagents stored on the microfluidic device will require stabilization, achieved, for example, in the case of antibodies by the addition of trehalose [9].

Microfluidic systems are now finding increasing use in the field of clinical diagnostics, for example, through viral genotyping of human papilloma virus (HPV) [10] and the testing of multiple metabolic parameters, such as glucose and lactate in a portable handheld device [11]. Fully integrated “digital” microfluidic devices have also been developed, which use the electrowetting effect to manipulate droplets. These droplets act as individual reaction chambers and have allowed a proof-of-principle colorimetric enzymatic glucose assay to be performed. The technique can be used to manipulate a wide variety of biological fluids, including whole blood, plasma and saliva, with the system being fully integrated from sample injection through to detection [12]. While such systems aid clinical diagnosis and provide an introduction to clinicians to the use of microfluidic systems, they do not represent personalized healthcare.

Those microfluidic systems that truly aid personalized diagnostics are just beginning to emerge and are aimed at analysis at different cellular levels. The ideal microfluidic device should have sample in-answer out capabilities, require minimal user intervention, be low cost and disposable. This review presents current research in the field of personalized medical diagnostics and considers future perspectives for microfluidic devices covering areas such as pharmacogenomics, transcriptomics and proteomics.

2 Genetic analysis

2.1 Viral detection

Direct nucleic acid amplification of clinically relevant diagnostic targets on microfluidic devices, made from cyclic olefin copolymer, has been reported by Gulliksen et al. [13], which exploits real-time nucleic acid sequence-based amplification for the detection of HPV. Using such a device for the identification of high-risk HPV mRNA transcripts will hopefully provide a more sensitive and reliable method for cervical cancer screening as compared with cytological testing. Reaction volumes were limited to 80 nL, which reduces the amount of reagents required; the associated control system was also designed for simplicity using a simple heating mechanism, as isothermal amplification was used, and a light emitting diode in combination with a photomultiplier tube for detection.

Kaigala et al. [14] developed a microfluidic device that combined polymerase chain reaction (PCR) amplification with capillary electrophoresis for the detection of BK virus (Fig. 1). High levels of BK virus can cause serious complications in renal transplant patients, such as graft loss in up to 80% of patients who develop BK-virus associated nephritis. No sample processing was required as urine samples were directly applied to the microfluidic device, which simplifies user intervention. Sensitive limits of detection, down to as few as 1–2 viral copies,

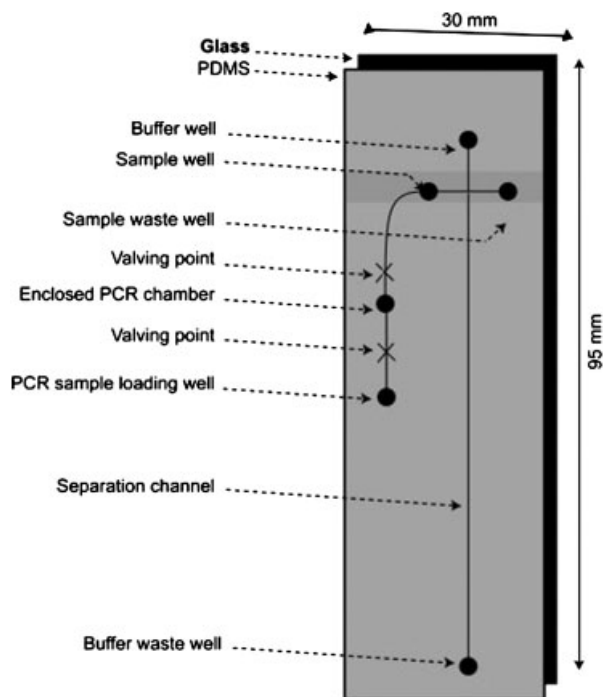


Figure 1. Schematic of a poly(dimethylsiloxane) (PDMS)/glass microfluidic device for PCR and capillary electrophoresis. Reproduced with permission from [14].

enabled the system to distinguish between different viral loads and inform the physician whether clinical intervention was required. Routine screening of patients for the recommended 2 years post-transplant is currently limited by cost considerations but may be improved if the patient can perform a self-test at home or in the doctor’s surgery using such a microfluidic system.

2.2 Gene expression profiling

Conventional transcriptome analysis is achieved by performing a reverse transcription-PCR (RT-PCR) followed by hybridization of the DNA products on a microarray. Such technology lends itself well to the detection of prognostic biomarkers to aid personalized medicine. For example, chronic lymphocytic leukemia can be divided into two prognostic subtypes depending upon the degree of mutation in immunoglobulin heavy-chain variable region (IgV_H) genes. Patients who have unmutated IgV_H genes have an average survival of 8 years from diagnosis compared to 25 years for those with mutated IgV_H genes. A custom-printed TaqMan Low Density Array microfluidics card has been successfully used to perform quantitative RT-PCR and distinguish between mutated and unmutated genes from samples of patients with this form of leukemia. Despite the clear prognostic value of such a system, extensive sample preparation was required off-chip which limits use at POC, although recently systems have emerged that show integration of sample preparation and subsequent genetic analysis to be possible [15].

Yokokawa et al. [16] have developed a poly(dimethylsiloxane) (PDMS) microfluidic device for transcriptome analysis to detect *c-fos* mRNA, an oncogene whose over-expression is involved in carcinogenesis. Sequence-specific mRNA detection is achieved by hybridization to a 2'-*O*-methyl oligonucleotide probe, resulting in a significant increase in fluorescence, which can be observed using a conventional epifluorescent microscope (Fig. 2). The advantage of this system over traditional microarrays is that the hybridization occurs in the liquid phase, which means that there is no need to purify the target mRNA and no wash steps are required to remove any unhybridized probes as these are not detectable, resulting in a decreased analysis time.

Direct profiling of cancer biomarkers in tumor tissue using a multiplexed nanostructured microelectrode integrated circuit was recently reported by Fang et al. [17]. mRNA from tumor biopsies was analyzed for prostate cancer-related gene fusions, which could be used to distinguish between aggressive and slower progressing forms of the disease. Following mRNA extraction, samples were added onto the device and direct, amplification-free analysis could be completed in less than 1 h. Microelectrodes were modified with thiolated peptide nucleic acid probes and upon hybridization of complementary sequences an electrical signal was observed. The clinical application of the approach is awaited.

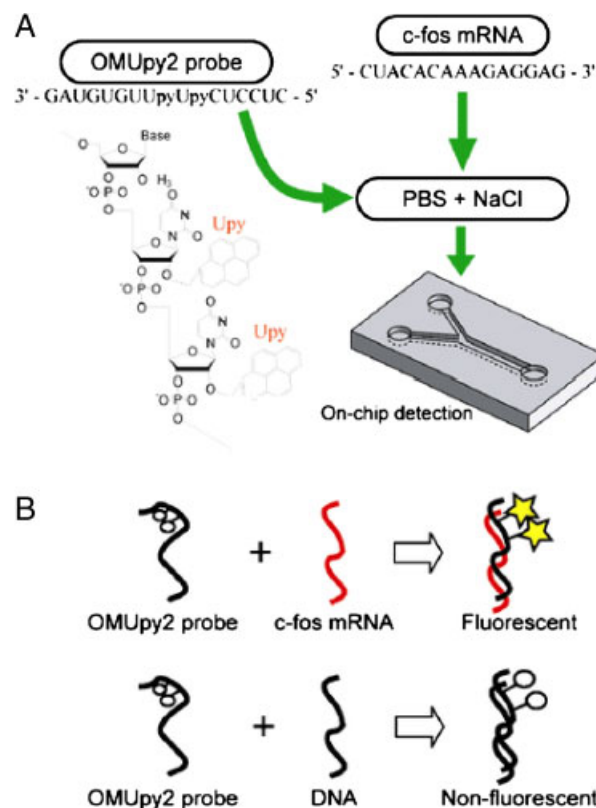


Figure 2. A schematic showing (A) the microfluidic device and (B) the mechanism of hybridization whereby fluorescence detection of only *c-fos* mRNA occurs. Reproduced with permission from Fig. 1 of [16].

2.3 Genotyping by fragment analysis

Miniaturized electrophoresis devices have been applied to a wide range of biomolecular analysis techniques that have the potential to be integrated into more complete systems for personalized medicine. SNP analysis has been applied in a microfluidic setting to evaluate the risk of adverse drug events. In patients undergoing thiopurine therapy, for conditions such as acute lymphoblastic leukemia, rheumatoid arthritis or organ transplantation, SNPs account for inter-patient variability in drug response. An inherited deficiency in thiopurine S-methyltransferase (TPMT), a cytosolic enzyme that catalyses S-methylation of thiopurines, leads to toxic metabolite accumulation and potentially fatal neutropenia. Approximately 0.3% of the population have two non-functional alleles and therefore have no detectable enzyme activity. If identified, such individuals can then be treated with a significantly lower thiopurine dose (10- to 15-fold reduction) to minimize any adverse effects. An integrated microfluidic device has been presented by Chowdhury et al. [18], which combines either restriction fragment length polymorphism analysis or allele-specific PCR with capillary electrophoresis for identification of the three most common SNP alleles associated with TPMT deficiency. The microfluidic device was partnered with a control system which was used to supply thermal cycling, electrokinetic movement and detection components. An estimated cost for such a system was proposed as less than \$10 per microfluidic device and approximately \$1000 for the control system. This represents a step forward toward POC systems compared to traditional methods where DNA microarrays were previously the best option [19], although in both these systems DNA extraction and quantification from whole blood samples was still performed off-chip.

Odenthal et al. [20] presented a microfluidic electrophoresis chip for the detection of microsatellite instability in patients with colorectal cancer. Carcinogenesis caused by genomic defects in the mismatch repair machinery, which occurs in 10–20% of patients with colorectal cancer, leading to microsatellite instability is associated with a better prognosis and therefore provides a useful diagnostic marker. Following off-chip DNA extraction and PCR, electrophoretic separation was carried out using commercially available DNA 1000 LabChip Kits and a 2100 Bioanalyser (Agilent, Germany) for the detection of five key microsatellite loci. Electropherograms of tumor and non-tumor tissue were overlaid to show any microsatellite instability present. The 2100 Bioanalyser has also been used in conjunction with a microfluidic device for the rapid mutation screening of *KIT* and *PDGFRA* genes in gastrointestinal stromal tumors. Insertion and deletion mutations frequently occur in both genes and their presence is directly related to treatment response to the kinase inhibitor imatinib mesylate (Gleevec®); therefore mutation detection aids in determining the optimum course of treatment. In a similar procedure to that described above, tissue samples have been subjected to conventional off-chip DNA extraction and RT-PCR procedures before the resulting products are applied to the microfluidic device. Electrophoresis was performed in the presence of an intercalating dye, which enabled fluorescence detection of the PCR products on-chip [21].

In addition, microfluidic electrophoresis chips have been used as a screening methodology to detect mutations in breast cancer susceptibility genes. Such mutations show higher frequency in certain ethnic populations, for example, mutations 185delAG and 5382insC in BRCA1 and 6174delT in BRCA2 are common in the Ashkenazi Jewish population, and women who have one or more of these mutations are at a high risk of developing breast or ovarian cancer in the future. After off-chip DNA extraction and PCR, mutations were detected by the incorporation of fluorescently labeled primers in less than 2 min [22], in an analogous way to that described by Zamo et al. [21].

3 Immunoassays

The use of immunoassays in diagnostic medicine is something that has gained great popularity, but these can be time consuming to perform (4–8 h) and require relatively large reagent volumes. Fortunately, the immunoassay format is highly compatible with microfluidic systems, which can be used to overcome these limitations and make immunoassays ideal for POC applications. Accordingly, research in this area has been extensive and varied, including detection of hormones, cancer markers and common pathogens. Immunoassays can be either heterogeneous, i.e. where antibodies are immobilized on a solid surface, or homogeneous, i.e. where the conjugation of antibody and antigen occurs in solution. Heterogeneous methodology is commonly employed as it brings with it greater sensitivity, achieved by an increased surface area for antibody–antigen binding. The use of sandwich immunoassays, commonly an ELISA, has been widely adapted for use in microfluidic systems. The principle involves using a primary antibody, attached to a solid support, to bind any antigen present in the sample. Following this, a secondary enzyme-conjugated antibody is added and which also binds to the antigen. Upon addition of the enzyme substrate, a signal is generated proportional to the amount of target antigen present.

Currently, microfluidic devices reported for performing immunoassays have focused on diagnosis and detection rather than personalized medicine. Examples include the diagnosis of celiac disease [23] and detection of *Helicobacter pylori* infection [24]. Despite not representing personalized biomolecular diagnostics, such systems enable faster detection and therefore swifter patient treatment. Yet one of the fields where immunoassay methodology has found great success is in the analysis of biomarkers associated with various forms of cancer. Differential expression of such biomarkers often provides an indication of disease state or phenotype. For example, the overexpression of EGFR is associated with early tumorigenesis and/or aggressive phenotypes in head and neck cancer [25]. Immunological techniques can be used to isolate different cell types, from complex biological fluids or biopsy suspensions, prior to interrogation of the cells for specific biomarkers. For example, this can be achieved by a polycarbonate membrane that acts as a microsiege to capture cells within a poly(methylmethacrylate) chip. The captured cells can then be interrogated by immunofluorescent assays in order to confirm their presence and determine the isotype [26]. Christodoulides

et al. [27] presented a microfluidic system which exploited antibody-based capture techniques for both cells and individual proteins from whole blood samples. Both increased serum concentration of C-reactive protein (CRP) and leukocyte count are predictors for the development of coronary heart disease and so are useful diagnostic markers, particularly in combination. Porous agarose microspheres, contained within an etched well array, coated in CRP-specific antibodies capture the CRP antigen if present. This was coupled with a polycarbonate membrane that captured the leukocytes while allowing deformable erythrocytes to pass through. Both predictors generate fluorescent signals, through a secondary labeled antibody, which are detected using a charge-coupled device and data analysis software. In addition, Lenshof et al. [28] showed that plasma could be separated from whole blood using an acoustic plasmapheresis chip and the resulting plasma transferred to a linked microarray for prostate-specific antigen detection without the need for any signal amplification.

A problem with microfluidic immunoassays is often the low sensitivity associated with widespread optical detection methods, accordingly techniques such as fluorescence or luminescence, are often coupled with expensive equipment for the analysis to counteract this. The detection of single biomarkers does not provide sufficient clinical information with regards to the large variety of cancerous diseases, so it is crucial that multiple biomarkers can be detected efficiently. Ko et al. [29] were able to capitalize on more recently developed electrochemical immunoassay detection methods to develop a device to detect multiple biomarkers. In this case, high sensitivity is achieved via an electrical signal produced from a redox reaction of an enzyme tagged with antibodies. The electrical signal is then amplified via a silver enhancer before detection. This methodology was integrated into a microfluidic device to provide a multiple electro-immunosensing system, and was used successfully to detect three cancer biomarkers. However, one of the main disadvantages of using electrochemical detection in immunoassay microarrays is the significant cross-talk that can occur. To overcome this, a disposable array has been developed for simultaneous detection of two tumor markers, carbohydrate antigen (CA19-9) and carcinoma antigen (CA125), by using a cellulose acetate membrane to co-immobilize a thionine mediator and two kinds of antigens on two carbon electrodes of a screen-printed chip. Corresponding horseradish peroxidase-labeled antibodies were then captured on the membranes and the immobilized thionine shuttled electrons between horseradish peroxidase and the electrodes for enzymatic reduction of H_2O_2 to produce detectable signals [30].

An alternative means of increasing the sensitivity of immunoassays is via the use of quantum dots. Multiplex cancer biomarker detection from serum has been shown to be possible, down to fM sensitivity, by employing secondary antibodies conjugated to luminescent CdTe/CdS quantum dots [31]. Jokerst et al. [7] also showed the ability to detect successfully three cancer biomarkers from serum, as well as from saliva. The discussed biomarkers are able to again provide early detection while providing extensive on-going information on treatment and metastasis developments. Whole saliva is an ideal fluid for sampling as it can be collected in high quantities with minimal patient invasion; however, biomarkers are often present at low

concentrations. Here, the high sensitivity of antibody-conjugated semi-conductor nanoparticle quantum dot fluorophores was used to overcome the lower levels of biomarkers present within saliva, while also being successfully integrated to a microfluidic device (Fig. 3). The low limits of detection provided by quantum dots, which can amplify the signal 30 times relative to that of standard fluorophores, showed the potential for fingerprinting from serum and more importantly saliva. In addition, the integration of sample processing, analyte capture and detection to produce a LOC device shows great hope for on-going POC analysis.

Another way to improve detection sensitivity has been demonstrated through the use of iridium oxide nanowires for the detection of inflammatory disease biomarkers, CRP and myeloperoxidase. During protein binding on the nanowires, a specific electrical parameter perturbation occurs during the immunoassay, which enables monitoring of disease biomarker proteins. The use of iridium oxide, and its capability to detect very small changes to the surface charge, forms the basis of the key innovations of this technology, which are improving the selectivity and sensitivity of detection [32].

4 Cell analysis

4.1 Isolation of specific cell populations

The immunological properties of cells can also be exploited to facilitate the capture of specific cell populations from complex biological matrices and such methodology has been widely demonstrated in microfluidic systems. Circulating tumor cells (CTCs), particularly those of the colorectal origin are characterized by an overexpression of epithelial cell adhesion molecule (EpCAM), are produced during tumorigenesis and

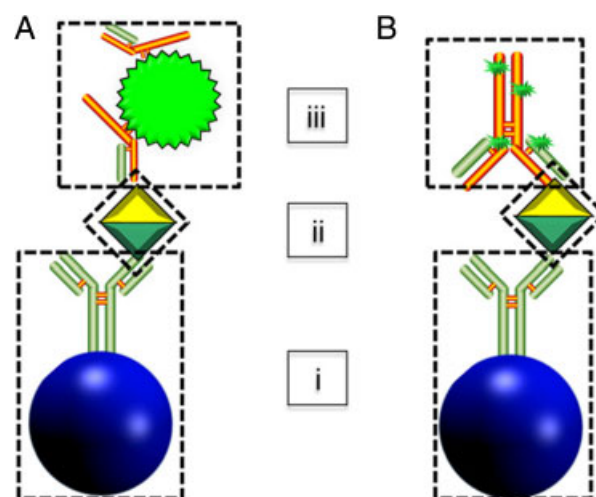


Figure 3. Schematic showing a comparison of (A) quantum dots and (B) fluorescent labels for detection in immunoassays where the following components are represented: (i) capture antibody on bead-based support, (ii) antigen and (iii) detection antibody–fluorophore complex. Reprinted from [7] with permission from Elsevier.

are an indicator of metastasis [33]. Isolation of CTCs from whole blood and saliva samples has been demonstrated by various forms of antibody-mediated capture using anti-EpCAM. This enables enrichment of CTCs, while allowing removal of hematological cells which do not express EpCAM. One of the simplest means is via the use of anti-EpCAM-coated microposts within a microfluidic device and this has been successfully demonstrated for the isolation of CTCs from whole blood samples from patients with lung, prostate, pancreatic, breast and colon cancers. Such systems are very sensitive, with the ability to detect 1 CTC per 10^9 hematological cells. Once captured the CTC may be subject to further interrogation, from simple counting of cells which can be indicative of treatment efficiency, to more complex off-chip mutational analysis by PCR, for example, the presence of a T790M mutation in the EGFR gene is associated with reduced survival [34]. A larger surface area for increased antigen capture efficiency can also be provided using a series of high-aspect ratio channels within the microfluidic device. For example, Adams et al. [35] demonstrated that following isolation of CTCs from 1 mL of whole blood, they could be released using trypsin and counted using a label-free conductivity route which was capable of detecting single tumor cells as they passed through detection electrodes, all of which was possible within 37 min. The number of CTCs was related to progression free survival rates, with an average of 7 months for patients with ≤ 5 CTCs/75 mL blood compared with 2.7 months when > 5 CTCs/75 mL blood were detected. The simplicity of the device makes it an attractive prospect for POC applications.

In addition to CTCs, antibody-mediated capture on microfluidic devices can be applied to other distinct cell populations. For example, Du et al. [36] reported a device for the capture of cervical cancer cells, which relies on up-regulation of $\alpha 6$ -integrin cell surface receptors as a result of HPV-16 infection in order to facilitate capture. Such techniques have also proved successful when combined with negative dielectrophoresis for cell trapping. Here, such methodology was combined with label-free impedance detection for counting of endothelial progenitor ($CD34^+$) cells from mature white blood cells. Further work aims to focus on the integration of cell isolation and detection with whole blood sample preparation for the development of a cardiovascular diag-

nostics system that can be implemented, for example, in urgent cases like stent deployment [37].

Isolation and enumeration of $CD4^+$ T lymphocytes from whole blood samples has been demonstrated, with analysis of needle stick samples possible in less than 1 h. More than 85% of the 33 million people worldwide infected with HIV live in developing countries, and as such the main aim of work was to present methodology that would be used in resource-limited settings. Such a device could enable clinicians to monitor T-cell populations to determine the degree of immunological deterioration and effectiveness of current retroviral therapies. The disposable device presented contained all the necessary reagents held within fluid holding blister packs, no refrigeration was necessary due to solid-layer storage of antibodies on the device and the inclusion of waste reservoirs on the microfluidic device limits the production of harmful waste products for external disposal. In addition, the use of quantum dot-antibody adducts enabled a reduction in the complexity of optical detection requirements due to increased sensitivity [38].

4.2 Cell culture and analysis

Microfluidic devices can be used to culture cell populations, to provide a more biomimetic microenvironment than traditional monolayer cultures. Komen et al. [39] developed a system of cell culturing for estrogen receptor positive human breast cancer cells, which were shown to be viable for up to 7 days by static culture on the microfluidic device (Fig. 4). Chemosensitivity of the cultured cells to the anticancer drug staurosporine was then evaluated and apoptosis was observed. Development of such techniques for use on individual patient cell populations would enable multiple drug testing and allow the optimum combination of drugs to be administered.

To further mimic the *in vivo* microenvironment, a droplet-based system has been reported for multicellular tumor spheroid formation and anti-cancer drug testing. Alginate beads were used to entrap breast tumor cells and continuous dynamic perfusion enabled long-term cell culture, permitting cell proliferation and spheroid formation. Dose-dependent response to the anticancer drug doxorubicin (anthracycline molecule that intercalates DNA, inhibiting topoisomerase II and therefore

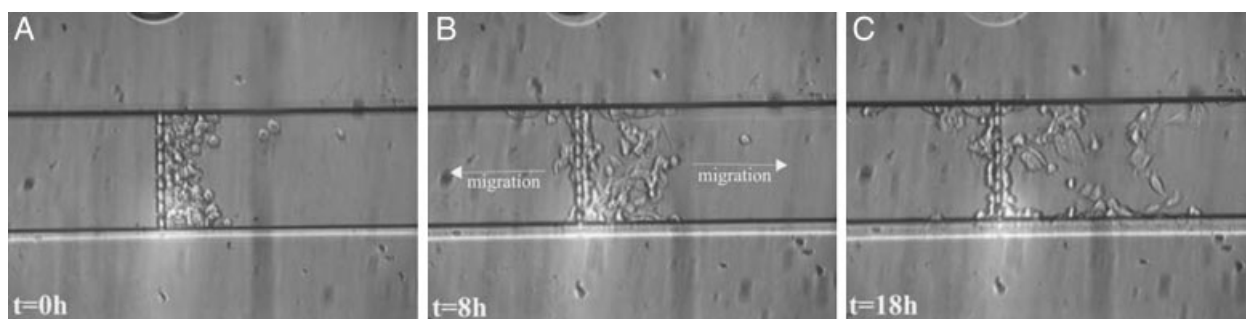


Figure 4. Static culture of MCF-7 cells on a microfluidic device developed by Komen et al. [39]. Cells were loaded onto the microfluidic device and held by a cell trap. Cell culture was achieved using a specific cell culture medium at a temperature of 37°C . Reproduced with permission from [39].

synthesis) was evaluated. Increased drug resistance was observed in the multicellular tumor spheroid compared with conventional monolayer culture hypothesized to be due to contact with the extracellular microenvironment [40].

Alternatively, tissue biopsy samples can be disaggregated by conventional laboratory techniques and then applied to a microfluidic device for analysis. Cell studies can provide a fully quantitative assessment of the molecular content of a tumor biopsy while requiring minimal tissue sampling [41]. In this case, single cell microfluidic image cytometry was utilized to isolate signaling protein biomarkers from within a brain tumor tissue sample. The phosphoinositide 3-kinase/Akt/mammalian target of the rapamycin signaling pathway is frequently deregulated in glioblastoma multiforme, the most lethal form of brain cancer in adults. Here, four critical signaling proteins within this oncogenic pathway were used as biomarkers. Following off-chip dissociation of brain tumor biopsies, between 1000 and 3000 cells were applied to the microfluidic device and subjected to immunolabeling. Bioinformatic analysis revealed clusters of molecular signatures that correlated with a prediction of tumor progression or poor patient survival; for example, high EGFR expression is associated with poor patient outcome. These biomarkers bring with them extensive detail on the progression of the cancer within the individual, providing further vital information about survival chances. Such data can influence key decisions regarding therapy or surgery for a particular individual [42].

5 Tissue analysis

While cellular analysis lends much valuable knowledge to the field of personalized medicine, it falls short in some aspects. Cells *in vivo*, with the exception of those in the vasculature, never exist in an isolated manner, but as part of a complex 3-D structure containing many constituent parts, all of which are continuously communicating and responding to external stimuli. Traditional cell culture fails to recreate this natural environment, as individual cell lines are routinely cultured in isolation, which can lead to experimental artifacts. For example, cells cultured in this way are more likely to undergo changes to cell surface markers in the longer term than when whole tissue biopsies are studied [43]. It is therefore beneficial in some situations to analyze tissue samples as whole entities, so that the physiology might be more akin to that seen *in vivo*.

The use of a microfluidic environment for tissue analysis provides many advantages over larger scale tissue analysis such as the requirement for only small quantities of tissue for experimentation. For tissue types that are highly perfused *in vivo* (such as liver and kidney), microfluidic devices can be superior in mimicking the natural extracellular environment, due to the close proximity of the “vascular” network [44]. The ability to add nutrients continuously and remove waste products on-chip is also preferable to the more static nature of traditional tissue culture [45]. Indeed, some cells, such as primary hepatocytes, are difficult to culture beyond 24 h in static medium, whereas continuous perfusion of tissue samples could significantly extend the time available for interrogation

[46]. This provides investigators with a pseudo-*in vivo* environment, which is easy to both alter and monitor.

Broadly speaking tissue samples can be interrogated on a microfluidic device in two ways. The first involves a biopsy being taken directly from a subject and maintained for analysis on-chip. The latter involves developing a scaffold that allows individual cells to aggregate in a manner that resembles that of a complex tissue structure. Examples of the preliminary work in both these fields will now be discussed.

5.1 Maintaining tissue on a microfluidic device

The direct addition of conventional paraffin embedded thin-film tissue sections into microfluidic devices for immunohistochemical analysis has been explored. For example, the successful detection of multiple biomarkers (estrogen receptor, HER-2, progesterone receptor and Ki-67) in breast cancer tissue [5]. However, as the tissue has been fixed and paraffin embedded this prevents dynamic, real-time measurements from being performed. To try and overcome such problems, a number of groups have begun to look at the maintenance of tissue samples directly within a microfluidic system.

Hattersley et al. [45] have described a microfluidic device capable of maintaining liver tissue in a viable state for a duration of up to 70 h. Small biopsies of liver tissue (4 mm³) were immersed in medium on a microfluidic device and placed in a 37°C incubator. Throughout the experiment, the continuing function of the tissue was demonstrated by the production of both albumin and urea, which are synthesized and secreted by liver hepatocytes. The retention of normal tissue architecture at the end of the time period was also demonstrated. On-chip cell disaggregation was performed, with 78% of cells remaining alive, a value comparable to traditional disaggregation methods.

Tissue maintenance has also been described by van Midwoud et al. [46] who have developed a microfluidic system for performing absorption, distribution, metabolism, excretion and toxicity studies on precision-cut liver slices (Fig. 5). Precision-cut liver slices provide a good alternative to traditional biopsies as not only is much of the architecture of the organ sampled maintained but also the thinness of the samples (~100 μm) leaves far shorter diffusion distance to the innermost cells, allowing better supply of nutrients throughout the tissue; however, the sample size does limit the number of cells that can be tested. Cell viability and hepatic metabolic activity were assessed and found to be comparable with that reported for conventional well-plate systems but with the added advantages previously described for microfluidic systems.

Interrogation of human colorectal tissue biopsies has also been demonstrated using neoplastic and normal tissues biopsies sectioned for use on a microfluidic device [43]. Examining both cancerous and normal tissue from the same subject provides an invaluable tool when investigating not only the desirable cytotoxic action but also any undesirable adverse effects of a chemotherapeutic agent. A hypoxic environment was created in the microfluidic device and levels of vascular endothelial growth factor in the supernatant were monitored at regular intervals. Enhanced production of vascular

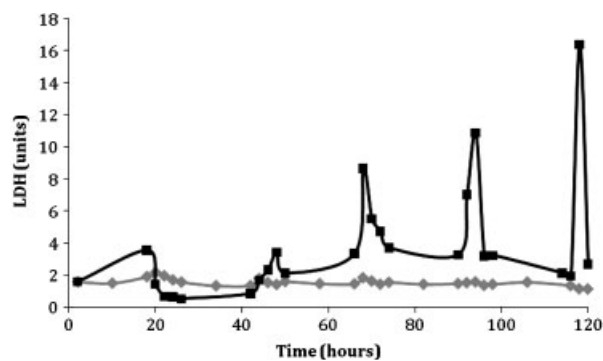


Figure 5. Control samples (—◆—) compared with samples treated with camptothecin (—■—) as analyzed using a lactate dehydrogenase (LDH) assay to evaluate cytotoxicity. The LDH signal intensity is directly proportional to the number of cells which have been lysed.

endothelial growth factor was observed in the neoplastic tissue when compared with the normal tissue, which is in keeping with known *in vivo* responses of colorectal neoplastic tissue to hypoxic environments [47]. In addition, a similar system has also been used to interrogate heart tissue for electrochemical observation of reactive oxygen species, which play a major role in conditions such as ischemia-reperfusion injury and neurodegenerative disorders [48]. Here, viable heart tissue was maintained within a microfluidic perfusion system allowing real-time monitoring in a biomimetic environment.

Professor Haswell's team at the University of Hull have used such microfluidic systems to investigate the effects of various anti-cancer drugs, including camptothecin, on colorectal tissue biopsies. Camptothecin is a cytotoxic quinoline alkaloid that inhibits human DNA topoisomerase I [49]. Blockage of the rejoining step of the cleavage/religation reaction results in accumulation of a covalent reaction intermediate, the topoisomerase I cleavable complex. Cell death primarily occurs due to lethal collisions between this complex and the advancing DNA replication forks. As demonstrated in Fig. 6, cell death occurs in a cyclic manner approximately every 24 h due to the cell cycle-specific action of camptothecin; cell death only occurs during the S phase. It is hypothesized that a replication wave sweeps through the tissue, resulting in semi-synchronous cell death through the sample. In addition to loss of dead cells from the outside of the tumor, further penetration of camptothecin over time results in increased cell death per cycle.

5.2 Engineered 3-D tissue

A microfluidic device for engineering 3-D liver tissue has been reported by Domansky et al. [50], consisting of an array of 12 fluidically isolated open-well bioreactors. Cells were pipetted onto the extracellular matrix-coated scaffolds contained in the reactor wells, where they self-assembled into 3-D tissue units. A micropump was then used to circulate medium from individual reservoir wells (one per reactor) in a continuous manner. Hepatocyte enriched populations attached to the scaffold within the first few hours and were shown to be

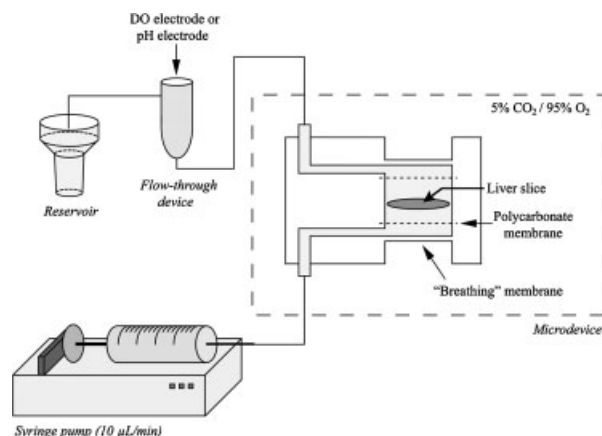


Figure 6. Schematic view of the set-up of the microfluidic device developed by van Midwoud et al. for the perfusion of precision-cut liver slices [46]. The device incorporates PDMS membranes to allow a sufficient supply of oxygen and carbon dioxide, while providing a suitable pressure resistance to the flow of medium through the chip, enabling good tissue perfusion without undesirable tissue damage. Reproduced with permission from [46].

predominately viable at 7 days. Retention of hepatocyte function was also demonstrated using albumin-specific antibodies. To investigate the possibilities of culturing non-parenchymal cells (to more closely mimic normal tissue composition), co-cultures of hepatocytes and liver sinusoidal endothelial cells were carried out. Liver sinusoidal endothelial cells normally show signs of de-differentiation within 1–3 days of static culture. When co-cultured using the extracellular matrix coated scaffolds, good morphology was seen at 3 days, with a decline in levels of de-differentiation occurring after 7 days. The authors suggest that the maintenance of function demonstrated in these “hard to culture” cells are likely to be attributable to the cell-cell interactions occurring in this 3-D engineered tissue, similar to those occurring in tissue *in vivo*. Functional marker staining as late as 13 days also showed Kupffer and stellate cells present, suggesting many of the normal liver cells types remain viable in this microfluidic device. If mass produced, the design of these devices is such that they could be disposable, allowing for single use for individual patients. The presence of multiple wells side by side would allow several drugs to be trialed simultaneously on cells from the same engineered tissue sample and the best candidate drug used clinically.

Taking the idea of engineered 3-D tissue a stage further, Hsiao et al. [51] generated prostate cancer spheroids on a microfluidic device (Fig. 7). The metastatic model includes surrounding cell types to closely mimic the bone micro-environment where prostate cancer metastasis is prevalent, including osteoblasts and endothelial cells. Uniform incorporation of the different cell types into the spheroids was observed with the ability to maintain cultures for at least 7 days. The rate of prostate cancer cell proliferation was lower in this 3-D cell culture model, compared with conventional 2-D cell culture techniques, which may more accurately reflect the true *in vivo* behavior of such cell types.

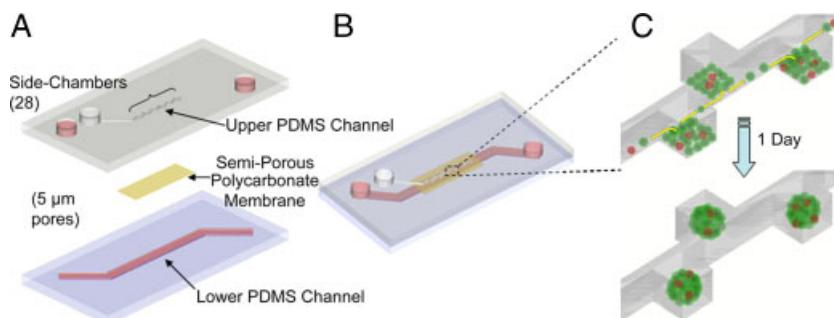


Figure 7. Schematic illustrations of (A and B) the microfluidic device and (C) co-culture spheroid formation process. The device consists of two PDMS microchannels separated by a semi-permeable polycarbonate membrane with 5 μm pores. The cells preferentially settle in side chambers and self-aggregate to form co-culture spheroids within 1 day of culture. Red represents fluorescently labeled metastatic prostate cancer cells and green represents live cells. Reprinted with permission from [51].

In a similar effort, Sung and Shuler [52] used hydrogels to embed cells for culture on microfluidic devices. To examine multi-organ interactions, three types of cells were cultured in interlinked compartments within the same device: colon cancer cells (tumor), hepatoma cells (liver) and myeloblasts (marrow). The channels which connected the tissue chambers and the use of hydrogels combine to create a more realistic physiological environment. Following successful cell culture, the cytotoxic effect of the anti-cancer drug Tegafur was examined. Tegafur is an oral pro-drug, which is metabolized to 5-fluorouracil in the liver. Successful reproduction of liver metabolism of Tegafur was achieved using the microfluidic device as demonstrated by a decrease in cell viability as visualized using a live/dead stain (5 μM calcein AM and 5 μM ethidium homodimer-1 in DPBS (Invitrogen)). The ability to study drug metabolism and organ interaction on a single system offers great potential for development of personalized therapeutics.

6 Concluding remarks

Genetic analysis is particularly useful as a tool for determining pre-disposition to certain diseases by identification of known risk factors. SNP analysis has also been used to identify patients with mutations that make them susceptible to adverse drug reactions; such information allows the clinician to alter drug choice or dosage. Biomarkers have shown great promise in informing treatment choice, particularly in cancer patients, and many microfluidic systems have been developed that exploit immunological properties for isolation and detection of these biomarkers to produce an individual patient profile to aid optimum treatment. While the detection of disease may not require an instant answer by the clinician, the choice of optimum drug treatment would prove invaluable. In addition, such systems would prove useful in monitoring the patient following treatment to access efficacy and determine if further action was necessary. Performing analysis at POC also brings with it a reduced cost of analysis, which opens up the possibility of large-scale screening and the ability to perform testing in resource-limited areas.

In an excellent review recently published by Wlodkowic and Cooper [53], the use of microfluidics for cancer research is discussed. Here, the advantages of using microfluidic systems are highlighted as they mimic the physiological environment within the human body due to the comparable dimensions. Many of the papers presented look at the development of cell culture methods for creating artificial tissues. While such methodology has significant advantages over traditional 2-D cell culture, it seems intuitive that if actual tissue sections could be incorporated into microfluidic device, this would enable much more representative analysis. The field of whole tissue analysis on microfluidic systems, despite being relatively new, holds many exciting possibilities regarding personalized medicine. The work reviewed here demonstrates the possibility that a biopsy taken from an individual could be analyzed to assess physiological responses (both desirable and adverse) of different tissue types to pharmacological interventions. Much of this work is however purely experimental, with few diagnostic or personalized medicine applications due to the difficulty in obtaining tissue and maintaining it thereafter for experimentation [54]. The smaller tissue quantities and closer to in vivo environments potentially possible on a microfluidic device could turn the area of functional human tissue assays from one confined to drug discovery and clinical trials, to one which could be applied to the individual patient.

Despite widespread research efforts, very few microfluidic systems for personalized biomolecular diagnostics have yet to find a place in clinical practice. Those microfluidic-based systems which have made it into clinical practice are predominantly not for personalized medicine but are designed for situations where rapid analysis is crucial, for example, the i-STAT[®], Triage[®] and ABORhCard[®] systems. The i-STAT[®] is a handheld device first evaluated in 1993 for the detection of sodium, potassium, chloride, glucose, urea nitrogen and hematocrit from a whole blood sample in 2 min [55]. A variety of electrochemical sensors are used for the detection of the different analytes, such as ion selective electrode potentiometry for sodium, potassium and chloride. Abbott now markets the handheld analyzer with a range of cartridges designed for evaluation of a wide range of clinical diagnostics including cardiac markers, blood gases and electrolytes. An example Triage[®] system, developed by Biosite, is their cardiac system that is used for the analysis of troponin I, CKMB and

myoglobin from blood samples [56]. ABORhCard[®] is an example of a microfluidic immunoassay device that is able to perform bloodtyping from a fingerstick blood sample in less than 1 min [57]. In terms of commercialized microfluidic systems specifically for personalized medicine, the Verigene[®] Warfarin Metabolism Nucleic Acid Test (Nanosphere US) provides an excellent example of what can be achieved and has received FDA approval [58]. Warfarin is a widely prescribed anticoagulant but genetic variations between individuals can lead to an increased risk of adverse reactions including hemorrhage. The Verigene[®] system utilizes gold nanoparticle technology to detect nucleic acid targets on a microfluidic test cartridge. Genotyping of CYP2C9 alleles and VKORC1 point mutations aids identification of individuals with an increased risk of warfarin sensitivity enabling treatment to be tailored accordingly. Such devices are leading the way toward the use of microfluidic devices in clinical settings for POC diagnostics.

One example of a microfluidic system for personalized medicine in a clinical setting was developed by Russom et al. [59] and tested in a hospital by nurses and laboratory staff. The microfluidic device has been designed for isolation of leukocyte nucleic acids for gene expression analysis. To assess the user friendliness of the microfluidic system, the research team provided a 4 h training session to research nurses who took samples from critically ill hospitalized patients with severe burn or trauma injuries. Generation of enriched leukocyte populations from whole blood samples using the microfluidic system was possible in less than 25 min. The leukocytes were then removed from the microfluidic device and gene expression analysis was performed. Gene expression profiles from samples processed using both the microfluidic system and conventional laboratory techniques were concordant, showing less variability than existed between individual patient samples. This provides an excellent example of the development of a user friendly system, which can be used in a clinical setting by medical professionals with limited training.

The ability to perform biomolecular analysis at the point-of-need in order to allow the physician to provide personalized medicine is a tantalizing prospect. As described throughout this review, there are many microfluidic devices aimed at achieving this situation, although there are still some gaps preventing widespread use in clinical settings. However, issues such as integration of multiple techniques on a single unit, storage of reagents at room temperature on microfluidic devices and ease of user interaction are all currently being addressed. In addition, coupling such technology with telemedicine would open up the market for such devices in resource-limited areas where simple tests could be performed at POC and results transferred remotely to a clinician who could interpret the results and advice the best course of treatment [60]. Moving the laboratory closer to the patient will revolutionize medicine over the next decade.

The authors would like to thank Dr. Abigail Webster for contributing to Fig. 5 and the BBSRC for funding (BB/E002722/1).

The authors have declared no conflict of interest.

7 References

- [1] Ross, J. S., Ginsburg, G. S., The integration of molecular diagnostics with therapeutics – implications for drug development and pathology practice. *Am. J. Clin. Pathol.* 2003, 119, 26–36.
- [2] Bates, S., Progress towards personalized medicine. *Drug Discov. Today* 2010, 15, 115–120.
- [3] Versmissen, J., Oosterveer, D. M., Yazdanpanah, M., Mulder, M. et al., A frequent variant in the ABCA1 gene is associated with increased coronary heart disease risk and a better response to statin treatment in familial hypercholesterolemia patients. *Eur. Heart J.* 2011, 32, 469–475.
- [4] Carrara, S., Nano-bio-technology and sensing chips: New systems for detection in personalized therapies and cell biology. *Sensors* 2010, 10, 526–543.
- [5] Kim, M. S., Kim, T., Kong, S. Y., Kwon, S. et al., Breast cancer diagnosis using a microfluidic multiplexed immunohistochemistry Platform. *PLoS One* 2010, 5, e10441.
- [6] Marko-Varga, G., Ogiwara, A., Nishimura, T., Kawamura, T. et al., Personalized medicine and proteomics: Lessons from non-small cell lung cancer. *J. Proteome Res* 2007, 6, 2925–2935.
- [7] Jakerst, J. V., Raamanathan, A., Christodoulides, N., Floriano, P. N. et al., Nano-bio-chips for high performance multiplexed protein detection: Determinations of cancer biomarkers in serum and saliva using quantum dot bioconjugate labels. *Biosens. Bioelectron.* 2009, 24, 3622–3629.
- [8] Ong, S. E., Zhang, S., Du, H. J., Fu, Y. Q., Fundamental principles and applications of microfluidic systems. *Front. Biosci.* 2008, 13, 2757–2773.
- [9] Chin, C. D., Linder, V., Sia, S. K., Lab-on-a-chip devices for global health: Past studies and future opportunities. *Lab Chip* 2007, 7, 41–57.
- [10] Xu, L., Yu, H., Akhras, M. S., Han, S. J. et al., Giant magnetoresistive biochip for DNA detection and HPV genotyping. *Biosens. Bioelectron.* 2008, 24, 99–103.
- [11] Do, J., Lee, S., Han, J. Y., Kai, J. H. et al., Development of functional lab-on-a-chip on polymer for point-of-care testing of metabolic parameters. *Lab Chip* 2008, 8, 2113–2120.
- [12] Srinivasan, V., Pamula, V. K., Fair, R. B., An integrated digital microfluidic lab-on-a-chip for clinical diagnostics on human physiological fluids. *Lab Chip* 2004, 4, 310–315.
- [13] Gulliksen, A., Solli, L. A., Drese, K. S., Sorensen, O. et al., Parallel nanoliter detection of cancer markers using polymer microchips. *Lab Chip* 2005, 5, 416–420.
- [14] Kaigala, G. V., Huskins, R. J., Preiksaitis, J., Pang, X. L. et al., Automated screening using microfluidic chip-based PCR and product detection to assess risk of BK virus-associated nephropathy in renal transplant recipients. *Electrophoresis* 2006, 27, 3753–3763.
- [15] Abruzzo, L. V., Barron, L. L., Anderson, K., Newman, R. J. et al., Identification and validation of biomarkers of IgV(H) mutation status in chronic lymphocytic leukemia using microfluidics quantitative real-time polymerase chain reaction technology. *J. Mol. Diagn.* 2007, 9, 546–555.

- [16] Yokokawa, R., Tamaoki, S., Sakamoto, T., Murakami, A., Sugiyama, S., Transcriptome analysis device based on liquid phase detection by fluorescently labeled nucleic acid probes. *Biomed. Microdevices* 2007, 9, 869–875.
- [17] Fang, Z. C., Soleymani, L., Pampalakis, G., Yoshimoto, M. et al., Direct profiling of cancer biomarkers in tumor tissue using a multiplexed nanostructured microelectrode integrated circuit. *ACS Nano* 2009, 3, 3207–3213.
- [18] Chowdhury, J., Kagiala, G. V., Pushpakom, S., Lauzon, J. et al., Microfluidic platform for single nucleotide polymorphism genotyping of the thiopurine S-methyltransferase gene to evaluate risk for adverse drug events. *J. Mol. Diagn.* 2007, 9, 521–529.
- [19] Nasedkina, T. V., Fedorova, O. E., Glotov, A. S., Chupova, N. V. et al., Rapid genotyping of common deficient thiopurine S-methyltransferase alleles using the DNA-microchip technique. *Eur. J. Hum. Genet.* 2006, 14, 991–998.
- [20] Odenthal, M., Barta, N., Lohfink, D., Drebbler, U. et al., Analysis of microsatellite instability in colorectal carcinoma by microfluidic-based chip electrophoresis. *J. Clin. Pathol.* 2009, 62, 850–852.
- [21] Zamo, A., Bertolaso, A., Franceschetti, I., Weirich, G. et al., Microfluidic deletion/insertion analysis for rapid screening of KIT and PDGFRA mutations in CD117-positive gastrointestinal stromal tumors – diagnostic applications and report of a new KIT mutation. *J. Mol. Diagn.* 2007, 9, 151–157.
- [22] Tian, H. J., Jaquins-Gerstl, A., Munro, N., Trucco, M. et al., Single-strand conformation polymorphism analysis by capillary and microchip electrophoresis: A fast, simple method for detection of common mutations in BRCA1 and BRCA2. *Genomics* 2000, 63, 25–34.
- [23] Pereira, S. V., Raba, J., Messina, G. A., IgG anti-gliadin determination with an immunological microfluidic system applied to the automated diagnostic of the celiac disease. *Anal. Bioanal. Chem.* 2010, 396, 2921–2927.
- [24] Pereira, S. V., Messina, G. A., Raba, J., Integrated microfluidic magnetic immunosensor for quantification of human serum IgG antibodies to *Helicobacter pylori*. *J. Chromatogr. B* 2010, 878, 253–257.
- [25] Shin, D. M., Ro, J. Y., Hong, W. K., Hittelman, W. N., Dysregulation of epidermal growth-factor receptor expression in premalignant lesions during head and neck tumorigenesis. *Cancer Res.* 1994, 54, 3153–3159.
- [26] Weigum, S. E., Floriano, P. N., Christodoulides, N., McDevitt, J. T., Cell-based sensor for analysis of EGFR biomarker expression in oral cancer. *Lab Chip* 2007, 7, 995–1003.
- [27] Christodoulides, N., Floriano, P. N., Acosta, S. A., Ballard, K. L. M. et al., Toward the development of a lab-on-a-chip dual-function leukocyte and C-reactive protein analysis method for the assessment of inflammation and cardiac risk. *Clin. Chem.* 2005, 51, 2391–2395.
- [28] Lenshof, A., Ahmad-Tajudin, A., Jaras, K., Sward-Nilsson, A. M. et al., Acoustic whole blood plasmapheresis chip for prostate specific antigen microarray diagnostics. *Anal. Chem.* 2009, 81, 6030–6037.
- [29] Ko, Y. J., Maeng, J. H., Ahn, Y., Hwang, S. Y. et al., Microchip-based multiplex electro-immunosensing system for the detection of cancer biomarkers. *Electrophoresis* 2008, 29, 3466–3476.
- [30] Wu, J., Zhang, Z., Fu, Z., Ju, H., A disposable two-throughput electrochemical immunosensor chip for simultaneous multianalyte determination of tumor markers. *Biosens. Bioelectron.* 2007, 23, 114–120.
- [31] Hu, M., Yan, J., He, Y., Lu, H. T. et al., Ultrasensitive, multiplexed detection of cancer biomarkers directly in serum by using a quantum dot-based microfluidic protein chip. *ACS Nano* 2010, 4, 488–494.
- [32] Venkatraman, V. L., Reddy, R. K., Zhang, F. Y., Evans, D. et al., Iridium oxide nanomonitors: Clinical diagnostic devices for health monitoring systems. *Biosens. Bioelectron.* 2009, 24, 3078–3083.
- [33] Khair, G., Monson, J. R. T., Greenman, J., Epithelial molecular markers in the peripheral blood of patients with colorectal cancer. *Dis. Colon Rectum* 2007, 50, 1188–1203.
- [34] Maheswaran, S., Sequist, L. V., Nagrath, S., Ulkus, L. et al., Detection of mutations in EGFR in circulating lung-cancer cells. *New England J. Med.* 2008, 359, 366–377.
- [35] Adams, A. A., Okagbare, P. I., Feng, J., Hupert, M. L. et al., Highly efficient circulating tumor cell isolation from whole blood and label-free enumeration using polymer-based microfluidics with an integrated conductivity sensor. *J. Am. Chem. Soc.* 2008, 130, 8633–8641.
- [36] Du, Z., Colls, N., Cheng, K. H., Vaughn, M. W., Gollahon, L., Microfluidic-based diagnostics for cervical cancer cells. *Biosens. Bioelectron.* 2006, 21, 1991–1995.
- [37] Ng, S. Y., Reboud, J., Wang, K. Y. P., Tang, K. C. et al., Label-free impedance detection of low levels of circulating endothelial progenitor cells for point-of-care diagnosis. *Biosens. Bioelectron.* 2010, 25, 1095–1101.
- [38] Jokerst, J. V., Floriano, P. N., Christodoulides, N., Simmons, G. W., McDevitt, J. T., Integration of semiconductor quantum dots into nano-bio-chip systems for enumeration of CD4+T cell counts at the point-of-need. *Lab Chip* 2008, 8, 2079–2090.
- [39] Komen, J., Wolbers, F., Franke, H. R., Andersson, H. et al., Viability analysis and apoptosis induction of breast cancer cells in a microfluidic device: effect of cytostatic drugs. *Biomed. Microdevices* 2008, 10, 727–737.
- [40] Yu, L. F., Chen, M. C. W., Cheung, K. C., Droplet-based microfluidic system for multicellular tumor spheroid formation and anticancer drug testing. *Lab Chip* 2010, 10, 2424–2432.
- [41] Hicks, D. G., Tubbs, R. R., Assessment of the HER2 status in breast cancer by fluorescence *in situ* hybridization: A technical review with interpretive guidelines. *Hum. Pathol.* 2005, 36, 250–261.
- [42] Sun, J., Masterman-Smith, M. D., Graham, N. A., Jiao, J. et al., A microfluidic platform for systems pathology: Multiparameter single-cell signaling measurements of clinical brain tumor specimens. *Cancer Res.* 2010, 70, 6128–6138.
- [43] Webster, A., Dyer, C. E., Haswell, S. J., Greenman, J., A microfluidic device for tissue biopsy culture and interrogation. *Anal. Methods* 2010, 2, 1005–1007.
- [44] Kim, L., Toh, Y. C., Voldman, J., Yu, H., A practical guide to microfluidic perfusion culture of adherent mammalian cells. *Lab Chip* 2007, 7, 681–694.

- [45] Hattersley, S. M., Dyer, C. E., Greenman, J., Haswell, S. J., Development of a microfluidic device for the maintenance and interrogation of viable tissue biopsies. *Lab Chip* 2008, 8, 1842–1846.
- [46] van Midwoud, P. M., Groothuis, G. M. M., Merema, M. T., Verpoorte, E., Microfluidic biochip for the perfusion of precision-cut rat liver slices for metabolism and toxicology studies. *Biotechnol. Bioeng.* 2010, 105, 184–194.
- [47] Brown, L. F., Berse, B., Jackman, R. W., Tognazzi, K. et al., Senger, Increased expression of vascular-permeability factor (vascular endothelial growth-factor) and its receptors in kidney and bladder carcinomas. *Am. J. Pathol.* 1993, 143, 1255–1262.
- [48] Cheah, L., Dou, Y., Seymour, A. L., Dyer, C. E. et al., Microfluidic perfusion system for maintaining viable heart tissue with real-time electrochemical monitoring of reactive oxygen species. *Lab Chip* 2010, 10, 2720–2726.
- [49] Liu, L. F., Desai, S. D., Li, T. K., Mao, Y. et al., Mechanism of action of camptothecin. *Ann. NY Acad. Sci.* 2000, 922, 1–10.
- [50] Domansky, K., Inman, W., Serdy, J., Dash, A. et al., Perfused multiwell plate for 3D liver tissue engineering. *Lab Chip* 2010, 10, 51–58.
- [51] Hsiao, A. Y., Torisawa, Y. S., Tung, Y. C., Sud, S. et al., Microfluidic system for formation of PC-3 prostate cancer co-culture spheroids. *Biomaterials* 2009, 30, 3020–3027.
- [52] Sung, J. H., Shuler, M. L., A micro cell culture analog (mu CCA) with 3-D hydrogel culture of multiple cell lines to assess metabolism-dependent cytotoxicity of anti-cancer drugs. *Lab Chip* 2009, 9, 1385–1394.
- [53] Wlodkowic, D., Cooper, J. M., Tumors on chips: oncology meets microfluidics. *Curr. Opin. Chem. Biol.* 2010, 14, 1–12.
- [54] Hillier, C., Bunton, D., Functional human tissue assays. *Drug Discov. Today* 2007, 12, 382–388.
- [55] Erickson, K. A., Wilding, P., Evaluation of a novel point-of-care system, the i-STAT portable clinical analyzer. *Clin. Chem.* 1993, 39, 283–287.
- [56] Schulte, T. H., Bardell, R. L., Weigl, B. H., Microfluidic technologies in clinical diagnostics. *Clin. Chim. Acta* 2002, 321, 1–10.
- [57] Weigl, B., Domingo, G., LaBarre, P., Gerlach, J., Towards non- and minimally instrumented, microfluidics-based diagnostic devices. *Lab Chip* 2008, 8, 1999–2014.
- [58] Verigene[®] Warfarin Metabolism Nucleic Acid Test, Nanosphere Inc, US. <http://www.nanosphere.us/VerigeneWarfarinMetabolismNucleicAcidTest.html> [Accessed 23rd February 2011].
- [59] Russom, A., Sethu, P., Irimia, D., Mindrinos, M. N. et al., Microfluidic leukocyte isolation for gene expression analysis in critically ill hospitalized patients. *Clin. Chem.* 2008, 54, 891–900.
- [60] Martinez, A. W., Phillips, S. T., Whitesides, G. M., Carrilho, E., Diagnostics for the developing world: Microfluidic paper-based analytical devices. *Anal. Chem.* 2010, 82, 3–10.

Development of microfluidic devices for biomedical and clinical application

Abigail Webster,^a John Greenman^b and Stephen J. Haswell^{a*}

Abstract

This review focuses on the development and use of microfluidic devices within a clinical setting. The underlying theoretical background of microfluidics is briefly elucidated. The materials and techniques used to fabricate the devices and their applicability to the clinical environment are described. The current research in this area is appraised and projections for future applications are discussed.

© 2010 Society of Chemical Industry

Keywords: body-on-a chip; lab-on-a-chip; microfluidics; organ-on-a-chip; point of care; tissue

NOMENCLATURE

5-fu: 5-fluorouracil
EB: Embryoid bodies
ECM: Extracellular matrix
EGFR: Epidermal growth factor receptor
EI: Elongation index
EOF: Electro-osmotic flow
ESCs: Embryonic stems cells
CAD: Computer aided design software
DRIE: Deep reactive ion etching
HLM: Human liver microsomes
 μ TAS: Miniaturized total chemical analysis system
MSC: Mesenchymal stem and progenitor cells
NMR: Nuclear magnetic resonance
PC-3: Prostate cancer cells
PCR: Polymerase chain reaction
PDMS: Polydimethylsiloxane
PMMA: Polymethyl methacrylate
POC: Point of care
UV: Ultraviolet

INTRODUCTION

The application of microfluidic devices to biomedical research, cell culture and medical diagnostics has the potential to facilitate a paradigm shift in methodology by offering a better representation of the physiological and pathological condition of complex biological systems. The technology has progressed a long way since its beginnings in the 1970s with the introduction of a miniaturised gas chromatography analyzer,¹ and the first cell culture in a microchannel.² This is in marked contrast with traditional cell culture techniques which have remained relatively unchanged over the intervening decades. Cell culture models are traditionally produced in large, homogenous, 2D plastic culture flasks that promote monolayer cellular growth, which is a very different from the dynamic, complex 3D counterparts that form biological tissues. Cultured cells are most commonly maintained as a single cell source, compared with the cellular community which typically forms tissues and where interactions with neighbouring

cells of different types significantly influences their growth, development and function. Furthermore, fluid movement within a culture flask is normally static or turbulent, if roller bottles are used to create fluid movement, whereas in the body, tissues are continually bathed in fluids that are moved hydrodynamically under pressure and with flow nominally laminar. In addition, *in vivo* cells respond to spatial and temporal signals from their multi-cellular community; by contrast cultured cells are often starved of concentration gradients and signal variety that are known to result in alterations in cell surface receptor density, together with autocrine and conditioning factors being lost when media are changed. It is also notable that cells in culture grow in their own metabolic 'waste', which leads to pH changes of the growth media; while *in vivo* cells perform constant housekeeping to keep waste levels and pH changes to a minimum. As cells adjust to and transform in culture conditions, over the long term, cultured cell lines often possess abnormal cell cycle control mechanisms, in part due to mutated genes. These defects are evident when cultured cells are transplanted back into an animal host, as they frequently form tumours.³

The concept of a 'miniaturized total chemical analysis system' or μ TAS was first proposed by Manz *et al.* in 1990,⁴ microfluidics, however, is a broad term used to describe the behaviour, precise control and manipulation of geometrically constrained fluids on a sub-millimetre scale. Microfluidic devices are characterised by small length scales, laminar flow regimes and diffusion dominated mass transport.⁵ These characteristics can be exploited to provide a biomimetic environment for cell and tissue culture, and thus advance traditional culture methodology with the creation of unique environments that mimic the intracellular environment. Continuous flow of fresh media within the culture system is one of

* Correspondence to: Stephen J. Haswell, Department of Chemistry, University of Hull, Cottingham Rd, Hull, UK. E-mail: s.j.haswell@hull.ac.uk

a Department of Chemistry, University of Hull, Cottingham Rd, Hull, UK

b Centre for Biomedical Research, University of Hull, Hull, UK

Table 1. Comparison of the biocompatibility offered by microfluidics versus cell culture flask, relating these comparisons to general biological functions where applicable

Cellular	Microfluidics	Cell culture flask
Large surface to volume ratio	Large surface to volume ratio	Small surface to volume ratio
Constant movement of fluids, replacement of nutrient and removal of waste	Constant renewal of media (replacement of nutrients and removal of waste)	Static until changed (build up of waste products with concomitant removal of nutrient)
Generally laminar (some turbulence in areas of high pressure i.e. ascending aorta)	Laminar flow of fluid	Turbulent (during movement or flask/roller flask) or static
Variable pressures	Variable pressures (controllable)	Set pressure
	Small media consumption/cell	Large media consumption/cell
	Integration to instrumentation/assay	No integration to instrumentation
	Rapid temperature changes	Slow temperature changes
	Control of shear stress	No shear stress

the advantages that microfluidics can bring to cell culture. Laminar flow replicates the normal fluid flow within the body, facilitating mass transport of solutes, simultaneously supplying consistent nutrient delivery, effective waste removal and downstream signalling resulting in a more *in vivo*-like environment. The small fluid volume required for the devices results in reduced reagent consumption when compared with static culture. This can be an important consideration with expensive reagents, for example, a microfluidic culture system at a flow rate of $1 \mu\text{L min}^{-1}$ would require only 10 mL of medium for an entire week. It is worth noting that the average flow of blood through tumour tissue is $\sim 0.8 \text{ mL g}^{-1} \text{ min}^{-1}$.⁶ Furthermore, recirculation of media can promote greater cell signalling as conditioning factors from the cells are secreted into the media; recirculation reduces media consumption too.⁷ Continual flow can result in shear stress, however, this feature can be controlled by the flow rate to stimulate cell growth in a biomimetic manner,⁸ or to investigate disease processes, for example, by mimicking cellular damage and disease progression.^{9,10} Constant fluidic loading is an important principle in many areas of biology, for example, in remodelling and bone shaping mechanisms during skeletal development;¹¹ a comparison of microfluidic to cell culture flask can be seen in Table 1.

One of the long-term goals of microfluidics is integrated, portable diagnostic devices; this approach would be especially useful in the clinical setting where point of care (POC) units for doctors' surgery, bedside, clinics or even operating theatre use could eliminate time consuming laboratory analysis procedures. The reduced scale of these devices negates the need for large laboratory facilities while integrated instrumentation and combined sample processing results in shorter assay times and higher sensitivity. The low cost manufacture of the devices permits

them to be single use and disposable, reducing the possibility of false results caused by contamination and mislabelling. When realised, one such use of the technology would be the ability of the surgeon to test biopsy tissue *in situ*, and choose the right course of treatment/action before the patient comes out of anaesthetic, negating the need for additional surgical procedures, both reducing the risk to the patient and offering a substantial cost saving. These benefits signify that personal medicine, for example 'individualised' patient therapy regimens is a goal worth pursuing.

Introduction to Microfluidics

Fluid flow through microfluidic channels is characterised by low Reynolds numbers, a dimensionless parameter, which when less than 2000 results in laminar flow dominating. In this flow regime, the mass transfer of solutes occurs transversely between the characteristic parallel flow profile. Accordingly, mixing of such solutes occurs by diffusive forces as described by Fick's second law. In a microfluidic device, this results in excellent spatial and temporal regulation of solute concentration, which is essential for the control of biomimetic processes.

In addition, the high surface to volume ratios found within the microfluidic channel further mimic the biological setting. This ratio also enables rapid temperature change and improves thermal transfer in two significant ways. Initially, convective heat transfer occurs at the solid/liquid interface, following Newton's law of cooling, thus the liquid flow is effectively cooling the device until the temperature of the liquid and the device equilibrate; and secondly, heat transfer in small fluid volumes, such as found in a microfluidic device, occurs rapidly. Improved thermal transfer results in rapid thermal homogeneity and reduced thermal cycling times, which is especially advantageous in techniques such as the polymerase chain reaction (PCR) used to amplify DNA sequencing.¹² Surface attachments also benefit from the spatial and temporal properties of the microchannel, which can be exploited to offer increased surface area for catalysts, resulting in improved antibody/enzymatic reactions useful for analyte detection and quantification.¹³

Fluid Delivery within a Microfluidic Device

Fluids behave differently at the microscale; factors such as energy dissipation, surface tension and fluid resistance dominate, and mixing is diffusional because there is no turbulence within the liquid as indicated above. Two of the most common methods to achieve fluid flow within a microfluidic device are pressure or hydrodynamic driven flow and electro-osmotic flow (EOF).^{14–18}

Pressure driven flow allows fluid to be moved via positive or negative displacement, such as syringe or peristaltic pumps. The static nature of the fluid at the boundary produces a parabolic velocity profile within the channel (see Fig. 1(a)).¹⁹ There are two broad categories of pressure driven flow, closed reservoir, such as that found within a syringe pump, where the whole fluid reservoir must be replaced when the fluid is exhausted. In contrast, peristaltic pumping, where the reservoir is external to the pump, enables the reservoir to be refilled without a break in the continuity of the fluid flow. This latter type is more suitable for continual gassing of fluids, which is a requirement of cell and tissue culture because most media, and the tissue that it bathes, require pH stabilisation by CO_2 .

Positive displacement pumps are highly amenable to miniaturisation, as these devices are relatively inexpensive and offer reproducible flow profiles, which is their major advantage. However, the parabolic velocity profile has significant implications for

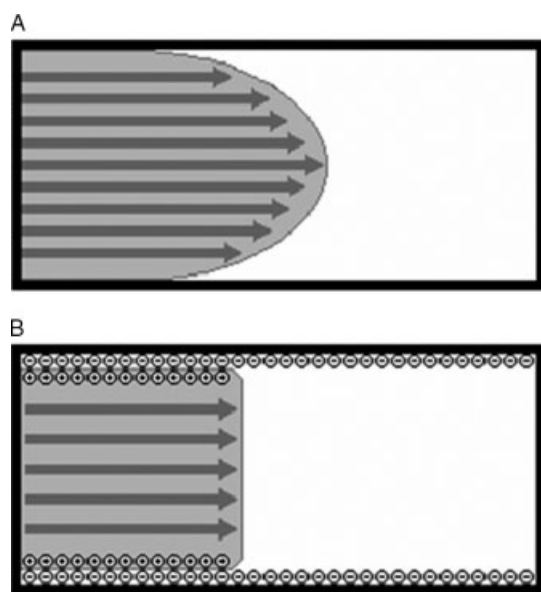


Figure 1. Graphic examples of the fluid profiles seen within a microchannel. (A) During pressure driven flow a parabolic profiles is observed. (B) During EOF, displaying the blunted fluid profile and the anionic surface charge, with the movement of cations from solution towards the charged wall.

the distribution of solutes transported within the channel, leading to non-uniformity of diffusion coefficients and greater dispersion of sample plugs.²⁰

EOF induces fluid flow by the application of an electrical potential across a microchannel. In brief, ions in solution migrate to the opposite charge lining the channel wall, creating an electrical double layer of counter ions. The velocity profile of electro-osmotic movement in an open channel is flat, exhibiting plug flow (see Fig. 1(b)), whereas in a closed channel the profile is slightly curved due to recirculation effects around the walls of the channel caused by back-pressure within the system.²¹

The advantages of EOF are that the velocity profile reduces the diffusional non-uniformity seen with pressure driven flow, although sample dispersion by band broadening still occurs.²⁰ EOF is simpler to couple to a device as there are no moving parts; flow velocity is constant and can be computer controlled. However, there are also a number of drawbacks, principally proteins in solution can adsorb to the walls of the channels, changing the surface characteristics and therefore fluid velocity, resulting in unpredictable flow. Additionally, flow characteristics are affected by other factors including the nature of the buffer, surface composition and hydrodynamic effects.

Fabrication of Microfluidic Devices, Methods and Materials

Materials used for fabrication of microfluidic devices vary; the commonest substrates being glass, polymers (both synthetic and natural) and hydrogels. The fabrication technologies used to create these devices are specific to the material used for the device, often requiring the use of computer aided design (CAD) software to produce photomasks prior to photolithography,²² and include techniques such as etching, cutting, embossing and moulding. Such methodologies can create highly complex, integrated devices, with cross-sectional dimensions of microchannels ranging between 10 and 500 μm . The device material is chosen to best suit the application, the substrate would then dictate the method used for the fabrication; Table 2 shows a number of materials that

Table 2. A selection of materials used for the fabrication of μTAS chips and the most commonly used method for fabrication in each material

Material	Channel etching technique	EOF
Glass	Chemical etch, laser cutting, DRIE	Y
Hydrogels	Photopolymerisation or microfluidic tectonics	
Polymeric films (Mylar)	Laminate laser cutting	Y
Silicon	Chemical wet etch, DRIE	Y
Silicone elastomer (PDMS)	Micromoulding or soft lithography	poor
Thermoplastic (PMMA, polycarbonate, etc.)	Hot embossing, injection moulding	

have been used for microfluidic devices and relevant applicable fabrication techniques and the native EOF compatibility.

Due to the close technical connections of microfluidics with the microelectronics industry, silicon and glass were the first substrates used to create microfluidic devices, and chemical etching is the most established method for creating channels in this substrate. However, this material is becoming largely overshadowed by the use of plastics and elastomers, due to the labour intensive, technically challenging method of creating the channels as well as the relative expense of the glass quality required. While glass is not gas permeable, it is easy to sterilise, chemically robust, and offers simple surface functionalisation, although optical devices can only be in the visible region.

Elastomers, based on the initial work of George Whitesides,²³ are popular for the creation of microfluidic devices owing to the ease and speed of fabrication. Some of the more important features of elastomers include gas permeability and optical transparency, although there is a slight fluorescence background signal with PDMS. The porous nature of the substrate can reduce its effectiveness when detection of trace elements is required as well as the propensity of fluorescent dyes adsorbing to the surface prior of the channels, which can be resolved by prior surface coating.²⁴ However, the relative ease of fabrication and cheap manufacture costs offers the prospect of the devices being of a disposable nature; as well as the ability for built-in valves and other fluid controlling devices.²⁵

Various plastics have also been used, including thermoplastics and thermo-set plastics. Thermoplastic polymers differ from thermo-set polymers in their ability to be reshaped upon heating, while retaining chemical and dimensional stability over a range of operational pressures and temperatures.²⁶ These polymers exhibit softening behaviour above a characteristic glass transition temperature resulting from the long-range motion of the polymer backbone; upon cooling they return to their original chemical state. Fabrication methodologies used for thermoplastics include injection moulding and embossing, which offer high throughput production of devices, facilitating their mass fabrication. In addition, the ease of tailoring chemophysical properties makes thermoplastics highly adaptable substrates giving this material a strong niche within microfluidic technology. Recently, biopolymers have started to make an impact as a material for microfluidic devices with substrates such as chitosan,²⁷

collagen,²⁸ silk²⁹ and hydrogels³⁰ being investigated for their potential as microfluidic platforms, principally due to their compatibility with biomolecules and cell culture, as well as ease of functionalisation with bioactive reagents.

TISSUE CULTURE WITHIN A MICROFLUIDIC DEVICE

There are many potential applications for microfluidic devices in the area of regenerative medicine, which include the disciplines of tissue engineering, biomaterials and cell and tissue transplantation. These disciplines all contribute to restoring function to diseased or damaged tissues through the use of cells and biomaterial scaffolds. The success of therapeutic strategies relies on an understanding of the complex cellular microenvironments that form functional tissue. Microfluidic devices can be utilised to create unique biomimetic platforms that enable the study of the cellular response, while micropatterning of cells allows for structural biomaterials to be formed.

One of the most fundamental aspects of tissue engineering is the isolation and enrichment of selected cell types from a heterogeneous cell suspension. Towards this goal, Green *et al.*³¹ developed a deterministic lateral displacement microfluidic device capable of separating large epithelial cells from smaller fibroblasts. They quoted rapid, high purity separations of >97% with a 90% yield in a single pass process. In a different approach to cell isolation, Plouffe *et al.*³² developed a microfluidic platform that utilised variable shear stress and a panel of conjugated antibodies and -von Willebrand factor to capture circulating endothelial progenitor cells by exploiting cell surface chemistry and adhesion profiles, in an endeavour to provide new tools to address challenges in cardiovascular disease and tissue engineering. A dielectrophoretic field-flow fractionation separator device was constructed by Vykoukal *et al.*³³ for the enrichment of a putative stem cell population derived from enzyme-digested adipose tissue using a microelectronic hybrid flex-circuit. They reported a 14-fold enrichment of an NG2-positive cell population (pericytes and/or putative progenitor cells) in a label-free fractionation of the cell subpopulation. Shafiee *et al.* presented two microfluidic prototypes capable of contactless dielectrophoretic separation. Both devices provided greater than 95% removal efficiency at 0.2–0.5 mm s⁻¹ with 100% selectivity between live/dead cells. The devices could be used, in conjunction with enrichment methodologies, for reliable, automated microfluidic cell sorting.³⁴

High density, 3D cultures are being recognised for their physical similarity to *in vivo* tissue, however, one of the limiting factors to the use of biologically relevant dense cell culture is that unassisted intra-culture transport is limited to just a few layers of thickness. If this form of culture could be developed it would provide an invaluable tool for pre-clinical therapeutic discoveries. Recently, a number of novel microfluidic approaches have been developed to investigate different aspects of tissue culture; these approaches include concentration of nutrient and catabolite movement at biologically relevant levels in structure and resembling tissue dimensions.

Song *et al.*³⁵ produced a novel 3D hydrogel tissue construct, and investigated O₂ and nutrients perfusion through the system with respect to efficient delivery to the cells determined by cell growth and viability. They found a channel radius within the scaffold of 400 μm with a large channel to channel distance (R = 7.5 mm, volume = 5 mL) allowed nutrients to diffuse further through the 3D hydrogel tissue construct than smaller channels and distances.

Their findings revealed a close correlation between nutrient diffusion profiles and cell viability throughout the hydrogel.

A simple approach for the preparation of cell attachable Janus microfibres in a microfluidic system was presented by Jung *et al.*³⁶ These microfibres consist of a porous region that promotes cellular adhesion and a nonporous region for scaffold strength. Janus fibres were synthesised using laminar flows to produce the formation of carbon dioxide bubbles, resulting in an asymmetrically porous microfibre, which provided improved cell adhesion, proliferation, and viability of cultured cells. The Janus microfibre can be used as an alternative to 2D cell culture plates providing a 3D scaffold for tissue engineering.

Vukasinovic *et al.*³⁷ cultured neural astrocytic constructs at a cell density close to that found in the brain (50,000 cells/mm³). They applied forced convection laminar flow to supply nutrients and remove catabolites, and determined that perfused cultures exhibited good viability (90% over 2 days), whereas unperfused cultures were mainly dead over the same period. Taking a different approach, Huang *et al.*³⁸ demonstrated a versatile microfluidic platform utilising mechanical and chemical 3D microenvironments using precise patterning of 3D biopolymer gels in well-defined geometries to observe extracellular matrix (ECM)–cell and cell–cell interactions in real time. During a 7 day experiment, they found that macrophages invaded neighbouring gels containing the breast carcinoma cell MDA-MB-231; however cell-deficient gels were not invaded. Toh *et al.*³⁹ developed a transparent 3D microfluidic channel-based system that enabled optical monitoring of cells and cellular events. Maximal cell–cell interaction was achieved by perfusion-seeding cells through an array of micropillars. 3D cell–cell and cell–matrix interactions supported and encouraged cell growth; this was achieved by a polyelectrolyte complex coacervation process. Carcinoma cell lines (HepG2, MCF7), primary differentiated (hepatocytes) and primary progenitor cells (bone marrow mesenchymal stem cells) were perfusion-cultured for up to a week in the channel and their 3D cyto-architecture, cell-specific functions and differentiation competence were well preserved.

Stem Cells and Tumour Spheroids

The pluripotent nature of embryonic stem cells (ESCs) means that they receive a great deal of interest as a renewable source for tissue regeneration and cellular replacement therapies, however controlling their differentiation is paramount to success. Fung *et al.*⁴⁰ developed a microfluidic device based on the most common technique to cause differentiation of ESCs, the *in vitro* aggregation of embryoid bodies (EB) with ESCs. The device encompassed a Y-channel design which allowed two different epidermal growth factors, fibroblast growth factor 2, and platelet-derived growth factor, to be flowed over an EB located centrally between the laminar streams. These factors successfully facilitated the dual differentiation of EBs.

Successful repair and regeneration of damaged and diseased tissues relies on good cell–matrix interactions. It has been proposed, due to the anisotropic nature of many tissues, that aligned ECM could guide and support differentiation of mesenchymal stem and progenitor cells (MSC). To address this, Lanfer *et al.*⁴¹ aligned collagen type 1 structures within a microfluidic device. It was found that such ECM structures enabled the maintenance of multilineage differentiation of MSCs with ordered matrix mineralisation in osteoblasts, while myotube organisation and length were enhanced in the mouse myoblast cell line, C2C12,

when compared with the control. In a similar vein, Khademhosseini *et al.*⁴² seeded cardiomyocytes onto hyaluronic acid subset patterned microfluidic chambers to create 3D cardiac tissue. The cells elongated and aligned along the pattern direction, attaching preferentially to the glass substrate, which once detached from the surface, formed contractile cardiac organelles. Tanaka *et al.*⁴³ in a related area, created a unique microspherical pump powered by cardiomyocyte-sheet contractions, which required no external energy source or stimuli. A sheet of beating cardiomyocytes were wrapped around a fabricated hollow elastomeric sphere fixed to inlet and outlet ports. The synchronously pulsating cardiomyocyte sheet induced fluid oscillations in a capillary connected to the hollow sphere confirming cellular contractions for 5 days, which could offer novel, non-mechanical pumping that could be applied for various purposes, for example, as a bioactuator for medical implant devices, as it relies solely on biochemical energy.

An alternative to 3D cell seeding within prepared tissue scaffolds is the formation and culture of cellular spheroids, classically formed by adding cells to an inverted media drop, held by surface tension so cells accumulate and develop at the free liquid–air interface forming a compacted tissue. These are complex multicellular constructs that can be described as an intermediate between monolayer culture and *in vivo* models such as xenografts. Tumour spheroids have been receiving attention recently as a tool to investigate cancer medication. Spheroids offer a better model of tumour tissue compared with cell line models as they more closely mimic the microenvironment prevalent within tumour tissue and the specific processes such as angiogenesis, invasion and metastasis. Torisawa *et al.*⁴⁴ first described multicellular spheroid culture within a microfluidic device. Their spheroid culture device consisted of an array of pyramid-like microholes constructed in a silicon device with elastomeric microchannels. Cells in suspension were introduced into the silicon microholes and microwells to enable the formation of cellular spheroids. The production of albumin from the hepatoma cell line (HepG2) was measured to demonstrate maintenance of liver-specific functions for 2 weeks. Cellular response to different chemical stimuli was detected simultaneously on the same device, demonstrating the independence of each channel and hence the ability to multiplex analysis. Hu *et al.*⁴⁵ utilised tumour spheroids to investigate 3D flow and nutrient transport within an avascular, multicellular tumour spheroid growth model. They showed that continuous-flow perfusion was more efficient for nutrient delivery than static culture. Further, they found that single spheroids were insensitive to flow rate increases (and hence increased nutrient delivery) but when more than one spheroid was in a chamber together, increased velocities were required to maintain growth rates. Hsiao *et al.*⁴⁶ engineered a multicellular metastatic prostate cancer model that mimicked the bone microenvironment found *in vivo* for prostate cancer cells. The model consisted of the prostate cancer cells (PC-3) osteoblasts and endothelial cells in a co-culture spheroid. They found during the 7 day culture time, that PC-3 cell proliferation rates were decreased without reduced cell viability, which could offer good insight to the *in vivo* growth of malignant prostate cancer and a possible drug model. In a similar manner, Wu *et al.*⁴⁷ created multicellular tumour spheroids for characterising anticancer treatments, which hydrodynamically trapped cancer cells in controlled geometries. Spheroid formation was enhanced by continuous perfusion maintaining compaction of the trapped cells. The average speed of spheroid formation was ~7 h, while size uniformity was found to increase with flow rate (up to 10 $\mu\text{m min}^{-1}$) and provided a much simpler approach to the classic 'hanging drop' method. In a different approach to

tissue modelling, Rosano *et al.*⁴⁸ developed a synthetic microvascular network on PDMS, capable of serving as an *in vitro* model of the bifurcations, tortuosities and cross-sectional changes found *in vivo* in the vascular network. The vascular system was computer-mapped using a graphical information system and manufactured as a physically realistic vascular network. The finished PDMS device was seeded with bovine aortic endothelial cells and cultured to confluency over 4 days. These cells were found to be viable, retaining cytokine responses and expression of anti-ICAM-1.

While cell culture in microfluidic devices is relatively well established, whole tissue or biopsy culture within a microfluidic device is still in its infancy; however there have been some inroads into this area, mostly utilising brain tissue. Passeraub *et al.*⁴⁹ first developed a microfluidic chamber for the maintenance of thick slice brain tissue using an array of micropillars to replace the mesh normally used in classical interfaces. Using a zero-Mg²⁺ model of epileptiform activity, they observed spontaneous single and multi-spike bursts in the CA3 region of a rat hippocampal brain slice for greater than 5 h. Blake *et al.*⁵⁰ produced a novel method to control the microenvironment of brain slices within a PDMS device. The device could accommodate brain slices approximately 700 μm thick and was used to culture the slices for up to 3 h, with viable active tissue capable of respiratory-related motor output. Similarly, Rambani *et al.*⁵¹ cultured thick brain slices in a custom-made perfusion chamber which facilitated laminar flow and interstitial perfusion of oxygenated nutrient supplemented medium with concomitant removal of depleted medium and catabolites. The method gave approximately 84% viability of functionally active tissue after 5 days *in vitro*. An alternative approach to culturing thick brain slices was explored by Choi *et al.*,⁵² who fabricated a microneedle based perfusion device for high cell density *in vitro* tissue culture. The device was fabricated from PDMS and used to test the sensitivity to nutrient supply disruptions. High viability of the tissue was confirmed visually by fluorescent live–dead staining and confocal microscopy. In a different approach to on-chip tissue culture, rat liver biopsies were cultured within a microfluidic device for 70 h, the tissue was finally disaggregated on-chip using a collagenase digestion to show cell viability by Trypan blue assay.⁵³

In summary, microfluidic technology has made a number of inroads into the areas of cell and tissue culture, offering specific environments that are not possible to provide by standard culture methodology; for example the dual differentiation of EB⁴⁰ and novel devices from cells, such as the cardiomyocyte pump,⁴³ while devices such as the tumour spheroid-forming microdevices^{44,47} offer simplistic solutions to technically challenging biology.

BIOCHEMICAL ANALYSIS OF CLINICALLY RELEVANT SAMPLES WITHIN A MICROFLUIDIC DEVICE

Monitoring disease and disease progression

Monitoring of clinical samples benefits from fast throughput, small sample size and accurate, single use analysis devices; microfluidic devices are in a unique position to offer all these benefits. The following section will show the breadth of approaches currently being researched. Alyassin *et al.*⁵⁴ presented an automated device for high throughput quantification of fluorescent cell image analysis using the data analysis program Matlab. HIV-infected whole blood samples were used to validate the method and the automatic microfluidic platform was found to perform similarly in speed and accuracy to manual counting with small cell numbers.

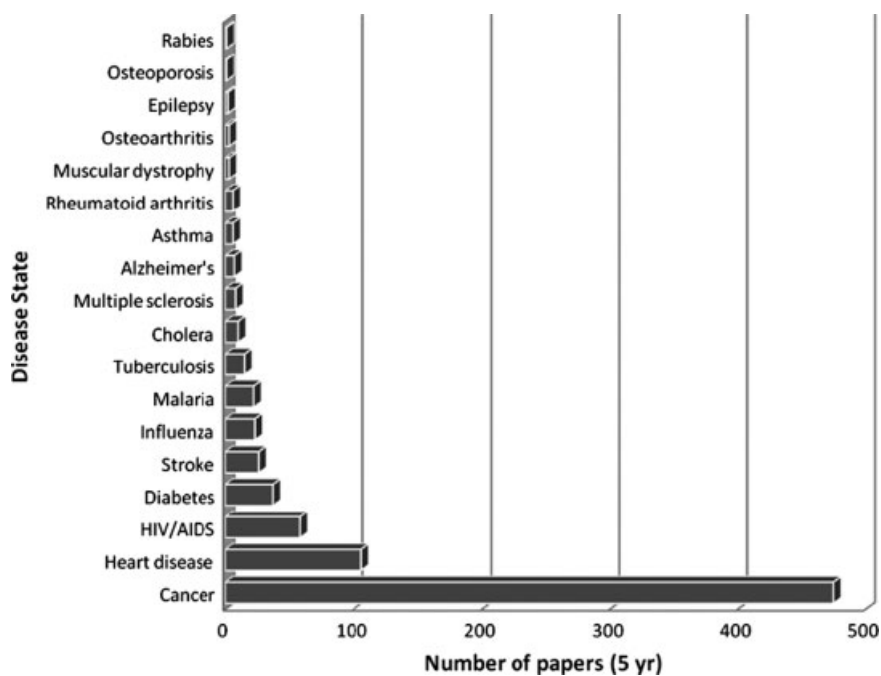


Figure 2. Bar chart showing the publications for microfluidic platforms developed for a number of common disease states over the past 5 years.

However, the microfluidic device was more accurate and >100 times faster for multiple-colour stained cells, or when relatively large numbers of cells were present (>500). The software programming accounted for general problems such as uneven fluorescent background, overlapping cell images and cell detection with multiple stains, to give accurate and precise data which the authors concluded that the methodology was suitable for many assays utilising fluorescent cell staining. Lee *et al.*⁵⁵ developed a diagnostic magnetic resonance sensor combining a miniaturised NMR probe with targeted magnetic nanoparticles for detection and molecular profiling of cancer cells. The sensor measured the transverse relaxation of water molecules in magnetic nanoparticle-labelled cells in biological samples. They quoted high sensitivity and a detection rate of as few as 2 cancer cells in 1 μL of unprocessed fine-needle tumour aspirates, with expression profiling taking less than 15 min. Shin *et al.*⁵⁶ compared blood samples for erythrocyte deformability from healthy and diabetic (diabetes mellitus) patients using a microfluidic ektacytometer to determine the elongation index (EI), which changes due to the hyperglycemic process. The measurement was performed in a viscous polyvinyl pyrrolidone solution within a disposable microchannel, and the results correlated well with the levels of creatinine and haemoglobin. EI decreased with chronic renal failure, end stage renal disease, retinopathy and with a combination of retinopathy and nephropathy. Further reductions were induced by the microangiopathy process despite drug therapy. The device offered a simple way to measure the progressive decrease seen in EI with respect to disease. Mohammed *et al.*⁵⁷ developed a microfluidic device to perfuse pancreatic islets while simultaneously characterising mitochondrial membrane potential and intracellular calcium, as well as quantification of secreted insulin by ELISA; offering a means for the rapid assessment of tissue quality immediately following donor isolation. Mohammed *et al.* believed this work could provide a new gold standard for comprehensive islet analysis and predictive value for islet functionality prior to transplantation into recipients.

Microfluidics has shown its versatility in the area of disease monitoring with small sample size, unique and tailored environments, whilst matching or even exceeding the speed and sensitivity of the standard protocols used in macro-system assays. A bar chart showing the breadth and depth of research applying microfluidic technology to various disease states is shown in Fig. 2.

Pharmaceutical applications

Microfluidic devices can offer a great many benefits to the pharmaceutical industry with faster assay times, unique microenvironments and small sample sizes. Research to explore the potential of microfluidic drug screening methodology is accumulating, from drug treatment strategies to toxicological studies.

Zhang *et al.*⁵⁸ investigated the viability of four human cell types (C3A, A549, HK2 and HPA) in compartmentalised microenvironments chosen to represent liver, lung, kidney and adipose tissues. Cellular functions were optimised by growth factor supplementation of the medium. The device demonstrated cell-cell cross-talk similar to the *in vivo* environment. This system could offer potential alternatives to animal testing in drug screening experiments. Similarly, Sung *et al.*⁵⁹ using an approach termed 'body-on-a-chip' produced a 3D hydrogel culture of three separate cell types, liver, tumour and bone marrow within a single microfluidic device connected by channels mimicking blood flow. The system investigated the cytotoxicity of anticancer drugs to gain pharmacokinetic and pharmacodynamic profiles of the drug. Colon cancer (HCT-116) and hepatoma cells (Hep G2/C3A) were encapsulated in matrigel and cultured in separate chambers within the device to assess the effect of 5-fluorouracil (5-fu). The device was able to reproduce the metabolism of the 5-fu pro-drug Tegafur in the liver, giving consistent results on cell death by 5-fu, while 96-well plate cultures were unable to demonstrate significant drug metabolism. Ma *et al.*⁶⁰ developed an integrated microfluidic device for the simultaneous characterisation of drug metabolites and cytotoxic assay of human liver microsomes (HLM). The multilayer PDMS device contained a three-microwell array of solgel

HLM bioreactors. Unit functionality was validated by monitoring UDP-glucuronosyltransferase metabolism based drug–drug interaction between acetaminophen and phenytoin and their effect on hepG2 cells, which demonstrated increased hepG2 cytotoxicity in response to the drug treatment.

Monodispersity of pharmaceutical colloid spheres is an important issue for the pharmaceutical industry. Zhang *et al.*⁶¹ investigated monodispersed pharmaceutical colloidal spheres of size-tunable atorvastatin calcium, synthesised in a continuous flow microfluidic system. It was found that altering drug concentration and flow rate could efficiently control particle size and improve polydispersity. The microfluidic-prepared spheres were amorphous and displayed an enhanced dissolution rate when compared with commercial preparations. The work offered a simple and economic way to prepare monodispersed pharmaceutical colloidal particles or nanoparticles of predetermined sizes.

In the area of drug testing, microfluidic devices are in a commanding position to offer faster throughput and greater sensitivity, as well as the ability to integrate the (3D) culture of cells and/or tissue to instrument analysis in real time. Body-on-a-chip and organ-on-a-chip will offer pharmaceutical companies viable alternatives to animal experimentation. Although some potential has already been realised, this field is bound to grow as our need for more reliable drug testing, without animal models, is becoming paramount due to public reaction and European dictate.

FUTURE PROSPECTS AND PERSONALISED MEDICINE

Microfluidics is an enabling technology that can be utilised for an almost limitless number of applications, many of which are beneficial to cell culture and tissue analysis, for example, reduced running costs, integrated technology and designer biomimetic environments. Constant fluid flow in laminar regimes enables transport of nutrient and waste products, as well as high surface to volume ratios. Manufacturing methodologies can create complex, compact and highly integrated platforms which enable on-chip cell separation and/or cell enriching, one-step sample to assay procedures and drug compatibility studies.

While glass and PDMS are popular substrates, the future of biomedical microfluidic device manufacture on a large scale will probably exploit thermoplastic substrates. This substrate enables cost effective, high throughput manufacture of disposable devices by injection moulding, while the substrate itself can be chemically designed with versatile functionalisation chemistries to offer a myriad of desirable surface properties. Studies into 'green' biodegradable thermoplastic and other 'natural' biocompatible polymers^{29,62,63} offer further reasons why this substrate is likely to become the more popular material for disposable devices, for example thermoplastic cornstarch blends have shown good potential for biomedical applications.⁶⁴ However, choice of device substrate will always remain a function of the properties needed for the specific application of the device.

In the light of strong international concern and the latest European directives to reduce the use of experimental animals for toxicological testing as well as the ban on cosmetic testing, cell and biopsy models should be considered for the development of alternative *in vitro* toxicity tests. Biomedical microfluidics is in a unique position to offer an acceptable alternative with the ability to create niche biomimetic environments for *in vitro* pharmacokinetic evaluation of drug candidates⁶⁵ and disease study that cannot be modelled by standard culture

technology, for example the effects of high shear stress on plaque formation within a biological system.²⁶ The wealth of applications envisioned for biomedical microfluidic platforms are limited at this stage only by the imagination. Advanced cell culture, where intrinsic control over the microenvironment is essential, can be realised by microfluidic technology in ways that standard culture methodology fails. Personalised medicine and POC devices will enable faster, individually relevant medical results and decisions, thus influencing medical interventions and drug therapy choices. These devices do not end with assay platforms but will extend to implantable devices that can for example, control drug delivery and dosing, without the need for internal circuitry, or on-going monitoring of disease recurrence. While still in its infancy, the application of microfluidics to medical analysis, intervention, diagnosis and cell culture is set to change the face of medicine on a level equivalent to the discovery of antibiotics in the 1930s or monoclonal antibodies in the 1970s.

ACKNOWLEDGEMENTS

The authors acknowledge financial support from the BBSRC (BB/E002722).

REFERENCES

- 1 Terry SC, Jerman JH and Angell JB, Gas-chromatographic air analyzer fabricated on a silicon-wafer. *IEEE Trans Electron Devices* **26**:1880–1886 (1979).
- 2 Doroszewski J, Skierski J and Prządka L, Interaction of neoplastic-cells with glass surface under flow conditions. *Exp Cell Res* **104**:335–343 (1977).
- 3 Davis JM (ed), *Basic Cell Culture: A Practical Approach*, 2nd edn. Oxford University Press, New York (2002).
- 4 Manz A, Graber N and Widmer HM, Miniaturized total chemical analysis systems: A novel concept for chemical sensing. *Sensors Actuators B: Chem* **1**:244–248 (1990).
- 5 Whitesides GM, The origins and the future of microfluidics. *Nature* **442**:368–373 (2006).
- 6 Tozer GM, Prise VE and Cunningham VJ, Quantitative estimation of tissue blood flow rate. *Methods Mol Biol* 271–286 (2009).
- 7 Futai N, Gu W, Song JW and Takayama S, Handheld recirculation system and customized media for microfluidic cell culture. *Lab on a Chip* **6**:149–154 (2006).
- 8 Leclerc E, *et al*, Study of osteoblastic cells in a microfluidic environment. *Biomaterials* **27**:586–595 (2006).
- 9 Gosgnach W, Challah M, Coulet F, Michel JB and Battle T, Shear stress induces angiotensin converting enzyme expression in cultured smooth muscle cells: possible involvement of bFGF. *Cardiovasc Res* **45**:486–492 (2000).
- 10 Beacham DA, *et al*, Arterial shear stress stimulates surface expression of the endothelial glycoprotein Ib complex. *J Cellular Biochem* **73**:508–521 (1999).
- 11 Bancroft GN, *et al*, Fluid flow increases mineralized matrix deposition in 3D perfusion culture of marrow stromal osteoblasts in a dose-dependent manner. *Proc Nat Acad Sci USA* **99**:12600–12605 (2002).
- 12 Wang F and Burns MA, Performance of nanoliter-sized droplet-based microfluidic PCR. *Biomed Microdevices* **11**:1071–1080 (2009).
- 13 Greenway GM and McCreedy T, Microreactor technology for biological applications. *Microreaction Technol: Ind Prospects* 72–79 (2000).
- 14 Chiu S-H and Liu C-H, An air-bubble-actuated micropump for on-chip blood transportation. *Lab on a Chip* **9**:2009 (2009).
- 15 Zhang K, Liang QL, Wang YM and Luo GA, A gravity-actuated technique for droplet microfluidics. *Aifpt'6: Progress on Post-Genome Technologies, Proceedings*, 106–107 (2009).
- 16 Li BW, *et al*, Development of micropump-actuated negative pressure pinched injection for parallel electrophoresis on array microfluidic chip. *Electrophoresis* **30**:3053–3057 (2009).
- 17 Mishchuk NA, Heldal T, Volden T, Auerswald J and Knapp H, Micropump based on electroosmosis of the second kind. *Electrophoresis* **30**:3499–3506 (2009).

- 18 Zhang W, *et al*, PMMA/PDMS valves and pumps for disposable microfluidics. *Lab on a Chip* **9**:2009.
- 19 Kamholz AE and Yager P, Theoretical analysis of molecular diffusion in pressure-driven laminar flow in microfluidic channels. *Biophys J* **80**:155–160 (2001).
- 20 Paul PH, Garguilo MG and Rakestraw DJ, Imaging of pressure- and electrokinetically driven flows through open capillaries. *Anal Chem* **70**:2459–2467 (1998).
- 21 Crabtree HJ, Cheong ECS, Tilroe DA and Backhouse CJ, Microchip injection and separation anomalies due to pressure effects. *Anal Chem* **73**:4079–4086 (2001).
- 22 McCreedy T, Fabrication techniques and materials commonly used for the production of microreactors and micro total analytical systems. *Trac – Trends Anal Chem* **19**:396–401 (2000).
- 23 Xia YN and Whitesides GM, Soft lithography. *Angewandte Chemie – Int Edn* **37**:551–575 (1998).
- 24 Han B, Xu Y, Zhang L, Yang X and Wang E, Surface modification of poly(dimethylsiloxane) microchips using a double-chained cationic surfactant for efficiently resolving fluorescent dye adsorption. *Talanta* **79**:959–962 (2009).
- 25 Kim D and Beebe DJ, Hydrogel-based reconfigurable components for microfluidic devices. *Lab on a Chip* **7**:193–198 (2007).
- 26 Dirksen MT, van der Wal AC, van den Berg FM, van der Loos CM and Becker AE, Distribution of inflammatory cells in atherosclerotic plaques relates to the direction of flow. *Circulation* **98**:2000–2003 (1998).
- 27 Cao Q, Xu Y, Song DF, Han WW and Dong XZ, study of microfluidic chip with in-situ prepared chitosan membrane immobilized with glucose oxidase. *Micro Nano Technol* **60–61**:194–197 (2009).
- 28 Puleo CM, Ambrose WM, Takezawa T, Elisseff J and Wang TH, Integration and application of vitrified collagen in multilayered microfluidic devices for corneal microtissue culture. *Lab on a Chip* **9**:2009.
- 29 Bettinger CJ, *et al*, Silk fibroin microfluidic devices. *Adv Mater* **19**:2847 (2007).
- 30 Golden AP and Tien J, Fabrication of microfluidic hydrogels using molded gelatin as a sacrificial element. *Lab on a Chip* **7**:720–725 (2007).
- 31 Green JV, Radisic M and Murthy SK, Deterministic lateral displacement as a means to enrich large cells for tissue engineering. *Anal Chem* **81**:9178–82 (2009).
- 32 Plouffe BD, Kniazeva T, Mayer JE, Murthy SK and Sales VL, Development of microfluidics as endothelial progenitor cell capture technology for cardiovascular tissue engineering and diagnostic medicine. *Faseb J* **23**:3309–3314 (2009).
- 33 Vykoukal J, Vykoukal DM, Freyberg S, Alt EU and Gascoyne PRC, Enrichment of putative stem cells from adipose tissue using dielectrophoretic field-flow fractionation. *Lab on a Chip* **8**:1386–1393 (2008).
- 34 Shafiee H, Sano MB, Henslee EA, Caldwell JL and Davalos RV, Selective isolation of live/dead cells using contactless dielectrophoresis (cDEP). *Lab on a Chip* **10**:438–445 (2010).
- 35 Song YS, *et al*, Engineered 3D tissue models for cell-laden microfluidic channels. *Anal Bioanal Chem* **395**:185–193 (2009).
- 36 Jung JH, Choi CH, Chung S, Chung YM and Lee CS, Microfluidic synthesis of a cell adhesive Janus polyurethane microfiber. *Lab on a Chip* **9**:2596–2602 (2009).
- 37 Vukasinovic J, Cullen DK, Laplaca MC and Glezer AA, Microperfused incubator for tissue mimetic 3D cultures. *Biomed Microdevices* **11**:1155–65 (2009).
- 38 Huang CP, *et al*, Engineering microscale cellular niches for three-dimensional multicellular co-cultures. *Lab on a Chip* **9**:1740–1748 (2009).
- 39 Toh YC, *et al*, A novel 3D mammalian cell perfusion-culture system in microfluidic channels. *Lab on a Chip* **7**:302–309 (2007).
- 40 Fung WT, Beyzavi A, Abgrall P, Nguyen NT and Li HY, Microfluidic platform for controlling the differentiation of embryoid bodies. *Lab on a Chip* **9**:2591–2595 (2009).
- 41 Lanfer B, *et al*, The growth and differentiation of mesenchymal stem and progenitor cells cultured on aligned collagen matrices. *Biomaterials* **30**:5950–5958 (2009).
- 42 Khademhosseini A, *et al*, Microfluidic patterning for fabrication of contractile cardiac organoids. *Biomed Microdevices* **9**:149–157 (2007).
- 43 Tanaka Y, *et al*, A microspherical heart pump powered by cultured cardiomyocytes. *Lab on a Chip* **7**:207–212 (2007).
- 44 Torisawa YS, *et al*, A multicellular spheroid array to and viability realize spheroid formation, culture, assay on a chip. *Biomaterials* **28**:559–566 (2007).
- 45 Hu GQ and Li DQ, Three-dimensional modeling of transport of nutrients for multicellular tumor spheroid culture in a microchannel. *Biomed Microdevices* **9**:315–323 (2007).
- 46 Hsiao AY, *et al*, Microfluidic system for formation of PC-3 prostate cancer co-culture spheroids. *Biomaterials* **30**:3020–3027 (2009).
- 47 Wu LY, Di Carlo D and Lee LP, Microfluidic self-assembly of tumor spheroids for anticancer drug discovery. *Biomed Microdevices* **10**:197–202 (2008).
- 48 Rosano JM, *et al*, A physiologically realistic in vitro model of microvascular networks. *Biomed Microdevices* **11**:1051–1057 (2009).
- 49 Passeraub PA, Almeida AC and Thakor NV, Design, microfabrication and analysis of a microfluidic chamber for the perfusion of brain tissue slices. *Biomed Microdevices* **5**:147–155 (2003).
- 50 Blake AJ, Pearce TM, Rao NS, Johnson SM and Williams JC, Multilayer PDMS microfluidic chamber for controlling brain slice microenvironment. *Lab on a Chip* **7**:842–849 (2007).
- 51 Rambani K, Vukasinovic J, Glezer A and Potter SM, Culturing thick brain slices: an interstitial 3D microperfusion system for enhanced viability. *J Neurosci Meth* **180**:243–254 (2009).
- 52 Choi Y, McClain MA, LaPlaca MC, Frazier AB and Allen MG, Three dimensional MEMS microfluidic perfusion system for thick brain slice cultures. *Biomed Microdevices* **9**:7–13 (2007).
- 53 Hattersley SM, Dyer CE, Greenman J and Haswell SJ, Development of a microfluidic device for the maintenance and interrogation of viable tissue biopsies. *Lab on a Chip* **8**:1842–1846 (2008).
- 54 Alyassin MA, *et al*, Rapid automated cell quantification on HIV microfluidic devices. *Lab on a Chip* **9**:2009.
- 55 Lee H, Yoon TJ, Figueiredo JL, Swirski FK and Weissleder R, Rapid detection and profiling of cancer cells in fine-needle aspirates. *Proc Nat Acad Sci USA* **106**:12459–12464 (2009).
- 56 Shin S, *et al*, Progressive impairment of erythrocyte deformability as indicator of microangiopathy in type 2 diabetes mellitus. *Clin Hemorheol Microcirculation* **36**:253–261 (2007).
- 57 Mohammed JS, Wang Y, Harvat TA, Oberholzer J and Eddington DT, Microfluidic device for multimodal characterization of pancreatic islets. *Lab on a Chip* **9**:97–106 (2009).
- 58 Zhang C, Zhao Z, Abdul Rahim NA, van Noort D and Yu H, Towards a human-on-chip: Culturing multiple cell types on a chip with compartmentalized microenvironments. *Lab on a Chip* **9**:3185–92 (2009).
- 59 Sung JH and Shuler ML, A micro cell culture analog (mu CCA) with 3-D hydrogel culture of multiple cell lines to assess metabolism-dependent cytotoxicity of anti-cancer drugs. *Lab on a Chip* **9**:1385–1394 (2009).
- 60 Ma B, Zhang GH, Qin JH and Lin BC, Characterization of drug metabolites and cytotoxicity assay simultaneously using an integrated microfluidic device. *Lab on a Chip* **9**:232–238 (2009).
- 61 Zhang HX, Wang JX, Shao L and Chen JF, Microfluidic fabrication of monodispersed pharmaceutical colloidal spheres of atorvastatin calcium with tunable sizes. *Ind Eng Chem Res* **49**:4156–4161 (2010).
- 62 Microfluidic spider silk. *Chemical and Engineering News* **86**:38 (2008).
- 63 Gross M, Natural materials – spider silk through microfluidics? *Chemie in Unserer Zeit* **42**:189–189 (2008).
- 64 Mano JF, Koniarova D and Reis RL, Thermal properties of thermoplastic starch/synthetic polymer blends with potential biomedical applicability. *J Mater Sci – Mater Med* **14**:127–135 (2003).
- 65 Maguire TJ, *et al*, Design and application of microfluidic systems for in vitro pharmacokinetic evaluation of drug candidates. *Curr Drug Metab* **10**:1192–1199 (2009).

Microscreening toxicity system based on living magnetic yeast and gradient chips

Javier García-Alonso · Rawil F. Fakhrullin · Vesselin N. Paunov · Zheng Shen · Joerg D. Hardege · Nicole Pamme · Stephen J. Haswell · Gillian M. Greenway

Received: 21 July 2010 / Revised: 16 September 2010 / Accepted: 21 September 2010 / Published online: 6 October 2010
© Springer-Verlag 2010

Abstract There is an increasing demand for easy and cost-effective methods to screen the toxicological impact of the growing number of chemical mixtures being generated by industry. Such a screening method has been developed using viable, genetically modified green fluorescent protein (GFP) reporter yeast that was magnetically functionalised and held within a microfluidic device. The GFP reporter yeast was used to detect genotoxicity by monitoring the exposure of the cells to a well-known genotoxic chemical (methyl methane

sulfonate, MMS). The cells were magnetised using biocompatible positively charged PAH-stabilised magnetic nanoparticles with diameters around 15 nm. Gradient mixing was utilised to simultaneously expose yeast to a range of concentrations of toxins, and the effective fluorescence emitted from the produced GFP was measured. The magnetically enhanced retention of the yeast cells, with their facile subsequent removal and reloading, allowed for very convenient and rapid toxicity screening of a wide range of chemicals. This is the first report showing magnetic yeast within microfluidic devices in a simple bioassay, with potential applications to other types of fluorescent reporter yeast in toxicological and biomedical research. The microfluidic chip offers a simple and low-cost screening test that can be automated to allow multiple uses (adapted to different cell types) of the device on a wide range of chemicals and concentrations.

Published in the special issue *Microorganisms for Analysis* with Guest Editor Gérald Thouand

Electronic supplementary material The online version of this article (doi:10.1007/s00216-010-4241-3) contains supplementary material, which is available to authorized users.

J. García-Alonso · J. D. Hardege
Department of Biological Sciences, University of Hull,
Cottingham Road,
Hull, England HU6 7RX, UK

V. N. Paunov · N. Pamme · S. J. Haswell · G. M. Greenway
Department of Chemistry, University of Hull,
Cottingham Road,
Hull, England HU6 7RX, UK

R. F. Fakhrullin
Department of Biochemistry,
Kazan (Idel-Ural) Federal University,
Kreml uramı 18,
Kazan 420008, Republic of Tatarstan

Z. Shen
Dalian Inst Chem Phys, Chinese Acad Sci,
Dalian 116023, China

J. García-Alonso (✉)
Trace Metal Research Group, Department of Zoology,
The Natural History Museum,
London SW75BD, UK
e-mail: j.garcia-alonso@nhm.ac.uk

Keywords Toxicity screening · GFP reporter yeast · Magnetic retention · Microfluidic devices

Introduction

There is an urgent need for simple toxicity screening systems for environmental and regulatory reasons. For instance, the introduction of the new European Union regulations for the Registration, Evaluation, Authorisation and Restriction of Chemicals which has placed a duty on manufacturers to assess the safety of the chemicals they manufacture, including formulations, for both humans and the environment [1]. There is a profound difference with respect to monitoring the safety of individual chemicals compared to mixtures, as synergistic effects from several compounds in a formulation or product can occur. Approved animal-based toxicity testing methods are expensive, and (Q)SAR methods are not designed to test

synergistic effects in mixtures. This creates a need for simple screening methods to identify products that may be of concern. Although fully automated commercial screening systems based on 96-well plate systems have been developed for the pharmaceutical industry, these are not relevant for companies that just want to check different formulations of a relatively low number of chemicals.

Toxicity screening using yeast is widely employed for detecting oxidative stress factors [2], genotoxic chemicals [3] or endocrine-disrupting chemicals [4]. Recombinant budding yeasts *Saccharomyces cerevisiae* have been developed, containing fluorescent markers such as green or red fluorescent protein (GFP or RFP), and have been proven to be extremely useful for microscreening because they release the fluorescence without the necessity of adding any substrates. For example, GreenScreen™ yeast cells have been genetically modified to express the GFP whenever the cells carry out repair of DNA damage, and this has been used to detect genotoxicity and cytotoxicity simultaneously [3]. Under genotoxic conditions, the fluorescence emission increases. GreenScreen™ is a well-established yeast reporter, and it has been employed for a range of applications including screening of industrial products and environmental samples [5, 6].

The incorporation of such screening tools within a miniaturised system has many advantages including a small sample and reagent volumes as well as the biomimetic microenvironment within microfluidic systems, which is ideal for microorganism maintenance. The microfluidic environment with its inherent high surface area-to-volume ratio provides a tool that creates a more *in vivo*-like cellular microenvironment *in vitro* than current methodology offers. A number of elegant microfluidic cell-based handling applications have been described for drug development, tissue engineering, molecular diagnostics and biosensors [7–9]. Microfluidic systems have been used to analyse single cells, including bacterial, fungal, yeast and mammalian cells [10–14]. It has also been shown that the gradient mixing can be employed to facilitate the screening process by automatically providing the range of reagent concentrations [13, 15].

Yeast cells are small (<12 μm) and can thus be easily loaded into microfluidic devices. However, it can be challenging to retain the cells within the device and in a viable condition [14]. One method of overcoming this problem is to coat the yeast with magnetic nanoparticles [16] and then employ magnetic fields to retain them inside the microfluidic devices [17].

In this communication, we present a simple, low-cost method for “on-chip” testing of toxicity, incorporating both gradient mixing of toxins and magnetic GFP reporter yeast cells retained and released by the application of external magnetic fields.

Experimental procedures

Chemicals and materials

GreenScreen™ yeast strains, specialist resuscitation and assay media were supplied by Gentronix Ltd. (Manchester, UK). A DNA-repair-competent strain of the brewer’s yeast *S. cerevisiae* was employed as the host strain for a reporter of DNA repair activity (the “test” strain). Viability test was carried out using fluorescein diacetate (F7378, Sigma-Aldrich). On exposure to a genotoxic agent, the cells become increasingly fluorescent as GFP accumulates. MMS (# M4016) was employed as the genotoxic standard and dimethyl sulfoxide (DMSO # D8418) as diluent (purchased from Sigma-Aldrich).

Microfluidic devices manufacture

“Glass-on-glass” and “polydimethylsiloxane (PDMS)-on-glass” microchips were designed with multi-gradient pattern (Fig. 1a). The design was drawn using auto-CAD software and transferred by a commercial process (J. D. PhotoTools, Oldham, UK) to a film photomask. Crown white glass (B270) plates coated with chrome and photoresist (Telic Co., CA, USA) were contacted with a photomask design and exposed to UV radiation. The plates were then treated with photoresist developer followed by chrome etch solution (Rohm-Haas Ltd. UK). The exposed glass channels were etched at a rate of 4 $\mu\text{m}/\text{min}$ in a 1% hydrofluoric acid/5% ammonium fluoride solution at 65 °C. A pine tree pattern of channels were designed in order to get a gradient from two inlets (one containing culture medium and the other containing a high concentration of standard or test sample). Channels (40 μm wide and 80 μm deep) with three series of serpentine consisting of four completed loops and the yeast chambers (up to 400 μm wide and 40 μm deep) were fabricated by wet etching the glass [14]. After a cleaning process, the etched plates were thermally bonded (595 °C for 3 h) to top plates with drilled access holes.

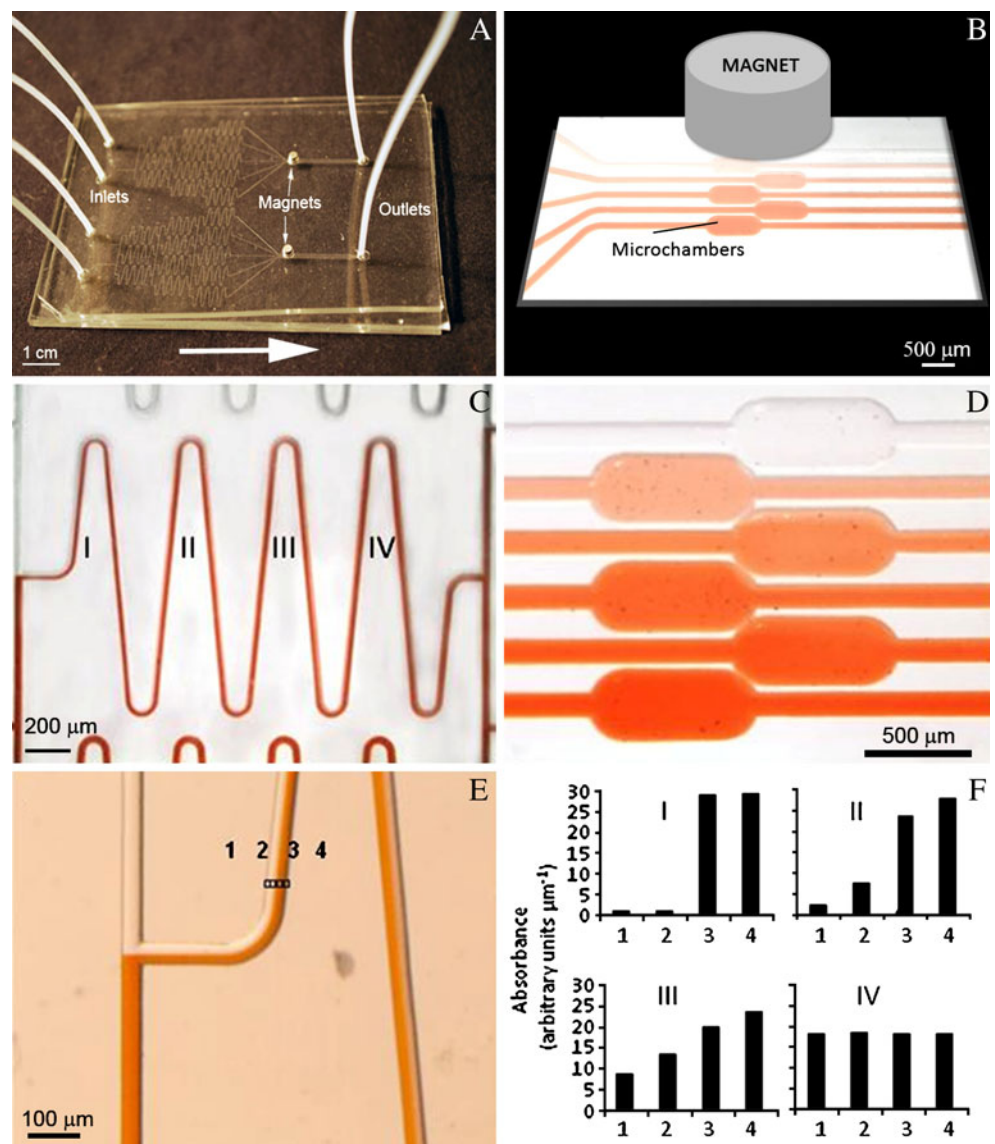
The fabrication of the PDMS glass microchips used the same methodology as described above for the glass base plates. Briefly, these microchips were developed using the etched glass bonded with two consecutive PDMS layers. PDMS (Sylgard 184 kit, IPA, HMDS) were polymerised in two layers. The upper layers of PDMS (0.1 and 5 mm, respectively) were polymerised and hardened for 2 h at 90 °C and plasma-bonded via Oxigen to the glass (Fig. 1a).

TFZL tubing (i.d. 1/16 in, Upchurch Scientific) was used to interface the chip with syringes containing culture medium.

Microscreening bioassay

The magnetisation of the GFP report yeast with nanoparticles, and the posterior viability test of the cells are

Fig. 1 The gradient microscreening system. **a** PDMS glass microscreening system. Two parallel systems are used, one to test an unknown sample and the second with a reference. The magnets were placed above the chambers to retain the yeast. *Arrow* shows the laminar flow direction. **b** A scheme showing the position of the magnet on the top of the chambers. **c** The details of the serpentine pattern visualised with safranin (dye) showing the four loops that contain each serpentine. **d** Generated concentration gradients in the microchambers visualised with red ink (safranin) at the working flow rate. **e** The first step in the pine-tree-shaped pattern, indicating the squares where the intensity (densitometry) was analysed to corroborate diffusion and complete homogenisation. **f** Densitometry of the squares at each loop indicating laminar flow and posterior diffusion at each serpentine



described in the Electronic Supplementary Material Fig. 1S. Based on the previous prototype, the devices allowed the performance of toxicity bioassays by placing the microchip under an inverted microscope, such that all the chambers could be observed at the same time at 40 times magnification. The specific assay culture medium was then pumped into the microfluidic device at a very low flow rate of $0.1 \mu\text{L min}^{-1}$ using two pumps (KDS-200CE, KD Scientific®). One inlet of the system was connected to a syringe containing culture medium + MMS at 0.005%, while the other inlet was connected to a syringe with culture medium and diluent (DMSO) (see Fig. 1SA).

Aliquots (50 μL) of magnetic yeast suspension were pumped into the microchip. The yeast were trapped in the chambers, and then the culture media (with or without the addition of MMS) was passed over the cells for 14–16 h at 25 °C. After exposure to MMS, yeast were excited at 485 nm, and the fluorescence emission detected at 520 nm under an

inverted microscope (Olympus IX71) using a $\times 4$ objective (UPLFLN). The induction of GFP fluorescence in exposed yeast was compared to the constitutive expression of GFP in the control cells, as they maintain their DNA integrity.

Fluorescence emission was quantified as intensity per area using Cell D™ software. Ten squares ($5,000 \mu\text{m}^2$) were analysed per chamber, obtaining mean intensity per treatment. Comparisons of the fluorescence intensity were performed by analyses of variance followed by Dunnett's T_3 post hoc test, using SPSS 16.0 software. Genotoxicity was corroborated when significant differences appeared ($p < 0.05$) between those cells exposed to MMS and those under the control condition (2% DMSO only). When the bioassay is finished, the yeast is easily discarded from the devices by removing the magnets on the top of the chambers and flowing culture medium through the channels and chambers. After that, the systems are ready to re-load yeast and start a bioassay again with very good reproducibility.

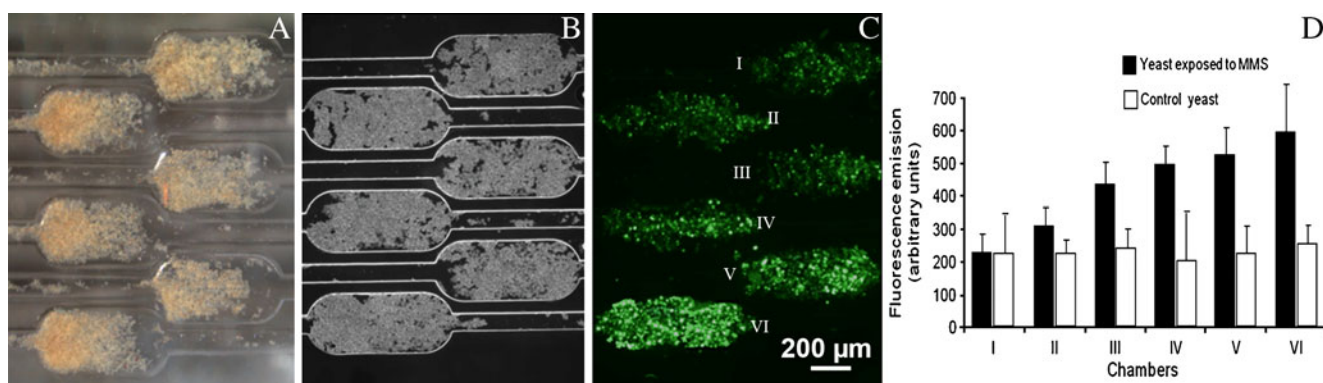


Fig. 2 A six-concentration microscreening system. **a** Yeast cells are loaded into the system and retained via the external magnetic field; **b** after the bioassay (14 h), yeast remained in the chamber (light microscopy image); **c** fluorescence emission from yeast, showing the GFP expression and intensity correlating with the amount of genotoxic

compound. **d** Fluorescence quantification (intensity per square millilitre, mean \pm SD). The concentration range of MMS were 0, 28, 56, 112, 225 and 450 μ M (*black columns*). White columns correspond to a control parallel system (not shown); chamber was exposed only to the diluent (culture media containing 2% DMSO)

Results and discussion

The microfluidic device, designed to generate concentration gradients and based on magnetically functionalised GFP reporter yeast, was evaluated using both glass and PDMS glass microchips. The devices were found to maintain a concentration gradient (Fig. 1c–f) and to retain the cells within the microchambers (Fig. 2a). The glass microchips were found to be more robust for handling, although the multilayer PDMS glass devices offer great potential to develop 3D microscreening devices with low cost of production.

Visualisation of concentration gradient was performed in the system by using the dye safranin instead of the genotoxic agent (Fig. 1c, d). The serpentine pattern increases the length of the channels, allowing the lateral diffusion and complete homogenisation for each concentration before reaching the chambers containing the yeast (Fig. 1c). As can be seen from Fig. 1d, the concentration gradient was well established in chambers that housed the yeast cells. A direct magnetisation of yeast with magnetite nanoparticles were achieved previous to the bioassay (Fig. 1SB, C). The nanoparticles were located at the surface of the cell walls and did not internalise into the cells (Fig. 1SC).

In this work, the utilisation of magnetically retained living fluorescent yeast was found to overcome cell retention problems commonly reported in microfluidic devices [14]. Yeast was successfully retained by placing a small neodymium magnet on the top of the chambers (Figs. 1b and 2a). The removal of the magnet led to sweeping of the yeast cells out of the microchip. The fluorescence emitted by GFP reporter yeast used indicates that the gene expression and synthesis of GFP were not affected either by the coating or the devices.

A genotoxicity bioassay was developed in the microscreening device, with a proportional increase of fluorescence upon increasing the genotoxic compound and statistically significantly higher than the control system (Fig. 2c, d).

At the level of the microchambers where the yeast are maintained, the speed of the culture medium flow was at $21 \mu\text{m s}^{-1}$, calculated as the flow rate/cross-sectional area. At this speed, the flow allows the magnetic fields to retain the yeast inside the chambers. As expected, an increase in fluorescence intensity was observed towards the chambers where the yeast was exposed to the higher concentration of genotoxic agent (MMS, Fig. 2d). Using selected areas for fluorescence intensity quantification, it was possible to clearly differentiate between the cells exposed to MMS and those in the control chamber (the yeast strain exposed to DMSO alone). Yeast exposed to the lowest concentrations of MMS showed the lowest values in arbitrary units of 75.57 ± 15 . Then, the increasing concentration generated by the gradient system proportionally increased the fluorescence until values of 455 ± 55 were reached (Fig. 2).

The methodology developed was found to offer an effective way of locating magnetically functionalised GFP reporter yeast on the chip, including magnet-facilitated loading of the cells, their retention during the toxicity tests and their release upon removal of the magnetic field (Fig. 1SB). Further optimisation of flow designs was carried out in order to fine-tune the system and avoid any uneven distribution of cells within all chambers. Based on its dynamic, this microscreening system presents several advantages over the static plate-based bioassays. It allows simple testing of different formulations and concentrations, regulated fresh nutrient and analytes inputs, adaptability to diverse conditions, keeping diverse cells types in optimum conditions and potential portability.

This screening test can be easily automated to allow multiple uses in biomedical, industrial and environmental monitoring studies. Miniaturisation of toxicity screening methods is very promising for toxicity testing of new formulations and for environmental monitoring. Future work will involve the spatial reduction of the microfluidic pattern and increase the number of toxicities to be tested in parallel.

Acknowledgements We thank Dr. Andrew Knight Gentrionix® for kindly supplying the yeast cells, Mr. Stephen Clark for technical support and Mrs. A. Lowry for the technical assistance with TEM. This work was funded by the European Commission, TESS COLLECT-2006 project. The support by the Government of the Republic of Tatarstan (Algarish Grantlar Programmasi) is gratefully acknowledged by R.F.F.

References

1. European Commission Regulation (2006) Regulation (EC) No 882/2004 of the European parliament and of the council as regards community reference laboratories. Official J Eur Union L136:3–8
2. de Souza PR, Geibel J (1999) Direct observation of oxidative stress on the cell wall of *Saccharomyces cerevisiae* strains with atomic force microscopy. Mol Cell Biochem 201:17–24
3. Cahill PA, Knight AW, Billinton N, Barker MG, Walsh L, Keenan PO, Williams CV, Tweats DJ, Walmsley RM (2004) The GreenScreen genotoxicity assay: a screening validation programme. Mutagenesis 19:105–119
4. Michelini E, Leskinen P, Virta M, Kart M, Roda A (2005) A new recombinant cell-based bioluminescent assay for sensitive androgen-like compound detection. Biosens Bioelectron 20:2261–2267
5. VanGompel JV, Woestenborghs F, Beerens D, Mackie C, Cahill PA, Knight AW, Billington N, Tweats DJ, Walmsley RM (2005) An assessment of the utility of the yeast GreenScreen assay in pharmaceutical screening. Mutagenesis 20:449–454
6. Knight AW, Keenan PO, Goddard NJ, Fielden PR, Walmsley RM (2004) A yeast-based cytotoxicity and genotoxicity assay for environmental monitoring using novel portable instrumentation. J Environ Monitor 6:71–79
7. MacDonald MP, Spalding GC, Dholakia K (2003) Microfluidic sorting in an optical lattice. Nature 426:421–424
8. Cho BS, Schuster TG, Zhu X, Chang D, Smith GD, Takayama S (2003) Passively driven integrated microfluidic system for separation of motile sperm. Anal Chem 75:1671–1675
9. Rhee SW, Taylor AM, Tu CH, Cribbs DH, Cotman CW, Jeon NL (2004) Patterned cell culture inside microfluidic devices. Lab Chip 5:102–107
10. Zeringue HC, Rutledge JJ, Beebe DJ (2004) Early mammalian embryo development depends on cumulus removal technique. Lab Chip 5:86–90
11. Tourovskaia A, Figueroa-Masot X, Folch A (2004) Differentiation-on-a-chip: a microfluidic platform for long-term cell culture studies. Lab Chip 5:14–19
12. Verdich AA, Lima EA, Ivanov B, Ges I, Anderson ME, Wikswow JP, Baudenbacher FJ (2004) A microfluidic device to confine a single cardiac myocyte in a sub-nanoliter volume on planar microelectrodes for extracellular potential recordings. Lab Chip 4:357–362
13. Hung PJ, Lee PJ, Sabounchi P, Lin R, Lee LP (2005) Continuous perfusion microfluidic cell culture array for high-throughput cell-based assays. Biotechnol Bioeng 89:1–8
14. García-Alonso J, Greenway G, Hardege J, Haswell S (2009) A prototype microfluidic chip using fluorescent yeast for detection of toxic compounds. Biosens Bioelectron 24:1508–1511
15. Ye N, Qin J, Shi W, Liu X, Lin B (2007) Cell-based high content screening using an integrated microfluidic device. Lab Chip 7:1696–1705
16. García-Alonso J, Fakhrullin RF, Paunov VN (2010) Rapid and direct magnetization of GFP-reporter yeast for micro-screening systems. Biosens Bioelectron 25:1816–1819
17. Pamme N (2006) Magnetism and microfluidics. Lab Chip 6(1):24–38
18. Breeuwer P, Drocourt J-L, Bunschoten N, Zwietering MC, Rombouts FM, Abee T (1995) Characterization of uptake and hydrolysis of fluorescein diacetate and carboxyfluorescein diacetate by intracellular esterases in *Saccharomyces cerevisiae*, which result in accumulation of fluorescent product. Appl Environ Microbiol 61:1614–1619

Scaling up of continuous-flow, microwave-assisted, organic reactions by varying the size of Pd-functionalized catalytic monoliths

Ping He¹, Stephen J. Haswell*¹, Paul D. I. Fletcher¹, Stephen M. Kelly¹
and Andrew Mansfield²

Full Research Paper

Open Access

Address:

¹Department of Chemistry, University of Hull, Hull HU6 7RX, UK and
²Pfizer Global Research & Development, Sandwich, Kent CT13 9NJ,
UK

Email:

Stephen J. Haswell* - s.j.haswell@hull.ac.uk

* Corresponding author

Keywords:

continuous flow; microwave heating; monolith; scaling-up;
Suzuki–Miyaura reaction

Beilstein J. Org. Chem. **2011**, *7*, 1150–1157.

doi:10.3762/bjoc.7.133

Received: 17 May 2011

Accepted: 02 August 2011

Published: 23 August 2011

This article is part of the Thematic Series "Chemistry in flow systems II".

Guest Editor: A. Kirschning

© 2011 He et al; licensee Beilstein-Institut.

License and terms: see end of document.

Abstract

A product-scalable, catalytically mediated flow system has been developed to perform Suzuki–Miyaura reactions under a microwave heating regime, in which the volumetric throughput of a Pd-supported silica monolith can be used to increase the quantity of the product without changing the optimal operating conditions. Two silica monoliths (both 3 cm long), with comparable pore diameters and surface areas, were fabricated with diameters of 3.2 and 6.4 mm to give volumetric capacities of 0.205 and 0.790 mL, respectively. The two monoliths were functionalized with a loading of 4.5 wt % Pd and then sealed in heat-shrinkable Teflon[®] tubing to form a monolithic flow reactor. The Pd-supported silica monolith flow reactor was then placed into the microwave cavity and connected to an HPLC pump and a backpressure regulator to minimize the formation of gas bubbles. The flow rate and microwave power were varied to optimize the reactant contact time and temperature, respectively. Under optimal reaction conditions the quantity of product could be increased from 31 mg per hour to 340 mg per hour simply by changing the volumetric capacity of the monolith.

Introduction

Interest in flow based reaction chemistry has grown over recent years with the realization that such systems can offer greater control over reaction conditions, such as catalyst and heating contact time, which in turn lead to improved product selectivity and yield when compared to batch based methods [1-7]. Much of this work has focused on continuous-flow microreactor

methodology for laboratory based organic synthesis, and has featured the development of inorganic and organic polymer based functionalized monolithic reactors that can operate at elevated temperatures and under high pressure [8,9]. Recently, application of magnetic nanoparticles as media that can be heated in an electromagnetic field, was reported to be ideal for

use inside microfluidic fixed-bed reactors for chemical synthesis [10]. A new concept to build the catalytic membrane inside a microchannel reactor was demonstrated by Uozumi et al. [11], where carbon–carbon bond forming reactions of aryl halides and arylboronic acids under microflow conditions can be achieved quantitatively within 4 s residence time. However, the stability of the catalytic membrane was not discussed. Monolith based devices have shown good flow characteristics when coupled with the highly controlled surface properties associated with the formation of nano-, micro- and mesoporous structures, and they therefore represent ideal supports for reagents and catalysts where contact time and temperature can be spatially and temporally mediated [12,13]. To this end, the use of microwave heating in conjunction with microporous monolithic reactors has attracted some interest for small-scale synthesis under continuous-flow conditions [14–16]. One obvious problem, however, when using microwaves to heat solvents/reagents and surface-functionalized monoliths in a flow microreactor, is the achievement of an efficient coupling of the microwave energy, which will be a function of both the absorbing species present and of the penetration depth of microwave irradiation into the reaction zone [17]. This is especially important in flow systems where the reactants are present in the irradiation chamber for a short period of time [18,19]. Therefore, the application of microwave chemistry to scalable, continuous-flow processes, with commercially available microwave equipment and suitable flow instrumentation, is becoming increasingly important [7,20]. Finally, the high surface-to-volume ratio and spatial and temporal control over the reactants and products, without the need for additional optimization, is of considerable interest [7,21–23] as these factors promise to increase the quantity of product to desirable levels whilst maintaining the intrinsic benefits of the reaction geometry offered when using microreactor methodology.

In this work we report a simple and effective approach for achieving volumetric scalability in a flow reaction system through the use of Pd-supported silica-based monolithic reac-

tors coupled with microwave heating. The practicality of this approach will be demonstrated using Suzuki–Miyaura reactions in which the Pd-supported silica-monolith catalysts exhibit excellent activities and the doubling of the monolith diameter, thus operating at four times the volumetric flow rate, increases product output without any observable change in the reaction conversion.

Results and Discussion

Synthesis of silica monolith and Pd-supported silica monolith catalyst

The reaction parameters, such as polymer concentration, acid strength, water content, amount of silicon alkoxide, reaction temperature and reaction time, all have an important impact on the physical properties of the silica monoliths prepared. Silica monoliths used as catalyst supports require not only a high surface area to maximize their catalytic activity, but also a high permeability to achieve good flow characteristics and enable fast mass transfer from the flowing reaction solutions to the catalytic surface. In addition, they must be mechanically strong enough to withstand the pressures required to drive fluid through the monolithic structure at the required flow rate. Silica monoliths were synthesized from PEO, tetraethoxysilane and nitric acid as supports for the Pd catalyst, as based on the results of previous studies [24]. Silica monoliths, i.e., monolith-3.2 and monolith-6.4 (diameters of 3.2 mm and 6.4 mm respectively), with two different diameters were synthesized using the same procedure, leading to structures with comparable surface characteristics but with different volumes for the solution-accessible connected pores. Characterization of these monoliths indicated that a 2-fold increase in the monolith diameter had little influence on the physical characteristics of the monoliths (see Table 1, entries 1 and 3, 2 and 4), except the total volume that was increased by a factor of almost four, as expected. In addition, the loading of metal particles within monoliths had no effect on either the nm-scale or μm -scale pore structures (see Table 1, entries 1 and 2, 3 and 4, also see Supporting Information File 1, Figure S1).

Table 1: The main characteristics of monoliths characterized by N_2 adsorption at 77 K.^a

Entry	Monolith	D_{N_2} (nm)	S_{BET} ($\text{m}^2 \text{g}^{-1}$)	V_{N_2} ($\text{cm}^3 \text{g}^{-1}$)	V_{water} (mL)	ϕ_t
1	monolith-3.2	16.0	164	0.70	0.205	0.85
2	Pd-monolith-3.2	15.9	169	0.67	0.202	0.84
3	monolith-6.4	16.1	161	0.73	0.791	0.82
4	Pd-monolith-6.4	16.0	166	0.67	0.790	0.82

^a D_{N_2} , S_{BET} and V_{N_2} are the pore diameter, specific surface area and pore volume, respectively, as determined by N_2 adsorption at 77 K. V_{water} is the total volume of the monoliths as measured by the adsorption of water at room temperature. ϕ_t is the total porosity as determined by equation $(W_{\text{M}} - W_{\text{T}})/dlr^2\pi$, here W_{T} and W_{M} are the weights of the dry and water filled monolith respectively, d is the density of water and l and r are the overall length and radius of the cylindrical monoliths. The palladium loading for entries 2 and 4 was ca. 4.5 wt %.

According to IUPAC [24] the measurements obtained from N₂ adsorption and desorption isotherms indicate a type H2 hysteresis, which is consistent with the disordered mesoporous structure seen in the micrograph shown in Figure 1 (also see Supporting Information File 1, Figure S2)

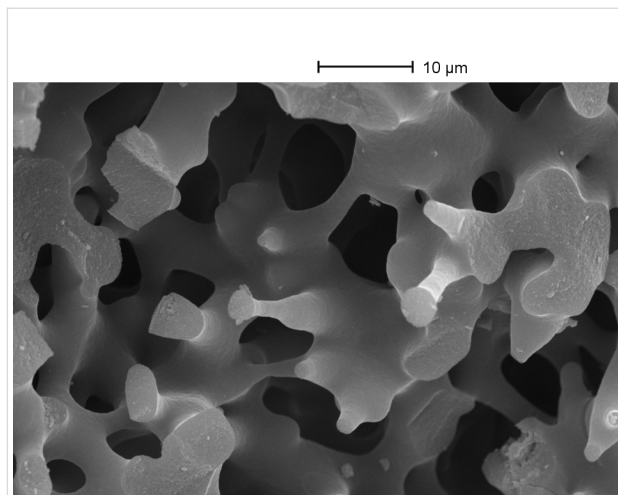
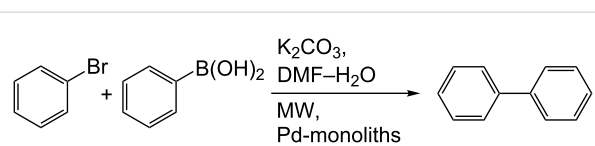


Figure 1: SEM image of silica monolith.

Effect of Pd precursor on the activity of the Pd-monolith catalyst

The Suzuki–Miyaura reaction is a widely used method in organic synthesis for the selective formation of aryl–aryl carbon–carbon bonds in the synthesis of high-value fine chemicals and intermediates in the pharmaceutical industry. This reaction requires a metal catalyst, such as palladium, in both homogeneous and heterogeneous reactions. In this study, the Suzuki–Miyaura reaction of bromobenzene with phenylboronic acid (Scheme 1) was initially used as a model heterogeneously catalyzed reaction for the evaluation of Pd-monolith activity under continuous flow conditions with microwave heating.



Scheme 1: Suzuki–Miyaura reaction of bromobenzene with phenylboronic acid.

The silica monoliths were impregnated with a range of Pd precursors, namely Na₂PdCl₄, Pd(OAc)₂, Pd(dba)₂ and Pd(NO₃)₂, by a standard method described previously for the preparation of Pd-monoliths. The Pd-monolith-3.2 catalysts were evaluated using the previously optimized solvent and basic reaction conditions [3,4]. The results of this study (Table 2, entries 1–4) indicate that, whilst all the Pd-monolith catalysts contain the same amount of palladium (around 4.5 wt %), their catalytic activity differs significantly even for similar reaction temperatures and contact times, showing a significant effect of the palladium precursor on the catalyst activity. The Pd-monolith catalyst that was synthesized from a Na₂PdCl₄ precursor showed the best activity and was therefore used as the Pd precursor for the preparation of a Pd-monolith catalyst to be employed in further investigations. As expected, reducing the reaction temperature and decreasing the catalyst contact time (see Table 2, entries 4–7) resulted in a corresponding reduction of the product yield.

Comparison of activity between Pd-monolith-3.2 and Pd-monolith-6.4

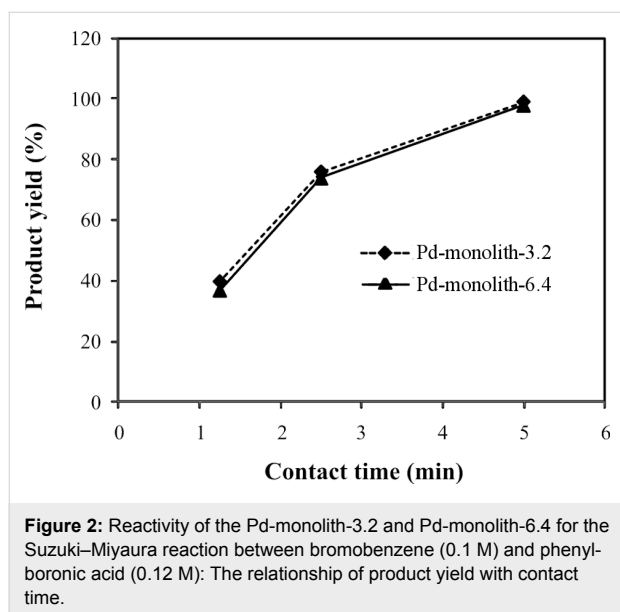
The main aim of this work is to develop a methodology to scale up the rate of product formation without a loss in the intrinsic reaction performance, by using a continuous-flow, microwave-assisted, Pd-supported silica-monolith reactor. The Pd-monolith-3.2 and Pd-monolith-6.4 (both with the same length of 3 cm) were used to perform the model reaction (1) to demonstrate this methodology. The total pore volume accessible to the

Table 2: Reactivity of Pd-monolith-3.2 synthesized using different Pd precursors in the Suzuki–Miyaura reaction between bromobenzene and phenylboronic acid under continuous flow conditions.^a

Entry	Pd precursor	MW power (W)	Temperature (°C)	Flow rate (μL min ⁻¹)	Contact time (min)	Conversion (%)
1	Pd(OAc) ₂	8	123	20	10	72
2	Pd(dba) ₂	8	123	20	10	55
3	Pd(NO ₃) ₂	15	123	20	10	28
4	Na ₂ PdCl ₄	5	123	20	10	97
5	Na ₂ PdCl ₄	3	99	20	10	70
6	Na ₂ PdCl ₄	10	116	40	5	66
7	Na ₂ PdCl ₄	5	109	40	5	45

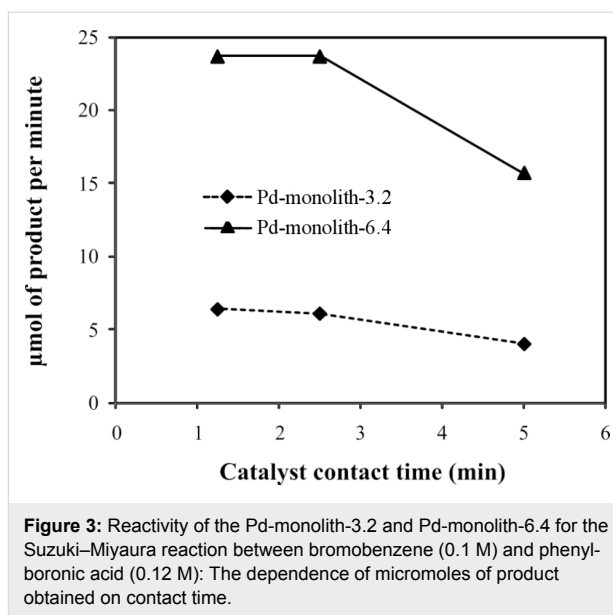
^aAll Pd-monolith catalysts have a Pd-loading of ca. 4.5 wt %. Conversions were determined using GC–MS versus internal standard. The main byproducts (1–3%) were formed by the debromination of halide reactants.

solution, determined by adsorption of water, was 0.20 mL for Pd-monolith-3.2 and 0.79 mL for Pd-monolith-6.4, which represents an almost 4-fold volume increase for the larger Pd-monolith-6.4. The activities of both monoliths for the Suzuki–Miyaura reaction (Scheme 1) are shown in Figure 2. It can be seen that Pd-monolith-6.4 produces a very similar percentage yield of product to that obtained using the Pd-monolith-3.2 under four times the flow rate to keep the same catalyst contact time. This observation is suggestive of virtually identical intrinsic properties for both monoliths in terms of flow rate and reaction conversion.



It can also be seen (Figure 3) that the rate of product formation scales up as expected, i.e., the larger catalyst monolith produces four times as much product compared to the smaller catalyst monolith under equivalent reaction conditions. However, it is also evident from the data that whilst shorter catalyst contact times (corresponding to higher solution flow rates) produce an increase in the rate of product formation, this increased rate of product formation is at the expense of reduced reagent conversion.

This methodology was also used to test Suzuki–Miyaura reactions with a variety of substrates, as shown in Table 3. It can be seen that this scale-up strategy also works very well, with the amount of product obtained with the Pd-monolith-6.4 being four times greater than that obtained with the Pd-monolith-3.2, under these conditions. Most reagents generated an excellent reaction conversion of the desired coupling product (see Supporting Information File 1, Figures S3, S4 and S5), even in the case of chlorobenzene, which is a notably poor substrate for the Suzuki–Miyaura reaction (entries 6 and 12). The



Suzuki–Miyaura reaction between bromobenzene and 4-bromobenzaldehyde with a higher concentration of reactants, i.e., 0.3 M, was also performed with the Pd-monolith-6.4 catalyst to evaluate the conversion ability. The reaction conversion was found to be high, i.e., 87–89 %, under these modified conditions.

The high catalytic activity of the Pd-monolith catalysts in Suzuki–Miyaura reactions can be attributed to the following three factors. First is the high dispersion of small Pd particles over the substrate surface within the monolith mesopores. The TEM image (Figure 4) shows that the catalyst sample incorporates metal particles, distributed over the substrate surface, with two different sizes: Small crystallites with dimensions of less than 2 nm (majority), and large crystallites with diameters of

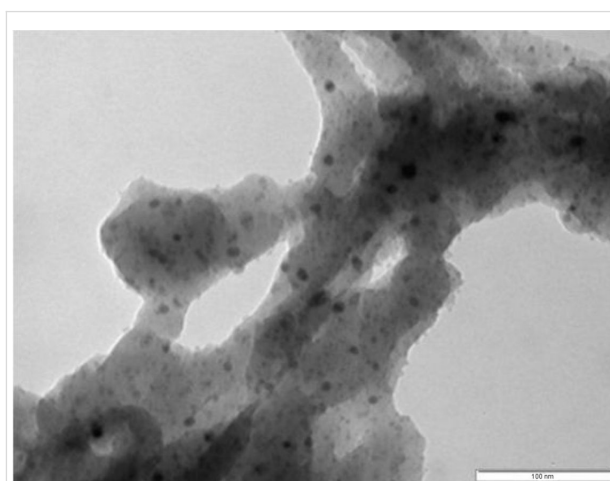
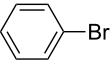
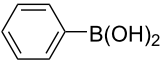
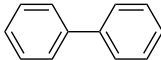
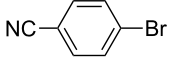
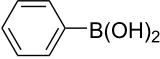
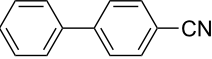
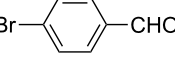
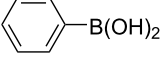
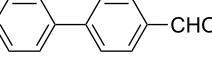
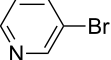
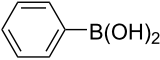
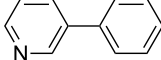
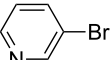
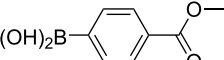
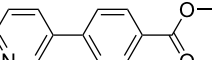
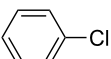
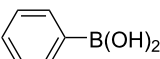
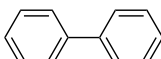
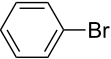
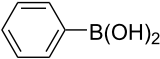
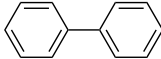
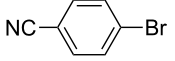
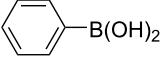
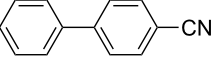
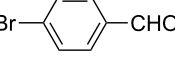
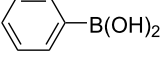
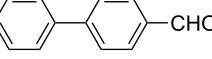
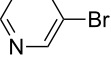
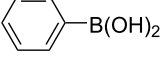
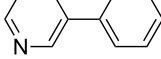
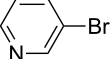
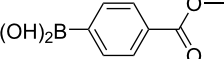
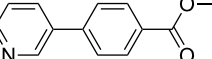
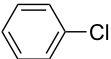
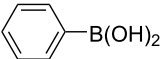
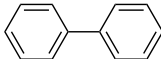


Figure 4: TEM image of Pd-monolith catalyst (scale bar: 100 nm).

Table 3: Reactivity of Pd-monoliths with different diameters, in the Suzuki–Miyaura reaction between various reactants under continuous-flow conditions.^a

Entry	Catalyst	Flow rate ($\mu\text{L min}^{-1}$)	Halide	Boronic acid	Product	Conversion (%)
1	Pd-monolith-3.2	40				99
2	Pd-monolith-3.2	20				100
3	Pd-monolith-3.2	30				95
4	Pd-monolith-3.2	20				65
5	Pd-monolith-3.2	20				60
6	Pd-monolith-3.2	20				99
7	Pd-monolith-6.4	160				99
8	Pd-monolith-6.4	80				99
9	Pd-monolith-6.4	120				95
10	Pd-monolith-6.4	80				65
11	Pd-monolith-6.4	80				59
12	Pd-monolith-6.4	80				98

^aMW power used was 5–10 W for Pd-monolith-3.2 and 1–2 W for Pd-monolith-6.4 to maintain reaction temperature of 125–130 °C. The backpressure valve was set up 75 psi for Pd-monolith-3.2 and 45 psi for Pd-monolith-6.4, respectively. The reaction conversion was determined by GC–MS with an internal standard and the main byproduct (1–3%) was formed by debromination of halide reactants.

around 10 nm. Second is the large surface-to-volume ratio of the monoliths. The values of the surface-area-to-volume ratio for the microchannels typically range from 10,000 to 50,000 m^2/m^3 , as a consequence of their decreased size. Based on BET characterization, the surface-area-to-volume ratio generated within the Pd-monolith-3.2 reactor was estimated to be $2.5 \times 10^8 \text{ m}^2/\text{m}^3$, which contributed greatly to the promotion of the reaction. The final factor relates to the combination of microwave heating and palladium nanoparticles. Kappe et al. found that smaller particles are more active in traditional heating whereas bigger particles perform better in microwave heating [25]. The monolithic structure used in this work takes

advantage of both these characteristics by having more reactive, nano-sized, Pd particles located within a strongly microwave-absorbing, meso-size, silica structure. Because it was difficult to measure the temperature inside the monolith, the outlet temperature measured by fiber probe was used, which gave a difference of at least 20 °C between the outlet temperature and the temperature of the outer surface of the monolith, as measured using the installed IR sensor. It was found that reaction conversion was only 40–50% with oil bath heating.

With supported Pd catalysts, leaching of palladium is always an issue of concern in terms of catalyst performance, cost and

recovery. Recent papers have shown that leaching from palladium catalysts is in the order of 1 to several tens of ppm [6,10,19,25] and that recovery of this palladium could be achieved with a scavenger column [6]. The tendency for leaching of palladium metal from the Pd-monoliths was measured through an ICP–OES analysis to determine the Pd concentration in the washing liquid, which immediately followed the first flow reaction experiment. This was achieved by pumping DMF/H₂O (3:1) solvent through the Pd-monolith at 0.1 mL/min for 20 min. For the Na₂PdCl₄ based monolithic catalyst, the amount of palladium present in the washing liquid was found to be as little as 74 ppb (Pd-monolith-3.2), corresponding to a loss of only 0.00011% of the initial amount of palladium added to the monoliths. The amount of palladium present in the final reaction sample was found still to be less than 100 ppb. This finding suggests that there is a highly specific and strong interaction between the impregnated metal nanoparticles and the monolith support surface, possibly through a combination of hydrogen bonding, ionic interactions and substitution of Cl by silanol groups present on the monolith surface, resulting in highly stable nanoparticle fixation [26,27]. The presence of a strong specific metal/support interaction is also supported by observations made during the impregnation process, where PdCl₄²⁻ uptake in the silica monolith body was seen to be fast, with the monolith turning a stable dark brown color after several hours. In contrast, the Pd(NO₃)₂ salt gave the monolith a lighter coloration, much more slowly, and was easily washed away. The PdCl₄²⁻ based Pd-monolith catalyst was in fact used for several runs (i.e., 6 runs representing 15–20 hours) with no deactivation being observed when the catalyst was washed with DMF, water or DMF/H₂O (3:1) after completion of each run.

Conclusion

It has been demonstrated that the combination of Pd-functionalized silica monolithic reactors with microwave heating results in a high percentage yield of the desired reaction products for Suzuki–Miyaura reactions under flow conditions. Yields can be scaled-up by increasing the diameter of the catalytic monolith used. The cylindrical catalyst monoliths were of a constant length, but of variable diameter and were produced to give the same intrinsic monolith activity and permeability properties, when operating under the same conditions of temperature and catalyst contact time. In this way the product formation rate scales quantitatively with the square of the catalyst monolith diameter. However, at least one alternative approach can be envisaged, i.e., changing the monolith length for scaling up whilst maintaining the required intrinsic properties. It is worth considering the relative advantages and disadvantages of these two possible approaches in light of the work presented. Increasing the diameter of a fixed length monolith, the scale-up

method as used here, offers the advantage that the pressure drop required to produce a certain flow rate decreases with increasing diameter. However, as microwave penetration is necessary to obtain reliable heating characteristics, there will come a point at which the monolith diameter will become larger than the penetration depth of the microwaves (estimated to be 4 cm), which will lead to an unheated, cold “core”. In addition for disc-shaped monoliths, where diameters are larger than the length, there will also come a point where the mechanical strength of the monolith will be a limitation with respect to the pressure drop required for flow. On the other hand, increasing the length of a fixed diameter monolith in order to achieve this scale-up offers the advantage that uniform microwave penetration/heating can be maintained. In addition, the catalyst contact time could be extended by increasing the length. The disadvantage, however, to this approach is related to the pressure drop required to produce the required flow rate, which will increase proportionally with the length. Hence, the mechanical strength of the monolith structure, i.e., the strength to resist collapse of the pores and/or the monolith casing material, ultimately limits the maximum length achievable.

Experimental

Materials

The reagents and solvents bromobenzene (99%), 4-bromobenzonitrile (99%), 4-bromobenzaldehyde (99%), 3-bromopyridine (99%), chlorobenzene (99%), phenylboronic acid (97%), 4-carboxyphenylboronic acid (97%), poly(ethylene oxide) (PEO) with average relative molar mass of 100 kDa, tetraethoxysilane (TEOS), *N,N*-dimethylformamide (99%, DMF), dichloromethane (99%, DCM), ammonium hydroxide (5 N) and nitric acid aqueous solutions (1 N) were purchased from Aldrich. All reagents were used as obtained, without further purification. Heat shrinkable Teflon[®] tubes (wall thickness 0.1 and 0.3 mm before and after shrinkage) with a shrinkage ratio of 2:1 were purchased from Adtech Polymer Engineering Ltd. (UK).

Synthesis of silica monolith supports

Silica based monoliths were prepared using a sol–gel process described in the literature [24]. The desired amount of PEO was added to an aqueous solution of nitric acid and the resultant mixture was cooled in an ice bath and stirred until a homogeneous solution formed. TEOS was then added to the reaction mixture, which was stirred vigorously in the ice bath for 30 min to form a transparent solution. Subsequently, the solution was poured into a plastic mould (diameter 4.8 mm and length 6 cm for monolith-3.2; and diameter 8.2 mm and length 5 cm for monolith-6.4). Both ends of the plastic mould were then closed and the sealed tube was incubated in an oven at 40 °C for 3 days, during which time a wet, semi-solid, gel monolith was

formed. Approximately 20% shrinkage occurred during this gel formation, which allowed easy removal of the wet gel monoliths from the plastic tube moulds. The wet gel monoliths were washed with copious amounts of water to remove any residues and then transferred to a 10 times larger volume of 0.5 M NH_4OH aqueous solution in an autoclave, where it was incubated at 80 °C for 24 h. The monoliths were again washed with copious amounts of water before drying in an oven at 90 °C for 24 h. Finally, the monoliths were calcined at 550 °C for 3 h (heating rate: 2 °C/min) in an air flow to remove the remaining PEO and form white silica-monolith rods (diameters 3.2 and 6.4 mm respectively) that were then cut to 3 cm long monoliths.

Preparation of Pd-supported silica-monolith catalyst (Pd-monolith)

An aqueous solution of 200 μL containing 0.017 g Na_2PdCl_4 (theoretical Pd loading 5.0 wt %) was adsorbed onto the monoliths, dried at 90 °C and calcined at 550 °C for 3 h (temperature ramp: 2 °C min^{-1}) under a flow of air, followed by reduction in a H_2 (10%)/ N_2 stream at 340 °C for 3 h (heating rate: 2 °C) to produce a black Pd-monolith rod with Pd loading of approximately 4.5 wt % as determined by ICP–OES (Perkin Elmer Optima 5300DV). The Pd-monolith rod obtained was then clad in a heat-shrinkable Teflon[®] tube with a glass connector at each end. The assembly was heated in a furnace up to 330 °C until the monolith was sealed within the Teflon[®] tube to form a flow Pd-monolith reactor system.

Sample characterization

Scanning electron microscopy (SEM) images were obtained by means of a Cambridge S360 scanning electron microscope operated at 20 kV. Each sample was sputter coated with a thin layer of gold–platinum (thickness approximately 2 nm) by a SEMPREP 2 Sputter Coater (Nanotech Ltd.). Transmission electron microscopy (TEM) was carried out on a JEOL-2010 operating at 200 kV. The BET surface area and nm-scale pore-size distribution were obtained by measuring N_2 adsorption and desorption isotherms at 77 K by means of a Micromeritics Surface Area and Porosity Analyzer. The pore volume and pore size distributions of the nm-scale pores within the monoliths were evaluated from the isotherms within the BJH (Barrett–Joyner–Halenda) model. The palladium content in the monoliths and washing liquid was determined by ICP–OES. Determination of the μm -scale porosity ϕ_t (which determines the monolith permeability) was determined from the equation $(W_M - W_T)/dlr^2\pi$, where W_T and W_M were the weights of the dry and water filled monolith respectively, d was the density of water, l and r were the overall length and radius of the cylindrical monolith. The μm -scale pore size was determined from SEM measurements.

Activity measurements

The experimental setup is shown schematically in Supporting Information File 1, Figure S6. The 30 mm long Pd-monolith reactor with a diameter of either 3.2 mm (Pd-monolith-3.2) or 6.4 mm (Pd-monolith-6.4) was positioned in the cavity of a Discover microwave system (CEM Ltd.) with the capability of delivering 0–300 W of microwave power at 2.45 GHz with mono-mode operation. The microwave cavity was fitted with an infrared sensor to monitor the temperature of the external surface of the monolith catalyst. A reactant solution containing an aryl halide (0.1 M), arylboronic acid (0.12 M), K_2CO_3 (0.3 M) in DMF/ H_2O (3:1) solvent was pumped through the reactor with an HPLC pump, and a backpressure valve (45–75 psi) was used to minimize the formation of gas bubbles (see Supporting Information File 1, Figure S6). The residence times of the reactants within the catalytic monoliths were determined based on the known monolith and pore volume and from the different flow rates. Product samples were collected at defined flow periods during a reaction run, weighed and a known amount of dodecane was added to the individual samples as an internal standard. Samples were treated with 1 M aqueous NaOH to remove unreacted arylboronic acid and extracted with DCM. The remaining organic material was then washed three times with distilled water, collected and dried over MgSO_4 . Individual samples were analyzed using GC–MS (Varian 2000) as described in literature [3,4].

Supporting Information

The Supporting Information File contains six parts, Figure S1: SEM image of Pd-monolith; Figure S2: BET characterization; Figure S3: GC–MS chromatogram for Suzuki–Miyaura reaction of bromobenzene and phenylboronic acid; Figure S4: GC–MS chromatogram for Suzuki–Miyaura reaction of 4-bromobenzaldehyde and phenylboronic acid; Figure S5: GC–MS chromatogram for Suzuki–Miyaura reaction of 4-bromobenzonitrile and phenylboronic acid; Figure S6: Schematic diagram of the setup for continuous-flow, microwave-assisted Suzuki–Miyaura reactions.

Supporting Information File 1

Additional material.

[<http://www.beilstein-journals.org/bjoc/content/supplementary/1860-5397-7-133-S1.pdf>]

References

- Vankayala, B. K.; Löb, P.; Hessel, V.; Menges, G.; Hoffmann, C.; Metzke, D.; Krtschil, U.; Kost, H.-J. *Int. J. Chem. React. Eng.* **2007**, *5*, A91. doi:10.2202/1542-6580.1463

2. de Mas, N.; Günther, A.; Kraus, T.; Schmidt, M. A.; Jensen, K. F. *Ind. Eng. Chem. Res.* **2005**, *44*, 8997. doi:10.1021/ie050472s
3. He, P.; Haswell, S. J.; Fletcher, P. D. I. *Lab Chip* **2004**, *4*, 38. doi:10.1039/b313057f
4. He, P.; Haswell, S. J.; Fletcher, P. D. I. *Appl. Catal., A* **2004**, *274*, 111. doi:10.1016/j.apcata.2004.05.042
5. Glasnov, T. N.; Kappe, C. O. *Adv. Synth. Catal.* **2010**, *352*, 3089. doi:10.1002/adsc.201000646
6. Mennecke, K.; Kirschning, A. *Beilstein J. Org. Chem.* **2009**, *5*, No. 21. doi:10.3762/bjoc.5.21
7. Razzaq, T.; Kappe, C. O. *Chem.–Asian J.* **2010**, *5*, 1274. doi:10.1002/asia.201000010
8. Comer, E.; Organ, M. G. *Chem.–Eur. J.* **2005**, *11*, 7223. doi:10.1002/chem.200500820
9. Gömann, A.; Deverell, J. A.; Munting, K. F.; Jones, R. C.; Rodemann, T.; Cauty, A. J.; Smith, J. A.; Guijt, R. M. *Tetrahedron* **2009**, *65*, 1450. doi:10.1016/j.tet.2008.12.007
10. Ceylan, S.; Friese, C.; Lammel, C.; Mazac, K.; Kirschning, A. *Angew. Chem., Int. Ed.* **2008**, *47*, 8950. doi:10.1002/anie.200801474
11. Uozumi, Y.; Yamada, Y. M. A.; Beppu, T.; Fukuyama, N.; Ueno, M.; Kitamori, T. *J. Am. Chem. Soc.* **2006**, *128*, 15994. doi:10.1021/ja066697r
12. Svec, F.; Huber, C. G. *Anal. Chem.* **2006**, *78*, 2100. doi:10.1021/ac069383v
13. Preinerstorfer, B.; Bicker, W.; Lindner, W.; Lämmerhofer, M. *J. Chromatogr., A* **2004**, *1044*, 187. doi:10.1016/j.chroma.2004.04.078
14. Smith, C. J.; Smith, C. D.; Nikbin, N.; Ley, S. V.; Baxendale, I. R. *Org. Biomol. Chem.* **2011**, *9*, 1927. doi:10.1039/c0ob00813c
15. Kunz, U.; Kirschning, A.; Wen, H.-L.; Solodenko, W.; Cecilia, R.; Kappe, C. O.; Turek, T. *Catal. Today* **2005**, *105*, 318. doi:10.1016/j.cattod.2005.06.046
16. Nikbin, N.; Ladlow, M.; Ley, S. V. *Org. Process Res. Dev.* **2007**, *11*, 458. doi:10.1021/op7000436
17. Kappe, C. O.; Dallinger, D.; Murphree, S. S. *Practical Microwave Synthesis for Organic Chemists – Strategies, Instruments, and Protocols*; Wiley-VCH: Weinheim, Germany, 2009; pp 138–160.
18. Comer, E.; Organ, M. G. *J. Am. Chem. Soc.* **2005**, *127*, 8160. doi:10.1021/ja0512069
19. Shore, G.; Morin, S.; Organ, M. G. *Angew. Chem., Int. Ed.* **2006**, *45*, 2761. doi:10.1002/anie.200503600
20. Singh, B. K.; Kaval, N.; Tomar, S.; Van der Eycken, E.; Parmar, V. S. *Org. Process Res. Dev.* **2008**, *12*, 468. doi:10.1021/op800047f
21. Glasnov, T. N.; Kappe, C. O. *Macromol. Rapid Commun.* **2007**, *28*, 395. doi:10.1002/marc.200600665
22. Mason, B. P.; Price, K. E.; Steinbacher, J. L.; Bogdan, A. R.; McQuade, D. T. *Chem. Rev.* **2007**, *107*, 2300. doi:10.1021/cr050944c
23. Pennemann, H.; Watts, P.; Haswell, S. J.; Hessel, V.; Löwe, H. *Org. Process Res. Dev.* **2004**, *8*, 422. doi:10.1021/op0341770
24. Fletcher, P. D. I.; Haswell, S. J.; He, P.; Kelly, S. M.; Mansfield, A. J. *Porous Mater.* **2010**, *18*, 501. doi:10.1007/s10934-010-9403-3
25. Mennecke, K.; Cecilia, R.; Glasnov, T. N.; Gruhl, S.; Vogt, C.; Feldhoff, A.; Vargas, M. A. L.; Kappe, C. O.; Kunz, U.; Kirschning, A. *Adv. Synth. Catal.* **2008**, *350*, 717. doi:10.1002/adsc.200700510
26. Bronstein, L. M.; Polarz, S.; Smarsly, B.; Antonietti, M. *Adv. Mater.* **2001**, *13*, 1333. doi:10.1002/1521-4095(200109)13:17<1333::AID-ADMA1333>3.0.CO;2-P
27. Kosslick, H.; Mönnich, I.; Paetzold, E.; Fuhrmann, H.; Fricke, R.; Müller, D.; Oehme, G. *Micro. Meso. Mater.* **2001**, *44-45*, 537. doi:10.1016/S1387-1811(01)00232-3

License and Terms

This is an Open Access article under the terms of the Creative Commons Attribution License (<http://creativecommons.org/licenses/by/2.0>), which permits unrestricted use, distribution, and reproduction in any medium, provided the original work is properly cited.

The license is subject to the *Beilstein Journal of Organic Chemistry* terms and conditions:

(<http://www.beilstein-journals.org/bjoc>)

The definitive version of this article is the electronic one which can be found at:

doi:10.3762/bjoc.7.133



Production of deuterium labelled (–)-epicatechin in a microreactor

Jonathan W. Betts^a, Stuart P. Kitney^a, Yiton Fu^b, Wei-Min Peng^c,
Stephen M. Kelly^a, Stephen J. Haswell^{a,*}

^a Department of Chemistry, The University of Hull, Hull, HU6 7RX, UK

^b Unilever R&D, Colworth, UK

^c Unilever R&D, Shanghai, China

ARTICLE INFO

Article history:

Received 14 April 2010

Received in revised form 29 August 2010

Accepted 31 August 2010

Keywords:

Microreactor
Epicatechin
Polyphenols
Deuterium
Labelling

ABSTRACT

Green tea catechins have been reported to have multiple health benefits. To understand their metabolic and toxicological interactions in the human body studies need to be undertaken using stable isotope labelled compounds, but they can be time consuming and expensive. Using microreactor technology labelling catechins could be produced more quickly and at a reduced cost. This research reports on a 2-step synthesis of deuterium labelled epicatechin developed using microreactor technology for the production.

© 2010 Elsevier B.V. All rights reserved.

1. Introduction

Green tea is produced from the plant *Camellia sinensis* and has been linked with many potential health benefits [1]. These benefits are linked to polyphenols compounds, which are part of the flavanoid group and include antioxidants such as theaflavin and catechins [2]. Previous studies have discovered their benefits include radical scavenging, anticancer and antimicrobial activity [3].

A number of studies have investigated the metabolites of catechins to gain metabolic and toxicological knowledge of these compounds [4]. However this requires labelling the compounds, which can often be expensive and time consuming. Labelling molecules in order to monitor their metabolic activity can be performed using various methods, such as tagging the molecule by fluorescence or by using stable carbon isotopes in the molecular structure [5]. Whilst fluorescent markers are very useful in biological studies, their structures are sensitive to environmental conditions such as temperature [6]. In addition, fluorescent labels can alter the overall structure and potentially the properties of the compound, which in turn could distort results in a metabolic study. The use of a ¹³C or ¹⁴C marker offers substantial benefits in metabolic studies due to their stability and integration into the overall structure of the compound investigated [7]. Although this

is an effective method of labelling a compound and has been used in flavanoids in previous research, it often involves many reaction steps and more complicated stereochemistry [8].

An alternative method to ¹³C or ¹⁴C labelling is to label the compound under investigation with deuterium. This approach has proven to be successful in various batch reactions including that for the labelling of the catechin epigallocatechin gallate [4]. Such synthesis has also been undertaken previously in microreactors for the production of labelled phenol compounds [9]. In this present study we extend this earlier work to the labelling of polyphenols using microreactor technology, which offers a more rapid, low volume methodology, with the capability of integrating chemical synthesis and biological testing [10]. Using microreactors in synthetic chemistry have been shown to have many advantages [11] including a greater level of reaction control, an increase in product yield and purity and a lower volume of reagents required. Further benefits of microreactors is in the area of health and safety where due to reduced reactants, factors such as managing heat transfer are more easily and safely controlled [12].

In this paper we report the use of a simple T-shaped microreactor to perform a 2-step synthesis route, based on a previous batch synthesis [13], to generate deuterium labelled epicatechin.

2. Experimental

In this 2-step procedure epicatechin was labelled in a T-shaped microreactor (Fig. 1a and b), which was fabricated using methods developed at the University of Hull [14]. The first step was a 1:1 iod-

* Corresponding author.

E-mail address: s.j.haswell@hull.ac.uk (S.J. Haswell).

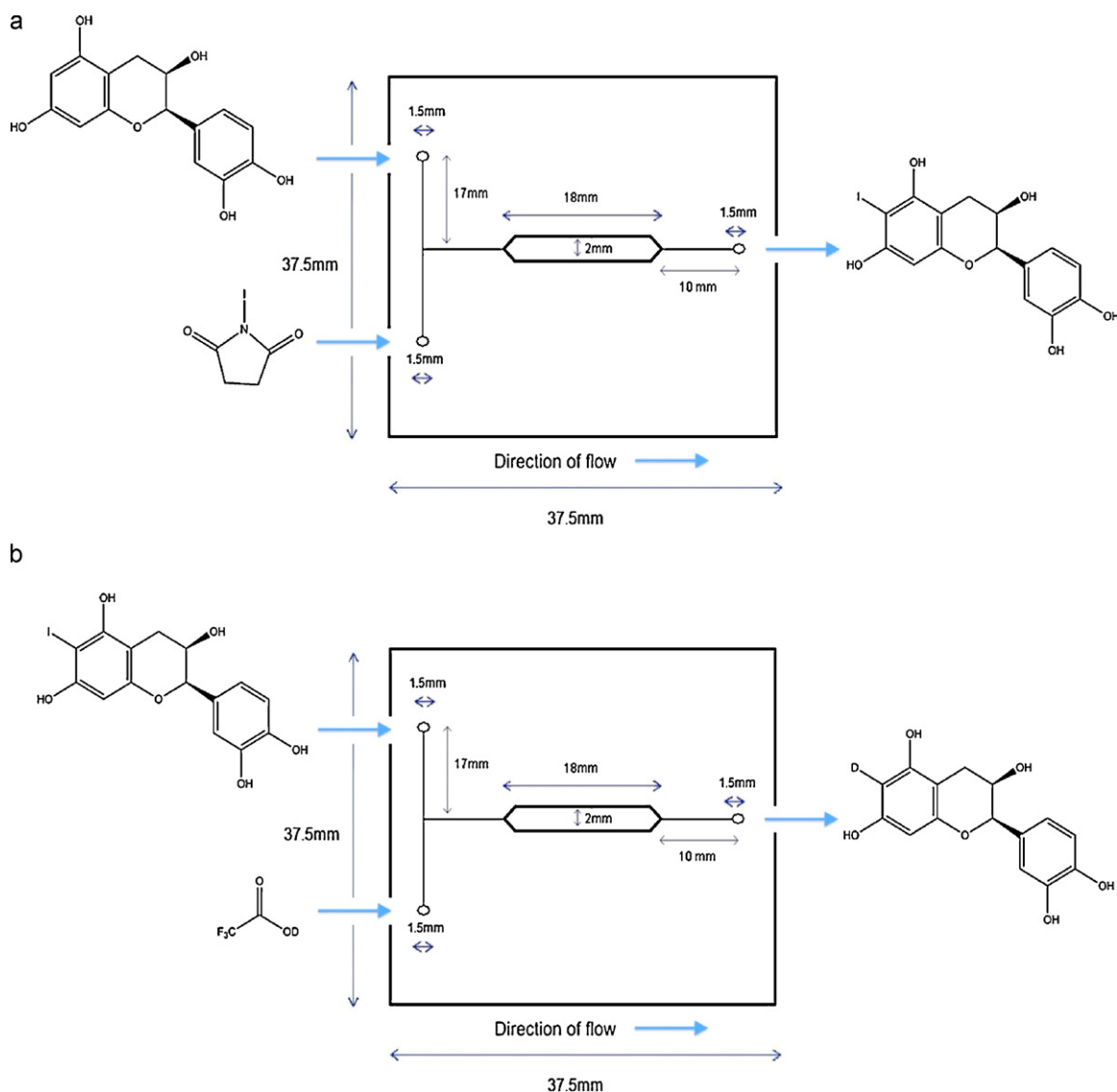


Fig. 1. (a and b) Showing a schematic of the microreactor. (a) Step 1 of the synthesis showing the conversion of (–)-epicatechin to 6-iodoepicatechin. (b) Step 2 of the synthesis showing the conversion of 6-iodoepicatechin to deuterium labelled epicatechin in position 6.

ination reaction (Fig. 1a), between epicatechin (0.058 g, 20 mmol) and N-iodosuccinimide (0.045 g, 20 mmol) in acetone at 30 °C controlled by a syringe pump at 10 $\mu\text{L}/\text{min}$. Products were collected into a vial containing methanol, which acted as a quencher. This was to confirm that the reaction actually occurred in the micro reactor and not in the collecting vial. Products were concentrated under reduced pressure leaving a brown/beige coloured powder (0.1 g). ^1H NMR and LC/MS data were then acquired.

Step 2 of the procedure was a 1:2 deuteration reaction between the crude 6-iodoepicatechin powder (0.1 g) and trifluoroacetic acid-d (0.046 g, 40 mmol), performed again in a T-shaped microreactor (Fig. 1b). The reaction was performed in acetone- d_6 and controlled by a syringe pump at 10 $\mu\text{L}/\text{min}$ and was at a temperature of 30 °C. Products were collected into a vial and then concentrated under reduced pressure leaving a purple/brown oil (0.105 g) which was analyzed via ^1H NMR and LC/MS.

The immediate stability of the labelled epicatechin was also tested in water at room temperature. LC/MS of the compound was performed at 0, 1 and 2 h after production.

An initial optimization of these reactions to establish the most appropriate flow rate in the range 20–5 $\mu\text{L}/\text{min}$ was carried out

(results not shown here) from which 10 $\mu\text{L}/\text{min}$ was found to be the optimal flow.

3. Results and discussion

The H NMR data from the crude products of both reactions showed that they were almost 100% complete. From the reaction in step 1 the following ^{13}C NMR and ^1H NMR data is reported where: d = doublets, dd = doublet of doubles, m = multiplet, s = singlet and bs = broad singlet.

^1H NMR (400 MHz, CD_3COCD_3) 6.95 (1H, d, $J=1.36$ Hz, H-2'), 6.81 (1H, d, $J=2.2$ Hz, H-6'), 6.14 (1H, d, $J=2.76$ Hz, H-8), 5.45 (1H, m, H-3), 4.87 (1H, bs, H-2), 2.90 (1H, dd, $J=19.2, 4.67$ Hz, H-4), 2.70 (1H, dd, $J=16.6, 2.2$ Hz, H-4).

^{13}C NMR (400 MHz, CD_3COCD_3) 157.4 (C-8a), 156.3 (C-7), 156.2 (C-5), 145.2, 141.1 (C-3', C-4'), 131.8 (C-1'), 119.2 (C-6'), 115.7 (C-2'), 115.0 (C-5'), 100.5 (C-4a), 96.2 (C-8), 79.8 (C-2), 67.2 (C-3), 66.4 (C-6), 29.6 (C-4).

From the H NMR data identifies the disappearance of a peak at 6.25 ppm indicating that the proton in that region had been lost. LC/MS confirmed a peak at 416.8 m/z (see supplementary data),

which was consistent with the loss of a proton and thus iodination had occurred giving 6-iodoepicatechin.

Due to the large variation between the H NMR peaks of epicatechin and catechin, a direct comparison of the data from the iodocatechin [13] could not be made with the iodoepicatechin produced. However, there is a clear indication that the iodination of epicatechin was successful. The high conversion in step 1 eliminated the need for purification prior to step 2.

From the reaction in step 2 the following ^{13}C NMR and ^1H NMR data was obtained where: d = doublets, dd = doublet of doublets, m = multiplet, s = singlet and bs = broad singlet.

^1H NMR (400 MHz, CD_3COCD_3) 6.95 (1H, d, $J = 1.36$ Hz, H-2'), 6.81 (1H, d, $J = 2.2$ Hz, H-6'), 6.14 (1H, d, $J = 2.76$ Hz, H-8), 5.45 (1H, m, H-3), 4.87 (1H, bs, H-2), 2.90 (1H, dd, $J = 18.1, 4.76$ Hz, H-4), 2.70 (1H, dd, $J = 16.2, 2.2$ Hz, H-4).

^{13}C NMR (400 MHz, CD_3COCD_3) 157.5 (C-8a), 157.0 (C-7), 156.6 (C-5), 145.2, 145.1 (C-3', C-4'), 132.4 (C-1'), 119.4 (C-6'), 115.7 (C-2'), 115.2 (C-5'), 100.1 (C-4a), 99.8 (C-8), 95.6 (C-6), 79.9 (C-2), 66.6 (C-3), 29.6 (C-4).

The H NMR spectra showed that only one peak remained at 6.14 ppm and the peak at 6.25 ppm had not returned. LC/MS of the product again showed main peaks at 292 m/z and 293 m/z (see supplementary data) indicating the mass of single and double D-labelled epicatechin with the additional deuterium most likely being from hydrogen transfer with one of the phenol groups.

The immediate stability tests of deuterium labelled compound showed that in water it was stable for up to 2 h. LC/MS performed at 0, 1 and 2 h after storage showed the main mass peak remained at 292 m/z . The peak at 293 m/z had been reduced indicating hydrogen transfer had again occurred. However this does not represent the stability in serum and this would need to be investigated further if it were to be used in toxicological studies.

4. Conclusions

This research shows for the first time that labelling polyphenols in a microreactor is possible and unlike batch reactions is more cost effective and could be used for a continuous flow process to monitor toxicological effects of various compounds in a microfluidic device. It is also the first time epicatechin has been labelled in the 6 position using a 2-step process. Due to the high conversion in step 1 and the need for no purification, it is clear that at a future date the labelling could be undertaken in a single microreactor. The unique structure of epicatechin allows iodination and deuteration in the positions we have shown. However, when applied to more complex polyphenols, iodination could occur in multiple positions thus complicating any *in vivo* analysis. We propose that future studies should investigate

the 24 h stability of this labelled compound in more depth for the preparation of its use in toxicological/metabolic studies.

Acknowledgements

EPSRC and Unilever, UK are gratefully acknowledged for funding. Dr. Steve Clark is also gratefully acknowledged for microreactor production.

Appendix A. Supplementary data

Supplementary data associated with this article can be found, in the online version, at doi:10.1016/j.cej.2010.08.093.

References

- [1] N.T. Zaveri, Green tea and its polyphenolic catechins: medical uses in cancer and noncancer applications, *Life Sciences* 78 (2006) 2073–2080.
- [2] M. Lorenz, S. Wessler, E. Follmann, W. Michaelis, T. Dusterhoft, G. Baumann, K. Stangl, V. Stangl, A constituent of green tea, epigallocatechin-3-gallate, activates endothelial nitric oxide synthase by a phosphatidylinositol-3-OH-kinase-, cAMP-dependent protein kinase-, and Akt-dependent pathway and leads to endothelial-dependent vasorelaxation, *The Journal of Biological Chemistry* 279 (2004) 6190–6195.
- [3] Y. Dobashi, T. Hirano, M. Hirano, Y. Ohkatsu, Antioxidant and photo-antioxidant abilities of catechins, *Journal of Photochemistry and Photobiology A: Chemistry* 197 (2008) 141–148.
- [4] T. Kohri, F. Nanjo, M. Suzuki, R. Seto, N. Matsumoto, M. Yamakawa, H. Hojo, Y. Hara, D. Desai, S. Amin, C.C. Conway, F.L. Chung, Synthesis of (–)-[4- ^3H]epigallocatechin gallate and its metabolic fate in rats after intravenous administration, *Journal of Agriculture and Food Chemistry* 49 (2001) 1042–1048.
- [5] E. Lundberg, M. Sundberg, T. Gräslund, M. Uhlén, H. Andersson Svahn, A novel method for reproducible fluorescent labelling of small amounts of antibodies on solid phase, *Journal of Immunological Methods* 322 (2007) 40–49.
- [6] W.J. Parak, T. Pellegrino, C. Plank, Labelling of cells with quantum dots, *Nanotechnology* 16 (2005) R9–R25.
- [7] S. Flores, G. Gosset, N. Flores, A.A. de Graaf, F. Bolivar, Analysis of carbon metabolism in *Escherichia coli* strains with an inactive phosphotransferase system by ^{13}C labelling and NMR spectroscopy, *Metabolic Engineering* 4 (2002) 124–137.
- [8] B. Nay, V. Arnaudinaud, J. Vercauteren, Total synthesis of asymmetric flavonoids: the development and applications of ^{13}C -labelling, *Comptes Rendus Chimie* 5 (2002) 577–590.
- [9] J. Hooper, P. Watts, C. Wiles, Deuterated isotope labelling of phenol derivatives within micro reactors, *Microfluidics and Nanofluidics* 5 (2008) 595–602.
- [10] S.J. Haswell, All together now, *Nature* 441 (2006) 705.
- [11] D. Janasek, J. Franzke, A. Manz, Scaling and the design of miniaturized chemical-analysis systems, *Nature* 442 (2006) 374–380.
- [12] S.J. Haswell, V. Skelton, Chemical and biochemical microreactors, *Trends in Analytical Chemistry* 19 (2000) 389–395.
- [13] E. Kiehlmann, N. Lehto, D. Cherniwchan, Iodination and deuteration of catechins derivatives, *Canadian Journal of Chemistry* 66 (1988) 2431–2439.
- [14] T. McCreedy, Rapid prototyping of glass and PDMS microstructures for micro total analytical systems and micro chemical reactors by microfabrication in the general laboratory, *Analytica Chimica Acta* 427 (2001) 39–43.

Permeability of silica monoliths containing micro- and nano-pores

Paul D. I. Fletcher · Stephen J. Haswell ·
Ping He · Stephen M. Kelly · Andrew Mansfield

Published online: 1 August 2010
© Springer Science+Business Media, LLC 2010

Abstract For applications as catalyst supports in flow reactors, porous silica monoliths require a combination of connected pores of micron-scale to enable fluid flow plus nm-scale pores to enable high catalyst area and activity. We have synthesised a range porous silica monoliths, characterised their micron and nm-scale pores and measured their permeability coefficients K . K can be controlled over the range 10^{-10} – 10^{-14} m², primarily by adjustment of the polymer/silane concentration ratio, whilst maintaining the specific surface area and nm-scale porosity approximately constant. For the majority of the silica monolith samples, the measured permeability coefficient K is 2–5 times smaller than K for a hypothetical reference system consisting of a monolith with uniform cylindrical pores aligned in the flow direction and with the same average pore diameter and volume fraction.

Keywords Silica · Porous · Monolith · Permeability

1 Introduction

Increasing interest in the development of miniaturised micro chemical systems has led to increased research in micro chemical engineering; embracing microfabrication, microfluidics and microreaction technology and their applications in chemical synthesis and analytical and

physical measurements. Such systems commonly have feature sizes in the range 1–1,000 μm and reagent flow channels are usually integrated with microsensors, microactuators and catalytic elements appropriate to the particular application [1–5]. Understanding and controlling microfluidics is key to controlling reagent delivery, mixing, separation, heat and mass transfer and reagent contact time with a heterogeneous catalyst. Most microchemical systems employ either electrokinetic mobilisation or pressure-driven pumping of reagents and, in previous studies, we have demonstrated the successful modelling of an electrokinetic system for the control of the spatial and temporal evolution of chemical reactions [6]. In the present study, we focus on the pressure-driven flow properties (i.e. the permeability) of porous silica monolithic catalyst supports integrated within flow systems.

Silica monoliths for use as catalyst supports require a high specific surface area (achieved with nm-sized pores) to maximise their catalytic activity but must also be highly permeable (achieved with micron-sized pores) to enable fast mass transfer to the catalytic surface. They must also be mechanically strong to withstand the pressures required to drive fluid through them at the required flow rate. Hence, effective monoliths must achieve a suitable compromise between these conflicting requirements which can be done using fabrication procedures yielding monoliths with both micron and nano-scale pores. Such monoliths are made by the sol–gel synthesis of silicon alkoxide precursors in the presence of additives such as organic solvents or polymers and there is an extensive literature on their synthesis and the control of the pore morphology, particularly with regard to fabricating chromatographic columns with enhanced performance [7–22]. Formation of a silica monolith proceeds in the following stages. Firstly, a homogeneous, single-phase aqueous solution containing a

P. D. I. Fletcher (✉) · S. J. Haswell · P. He · S. M. Kelly
Department of Chemistry, University of Hull,
Hull HU6 7RX, UK
e-mail: P.D.Fletcher@hull.ac.uk

A. Mansfield
Pfizer Global Research & Development, Sandwich,
Kent CT13 9NJ, UK

silicon alkoxide, a catalyst (commonly an acid or a base) and an organic additive such as a water-miscible co-solvent or water-soluble polymer is prepared. The alkoxide then undergoes hydrolysis to produce -Si-OH species followed by their polymerisation to yield polycondensed species containing -Si-O-Si- linkages. The polymerisation induces phase separation of a silica-rich phase which, depending on conditions, can occur either by nucleation and growth or by spinodal decomposition. Additionally, the polymerisation also causes gelation of the silica-rich phase which “freezes” the morphology of the silica-rich phase. The aged wet gel is washed and treated with ammonium hydroxide solution before washing, drying and calcination to produce the final porous silica monolith in which the morphology of the silica “skeleton” is determined by that of the silica-rich phase of the wet gel, albeit with some shrinkage. According to this mechanism, the micron-size pore structure is determined by the composition of the initial solution and reaction conditions which, in turn, control the type (nucleation and growth or spinodal decomposition) and rate of the phase separation and the subsequent coarsening of the multi-phase system before gelling occurs to “freeze” the structure. The nm-size pores are thought to be formed by dissolution/re-precipitation on the rough surface of the gel network during the treatment with base and the average nano-pore size can be controlled by varying the pH and temperature of this treatment step. A detailed discussion of these processes and how to control them is given in the elegant review by Nakanishi [8].

Although the extensive literature on silica monoliths provides much elegant and systematic information on the mechanism of formation, the control of pore morphology and monolith performance in chromatography applications, direct information on fluid permeability through monoliths is somewhat scattered (see, for example, [11]). In this work we focus on two main questions. Firstly, how does the permeability coefficient of a monolith depend on its porosity and pore size and, secondly, how do measured permeability coefficients compare with that of a hypothetical monolith containing monodisperse, uniform, cylindrical micron-scale pores of the same micron-scale porosity and pore size.

2 Experimental

2.1 Materials

Poly(ethylene oxide) (PEO) with average relative molar masses of 10, 35, 100, 200 and 300 kDa, poly(ethylene oxide)-*block*-poly(propylene oxide)-*block*-poly(ethylene oxide) (P123, $\text{EO}_{20}\text{PO}_{70}\text{EO}_{20}$ and F127, $\text{EO}_{106}\text{PO}_{70}\text{EO}_{106}$), tetramethoxysilane (TMOS), tetraethoxysilane (TEOS),

ammonium hydroxide (5 N), and nitric acid aqueous solutions (1 N) and acetic acid were purchased from Aldrich. All reagents are AR grade and were used as obtained without further purification. Heat Shrinkable Teflon tubes with a shrinkage ratio of 2:1 were purchased from Adtech Polymer Engineering Ltd., UK.

2.2 Synthesis of silica monoliths

The silica monoliths were prepared using a procedure similar to that described by Nakanishi [8]. The desired amount of polymer was added to aqueous solution of acid, the mixture was cooled in an ice bath and stirred until a homogeneous solution formed. Then the required amount of silicon alkoxide was added and the mixture was stirred vigorously in the ice bath for 30 min to form a transparent solution. Subsequently, the solution was poured into a plastic tube (diameter 4.8 mm and length 6 cm), both ends were closed and the tube was incubated in a water bath at 40 °C for 3 days, during which a wet, semi-solid gel monolith was formed. Approximately 20% shrinkage occurred during this gel formation which allowed easy removal of the wet gel monoliths from the plastic tube moulds. The wet gel monoliths were washed with copious amounts of water to remove any possible residues and then transferred to a 10 times volume of 1 M NH_4OH aqueous solution in an autoclave where it was incubated at 90 °C for 16 h. The monoliths were again washed with lots of water before drying in an oven at 60 °C for 2 days. Finally, the monoliths were calcined at 550–650 °C for 16 h under air flow to remove any remaining organic material.

The desired application for these silica monoliths is as catalyst supports within continuous flow chemical reactors. For both this application and the fluid permeability measurements described here, it is essential they can be mounted tightly with no leakage in a flow system. The following method was found to be effective. The silica monolith rod was clad in a heat shrinkable Teflon tube which was also connected to the ends of the flow system. The assembly was then heated in an oven at 320 °C until the monolith was sealed within the Teflon tube which also formed leak-tight connections with the flow system.

2.3 Characterization

Scanning electron microscopy (SEM) images were obtained using a Cambridge S360 scanning electron microscope operated at 20 kV. Each sample was sputter-coated with a thin layer of gold-platinum (thickness approximately 2 nm) using a SEMPREP 2 Sputter Coater (Nanotech Ltd.). Mean micron-scale pore diameters were estimated by averaging >20 pore diameters measured from the SEM images.

Nitrogen adsorption and desorption isotherms were measured at 77 K using a Micromeritics Surface Area and Porosity Analyzer. The isotherms were analysed to obtain the specific surface area according to the Brunauer-Emmett-Teller (BET) model. The pore volume and pore size distributions of the nm-scale pores within the monoliths were evaluated from the isotherms using the BJH (Barrett-Joyner-Halenda) model. The micron-scale pores are too large to significantly affect the adsorption isotherms.

Permeability coefficients (K) of the monoliths were determined by measuring the variation of the pressure drop across the monolith (ΔP) with liquid volumetric flow rate (Q). A syringe pump (KDS 200) was used to drive a set flow rate of either water or hexane through the monolith and a miniature pressure sensor (Entran Sensors and Electronics with range 0–35 bar) was used to measure ΔP . Measurement data sets were converted into values of the permeability coefficient K for each monolith using Darcy's law.

$$K = \frac{Q\mu L}{A\Delta P} \quad (1)$$

where Q is the volumetric flow rate (units $\text{m}^3 \text{s}^{-1}$), μ is the fluid viscosity (units Pa s), L is the monolith length in the direction of the fluid flow and A is the overall monolith cross-sectional area.

The total porosity (ϕ_t , equal to the volume fraction of both the micron-scale and nm-scale pores) of the cylindrical monolith samples were determined by weighing the monoliths when dried (i.e. with all pores containing only air) and when filled with water. The total porosity was obtained from the weight measurements using Eq. 2.

$$\phi_t = \frac{W_M - W_T}{dLR^2\pi} \quad (2)$$

where W_T and W_M are the weights of the dry and water-filled monolith respectively, d is the density of water and L and R are the overall length and radius of the cylindrical monolith. The measurements were normally carried out five times and an average taken. Several points should be noted about the value of total monolith porosity estimated in this way. Firstly, the assumption of air-filled pores initially is likely to be valid owing to the long drying time and high temperature calcination in air used in the preparation of the monoliths. Secondly, water is expected to be fully imbibed in all micron and nano-sized pores since water virtually completely wets silica (i.e. the contact angle of a water drop on silica is close to zero) which makes complete filling energetically favourable. In principle, despite thermodynamic favourability, complete water filling may be kinetically-limited by the monolith structure. However, the monoliths here contain a combination of micron and

nano-sized pores which are likely to ensure rapid water filling. Finally, it is noted that the measured values of ϕ_t reported here will *not* include any micro- or nano-pores which are closed, i.e. not connected with the main pore network which is continuous through out the monolith.

3 Results and discussion

The range of liquid mixture compositions, including polymer, acid, water and silicon alkoxide, used for the synthesis of silica monoliths are summarized in Table 1 together with the values of the key characterisation parameters.

SEM images of examples of the various final monolith morphologies after calcination are shown in Fig. 1. The nm-scale pores are not visible at this magnification. As discussed in [8], the final silica skeleton is dictated by the point at which the phase separation and subsequent coarsening of the silica-rich phase becomes “frozen-in” by solidification. The interplay between these processes can result in the different morphologies exemplified by the sample images in Fig. 1. These include (1) fully or partially discontinuous voids in a continuous silica matrix (“air-in-silica”), (2) fully or partially discontinuous silica particles in a continuous gas phase (“silica-in-air”) and (3) “sponge-like” structures which are continuous in both the silica and gas phases (“bicontinuous”). Of the monolith samples prepared and investigated here, the majority were of the bicontinuous type with only samples 17 and 39 being of the silica-in-air type and samples 24, 42 and 43 being air-in-silica.

Figure 2 shows a representative nitrogen adsorption/desorption isotherm and the corresponding size distribution of the nano-scale pores for monolith sample 20. The nm-pore distributions are fairly broad and show significant hysteresis between adsorption and desorption indicating the pores are not uniform cylinders in shape. The physisorption analysis illustrated in Fig. 2 shows that the monolith exhibits a type 4 nitrogen adsorption isotherm, which is typical of mesoporous materials with a large surface area. As shown in Table 1 for all the different monolith systems made here, the variations in mean nano-pore diameter (11–19 nm), nanopore volume per gram of monolith (0.53–0.95) and specific surface area (164–252 $\text{m}^2 \text{g}^{-1}$) are (relatively) not very large, even though the compositions, the polymer, acid and the silicon alkoxide used in the preparations all differ. The variation is even less within the subsets of systems all containing the same components. This lack of wide variation is a consequence of the fact that the nano-pores in the silica skeleton are mainly created by the treatment step with ammonium hydroxide which is constant for all the monoliths described here. The treatment

Table 1 Components and compositions of the initial liquid mixtures used for the synthesis of silica monoliths and the physical properties of the final monoliths

No.	WF _{polymer}	WF _{water}	WF _{silane}	[acid] _{ov} / [M]	Calcin. Temp (°C)	Pore diam (nm)	Surface area (m ² g ⁻¹)	Porosity (nm)	Porosity (micron)	Pore diam (μm)	10 ¹⁴ (K/m ²)	K/K _{ref}
<i>F127 13k, acetic acid, TMOS</i>												
1	0.067	0.622	0.311	0.0124	550	14.6	183	0.119	0.801	2	3.5	0.35
2	0.062	0.577	0.361	0.0115	–	–	–	–	–	–	–	A
3	0.051	0.474	0.474	0.0095	–	–	–	–	–	–	–	A
4	0.058	0.538	0.404	0.0108	–	–	–	–	–	–	–	A
5	0.067	0.622	0.311	0.0124	550	12.7	197	0.154	0.736	3	6.2	0.30
6	0.067	0.622	0.311	0.0124	600	13.5	205	0.153	0.747	3	6.6	0.31
7	0.067	0.622	0.311	0.0124	650	13.9	201	0.171	0.719	2	4.5	0.50
<i>P123 6k, acetic acid, TMOS</i>												
8	0.184	0.588	0.228	0.0118	550	16.2	234	0.211	0.689	7	2.5	0.02
9	0.184	0.588	0.228	0.0118	550	12.8	252	0.200	0.690	7	2.5	0.02
10	0.184	0.588	0.228	0.0118	600	14.6	236	0.115	0.825	5	–	–
11	0.184	0.588	0.228	0.0118	650	14.9	236	0.113	0.827	4	–	–
12	0.171	0.548	0.281	0.0110	–	–	–	–	–	–	–	A
13	0.229	0.556	0.215	0.0111	–	–	–	–	–	–	–	A
<i>PEO 100k, acetic acid, TMOS</i>												
14	0.047	0.667	0.286	0.0133	–	–	–	–	–	–	–	A
<i>F127 13k, nitric acid, TEOS</i>												
15	0.059	0.550	0.391	0.5498	–	–	–	–	–	–	–	A
16	0.053	0.527	0.420	0.4728	–	–	–	–	–	–	–	A
17	0.058	0.586	0.355	0.5261	550	10.5	207	0.134	0.756	–	–	–
18	0.058	0.586	0.355	0.5261	550	10.5	207	0.122	0.778	–	140	–
<i>P123 6k, nitric acid, TEOS</i>												
19	0.165	0.527	0.309	0.4739	–	–	–	–	–	–	–	A
<i>PEO 100k, nitric acid, TEOS</i>												
20	0.053	0.527	0.420	0.4728	550	16	164	0.249	0.591	10	140	0.76
21	0.057	0.525	0.418	0.4713	550	16.6	199	0.240	0.630	4	10	0.32
22	0.057	0.525	0.418	0.4713	600	14.9	194	0.160	0.740	4	5.9	0.16
23	0.057	0.525	0.418	0.4713	650	14.8	192	0.205	0.665	3	8.3	0.44
24	0.044	0.404	0.553	0.3623	550	15.6	172	1.058	0.300	30	37,000	43.85
25	0.043	0.802	0.155	0.7191	–	–	–	–	–	–	–	A
26	0.022	0.820	0.158	0.7353	–	–	–	–	–	–	–	A
27	0.065	0.604	0.331	0.5417	–	–	–	–	–	–	–	A
28	0.028	0.260	0.712	0.2334	–	–	–	–	–	–	–	A
29	0.057	0.576	0.367	0.5167	550	18	187	0.189	0.711	4	12	0.34
30	0.057	0.576	0.367	0.5167	600	16.8	190	0.213	0.667	4	14	0.42
31	0.057	0.576	0.367	0.5167	650	17.1	190	0.090	0.860	3	11	0.45
<i>PEO 200k, nitric acid, TEOS</i>												
32	0.053	0.527	0.420	0.4728	550	13.2	201	0.220	0.630	4	10	0.32
33	0.053	0.527	0.420	0.4728	600	13.6	181	0.193	0.667	3	8.3	0.44
34	0.053	0.527	0.420	0.4728	650	19.2	181	0.249	0.611	3	7.1	0.41
35	0.027	0.541	0.432	0.4856	–	–	–	–	–	–	–	A
<i>PEO 300k, nitric acid, TEOS</i>												
36	0.032	0.713	0.255	0.2865	–	–	–	–	–	–	–	A
37	0.018	0.546	0.436	0.4898	–	–	–	–	–	–	–	A

Table 1 continued

No.	WF _{polymer}	WF _{water}	WF _{silane}	[acid] _{ov} / [M]	Calcin. Temp (°C)	Pore diam (nm)	Surface area (m ² g ⁻¹)	Porosity (nm)	Porosity (micron)	Pore diam (µm)	10 ¹⁴ (K/m ²)	K/K _{ref}
<i>F127 13k, nitric acid, TMOS</i>												
38	0.067	0.622	0.311	0.6219	–	–	–	–	–	–	–	A
<i>PEG 10k, nitric acid, TMOS</i>												
39	0.058	0.586	0.355	0.5261	550	10.5	195	0.200	0.630	–	–	–
40	0.058	0.586	0.355	0.5261	550	–	–	–	0.830	–	240	–
<i>PEG 35k, nitric acid, TMOS</i>												
41	0.058	0.586	0.355	0.5261	550	13.3	191	0.650	0.570	4	–	–
42	0.058	0.586	0.355	0.5261	550	13.3	191	0.650	0.570	4	350	12.28
<i>PEO 100k, nitric acid, TMOS</i>												
43	0.058	0.586	0.355	0.5261	550	14.9	184	0.828	0.460	–	–	A

WF signifies the weight fraction of the component

The entry “A” in the final column indicates that either the monolith did not form or it was too easily cracked to enable permeability measurements

with base is thought to create the nanopores through a process of dissolution/re-adsorption, see [8] and references therein.

Monolith permeability was determined from measurements of pressure drop as a function of liquid volumetric flow rate (using either water or hexane as liquid) and representative plots are shown in Fig. 3. The plots for all samples were found to be linear indicating that Darcy’s law (Eq. 1) is obeyed, at least up to driving pressures of 60 psi. The silica monoliths made here contain both micron and nanoscale pores. Because it is likely that only the micron-scale pores contribute to the permeability, in order to determine how the permeability varies with porosity, it is useful to separate the total porosity ϕ_t (measured by water imbibition) into the micron-scale porosity ϕ_m and nano-scale porosity ϕ_n (measured by BET). We assume that all pores are accessible to water imbibition, i.e. there are no sealed voids in the monoliths. In this case, we have:

$$\phi_t = (\phi_m + \phi_n) = \frac{V_n + V_m}{V_n + V_m + V_{Si}} \tag{3}$$

where V_n , V_m and V_{Si} are the volumes per unit mass of monolith of nano-scale pores, micron-scale pores and silica respectively. Noting that V_n is obtained directly from the nitrogen adsorption isotherms and that $V_{Si} = 1/\rho_{Si}$ (where ρ_{Si} is the density of silica), the final expression for ϕ_m in terms of the measured quantities ϕ_t and V_n is:

$$\phi_m = \frac{((\phi_t - 1)V_n + \phi_t V_{Si}) / (1 - \phi_t)}{V_n + V_{Si} + ((\phi_t - 1)V_n + \phi_t V_{Si}) / (1 - \phi_t)} \tag{4}$$

Table 1 summarises the values of nano- and micron-scale porosities, average micron-scale pore sizes and permeability coefficients for all monolith samples. For some monoliths, (samples 24, 41 and 42), the apparent values of ϕ_m estimated using Eq. 4 were found to be negative which

indicates that one or both of the assumptions underpinning Eq. 4 (i.e. that water is imbibed into both the micron- and nm-scale pores and that no pores are closed) must be invalid in some cases. For these samples, the micron porosity values in Table 1 refer to the total porosities.

The permeability coefficient K of a monolith is expected to depend on the porosity, the average pore diameter and factors dependent on the detailed geometry of the pore network such as tortuosity and inter-connectivity (see, for example, [21, 22]). In order to estimate the relative importance of these different factors, it is useful to compare the measured permeability coefficients with a hypothetical reference system consisting of a monolith containing a volume fraction ϕ_m of uniform, cylindrical pores of radius r aligned parallel to the flow direction [23]. The number of pores in the monolith (n) is

$$n = \frac{\phi_m A}{\pi r^2} \tag{5}$$

Assuming the fluid flow through the cylindrical pores is laminar, the Hagen-Poiseuille equation yields the volumetric flow rate Q as:

$$Q = \frac{n \Delta P \pi r^4}{8 \mu L} \tag{6}$$

Substituting for n in Eq. 6 followed by substitution for Q in Eq. 1 yields the final expression for the permeability coefficient of this reference system of monodisperse, uniform, cylindrical pores (K_{ref}).

$$K_{ref} = \frac{\phi_m r^2}{8} \tag{7}$$

Values of K_{ref} provide an upper limit to the permeability coefficient expected for a monolith with micron-scale porosity ϕ_m and average pore radius r since factors such as

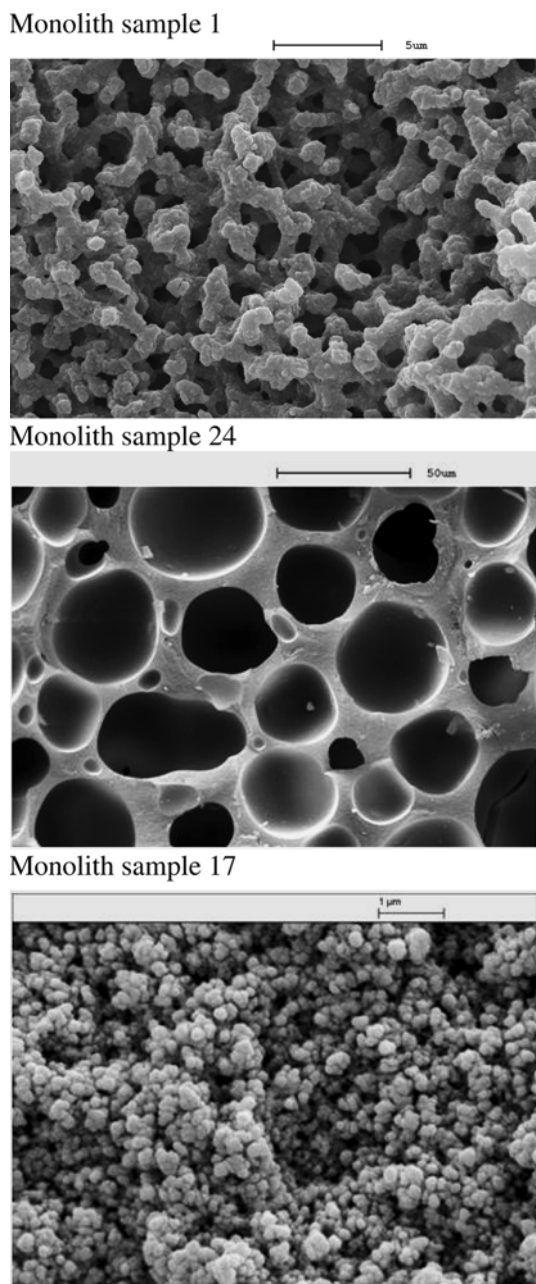


Fig. 1 SEM micrographs showing examples of the main structural types: bicontinuous (sample 1), air-in-silica (sample 24) and silica-in-air (sample 17)

the tortuosity of the micron-scale pores in real monoliths are expected to reduce the observed permeability coefficient.

Figure 4 shows how the measured monolith permeability coefficients listed in Table 1 compare with values of K_{ref} calculated using Eq. 7. For most of the monoliths, the experimental values of K scale with $\phi_m r^2$ but have absolute values which are a factor of 2–5 below the behaviour predicted by Eq. 7. For these monoliths, the variation in

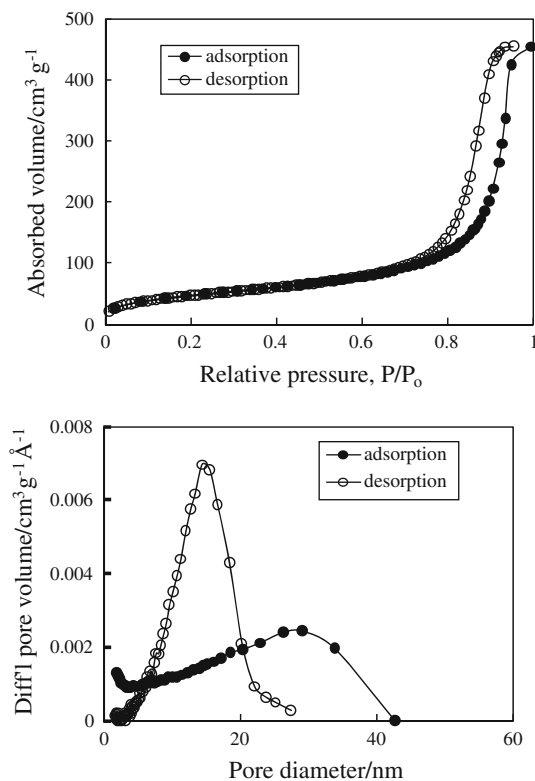


Fig. 2 Nitrogen adsorption isotherms and derived nm-scale pore size distributions for monolith sample number 20

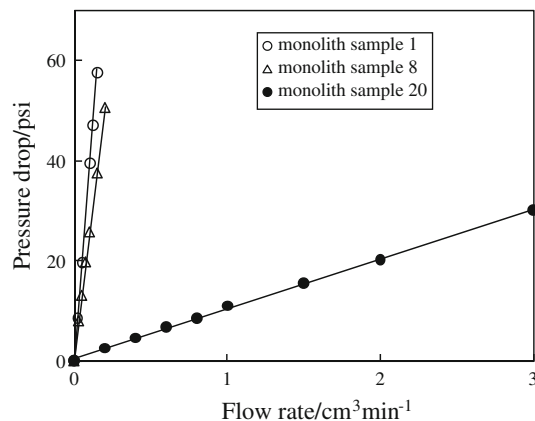


Fig. 3 Representative plots of pressure drop versus liquid volumetric flow rate for monolith samples 1, 8 and 20

K is dominated by changes in average pore radius r since the extent of variation in micron-scale porosity is relatively small (Table 1). A key overall conclusion is that (apart from the exceptional cases discussed below) the factors dependent on the pore network geometry (tortuosity, etc.) reduce the permeability by only a factor 2–5 below that for a monolith with uniform, cylindrical pores of the same porosity and pore size.

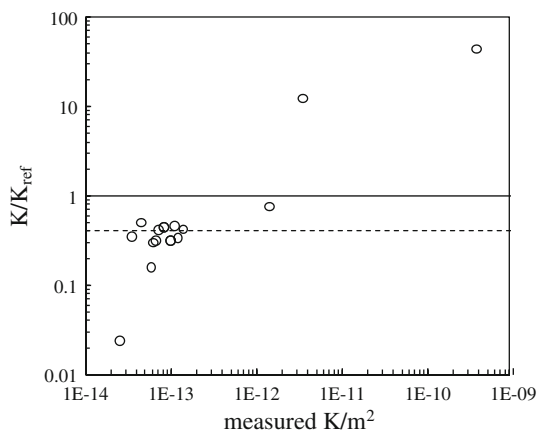


Fig. 4 Comparison of measured monolith permeability coefficients with K_{ref} calculated using Eq. 7. The *solid line* shows the values expected for monoliths containing *uniform cylindrical pores*, i.e. $K/K_{\text{ref}} = 1$. The *horizontal dashed line* shows the average value of K/K_{ref} for all monolith samples except those with anomalously high values (samples 24 and 42) and anomalously low values (samples 8 and 9)

Figure 4 shows two monoliths (samples 24 and 42) with anomalously *high* values of K , i.e. K/K_{ref} is greater than 1. Both these samples are of the “air-in-silica” type (see Fig. 1) containing fully or partially discontinuous air voids in a continuous silica matrix. They also showed apparently negative values of ϕ_m estimated using Eq. 4 which indicates that one or both of the assumptions (i.e. that water is imbibed into both the micron- and nm-scale pores and that no pores are closed) must be invalid for these monoliths. In principle, the anomalously high values of K could be a consequence of either incomplete sealing of the monoliths within the heat shrink Teflon cladding or pressure-driven collapse of the silica skeleton of the monoliths leading to large diameter pathways through the monoliths. Pressure driven breakthrough into initially closed air voids (=pores) could account for both the anomalously high values of K and negative values of ϕ_m and therefore appears to be the most likely explanation.

Two monolith samples (8 and 9) show unusually *low* values of K/K_{ref} of approximately 0.02. Both these samples appear to be of the “bicontinuous” structural type and it is presently unclear why K/K_{ref} is low for these samples. It is noteworthy that sample 17, showing “silica-in-air” morphology (Fig. 1), had a very low permeability coefficient ($<10^{-15} \text{ m}^2$), too low to be measured by the method used here. For samples 8 and 9, although the SEM images of the monolith surfaces indicate a bicontinuous structure, it may be that their internal structure has partially collapsed.

As noted above, monolith permeability is primarily controlled by the average micron-scale pore size r . As discussed in [8], the key compositional variable affecting r is the ratio of concentrations of the polymer to silicon

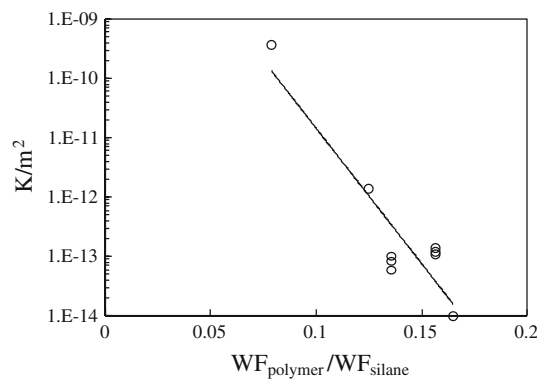


Fig. 5 Variation of permeability coefficient for monoliths containing PEO 100k, nitric acid and TEOS (samples 20–31) with the ratio of weight fractions of polymer/silicon alkoxide

alkoxide, i.e. r decreases as $\text{WF}_{\text{polymer}}/\text{WF}_{\text{silane}}$ increases. Hence, it is expected that K will decrease sharply with increasing $\text{WF}_{\text{polymer}}/\text{WF}_{\text{silane}}$. Figure 5 shows this expectation is indeed realised for monoliths containing PEO 100k, nitric acid and TEOS (samples 20–31) and K can be “tuned” over 4 orders of magnitude by adjustment of this concentration ratio.

4 Conclusions

The key conclusion from this study is that the permeability coefficient K of silica monoliths can range from 10^{-14} to 10^{-10} m^2 and approximately scales with $\phi_m r^2$. Using the synthesis method described here, K can be controlled, primarily by adjustment of the polymer/silane concentration ratio, whilst maintaining the specific surface area and nanopore diameter and volume approximately constant. For the majority of monolith samples, the value of K is a factor of 2–5 smaller than a corresponding monolith with uniform cylindrical micron-scale pores with the same porosity and size. Some exceptions to this behaviour are seen and probably caused by either pressure driven breakthrough into initially closed pores (producing anomalously high K monoliths) or either initial formation or partial collapse to a silica-in-air morphology (producing anomalously low K monoliths).

Acknowledgments We thank Pfizer and the Engineering & Physical Sciences Research Council of the UK for funding this research.

References

1. A.J. Cabty, J.A. Deverell, A. Gomann, R.M. Gujit, T. Rodemann, J.A. Smith, *Austral. J. Chem.* **61**, 630–633 (2008)
2. P.D.I. Fletcher, S.J. Haswell, P. Watts, X. Zhang, in *Dekker Encyclopedia of Nanoscience and Nanotechnology*, ed. by

- J.A. Schwarz, C.I. Contescu, K. Putyera (Marcel Dekker, Amsterdam, 2004), pp. 1547–1564
3. V. Hessel, *Chem. Eng. Technol.* **32**, 1655–1681 (2009)
 4. P. He, G.M. Greenway, S.J. Haswell, *Microfluid. Nanofluid.* **8**, 565–573 (2010)
 5. M. Volder, D. Reynaerts, *J. Micromech. Microeng.* **20**, 043001 (2010)
 6. P.D.I. Fletcher, S.J. Haswell, X. Zhang, *Lab. Chip* **2**, 102–112 (2002)
 7. R. Takahashi, K. Nakanishi, N. Soga, *J. Non-Cryst. Solids* **189**, 66–76 (1995)
 8. K. Nakanishi, *J. Porous. Mater.* **4**, 67–112 (1997)
 9. K. Nakanishi, R. Takahashi, T. Nagakane, K. Kitayama, N. Koheiya, H. Shikata, N. Soga, *J. Sol-Gel, Sci. Technol.* **17**, 191–210 (2000)
 10. F.C. Leinweber, D. Lubda, K. Cabrera, U. Tallarek, *Anal. Chem.* **74**, 2470–2477 (2002)
 11. M. Motokawa, H. Kobayashi, N. Ishizuka, H. Minakuchi, K. Nakanishi, H. Jinnai, K. Hosoya, T. Ikegami, N. Tanaka, *J. Chromatogr. A* **961**, 53–63 (2002)
 12. A.-M. Siouffi, *J. Chromatogr. A* **1000**, 801–818 (2003)
 13. Z.-G. Shi, Y.-Q. Feng, L. Xu, S.-L. Da, Y.-Y. Ren, *Microporous Mesoporous Mater.* **68**, 55–59 (2004)
 14. T. Amatani, K. Nakanishi, K. Hirao, T. Kodaira, *Chem. Mater.* **17**, 2114–2119 (2005)
 15. T. Hara, H. Kobayashi, T. Ikegami, K. Nakanishi, N. Tanaka, *Anal. Chem.* **78**, 7632–7642 (2006)
 16. K. Nakanishi, N. Tanaka, *Acc. Chem. Res.* **40**, 863–873 (2007)
 17. J. Babin, J. Iapichella, B. Lefevre, C. Biolley, J.-P. Bellat, F. Fajula, A. Galarneau, *New J. Chem.* **31**, 1907–1917 (2007)
 18. H. Zhong, G. Zhu, P. Wang, J. Liu, J. Yang, Q. Yang, *J. Chromatogr. A* **1190**, 232–240 (2008)
 19. E.I. Trilisky, H. Koku, K.J. Czymmek, A.M. Lenhoff, *J. Chromatogr. A* **1216**, 6365–6376 (2009)
 20. J. Chamieh, Y. Zimmermann, A. Boos, A. Hagege, *J. Colloid Interface Sci.* **340**, 225–229 (2009)
 21. N. Vervoort, P. Gzil, G.V. Baron, G. Desmet, *Anal. Chem.* **75**, 843–850 (2003)
 22. H. Saito, K. Nakanishi, K. Hirao, H. Jinnai, *J. Chromatogr. A* **1119**, 95–104 (2006)
 23. J.A. Petty, *J. Expt. Bot.* **29**, 1463–1469 (1978)

Jane Woods^{1,2}
Peter T. Docker¹
Charlotte E. Dyer²
Stephen J. Haswell¹
John Greenman²

¹Department of Chemistry,
University of Hull, Hull, UK
²Postgraduate Medical Institute,
University of Hull, Hull, UK

Received March 16, 2011
Revised July 28, 2011
Accepted August 23, 2011

Research Article

On-chip integrated labelling, transport and detection of tumour cells

Microflow cytometry represents a promising tool for the investigation of diagnostic and prognostic cellular cancer markers, particularly if integrated within a device that allows primary cells to be freshly isolated from the solid tumour biopsies that more accurately reflect patient-specific *in vivo* tissue microenvironments at the time of staining. However, current tissue processing techniques involve several sequential stages with concomitant cell losses, and as such are inappropriate for use with small biopsies. Accordingly, we present a simple method for combined antibody-labelling and dissociation of heterogeneous cells from a tumour mass, which reduces the number of processing steps. Perfusion of *ex vivo* tissue at 4°C with antibodies and enzymes slows cellular activity while allowing sufficient time for the diffusion of minimally active enzymes. *In situ* antibody-labelled cells are then dissociated at 37°C from the tumour mass, whereupon hydrogel-filled channels allow the release of relatively low cell numbers (<1000) into a biomimetic microenvironment. This novel approach to sample processing is then further integrated with hydrogel-based electrokinetic transport of the freshly liberated fluorescent cells for downstream detection. It is anticipated that this integrated microfluidic methodology will have wide-ranging biomedical and clinical applications.

Keywords:

Electrokinetic / Head and neck squamous cell carcinoma / Hydrogel / Lab on a chip / Microflow cytometry
DOI 10.1002/elps.201100172

1 Introduction

Flow cytometry is an invaluable biomedical tool for research into the cellular mechanisms of cancer malignancy [1]. Microflow cytometry, an emerging technology in cancer research, has advantages over conventional flow cytometry; these include compactness, reduced sample size requirements, prevention of cross-contamination by containment of biohazardous samples in disposable microfluidic devices and possibilities for integrated analyses [2]. The first instance of microflow cytometry on patient-derived solid tumour cells was reported over four decades ago, where fixed cells were detected and sorted according to the size and nucleic acid content by differences in light absorption and scattering properties [3].

Despite the inherent promise of this early success, microflow (and flow) cytometry for cancer research remains

largely restricted to the analysis of cultured cell lines selected to represent the tissue of origin. However, the risk of phenotypic alteration brings interpretive problems, *i.e.* insights gained through cell line work cannot be confidently extrapolated to explain *in vivo* tumour behaviour. Even 3-D co-cultures or artificial tissue constructs do not fully represent tissue complexity, in which multiple cell types continuously interact with one another and with the extracellular matrix (ECM [4]). Furthermore, the tumour ECM and stroma are known to exhibit patient-to-patient heterogeneity even among tumours of the same histopathological type, and this has a significant influence upon metastatic potential and thus upon patient prognosis [5].

Consequently, fresh biopsies comprising patient-specific tumour cells and stromal cells within their native ECM milieu constitute more physiologically relevant samples for the exploration of solid tumour biology at the cellular level [6, 7]. It is postulated that cells directly liberated from this microenvironment would more reliably retain their phenotypes; however, the labelling of cell-membrane markers entails several sequential steps – tissue disaggregation, incubation of dissociated cells with fluorescently conjugated antibody, and removal of unbound antibody – each necessitating cell washing and centrifugation [8]. Inevitable cell losses during these procedures render flow cytometry

Correspondence: Professor John Greenman, Centre for Biomedical Research, Postgraduate Medical Institute, University of Hull, Cottingham Road, Hull, HU6 7RX, UK
E-mail: j.greenman@hull.ac.uk
Fax: +44-1482-466996

Abbreviations: ECM, extracellular matrix; EPF, electrophoretic flow; HNSCC, head and neck squamous cell carcinoma

Colour online: See the article online to view Figs. 3, 4 and 6 in colour.

impractical for small biopsy samples [9]. Microflow cytometry meanwhile has the capability to analyse small numbers of cells; nonetheless, there is an acknowledged need for simplified, robust, integration of pre-analytical sample processing if such a technology is to be widely adopted by biomedical researchers [10–12]. Progress in this area has been demonstrated, for example, by antibody labelling of primary human blood cells in Lab-on-a-chip (or micro Total Analysis Systems); accordingly, the ability to label solid tumour cells on microfluidic-based devices would represent a further significant step [13].

Other advantageous features of a microflow cytometer for biomedical research include a reduced footprint and fewer moving parts; advantages afforded by utilising an electrokinetic (EK) system for cell movement that can be rapidly switched for accurate cell sorting. Early work on EK cytometry explored the manipulation of unlabelled bacteria, yeasts and red blood cells, employing combinations of microchannel layouts and voltage switching [14]. Since then, applications have extended to encompass the labelling of bacteria on-chip prior to sorting [15] but for tumour cell manipulation the greater convenience of EK has yet to be exploited.

We present here an innovative and integrated approach to pre-analytical tumour tissue disaggregation, single cell isolation and antibody cell labelling that represents a departure from conventional protocols such as FACS which is designed for large cell numbers and high throughput [16]. This methodology allows in situ labelling of cells within a tumour mass during interactions with neighbouring cells and with the tumour-specific ECM, prior to cell dissociation. Moreover, this pre-analytical sample processing is then integrated with EK transport and detection of relatively small numbers of freshly liberated tumour cells, as illustrated in Fig. 1A which can be used for subsequent analysis, e.g. polymerase chain reaction (PCR) measurement of changes in gene transcription.

2 Materials and methods

2.1 Microfluidic devices

Glass microfluidic devices were fabricated using standard photolithography and wet etching techniques to produce the design shown in Fig. 2. Channels 70 μm deep \times 150 μm wide were etched in 1 mm glass. A 3-mm diameter tissue chamber and 1.5 mm holes for sample, reagent and electrode access were drilled in a 3-mm glass top plate before thermally bonding it to the etched base plate to form the device. Prior to each use, devices were sterilised by flushing with ethanol and autoclaving, and fresh reservoirs glued around the access ports using epoxy resin (Perma-bond, UK). Lids reduced evaporation and housed 0.5 mm diameter Pt electrodes. Channels were flushed with deionised H_2O , then 0.1 M NaOH for 5 min, followed by deionised H_2O and then finally media. All fluids were

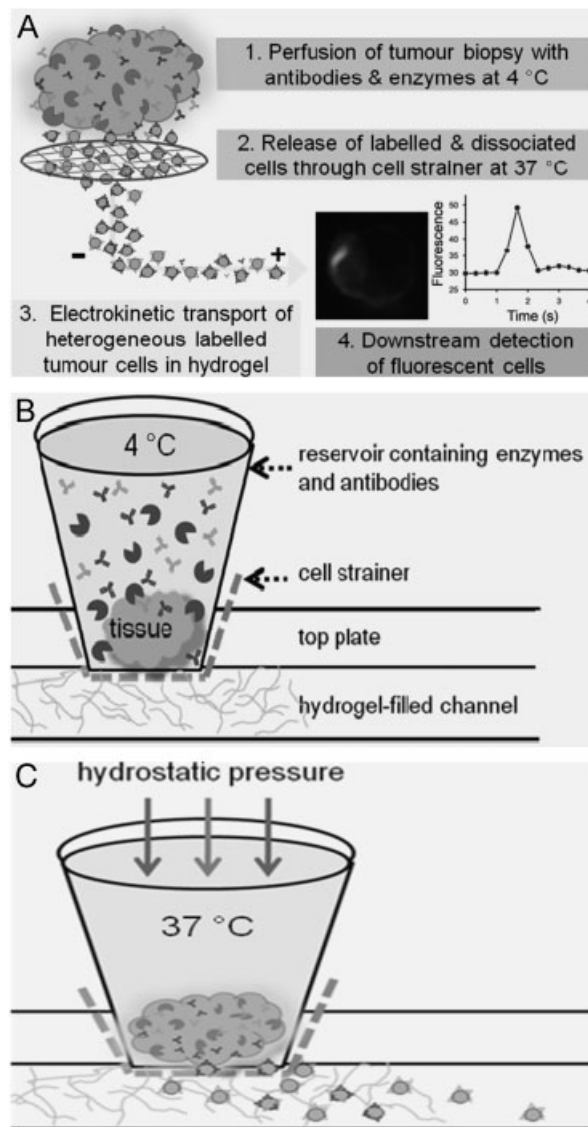


Figure 1. (A) Schematic of integrated microfluidic processes from biopsy to detection of antibody-labelled tumour cells. Labelling is achieved during in situ interactions with native ECM and neighbouring cells. Following controlled release, labelled tissue cells are transported electrokinetically in small numbers for detection and imaging. (B) HNSCC tissue ($\approx 1 \text{ mm}^3$) placed upon cell strainer in tissue chamber, submerged in enzyme/antibody mixture. At 4 °C, solid hydrogel acts to contain fluid in reservoir. (C) A combination of melting hydrogel and hydrostatic pressure allows in situ antibody-labelled, dissociated cells to pass through the cell strainer and hydrogel macropores in the microchannel.

filtered prior to use through a 0.22- μm syringe filter (Millipore, UK). After filling microchannels with hydrogel (formulated as described below), excess hydrogel was removed from the tissue chamber, and to prevent tissue debris from entering and clogging the channels, a 50- μm mesh cell strainer (340632, BD Falcon, UK) was secured above the main channel as shown in Fig. 2C.

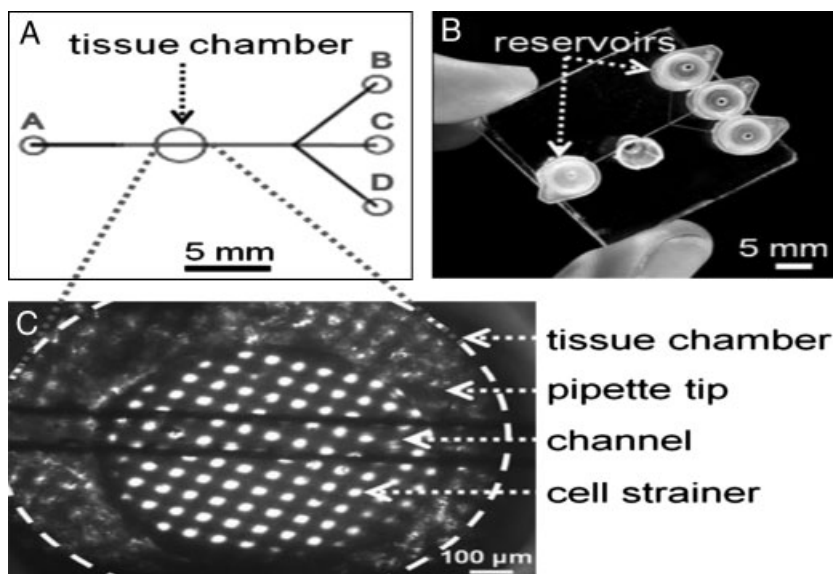


Figure 2. (A) Scale drawing of microfluidic device showing tissue chamber above main channel, and access ports A–D above channel ends; (B) photograph of device with reservoirs in place; (C) photograph taken on inverted microscope showing 50 μm mesh cell strainer secured in tissue chamber $\approx 100 \mu\text{m}$ above main channel.

2.2 Preparation of hydrogel for tumour cell electrokinesis

As fluid flow in tissues occurs within a gel-like matrix [17, 18], low melting point (LMP) agarose hydrogel (A9419, Sigma-Aldrich, UK) was used in the microchannels to provide a biometric microenvironment and also to suppress the hydrodynamic back pressure during EK transport. 4-(2-Hydroxyethyl)-1-piperazineethanesulfonic acid (HEPES)/sucrose mixture was first prepared by dissolving acid and base components of HEPES in deionised water giving a 0.1 M stock solution, pH 7.4, at 25°C (<http://www.liv.ac.uk/buffers/buffercalc.html>). This was diluted 1:1 with deionised water and then mixed with 0.50 M sucrose 1:1 to give 0.025 M HEPES/0.25 M sucrose (final concentrations). Hydrogel was then prepared by dissolving 0.25 or 0.50% w/v LMP agarose in the above HEPES/sucrose buffer, which was specifically formulated to meet the following criteria:

- (i) EK linear velocity is proportional to zeta potential ζ and field strength. Applied potentials should be kept at minimal levels to prevent high currents, Joule heating and cell lysis [19]. To maximise bulk flow and cell viability at a given voltage, it is desirable to maximise ζ which is affected by pH and inversely proportional to ionic strength [20–22]. Well-buffered fluids at low ionic strength are thus essential for EK at low voltages in microfluidic cellular applications.
- (ii) Biocompatible osmolality for human tumour cells is $\approx 297 \text{ mOsm/kg}$ [23]. To prevent artefacts arising from hypo- or hyper-tonic shock, osmolality in vitro is commonly controlled using salts, e.g. phosphate-buffered saline (PBS). The requirement for low ionic strength precludes the use of salts, so an isotonic sucrose solution was used in place of PBS [24].

- (iii) Biocompatible extracellular pH is 6.8–7.8 [25]. Adequate pH buffering is especially important in EK, as electrolysis and other interactions can alter the local pH, reduce the zeta potential and even reverse the direction of flow [26–29]. A 0.025 M HEPES buffer was selected as optimal for this application [30, 31].

A PBS-based hydrogel was also used in all the comparative EK mobility experiments.

2.3 Tissue and cell samples

Tumour samples from patients with head and neck squamous cell carcinoma (HNSCC) were selected as representative of small clinical biopsies typically consisting of tiny pieces of tissue ≈ 0.1 –3.0 g in mass. Anonymised samples from HNSCC lesions were obtained from patients undergoing surgery, having gained ethical approval from Hull and East Yorkshire Research Ethics Committee (07/H1304) and the Hull and East Yorkshire Hospitals NHS Trust (RO568). Samples were stored in Dulbecco's modified Eagle's medium (DMEM; E15-009, PAA Laboratories, UK) supplemented with 10% v/v foetal calf serum (FCS; S1900, Biosera, UK) and antibiotic solution [10 000 U/mL penicillin and 10 mg/mL streptomycin in 0.9% w/v NaCl; P11-010, Sigma, UK], at 4°C, and if not used immediately, snap frozen and cryopreserved in liquid nitrogen at -196°C .

K562 human erythroleukaemic cells were selected for proof of principle in EK studies, as it was experimentally easier to work with cell lines than fresh cells derived from a tumour. Cells were cultured in Roswell Park Memorial Institute medium (RPMI 1640; E15-840, PAA Laboratories) supplemented as above and harvested by centrifugation at $400 \times g$. Cell and tissue preparation was carried out in a class II biological safety cabinet.

2.4 Antibodies

Integrin subunits $\beta 1$ and $\alpha 6$ were selected as ubiquitously expressed cell membrane targets that are reported to be upregulated in metastatic HNSCC cells [32, 33]. Monoclonal antibodies conjugated with red or green fluorophores were used: anti-CD29 (integrin $\beta 1$) PerCPe-Fluor[®]710 (46-0299, eBioscience, UK) and anti-CD49f (integrin $\alpha 6$) Alexa Fluor[®]488 (313608, Cambridge Bioscience Ltd, UK), each at 5 μL per mm^3 of tissue ($\approx 400\,000$ cells).

2.5 Integrated antibody labelling and cell release

A 1 mm^3 piece of HNSCC biopsy tissue was placed in the tissue reservoir upon the cell strainer and submerged in 200 μL of enzyme solution. Antibodies as described above were added to the collagenase solution (see below) after 3 h, and the tissue incubated at 4°C for a further 5–21 h as shown in Fig. 1B. The reduction in temperature and extended time frame, compared with conventional methodology, was designed to minimise enzyme and cellular metabolic activity while permitting sufficient time for diffusion of reagents to occur into centre of the tissue.

In preliminary experiments, cells were retrieved at various stages for imaging, to assess the effectiveness of the labelling and dissociation method, to optimise the duration of the cold perfusion required for saturation of tissue with enzymes and antibodies, and to check whether the enzymes affect antibody labelling. Reservoir contents were gently pushed through a 50 μm mesh cell strainer using a syringe plunger, centrifuged at 400 $\times g$ for 3 min; 10 μL from the reservoir was observed on a microscope slide by inverted fluorescence microscopy (Axiovert S100, Carl Zeiss, UK) using a 20 \times objective lens. Identical excitation filters of band pass 470/40 nm allowed excitation at 488 nm. To collect the red signal, a 660-nm beam splitter and emission filter band pass 690/50 nm excluded green fluorescence. To collect the green signal, a 495 nm beam splitter and emission filter band pass 540/50 nm excluded red fluorescence. Dual-labelled cells were separately imaged by monochrome CCD camera [Orca ER, Hamamatsu Photonics UK] for analysis in ImageJ software [34].

After an allotted time span for incubation in enzyme/antibody mixture, the solution was replaced with HEPES/sucrose buffer and cell release from the tumour mass was instigated by incubating the device at 37°C for 30–60 min. The device was then placed upon the microscope stage for observation of tissue cells passing through the cell strainer, under gravity and hydrodynamic pressure, and into the microchannel.

2.6 EK cell transport

Once the optimal conditions for effective in situ labelling of cell-membrane integrins and the dissociation of labelled

cells had been established, the optimal field strength required for controlled cell manipulation enabling subsequent cell sorting (10–100 V/cm) was determined using K562 cells. After functionalising the device by rinsing with NaOH and buffer as described, channels were filled with hydrogel made with either PBS or HEPES/sucrose buffer, and containing either labelled or unlabelled cells suspended at $\approx 0.5\text{--}1.0 \times 10^6 \text{ mL}^{-1}$. The device was placed on the stage of an inverted fluorescence microscope, and a voltage applied between access ports A and B (Fig. 2A) using 0.5 mm Pt electrodes connected to a 1-kV DC power supply (Kingfield Electronics, UK). Fluorescent image sequences were analysed in ImageJ to derive apparent linear velocity (v_{app}) which was converted to apparent mobility (μ_{app}); $\mu_{\text{app}} = \mu_{\text{epf}} + \mu_{\text{eof}}$. Cell diameters were measured in ImageJ and plotted against corresponding μ_{app} .

Having established cell flow characteristics using the K562 cells, the integrated device was then used to study freshly dissociated antibody-labelled tumour cells from a tissue biopsy. Cells were initially observed entering the channel under gravitational and hydrodynamic forces, and when this cell movement had subsided, the cells were then moved through the microchannel to the detection window by EK with a field strength of 70 V/cm. Again, μ_{app} was derived from v_{app} using ImageJ analysis.

3 Results

3.1 Integrated antibody labelling and cell release

Antibody labelling and dissociation of cells from tumorous and normal (peripheral) regions of HNSCC biopsies was undertaken both ‘off-chip’ and ‘on-chip’ on a series of different biopsies, testing different incubation periods of the enzyme and antibody mixture. An example of an ‘off-chip’ experiment is shown in Fig. 3. It was found that incubation periods >20 h were required to elicit relatively small clumps of cells and sufficient single cells for downstream analysis; tumour biopsies tended to yield more single cells than the peripheral tissue although as expected there were difference in the dissociation reflecting tumour heterogeneity. Greater incubation times were not pursued as the aim was to label and analyse as contemporaneously as possible. This methodology enables minimally disruptive in situ antibody labelling of cell membrane targets and moreover is able to reflect the dynamic behaviours of ex vivo human cancer cells within both normal and malignant functional tissues.

The rationale behind the cold perfusion approach for antibody labelling and tissue disaggregation is the total suffusion of the tissue ECM with minimally active collagenase, and simultaneous saturation of antigen binding sites with antibody. In contrast to conventional methods, this relatively prolonged incubation at 4°C preserves the tissue, antibodies and enzymes, and slows cellular activity; while

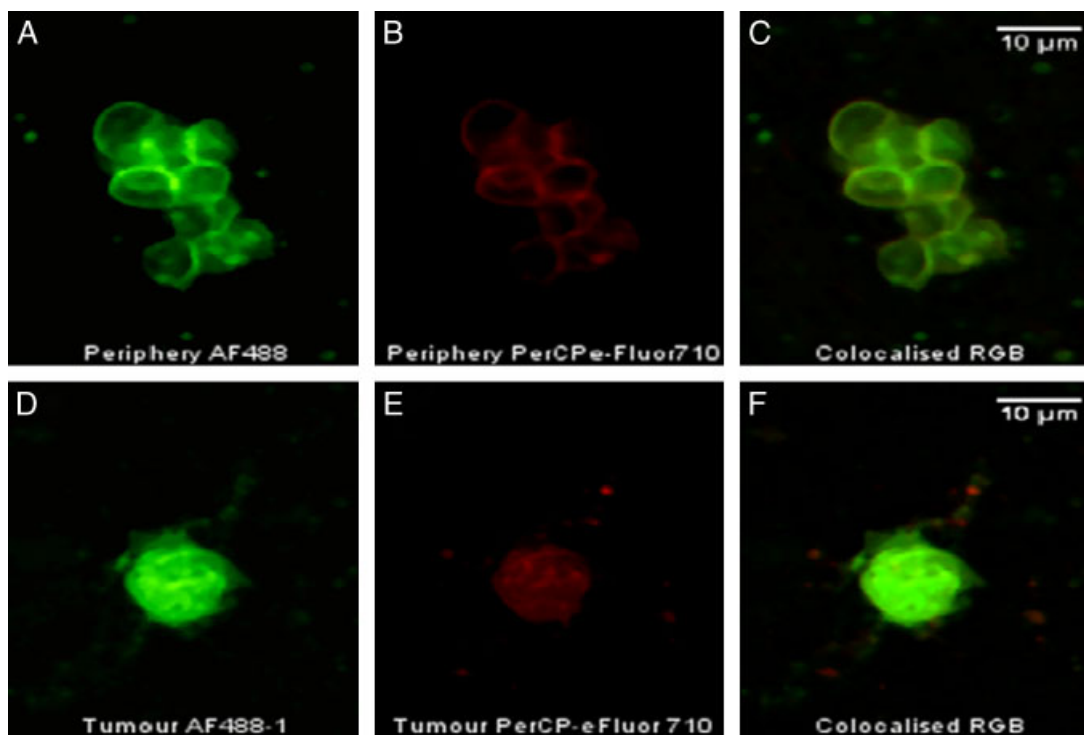


Figure 3. Fluorescent pseudo-coloured micrographs of peripheral cells (A–C) and tumour cells (D–F) from a patient with HNSCC. Cells were dual-labelled and dissociated ‘off-chip’ by the combination method. Antibodies to two integrin subunits were used: (A and D) anti-CD49f ($\alpha 6$) conjugated with Alexa Fluor[®] 488 (green), (B and E) anti-CD29 ($\beta 1$) conjugated with PerCPe-Fluor[®] 710 (red). Monochrome images were combined to show co-localisation of $\alpha 6$ and $\beta 1$ (C and F). Pseudopodia are just apparent upon the tumour cells, with clusters of $\beta 1$ at the leading edges. Results are representative of three separate experiments.

allowing sufficient time for diffusion to the centre of the tissue. The diffusion coefficient D in free solution at 20°C is dependent upon both medium and solute, and inversely proportional to solute molecular weight. Diffusion into tissue, however, is more complex than in free solution, as extracellular space is non-homogeneous, and tissue porosity affects diffusion rate [35]. Tumour tissue is often composed of very densely packed cells, in the region of $2\text{--}4 \times 10^5$ cells/ μL (mm^{-3} [36]). D for IgG₁ and collagenase in tumour tissue is typically $\approx 1 \times 10^{-11}$ m²/s, or 10 μm^2 /s [36, 37] compared with 4.2×10^{-11} and 4.5×10^{-11} m²/s for IgG₁ and collagenase in free solution at 20°C [38]. For a 1-mm³ piece of tumour tissue, diffusion distance to the centre is 5×10^{-4} m, giving an approximate diffusion time of $\approx 12\,500$ s or 3.5 h at 20°C. However, diffusion is also temperature dependent, resulting in significantly longer time scales at 4°C [39].

In the case of antibody diffusion, as the antibody front progresses, the effective diffusion rate is influenced not only by the above factors but also by antibody–antigen binding and is thus inversely proportional to antigen density [40]. Pre-treatment with collagenases has been shown previously to enhance the diffusion of large molecules into in vivo tissue [40]. Accordingly in this current work, collagenase – whose activity at 4°C is much reduced [41] – was incubated for 24 h to allow diffusion into the tissue with only residual

collagenase activity. Since this may nonetheless go some way toward preconditioning the tissue to facilitate entry of IgG₁, a 3-h delay was incorporated before adding the antibody. Although 24 h incubation was used for the following proof of concept studies, shorter incubation time periods also gave effective antibody labelling but less efficient dissociation.

After incubation of tissue biopsies ‘on-chip’ with the antibodies and enzymes, the excess mixture was replaced with HEPES/sucrose buffer. Incubation at 37°C then increased enzymatic activity within the tissue, cleaving the ECM and releasing labelled cells. Concurrently, as the temperature was raised from 4 to 37°C, the hydrogel underwent partial melting without reaching the total fluid phase (50°C). Heating the microdevice to 37°C thus realised two desired outcomes – dissociation of labelled cells from the tissue, and flow of cells vertically through the strainer and laterally into the hydrogel-filled channel by gravitational and hydrodynamic forces, as shown in Fig. 1C. The 0.25% hydrogel was found to be superior to the 0.5% hydrogel in terms of allowing cells to cross from a fluidic medium into the hydrogel macropores, whereupon it was found to adequately control the hydrodynamic back flow and stabilise cell motion in the microchannel. Eight independent experiments were undertaken to test the labelling and dissociation aspects of the device.

3.2 EK cell transport

In preparation for transporting dissociated cancer cells, the interplay between electroosmotic flow (EOF) and electrophoretic flow (EPF) in hydrogel-based EK was explored. Figure 4A shows a scatter plot for μ_{app} versus cell diameter for unlabelled K562 cells in PBS-based hydrogel in a field of 70 V/cm. Figure 4B shows the experimental set-up in which a range of EK field strengths were studied. The levels below 50 V/cm did not reproducibly cause movement with all cell types studied (data not shown). The levels in excess of 70 V/cm, although causing more rapid movement, commonly induced extensive cell lysis, particularly in the freshly isolated tumour cells. The data show a positive correlation between cell diameter and EK mobility indicating that in this application, μ_{app} is generally higher for larger cells than for smaller ones. These results suggest that cells can be discriminated on the basis of size alone, a factor that could be useful in future applications of this technology.

Figure 5 shows μ_{app} for fluorescent antibody-labelled versus unlabelled cells in HEPES/sucrose hydrogel. This result indicates that μ_{app} is much higher for unlabelled cells ($>2.0 \times 10^{-8} \text{ m}^2/\text{Vs}$) than for labelled cells ($<1.0 \times 10^{-8} \text{ m}^2/\text{Vs}$). These variations in overall EK mobilities for cells of varying size and for labelled and unlabelled cells reveal the part played by EPF. The negatively charged membrane attracts cations to form an electric double layer and cellular zeta potential ζ_c . Simultaneous to cell movement within the EOF bulk flow, cell movement relative to the fluid occurs by EPF, with linear velocity v_{epf} dependent upon charge-to-size ratio. Smaller cells possess higher charge-to-size ratios and thus experience greater cathodic EPF. In the case of labelled cells, antibody charge is pH dependent and governed by the isoelectric point. For monoclonal IgG₁, the isoelectric point is highly heterogeneous but lies in the range 7.0–9.0, and so IgG₁ has a net positive charge at pH 7.4 [42]. The overall charge on conjugated antibodies should include fluorophore charge; however, this information is not readily available. However, what is known is that cells with bound conjugated antibody have increased ζ_c and greater charge-to-size ratios than unlabelled cells [43]. Labelled cells are consequently more electrophoretically mobile, a phenomenon used for the characterisation of lymphocyte phenotypes, zeta potential calculation and immunoelectrophoresis of erythrocytes [43, 44].

If μ_{epf} and μ_{eof} are in the same direction, μ_{app} is increased; conversely, if they are in opposite directions μ_{app} is decreased. As a consequence of microchannel fouling, due to the deposition and adsorption of proteins and other cellular debris, it is known that normally negative channel surfaces become positively charged resulting in reverse EOF, i.e. bulk flow is towards the anode [45, 46]. Following release into the microchannel as described above, antibody-labelled dissociated tumour cells were transported by hydrogel-based EK for detection by fluorescence microscopy. Figure 6A shows a stationary integrin β 1-labelled cell in the

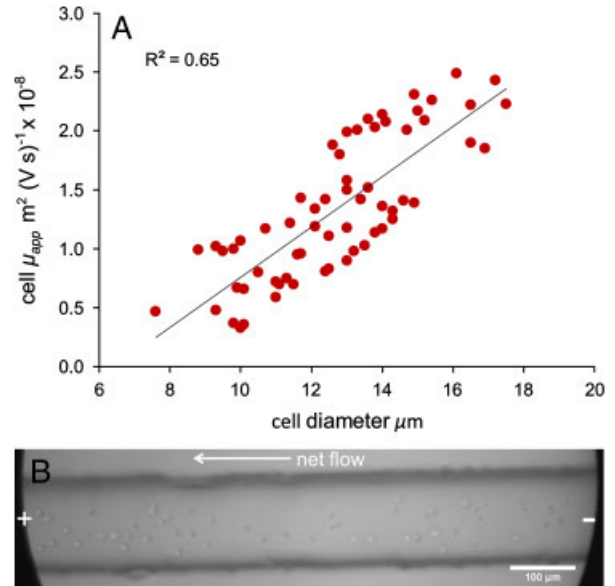


Figure 4. (A) Scatter plot of EK mobility (μ_{app}) versus cell diameter for unlabelled K562 cells in PBS-based hydrogel. Each point represents an individual cell, data shown are representative of over 150 cells. Mean $v_{\text{app}} \approx 9.0 \times 10^{-5} \text{ m/s}$. Mean $\mu_{\text{app}} \approx 1.34 \times 10^{-8} \text{ m}^2/\text{Vs}$; (B) K562 cells moving by EK in a hydrogel-filled microchannel. All observed cell velocities are toward the anode.

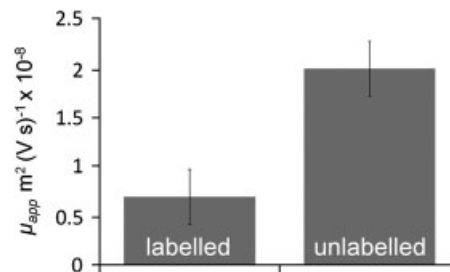


Figure 5. EK mobility (μ_{app}) for antibody-labelled and unlabelled cells in HEPES/sucrose hydrogel. Error bars are SE for four repeats.

0.25% hydrogel-filled channel, just prior to application of an electric field. The fluorescent signal is sufficiently bright to be easily detectable, showing that antibody remains bound to cells while in motion within the hydrogel, and that the hydrogel is a suitably transparent medium. In addition, the levels of unbound antibody in the hydrogel are low in contrast with antibody bound to the cells.

Figure 6B shows a plot of intensity versus time for the same cell (representative of many cells) traversing a region of interest (ROI; marked on Fig. 6C) upon the application of 45 V/cm. The fluorescence peak for the cell is distinct from that of the background, indicating that washing off excess antibody is unnecessary, and also that the selected fluorophores are sufficiently bright and photostable to give prolonged, detectable signals from moving cells.

The sequence in Fig. 6C shows cells moving by hydrogel-based EK, with dominant anodic EOF. The overall

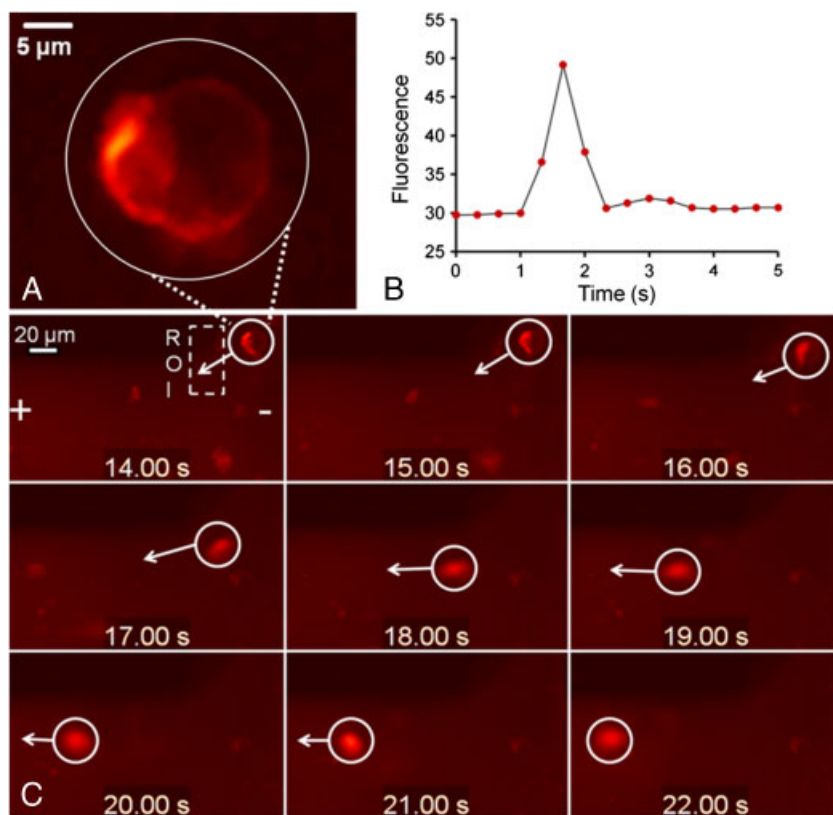


Figure 6. Electrokinesis of antibody-labelled and dissociated HNSCC tumour cells in 0.25% hydrogel-filled microchannel: (A) stationary β 1-labelled cell immediately prior to application of electric field; 45 V/cm applied at 14 s; (B) plot of intensity versus time for same cell traversing ROI marked on (C). [(B) $t = 0\text{--}4$ s corresponds approximately to (C), $t = 14\text{--}18$ s]; (C) fluorescent micrograph sequence of EK cell transport. $v_{\text{app}} \approx 5.9 \times 10^{-5}$ m/s; $\mu_{\text{app}} \approx 1.3 \times 10^{-8}$ m²/Vs.

mobility of these cells showed no difference from that observed in initial experiments characterising the flow system with the K562 cell line. Agarose hydrogel is mechanically similar to ECM and supports the cells in motion, preventing settling out, while permitting continued paracrine interactions via soluble signalling factors [18, 47, 48].

4 Discussion

This study has demonstrated the feasibility of using ex vivo human tumour tissue as a source of primary cells for EK microflow cytometry. Furthermore, it has enabled the integration of solid tumour cell dissociation, antibody labelling, cell transportation and fluorescence-based cell detection to be achieved on a single microfluidic platform. The demonstration that these procedures can be successfully assimilated will lead to future devices containing these processes in portable units as the existing components can all be miniaturised without loss of function or sensitivity [2]. The innovative tissue processing approach reduces cell handling, simplifies the pre-analytical stage of microflow cytometry and thus minimises the potential for generating experimental artefacts. In addition, cell labelling can be achieved alongside complex dynamic signalling and adhesion events with neighbouring cells and with the ECM. The work demonstrates the value of microfluidics as a tool for solid tumour research at the cellular level. Cells released

directly from this vital and information-rich tumour microenvironment provide unique data on individual patient tumours. Finally, the use of EOF and EPF to transport antibody-labelled and unlabelled heterogeneous tumour cells suggests that through careful selection of field strength and flow direction, some degree of cell separation may also be achievable. Future studies using multiple fluorescently labelled antibodies to validate the detection of known diagnostic/prognostic markers on tumour samples in the microfluidic device are planned, e.g. detection of epidermal growth factor receptor on HNSCC, in parallel with technological developments of the integrated microfluidic device.

The authors thank Dr. S. Clark, Dr. S. Hattersley, L. Houghton, M. Park, Dr. K. Shaw, M. Tarn, and Dr. X. Zhang for technical assistance, Professor N. Stafford for HNSCC tumour samples and the BBSRC (BB/E002722) and the University of Hull for financial support.

The authors have declared no conflict of interest.

5 References

- [1] Bonetta, L., *Nat. Methods* 2005, 2, 785–794.
- [2] Chung, T. D., Kim, H. C., *Electrophoresis* 2007, 28, 4511–4520.

- [3] Kametsky, L. A., Melamed, M. R., *Science* 1967, 156, 1364–1365.
- [4] Schwartz, M. P., Fairbanks, B. D., Rogers, R. E., Rangarajan, R., Zaman, M. H., Anseth, K. S., *Integr. Biol.* 2010, 2, 32–40.
- [5] Joyce, J. A., Pollard, J. W., *Nat. Rev. Cancer* 2009, 9, 239–252.
- [6] Webster, A., Dyer, C. E., Haswell, S. J., Greenman, J., *Anal. Methods* 2010, 2, 1005–1007.
- [7] Hattersley, S. M., Dyer, C. E., Greenman, J., Haswell, S. J., *Lab Chip* 2008, 8, 1842–1846.
- [8] Ailles, L., Prince, M., in: Yu, J. S. (Ed.), *Cancer Stem Cells: Methods and Protocols*, Humana Press, London 2009, pp. 175.
- [9] Fitzpatrick, E., McBride, S., Yavelow, J., Najmi, S., Zanzucchi, P., Wieder, R., *Clin. Chem.* 2006, 52, 1080–1088.
- [10] Ateya, D. A., Erickson, J. S., Howell, P. B., Jr., Hilliard, L. R., Golden, J. P., Ligler, F. S., *Anal. Bioanal. Chem.* 2008, 391, 1485–1498.
- [11] Sims, C. E., Allbritton, N. L., *Lab Chip* 2007, 7, 423–440.
- [12] Whitesides, G. M., Woodford, L., Flowers, A. A., *Lab Chip* 2010, 10, 2317–2318.
- [13] Lancaster, C., Kokoris, M., Nabavi, M., Clemmens, J., Maloney, P., Capadanno, J., Gerdes, J., Battrell, C. F., *Methods* 2005, 37, 120–127.
- [14] Li, P. C. H., Harrison, D. J., *Anal. Chem.* 1997, 69, 1564–1566.
- [15] Dittrich, P. S., Schwille, P., *Anal. Chem.* 2003, 75, 5767–5774.
- [16] Wang, M. M., Tu, E., Raymond, D. E., Yang, J. M., Zhang, H. C., Hagen, N., Dees, B., Mercer, E. M., Forster, A. H., Kariv, I., Marchand, P. J., Butler, W. F., *Nat. Biotechnol.* 2005, 23, 83–87.
- [17] Rutkowski, J. M., Swartz, M. A., *Trends Cell Biol.* 2007, 17, 44–50.
- [18] Ling, Y., Rubin, J., Deng, Y., Huang, C., Demirci, U., Karp, J. M., Khademhosseini, A., *Lab Chip* 2007, 7, 756–762.
- [19] Gabi, M., Sannomiya, T., Larmagnac, A., Puttaswamy, M., Voros, J., *Integr. Biol.* 2009, 1, 108–115.
- [20] Barz, D. P. J., Ehrhard, P., *Lab Chip* 2005, 5, 949–958.
- [21] Sparks, D. L., *Environmental Soil Chemistry*, Academic Press, San Diego 2003.
- [22] Li, D., *Electrokinetics in Microfluidics*, Elsevier, London 2004.
- [23] You, J., Aznavoorian, S., Liotta, L. A., Dong, C., *J. Cell. Physiol.* 1996, 167, 156–163.
- [24] Shier, W. T., Olsen, S. G., *In Vitro Cell Dev. Biol. Anim.* 1995, 31, 336–337.
- [25] Wu, M. H., Lin, J. L., Wang, J., Cui, Z. F., Cui, Z., *Biomed. Microdevices* 2009, 11, 265–273.
- [26] Persat, A., Suss, M. E., Santiago, J. G., *Lab Chip* 2009, 9, 2454–2469.
- [27] Hsieh, S. S., Lin, H. C., Lin, C. Y., *Colloid Polym. Sci.* 2006, 284, 1275–1286.
- [28] Minerick, A. R., Ostafin, A. E., Chang, H. C., *Electrophoresis* 2002, 23, 2165–2173.
- [29] Xuan, X., Li, D., *J. Micromech. Microeng.* 2004, 14, 1171–1180.
- [30] Good, N. E., Winget, G. D., Winter, W., Connolly, T. N., Izawa, S., Singh, R. M. M., *Biochemistry (NY)* 1966, 5, 467–477.
- [31] Beynon, R. J., Easterby, J. S., *Buffer Solutions*, IRL Press, Oxford 1996.
- [32] Shinohara, M., Nakamura, S., Sasaki, M., Kurahara, S., Ikebe, T., Harada, T., Shirasuna, K., *Am. J. Clin. Pathol.* 1999, 111, 75–88.
- [33] Zhang, X., Liu, Y., Gilcrease, M. Z., Yuan, X. H., Clayman, G. L., Adler-Storthz, K., Chen, Z., *Cancer* 2002, 95, 1663–1672.
- [34] Rasband, W. S., *ImageJUSA*, U.S. National Institutes of Health, Bethesda, MD 1997–2009.
- [35] O'Sullivan, D. G., *J. Theor. Biol.* 1962, 2, 117–128.
- [36] Thurber, G. M., Schmidt, M. M., Wittrup, K. D., *Adv. Drug Deliv. Rev.* 2008, 60, 1421–1434.
- [37] Ackerman, M. E., Pawlowski, D., Wittrup, K. D., *Mol. Cancer Ther.* 2008, 7, 2233–2240.
- [38] Freitas, R. A., Jr, *Nanomedicine Volume 1: Basic Capabilities*, Landes Bioscience, Georgetown 1999.
- [39] McCabe, M., Adam, K., Maguire, D., *J. Theor. Biol.* 1979, 78, 51–59.
- [40] Magzoub, M., Jin, S., Verkman, A. S., *FASEB J.* 2008, 22, 276–284.
- [41] Dono, K., Gotoh, M., Monden, M., Kanai, T., Fukuzaki, T., Mori, T., *Transplantation* 1994, 57, 22–26.
- [42] Prin, C., Bene, M. C., Gobert, B., Montagne, P., Faure, G. C., *Biochim. Biophys. Acta* 1995, 1243, 287–290.
- [43] Wall, J., Ayoub, F., O'Shea, P., *J. Cell Sci.* 1995, 108, 2673–2682.
- [44] Ichiki, T., Ujiie, T., Shinbashi, S., Okuda, T., Horiike, Y., *Electrophoresis* 2002, 23, 2029–2034.
- [45] Mukhopadhyay, R., *Anal. Chem.* 2005, 77, 429A–432A.
- [46] Kirby, B. J., Wheeler, A. R., Zare, R. N., Fruetel, J. A., Shepodd, T. J., *Lab Chip* 2003, 3, 5–10.
- [47] Walker, G. M., Zeringue, H. C., Beebe, D. J., *Lab Chip* 2004, 4, 91–97.
- [48] Domenech, M., Yu, H., Warrick, J., Badders, N. M., Meyvantsson, I., Alexander, C. M., Beebe, D. J., *Integr. Biol.* 2009, 1, 267–274.

Study of ethanol induced toxicity in liver explants using microfluidic devices

Samantha M. Hattersley · John Greenman ·
Stephen John Haswell

Published online: 29 July 2011
© Springer Science+Business Media, LLC 2011

Abstract Current *in vitro* methodologies for the culture and analysis of liver specific responses lack the sophistication of *in vivo* dynamics. In this work, a microfluidic based experimental methodology has been utilized to reproduce a biomimetic microenvironment in which pseudo *in vivo* liver tissue studies can be carried out under *in vitro* conditions. This innovative technique, which exploits the inherent advantages of microfluidic technology, has been utilised to study the viability and functionality of explant liver tissue over four days in the presence of varying concentrations of ethanol. Concentrations of ethanol as low as 20 mM have produced a decrease in WST-1 metabolism, a marker of mitochondrial activity, and an increase lactose dehydrogenase release, reflecting cell death, in the explant samples; these effects increase with higher ethanol concentrations. A concomitant decrease in albumin and urea synthesis was also observed. We believe the proposed methodology is widely applicable and is clearly of relevance to biological and clinical research including drug development and toxicity, as well as enabling better fundamental understanding of tissue/cell processes.

Keywords Alcohol induced injury · Liver biopsy · Liver metabolism

1 Introduction

The association of alcohol abuse with liver tissue damage has been the focus of considerable research that has shown ethanol to be the direct cause of various abnormalities in liver architecture and functionality such as fatty liver, apoptosis, necrosis, cancer, fibrosis and cirrhosis (Albano 2008; Clemens 2007; Seitz and Becker 2007). However, the understanding of the mechanisms of alcoholic liver disease (ALD) progression has been protracted due to the lack of appropriate *in vitro* models that accurately simulate the microenvironment of the liver organ itself. Whilst extensive knowledge has been gained through the application of primary hepatocytes in culture and hepatoma cells lines, both in tandem and isolation, these studies cannot provide a complete understanding of the complex intracellular interactions and regulatory factors that are exhibited in native tissue (Emami et al. 2009; Jones et al. 2010; Ruan et al. 2010). Indeed many liver cells cultured by traditional methods, which do not replicate *in vivo* flow and transport dynamics, rapidly lose their specific liver gene expression and consequently their ability to produce tissue specific functions (Boess et al. 2003; Mathijs et al. 2009). Traditionally to overcome many of the limitations associated with cell-based methodology, animal models have been utilised to study physiological and pathological effects however, due to differences between organisms these models are limited (King et al. 2010; Mortensen et al. 2008). The maintenance of human liver tissue *in vitro* represents a more attractive approach to studying biological processes,

S. M. Hattersley (✉) · J. Greenman
Centre for Biomedical Research,
University of Hull, Cottingham Road,
Hull HU6 7RX, UK
e-mail: samantha.hattersley@hull.ac.uk

J. Greenman
e-mail: j.greenman@hull.ac.uk

S. J. Haswell
Department of Chemistry, University of Hull,
Cottingham Road,
Hull HU6 7RX, UK
e-mail: s.j.haswell@hull.ac.uk

compared with isolated and cultured primary hepatocytes, as the former offers the complexity and interactions of multiple different cell types arranged in their specific *in vivo* architectural patterns.

In the liver, hepatocytes are the main functional element responsible for toxicity elimination, xenobiotic and fatty acid metabolism, glucose storage, and protein synthesis. Accordingly, realizing a method for the maintenance of liver-specific functions of hepatocytes and other liver cells in a tissue environment would represent a useful tool for investigating functional changes through toxicological damage. A number of *in vitro* models for liver function have used precision-cut liver slices (PCLS). PCLS represent fractions of the whole liver in the form of thin sections (150–250 μm) of tissue. PCLS have been used to study a variety of metabolic and toxicological studies and have been effectively used to model ethanol hepatotoxicity. An *in vitro* method, for example, has recently been developed of ethanol-induced injury using PCLS from Wistar rats, cultured with and without 25 mmol/L ethanol using a roller system under 95% O_2 (Klassen et al. 2008). However, the PCLS used in this study were dimensionally only a few hundred microns in scale and would contain therefore approximately 8–10 hepatocytes, which may in fact be too thin to include all of the relevant cell types and 3D structure necessary to model the whole organ effectively, e.g. cell types that are sparsely represented within the tissue such as cholangiocytes may not be present. A further problem with such methodology is that it lacks *in vivo* flow dynamics as nutrients are typically supplied in discreet batches, which then decrease as metabolism occurs generating a build-up of waste products (Kim et al. 2007; Walker et al. 2004; Warrick et al. 2007). Under normal physiological conditions the flow within vascular capillaries and tissues is known to have Reynolds numbers <100 , resulting in predominantly diffusion based characteristics, over spatial distances of approximately 100 μm , (Kim et al. 2007; Ling et al. 2007) conditions under which cellular metabolite uptake, gaseous exchange and waste removal occur (Nevill et al. 2007).

Given that the flow and spatial parameters which exist in tissue are very similar to those of the microfluidic environment, the opportunity to carry out continuous perfusion of tissue samples (Kim et al. 2006; Nevill et al. 2007) offers an experimental approach that may overcome some of the limitations of current standard batch culture systems (Yu et al. 2007). The benefits of microfluidic techniques for cell/tissue culture that have been demonstrated previously include laminar flow conditions, small length scales, large surface to volume ratios, diffusion dominant transport, portability, reusability or disposability and reduced cost (El-Ali et al. 2006, Meyvantsson and Beebe 2008). In addition, by exploiting the flow conditions present in a microfluidic device, unprecedented spatial and

temporal control over materials entering and leaving an experimental system can be achieved (Hattersley et al. 2008; Takayama et al. 2003; Zhang et al. 2008). Accordingly the ability to place a viable tissue biopsy in a microfluidic device will offer the opportunity to control, probe and monitor complex cell functions in diseased and healthy tissue whilst maintaining *in vivo* architecture (El-Ali et al. 2006; Weibel and Whitesides 2006; Puleo et al. 2007; Nakanishi et al. 2008).

In this paper, we build on previous work (Hattersley et al. 2008) to describe an innovative approach for studying rat liver tissue that exploits the benefits of the microfluidic environment to create pseudo *in vivo* conditions *in vitro* and apply it to an investigation of ethanol hepatotoxicity.

2 Material and methods

2.1 Design and microfabrication of the microfluidic device

The microfluidic chips were fabricated using photolithography techniques as described previously (Broadwell et al. 2001; McCreedy 2001). AutoCAD LT software, a computer assisted design package, was used to design the microdevice from which a photomask was generated. The final device was generated in glass by transferring the design produced on the photomask using standard photolithography and wet-etching techniques (Broadwell et al. 2001). Access holes and a central chamber (diameter 3 mm) were drilled in the top plate. The top plate was then thermally bonded to the etched bottom plate in a furnace at 590°C for 3 h (Tarn 2008). The channel design used in this device consisted of a single channel, which diverged into two outlet channels as shown in Fig. 1.

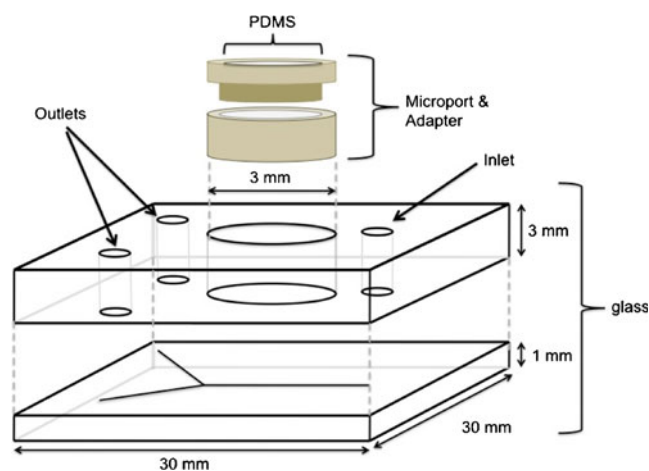


Fig. 1 (a) Image of the microfluidic device, tissue was placed in the 3 mm circular cavity in the centre of the device. (b) Image of four microdevices in operation within a single experiment (c) Schematic of the microfluidic device used in these studies

2.2 Microfluidic system for maintaining tissue biopsies

The microfluidic device as described above had a microport (Anachem, UK) glued to the surface of the top glass layer such that the circular tissue cavity could be sealed using an English threaded adapter (Anachem, UK). The adapter was filled with poly-dimethylsiloxane (PDMS) (Dow Corning, UK) to allow gaseous exchange (Kane et al. 2006). The tissue cavity is cylindrical with a volume of approximately 20 μl . A Harvard PhD 2000 syringe pump (Harvard, UK) was connected to the device via 0.8 mm ID \times 1.58 mm OD TFE Teflon[®] tubing (Anachem, UK). The length of the tubing from syringe to the device was 30 cm. This allowed sufficient time for the media to be heated to 35–37°C before reaching the tissue. A 0.22 μm syringe filter (Millipore, UK) was fitted in line to remove any bacterial contamination; this also minimised the generation of gas bubbles in the media. A 1.5 ml microcentrifuge tube, with a hole in the lid covered with parafilm to stop contamination and leakage, was placed on each end of the outlet tubing to collect eluate. The entire system was placed in a portable incubator at 37°C.

2.3 Animal and tissue preparation

All samples for the following experiments were taken from a single male rat (Wistar, B&K Universal Ltd, UK). The animal was fed and watered *ad libitum* until anaesthetized (10 ml kg^{-1} of 10 mM sodium thiopentone, intraperitoneal) and killed under a Schedule 1 procedure prior to liver extraction. The liver was immediately sectioned into pieces, approximately 1 cm^3 using a scalpel, and placed in 1 ml cryovials (Alpha Laboratories, UK), which were then plunged into liquid nitrogen and stored for subsequent experimentation.

Six microfluidic devices were sterilized prior to use by pumping 70% (v/v) ethanol/water through the devices for 15 min at 10 $\mu\text{l min}^{-1}$ followed by a rinse with sterile, distilled water. The devices were then primed with Williams Media E (WME) (Gibco, UK) supplemented with 1% (w/v) penicillin/streptomycin (Sigma, UK) at a flow rate of 20 $\mu\text{l min}^{-1}$ and set in a 37°C incubator. The frozen tissue was removed from the cryovial, cut into approximately 4 mm^3 sized sections, allowed to thaw, weighed and placed into the tissue cavities pre-filled with medium. To ensure that all cells in such a tissue sample have time to come into contact with media or ethanol/media it was found that a period of approximately 2 h was required for the tissue sample to become fully diffused. This was determined through the application of Brilliant Blue Dye (Sigma, UK) to the sample through the system at 2 $\mu\text{l min}^{-1}$, then removing the tissue and cutting it in half to visualize the diffusion profile. The flow rate through the tissue cavities was maintained at 2 $\mu\text{l min}^{-1}$. A visual check was made to

ensure no bubbles were trapped in any of the chambers; if observed they were removed using a sterile hypodermic needle. WME was replaced with WME supplemented with 20, 50, 100, 150 and 200 mM ethanol in five independent parallel devices. In the sixth device, WME only was run and acted as a negative control. The eluent from the outlets of each of the microfluidic device was collected every hour in 0.5 ml microcentrifuge tubes for cell viability and functionality analysis.

2.4 Viability analysis

To quantify cell viability and cell death within the tissue sample, a colorimetric cytotoxicity assay (Cytotoxicity Detection Kit Plus, Lactate dehydrogenase (LDH) Roche, UK) and a colorimetric cell proliferation assay using a tetrazolium salt, 4-[3-[4-Iodophenyl]-2-(4-nitrophenyl)-2H-5-tetrazolio-1, 3-benzene disulfonate (WST-1) (Roche, UK) were carried out following the manufacturer's protocols. Aliquots were collected every hour over 8 h period and analysed individually in triplicate. The daily results represent the average absorbance of these samples, which are then subsequently divided by the mass of liver tissue (mg) in each microfluidic device. The absorbances of the samples were determined at 492 nm (LDH) and 450 nm (WST-1), using 690 nm as a reference in both cases. The spectrophotometer was blanked using WME media alone. The samples were refrigerated and analyzed after every 8 h period was completed.

2.5 Functionality analysis

To assess the functionality of the tissue within the microfluidic device production of albumin and urea was investigated. Albumin levels in the eluent were obtained by the use of an enzyme-linked immunosorbant assay (ELISA) (Bethyl Laboratories Inc., USA) according to the manufacturer's guidelines. A 96-well flat bottom ELISA plate (SLS, UK) was coated overnight with 100 μl primary sheep anti-rat albumin antibody diluted in 0.05 M carbonate-bicarbonate buffer, pH 9.6 at 4°C. A 200 μl wash solution containing 50 mM Tris, 0.14 M NaCl, and 0.05% (v/v) Tween 20, pH 8.0 was used after each step and repeated three times. Plates were subsequently blocked with 200 μl 50 mM Tris, 0.14 M NaCl, containing 1% (w/v) Bovine Serum Albumin (BSA) pH 8.0 for 30 min at ambient temperature. The rat serum reference standards (10,000, 500, 250, 125, 62.5, 31.25, 15.625 and 7.8 ng ml^{-1}) were diluted in 50 mM Tris, 0.14 M NaCl and 0.05% (v/v) Tween 20, pH 8.0 and 100 μl of each dilution was incubated on the plate with eluent samples for 1 h. The plates were subsequently incubated with 100 μl Horseradish Peroxidase-conjugated detection antibody 1:5,000 in 50 mM Tris, 0.14 M NaCl and 0.05% (v/v) Tween 20, pH 8.0 for

1 h. Finally, a colorimetric reaction was carried out by the addition of 50 μ l undiluted tetramethyl benzidine solution. The reaction was stopped with 25 μ l of 2 M sulphuric acid and the absorbances were measured at $\lambda = 450$ nm.

Urea concentrations in the media were determined using a colorimetric assay (QuantiChrom™ Urea Assay Kit, BioAssay Systems, USA) carried out using the manufacturer's protocol.

2.6 Morphology analysis

To visualize cell architecture within the tissue, it was first embedded on a cork tile covered with Tissue-Tek® (Sakura, Netherlands) and plunged immediately in liquid nitrogen-cooled 2-methyl butane solution. Frozen sections (12 μ m thick) were then cut using a Microm HM505E cryostat. Sections were selected from the centre of the sample and these were stained with Haematoxylin and Eosin (H&E). The sections were then fixed with 10% (v/v) formalin for 10 min in a fume cupboard, stained with Delafield's Haematoxylin for 5 min before rinsing with running cold tap water. After rinsing for 10 min the tissue was dehydrated with sequentially higher concentrations of 25%, 50%, 75%, 85% and 95% (v/v) ethanol over 8 min. The tissue was then stained with 100% Eosin for 1 min before being quickly dipped in 95% (v/v) and absolute ethanol. The tissue was finally placed in HistoClear for five minutes to remove any excess, non-specific stain and mounted in Depex using a coverslip. The tissue was imaged by light microscopy.

2.7 Fatty liver

The first pathologic alteration that occurs to the liver as a consequence of ethanol consumption is the development of fat in the liver, a condition called steatosis. It has been proposed that ethanol sensitizes the liver through the accumulation of fat to additional oxidative injury that leads to alcoholic liver disease (Tsukamoto et al. 2009). The increase in fat in the liver has been recognized as a factor that can be involved in more serious liver injury (Zeng and Xie 2009). To discover whether there was a build up of fat in cells of the rat liver tissue after interrogation with increasing ethanol concentrations, a lipid stain was used. Oil Red O is a lysochrome (fat-soluble dye) diazo dye used for staining of neutral triglycerides and lipids.

Frozen sections (12 μ m thick) were cut from the liver samples after maintenance in the microfluidic system using a Microm HM505E cryostat. Sections were selected from the centre of the sample and these were allowed to dry for 60 min and subsequently fixed with 10% (v/v) formalin for 10 min in a fume cupboard, then allowed to dry again for another 60 min. The slides were placed in absolute

propylene glycol for 2 min before being immersed in Oil Red O for 10 min before rinsing with distilled water. The tissue was then placed in 85% (v/v) propylene glycol for five minutes to remove any excess stain, rinsed under running water and finally mounted in Depex using a coverslip. The tissue was then imaged using light microscopy using 40 \times magnification.

2.8 Statistical analysis

The results are expressed as standard error of the mean (S.E.M.) All statistical analysis was performed using statistical analysis software SPSS 17 (SPSS Inc. UK).

3 Results

A 20 mM concentration of ethanol, roughly equates to the legal drink drive limit in a blood sample in the United Kingdom (18.5 mM). Levels over 100 mM ethanol equate to a blood concentration associated with a heavy consumer of alcohol (Wu et al. 2006). The tissue sample perfused with WME alone (negative control) established the 'normal' baseline for WST-1 and LDH measurements within the device. The WST-1 results determined for each of the individual different concentrations of ethanol are represented as percentages of the negative control (Fig. 2). All samples show an initial decrease in WST-1 metabolism however by the fourth day, the liver tissue treated with the lowest concentration of ethanol is 20% lower than the untreated liver samples. Increasing concentrations of ethanol show a dose dependant decrease in WST-1 metabolism.

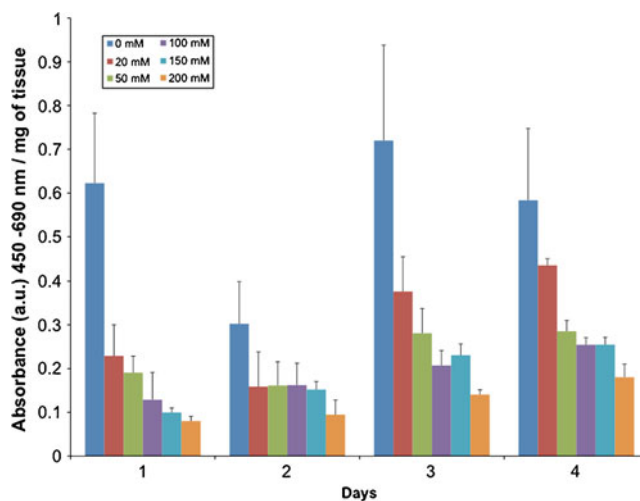


Fig. 2 Percentage of viable rat liver tissue using WST-1 metabolism as an indicator after interrogation with 20, 50, 100, 150 and 200 mM compared with negative control of untreated liver samples (from aliquots collected over 8 h period). Data are expressed as the mean % of three separate experiments

Ethanol is known to be a significant source of energy through its NAD metabolism. NADH rapidly reduces WST-1 to formazan however; this reduction is strongly inhibited by superoxide dismutase (SOD), which is also upregulated in ethanol metabolism to detoxify superoxide radicals (Berridge et al. 1996). As SOD is upregulated, inhibition of WST-1 occurs resulting in potentially a lower formazan production. This may impact the results of the test samples giving a lower indication of viability of the tissue than may actually be present. Measurement of LDH activity in the eluent showed that cell death in the control liver sample remained at low levels for the 96 h studied in the perfusion period in Fig. 3. Exposure to ethanol levels above 100 mM resulted in an increase in LDH release compared to the untreated tissue, indicative of increased levels of cell death at these concentrations over the time periods assayed. LDH activity at 20 and 50 mM show no marked difference compared with the control. These results corresponds to the findings of an earlier study, which demonstrated that exposure to low ethanol concentrations reduces cell necrosis through the reduction of intracellular oxidative stress (Castilla et al. 2004). Both the LDH and WST-1 data signifies that ethanol concentrations in excess of 50 mM, after a period of two days resulted in a marked decrease in cell viability.

The ability of the liver tissue sample to continue to produce both serum albumin and urea under interrogation from increasing ethanol concentrations are shown in Figs. 4 and 5. Increases in ethanol concentration are known to

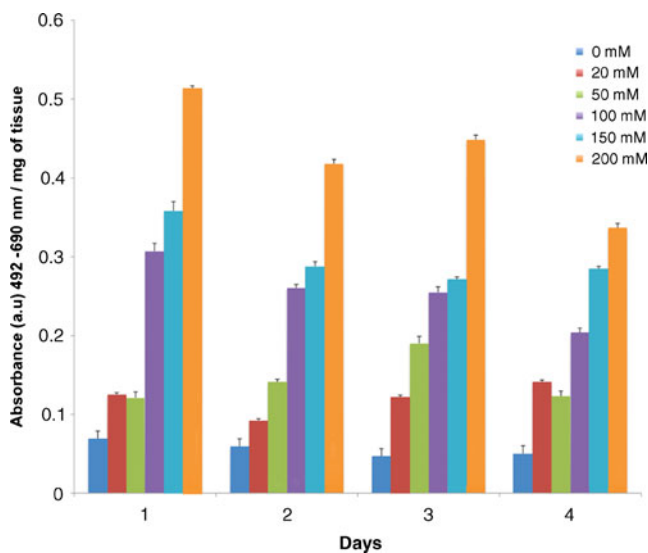


Fig. 3 LDH activities in rat liver tissue samples after maintenance within a micro fluidic device during interrogation with increasing ethanol concentrations. Liver samples were maintained at t_0 , 24, 48, 72, 96 h in the absence of ethanol, control (dashed line, black), and in the presence of 20 mM (solid line, purple), 50 mM (dashed line, blue), 100 mM (solid line, green), 150 mM (dashed line, orange) and 200 mM (solid line, red) ethanol. Data are expressed as the mean % of three separate experiments, repeated in duplicates. \pm S.E.M. of three separate experiments

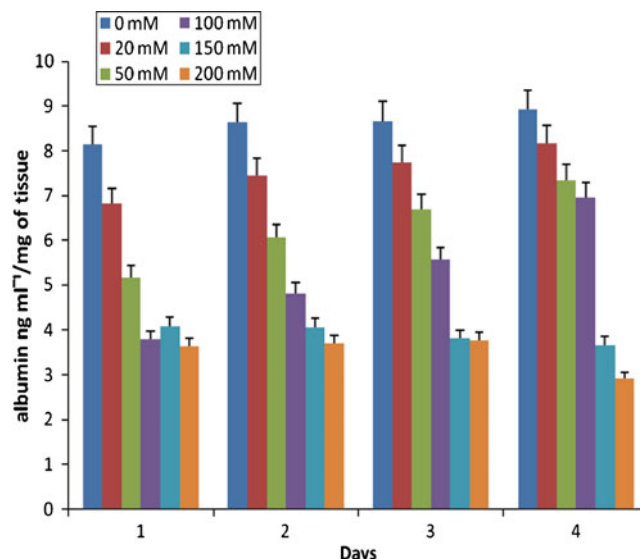


Fig. 4 Albumin secretion by of rat liver tissue samples after maintenance within a micro fluidic device and incubated with increasing ethanol concentrations. Data are expressed as the mean albumin levels ng ml^{-1} in the liver sample eluent \pm S.E.M. of three separate experiments

affect protein synthesis (Ohtake et al. 1986). As shown in Fig. 4, albumin was secreted by all the liver samples despite the interrogation with ethanol. As the ethanol concentration increased, the albumin synthesis decreased, with relatively little difference over time. Liver samples interrogated with 100 mM ethanol concentrations and below showed a steady increase over the four-day exposure period although this level always remained below the control (0 mM). Ethanol concentrations of 150 mM and 200 mM show depressed

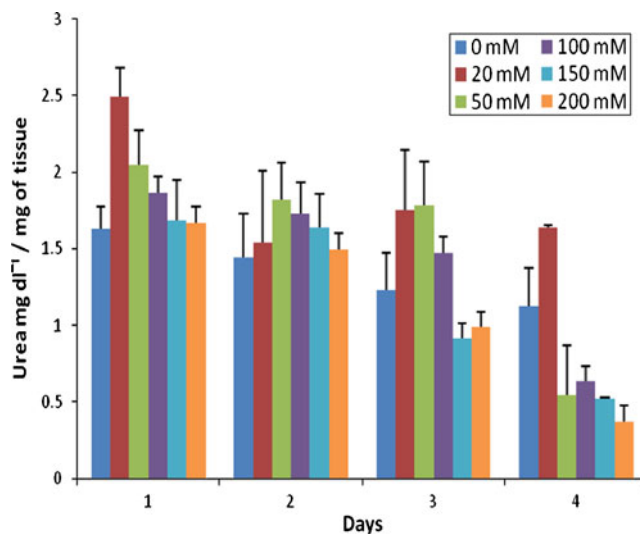


Fig. 5 Urea production by of rat liver tissue samples after maintenance within a micro fluidic device and incubated with increasing ethanol concentrations. Data are expressed as the mean albumin levels ng ml^{-1} in the liver sample eluent \pm S.E.M. of three separate experiments

secretion. The maximum concentration (200 mM) shows a decline of albumin secretion of two-thirds compared with the control. It can be seen from Fig. 5 that urea, like albumin, was secreted by all liver samples regardless of their treatment. The control shows a 30% decrease of urea production from the start to the finish of the experiment. The sample treated with 20 mM ethanol exhibited an initial 80% increase, which dropped to a 37% increase over the four-day exposure period but consistently remained higher than the control. Ethanol treatment at 50 mM and 100 mM demonstrates an increase of urea production over the first three days however by day four, urea levels have dropped to between 50–75% compared with the control. Urea production in liver samples interrogated with 150 mM and 200 mM initially remain stable and comparable with the control. However by day three, urea levels are depressed by 25–30% and at the end of day four; the levels were only 45% and 33% respectively. These results suggest that the metabolism of ethanol is involved in the decrease of albumin secretion and the increase of urea production at relatively low ethanol concentrations however; constant exposure over the period with concentrations above 50 mM causes urea levels to drop. These results correlate with the viability of the cells as cell death is increasing over time. This is supported through finding from a previous study using isolated perfused liver (Rothschild et al. 1983).

H&E staining of the rat liver tissue after maintenance and interrogation with different concentrations of ethanol was used to analyze the integrity of the tissue and cell morphology. Figure 6(a) shows the control liver sample after four days maintenance in the microfluidic device. These samples were taken from the centre of the sample between 120 μm and 180 μm from the periphery. As shown the cell nuclei of the hepatocytes have maintained their rounded appearance, with little or no shrinkage after 96 h of culture in the microfluidic device. The cell membranes can be seen in several places, with the hepatocytes preserving their original hexagonal shape. In addition there is no discernible loss of the extracellular matrix between the cells. However, as ethanol concentration increases, there are small gaps seen appearing in the structure of the tissue and the cells are beginning to look misshaped and there is evidence of some loss of cytoplasm (Fig. 6(b)) as reported in a previous study (Gavaler et al. 1984). The loss of ECM can be seen to increase with larger gaps appearing (Fig. 6(c), (d), (e), (f)) and the cells begin to lose their shape, structure and cohesion this is exacerbated by the lost of viable hepatocytes. Ethanol has been shown to arrest the cell cycle and impair the replication of normal hepatocytes, even though the liver usually has a tremendous capacity to replace cells that are lost or damaged from other cytotoxic injuries (Clemens 2007).

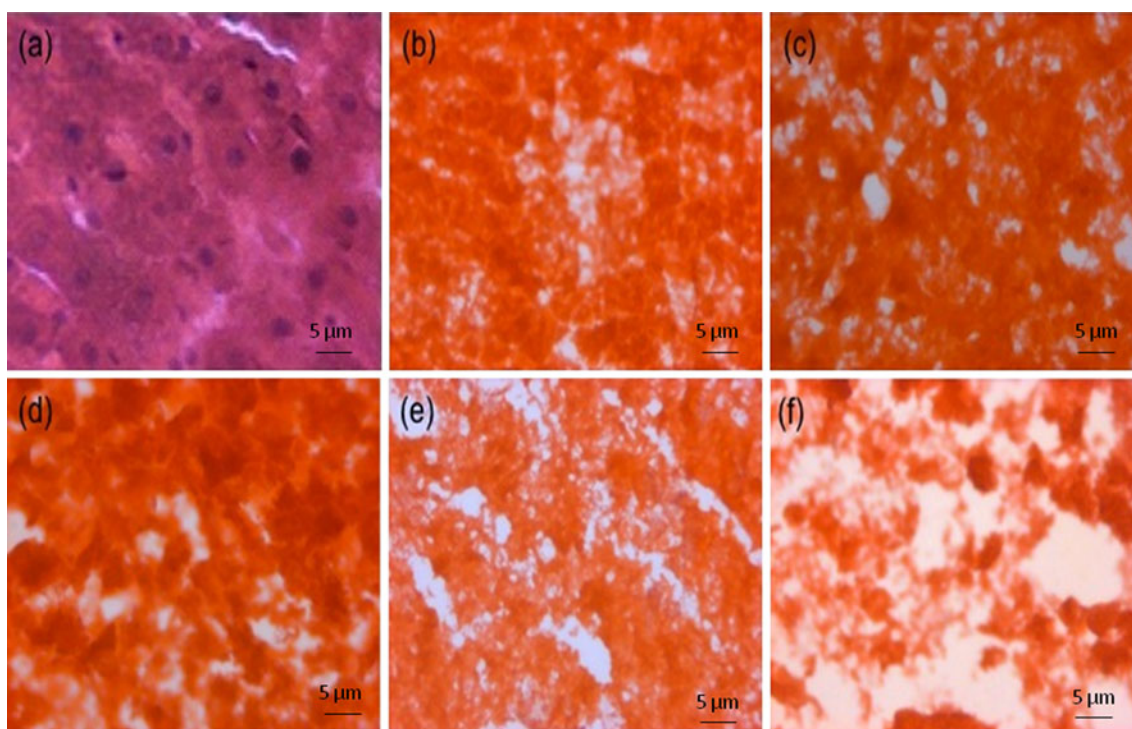


Fig. 6 Haematoxylin and Eosin (H&E) staining of rat liver tissue samples after maintenance within a microfluidic device and incubated with increasing concentrations after maintenance in a microfluidic device. Liver samples were maintained in (a) 0 mM ethanol, (b) 20 mM ethanol, (c)

50 mM ethanol, (d) 100 mM ethanol, (e) 150 mM ethanol and (f) 200 mM ethanol. Samples were chosen between 200 μm and 300 μm from edge of tissue. Light microscopy images were taken at random on under $\times 40$ magnification and are representative of three separate experiments

Fatty liver is a reversible condition associated with alcohol consumption where the liver stores triglycerides (Iseri et al. 1966). Oil Red O staining of the rat liver tissue biopsies treated with increasing ethanol concentrations are shown in Figure 7. No staining of fatty infiltration was observed in samples interrogated with 20, 50 and 100 mM over the exposure period (not shown). In contrast with the control (Fig. 7(a)), the liver sample exposed to 150 mM ethanol demonstrates a small increase in staining by Oil Red O (Fig. 7(b)) and the liver sample exposed to 200 mM ethanol showed a marked increase in staining (Fig. 7(c)).

A recent study using PCLS and traditional explant culture methods, demonstrated that there was an increase in Oil Red O staining after the slices were incubated for over 48 h with 25 mM ethanol compared to the control (Klassen et al. 2008). However, they also noted that there was an increase of Oil Red O staining in the control PCLS after culture compared with the PCLS examined before culture. High (>100 mM) concentrations of ethanol decrease the viability and functionality of the cells in the liver biopsy. Histological analysis of the liver sections showed the loss of ECM in the tissue and the increase of fatty deposits in the cells. Further analysis of the effects of ethanol on liver tissue in the microfluidic system could in the future give more information on the mechanisms involved in ethanol metabolism and how these can be used to treat ALD.

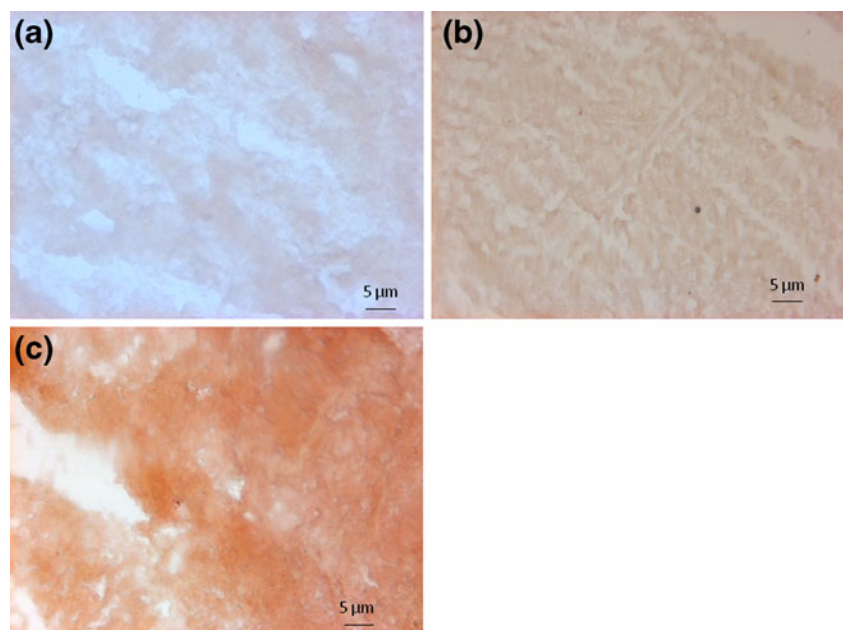
4 Discussion and conclusion

The responses of defined cell types to specific physiological stimuli can be manipulated within the microfluidic cell culture

environment to provide greater knowledge of key cellular responses. The high degree of fluidic control within a microsystem makes it possible to pinpoint different environmental conditions to a particular cell or groups of cells (Takayama et al. 2003). Conventional cell analysis is usually based on bulk averages of multiple cellular responses where it is impossible to isolate a single cell to analyse its output (Rao et al. 2002). This is due to the fact that vessels used to culture, store, interrogate and analyse cell responses are considerably larger than the individual cell. The microfluidic environment can facilitate the continuous perfusion of fresh media at a scale that enables the contents of the microchannels to be continually replaced and analysed without disturbing individual cell dynamics (Kim et al. 2006; Nevill et al. 2007). With these advantages, microfluidic devices have the potential to revolutionize the field of cell biology and open up new avenues of research which are currently inaccessible such as for example; pinpointing individual signalling pathways in response to a single stimulus or the response of different cells to extracellular matrices (Lee et al. 2006; Takayama et al. 2003). Growth in the use of microscale systems in the field of cell biology has been rapid over the past few years, largely due to the many practical advantages offered by such methodology. In addition to the fundamental fluidic properties further advantages such as; portability, reusability or disposability of equipment, reduced costs and low cell number requirement make micro fluidic devices superior to conventional cell culture in many assays.

Microfluidic technology is currently being used to extend the viability and functionality of explants in culture. Explant culture which can be defined as an *in vitro* technique that maintains sections or whole organs in culture

Fig. 7 Oil Red O staining of rat liver tissue samples after maintenance within a microfluidic device and incubated with increasing ethanol concentrations. Liver samples were maintained in (a) 0 mM ethanol, (b) 150 mM ethanol and (c) 200 mM ethanol. Samples were chosen between 200 μm and 300 μm from edge of tissue. Light microscopy images were taken at random under $\times 40$ magnification and are representative of three separate experiments



using specialised media, vessels and atmosphere (Jones et al. 1981). Such an approach would enable the normal architecture of the tissues with its three-dimensional intercellular complex relationships to be maintained in culture conditions (Jones et al. 1981). Traditionally explant culture is carried out in vessels submersed with media in rocking chambers, platforms or roller bottle equipment to improve diffusion of nutrients into the tissue (Resau et al. 1991). The methodology is however problematical when used in biological laboratories as it lacks the ability to maintain the tissue morphology and functionality during culture, due to a lack of oxygen diffusion of into the explant coupled with the diffusive removal of toxic metabolites (Sundstrom et al. 2005). The microenvironment cells occupy, can dramatically alter the genotype and consequently the phenotype of the cells, such as the addition of serum to fibroblast culture can alter the gene expression of the cell (Iyer et al. 1999). The chemical composition of the microenvironment is rigidly controlled by the release of signals from different cells, which may or may not be in close proximity. Therefore, a number of different cells are needed within an experimental model in order to give a greater approximation of typical cellular responses to external stimuli.

Many of the cell lines used in cell culturing both in traditional and microfluidic systems have been immortalized or are tumour-derived, which are genetically unstable, have intrinsic changes in gene expression, loss of proliferative regulation and signaling transduction pathways. These cells therefore are not a replicate of the typical *in vivo* cell (Balis 2002). It has also been shown lately the importance of the ECM and its components. ECM is composed of structural proteins such as collagen and elastin, specialized proteins such as fibrillin, fibronectin, and laminin and proteoglycans. There are at least 19 different vertebrate collagens with tissue-specific distributions and unique functional properties (Koch et al. 2003). Proteoglycans, for example, are a diverse multifunctional component of the ECM, playing roles in regulating matrix organization, growth factor activity, cell proliferation, and differentiation (Cattaruzza and Perris 2005). The research into the relationships between cardiac myocytes, fibroblasts, endothelial cells and the surrounding ECM, highlights the importance of particular cardiac cell populations and extracellular matrix factors that are critical to the development and regulation of heart function. These include the differences in ECM in conditions such as hypertrophy and aortic valve stenosis. These differences include increased fibronectin and collagens I, III, IV, compared with physiological hypertrophy where there is no such increase in ECM expression (Bowers et al. 2010). The ECM used in both traditional and microfluidic 3D cell culture lacks these *in vivo* complexities (Chatterjee et al. 2010; Kievit et al. 2010).

It is also widely acknowledged that there is a need for preclinical models of human disease which better reflect the *in vivo* environment incorporating all components of the tissue in their *in vivo* configurations (Thompson et al. 2008). However, tissue-based microfluidic applications are still in their infancy. The first micro fluidic studies using tissue slices were the culture of *ex vivo* brain tissue employing either a hollow SU-8 microneedles on 2.7 mm circular disks within a micro fluidic system (Choi et al. 2007) to perfuse 400 μm thick hippocampal rat brain tissue at 40 $\mu\text{l min}^{-1}$ or a three-layer PDMS device incorporating 530–700 μm thick medullary brain slices from neonatal rats perfused at 1 ml min^{-1} (Blake et al. 2007). Using these approaches cell viability was found to be lost after 4 h at 36°C in the case of the microneedle device and 3 h in the PDMS system, this is a shorter viability period than traditional methods as shown in a earlier section. Liver explant culture is the latest development in microfluidic tissue studies. The first was published by our group (Hattersley et al. 2008); the second study used precision cut tissue slices (PLCS), in a 10 layer PDMS micro fluidic device. The PLCS had 4 mm diameter and were 100 μm thick and perfused at 10 $\mu\text{l min}^{-1}$, and maintained viability for 24 h. The PLCS were subsequently interrogated with 7-ethoxycoumarin (7-EC) and exhibited results comparable to PLCS cultured in 1.3 ml well plates (Van Midwoud et al. 2010). This study however only maintained the explants for up to 24 h. Interrogating tissues within a microfluidic system couples the benefits of tissue-based methodologies; the different phenotypes of cells, mechanical forces and extracellular matrix, with the additional advantages of replicating the transport and flow mechanisms that are found within *in vivo* dynamics.

In conclusion, liver samples were kept viable and functional over 4 days, and with the addition of ethanol, the samples exhibited many of the same characteristics noted in previous studies which have used isolated hepatocytes and *in vivo* models of chronic ethanol intoxication. These included the decrease in viability of the tissue over the concentration range, with the reduction of albumin production and decrease in urea levels. This tissue model could offer a novel route to deciphering the multitude of interactions between cells and extracellular matrix, cell signaling pathways and toxicology in a more biologically relevant environment. Tissue-based microfluidic methodology could have a wide impact on biological and clinical research in the modeling hepatotoxicity, as well as enabling better fundamental research into cell processes within the microenvironment. The direct use of native tissue offers a more clinically relevant experimental system, which can potentially replace less relevant animal-based models.

Acknowledgements The authors acknowledge the support of Biotechnology and Biological Sciences Research Council (Grant no. BB/E002722/1) and University of Hull for SMH studentship funding.

Competing interest None to declare.

References

- E. Albano, Oxidative mechanisms in the pathogenesis of alcoholic liver disease. *Mol. Aspects Med.* **29**, 9–16 (2008)
- F.M. Balis, Evolution of anticancer drug discovery and role of cell-based screening. *J. Natl. Cancer Inst.* **94**, 78–79 (2002)
- M.V. Berridge, A.S. Tan, K.D. McCoy, R. Wang, The biochemical and cellular basis of cell proliferation assays that use tetrazolium salts. *Biochimica* **4**, 15–20 (1996)
- A.J. Blake, T.M. Pearce, N.S. Rao, S.M. Johnson, J.C. Williams, Multilayer PDMS microfluidic chamber for controlling brain slice microenvironment. *Lab Chip* **7**, 842–849 (2007)
- F. Boess, M. Kamber, S. Romer, R. Gasser, D. Muller, S. Albertini, L. Suter, Gene expression in two hepatic cell lines, cultured primary hepatocytes, and liver slices compared to the *in vivo* liver gene expression in rats: Possible implications for toxicogenomics use of *in vitro* systems. *Toxicol. Sci.* **73**, 386–402 (2003)
- S.L.K. Bowers, I. Banerjee, T.A. Baudino, The extracellular matrix: at the center of it all. *J. Mol. Cell. Cardiol.* **48**, 474–482 (2010)
- I. Broadwell, P.D.I. Fletcher, S.J. Haswell, T. McCreedy, X.L. Zhang, Quantitative 3-dimensional profiling of channel networks within transparent ‘lab-on-a-chip’ microreactors using a digital imaging method. *Lab Chip* **1**, 66–71 (2001)
- R. Castilla, R. Gonzalez, D. Fouad, E. Fraga, J. Muntane, Dual effect of ethanol on death in primary culture of human and rat hepatocytes. *Alcohol Alcohol.* **39**, 290–296 (2004)
- S. Cattaruzza, R. Perris, Proteoglycan control of cell movement during wound healing and cancer spreading. *Matrix Biol.* **24**, 400–417 (2005)
- K. Chatterjee, S. Lin-Gibson, W.E. Wallace, S.H. Parekh, Y.J. Lee, M. T. Cicerone, M.F. Young, C.G. Simon Jr., The effect of 3D hydrogel scaffold modulus on osteoblast differentiation and mineralization revealed by combinatorial screening. *Biomaterials* **31**, 5051–5062 (2010)
- Y. Choi, M.A. McClain, M.C. LaPlaca, A.B. Frazier, M.G. Allen, Three dimensional MEMS microfluidic perfusion system for thick brain slice cultures. *Biomed. Microdevices* **9**, 7–13 (2007)
- D.L. Clemens, Effects of ethanol on hepatic cellular replication and cell cycle progression. *World J. Gastroenterol.* **13**, 4955–4959 (2007)
- J. El-Ali, P.K. Sorger, K.F. Jensen, Cells on chips. *Nature* **442**, 403–411 (2006)
- S.A. Emami, N. Vahdati-Mashhadian, R. Vosough, M.B. Oghazian, The anticancer activity of five species of artemisia on Hep2 and HepG2 cell lines. *Pharmacologyonline* **3**, 327–339 (2009)
- J.S. Gavalier, H.A. Perez, L. Estes, D.H. Van Thiel, Morphologic alterations of rat Leydig cells induced by ethanol. *Pharmacol. Biochem. Behav.* **18**, 341–347 (1984)
- S.M. Hattersley, C.E. Dyer, J. Greenman, S.J. Haswell, Development of a microfluidic device for the maintenance and interrogation of viable tissue biopsies. *Lab Chip* **8**, 1842–1846 (2008)
- O.A. Iseri, C.S. Lieber, L.S. Gottlieb, The ultrastructure of fatty liver induced by prolonged ethanol ingestion. *Am. J. Pathol.* **48**, 535–555 (1966)
- V.R. Iyer et al., The transcriptional program in the response of human fibroblasts to serum. *Science* **283**, 83–87 (1999)
- R.T. Jones, E.A. Hudson, J.H. Resau, A review of *in vitro* and *in vivo* culture techniques for the study of pancreatic carcinogenesis. *Cancer* **47**, 1490–1496 (1981)
- C.N. Jones, N. Tuleuova, J.Y. Lee, E. Ramanculov, A.H. Reddi, M. A. Zern, A. Revzin, Cultivating hepatocytes on printed arrays of HGF and BMP7 to characterize protective effects of these growth factors during *in vitro* alcohol injury. *Biomaterials* **31**, 5936–5944 (2010)
- B.J. Kane, M.J. Zinner, M.L. Yarmush, M. Toner, Liver-specific functional studies in a microfluidic array of primary mammalian hepatocytes. *Anal. Chem.* **78**, 4291–4298 (2006)
- F.M. Kievit, S.J. Florczyk, M.C. Leung, O. Veishe, J.O. Park, M.L. Disis, M. Zhang, Chitosan-alginate 3D scaffolds as a mimic of the glioma tumor microenvironment. *Biomaterials* **31**, 5903–5910 (2010)
- L. Kim, M.D. Vahey, H.Y. Lee, J. Voldman, Microfluidic arrays for logarithmically perfused embryonic stem cell culture. *Lab Chip* **6**, 394–406 (2006)
- L. Kim, Y.C. Toh, J. Voldman, H. Yu, A practical guide to microfluidic perfusion culture of adherent mammalian cells. *Lab on a Chip* **7**, 681–694 (2007)
- A.L. King, T.M. Swain, D.A. Dickinson, M.J. Lesort, S.M. Bailey, Chronic ethanol consumption enhances sensitivity to Ca²⁺ mediated opening of the mitochondrial permeability transition pore and increases cyclophilin D in liver. *Am. J. Physiol.—Gastrointest. Liver. Physiol.* **299** (2010)
- L.W. Klassen, G.M. Thiele, M.J. Duryee, C.S. Schaffert, A.L. DeVény, C.D. Hunter, P. Olinga, D.J. Tuma, An *in vitro* method of alcoholic liver injury using precision-cut liver slices from rats. *Biochem. Pharmacol.* **76**, 426–436 (2008)
- M. Koch, F. Laub, P. Zhou, R.A. Hahn, S. Tanaka, R.E. Burgeson, D.R. Gerecke, F. Ramirez, M.K. Gordon, Collagen XXIV, a vertebrate fibrillar collagen with structural features of invertebrate collagens: selective expression in developing cornea and bone. *J. Biol. Chem.* **278**, 43236–43244 (2003)
- P. Lee, R. Lin, J. Moon, L.P. Lee, Microfluidic alignment of collagen fibers for *in vitro* cell culture. *Biomed. Microdevices* **8**, 35–41 (2006)
- Y. Ling, J. Rubin, Y. Deng, C. Huang, U. Demirci, J.M. Karp, A. Khademhosseini, A cell-laden microfluidic hydrogel. *Lab Chip* **7**, 756–762 (2007)
- K. Mathijs, A.S. Kienhuis, K.J.J. Brauers, D.G.J. Jennen, A. Lahoz, J. C.S. Kleinjans, J.H.M. Van Delft, Assessing the metabolic competence of sandwich-cultured mouse primary hepatocytes. *Drug Metab. Dispos.* **37**, 1305–1311 (2009)
- T. McCreedy, Rapid prototyping of glass and PDMS microstructures for micro total analytical systems and micro chemical reactors by microfabrication in the general laboratory. *Anal. Chim. Acta* **427**, 39–43 (2001)
- I. Meyvantsson, D.J. Beebe, Cell culture models in microfluidic systems. *Annu. Rev. Anal. Chem.* **1**, 423–449 (2008)
- A. Mortensen, I.K. Sorensen, C. Wilde, S. Dragoni, D. Mullerova, O. Toussaint, Z. Zloch, G. Sgaragli, J. Ovesna, Biological models for phytochemical research: from cell to human organism. *British J. Nutr.* **99** (2008)
- J. Nakanishi, T. Takarada, K. Yamaguchi, M. Maeda, Recent advances in cell micropatterning techniques for bioanalytical and biomedical sciences. *Anal. Sci.* **24**, 67–72 (2008)
- J.T. Nevill, R. Cooper, M. Dueck, D.N. Breslauer, L.P. Lee, Integrated microfluidic cell culture and lysis on a chip. *Lab Chip* **7**, 1689–1695 (2007)
- H. Ohtake, S. Kato, Y. Murawaki, Acute and chronic effect of ethanol on hepatic albumin synthesis in rat liver *in vitro*. *Res. Commun. Chem. Pathol. Pharmacol.* **53**, 213–231 (1986)
- C.M. Puleo, H.C. Yeh, T.H. Wang, Applications of MEMS technologies in tissue engineering. *Tissue Eng.* **13**, 2839–2854 (2007)
- C.V. Rao, D.M. Wolf, A.P. Arkin, Control, exploitation and tolerance of intracellular noise. *Nature* **420**, 231–237 (2002)

- J.H. Resau, K. Sakamoto, J.R. Cottrell, E.A. Hudson, S.J. Meltzer, Explant organ culture: a review. *Cytotechnology* **7**, 137–149 (1991)
- M.A. Rothschild, M. Oratz, S.S. Schreiber, Effects of nutrition and alcohol on albumin synthesis. *Alcohol. Clin. Exp. Res.* **7**, 28–30 (1983)
- X. Ruan, C. Shen, Q. Meng, Establishment of a methodology for investigating protectants against ethanol-induced hepatotoxicity. *Food Chem. Toxicol.* **48**, 1145–1151 (2010)
- H.K. Seitz, P. Becker, Alcohol metabolism and cancer risk. *Alcohol Res. Health* **30**, 38–47 (2007)
- L. Sundstrom, B. Morrison Iii, M. Bradley, A. Pringle, Organotypic cultures as tools for functional screening in the CNS. *Drug Discov. Today* **10**, 993–1000 (2005)
- S. Takayama, E. Ostuni, P. LeDuc, K. Naruse, D.E. Ingber, G.M. Whitesides, Selective Chemical Treatment of Cellular Microdomains Using Multiple Laminar Streams. *Chem. Biol.* **10**, 123–130 (2003)
- M.D. Tarn. *Standard Operating Procedures for the Fabrication of Glass Microchips: University of Hull* (2008)
- A. Thompson, K. Brennan, A. Cox, J. Gee, D. Harcourt, A. Harris, M. Harvie, I. Holen, A. Howell, R. Nicholson, M. Steel, C. Streuli, Evaluation of the current knowledge limitations in breast cancer research: a gap analysis. *Breast Canc. Res.* **10** (2008)
- H. Tsukamoto, K. Machida, A. Dynnyk, H. Mkrtchyan, “Second hit” models of alcoholic liver disease. *Semin. Liver Dis.* **29**, 178–187 (2009)
- P.M. Van Midwoud, G.M.M. Groothuis, M.T. Merema, E. Verpoorte, Microfluidic biochip for the perfusion of precision-cut rat liver slices for metabolism and toxicology studies. *Biotechnol. Bioeng.* **105**, 184–194 (2010)
- G.M. Walker, H.C. Zeringue, D.J. Beebe, Microenvironment design considerations for cellular scale studies. *Lab Chip* **4**, 91–97 (2004)
- J. Warrick, I. Meyvantsson, J.I. Ju, D.J. Beebe, High-throughput microfluidics: improved sample treatment and washing over standard wells. *Lab Chip* **7**, 316–321 (2007)
- D.B. Weibel, G.M. Whitesides, Applications of microfluidics in chemical biology. *Curr. Opin. Chem. Biol.* **10**, 584–591 (2006)
- D.M. Wu, Q.W. Zhai, X.L. Shi, Alcohol-induced oxidative stress and cell responses. *J. Gastroenterol. Hepatol.* **21**, S26–S29 (2006)
- H.M. Yu, C.M. Alexander, D.J. Beebe, Understanding microchannel culture: parameters involved in soluble factor signaling. *Lab Chip* **7**, 726–730 (2007)
- T. Zeng, K.Q. Xie, Ethanol and liver: Recent advances in the mechanisms of ethanol-induced hepatosteatosis. *Arch. Toxicol.* **83**, 1075–1081 (2009)
- X.L. Zhang, H.B. Yin, J.M. Cooper, S.J. Haswell, Characterization of cellular chemical dynamics using combined microfluidic and Raman techniques. *Anal. Bioanal. Chem.* **390**, 833–840 (2008)

Direct processing of clinically relevant large volume samples for the detection of sexually transmitted infectious agents from urine on a microfluidic device

Cordula Kemp,^a Christopher Birch,^a Kirsty J. Shaw,^c Gavin J. Nixon,^b Peter T. Docker,^c John Greenman,^a Jim F. Huggett,^b Stephen J. Haswell,^c Carole A. Foy^b and Charlotte E. Dyer^{*a}

Received 20th January 2012, Accepted 9th May 2012

DOI: 10.1039/c2ay25075f

Urine is a preferred specimen for nucleic acid-based detection of sexually transmitted infections (STIs) but represents a challenge for microfluidic devices due to low analyte concentrations. We present an extraction methodology enabling rapid on-chip nucleic acid purification directly from clinically relevant sample volumes up to 1 ml and subsequent PCR amplification detection.

Introduction

An estimated 1 million new cases of curable bacterial STIs occur daily worldwide.¹ As such, STIs present a major challenge to global healthcare, highlighting the need for the development of novel technologies offering rapid point-of-care (POC) detection and diagnosis, to improve disease control and inform therapeutic intervention. Emerging microfluidic lab-on-a-chip (LOC) analytical technologies offer advanced alternatives to conventional diagnostic methods, as they facilitate automated integration of several sample processing and analysis techniques. In addition, the potential for system miniaturisation using microfluidic technologies offers a number of advantages for the development of POC platforms, including increased speed of analysis, reduction in sample and reagent volumes used, reduced power consumption compatible with non-mains power sources and minimal user intervention.

For the detection of STIs, urine provides a favourable choice as patient specimen, as it can be easily self-collected and is non-invasive. However, urine has not been widely investigated as a sample matrix for microfluidic LOC analysis. In the case of BK virus (BKV) infection, 1000 fold dilutions of fresh urine samples were used in an automatic microchip screening platform directly in the PCR reaction.² This approach avoids prior extraction or purification of the target nucleic acid but is only suitable for infections such as BKV that accumulate in the urine at high levels (10^7 to 10^{10} BKV particles per ml). Many STIs, however, such as *Neisseria gonorrhoeae* which shows considerably lower titers in the estimated range of 10^3 to 10^5 CFU per ml, are not suitable for this direct approach.³

Current clinically validated nucleic acid-based diagnostic systems, such as BD ProbeTec™ *Chlamydia trachomatis* (CT) Q^x Amplified DNA Assay (Becton, Dickinson and Company, USA), use 2 to 3 ml of first void urine for initial processing and around 400 μ l of urine for the actual test procedure, whereas the Gen-probe APTIMA COMBO 2[®] Assay (Gene Probe Incorporated, USA) requires sample volumes of 300–500 μ l urine. Such large specimen volumes represent a significant challenge for microfluidic LOC devices. Ideally, little or no prior processing of clinical samples at the bench should be required in order to provide simple and cost-effective POC diagnostics.

Here, we present an efficient sample loading methodology for performing DNA extraction directly from an artificial urine matrix (AUM) on a microfluidic device that demonstrates the successful processing of specimen volumes of up to 1 ml, with reduced processing time. This system differs significantly from others reported, since it provides the processing of clinically relevant large volumes on a microfluidic device without pre-concentrating the biological matrix or adding buffering reagents.^{4,5}

Theory

The development of the rapid DNA extraction methodology reported in this work utilises silica-based monoliths integrated within a microfluidic device. Solid-phase nucleic acid extraction relies on the binding of nucleic acids to a silica support in the presence of a chaotropic salt at pH \leq 7.5; this is below the pK_a of the surface silanol groups and so reduces the negative charge at the surface thereby decreasing electrostatic repulsion and facilitating nucleic acid adsorption. The presence of a high capacity solid phase is characterised by a high surface area for binding and several approaches are available to achieve this, including the generation of porous monolithic silica structures or the high density packing of silica beads.⁶ The removal of proteins and other contaminating macromolecules present in a sample is achieved using an alcohol wash and subsequent retrieval of

^aPostgraduate Medical Institute, University of Hull, Cottingham Road, Hull, HU6 7RX, UK. E-mail: c.e.dyer@hull.ac.uk; Fax: +44 (0)1482 466996; Tel: +44 (0)1482 466993

^bMolecular and Cell Biology Team, LGC Ltd, Queens Road, Teddington, TW11 0LY, UK

^cDepartment of Chemistry, University of Hull, Cottingham Road, Hull, HU6 7RX, UK

purified nucleic acids from the solid phase is brought about by elution in a low ionic strength medium.

Purification of DNA from biological specimens by solid-phase extraction on microfluidic devices is commonly performed by addition of a chaotropic salt, such as guanidine hydrochloride (GuHCl) in solution. Typically this is added directly to the sample, thus increasing the total sample volume for loading and so lengthening the processing time. Through optimisation of the microfluidic DNA extraction system reported here, novel methodologies have been developed which minimise sample volumes for processing in addition to increasing loading speed, without loss of DNA extraction efficiency.

Experimental

Glass microfluidic devices were manufactured using standard photolithography and wet etching techniques to produce the design shown in Fig. 1. Thermally activated silica monoliths were prepared in the DNA extraction chambers by curing a mixture of potassium silicate and formamide at 90 °C overnight.⁷ Initial validation experiments were performed using a glass capillary flow system. All DNA extractions were performed using hydrodynamic pumping, allowing sample loading and recovery *via* inlet and outlet channels. Silica monoliths were activated by flowing through 10 mM TE buffer (10 mM Tris, 1 mM EDTA, pH 6.7) for 30 minutes at 5 $\mu\text{l min}^{-1}$. An AUM medium was prepared in order to assess the compatibility of the proposed system with direct analysis of urine specimens.⁸ Standard DNA extractions were performed using samples comprising 5 ng μl^{-1} human genomic DNA (gDNA) prepared in either water or AUM. This was then added to a 5 M GuHCl solution prepared in either 10 mM TE buffer or AUM. The sample was then loaded onto the silica monolith at a flow rate of 2.5 $\mu\text{l min}^{-1}$ followed by a washing phase with 80% (v/v) isopropanol (5 $\mu\text{l min}^{-1}$). Finally, the bound DNA was eluted with water at 1 $\mu\text{l min}^{-1}$. Throughout the extraction process, 2 μl fractions were continuously collected and double-stranded DNA (dsDNA) content was quantified using a Quant-iT™ Picogreen® assay [Invitrogen, UK] and FLUOstar Optima Plate Reader [BMG Labtech, UK].

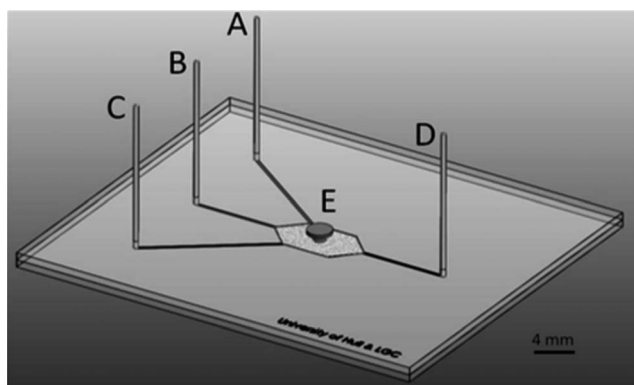


Fig. 1 Three dimensional representation of the DNA extraction microfluidic device. The DNA extraction chamber was etched to a depth of 100 μm resulting in a volume of 2.4 μl . Channels were connected, *via* holes in the top plate, to 360 μm diameter PEEK tubing enabling hydrodynamic pumping (A)–(D). A 1 mm port was incorporated in the centre of the DNA extraction chamber to permit addition of the solid-phase reagents (E).

Optimisation of the system to achieve rapid, large volume sample processing was performed through a series of DNA extractions investigating the effects of varying the quantity of 5 M GuHCl solution added to the sample prior to loading and also the rate of sample loading onto the monolith. Validation of the system was performed by processing model samples simulating concentrations of patient and pathogen nucleic acids found in clinical urine specimens. For the model sample, 1 ml AUM was spiked with 25 ng human gDNA plus 10^5 copies of a plasmid-based multi-STI pathogen target (pSTI) [designed and constructed by LGC Ltd, UK]. The pSTI contained cloned sequences from *Chlamydia trachomatis*, *Neisseria gonorrhoeae* and *Mycoplasma genitalium*, providing targets for amplification and detection by quantitative real time PCR (qPCR). Following DNA extraction, eluted samples were analysed by both PicoGreen® assay, to determine the total dsDNA content, and by qPCR, to determine plasmid copy number. qPCR was carried out using GoTaq® Hot Start DNA Polymerase, 3 mM MgCl_2 [Promega], and custom Taq-Man® probes and primers for the Pa gene of *Mycoplasma genitalium* [forward primer 5'-GGCGAGCCTATCTTTGATCCT-3', reverse primer 5'-AACTTACCTTTGATCTCATTC CAATC-3' probe 5'-FAM-AAAGGCTTTGGTTAACTGG TAATGCCCT-TAMRA-3', designed by LGC Ltd, UK and supplied by Applied Biosystems, UK]. Thermal cycling was performed on a StepOnePlus™ Real-Time PCR instrument [Applied Biosystems, UK] using an initial denaturation step of 95 °C for 10 minutes, followed by 50 cycles of 95 °C for 15 seconds and 60 °C for 1 minute.

Results and discussion

For all experiments the DNA extraction efficiency was assessed by calculating the quantity of DNA eluted as a percentage of the quantity of DNA initially loaded onto the system. Investigations comparing DNA extraction using either water or AUM as the sample matrix were performed in the flow system with added 5 M GuHCl solution prepared in either TE buffer or AUM (1 volume sample : 9 volumes GuHCl). The presence of the AUM did not appear to inhibit the extraction process as comparable DNA extraction efficiencies were obtained using either AUM or water (Table 1). The demonstration that DNA extraction efficiency was not adversely affected by using an AUM sample matrix suggests the proposed system is suitable for direct processing of clinical urine specimens.

In order to minimise sample volumes for loading onto the device, experiments were performed using the standard conditions described but varying the ratio of the volume of biological sample : volume of GuHCl solution (5 M in TE buffer). Little

Table 1 DNA extraction efficiencies using various sample-GuHCl matrices. Values shown represent the mean and standard deviation of 6 independent experiments. In all experiments, the DNA : GuHCl ratio was 1 : 9, representing a final concentration of GuHCl of 4.5 M

Sample matrix	GuHCl solution	DNA extraction efficiency [%]
Water	TE buffer	21.7 \pm 7.8
AUM	TE buffer	22.0 \pm 4.2
AUM	AUM	21.6 \pm 6.2

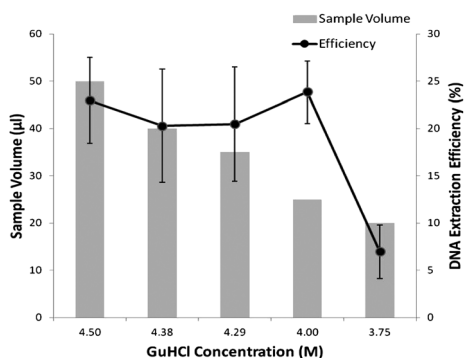


Fig. 2 Effects of varying the amount of GuHCl added to the biological sample on DNA extraction efficiency ($n = 6$).

variation in DNA extraction efficiency was observed for ratios of 1 : 9, 1 : 7, 1 : 6 and 1 : 4 (corresponding to final GuHCl concentrations of 4.5 M, 4.38 M, 4.29 M and 4 M) (Fig. 2). A dramatic reduction in efficiency was found to occur, however, once the ratio was reduced to 1 : 3 (3.75 M GuHCl), indicating insufficient quantity of chaotrope to achieve successful DNA binding to the silica-based monolith. Subsequently, experiments were conducted which indicated that GuHCl could be dissolved directly in the urine-based sample to give a final concentration of 5 M without compromising DNA extraction efficiency. Samples were subsequently prepared using this technique in all further experiments allowing sample volumes to be minimised by eliminating addition of GuHCl in solution.

Further characterisation of the system was performed using the microfluidic device to investigate the effects of increasing the rate of sample loading on to the monolith on DNA extraction efficiency. Experiments were carried out using the standard conditions described but with sample loading flow rates increased from $2.5 \mu\text{l min}^{-1}$ to 5, 10 and $25 \mu\text{l min}^{-1}$. Flow rates for DNA loading could be increased by up to 4 fold ($10 \mu\text{l min}^{-1}$) without apparent reduction in DNA extraction efficiency, permitting more rapid processing of large volume samples (Fig. 3). At a flow rate of $25 \mu\text{l min}^{-1}$, however, DNA binding to the silica monolith was found to decrease markedly associated with a reduction in DNA extraction efficiency.

Validation experiments using the biological model described above were performed by dissolving GuHCl directly in the simulated urine sample to give a final concentration of 5 M and loading on to the monolith at $10 \mu\text{l min}^{-1}$. Analysis of extracted

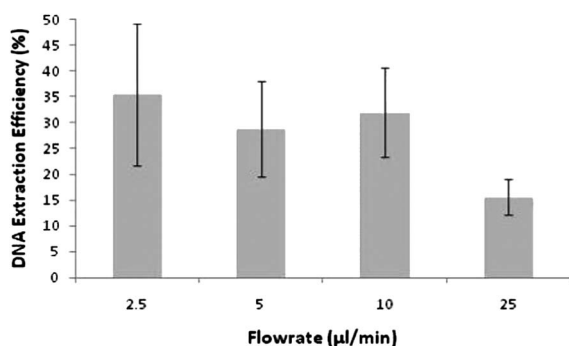


Fig. 3 Effect of the sample loading flow rate on DNA extraction efficiencies ($n = 6$).

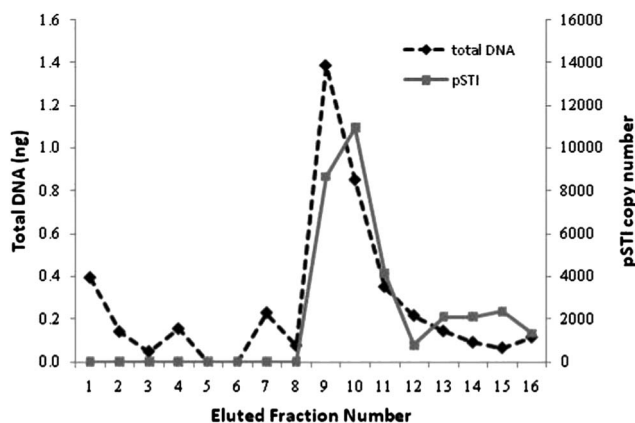


Fig. 4 A typical DNA elution profile illustrating co-elution of host (total dsDNA (black dotted line)) and pathogen DNA (number of pSTI copies as determined by qPCR (grey solid line)) from the microfluidic system.

DNA by qPCR showed the DNA to be of sufficient quantity and quality for successful amplification to be achieved (Fig. 4). In addition, these findings suggest that any AUM components potentially co-purified with the extracted DNA do not inhibit quantitation. Comparison of results from the PicoGreen[®] assay of total dsDNA and pSTI plasmid detection by qPCR showed co-elution of human gDNA with pSTI (Fig. 4).

Furthermore, studies varying the amount of human gDNA ($25\text{--}50 \text{ ng}$) and pSTI (10^4 to 10^5 plasmid copies) contained in the model sample did not affect the ability of the system to extract DNA suitable for analysis by qPCR (results not shown).

Conclusions

A novel method for DNA extraction on a microfluidic device directly from a urine-based sample is reported which addresses issues associated with processing large sample volumes and speed of analysis, critical for the development of a POC diagnostic platform. Current clinically validated molecular diagnostic kits use around $400 \mu\text{l}$ of urine, which are volumes that lie well within the sample loading capacity of the microfluidic system described. Being able to process up to 1 ml of sample using this system provides potential for specific tailoring of the specimen volume according to the target organism, in order to achieve the required sensitivity for detection even at low target copy numbers. The capacity to process such a large volume sample of potentially low target concentration will facilitate earlier presymptomatic disease diagnosis as well as detection of low target number coinfections, key goals in the prevention of STI transmission through earlier diagnosis and appropriate treatment. Furthermore, the system described successfully accommodated variations in both host and pathogen DNA quantity as occurs in clinical samples, where typical human gDNA concentrations range from $14\text{--}200 \text{ ng ml}^{-1}$ in females and $4\text{--}60 \text{ ng ml}^{-1}$ in males.⁹

The use of a non-infectious biological model system as a target in conjunction with an artificial urine medium in this study has permitted the validation of the on-chip sample processing and DNA extraction techniques under standardised conditions which are not achievable using clinical samples, that can be of highly variable composition and present potential infection hazards. Further studies are now required to demonstrate the efficiency of

this system for the analysis of clinical samples in order to account for variations in sample composition, including variable levels of host genomic background DNA and the stage of infection affecting concentration of infectious agent DNA.

Since the extracted DNA was shown to be suitable for PCR amplification there is potential for the methodology described here to be integrated with downstream processes, such as qPCR or isothermal amplification, in a single microfluidic device. Such a device could offer a POC platform for STI detection in a clinical setting enabling sample analysis, diagnosis and treatment in a single visit.

Acknowledgements

The authors would like to thank Dr Steve Clark, University of Hull for manufacturing the microfluidic devices. This work was funded, in part, by the UK National Measurement System.

Notes and references

- 1 L. Greer and G. Wendel, *Infect. Dis. Clin. North Am.*, 2008, **22**, 601–617.
- 2 G. V. Kaigala, R. J. Huskins, J. Preisaitis, X. L. Pang, L. M. Pilarski and C. J. Backhouse, *Electrophoresis*, 2006, **27**, 3753.
- 3 J. Schirm and W. G. MacKay, *QCMD Neisseria gonorrhoeae (NgDNA08) EQA Programme*, 2008.
- 4 T. Baier, T. E. Hansen-Hagge, R. Gransee, A. Crombé, S. Schmahl, C. Paulus, K. S. Drese, H. Keegan, C. Martin, J. J. O'Leary, L. Furberg, L. Solli, P. Grønn, I. M. Falang, A. Karlgård, A. Gulliksen and F. Karlsen, *Lab Chip*, 2009, **9**, 3399–3405.
- 5 M. D. Kulinski, M. Mahalanabis, S. Gillers, J. Y. Zhang, S. Singh and C. M. Klapperich, *Biomed. Microdevices*, 2009, **11**, 671–678.
- 6 J. Wen, L. A. Legendre, J. M. Bienvenue and J. P. Landers, *Anal. Chem.*, 2008, **80**, 6472–6479.
- 7 K. J. Shaw, D. A. Joyce, P. T. Docker, C. E. Dyer, J. Greenman, G. M. Greenway and S. J. Haswell, *Lab Chip*, 2009, **9**, 3430–3432.
- 8 T. Brooks and C. W. Keevil, *Lett. Appl. Microbiol.*, 1997, **24**, 203–206.
- 9 N. Vu, A. Chaturvedi and D. Canfield, *Forensic Sci. Int.*, 1999, **102**, 23–34.

Integrated DNA extraction and amplification using electrokinetic pumping in a microfluidic device

Joseph Parton, Christopher Birch, Cordula Kemp, Stephen J. Haswell, Nicole Pamme and Kirsty J. Shaw*

Received 2nd September 2011, Accepted 7th October 2011

DOI: 10.1039/c1ay05552f

An integrated system employing anion exchange for the extraction of DNA from biological samples prior to polymerase chain reaction DNA amplification has been developed, based on microfluidic methodology utilising electrokinetic pumping. In this system, the biological samples were added directly to chitosan-coated silica beads to facilitate DNA immobilisation. The purified, pre-concentrated DNA was then eluted using a combination of electro-osmotic flow enhanced with electrophoretic mobility, which enable DNA to be transported by both mechanisms into the DNA amplification chamber. Through optimisation of the DNA elution conditions, average DNA extraction efficiencies of 69.1% were achievable. Subsequent DNA amplification performed on the microfluidic system demonstrated not only the ability to use electrokinetic movement to integrate the two processes on a single device, but also that the quality and quantity of DNA eluted was suitable for downstream analysis. This work offers an attractive real-world to chip interface and a route to simpler Lab-on-a-Chip technology which eliminates the need for moving parts.

Introduction

Microfluidics has been widely exploited for genetic analysis in order to advance developments in areas such as clinical diagnostics and forensics.^{1,2} Across this wide range of potential applications, it is often necessary to first isolate the nucleic acids from the sample matrix using an extraction step. This allows the target DNA to be purified and/or pre-concentrated.

At present, DNA extraction methodologies employed in microfluidic systems are predominantly silica-based, in which the addition of chaotropic salts to the sample matrix generates the necessary conditions for cell lysis and subsequent denaturing of the free DNA. This in turn leads to the binding of the DNA to a high surface area, solid silica phase.^{3,4} Any biological contaminants or potential inhibitors of downstream processes, such as the polymerase chain reaction (PCR), can then be removed using an alcohol wash and the purified DNA can be eluted in a low ionic strength buffer. While such methodologies have consistently provided a high yield of purified DNA, chaotropic salts and organic solvents have been found to substantially hinder the PCR process. As a result, attempts to integrate silica-based nucleic acid extraction to downstream processes on a single microfluidic device has carried with it the added complication of additional wash steps. In order to experimentally simplify the extraction procedure, modified materials such as movable magnetic silica particles, which carry the bound target

DNA to the elution buffer rather than introducing sample and reagents consecutively, have been reported.⁵

The use of anion exchange resins presents an attractive alternative to silica-based methodologies as they bypass the need for chaotropic salts and organic solvents by utilising surface chemistries which facilitate binding and elution of DNA to/from the solid-phase matrix by pH manipulation. Nakagawa *et al.* developed a microfluidic device which integrated a silicon wafer coated with amino groups to allow DNA recoveries of 40% from whole blood by the capture and release of DNA at pH 7.5 and 10.6 respectively.⁶ More recently, the field has capitalised on a similar surface activity provided by the increasingly popular and highly versatile biomaterial chitosan ($\alpha(1 \rightarrow 4)$ -linked 2-amino-2-deoxy- β -D-glucopyranose). The bioactive polymer, synthesised from the partial deacetylation of naturally occurring chitin, possesses a variety of physical characteristics, such as high solubility, viscosity and biodegradability.⁷ Importantly, the presence of reactive amino side groups with a pK_a of 6.3 makes chitosan an ideal solid-phase matrix for DNA extraction as deprotonation, and hence DNA release, can occur at pH 9 leaving the DNA in a suitable media for subsequent PCR. Furthermore, the ability to treat silica surfaces with chitosan directly has inspired a number of microfluidic applications and several high performing DNA purification methodologies have emerged. Cao *et al.*, for example, were able to integrate chitosan-coated beads into a microfluidic device and obtained DNA recoveries from whole blood as high as 75%.⁸ Simple hydrodynamic pumping techniques were implemented to flow sample and reagents through the bead-packed extraction chamber allowing easy retrieval of target DNA for further analysis. Reedy *et al.*

Department of Chemistry, University of Hull, Cottingham Road, Hull, HU6 7RX, UK. E-mail: k.j.shaw@hull.ac.uk; Fax: +44 (0)1482 466416; Tel: +44 (0)1482 466746

used a similar approach in conjunction with a preceding silica-based step, highlighting chitosan as an especially effective tool for nucleic acid preconcentration. This additional step provided a significant 50-fold reduction in elution volume which is highly appealing as it is more manageable for PCR.⁹ In further work, Reedy and colleagues adopted a modified approach by using pre-fabricated polymeric micro-posts functionalised with chitosan. Also using hydrodynamic pumping, the work demonstrated the ability to functionalise a wider variety of materials (*e.g.* poly (methyl methacrylate)) with chitosan for DNA extraction.¹⁰

The use of electrokinetic movement of reagents, *i.e.* electroosmotic flow (EOF) and/or electrophoresis, in microfluidic devices is a desirable alternative to hydrodynamic pumping, as it eliminates the need for moving parts and simplifies the experimental process both mechanically and spatially. Such techniques have been used to successfully integrate DNA extraction and amplification steps, demonstrating the process as a suitable real-world to chip interface.¹¹ In addition to this, Shaw *et al.* showed how a reversal of normal EOF (*i.e.* using a net positive charge on the surface generating bulk flow towards the positive electrode) using a suitable surface functional group (*e.g.* hexadimethrine bromide) is especially welcome in analysis of nucleic acids, as the negatively-charged sugar-phosphate backbone ensures an electrophoretic movement which compliments the direction of the bulk flow. This combined electrokinetic movement can be advantageous, in terms of both experimental timescale and energy usage.¹¹

In the work presented here, an integrated microfluidic device for performing DNA extraction and amplification is described in which all sample and reagent movement within the system is controlled electrokinetically. For the first time, the processes support an anion exchange methodology using chitosan-coated silica beads for the initial DNA purification step. Furthermore, the observed reverse-EOF in the presence of chitosan-treated surfaces is capitalised on for optimum experimental performance.

Experimental

Manufacture and functionalisation of microfluidic devices

Glass microfluidic devices were produced using standard photolithography and wet-etching techniques to produce the design shown in Fig. 1. The 1 mm base plate was etched to a depth of 100 μm and then thermally bonded to a 3 mm top plate containing 3 mm access ports. Silanisation of the PCR chamber was performed in order to prevent DNA polymerase adsorption which would otherwise lead to PCR inhibition.¹² This was achieved by adding a 150 mM solution of trichloro(1*H*,1*H*,2*H*,2*H*-perfluorooctyl)silane [Sigma-Aldrich, UK] in 2,2,4-trimethylpentane [Fisher Scientific, UK] to the PCR chamber for 10 min. Solutions of 2,2,4-trimethylpentane, acetone and distilled water were then sequentially used to wash the device.¹³

Silica beads (40–60 μm diameter) [Sigma-Aldrich, UK] were thoroughly cleaned using piranha solution (2 : 1, $\text{H}_2\text{SO}_4/\text{H}_2\text{O}_2$), washed with water and dried prior to use. The beads were then incubated with a solution of 1% low molecular weight chitosan oligosaccharide lactate [Sigma-Aldrich, UK] and 0.1% (3-glycidyloxypropyl) trimethoxysilane [Sigma-Aldrich, UK] for 8 h at

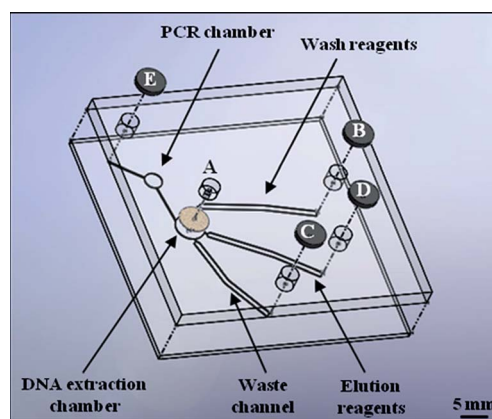


Fig. 1 Schematic of the microfluidic device design used to perform integrated DNA extraction and amplification experiments. The position of the DNA extraction chamber packed with chitosan-coated silica beads, DNA amplification chamber and electrodes (B–E) for performing electrokinetic movement are all illustrated.

room temperature. After chitosan coating, the beads were washed in 10 mM acetic acid and dried at 60 °C prior to use.⁸ When required, the chitosan-coated beads were injected through Port A into the DNA extraction chamber on the microfluidic device, which was designed such that the beads were held in place *via* the keystone effect.

DNA extraction and amplification procedure

In order to enable calculation of the DNA extraction efficiency of the system, human genomic DNA samples were prepared to a final concentration of 5 ng μL^{-1} in an artificial urine matrix.¹⁴ To further evaluate the system real urine samples were used during the integrated DNA extraction and amplification phase. The urine samples were thermally lysed and 50 μL aliquots used for analysis. The biological samples were then added to 10 mM 2-(*N*-morpholino)ethanesulfonic acid (MES) buffer (pH 5) prior to manual injection through Port A onto the solid-phase matrix in order to facilitate DNA binding, with any residual sample directed into the waste channel. Once the biological sample had been loaded, the microfluidic device was sealed with carbon-filled polystyrene electrodes positioned within the ports of the device and connected to an external Paragon 3B Power Supply Unit [Kingfield Electronics, UK] in order to facilitate electrokinetic movement.

Following this, the solid-phase was washed with 10 mM MES buffer, contained within channel B, in order to remove any potential contaminants of downstream processes. This was achieved by applying a voltage between electrodes B and C. The pre-concentrated, purified DNA was then eluted using 10 mM Tris buffer with 50 mM KCl (pH 9), contained within channel D, by applying a voltage between electrodes D and E. Whilst optimising the electrokinetic movement it was found that cooling the microfluidic device to 4 °C increased the efficiency of the process by reducing Joule heating, which in turn minimized sample evaporation/diffusion.

Subsequently DNA amplification *via* PCR was performed on the microfluidic device. The PCR solution consisted of: 1x

GoTaq[®] buffer, 2 mM MgCl₂, 1 unit GoTaq[®] Hot Start DNA polymerase [Promega, UK], 10 mg ml⁻¹ bovine serum albumin [NEB Inc., UK], 0.01% (w/v) poly(vinylpyrrolidone), 0.1% (v/v) Tween-20 [Sigma-Aldrich, UK], 200 μM each deoxyribonucleotide triphosphates [Biolone, UK] and 0.1 μM Amelogenin forward and reverse primers¹⁵ [Eurofins MWG Operon, Germany]. Thermal cycling was performed using a thermoelectric Peltier element, which provided both the heating and cooling required. The following program was used: an initial denaturation step of 95 °C for 2 min, 35 cycles of 94 °C for 30 s, 60 °C for 30 s and 72 °C for 30 s, with a final extension step of 60 °C for 7 min. Control PCR samples were also run on a Techne TC-312 thermal cycler.

DNA quantification and capillary electrophoresis

DNA quantification was performed using a Quant-iT[™] PicoGreen[®] double stranded DNA Assay Kit [Invitrogen, UK] and analysed using a FLUOstar Optima Plate Reader [BMG Labtech, UK]. All amplified DNA samples were analysed off-chip by capillary gel electrophoresis using a 3500 Genetic Analyzer [Applied Biosystems, UK]. Samples (1 μL) were added to 12 μL of Hi-Di[™] Formamide and 0.5 μL GeneScan[™] 500 LIZ[®] Size Standard [Applied Biosystems, UK] and denatured for 5 min at 95 °C before being snap-cooled on ice and loaded onto the instrument.

Results and discussion

Movement of reagents within the microfluidic device

Initial experiments were designed to assess the compatibility of the different reagents required for chitosan-based anion exchange methodology with EOF movement. It was found that all solutions were capable of supporting EOF and so a range of voltages (50–500 V cm⁻¹) were examined to evaluate flow rates. The EOF mobilities for the wash and elution buffers were found to be 3.70×10^{-4} cm² V⁻¹ sec⁻¹ and 3.95×10^{-4} cm² V⁻¹ sec⁻¹, respectively (Fig. 2).

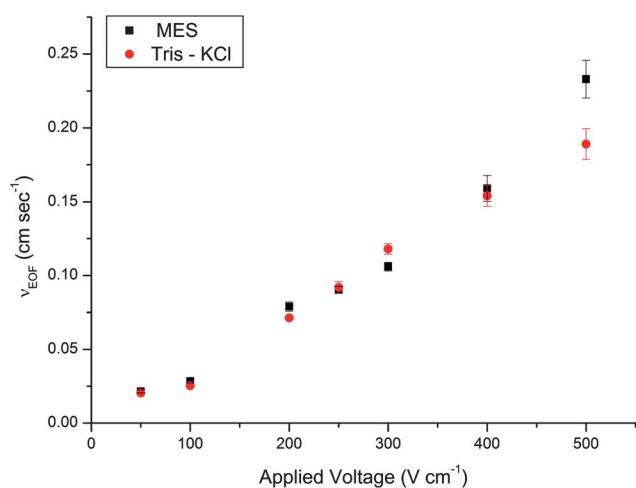


Fig. 2 Graph showing the average v_{EOF} at different applied voltages for the binding/wash solution [MES buffer pH 5 (■)] and elution solution [Tris-KCl buffer pH 9 (●)] for anion exchange-based DNA extraction.

Due to the anionic nature of the chitosan surface, bulk movement of solutions *via* EOF occurs towards the positive electrode. As the electrophoretic mobility of DNA in free solution is 3.75×10^{-4} cm² V⁻¹ sec⁻¹, this combines with EOF to generate efficient movement of DNA within the microfluidic device.¹⁶

DNA extraction capability

The efficiency of the DNA extraction process was evaluated as a function of the time over which the elution buffer was pumped over the solid-phase. DNA extraction efficiency was calculated as the amount of DNA recovered during the elution expressed as a percentage of the amount of DNA initially loaded onto the system. Maximum DNA yields were obtained when a 20 min elution was used, resulting in an average DNA extraction efficiency of 46.6% ($\pm 5.6\%$) when a potential of 100 V cm⁻¹ was applied (Fig. 3).

The DNA extraction efficiency was also evaluated as a function of the voltage applied during the DNA elution phase using the optimised 20 min elution time (Fig. 4). The data showed a Gaussian shaped distribution, peaking at 100 V cm⁻¹ with an average DNA extraction efficiency of 69.1% ($\pm 10.7\%$). The increase in average efficiency from Fig. 3 is due to the introduction of cooling the microfluidic device in order to minimize the effects of Joule heating.

During the evaluation of DNA extraction efficiency, PCR reagents were loaded onto the microfluidic device within the DNA amplification chamber. Following the extraction process, the PCR reagents were removed and subject to DNA amplification on a conventional thermal cycler in order to assess whether the use of electrokinetic movement had any adverse affect on the reagents. An evaluation of these samples confirmed that the use of electrokinetic movement did not have an inhibitory effect on the PCR reagents. However, it was found that altering the voltages affected the relative PCR efficiency, as observed from a change in fluorescence intensity of the PCR

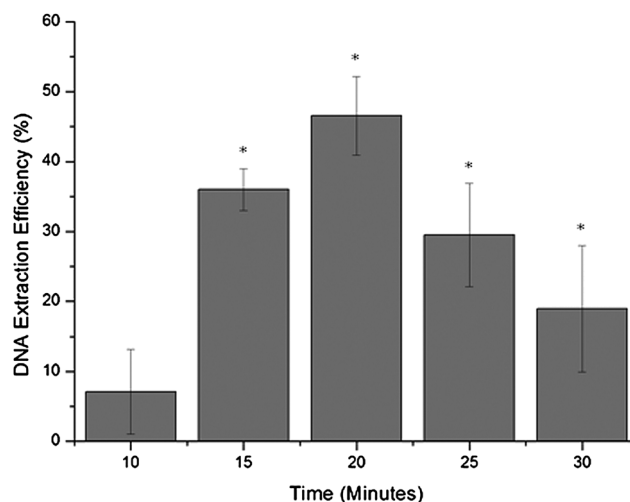


Fig. 3 Graph showing DNA extraction efficiency as a function of the time the voltage was applied in order to perform the elution phase of the DNA extraction process on the microfluidic device, where * denotes eluted DNA samples which were successfully amplified by PCR (n = 3).

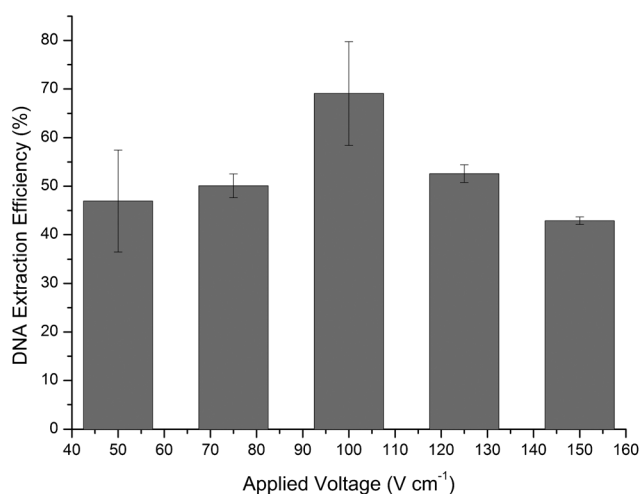


Fig. 4 DNA extraction efficiencies expressed as a function of applied voltage for electrokinetic movement of reagents within the microfluidic system ($n = 3$).

products produced. The most efficient DNA amplification results were obtained when 100 V cm^{-1} was used, as this resulted in an average signal intensity at least 21% higher than at any other applied voltage.

Optimal conditions were achieved using an applied voltage of 100 V cm^{-1} for both DNA extraction and PCR efficiency. Whilst it is clear that the application of different voltages during the DNA extraction step has a direct effect on the efficiency of the process, there maybe direct and/or indirect influences on PCR efficiency. It is hypothesized that both play an important role, whereby the voltage can directly affect the PCR reagents and can also indirectly influence the efficiency of the upstream DNA extraction process resulting in differing quality and quantity of DNA for amplification.

Integrated DNA extraction and amplification

Following optimisation of the DNA extraction process and the confirmation that the PCR reagents were not inhibited by the electrokinetic movement, integration of DNA extraction and amplification on the microfluidic device was evaluated. Control of DNA movement between the DNA extraction and amplification chambers was driven electrokinetically and the eluted DNA was transferred directly into the PCR chamber. The PCR chamber was positioned on a thermoelectric Peltier which was used to provide the thermal cycling. The eluted DNA was successfully amplified on the integrated microfluidic system, as confirmed by off-chip capillary gel electrophoresis (Fig. 5).

Conclusions

Exploitation of EOF with enhanced electrophoretic mobility to achieve electrokinetic pumping provided high DNA extraction efficiencies, using a chitosan-based solid-phase, along with successful DNA amplification. The DNA extraction efficiencies presented are comparable to those summarized in a recent review, which reported average efficiencies of between 60 and

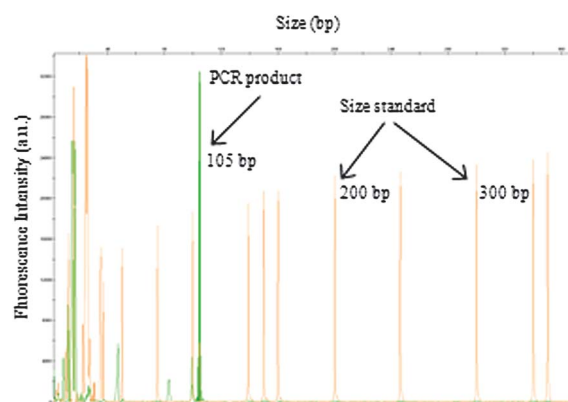


Fig. 5 Electropherogram showing PCR products from the amplification of the Amelogenin locus ($X = 105 \text{ bp}$) from a human urine sample, using DNA extracted and amplified on the integrated microfluidic device as confirmed on an ABI 3500 Genetic Analyzer.

70% for the majority of silica-bead and anion exchange-based microfluidic devices.³

The ability to integrate both DNA extraction and amplification on a single device offers several advantages, including a reduction in the potential for contamination of the biological sample and reduced reagent consumption. While the DNA extraction efficiencies reported here are comparable to those previously described for electrokinetically driven systems, the integration with PCR was improved. By using an anion exchange matrix rather than silica one, the solutions used are more compatible for integration with downstream processes as the use of chaotropic salts and organic solvents can be avoided.¹¹ Moreover, the opportunity exists for further integration with downstream detection techniques such as DNA hybridisation or capillary electrophoresis.

By controlling the movement of reagents electrokinetically, moving components either on- or off-chip are eliminated which greatly reduces the complexity of the design and the footprint of the system. The possibility of incorporating reagent storage as previously described could also increase the application of the system described into 'ready-to-use' microfluidic devices.¹¹

Acknowledgements

The authors would like to thank Dr Steve Clark for manufacturing the microfluidic devices, Dr Peter Docker for development of the Peltier thermal cycling system and Professor Nick Goddard for the kind gift of the carbon filled polystyrene electrodes.

Notes and references

- 1 G. M. Whitesides, *Nature*, 2006, **442**, 368–373.
- 2 K. M. Horsman, J. M. Bienvenue, K. R. Blasier and J. P. Landers, *J. Forensic Sci.*, 2007, **52**, 784–799.
- 3 J. Wen, L. A. Legendre, J. M. Bienvenue and J. P. Landers, *Anal. Chem.*, 2008, **80**, 6472–6479.
- 4 K. A. Melzak, C. S. Sherwood, R. F. B. Turner and C. A. Haynes, *J. Colloid Interface Sci.*, 1996, **181**, 635–644.
- 5 S. M. Berry, E. T. Alarid and D. J. Beebe, *Lab Chip*, 2011, **11**, 1747–1753.

- 6 T. Nakagawa, T. Tanaka, D. Niwa, T. Osaka, H. Takeyama and T. Matsunaga, *J. Biotechnol.*, 2005, **116**, 105–111.
- 7 P. K. Dutta, J. Dutta and V. S. Tripathi, *Journal of Scientific & Industrial Research*, 2004, **63**, 20–31.
- 8 W. D. Cao, C. J. Easley, J. P. Ferrance and J. P. Landers, *Anal. Chem.*, 2006, **78**, 7222–7228.
- 9 C. R. Reedy, K. A. Hagan, B. C. Strachan, J. J. Higginson, J. M. Bienvenue, S. A. Greenspoon, J. P. Ferrance and J. P. Landers, *Anal. Chem.*, 2010, **82**, 5669–5678.
- 10 C. R. Reedy, C. W. Price, J. Sniegowski, J. P. Ferrance, M. Begley and J. P. Landers, *Lab Chip*, 2011, **11**, 1603–1611.
- 11 K. J. Shaw, D. A. Joyce, P. T. Docker, C. E. Dyer, G. M. Greenway, J. Greenman and S. J. Haswell, *Lab on a Chip*, 2011.
- 12 I. Erill, S. Campoy, N. Erill, J. Barbe and J. Aguilo, *Sens. Actuators, B*, 2003, **96**, 685–692.
- 13 H. Hartshorne, C. J. Backhouse and W. E. Lee, *Sens. Actuators, B*, 2004, **99**, 592–600.
- 14 T. Brooks and C. W. Keevil, *Lett. Appl. Microbiol.*, 1997, **24**, 203–206.
- 15 B. E. Krenke, A. Tereba, S. J. Anderson, E. Buel, S. Culhane, C. J. Finis, C. S. Tomsey, J. M. Zachetti, A. Masibay, D. R. Rabbach, E. A. Amriott and C. J. Sprecher, *Journal of Forensic Sciences*, 2002, **47**, 773–785.
- 16 J. Chen, M. Wabuye, H. Chen, D. Patterson, M. Hupert, H. Shadpour, D. Nikitopoulos and S. A. Soper, *Anal. Chem.*, 2005, **77**, 658–666.

A Microfluidic System for Testing the Responses of Head and Neck Squamous Cell Carcinoma Tissue Biopsies to Treatment with Chemotherapy Drugs

SAMANTHA M. HATTERSLEY,^{1,2} DEBORAH C. SYLVESTER,¹ CHARLOTTE E. DYER,¹ NICHOLAS D. STAFFORD,¹ STEPHEN J. HASWELL,² and JOHN GREENMAN¹

¹Centre for Biomedical Research, Postgraduate Medical Institute, University of Hull, Cottingham Road, Kingston upon Hull HU6 7RX, UK; and ²Department of Chemistry, University of Hull, Cottingham Road, Kingston upon Hull HU6 7RX, UK

(Received 4 July 2011; accepted 1 October 2011; published online 15 October 2011)

Associate Editor Michael Shuler oversaw the review of this article.

Abstract—Tumors are heterogeneous masses of cells characterized pathologically by their size and spread. Their chaotic biology makes treatment of malignancies hard to generalize. We present a robust and reproducible glass microfluidic system, for the maintenance and “interrogation” of head and neck squamous cell carcinoma (HNSCC) tumor biopsies, which enables continuous media perfusion and waste removal, recreating *in vivo* laminar flow and diffusion-driven conditions. Primary HNSCC or metastatic lymph samples were subsequently treated with 5-fluorouracil and cisplatin, alone and in combination, and were monitored for viability and apoptotic biomarker release ‘off-chip’ over 7 days. The concentration of lactate dehydrogenase was initially high but rapidly dropped to minimally detectable levels in all tumor samples; conversely, effluent concentration of WST-1 (cell proliferation) increased over 7 days: both factors demonstrating cell viability. Addition of cell lysis reagent resulted in increased cell death and reduction in cell proliferation. An apoptotic biomarker, cytochrome *c*, was analyzed and all the treated samples showed higher levels than the control, with the combination therapy showing the greatest effect. Hematoxylin- and Eosin-stained sections from the biopsy, before and after maintenance, demonstrated the preservation of tissue architecture. This device offers a novel method of studying the tumor environment, and offers a pre-clinical model for creating personalized treatment regimens.

Keywords—Head and neck squamous cell carcinoma, 5-fluorouracil, Cisplatin, Lactate dehydrogenase, Cytochrome *c*.

INTRODUCTION

Discovering improved prognostic models remains a high priority for clinicians. At present, the vast majority of pre-clinical models use cell-based methodologies or animal models. Although these models have given invaluable information for the prognosis and diagnosis of several pathological and physiological conditions, as yet, most of these questions remain largely unanswered because of the complexity of disease progression.^{14,19} While cell-based models make use of human-derived cell types, these have been modified and transformed for *in vitro* culture conditions. In recent years, protocols have changed to include extracellular matrix (ECM) and different cell types; however, these models still lack the complexity of *in vivo* microenvironment.¹⁹ The alternative to cell-based methods has been the use of animal models which too have major drawbacks as a number of pathological and physiological pathways can differ from animal to animal, and animal to human, leading to results that cannot be translated to the clinical setting as well as the additional ethical and moral considerations.^{14,24}

The major biological benefit of microfluidics is the ability to replicate the *in vivo* environment, which is lost when using traditional macroscopic vessels. Parameters, such as laminar flow, mass transport driven by diffusion rather than turbulence, constant removal of waste products, while maintaining cell-to-cell interactions *via* paracrine- and autocrine-signaling molecules, can all be incorporated into such devices. The ability to replicate the *in vivo* dynamics of biological tissue is

Address correspondence to John Greenman, Centre for Biomedical Research, Postgraduate Medical Institute, University of Hull, Cottingham Road, Kingston upon Hull HU6 7RX, UK. Electronic mail: j.greenman@hull.ac.uk

revolutionary and when applied to tumor biology provides a unique platform to explore the pathological microenvironment with the analysis of released paracrine and autocrine molecules. Ultimately, this technology will permit a better understanding of biological mechanisms operating within pathological and normal tissues as well as providing a gateway to novel point of care devices for biomarker monitoring.

Current studies of cancer dynamics within microfluidic systems have principally focused on evaluating the steps involved in cancer cell metastasis, with a benefit of these studies being that these factors make ideal biomarkers in many instances. In such studies, tumor cells have been exposed to differing shear stresses and chemokine gradients, parameters that change in capillaries *in vivo*, to study factors thought to be involved in generating circulating tumor cells.^{34,35} Others have examined the site of attachment and adhesion itself through the use of isotropic silicon microstructures and matrigel lined with human microvascular endothelial cells—highlighting the biomechanical properties of normal and cancer cells.^{9,21} A third group of studies have examined cell deformability, to distinguish between normal, benign, and metastatic cancer cells using antibody-coated microchannels, to develop a test for metastatic disease.^{5,15}

In this article, we describe a microfluidic platform that will address many of these parameters, using head and neck tumor biopsies to demonstrate proof of concept. Worldwide, head and neck cancer is the sixth most frequent solid tumor with about 90% of these being squamous cell carcinomas (HNSCC).⁸ These cancers are more frequent in people over the age of 50 and are more common in males.²⁰ However, there is evidence of an increase in incidence in the younger population; such a group would most likely benefit from targeted therapy.⁸ Despite advances in chemotherapy, radiotherapy, and surgical techniques, 5-year survival rates remain largely unchanged for the last 3 decades. HNSCC encompasses a heterogeneous group of tumors with distinct epidemiology, biology, and clinical behavior, with each subsite differing greatly in management and prognosis; however, they are often grouped together in research studies because of limited amounts of tissue and inadequate culture techniques. The relatively small biopsy-sizes available and the lack of advances in treatment make this malignancy ideally suited to a microfluidic-based analysis approach.

Rapid and easily detected markers of cell death are needed for appraising early therapeutic efficiency for chemotherapy, so that patients and their oncologists can make better informed decisions regarding treatment strategies. In recent laboratory studies, it has been shown that tumor cells undergoing apoptosis release cellular components into the culture media, for

example, cytochrome *c*.^{3,31,33} Ideally, such markers should be detected within hours or days, giving a specific response that relates to positive or negative outcome of on-going or completed treatment, and to determine the continuing effectiveness of targeted therapies saving the expense of long term (>5 years) follow-up studies.^{7,36} The main objective of this study is the demonstration that an explant-based microfluidics device can be used effectively to analyze apoptosis-related biomarkers offering a new type of technology with wide-spread applications.

MATERIALS AND METHODS

Design and Microfabrication of the Microfluidic Device

The microfluidic devices were fabricated using photolithography techniques as described previously.^{4,23} AutoCAD LT software, a computer-assisted design package, was used to design the microdevice from which a photomask was generated. The final device was generated in glass using standard photolithography and wet-etching techniques.⁴ Access holes and a central chamber (diameter 3 mm) were drilled in the top plate and was then thermally bonded with the etched bottom plate in a furnace at 590 °C for 3 h. The channel network was etched into the bottom 1-mm glass layer to produce channels of 190- μ m width and 70- μ m depth, which diverged into two channels as shown in Fig. 1.

Microfluidic System for Maintaining Tissue Biopsies

As described in previous study,¹² the microfluidic device had a microport (Anachem, UK) glued to the surface of the top glass layer such that the circular tissue cavity could be sealed using an English-threaded adapter (Anachem, UK). The adapter was filled with poly-dimethylsiloxane (PDMS; Dow Corning, UK) to allow gaseous exchange to occur. The tissue chamber is cylindrical with a volume of approximately 20 μ L. A Harvard PhD 2000 syringe pump (Harvard, UK) was connected to the device *via* 0.8 mm (internal diameter) \times 1.58 mm (external diameter) TFE Teflon[®] tubing (Anachem, UK). The length of the tubing from syringe to the device was 30 cm, and this allowed sufficient time for the media to be heated to 37 °C before reaching the tissue. A 0.22- μ m syringe filter (Millipore, UK) was fitted in-line to remove any bacterial contamination; this also minimized the generation of gas bubbles in the media. A 1.5-mL microcentrifuge tube (Sarstedt, UK) with a hole in the lid covered with parafilm to stop contamination and leakage was placed on each end of the outlet tubing to

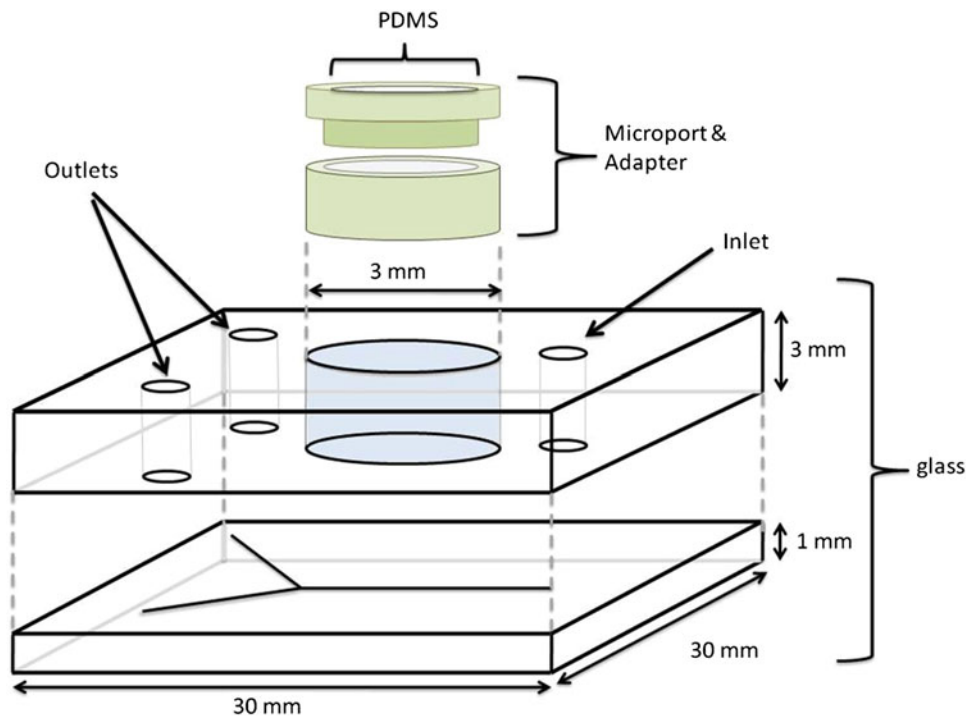


FIGURE 1. Schematic of glass microfluidic device used in these studies. Access holes and a central chamber (diameter 3 mm) were drilled in the top plate. The channel network was etched into the bottom 1-mm glass layer to produce channels of 190- μm width and 70- μm depth, which diverged into two channels. The tissue chamber, shaded blue, was sealed with a threaded adaptor filled with PDMS during perfusion.

collect eluate. The entire system was placed in a portable incubator at 37 °C.

Establishment of HNSCC Tissue Biopsies

In this study, histopathological-confirmed samples from 23 patients undergoing surgery for HNSCC were studied within 107 microfluidic devices. Samples were provided in an anonymous manner, apart from the type of tumor, in accordance with Local Research Ethics Committee and NHS Trust R&D approval (LREC-07/H1304/105; R0568). Tissue biopsies obtained during neck lymph node dissection or primary tumor resection were transported to the laboratory in media at 4 °C. Within 40 min of resection, the tissue was cut into approximately 3 mm³ sections, with the weight of each individual sample recorded. The microfluidic system was cleaned before use by pumping 70% (v/v) ethanol/water through the device for 15 min at 10 $\mu\text{L min}^{-1}$ followed by a rinse with autoclaved, distilled water. The device was then primed with Dulbecco's Modified Eagle's medium, DMEM (Gibco, UK) supplemented with 1% (w/v) penicillin/streptomycin (Sigma, UK) at a flow rate of 20 $\mu\text{L min}^{-1}$ for 30 min and set in the incubator. DMEM uses phenol red as a pH indicator that gradually changes from yellow to red over the pH range of 6.8–8.2 that is routinely used in cell culture.

When cells are necrotic, released cell products cause acidification of the media, turning this to turn from pink to yellow.¹⁷ In addition, waste products produced by mammalian cells will slowly decrease the pH if accumulation occurs;²⁹ inclusion of the indicator within media is a simple way to confirm the health of cultured cells. The tumor sample was then added to the central well of the microchip giving a ratio of chamber to tissue volume of approximately 1:0.8. The cavity was sealed using the threaded adaptor, and the flow rate reduced to 2 $\mu\text{L min}^{-1}$. A visual check was made to ensure no bubbles were trapped in the chamber; any bubbles observed were removed using a sterile hypodermic needle. The effluent from both outlets of the microfluidic device was collected for a period of 30 min and then combined in a 0.5 mL microcentrifuge tubes for analysis. Samples were stored at 4 °C for up to 6 h before the appropriate assays were performed.

Analysis of HNSCC Samples Incubated in the Microfluidic Device

Histological Examination of Tissue Sections Using H&E Staining

To visualize cell architecture samples were taken before, and after, perfusion in the microfluidic device. Tissue was embedded on a cork tile covered with

Tissue-Tek® (Sakura, Netherlands) and plunged immediately in liquid-nitrogen-cooled 2-methyl butane solution (Sigma, UK). Frozen sections (12 μm) were cut using a Microm HM505E cryostat, fixed with 10% (v/v) formalin and stained with Hematoxylin and Eosin (H&E) using standard protocols.² Stained sections were reviewed by Dr. L. Karsai (Consultant Histopathologist, Hull & East Yorkshire NHS Trust).

Measurement of Viability Using Lactose Dehydrogenase Release and WST-1 Metabolism

To quantify cell viability and proliferation, a colorimetric cytotoxicity assay (Cytotoxicity Detection Kit Plus, LDH, Roche, UK) and a Water Soluble Tetrazolium (WST-1) Cell Proliferation Assay (Roche, UK) were used, respectively. Analyses were carried out according to the manufacturer's protocols with the exception that all LDH test samples were diluted 1:10 before analysis—based on preliminary experiments. The results are expressed as an average determined from triplicate samples. The background LDH and WST-1 levels present within the media were subtracted, and the data normalized per mg of tissue. For the determination of viability after perfusion (up to 72 h), tissue samples were incubated with 10% (v/v) lysis buffer from the Cytotoxicity Detection Kit introduced at $2 \mu\text{L min}^{-1}$ for 4.5 h.

Chemotherapy Treatments

Eight microfluidic systems were used in parallel allowing all the variables of chemotherapy treatments to be explored on a single cancer biopsy from a single patient. Before the tissue was placed in the microfluidic systems, these were sterilized by the passage of 70% (v/v) ethanol for 20 min at $10 \mu\text{L min}^{-1}$ then rinsed with sterile, distilled water as described above.

For the first 12 h of the experiment, only DMEM flowed through the system. After 12 h, the media were changed in six of the microfluidic systems (two systems remained as controls with media only flowing through the tissue). For the six systems receiving drugs: two systems had $0.2 \mu\text{g mL}^{-1}$ cisplatin (CDDP) in DMEM, two systems had $1.0 \mu\text{g mL}^{-1}$ 5-fluorouracil (5-FU) in DMEM; and the remaining two had both $0.2 \mu\text{g mL}^{-1}$ CDDP and $1.0 \mu\text{g mL}^{-1}$ 5-FU in DMEM. These concentrations were used in a previous study that examined a 3D cell culture system, constructed from silicon and PDMS with multi-microchannels, for evaluating the effect of chemotherapy drugs on cancer cells and closely resemble the concentrations found in a patient's plasma undergoing chemotherapy treatment.³² The treatment period was 7 days with the total experiment lasting 8 days.

Effluent was collected constantly in 4-hourly aliquots throughout the day and night for the 7 days of treatment. These samples, six for every 24 h, were analyzed in duplicate, and then the results were averaged for the whole 24 h to give daily values.

Viability Analysis of Single Cells Released from the Biopsy During Incubation

Cancer cells were collected in the effluent from the microfluidic system after the 7-day incubation period. This was collected for 3 h in a 1.5 mL micro centrifuge tubes and centrifuged at 100 g for 5 min. The supernatant containing cell debris was removed by aspiration, and then the cells were resuspended in DMEM. To quantify cell viability equal volumes of 2% (w/v) trypan blue and cell solution were mixed, and the cell count enumerated using a hemocytometer. Counts were measured in duplicate and the percentage viability determined.

Cytochrome c Analysis

Cytochrome *c* is a 14.5 kDa protein that is located in the inner mitochondria membrane in healthy cells and is a key component of the electron transport chain in the respiration, functioning as an electron shuttle.³⁰ During apoptosis, cytochrome *c* is liberated from the mitochondria into the cytoplasm, where it is then released into the culture media.³⁸ Within 1 h of treatment, cytochrome *c* was found in the media whereas LDH was released only after 15 h.²⁸ In necrosis it was shown that cytochrome *c* remains within the cell and is not released into the media. There is much speculation of the biological significance of the release of cytochrome *c*, with studies showing various anti-inflammatory effects, e.g., guiding phagocytes to sites of injury, and increasing the effect of apoptosis and cell shrinkage by inducing K^+ efflux from cells.^{1,25,28} To quantify the release of cytochrome *c* within the tissue sample, a quantitative sandwich enzyme immunoassay technique (Quantikine®, Human Cytochrome *c*, R&D Systems, USA) was carried out following the manufacturer's protocol. Cytochrome *c* has a half-life of 8 days²², and therefore samples were kept at 4 °C until the experiment was completed, and all samples were analyzed on the same plate.

RESULTS

Characterization of Tissue Viability and Metabolic Activity

To validate the microfluidic device's ability to model the *in vivo* cancer microenvironment, HNSCC tissue

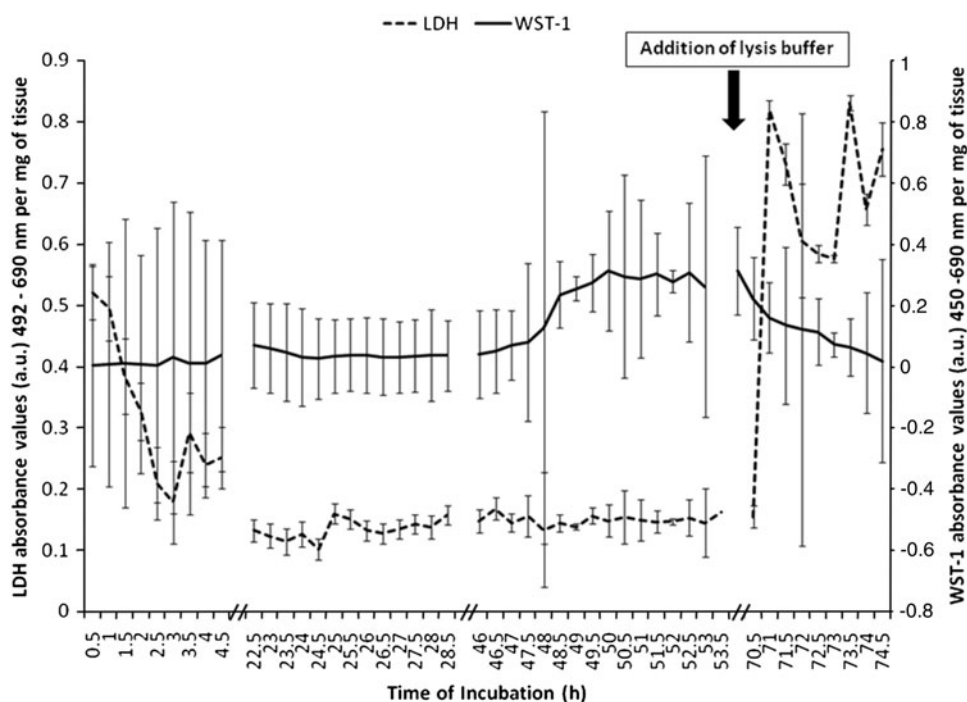


FIGURE 2. LDH release and WST-1 metabolism of primary HNSCC tissue with the addition of 10% lysis buffer after 70 h. Aliquots of effluent were collected every 30 min for determination of LDH and WST-1 concentration in duplicate; all values were then standardized per mg of biopsy. Data are expressed as the mean (\pm S.E.M) of 22 separate experiments.

samples were placed in a microfluidic system, while the viability was examined using biochemical biomarkers: water soluble tetrazolium (WST)-1 metabolism and lactate dehydrogenase (LDH) release over a 75-h time period. WST-1 metabolism is achieved by the mitochondrial enzyme succinate-tetrazolium reductase, and increases in proportion with the number of viable cells. LDH is a cytoplasmic enzyme that is constitutively expressed in most mammalian cells, enabling its widespread use for assessing plasma membrane integrity by detecting the amount of LDH released into the supernatant. During the subsequent experiments, only two cases of media color change were recorded, and these samples were removed from the study as this change was caused by bacterial contamination.

After an initial peak of LDH release at the beginning of the experiment, thought to be due to the damage caused to the surface of the tissue in harvesting and handling, levels decreased and remained low for the next 48 h (Fig. 2). On application of the lysis buffer, that ruptures cell membranes, after 70 h there was a marked rise in LDH release. LDH levels remained high for the next 5 h as more cells became exposed to the lysis buffer as this diffused through the tissue. In contrast to LDH release, WST-1 metabolism only showed an increase in detectable formazan product after approximately 40 h. The delay in detection of product is most probably due to the fact that only the outer layers of cells would initially be exposed

to the WST-1 reagent, therefore relatively small amounts of substrate would be actively metabolized. As the reagent diffuses further into the tissue, through the extracellular spaces, more cells would become exposed hence increasing the amount of metabolized product. Furthermore, the formazan salt would also take time to diffuse out of the tissue sample into the effluent. Extensive analysis of more than 40 different biopsies of normal²³ and malignant tissues,² from various types of tissues has always shown a 35–50 h delay in WST-1 detection. After the application of lysis buffer at 70 h of tissue maintenance, the amount of formazan salt detected decreases rapidly as the number of viable cells is reduced mirroring the increase in LDH concentration.

To understand whether the characteristics of the tumor tissue had an effect on the results, primary tumor tissue was compared with biopsies from metastatic lymph nodes again using LDH leakage and WST-1 metabolism. When comparing the absorbance values for the LDH release between the primary tumors and nodal tissue, no significant differences were detected (Fig. 3). However, when comparing the metabolism of WST-1 in the primary and secondary tumors, there was a marked difference in the amount of formazan released after 46 h. This could indicate higher proliferation of cells in the primary tumor in comparison with the metastatic node as more cells would produce more formazan. Another factor to be

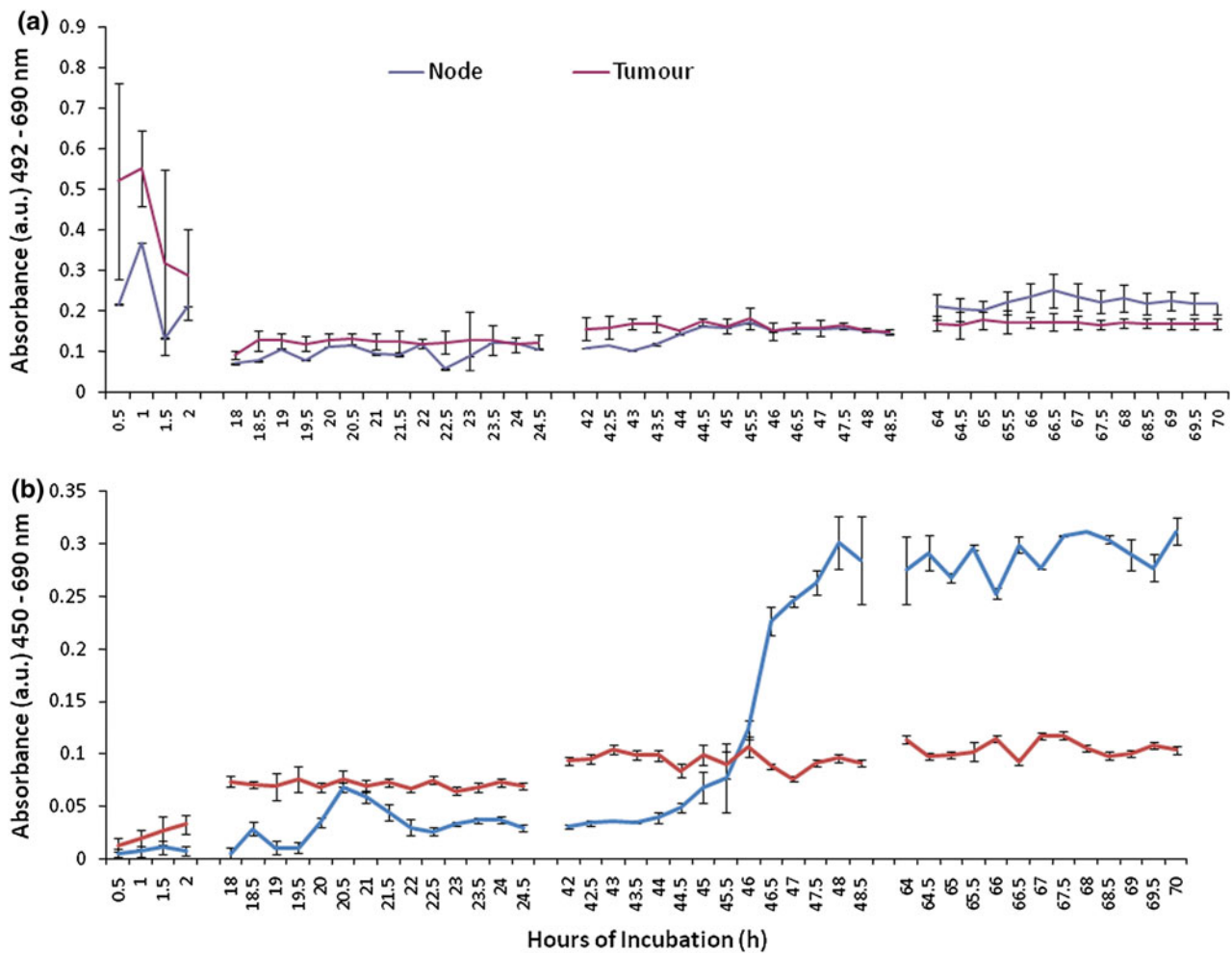


FIGURE 3. Comparison of LDH release and WST-1 metabolism between primary HNSCC and nodal tissue. Aliquots of effluent are collected every 30 min for determination of (a) LDH and (b) WST-1 concentration in duplicate; all values were then standardized per mg of biopsy. Data are expressed as the mean (\pm SEM) of 22 separate experiments.

taken into consideration is the potential difference in the architecture of the biopsies. As tumors develop, the basic morphology of the tissue breaks down with the loss of structure, cohesion, and ECM, causing the tumor tissue to become fenestrated allowing greater diffusion between cells and hence greater access to WST-1 for metabolism and subsequent release. Although this is true for primary tumor, lymph nodes are bounded by a capsule, and thus metastatic deposits are likely to possess a more compact, dense, structure than the primary malignancy; this could contribute to the observed differences in the biochemical markers.

H&E-stained Cryostat Sectioning of HNSCC Biopsy Tissue

A comparison of H&E-stained tissue sections taken before placement in the microfluidic device (Figs. 4a, 4b) and after 72 h of continuous perfusion within the device (Figs. 4c, 4d), indicated that the architecture of

the samples has been maintained. The nuclei appear intact and loss of cell cohesion is minimal. It is notable that there was no evidence of necrosis in the center of the biopsy, supporting the evidence that the microfluidic diffusion properties can facilitate the passage of nutrients, and removal of waste throughout the biopsy.

Analysis of LDH Release and WST-1 Metabolism in Primary HNSCC Biopsies Treated with Chemotherapeutic Drugs

The aim of these preliminary experiments was to determine the viability of tumor tissue after treatment with chemotherapeutic agents within a microfluidic system. All chemotherapy treatments invoked a greater release of LDH than untreated tumor tissue, from the same biopsy, over the 7 day treatment period (Fig. 5).

LDH was released in the greatest concentration in the combination therapy of 5-FU and CDDP. In the first 5 days of treatment, the amount of LDH released

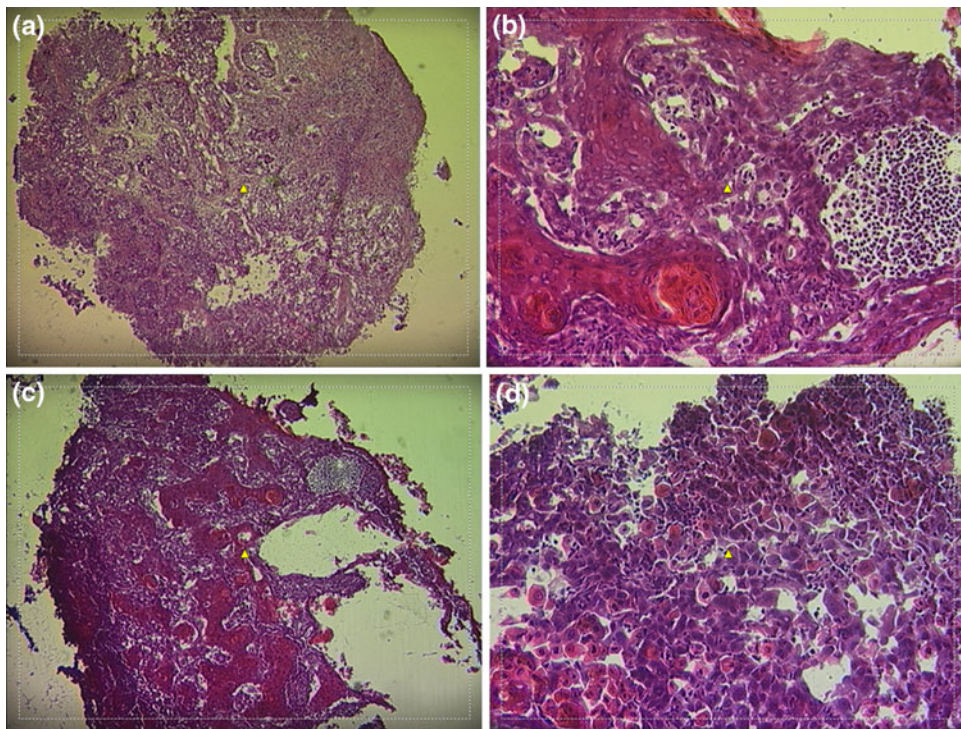


FIGURE 4. H&E-stained cryostat sections of HNSCC. Tumor biopsies before perfusion at 5 \times (a) and 20 \times (b) magnification, and after 72 h of perfusion in media alone at 5 \times (c) and 20 \times (d) magnification were cryostat sectioned (12 μ m) and stained with H&E. Representative images of sections from three separate tumors are shown.

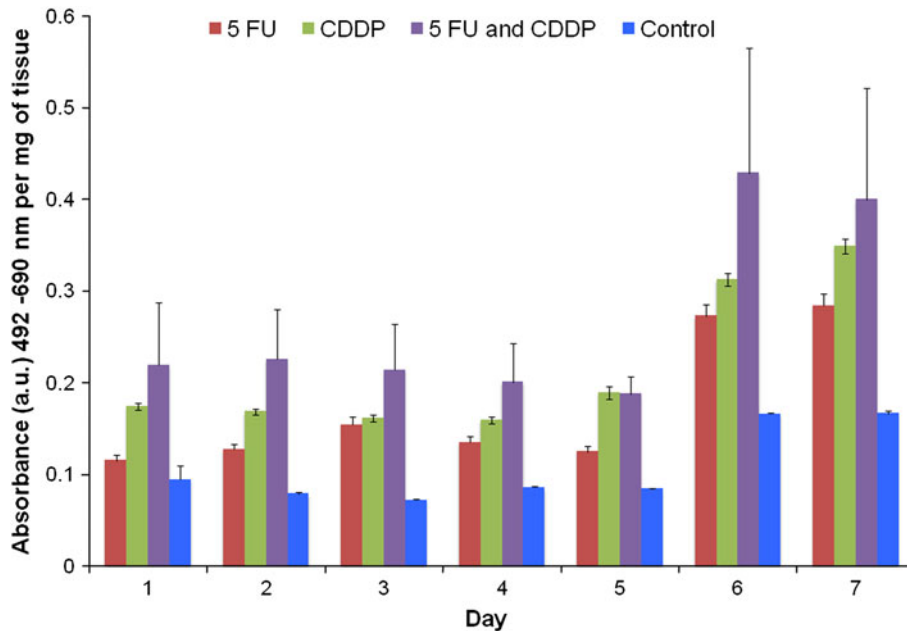


FIGURE 5. LDH released from primary HNSCC tissue during treatment with different chemotherapy treatments (5-FU, cisplatin, and 5-FU with cisplatin) compared with untreated cancer tissue biopsies. Aliquots of effluent are collected each 24 h over 7 days for determination of LDH concentration; all values were then standardized per mg of biopsy. Data are expressed as the mean (\pm SEM) absorbance levels of LDH in the effluent from three separate experiments performed in duplicate.

was approximately double the amount released by the untreated sample, and for the final two days, this increased further. CDDP induced a greater death

response than 5-FU alone; on average, 30% more LDH was released over the exposure period. The combination therapy, however, showed the greatest

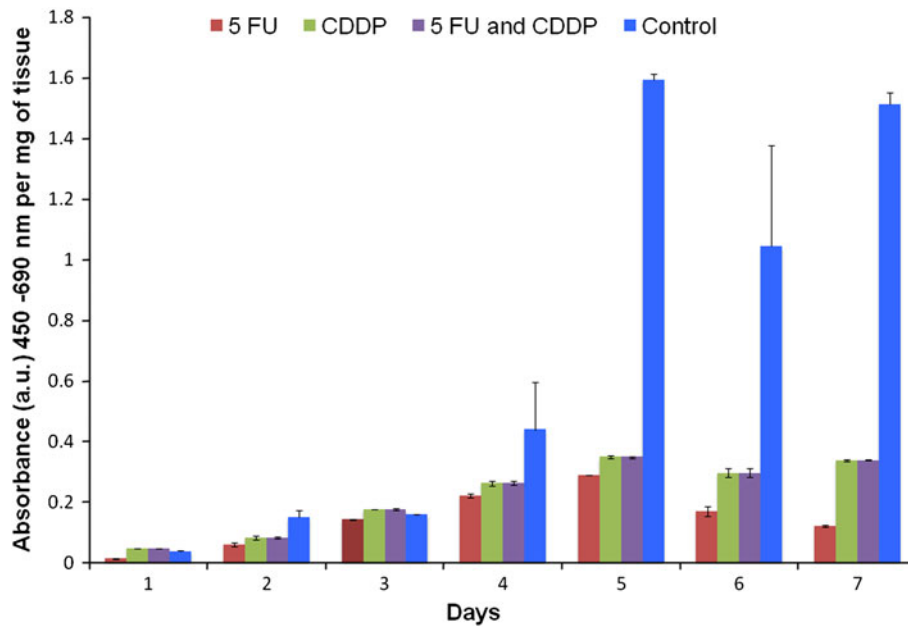


FIGURE 6. WST-1 metabolism in primary HNSCC tissue during treatment with different chemotherapy treatments (5-FU, cisplatin, and 5-FU with cisplatin) compared with untreated cancer tissue biopsies. Aliquots of effluent are collected each 24 h over 7 days for determination of LDH concentration; all values were then standardized per mg of biopsy. Data are expressed as the mean (\pm SEM) absorbance levels of LDH in the effluent from three separate experiments performed in duplicate.

variation between samples as shown by relatively wide error bars (Fig. 5). All treatments over the interrogation period significantly affected the viability of the tissue, as assessed by LDH release, compared with the control (ANOVA, $p < 0.01$). *Post hoc* comparisons using the Tukey test indicated that only the combination treatment was significantly different from the untreated control.

In Fig. 6, the effects of the chemotherapeutic agents on WST-1 metabolism are highly noticeable from Day 5. In the untreated control samples, WST-1 metabolism at Day 5 is over four-and-a-half times more than the samples treated with the chemotherapy drugs, and this is maintained over the next 2 days of treatment. Interestingly, there is no marked difference in the amount of WST-1 metabolized between the three different regimes, however, in these tests, 5-FU treated samples seem to have a slightly greater effect than the two other treatments. This could be a reflection of the 5-FU and CDDP acting *via* different mechanistic pathways and/or differences in the tumor biology. A one-way between-subjects ANOVA showed there was no significant effect of different drug treatments on the tumor samples.

Analysis of Single Cell Viability After Chemotherapeutic Intervention

The aim of this experiment was to determine whether chemotherapeutic agents destroyed cells released

TABLE 1. Percentage of viable single cancer cells recovered after primary tumor tissue was maintained and interrogated in microfluidic system for 7 days.

Drug treatment	Percentage of viable cells collected in eluent from microfluidic system. Number of cells collected in total in brackets
Untreated samples	72% \pm 15.6 (32 \pm 3.27)
5-FU only	45% \pm 22.3 (29 \pm 8.64)
CDDP only	44% \pm 20.2 (32 \pm 2.83)
5-FU and CDDP combination	30% \pm 23.7 (35 \pm 7.48)

Mean (\pm SEM) from three separate experiments.
5-FU, 5-fluorouracil; CDDP, cisplatin.

from the tumor tissue in the microfluidic system. The cells collected at the end of experiment resulted in approximately 3000 cells being liberated from an untreated 3 mm³ biopsy; based on hemocytometer measurements. Cells were removed from the primary tissue by increasing the flow rate to 10 μL^{-1} min. The percentage of cancer cells which survived the chemotherapy interrogation as assessed by Trypan blue exclusion, is shown in Table 1. The results indicate that an average of 72% ($n = 3$ patients) of cells were alive from the untreated tumor biopsy, which is comparable with viability levels obtained in cell culture.

The viability of the cancer cells treated with the chemotherapy decreased compared with the untreated tumor biopsy, the combination therapy again showed

the greatest effect of all the treatment regimens, correlating favorably with the results from the LDH and WST-1 assays.

Determination of Cytochrome *c* Release from Primary HNSCC Biopsies

The aim of this experiment was to determine whether cytochrome *c* was released from primary tumor biopsies maintained within a microfluidic system providing a second marker of cell death. Effluent collected from the microfluidic system was analyzed using a commercial immunoassay. All treatments incurred an immediate response as cells were damaged incorporating the tissue into the device. However, by the second day of treatment, the amount of cytochrome *c* released from the control sample had decreased and was maintained at a low level through the rest of the experiment. The tissue treated with 5-FU alone showed the highest release of cytochrome *c* within the first 2 days with the combination therapy showing a sustained effect over the first 6 days of the experiment (Fig. 7). CDDP alone showed little effect within the first 24 h of the samples studied; however, a measurable response from the tissue was shown after this time. All treatments showed a higher release of cytochrome *c* throughout the experiment than the control samples. A one-way between-subjects ANOVA showed there was a significant effect of drug action on the tumor samples at all three conditions ($p < 0.01$).

DISCUSSION

In the current investigation, an *in vitro* cancer explant tissue model was used to maintain viability and architecture of 23 independent HNSCC tissue biopsies: 14 primary tumors and nine metastatic nodes, using microfluidic technology. By using biochemical assays and basic histological techniques, HNSCC primary and secondary cancer tumor biopsies have been shown viable with little or no loss of morphology and viability after 7 days within a microfluidic system. Although differences in the magnitude of responses between primary tumors and metastatic deposits have been shown, their patterns of behavior are very similar. Traditional *in vitro* cancer models have been used extensively to study cancer proliferation and key genetic events, however, it has been noted by many that these models do lack the complex *in vivo* structure and dynamic kinetics of nutrients and signaling molecules. Viability of *in vitro*-cultured cancer explants using WST-1 and LDH as biomarkers in the effluent of the tissue exposed medium has not been previously investigated; however, it has been reported that LDH levels in serum could have diagnostic and prognostic values in a number of clinical studies.³⁷

Histology of the tumor explants was analyzed before and after maintenance in the microfluidic system by H&E staining of sections taken through the full depth of the biopsy. There is little or no shrinkage in the nuclei or cytosol of the cells in the biopsy after 72 h of culture in a microfluidic system. The nuclei of the

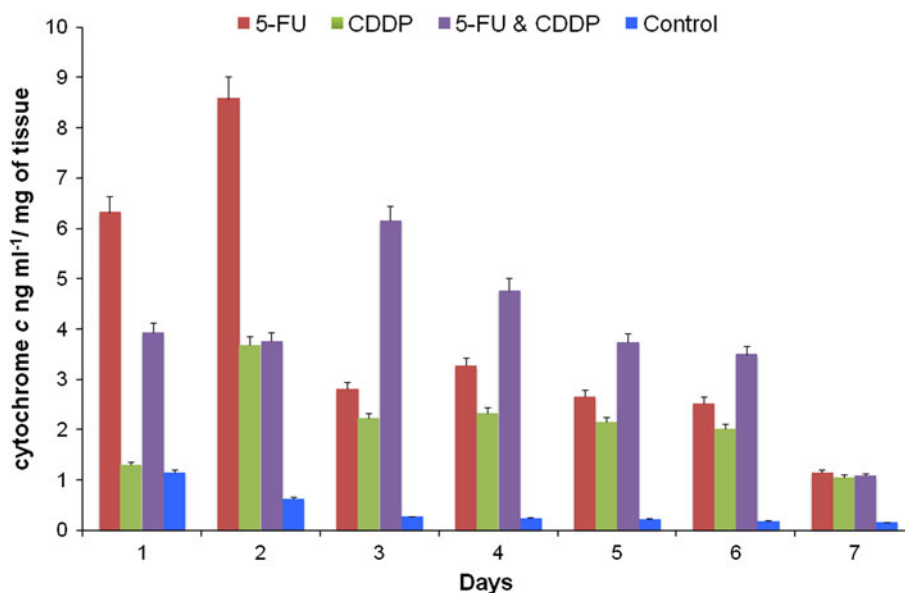


FIGURE 7. Cytochrome *c* released from primary HNSCC tissue during treatment with different chemotherapy treatments (5-FU, cisplatin, and 5-FU with cisplatin) compared with untreated cancer tissue biopsies. Aliquots of effluent are collected every 24 h over 7 days. Data are expressed as the mean (\pm SEM) of cytochrome *c* levels $\text{ng mL}^{-1} \text{mg}^{-1}$ of tissue from three separate experiments.

tumor cells maintained their spherical appearance and, as with all cancer cells, a variable degree of dysplasia was seen, which did not change after culture. The cell membranes remain intact and clearly visible, and there is no discernible loss of the extracellular matrix between the cells. Preservation of the morphology of the tissue was also seen when culturing brain slices ($>700\ \mu\text{m}$) in microfluidic perfusion chambers.²⁶ Rambani and colleagues demonstrated, as in the current study, that the overall structure, cell sizes, and shapes of the perfused slices were comparable to the baseline slices. In comparison, their unperfused slices showed the health of the cells to be compromised, with cell death occurring from the center outwards. The combination of the histology with the anticipated responses of WST-1 and LDH provide convincing evidence that tissue was being maintained in a viable state in the glass device.

Although the tissue-containing device was maintained in a $37\ ^\circ\text{C}$ incubator, the media were not continuously oxygenated. Analyses of the biochemical and histological results have shown a continuous flow rate of $2\ \mu\text{L}\ \text{min}^{-1}$, meaning that, the total volume of the tissue chamber is theoretically changed every 2 min was sufficient to ensure maintenance of the cancer biopsies without obvious changes in tissue architecture being observed. This differs from many reported explant cultures that required the use of 5% CO_2 incubators or other complex gaseous parameters.^{10,16} The relative simplicity of the set-up in terms of apparatus is an important consideration that should facilitate widespread use of the technology. With minor alterations to the device, we have already demonstrated that liver and cardiac tissues of similar size to the malignant biopsies can be maintained and studied; the latter being electrically stimulated.^{6,13} The benefit of explant-based microfluidics other than allowing the replication of the *in vivo* microenvironment is that it also permits numerous analyses to be undertaken on a single biopsy over several days.

In this study, the analysis of different biomarkers of viability and cell death, involving distinct cell processes, in effluent from a tissue sample maintained in a microfluidic was achieved. LDH is released from both necrotic and apoptotic cells, whereas cytochrome *c* is released almost immediately during necrosis, but only later in apoptosis.¹⁸ Release of cytochrome *c* was low in the first day of the treatment, compared to the control, in all except those samples treated with 5-FU alone. In days two and three, the release of cytochrome *c* peaked in all the treated biopsies with a gradual decrease over the next 4 days. This correlates with previous studies into the temporal release of cytochrome *c* and suggests that the mechanism of death is largely apoptotic rather than necrotic.¹⁸

Research into cytochrome *c* as a biomarker of cancer response to chemotherapeutic agents is in its infancy, although some encouraging data have been published. Cancer patients that responded to treatment and survived for 3 years had lower serum levels of cytochrome *c* ($25\ \text{ng}\ \text{mL}^{-1}$) within the first 3 days than those patients that died.²⁸ Conversely, a study aimed at testing the prognostic significance of several biomarkers, including cytochrome *c*, in surgically treated parotid cancer patients treated with adjuvant radiotherapy showed that, through immunohistochemical examination of paraffin-embedded tissue specimens, cytochrome *c* expression did not predict survival.¹¹ These results might indicate that the use of cytochrome *c* as a biomarker is limited to specific types of cancer and/or chemotherapy regimens.

In the current study, explant culture was used, as it has all the relevant cell types alongside the specialized and complex extracellular matrix found in a specified locale, which can be either normal or pathological in nature. Using microfluidic technology, these tissue samples have been maintained for a significant period of time with little loss of viability or structures. The microfluidic experiments, although relatively small in size, have shown the ability to model cell death by chemotherapeutic agents in HNSCC biopsies, and the results are in agreement with those published using cell models, and, more importantly, those found in cancer patients themselves, i.e., that combination drug therapy is most effective in causing cell death.

Head and neck cancer, like many others, has a low survival rate, and while there have been advances in clinical treatment regimens, translation of these improvements into decreases in the mortality rate have not been achieved.²⁷ This study provides an important first step into the development of a pre-clinical microfluidic device, which can be used to provide further understanding into the progression and treatment of solid tumors. It is envisaged that the approach will be extremely powerful in studying the metastatic process as well as allowing therapeutic regimens to be tested on biopsies from primary tumor, permitting therapy to be tailored in terms of specific drug combinations and concentrations on a personalized basis directing the oncologist's choice of first-line therapy.

ACKNOWLEDGMENTS

The authors thank Mrs Ann Lowry and Dr. Patrick Murray for their technical expertise, and Dr. L. Karzai (Consultant Histopathologist) for reviewing the stained sections; the financial supports from the University of Hull student scholarship programme and BBSRC (BB/E002722) are gratefully acknowledged.

REFERENCES

- ¹Ahlemeyer, B., S. Klumpp, and J. Krieglstein. Release of cytochrome c into the extracellular space contributes to neuronal apoptosis induced by staurosporine. *Brain Res.* 934:107–116, 2002.
- ²Bancroft, J. D., and A. Stevens. *Theory and Practice of Histological Techniques*. New York: Churchill Livingstone, 766 pp, 1996.
- ³Barczyk, K., M. Kreuter, J. Pryjma, E. P. Booy, S. Maddika, *et al.* Serum cytochrome c indicates *in vivo* apoptosis and can serve as a prognostic marker during cancer therapy. *Int. J. Cancer* 116:167–173, 2005.
- ⁴Broadwell, I., P. D. I. Fletcher, S. J. Haswell, T. McCreedy, and X. L. Zhang. Quantitative 3-dimensional profiling of channel networks within transparent ‘lab-on-a-chip’ microreactors using a digital imaging method. *Lab Chip* 1:66–71, 2001.
- ⁵Chaw, K. C., M. Manimaran, E. H. Tay, and S. Swaminathan. Multi-step microfluidic device for studying cancer metastasis. *Lab Chip* 7:1041–1047, 2007.
- ⁶Cheah, L. T., Y. H. Dou, A. M. Seymour, C. E. Dyer, S. J. Haswell, *et al.* Microfluidic perfusion system for maintaining viable heart tissue with real-time electrochemical monitoring of reactive oxygen species. *Lab Chip*. 11:1240–1248, 2010.
- ⁷Cho, W.C.S. 2007. Contribution of oncoproteomics to cancer biomarker discovery. *Molecular Cancer* 6.
- ⁸Curado, M. P., and M. Hashibe. Recent changes in the epidemiology of head and neck cancer. *Curr. Opin. Oncol.* 21:194–200, 2009.
- ⁹Du, Z., K. H. Cheng, M. W. Vaughn, N. L. Collie, and L. S. Gollahon. Recognition and capture of breast cancer cells using an antibody-based platform in a microelectromechanical systems device. *Biomed. Microdevices* 9:35–42, 2007.
- ¹⁰Gabriel, N., J. F. Innes, B. Caterson, and A. Vaughan-Thomas. Development of an *in vitro* model of feline cartilage degradation. *J. Feline Med. Surg.* 12:614–620, 2010.
- ¹¹Giotakis, J., I. P. Gomas, L. Alevizos, A. N. Georgiou, E. Leandros, *et al.* Bax, cytochrome c, and caspase-8 staining in parotid cancer patients: markers of susceptibility in radiotherapy? *Otolaryngol. Head Neck Surg.* 142:605–611, 2010.
- ¹²Hattersley, S. M., C. E. Dyer, J. Greenman, and S. J. Haswell. Development of a microfluidic device for the maintenance and interrogation of viable tissue biopsies. *Lab Chip* 8:1842–1846, 2008.
- ¹³Hattersley, S. M., J. Greenman, and S. J. Haswell. Study of ethanol induced toxicity in liver explants using microfluidic devices. *Biomed. Microdevices* 2011. doi:10.1007/s1044-011-9570-2.
- ¹⁴Holmes, A. M., R. Solari, and S. T. Holgate. Animal models of asthma: value, limitations and opportunities for alternative approaches. *Drug Discov. Today*. doi:10.1016/j.drudis.2011.05.014.
- ¹⁵Hou, H. W., Q. S. Li, G. Y. H. Lee, A. P. Kumar, C. N. Ong, and C. T. Lim. Deformability study of breast cancer cells using microfluidics. *Biomed. Microdevices* 11:557–564, 2009.
- ¹⁶Humphreys, P., S. Jones, and W. Hendelman. Three-dimensional cultures of fetal mouse cerebral cortex in a collagen matrix. *J. Neurosci. Methods* 66:23–33, 1996.
- ¹⁷Jauregui, H. O., P. N. McMillan, J. Driscoll, and S. Naik. Attachment and long term survival of adult rat hepatocytes in primary monolayer cultures: comparison of different substrata and tissue culture media formulations. *In Vitro* 22:13–22, 1986.
- ¹⁸Jemmerson, R., B. LaPlante, and A. Treeful. Release of intact, monomeric cytochrome c from apoptotic and necrotic cells. *Cell Death Differ.* 9:538–548, 2002.
- ¹⁹Kaji, H., G. Camci-Unal, R. Langer, and A. Khademhosseini. Engineering systems for the generation of patterned co-cultures for controlling cell–cell interactions. *Biochim. Biophys. Acta* 1810:239–250, 2011.
- ²⁰Lalami, Y., G. De Castro Jr, C. Bernard-Marty, and A. Awada. Management of head and neck cancer in elderly patients. *Drugs Aging* 26:571–583, 2009.
- ²¹Lindstrom, S., K. Mori, T. Ohashi, and H. Andersson-Svahn. A microwell array device with integrated microfluidic components for enhanced single-cell analysis. *Electrophoresis* 30:4166–4171, 2009.
- ²²Matapurkar, A., and Y. Lazebnik. Requirement of cytochrome c for apoptosis in human cells. *Cell Death Differ.* 13:2062–2067, 2006.
- ²³McCreedy, T. Rapid prototyping of glass and PDMS microstructures for micro total analytical systems and micro chemical reactors by microfabrication in the general laboratory. *Anal. Chim. Acta* 427:39–43, 2001.
- ²⁴Parsons, B. A., and M. J. Drake. Animal models in overactive bladder research. In: Citation: Handbook of Experimental Pharmacology, edited by K. E. Andersson, and M. C. Michel. Bristol: Bristol Urological Institute, Southmead Hospital, 2011, pp. 15–43.
- ²⁵Platoshyn, O., S. Zhang, S. S. McDaniel, and J. X. J. Yuan. Cytochrome c activates K⁺ channels before inducing apoptosis. *Am. J. Physiol. Cell Physiol.* 283:C1298–C1305, 2002.
- ²⁶Rambani, K., J. Vukasinovic, A. Glezer, and S. M. Potter. Culturing thick brain slices: an interstitial 3D microperfusion system for enhanced viability. *J. Neurosci. Methods* 180:243–254, 2009.
- ²⁷Remmerbach, T. W., K. Maurer, S. Janke, W. Schellenberger, K. Eschrich, *et al.* Oral brush biopsy analysis by matrix assisted laser desorption/ionisation- time of flight mass spectrometry profiling—a pilot study. *Oral Oncol.* 47:278–281, 2011.
- ²⁸Renz, A., W. E. Berdel, M. Kreuter, C. Belka, K. Schulze-Osthoff, and M. Los. Rapid extracellular release of cytochrome c is specific for apoptosis and marks cell death *in vivo*. *Blood* 98:1542–1548, 2001.
- ²⁹Richards, J., W. Imagawa, A. Balakrishnan, M. Edery, and S. Nandi. The lack of effect of phenol red or estradiol on the growth response of human, rat, and mouse mammary cells in primary culture. *Endocrinology* 123:1335–1340, 1988.
- ³⁰Schultz, D. R., and W. J. Harrington, Jr. Apoptosis: programmed cell death at a molecular level. *Sem. Arthritis Rheum.* 32:345–369, 2003.
- ³¹Sheard, M. A., B. Vojtesek, M. Simickova, and D. Valik. Release of cytokeratin-18 and -19 fragments (TPS and CYFRA 21-1) into the extracellular space during apoptosis. *J. Cellular Biochem.* 85:670–677, 2002.
- ³²Torisawa, Y. S., A. Takagi, Y. Nashimoto, T. Yasukawa, H. Shiku, and T. Matsue. A multicellular spheroid array to and viability realize spheroid formation, culture, assay on a chip. *Biomaterials* 28:559–566, 2007.
- ³³Trejo-Becerril, C., E. Perez-Cardenas, H. Trevino-Cuevas, L. Taja-Chayeb, P. Garcia-Lopez, *et al.* Circulating nucleosomes and response to chemotherapy: an *in vitro*, *in vivo* and clinical study on cervical cancer patients. *Int. J. Cancer* 104:663–668, 2003.

- ³⁴Verdier, C., C. Couzon, and A. Duperray. Critical stresses for cancer cell detachment in microchannels. *Eur. Biophys. J.* 38:1035–1047, 2009.
- ³⁵Walker, G. M., J. Sai, A. Richmond, M. Stremler, C. Y. Chun, and J. P. Wikswo. Effects of flow and diffusion on chemotaxis studies in a microfabricated gradient generator. *Lab Chip* 5:611–618, 2005.
- ³⁶Yeom, Y. I., S. Y. Kim, H. G. Lee, and E. Y. Song. Cancer biomarkers in omics age. *Biochip J.* 2:160–174, 2009.
- ³⁷Ziebart, T., S. Walenta, M. Kunkel, T. E. Reichert, W. Wagner, and W. Mueller-Klieser. Metabolic and proteomic differentials in head and neck squamous cell carcinomas and normal gingival tissue. *J. Cancer Res. Clin. Oncol.* 137:193–199, 2010.
- ³⁸Zou, H., W. J. Henzel, X. Liu, A. Lutschg, and X. Wang. Apaf-1, a human protein homologous to *C. elegans* CED-4, participates in cytochrome c-dependent activation of caspase-3. *Cell* 90:405–413, 1997.

Evaluation of Heart Tissue Viability Under Redox-Magnetohydrodynamics Conditions: Toward Fine-Tuning Flow in Biological Microfluidics Applications

Lih Tyng Cheah,¹ Ingrid Fritsch,² Stephen J. Haswell,³ John Greenman¹

¹Centre for Biomedical Research, Postgraduate Medical Institute, University of Hull, Cottingham Road, Kingston-Upon-Hull, HU6 7RX, UK; telephone: +44 (0) 1482466032; fax: +44 (0) 1482465458; e-mail: j.greenman@hull.ac.uk

²Department of Chemistry and Biochemistry, University of Arkansas, Fayetteville, Arkansas 72701; telephone: +1 (479) 575-6499; fax: +1 (479)-575-4049; e-mail: ifritsch@uark.edu

³Department of Physical Sciences, University of Hull, Cottingham Road, Kingston-Upon-Hull, HU6 7RX, UK

Received 13 September 2011; revision received 18 December 2011; accepted 20 December 2011

Published online 24 January 2012 in Wiley Online Library (wileyonlinelibrary.com). DOI 10.1002/bit.24426

ABSTRACT: A microfluidic system containing a chamber for heart tissue biopsies, perfused with Krebs–Henseleit buffer containing glucose and antibiotic (KHGB) using peristaltic pumps and continuously stimulated, was used to evaluate tissue viability under redox-magnetohydrodynamics (redox-MHD) conditions. Redox-MHD possesses unique capabilities to control fluid flow using ionic current from oxidation and reduction processes at electrodes in a magnetic field, making it attractive to fine-tune fluid flow around tissues for “tissue-on-a-chip” applications. The manuscript describes a parallel setup to study two tissue samples simultaneously, and 6-min static incubation with Triton X100. Tissue viability was subsequently determined by assaying perfusate for lactate dehydrogenase (LDH) activity, where LDH serves as an injury marker. Incubation with KHGB containing 5 mM hexaammineruthenium(III) (ruhex) redox species with and without a pair of NdFeB magnets (~0.39 T, placed parallel to the chamber) exhibited no additional tissue insult. MHD fluid flow, viewed by tracking microbeads with microscopy, occurred only when the magnet was present and stimulating electrodes were activated. Pulsating MHD flow with a frequency similar to the stimulating waveform was superimposed over thermal convection (from a hotplate) for Triton-KHGB, but fluid speed was up to twice as fast for ruhex-Triton-KHGB. A large transient ionic current, achieved when switching on the stimulating electrodes, generates MHD perturbations visible over varying peristaltic flow. The well-controlled flow methodology of redox-MHD

is applicable to any tissue type, being useful in various drug uptake and toxicity studies, and can be combined equally with on- or off-device analysis modalities.

Biotechnol. Bioeng. 2012;109: 1827–1834.

© 2012 Wiley Periodicals, Inc.

KEYWORDS: heart tissue; microfluidics; redox-magnetohydrodynamics; lactate dehydrogenase; Triton X100; hexaammineruthenium(III) chloride

Introduction

Redox-magnetohydrodynamics (redox-MHD) possesses unique capabilities to control fluid flow using the ionic current resulting from oxidation and reduction processes produced at electrodes in the presence of a magnetic field. This makes it attractive to fine-tune fluid flow for “tissue-on-a-chip” applications. This is the first study where the impact of redox-MHD conditions on the viability of heart tissue has been examined. Viability was indicated by the cell membrane integrity, determined by lactate dehydrogenase (LDH) release from the cardiomyocytes. Studies involved the presence and absence of the redox species and magnetic field, which are considered necessary for pumping fluid by redox-MHD.

There has been a rapid growth of microfluidic and lab-on-a-chip technologies to conduct biological research. They offer several advantages over conventional, non-microfluidic-based techniques, including the use of a very small amount of sample and reagent, portability, low production cost per device, and fast sampling and assay time (Manz et al., 1990).

Correspondence to: I. Fritsch and J. Greenman

Contract grant sponsor: Heart Research UK

Contract grant number: RG2538/07/10

Contract grant sponsor: University of Hull (Overseas Research Scholarship)

Contract grant sponsor: National Science Foundation USA

Contract grant number: CHE-0719097

Additional Supporting Information may be found in the online version of this article.

Furthermore, the existing apparatus is commonly expensive and requires highly trained personnel.

Several tissue interrogation studies within microfluidic devices have been reported, involving for instance liver tissue (Hattersley et al., 2008; van Midwoud et al., 2010), colorectal tissue (Webster et al., 2010), and brain tissue (Caicedo et al., 2010; Choi et al., 2007). Moreover, a microfluidic perfusion system has been developed and optimized to maintain the viability of heart tissue samples (Cheah et al., 2010), where the tissue was continuously supplied with enriched media and waste products were removed. This kind of fluid exchange resembles the human circulatory in vivo conditions (Hung et al., 2005; Yeon and Park, 2007). In addition, the heart tissue samples were also electrically stimulated using platinum electrodes to mimic the in vivo situation.

Low Reynolds numbers of flow in microfluidic devices with channels of 100- μm width indicate that the flow is predominately laminar with limited mixing, except for density and thermal gradients (Chapman, 1987; Gao et al., 1995) and diffusion (Ottino and Wiggins, 2004), between two streams of fluids. Mixing is particularly essential in biological processes, therefore microstirrers or micromixers are often integrated with these devices to facilitate and enhance mixing (Miyake et al., 1993; Voldman et al., 2000; Wong et al., 2004). MHD offers mixing capability by controlling fluid flow locally using ionic currents in a magnetic field (Qian and Haim, 2009; Weston et al., 2010b). A force, F_B (the magnetic portion of the Lorentz force) on ions that have velocities at a right angles to a magnetic field, B , moves them in the third direction, according to the cross product, $F_B = j \times B$, where j is the ionic current density. A momentum transfer to the solution surrounding those ions also causes that volume element to move in the direction of F_B . The actual velocity of that volume element is further influenced by other forces and the no slip boundary condition at surfaces of walls and objects in the chamber. By having programmable electrodes patterned in a small space and by adding chemical species (redox species) to the solution that can be oxidized or reduced by them, one can tune the density and location of the ionic current, and thus the patterns of fluid motion on the small scale without the use of channel walls to direct this, causing little or no bubble formation or electrode corrosion (Anderson et al., 2010; Weston et al., 2010a).

Redox-MHD has features that are not possible with other microfluidic pumps. These include the capability to stir without moving parts or specially fabricated obstacles (Fahidy, 1983; Qian and Bau, 2005; Tacke and Janssen, 1995; Weston et al., 2006); to control the flow pattern in a small volume by activating different microelectrodes patterned on a chip; and to move a plug of solution of a different composition without the need for channel walls (Weston et al., 2010a). Although this latter study also showed that the activity of alkaline phosphatase, an enzyme used in ELISA, was maintained in the presence of low concentrations (5 mM) of the redox species, $[\text{Ru}(\text{NH}_3)_6]^{3+}$

(ruhex), there remains concern for reactivity and interference of the redox species with biological samples. Consequently, we set out to determine the impact of the presence of the redox species and MHD on probably the most complex of biological tissue samples, that is, heart tissue biopsies. The maintenance of heart tissue has additional consideration, in that it requires electrical stimulation to replicate the in vivo environment, thus offering an intrinsic source of ion current that in the presence of an orthogonal magnetic field can produce MHD.

In addition, modifications were implemented in the perfusion setup shown previously (Cheah et al., 2010) to improve reproducibility and time efficiency within a set of experiments to test the effect of a variable on heart viability. The LDH assay was chosen as it is a simple and rapid test for membrane integrity, which is compromised when cells die. Other assays that could be used, for example, M30 CytoDEATH (Fayad et al., 2011) and cellular DNA fragmentation (Niemi et al., 2011), are more complicated, expensive, and time-consuming. An alternative approach would be to assess the tissue response by immunohistochemical staining for markers of cell death (TUNEL) or proliferation, for example, Ki-67. However, this is not suitable for the current study that needs to be undertaken repeatedly over the assay duration and in real-time. A parallel setup has been established so that two tissues cut from the same heart could be studied simultaneously, having aged for the same time before use. Repeated experimentation on the same tissue sample was performed to eliminate inherent variations between tissue samples due to cutting ($\sim 2 \text{ mm} \times 4 \text{ mm} \times 4 \text{ mm}$), or the region where the tissue sample was taken from the same heart.

Materials and Methods

Chemicals

All chemicals were reagent grade and used as received, unless otherwise specified. The sodium thiopentone was obtained from Link Pharmaceutical Ltd (UK). The sodium chloride, sodium hydrogen carbonate, potassium chloride, potassium dihydrogen phosphate, magnesium sulfate heptahydrate, calcium chloride dihydrate, Triton X100, glucose, and hexaammineruthenium(III) chloride (98%) were acquired from Sigma-Aldrich (Dorset, UK). The gas consisting of 95% O_2 and 5% CO_2 was purchased from BOC (South Yorkshire, UK).

Animal Model

This investigation conforms to the UK Animals (Scientific Procedures) Act 1986. Male Sprague Dawley rats (Charles River Laboratories International Inc, Margate, UK) were all housed under conditions with a 12:12 h light–dark cycle and provided with food and water ad libitum. Animals were anaesthetized via intraperitoneal injection of 0.5 mL sodium

thiopentone/100 g and the hearts were excised under a Schedule 1 procedure.

Microfluidic Perfusion System

A microfluidic perfusion device was constructed from polydimethylsiloxane (PDMS) on a polystyrene base (Cheah et al., 2010). The perfusion system was set up as shown in Figure 1a so that it could perform perfusion studies on two samples of heart tissue (A and B) simultaneously. Tubing lengths between different components of the system were identical for A and B so that arrival and departure times of perfusing solutions were the same in both chambers; this was confirmed by control experiments. One peristaltic pump served as the pushing pump and another as the withdraw pump for A and B. Before introduction of a tissue sample, the microfluidic system was sterilized with 70%

(v/v) ethanol/water by perfusion at 120 $\mu\text{L}/\text{min}$ for 10 min and rinsed with sterile double distilled water. The microfluidic device was then primed with Krebs–Henseleit buffer (KH) containing glucose (G) and antibiotic (B) (pH 7.4). KHGB buffer consisted of 118 mM NaCl, 25 mM NaHCO_3 , 4.8 mM KCl, 1.2 mM KH_2PO_4 , 1.2 mM $\text{MgSO}_4 \cdot 7 \text{H}_2\text{O}$, 2.5 mM $\text{CaCl}_2 \cdot 2 \text{H}_2\text{O}$, 5 mM glucose, which was supplemented with 100 U/mL Penicillin and 0.1 mg/mL Streptomycin (Sigma–Aldrich) and then filtered using 0.22 μm syringe driven filter unit (Millipore Corporation, Billerica, MA) prior to use. The buffer solution containing redox species consisted of 5 mM $\text{Ru}(\text{NH}_3)_6\text{Cl}_3$ in KHGB (ruhcx-KHGB). The non-ionic surfactant Triton X100 was added to the buffer to reach 2% (w/v) to cause solubilization of phospholipid membranes, and release of the intracellular contents, measured by LDH activity.

In brief, rat hearts were rapidly excised and a piece ($\sim 2 \text{ mm} \times 4 \text{ mm} \times 4 \text{ mm}$) of right ventricular tissue was placed directly into the chamber of the perfusion device. The perfusion chamber was positioned on a 37°C hotplate connected to a Carel IR Thermostat controller (World Precision Instruments, Hertfordshire, UK). Care was taken to ensure that the chamber was level. Buffer was introduced to the chamber via the inlet and was removed from the chamber through the outlet. In this way, the heart tissue was supplied with fresh nutrients throughout the experiment. The inlet and outlet were connected to separate Minipuls3 peristaltic pumps (Gilson Inc, Villiers-le-Bel, France) at a flow rate of 120 $\mu\text{L}/\text{min}$. All solutions pumped through the chamber were gassed with 95% O_2 , 5% CO_2 in a water bath of 37°C throughout the experiment (Grant Instruments Ltd, Cambridgeshire, UK), with a residence time of 6.9 min. Heart tissue was electrically stimulated via two platinum wire electrodes (0.4 mm diameter) using a programmable function generator to produce a square wave, 2 V, 1.5 Hz (Thurlby Thandar Instruments Ltd, Cambridgeshire, UK). Contraction of the heart tissue was monitored using a microscope-based camera (Veho, Hampshire, UK).

After introduction of the heart sample into the microfluidic device, the tissue was perfused with KHGB for 90 min, followed by static incubation of KHGB, Triton-KHGB, or ruhcx-Triton-KHGB for 6 min in the presence or absence of a magnetic field (described below). After that, the incubation solution was washed away from the tissue chamber by again perfusing with oxygenated KHGB for another 90 min. At this point, if stated, a second static incubation period may have been performed and the KHGB washing/perfusion repeated. For the last 30 min of all experiments, the heart tissue sample was perfused with Triton-KHGB. Approximately 200 μL effluent was collected every 5 min. Effluent samples were stored at -20°C for subsequent LDH analysis. The tissue sample was discarded after each experiment.

Polystyrene latex microspheres (10- μm diameter, 2.5 wt% dispersion, stabilized with slight anionic charge from surface sulfate groups, Alfa Aesar, Lancashire, UK) were added to the solution in a 1:30 dilution for monitoring

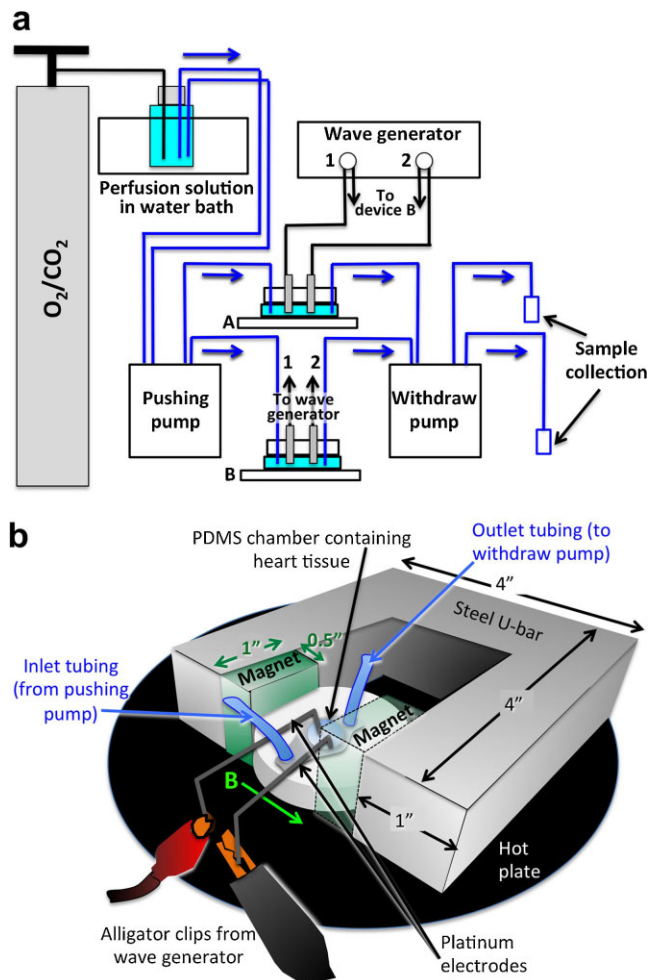


Figure 1. Schematics of the experimental setup. **a:** The overall system for parallel studies that simultaneously perfuses two tissue chambers (A and B) and applies a square wave potential to both sets of stimulating electrodes (modified from the single-tissue setup of Cheah et al., 2010). **b:** An enlarged view of a device for studies involving the magnet, showing placement of hot plate, chamber, perfusion tubing, platinum stimulating electrodes, and clips from wave generator.

fluid flow caused by MHD and other convection sources (thermal gradients and perfusion) under an inverted microscope.

LDH Measurement

To quantify the extent of cell damage, and thereby, provide a measure of viability, a colorimetric cytotoxicity assay using LDH as a marker of injury (Cytotoxicity Detection Kit^{Plus} (LDH), Roche, West Sussex, UK) was carried out according to manufacturer's instructions. Absorbance of the samples was measured at 490 nm using a microplate reader (BioTek Instruments, Inc., Winooski, VT). The results were expressed as the average determined from triplicate samples. The absorbance value obtained from the background control (KHGB alone) was subtracted from all test values. Absorbance values of the samples were converted to LDH activity (U/mL) according to the LDH standard curve. The ruhex is pale yellow, and it exhibits negligible absorbance at 490 nm. However, its presence at 5 mM concentration decreased the sensitivity of the LDH assay to 54%. Thus, for effluent samples expected to contain ruhex, the LDH activity determined by using the standard method was first corrected, before accounting for the dilution factor and tissue weight. Throughout the studies reported here, there were fluctuations in LDH activity from tissue to tissue and from experiment to experiment. Therefore, data analysis was confined to evaluating relative trends.

Magnet Setup

A magnet configuration was chosen to allow viewing of bead motion to monitor fluid flow in the chamber of the chip with an inverted microscope (Axiovert S100, Zeiss, Hertfordshire, UK). A similar setup was used for viability experiments, although viewing of microbeads was not performed in those studies. Two permanent NdFeB sintered magnets (1 in. × 1 in. × 0.5 in.) were placed at the ends of a steel U-shaped bar in an attracting arrangement with the magnetic field parallel to the plane of the chip (see Fig. 1b). A dc magnetometer (AlfaLab, Inc., Salt Lake City, UT) was used to measure the magnetic field at the surface of each magnet to be 0.39 T. The magnet apparatus was placed on top of the hotplate, with the chamber centered horizontally between the poles and placed vertically about ¼ the way up from the bottom of the magnet. The chamber had to be centered over the hole (0.6 cm diameter) in the hotplate to monitor fluid flow via bead movement with the inverted microscope. The chamber was shielded during bead studies to minimize air currents which otherwise added to the overall convection of the fluid.

Results and Discussion

Multiple Experiments With a Single Tissue

In order to enhance time efficiency, a tissue sample was subjected to two 6-min static incubations with Triton-

KHGB during the experiment, followed by final Triton-KHGB perfusion. The LDH release following the brief incubation with Triton-KHGB was determined and served several purposes: (1) to indicate whether the tissue remains viable after an experiment; and (2) as a marker of the end of an experiment and the start of another. A lack of LDH release is an inverse measure of tissue viability. Figure 2 shows that LDH activities were high initially (0–30 min), most probably due to the damage of cells at the edge or surface of the tissue when excised from the heart. The relatively high initial LDH leakage was also observed by Obatomi et al. (1998), Hattersley et al. (2008), and van Midwoud et al. (2010). As perfusion proceeded, this trauma associated LDH was washed away (~45 min) and then remained at relatively low levels. LDH activity increased at 100 min, after the short Triton-KHGB static incubation (84–90 min), but decreased to low levels with time. The delay from the end of the incubation period and the LDH peak is attributed to a combination of chamber-emptying time (~4 min) and a 6.9-min travel time of solution from the chamber to collection tube. The LDH spike suggests that the tissue was viable during the first perfusion period. A second Triton-KHGB incubation (174–180 min) produced a similar LDH response, with a spike at 185 min. This indicates that the tissue had remained viable after the first Triton-KHGB incubation and second perfusion periods. A final Triton-KHGB perfusion (≥ 270 min) elicited a larger LDH peak, revealing that the sample was still viable after the second Triton-KHGB incubation and third perfusion periods.

This result suggests that a series of experiments can be carried out on the same piece of tissue sample. During static

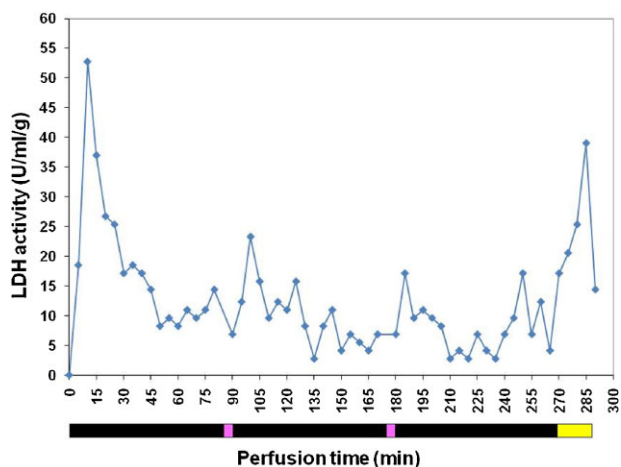


Figure 2. A representative study of LDH release from heart tissue resulting from two brief exposures to Triton, each followed by a recovery period. Black and pink bars indicate oxygenated KHGB perfusion and 6-min static Triton-KHGB incubation, respectively. The yellow bar (from 270 min) shows the final Triton-KHGB perfusion used to confirm viability of the tissue at the end of experiment; the time corresponds to when solution filled the tissue chamber. $N = 2$.

incubation, the peristaltic pump was turned off to maximize the influence of redox-MHD fluid flow on the tissue without the overriding fluid flow and diluting effects from a perfusion stream. A 6-min Triton-KHGB incubation time was long enough to produce tissue insult and induce LDH release, but short enough to avoid complete tissue death. Other incubation periods were not investigated.

Heart tissue has been shown viable in the present device for up to 5 h (Cheah et al., 2010). In a sealed glass microfluidic device developed in our group, the tissue sample was viable for up to 24 h in a chamber with diameter 3 mm (data not shown). Clinically, heart biopsies are preserved *ex vivo* for no longer than 4–6 h (Ozeki et al., 2007); therefore, a 5-h perfusion period in this microfluidic system is considered sufficient. Conventional methods such as the whole heart perfusion, for example, the Langendorff preparation, and isolated cardiomyocyte culture studies will commonly maintain viability for several hours and have been very useful for measuring heart contraction activity. However, these approaches possess major drawbacks attributed to the limitations in replicating *in vivo* microenvironments and are considered “dying models”.

Influence of Redox Species and Magnetic Field on Viability

Many possible redox species can be used in electrochemically generating the current, and therefore the ion flux necessary to induce MHD in a magnetic field. Those redox species can be native to the fluid of interest (e.g., oxygen, solvent, components in a buffer, or electrolyte), added (as was done here), or components of the electrode material itself (e.g., dissolution of easily oxidizable metals, such as copper, silver, and nickel).

Selection of an appropriate redox species for redox-MHD microfluidics depends on the application. The factors that should be considered are: (1) an acceptable range of potentials or currents that can be applied at the electrodes; (2) solubility in and chemical reactivity (compatibility) with the solutions; (3) possible interference with detection methods; and (4) chemical reactivity with the sample. The latter point is the main focus of this paper.

To address (1), we chose three typical redox species that are relatively stable, commonly used in electrochemical studies, easily obtainable from a commercial source, and require voltages for oxidation and reduction that minimize water electrolysis (and therefore, bubble formation) and corrosion of the electrodes. We used two of these in previous redox-MHD studies: ruhex (Weston et al., 2010a) and a mixture of a 1:1 mole ratio of potassium ferricyanide and potassium ferrocyanide (Aguilar et al., 2006; Anderson et al., 2010; Arumugam et al., 2006). The third was hydroquinone, a structure present in some biochemical compounds, and therefore compatible with physiological conditions.

To address (2), we evaluated the electrochemical behavior of the three species in the KHGB solution that would be used

for the heart tissue. All three tested chemicals were stable and provided expected responses.

We screened these redox species in solutions of KHGB for interference with the detection method (the LDH assay). This step addresses (3). We already knew that 5 mM ruhex was compatible with alkaline phosphatase activity from our previous work (Weston et al., 2010a). Thus, we also chose redox concentrations of 5 mM for hydroquinone, and 2.5 mM of each form in the ferricyanide/ferrocyanide mixture. The ruhex decreased the assay sensitivity to about half (a factor of 0.542), whereas, the other two redox species adversely affected the assay results. Thus, ruhex was chosen for subsequent studies on tissue viability. Separate calibration curves, then, were obtained for LDH with and without ruhex.

The effect of 5 mM ruhex on heart tissue samples was investigated before redox MHD was performed. Using the parallel setup in Figure 1a, two tissues excised from the same heart were evaluated simultaneously with a 6-min incubation period in KHGB (84–90 min). Ruhex was only present during this “static” period for one of the tissues (red squares in Fig. 3). Figure 3 shows that the trends of LDH activities with time are similar, with the appearance of a small LDH spike at 100 min (with ruhex) and 95 min (without ruhex), followed by low LDH activities. This result indicates that insult on the tissue during the static period is not further affected by the presence of ruhex. Also, the increase in LDH activity after Triton-KHGB perfusion at the end of the experiments confirmed the tissue remained viable in the presence of the redox species. Two sets of parallel studies were performed. A previous study by Schoenfisch et al.

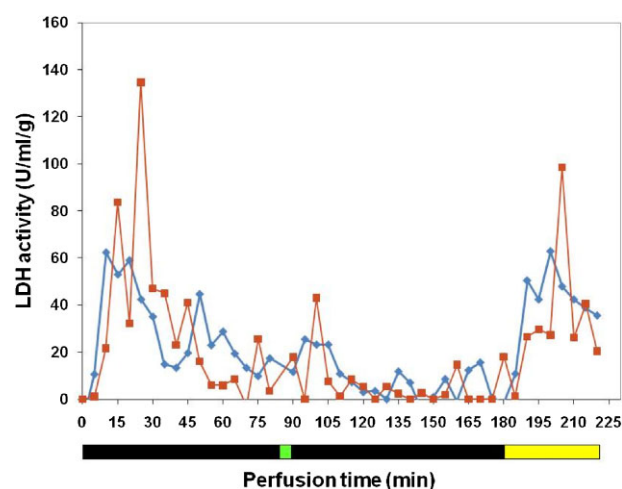


Figure 3. The effect of ruhex on LDH release from the heart tissue sample during perfusion. A representative parallel study was performed in which the 6-min incubation step (green bar) involved 5 mM ruhex in KHGB for one tissue (red squares) and only KHGB for the other (blue diamonds). Black bars indicate oxygenated KHGB perfusion. The yellow bar (from 180 min) shows the final Triton-KHGB perfusion used to confirm viability of the tissue at the end of experiment; the time corresponds to when solution filled the tissue chamber. $N=2$.

(2005) used 1–5 mM Ruhex in a rat heart perfusion system to carry out in situ electrochemical measurements. The tissue was considered to be “living” based on the criterion that the heart was still metabolizing nutrients and generating a heartbeat.

The effect of the magnetic field during the incubation period (84–90 min) with ruhex-Triton present was determined using the parallel tissue setup (Fig. 1a). The magnet was inserted across one of the chambers at the beginning of the incubation period (see Fig. 1b) and removed at the end. Two sets of parallel studies were carried out. Figure 4 shows that the magnet had no perceptible impact on LDH release from the heart tissue. In fact, the LDH variation with time was similar for both tissues, showing an increase in LDH activity at 95 min, as in the other cases investigated. The slower drop in LDH activity after 95 min was not typical, but because it occurred for both tissues, it was likely due to the flow apparatus behavior, and not the chemistry with the tissue. The tissue still remained viable as determined by the prolonged perfusion in Triton at the end of the experiments, causing marked LDH release. Because of the significant variations of LDH activity following Triton-KHGB incubation in Fig. 4, it cannot be confirmed here whether the redox-MHD stirring had an enhancing or diminishing effect on tissue lysis in the presence of Triton. A closed chip and patterned electrodes throughout the chamber (instead of only using the stimulating electrodes) would provide a platform to fine-tune fluid flow around the tissue with the goal of affecting concentration gradients at the tissue surface, and therefore enhance release and uptake of chemical species.

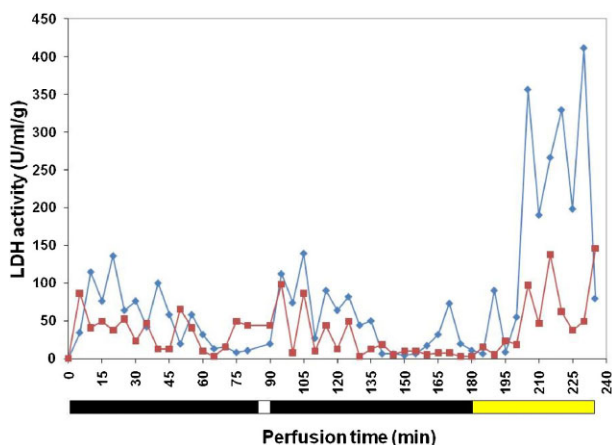


Figure 4. The effect of redox MHD on LDH release from heart tissue sample during the perfusion. A representative parallel study was performed in which the 6-min ruhex-Triton-KHGB incubation step (white bar) included the presence of the magnet for one tissue (red squares) but not for the other (blue diamonds). Black bars indicate oxygenated KHGB perfusion. The yellow bar (from 180 min) shows the final Triton-KHGB perfusion used to confirm viability of the tissue at the end of experiment; the time corresponds to when solution filled the tissue chamber. $N = 2$.

MHD Fluid Flow Under Perfusion and Heating Conditions

Fluid flow under heart tissue conditions was qualitatively investigated in a single-chamber apparatus on the stage of an inverted microscope, by adding microbeads to the solution to track the flow. These studies confirm that MHD flow occurs because of the stimulating electrodes alone in the presence of a magnetic field. Video clips (of 5 and 10 s duration) are provided as Supplementary Information online. Because a magnet was only present during the 6-min incubation period in the tissue studies and because Triton was usually present during that time, the available video clips are only shown on Triton-KHGB and ruhex-Triton-KHGB solutions. Similar trends were also observed in KHGB and ruhex-KHGB (without Triton).

Video 1 (see Supplementary Information online) shows natural agitation of Triton-KHGB solution from thermal gradients caused by the 37°C hot plate located beneath the chamber. When the wave generator was turned on at 2 s to activate the stimulating electrodes, there was no significant change in fluid flow. However, when the wave generator was on in the presence of the magnet, MHD flow was superimposed on the thermal convection as shown in Video 2 (see Supplementary Information online). Slight pulsating movement of microbeads seemed to occur at about 1.5 Hz, in synchrony with the alternating ionic current produced by the square wave potential at the stimulating electrodes. The applied voltage was large enough in the weak magnetic field to generate enough ionic current without ruhex to produce the MHD flow. The orientation of the chamber, its tubing, and placement of the stimulating electrodes relative to the magnet was chosen because of its convenience for performing the tissue studies, but is not optimal for MHD. (A 90-degree rotation of the pair of stimulating electrodes around the chamber would have been expected to provide maximum MHD force.) The net ion flux between the stimulating electrodes (see Fig. 1b) was approximately parallel to the magnetic field. Thus, in the evaluated configuration there must have been sufficient radially-directed, ionic current along the axis of the Pt wires and the wires must not have been directly across from each other and aligned along the magnetic field lines. It was difficult to track the MHD fluid flow when perfusion was then turned on, as in Video 3 (see Supplementary Information online). There was a slow pulsating (forward and slight reversal) motion that is consistent with the peristaltic pump roller frequency of about 5.5 s (determined by dividing the time for one rotation of the pump, 55 s, by the number of rollers, 10; 0.18 Hz).

The presence of ruhex in the Triton-KHGB made the MHD more noticeable over thermal convection (see Video 4 in Supplementary Information online) than without added ruhex. An initial surge of flow occurred in a direction different than motion from thermal convection when the wave generator was turned on at 2.0 s. This observation is attributed to the transient faradaic current in the presence of

the magnetic field. The MHD flow which decreased was clearly visible over the thermal convection and about ~ 1.5 to 2 times greater (based on net bead displacement for a fixed time) compared to that in the absence of redox. Pulsating bead movement appeared to be synchronized with the alternating ionic current at the stimulating electrodes. There was a noticeable surge of redox-MHD fluid flow even during perfusion at the moment when the wave generator was switched on in the presence of the magnet (at 2.2 s in Video 5, see Supplementary Information online) due to the large transient faradaic current. Microbeads slowed after the initial surge and their movement due to MHD became difficult to distinguish over the highly variable convection from perfusion. (Because the heart sample only occupied a fraction of the chamber, we observed redox-MHD fluid flow without perfusion even when the tissue was added to the chamber; not shown.)

Conclusions

Redox-MHD conditions have unnoticeable effects on heart tissue viability as determined by the LDH analysis. Fluid flow resulting from MHD in this system is evident over thermal convection when stimulating electrodes were used to produce the ionic current in the presence of a magnetic field, without addition of redox species, presumably because the applied voltage was sufficiently large enough to electrolyze water ($\Delta E = 2\text{ V}$). However, MHD fluid flow was higher in the presence of redox species. The transient current achieved when turning on the stimulating electrodes produced a MHD movement visible over perfusion, as well.

Surprisingly, although the presence of redox did not adversely affect the viability of the heart tissue, it did influence the LDH assay sensitivity. However, it was possible to account for the change in sensitivity by calibration. Thus, the entire study must be considered when choosing a redox species to induce redox-MHD. An alternative is to apply potentials that might electrolyze water or electrolyte, but where the current is so small that resulting gaseous products remain dissolved in the solution and bubbles are not problematic.

This system is actually more challenging than a laminar flow platform, because it had not been demonstrated whether redox-MHD could exhibit a perceptible effect over perfusion which was driven by peristaltic pumps. However, it was still possible to stop the perfusion briefly during a redox-MHD event to separate out the effect of perfusion and the effect of redox-MHD on the tissue.

The convection caused by redox MHD using the stimulating electrodes alone did not appear to change the effect of Triton on tissue viability during the 6-min incubation period. Avenues to pursue the effects of additional stirring on release or uptake of species or drugs by tissue could include orienting the magnetic field perpendicular to the path between stimulating electrodes to maximize the cross product, and using chips patterned

with arrays of individually addressable electrodes to fine-tune fluid flow around the tissue to offset dead volumes and eddies.

The described methodology can be adopted for any tissue type, permitting direct in vitro experimentation on primary clinical tissue, even when just a biopsy-sized sample is available, while retaining the in vivo environment. Efficient mixing around the tissue sample controlled by redox-MHD allows defined uptake of drugs as well as monitoring release of chemical species; facilitating drug availability and toxicity investigations. Furthermore, the redox-MHD methodology allows local concentrations of solutes to be specifically generated for known time periods, after which tissue responses can be measured. The fine control of the environment can be coupled with subsequent analysis of the tissue biopsy, either on the device or after additional labeling and study, for example, confocal microscopy.

L.-T. C. was supported by Heart Research UK (RG2538/07/10) and the University of Hull (Overseas Research Scholarship). The National Science Foundation (USA) is also acknowledged for financial support through grant CHE-0719097.

References

- Aguilar ZP, Arumugam PU, Fritsch I. 2006. Study of magnetohydrodynamic driven flow through LTCC channel with self-contained electrodes. *J Electroanal Chem* 591:201–209.
- Anderson EC, Weston MC, Fritsch I. 2010. Investigations of redox magnetohydrodynamic fluid flow at microelectrode arrays using microbeads. *Anal Chem* 82:2643–2651.
- Arumugam PU, Fakunle ES, Anderson EC, Evans SR, King KG, Aguilar ZP, Carter CS, Fritsch I. 2006. Redox magnetohydrodynamics in a microfluidic channel: Characterization and pumping. *J Electrochem Soc* 153:E185–E194.
- Caicedo HH, Hernandez M, Fall CP, Eddington DT. 2010. Multiphysics simulation of a microfluidic perfusion chamber for brain slice physiology. *Biomed Microdevices* 12:761–767.
- Chapman AJ. 1987. *Fundamentals of heat transfer*. New York: Macmillan.
- Cheah L-T, Dou Y-H, Seymour A-ML, Dyer CE, Haswell SJ, Wadhawan JD, Greenman J. 2010. Microfluidic perfusion system for maintaining viable heart tissue with real-time electrochemical monitoring of reactive oxygen species. *Lab Chip* 10:2720–2726.
- Choi Y, McClain MA, LaPlaca MC, Frazier AB, Allen MG. 2007. Three dimensional MEMS microfluidic perfusion system for thick brain slice cultures. *Biomed Microdevices* 9:7–13.
- Fahidy TZ. 1983. Magneto-electrolysis. *J Appl Electrochem* 13:553–563.
- Fayad W, Rickardson L, Haglund C, Olofsson MH, D'Arcy P, Larsson R, Linder S, Fryknes M. 2011. Identification of agents that induce apoptosis of multicellular tumour spheroids: Enrichment for mitotic inhibitors with hydrophobic properties. *Chem Biol Drug Des* 78:547–557.
- Gao X, Lee J, White HS. 1995. Natural convection at microelectrodes. *Anal Chem* 67:1541–1545.
- Hattersley SM, Dyer CE, Greenman J, Haswell SJ. 2008. Development of a microfluidic device for the maintenance and interrogation of viable tissue biopsies. *Lab Chip* 8:1842–1846.
- Hung PJ, Lee PJ, Sabounchi P, Lin R, Lee LP. 2005. Continuous perfusion microfluidic cell culture array for high-throughput cell-based assays. *Biotechnol Bioeng* 89:1–8.
- Manz A, Graber N, Widmer HM. 1990. Miniaturized total chemical analysis systems: A novel concept for chemical sensing. *Sens Actuators B* 1:244–248.

- Miyake R, Lammerink TSJ, Elwenspoek M, Fluitman JHJ. 1993. Micro mixer with fast diffusion. Proc. MEMS'93, Pages 248–253. 6th IEEE Int. Workshop Micro Electromechanical System. San Diego, CA.
- Niemi NM, Lanning NJ, Klomp JA, Tait SW, Xu Y, Dykema KJ, Murphy LO, Gaither LA, Xu HE, Furge KA, Green DR, MacKeigan JP. 2011. MK-STYX, a catalytically inactive phosphatase regulating mitochondrially dependent apoptosis. *Mol Cell Biol* 31:1357–1368.
- Obatomi DK, Brant S, Anthonypillai V, Early DA, Bach PH. 1998. Optimizing preincubation conditions for precision-cut rat kidney and liver tissue slices: Effect of culture media and antioxidants. *Toxicol In Vitro* 12:725–737.
- Ottino JM, Wiggins S. 2004. Introduction: Mixing in microfluidics. *Phil Trans R Soc Lond A* 362:923–935.
- Ozeki T, Kwon MH, Gu J, Collins MJ, Brassil JM, Miller MB, Gullapalli RP, Zhuo J, Pierson RN, Griffith BP, Poston RS. 2007. Heart preservation using continuous ex vivo perfusion improves viability and functional recovery. *Circ J* 71:153–159.
- Qian S, Bau HH. 2005. Magneto-hydrodynamic stirrer for stationary and moving fluids. *Sens Actuat B* 106:859–870.
- Qian S, Haim HH. 2009. Magneto-hydrodynamics based microfluidics. *Mech Res Commun* 36:10–21.
- Schoenfisch MH, Pemberton JE, Ovadia M, Levy M. 2005. In situ electrochemistry of $\text{Ru}(\text{NH}_3)_6^{3+}$ in a perfused rat heart. *Electroanalysis* 9:135–140.
- Tacken RA, Janssen LJJ. 1995. Applications of magnetoelectrolysis. *J Appl Electrochem* 25:1–5.
- van Midwoud PM, Groothuis GMM, Merema MT, Verpoorte E. 2010. Microfluidic biochip for the perfusion of precision-cut rat liver slices for metabolism and toxicology studies. *Biotechnol Bioeng* 105:184–194.
- Voldman J, Gray ML, Schmidt MA. 2000. An integrated liquid mixer/valve. *J Microelectromech Sys* 9:295–302.
- Webster A, Dyer CE, Haswell SJ, Greenman J. 2010. A microfluidic device for tissue biopsy culture and interrogation. *Anal Methods* 2:1005–1007.
- Weston MC, Anderson EC, Arumugam PU, Yoga Narasimhan P, Fritsch I. 2006. Redox magnetohydrodynamic enhancement of stripping voltammetry: Toward portable analysis using disposable electrodes, permanent magnets, and small volumes. *Analyst* 131:1322–1331.
- Weston MC, Nash CK, Fritsch I. 2010a. Redox-magnetohydrodynamic microfluidics without channels and compatible with electrochemical detection under immunoassay conditions. *Anal Chem* 82:7068–7072.
- Weston MC, Gerner MD, Fritsch I. 2010b. Magnetic fields for fluid motion. *Anal Chem* 82:3411–3418.
- Wong SH, Ward MCL, Wharton CW. 2004. Micro T-mixer as a rapid mixing micromixer. *Sens Actuat B* 100:365–385.
- Yeon JH, Park J-K. 2007. Microfluidic cell culture systems for cellular analysis. *Biochip J* 1:17–27.



Improved DNA extraction efficiency from low level cell numbers using a silica monolith based micro fluidic device

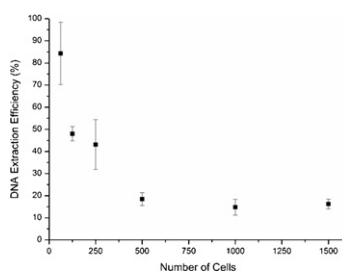
Loay Kashkary, Cordula Kemp, Kirsty J. Shaw*, Gillian M. Greenway, Stephen J. Haswell

Department of Chemistry, University of Hull, Cottingham Road, Hull HU6 7RX, UK

HIGHLIGHTS

- ▶ In situ fabrication of silica monoliths within micro fluidic devices.
- ▶ Improved DNA extraction efficiency from low cell numbers.
- ▶ Relevant to forensic or clinical diagnostics applications.

GRAPHICAL ABSTRACT



ARTICLE INFO

Article history:

Received 15 March 2012
 Received in revised form 10 May 2012
 Accepted 12 May 2012
 Available online 22 May 2012

Keywords:

DNA extraction
 Monolith
 Micro fluidic

ABSTRACT

The evaluation of a micro fluidic system with an integrated silica monolith for performing DNA extraction from limited biological samples has been carried out. Low DNA target concentrations usually require the addition of carrier RNA to ensure desired extraction efficiencies. Here, we demonstrate a micro fluidic extraction system with increasingly efficient extraction performances for biological samples containing <15 ng of total DNA without the need of adding carrier nucleic acids. All extracted DNA showed successful amplification via the polymerase chain reaction demonstrating both the effectiveness of the proposed system at removing potential inhibitors and yielding good quality DNA. The work presented here beneficially identifies reduced sample volumes/concentrations as suitable for processing with respect to downstream analysis by enabling pre-concentration of the biological sample, particularly important when dealing with clinical or forensic specimens.

© 2012 Elsevier B.V. All rights reserved.

1. Introduction

Biological samples recovered for forensic analysis or clinical diagnostic applications are often limited in terms of the amount of target analyte present. As a result, methodologies which enable concentration of target molecules as well as isolation from the

complex biological matrix offer distinct advantages and increase the likelihood of achieving positive results during downstream analyses. The use of solid-phase extraction matrices facilitates such sample processing.

Micro fluidics enables the manipulation of microlitre volumes of liquids within a micron scale environment to be carried out. The rapid expansion of this field over the past two decades has been driven by the advantages offered in the development of integrated 'Lab-on-a-Chip' systems. Micro fluidic devices offer numerous advantages over conventional systems as they enable the use of reduced sample and reagent volumes, alongside easier integration of multiple processes on a single device. The ability to integrate sequential processes within a micro fluidic system, that is completely sealed once the samples have been added, offers significant advantages in terms of a reduced risk of contamination [1]. Such

Abbreviations: EDTA, ethylene diaminetetraacetic acid; EMEM, Eagle's minimum essential medium; GuHCl, guanidine hydrochloride; PCR, polymerase chain reaction; TBE, Tris–borate–EDTA buffer; TE, Tris–EDTA buffer.

* Corresponding author. Tel.: +44 1482 466746; fax: +44 1482 466410.

E-mail addresses: l.kashkary@2008.hull.ac.uk (L. Kashkary), cordula.kemp@hull.ac.uk (C. Kemp), k.j.shaw@hull.ac.uk (K.J. Shaw), g.m.greenway@hull.ac.uk (G.M. Greenway), s.j.haswell@hull.ac.uk (S.J. Haswell).

inherent characteristics make micro fluidic systems highly suited for dealing with limited or degraded samples, as is frequently the case for forensic specimens.

Integrating solid-phase nucleic acid extraction techniques into a micro fluidic system enables efficient isolation of target analytes due to beneficial surface area characteristics. Isolation of nucleic acids can be achieved using a silica-based solid-phase onto which the nucleic acids bind in the presence of a chaotropic reagent, such as a guanidine salt. The residual biological matrix, plus any exogenous contaminants, can then be removed by washing the solid-phase with an alcohol. Removal of the purified nucleic acids from the solid-phase matrix is then carried out in a low strength ionic buffer. A more detailed account of the mechanisms involved in the interaction of nucleic acids with silica surfaces is presented in an excellent review by Wen et al. [2]. The use of a small volume of elution buffer can enhance the effective concentration of the nucleic acids from the original total sample volume [3]. This methodology provides additional benefits in that the chaotropic agent used to facilitate DNA binding also serves to lyse any cells present, releasing the nucleic acids, and eliminating the need for a separate lysis step thereby simplifying the extraction procedure.

While conventional DNA extraction kits often rely on bulky equipment for centrifugation or manipulation of magnetic particles to enable washing of the solid-phase, micro fluidic system can use hydrodynamic pumping [4], electro-osmotic pumping [5] or centrifugal forces [6] to control fluid flow within the device. For hydrodynamic pumping, a simple syringe pump can be connected to the micro fluidic device to deliver sample and reagents at precisely controlled volumes and flow rates.

The use of micro fluidic devices offers an increased surface area available for nucleic acid binding resulting in an efficient DNA extraction process. Manipulation of channel geometries or addition of a solid-phase matrix can further enhance these beneficial properties. Pillars, or similar structures, can be fabricated into the micro fluidic device during the manufacturing process and provide an integral means of increasing the surface area available, although DNA extraction efficiencies are limited [7]. The introduction of silica coated particles offers an increased surface area with improved DNA extraction efficiencies of 56% in a micro fluidic device [8]. The challenges of this methodology are in holding the beads in place within the device, using channel geometries or weir-type structures, reducing the reproducibility of the system. More recently, silica-coated magnetic particles have been shown to be successfully manipulated within micro fluidic device via the use of external magnets [9].

In order to achieve more reproducible extraction efficiencies on micro fluidic devices, methodologies which rely on the in situ fabrication of monolithic, i.e. continuous polymeric, structures have been developed [10]. The availability of different monomers and porogens leads to the creation of monolithic structures with different surface properties and pore structures. An ideal monolith has a bimodal pore structure containing macropores (>50 nm) enabling unhindered flow of solutions in addition to micropores (<2 nm) which provide the high surface area required for DNA binding [11]. For example, the use of tetramethyl orthosilicate as the monomer rather than tetraethyl orthosilicate offers higher DNA extraction efficiencies and reduced problems with high backpressures [12]. Precision placement of the monolith within the micro fluidic device can be achieved using photopolymerisation [13] or controlled heating [14].

Further improvements can be made for the extraction of low quantities of nucleic acids by including carrier molecules as part of the binding solution. While a number of carrier molecules exist depending on the application, poly-A carrier RNA has commonly been used in commercially available DNA extraction kits, e.g. Qiagen, and can increase DNA yields by an average of 24% [15]. Such

methodology has also been adapted for inclusion within micro fluidic DNA extraction protocols and showed a significant increase in DNA extraction efficiencies particularly at lower starting amounts of DNA [4].

Here we present an evaluation of a micro fluidic system containing an integrated silica monolith for the extraction of DNA from biological samples. The extraction efficiency of the system improved with minimal cell samples containing less than 15 ng of total DNA, without the need of the addition of carrier RNA. The robustness of the system shows potential for situations where samples are limited, such as in a forensic setting.

2. Experimental

2.1. Micro fluidic device fabrication

Micro fluidic devices were produced in borosilicate glass using standard photolithography and wet etching techniques to generate the design shown in Fig. 1. The features were etched to a depth of 100 μm using a 1% hydrofluoric acid/5% ammonium fluoride solution. In order to allow poly(etheretherketone) tubing to be attached to the micro fluidic device, 360 μm diameter holes were drilled in a 1 mm thick top plate which was then thermally bonded to the etched glass wafer (1 mm thick) to produce the complete micro fluidic device.

The thermally activated silica-based monolith was produced by mixing potassium silicate solution (21% SiO_2 and 9% K_2O [VWR International, UK]) and formamide [Alfa Aesar, UK] in a 10:1 ratio [4]. In order to ensure the monolith was only produced in the DNA extraction chamber, the entire device was first filled with glycerol [Sigma-Aldrich, UK]. The monolith solution was then injected into the DNA extraction chamber, displacing the glycerol, and the micro fluidic device placed in an oven at 90 $^\circ\text{C}$ for 15 min. After this initial heating step, the remaining glycerol was removed and the micro fluidic device placed back in the oven overnight for complete polymerisation to occur. Once polymerised, the monoliths were washed with ethanol to remove any unreacted solution and glycerol residue. Prior to DNA extraction the monoliths were washed with 10 mM TE buffer (10 mM Tris and 1 mM ethylenediaminetetraacetic acid (EDTA) in distilled water, adjusted to pH 6.7 using hydrochloric acid [Sigma-Aldrich, UK]) at 5 $\mu\text{L min}^{-1}$ for 30 min.

2.2. DNA extraction

DNA extractions were carried out on *Mus musculus* cells [Neuro-2a, LGC, UK] grown in ATCC-formulated Eagle's minimum essential medium (EMEM). Cell populations were counted using an improved Neubauer haemocytometer [Weber Scientific International Ltd., UK] and then diluted in EMEM to produce a range of cell numbers (diluted down from a maximum working concentration of 1500 cells mL^{-1}). Cells were then pelleted and the supernatant removed prior to the cells being frozen at -20 $^\circ\text{C}$ until required. The cells were then added to a solution of 5 M guanidine hydrochloride (GuHCl) [Sigma-Aldrich, UK] in 10 mM TE buffer, pH 6.7, and applied to the monolith at 2.5 $\mu\text{L min}^{-1}$. The monolith was washed with 100% ethanol to remove proteinaceous debris along with other potential contaminants of downstream processes at 5 $\mu\text{L min}^{-1}$. Finally, the purified DNA was then eluted from the monolith in 10 mM TE buffer, pH 8.5 at 1 $\mu\text{L min}^{-1}$. All solutions that flowed through the monolith were collected in 4 μL fractions and then analysed by both quantification and amplification techniques.

2.3. DNA quantification

Quantification of the DNA obtained from the extraction procedure was assessed using a Quant-iTTM PicoGreen[®] double stranded

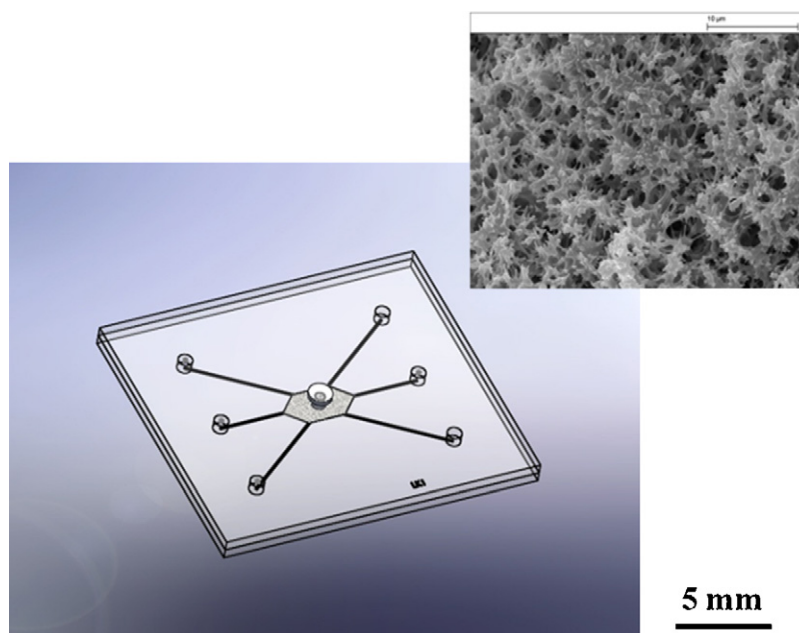


Fig. 1. Schematic showing the micro fluidic device and a close-up of the monolith structure as seen using scanning electron microscopy (10,000 \times resolution).

(ds) DNA Assay Kit [Invitrogen, UK]. To each 2 μL aliquot of sample from the DNA extraction process a 100 μL of the PicoGreen[®] working stock solution was added, based on manufacturer's protocol, in a black microtitre plate. DNA standards were used to provide a calibration curve at the following concentrations: 10, 5, 2.5, 1.25, 0.625, 0.313 and 0.156 $\text{ng } \mu\text{L}^{-1}$. A blank containing no DNA was also used to account for any background fluorescence. All samples were analysed using a FLUOstar Optima Plate Reader [BMG Labtech, UK].

In order to enable calculation of DNA extraction efficiencies, it was necessary to determine the total amount of DNA initially added to the system. Diluted cell populations were thermally lysed by heating to 100 $^{\circ}\text{C}$ and the total amount of DNA released quantified. DNA extraction efficiencies were then expressed as a percentage of the amount of DNA recovered during the elution step compared to the initial amount of DNA added to the system.

2.4. DNA amplification

In order to ensure that the eluted DNA was free of inhibitors and was of sufficient quality for downstream processing, DNA amplification using the polymerase chain reaction (PCR) was performed. The PCR reagent mixture was composed of: 1 \times GoTaq[®] buffer, 2 mM MgCl_2 , 1 unit GoTaq[®] Hot Start DNA polymerase [Promega, UK], 10 mg mL^{-1} bovine serum albumin [NEB Inc., UK], 0.01% (w/v) poly(vinylpyrrolidone), 0.1% (v/v) Tween-20 [Sigma–Aldrich, UK], 200 μM each deoxyribonucleotide triphosphate [Bioline, UK] and 0.1 μM primers for amplification of murine β -actin (forward: 5'-GCAGTCCTTCGTTGCCGGT-3'; 5'-CCCGCCCATGGTGT-CCGTTCC-3') [Eurofins MWG Operon, Germany]. Samples were run on a Techne-32 conventional thermal cycler using the following programme: an initial denaturation of 94 $^{\circ}\text{C}$ for 5 min, followed by 35 cycles of 94 $^{\circ}\text{C}$ for 30 s, 60 $^{\circ}\text{C}$ for 30 s and 72 $^{\circ}\text{C}$ for 30 s, with a final extension step of 60 $^{\circ}\text{C}$ for 5 min.

PCR products were then analysed using slab-gel electrophoresis. A 1.5% (w/v) agarose gel was prepared by dissolving 1.5 g agarose [Bioline, UK] in 100 mL 0.5 \times TBE buffer (0.09 M Tris–HCl, 0.09 M boric acid and 0.002 M EDTA [Sigma–Aldrich, UK] in distilled water). PCR products were mixed with loading dye [Fermentas, UK] and added to the gel, along with a DNA molecular weight standard, GeneRuler[™] 100 bp Plus DNA Ladder [Fermentas, UK], before being

subjected to electrophoresis at 120 V until adequate separation was achieved. Gels were then stained using 0.5 mg mL^{-1} ethidium bromide [CLP, UK] in 0.5 \times TBE buffer for 20 min and then visualized using a UV transilluminator.

3. Results and discussion

3.1. Monolith characterisation

The nucleic acid binding capacity of monoliths formed within the micro fluidic device was initially established. Purified human genomic DNA in 5 M GuHCl in 10 mM TE buffer (pH 6.7) was continuously loaded onto the pre-conditioned monolith for 30 min at a flow rate of 2.5 $\mu\text{L min}^{-1}$. All solutions that passed through the monolith were collected and the amount of DNA present was quantified in order to determine the point at which nucleic acid binding sites on the solid-phase became saturated. Evaluation of the breakthrough curve, showed this point to be approximately 620 ng. However, given the limited biological samples that this proposed system aims to analyse, the DNA present will be well below the binding capacity of the monolith so no potential loss of analyte is anticipated at the binding stage.

3.2. DNA extraction

DNA extraction was performed using decreasing cell numbers in order to evaluate the efficiency of the process when dealing with limited sample populations. An example of a typical elution profile is shown in Fig. 2. As can be seen, minimal DNA passes through the system during the binding and wash phases indicating successful adsorption. A distinct peak, showing release of DNA, is present during the elution step, which is used to calculate the efficiency of the extraction process.

At reduced cell numbers, the efficiency of the DNA extraction process was shown to increase, particularly at 250 cells or less (Fig. 3). Previous research, using micro fluidic devices containing a silica-coated paramagnetic particles, has shown a linear relationship between DNA loaded onto the system and DNA recovered in the range of 25–400 ng [16]. The work presented here is in concordance with that data but goes further to show that when DNA

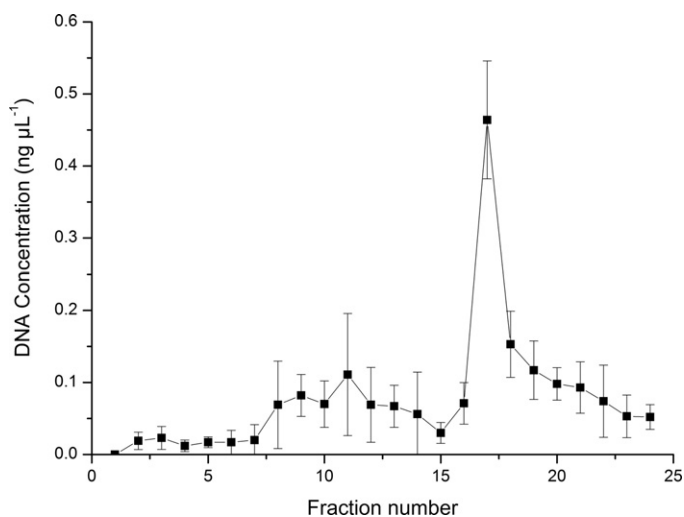


Fig. 2. Average DNA elution profile from DNA extracted from 1000 cells using a silica-based monolith within a micro fluidic device showing binding (1–7), wash (8–15) and elution (16–24) stages ($n=3$).

is loaded in amounts less than 15 ng, equivalent to 250 cells, DNA extraction efficiencies increase and the system is more effective at dealing with limited samples.

Analysis of the DNA elution profiles show that adsorption of DNA is occurring during the binding phase, regardless of the number of cells which are initially added to the system. However, the amount of DNA that is recovered during the elution phase increases in a linear fashion, as lower cell numbers are used. This trend is thought to be due to the low levels of DNA binding initially to reversible rather than irreversible binding sites on the silica monolith [15], a trend which diminishes with increasing amounts on DNA as the reversible sites preferentially fill. Accordingly with low DNA concentrations more reversible binding occurs giving a corresponding higher release efficiency. This hypothesis is in good agreement with the observation that in the presence of carrier RNA, the DNA extraction efficiency increases due to selective irreversible binding of the RNA which in turn improves the elution efficiency of DNA.

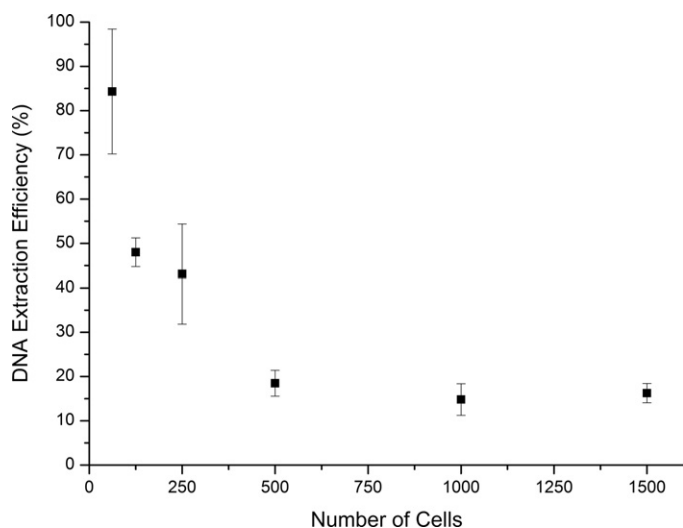


Fig. 3. Comparison of DNA extraction efficiency from varying cell populations, using thermally activated silica monoliths in a micro fluidic device ($n=3$).

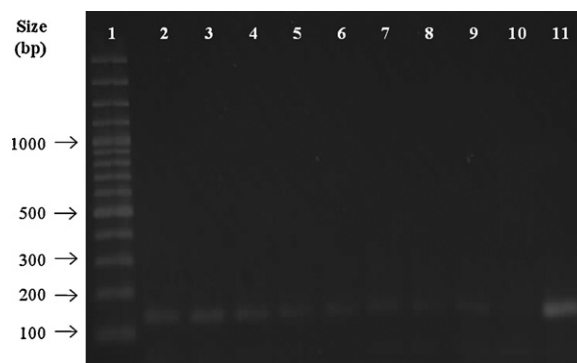


Fig. 4. Example of a gel image showing successful amplification of β -actin gene a micro fluidic DNA extraction from ~ 62 murine cells: (1) DNA size ladder; (2–9) sequentially eluted samples; (10) negative control; (11) β -actin positive control.

3.3. DNA amplification

DNA amplification was performed on the extracted DNA in order to confirm that the extraction process was suitable for removing inhibitors of PCR and the eluted DNA was of suitable quality for analysis. PCR products of the expected size, 135 bp for β -actin, were detectable from DNA extracted using the micro fluidic system (Fig. 4).

4. Conclusion

The evaluation of a micro fluidic device with an integrated silica monolith for the extraction of DNA from limited biological samples has been performed. The high surface area and preferential use of reversible binding sites afforded by the silica monolith when low quantities of DNA are present, were found to enhance the recovery of nucleic acids from complex biological samples. In particular, it has been shown that at lower cell numbers, high DNA extraction efficiencies were achieved without the need of additional carrier RNA. The system developed showed robust performance for limited samples containing less than 15 ng total DNA, which in combination with its ability to use a low volume, relatively closed system to maximise the amount of DNA recovered from limited sample types greatly increases the potential for reducing contamination. Given the low cell numbers that can be successfully extracted, this system lends itself to the examination of clinical or forensic specimens where samples are often limited, such as DNA profiling from crime scene samples. These samples can be directly applied to the micro fluidic device, DNA extraction performed and then analysed either using conventional downstream methodologies or, as hoped in the future, as part of an integrated Lab-on-a-Chip system.

Acknowledgements

The authors would like to thank Dr. Steve Clark for fabrication of the micro fluidic device and the Government of Saudi Arabia for funding.

References

- [1] S.E. Ong, S. Zhang, H.J. Du, Y.Q. Fu, *Front. Biosci.* 13 (2008) 2757.
- [2] J. Wen, L.A. Legendre, J.M. Bienvenue, J.P. Landers, *Anal. Chem.* 80 (2008) 6472.
- [3] R. Boom, C.J.A. Sol, M.M.M. Salimans, C.L. Jansen, P.M.E. Wertheimvanden, J. Vandernoordaa, *J. Clin. Microbiol.* 28 (1990) 495.
- [4] K.J. Shaw, L. Thain, P.T. Docker, C.E. Dyer, J. Greenman, G.M. Greenway, S.J. Haswell, *Anal. Chim. Acta* 652 (2009) 231.
- [5] J. Parton, C. Birch, C. Kemp, S.J. Haswell, N. Pamme, K.J. Shaw, *Anal. Methods* 4 (2012) 96.
- [6] Y.K. Cho, J.G. Lee, J.M. Park, B.S. Lee, Y. Lee, C. Ko, *Lab Chip* 7 (2007) 565.

- [7] B.J. Hindson, D.M. Gutierrez, K.D. Ness, A.J. Makarewicz, T.R. Metz, U.S. Setlur, W.B. Benett, J.M. Loge, B.W. Colston, P.S. Francis, N.W. Barnett, J.M. Dzenitis, *Analyst* 133 (2008) 248.
- [8] K.A. Wolfe, M.C. Breadmore, J.P. Ferrance, M.E. Power, J.F. Conroy, P.M. Norris, J.P. Landers, *Electrophoresis* 23 (2002) 727.
- [9] S.M. Azimi, G. Nixon, J. Ahern, W. Balachandran, *Microfluid. Nanofluid.* 11 (2011) 157.
- [10] K.J. Shaw, D.A. Joyce, P.T. Docker, C.E. Dyer, J. Greenman, G.M. Greenway, S.J. Haswell, *Lab Chip* 9 (2009) 3430.
- [11] X. Chen, D.F. Cui, C.C. Liu, H. Li, *Microsyst. Technol.: Micro- Nanosyst. Inform. Storage Process. Syst.* 14 (2008) 51.
- [12] Q.R. Wu, J.M. Bienvenue, B.J. Hassan, Y.C. Kwok, B.C. Giordano, P.M. Norris, J.P. Landers, J.P. Ferrance, *Anal. Chem.* 78 (2006) 5704.
- [13] J. Wen, C. Guillo, J.P. Ferrance, J.P. Landers, *Anal. Chem.* 78 (2006) 1673.
- [14] K.J. Shaw, D.A. Joyce, P.T. Docker, C.E. Dyer, G.M. Greenway, J. Greenman, S.J. Haswell, *Lab Chip* (2011).
- [15] R. Kishore, W.R. Hardy, V.J. Anderson, N.A. Sanchez, M.R. Buoncristiani, *J. Forensic Sci.* 51 (2006) 1055.
- [16] C.R. Reedy, J.M. Bienvenue, L. Coletta, B.C. Strachan, N. Bhatni, S. Greenspoon, J.P. Landers, *Forensic Sci. Int.: Genet.* 4 (2010) 206.

Acetylation of Alcohols and Phenols Using Continuous-Flow, Tungstosilicic Acid-Supported, Monolith Microreactors With Scale-Up Capability

Ping He¹, Stephen J. Haswell^{1*}, Paul D. I. Fletcher¹, Stephen M. Kelly¹ and Andrew Mansfield²

¹Department of Chemistry, University of Hull, Hull HU6 7RX, UK

²Pfizer Global Research and Development, Sandwich, Kent CT13 9NJ, UK

A highly scalable and efficient flow-system has been developed to perform the catalyzed acetylation of alcohols and phenols, such as salicylic acid, at room temperature in excellent yield. The volumetric throughput and the amount of product can be increased simply by increasing the diameter of a versatile catalytic 12-tungstosilicic acid-supported, silica monolith can be used to increase the quantity of product produced without having to change the optimal operating reaction conditions.

Keywords: micro reactor, continuous-flow, monolith

1. Introduction

The acetylation of alcohols and phenols to form alkyl or aryl acetates (methanoates; Ac = CH₃CO–) represents a very important and routinely utilized transformation in organic chemistry and is commonly carried out in the presence of acetic anhydride as an acetylating agent and either a liquid acid or base catalyst (Scheme 1) [1]. One of the most well known and industrially important chemical reactions is the acetylation of salicylic acid in the presence of acetic anhydride and mineral acid to produce acetyl salicylic acid (aspirin). Since Dresser introduced the clinical use of aspirin in 1899, it has become one of the most widely used medications in the world, still relevant today as an analgesic and prophylactic for several serious medical conditions, with an estimated annual production of 40,000 tons [2]. Various metal chlorides [3] and triflates [4] have been investigated in attempts to develop more efficient and selective acetylation reaction protocols. Unfortunately, these catalysts are often toxic, corrosive, and difficult to recover from the reaction solution.



Due to an advantageous combination of strong acidity and an environmentally friendly nature, heteropoly acids (HPAs) have found numerous applications as versatile, green catalysts for a wide variety of organic reactions, such as acetylation of alcohols and phenols [5], oxidation of alcohols [6], Friedel–Crafts and Mannich reactions [7], cyanosilylation [8], ring-opening reactions of epoxides [9], dehydration [10], and hydrolysis reactions in the manufacture of biofuels [11]. HPAs generally exhibit higher catalytic activity than that of conventional liquid mineral acid catalysts, offering many advantages including high flexibility in the modification of the acid strength, ease of handling, reusability, experimental simplicity, minimal environmental pollution, and limited corrosion problems [12]. However, notable disadvantages of HPAs, which limit their application, are their low surface area and high solubility in polar solvents. These problems can be overcome by the use of a support material, such as porous silica or mobile crystalline material (MCM)-41 [13]. Currently, supported HPA catalysts are used as particles suspended in a reaction mixture which makes it difficult to control

reaction parameters and conditions when attempting to scale-up the reaction. In addition, a reduction in the activity of supported HPA catalysts over several reaction cycles has been observed due to loss of the supported HPAs [14].

Recently, the use of continuous-flow micro reactors for chemical synthesis has been shown to offer greater control over reaction conditions, e.g., catalyst, reagent, and contact time, with the ability to optimize and scale-up chemical reactions without the need for additional optimization [15]. This combination of reactor attributes leads to lower cycle times, greater selectivity, and higher yield compared to those using batch-based methods [16]. In particular, so-called “monolith flow reactors” have been shown to offer good flow characteristics, associated with the presence in the monolith of nano- and micro-scale pores, while representing ideal supports for reagents and catalysts [15c].

We report in this paper the development of an heteropoly acid, 12-tungstosilicic acid (H₄SiW₁₂O₄₀)-supported silica-based monolithic reactor and the results of testing it by the acetylation of alcohols and phenols, such as salicylic acid, in the presence of acetic anhydride as a model reaction to demonstrate the practicality of this approach and to extend the scope of continuous-flow monolithic reactors. The results reported here indicate that HPAs-supported monoliths not only minimize the pollution and corrosion problems of the traditional reactions but also facilitate the optimization and scaling up of chemical reactions with precise control over the reaction parameters without the need for additional optimization. The results of this model reaction indicate that the use of continuous-flow monoliths allows scale-up of chemical reactions without any material change in the product yield or reaction conditions, by the simple expedient of increasing the diameter of the monolith, e.g., a doubling of the monolith diameter results in a four-fold increase in the flow rate and corresponding four-fold increase in product output. This scaling-up process is particularly attractive because as the dimensions of the nano- and micro-pores in both monolithic structures are the same, the corresponding permeability coefficient will remain constant resulting in no change in the pressure drop for the larger monolith, which will, however, produce a larger volumetric throughput for an identical flow rate or catalyst contact time [15c]. Furthermore, the continuous-flow process eliminates the requirement of the separation of heterogeneous catalysts from the reaction mixture and minimizes the environmental pollution and corrosive problems often encountered using the traditional methodologies involving the use of toxic and corrosive liquid acids, such as hydrofluoric and sulfuric acids.

* Author for correspondence: s.j.haswell@hull.ac.uk

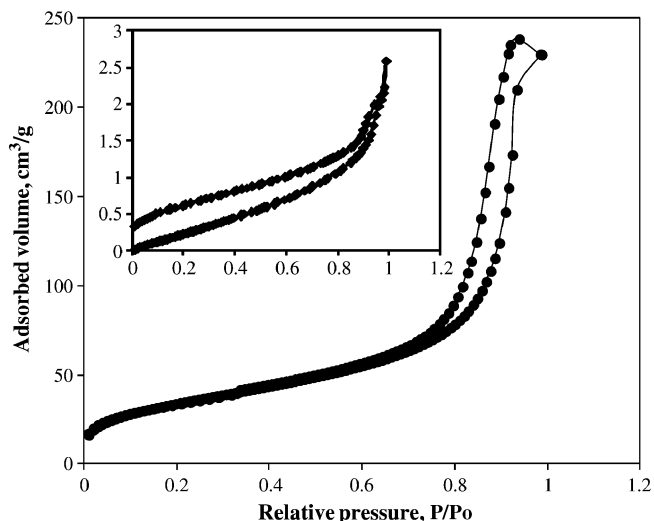


Figure 1. N_2 adsorption–desorption isotherms of the $H_4SiW_{12}O_{40}$ -monolith at 77 K. Inset: N_2 adsorption–desorption isotherms of bulk $H_4SiW_{12}O_{40}$

2. Results and Discussion

2.1. Immobilization and Characterization of the Monolithic Catalysts. The preparation of silica-based monoliths and 12-tungstosilicic acid-supported monoliths ($H_4SiW_{12}O_{40}$ -monolith) is described in the Experimental. Characterization of these monoliths by N_2 adsorption and desorption isotherms indicates type H2 hysteresis (see Figure 1), which is consistent with the disordered mesoporous structure seen in the micrograph shown in Figure 2.

The Brunauer, Emmett and Teller (BET) surface area, pore volume and size for the $H_4SiW_{12}O_{40}$ -monolith and bulk $H_4SiW_{12}O_{40}$ catalysts are shown in Table 1. The BET surface area for the $H_4SiW_{12}O_{40}$ -monolith was $\sim 131 \text{ m}^2/\text{g}$ compared to only $\sim 0.95 \text{ m}^2/\text{g}$ for bulk $H_4SiW_{12}O_{40}$, resulting in a catalytic monolith with approximately 138 times higher surface area. It can be seen from the powder X-ray diffraction (XRD) patterns of pure $H_4SiW_{12}O_{40}$ and the $H_4SiW_{12}O_{40}$ -monolith (Figure 3) that there is no indication of the presence of $H_4SiW_{12}O_{40}$ crystals in the XRD patterns of the $H_4SiW_{12}O_{40}$ -monolith, indicating that the 12-tungstosilicic acid species are highly dispersed within the mesoporous structure of the silica monoliths [14a], as shown in Figure 2.

2.2. Acetylation of Alcohols and Phenols. A variety of hydroxyl substrates including primary, secondary, benzylic alcohols, and phenols has been used as reactants in a model acetylation

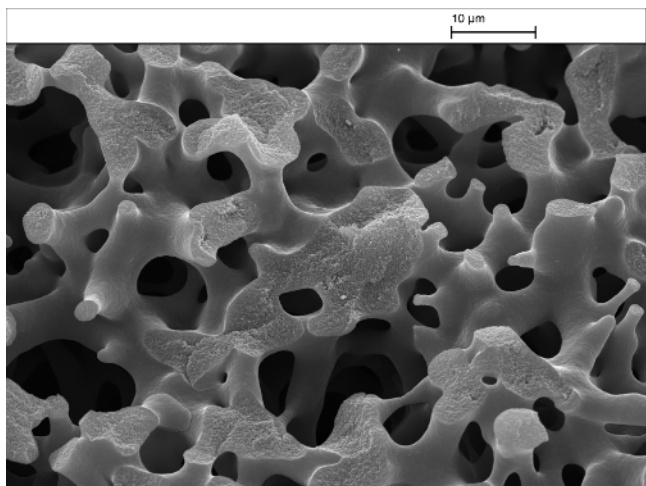


Figure 2. SEM image of 12-tungstosilicic acid-supported monolith

Table 1. BET characterization of bulk $H_4SiW_{12}O_{40}$ and $H_4SiW_{12}O_{40}$ -monolith catalysts

Sample	Surface area (m^2/g)	Pore volume (cm^3/g)	Pore size (nm)
$H_4SiW_{12}O_{40}$ -monolith-3.2	130.9	0.35	11.4
$H_4SiW_{12}O_{40}$ -monolith-6.4	130.1	0.36	11.5
Bulk $H_4SiW_{12}O_{40}$	0.95	0.0034	8.8

reaction using the 12-tungstosilicic acid $H_4SiW_{12}O_{40}$ -monolith-3.2 in the presence of acetic anhydride as acetylating agent without solvent and at room temperature under continuous-flow conditions. It can be seen from Table 2 that all of these acetylation reactions are efficient, giving a high yield with negligible formation of by-products (see GC–MS chromatograms of samples in the Supporting Information). This HPA-supported monolith is a more active catalyst than that used in conventional batch reactions, e.g., see that reported by Heravi et al. [5a] where the use of free HPA in a batch acetylation reaction gave an 89% yield using 4-nitrophenol and 97% yield using 4-methoxy benzyl alcohol as the reactants, with a reaction time of 15 min, compared to the results reported here using the HPA-supported monolith catalyst in a continuous-flow microreactor where the acetylation is 100% complete within a residence time of 3 min (see entries 3 and 4). The high activity of the supported 12-tungstosilicic acid can be attributed to the high dispersion of the acid in the monolith mesopores. However, when the reagent flow rate is increased from 80 to 160 and then 320 $\mu\text{L}/\text{min}$, corresponding to contact times of 3, 1.5, and 0.75 min, respectively, the product yield, for example, of the acetylation of 2,4,6-trichlorophenol decreases from 100% to 68% and then 36% due to the shorter contact times. This continuous-flow method tolerates other functional groups on the reactants such as double bonds (entry 9) and gives the quantitative acetylated product. A deactivating group in the reactants reduces their reactivity towards acetylation. It is also very interesting to note that 3-hydroxyphenol (entry 6) mainly gives mono-acetylated product (97%) with only 3% di-acetylated product, while the acetylation of 1,4-dihydroxybutane (entry 7) only generates the di-acetylated product and none of the mono-acetylated product. These results suggest that the presence of the acetyl group added by acetylation reaction reduces the activity of the second hydroxyl group in phenols, while there is little effect on the

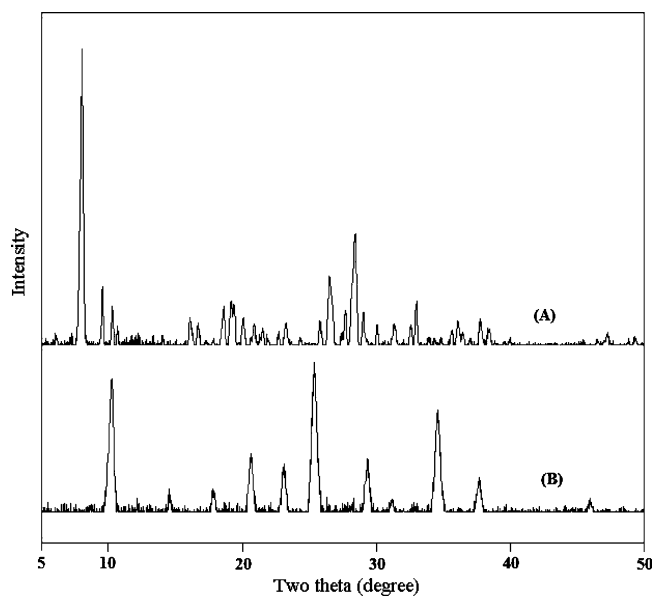
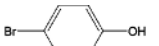
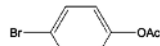
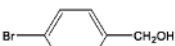
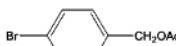
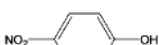
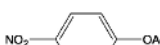
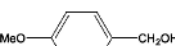
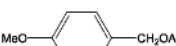
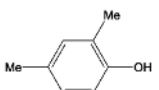
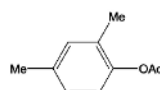
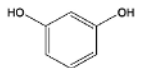
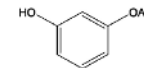
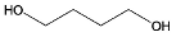
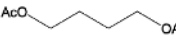
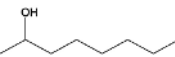
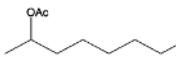
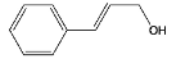
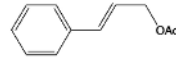
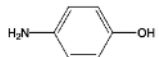
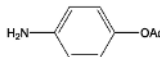
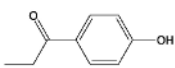
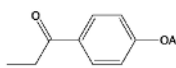
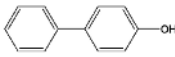
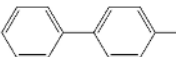
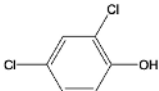
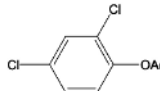
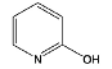
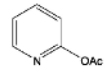
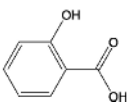
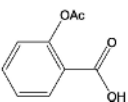


Figure 3. XRD patterns of pure $H_4SiW_{12}O_{40}$ (A) and $H_4SiW_{12}O_{40}$ -monolith (B)

Table 2. Activity of $\text{H}_4\text{SiW}_{12}\text{O}_{40}$ -monoliths with different diameters in acetylation reactions with a variety of substrates under continuous-flow conditions^a

Entry	Substrate	Product	$\text{H}_4\text{SiW}_{12}\text{O}_{40}$ -monolith-3.2	$\text{H}_4\text{SiW}_{12}\text{O}_{40}$ -monolith-6.4
			Yield (%)	Yield (%)
1			100	100
2			100	100
3			100	100
4			100	100
5			100	100
6 ^b			97	97
7			100	100
8			100	100
9			100	100
10			100	100
11			100	100
12			100	100
13			99	99
14			100	100
15			100	100

^aAll reactions were carried out at room temperature (~ 25 °C). Reactant (0.3 M) was premixed in acetic anhydride, and the reactant solution was pumped through the reactor using an HPLC pump. Yields were determined by GC–MS versus internal standard. Substrate contact time for both monolithic reactors was 3 min. Flow rates were 80 $\mu\text{L}/\text{min}$ for $\text{H}_4\text{SiW}_{12}\text{O}_{40}$ -monolith-3.2 and 320 $\mu\text{L}/\text{min}$ for $\text{H}_4\text{SiW}_{12}\text{O}_{40}$ -monolith-6.4.

^b3% di-acetylated product was formed.

activity of the second hydroxyl group in 1,4-dihydroxybutane. This may be attributable to mesomeric effects in (aromatic) phenols, which are not present in (aliphatic) alcohols. Similar results to those reported in Table 2 using a very large excess of acetic anhydride can also be obtained using 1.0–1.5 M equivalent of acetic anhydride to reactant when the reactant is soluble in acetic anhydride. However, some reactants have limited solubility in acetic anhydride and a high concentration of acetic anhydride, e.g., 0.3 M for salicylic acid is used to make a homogeneous reaction mixture. Therefore, this concentration was used for all reactions in this work (see Table 2) to eliminate the effect of changing the concentration of reagents and reactants, so that valid comparisons of the results can be made.

2.3. The Scalability of the Monolithic Catalysts. To evaluate the scalability of the methodology, a larger-diameter monolith, $\text{H}_4\text{SiW}_{12}\text{O}_{40}$ -monolith-6.4 (6.4 mm in diameter, 35-mm long and void volume of 0.95 mL), was prepared and used to perform the same reactions as carried out by the $\text{H}_4\text{SiW}_{12}\text{O}_{40}$ -monolith-3.2 in Table 2. The results confirm that the larger monolith with a two-fold increase in diameter (3.2 to 6.4 mm both 35-mm long) gives correspondingly high yields with an almost four-fold increase in product quantity. The $\text{H}_4\text{SiW}_{12}\text{O}_{40}$ -monoliths were also tested for acetylation of salicylic acid (entry 15) to produce acetylsalicylic acid (aspirin) which demonstrates that 1 g acetylsalicylic acid can be produced within 1 h using a flow rate of 0.32 mL/min. A control experiment was also carried out

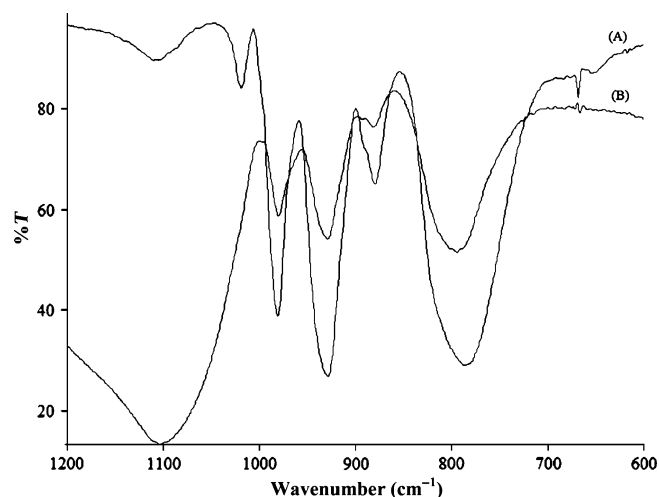


Figure 4. Infrared spectra of bulk $\text{H}_4\text{SiW}_{12}\text{O}_{40}$ (A) and 40 wt% of $\text{H}_4\text{SiW}_{12}\text{O}_{40}$ -monolith (B)

using a conventional batch reactor. The same amount of free HPA as supported HPA (0.039 g), salicylic acid and acetic anhydride, used in the flow reaction, was used, and a yield of 0.96 g acetylsalicylic acid was obtained within 1 h. A similar result was also reported by Heravi et al. [5b] using free HPA. However, the monolithic reactor can be continuously used for many hours, while the free $\text{H}_4\text{SiW}_{12}\text{O}_{40}$ is difficult to remove from the batch reaction mixture.

2.4. The Stability of the Monolithic Catalysts. The stability of the $\text{H}_4\text{SiW}_{12}\text{O}_{40}$ -monoliths is indicated through their repeated use which, in this investigation, represented 15 reactions, each requiring five optimization reactions (total reaction number 75) carried out using one monolithic reactor without any distinguishable loss in reaction performance. In addition, the monolith catalyst was washed with methanol (see washing treatment in the Supporting Information) between each acetylation reaction, and the turnover frequency (TOF) for salicylic acid was 130/h. This stability can be attributed to the surface interaction between 12-tungstosilicic acid and the monolith support, which is confirmed by infrared characterization. As seen in Figure 4, the main infrared (IR) bands of $\text{H}_4\text{SiW}_{12}\text{O}_{40}$ -monolith are 978 (W=O), 929 (Si-O), 885, and 795 cm^{-1} (W-O-W), which corresponds to characteristic 12-tungstosilicic acid vibrations [17], indicating that the Keggin structure of HPA remains after the silica monoliths are impregnated with HPA. The absorption band for W=O shows a small (3 cm^{-1}) red shift, and the bands for W-O-W show more significant blue shifts (up to 13 cm^{-1}) compared to the corresponding peaks in the IR spectrum of bulk 12-tungstosilicic acid (see Table 3). The presence of these shifts is indicative of the interaction of the monolith support with the most external oxygen atoms of the Keggin anion and stabilization of the 12-tungstosilicic acid supported on the mesoporous silica monoliths [18].

3. Conclusion

In summary, it has been demonstrated that the 12-tungstosilicic acid-supported silica monolithic reactors show excellent yields

Table 3. IR characteristics of bulk and monolith-supported 12-tungstosilicic acid^a

Sample	W=O	Si-O	W-O _d -W	W-O _b -W
$\text{H}_4\text{SiW}_{12}\text{O}_{40}$ -monolith	978 cm^{-1}	929 cm^{-1}	885 cm^{-1}	795 cm^{-1}
Bulk $\text{H}_4\text{SiW}_{12}\text{O}_{40}$	981 cm^{-1}	927 cm^{-1}	880 cm^{-1}	782 cm^{-1}

^aSee Ref. [18] for the identification of the infrared absorption bands.

for acetylation of alcohols and phenols, such as salicylic acid, under continuous-flow conditions. One of the important features of the monolithic reactor is that the amount of product can be scaled-up simply by increasing the diameter of the catalytic monolith without changing the optimal reaction conditions. The high activity and strong stability of the supported 12-tungstosilicic acids are attributed to high dispersion of 12-tungstosilicic acids on silica monolith supports and the surface interaction between the monolith and the most external oxygen atoms of the Keggin anions. No problems were encountered in the scale-up of the monolith with a diameter of 3.2-mm to a 6.4-mm monolith, i.e., there was no shrinkage, and the flow reaction worked perfectly well. However, it was more difficult to maintain a uniform temperature across the larger monolith during the gelation reaction, and this difference in gelation temperature resulted in a change in the nano- and micro-structure of monoliths.

4. Experimental

4.1. Materials. All reagents and solvents, such as poly(ethylene oxide) (PEO) with average relative molar mass of 100 kDa, tetra-ethoxysilane (TEOS), acetic anhydride (99%), dichloromethane (99%, DCM), ammonium hydroxide (5 N), and nitric acid aqueous solutions (1 N), were purchased from Aldrich. All reagents were used as obtained without further purification. Heat-shrinkable Teflon tubes (wall thickness of 0.1 and 0.3 mm before and after shrinkage) with a shrinkage ratio of 2:1 were purchased from Adtech Polymer Engineering Ltd. (UK).

4.2. Synthesis of Silica Monolith Supports. Silica-based monoliths were prepared using a sol-gel process described in the literature [19]. The desired amount of PEO was added to an aqueous solution of nitric acid, and the resultant mixture was cooled in an ice bath and stirred until a homogeneous solution formed. TEOS was then added to the reaction mixture, which was stirred vigorously in an ice bath for 30 min to form a transparent solution. Subsequently, the solution was poured into a plastic mold (diameter of 4.8 mm and length of 6 cm for monolith-3.2 and diameter of 8.2 mm and length of 5 cm for monolith-6.4). Both ends of the plastic mold were then closed, and the sealed tube was incubated in an oven at 40 °C for 3 days, while a wet, semi-solid gel monolith was formed. Approximately 20% shrinkage occurred during this gel formation, which allowed easy removal of the wet gel monoliths from the plastic tube molds. The wet gel monoliths were washed with copious amounts of water to remove any residues and then transferred to a 10 times volume of 1 M NH_4OH aqueous solution in an autoclave where it was incubated at 80 °C for 24 h. The monoliths were again washed with copious amounts of water before drying in an oven at 90 °C for 24 h. Finally, the monoliths were calcined at 550 °C for 3 h (heating rate: 2 °C/min) in an air flow to remove the remaining PEO and form white silica-monolith rods (diameters of 3.2 and 6.4 mm, respectively), which were then cut to 35-mm-long monoliths.

4.3. Preparation of 12-Tungstosilicic Acid-Supported Silica-Monolith ($\text{H}_4\text{SiW}_{12}\text{O}_{40}$ -Monolith). An aqueous solution of 240 μL containing 40 wt% $\text{H}_4\text{SiW}_{12}\text{O}_{40}$ relative to silica monolith was totally adsorbed onto the monoliths, dried at 90 °C and calcined at 200 °C for 2 h (temperature ramp: 1 °C/min) under a flow of air. The $\text{H}_4\text{SiW}_{12}\text{O}_{40}$ -monolith rod obtained was then clad in a heat-shrinkable Teflon tube with a glass connector at each end. The assembly was heated in a furnace at 330 °C until the monolith was sealed within the Teflon tube to form a flow- $\text{H}_4\text{SiW}_{12}\text{O}_{40}$ -monolith reactor system.

4.4. Activity Measurements. The 35-mm-long $\text{H}_4\text{SiW}_{12}\text{O}_{40}$ -monolith reactor with a diameter of either 3.2 mm ($\text{H}_4\text{SiW}_{12}\text{O}_{40}$ -monolith-3.2) or 6.4 mm ($\text{H}_4\text{SiW}_{12}\text{O}_{40}$ -monolith-6.4) was connected to a high performance liquid chromatography (HPLC) pump.

A reaction solution containing reactant (0.3 M) in acetic anhydride was pumped through the reactor at room temperature. The residence times of the reactants within the catalytic monoliths were determined using the known void volume of monoliths and different flow rates. Product samples were collected at defined flow periods during a reaction run and weighed, and a known amount of dodecane was added to the individual samples as an internal standard. Samples were treated with distilled water to remove excess acetic anhydride and extracted with DCM. The remaining organic material was then washed three times with distilled water, collected and dried over MgSO₄. Individual samples were analyzed using GC–MS (Varian 2000) as described in literature [20].

4.5. Sample Characterization. Scanning electron microscopy (SEM) images were obtained using a Cambridge S360 scanning electron microscope operated at 20 kV. Each sample was sputter coated with a thin layer of gold-platinum (thickness approximately 2 nm) using a SEMPREP 2 Sputter Coater (Nanotech Ltd.). Transmission electron microscopy (TEM) was carried out on a JEOL-2010 operating at 200 kV. The BET surface area and nanometer-scale pore-size distribution were obtained by measuring N₂ adsorption and desorption isotherms at 77 K by using a micromeritics surface area and porosity analyzer. The pore volume and pore size distributions of the nanometer-scale pores within the monoliths were evaluated from the isotherms using the BJH (Barrett–Joyner–Halenda) model. The powder XRD patterns and the IR spectra of the H₄SiW₁₂O₄₀ monolith and pure H₄SiW₁₂O₄₀ were obtained by using SIEMENS D5000 and PerkinElmer Paragon1000 instrument, respectively. Determination of the micrometer-scale porosity φ_t (which determines the monolith permeability) was determined from the equation $(W_M - W_T)/dlr^2\pi$, where W_T and W_M were the weights of the dry and water-filled monolith, respectively, d was the density of water, and l and r were the overall length and radius of the cylindrical monolith. The micrometer-scale pore size was determined from SEM measurements.

References

- (a) Sartori, G.; Bellini, R.; Bigi, F.; Bosica, G.; Maggi, R.; Righi, P. *Chem. Rev.* **2004**, *104*, 199–250; (b) Pearson, A. L.; Roush, W. J. *Handbook of Reagents for Organic Synthesis: Acetylating Agents and Protecting Groups*; John Wiley: Chichester, U.K., 1999.
- Warner, T. D.; Mitchell, J. A. *Proc. Natl. Acad. Sci. USA* **2002**, *99*, 13371–13373.
- (a) Heravi, M. M.; Behbahani, F. K.; Shoar, R. H.; Oskooie, H. A. *J. Mol. Catal. A: Chem.* **2006**, *244*, 8–10; (b) Kantam, M. L.; Aziz, K.; Likhar, P. R. *Catal. Commun.* **2006**, *7*, 484–487.
- Orita, A.; Tanahashi, C.; Kakuda, A.; Otera, J. *Angew. Chem. Int. Ed.* **2000**, *39*, 2877–2879.
- (a) Heravi, M. M.; Behbahani, F. K.; Bamoharram, F. F. *J. Mol. Catal. A: Chem.* **2006**, *253*, 16–19; (b) Heravi, M. M.; Behbahani, F. K.; Bamoharram, F. F. *ARKIVOC* **2007**, *xvi*, 123–131.
- Firouzabadi, H.; Iranpoor, N.; Amani, K. *Synthesis* **2003**, 408–412.
- (a) Kaur, J.; Griffin, K.; Harrison, B.; Kozhevnikov, I. V. *J. Catal.* **2002**, *208*, 448–455; (b) Azizi, N.; Torkiyani, L.; Saidi, M. R. *Org. Lett.* **2006**, *8*, 2079–2082.
- Firouzabadi, H.; Iranpoor, N.; Jafari, A. A. *J. Organomet. Chem.* **2005**, *690*, 1556–1559.
- Azizi, N.; Saidi, M. R. *Tetrahedron* **2007**, *63*, 888–891.
- Dias, A. S.; Lima, S.; Pillinger, M.; Valente, A. A. *Carbohydr. Res.* **2006**, *341*, 2946–2953.
- Zhao, S.; Cheng, M.; Li, J.; Tian, J.; Wang, X. *Chem. Commun.* **2011**, *47*, 2176–2178.
- (a) Kozhevnikov, I. V. In *Catalysis for Fine Chemical Synthesis, Catalysis by Polyoxometalates 2*; Derouane, E., Eds.; Wiley: New York, **2002**; (b) Romanelli, G. P.; Bennardi, D.; Ruiz, D. M.; Baronetti, G.; Thomas, H. J.; Autino, J. C. *Tetrahedron Lett.* **2004**, *45*, 8935–8939.
- (a) Popa, A.; Sasca, V.; Kiš, E. E.; Marinković-Nedučin, R.; Bokorov, M. T.; Halasz, J. *J. Opt. Adv. Mater.* **2005**, *7*, 3169–3177; (b) Damayanova, S.; Gomez, M. L.; Banares, M. A.; Fierro, J. L. G. *Chem. Mater.* **2000**, *12*, 501–510; (c) Liu, Y.; Xu, L.; Xu, B.; Li, Z.; Jia, L.; Guo, W. *J. Mol. Catal. A: Chem.* **2009**, *297*, 86–92; (d) Xia, Q. H.; Hidajat, K.; Kawi, S. *J. Catal.* **2003**, *209*, 433–444; (e) Juan, J. C.; Zhang, J. C.; Yarmo, M. A. *J. Mol. Catal. A: Chem.* **2007**, *267*, 265–271.
- (a) Zhang, F.; Yuan, C.; Wang, J.; Kong, Y.; Zhu, H.; Wang, C. *J. Mol. Catal. A: Chem.* **2006**, *247*, 130–137; (b) Zhu, Z.; Yang, W. *J. Phys. Chem. C* **2009**, *113*, 17025–17031; (c) Javid, A.; Heravi, M. M.; Bamoharram, F. F. *E-J Chem.* **2011**, *8*, 910–916.
- (a) Mason, B. P.; Price, K. E.; Steinbacher, J. L.; Bogdan, A. R.; McQuade, D. T. *Chem. Rev.* **2007**, *107*, 2300–2318; (b) Pennemann, H.; Watts, P.; Haswell, S. J.; Hessel, V.; Löwe, H. *Org. Process Res. Dev.* **2004**, *8*, 422–439; (c) He, P.; Haswell, S. J.; Fletcher, P. D. I.; Kelly, S. M.; Mansfield, A. *Beilstein J. Org. Chem.* **2011**, *7*, 1150–1157.
- (a) Vankayala, B. K.; Löb, P.; Hessel, V.; Menges, G.; Hoffman, C.; Metzke, D.; Krtischil, U.; Kost, H. *J. Int. J. Chem. React. Eng.* **2007**, *5*, A91; (b) De Mas, N.; Günther, A.; Kraus, T.; Schmidt, M. A.; Jensen, K. F. *Ind. Eng. Chem. Res.* **2005**, *44*, 8997–9013; (c) He, P.; Fletcher, P. D. I.; Haswell, S. J. *Lab. Chip* **2004**, *4*, 38–41.
- Bielanski, A.; Lubanska, A.; Pozniczek, J.; Micek-Ilnick, A. *Appl. Catal. A: Gen.* **2003**, *238*, 239–250.
- Nasr-Esfahani, M.; Montazerzohori, M.; Moghadam, M.; Akhlaghi, P. *ARKIVOC* **2010**, *ii*, 97–107.
- Fletcher, P. D. I.; Haswell, S. J.; He, P.; Kelly, S. M.; Mansfield, A. *J. Porous Mater.* **2011**, *18*, 501–508.
- He, P.; Fletcher, P. D. I.; Haswell, S. J. *Appl. Catal. A: Gen.* **2004**, *274*, 111–114.



Sex identification of ancient DNA samples using a microfluidic device

Joseph Parton^a, Naglaa Abu-Mandil Hassan^b, Terence A. Brown^b, Stephen J. Haswell^a, Keri A. Brown^b, Kirsty J. Shaw^{a,*}

^a Department of Chemistry, University of Hull, Cottingham Road, Hull HU6 7RX, UK

^b Manchester Institute of Biotechnology, Faculty of Life Sciences, University of Manchester, 131 Princess Street, Manchester M1 7DN, UK

ARTICLE INFO

Article history:

Received 8 June 2012

Received in revised form

17 July 2012

Accepted 19 July 2012

Keywords:

Amelogenin

Ancient DNA

Biomolecular archaeology

Microfluidics

Sex identification

ABSTRACT

A microfluidic device has been developed for the sex identification of ancient DNA samples and works by manipulating liquids within an environment of micrometer dimensions. In this work a range of microfluidic DNA extraction methods were evaluated for their compatibility with ancient DNA samples, and the use of streptavidin-coated super paramagnetic particles to isolate biotin-labeled abasic sites within damaged DNA was shown to be the most reproducible. Polymerase chain reaction-based DNA amplification was possible on the microfluidic device when less than 50 pg of template DNA was added. As a proof-of-principle, powdered bone samples were analysed using the integrated methodology developed. Following conventional capillary gel electrophoresis, two out of the three samples produced positive amplification results and were successfully identified as female. These sex identifications were corroborated by independent Amelogenin, anthropological and Y chromosome analysis. The work reported here is the first step in the development of a complete miniaturized microfluidic system that would enable on-site ancient DNA analysis.

© 2012 Elsevier Ltd. All rights reserved.

1. Introduction

Ancient DNA is the name given to the degraded, fragmented and chemically damaged biomolecules that can be recovered from archaeological remains of plants, animals and humans. Its preservation and survival are not fully understood. Where it does survive, it can give valuable information, and ancient human DNA from archaeological sites is especially useful for its potential to identify kinship, population affinities, pathogens and biological sex (Brown and Brown, 2011).

However, ancient human DNA analysis is still not routinely applied in archaeology because of three major problems. Firstly there is the issue of contamination with modern human DNA, derived from handling of human remains by archaeologists and osteoarchaeologists. This can largely be overcome by adopting precautions during excavation to minimise contamination and by careful cleaning and treatment of the samples when they reach the

laboratory (Brown and Brown, 2011). Secondly there is the issue of cost. Ancient human DNA analysis requires specialist clean room facilities, laboratory equipment and is labour intensive – for results to be credible highly technically skilled and reputable scientists should carry out the work. Finally there is a limited range of analytical methods available for ancient DNA analysis. Although Next Generation Sequencing (NGS) techniques are becoming increasingly utilised, the bioinformatic analysis of the DNA sequences obtained is time consuming. The more traditional polymerase chain reaction (PCR) methods do not seem amenable to multiplexing with ancient DNA templates, so for each DNA target one PCR at a time must be carried out, with additional cloning and sequencing experiments to confirm the authenticity of the DNA sequences obtained. A way forward would seem to be a method that incorporates the ability to perform multiple PCRs on a device that also allows DNA extraction in one operation. The problems of contamination could also be minimised or eradicated if these procedures could be performed in an enclosed system.

Microfluidics concerns the manipulation of small amounts of fluids within channels of micron dimensions (Whitesides, 2006). This spatial and temporal fluidic control is coupled with efficient mass and thermal energy transfer providing microfluidic platforms with the potential to not only miniaturise existing methodologies but also to develop novel techniques which benefit from this reduced scale. Inherent benefits include a reduction in sample and

* Corresponding author. Present address: School of Science and the Environment, Manchester Metropolitan University, Chester Street, Manchester M1 5GD, UK. Tel./fax: +44 (0)161 247 1538.

E-mail addresses: j.parton@2008.hull.ac.uk (J. Parton), Naglaa.Abu-MandilHassan@postgrad.manchester.ac.uk (N. Abu-Mandil Hassan), terry.brown@manchester.ac.uk (T.A. Brown), s.j.haswell@hull.ac.uk (S.J. Haswell), keri.brown@manchester.ac.uk (K.A. Brown), k.shaw@mmu.ac.uk (K.J. Shaw).

reagent consumption, increased speed of analysis, reduced cost and increased portability. Of particular advantage is the ability to integrate multiple techniques onto a single microfluidic device, known as micro-total analysis systems (μ TAS) or Lab-on-a-Chip (LOC).

Microfluidic devices can be produced in a broad range of materials depending upon the specific application. Glass, for example, has been widely used in the production of microfluidic devices for genetic analysis as it has good thermal properties for PCR-based DNA amplification and optical transparency enabling a number of detection techniques to be used. However, the high surface area to volume ratio present within microfluidic devices coupled with the lack of biocompatibility of glass often requires surface treatment to minimise adsorption of reagents, such as DNA polymerase (Erill et al., 2003). Alternatively, polymers such as poly(methyl methacrylate) can be utilised as they often exhibit good biocompatibility but are less well suited to high temperature requirements (Zhang and Xing, 2007).

Movement of reagents around microfluidic devices can be achieved using a variety of different mechanisms, the most common being hydrodynamic and electrokinetic pumping techniques. Hydrodynamic pumping is a well established methodology that uses syringe pumps in either infusion or withdrawal mode, attached to the microfluidic device by tubing and connectors, to achieve reagent movement. This generates a parabolic flow profile within the channel which means that the flow of solutions is faster in the centre of the channel due to frictional forces at the surface (Taylor and Yeung, 1993). Electrokinetic pumping can occur due to the electrophoretic movement of charged species within the microfluidic device or the bulk flow of solutions via electro-osmotic flow (EOF). In EOF, an electrical double layer is generated at the glass surface due to an electrostatic attraction of cations to the deprotonated silanol groups. The more diffuse mobile layer is pulled towards the cathode, in the presence of an applied electric field, dragging with it the bulk solution. In the absence of a pressure difference across the length of the microfluidic channel, a flat flow profile is produced which means that all molecules exhibit the same velocity, except for those very close to the internal surface wall (Taylor and Yeung, 1993).

The use of microfluidic technology for carrying out genetic analysis has received much attention in the literature for clinical diagnostic (Shaw et al., 2011a) and forensic applications (Horsman et al., 2007). Isolated sample preparation, amplification and detection techniques within microfluidic systems have been demonstrated in a wide range of forms, with the integration of two or more components being developed more recently (Njoroge et al., 2011).

Nucleic acid isolation on microfluidic devices is commonly achieved using solid-phase extraction protocols (Wen et al., 2008). The general principle involves the binding of nucleic acids to a solid-phase support, washing to remove any cellular debris or potential contaminants and finally elution of the concentrated, purified nucleic acids. The use of silica as the solid-phase has been shown to be highly compatible with microfluidic environments and produces high yields of purified DNA. However, the requirement for chaotropic salts and organic solvents can lead to problems in terms of integration with sensitive downstream applications such as PCR. Anion exchange resins can be used to overcome these challenges as they utilise pH changes to bind and release nucleic acids from the solid-phase. In particular chitosan, $\alpha(1\rightarrow4)$ -linked 2-amino-2-deoxy- β -D-glucopyranose, can be coated either directly onto the surface of the microfluidic device or on beads/particles or monoliths which can be incorporated after fabrication (Reedy et al., 2011). DNA binding occurs at pH 5, with release facilitated by increasing the pH of the buffer used to pH 9.

DNA amplification lends itself well to a microfluidic format and as such has received widespread attention in the literature, in particular with reference to PCR-based amplification techniques (Zhang et al., 2006). More recently, biochemical advances have led to the development of a range of novel isothermal amplification techniques and these have also been successfully applied on a microfluidic scale (Asiello and Baeumner, 2011). There are three main types of microfluidic PCR systems; stationary, flow-through and droplet. In stationary PCR, one or more PCR chambers are cycled through the required temperature zones in a similar way to a conventional thermal cycler. Thermal cycling can be provided by direct contact with a simple block heater, such as a Peltier element, or via non-contact methods like infra-red (Zhang et al., 2006). Flow-through PCR relies on the movement of the PCR reagents through distinct temperature zones resulting in thermal cycling. Amplification in such systems is governed by the flow rate of solutions and the layout of the microfluidic device (Zhang et al., 2006). More recently, droplet-based PCR has emerged due to the need for higher throughput amplification techniques. Water-in-oil droplets containing all the necessary PCR reagents are applied to flow-through devices, with the possibility for encapsulation and analysis of single molecules (Schaerli et al., 2009).

Integration of purification and amplification techniques is not without its challenges; in particular those issues raised by confinement of the solid-phase matrix, chemical compatibility and surface properties of the device required for the different stages (Ferrance et al., 2003). One solution used to overcome these challenges is to combine the flow of DNA eluted from the solid-phase with a concentrated PCR reagent mixture from a side channel and direct the combined solutions into a PCR chamber for amplification (Bienvenue et al., 2010). Alternatively, the use of suitably functionalised magnetic particles as the solid-phase can facilitate nucleic acid movement within microfluidic systems. Pipper et al., developed a device for the detection of the H1N1 (bird flu) virus by using superparamagnetic particles to move viral RNA between aqueous droplets in an oil environment (Pipper et al., 2007). Each droplet contained a different reagent for sequential nucleic acid purification and reverse transcription-PCR. Previous work by the authors has demonstrated the successful use of electrokinetic pumping to integrate DNA extraction and amplification techniques on a single glass microfluidic device for forensic applications (Shaw et al., 2011b). All necessary reagents were pre-loaded into the microfluidic device in a gel encapsulated form and, upon addition of the sample, the device was sealed with polymer electrodes. This enclosed system was designed so that potential contamination was reduced and that the input required from the user was minimal.

While integrated genetic analysis on microfluidic systems has been reported for a wide range of sample types (Liu and Mathies, 2009), archaeological samples have yet to receive attention in the literature. The concerns regarding contamination issues, in particular with modern DNA, make integrated microfluidic systems an ideal choice for analysis of such specimens. The LOC theory provided the inspiration to devise a new method for ancient DNA analysis that utilises microfluidics and miniaturisation of standard ancient DNA protocols as described in this paper. We report the first successful application of these methods with ancient DNA templates, from a relatively recent (19th century) set of skeletons chosen for this proof-of-concept project. A range of DNA extraction methodologies were evaluated and integration with DNA amplification was performed. In particular, we report the sex identification of bone samples from analysis of the Amelogenin locus using the developed microfluidic protocol.

2. Materials & methods

2.1. Bones

Bones were excavated by Oxford Archaeology North from a site in Darwen, Lancashire, UK that was used as a burial ground in the mid 19th century, 1832–1862. The burials were excavated in 2008. Bone samples from three individuals were prepared in a laminar flow cabinet in an ultraclean room dedicated for ancient human DNA work. The outer surface of the bones were UV irradiated and a dental pick was used to remove 0.1 g of powdered bone from the spongy matrix within a broken end of the bone.

2.2. Conventional DNA extraction

Powdered bone samples were added to 1 mL of extraction buffer (0.5 M EDTA pH 8.0, 0.5% SDS and 100 µg Proteinase K) and incubated on a shaking incubator at 650 rpm at 55 °C for 24 h in preparation for extraction using an adapted Qiagen protocol (Bouwman and Brown, 2005). Briefly, samples were then centrifuged at 2000 rpm for 5 min and 0.5 mL of the supernatant transferred to a small Falcon tube, prior to addition of 2.5 mL of PB (binding) buffer [Qiagen, UK]. A 0.5 mL aliquot of this solution was then placed onto a silica spin column [Qiagen, UK] and centrifuged for 1 min. This centrifugation step was repeated until all the sample had been passed through the column. Then 0.75 mL PE (wash) buffer [Qiagen, UK] was added to the spin column and centrifuged for 1 min. The flow through was discarded and the DNA was eluted from the spin column by adding 50 µL of EB (elution) buffer [Qiagen, UK] and centrifuging for 14,000 rpm for 1 min after 1 min of room temperature incubation.

2.3. Conventional DNA amplification

2.3.1. Polymerase chain reaction (PCR)

Conventional DNA amplification was carried out using PCR. A 50 µL reaction contained 2.5 µL of bone extract, 1× buffer (150 mM Tris–HCl pH 8.0, 500 mM KCl), 2 mM MgCl₂, 200 µM each dNTPs, 100 ng each primer, 1% bovine serum albumin and 1.25 units AmpliTaq Gold DNA polymerase [Life Technologies, UK]. Primer sequences for the amplification of the Amelogenin locus were 5'-FAM-CCC TGG GCT CTG TAA AGA A-3' and 5'-ATC AGA GCT TAA ACT GGG AAG CTG-3' [Eurofins MWG Operon, Germany]. Thermal cycling was carried out under the following conditions: 4 min at 94 °C; followed by 44 cycles of 1 min at 55 °C, 1 min at 72 °C and 1 min at 94 °C; followed by 1 min at 55 °C and 10 min at 72 °C.

2.3.2. Real-time (quantitative) polymerase chain reaction (qPCR)

qPCR was used to assess the efficiency of the DNA extraction methodologies performed on the microfluidic device. Eluted DNA (1 µL) was added to a solution of 1× GoTaq[®] qPCR Master Mix [Promega, UK] with 0.5 µM forward and reverse Amelogenin primers, made up to a total volume of 50 µL with nuclease-free water. Samples were then run using the following program on a StepOnePlus[™] Real-Time PCR System [Life Technologies, UK]: Hot-Start activation of 95 °C for 2 min, followed by 40 cycles of denaturation at 95 °C for 15 s and annealing/extension at 60 °C for 1 min, then melt-curve analysis from 60 to 95 °C.

2.4. Gel electrophoresis

Both slab-gel and capillary gel electrophoresis techniques were used for the analysis of PCR products. Slab-gel electrophoresis was

performed using 3% (w/v) agarose gels. Samples were electrophoresed at 120 V until adequate separation was achieved, stained using ethidium bromide and visualised using a UV trans-illuminator. Capillary gel electrophoresis was carried out using a 3500 Genetic Analyzer [Applied Biosystems, UK]. Samples (1 µL) were added to 12 µL of Hi-Di[™] Formamide and 0.5 µL GeneScan[™] 500 LIZ[®] Size Standard [Applied Biosystems, UK] and denatured for 5 min at 95 °C before being snap-cooled on ice and loaded onto the instrument.

2.5. Microfluidic device manufacture

Glass microfluidic devices were produced using standard photolithography and wet etching techniques to produce the design shown in Fig. 1a and b (McCreeley, 2000). The 1 mm bottom glass layer was isotropically etched to a depth of 100 µm, using a solution of 1% hydrofluoric acid/5% ammonium fluoride at 65 °C, creating channels of 250 µm width. Access holes, of 1, 3 and 5 mm diameter, were drilled in the 3 mm top glass layer. The two layers were then thermally bonded at 595 °C for 3 h. Silanisation of the PCR chamber was performed in order to minimise DNA polymerase adsorption. A 150 mM solution of trichloro(1H,1H,2H,2H-perfluorooctyl)silane [Sigma-Aldrich, UK] in 2,2,4-trimethylpentane [Fisher Scientific, UK] was added to the PCR chamber and incubated at room temperature for 10 min. The microfluidic device was then sequentially washed with solutions of 2,2,4-trimethylpentane, acetone and distilled water.

2.6. Microfluidic DNA extraction

A number of different DNA extraction techniques were evaluated on the microfluidic device for their compatibility with dealing with the typically limited sample amounts found with ancient DNA specimens. These included anion exchange facilitated by both hydrodynamic and EOF and selective enrichment of DNA containing abasic sites (which are present in ancient DNA but rare in modern DNA) using 1 µm streptavidin-coated superparamagnetic polystyrene particles [Sigma-Aldrich, UK]. A schematic showing the generic operation of the microfluidic device is shown in Fig. 1c–e. In order to evaluate the different methodologies, experiments were carried out using a known concentration of DNA (50 pg) which had already been purified using the conventional technique described in Section 2.2. allowing DNA extraction efficiencies to be calculated. Following DNA extraction, all eluted samples were collected and analysed by qPCR.

2.6.1. Anion exchange using hydrodynamic pumping

Anion exchange was performed using chitosan coated silica beads, prepared as previously described (Parton et al., 2012), which were added to the DNA extraction chamber (B in Fig. 1) on the microfluidic device. Following addition to the chamber, using a pipette, the beads were held in place via the “keystone effect” and the chamber sealed using a polytetrafluoroethylene (PTFE) plug. PTFE tubing [Kinesis, UK] was attached to the outlets of the microfluidic device, using epoxy resin, to facilitate attachment to a PHD syringe pump [Harvard Apparatus, UK]. Purified DNA was diluted to a total volume of 20 µL in a solution of 10 mM 2-(N-morpholino) ethanesulfonic acid (MES) buffer (pH 5) [Sigma-Aldrich, UK] and then pumped over the beads, from inlet A to outlet C (Fig. 1) using the syringe pump operated in withdrawal mode at a rate of 1 µL min⁻¹. Washing was then achieved by pumping 10 mM MES buffer alone over the silica beads, again from inlet A to outlet C. Elution of the DNA was then carried out by flowing a solution of 10 mM tris(hydroxymethyl)aminomethane

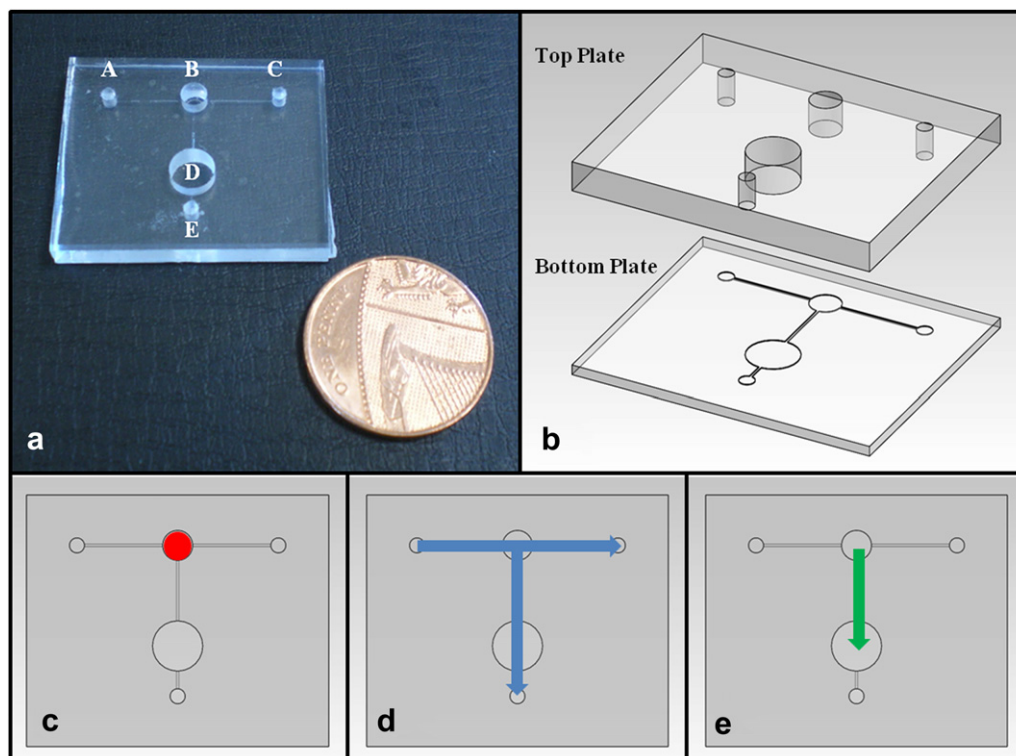


Fig. 1. a) Photograph showing the microfluidic device used for integrated DNA extraction and amplification experiments, where A, C and E are the 1 mm inlet/outlet holes for reagent/electrode addition; B is the DNA extraction chamber and D is the PCR chamber; b) diagram showing the composition of the two layer microfluidic device; Schematic showing the genetic operation of the microfluidic device for DNA extraction and amplification where c) is the location for introduction of the solid-phase (beads or particles) and DNA sample binding; d) shows the flow path of the wash solution depending on the pumping mechanism used (hydrodynamic: A to C, EOF: A to E) and e) demonstrates the movement of eluted DNA (anion exchange) or magnetic particles (selective enrichment) into the PCR chamber for subsequent DNA amplification.

(Tris) buffer supplemented with 50 mM KCl (pH 9) [Sigma-Aldrich, UK] from inlet A to outlet E, thereby transferring the eluted DNA into the PCR chamber.

2.6.2. Anion exchange using EOF

The principles of the anion exchange methodology are as described in Section 2.6.1. but with the movement of reagents controlled electrokinetically. Purified DNA in 10 mM MES buffer was manually added to the DNA extraction chamber containing the packed chitosan-coated silica beads and incubated for 10 min at room temperature. Chamber A was filled with 10 mM MES buffer and chambers C, D and E were filled with 10 mM Tris buffer (Fig. 1). Platinum wire electrodes were positioned within inlets A, C and E and connected to an external Paragon 3B Power Supply Unit [Kingfield Electronics, UK]. The beads were washed using 10 mM MES buffer by applying a voltage of 100 V cm^{-1} between electrodes A and E. Subsequently the purified DNA was eluted using 10 mM Tris buffer by applying a voltage of 100 V cm^{-1} between electrodes C and E resulting in transfer of eluted DNA into the PCR chamber. While carrying out electrokinetic movement, the microfluidic device was cooled to around $4 \text{ }^{\circ}\text{C}$, using a thermoelectric Peltier element, in order to reduce Joule heating and minimise sample evaporation.

2.6.3. Selective enrichment using magnetic particles

DNA was incubated for 1 h at room temperature with 5 mM of biotinylated aldehyde reactive probe (ARP) [Invitrogen, UK] within the DNA extraction chamber (B in Fig. 1). ARP undergoes a Schiff's base reaction resulting in biotin labelling of any abasic sites present within the DNA structure (Fundador and Rusling, 2007). A $5 \mu\text{L}$ aliquot of streptavidin-coated superparamagnetic

polystyrene particles was manually pipetted into the solution within the DNA extraction chamber located on the microfluidic device and incubated for an hour at room temperature to allow binding of biotinylated DNA. Following binding, the magnetic particles were immobilised by placing a NdFeB permanent magnet [Magnet Sales, UK] underneath the extraction chamber and washed using distilled water, pumped over the particles using the syringe pump operated in withdrawal mode at a rate of $1 \mu\text{L min}^{-1}$ from inlet A to outlet C (Fig. 1), to remove and contaminants or unbound DNA. The washed magnetic particles were then transferred directly into the PCR reagent solution (chamber D, Fig. 1), facilitated by manual movement of the NdFeB permanent magnet, for combined elution and amplification of the DNA.

2.7. Microfluidic DNA amplification

DNA amplification was performed on a microfluidic device using the following PCR reagent mixture: $1 \times$ GoTaq[®] buffer, $0.1 \text{ U } \mu\text{L}^{-1}$ GoTaq[®] DNA polymerase, 2 mM MgCl_2 [Promega, UK], 200 μM each dNTPs [Bioline, UK], 0.5 μM forward and reverse Amelogenin primer, 0.2 $\mu\text{g } \mu\text{L}^{-1}$ bovine serum albumin, 0.01% (w/v) poly(vinylpyrrolidone) and 0.1% (v/v) Tween-20 [Sigma-Aldrich, UK]. Once the PCR reagents were added to the microfluidic device, along with the extracted DNA, the inlets were covered with a drop of mineral oil [Sigma-Aldrich, UK] to prevent evaporation during the thermal cycling process. The microfluidic device was then positioned on a thermoelectric Peltier element which was used to provide thermal cycling at the same conditions as described in Section 2.3.1.

3. Results & discussion

3.1. Comparison of microfluidic DNA extraction methods

Extraction was performed, from 50 pg of DNA, using both anion exchange and the magnetic bead enrichment techniques. Following DNA extraction, all samples were analysed by qPCR enabling the DNA extraction efficiency to be determined (Fig. 2). The results showed that EOF did not produce any quantifiable results, demonstrating either a poor DNA extraction efficiency resulting in insufficient DNA for amplification or that inhibitors remained which prevented successful amplification. Anion exchange using hydrodynamic pumping demonstrated ~35% DNA extraction efficiencies but lacked reproducibility. Magnetic enrichment based on selectively isolating labelled abasic sites on the DNA showed good reproducibility. In addition, as it provides enrichment, the low percentage can be attributed to any non-damaged DNA not being captured.

3.2. Limits of detection for microfluidic DNA amplification

While DNA levels present in ancient bone samples are widely variable due to localised environmental conditions, most ancient DNA analyses are optimised to work on 50 pg or less of DNA. A feasibility study was carried out in order to establish the limits of amplification on the microfluidic system. PCR was performed using different levels of template DNA, ranging from 1 to 1000 pg, and analysed using capillary gel electrophoresis (Fig. 3). Although DNA amplification was more efficient at DNA amounts of ≥100 pg, DNA amplification was possible down to 1 pg, well within the desired range for typical ancient DNA samples.

3.3. Integrated DNA extraction and amplification

From comparison of the different DNA extraction techniques, selective enrichment was used for the integrated microfluidic system as it offered good reproducibility. In addition, extraction of only DNA containing abasic sites reduces the likelihood of contamination from modern DNA samples as these are less likely to contain abasic sites and will be removed during the wash step. Integration of the DNA extraction and amplification methodologies described above for the analysis of powdered bone samples were performed on the microfluidic device (Fig. 4).

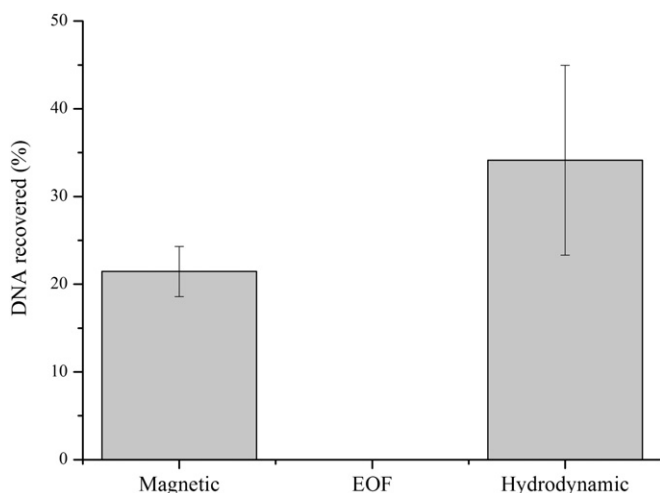


Fig. 2. Comparison of DNA extraction efficiencies, as determined by qPCR, for the different extraction methodologies (n = 3).

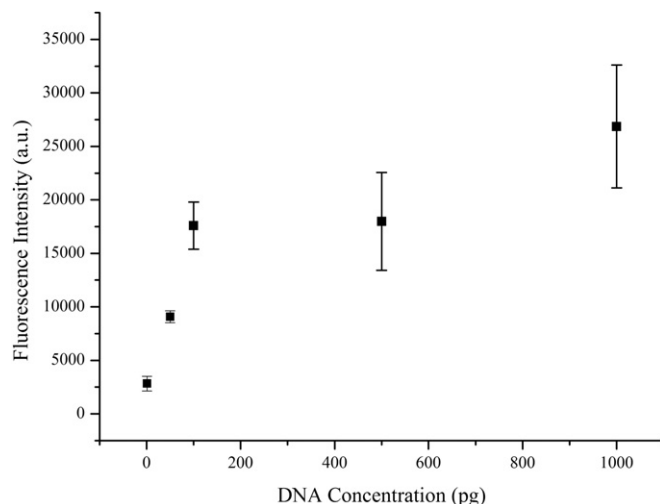


Fig. 3. Intensity of PCR products amplified on the microfluidic system from varying levels of template DNA (n = 3).

Three different bone samples (SK095, SK091 and SK116) were analysed in triplicate on the microfluidic system and the results analysed by conventional capillary gel electrophoresis. The PCR target was the Amelogenin gene, which is present on the X and Y chromosomes. A 6 bp deletion within the amplified region of the X version of the gene means that the sizes of the PCR products indicate which chromosomes are present, the X product being 104 bp and the Y version 110 bp (Sullivan et al., 1993). Samples SK091 and SK116 produced detectable results and indicated the sex of both sets of bones to be female (XX) for all replicates performed (Fig. 5). Sample SK095 however did not produce any detectable results upon repeated analysis.

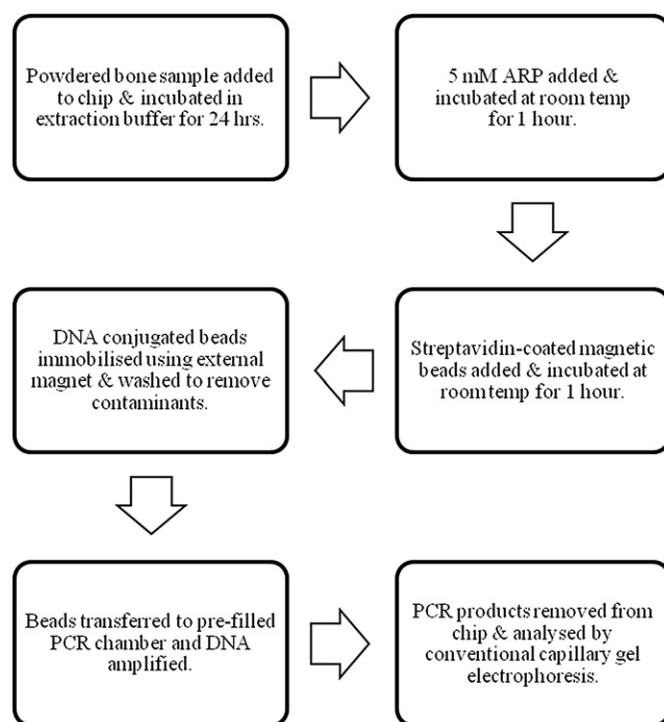


Fig. 4. Schematic showing the operational process for integration of DNA extraction and amplification on the microfluidic device.

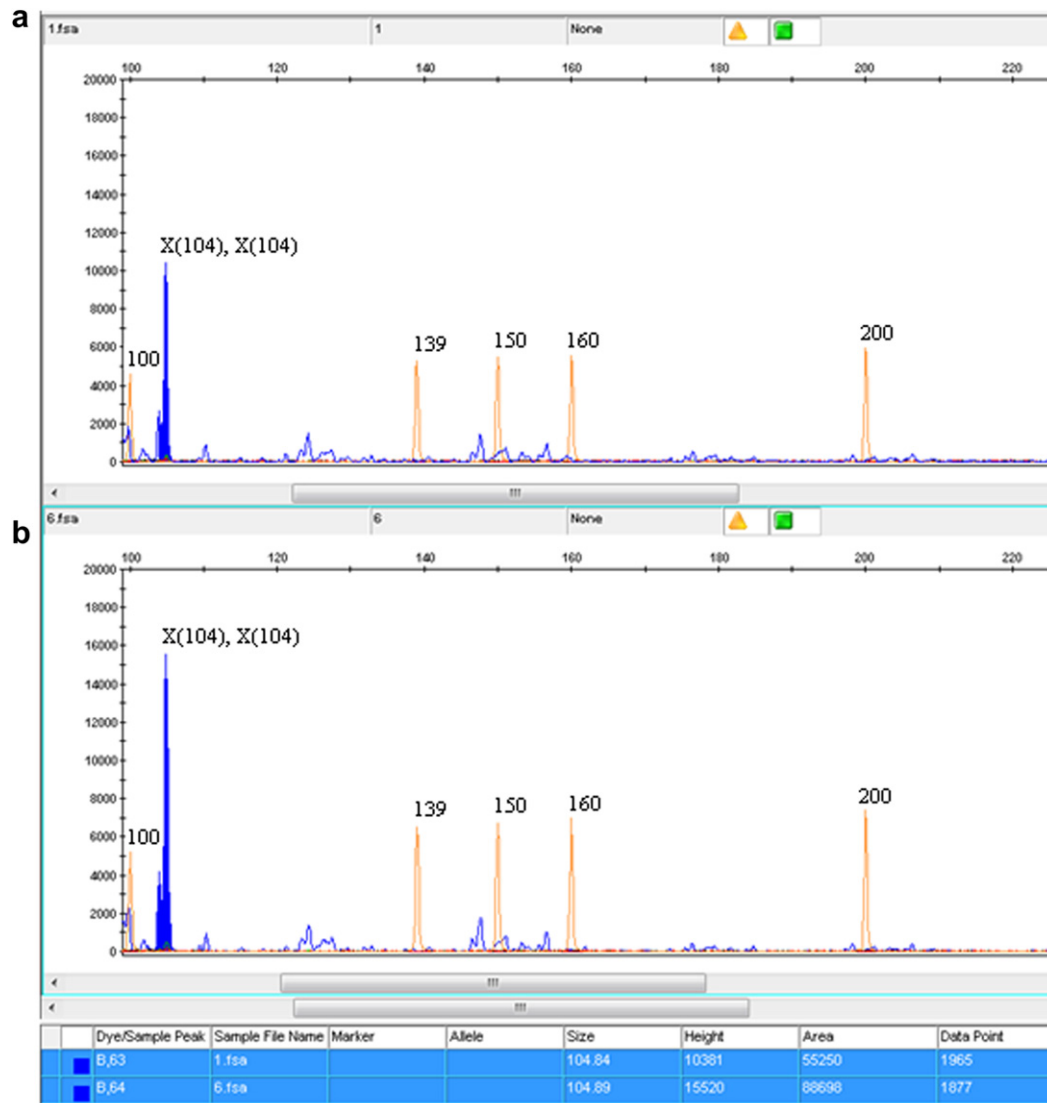


Fig. 5. Electropherograms showing sex identification of bone samples a) SK091 and b) SK116, following DNA extraction and amplification on the microfluidic system. The size (bp) is shown on the x axis and the fluorescent intensity of given on the y axis. PCR product (blue) and DNA size ladder (orange) peaks are labelled with their relative sizes. (For interpretation of the references to colour in this figure legend, the reader is referred to the web version of this article.)

3.4. Comparison of conventional and microfluidic methodologies

In order to corroborate the finding obtained on the microfluidic system at the University of Hull, the results were compared with the anthropological sex identifications made by Oxford Archaeology North, and with molecular sex identifications using conventional PCR techniques, directed at the Amelogenin gene and various markers on the Y chromosome, performed independently at the University of Manchester (Table 1). The result obtained for SK091 is encouraging as SK091 could not be assigned sex on osteological grounds. Although the Y chromosome was detected by

Table 1

Summary of sex identification results obtained from 3 bone samples as analysed by anthropological and biomolecular techniques (†Y chromosome marker DYS446; ‡Y chromosome markers DYS446 and DYS388; Ag, Amelogenin).

Burial reference	Conventional Ag sex ID	Anthropological sex ID	Y chromosome sex ID	Microfluidic Ag sex ID
SK091	Female	Unknown	Positive [†]	Female
SK095	Male	Male	Positive [‡]	–
SK116	Female	Female	Negative	Female

conventional PCR with this sample, this result was for a single marker, DYS446, that is no longer looked on as male-specific because of the discovery of a similar DNA sequence in the Xq21 region of the X chromosome (Asamura et al., 2008). The non-specific Y detection must therefore be weighed against the Amelogenin result indicating a female and the microfluidic system result corroborating this. Although SK095 did not provide a result with the microfluidic system, paradoxically this may be because of the good preservation of the nuclear DNA in this sample, which gave a Y chromosome PCR result for both DYS446 and DYS388 loci. It may be that there was a lack of abasic DNA fragments in this particular template. All the results, whether osteological or biochemical, obtained for SK116 were in agreement that the sample was female.

4. Conclusions

The work presented here describes the first steps in the development of a microfluidic system for the analysis of ancient DNA samples. A number of DNA extraction methodologies were

evaluated for their suitability at dealing with limited, possibly degraded DNA samples, as is often the case with ancient archaeological specimens. Both anion exchange and the enrichment of labelled abasic sites have been demonstrated as feasible techniques. However, the use of a method which allows selective extraction of damaged DNA offers advantages in the reduction of contamination by modern DNA. Amplification from less than 50 pg of DNA was shown to be successful within silanised glass microfluidic devices, thermally cycled using a custom-built Peltier-based heating/cooling system. Direct analysis of three powdered bone samples was carried out as a proof-of-principle. Two out of the three samples produced positive results and were identified as female which was found to be in keeping with sex identification results independently obtained at the University of Manchester.

The use of a microfluidic system offers a number of advantages over conventional ancient DNA analysis techniques. Integration of several analysis techniques within a single microfluidic device reduces the likelihood of contamination as the device can be sealed once the sample has been added. By miniaturising the associated control systems, such as the Peltier heater, it will be possible to create a portable operating system that could be used at an archaeological excavation enabling on-site results to be generated. Further work will aim at establishing a robust methodology with integrated detection system. Development of a “sample in-answer out” system would enable use by non-specialised staff and therefore increase the convenience and acceptance of genetic testing of ancient DNA samples. The possibilities can then be extended from relatively simple sex identification to mitochondrial DNA haplotyping or more complex trait analysis.

Acknowledgements

The authors would like to thank Dr. Steve Clark at the University of Hull for manufacture of the microfluidic devices and Stephen Rowland, Project Manager, Oxford Archaeology North, for permission to take samples for ancient DNA analysis. Naglaa Abu-Mandil Hassan was supported by a studentship from the Egyptian Cultural and Educational Bureau, London.

References

- Asamura, H., Fujimori, S., Ota, M., Oki, T., Fukushima, H., 2008. Evaluation of miniY-STR multiplex PCR systems for extended 16 Y-STR loci. *International Journal of Legal Medicine* 122, 43–49.
- Asiello, P.J., Baemner, A.J., 2011. Miniaturized isothermal nucleic acid amplification, a review. *Lab on a Chip* 11, 1420–1430.
- Bienvenue, J.M., Legendre, L.A., Ferrance, J.P., Landers, J.P., 2010. An integrated microfluidic device for DNA purification and PCR amplification of STR fragments. *Forensic Science International: Genetics* 4, 178–186.
- Bouwman, A.S., Brown, T.A., 2005. The limits of biomolecular palaeopathology: ancient DNA cannot be used to study venereal syphilis. *Journal of Archaeological Science* 32, 703–713.
- Brown, T.A., Brown, K.A., 2011. *Biomolecular Archaeology: an Introduction*. Wiley-Blackwell.
- Erill, I., Campoy, S., Erill, N., Barbe, J., Aguilo, J., 2003. Biochemical analysis and optimization of inhibition and adsorption phenomena in glass-silicon PCR-chips. *Sensors and Actuators B-Chemical* 96, 685–692.
- Ferrance, J.P., Wu, Q.R., Giordano, B., Hernandez, C., Kwok, Y., Snow, K., Thibodeau, S., Landers, J.P., 2003. Developments toward a complete micro-total analysis system for Duchenne muscular dystrophy diagnosis. *Analytica Chimica Acta* 500, 223–236.
- Fundador, E., Rusling, J., 2007. Detection of labeled abasic sites in damaged DNA by capillary electrophoresis with laser-induced fluorescence. *Analytical and Bioanalytical Chemistry* 387, 1883–1890.
- Horsman, K.M., Bienvenue, J.M., Blasler, K.R., Landers, J.P., 2007. Forensic DNA analysis on microfluidic devices: a review. *Journal of Forensic Sciences* 52, 784–799.
- Liu, P., Mathies, R.A., 2009. Integrated microfluidic systems for high-performance genetic analysis. *Trends in Biotechnology* 27, 572–581.
- McCreeedy, T., 2000. Fabrication techniques and materials commonly used for the production of microreactors and micro total analytical systems. *Trac-Trends in Analytical Chemistry* 19, 396–401.
- Njoroge, S.K., Chen, H.W., Witek, M.A., Soper, S.A., 2011. *Integrated Microfluidic Systems for DNA Analysis*, pp. 203–260.
- Parton, J., Birch, C., Kemp, C., Haswell, S.J., Pamme, N., Shaw, K.J., 2012. Integrated DNA extraction and amplification using electrokinetic pumping in a microfluidic device. *Analytical Methods* 4, 96–100.
- Pipper, J., Inoue, M., Ng, L.F.-P., Neuzil, P., Zhang, Y., Novak, L., 2007. Catching bird flu in a droplet. *Nature Medicine* 13, 1259–1263.
- Reedy, C.R., Price, C.W., Sniogowski, J., Ferrance, J.P., Begley, M., Landers, J.P., 2011. Solid phase extraction of DNA from biological samples in a post-based, high surface area poly(methyl methacrylate) (PMMA) microdevice. *Lab on a Chip* 11, 1603–1611.
- Schaerli, Y., Wootton, R.C., Robinson, T., Stein, V., Dunsby, C., Neil, M.A.A., French, P.M.W., deMello, A.J., Abell, C., Hollfelder, F., 2009. Continuous-flow polymerase chain reaction of single-copy DNA in microfluidic microdroplets. *Analytical Chemistry* 81, 302–306.
- Shaw, K.J., Birch, C., Hughes, E.M., Jakes, A.D., Greenman, J., Haswell, S.J., 2011a. Microsystems for personalized biomolecular diagnostics. *Engineering in Life Sciences* 11, 121–132.
- Shaw, K.J., Joyce, D.A., Docker, P.T., Dyer, C.E., Greenway, G.M., Greenman, J., Haswell, S.J., 2011b. Development of a Real-World Direct Interface for Integrated DNA Extraction and Amplification in a Microfluidic Device.
- Sullivan, K.M., Mannucci, A., Kimpton, C.P., Gill, P., 1993. A rapid and quantitative DNA sex test: fluorescence-based PCR analysis of X–Y homologous gene amelogenin. *BioTechniques* 15, pp. 636–638 ± 640–641.
- Taylor, J.A., Yeung, E.S., 1993. Imaging of hydrodynamic and electrokinetic flow profiles in capillaries. *Analytical Chemistry* 65, 2928–2932.
- Wen, J., Legendre, L.A., Bienvenue, J.M., Landers, J.P., 2008. Purification of nucleic acids in microfluidic devices. *Analytical Chemistry* 80, 6472–6479.
- Whitesides, G.M., 2006. The origins and the future of microfluidics. *Nature* 442, 368–373.
- Zhang, C.S., Xing, D., 2007. Miniaturized PCR chips for nucleic acid amplification and analysis: latest advances and future trends. *Nucleic Acids Research* 35, 4223–4237.
- Zhang, C.S., Xu, J.L., Ma, W.L., Zheng, W.L., 2006. PCR microfluidic devices for DNA amplification. *Biotechnology Advances* 24, 243–284.

Development and Evaluation of a Raman Flow Cell for Monitoring Continuous Flow Reactions

Grant Chaplain,^A Stephen J. Haswell,^{A,C} Paul D. I. Fletcher,^A
Stephen M. Kelly,^A and Andrew Mansfield^B

^ADepartment of Chemistry, University of Hull, Hull, HU6 7RX, UK.

^BFlow Chemistry Solutions, Room F 238, Building 130, Abbott Drive, Kent Science Park, Sittingbourne, Kent, ME9 8AZ, UK.

^CCorresponding author. Email: s.j.haswell@hull.ac.uk

We show how in-line Raman spectroscopy can be used to monitor both reactant and product concentrations for a heterogeneously catalysed Suzuki cross reaction operating in continuous flow. The flow system consisted of an HPLC pump to drive a homogeneous mixture of the reactants (4-bromobenzonitrile, phenylboronic acid, and potassium carbonate) through an oven heated (80°C) palladium catalyst immobilised on a silica monolith. A custom built PTFE in-line flow cell with a quartz window enabled the coupling of an Ocean Optics Raman spectrometer probe to monitor both the reactants and product (4-cyanobiphenyl). Calibration was based on obtaining multivariate spectral data in the range 1530 cm⁻¹ and 1640 cm⁻¹ and using partial least-squares regression (PLSR) to obtain a calibration model which was validated using gas chromatography–mass spectrometry (GCMS) analysis. In-line Raman monitoring of the reactant and product concentrations enable (i) determination of reaction kinetic information such as the empirical rate law and associated rate constant and (ii) optimisation of either the product conversion (61 % at 0.02 mL min⁻¹ generating 17 g h⁻¹) or product yield (14 % at 0.24 mL min⁻¹ generating 53 g h⁻¹).

Manuscript received: 15 August 2012.

Manuscript accepted: 4 December 2012.

Published online: 11 January 2013.

Introduction

The application of flow chemistry to a range of organic syntheses has been demonstrated to offer several benefits including improvements in reaction yields, product selectivity, and scalability.^[1–3] These benefits are mainly associated with the good spatial, thermal, and temporal control offered by flow methodology.^[4–7] Reactions such as acetylation, Suzuki, Heck, amide synthesis, Knoevenagel condensation, and many more, which have utilised flow reaction chemistry, all report more efficient processes.^[8–11] In such systems, it has also been common to utilise catalysts such as palladium configured in both homogeneous and heterogeneous reaction states.^[12,13] For example, He et al. reported using heterogeneous palladium coupled with microwave heating in a flow system to carry out Suzuki reaction chemistry which produced yields in excess of 70 % in 60 s.^[14] Whilst microwave heating has been reported to improve such reactions due to localised heating generated at the surface of the catalyst during exposure,^[15] other heating methods such as oil baths, water baths, infrared, and column heating^[16–19] are all equally suitable for implementation into flow systems where contact times can easily be controlled by flow rate.

One aspect of flow chemistry which has received less attention to date has been in-line or in-channel reaction monitoring. When coupled with flow rate feedback, this offers the potential of controlling variables such as reagent mixing and catalyst contact times, which would clearly be beneficial in optimising reaction yields.^[20,21] In-line monitoring using

various spectroscopic techniques coupled, using a flow cell configuration to flow systems have been reported; these include infrared,^[22] ultraviolet,^[23] nuclear magnetic resonance,^[24] and Raman.^[25] For example, Carter et al. have reported the incorporation of an ATR-IR spectral window in a flow reactor to monitor hydrogenation, Curtius rearrangement, azide formation, peptide coupling, butane-2,3-diacetal protection, addition of allenylstannanes to aldehydes, and fluorination reactions.^[26] Raman spectroscopy however, which offers a greater tolerance to water than IR, has the potential to realise a much more robust methodology capable of acquiring molecular identification. In addition, fibre optic probes coupled with Raman spectroscopy are able to provide remote monitoring with good spatial resolution.^[27] Mozharov et al. have used Raman spectroscopy very effectively for monitoring base-catalyzed Knoevenagel condensation between ethyl cyanoacetate and benzaldehyde.^[28] Their findings allowed quantification and kinetic reaction studies to be performed, without the need for multiwavelength chemometric calibration. Most Raman spectroscopic systems however, utilise chemometric techniques to extract the relevant chemical information from multiwavelength spectral measurements. This is necessary in part to remove contributing factors such as fluorescence. Walmsley et al. for example, used principal component analysis (PCA) to identify and remove the underlying fluorescence signal in Raman measurements from esterification reactions to obtain pure Raman spectra.^[29] Other multivariate chemometric techniques have been coupled with regression

analysis to allow quantification of Raman spectra to be achieved.^[30]

In this paper, we describe the development of a novel in-line Raman flow cell which has been evaluated using the Suzuki cross coupling reaction between 4-bromobenzonitrile and phenylboronic acid, using a heated heterogeneous palladium-silica monolithic catalyst.

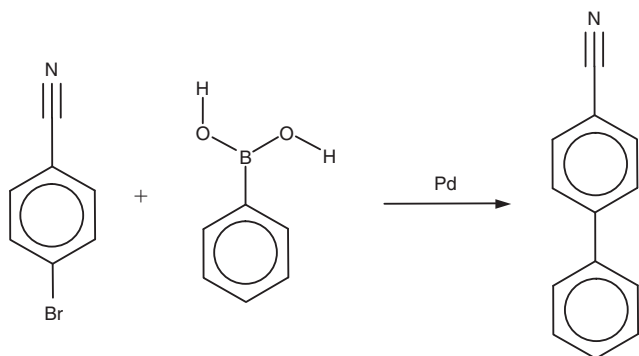


Fig. 1. Scheme for the Suzuki reaction used to develop and test the reported flow system, which consists of 4-bromobenzonitrile (0.1 M), phenylboronic acid (0.12 M), and potassium carbonate (0.24 M). The catalyst used was an in-house produced palladium/silica monolith enclosed in an HPLC column heater device.

Results and Discussion

Experimental Set-Up

The reaction used to illustrate the potential of the flow reaction system developed is shown in Fig. 1. The Suzuki cross coupling was carried out by pumping a homogeneous reaction mixture containing 4-bromobenzonitrile (0.1 M), phenyl boronic acid (0.12 M), and potassium carbonate (0.24 M) through a heated column containing palladium catalyst immobilised on a silica monolith, with in-line product and reactant quantification using Raman spectroscopy (Fig. 2). Optimisation of the product generated could be achieved by either changing the temperature of the catalyst column or the catalyst contact time, which was varied by altering the solution flow rate using a calibrated HPLC pump (See Fig. S1 in the Supplementary Material).

Calibration of Raman and GCMS Validation

In order to ensure the Raman flow cell could detect quantitative reactant and product concentrations from the reaction, a series of matrix match standards were prepared and introduced into the flow cell sequentially and measured. As the signal response was found to be unaffected by flow (see Fig. S2 in the Supplementary Material) the calibration was carried out in static mode to simplify the experimental methodology. Raman spectral data obtained for the calibration was based on the greatest spectral variance which occurred in the range between 1530 cm^{-1} and 1640 cm^{-1} (see Fig. S3 in the Supplementary Material) and is

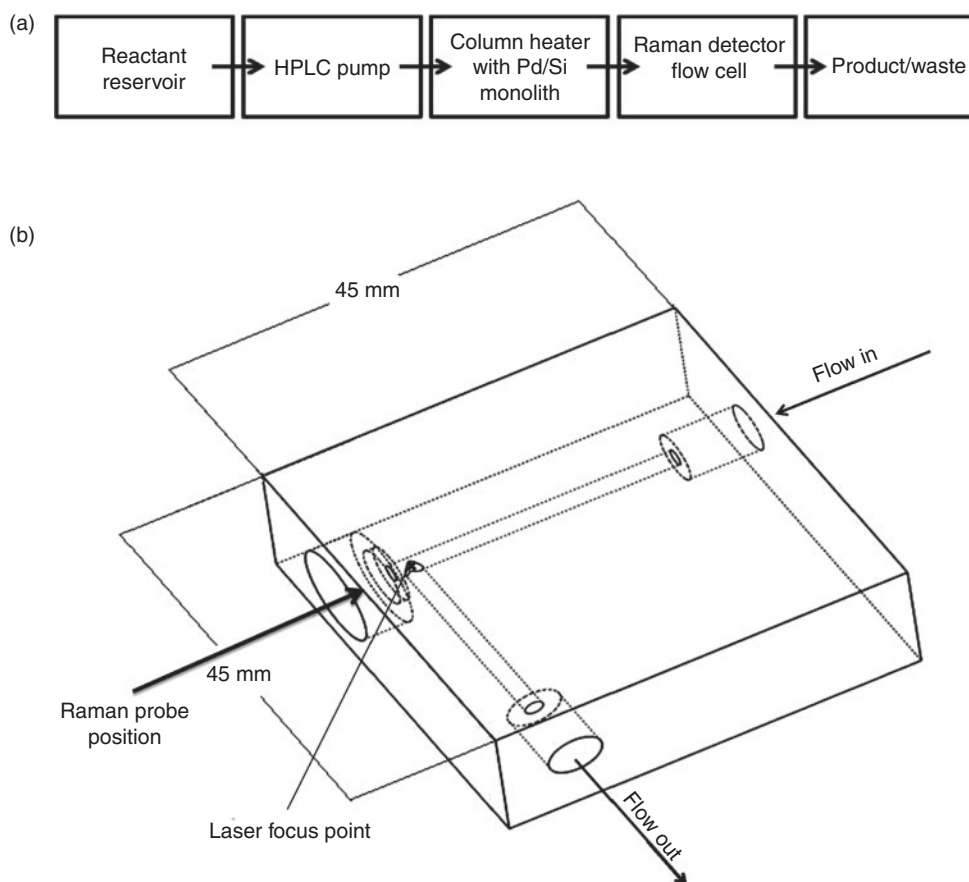


Fig. 2. (a) Schematic of the flow reaction system used which incorporates a reactant reservoir, HPLC pump, palladium/silica monolithic catalyst inside a column heater, Raman detector, and product/waste reservoir. (b) Details of the in-house built PTFE Raman flow cell incorporating a quartz window ($10.0\text{ mm } \varnothing \times 2.0\text{ mm}$). The focal point of the laser is 7.5 mm into the channel with a spot size of $135\text{ }\mu\text{m}$ and a depth of field of 2.2 mm .

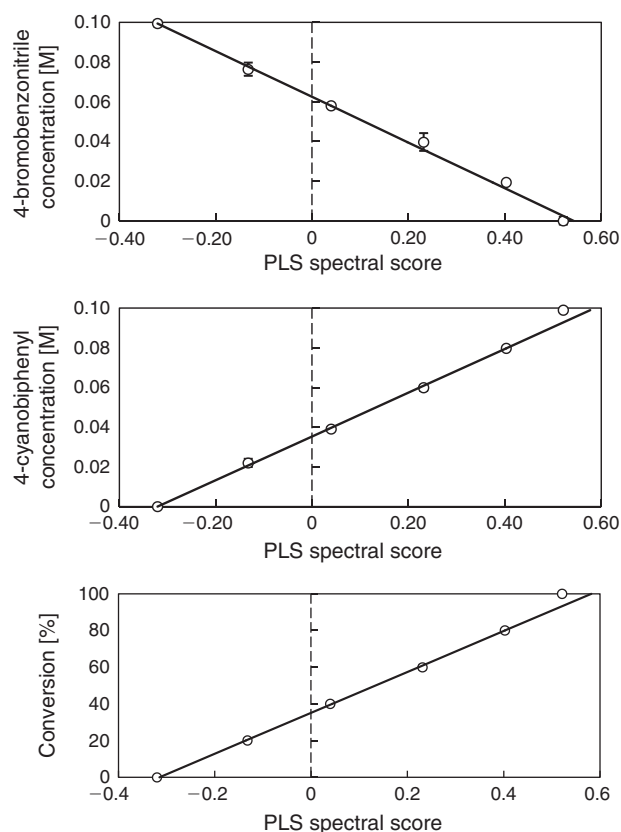


Fig. 3. Raman calibration for matrix match standards consisting of 0.00–0.099 M solutions for both 4-bromobenzonitrile and 4-cyanobiphenyl. Each calibration solution was measured in the Raman flow cell under static conditions at a temperature of 20°C with no catalyst present. Raman spectra in the range 1530 cm^{-1} and 1640 cm^{-1} were recorded as the average of five measurements, each with a 1 s integration time. A 785 nm laser set at 340 mW was used. All spectra were subjected to default dark signal and stray light corrections.

attributed to the presence of the nitrile group on the 4-bromobenzonitrile and 4-cyanobiphenyl. The two compounds are however distinguishable from each other due to the fact that the induced dipole associated with the nitrile group of the 4-bromobenzonitrile is slightly more hindered than in the case of 4-cyanobiphenyl, resulting in a weaker Raman shift when using the 785 nm light source. This data was used in conjunction with partial least-squares regression (PLSR) to obtain calibration plots of the PLS scores for 4-bromobenzonitrile (starting material) and 4-cyanobiphenyl (product) as shown in Fig. 3. In this case, the scores represent the coordinates in space of the Eigenvectors from the spectral data variance. Using the calibration plots it was possible to predict the conversion and concentrations of compounds in the reaction mixture against scores.

The PLSR Raman calibration model was validated using GCMS analysis performed using the same reaction solutions (see Fig. S4 in the Supplementary Material). The results indicated that the Raman and GCMS measurements gave calibration predictions within $\pm 10\%$.

Having established that in-line Raman spectroscopy will offer access to quantitative data on both the reactant and product for the Suzuki reaction shown in Fig. 1, the opportunity to acquire direct reaction information related to reaction rates and product yield/conversion represents an attractive aspect of the

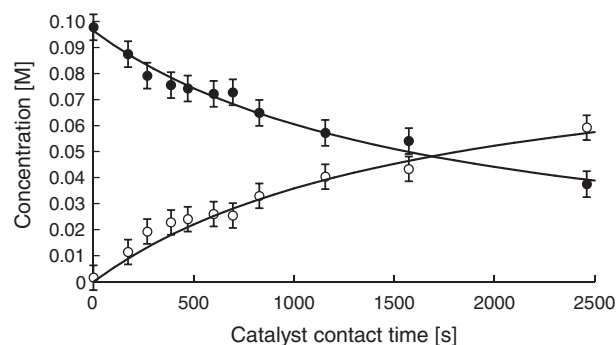


Fig. 4. Plots of the concentrations of 4-bromobenzonitrile (●) and 4-cyanobiphenyl (○) determined by the Raman spectrometer as a function of the catalyst contact time. The reaction was performed at volumetric solution flow rates of 0 to 0.38 mL min^{-1} and the temperature in the column heater was set at 80°C. The solid lines show the best fit to the second-order integrated rate Eqn 2 with $k = 4.8 \times 10^{-3} \text{M}^{-1} \text{s}^{-1}$.

methodology developed. To illustrate this aspect of flow reaction monitoring a brief example of how kinetic data and reaction optimisation can be obtained is presented in the following sections. It should be stressed however, that as the main thrust of this paper has been to report the development of Raman flow monitoring methodology, the applications reported here of how the measured data can be used to extract kinetic and reaction optimisation information is intended to illustrate the principles involved rather than to provide a definitive and comprehensive study.

Kinetic Data

Reaction kinetic studies were conducted by varying flow rates and hence catalyst contact times, for the Suzuki cross coupling reaction outlined in Fig. 1. Volumetric flow rates of between 0.02 and 0.38 mL min^{-1} , producing catalyst contact times of between 2461 and 130 s were used. The monolith was estimated to have a pore volume of 1.09 mL determined from the difference in dry and water filled weights of the monolith. Fig. 4 shows the concentration of 4-bromobenzonitrile and 4-cyanobiphenyl as a function of catalyst contact time. As expected, as the contact time increased, the concentration of 4-bromobenzonitrile decreased and that for 4-cyanobiphenyl increased.

In order to derive kinetic information about the heterogenous Suzuki reaction, the concentration data shown in Fig. 4 was fitted to various integrated rate equations corresponding to alternative empirical rate laws. The best-fit (shown as the solid lines Fig. 4) was found to correspond to the second-order rate law (Eqn 1: rate law for the Suzuki reaction between 4-bromobenzonitrile (BBN) and phenylboronic acid (PBA)) and the corresponding integrated rate Eqn 2 (reaction kinetic equation for an overall second order reaction with phenylboronic acid (PBA) and 4-bromobenzonitrile (BBN) being both first order^[31]), i.e. the rate of reaction was found to be first order with respect to both 4-bromobenzonitrile (BBN) and phenylboronic acid (PBA). For the reaction conditions used, the overall second-order rate constant k is $4.8 \times 10^{-3} \text{M}^{-1} \text{s}^{-1}$.

$$\text{Rate of reaction} = k[\text{BBN}][\text{PBA}] \quad (1)$$

$$\frac{1}{[\text{PBA}]_0[\text{BBN}]_0} \cdot \ln \frac{[\text{PBA}]_0}{[\text{BBN}]_0} \cdot \frac{[\text{BBN}]}{[\text{PBA}]} = kt \quad (2)$$

Table 1. Optimisation of product yield and product formation for the Suzuki cross coupling reaction between 4-bromobenzonitrile (0.1001 M) and phenylboronic acid (0.1196 M) in the presence of potassium carbonate (0.2391 M) and palladium catalyst immobilised on a silica monolith as a function of flow rate

The temperature in the column heater was set at 80°C; 4-cyanobiphenyl concentrations were determined by the Raman spectrometer

Flow rate [mL min ⁻¹]	Reaction time [s]	4-cyanobiphenyl produced [g h ⁻¹]	Conversion [%]
0.02	2461	17.02	61
0.04	1573	19.49	44
0.05	1156	24.69	41
0.08	827	28.2	33
0.09	696	25.87	25
0.11	600	30.67	26
0.14	471	36.14	24
0.17	387	41.67	23
0.24	268	50.98	19
0.38	173	46.83	11

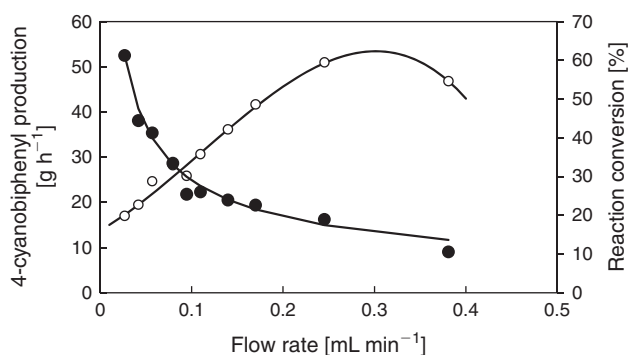


Fig. 5. The influence of flow rate on 4-cyanobiphenyl production (○) and conversion (●) in the Suzuki cross coupling reaction between 4-bromobenzonitrile (0.1 M) and phenylboronic acid (0.12 M) in the presence of potassium carbonate (0.24 M) using a palladium catalyst immobilised on a silica monolith at a temperature of 80°C. 4-Cyanobiphenyl concentrations and reaction conversions were determined by the Raman spectrometer.

Reaction Optimisation for Conversion and Product Production Per Hour

Based on the concentration data obtained for the kinetics study we illustrate here how the optimal flow rate (catalyst contact time) for the production of both the maximum conversion and maximum output in grams per hour for 4-cyanobiphenyl can be determined. From the data presented in Table 1 it can be seen that maximum conversion of 4-cyanobiphenyl occurred at 0.02 mL min⁻¹ whilst the maximum output of the product in grams per hour was produced at 0.24 mL min⁻¹. Once again this illustrates an interesting aspect of flow chemistry, namely that whilst the percentage conversion of a catalytic product is proportional to contact time of reactants, production of product as a function of time continues to increase even with decreasing conversions up to a maximum; after this the conversion drops as the conversion becomes too low to warrant sufficient product generation. The product production in grams per hour is shown in Fig. 5 and indicates the optimal flow rate for the production of 4-cyanobiphenyl at 53 g h⁻¹ even though the conversion is only around 14%.

Conclusions

An in-line flow cell for the acquisition of Raman spectral data has been shown to offer an attractive information rich approach for monitoring chemical reactions under flow control. Whilst the main thrust of this present paper has been directed towards the development of the in-line Raman detection system and its calibration capability, two examples of how such data could potentially be used have been presented to illustrate the wider potential of the approach. Such methodology is considered key to the ongoing development of flow chemical reactors as it not only offers the possibility of optimisation feedback control but also enables such experimental platforms to access important physical organic data relating to often complex reaction mechanisms.

Experimental

Chemicals

Dimethylformamide (99%), 4-bromobenzonitrile (99%), phenylboronic acid (>97%), potassium carbonate (99%), and 4-cyanobiphenyl (95%) were used for the Suzuki cross coupling reaction. The heterogeneous catalyst was prepared using tetraethyl orthosilicate (TEOS, 98%), nitric acid (volumetric standard 1.000 N), polyethylene oxide (PEO, 100000 M_v), ammonium hydroxide (volumetric standard 5.0 N), and sodium tetrachloropalladate (98%) fabricated the silica monolithic reactor. Hydrogen (10%) in nitrogen was used to reduce the sodium tetrachloropalladate. Magnesium sulfate (99.5%) and dichloromethane (>99.8%) were used for purification of reaction products for GCMS analysis using decane (99%) as internal standard. All chemicals were purchased from Sigma Aldrich except the hydrogen (10% in nitrogen) which was purchased from Energas.

Equipment

The flow reaction system was made from 1/16 inch internal diameter (ID) polyether ether ketone (PEEK) tubing, valves, connectors (Upchurch Scientific), and HPLC pump (Jasco Pu-1580). Flow reaction heating was achieved with a column heater (Jones Chromatography, Column Block Heater). A furnace (ESF Carbolite), hotplate (Stuart CB162), oven (Hotbox size 1 Gallenkamp), and syringes (BD Plastipack) were used to create the palladium/silica-monoliths. Polytetrafluoroethylene (PTFE) heat shrink tubing (Adtech Polymer Engineering) was used to encase the monoliths into flow geometry. Detection was carried out using an in house PTFE flow cell with a quartz window to enable optical access for a Raman probe fibre optic connected to a 785 nm laser (350 mV) and a Raman spectrometer QE65000 (all provided by Ocean Optics). Raman data was collected and analysed using Spectra Suite software. Analysis of the reaction yield was confirmed by gas chromatography (Perkin Elmer Gas Chromatograph) in gas chromatograph mass spectrometer (GCMS, Varian Saturn 2000) with a GCMS column (30 m × 0.25 mm, Phenomenex Zebron ZB-5 capillary column).

Flow Suzuki Reaction System

Each reaction consisted of a mixture containing 4-bromobenzonitrile (0.1 M), phenylboronic acid (0.12 M), and potassium carbonate (0.24 M) in DMF (66.7%). The mixture was placed in the reactant reservoir and pumped through the HPLC pump into the palladium/silica monolith where it was heated at 80°C. From here the reaction mixture passed through the Raman flow cell where spectral recording was obtained. The total volume of the flow manifold including the monolithic reactor and glass connectors was 0.900 mL. Within this volume

the Raman flow cell represented a volume of 0.182 mL of which 0.094 mL was the measurement zone. The effluent of the cell was subjected to liquid-liquid separation and GCMS analysis.

Palladium/Silica Monolith Preparation

The catalyst was prepared by previously reported literature methods.^[14]

Raman Analysis

Calibration solutions representing reaction product conversions of 0, 20, 40, 60, 80, and 100% were produced using 4-bromobenzonitrile, phenylboronic acid, potassium carbonate, and 4-cyanobiphenyl. Solutions prepared contained 0.0994, 0.0764, 0.0579, 0.0397, 0.0193, and 0 M 4-bromobenzonitrile, 0.1156, 0.0957, 0.0802, 0.0677, 0.0413, and 0.0205 M phenylboronic acid, 0.2485, 0.2544, 0.2440, 0.2394, 0.2400, and 0.2438 M potassium carbonate, and 0.0000, 0.0220, 0.0391, 0.0598, 0.0797, and 0.0989 M 4-cyanobiphenyl in 66.7% DMF respectively. A total of five spectra were obtained for each solution in the Raman flow cell under static conditions. The averages of the five spectra were placed into PyChem software and data regression performed. Row-mean centring and baseline correction of the calibration and reaction data were performed simultaneously. The spectral data between 1530 cm^{-1} and 1640 cm^{-1} was subject to partial least-squares regression (PLSR) accounting for four factors contributing to the Raman signal. The scores for the calibration solutions were used to create calibration plots. Calibration plots of the conversion (%), 4-bromobenzonitrile concentration (M), and 4-cyanobiphenyl concentration (M) were obtained.

GCMS Analysis

The calibration solutions described above were subjected to liquid-liquid extraction with dichloromethane and water. 10 μL of decane (>99%) was added as an internal standard to 400 μL of the standard or sample. Sample preparation required liquid-liquid extraction of the reaction product in CH_2Cl_2 (Analar Grade) with three separate washes in water. This was followed by drying with magnesium sulfate; the samples were filtered and injected directly in the GCMS (Perkin Elmer Gas Chromatograph and a Varian Saturn 2000 mass spectrometer). A Phenomenex Zebron ZB-5 30 m \times 0.25 mm capillary column was used for separation. The separation conditions were split injection (50:1) of a 1 μL extract, helium flow rate of 1 mL min^{-1} , injection temperature of 250°C, initial oven temperature of 50°C with a ramp of 35°C min^{-1} to 70°C and held for 7.43 min, followed by a further ramp of 20°C min^{-1} to 250°C held for 6.00 min. The resulting GC-MS retention times were observed at 6.44 min for decane, 11.13 min for 4-bromobenzonitrile, and 15.35 min for 4-cyanobiphenyl (see Fig. S5 in the Supplementary Material). The mass spectra confirmed these peaks as decane, 4-bromobenzonitrile, and 4-cyanobiphenyl respectively (See Figs 6–8 in the Supplementary Material). PLSR was also performed on the chromatograph between 5 and 20 min for the calibration and the reaction solutions.

Supplementary Material

HPLC pump calibration, Raman spectra and PLS calibration and GCMS data are available on the Journal's website.

Acknowledgements

Financial support from Engineering and Physical Sciences Research Council (EPSRC) grant EP/G027765 is gratefully acknowledged.

References

- [1] B. Ahmed-Omer, J. C. Brandt, T. Wirth, *Org. Biomol. Chem.* **2007**, *5*, 733. doi:10.1039/B615072A
- [2] T. Noel, J. R. Naber, R. L. Hartman, J. P. McMullen, K. F. Jensen, S. L. Buchwald, *Chem. Sci.* **2011**, *2*, 287. doi:10.1039/C0SC00524J
- [3] A. Sniady, M. W. Bedore, T. F. Jamison, *Angew. Chem.* **2011**, *123*, 2203. doi:10.1002/ANGE.201006440
- [4] J. Moorthy, C. Khoury, J. S. Moore, D. J. Beebe, *Sens. Actuators B Chem.* **2001**, *75*, 223. doi:10.1016/S0925-4005(01)00557-3
- [5] K. J. Shaw, P. T. Docker, J. V. Yelland, C. E. Dyer, J. Greenman, G. M. Greenway, S. J. Haswell, *Lab Chip* **2010**, *10*, 1725. doi:10.1039/C000357N
- [6] D. Cantillo, H. Sheibani, C. O. Kappe, *J. Org. Chem.* **2012**, *77*, 2463. doi:10.1021/JO3001645
- [7] Y. Matsushita, N. Ohba, T. Suzuki, T. Ichimura, *Catal. Today* **2008**, *132*, 153. doi:10.1016/J.CATTOD.2007.12.078
- [8] P. He, P. Watts, F. Marken, S. J. Haswell, *Green Chem.* **2007**, *9*, 20. doi:10.1039/B610415K
- [9] Y. Kikutani, T. Kitamori, *Macromol. Rapid Commun.* **2004**, *25*, 158. doi:10.1002/MARC.200300192
- [10] S. Liu, T. Fukuyama, M. Sato, I. Ryu, *Org. Process Res. Dev.* **2004**, *8*, 477. doi:10.1021/OP034200H
- [11] P. He, S. J. Haswell, P. D. I. Fletcher, *Appl. Catal. A Gen.* **2004**, *274*, 111. doi:10.1016/J.APCATA.2004.05.042
- [12] M. Larhed, C. Moberg, A. Hallberg, *Acc. Chem. Res.* **2002**, *35*, 717. doi:10.1021/AR010074V
- [13] N. T. S. Phan, J. Khan, P. Styring, *Tetrahedron* **2005**, *61*, 12065. doi:10.1016/J.TET.2005.07.109
- [14] P. He, S. J. Haswell, P. D. I. Fletcher, S. M. Kelly, A. Mansfield, *Beilstein J. Org. Chem.* **2011**, *7*, 1150. doi:10.3762/BJOC.7.133
- [15] A. de la Hoz, A. Diaz-Ortiz, A. Moreno, *Chem. Soc. Rev.* **2005**, *34*, 164. doi:10.1039/B411438H
- [16] M. N. Slyadnev, Y. Tanaka, M. Tokeshi, T. Kitamori, *Anal. Chem.* **2001**, *73*, 4037. doi:10.1021/AC010318P
- [17] C. D. Smith, I. R. Baxendale, S. Lanners, J. J. Hayward, S. C. Smith, S. V. Ley, *Org. Biomol. Chem.* **2007**, *5*, 1559. doi:10.1039/B702995K
- [18] J. Stripeikis, P. Costa, M. Tudino, O. Troccoli, *Anal. Chim. Acta* **2000**, *408*, 191. doi:10.1016/S0003-2670(99)00881-8
- [19] G. Shore, S. Morin, M. G. Organ, *Angew. Chem.* **2006**, *118*, 2827. doi:10.1002/ANGE.200503600
- [20] J. W. Schoppelrei, M. L. Kieke, X. Wang, M. T. Klein, T. B. Brill, *J. Phys. Chem.* **1996**, *100*, 14343. doi:10.1021/JP960396U
- [21] J. A. Banister, P. D. Lee, M. Poliakoff, *Organometallics* **1995**, *14*, 3876. doi:10.1021/OM00008A039
- [22] D. Ferri, A. Baiker, *Top. Catal.* **2009**, *52*, 1323. doi:10.1007/S11244-009-9310-5
- [23] A. Ruiz-Medina, E. J. Llorent-Martínez, *J. Pharm. Biomed. Anal.* **2010**, *53*, 250. doi:10.1016/J.JPBA.2010.04.020
- [24] S. Xu, W. Zhang, X. Liu, X. Han, X. Bao, *J. Am. Chem. Soc.* **2009**, *131*, 13722. doi:10.1021/JA904304H
- [25] P. D. I. Fletcher, S. J. Haswell, X. Zhang, *Electrophoresis* **2003**, *24*, 3239. doi:10.1002/ELPS.200305532
- [26] C. F. Carter, H. Lange, S. V. Ley, I. R. Baxendale, B. Wittkamp, J. G. Goode, N. L. Gaunt, *Org. Process Res. Dev.* **2010**, *14*, 393. doi:10.1021/OP900305V
- [27] S. Farquharson, W. Smith, R. M. Carangelo, C. Brouillette, *Proc. SPIE* **1999**, *3859*, 14. doi:10.1117/12.372937
- [28] S. Mozharov, A. Nordon, D. Littlejohn, C. Wiles, P. Watts, P. Dallin, J. M. Girkin, *J. Am. Chem. Soc.* **2011**, *133*, 3601. doi:10.1021/JA1102234
- [29] R. J. Ampiah-Bonney, A. D. Walmsley, *Analyst (Lond.)* **1999**, *124*, 1817. doi:10.1039/A907200D
- [30] A. Fiedler, M. Baranska, H. Schulz, *J. Raman Spectrosc.* **2011**, *42*, 551. doi:10.1002/JRS.2726
- [31] K. J. Laidler, J. H. Meiser, B. C. Sanctuary, *Physical Chemistry* **2003**, 4th edn (Houghton Mifflin: Boston, MA).

Integrated RNA extraction and RT-PCR for semi-quantitative gene expression studies on a microfluidic device

Kirsty J Shaw¹, Elizabeth M Hughes², Charlotte E Dyer³, John Greenman³ and Stephen J Haswell⁴

This paper describes the development of a microfluidic methodology, using RNA extraction and reverse transcription PCR, for investigating expression levels of cytochrome P450 genes. Cytochrome P450 enzymes are involved in the metabolism of xenobiotics, including many commonly prescribed drugs, therefore information on their expression is useful in both pharmaceutical and clinical settings. RNA extraction, from rat liver tissue or primary rat hepatocytes, was performed using a silica-based solid-phase extraction technique. Following elution of the purified RNA, amplification of target sequences for the housekeeping gene, glyceraldehyde-3-phosphate dehydrogenase (GAPDH) and the cytochrome P450 gene CYP1A2, was carried out using a one-step reverse transcription PCR. Once the microfluidic methodology had been optimized, analysis of control and 3-methylcholanthrene-induced primary rat hepatocytes were used to evaluate the system. As expected, GAPDH was consistently expressed, whereas CYP1A2 levels were found to be raised in the drug-treated samples. The proposed system offers an initial platform for development of both rapid throughput analyzers for pharmaceutical drug screening and point-of-care diagnostic tests to aid provision of drug regimens, which can be tailor-made to the individual patient.

Laboratory Investigation (2013) **93**, 961–966; doi:10.1038/labinvest.2013.76; published online 27 May 2013

KEYWORDS: diagnostic; metabolism; microfluidics; point-of-care

Cytochrome P450 enzymes (P450s) are a superfamily of haem-containing monooxygenase enzymes, which have specific roles in numerous metabolic and synthetic pathways.¹ P450s are the major enzymes involved in phase I metabolism of xenobiotics, ie, any foreign chemicals that can be introduced into an organism, including deliberately administered pharmaceutical agents.² Phase I metabolism involves the oxidation, hydroxylation, reduction, and hydrolysis of drug molecules making them more water soluble for easy removal from the body. P450 enzymes, as well as metabolizing drugs, are also involved in drug–drug interactions, in which induction or inhibition of P450 expression can result in a greater production of toxic metabolites, or a decrease in efficacy of a drug due to increased clearance.¹ There are situations in which, instead of assisting in the elimination of drugs, P450s can activate prodrugs or procarcinogens, causing them to become toxic.³ This is the case with polycyclic aromatic hydrocarbons (PAHs), which

are found in compounds such as tar. PAHs by themselves cannot damage DNA, but once hydroxylated by P450 they become activated and have a carcinogenic role.⁴

Measuring P450 gene expression levels can be beneficial in the development and administration of pharmaceutical drugs. For example, the levels of P450 enzymes found in cells after exposure to a new drug could indicate the likely outcome of that drug due to a fast metabolism of the drug, or its conversion to undesirable by-products. Specifically, an individual patient's likely response to a particular drug could be determined before use through testing on a biopsy taken from the patient. A tailored dosage could then be administered taking into consideration the metabolic effects of the P450 enzymes, and reducing the risk of any adverse effects to the patient.⁵

CYP1A2 is a cytochrome P450 enzyme associated with the metabolism of a number of clinically relevant drugs, such as clozapine (an antipsychotic), which is released from the cell

¹School of Science and the Environment, Manchester Metropolitan University, Manchester, UK; ²Hull York Medical School, Hull, UK; ³Department of Biology, University of Hull, Hull, UK and ⁴Department of Chemistry, University of Hull, Hull, UK
Correspondence: Dr KJ Shaw, PhD, School of Science and the Environment, Manchester Metropolitan University, Chester Street, Manchester M1 5GD, UK.
E-mail: k.shaw@mmu.ac.uk

Received 8 April 2013; revised 6 May 2013; accepted 7 May 2013

under the induction of various chemicals. One way in which P450 induction can be assessed is via the 7-ethoxyresorufin O-dealkylation (EROD) assay.⁶ In this assay, 7-ethoxyresorufin is converted, by CYP1A2, to resorufin that can then be quantified fluorescently.⁷ Hepatotoxicity studies have been carried out previously within a microfluidic environment using *in situ* quantification of the fluorescent intensity of cells and their surrounding media via the EROD assay to compare CYP1A2 expression in control and 3-methylcholanthrene (3-MC)-induced primary rat hepatocytes.⁸ Assessment of the catalytic action of CYP1A2 provides information as to the action of the protein but does not measure gene expression levels. Information about changes to specific gene expression levels, in response to certain conditions, can only be obtained by analyzing levels of messenger RNA (mRNA).

To obtain this information, mRNA must first be extracted from the biological matrix that is being investigated. The purified mRNA is then converted to complementary DNA (cDNA) by a reverse transcriptase enzymatic reaction. The cDNA can then be amplified using the PCR, which enables either end-point or real-time detection.

The increasing ability to miniaturize laboratory techniques onto a 'Lab-on-a-Chip' format using microfluidic technology has opened the door to many varied and far-reaching applications. It is now possible to integrate reactions in a way not possible before, so that instead of products being moved from one reaction vessel to another, risking contamination and loss of product, two or more reactions can happen on the same enclosed microfluidic device.⁹

Although nucleic acid analysis on microfluidic devices has received great interest in the literature, the majority of publications are focussed on DNA presumably because of the less-stable nature of RNA and its susceptibility to RNases. However, analysis of RNA is vital for gene expression studies. Total RNA can be extracted from biological samples using a solid-phase matrix to which nucleic acids bind under selective conditions. The most common methods involve either a silica- or anion exchange-based solid phase. When using silica, nucleic acids bind to the solid phase in the presence of a chaotropic salt such as guanidine hydrochloride, and unbound contaminants are then removed with an alcohol wash before the purified nucleic acids are eluted in a low ionic strength buffer.¹⁰ Chitosan is an example of an anion exchange matrix that can be used to bind nucleic acids in solution at pH 5 and elute them at pH 9 once unbound contaminants have been removed.¹¹ Alternatively, mRNA can be isolated via the poly(A) tail using tethered poly(T) sequences, eg, directly immobilized onto the channel surface¹² or on superparamagnetic beads enabling the captured mRNA sequences to be manipulated around the microfluidic device using an external magnet.¹³ More recent developments have enabled even more selective extraction of RNA using sequence-specific probes. Root *et al*¹⁴ presented an innovative method for the purification of RNA from serum using a polymer capture matrix containing covalently

bound oligonucleotides. The capture, wash, and elution of target RNA sequences were controlled by electrophoresis, with an additional heating step required for elution.

A variety of amplification methods have been applied to microfluidic devices to analyze RNA. Amplification of RNA viruses, as well as the more traditional single chamber for aqueous RT-PCR, has been achieved using both continuous flow¹⁵ and solid-phase microarrays.¹⁶ Isothermal techniques, such as nucleic acid sequence-based amplification¹⁷ and loop-mediated isothermal amplification,¹⁸ have also been successfully used.

The integration of RNA purification and amplification processes is a challenge that has led to the development of a number of inventive solutions. For example, Pippier *et al*¹⁹ used a series of aqueous droplets in oil on a perfluorinated surface. Silica-coated superparamagnetic particles were incubated with a biological sample and then dragged through droplets containing wash and elution reagents for RT-PCR before amplification and real-time detection. Lateral flow strips have also been incorporated into a microfluidic device for detection of RT-PCR products for HIV.²⁰ Amplicons are labeled with digoxigenin and biotin that bind to immobilized streptavidin and are then detected using up-converting phosphor reporter particles. Another alternative approach was presented by Ferguson *et al*²¹ who used immunomagnetic target capture combined with sequence-specific electrochemical detection for identification of the H1N1 influenza virus from throat swab samples within 3½ h.

Microfluidic devices provide a biomimetic microenvironment that allows tissue samples/biopsies to be maintained for up to 8 days.^{22,23} This enables investigation of the tissue as a whole or of individual cells following disaggregation.²⁴ Here we demonstrate the integration of RNA extraction with RT-PCR on a single microfluidic device that could be used for the analysis of tissue samples. CYP1A2 gene expression levels, from 3-MC-induced and non-induced cell populations, were compared with gene expression levels of glyceraldehyde-3-phosphate dehydrogenase (GAPDH) as an internal control.

MATERIALS AND METHODS

Preparation of Microfluidic Devices

The microfluidic device used was made of borosilicate glass and prepared using standard photolithography and wet etching techniques to produce the design shown in Figure 1. The etched bottom plate was then thermally bonded to a top plate containing 360 µm holes drilled to act as inlets and outlets for the channels.

The internal surfaces of the microfluidic device were silanized to minimize DNA polymerase adsorption. The channels were washed overnight with 10% (w/v) NaOH, then sequentially with 10 ml water and ethanol before being dried thoroughly in an oven at 90 °C. Sigmacote (Sigma-Aldrich, UK) was then applied to the channels for 5 min, following which the microfluidic devices were dried in an oven for 30 min. Porous thermally activated silica monoliths were

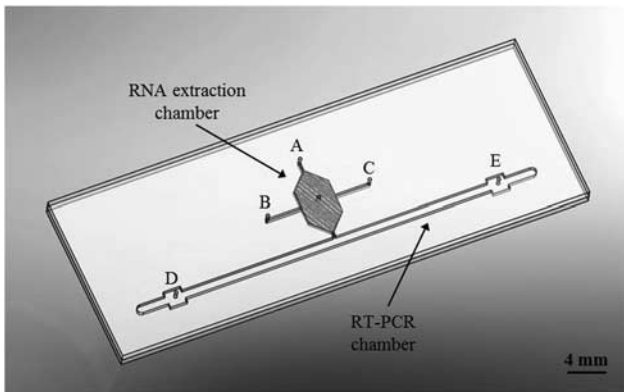


Figure 1 Schematic diagram of the microfluidic device used for the integration of RNA extraction and RT-PCR. All features were etched to a depth of 500 μm . (a) Monolith solution inlet. (b) Sample, wash and elution reagent inlet. (c) Waste outlet. (d) PCR reagent inlet. (e) Waste outlet.

generated in the RNA-extraction chamber. The monoliths were made from potassium silicate (K_2SiO_3 (21% SiO_2 , 9% K_2O)) (VWR International, UK) and formamide (Alfa Aesar, UK) in a 10:1 ratio, and cured in an oven overnight at 90 $^\circ\text{C}$.²⁵ The monoliths generated are contained within the hexagonal RNA-extraction chamber. Porous silica monoliths have been shown to contain both micron and nm-scale pores, resulting in *facile* flow of solutions through the micron pores and generation of a large surface area for reactions due to the nm-scale pores.²⁶ In this instance, the micron pores have an average diameter of 1.6 μm (Supplementary Material, Supplementary Figure S1). Agarose gel encapsulated RT-PCR reagents were then filled into half of the PCR chamber and the microfluidic device stored at 4 $^\circ\text{C}$ until required.²⁷

Sample Preparation

Experiments used either rat liver tissue or primary rat hepatocytes. Male Wistar rats were housed under standard conditions. All animals were fed and watered *ad libitum* until anaesthetized and killed under schedule 1 procedure for liver extraction. Total hepatectomy was performed, and tissue sections of approximately 1 mm^3 were stabilized in RNAlater solution (Qiagen, UK) to prevent degradation of RNA and were stored at -20°C . Control and 3-MC-induced primary rat hepatocytes were provided by LGC (Teddington, UK) and were stored in Trizol (Invitrogen, UK) at -80°C until required.

Conventional RNA Extraction

All solutions were prepared using diethylpyrocarbonate (Sigma-Aldrich) treated water. RNA extraction was carried out from the stabilized liver tissue, following the Qiagen RNeasy Mini Kit (Qiagen) protocol. Briefly, tissue sections were homogenized in RLT buffer supplemented with 2 M dithiothreitol (Fluka, UK) using a 1 ml syringe and a needle. Homogenized cells were applied to an RNeasy spin column, washed, and then eluted in 50 μl of water and stored at

-20°C until required. RNA extraction from primary rat hepatocytes ($\sim 0.4 \times 10^6$ cells) was carried out using conventional Trizol methodology.

Microfluidic RNA Extraction

Before sample addition, the monoliths were pretreated with 10 mM TE buffer (10 mM Tris, 1 mM EDTA, adjusted to pH 6.7), which was hydrodynamically pumped through at 5 $\mu\text{l}/\text{min}$. Rat liver tissue (1 mm^3) or primary hepatocytes ($\sim 0.4 \times 10^6$ cells) were homogenized in 40 μl 5 M guanidine hydrochloride (Sigma-Aldrich) in 10 mM TE buffer, and then pumped through the monolith at 2.5 $\mu\text{l}/\text{min}$. The optional addition of DNase I (Invitrogen) to this lysis/binding buffer was also evaluated. A 50 μl solution of 80% (v/v) isopropanol (Sigma-Aldrich) was then used to wash the monolith and remove cellular debris and potential contaminants of downstream processes. The concentrated RNA was eluted from the monolith using 50 μl of water at a flow rate of 1 $\mu\text{l}/\text{min}$. Fractions of 5 μl were continuously collected throughout the extraction procedure for RNA quantification and downstream analysis using RT-PCR.

RNA Quantification

RNA quantification was carried out using a Nanodrop spectrometer (ThermoScientific, UK) using 1 μl aliquots taken from each collected fraction.

RT-PCR

Intron spanning primers were used for GAPDH and CYP1A2 to facilitate amplification of transcribed mRNA and not genomic DNA (Table 1). GAPDH primers were previously published,¹ whereas CYP1A2 primers were designed using Primer-BLAST software and synthesized *de novo*. GAPDH, a housekeeping gene, was used as a positive control because of its constitutive expression.

A one-step RT reaction and PCR were combined for generation of cDNA and subsequent amplification. RT-PCR was carried out using the following reagent mixture: 2.5 μM forward primers, 2.5 μM reverse primers, 0.5 μM probes, 1 \times M-MLV reaction buffer, 200 U M-MLV reverse transcriptase, 200 μM each deoxyribonucleotides, 2 mM MgCl_2 , 20 $\mu\text{g}/\text{ml}$ bovine serum albumin, and 0.2 U GoTaq DNA polymerase (Promega, UK).

After the RNA was eluted from the monolith, the inlets/outlets of the microfluidic device were covered with a drop of mineral oil to prevent evaporation of reagents during thermal cycling. The microfluidic device was placed on a thermoelectric Peltier element, which provided heating and cooling for RT-PCR. Control samples were run on a conventional TC-312 (Techne, UK) thermal cycler. All samples were run under the following conditions: reverse transcription (70 $^\circ\text{C}$ for 5 min, 4 $^\circ\text{C}$ for 30 s, and 37 $^\circ\text{C}$ for 15 min) and PCR (28 cycles of 94 $^\circ\text{C}$ for 30 s, 59 $^\circ\text{C}$ for 30 s, and 72 $^\circ\text{C}$ for 30 s). Amplified samples were analyzed either by agarose gel electrophoresis or capillary gel electrophoresis.

Table 1 Primer sequences for GAPDH and CYP1A2

Target	Sequence (5' – 3')	Product size
GAPDH (forward)	5'-FAM-CAAGGTCATCCATGACAACCTTTG-3'	91 bp
GAPDH (reverse)	5'-GGGCCATCCACAGTCTCTCTG-3'	
CYP1A2 (forward)	5'-JOE-ACAGCACAACGAGGGACAC-3'	129 bp
CYP1A2 (reverse)	5'-CTCTGGGCGGAACACAAA-3'	

Gel Electrophoresis

Products of RT-PCR were analyzed using agarose gel electrophoresis. Agarose gels of 2% (w/v) concentration were made in $0.5 \times$ Tris/Borate/EDTA buffer. Loading dye was added to the RT-PCR products before being run at 120 V for 90 min alongside Hyperladder II (BioLine, UK) for comparison. Ethidium bromide at a concentration of $0.5 \mu\text{g/ml}$ (CLP, US) was used to stain the DNA for visualization using a UV transilluminator.

RT-PCR products were alternatively analyzed using a standard procedure on a Capillary Gel Electrophoresis CEQ 8000 Genetic Analyser (Beckman-Coulter, UK).

RESULTS

RNA Extraction

As silica is known to bind all nucleic acids, DNase I was used to remove any potentially contaminating DNA and maximize RNA-extraction efficiency. This was carried out by adding DNase I, at a range of $0.01\text{--}10 \text{ mg/ml}$, to the binding buffer. Optimization of this process showed that a concentration of 1 mg/ml removed the maximum amount of DNA (data not shown).

Preconditioning of the silica monolith using 10 mM TE buffer, pH 6.7, was performed in order to confer the most appropriate level of protonation to the surface in order to maximize nucleic acid adsorption/desorption²⁸. A 30-min conditioning step was found to be optimal as it resulted in maximal RNA yields during the elution phase, approximately 32% greater total yield than with no preconditioning (Figure 2). Longer incubation times, 60 min, resulted in loss of RNA during the washing phase, suggesting an inefficient binding process.

Following optimization of the RNA-extraction process on the proposed microfluidic system, whole tissue was homogenized directly in the lysis/binding buffer and RNA extracted. RNA was successfully extracted from rat liver tissue using this technique, and the eluted fractions are shown to be of sufficient quantity and quality for amplification using RT-PCR on the microfluidic device (Figure 3).

RT-PCR

Combined RT-PCR for multiplex amplification was optimized on the benchtop and then transferred onto the microfluidic system. Successful amplification of both

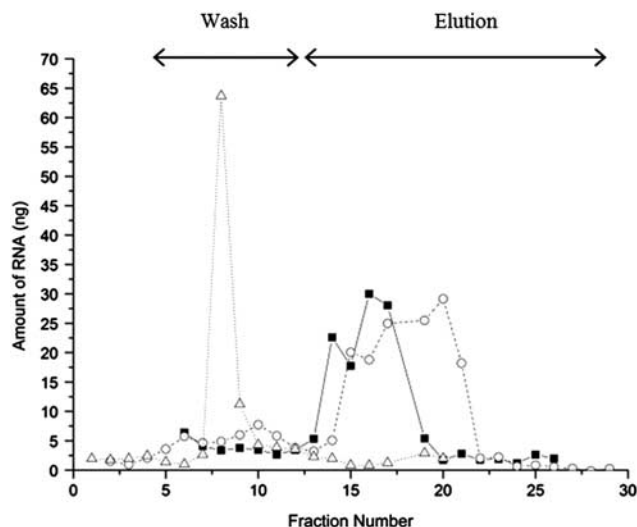


Figure 2 Graph showing an example of the RNA-elution profile results obtained when the monolith was subjected to different preconditioning times of 0 (—■—), 30 (---○---), and 60 min (···Δ···) ($n=3$ for each condition tested).

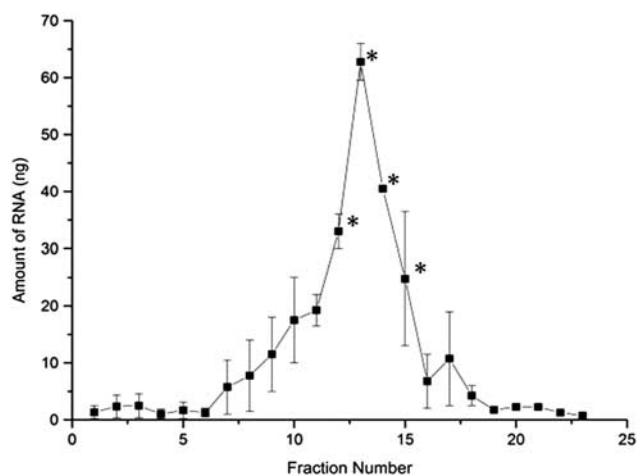


Figure 3 Graph showing average elution profile from RNA extracted from rat liver tissue on a microfluidic device. *Denotes samples that were successfully amplified by RT-PCR ($n=3$).

targets was demonstrated on the microfluidic device as demonstrated by the generation of PCR products of the expected sizes for GAPDH and CYP1A2 (Figure 4).

Process Integration on a Microfluidic Device

To facilitate integration of the RNA extraction and RT-PCR process on a single microfluidic device, the RT-PCR reagents were encapsulated in a 1.5% (w/v) agarose gel and filled into half of the amplification chamber. Once the RNA was eluted from the monolith, the flow was directed toward the amplification chamber, whereupon it filled the second half of the amplification chamber. The inlets and outlets of the microfluidic device were then covered with a layer of mineral oil to

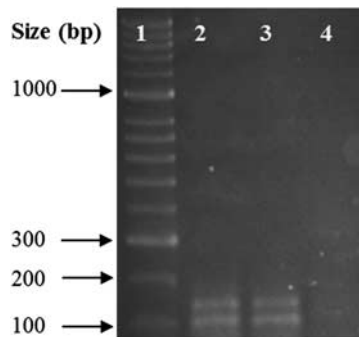


Figure 4 Gel electropherogram showing RT-PCR products: (1) DNA size ladder; (2) positive control samples amplified on a conventional thermal cycler; (3) RT-PCR samples amplified on the microfluidic device, GAPDH (91 bp), and CYP1A2 (129 bp); and (4) negative control ($n=3$).

prevent evaporation. Upon the initial reverse transcription heating step, the agarose gel melts to release the RT-PCR reagents, which combine with the eluted RNA. Following amplification on the microfluidic device, RT-PCR products were analyzed by capillary gel electrophoresis, and the relative fluorescent intensities of the products were compared to enable qualitative analysis of the end-point RT-PCR. This technique was successfully used to compare basal gene expression levels of CYP1A2 with those induced by 3-MC, using GAPDH as a constitutively expressed control (Figure 5). As expected, treatment with 3-MC led to induction of CYP1A2 resulting in increased gene expression levels; $P=0.008$, two-tailed paired t -test, which was in agreement with Baldwin *et al.*¹

DISCUSSION

The ability to monitor drug effects on tissue samples using a microfluidic system offers numerous advantages over conventional drug-examination methods. First, multiple experiments could be carried out on a single biopsy sample, reducing the number of animals required for basic research or enabling a patient biopsy to be used enabling individually tailored medications and treatment plans to be devised.^{5,29} Furthermore, as the effect of the drug can be monitored not only at an observable cellular level but also at the level of gene expression, the pharmacological effect can be monitored looking at potential unwanted side effects caused by the activation of prodrugs or carcinogens. Integration of the proposed system with other techniques, such as the EROD assay, would allow more information to be obtained from individual biopsy samples, eg, protein activity and gene expression levels, in the development of techniques for patient-specific treatments. Most important is the ability to integrate analysis directly from a biopsy of tissue. This allows direct interrogation in the most appropriate manner depending on the type of analysis to be performed, allowing extraction and quantification of the mRNA within approximately 100 min from the time of sample input

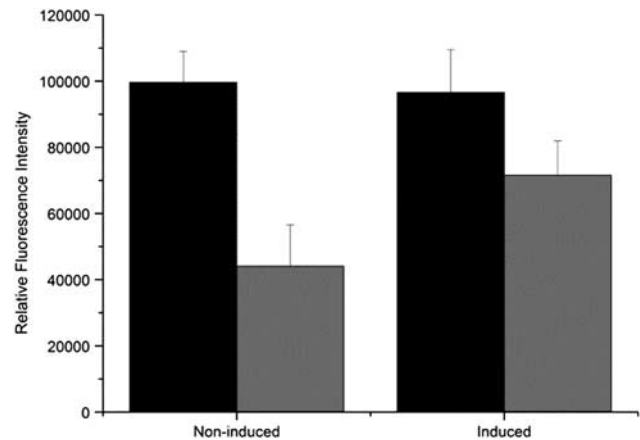


Figure 5 Comparison of 3-MC-induced and non-induced primary rat hepatocytes as extracted and amplified for GAPDH (black) and CYP1A2 (gray) using the integrated microfluidic system ($n=3$). A statistically significant difference in CYP1A2 induction by 3-MC was observed.

into the microfluidic device. Integration minimizes contamination and loss of sample, making the whole process more reliable and applicable to small samples—useful in many clinical settings where the tissue is often limited. In addition to measuring changes in mRNA expression, the tissue-based microfluidic system can be coupled to other ‘downstream’ analysis modules, eg, spectrophotometric/fluorescent detection of protein release,³⁰ individual cells can be liberated and changed to the cell surface analyzed by on-chip flow cytometry,²⁴ and oligonucleotide hybridization arrays can be used to assess global changes in gene expression.³¹ The combination of these technologies together with the RT-PCR described here has the potential to offer a new platform technology for studying normal or diseased tissue.

Supplementary Information accompanies the paper on the Laboratory Investigation website (<http://www.laboratoryinvestigation.org>)

ACKNOWLEDGEMENTS

The authors would like to thank Dr Steve Clark for fabrication of the microfluidic devices, LGC for providing rat hepatocytes, and HYMS for funding.

DISCLOSURE/CONFLICT OF INTEREST

The authors declare no conflict of interest.

1. Baldwin SJ, Bramhall JL, Ashby CA, *et al*. Cytochrome P450 gene induction in rats *ex vivo* assessed by quantitative real-time reverse transcriptase-polymerase chain reaction (taqman). *Drug Metab Dispos* 2006;34:1063–1069.
2. Ek M, Soderdahl T, Kupperts-Munther B, *et al*. Expression of drug metabolizing enzymes in hepatocyte-like cells derived from human embryonic stem cells. *Biochem Pharmacol* 2007;74:496–503.
3. Baudoin R, Corlu A, Griscorn L, *et al*. Trends in the development of microfluidic cell biochips for *in vitro* hepatotoxicity. *Toxicol In Vitro* 2007;21:535–544.

4. Xue W, Warshawsky D. Metabolic activation of polycyclic and heterocyclic aromatic hydrocarbons and DNA damage: A review. *Toxicol Appl Pharmacol* 2005;206:73–93.
5. Bates S. Progress towards personalized medicine. *Drug Discov Today* 2010;15:115–120.
6. Vakharia DD, Liu N, Pause R, *et al*. Effect of metals on polycyclic aromatic hydrocarbon induction of CYP1A1 and CYP1A2 in human hepatocyte cultures. *Toxicol Appl Pharmacol* 2001;170:93–103.
7. Kennedy SW, Jones SP, Bastien LJ. Efficient analysis of cytochrome P450A catalytic activity, porphyrins, and total proteins in chicken embryo hepatocyte cultures with a fluorescence plate reader. *Anal Biochem* 1995;226:362–370.
8. Anderson K, Cooper JM, Haswell SJ, *et al*. Microfluidic-based measurements of cytochrome P450 enzyme activity of primary mammalian hepatocytes. *Analyst* 2010;135:1282–1287.
9. Whitesides GM. The origins and the future of microfluidics. *Nature* 2006;442:368–373.
10. Wang C, Kim T, Gao D, *et al*. Rapid high-yield mRNA extraction for reverse-transcription PCR. *J Biochem Biophys Methods* 2006;70:507–509.
11. Hagan KA, Meier WL, Ferrance JP, *et al*. Chitosan-coated silica as a solid phase for RNA purification in a microfluidic device. *Anal Chem* 2009;81:5249–5256.
12. Hughes-Chinkhota CN, Banda M, Smolinski JM, *et al*. Oligonucleotide immobilization using 10-(carbomethoxy)decyl- dimethylchlorosilane for mRNA isolation and cDNA synthesis on a microfluidic chip. *Sensors Actuators B: Chem* 2011;155:437–445.
13. Jiang GF, Harrison DJ. mRNA isolation in a microfluidic device for eventual integration of cDNA library construction. *Analyst* 2000;125:2176–2179.
14. Root BE, Agarwal AK, Kelso DM, *et al*. Purification of HIV RNA from serum using a polymer capture matrix in a microfluidic device. *Anal Chem* 2011;83:982–988.
15. Li Y, Zhang C, Xing D. Fast identification of foodborne pathogenic viruses using continuous-flow reverse transcription-PCR with fluorescence detection. *Microfluid Nanofluid* 2011;10:367–380.
16. Sun Y, Dhumpa R, Bang DD, *et al*. A lab-on-a-chip device for rapid identification of avian influenza viral RNA by solid-phase PCR. *Lab on a Chip* 2011;11:1457–1463.
17. Dimov IK, Garcia-Cordero JL, O'Grady J, *et al*. Integrated microfluidic tmRNA purification and real-time NASBA device for molecular diagnostics. *Lab on a Chip* 2008;8:2071–2078.
18. Wang CH, Lien KY, Wang TY, *et al*. An integrated microfluidic loop-mediated-isothermal-amplification system for rapid sample pre-treatment and detection of viruses. *Biosens Bioelectron* 2011;26:2045–2052.
19. Pipper J, Inoue M, Ng LF-P, *et al*. Catching bird flu in a droplet. *Nat Med* 2007;13:1259–1263.
20. Chen D, Mauk M, Qiu X, *et al*. An integrated, self-contained microfluidic cassette for isolation, amplification, and detection of nucleic acids. *Biomed Microdevices* 2010;12:705–719.
21. Ferguson BS, Buchsbaum SF, Wu TT, *et al*. Genetic analysis of H1N1 influenza virus from throat swab samples in a microfluidic system for point-of-care diagnostics. *J Am Chem Soc* 2011;133:9129–9135.
22. Hattersley SM, Dyer CE, Greenman J, *et al*. Development of a microfluidic device for the maintenance and interrogation of viable tissue biopsies. *Lab on a Chip* 2008;8:1842–1846.
23. Hattersley SM, Sylvester DC, Dyer CE, *et al*. A microfluidic system for testing the responses of head and neck squamous cell carcinoma tissue biopsies to treatment with chemotherapy drugs. *Ann Biomed Eng* 2012;40:1277–1288.
24. Woods J, Docker PT, Dyer CE, *et al*. On-chip integrated labelling, transport and detection of tumour cells. *Electrophoresis* 2011;32:3188–3195.
25. Oakley JA, Shaw KJ, Docker PT, *et al*. Development of a bi-functional silica monolith for electro-osmotic pumping and DNA clean-up/extraction using gel-supported reagents in a microfluidic device. *Lab on a Chip* 2009;9:1596–1600.
26. Fletcher PDI, Haswell SJ, He P, *et al*. Permeability of silica monoliths containing micro- and nano-pores. *J Porous Mater* 2011;18:501–508.
27. Shaw KJ, Joyce DA, Docker PT, *et al*. Development of a real-world direct interface for integrated DNA extraction and amplification in a microfluidic device. *Lab on a Chip* 2011;11:443–448.
28. Melzak KA, Sherwood CS, Turner RFB, *et al*. Driving forces for DNA adsorption to silica in perchlorate solutions. *J Colloid Interface Sci* 1996;181:635–644.
29. Shaw KJ, Birch C, Hughes EM, *et al*. Microsystems for personalized biomolecular diagnostics. *Eng Life Sci* 2011;11:121–132.
30. Martino C, Zagnoni M, Sandison ME, *et al*. Intracellular protein determination using droplet-based immunoassays. *Anal Chem* 2011;83:5361–5368.
31. Demarest TG, Murugesan N, Shrestha B, *et al*. Rapid expression profiling of brain microvascular endothelial cells by immuno-laser capture microdissection coupled to TaqMan[®] low density array. *J Neurosci Methods* 2012;206:200–204.